東京帝國大學

地震研究所彙報

第15號

昭和12年

BULLETIN

OF THE

EARTHQUAKE RESEARCH INSTITUTE

TOKYO IMPERIAL UNIVERSITY

Vol. XV

1937

目　次

第 15 號

第1册（昭和12年3月）

			頁
1.	半無限體の振動に於ける共振現象及び逸散波（英文）…	妹澤克惟 金井清	1
2.	球窩面の振動に於ける共振現象及び逸散波（英文）……	妹澤克惟 金井清	13
3.	構造物の震動を防止する一つの方法（英文）……………	妹澤克惟 金井清	21
4.	五重塔の耐震性に關する研究（英文）…………………	妹澤克惟 金井清	33
5.	彈性波の生成及び傳播に關する實驗（英文）……………	木下潤一	41
6.	淺間火山近傍に於ける重力偏差の觀測（其1）（英文）…	水上武	50
7.	振動方法による土の彈性測定第2報剛性率及びポアソン比の測定（英文）…………………………	石本巳四雄 飯田汲事	67
8.	土壤層中に於ける人工地震波の傳播並に土壤の彈性に關する研究（其2）（邦文）…………………………	那須信治 萩原尊禮 表俊一郎	87
9.	發震機構に就いて（第II報）（英文）……………………	井上宇胤	90
10.	江東地域に於ける地盤沈下の原因に就て（I）（英文）……	宮部直巳	102
11.	昭和11年6月19日の日食時に於ける地電流の觀測（英文）…………………………	高橋龍太郎	109
12.	伊豆，熱海溫泉に就て（英文）………………………	福富孝治	113
13.	淺間山麓千ケ瀧溫泉と地下水（英文）…………………	水上武	134
14.	地震回數の統計的研究（英文）………………………	井上宇胤	142
15.	世界に於ける深層地震の分布（英文）…………………	山口生知	170
16.	昭和11年11月3日金華山沖地震被害調査報告（邦文）…	高山威雄	179
17.	磁氣伏角變化計（英文）………………………………	永田武	185
18.	房總半島に於ける一デツケン構造（英文）……………	大塚彌之助	193
19.	日本群島附近の古第三紀の海岸線の變化（邦文）………	大塚彌之助	198

20. 富士火山帶の火山活動，特に伊豆及び南方諸島の地質及び岩石に就いて（英文）…………………………… 津屋弘逵 215

第2冊（昭和12年6月）

21. 地表層が鉛直荷重を受ける場合の彈性的變形分布に就て（英文）…………………………… 妹澤克惟 金井清 359
22. 震源に於ける異型の發振に伴ふその同型の定常振動（英文）…………………………… 妹澤克惟 金井清 370
23. 斜のディスターバンスによつて誘起する表面層の自由振動に就で（英文）…………………………… 妹澤克惟 金井清 385
24. 橋梁の振動に於ける勢力の逸散性（第1報）（英文）……… 妹澤克惟 金井清 385
25. 斜めの入射波による表面層の振動とその共振れ性質（英文）…………………………… 西村源六郎 高山威雄 394
26. 伊豆大島三原火山の地球物理學的研究，火口の地形測量及大島磁氣測定（英文）…………………………… 高橋龍太郎 水上武 441
27. 最近の淺間火山の活動と地表傾斜變化（英文）………… 高橋龍太郎 水上武 463
28. 最近の活動に伴へる淺間火山の火口底深さの變化（英文）…………………………… 水上武 492
29. 新島地震前後に於る，同地方磁氣伏角測定値の比較（邦文）…………………………… 永田武 497
30. 伊豆伊東溫泉に就て（邦文）…………………………… 福富孝治 藤井次郎 506
31. 震央距離の比較的大なる地震による東京近傍卓越振動周期（邦文）…………………………… 石本巳四雄 536
32. 土の收縮に關する二三の實驗（邦文）…………………… 飯田汲事 544
33. 昭和11年12月27日伊豆新嶋地震餘震觀測並に踏査報告（邦文）…………………………… 萩原尊禮 表俊一郎 559
34. 大分縣坂の市—鹿兒島縣伊集院村間並に宮崎縣細島町—熊本縣熊本市間の水準改測結果（邦文）…………………………… 569

第3冊（昭和12年9月）

35. 地表層の厚さとラブ波の振幅との關係（英文）………… 妹澤克惟 金井清 577
36. 地球の核のプラスチック性に就て（英文）……………… 妹澤克惟 582
37. 橋梁の振動に於ける勢力の逸散性（第2報）（英文）…… 妹澤克惟 金井清 590

38. 構造物震動の力學的制振法の模型實驗的確め（英文）…… 妹澤克惟 金井清 598

39. 彈性體內に在る球狀空窩の內面に作用する壓力變化によつて生ずる彈性波（英文）…… 西村源六郎 614

40. 重力と地下構造との關係（英文）…… 坪井忠二 淵田隆門 636

41. 鉛直線偏倚，ジオイドの凹凸と重力異常（英文）…… 坪井忠二 650

42. 丹後地方の地殼變形研究補遺（英文）…… 宮部直巳 654

43. 淺間及三原火山熔岩の物理的性質
I. 電氣傳導度及び其の溫度變化（英文）…… 永田武 663

44. 發震機構に就いて（第3報）（英文）…… 井上宇胤 674

45. 發震機構に就いて（第4報）（英文）…… 井上宇胤 686

46. 東京地方微動の觀測（佛文）…… 石本巳四雄 697

47. 所謂椋平虹に就て（英文）…… 藤原咲平 706

48. 日本に於ける地震發生の一年變化（獨文）…… 松澤武雄 仲町容 西川與志男 吉村慶丸 711

49. 昭和5年伊東地震群の頻度分布（英文）…… 岸上冬彥 785

50. 丸の內に於ける表面土と基盤岩との彈性係數測定（邦文）…… 飯田汲事 828

51. 昭和11年11月3日の三陸地方の地震に伴つた津浪（英文）…… 宮部直巳 837

第4冊（昭和12年12月）

52. 地表層の厚さと分散性レーレー波の振幅との關係（英文）…… 妹澤克惟 金井清 845

53. 極座標上から出した地球の彈性的安定の問題（英文）…… 妹澤克惟 金井清 860

54. 重力を受ける地球のプラスチツク釣合（英文）…… 妹澤克惟 878

55. 振動性津浪の卓越周期（英文）…… 妹澤克惟 金井清 888

56. 昭和5年11月26日の北伊豆烈震に伴へる同地方の地殼變動（英文）…… 山口生知 899

57. 琵琶湖の水位に就いて（英文）…… 坪井忠二 935

58. 車輛，航空機用加速度計の製作（邦文）…… 萩原尊禮 945

59. 發震機構に就いて（訂正）（英文）…… 井上宇胤 956

60. 本郷に於ける観測より推定し得たる地殼表層の配列（第1報）（英文）…………………… 木下潤一 965

61. 關東地方南部の地質構造（I）〔横濱—藤澤間〕（邦文）… 大塚彌之助 974

62. 日本の第三紀皺曲帶の或る地質學的考察（豫報）（英文）…………………… 大塚彌之助 1041

63. 伊豆大島三原火山の地球物理學的研究，火口内の物理的性質の概況（英文）…………………… {高橋龍太郎 永田武} 1047

Contents.

Vol. XV.

Part 1.—March, 1937.

Page

1. K. SEZAWA and K. KANAI, Resonance Phenomena and Dissipation Waves in the Stationary Vibrations of a Semi-infinite Body. (in English) 1
2. K. SEZAWA and K. KANAI, Resonance Phenomena and Dissipation Waves in the Stationary Vibration of the Surface of a Spherical Cavity. (in English) 13
3. K. SEZAWA and K. KANAI, A Method of Minimizing the Seismic Vibrations of a Structure. (in English) 21
4. K. SEZAWA and K. KANAI, Further Studies on the Seismic Vibrations of a Gozyûnotô (Pagoda) (in English) 33
5. Z. KINOSITA, Some Experiments on the Generation and Propagation of Elastic Waves. (in English) 41
6. T. MINAKAMI, Torsion Balance Surveys on Volcano Asama. (Part 1.) (in English) 50
7. M. ISHIMOTO and K. IIDA, Determination of Elastic Constants of Soils by means of Vibration Methods. Part II. Modulus of Rigidity and Poisson's Ratio. (in English) 67
8. N. NASU, T. HAGIWARA and S. OMOTE, Studies of the Propagation of the Artificial Earthquake Waves through Superficial Soil or Sand Layers and the Elasticity of Soil and Sand. (Part 2). (in Japanese) 87
9. W. INOUYE, Notes on the Origins of Earthquakes. (Second paper.) (in English) 90

10. N. **Miyabe**, The Cause of the Subsidence of the Earth's Surface in the Kôtô Region, Tokyo. I. (in English) 102

11. R. **Takahasi**, Observations on Earth Current during the Solar Eclipse of June 19, 1936. (in English) 109

12. T. **Fukutomi**, On the Hot Springs of Atami, Izu Peninsula. (in English) 113

13. T. **Minakami**, The Sengataki Thermal Spring and Underground Mineral Water at the Foot of Volcano Asama. (in English) 134

14. W. **Inouye**, Statistic Investigations of Earthquake Frequencies. (in English) 142

15. S. **Yamaguti**, World Distribution of "Deep" Earthquakes. (in English) 170

16. T. **Takayama**, Report on the Field Investigation of the Earthquake of November 3, 1936. (in Japanese) 179

17. T. **Nagata**, A Dip Variometer. (in English) 185

18. Y. **Otuka**, "Decken" Structure in the Bôsô Peninsula, Japan. (in English) 193

19. Y. **Otuka**, Palaeogene Palaeogeography near Japan. (in Japanese) 198

20. H. **Tsuya**, On the Volcanism of the Huzi Volcanic Zone, with Special Reference to the Geology and Petrology of Idu and the Southern Islands. (in English) 215

Part 2.—June, 1937.

21. K. **Sezawa** and K. **Kanai**, On the Elastic Deformation of a Stratified Body Subjected to Vertical Surface Loads. (in English) 359

22. K. **Sezawa** and K. **Kanai**, The Same Stationary Vibration of an Origin Accompanying Different Types of Disturbances Therefrom. (in English) 370

23. K. **Sezawa** and K. **Kanai**, On the Free Vibrations of Sur-

face Layer due to an Obliquely Incident Disturbance. (in English) 377

24. K. SEZAWA and K. KANAI. Energy Dissipation in the Vibrations of a Bridge. I. (in English) 385

25. G. NISHIMURA and T. TAKAYAMA, The Vibration due to Obliquely Incident Waves of a Surface Stratum Adhering Closely to the Subjacent Medium, and the Properties of its Resonance Condition. (in English) 394

26. R. TAKAHASI and T. NAGATA, Geophysical Studies of Volcano Mihara, Oosima Island; Topographic Survey of the Crater of Mihara and the Magnetic Survey of Oosima. (in English)... 441

27. R. TAKAHASI and T. MINAKAMI, Tilt Observations during the Recent Activities of Volcano Asama. (in English) 463

28. T. MINAKAMI, Changes in the Depth of the Crater Floor of Volcano Asama in the Recent Activities. (in English) 492

29. T. NAGATA, A Comparison of the Results of Magnetic Surveys before and after the Niizima Earthquake of December, 27th, 1936. (in Japanese) 497

30. T. FUKUTOMI, and Z. HUZII, On the Thermal Springs of Itô, Izu Peninsula. (in Japanese) 506

31. M. ISHIMOTO, Observations des périodes prédominantes dans les secousses séismiques dont la distance épicentrale est assez grande. (en japonais) 536

32. K. IIDA, Some Experiments on the Shrinkage of Soil. (in Japanese) 544

33. T. HAGIWARA and S. OMOTE, The Niizima Earthquake of December 27, 1936. (in Japanese) 559

34. The Results of Precise Levelling along the Line between Sakanoiti and Izyuin, via Kokura, Hukuoka, and Kumamoto, and the Line between Hosozima and Kumamoto, via Nobeoka. (in Japanese) 569

Part 3.—September, 1937.

35. K. **Sezawa** and K. **Kanai**, Relation between the Thickness of a Surface Layer and the Amplitudes of Love-waves. (in English) 577

36. K. **Sezawa**, On the Plastic Properties of the Earth's Core. (in English) 582

37. K. **Sezawa** and K. **Kanai**, Energy Dissipation in the Vibrations of a Bridge. II. (in English) 590

38. K. **Sezawa** and K. **Kanai**, Model Experiment Confirmations of a Dynamic Method of Minimizing the Seismic Vibrations of a Structure. (in English) 598

39. G. **Nishimura**, On the Elastic Waves due to Pressure Variation on the Inner Surface of a Spherical Cavity in an Elastic Solid. (in English) 614

40. C. **Tsuboi** and T. **Fuchida**, Relations between Gravity Values and Corresponding Subterranean Mass Distribution. (in English) 636

41. C. **Tsuboi**, The Deflections of the Vertical, the Undulation of the Geoid, and Gravity Anomalies. (in English) 650

42. N. **Miyabe**, Supplementary Notes to the Study of Crustal Deformation in the Tango District. (in English) 654

43. T. **Nagata**, Some Physical Properties of the Lava of Volcanoes Asama and Mihara. I. Electric Conductivity and Its Temperature-Coefficient. (in English) 663

44. W. **Inouye**, Notes on the Origin of Earthquakes. (Third paper) (in English) 674

45. W. **Inouye**, Notes on the Origin of Earthquakes. (Fourth paper) 686

46. M. **Ishimoto**, Observations sur des secousses d'une petite amplitude. (en français) 697

47. S. **Fujiwhara**, On the So-called Mukuhira's Arc as the Foreshadow of an Earthquake. (in English) 706

48. T. **MATUZAWA**, H. **NAKAMATI**, Y. **NISIKAWA** und Y. **YOSIMURA**, Über die Jahresschwankung der Erdbebenhäufigkeit in Japan. (in deutsch) 711

49. F. **KISHINOUYE**, Frequency-distribution of tho Itô Earthquake Swarm of 1930. (in English) 785

50. K. **IIDA**, Determination of the Elastic Constants of Superficial Soil and Base-rock at Maru-no-uti in Tôkyô. (in Japanese)... 828

51. N. **MIYABE**, Tunami associated with the Sanriku Earthquake that occurred on November 3, 1936. (in English) 837

Part 4.—December, 1937.

52. K. **SEZAWA** and K. **KANAI**, Relation between the Thickness of a Surface Layer and the Amplitudes of Dispersive Rayleigh-waves. (in English) 845

53. K. **SEZAWA** and K. **KANAI**, The Problem of Elastic Stability of the Earth treated in Polar Coordinates. (in English) ... 860

54. K. **SEZAWA**, The Plastic State of the Earth under Gravitational Forces. (in English) 878

55. K. **SEZAWA** and K. **KANAI**, Prevalent Periods of Oscillation in Tidal Waves. (in English) 888

56. S. **YAMAGUTI**, Deformation of the Earth's Crust in Idu Peninsula in Connection with the Destructive Idu Earthquake of Nov. 26, 1930. (in English) 899

57. C. **TSUBOI**, The Water Surface of a Lake as an Indicator of Crustal Deformation. (in English) 935

58. T. **HAGIWARA**, An Accelerograph for Measuring the Shaking of Railroad Trains, Automobiles and Airoplanes, etc. (in Japanese) 944

59. W. **INOUYE**, Revisions of my "Notes on the Origins of Earthquakes." (in English) 956

60. Z. **KINOSITA**, The Arrangement of Layers in the Earth's Crust as deduced from Seismometrical Observations at Hongô,

Tokyo (first paper). (in English) 965
61. Y. OTUKA, Geologic Structure of the South Kwanto Region, Japan. (1) (Yokohama-Hudisawa districts.) (in Japanese) ... 974
62. Y. OTUKA, Some geologic considerations of the folded Tertiary zones in Japan (advanced paper). (in English) 1041
63. R. TAKAHASI and T. NAGATA, Geophysical Studies of Volcano Mihara, Oosima Island; the General Aspect of Physical Conditions in the Crater. (in English) 1047

1. *Resonance Phenomena and Dissipation Waves in the Stationary Vibrations of a Semi-infinite Body.*

By Katsutada SEZAWA and Kiyoshi KANAI,

Earthquake Research Institute.

(Read Oct. 20, 1936.—Received Dec. 21, 1936.)

1. *Introduction.*

It seems the prevalent belief that the surface vibration of a semi-infinit body caused by usual disturbances of a local type is present only in the form of propagated waves; the chances of general acceptance of the idea of resonance phenomena in such a vibration being rather remote. We shall however show that if certain periodic surface disturbances were distributed in a special way on a certain area of the surface of a semi-infinite body, it would excite a standing vibration of the body, at least within the area of disturbances, so long as the frequency of the disturbances is relatively low. The vibration under consideration naturally assumes the type of resonance at a certain frequency. Beyond another assigned frequency, however, the movement of the body changes from a state of standing vibration to one of wave motion. In some kinds of surface disturbances, on the other hand, the vibration never becomes stationary at any frequency, being present only if no surface wave can possibly exist. The various cases will be described in the sections to which they belong.

2. *Elementary solutions.*

The case in which the disturbances are distributed in the form of cylindrical coordinates will first be discussed. The solution is the same as that given in our preceding papers.[1]

When the surface vibrations are composed of both dilatational and distortional movements, the solutions assume the forms

$$\left.\begin{aligned} \Delta &= A_m J_m(kr)\, e^{-\alpha z - ipt} \cos m\theta\,, \\ u_1 &= -\frac{A_m}{h^2}\frac{\partial J_m(kr)}{\partial r}\, e^{-\alpha z - ipt} \cos m\theta\,, \end{aligned}\right|$$

---

[1] K. SEZAWA, *Proc. Imp. Acad.*, **4** (1928), 267; *Bull. Earthq. Res. Inst.*, **6** (1929), 1—18.

$$\left.\begin{aligned} v_1&=\frac{A_m}{h^2}\frac{J_m(kr)}{r}e^{-\alpha z-ipt}m\sin m\theta\,,\\ w_1&=\frac{A_m}{h^2}\alpha J_m(kr)e^{-\alpha z-ipt}\cos m\theta\,,\end{aligned}\right\} \tag{1}$$

$$\left.\begin{aligned} u_3&=-\frac{C_m}{j^2}\frac{\partial J_m(kr)}{\partial r}e^{-\beta z-ipt}\cos m\theta\,,\\ v_3&=\frac{C_m}{j^2}\frac{J_m(kr)}{r}e^{-\beta z-ipt}m\sin m\theta\,,\\ w_3&=\frac{C_m}{j^2}\frac{k^2}{\beta}J_m(kr)e^{-\beta z-ipt}\cos m\theta\,,\end{aligned}\right\} \tag{2}$$

$$\left.\begin{aligned} u_2&=\frac{B_m}{k^2}\frac{J_m(kr)}{r}e^{-\beta z-ipt}m\sin m\theta\,,\\ v_2&=\frac{B_m}{k^2}\frac{\partial J_m(kr)}{\partial r}e^{-\beta z-ipt}\cos m\theta\,,\\ w_2&=0\,,\end{aligned}\right\} \tag{3}$$

where

$$k^2=\alpha^2+h^2=\beta^2+j^2,\quad h^2=\rho p^2/(\lambda+2\mu),\quad j^2=\rho p^2/\mu. \tag{4}$$

The surface disturbances may be classified into two kinds, the first of which is expressed by

$$\left.\begin{aligned} \widehat{zz}&=\lambda\Delta+2\mu\frac{\partial w}{\partial z}=P_m J_m(kr)\cos m\theta e^{-ipt}\,,\\ \widehat{rz}&=\mu\left(\frac{\partial w}{\partial r}+\frac{\partial u}{\partial z}\right)=Q_m\frac{\partial J_m(kr)}{\partial(kr)}\cos m\theta e^{-ipt}\,,\\ \widehat{\theta z}&=\mu\left(\frac{1}{r}\frac{\partial w}{\partial\theta}+\frac{\partial v}{\partial z}\right)=-Q_m\frac{J_m(kr)}{kr}m\sin m\theta e^{-ipt}\,,\end{aligned}\right\} \tag{5}$$

where $u=u_1+u_3$, $v=v_1+v_3$, $w=w_1+w_3$, and the second by

$$\left.\begin{aligned} \widehat{zz}&=0\,,\\ \widehat{rz}&=\mu\frac{\partial u_2}{\partial z}=R_m\frac{J_m(kr)}{kr}m\sin m\theta e^{-ipt}\,,\\ \widehat{\theta z}&=\mu\frac{\partial v_2}{\partial z}=R_m\frac{\partial J_m(kr)}{\partial(kr)}\cos m\theta e^{-ipt}\,.\end{aligned}\right\} \tag{6}$$

The second kind of disturbances never gives rise to vertical displacement, nor normal surface stress, nor even volume change of body.

Solving (5), (6) we obtain

$$\left.\begin{aligned} -\frac{\mu A_m}{h^2} &= \frac{1}{k^2}\left\{\frac{P_m(2-j'^2)+Q_m 2\beta'}{(2-j'^2)^2-4\alpha'\beta'}\right\}, \\ \frac{\mu C_m}{j^2} &= \frac{1}{k^2}\left\{\frac{P_m 2\alpha'\beta'+Q_m\beta'(2-j'^2)}{(2-j'^2)^2-4\alpha'\beta'}\right\}, \end{aligned}\right\} \qquad (7)$$

$$-\frac{B\mu_m}{k^2} = \frac{R_m}{\beta}, \qquad (8)$$

where $j'=j\ k$, $\alpha'=\alpha/k$. $\beta'=\beta/k$.

3. *Vibration of the first kind.*

From disturbances of the first kind we obtain the vibration of the first kind, in which case the displacement is expressed by

$$u=u_1+u_3, \quad v=v_1+v_3, \quad w=w_1+w_3. \qquad (9)$$

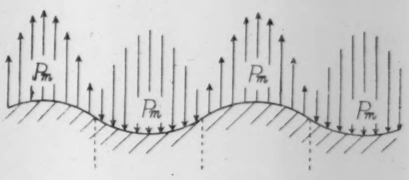

Fig. 1.

We shall assume that the nodal planes with respect to the vibrations or the nodal lines of disturbances are of a given distribution, whereas the frequency of the vibrational disturbances are varied, the vibrational character of different ranges of j', namely of frequency p, being considered separately.

(a) $0 < j' < 1 \quad \left(0 < \sqrt{\frac{\rho}{\mu}}\frac{p}{k} < 1\right);$

The vibration is of the surface type and standing under the periodic surface disturbance.

(b) $(2-j'^2)^2-4\alpha'\beta'=0$, namely $j'=0{\cdot}9194$ for $\lambda=\mu$;

The displacement becomes such that

$$u \to \infty, \quad v \to \infty, \quad w \to \infty,$$

the standing vibration is in resonance condition.

(c) $1 < j' < \sqrt{\frac{\lambda+2\mu}{\mu}} \quad \left(1 < \sqrt{\frac{\rho}{\mu}}\frac{p}{k} < \sqrt{\frac{\lambda+2\mu}{\mu}}\right);$

In this case u_1, v_1, w_1 form standing surface vibrations, whereas u_3, v_3, w_3 become waves transmitted downwards with velocity

$$\sqrt{\frac{\mu}{\rho}}\frac{1}{\sqrt{1-\frac{\mu}{\rho}\frac{k^2}{p^2}}}.$$

This results directly from the condition in (4).

(d) $$\sqrt{\frac{\lambda+2\mu}{\mu}}<j' \qquad \left(\sqrt{\frac{\lambda+\mu}{\mu}}<\sqrt{\frac{\rho}{\mu}}\frac{p}{k}\right);$$

u_1, v_1, w_1 and u_3, v_3, w_3 both form waves that are transmitted downwards with velocities

$$\sqrt{\frac{\lambda+2\mu}{\rho}}\frac{1}{\sqrt{1-\frac{\lambda+2\mu}{\rho}\frac{k^2}{p^2}}}, \quad \sqrt{\frac{\mu}{\rho}}\frac{1}{\sqrt{1-\frac{\mu}{\rho}\frac{k^2}{p^2}}}$$

respectively in consequence of conditions in (4).

4. *Vibration of the second kind.*

Vibrations of this kind correspond to disturbances of the second kind. The nature of the vibration for different ranges of j' is

(a) $$0<j'<1 \qquad \left(0<\sqrt{\frac{\rho}{\mu}}\frac{p}{k}<1\right);$$

These vibrations are of surface type and standing under the periodic surface disturbances.

(b) Without resonance conditions.

(c) $$1<j' \qquad \left(1<\sqrt{\frac{\rho}{\mu}}\frac{p}{k}\right);$$

u_2, v_2 form waves that are transmitted downwards with velocity

$$\sqrt{\frac{\mu}{\rho}}\frac{1}{\sqrt{1-\frac{\mu}{\rho}\frac{k^2}{p^2}}}.$$

5. *Vibration of the second kind in a stratified body.*

While the vibration of the second kind in a semi-infinite body does not show any resonance phenomenon, the same vibration in a stratified body has resonance conditions. Let the thickness of the layer be H, and let the axis of z be directed vertically downwards from the upper surface of the layer. The displacement u_2, v_2 in the layer and the displacement u_2', v_2' in the subjacent medium are such that

$$\left.\begin{array}{l} u_2=\dfrac{-R_m}{\mu k\beta}\dfrac{J_m(kr)}{r}\dfrac{\{(\mu\beta+\mu'\beta')e^{\beta(H-z)}+(\mu\beta-\mu'\beta')e^{-\beta(H-z)}\}}{\{(\mu\beta+\mu'\beta')e^{\beta H}-(\mu\beta-\mu'\beta')e^{-\beta H}\}}m\sin m\theta e^{-ipt}, \\ v_2=\dfrac{-R_m}{\mu k\beta}\dfrac{\partial J_m(kr)}{\partial r}\dfrac{\{(\mu\beta+\mu'\beta')e^{\beta(H-z)}+(\mu\beta-\mu'\beta')e^{-\beta(H-z)}\}}{\{(\mu\beta+\mu'\beta')e^{\beta H}-(\mu\beta-\mu'\beta')e^{-\beta H}\}}\cos m\theta e^{-ipt}, \\ w_2=0, \end{array}\right\} \quad (10)$$

$$\left.\begin{array}{l} u_2'=\dfrac{-2R_m}{k}\dfrac{J_m(kr)}{r}\dfrac{e^{\beta'(H-z)}}{\{(\mu\beta+\mu'\beta')e^{\beta H}-(\mu\beta-\mu'\beta')e^{-\beta H}\}}m\sin m\theta e^{-ipt}, \\ v_2'=\dfrac{-2R_m}{k}\dfrac{\partial J_m(kr)}{\partial r}\dfrac{e^{\beta'(H-z)}}{\{(\mu\beta+\mu'\beta')e^{\beta H}-(\mu\beta-\mu'\beta')e^{-\beta H}\}}\cos m\theta e^{-ipt}, \\ w_2'=0, \end{array}\right\} \quad (11)$$

where $k^2=j^2+\beta^2=j_1^2+\beta'^2$, $j^2=\rho p^2/\mu$, $j_1^2=\rho' p^2/\mu'$; ρ, ρ', μ, μ' being densities and rigidities of the surface layer and the subjacent medium. We shall now discuss the problem of different frequencies of vibrations.

(a) $0<j_1'<1 \quad \left(0<\sqrt{\dfrac{\rho'}{\mu'}}\dfrac{p}{k}<1\right)$, j_1' being j_1/k;

This vibration is of surface type, and standing.

(b) $(\mu\beta+\mu'\beta')e^{\beta H}-(\mu\beta-\mu'\beta')e^{-\beta H}=0$;

This standing vibration is under resonance condition.

(c) $1<j' \quad \left(1<\sqrt{\dfrac{\rho'}{\mu'}}\dfrac{p}{k}\right)$;

u_2', v_2' are waves transmitted vertically downwards with velocity

$$\sqrt{\frac{\mu'}{\rho'}}\frac{1}{\sqrt{1-\dfrac{\mu'}{\rho'}\dfrac{k^2}{p^2}}}.$$

6. *Periodic arbitrary disturbances.*

(i) For the arbitrary disturbance of the first kind on $z=0$

$$\widehat{zz}=f(r)\cos m\theta e^{-ipt}, \quad \widehat{rz}=0, \quad \widehat{\theta z}=0, \qquad (12)$$

we generalize the result shown in Section 4 as follows:

$$u_1=\frac{\cos m\theta e^{-ipt}}{\mu}\int_0^\infty\frac{(2k^2-j^2)e^{-\alpha z}}{(2k^2-j^2)^2-4k^2\alpha\beta}\frac{\partial J_m(kr)}{\partial r}kdk\int_0^\infty f(R)J_m(kR)RdR,$$

$$v_1=\frac{-m\sin m\theta e^{-ipt}}{\mu}\int_0^\infty\frac{(2k^2-j^2)e^{-\alpha z}}{(2k^2-j^2)^2-4k^2\alpha\beta}\frac{J_m(kr)}{r}kdk\int_0^\infty f(R)J_m(kR)RdR\,,$$

$$w_1=\frac{\cos m\theta e^{-ipt}}{\mu}\int_0^\infty\frac{\alpha(2k^2-j^2)e^{-\alpha z}}{(2k^2-j^2)^2-4k_2\alpha\beta}J_m(kr)kdk\int_0^\infty f(R)J_m(kR)RdR\,, \qquad (13)$$

$$u_3=\frac{-\cos m\theta e^{-ipt}}{\mu}\int_0^\infty\frac{2\alpha\beta e^{-\beta z}}{(2k^2-j^2)^2-4k^2\alpha\beta}\frac{\partial J_m(kr)}{\partial r}kdk\int_0^\infty f(R)J_m(kR)RdR\,,$$

$$v_3=\frac{m\sin m\theta e^{-ipt}}{\mu}\int_0^\infty\frac{2\alpha\beta e^{-\beta z}}{(2k^2-j^2)^2-4k^2\alpha\beta}\frac{J_m(kr)}{r}kdk\int_0^\infty f(R)J_m(kR)RdR\,,$$

$$w_3=\frac{\cos m\theta e^{-ipt}}{\mu}\int_0^\infty\frac{2k^2\alpha e^{-\beta z}}{(2k^2-j^2)^2-4k^2\alpha\beta}J_m(kr)\,kdk\int_0^\infty f(R)J_m(kR)RdR\,. \qquad (14)$$

(ii) For arbitrary disturbances of the second kind on a semi-infinite body,

$$\left.\begin{aligned}\widehat{rz}&=\frac{\phi(r)}{kr}m\sin m\theta e^{-ipt}\,,\\ \widehat{\theta z}&=\frac{\partial\phi(r)}{\partial(kr)}\cos m\theta e^{-ipt}\,,\end{aligned}\right\} \qquad (15)$$

we get

$$\left.\begin{aligned}u_2&=\frac{m\sin m\theta e^{-ipt}}{\mu}\int_0^\infty\frac{e^{-\beta z}}{\beta}\frac{J_m(kr)}{r}kdk\int_0^\infty\phi(R)J_m(kR)RdR\,,\\ v_2&=\frac{\cos m\theta e^{-ipt}}{\mu}\int_0^\infty\frac{e^{-\beta z}}{\beta}\frac{\partial J_m(kr)}{\partial r}kdk\int_0^\infty\phi(R)J_m(kR)RdR\,,\\ w_2&=0\,.\end{aligned}\right\} \qquad (16)$$

(iii) For arbitrary disturbances of the second kind on a stratified body we get

$$u_2=\frac{-m\sin m\theta e^{-ipt}}{\mu}\int_0^\infty\frac{\{(\mu\beta+\mu'\beta')e^{\beta(H-z)}+(\mu\beta-\mu'\beta')e^{-\beta(H-z)}\}}{\beta\{(\mu\beta+\mu'\beta')e^{\beta H}-(\mu\beta-\mu'\beta')e^{-\beta H}\}}\Phi(k)\frac{J_m(kr)}{r}kdk\,,$$

$$v_2=\frac{-\cos m\theta e^{-ipt}}{\mu}\int_0^\infty\frac{\{(\mu\beta+\mu'\beta')e^{\beta(H-z)}+(\mu\beta-\mu'\beta')e^{-\beta(H-z)}\}}{\beta\{(\mu\beta+\mu'\beta')e^{\beta H}-(\mu\beta-\mu'\beta')e^{-\beta H}}\Phi(k)\frac{\partial J_m(kr)}{\partial r}kdk\,,$$

$$w_2=0\,, \qquad (17)$$

$$u_2'=\frac{-2m\sin m\theta e^{-ipt}}{\mu}\int_0^\infty\frac{e^{\beta'(H-z)}}{(\mu\beta+\mu'\beta')e^{\beta H}-(\mu\beta-\mu'\beta')e^{-\beta H}}\Phi(k)\frac{J_m(kr)}{r}kdk\,,$$

$$v_2'=\frac{-2\cos m\theta e^{-ipt}}{\mu}\int_0^\infty\frac{e^{\beta'(H-z)}}{(\mu\beta+\mu'\beta')e^{\beta H}-(\mu\beta-\mu'\beta')e^{-\beta H}}\Phi(k)\frac{\partial J_m(kr)}{\partial r}kdk\,,$$

$$w_2'=0\,, \tag{18}$$

where

$$\Phi=\int_0^\infty\phi(R)J_m(kR)RdR. \tag{19}$$

7. *Movements of the body outside the region of disturbances.*

Although the vibrations of a body due to disturbances of local type are never standing outside the region of those disturbances, they become waves that are transmitted outwards, as will be seen upon evaluating the integrals (13)∼(19) for a large value of r. As, however, the matter of evaluating these integrals has frequently been discussed, we shall not go further into the subject. The conclusion, which may be arrived at very easily, is as follows:

(i) Disturbances of the first kind.

The waves that are transmitted outwards are composed of Rayleigh-waves, longitudinal waves, and transverse waves, the amplitudes of which at a large epicentral distance are respectively proportional to[2]

$$\frac{1}{\sqrt{r}}\,,\quad\frac{1}{r^2}\,,\quad\frac{1}{r^2}\,.$$

(ii) Disturbances of the second kind on a semi-infinite body.

The transmitted waves are only bodily transverse waves, the amplitude of which at a long epicentral distance is proportional to $\frac{1}{r}$, the proof of which is very simple.[3]

(iii) Disturbances of the second kind on a stratified body.

The transmitted waves are Love-waves and bodily transverse waves, the amplitudes of which waves at a great epicentral distance are respectively proportional to[4]

---

[2] H. Lamb, *Phil. Trans. Roy. Soc.*, **203** (1904), etc.

[3] One method of evaluating (16) is obtained by writing $\int_0^\infty\phi(R)J_m(kR)RdR=\Phi(k)=C$, and using formula $\int_0^\infty\frac{e^{-\beta z}}{\beta}J_m(kr)kdk=\frac{e^{-ijr_1}}{r_1}$ where $r_1^2=r^2+z^2$.

$$\frac{1}{\sqrt{r}}, \quad \frac{1}{r^2}.$$

The velocity of transmission of the bodily waves is that of transverse waves in the subjacent medium.

8. *Movements of the ground within the region of disturbances.*

An important part of the present problem is the movement of the ground within the region of disturbance, particularly for the case wherein the disturbance is distributed in some periodic manner. Let the disturbance be distributed such that

$$\left.\begin{aligned} \widehat{zz} &= P_m J_m(Kr)\cos m\theta e^{-ipt}, \\ \widehat{rz} &= Q_m \frac{\partial J_m(Kr)}{\partial(Kr)}\cos m\theta e^{-ipt}, \\ \widehat{\theta z} &= -Q_m \frac{J_m(Kr)}{Kr} m\sin m\theta e^{-ipt}, \end{aligned}\right\} \quad (z=0;\quad r<a) \qquad (20)$$

$$\widehat{zz}=0, \quad \widehat{rz}=0, \quad \widehat{\theta z}=0 \qquad (z=0;\quad r>a) \qquad (21)$$

in the first kind; and

$$\left.\begin{aligned} \widehat{rz} &= R_m \frac{J_m(Kr)}{Kr} m\sin m\theta e^{-ipt}, \\ \widehat{\theta z} &= R_m \frac{\partial J_m(Kr)}{\partial(Kr)}\cos m\theta e^{-ipt}, \end{aligned}\right\} \quad (z=0,\quad r>a) \qquad (22)$$

$$\widehat{rz}=0, \quad \widehat{\theta z}=0 \qquad (z=0;\quad r>a) \qquad (22)$$

in the second kind, when from (7), (8)

$$\left.\begin{aligned} u_1 &= \frac{1}{\mu K^2}\left\{\frac{P_m(2-j'^2)+Q_m 2\beta'}{(2-j'^2)^2-4\alpha'\beta'}\right\}\frac{\partial J_m(Kr)}{\partial r}\cos m\theta e^{-ipt}, \\ v_1 &= \frac{-1}{\mu K^2}\left\{\frac{P_m(2-j'^2)+Q_m 2\beta'}{(2-j'^2)^2-4\alpha'\beta'}\right\}\frac{J_m(Kr)}{r} m\sin m\theta e^{-ipt}, \\ w_1 &= \frac{-\alpha}{\mu K^2}\left\{\frac{P_m(2-j'^2)+Q_m 2\beta'}{(2-j'^2)^2-4\alpha'\beta'}\right\} J_m(Kr)\cos m\theta e^{-ipt}, \end{aligned}\right\} \qquad (25)$$

---

[4] If we were to assume $\int_0^\infty \phi(R)J_m(kR)RdR=\Phi(k)=C$ in (17), (18), the integrals to be evaluated have the same form as those in the paper: K. SEZAWA, "Love-waves generated from a Source of certain Depth", *Bull. Earthq. Res. Inst.*, **13** (1935), 17; the result being the conclusion shown in (iii).

$$\left.\begin{aligned} u_3 &= \frac{-1}{\mu K^2}\left\{\frac{P_m 2\alpha'\beta' + Q_m\beta'(2-j'^2)}{(2-j'^2)^2-4\alpha'\beta'}\right\}\frac{\partial J_m(Kr)}{\partial r}\cos m\theta e^{-ipt}, \\ v_3 &= \frac{1}{\mu K^2}\left\{\frac{P_m 2\alpha'\beta' + Q_m\beta'(2-j'^2)}{(2-j'^2)^2-4\alpha'\beta'}\right\}\frac{J_m(Kr)}{r} m\sin m\theta e^{-ipt}, \\ w_3 &= \frac{1}{\beta}\left\{\frac{P_m 2\alpha'\beta' + Q_m\beta'(2-j'^2)}{(2-j'^2)^2-4\alpha'\beta'}\right\} J_m(Kr)\cos m\theta e^{-ipt}, \end{aligned}\right\} \tag{25}$$

$$\left.\begin{aligned} u_2 &= \frac{-R_m}{\mu\beta}\,\frac{J_m(Kr)}{r} m\sin m\theta e^{-ipt}, \\ v_2 &= \frac{-R_m}{\mu\beta}\,\frac{\partial J_m(Kr)}{\partial r}\cos m\theta e^{-ipt}, \\ w_2 &= 0, \end{aligned}\right\} \tag{26}$$

all within $r < a$ and on $z=0$, where

$$K^2 = \alpha^2 + h^2 = \beta^2 + j^2, \quad j' = j/K, \quad \alpha' = \alpha/K, \quad \beta' = \beta/K. \tag{27}$$

Although these expressions have been given without any proof, they are direct consequences of the relations (1), (2), (3), (20), (21), (22), (23), which could be shown by accurately evaluating the integrals (13) ~(19).

Now vibrations (u_1, v_1, w_1) and (u_3, v_3, w_3) for $r < a$, $z=0$ are in resonance condition when the frequency of the disturbance satisfies the condition

$$(2-j'^2)^2 - 4\alpha'\beta' = 0. \tag{28}$$

Vibration (u_2, v_2, w_2), on the other hand, is never under resonance, even if $r < a$.

Although the answer to the question whether or not the movement in $r > a$ or $z \neq 0$ is in standing vibration cannot be strictly obtained with the aid of our present simple calculation, the probability is that movement in such a region is almost a wave motion.

9. *Numerical calculation of displacement distribution for a two-dimensional vibration of the first kind.*

With a view to ascertaining the numerical values of the displacements, we calculated a two-dimensional vibration of the first kind. Let the axis of x be drawn horizontally on the free surface and that of z vertically downwards. We then get

$$\left.\begin{aligned} \Delta &= Ae^{i(pt+\alpha z)}\cos kx\,, \\ u_1 &= \frac{kA}{h^2}e^{i(pt+\alpha z)}\sin kx\,, \\ w_1 &= \frac{\alpha A}{h^2}e^{i(pt+\alpha z)}\cos kx\,, \end{aligned}\right\} \tag{29}$$

$$\left.\begin{aligned} u_2 &= \frac{\beta}{j^2}Be^{i(pt+\beta z)}\sin kx\,, \\ w_2 &= \frac{k}{j^2}Be^{i(pt+\beta z)}\cos kx\,, \end{aligned}\right\} \tag{30}$$

where $k^2=\alpha^2+h^2=\beta^2+j^2$. The boundary conditions in the present calculation are such that

$$\lambda\Delta+2\mu\frac{\partial w}{\partial z}=P\cos kxe^{ipt}\,,\quad \frac{\partial u}{\partial z}+\frac{\partial w}{\partial x}=0 \tag{31}$$

at $z=0$ where $u=u_1+u_2$, $w=w_1+w_2$. These give the values of the constants, the result for the case $\lambda=\mu$ being

$$\left.\begin{aligned} \frac{\mu}{P}u_1 &= \frac{-(2-j'^2)}{k\Phi}e^{i(pt+\alpha z)}\sin kx\,, \\ \frac{\mu}{P}w_1 &= \frac{-\alpha'(2-j'^2)}{k\Phi}e^{i(pt+\alpha z)}\cos kx\,, \end{aligned}\right\} \tag{32}$$

$$\left.\begin{aligned} \frac{\mu}{P}u_2 &= \frac{2\alpha'\beta'}{k\Phi}e^{i(pt+\beta z)}\sin kx\,, \\ \frac{\mu}{P}w_2 &= \frac{2\alpha'}{k\Phi}e^{i(pt+\beta z)}\cos kx\,, \end{aligned}\right\} \tag{33}$$

where

$$\Phi=(2-j'^2)^2-4\alpha'\beta'. \tag{34}$$

The nature of the problem is the same as that for the three-dimensional problem. Fig. 2 indicates the surface displacement, and Fig. 3 the amplitudes of the dissipation waves.

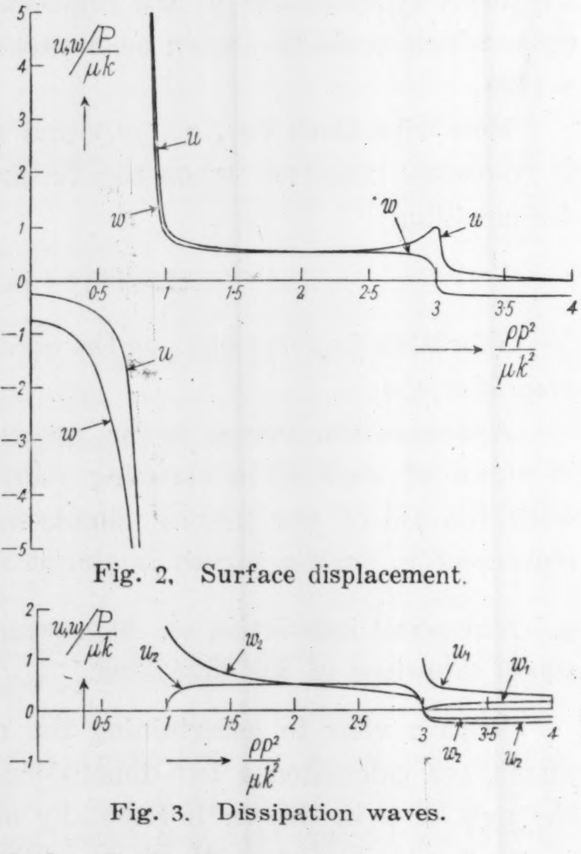

Fig. 2. Surface displacement.

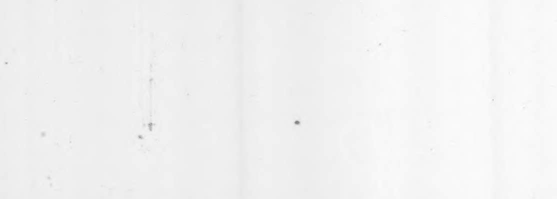

Fig. 3. Dissipation waves.

(a) If $0 < \sqrt{\frac{\rho}{\mu}}\frac{p}{k} < 1$, there exists a standing vibration without any wave dissipation.

(b) If $\sqrt{\frac{\rho}{\mu}}\frac{p}{k} = 0.9194$, the standing vibration is under resonance, so that $u = u_1 + u_2$, $w = w_1 + w_2$ then become infinitely large as will be seen from Fig. 1.

(c) If $1 < \sqrt{\frac{\rho}{\mu}}\frac{p}{k} < \sqrt{3}$, the transverse waves (u_2, v_2) are dissipating, the dilatational component of the displacement still forming stationary vibrations near the surface. The numerical relation will be seen from Fig. 1, 2.

(d) If $\sqrt{3} < \sqrt{\frac{\rho}{\mu}}\frac{p}{k}$, the longitudinal as well as the transverse waves are dissipating, without any standing wave on the surface.

10. *Concluding remarks.*

It will be seen from these studies that, while the movement of the ground within the region of the applied disturbance is in stationary vibration or in wave motion according as the frequency of the vibratory disturbance is relatively low or relatively high for a given distribution of the same disturbance, movement outside the region under consideration is almost a wave motion for any frequency of the periodic disturbance. In that case wherein it is possible for the surface waves to exist outside the region of disturbance, there is such a frequency of periodic disturbances that the surface movement is under resonance conditions. On the other hand, in the case wherein no surface wave can possibly exist outside the region of disturbance, the surface movement is never under resonance condition for any periodic disturbance.

A number of writers have discussed with various conclusions whether microseismic movement, under certain weather conditions, is of wave motion or a standing vibration of the ground. Even should the movement under consideration be a standing vibration, its type would be of such surface vibration as has been shown in the present paper, it therefore being possible for resonance conditions to exist.

For resonance conditions to occur in the vibration of the ground surface, the presence of a superficial layer has no place in any important part of the problem unless the vibration of the second kind, namely, the case of pure shearing disturbance applied to the surface, is taken into consideration. The effect of surface layers on vibration under reso-

nance in the case of the first kind of vibrations merely results some modification in the frequency of that resonance, as is the case for differences in velocity between Rayleigh-waves on a semi-infinite body and those on a stratified body.

---

1. 半無限體の振動に於ける共振現象及び逸散波

地震研究所 ｛妹澤克惟
　　　　　 ｛金井清

半無限體の表面にディスターバンスが加つてもその振動は波動の形としてだけ存在すると考へられるから，その共振現象などといふ事は簡單には想像できにくい．しかしながらディスターバンスが表面上に週期的に配列し且つそのディスターバンスの振動週期が極く緩い場合には固體の表面だけの定常振動が現れ，且つ共振の振動狀態にもなり得るものである．

ディスターバンスが固體に振り變形の外に壓縮變形をも起すやうな振動を與へる場合には極めて低い振動週期，卽ち $0<\sqrt{\rho/\mu}(p/k)<1$ に於て勢力が固體表面にのみ集中する定常振動を起し，且つ Rayleigh 波に相當する波長と振動數との關係のときに振動の共振現象が起るものである．振動週期が少しく急になり，$1<\sqrt{\rho/\mu}(p/k)<\sqrt{(\lambda+2\mu)/\mu}$ の狀態になると横波が下方へ傳播するやうになる．しかし縱波の振動はやはり定常振動として表面近くに集つてをるものである．$\sqrt{(\lambda+2\mu)/\mu}<\sqrt{\rho/\mu}(p/k)$ の如き高い振動數になると定常振動は無くなり，縱波も横波も傳搏する部分のみとなる．

ディスターバンスが振り變形のみを起すやうな場合には，$0<\sqrt{\rho/\mu}(p/k)<1$ に於て表面の定常振動型のものが，$1<\sqrt{\rho/\mu}(p/k)$ になると全部横波として傳播するものである．この場合には共振が存在しない．

固體の表面に層のある場合にも同樣な性質があるが，ただディスターバンスが振り變形を與へるやうな場合でも表面波の存在し得るときには共振現象のあることは非常に違つた點である．從て固體に表面波の存在し得る場合には必ず共振現象のあり得る譯である．

以上述べた事柄が成立つには必しも固體表面の全體に渉つてディスターバンスが分布してをる必要がないのであつて，固體表面の一部分にディスターバンスがあつても，その部分の中だけについては前述の事柄が行はれる．しかしその部分の外では寧ろ波動現象のみが存在するものである．

地表面の脈動は波動であるか定常振動であるかといふ事が屢々問題となるが，脈動が大氣中でのディスターバンスによるとしても，それはこの論文の結果の如くその分布と振動週期如何によつて或は波動となり，或は定常振動となり，又特に共振振動ともなる事が知られるのである．

2. *Resonance Phenomena and Dissipation Waves in the Stationary Vibration of the Surface of a Spherical Cavity.*

By Katsutada SEZAWA and Kiyoshi KANAI,

Earthquake Research Institute.

(Read Nov. 17, 1936.—Received Dec. 21, 1936.)

1. In the preceding paper,[1] we discussed the possibility of resonance phenomena in the stationary vibration of a semi-infinite body. Since then the question has arisen whether or not such a perfect resonance condition is possible also in the forced stationary vibration of the surface of a spherical cavity. When the wave length of the standing vibration is very short compared with the radius of the sphere, a resonance condition is, in the nature of things, possible, seeing that the problem is virtually the same as that for a semi-infinite body. The problem of a finite number of wave lengths of vibration along the spherical surface of the cavity, however, is totally different. In this case, the distance from one nodal surface of the vibration to the next increases with increase in radial distance from the cavity, the result being that the wave energy is likely to dissipate outwards. Our mathematical examination of the subject shows, however, that for a certain value of the frequency in the vibration there still exists a resonance-like condition such that the displacement of the movement becomes relatively large, though not excessively so.

In our last year's paper[2] on wave generation from a spherical cavity, we questioned why resonance-like conditions should exist at certain frequencies, notwithstanding that the body has no any outer boundary. The present paper, which is an extension of the preceding one,[3] is also an answer to the question just mentioned that was raised in last year's paper. Although the existence of the resonance-like character in question has been suggested in a way by the calculation of a certain problem due to

---

[1] K. SEZAWA and K. KANAI, "Resonance Phenomena and Dissipation Waves in the Stationary Vibrations of a Semi-infinite Body", *Bull. Earthq. Res. Inst.*, **15** (1937).

[2] K. SEZAWA, "The Effect of Differences in the Media on the Distribution of Displacements in a Seismic Wave Front", *Bull. Earthq. Res. Inst.*, **14** (1936), 506—513.

[3] K. SEZAWA and K. KANAI, *loc. cit.*, 1).

Kawasumi and Yosiyama[4] and of another one due to Inouye,[5] both of which are based on our mathematical formulae,[6][7] no systematic study has yet been made to ascertain the possible extent of the resonance-like condition and the corresponding frequency of vibrations. As a matter of fact, the frequency of vibration for giving large amplitudes at the surface of the cavity does not perfectly agree with that of dissipation waves. It has also been shown that at a certain high frequency the amplitudes of the dissipation waves become fairly large, even beyond that of the said resonance frequency, notwithstanding that the vibration amplitude on the surface of the cavity is very small.

2. We shall take a disturbance of the first kind, namely, that quite similar to the case of a semi-infinite body. The solution then assumes the forms

$$\varDelta = A_n \frac{H^{(2)}_{n+\frac{1}{2}}(hr)}{\sqrt{r}} P_n(\cos\theta)e^{ipt}, \tag{1}$$

$$\left.\begin{aligned} u_1 &= \frac{-A_n}{h^2}\frac{d}{dr}\frac{H^{(2)}_{n+\frac{1}{2}}(hr)}{\sqrt{r}} P_n(\cos\theta)e^{ipt}, \\ v_1 &= \frac{-A_n}{h^2}\frac{H^{(2)}_{n+\frac{1}{2}}(hr)}{r^{3/2}}\frac{dP_n(\cos\theta)}{d\theta}e^{ipt}, \end{aligned}\right\} \tag{2}$$

$$\left.\begin{aligned} u_2 &= \frac{-n(n+1)}{j^2}B_n\frac{H^{(2)}_{n+\frac{1}{2}}(jr)}{r^{3/2}}P_n(\cos\theta)e^{ipt}, \\ v_2 &= \frac{-B_n}{j^2}\frac{1}{r}\frac{d}{dr}\{\sqrt{r}\,H^{(2)}_{n+\frac{1}{2}}(jr)\}\frac{dP_n(\cos\theta)}{d\theta}e^{ipt}. \end{aligned}\right\} \tag{3}$$

We shall furthermore take a special conditions of the boundary, such as

$$\widehat{rr} = p_n P_n(\cos\theta)e^{ipt}, \quad \widehat{r\theta} = 0\,, \tag{4}$$

at $r=a$. Since

$$\widehat{rr} = \lambda\varDelta + 2\mu\frac{\partial u}{\partial r}\,, \quad \widehat{r\theta} = \mu\left(\frac{\partial v}{\partial r} - \frac{v}{r} + \frac{1}{r}\frac{\partial u}{\partial \theta}\right), \tag{5}$$

---

4) H. KAWASUMI and R. YOSIYAMA, "On an Elastic Wave animated by the Potential Energy of Initial Strain", *Disin*, **7** (1935), 367.

5) W. INOUYE, "On the Mechanism of a Seismic Origin," *Disin*, **8** (1936), 387—403.

6) K. SEZAWA, "Dilatational and Distortional Waves generated from a Cylindrical or Spherical Origin," *Bull. Earthq. Res. Inst.*, **2** (1927), 13—20.

7) K. SEZAWA and K. KANAI, "Amplitudes of P- and S-waves at Different Focal Distances", **10** (1932), 299—334.

where $u=u_1+u_2$, $v=v_1+v_2$, we find from (1)~(5)

$$2A_n\left\{-\frac{(n-1)}{h^2r^2}H^{(2)}_{n+\frac{1}{2}}(hr)+\frac{1}{hr}H^{(2)}_{n+\frac{3}{2}}(hr)\right\}$$

$$+B_n\left\{-\frac{2(n^2-1)}{j^2r^2}H^{(2)}_{n+\frac{1}{2}}(jr)+\frac{2n+1}{jr}H^{(2)}_{n+\frac{3}{2}}(jr)-H^{(2)}_{n+\frac{5}{2}}(jr)\right\}=0, \quad (6)$$

$$A_n\left\{\left(\frac{\lambda}{\mu}-\frac{2n(n-1)}{h^2r^2}\right)H^{(2)}_{n+\frac{1}{2}}(hr)+2\left(\frac{2n+1}{hr}H^{(2)}_{n+\frac{3}{2}}(hr)-H^{(2)}_{n+\frac{5}{2}}(hr)\right\}\right.$$

$$+2B_n n(n+1)\left\{-\frac{n-1}{j^2r^2}H^{(2)}_{n+\frac{1}{2}}(jr)+\frac{1}{jr}H^{(2)}_{n+\frac{3}{2}}(jr)\right\}=\frac{p_n\sqrt{r}}{\mu} \quad (7)$$

at $r=a$. Solving (6), (7) we obtain A_n, B_n.

3. We shall take the case $\lambda=\mu$ and calculate the displacement at the surface $r=a$ as well as the amplitudes of the dissipation waves at $r=\infty$ for three cases of n, namely $n=1, 2, 4$, the results being plotted in Figs. 1~6. It should been borne in mind that in the results for the three cases $P_n(\cos\theta)$ in u or $dP_n(\cos\theta)/d\theta$ in v was conventionally replaced by unity.

We have already shown that the displacement of the dissipation waves at $r=\infty$ consists only of the radial component of the dilatational waves and the transverse component of the distortional waves. These figures show that the higher the value of n, the greater the value of ka that assumes maximum displacement at $r=a$ or the maximum amplitude of the dissipation waves at $r=\infty$[8]. The value of ka that corresponds to the said maxima cannot be obtained by the minimum condition of the expression

$$\frac{4n(n+1)}{hja^2}\left\{-\frac{n-1}{ha}H^{(2)}_{n+\frac{1}{2}}(ha)+H^{(2)}_{n+\frac{3}{2}}(ha)\right\}\left\{-\frac{n-1}{ja}H^{(2)}_{n+\frac{1}{2}}(ja)+H^{(2)}_{n+\frac{3}{2}}(ja)\right\}$$

$$-\left\{-\frac{2(n^2-1)}{j^2a^2}H^{(2)}_{n+\frac{1}{2}}(ja)+\frac{2n+1}{ja}H^{(2)}_{n+\frac{3}{2}}(ja)-H^{(2)}_{n+\frac{5}{2}}(ja)\right\}$$

$$\cdot\left\{\left(\frac{\lambda}{\mu}-\frac{2n(n-1)}{h^2a^2}\right)H^{(2)}_{n+\frac{1}{2}}(ha)+2\left(\frac{2n+1}{ha}H^{(2)}_{n+\frac{3}{2}}(ha)-H^{(2)}_{n+\frac{5}{2}}(ha)\right)\right\}, \quad (8)$$

which is the denominator for both A_n, B_n. The maximum values in question were obtained merely as final results of all the calculations, whence it follows that the criterion of the resonance condition is somewhat ambiguous, at any rate in the case of vibration of the surface of a spherical cavity. The fact that the vibrational frequency for maximum amplitude at the spherical surface does not perfectly agree with that for maximum amplitudes of the dissipation waves, will now be understood.

---

[8] It appears that in the case of Inouye's investigation *loc. cit.* 5) for $n=2$, the amplitude of dissipation waves assumes its maximum at a somewhat different value of ja and that the maximum value in question is too conspicuous.

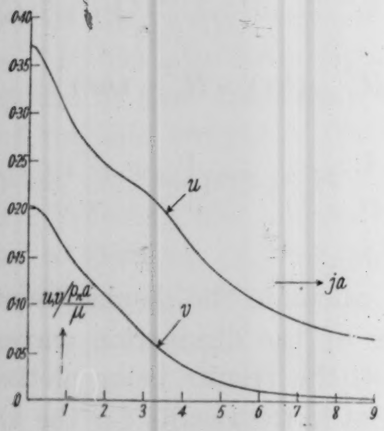

Fig. 1. Displacement at $r=a$, $n=1$.

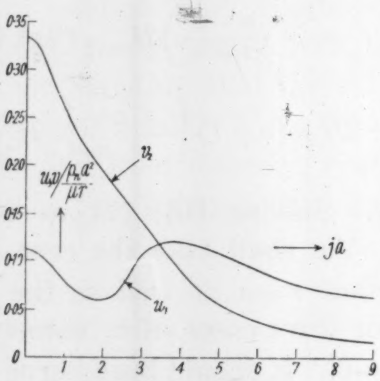

Fig. 2. Amplitudes of dissipation waves, $n=1$.

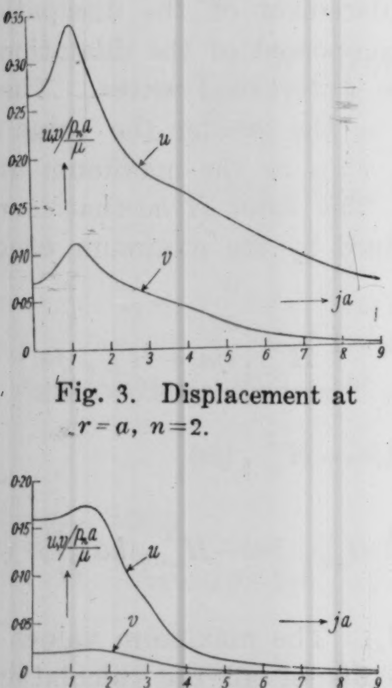

Fig. 3. Displacement at $r=a$, $n=2$.

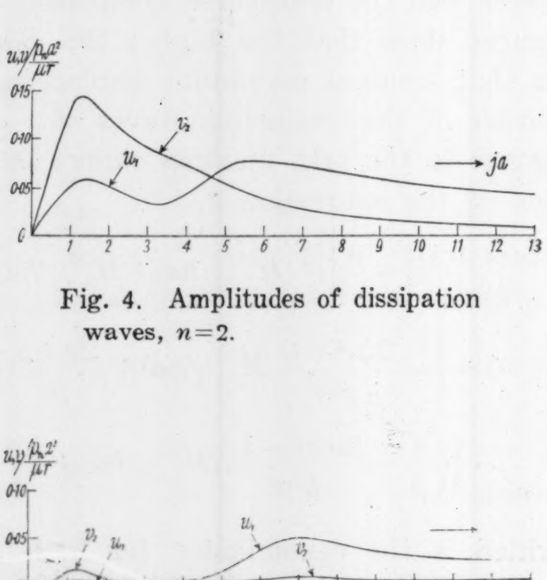

Fig. 4. Amplitudes of dissipation waves, $n=2$.

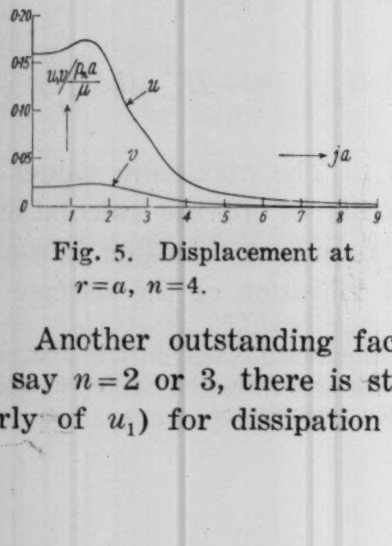

Fig. 5. Displacement at $r=a$, $n=4$.

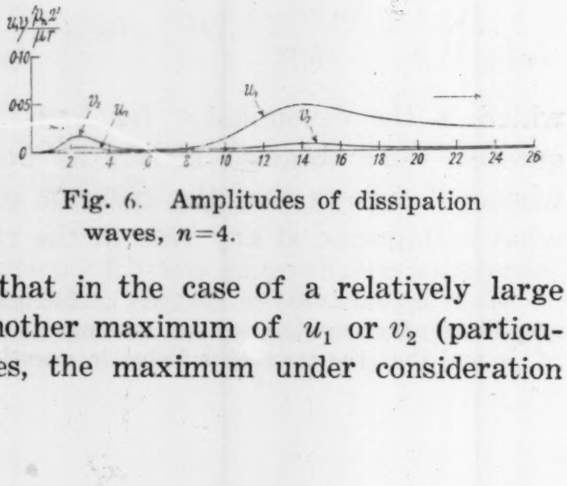

Fig. 6. Amplitudes of dissipation waves, $n=4$.

Another outstanding fact is that in the case of a relatively large n, say $n=2$ or 3, there is still another maximum of u_1 or v_2 (particularly of u_1) for dissipation waves, the maximum under consideration being greater even than the maximum value for the assumed resonance condition of the vibration.

4. In the case $n=\infty$, the Bessel functions assume the forms[9]

$$\left.\begin{aligned} H^{(2)}_{n+\frac{1}{2}}(hr) &= \frac{1}{\pi} e^{-ihr(\sin\tau-\tau\cos\tau)} \sum_{m=0}^{m=q} A_m(\tau) e^{i(2m+1)\frac{\pi}{4}} \frac{\Gamma\left(m+\frac{1}{2}\right)}{\left(\frac{hr}{2}\sin\tau\right)^{m+\frac{1}{2}}}, \\ &\qquad \left\{\cos\tau = \left(n+\frac{1}{2}\right)\Big/(hr) < 0\right\} \\ H^{(2)}_{n+\frac{1}{2}}(jr) &= \frac{1}{\pi} e^{-ijr(\sin\tau'-\tau'\cos\tau')} \sum_{m=0}^{m=q'} A_m(\tau') e^{i(2m+1)\frac{\pi}{4}} \frac{\Gamma\left(m+\frac{1}{2}\right)}{\left(\frac{jr}{2}\sin\tau'\right)^{m+\frac{1}{2}}} \\ &\qquad \left\{\cos\tau' = \left(n+\frac{1}{2}\right)\Big/(jr) < 0\right\} \end{aligned}\right\} \quad (9)$$

where both of the series perfectly converge within the terms q and q' respectively, and A_m's are of the type such that

$$\left.\begin{aligned} &A_0(\tau)=1, \quad A_1(\tau) = \frac{1}{8} + \frac{5}{24}\cot^2\tau, \\ &A_2 = \frac{3}{128} + \frac{77}{576}\cot^2\tau + \frac{385}{3456}\cot^4\tau, \end{aligned}\right\} \quad (10)$$

$$\left.\begin{aligned} H^{(2)}_{n+\frac{1}{2}}(hr) &= \frac{i}{\pi} e^{hr(\tau\cosh\tau-\sinh\tau)} \sum_{m=0}^{m=q} (-1)^m B_m(\tau) \frac{\Gamma\left(m+\frac{1}{2}\right)}{\left(\frac{hr}{2}\sinh\tau\right)^{m+\frac{1}{2}}}, \\ &\qquad \left\{\cosh\tau = \left(n+\frac{1}{2}\right)\Big/(hr) > 0\right\} \\ H^{(2)}_{n+\frac{1}{2}}(jr) &= \frac{i}{\pi} e^{jr(\tau'\cosh\tau'-\sinh\tau')} \sum_{m=0}^{m=q'} (-1)^m B_m(\tau') \frac{\Gamma\left(m+\frac{1}{2}\right)}{\left(\frac{jr}{2}\sinh\tau'\right)^{m+\frac{1}{2}}}, \\ &\qquad \left\{\cosh\tau' = \left(n+\frac{1}{2}\right)\Big/(jr) > 0\right\} \end{aligned}\right\} \quad (11)$$

where q, q' are of the same meanings as before and

---

[9] E. Jahnke u. F. Emde, *Funktionentafeln*, 103.

$$\left.\begin{aligned} &B_0(\tau)=1\,,\quad B_1(\tau)=\frac{1}{8}-\frac{5}{24}\coth^2\tau\,,\\ &B_2(\tau)=\frac{3}{128}-\frac{77}{576}\coth^2\tau+\frac{385}{3456}\coth^4\tau\,. \end{aligned}\right\} \tag{12}$$

From these expressions and (1), (2), (3), it follows that

(i) For $hr<n+\frac{1}{2}$ and $jr<n+\frac{1}{2}$, the movement of the body is in standing vibration. (The region within the second sphere in Fig. 7).

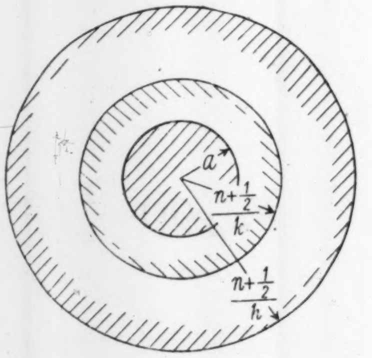

Fig. 7 [10]

(ii) As a special case of (i), *ha* and *ja* satisfy the condition that the expression in (8) vanishes, the equation thus formed being the same as the frequency equation for determining the velocity of Rayleigh-waves on a semi-infinite body. The standing vibration of the present problem is then under resonance condition.

(iii) For $hr<n+\frac{1}{2}$ and $jr>n+\frac{1}{2}$, transverse waves dissipate outwards, while the standing vibration, due to compressional displacement, still exists. (The region between the second and the third spheres in Fig. 7).

(iv) For $hr>n+\frac{1}{2}$ and $jr>n+\frac{1}{2}$, longitudinal and transverse waves dissipate outwards and no standing vibration exists. (The region outside the third sphere in Fig. 7).

5. We shall now compare the apparent resonance conditions for the movements at $r=a$ as well as the amplitudes of dissipation waves at $r=\infty$ for different values of n, the results being arranged as follows:

A maximum of the displacement at $r=a$ is present when

$n=1$	2	4	∞
$ja=0$	1·15	1·5	$0.9194\,n$

Maxima of u_1 at $r=\infty$ is present when

$n=1$	2	4	∞
$ja=$ 0 3·8	1·3 6	2·5 14	—

---

[10] The letter *k* in this figure was misused; indeed, the letter *j* had to be written in lieu of *k*.

Maxima of v_2 at $r=\infty$ is present when

$n=1$	2	4	∞
$ja=0$	1.3	$\begin{cases} 2.6 \\ 14 \end{cases}$	—

It should be borne in mind that the resonance condition of a solid vibrating sphere for $n=2$ is $ja=0{\cdot}840\pi=2{\cdot}64$,(11) which obviously differs from that for a body having a spherical cavity of the same radius.

It will be seen that the condition of maximum of dissipation waves is not likely to agree with the apparent resonance of surface vibration of the spherical cavity. It is possible to confirm whether the apparent resonance is the actual one or not by investigating the same mode of vibration under different exciting forces of the same frequency.

In the present problem the ratio of the transverse component v_2 of distortional waves to the radial component u_1 of dilatational waves, both at great distances from the origin, invariably vanishes in a linear order of zero. This is because the applied force at the surface of the spherical cavity is of normal pressure type. If, on the other hand, the applied force at the cavity were of the tangential force type, the result would probably be reversed, that is, the ratio of u_1/v_2 at great distances would then be in a linear order of zero. Since this case is also being investigated, the result will be available before long.

It is remarkable, at all events, that even under resonance conditions, the surface vibration of the cavity does not assume an infinitely large amplitude for a finite value of n. Nevertheless, the matter can be accounted for very simply. In the case of a finite value of n_1 the vibrational energy dissipates outside a certain radial distance, which contributes to the vibration damping, the result being very similar to that of the resonance-like but fairly damped vibration of a stratified body.[12]

---

11) H. LAMB, *Proc. Math. Soc., London,* **13** (1882).

12) K. SEZAWA and K. KANAI, "Decay Constants of Seismic Vibrations of a Surface Layer", *Bull. Earthq. Res. Inst.,* **13** (1935), 251~265.

It should be borne in mind that Saita's data, which we referred in the paper cited, are not complete owing to the fact that he took the ratio of the surface displacement to that beneath the surface layer. Notwithstanding the latter displacement should be nearly zero under resonance, since his result shows that the ratio under consideration is rather too small, so that it would hardly be possible to ascertain whether or not the amplitude under resonance is actually large.

2. 球窩面の振動に於ける共振現象及び逸散波

地震研究所 {妹澤克惟
金井清

半無限體の表面にディスターバンスを與へた場合に共振現象の存在し得ることがわかつたが，球窩面にディスターバンスを與へる場合にも同樣な事があり得るかどうかを研究して見たのである．

以前に出した球帶函數による解を應用して $n=1, 2, 4$ の場合を取り，且つディスターバンスは壓力型である場合を取つて見る．この場合にはいつでも逸散波が存在することがわかつた．之はよく考へると當然な事であつて，球窩の附近では一つの節面から次の節面までの距離が近くても遠方ではこの距離がいくらでも大きくなり遂には節面の影響がきかなくなるから從て逸散波が必ず存在する次第である．

以上のやうな機構があるから，共振現象も極めて不明瞭になるものである．或る振動週期で振幅がいくらか大きくなるやうに見えるけれども，しかし球窩面での振幅が最も大きくなる振動週期と無限の距離で逸散波の振幅が大きくなる振動週期とには多少喰ひ違ひがある．而も之等の週期は球體の表面の自由振動週期とも一致してをらぬものである．

尚特に變つてをることは，上の週期とは別に相當高い週期で逸散波の振幅が著しく大きくなることである．しかしその場合に球窩面では振幅が殊更大きくはならない．

只今の問題では，球窩面の振幅はその半徑方向のものが大きく，極く長い週期でも n が大きければ大きい程その方向のものが大きい，極く短い週期になると振幅は殆ど半徑方向のもののみとなるものである．無限大の距離での逸散波の振幅は，極く長い週期の振動では直角の方向の振幅の方が半徑の方向のものよりも大きいけれども，短い週期になると殆ど半徑方向の振幅のみとなるものである．この問題は球窩面に壓力型のディスターバンスの働いた場合の結果である．只今剪力型のものを研究中であるがその結果は著しく違つてをるやうである．

$n=\infty$ の場合を研究すると半無限體の場合のそれと非常によく一致した結果が現れる．

何れにしても n が有限の場合には球窩面の振幅が無限大になることのないのは注意すべき事柄である．之は逸散波が存在するためであつて，地表層の振動が如何に共振に相當する週期になつてもある減衰された狀態になるといふ我々の以前の研究と深く關聯してゐる事柄である．

3. *A Method of Minimizing the Seismic Vibrations of a Structure.*

By Katsutada SEZAWA and Kiyoshi KANAI,

Earthquake Research Institute.

(Read Dec. 15, 1936.—Received Dec. 21, 1936.)

I. *Introduction.*

1. Although the usual way of stiffening a structure as rigidly as possible seems to be based on the simple idea of practical safety, the method however cannot be commended from the dynamical point of view. Even should a structure be very rigidly stiffened and made earthquake-proof, namely, against seismic vibrations of relatively low frequencies, its conditions under resonance, that is to say, the very pronounced peaks in the resonance curves of its vibration can never be eliminated.

We believe that there are at least two practical ways of flattening the resonance curve, the one being to render more effective the dissipation of vibrational energy into the ground and the other to fit up a certain vibration damper inside the structure. If the foundation of the structure were in a satisfactory condition the former would be inherently present in the vibration phenomena of the structure in any earthquake. From our new investigations[1] of the last two years, it appears that in almost every structure of European style in the down-town of Tokyo, its serious vibration is fairly damped by the dissipation under consideration. The phenomenon being however self-existent, it is scarcely reasonable to expect a favourable condition of dissipation in any kind of structure.

The vibration damper that we propose here is a coupled oscillator with viscous damping. The principle of the method however is not new; the anti-rolling tank invented about thirty years ago for minimizing the rolling of ships and the Lanchester damper recently used for absorbing the vibrational energy of a machine being good examples. We found for the first time that the application of the same principle to the case of seismic vibrations of a structure is more effective and practicable than if applied to the case of rolling of ships or of machine vibrations.

---

[1] K. SEZAWA and K. KANAI's various papers on the decay of seismi cvibrations of a structure by dissipation of vibrational energy into the ground in the form of elastic waves, *Bull. Earthq. Res. Inst.* **13** (1935), **14** (1936).

Although we have already pointed out the feasibility of applying the coupled oscillator to minimizing the vibration of a structure,[2] in order to simplify matters we did not take into account viscous damping, with the result that it was not possible to obtain a solution showing a condition that is free from resonance for any vibrational frequency. In the present case we shall consider both restitutive and damping resistances in order to obtain a condition for minimizing the vibration for any frequency.

Since, generally speaking, the amplitude of seismic vibrations is particularly large in the horizontal sense, and since furthermore the vibration of a structure is most sensible to the same horizontal movement of the ground, the damper in question should be used mainly to resist the horizontal seismic vibrations.

Throughout this paper the discussion is theoretical, model experiments to confirm the theory being now in course of prgress. Bearing on the first and second sections of this paper, the case of a single-storied structure with a vibration damper and one with a damper similar to that of a seismograph were separately studied and the two cases then compared, whereas for the third section, we investigated the case of an actual three-storied structure, in which the roof, with certain modifications in the conditions of the columns just underneath it, was availed of as a vibration damper.

II. *A single-storied structure with a vibration damper.*

2. We shall use the following symbols.

l=height of the structure,

E, I=Young's modulus and sum of moments of inertia of sections of all columns,

x=coordinate taken along columns from their lower ends,

y=deflection of columns at x,

m=mass concentrated at the roof,

M, c, μ'=mass, stiffness, and the damping constant of the vibration damper,

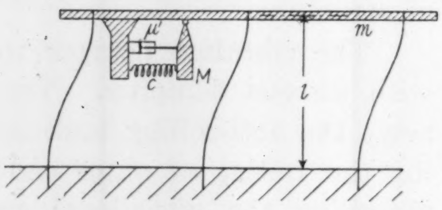

Fig. 1.

ξ=horizontal displacement of the damper mass relative to the roof of the structure,

---

[2] K. SEZAWA and K. KANAI, "Some New Problems of Forced Vibrations of a Structure", *Bull. Earthq. Res. Inst.*, **13** (1935), 848.

be^{ipt} = horizontal movement of the ground.

If the columns of the structure were assumed to be massless, the solution of their deflections would be written

$$y=(A+Bx+Cx^2+Dx^3)e^{ipt}. \tag{1}$$

When both ends of each column are in a fixed condition and no vibrational energy dissipates into the ground, the boundary conditions are

$$x=0; \qquad y=be^{ipt}, \quad \frac{\partial y}{\partial x}=0, \qquad (2),\ (3)$$

$$x=l; \qquad \frac{\partial y}{\partial x}=0, \tag{4}$$

$$-EI\frac{\partial^3 y}{\partial x^3}+m\frac{\partial^2 y}{\partial t^2}-c\xi-\mu'\frac{\partial \xi}{\partial t}=0, \tag{5}$$

$$\mathrm{M}\left(\frac{\partial^2 \xi}{\partial t^2}+\frac{\partial^2 y}{\partial t^2}\right)+c\xi+\mu'\frac{\partial \xi}{\partial t}=0. \tag{6}$$

Solving (1) ~ (6) we get

$$y=be^{ipt}\left[1+\left(-3\frac{x^2}{l^2}+2\frac{x^3}{l^3}\right)\frac{\left\{-\frac{mMl^3p^4}{EIc}+\frac{(m+M)l^3p^2}{EI}\right\}+i\frac{(m+M)\mu'l^3p^3}{EIc}}{\Phi}\right], \tag{7}$$

$$\frac{\partial^2 y}{\partial x^2}=\frac{6be^{ipt}}{l^2}\left[\left(-1+\frac{2x}{l}\right)\frac{\left\{-\frac{mMl^3p^4}{EIc}+\frac{(m+M)l^3p^2}{EI}\right\}+i\frac{(m+M)\mu'l^3p^3}{EIc}}{\Phi}\right], \tag{8}$$

where

$$\Phi=\left[\left\{\frac{(m+M)l^3p^2}{EI}-12\right\}-\frac{Mp^2}{c}\left\{\frac{ml^3p^2}{EI}-12\right\}\right]+i\frac{\mu'p}{c}\left\{\frac{(m+M)l^3p^2}{EI}-12\right\}, \tag{9}$$

$$\xi=\frac{Mp^2y_{x=l}}{(-Mp^2+c)+i\mu'p}. \tag{10}$$

In the special case, $x=l$, we have (taking the real parts)

$$y=\frac{12b\sqrt{(\eta\gamma-1)^2+\zeta\gamma}}{\sqrt{P^2+Q^2}}\cos\left(pt+\tan^{-1}\frac{\sqrt{\zeta\gamma}}{1-\eta\gamma}-\tan^{-1}\frac{Q}{P}\right), \tag{11}$$

$$\frac{EI\dfrac{\partial^2 y}{\partial x^2}}{(m+M)lp^2} = \frac{6b\sqrt{\left(\dfrac{m}{m+M}\eta\gamma-1\right)^2+\zeta\gamma}}{\sqrt{P^2+Q^2}}$$

$$\cdot\cos\left(pt+\tan^{-1}\frac{\sqrt{\zeta\gamma}}{1-\dfrac{m}{m+M}\eta\gamma}+\tan^{-1}\frac{Q}{P}\right), \qquad (12)$$

where

$$P=(\gamma-12)-\eta\gamma\left(\frac{m}{m+M}\gamma-12\right), \quad Q=\sqrt{\zeta\gamma}(\gamma-12), \qquad (13)$$

$$\gamma=\frac{(m+M)l^3p^2}{EI}, \quad \eta=\frac{EI}{(m+M)l^3}\frac{M}{c}, \quad \zeta=\frac{EI}{(m+M)l^3}\left(\frac{\mu'}{c}\right)^2, \qquad (14)$$

corresponding to the movement of the ground $y=b\cos pt$.

In the case, $\mu'\to\infty$, Q is the important term of the denominator of both y and $\partial^2y/\partial x^2$, whereas in the case, $\mu'\to 0$, P participates chiefly in the value of that denominator. In the former case the vibration is no more than an uncoupled one, the resonance frequency then being given by $\gamma=12$. In the latter case, on the other hand, the vibration is a coupled one of two degrees of freedom and the two resonance frequencies are indicated by the two values of p^2 in the equation $P=0$. These two extreme cases, namely $\zeta=\infty$, $\zeta=0$, are shown by the broken and chain lines respectively in both Figs. 2 and 4. For moderate values of μ' there are generally two resonance conditions.

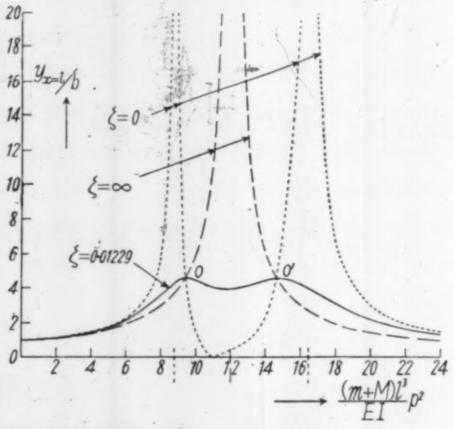

Fig. 2. The floor displacement.

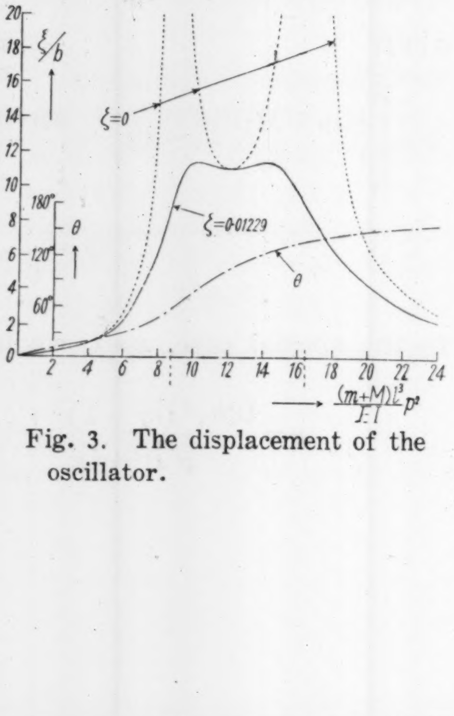

Fig. 3. The displacement of the oscillator.

3. It appears that the two intersection points 0, 0′ of the resonance curves of the two extreme cases in Fig. 2 and in Fig. 4 are independent of the value of μ', not being limited to the case $\mu'=\infty$; and that $\mu'=0$. These two points are obtained by a simple equation such as

$$\frac{Mp^2}{c}-1:\frac{\mu p}{c}=P:Q \qquad (15a)$$

in the case of the resonance curve for y, and

$$1-\frac{mMp^2}{(m+M)c}:\frac{\mu p}{c}=P:Q \qquad (15b)$$

in the case of the resonance curve for $\partial^2 y/\partial x^2$. The two values of y and the corresponding vibration frequecies thus found (for (15 a)) are

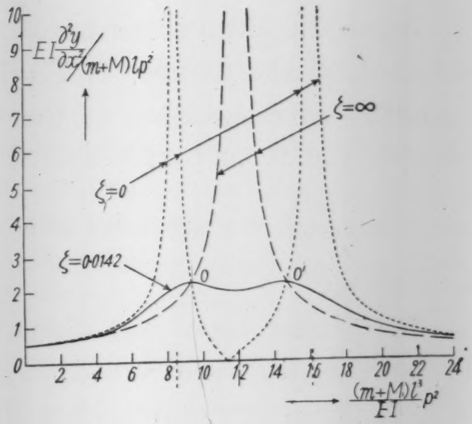

Fig. 4. The bending moments in columns.

$$\left.\begin{aligned}&\frac{y}{b}=\frac{12}{\gamma-12},\\ &\gamma=\frac{m+M}{2m+M}\left(\frac{1}{\eta}+21\right)\pm\sqrt{\left\{\frac{m+M}{2m+M}(\eta+12)\right\}^2-\frac{24}{\eta}\,\frac{m+M}{2m+M}}\end{aligned}\right\} \qquad (16a)$$

respectively. The two values of EId^2y/dx^2 and the corresponding vibration frequencies under similar condition (for (15 b)) are such that

$$\left.\begin{aligned}&EI\frac{d^2y}{dx^2}\Big/b(m+M)lp^2=\frac{6}{\gamma-12},\\ &\gamma=\left\{3\left(2+\frac{M}{m}\right)+\frac{1}{2\eta}\left(1+\frac{M}{m}\right)\right\}\pm\sqrt{\left\{3\left(2+\frac{M}{m}\right)+\frac{1}{2\eta}\left(1+\frac{M}{m}\right)\right\}^2-\frac{12}{\eta}\left(1+\frac{M}{m}\right)}.\end{aligned}\right\} \qquad (16b)$$

The resonance curve for any value of μ' should pass through the two points thus found in the case of either y or of d^2y/dx^2.

4. It is possible to make the ordinates of both 0 and 0′ of the same height. This is very easily attained by substituting the two values of γ in y in (16a) or in $d^2y\,dx^2$ in (16b) in either case and equating both values of y or of d^2y/dx^2, the result being such that

$$\eta=\frac{m+M}{12m},\quad \gamma=12\left\{1\pm\sqrt{\frac{M}{2m+M}}\right\},\quad \frac{y}{b}=\sqrt{\frac{2m+M}{M}} \qquad (17a)$$

for the case of y, and

$$\eta=\frac{m+M}{6(2m-M)},\quad \gamma=12\left(1\pm\sqrt{\frac{M}{2m}}\right),\quad \frac{EI\frac{d^2y}{dx^2}}{b(m+M)lp^2}=\sqrt{\frac{m}{2M}} \qquad (17b)$$

for the case of d^2y/dx^2.

Since the natural period of the structure is $T=2\pi\sqrt{12(m+M)l^3/EI}$ and that of the damper is $T'=2\pi\sqrt{M/c}$, we obtain the relation between T and T' corresponding to the values of η in (17a) or (17b), the relation for the former and that for the latter being

$$T'/T=\sqrt{(m+\text{M})/m}\,, \quad T'/T=\sqrt{(m+M)/6(2m-M)} \tag{18}$$

respectively.

5. Under these conditions we have calculated the resonance curves for both cases, the results being shown by full lines in Figs. 2, 3, 4. In both these cases we have taken $M/m=1/10$, whereas the values of c, μ' availed of are such that $\zeta=0.01229$, $T'/T=1.0488$ for y and ξ in Figs. 2, 3 and $\zeta=0.0142$, $T'/T=1.0765$ for EId^2y/dx^2 in Fig. 4. With a view to gaining an idea of the stiffness and the damping coefficient of the damper corresponding to the resonance curve in Fig. 3, we shall suppose that a single floor height of the Mitsubishi Naka 13go-kan forms a single-storied structure. The constants belonging to the damper which corresponds to the resonance curve of the full line in Fig. 4 are then such that $c=0{\cdot}998.10^{12}$ gr. mass/sec^2 and $\mu'=0{\cdot}296.10^{10}$ gr. mass/sec.

It will be seen that, by a suitable choice of c and μ', the amplitudes of vibrations or bending moments are strongly damped even under resonance conditions, and furthermore that the displacement of the damper itself is not necessarily too large. The ratio of $M/m=1/10$ is not practically too large. It appears that such ratio of masses also applies to the case of a high building.

III. *A single-storied structure with a damper similar to that used for seismographs, and its comparison with the preceding case.*

6. The question may arise whether or not the vibration damper of the preceding case is more effective than a damper used in the same way as for seismographs, namely, in such a way that the vibration of the floor is directly resisted by a damper resting on the moving ground. To answer it, we shall first obtain its mathematical solution and, using the same value of μ', we shall compare its nature with that of the preceding case. The boundary conditions in this case have the forms

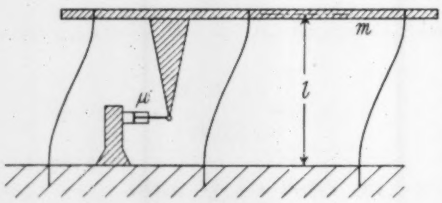

Fig. 5.

$$x=0;\qquad y=be^{ipt},\quad \frac{\partial y}{\partial x}=0, \tag{19), (20}$$

$$x=l;\quad \frac{\partial y}{\partial x}=0,\quad -EI\frac{\partial^3 y}{\partial x^3}+m\frac{\partial^2 y}{\partial t^2}+\mu'\frac{\partial}{\partial t}(y_l-y_0)=0. \tag{21), (22}$$

Substituting (1) in (19) ~ (22) we obtain the maximum values of y and $\partial^2 y/\partial x^2$ as follows:

$$y=b\sqrt{\frac{12^2+\gamma\zeta}{(12-\gamma)^2+\gamma\zeta}}\cos\left(pt+\tan^{-1}\frac{\sqrt{\gamma\zeta}}{12}-\tan^{-1}\frac{\sqrt{\gamma\zeta}}{12-\gamma}\right). \tag{23}$$

$$\frac{EI\dfrac{\partial^2 y}{\partial x^2}}{mlp^2}=\frac{-6b}{\sqrt{(12-\gamma)^2+\gamma\zeta}}\cos\left(pt-\tan^{-1}\frac{\sqrt{\gamma\zeta}}{12-\gamma}\right), \tag{24}$$

where

$$\gamma=\frac{ml^3p^2}{EI},\quad \zeta=\frac{\mu'^2l^3}{mEI} \tag{25}$$

corresponding to the ground vibration $y=b\cos pt$, the result for bending moments being plotted in Fig. 6. Notwithstanding that the value of μ' used in this case is the same as that for the resonance curve shown by the full line in Fig. 4, the peak of the resonance curve is very pronounced in this case. It will therefore be seen how ineffective the damping action would be were the damper used in the same manner as in the case of a seismograph.

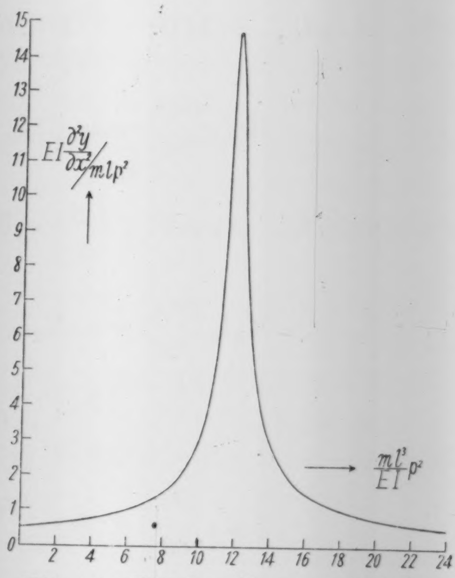

Fig. 6. The bending moment in columns.

IV. *A three-storied structure, with its roof used as a vibration damper.*

7. With a view to obtaining a more practical confirmation of the problem, we shall consider the case of the Mitsubishi Naka 13go-kan, with however certain modifications in the dimensions of the columns between the second floor and the roof, the original data of the structure being as shown in an earlier paper.[3]

---

[3] K. SEZAWA and K. KANAI, *Bull. Earthq. Res. Inst.*, **13** (1935), 930.

Let a viscous damper of constant μ' be placed between the second floor and the roof. Then the equations of the deflections of the columns in the respective floors are such that

$$y_n=(A_n+B_nx_n+C_nx_n^2+D_nx_n^3). \quad (n=1,2,3) \tag{26}$$

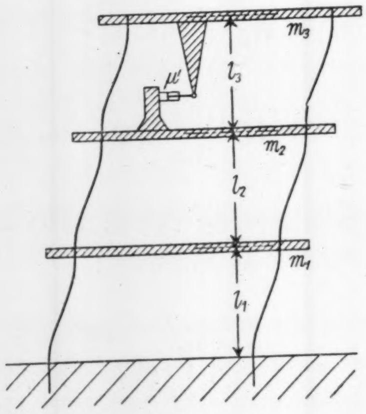

Fig. 7.

The boundary conditions in the case of no dissipation of energy into the ground have the forms

$$x_1=0; \qquad y_1=be^{ipt}, \quad \frac{\partial y_1}{\partial x_1}=0, \qquad (27),\ (28)$$

$$x_1=l_1, \quad x_2=0; \quad \frac{\partial y_1}{\partial x_1}=0, \quad \frac{\partial y_2}{\partial x_2}=0, \quad y_1=y_2, \qquad (29),\ (30),\ (31)$$

$$-E_2I_2\frac{\partial^3 y_2}{\partial x_2^3}=-E_1I_1\frac{\partial^3 y_1}{\partial x_1^3}+m_1\frac{\partial^2 y_1}{\partial t^2}, \tag{32}$$

$$x_2=l_2, \quad x_3=0; \quad \frac{\partial y_2}{\partial x_2}=0, \quad \frac{\partial y_3}{\partial x_3}=0, \quad y_2=y_3, \qquad (33),\ (34),\ (35)$$

$$-E_3I_3\frac{\partial^3 y_3}{\partial x_3^3}=-E_2I_2\frac{\partial^3 y_2}{\partial x_2^3}+m_2\frac{\partial^2 y_2}{\partial t^2}-\mu'\frac{\partial}{\partial t}(y_3-y_2), \tag{36}$$

$$x_3=l_3; \qquad \frac{\partial y_3}{\partial x_3}=0, \tag{37}$$

$$-E_3I_3\frac{\partial^3 y_3}{\partial x_3^3}+m_3\frac{\partial^2 y_3}{\partial t^2}+\mu'\frac{\partial}{\partial t}(y_3-y_2)=0. \tag{38}$$

Substituting (26) in (27) ~ (38) we eventually obtain

$$A_1=b,$$

$$\Phi l_1^3D_1=2b\Big\{[12(12\eta_1-\gamma_1)\eta_2\gamma_3+(12-\gamma_3)\{\gamma_1(12-\gamma_2)+12\eta_1\gamma_2\}]$$
$$+i\sqrt{\zeta_1\gamma_3}\{\eta_2\gamma_3(12\eta_1-\gamma_1)+\gamma_1(12-\gamma_2)+12\eta_1\gamma_2\}\Big\},$$

$$\Phi A_2=12b[\{12\eta_2\gamma_3-(12-\gamma_2)(12-\gamma_3)\}+i\sqrt{\zeta_1\gamma_3}\{\eta_2\gamma_3-(12-\gamma_2)\}],$$

$$\Phi l_2^3D_2=2.12b[\{12\eta_2\gamma_3+\gamma_2(12-\gamma_3)\}+i\sqrt{\zeta_1\gamma_3}(\eta_2\gamma_3+\gamma_2)],$$

$$\Phi A_3=-12^2b\{(12-\gamma_3)+i\sqrt{\zeta_1\gamma_3}\},$$

$$\Phi l_3^3D_3=2.12^2b\gamma_3,$$

$$\Phi=12[\{12(\eta_1+1)-\gamma_1\}\eta_2\gamma_3-(12-\gamma_3)\{(12-\gamma_1)(12-\gamma_2)-12\eta_1\gamma_2\}]$$

$$+\,i\sqrt{\zeta_1\gamma_3}[\{12(\eta_1+1)-\gamma_1\}\eta_2\gamma_3-(12-\gamma_1)(12-\gamma_2)+12\eta_1\gamma_2],$$

$$\gamma_1=\frac{m_1l_1^3p^2}{E_1I_1},\quad \gamma_2=\frac{m_2l_2^3p^2}{E_2I_2},\quad \gamma_3=\frac{m_3l_3^3p^2}{E_3I_3},$$

$$\eta_1=\frac{E_2I_2l_1^3}{E_1I_1l_2^3},\quad \eta_2=\frac{E_3I_3l_2^3}{E_2I_2l_3^3},\quad \zeta_1=\frac{\mu'^2l_3^3}{m_3E_3I_3},$$

$$B_1=B_2=B_3=0\,,\quad C_1=-\frac{3}{2}l_1D_1,\quad C_2=-\frac{3}{2}l_2D_2,\quad C_3=-\frac{3}{2}l_3D_3\,. \tag{39}$$

When $l_1=l_2=l_3\equiv l$, $m_1=m_2=m_3\equiv m$, $E_1I_1=E_2I_2\equiv EI$, $EI/E_3I_3\equiv\beta$, the maximum values of $\partial^2y_1/\partial x_1^2$, $\partial^2y_2/\partial x_2^2$, $\partial^2y_3/\partial x_3^2$ are such that

$$EI\frac{\partial^2y_1}{\partial x_1^2}\Big/bmlp^2=6\sqrt{\frac{R^2+S^2}{P^2+Q^2}}\cos\left(pt-\tan^{-1}\frac{Q}{P}+\tan^{-1}\frac{S}{R}\right), \tag{40}$$

$$EI\frac{\partial^2y_2}{\partial x_2^2}\Big/bmlp^2=6.12\sqrt{\frac{R'^2+S'^2}{P^2+Q^2}}\cos\left(pt-\tan^{-1}\frac{Q}{P}+\tan^{-1}\frac{S'}{R'}\right); \tag{41}$$

$$EI\frac{\partial^2y_3}{\partial x_3^2}\Big/bmlp^2=\frac{6.12^2\beta}{\sqrt{P^2+Q^2}}\cos\left(pt-\tan^{-1}\frac{Q}{P}\right), \tag{42}$$

where

$$\left.\begin{aligned}
&P=12\gamma(24-\gamma)-(12-\beta\gamma)\left\{(12-\gamma)^2-12\gamma\right\},\\
&Q=\sqrt{\beta\zeta\gamma}\left\{\gamma(24-\gamma)-(12-\gamma)^2+12\gamma\right\},\\
&R=12(12-\gamma)+(24-\gamma)(12-\beta\gamma),\\
&S=2\sqrt{\beta\zeta\gamma}(18-\gamma),\\
&R'=24-\beta\gamma,\quad S'=2\sqrt{\beta\zeta\gamma}\,.
\end{aligned}\right\} \tag{43}$$

8. Since it is rather difficult in the present case to determine the fixed points in the resonance curves similar to 0, 0′ in the case of a single-storied structure, we have tentatively chosen two particular cases, namely, (i) $\mu'^2l^3/mEI=6.91$, $EI/E_3I_3=2.617$; (ii) $\mu'^2l^3/mEI=0.929$, $EI/E_3I_3=20$. The values of EI and m are the same as those in the calculation for the Mitsubishi Naka 13go-kan[4] that is, $E=2{\cdot}1.10^9$ kg/m², $I=2{\cdot}54$ m⁴, $l=3{\cdot}67$ m, $m=5{\cdot}976.10^5$ kg. mass. Then $\mu'=0{\cdot}247.10^7.9{\cdot}8$kg. sec/$m=2{\cdot}42.10^{10}$ gr. mass/sec. The results in both cases (i), (ii) are

---

4) K. SEZAWA and K. KANAI, *loc. cit.* 3).

plotted in Fig. 8, 9. In every case, the short vertical strips marked on each base linere present the condition $P=0$ and that $Q=0$ respectively.

It will be seen that in the second case (ii), the bending moments in columns below the first floor and those below the second floor become as small as merely twice the values at zero frequency, even under resonance conditions

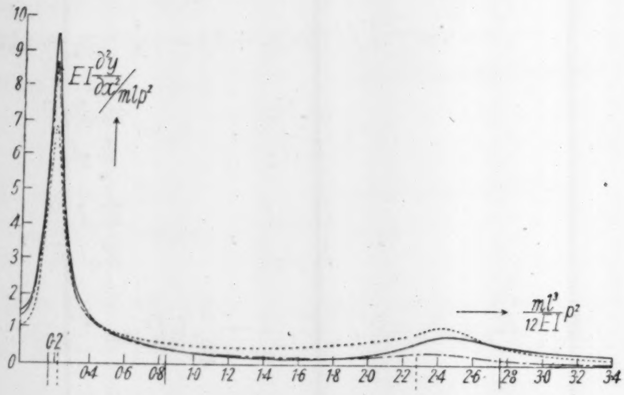

Fig. 8. The bending moments. $\mu'^2 l^3/mEI=6{\cdot}91$, $EI/E\,I=2{\cdot}617$. Full and broken lines represent the moments in columns beneath the first and second floors respectively, whereas the chain line the moment in columns for the oscillator.

Although, from the nature of the problem, the bending moments in columns between the second floor and the roof in case (ii) is naturally very large, its value under resonance conditions is never large compared with that at zero frequency. The construction of the columns under consideration should rather be constructed so that they shall resist high bending moments. A satisfactory method probably would be to use columns of mere steel frames with very little concrete attached. It is not a difficult matter to make $E_3 I_3/EI=1/10\sim 1/20$ by replacing the concrete columns with steel frame columns. The great advantage lies in the fact that the higher the resonance condition, the greater the diminution in value of the bending moment in every case.

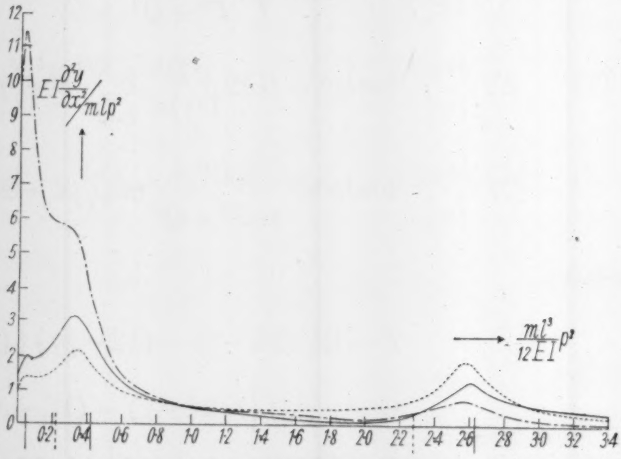

Fig. 9. The bending moment. $\mu'^2 l^3/mEI=0{\cdot}929$, $EI/E\,I_3=20$. Full and broken lines represent the moment in columns beneath the first and second floors respectively, whereas the chain line the moment in columns for the oscillator.

It should be borne in mind however that, although in the present example m_3 has been assumed to be equal to m_1 or m_2, it was merely for obtaining an easy confirmation of the practicability of the problem in an actual case. In order to use a smaller value of m_3, as was done in the case of a single storied structure in Section II, some changes in the value of E_3I_3 as well as in μ' was deemed suitable and sufficient in the attempt to obtain a virtually analogous result in minimizing the the seismic vibration of the structure.

9. With a view to ascertaining the amount of μ' that would be necessary for obtaining the damped condition in case (ii), we shall take viscous friction as an example. From the experiments of Ishimoto and Iida,[5] a certain soil of 48% water content has a viscosity $\mu = 1\cdot6.10^5$ (C. G. S.). If we were to use a thin box of thickness $2h = 2$ cm as a damper which contains the soil under consideration, a sliding vane inserted in the box for generating a shearing resistance to the relative movements of the second floor and the roof should have an area of $A = 7.6\ \mathrm{m}^2$, which is immediately determined from the expression for the damping force, namely,

$$\mu \frac{2A}{h} \frac{\partial}{\partial t} (y_3 - y_2)\,, \tag{44}$$

where

$$\mu 2A/h = \mu'. \tag{45}$$

The above damping mechanism may be replaced by a Coulomb friction, a device rather easily constructed.

As already said, we are trying to confirm the present result by means of model experiments.

In conclusion we wish to express our thanks to the Council of the Japan Society for the Promotion of Scientific Research, with whose aid the present investigation has been made possible.

---

3. 構造物の震動を防止する一つの方法

地震研究所 {妹澤克惟
　　　　　 {金井清

構造物を耐震的にする爲にできるだけ剛くすることは實際上には簡單であるけれども之は力學的に考へて餘り賢い方法とはいはれない．理論的に面白く且つ今まで餘り氣のつかなかつた方法は，その一つとして震動勢力が地中によく逸散するやうにすることであり，他の一つは減衰聯成振動器を附加へることである．始めの方法は我々が初めて研究したものであるが，それは自然の

---

[5] M. Ishimoto et K. Iida, "Experiences sur le sol", *Bull. Earthq. Res. Inst.*, **14** (1936), 537.

狀態で減衰させるのであるからその減衰性には限度がある．然るに第二の方法は他の工學的方面，例へば造船學や回轉機械では以前から用ひられてをつたものであつて餘り新しくはないけれども，之は構造物震動の制振法には特に有効に働くことがわかつたのである．尤も之は人工的の方法であるから有効なことは當然とも思はれる．この論文では主として力學的研究のみを行ひ模型實驗は只今計畫中である．

最も簡單な場合として1階建を取り，之に第1圖の如き震動制振器（その質量は構造物のそれの1/10とす）を附加へる．減衰器の粘性が零の場合には第2圖（振幅）第4圖（屈曲モーメント）の$\zeta=0$ 如き共振曲線となり，粘性が無限大になると$\zeta=\infty$ の如き共振曲線となる．然るに減衰器の彈性と粘性とを適當に調整するとそれ等の圖の實線の如き共振曲線となり，共振に於ける振幅や屈曲モーメントが零振動數の場合のそれの4倍位にしかならぬものである．尙震動減衰器の振子の振幅もそれ程は大きくはなく第2圖に相當して第3圖の如き割合となるのに過ぎぬものである．

震動制振器を地震計の制振器のやうな狀態卽ち第5圖の如く配置すると減衰性がもつとよくはならぬかをしらべて置く．第4圖の場合と同じ數値を用ひると（粘性も同じにする），第6圖のやうな共振曲線が得られる．これで見ると地震計のやうな方法にする方がむしろ効果の少いことがわかる譯である．

實在の建物の一部分を變更して震動制振器が造り得ぬかを見る爲に三菱仲 13 號館の3階の柱を細くして見る．例へばそのコンクリート柱を鐵柱に直せばよい譯である．3階の柱の應力は少いけれどもその振幅は大きい．而して粘性抵抗器を3階の床と屋根との間に挾んで見る．その鐵柱の大さの割合によつて第8圖，第9圖の如き屈曲モーメントの共振曲線が得られる譯である．第9圖の場合には振子として用ひた3階の柱のモーメントは相當に大きいけれども，1階2階のモーメントは共振週期でも非常に小さくなることが知られる．

この3階建の例では屋根の質量を態とその儘にして3階の柱の寸法だけを變へて見たのである．之は變數を二重に作るのを避ける爲である．震動制振器の振子を特に附加へるにはこの質量をなるべく小さくしなければならぬ．それにはその彈性卽ち柱の抵抗を遙かに少しく且つ粘性の値を適當に與へればよい．この例もそのうちに出すけれども，只今の例について誤解のない事を望む次第である．この論文の結果でも1階の場合の質量比を見れば容易に想像がつくものと思ふ．

尙，振動制振器中の粘力器は可なり小なるもの例へば三菱仲 13 號館の場合に數米平方位の寸法のものでも役立つことがわかつたのである．

4. *Further Studies on the Seismic Vibrations of a Gozyûnotô (Pagoda).*

By Katsutada SEZAWA and Kiyoshi KANAI,

Earthquake Research Institute.

(Read Dec. 15, 1936.—Received Dec. 21, 1936.)

1. *Introduction.*

In our previous paper[1] we discussed the earthquake-proof properties of a gozyûnotô mainly from the standpoint of dissipation of the vibrational energy into the ground. The data of numerous experiments, due to Omori,[2] that we used in our calculation in the previous paper, were restricted to structural dimensions and the vibration frequency of the tower. Upon reexamining the problem, however, we found that application of such data implied the condition that the mass of the tower is disproportionately large, with the result that the dissipation of vibrational energy forms an important part of the damping phenomena. If, on the other hand, we were to take the most probable mass of the tower, the dissipation would be negligible, the nature of the problem thus differing entirely from that of a concrete structure of European style. We are therefore now in a position to reinvestigate the problem from a different point of view.

The deformation damping resistance of a structure as worked out by us[3] is not more effective on the damping phenomena of the structure here treated than in others. The conclusions arrived at after our inspection of actual towers, particularly of the Ueno Gozyûnotô, is that Coulomb's damping is the principal resistance and, furthermore, that the damping should increase with increase in the relative displacements between the respective adjacent roof truss parts for the reason that the structural members in every columnar part between the roof truss parts under consideration are connected by joggle joints, but not by simple slip joints. Aside from this fact, it is possible for the Coulomb damping in a vibrating body to increase with increase in the relative displacements in consequence of the diminution in the moving velocity with increase in the displacements in question. Under these considerations we assumed that the Coulomb damping approximately increases linearly as the relative displacements.

---

[1] K. SEZAWA and K. KANAI, "On the Vibrations of a Gozyûnotô (Pagoda)", *Bull. Earthq. Res. Inst.*, **14** (1936), 525~533.

[2] F. OMORI, *Bull. Earthq. Inv. Comm.*, **9** (1918~21), 110~150.

[3] K. SEZAWA, *Bull. Earthq. Res. Inst.*, **3** (1927), 50.

It should be borne in mind that, since not only gozyûnotôs but also almost all Japanese style structures, including a palace and a buddhist temple, are more or less similar in type, the correct treatment of Coulomb damping is extremely important over a wider range of problems. All we can add here is that this form of damping is very far-reaching in the case of the gozyûnotô.

2. *The solution of the problem.*

Let $y_1, y_2, \cdots, y_5$ be horizontal displacements of the first, second, $\cdots$, fourth and fifth roof truss parts respectively, and y_0 the horizontal movement of the ground. If the elastic resistance is proportional to the relative displacements of adjacent roof truss parts and the damping resistance is a certain function of the relative velocities of the same roof truss parts, then the equations of vibrations are expressed by

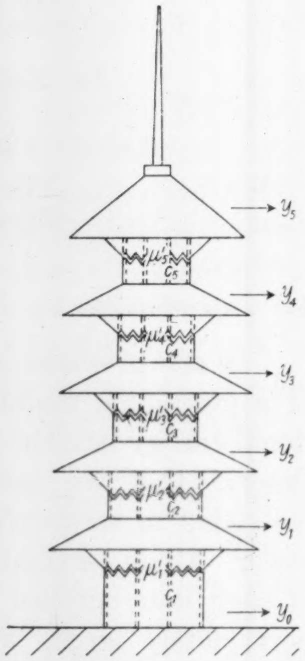

Fig. 1.

$$\left.\begin{aligned}
&M_1\ddot{y}_1+f_1(\dot{y}_1-\dot{y}_0)-f_2(\dot{y}_2-\dot{y}_1)+c_1(y_1-y_0)-c_2(y_2-y_1)=0\,,\\
&M_2\ddot{y}_2+f_2(\dot{y}_2-\dot{y}_1)-f_3(\dot{y}_3-\dot{y}_2)+c_2(y_2-y_1)-c_3(y_3-y_2)=0\,,\\
&\cdots\cdots\cdots\cdots\cdots\cdots\cdots\cdots\cdots\cdots\cdots\cdots\cdots\cdots\\
&M_5\ddot{y}_5+f_5(\dot{y}_5-\dot{y}_4)+c_5(y_5-y_4)=0,
\end{aligned}\right\} \qquad (1)$$

where $M_1, M_2, \cdots, M_5, c_1, c_2, \cdots, c_5$ are masses concentrated on the respective roof truss parts and the stiffnesses of the columnar parts between the successive roof truss parts, whereas $f_1, f_2, \cdots, f_5$ are functions corresponding to the damping. Rewriting the above equations and putting $M_1=M_2=\cdots=M_5\equiv M$, $f_1=f_2=\cdots=f_5\equiv f$, $c_1=c_2=\cdots=c_5\equiv c$, we get

$$\left.\begin{aligned}
&f(\dot{y}_1-\dot{y}_0)+c(y_1-y_0)=-M(\ddot{y}_1+\ddot{y}_2+\cdots+\ddot{y}_5)\,,\\
&f(\dot{y}_2-\dot{y}_1)+c(y_2-y_1)=-M(\ddot{y}_2+\ddot{y}_3+\cdots+\ddot{y}_5)\,,\\
&\cdots\cdots\cdots\cdots\cdots\cdots\cdots\cdots\cdots\cdots\\
&f(\dot{y}_5-\dot{y}_4)+c(y_5-y_4)=-M\ddot{y}_5\,.
\end{aligned}\right\} \qquad (2)$$

The expressions of types (2) for a special case, $f=0$, was obtained by

Martel.4)

The simplest way to express f is to write

$$f(\dot{y}_n-\dot{y}_{n-1})=\mu'(\dot{y}_n-\dot{y}_{n-1}) \tag{3}$$

where μ' is a constant depending on the frequency of the vibration. By adjusting the form of μ', it is possible to have a damping force in agreeing with Coulomb's friction. From the condition assumed we have

$$f(\dot{y}_n-\dot{y}_{n-1})=Fi(y_n-y_{n-1}), \tag{4}$$

where F is a constant independent of the vibrational frequency. The nature of the damping resistance and that of the elastic resistance differ only in the term of i. Let

$$y_0=A_0e^{ipt},\quad y_1=A_1e^{ipt},\ \cdots\cdots,\quad y_5=A_5e^{ipt}. \tag{5}$$

Equating (3), (4) by means of (5), we get

$$\mu'=F/p. \tag{6}$$

Now substituting (5) in (2) under the condition $\mu'=F/p$, we get

$$\begin{aligned}\frac{A_1\Phi}{A_0}=&\Bigg[\left\{-1+10\left(\frac{p\mu'}{c}\right)^2-5\left(\frac{p\mu'}{c}\right)^4\right\}+10\left(\frac{Mp^2}{c}\right)\left\{1-6\left(\frac{p\mu'}{c}\right)^2+\left(\frac{p\mu'}{c}\right)^4\right\}\\&+15\left(\frac{Mp^2}{c}\right)^2\left\{-1+3\left(\frac{p\mu'}{c}\right)^2\right\}+7\left(\frac{Mp^2}{c}\right)^3\left\{1-\left(\frac{p\mu'}{c}\right)^2\right\}-\left(\frac{Mp^2}{c}\right)^4\Bigg]\\&+i\left(\frac{p\mu'}{c}\right)\Bigg[\left\{-5+10\left(\frac{p\mu'}{c}\right)^2-\left(\frac{p\mu'}{c}\right)^4\right\}+40\left(\frac{Mp^2}{c}\right)\left\{1-\left(\frac{p\mu'}{c}\right)^2\right\}\\&+15\left(\frac{Mp^2}{c}\right)^2\left\{-3+\left(\frac{p\mu'}{c}\right)^2\right\}+14\left(\frac{Mp^2}{c}\right)^3-\left(\frac{Mp^2}{c}\right)^4\Bigg],\end{aligned} \tag{7}$$

$$\begin{aligned}\frac{A_2\Phi}{A_0}=&\Bigg[\left\{-1+10\left(\frac{p\mu'}{c}\right)^2-5\left(\frac{p\mu'}{c}\right)^4\right\}+6\left(\frac{Mp^2}{c}\right)\left\{1-6\left(\frac{p\mu'}{c}\right)^2+\left(\frac{p\mu'}{c}\right)^4\right\}\\&+5\left(\frac{Mp^2}{c}\right)^2\left\{-1+3\left(\frac{p\mu'}{c}\right)^2\right\}+\left(\frac{Mp^2}{c}\right)^3\left\{1-\left(\frac{p\mu'}{c}\right)^2\right\}\Bigg]\\&+i\left(\frac{p\mu'}{c}\right)\Bigg[\left\{-5+10\left(\frac{p\mu'}{c}\right)^2-\left(\frac{p\mu'}{c}\right)^4\right\}+24\left(\frac{Mp^2}{c}\right)\left\{1-\left(\frac{p\mu'}{c}\right)^2\right\}\\&+5\left(\frac{Mp^2}{c}\right)^2\left\{-3+\left(\frac{p\mu'}{c}\right)^2\right\}+2\left(\frac{Mp^2}{c}\right)^3\Bigg],\end{aligned} \tag{8}$$

$$\begin{aligned}\frac{A_3\Phi}{A_0}=&\Bigg[\left\{-1+10\left(\frac{p\mu'}{c}\right)^2-5\left(\frac{p\mu'}{c}\right)^4\right\}+3\left(\frac{Mp^2}{c}\right)\left\{1-6\left(\frac{p\mu'}{c}\right)^2+\left(\frac{p\mu'}{c}\right)^4\right\}\\&+\left(\frac{Mp^2}{c}\right)^2\left\{-1+3\left(\frac{p\mu'}{c}\right)^2\right\}\Bigg]+i\left(\frac{p\mu'}{c}\right)\Bigg[\left\{-5+10\left(\frac{p\mu'}{c}\right)^2-\left(\frac{p\mu'}{c}\right)^4\right\}\end{aligned}$$

---

4) R. R. MARTEL, "The Dynamic Behaviour of Some Simple Bents Subjected to Established Simple Harmonic Motion", *World Eng. Congr. Tokyo*, 1929, 3, Paper No. 490.

$$+12\left(\frac{Mp^2}{c}\right)\left\{1-\left(\frac{p\mu'}{c}\right)^2\right\}+\left(\frac{Mp^2}{c}\right)^2\left\{-3+\left(\frac{p\mu'}{c}\right)^2\right\}\Bigg], \quad (9)$$

$$\frac{A_4\Phi}{A_0}=\left[\left\{-1+10\left(\frac{p\mu'}{c}\right)^2-5\left(\frac{p\mu'}{c}\right)^4\right\}+\left(\frac{Mp^2}{c}\right)\left\{1-6\left(\frac{p\mu'}{c}\right)^2+\left(\frac{p\mu'}{c}\right)^4\right\}\right]$$

$$+i\left(\frac{p\mu'}{c}\right)\left[\left\{-5+10\left(\frac{p\mu'}{c}\right)^2-\left(\frac{p\mu'}{c}\right)^4\right\}+4\left(\frac{Mp^2}{c}\right)\left\{1-\left(\frac{p\mu'}{c}\right)^2\right\}\right], \quad (10)$$

$$\frac{A_5\Phi}{A_0}=\left\{-1+10\left(\frac{p\mu'}{c}\right)^2-5\left(\frac{p\mu'}{c}\right)^4\right\}+i\left(\frac{p\mu'}{c}\right)\left\{-5+10\left(\frac{p\mu'}{c}\right)^2-\left(\frac{p\mu'}{c}\right)^4\right\}, \quad (11)$$

where

$$\Phi=P+iQ$$

$$=\Bigg[\left\{-1+10\left(\frac{p\mu'}{c}\right)^2-5\left(\frac{p\mu'}{c}\right)^4\right\}+15\left(\frac{Mp^2}{c}\right)\left\{1-6\left(\frac{p\mu'}{c}\right)^2+\left(\frac{p\mu'}{c}\right)^4\right\}$$

$$+35\left(\frac{Mp^2}{c}\right)^2\left\{-1+3\left(\frac{p\mu'}{c}\right)^2\right\}+28\left(\frac{Mp^2}{c}\right)^3\left\{1-\left(\frac{p\mu'}{c}\right)^2\right\}-9\left(\frac{Mp^2}{c}\right)^4$$

$$+\left(\frac{Mp^2}{c}\right)^5\Bigg]+i\left(\frac{p\mu'}{c}\right)\Bigg[\left\{-5+10\left(\frac{p\mu'}{c}\right)^2-\left(\frac{p\mu'}{c}\right)^4\right\}+60\left(\frac{Mp^2}{c}\right)\left\{1-\left(\frac{p\mu'}{c}\right)^2\right\}$$

$$+35\left(\frac{Mp^2}{c}\right)^2\left\{-3+\left(\frac{p\mu'}{c}\right)^2\right\}+56\left(\frac{Mp^2}{c}\right)^3-9\left(\frac{Mp^2}{c}\right)^4\Bigg\}. \quad (12)$$

Rewriting these expressions we get

$$\left(\frac{p\mu'}{c}\right)^2=\alpha, \quad \frac{Mp^2}{c}=\beta; \quad (13)$$

$$\frac{A_1\Phi}{A_0}=\left\{(-1+10\alpha-5\alpha^2)+10\beta(1-6\alpha+\alpha^2)+15\beta^2(-1+3\alpha)+7\beta^3(1-\alpha)-\beta^4\right\}$$

$$+i\sqrt{\alpha}\left\{(-5+10\alpha-\alpha^2)+40\beta(1-\alpha)+15\beta^2(-3+\alpha)+14\beta^3-\beta^4\right\}, \quad (7')$$

$$\frac{A_2\Phi}{A_0}=\left\{(-1+10\alpha-5\alpha^2)+6\beta(1-6\alpha+\alpha^2)+5\beta^2(-1+3\alpha)+\beta^2(1-\alpha)\right\}$$

$$+i\sqrt{\alpha}\left\{(-5+10\alpha-\alpha^2)+24\beta(1-\alpha)+5\beta^2(-3+\alpha)+2\beta^3\right\}, \quad (8')$$

$$\frac{A_3\Phi}{A_0}=\left\{(-1+10\alpha-5\alpha^2)+3\beta(1-6\alpha+\alpha^2)+\beta^2(-1+3\alpha)\right\}$$

$$+i\sqrt{\alpha}\left\{(-5+10\alpha-\alpha^2)+12\beta(1-\alpha)+\beta^2(-3+\alpha)\right\}, \quad (9')$$

$$\frac{A_4\Phi}{A_0}=\left\{(-1+10\alpha-5\alpha^2)+\beta(1-6\alpha+\alpha^2)\right\}$$

$$+i\sqrt{\alpha}\left\{(-5+10\alpha-\alpha^2)+4\beta(1-\alpha)\right\}, \quad (10')$$

$$\frac{A_5\Phi}{A_0}=(-1+10\alpha-5\alpha^2)+i\sqrt{\alpha}\,(-5+10\alpha-\alpha^2)\,, \tag{11'}$$

$$\begin{aligned}\Phi=&\Big\{(-1+10\alpha-5\alpha^2)+15\beta(1-6\alpha+\alpha^2)+35\beta^2(-1+3\alpha)\\ &+28\beta^3(1-\alpha)-9\beta^4+\beta_5\Big\}+i\sqrt{\alpha}\,\Big\{(-5+10\alpha-\alpha^2)+60\beta(1-\alpha)\\ &+35\beta^2(-3+\alpha)+56\beta^3-9\beta^4\Big\}\,.\end{aligned} \tag{12'}$$

3. *Some numerical examples.*

Omori's report[5] contains, though not always perfectly accurate, a good deal of experimental data regarding free vibrations as well as artificial forced vibrations of the gozyûnotôs, from which it is possible to estimate roughly the values of the damping constants peculiar to the vibrations of various towers. In the case of the Ueno Gozyûnotô, the amplitude of the free vibration diminishes to about one-half its initial value after three or four cycles of vibrations, whereas the amplitude of the forced vibration at a frequency of about two-thirds of the natural one is nearly one-tenth or one-fifteenth of the amplitude under resonance conditions. After a number of tentative calculations we found that the following two examples represent extreme cases of the mostly probable conditions which actual towers of the natural period 1 sec should assume; the case of Ueno Gozyûnotô seeming to correspond to the first of the examples.

(i) $M/c=0{\cdot}002052\,\mathrm{sec}^2$, $F/Mg=0{\cdot}02547\,\mathrm{cm}^{-1}$;

(ii) $M/c=0{\cdot}002052\,\mathrm{sec}^2$, $F/Mg=0{\cdot}2487\,\mathrm{cm}^{-1}$.

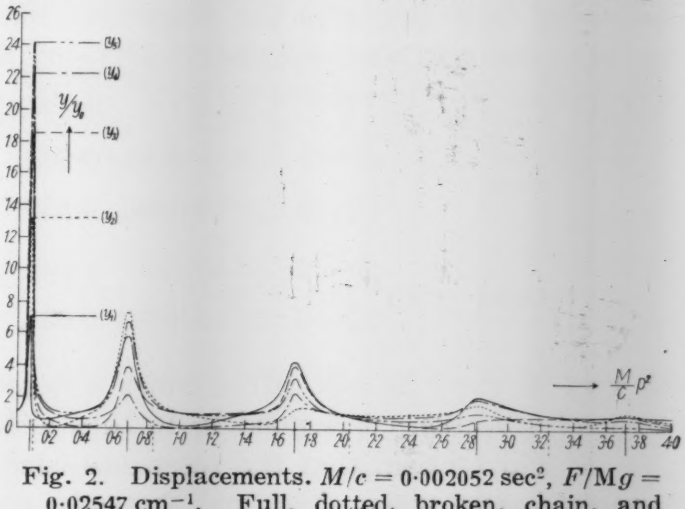

Fig. 2. Displacements. $M/c=0{\cdot}002052\,\mathrm{sec}^2$, $F/Mg=0{\cdot}02547\,\mathrm{cm}^{-1}$. Full, dotted, broken, chain, and double chain lines represent the displacements of the first, second, third, forth, and fifth roof truss parts respectively.

The relation $M/c=0{\cdot}002052\,\mathrm{sec}^2$ gives the condition that the fundamental natural period of the tower is about 1 sec, whereas $F/Mg=0{\cdot}02547\,\mathrm{cm}^{-1}$ and $F/Mg=0{\cdot}2487\,\mathrm{cm}^{-1}$ indicate the conditions that the ratios of the tangential friction to the weight of a one story for relative displacements of 1 cm are 0·02547 and 0·2487 respectively. These ratios are rather too small when compared with the results of other kinds of experiments. The result of calculation for these two cases are shown in Figs. 2, 3. The full, dotted, broken, chain, and double-chain lines represent the displacement ratios of the first, second, third, fourth, and the fifth roof truss parts to the ground vibration, namely y_1/y_0, y_2/y_0, y_3/y_0, y_4/y_0, y_5/y_0 respectively. The short vertical strips of full line and those of dotted line marked on every base line give the respective conditions, $P=0$, $Q=0$, that is to say, the real and imaginary parts of Φ become zero respectively; the values of β corresponding to $P=0$, $Q=0$ being shown below.

---

[5] F. Omori, *loc. cit.* 2)

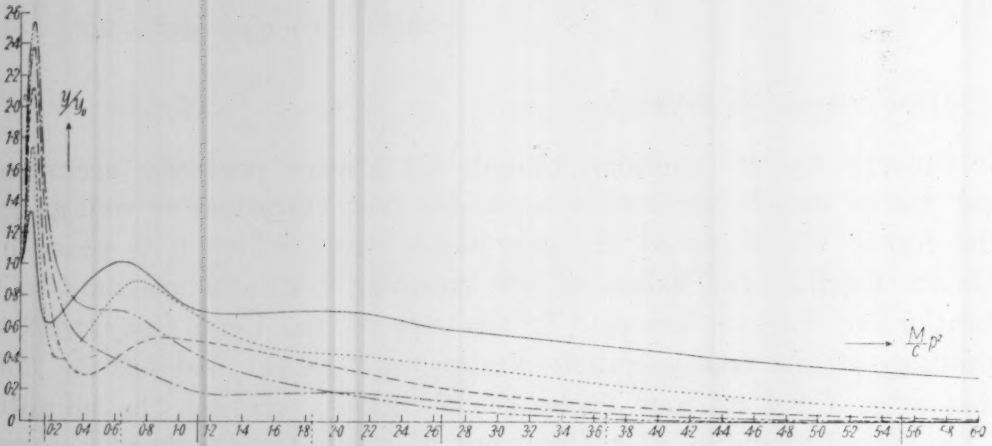

Fig. 3. Displacements. $M/c = 0{\cdot}002052\ \mathrm{sec}^2$, $F/Mg = 0{\cdot}2487\ \mathrm{cm}^{-1}$. Full, dotted, broken, chain and double chain lines represent the displacements of the first, second, third, forth, and fifth roof truss parts respectively.

$$\text{Case (i)}\begin{cases} P=0;\ \beta=0{\cdot}0803,\ 0{\cdot}681,\ 1{\cdot}705,\ 2{\cdot}816,\ 3{\cdot}717; \\ Q=0;\ \beta=0{\cdot}0996,\ 0{\cdot}839,\ 2{\cdot}038,\ 3{\cdot}25. \end{cases}$$

$$\text{Case (ii)}\begin{cases} P=0;\ \beta=0{\cdot}159,\ 1{\cdot}123,\ 2{\cdot}65,\ 5{\cdot}521,\ -0{\cdot}45; \\ Q=0;\ \beta=0{\cdot}0659,\ 0{\cdot}638,\ 1{\cdot}839,\ 3{\cdot}679. \end{cases}$$

A root of $P=0$ in case (ii) assumes a negative value, showing that the natural vibration corresponding to this, should it exist, is aperiodic.

It will be seen that the resonance condition in case (i) takes place approximately when $P=0$ and the same condition in case (ii) approximately when $Q=0$. At all events, the frequency of the fundamental resonance was adjusted to 1 sec in both cases.

4. *Interpretation of the result.*

It will be seen from the results given here that, although in case (i), the amplitude of the uppermost roof truss part at frequency near the first resonance is about 24 times that of the ground movement, a similar amplitude in case (ii) is only about 2·5 times that of the ground movement.

In both examples, the lower the roof truss part the smaller the amplitude of the same part at relatively low frequency. For higher vibration frequencies, on the other hand, the amplitudes of the higher roof truss parts become smaller, the feature of the displacement distribution for a fairly high frequency being the very reverse of that of the fundamental resonance condition. In case (i), displacement of the first roof truss part becomes the largest at frequencies near the third resonance, whereas in case (ii) the same displacement becomes the largest one even at frequency below the second resonance.

It is a remarkable fact that, while the large amplitude under all resonance conditions is fairly pronounced in case (i), amplitude under any resonance higher than the third in case (ii) is scarcely noticeable, with the result that it is almost impossible to identify the resonance frequencies from the resonance curves.

It seems that the property of vibration damping in a structure of the present type is not only restricted to a gozyûnotô, but, is also found in the case of a buddhist temple, and even in a house of palace style of construction in Japan. It may however be concluded that the property under consideration is particularly pronounced in the case of the gozyûnotô.

In conclusion we wish to express our thanks to the Council of the Japan Society for the Promotion of Scientific Research, with whose aid progress in the present investigation was considerably furthered.

4. 五重塔の耐震性に關する研究

地震研究所 妹澤克惟
地震研究所 金井清

この前の報告に於て五重塔の耐震性に關する問題を論じて置いた．しかしその議論に必要なる數値的材料は主さして大森博士が試みた振動週期についての試験結果さ塔の幾何學的寸法のみであつて，塔の重さについては直接考へて見なかつた爲に，五重塔の耐震性がコンクリートの建物

と同様に震動勢力の地中逸散といふことで見た所は相當に説明がついたのである．しかしその結果として塔の重量が非常に大きなものでないと成立たぬことに氣がついたので，その耐震性を更に見直して見ることにした譯である．

構造物中の粘性抵抗が五重塔の場合に限つて特に大きいとは考へられぬ．五重塔の構造をよくしらべて見ると Coulomb の固體摩擦がよく働いてをることがわかつた．而も之は塔の順々の屋根及斗組の間にある軸部に於ける結合部が主として嚙合接となつてをる爲に軸部の比較變性の大さに比例してこの摩擦が增加することがわかつたのである．接合せが嚙合でなく突附接の場合でも比較變位速度の增加と共に Coulomb の摩擦が減少するから，從て軸部の比較變位の大さと共に摩擦の增加するのは寧ろ一般的の性質のやうである．

このやうな考のもとに震動の理論的研究を試みたのであるが，その彈性的及び摩擦的常數は如何にして定めたかといふと，それには大森博士の五重塔の强制振動及び自由振動の試驗結果を比較して見た上でのことである．即ち自由振動では3週期か4週期の繰返しの後に振幅が半減すること，强制振動では共振の振動數の約 2/3 の振動數に於ける振幅が同じ强制力のもとの共振に於ける振幅の 1/10 乃至 1/15 位であるといふことから推定したのである．

このやうにして實際の五重塔に最も可能でありさうな範圍の二つの極端な場合について共振曲線を出して見た．摩擦の少い方の極端では共振の振幅が零振動數の場合のそれの約 24 倍となり，摩擦の多い方の極端ではその値が約 2·5 倍となる．實際の塔はこの始めの方に近いやうである．それにしても摩擦力が力學的にむしろ少な過ぎる位であるにも拘らず，前回の論文では容易に近づき得なかつたやうな減衰振幅に到達し得たのである．

低い振動數では五重塔の下部程振幅が少くなり，稍高い振動數では逆に上部程振幅が少くなるのである．之は當然なこととはいひながら，五重塔の場合に特に目立つてをるやうに思はれる．

このやうに上部程振幅が少くなることは摩擦力の少い方の例では第3共振以上の振動數で現れ，摩擦力の多い方の例では第2共振よりも低い振動數で旣に現れるものである．

尙注目に値することは，摩擦の少い方の例では殆ど何れの共振も共振曲線中にはつきりと見えるのに，摩擦の多い方の例では第3共振以上はどれが共振であるか判別がつかぬ程度になる事柄である．

只今述べたやうな摩擦のための振動減衰性は五重塔にのみ限つたことでなく日本の寺院や御殿風の建等には何れにも存在するもののやうである．しかし柱や重量の割合から見て五重塔に特別に著しく現れるものであることが知られた次第である．心柱はそれに何か特別の摩擦裝置を與へぬ限り効力のないことは依然として同樣である．

5. *Some Experiments on the Generation and Propagation of Elastic Waves.*[*]

By Zyun'iti KINOSITA,

Earthquake Research Institute.

(Read March 17, 1936.—Received Dec. 21, 1936.)

1. Introduction.

A number of investigations on the generation and the propagation of elastic waves have been accomplished in the field of mathematical physics, and the results are already applied in the elucidation of seismic waves generated and propagated in the crust of our planet, throwing remarkable light on the nature and the origin of earthquakes. The investigations so far attained in these branches could sufficiently explain the regional distribution of the initial dilatation and compression as well as the magnitude of the first impulsion, though the character of the first impulsion, whether it is of shock type or not, is still to be explained.

As to experimental studies of elastic waves, we have only a few works as compared with those on theoretical studies. The experimental difficulties owing to the high velocity of propagation seems to have prevented the developement of studies in this branch of investigation. But in view of the bearing of the experimental studies in the elucidation of seismic waves and the verification of theoretical results, some step forward is to be made in the domain of experimental studies no matter how difficult the realisation may be.

With this in view, we have first studied, for simplicity's sake, the generation and propagation of elastic waves along metallic wires. We certainly aware that the nature of waves propagated in three dimensions is not immeadiately inspected from the mere knowledge of that of one dimensional waves, and the extension of our experiments to more general cases will be made in future.

The results of our preliminary study, however, contains points of some importance as will be seen from the descriptions in the following.

2. Experimental Arrangement.

Experiments were made on the generation and propagation of distor-

---

[*] Communicated by Prof. M. Ishimoto.

tional waves along metallic wires attached with a number of wooden pieces in equal distances.[1] (See Fig. 1. PL. I.) This disposition is not what we have aimed at, but this contrivance reduced the velocity of propagation to so small a value that we can easily observe the phenomena in the laboratory. The dimensions of wooden pieces used are 11·94 cm × 1·65 cm × 1·20 cm, and the weight of which were 13·0 gr in the mean, the deviation being within ±1 gr.

Two kinds of wires were used in the present experiment, the one being a brass wire with a diameter 0·059 cm, and the other steel wire of 0·064 cm dia. The length of wire between consecutive wooden pieces were 1·89 cm in each experiment. The wire was hung from the ceiling and clumped at the lower end. The lengths of wire between wooden pieces and the upper and the lower clumps were also made 1·89 cm, equal to the distance of consecutive wooden pieces.

The motion of a wooden piece was recorded on smoked paper (arround a drum driven by a synchronous moter) with an indicator of straw arm which is directly connected to the wooden piece. This recording device is the same with those used in the Ishimoto acceleration seismometer and Hagiwara velocity seismograph, with the credit of the smallness of the weight of the arm and the friction at the indicator end. The driving rate of the smoked paper was 0·94 cm/sec.

At both ends of a certain wooden piece small iron pieces so light that they exerted no appreciable influence were attached in order to pull by electromagnets in case of giving impulsive couple to the suspended wire or clumping the wooden piece at required positions. But in some cases wooden pieces move to and fro through the position of electromagnets in the above arrangement. In such cases wooden pieces were connected by silk thread with iron pieces, which after leaving the electromagnets did not hinder the motion of wooden pieces.

The forces applied were couples in each case, and lateral vibrations of the wire were never excited when the positions of the magnets were properly adjusted.

3. Measurement of Velocity of Propagation.

First using the brass wire model, an impulsive couple was given at the lower end of the wire, and travel times were observed at various points. From the travel time curve (Fig. 2) the velocity of propagation was obtained as 35·9 sections/sec. Since the length of one section consisting of the wire of length $l = 1·89$ cm and wooden piece of breadth $l =$

---

[1] This contrivance was invented by Prof. M. Ishimoto and a model was constructed by him.

1·65 cm is 3·54 cm the velocity comes out $35{\cdot}9\times3{\cdot}54=127$ in cm/sec.

On the other hand, the equation of motion refered to x-axis taken in the direction of wire and measured by the length of one section $(l+l')$ is

$$I\frac{\partial^2\xi}{\partial t^2}=\tau\frac{\partial^2\xi}{\partial x^2}\,,\ \left(\tau=\frac{\pi n a^4}{2l}\right)\qquad(1)$$

where ξ represents angular displacement, τ the moment of couple of the wire of length l when the one end of the wire is rotated through one radian, and n and a denote the rigidity and radius of wire, while I is the moment of inertia arround the axis of rotation of one section and practically equal to that of the wooden piece as the part due to the wire is negligibly small. Then $c=\sqrt{\tau/I}$ is the velocity of propagation and $v=c(l+l\ )$ is the velocity in c. g. s. unit. Introducing the dimensions already mensioned and the value of $n=3{\cdot}43\times10^{11}$ c. g. s. as determined experimentally, we have $v=132$ cm/sec in good accord with the observed value 127 cm/sec.

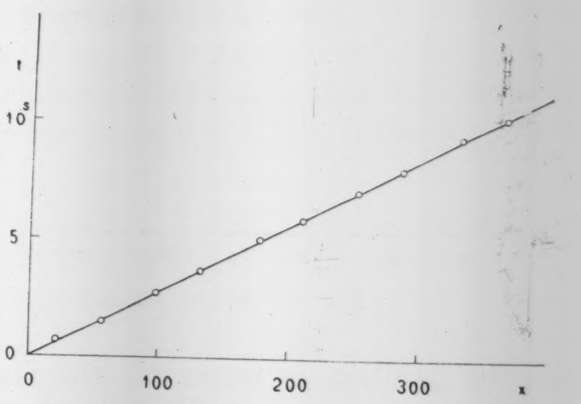

Fig. 2. Time distance curve for brass wire model.

Similar determination with the steel wire model gave (Fig. 3) $c=62{\cdot}35$ sections/sec or $v=220{\cdot}7$ cm/sec.

4. Energy of waves Generated from the Release of Statical Strains.[2]

The upper and the lower end of the wire as well as the fourth wooden piece from the lower end were clumped in strainless positions. Then the lower end was rotated through a certain angle θ, so that strain energy was stored between the lower end and the fourth wooden piece. (Fig. 4 represents the angular displacement of the wire.)

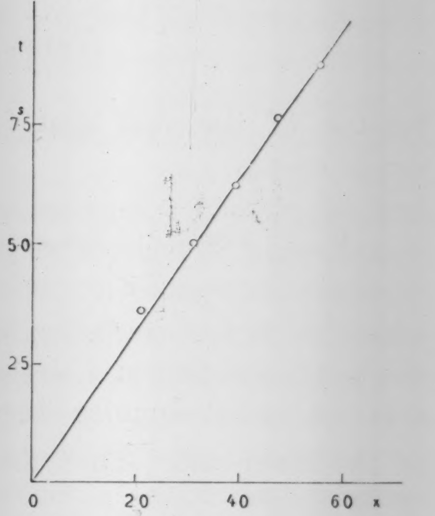

Fig. 3. Time distance curve for steel wire model.

---

2)—The possibility of the generation of earthquakes from the release of statical strain has often been suggested since the beginning of seismology, and recently Prof. Ishimoto called attension of this fact and Messrs. H. Kawasumi and K. Yosiyama [Bull. Earshq. Res. Inst., **13** (1935),496~503, & Disin, **7** (1935), 359~375.] could for the first time prove it theoretically although Prof. K. Sezawa and Mr. K. Kanai [Bull. Esrthq. Res.Inst., **13** (1935), 740~749; **14** (1936), 10~18.] contested against this conclusion.

When the couple which has kept the fourth wooden piece in its original position is taken off, the statical strain energy stored in the lower part is transported by the elastic waves then generated and propagated upward. Fig. 5 (PL.II) is the record of this wave at 36th piece from the lower end. From this record we see a wave with permanent displacement in one direction. The small undulation following the large displacement seems to be the free oscilation of one section, since the calculated period $2\pi/\sqrt{\tau/I}=0{\cdot}17$ sec is equal to the observed period.

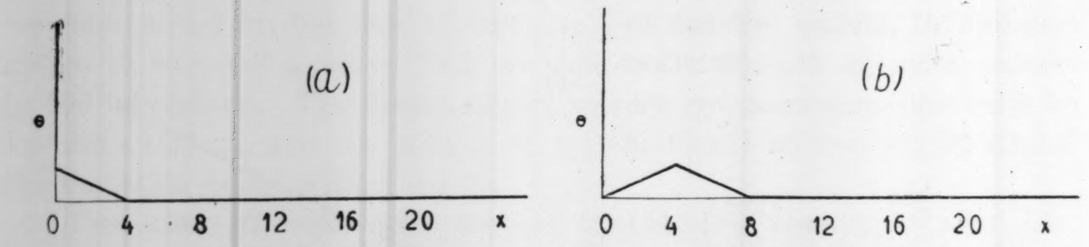

Fig. 4. Initial strain. (a): Type A. (b): Type B.

The energy flux through a point is $\tau\frac{\partial\xi}{\partial x}\frac{\partial\xi}{\partial t}$,and the total energy E transported across a point is

$$E=\int\tau\frac{\partial\xi}{\partial x}\frac{\partial\xi}{\partial t}\,dt\doteq\frac{\tau}{c}\int\left(\frac{\partial\xi}{\partial t}\right)^2 dt\,, \tag{2}$$

because of the fact that $\xi=f(x-ct)$. On the other hand the initial strain energy

$$V=\frac{1}{2}\tau'\theta^2=\frac{1}{2}\frac{\tau}{4}\theta^2=\frac{\tau}{8}\theta^2\,, \tag{3}$$

where τ' is the coefficient of couple due to the rotation of 4 sections, while θ is the initial angular displacement at the lower end. Then the ratio of energies

$$\frac{E}{V}=\frac{1}{c}\int\left(\frac{\partial\xi}{\partial t}\right)^2 dt\Big/\frac{\theta^2}{8}. \tag{4}$$

Since the result of comparison (Fig. 6) of the deflections ξ by waves with θ shows a linear inter-relation, the wave energy E and the strain energy V seem also to be linearly proportional through the relation (4).

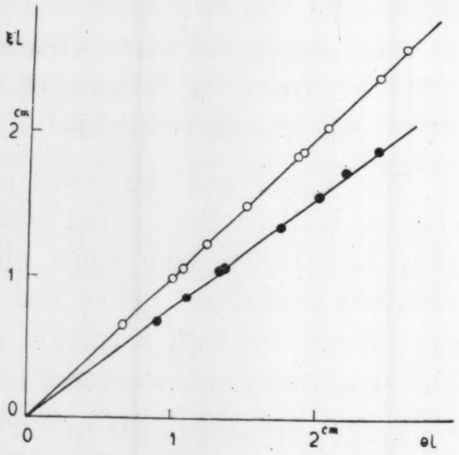

Fig. 6. Correlation between the angular displacement ξ and initial strain θ. (L=15 cm is the length of indication arm.)

● Brass wire model.

○ Steel wire model.

Then in order to calculate the energy of wave by the formula (2) the original record was enlarged photographically and the deflections were read off at every 1/200 sec. As the indicator end moves on a circular arc, due corrections to the amplitude and time are applied. Full line curve in Fig. 7 represents the corrected curve, while the curve in broken line is the corresponding velocity obtained by numerical differentiation by means of the formula[3]

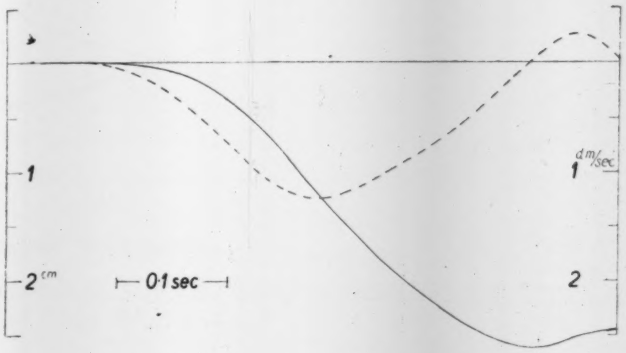

Fig. 7. Corrected displacement ξL (full line curve) and its time derivative $\frac{d\xi L}{dt}$ (broken line curne) due to waves generated by the initial strain of type A. (Brass wire model).

$$\dot{y}_n=\frac{2}{3}(y_{n+1}-y_{n-1})-\frac{1}{12}(y_{n+2}-y_{n-2})\,, \tag{5}$$

where y's are deflections at equal (unit) time interval. This is the first derivative of a cubic equation determined by the method of least squares using five consecutive values at the central point. Although the displacements and velocities required are angular displacements and velocities, all the arms of indicators being of equal length the readings from the records were used as they were without reducing to the angular ones. From these values of velocities, energy of wave E was calculated by the equation (2) by means of Sympson's method of numerical integration. The comparision of the result with the initial strain energy shows that they are nearly equal in magnitude although the wave energy is a little less than the strain energy. This may naturally be attributed to the loss in the excitation of the free oscillations of wooden pieces as well as damping of surrounding air. To make clear of this relation, observations were made at five positions. The results of calculation from five observations of the primary wave as well as five values corresponding to the reflected wave at the upper end are plotted in Fig. 8 (a) aginst the distances from the lower end. From this diagram we see that the wave energy is dissipated nearly exponentially with distance from the initial values which is equal to the initial strain energy.

---

[3] This formula was obtained by Mr. H. Kawasumi.

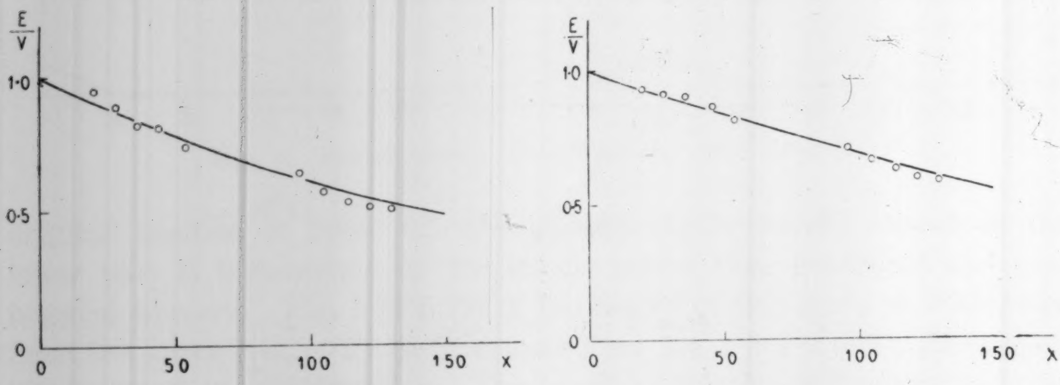

(a): Brass wire model. (b): Steel wire model.

Fig. 8. Dissipation of wave energy E with distance of the wave generated by the initial strain of type A (Fig. 4). The ordinates are measured in fraction of initial strain energy V.

Fig. 8 (b) for the steel wire model also indicates the same relation.

Next, the upper and the lower ends as well as the 8th piece from the lower end were clumped at strainless positions and the fourth one was rotated through a certain angle. Fig. 4 b represents the angular displacement of the wire (Type B). Then the couples which were acting to the fourth and the 8th pieces were suddenly taken off at the same time. In this case the strain energy stored between 8th piece and the lower end is transmitted upward. The wave form is shown in Fig. 9 (PL. III). With this wave, the calculation of energy were done as in the former example. Curves in Fig. 10 represent corrected displacement and velocity. Ratios of energies (E/V) at five positions were found for primary as well as the reflected waves. Fig. 11 (a) and 11 (b) represent the dissipations of waves as they are propagated along the brass and steel wires respectively.

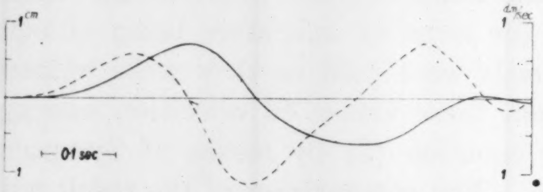

Fig. 10. Corrected displacement ξL (full line curve) and its time derivative $\frac{d\xi L}{dt}$ (broken line curve) due to waves generated by the initial strain of type B. (Brass wire model.)

Thus we see from Figs. 8 (a), 8 (b), 11 (a), and 11 (b) that the wave Energy E is dissipated nearly exponentially, and extrapolation to $x=0$ shows in each case that the wave energy is practically equall to the energy released from the initial statical strain. We may, therefore,

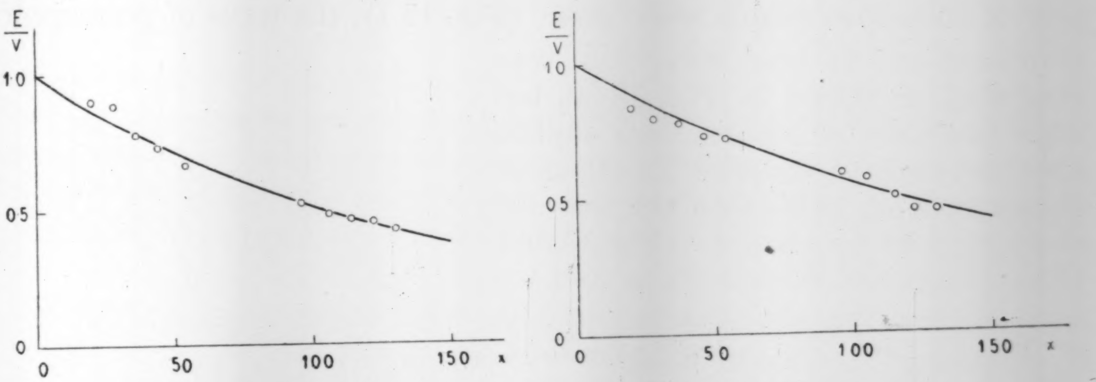

(a): Brass wire model. (b): Steel wire model.

Fig. 11. Dissipation of energy E with distance of the waves generated from the initial strain of type B (Fig. 4).

safely conclude that the whole statical strain energy is converted into wave energy and transmitted to distances, although a part of which is gradually dissipated in exciting the free oscillations of wooden pieces and owing to the damping effect of surrounding air. If the medium were perfectly homogeneous and there were no oscillators, the waves generated from the release of statical strains would keep their propagation without loss of energy but for the air damping.

These results are nothing but the experimental proof of the principle of the conservation of energy.

5. Forms of Waves Generated from the Release of Statical Strains or by Actions of Impulsive Forces.

Recent investigations revealed that the frequent occurrences of a kind of wave forms usually called a shock type at the very commencement of earthquakes, and methods of deducing actual amplitudes from the observed first impulsions on the seismograms have been worked out assuming the ground motion of such type. But no explanation on the mechanism of occurrence of waves of this type has been given. We have tried and succeeded to generate waves of such form propagated along metallic wires, as will be described in the following. Of course, as the writer has already stated, some precaution and restriction will be necessary in the application of the present result to the interpretation of seismic waves which are propagated in three dimensions.

In the experiments described in the above sections, the waves reflected at the lower end were superposed on the primary waves, and the results are not applicable to the present problem directly. In roder to avoid the boundary effect, impulsive couples or the initial strains were given in the present experiments at the central part of the wire. When a pair of impulsive couple were given (Fig. 12 I), the wave of permanent displacement to one direction was generated as shown in Fig. 13 (a), but when two pairs of couples were applied simultaneously in opposite directions as shown in Fig. 12 II, then the wave of shock type was generated. (Fig. 13 (b).) Other forms of initial strains and the waves therefrom are indicated in Fig. 12 III, IV, and Figs. 13 (c) and 13 (d) (PL. IV) respectively.

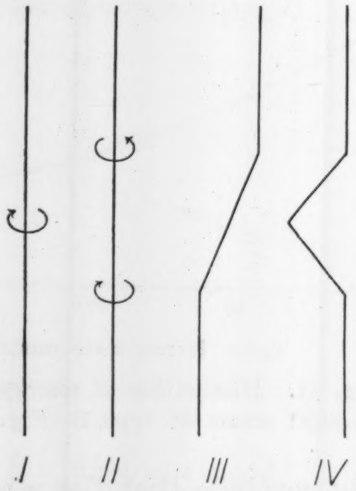

Fig. 12. Types of initial disturbances.
I, II: Impulsive couple(s).
III, IV: Initial strain.

The waves generated by mechanisms of type I and type III are almost identical while those of type II and type IV are irrespectively of shock type. It is interesting to note that the number of couples required to obtain a type of wave form are always less than the number of couples required to obtain the statical strain which give rise the same type of waves when the strain is released. It is also to be noted that the directions of initial motions above and below the central part where the disturbances are given are the same in the mechanism of type I and IV, while it is oposite in types II and III. The consequence is that the motions by the impulses and the release of strain are not equal when the reflected waves arrived.

By the superpositions of these mechanisms, waves of various types are to be generated. But the waves of complex types were not tried, as the adjustments of appratus were very difficult and such waves are of no practical value at present.

6. Conclusions.

In the present experiments, the distortional waves along metallic wires were studied. In order to diminish the velocity of propagation many wooden pieces were successfully attached to the wire, although the consequentious free oscillations of elementary parts were excited with some inconvenience. But the dissipation of the wave energy in this way was nearly exponential with the distance. Taking this into consideration following results were obtained.

1. Energy of wave generated from the release of statical strain is equal to the energy of the statical strain then released.

2. Forms of waves generated from the release of statical strains or

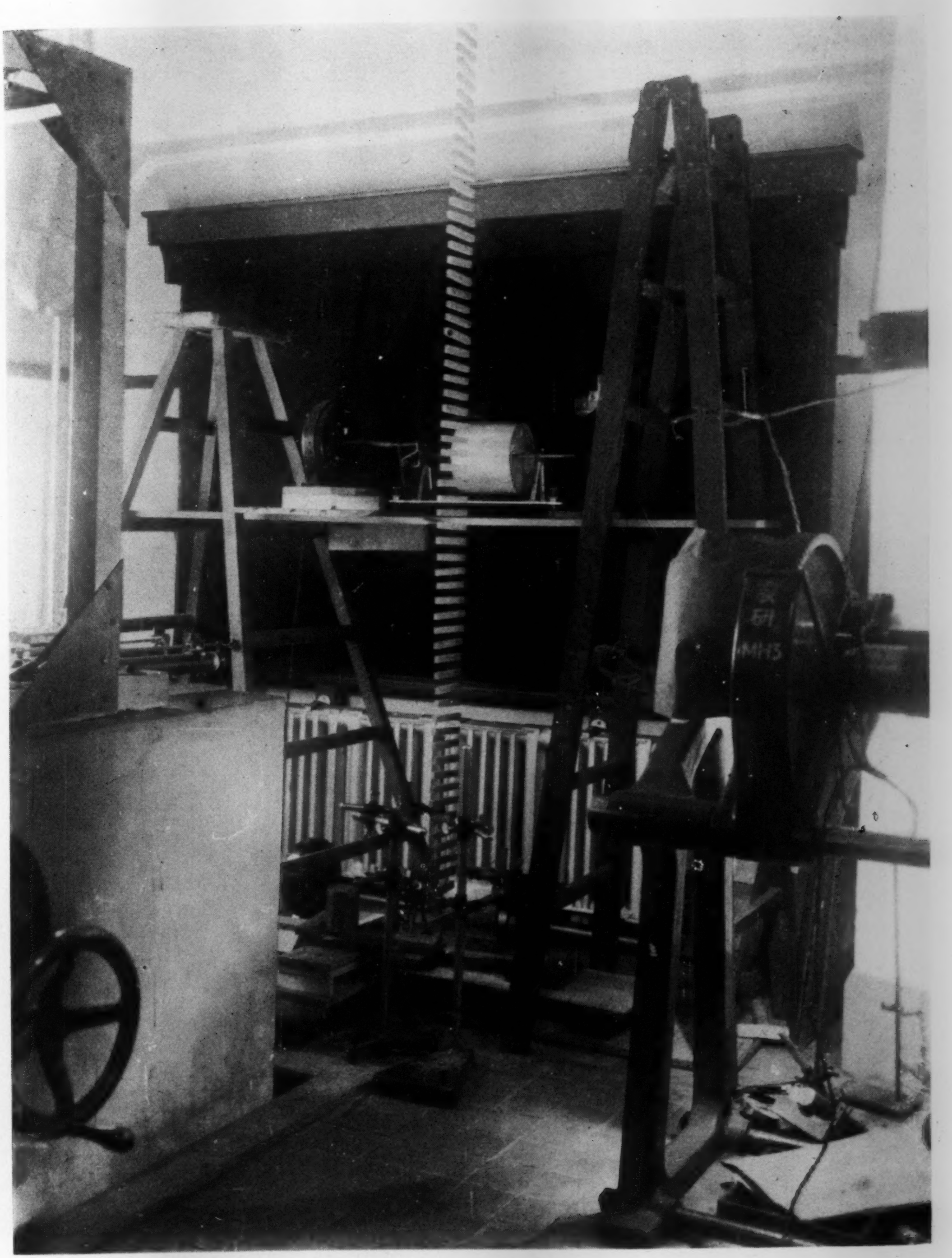

Fig. 1. Experimental arrangement.

（震研彙報 第十五號 圖版 木下）

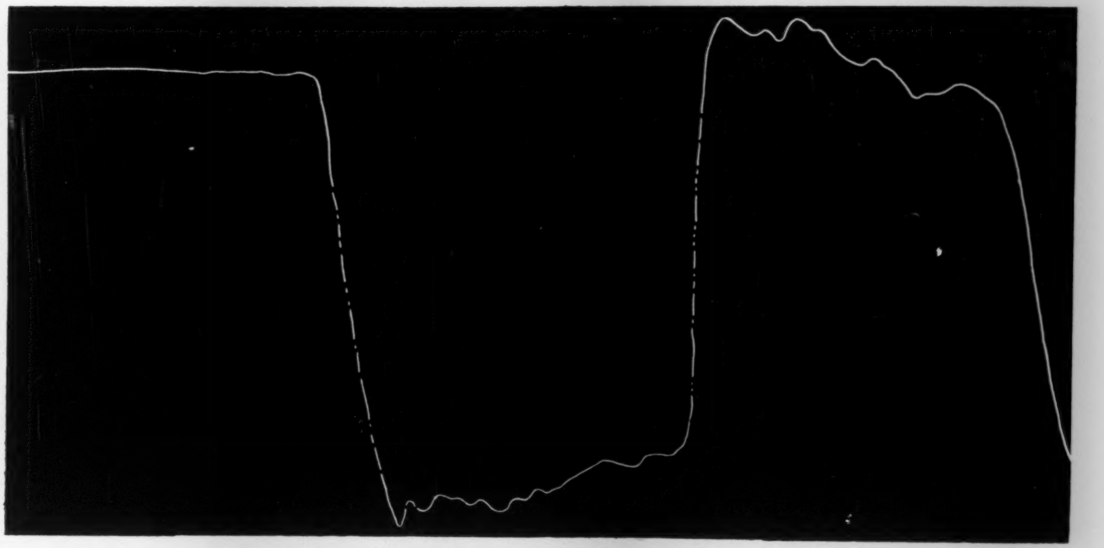

(a): Brass wire model.

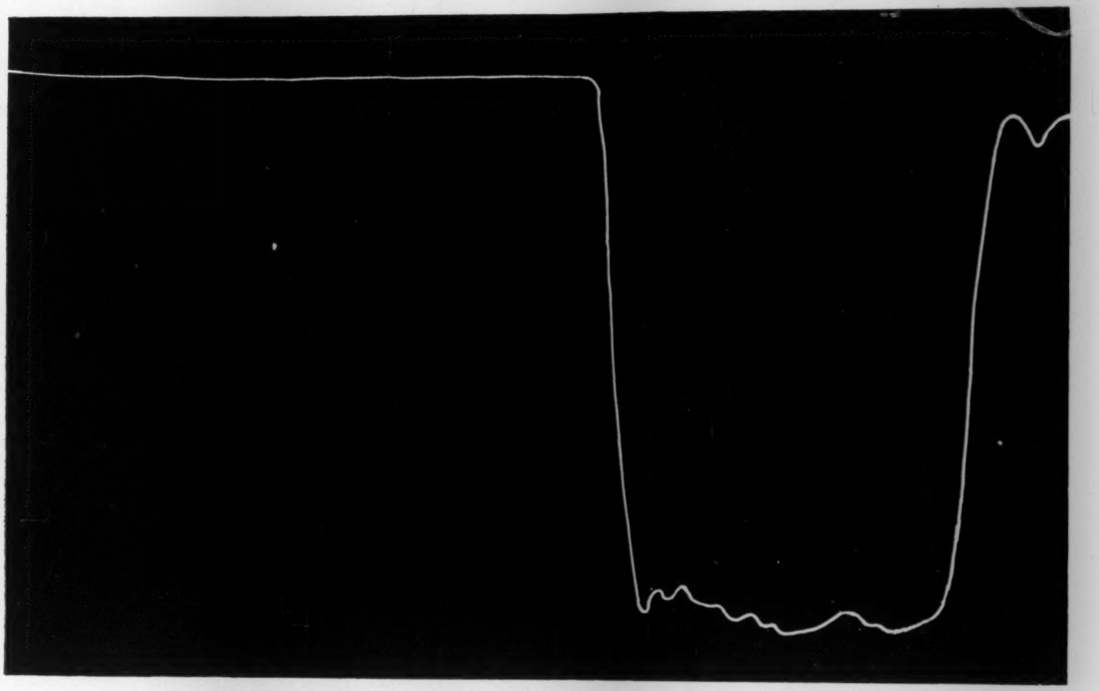

(b): Steel wire model.

Fig. 5.

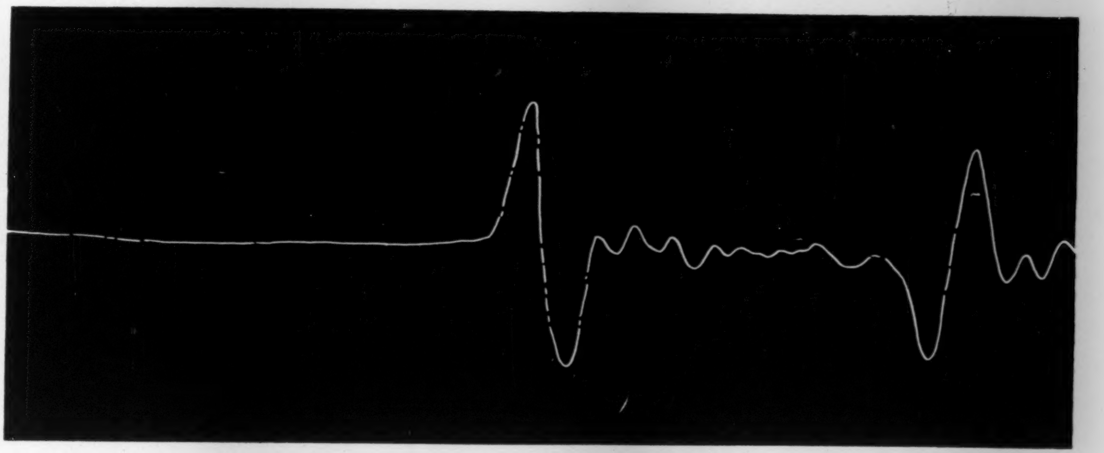

(a): Brass wire model.

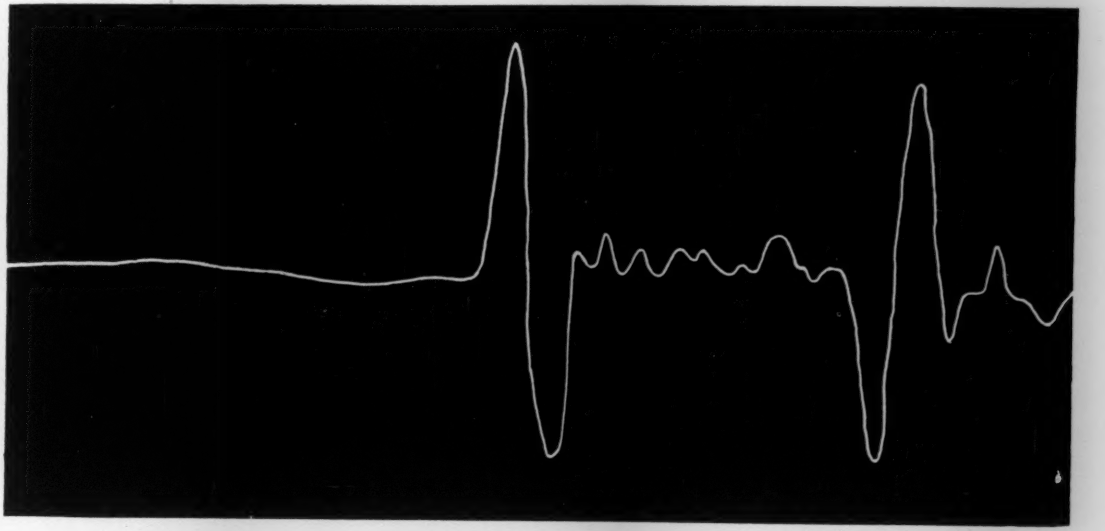

(b): Steel wire model.

Fig. 9.

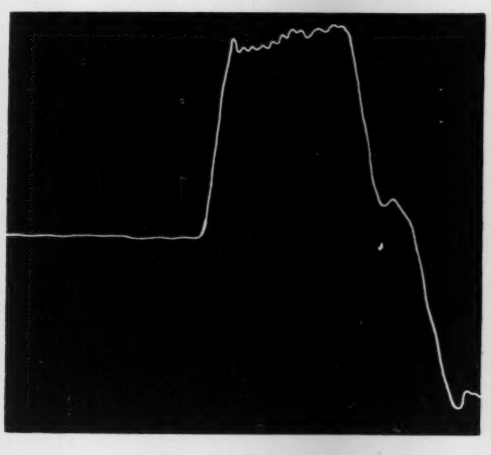

(a): type I.

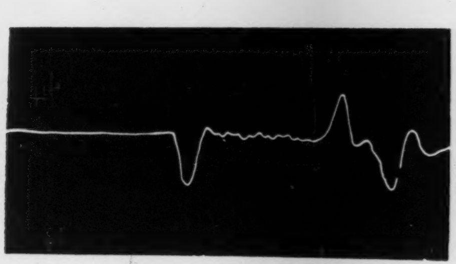

(b): type II.

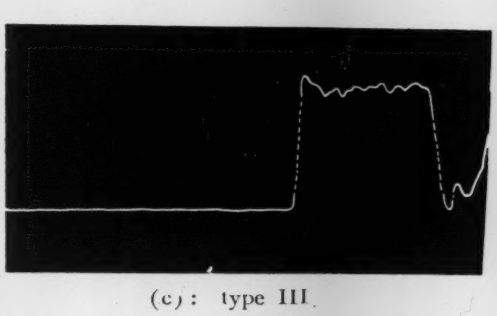

(c): type III.

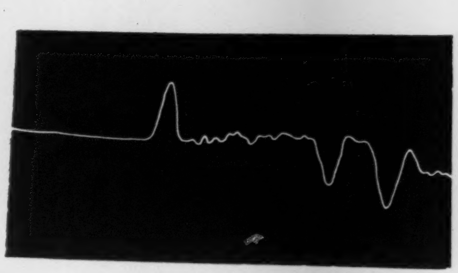

(d): type IV.

Fig. 13. Waves due to various initial localized disturbances at the central part of the wire.

(a): (b), Initial impulsive couple(s).
(c): (d), Initial strain (See Fig. 9).

（震研彙報 第十五號 圖版 木下）

by the actions of the impulsive forces at a part of one dimensional medium were found. Special attension was paid to the mechanism by which waves of shock-type were generated.

In conclusion, the writer wishes to express his best thanks to Prof. M. Ishimoto for his kind suggestions and guidance, and deep thanks are also due to Mr. H. Kawasumi for his valuable discussions.

---

5. 彈性波の生成及び傳播に關する實驗

地震研究所　木下潤一

彈性波の生成及び傳播に關する理論的研究は主として我國に於て最近著しい進歩を遂げたが，實驗的研究は未だ全く微々たるものである．此れは其の實驗の極めて困難なるに因るが，理論的に得られたる結果を實驗的に實證し，此れによつて理論の進展に資する事も又必要なるを以て，先づ簡單なる一次元的波動の生成及び傳播に關する實驗を行つて見た．

此の實驗に於ては針金に傳る捻れ波の傳播を實驗したが，多數の木片を等間隔に取り付ける事により傳播速度を小さくする事を得て實驗の困難の大部分は解消し，波動の傳播を肉眼にても見得る程度になつた．眞鍮の針金（直徑 0·059 cm）を用ひた場合には傳播速度は 132 cm/sec となり，鋼鐵線（直徑 0·064 cm）の場合には 221 cm/sec となつた．

種々の擾亂によつて起される波動を數箇所にて記錄測定し，波動の形を得，其れによりて運ばれる波動の勢力を計算した．例へば歪の潛勢力が波動を起し，其の際勢力の保存則があてはまる事を實證する事が出來た．

此の實驗は石本教授の指導鞭撻によつて出來たものである事を此處に銘記して厚く感謝の意を表する．

6. *Torsion Balance Surveys on Volcano Asama.* (*Part 1.*)

By Takeshi MINAKAMI,

Earthquake Research Institute.

(Read Nov. 17, 1936—Received Dec. 21, 1936.)

1. Introduction.

Precise levellings and triangulations showed that large scale topographical deformations in the neibourhood of active volcanoes are usually followed by explosive activities of the volcano. Examples are the remarkable crustal deformations that occurred at the time of the explosive activities of Sakuradima[1] in 1914 and of the quite recent explosions of Volcano Asama.[2]

Any displacement of mass, such as topographical deformations and ejections of lava, it is obvious, will evitably be followed by changes in the gravity potential.

In studying the second derivatives of gravity potential near active volcanoes in Japan, it is well to bear in mind the following facts.

M. Matsuyama,[3] in 1923, made gravimetric observations with an Eötvös gravity variometer at 28 stations in Sakuradima and the periphery of Kagoshima bay, and studied the subterranean formation of that region.

C. Tsuboi,[4] at the time of the explosive activities of Volcano Komagadake in Hokkaido, installed a pair of quatz torsion balances of his own construction at the foot of the volcano and continued observations for six months from June, 1929. His report was that no trace of change in the gravity potential could be detected, notwithstanding that his instrument had the high sensibility of 10^{-10} C. G. S..

As to Volcano Asama, I. Yamamoto,[5] who observed with an Eötvös gravity variometer in 1921 and 1922 at 13 stations, reported after comparing these two series of observations, that in one year the maximum time variation in the second derivatives of the gravity potential amounted to 200×10^{-9} C. G. S..

---

[1] F. ŌMORI, *Bull. Imp. Earthq. Inv. Comm.*, **8** (1914~1922), 158.

[2] R. TAKAHASI, *Bull. Earthq. Res. Inst.*, **14** (1936), 18.
T. MINAKAMI, *Bull. Earthq. Res. Inst.*, **14** (1936), 222.

[3] M. MATSUYAMA, *Nat. Res. Coun. Jap.*, **4** (1927), 121.

[4] C. TSUBOI, *Bull. Earthq. Res. Inst.*, **8** (1930), 301.

[5] I. YAMAMOTO, *Rep. Imp. Jap. Geod. Comm.*, No. 111, (1923).

At the same time, R. Takahasi,[6] in 1935, studied from the astronomical observations the form of the geoid at Volcano Asama and found at two triangulation points at the distance of 4 km from the crater, deviations in the plumb line of 12 secondes and 4 secondes.

On the other hand, since Yamamoto's observations in 1922, Asama has been the scene of violent explosions in 1927, 1928, 1931, 1932, 1935 and 1936. The present activity, which began in April 1935, still, at the close of 1936, shows no signs of complete abatement. In these violent explosions, a large quantity of lava is ejected from the crater in the form of volcanic bombs and volcanic ash. As already reported by the writer during active periods, the crater floor rises and falls 200 m and more.

The main purpose of the present observations was to measure the second derivatives of the gravity potential around the volcano, and, if possible, to detect any time variation in these quantities at the time of volcanic activity, to accomplish which it is necessary to repeat the observations at the same station at suitable time intervals. Of the 22 stations selected by the writer for this purpose, 12 are those that were used by I. Yamamoto in his investigations already referred to.

Although, obviously, determination of the surface form of the gravity equi-potential and mass distribution is an interesting problem, the results of such observations involve all the quantities due to the attracting masses surrounding the points observed. The final result free from the effects of the terrain and of the topography in the neibourhood of a station, is therefore a quantity that depends upon the density distribution underneath the region near the station. Unfortunately, however, the topography around our present stations is too complex to allow of the effects due to it being completly reduced, for which reason it is more convenient to defer the study of mass distribution until after the observations of gravity (g) have been completed.

2. Instrumental and Calculation Formulas.

The instrument used in our present observations was a "Grosse Drehwaage nr. 2021," made in Askania, Germany. In most of our observations, of the two balances I and II, only the former was used. In order to reduce possible errors of observations to the minimum, the records at all the stations were obtained photographically.

---

[6] R. Takahasi, *Bull. Earthq. Res. Inst.*, **14** (1936), 26. (in Japanese.)

The fundamental formula for the gravity-variometer is

$$d-d_0=\frac{K}{2\tau}\left(\frac{\partial^2 V}{\partial y^2}-\frac{\partial^2 V}{\partial x^2}\right)\sin 2\alpha+\frac{K}{\tau}\left(\frac{\partial^2 V}{\partial x\partial y}\right)\cos 2\alpha$$

$$-\frac{mhs}{\tau}\left(\frac{\partial^2 V}{\partial x\partial z}\right)\sin\alpha+\frac{mhs}{\tau}\left(\frac{\partial^2 V}{\partial y\partial y}\right)\cos\alpha \qquad (1)$$

where

K; moment of inertia of balance.
τ; restitutive force of torsion wire.
V; gravity potential.
m; mass of a weight.
h; distance from horizontal axis of balance to center of gravity of lower mass.
S; horizontal distance of lower and upper weights.
α; azimuth of balance referred magnetic meridian.
d_0; null position of balance.
d; equilibrium position of balance for each azimuth.

In the preceding formula, the directions of x, y, z are in the magnetic north, magnetic east, and downward at each station. As will be seen from the foudamental formula (1), $\frac{\partial^2 V}{\partial y^2}-\frac{\partial^2 V}{\partial x^2}$, $\frac{\partial^2 V}{\partial x\partial y}$, $\frac{\partial^2 V}{\partial x\partial z}$, $\frac{\partial^2 V}{\partial y\partial z}$ and d_0 are unknown, so that in using balance I alone, observation must be made in five azimuths.

The calculation formulas(7) for five azimuths, say, 0, $\frac{2\pi}{5}$, $\frac{4\pi}{5}$, $\frac{6\pi}{5}$, and $\frac{8\pi}{5}$ are

$$\frac{\partial^2 V}{\partial y^2}-\frac{\partial^2 V}{\partial x^2}=\frac{1}{a}\times 0{\cdot}5257\Big[\{(d_1-d_2)-(d_1-d_5)\}-1{\cdot}6180\,\{(d_1-d_3\;-\;d_1-d_4)\}\Big],$$

$$2\,\frac{\partial^2 V}{\partial x\partial y}=\frac{1}{a}\times 0{\cdot}3225\Big[\{(d_1-d_2)+(d_1-d_5)\}-0{\cdot}3820\,\{(d_1-d_3)+(d_1-d_4)\}\Big],$$

$$\frac{\partial^2 V}{\partial z\partial x}=\frac{1}{b}\times 0{\cdot}3803\Big[\{(d_1-d_2)-(d_1-d_5)+\}+\frac{1}{1{\cdot}6180}\{(d_1-d_3)-(d_1-d_4)\}\Big],$$

---

7) Handbuch der Experimentalphysik, 15 (2)
C. TSUBOI, *Gravity*, (in Japanese)

$$\frac{\partial^2 V}{\partial z \partial y} = \frac{1}{b} \times 0{\cdot}1235\left[\{(d_1-d_2)+(d_1-d_5)\} - \frac{1}{0.3820}\{(d_1-d_3)+(d_4-d_4)\} \right],$$

where

$$a = \frac{2l}{\pi r^4 n} DK = 0{\cdot}08077 \times 10^9 ,$$

$$b = \frac{2l}{\pi r^4 n} \times 2Dshm = 0{\cdot}23055 \times 10^9$$

l ; length of wire.
r ; radius of wire.
n ; rigidity of wire.
D ; distance between light source and registering plate.

In the above four formulas, d_1, d_2, d_3, d_4 and d_5 are scale-readings refered to fixed points on the registering plate in the five azimuthal observations. If the errors of 0·1 mm in each scale-reading on the plate are expected, the maximum errors in the values for the four second derivatives can be derived from the following formulas:

$$\partial\left(\frac{\partial^2 V}{\partial y^2} - \frac{\partial^2 V}{\partial x^2}\right) = \pm\left\{6{\cdot}508 \times (0{\cdot}1 \times 2) + 10{\cdot}531 \times (0{\cdot}1 \times 2)\right\} = \pm 3{\cdot}40 ,$$

$$\partial\left(2\frac{\partial^2 V}{\partial x \partial y}\right) = \pm\left\{4{\cdot}005 \times (0{\cdot}1 \times 4) + 1{\cdot}529 \times (0{\cdot}1 \times 4)\right\} = \pm 2{\cdot}21 ,$$

$$\partial\left(\frac{\partial^2 V}{\partial z \partial x}\right) = \pm\left\{1{\cdot}649 \times (2 \times 0{\cdot}1) + 1{\cdot}019(0{\cdot}1 \times 2)\right\} = \pm 0{\cdot}53 ,$$

$$\partial\left(\frac{\partial^2 V}{\partial y \partial z}\right) = \pm\left\{0{\cdot}535 \times (0{\cdot}1 \times 4) + 1{\cdot}402(0{\cdot}1 \times 4)\right\} = \pm 0.77 .$$

The above derived values are maximum errors in the calculated values of the second derivatives of the gravity potential for single observations. From these formulas it is clear that the gradient term is obtained with greater accuratly than the curvature term, but in reviewing the observational data of the 22 stations, the errors in the four values were regarded as being less than 1 Eötvös. Although the temperature both in the instrument and outside of it varies with the time at which the observations are made, the effects of temperature changes on the observed values are much smaller than the maximum errors obtained above, so that it is not necessary to correct the effects of changes in temperature.

3. Observations.

The observations, which were begun April 16, 1936, were concluded on July 30, 1936. There were in all 26 stations, but as the records from 4 of the stations were incomplete, observations of only 22 stations were studied. In the observations, carefull attention was paid to the following points. In order to obtain stability, the instrument at each station was set up on concreate pedestal. Since the rays from light source to the dry plate are first refracted by a prism and then reflected three times by means of mirrors, should the prism and mirrors be blurred by sudden changes in atmospheric temperature and another causes, the dry plate will be insufficiently exposed, for which reason a very sensible plate was used and observations were made only from sunset to dawn. In order however to prolong the time of observation, the interior of the tent in which the instrument was set was kept dark to a certain extent by means of black curtains. Of the various hindrances to observation, the worst was wind which made it difficult to keep the balance in equilibrium.

Moreover at noon, the instrument and other accessories had to be transported by wagon, horse-back, and by man from station to station. Owing to the heat of the sun, the interior of the instrument rose in temperature, so that sometimes the instrument had to be cooled by ice.

As already mentioned, in the course of the present observations, the volcano was showing sign of activity. At the station 19 (Yunotaira Sainokawara) on July 22, violent explosions continued for about 3 hours in the middle of the night. Fortunatly, since at the station 18 (Yosinotaira), observations had been made the preceding day immedately after this violent explosion, it was possible from these two series of observations to arrive at the variations in the second derivatives of the gravity potential immediately followed by the explosion on July 22.

The records of observation at the stations 5, 6, and 8 are shown in Fig. (3) in which F, T_i and I, signify fixed points, internal temperature of the instrument, and the records of balance I. As to the internal temperature of the instrument, a displacement of 0·5 mm on the recording plate corresponds to a change of temperature of 1°C.

In the following Table I, are shown the results of observations at 22 stations. The station number follows the order of date of

Table I.

Station No. 1 研究所前
$\varphi=36^\circ\ 24'{\cdot}0$ May 24~25

date	Setting	T_e	T_i	d
h m				
8 10 p.m.	20°		8·7°C	46·9
8 50	92		8·6	42·2
9 30	164		8·5	40·2
10 10	236		8·4	43·4
10 50	308		8·3	47·4
11 30	20		8·1	47·0
0 10 a.m.	92		7·9	42·2
0 50	164		7·6	40·2
1 30	236		7·3	43·3
2 10	308		7·1	47·5
2 50	20		7·0	46·9
3 30	92		6·9	42·0
4 10	164		6·7	40·1
4 50	236		6·4	43·3

Station No. 1 研究所前
$\varphi=36^\circ\ 24'{\cdot}0$ May 25~26

date	Setting	T_e	T_i	d
h m				
9 05 p.m.	236°		26·0°C	23·5
9 45	308		25 3	23·3
10 25	20		24·9	18·5
11 05	92		24·7	16·1
11 45	164		24·5	19·0
0 25 a.m.	236		24·2	23·7
1 05	308		23·9	23·1
1 45	20		23·6	18·2
2 25	92		23·4	15·9
3 05	164		23·2	19·1
3 45	236		23·0	23·4
4 05	308		22·9	23·2

Station No. 1 研究所前
$\varphi=36^\circ\ 42'{\cdot}0$ May 28~29

date	Setting	T_e	T_i	d
h m				
7 30 p.m.	92°		48·6°C	21·8
8 10	164		48·4	24·8
8 50	236		48·2	29·6
9 30	308		48·0	29·5
10 10	20		47·8	24·3
10 50	92		47·7	21·8
11 30	164		47·5	24·9
0 10 a.m.	236		47·4	29·4
0 50	308		47·3	29·6
1 30	20		47·2	24·4
2 10	92		47·1	21·7
2 50	164		47·0	24·7
3 30	236		46·9	29·6
4 10	308		46·8	29·1

Station No. 2 上信國境
$\varphi=36^\circ\ 25'{\cdot}1$ May 29~30

date	Setting	T_e	T_i	d
h m				
8 40 m.p.	308°	6·5°C	25·6°C	30·8
9 20	20	6·7	21·6	30·1
10 00	92	7·0	18·9	35·9
10 40	164	6·5	15·2	40·2
11 20	236	6·2	13·2	37·3
0 00 a.m.	308	5·9	11·6	30·9
0 40	20	5·4	10·2	30·3
1 20	92	5·0	9·2	36·2
2 00	164	6·0	9·4	39·8
2 40	236	6·5	9·0	36·6
3 20	308	6·2	8·0	30·8
4 00	20	5·3	7·0	30·6
4 40	92	5 0	6·0	36·0

(to be continued.)

Table I. (*continued.*)

Station No. 3 分去茶屋
$\varphi=36°\ 25'·9$ May 30~31

date	Setting	T_e	T_i	d
h m				
8 04	236°	6·8°C	12·0°C	31·8
8 44	308	5·0	11·4	30·0
9 24	20	5·0	10·2	30·8
10 04	92	4·9	9·6	33·4
10 44	164	4·1	9·0	33·8
11 24	236	3·2	8·2	31·4
0 04	308	2·4	7·4	29·7
0 44	20	2·0	6·0	31·0
1 24	92	1·7	5·4	33·7
2 04	164	1·0	4·2	34·3
2 44	236	0·5	3·0	31·8
3 24	308	1·0	2·0	29·7

Station No. 1 北輕井澤，大笹新道交點
$\varphi=36°\ 27'·2$ June 1~2

date	Setting	T_e	T_i	d
h m				
8 00 p.m.	20°	14·8°C	21·9°C	37·0
8 40	92	14·4	20·8	33·5
9 20	164	14 0	19·7	33·7
10 00	236	13·5	18·6	38·2
10 40	308	13·0	17·4	40·7
11 20	20	12·5	16·5	37·3
0 00 a.m.	92	12·0	15·6	33·4
0 40	164	11·5	14·5	33·8
1 20	236	11·0	13·7	38·2
2 00	308	10·5	12·5	40·7
2 40	20	10·0	11·6	37·2
3 20	92	9·9	10·5	33·5
4 00	164	9·8	9.5	33·4

Station No. 5 鬼押出茶屋
$\varphi=36°\ 26'·7$ June 4~5

date	Setting	T_e	T_i	d
h m				
7 40 p.m.	308°	13·4°C	19·5°C	40·7
8 20	20	12·9	18·7	41·6
9 00	92	12·7	17·9	38·0
9 40	164	12·6	17·5	34·9
10 20	236	12·6	17·3	36·5
11 00	308	12·3	16·5	40·7
11 40	20	12·2	15·9	41·8
0 20 a.m.	92	11·6	14·9	38·0
1 00	164	11·1	13·5	34·9
1 40	236	10·9	12·7	36·7
2 20	308	9·5	12·3	40·8
3 30	20	9·1	11·5	41·6
3 40	92	9·5	11·1	38·0

Station No. 6 鬼押出茶屋北方 2 粁
$\varphi=36°\ 27·2'$ June 5~6

date	Setting	T_e	T_i	d
h m				
7 55 p.m.	20°		27·9°C	35·8
8 35	92		25·1	33 5
9 15	164		22·1	38·5
9 15	236		19·3	43·5
10 85	308		16·9	42·2
11 15	20		13·9	35·6
11 55	92		11·3	33·7
0 35 a.m.	164		9·3	38·4
1 15	236		7·5	43·5
1 55	308		6·3	42·4
2 35	20		5·3	35·7
3 15	92		4·3	33·4
3 55	164		3·3	38·4

(*to be continued.*)

Table I. (*continued.*)

Station No. 7 新 鹿 澤
$\varphi=36^\circ\ 28'\cdot4$ June 7～8

date	Setting	T_e	T_i	d
h m				
7 30 p.m.	236°	5·9°C		35·4
8 10	308	2·1		33·9
8 50	20	0·7		38·3
9 30	92	−0·6		42·7
10 10	164	−0·7		40·4
10 50	236	−1·7		35·5
11 30	308	−2·2		34·3
0 10 a.m.	20	−2·3		38·7
0 50	92	−1·7		42·5
1 30	164	−2·8		40·5
2 10	236	−3·6		35·6
2 50	308	−3·3		34·4
3 50	20	−3·5		38·7

Station No. 8 分去茶屋西方地藏川
$\varphi=36^\circ\ 25'\cdot5$ June 13～14

date	Setting	T_e	T_i	d
h m				
7 55 p.m.	92°	12·6°C	19·7°C	33·5
8 35	164	12·0	18·5	25·5
9 15	236	10·9	17·3	30·2
9 55	308	10·8	16·1	41·8
10 35	20	10·3	14·9	44·5
11 15	92	10·1	13·7	33·5
11 55	164	9·6	12·9	25·4
0 35 a.m.	236	9·4	11·9	30·2
1 15	3 8	9·3	11·1	42·1
1 55	20	9·0	10·5	44·3
2 35	92	8·6	9·7	33·2
3 15	164	8·6	9·5	25·5
3 55	236	9·3	9·3	30·1

Station No. 9 小淺間水準點
$\varphi=36^\circ\ 24'\cdot1$ June 26～27

date	Setting	T_e	T_i	d
h m				
6 40 p.m.	236°	11·0°C	22·4°C	20·0
7 20	308	10·5	20·4	16·2
8 00	20	10·3	18·4	17·8
8 40	92	9·8	17·0	21·6
9 20	164	9·5	15·8	22·3
10 00	236	9·3	15·4	19·5
10 40	308	9·2	14·4	15·6
11 20	20	8·8	13·8	17·6
0 00 a.m.	92	8·5	12·8	21·3
0 40	164	8·5	12·4	22·1
1 20	236	7·8	11·0	19·7
2 00	308	7·3	10·6	15·6
2 40	20	6·9	10·0	17·4
3 20	92	6·2	8·6	21·5
4 00	164	5·5	7·8	22·3

Station No. 10 草水三角點
$\varphi=36^\circ\ 23'\cdot6$ June 28～29

date	Setting	T_e	T_e	d
h m				
6 40 p.m.	308°	15·1°C	14·0°C	14·1
7 20	20	15·0	13·6	16·3
8 00	92	14·8	13·2	15·7
8 40	164	14·9	13·0	12·7
9 20	236	15·4	13·2	12·2
10 00	308	15·4	13·4	14 4
10 40	20	15·3	13·6	16·4
11 20	92	15·2	13·6	15·6
0 00 a.m.	164	15·4	13·6	12·7
0 40	236	15·4	13·8	12·2
1 20	308	15·8	14·2	14·1
2 00	20	15·1	14·6	15·9
2 40	92	15·3	15·4	15·7
3 20	164	15·4	15·6	12·8
4 00	236	15·4	15·8	12:3

(*to be continued.*)

Table I. (*continued.*)

Station No. 11 千ケ瀧クラブ前
$\varphi=36°\ 23'\cdot0$ July 8~9

date	Setting	T_e	T_i	d
h m				
6 05 p.m.	308°	17·0°C	19·1°C	22·4
6 45	20	16·7	18·9	19·1
7 25	92	17·0	18·7	15·4
8 05	164	17·0	18·5	16·5
8 45	236	16·8	18·1	21·5
9 25	308	16·5	17·9	22·5
10 05	20	16·5	17·7	19·5
10 45	92	16·5	17·7	15·7
11 25	164	16·5	17·5	16·6
0 05 a.m.	236	16·4	17·3	21·5
0 45	308	16·1	17·1	22·6
1 25	20	16·1	16·9	19·3
2 05	92	16·0	16·7	15·5
2 45	164	15·0	16·5	17·1
3 25	236	15·7	16·3	21·6
4 05	308	15·5	16·1	22·4

Station No. 12 千ケ瀧避暑地入口
$\varphi=36°\ 21'\cdot7$ July 9~10

date	Setting	T_e	T_i	d
h m				
7 05 p.m.	20°	16·2°C	19·5°C	14·7
7 45	92	16·0	19·3	12·5
8 25	164	16·0	18·9	16·4
9 05	236	15·8	18·7	21·4
9 45	308	15·7	18·3	20·0
10 25	20	15·7	17·7	14·7
11 05	92	15·6	17·3	12·4
11 45	164	15·4	17·1	16·1
0 25 a.m.	236	15·3	16·7	21·2
1 05	308	15·3	16·5	20·1
1 45	20	15·1	16·1	14·6
2 25	92	15·0	15·9	12·4
3 05	164	15·0	15·5	16·3
3 45	236	14·9	15·3	21·2

Station No. 13 沓掛
$\varphi=36°\ 20'\cdot8$ July 10~11

date	Setting	T_e	T_e	d
h m				
9 45	92°	14·6°C	18·9°C	12·4
10 25	164	14·7	18·5	16·1
11 05	236	15·0	18·1	20·7
11 45	308	15·1	17·7	19·9
0 25 a.m.	20	15·1	17·3	16·4
1 05	92	14·9	16·9	12·8
1 45	164	14·4	16·5	16·0
2 25	236	14·1	16·1	20·8
3 05	308	14·2	15·7	19·8
3 45	20	14·5	14·9	16·4

Station No. 14 追分淺間神社
$\varphi=36°\ 20\cdot3'$ July 11~12

date	Setting	T_e	T_i	d
h m				
7 15 p.m.	92°	17·9°C	27·7°C	16·0
7 55	164	18·1	25·3	13·4
8 35	236	17·8	23·1	16·8
9 15	308	17·6	21·7	21·3
9 55	20	17·4	20·5	20·7
10 35	92	17·1	19·5	16·0
11 15	164	16·9	18·7	13·3
11 55	236	16·5	17·9	16·8
0 35 a.m.	308	15·6	17·3	21·2
1 15	20	15·7	16·7	20·7
1 55	92	15·9	16·3	16·0
2 35	164	15·3	16·1	13·5
3 15	236	15·4	15·9	17·0
3 55	308	15·1	15·7	21·3

(*to be continued.*)

Table I. (*continued.*)

Station No. 15 鹽野新道追分北方
φ=36° 21′·9 July 12～13

date	Setting	T_e	T_i	d
h m				
6 15 p.m.	236°	18·6°C	30·0°C	17·8
6 55	308	18·0	27·6	14·2
7 35	20	17·8	25·4	17·0
8 15	92	17·4	23·6	22·1
8 55	164	17·0	22·2	22·5
9 35	236	16·9	21·2	17·8
10 15	308	18·8	20·6	14·7
10 55	20	16·2	20·2	17·5
11 35	92	16·1	19·4	22·3
0 15 a.m.	164	15·9	18·2	22·4
0 55	236	15·9	17·8	17·5
1 35	308	15·8	17·4	15·0
2 15	20	15·6	17·2	18·1
2 55	92	15·3	16·8	22·2
3 35	164	14·7	16·2	21·9
4 15	236	14·5	15·8	17·7

Station No. 16 淸 萬
φ=36° 20′·3 July 16～17

date	Setting	T_e	T_i	d
h m				
9 15 m. p.	164°	19·0°C	30·3°C	22·5
9 55	236	19·1	28·1	21·2
10 35	308	19·3	26·9	24·8
11 15	20	19·6	25·7	29·2
11 55	92	19·7	23·9	28·0
0 35 a.m.	164	19·9	23·1	22·5
1 15	236	20·1	22·9	20·9
1 55	308	20·1	21·9	24·6
2 35	20	20·3	21·3	29·4
3 15	92	20·8	20·9	28·0
3 55	164	21·0	20·5	22·4
4 35	236	21·1	20·1	20·8

Station N. 17 小沼村小學校
φ=36° 19′·6 July 17～18

date	Setting	T_e	T_i	d
h m				
7 10 p.m.	308°	27·9°C		25·0
7 50	20	26·3		28·5
8 30	92	25·4		35·8
9 10	164	24·8		37·4
9 50	236	24·5		30·5
10 30	308	23·8		25·0
11 10	20	23·6		28·7
11 50	92	23·3		36·0
0 30 a.m.	164	23·0		37·3
1 10	236	22·4		30·3
1 50	308	22·0		25·0
2 30	20	21·7		28·5
3 10	92	21·7		35·5
3 50	164	21·5		37·0
4 30	236	21·4		30·5
5 10	308	21·3		25·0

Station No. 18 芦ノ平淺間館
φ=36° 22′·5 July 21～22

[illegible]	Setting	T_e	T_i	d
h m				
7 00 p.m.	92°	16·6°C	30·8°C	1·8
7 45	164	16·0	27·8	4·0
8 25	236	15·0	25·2	11·6
9 05	308	14·2	22·8	14·4
9 45	20	13·6	20·4	9·3
10 25	92	13·0	18·6	1·9
11 05	164	13·2	16·8	3·9
11 45	236	12·9	15·8	11·6
0 25	308	12·6	14·6	14·1
1 05	20	12·5	13·8	9·2
1 45	92	12·5	13·4	2·0
2 25	164	12·3	13.0	3·7
3 05	236	12·2	12·6	11·4
3 45	308	12·3	12·4	14·2
4 25	20	12·4	12·2	9·3
5 05	92	12·4	12·2	2·0
5 45	164	12·2	12·2	4·0

(*to be continned.*)

Table I. (*continued.*)

Station No. 18 芦ノ平淺間館
$\varphi=38°\ 22'{\cdot}5$ July 25～26

date	Setting	T_e	T_i	d
h m				
5 35 p.m.	20°	25·8°C		25·3
6 15	92	25·0		18·7
6 55	164	23·3		21·0
7 35	236	22·0	32·3°C	29·8
8 15	308	20·4	30·3	31·5
8 55	20	19·9	27·9	25·4
9 35	92	18·8	26·3	19·0
10 15	164	18·6	24·7	21·0
10 55	236	18·0	23·7	29·7
11 35	308	17·4	22·5	31·5
0 15 a.m.	20	17·3	21·7	25·5
0 55	92	16·3	20·5	18·9
1 35	164	15·7	18·9	21·0
2 15	236	15·1	18·1	29·8
2 55	308	14·7	17·5	31·5
3 35	20	14·3	16·7	25·4
4 15	92	14·3	15·7	19·0

Station No. 19 湯ノ平賽ノ河原
$\varphi=36°\ 23'{\cdot}9$ July 22～23

date	Setting	T_e	T_i	d
h m				
7 35 p.m.	20°	14·9°C	30·6°C	22·5
8 15	92	14·2	27·2	18·5
8 55	164	14·0	23·4	20·5
9 35	236	13·0	22·2	25·4
10 15	308	12·2	21·0	27·1
10 55	20	10·9	19·2	22·5
11 35	92	9·5	17·8	18·2
0 15 a.m.	164	8·5	16·0	20·3
0 55	236	7·9	14·0	25·5
1 35	308	9·3	12·6	27·1
2 15	20	8·5	11·8	22·5
2 55	92	6·8	11·2	18·4
3 35	164	6·5	9·6	20·1
4 15	236	6·2	8·4	25·5
4 55	308	5·9	7·4	27·1
5 35	20	7·0	6·8	22·5

Station No. 20 天狗ノ露路
$\varphi=36°\ 23'{\cdot}6$ July 23～24

date	Setting	T_e	T_i	d
h m				
5 35 p.m.	164°	16·8°C	26·0°C	19·6
6 15	236	16·3	24·0	24·5
6 55	308	16·0	22·0	31·0
7 35	20	15·6	20·6	31·2
8 15	92	15·3	19·4	23·3
8 55	164	15·1	18·6	19·6
9 35	236	14·9	17·8	24·5
10 15	308	14·8	16·4	31·0
10 55	20	14·8	16·0	31·1
11 35	92	14·6	15·6	23·4
0 15 a.m.	164	14·6	15·2	19·5
0 55	236	14·5	15·2	24·3
1 35	308	14·6	15·0	31·2
2 15	20	14·7	15·0	31·1
2 55	92	14·8	15·0	23·2
3 35	164	14·8	15·0	19·5
4 15	236	14·8	15·0	24·5
4 55	308	14·8	14·8	31·1
5 35	20	14·8	14·8	31·0

Station No. 21 湯ノ平火山觀測所
$\varphi=36°\ 23'{\cdot}9$ July 24～25

date	Setting	T_e	T_i	d
h m				
0 25 p.m.	92°	17·0°C	15·0°C	29·1
1 05	164	16·8	15·8	
1 45	236	16·9	16·4	19·0
2 25	308	16·9	16·6	
3 05	20	17·0	16·6	
3 45	92	17·1	16·8	29·2
6 05 p.m.	20	16·9	19·0	28·8
6 45	92	16·8	18·8	29·1
7 25	164	16·8	18·6	22·6
8 05	236	16·7	18·4	18·8
8 45	308	16·7	18·2	22·3
9 25	20	16·6	18·0	28·7
10 05	92	16·4	17·8	29·0
10 45	164	16·3	17·6	22·6
11 25	236	16·2	17·4	18·9
0 05 a.m.	308	16·0	17·2	22·3
0 45	20	16·0	17·0	28·8
1 25	92	16·0	16·8	29·2
2 05	164	16·0	16·6	22·5
2 45	236	16·0	16·4	18·9
3 25	308	15·9	16·2	22·4
4 05	20	15·7	16·2	28·6
4 45	92	15·3	16·0	29·0
5 25	164	15·0	16·0	22·7

(*to be continued.*)

Table I. *(continued.)*

Station No. 22 岩村田農學校
$\varphi=36^\circ\ 16'{\cdot}7$ July 28～29

date	Setting	T_e	T_i	d
h m				
7 05 p.m.	308°	26·9°C		31·5
7 45	20	26·2		29·6
8 25	92	25·2		22·6
9 05	164	24·7		20·5
9 45	236	24·3		26·5
10 25	308	24·1		31·6
11 05	20	23·7		29·8
11 45	92	23·5	27·1°C	22·2
0 25 a.m.	164	23·2	26·3	20·5
1 05	236	22·7	25·3	26·5
1 45	308	22·2	24·9	31·5
2 25	20	21·7	24·1	29·6
3 05	92	21·7	22·7	22·3
3 45	164	21·6	22·5	20·4
4 25	232	21·5	22·1	26·5
5 05	308	21·3	21·7	31·5

observation, T_e, T_i, and d being the atmospheric temperature, internal temperature of the instrument and scale-readings of the equilibirum position of the balance. In the same table, "setting" shows the azimuths of balance I referred to the magnetic meridian.

4. Reduction of Co-ordinate.

In setting up the instrument at the stations, the azimuth of the balance was determined by the magnetic north at each station. For convenience of reduction to effects due to the form of the geoid, it is necessary to transform the observed values to a rectangular co-ordinate in which the astronomical north, say the x'-axis, the astronomical east, say the y'-axis, and the direction of gravity, say the z'-axis, will have to be determined.

The magnetic declination for none of the stations being known, the values of the magnetic declination at Ueda [5° 36′ W] which lies 25 km N-W from the volcano and Matuida [5° 49′ W] which lies 20 km S-E from the volcano, have been used in this study. Since all the present stations lie between Ueda and Matuida, the 5° 43′ W was adopted as the common value of declination in the following calculations.

$$\left.\begin{aligned} x&=y'\sin\alpha+x'\cos\alpha\,,\\ y&=y'\cos\alpha-x'\sin\alpha\,,\\ z&=z', \end{aligned}\right\} \tag{3}$$

whence formulas (2) are transformed into

$$\left.\begin{aligned} \frac{\partial^2 V}{\partial y'^2}-\frac{\partial^2 V}{\partial x'^2}&=\left(\frac{\partial^2 V}{\partial y^2}-\frac{\partial^2 V}{\partial x^2}\right)\cos 2\alpha+2\frac{\partial^2 V}{\partial x\partial y}\sin 2\alpha\,,\\ \frac{\partial^2 V}{\partial x'\partial y'}&=-\frac{1}{2}\left(\frac{\partial^2 V}{\partial y^2}-\frac{\partial^2 V}{\partial x^2}\right)\sin 2\alpha+\frac{\partial^2 V}{\partial x\partial y}\cos 2\alpha\,,\\ \frac{\partial^2 V}{\partial x'\partial z'}&=\frac{\partial^2 V}{\partial x\partial z}\cos\alpha-\frac{\partial^2 V}{\partial y\partial z}\sin\alpha\,, \end{aligned}\right| \tag{4}$$

$$\left.\frac{\partial^2 V}{\partial y'\partial z'}=\frac{\partial^2 V}{\partial x\partial z}\sin\alpha+\frac{\partial^2 V}{\partial y\partial z}\cos\alpha\,.\right\}$$

5. Corrections for Ellipsoidal Form.[8]

The Eötvös quantities due to the form of the geoid are obtained as following:

$$\left.\begin{aligned}\frac{\partial^2 V}{\partial y'^2}-\frac{\partial^2 V}{\partial x'^2}&=g\left(\frac{1}{\rho_1}-\frac{1}{\rho_2}\right),\\ \frac{\partial^2 V}{\partial x'\partial y'}&=0\,.\end{aligned}\right\}\qquad(5)$$

$$\frac{1}{\rho_1}-\frac{1}{\rho_2}=\frac{(1-\xi)^3\{1-(1-\xi)^2\}\{\sin^2\varphi+(1-\xi)^2\cos^2\varphi\}^{\frac{1}{2}}\cos^2\varphi}{a[1-\{1-(1-\xi)^4\}\cos^2\varphi]^{\frac{3}{2}}}\,,$$

$$\xi=\frac{1}{296\cdot 96}$$

$a=6378388$ m,

$\varphi=$latitude,

ρ_1, $\rho_2=$principal radii of curvature.

In the present calculation of gradient term, the Bowie's gravity formula is adopted.

$$\gamma_0=978\cdot 039(1+0\cdot 005294\sin^2\varphi-0\cdot 000007\sin^2 2\varphi)\,.$$

Therefore,

$$\frac{\partial^2 V}{\partial x'\partial z'}=\frac{1}{\rho_1}\times 978\cdot 039(0\cdot 005294\sin 2\varphi-0\cdot 000014\sin 4\varphi)\,,$$

$$\frac{\partial^2 V}{\partial y'\partial z'}=0\,.$$

The values of the curvature and gradient due to the form of the geoid for every latitude were therefore obtained from the above formu-

---

8) N. KUMAGAI, *Nat. Res. Coun. Jap.* 4 (1926), 109.
C. TSUBOI, *loc. cit.*

las, the results of which are shown in Fig. 1.

As the final values given in Table 2 have only been corrected for the ellipsoidal form, they involve the effects due to topography, etc.

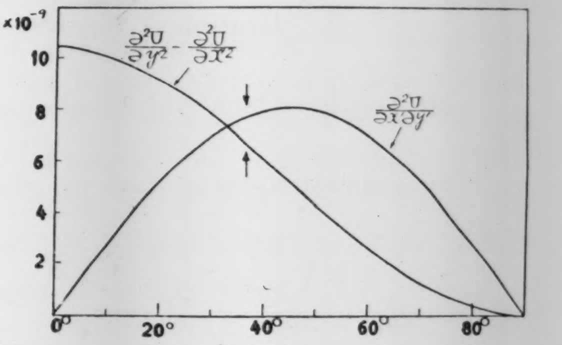

Fig. 1.

Table II. Final results.

Station No.	date	$\frac{\partial^2 V}{\partial y'^2} - \frac{\partial^2 V}{\partial x'^2}$	$2\frac{\partial^2 V}{\partial x' \partial y'}$	$\frac{\partial^2 V}{\partial x' \partial z'}$	$\frac{\partial^2 V}{\partial y' \partial z'}$
1	May 24∼25	− 5·49	−1·08	9·00	3·60
1	″ 25∼26	− 6·47	−0·96	9·88	2·64
1	″ 28∼29	− 6·18	−1·10	10·74	2·10
2	″ 29∼30	− 8·27	−0·26	−14·21	21·86
3	″ 30∼31	− 0·01	−0·04	−14·45	8·51
4	June 1∼ 2	− 5·06	−2·65	7·41	− 7·17
5	″ 4∼ 5	− 6·96	0·27	− 5·19	−15·23
6	″ 5∼ 6	− 2·67	−0·55	14·32	7·16
7	″ 7∼ 8	− 8·69	−1·00	−26·40	3·23
8	″ 13∼14	− 2·77	4·20	0·87	−42·74
9	″ 26∼27	−16·10	−0·34	−17·27	11·20
10	″ 28∼29	− 9·87	−2·11	−12·80	− 8·07
11	July 8∼ 9	−12·22	0·35	8·07	3·88
12	″ 9∼10	− 8·98	−0·85	11·79	5·13
13	″ 10∼11	−12·31	6·05	9·91	1·48
14	″ 11∼12	− 8·44	−0·95	0·81	−15·98
15	″ 12∼13	− 7·04	0·48	−22·95	10·14
16	″ 16∼17	−11·89	−0·97	−18·93	−15·81
17	″ 17∼18	− 6·11	1·73	−18·80	16·03
18	″ 21∼22	− 5·23	5·20	18·68	− 9·90
18	″ 25∼26	−16·90	−1·61	20·91	− 7·17
19	″ 22∼23	− 5·12	−0·44	11·57	− 4·20
20	″ 23∼24	− 9·20	2·82	4·26	−25·06
21	″ 24∼25	−10·90	−1·33	−26·91	−14·91
22	″ 28∼29	−11·58	1·57	9·31	−19·21

Eötvös unit.

6. Graphical Representation and Conclusion.

The results from the final values are graphically represented in Fig. 2.

The curvature-term may be given by

$$\sqrt{\left(\frac{\partial^2 V}{\partial y'^2}-\frac{\partial^2 V}{\partial x'^2}\right)^2+4\left(\frac{\partial^2 V}{\partial x'\partial y'}\right)^2}=g\left(\frac{1}{\rho_1}-\frac{1}{\rho_2}\right),$$

$$\frac{-2\dfrac{\partial^2 V}{\partial x'\partial y'}}{\dfrac{\partial^2 V}{\partial y'^2}-\dfrac{\partial^2 V}{\partial x'^2}}=\tan 2\theta.$$

In the foregoing formula, 2θ is an acute angle determined by $\tan^{-1}\dfrac{-2\dfrac{\partial^2 V}{\partial x'\partial y'}}{\dfrac{\partial^2 V}{\partial y'^2}-\dfrac{\partial^2 V}{\partial x'^2}}$ and measured clock-wise from the astronomical north but the required azimuth is θ or $\theta+\frac{\pi}{2}$ according as $\dfrac{\partial^2 V}{\partial y'^2}-\dfrac{\partial^2 V}{\partial x'^2}$ is positive or negative.

The horizontal projection of the gradient is given by

$$\sqrt{\left(\frac{\partial^2 V}{\partial x'\partial z'}\right)^2+\left(\frac{\partial^2 V}{\partial y'\partial z'}\right)^2}=\frac{\partial g}{\partial s} \qquad \sqrt{(\partial x')^2+(\partial y')^2}=\partial s,$$

$$\frac{\dfrac{\partial^2 V}{\partial x'\partial z'}}{\dfrac{\partial^2 V}{\partial y'\partial z'}}=\tan\gamma$$

where γ is an acute angle determined by $\tan^{-1}\dfrac{\dfrac{\partial^2 V}{\partial x'\partial z'}}{\dfrac{\partial^2 V}{\partial y'\partial z'}}$ and measured clock-wise from the astronomical north as well as θ. Naturally, the horizontal direction of the gradient shown in Fig. 2, which points to the direction of increase of gravity, is determined by γ or $\gamma+\pi$ according as to whether $\dfrac{\partial^2 V}{\partial y'\partial z'}\Big/\dfrac{\partial^2 V}{\partial x'\partial z'}$ is positive or negative.

A glance at the resulting values shows conspicuously that the curvature at all the stations are remarkably small and negative, which, no doubt, are the effects of topography, seeing that the present stations are all situated either at the foot of the volcano or in the valleys of Zyabori and Sengataki. Thus, from the topography of volcano Asama, which is a sort of "Konide" type, we may regard the surface of the gravity potential as having an inflection line at the foot of the volcano. Further, the mountain mass lies rather at higher levels than the stations, so that the concave side of the equi-potential surface points upward, that is to say, the curvature-term is negative.

On the other hand, although the gradient term shows itself to be larger than the curvature term, the direction of increase at all the stations does not always point to the crater or in the opposite direction. It is however believed to be influenced by near topography around the station. To illustrate, the gradients at stations situated in the ancient crater point rather in the opposite direction towards the present crater; whence no doubt they exhibit the remarkable effects due to the mountain masses of Kurohu-Yama and Gippa-Yama.

At the station 18 (Yosinotaira), lying only 3 km W-S from the crater, observations were made both before and after the violent explosion of July 22. According to the two series of observations, the variations in the gravity potential at this station which accompanied the explosion are as follows:

$$\varDelta\left(\frac{\partial^2 V}{\partial y'^2}-\frac{\partial^2 V}{\partial x'^2}\right)=11{\cdot}67\times 10^{-9},$$

$$\varDelta\left(\frac{\partial^2 V}{\partial x'\partial y'}\right)=6{\cdot}81\times 10^{-9},$$

$$\varDelta\left(\frac{\partial^2 V}{\partial x'\partial z'}\right)=-2{\cdot}13\times 10^{-9},$$

$$\varDelta\left(\frac{\partial^2 V}{\partial y'\partial z'}\right)=-2{\cdot}73\times 10^{-9}.$$

These quantities exceed the maximum errors for a single observation. As already mentioned, I. Yamamoto made gravimetric observations with the same kind of instrument and reported the results of his work, but in this paper, the writer did not dare to compare his results with Yamamoto's, as they do not appear to the writer to be accurate enough for the purpose.

In conclusion, the writer wishes to express his hearty thanks to

Professor M. Ishimoto and Doctor R. Takahasi for their interest and encouragement in this study. He also acknowledges his great indebtedness to the Foundation of the Promotion of Scientific and Industrial Research of Japan, with whose grant this study was made possible.

---

6. 淺間火山近傍に於ける重力偏差の觀測（其の1）

地震研究所　水上　武

1. 活火山近傍の著しい地形變動，熔岩の噴出等に依る多量の質量移動は必然的に重力ポテンシャルの變化を引き起す．今回の觀測の目的は重力ポテンシャルの第二次微分係數が火山活動に伴ひ如何に變化するかを明かにするにあつた．

2. 觀測は昭和11年4月より7月に亘つて26ケ所の地點に於いて行つた．火山は當期間內度々大爆發を行つた．特に7月22日，湯の平に於いて觀測中，數時間に亘つて噴火し，無數の火山彈は400～500米の近く迄飛來する有樣であつた．然し，この爆發の前日芦の平の觀測を終了して居たので，爆發後直ちに再測して，この爆發に直接伴つた變化を知る事が出來た．

3. 觀測の結果を通覽して見ると地形による影響が極めて顯著な事が判る．曲率項が著しく小さい事も特に注目される．2，3年後，再び同じ地點に於いて觀測し，兩回の觀測を比較研究して見度いと思つてゐる．尙今回の結果には，ゲオイドの形による補正以外には，何等の補正をも加へて無い．

今回の觀測を施行するに當り，多大の研究費を支給されたる日本學術振興會に對し，深甚の感謝の意を表する次第である．

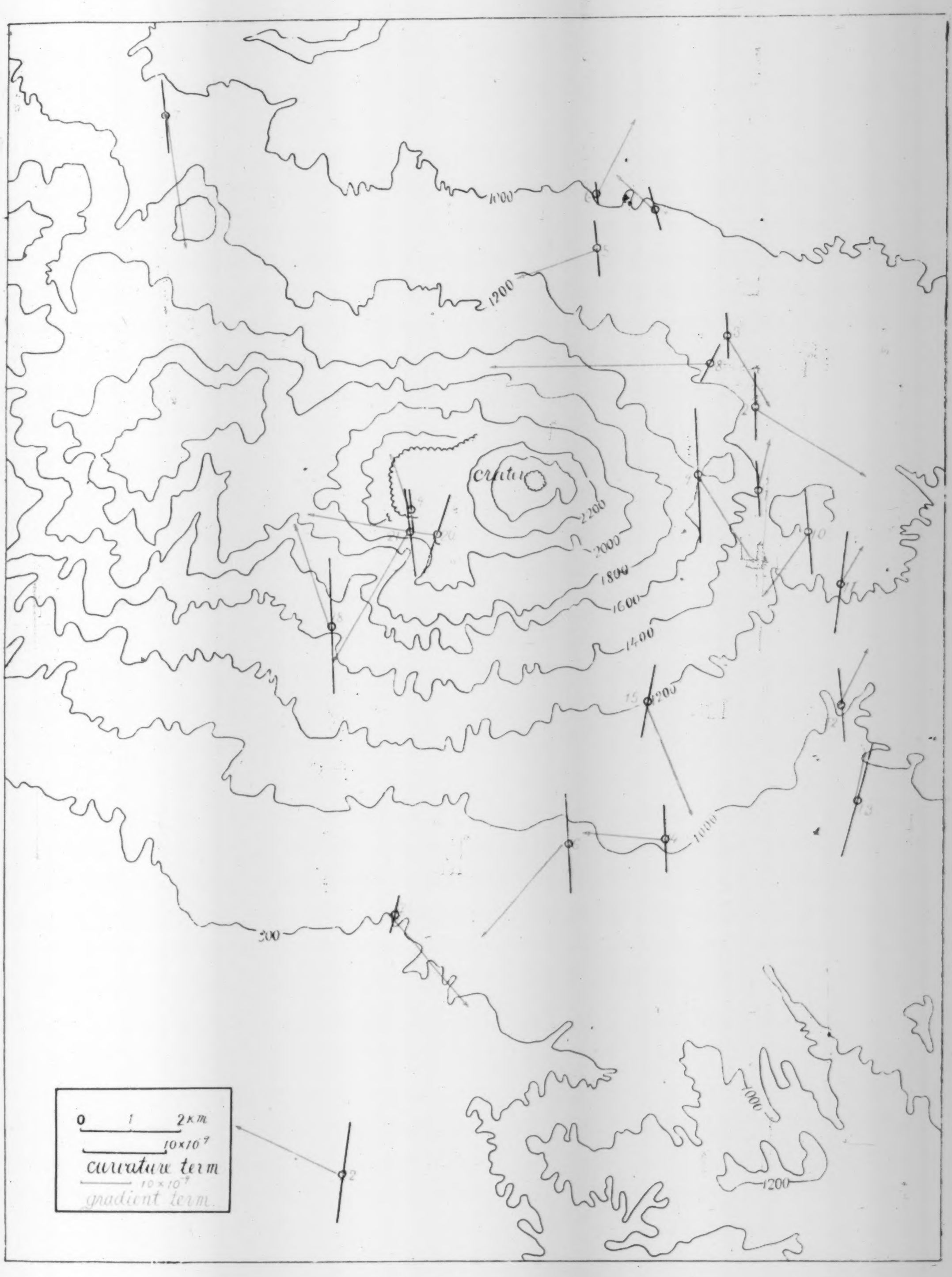
1000
1200
crater
2200
2000
1800
1600
1400
1200
1000
800
1000
1200
0 1 2 km
10×10⁻⁹
curvature term
10×10⁻⁹
gradient term

Fig. 2

Graphical Representation of Eötvös Quantities.

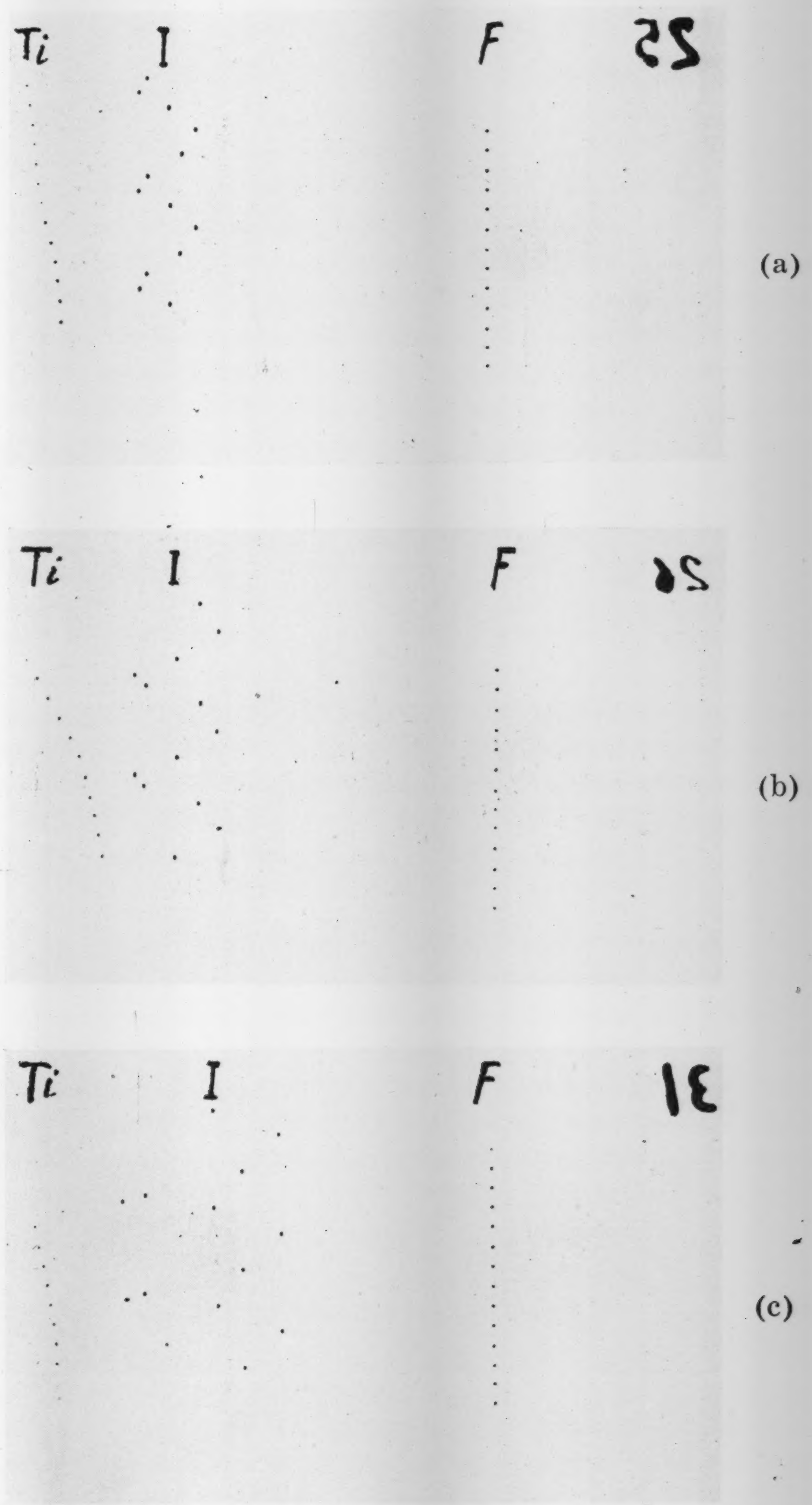

（震研彙報 第十五號 圖版 水上）

Fig. 3.
Records at the Stations No. 5. No. 6. and No. 8

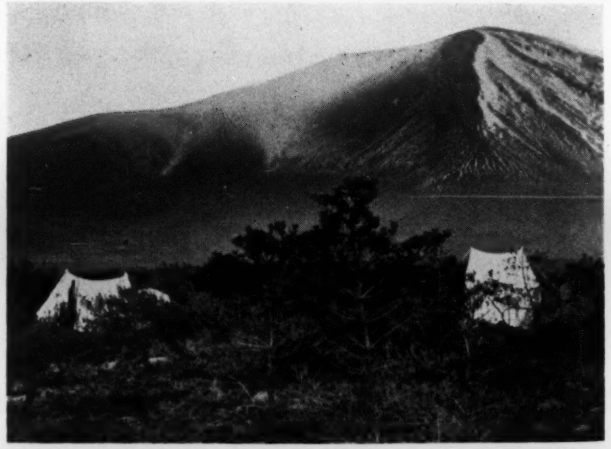

Fig. 4. a.
Wakasari-Tyaya (St. No. 3)

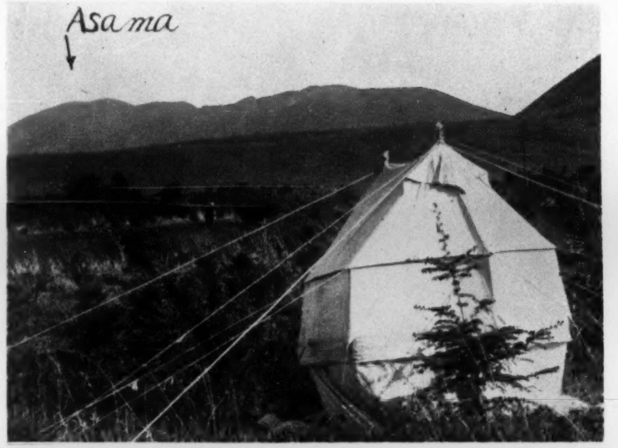

Fig. 4. b.
Sinkazawa (St. No. 7)

Fig. 4. c.
Yunotaira Sainokawara (St. No. 19)

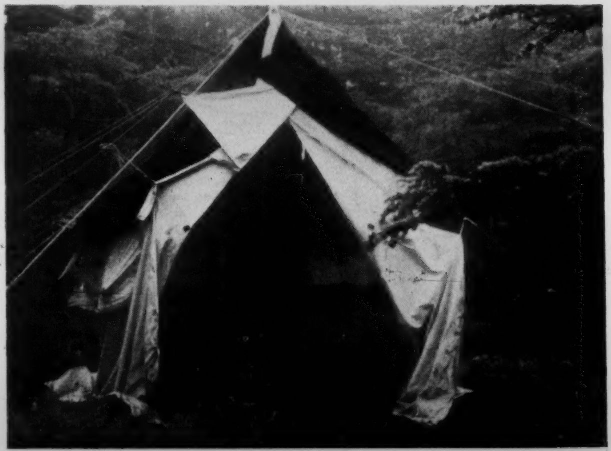

Fig. 4. d.
Tengunorodi (St. No. 20)

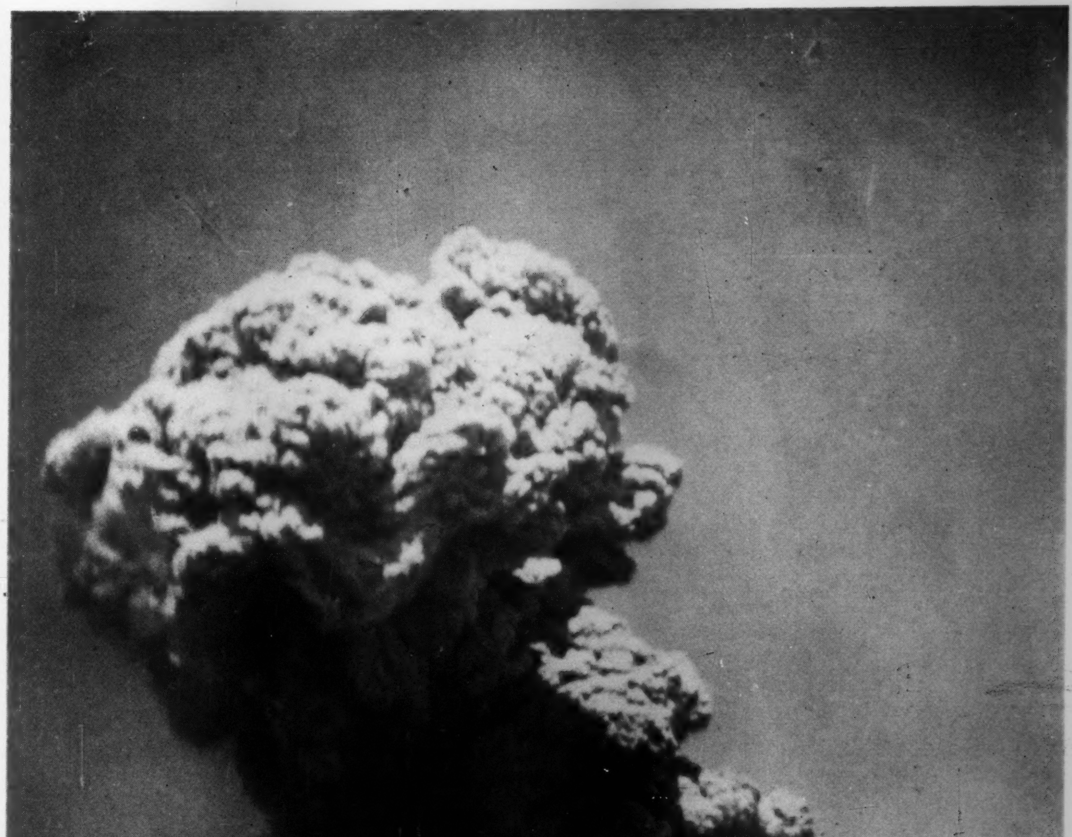

Fig. 5.
An explosion occurred in the midst of the present surveys.

7. *Determination of Elastic Constants of Soils by means of Vibration Methods.*

Part 2. Modulus of Rigidity and Poisson's Ratio.

By Mishio ISHIMOTO and Kumizi IIDA,

Earthquake Research Institute.

(Read Dec. 15, 1936 and Jan. 19, 1937.—Received Dec. 21. 1936.)

1. Introduction.

In the preceding paper[1], we reported our study of the elastic properties, such as longitudinal wave-velocities or Young's moduli as well as their solid viscosity coefficients of soils obtained by means of vibration method; these soils were taken from various depths in several sections of Tôkyô. From the results of our preceding experiments[2], we were able to ascertain that the elastic properties of these soils differ according to their kinds, their moisture contents, and their natural and recomposed states. To apply our results to geophysical problems, such as the propagation of seismic waves, especially in the most superficial layer of the earth's crust, we wished to carry out further experiments in this field, for the determination of other elastic properties of every kind of soil.

One of the objects of our present investigation was to find the elastic properties, such as the moduli of rigidity and Poisson's ratios[3], for the same kinds of soils as those adopted in the previous studies. Moreover we desired to ascertain whether or not the elastic constants of the soils vary according to their conditions.

The method of our present experiment is briefly described as follows; we continuously induced a variable frequency of torsional vibration at the foot of the soil specimen, and detected its fundamental resonance frequency. From that we then calculated its modulus of rigidity.

In order to obtain Poisson's ratio σ of the soil specimen, we measured the transverse wave-velocity as well as the longitudinal wave-velocity for the same specimen, and then computed these constants from the following equation

---

[1] M. ISHIMOTO and K. IIDA, *Bull. Earthq. Res. Inst.*, **14** (1936), 632~657.

[2] M. ISHIMOTO and K. IIDA, *ditto.* It is quoted in appropriate places.

[3] These same elastic properties, especially for the rock specimens, were dynamically studied by John M. IDE. *Proc. Nat. Acad. Sci.*, **22** (1936), 482.

$$\sigma=\frac{1}{2}\left\{\left(\frac{V_l}{V_t}\right)^2-2\right\}, \text{ or } \sigma=\frac{1}{2}\left\{\frac{E}{\mu}-2\right\},$$

$$V_l=\sqrt{\frac{E}{\rho}}, \qquad V_t=\sqrt{\frac{\mu}{\rho}},$$

in which V_l is the longitudinal wave-velocity, V_t the transverse wave-velocity, E Young's modulus, μ the modulus of rigidity, and ρ the density of the soil specimen. We studied also the elastic constants of soils, considering the effects of moisture content. Moreover, in the present experiments we investigated two kinds of solid viscosity coefficients, namely, the normal and the tangential ones.

As we adopted the same kinds of soil as were employed in the experiments reported in the previous paper, we have therefore omitted dealing with their mechanical analysis here.

2. Experiments.

(a) Apparatus for the experiment.

To carry out our experiment, we adopted two apparatuses, one of which we had already used in our preceding study, whereas the other

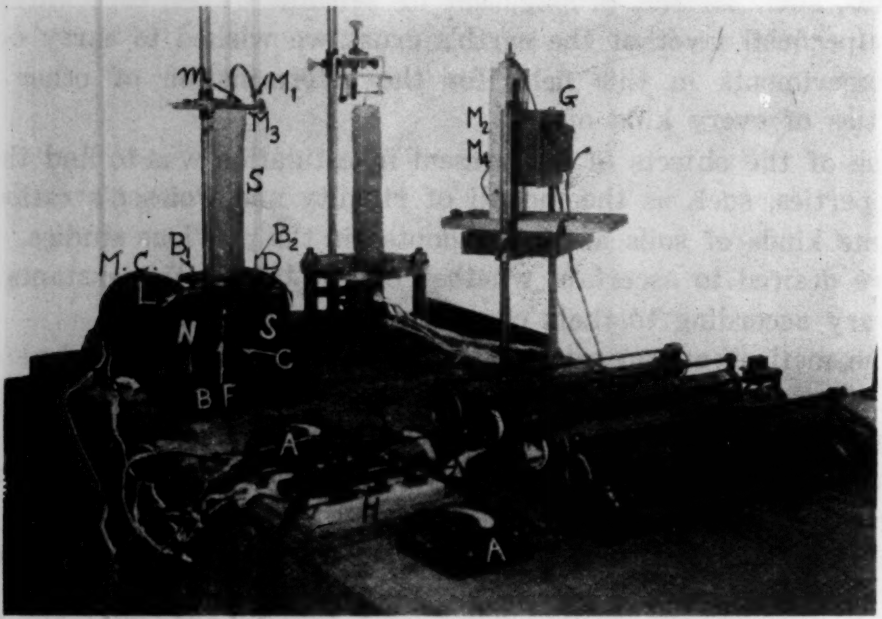

Fig. 1. Apparatuses for the experiment. (The symbols in this figure have the same meaning as in Fig. 2.)

was newly constructed for the present purpose; the photograph of both is shown in Fig. 1. A schematic diagram of the arrangement of these apparatuses is shown in Fig. 2. It is necessary to describe the particular details of our new apparatus.

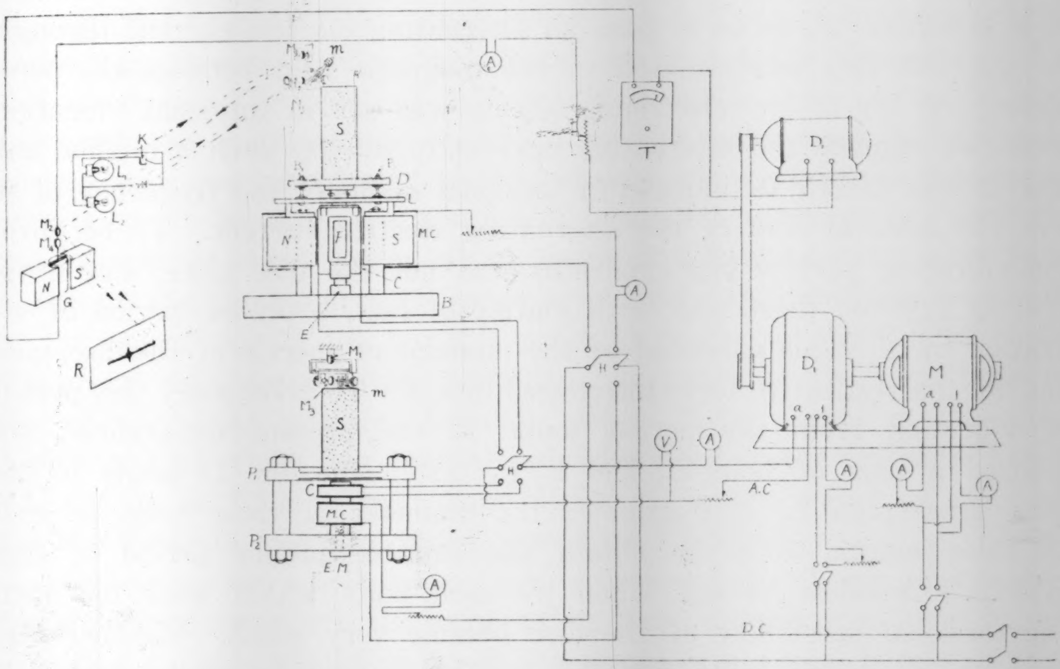

Fig. 2. Schematic diagram of arrangement of the apparatuses for producing the torsional and the longitudinal vibrations of soils.

a: Armature terminal.
A: Ampere-meter.
$A.C.$: Alternating current circuit.
B: Steel block.
B_1, B_2: Brass bolt.
C: $A.C.$ coil.
D: Circular brass disc.
D_1: Alternating generator.
D_2: Dynamo of the Weston tachometer.
$D.C.$: Direct current circuit.
E: End of the pivot.
$E.M.$: Electromagnet.
F: Solid cylindrical iron stick.
f: Field terminal.
G: Galvanometer.
H: Switch.
K: Key.
L_1, L_2: Light source.
m: Magnet.
M: $D.C.$ motor.
M_1, M_3: Lens mirror.
M_2, M_4: Plane mirror.
$M.C.$: $D.C.$ coil for electromagnet.
N, S: Pole piece of electromagnet.
P_1: Circular iron disc for vibration.
P_2: Circular iron disc with electromagnet.
R: Bromide paper for record.
S: Soil specimen.
T: Voltmeter of the Weston tachometer.

Vibrating disc. We employed a circular brass disc D for a vibrating disc, with a diameter of 14 cm and a thickness of 0·5 cm. On this vibrating disc, the soil column S stood upright. In order to avoid the slip, certain to occur during its torsional vibration, at the contact surface of this disc D and the soil specimen S, we notched its disc-surface so that it was like a rasp. There was a coil C attached firmly beneath the vibrating disc D, which was connected with the circuit of a generator D_1 so as to pass an alternating electric current through it. As this coil was situated in the magnetic field between the pole-pieces (N, S) of an electromagnet, it was set in torsional vibration when we applied the alternating current to it. By such a method the disc D was forced to vibrate in torsional manner; the frequency of it was the same as that of the alternating electric current. To be sure, the vibrating part of the apparatus was not the disc alone, but a vibrating system; there was, as a matter of fact, a proper period of vibration in it. This consisted of the moment of inertia of the disc, etc., and of the restitutive force introduced into it. To drive away this period of vibration from the period found in the present experiment, we utilized a pair of bolts B_1 and B_2 to fasten the disc D firmly to the fixed brass plate L. We adjusted the diameter of these bolts as well as their length, so as to obtain the suitable proper period of this system. Needless to say, when we used bolts which were too stiff, the torsional sensibility of the disc became very small. We therefore made a choice of bolts for this system, having its proper period of vibration just at the edge of the field in which we wished to carry out our experiment.

To succeed in obtaining the pure torsional vibration of this disc D, we controlled the vibration with the part of a pivot, its sharpened end E touching a conical support on the brass plate L, through which the shaft of this disc rotated freely during torsional vibrations.

The magnetic field, in which we inserted the coil C, was regulated by the amount of the direct current which passed through the exciting coil $M.C.$ of the electromagnet.

Magnification of vibration amplitude of the top of soil specimen. In the present experiment, as we intended to determine the amplitude of the torsional vibration of the soil specimen, we adopted its magnification device as being almost the same as that described in our preceding paper. However, we changed this device to fit our purpose. The vibration amplitude of the top of the soil specimen attained its maximum, when the vibration frequency of this vibrating disc reached a condition to provoke a stationary wave in the soil specimen. Even in this case, the vibration of its top was, of course, perceptible to the tip of one's finger; but we had to magnify it by some device in order to record continuously the variation of its vibration amplitude and to determine accurately the position of its maximum amplitude. We therefore adopted the same device, a pair of small pivot and small magnet *m*, to get a sufficient magnification of it. A part of the frame of this small pivot was inserted into one side of the top of the soil specimen *S*. As the weight of this small pivot and its frame amounted only to about 5 gr, it seemed to us that it did not disturb the vibration of the soil specimen. The pivot of 1·77 mm in diameter was always in contact with the small magnet *m*, which rotated easily upon its own axis. In this way, the pivot could be rotated with the smallest possible degree of friction. On this pivot there was a small lens-mirror M_3 with the focal length of about 50 cm, which reflected a light-beam radiated from a slit of the light-source L_2 so as to magnify the vibration amplitude of the top of soil on the bromide paper as much as about 2200 times. We could then register the continuous variation of the amplitude on the photographic sensitive bromide paper *R*, by means of the same device as that which has been already described in the preceding paper. We had, in addition, a fixed plane-mirror M_1 which served as the scale for the accurate measure of the resonance frequency.

Motor-generator, tachometer, and galvanometer. These apparatuses for the experiments are the same as we have already mentioned in our preceding paper. Therefore it will not necessary to repeat here a description of them.

(b) Testing of the apparatus.

Proper period of the vibrating disc. As the effect of the proper period of the vibrating disc on resonance frequency of the soil specimen is always considerable, we endeavoured to eliminate the proper period from the field of our experiment.

In our apparatus preliminary constructed, we noticed that at the frequency of about 30 vibrations per second the vibration amplitude of the disc became to the maximum. This was the natural effect of the proper period of the disc, together with the vibrating system consisting of the moment of inertia of the disc, etc., and the restitutive force mainly due to the bolts which connected the disc with the fixed brass plate *L*. In order to discount the effect of this proper period from the present experiment, we selected a pair of bolts one after another, until at last we decided upon those with a diameter of 0·6 cm and a length of 1·5 cm. By the employment of these two bolts we conclusively proved that the proper period of this vibrating system was eliminated from the field of our use. We found, at any rate, that this fundamental vibration frequency of our disc system was about 270 vibrations per second. In order to find whether or not this proper period might be varied by the moment of inertia of a dead weight of metal loaded on the vibrating disc, we repeated the same experiment with several different sizes of metal, the weights of which were up to the limit of 2 kg. From the results of these experiments, we also ascertained that the proper period is scarcely affected by the additional moment of inertia. We may, therefore, conclude from the above experiments that no effect was found which needs to be taken into consideration. We can thus pick out the pure characteristics of the soil specimens.

Calibration of the tachometer. In the present study we also employed the same calibration curve as that shown in our preceding paper. We have taken into consideration the correction of the readings of the Weston tachometer.

(c) Methods of the experiment.

The methods of the present experiment were also about the same as those employed in the previous experiments. We experimented on the soil specimens in the natural state and sometimes in the recomposed state; the form of which was a cylinder with the initial height of 20 cm∼40 cm, and the diameter of about 5 cm. At that time we took the same kind of commercial rubber as that used in the previous experiment, for the purpose of comparing its elastic properties with those of the soils. The dimension of this specimen was the same as before. We measured the density and the moisture content of the soil specimen by the same process as before.

In order to determine Poisson's ratio of the soil specimen, we employed both apparatuses together, one being the longitudinal-vibration apparatus which had already been adopted in our previous experiment. First of all, setting the soil specimen on the vibrating disc of the new torsional-vibration apparatus, we made a photographic record while applying the forced transverse vibration to the soil up to the limit; and then setting this same specimen on the vibrating plate of the longitudinal-vibration apparatus, we again made a photographic record while applying the forced longitudinal vibration up to the same limit. To apply the direct and the alternating electric currents, one after the other, to the two different apparatuses, we employed two switches H which served for our purpose very well. We repeated the procedure on the identical material arranged in various heights that were diminished in equal amounts. We thus got the reducing curves in the two cases of the longitudinal and the torsional vibrations, for soils of the same condition. We succeeded finally in computing the two constants of elasticity and of Poisson's ratio of the tested soils.

3. Results of the Experiments.

(a) Photographic records.

Actual photographs thus obtained of the two kinds of soil specimens collected at Hongô and at Maru-no-uti in Tôkyô are shown in Figs. 3 and 4. The photographs are shown in pairs, according to the two kinds of vibrations, namely, the torsional and the longitudinal, in the different heights of the soil specimens. As will be seen from these figures, the characteristics of these resonance curves are almost identical; and the frequency, corresponding to the resonance position in the case of the torsional vibration, is generally smaller than that in the case of the longitudinal vibration. Merely from this appearance we have reached the conclusion that the transverse wave-velocity is always less than that of the longitudinal wave-velocity. In some of these photographs, we can also detect the resonance of higher orders; this is due to the size and condition of the soil specimens, such as their height, or their moisture content. We observe also the fact that the resonance curves tended to flatten when the height or the moisture content was diminished.

(b) Determination of two kinds of wave-velocities, Poisson's ratio, and two kinds of solid viscosity coefficients.

As was already set forth in our preceding paper, the equation of motion for the longitudinal wave in the soil specimen is expressed by

$$\rho\frac{\partial^2\zeta}{\partial t^2}=E\frac{\partial^2\zeta}{\partial z^2}+\gamma_l\frac{\partial^3\zeta}{\partial z^2\partial t}, \tag{1}$$

where ζ is the displacement in the direction of the height z, t the time, ρ the density, E the Young's modulus, and γ_l the coefficient of normal solid viscosity. We have also the similar equation of motion for the transverse wave in the soil specimen such as

$$\rho\frac{\partial^2\xi}{\partial t^2}=\mu\frac{\partial^2\xi}{\partial z^2}+\gamma_t\frac{\partial^3\xi}{\partial z^2\partial t}, \tag{2}$$

in which ξ is the displacement in the direction of the horizontal, μ the modulus of rigidity, and γ_t the coefficient of tangential solid viscosity.

The solutions of (2) in the case of the free and the forced vibrations of the soil specimen are the same as those obtained in our previous paper, provided μ and γ_t are in the place of E and γ_l respectively.

Namely, the solution in the case of free vibration of the soil specimen is given by

$$\left.\begin{aligned} \xi &= Ae^{-\frac{\gamma_t f^2}{2\rho}t}\cos\left\{\sqrt{\frac{\mu f^2}{\rho}-\left(\frac{\gamma_t f^2}{2\rho}\right)^2}\,t-\alpha\right\}\sin fz, \\ f &= \frac{2r-1}{2h}, \quad r\ \ 1,\ 2,\ldots\ldots \end{aligned}\right\} \tag{3}$$

We have also the following solution in the case of their forced vibration

$$\left.\begin{aligned} \xi &= C(\xi_1+i\xi_2)e^{ipt}, \\ \xi_1 &= \cos f_1 z\cosh f_2 z+\frac{1}{\vartheta}(\sin f_1 h\cos f_1 h\sin f_1 z\cosh f_2 z \\ &\quad -\cos f_1 z\sinh f_2 z\sinh f_2 h\cosh f_2 h), \\ \xi_2 &= \sin f_1 z\sinh f_2 z-\frac{1}{\vartheta}(\sin f_1 h\cos f_1 h\cos f_1 z\sinh f_2 z \\ &\quad +\sin f_1 z\cosh f_2 z\sinh f_2 h\cosh f_2 h), \end{aligned}\right\} \tag{4}$$

where, $\vartheta=\cos^2 f_1 h\cosh^2 f_2 h+\sin^2 f_1 h\sinh^2 f_2 h,$

$$f_1-if_2=\frac{fp}{(n^4+4p^2\varepsilon^2)^{\frac{1}{4}}}\left\{\sqrt{\frac{1}{2}\left(1+\frac{n^2}{\sqrt{n^4+4p^2\varepsilon^2}}\right)}-i\sqrt{\frac{1}{2}\left(1-\frac{n^2}{\sqrt{n^4+4p^2\varepsilon^2}}\right)}\right\},$$

and $\varepsilon=\dfrac{1}{2}\dfrac{\gamma_t}{\rho}f^2, \quad n^2=\dfrac{\mu}{\rho}f^2.$

The resonance period T_t in the case of the torsional vibration is given by

$$T_t=\frac{4h}{(2r-1)\sqrt{\dfrac{\mu}{\rho}-\dfrac{(2r-1)^2\pi^2\gamma_t^2}{16\rho^2h^2}}}, \quad r=1,\ 2,\ 3,\ldots\ldots \tag{5}$$

This formula showing the relation between the resonance period T_t and the height h of the soil specimen are almost the same as before.

The process of determining the transverse wave-velocity and the tangential solid viscosity coefficient is also the same as that set forth in our previous paper. The diagrams showing the relation between the fundamental resonance period T_t or T_l (resonance period in the case of longitudinal vibration) and the height h of the soil specimens are shown in Figs. 5~9, in which the pepiod, T_t or T_l is taken as ordinate and the height h as abscissa. These figures are the reducing curves, by which the transverse and the longitudinal wave-velocities and the normal and the tangential solid viscosity coefficients are all determined. Also the reducing curves of rubber are shown in Fig. 10. In every experiment it is also believed that the mode of vibra-

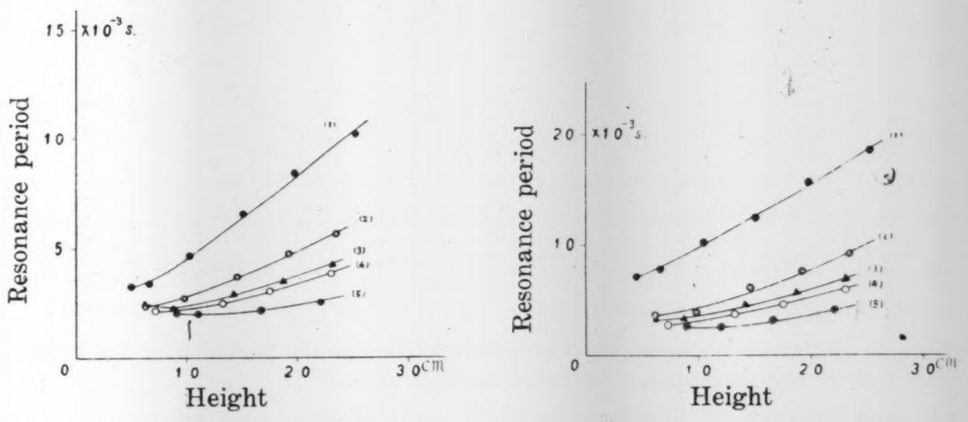

(a) Longitudinal vibration. (b) Torsional vibration.

Fig. 5. Relation between the fundamental resonance period and the height of soil in the natural state taken from Maru-no-uti.
(1) Moisture content 48·7%. (2) 42·6%. (3) 3 ·4%. (4) 37·6%. (5) 31·8%.

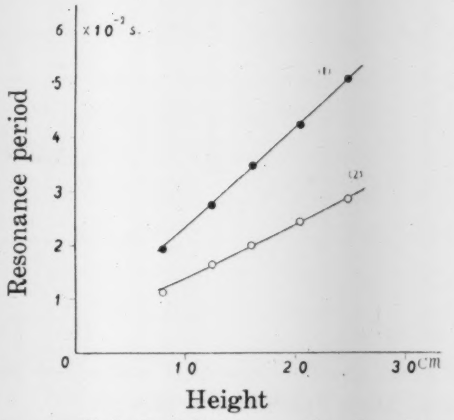

Fig. 6. Relation between the fundamental resonance period and the height of soil in the recomposed state taken from Maru-no-uti.
Moisture content 47·7%.
(1) Case of torsional vibration.
(2) 〃 longitudinal vibration.

tion of the soil specimens corresponds to that of the clamped- and free-end bar, the reason for which will be explained later. As the mode of vibration has been determined, we have succeeded in finding out from these reducing curves the values of the longitudinal and the transverse wave-velocities, namely V_l and V_t ; and the normal and the tangential solid viscosity coefficients, namely γ_l and γ_t, of the soil specimens. These values thus obtained are all tabulated in Table I.

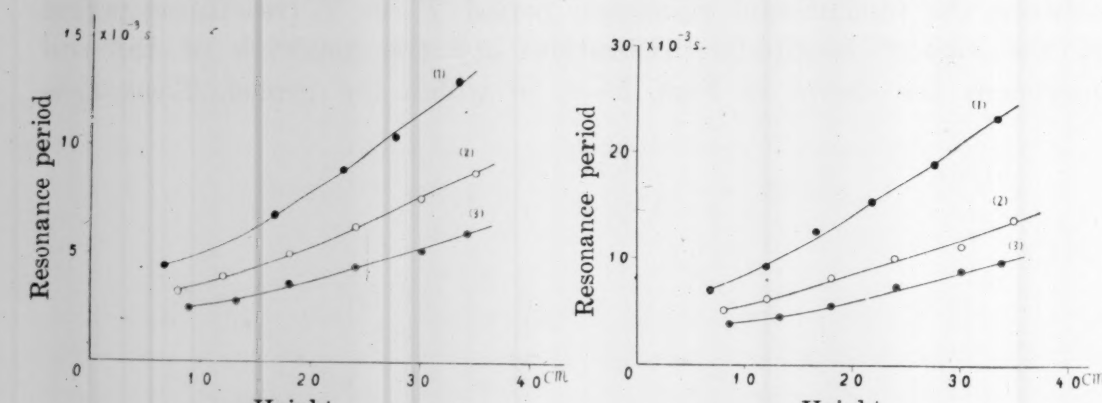

(a) Longitudinal vibration. (b) Torsional vibration.

Eig. 7. Relation between the fundamental resonance period and the height of soil in the recomposed state of Komatugawa.
(1) Moisture content 27·0%. (2) 24·5%. (3) 21·2%.

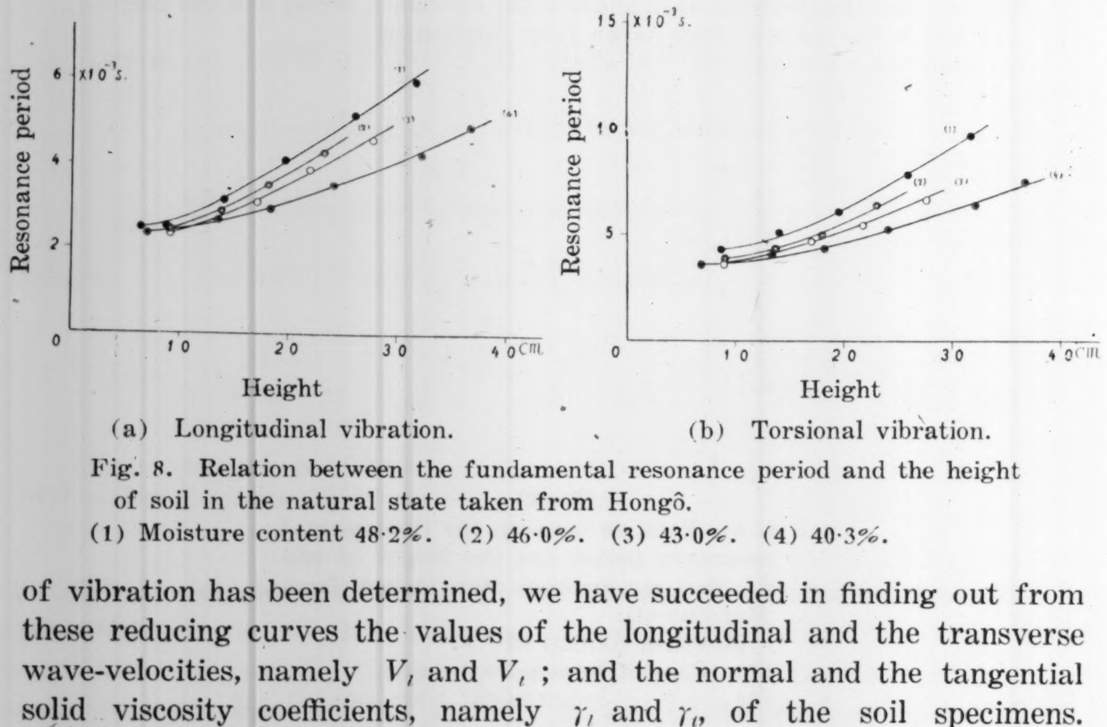

(a) Longitudinal vibration. (b) Torsional vibration.

Fig. 8. Relation between the fundamental resonance period and the height of soil in the natural state taken from Hongô.
(1) Moisture content 48·2%. (2) 46·0%. (3) 43·0%. (4) 40·3%.

The moduli of rigidity of the soil specimens were then computed from the equation $\mu=\rho V_t^2$, and their Young's moduli E were also calculated from the equation $E=\rho V_l^2$. As V_l and V_t, or E and μ are thus obtained, Poisson's ratio σ was then calculated from the equation $\sigma=$

$\frac{1}{2}\left\{\left(\frac{V_l}{V_t}\right)^2-2\right\}$ or $\sigma=\frac{1}{2}\left\{\frac{E}{\mu}-2\right\}$. These computed values of E, μ, and σ are all shown in Table II.

All of Young's moduli, the moduli of rigidity, and the solid viscosity coefficients of these soil specimens in the natural state show greater values than those in the recomposed state. These phenomena could be seen in the soils taken from Maru-no-uti, from Komatugawa, and in a kind of clay; these are shown in the reducing curves in Figs. 6~7 and 9 (a), (b) and in Tables I and II. It seems to us that Poisson's ratio of loam at Hongô is smaller than that of the silty-clay at Maru-no-uti within a certain moisture content limit.

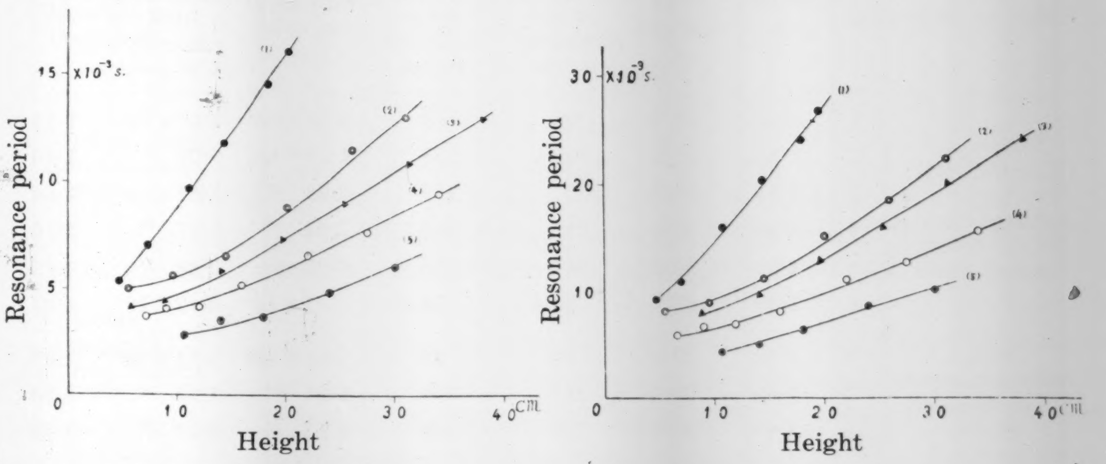

(a) Longitudinal vibration. (b) Torsional vibration.

Fig. 9. Relation between the fundamental resonance period and the height of a kind of clay in the recomposed state.
(1) Moisture content 32·6%. (2) 28·3%. (3) 27·8%. (4) 25·1%. (5) 22·0%.

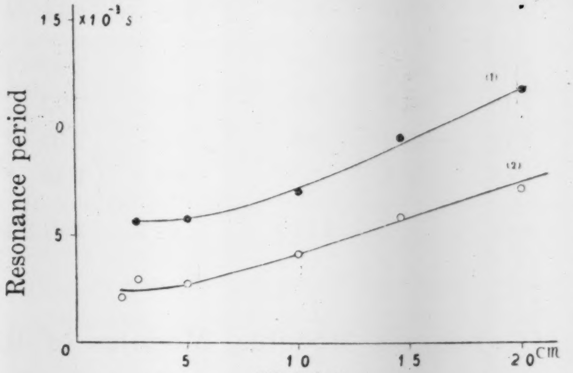

Fig. 10. The relation between the fundamental resonance period and the height of a kind of rubber, the result being obtained by torsional and longitudinal vibrations.
(1) Case of torsional vibration.
(2) 〃 longitudinal vibration.

Table I. Longitudinal and Transverse Wave-Velocities, Coefficients of Normal and Tangential Solid Viscosities, Density, and Moisture Content of Soils.

Kinds of soils	No.	Density ρ	Moisture content %	Longitudinal wave velocity m/sec	Transverse wave velocity m/sec	Coef. normal solid viscosity γ_l (c.g.s.)	Coef. tangential solid viscosity γ_t (c.g.s.)	$\frac{\gamma_l}{\gamma_t}$
Silty-clay (Maru-no-uti) (No. 1~5: natural state. No.6: recomposed state.)	1	1·50	48·7	98	58	4·58×10^{4}	4·02×10^{4}	1·14
	2	1·56	42·6	169	103	1·29×10^{5}	9·20 ″	1·40
	3	1·56	39·4	222	138	2·65 ″	1·62×10^{5}	1·64
	4	1·56	37·6	253	160	2·94 ″	1·67 ″	1·76
	5	1·59	31·8	364	237	4·90 ″	2·80 ″	1·75
	6	1·49	47·7	34·4	20·0	5·31×10^{3}	6·12×10^{3}	0·87
Silt (Komatugawa) (Recomposed state)	1	1·94	27·0	94	58	1·66×10^{5}	1·11×10^{5}	1·49
	2	1·89	24·5	163	104	2·34 ″	1·48 ″	1·58
	3	1·96	21·2	237	149	3·73 ″	2·21 ″	1·69
A kind of clay (Recomposed state)	1	1·89	32·6	51·0	29·6	3·33×10^{4}	2·90×10^{4}	1·15
	2	1·89	28·3	96·0	56·5	1·28×10^{5}	9·35×10^{4}	1·37
	3	1·89	27·8	116	68	1·38 ″	1·09×10^{5}	1·27
	4	1·90	25·1	150	91	2·18 ″	1·31 ″	1·66
	5	1·91	22·0	211	132	2·55 ″	1·60 ″	1·60
Loam (Hongô) (Natural state)	1	1·24	48·2	212	132	2·01×10^{5}	1·45×10^{5}	1·39
	2	1·19	46·0	232	148	2·13 ″	1·55 ″	1·38
	3	1·16	43·0	255	167	2·20 ″	1·56 ″	1·41
	4	1·09	40·3	303	200	2·18 ″	1·47 ″	1·48
Rubber		1·77		114·5	69·0	1·41×10^{5}	1·06×10^{5}	2·01

Table II. Young's Modulus, Modulus of Rigidity, Poisson's Ratio, and Moisture Content of Soils.

Kinds of soils	No.	Moisture Content %	Young's modulus E (c.g.s.)	Modulus of rigidity μ (c.g.s.)	Poisson's ratio σ
Silty-clay (Maru-no-uti) (No. 1~5: natural state. No. 6: recomposed state.)	1	48·7	1·44×10^{8}	5·05×10^{7}	0·43
	2	42·6	4·46 ″	1·65×10^{8}	0·35
	3	39·4	7·69 ″	2·97 ″	0·30
	4	37·6	1·00×10^{9}	3·99 ″	0·25
	5	31·8	2·11 ″	8·93 ″	0·19
	6	47·7	1·76×10^{7}	5·96×10^{6}	0·48

(to be continued.)

Table II. (*continued*).

Kinds of soils	No.	Moisture Content %	Young's modulus E (c.g.s.)	Modulus of rigidity μ (c.g.s.)	Poisson's ratio σ
Silt (Komatugawa) (Recomposed state)	1	27·0	$1{\cdot}71\times10^{8}$	$6{\cdot}52\times10^{7}$	0·32
	2	24·5	5·02 〃	$2{\cdot}04\times10^{8}$	0·28
	3	21·2	$1{\cdot}10\times10^{9}$	4·35 〃	0·26
A kind of clay (Recomposed state)	1	32·6	$5{\cdot}02\times10^{7}$	$1{\cdot}66\times10^{7}$	0·48
	2	28·3	$1{\cdot}74\times10^{8}$	6·03 〃	0·47
	3	27·8	2·54 〃	7·45 〃	0·41
	4	25·1	4·27 〃	$1{\cdot}57\times10^{8}$	0·35
	5	22·0	8·50 〃	3·28 〃	0·29
Loam (Hongô) (Natural state)	1	48·2	$5{\cdot}48\times10^{8}$	$2{\cdot}16\times10^{8}$	0·30
	2	46·0	6.41 〃	2·60 〃	0·22
	3	43·0	7·56 〃	3·23 〃	0·17
	4	40·3	$1{\cdot}01\times10^{9}$	4·36 〃	0·15
Rubber			$2{\cdot}35\times10^{8}$	$8{\cdot}43\times10^{7}$	0·38

(c) Effect of moisture content on the constants of elasticity and solid viscosity.

To observe the effect of moisture content on the physical properties of soils, we plotted the computed values (Tables I and II) from the

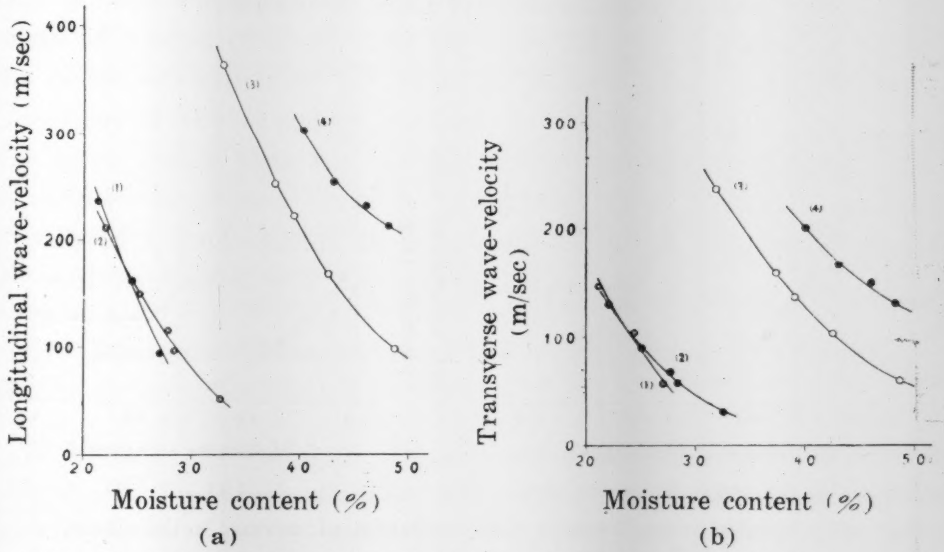

Fig. 11. (a) Relation between the longitudinal wave-velocity and the moisture content.
(b) Relation between the transverse wave-velocity and the moisture content.
(1) Silt of Komatugawa. (2) A kind of clay. (3) Silty-clay of Maru-no-uti. (4) Loam of Hongô.

results of the experiments shown in several diagrams, such as in Figs.

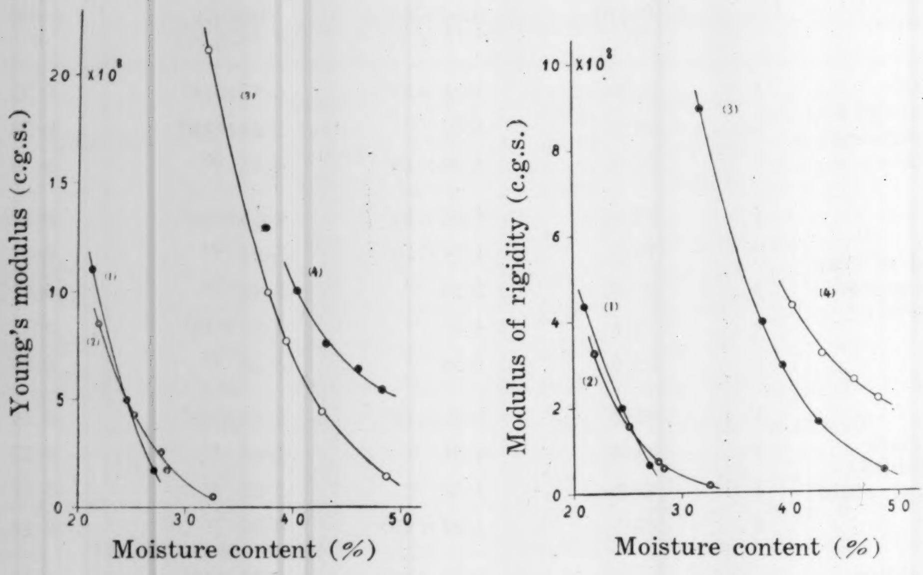

(a) (b)

Fig. 12. (a) Relation between Young's modulus and the moisture content.
(b) Relation between the modulus of rigidity and the moisture content.
(1) Silt of Komatugawa. (2) A kind of clay. (3) Silty-clay of Maru-no-uti. (4) Loam of Hongô.

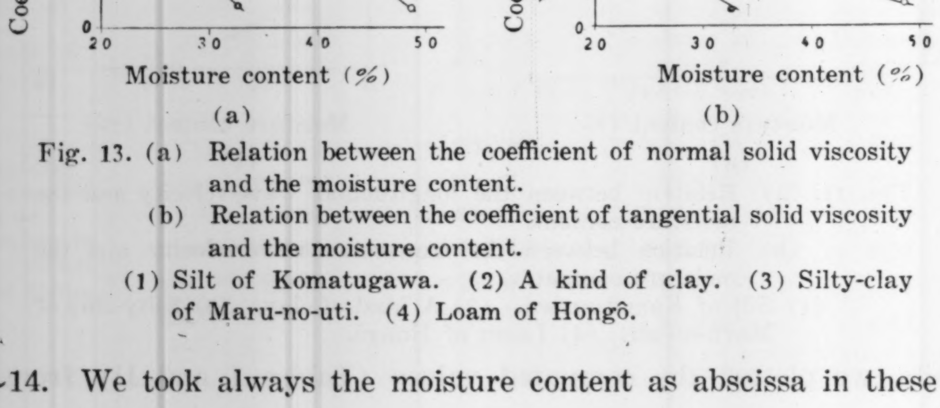

(a) (b)

Fig. 13. (a) Relation between the coefficient of normal solid viscosity and the moisture content.
(b) Relation between the coefficient of tangential solid viscosity and the moisture content.
(1) Silt of Komatugawa. (2) A kind of clay. (3) Silty-clay of Maru-no-uti. (4) Loam of Hongô.

11∼14. We took always the moisture content as abscissa in these diagrams; and the transverse wave-velocity, the longitudinal wave-velocity, Young's modulus, Poisson's ratio, and the tangential or the normal solid viscosity coefficient are all considered as ordinate in each case in these diagrams. As will be seen from these figures, all the values, such as V_l, V_t, E, and μ decrease somewhat rapidly with the increase of the moisture content, especially is the rate of this decrease of V_l and E greater than that of V_t and μ. Evidently the manner of the decrease differs according to each soil specimen. The degree of decrease of all these things in the soil taken from Maru-no-uti seems to be greater than in that of Hongô.

The solid viscosity coefficients of the finer grained soils, such as that of Maru-no-uti, Komatugawa, and a kind of clay, seem to decrease also somewhat rapidly with the increase of the moisture content; these coefficients are of the order of $10^4 \sim 10^5$ (c.g.s.) at the moisture content ranges of about 50% ~ 20%; while in the case of coarse grained soils such as that of Hongô, the coefficients, of the order of which is 10^5 (c.g.s.), is somewhat constant even with the increase of the moisture content to a certain limit.

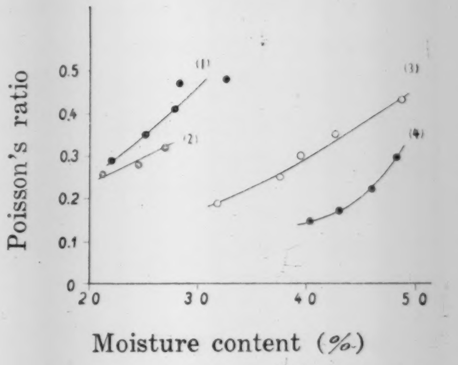

Fig 14. Relation between Poisson's ratio and the moisture content.
(1) A kind of clay. (2) Silt of Komatugawa. (3) Silty-clay of Maru-no-uti. (4) Loam of Hongô.

We have found that the normal solid viscosity coefficient γ_l of every soil specimen is greater than its tangential solid viscosity coefficient γ_t. The ratio of γ_l to γ_t seems to approach 1·0 when the moisture content of the soil increases, and *vice versa*.

(d) Resonance frequencies of the higher orders of vibration. (Partials)

As already described in the preceding paper, the determination of the mode of vibration of the soil specimen is one of the most important matters of investigation. We, therefore, studied the resonance frequencies of the higher orders in every case. Five examples of the relation between the resonance frequencies of the torsional vibrations and the order of their successive maximum amplitude are shown in Table III and Fig. 15, in which we took the frequency as ordinate and the order as abscissa. We also found that these points are not in a straight line, owing to the effect of the solid viscosity of the soil speci-

Table III. Resonance Frequencies of the Fundamental and the Higher Orders.

Soil specimen		Height h	Transverse and longitudinal resonance frequencies.			
Kind	State		Fundamental	2nd order	3rd order	4th order
		cm	per sec	per sec	per sec	per sec
Silty-clay (Maru-no-uti)	Natural	25·1	54 93	149 280	247 468	330 ——
	Recomposed	24·7	19 35	53 98	84 162	110 214
Silt (Komatugawa)	Recomposed	33·2	43 73	112 198	187 327	263 ——
A kind of clay	Recomposed	38·0	42 77	111 213	187 352	288 ——
Loam (Hongô)	Natural	31·5	104 165	296 463	486 ——	

mens. As will be seen in Fig. 15 or Table III, the successive resonance frequencies of the higher orders are about an odd number of times that of the fundamental resonance frequency. We ascertained, therefore, that the observed vibration of the soil specimen is revealed by the transverse vibration in a clamped- and free- end bar, a fact which has already been pointed out in the preceding paper.

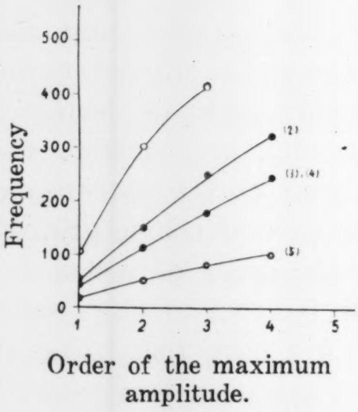

Fig. 15. Relation between the resonance frequency and the order of resonance position. (1) Loam of Hongô in the natural state, $h=31{\cdot}5$ cm. (2) Silty-clay of Maru-no-uti in the natural state, $h=25{\cdot}1$ cm. (3) Clay in the recomposed state, $h=38$ cm. (4) Silt of Komatugawa in the recomposed state, $h=33{\cdot}2$ cm. (5) Silty-clay of Maru-no-uti in the recomposed state, $h=24{\cdot}7$ cm.

4. Remarks.

In the process of determining the velocity of elastic waves in the soil specimen, the investigation of the mode of its vibration is certainly one of the most important matters. If the mode of vibration of the soil specimen corresponds to that of the bar with both ends free, the loop of which is at both ends and the node at its center, then the elastic wave-velocity computed therefrom is, of course, reduced to half that computed from the conditions corresponding to the mode of vibration of a clamped-free bar. However, in most of our present examples, the mode of vibration of the soil specimen corresponds, unquestionably, to that of a clamped-free bar, because the resonance frequencies of the higher orders are about an odd number of times that of the fundamental frequency. In the process of determining the velocity of elastic waves in the soil specimen, we trace, therefore, a straight line, which is to be an asymptote to the reducing curve passing through the point of origin. This straight line represents the relation between the fundamental resonance period T_t and the height h, such as $T_t = \frac{4h}{\sqrt{\frac{\mu}{\rho}}}$, from which we can determine the transverse wave-velocity V_t.

When the soil specimen becomes hard by reason of the diminishing of its moisture content, it is, however, difficult to observe resonance frequencies of the higher orders within the limit of our field of experiment, owing to the increase of fundamental resonance frequency. In such a case the mode of vibration of the soil specimen is not to be determined, but, at any rate, we adopted the mode of vibration corresponding to the vibration in a clamped-free bar. Here, we remark that in the case of hard material, the boundary conditions must be changed. These problems are to be dealt with in future experiments.

In our laboratory, we endeavoured not to allow a decrease of moisture in the soil, so it is probable that moisture values were always constant in the interval of each of our experiments; since each allowed for no more than half an hour of exposure. We noticed during our other investigations that the finer grained soils, such as that of Maru-no-uti, have a tendency to great shrinkage in height with the decrease of moisture content and the density was almost constant; while in the case of coarse grained soils, such as that of Hongô, this tendency is not so conspicuous, but the density became small; this difference may be chiefly due to the state of the internal structure of the soils.

5. Summary and Conclusion.

1) We studied the elastic properties of the same kinds of soil taken from several sections in Tôkyô as those adopted in our preceding studies. The soils were taken out in the natural state from various depths underground in Hongô, Maru-no-uti, and Komatugawa, by means of the boring process. All of specimens, which were divided into 4 classes, namely, clay, silt, silty-clay, and loam, were made into the form of a cylinder, and tested in both the natural and the recomposed states.

2) We obtained the transverse wave-velocity in these soil specimens as well as the longitudinal wave-velocity, by means of the vibration

methods, and then computed their moduli of rigidity and Young's moduli from the following equations, respectively $\mu=\rho V_t^2$, and $E=\rho V_l^2$.

We calculated Poisson's ratio of these soils from the following equation.

$$\sigma=\frac{1}{2}\left\{\left(\frac{V_l}{V_t}\right)^2-2\right\}, \text{ or } \sigma=\frac{1}{2}\left\{\frac{E}{\mu}-2\right\}.$$

The values of these constants are shown in Tables I and II.

3) We determined the normal and the tangential solid viscosities, namely γ_l and γ_t, from the curved portions near the origin of each reducing curve, by means of the following equations

$$T_t=\frac{4h}{\sqrt{\dfrac{\mu}{\rho}-\dfrac{\pi^2\gamma_t^2}{16\rho^2h^2}}}, \text{ and } T_l=\frac{4h}{\sqrt{\dfrac{E}{\rho}-\dfrac{\pi^2\gamma_l^2}{16\rho^2h^2}}},$$

in which the symbols have the same meaning as before. The normal solid viscosity coefficients of these soils are greater than their tangential solid viscosity coefficients, and the greater the decrease of moisture content in the soil specimen, the less difference there is between normal and tangential viscosities. The ratio of γ_l to γ_t seems to be about 2·0 in the case of diminishing the moisture content of the soil, while it approches about 1·0 when the moisture content increases.

4) The transverse wave-velocity, the modulus of rigidity, and the tangential solid viscosity coefficient, as well as the londitudinal wave-velocity, Young's modulus, and the normal solid viscosity coefficients of the soils in the natural state are greater than those obtained in the recomposed state.

5) The elastic constants, such as Young's modulus and the modulus of rigidity, decrease somewhat rapidly with the increase of moisture content. These are of the order of $10^7\sim10^8$ (c.g.s.) at the moisture content ranges of about 50%～30%; the solid viscosity coefficients of these soils are of the order of $10^4\sim10^5$ (c.g.s.); and also the transverse wave-velocity varies from about 60 m per sec to about 250 m per sec at the above moisture content ranges.

Poisson's ratio of these soils, however, increases with the increase of the moisture content; the variation of which is 0·43～0·19 at the moisture content ranges of about 49%～32% in the case of silty-clay at Maru-no-uti; while 0·30～0·15 at the moisture content ranges of about 48%～40% in the case of soils at Hongô. It seems to us that Poisson's ratio of loam at Hongô is smaller than that of silty-clay at Maru-no-uti within a certain moisture content limit. This difference may be chiefly due to the state of the internal structure of the soils.

6) The resonance frequencies of the second maximum amplitude attain about three times the frequency of the fundamental resonance, a fact of which was already pointed out in our preceding paper. The observed vibration of the soil specimen can be, therefore, revealed by the transverse vibration in a clamped- and free-end bar.

In conclusion, our sincerest thanks are due to Dr. T. Watanabe, member of Geotechinical Committee, Government Railways of Japan, who kindly gave us the soils of Mar-no-uti and a kind of clay adopted in our experiments. We also wish to express our thanks to Dr. N. Miyabe, member of our institute, who gave us a permission to study the soil specimen of Komatugawa which was recently collected himself.

7. 振動方法による土の彈性測定

第 2 報 剛性率及びポアソン比の測定

地震研究所 石本巳四雄
飯田汲事

表面土中の縱波の傳播速度及び其のヤング率に關する報告は既に前號に示したが，其の實驗結果よりすれば，土の彈性は土の種々なる狀態，特に其の含水率によつて著しく異る事が判明した．

本論文は表面土の彈性に關する續研究にして，特に土中の橫波の傳播速度或は其の剛性率及びポアソン比等を取扱ひ，且つ此等の彈性係數が土の種々なる狀態によつて如何に變化するかをも調べたものである．試驗土は前囘と全く同種類のものを採用し，其の試驗方法も亦前囘と殆んど同樣である．實驗裝置は第 1 圖に示す如く電磁的方法によつて振振動をなし，且つ每秒 0〜700 の範圍に連續的に振動數を變化せしめ得る振動盤を採用した．先づ土柱を其の上に乘せ，其の共鳴する振動數を求めて結局土中に於ける橫波の速度を測定した．次いで $V_t=\sqrt{\frac{\mu}{\rho}}$ の式より其の剛性率 μ を計算し，猶ほ同時に前囘採用した實驗裝置を併用する事によつて同一物質の縱波の速度 V_l 及びヤング率 E を知り，斯くて次式 $\sigma=\frac{1}{2}\left\{\left(\frac{V_l}{V_t}\right)^2-2\right\}$ により其のポアソン比 σ を算出した．

實驗結果の主なるものを擧ぐれば次の如くである．

自然狀態に於ける土の縱波，橫波の傳播速度或はヤング率，剛性率及び固體粘性係數等は其のねり直し狀態のものより大なる値を示す事が判明した．又此等の諸量は含水量の增加に從つて減少する．含水率の變化範圍が約 50%〜30% なる場合に，橫波の傳播速度は約 60 m/sec〜250 m/sec 程度，剛性率は 10^7〜10^8 (c.g.s.) 程度及び固體粘性係數は 10^4〜10^5 (c.g.s.) 程度の間に變化する．

橫振動より求めた固體粘性係數は縱振動より求めたものに比して一般に小さく，其の比は含水量が小であると 2 に近いが，含水量の增加と共に 1 に接近する．

ポアソン比は含水量の增加と共に大きくなる．例へば丸の內の土（沈泥質粘土）に於ては含水率の變化の範圍が約 49%〜32% に對して，ポアソン比は約 0·43〜0·19 の中に變化する．本鄕大學構內の土（赤土）に於ては含水率の變化の範圍が約 48%〜40% に對して，ポアソン比の變化は約 0·30〜0·15 である．赤土が沈泥質粘土に對してポアソン比の小であるのは其等を形成する土の粒子の大小によるものと思はれる．

振動の mode は前論文に示せる如く，一端固定，他端自由な棒の振動樣式と見做してゐるが，高次の固有振動の周期からも其の差支へ無き事が證明される．

土の含水量を減ぜしめた場合，丸の內の沈泥質粘土は比重の變化は左程なく高さを減ずる．本鄕の土は高さは左程變化しないが，比重は非常に小となり多孔質となるやうである．此の事は物質の內部構造組織卽ち海綿構造であるや否やの問題と思考される．

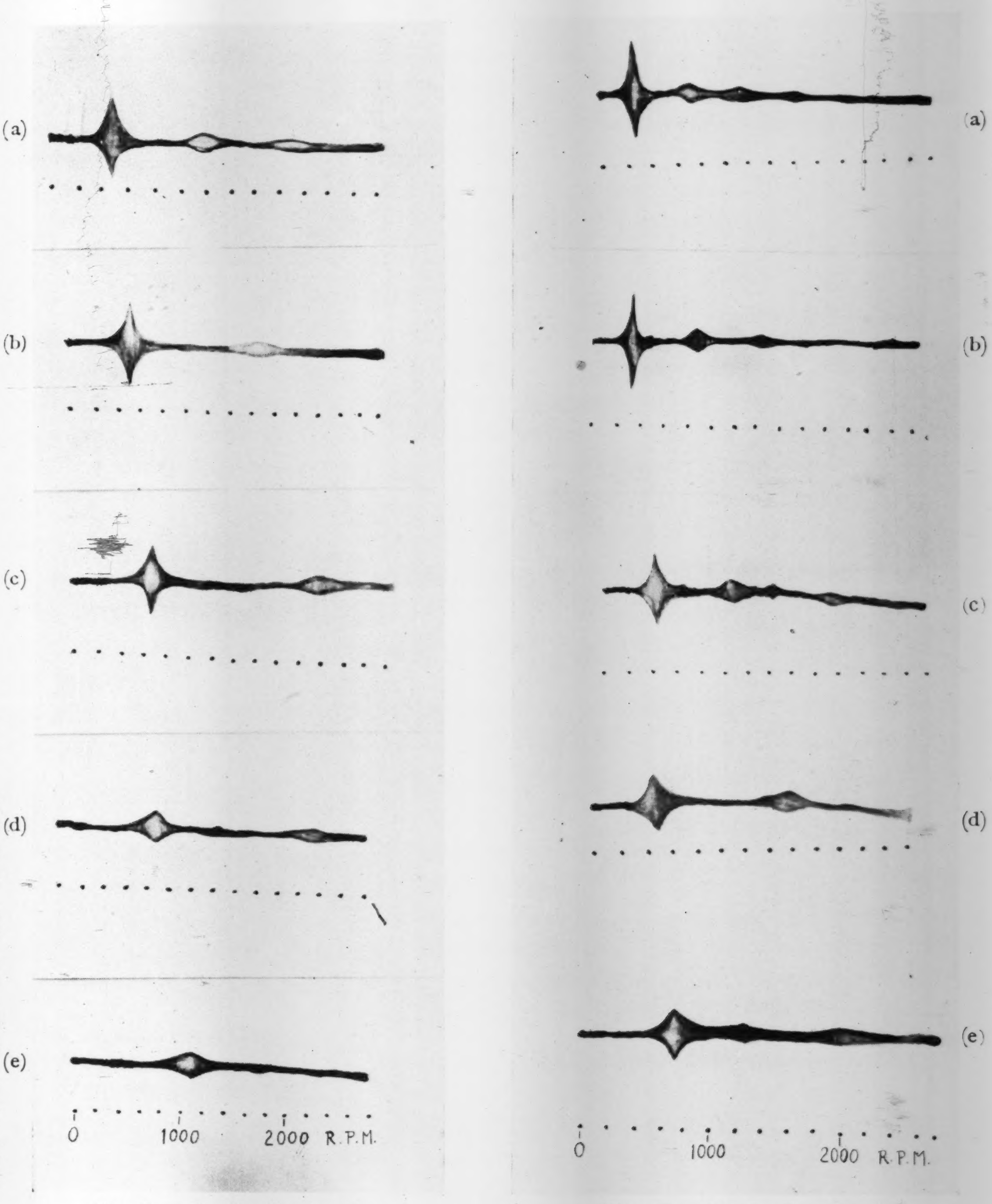

(i) Longitudinal vibration. (ii) Torsional vibration.

Fig. 3. Resonance curves of soils taken from Maru-no-uti. Moisture content 48·7% $\rho=1{\cdot}50$, h=height, N=frequency.

(i)
(a) $h=25{\cdot}0$ cm, $N=98$ vib. per sec.
(b) $h=19{\cdot}7$, $N=118$.
(c) $h=15{\cdot}0$, $N=153$.
(d) $h=10{\cdot}4$, $N=213$.
(e) $h=\ 6{\cdot}6$, $N=298$.

(ii)
(a) $h=25{\cdot}1$ cm, $N=54$ vib. per sec.
(b) $h=19{\cdot}7$, $N=64$.
(c) $h=15{\cdot}0$, $N=81$.
(d) $h=10{\cdot}4$, $N=98$.
(e) $h=\ 6{\cdot}6$, $N=128$.

（震研彙報 第十五號、圖版 石本・飯田）

（震研彙報 第十五號 圖版 石本・飯田）

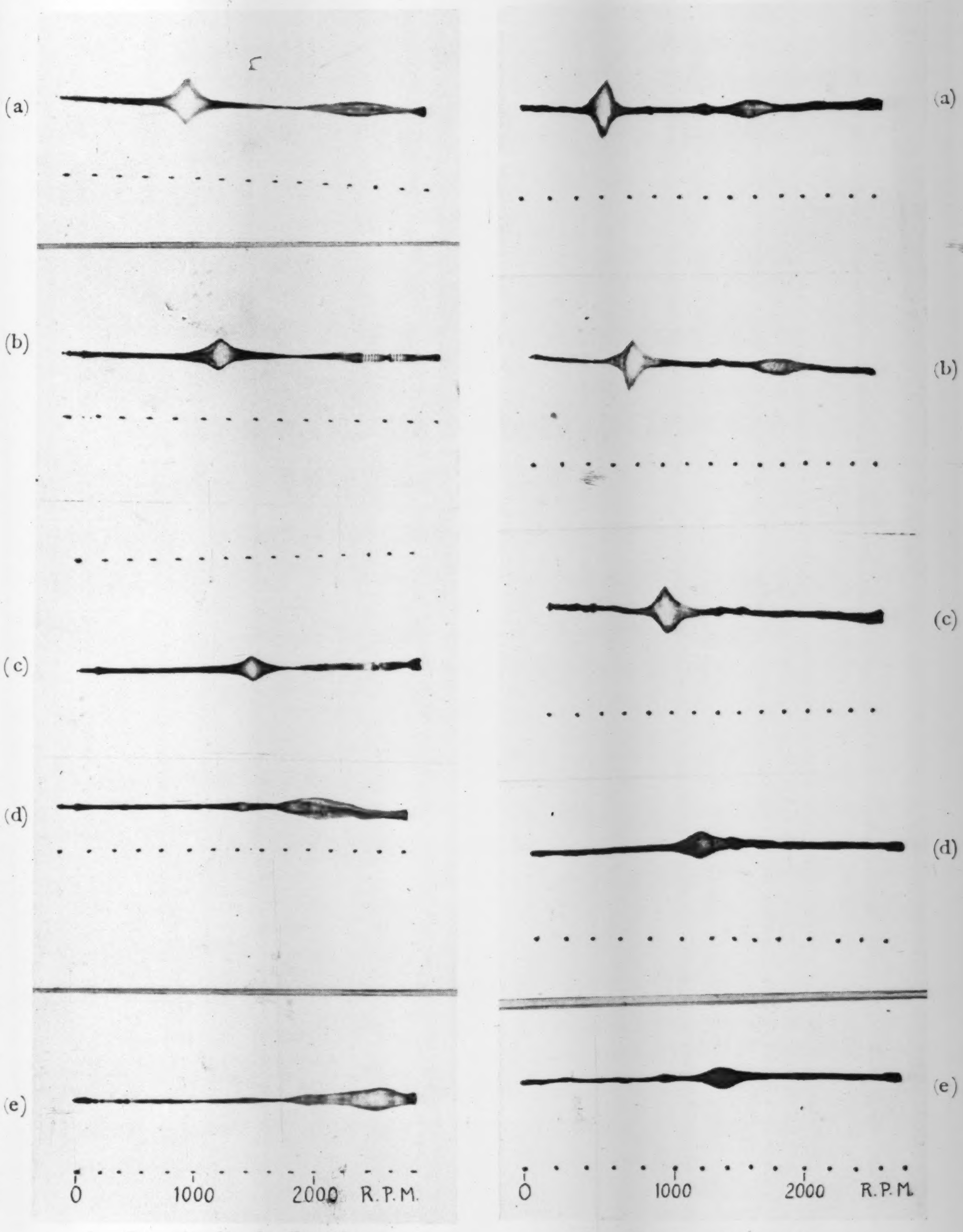

(i) Longitudinal vibration.

(ii) Torsional vibration

Fig. 4. Resonance curves of soils taken from Hongô, Imperial University. Moisture content 48·2%, $\rho=1{\cdot}24$, h=height, N=frequency.

(i)
(a) $h=31{\cdot}4$ cm, $N=168$ vib. per sec.
(b) $h=25{\cdot}7$, $N=193$.
(c) $h=19{\cdot}5$, $N=243$.
(d) $h=14{\cdot}0$, $N=310$.
(e) $h=8{\cdot}7$, $N=433$.

(ii)
(a) $h=31{\cdot}5$ cm, $N=104$ vib. per sec.
(b) $h=25{\cdot}8$, $N=128$.
(c) $h=19{\cdot}5$, $N=167$.
(d) $h=14{\cdot}0$, $N=198$.
(e) $h=8{\cdot}7$, $N=236$.

8. 土壤層中に於ける人工地震波の傳播並に土壤の彈性に關する研究（其 2）

地震研究所 那須信治
萩原尊禮
表俊一郎

（昭和11年9月15日發表──昭和11年12月20日受理）

9. 福島縣白河町に於ける彈性波式地質調査の結果と鑿井による地質調査との比較

福島縣白河町，東北本線白河驛構內機關庫及び其の他停車場用水のため新に鑿井工事を施行することゝなり，工事に先立つて地下水面及び岩盤層の位置を探査するため鐵道省の依囑により彈性波式地質調査法を行つた事は既報の通りである．[1]

其後愈々鑿井工事が I の觀測線附近で（前論文中第 12 圖參照）實施され地下層の分布狀態が明瞭になつたので彈性波式調査法によつて求めた岩盤の位置を實際のものと比較する機會を得たのである．前の論文中岩盤は周圍の地質から推定すれば石英粗面岩の層であらうと記しておいたが實際は此の層は現在の鑿井の深度では現はれなかつた．第 23 圖は鑿井工事の進捗度及び地層の分布を示す．此の圖に見られる如く地表より 51 m 附近までは砂礫及砂礫を交へた硬質粘土或は砂層であつて岩盤層とも稱すべきものは凝灰岩層である．

前論文中に記しておいた彈性波の反射波中 ${}_sR_1$ 波（I の觀測線に於ては 24·2 m，II の觀測線に於ては 20·0m の深さに於て反射した波）は或は此の圖に示されてある硬質粘土層中に於て反射したものらしく思はれる．同じ粘土層といつても深さによつては硬度が多小異るであらうから圖に示された地質の境界面が必ずしも彈性波の反射面に一致するとは言ひ得ないが此の場合は地下 20～25 m 附近に硬いところがあり更にそれより下は稍軟弱な地層が岩盤を覆つてゐることだけは確かであらう．

${}_sR_2$ 波（I の觀測線に於ては 57 m，II の觀測線に於ては 51 m の深さに於て反射した波）の觀測は前論文中にも示した如く現在の目的たる岩盤層の位置を求めるためには重要であるから前論文中に省略した事柄の補訂のため少しく附け加へておく．

---

[1] 那須信治・萩原尊禮・表俊一郎 震研彙報 **14** (1936), 560.

第 IX 表　$_sR_2$ 波の走時

（I の觀測線に就いて）

距　離	走　時	距　離	走　時
m	sec	m	sec
10	0·71	40	0·73
15	0·72	50	0·76
20	0·73	60	0·82

この値を用ひ a, b 曲線（第 24 圖）を引けば直線の傾斜より $_sR_2$ 波の平均傳播速度は 162 m/sec となり距離（$\sqrt{b}$）が O なる場所に於ける走時（$\sqrt{a}$）は 0·70 sec となり從つて上層の厚さは約 57 m となる．

II の觀測線に就いて以上の如き方法によつて得たる岩盤層の深さは地表下 51 m であつた事は既に述べた通りである．

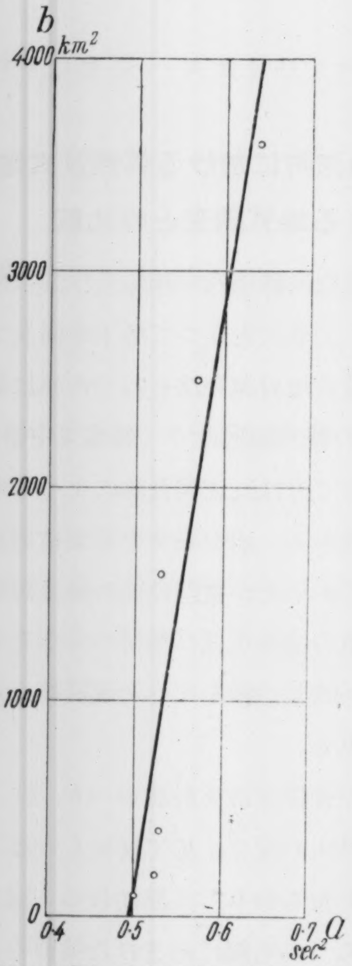

第 24 圖　白河の觀測線 I に於ける SR_2 波に對する a-b 曲線

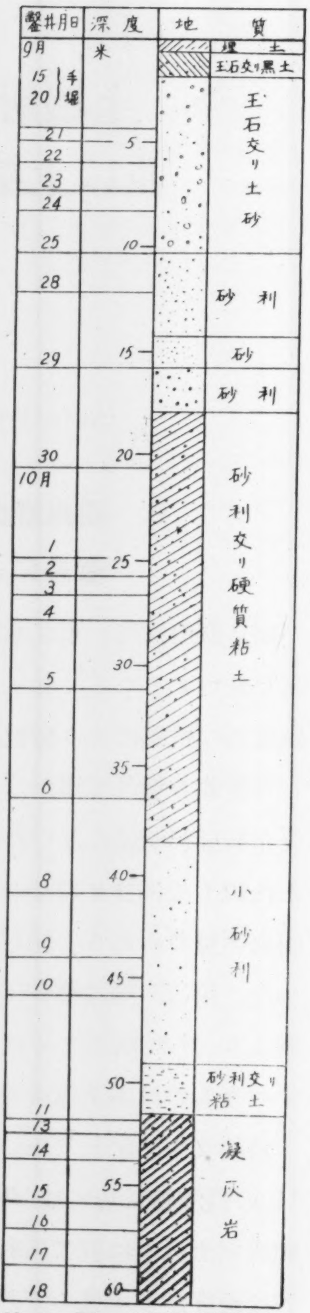
鑿井月日
深度
地　質
9月
米
15
20
手堀
埋土
王石交り黒土
王石交り土砂
21
22
23
24
25
28
29
30
10月
1
2
3
4
5
6
8
9
10
11
13
14
15
16
17
18
5
10
15
20
25
30
35
40
45
50
55
60
砂利
砂
砂利
砂利交り硬質粘土
小砂利
砂利交り粘土
凝灰岩

第 23 圖　白河驛（機關庫）給水設備箇所地質斷面圖（請負人　大正鑿泉株式會社）

I と II の觀測線に就いて求めた上層の厚さには約 6 m の差があるがこれは岩盤面が地表と必ずしも平行でないためでもあらうが I の觀測線と II の觀測線とでは肉眼で見てもこれ位の地表の高低差がある．卽ち I は鐵道線路の築堤の路面と略同じ高さであり，II はこれよりは一段低い水田の畦道である．又實際に鑿井された場所は I よりは 2～3 米低い場所であり，第 23 圖の地質斷面圖に示してある深度 O なる所謂地表は I に於ける地表より 2～3 米低い位置を指示するものである．

岩盤層とその上に位する層とは可成り硬さに於て差があるらしい．その證據の一つ

として第23圖中鑿井の進捗度を比較すれば格段の差があることが見られるであらう.

同地質圖に於ては 51·5 m より深いところは凝灰岩層であり，この面に於て sR_2 波が反射したのであらう.

I に於て求めた岩盤の深さ 57 m，II に於て求めた 51 m は何れもこの凝灰岩層の深さであることは間違ない.

彈性波式地質調査法に依つて求める岩盤層の深さは現在の如き比較的淺く，且つ岩盤と上層との彈性に格段の差のある場合は，相當正しく岩盤層の位置を求めることが出來るであらう.

---

8. *Studies on the Propagation of the Artificial Earthquake Waves through Superficial Soil or Sand Layers and the Elasticity of Soil and Sand. (Part 2)*

By Nobuji NASU, Takahiro HAGIWARA and Syun'itiro OMOTE,

Earthquake Research Institute.

Comparison of the results of the seismic prospecting with those of the boring made at Sirakawa.

The travelling times of the reflected wave (sR_2) which underwent reflection on the surface of the bed rock, being agglomerate in this case, are shown in Table IX.

The depth of the bed rock which was determined by the seismic method at two places I and II were 57 m and 51 m, respectively. The result of the boring shows that the depth of the bed rock is 51·5 m from the ground surface at a place near point I. The ground where the boring was made, however, is lower than the place I by 2～3 m.

The columnar section of the superficial layers determined by the boring is shown in Fig 23.

---

9. *Notes on the Origins of Earthquakes. (Second paper.)*

By Win INOUYE,

Earthquake Research Institute.

(Read Oct. 20, 1936.—Received Dec. 21, 1936.)

1. *Introduction*

In his previous paper,[1] the author discussed the elastic waves radiated from a spherical cavity in a homogeneous isotropic elastic medium when the normal pressure on the surface of the cavity changed periodically; and two cases in which the azimuthal distribution of the normal pressure on the surface of the spherical cavity could be expressed either by $P_0(\cos\theta)$ or $P_2(\cos\theta)$ were studied theoretically.

In such a case, the normal component of displacement of the dilatational waves that originated from the single source ($P_0(\cos\theta)$) far exceeds that originated from the quadruple source ($P_2(\cos\theta)$), so long as the wave length of the dilatational waves is greater than the dimension of the spherical cavity, assuming that the range of pressure variation in the two cases are the same. Should the wave length be comparable with the dimension of the spherical cavity, the two normal components of the displacements in question become comparable to each other in magnitude.

Now, as the single source is the most simplest one and liable to occur accompanied with the rather complex quadruple source. Professor M. Ishimoto[2] has already shown that the geographical distribution of the initial motions of an earthquake could well be explained by assuming that the quadruple source co-acted with the single source at the hypocenter.

If so, then the wave lengths of the dilatational waves emanating from the seismic origin must be comparable with the dimension of the diameter of the origin in order that it shall accord with the observed distribution of the initial motions.

In this paper, the writer investigates the case in which the normal stress on the surface of the spherical cavity changes with different rapidities. In this case, the elastic waves of shock type are radiated from the origin and the durations of the shocks of the dilatational and distortioal waves differ, the former usually being shorter than the latter.

---

[1] W. INOUYE, *Bull. Earthq. Res. Inst.*, **14** (1936), 582.

[2] M. ISHIMOTO, *Bull. Earthq. Res. Inst.*, **10** (1932), 449~471.

2. The case in which there is no azimuthal difference in the normal pressures on the surface of the cavity, that is the one in which the azimuthal distribution of the normal pressure takes the form $P_0(\cos\theta)$, has been already studied by Professor K. Sezawa,[3] who found the expression for the displacement (normal) of the medium as follows:

The change in the pressure at $r=a$,

$$\left.\begin{aligned} &P=o, && (r=a,\ t<o) \\ &P=Ne^{-ct}(1-e^{-qt}), && (r=a,\ t>o) \end{aligned}\right\}$$

in which $c\rightarrow 0$, and q indicates the rapidity of the stress change.

The displacement at $r\rightarrow\infty$ can be determined from the following equation, written in convenient form by the writer,

$$u=\frac{a^3N}{4\mu r^2}+\frac{a^2NR\dfrac{\mathfrak{v}}{v}}{\mu r\left(4-4R\dfrac{\mathfrak{v}}{v}+R^2\right)}\left[e^{-R\tau}-e^{-2\frac{\mathfrak{v}}{v}\tau}\left\{\cos 2\sqrt{1-\left(\frac{\mathfrak{v}}{v}\right)^2}\,\tau\right.\right.$$

$$\left.\left.+\frac{2-\dfrac{v}{\mathfrak{v}}R}{2\sqrt{\left(\dfrac{v}{\mathfrak{v}}\right)^2-1}}\sin 2\sqrt{1-\left(\frac{\mathfrak{v}}{v}\right)^2}\,\tau\right\}\right],$$

where $$R=\frac{aq}{\mathfrak{v}},\quad \tau=\frac{\mathfrak{v}}{a}\left(t-\frac{r-a}{v}\right),$$

v and $\mathfrak{v}$ are the velocities of the dilatational and the distortional waves respectively.

We shall consider now only that case in which the Poisson's ratio $\sigma=\dfrac{1}{4}$, that is $\lambda=\mu$, and in which the displacement at $r\rightarrow\infty$ can be expressed by

$$u=\frac{a^3N}{4\mu r^2}+\frac{a^2NR}{1{\cdot}732\mu r(4-2{\cdot}309R+R^2)}$$

$$\times\left[e^{-R\tau}-e^{-1{\cdot}155\tau}\left\{\cos 1{\cdot}633\tau+(0{\cdot}7072-0{\cdot}6124R)\sin 1{\cdot}633\tau\right\}\right].$$

---

3) K. SEZAWA, and K. KANAI, *Bull. Earthq. Res. Inst.*, **14** (1936), 10~17.

We will consider two cases in which $\frac{aq}{\mathfrak{v}}=\infty$ and $\frac{aq}{\mathfrak{v}}=1$. The rapidities of changes in the pressure on the surface of the spherical cavity are shown graphically in Fig. 1, from which it will be seen that in the case in which $\frac{aq}{\mathfrak{v}}=1$, the pressure almost attains to its final value in the period during which the dilatational wave travels a distance that is three or four times longer than the radius of the cavity.

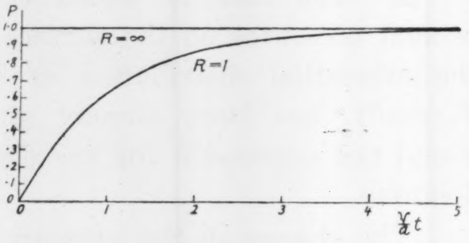

Fig. 1.

The displacement variation in time in the case $r\rightarrow\infty$, due to stress change in two different rapidities at $r=a$, is shown in Fig. 2, from which it will be seen that the displacements manifest shock types.

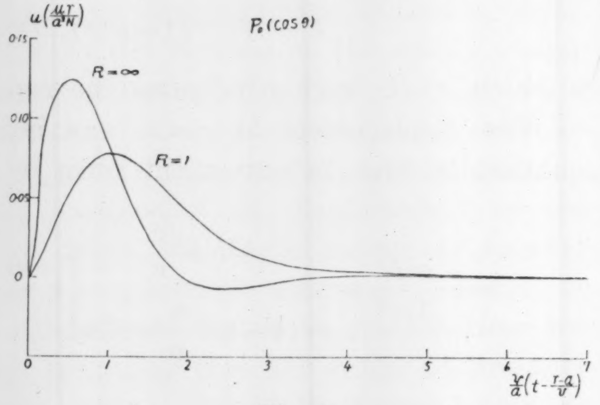

Fig. 2.

3. The general case in which the azimuthal distribution of normal stresses on the spherical cavity is expressed by a certain spherical function has already been treated by Dr. H. Kawasumi,[4] according to whose result, under the conditions at $r=a$

$$\widehat{rr}=N\varphi(t)P_n^m(\cos\theta)\quad\left.\begin{matrix}\cos m\varphi\\-\sin m\varphi\end{matrix}\right\}$$

$$\widehat{r\theta}=T\varphi(t)\frac{dP_n^m(\cos\theta)}{d\theta}\quad\left.\begin{matrix}\cos m\varphi\\-\sin m\varphi\end{matrix}\right\}$$

$$\widehat{r\varphi}=-mT\varphi(t)\frac{P_n^m(\cos\theta)}{\sin\theta}\quad\left.\begin{matrix}\sin m\varphi\\\cos m\varphi\end{matrix}\right\},$$

the normal, co-latitudinal, and longitudinal components of displacements being given respectively by

---

4) H. KAWASUMI and R. YOSIYAMA, *Jisin*, **7** (1935), 359.

$$u=\frac{1}{2\pi}\int_{-\infty}^{\infty}\frac{1}{\Delta}\left\{\Delta_1\frac{1}{dr}\frac{H^{(2)}_{n+\frac{1}{2}}(hr)}{\sqrt{r}}+n(n+1)\Delta_2\frac{H^{(2)}_{n+\frac{1}{2}}(kr)}{r^{3/2}}\right\}e^{ipt}dp$$

$$\times\int_{-\infty}^{\infty}\varphi(w)e^{-ipw}dwP^m_n(\cos\theta)\quad\left.\begin{matrix}\cos m\varphi\\ -\sin m\varphi\end{matrix}\right\}$$

$$v=\frac{1}{2\pi}\int_{-\infty}^{\infty}\frac{1}{\Delta}\left[\Delta_1\frac{H^{(2)}_{n+\frac{1}{2}}(hr)}{r^{3/2}}+\Delta_2\frac{1}{r}\frac{d}{dr}\left\{\sqrt{r}\,H^{(2)}_{n+\frac{1}{2}}(kr)\right\}\right]e^{ipt}dp$$

$$\times\int_{-\infty}^{\infty}\varphi(w)e^{-ipw}dw\frac{dP^n_n(\cos\theta)}{d\theta}\quad\left.\begin{matrix}\cos m\varphi\\ -\sin m\varphi\end{matrix}\right\}$$

$$w=-\frac{m}{2\pi}\int_{-\infty}^{\infty}\frac{1}{\Delta}\left[\Delta_1\frac{H^{(2)}_{n+\frac{1}{2}}(hr)}{r^{3/2}}+\Delta_2\frac{1}{r}\frac{d}{dr}\left\{\sqrt{r}\,H^{(2)}_{n+\frac{1}{2}}(kr)\right\}\right]e^{ipt}dp$$

$$\times\int_{-\infty}^{\infty}\varphi(w)e^{-ipw}dw\frac{P^m_n(\cos\theta)}{\sin\theta}\quad\left.\begin{matrix}\sin m\varphi\\ \cos m\varphi\end{matrix}\right\},$$

where

$$\Delta=-\left(\lambda h^2\frac{H^{(2)}_{n+\frac{1}{2}}(ha)}{\sqrt{a}}-2\mu\frac{d^2}{da^2}\frac{H^{(2)}_{n+\frac{1}{2}}(ha)}{\sqrt{a}}\right)$$

$$\times\mu\left[\frac{d}{da}\left(\frac{1}{a}\frac{d}{da}\left\{\sqrt{a}\,H^{(2)}_{n+\frac{1}{2}}(ka)\right\}\right)-\frac{1}{a^2}\frac{d}{da}\left\{\sqrt{a}\,H^{(2)}_{n+\frac{1}{2}}(ka)\right\}\right.$$

$$\left.+n(n+1)\frac{H^{(2)}_{n+\frac{1}{2}}(ka)}{a^{5/2}}\right]-2\mu^2n(n+1)\left\{\frac{d}{da}\frac{H^{(2)}_{n+\frac{1}{2}}(ha)}{a^{3/2}}\right.$$

$$\left.-\frac{H^{(2)}_{n+\frac{1}{2}}(ha)}{a^{5/2}}+\frac{1}{a}\frac{d}{da}\frac{H^{(2)}_{n+\frac{1}{2}}(ha)}{\sqrt{a}}\right\}\frac{d}{da}\frac{H^{(2)}_{n+\frac{1}{2}}(ka)}{a^{3/2}},$$

$$\Delta_1=-N\mu\left[\frac{d}{da}\left(\frac{1}{a}\frac{d}{da}\left\{\sqrt{a}\,H^{(2)}_{n+\frac{1}{2}}(ka)\right\}\right)-\frac{1}{a^2}\frac{d}{da}\left\{\sqrt{a}\,H^{(2)}_{n+\frac{1}{2}}(ka)\right\}\right.$$

$$\left.+n(n+1)\frac{H^{(2)}_{n+\frac{1}{2}}(ka)}{a^{5/2}}+\right]-2T\mu n(n+1)\frac{d}{da}\frac{H^{(2)}_{n+\frac{1}{2}}(ka)}{a^{3/2}},$$

$$\Delta_2=+N\mu\left\{\frac{d}{da}\frac{H^{(2)}_{n+\frac{1}{2}}(ha)}{a^{3/2}}-\frac{H^{(2)}_{n+\frac{1}{2}}(ha)}{a^{5/2}}+\frac{1}{a}\frac{d}{da}\frac{H^{(2)}_{n+\frac{1}{2}}(ha)}{\sqrt{a}}\right\}$$

$$-T\left(\lambda h^2\frac{H^{(2)}_{n+\frac{1}{2}}(ha)}{\sqrt{a}}-2\mu\frac{d^2}{da^2}\frac{H^{(2)}_{n+\frac{1}{2}}(ha)}{\sqrt{a}}\right).$$

4. We shall next take the case $n=2$, $m=0$, tangential stresses $\widehat{r\theta}=0$, $\widehat{r\varphi}=0$, and the change in the normal stress at $r=a$

$$\left.\begin{aligned}\widehat{rr}&=0 && (r=a,\ t<0)\\ \widehat{rr}&=Ne^{-ct}(1-e^{-qt})P_2(\cos\theta), && (r=a,\ t>0)\end{aligned}\right\}$$

in which $c\rightarrow 0$.

The normal component of displacement of the dilatational wave at a point distant from the origin as compared with the radius of the origin is given by

$$u=\frac{1}{2\pi}\int_{-\infty}^{\infty}\frac{\Delta_1}{\Delta}\frac{d}{dr}\frac{H^{(2)}_{\frac{5}{2}}(hr)}{\sqrt{r}}e^{ipt}dp\int_{-\infty}^{\infty}\varphi(w)e^{-ipw}dwP_2(\cos\theta)$$

$$=\frac{1}{2\pi}\frac{N\mathfrak{v}^4}{\rho ar^2}P_2(\cos\theta)i\left[\int_{-\infty}^{\infty}\frac{f(p)e^{ip\left(t-\frac{r-a}{v}\right)}}{(p-ic)g(p)}dp\right.$$

$$\left.-\int_{-\infty}^{\infty}\frac{f(p)e^{ip\left(t-\frac{r-a}{v}\right)}}{(p-iq)g(p)}dp\right],$$

where

$$\varphi(w)=e^{-ct}(1-e^{-qt}) \text{ in which } c\rightarrow 0,$$

$$f(p)=\left[5\frac{a}{\mathfrak{v}}p^2-48\frac{\mathfrak{v}}{a}+i\left\{\frac{a^2}{\mathfrak{v}^2}p^3-21p+48\frac{\mathfrak{v}^2}{a^2p}\right\}\right]$$

$$\left[-\frac{1}{\sqrt{3}}\frac{r}{\mathfrak{v}}p^2+9\sqrt{3}\frac{\mathfrak{v}}{r}+i\left\{4p-27\frac{\mathfrak{v}^2}{r^2p}\right\}\right]$$

$$\doteq\frac{r}{\sqrt{3}}\left(-i\frac{a^2}{\mathfrak{v}^3}p^5-5\frac{a}{\mathfrak{v}^2}p^4+i21\frac{1}{\mathfrak{v}}p^3+48\frac{1}{a}p^2-i48\frac{\mathfrak{v}}{a^2}p\right)$$

$$-i4\left(-i\frac{a^2}{\mathfrak{v}^2}p^4-5\frac{a}{\mathfrak{v}}p^3+i21p^2+48\frac{\mathfrak{v}}{a}p-i48\frac{\mathfrak{v}^2}{a^2}\right),$$

$$g(p)=p^6-i12{\cdot}505\frac{\mathfrak{v}}{a}p^5-81{\cdot}67\frac{\mathfrak{v}^2}{a^2}p^4+i326\frac{\mathfrak{v}^3}{a^2}p^3$$

$$+760\frac{\mathfrak{v}^4}{a^4}p^2-i872\frac{\mathfrak{v}^5}{a^5}p-552\frac{\mathfrak{v}^6}{a^6}$$

$$=\left\{p-(i1\cdot800+4\cdot185)\frac{\mathfrak{v}}{r}\right\}\left\{p-(i1\cdot800-4\cdot185)\frac{\mathfrak{v}}{a}\right\}$$

$$\left\{p-(i3\cdot640+1\cdot432)\frac{\mathfrak{v}}{a}\right\}\left\{p-(i3\cdot640-1\cdot432)\frac{\mathfrak{v}}{a}\right\}$$

$$\left\{p-(i0\cdot807+1\cdot040)\frac{\mathfrak{v}}{a}\right\}\left\{p-(i0\cdot807-1\cdot040)\frac{\mathfrak{v}}{a}\right\}.$$

The co-latitudinal component of displacement of the distortional wave at $r\rightarrow\infty$ is expressed by

$$v=\frac{1}{2\pi}\int_{-\infty}^{\infty}\frac{1}{\Delta}\left\{\Delta_2\frac{1}{r}\frac{d}{dr}\left\{\sqrt{r}\,H_{\frac{5}{2}}^{(3)}(kr)\right\}e^{ipt}dp\right.$$

$$\times\int_{-\infty}^{\infty}\varphi(w)e^{-ipw}dw\frac{dP_2(\cos\theta)}{d\theta}$$

$$=-\frac{1}{2\pi}\frac{2N\mathfrak{v}^4}{\mu ar^2}\frac{dP_2(\cos\theta)}{d\theta}i\left[\int_{-\infty}^{\infty}\frac{f'(p)e^{ip\left(t-\frac{r-a}{\mathfrak{v}}\right)}}{(p-ic)g(p)}dp\right.$$

$$\left.-\int_{-\infty}^{\infty}\frac{f'(p)e^{ip\left(t-\frac{r-a}{\mathfrak{v}}\right)}}{(p-iq)g(p)}dp\right],$$

where

$$f'(p)=\left[\frac{12v}{a}-\frac{ap^2}{v}+i\left(-\frac{12v^2}{a^2p}+5p\right)\right]\left[\frac{6\mathfrak{v}}{r}-\frac{rp^2}{\mathfrak{v}}+i\left(-\frac{6\mathfrak{v}^2}{r^2p}+3p\right)\right]$$

$$=r\left(0\cdot5774\frac{a}{\mathfrak{v}^2}p^4-i5\frac{1}{\mathfrak{v}}p^3-20\cdot78\frac{1}{a}p^2+i36\frac{\mathfrak{v}}{a^2}p\right)$$

$$+3\left(-i0\cdot5774\frac{a}{\mathfrak{v}}p^3-5p^2+i20\cdot78\frac{\mathfrak{v}}{a}p+36\frac{\mathfrak{v}^2}{a^2}\right).$$

Upon evaluating the integrations by applying the theory of residues, the final results for the normal component of displacement of the dilatational wave and the co-latitudinal component of displacement of the distortional wave are given respectively by u and v as follows:

$$u=-0\cdot3478\frac{Na^3}{\mu r^2}P_2(\cos\theta)$$

$$+\frac{Na^2}{\sqrt{3}\,\mu r}P_2(\cos\theta)$$

$$\times\left[\frac{(R^5-5R^4+21R^3-48R^2+48R)e^{-R\tau}}{-R^6+12\cdot505R^5-81\cdot67R^4+326R^3-760R^2+872R-552}+2\frac{e^{-1\cdot800\tau}}{8\ 370}\right.$$

$$\times\Bigg\{\frac{(1\cdot225\times10^6-8\cdot487\times10^4R)\cos(4\cdot185\tau)-(-1\cdot057\times10^5+2\cdot559\times10^5R)\sin(4\cdot185\tau)}{(1564-137\cdot5R)^2+(9\cdot5+314\cdot4R)^2}$$

$$-\frac{1\cdot225\times10^6\cos(4\cdot185\tau)+1\cdot057\times10^5\sin(4\cdot185\tau)}{2\cdot446\times10^6}\Bigg\}$$

$$+2\frac{e^{-3\cdot640\tau}}{2\cdot864}$$

$$\times\Bigg\{\frac{(-1\cdot689\times10^5+7\cdot050\times10^4R)\cos(1\cdot432\tau)-(-3\cdot237\times10^5+6\cdot121\times10^4R)\sin(1\cdot432\tau)}{(821\cdot5-190\cdot2R)^2+(56\cdot1-90\cdot24R)^2}$$

$$-\frac{-1\cdot689\times10^5\cos(1\cdot432\tau)+3\cdot237\times10^5\sin(1\cdot432\tau)}{6\cdot780\times10^5}\Bigg\}$$

$$+2\frac{e^{-0\cdot807\tau}}{2\cdot080}$$

$$\times\Bigg\{\frac{(3490+2214R)\cos(1\cdot040\tau)-(-6397+5073R)\sin(1\cdot040\tau)}{(52\cdot41+121\cdot3R)^2+(242\cdot8-144\cdot5R)^2}$$

$$-\frac{3490\cos(1\cdot040\tau)+6397\sin(1\cdot040\tau)}{61697}\Bigg\}\Bigg],$$

$$v=-0\cdot3912\frac{Na^3}{\mu r^2}\frac{dP_2(\cos\theta)}{d\theta}$$

$$-\frac{2Na^2}{\mu r}\frac{dP_2(\cos\theta)}{d\theta}$$

$$\times\Bigg[\frac{(0\cdot5774R^4-5R^3+20\cdot78R^2-36R)e^{-R\tau}}{-R^6+12\cdot505R^5-81\cdot67R^4+326R^3-760R^2+872R-552}$$

$$+2\frac{e^{-1\cdot800\tau}}{8\cdot370}$$

$$\times\Bigg\{\frac{(1\cdot088\times10^5+1\cdot477\times10^4R)\cos(4\cdot185\tau)-(-1\cdot200\times10^5+3\cdot235\times10^4R)\sin(4\cdot185\tau)}{(1564-137\cdot5R)^2+(9\cdot5+314\cdot4R)^2}$$

$$-\frac{1\cdot088\times10^5\cos(4\cdot185\tau)+1\cdot200\times10^5\sin(4\cdot185\tau)}{2\cdot446\times10^6}\Bigg\}$$

$$+2\frac{e^{-3\cdot640\tau}}{2\cdot864}$$

$$\times\Bigg\{\frac{(-16290+6091R)\cos(1\cdot432\tau)-(-23650+4101R)\sin(1\cdot432\tau)}{(821\cdot5-190\cdot2R)^2+(56\cdot1-90\cdot24R)^2}$$

$$-\frac{-16290\cos(1\cdot432\tau)+23650\sin(1\cdot432\tau)}{6\cdot780\times10^5}\Bigg\}$$

$$+2\frac{e^{-0\cdot807\tau}}{2\cdot080}$$

$$\times\Bigg\{\frac{(399-4671R)\cos(1\cdot040\tau)-(7476-3241R)\sin(1\cdot040\tau)}{(52\cdot41+121\cdot3R)^2+(242\cdot8-144\cdot5R)^2}$$

$$-\frac{399\cos(1\cdot040\tau)-7476\sin(1\cdot040\tau)}{61697}\Bigg\}\Bigg].$$

In both above two equations, the first term is the displacement that remains after the passage of the elastic waves as elastic deformation, and the second the oscillatory part that travels as elastic waves. It must be remembered that the terms representing the elastic deformation decrease as the inverse square of the distance from the origin, while those representing the propagating waves diminish in inverse ratio to the distance.

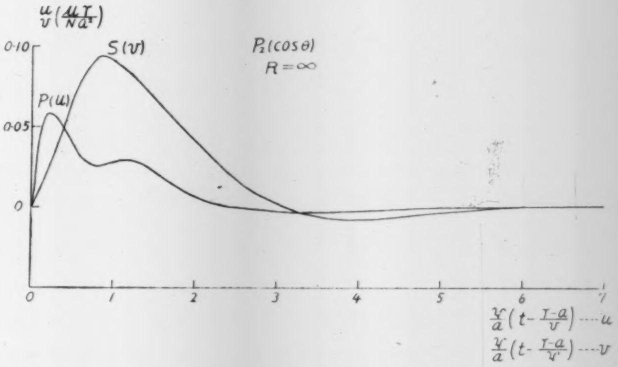

Fig. 3.

The displacements u (P phase) and v (S phase) in the above equations at $r\rightarrow\infty$ in the two cases, $R=\frac{aq}{\mathfrak{v}}=\infty$ and $R=1$, are shown respectively in Figs. 3, 4, from which it will be seen that the waves are of shock type, the duration of shock of distortional waves being usually longer than those of dilatational waves.

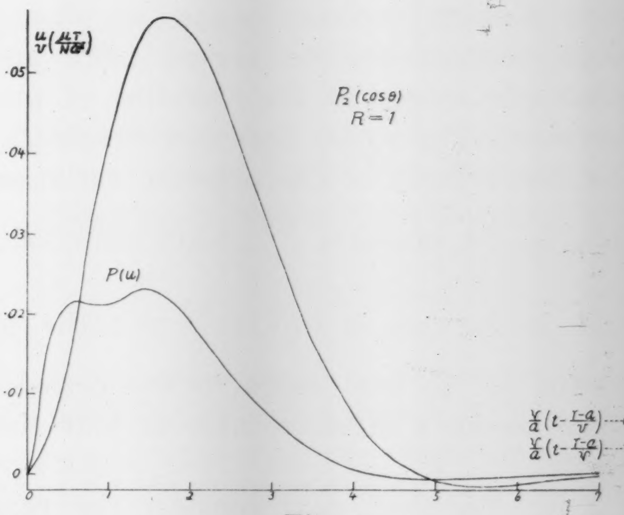

Fig. 4.

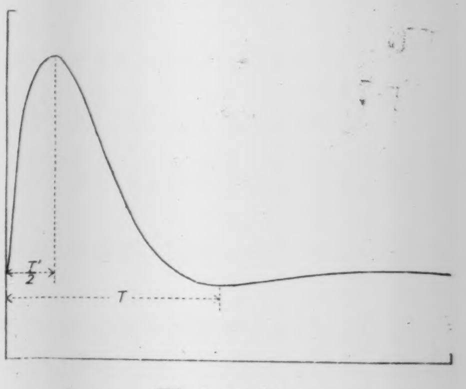

Fig. 5

5. The wave lengths calculated for cases in which the periods have been taken as shown in Fig. 5, the ratios of the amplitudes of the P phases due to a single source $P_0(\cos\theta)$ to those that have resulted from a quadruple source $P_2(\cos\theta)$ as well as the ratios of the amplitudes of the S phases to those of the P phases in the cases of a quadruple source, are all given in Table 1. As will be seen from the table, the wave lengths become longer as the velocity of change in pressure in the cavity decreases, and further that they are several times greater than the radius of the spherical cavity. The ratios of the amplitudes of displacement of the P phases due to a single source to those due to

Table I.

$R = \infty$

Source	Phase	λ (VT)	λ' (VT′)	Up_0/Up_2	Vp_2/Up_2
$P_0(\cos\theta)$	P	$4{\cdot}15a$	$1{\cdot}73a$	2·11	1·54
$P_2(\cos\theta)$	P	$5{\cdot}88a$	$0{\cdot}87a$		
,,	S	$4{\cdot}0a$	$1{\cdot}7a$		

$R = 1$

Source	Phase	λ(VT)	λ' (VT′)	Up_0/Up_2	Vp_2/Up_2
$P_0(\cos\theta)$	P	——	$3{\cdot}47a$	3·08	2·44
$P_2(\cos\theta)$	P	$8{\cdot}66a$	$4{\cdot}85a$		
,,	S	$5{\cdot}5a$	$3{\cdot}4a$		

a quadruple source have the tendency to become greater as the wave lengths become longer, so that the displacements due to a single source come to prevail more and more over those due to a quadruple source as the velocities of pressure varitaions in the cavity decrease. The writer therefore considers it quite in order to assume that the velocity of the pressure variation in the cavity is fairly great, that is, for example, $\frac{aq}{\mathfrak{v}}$ takes some value between ∞ and 1. As just said, in the case in which $\frac{aq}{\mathfrak{v}} = 1$, the pressure in the cavity almost attains to its final value in the period during which the longitudinal wave travels a distance three or four times that of the radius of the cavity.

6. We shall next consider the range of the pressure changes in the origins, assuming that the quadruple source in the case in which $\frac{aq}{\mathfrak{v}} = 1$ corresponds to an actual earthquake.

According to Dr. H. Honda,5) the normal component of the dilatational wave when r is large is given by

$$u_1 = \mathfrak{A}\frac{1}{r}\sin 2\theta\cos\varphi\cos(pt - hr).$$

In the deep-focus earthquake of June, 2, 1929 (focal depth ≒ 300 km),6) the observed amplitudes in the P phases are well given by assuming

---

5) H. HONDA, *Geophys. Mag.*, **8** (1934), 153~164.

6) H. HONDA, *loc. cit.*

$$\mathfrak{A} = -7{\cdot}58 \times 10^5 \text{ cm}^2.$$

While, in our case and also in the case $P_2^1(\cos\theta)$ in which $\dfrac{aq}{\mathfrak{b}} = 1$,

$$\mathfrak{A} = 0{\cdot}02521 \frac{Na^2}{\mu},$$

whence

$$N = -7{\cdot}58 \times 10^5 \text{ cm}^2 \frac{\mu}{2{\cdot}521 \times 10^{-2} a^2}.$$

According to Dr. K. Sagisaka,[7] we assume $T' \fallingdotseq 1{\cdot}7$ sec.

Assuming

$$v = 8{\cdot}57 \text{ km/sec},$$

we obtain

$$\lambda' = 8{\cdot}57 \times 1{\cdot}7 = 14{\cdot}6 \text{ km},$$

while

$$\lambda' = 4{\cdot}85a,$$

whence

$$a = 3{\cdot}03 \text{ km}.$$

Assuming

$$\mu = 8{\cdot}4 \times 10^{11} \text{ dyne/cm}^2,$$

$$\begin{aligned} N &= -7{\cdot}58 \times 10^5 \frac{8{\cdot}4 \times 10^{11}}{2{\cdot}521 \times 10^{-2}(3{\cdot}03 \times 10^5)^2} \\ &= -2{\cdot}76 \times 10^8 \text{ dyne/cm}^2 = -273 \text{ atms.} \end{aligned}$$

In the deep-focus earthquake of Nov. 13, 1932 (focal depth $\fallingdotseq$ 300 km),[8] the observed amplitudes in the P phases are well expressed by assuming

$$\mathfrak{A} = -3{\cdot}22 \times 10^6 \text{ cm}^2.$$

The writer estimated $\dfrac{T'}{2} = 1{\cdot}92$ sec on the seismogram obtained by Dr. N. Nasu's vertical component seismometer installed at Tokyo. The proper period of this pendulum is 28 sec.

Whence we obtain $a = 6{\cdot}8$ km,

and

$$N = -2{\cdot}32 \times 10^8 \text{ dyne/cm}^2 = -228 \text{ atms.}$$

---

[7] T. ISHIKAWA, *Kishô-Syûsi*, [ii], **10** (1932), 261.

[8] H. HONDA, *Geophys. Mag.*, **8** (1934), 173.

The pressures thus obtained are quite of the same orders of magnitude as the pressure of gases (mainly water vapour), which are from 200 to 500 atms in the case of volcanic eruptions[9].

7. As already noted, the apparent periods of the *S* phases exceed those of the *P* phases (see Figs. 3, 4).

The writer thinks it of interest to refer to the observed periods in the *P* phases and the *S* phases of actual earthquakes.

According to Dr. T. Ishikawa,[10] in the deep-focus earthquake of Feb. 20, 1931, the observed periods of the *S* phases were in the mean 1·77 times greater than those of the *P* phases.

8. Summary.

In the present paper, the writer, following his previous investigations in which it is assumed that normal stress causes periodic changes, investigates the case in which the normal stress on the surface of a spherical cavity changes with different rapidities.

The main results are as follow:

1) In such a case, elastic waves of shock type emanate from the origin, the duration of shock in distortional waves being usually longer than those in dilatational waves.

2) It is plausible to assume that the origins send forth elastic waves, the wave lengths of which are comparable (several times the radius) with the dimension of the origins.

3) The range of pressure changes in the seismic origins (spherical cavity) may be of the same order of magnitudes as the pressure of gases in the case of volcanic eruptions, namely from 200 to 500 atms.

---

[9] T. MATUZAWA, *Bull. Earthq. Res. Inst.*, **11** (1933), 347.

[10] T. ISHIKAWA, *loc. cit.*

9. 發震機構に就いて（第2報）

地震研究所　井上宇胤

第一報に於ては球形空窩の表面に週期的垂直應力が働く場合を數理的に研究したが此處では其の續きとして空窩の表面に働く垂直應力が種々なる早さを以て變化する場合を調査してある。

主なる結果を擧げれば次の如きものである。

（イ）以上の樣な場合に於ては震源から遠い所に於ては衝擊性の波を記錄する事となり且橫波の週期の方が縱波の週期より相當延びる事となる，此れは旣に觀測されては居たが今日迄理論的の說明の附かなかつた事である。

（ロ）震源から出る波の波長は震源を球形であると考へた時に其の半徑の數倍のものであると考へられる。

（ハ）二つの深發地震に於て震源に於ける壓力變化の程度を吟味して見た所大略數百氣壓であれば觀測された縱波や橫波の說明が附く事を知つた，此の値は丁度火山爆發の際のガスの壓力と同程度のものである。

10. The Cause of the Subsidence of the Earth's Surface in the Kôtô Region, Tokyo. I.

By Naomi MIYABE.

Earthquake Research Institute.

(Read Oct. 17, 1936.—Received Dec. 21, 1936.)

1. In several parts of Tokyo, namely, the districts of Kôtô, Marunouti, Kanda, Tameike Valley in Akasaka, Senzyu (northern part of Asakusa) ect., the ground was found to have subsided considerably as shown by relevellings[1].

As to the cause of these remarkable subsidences there are two alternatives, the one is crustal disturbance, as, for example, local down-warping or down-ward movement of a block or blocks of small horizontal dimensions. The other is contraction of the soil composing the surface layer to a considerable thickness.

In the latter case even were the subsidence put down to contraction of the soil, the thickness of that soil which contracts itself raises certain problems. In estimating the thickness of this soil layer, the following points are important.

In Honzyo and Hukagawa, where the subsidence was very marked, the surface of the earth's crust is covered by an Alluvial deposit, about 30 metres thick, underneath which are harder Tertiary rocks[2]. The probability is that the loosely packed Alluvial soil contracted as the result of changes either physical or chemical or both in the soil itself.

It is notable that buildings situated in the neighbourhood of Marunouti and Hibiya, in the central part of the city of Tokyo, were found to have been pushed up considerably.

These apparent uplifts of buildings can be measured easily, since, they have been pushed up in the manner shown in Fig. 1. The apparent uplifts of a number of buildings were measured in October, 1936, the results being shown in Table I. The distribution of the buildings is shown in Fig. 2, in which the bracketted numerals against the marks indicating the buildings give the amounts of apparent uplift of the respective buildings.

---

[1] N. MIYABE, *Proc. Imp. Acad.*, **8** (1932), 417~420; **9** (1933), 588~591. *Bull. Earthq. Res. Inst.*, **10** (1932), 844~857; **13** (1933), 587~591; **13** (1935), 773~771.

[2] Reconstraction Bureau, *Report on the Results of Geological Survey in Tokyo and Yokohama*, 1925.

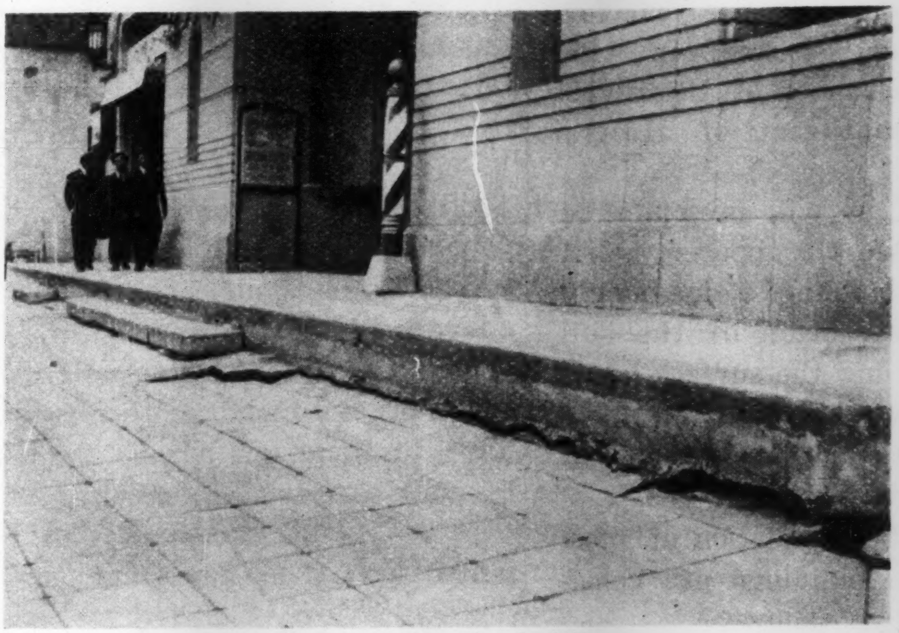

Fi. 1. Uprise of a building.

Table I. Amounts of uprise of several buildings

Name of Buil.	Amount of Uprise	Name of Buil.	Amount of Uprise
Tokyo Marine Insurance.	14 cm	Hibiya Cine. Theatre.	4 cm ?
Syôwa	14	Kangyô Ginkô	34
Zizi-Sinpô	10	Hukoku Tyôhei	30
Tokyo Kwaikwan	18	Sisei Kwaikwan	43
Main Depo. Industr. Assoc.	44	Tokyo Dentô	78
Sansi Kwaikwan	40	Tyôsen Sôtokuhu	15 ?
Marunouti Police Office.	30	Syôkyûdô	20 ?
Sansin	40	Zinzyu Seimei.	41
Tôhô Theatre	12		

From the result obtained above, the rates of apparent uplift can be calculated for several buildings, as given in Table II.

Table II. Mean velocity of uprise of several buildings

Name of buil.	Velocity of uprise cm/year.
Tokyo Dentô	7·4
Zinzyu Seimei	5·6
Sisei Kwaikwa	5·9
Kangyô Ginkô	4·9
Tôhô Theatre	4·4
Tokyo Kwaikwan	1·2
Tokyo Marine Ins.	1·4
Syôwa	2·2
Hibiya Cine. Theatre	1·6

The rates of apparent uplift, as shown in the foregoing Table, work out to $7\sim4$ cm per year for buildings situated in the neighbourhood of Utisaiwai-tyô, southeast of Hibiya Park.

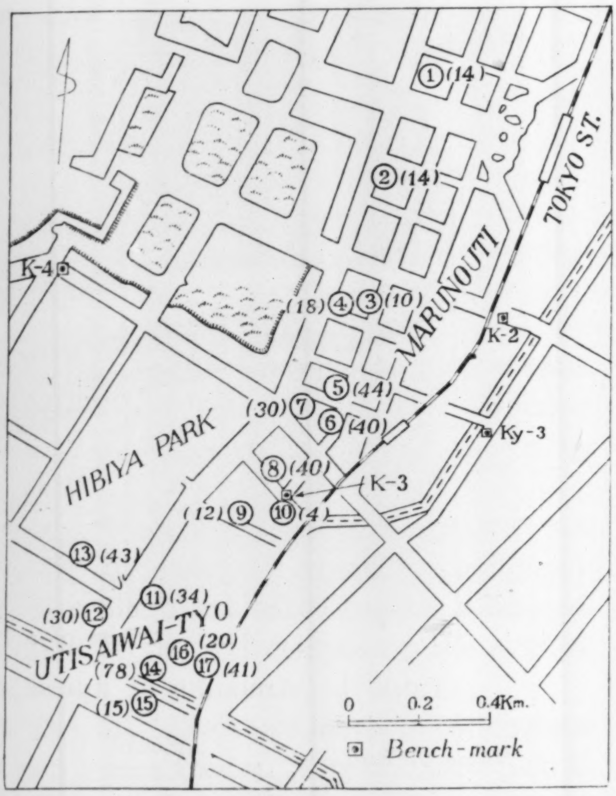

Fig. 2. Distribution of buildings, uprise of which being measured.(The bracketted numerals denote the amounts of uprise in cm)

1. Tokyo Kaizyô Hoken Kaisya Tokyo Marine-Insurance Co.)
2. Syôwa-Building.
3. Zizi-Sinpô-Sya.
4. Tokyo Kwaikwan.
5. Sangyô Kumiai Tyûô Kinko (Main Depository of Industry Assoc.)
6. Sansi-Kwaikwan.
7. Marunouti Police office.
8. Sansin-Building.
9. Tôhô (Tokyo Takaraduka) Theatre.
10. Hibiya Cinema-Theatre.
11. Kangyô Ginkô (Bank.).
12. Hukoku-Tyôhei Hoken Kaisya.
13. Sisei Kwaikwan.
14. Tokyo Dentô Kaisya.
15. Tyôsen Sôtokuhu.
16. Seikyûdô.
17. Zinzyu Seimei Hoken Kaisya (Zinzyu Life Insurance Co.)

If, as will presently be discussed, the apparent uplift of the buildings is due mainly to contraction of the soil composing the surface layer, the rates obtained above will be that of the contraction of the soil.

The foundation of most of the buildings are constructed as follows.

The ground was first excavated to a depth of several metres, and piled driven into a depth of about 20 metres. The number of piles driven is from 1 to 2 for every $4\ m^2$. The piles are usually concrete rods or pine logs, 20 metres long and from 10 to 20 cm in diameter.

As the thickness of the soil layer of Alluvium here is about 20 metres, these piles may reach the underlying hard Tertiary rocks, from which it may be concluded that buildings, the foundations of which are constructed as just described, are rigidly connected to the stable hard Tertiary rocks.

The apparent uprise of the buildings may therefore be regarded as due mainly to the contraction of the soil composing the surface layer and surrounding the buildings and their foundations.

These phenomena led to our constructing special bench-marks for studying the cause of the remarkable subsidence of the earth's surface in Honzyo and Hukagawa.

2. One of these special bench-marks (numbered S–1) was imbedded in the playground of the Kazuya Primary School in Hukagawa and the other (S–2) in the playground of the Kayaba Primary School in Honzyo.

They were long iron tubes, 10 cm in diameter, with a mark on the top made of stainless steel, driven to a depth of 35 metres through the soft Alluvial soil, 30 metres thick. A sectional view of the bench-mark and the soil composing the layer as obtained by boring is shown in Fig. 3.

Soon after the bench-marks were constructed, their heights relative to the nearest bench-marks were measured in April, 1936. The height of S–1 was measured relative to that of B. M. M–9831, and the height of S–2 to those of B. M.'s M–3378 and Sy–7.

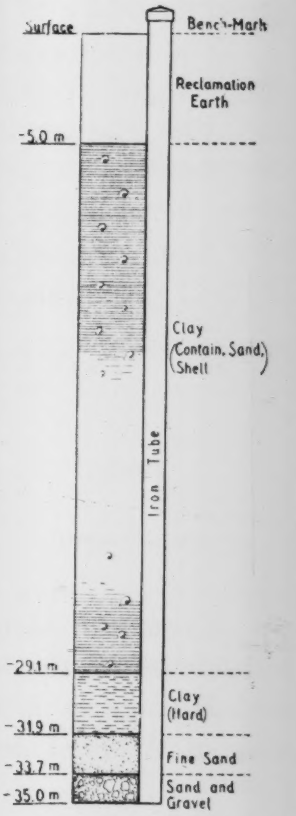

Fig. 3. Sectional view of the bore hole at Kazuya Primary School and B. M. S-1.

3. The precise levelling was revised in October, 1936, about six months after the bench-marks were established, the changes in height of B. M. S–1 relative to M–9831 and those of S–2 relative to M–3378 and Sy–7 being shown in Table III.

Table III. Heights and the changes in heights of S–1 and S–2 relative to nearest bench-marks.

Date	S1—M9831	M3378—S2	S2—Sy. 7.
	m	m	m
Oct. 1936	1·3874	−0·5352	1·3536
Apr. 1936	1·3077	−0·5692	1·3216
Change	79·7 mm	34·0 mm	32·0 mm

It may be deduced from the foregoing Table that, if the heights of the new bench-marks, S–1 and S–2, are assumed not to have changed during the interval April-October, 1936, the surface of the ground represented by the heights of B.M.'s M–9831, M–3378 and Sy–7,may be regarded as having subsided from 30 to 80 mm, relative to the surface of the Tertiary layer, which extends up to about 30 metres below the present surface of the ground.

The assumption that the heights of bench-marks S–1 and S–2 have not changed during the period mentioned is probably confirmed by the fact that the vertical displacement of B. M. M–9831 with reference to the standard datum point[3] was found to be nearly equal to that of the same bench-mark relative to S-1 during the same period, as will be seen upon comparing Table III with Table IV, in which are shown the vertical displacements of M–9831 for various periods.

Table IV. Vertical displacements of B.M. M–9831 referred to the standard datum point.

Period	Nov.1929—Jan.1932	Jan.1935—Apr.1936	Apr.—Oct., 1936
Displacement	−156·0 mm	−282·6 mm	77·1 mm

From the facts cited above, it may be deduced that the remarkable subsidence of the surface of the earth noticed in the region of Honzyo and Hukagawa is largely due to contraction of the surface soil consisting of Alluvial deposits about 30 metres thick.

4. The relevelling of October 1936 was carried out over the line from the standard datum point to S–1 and over the line from M3378–S2–Sy7, the distribution of which is shown in Fig. 4. The vertical displacements of the bench-marks on these lines found by this relevelling are given in Table V.

Table V. Vertical displacements of bench-marks in Tokyo found by relevelling as in Oct., 1936.

Bench-mark	Displacements	Period	Bench-mark	Displacements	Period
K-4	− 10·9 mm	1929—Oct.1936	Ky-4	− 11·9 mm	1929—Oct.1936
K-3	−386·9	〃	M-J-O	− 6·4	〃
K-2	− 43·8	〃	H-1	−257·7	〃
Ky-3	−167·1	〃	R-35	−568·1	〃
R-12	− 26·6	〃	M-9831	−515·7	〃

---

[3] Although strictly speaking, the vertical displacement of the standard datum point is not zero, it may not be sensibly large during such a short period of time as mentioned above, i. e., about six months, as estimated from the results of relevellings on the line between Tokyo and Aburatubo, where the tide gauge is constantly working. The vertical displacement of the standard datum point may therefore be ignored in the present study.

[4] It will be seen that the vertical displacement, −77·1 mm, of M-9831 is approximately equal to that of the same bench-mark relative to S-1, −79·7 mm.

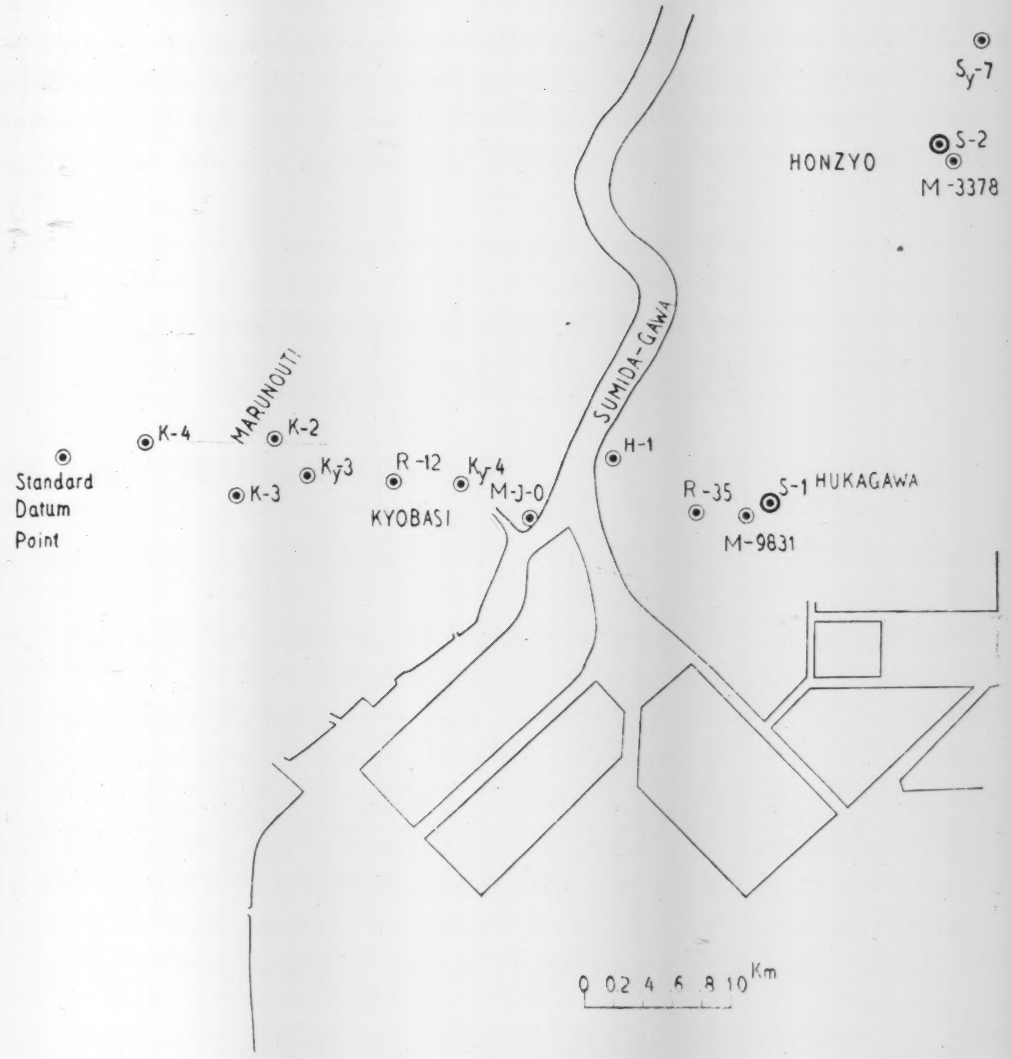
Sy-7
S-2
HONZYO
M-3378
SUMIDA-GAWA
MARUNOUTI
K-4
K-2
Standard
Datum
Point
K-3
Ky3
R-12
Ky4
M-J-0
KYOBASI
H-1
R-35
S-1
HUKAGAWA
M-9831
0 0.2 .4 .6 .8 1.0 Km

Fig. 4. Distribution of bench-marks.

As will be seen from the foregoing table, bench-mark K–3, situated very close to the Sansin-Building, sank 386·9 mm during the period from Aug., 1929 to Oct., 1936, which agrees well with the amount of apparent uprise of the building measured in October 1936. This fact seems to support the conclusion that the apparent uprise of the buildings in the neighbourhood of Marunouti and Hibiya is due to contraction of the soil composing the surface layer. It also implies that the time elapsed since the soil of the surface layer had began to contract, probably does not exceed 10 years.

Further studies of the physical properties of the soil taken from borings for bench-marks S–1 and S–2 are now proceeding so that the results will be available in due course.

The writer wishes to express his sincere thanks to the council of the Hattori Hôkôkwai for the grant of the research fund by means of which the present study was carried out. The writer's cordial thanks are also due to the Municipal Authorities of Tokyo for their courtesy in constructing the bench-marks and in carrying out the relevellings.

10. 江東地域に於ける地盤沈下の原因に就て I.

地震研究所　宮部直巳

東京市内の一部，殊に江東地域に於いて，著しい地盤沈下の現象の認められることは既に屡々報告された所である．

この沈下現象の原因として可能なる 2〜3 の事項も既に報じておいたが，江東地域における地盤の沈下がその中の何れの事項に該當するかは未だ明かではない．

一方に於いて，種々な點から，沈下の原因が，表面に在る比較的軟弱なる地層の收縮にあるらしく思はれる．それで，先づ，表面にある地層の收縮とすれば，それが如何なる程度に沈下現象と關聯を持つかといふことを明かにする目的を以て，次の様なことを試みてみた．

深川及び本所の地域に於いて，表面にある軟弱なる地層は大約 30m の厚さを有することが知られてゐる．そこで，地表から約 35m の深さに達する鐵管を埋設し，その頂部を水準標とした．鐵管の徑は約 10cm である．若しも，沈下現象が主として表面の軟弱地層の收縮に因るものであるならば，江東地域にある他の水準點と，新に埋設した水準點との間の比高は次第に增加すべき筈である．

この水準點は，深川では數矢小學校々庭に，本所では茅場小學校々庭に埋設することを得て，其等を夫々 S–1 號及び S–2 號と名けた．この水準點の埋設をすると同時に附近の水準點との間の比高を測量したのが昭和 11 年 4 月であつた．

最近卽ち昭和 11 年 10 月其等の水準點を含む水準線に就き改測を施行した結果によると，S–1 號は附近の M–3378 號に比して 79·7mm 上昇し，S–2 號は，M–3378 號に比して 34·0mm，SY–7 號に比して 32·0mm 夫々上昇したことが明かとなつた．尙，M–9831 號は同期間に於いて，陸地測量部構內に在る水準原點に比して，77·1mm の沈下を示して居るので，これ等の結果から見ると，S–1 號水準點は，原點に比較して殆ど動かなかつた事と，従つて，M–9831 號その他の水準點によつて代表される深川附近の地表面が全體として約 80mm 沈下した事，及びその沈下が主として表面に在る厚さ約 30m の地層の收縮によるものであらうと思つてよいやうである．

尙，丸の內附近においても殆ど同樣の現象の存することが，例へば，三信ビルデイングの拔上り高約 40cm と，これに程近い水準點 K–3 號の沈下量 386·9mm とを比較することによつて知れるであらう．

11. Observations on Earth Current during the Solar Eclipse of June 19, 1936.

By Ryûtarô TAKAHASI,

Earthquake Research Institute.

(Read July 7, 1936.—Recived Dec. 21, 1936.)

1. Variations in the intensity and direction of the earth current which are expected to accompany solar eclipses should be observed not only in the belt of total eclipse but also in zones of partial eclipse as well as in localities where the eclipse is invisible, although obviously, the amount of variation decreases with distance from the total eclipse belt. Since in the case of the total eclipse of June 19, 1936, totality in the Kwanto district was from 75 to 80%, it was decided to carry out simultaneous observations with instruments of increased sensitivity and recording speed at our permanent earth current stations that had been set up in different localities in the Kwanto district primarily with the object of detecting variations in the earth current in connexion with earthquakes and volcanic eruptions.

In conformity with this plan, Drs. T. Hagiwara, T. Minakami, W. Inouye, T. Nagata, and the writer tcok charge of the instruments respectively at Tukuba, Asama, Komaba and Kiyosumi.

2. All these stations had virtually the same equipment for observing the earth current. For electrode, a lead tube, with an inner diameter of from 1/2″ to 1/4″ and from 5 to 10 meters long, is bent in the form of a spiral and imbedded horizontally in the ground at a depth of 2 meters. The leading wire, usually rubber-covered copper, is soldered to the electrode. The junction of the copper wire and the lead tube is perfectly protected with a compound insulating material (asphalt). To minimize the thermoelectric effect caused by temperature variations, this junction is placed about 1·5 m below the ground surface. The leading wire is brougt to the ground surface through a conduit-tube filled with asphalt. The arrangement of the electrode is shown schematically in Fig. 1.

At Kiyosumi, each pole consisted of two such electrodes imbedded 5 meters apart from each other, and with a view to balance local polarization effects connected in parallel. At the other stations, each pole consisted of only one electrode. Particular care was exercised in installing the electrodes in order to have the conditions at each pole the same as far as possible.

The distance between poles at the different stations differed with the topography of the particular station. The method of observation was almost the same in all the stations: a gavanometer was inserted between the poles, togather with a high resistance of $10^4 \sim 10^5$ ohms connected in series. The deflection of the galvanometer was recorded photographically on a sheet of bromide paper wound on a drum which revolved once a day. At the Asama Volcano Observatory, recording drums that revolved twice a day were used. Details of the apparatus at each station are given in the annexed table.

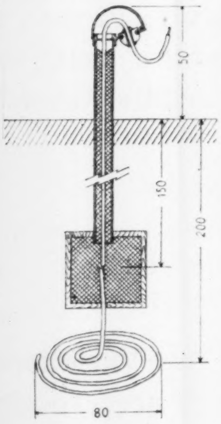

Fig. 1. The electrode.

Name of Station	Latitude	Longitude	Component	True Direction	Distance btw. Poles
Kiyosumi	35°·2	140°·2	E-W	Due E	130 m
			N-S	Due N	150
Tukuba	36·2	140·1	N-S	Due N	65
Asama	36·4	138·5	E-W	E 10°S	80
			N-S	N 15°E	100
Komaba	35·6	139·7	N-S	Due N	50

3. Simultaneous observations were caraied out from June 17 to June 30. Parts of the records obtained at each station, and which correspond to several hours both before and after the eclipse are shown in Fig. 2, Pl. XI. The time shown in the figure is Japan Central Standard Time (135°E meridian). The beginning and ending of the eclipse are shown by white circles under the time marks, and the center of the eclipse by a black circle.

As will be seen from the figure, a remarkable earth current storm broke out on June 19 about 6 hours before the eclipse and lasted till 2 h the next day, that is, 8 hours after the end of the eclipse. The records of the E–W and N–S components obtained at Kiyosumi station closely resemble one another in form with respect to the variation, although in the N–S component there is a marked shift of zero (the daily variation). The corresponping pronounced peaks in each record are shown by capital letters.

It is worthy of note that the form of the record obtained at Tukuba station is identical with that obtained at Kiyosumi station, notwithstanding that a distance of 100 km separates the two stations. These variations are not therefore the result of local disturbances, but of some other general causes.

The form of the records obtained at the Asama Volcano Observatory somewhat resembles those obtained at Kiyosumi, although the former was disturbed severely by short-period disturbances that are probably due to the electric trains at Usui Pass, near Karuizawa.

The records of earth current obtained at Komaba turned out to be quite useless for the present purpose, owing to serious disturbances by the electric railway that passes within 100 meters of the station.

4. According to T. Okada[1], M. Hasegawa[2], S. Ono[3], T. Otagaki[4], S. Shinjo[5], and others, a remarkable magnetic storm was observed on June 19 for many hours both before and after the eclipse, in Hokkaido as well as in Manchoukuo. The forms of variations in these magnetic storm exhibit many similarities with those of the earth current observed by us, whence it is not possible to conclude that the observed variations in the earth current were all due to the eclipse, although it can be said that it is very intimately related to the magnetic storm. In this connection it will be noticed that a magnetic storm has usually little effect on the earth current at Kiyosumi and Tukuba. It is therefore worth noting that on the case of the solar eclipse, the earth current underwent a variation the same as did terrestrial magnetism.

If, however, the intensity and the height of the ionized layers in the upper atmosphere vary with the eclipse, there must necessarily occur variations in terrestrial magnetism as well, while at the same time the quantity of electric charge induced on the surface of the earth must also vary, resulting in variations in the earth current. According to the theory of Chapman[6], and others, these variations should be of comparatively simple forms. We understand from the Electrotechnical Laboratory, Ministry of Communication, that the ionic densities of the E and F_1 layers diminished during the eclipse, so that certain phases of the observed variation in the earth current may have been due to the eclipse.

The difficulties at present in identifying such phases in the records

---

1), 2), 3), 4), 5), Preliminary short reports of magnetic and electric observations made in the Far-East during the total solar eclipse of June 19th, 1936. Communication by the National Committee of Japan on Terrestrial Magnetism and Electricity.

[6] S. CHAPMAN, *Terr. Mag.*, **38** (1933), 175.

of the earth current are however so great that conclusive discussions will have to await publication of the detailed observational data of terrestrial magnetism and of the ionospheric phenomena.

In conclusion, the writer wishes to express his sincere thanks to Professer M. Ishimoto, the director of this Institute, for his encouragement, and also to Drs. T. Hagiwara, T. Minakami, W. Inouye and T. Nagata, who have put the results of their observations at the writer's disposal.

11. 昭和11年6月19日の日食時に於ける地電流の觀測

地震研究所 高橋龍太郎

昭和11年6月19日北海道に於ける皆既日食に際し，關東地方に於ては大凡80%の食分なりしを以て，地震研究所支所の內，地電流觀測設備を有す所に於ては，平常よりも器械の感度を增大し，記錄速度を增大して，日食に原因する地電流の變化を觀測せんと試み，同時觀測を行ひたり．本文第2圖は其の記錄の一部分にして日食の前後數時間に相當するものなり．

各地に於ける地電流の變化の模樣は大凡相似なれども，生憎日食當日は日食の數時間前より日食後十數時間に亘りて地磁氣嵐ありて第2圖に示せる地電流の變化が悉く日食に原因するものと言ふ可からず．此の內に日食と直接關係を有するもの有りや無しやは他日地磁氣，イオン層等に關する觀測結果の發表を俟ちて更に是を研究せんとす．

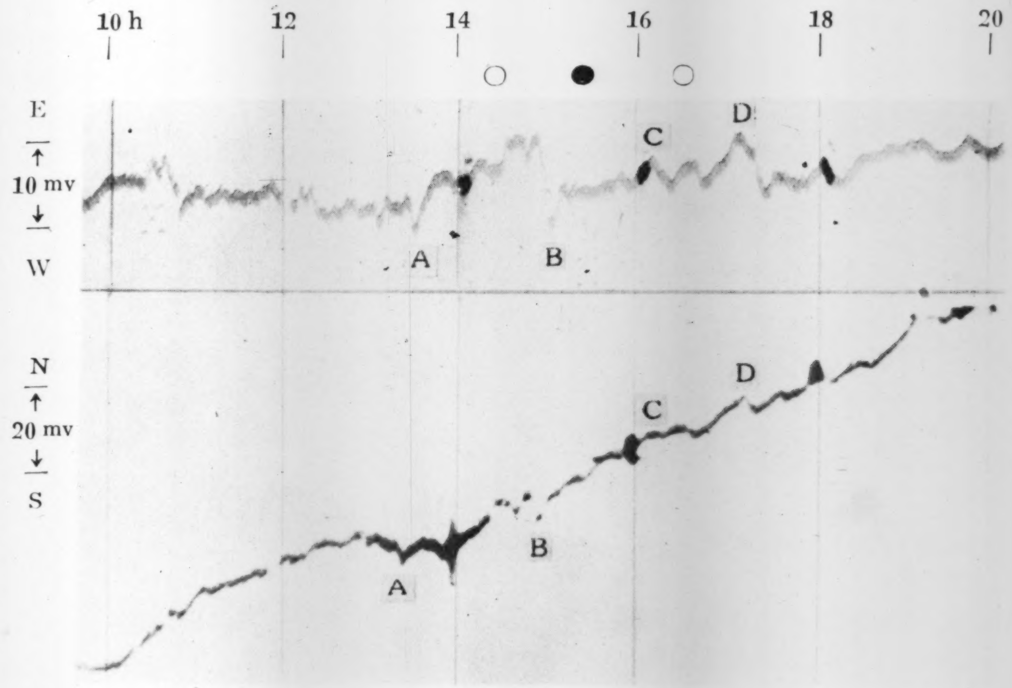

KIYOSUMI.

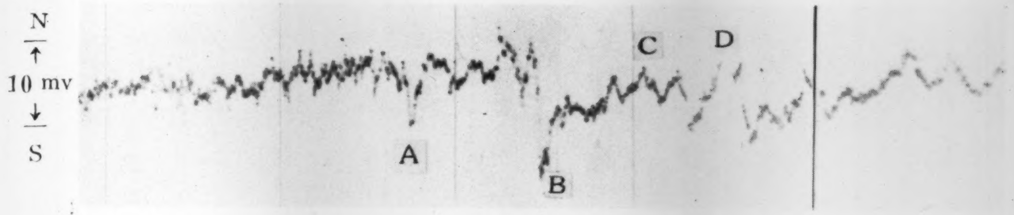

TUKUBA.

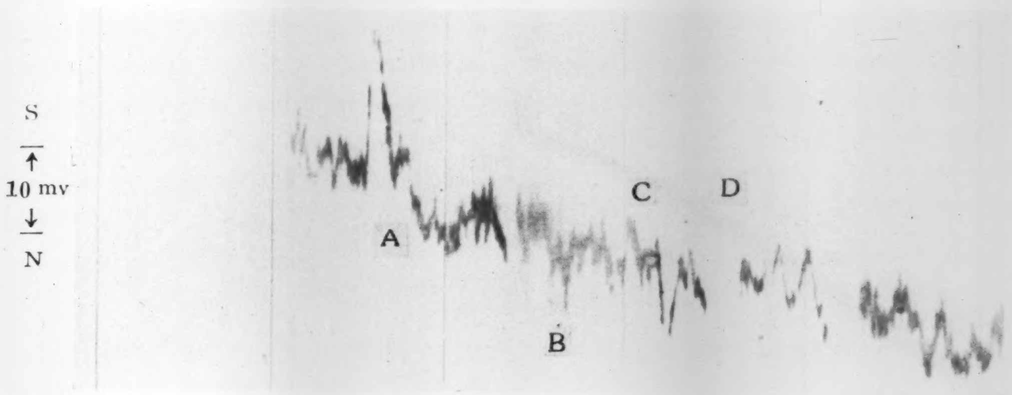

ASAMA.

Fig. 2. Records of the earth current obtained at Kiyosumi, Tukuba and Asama, during the solar eclipse of June 19, 1936.

12. *On the Hot Springs of Atami, Izu Peninsula.*

By Takaharu FUKUTOMI,

Mitsui Geophysical Observatory,
(Susaki, Kamo-gun, Sizuoka prefecture)

(Read Sept. 15, 1936.—Received Dec. 20, 1936.)

I. Introduction.

Atami, situated on the eastern slope of the coastal mountain range in Izu Peninsula, is one of the oldest and most famous hot spring resorts in Central Japan. In the latter part of the Tokugawa era (about 100 years ago), there were 8 natural springs, the so-called "Seven Spas of Atami"[1] which consisted of the "ôyo geyser" (the most famous in Japan and the subject of many interesting studies by the foremost authorities[2]), the "Seizaemon-spring", "Hôsai-spring", "Huro-spring", "Kawara-spring", "Sazirô-spring" and the "Nonaka-spring", all close to one another in the central part of the town of Atami, and one called the "Izusan-hasiri-spring" in a northern suburb of the town as shown in Fig. 1. According to old records, at that time, at low tide, some hot springs used to flow from the

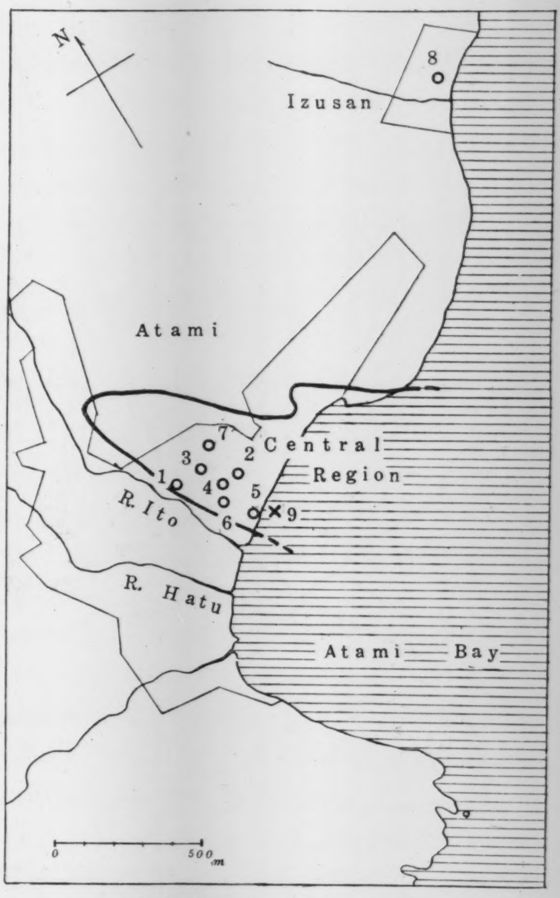

Fig. 1. Distribution of Atami hot springs in the latter part of the Tokugawa era, about 100 years ago.
1. Ôyu-geyser. 2. Seizaemon-spring. 3. Hôsai-spring. 4. Huro-spring. 5. Kawara-spring. 6. Sazirô-spring. 7. Nonaka-spring. 8. Izusan-hasiri-spring.

---

[1] "*Zôtei-zusyûsikô*" **3-A**, 16~20; **6**, 35~39.

[2] K. HONDA and T. TERADA, *Publ. Earthq. Inv. Comm.*, **22-B** (1906), 51; H. ISHIWARA. *Rep. Earthq. Inv. Comm.*, **17** (1898), 41; T. OGAWA, *Globe*, **2** (1924), 16; T. KÔZU, *Rep. Geol. Surv.*, **36** (1912).

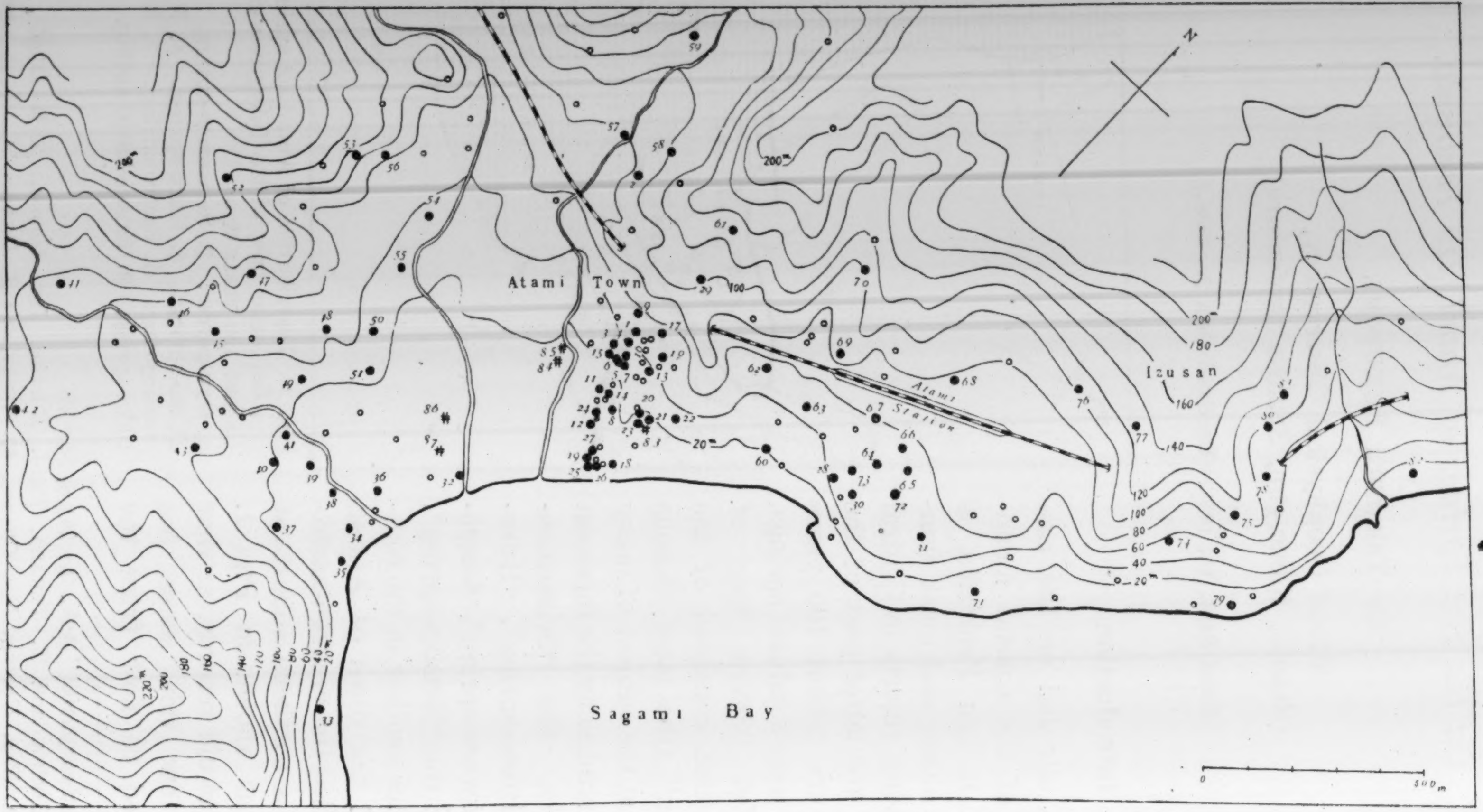
N
Atami Town
Izusan
Atami Station
Sagami Bay
200
180
160
140
120
100
80
60
40
20
220
0
500m

Fig. 2. Distribution of the Atami hot springs in the recent years.
● observed hot spring, ○ unobserved hot spring, # ordinary well. (Numeral attached to black circle denotes hot spring number in Table I.)

sandy beach, the approximate positions of which are marked × in Fig. 1. Since then, about 30 years ago, from some 20 to 30 shallow hot springs have been bored by primitive methods not far from the foregoing "Seven Spas of Atami". At present, thanks to the great strides made in boring technic which make it possible to reach great depths, we find today some 180 orifices of hot spring in the town and neighbourhood, with depths ranging from 0 to 400 m as shown in Table I. (Black circles and plain circles in Fig. 2 indicate the sites of spring orifices that were studied and the other hot springs respectively. The numerals affixed to each black circle correspond to the numbers of the hot spring in Table I.)

The writer recently had the opportunity of observing the orifice temperatures and analysing some of the chief chemical constituents of 82 of these hot springs and of some ordinary wells, the results of which, together with the physical properties of these already known, enable us to distinguish two different systems of springs in the locality.

II. Methods and results of investigation.

The observation was carried out by the writer with the aid of Mr. M. Ôtuka, a member of the Atami Hot Spring Owners' Association, during the period from June 2 to June 6, 1936.

For the temperature, a maximum thermometer graduated to 150°C was used. The volume output of these hot springs was not estimated for the reason that to estimate the output of these so-called "Boiling springs" in the central part of the town without suitable equipment would involve no little personal danger, and further because in the case of hot springs situated away from the central part of the town, the hot water was drawn through artesian wells by artificial methods, hence no representing the natural condition of the springs.

As to the chemical analyses of the hot spring, we measured the amounts of Cl, Ca, SO_4, SiO_2 and the alkalinity, seeing that the analyses of several Atami springs made by the Tôkyô Hygienic Laboratory indicate that the chief mineral constituents of these springs are NaCl, $CaCl_2$, $CaSO_4$. The methods of analysis were briefly as follows:

(1) Determination of Cl. The normal titration method for sea water with a $AgNO_3$-solution of known strength (71·866 g/L) was added to 15 cc of the sample in the presence of a few drops of 8%-solution of K_2CrO_4 from a microburette. For calibration of the method, the writer analysed ten times a solution containing 1·65 g of NaCl in 1 litre of pure water (Cl=1·003 g/L). With this method, a Cl content

of $1{\cdot}005 \pm 0{\cdot}001$[3] g/L was obtained.

(2) Determination of Ca. From 2 cc of the sample (neutral or mildly basic) and 1 cc of $(NH_4)_2C_2O_4$, a white precipitate of C_2O_4Ca was obtained. The precipitate was centrifuged and the upper liquid decanted. The precipitate after washing with pure water was again centrifuged, the process being repeated two or three times. With the C_2O_4Ca precipitate and 5 cc of N–H_2SO_4, oxalic acid ($C_2O_4H_2$) was formed, the volume of which was measured by the normal titration method for oxalic acid using $N/100$-$KMnO_4$ at a temperature of about 80°C. For calibration of the method, the writer analysed ten times a solution of $CaCl_2$ containing 11·13 g/L (Ca=4·02 g/L) with the method, and obtained Ca=4·042 ± 0·034 g/L.

(3) Determination of SO_4. 20 cc of the sample (neutral or mildly basic) were diluted to 50 cc with pure water, from which solution and 10 cc of $BaCl_2$ solution ($BaCl_2+2H_2O$-content=4·88 g/L), a white precipitate of $BaSO_4$ was obtained. Then from the $BaCl_2$ residue and 10 cc of $N/50$-K_2CrO_4, $BaCrO_4$ (colourless, no precipitate) resulted. The solution was pale yellowish owing to the presence of residual K_2CrO_4. The amount of K_2CrO_4 residue was determined by comparing the concentration of this colour with that of a solution of $N/50$-K_2CrO_4 by means of Hehner's cylinder and the amount of SO_4 in 1 litre of the sample calculated. For calibration of the method, the writer analysed ten times a solution of $(NH_4)_2SO_4$ containing 0·688 g/L of $(NH_4)_2SO_4$ (SO_4=0·500 g/L) with this method and obtained SO_4-content=0·501 ± 0·003 g/L. The writer here wishes to acknowledge his indebtedness to Mr. S. Yoshimura, a member of Geographical Institute, College of Literature and Science, Tôkyô, for his kind advices on the methods here described.

(4) Determination of silicate. 15 cc of the sample were diluted to 50 cc with pure water, from which solution, with 1 cc of a 10%-solution of ammonium molybdate and 4 drops of a 50%-solution of H_2SO_4, a pale yellowish solution of silico-molybdates was obtained. The amount of silicate in 1 litre of the sample was determined by comparing the colour of this solution by means of Hehner's cylinder with a yellowish solution of picric acid (picric acid made by E. Merck, Darmstadt, Germany, 25·6 mg/L) the colour of which corresponded to that of the sample of 50 mg/L of SiO_2 obtained by the foregoing method.

(5) Determination of alkalinity. The normal titration method for the so-called "temporary hardness of water" was used. A sufficient volume of $N/10$-HCl to change such compounds as XCO_3, $X(HCO_3)_2$ (X=Ca, Mg, or Fe, etc.) in 10 cc of the sample into XCl_2, CO_2, and H_2O, was measured in the presence of a few drops of a 0·1%-solution

---

[3] probable error.

of methyl orange, and the alkalinity as the amount of $CaCO_3$ in 1 litre of the sample calculated from the required volume of $N/10$-HCl.

The results of temperature measurements and of chemical analyses of 82 hot springs and 5 ordinary wells in Atami, determined by the foregoing methods, are shown in Table I.

Table I.

NO.	Name of hot spring (温泉名)	Height of * orifice above mean sea-level (湧出口海面上高)	Depth* of artesian well (溫泉井の深さ)	Orifice temperature (湧出溫度)	Chemical constituents (化學成分)					Remarks
					$Ca^{\cdot\cdot}$	Cl'	SO_4''	SiO_2	Alkalinity as $CaCO_3$	
		m	m	°C	mg L	g/L	mg/L	mg/L	mg/L	
1	Hachisuka-yu	37·7	45·4	100	957	4·09	203	173	22	Suction-pump working
2	Kinomiya-yu	——	272·7	99	971	3·80	205	200	29	
3	Yamanasi-yu	27·4	60·0	100	926	3·79	141	182	24	
4	Aonuma-yu	30·0	63·6	100	1093	3·78	269	199	20	
5	Huzii-yu	23·0	66·7	100	853	3·54	238	192	19	
6	Aoki-yu	22·9	72·7	100	812	3·33	278	189	20	
7	Ozawa-yu	22·8	74·5	100	813	3·27	265	202	45	
8	Tenzin-yu	17·4	36·4	100	820	3·27	259	167	19	Ditto
9	Miura-yu	48·8	121·8	100	847	3·22	261	190	21	
10	Nonaka-yu	42·4	90·9	100	874	3·15	307	206	26	Ditto
11	Hukusimaya-yu	17·7	29·1	100	755	2·95	275	202	16	
12	Uzawa-yu	6·4	——	100	576	2·75	186	196	49	
13	Komatu-yu	31·5	60·0	100	650	2·58	310	173	17	Ditto
14	Mizu-no-yu	13·0	16·7	100	643	2·55	368	176	15	
15	Nisi-yu	22·1	10·9	100	610	2·49	134	147	11	Ditto
16	Yonekura-yu	24·0	72·7	100	665	2·35	394	180	18	〃
17	Hurukawa-yu	38·8	90 9	100	604	2·25	426	190	24	〃
18	Iseya-no-yu	4·1	5·8	85	370	1·89	279	171	25	〃
19	Noda-yu-2	3·8	4·5	100	458	1·71	202	114	35	〃
20	Kawarai-yu	19·2	10·9	98	552	1·58	331	153	16	〃
21	Huruya-yu	16·8	7·3	92	560	1·57	448	163	21	〃
22	Suzukiya-yu	32·3	100·0	94	490	1·57	443	147	19	〃
23	Seizaemon-yu	17·6	33·6	93	510	1·53	475	152	22	
24	Owariya-yu	9·6	40·0	84	382	1·44	209	92	47	Ditto
25	Nakadama-yu	4·5	3·6	85	350	1·40	191	111	29	〃
26	Tama-no-yu	3·8	2·4	70	365	1·16	193	109	28	〃
27	Naka-no-yu	4·5	2·2	66	208	1·12	150	114	64	〃
28	Yokoiso-yu	45·7	181·8	78	1595	4·02	655	104	29	〃
29	Sano-yu	108·5	245·5	87	570	1·55	476	128	14	〃

(*to be continued.*)

Table I. (*continued.*)

No.	Name of hot spring (溫泉名)	Height of* orifice above mean sea-level (湧出口海面上高)	Depth* of artesian well (溫泉井の深さ)	Orifice tem-perature (湧出溫度)	Chemical constituents (化學成分)					Remarks
					$Ca^{\cdot\cdot}$	Cl'	SO_4''	SiO_2	Alkalinity as $CaCO_3$	
		m	m	°C	mg/L	g/L	mg/L	mg/L	mg/L	
30	Siomi-yu	53·6	218	80	680	1·18	534	77	21	Suction-pump working
31	Eizyu-byôin-1	10·6	63	72	390	1·18	567	77	31	Ditto
32	Atamien-yu	3·8	270	41	135	0·081	229	33	41	〃
33	Uomigasaki-yu	10·5	300	55·5	433	0·414	741	49	21	〃
34	Oonoya-yu-1	4·5	110	60·5	375	0·348	663	47	19	
35	Oonoya-yu-2	4·2	160	57·7	398	0·357	706	48	26	
36	Horikosi-yu	6·0	90	40·5	144	0·118	379	45	30	
37	Hatiman-onsen	16·2	270	56	360	0·291	821	51	21	Ditto
38	Takeuti-yu	13·9	240	60·7	370	0·309	778	48	28	〃
39	Mitueda-A-yu	12·7	240	58·5	235	0·183	289	49	18	〃
40	Nakazaki-yu	28·4	220	49·7	50	0·030	63	46	38	〃
41	Wada-yu (Ku-yû)	24·8	360	58	398	0·392	734	49	20	〃
42	Tamanoi-yu	83·0	270	54·8	390	0·270	781	49	26	〃
43	Nasaka-kuzu-yu	42·4	360	48·2	189	0·134	374	41	38	〃
44	Itikawa-yu	71·3	360	54	352	0·258	951	51	——	〃
45	Murayama-yu	46·1	270	52·3	360	0·235	926	46	20	〃
46	Watanabe-yu	57·6	270	38·3	249	0·080	663	33	33	〃
47	Sankairô-yu	42·8	360	44·3	282	0·189	643	52	31	〃
48	Midori-yu	39·1	300	51·8	331	0·221	1011	49	21	〃
49	Huzita-yu	20·9	420	57	460	0·563	1002	46	——	〃
50	Hayasi-yu	30·2	240	59	350	0·240	725	45	34	〃
51	Tenzinyama-yu	24·9	360	63	362	0·212	811	55	36	〃
52	Kitazawa-yu	66·3	360	64	382	0·253	704	49	34	〃
53	Minaguti-yu	97·0	300	67·8	495	0·256	754	55	31	〃
54	Huku-no-yu	28·4	310	60·5	334	0·213	694	54	14	〃
55	Mizutani. K-yu	23·9	220	65	355	0·251	736	57	15	〃
56	Sanbonmatu-yu-2	——	——	65	340	0·207	586	48	16	〃
57	Kusunoki-yu	77·3	303	80	383	0·244	203	69	34	〃
58	Tateisi-yu	100·0	273	83·8	229	0·590	167	126	30	〃
59	Nisiyama-yu	117·5	54	57·5	64	0·030	47	53	50	〃
60	Kawamoto-yu-2	20·8	127	96	235	0·815	383	150	34	〃
61	Iwasaki-yu	128·2	336	79	104	0·173	119	67	43	〃
62	Kômyô-yu	49·5	236	97	187	0·697	211	185	31	〃
63	Kawamoto-yu-1	44·7	272	88	270	0·651	458	55	23	〃

(*to be continued.*)

Table I. (*continued.*)

No.	Nome of hot spring (温泉名)	Height of* orifice above mean sea-level (湧出口海面上高)	Depth* of artesian well (温泉井の深さ)	Orifice temperature (湧出溫度)	Chemical constituents (化學成分)					Remarks
					Ca··	Cl'	SO_4''	SiO_2	Alkalinity as $CaCO_3$	
		m	m	°C	mg/L	g/L	mg/L	mg/L	mg/L	
64	Murakami-yu	71·8	218	74	345	0·442	657	82	24	Suction-pump working
65	Sayama-yu	70·9	252	73	287	0·406	422	88	48	〃
66	Asahi-yu (Iinuma)	64·4	218	69·8	313	0·418	718	97	38	〃
67	Atami-eki-yu	60·7	273	82	330	0·537	629	82	23	〃
68	Takeuti-yu	80·0	——	75	335	0·460	757	80	28	〃
69	Wakôen-yu	81·5	282	71·5	242	0·410	399	75	79	〃
70	Inouye-yu	90·0	364	73	255	0·455	504	76	28	〃
71	Eizyu-byôin-2	51·3	179	78	282	0·433	691	89	33	〃
72	Siomisaki-yu	56·0	276	79·3	301	0·451	664	83	24	〃
73	Kosuge-yu	63·3	268	72	300	0·574	563	85	31	〃
74	Atami-hotel-yu	28·9	127	72·7	326	0·393	673	78	35	〃
75	Kisi-yu	106· –	——	——	217	0·278	398	67	93	〃
76	Hukusima-yu	95·7	——	70	325	0·423	648	118	45	〃
77	Harumi-yu	111·3	327	62	225	0·423	1045	60	95	〃
78	Hosono-yu(Ôki?)	87·0	——	65	263	0·392	583	81	34	〃
79	Higuti-yu	6·7	200	64·8	256	0·377	577	81	29	〃
80	Suzuki-yu	92·8	280	62	328	0·402	598	82	34	〃
81	Kôbô-yu	123·3	——	68	352	0·416	534	99	40	〃
82	Izusanhasiri-yu	11·8	0	59·5	284	0·304	556	43	31	Natural spring
	normal well									
83	Huruya-izumi	17	——	18	14	0·015	27	36	31	
84	Narihira-ido	18	——	23	44	0·233	38	42	37	
85	Onsenzi-ido	19	——	21	42	0·086	47	31	8	
86	Aokikwan-ido	4	——	20	30	0·118	42	32	50	
87	Atamien-ido	4	——	19	12	0·013	22	35	26	

* Investigation made by the Hygienic Department, Sizuoka Prefecture.

III. Discussion of the results.

(1) Geographical distribution of hot springs by depth.

As it seems that the depths of hot springs indicate approximately the depth of the source of the hot water, it may be interesting to know their geographical distribution. This geographical distribution of the depths of hot spring was investigated from the records of the Atami

Hot Spring Owners' Association[4]. The total area was divided into a number of imaginary meshes, each representing 100 m × 100 m, and the depths of the wells in the central one of every nine meshes multiplied by 2 and those in other meshes by 1. Thus the calculated weighted mean was assumed to be the mean depth of the wells in the central mesh. After repeating this process with all the meshes, contour lines of the assumed depths below mean sea-level were drawn as shown in Fig. 3.

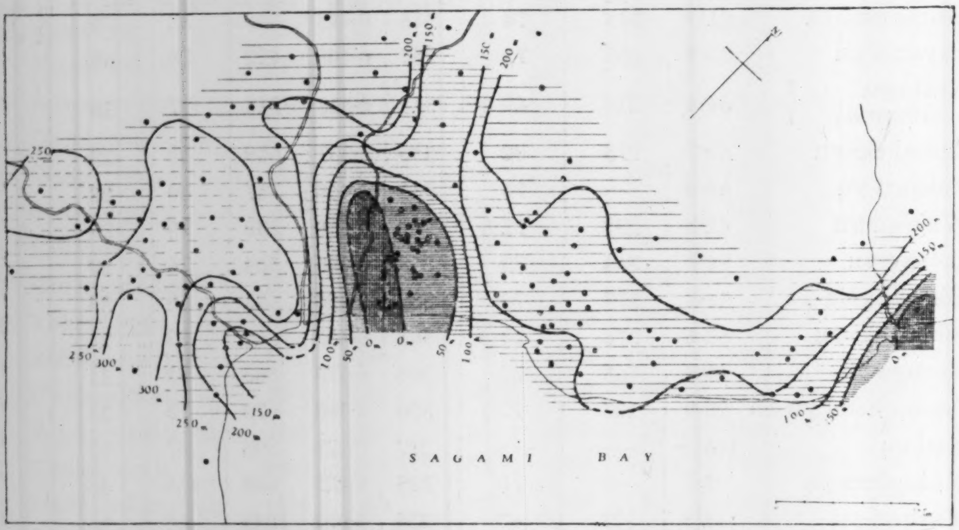

Fig. 3. Geographical distribution of depth of well in metre of hot spring below the mean sea-level.

It will be seen from this figure that hot water flows from shallow depths above mean sea-level in the central part and the north-eastern suburb of the town, and that the greater the distance from this region the greater the depth of the well. On the other hand, in the north-western and south-western suburbs of the town, at about 200∼300 m below mean sea-level, the hot water flows out with difficulty.

An interesting coincidence is that the natural springs shown in Fig. 1 are in regions where the wells are very shallow.

According to the geological studies of Messrs. Y. Ôtuka and H. Kuno[5], the Sogayama beds of lower Miocene age, which are chiefly decomposed green andesitic rocks and tuff, form the base of Izu Peninsula, at any rate the region near the town of Atami and neighbourhood. The younger volcanic material do not cover this basal rock to any great depth. It is therefore highly probable that these hot springs have their source in the Sogayama beds.

---

4) "Atami Onsen Kumiai".

5) Y. OTUKA and H. KUNO, *Bull. Earthq. Res. Inst.*, **10** (1932), 472.

(2) Geographical distributions of orifice temperature and of the Cl and SO_4 contents of hot springs.

The geographical distribution of orifice temperature was found to be as shown in Fig. 4. The places where the temperature attains to 100°C are comfined to a narrow area in the central part of the town where the phenomena of "Boiling spring" may be witnessed, ejecting great quantities of hot water of about 100°C and volumes of steam. The temperature of the water diminishes with distance from the region of high temperature, just mentioned, there being places in the southern suburb of the town where the temperature falls below 40°C.

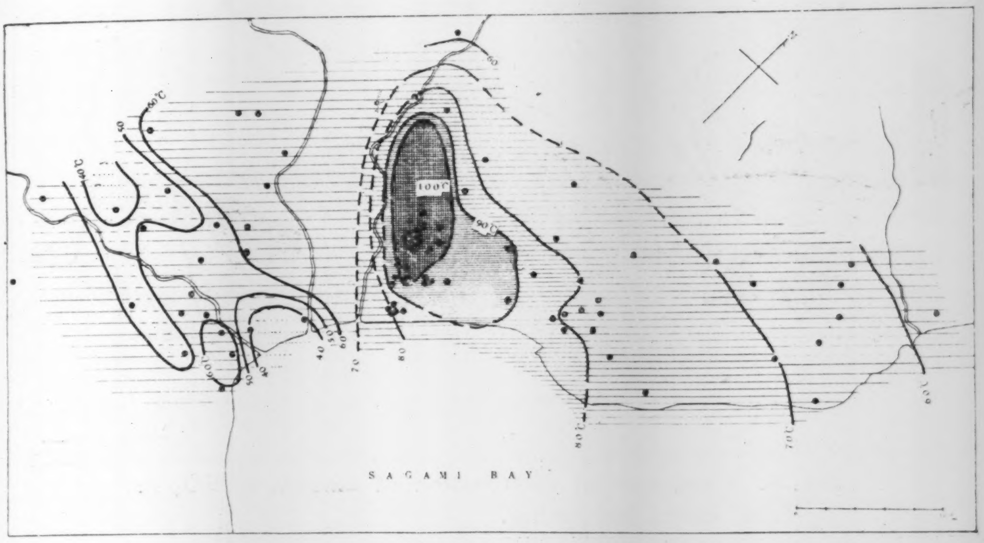
60°C
50
40°C
100°C
90°C
60
40
50
60
70
80
80°C
70°C
60°C
SAGAMI BAY

Fig. 4. Geographical distribution of orifice temperature in degree C of Atami hot spring.

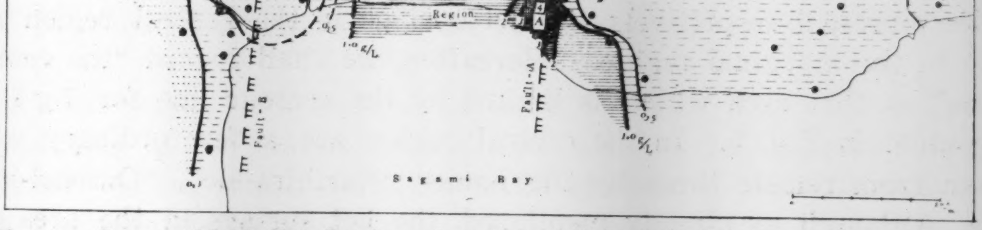
Central
Region
0.5
1.0 g/L
4
A
Fault-A
Fault-B
0.1
Sagami Bay

Fig. 5. Geographical distribution of amount of Cl in g/L of Atami hot spring.

The geographical distribution of the Cl and SO_4 contents were found to be as shown in Figs. 5 and 6. Large Cl content was also found in the central part of the town, the water being highly saline and containing a maximum of about 4·1 g/L, that is, about one fifth of that contained in sea water, and the longer the distance from the central region the lower the salinity, until in the southern suburb, we find places where the amount of Cl is only about 0·2 g/L. As to the SO_4 content, its geographical distribution shows it to be inversely related to that of Cl.

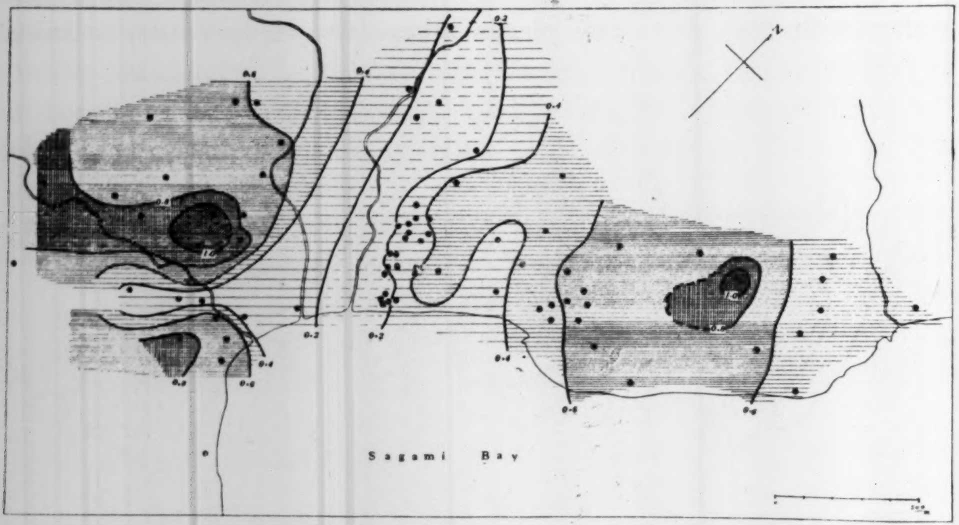

Fig. 6. Geographical distribution of amount of SO_4 in g/L of Atami hot spring.

(3) Relation between orifice temperature and the amount of Cl and that between the latter and the various chemical constituents.

Figs. 4 and 5 show the existence of some analogy between the change in temperature and that of the Cl content of hot springs. If, in order to ascertain more exactly the relation between these two quantities, the points be plotted on a diagram with the temperature of the springs as abscissae and the amounts of Cl in 1 litre of the corresponding water as ordinates, we obtain Fig. 7, in which the plain circles and black circles represent respectively the hot springs in the central region and those in the marginal region. Hereafter, we shall regard "the central region" as that area which is limited by the contour line for 1 g L of Cl content in Fig. 5. In the central region are a few ordinary wells known from remote times by the names "Narihira-ido", "Onsenzi-ido", etc. Although as already mentioned, the hot springs in the area are not so deep compared with ordinary wells, we find no differences in the original characters of these two kinds of wells. In Fig. 7, therefore, the values of the temperature and Cl content of these ordinary wells

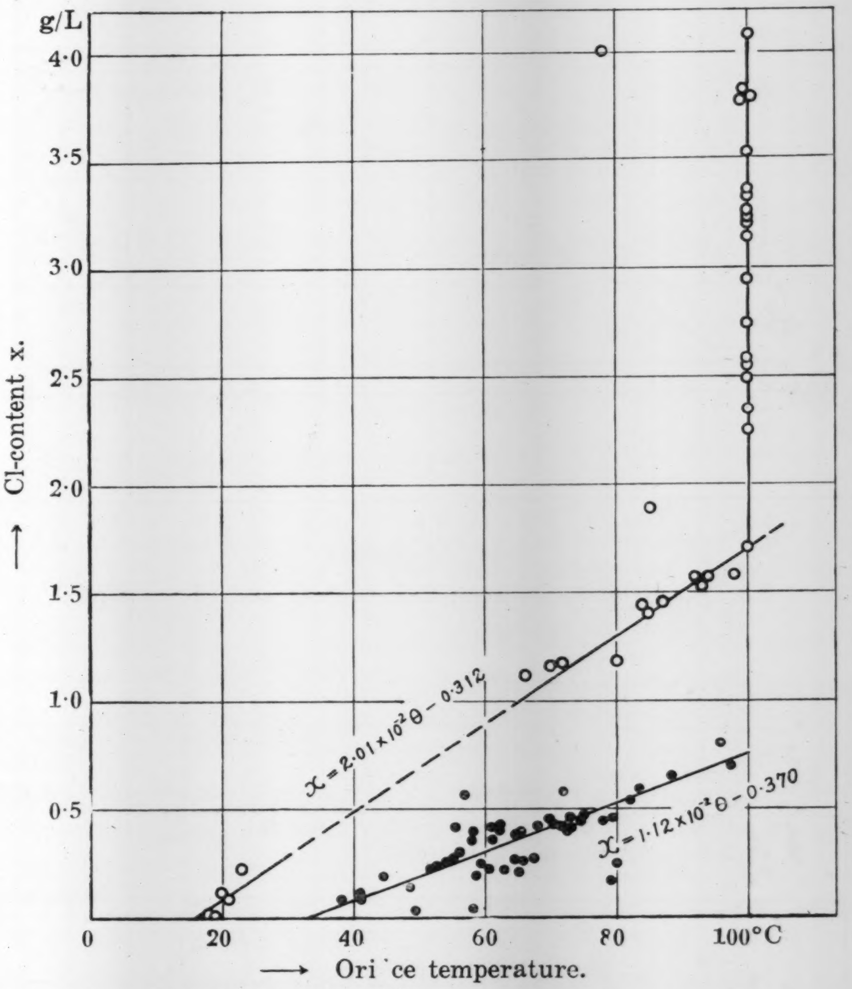

Fig. 7. Relation between Cl-content and orifice temperature of Atami hot springs.

○ hot spring of the central region.

● hot spring of the marginal region.

are plotted the same as those of the hot springs in the central region.

Fig. 7 reveals the remarkable fact of the existence of two series of hot springs in Atami. Those in the central region, which contain a moderate amount of Cl with comparatively high temperature, belong to the first series. In contrast to them, those in the widely spread area consisting of the town of Atami and neighbourhood except those in the central region, which contain a small amount of Cl with comparatively low temperature, belong to the second series.

Other evidences pointing to the existence of these two series are found also in Figs. 8 to 12. Figs. 8 to 10 show the relation in the amounts of Cl to those of silicate, sulphate, and alkalinity as $CaCO_3$,

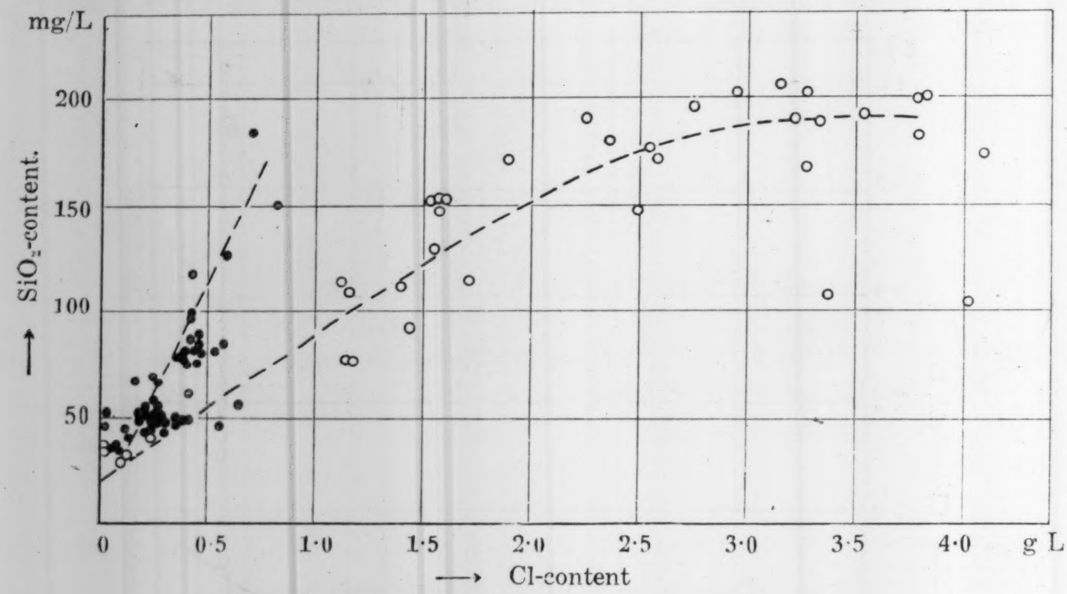

Fig. 8. Relation between SiO_2-content and Cl- content of Atami hot springs.

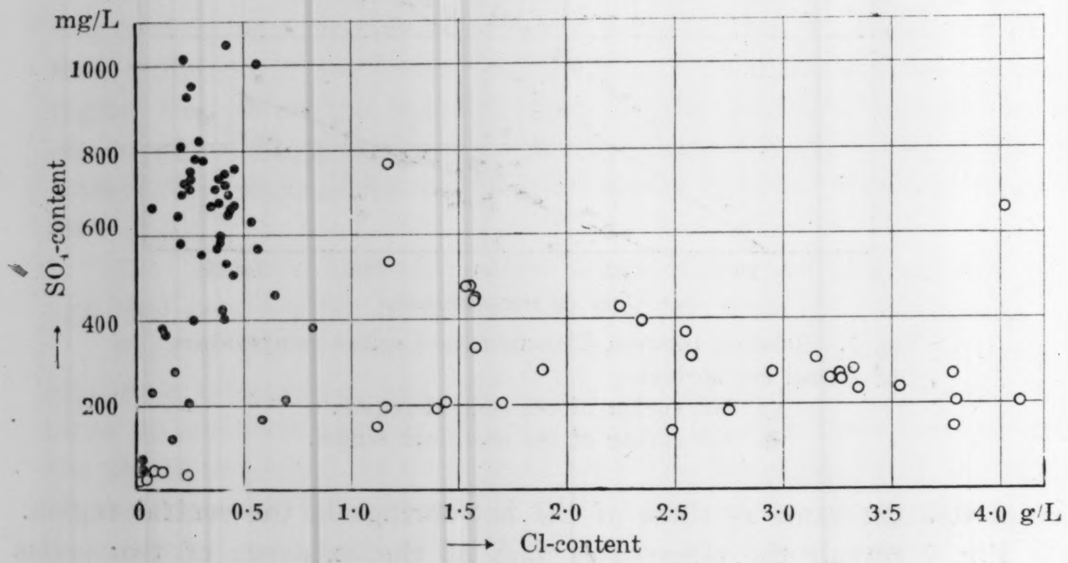

Fig. 9. Relation between SO_4-content and Cl-content of Atami hot springs.

respectively. In these figures, the points seem to be distributed more or less systematically, that is, the points indicated by the same kind of mark cluster into rather definite groups.

According to the analysis of the Tôkyô Hygienic Laboratory, the mineral constituents per litre of the water of the several springs in Atami are shown in the following table.

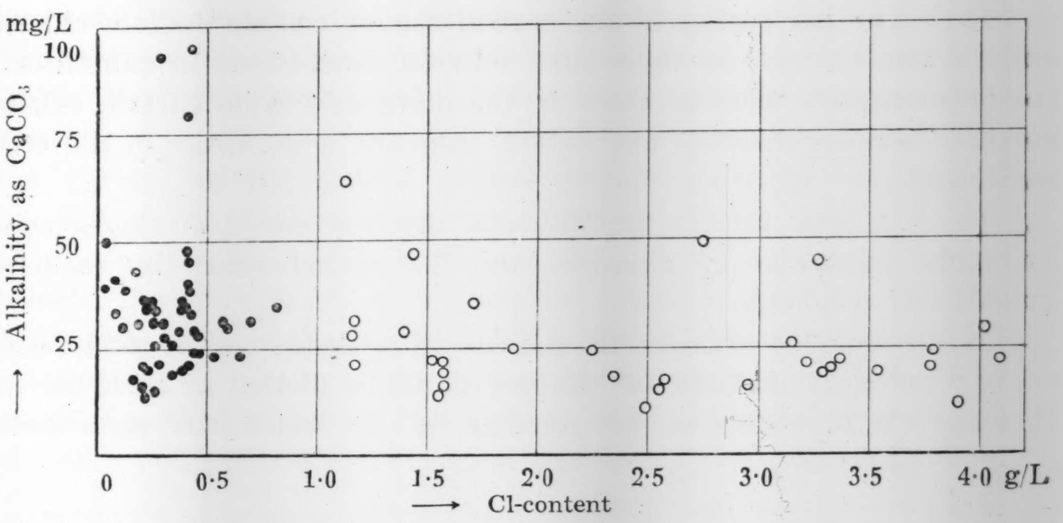

Fig. 10. Relation between alkalinity as $CaCO_3$ and Cl-content of Atami hot springs.

Table II. Comparison of the Chief Mineral Constituents contained per Litre of Water in the Hot Springs of Atami as analyzed by Tôkyô Hygienic Laboratory.

Mineral constituents ↓ (含有成分)	Hot springs in the central region (中心地の溫泉)		Hot springs in the marginal region. (中心地以外の溫泉)					
	Nonaka-yu (野中湯)	Aoki-yu (青木湯)	Atami-en-yu (熱海園湯)	Huzita-yu (戸倉湯)	Kitazawa-yu (牡丹臺湯)	Siomisaki-yu (潮見崎湯)	Suzuki-yu (鈴木湯)	Izusanhasiri-yu (伊豆山走湯)
Spring number in Fig. 2. →	(10)	(6)	(32)	(49)	(52)	(72)	(80)	(82)
	g/L	g/L	g/L	g/L	g/L	g/L	g/L	g/L
NaCl	**5·4090**	**5·4623**	0·1140	0·4748	0·3330	0·7655	0·6624	0·4537
$CaCl_2$	2·8930	2·5647	——	——	——	——	——	——
KCl	0·3540	0·5133	0·0089	0·0277	0·0746	0·0257	0·0324	0·0108
$MgCl_2$	0·0145	0·2740	——	——	——	——	——	——
$CaSO_4$	0·1313	0·1729	**0·3445**	**1·1735**	**0·9416**	**0·9913**	**0·8491**	**0·7619**
Na_2SO_4	——	——	0·0702	0·2323	0·3688	0·0506	0·1384	0·0577
$CaCO_3$	——	0·3793	——	——	——	——	——	——
$Ca(HCO_3)_2$	——	——	0·0466	——	0·1232	——	——	0·0294
$Mg(HCO_3)_2$	——	——	0·0105	——	0·0114	0·0024	0·0412	0·0259
H_2SiO_3	0·6813	0·1985	0·0403	0·0527	0·0387	0·0831	0·0774	0·0488
Chemical classification	Muriated spring (食鹽泉)	Muriated spring (食鹽泉)	Simple thermal spring (單純泉)	Bitter spring (苦土泉)	Bitter spring (苦土泉)	Bitter spring (苦土泉)	Bitter spring (苦土泉)	Bitter spring (苦土泉)

Numerals in heavy style and those underlined denote the largest amount and the largest but one of the mineral constituent respectively.

From Table II we may infer the following facts:

(a) The hot spring in the central region contain sodium chloride and calcium chloride as their chief mineral constituents in quantities in the order named, whereas those in the marginal region contain calcium sulphate, sodium chloride, and sodium sulphate in quantities in the order mentioned.

(b) In their mineral constituents, the first series is characterised by large quantities of chloride, and the second series by moderate amounts of sulphate.

If, in order to examine these facts more closely as the total results of our chemical analysis, the amount of Cl be plotted as abscissae and those of Ca as ordinates, we get Fig. 11, in which the plain circles and black circles show respectively the hot springs in the central region and those in the marginal region. The curve thus obtained indicates

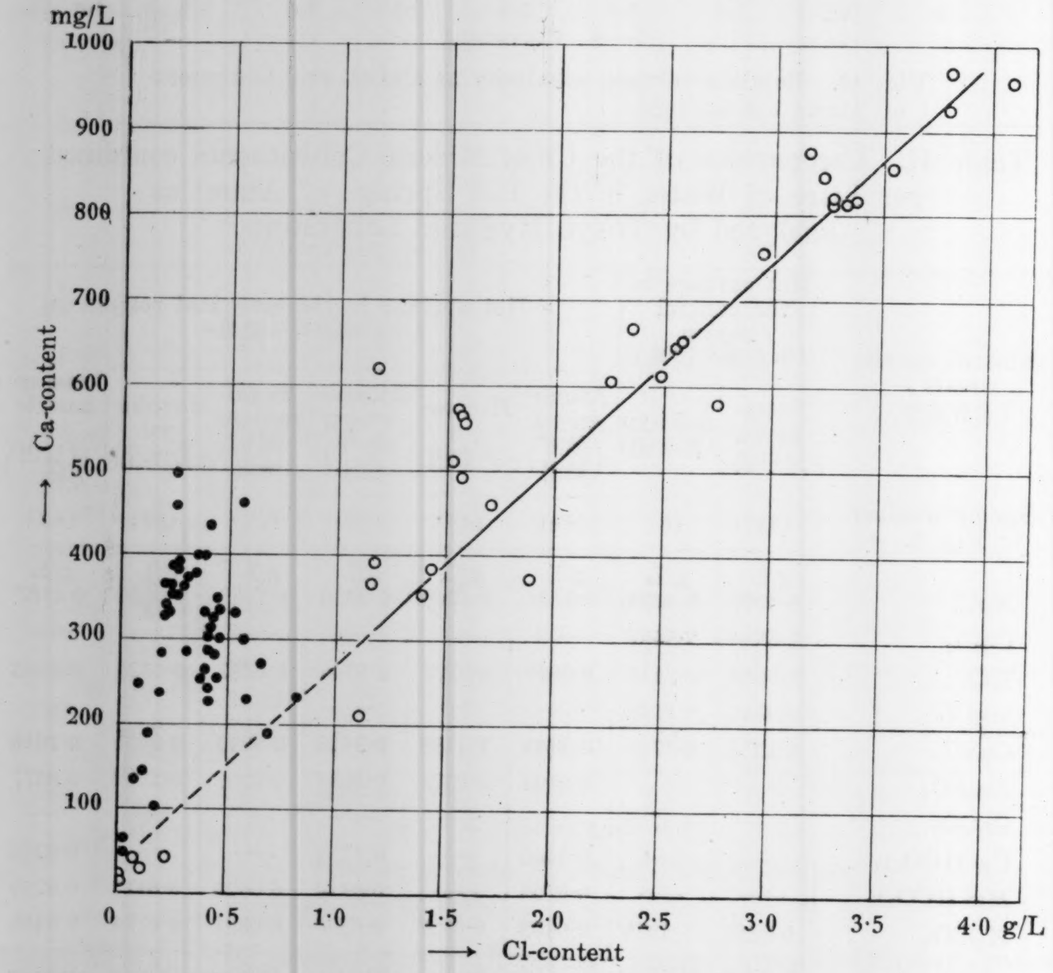

Fig. 11. Relation between Ca-content and Cl-content of Atami hot spring.
○ hot spring of the central region.
● hot spring of the marginal region.

a linear relation between the amounts of Cl and those of Ca for the hot springs in the former, whereas the points show rather a scattered distribution for those in the latter. The linear relation between these two quantities would seem obvious from the reason just stated that the hot springs in the central region contain moderate amounts of $CaCl_2$. From the analysis just mentioned of a hot spring in the central region (see Table II), NaCl and $CaCl_2$ were its chief chemical constituents, the amounts of other chemical constituents being negligble compared with those of NaCl and $CaCl_2$. We therefore calculated the residual amounts of Cl in every spring subtracting the amounts of Cl that combine with Ca to form $CaCl_2$ from the total amounts of Cl and Ca that were obtained by our chemical analyses. The relation between

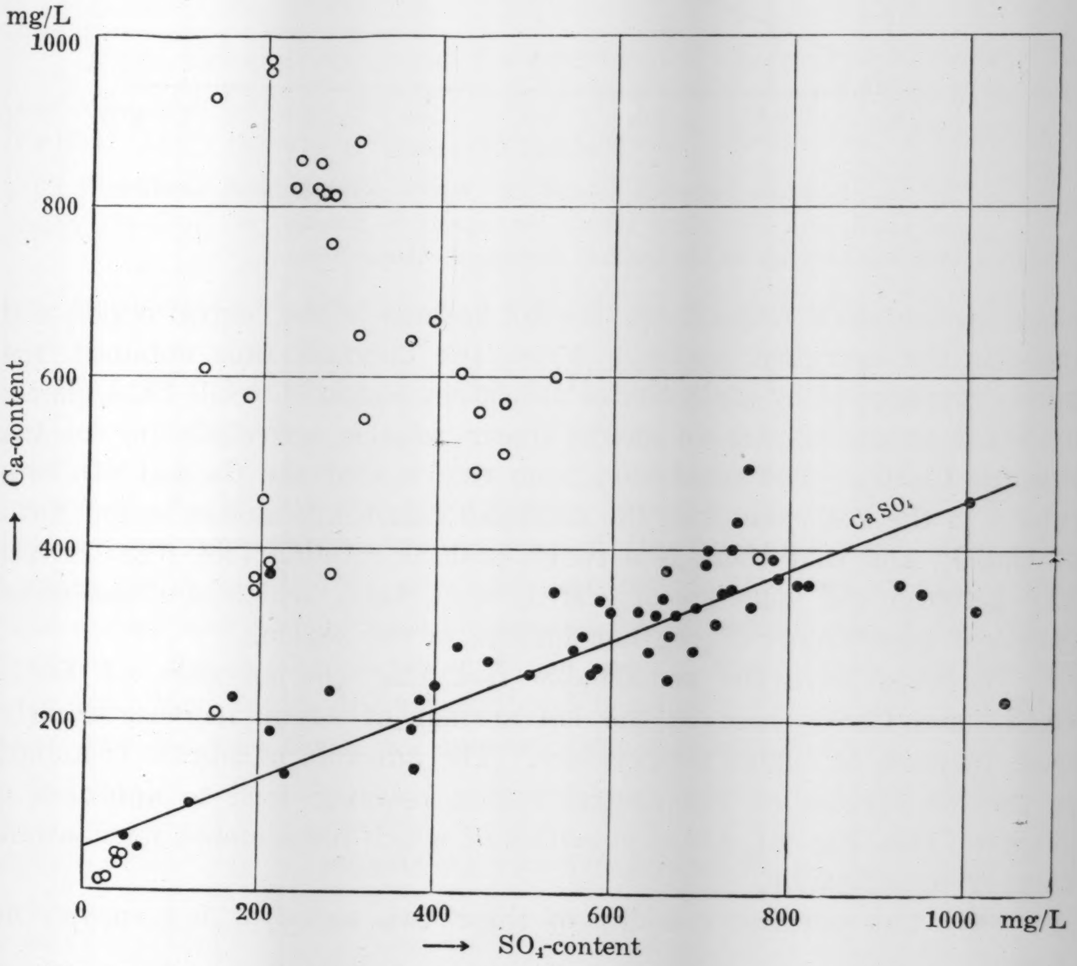

Fig. 12. Relation between Ca-content and SO_4-content of Atami hot springs.
○ hot spring of the central region.
● hot spring of the marginal region.

the residual amounts of Cl that correspond to the amounts of NaCl and the amounts of Ca corresponding to the amounts of $CaCl_2$ are shown in Fig. 13, from which it will be clearly seen that a rough linear relation exists between the amounts of NaCl and those of $CaCl_2$.

On plotting next the amounts of Ca as abscissae and the amounts of SO_4 as ordinates, we get Fig. 12, in which the plain circles and black circles show respectively the hot springs in the central region and those in the marginal region. From the diagram thus obtained, the points represented by plain circles are rather scattered, while those shown by black circles exhibit an almost linear relation, corresponding to the line for $CaSO_4$. The conclusion from this is that the Ca and SO_4 contained in the hot springs of the marginal region are almost in the form of $CaSO_4$, and that there is a rough positive relation (see Figs. 11 and 12) between the amounts of $CaSO_4$ and NaCl, which are the chief chemical constituents of the hot springs in the region.

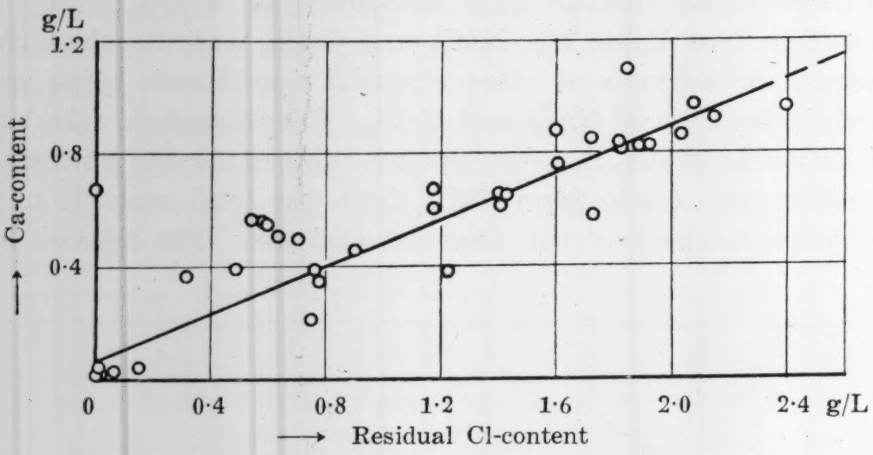

Fig. 13. Relation between Ca-content which correspond to amount of $CaCl_2$ and Cl-content which correspond to amount of NaCl of the hot springs in the central region of Atami town.

We thus have the remarkable fact that the amounts of NaCl, $CaCl_2$, and $CaSO_4$ held in the hot springs of Atami increase linearly with increase in orifice temperature. The amounts of silicate contained in the hot springs of the central region however tend to approach a constant (see Fig. 8), the explanation of which phenomenon must await further investigation.

(4) The physical meaning of these two series of hot springs in Atami.

The conclusion from the foregoing results is that two different series of hot springs exist in Atami and neighbourhood. The first series, to which the hot springs in the central region belong, has comparatively high temperature and contains moderate amounts of NaCl and $CaCl_2$, while the second series differs from it in having a low temperature and containing as its chief chemical constituents, relatively small amount of $CaSO_4$ and NaCl. The comparatively great depth of the hot springs is an additional feature of the second series.

The fact that hot springs of a character intermediate between the first and the second series are rare may be attributed to the characteristic properties of these two series and to the underground structure of the district.

The remarkable fact that the amounts of Cl increase with increase in orifice temperature in both series, and the existence of a simple linear relation between the amounts of NaCl and that of $CaCl_2$ in the first series, and between the $CaSO_4$ and NaCl contents in the second series, is very similar to the general conditions described in the previous paper[6].

As to the explanation of the phenomena, the prevalent theory that the cold underground water mixes with a hot spring in the superficial crustal layer, assuming that neither chemical change nor deposition of the materials accompany the mixing, seems the most probable in this case.

Then for the relational equation between the amounts of the chemical constituents of the spring x and orifice temperature θ, we get

$$x=\frac{(N-n)(1+\lambda)}{\theta_1-k\theta_0}\theta+\left[n-\frac{(N-n)(1+\lambda)\theta_0}{\theta_1-k\theta_0}\left\{1+\frac{k-1}{1+\lambda}\right\}\right],\quad \lambda=\frac{KS}{Vc\rho}. \qquad (1)$$

where θ_1, θ_0, $k\theta_0$ are the underground temperature of the original hot spring, air temperature, temperature of the cold underground water, N and n the amount of a chemical constituent dissolved in the original hot spring and that in the underground water respectively, V the volume output, ρ the density of water, c the specific heat, S the effective area for heat loss, and K the proportional constant.

For the first series we can estimate approximately

$$\theta_1 \geqq 180^\circ\mathrm{C}, \quad N \geqq 3{\cdot}34\ \mathrm{g/L\ of\ Cl},$$
$$k\theta_0 = 20^\circ\mathrm{C}, \quad n = 0{\cdot}08\ \mathrm{g/L\ of\ Cl}.$$

For the second series we also obtain

$$\theta_1 \geqq 98^\circ\mathrm{C}, \quad N \geqq 0{\cdot}7\ \mathrm{g/L\ of\ Cl},$$
$$33^\circ\mathrm{C} \leqq k\theta_0 \leqq 37^\circ\mathrm{C}, \quad 0 \leqq n \leqq 0{\cdot}06\ \mathrm{g/L\ of\ Cl}.$$

---

[6] T. FUKUTOMI, *Bull. Earthq. Res. Inst.*, **14** (1936), 259.

That the temperature of the mixed underground water in the second series is higher than that of the mixed underground water in the first series harmonises fairly well with the fact that the hot spring of the second series are deeper than those of the first series.

As to springs of the first series, the Cl contents of which are less than 1·7 g/L, a positive linear relation exists between the Cl contents and the orifice temperatures as just mentioned (see Fig. 7). In spring, the Cl contents of which are more than 1·7 g/L, the orifice temperature is always constant at about 100°C, displaying the phenomenon of a "Boiling spring". This may be attributed to loss of the excess heat from water of high temperature, which is below that of boiling point under high pressure at depth as latent heat of evaporation due to smaller pressure at the earth's surface. Before the boiling occurs at depth, we may assume that the linear relation $x=A\theta+B$ as shown in Fig. 7 between the Cl contents and the temperatures must be satisfied. The temperature of the original source of the hot spring can be roughly estimated as follows: Let m be the amount of Cl in the water at the orifice and l the latent heat of evaporation. We then get the approximate temperature θ' of the spring before boiling from the equation

$$\theta'=\frac{m-B\left(1-\frac{c}{l}100\right)}{m\frac{c}{l}+A\left(1-\frac{c}{l}100\right)} \tag{2}$$

Putting $c=1{\cdot}007$, $l=539{\cdot}1$ cal, $A=2{\cdot}01\times10^{-2}$, $B=-3{\cdot}12\times10^{-1}$, and taking for m the maximum value of m 4·1 g/L in the Atami hot springs, we get $\theta'=181$°C. According to measurements made by Prof. K. Honda and Prof. T. Terada[7] in 1906, the temperature of Suzukiya's well (No. 22 in Fig. 2) reached 140°C at 35 m depth. From recent measurements, Cl content and its temperature at the orifice of this well are 1·57 g/L and 94°C respectively. Since the temperature of a spring and the amount of its mineral constituents may vary more or less with lapse of time, old measurements of temperature are likely to differ from what they are today. But now in arriving at the temperature of the original source of springs of the first series, an actual measurement at 35 m depth, as already mentioned, may give, in approximation, a minimum of 140°C, in view of the fact that the Cl-content of Suzukiya's well is fairly less than that of the maximum value 4·1 g/L of the hot spring of first series. And with more accurate data now available we shall not be far wrong in estimating the temperature of the original source of hot springs of the first series to be not less than 180°C (as shown by our calculations). We thus have the remarkable fact that in the central region of the town there are layers near the surface with very high temperatures.

---

[7] K. HONDA and T. TERADA, *Publ. Earthq. Inv. Comm*, **22-B** (1906), 51.

Regarding the distribution of hot springs belonging to the first series, there are, as shown in Fig. 5, two areas, *A* and *B*, where their Cl contents are very large. These areas may be assumed to contain the outlets for the original source of the hot spring of the first series. According to geological investigations made by Messrs. Y. Ôtuka and H. Kuno[8], there are two faults in the district in question, the positions of which are shown in Fig. 5. Comparing the positions of these areas with those of the faults, we find interesting coincidences in the position of the northern area *A* and that of fault-*A*, and in that of the direction of the elongated axis of the southern area *B* and those of the faults. The hot water of the first series may therefore be regarded as having ascended from depths along these fissures.

As to the springs of the second series, although the hot water issues from depths of from 100 to 300 m, their sites are spread over a wide area in the town of Atami and neighbourhood. We cannot, however, at present positively indicate the position of the original source of the hot springs of the second series, so that the matter must be held in abeyance until further investigations have been made.

IV. Conclusions.

There is no doubt of the existence in the town of Atami and neighbourhood of two series of hot springs of entirely different character—the one characterised by high temperature, large amounts of chloride, and ascent of water along fissures from an origin of much greater depth than the latter, and the other, differing from the preceding in its relatively low temperature, moderate quantity of sulphate and the availability of hot springs of this series over a wide area, although the relation between the two is not so simple as this. It is also worthy of note that in these two series, the relation between their chemical constituents and temperature tends to obey Deville's law[9] with respect to the chemical nature of volcanic fumaroles.

There seems to be little doubt that, for identifying these systems of hot springs in a locality, curves showing the relation between the chemical constituents, specially, the Cl content and the orifice temperature, are very useful, so that the line of investigation here adopted promises to be of aid in studies of hot springs if done with more ample data and more refined methods.

---

[8] Y. Otuka and H. Kuno, *loc. cit.*

[9] M. Ch. Saint-Claire-Deville, *Bull. Soc. G ol. France*, **14-II** (1856~57), 257. (F. Wolff, *Handbuch der Geophysik*, Bd. III, Lief. 1, 282.)

In conclusion, the writer expresses his cordial thanks to Mr. H. Mizukosi and Mr. M. Ôtuka, members of the Atami Hot Spring Owners' Association, for their numerous courtesies, and to the owners of the hot springs in Atami for their kind permission to make the various measurements. Further, the writer wishes to express his thanks to Mr. Z. Huzii and Mr. M. Komono, assistants in the Mitsui Geophysical Observatory, for valuable aid rendered in carrying out the chemical analyses.

---

12. 伊豆，熱海溫泉に就て

三井地球物理研究所 福富孝治

古來熱海溫泉は我國でも最も有名な溫泉の1に數へられ，其泉源として大湯間歇泉，清左衞門湯，法齋湯，風爐湯，瓦湯，左次郎湯，野中湯，伊豆山走湯等は就中古くから有名であつた(Fig. 1). 近年溫泉掘鑿の技術の長足の進歩に依つて可成りの深さの掘抜井戸が得られる樣になつたので，今日では（Fig. 2）に示す如く熱海町及其近郊に 180 にも及ぶ溫泉穿井が存在して居る．最近筆者は之等の中 82 の溫泉，5 の普通井戸の採水，測溫を行ひ，主要なる化學成分として Ca，Cl，SO_4，SiO_2，Alkalinity（$CaCO_3$ で便宜上表した）の分析を行つた (Table I). 之等の結果に就ての報告である．其概括を述べれば次の樣である．

1. 溫泉穿井の深さは大體溫泉の湧出する深さを示すと考へられるが，其分布は（Fig. 3）に示す如く町の中心附近並に伊豆山の一部で極めて淺く海面よりも高い所もある．古來の溫泉は何れも此部分に存在する．此部分から遠ざかると段々深くなつて町の南方，又は北西方では 200〜300 m にも達する．
2. 湧出溫度も町の中心附近が最も高く 100°C に達し（Fig. 4)，所謂沸騰泉の現象を呈する．此處を遠ざかると溫度低下し南方では 40°C 以下の部分もある．
3. 鹽分の分布（Fig. 5）も稍々溫度の分布と相似であつて中心地附近に Cl が 4 g/L 以上の含有量で極大を示す 2 の面積が存在する．硫酸鹽の分布 (Fig. 6) は鹽分と略々逆の關係を示す．
4. Cl 含有量と湧出溫度との量的關係（Fig. 7）から，熱海溫泉には性質の異つた 2 の系統の溫泉が存在する事が判つた．之は Ca 含有量と鹽分含有量との關係 (Fig. 11)，Ca 含有量と SO_4 含有量（Fig. 12)，SiO_2 含有量と鹽分含有量との關係等（Fig. 8, Fig. 9, Fig. 10）からも推定に難くない．尙內務省東京衞生試驗所の分析に依る熱海溫泉の分析結果 (Table II)

に徵しても明である．卽中心地の溫泉では NaCl と $CaCl_2$ とが其主成分であるが，周緣の溫泉では $CaSO_4$ と NaCl 等が主成分である．尙中心附近に湧出する第1系統の溫泉では其主成分 NaCl と $CaCl_2$ の量の間に直線的關係があり，周緣の第2系統の溫泉でも其主成分 $CaSO_4$ と NaCl の量の間に略々正の相關が伺はれる．

5. 第1，第2各々の溫泉系統では其溫度と鹽分含有量，又は主成分間に直線的關係が存在する事が判つたが，此說明としては從來の硏究と同樣に1の源溫泉と地下水との混合結果であると考へると最も都合良く說明される．然して第1系統の源溫泉は 180°C 以上の溫度を有し，中心附近の地下より湧出する事が判つた．第2系統の源溫泉は 98°C 以上の溫度を有する．混入する地下水の溫度は第2系統のもの 33°C で第1系統のものが略々 20°C であるに比較して可成り溫度が高いが，溫泉穿井の深さが第2系統では第1系統に比較して遙に深い事を考へると都合が宜しい．又第2系統の溫泉は 200～300 m の深さに掘ると可成りの廣範圍の面積から湧出するが，第1系統の溫泉は極限された小區域にのみ湧出する事，然かも此部分が斷層と密接な關係を持つ事から，恐くは第1系統の溫泉は構造線に沿ひ地下深所より湧出するものであらうと推定した．

13. The Sengataki Thermal Spring and Underground Mineral Water at the Foot of Volcano Asama.

By Takeshi MINAKAMI,

Earthquake Research Institute.

(Read Sept. 15, 1936.—Received Dec. 21, 1936.)

1. Introduction.

T. Fukutomi[1], quite recently, dealt with the geophysical and geochemical properties of some of the thermal springs in the Idu peninsula. His results elucidate the various interesting relations that hold between the crustal movements, meteorological elements, the orifice temperatures, and the volume of water, while T. Nomitsu[2], who studied the Beppu thermal springs, Kyusyu, has discussed the problem of distribution of the original sources and their geophysical properties. According to T. Fukutomi, the water table of the Rendaidi thermal spring in south Idu underwent a change on the occasion of the earthquake of July 11, 1935. In the light of this phenomenon, it will not be unresonable to suppose that in the neighbourhood of Volcano Asama as well, thermal springs and underground water will undergo changes as the result of volcanic activities.

Information supplied by the villagers living at the foot of the volcano urged us to investigate the thermal springs and underground waters in the neighbourhood of this volcano, Asama, which although very quiet up to 1934, became the scene of violent explosions in 1935 and 1936.

Of the thermal and mineral springs found near the volcano, the writer specially studied the Sengataki thermal spring and the Sengataki underground water by continuous observations of their orifice temperatures and volume of issue. These two original sources of springs are situated in a deep valley, at the distance of 6 km southeast from the crater. Our main object was to ascertain if these springs undergo any change with activities of the volcano, seeing that the results of Noguti's[3] studies are based on too small a number of observations.

---

[1] T. FUKUTOMI and M. NAKADA, *Bull. Earthq. Res. Inst.*, **13** (1935), 616; **14** (1936), 259.

[2] He reported at the annual meeting of Physico-Mathematical Society of Japan in 1936.

[3] K. NOGUTI, 日本化學會誌, **56** (1935), 1495; **57** (1936), 920.

2. Distribution of Thermal and Mineral Springs.

In the neighbourhood of volcano Asama, especially at Karuizawa, the popular summer resort, attempts have been made from time to time to locate a thermal spring with high temperature, with which object borings were frequently resorted to, particularly as the thermal springs already known, the Sengataki, Hosino, Siotubo, and Kosé springs, are all under 35°C in orifice temperature.

The topographical distribution of the original sources of these thermal springs and underground water is shown in Fig. 1. As will be seen from Fig. 1, cold springs have their origins on the slopes of volcano, where the water table cuts the surface of the ground. Springs 5, 7, and 8 are the sources of the Zyabori, the Nigori, and the Yukawa rivers.

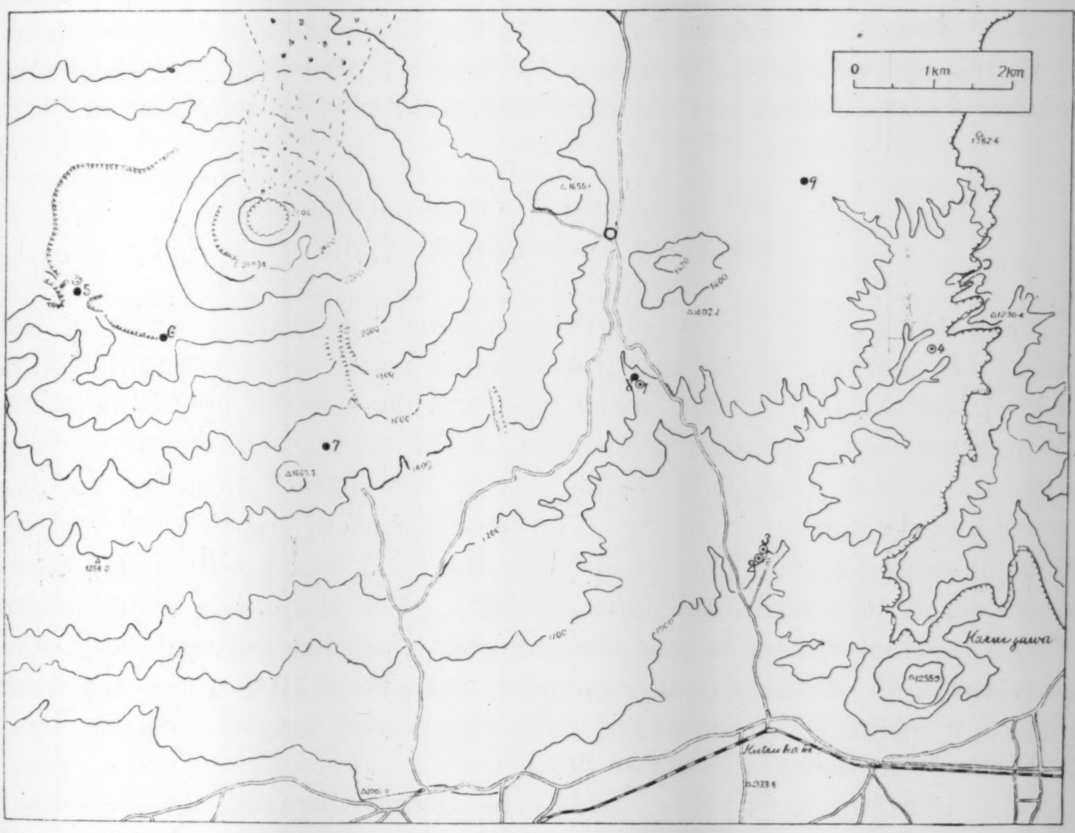
0
1km
2km
△1382.6
9
△1655
1420
1400
△1402.2
△1230.4
4
5
6
2000
1800
1600
1400
8
1
7
△1667.3
1200
△1254.0
1100
1000
3
2
Karuizawa
△1255.9
Kutsukake
△1001.9
△933.8

Fig. 1

◉ thermal spring. 1. Sengataki. 2. Hosino. 3. Siotubo. 4. Kosé.

● cold spring.

In order to make clear the relation between the situation of spring origins and their heights above sea-level, an E–W section through

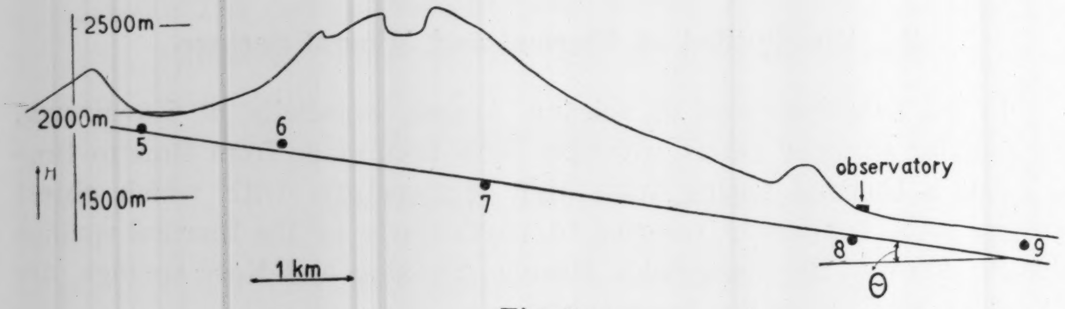

Fig. 2.

E-W section of volcano Asama. H: height above sea-level.

the crater is shown in Fig. 2. The heights of the origins, change linearly toward E–W derection, that is, the water table inclines by about 5° to the east side of the volcano. H· Tsuya4), Who studied geologically volcano Asama pointed out the same fact in the field investigation in 1932.

3. The Sengataki Thermal Spring and Sengataki Underground Water.

Observations of the orifice temperature and rate of flow of the Sengataki thermal spring and underground water were begun in May, 1934. The thermal spring, which issues from a depth of 100 m below the surface of the ground is brought to the surface by means of iron pipe, for which reason, in its passage to the surface from the bottom, no cold water can mix with it. The temperature of the thermal springs were measured in the pipe 10 m below the head water with a Hg thermometer, at first daily and later weekly. For the orifice temperature of the thermal spring, a gas thermometer recorded automatically, and since the bulb of the gas thermometer was placed 10 m under the head water by means of a connection tube, the record agreed with the temperature 10 m below the water head.

In addition, since May, 1934, the temperature of the Sengataki underground water which issues near the Sengataki thermal spring and the atmospheric temperature at the same time were observed, sometimes personally, and at other times by means of an automatic apparatus.

Table II and Fig. 3 show the temperatures of the Sengataki thermal and cold springs, atmospheric temperature, and an outline of volcanic activities with their dates and times of observation, from which it will

---

4) H. TSUYA, Reported at the meeting of the Earthquake Research Institute on April 18, 1932.

Table I.

Date	Time	Atmospheric temperature	Orifice temp. of Sengataki thermal spr.	Temp. of Sengataki underground water	Δy	Remark
1934	h m	°C	°C	°C	°C	
July 11	10 30	20·3	32·5	14·0	0·0	Since autumm of 1931, the volcano had been very inactive, with neither eruption of any violence nor volcanic micro-earthquake.
13	10 30	14·5	33·0	13·5	+0·5	
14	10 20	16·5	33·2	13·3	0·0	
16	11 30	15·1	33·5	13·7	+0·6	
17	10 00	18·2	33·0	14·2	+0·6	
18	10 00	15·7	32·5	13·5	+0·2	
19	11 00	25·6	33·3	14·5	−0·4	
20	11 15	24·0	33·0	15·0	+0·4	
21	10 25	18·0	33·0	14·0	+0·4	
22	10 15	22·2	33·2	14·2	−0·1	
23	10 15	21·5	33·3	14·5	+0·3	
24	10 30	19·0	33·0	14·4	+0·7	
25	9 45	18·8	33·0	14·5	+0·8	
26	10 35	15·6	33·0	13·6	+0·4	
27	10 40	19·2	33·2	14·0	+0·2	
28	10 40	22·4	33·3	14·5	+0·9	
29	10 30	20·5	33·3	14·0	0·0	
30	10 50	18·0	33·1	14·5	+0·9	
31	11 05	17·5	32·6	13·1	−0·4	
Aug. 1	10 15	18·9	33·1	14·0	+0·3	
2	11 20	19·0	33·3	14·3	−0·4	
3	16 00	22·0	33·3	14·5	+0·3	
4	16 25	21·0	33·5	14·2	+0·1	
5	17 00	18·4	33·4	14·0	+0·4	
10	14 00	21·5	33·3	14·5	+0·3	
21	17 00	18·5	33·4	14·0	+0·4	Volcanic micro-earthquakes were observed for the first time on January 2, 1935, and thereafter.
28	10 00	23·0	33·4	14·7	+0·3	
Sept. 4	15 30	16·5	33·3	14·5	+1·2	
11	16 00	16·0	33·4	13·7	+0.5	
18	14 00	15·5	33·4	13·5	+0·4	
25	16 40	11·7	33·4	12·5	0·0	
Oct. 2	16 30	9·2	33·3	12·0	−0·1	
11	15 00	13·4	33·3	12·5	−0·3	
31	14 00	8·7	33·5	10·5	−1·5	
Nov. 7	15 00	10·0	33·3	11·5	−0·7	

(*to be continued.*)

Table I. (*continued.*)

Date	Time	Atmospheric temperature	Orifice temp. of Sengataki thermal spr.	Temp. of Sengataki underground water	Δy	Remark
	h m	°C	°C	°C	°C	
1934						
Nov. 13	16 00	1·5	33·3	10·5	−0·3	On April 20, 1935, the violent explosion occurred.
1935						
Aug. 24	15 25	21·0	33·2	14·5	+0·4	On May 5, 11, 15, 16, 21, 22 and 28, the remarkable explosions occurred.
Sept. 1	10 10	15·0	33·2	13·5	+0·4	
7	15 30	21·2	33·2	14·0	−0·1	
15	9 25	11·2	33·2	12·8	+0·4	
27	9 45	16·5	33·2	13·0	−0·3	During April and May the volcano was unusually active, quieting down from the early part of June, but resuming its activities in August.
Oct. 9	13 20	13·0	33·2	11·0	−1·7	
20	15 00	12·8	33·2	11·5	−1·2	
Nov. 1	8 40	5·5	33·1	11·1	−0·3	
15	9 30	4·5	33·2	12·0	+0·7	
26	8 20	3·0	33·1	11·0	0·0	On August 4, 17 and 28, the remarkable eruptions occurred.
Dec. 16	13 40	0·1	33·2	10·0	−0·3	
24	11 05	4·0	33·0	10·5	−0·7	On September 19, and November 7 the violent explosions occurred.
31	11 45	1·5	33·1	10·6	−0·2	
1936						
Jan. 7	11 15	−2·5	33·1	10·5	+0·4	
14	11 20	−1·2	33·2	10·5	+0·2	
21	13 50	−4·0	33·2	9·9	+0·1	
27	14 20	−6·5	33·2	9·5	+0·1	
Feb. 4	11 50	−7·7	33·3	9·0	−0·2	
9	12 45	1·5	33·4	10·6	−0·2	
16	15 00	0·5	33·2	10·1	−0·5	The explosions occurred frequently in February and March in 1936.
25	11 55	−2·5	33·2	10·5	+0·4	
Mar. 2	10 40	−4·5	33·2	9·9	+0·2	
9	13 00	−3·0	33·2	10·3	+0·3	
16	10 40	1·0	33·3	11·0	+0·3	
23	12 05	1·0	33·3	11·2	+0·5	
30	13 50	−3·0	33·2	10·2	+0·2	
Apr. 6	10 50	15·2	33·3	13·0	−0·1	
13	10 50	1·5	33·3	10·5	−0·3	
20	12 00	15·6	33·3	13·5	+0·3	
26	14 15	13·5	33·3	12·2	−0·6	
May 4	15 15	15·3	33·3	12·6	−0·5	
11	8 35	14·5	33·3	12·5	−0·5	
18	9 10	12·0	33·3	12·4	−0·1	

(*to be continued.*)

Table I. (*continued.*)

Date	Time	Atmospheric temperature	Orifice temp. of Sengataki thermal spr.	Temp. of Sengataki underground water	Δy	Remark
1936	h m	°C	°C	°C	°C	
May 22	16 15	14·3	33·2	12·2	−0·7	
30	9 00	11·0	33·2	12·0	−0·4	
June 6	7 40	10·5	33·2	12·4	+0·1	
13	8 45	16·4	33·2	13·5	+0·2	
20	9 00	19·3	33·2	13·0	−0·7	
27	12 50	18·8	33·2	13·0	−0·7	
July 4	10 15	17·0	33·2	13·3	−0·1	
12	14 00	20·5	33·2	12·8	−1·2	
19	10 00	25·2	33·1	13·0	−1·3	
26	14 07	25·2	33·2	13·0	−1·3	
Aug. 2	10 30	21·0	33·2	12·5	−1·3	
18	13 25	25·2	33·2	12·8	−1·9	Until the end of 1936, explosions sometimes occurred.
Sept. 1	10 50	22·8	33·2	13·2	−1·1	
17	13 00	13·0	33·2	12·0	−0·7	
Oct. 1	8 15	11·5	33·1	12·0	−0·4	

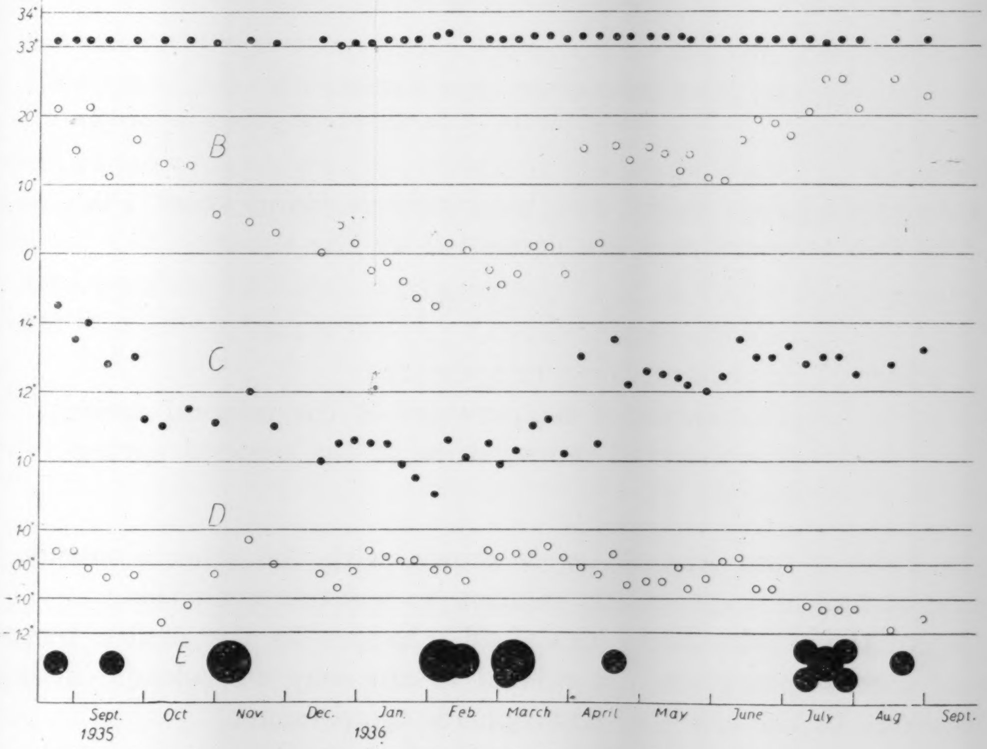

Fig. 3. A; Orifice temperature of Sengataki thermal spring.
B; Atmospheric temperature.
C; Temperature of Sengataki Underground water.
D; $\Delta y = y_o - y_c$.
E; Explosion.

be seen that the temperature of the thermal spring showed no changes, daily nor annually, nor any other changes during the volcano's inactive period of 1934 nor in its active periods in 1935 and 1936, whereas Sengataki, a cold spring, showed 15°C and 10°C as the maximum and minimum temperatures.

As will be seen from Fig. 4, the orifice temperature of the Sengataki cold spring and the atmospheric temperature changes in parallel, the rate of variation in the two temperatures being about 1/6.

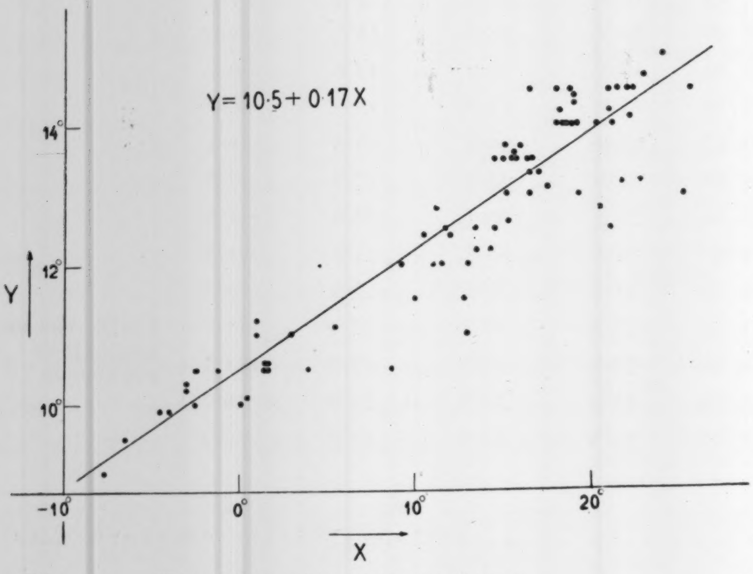

Fig. 4. X; Atmospheric temperature.
Y; Temperature of Sengataki underground water.

The two temperatures are connected by the equation

$$y_c = 10{\cdot}50 + 0{\cdot}17x,$$

where x = atmospheric temperature,
y_c = calculated temperature of the mineral spring,
y_o = observed temperature of the mineral spring,
$\Delta y = y_o - y_c$.

In Table I and Fig. 3, Δy is shown with the other elements, but we cannot find any systematic relation to volcanic activities.

From the results above described, changes in the orifice temperature of a cold spring are not related in any way to volcanic activities but are due to the effect of atmospheric temperature.

As to the Hosino, Siotubo, and Kosé thermal springs, no changes were observed either in the orifice temperature or in the rate of flow.

4. Conclusion.

Although the writer had expected that terrestrial heat in the vicinity of a volcano would change with volcanic activity, as the result of which the temperature of thermal springs would be affected by some variation in volcanic activity, the present observations gave a negative answer.

In his papers on the Rendaidi and other thermal springs, T. Fukutomi[5] concluded that changes in the orifice temperature of thermal springs are due to changes in the intermixture of underground water, escape of heat by conduction, and other causes. The results of our present observations in no way contradict his theory.

13. 淺間山麓千ヶ瀧温泉さ地下水

地震研究所　水上　武

1） 淺間火山の火口より 15 粁以内に湧出する温泉さして千ケ瀧，小瀬，星野，鹽壺の諸温泉を擧げる事が出來る．此等の温泉中特に火口に最も近い千ケ瀧温泉に就き昭和9年5月より，昭和 11 年 9 月迄，湧出温度，湧出量の觀測を行つた．

淺間火山は昭和9年は極めて靜穩であつたが昭和 10 年4月以來度々爆發した．火山の靜穩，活動兩期に於いて，山麓温泉に何等かの異常を期待されたが，湧出量，湧出温度共に變化が現れなかつた．

2） 淺間火山附近の地下水が地表を切る諸點を調査して見るさ地下水面は火山の西側から東側に向つて約 5° の傾斜をしてゐる事が判つた．この事實は津屋博士の調査さ一致する．

---

[5] T. FUKUTOMI, *loc. cit.*

14. *Statistic Investigations of Earthquake Frequencies.*

By Win INOUYE,

Earthquake Research Institute.

(Read April 21, 1936.—Received Dec. 21, 1936.)

1. *Introduction*

The writer in his previous paper,[1] investigated how earthquake frequencies coincide with or deviate from the frequency distributions in cases of rare events, or in those of independent events with very small probabilities of occurrence. He further tried to explain such cases as deviate from the law of rare events (the Poisson's law) by assuming that the mean earthquake frequency had varied from time to time during the period of observation instead of being constant throughout the period.

In the following, more fully investigations are made in quantitative sense.

2. The probability of r occurrences of a certain event, the probability of occurrence of which is p, in n independent trials is given by

$$P(r)=\frac{n!}{(n-r)\,!r!}\,p^r q^{n-r},$$

where $q=1-p$.

If n is very Large and p very small, and np, the product of the two, is finite, the above equation can be transformed into

$$p\leqslant 1,\ n\geqslant 1,\ pn=m,$$

$$P(r)=e^{-np}\frac{(np)^r}{r!}=e^{-m}\frac{m^r}{r!}\quad \text{(the Poisson's formula)},$$

where m is the mean frequency.

Although Poisson's formula differs considerably from the Gaussian law of error distribution provided m is small, it approaches the Gaussian as m becomes larger.

The writer thinks it is quite in order to compare earthquake frequencies with Poisson's formula, since there is a possibility of a great number of earthquakes occuring at certain epochs, although a few earthquakes do occur at ordinary times.

---

[1] W. INOUYE, *Bull. Earthq. Res. Inst.*, **10** (1932), 43.

The writer has shown in his previous paper that the probability function of earthquake frequencies may be expressed by

$$P(r)=\frac{1}{n_1}e^{-m_1}\frac{m_1^r}{r!}+\frac{1}{n_2}e^{-m_2}\frac{m_2^r}{r!}+\cdots\cdots+\frac{1}{n_n}e^{-m_n}\frac{m_n^r}{r!},$$

where $\frac{1}{n_1}+\frac{1}{n_2}+\cdots\cdots+\frac{1}{n_n}=1.$

It will be seen from the above equation that the mean frequency, about which the actual frequencies fluctuate, does not remain constant for any long period but varies from time to time.

3. The earthquake frequencies will now be considered in detail, but before doing so, we shall consider K. Pearson's procedure.

The Gaussian frequency curve is expressed by

$$y=\frac{1}{\sqrt{2\pi}\sigma}e^{-\frac{(x-a)^2}{2\sigma^2}}.$$

K. Pearson, in generalizing this equation into the form

$$\frac{1}{y}\frac{dy}{dx}=\frac{x-a}{f(x)},$$

writes,[2] "We may suppose $f(x)$ expanded in a series of powers of x and we stop at x^2, then our differential equation is of the form

$$\frac{1}{y}\frac{dy}{dx}=\frac{x-a}{c_0+c_1x+c_2x^2}$$

and we need only $\beta_1=\mu_3^2/\mu_2^3$ and $\beta_2=\mu_4/\mu_2^2$, where μ_2, μ_3, μ_4 are the second, third, and fourth moment coefficients about the mean.

If we take the form $\frac{1}{y}\frac{dy}{dx}=\frac{x-a}{c_0}$, we reach the Gaussian, in which each contributory cause-group is independent, and if the number of groups be not very large, each cause-group is of equal valency and contributes with equal frequency results in excess and in defect of its mean contribution. If we take $\frac{1}{y}\frac{dy}{dx}=\frac{x-a}{c_0+c_1x}$, then each contributory cause-group is still of equal valency and independent, but does not give contribution in excess and defect of equal frequency. Finally if we take $\frac{1}{y}\frac{dy}{dx}=\frac{a-x}{c_0+c_1x+c_2x^2}$, then contributory cause-groups are not of equal valency, they are not independent, but their results correlated, and further contributions in excess and defect are not equally probable. The use of this form $\frac{1}{y}\frac{dy}{dx}=\frac{x-a}{c_0+c_1x+c_2x^2}$ was adopted to allow of this wide generalisation of the Gaussian hypothesis."

---

[2] K. PEARSON, Table for Statisticians and Biometricians, I, lxi.

According to the value of the criterias β_1, β_2 and

$$K_2=\frac{\beta_1(\beta_2+3)^2}{4(4\beta_2-3\beta_1)(2\beta_2-3\beta_1-6)},$$

there are eleven types of frequency curves. Any arbitrary frequency curve may belong to one of these types, but it frequently happens that the given frequency curve may be represented by several types in the same way, and there is no physical meaning to any given frequency curve expressed by one of these types.

The data of earthquake frequencies are as follow:

1) The strong earthquakes that occurred in Japan and its vicinity during the 14 years from 1912 to 1925, taken from the table[3] published by the Central Meteorological Observatory of Japan.

2) The Itô earthquake swarms that occurred between Feb. 24 and April 10, 1930, taken from the report[4] based on the records obtained instrumentally at Misaki.

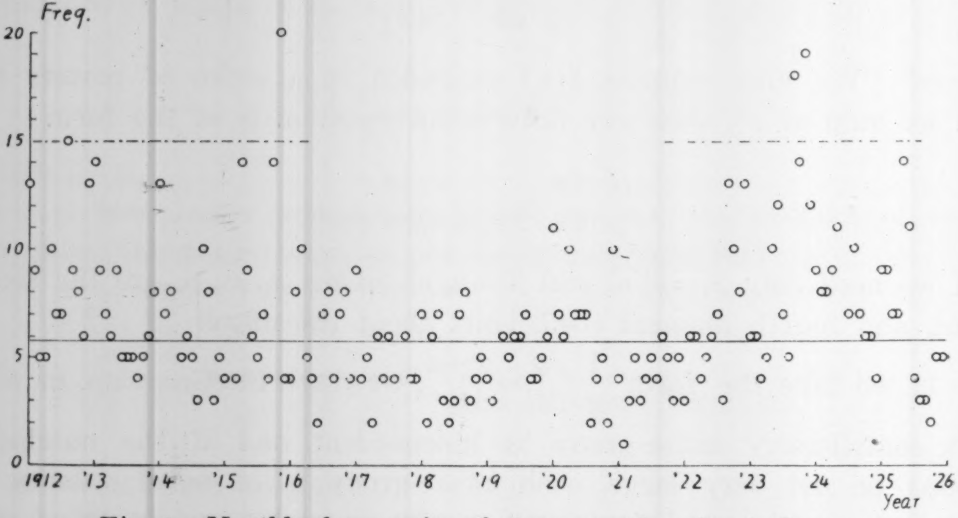

Fig. 1. Monthly frequencies of strong earthquakes in Japan represented chronologically.

---

[3] *Kensin-Jihô*, **2** (1926), 87.

[4] *Jisin*, **2** (1930), 281.

3) The Asama volcanic earthquakes, taken from the report of Prof. F. Omori.[5)]

The monthly frequencies of strong earthquakes in Japan are shown in Table 1, and chronologically in Fig. 1.

The frequency distribution is shown in Fig. 2, with frequency curve as calculated with Poisson's formula.

Although the actual frequency curve diverges systematically from the calculated curve, upon considering only the period of 6 years from 1916 to 1921, we find that the earthquake frequency distribution agrees fairly well with the theoretical curve calculated with Poisson's formula as shown in Fig. 3. Moreover, if we divide Japan and its vicinity

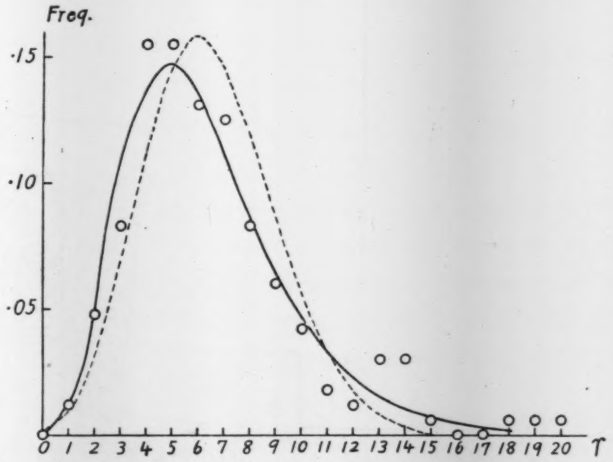

Fig. 2. Monthly frequencies of strong earthquakes in Japan.

Circle: Observed monthly frequencies.

Dotted line: Frequency curve calculated with Poisson's formula.

Full line: $\varphi(r)=\dfrac{1}{\sqrt{2\pi}\,0{\cdot}37(2+r)}e^{-\frac{[\log(2+r)-2{\cdot}06]^2}{2(0{\cdot}37)^2}}$.

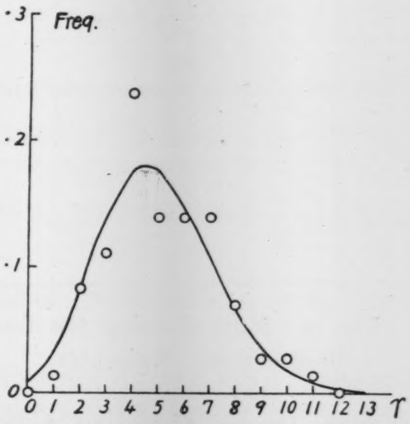

Fig. 3. Monthly frequencies of strong earthquakes in Japan during the period from 1916 to 1921.

Circle: Observed frequencies.

Full line: Frequency curve calculated with Poisson's formula.

---

5) F. Omori, *Bull. E.I.C.*, **6** (1912~14); **7** (1914~19).

into four regions as shown in Fig. 4, the frequency distributions (10 a day, monthly, and bimonthly) in region *a* are also satisfactorily expressed by Poisson's simple formula as will be seen from Fig. 5.

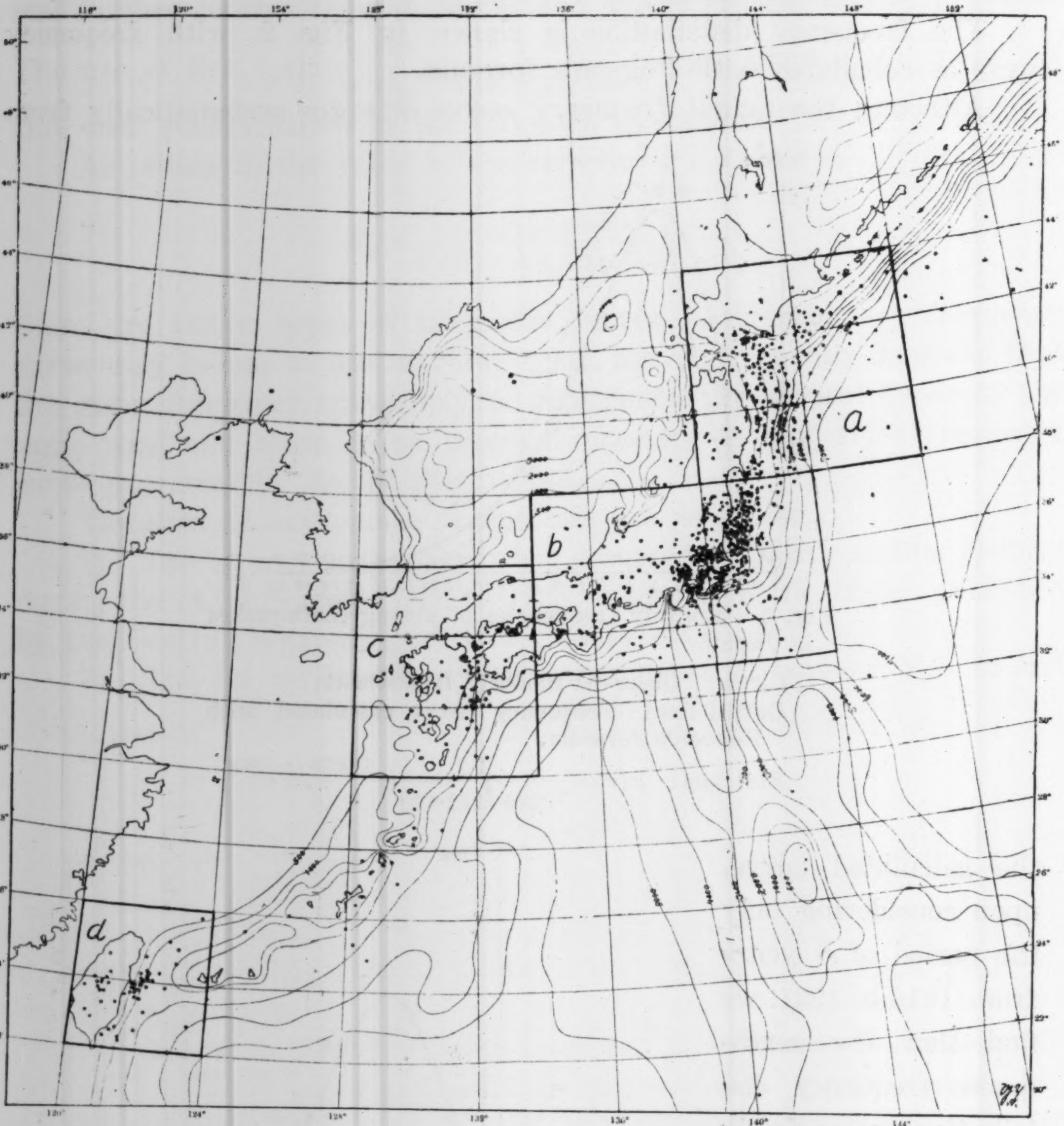

Fig. 4. Map showing the four regions seismically active.
Black circle: Epicenter.

These facts show that, in these cases, the earthquakes occurred independently of one another. Moreover, they suggest that, in general, even such cases as exhibit more complex forms of frequency distribution could be decomposed into elementary Poisson types.

We may assume, therefore, that in a general case, the mean frequency *m* in Poisson's formula is not constant throughout the period under consideration, but varies from time to time, that is several epochs, each of which has a certain mean freyuency m_i, mixed together in the period.

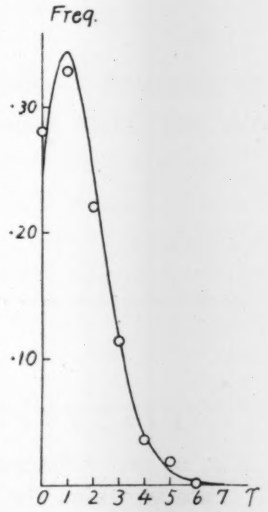

Fig. 5_1. Monthly frequencies of earthquakes in region a.

Circle: Observed frequencies.
Full line: Frequency curve calculated with Poisson's formula.

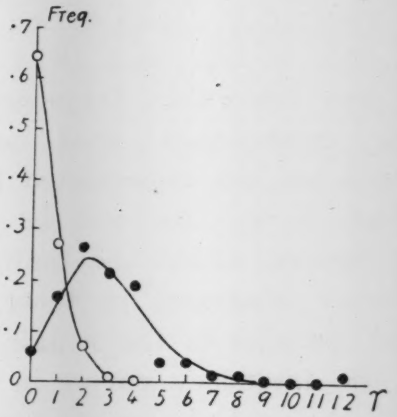

Fig. 5_2. Frequencies of earthquakes in region *a*.

Circle: 10 a day frequencies.
Black circle: Bimonthly frequencies.
Full lines: Frequency curves calculated with Poisson's fromulas.

We shall now let the observed frequencies of r_1, r_2, $\cdots\cdots$ r_n occurrences be $W(r_1)$, $W(r_2)$, $\cdots\cdots$ $W(r_n)$.

By putting these values into Poisson's formula, we obtain the mean frequencies m_1, m_2, $\cdots\cdots$ m_n, each satisfying the corresponding equation

$$e^{-m_1}\frac{m_1^{r_1}}{r_1!}=W(r_1),\ e^{-m_2}\frac{m_2^{r_2}}{r_2!}=W(r_2),\ \cdots\cdots\ e^{-m_n}\frac{m_n^{r_n}}{r_n!}=W(r_n).$$

The $m_i s$ thus obtained are next represented graphically as the function of $r_i s$.

If the observed frequency distribution agrees with Poisson's formula, all the m_i become equal to one another and equal to a constant that is the mean frequency throughout the period as follows:

$$m_1=m_2\ \cdots\cdots\ =m_n=m,$$

and the $m-r$ diagram becomes a straight line parallel to the r axis. For example, the $m-r$ diagram is shown in Fig. 6 for the case in which the frequency curve is represented by Poisson's formula ($m=4{\cdot}3$).

The $m-r$ diagrams for the monthly frequencies of the strong earthquakes that occurred in Japan during the period from 1916 to 1921, and 10 a day, monthly, and bimonthly frequencies of the strong earthquakes that occurred in region a are also represented graphically in Figs. 7, 8. As will be seen from these figures, within the limit of errors, the $m-r$ diagrams in these cases are almost parallel to the r axis, and show that the frequency curves in these cases might be satisfactorily expressed by Poisson's formula.

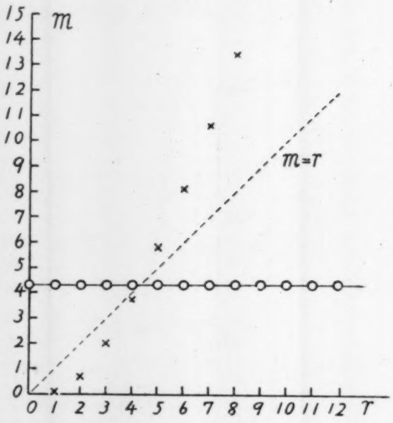

Fig. 6. $m-r$ diagram for the case in which the frequency curve is represented by Poisson's forumla ($m=4{\cdot}3$).

Next, if epochs, each of which have a certain mean frequency of earthquake occurrence, are mixed together, the frequency curve may be expressed by

$$W(r)=\frac{1}{n_1}e^{-m_1}\frac{m_1^r}{r!}+\frac{1}{n_2}e^{-m_2}\frac{m_2^r}{r!}+$$

$$\cdots\cdots+\frac{1}{n_n}e^{-m_n}\frac{m_n^r}{r!}.$$

By putting this equation into Poisson's formula

$$e^{-m}\frac{m^r}{r!}=W(r),$$

and solving it, we get the $m-r$ relation

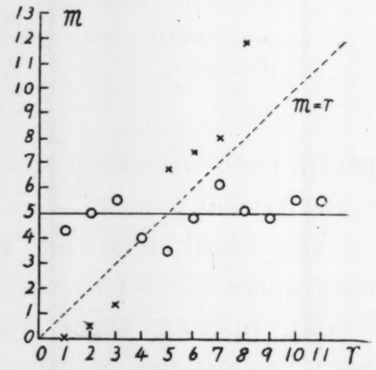

Fig. 7. $m-r$ diagram for the monthly frequencies of the strong earthquakes that occurred in Japan during the period from 1916 to 1921.

By assuming various forms for function $W(r)$, we get various theoretical $m-r$ diagrams.

Then upon comparing any actual $m-r$ diagram with these theoretical $m-r$ diagrams, it will be possible to deduce function $W(r)$ which represents the observed frequency distribution.

We shall first take the case in which the mean frequency increases temporarily during the period under consideration, and assume for example that the frequency function is of the form

$$W(r)=\frac{10}{11}e^{-6\cdot0}\frac{6\cdot0^r}{r!}+\frac{1}{11}e^{-15\cdot0}\frac{15\cdot0^r}{r!}.$$

The $m-r$ diagram in this case is showm in Fig. 9, from which it will be seen that the diagram assumes a nearly straight line parallel to the r axis, provided r is small, that is, m_i is nearly constant; but m_i increases rapidly after a certain large value of r.

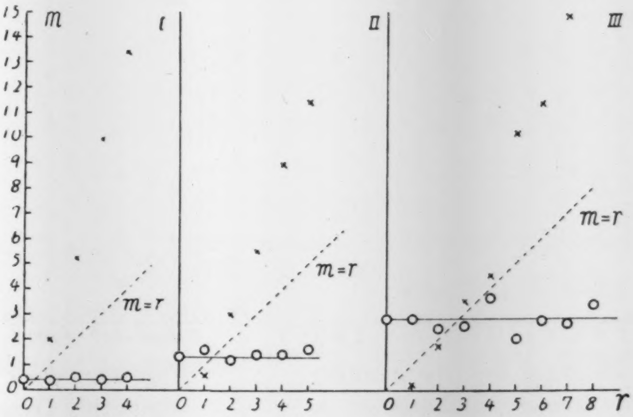

Fig. 8. $m-r$ diagrams for the strong earthquakes that occurred in region a.
I: 10 a day frequencies.
II: Monthly frequencies.
III: Bimonthly frequencies.

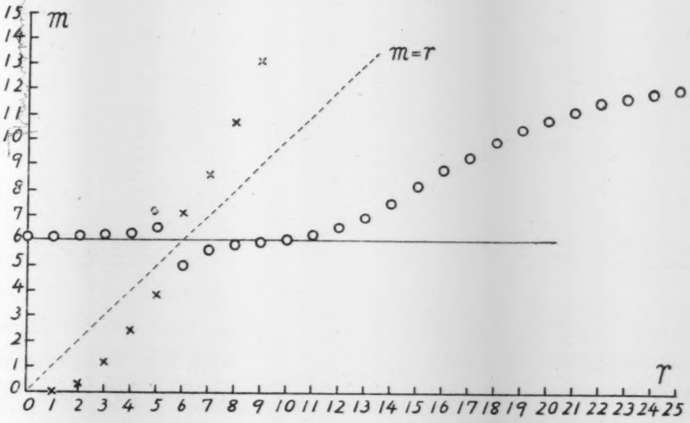

Fig. 9. $m-r$ diagram for the case in which the frequency function is of the form,

$$W(r)=\frac{10}{11}e^{-6\cdot0}\frac{6\cdot0^r}{r!}+\frac{1}{11}e^{-15\cdot0}\frac{15\cdot0^r}{r!}.$$

The $m-r$ diagrams for the case of earthquakes for the whole of Japan and of regions b, c, and d are shown respectively in Figs. 10–13. All these diagrams show that the frequency curves for these cases belong in the above category. The observed frequency curves and the theoretical curves calculated on this assumption are shown respectively in Figs. 14–17.

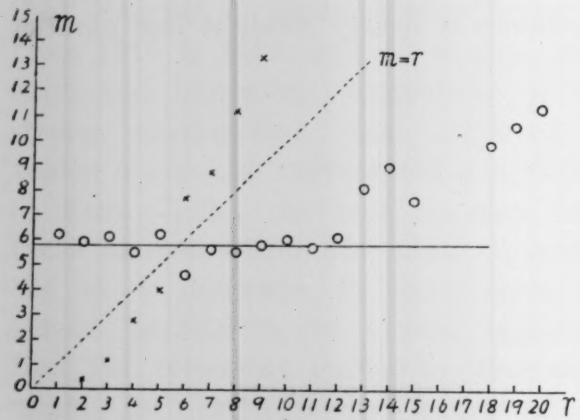

Fig. 10. $m-r$ diagram for the monthly frequencies of strong earthquakes in Japan.

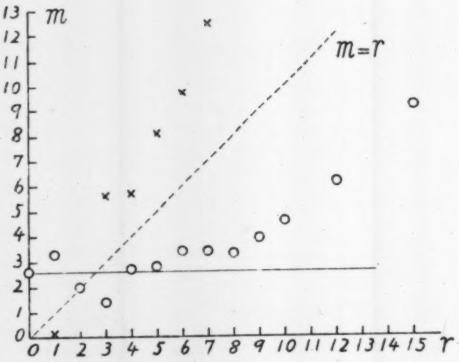

Fig. 11. $m-r$ diagram for the monthly frequencies of earthquakes in region b.

The monthly frequencies of earthquakes in regions a, b, c, and d will be found in Table II.

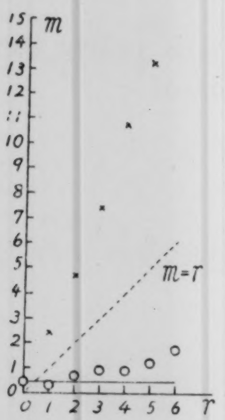

Fig. 12. $m-r$ diagram for the monthly frequencies of earthquakes in region c.

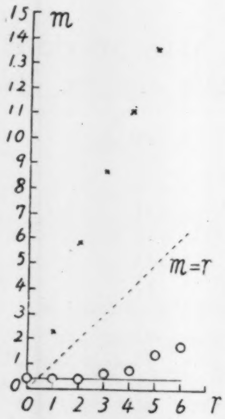

Fig. 13. $m-r$ diagram for the monthly frequencies of earthquakes in reigon d.

For reference, the monthly frequencies of earthquakes felt in Tokyo during 48 years from 1876 to 1932 will now receive brief attention. The $m-r$ diagram in this case is shown in Fig. 18, from which it will be found that the frequency curve may be expressed on the assumption that there are two epochs during the period under consideration, one of which has a mean frequency of about 3·5 and the other about 8·0. The observed curve and a theoretical one calculated on this assumption are shown in Fig. 19. A full account of these earthquakes was published by Prof. M. Ishimoto.[6]

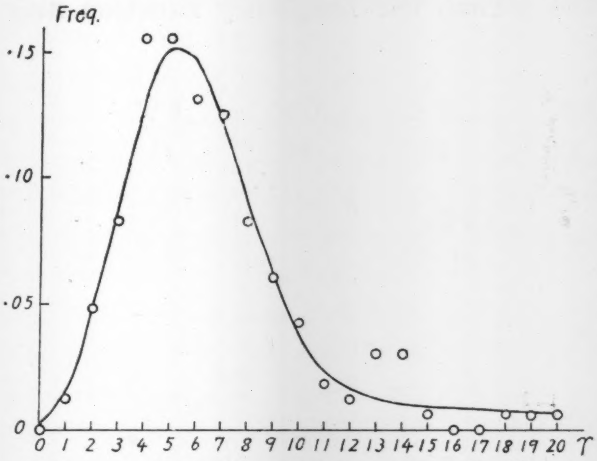

Fig. 14. Monthly frequencies of the strong earthquakes in Japan.
Circle: Observed frequencies.
Full line:

$$W(r)=\frac{10}{11}e^{-5\cdot8}\frac{5\cdot8^r}{r!}+\frac{1}{11}e^{-15\cdot0}\frac{15\cdot0^r}{r!}$$

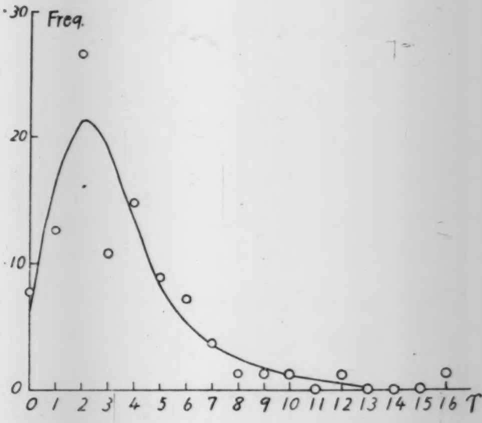

Fig. 15. Monthly frequencies of the earthquakes in region *b*.
Circle: Observed frequencies.
Full line:

$$W(r)=\frac{5}{6}e^{-2\cdot6}\frac{2\cdot6^r}{r!}+\frac{1}{6}e^{-7\cdot0}\frac{7\cdot0^r}{r!}$$

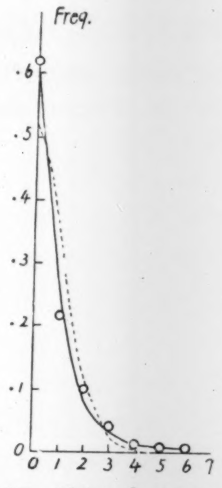

Fig. 16. Monthly frequencies of the earthquakes in region *c*.
Circle: Observed frequencies.
Dotted line: Frequenrcy curve calculated with Poisson's formula.
Full line:

$$W(r)=\frac{10}{11}e^{-0\cdot4}\frac{0\cdot4^r}{r!}+\frac{1}{11}e^{-3\cdot0}\frac{3\cdot0^r}{r!},\quad \text{or}$$

$$\varphi(r)=\frac{1}{\sqrt{2\pi}0\cdot643(1+r)}e^{-\frac{\{\log(1+r)-0\cdot253\}^2}{2(0\cdot643)^2}}$$

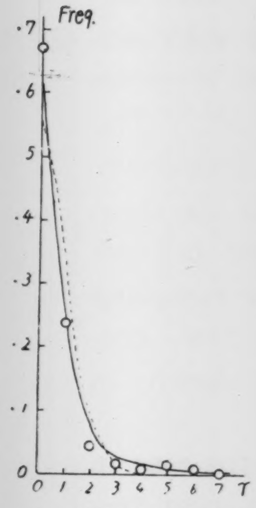

Fig. 17. Monthly frequencies of the earthquakes in region *d*.
Circle: Observed frequencies.
Dotted line: Frequency calculated with Poisson' formula.
Full line:

$$W(r)=\frac{10}{11}e^{-0\cdot4}\frac{0\cdot4^r}{r!}+\frac{1}{11}e^{-3\cdot0}\frac{3\cdot0^r}{r!},\quad \text{or}$$

$$\varphi(r)=\frac{1}{\sqrt{2\pi}0\cdot60(1+r)}e^{-\frac{\{\log(1+r)-0\cdot253\}^2}{2(0\cdot60)^2}}$$

---

[6] M, ISHIMOTO, *Bull. Earthq. Res. Inst.*, **14** (1936), 610.

Should the mean frequency increase or decrease exponentially, that is, makes rapid changes during the period, the frequency function may be given, for example, by

$$W(r)=\frac{1}{8}\Big(e^{-0\cdot1}\frac{0\cdot1^r}{r!}+e^{-0\cdot2}\frac{0\cdot2^r}{r!}+e^{-0\cdot4}\frac{0\cdot4^r}{r!}+e^{-0\cdot8}\frac{0\cdot8^r}{r!}+e^{-1\cdot6}\frac{1\cdot6^r}{r!}$$

$$+e^{-3\cdot2}\frac{3\cdot2^r}{r!}+e^{-6\cdot4}\frac{6\cdot4^r}{r!}+e^{-12\cdot8}\frac{12\cdot8^r}{r!}\Big).$$

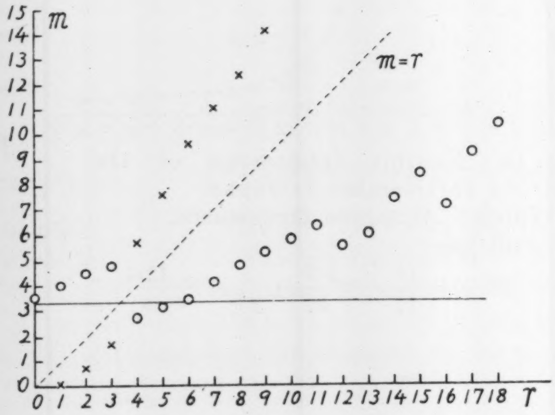

Fig. 18. $m-r$ diagram for the monthly frequencies of the earthquakes felt in Tokyo during the period from 1876 to 1923.

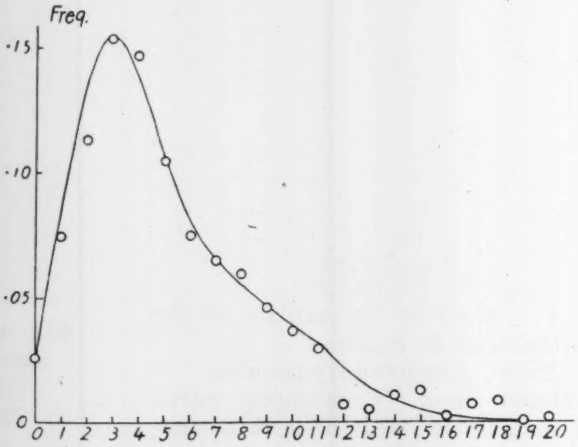

Fig. 19. Monthly frequencies of the earthquakes felt in Tokyo.
Circle: Observed frequencies.
Full line: $W(r)=\frac{2}{3}e^{-3\cdot3}\frac{3\ 3^r}{r!}+\frac{1}{3}e^{-8\cdot5}\frac{8\cdot5^r}{r!}$

The $m-r$ diagram for this case is shown in Fig. 20.

The $m-r$ diagram for the 3-hourly frequency of the Itô earthquakes swarms is shown in Fig. 21, which agrees well with the theoretical, is shown in Fig. 20. The actual frequency curve and the theoretical one calculated by the foregoing equation are graphically shown in Fig. 22.

For the case in which the mean freqnuency changes linearly during the period under consideration, the frequency curve may be expressed, for example, by

$$W(r)=\frac{1}{10}\Big(e^{-1}\frac{1^r}{r!}+e^{-2}\frac{2^r}{r!}+e^{-3}\frac{3^r}{r!}\cdots\cdots+e^{-10}\frac{10^r}{r!}\Big).$$

The $m-r$ diagram in this case is shown in Fig. 23.

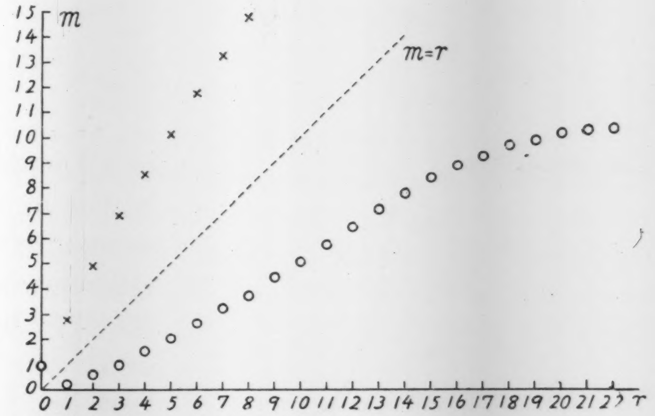

Fig. 20. $m-r$ diagram for the case in which the frequency function is of the form

$$W(r)=\frac{1}{8}\Big(e^{-0\cdot1}\frac{0\cdot1^r}{r!}+e^{-0\cdot2}\frac{0\cdot2^r}{r!}+e^{-0\cdot4}\frac{0\cdot4^r}{r!}+e^{-0\cdot8}\frac{0\cdot8^r}{r!}$$
$$+e^{-1\cdot6}\frac{1\cdot6^r}{r!}+e^{-3\cdot2}\frac{3\cdot2^r}{r!}+e^{-6\cdot4}\frac{6\cdot4^r}{r!}+e^{-12\cdot8}\frac{12\cdot8^r}{r!}\Big).$$

4. We shall now consider the other method for obtaining the functional form representing arbitrary frequency distribution.

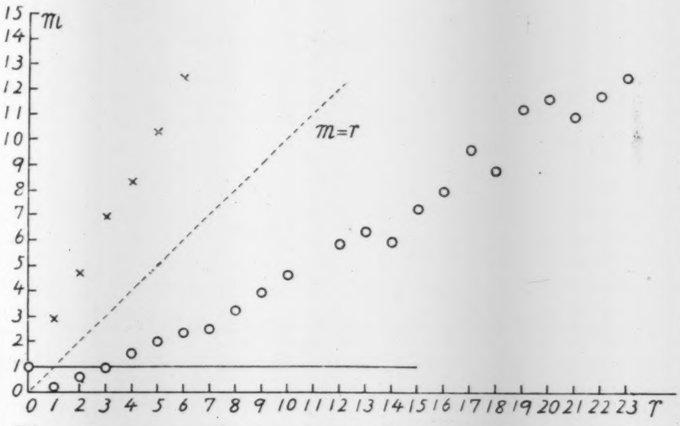

Fig. 21. $m-r$ diagram for the 3-hourly frequencies of the Itô earthquake swarm.

A certain frequency distribution can be transformed into the normal type (Gaussian law) by substituting the variable with another variable.

The given frequency function $p(t)$ can be transformed to $\frac{1}{\sqrt{2\pi}}e^{-\frac{x^2}{2}}$ by substituting variable t with $t(x)$.

To obtain function $t(x)$ it is necessary to find the relation between t and x in the equation

$$\int_{t_0}^{t} p(t)\,dt = \frac{1}{\sqrt{2\pi}}\int_{-\infty}^{x} e^{-\frac{x^2}{2}}\,dx,$$

where t_0 is the smallest value of t.

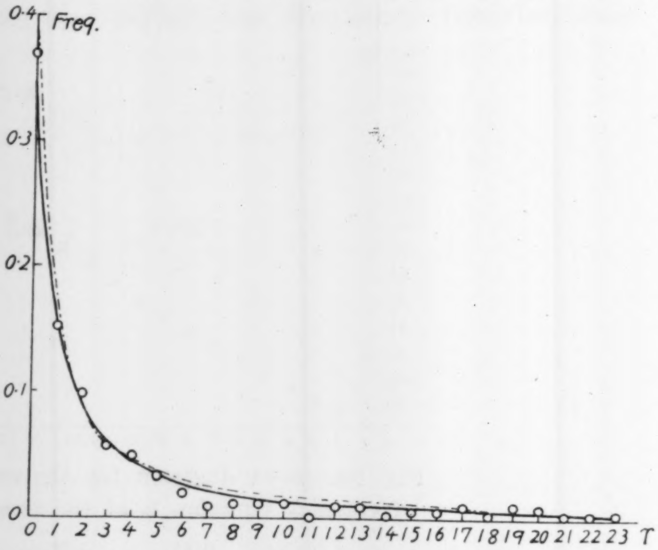

Fig. 22. 3-hourly frequencies of the Itô earthquake swarm.

Circle: Observed frequencies.

Dotted line:

$$W(r)=\frac{1}{8}\Big(e^{-0\cdot1}\frac{0\cdot1^r}{r!}+e^{-0\cdot2}\frac{0\cdot2^r}{r!}+e^{-0\cdot4}\frac{0\cdot4^r}{r!}+e^{-0\cdot8}\frac{0\cdot8^r}{r!}$$
$$+e^{-1\cdot6}\frac{1\cdot6^r}{r!}+e^{-3\cdot2}\frac{3\cdot2^r}{r!}+e^{-6\cdot4}\frac{6\cdot4^r}{r!}+e^{-12\cdot8}\frac{12\cdot8^r}{r!}\Big).$$

Full line:

$$\varphi(r)=\frac{1}{\sqrt{2\pi}\,1\cdot77\,(r+0\cdot5)}e^{-\frac{\{\log(r+0\cdot5)-0\cdot60\}^2}{2(1\cdot77)^2}}.$$

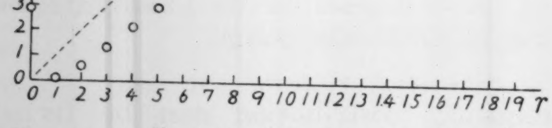

Fig. 23. $m-r$ diagram for the case in which the frequency function is of the form,

$$W(r)=\frac{1}{10}\Big(e^{-1}\frac{1^r}{r!}+e^{-2}\frac{2^r}{r!}+e^{-3}\frac{3^r}{r!}\cdots\cdots+e^{-10}\frac{10^r}{r!}\Big).$$

Upon finding the functional relation $x=x(t)$ or $t=t(x)$ by means of the above equation, we obtain the frequency function under consideration as

$$p(t) = \frac{1}{\sqrt{2\pi}} e^{-\frac{[x(t)]^2}{2}} x'(t).$$

The functional forms thus obtained in actual earthquake frequencies are shown graphically in Figs. 2, 16, 17, 22, 24, 25, and 26, from which it will be seen that earthquake frequencies can generally be expressed by

$$p(t) = \frac{1}{\sqrt{2\pi}\sigma t} e^{-\frac{(\log t - c)^2}{2\sigma^2}},$$

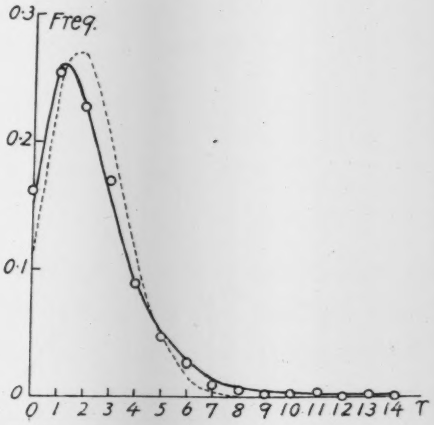

Fig. 24. 10 a day frequencies of the strong earthquakes in Japan.

Circle: Observed frequencies,

Dotted line: Frequency curve calculated with Poisson's formula.

Full line:

$$\varphi(r) = \frac{1}{\sqrt{2\pi}\,0\cdot44(r+2)} e^{-\frac{\{\log(r+2)-1\cdot34\}^2}{2(0\cdot44)^2}}.$$

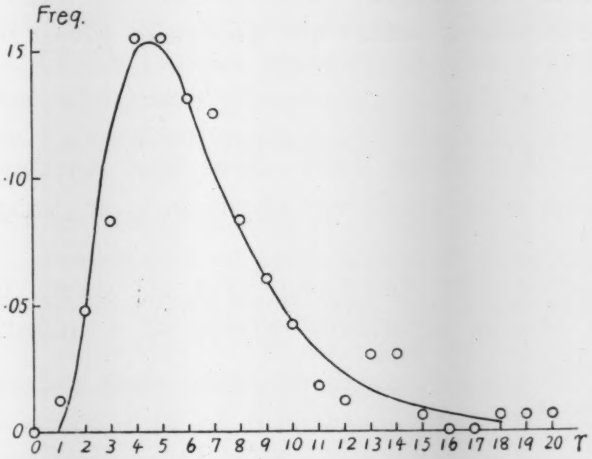

Fig. 25. Monthly frequencies of the strong earthquakes in Japan.

Circle: Observed frequencies.

Full line: $\varphi(r) = \frac{1}{\sqrt{2\pi}\,0\cdot51r} e^{-\frac{(\log r - 1\cdot75)^2}{2(0\cdot51)^2}}$.

for the case in which frequencies of O occurrences may be neglected. If however $p(o)$ cannot be ignored, the frequency function may be given by

$$p(t) = \frac{1}{\sqrt{2\pi}\sigma(t+k)} e^{-\frac{[\log(t+k)-c]^2}{2\sigma^2}}.$$

Now, as t is a function of x, and x fluctuates under Gaussian law, that is, results in normal dispersion, we can suppose that earthquake frequencies fluctuate as certain functions of the fluctuating secondary cause x. These functional forms are generally given by

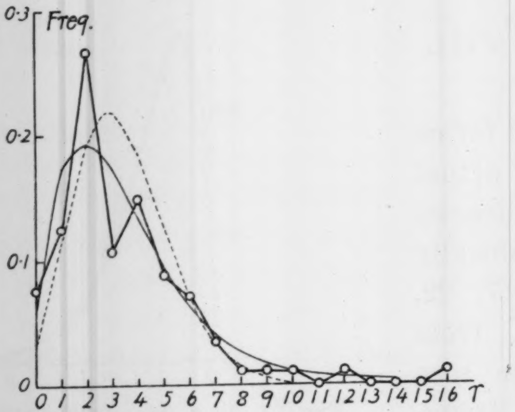

Fig. 26. Monthly frequencies of the earthqukes in region b.
Circle: Observed frequencies.
Dotted line: Frequency curve calculated with Poisson's formula.
Thin full line:

$$\varphi(r)=\frac{1}{\sqrt{2\pi}0\cdot46(r+2)}e^{-\frac{[\log(r+2)-1\cdot6]^2}{2(0\cdot46)^2}}.$$

$$t=e^{\sigma x+c},\qquad t=e^{\sigma x+c}-k.$$

We may suppose that these facts show that earthquake frequencies make rapid changes with small variations in x, or imaginary secondary cause.

The above probability functions have the same form as the probability function of the secondary effects of a number of many independent variables.

For example, let

$$y=y_1y_2\cdots\cdots y_n,\ n\gg1$$

where y_1, y_2, $\cdots\cdots$, y_n are independent variables, then the probability function of y is given by

$$\varphi(y)=\frac{1}{\sqrt{2\pi}\sigma y}e^{-\frac{(\log y-\bar{x})^2}{2\sigma^2}},\ (0<y<\infty),$$

where $\bar{x}=\overline{\log y}$.

From this standpoint, we may also suppose that earthquake occurrences are affected by the secondary effects of many causes.

This fact, moreover, reminds us that in counting the number of earthquake occurrences, many factors control the final results.

Here, for comparison, we shall refer to the frequency law of the space velocities of stars.7) In this case, the observed distribution of space velocities are expressed by

$$\varphi(v) = \frac{h\,Mod.}{\sqrt{\pi}\ v} e^{-h^2(\log v - \overline{\log v})^2}.$$

It is of interest to note that this form is very similar to the frequency functions of earthquake numbers. It seems to the writer that in this case also, the frequency distribution can well be represented by the sum of the two Gaussian formulae, suggesting that there are two main groups in the velocities of stars.

In the case of a large mean frequency, the Gaussian formula corresponds to Poisson's formula. The latter has only one variable, that is the mean frequency, while the former has two, the mode and the standard deviation, for which reason the writer has not been able to find a method of denoting any given frequency function as the sum of some numbers of the Gaussian formula.

5. We shall next consider the volocity of fluctuation.

The velocity of fluctuation depends on the order the frequencies follow one another in time.

Let n_1, n_2 be successive frequencies; the velocity of fluctuation is then given by $\Delta(n_1) = n_1 - n_2$.
The mean velocity is $\overline{\Delta(n_1)} = \overline{n_1 - n_2} = n_1 - \overline{n_2}$.
In n_1 and n_2 are independent of each other, it becomes $\overline{\Delta(n_1)} = n_1 - \nu$, where ν is the mean n, where as if they are dependent, $\overline{n_2}$ varies as a function of n_1.

If the events are rare (Poisson's law), it is given by $\overline{\Delta(n)} = P(n - \nu)$, where P8) is the probability of occurrence of an unfavourable event in a trial which was favourable in the immediately preceding trial.

The frequency distribution of Δ in the case of 10 day frequencies of strong Japanese earthquakes is shown in Fig. 27, from which it will be seen that there are no very noticeable points in the frequency distribution of Δ in this case, although the writer thinks it desirable to examine the frequency distributions of Δ in a number of other cases.

$\overline{n_2}$ is represented as a function of n_1 for saveral cases in Figs. 28-30. As will be seen from these figures, there is a tendency for

---

7) M. Kaburaki, *Jour. Fac. Sci. Tokyo*, [i], **1** (1926), 285.

8) R. Fürth, Schwankungserscheinungen in der Physik, 27.

great frequencies to be accompanied with greater frequencies than the mean frequency and *vise versa,* besides the case of region a in which

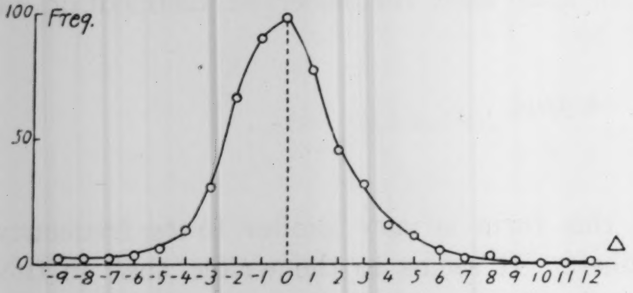

Fig. 27. Frequency distribution of Δ in the case of 10 a day frequencies of strong Japanese earthquakes.

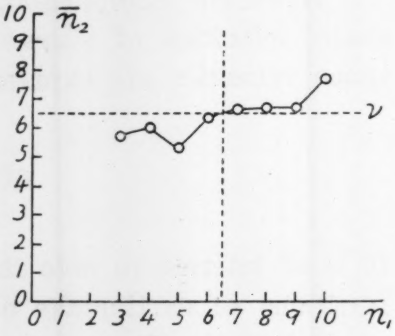

Fig. 28. $\overline{n}_2$ as a function of n_1 in the case of the monthly frequencies of strong earthquakes in Japan.

$\overline{n}_2$ is constant, namely, the mean frequency, suggesting that they occurred at random in the course of time.

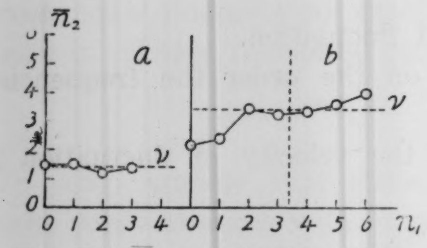

Fig. 29. $\overline{n}_2$ as a function of n_1.
a: Monthly frequencies of the earthquakes in region a.
b: Monthly frequencies of the earthquakes in region b.

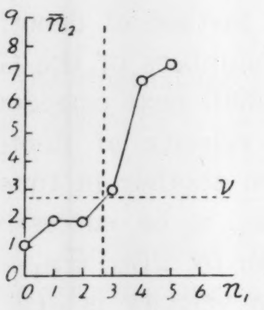

Fig. 30. $\overline{n}_2$ as a function of n_1 in the case of hourly frequencies of the Itô earthquake swarm.

We shall now take dn the square of the velocities of fluctuatious.

$$\overline{\Delta^2}=\overline{(n_1-n_2)^2}=\overline{(n_1-\nu)^2}+\overline{(n_2-\nu)^2}-2\overline{(n_1-\nu)(n_2-\nu)}$$

$$=2\nu^2\overline{\delta^2}-2\overline{(n_1-\nu)(n_2-\nu)},$$

where $\delta=\frac{n-\nu}{\nu}$ (relative deviation),

Putting $P=\frac{1}{2}\frac{\overline{\Delta^2}}{\overline{s^2}}=\frac{1}{2}\frac{\overline{\Delta^2}}{\nu^2\overline{\delta^2}}=1-\frac{\overline{(n_1-\nu)(n_2-\nu)}}{\nu^2\overline{\delta^2}},$

where $s=n-\nu$ (absolute deviation).

Let r be the correlation coefficient between n_1 and n_2;

then $$r=\frac{1}{\sigma n_1 \sigma n_2}\left(\frac{\sum(n_1-\nu)(n_2-\nu)}{N}\right),$$

where N is the total number of the pairs n_1 and n_2.

Since $\sigma n_1=\sigma n_2=\sqrt{\overline{s^2}}$,

$$r=\frac{1}{s^2}\overline{(n_1-\nu)(n_2-\nu)}=\frac{\overline{(n_1-\nu)(n_2-\nu)}}{\nu^2\delta^2}.$$

We thus get the relation between r and P', namely,

$$r=1-P'=1-\frac{1}{2}\frac{\overline{\Delta^2}}{\overline{s^2}},$$

with which equation it is possible to calculate easily the correlation coefficient between n_1 and n_2.

The probable error in r is given by

$$\text{the probable error in } r=\pm 0{\cdot}67\frac{1-r^2}{\sqrt{N}}.$$

For the case of rare events, we have $\overline{\Delta^2}=2\nu P$ and $\overline{s^2}=\nu$, whence $P'=P$. We have therefore $P=1-r$, that is to say, quantity P, which is usually used in statistics as a measure of the degree of the after-effect, is in inverse relation to quantity r which measures the degree of correlation between the succeeding events.

The correlation coefficients r between the monthly frequency in any arbitrary month and the frequency in the next month, in the month next but one, in the month next but two and so on, with the range of probable errors in r, are shown in Fig. 31. As will be seen from these figures that there is some correlation between the monthly frequencies of strong Japanese earthquakes and the succeeding frequencies, excepting the cases in region *a* and *c*, in which there is no appreciable correlation. Moreover, since the correlation curves have periodic forms, the monthly frequencies for the whole of Japan and those of region *b* tend to fluctuate periodically in 3-4 months.

The correlation coefficients between the successive frequencies in variable periods during which the frequencies are counted are shown in Figs. 32 and 33, from which it will be seen that the values of correlation coefficients differ fairly widely under numerous circumstances. In the case of strong earthquakes for the whole of Japan, the frequencies in shorter periods, contrary to what would be expected, had no correlation with frequencies that immediately preceded or followed them. In the case of the Itô earthquake swarm, the frequencies in periods longer than 3 hours had little correlation with the frequencies that immediately preceded or followed them.

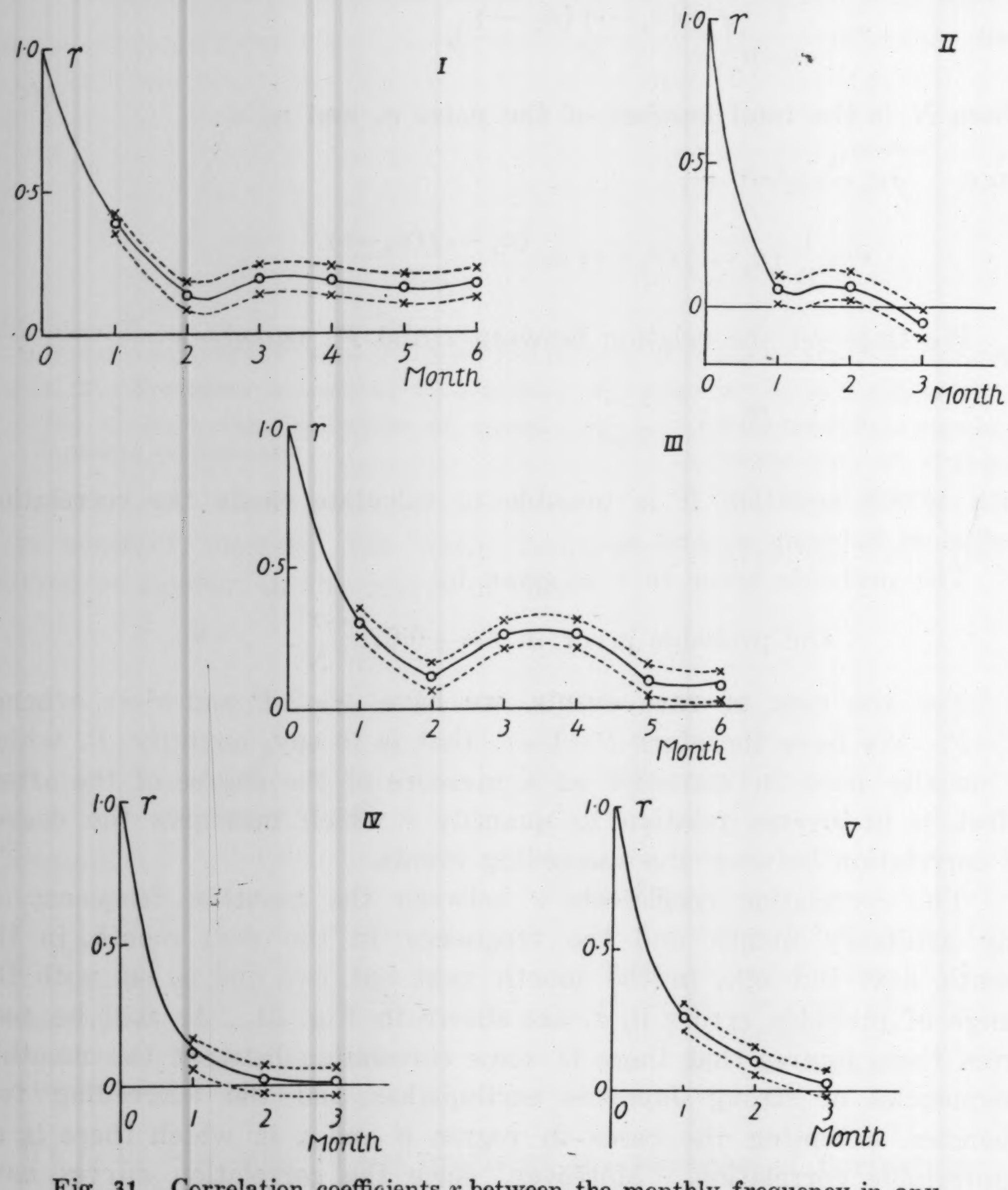

Fig. 31. Correlation coefficients r between the monthly frequency in any arbitrary month and the frequency in the next month, in the month next but one, in the month next but two and so on.

Two dotted lines: Range of probable error in r.

I: Earthquakes in the whole of Japan.
II: Earthquakes in Region *a*.
III: Earthquakes in Region *b*.
IV: Earthquakes in Region *c*.
V: Earthquakes in Region *d*.

The correlation coefficients between two successive hourly frequencies of the Itô earthquakes calculated separately for 7 day periods

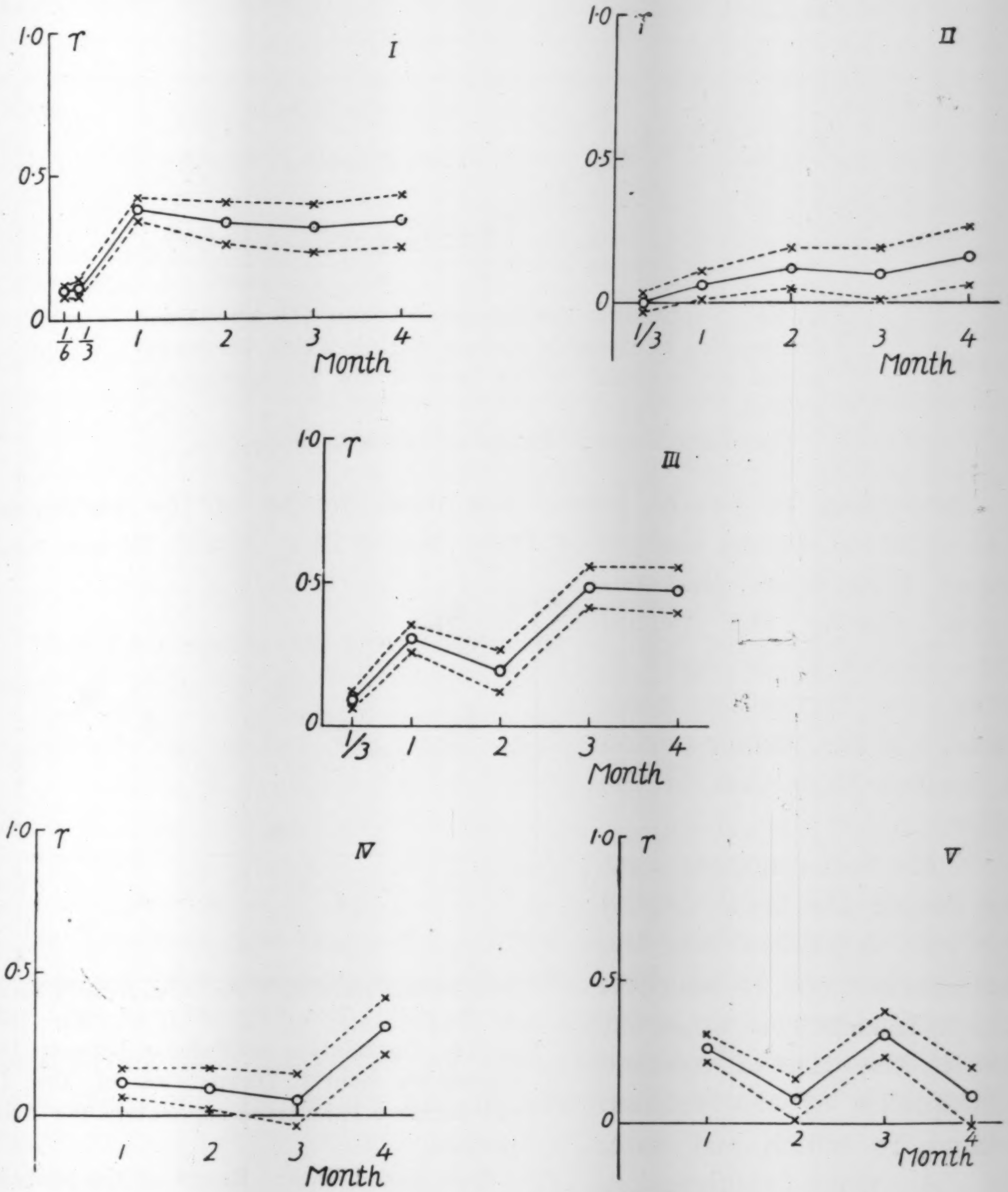

Fig. 32. Correlation coefficients between the successive frequencies in variable periods during which the frequencies are counted.

Two dotted line: Range of probable error in r.

I: Earthquakes in the whole of Japan.
II: Earthquakes in Region *a*.
III: Earthquakes in Region *b*.
IV: Earthquakes in Region *c*.
V: Earthquakes in Region *d*.

are shown in Fig. 34, which also shows the mean frequency for every

7 days. As will be seen from the figure, the correlation coefficient fluctuate with the epochs under consideration.

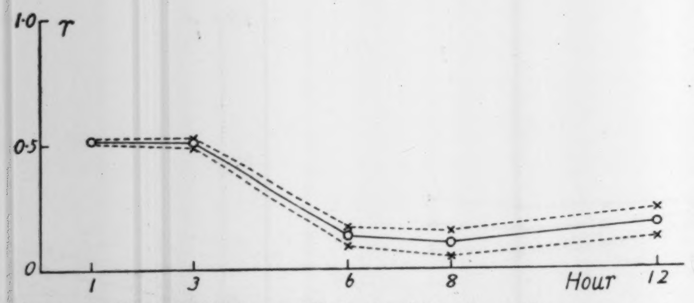

Fig. 33. Correlation coefficients between the successive frequencies in variable periods during which the frequencies are counted in the case of the Itô earthquake swarm.

Two dotted lines: Range of probable error in r.

According to Dr. N. Nasu,[9] the focal depths of the earthquakes that occurred during the period from March 14 to March 20 are rather deeper than those that occurred during the period from March 21 to April 3, while the correlation coefficient r in the former period is smaller than that in the latter.

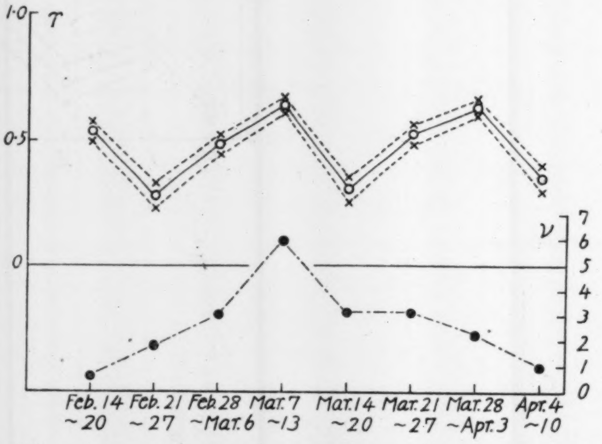

Fig. 34. Correlation coefficients between two successive hourly frequencies of the Itô earthquakes calculated separately for 7 day periods.

Two dotted lines: Range of the probable error in r.

Black circle: Mean frequency for every 7 days.

This fact suggests that the deeper the focal depths the less dependent are the earthquakes one to another, which tendency is apparent also in the case of volcanic earthquakes of the Volcano Asama, in which last case, the *A* type earthquakes (accompanied by no eruptions) seem to have rather deeper origins than the *B* type (accompanied by eruptions), while the correlation coefficients in the former are smaller than those in the latter. (see Table III).

6. We shall next consider briefly the successive time intervals in the occurrence of earthquakes.

---

[9] N. NASU, *Bull. Earthq. Res. Inst.*, **13** (1935), 400.

Table III.

The Correlation Coefficients r in the Cases of Volcanic Earthquakes of Asama.

Type	Period of Observation	r	Remark
A	June 25 to Oct. 20, 1911	0·23	daily frequency
B	,, ,,	0·355	,, ,,
A	May 16 to Aug. 16, 1912	0·225	,, ,,
B	,, ,,	0·465	,, ,,
A	June 17, 1912	0·64	10 minutes frequency
A	June 25, 1912	0·45	,, ,,
A	July 16, 1912	0·785	,, ,,
B	Oct. 5, 1912	0·805	,, ,,
B	July 5~6, 1913	0·77	,, ,,
B	Aug. 27~28, 1913	0·805	,, ,,
B	Sep. 1~2, 1913	0·765	,, ,,
B	Oct. 15, 1913	0·61	,, ,,

The frequencies of time intervals in the cases of independent events are given by

$$W(t)=\int_{t_1}^{t_2} c_1e^{-c_1t}dt=e^{-c_1t_1}-{}^{-c_1t_2},$$

where $c_1=\dfrac{1}{\theta}$ (θ is the mean successive time interval).[10]

To illustrate, the frequency curves of successive time intervals in the case of strong Japanese earthquakes are shown in Figs. 35, 36, from which it will be seen that the observed frequency curves are comparatively well expressed by the formula of independent events within the limits of errors due to the small number of observations made.

7. Discussion

There being certain uncertainties in the counting of earthquakes under a variety of circumstances, the writer thinks it desirable to inquire and ascertain how the observed frequency distributions might be disturbed by these factors.

We shall first take the case in which we are observing some fractions (r) of actual frequencies x, like $u=rx$. Here we assume that x disperses normally that is, the probability function of x is given by

---

[10] R. FÜRTH, *loc. cit*, 37.

$$p(x)=\frac{1}{\sqrt{2\pi}\sigma_x}e^{-\frac{(x-\bar{x})^2}{2\sigma_x^2}}.$$

We shall consider the two following cases:

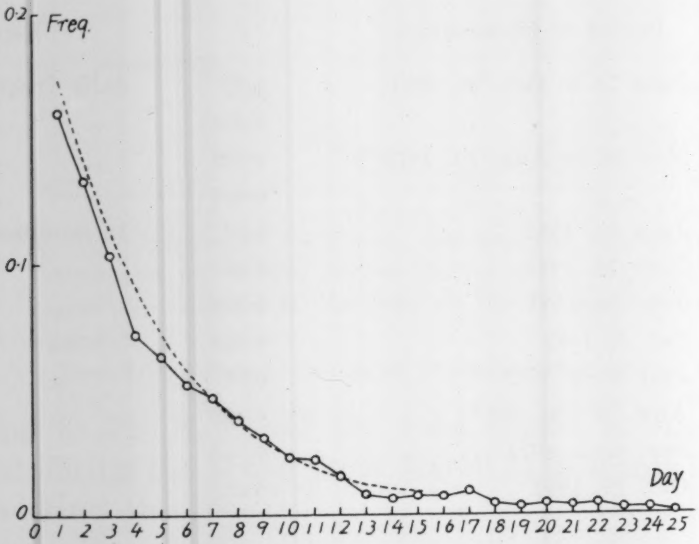

Fig. 35. Frequencies of the successive time intervals in the case of strong Japanese earthquakes.

Full line: Observed frequencies.
Dotted line: Calculated frequencies.

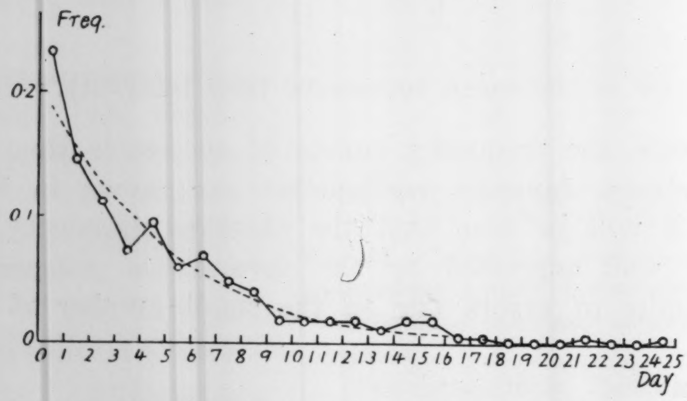

Fig. 36. Frequencies of the successive time intervals in the case of the earthquakes in region a.

Full line: Observed frequencies.
Dotted line: Calculated frequencies.

1) r is a constant.

$$\varphi(u)=\frac{p(x)}{\dfrac{\partial u}{\partial x}}=\frac{1}{\sqrt{2\pi}\sigma_u}e^{-\frac{(u-\bar{u})^2}{2\sigma_u^2}}.$$

The probability function in this case assumes a form similar to the Gaussian law.

2) r also disperses normally.

Although the writer has not yet been able to obtain the probability function in this case, it may assume a form similar to the Gaussian.

We shall next consider the case in which we are observing seismic activities simultaneausly in several localities. Here we assume that the frequency distribution in each locality disperses normally.

1) There are two seismically active localities.

$$u=x+y.$$

$$A(x)=\frac{1}{\sqrt{2\pi\sigma_x}}e^{-\frac{(x-\bar{x})^2}{2\sigma x}},$$

$$B(y)=\frac{1}{\sqrt{2\pi\sigma_y}}e^{-\frac{(y-\bar{y})^2}{2\sigma y}}.$$

$$\varphi(u)=\int_{-\infty}^{\infty}A(u-y)B(y)dx=\frac{1}{\sqrt{2\pi\sigma_u}}e^{-\frac{(n-\bar{u})^2}{2\sigma u^2}}.$$

2) The number of localities seismically active is infinite.

$$u=y_1+y_2\cdots\cdots+y_n,\ n\gg 1.$$

$$\varphi(u)=\frac{1}{\sqrt{2\pi\sigma_u}}e^{-\frac{(u-u)^2}{2\sigma u^2}}.$$

In all these cases the probability functions are exactly the same as that of the Gaussian.

We shall next consider the case in which an unknown number of earthquakes is caused to occur by a larger earthquake or by other causes, such as a cyclone, while the frequency in occurrence of these causes changes from time to time.

In this case we obtain the equation

$$u=k_1+k_2\cdots\cdots+k_n,$$

where k_1 is the number of earthquakes induced by the first large earthquake, k_2 is that induced by the second large earthquake, and so on. The probability function in this case has not yet been found, by the writer, but the relative deviation is given by

$$\overline{\delta_u^2}=\frac{1}{\nu}\overline{\delta_k^2}+\overline{\delta_n^2},\ \text{where}\ \delta_k=\frac{k-x}{x}\ \text{and}\ \delta_n=\frac{n-\nu}{\nu}.$$

8. *S*ummary

1) Generally speaking, in the case of rare events, the frequency distribution of earthquakes in a region and during the initial epoch may be satisfactorily expressed by the probability function, or Poisson's formula, although we have rather complex frequency distributions as the result probably of counting the number of earthquakes in several locatities and in several epochs of varying simultaneous activities.

2) There are some correlations between two successive frequencies, besides the tendency that the deeper the focal depths the fewer the earthquakes that are dependent on one another.

The writer thinks it desirable to examine the correlations between successive frequencies in the cases of after-shocks and preparatory shocks for the purpose of gaining knowledge of conditions in regions seismically active.

The writer's cordial thanks are due to Prof. M. Ishimoto and Dr. N. Nasu for their kind advice and encouragement in the course of this study.

Table I.

Monthly Frequencies of the Strong Earthquakes in Japan and its Visinity.

Year / Month	1912	1913	1914	1915	1916	1917	1918	1919	1920	1921	1922	1923	1924	1925
January	13	14	13	4	4	9	7	4	11	4	3	6	9	9
February	9	8	7	2	8	4	2	3	7	1	6	6	8	9
March	5	7	8	4	10	5	6	8	6	3	6	4	8	7
April	5	6	1	14	5	2	7	6	10	5	4	5	9	7
May	10	9	5	9	4	6	3	5	7	3	5	10	11	14
June	7	5	6	6	2	4	2	6	7	4	6	12	5	11
July	7	5	5	5	7	6	3	6	7	5	7	7	7	4
August	15	5	3	7	8	4	7	4	2	4	3	5	10	3
September	9	4	10	4	4	3	8	4	4	6	13	18	7	3
October	8	5	8	14	7	6	3	4	5	5	10	14	6	2
November	6	6	3	20	8	4	4	5	2	3	8	19	6	5
December	13	8	5	4	4	4	5	6	9	5	13	12	4	5

$\nu=6{\cdot}5$, $\overline{|n-\nu|}=2{\cdot}56$, $\overline{(n-\nu)^2}=11{\cdot}7$.

Table II_1.

Monthly Frequencies of the Strong Earthquakes in Region *a*.

Month \ Year	1912	1913	1914	1915	1916	1917	1918	1919	1920	1921	1922	1923	1924	1925
January	2	3	5	1	2	0	1	2	0	1	0	0	2	1
February	1	1	3	1	2	1	1	0	2	0	1	0	0	4
March	1	0	4	2	5	3	1	3	2	0	0	1	2	0
April	1	0	0	2	2	1	0	1	2	2	0	3	2	2
May	2	1	3	0	2	0	1	1	1	0	1	1	3	0
June	2	0	0	3	0	1	0	1	1	2	2	2	0	3
July	0	1	2	1	2	3	0	2	2	0	2	2	1	1
August	3	2	0	1	0	1	2	1	1	3	1	1	0	0
September	2	0	3	1	0	1	2	4	3	3	0	0	1	1
October	0	3	0	11	4	0	1	1	3	1	2	1	0	1
November	1	1	1	4	1	1	1	0	0	0	1	0	2	1
December	3	4	3	2	0	2	1	0	1	2	5	0	2	1

$\nu=1{\cdot}4,\ \overline{|n-\nu|}=1{\cdot}05,\ \overline{(n-\nu)^2}=2{\cdot}02.$

Table II_2.

Monthly Frequencies of the Strong Earthquakes in Region *b*.

Month \ Year	1912	1913	1914	1915	1916	1917	1918	1919	1920	1921	1922	1923	1924	1925
January	6	6	5	2	2	4	4	2	4	1	2	3	7	7
February	7	6	4	1	4	2	0	3	3	1	4	5	7	4
March	3	5	4	1	2	2	4	2	3	2	5	0	3	4
April	4	2	1	12	3	1	3	5	6	0	4	0	4	4
May	7	5	2	8	2	4	2	1	2	2	3	6	6	10
June	5	2	6	3	2	3	2	4	0	1	3	7	4	5
July	5	1	1	4	4	2	2	2	4	0	1	0	2	2
August	9	3	2	4	5	2	3	5	1	0	1	2	9	3
September	5	2	5	2	2	2	2	1	1	0	2	16	6	2
October	6	1	6	2	2	6	2	2	0	1	1	12	6	0
November	3	2	1	16	5	3	1	0	2	0	4	10	2	3
December	8	4	2	2	2	2	2	2	4	2	1	5	2	4

$\nu=3{\cdot}4,\ \overline{|n-\nu|}=2{\cdot}0,\ \overline{(n-\nu)^2}=7{\cdot}4.$

Table II$_3$.

Monthly Frequencies of the Strong Earthquakes in Regiqn *c*.

Year Month	1912	1913	1914	1915	1916	1917	1918	1919	1920	1921	1922	1923	1924	1925
January	4	1	3	0	0	1	0	0	0	1	0	2	0	0
February	1	1	0	0	0	0	0	0	1	0	1	0	1	0
March	0	0	0	0	3	0	0	1	0	0	0	0	1	1
April	1	4	0	0	0	0	2	0	1	2	0	0	1	0
May	0	2	0	0	0	0	0	3	2	0	0	0	0	2
June	0	3	0	0	0	0	0	0	0	0	0	0	1	0
July	0	2	0	0	0	0	1	1	0	0	1	2	1	1
August	1	0	1	0	2	0	0	0	0	0	1	0	1	0
September	2	2	2	1	1	0	1	0	0	0	0	1	0	0
October	2	1	1	1	0	0	0	0	0	2	0	1	0	0
November	0	2	0	0	0	0	1	3	0	3	0	1	1	0
December	0	0	0	0	2	0	1	2	3	0	5	6	0	0

$\nu=0{\cdot}65,\ \overline{|n-\nu|}=0{\cdot}82,\ \overline{(n-\nu)^2}=1{\cdot}13.$

Table II$_4$.

Monthly Frequencies of the Strong Earthquakes in Region *d*.

Year Month	1912	1913	1914	1915	1916	1917	1918	1919	1920	1921	1922	1923	1924	1925
January	0	3	0	1	0	3	1	0	2	0	1	1	0	0
February	0	0	0	0	0	0	0	0	0	0	0	0	0	0
March	1	0	0	1	0	0	1	0	1	0	0	1	0	1
April	0	0	0	0	0	0	0	0	0	1	0	1	0	1
May	0	0	0	0	0	1	0	0	1	0	1	0	0	1
June	0	0	0	0	0	0	0	1	5	0	0	0	0	3
July	1	1	1	0	0	0	0	1	1	4	2	1	2	0
August	1	0	0	1	1	0	0	1	0	1	0	1	0	0
September	0	0	0	0	0	0	0	0	0	0	11	0	0	0
October	0	0	0	0	1	0	0	1	2	0	6	0	0	0
November	2	1	0	0	1	0	0	1	0	0	2	5	1	0
December	1	0	0	0	0	0	1	2	0	1	1	0	0	0

$\nu=0{\cdot}56,\ \overline{|n-\nu|}=0{\cdot}77,\ \overline{(n-\nu)^2}=1{\cdot}6.$

14. 地震回數の統計的研究

地震研究所　井上　宇胤

一般に地震回數の頻度曲線はガウスの誤差分布の法則とは異なり非對稱曲線をなして居つて

$$p(t)=\frac{1}{\sqrt{2\pi}\,\sigma(t+k)}e^{-\frac{[\log(t+k)-c]^2}{2\sigma^2}}$$

なる式で頁く表はされる.

然し地震は時に多數起る可能性があるが平常は稀に發生して居るものであるから小確率の場合の統計論であるポアソンの法則と比較して見る事にした.

實際或る小區域に發生した地震のみを問題とした場合や又は廣範圍の地震活動に於ても問題とした期間を適當に短かく取つた場合等では地震回數の頻度分布は全くポアソンの法則に從つて居るものである.

從つて一般に問題の地震の回數の頻度分布が相當複雜である場合に於ても幾つかの短期間に分ければポアソンの法則に從ふものと考へて一般の地震回數の頻度分布を幾つかのポアソンの法式の和に依つて表はす方法を示して置いた.

尙一般に次々の地震回數の間には相當な相關關係があるものであつて此の事は淺い地震程著しいものらしい.

15. *World Distribution of "Deep" Earthquakes.*

By Seiti YAMAGUTI,

Earthquake Research Institute.

(Read Oct. 20, 1936.—Received Dec. 21, 1936.)

Introduction.

The object of the present investigation was to ascertain the vertical distribution of foci of "deep" earthquakes, especially of the world's "deepest" earthquakes.

It was also hoped that some knowledge regarding the existence of "weak lines" in the earth's crust and their locations.

The statistical periodicity of "deep" earthquakes was also investigated and the probable "periods" of occurrence obtained.

V. Conrad[1], who has made similar investigations, in summarizing his paper entitled "Die Zeitliche Folge von Beben mit tiefem Herd", writes:

"From the frequency of deep-focus earthquakes given in the I. S. S. (International Seismological Summaries 1919$\sim$28) it is not possible to find any periodicity for a day's length, whether the epicentral-time given be local or world-time. No clustering of earthquakes near days of full or new moon could be found.

Although a real periodicity for a whole year calculated on the basis of monthly frequencies is not improbable, that for a length of six months is probable—a fact seemingly important since all the writer's previous studies of earthquakes with shallow focus have shown such periodicity.

A periodogram of the frequency of these earthquakes (grouped in this case in tenths of a year) does not, it is true, show a trial-period for which A. Schuster's criterion would indicate reality. But there are in the periodogram three sharp peaks at five-, ten-, and twelve-tenths of a year. The half-year periodicity found in the first part of this and previous studies on this subject seems to point to rotation of the earth's pole as the cause of the variations in frequency, the probability of which seems to be supported by the fact as pointed out by Pollak that the only harmonic components in the rotation of the earth's pole are the two periods of ten- and twelve-tenths of a year. It is therefore likely that in the future increased statistical material will enable one to see in the rotation of the pole one of the causes of both deep- and shallow-focus earthquakes.

---

[1] V. CONRAD, *Gerl. Beitr. Geophys.*, **40** (1933).

Of the series obtained by dividing the scanty *eo ipso* material in two halves, the frequency of earthquakes of more shallow focus shows half-year periodicity in a fairly clear manner."

The data of the world's "deep" earthquakes during the period of twelve years from 1919 to 1930 were taken from the International Seismological Summary, collected by H. H. Turner. In Turner's list of earthquakes (I. S. S.), such terms as *normal depth, below normal, above normal,* are used for roughly classifying the depths of earthquakes, the *normal depth* and the earth's radius for calculating the focal depths having probably been taken as 255 and 6370 kilometres respectively.

Method of Investigation and Results.

1. Geographical and Vertical Distribution.

The epicentres, as many as 241, are plotted on a map of the world. The numerals against the points that represent the hypocentres show their focal depths, h, in kilometres. The points thus plotted for many regions of the world were separated into four parts with contour lines of 700 km, 500 km, and 300 km, such as $h \geq 700$, $700 > h \geq 500$, $500 > h \geq 300$, and $300 > h \geq 100$, for the respective regions as shown in Fig. 1.

A mere glance will show that the deepest regions are near Japan, in the middle part of South America, the southern part of the Philippines, and the ocean east of Australia. Of these, there are several "deep" earthquakes with greater depth of foci than 800 kilometres, although it is possible that the depths of earthquakes, as estimated by Turner exceed somewhat those made by a number of seismologists in Japan. Near Japan, two of the three deepest regions are situated at each end of the so-called "deep" earthquake zone, i. e., in the ocean beds near the Ogasawara (Bonin) Islands and on the main land of Manchuria, the third being in the Okhotsk Sea. Comparatively shallow earthquakes occur in the middle of the Asiatic continent, in Africa, and in the southern sea bed of the island of Sumatra.

We also notice a distinct difference between the geographical distribution of "deep" earthquakes and that of "shollow" earthquakes. Deep focus earthquakes do not occur on the Mediterranean Coast; they rarely occur in North America, especially on its Pacific Coast, while shallow earthquakes frequently occur in the regions just mentioned as well as in other regions of the world.

By projecting the centres of the "deep" earthquakes in South America on a vertical plane containing the equator, which diagram is omitted here, we notice that a number of points tend to lie in a zone, through the deepest region, i. e. the middle part of South America, and inclined toward the Pacific Ocean with a slope of about 1/5 from the horizontal.

As for the "deep" earthquakes that occurred in the Continent of Asia, we notice a similar tendency, i. e. the focal depths become shallower as the longitude eastward increases, from the Plateau of the Pamirs to the eastern part of Tibet.

2. Hypocentral "transfer" in Vertical direction.

i) For the world's "deep" earthquakes.

Owing to the data being very scanty, we had to calculate the preferential ratios for the case of hypocentral "transfer" in radial direction of the earth, regardless of the geographical distribution of earthquakes. By preferential ratio, r, is meant the ratio of the actual number of times the "transfers" have occurred, N_0, to, N', the expected number obtained by calculation, that is $r=N_0/N'$, as already explained in a previous paper[2]. The values of the ratios r's were calculated for six layers separated according to their depths, such as $100 \leqq h < 300$, $300 \leqq h < 400$, ... $600 \leqq h < 700$, and $h \geqq 700$, in kilometres, as shown in Table I.

Table I. Radial hypocentral "transfer" of the world's "deep" earthquakes. Jan., 1919∼Dec., 1930 (whole 12 years).

		Region of the second of the two earthquakes					
		100∼300 km	300∼400 km	400∼500 km	500∼600 km	600∼700 km	700→ km
Region of the first of the two earthquakes	100∼300	**5·33**	*0·38*	0·67	1·21	0·67	*0·58*
	300∼400	0·57	1·25	0·89	0·80	1·02	*0·66*
	400∼500	*0·33*	0·82	**1·63**	**1·33**	0·65	1·12
	500∼600	*0·30*	1·03	1·03	1·23	0·91	1·04
	600∼700	1·33	0·76	0·98	0·91	**2·00**	1·16
	700→	*0·58*	0·99	*0·56*	0·78	1·16	**2·49**

Judging from this table, we may say that

(*a*) When an earthquake occurs in a certain layer, other earthquakes are liable to occur immediately in the same layer.

---

[2] S. Yamaguti, *Bull. Earthq. Res. Inst.*, **11** (1933), 50.

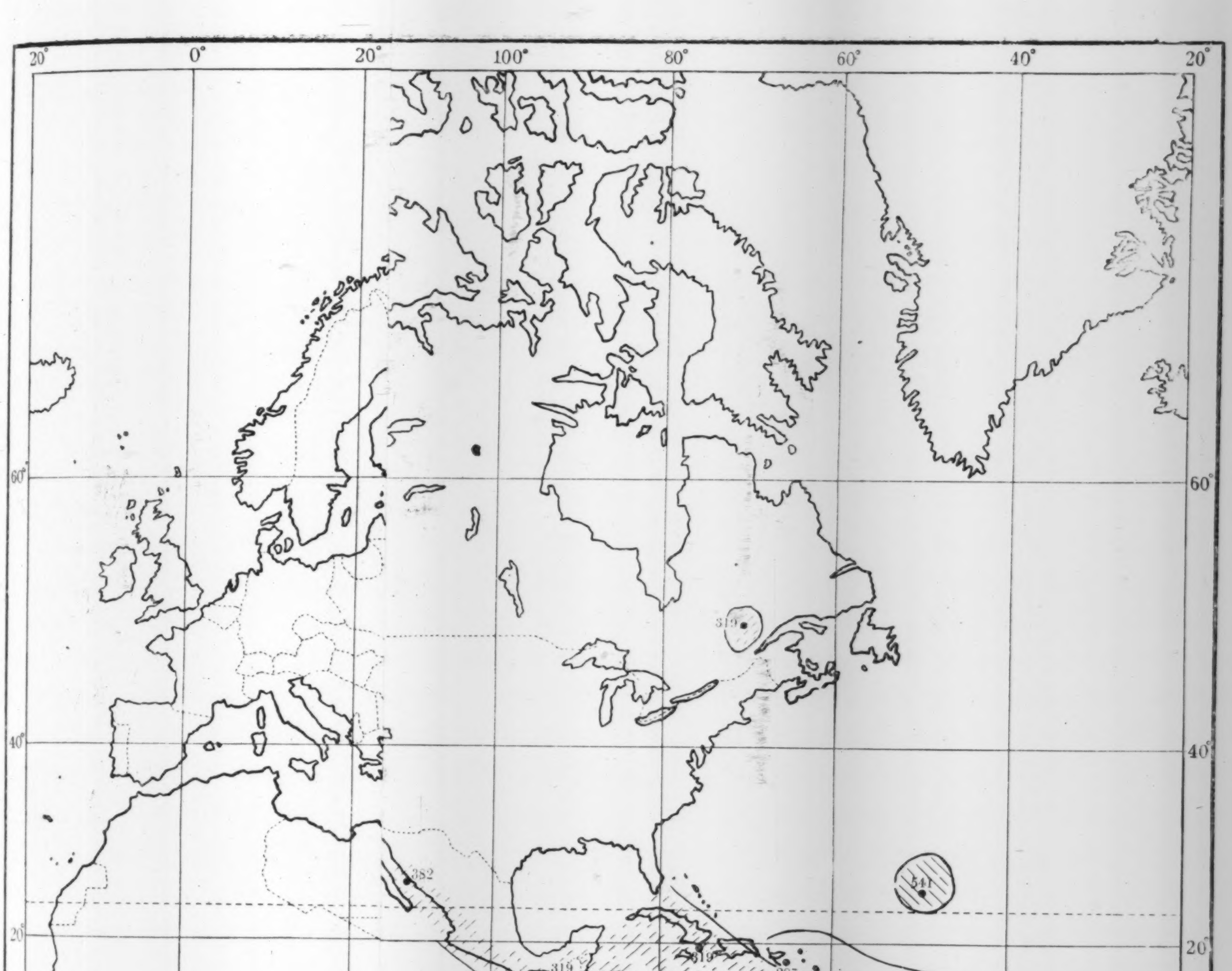
20°
0°
20°
100°
80°
60°
40°
20°
60°
40°
20°
0°
20°
40°
319
382
319
350
382
382
319
287
319
287
287
414
414
319
541
414
510
764
764
510
764
764
764
510
510
382
573
764
319
319
351
573
350
414
414
764
350
350
350
350
382
382
382
541
382
217

ocal depths, *h*, in kilometres.

b

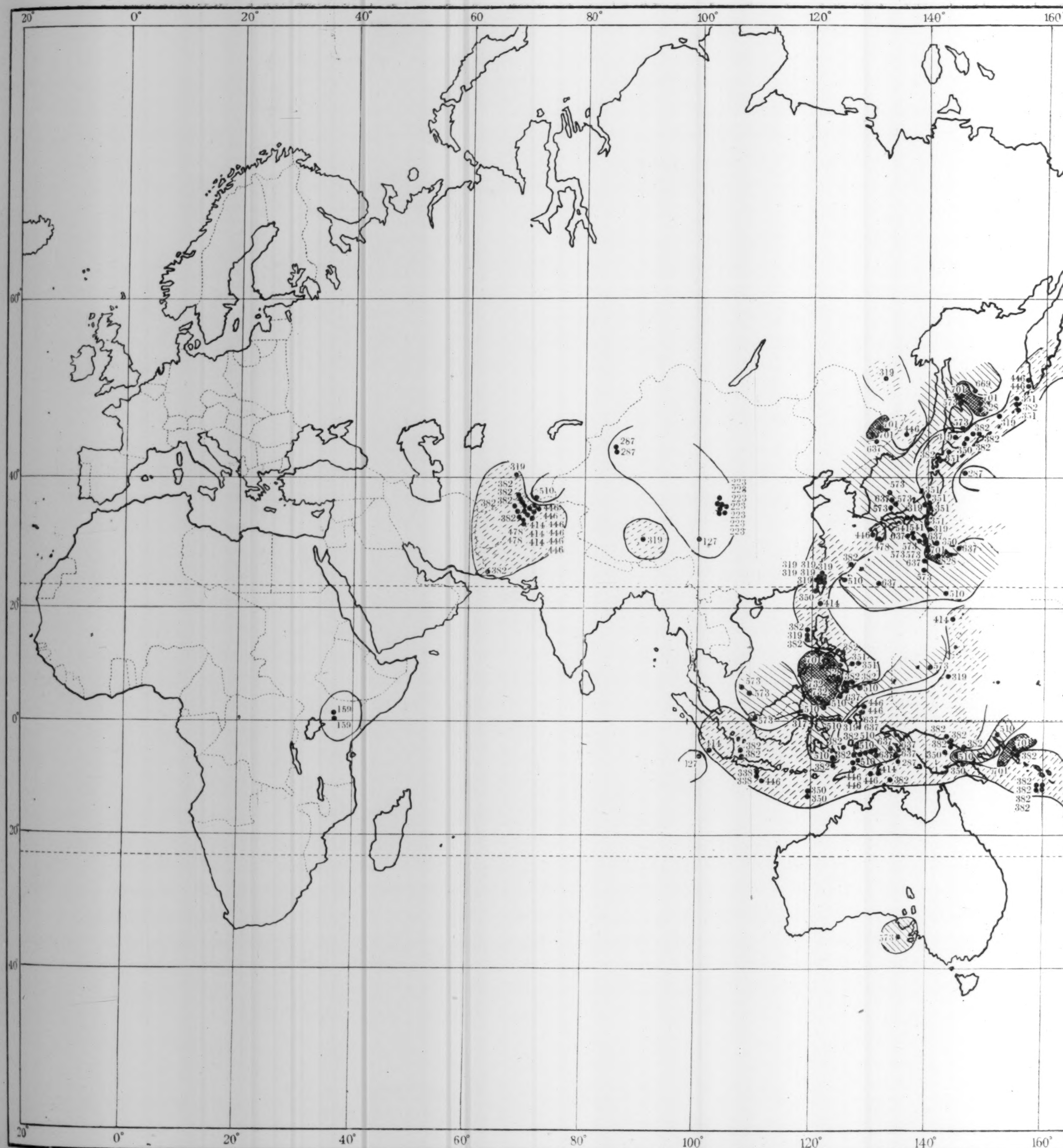
20°
0°
20°
40°
60
80°
100°
120°
140°
160
60°
40°
20°
0°
20°
40°
20
319
669
701
446
351
382
573
637
287
319
382
510
446
414
478
382
287
287
223
319
127
319
350
414
510
573
159
159
573
127
414
382
338
446
350
382
510
637
701
382
573

Fig. 1. Geographical and Vertical distribution of "Deep" earthquakes. The numerals agai

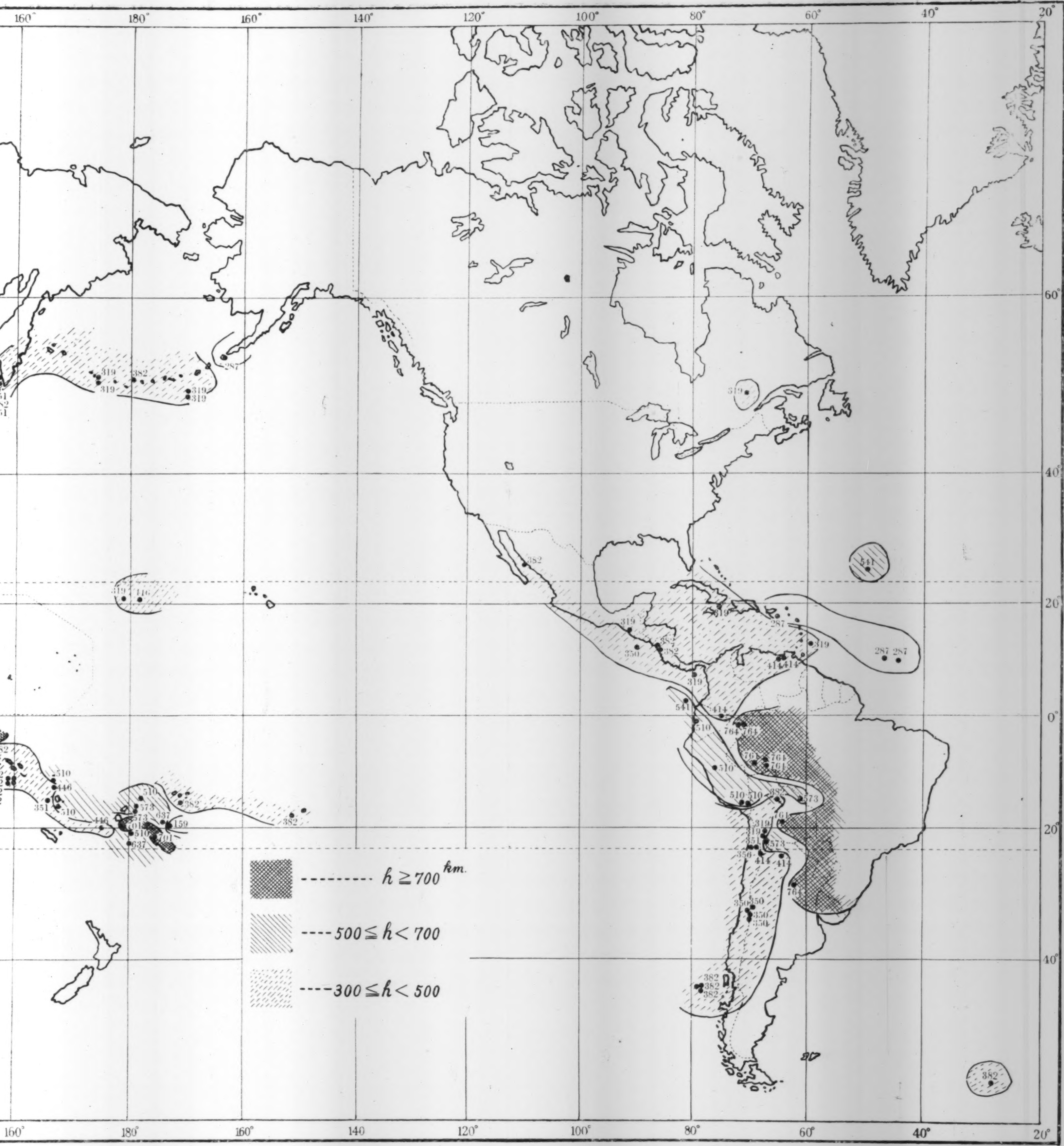

160°
180°
160°
140°
120°
100°
80°
60°
40°
20°
60°
40°
20°
0°
20°
40°
$h \geq 700$ km.
$500 \leq h < 700$
$300 \leq h < 500$

against the points that represent the hypocentres show their focal depths, h, in kilometres.

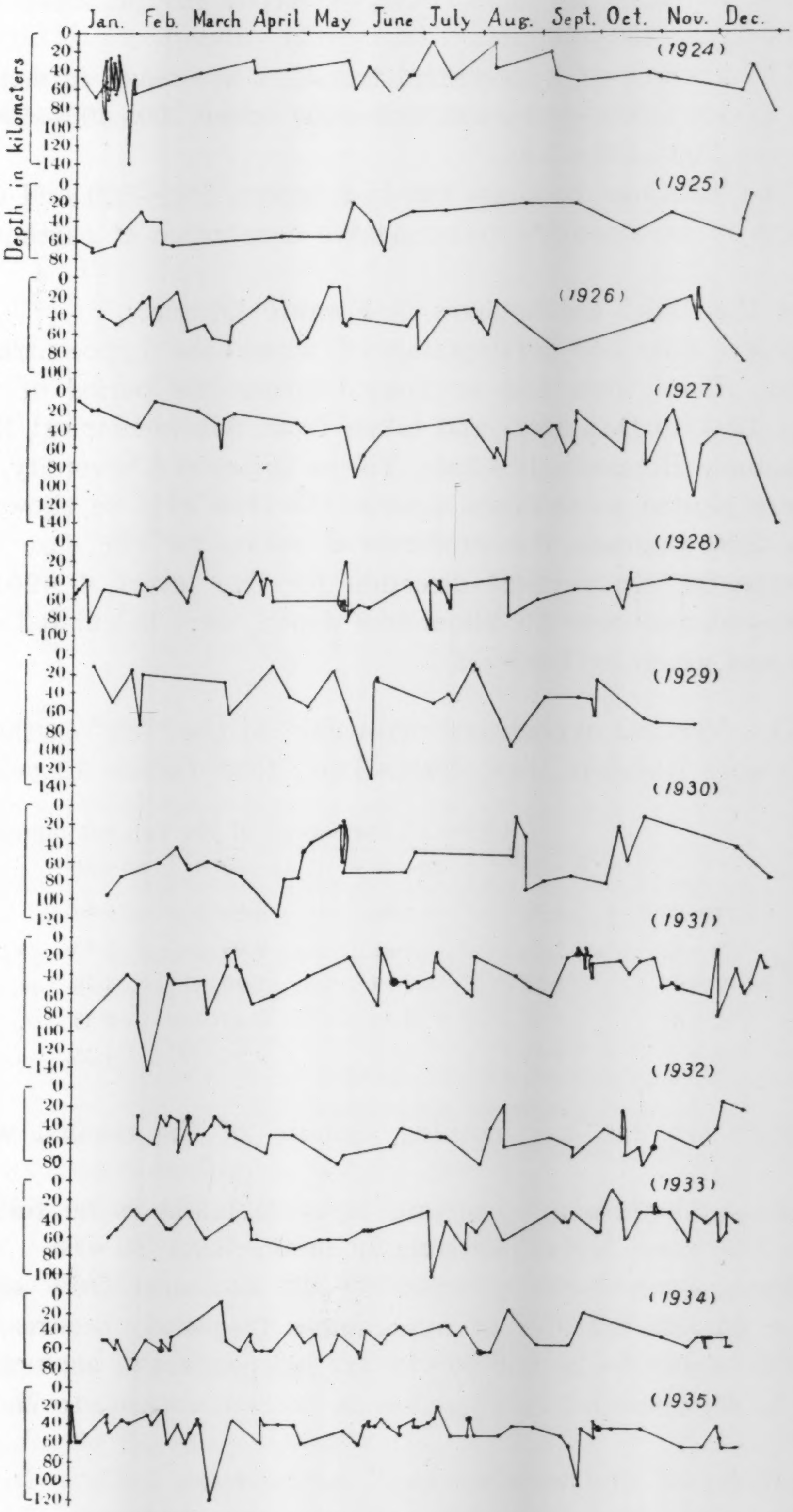

Fig. 2. Depth Time diagram for the "felt" earthquakes in Kwantô Districts.

(*b*) Earthquakes are most likely to occur in the layer 500~600 next to the layer 400~500.

(*c*) The chances of hypocentral transfers are small in such ranges of layers as 100~300→300~400, 300~400→over 700, 400~600→100~300 and over 700→400~500.

(*d*) The relations between the two layers, 100~300 and over 700, do not seem to be amenable to successive occurrence of earthqukes.

ii) For the "felt" earthquakes in Kwantô Districts.

There are only 553 earthquakes of which the hypocentral depths are known. They were felt in Tokyo during the period of 12 years from Jan. 1924 to Dec. 1935 and taken from Seismometrical Report of the Earthquake Research Institute, Tokyo Imperial University, and the depths were plotted as ordinate against the time axis, as shown in Fig. 2. From this diagram, the preferential ratios for the case of hypocentral "transfer" in vertical direction for five layers, 0~20, 20~40, 40~60, 60~80, and over 80, kilometres depth, were calculated similarly as before and given in Table II.

Table II. Vertical hypocentral "transfer" of the "felt" earthquakes in Kwantô Districts. Jan., 1924~Dec., 1935 (whole 12 years).

		Region of the second of the two earthquakes				
		0~20^{km}	20~40^{km}	40~60^{km}	60~80^{km}	80^{km} →
Region of the first of the two earthquakes	0~20 ^{km}	1·38	**1·68**	0·83	0·34	1·46
	20~40	1·26	1·05	0·95	0·93	1·19
	40~60	1·15	0·99	1·13	0·78	0·85
	60~80	*0·56*	0·80	0·88	**1·53**	0·90
	80→	0·49	0·75	0·94	**1·35**	1.36

Although we can say nothing definite of the results, we might say that

(*a*) An earthquake in a certain layer is liable to be followed by another in the same layer, particularly in the layer 60~80.

(*b*) From layer 0~20 to layer 20~40, and also from layer over 80 to layer 60~80, transfer of hypocentres frequently occurs.

(*c*) The layers 0~20 and 60~80 are independent of each other with reference to sequences of earthquakes in both directions, to and from.

3. Periodicity of the world's "deep" earthquakes.

Not only the time intervals between the occurrence of a "deep" earthquake and the next one, the number of which is $N=240$, but also the time intervals between the occurrence of a "deep" earthquake and the second, third, fourth, fifth, and sixth, the number of which is $N'=1168$, were taken, and the frequencies of these intervals for every 10 days counted and plotted as ordinates, the intervals being taken as

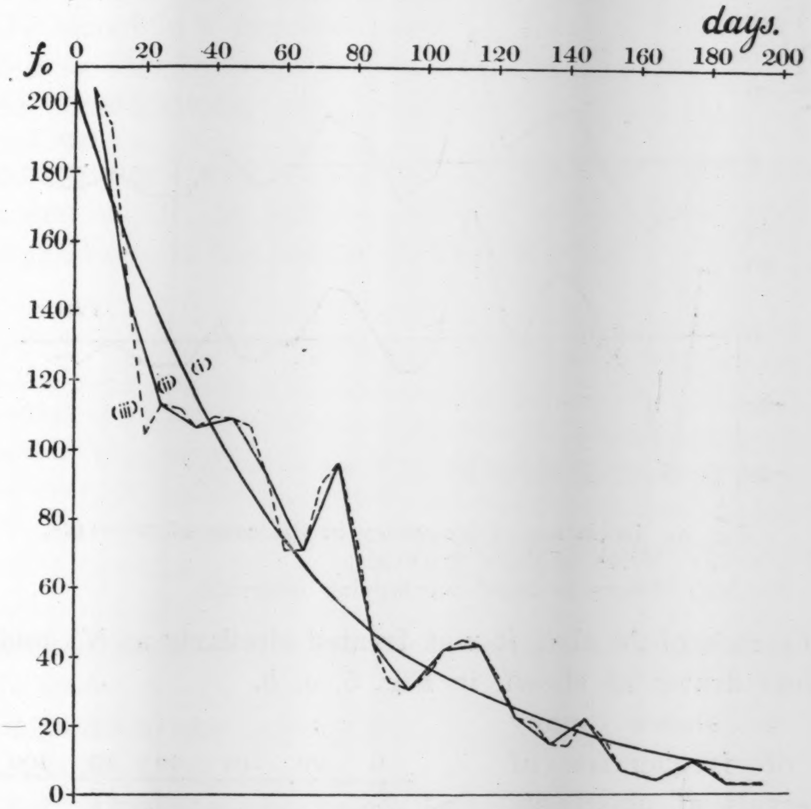

Fig. 3. Frequency of time intervals between the occurrence of a "deep" earthquake and the second, third, fourth, fifth, and sixth, the number of which is $N'=1168$.

(i) $f_t=204\,e^{-0.017t}$

(ii) Every 10 days' intervals.

(iii) Every 10 days' overlapping intervals.

abscissa, as shown in Fig. 3. for the case of N'. The intervals of time for N' were especially taken in this case in order not to miss such particular series of earthquakes as are intimately connected with one another in bringing about the sequences of earthquake occrrence, if such sequences do exist.

The general trend of the curve shows that earthquakes occur at random. We calculated the frequency f_t for purely random occurrences, assuming $f_t=a\,e^{-bt}$, and obtained the deviations in actual frequencies from the theoretical value of f. In order to satisfy ourselves that the periodicity of the deviation curve is not due to an apparent one common to any accidental phenomena, we also tried to take the overlapping intervals of days for comparison. The deviation curves for N' are shown in Fig. 4, *a*, and *b*.

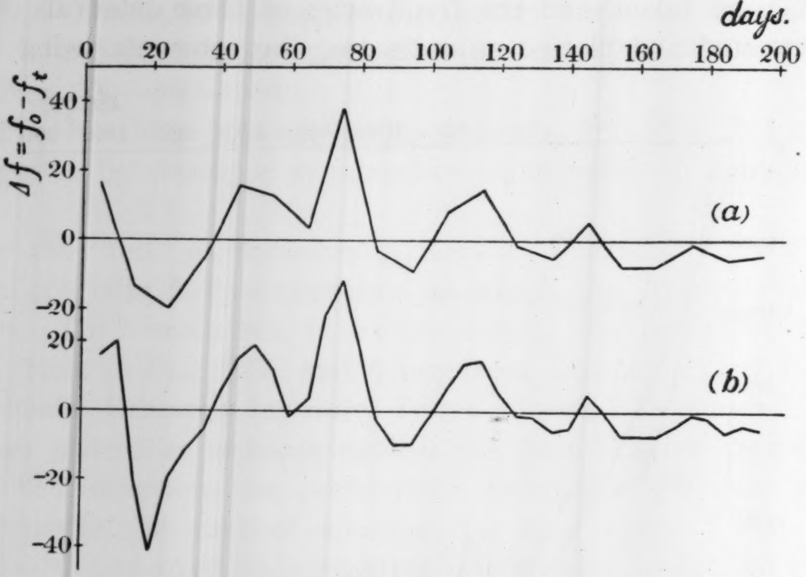

Fig. 4. Deviation of frequency in the case of $N' = 116^8$.
(*a*) Every 10 days' intervals.
(*b*) Every 10 days' overlapping intervals.

In the case of N also, it was treated similarly as N', and deviation curves were drawn as shown in Fig. 5, *a*, *b*.

Fig. 4 shows many maxima of frequencies of time intervals at about 45, 75, 115, 145, and 175 days. The period of 175 days corresponds nearly to V. Conrad's semi-annual period, which was regarded by him as being likely, and which may correspond to the rotation period of the earth's pole.

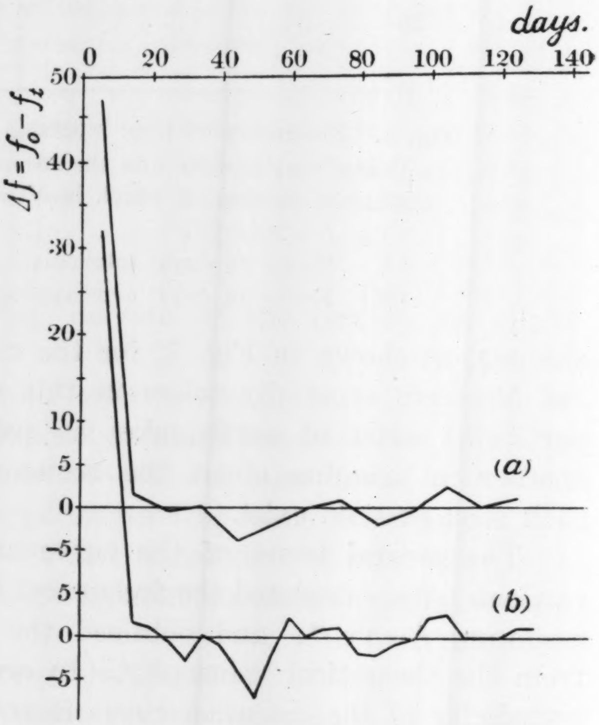

Fig. 5. Deviation of frequency in the case of the time intervals between successive two earthquakes ($N = 240$).
(*a*) Every 10 days' intervals.
(*b*) Every 10 days' overlapping intervals.

Although the amplitude of the deviation curve is rather small, we can still see from Fig. 5 large frequencies of time intervals in a conspicuous manner at about 5 days, besides which we may observe three maxima of frequencies at abont 35, 75, and 105 days. This last period of 105 days was also seen in the world's destructive shallow earthquakes as already stated in a previous paper[3]. These identical results may be regarded as a clue to some hidden physical meaning to be unravelled by future investigations.

In conclusion, I wish to express my heartiest thanks to Prof. M. Ishimoto and to Dr. N. Miyabe, both of whom have given me many useful suggestions in the course of these studies.

---

15. 世界に於ける深層地震の分布

地震研究所 山口生知

1919年より1930年に至る滿12ケ年間に起つた世界に於ける深層地震の分布，特にその鉛直分布を調査して見た.

世界深層地震の週期性に就いても研究を試みた.

其の結果は次の通りである.

1. 世界に於ける淺層地震は地中海沿岸，亞細亞大陸，日本附近，フィリッピン群島附近，濠洲及びその附近の海底，北米，中米及び南米等廣範圍に分布してをるが，深層地震は之と異なつて地中海沿岸には全く起らない. 又北米特にその大平洋沿岸には極めて稀にしか起らない.
2. 震源の深さが700kmといふ最も深い地震は日本附近，南米の中部，フィリッピン群島南部及び濠洲の東方海中に起つて居る. 亞細亞大陸の深層地震は比較的淺いものが多い.
3. 地球半徑方向の震源移動に關しては，
   (*a*) 或る深さの層に地震が起るとその層の中で引き續いて起る場合が多い.
   (*b*) 400～500kmの層から300～400kmの層には震源が移り易い.
   (*c*) 300km以下の層より300～400kmの層へ又400～600kmの層より300km以下の層へは移動することが稀である.
4. 序でに1924年から1935年に至る滿12ケ年間に關東地方に起つた有感地震について，鉛直方向に於ける震源移動を調べた結果は次の通りである.
   (*a*) 同一深さの層に於いて，地震は引續いて起り易い. 特に60～80kmの層に於いてその傾向が著しい.
   (*b*) 20km以下の層から20～40kmの層へ又80km以上の層から60～80kmの層へは震源が移り易い.

---

3) S. YAMAGUTI, *loc. cit.*, 2), 59.

(*c*) 20 km 以下の層から 60～80 km の層へ又その反對の 60～80 km より 20 km 以下の層へは移動することが稀である．卽ちその二つの層は，地震が相次いで起ることに關してお互に無關係である．

5. 世界深層地震の週期性については，175日と云ふ週期が出て來るが，之は V. Conrad が著者とは異なつた方法で調べられた結果指摘されて居るところの半年週期に相當する．

105日と云ふ週期も表はれて居るが，この週期は世界の破壞的淺層地震にも共通であると云ふことは何か或る物理的意義を有するものと思はれる．

長岡博士は地軸變動の週期のhigher harmonics に相當するものではないかと云ふ疑問を懷いて居られる．何れ將來の研究を待つて其の意義が明瞭にされるものと思ふ．

16.　昭和11年11月3日金華山沖合地震被害調査報告

地震研究所　高山威雄

（昭和11年12月21日受理）

昭昭11年11月3日5時46分頃東北地方關東地方の表日本の地は近年稀な强震に見舞れた．

氣象要覽1)によれば震央は東經142°0北緯38°4金華山の東微北約35 km の沖合にあり．强震地域は廣範圍に亘りその中主なものを擧ぐれば釜石，氣仙沼，石卷，仙臺亘理，中村，富岡，小名濱等の沿岸地方及鬼首，棚倉，三春，會津，佐原，笹川等內陸地方である．

筆者の踏査した地は福島縣の北部より宮城縣に至る强震地域內で福島縣相馬郡小高町より北上して原ノ町鹿島町磯部村磯部中村町中村町原釜宮城縣亘理郡亘理町荒濱村名取郡岩沼町增田町閖上町仙臺市鹽釜町桃生郡小野村石卷市牡鹿郡女川町等以上16市町村である以上の市町村を通じて被害の著しきものは殆どなく商品（陶器類罎詰類）の顚倒に因る破損及土藏の壁の龜裂脫落等がその主なるものであつた．後者の被害にしても古き土藏或は古き土藏造住家に限られ新らいのは勿論古くとも建築の堅固なものには少の被害もなかつた．住家の壁の落ちたと云ふものも殆どなかつた．唯例外として磯部部落地先の魚市場の吹拔小屋の倒潰したものがあつた．

各地に於ける土藏の被害を比較するに中村町が最も著しく鹿島町これに次ぎ閖上町仙臺市鹽釜町等では何れも同じ樣な狀態で多少の被害があつた．原ノ町亘理町岩沼町小高町等には殆ど被害が見られなかつた．

堤防橋梁道路等の被害も殆どなく僅かに仙臺市小野村石卷市附近に見られたに過なかつた井戶水の變化の認められた處は小高町鹿島町で一時（堀拔井戶の自然湧出）濁り或は多少の增水したらしい樣であつた．

發光現象は何處でも認められなかつた．2)

---

1) 氣象要覽447號（1936）．1166頁

2) 武者金吉氏の調査によれば，岩手縣田の濱にて11月3日地震直後沖に海光を認めた漁師があるさいふこさである．

音（地震前）は鹿島ではゴート云ふ音に續いて地震動を感じたと云ふ者多く磯部，原釜では聞へたと云ふ者聞へなかつたと云ふ者があつた．其他の地方では殆ど聞へなかつた様である．

津浪は荒濱磯部閖上等では全く認められなかつた．鹽釜に至りて漸く港内の渡船場の渡守がそれらしきものを認めた，港内設置の驗潮記象にも地震後數十分を經て海面の昇降のあつたことが現れてゐた．石巻港では全く氣付かれなかつた．女川港では地震後2尺位海面の昇降があつた模様である．

次に各地の踏査報告を記す．

福島縣相馬郡小高町 被害としては商品の被損が著しいものがあつた．建築物の被害は殆ど無く壁の亀裂等も聞ない時計は止た方が多かつたらしい．町内では飲料として掘抜井戸（深さ 60 間位）が多數使用されて居るが地震の時丈け其湧出量の少し増したもの及多少の青砂を出したもの數箇あつた．居住者の話では小高町は地盤が悪いので何時の地震でも原ノ町より多く搖れるとのことであつた．

原ノ町 時計は止たと云ふもの少なく井戸水にも變化無く墓石は多少回轉又は移動して居た．原ノ町警察署調査によれば商品の被害が小高町 2 件，原ノ町に 1 件，又原ノ町には紡績工場の電話不通 1 件あつた．

鹿島町 鹿島驛（田面埋立地）時計止り壁に數ヶ所亀裂を生じ其他にも多少の被害を蒙た驛前の石藏の一角の一部が破損した．土藏の屋根瓦が少し痛だ．町内に入て古い土造の住家（第1圖）の軒蛇腹の損傷したもの及土藏壁の少し損だもの等あつた．墓石は轉倒したものは無かつたが何れも多少回轉又は移動して居た．その程度は原ノ町及仙臺市の或ものよりは著しかつた．

時計は止た家が多つた地震の時野良で働いて居た農夫の話ではゴ1と北の方から（急行を遠くで聞いた様な音）鳴てから地面が動き出し立て居られぬ程で杉の立木は音をたてゝ搖れ出した光物等には別に氣付かなかつたと．音を聞いたと云ふ者は他に 2~3 人あつた．

掘抜井戸（深さ約 120 間）湧出量が地震直後暫くの間多少増し又濁たものが 2~3 あつた．

町の裏の小川の堤防道路上に數ヶ所亀裂が生じたとて筆者を案内してくれた者があつたが其の時には僅かにそれらしいものが見られたに過なかつた．

駐在所巡査の話では擔當區域内では報告する程の被害は無く只土藏に亀裂が入り又多少壁が落ちた位のことであり堤防其他にも被害はなかつたと．

幾部村幾部 部落内人家には被害なし，ゴーと云ふ音を聞いた者もあつた，井戸水

には變化無かつた．海岸の埋立地にある魚市場の吹拔小屋が1箇倒潰した，（第2圖）丁度其時管理人が魚船を送り出して岸壁に立て居た折だつたのでその時の模樣を仔細に觀察することが出來た．その話ではゴーと音がしてからぐらぐらと急に搖れて來たその中小屋の柱 2～3 本のものが土台から足を脫してゆらゆらして居る內地動の終る頃遂に倒潰した，海面には別に異狀は見られなかつたと．岸壁とコンクリート打ちの斜面との間に 4 cm の位の開きが出來斜面の處々に亀裂を生じた．

小屋に隣れる事務所及住宅（二階）のモルタルに龜裂を生じたが屋根瓦には異常はなかつた，土臺の周圍の地盤が 6 cm 位一樣に低下した地面には龜裂は生じなかつたが一時水を噴出した處もあつた．近くの掘拔井戶（600 尺）は地震後1時間位の間增水した，この市場は3年程前に海岸の葦原を埋立てゝ舟入場と共に建設したものである．

中村町　古い土藏及土藏造の住家の壁の龜裂，一部の脫落屋根瓦の損傷等が數ケ所で見られた（第3圖，第5圖）相隣れる土藏で古い方には相當被害を受けてゐるにもかゝはらず新しいものにはひゞ一つ入て居ないものもあつた又被害を蒙た土藏に續く住家の外觀相當古く見へても屋內の壁等には殆ど被害のないのも多かつた．

時計の停止戶障子の脫離棚の物の轉落等も隨所にあつた，或時計屋では振子が南北に動いてゐたものの中には止たものもあつたが東西のものは一つも止らなかつたと．

中村警察署の調査によれば，（1）中村町土藏壁の脫落3件石塀約 17 間倒潰1件，その他1件．（2）磯部漁業組會の魚市場倒壞1件，（3）大野村石上字蛇山住宅の裏の高さ約 20 尺の山崩壞，家屋（間口5間奧行3間セメント瓦ぶきの平家）半壞せるも人畜に被害無し，（4）駒ケ嶺村土藏の壁の落ちたもの（約半分）1 ケ所，土藏の壁の被損したるもの2ケ所硝子破損6ケ所，（5）八澤小學校の壁おちたる所 2,3，（6）尾濱土藏壁外面5坪崩落，松川築港園（カコヒ）堤には所々に龜裂を生じたり船舶には何等の被害なし，海上津浪なし．

中村町原釜，尾濱　原釜では住家非住家共に被害なし．ゴ1と云ふ音があつたと云ふ者2人音は聞へなかつたと云ふ者4人あつた，時計は止つたり止らなかつたりであつた．尾濱で土藏の壁の剝落したもの1棟（第6圖）外に龜裂の入たもの1棟あつた．猶ほこの部落內には暴風雨の日に壁が剝落したと云ふ土藏が1棟あつた．

宮城縣亘理郡亘理町　被害無し，時計は大方は止らなかつた．亘理警察署の調べでは管內で被害の報ずべきものは無かつた．唯海岸の道路に多少龜裂した箇所があつたと．

荒濱村　亘理町と同樣．可成粗末な荒壁造りの漁師の住宅ですら何等の被害を蒙てゐなかつた．音はなく，急激に短時間の間搖れたと，只變た事は阿武隈河口近くに水

路の轉向を計る爲めに河中に打込んだ沈床の杭の一部が約3尺位地震後抜出た，これと少しく離れた箇所の沈床數本のものが7尺位抜出たと土地の者の話であつた．

岩沼町　亘理町と同様，墓石の廻轉運動の模様は小高町と似寄て居た．竹駒神社前賣店の陳列品も殆ど倒れなかつた．

増田町　岩沼町と同じ程度であつた．

閖上町　岩沼町よりは多少被害が多い様に見えた．古い土藏の壁にひびの入つたもの又少し脱落したもの等 2～3 あつたが一方には荒壁造りの極く粗末な住宅ですら無難なものも少くなかつた．船着場の魚市場の邊りの道路が 10 數間の間 2～3 寸下り多少の龜裂が生じたと．岸壁には別に異常は認められなかつた．

仙臺市　住家非住家の被害も殆どなく古い土藏の壁の痛んだものは多少あつた，仙臺警察署前の墓地の墓石等の廻轉度は原ノ町それと大差なかつた．八幡神社（高臺にあり）の本殿の前の石燈籠中1基が北方に倒れた外に5～60基ある中笠石の落ちたもの 2～3，根本から倒れたもの（北方）1 基あつた，坂の途中で倒れたもの 1 基あつた．凡ての笠石は多少の回轉は免れ得なかつた．天主臺の昭忠碑の金鵄の片翼が羽先を先にして落下土中に喰込んだ，臺石にも多少龜裂を生じたとのことである．(第7圖)

愛宕橋の南の橋脚に龜裂を生じ欄干の處で左方 2·5 cm 右方 3·0 cm 外側に辷り出た路面にも亀裂を生じたが交通には支障を及ほす程のことはなかつた．

仙臺市中の被害の主なものは窓硝子の破損及商品（酒類，陶器類等の顚倒による破損）及住家，非住家の損傷等で仙臺警察署の調べによれば，住家の損傷 90 件（損害見積 800 圓） 非住家損傷，75 件（損害見積 9000 圓）其他損害件數 2（損害見積 3000 圓）道路決潰 2 件（損害見積 1500 圓）其他の損害件數 5（損害見積 500 圓）商品 80 件（損害價額 8000）合計 254 件 30000 圓である，猶同署の調査より商品被害を除き他の主なものを次に抄出す．

連坊小路小學校々庭建設中の二宮尊德翁の石像倒れた．「瑞鳳殿の石燈兩側の中五輪燈籠 2 基倒壊火袋等別個に離れ横たはり他に五輪のみ轉げ落ちたるもの 3 基あり且感仙殿東南隅石垣 1 坪程崩壊五輪燈籠 1 基横倒せり，殉死者の墓全部は倒れたるも直に原狀に復舊なし居りたり．

霊屋橋全體に渉りさしたるものに非らざるも 4,5 米位づゝ亀裂數十本生じ且全橋西袂に 10 米位の亀裂生じたり．

市役所サイレン塔の壁約 $^{1}/_{3}$ 崩壊せり．

愛宕橋南阿元約 3,4 寸位の横斷せる喰違を生じたるも云々．

（荒井巡査派出所管內）土藏の壁破損せるもの及物置土臺石垣の破損せるもの各々 1

あり.

宮城縣農學校舍の壁破損及窓ガラス600枚の破損せり.

八幡神社鳥居1破損

仙臺驛三等待合室壁亀裂を生じ5ケ所脱落二等待合室煉瓦の煙突上部より約6尺折損便所の煙突倒潰，驛前仙臺ホテル廊下の壁脱落.

（下愛宕巡査派出所）山形に通ずる縣道にて白澤野川間秋保村の分なるも約 20 間位の場所岩石崩壊し諸車交通不能なり云々，該場所附近に道路の亀裂2ケ所あるも交通に支障なき程度なり.

（芋澤巡査駐在所）村社宇那彌神社境內の石燈籠の笠倒壊したるも破損を免れたり，芋澤宿川橋の北阿元石垣崩壊せるも交通上支障なき程度なり.

（原之町巡査駐在所）平田神社鳥居破損及土藏屋根及壁の破損3件あり.

鹽釜町　被害狀況は仙臺と殆ど同様で土藏の壁及家屋の痛んだのも 2.3 見られた. 津浪，一般の人は注意しなかつたが港內の渡船場の渡守が6時から8時までの內1時間に 4～5 回潮がスーと上て來てはスーと下るのを注意した，最も大きく上下したものが 1尺5.6寸あつたと.

鹽釜警察署の調査に依れば被害は窓硝子及瀬戸物類を除いては，

七ケ濱村菖蒲田濱　で石藏の半潰1件，

松島町　で住家壁落2件屋根瓦の損傷1件，土藏2棟壁落下，

浦戸村　で土藏瓦落下2件，崖の決潰により破損1件，

（八幡村駐在所） 仙鹽道路東側高1丈崩壊.

石巻市　鹽釜町と同程度で古い土藏の壁の離れたもの 2～3 あつた(第8圖). 市役所（第4圖）の木骨帖付裝飾瓦處々が剝落した內部の壁體にも多少亀裂を生じた（古い建物である).

石巻警察署調査によれば商品を除き屋根，壁の被害は石巻市 44 件，鹿又7件，蛇田3件，稲井1件渡波2件大原1件，赤井3件，鷹來1件、小野1件，廣淵1件，前谷地2件. 道路欠壞箇所及間數は石巻市3ケ所3間，稲井 17 ケ所 60 間，女川1ケ所（女川港灣）70 間，荻濱 2 ケ所 23 間，大原1ケ所 10 間，須江 2 ケ所 2 間，廣淵 2 ケ所 5 間あつた.

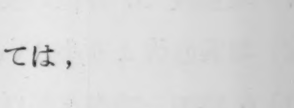

第 9 圖

石巻縣工務所主任によれば管內で被害の最も大きかつたものは，(1) 小野橋（全長247 m）左岸から 110 m 位の處で 5 cm 以上の喰違ひが生じボールトも多數損傷を蒙た，併し車馬の交通には支障なかつた. 又川床の水ぎはの芝地

に龜烈を生じた.

(2) 大鹽村内縣道に於て亀裂を生じ，長さ80 間，開口約1尺，且つ，20 cm 位低下した. これは改修をして幅員を増したので其の境ではないかと思はれる（第9圖).

(1),(2) が比較的著しい被害で以下は大いしたものではない.

(3) 定川赤井村の堤防が 30 m 位小亀裂を生じた.

(4) 石巻市對岸で湊より藤巻ノ渡に至る間堤防に多少の亀裂が生じた.

(5) 前谷地村縣道で鐵道踏切近くで 5 m 位盛土した道路に 40m 位の間に龜裂が生じた.

(2) 蛇田村で新橋（縣道に架設）コンクリート橋が其の方向にそのまゝ 1·5 cm 移動した(第10圖).

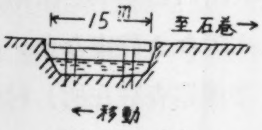

第 10 圖

女川港 被害狀況は石巻市と大差なし，この地は昭和8年3月3日の津浪で大いに痛められた處であるから，今回も人々は其點は十分に警戒して居た. 津浪のことに關し岸壁に臨んで住居して居た數人に就きたゞして見た.

(1) 地震後 20 分位の後岸壁より急に3尺位ひいたが5分間位して元通りになつた.

(2) 地震直後より小さい波が立ち海水の動揺があつた.

(3) 6 時頃一時海水がひいたが其後岸壁の面上すれすれに上つた（3尺位高まつたことになる）10 分頃で元通にひいた.

---

16. *Report on the Field Investigation of the Earthquake of November 3, 1936.*

By Takeo TAKAYAMA,

Earthquake Research Institute.

On November 3, 1936 at 5th 46m a.m. a comparatively large region along the Pacific Coast from Kamaisi in Iwate prefecture to Onahama in Fukusima prefecture was visited by a strong earthquake. The epicentre [1] was determined to be $\lambda=142°0$ and $\varphi=38°4$. The paper reports the seismic damages in these districts and the tunami affair along the coast caused by the present earthquake.

---

[1] Kishoyoran, No. 447 (1936). 1166.

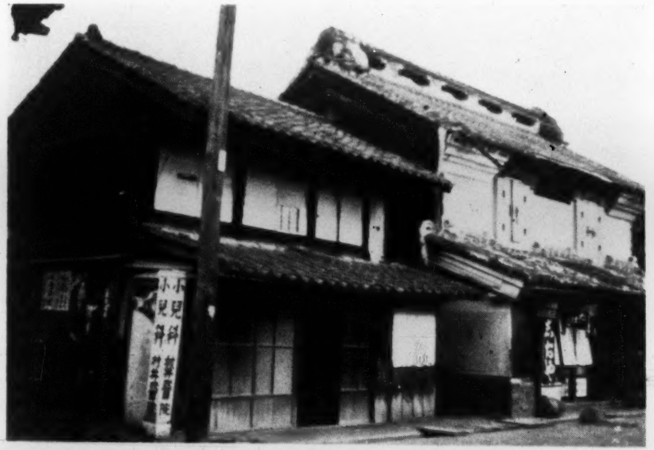

第 1 圖　鹿島町 古い土藏造住家の軒蛇腹の一部損傷

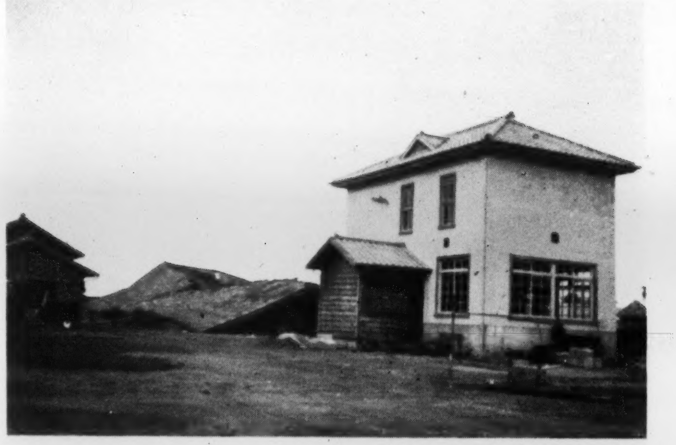

第 2 圖　磯部 魚市場の吹拔き小屋の倒潰

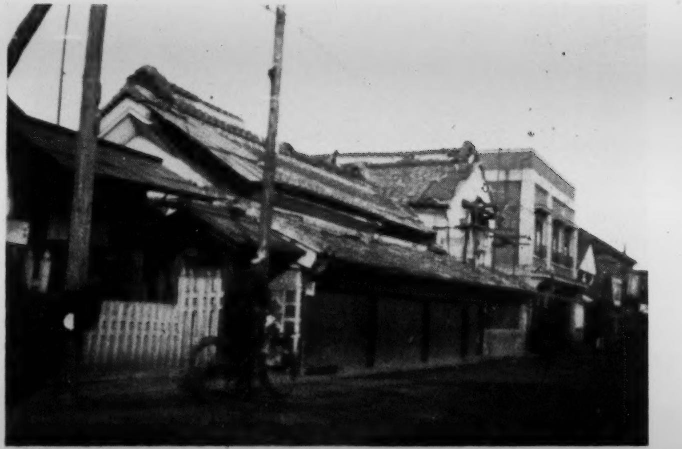

第 3 圖　中村町 古い土藏造の住家の棟瓦の辷り落ち

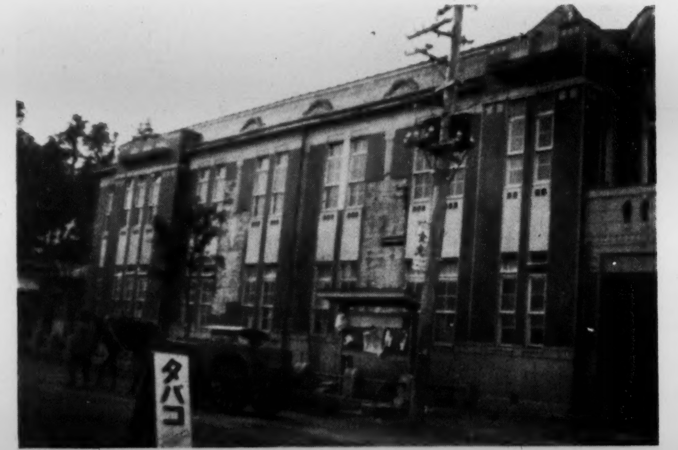

第 4 圖　石巻市 市役所古い木骨帖付裝飾瓦の一部剝落，內部の壁體にも亀裂生ず

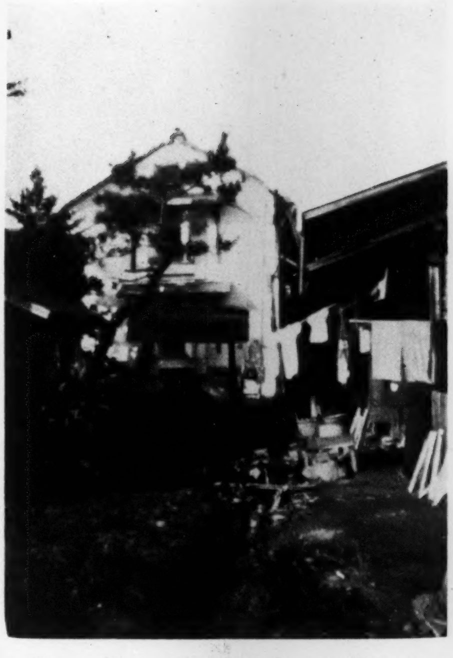

第 5 圖　中村町 古い土藏の壁の角の損傷

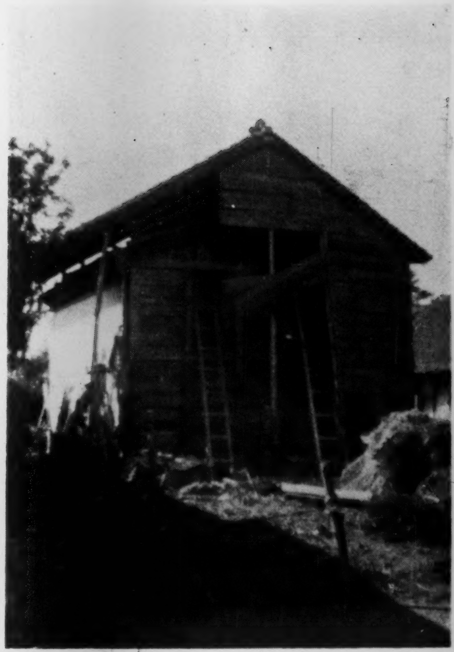

第 6 圖　尾濱村 古い土藏の壁の剝落

（震研彙報 第十五號 圖版 高山）

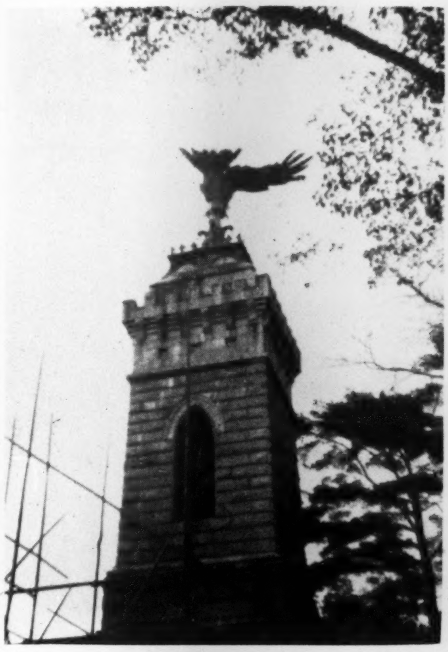

第 7 圖　仙臺市 天主臺の昭忠碑の金鵄の片翼墜落（脊面より撮影）

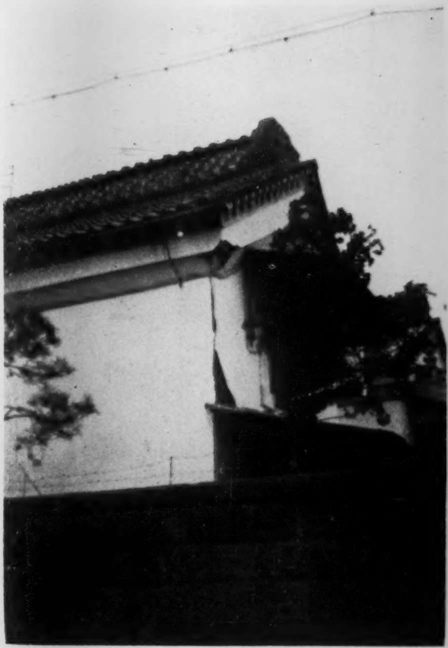

第 8 圖　石卷市 塗り替へた土藏の壁の角の損傷

17. *A Dip-Variometer.**

By Takesi NAGATA,

(Read Nov. 17, 1936.—Received Dec. 21, 1636.)

1. Introduction

The question of variations in terrestrial magnetic field in connection with seismic and volcanic activities occupied the attention of a number of investigators. Recently, S. T. Nakamura and Y. Kato,[1] who measured the dip of the terrestrial magnetic field with a Barrow-type dip circle both before and after earthquakes and eruptions of volcanoes, recognized a certain relationship between the two phenomena. According to these two authors, the variations in dip that accompany earthquakes are not always invariable in character, merely increasing or decreasing, but frequently of a complex oscillating nature.

The equi-variation lines of magnetic dip as given by these two investigators may therefore not be exact, since they were obtained from measurements extending to several days, and not from simultaneous ones. In addition, magnetic storms and daily variations must first be eliminated from the results of their observations, before any relation between the variation in magnetic field and earthquakes can be established.

In the case of a volcanic eruption, an observatory at the foot of the mountain would be an ideal place for observing the time variations, if any, in a terrestrial magnetic field following volcanic activities,[2] for which purpose continuous observation of dip would seem to give the best results.

Instead of a dip-variometer, magnetometers for horizontal and vertical intesities could be used. Askania's station variometer[3] has devices for recording both horizontal and vertical components, while Terada's instrument[4] is for horizontal intensity. Recently H. Nagaoka[5] constructed a variometer for recording the rate of variation in field intentsity; although a time variometer of the inclination itself, if such could be made, would be the most suitable.

---

* Communicated by M. Ishimoto.

[1] S. T. NAKAMURA, *Proc. Imp. Acad., Japan,* **11** (1935), 102.
S. T. NAKAMURA and Y. KATO, *Proc. Imp. Acad., Japan,* **10** (1935), 456; **12** (1936), 64.
Y. KATO, *Jap. Journ. Astro. Geophys.,* **10** (1933), 249; **12** (1934), 1; **12** (1934), 237.

[2] T. MINAKAMI, *Bull. Earthq. Res. Inst.,* **13** (1935), 790.

[3] *Handb. d. Exp. Phys.,* XXV, I Teil, pp. 579~585.

[4] T. TERADA, *Jaurn. Coll. Scien., Tokyo Imp. Univ.,* **38** (1919).

[5] H. NAGAOKA, *Read at annual meeting of Phys. Chem. Res. Inst.,* (1936), Not yet published.

2. Design and Construction

Sensibility. According to S. T. Nakamura,[6] the variation in dip that accompanies earthquakes and volcanic eruptions is, at maximum amplitude, about 10 minutes of arc, the minimum clearly recorded variation in dip necessary for analysis being 0·2 min. of arc. In the writer's instrument, therefore, the designed sensibility in 5 mm/minute in the scale value of the recorder.

System of magnification. If the system of recording is optical, the most convenient length for the optical lever is about one meter, for which reason a second magnification is necessary.

The bifilar suspension, shown in Fig. 1, which was adopted for the second magnifying device, proved satisfactoay. In Fig. 1, AB is a bar magnet supported at its center of gravity, and OC an arm fixed to the magnet in such a direction that when the magnet is free, it points downwards. D is the top of another arm fixed to the base of the instrument, a mirror M being suspended with quartz fibre from C and D.

Denoting the deflection angle of magnet AB and mirror M by Θ and Ψ respectively,

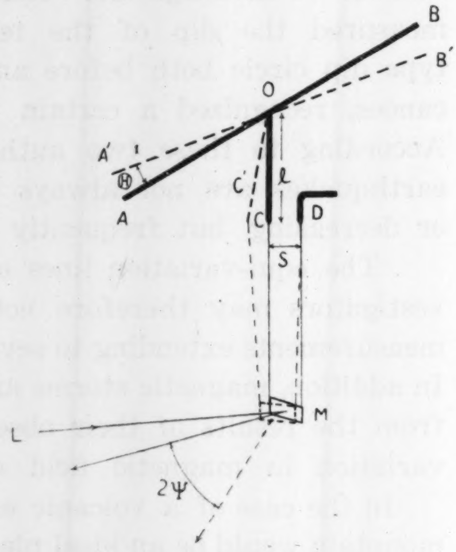

Fig. 1. Sketch of the system of magnifcation
AB; Bar magnet
M; Mirror
L; Light source.

$$\text{the displacement of } C = CC' = l\Theta, \qquad \tan\Psi = \frac{l\Theta}{S},$$

whrer l is the length of OC, and S the distance between C and D.

Since $\Theta \ll 1$, $\Psi \ll 1$, We have from the above equation

$$\Psi = \frac{l}{S}\Theta. \tag{1}$$

---

[6] *loc. cit.*.

In the writer's instrument, it has been designed that in order to secure the necessary sensibility, l/S shall be 8.

Intensity of magnet. In the design of this dip-variometer, one of the greatest difficulties was to eliminate the errors caused by displacement of the center of gravity of the magnet system through the knife edge, by means of which the magnet is supported of horizontal agate plates. We shall now estimate the magnitude of the error arising from this cause in the case shown in Fig. 2.

At the initial state, where the direction of the magnetic field is OH in the magnetic meridian and its intenstiy H, thd equation of equilibrium of the needle is

$$MH\sin\theta = mgp\sin\varphi\,, \qquad (2)$$

where M is the magnetic moment of the magnet, m its mass, and θ and φ tho angles shown in the figure. When the direction of the magnetic field changes by amount δ from its initial direction, becoming OH' in the figure, the equation of equilibrium in this state is

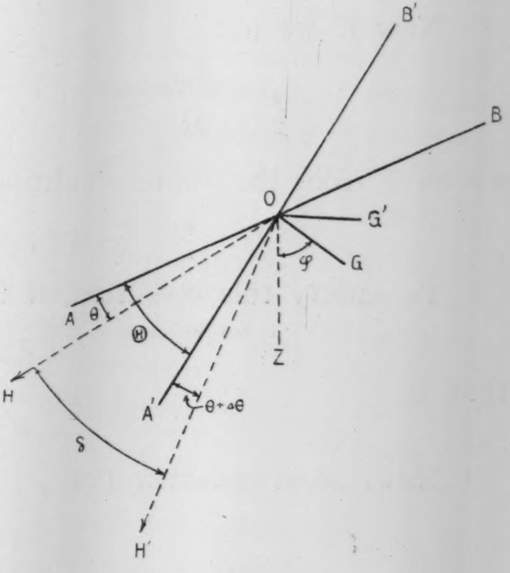

Fig. 2.

$$M(H+\varDelta H)\sin(\theta+\varDelta\theta) = mgp(\varphi+\Theta)\,, \qquad (3)$$

where Θ is the angle of deflection of the magnet. Beside this, there is a relation between δ and Θ, as shown in the next equation

$$\delta - \Theta = \varDelta\theta\,. \qquad (4)$$

From equations (2), (3), (4), we can get, neglecting small quantities, the relation

$$\Theta = \frac{\delta}{1+\dfrac{mgp\cos\varphi}{MH\cos\theta}} + \tan\theta\,\frac{\dfrac{\varDelta H}{H}}{1+\dfrac{mgp\cos\varphi}{MH\cos\theta}}\,, \qquad (5)$$

As will be seen from equation (5), the deflecting angle Θ of the magnet depends not only upon δ, but also upon $\varDelta H/H$. From records obtained in observations of the terrestrial magnetic field, the maximum daily variation in dip is usually only from 1 to 2 minutes, while the total intensity amounts sometimes to 100 γ. As the magnitude of H in

Japan is about 35,000 γ, the maximum value of the daily variation in $\Delta H/H$ may be of the order of $3\ 10^{-3}$. For recording the variation in dip itself, the part of the deflection of the magnet that is due to $\Delta H/H$ must be negligible cempared with that due to δ.

Consequently the writer designed his instrument to satisfy the next condition in equation (5), namely.

$$\delta \gg \tan\theta \frac{\Delta H}{H}.$$

Now if we put,

$$\frac{\Delta H}{H} \sim 3\cdot 10^{-3}, \qquad \delta \sim 0\cdot 0003 = 1',$$

we have from the above condition,

$$3\cdot 10^{-4}, \gg 3\cdot 10^{-3}\tan\theta.$$

To satisfy this condition, it is suficient if we have,

$$\theta \lesssim 10^{-2},$$

that is,

$$\theta \lesssim 30'.$$

Now, from equation (2)

$$\theta \simeq \frac{\rho g}{IH} p\sin\varphi, \tag{6}$$

where ρ is the density of the magnet, and I the magnetic intensity per unit volume. Since in Japan,

$$\frac{g}{H} \simeq 3\cdot 10^{3},$$

the next relation can be obtained from equation (6),

$$p\sin\varphi \sim 3\cdot 10^{-4}\frac{I}{\rho}\theta \lesssim 3\cdot 10^{-3}\frac{I}{\rho}. \tag{7}$$

As will be easily seen, it is difficult to adjust $p\sin\varphi$ so that it shall satisfy the condition expressed by equation (7) unless quantity I/ρ is larger than 10^3. To fulfil this requirement, we used "Mishima" steel, the intensity and magnetic stability of which are large enough for this purpose. The stable magnetic intensity $\sigma\left(\sigma = \frac{I}{\rho}\right)$ of magnetized Mishima steel is about $7\cdot 10^3$, *C. G. S.* units, whence from equation (7) we have

$$p\sin\varphi \lesssim 2\cdot 10^{-2}.$$

Condition (7) is therefore easily satisfied. In the denominator of equation (5), $\frac{mgp}{MH}$ then becomes as small as 10^{-2}, with the result that the effect of this 2nd term on sensibility may be disregarded.

Details of the instrument. Based on these principles, the writer designed and constructed a dip-variometer as follows:—

a) The magnet is supported on agate plates by the usual steel knife-edge fixed to the magnet. The magnet is of cylindrical shape, 1 cm in diameter, 10 cm long. Although these dimensions of the magnet seem to exceed somewhat those of usual magnetometers, it was inevitable in order to overcome errors due to displacement of centre of gravity of the magnet owing to the knife edge.

b) To bring the centre of gravity into line with the knife edge, three counter weights are attached to the magnet as shown in Fig. 3.

An arm holder, supporting an arm made of fuzed silica, is also attached to the magnet making an angle of 50° with the axis of the magnet, that is, in such a direction that it becomes vertical when the magnet is free.

Since in the Kwanto district and vicinity, the dip ranges from 45° to 55°, it is necessary for our purpose that the direction of the arm may be varied within this range, adjustment being made by a pair of screws attached to the arm-holder.

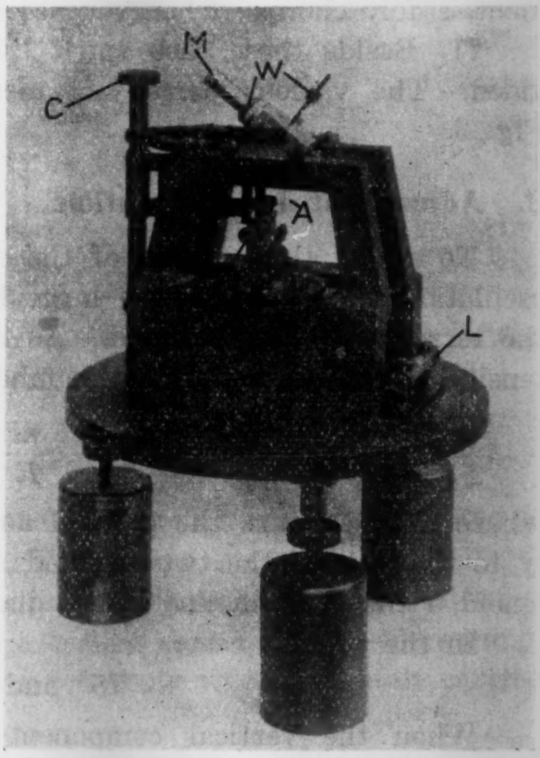

Fig. 3. General view of the instrument. Cover and lens removed.
M; Bar magnet
W; Counter Weight
A; Arm made of fuzed silica
C; Clamping
S; Screw for adjustment of sensibility
L; Spirit level.

c) As will be seen from equation (1), the magnification can be varied by changing S, namely, the distance between C and D. Arm D, made of fuzed silica, is affixed to the metal pieces shown in Fig. 3, the metal piece being adjustable in 3 directions by means of three screws, so that not only the sensibility of the instrument, but also the deflection of the suspended mirror can be adjusted.

d) As the weight of the suspended mirror must be the smallest possible, in the case of this instrument a plane mirror $3^{\mathrm{mm}} \times 5^{\mathrm{mm}}$ in size and weighing only 0·1 gram is suspended by means of two thin fibres ot fuzed silica of $5 \sim 6\,\mu$ diameter.

The torsional effect of these fibres is therefore negligible, provided the angle of deflection Ψ does not exceed one degree.

e) A clamping, device provided on the left-hand of the instrument, safely clamps, whenever necessary, both mirror and magnet.

f) Beside these, two spirit livels and a converging lens are provided. The various parts just mentioned are arrangeed as shown in Fig. 3.

3. Adjustment and Calibration

To adjust the position of the centre of gravity of the magnet, the oscillation method is used, a large Helmholtz's coil being used to nullify the terrestrial magnetic field. As is well known, the magnetic field intensity at the centre of the Helmholtz's coil is approximately,

$$X = \frac{8}{5\sqrt{5}} \frac{ni}{R}, \qquad Y = 0, \tag{8}$$

where X and Y are the parallel and orthogonal components respectively to the axis of the two solenoids, n the number of turns of each solenoid, i the current, ane R the diameter of the coil.

In the present case,

$$n = 75 \quad \text{and} \quad R = 50\,\text{cm}.$$

When the vertical component of the terrestrial magnetic field is compensated by this coil, which is installed vertically as shown in Fig. 5 (Plate I), it is possible to obtain a space that is free from terrestrial magnetism in the neighbourhood of its centre and in the plane perpendicular to the magnetic meridian.

In this plane, the magnet can oscillate on the knife edge under the force of gravity alone, and its period T can be determined by the equation

$$T = 2\pi \sqrt{\frac{J}{mgp}},$$

where J is the moment of inertia of the magnet around the axis of its rotation. As to the present instrument, since we have

$$m = 65, \qquad J \simeq 6 \cdot 10^2,$$

if the period T is 15 sec, we have

$$p \simeq 2 \cdot 10^{-2}, \quad \therefore \quad p \sin\varphi \lesssim 2 \cdot 10^{-2}.$$

This is small enough to offset the errors mentioned in section 2. Since the longer the period T the better, the writer adjusted the period to 20 sec.

The sensibility was calibrated by deflecting the magnet placed in the magnetic meridian with the Helmholtz's coil. The field intensity in the neighbourhood of the center of the coil was calculated from equation (8) and the total intensity and dip of the natural field measured with another magnetometer. The procedure in this calibration was checked by absolute measurements, using a "Suirobu" type magnetometer.[7]

A sensibility curve, when $l S$ is 8·3, is shown in Fig. 4. If necessary, the sensibility can be increased up to 10^{mm}/minute.

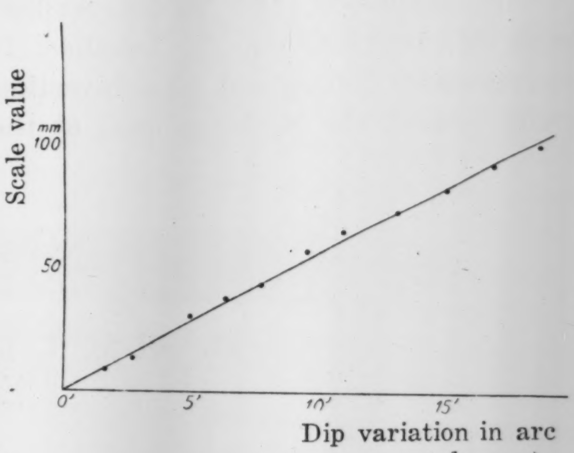

Fig. 4. Sensibility Curve. $\left(\frac{l}{S}=8\cdot3\right)$

4. Results of Obsrvation in Tokyo.

As is well known, the magnetic field in such a place like Tokyo is always disturbed by eletric railways, motor cars, etc.[8]

The disturbance, however, is comparatively small during the hours from 2^h to 4^h a. m., when the electric trolley cars have ceased running. The adjustment and calibration mentioned above were invariably carried out during this period.

In Fig. 6. (Plate II) are shown several records of dip variations obtained at the Earthquake Research Institute, Hongo, Tokyo. Seeing that the disturbance was very pronounced, the optical lever in this case was shortened to 30 cm, the sensibility being accordingly 1·5^{mm}/minute.

In the case of observations made in an Institute such as ours, the artificial disturbance is so large and the oscillation so pronounced, that care is necessary te see that the magnet shall faithfully follow even such quick oscillating disturbances.

For this purpose, two copper plates were placed near both sides of the magnet to act as a magnetic damper, the gap between them being adjusted so as to give almost critical damping.

Although the present observations made in Tokyo cannot be expected to supply any knowledge of the daily variations in the magnetic field or other geophysical phenomena, it is hoped that observations now being made with the instrument at the foot of Mt. Asama and other volcanoes, will yield much fruit.

---

[7] *Bull. Hydrogr. Dep., I. Jap. Navy.*, **5** (1926).

[8] S. Ono, *Geoph. Mag.*, **3** (1930), 229.

In conclusion, the writer wishes to express his sincere thanks to profs. M. Ishimoto ond R. Takahasi for their kind guidance and encouragement throughout this investigation, and to Mr. M. Hirose, who kindly placed the Mishima steel at the writer's disposal.

---

17. 磁氣伏角變化計

永田　武

Milne, 田中館, 長岡博士等によつて最初に注目された地震及火山爆發による地球磁場の擾亂に就て, 最近中村(左)博士. 加藤學士等はその多くの實例に就て伏角の測定を行ひ, 注目すべき結果を擧げてゐられる. 筆者は之等の測定にあたつて, 少くとも一地點に於ては連續的に時間的變化の觀測を行ふ必要を感じ, 伏角の時間變化の記錄裝置製作を試みた.

伏角計の製作にあたつて, 先づ二つの困難に相遇する. 一つは, 倍率の問題であり, 他の一つは, 地磁氣の强さに比して, 重力加速度が著しく大である爲に, 磁針を充分その重心近くで支持する事に於ける困難である. 筆者は, 前者に對して. 普通の光挺による擴大裝置の上に, 更にその反射鏡を二本吊方法を用ひて第二段の擴大を爲さしめる事により, 又後者に對しては磁針の材料として“三鳥鋼”を用ひる事により, 夫々の目的を達する事を得た.

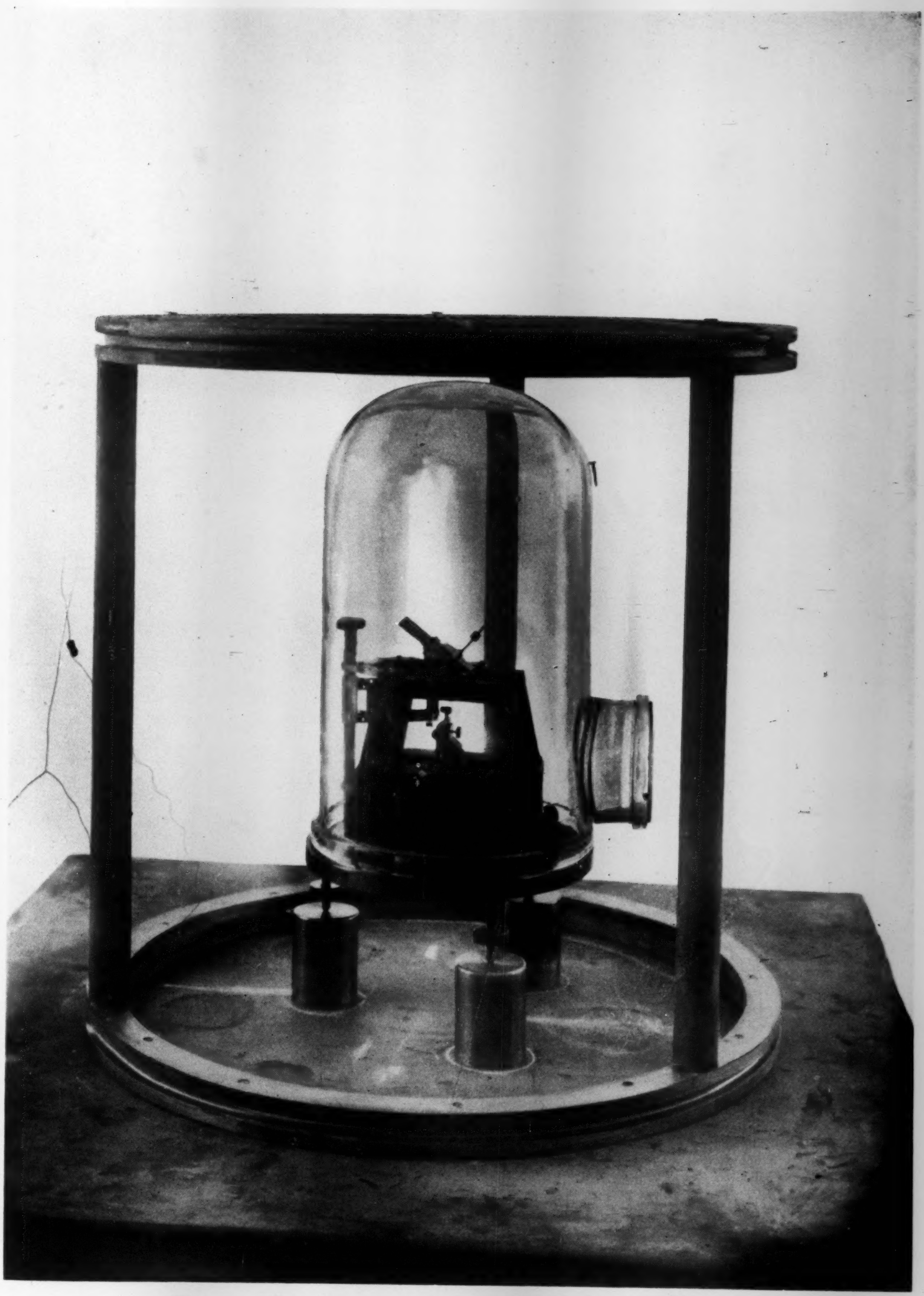

Fig. 5. The dip-variometer and Helmholtz's coil.

（震研彙報 第十五號 圖版 永田）

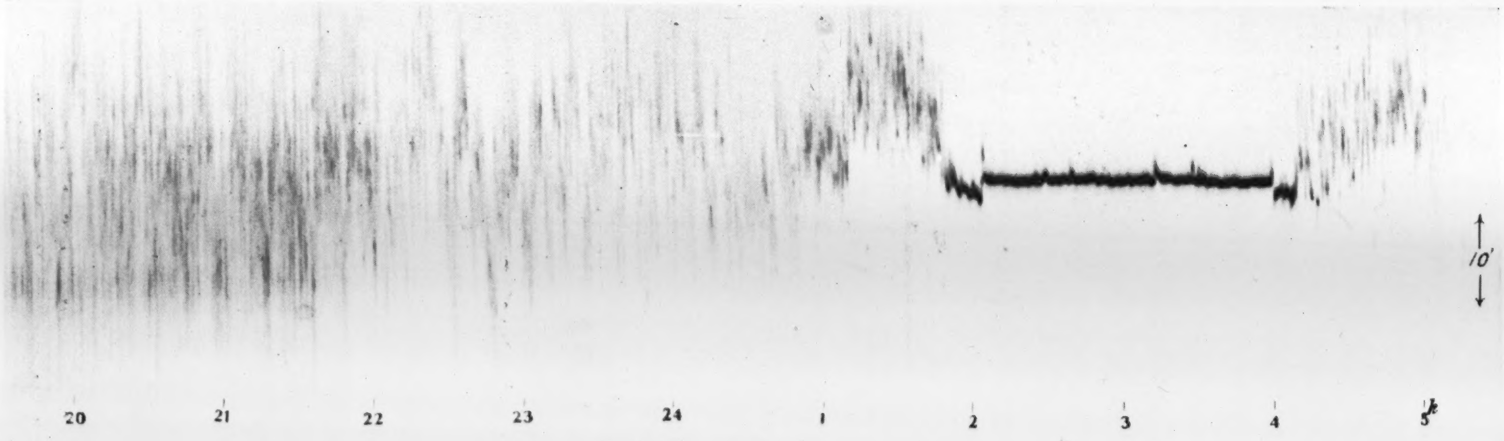

(a) 20 h~5 h

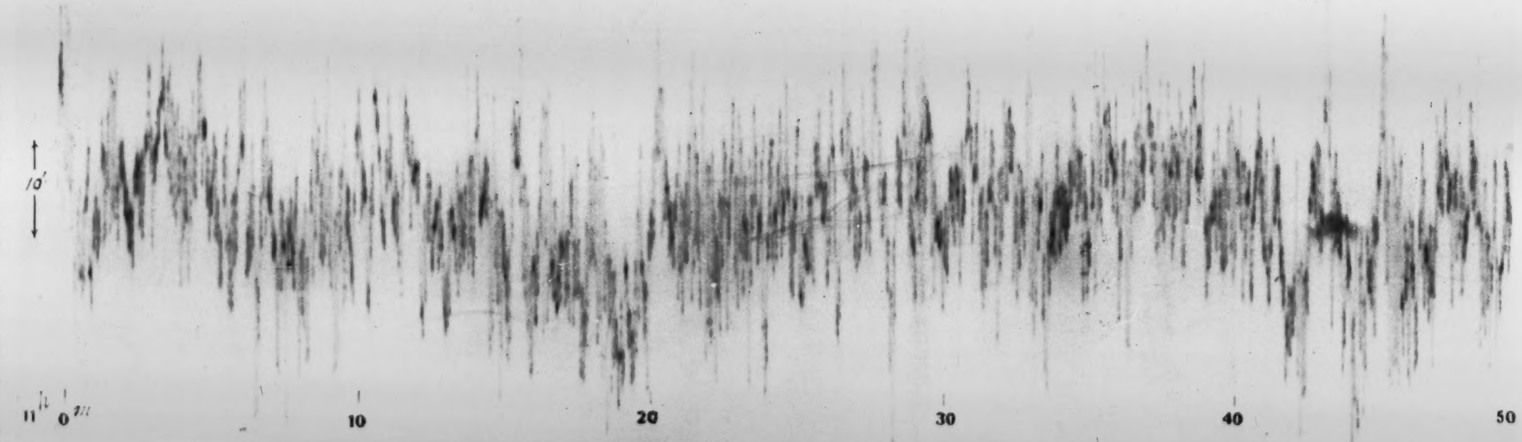

(b) 11 h 00 m~11 h 50 m

Fig. 6. Records of dip variation obtained at E. R. I.

18. *"Decken" Structure in the Bôsô Peninsula, Japan.*

By Yanosuke OTUKA,

Earthquake Research Institute.

(Read Dec. 15, 1936.—Received Dec. 21, 1936.)

The writer, here discusses the probable existence of "Decken" structures in the Bôsô Peninsula, and suggests certain points to be considered in any tectonical study of this region.

The Bôsô Peninsula is the eastern arm that surrounds Tôkyô bay, its southern part being divided into the Kiyosumi and Awa mountainlands by a tectonic valley running in an E–W trend from Hota (保田) to Kamogawa (鴨川). The tectonic line that forms this valley may be called the *Kamogawa tectonic line.*

The watershed of the Kiyosumi mountainland is in the southern part of this mountainland, almost parallel to the Kamogawa tectonic line, the northern slope of which gradually becomes lower, forming many *cuesta* like topographies owing to the simple monoclinal structure of the Neogene, where as its southern slope goes steeply down to the lowland of Kamogawa tectonic valley and the Pacific Ocean.

The Awa mountainland, which is lower than the Kiyosumi, consists of complicated structures of Neogene and other rocks.

The Kiyosumi mountainlands have been studied geologically by Dr. WAKIMIZU[1], the late Dr. N. YAMASAKI[2], Dr. H. YABE[3], and F. UEDA[4], and in detail recently by T. MITSUCHI[5] and the writer.

The stratigraphic succession exposed near Mt. Kiyosumi is as follow in descending order:

- Neogene
  - Kiyosumi sandstone bed.
  - Amatu bed
    - Amatu upper mud.
    - Amatu upper tuff.
    - Amatu middle mud.
    - Amatu lower tuff.
    - Amatu lower mud.
    - Utusumi alternation.
  - Sakuma bed

---

[1] T. WAKIMIZU: *Jour. Geol. Soc. Tokyo,* **8** (1901).

[2] N. YAMASAKI: *Jour. Fac. Sci. Imp. Univ. Tokyo,* sec. II, (1926) pp. 77—119.

[3] H. YABE: *Gendai no Kagaku,* **2**, 4 (1914).

[4] F. UEDA: *Jour. Geol. Soc. Tokyo,* **37** (1930), pp. 250—253; **30** (1933) pp. 799—801.

[5] T. MITSUCHI: *MS. of Geol. Sheet,* 1/75000, *Imp. Geol. Surv.*

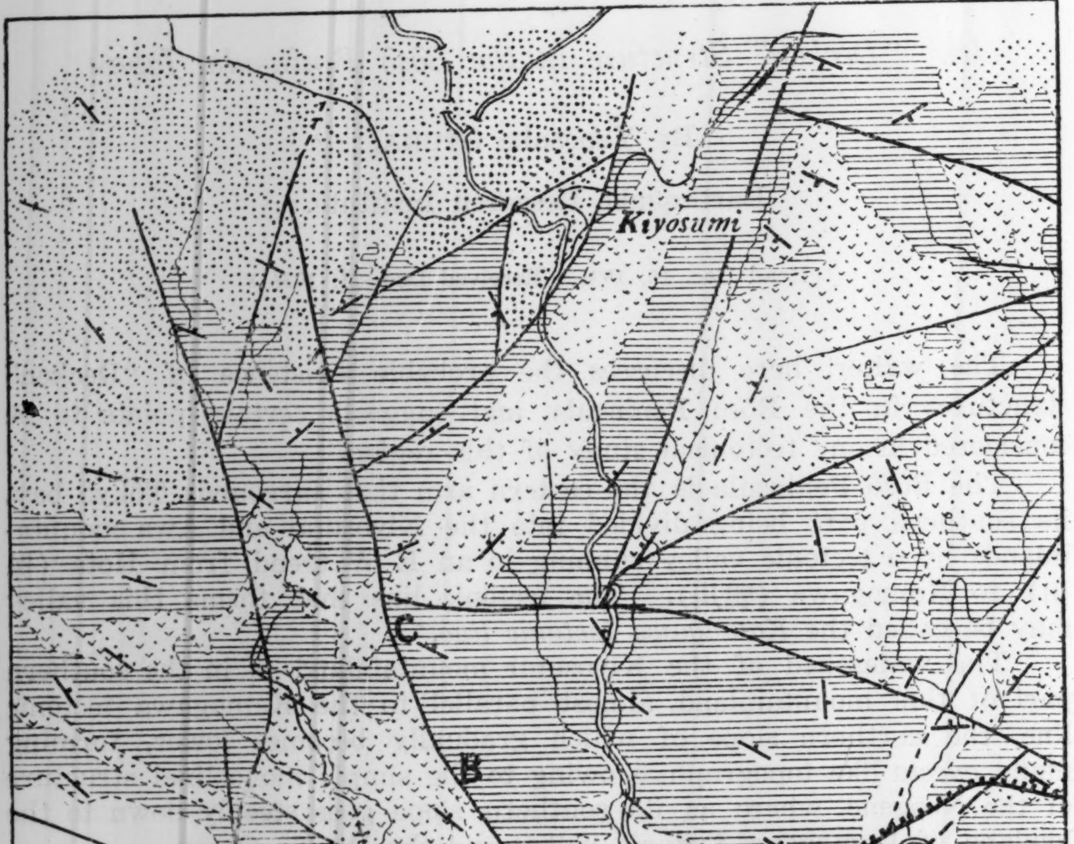
Kiyosumi
C
B
A
Amatu
Alluvium
Kiyosumi sand bed
mud
tuff
mud
tuff
mud
Amatu bed
Utusumi sand. mud and conglomerate bed
Fault

Fig. 1. Geologic map near Mt. Kiyosumi [Surveyed by T. MITSUCHI and Y. OTUKA, 1936.]

This stratigraphic column is that partly given by T. MITSUCHI and F. UEDA. Their stratigrahic division embraces more geologic formations, but they will not be discussed here.

Fig. 1 is a geologic map of the region near Amatu, Tiba prefecture. According to the geologic map, the Kiyosumi and Amatu regions consist of the Amatu and the Kiyosumi beds, forming a synclinal structure (distance from limb to limb of fold about 5 km), cut obliquely by faults. In this strucutre the writer found a low angle thrust as shown in fig. 3. This exposure has increased the probability of the existence of "Decken" structure in the Bôsô Peninsula. At localities A, B, C fig. 1, the writer found outcrops of a normal fault cutting the synclinal structure just mentioned. This fault dips 60° westward, a tuffaceous coarse sandstone bed being the down-throw, the horizon of which is higher than that of the mudstone bed which is the upthrow side, and exposed at the Amatu shore. The stratigraphic relation of this tuffaceous sandstone bed to the mudstone bed may be seen on the road from Amatu to Kiyosumi, where the former is conformably underlain by the latter. Although, the geologic structure of Mt. Kiyosumi, as already mentioned, is complicated, if compared with that of the Awa mountainland, the former is so simple that a detailed field geologic survey of the scattered exposures is sufficient to enable one to construct an almost exact geologic structural map, where as in the case of the latter it may not be possible to do the same owing to the apparent lack of continuous geologic exposures.

Fortunately, however, the eastern coast of the Awa mountainland is fringed with broad upheaved wave-cut platforms (Fig. 4) on which parts of the complicated structure of the Awa mountainland are continuously exposed, with the result that the writer, succeeded in con-

INDEX MAP

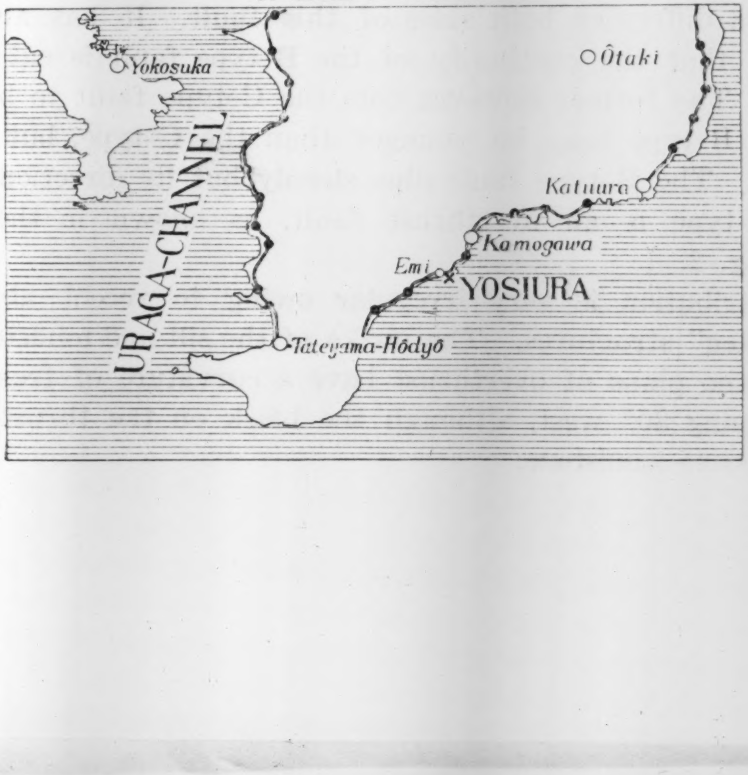

structing a geologic map (1/100) of this raised wave-cut platform southeast of Yosiura (吉浦), in Hutomi-mura (太海村), Awa-gun (see index map).

Fig. 2 is a geologic map of the platform, in constructing which it took the writer and his assistant, S. INOMATA, 5 days. Loc. 1, fig. 2, × in fig. 5 are the basal point shown in index map.

Geologic interpretation of fig. 2.

The most remarkable faults in fig. 2 are those that have trends of about N 60° E as AB fault, fig. 2. They are grouped here into the writer's type A, which are those most recently formed, and which have affected the positions of other types of faults as seen in loc. 2 and 3, fig. 2. It will be noticed however that the strata on each sides of a fault of type–A are neither altered in strike nor in direction of dip. That is, as seen in the northeast corner of fig. 2, neither strike nor dip of the strata are affected by the A-type of faults, nor are they deformed through "Schreppung", or drag. From these facts, the writer concludes that the A-type faults occurred with greater suddenness compared with the other two types of faults to be described presently.

On account of its small resistance to wave-action, the A-type faults on the Yosiura wave-cut platform are grooved deeply along the A-type faults, although the characteristic fault topography which seems to be due to the A-type of faults is not found in the Awa mountainland. The A-type faults dip variously ranging from 70° to vertical.

Further conspicuous faults run in an E-W trend, called here the B-type, the most prominent of which is the CD fault, fig. 2, and which runs through the centre of figure 2 in an E-W trend. The position of the strata differs on both sides of this fault. It has already been pointed out that the continuity of the B-type fault is cut by the A-type fault. The former however cuts the C-type fault to be described later. The B-type may be younger than the C-type, but older than the A-type. The B-type fault dips steeply but its direction changes.

The C-type is an overthrust fault, as shown in the northeast corner of fig. 2.

Its distribution is very irregular owing to recent abrasion into small "Decken" structures. The strike of the silt and mudstone alternation below the plane of overthrust have a curvature of from NS to N 60° W, dipping 30° west, although the block on the thrust plane consists of massive sandstone.

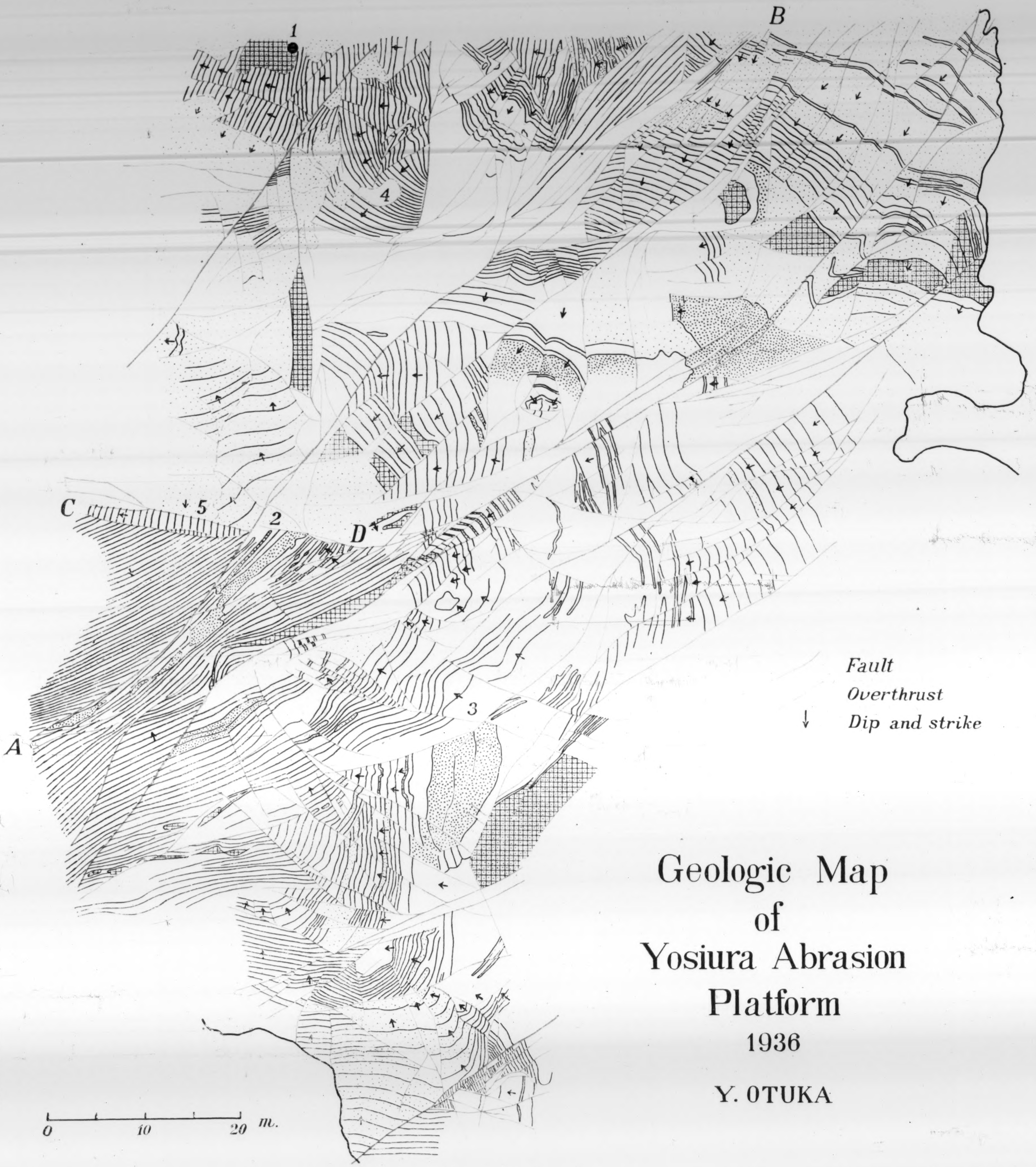
B
1
4
C
5
2
D
3
A
Fault
Overthrust
Dip and strike
Geologic Map
of
Yosiura Abrasion
Platform
1936
Y. OTUKA
0
10
20 m.

（震研彙報 第十五號 圖版 大塚）

Fig. 2. Geologic Map.

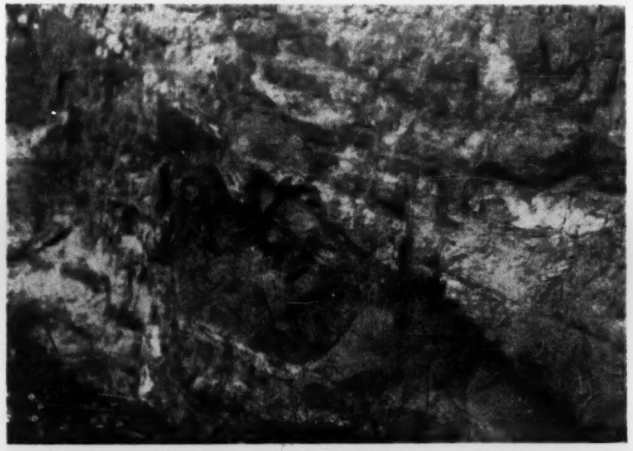

Fig. 3. Low angle thrust in Mt. Kiyosumi.

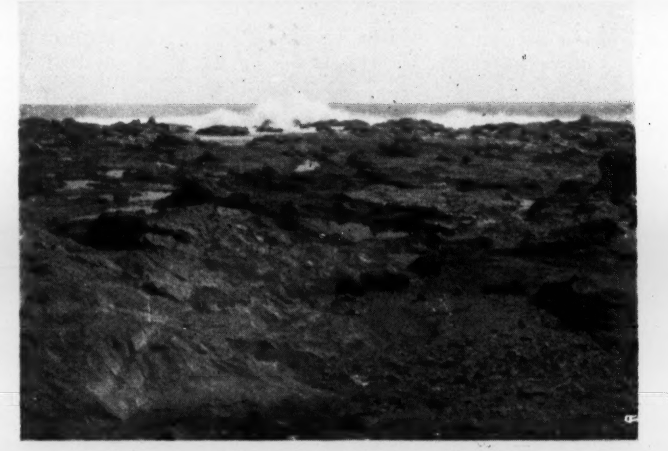

Fig. 4. Yosiura abrasion platform.

（震研彙報 第十五號 圖版 大塚）

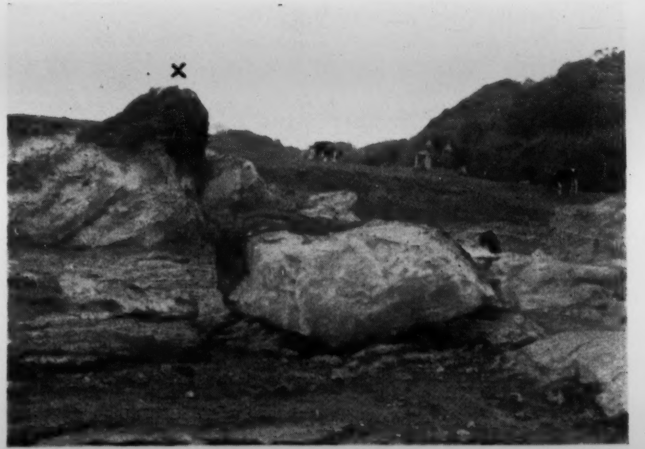

Fig. 5. Yosiura overthrust. × is the locality 1 in fig. 2.

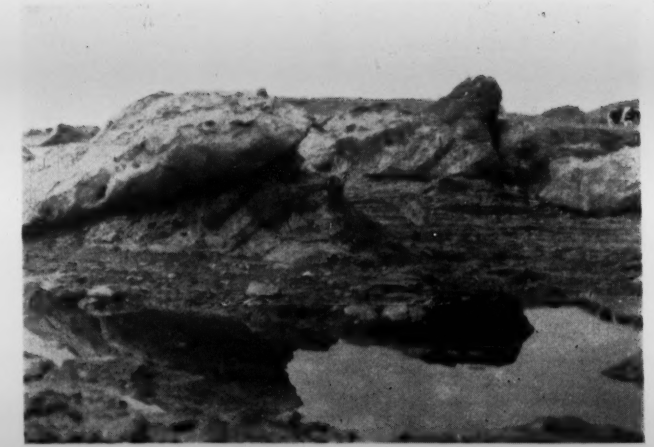

Fig. 6. Yosiura "Klippe". (Loc. 4 in fig. 2.)

A "Klippe" exposure at loc. 4, fig. 2, is shown in fig. 6. It was photographed from the east. This "Klippe" was formed by abrasion after movements of the B- and A-type faults which shifted the plane of the overthrust.

The C-type fault is the oldest fault of all, but the structure below the thrust plane must have been deformed before thrusting. Were these three types of faults disregarded in figure 2, the structure below the thrust plane would show a syncline, the axis of which trends E-W as seen in figure 2. That is, the overthrusted block covered this synclinal structure after the latter had already formed.

The tectonic development as interpreted from the geologic structure exposed on the abrasion platform at Yosiura is as follows:

1. Formation of synclinal structure.
2. Formation of overthrust structure.
3. Formation of B-type fault.
4. Formation of A-type fault.

As already mentioned, the writer is of opinion that overthrust structure may exist in the Awa mountainland.

The geologic age of this overthrust may be Late Miocene or Early Pliocene seeing that, as is known from previous studies, the southern part of the Bôsô and Miura Peninsulas greatly contracted during Later half of Miocene and Early Pliocene, so that the overthrust structure must have been formed at the time this contraction occurred, although the A and B-type faults may be younger than the C-type. The Awa mountainland therefore may consist not only of block structure as explained by previous writers, but also of folded and overthrusted structures. Those intending to study the Awa mountainland, would do well to take these structural characteristics into consideration.

---

18. 房總半島に於けるーデッケン構造

地震研究所　大塚彌之助

房總半島清澄山地．安房山地の地質構造の特徵を述べ，安房郡太海村吉浦海岸波蝕臺地面上に露出する複雜なる地質構造から安房山地にデッケン構造存在の可能性を知れり．

19. 日本群島附近の古第三紀の海岸線の變化

地震研究所　大塚彌之助

（昭和11年12月21日受理）

東亞の古地理圖，特に日本群島附近の古第三紀以來の海岸線の變化に就いては既に筆者は簡單に圖示したことがあつた[1]．尤も之より以前に多くの歐米の學者，例へば Arldt[2], Dacqué[3], Grabau 等が日本群島附近を含んで古地理圖を作製してゐたが，多くは東亞の事情に暗いため我々にとつては不滿足なものに了つてゐた．筆者が上記の古地理圖の作製を試みた當時も既に述べた如く，筆者の知識は極めて貧弱で，その作製に當つて，大膽な假定を多數に設けなければならなかつた．併しその後數年間多くの日本の層位學者・古生物學者の眞摯な努力によつて，遂に數年前筆者が試みた古地理圖に大修正を施すの餘儀なきに至らしめた．次に示す古地理圖も之等の貴重な研究結果の集積であつて，之からも益々進歩して行く，各地質時代に於ける古地理學的狀態の知識によつて，更に大改良が試みられる筈の原稿圖の樣なものである．之等の古地理圖に順次に示される變化は我々をして種々な地殼の習性を知らしめ我々の一生によつては充分に經驗することのできぬ將來の地變に對しても多くの關心を持たしめるに至るに違ひない．我々は假に過去から現在への地殼變化の狀をシネマで撮影し得たとするならば，古地理圖はその長い變化の一狀態を描出してゐるフイルムの數齣を重ねて見たものに過ぎないから，地殼變化の狀態を詳細に，且つ連續的に觀察するためには將來多くの古地理圖を作製する必要があらう．

古地理圖作製方針

古地理圖作製の方針に就いては既に Arldt, Dacqué, Schuchert[4] 氏等の詳細な論述があり，再説する必要もあるまいが，簡單に筆者の採つた方針を説明しておかう．

1. 各地に發達してゐる地層・岩石が持つてゐる過去の地理學的狀態を知るに必要な，資料を充分に知悉して組み立てられた夫々の地方の地史が先づ必要である．

2. 次に夫々各地で組み立てられた地史に就いてお互の同時性を嚴密に確めなけれ

---

[1] 望月勝海，大塚彌之助　地形發達史　岩波地理學講座 (1932).

[2] Arldt, *Handbuch der Palaeogeographie*, (1919), pp. 407, 413, 416, & 419.

[3] Dacqué, *Grundlagen und Methoden der Paläogeographie*, (1915).

[4] Schuchert, *Bull. Geol. Soc. Am.* **20**, (1910).

ばならない.

3. 斯して同時性の確められた各地の地史を參照して，我々は各地質時代の古地理圖を描き表はすことができる.

4. 故に各地に發達する地層の同時性の解釋の相異は，古地理圖に重大な變化を來すに違ひない. この同時性を確める方法は種々あるが，今日之を古生物學的證左にたるより他に信頼すべき方法はない.

日本の第三系の如く，從來日本の層位學者によつて殆ど顧られなかつた地層に於ける同時性の問題は，自ら第三系中に多數に含まれる貝化石の研究から開拓して行かねばならぬ. 筆者は更に更に各地の新生代地層中の層位・構造の實際・化石の詳細を確めて，從來知ることのできなかつた新しい地殼の習性を知つて行きたい.

5. 併し古生物學的方法が現在の如く不充分にしか研究されてゐないやうな場合には，各地の地層の同時性は尙“紀”又は“世”の範圍にしか知られず，よく知られた場合にのみ“世”の前半・後半の程度にしか確め得られない. 故に古地理圖によつて代表される地理學的狀態は少くともそれが代表する地質時代の期間中に存在したと言ふことを示すに過ぎない. 又侵蝕作用によつて，古地理圖に必要な資料が洗ひ盡されてゐる場合もあるから，海岸線なるものも決して現在の地形圖に示されるやうなものとは異り，海岸線の位置に就いてもかなり精度を缺いてゐる. 併し化石や堆積物質の性質から，それぞれの地層の陸成，又は海濱性，又は純海性等の區別ができるから，著しい誤を生ずることは殆どあり得ない. 卽ち古地理圖は或る地質時代中に起つた地理學的狀態を總和したものの分布圖を示してゐるに過ぎない. 次に上記の方針に從つて古第三紀の海岸線の變化を追求してみやう.

古第三紀層の層序及び對比論

東亞に發達してゐる古第三系には夾炭層が發達してゐるために比較的よくその層位・分布が研究されてゐる. その內，海成層は樺太・北海道・常磐・北西部九州・琉球・臺灣・小笠原島・伯耆・長門等に知られてゐる.

樺　太

樺太の古第三系に關する文獻は長尾巧博士の「古第三紀」(岩波地質學講座)[5] に掲げてある. 從來の研究から南北樺太の古第三系は次の樣に區分され，その各々の層序は筆者の現在の知識に於いて第Ⅰ表の如く對比できると思つてゐる. この對比表は從來先輩の試みられたものと稍々異にしてゐる點があるが，之等の矛盾は何れ此の地方の層位學的研究の進捗と共に解決されるであらうから筆者は暫く筆者の信ずる儘をこ

---

5) 長尾巧　古第三紀　岩波地質學講座.

ゝに記して，先輩の御批評を乞ふ積である．

北樺太の古第三系は嘗て矢部長克・清水三郎兩博士[6]によつてアレキサンドロフスク附近に就いて研究されて，次の様な層序が決定されてゐる．即ち上部から

ヅーヱ夾炭層群 (Dui coal bearing group).
ホインジユ火山岩及その集塊岩 (Khoinju volcanic group).
ヅーヱ玄能石泥板岩 (Dui gennô-isi shale).
カメンナヤ層群 (Kamennaya beds).
………(平行不整合)……
上部白堊系.

上記の内ヅーヱ夾炭層群とカメンナヤ層群とから，矢部博士[7]は次表の如き植物化石を報告されてゐる．〔表中「ヅ」はヅーヱ夾炭層，「カ」はカメンナヤ層群，「ヱ」はヱストル夾炭層群産のものである．〕重複するが表示する．

ヅーヱ・カメンナヤ兩夾炭層植物化石表

Sequoia langsdorfii	ヅ	カ	ヱ	*Fagus antipofi*	ヅ	カ	ヱ
Taxodium distichum miocenum	ヅ	カ	ヱ	*Ficus tiliaefolia*	—	カ	ヱ
Acer arcticum	—	カ	—	*Ficus* cf. *tiliaefolia*	ヅ	—	—
Acer trilobatum	ヅ	—	—	*Ficus* sp. (*Dombeyosis* type)	—	カ	—
Acer sp. (seed)	ヅ	—	—	*Hedera* cf. *cuneata*	—	カ	—
Alnus kefersteinii	ヅ	—	—	*Hedera* sp.	ヅ	—	—
Betula brongniarti	ヅ	カ	ヱ	*Juglans nigella*	ヅ	—	—
Betula elliptica	ヅ	カ	—	*Juglans* cf. *rostrata*	ヅ	—	—
Betula prisca	ヅ	—	—	*Juglans* (*Carya*) *picroides*	ヅ	—	—
Betula cf. *macrophylla*	ヅ	—	—	*Liquidamber formosana* ?	ヅ	—	—
Betula sachalinensis	ヅ	—	—	*Magnolia nordenskiordi* ?	ヅ	—	—
Carpinus grandis	ヅ	—	ヱ	*Nelumbo nipponica*	ヅ	—	ヱ
Carpinus atauia	ヅ	カ	—	*Populus gaudini*	—	カ	—
Carpinus sp.	ヅ	—	—	*Populus zaddachi*	—	カ	—
Cerastrus ? sp. cf. *borealis*	ヅ	—	—	*Populus balsamoides*	ヅ	—	—
Comptoniphyllum naumanni	ヅ	—	—	*Populs* ? sp.	ヅ	—	—
Comptoniphyllum andersonii	ヅ	—	—	*Prunus serrulata* ?	—	カ	—
Corylus insignis	—	カ	—	*Pterospermites spectcbilis*	—	カ	—
Castanea kubinyi ?	—	カ	—	*Quercus dyrmeia* ?	ヅ	—	—
Castanea atavia	ヅ	—	—	*Sophora schmidtiana*	ヅ	—	—
Castanea sp.	—	カ	—	*Trapa borealis*	ヅ	—	ヱ
Cerastrus sp. (cf. *borealis*)	ヅ	—	—	*Tilia sachalinensis*	ヅ	—	ヱ
Corylus macquarrii macrophylla	—	カ	—	*Ulmus plurinervia*	ヅ	—	ヱ
Crataegus cf. *kornerupi*	ヅ	—	—	*Ulmus plurinervia* ?	—	カ	—
Cupania longipes	ヅ	—	ヱ				

---

6) 矢部長克，清水三郎「北樺太亞港封鎖炭田南部に發達せる第三紀及白堊紀兩層の層序」東北帝大，地質學古生物學教室　邦文報告　第5號 (1924).

7) H. YABE, "Palaeogene Stratigraphy of Russian Saghalin" *Proc. Imp. Acad.* **10**, (1934), 166.

上表から判斷してヅーエ夾炭層群と後に述べるエストル夾炭層との間には共通種10種に及ぶがカメンナヤ夾炭層とヅーエ又はエストルとの間には共通種夫々5種に過ぎないことは注意すべき點で，ヅーエとエストルとの兩夾炭層に於いてより多く近緣であることを示しゐる．上記の植物化石は所謂 “Arctic Miocene Flora”〔極地中新世植物群〕中の要素からなつてゐて，後者は今日の知識では極地古第三紀植物群と呼ばれる方が適當であると考へられてゐる．

之より先 A. KRYSHTOFOVICH[8] 氏は北樺太 Alexandrovsk 及び Tangi 岬間の地方に發達してゐる第三系を Mgachi 統と名付け，その上部は Machi 層と呼んだ．Mgachi 統の下部は所謂 “Arctic Miocene Flora” を含んでゐる夾炭層であるが，KRYSHTOFOVICH 氏は之を矢部・清水兩博士のカメンナヤ層に該當せしめられてゐる．然れども KRYSHTOFOVICH 氏の揭げた僅數種の植物化石では，同氏の Mgachi 統下部は矢部・清水兩博士のヅーエ夾炭層群及びカメンナヤ夾炭層群の何れに對比しても差支えないのである．

KRYSHTOFOVICH 氏の Machi 層は最近槇山博士[9] によつて硏究された Matchgar の貝化石層を含む地層に略々該當し，Matchgar 層は東北日本の東岸常磐炭田地方に發達する淺貝砂岩との間に次の様に多數の貝化石を共通してゐることがわかつた．〔表中「A」は淺貝砂岩層產，M は Matchgar 產のものである．〕

淺貝砂岩及び北樺太 Matchgar 產化石表〔槇山博士による．〕

Yoldia asagaiensis MAKIYAMA	A. M.	*Liocyma furtiva* (YOKOYAMA)	A. M.
Yoldia laudabilis YOKOYAMA	A. M.	*Liocyma terrera* MAKIYAMA	A. —
Chlamys matchgarensis MAKIYAMA	— M.	*Periploma besshoensis* (YOKOYAMA)	A. —
Brachidontes matchgarenis MAKIYAMA	— M.	*Macoma sejugata* MAKIYAMA	A. —
Volsella yamasakii MAKIYAMA	— M.	*Macoma asagaiensis* MAKIYAMA	A. M.
Cardium matchgarensis MAKIYAMA	— M.	*Mya grewingki* MAKIYAMA	A. M.
Cardium yamasakii MAKIYAMA	— M.	*Turritella tokunagai* YOKOYAMA	A. M.
Cardium asagaiense MAKIYAMA	— M.	*Turritella importuna* YOKOYAMA	A. M.
Cardium harrimani (DALL)	A. M.	*Ampullina asagaiensis* MAKIYAMA	A. M.
Cardium iwakiense MAKIYAMA	A. M.	*Colus asagaiensis* MAKIYAMA	A. M.
Venericardia laxata YOKOYAMA	A. M.	*Buccinum nakamurai* MAKIYAMA	A. M.
Thyasira bisecta (CONRAD)	A. M.	*Buccinum matchgarense* MAKIYAMA	A. M.

之等の貝化石は寒流の影響を多分に持ち，當時ベーリング海峽が存在してゐたと言ふ說に對しては都合のよい資料である．この動物群を槇山博士は淺貝動物群と呼んだ．

この淺貝動物群を含む地層は次に述べる南樺太の長島砂岩層，北海道の幌內統下部

---

[8] A. KRYSHTOFOVICH, *Jour. Coll. Sci. Imp. Univ. Tokyo*, **40** (1918), 7, 及び *Rec. Geol. Comm. Russ. Far, East*, No. 18 (1921).

[9] J. MAKIYAMA, *Mem. Coll. Sci., Kyôto Imp. Univ.* ser. B., **10** (1934), 2.

に發見せられてゐる．槇山博士によれば淺貝動物群は上部漸新統か又は Aquitanian 階を代表するものと結論されたが，この結論は後に述べる理由から筆者の贊意を表する處である．

南樺太

南樺太の古第三系は今井半次郎博士[10]・室井渡理學士[11]其他諸先輩等の研究があり村山賢一學士[12]によつて紹介されてゐる．

今井博士のエストル地方に發達する古第三系の層序は次の様である．即ち上部より

エストル挾炭層
〔フレイ頁岩〕
長島貝殼化石層
間宮挾炭層
〰〰〰〰〰
白堊紀層

の順序に堆積し，矢部博士・今井博士・渡邊久吉博士等は何れも貝化石及びその層序から長島貝殼化石層を北樺太のヅーエ玄能石泥板岩及び Machi，又は Matchgar 化石層と略ぼ同時代であらうと結ばれた．

室井理學士は南樺太西柵丹地方の地質を調査されて次の如き層序を知ることができた．即ち上部より

新第三紀	恩内頁岩層
	名好夾炭層
古第三紀	握珠火山岩層
	西柵丹層
	立岩夾炭層
	沃内礫岩層
〰〰〰〰〰	
	白堊系

室井氏の立岩夾炭層と沃内礫岩層とはその層準・植物化石等より前述のカメンナヤ夾炭層及び間宮夾炭層に該當する．西柵丹層の動物群は近頃この地方の地質調査をされた採集品を檢して略ぼ長島・Matchgar 等と同樣淺貝動物群を含むことが明となつた．次に室井學士の採集鑑定せる植物化石名を擧げて參考に資す．

室井學士採集名好炭層產植物化石〔室井氏による〕

Alnus Kefersteinii, *Alnus Kefersteinii* var., *Alnus* cfr. *gastaldii*. *Acer pictum*, *Acer*. sp., *Betula prisca*, *Betula macrophylla*. *Betula brongniartii*, *Betula grandifolia*, *Betula grönlandifolia*, *Betula* sp., *Cassia phasoealites*, *Cassia* sp., *Cerastrus borealis*, *Corylus macquarrii*, *Castanea ungerii*, *Castanea vulgaris*, *Carpania longipes*, *Carpinus grandis*, *Carpinus* sp., *Fagus antipofi*,

---

10） 今井半次郎 「南樺太炭田の層位に就て」 地學雜誌 41 (1929).
11） 室井渡　東京帝大地質學教室卒業論文 (1931).
12） 村山賢一 「日本地質鑛產誌」 地質調査所 (1933).

Fagus feroniae, *Fagus* cfr. *deucalinis*, *Fagus subjaponica*, *Fagus ferruginea*. *Fagus antipofi* var. *Fagus macrophylla*, *Ficus tiliaefolia*. *Ficus crassipis*, *Ficus* sp., *Equisetum* sp., *Glyptostrobus europaeus*, *Ginkgoites adiantoides*, *Encalyptus borealis*, *Diospirus* sp., *Juglans nigella*, *Juglans acuminata*, *Juglans arctica*, *Juglans* sp., *Laurus* cfr. *plutonia*, *Laurus* sp., *Myrica* sp., *Myrica* sp., *Nelumbium* sp., *Platanus heeri*, *Planera ungeri*, *Planera aceroides*, *Populus latior*, *Populus arctica*, *Populus zaddachi*. *Populus glandulifera*, *Populus balsamoides*. *Pinus* sp., *Phyllites* sp., *Phyllites* sp., *Quercus stuxbergi*, *Quercus pironae*, *Quercus myrtillus*, *Quercus* sp., *Rhamnus Eridani*, *Rhamnus* sp., *Salix varians*, *Salix longa*, *Sequoia langsdorfii*, *Sequoia langsdorfii* var., *Salvinia* sp., *Taxodium distichum miocenum*, *Taxodium Tinajorum*, *Taxites olriki*, *Trapa borealis*, *Ulmus plurinervia*, *Ulmus speciosa*, *Vitis crenata*, *Vitis* sp., *Tilia alaskana*, *Viburnum odoardi*, *Viburnum Nordenskiordi*, *Ilex*. sp., *Iris* sp.

坂倉理學士は昭和 10～13 年度樺太廳石油地質調査の結果次の如き層名の層序を以て一般に協定用ひやうとする機運に向つてゐることを述べられた．卽ち上から

圓山層
〰〰〰〰〰〰
久良志硬質頁岩層
內幌夾炭層
野田噴出岩層
吐鯤保層
八眺嶺硬質頁岩層
荒貝噴出岩層
西柵丹層
〰〰〰〰〰〰
內淵夾炭層
〰〰〰〰〰〰
白堊系

に分たれてゐる．

內淵夾炭層は矢部清水兩博士の間宮夾炭層に該當する下部夾炭層にのみ限つて呼び，西柵丹層は室井學士の命名した地層に大部分該當し，矢部博士の記載された意味の長島層と略ぼ同時代として之を取扱つてゐる．內幌夾炭層は *Desmostylus mirabilis* NAGAO を産し，新第三紀に屬することが推定される．吐鯤保層は貧弱な炭層又は植物化石を有するを以てエストル夾炭層等の同時代異相と考へることが許される．荒貝噴出岩層以上野田噴出岩層に至る迄は火山物質の豐富な堆積層である．

西柵丹層と略ぼ同時代であると考へられてゐる能登呂附近の十和田層からは，南雲

南雲學士採集十和田層産貝化石〔長尾博士による〕

Chrysodomus intersculptus var. *fiata* PILSBRY
Ocinebra? tuzurensis YOKOYAKA
Natica janthostoma DESHAYES
Turritella cf. *importuna* YOKOYAMA
Turritella cf. *tokunagai* YOKOYAMA
Yolpia yabei (YOKOYAMA)
Yoldia cf. *laudabilis* YOKOYAMA
Yoldia cf. *limatula* SAY
Cardim cf. *zristiculum* YOKOYAMA
Venericardia paifica YOKOYAMA
Venericardia laxata YOKOYAMA
Periploma besshoeusis (YOKOYAMA
Mya grewingki MAKIYAMA

理學士[13]は上の様な貝化石を報告された.

上表から 13 種中 12 種が淺貝砂岩層にも產してゐる.

上記の如く南北兩樺太の古第三系には Matchgar, 西柵丹, 及び長島貝殼層等の如き淺貝動物群を含む地層が橫はり層序上も互に略ぼ同時代であると考へることができる海成層によつて, 上下二夾炭層に分つてゐる事は重要な事實である.

第一表は樺太古第三系の對比表である.

第 I 表

北海道と樺太との古第三系の對比

ヅーエ炭層	エストル炭層	名好炭層	吐鯤保層
ホインジユ火山層		提珠火山岩層	八眺嶺硬質頁岩層 荒貝火山碎屑岩
ヅーエ玄能石層	フレイ頁岩層 長島貝殼層	西棚丹層	西柵丹層
カメンナヤ層	間宮夾炭層	立岩炭層 沃内礫層	内淵層
上部白堊系	白堊系	白堊系	白堊系

今迄述べてきたやうに, Matchgar, 西柵丹, 及び長島層等が互に略ぼ同時代を代表してゐるとすれば, 之等は何れも常磐の淺貝砂岩層・北海道の幌內統の下半によく產出する淺貝動物群を含む地層と對比できることとなり, 之等南北兩樺太の含化石層は幌內統と略ぼ近き層準であることゝなる. 先輩諸兄の觀察によると, 上記の含化石層（淺貝動物群を含む）に該當する層準又はその上部に幌內統に類似する岩相が發達してゐることは略ぼ確實にして, (例へばヅーエ玄能石頁岩層, フレイ (Furei) 頁岩等), 之等は幌內頁岩に略ぼ近いものであらう.

從つてヅーエ夾炭層・エストル夾炭層・室井氏の名好夾炭層・吐鯤保層等は幌內統より上位の夾炭層と考へられる譯で, 之等は北海道雨龍幌新炭田地方に於いて, 宇佐美衛學士[14]が研究された幌新層下部の夾炭層に該當するものであらう. この幌新層は幌內層の上位に橫はり, 所謂 "Arctic Miocene Flora" の種類を多數に含んでゐる. この層序關係は雨龍・幌新炭田地方の地質構造が極めて複雜なため, 細部に亙つては後の研究に俟つところが多いが, 近年北海道帝國大學の諸兄によつて, 北海道の他の地方の層序の研究によつて更に確められつゝあるが, 筆者は當分宇佐美學士の研究をその儘々引用する.

カメンナヤ夾炭層, Mgachi 夾炭層, 間宮夾炭層, 內淵夾炭層, (又は立岩・沃內層) 等は幌內統の層準より下位で, 白堊系を平行不整合に被うてゐる. 故に之等の夾

---

13) 長尾巧 前揭 "古第三紀" による.

14) 宇佐美衛 東大卒論 (OTUKA, *Earthq. Res. Inst.*, 13 に引用)

炭層はたとへその厚さその動物群によつて明な特徴が示されないにしても，北海道地方の石狩統又は常磐炭田の石城・白水兩層と略ぼ同時代の陸成層を代表してゐるものとも解せらる.

即ち樺太地方は白堊紀以後漸新世に至るまで，夾炭層が堆積するやうな狀態としてのみ經過し，漸新世に至つて漸く Matchgar, 西柵丹，長島等の各海成層によつて示される海進を東から受けた. 而してこの海進はヅーエ玄能石頁岩，フレイ頁岩等で代表されるやうな玄能石を成生し得らるるやうな深い狀態に迄達する樣になつた時に，Khoinju, 握珠，荒貝一野田等の各火山岩層で代表される安山岩の火山活動が起り，樺太地方の大部は陸化した. ヅーエ・エストル・吐鯤保等の各夾炭層を堆積せしめた時代は即ちこの陸化後の時代であつた. この時代は別に詳しく論ずるであらうところの筆者の“幌內海進と門澤海進との間の移過層 (Transitional formation) 時代”に略ぼ該當する. 因みに上記の火山活動に引續いて，火山活動の一部は新生代初期に迄繼續した證左も認められてゐる.

北海道の古第三系

北海道の古第三系は幌內統と石狩統とによつて代表されてゐる.

“石狩炭田附近の層序は矢部長克・大井上義近・今井半次郎・村田析・田上政敏等諸先輩の詳細な研究が公にされてゐる. 矢部・今井兩博士によれば，石狩炭田地方の地層は次の如く分類されてゐる.

追　分　統
川　端　統
〔紅葉山中間層〕
幌　內　統
石　狩　夾　炭　統
～～～～～～～～
上　部　白　堊　系

村田學士はその後一つの中間層を川端統と幌內統との間に設けて，紅葉山層と名付けた. 幌內統は黑灰色の泥岩層で，薄い泥灰岩塊を含み下部は砂質又は海綠石砂質に變化してゐる. 泥岩層中からは *Bulimina* sp., *Venericardia compressa* YOKOYAMA, *Nucula poronaica* YOKOYAMA, *Nucula* (*Acila*) *picturata* YOKOYAMA, *Nuculana* sp. *Tapes ezoensis* YOKOYAMA, *Turritella wadana* YOKOYAMA 等を含んでゐる.”

長尾博士によれば幌內統の下部の砂質部分には上記の貝化石の他に淺貝動物群が發見せられてゐるし，小平蘂地方の幌內統下部にも同樣な淺貝動物群が發見せられてゐる.

“前に述べた如く，宇佐美衛學士は雨龍・幌新炭田を調査して，そこに發達する幌內統から *Bulimina* sp., *Venericardia compressa* YOKOYAMA, *Nucula* (*Acila*) *picturata* YOKOYAMA, *Nucula poronaica* YOKOYAMA, *Turritella wadana* YOKOYAMA, *Yoldia tokunagai* YOKOYAMA, *Callianassa* *muratai* NAGAO 等を採集され，その上位の幌新炭田層の上部からは *Dosinia nagaii* OTUKA, *Dosinia japonica nomurai* OTUKA, *Siratoria siratoriensis* (OTUKA), その他產出層準は稍々不明であるが，*Ancistrolepis yudaensis* OTUKA をも採集せられた．之等の幌新炭田層產の貝化石は幌內統產の動物群とも淺貝動物群とも類似せぬ特徵を示し”，

嘗て筆者が調査研究した中下部中新統の下部門澤統や中國濱田町附近の唐鐘中新統や野村七平氏の研究された仙臺市附近の鹽釜中新層等に普通に產する特徵的化石であつて，幌新炭田層下部に發達する夾炭層は日本群島の中下部中新統下に普通に橫はる所謂 “Arctic Miocene Flora” を含む植物群と略ぼ同時代であらうことを示してゐる．故に幌內統は明に古第三系に屬せしめるべきもので，この下部に產する淺貝動物群を漸新統とされた槇山博士に賛意を表するものである．前に述べた樣に筆者は上記の層序と化石の知識とから，幌內統によつて代表される海進と，幌新統によつて代表される海進とを夫々幌內海進，門ノ澤海進と呼んだ．故に小石源藏學士が幌新夾炭層を以て，前に述べた石狩炭田地方の紅葉山中間層及び川端統の一部と同時代の堆積物なりと主張されたことは，略ぼ正しき意見と言はなければならない．

石狩統　石狩統の細分は今井博士により調査次の如く決定されてゐる．

蘆別夾炭層
上部幌貝層
羊齒砂岩帶及幾春別夾炭層
下部幌貝層
美唄夾炭層
若鍋層
夕張夾炭層
幌加別頁岩層
登川層
白堊紀層

上記各層の內若鍋頁岩層又は若鍋貝殼層と呼ばれたもので，時に淡水棲化石を含んでゐるが，*Crassatellites yabei* var. *ezoensis* NAGAO & OTATUME を最も普通に產する他長尾博士によれば，

Cyrena aff. *incompta* DESHAYES
Macrocallista cf. *matsuraensis* NAGAO
Pitaria aff. *kyushuensis* NAGAO
Modiola aff. *ambiqus* DESHAYES
Soletellina n. sp.
Venericardia sp.
Cyrena n. sp.
Macrocallista hanzawai NAGAO
Mytilus rigaulti DESHAYES
Papyridea sp.
Pecten aff. *ashiyaensis* NAGAO

等を產し，純海成層と見做すことができる．上記の化石は長尾博士の豫報的な表であつたが掲載した．之に依れば九州北部蘆屋層群の化石種と共通なものが多く，兩層は略ぼ同時代のものであらうとの事である．

若鍋層は淡水棲貝化石等を含んだ地層であるが，若鍋層の上位は炭層を含み半淡水性又は海棲の貝化石等を含んでゐて，若鍋海進後の海退現象を示してゐる樣に見える．之等の植物化石中には *Woodwardia ezoana* Endo, *Sabal nipponica* Kryshtofovich, その他 *Nelumbo, Trapa* 等を含んでゐる，所謂 “Arctic Miocene Flora からなつてゐる．

橫山博士が記載報告された北海道雨龍炭田よりの貝化石は長尾博士によれば石狩統上部を代表してゐる樣に見え主なものとして次の樣な種類が報告さててゐる．之等は大體石狩統の若鍋層及びその上部層中から產するものと共通なものが少くない．

Cerithidea ishikariensis Yokoyama
“*Venus*”? *sanosawaensis* Yokoyama
Cyrena sp.
Cyrena verecunda Yokoyama
Anodonta suavis Yokoyama
Thiara fiscina Yokoyama
Nodularia subjapanensis Yokoyama
Modiola cf. *barbata* Linné
Martesia pulchella Yokoyama
“*Pophia*”? *muroei* Yokoyama
Cardita mandaica Yokoyama
Nodularia cf. *biwae* Kobelt
Viviparus uryuensis Yokoyama
Crassatellites heteroglyptus Pilsbry
“*Circe*” *tokudai* Yokoyama
Yoldia breviscapha Yokoyama

上述した層序から北海道の古第三系の分布を調べると，若鍋貝殼化石層に略ぼ該當する地層は北海道中央脊稜山地の西側及び十勝・釧路地方に迄分布してゐるが，石狩低地帶の西部には知られてゐない．

幌內統も大體上と同樣な分布をしてゐる．卽ち北海道白堊紀末以後始新世中期頃まで陸成層のみを推積する狀態として經過し，始新世末期より若鍋層によつて代表される若鍋海進と幌內統によつて代表される幌內海進とによつて漸新世を經過して，その後陸化狀態の儘々新第三紀へと移過した樣に見える．

本 州 島

日本群島本州島に分布する古第三紀層は從來津輕半島・岩手縣久慈・常磐炭田・信濃北相木・東美濃・新宮・木本・伯耆その他に知られてゐたが，之等の一部は植物化石のみによつて決定せられたり，一部は不完全な僅な化石によつて推定せられたりしてゐて，改良の餘地を殘してゐる．

津輕半島の所謂古第三系は半島の西側にあつて，櫻井理學士の研究になるもの

で，基盤岩層上に整合にのり，綠色岩層に被はれてゐる地層であるが，近頃野村七平・畑井小虎兩氏はこの地層の轉石から次の様な貝化石を記載報告されてゐる．

津輕半島の所謂古第三系產の貝化石（野村・畑井兩氏による）

Mytilus k-sakurai NOMURA et HATAI
Mytilus sp.
Volsella tugaruana NOMURA et HATAI
Cardium (*Clinocardium*) *mutuense* NOMURA et HATAI
Lyocyma aomori NOMURA et HATAI
Clementia aiutiensis NOMURA et HATAI
Macoma sp.
Turritella sp.

櫻井學士は *Venericardia nipponica* 又は *V. subnipponica* に似た *Venericardia* を採集されてゐるが，上表の化石類では充分に時代決定をすることは未だ望めない．

岩手縣久慈地方の古第三系は佐々學士の調査で明になつた．上位から

久喜層群｝野田古第三系
港層群　｝
～～～～～～～～～～
久慈海成白堊系

に分れ，港層群は大體海岸性又は淡水性の地層で上部には炭層を含み，下部には植物化石を含んでゐる．佐々學士は港層群から 24 種の植物化石を採集され北海道石狩統の植物化石と略ぼ同時代であることが確められた．

上記の植物化石は所謂 “Arctic Miocene Flora” を含み佐々學士は石狩統の羊齒砂岩帶附近に對比されやうとしてをられる． この古第三紀は厚さ 400 米以上を有するが，海進の證左が見出だされてゐない．之に反してこの下位の上部白堊系は明に海成層である．

北上山地北部岩泉四近に古生層中に西北一東南の帶狀をなした fault angle basin に第三系があり，炭層及び植物化石貝化石を含んでゐて，久慈の白堊系・古第三系に對比されさうであるが未だ古生物學上確たる證明はできてゐない．

常磐地方の古第三系は中村新太郎敎授の詳細な層序研究があり，その後德永・靑木・渡邊・槇山等諸先輩の研究により明にされてきた．

常磐炭田の層序は前記諸先輩の研究により，次の如く分けられてゐる．

多賀統（鮮新統）
白土統（中上部中新統）
湯長谷統（下部中新統）

亀ノ尾層
水野谷層
四ツ波層
五安層
淺貝層（漸新統か又は Aquitanian）
白坂頁岩層
淺貝砂岩層
石城層（漸新統）
白水層

淺貝砂岩層は石城層に整合してゐて，その化石群は既に述べた如く，横山・槇山兩博士の研究があり，北樺太の Matchgar 產の貝化石群と類似してゐることを示してゐる．

石城層は中粒綠色の wacke sandstone で，礫岩を介在し，*Ostrea takiensis* YOKOYAMA, *Glycymeris* sp. 等を含み，海成，海濱成の堆積物である．

最下位の白水層は砂岩で主要炭層を含み，その上部からは *Venericardia tokunagai* YOKOYAMA, *Turritella importuna* YOKOYAMA, *Cerithium* sp. 等を產することがあり，海成の部分もある．

石城層の植物化石は槇山博士[15]により所謂 "Arctic Miocene Flora" からなりたつてゐて，石狩統に比ぶべきことが主張されてゐる．

上述した樣に常磐炭田層は北海道・樺太等と密接な關係にあるが，それより以南の古第三系は全く上述の如き特色を持たないので一先づこゝで東北日本・北海道・樺太の古第三系の特徵を概括對比しておかうと思ふ．

1. 淺貝動物群と幌内層中に見られる幌内動物群とは何れも同一地質時代の生態學的條件の相異に基く特徵を示すものと解せられる．上記兩動物群は同一地質系統中の上下に產し，泥質部には玄能石と共に幌内動物群を產し，砂質部（主として下部を占める．）からは淺貝動物群を產してゐる．上記の動物群を含む地層は幌内海進の存在を示してゐる．淺貝砂岩層とその上位の白坂頁岩層，北海道の幌内統，樺太の長島貝殼層とその上のフレイ頁岩層，玄能石頁岩層，Matchgar 砂岩層，西柵丹層等は何れも幌内海進の產物と解することができる．この海進は附圖の東北部にて○印及び－・－線で示した範圍に達した．

幌内海進の地質時代は既に筆者が指摘した樣に東北日本油田地方に發達する新第三系の下部層で代表される時代より以前のものであつて，即ち *Lepidocyclina*, *Miogypsina*, *Operculina*, *Desmostylus japonicus* TOKUNAGA et IWASAKI, 及び *Desmostylus mirabilis* NAGAO を含む地層より明に下位の地層で代表されるものであつて，上記の高等有孔蟲又は哺乳動物化石を含む地層と幌内海進を代表する地層との間には一般に

---

15) 槇山次郎 地質學雜誌 27 卷，318 號 (1920).

mirabilis NAGAO を含む地層より明に下位の地層で代表されものであつて，上記の高等有孔虫又は哺乳動物化石を含む地層と幌内海進を代表する地層との間には一般に植物化石層又は火山碎屑岩層を介在してゐる．この陸成層は樺太ではヅーエ炭層・エストル炭層・吐鯤保層等となり，北海道では紅葉山中間層・幌新層下部等となり，本州島では岩手縣の四ツ役層16)，山形縣小國植物化石層17)，新潟縣觀音澤の植物化石層18)等多くの植物化石層として代表せられてゐる．

長尾博士の *Desmcstylus mirabilis* NAGAO は上記のヅーエ・エストル炭層に該當する炭層の上位の海成層である内淵層から産したもので，最近には常磐炭田に於いて，淺貝層の上位に不整合に横はる湯長谷統から *Desmcstylus mirabilis* NAGAO19) が產し，淺貝層の海をも含む幌内海進が漸新世なることを立證するに更に有利となつた．

石狩統によつて代表された海進は常磐炭田・石城・白水各統によつて代表されるやうに見える．石狩統若鍋層の貝化石は長尾博士によれば蘆屋層群のものに類似してゐて，漸新統下部の疑がある．近年北アメリカ西部の始新統の總括的研究を行つた B. L. CLARK 及び H. E. VOKES20) によれば，北アメリカ西部の始新世動物群は北方・北極海動物群の移入が認められないとのことである．若鍋層の貝化石は長尾博士の豫報的表中には南方種と共に北方種もかなり見受けられるので，若鍋層は少くとも漸新世の初期の堆積と見做す方がよい様な點がある．筆者は若鍋層を蘆屋層群と大體比較された長尾博士の意見に贊意を表する譯である．故に東北日本では始新統と確定した海

第 II 表

日本古第三系對比表

	北樺太	南樺太	北海道	岩手	常磐	北九州
中新統		内淵層	川端層	門ノ澤統	湯長谷統	
	ヅーエ炭層	エストル炭層	(紅葉山中間層)	四ツ役層		
漸新統	ヅーエ玄能石頁岩	フレイ頁岩 長島貝層	幌内層		白坂頁岩 淺貝砂岩 石城層 白水層	佐世保層群
	カメンナヤ炭層	間宮炭層	石狩統 若鍋層	野田層群		蘆屋層群
始新統						大辻 伊王島 坂瀬川 本渡 白岳 層群
曉新						赤崎
白堊系	上部白堊系	島岩層	函淵砂岩	久慈白堊系	双葉白堊系	天草白堊系

---

16) Y. OTUKA, *Bull. Earthq. Res. Inst.* **12**, 3 (1934). 599—602.
17) H. MORITA, *Jap. Jour. Geol. Geogr.* **9**, 1—2 (1931), 1—8.
18) A. KRYSHTOFOVICH, *Ejegodnik Russk. Paleontol. Obsh.* t. vi, 1926 g.
19) 德永重康 地學雜誌 **48**, 572 (1936). 473—484.
20) CLARK & VOKES. *Bull. Geol. Soc. America* **47**, 6 (1936), 851—877.

成層は未だ發見されない．石狩海進の範圍は附圖にて實線で示してある．

上掲の第 II 表によつて氣付くことは，前にも屢々述べたやうに東北日本の西側に海成古第三系の確實な分布がないことで，始新世末か漸新世初期の海は北海道中央脊稜及びその周圍に，漸新世末期には海は樺太・北海道・常磐に分布した樣である．

北朝鮮の吉州・明川の古第三系なるものはその後槇山博士により中新統なることが確められ，最下の植物化石層のみが古第三系として考慮され得る餘裕を殘した．南朝鮮迎日灣附近の第三系も最下の植物化石層のみが古第三系として考へ得る餘地を殘してゐることが金原均二學士によつて確められた．

信濃北相木の植物化石層は植物化石のみでは未だ第三系の何れの時代に決定するかは不可能なやうであるが，藤本教授によれば，厚殼の *Ostrea* sp. と *Phacoides* sp., *Nuculana penula* YOKOYAMA 等の產出を報じてをられる．之等貝化石は少くとも漸新世・始新世を代表してゐるやうには考へられない．

大 陸 地 域

古地理圖作製に當つて大陸地方の知識を參考する必要もある．シベリア大陸地方に於いても，OBRUTSCHEW, MALJAWKIN, KONSTANTOV 等の報告からアムール地方の Seja 河—Bureja 河の下流盆地地方に淡水成層の始新統が存在することが報告されてゐて，

Viburnum lesquereuxi WARD.
Viburnum multinerve HEER
Zizyphus meckii LESQ.
Zizyphus hyperboreus HEER
Grevia obovata HEER
Gingkoites adiantoides HEER
Ficus planicostata LESQ.
Corylus m'quarri FORB.

等の植物化石が報告されてゐる．KONSTANTOW は之等から上部始新統の陸成層と考へてゐるやうである．

南ウスリ地方では Ugolnaja 驛地方に漸新統と考へられる地層があることが STEMPEL によつて研究されてゐる．下部の亞炭層からは

Carpinus grandis UNGER
Sequoia langsdorfii BRONGNIART
Taxodium distichum miocenum HEER

等を產し，その上位には淡水貝を含む地層が横はつてゐる．之等は何れも海成層である．

ウラヂホストツクに含植物化石漸新統の存在することは PALIBIN の研究によつて知られてゐる．之等の文獻は何れも親しく手にとつて閲讀することができないで，唯

だ OBRUTSCHEW や F. RAUPACH の記事より知り得たのである．

撫順炭田・朝鮮各地にも古第三紀植物化石を含む地層が報告されてゐるが未だ海成層は見出されてゐない．

上記の様に大陸地方には陸成の資料のみしか知られてゐない．支那本土に於いても海成古第三系の存在は從來知られてゐない．

北九州

北九州地方に古第三系の發達してゐることは既に前述した通であるが，この地方の層位は長尾博士の詳細な研究があり，各地層は九州各地で夫々細分命名されてゐるが，大體次の如き層準が知られてゐる．即ち上部から

佐世保層群
蘆屋層群
大辻層群
伊王島層群
坂瀬川層群
本渡層群
白岳砂岩
赤崎層

最上部の佐世保層群は半淡水・半海成層で *Brachyodus japonicus* TOKUNAGA が報告されてゐるが，*Brachyodus* 屬の哺乳動物化石は歐州では漸新世から中世新初期にかけて生存してゐたものであるから，佐世保層群は大體上記の地質時代を代表するものと考へられる．

蘆屋層群は佐世保層群と同樣な動物群を含み，特に *Crassatellites yabei* NAGAO, *Venericardia subnipponica* NAGAO, *Macrocallista matsuraensis* NAGAO, *Glycymeris cisshuensis* NAGAO 等を產してゐる．長尾博士はこの層群を北海道石狩統の若鍋層の附近に對比せられたが，北九州では大辻層群以下赤崎層迄には始新統と確實に言ひ得る含化石海成層が存在する點で，北海道地方と稍々異つてゐる．

北九州の始新統漸新統の分布をみると，漸新統は始新統を明に累積 (overlap) してゐて，北九州古第三系の分布區域の東北部では漸新統のみが不整合に古期岩層上に横はるところも少くない．古第三紀の海は西南から東北へ向つて一進一退を繰回しつゝ進み，遂に山口縣の北側へ迄も分布したやうである．最近山口縣豐浦郡彥島市獅子ケ鼻產の貝化石を檢したところ，大體北九州の漸新統のものと一致することが確められたし，酒井榮吾氏は宍道半島から *Lamprotula nojimensis* UEJI[22] を報じ，宍道半島の第三系が北九州の佐世保層群に近きことが明となつたので，漸新世の堆積區がこの地

---

21) 德永重康 地學雜誌 **37** 440, (1925), p. 557.
22) 酒井榮吾 地質學雜誌 **43** (1936), 633.

方に迄分布したことも明となつた．富田達博士によればこの化石を含む地層は厚い火山碎屑岩層に被はれ，その上に *Desmostylus* を含む來待，布志名の地質系統が横はつてゐる。

伯耆國（鳥取縣）には多里の古第三紀層と言ふものが知られ，横山博士は *Pholadomya* 等を報ぜられてゐるが，筆者が多里で採集した化石の內には，金原學士が南朝鮮延日中新統，廣島縣庄原町附近の庄原中新統から產する *Cerithium sp, Cardiumsp.* 等が *Ostrea* と共に產してゐるので，その地質時代に就いては再考の要がある．多里第三系の堆積狀態は庄原附近と同樣に溺れ谷堆積物である．

臺灣・小笠原島・石垣島に始新統及び漸新統の純海成層のあることはよく知られてゐるし，臺灣及び西南琉球諸島では更に炭層もあり，この地方の含炭層が略ぼ古第三紀末期から新第三紀初期へのものであることも確められてゐる．

東亞の第三紀海岸線の變化

上に述べてきた多數の地史學的事實とその對比論とによつて，我々は次の樣な概念圖的古地理圖及び柱狀圖で，日本の周圍に於ける古第三紀海岸線の變化を示すことができやう．第1圖はその古地理圖であり，第3表は古地理學的柱狀圖である．

この柱狀圖から知られることは中央日本は朝鮮と共に大陸式の地史をとつてゐることがわかる．又中新統下部を A, 中新・漸新間の移過層を B, 幌內統を C, 石狩統上部炭層を D, 蘆屋層群を E, 始新世海進を代表する地層を F, 白堊系上部を G とすれば，第1表柱狀斷面圖に於いて，A 期の海成層 (M) は 9 ケ所，小笠原は稍々疑問，陸成層 (L) は 3 ケ所，B 期の海成層は稍々疑問なもの 1 ケ所，他は陸成層 11 ケ所，C 期の海成層は臺灣他 8 ケ所，陸成層 5 ケ所，D 期の海成層は 3 ケ所，陸成 10 ケ所，E 期の海成 4 ケ所，陸成 7 ケ所，F 期は海成の疑問 2 ケ所，海成 2 ケ所，陸成 9 ケ所，G 期は海 5 ケ所，海の疑問 3，陸 5 ケ所で，海陸分布の割合を時代順に求めてみると，日本群島周緣の海岸線は白堊紀末海進後，始新世初期には著しく海退の現象を示したが，その後海進は逐次その分布範圍を擴めたやうに見える．而して中新世初期に極めて擴大した海岸線を有したやうに見える．勿論この推定は上記の材料では未だ嚴密な意味ではなりたたないが，唯だ第1表の柱狀斷面圖の知識に基いたものに過ぎない．又海進の範圍が擴がるに從つて，次の海進との間の海退の範圍が擴がつてゐるやうに見え，海成層の堆積輪廻の變動が大きくなつてゐることも看取できる．この事實は今迄知られてゐなかつた事實のやうに見えるので，も少し愼重に研究してみたいと思つてゐる．

第1圖の古地理圖から判斷されることは日本島が古第三紀には尙大陸の緣邊部として存在し，次第に中新世に近付くに從つて海に被はれる部分が擴がつてゐた．北九州では日本海方面へ向つて一つの地向斜狀の窪みが生じ始め，漸新世末期には宍道半島

方面に迄灣入が擴大してゐた．前述したＣ期からＡ期へ至る移化期Ｂ期前後には壯に各地に火山活動が起つてゐた．東北日本の西部から所謂 Fossa Magna 地方に亘る古第三紀末か又は中新世初期かを代表する火山碎屑岩層の大部分はこのＢ期前後に成生されてゐる．

多くの先輩に指摘されてゐるやうに，白堊系から始新統への層位學的關係は各地で著しい傾斜不整合關係を伴つてゐないで侵蝕間隙[23]のみである．之は白堊紀末より始新世初期へかけて著しい造山運動の時期が存在してゐなかつた事を示してゐる．併しその分布から判斷して白堊系と始新統・漸新統の堆積區は著しく相異してゐる．即ち地殼は堆積を許容する窪みを各地質時代によつて場所を更へて作つてゐる．この變化は何に原因してゐるかはも少し研究を進めてからにしたい．この樣な海進，海退を引起す地殼運動は造陸運動的地殼運動と呼ぶことができやう．

19. *Palaeogene Palaeogeography of Japan and its Vicinity.*

Yanosuke Otuka

Earthquake Research Institute.

In this paper, the writer discusses the stratigraphic chronology of the Palaeogene strata exposed in Japan, and shows a palaeogeographic map of Palaeogene in Japan. He has schemed following table (Table III.) deduced from many literatures hitherto published by the previous authours. Fig. 1 is the palaeogeographic map of the Palaeogene of Japan, and its vicinity. Full description of this map in occidental language will be published in the Proc. Intern. Geol Cong. 1937.

Pl. III Palaeogene palaeogeographic Column near Japan. (Y. Otuka)

(M=marine condition. L=land condition.)	**A.** Lower Miocene	**B.** Transit. bed A. & B.	**C.** Poronai stage	**D.** Upper Isikari st.	**E.** Asiya stage	**F.** Eocene	**G.** Upper Cretaceous
Karahuto (1, 2, 3, in fig. 1)	M	L	M	L	L	L	M
Hokkaido (4, 5, 6)	M	L	M	L	M	L	M
Iwate (7, 8)	M	L	L	L	L	L	M
Zyoban (9)	M	L	M	L	M	L	M
Nagano-Niigata (31, 10)	M	L	L	L	L	L	L
Siberia (28, 23)	L	L	L	L	L	L	L
Manchoucou (29)	L	L	L	L	L	L	L
Tyosen (24, 25, 26, 27)	M	L	L	L	L	L	L
Yamaguti (13, 14)	M	L	M	L	L	L	L
Kyûsyû (15, 16, 17)	L	L	M	L	M	M	M
S. W. Ryûkyû (18)	M?	L	M?	M	?	?	?
Ogasawara (21)	?	?	M?	M	?	?	?
Taiwan (19, 20)	M	L	M	M	M	M	?

---

23) H. Yabe, *Proc Imp. Acad.*, **2** (1926), 417～418.

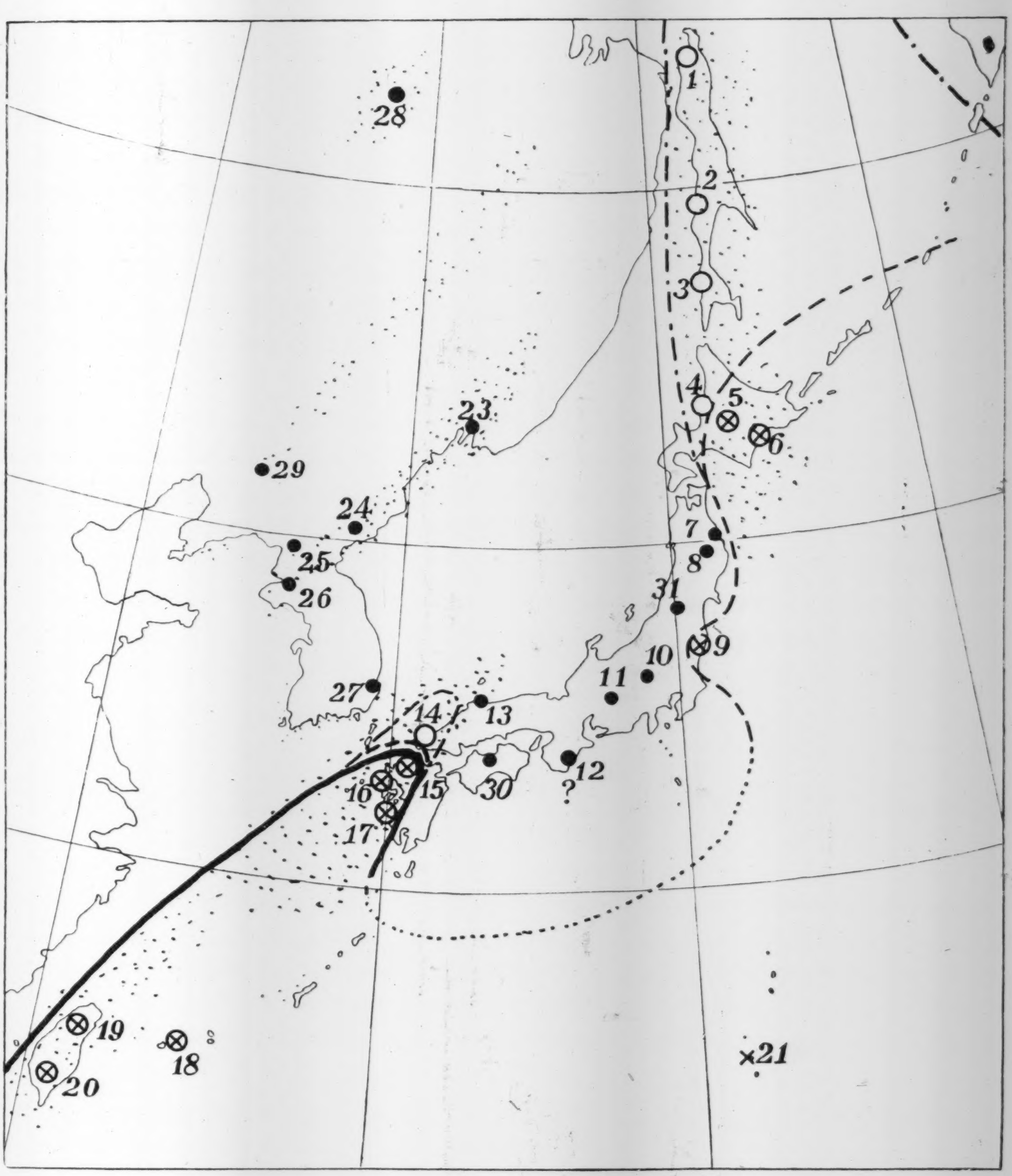
1
2
3
4
5
6
7
8
9
10
11
12
?
13
14
15
16
17
18
19
20
21
23
24
25
26
27
28
29
30
31

（震研彙報 第十五號 圖版 大塚）

Fig. 1. 古第三紀古地理圖 (Palaeogene palaeogeographic map.) (OTUKA, 1937)

× 海成始新統及び下部漸新統 (Marine Eocene and Lower Oligocene).

○ 海成上部漸新統 (Marine Upper Oligocene).

● 陸成古第三系及び新第三系最下層 (Continental Palaeogene and Earliest Neogene).

⁘ 古第三紀地向斜（又は堆積區）(Palaeogene Geosyncline or sedimentation area).

━━ 始新世海岸線 (Eocene shore-line).

- - - - 漸新世期海岸線 (Early Oligocene shore-line).

—·—·— 漸新世末期海岸線 (Late Oligocene shore-line).

·········· 推定海岸線 (Presumptive shore-line).

20. *On the Volcanism of the Huzi Volcanic Zone, with Special Reference to the Geology and Petrology of Idu and the Southern Islands.*

By Hiromichi TSUYA,

Earthquake Research Institute.

(Received Dec. 21, 1936.)

CONTENTS.

	Page
Introduction	216
I. Tertiary volcanism	219
General statement	219
A. Palaeogene volcanism of the Ogasawara (Bonin) Islands	222
1. Eocene volcanics of Haha-sima	222
2. Upper Eocene or lower Oligocene volcanics of Titi-sima	225
B. Neogene volcanism of Idu	228
General statement	228
3. Miocene effusives	233
4. Pliocene effusives	237
5. Minor Tertiary intrusives	240
II. Quaternary volcanism	243
General statement	243
A. Complex volcanoes	252
1. Amagi-san Volcano	252
2. Hakone-yama Volcano	259
B. Basaltic and andesitic volcanoes	260
3. Tensi-yama Volcano	260
4. Usami Volcano	264
5. Taga Volcano	270
6. Asitaka-yama Volcano	275
7. Mikura-sima Volcano	277
8. Tori-sima Volcano	280
9. Kita Io-sima Volcano	282
10. Aoga-sima Volcano	285
11. Hatizyo-sima Volcano	287
12. Miyake-sima Volcano	290
13. O-sima Volcano	296
14. Omuro-yama volcano group	300
15. Huzi-san Volcano	302
C. Dacitic and liparitic volcanoes	308
16. Nii-sima group	309

Page
D. Trachyandesitic volcanoes 316
17. Io-sima Volcano 316
18. Sin Io-sima Volcano (a submarine volcano near Minami Io-sima) 320
III. General petrology 321
A. Mineralogical characters 322
B. Chemical characters 334
IV. Summary and conclusions 350

Introduction.

On the "fossa magna", a well-known tectonic zone traversing central Japan from the Japan Sea coast to the Pacific coast in a NNW.–SSE. direction, are arranged many volcanoes in a zone called the "Huzi Volcanic Zone" after the celebrated volcano. Since early Pleistocene this zone has been the seat of volcanism, the rocks of which are chiefly basalt followed by andesite. In this zone, which extends far south into the Pacific, we find a group of insular volcanoes, linearly-arranged, a group that comprises the Seven Idu Islands and the Southern Islands (except the Ogasawara), all of which rise up from a submarine ridge of what may be an underground manifestation of the geotectonic structure of the zone.

So far as we know, the volcanoes of this zone on the fossa magna are underlain largely by Neogene Tertiary formations, all the members of which, excepting a few clastic sediments and limestones, are volcanic in character, and include, in addition to pyroclastic beds, various lavas and minor intrusives. Although, structurally, the Ogasawara Islands appear to lie outside the zone, they are mostly composed of volcanic rocks which, with the intercalated limestones, have been assigned to Palaeogene, and which, petrologically, may be treated together with the rocks of the adjoining shores of that zone as a connected whole. Consequently, there is in the Huzi volcanic zone a profusion of petrological phenomena portraying the intensive volcanic activities that characterized the entire zone since the time of the early Tertiary.

In this paper the writer presents in some detail the results of his studies in the field as well as in the laboratory of the volcanic rocks with special reference to the Idu region and the Southern Islands. Although the area studied forms but a fraction of that vast region wherein similar geologic conditions prevailed contemporaneously, it may be wide enough for our purpose considering the large amount of data that studies of the region have yielded us. Indeed, in some respects the region studied typifies the whole, especially as it contains the principal centres, both of Quaternary and Recent volcanic activity—Huzi, O-sima, Miyake-sima, Hatizyo-sima, etc.—and one of the regions in which the Tertiary forerunner of the volcanic zone is most typically developed, namely, the Idu peninsula which is the southern expression of the fossa magna.

The writer has endeavoured to range the volcanic rocks in natural groups each belonging to a definite epoch, and these are treated, generally, in chronological sequence. Matters of convenience, however, sometimes make adherence to this intended order impossible, such for instance as when certain repetitions have to be avoided, although more often the reason for it is the lack of evidence to substantiate the particular order. As the principal object of this paper is to present both the general sequence and a general petrology of the region under discussion, petrographic descriptions must of necessity be concise with many details of the common and most widely represented rocks omitted in order not to emphasize unduly the rarer and more interesting rocks.

Most of the chemical analyses of rocks presented in this paper were made specially for this study by S. Tanaka. Petrographic descriptions have been given of the specimens that have been analyzed, although, for the sake of completeness, some additional specimens have been described unaccompanied by any chemical analyses. In the descriptions, the chemical compositions of both porphyritic minerals and groundmass constituents have been given, so far as they could be determined by measuring some of their optical constants. Plagioclase was determined by Tsuboi's method[1], monoclinic pyroxene by measuring both 2V and β (or n_1 on 110) and by means of Tomita's diagrams[2], hypersthene by measuring n_1 or n_2 on (110) and by means of curves for the indices of refraction of rhombic pyroxene as proposed by Bowen and Schairer[3], and olivine by measuring both 2V and the indices of refraction and by means of Winchell's diagram[4], but reduced to wt. % of the components. Excepting a few measurements of minute groundmass constituents, which were made by the ordinary

---

1) S. TSUBOI, *Jap. Jour. Geol. Geogr.*, **11** (1934), 325.

2) T. TOMITA, *Jour. Sanghai Sci. Inst.*, Sec. II, **1** (1934), 41. H. Kuno has proposed a similar diagram useful for the same purpose. His diagram differs but slightly from Tomita's diagram in that the curves for β are chiefly based on common pyrogenic monoclinic pyroxenes with moderate amounts of sesquioxides and titania. H. KUNO, *Jap. Jour. Geol. Geogr.*, **13** (1936), 110.

3) N. L. BOWEN and J. F. SCHAIRER, *Am. Jour. Sci.*, **29** (1935), 198.

4) N. WINCHELL, Elements of Optical Mineralogy, Part II (1927), 168.

immersion method, the indices of refraction in all cases were measured by Tsuboi's dispersion method[5]. The optic angles were measured in all cases by using Fedorow's universal stage.

It should be emphasized that, in classifying the rocks into various rock types, the normative composition has been taken into account in the choice of rock names, especially those for the "basaltic" rocks that predominate in the region studied. To discriminate basalt and andesite from microscopical characters alone was found to be impracticable, seeing that there is every gradation of that character from normal basalt to andesite. Neither would we be justified in taking the presence or absence of olivine as a criterion for discriminating basalt and andesite; many rocks destitute of that mineral are probably quite as basic in composition as some of those with olivine. Tsuboi has proposed the term "miharaite" for the basaltic rocks from Mihara-yama, O-sima, which are characterized modally by some phenocrysts of bytownite and pyroxenes in a groundmass containing labradorite and monoclinic pyroxene[6]. As will be discussed later, similar rocks—most of them almost non-porphyritic (aphyric)—occur in several volcanoes, such as Hatizyo-sima, Miyake-sima, Taga. etc. The groundmass of the porphyritic (phyric) rocks from these volcanoes also greatly resembles miharaite in composition. Like the miharaite, similar non-porphyritic rocks may be called basalt (tholeiitic basalt)[7], which is also true for the porphyritic rocks, the groundmass of which is similar chemically to miharaite.

Washington, who distinguishes basalt from andesite on the basis of the relative amounts of the salic and the femic minerals shown in the norm, writes: "...andesite, in which plagioclase dominates over femic minerals, that is, plagioclase constitutes from 87·5 to 62 per cent of the norm; and basalt, in which the amounts of plagioclase and femic minerals are about equal, that is, the percentage of feldspar lies between 62·5 to 37·5, and conversely with femic minerals".[8] This scheme, however, fails to discriminate basalt and andesite among our rocks. Although no good purpose would be served by discussing them separately, the writer, for convenience of description, uses the term basalt for rocks in which $(Q+F)/(M+F)$ is less than 0·75 (3/4), and andesite for rocks in which $(Q+F)/(M+F)$ lies between 0·75 to 1·33 (4/3). Basalt thus includes, in addition to all the basic rocks characterized by phenocrysts of calcic plagioclase (anorthite and/or bytownite), either together with or without olivine and pyroxenes, the miharaite and allied rocks which some writers might prefer to call "basaltic andesite" or "basaltic bandaite".

---

[5] S. Tsuboi, *Jour. Fac. Sci., Imp. Univ., Tokyo*, Sec. II, **1**~5 (1926), 139.

[6] S. Tsuboi, *Jour. Col. Sci., Imp. Univ., Tokyo*, Art. 6, **43** (1920), 87.

[7] W. Q. Kennedy, *Am. Jour. Sci.*, **25** (1933), 239.

[8] H. S. Washington, *Ibid.*, **5** (1923), 469.

Some of the volcanoes in the region under study, especially those of the Idu peninsula and the outlying Seven Idu Islands, have been studied by a number of authors, whose works have been referred to in their proper places in this paper.

The writer desires to express his sincere thanks to Dr. S. Tsuboi, who went over this paper in manuscript, and also to Mr. H. Kuno, who supplied him with new analyses of rocks from the volcanoes Hakone and Taga. He is also greatly indebted to Mr. S. Tanaka, analyst of this Institute, who kindly made chemical analyses of a large number of rocks for this paper.

I. TERTIARY VOLCANISM.

General statement.

It is perhaps well to state at the outset that in none of the regions dealt with in this paper are there any rocks older than the Tertiary. They are all completely buried under more recent formations: not even fragments of pre-Tertiary rocks have ever been found among either the volcanics or the sedimentaries of these regions. What happened there during the Mesozoic and still older times is therefore at present a perfect blank. The oldest event known to us is Tertiary volcanism, which may be divided into the Palaeogene volcanism of the Ogasawara Islands and the Neogene volcanism of the Idu peninsula.

The Ogasawara Islands occupy in the Pacific an isolated position of exceptional interest, both structurally and geologically. Situated about 150 km east of Nisino-sima (Rosario I.)[9], and flanked on the east by the great depression—the Japan Trough—which within 400 km of the shores of the islands has a depth of more than 8000 m. These islands form a linearly-arranged chain stretching in N.–S. direction from 28°30′N. to 26°30′N. As shown in Fig. 1, they are the only peaks projecting from the submarine ridge that runs parallel to the much longer and larger submarine ridge lying beneath the insular volcanoes of the Huzi volcanic zone, there being a depression of more than 4000 m between the two ridges just mentioned. Although the islands are largely composed

---

[9] A dissected volcanic island, situated 27°14′N. and 140°53′E., between Sohu-gan (Lots Wife Rocks) and Kita Io-sima (San Alessandro I.) on the southern extension of the Huzi volcanic zone.

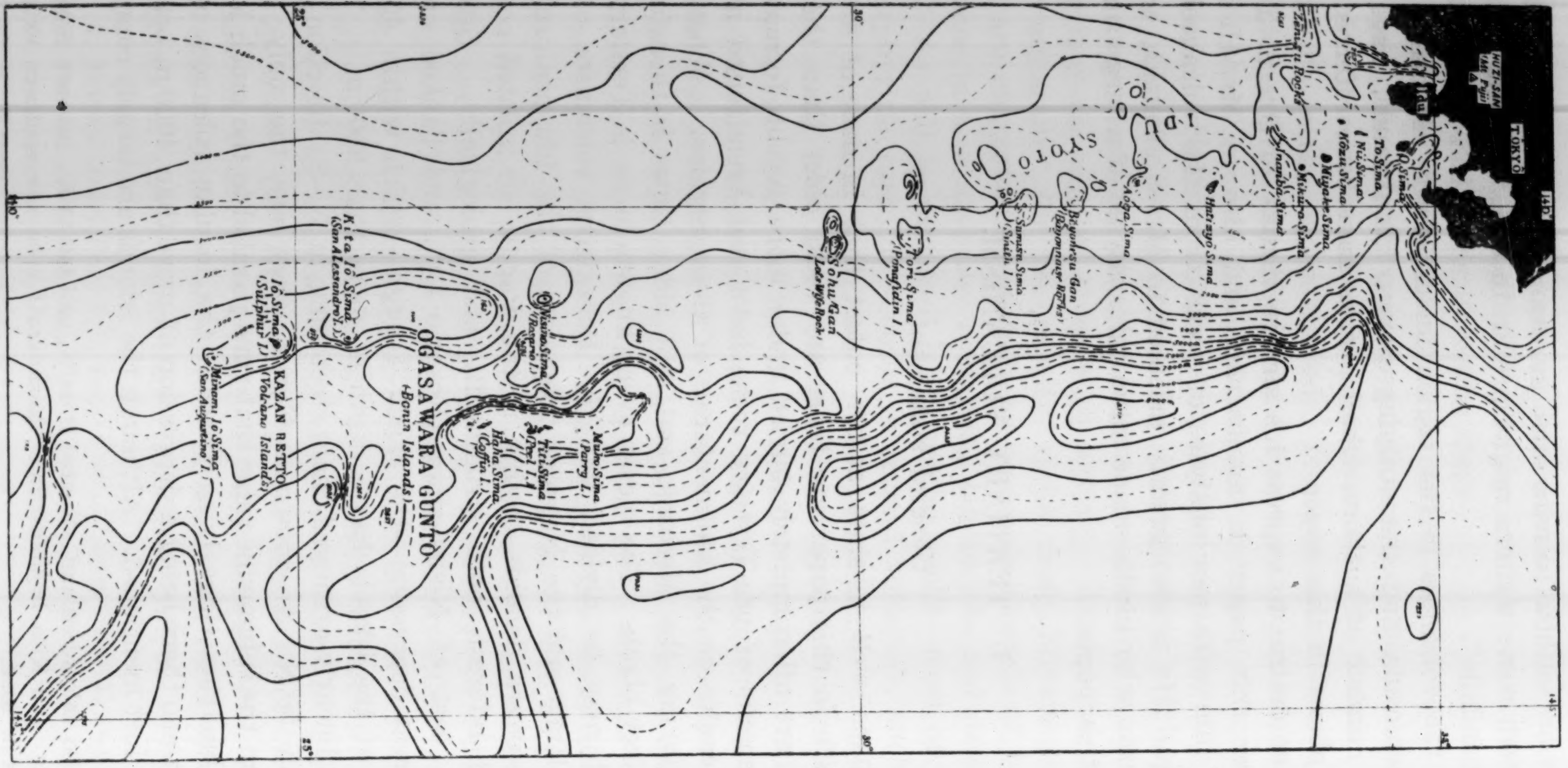
140°
145°
TOKYO
HUZI-SAN
(Mt. Fuji)
Idu
O Sima
To Sima
Nii Sima
Kôzu Sima
Miyake Sima
Mikura Sima
Zenisu Rocks
Inanba Sima
Hatizyô Sima
I-DU
SYOTO
Aoga Sima
Beyonesu Gan
(Bayonnaise Rocks)
Sumisu Sima
(Smith I.)
Tori Sima
(Ponafidin I.)
30°
Sohu Gan
(Lot's Wife Rock)
Muko Sima
(Parry I.)
Titi Sima
(Peel I.)
Haha Sima
(Coffin I.)
Nisino Sima
(Rosario I.)
OGASAWARA GUNTO
(Bonin Islands)
Kita Iô Sima
(San Alessandro I.)
25°
Iô Sima
(Sulphur I.)
KAZAN RETTO
(Volcano Islands)
Minami Iô Sima
(San Augustino I.)

Fig. 1. Map showing the Seven Idu Islands and the Southern Islands in relation to the submarine areas about them (based on the chart Nos. 81, 83, and 86, of the Hydrographic Office, Imp. Japanese Navy).

of volcanic rocks of an andesitic character, none of them has that appearance, structural and morphological, characteristic of central volcanoes. The volcanics are locally intercalated with sedimentary rocks whose Paleogene age has definitely been proved by fossil evidence. Neither volcanics nor sediments of younger age, except the beach deposits on the present sea-shore, are represented. So far as observed, they appear to be tilted blocks traversed by numerous faults. They may thus be interpreted as relics of fault-blocks that have emerged since the end of the Palaeogene.

The Idu peninsula projects into the Pacific from the southern coast of the central Japan, separating the Suruga bay on the west from the Sagami bay on the east. Geologically speaking, this peninsula is the southernmost expression of the much larger region of the fossa magna. The southern half of the peninsula is composed largely of the so-called Idu Neogene formations, which continue beneath the Quaternary volcanoes (Amagi, Daruma, Usami, Taga, etc.) of the northern part of the peninsula into the Asigara mountains that border the peninsula on the north. Various volcanics are represented in the formations, together with contemporaneous sedimentary rocks composed practically of volcanic material. Consequently one finds here a wealth of phenomena testifying to the intensive volcanic activities that have characterized this region since the time of the Neogene. This is the case not only with the Idu peninsula, but also with the whole region of the fossa magna, of which the Idu peninsula forms but a very small part. The sequence of volcanic activities as inferred from the rock-sequence in various parts of the fossa magna are correlative with each other, although in detail the sequence of one part may be more complicated than that of another⁽¹⁰⁾. Throughout the region of the fossa magna the Neogene volcanism dates from the lower Miocene, which appear to have been concurrent with the period during which the fossa magna was formed. It is probable that the tectonic disturbance that brought about the fossa magna was responsible for the volcanism.

The Neogene formations of the Idu peninsula seem to continue farther south into the submarine ridge on which the Quaternary insular volcanoes of the Seven Idu Islands rest, seeing that the Zenisu Rocks⁽¹¹⁾, which are nothing but erosion-relics of a peak projecting from the submarine ridge (Fig. 1), are composed of volcanics (lava and agglomerate) similar to the altered lower Miocene andesites from the Idu

---

10) H. Tsuya, *Bull. Earthq. Res. Inst.*, **10** (1932), 253.

11) A group of small reefs, about 150 km off the suthern point of the Idu peninsula.

peninsula.

The structural relation of the Ogasawara Islands to the Idu peninsula and to other parts of the fossa magna is unknown at present. As will be described later, however, volcanics petrographically similar to the Palaeogene volcanics of Ogasawara are found amongst the Neogene volcanics of Idu. Moreover, many petrographic evidences show that most of the Tertiary volcanics of these two regions are comagmatic with the Quaternary volcanics of the Huzi volcanic zone. Accordingly, the Palaeogene volcanism of Ogasawara may be regarded as the forerunner of the Quaternary volcanism of the Huzi volcanic zone as well as of the Neogene volcanism of the entire region within the fossa magna.

A. *Palaeogene Volcanism of the Ogasawara (Bonin) Islands.*

The Palaeogene volcanics, which represent the oldest recognized volcanism in the region now under consideration, occupy the greater part of the Ogasawara island-group that comprises, in addition to the two larger islands, Titi-sima (Peel I.) and Haha-sima (Coffin I.), many uninhabited islets.

1. Eocene Volcanics of Haha-sima.

Haha-sima, situated 26°38′N. and 142°E., is an island with a very uneven profile, 250 m above the sea at its highest part, with an indented outline extending 17 km in a due N.–S. direction and 2 km in an E.–W. direction. The island is practically composed of volcanic rocks of an andesitic nature, with calcareous rocks next in abundance. Although the strata of these rocks throughout the island do not show any regular disposition, most of them dip at an angle of less than 20° south or north of west. The calcareous rocks (calcareous tuff and limestone) that are exposed patchwise and mostly in the central part of the island, yield abundant marine Eocene fossils. These fossils, which were examined first by S. Tokunaga (Yoshiwara)[12], were later revised by H. Yabe[13] and S. Hanzawa[14]. The last-named author divided them into two horizons—the Priabonian and the upper Lutetian stages. The Priabonian stage is represented by the *Pellatispira* limestone which is the youngest formation in the island. The upper Lutetian stage is represented by the *Nummulites* beds and the *Orthophragmina*-bearing

---

12) S. Yoshiwara, *Geol. Mag.*, **9** (1902), 297.
13) H. Yabe, *Jour. Geol. Soc., Tokyo*, **27** (1920), 19.
14) S. Hanzawa, *Ibid.*, **32** (1925), 470.

Globigerina beds, both of which are intercalated in the volcanic formations underlying the *Pellatispira* limestone.

These volcanic formations, which consist of lava, agglomerate, tuff-breccia, and tuff, are therefore of submarine eruptional origin ranging in age from middle to upper Eocene. The eruptions were probably of the central paroxysmal type that took place on the floor of the Eocene sea in the area adjoining the present island, seeing that the greater part of the formations consists of agglomerate and tuff, the agglomerate carrying abundant lava-blocks which are so large (1 m or more dia.) that they could scarcely have been derived from any remote eruption-centre.

So far as the writer's observations go, the volcanic formations comprise three kinds of andesitic rocks—two-pyroxene-andesite, quartz-bearing two-pyroxene-andesite, and olivine-bearing two-pyroxene-andesite. The following petrographic descriptions are those of eight specimens collected by the writer from the lava- and agglomerate-beds exposed along the road from Nankin-hama to Nisi-ura.

No. 1. *Two-pyroxene-andesite.* This rock, which forms the bulk of the volcanic formations, occurs as lava-flows, agglomerates, and as fragments in the tuff. Six specimens of the rock from various parts of the formations have generally similar petrographic characters, being porphyritic with many phenocrysts of plagioclase, augite, and hypersthene in an aphanitic groundmass. They are black to dark gray with a greenish tint that varies with the extent of alteration to which the rock has been more or less subjected. The freshest specimen of the rock that was collected south of Okimura has the following microscopic characters.

Phenocrysts: The plagioclase is distinctly zoned. Of the two kinds of the mineral distinguished, the one that occurs as the larger phenocrysts (2~5 mm dia.), is anorthite 99~91 An ($n_1=1{\cdot}5797\sim1{\cdot}5756$), and the other, the lesser one (0·1~1·0 mm dia.) is labradorite 68~54 An ($n_1=1{\cdot}5638\sim1{\cdot}5560$). The augite (0·1~0·5 mm dia.), which is pale brownish and non-pleochroic, has $n_1=1{\cdot}6910\sim1{\cdot}6953$ and $2V(+)=55°\sim51°$. It often exhibits zonal structure as observed by differences in the optic angles in the manner: $2V(+)=55°$, 52°, and 49° in the core, middle zone, and at the margin respectively. Average composition: $Wo_{35}En_{43}Fs_{22}$, assuming $n_1=1{\cdot}693$ and $2V=52°$. The hypersthene (0·1~0·5 mm long) is pale greenish with distinct pleochroism. $n_1=1{\cdot}6960$, $n_2=1{\cdot}7080$. $2V(-)=65°$. Composition: $En_{62}Fs_{38}$. The mineral has a thin rim of monoclinic pyroxene in parallel intergrowth. The magnetite forms very small phenocrysts 0·2 mm across.

Groundmass: The groundmass is a dark-brown glass packed with plagioclase prismoids (0·05 mm long) and very minute granules of monoclinic pyroxene and magnetite.

The chemical composition of the rock just described is shown in column No. 1, Table I, where it is compared with a Tertiary (lower Miocene or older)[15] volcanic rock described by K. Tsuboya[16] as a hypersthene-andesite from Laulau Bay, Saipan

---

[15] R. TAYAMA, *Sci. Rep. Geol. Palaeont. Inst., Tohoku Imp. Univ.*, **21** (1936), 43.

[16] K. TSUBOYA, *Jap. Jour. Geol. Geogr.*, **9** (1932), 210.

Island, Marianas, and with a Tertiary andesite17) from the top of Malakal Island, Palau18). As shown in the table, the Haha-sima andesite resembles in chemical composition the Tertiary pyroxene-andesites form the Marianas and Palau Islands. Still closer resemblances are found with some of the Tertiary pyroxene-andesites from the Idu peninsula (No. 12, Table V). As to its alkalies, the Haha sima rock is a normal andesite that is commonly met with in Japan, its normative plagioclase being labradorite 51 An. The normative pyroxene also is very close to that of the common Japanese pyroxene-andesite, its composition being $Wo_{20}En_{45}Fs_{35}$. As thus, plotted on the Wo-En-Fs diagram (or Di-Hd En Fs diagram), it falls within the area of the diagram, which, being occupied by the normative pyroxenes of the Japanese pyroxene-andesites, lies more to the En Fs side compared with the area representing the normative pyroxenes of the intra Pacific lavas.20)

Table I.

	No. 1	A	B
SiO_2	58·47	56·45	56·69
Al_2O_3	16·47	18·97	16·47
Fe_2O_3	2·08	3·61	2·67
FeO	5·46	3·56	4·87
MgO	3·90	3·55	5·07
CaO	7·68	7·02	9·06
Na_2O	3·16	2·50	2·08
K_2O	0·91	0·43	0·43
H_2O+	0·75	1·68	0·74
H_2O-	0·33	1·14	0·60
TiO_2	0·80	0·61	0·64
P_2O_5	0·06	0·07	0·09
MnO	0·18	0·10	0·16
Total	100·25	99·69	99·57

Norm of No. 1.19)

Q	12·85	QFM	Q	13
Or	5·57		F	61
Ab	26·74		M	26
An	28·09	NF	Or	9
Wo	4·18		Ab	44
En	9·74		An	47
Fs	7·39	NPl	An	51
Mt	3·01	NPy	Wo	20
Il	1·52		En	45
Ap	tr.		Fs	35
		Fe		65

No. 1. *Two-pyroxene-andesite.* Okimura, Haha-sima, Ogasawara (Bonin) Islands. S. Tanaka, analyst.

A. Hypersthene andesite. Laulau Bay, Saipan Island, Marianas Islands. S. Tanaka, analyst.

B. Pyroxene-andesite, Top of Malakal Island, Palau Islands. A. Soule, analyst.

---

17) R. TAYAMA, *Sci. Rep. Geol. Palaeont. Inst., Tohoku Imp. Univ.*, **18** (1935), 25.

18) W. H. HOBBS and W. F. HUNT, *Proc. Third Pan-Pacific Sci. Congr., Tokyo*, **1** (1926), 715.

19) For the convenience' sake, the following abbreviated words are used in the tables of analyses throughout this paper.
QFM means the ratio (wt.%) Q: F: M in norm.
NF means normative feldspar (wt.%).
NPl means normative plagioclase (wt.%).
NPy means normative pyroxene (wt.%).
Fe means 100 × $(FeO+Fe_2O_3)/(FeO+Fe_2O_3+MgO)$.

20) S. TSUBOI, *Jap. Jour. Geol. Geogr.*, **10** (1932~33), 79.

No. 2. *Olivine-bearing two-pyroxene-andesite.* This rock, which is exposed as a weathered lava-flow south of Hyogo taira, is similar in texture and mineral constituents to the rock just described, except that it carries subordinate olivine phenocrysts that have been completely pseudomorphed by a chloritic substance.

No. 3. *Quartz-bearing two-pyroxene-andesite.* This rock was found as lava-blocks composing the bulk of the agglomerate bed exposed on the shore at Nisi-ura. Microscopically, it consists of phenocrysts of plagioclase, quartz, augite, hypersthene, and a light-greenish devitrified groundmass rich in secondary silica and zeolitic material. The agglomerate bed carries, in addition to the rock just mentioned, a few fragments of completely altered andesites which resemble microscopically some of the lower Miocene rocks from the Idu peninsula.

2. Upper Eocene or Lower Oligocene Volcanics of Titi-sima.

Titi-sima, situated about 30 km north of Haha-sima, in 27°N. and 142°E., is an indented island measuring about 8 km in a N.–S. direction and 4 km in a E.–W. direction. This island is virtually composed of a volcanic series of andesitic nature, although a small area in its southern extremity is occupied by a limestone bed. The lower part of the volcanic series is chiefly lava-flows, while the upper part consists of agglomerates (locally conglomeratic), tuff-breccia, and tuffs. The strata of these rocks, which generally dip gently southwest, are intruded in several parts of the island by small masses of a dacitic rock. According to Hanzawa[21], one of the lavas is conformably overlain by the limestone bed that is exposed at the southern extremity of the island as well as in the adjoining islets, and contains *Lepidocyclina* (*Eulepidina*) with some other foraminifera, for which reason it is referred to the Oligocene age. The volcanic series, therefore, is mostly lower Oligocene or upper Eocene, while the eruptions that gave rise to them were probably submarine, although the centre of eruptions cannot be traced at present.

The volcanic rocks are usually greatly altered, the alteration being exhibited in various ways. The commonest alteration product is a whitish to greenish flinty rock, infiltrated with calcedony, calcite, and zeolite. The following petrographic descriptions are those of ten of the least-altered specimens that were collected by the writer in 1935 from the volcanic series exposed near Omura and Okumura on the northern side of port Hutami. The alteration products and secondary minerals that were collected at the same time from the same series will form the subject of further study, although in a petrographic study of the island, they are quite important. Among the specimens examined, six are two-pyroxene-andesite, one aphyric andesite, one quartz-two-pyroxene-andesite, and the remainder tuff and tuff-breccia.

No. 4. *Two-pyroxene-andesite.* This rock, which, so far as observed, occupies the greater part of the volcanic series, occurs as massive lava and agglomerate. Mega-

---

21) S. HANZAWA, *loc. cit.*

scopically, the least-altered specimen, which is one of the angular lava-blocks composing an agglomerate bed exposed midway between Omura and Okumura, is pitch-black and more or less vesicular, the round vesicles (up to 3 mm dia.) of which are lined with a whitish zeolite. Although the rock carries megascopic phenocrysts of plagioclase and pyroxene, its porphyritic structure is rather inconspicuous. Microscopically, it contains phenocrysts of plagioclase, augite, and hypersthene scattered through a glassy groundmass packed with prismoids of plagioclase and monoclinic pyroxene and a few magnetite granules.

Phenocrysts: The plagioclase, which is very faintly zoned, is bytownites 87 An ($n_1=1{\cdot}5737$). The pale-brownish and non-pleochroic augite has $n_1=1{\cdot}6910$ and $2V(+)=53°$. Composition: $Wo_{36}En_{43}Fs_{21}$. The hypersthene, which is greenish with distinct pleochroism, shows $n_1=1{\cdot}6982$ and $2V(-)=65°$. Composition: $En_{61}Fs_{39}$. The mineral occurs either as isolated individuals or in parallel intergrowth with a monoclinic pyroxene ($c \wedge Z=39°$), the latter being usually on the outside.

Groundmass: Although the plagioclase appears to be a sodic bytownite, its composition could not be exactly made out, owing to its minute size. The optic angle of the monoclinic pyroxene, which last is rather pigeonitic, is about 44°.

Another specimen of the two-pyroxene-andesite is a lava-ball, 5∼10 cm in diameter, a number of which occur in agglomerate exposed along a road at the eastern end of Omura. Megascopically, it is pitch-black with a resinous luster. Microscopically, it carries phenocrysts of plagioclase, augite, and hypersthene, all of which have the same optical properties as those in the preceding specimen. The groundmass is more glassy than that of the preceding rock, the greenish-brown glass ($n=1{\cdot}5198\sim1{\cdot}5245$) being packed with incipient crystals of plagioclase, monoclinic pyroxene and iron-ore, together with a few microphenocrysts of a pigeonitic pyroxene ($n_1=1{\cdot}7035$).

No. 5. *Aphyric andesite.* This rock, exposed on a cliff by the road immediately north of Okumura, occurs as a lava-flow, about 2 m thick, intercalated between agglomerate beds. Megascopically, it is black, aphanitic, and more or less vesicular, the vesicular cavities being lined with zeolites. When altered, it is grayish with various tints of green. Microscopically, the rock is entirely devoid of phenocrysts, except for a few augite (0·3 mm dia., $2V(+)\doteqdot52°$), the whole mass being a greenish-brown glass densely packed with minute prismoids (0·05∼0·1 mm long) of plagioclase and monoclinic pyroxene, and dusty magnetite granules, together with a few microphenocrystic laths of plagioclase and multiple-twinned monoclinic pyroxene. The plagioclase, as measured on one of the minute laths of the mineral is labradorite 68 An ($n_1=1{\cdot}564$). The monoclinic pyroxene is pigeonite, its optic angle being 30° and smaller and $\beta=1{\cdot}7026$. Composition: $Wo_{13}En_{47}Fs_{40}$.

The freshest part of the aphyric andesite was chemically analyzed by Tanaka, with the results shown in column No. 5 of Table II, where it is compared with three earlier analyses of samples from the same island, one from the neighbouring island, Ototo-sima, and with an analysis of augite-andesite obsidian from Saipan Island, Marianas. As the analysis No. 5 shows, the aphyric andesite just described is rather high in silica content, its norm showing abundant quartz. The normative plagioclase and pyroxene are 50 An and $Wo_{19}En_{26}Fs_{55}$ respectively. Hobbs and Hunt[22] give an analysis (A of Table II) of a specimen that they collected from "near the Church of England in the town of Bonin", and to which they refer with two other specimens as an augite-hypersthene-andesite with "large phenocrysts and broken crystals of hypersthene, augite (slightly sodic), andesine-labradorite-feldspar and large magnetite grains ……in a brownish glass containing numerous microlites of feldspar, green amphibole,

---

[22] W. H. HOBBS and W. F. HUNT, *loc. cit.*

Table II.

	No. 5	A	B	C	D	E
SiO_2	62·22	59·65	54·44	53·92	53·18	63·58
Al_2O_3	13·81	13·24	12·90	17·98	16·18	14·57
Fe_2O_3	1·73	1·96	7·08	n.d.	10·30	1·52
FeO	6·54	5·66	n.d.	4·88	n.d.	5·92
MgO	2·07	5·92	12·75	4·57	6·72	1·60
CaO	6·51	6·70	5·12	7·59	10·12	4·58
Na_2O	2·70	2·51	2·06	3·92	1·85	4·86
K_2O	0·65	1·04	0·35	1·14	0·35	2·02
H_2O+	3·22	2·00	5·54	4·64	1·65	0·31
H_2O-	0·22	1·10				
TiO_2	0·24	0·29	n.d.	n.d.	n.d.	0·71
P_2O_5	tr.	0·06	n.d.	n.d.	n.d.	0·34
MnO	0·20	0·12	n.d.	n.d.	n.d.	tr.
Total	100·11	100·25	100·24	98·64	100·35	100·01

Norm of No. 5.

Q	23·96	QFM	Q	25
Or	3·90		F	52
Ab	23·07		M	23
An	23·36	NF	Or	8
Wo	3·72		Ab	46
En	5·12		An	46
Fs	10·55	NPl	An	50
Mt	2·55	NPy	Wo	19
Il	0·46		En	26
Ap	tr.		Fs	55
		Fe		80

No. 5. *Aphanitic andesite.* Okumura, Titi-sima, Ogasawara (Bonin) Islands. S. Tanaka, analyst.

A. Augite-hypersthene-andesite. Town of Bonin, Bonin Islands. K. McAlpine, analyst.

B. Andesite. Miyanoura, Titi-sima. Fukuda, analyst.

C. Bronzite-limburgite ("boninite"). Ogiura, Titi-sima. J. Petersen, analyst.

D. Andesite perlite. Kurose, Ototo-sima, Ogasawara (Bonin) Islands. Fukuda, analyst.

E. Augite-andesite obsidian. Saipan Island, Marianas Islands. Eyme, analyst.

minute grains of magnetite and prisms of apatite". The two analyses, columns 5 and A, are much alike, the only notable differences between them being the lower magnesia and the little higher silica of the aphyric andesite. Compared with these two analyses, the three old ones (B, C, and D of Table II) are certainly lower in silica, the other oxides showing diverse relations. Altogether, these three analyses are so incomplete and unsatisfactory that we cannot rely much upon them. The aphyric andesite is higher in silica and lower in alumina than the two-pyroxene-andesite from Haha-sima (No. 1 of Table I), the other oxides being approximately alike in both, if the higher water content of the former is taken into consideration. Containing almost the same amounts of silica and alumina, the aphyric andesite is more calcic and less alkalic than the augite-andesite obsidian (E of Table II) from Saipan Island, Marianas. Furthermore, in the matter of analyses of the Idu Neogene rocks, the aphyric andesite does not match in chemical composition with any of them. It is worth noting, however, as will be discussed presently, that the latter closely fits the variation diagram which, owing to its having been constructed exclusively from analyses of aphyric and aphanitic rocks from the Neogene and Quaternary volcanic rocks of Idu and the Southern Islands, represents variations in the magmatic liquids that have possibly characterized the volcanism of the region since the Neogene.

No. 6. *Two-pyroxene-dacite* (or *quartz-two-pyroxene-andesite*). This type of rock occurs in several parts of the island either as dikes or necks intruding into the two-pyroxene-andesite masses. The specimen which the writer collected from a dike (?) exposed on the sea-cliff, about 1·5 km south of Okumura, is megascopically pale-gray, compact, glassy, and porphyritic with phenocrysts of plagioclase and pyroxene. Microscopically, it contains phenocrysts of bytownite-labradorite 78∼55 An ($n_1 = 1{\cdot}569 \sim 1{\cdot}557$), augite ($n_1 = 1{\cdot}703$), hypersthene ($n_1 = 1{\cdot}7165$), and indented quartz, in a glassy groundmass packed with microphenocrystic plagioclase, pyroxenes (both monoclinic and rhombic), and magnetite, besides incipient crystals of plagioclase and pyroxene.

B. *Neogene Volcanism of Idu.*

General statement.

The Neogene Tertiary volcanics, which are distributed extensively over the Idu peninsula, and which range in age from lower Miocene to upper Pliocene, comprise various rock-types from olivine-basalt to biotite-liparite, all accompanying their own pyroclastics, besides solid lavas. Since the sequence of these rocks has been given by the writer in his earlier papers(32), it will not be repeated here. However, in order to present in one whole view, the leading rock-types that erupted during the Neogene, the general rock-sequence as they erupted is given in Table III in a more or less revised form, together with the stratigraphic sequences as proposed by previous writers. This table may by taken as giving the sequence, generally, although in detail the sequence would naturally be much more complicated.

The oldest series in the Neogene volcanic sequence is represented by greenish andesitic rocks referred to as the so-called propylite, and their pyroclastics (green tuff, tuff-breccia, and agglomerate), intercalated with shale, sandstone, and conglomerate, all of which are mostly composed of volcanic material. The volcanic rocks of the series, which vary considerably in megascopical as well as in microscopical charac-

---

23) H. TSUYA, *Bull, Earthq. Res. Inst.*, 10 (1932), 247; *Proc. Fifth Pan-Pacific Sci. Congr.*, Victoria and Vancouver, B.C., Canada, (1933), 2385.

ters, have been subjected to various degrees of "propylitization". Those in which the primary constituents (plagioclase and mafic minerals) are entirely replaced by secondary calcite, chlorite, zeolite, epidote, silica, etc., are frequently met with, while highly albitized or highly silicified rocks are also represented. As may be judged from the less-altered parts of these rocks, most of them are altered pyroxene-andesite (and basalt), but some of them have certainly been derived from dacitic (or liparitic) rocks. Thus the oldest series, which is exposed in the upper course of the Kano-gawa (river) from Yugasima to Amagi-toge in central Idu, is regarded by Tayama and Niino[24] as the most typical representative of their "Yugasima series" (see Table III), which consists of altered dacitic rocks, besides altered andesites, together with green tuff and tuff-breccia containing abundant quartz fragments.

The oldest series is invaded by minor intrusives (dike and intrusive sheet) of basalt, diabase, altered andesite, dacite and liparite (or quartz-porphyry). It is worth noting that both the intrusives and their wall-rocks are altered in the same way, while the alteration in the wall-rocks is more intensive at their contacts with the intrusives than at distances from them.

Although the age of the oldest series has not yet been definitely determined, the upper limit to the possible range of the age is fixed by a lower Miocene series which consists chiefly of strata of more or less altered andesite, dacite, and their tuffs, intercalated with foraminifera limestones (Nasimoto beds and Simo-Siroiwa beds)[25], and which appear to overlie the oldest series. The writer has still no definite evidence that would enable him to determine the stratigraphic relation between the oldest series and the limestone-bearing series. Whether the former underlies the latter with unconformity between them, or without, it is possible that they are of about the same age. Notwithstanding that the limestone-bearing series has been assigned by Tayama and Niino to the "Sirahama group", the writer believes that the former is older than the Sirahama beds which, as developed in the vicinity of Sirahama, south Idu, are regarded as type-horizons of the Sirahama group.

The volcanic series next to the oldest one (including the limestone-bearing series), which is distributed extensively in the southern part, and rather locally in the northern part, of the Idu peninsula, consists largely of alternations of pumiceous tuff, tuff-breccia, and agglomerate,

---

[24] R. TAYAMA and H. NIINO, *Rep. Sci. Res., Saito Gratitude Foundation*, Nos. **11**, **13** (1931).

[25] *Miogypsina* limestone of Nasimoto and *Lepidocyclina* limestone of Simo-Siroiwa. Cf. S. HANZAWA, *Sci. Rep., Tohoku Imp. Univ.*, **12** (1928~33), 159.

Table III. Tertiary Volcanic Sequence of Idu.

	Idu (Tsuya)		Idu (Tayama and Niino)			Atami, Yugawara, Hakone (Kuno)	
	Effusives	Minor Intrusives	Volcanics	Formations		Volcanics	Formations
Pliocene	Pyroxene-dacite Pyroxene-andesite Basalt					Basalt Basalt Pyroxene-andesite	Hata beds Aziro beds
	Hornblende-pyroxene-dacite (Hiyekawa beds)					Hornblende-dacite	Tensyozan beds
		Pyroxene-porphyrite (dike)				Basalt	Mikasayama bed
						Olivine-pyroxene-andesite	Ainohara beds
	Pyroxene-andesite					Pyroxene-andesite	Inamura beds
Miocene	Pyroxene-andesite		Pyroxene-andesite	Matuzaki group	Simoda series	Pyroxene-andesite	Sukumogawa beds
	Hornblende-dacite		Andesite-tuff	Sirahama group		Dacite-tuff	Hayakawa beds
	Biotite-plagioliparite Potash-liparite (Simoda beds)	Dacite Liparite (or quartz-porphyry)	Liparite-tuff				
			Liparite Dacite White tuff	Tateiwa group			
	Dacite, Pyroxene-andesite and tuffs*		Pyroxene-andesite	Aoiti group			
		Altered pyroxene-andesite Basalt Diadase Diabase-porphyrite	Dolerite Diabase Porphyrite		Yugasima series	Quartz-gabbro Quartz-diorite	
	Propylite series Dacite and/or liparite Andesite Basalt (Yugasima beds)		Propylite Green tuff	Yugasima group		Green andesite Green tuff-breccia	Dogasima beds Hirogawara beds Sogayama beds

* Includes horizons of *Miogypsina* limestone (Nasimoto) and *Lepidocyclina* limestone (Simo-Siroiwa).

together with a few tufaceous shales and sandstones. Lavas are comparatively insignificant in amount and local in origin, though minor intrusives frequently occur. The rocks of this series are mostly of rather acid type, including varieties that range from potash-liparite, through plagioliparite, into dacite, although certain andesites are also represented, especially in the upper horizons of the series.

The oldest series is clearly distinguished from the last-mentioned one. The former has been subjected to more intense alteration than the latter, and although the rocks of the former are generally devoid of most of their primary constituent minerals, the rocks of the latter usually retain their primary structure with the least-altered minerals (feldspar, pyroxene, hornblende, biotite, etc.), while the pumiceous tuff of the former series contains much devitrified pumice, in contrast to which the allied rock of the latter consists of fresh pumice. The boundaries of the two series are often defined by faults. Were it not the case, they should lie one above the other unconformably, since certain rock-fragments belonging to the oldest series are contained in the tuff ane tuff-breccia of the other series.

Tayama and Niino mention the "Aoiti group" and "Tateiwa group", both of which, included in the "Simoda series", are supposed to be younger than the Yugasima series, but older than the Sirahama group. They refer to the Aoiti group as a bed of agglomerate consisting chiefly of hypersthene-andesite and two-pyroxene-andesite, while according to them, the Tateiwa group consists of alternating layers of dacitic and liparitic tuffs. So far as the writer's observations in northern Idu go, there is no need to place these two groups between the Yugasima and Sirahama group, seeing that, of the beds to which they have assigned the one or the other of these two groups, one may be correlated to the Yugasima group and the rest to the Sirahama group.

Only a few areas of upper Miocene and lower Pliocene volcanics have been recognized in Idu. This may be due largely to the difficulty of distinguishing between lower and upper Miocene, and between Miocene and Pliocene, particularly when there are only a few sedimentary rocks that probably belong to these periods, and which, so far, have yielded only fossils of small value as age markers. The upper horizons of the Tayama and Niino's Sirahama group, which, contrary to the dacitic and liparitic rock-types of its lower horizons, are chiefly represented by andesitic rock-types (tuff and tuff-breccia of pyroxene-andesite), are possibly upper Miocene, although there may be marked unconformity between the upper and lower horizons. Indeed, according to Y. Otuka[26], the shell beds at Sirahama (type locality of the Tayama and Niino's Sirahama group) may be correlated with the shell beds in the Hayakawa tuffite beneath the Hakone volcano, both of which contain fossils that point to their age as being upper Miocene or lower Pliocene.

The Tertiary beds exposed on the wall of the Tanna tunnel near its western entrance are examples of upper Miocene or lower Pliocene volcanics. These volcanics are divided into upper and lower horizons (Fig. 3, Table XII). The lower horizon consists of loosely-coherent sand beds containing abundant sandy pebbles of hornblende-dacite, one of the lower Miocene volcanics. According to Otuka[27], judging from the fossils they contain, the sand beds may be middle Neogene (upper Miocene or lower Pliocene). The upper horizon, which overlies unconformably (?) the lower, is represented by a volcanic series consisting of a glassy two-pyroxene-andesite lava, with its agglomerate and tuff-breccia[28]. A dike of similar andesite occurs as an intrusive into the lower horizon. These volcanics, which underlie another and wholly different series of volcanics and sedimentaries (lower Pleistocene beds referred to as the Simo-Tanna beds), may be lower Pliocene or slightly younger. They probably extend southward underneath the lavas from the Taga volcano into the Tertiary terrane in the vicinity of Nirayama, for similar rocks are exposed patchwise in this terrane. Here, however, they overlie lower Miocene rocks (green tuff-breccia, propylite, dacite, etc.), both forming steep slopes that border the overlying lavas from the Taga volcano on the east. The Tertiary volcanics, that is, those located west of the last-mentioned locality across the Kano-gawa Alluvial plain, and which form Wasidu-yama and Katuragi-yama, may also be of the same age. Besides these, similar volcanics are found in several Tertiary terranes of central and south Idu, although their age is not yet certain.

Upper Pliocene volcanics occur in the Tertiary terrane that borders the Amagi volcano on the north, their type localities being Hiyekawa, Kasiwa-toge, and thereabouts. Covered unconformably by the lower Pleistocene beds (Zyo beds) and by lavas from the Pleistocene volcanoes (Tensi-yama, Usami, and Amagi-san), they rest on the Mio-

---

26) Y. OTUKA, *Jour. Geol. Soc., Tokyo*, **41** (1934), 564.

27) Y. OTUKA, *Bull. Earthq. Res. Inst.*, **11** (1933), 548.

28) This series may possibly be correlated with the Asigara formation which is distributed extensively in the Tertiary terrane that borders the Hakone volcano on the north, as rocks closely resembling the former are found among the volcanics from the latter.

cene beds exposed in the same district. Basalt, andesite, dacite, and plagioliparite are the rock-types represented in them. These upper Pliocene volcanics occur as solid lavas accompanying their own tuffs, tuff-breccias, and agglomerates, with a few intercalated tufaceous shales and mudstones. Of these, tuff, shale, and mudstone have yielded fossil shells and foraminifera. According to Otuka, the fossil shells that the writer collected from a tufaceous shale exposed along the driveway south of Kasiwa-toge, are either lower Pleistocene or upper Pliocene. They may be assigned more probably to the upper Pliocene, seeing that the beds in which they occur are older and more deformed than the lower Pleistocene Zyo beds. The Matuzaki group which, according to Tayama and Niino, consists practically of pyroxene-andesite (tuff and agglomerate), may be partly at any rate of the same age.

To summarize, since all the Neogene Tertiary volcanics from lower Miocene to upper Pliocene have yielded marine fossils in the intercalated tuffs and tufaceous sediments, they can be assigned to submarine eruptions during the Neogene. Now volcanics that thicken toward their centres have been taken to mark volcanoes of the central eruption type, but none of these volcanics do so sufficiently to warrant the supposed association. It is thus possible that the eruptions of the Tertiary age took place from numerous local vents. Some of the dikes and necks that occur among the Tertiary volcanic masses are probably indications of it.

The petrography of the Neogene Tertiary volcanics was studied with a few representative specimens from the large number that the writer collected, mostly from the Tertiary terrane round and about the Amagi volcano, and which include several rock-types ranging from basalt to plagioliparite. As to the acid rocks which, distributed extensively in the southern and southwestern parts of the peninsula, include dacite, plagioliparite, and potash-liparite(29), the writer reserves his comments as brief reference to them has already been made elsewhere(30).

3. Miocene Effusives.

Seven specimens of the Miocene effusives(31) were studied, both micro-

---

29) Although the type-locality of the potash-liparite is Manzo-yama, near Simoda, a similar rock occurs at Kisami and Sitaru, about 1·5 km and 10 km southwest of Simoda. To these may be added the biotite-liparite exposed immediately south of Hama, Simo-Kawadumura, since the rock is similarly rich in potash (8·54% K_2O), Cf. T. YAMAGISHI, *Jour, Geol. Soc., Japan*, **43** (1936), 384.

30) H. TSUYA, *Bull. Earthq. Res. Inst.*, **7** (1929), 329.

31) The localities of the specimens examined are shown in Fig. 2 by corresponding numbers.

scopically and chemically, with results as shown in Tables IV and V. They are of the following rocks.

Table IV. Constituent Minerals of the Miocene Effusive Rocks, Idu.

		No. 7	No. 9	No. 10	No. 12	No. 13
Porphyritic Minerals	Plagioclase	$n_1=1{\cdot}5795\sim$ $1{\cdot}5759$ 93~91 An	$n_1=1{\cdot}5660$ 72 An	$n_1=1{\cdot}5800\sim$ $1{\cdot}5762$ 100~92 An	$n_1=1{\cdot}5615\sim$ $1{\cdot}5560$ 47~37 An	$n_1=1{\cdot}5582\sim$ $1{\cdot}5542$ 58~50 An
	Augite	—	$n_1=1{\cdot}6975$ $2V(+)=56°$ $Wo_{40}En_{37}Fs_{23}$	$n_1=1{\cdot}6846\sim$ $1{\cdot}6910$ $2V(+)=54°$ (core) $2V(+)=49°$ (margin) $Wo_{33}En_{42}Fs_{25}$	$n_1=1{\cdot}6914\sim$ $1{\cdot}6938$ $2V(+)=52°$ (core) $2V(+)=56°$ (margin) $Wo_{38}En_{42}Fs_{20}$	—
	Hypers-thene	—	Completely replaced by chlorite	$n_1=1{\cdot}6864\sim$ $1{\cdot}6916$ $2V(-)=60°$ (core) $2V(-)\ 72°$ (margin) $En_{69}Fs_{31}$	$n_1=1{\cdot}7045\sim$ $1{\cdot}7087$ $2V(-)=62°$ (core) $2V(-)=57°$ (margin) $En_{54}Fs_{46}$	—
	Olivine	Completely replaced by chlorite	—	Largely replaced by chlorite	—	—
	Hornblende	—	—	—	—	$n_1=1{\cdot}6610$ $n_2=1{\cdot}6727$ $2V(-)=83°$ Largely replaced by chlorite
	Accessories	—	—	Quartz Magnetite	Quartz Magnetite	Quartz Magnetite Apatite
Groundmass	Plagioclase	$n_1=1{\cdot}5652$ 70 An	$n_1=1{\cdot}5630$ 66 An	$n_1=1{\cdot}5710$ 82 An	n.d.	n.d.
	Pyroxene	$\beta=1{\cdot}7114$ $2V(+)=43°$ $Wo_{24}En_{36}Fs_{40}$	n.d.	$n_1=1{\cdot}6952$ $2V(+)=52°$ (core) $2V(+)=35°$ (margin) $Wo_{34}En_{42}Fs_{24}$	Augite: $n_1=1{\cdot}6965$ $2V(+)=50$ Hypersthene: $2V(-)=61°\sim$ 69°	—
	Accessory and interstitial materials	Magnetite Cristobalite Glass base	Glass	Glass	Magnetite Apatite Acid feldspar Quartz Secondary chlorite and zeolite	Magnetite Apatite Acid feldspar Quartz

Table V. Analyses of the Miocene Effusive Rocks from Idu. S. Tanaka, analyst.

		No. 7	No. 8	No. 9	No. 10	No. 11	No. 12	No. 13
SiO_2		49·62	53·13	54·40	54·55	55·72	59·91	63·16
Al_2O_3		20·37	17·75	18·00	16·54	16·08	16·42	15·68
Fe_2O_3		2·61	5·14	1·77	1·47	4·16	3·52	3·11
FeO		6·71	3·90	6·76	7·10	4·62	3·71	2·55
MgO		4·05	3·24	4·08	5·76	3·30	2·81	2·36
CaO		11·97	7·58	8·02	8·85	6·73	6·82	4·48
Na_2O		1·89	2·52	2·61	2·06	2·78	3·17	2·77
K_2O		0·31	0·23	1·19	0·62	0·48	1·07	2·33
H_2O+		0·39	1·71	1·63	1·41	1·44	0·74	1·30
H_2O-		0·71	3·80	0·91	0·87	3·38	0·73	1·20
TiO_2		0·87	0·87	0·78	0·70	0·82	0·72	0·52
P_2O_5		0·07	0·12	0·13	tr.	0·10	0·13	0·10
MnO		0·17	0·09	0·16	0·16	0·12	0·14	0·05
Total		99·74	100·08	100·44	100·09	99·73	99·89	99·61
Q		4·93	16·34	8·29	9·73	17·48	18·92	24·56
Or		1·67	1·11	7·23	3·90	2·78	6·12	13·91
Ab		15·73	21·50	22·02	17·30	23·59	26·74	23·59
An		46·45	36·44	33·93	33·93	30·04	27·54	21·42
Wo		5·11	0·12	2·09	4·18	1·05	2·32	C=0·71
En		10·04	8·03	10·13	14·36	8·23	7·03	5·92
Fs		8·97	1·59	9·90	10·95	3·96	3·03	1·32
Mt		3·70	7·41	2·55	2·08	6·02	5·09	4·40
Il		1·67	1·67	1·52	1·37	1·52	1·37	1·06
Ap		tr.	0·33	0·33	tr.	0·33	0·33	0·33
QFM	Q	5	17	8	10	18	19	25
	F	64	62	64	56	59	61	61
	M	31	21	28	34	23	20	14
NF	Or	2	2	11	7	5	10	24
	Ab	24	36	35	31	42	44	40
	An	74	62	54	62	53	46	36
NPl	An	75	63	61	66	56	51	48
NPy	Wo	21	2	9	14	8	19	—
	En	42	82	46	49	62	57	82
	Fs	37	16	45	37	30	24	18
Fe		69	72	67	59	72	71	69

No. 7. *Olivine-basalt.* Compact, greenish-gray, and porphyritic with plagioclase phenocrysts. Agglomerate in Kuno's Soga-yama beds (lower Miocene) underlying the two-pyroxene-andesite lave from the Taga volcano. Locality: about 1 km south of Atami along the driveway leading from Atami to Aziro, north Idu.

No. 8. *Two-pyroxene-andesite.* Compact to vesicular, greenish-gray, and slightly porphyritic with plagioclase phenocrysts and rare augite. Microscopically, the porphyritic minerals are anorthite 92 An ($n_1=1{\cdot}5763$), augite ($n_1=1{\cdot}698$), and chloritized hypersthene. The groundmass is occupied largely by a chloritic substance, besides a few plagioclase laths and magnetite grains. Lava, about 5 m, thick, intercalated between fossiliferous gray-tuff beds (lower Miocene) a short distance below the *Lepidocyclina*-limestone horizon. Locality: Simo-Siroiwa, Simo-Omimura, north Idu.

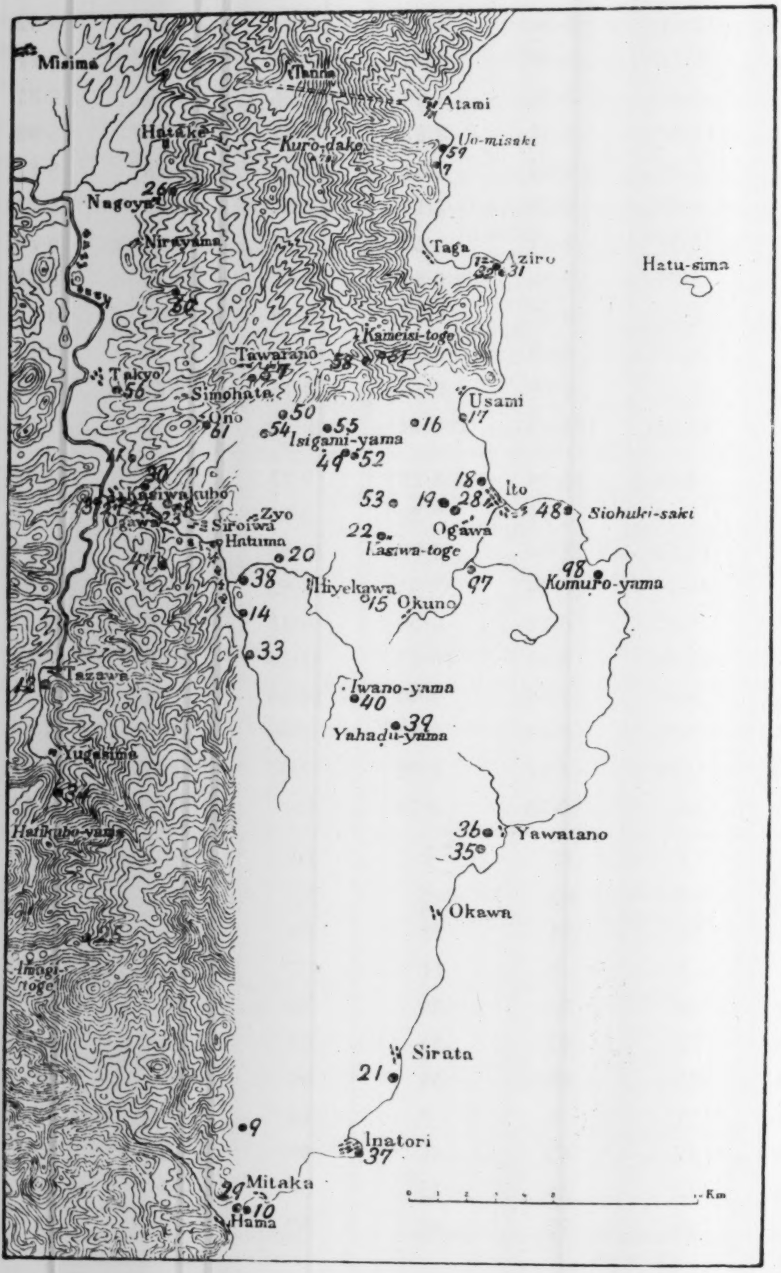
Misima
Tanna
Atami
Uo-misaki
57
7
Hatake
Kuro-dake
26
Nagoya
Nirayama
Taga
Aziro
32
31
Hatu-sima
60
Kameisi-toge
Tawarano
51
58
Takyo
56
Simohata
Usami
17
50
Ono
61
55
54
Isigami-yama
16
49
52
18
Ito
53
19
28
48
Siohuki-saki
Zyo
Siroiwa
Ogawa
Hatuma
22
Kasiwa-toge
Ogawa
20
38
97
98
Komuro-yama
Hiyekawa
15
Okuno
14
33
Tazawa
Iwano-yama
40
39
Yahadu-yama
Yugasima
Hatikubo-yama
36
35
Yawatano
Okawa
Imagi-toge
Sirata
21
9
Inatori
37
Mitaka
29
10
Hama
Km

Fig. 2. Northeastern part of the Idu peninsula, showing the localities of the rock-specimens described in the text.

No. 9. *Two-pyroxene-andesite.* Compact, greenish-gray, and porphyritic with phenocrysts of plagioclase and pyroxene. Lava underlies a Miocene (lower ?) series composed of liparite and dacite, together with their tuff and tuff-breccia. Locality: about 2 km inland from Mitaka, Simo-Kawadumura, south Idu.

No. 10. *Quartz-olivine-bearing two-pyroxene-andesite.* Compact to slightly vesicular, dark-gray to black, and porphyritic with phenocrysts of plagioclase, pyroxene, olivine, and quartz. Agglomerate in the fossiliferous tuff and sandstone beds (Miocene, lower ?). Locality: sea-shore immediately north of Hama, Simo-Kawadumura, south Idu.

No. 11. *Two-pyroxene-andesite.* Vesicular, greenish-gray, and slightly porphyritic with plagioclase phenocrysts and a few pyroxene. Microscopically, it contains phenocrysts of faintly-zoned anorthite-bytownite 93~85 An ($n_1=1{\cdot}5766\sim1{\cdot}5727$) and partially-chloritized augite ($n_1=1{\cdot}6952$), with completely chloritized hypersthene, all in a groundmass consisting of labradorite 60 An ($n_1=1{\cdot}5596$), magnetite, and tridymite, with a base impregnated by a chloritic substance. The vesicles are lined with zeolite. Agglomeratic lava intercalated between fossiliferous tuff and tuff-breccia beds (Miocene, lower ?). Locality: mountain-side, 1·5 km east of Makinogo, Kita-Kanomura, north Idu.

No. 12. *Quartz-bearing two-pyroxene-andesite.* Compact to vesicular, pale-gray, and porphyritic with phenocrysts of plagioclase and pyroxene. Lava and agglomerate unconformably overlie the propylite series. Locality: east bank of Kano-gawa, midway between Tazawa and Itiyama, Kami-Kanomura, north Idu.

No. 13. *Hornblende-dacite.* Compact, greenish-gray, and porphyritic with phenocrysts of plagioclase, quartz, and hornblende. The agglomerate of this rock is overlain by strata of siliceous sandstone and tuff (lower Miocene), and intruded by dikes of green andesite. Locality: floor of the Kano-gawa, at Ko-Tatino, Kita-Kanomura, north Idu.

4. Pliocene Effusives.

Ten specimens of the Pliocene effusives were examined both microscopically and chemically, with the results as shown in Tables VI and VII. They are of the following rocks[32].

No. 14. *Hypersthene-bearing augite-olivine-basalt.* Compact, greenish-gray to black, and porphyritic with phenocrysts of plagioclase and olivine. Microscopically, augite phenocrysts are surrounded by sharp, narrow rim of pigeonite. The hypersthene occurs only in parallel intergrowth with the phenocrystic augite. The agglomerate, which overlies dacite (lava and agglomerate) and pumiceous tuff (upper Pliocene), is unconformably overlain by the Zyo beds and a lava-flow from the Amagi volcano. Locality: about 500 m south of Hatuma, Simo-Omimura, north Idu.

No. 15. *Olivine-basalt.* Compact, gray, and porphyritic with abundant plagioclase phenocrysts and a few olivine. Lava resting upon another lava (pyroxene-andesite, No. 16) which in turn overlies dacitic agglomerate. Locality: 3 km southeast of Hiyekawa along the mountain path from Hiyekawa to Okuno, Ito-mati, north Idu.

No. 18. *Two-pyroxene-andesite.* Compact, greenish-gray to black, and porphyritic with phenocrysts of plagioclase and pyroxene. Lava with platy joints. It is covered by the lavas from the Usami volcano. Petrographically, it closely resembles the

---

[32] The localities of the specimens examined are shown in Fig. 2 by corresponding numbers.

Table VI. Constituent Minerals of the Pliocene Effusive Rocks, Idu.

		No. 14	No. 15	No. 18	No. 20	No. 21	No. 22
Porphyritic Minerals	Plagioclase	$n_1=1\cdot5748$ 89 An	$n_1=1\cdot5770\sim$ 1·5749 94~90 An	$n_1=1\cdot5769\sim$ 1·5684 93~77 An	$n_1=1\cdot5568\sim$ 1·5537 55~49 An	$n_1=1\cdot5546\sim$ 1·5515 50~46 An	$n_1=1\cdot5660\sim$ 1·5540 70~50 An
	Augite	core margin 2V(+)=60°→53° →16° $n_1=1\cdot6970\sim1\cdot6995$ $c\wedge Z \doteqdot 45°$ $Wo_{40}En_{37}Fs_{23}$	—	2V(+)=50° $n_1=1\cdot6905$ $Wo_{32}En_{45}Fs_{23}$	2V(+)=53° $n_1=1\cdot6950$ $Wo_{37}En_{41}Fs_{22}$	$n_1=1\cdot6910$	2V(+)=46°(min.) $n_1=1\cdot6965\sim1\cdot6980$ $Wo_{27}En_{43}Fs_{30}$
	Hypersthene	2V(−)≑79° (very rare)	—	2V(−)=64° $n_1=1\cdot6992$ $En_{60}Fs_{40}$	2V(−)=61° $n_1=1\cdot7074$ $En_{53}Fs_{47}$	2V(−)=63° $n_1=1\cdot6955$ $En_{63}Fs_{37}$	2V(−)=62°
	Olivine	$\alpha=1\cdot6715$ $\beta=1\cdot6920$ $Fo_{74}Fa_{26}$	2V(−)≑86° Largely replaced by chlorite	—	—	—	—
	Accessories	—	—	Magnetite Apatite	Hornblende Quartz Magnetite Apatite	Magnetite	Quaartz Magnetite
Groundmass	Plagioclase	n.d.	$n_1=1\cdot5633$ 67 An	$n_1=1\cdot5628$ 65 An	n.d.	Greenish-brown glass packed with microlites and spherulites (acicular tridymite, feldspar, and hornblende). Tridymite patches	Glass (n=1·491) packed with microlites, spherulites, and magnetite dust.
	Pyroxene	2V(+)=18°~0° $\beta=1\cdot7050$ $Wo_{11}En_{40}Fs_{49}$	2V(+)=51°(core) −37°(margim) 17·30 $Wo_{24}En_{36}Fs_{40}$	Augite Hypersthene	Augite Hypersthene		
	Accessory and interstitial materials	Magnetite	Magnetite Tridymite	Magnetite Tridymite Quartz Acid feldspar	Magnetite Tridymite Glass		

Table VII. Analyses of the Pliocene Effusive Rocks from Idu.
S. Tanaka, analyst,

		No. 14	No. 15	No. 16	No. 17	No. 18	No. 19	No. 20	No. 21	No. 22
SiO_2		48·57	50·82	56·42	57·19	60·70	61·25	65·85	70·00	75·63
Al_2O_3		19·25	20·54	17·01	16·85	16·10	16·34	15·95	14·89	12·80
Fe_2O_3		2·56	3·78	3·06	3·91	2·79	3·28	2·84	2·03	0·47
FeO		7·70	5·44	4·97	3·97	3·92	3·30	1·89	1·32	1·95
MgO		6·38	3·30	4·36	4·28	2·78	2·35	1·92	0·73	0·28
CaO		11·21	10·60	8·49	7·74	6·26	6·02	4·44	3·05	2·20
Na_2O		1·73	2·29	2.12	2·46	3·39	3·51	3·51	4·14	3·71
K_2O		0·16	0·28	0·66	0·41	0·97	0·99	1·56	2·09	2·35
H_2O +		0·74	0·70	0·58	1·16	0·68	0·96	0·78	0·50	0·25
H_2O −		0·85	1·20	0·97	0·64	1·06	0·80	0·80	0·54	0·07
TiO_2		0·75	0·78	0·70	0·68	0·69	0·71	0·48	0·45	0·26
P_2O_5		0·10	0·04	0·06	0·09	0·27	0·18	tr.	0·13	tr.
MnO		0·15	0·14	0·16	0·19	0·11	0·11	0·11	0·09	0·06
Total		100·15	99·91	99·56	99·57	99·72	99·80	100·13	99·96	100·03
Q		1·86	7·81	15·92	18·08	19·40	20·42	26·55	30·75	38·56
Or		1·11	1·67	3·90	2·23	5·57	6·12	9·46	12·24	13·91
Ab		14·68	19·40	17·83	20·97	28·84	29·89	29·89	35·13	31·46
An		44·23	44·78	35·05	33·66	25·87	25·59	21·97	14·19	10·85
Wo		4·41	3·25	2·91	1·63	1·39	1·39	C=0·31	C=0·61	C=0·20
En		15·86	8·23	10·84	10·64	6·92	5·82	4·82	1·81	0·70
Fs		11·08	5·80	5·67	3·30	4·09	2·38	0·53	——	2·90
Mt		3·70	5·56	4·40	5·56	3·94	4·86	4·17	3·01	0·69
Il		1·37	1·52	1·37	1·37	1·37	1·37	0·91	0·91	0·46
Ap		0·33	tr.	tr.	0·33	0·65	0·33	tr.	0·33	tr.
QFM	Q	2	8	16	18	20	21	27	31	39
	F	61	67	58	58	61	63	62	63	56
	M	37	25	26	24	19	16	11	6	5
NF	Or	2	3	7	4	9	10	15	20	25
	Ab	24	29	31	37	48	49	49	57	56
	An	74	68	62	59	43	41	36	23	19
NPl	An	75	70	66	62	47	46	42	29	25
NPy	Wo	14	19	15	10	11	14	——	——	——
	En	51	48	56	68	48	61	90	100	19
	Fs	35	33	29	22	41	25	10	——	81
Fe		65	73	64	64	70	73	70	81	89

two-pyroxene-andesite agglomerate (lower Pliocene? or Otuka's middle Neogene) found on the wall near the west entrance of the Tanna tunnel. Locality: northern outskirt of Ito-mati, north Idu.

No. 16. *Two-pyroxene-andesite*. Lava-flow. Locality: about 2 km west of Nakazato, Usamimura, north Idu.

No. 17. *Two-pyroxene-andesite*. Lava-flow. Locality: sea-shore of Hadu, Usamimura, north Idu.

No. 19. *Two-pyroxene-andesite*. Lava and agglomerate intruded by a dike of quartz-bearing two-pyroxene-porphyrite (No. 28). Locality: Ogawa, immediately northwest of Ito-mati, north Idu.

Microscopically, these three rocks resemble the last-mentioned one (No. 18), so that the petrographic notes on them may be omitted, only their chemical analyses being given respectively in columns Nos. 16, 17, and 19, of Table VII.

No. 20. *Hornblende-augite-bearing hypersthene-dacite*. Pale-gray, compact but fragile, and porphyritic with abundant phenocrysts of plagioclase and pyroxene, besides a few hornblende and quartz. Glomeroporphyritic grouping of the phenocrysts, except the hornblende and quartz, is common. Lava and agglomerate, both associated with pumiceous tuff, are overlain by the basalt agglomerate (No. 14). Locality: Hiyekawa, Naka-Omimura, north Idu.

No. 21. *Two-pyroxene-dacite*. Pale-gray, compact but fragile, partly spherulitic, and porphyritic with phenocrysts of plagioclase and pyroxene. Lava with flow-banding, is unconformably overlain by both pyroclastic deposits and lava of the Amagi volcano. Locality: sea-cliff, 500 m south of Sirata, Kitomura, east coast of middle Idu.

No. 22. *Two-pyroxene-plagioliparite*. Obsidian with phenocrysts of plagioclase and pyroxene. Lava overlies a two-pyroxene-andesite lava, similar to rock No. 19, with ash beds between them. Although the basal part near the contact with the underlying ash beds is obsidian, the main upper bulk of the lava is pale-gray to white, and lithoiditic. Locality: Kasiwa-toge, midway between Ito-mati and Hiyekawa, north Idu.

5. Minor Tertiary Intrusives.

Of the minor Tertiary intrusives in the Idu peninsula, the following eight[33] were examined microscopically and chemically, with results as shown in Tables VIII and IX.

No. 23. *Diabase*. Black to greenish-gray, crystalline, medium-grained, and porphyritic with abundant plagioclase phenocrysts. Intrusive sheet into a pumiceous tuff-breccia (lower Miocene). Locality: Simo-Siroiwa, Simo-Omimura, north Idu.

No. 24. *Aphric basalt*. Compact, black, and almost aphyric with negligible plagioclase phenocrysts. Intrusive sheet, about 10 m thick, into a pumiceous tuff carrying blocks of liparite (lower Miocene). Locality: southern bank of the Tosi-kawa (river), near Kadono, Simo-Kanomura, north Idu.

No. 25. *Diabase-porphyrite*. Greenish-gray, crystalline, medium-grained, and slightly porphyritic. Intrusive sheet (?) into a green tuff (lower Miocene, propylite series). Locality: northern side of the Amagi tunnel, Amagi-toge, Kita-Kanomura, middle Idu.

No. 26. *Green andesite*. Compact, greenish, and slightly porphyritic with phenocrysts of plagioclase. Microscopically, the plagioclase phenocrysts are almost unaltered, with the composition of bytownite 85 An ($n_1 = 1{\cdot}573$). The mafic phenocrysts

---

33) The localities of the specimens examined are shown by corresponding numbers in Fig. 2.

(augite ?) are completely altered, their place being occupied by chlorite, calcite, and quartz. The groundmass consists of plagioclase laths and magnetite dust, together with chlorite, calcite, and quartz. One of the dikes intrude into a green tuff (lower Miocene . Locality: mountain side, east of Nagoya, Nirayamamura, north Idu.

No. 27. *Green andesite.* Compact, greenish, and porphyritic with plagioclase phenocrysts. Microscopically, the plagioclase phenocrysts are almost unaltered, with the composition of labradorite 54 An ($n_1=1{\cdot}5564$), while the mafic phenocrysts (hornblende ?) are completely altered to an aggregate of feldspar, magnetite, and chlorite. Accessory minerals: magnetite and apatite. The groundmass is a granular aggregate of quartz and feldspar, besides a few plagioclase prismoids and magnetite dust. The rock occurs as an intrusive sheet into a sandy tuff (lower Miocene) a short distance below the basalt sheet (No. 24). Locality: southern bank of the Tosi-kawa, Kadono, Simo-Kanomura, north Idu.

No. 28. *Quartz-bearing two-pyroxene-porphyrite.* Pale-gray, crystalline, medium to fine-grained, and slightly porphyritic. A dike intrudes into agglomerate of two-pyroxene-andesite (No. 19). Locality: quarry, immediately north of Ogawa, Ito-mati, north Idu.

No. 29. *Quartz-bearing two-pyroxene-porphyrite.* Dark-green, crystalline, medium-graind, and porphyritic. A dike intrudes into fossiliferous tuff and agglomerate

Table VIII. Constituent Minerals of the Minor Tertiary Intrusive Rocks, Idu.

		No. 23	No. 24	No. 25	No. 28	No. 29
Porphyritic Minerals	Plagioclase	$n_1=1{\cdot}5774\sim1{\cdot}5750$ 95~90 An	$n_1=1{\cdot}5795\sim1{\cdot}5749$ 98~90 An	$n_1=1{\cdot}5778\sim1{\cdot}5665$ 95~73 An	$n_1=1{\cdot}5654$ $1{\cdot}5620$ 71~65 An	$n_1=1{\cdot}5594$ 40 An
	Augite	——	——	$2V(+)=52°$ $n_1=1{\cdot}700$ $Wo_{34}En_{40}Fs_{26}$	$2V(+)=50°$ $n_1=1{\cdot}694$ $Wo_{32}En_{43}Fs_{25}$	$2V(+)=57\sim53°$ $n_1=1{\cdot}6925\sim1{\cdot}6952$ $c\wedge Z=43°$ $Wo_{38}En_{40}Fs_{22}$
	Hypers-thene	——	——	$2V(-)=65°$ $n_1=1{\cdot}698$ $n_2=1{\cdot}702$ $En_{61}Fs_{39}$	$2V(-)\fallingdotseq77°$	Completely replaced by chlorite.
	Accessories	——	——	Magnetite	Magnetite Quartz	Magnetite Quartz Apatite
Groundmass	Plagioclase	n.d.	$n_1=1{\cdot}562$ 65 An	$n_1=1{\cdot}5599$ 60 An	$n_1=1{\cdot}5540$ 50 An	n.d.
	Pyroxene	$2V(+)=50°$ $n_1=1{\cdot}696$ $Wo_{31}En_{42}Fs_{27}$	Pigeonite 2V very small	——	Augite Hypersthene $2V(-)\fallingdotseq67°\sim72°$	Largely replaced by chlorite
	Accessory and interstitial material	Magnetite Secondary chlorite and zeolite	Magnetite Interstitial quartz Secondary chlorite	Interstital quartz Secondary chlorite	Magnetite Tridymite	Magnetite Interstitial quartz and feldspar

Table IX. Analyses of the Minor Tertiary Intrusive Rocks, Idu.
S. Tanaka, analyst.

		No. 23	No. 24	No. 25	No. 26	No. 27	No. 28	No. 29	No. 30
SiO_2		49·23	49·30	50·23	55·38	60·76	61·58	61·61	66·00
$Al O_3$		18·81	14·69	17·59	18·04	16·70	16·06	15·81	15·12
Fe_2O_3		4·16	5·27	2·44	2·69	2·76	3·92	2·84	3·70
FeO		5·85	7·70	6·69	4·07	3·31	2·75	3·75	0·91
MgO		4·64	5·75	5·84	2·42	3·71	2·45	2·67	1·38
CaO		9·82	7·58	10·28	7·84	4·18	6·36	5·88	3·73
Na_2O		1·97	1·89	2·13	2·40	2·98	3·31	3·53	4·13
K_2O		0·21	0·24	0·27	0·52	1·38	0·89	1·04	0·78
H_2O +		1·19	1·89	2·13	2·40	2·98	3·31	3·53	4·13
H_2O −		3·17	3·57	1·25	0·66	1·20	1·00	1·23	1·94
TiO_2		0·75	1·08	0·93	0·76	0·53	0·66	0·70	0·65
P_2O_5		0·08	0·06	0·06	0·13	0·05	0·08	0·08	0·15
MnO		0·18	0·13	0·27	0·11	0·08	0·13	0·17	0·08
Total		100·06	99·50	100·10	99·94	100·01	100·03	100·35	100·12
Q		7·81	10·33	4·80	21·86	22·16	22·76	20·18	29.25
Or		1·11	1·67	1·67	3·34	8·35	5·01	6·12	4·45
Ab		16·78	15·73	17·83	20·45	25·17	27·79	29·89	35·13
An		42·00	30·88	37·83	27·26	20·86	26·70	24·20	17·80
Wo		2·44	2·79	5·46	C=3·47	C=2·65	1·63	1·74	C=0·92
En		11·55	14·36	14·55	6·02	9·23	6·13	6·62	3·41
Fs		6·33	8·17	9·23	4·22	3·03	0·93	3·56	——
Mt		6·02	7·64	3·47	3·94	3·94	5·79	4·17	1·39
Il		1·37	2·12	1·82	1·52	1·06	1·21	1·37	1·21
Ap		0·33	tr.	tr.	0·33	tr.	0·33	0·33	0·33
Cc		——	——	——	3·90	——	——	——	Hm2·71
QFM	Q	8	11	5	24	24	23	21	31
	F	63	52	59	55	58	61	61	60
	M	29	37	36	21	18	16	18	9
NF	Or	2	3	3	7	15	8	10	8
	Ab	28	33	31	40	46	47	50	61
	An	70	64	66	53	39	45	40	31
NPl	An	71	66	68	57	45	49	45	34
NIy	Wo	12	11	19	——	——	19	15	——
	En	57	57	50	59	75	71	56	100
	Fs	31	32	31	41	25	10	29	——
Fe		67	69	60	73	61	70	70	75

beds (Miocene, lower ?). Locality: sea-cliff, immediately north of Hama, Simo-Kawadumura, south Idu.

No. 30. *Green andesite.* More or less vesicular, greenish, and almost aphanitic. Microscopically, the rock consists of plagioclase laths, magnetite granules, tridymite, and apatite, with a chloritic material, besides a few microphenocrysts of partially-altered labradorite 65 An ($n_1 = 1{\cdot}562$). A dike intrudes into siliceous tuff and tuff-breccia (lower Miocene). Locality: top of Siro-yama, Kasiwakubo, Kita-Kanomura, north Idu.

II. QUATERNARY VOLCANISM.

General statement.

So far as could be observed in northern Idu, the earliest volcanism of Quaternary age is represented by the volcanics contained in the lower Pleistocene deposits, These deposits, which furnish a good horizon marker, enable the Quaternary volcanism to be dated with some degree of certainty. They are divided into the following two horizons:

The lower horizon of the lower Pleistocene deposits may be referred to as Zyo beds, named after the type-locality near the northern foot of Amagi volcano (see Fig. 2). It is an alternation of gravel, sand, and mud, containing numerous fossil shells and foraminifera, besides fossil leaves. According to Otuka[34], who made an exhausitive examination of these fossils, the Zyo beds may be either uppermost Pliocene or lowest Pleistocene, most probably his Dl. So far as examined, the constituent rock-materials of the Zyo beds are what may be expected to have been derived from the Tertiary rocks on which the beds rest unconformably. It is however worth noting that the mud carries not a few fragments of pumice—a possible indication that it is one of the earliest volcanics of the Pleistocene. The Zyo beds at the type-locality which, owing to dislocation by faulting dip generally 10°~20°E. or NE. are overlain unconformably by lava-flows from the Usami volcano on the east.

The upper horizon of the lower Pleistocene deposits is an alternation of gravel, sandy tuff, and mud, and referred to as Ono beds, are typically exposed at Ono, about 6 km north of Zyo. There one of the typical exposures is seen on the northern bank of the Ono valley, where a landslide occurred at the time of the north Idu earthquake of 1931. Table X shows a detailed section of the exposure as actually measured by the writer.

The Ono beds, which at the type-locality are badly dislocated by faulting, overlie unconformably the tuff and tuff-breccia of lower Mio-

---

[34] Y. OTUKA, *Bull. Earthq. Res. Inst.*, **11** (1933), 557.

Table X.

Thickness in meters	Rocks
8	Lava-flow (olivine-bearing two-pyroxene-andesite, No. 61).
0·05	Lapilli (olivine-bearing augite-andesite).
1	Ash containing plagioclase, pyroxene, and hornblende.
0·3	Gravel (aphanitic andesite, pyroxene-andesite, olivine-two-pyroxene-andesite, etc.).
	Unconformity.
0·5	Grayish mud.
0·1	Sandy tuff containing plagioclase, pyroxene, and olivine.
0·3	Grayish mud containing *Diatoms*.
0·2	Sandy tuff containing plagioclase, pyroxene, and fragments of pyroxene-andesite.
0·05	Grayish mud.
0·4	Sandy tuff containing plagioclase, pyroxene, and fragments of pyroxene-andesite.
5	Gravel (silicified dacite or liparite, aphanitic andesite, two-pyroxene-andesite, two-pyroxene-dacite, silicified rocks, etc.).
5	Yellowish mud.
2·5	Gravel (two-pyroxene-andesite, aphanitic andesite, quartz-porphyry, green rocks, etc.).
>15	Yellowish mud.
?	Gravel?
	Unconformity.
	Tertiary rocks (tuff and tuff-breccia).

cene, and are covered unconformably by lava-flow and pyroclastics from the Taga volcano. As will be seen from the foregoing table, volcanic materials become increasingly important upward, pyroxene-andesite being the rock-type represented.

The Ono beds may be correlated with the Simo-Hata beds which are typically exposed at Simo-Hata, about 2 km north of Ono, and which consist of gravel, mud, tufaceous shale, tuff, and tuff-breccia, all except the gravel containing fossil leaves and diatoms. Like the former, the latter, which dip 10°～30°NW. or SE., are unconformably underlain by Tertiary rocks, and underlie unconformably lava-flows from the Taga volcano. Table XI shows the rock-types represented in the beds.

Further north, at Simo-Tanna, are exposed Pleistocene deposits, referred to as the Simo-Tanna beds, and consisting of gravel, tufaceous sand, tufaceous shale, and tuff-breccia, all with fossil leaves except the gravel. These beds continue underground to beds similar to those found on the wall of the Tanna tunnel at a distance of 7000 ft and

Table XI.

Rocks	Volcanic Constituents and Fossils
Grayish tuff	Plagioclase, augite, olivine, and andesite scoria.
Volcanic sand	Olivine-two-pyroxene-andesite scoria and isolated crystals.
Tufaceous shale	Plagioclase, augite, hypersthene, and hornblende, with fossil leaves and diatoms.
Sandy tuff	Plagioclase, augite, and hypersthene.
Tufaceous mud	Plagioclase, augite, hornblende, and fragments of pyroxene-andesites, with fossil leaves and *diatoms*.
Gravel	

near it from its west entrance (Fig. 3). The latter consists of agglomerate, tufaceous shale, and sand, besides lapilli. The tufaceous shale contains fossil leaves and diatoms. Table XII shows the rock-types of the Simo-Tanna beds, together with the underlying Tertiary rocks and the overlying lava and agglomerate, all as found on the wall of the tunnel[35]. Though detached from the outcrops of the Ono beds and the Simo-Hata beds, there is little doubt, as a comparison of Tables X, XI, and XII will show, that the Simo-Tanna beds are of the same age.

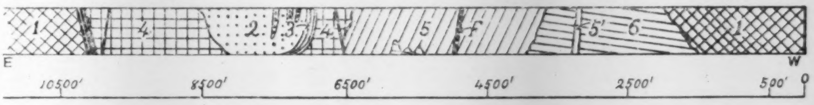

Fig. 3. Diagrammatic section showing the wall of the western half of the Tanna tunnel, north Idu.

1. Lava and agglomerate (olivine-basalt and olivine-pyroxene-basalt) from the Taga volcano.
2. Volcanic sand and agglomerate.
3. Pumice-tuff, lapilli, and gray tuff with diatoms.
4. Lava and agglomerate (two-pyroxene-andesite).

} Simo-Tanna beds.

5. Lava, agglomerate, and tuff (two-pyroxene-andesite — lower Pliocene.

5'. Dike of two-pyroxene-andesite.

6. Sand and tuff with fossil shells—upper Miocene.

It is worth noting that the Simo-Tanna beds are possibly correlated, both petrographically and stratigraphically, with the Tutizawa beds that are distributed in the Oiso geologic province adjoining the north-

---

35) The writer is indebted to Y. Otuka for the rock-specimens from the tunnel wall.

Table XII. Stratigraphic Sequence and Volcanic Rocks as observed in the Wall of the Western Part of the Tanna Tunnel.

	Rocks represented	Locality of the specimens examined (distance in ft from the W. entrance of the tunnel.	Petrographic rock-types represented	Porphyritic minerals					
				Plagioclase	Augite	Hypersthene	Olivine	Hornblende	Quartz
Taga volcano	Lava and agglomerate	10923′	Olivine-augite-basalt	+	+	−	+	−	−
		10791′	Olivine-two-pyroxene-basalt	94 An $n_1=1{\cdot}5572$	$n_1=1{\cdot}6929$	$n_1=1{\cdot}6892$	n.d.	−	−
		10461′	Olivine-basalt	92 An $n_1=1{\cdot}5760$	$n_1=1{\cdot}6983$	n.d.	$\alpha=1{\cdot}6680$	−	−
Simo-Tanna beds	Pumice-tuff*	7821′	Hornblende-two-pyroxene-dacite	57~48 An $n_1=1{\cdot}5579$ $\sim 1{\cdot}5527$	$n_1=1{\cdot}6930$	$n_1 1{\cdot}6992\sim$ $1{\cdot}7040$	−	$n_1=1{\cdot}6617$ $n_2=1{\cdot}6757$	+
	Lapilli and gray tuff** with *diatoms*	7000′ 6963′	Olivine-two-pyroxene-basalt	+	+	+	+	−	−
	Lava and agglomerate	9669′	Two-pyroxene-andesite	92 An $n_1=1{\cdot}5762$	$n_1=1{\cdot}6928$	n.d.	−	−	−
		8283′	Do	96 An $n_1=1{\cdot}5780$	$n_1=1{\cdot}6925$	n.d.	−	−	−
		9141′	Do						
		6963′	Do						
Lower Pliocene or upper Miocene	Lava and agglomerate	4587′ (6435′)	Two-pyroxene-andesite	86 An $n_1=1{\cdot}5730$	$n_1=1{\cdot}6967$	n.d.	−	−	−
	Pumice-tuff	6435′	Two-pyroxene-andesite	87 An $n_1=1{\cdot}5735$	$n_1=1{\cdot}6970$	$n_1=1{\cdot}6998$	−	−	−
	Agglomerate and tuff-breccia	5841′	Two-pyroxene-andesite	+	+	+	−	−	−
Miocene (Otuka's middle Neogene)	Tuff and sandstone with *fossil shells*	(6000′) 2145′	Hornblende-dacite (pebble)	57 An $n_1=1{\cdot}5579$	−	$n_1\doteqdot 1{\cdot}712$	−	$n_2=1{\cdot}680$	+

* Pumice glass $n=1{\cdot}5705$.

** Carries fragments of olivine-basalt and pyroxene-andesite, besides isolated fragments of plagioclase, augite, hypersthene, olivine, and hornblende.

east foot of the Hakone volcano[36]. The Tutizawa beds are recognized by Otuka as lower Pleistocene (his Dl_{I})[37].

Beneath the Taga volcano, in the vicinity of Aziro and Hata, lies a volcanic series which is composed of lavas and pyroclastic beds of basaltic nature, and is referred to by H. Kuno respectively as the Aziro beds and the Hata beds[38]. Although he has assigned these to upper Pliocene, definite evidence to justify the assignment is lacking. The writer believes them to be lower Pleistocene, seeing that the basaltic rocks in Kuno's Aziro beds and Hata beds are petrographically similar to some of the juvenile volcanic materials in the Simo-Hata beds as well as in the Simo-Tanna beds. Chemical analyses of two basaltic rocks from the Aziro beds are given in Table XIII[39].

From the foregoing remarks it may be said that either at the close of the Tertiary or in the beginning of the Pleistocene the Idu peninsula was subjected to crustal movement, generally in the sense of

Table XIII. Analyses of the Lower-Pleistocene Basalt and Andesite (Aziro beds) from Aziro.
S. Tanaka, analyst.

	No. 31	No. 32
SiO_2	51·10	56·62
Al_2O_3	18·90	15·49
Fe_2O_3	3·56	4·58
FeO	6·52	7·09
MgO	5·03	3·00
CaO	10·80	7·33
Na_2O	2·14	2·95
K_2O	0·32	0·55
H_2O +	0·50	0·35
H_2O −	0·28	0·72
TiO_2	0·83	0·96
P_2O_5	0·13	0·08
MnO	0·13	0·22
Q	6·01	15·50
Or	1·67	3·34
Ab	18·35	25·17
An	40·89	27·26
Wo	4.99	3·48
En	12·55	7·43
Fs	8·05	8·05
Mt	5·09	6·71
Il	1·52	1·82
Ap	0.33	0·33

		No. 31	No. 32
QFM	Q	6	16
	F	61	56
	M	33	28
NF	Or	3	6
	Ab	30	45
	An	67	49
NPl	An	69	52
NPy	Wo	19	18
	En	49	39
	Fs	32	43
Fe		66	79

No. 31. *Olivine-augite-hypersthene-bytownite-basalt.* Lava, south of Aziro-mati, north Idu. H. Kuno, Bull. Earthq. Res. Inst., **11** (1933), 400.

No. 32. *Aphyric andesite.* Lava, south of Aziro-mati, north Idu. H. Kuno, Bull. Volc. Soc., Japan, **3** (1936), 62.

---

[36] H. TSUYA, *Bull. Earthq. Res. Inst.*, **9** (1931), 353.

[37] Y. OTUKA, *Jour. Geol. Soc., Tokyo*, **36** (1929), 435, 479.

[38] H. KUNO, *Bull. Earthq. Res. Inst.*, **14** (1936), 96.

[39] H. KUNO, *Bull. Earthq. Res. Inst.*, **11** (1933), 400; *Bull. Volc. Soc., Japan*, **3** (1936), 62.

uplift, followed during lower Pleistocene by marine and lacustrine deposition of the Zyo beds, and then by lacustrine depositions of the Ono, Simo-Hata, and Simo-Tanna beds in certain basins on the erosion relief of the Tertiary rocks. Quaternary volcanism became increasingly vigorous as the deposition of these lower Pleistocene beds proceeded, pyroxene-andesite, pyroxene-hornblende-dacite, and olivine-two-pyroxene-andesite (or basalt) being the rock-types represented. Since these rocks, except the dacite, resemble certain lavas of volcanoes Usami and Taga, it is possible that these volcanoes began their activities during the deposition of the lower Pleistocene beds. What is certain however is that the great subaerial volcanism in Idu occurred in full force after the lower Pleistocene beds had been more or less deformed, with the consequent formation of numerous volcanic cones.

Quaternary volcanism in the Idu peninsula was active mostly in its northern part; while in the southern part, Tertiary volcanism was succeeded by the relative quiescence of the Quaternary, whence it follows that the principal volcanoes in north Idu are Amagi, Omuro, Usami, Taga, and Yugawara (see Fig. 4), although there are some that have not yet been studied (Daruma, Tanabe, Nekko, and Tyokuro[40]). These volcanoes are all Pleistocene, Usami and Omuro representing the oldest and the youngest ones respectively. Taga is younger than Usami but older than Yugawara. Omuro-yama, together with its neighbours that are included in a volcano group of that name might have been formed by volcanism of a late date when the volcanoes Amagi, Usami, Taga, and Yugawara had already been more or less dissected and dislocated. Considering the youngest volcano, the volcanism in this group seems to have been the last to occur in the Idu peninsula, the time being the late-Pleistocene, although the present numerous hot-springs there represent a stage of post-volcanic thermal activity.

The volcanoes Hakone, Asitaka, and Huzi in the terrane adjoining the northern part of the Idu peninsula are also Quaternary. Of these, Hakone is younger than the Yugawara volcano on the south, and possibly younger than Asitaka; while Huzi whose eruptions have been recurrent in historical times, is the youngest.

The Seven Idu Islands and the Southern Islands, except the Ogasawara Islands, are all Quaternary insular volcanoes that rest upon a submarine ridge which, as will be seen from Fig. 1, runs in a NNW.–SSE. from the Idu region through the Volcano Islands toward the

---

[40] R. TAYAMA and H. NIINO, *Rep. Sci. Res., Saito Gratitude Foundation*, No. **13** (1931).

Marianas. The ridge instead of being gentle and undulating, consists of several banks that are separated the one from the other by deeps

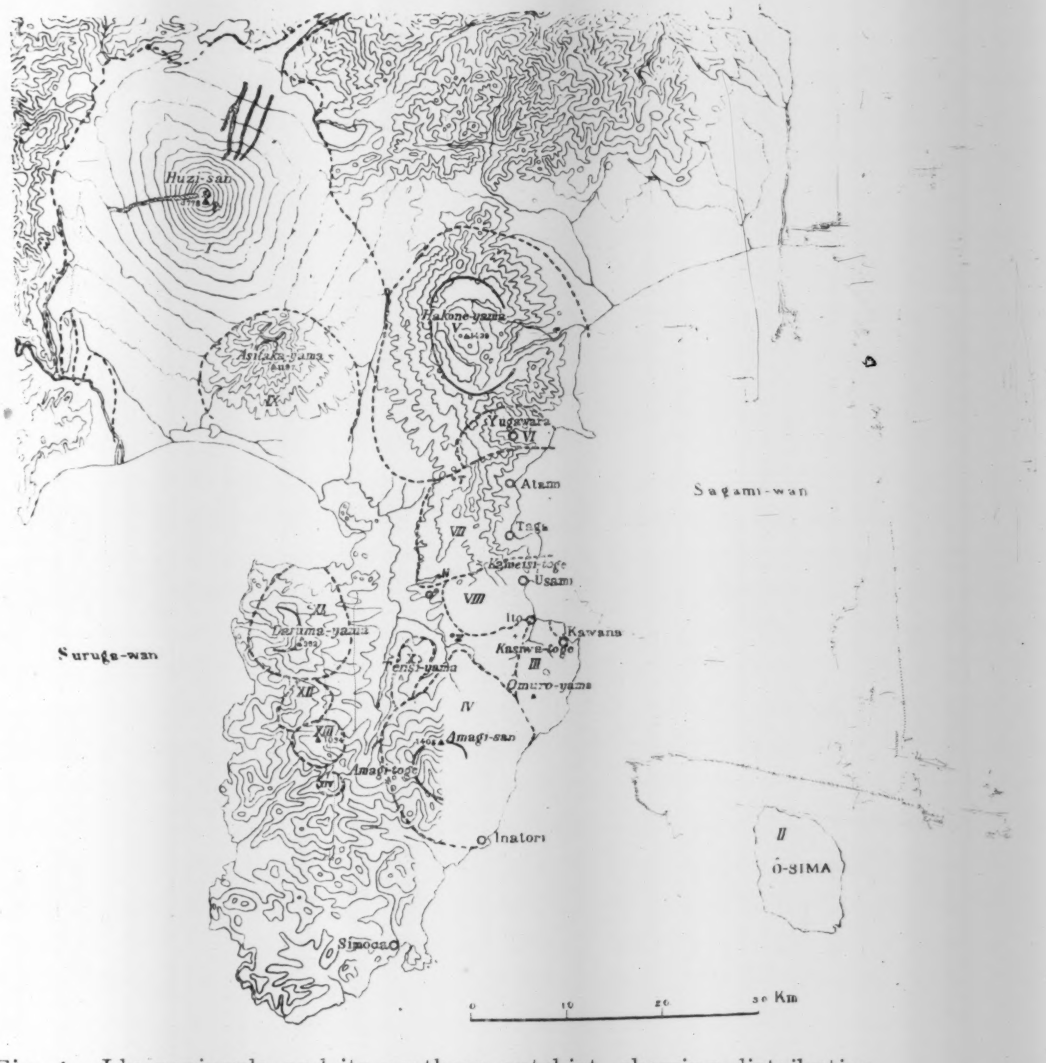
Huzi-san
Hakone-yama
V
Asitaka-yama
IX
Yugawara
VI
Atami
Sagami-wan
VII
Taga
Kameisi-toge
Usami
VIII
Ito
Kawana
Kasiwa-toge
III
Omuro-yama
XI
Daruma-yama
X
Tensi-yama
XII
IV
Amagi-san
XIII
Amagi-toge
XIV
Suruga-wan
Inatori
II
O-SIMA
Simoda
0
10
20
30 Km

Fig. 4. Idu peninsula and its northern outskirt, showing distribution of the Quaternary volcanoes. I—Huzi, II—O-sima, III—Omuro-yama volcano group, IV—Amagi, V—Hakone, VI—Yugawara, VII—Taga, VIII—Usami, IX—Asitaka, X—Tensi-yama, XI—Daruma, XII—Tanaba, XIII—Nekko, and XIV—Tyokuro-yama.

and arranged *en echelon.* It is only by comparison with the much profounder depression of the adjacent Japan Trough that these banks can be recognized as belonging to the submarine ridge. The genesis of the insular volcanoes seems to be closely related to the geotectonic history of the underlying submarine ridge and the Japan Trough, although what that actual relation is, is a question we have no means

Table XIV. Quaternary Volcanoes in Idu and the Southern Islands in Relation to the Quaternary Stratigraphic Sequence.

	Diluvium			Alluvium	
	Lower		Upper		
	Zyo beds Simo-Tanna beds Simo-Hata beds Ono beds Kuno's Hata and Aziro beds		Kano-gawa terrace deposits		Kano-gawa flood plain deposits
Volcanoes of Idu Peninsula and Vicinity		Usami Taga Yugawara Hakone (Sommas)	Hakone (Central cones)		
		Asitaka-yama			
		Tensi-yama Amagi (Main body)	Amagi (Parasitic cones)	Huzi (Earliest visible lavas)	Huzi (Uppermost part)
			Omuro-yama		
Volcanoes of the Seven Idu Islands and Southern Islands		Utone-sima To-sima			
		O-sima (Demolished bodies near Okada)	O-sima (Somma)		O-sima (Mihara-yama)
		Mikura-sima	Miyake-sima (somma)		Miyake-sima (Central cone and some flank openings)
		Hatizyo-sima (Higasi-yama)			Hatizyo-sima (Nisi-yama)
			Aoga-sima (Somma)		Aoga-sima (Central cone)
		Kita-Io-sima			
		Tori-sima (Somma)	Tori-sima (Central cone)		
			Minami-Io-sima		
					Kodu-sima (Tenzyo-san)
					Nii-sima (Muko-yama)
			Io-sima		Submarine volcano near Minami-Io-sima

Table XV. Quaternary Stratigraphic Schemes of North Idu, as proposed by Previous Writers.

	Tayama Niino	Ishii and Ihara	Otuka	Kuno
Alluvium	Recent deposits PL-terrace beds	Alluvial deposits	Kanogawa Alluvial deposits Misima fan } a	Talus, gravel, volc. ash, and lake-deposits
Diluvium (upper)	Loam M-terrace beds T-terrace beds	Terrace deposits	Hirai terrace deposits Hatake terrace deposits Kasiwanokubo terrace deposits } du	Central cone ejecta of Hakone volcano Younger-somma ejecta of Hakone volcano
	Atami group	Talus and boulder deposits Kasiwatoge beds	Darumayama volc. deposits Hakone volc. deposits Yugawara volc. deposits Tanakayama volc. deposits } $\mathrm{dl_{II}}$	Ejecta of Kintokiyama parasitic cone Makuyama dome Older-somma ejecta of Hakone volcano Ejecta of Yugawara volcano Local dacite lavas
Diluvium (lower)	Zyo group	Aziro beds Zyo beds	Zyo beds Simotanna beds (Hata beds of Kuno) } $\mathrm{dl_{I}}$	Ejecta of Taga volcano Ejecta of Usami volcano Simotanna beds
	Tertiary	Tertiary	Idu old Neogene Tertiary	Hata and Aziro beds (Pliocene)

of answering at present. Whatever the relation may be, there can be little doubt that the insular volcanoes are all products of Quaternary volcanism. Of these, history records the eruptions of O-sima, Miyake-sima, Hii-sima, Kodu-sima, Hatizyo-sima, Aoga-sima, and Tori-sima. Table XIV shows the representative Quaternary volcanoes in relation to the Quaternary stratigraphic divisions of north Idu. For comparison, Quaternary stratigraphic schemes of north Idu, as proposed by previous writers, are shown in Table XV.

The Quaternary volcanoes, which, omitting those yet unstudied, may be divided into four groups, will now be described in the following order:

A. Complex volcanoes...1. Amagi-san and 2. Hakone-yama.

B. Basaltic and andesitic volcanoes...... 3. Tensi-yama, 4. Usami volcano, 5. Taga volcano, 6. Asitaka-yama, 7. Mikura-sima. 8. Tori-sima, 9. Kita Io-sima, 10. Aoga-sima, 13. O-sima, 14. Omuro-yama volcano group, and 15. Huzi-san.

C. Liparitic volcanoes...16. Nii-sima group (Nii-sima and Kodu-sima).

D. Trachyandesitic volcanoes ....17. Io-sima and 18. "Sin-to" volcano.

A. *Complex Volcanoes.*

This group of Quaternary volcanoes includes those that have yielded various rock-types ranging in microscopical and chemical characters from basalt to dacite; namely, the volcanoes Amagi and Hakone.

1. Amagi-san volcano.

Amagi-san, which is the largest and highest volcano in Idu, occupies the eastern half of the central part of the peninsula, and consists, besides the main body, of numerous parasitic volcanoes. This volcano, which differs in structure from most of the basaltic and andesitic volcanoes in the region under investigation, is a complex volcano built up of various rock-types ranging from basalt to liparitic dacite. The main body, which consists rather of accumulations without any particular structure of both agglomerates and lavas of andesitic nature, is a gigantic cone with a base about 15 km across. Its top forms a circular ridge—a ring-wall—surrounding a circular caldera about 6 km across. The highest point of the volcano is the top of Manzabro-dake, 1405 m above the sea, on the northeastern segment of the ring-wall.

The outer flanks of the main body do not show the regular slopes usual with conical volcanoes, not only because they are deeply dissected by valleys, but because numerous parasitic volcanoes protrude from them. Thus, several parasitic cones, composed of scoria and ash with lava-flows of basaltic nature, occur lower down the slopes, near the base, of the main body, the most typical of them being Hatikubo-yama on the northwest, Noboruo-yama and Hati-yama on the southwest, and Oike-Koike on the south. The two distinct lava-domes—Yahadu-yama and Iwano-yama—rise up from the northeastern skirt of the main body, and probably belonging to the same group, is a mass of glassy lava (pumice and obsidian) that issued from the Kawago-taira crater on the northwestern flank, near the summit of the main body. Besides these two groups of parasitic volcanoes—basaltic and dacitic—, is another group of parasitic cones situated near the snmmit and half way down the flanks, which cones are composed of andesitic rocks, practically similar to those of the main body. Toogasa-yama on the northeast flank is the largest of this group[41].

The base upon which the present volcano immediately rests is mostly composed of the Idu Neogene Tertiary rocks that are exposed in the terranes about the volcano. The western and southern skirts of the volcano rest directly on the lower Miocene rocks, while the northern skirt rests either directly on these rocks or with upper Pliocene rocks interposed between them. The eastern skirt, which is washed by the sea of Sagami bay, does not disclose its base rocks anywhere, although along the lower and the middle course of the Sirata-gawa (river), which rises in the caldera and flows through the eastern gap in the ring mountains eastward into Sagami bay at Sirata, we find exposed a Tertiary series composed of greenish, silicified tuff and tuff-breccia and lavas of a greenish pyroxene-andesite, dipping 10° or more E. Though detached from the main outcrop of the lower Miocene rocks about the volcano, there is little doubt that this series is of the same age. It is comparable in many respects to the lower Miocene volcanics exposed in the terrane that adjoins the northeastern part of the volcano near Okuno, and undoubtedly continues underneath the volcano into the latter. The northwestern skirt of the volcano covers, besides the Tertiary rocks, certain lavas from a lower Pleistocene volcano called the Tensi-yama volcano, whose centre seems to lie farther northwest near Tensi-yama. On the other hand, large quantities of pumice and obsidian that were

---

41) J. SUZUKI, *Jour. Geol. Soc., Tokyo.* 28 (1921), 431.

ejected from the Kawago-taira crater (one of the youngest parasitic craters of Amagi) are contained, together with gravels of older lavas from the main body of Amagi and of the Tertiary rocks, in the river-terraces that develop at a height of 5~10 m above the present stream-level in the upper courses of the Kano-gawa and its tributary Omi-gawa. These terraces are possibly correlative with those in the lower course of the Kano-gawa in the vicinity of Syuzendi and Ohito, which, according to Otuka, are of upper Pleistocene age (his Du)[42]. In view of these facts, it appears that the most, if not the whole, of the Amagi volcano was formed during the later half of the Pleistocene.

The surface of the foundation rock upon which the Amagi lavas rest is planed across the steeply dipping Tertiary beds. It lies at various altitudes; west of the volcano, near the Amagi pass, it is about 1000 m above the sea; in the Sirata-gawa valley, it is only 300 m at the highest; while in the Tertiary terranes bordering the south and northeast margins of the volcano, it is again 300 m. Very possibly, this surfaces, which at one time before the birth of the volcano, might have been an extensively continuous erosion-plane of low relief, was dislocated along faults at the base of the volcano, and the lavas that were consequently erupted through one of these faults, spread down a farther distance to the eastern terrane where the downthrown base-surface was much less in altitude than was the upthrown surface of the base west of the volcano.

The rock specimens studied are those which the writer collected mostly from the lower flanks of the volcano,[43] and which, however, include most of the representative rock-types of both the main body and the parasitic volcanoes. These are olivine-basalt, two-pyroxene-andesite, and olivine-bearing two-pyroxene-hornblende-dacite. They have the following petrographic characters.

(A) Basalts. The rocks of this type were studied from two specimens:

No. 33. *Olivine-basalt* (Zizodo lava).
No. 34. *Olivine-basalt* (Hatikubo-yama lava).

The Zizodo lava, intercalated between pyroclastic beds, is exposed at Zizodo, Kami-Omimura, and is a lava-flow that poured out of the parasitic volcano, Marunoyama on the northern flank of Amagi. Megascopically, it is compact, dark-gray, and porphyritic with phenocrysts of plagioclase and olivine. Microscopically, the plagioclase of the phenocrysts is slightly zoned with an anorthite core 92 An ($n_1=1.5760$) surrounded by a bytownite shell 82 An ($n_1=1.5709$), while that in the groundmass is a bytownite 77 An ($n_1=1.5684$). The olivine phenocrysts, which show slight zoning, have 2 V=90° in the core and 2 V(−)=86° at the margin. $\beta=1{\cdot}6935$ (mean). Composition: $Fo_{76}Fa_{24}$. The pyroxene in the groundmass is a pigeonite with 2 V(+)= 40°∼38°. The groundmass, besides the glass base, contains a little interstitial quartz.

---

[42] Y. OTUKA, *Bull. Earthq. Res. Inst.*, **11** (1933), 539.

[43] The localities of the specimens examined are shown in Fig. 2 by corresponding numbers.

The Hatikubo-yama lava that issued from the parasitic volcano Hatikubo-yama on the northwestern flank of Amagi, flowed northward into the steep-sided Kano-gawa valley and ran along the valley for about 2 km northward toward Yugasima. In this valley the lava occurs in two flows, separated from each other by a scoria bed, 3 m thick. The lower lava rests on the lower Miocene series (dacitic agglomerate, green tuff, and altered andesite) either directly or together with an agglomeratic two-pyroxene-andesite lava of the main body of Amagi interposed between them. The specimen examined was collected from the upper flow that is exposed at Yoitizaka along the driveway from Yugasima to the Amagi pass.

Megascopically, the rock is compact, dark-gray, and slightly prophyritic with phenocrysts of lath-shaped plagioclase and granular olivine. Microscopically, we find phenocrysts of plagioclase (0·2∼0·5 mm long) and olivine (0·5∼1·0 mm dia.) in a groundmass consisting of plagioclase laths, microphenocrystic olivine grains, microphenocrystic and smaller pyroxene grains, magnetite granules, cristobalite aggregates, and pale-brown interstitial glass.

Phenocrysts: The plagioclase is a slightly zoned bytownite 78 An ($n_1=1{\cdot}5689$). Besides this, there are a few larger crystals of plagioclase (1∼3 mm dia.), which, identified as labradorite 58 An ($n_1=1{\cdot}5585$), may be regarded as xenocrysts, possibly captured from the underlying two-pyroxene-andesite lava of the main body of Amagi when the present rock was being forced upward through this lava. Olivine, which is generally anhedral with a rim of iron-oxide, has 2 V(−)=88° and $\beta=1{\cdot}7020$. Composition: $Fo_{76}Fa_{24}$.

Groundmass: The plagioclase may be either sodic bytownite or calcic labradorite, although its accurate composition could not be determined. The microphenocrystic olivine is identical with the phenocrystic one. The microphenocrystic pyroxene is augite with 2 V(+)=50° and $\beta=1{\cdot}7020$. Composition: $Wo_{30}En_{38}Fs_{32}$. But the augite sometimes exhibits faint zoning, its optic angle becoming smaller outward. Thus, in a zoned crystal, the core has 2 V(+)=55∼51°, while the margin 2 V(+)=43°. The minute pyroxene grains in the groundmass may possibly be pigeonite with much smaller optic angle.

The chemical composition of the above two lavas are much alike as shown under columns Nos. 33 and 34 of Table XVII, although the Zizodo lava is slightly more basic than the other. Both have normative olivine instead of normative quartz, and in both the normative plagioclase is labradorite.

(B) Andesites. The rocks of this type were studied from four specimens:

No. 35. *Olivine-two-pyroxene-bearing andesite* (Akasawa lava).
No. 36. *Quartz-olivine-bearing two-pyroxene-andesite* (Yawatano lava).
No. 37. *Olivine-bearing two-pyroxene-andesite* (Inatori lava).
No. 38. *Two-pyroxene-andesite* (Yanagase lava).

The olivine-two-pyroxene-bearing andesite (No. 35), which was collected on the driveway about 1 km south of Akasawa on the northeast coast of the volcano, occurs as a lava-flow, about 10 m thick and 20 m wide, that poured out of a parasitic volcano-either Toogasa-yama or Iio-yama of the northeastern flank of Amagi. Megascopically, the rock is compact, dark-gray, and very slightly porphyritic with a few plagioclase phenocrysts. Microscopically, we find, besides the plagioclase, very sporadical phenocrysts of olivine and pyroxenes (augite and hypersthene) in a groundmass consisting of plagioclase, pigeonite, and magnetite, with a few silica mineral (tridymite?) and interstitial glass base. Although the optical properties of these constituent minerals are not yet studied, the chemical composition of the rock is shown in column No. 35 of Table XVII.

The quartz-olivine-bearing two-pyroxene-andesite (No. 36), which occurs as lava and agglomerate on the northeastern flank of Amagi, is widely exposed on the sea-cliff bounding the northeastern foot of the volcano. A specimen collected from the lava exposed along the driveway between Yawatano and Akasawa is, megascopically, pale-gray, compact, and porphyritic with phenocrysts of plagioclase and pyroxene. Microscopically, it contains phenocrysts of plagioclase, augite, and hypersthene, with negligible quantities of olivine, quartz, magnetite, and apatite, in a groundmass of very minute aggregates of plagioclase prismoids, monoclinic pyroxene granules, and magnetite dust, besides tridymite in druse. Phenocrysts occasionally occur in glomeroporphyritic patches.

The olivine-bearing two-pyroxene-andesite (No. 37) occurs as a lava-flow forming a terrace at Inatori on the southeastern foot of Amagi. The specimen examined was collected from the sea-cliff that bounds the terrace on the east. Megascopically, it is compact, pale-gray, and porphyritic with phenocrysts of plagioclase and pyroxene. Microscopically, the phenocrysts are plagioclase, augite, and hypersthene, together with subordinate olivine, magnetite, and apatite. These phenocrysts form occasionally glomeroporphyritic patches. Besides these, there are occasional aggregates, which,

Table XVI. Porphyritic Minerals in the Pyroxene-andesites from Volcano Amagi.

	No. 36	No. 37	No. 38
Plagioclase	n. d.	$n_1=1.5605\sim1.5565$ 62~54 An	$n_1=1.5563$ 54 An
Augite	core margin 2V(+)=57° — 47° 49° — 50° — 53° — 2V(+)=43° (rim enclosing the core of hypersthene)	$n_1=1{\cdot}6928$ (mean) core margin 2V(+)=55° — 45° 55° — 48° 57° — 45° Average 2V=51° $Wo_{32}En_{44}Es_{24}$	$n_1=1{\cdot}6921$ (mean) 2V(+)=55°~50° $c \wedge z=46°$ $Wo_{37}En_{43}Fs_{20}$ Rim of green hornblende rarely present. Hypersthene inclusion present.
Hypersthene	core margin 2V(−)=63° — 75° 64° — 75° 2V(−)=65° (core enclosed by a rim of augite) 2V(−)=73° 78° — 63° (inner) (outer) (rim enclosing the core of olivine)	$n_1=1{\cdot}7000$ (mean) $n_2=1{\cdot}7085$ core margin 2V(−)=65° — 78° 67° — 75° 65° — 69° Average 2V=72° $En_{60}Fs_{10}$	n =1·6975 (mean) core margin 2V(−)=67°—82°—69° 77° — 75° 2V(−)=75° (inclusion in the augite) Average 2V=71° $En_{52}Fs_{38}$
Olivine	2V(−)≒90°~84°	2V(−)≒86°	—
Accessories	Magnetite Apatite Quartz	Magnetite Apatite	Magnetite Apatite

Table XVII. Analyses of Rocks from the Amagi Volcano.

S. Tanaka, analyst.

		No. 33	No. 34	No. 35	No. 36	No. 37	No. 38	No. 39	No. 40
SiO_2		49·51	51·48	54·81	59·11	60·09	62·60	68·87	71·16
Al_2O_3		18·19	18·25	18·09	16·31	16·64	15·98	14·78	14·72
Fe_2O_3		2·89	1·92	1·54	3·94	3·03	2·66	1·25	1·12
FeO		7·66	6·77	7·00	2·86	3·30	3·40	2·32	2·15
MgO		7·07	5·93	4·50	3·49	3·27	2·84	1·62	1·30
CaO		9·83	10·32	9·03	6·02	6·59	5·84	4·10	3·50
Na_2O		2·49	3·21	2·92	2·97	3·60	3·00	3·74	3·61
K_2O		0·48	0·34	0·57	1·47	1·40	1·66	2·00	2·06
H_2O +		0·45	0·43	0·50	1·48	0·68	0·45	0·68	0·27
H_2O −		0·27	0·25	0·50	1·00	0·70	0·24	0·10	0·10
TiO_2		0·64	1·03	0·79	0·76	0·80	0·65	0·40	0·36
P_2O_5		0·17	0·12	0·13	0·17	0·19	0·17	0·08	0·08
MnO		0·28	0·27	0·14	0·13	0·11	0·11	0·13	0·08
Total		99·93	100·32	100·18	99·71	100·40	99·60	100·07	100·51
Q		——	——	7·33	18·38	15·44	21·62	27·99	32·19
Or		2·78	2·23	3·34	8·90	8·35	10·02	11·69	12·24
Ab		20·97	27·26	24·64	25·17	30·41	25·17	31·46	30·41
An		36·99	34·21	34·49	26·70	25·03	25·31	17·80	16·41
Wo		4·53	6·74	3·95	0·93	2·91	1·16	0·70	C=0·51
En		16·06	14·30	11·24	8·73	8·13	7·02	4·01	3·21
Fs		10·29	9·30	10·42	0·92	2·51	3·17	2·77	2·51
Fo		1·06	0·39	——	——	——	——	——	——
Fa		0·71	0·25	——	——	——	——	——	——
Mt		4·17	2·55	2·32	5·79	4·40	3·94	1·85	1·52
Il		1·21	1·97	1·52	1·52	1·52	1·21	0·76	0·76
Ap		0·33	0·33	0·33	0·33	0·33	0·33	0·33	0·33
QFM	Q	——	——	7	19	16	22	28	32
	F	61	64	63	62	64	61	61	60
	M	39	36	30	19	20	17	11	8
NF	Or	5	4	5	15	13	17	19	21
	Ab	35	43	39	41	48	42	52	51
	An	60	53	56	44	39	41	29	28
NPl	An	64	56	58	51	45	50	36	35
NPy	Wo	15	22	15	9	21	10	9	——
	En	52	47	44	82	60	62	54	56
	Fs	33	31	41	9	19	28	37	44
Fe		59	59	65	65	65	67	67	71

composed of plagioclase, monoclinic pyroxene, and magnetite, have outlines suggesting a hornblende ancestry. The groundmass is a very minute aggregate of plagioclase laths, monoclinic pyroxene granules, and magnetite dust, with interstitial quartz and acid feldspar.

The two-pyroxene-andesite (No. 38), which occurs as a lava-flow on the northern flank of Amagi, is exposed on the southern side of the Omi-gawa valley between Hatuma and Hiyekawa, where it forms a lava-scarp, 20 m or more in height, resting on a Tertiary series (upper Pliocene). A specimen collected from lava exposed on a cutting near Hatuma is megascopically compact, light-gray, and porphyritic with phenocrysts of plagioclase and pyroxene. Microscopically, we find phenocrysts of plagioclase, augite, and hypersthene, with subordinate magnetite and apatite in a groundmass of plagioclase prismoids (0·05 mm long), pyroxene and magnetite granules, and tridymite prisms. The phenocrysts occasionally show glomeroporphyritic grouping.

The last-mentioned three lavas—Yawatano lava, Inatori lava, and Yanagase lava—, which are the typical ones from the main body of Amagi, resemble each other in the optical properties of the porphyritic minerals that they contain in common. These are given in Table XVI. They are also greatly alike in chemical composition as shown in columns Nos. 36, 37, and 38 of Table XVII.

(C) Dacites. The rocks of this type were studied from two specimens:

No. 39. *Olivine-bearing two-pyroxene-hornblende-dacite* (Yahadu-yama lava).
No. 40. *Olivine-bearing two-pyroxene-hornblende-dacite* (Iwano-yama lava).

The Yahadu-yama lava forms a twin dome of that name, about 5 km NW. of Yawatano on the northeast foot of Amagi. The specimen, which the writer collected from the northern steep slope of the dome, resembles both megascopically and microscopically the Iwano-yama dacite next to be described. Microscopically, we find phenocrysts of andesine, hornblende ($2V(-) \doteqdot 70°$), hypersthene ($2V(-) \doteqdot 67°$), augite ($2V \doteqdot (+) \doteqdot 57° \sim 54°$ in the core and $2V(+) \doteqdot 48°$ at the margin) and olivine ($2V(-) \doteqdot 85°$), with quartz surrounded by a corona of pyroxene grains in a glassy groundmass packed with microlites of plagioclase, hornblende, and pyroxene, besides a few apatite and magnetite.

The Iwano-yama lava forms a parasitic lava-dome of that name, which, situated about 3 km SE. of Hiyekawa on the northern flank near the base of Amagi, is a small hill with steep sides and a slight crater-like depression on its summit. Megascopically, the specimen, which was collected from the east foot of the hill, is light-gray, glassy, and porphyritic with abundant phenocrysts of plagioclase, pyroxene, and hornblende. Microscopically, it contains phenocrysts of plagioclase (0·3~1·5 mm dia.), augite (0·3~0·5 mm dia.), hypersthene (0·1~0·5 mm long), and hornblende (0·1~0·5 mm long), with subordinate olivine and quartz, scattered through a glassy groundmass packed with minute prismoids of plagioclase, hornblende, augite, and hypersthene, besides a few apatite needles and magnetite grains.

Phenocrysts: The plagioclase is an andesine 48 An ($n_1 = 1·5530$). The augite shows $2V(+) = 54°$ and $n_1 = 1·696$. Composition: $Wo_{40}En_{38}Fs_{22}$. The hypersthene shows $2V(-) = 71°$ and $n_1 = 1·6985$. Composition: $En_{62}Fs_{38}$. The hornblende, which is greenish-brown with moderate pleochroism, shows a slight zoning with $2V(-) = 75°$ in the core and $2V(-) = 70°$ at the margin. $n_1 = 1·6740$, $n_2 = 1·6915$. The olivine has $2V(-) = 87°$ and $\alpha = 1·6740$, $\beta = 1·6950$. Composition: $Fo_{72}Fa_{28}$,

The chemical composition of the above two dacites is shown in columns Nos. 39 and 40 of Table XVII. The two analyses are very much alike. Although the Yahadu-yama lava is slightly less acid than the Iwano-yama lava, the difference is rather small, both lavas having the usual composition of dacitic rocks.

2. Hakone-yama Volcano.

Hakone-yama, which lies immediately north of the Idu peninsula, is a great composite volcano measuring 25 km across the base and standing 1439 m above the sea. The geology and petrology of the volcano, which were studied by T. Hirabayashi,44) are being restudied in detail by Kuno, who has already published a series of valuable notes on them.45) According to him, the structural scheme of the volcano may be summarized as follows:

- (A) Older somma
  - Main body—a strato-volcano with a gigantic caldera whose walls are an ovally-arranged group of high peaks—Toga-mine, Myozyodake, Kintoki-yama, Mikuni-yama, and Hakugin-zan.
  - Parasitic volcanoes
    - Kintoki-yama—a strato-volcano on the NW. slope of the main body.
    - Maku-yama—a hybrid lava-dome protruding the SE. slope of the main body.
- (B) Younger somma—a shield volcano composed for the most part of lava-flows that erupted within the caldera of the older somma. Its western half has vanished by down-faulting, the eastern half consisting of Byobu-yama, Takanosu-yama, and Sengen-zan.
- (C) Central cones—six lava-domes (Hutago-yama, Komaga-take, Kami-yama, Daiga-take, and Koduka-yama) occupying the vanished portion of the younger somma.

It is noteworthy that the six central volcanoes are aligned, together with the parasitic cones on the older somma, in a NW.-SE. zone that coincides with the Huzi volcanic zone. Kuno regarded this zone as being the principal fracture line in the volcano, which is referred to as the Niizaki-gawa fault line. According to him, it was formed during the middle stage of the older somma's activities.

Hakone rests on Neogene Tertiary rocks that crop out not only in the valleys (Haya-kawa and Sukumo-gawa) that deeply cut its eastern slopes, but also in the Asigara mountains that border the volcano on the north. To the south, in the vicinity of Yugawara and Atami, lavas

---

44) T. Hirabayashi, *Rep. Earthq. Inv. Com.*, **16** (1898).

45) H. Kuno, *Jour. Geol. Soc., Japan*, **41** (1934), 347; *ibid.*, **42** (1935), 310; *ibid.*, **43** (1936), 376.

from the older somma of Hakone overlie the Yugawara volcano which in turn stands on the northern portion of the Taga volcano. In the valley of Kisegawa that borders Hakone on the northwest, the lower slope of the older somma is seen to be buried underneath lava-flows from Huzi either directly or with river-terrace deposits between them. At Oziri, which lies midway between Gotemba and Misima, one of the oldest visible lava-flows from Huzi is exposed on the southern bank of that valley, being directly underlain by the products (pumiceous breccia) of Hakone. In view of these facts, it seems reasonable to infer that, so far as the older somma is concerned, Hakone was active during the period between the upper half of lower Pleistocene and the upper Pleistocene. Although the younger somma and the central cones are in all probability upper Pleistocene. the latest volcanic activity that resulted in the explosion-craters and the mud-flows on the northwest flank of Kami-yama (one of the central cones) must surely be referred to a much later age. One of the explosion-craters—Owakudani—is still displaying solfataric activity.

According to Kuno, the rocks of the volcano are mostly two-pyroxene-andesite, although some of them are either basaltic or dacitic. He has published his petrological notes on six pyroxene-andesites from the older somma, special mention being made of those carrying phenocrysts of pigeonite.[46] Of the six andesites, three have the mineral compositions given in Table XVIII. Their chemical compositions are contained in Table XIX.

B. *Basaltic and Andesitic Volcanoes.*

Most of the Quaternary volcanoes in the region studied are composed of basaltic rocks or of basaltic and basic andesitic rocks. Since the classification of the rocks of these volcanoes into two kinds - basaltic and basic andesitic—is quite optional, it being immaterial which class is used, they may be treated as belonging to one group, whether basaltic or basic andesitic volcanoes.

3. Tensi-yama Volcano.

Lying northwest of the Amagi volcano is a dissected volcano, called the Tensi-yama volcano after its highest and most conspicuous remnant, 608 m above the sea, or about 250 m above the surrounding ground.

---

[46] H. KUNO, *Jap. Jour. Geol. Geogr.*, Nos. 1~2, **13** (1936), 107.

Table XVIII. Constituent Minerals of Hakone Andesites (H. Kuno).

		No. 41	No. 44	No. 45
Porphyritic Minerals	Plagioclase	core margin n_1=1·574—1·557—lower 88—55 An	core margin n_1=1·576—1·552—$\begin{cases}1{\cdot}571\\1{\cdot}567\end{cases}$ 92—47 $\begin{cases}81\\74\end{cases}$ An	core margin n_1=1·580—1·566—lower 98—72 An
	Hypersthene	2V(−)= core margin 66°—58°—58°—47° γ=1·703—1·713 $En_{61}Fs_{39}$ (average)	2V(−)= core margin 62°—57°—72°—68° $\left.\begin{array}{l}\alpha=1{\cdot}699-1{\cdot}704\\\beta=1{\cdot}709-1{\cdot}714\\\gamma=1{\cdot}712-1{\cdot}717\end{array}\right\}$ core $En_{55}Fs_{45}$ (average)	2V(−)=66°—53° γ=1·703—1·715 $En_{60}Fs_{40}$ (average)
	Augite	core margin 2V(+)=50°—48°—42° n_1=1·693—1·699 (β=1·699) $c\wedge Z$=42° $Wo_{30}En_{43}Fs_{22}$(average)	2V(+)= core margin 48°—43°—47°—43° $\left.\begin{array}{l}\alpha=1{\cdot}701\\\beta=1{\cdot}706\\\gamma=1{\cdot}729\end{array}\right\}$ core n_1=1·704, $c\wedge Z$=43° $Wo_{32}En_{37}Fs_{31}$(average)	2V(+)=49°—46° n_1=1·694—1·697 (β=1·698) $c\wedge Z$=43° $Wo_{34}En_{43}Fs_{23}$(average)
	Pigeonite	—	core margin 2V(+)=17°—10°—48° $\alpha\doteqdot\beta$=1·704 γ=1·728 $c\wedge Z$=43° $Wo_{13}En_{39}Fs_{48}$(average)	—
	Anorthoclase	Magnetite	Hornblende, Quartz, Magnetite, Apatite	Magnetite
Groundmass	Plagioclase	n_1=1·565—1·560—1·549 69—60—42 An	n_1=1·562—1·558 65—55 An	n_1=1·558—1·547 57—39 An
	Anorthoclase	$\alpha\leqq$1·525, γ=1·529	+	α=1·524, 2V(−)$\doteqdot$40°
	Pyroxene	Pigeonite 2V(+)=43° 2V(+)$\doteqdot$0° α=1·698 (min.) β=1·710 (max.) $c\wedge Z$=40° $Wo_{20}En_8Fs_{42}$(average)	Hypersthene 2V(−)=55° Augite 2V(+)=46° α=1·699 (min.) β=1·705 (max.) $c\wedge Z$=43° $Wo_{32}En_{38}Fs_{30}$(average)	Pigeonite 2V(+)$\doteqdot$0° $\alpha\doteqdot\beta$=1·710—1·715 $c\wedge Z$=42° $Wo_9En_{34}Fs_{57}$(average)
	Accessories	Magnetite, Ilmenite, Quartz, tridymite, Biotite, Apatite	Magnetite, Ilmenite, Quartz, tridymite, Cristobalite, Biotite, Apatite	Magnetite, Ilmenite, Quartz, tridymite, Biotite, Apatite

Table XIX. Analyses of Rocks from Hakone[47]
S. Tanaka, analyst.

		No. 41	No. 42	No. 43	No. 44	No. 45	No. 46
SiO_2		55·83	56·70	57·07	57·22	59·77	67·37
Al_2O_3		17·75	15·90	17·53	17·46	17·00	15·28
Fe_2O_3		2·76	2·94	2·59	2·45	2·49	1·13
FeO		6·01	7·74	5·44	6·15	5·59	3·86
MgO		3·90	3·34	3·87	3·77	2·24	1·20
CaO		8·62	7·77	8·77	7·93	7·05	4·46
Na_2O		2·98	3·13	2·80	2·87	3·29	4·67
K_2O		0·55	0·74	0·52	0·75	0·62	0·92
H_2O +		0·19	0·36	0·27	0·30	0·41	0·14
H_2O −		0·17	0·09	0·12	0·23	0·51	0·09
TiO_2		0·61	1·24	0·77	0·73	0·63	0·72
P_2O_5		0·13	0·16	0·08	0·11	0·10	0·18
MnO		0·17	0·18	0·14	0·16	0·16	0·15
Total		99·67	100·29	99·97	100·13	99·86	100·17
Q		10·63	12·13	13·33	12·97	17·60	24·02
Or		3·34	4·45	3·34	4·45	3·90	5·57
Ab		25·17	26·22	23·59	24·12	27·79	39·32
An		33·38	27·26	33·66	32·54	29·76	18·08
Wo		3·60	4·41	3·72	2·44	1·86	1·39
En		9·74	8·33	9·64	9·44	5·62	3·01
Fs		8·04	10·15	6·86	8·44	7·39	5·27
Mt		3·94	4·17	3·70	3·47	3·70	1·52
Il		1·21	2·43	1·52	1·37	1·21	1·37
Ap		0·33	0·33	0·33	0·33	0·33	0·33
QFM	Q	11	12	13	13	18	24
	F	62	58	61	61	62	63
	M	27	30	26	26	20	13
NF	Or	5	8	6	7	6	9
	Ab	41	45	39	39	45	62
	An	54	47	55	54	49	29
NPl	An	57	53	59	57	52	31
NPy	Wo	16	20	18	12	9	15
	En	46	36	48	46	38	31
	Fs	38	44	34	42	53	54
Fe		69	76	67	69	78	80

No. 41. *Augite-hypersthene-labradorite-andesite* (33022003). One of upper lavas of the older somma of Hakone.

No. 42. *Aphyric andesite* (33081909a). One of the middle lavas of the older somma of Hakone.

No. 43. *Olivine-bearing hypersthene-augite-labradorite-andesite* (33082410). Hutago-yama lava, Hakone.

No. 44. *Quartz-hornblende-bearing augite-pigeonite-hypersthene-labradorite-andesite* (33022001). One of the upper lavas of the older somma of Hakone.

No. 45. *Augite-hypersthene-bytownite-andesite* (31072908). One of the upper lavas of the older somma of Hakone.

No. 46. *Hypersthene-augite-andesite* (33090504). The uppermost lava of the older somma of Hakone.

---

[47] H. KUNO, *Bull. Volc. Soc., Japan*, **3** (1936), 53.

Tayama and Niino, who mention this volcano in their paper,[48] recognized the occurrence of a ruined, circular crater, about 1 km across, whose southern wall is the summit of Tensi-yama. Whether this crater is still in actual existence is not known for certain, because the original conical form of the volcano has suffered great changes through erosion and faulting, but that the principal vent was located probably close to, if not immediately on, the summit of Tensi-yama, is clear from the fact that the lavas usually dip outward from the latter and the neighbourhood as centre.

Of the many faults that traverse the volcano in various directions, the most remarkable is the Kumogane-Himenoyu fault that runs due W.-E. through the northern side near the summit of Tensi-yama. An earthquake fault (Himenoyu fault) appeared on this geologic fault-line at the time of the destructive north Idu earthquake of November 26, 1930.

The volcano is covered with a thin bed of pumice from the Amagi volcano. This bed thickens as one goes south toward Amagi, while at the northwest foot of the latter the products of the present volcano are covered with lavas from Amagi and the pumice bed. Underneath the pumice bed is a loam-like ash bed, which in turn rests on layers of lavas, agglomerates, and pyroclastics from Tensi-yama. The volcano, which is composed of these layers, rests either directly on the lower Miocene formation or with the upper Pliocene deposits interposed between them. These facts indicate that the volcano is of lower Pleistocene age.

The rocks of this volcano may be divided into three kinds: olivine-basalt, olivine-pyroxene-andesite, and two-pyroxene-andesite, of which only the last type will now be described.

No. 47. *Two-pyroxene-andesite.* This rock, which is one of the earliest lavas of the volcano, occurs as several flows and also as agglomerate and pyroclastic beds in the lower part of the mass. The specimen examined was collected at Ogawa (see Fig. 2), Naka-Omimura, on the northern slope near the base of the volcano, where, covered by an olivine-augite-andesite lava, it forms a flow about 10 m thick, overlying an agglomerate bed which in turn rests on Neogene Tertiary. Megascopically, the rock is compact, gray with a greenish tint, and porphyritic with phenocrysts of plagioclase and pyroxene. Microscopically, it contains two types of plagioclase phenocrysts, the one being the larger phenocrysts (10 mm dia.) of anorthite 94 An ($n_1 = 1{\cdot}577$) and the other the smaller ($0{\cdot}2 \sim 0{\cdot}5$ mm dia.) of faintly zoned bytownite $88 \sim 83$ An ($n_1 = 1{\cdot}5742 \sim 1{\cdot}5718$). They are surrounded by narrow rims of the groundmass plagioclase. The porphyritic augite ($0{\cdot}3 \sim 2{\cdot}0$ mm dia.) has $c \wedge Z = 46°$, $2V(+) = 49°$, and $n_1 = 1{\cdot}6976$. Composition: $Wo_{31}En_{42}Fs_{27}$. The porphyritic hypersthene ($0{\cdot}1 \sim 0{\cdot}5$

---

48) R. TAYAMA and H. NIINO, *Rep. Sci. Res., Saito Gratitude Foundation* No. **11** (1931).

mm dia.), which is always surrounded by pigeonite grains in the groundmass, has 2V(−)=66° and n =1·6992. Composition: $En_{60}Fs_{40}$. A few porphyritic magnetite grains adhere to the pyroxene phenocrysts. The groundmass consists of faintly-zoned laths (0·05∼0·1 mm long) of labradorite 63∼55 An (n_1=1·5615∼1·5575), pigeonite grains (β=1·7067), and magnetite cubes, besides interstitial tridymite and a little chloritized base.

The chemical composition of this rock is shown in Table XX.

Table XX. Analysis of the Two-pyroxene-andesite, No. 47, from the Tensi-yama Volcano. S. Tanaka, analyst.

	No. 47	Norm				
SiO_2	53·95	Q	11·11	QFM	Q	11
Al_2O_3	18·93	Or	1·67		F	64
Fe_2O_3	3·73	Ab	22·55		M	25
FeO	5·55	An	38·94			
MgO	3·48	Wo	2·91	NF	Or	6
CaO	9·42	En	8·64		Ab	36
Na_2O	2·68	Fs	6·07		An	61
K_2O	0·28	Mt	5·33			
H_2O +	0·63	Il	1·52	NPl	An	63
H_2O −	0·84	Ap	0·33			
TiO_2	0·81			NPy	Wo	17
P_2O_5	0·09				En	49
MnO	0·16				Fs	34
Total	100·55			Fe		72

4. Usami Volcano.

Adjoining the southern part of the basaltic Taga volcano in the northeastern Idu lies a number of dissected mountains that are composed of andesitic lavas and pyroclastics, and which form a sinuous ridge, nearly 5 km long with a maximum elevation of 577 m (Ogawasawa-yama), running N.–S. from near Kameisi-toge to Kasiwa-toge. The western side of this ridge is a long, gentle slope having the appearance so usual to lower slopes of conical volcanoes, although it is badly dissected by ravines radiating from the crest of the ridge. The strata of andesitic lavas and pyroclastics that are exposed in the ravines show a gentle westward dip that coincides with the surface slope, gradually sweeps up to the crest of the ridge where it ends abruptly, overlooking the steeper eastern side of the ridge. The upper part, near the crest of the eastern slope, forms a scarp terminating in many branching spurs lower down the slope. Andesitic lavas and pyroclastics are well exposed on the scarp, their strata ending abruptly with the cliff. The volcanic mass may therefore be interpreted as the remnant of a huge conical volcano, the old centre of activity of which lay to the east, the greater part of the eastern half of the volcano having eroded away. It seems best to refer to this volcano as the Usami volcano, naming it after a village that lies east of it.

The foundation on which the present volcano rests consists of the Idu Neogene Tertiary formations, besides the lower Pleistocene deposits referred to as the Zyo beds. The Tertiary formations that border the volcano on the east and the south extend underneath the lavas, forming the ridge just mentioned. The Zyo beds, which are to be seen only to the west of the volcano, continue with the underlying Neogene Tertiary formations, eastward underneath the western slope of the latter. On the north, the volcano is bordered by the southern slope of the northerly Taga volcano, the lavas of which cover that of the former. At Kameisi-toge, close to the northern margin of the Usami volcano, is a fault that traverses the southern slope of the Taga volcano with a WNW–ESE trend, and forming a northward fault-scarp a few score meters high. The southeasterly extension of this fault is indicated by a valley which, taking a straight course southeast, opens into the sea at Usami. This valley in its upper and middle courses cuts into lavas of both the Usami and the Taga volcanoes, while in its lower course it cuts into the underlying Tertiary rocks (altered andesites and siliceous tuffs). Although the terrane adjoining the north of the valley is for the most part covered by lavas of the Taga volcano, there is a small outlier close to the north of Usami that belongs to the Usami volcano. In view of these facts, it seems reasonable to infer that the Usami volcano is one of the lower Pleistocene volcanoes of northern Idu, and that it is older than the Taga volcano. There is little doubt that the Usami volcano is older than the Omuro-yama volcano group, seeing that the southern part of the former is locally covered by a thin bed of basaltic scoria (Ito scoria bed) that came from a vent in the latter, and that the hill bordering the sea between Ito-mati and Kawana, which is regarded as an outlier detached itself from the main mass of the Usami volcano, is partly covered by basaltic lavas and pyroclastic beds of the Omuro-yama volcano group.

About 1 km south of Kameisi-toge is a dome-shaped, basaltic cinder-cone (Sukumo-yama), 581 m above the sea, or about 150 m above the surrounding ground, standing on the slope of the Usami volcano. This cinder-cone, which is underlain by an olivine-basalt lava and traversed by dikes of similar rock, seems much younger than the Usami volcano.

So far as examined, the rocks of the present volcano are all andesitic, though of varying petrographic characters. Eight specimens of rocks from the volcano (see Fig. 2) were examined microscopically and chemically with results as shown in Tables XXI and XXII. They are of the following rocks:

No. 48. *Olivine-bearing two-pyroxene-andesite.* This rock occurs in alternating layers of lava-flows and pyroclastics with a general southwestward dip, forming the hill that lies between Ito-mati and Kawana. The specimen examined was collected from lava exposed near the base of the sea-cliff at Siohuki-zaki, 3 km east of Ito.

Megascopically, the rock is gray, compact to slightly vesicular, and porphyritic with abundant phenocrysts of plagioclase and pyroxene. Microscopically, we find, besides the phenocrysts of plagioclase (0·3~0·5 mm dia.), hypersthene (0·5~1·0 mm), and augite (0·5~1·0 mm), a few microphenocrysts of olivine, hypersthene, and accessory magnetite, in a groundmass of plagioclase, pigeonite, and magnetite,. together with interstitial tridymite and a little glass base.

There are two types of plagioclase phenocrysts; the larger ones being anorthite 95 An ($n=1{\cdot}5778$) and the smaller anorthite-bytownite 93~88 An ($n_1=1{\cdot}5766\sim1{\cdot}5742$). The groundmass plagioclase is bytownite 77 An ($n_1=1{\cdot}5686$). The hypersthene pheno-

Table XXIa. Constituent Minerals of the Andesites of the Usami Volcano.

		No. 49	No. 50	No. 51
Porphyritic Minerals	Plagioclase	$n_1=1{\cdot}5762\sim1{\cdot}5745$ 93~89 An	$n_1=1{\cdot}5776\sim1{\cdot}5745$ 95~89 An	$n_1=1{\cdot}5784\sim1{\cdot}5755$ 96~90 An
	Augite	$2V(+)=50°$ $n_1=1{\cdot}6970$ $c\wedge Z=45°$ $Wo_{33}En_{42}Fs_{25}$	$2V(+)=51°$ $n_1=1{\cdot}6975$ $Wo_{32}En_{42}Fs_{26}$	core margin $2V(+)=56°-54°-37°$ $n_1=1{\cdot}6949\sim1{\cdot}6982$ $Wo_{39}En_{39}Fs_{22}$(average)
	Hypersthene	$2V(-)\doteqdot75°$	$2V(-)=70°$ $n_1=1{\cdot}6926$ $En_{65}Fs_{35}$	$2V(-)=69°$ $n_1=1{\cdot}700$ $En_{60}Fs_{40}$
	Olivine	core margin $2V=89°(+)\sim82°(-)$	——	——
	Accessories	——	——	——
Groundmass	Plagioclase	n.d.	n.d.	$n_1=1{\cdot}5637$ 68 An
	Pyroxene	Microphenocrysts $2V(+)\doteqdot48°$(core)–20°(margin) Pigeonite prisms $2V(+)\doteqdot0°$	Pigeonite	Hypersthene Pigeonite
	Accessory and interstitial materials	Magnetite Tridymite Glass base	Magnetite Cristobalite (?) Tridymite Glass base	Magnetite Tridymite Acid feldspar Glass base

Table XXIb. Constituent Minerals of the Andesites of the Usami Volcano.

		No. 52	No. 53	No. 54	No. 55
Porphyritic Minerals	Plagioclase	$n_1=1·5778\sim$ 1·5754 95~90 An	$n_1=1·5798\sim$ 1·5767 99~93 An	$n_1=1·5690$ 78 An	$n_1=1·5716$ 83 An
	Augite	core margin 2V(+)=55°−50° $n_1=1·6970\sim$ 1·6998 c∧Z=45° $Wo_{35}En_{40}Fs_{25}$ (average)	core margin 2V(+)=50°−45° $n_1=1·6946\sim$ 1·6985 $Wo_{28}En_{43}Fs_{29}$ (average)	2V(+)=46° $n_1=1·6996$ $Wo_{27}En_{42}Fs_{31}$	core margin 2V(+)=47°−50° 50°−40° 52°−40° $n_1=1·6966$(mean) $Wo_{28}En_{43}Fs_{29}$ (average)
	Hypersthene	core margin 2V(−)=60°−67° $n_1=1·7070$(mean) $En_{54}Fs_{45}$ (average)	core margin 2V(−)=63°−70° −63°, 61°−70° $n_1=1·6980\sim$ 1·7068 $En_{57}Fs_{43}$ (average)	2V(−)≒65°~62°	2V(−)=65° $n_1=1·7007$ $En_{59}Fs_{41}$
	Olivine	2V(−)=88° $\alpha=1·6695$ $\beta=1·6885$ $Fo_{75}Fa_{25}$	2V(−)=87° $\beta=1·6830$ $Fo_{72}Fa_{28}$	——	——
	Accessories	Magnetite Apatite	Magnetite Apatite	Magnetite	Magnetite
Groundmass	Plagioclase	$n_1=1·5707$ 81 An	$n_1=1·5678$ 75 An	n.d.	$n_1=1·554$ 50 An
	Pyroxene	Micro-phenocrysts: Augite Hypersthene Small grains: Pigeonite	Augite 2V(+)≒46° Hypersthene 2V(−)≒61°	Pigeonite	Pigeonite
	Accessory and interstitial materials	Magnetite Tridymite Glass base	Magnetite Tridymite Acid feldspar	Magnetite Tridymite Acid feldspar	Magnetite Tridymite (?) Acid feldspar

Table XXII. Analyses of Rocks from the Usami Volcano. S. Tanaka, and analyst.

	No. 48	No. 49	No. 50	No. 51	No. 52	No. 53	No. 54	No. 55
SiO_2	50·57	50·59	51·67	53·08	55·96	57·61	59·00	62·70
Al_2O_3	19·38	19·73	19·88	20·01	16·92	15·88	15·26	16·09
Fe_2O_3	3·81	3·18	3·25	3·48	2·76	2·79	4·60	2·61
FeO	7·25	6·73	6·97	5·70	6·03	5·28	5·90	4·61

(*to be continued.*)

Table XXII. (*continued.*)

		No. 48	No. 49	No. 50	No. 51	No. 52	No. 53	No. 54	No. 55
MgO		3·89	4·15	3·30	2·80	4·39	5·92	2·14	1·49
CaO		11·43	10·31	9·46	9·80	8·06	7·58	6·36	5·25
Na_2O		1·86	1·94	2·18	2·29	2·07	2·59	2·83	3·26
K_2O		0·16	0·24	0·40	0·31	0·57	0·71	0·58	0·86
H_2O +		0·45	1·13	1·26	0·47	1·07	0·36	0·90	1·25
H_2O −		0·30	0·88	1·00	0·75	1·18	0·28	0·69	0·85
TiO_2		0·76	0·35	0·92	0·73	0·73	0·71	1·04	0·82
P_2O_5		0·10	0·10	0·10	0·06	0·08	0·07	0·11	0·17
MnO		0·13	0·15	0·16	0·17	0·17	0·15	0·18	0·12
Total		100·09	99·98	100·55	99·65	99·99	99·93	99·59	100·08
Q		7·57	7·75	9·31	11·65	15·68	13·33	21·98	24·80
Or		1·11	1·67	2·23	1·67	3·34	4·45	3·34	5·01
Ab		15·73	16·25	18·35	19·40	17·30	22·02	24·12	27·79
An		43·95	44·50	43·39	43·39	35·33	29·48	27·26	25·31
Wo		4·99	2·44	1·16	2·21	1·63	3·37	1·39	C=0·51
En		9·64	10·33	8·23	6·92	10·94	14·76	5·32	3·71
Fs		9·10	8·58	8·83	6·60	7·91	6·36	6·67	5·28
Mt		5·56	4·63	4·63	5·09	3·94	3·94	6·71	3·70
Il		1·52	1·67	1·82	1·37	1·37	1·37	1·97	1·52
Ap		0·33	0·33	0·33	0·33	0·33	0·33	0·33	0·33
QFM	Q	8	8	9	12	16	13	22	25
	F	61	64	65	65	57	56	56	60
	M	31	28	26	23	27	31	22	15
NF	Or	2	3	3	3	6	8	6	9
	Ab	26	26	29	30	31	39	44	48
	An	72	71	68	67	63	53	50	43
NPl	An	74	73	70	69	67	57	53	48
NPy	Wo	21	11	7	14	8	14	11	—
	En	40	48	45	44	53	60	43	41
	Fs	39	41	48	42	39	26	46	59
Fe		73	70	73	76	66	57	82	82

crysts, which are always surrounded by a thin rim of a monoclinic pyroxene ($c \wedge Z=$ 44), shows distinct zoning, their optic angles varying from core to margin in the manner: $2V(-)=78° \rightarrow 70°$ and $79° \rightarrow 68° \rightarrow 79° \rightarrow 68°$. $n_1=1·6922 \sim 1·6949$. Average composition: $En_{65}Fs_{35}$. The microphenocrystic hypersthene, which occurs in parallel intergrowth with a monoclinic pyroxene, shows $2V(-)=68°$. The augite phenocrysts, which are far less in amount than the hypersthene, has $n_1=1·6965$. The groundmass pigeonite has $2V(+)=20°$, $c \wedge Z=37°$, and $\beta=1·7048$. Composition: $W_{13}En_{40}Fs_{47}$. The olivine is anhedral and negligible in amount.

The chemical composition of the above-described rock is given in column No. 48 of Table XXII.

No. 49. *Hypersthene-bearing olivine-augite-andesite.* This rock occurs on the southwest slope of the volcano as a lava-flow, about 10 m thick, lying under another lava of olivine-bearing two-pyroxene-andesite (No. 52), with pyroclastic beds interposed between them. The specimen examined was collected from the eastern wall of the valley that bounds Isigami-yama on the east (4 km northeast of Zyo). Megascopically, it is compact, gray, and studded withlarge plagioclase phenocrysts (10 mm dia). Microscopically, it contains, besides the large plagioclase, phenocrysts of smaller plagioclase, olivine, and augite, with negligible quantities of hypersthene, in a groundmass consisting of plagioclase, microphenocrystic augite-pigeonite, pigeonite, and magnetite, together with interstitial tridymite and a little glass base.

No. 50. *Olivine-bearing two-pyroxene-andesite.* This rock occurs on the west slope of the volcano as a lava-flow, 10 m thick, intercalated between pyroclastic beds. The specimen examined was collected from the flow that is exposed at the southwest exit of the Tyozyaga-hara basin, about 2·5 km southwest of Kameisi-toge, on the north bank of the river that drains the basin. Megascopically, it is compact, dark-gray, and densely crowded with small plagioclase phenocrysts. Microscopically, the rock carries phenocrysts of augite and hypersthene, besides the plagioclase. Olivine is detected only as inclusions in the hypersthene phenocrysts, which in turn are usually surrounded by a thin rim of a monoclinic pyroxene. The groundmass is composed of plagioclase laths, pigeonite prisms, and magnetite granules, with interstitial tridymite and a little glass base.

No. 51. *Augite-hypersthene-andesite.* This rock occurs as a massive lava and agglomerate in the valley, which, situated between Usami and Kameisi-toge, separates the terrane of the Usami volcano from that of the Taga volcano. The specimen examined was collected from the floor of the valley that is situated midway between Usami and Kameisi-toge, where it forms a lava underlying a basaltic lava from the Taga volcano. Megascopically, the rock is gray with a greenish tint, compact to slightly vesicular, and porphyritic with plagioclase and pyroxene phenocrysts. Microscopically, the porphyritic minerals are anorthite with a narrow rim of labradorite similar to the groundmass plagioclase; hypersthene with a rim of pigeonite; and zoned augite with also a rim of pigeonite. The groundmass consists of labradorite laths, microphenocrystic hypersthene with pigeonite prisms, and magnetite granules, together with interstitial tridymite (?) and a little dusty glass base.

No. 52. *Olivine-two-pyroxene-andesite.* Rock of this type is distributed extensively in the southern and southwestern parts of the volcano, forming several lava-flows intercalated with pyroclastic beds. The specimen examined was collected at the same place as the locality of andesite No. 49, where it occurs as a lava above the last named. Megascopically, the rock is gray, compact, and porphyritic with phenocrysts of plagioclase and pyroxene. Glomeroporphyritic grouping of the phenocrysts is occasionally met with. Microscopically, we find phenocrysts of faintly zoned anorthite, zoned augite, zoned hypersthene with a rim of augite, and anhedral olivine, besides accessory magnetite and apatite, in a groundmass consisting of bytownite laths, microphenocrystic prisms of augite and hypersthene, pigeonite grains, and magnetite granules, together with tridymite and a little interstitial glass base.

No. 53. *Augite-bearing olivine-hypersthene-andesite.* Petrographically, this rock closely resembles the one just mentioned. The specimen examined was collected 5 km northeast of Hiyekawa, where it occurs as a lava about 15 m thick, intercalated between pyroclastic beds. Microscopically, the phenocrysts are slightly zoned anorthite;

zoned hypersthene with a rim of augite; anhedral olivine with a hypersthene rim; and augite in parallel intergrowth with the hypersthene, besides accessory magnetite and apatite. The groundmass consists of bytownite laths, hypersthene and augite prisms, and magnetite grains, together with interstitial tridymite and acid feldspar.

No. 54. *Aphyric two-pyroxene-andesite.* This rock, which is one of the earlier lavas of the volcano, occurs as a flow forming the lower part of the western slope. The specimen examined was collected from a lava exposed on the south wall of the valley that drains the Tyozyaga-hara basin, about 2 km southwest of that basin, where it rests upon gravel and sand beds (lower Pleistocene) which in turn rest on the Tertiary. Megascopically, it is dark-gray to black, compact, and carries negligible quantities of plagioclase phenocrysts. Microscopically, it contains, besides the plagioclase phenocrysts, a few microphenocrysts of augite and hypersthene, and accessory magnetite. The groundmass, which forms the bulk of the rock, is composed of plagioclase laths (0·01~0·03 mm long), pigeonite granules, and magnetite dust, with interstitial tridymite and feldspar,

No. 55. *Two-pyroxene-andesite.* This rock occurs as a lava-flow in a small area immediately north of Isigami-yama, where it forms the uppermost part of the central volcano. Megascopically, it is dark-gray to black, compact, and studded with plagioclase phenocrysts. Microscopically, it contains phenocrysts of faintly zoned bytownite with narrow rims of labradorite, zoned augite-pigeonite, hypersthene with thin rims of pigeonite, and accessory magnetite. The groundmass is composed of labradorite laths, pigeonite grains, and magnetite granules, together with interstitial tridymite and feldspar.

5. Taga Volcano.

The Taga volcano, which adjoins the northern part of the Usami volcano, occupies a wide tract extending from the mountains between Usami and Aziro to beyond Kuro-dake, and forms a long, semi-circular ridge, which at the last-mentioned mountain, reaches a maximum height of 799 m above the sea. The outer (western) side of this ridge slopes with a gentle sweep up to the crest of the ridge, where it ends abruptly overlooking the steeper inner (eastern) side. The upper part, near the crest of the inner side, are precipitous cliffs on which lavas and pyroclastics are clearly exposed, their strata ending in cliffs; while the lower part consists of numerous branching arêtes that separate deep valleys, on the walls of which older lavas and pyroclastics are exposed together with the bedrocks of this region. This volcanic mass, like the Usami volcano, is a remnant of a huge conical volcano, which H. Kuno calls the Taga volcano, naming it after the village near the probable former centre of activity.

Westward, the slopes of the volcano lead far down to the eastern margin of the Kano-gawa alluvial plain, although they are greatly dislocated by faults, the most striking being the Tanna fault which, connecting the tectonic basins of Tasiro, Ukihasi, and Tawarano, extends half way down the western slopes of the volcano from north to south. Southward, the slopes of the volcano end at the Usami volcano a short distance down the slopes of the latter, while northward they go under the volcano Yugawara, the slopes of which last in turn go underneath the Hakone volcano. Although the eastern half of the volcano has disappeared, it is possible that the vanished portions dropped down along a fault line into the sea that borders the volcano on the east.

The volcano rests on lower Pliostocene beds (Simo-Tanna beds, Simo-Hata beds, and Ono beds), besides the Neogene Tertiary (Kuno's Soga-yama beds, Nonaka beds, etc.). The volcano is of lower Pleistocene age. Although younger than the Usami volcano on its south, it is older than the Yugawara volcano on its north.

The rocks of this volcano show various types of basalt and andesite. The petrology of the volcano, together with its geology, will presently be published by H. Kuno[49], who made a detailed survey of the mass while he was studying the volcanoes of north Idu, in which study he is still engaged. The writer examined six rock-specimens from the volcano both microscopically and chemically, with results as shown in Tables XXIII and XXIV. The examined specimens, of which five were collected from the southwestern slope of the volcano and the remainder from Uomi-saki near Atami, are as follows:

No. 56. *Augite-olivine-basalt.* This rock occurs on the southwest slope of the volcano as a lava-flow resting on lower Pleistocene rocks (Simo-Hata beds). The specimen examined was collected from the northern bank of the Hukazawa, near Takyo, Kita-Kanomura, where it occurs as a flow about 15 m thick with columnar joints, overlying a gravel bed which in turn rests on Neogene Tertiary rocks (silicified tuff and green andesite, lower Miocene). Megascopically, the rock is compact, dark-gray, and porphyritic with abundant plagioclase phenocrysts, besides a few olivine and augite. Microscopically, it contains phenocrysts of anorthite, zoned augite-pigeonite, and zoned olivine, in a groundmass consisting of bytownite laths, zoned pigeonite prisms and magnetite cubes, besides cristobalite patches and a little dusty base.

No. 57. *Augite-bearing olivine-basalt.* This rock which also occurs as a lava-flow on the southwest slope of the volcano, resembles the foregoing, the only difference being in the amount of the porphyritic augite. The specimen examined was collected from the flow exposed near the southwest exit of the Tawarano basin, on the banks of the valley that drains this basin.

No. 58. *Two-pyroxene-olivine-basalt.* This rock occurs as a lava-flow, together wish its agglomerate, on the south slope of the volcano. The specimen examined was collected from the flow exposed on a ridge, 1 km southeast of Kameisi-toge, where it rests on products of the Usami volcano. Megascopically, the rock is compact, gray, and rich in phenocrysts of plagioclase, olivine, and pyroxene. Microscopically, the phenocrysts are anorthite-bytownite with narrow rims of the groundmass plagioclase, anhedral olivine with rims of augite grains, augite, and zoned hypersthene with augite

---

[49] H. Kuno, *Jour. Geol. Soc., Tokyo,* **40** (1933), 376.

Table XXIII. Constituent Minerals of the Rocks of the Taga Volcano, Idu.

		No. 56	No. 57	No. 58	No. 59	No. 60	No. 61
Porphyritic Minerals	Plagioclase	$n_1=1{\cdot}5794\sim1{\cdot}5757$ 98~91 An	$n_1=1{\cdot}5786\sim1{\cdot}5748$ 97~90 An	$n_1=1{\cdot}5790\sim1{\cdot}5745$ 98~89 An	$n_1=1{\cdot}5765$ 93An	—	$n_1=1{\cdot}5757$ 91An
	Augite	core margin $2V(+)=54°-38°$ $n_1=1{\cdot}6988\sim1{\cdot}7030$ $Wo_{27}En_{41}Fs_{32}$ (average)	core margin $2V(+)=58°-52°$ $n_1=1{\cdot}6968$ (mean) $Wo_{38}En_{39}Fs_{23}$ (average)	$2V(+)=55°$ $n_1=1{\cdot}6944$ $Wo_{38}En_{39}Fs_{23}$	$2V(+)=50°$ $n_1=1{\cdot}6899$ $Wo_{34}En_{46}Fs_{20}$	—	$n_1=1{\cdot}6976$
	Hypersthene	—	—	core margin $2V(-)\fallingdotseq77°-65°$ $72°-65°$	core margin $2V(-)=70°-75°$ $71°$ $n_1=1{\cdot}6942$ (mean) $En_{65}Fs_{35}$	—	$n_1=1{\cdot}700$
	Olivine	core margin $2V(-)=88°-82°$ $\alpha=1{\cdot}672,\beta=1{\cdot}6915$ $Fo_{74}Fa_{26}$	core margin $2V(-)=85°-79°$ $\beta=1{\cdot}7122$ $Fo_{62}Fa_{38}$	$2V\fallingdotseq90°$	—		$2V(-)\fallingdotseq78°$
Groundmass	Plagioclase	$n_1=1{\cdot}5698\sim1{\cdot}5643$ 79~69 An	$n_1=1{\cdot}5640$ 68 An	$n_1=1{\cdot}5718$ 84 An	$n_1=1{\cdot}5726$ 84 An	$n_1=1{\cdot}5615$ 64 An	$n_1=1{\cdot}5655\sim1{\cdot}5597$ 71~60 An
	Pyroxene	core margin $2V(+)=41°-30°$ $48°-30°$ $\beta=1{\cdot}7154$ (max.) $Wo_{16}En_{35}Fs_{49}$	$2V(+)=38°\sim20°$ $\beta=1{\cdot}715$ (max.) $Wo_{12}En_{35}Fs_{53}$	$2V(-)\fallingdotseq41°\sim36°$	$\beta=1{\cdot}703$	$2V(+)=40°$ $\beta=1{\cdot}715$ $Wo_{19}En_{35}Fs_{46}$	$2V(+)=39°$ $\beta=1{\cdot}716$ $Wo_{19}En_{34}Fs_{47}$
	Accessory and interstitial materials	Magnetite Cristobalite Glass base	Magnetite Cristobalite Tridymite Glass base	Magnetite Tridymite Glass base	Magnetite Cristobalite Glass base	Magnetite Tridymite Glass base	Magnetite Cristobalite Tridymite Glass base

Table XXIV. Analyses of Rocks from the Taga Volcano. S. Tanaka, analyst.

		No. 56	No. 57	No. 58	No. 59	No. 60	No. 61	No. 62	No. 63	No. 64	No. 65	No. 66
SiO_2		50·17	50·38	50·71	50·94	52·13	52·85	50·45	51·68	52·35	54·00	57·85
Al_2O_3		19·65	20·36	18·84	19·32	15·68	18·37	19·45	19·70	20·35	18·84	16·94
Fe_2O_3		2·54	2·86	2·42	4·14	4·36	3·48	2.27	2·69	2·23	2·07	2·23
FeO		7·92	7·26	7·13	5·52	9·81	7·83	8·41	6·78	6·25	7·71	5·30
MgO		4·54	4·45	6.08	4·20	4·08	2·96	3·73	4·15	3·72	2·72	4·31
CaO		11·29	11·28	10·05	10·62	8·87	10·12	11·23	10·78	9·62	9·74	7·80
Na_2O		1·66	1·95	2·03	2·15	2·44	2·07	1·75	1·94	2·74	2·95	3·32
K_2O		0·29	0·33	0·24	0·32	0·32	0·36	0·33	0·32	0·44	0·41	0·60
H_2O +		0·41	0·36	0·69	0·73	0·67	0·39	0·42	0·22	0·90	0·30	0·26
H_2O −		0·20	0·25	0·38	1·04	0·50	0·16	0·30	0·20	0·41	0·20	0·32
TiO_2		0·87	0·84	0·67	0·78	0·74	0·93	1·04	0·81	1·19	1·02	0·80
P_2O_5		0·10	0·10	0·13	0·07	tr.	tr.	0·09	0·13	0·15	0·11	0·13
MnO		0·17	0·15	0·15	0·18	0·32	0·17	0·20	0·16	0·13	0·29	0·15
Total		99·81	100·57	99·52	100·01	99·92	99·69	99·67	99·56	100·41	100·36	100·04
Q		5·77	4·93	4·44	7·87	8·35	11·11	6·37	8·17	6·49	7·87	12·07
Or		1·67	2·23	1·67	1·67	1·67	2·23	2·23	1·67	2·78	2·23	3·34
Ab		14·16	16·25	17·30	18·35	20·45	17·30	14·68	16·25	23·07	25·17	28·31
An		45·34	45·89	41·44	42·28	31·15	39·78	44·23	44·23	41·44	36·90	29·48
Wo		4·06	3·83	3·14	4·30	5·34	4·30	4·11	3·48	2·32	4·41	3·48
En		11·35	11·04	15·16	10·44	10·14	7·33	9·34	10·34	9·23	6·73	10·84
Fs		11·21	9·77	10·29	5·80	13·93	10·16	12·27	9·10	7·92	11·21	6·86
Mt		3·70	4·17	3·47	6·02	6·25	5·09	3·24	3·94	3·24	3·01	3·24
Il		1·67	1·67	1·21	1·52	1·37	1·82	1·97	1·52	2·38	1·97	1·52
Ap		0·33	0·33	0·33	0·33	tr.	tr.	0·33	0·33	0·33	0·33	0·33
QFM	Q	6	5	5	8	8	11	6	8	7	8	12
	F	62	64	61	63	54	60	62	63	68	64	61
	M	32	31	34	29	38	29	32	29	25	28	27
NF	Or	3	3	3	3	3	4	4	3	4	3	5
	Ab	23	25	29	29	38	29	24	26	34	39	46
	An	74	72	68	68	59	67	72	71	62	58	49
NPl	An	76	74	71	70	60	70	75	72	64	60	51
NPy	Wo	15	15	11	21	18	19	17	15	12	20	16
	En	43	45	53	51	34	34	36	45	47	30	51
	Fs	42	40	36	28	48	47	47	40	41	50	33
Fe		69	69	60	69	77	79	74	69	69	78	63

in parallel intergrowth. The groundmass consists of bytownite, microphenocrystic hypersthene and augite in parallel intergrowth, pigeonite, and magnetite, together with interstitial tridymite and a dusty glass base.

No. 59, *Two-pyroxene-andesite*. This rock, which is one of the earlier lavas of the volcano, occurs as a lava-flow, besides agglomerate, resting on lower Miocene rocks (Kuno's Sogayama beds). The specimen examined was collected from the lava exposed on a sea-cliff, near Uomi-saki, along the road from Atami to Aziro. Megascopically, the rock is compact, gray with a greenish tint, and studded with large plagioclase phenocrysts, besides a few pyroxene. Microscopically, we find phenocrysts of anorthite, zoned hypersthene with rims of augite grains, and augite, in a groundmass consisting of bytownite laths, pigeonite prisms, and magnetite granules, together with cristobalite, interstitial feldspar, and a little glass base.

No. 60. *Aphanitic basalt*. This rock occurs on the western foot of the volcano, near Nirayama, as a lava-flow sandwitched between lavas of porphyritic augite-olivine-basalt. The specimen examined was collected from the flow exposed on the south wall of a dale, about 1 km east of Hansyaro, Nirayama. Megascopically, it is compact, gray, and wholly aphanitic. Microscopically, it consists of labradorite laths (up to 0·2 mm long), pigeonite prisms (0·1 mm), and magnetite granules, together with interstitial tridymite and a little glass base, except a few microphenocrystic traces of olivine completely replaced by iron-ore.

No. 61. *Olivine-two-pyroxene-bearing andesite*. This rock occurs in the vicinity of Ono, Kita-Kanomura, as a massive lava, about 15 m thick, resting on the Ono beds (lower Pleistocene), either directly or with pyroclastic beds interposed between them. The specimen examined was collected from the lava exposed on the Ono landslide (cf. Table X). Megascopically, the rock is compact, gray, and densely packed with plagioclase phenocrysts. Microscopically, it contains in addition to the anorthite phenocrysts, a few olivine, augite, and negligible hypersthene in a groundmass consisting of labradorite laths, pigeonite prisms, and magnetite cubes, together with interstitial cristobalite, tridymite, and a little glass base.

Table XXIV contains in addition to the analyses of the foregoing rocks, five analyses[50] of specimens collected by Kuno from the volcano. These are as follows:

No, 62. *Augite-bearing olivine-bytownite-basalt* (31041812). The uppermost lava of the Taga volcano. Locality: middle course of a dale northwest of Usami, Idu.

No. 63. *Hypersthene-augite-olivine-bytownite-andesite* (31050201). An upper lava of the middle stage lavas of the Taga volcano. Locality: upper course of a dale southwest of Simo-Taga, Idu.

No. 64. *Olivine-bearing augite-hypersthene-labradorite-andesite* (31041909). A middle lava of the middle stage lavas of the Taga volcano. Locality: midway between Usami and Kameisi-toge, Idu.

No. 65. *Two-pyroxene-andesite* (32090104). The lowest lava of the middle stage lavas of the Taga volcano. Locality: midway between Taga and Yamabusi-toge, Idu.

No. 66. *Olivine-augite-hypersthene-labradorite-andesite* (32082002). The lowest lava (Wada lava) of the Taga volcano. Locality: upper course of a dale west of Wada, Atami-mati, Idu.

---

[50] The analyses Nos. 58, 60, 62~64, 66, were published in H. KUNO, *Bull. Volc. Soc., Japan*, **3** (1936), 55. No. 65 is yet unpublished analysis, for which the writer is indebted to Kuno.

6. Asitaka-yama Volcano.

Adjoining the southern part of Huzi is a large ruined volcano, Asitaka-yama, whose base is more than 15 km across. If this ruined volcano is viewed from the southwest, its gently sloping and almost symmetrical flanks sweeping to its summit, are seen to be excellently preserved. The lower half of the northern flank is entirely buried under the lava-flows from Huzi. The summit of the volcano is divided into five peaks —Etizen-dake (1504 m), Yobiko-dake (1313 m), O-dake (1253 m), Ihai-dake (1457 m), and Asitaka-yama (1187 m)—which form a sinuous, serrated range extending N.–S. According to T. Hirabayashi[51], these peaks, except the northernmost Etizen-dake, are remains of the ring-wall that surrounds a horseshoe-shaped, central crater, about 2 km across, and opening toward the southwest. He also mentions another explosion-crater adjoining the central crater on the northeast, which, surrounded by Etizen-dake, Yobiko-dake, and Nokogiri-dake, in a horseshoe-shape, opens toward the northeast.

The volcano is composed of lava-flows and pyroclastics of andesitic nature. According to Hirabayashi, the lavas are divided into three kinds: Nagakubo lava (two-pyroxene-andesite), Kamiya lava (olivine-two-pyroxene-andesite), and Asitaka lava (augite-bearing hypersthene-olivine-andesite). In addition, He mentions more than fifty dikes, most of which are inside the craters, and which are classified petrographically into seven types, namely olivine-two-pyroxene-andesite, augite-andesite, hypersthene-vitroandesite, aphyric andesite, and three subtypes of two-pyroxene-andesite.

The bedrock beneath the volcano is entirely hidden and no outcrops of it have been seen in the terranes bordering it. There can be no doubt, however, that the lower Neogene rocks (referred to as the Misaka series) which border the Huzi volcano on the east, north, and west, continue underneath the Huzi-Asitaka region into the Tertiary mountains of north Idu. It therefore seems permissible to infer that this volcano, situated at the northern extremity of the trough depression of the Suruga Bay, together with Huzi, rests on down-faulted lower Neogene rocks, either directly or together with certain younger rocks interposed between them.

This volcano is older than its neighbours—Huzi and Hakone. It is certainly older than the Huzi basalts that bound it on all sides except the southwest; indeed its lower flanks were eroded before the eruption of the latter, as an inspection of their observable contacts will indicate. The southeastern skirt of the volcano is separated from the northwestern slope of Hakone by the Huzi lavas that run into the valley (Kise-gawa valley) between them. It is possible, however, that the former is covered by the latter at the base of the Huzi lavas, as shown in Fig. 5, seeing that there are, close to and at a higher level than former, several small hills which, composed of loosely coherent pyroclastics (pumice, scoria, ash, etc.) may be regarded as outliers of the latter. On the evidence of erosion alone, it may be supposed that the Asitaka-yama volcano, most if not all of it, is older than Hakone. As far as can be judged from these rather meager evidences, it may be said that the present volcano is of lower Pleistocene age, although at present there is no means of telling when its activity began.

---

[51] T. HIRABAYASHI, *Rep. Earthq. Inv. Com.*, **24** (1899).

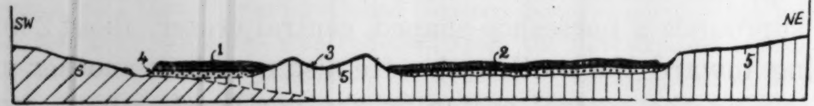

Fig. 5. Diagrammatic section across the valley of the Kise-gawa, showing the geological relation of the visible oldest lava-flows from Huzi to the NW. and SE. slopes respectively of Hakone and Asitaka. 1, 2: Lava-flows from Huzi. 3: Loam-like ash bed. 4: Gravel bed. 5: NW. slope of Hakone. 6: SE. slope of Asitaka.

The rocks of this volcano, which, so far as they are represented by the writer's specimens, are all andesitic, may be referred to two types, hypersthene-olivine-basalt and hypersthene-andesite.

No. 67. *Hypersthene-olivine-basalt.* This rock, which was collected from the northwestern foot of the volcano, 1 km west of Suyama, occurs as a lava-flow interposed between pyroclastic beds. Megascopically, it is compact, dark-gray, and porphyritic with abundant small phenocrysts of plagioclase. Microscopically, we find in addition to the plagioclase, phenocrysts of olivine and hypersthene in a groundmass of plagioclase laths, hypersthene prisms, augite and magnetite granules, and apatite needles, with interstitial tridymite.

Phenocrysts: There are two types of plagioclase phenocrysts; the megascopic phenocrysts, which microscopically exhibit faint zoning, are anorthite 98~90 An (n_1 = 1·5794~1·5753), and the microphenocrysts (up to 0·3 mm dia.) which are bytownite 74 An (n_1=1·568). The olivine, which is partly replaced by greenish antigorite and iron oxide, has $2V(-)\fallingdotseq 75^\circ$. The hypersthene shows $2V(-)=77^\circ$ and $\gamma=1{\cdot}699$. Composition: $En_{70}Fs_{30}$. The mineral contains inclusions of olivine grains.

Groundmass: The plagioclase is labradorite 67 An (n_1=1·563). The hypersthene, which occurs as microphenocrysts in the groundmass, has $2V(-)=61^\circ$. The monoclinic pyroxene is so small so that no accurate measurement of its optical properties could be made.

No. 68. *Hypersthene-andesite.* This rock, which occurs as a lava-flow on the eastern slope of the volcano, is well exposed in the valley between Imasato and Simo-

Wada that borders the volcano on the east. There, the lava, about 3 m thick, is sandwitched between ash beds, both overlain by a lava-flow (olivine-basalt) from Huzi. Megascopically, the rock is compact, gray, and densely packed with plagioclase phenocrysts. Microscopically, it contains in addition to the plagioclase (1~3 mm dia.), phenocrysts of hypersthene (0·5~1·0 mm dia.) in a groundmass consisting of plagioclase laths (0·1~0·3 mm long), pyroxene grains (0·1~0·2 mm eia.), and magnetite granules, with interstitial feldspathic material (alkali feldspar?) and a little glass base.

Table XXV. Analysis of the Hypersthene-andesite, No. 68, from Asitaka-yama.
S. Tanaka, analyst.

	No. 68	Norm				
SiO_2	54·70	Q	7·21	QFM	Q	7
Al_2O_3	20·18	Or	4·45		F	72
Fe_2O_3	2·40	Ab	30·93		M	21
FeO	5·10	An	36·16			
MgO	2·67	Wo	1·74	NF	Or	6
CaO	8·33	En	6·63		Ab	43
Na_2O	3·65	Fs	6·07		An	51
K_2O	0·77	Mt	3·47			
H_2O +	0·75	Il	1·82	NPl	An	54
H_2O −	0·40	Ap	0·33			
TiO_2	0·93			NPy	Wo	12
P_2O_5	0·20				En	46
MnO	0·10				Fs	42
Total	100·22					
				Fe		73

Phenocrysts: The plagioclase is faintly zoned, its average composition being bytownite 72 An (n_1=1·5657). The hypersthene, which is surrounded by pigeonite grains, is distinctly zoned with 2V(−)=74° in the core and 2V(−)=65° at the margin. γ= 1·7065 (mean). Composition: $En_{57}Fs_{33}$.

Groundmass: The plagioclase, which exhibits distinct zoning, is labradorite 68~58 An (n_1=1·522~1·5585). The hypersthene is identical in composition with the margin of the phenocrystic hypersthene, its optic angle being 2V(−)=64°. The pigeonite, which occurs in the corona surrounding the hypersthene and as prisms dispersed through the groundmass, has 2V(+)=44°~38° and β=1·706. Composition: $Wo_{21}En_{39}$-Fs_{40}.

The chemical composition of this rock is shown in Table XXV.

7. Mikura-sima Volcano.

Mikura-sima, which is one of the Seven Idu Islands, lying about 100 km SSE. of Miyake-sima, in 35°52′N. and 139°37′E., is an extinct insular volcano, 851 m above the sea, and about 5 km in diameter at its visible base. The volcano is greatly dissected; its flanks are cut by numerous radial valleys, while its skirt is cut into precipitous sea-cliffs varying in height from 250∼350 m on the southwest shore to about 150 m on the opposite side. The summit of the volcano is a truncated horseshoe-shaped ring-wall surrounding a deep valley (Kawaguchi-no-sawa or Hirasimizu-gawa) which, opening toward the south, suggests a former caldera. The northeastern segment of the ring-wall forms a saddle between the northern ridge (Oyama) and the eastern ridge (850m peak). This saddle may be the result of a side explosion that probably occurred on the northeastern flank at the head of a deep valley (Simawakono-sawa), as a result of which the upper part of the northeastern ring-wall might have been blown away. On the southwestern flank, near the shore, is a knob (Akasawa-yama or Takao-yama) suggestive of a parasitic cone.

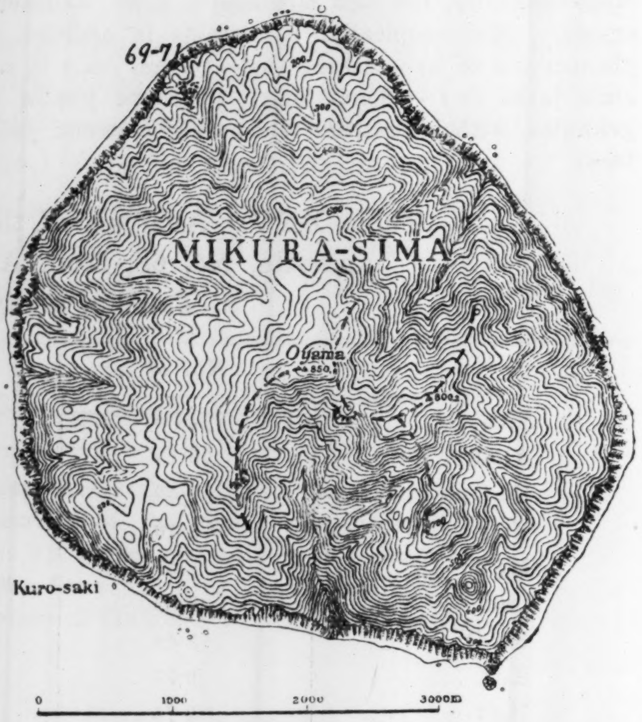

Fig. 6. Mikura-sima, showing the locality of the rock-specimens described in the text.

The volcano is composed of alternating layers of lava-flows and pyroclastic products of a basaltic nature. These layers are cut by numerous dikes of allied rocks, as is seen from exposures in the sea-cliffs around the island. According to N. Fukuchi[52], similar dikes occur in the walls of the caldera.

The following petrographic descriptions are of four specimens, all of which were collected by the writer in 1925 from the lava-flows exposed on the sea-cliff near the landing place on the northern shore of the island (see Fig. 6). Of these, two are olivine-basalt, one hypersthene-bearing olivine-basalt, and the remainder olivine-two-pyroxene-andesite.

---

[52] N. Fukuchi, *Jour. Geogr., Geogr. Soc., Tokyo*, **14** (1902), 854.

No. 69. *Olivine-basalt.* Of the two specimens of this type, one is grayish, compact, and only slightly porphyritic with very sporadic phenocrysts of plagioclase and olivine, while the other, which also is grayish and compact, is strongly porphyritic with abundant plagioclase and less conspicuous olivine phenocrysts.

(a) Almost-aphyric olivine-basalt. Microscopically, we find a few phenocrysts of plagioclase (0·5∼2·0 mm dia.) and lesser microphenocrysts of olivine (0·05∼0·2 mm dia.) in a groundmass of plagioclase laths (0·1∼0·3 mm long), pigeonite prisms (0·1 mm long), magnetite granules, tridymite aggregates, and a little interstitial glass base.

Phenocrysts: The plagioclase is slightly zoned, its composition varying from anorthite 96 An ($n_l=1{\cdot}5783$) to calcic bytownite 88 An ($n_l=1{\cdot}5741$). The olivine, which is surrounded by pigeonite grains, shows a faint zoning with 2V(−) varying from 88° in the core to 81° at the margin.

Groundmass: Plagioclase zonally built, the most sodic part being labradorite 66 An ($n_l=1{\cdot}5627$). The pigeonite shows $c\wedge Z=38°$ and 2V(+) smaller than 30°.

Table XXVI. Analysis of the Olivine-basalt, No. 69 (a),
from Mikura-sima, Seven Idu Islands.
S. Tanaka, analyst.

	No. 69(a)	Norm				
SiO_2	50·50	Q	6·55	QFM	Q	7
Al_2O_3	15·86	Or	2·78		F	55
Fe_2O_3	4·03	Ab	19·40		M	38
FeO	10·00	An	31·31			
MgO	4·64	Wo	4·30	NF	Or	5
CaO	8·63	En	11·54		Ab	36
Na_2O	2·28	Fs	13·19		An	59
K_2O	0·51	Mt	5·79			
H_2O +	1·26	Il	2·58	NPl	An	62
H_2O −	0·86	Ap	0·33			
TiO_2	1·33			NPy	Wo	15
P_2O_5	0·11				En	40
MnO	0·23				Fs	45
Total	100·24					
				Fe		75

The chemical composition of this rock is shown in Table XXVI.

(b) Porphyritic olivine-basalt. Microscopically, this rock carries abundant phenocrysts of plagioclase and olivine. We find two types of plagioclase phenocrysts, the larger one being a slightly zoned anorthite 97∼91 An ($n_l=1{\cdot}5786\sim1{\cdot}5757$), and the smaller one bytownite 82 An ($n_l=1{\cdot}5712$). The olivine, which is surrounded by minute pigeonite grains, has $2V(-)\fallingdotseq89°$. The groundmass consists of bytownite 75 An ($n_l=1{\cdot}568$), pigeonite $Wo_{13}En_{40}Fs_{47}$ ($\beta=1{\cdot}7053$, $c\wedge Z=40°$, and 2V(+)=27° or smaller), magnetite, cristobalite, and a little interstitial glass base.

No, 70. *Hypersthene-bearing olivine-basalt.* Megascopically, this rock is grayish, compact, and studded with conspicuous plagioclase and less conspicuous olivine phenocrysts. Microscopically, the phenocrysts are zoned anorthite-bytownite 95∼81 An

($n_1 = 1{\cdot}5772 \sim 1{\cdot}5705$) and zoned olivine ($2V(-) \doteqdot 87°$ in the core and $2V(-) \doteqdot 81°$ at the margin). The groundmass consists of bytownite 71 An ($n_1 = 1{\cdot}5655$), anhedral olivine surrounded by pigeonite grains either directly or with hypersthene between them, hypersthene ($2V(-) = 66°$) with a rim of pigeonite in parallel intergrowth, pigeonite $Wo_{12}En_{41}Fs_{47}$ ($\beta = 1{\cdot}7027$, $2V(+) = 17°$ or smaller), and tridymite, with a little interstitial glass.

No. 71. *Olivine-two-pyroxene-andesite.* Megascopically, this rock also is grayish, compact, and strongly porphyritic with phenocrysts of plagioclase and pyroxene. Microscopically, we find phenocrysts of faintly-zoned anorthite-bytownite 94~85 An ($n_1 = 1{\cdot}5770 \sim 1{\cdot}5724$) with a thin rim of the groundmass plagioclase, hypersthene $En_{62}Fs_{38}$ ($2V(-) = 71°$, $\gamma = 1{\cdot}7031$ or $n_1 = 1{\cdot}6966$) with a thin rim of monoclinic pyroxene, augite ($2V(+) = 48°$), olivine ($2V(-) \doteqdot 87°$) surrounded by pigeonite grains, and accessory magnetite. The groundmass consists of labradorite 62 An ($n_1 = 1{\cdot}5603$), pigeonite $Wo_{12}En_{40}Fs_{48}$ ($2V(+) = 18° \sim 10°$, $\beta = 1{\cdot}705$), magnetite, and cristobalite, with a little interstitial glass base.

8. Tori-sima (Mitugo-sima or Ponafidin I.) Volcano.

Tori-sima, in 30°28′N. and 140°14′E., is an insular volcano with a circular outline of about 2·5 km in diameter, and consisting of a somma and a central cone. The somma has a circular crater, 1 km in diameter, surrounded by a ring-wall, the east and west segments of which are clearly the respective crest-lines around them—Asahi-yama (387 m) on the east and Tukiyo-yama (374 m) on the west. The central cone, Komoti-yama (361 m above the sea or about 100 m above the eastern atrio of the somma), stands in the centre of the caldera, its top, with the walls of two circular craters, being truncated. These craters, together with two other smaller ones in the atrio—Kitano-kubo in the northern atrio and Butano-kubo in the southern—, besides a horseshoe-shaped depression (Titose Bay) on the northern shore, rest on a line that suggests a fissure and traverses the island in a N.–S. direction through the central cone. In addition, there are two explosion-craters that were formed by the disasterous explosions of August 1902, which were the last and only recorded explosive activity on the island. One of these, A, is a rift-crater, 900 m long, 300 m wide, and 100 m deep, stretching in a N.–S. direction on the west flank of

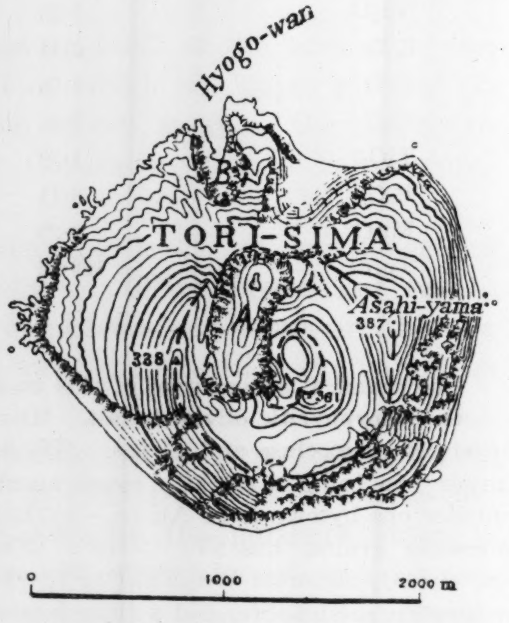

Fig. 7. Tori-sima.

the central cone; and the other, B, a horseshoe-shaped explosion-crater (Hyogo Bay) on the NNW. shore of the island⁵³⁾ (see Fig. 7).

The volcano is composed of alternating layers of lava, agglomerate, and other pyroclastic products. Although the writer did not landed on the island, he examined two out of a number of specimens that were collected by T. Akagi from the shore of the Bay of Hyogo, and which are preserved in the collection of the Geological Institute of the Tokyo Imperial University. One of these is augite-olivine-basalt and the other two-pyroxene-andesite, their respective petrographic characters being as follows:

No. 72. *Augite-olivine-basalt.* This rock is grayish, rather compact with a few round vesicular cavities and strongly porphyritic with abundant phenocrysts of plagioclase, olivine, and pyroxene. Microscopically, we find phenocrysts of plagioclase (0·5~1·0 mmd ia.), olivine (0·5~2·0 mm dia.) and augite (0·5~2·0 mmd ia.), in a groundmass of plagioclase laths (0·1~0·2 mm long), augite prisms (0·1~0·2 mm long), magnetite grains, and a few tridymite, with a little interstitial glass base packed with dust material.

Phenocrysts: The plagioclase may be referred to two types: the larger crystals of anorthite 97 An ($n_1=1{\cdot}5790$) and the smaller ones of less calcic anorthite 91 An ($n_1=1{\cdot}5760$). They are surrounded by a thin rim of the groundmass plagioclase. The olivine, which occurs as anhedral round crystals enclosed by pyroxene grains, has $2V(-)=86°$ and $\beta=1{\cdot}7067$. Composition: $Fo_{67}Fa_{33}$. The augite is faintly zoned, its optic angle varying from the core to the margin in the manner: $2V(+)=51° \rightarrow 42°$

Table XXVII. Analysis of the Augite-olivine-basalt, No. 72, from Tori-sima, Southern Islands. S, Tanaka, analyst.

	No. 72	Norm				
SiO_2	48·70	Q	0·60	QFM	Q	1
Al_2O_3	20·08	Or	1·11		F	61
Fe_2O_3	1·80	Ab	13·11		M	38
FeO	8·14	An	47·29			
MgO	5·53	Wo	7·55	NF	Or	2
CaO	13·20	En	13·75		Ab	21
Na_2O	1·56	Fs	12·79		An	77
K_2O	0·17	Mt	2·55			
H_2O +	0·20	Il	1·21	NPl	An	78
H_2O −	0·13	Ap	0·33			
TiO_2	0·64			NPy	Wo	22
P_2O_5	tr.				En	40
MnO	0·20				Fs	38
Total	100·35					
				Fe		64

---

53) K. JIMBO, *Rep. Earthq. Inv. Com.*, **43** (1903).

or $58^\circ \rightarrow 48^\circ \rightarrow 36^\circ$. $n_1 = 1{\cdot}6906$ (mean). Average composition: $Wo_{23}En_{47}Fs_{25}$.

Groundmass: The plagioclase is bytownite 85~81 An ($n_1 = 1{\cdot}5776 \sim 1{\cdot}5758$). The monoclinic pyroxene is zonally built, its optic angle varying from $2V(+) = 50^\circ \sim 45^\circ$ in the core to 34° or smaller at the margin. $\beta = 1{\cdot}7020$ (mean). Average composition: $Wo_{20}En_{41}Fs_{39}$. The magnetite occurs either as isolated equant individuals or in an ophitic intergrowth with the plagioclase and pyroxene laths.

The chemical composition of this rock is given in No. 72 of Table XXVII. The rock is high in alumina and lime, and low in alkalies, indicating a predominance of the calcic plagioclase. The normative plagioclase has the composition of bytownite 78 An which is a little more sodic than the modal plagioclase. The analysis closely resembles that of the augite-olivine-basalt from Kita Io-sima (No. 75, Table XXVIII), although the former is more aluminous and more calcic, but less alkalic, compared with the latter, and although the former shows a little normative quartz instead of the normative olivine which appears a little in the latter. The present rock is also very similar in chemical composition to the porphyritic olivine-basalt from the demolished igneous body of the northwestern coast of O-sima (No. 90, Table XXXIII).

No. 73. *Two-pyroxene-andesite.* This rock is dark-gray, compact, and less porphyritic than the rock above described, with sporadic phenocrysts of plagioclase and pyroxene. Microscopically, the phenocrysts are two types of plagioclase—anorthite ($n_1 = 1{\cdot}578$) and calcic bytownite 86 An ($n_1 = 1{\cdot}574$)—, faintly zoned augite Wo_{32}-$En_{43}Fs_{25}$ ($2V(+) = 53^\circ$ in the core and $2V(+) = 48^\circ$ at the margin, $\beta = 1{\cdot}6964$ or $n_1 = 1{\cdot}6933$), and hypersthene $En_{65}Fs_{35}$ ($2V(-) = 73^\circ$, $n_1 = 1{\cdot}6942$). Most of the hypersthene phenocrysts are enclosed in a rim of augite ($c \wedge Z = 47^\circ$) in parallel intergrowth, while a few occur as randomly-oriented inclusions in the aguite phenocrysts. The groundmass consists of bytownite 84 An ($n_1 = 1{\cdot}5720$), monoclinic pyroxene ($\beta = 1{\cdot}710$), Magnetite, and tridymite, with a little interstitial glass base. The tridymite, as minute grouped crystals, is more plentiful in this than in the preceding rock.

9. Kita Io-sima (San Alessandro I.) Volcano.

Kita Io-sima, situated 25°25′N. and 141°16′E., is the northernmost member of the Volcano Islands, southwest of the Bonin Islands. Its elliptical coastline, the major and minor axes of which are 3 km from NNW. to SSE. and 2 km from ENE. to WSW., respectively, has but few indentations. The island is a much dissected volcanic cone; its summit, instead of being a pointed peak as in the usual conical volcano, is a ridge stretching in a NNW.–SSE. direction along the major axis of the island from the highest southern peak, Sakakiga-mine (804 m above the sea) to the lowest northern peak, Aono-mine (523 m), through the 665 m peak that lies between them. The lateral slopes of the ridge, which are generally inclined more than 35°, showing numerous slips and scars, are broken in an irregular manner and deeply dissected by ravines, of which the Isino valley on the northeast slope between the south and north peaks, is the largest and most striking. The steep slopes of the upper part of the ridge end abruptly with precipitous sea-cliffs up to 400 m high and are fringed with narrow gravel beaches along the whole coast. The gravel beach, which, at the base of the sea-cliffs rises a few meter above the sea, gradually descends seaward without being cut by coastal terraces of any height, and continues to a shallow-water wave-cut platform offshore.

So far as the writer's observations go, the volcano is built up of much agglomerate, a few lava sheets, and numerous dikes, all of basaltic nature. Thus, the precipitous cliff near the landing place on the north-east side shows strata of agglomerate which, dipping apparently to the south, are traversed by numerous dikes. In places the agglomerate carries huge lava-blocks (2 m or more in diameter), but in others it is a bed of material so fine that it may be called an ash bed. Dikes of thicknesses up to several meters stand almost vertically with a NW.–SE. strike, some of them extending for more than 300 m from the base to the upper edge of the cliff.

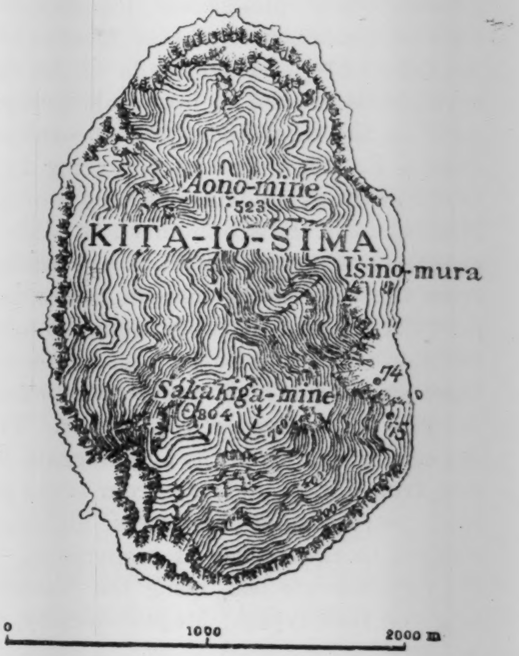

Fig. 8. Kita Io-sima, showing the localities of the rock-specimens described in the text.

On the top of the south peak is a small depression suggestive of a former crater, which however can scarcely be the main crater of the volcano, seeing that the strata of agglomerate do not show a quaquaversal dip from the top of the south peak as the centre. It is possible that the former main crater of activity of the volcano is at the head of the Isino valley already referred to. T. Wakimizu[54] regarded the valley as an old explosion-crater. The steep wall that surrounds the valley in a horseshoe-shape is covered in places with a whitish to yellowish material that may owe its origin to a former solfatara—a vestige of the last phase of volcanic activity. A rocky pinnacle suggestive of a neck rises above the steep wall adjoining the southern part of the valley. There is no historic record either of a volcanic eruption or of active solfataras of any extent in the supposed crater nor elsewhere else in the island, although a submarine volcano, about 2 km northwest of the island, continued activities for a number of years until 1889.

Six rock specimens were collected by the writer in 1935 from the

---

54) T. Wakimizu, *Publ. Earthq. Inv. Com.*, No. 22 C (1908).

northeastern part of the island. Petrographically, they may be referred to two types, olivine-basalt and augite-olivine-basalt.

No. 74. *Olivine-basalt.* This rock is represented by lava-blocks collected from an agglomerate bed exposed on the precipitous cliff on the northeast coast. Megascopically, it is grayish, either compact or slightly vesicular, and porphyritic with abundant phenocrysts of plagioclase, together with a few olivine. Microscopically, the plagioclase of the phenocrysts is faintly zoned, its composition varying from anorthite 99 An ($n_t=1{\cdot}5797$) to bytownite 82 An ($n_t=1{\cdot}5715$). The olivine, which occurs in rounded crystals, is altered to brownish iddingsite along its cracks. Zoning is distinct: $2V(-)=88°$ in the core, and $2V=80°\sim78°$ at the margin. $\beta=1{\cdot}7180$ (mean). Average composition: $Fo_{62}Fa_{38}$. Besides occurring in comparatively larger phenocrysts, the olivine is found in the groundmass as very minute crystals surrounded with pyroxene grains. The plagioclase in the groundmass is calcic labradorite 66 An ($n_t=1{\cdot}5627$). The monoclinic pyroxene, which occurs in the groundmass only, is zonally built, its optic angle varying from the core to the margin in the manner: $2V(+)=46°\rightarrow34°$, $52°\rightarrow40°$, or $52\rightarrow35°$. $\beta=1{\cdot}711$ (mean). Average composition: $Wo_{24}En_{37}Fs_{39}$. The groundmass contains in addition to the plagioclase and pyroxene, magnetite granules and interstitial tridymite, together with a little dusty glass base.

No. 75. *Augite-olivine-basalt.* This rock occurs both as lava-sheets and dikes, besides occurring also in the agglomerate bed. The four specimens (one from agglomerate, two from dikes, and one from lava) belonging to this rock type are greatly alike in their petrographic characters, although megascopically they differ from each other according to their mode of occurrence. One of them, collected from a dike traversing the agglomerate bed, being the freshest specimen, will be described here as representing the rock-type. Megascopically, the specimen is dark-gray with a greenish tint,

Table XXVIII. Analysis of the Augite-olivine-basalt,
No. 75, from Kita Io-sima, Volcano Islands.
S. Tanaka, analyst.

	No. 75	Norm				
SiO_2	48·49	Q	—		Q	—
Al_2O_3	18·72	Or	2·23	QFM	F	61
Fe_2O_3	2·77	Ab	17·30		M	39
FeO	8·18	An	40·89			
MgO	5·17	Wo	8·71		Or	4
CaO	12·47	En	12·60	NF	Ab	29
Na_2O	2·02	Fs	11·67		An	67
K_2O	0·33	Fo	0·18			
H_2O +	0·38	Fa	0·15	NPl	An	70
H_2O −	0·60	Mt	3·94			
TiO_2	0·76	Il	1·52		Wo	26
P_2O_5	0·05	Ap	tr.	NPy	En	38
MnO	0·22				Fs	36
Total	100·16					
				Fe		67

vesicular to compact, and porphyritic with phenocrysts of plagioclase, pyroxene and olivine. Microscopically, the phenocrysts of plagioclase (0·5~3·0 mm dia.), augite (0·3~1·5 mm dia.) and olivine (0·1~1·0 mm dia.) are scattered through a groundmass of plagioclase (0·1 mm), augite (0·03~0·1 mm) and magnetite, with a greenish-brown interstitial glass.

Phenocrysts: The plagioclase is anorthite 95~90 An (n_1=1·5774~1·5752) surrounded by a thin rim of the groundmass plagioclase. The olivine, which is partly serpentinized, has 2V(−)=86° in the core and 2V(−)=82° at the margin. β=1·7038 (mean). Average composition: $Fo_{65}Fa_{35}$. The augite shows a distinct zoning, its optic angle varying from the core to the margin in the manner: 2V(+)=50°→58°→→50°, 58°→52°→45°, or 53°→50°. n_1=1·6953 (mean). Average composition: Wo_{32}-$En_{33}Fs_{35}$.

Groundmass: The plagioclase, which occurs either as stout prismoids or as equant grains, is bytownite 78 An (n_1=1·5692). The augite has 2V(+)=50→46° and n_1=1·6982. Approximate composition: $W_{30}En_{42}Fs_{28}$. The magnetite, which occurs rather sporadically, is ophitically intergrown with the groundmass plagioclase laths and pyroxene grains. No silica mineral was observed in the groundmass.

The specimen just described was chemically analyzed with results as given in Table XXVIII. It is low in silica, but high in alumina and lime. The norm shows a little olivine instead of quartz.

10. Aoga-sima Volcano.

Aoga-sima, situated about 50 km SSE. of Hatizyo-sima, in 31°28′N. and 139°45′E., has an elliptical outline measuring 3·5 km from NNW. to SSE. and 2 km from ENE. to WSW. It is a composite insular volcano consisting af a somma and a central cone. The somma, 423 m above the sea, is deeply eroded, resulting in the formation of steep outer slopes surrounded by high sea-cliffs on all sides except in the northwest, where a gentle slope of the original conical volcano has been left intact. The top of the somma is truncated, with a ring-wall surrounding a circular crater (Ikeno-sawa), about 1 km in diameter and 300 m deep from the highest crest of the ring-wall. The central cone, which rises 100 m above the floor of the crater of the somma, is a truncated cone with a circular crater, 200 m in diameter, having very young morphological features. Recent known

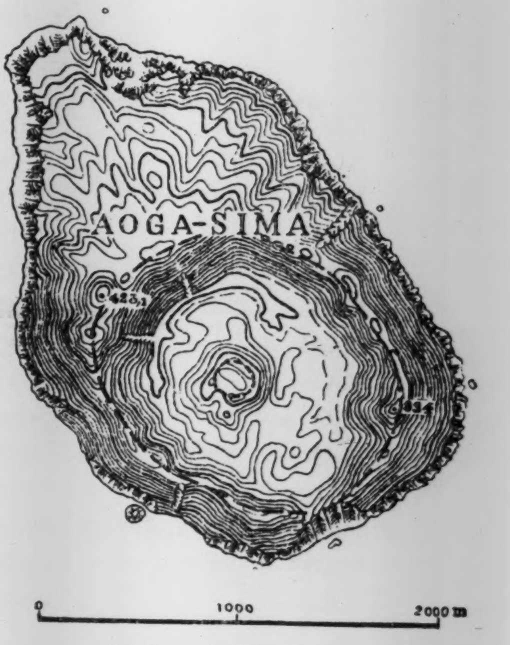

Fig. 9. Aoga-sima.

eruptions of the volcano occurred in 1780∼1785 when the central cone was formed; and if the records are trustworthy, what may be guessed as an eruption occurred in 1652[55].

As to the geologic structure of the volcano, and its rocks, our knowledge is very meagre, for the mountain has rarely been visited and what descriptions we have of it are of the briefest. The following petrographic descriptions refer to four specimens, all of which were collected by T. Akagi from the island, and which are in the collection of the Geological Institute of the Tokyo Imperial University. Of the specimens, two are olivine-bearing two-pyroxene-andesite, and the remainder olivine-basalt. Their petrographic characters are as follows:

No. 76. *Olivine-bearing two-pyroxene-andesite.* Megascopically, this rock is black and almost aphyric, but occasionally contains small phenocrysts of plagioclase and pyroxene. One part of the rock is scoriaceous with small vesicular cavities, while the other part is compact, showing that luster so characteristic of obsidian. Microscopically, we find a few phenocrysts of plagioclase (0·1∼1·0 mm dia.), augite (0·1∼1·0 mm dia.), hypersthene (0·1∼1·0 mm), and olivine (0·1∼0·2 mm dia.), in a glassy groundmass. Angular, accessory xenoliths (1∼5 mm dia.) of more crystalline andesite are sporadically found. The plagioclase of the phenocrysts is bytownite 80∼74 An ($n_1=1{\cdot}5701\sim1{\cdot}5670$). The augite shows $n_1=1{\cdot}7015$, $2V(+)=50°$, and $c\wedge Z=45°$. Composition: $\mathrm{Wo_{29}En_{35}Fs_{36}}$. The hypersthene, which is greenish brown with distinct pleochroism, has $n_1=1{\cdot}715$. Composition: $\mathrm{En_{47}Fs_{53}}$. The amount of olivine is negli-

Table XXIX. Analysis of the olivine-bearing two-pyroxene-andesite, No. 76, from Aoga-sima.
S. Tanaka, analyst.

	No. 76	Norm				
SiO_2	61·73	Q	20·36	QFM	Q	21
Al_2O_3	14·60	Or	2·78		F	56
Fe_2O_3	1·75	Ab	29·89		M	23
FeO	7·70	An	22·53			
MgO	1·82	Wo	2·79	NF	Or	5
CaO	6·07	En	4·52		Ab	54
Na_2O	3·52	Fs	11·34		An	41
K_2O	0·47	Mt	2·55			
H_2O +	0·48	Il	1·97	NPl	An	43
H_2O −	0·22	Ap	0·33			
TiO_2	1·05			NPy	Wo	15
P_2O_5	0·20				En	24
MnO	0·22				Fs	61
Total	99·83					
				Fe		84

---

55) F. Omori, *Rep. Earthq. Inv. Com.*, **43** (1903).

gible. The groundmass is a pale to dark brown glass with $n = 1{\cdot}5443 \sim 1{\cdot}5660$. It carries a few plagioclase microlites (0·05 mm long). The chemical composition of this rock is shown in Table XXIX.

No. 77. *Olivine-basalt.* Megascopically, this rock is black, vesicular, and porphyritic with abundant phenocrysts of plagioclase. Microscopically, besides the plagioclase, it contains a few phenocrysts of olivine. The plagioclase is faintly zoned, its composition varying from anorthite 93 An ($n_1 = 1{\cdot}5770$) to calcic bytownite 87 An ($n_1 = 1{\cdot}5735$). The olivine has $2V \doteqdot 90°$. The groundmass is an opaque glass carrying a few plagioclase microlites.

11. Hatizyo-sima Volcano.

Hatizyo-sima, which is the southernmost member of the Seven Idu Islands, lying in 139°50′E. and 33°05′N., is a gourd-shaped volcanic island measuring about 14 km in a NNW.–SSE. direction and 7·5 km E.–W. It is composed of two volcanoes—Higasi-yama (Mihara-yama) and Nisi-yama (Hatizyo-huzi). Higasi-yama, which occupies the southeastern half of the island, is a dissected composite volcano consisting of a somma (Todaisi-yama, 837 m above the sea) and a central cone (Higasi-yama proper, 701 m). Besides these, there are, near the skirt of the somma, several small dissected hills, 100∼300 m high above the sea, which are morphologically separated from the main body of the somma, and which suggest remains of an old volcano buried beneath the somma. K. Niinomi[56] regarded them as representing detached segments of the ring-wall of an older somma. Nisi-yama, a typical volcanic cone, 854 m above the sea, occupies the rest of the island. It is in marked contrast with the preceding volcano in that its morphological features are quite young. The top of the cone is truncated, with a ring-wall surrounding the circular crater (O-ana), which is about 400 m in diameter. In the crater is a small central

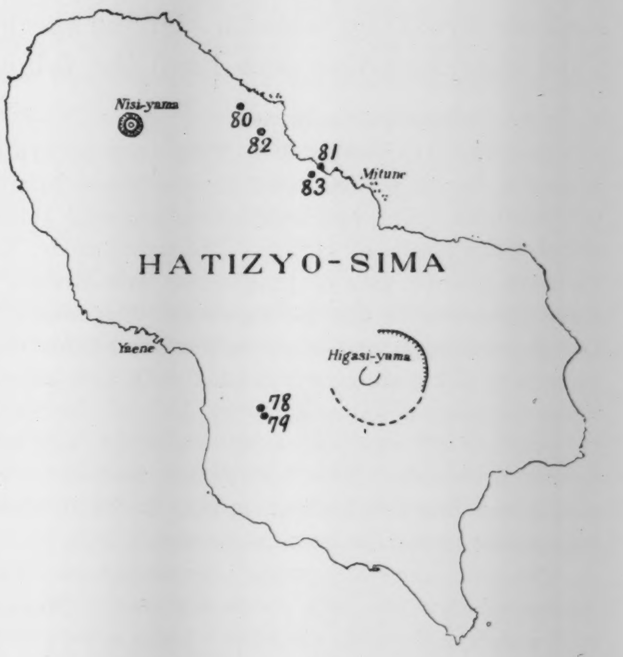

Fig. 10. Hatizyo-sima, showing the localities of the rock-specimens described in the text.

---

[56] K. Niinomi, *Jour. Geogr., Geogr. Soc., Tokyo*, **24** (1912), 45.

cone (Naka-yama). There are several parasitic cones and vents on the flanks of the Nisi-yama volcano. History records a number of eruptions from this volcano, which at present is dormant without any sign of activity. The last known eruption occurred in 1605, when, according to Niinomi, a lava-flow that issued from the southeast slope of Nisi-yama reached the sea at Mitune on the east side of the island, while other eruptions are recorded as having occurred in 1487, 1518, and 1522.

Both volcanoes—Higasi-yama and Nisi-yama—are composed of alternate layers of lavas and pyroclastic products of basaltic nature. The Higasi-yama lavas are olivine-basalt and augite-bearing olivine-basalt, so far as they are represented by the specimens which the writer collected in 1935 from the lower part of the northwest flank of the volcano, although Niinomi speaks of olivine-two-pyroxene-andesite as being among them. The Nisi-yama lavas, which generally appear to be a little less basic than the Higasi-yama lavas, are poor in phenocrysts of mafic minerals. These lavas may however be referred to three types: aphyric basalt, two-pyroxene-basalt, and olivine-basalt. Besides these, Niinomi mentions hypersthene-andesite and olivine-bearing two-pyroxene-andesite from the volcano. Of the specimens collected by the writer, the most representative ones have the following petrographic characters:

(A) Higasi-yama lavas.

No. 78. *Olivine-basalt.* This rock occurs on the northwest flank of Higasi-yama, where it forms a lava-flow, 10 m or more in thickness, intercalated between pyroclastic products. The specimen examined was collected from the lava exposed on the road about 2 km south of Ogago. Megascopically, the rock is gray, compact, and porphyritic with phenocrysts of plagioclase and olivine. Microscopically, two types of plagioclase phenocrysts are distinguished: the larger phenocrysts are anorthite 95 An, while the smallar ones are calcic bytownite 88 An ($n_1 = 1.574$). The olivine, which occurs as anhedral crystals surrounded with pyroxene grains, has $2V(-) \doteqdot 86°$. The groundmass consists of labradorite 75 An ($n_1 = 1{\cdot}5678$), zoned augite $Wo_{26}En_{40}Fs_{34}$ ($2V(+) = 50° \rightarrow 43°$ or $52° \rightarrow 47°$, $\beta = 1{\cdot}7015$ (mean)), and magnetite, with a little interstitial feldspathic material. The feldspathic material, which has very weak double refraction and low refractive indices, appear to be an alkali-feldspar; definite identification being impossible owing to its minute size.

No. 79. *Augite-bearing olivine-basalt.* This rock occurs as a lava-flow some distance below the lava above described. Megascopically, the rock is grayish, compact, and porphyritic with abundant phenocrysts of plagioclase and olivine and subordinate ones of pyroxene. Microscopically, it contains phenocrysts of anorthite 98~91 An ($n_1 = 1{\cdot}5790 \sim 1{\cdot}5766$), olivine ($2V(-) \doteqdot 86°$) with rims of pyroxene grains, and faintly zoned augite. The optic angle of the last-named mineral varies from the core to the margin in the manner: $2V(+) = 52° \rightarrow 45°$, $50° \rightarrow 44°$, or $52° \rightarrow 43°$. The groundmass consists of bytownite 75 An ($n_1 = 1{\cdot}5675$), monoclinic pyroxene $Wo_{27}En_{41}Fs_{32}$ ($2V(+) = 46° \sim 43°$ and $\beta = 1{\cdot}700$), and dusty magnetite, with a little interstitial, colorless material exhibithing weak double refraction and low refractive indices.

(B) Nisi-yama lavas.

No. 80. *Two-pyroxene-bearing basalt.* Covered with beds of pyroclastic products, about 2 m in thickness, this rock occurs as a lava-flow on the east-southeast slope of Nisi-yama, about 2·5 km north of Mitune. It is a vesicular, black, slightly porphyritic rock with a few phenocrysts of plagioclase. Microscopically, it contains, besides the plagioclase, a few microphenocrysts of a monoclinic pyroxene. Although no hypersthene could be detected in the thin section, the mineral must be present as very rare phenocrysts in the rock, for a pyroxene megacryst picked out of the rock was identified through its optical characters as that mineral. The plagioclase phenocrysts are a faintly zoned bytownite 90∼83 An ($n_1=1{\cdot}5758\sim1{\cdot}5716$). The microphenocrystic pyroxene is pigeonitic, with $n_1=1{\cdot}702$. The hypersthene, which was picked out of the rock, showed $n_1=1{\cdot}6975$. Composition $En_{65}Fs_{35}$. The groundmass consists of very minute plagioclase microlites, pigeonite prisms, and magnetite cubes, with tridymite (?) and interstitial feldspar.

No. 81. *Olivine-bearing basalt.* This rock occurs on the beach adjoining the northern side of the landing place, Mitune, as a lava-flow underlying the lava of aphyric basalt, No. 83. A similar lava is exposed extensively on the rear side of the island, near the landing place, Yaene. Megascopically, the rock is dark-gray, vesicular, and strongly porphyritic with numerous phenocrysts of plagioclase. Microscopically, we find a few phenocrysts of olivine, besides the plagioclase. The plagioclase is distinctly zoned, its composition varying from anorthite 94 An ($n_1=1{\cdot}5769$) to bytownite 86 An ($n_1=1{\cdot}5730$). The olivine has $2V(-)=88°$ and $\beta=1{\cdot}7180$. Composition: $Fo_{60}Fa_{10}$. The groundmass consists of minute laths of sodic bytownite 70 An ($n_1=1{\cdot}5648$), pigeonite (2V small, $\beta=1{\cdot}718$), and magnetite grains, with cristobalite and interstitial brown glass.

No. 82. *Basalt free from phenocrysts of mafic minerals.* This rock occurs as a lava-flow covering the surface of the lower part of the southeast slope adjoining the southern part of the area occupied by the lava, No. 80. Megascopically, it is vesicular, gray to black, and porphyritic with plagioclase phenocrysts. Microscopically, it contains abundant phenocrysts of plagioclase only, the composition of which is anorthite-bytownite 92∼84 An ($n_1=1.5760\sim1{\cdot}5721$). The groundmass is a dark-brownish glass packed with bytownite laths (80 An, $n_1=1{\cdot}5698$), pigeonite prisms ($\beta\fallingdotseq1{\cdot}700$, 2V very small or nearly zero), and magnetite dust.

No. 83. *Aphyric basalt.* This rock occurs as a lava-terrace, 5∼10 m high above the sea, on the eastern coast near the landing place, Mitune. The lava, which is the youngest flow exposed on that coast, may possibly be what Niinomi regarded as having issued in 1605 from the southeastern slope of the Nisi-yama cone. The specimen examined was collected from a cliff cut in the terrace-forming lava about 100 m north of the landing place. Megascopically, the rock is compact, dark-gray to black, and almost completely aphyric without any noticeable phenocrysts except a few small plagioclase. Microscopically, it consists of plagioclase, pigeonite, and magnetite, with a little interstitial material. The plagioclase occurs, rarely, as microphenocrysts (0·5 mm dia.), besides minute laths (0·03∼0·1 mm long). The microphenocrystic plagioclase is bytownite 87 An ($n_1=1{\cdot}5735$) with a thin rim of a little less calcic bytownite; while the minute lath-shaped plagioclase is bytownite 80 An ($n_1\fallingdotseq1{\cdot}570$). The pigeonite also occurs as microphenocrysts (0·5 mm long), besides minute slender prisms (0·1 mm long). The microphenocrystic pigeonite has $\beta=1{\cdot}7045$ ($n_1=1{\cdot}7025$), while the minute pigeonite $\beta=1{\cdot}7070$. Their optic angles are very small. The magnetite is found as equant granules, 0·01 mm in diameter. There is a small amount of colorless base, which is almost isotropic and has a refractive index smaller than that of balsam.

Table XXX. Analysis of the Aphyric Basalt, No. 83, from Nisi-yama, Hatizyo-sima. S. Tanaka, analyst.

	No. 83	Norm				
SiO_2	54·67	Q	10·51	QFM	Q	11
Al_2O_3	14·47	Or	2·78		F	51
Fe_2O_3	1·86	Ab	22·02		M	38
FeO	12·30	An	26·42			
MgO	3·03	Wo	5·23	NF	Or	5
CaO	8·03	En	7·53		Ab	43
Na_2O	2·59	Fs	18·86		An	52
K_2O	0·50	Mt	2·78			
H_2O +	0·45	Il	3·19	NPl	An	54
H_2O −	0.09	Ap	0·33			
TiO_2	1·64			NPy	Wo	17
P_2O_5	0·16				En	23
MnO	0·32				Fs	60
Total	100·11					
				Fe		82

The results of Tanaka's analysis of this rock are given in Table XXX. The analysis closely resembles those of the basaltic rocks from O-sima and Miyake-sima, although the former is slightly more acidic than the latter. Thus the present rock, like the analyzed rocks from O-sima and Miyake-sima, is rather low in alumina and high in iron-oxides compared with the porphyritic basalts from Tori-sima, Kita Io-sima, etc. The norm shows abundant quartz. The normative plagioclase and pyroxene are 54 An and $Wo_{17}En_{23}Fs_{60}$ respectively. In the analyses of basaltic rocks from the region now under investigation, the present analysis shows the highest percentage of ferrosilite molecule in the normative pyroxene.

12. Miyake-sima Volcano.

Miyake-sima, situated in 34°03′N. and 139°30′E., is an insular volcano with a circular outline measuring about 7 km in diameter. It is a composite stratified volcano consisting of a somma and a central cone. The somma is truncated at the top, with a ring-wall whose northern segment is clearly seen as a semi-circular crest-line around it. The highest point (815 m above the sea) of the somma is the northern crest of this ring-wall. The caldera, whose northern part is preserved as a crescentic atrio encircled by the ring-wall, must have originally been about 1·5 km in diameter. The central cone (O-yama), which is 814 m above the sea or about 120 m above the floor of the atrio, lies slightly south of the caldera. Its top is truncated, with walls surrounding a composite crater consisting of four crater-bowls aligned in an E.–W. direction. Of these, the easternmost crater (the first crater), the principal one of the central cone, is the largest (about 400 m in diameter); the second crater (200 m dia.) lying immediately west of the first, is the deepest (about 115 m below the highest rim of the crater-wall), while the others are smaller and shallower than those just mentioned (see Fig. 11).

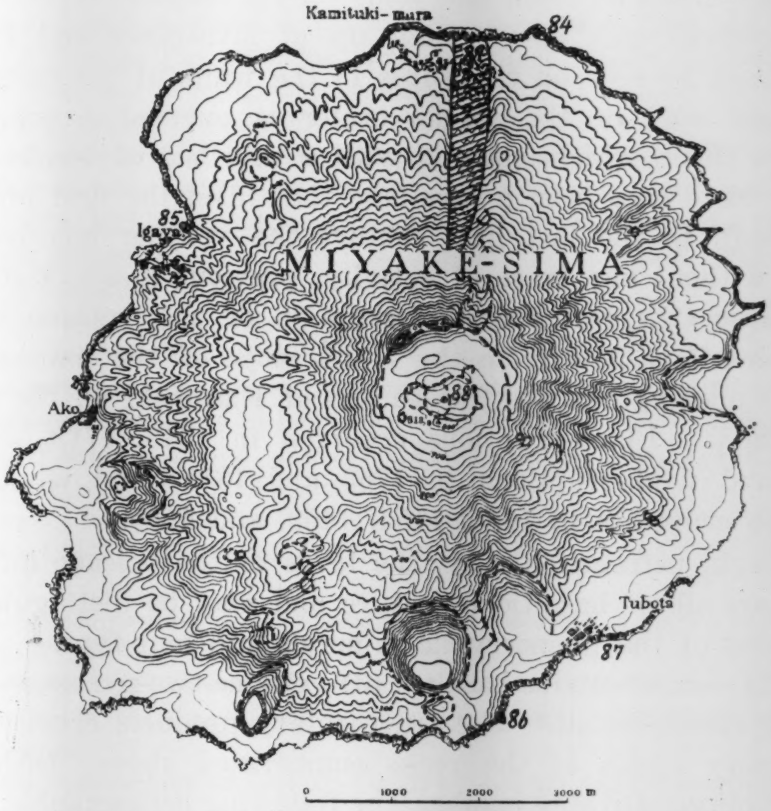

Fig. 11. Miyake-sima, showing the localities of rock-specimens described in the text. Hatched area is the lava of 1874.

The somma has more than twenty parasitic knobs and flank-vents, most of which lie on the NNE. snd SSW. slopes, but none of them are large enough to affect much the regular outline of the somma. The central cone also has a parasitic knob on its southwest slope.

The somma is composed of alternate accumulations of lava-flows and fragmentary material. Although the thick accumulation of fragmentary ejecta and the absence of deep ravines on the slopes preclude detailed study of the earlier products lower down the somma, the best exposures of its inner structure are to be seen on the sea-cliffs around the island and on the ring-wall surrounding the caldera, where many superposed lava-flows, most of them only a few meters thick, are exposed, intercalated by layers of fragmentary ejecta. Some of the flows, especially those exposed on the southwest shore, must have come from the parasitic cones or from the vents on the slopes.

The central cone also is built up of lava-flows and fragmentary ejecta as may be seen on exposures in the walls of the summit-craters. On the east wall of the second crater is exposed a columnar lava, about 20 m thick, which, covered with a thin bed of bombs, lapilli and ash, must have once been a lava-lake that filled the first crater[57].

Although in the last half century the volcano has been entirely quiescent without any trace of activity, previous to which it was active several times, the last recorded eruption of the volcano occurred in 1874, when a lava-flow from the NNE. slope of the somma through a fissure-like opening, reached the sea east of Kamituki on the north coast of the island. Flank-eruptions occurred in 1643, 1712, and in 1835, summit- and flank-eruptions in 1763 and 1811; and what have been reported as eruptions in 1085, 1154, 1469, and 1595.

Although, petrographically, the lavas of the volcano differ more or less, they are all of basaltic in nature and may be distinguished by the combinations of the phenocrystic minerals into four types: (1) olivine-basalt, (2) augite-olivine-basalt, (3) olivine-two-pyroxene-basalt, and (4) two-pyroxene-basalt. The fragmentary products consist of juvenile and accessory ejecta of the rocks enumerated above, besidesanorthite lapilli and micro-allivalite bombs. The following petrographic descriptions refer to six representative specimens from the seventy that the writer collected in 1925, when studying the structural details of the volcano.

(A) Somma lavas.

No. 84. *Olivine-basalt.* This rock occurs in several superposed lava-flows exposed on the northeast coast between Akon-saki and Ano-saki. The specimen examined was collected from the lowest of the three flows exposed at Akon-saki. It is grayish, compact, and porphyritic with phenocrysts of plagioclase and olivine. Microscopically, the plagioclase phenocrysts are faintly zoned with composition varying from 98 An ($n_1 = 1{\cdot}5793$) to 92 An ($n_1 = 1{\cdot}5764$). The olivine shows very faint zoing: $2V(-)88°$ in the core, and $2V(-) = 79°$ at the margin. $\beta = 1{\cdot}7033$ (mean). Composition: $Fo_{65}Fa_{35}$. The groundmass, which is highly crystalline, consists of bytownite 77 An ($n_1 = 1{\cdot}5684$), monoclinic pyroxene, and magnetite, with a very little interstitial glass base. The monoclinic pyroxene is zonally built, the variation in its optic angle from core to margin being: $2V(+) = 49° \rightarrow 36°$, $48° \rightarrow 37°$, or $52° \rightarrow 41°$. $\beta = 1{\cdot}711$ (mean). Average composition: $Wo_{24}En_{37}Fs_{39}$.

In another specimen of the same rock type collected from the sea-cliff, about 2 km southeast of Akon-saki, the phenocrystic olivine has $2V = 90°$, and the groundmass pyroxene is zonally built, its optic angle varying from $2V(+) = 49° \sim 47°$ in the core to $2V(+) = 34° \sim 0°$ at the margin.

---

57) I. FRIEDLAENDER, *Mitteil. d. Deutch. Gesell. f. Natur- u. Volkerkunde Ostasiens*, **12** (1909), 76.

No. 85. *Augite-olivine-basalt.* This rock, which is the most abundant of the somma lavas, occurs as lava-flows at several places on sea-cliffs around the island as well as in the ring-wall surrounding the caldera. A specimen from the lava exposed on the shore of Ohunato Bay adjoining Igaya (a village on the northeast coast) on its north, was examined as being a representative of this type. Megascopically, it is grayish, compact, and slightly porphyritic with a few inconspicuous phenocrysts of plagioclase and pyroxene. Microscopically, it contains phenocrysts of plagioclase (1~1·5 mm dia.) and augite (0·5~1·0 mm dia.), and microphenocrysts of olivine (0·1~0·2 mm dia.), in a highly crystalline groundmass of plagioclase laths (0·05~0·3 mm long), pigeonite prisms (0·05 mm long), and magnetite granules, with interstitial cristobalite and negligible amount of glass base.

Phenocrysts: The plagioclase is faintly zoned, its composition varying from anorthite ($n_1=1{\cdot}5798$) to calcic bytownite 89 An ($n_1=1{\cdot}5746$). The olivine, which occurs only as anhedral microphenocrystic individuals surrounded by minute grains of the groundmass pyroxene, has $2V(+)\doteqdot 86°$. The augite is zoned with 2V varying from the core to margin in the manner: $2V(+)=52°\rightarrow 46°$, or $50°\rightarrow 40°$. $n_1=1{\cdot}6933$ (mean). Average composition: $Wo_{28}En_{45}Fs_{27}$.

Groundmass: The plagioclase is bytownite 74 An ($n_1=1{\cdot}5670$) to calcic labradorite 69 An ($n_1=1{\cdot}5643$). The pigeonite has $2V(+)=38°$ and $\beta=1{\cdot}7148$. Composition: $Wo_{18}En_{35}Fs_{47}$.

The chemical composition of the specimen just described is shown in column No. 85 of Table XXXI.

Another specimen of the same rock-type, which was collected from a lava exposed some distance above the base of the northern ring-wall, consists of the following mineral ingredients:

Phenocrysts: Anorthite 95 An ($n_1=1{\cdot}5774$), olivine ($2V(-)\doteqdot 88°$), and augite $Wo_{31}En_{43}Fs_{26}$ ($n_1=1{\cdot}6934\sim 1{\cdot}6963$, $2V(+)=52°\sim 47°$) with pigeonite rim ($2V(+)=43°-15°$). Groundmass: Bytownite 79 An ($n_1=1{\cdot}5694$), pigeonite ($\beta=1{\cdot}7124$, 2V very small), magnetite, and interstitial brown glass.

No. 86. *Olivine-two-pyroxene-basalt.* Somma lavas of this type occur on the southeast coast near Tubota, where they underlie the lavas of two-pyroxene-basalt next to be described. The specimen studied was collected from a lava-flow exposed on the sea-cliff adjoining the southern part of Tubota. Megascopically, it is gray to almost black, more or less vesicular, and porphyritic with phenocrysts of plagioclase, pyroxene, and olivine. Microscopically, the phenocrysts are anorthite ($n_1=1{\cdot}579$) surrounded by a thin rim of bytownite 88 An ($n=1{\cdot}574$), faintly zoned augite $Wo_{30}En_{43}Fs_{27}$ ($2V(+)=55°$ in the core and 43° at the margin. $n_1=1{\cdot}6964$ (mean)), hypersthene $En_{57}Fs_{43}$ ($2V(-)=60°\sim 70°$ and $n_1=1{\cdot}700$), and olivine ($2V(-)\doteqdot 87°$). The groundmass consists of bytownite (the same as the rim of the phenocrystic plagioclase), monoclinic pyroxene ($\beta=1{\cdot}70$), and magnetite, with a brown glass base.

No. 87. *Two-pyroxene-basalt.* The lavas of this type occur on the south, southeast, and southwest coast in several lava-flows. Megascopically, they are usually dark to light gray, compact to slightly vesicular, and almost aphyric without any conspicuous phenocrysts except very sporadical ones of plagioclase and pyroxene. Microscopically, one specimen collected from a lava-flow on the southeast coast, about 2 km northeast of Tubota, is dark-gray and slightly vesicular and carries a few phenocrysts of plagioclase (0·3~1·0 mm dia.), and microphenocrysts (up to 0·2 mm dia.) of augite and hypersthene. The plagioclase phenocrysts show two types: the larger anorthite phenocrysts 94 An ($n_1=1{\cdot}5773$) and tne microphenocrysts of bytownite 79 An ($n_1=1{\cdot}5692$). The augite has the composition $Wo_{30}En_{42}Fs_{28}$ ($2V(+)=49°$ and

$n_1=1{\cdot}697$). The hypersthene, which occurs either as isolated individuals or in parallel growth with a monoclinic pyroxene, the latter being usually outside, is identified as $En_{65}Fs_{35}$ with $n_1=1{\cdot}698$. The groundmass is a dark-brown glass packed with slender laths of plagioclase and very minute grains of pyroxene and magnetite.

Another specimen of the same rock-type collected from a lava-flow exposed on the sea-cliff at Tubota, when compared with the preceding one, is more compact, more crystalline, and less porphyritic. Microscopically, we find very sporadic phenocrysts of plagioclase (0·5~1·0 mm dia.), augite (0·1~0·3 mm dia.), hypersthene (0·1~0·3 mm long), and accessory magnetite. The plagioclase is bytownite 84 An ($n_1=1{\cdot}572$.) The augite has $2V(+)=49°\sim47°$ and $n_1=1{\cdot}698$. Some individuals of the augite are distinctly zoned with a rim of pigeonite ($2V(+)=30°$ or smaller). The hypersthene, which is usually enclosed in a thin rim of monoclinic pyroxene in parallel growth, has $2V(-)=72°$. The groundmass consists of plagioclase laths (0·1 mm long), minute grains of pyroxene and magnetite, tridymite, and a little interstitial glass base.

The specimen just mentioned was analyzed by Tanaka, with results as given in column No. 87 of Table XXXI.

(B) Central cone lavas.

No. 88. *Augite-olivine-basalt.* The central cone lavas are exclusively augite-olivine-basalt. A specimen collected from the east wall of the second crater, and representing the rock of the solidified lava-lake in the first crater of the central cone, is grayish, compact, and almost aphyric without any conspicuous megascopic phenocrysts except a few very small plagioclase and olivine. Microscopically, we find phenocrysts of faintly zoned anorthite-bytownite 94~82 An ($n_1=1{\cdot}577\sim1{\cdot}571$), olivine ($2V(-)=86°$) with a rim of iron-oxide, and augite ($2V(+)=53°\sim48°$ in the core and 43° at the margin), all scattered sporadically through a groundmass of bytownite 78 An ($n_1=1{\cdot}5692$), pigeonite ($\beta=1{\cdot}708$), magnetite, and cristobalite, with a little interstitial glass base.

Another specimen collected from a lava in the northern wall of the second crater of the central cone is more porphyritic, compared with the preceding one, with magascopic phenocrysts of plagioclase, pyroxene and olivine. Microscopically, it contains phenocrysts of anorthite 95 An ($n_1=1{\cdot}5775$) with a rim of bytownite 87 An ($n_1=1{\cdot}5735$), augite $Wo_{26}En_{12}Fs_{32}$ ($2V(+)=45°$, $\beta=1{\cdot}698$) with a rim of pigeonite ($2V(+)=34°$ or smaller) and olivine ($2V(-)\doteqdot80°$) in a groundmass of bytownite 76 An ($n_1=1{\cdot}568$), pigeonite $Wo_{11}En_{36}Fs_{53}$ ($2V(+)=10°$, $\beta=1{\cdot}7125$), magnetite, cristobalite, and interstitial glass base.

The chemical composition of one of the central cone lavas is shown in the analysis (No. 88, Table XXXI) made by M. Dittrich of a specimen that was collected by I. Friedlaender and described by C. Bacher as augite-andesite[58]. As will be seen from the analysis, the central cone lava resembles chemically the lavas from O-sima and Hatizyo-sima (Nisi-yama). Thus, it is rather low in alumina but high in iron-oxides. The norm shows plagioclase 62 An and pyroxene $Wo_{20}En_{39}Fs_{41}$, with considerable quartz.

(C) Lava of 1874.

No. 89. *Olivine-augite-basalt.* This lava occupies a narrow area on the northern slope of the somma, stretching for about 3 km from its vent half way down the slope to the northern sea-shore, with a maximum width of 800 m. Although the slope adjoining the east of the lava field on the east is covered with scoriae and anorthite lapilli

---

58) C. BACHER, Über die Laven der Kleineren Izu-Inseln. Ein Beitrag zur Petrographie Japans. München (1914), 20.

Table XXXI. Analyses of Rocks from Miyake-sima.

		No. 85	No. 87	No. 88	No. 89
SiO_2		53·25	54·10	54·55	53·35
Al_2O_3		16·30	15·24	16·26	15·62
Fe_2O_3		2·89	2·87	4·07	4·21
FeO		9·00	10·38	8·02	8·12
MgO		4·51	3·63	3·66	4·44
CaO		9·52	8·38	8·91	9·68
Na_2O		2·67	2·86	2·44	2·18
K_2O		0·38	0·49	0·32	0·84
H_2O +		0·30	0·30	0·29	0·40
H_2O −		0·18	0·16	n.d.	n.d.
TiO_2		1·12	1·38	1·19	1·18
P_2O_5		0·06	0·11	——	——
MnO		0·22	0·23	——	tr.
Total		100·40	100·13	99·95*	100·02
Q		6·85	8·95	12·97	9·61
Or		2·23	2·78	1·67	5·01
Ab		22·55	24·12	20·45	18·35
An		31·43	27·26	32·82	30·32
Wo		6·62	5·57	4·76	7·43
En		11·24	9·03	9·14	11·05
Fs		12·66	14·77	9·49	9·50
Mt		4·17	4·17	5·79	6·02
Il		2·12	2·58	2·28	2·28
Ap		tr.	0·33	——	——
QFM	Q	7	9	13	10
	F	56	54	55	54
	M	37	37	32	36
NF	Or	4	5	3	9
	Ab	40	45	37	34
	An	56	50	60	57
NPl	An	58	53	62	62
NPy	Wo	22	19	20	27
	En	37	31	39	39
	Fs	41	50	41	34
Fe		72	78	76	73

* includes CO_2 0·24.

ejected at the time of the lava outflow, the lava still remains almost bare.

This lava, which mostly occurs in the aa form, is dark-gray to black, vesicular, and either almost aphyric or porphyritic with conspicuous phenocrysts of anorthite and less conspicuous ones of pyroxene and olivine, according to the part of the flow whence the specimen came. Microscopically, the porphyritic specimen carries phenocrysts of plagioclase, augite, and olivine, scattered through a glassy groundmass packed with plagioclase prismoids ($0{\cdot}05\sim0.1$ mm long), and minute grains of monoclinic pyroxene and magnetite; while the aphyric specimen is a brownish glass in which, besides a few microphenocrysts of plagioclase, augite, and olivine, numerous minute plagioclase laths and dusty grains of pyroxene and magnetite are found.

Phenocrysts: There are two types of plagioclase phenocrysts. One type is represented by anorthite 95 An ($n_1=1{\cdot}5775$), which occurs only in the porphyritic specimen as megascopic phenocrysts ($2\sim15$ mm dia.); and the other as bytownite 88 An ($n_1=1{\cdot}5741$), which is found both in the porphyritic and the aphyric specimens, mostly forming microphenocrysts up to $0{\cdot}5$ mm in diameter. The olivine ($0{\cdot}3$ mm dia.) has $2V(-)\doteqdot88^\circ\sim82^\circ$. The augite is identified as $Wo_{33}En_{39}Fs_{28}$, with $2V(+)=53^\circ\sim51^\circ$ and $n_1=1{\cdot}6972$ ($\beta=1{\cdot}700$).

Although the groundmass minerals could not be analyzed optically, the plagioclase laths appear to be a calcic labradorite, and the pyroxene grains a pigeonite.

The chemical composition of the 1874 lava is given by the analysis (No. 89, Table XXXI) made by M. Dittrich of a specimen collected by I. Friedlaender and described by C. Bacher as olivine-bearing feldspar-basalt[59]. Chemically, the lava closely resembles the central cone lava just described, and consequently to the lavas of O-sima and Hatizyo-sima. S. Kozu speaks of a chemical analysis of the lapilli that were ejected at the same time as the 1874 lava[60]. It is much like Dittrich's analysis of the lava, the only notable difference being the lower magnesia in the former as compared with the latter.

13. O-sima Volcano.

O-sima, situated in the bay of Sagami, and the largest of the Seven Idu Islands, is an insular volcano consisting of a somma and a central cone, with numerous parasitic knobs and explosion-pits on the flanks of the somma, besides the ruins of volcanic bodies underlying the northwestern skirt of the somma. According to S. Tsuboi[61], who studied the volcano in detail, this volcano came into being at a late date, probably late Diluvium. The central cone, Mihara-yama, seems to have been continuously active for many centuries, the activities culminating, whenever they did so, in spasmodic eruptions of a rather minor explosive character. Its earliest recorded eruption dates back to 684 A.D. Of its many subsequent eruptions, that in 1777～1778 poured out tremendous lava-flows (An'ei lavas), one of which reached the sea on the east. In the last period of eruption, which lasted for three years from 1912, newly erupted lava (Meidi-Taisyo lava) filled the

---

59) C. Bacher, *loc. cit.*, mentions two specimens representing the 1874 lava: the one being olivine-bearing feldspar-basalt and the other a "hypersthene-basalt transitional to hypersthene-andesite". So far as the writer's observations go, no part of the lava is represented by the latter rock-type.

60) S. Kozu, *Bull. Volc. Soc., Japan*, **1** (1932), .

61) S. Tsuboi, *Jour. Col. Sci., Imp. Univ. Tokyo*, *Art.* 6, **43** (1920), 139.

crater of the central cone to only a short distance below the lowest part of its rim. Its activity today is confined to the pit-crater (about 250 m across and 350 m deep as measured in May, 1933) situated in the center of the old summit-crater, with incandescent lava in its bottom. Occasionally sharp staccato sounds like those of a pistol discharged in the open air are heard at intervals of a few minutes, accompanying emissions of whitish vapor-clouds mixed with small quantities of magma-ash.

The rock of the volcano are exclusively basaltic. Tsuboi divided them into three main types: basalt, basaltic bandaite, and miharaite.

Table XXXII. Constituent Minerals of O-sima Basalts.

		1	2	3
Porphyritic Minerals	Plagioclase	$n_1=1{\cdot}5780\sim1{\cdot}5747$ 96~89 An	$n_1=1{\cdot}5776\sim1{\cdot}5740$ 95~88 An	$n_1=1{\cdot}5780\sim1{\cdot}5740$ 96~88 An
	Hypersthene	$2V(-)\doteqdot74^\circ$	——	$2V(-)=73^\circ$ $n_1=1{\cdot}6927$ $n_2=1{\cdot}7000$ $En_{66}Fs_{34}$
	Augite	$2V(-)\doteqdot\overset{\text{core}}{49^\circ}-\overset{\text{margin}}{30^\circ}$	——	$n_1=1{\cdot}6927$ (very rare)
	Olivine	$2V\doteqdot\overset{\text{core}}{88^\circ(+)}-\overset{\text{margin}}{86(-)}$	——	——
Groundmass	Plagioclase	$n_1=1{\cdot}5695$ 79 An	$n_1=1{\cdot}5675$ 75 An	$n_1=1{\cdot}568\sim1{\cdot}571$ 76~82 An
	Pyroxene	Pigeonite $2V=0^\circ$ $\beta=1{\cdot}7078$ $Wo_{10}En_{38}Fs_{52}$	Pigeonite $2V(+)=30^\circ\sim10^\circ$ $\beta=1{\cdot}707$ (mean) $Wo_{12}En_{39}Fs_{19}$ $\left.\begin{array}{l}\text{Augite}\\ \text{Hypersthene}\end{array}\right\}$ microphenocrysts	Pigeonite $2V(+)=30^\circ\sim0^\circ$ $\beta=1{\cdot}7067$ (mean) $Wo_{12}En_{38}Fs_{50}$
	Accessory and interstitial materials	Magnetite Cristobalite Glass absent	Magnetite Glass	Magnetite Glass

1. "Basaltic bandaite" (Tsuboi's fourth type of the somma lava). Dark-gray, vesicular, and slightly porphyritic with a few plagioclase and olivine phenocrysts. Locality: Lava-cascade exposed on the road from Motomura to the summit, about 250 m above the sea.
2. "Miharaite" (lava of 1778). Dark-gray, vesicular, and slightly porphyritic with a few phenocrysts of plagioclase. Locality: Lava-field on the northern foot of the central cone, Mihara-yama.
3. "Miharaite" (lava of 1912~14). Black, vesicular, and porphyritic with moderate phenocrysts of plagioclase. Locality: Northern lava-field within the crater of the central cone, Mihara-yama.

Table XXXIII. Analyses of Rocks from O-sima.

		I. Iwasaki, analyst.					Imp. Geol. Surv. analyst.	
		No. 90	No. 91	No. 92	No. 93	No. 94	No. 95	No. 96
SiO_2		48·02	51·25	51·23	52·45	52·53	51·45	53·01
Al_2O_3		20·48	14·73	15·24	13·48	15·25	16·84	14·73
Fe_2O_3		2·13	3·82	4·18	4·60	2·69	1·49	3·38
FeO		7·05	10·22	8·99	10·02	10·57	10·95	9·42
MgO		5·79	5·47	4·85	4·78	4·54	4·48	4·97
CaO		14·14	11·73	11·14	10·23	10·76	10·71	9·09
Na_2O		1·28	1·85	2·19	1·99	1·89	1·23	2·09
K_2O		0·30	0·26	0·54	0·52	0·43	0·37	0·44
H_2O +		n.d.	n.d.	n.d.	n.d.	n.d.	0·72	1·22
TiO_2		0·78	0·81	0·83	1·39	0·74	1·27	1·03
P_2O_5		0·01	0·13	0·03	0·33	0·41	0·26	0·11
MnO		0·26	0·28	0·33	0·31	0·24	0·19	0·34
Total		100·363(a)	100·708(b)	99·68(c)	100·319(d)	100·157(e)	99·96	99·87(f)
Q		0·24	5·41	5·35	9·61	7·87	8·83	9·61
Or		1·67	1·67	3·34	3·34	2·78	2·23	2·78
Ab		11·01	15·73	18·35	16·78	15·73	10·49	17·83
An		49·23	30·88	30·04	26·15	31·99	39·22	29·21
Wo		8·71	11·03	10·57	9·41	7·78	4·99	6·24
En		14·46	13·65	12·05	11·95	11·34	11·14	12·35
Fs		10·42	14·77	12·01	12·80	16·36	17·14	13·46
Mt		3·01	5·56	6·02	6·71	3·91	2·08	4·86
Il		1·52	1·52	1·52	2·58	1·37	2·43	1·97
Ap		tr.	0·33	tr.	0·65	0·99	0·65	0·33
QFM	Q	tr.	5	5	10	8	9	10
	F	62	48	52	46	50	52	51
	M	38	47	43	44	42	39	39
NF	Or	3	3	6	7	6	4	6
	Ab	18	33	35	36	31	20	36
	An	79	64	59	57	63	76	58
NPl	An	82	66	62	61	67	79	62
NPy	Wo	26	28	31	28	22	15	20
	En	43	35	35	35	32	33	38
	Fs	31	37	34	37	46	52	42
Fe		61	71	72	75	74	73	71

(a) includes $(CeY)_2O_3$ 0·003, ZrO_2 0·002, BaO 0·010, S 0·108.
(b) includes $(CeY)_2O_3$ 0·002, ZrO_2 0·005, BaO 0·014, S 0·137.
(c) includes $(CeY)_2O_3$ 0·003, ZrO_2 0·002, BaO 0·025, S 0·100.
(d) includes $(CeY)_2O_3$ 0·003, ZrO_2 0·004, BaO 0·030, S 0·182.
(e) includes $(CeY)_2O_3$ 0·004, ZrO_2 0·002, BaO 0·023, S 0·078.
(f) includes ZrO_2 0·04.

No. 90. *Hypersthene-bearing olivine-basalt* (old lava of O-sima, I). Phenocrysts: anorthite-bytownite, olivine, and hypersthene. Groundmass: plagioclase, pigeonite (2V(+)=40°∼0°), magnetite, and cristobalite. Locality: sea-cliff immediately west of Okada, O-sima.

No. 91. *Aphyric basalt* (old lava of O-sima, II). Phenocrysts (very few): plagioclase and olivine. Groundmass: plagioclase, monoclinic pyroxene (2V (−)=45° or smaller), magnetite, and cristobalite. Locality: sea-cliff immediately west of Okada, O-sima.

No. 92. *Hypersthene-bearing olivine-basalt* (somma lava of O-sima). Phenocrysts: plagioclase, olivine, and hypersthene. Groundmass: plagioclase, pigeonite (2V(+)=30°∼0°), magnetite, ilmenite, tridymite, and calcite. Locality: southwestern part of the ring-wall of the somma, O-sima.

No. 93. *Hypersthene-bearing basalt* (Mihara-yama lava, I—An′ei lava). Phenocrysts: plagioclase and hypersthene. Groundmass: plagioclase, pigeonite (2V(+)=30°∼0°), magnetite, and cristobalite (tridymite?), with brownish glass. Locality: northern foot of Mihara-yama, O-sima.

No. 94. *Basalt* (Mihara-yama lava, II—Meidi-Taisyo lava. Phenocrysts: plagioclase. Groundmass: plagioclase, pigeonite (2V(+)=30°∼0°), and magnetite, with brownish glass. Locality: northwestern part of the floor of the old summit-crater of Mihara-yama, O-sima.

No. 95. *Miharaite*. Average of four analyses of the lavas of 1912∼14.

No. 96. *Basaltic bandaite almost free from phenocrysts of mafic minerals* (the first type of the somma lavas). Locality: southern coast east of Sasikidi, O-sima.

The petrographic characters of these rocks are described by him with a petrogenic discussion. A few additional data obtained by the writer are given in Table XXXII.

The chemical composition of the O-sima rocks may be seen from the seven analyses shown in Table XXXIII, of which two (Nos. 95, 96) are referred to by Tsuboi and the remainder by Iwasaki(62). Besides these, are analyses of the lavas of 1912–14, which however are not cited here, because, so far as the determinations go, they are almost duplicates of the two analyses (Nos. 94, 95) given in the above table. As will be seen from the table, all the analyses but one (No. 90) —namely, that of a hypersthene-bearing olivine-basalt from the ruins of the old volcanic bodies near Okada - are in most respects greatly alike, alumina being the most variable constituent. Although the iron-oxides show more marked differences, their total amounts are about the same in the six analyses. Iwasaki's analyses, except in the case of the basalt just mentioned, concerned specimens in which porphyritic minerals were either absent or were very few. They, together with the other two analyses (Nos. 95, 96), may therefore be regarded as representing approximately the composition of magmatic liquids. The analysis of

---

62) I. IWASAKI, *Jour. Chem. Soc., Japan*, **56** (1935), 1511.

basalt No. 90 differs considerably from the remaining ones, the former, compared with the latter, showing much higher alumina and lime and lower iron-oxides. This may be ascribed to the effect of porphyritic minerals, seeing that the basalt contains abundant phenocrysts of calcic plagioclase and olivine, both of which are either absent or are very few in the other rocks.

14. Omuro-yama Volcano Group.

Outside the boundary of the northeastern foot of the Amagi volcano, there is a group of basaltic volcanoes—the Omuro-yama volcano group—which, ramparted on the west and northwest by dissected Tertiary mountains, forms a less dissected hill-land extending to the southern part of the Ito hot-spring resort on the northeastern coast of the Idu peninsula. As already described in an earlier paper(63), this group comprises, besides the Ito scoria bed, four volcanoes: Omuro-yama, Komuro-yama, Zyobosi, and Umenoki-taira, of which Omuro-yama is the youngest and Umenoki-taira the oldest. A structural characteristic, common to these volcanoes, is that they are built up of lava-flows that had effused at an earlier stage and pyroclastics that were ejected at a later stage of their respective volcanic activities. The Omuro-yama and Komuro-yama volcanoes are much alike in structure, each representing a typical aspi-conide. Zyobosi is a plateau-like volcano, consisting of lava-flows with some overlying pyroclastics. The Umenoki-taira volcano consists of a somma and a central cone. Although the cone is composed practically of pyroclastics, the somma is built up of superposed lava-flows overlain by a thick accumulation of pyroclastics. On the southwest flank of the somma lies a parasitic volcano called Takamuro-yama, which consists of twin cinder-cones. The Ito scoria bed, which covers a wide area west of Ito-mati without forming an outstanding volcanic cone, has its own vent located about 1 km northwest of the town.

Of the four volcanoes referred to, one (Umenoki-taira) is composed of both olivine-basalt and olivine-two-pyroxene-basalt, and the others entirely of olivine-basalt. The Ito scoria bed also is composed of fragmentary products of olivine-basalt (bombs, lapilli, sand and ash).

No. 97. *Olivine-two-pyroxene-basalt.* This rock occurs as several lava-flows composing the lower parts of the Umenoki-taira volcano. Megascopically, these lavas are usually dark-gray to black, either vesicular or compact, and porphyritic with abundant phenocrysts of plagioclase, pyroxene, and olivine. They often contain like the olivine-basalt next to be described, sporadic xenocrysts of quartz, andesine, and hornblende. The following petrographic description is of a specimen that was collected from a lava-flow on the northwestern foot, near the base of the volcano (see Fig. 2).

---

(63) H. TSUYA, *Bull. Earthq. Res. Inst.*, **8** (1930), 409.

The specimen studied is dark-gray, compact, and strongly porphyritic with conspicuous phenocrysts of plagioclase, olivine, and pyroxene. Microscopically, the phenocrysts of plagioclase (1~10 mm dia.), olivine (0·2~1·0 mm dia.), hypersthene and augite (0·5~2·0 mm dia.), are thickly packed in a groundmass, which is merely interstitial relative to the phenocrysts, consisting of plagioclase laths (0·05 mm dia.), pyroxene grains (0·05 mm dia.) and magnetite granules, with interstitial cristobalite and a little dusty glass, besides some microphenocrysts of hypersthene and pigeonite.

Phenocrysts: The plagioclase occurs in two types: the larger phenocrysts are anorthite 98~94 An (n_1=1 5795~1·5770), and the smaller ones (0·5 mm dia.) anorthite-bytownite 91~87 An (n_1=1·5756~1·5736). The olivine, which is occasionally altered to iddingsite, shows a distinct zoning, with 2V(−)=88° in the core and 2V(−)=84° at the margin. β=1·706 (mean). Composition: $Fo_{67}Fa_{33}$. The hypersthene is very faintly zoned, its optic angle varying from 2V(−)=78° in the core to 2V)−)=76° at the margin. n_1=1·6892~1·6932. Average composition: $En_{67}Fs_{33}$. The mineral, which carries inclusions of olivine, is almost always surrounded by a thin rim of augite ($c \wedge Z$=47°). The augite also is faintly zoned, its optic angle varying from 2V(+)=53° in the core to 2V(+)=43° at the margin. n_1=16938−1·700. Average composition: $Wo_{30}En_{43}Fs_{27}$.

Groundmass: The plagioclase is bytownite 75 An (n =1·528). The hypersthene microphenocrysts (n_1=1·6983, $En_{64}Fs_{36}$) is always surrounded by pigeonite (2V(+)=43°~41°) in parallel intergrowth. The pigeonite occurs as minute prisms, besides as microphenocrysts. The cristobalite, together with the dusty glass base, fills the interstices of the other minerals in the groundmass.

This rock was chemically analyzed by Tanaka, with results as shown in column No. 97 of Table XXXIV. The analysis differs from that of the olivine-basalt next to be described in its lower silica and alkalies, and higher alumina, lime, magnesia, and iron-oxides. The nearest approach to it is found in the analyses of some porphyritic

Table XXXIV. Analyses of the Basalts from the Omuro-yama Volcano Group. S. Tanaka, analyst.

	No. 97	No. 98	Norms						
				No. 97	No. 98			No. 97	No. 98
SiO_2	50·17	56·03	Q	4·62	9·85	QFM	Q	5	10
Al_2O_3	19·30	17·90	Or	1·11	5·01		F	60	63
Fe_2O_3	2·60	1·69	Ab	14·68	24·12		M	35	27
FeO	8·52	6·16	An	44·23	33·66	NF	Or	2	8
MgO	5·60	4·33	Wo	2·91	2·55		Ab	24	38
CaO	10·30	8·40	En	13·96	10·74		An	73	54
Na_2O	1·72	2·83	Fs	12·66	8·97	NPl	An	75	58
K_2O	0·15	0·83	Mt	3·70	2.55	NPy	Wo	10	11
H_2O +	0·87	0·60	Il	1·37	1·37		En	47	48
H_2O −	0·42	0·27	Ap	tr.	0·65		Fs	43	41
TiO_2	0·73	0·74				Fe		66	64
P_2O_5	0·05	0·22							
MnO	0·16	0·11							
Total	100·60	100·11							

lavas from the Usami and Taga volcanoes adjoining the northern part of the present volcano group.

No. 98. *Olivine-basalt.* In their important petrographic characters, the olivine-basalts of the group are much alike, although megascopically they vary from vesicular to compact, and from dark-gray to black. They are almost aphyric with very few, or usually with no, megascopic phenocrysts. Almost all of them, except the olivine-basalt composing the Ito scoria bed, carry sporadic xenocrysts, either megascopic or microscopic, of quartz and andesine, probably derived from a hornblende-dacite, the presence of which at the base of the volcano group is inferred from the fact that blocks of this rock are frequently met with in the pyroclastics of the Umenoki-taira volcano. A specimen that was collected from a lava-flow on the east side of the Komuro-yama volcano, and which represents this rock-type will next be described.

Megascopically, the rock is black, more or less vesicular, containing a few conspicuous crystals of plagioclase and quartz, with less conspicuous ones of olivine. Microscopically, we find phenocrysts of plagioclase (1~3 mm dia.) and olivine (1~2 mm dia.), with quartz (0·5~1·0 mm dia.), scattered through a groundmass consisting of plagioclase laths (0·05~0·1 mm long), pyroxene prisms (0·05~0·1 mm long), magnetite granules, and interstitial pale-brown glass, besides microphenocrysts of plagioclase (0·3~0·5 mm dia.), olivine (0·1~0·3 mm dia.), augite (0·1~0·2 mm dia.), and hypersthene (0·1~0·5 mm long).

Phenocrysts: The plagioclase, which occurs sporadically as faintly zoned euhedral phenocrysts, is anorthite varying in composition from anorthite to calcic bytownite 99~90 An ($n_1=1{\cdot}5799\sim1{\cdot}5755$). The olivine has the composition $Fo_{77}Fa_{23}$, as identified from $2V(-)=89°$ and $\beta=1{\cdot}6693$. Besides these phenocrysts, we find a few xenocrysts of andesine 46 An ($n_1=1{\cdot}5518$) and quartz. The quartz, which is either round or indented with inlets of the groundmass, has a corona consisting of a granular aggregate of the groundmass augite.

Groundmass: The plagioclase is bytownite 76 An ($n_1=1{\cdot}568$). The augite shows undulatory extinction, with $2V(+)=46°$, $n_1=1{\cdot}700$, and $c\wedge Z=45°$. Composition: $Wo_{27}En_{42}Fs_{31}$. The hypersthene, which is surrounded with a thin rim of monoclinic pyroxene, shows a very faint zoning, with $2V(-)=75°$ in the core and $2V(-)=69°$ at the margin. The olivine is identical with the phenocrystic one.

The results of Tanaka's analysis of this rock are given in column No. 98 of Table XXXIV. D. Sato[64] speaks of an analysis of "pyroxene-andesite" from the Komuro-yama volcano. Regard its silica content, the new analysis, like Sato's one, may be referred to as andesite rather than normal basalt. The norm thus shows considerable quartz, the normative plagioclase and pyroxene having the compositions respectively of 58 An and $Wo_{11}En_{48}Fs_{11}$. Compared with the new, the old analysis is still higher in silica with more abundant normative quartz, although the normative plagioclase and pyroxene, which are respectively 59 An and $Wo_{14}En_{11}Fs_{45}$, closely approach those of the former. The high silica contents of the analyses, both new and old, may be due, partly at any rate, to the presence of quartz xenocrysts in the basalt.

15. Huzi-san Volcano.

Huzi-san, situated near the shore of Suruga Bay, is a large conical volcano, 3776 m above the sea, measuring 50 km across the base, with gracefully curving slopes diminishing from 34° near the summit to 25°

---

[64] D. SATO, Ganseki-tisitugaku (Textbook of Petrological Geology). Tokyo, (1925), 339.

~17° in the middle to almost level at the base. Of the geology and petrology of this volcano, full details are expected to be published shortly when the investigation now being made of them is completed; an investigation in which the writer has been engaged alone, since July 1935 under the auspieces of the Nippon Gakuzyutu-sinkokwai. A brief summary, however, of the results already found[65], together with some additional remarks, will be given here.

As the volcano is still in the earlier stages of dissection, its lower bulk is inaccessible to observation. So far as the visible parts are concerned, however, the volcano is composed of many superposed lava-flows, mostly a few meters thick, with intercalations of pyroclastic beds. Most of the lava-flows end abruptly, forming a series of lava-coulee, the length of each successive flow being shorter with diminishing distance from the summit crater. In volume, the lava-flows as a whole appear to exceed the pyroclastic beds. It should be remembered, however, that the core of the volcano may be composed for the most part of pyroclastic material, seeing that underneath the lowest visible lavas (Hirabayashi's Misima-Omiya lavas[66]) that form the lower slopes of the southern half of the volcano, there lie in places thick mud-flow deposits.

On the outer slopes of the volcano are a number of bare lava-flows not covered by any pyroclastic ejecta. Most of these flows, except those on the upper slopes near the summit, originated either in parasitic cones or in flank openings. Of these recent flows, the Aokiga-hara lava which, in 864 A. D., poured out of the boccas on the northwest flank (Koori-ike and Hakudai-ryuo), about 1500 m above the sea, and flowed down toward the northwestern foot, is the most conspicuous, covering as it does an area of about 32 sq. km with an average thickness of more than 10 m. Another lava, which probably dates from the same time as the Aokiga-hara lava, is the "Ken-marubi" lava that poured out of the northwest flank and descended northeastward near the town of Yosida.

Most of the parasitic cones and flank vents, of which there are more than forty in all, occur halfway down the slopes of the main volcano. There are no such parasitic bodies on the upper slopes near the summit, the Hoei explosion-crater of the last eruption in 1707 on the southeast slope being the highest, lying about 1000 m below the summit. Many of the parasitic cones are probably arranged either con-

---

65) H. Tsuya, *Bull. Earthq. Res. Inst.*, **13** (1935), 645; *Bull. Volc. Soc., Japan*, **2** (1935), 149.

66) T. Hirabayashi, *Rep. Earthq. Inv. Com.*, **24** (1899).

centrically or spirally with the summit crater as the centre[67], while many others are aligned in a zone which, running NW.-SE. through the summit and coinciding with the Huzi volcanic zone, represents in all probability the principal fracture in the ground beneath the volcano. The parasitic cones on the lower slopes are generally larger than those on the upper slopes, mainly because material ejected through vents on the gentler lower slopes fall within a smaller area than if they had been thrown out from greater heights.

Although the inner structure of the parasitic cones is rarely exposed to view, most of them may be known at once from their morphological features. There are, however, a number of knobs which, morphologically and structurally, differ considerably from the parasitic cones. Of these knobs, the two that deserve special mention are Hoei-zan and Komitake, lying respectively on the SE. and N. flanks of the volcano.

Hoei-zan, situated about 1000 m below the summit, is a prominent shoulder forming the south wall of the Hoei explosion-crater. The projection is an obtuse-angled ridge, without any trace of a former parasitic cone. The inner side of the ridge slopes about 35° toward the bottom of the Hoei crater, while the outer side (southeastern side) is bounded by steep cliffs overlooking the lower SE. slope of the volcano. Although the ridge is thinly covered by the Hoei ejecta (bombs, lapilli, accessory lava-blocks, and accidental ejecta of both volcanic and sedimentary rocks), its main, lower mass is composed of loosely-coherent beds of yellowish ash and sandy breccia carrying a few blocks of a black, scoriaceous lava. These beds, which are discordantly overlain by the structureless accumulation of the Hoei ejecta, show evident stratification, and are traversed by numerous minor faults mostly striking NE.-SW. and less so N.-S. The ridge is thus divided into several minor blocks, the steep cliffs of its outer side being fault-scarps. The dips of the beds differ with the block, although within the block itself it is quite regular. They vary from 40° to 20°, with an E., W., SW., or SE. direction. Thus the beds do not dip away from the summit of Huzi, nor from the Hoei crater. Neither lava-flows nor intrusive bodies of any sort have been found in the beds. S. Kambara's hypothesis[68] is that the ridge is an upturned block that detached itself from the northern wall of the Hoei crater on the occasion of the Hoei explosion in 1707. Nowhere on the wall do we see similar beds, the wall being

---

67) S. FUJIWARA, *Proc. Fifth Pan-Pacific Sci. Congr.*, Victoria and Vancouver, B. C., Canada (1933).

68) S. KAMBARA, *Jour. Geogr., Geogr. Soc. Tokyo*, **47** (1934).

composed entirely of alternating strata of lava-flows and pyroclastic beds that came from the summit crater, besides numerous dikes that traverse the strata. It is probable that the Hoei-zan beds are much older than any that are exposed in the Hoei crater or on the outer slopes in its vicinity. Evidently one is dealing here with an older volcanic body that had largely, if not wholly, been demolished by block-faulting and much erosion before the explosion of 1707 opened the Hoei crater on the northwest side of that body. It is suggested that the Hoei-zan ridge is what remains of a former parasitic cinder-cone of comparatively early date lying on a former slope of the main volcano, which last is now buried deep, although definite evidence in support of this suggestion is yet lacking.

Komitake, stuated about 1500 m below the summit, is a deeply dissected knob projecting above the northern slope of the volcano. The knob, which is discordantly overlain by younger ejecta from the summit crater, is composed of several lava-flows, besides pyroclastic beds interposed between them. The strata of these lava-flows and pyroclastic beds that are exposed in the deep ravines on the northern side of the knob show a steep northward dip (about 35°) that coincides with the surface slope on that side. Petrographically, the lava-flows are quite identical with some of the oldest lava-flows that are exposed on the lower slopes of the southern half of the volcano. In view of these facts, it seems reasonable to infer that the knob is a remain of an older volcano—Komitake volcano—which had been badly dissected before the present cone of Huzi was formed. The volcanism of Huzi may therefore be divided broadly into two periods—earlier activities of the Komitake volcano and later activities of the present Huzi volcano—interposed by a dormant period, during which period the Komitake volcano was subjected to deep erosion. Kambara believes that Komitake and another, Kohuzi, on the east slope, are ruins of the rim of an ancient somma volcano that may underlie the top part of the present cone of Huzi.

The terrane through which the lavas of Huzi have been erupted is a depression in the Tertiary (lower Miocene) mountains that lies at the northern extremity of the fault trough represented by Suruga Bay. The bedrock underneath the volcano are thus continuations of the Tertiary rocks (Misaka series) that bound the volcano on the east, north, and west. That Huzi is younger than the neighbouring volcanoes, Asitaka and Hakone, is evident from the fact that some of the earliest visible lavas of Huzi flow southeastward into the intervale, Kise-gawa valley, between Asitaka and Hakone (see Fig. 5). So far as fhe visible parts are concerned, therefore, it is inferred that Huzi began its activity at a late date, probably later than the uppermost Pleistocene. During historical times, there were at least fifteen outbursts from Huzi, the earliest and the last ones being the eruptions of 781 and 1707 respectively. At present the volcano is entirely dormant, although there is a feeble fumarole (77° ~ 85°C. in August, 1935) in the rocks on the eastern rim of the summit crater.

The rocks composing the volcano are mostly olivine-bytownite-basalts with or without phenocrysts of pyroxenes. Six basalts from the volcano, the petrography of which was already published in the earlier papers, have the mineral compositions as shown in Table XXXV. Their chemical compositions are contained in Table XXXVI, where they are accompanied by three yet unpublished analyses of rocks from the volcano. From the table it will be seen that the Huzi basalts are generally slightly richer in potash than any of the basalts from the Idu region, the former bearing a closer resemblance to the "plateau basalt" (Deccan basalt, Oregonian basalt, etc.) than to the latter. It

Table XXXV. Constituent Minerals of Huzi Basalts.

		No. 101	No. 102	No. 103	No. 104	No. 105	No. 106
Porphyritic Minerals	Plagio-clase	$n_1=1.5663$ 73 An	$n_1=1{\cdot}5776$ $n_1=1{\cdot}5710$ 95 An, 84 An	$n_1=1{\cdot}5676$ 75 An	$n_1=1{\cdot}5660$ 72 An	$n_1=1{\cdot}5744$ $n_1=1{\cdot}5717$ 95 An, 83 An	$n_1=1{\cdot}5655$ 71 An
	Augite	——	$n_1=1{\cdot}6967$	$2V(+)=52^\circ$ $n_1=1{\cdot}6956$	n.d.	n.d.	$n_1=1{\cdot}6979$
	Hyper-sthene	——	$n_1=1{\cdot}6987$ $n_2=1{\cdot}7077$ $En_{60}Fs_{40}$	——	$n_1=1{\cdot}6983$ $n_2=1{\cdot}7078$ $2V(-)=71^\circ$ $En_{61}Fs_{39}$	——	$n_1=1{\cdot}6983$ $n_2=1{\cdot}7076$ $2V(-)=71^\circ$ $En_{61}Fs_{39}$
	Olivine	$2V(-)\doteqdot 89^\circ$ $\sim 84^\circ$	$2V(-)=85^\circ$ $\alpha=1{\cdot}6794$ $\beta=1{\cdot}6985$ $Fo_{69}Fa_{20}$	$2V=90^\circ$ $\alpha=1{\cdot}6667$ $\beta=1{\cdot}6843$ $Fo_{80}Fa_{20}$	$2V\doteqdot 90^\circ$	$2V(-)=84^\circ$ $\alpha=1{\cdot}6788$ $\beta=1{\cdot}7002$ $Fo_{67}Fa_{33}$	$2V\doteqdot 90^\circ\sim$ $86^\circ(-)$
Groundmass	Plagio-clase	$n_1=1{\cdot}5630$ 67 An	$n_1=1{\cdot}5670$ 74 An	$n_1=1{\cdot}5654$ 71 An	n.d.	$n_1=1{\cdot}5695$ 78 An	n.d.
	Olivine	n.d.	——	n.d.	——	——	——
	Pyroxene	$2V(+)\doteqdot 52^\circ$ $\sim 46^\circ$	$2V(+)\doteqdot 51^\circ$ $\sim 41^\circ$	$2V(+)\doteqdot 49^\circ$	n.d.	——	$2V(+)\doteqdot 40^\circ$
	Accessory and inter-stitial materials	Magnetite Glass	Magnetite Glass	Magnetite Glass	Magnetite Glass	Dark-brown glass packed with dust material.	Magnetite Glass

Table XXXVI. Analyses of Rocks from Huzi.

S. Tanaka, analyst.

		No. 99	No. 100	No. 101	No. 102	No. 103	No. 104	No. 105	No. 106	No. 107
SiO_2		49·60	49·60	50·28	50·64	50·66	51·05	51·09	51·30	63·84
Al_2O_3		16·96	16·14	18·30	18·58	18·25	18·35	17·62	18·74	15·82
Fe_2O_3		5·40	3·67	4·50	3·04	4·78	2·76	2·64	1·83	0·95
FeO		6·65	9·90	6·89	7·29	5·72	7·72	8·42	8·34	5·02
MgO		5·92	4·79	3·80	5·58	4·94	4·63	5·09	4·80	1·67
CaO		10·03	8·80	9·76	10·00	9·98	9·90	9·68	9·76	4·88
Na_2O		2·48	2·90	2·87	2·64	2·78	2·81	2·80	2·55	3·88
K_2O		0·58	0·93	0·94	0·61	0·77	0·81	0·76	0·71	2·12
H_2O +		0·50	0·55	0·20	0·20	0·38	0·40	0·28	0·22	0·45
H_2O −		0·12	0·14	0 08	0·06	0·13	0·11	0·06	0·06	—
TiO_2		1·40	1·97	1·78	1·15	1·38	1·41	1·38	1·43	0·87
P_2O_5		0·20	0·31	0·34	0·16	0·25	0·24	0·26	0·29	0·22
MnO		0·21	0·23	0·20	0·17	0·17	0·18	0·21	0·28	0·17
Total		100·05	99·93	99·94	100·12	100·19	100·37	100·29	100·31	99·89
Q		3·78	1·26	3·96	1·98	4·14	2·34	2·04	2·82	18·14
Or		3·34	5·57	5·57	3·34	4·45	5·01	4·45	4·45	12·80
Ab		20·97	24·64	24·14	22·55	23·59	23·59	23·59	21·50	33·03
An		33·38	28·09	34·49	36·99	35·05	35·05	33·38	37·55	19·19
Wo		6·50	5·69	5·11	4·88	5·34	5·23	5·46	3·83	1·28
En		14·76	11·95	9·43	13·85	12·34	11·54	12·65	11·95	4·11
Fs		5·80	12·27	6·47	9·24	4·62	9·89	11·35	12·01	7·25
Mt		7·87	5·33	6·48	4·40	6·95	3 94	3·94	2·55	1·39
Il		2·73	3·79	3·34	2·12	2·58	2·73	2·58	2·73	1·67
Ap		0·33	0·65	0·65	0·33	0·65	0·65	0·65	0·65	0·65
QFM	Q	4	1	4	2	4	2	2	3	18
	F	58	59	64	63	63	64	61	64	65
	M	38	40	32	35	33	34	37	33	17
NF	Or	6	10	9	5	7	8	7	7	20
	Ab	36	42	38	36	37	37	38	34	51
	An	58	48	53	59	56	55	55	59	29
NPl	An	61	53	59	62	60	60	59	64	37
NPy	Wo	24	19	24	17	24	19	18	14	10
	En	55	40	45	50	56	44	49	49	33
	Fs	21	41	31	33	20	37	33	37	57
Fe		66	73	74	64	67	69	68	68	78

No. 99. *Olivine-basalt* (almost aphyric). One of the lava-flows exposed on the western wall of the Hoei explosion-crater, Huzi.

No. 100. *Olivine-basalt* (almost aphyric). Lava-flow at Tawarano-taki (water-fall , Toka-itiba.

No. 101. *Olivine-basalt*, F$_{67\text{-}a}$.
No. 102. *Two-pyroxene-bearing olivine-basalt*, F$_{67\text{-}b}$.
No. 103. *Augite-bearing olivine-basalt*, F$_{67\text{-}d}$.
No. 104. *Hypersthene-augite-olivine-basalt*, F$_{67\text{-}e}$.
Lava-flows at Makuiwa on the SE. slope of Huzi.
No. 105. *Augite-bearing olivine basalt*. Scoriaceous lava-block, one of the ejecta of 1707 explosion of the Hoei crater.
No. 106. *Two-pyroxene-olivine-basalt*. Aokiga-hara lava of 864 eruption, NW. foot of Huzi.
No. 107. *Aphanitic andesite* (pitchstone). Karasuisi lava at Nagamine on the SE. slope.

is worth noting that, although the Huzi rocks are mostly basalts, a few of them are evidently andesitic. Analysis No. 107 shows the composition of one of these andesitic rocks. The specimen analyzed was collected at Nagamine, a short distance down the southwest slope of Hoei-zan, where it occurs in an agglomerate bed and is also found scattered here and there. Although not a single massive lava-flow of the rock has been found, the rock is evidently juvenile, and comparable with Hirabayashi's "Karasuisi lava". Megascopically, it is pitch-black and densely aphanitic. Microscopically, it is composed wholly of dark-brownish glass densely packed with minute microlites. The analysis shows that, like the basalts, the andesite is richer in potash than any andesite with corresponding silica content from the Idu region.

C. *Dacitic and Liparitic Volcanoes*.

Dacitic and liparitic rocks play but a very subordinate part among the Quaternary volcanics of the region under consideration. It has already been mentioned that the Simo-Tanna beds in north Idu contain, besides basaltic pyroclastics, a quantity of pyroxene-hornblende-dacitic pumice which may be correlated, both petrographically and stratigraphically, with similar pumice from the Tutizawa beds in the Oiso geologic province. The pumice therefore suggests the former existence of one or more lower Pleistocene dacitic volcanoes that yielded it, although, so far as the observations in north Idu go, there is no sign of such a volcano to which the pumice can be traced. Dacites occur in parasitic domes on the Amagi volcano, Iwano-yama and Yahadu-yama being the representative ones. Reference has also been made to the fact that, according to Kuno, the Hakone volcano has some dacitic masses, of which the Maku-yama dome (Kuno's Quellkuppe) is the most striking. In addition to the foregoing, we find several dacitic masses in the vicinity of Atami (pyroxene-dacite of Hikane-yama, pyroxene-hornblende-dacite of Idusan and Kami-Taga), which, according to Kuno, extruded later than the products of the Taga volcano, but earlier than those of the Yugawara volcano. The limited spread and volume of every one of these masses suggest that they are nothing but local lavas, possibly representing domical protrusions, although none of them retain the original form that we associate with dome-shaped volcanoes.

The above-mentioned masses comprise all the Quaternary dacitic volcanoes, recognized so far in the Idu peninsula. Leaving aside for a while these masses, we have now to refer more particularly to the Quaternary liparitic volcanoes, Nii-sima group, in the Seven Idu Islands, which in many respects are undoubtedly the most important group in the acidic suite of the Quaternary volcanic rocks in the region studied.

16. Nii-sima Group.

The Nii-sima group consists of three main islands, Nii-sima, Sikine-sima, and Kodu-sima, besides several dependent islets which, being aligned NE.-SW. off the southern point of the Idu peninsula, form a short but distinct volcanic chain, called by B. Koto the Kodu-sima Volcanic Chain.[69] The volcanism of this group has already been discussed in an earlier paper[70], with special reference to the geology and petrology of Kodu-sima, which leaves little to added here. It seems desirable, however, for the sake of completeness, to give a brief summary of the structure and the rock sequence of this group.

Nii-sima consists of several liparitic masses (lava-dome, lava-mesa, pumice-cone, and pumiceous ejecta bed), of which the Muko-yama double volcano (central lava-dome, Muko-yama, and outer pumice-cone, Omine)[71] in the southern part of the island and the Miyatuka-yama lava-dome, slightly north of the central part, are the most striking. The rocks constituting these masses are grouped under three main headings—pyroxene-plagioliparite, hornblende-plagioliparite, and biotite-plagioliparite—in order of eruption.[72] Biotite-plagioliparite forms both the Muko-yama and Miyatuka-yama volcanoes, besides a number of relatively younger masses in the island, while the rocks of the remaining two types occur in older, local masses, most of which are overlain by one or more masses of biotite-plagioliparite. Besides these liparites, in the northernmost part of the island, we find basaltic scoria and ash piled up in beds, 10 m or more in thickness, covering oldest pyroxene-plagioliparite mass (Fukuchi's Nebu-saki type), and forming the coastal terrace that borders the mass on the west on the coast of Wakago village. In the island itself there is no sign of a volcanic centre to which the basaltic ejecta can be traced. I. Friedlaender[73] inferred that they came from the ruined volcano Utone-sima lying 3 km off the northern point of the island. But, as may be seen on the coast of Wakago, the basaltic ejecta bed thickens toward the south, and the fragments in the bed increase their sizes in the same direction. Although, petrographically, the ejecta closely resemble the basalt of Utone-sima, it is unlikely that the former came from the vent of the latter. The ejecta could only have come from a vent lying somewhere south, and while this obviously does not prove that the source is in Nii-sima itself, it is not impossible that the basaltic ejecta were erupted by a volcano that subsequently broke up to form the base of some younger liparitic masses bordering the ejecta bed on the south.

---

[69] B. Koto, *Jour. Fac. Sci., Imp. Univ. Tokyo*, **3** (1929~34), 205.

[70] H. Tsuya, *Bull. Earthq. Res. Inst.*, **7** (1929), 269.

[71] T. Tsujimura, *Rep. Earthq. Inv. Com.*, **89** (1918).

[72] N. Fukuchi, *ibid.*, **39** (1902).

Sikine-sima, situated immediately south of Nii-sima, and which was once in land-connection with the latter, is nothing but a single lava-plateau of biotite-plagioliparite.

Kodu-sima consists, like Nii-sima, of several liparitic masses, of which the Tenzyo-san lava-dome in the centre of the island is the youngest as well as the largest. The structural scheme, together with the rock-types represented may be summarized as follows:

1. Lavas forming the lowest visible part of Kodu-sima (the first period lavas)	Potash-liparite. Hypersthene-plagioliparite. Hornblende-bearing hypersthene-plagioliparite. Hornblende-plagioliparite. Biotite-plagioliparite. Aphanitic liparite.	
2. Titibu-yama ejecta bed	Biotite-plagioliparite (juvenile pumice).	
	Liparite Quartz-porphyry Porphyritic hornblende-diorite Hornblende-andesite	Accessory or accidental ejecta.
3. Takodo-yama and Nati-san domes (the second period lavas)	Biotite-plagioliparite.	

---

[73] I. FRIEDLAENDER, *loc. cit.*

4. Zyogoro-yama, Anagi-yama, and Kobe-yama domes (the third period lavas) ... Do.
5. Sriomama ejecta bed........... Biotite-plagioliparite (juvenile ejecta).
6. Siro-sima and Kusigamine pumice cones .... Do.
7. Tenzyo-san dome (the fourth and last period lava .... Biotite-plagioliparite.

As will be seen from the foregoing, the first period of activity is represented by liparites of various types and the subsequent ones exclusively by biotite-plagioliparite. This accord generally with the sequence observed in Nii-sima.

Although within the islands of the group themselves, pre-volcanic bedrocks are nowhere exposed, there can be no doubt that the Neogene Tertiary rocks of the Idu peninsula extend southward to the sea-floor in the vicinity of the group, seeing that the Zenisu bank, situated 40 km SW. of Kodu-sima, consists of these rocks. This bank is a projected peak in the submarine ridge trending NE.-SW. upon which the Nii-sima group rests, and according to H. Niino,[74] it is headed by several stacks, besides shoals, consisting of lava and agglomerate. The specimens collected by him from these masses are exclusively of altered pyroxene-andesites that are comparable in many respects to allied rocks in the lower Miocene series of the Idu peninsula. Similar rocks were also found among the pebbles collected by dredgings made by Niino on the same bank. With these facts in view, it is inferred that similar rocks underlie the whole of the Nii-sima group. Some support is lent to this inference by the finding of not a few fragments of Tertiary volcanic rocks from the pyroclastic beds of Kodu-sima and Nii-sima. The accessory or accidental rock-fragments (quartz-porphyry, hornblende-andesite, two-pyroxene-andesite, etc.) in the Titibu-yama ejecta bed of Kodu-sima closely resemble the allied rocks in the Tertiary volcanics of the Idu peninsula. So also do some of the accessory or accidental rocks (silicified tuff, diabase, propylite, pyroxene-andesite, etc.) that are contained in the pyroclastic ejecta bed (Fukuchi's siromama bed) of Nii-sima. It is also worth noting that the potash-liparite of Kodu-sima, which occurs as a small mass underlying the Anagi-yama plagioliparite dome on the northern coast of the island, is quite similar chemically to the potash-liparite of Manzo-yama and vicinity in the southern part of the Idu peninsula.

---

[74] H. Niino, *Jour. Geogr., Geogr. Soc. Tokyo,* **47** (1935), 32.

Nothing can be said concerning the time of genesis of the liparitic volcanoes of the Nii-sima group, except that most of them appear to have been formed by subaerial eruptions during the Quaternary. In this connection we may repeat the statement that in Nii-sima the biotite-liparite masses are nowhere covered by the Quaternary basaltic ejecta, although the latter overlie the oldest pyroxene-plagioliparite mass. Further evidence for the age of the group has been supplied by the basic xenoliths found in some of the lavas from Nii-sima and Kodu-sima. The biotite-plagioliparite exposed on Awaiura (east coast of the northern part of Nii-sima) is packed with not a few basic xenoliths. So also is the hypersthene-plagioliparite that forms the southwest headland of Kodu-sima. Most of these xenoliths are basaltic, consisting of a few phenocrysts of calcic plagioclase and augite, with a groundmass of plagioclase. augite, magnetite, and interstitial glass, although the pyroxenes, both of the phenocrysts and in the groundmass, are partially transformed to greenish-brown hornblende (Table XXXVII). One of the xenoliths is, chemically, much like the basalts from Utone-sima and To-sima (Table XXXVIII). While this obviously does not prove a common source, the possibility arises that most of the xenoliths are fragments of basalts that were torn from certain Quaternary basaltic masses during the eruptions of the liparites in which they were caught.

Table XXXVII. Constituent Minerals of the Basaltic Xenoliths in Liparites from Kodu-sima and Nii-sima.

	1	2	3
Plagioclase	$n_1=1{\cdot}5615$ 63 An	$n_1=1{\cdot}5667$ 71 An	$n_1=1{\cdot}572$ 85 An (phenocrysts) $n_1=1{\cdot}552$ 46 An (groundmass)
Augite	$n_1=1{\cdot}6965$	$n_1=1{\cdot}6945$ $2V(+)=56^\circ\sim52^\circ$	Phenocrysts n.d. $n_1=1{\cdot}659$ (groundmass)
Hornblende	$n_1=1{\cdot}682$ $c\wedge Z'=7^\circ$ Greenish-brown	$n_1=1{\cdot}6725$ (mean) $c\wedge Z'=15^\circ$ Greenish-brown	$n_1=1{\cdot}713$ Reddish-brown
Accessories	Magnetite Glass	Magnetite Glass	Magnetite Glass

1, 2. Xenoliths in the hypersthene-plagioliparite, Himmasi-hana, Kodu-sima.
3. Xenolith in the biotite-plagioliparite, Awai-ura, Nii-sima.

Table XXXVIII.

		A	No. 108	No. 109
SiO_2		50·74	50·79	49·91
Al_2O_3		18·59	16·61	18·13
Fe_2O_3		9·23	6·96	3·87
FeO		1·01	3·51	5·48
MgO		5·37	7·63	6·16
CaO		10·21	10·03	9·90
Na_2O		2·35	2·58	2·33
K_2O		0·57	0·55	0·37
H_2O+		0·74	0·38	0·78
H_2O-		0·16		
TiO_2		0·98	1·01	0·87
P_2O_5		0·06	——	——
MnO		0·16	——	——
Total		100·31*	100·24**	99·80
Q		7·69	4·50	4·32
Or		3·34	3·34	2·23
Ab		19·92	32·02	19·92
An		38·38	31·99	37·83
Wo		5·11	7·43	4·76
En		13·35	18·97	15·36
Fs		——	——	5·41
Mt		0·46	8·33	5·56
Il		1·82	1·97	1·67
Ap		tr.	——	——
Hm		8·62	1·28	——
QFM	Q	8	5	4
	F	62	57	62
	M	30	38	34
NF	Or	5	6	4
	Ab	32	38	33
	An	63	55	63
NPl	An	66	59	65
NPy	Wo	28	28	19
	En	72	72	60
	Fs	——	——	21
Fe		63	56	59

* includes NaCl 0·14. ** includes CO_2 0·19.

A. Basaltic xenolith (Table XXXVII, 1) in the hypersthene-plagioliparite. Himmasi-hana, Kodusima.

No. 108. "*Olivine-bearing feldspar-basalt*". Phenocrysts: labradorite-bytownite, augite, and olivine. Groundmass: plagioclase, augite, magnetite, and olivine. Utone-sima. M. Dittrich, analyst. C. Bacher, *loc. cit.*

No. 109. *"Olivine-bearing feldspar-basalt"*. Phenocrysts: labradorite-bytownite, augite, olivine, and biotite. Groundmass: plagioclase, augite, magnetite, and glass. Lava, 100 m north of the top of Tosima. M. Dittrich, analyst. C. Bacher, *loc. cit.*

From what has been said, it is indisputable that the Nii-sima group is as young as the basaltic volcanoes (O-sima group) in the Seven Idu Islands. Both Nii-sima and Kodu-sima, according to records, have had only one eruption each, namely Nii-sima in 886 and Kodu-sima in 838. It is not certain whether these eruptions were of such a nature as to erupt new lavas in quantity sufficient to form distinct volcanic masses, but both Muko-yama in Nii-sima and Tenzyo-san in Kodu-sima have morphological features so youthful that they were probably formed by the last known eruptions. If so, the major eruptions that resulted

Table XXXIX. Constituent Minerals of the Liparites from Kodu-sima.

		No. 110	No. 111	No. 112	No. 113	No. 114
Porphyritic Minerals	Quartz	+	—	+	+	—
	Sanidine	$n_1=1{\cdot}520$	—	—	—	+
	Plagioclase	—	—	$n_1=1{\cdot}540$ 24 An	$n_1=1{\cdot}539\sim1{\cdot}544$ 23 ~ 32 An	$n_1=1{\cdot}533\sim1{\cdot}535$ 12 ~ 15 An
	Biotite	—	—	—	—	$\gamma=1{\cdot}665$ $2E=37°38'$ $\gamma>1{\cdot}700$ 2E large
	Hornblende	—	—	$2V(-)=87°\sim83°$ $n_1=1{\cdot}644$ $c\wedge Z'=11°$ Greenish-brown	—	—
	Hyper-sthene	—	—	—	$2V(-)=52°$ (core) ~ 62° (margin) $n_1=1{\cdot}7005$ (mean) $En_{59}Fs_{41}$	—
Groundmass		Sanidine Quartz Magnetite Secondary pyrite and epidote	Glass Microlites of feldspar and biotite	Glass ($n=1{\cdot}497$) Microlites of feldspar and biotite	Glass ($n=1{\cdot}497$) Microlites of feldspar and biotite	Glass ($n=1{\cdot}490$)

Table XL. Analyses of Liparites from Idu. S. Tanaka, analyst.

		No. 110	No. 111	No. 112	No. 113	No. 114	No. 115	No. 116
SiO_2		71·64	74·93	75·10	75·35	76·60	76·05	76·05
Al_2O_3		14·13	13·52	13·36	13·49	13·22	12·44	12·79
Fe_2O_3		0·34	0·76	0·30	0·95	0·27	0·84	1·47
FeO		0·50	0·72	0·74	0·55	0·43	0·22	0·31
MgO		0·08	0·32	0·27	0·36	0·19	0·17	0·08
CaO		0·17	0·93	1·43	1·61	0·75	0·87	1·60
Na_2O		0·50	4·50	4·21	4·28	4·62	4·31	3·89
K_2O		10·77	3·39	1·58	2·52	1·61	2·88	1·82
H_2O +		0·80	0·46	2·27	0·61	1·50	1·66	0·74
H_2O −		0·23	0·33	0·17	0·06	0·11	0·11	0·52
TiO_2		0·55	0·13	——	0·20	——	0·12	0·19
P_2O_5		0·08	0·08	——	——	——	tr.	tr.
MnO		tr.	0·08	0·10	0·08	0·16	0·07	0·05
Total		99·97*	100·15	99·53	100·06	99·46	99·74**	99·51
Q		27·57	33·27	40·36	36·76	41·20	37·48	42·88
Or		63·44	20·04	9·46	15·03	9·46	17·25	10·57
Ab		4·19	38·27	35·65	36·18	39·32	36·70	33·03
An		——	3·89	7·23	8·07	3·61	4·45	8·07
C		1·73	1·02	2·04	0·71	2·55	0·51	1·43
En		0·20	0·80	0·70	0·90	0·50	0·40	0·20
Fs		——	0·53	1·19	——	0·79	——	——
Mt		——	1·16	0·46	1·39	0·46	0·46	0·69
Il		1·06	0·30	——	0·46	——	0·30	0·30
Ap		0·33	0·33	——	0·33	——	tr.	tr.
Hm		0·32	——	——	——	——	0·48	0·96
QFM	Q	28	35	42	37	43	38	44
	F	70	62	55	60	55	60	53
	M	2	3	3	3	2	2	3
NF	Or	94	32	18	25	18	30	20
	Ab	6	62	68	61	75	63	64
	An	——	6	14	14	7	7	16
NPl	An	——	9	17	18	8	11	20
NPy	En	100	60	37	100	39	100	100
	Fs	——	40	63	——	61	——	——
Fe		91	81	79	80	78	85	95

* includes S 0·18. ** includes NaCl 0·47.

No. 110. *Potash-liparite.* Kaesu-hama, northerne coast of Kodu-sima.

No. 111. *Aphanitic liparite.* Ombasi-zima, 4 km southwest of Kodu-sima.

No. 112. *Hornblende-plagioliparite.* Ko-hama, southern part of Naga-hama, Kodu-sima.

No. 113. *Hypersthene-plagioliparite.* Himmasi-hana, southwestern point of Kodu-sima.

No. 114. *Biotite-plagioliparite.* Top of Tenzyo-san, Kodusima.

No. 115. *Biotite-plagioliparite.* Muko-yama, southern part of Nii-sima.

No. 116. *"Augite-hypersthene hornblende-andesine-dacite".* Kami-Taga, north Idu. H. Kuno, Bull. Volc. Soc., Japan, **3** (1936), 55.

in the Nii-sima group must surely be referred to Pleistocene and Recent.

The mineral constitution and chemical composition of the representative rock-types of Kodu-sima are shown in Table XXXIX and Table XL respectively. The three rock-types of Nii-sima are, petrographically, much like the corresponding types of Kodu-sima.

D. *Trachyandesitic Volcanoes.*

In the Volcano Islands group are two volcanoes composed of andesitic rocks instead of basalt, the rocks showing a distinct alkalic tendency as indicated by their microscopical and chemical characters. One of them is the insular volcano Io-sima (Sulphur Island) situated midway between Kita Io-sima and Minami Io-sima[75] and the other, that submarine volcano which, situated about 3 miles off the northeastern coast of Minami Io-sima, displayed violent eruptions twice (in 1905 and 1914), forming in each case an ephemeral volcanic island "Sin-to" or "Sin Io-sima" (New Sulphur Island).

17. Io-sima Volcano.

Io-sima, situated 24°47′N. and 141°18′E., or Naka Io-sima, as it is frequently called to distinguish it from Kita Io-sima and Minami Io-sima, is a gourd-shaped island measuring about 8 km NE.-SW. and 1∼5 km NW.-SE. Morphologically, the island may be divided into three parts: Moto-yama, Suribati-yama, and Tidoriga-hara. Occupying the northeastern half of the island, Moto-yama is a flat-topped, dome-shaped hill (116 m above the sea) surrounded by uplifted wave-cut terraces on all sides, except at its southwest side where it is connected by a flat (Tidoriga-hara) with Suribati-yama. Suribati-yama (Mt. Pipe), which occupies a small area in the southwestern part of the island, is a truncated conical volcano, 165 m above the sea, with a funnel-shaped crater (300 m in diameter and 100 m deep) at its summit. Tidoriga-hara, by means of which the preceding two parts are connected with each other, is a flat (40 m～100 m above the sea) veneered with drifting dune sand.

---

[75] Minami Io-sima (San Augustino Island), situated 24°14′N. and 141° 29′E., is an insular, conical volcano measuring 3 km across the visible base, with a pointed peak (926 m above the sea) and steep lateral slopes (40° or steeper) ending abruptly with precipitous sea-cliffs. As to the rocks of the volcano, our knowledge is very meagre, for the desert island has rarely been visited, and what descriptions we have of it are of the briefest.

Of the geologic structure and the rocks of the island, a brief summary of the results already found[76] will be given here. The island is formed entirely of volcanic rocks and their detritus, which may be separable from older to younger into the following seven formations: (1) Moto-yama bluff tuff and Suribati-yama bluff tuff, (3) Moto-yama intrusive rock and Suribati-yama lava, (3) Suribati-yama cone ejecta, (4) Tidoriga-hara sand bed, (5) terrace deposits, (6) dune sand, and (7) beach deposit. These formations are, geologically speaking, very recent. The Moto-yama and Suribati-yama bluff tuffs, which are the visible oldest beds of the island, show that the volcanic activity began with the submarine explosive outbursts that gave rise to these beds. From a central vent, now represented by Suribati-yama, a submarine outflow of the Suribati-yama lava followed. Almost contemporaneously with the outflow began an injection of the Moto-yama intrusive rock into the previously deposited Moto-yama tuff. The intrusion, which might have originated satellitically at moderate depth from the conduit of the Suribati-yama, rose apparently through one or a number of fissures until it reached the lower horizon of the Moto-yama tuff, where it spread laterally and upward to form a laccomorphic intrusive mass. The beginning of the extensive uplift that brought the Moto-yama tuff above the sea and changed it into a dome of much the same form as we now see, appear to date back to the time of that intrusion. By continued upwarping of the ocean-bottom, both the Moto-yama dome and the basal part (Suribati-yama tuff and Suribati-yama lava) of Suribati-yama rose above the water. But a small part between them, now represented by Tidoriga-hara, would have remained as a shallow water. The sandy material transported by the waves from the shores of Moto-yama and Suribati-yama of that time, were deposited on the shallow-sea platform as the Tidoriga-hara sand bed. It was to the time of the deposition of this bed that subaerial eruptions took place from a central vent, now represented by the Suribati-yama crater. The Suribati-yama cone ejecta are the products of these eruptions. Together with the subsequent uplift of both Moto-yama and Suribati-yama, Tidoriga-hara also emerged, the three parts having joined together into one

---

[76] H. TSUYA. *Bull. Earthq. Res. Inst.*, **14** (1936), 453; *Bull. Volc. Soc., Japan*, **3** (1936), 28.

Table XLI. Constituent Minerals of the Trachyandesites from Io-sima, Volcano Islands.

		No. 117	No. 118	A	B
Porphyritic Minerals	Plagioclase	$n_1=1{\cdot}5493$ $n_2=1{\cdot}5567$ 43 An Anorthoclase rim $2V(-)=62^{\circ}, 49^{\circ}, 46^{\circ}$	$n_1=1{\cdot}5499$ $2V(+)=83^{\circ}$ 45 An Anorthoclase rim absent	Extinction angle on $(010)=-7{\cdot}5^{\circ}$ 23 An	n (mean) $=1{\cdot}5525$ 36 An Extinction angle on $(010)=-2^{\circ}$ (core), $-8{\cdot}5^{\circ}$ (margin) 34~42 An
	Augite	$2V(+)=55^{\circ}$ (core), 48° (margin) $2V(+)=57^{\circ}, 61^{\circ}$ $n_1=1{\cdot}6974$ (core) $Wo_{40}En_{37}Fs_{23}$	$2V(+)=54{\cdot}5^{\circ}$ $n_1=1{\cdot}6970$ $Wo_{40}En_{37}Fs_{23}$	$c\wedge Z=46^{\circ}\sim48^{\circ}$ Pleochroism weak X—yellowish-gray Y=Z—yellowish-green	$n>1{\cdot}700$ $c\wedge Z=45^{\circ}$ Deep to pale green
	Olivine	$2V(-)=84^{\circ}$ $\beta=1{\cdot}7020$ $Fo_{66}Fa_{34}$	$2V(-)\doteqdot83^{\circ}$	+	n (mean) $=1{\cdot}671$ Opt. ch. negative
	Accessories	Magnetite Apatite	Magnetite Apatite	Magnetite Apatite	Magnetite
Groundmass	Anorthoclase	$\alpha=1{\cdot}5253$ $\gamma=1{\cdot}5325$ $2V(-)=71^{\circ}$ (core), 48° (margin)	Pale to dark-brown glass ($n=1{\cdot}5237\sim1{\cdot}5277$) packed with microlites of feldspar and pyroxene.	Pale-brown glass packed with microlites of monoclinic pyroxene (pale yellowish-green, maximum extinction angle $=52^{\circ}$).	Magnetite Apatite Monoclinic pyroxene Glass
	Plagioclase	$n_1=1{\cdot}5439$ $2V(-)=82^{\circ}\sim86^{\circ}$ 28 An			
	Pyroxene	Augite $2V(+)=55^{\circ}$ $n_1=1{\cdot}6997$ $c\wedge Z'=51{\cdot}5^{\circ}$ (max.) $Wo_{40}En_{36}Fs_{24}$ Acmite X—pale green Y—green Z—greenish-brown $X>Y>Z$ $2V(-)=68^{\circ}\sim73^{\circ}$ $\alpha>1{\cdot}750$ $c\wedge X$ small			
	Hornblende	$n_1=1{\cdot}6465$ $n_2=1{\cdot}6552$ Z (or Y)—reddish-brown Z (or Y) $>$ X $c\wedge Z'=21^{\circ}$ (max.)			
	Accessories	Magnetite			

A. "Olivine-pyroxene-andesite". Pumice and obsidian of 1904 eruption, "Sin-to", Volcano Islands. According to Wakimizu (*loc. cit.*), the rock contains, in addition to the minerals given under column A of the above table, a few phenocrysts of rhombic pyroxene.

B. "Olivine-bearing augite-vitroandesite". Pumice, obsidian, and lava, of 1914 eruption, "Sin Io-sima", Volcano Islands. T. Ogura, *loc. cit.*

Table XLII. Analyses of the Trachyandesites from Io-sima, Volcano Islands.

	No. 117	No. 118	No. 119			Norms		
						No. 117	No. 118	No. 119
SiO_2	58·91	59·60	60·82	Q		1·62	——	1·98
Al_2O_3	17·71	16·81	16·63	Or		23·37	24·49	25·04
Fe_2O_3	2·81	0·83	1·15	Ab		50·83	51·91	47·71
FeO	2·67	5·87	3·46	An		9·74	6·12	7·51
MgO	0·88	1·34	1·79	Wo		1·97	2·32	3·02
CaO	3·47	3·10	3·35	En		2·20	1·10	4·42
Na_2O	6·01	6·11	5·62	Fs		1·45	3·43	5·27
K_2O	3·94	4·17	4·21	Fo		——	1·55	——
H_2O +	0·34	0·25	1·84	Fa		——	4·48	——
H_2O −	0·30	0·10	(ign. l.)	Mt		4·17	1·16	1·52
TiO_2	0·82	0·86	0·45	Il		1·52	1·67	0·91
P_2O_5	0·49	0·50	0·22	Ap		0·99	1·32	0·65
MnO	0·16	0·26	0·39	QFM	Q	2	——	2
Total	100·23*	99·80	99·93		F	86	83	82
					M	12	17	16
				NF	Or	28	30	31
					Ab	61	63	59
					An	11	7	10
				NPl	An	16	11	14
				NPy	Wo	35	16	24
					En	39	22**	34
					Fs	26	62	42
				Fe		86	83	71

* includes S 1·71.

No. 117. *Olivine-augite-andesine-trachyandesite.* Suribati-yama (Mt. Pipe), Io-sima. *S.* Tanaka, analyst.

No. 118. Do. Moto-yama, Io-sima. S. Tanaka, analyst.

No. 119. "*Olivine-pyroxene-andesite.*" Pumice of 1914 eruption, "Sin Io-sima". Imp. Geol. Surv., analyst.

** includes olivine as metasilicate.

island as we see at present. The uplift of the island was not continuous, but occurred intermittently for a long period with frequent halts of the sea, during which intervals marine erosion was active on weaker rock like the Moto-yama tuff, giving to the island its present terraced feature. Such stepwise uplift will be naturally expected, it being likely that the intrusion of the Moto-yama intrusive rock occurred recurrently through a long period of volcanic activities.

There is no volcanic material that was ejected since the Suribati-yama cone ejecta had been formed, nor is there any historic record of an eruption in the island. But volcanic activity is manifested in the island even at the present day by numerous solfataras. One of these solfataras on the northwestern side of Moto-yama is said to have been culminated a few years ago in ejecting a small volume of solid material. It is also said that detonations are often heard from the sea northeast of the island.

The rocks of the island may be called trachyandesite since they are close in petrographic characters, microscopical as well as chemical, to some trachytes from the Pacific islands rather than to the common Japanese pyroxene-andesites. Thus, as will be seen from Tables XLI and XLII, the Suribati-yama lava and the Moto-yama intrusive rock are crystalline olivine-augite-andesine-trachyandesite and vitrophyric olivine-augite-andesine-trachyandesite respectively. Both the tuffs andt he Suribati-yama cone ejecta are petrographically very similar to either the Suribati-yama lava or the Moto-yama intrusive, although of diverse appearances such as pumiceous, vitreous, scoriaceous, and felsitic.

18. Sin Io-sima Volcano (a submarine volcano near Minami Io-sima).

Sin Io-sima volcano, lying about 3 miles off the NE. shore of Minami Io-sima, might have existed for untold ages, but its actual existence was ascertained for the first time on Nov. 28, 1904, when it violently erupted. These eruptions continued for more than two months, from Nov. of the year to the following January, culminating in forming a new volcanic island "Sin Io-sima" or "Sin-to". According to T. Wakimizu,[77] the new island, which was composed of pumice and obsidian, all but disappeared after 135 days of existence. Thus while in Feb., 1905, it measured about 150 m above the sea and 5 km in circumference, in June of that year only a shoal about 100 m in diameter remained to mark the site of the island. In subsequent years, the shoal also disappeared, while in 1910 there was about 424 m of water where the island once stood. On Jan. 34, 1914, after ten years of quiescence, the submarine volcano was again in eruption, culminating in the formation of the second new volcanic island at the site of the 1904 island. According to T. Ogura[78], who visited the scene of the eruptions the following month, the island, which was a conical volcano of pumice and obsidian, stood about 120 m above the sea and 3.5 km in circumference. Nearly tow years later, the island

---

77) T. WAKIMIZU, *Publ. Earthq. Inv. Com.*, 22-C (1908), 15; *Rep. Earthq. Inv. Com.*, **56** (1907).

78) T. OGURA, *Rep. Earthq. Inv. Com.*, **79** (1914).

also had disappeared. The submarine volcano has not erupted since, its site being marked only by a submarine bank about 200 m deep which drops abruptly to the much more profounder depression of the adjoining sea. In 1935, when the writer sailed round Minami Io-sima, nothing out of the ordinary could be noticed from the sea above the submarine volcano.

The rocks ejected from the volcano in 1904 and 1914 are described by Wakimizu and Ogura respectively as olivine-augite-andesite and olivine-bearing augite-andesite. Petrographic characters of these rocks are excerpted from the descriptions of the respective authors in A and B, Table XLI, where they are compared with those of the trachyandesites from Iosima. The table shows that the products of the submarine volcano resemble petrographically the glassy type of the trachyandesites from Io-sima. Whereas, therefore, they are characterized by phenocrysts of andesine, olivine, and augite, they may be called trachyandesite, instead of andesite. This is justified from the chemical side also, as an analysis (No. 119, Table XLII) of a pumice[79] ejected from the submarine volcano in 1914 was found to agree practically with analyses of the trachyandesites from Io-sima, and because of the large quantity of alkalies, especially soda.

III. GENERAL PETROLOGY.

The foregoing descriptions practically cover all the important volcanic bodies of the region under investigation. The rocks composing these bodies show a fairly wide range of petrographic characters according to which they may be divided into the following principal rocks-types:

1. Basalts ......
    - phyric basalts ...
        - olivine-basalt.
        - augite-olivine-basalt.
        - hypersthene-olivine-basalt.
        - two-pyroxene-olivine-basalt.
        - two-pyroxene-basalt.
        - feldspar-phyric basalt.
    - aphyric basalt.
2. Andesites...
    - phyric andesites...
        - olivine-two-pyroxene-andesite.
        - two-pyroxene-andesite.
        - hypersthene-andesite.
    - aphyric or aphanitic andesite.
3. Dacites.............................
    - two-pyroxene-dacite.
    - two-pyroxene-hornblende-dacite.
    - hornblende-dacite.

---

[79] T. WAKIMIZU, *Toyo Gakugei-zassi*, **37** (1919), 257.

4. Liparites ...
    - plagioliparites ...
        - augite-plagioliparite.
        - hypersthene-plagioliparite.
        - pyroxene-hornblende-plagioliparite.
        - hornblende-plagioliparite.
        - hornblende-biotite-plagioliparite.
        - biotite-plagioliparite.
    - aphanitic liparite.
    - potash-liparite.
5. Trachyandesite .... olivine-augite-trachyandesite.

All the above rock-types are represented; basalts and andesites predominating the dacites and liparites, both of which occur mostly as local masses in the Teriary terrane of the southern half of the Idu peninsula, excepting however the liparites of the Nii-sima group, the last-named constituting only a small proportion of the total volume of the volcanics in the region studied. Trachyandesite is found only in the Volcano Islands group—in Io-sima. Besides the five rock-types enumerated, we find diabase, porphyrite, and quartz-porphyry among the minor Tertiary intrusives from the Idu peninsula. Gabbro and quartz-diorite have been reported from near Atami[80].

A. *Mineralogical Characters.*

There are not many rock-forming minerals; the salic minerals are feldspar, quartz, tridymite, and cristobalite, while the mafic minerals are olivine, pyroxene, hornblende, and biotite, with accessory magnetite and apatite, the first-named two being the most usual. The general characters of these minerals may be briefly summarized as follows:

Plagioclase. The plagioclase in the various rock-types as determined by measuring the indices of refraction exhibits a large rang of composition. The porphyritic plagioclase varies from anorthite add bytownite in basalt and basic andesite, through labradorite and andesine in acid andesite and dacite, to oligoclase in liparite. The groundmass plagioclase is naturally less calcic than the porphyritic plagioclase in the same rock. The porphyritic plagioclase in basalts from the region studied is, generally speaking, more calcic than that in allied rocks from other regions of the world[81]. So also do the porphyritic plagioclases that are contained in the other rock-types. Some porphyritic basalts contain large plagio.

---

[80] H. Kuno, *Jour. Geol. Soc., Tokyo*, **40** (1933), 379.

[81] The porphyritic plagioclases in lime sub-basalt and lime basalt from Hawaii are bytownite (75 An) to labradorite (51 An) and labradorite (65~70 An) respectively. T. F. W. Barth, *Am. Jour. Sci.*, **21** (1931), 517. The porphyritic plagioclase in some of the Deccan traps is labradorite.

clase phenocrysts (usually 1∼1·5 cm dia.), together with or without phenocrysts of olivine and pyroxene. When such largep lagioclase occurs in basalts, it is invariably anorthite, though with a certain range of composition according to the particular rocks. Thus, on Miyake-sima, anorthite (95 An) occurs as crystal-bombs among pyroclastic ejecta besides as phenocrysts in some of the porphyritic lavas. A similar anorthite is also found in some porphyritic basalts from Taga and Tori-sima as well as in some porphyritic andesites from Usami and Tensi-yama. Although the plagioclase phenocrysts in numerous Huzi lavas are bytownite, nearly 75 An by chemical composition, large anorthite phenocrysts are also found in some lavas from the volcano. The trachyandesite from Io-sima carries plagioclase phenocrysts of large size, but in this case the mineral is andesine (43 An).

The plagioclase, both of the phenocrysts and in the groundmass, often exhibits zoning due to chemical differences, in which case the marginal part of the mineral is usually less calcic than the core of the same crystal, although reverse or recurrent zoning also occurs. The zoning of plagioclase in the basic rock-types is in most cases rather faintly exhibited, the variation in composition in different parts of the same crystal being small—that is, anorthite to anorthite-bytownite, calcic bytownite to sodic bytownite, or sodic bytownite to calcic labradorite. In some cases, however, a broad core, either homogeneous or very slightly zoned, of porphyritic plagioclase, is sharply bordered by a rim of some other feldspar, usually the plagioclase in the groundmass, which is considerably less calcic than the core. In the trachyandesite from Io-sima, the almost homogeneous andesine phenocrysts are surrounded by a thin rim of an anorthoclase which is an essential constituent of the groundmass of the same rock. The zoning of the plagioclase in acid andesites and dacites is generally more pronounced than that in basalts and basic andesites. Thus, porphyritic

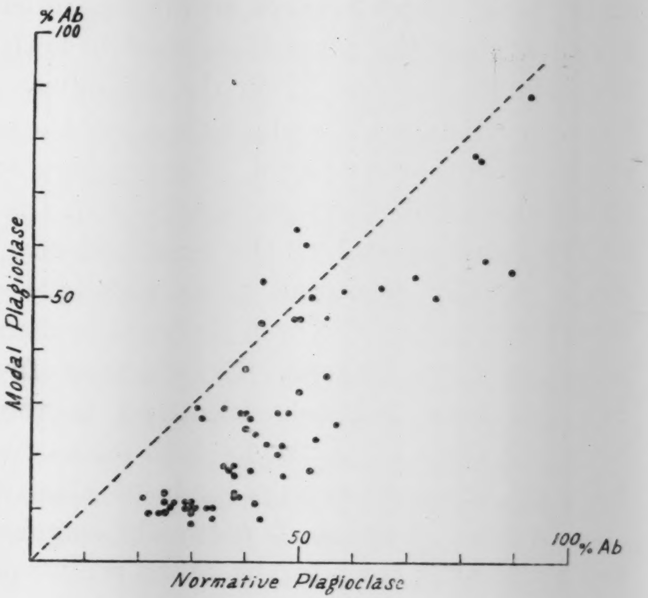

Fig. 12. Composition-relation between normative plagioclase and modal plagioclase (most sodic part).

plagioclases with a large range of composition in the same crystal have been described from Hakone. The core, for instance, may be anorthite (95 An), while the margin is labradorite (60 An).

The modal plagioclase is usually more calcic than the normative plagioclase in the same rock. But, in some rocks, such as those from Hakone, in which the groundmass is highly crystalline and the plagioclase is strongly zoned, the most sodic part of the mineral may naturally be less calcic than the normative plagioclase. Fig. 12 shows the composition relation between the most sodic part of the porphyritic plagioclase and the normative plagioclase of the same rock.

The plagioclase is usually quite fresh; even in Tertiary rocks, this mineral, except in some highly altered rocks the plagioclase of which has been subjected to saussuritization, is in most cases unaltered.

Alkali-feldspar. Alkali-feldspar is less in quantity than plagioclase, although different kinds of it are sometimes met with in certain acid and sub-acid rocks. Porphyritic sanidine with small optic angle occurs in the potash-liparite from Kodu-sima. Similar feldspar is also found in the potash-liparite from Manzo-yama and vicinity, south Idu, but the mineral is not fresh enough for precise examination of its optical properties. The plagioliparites from both Nii-sima and Kodu-sima also carry phenocrysts of sanidine, although they are usually far less in quantity than the plagioclase phenocrysts (oligoclase) contained in the same rock. Anorthoclase occurs in the trachyandesite from Io-sima as a rim around the plagioclase that is both in the phenocrysts and in the groundmass, besides filling the interstices of the other minerals. The boundary between the plagioclase and the associated anorthoclase is either sharp or rather continual. Zoning due to chemical difference is sometimes discernible through variations in the optic angle in different parts of the same crystal of the anorthoclase. When this is shown, the optic angle usually decreases from core ($2V=70°$) to margin ($2V=40°$). Anorthoclase has also been observed in the groundmass of some pyroxene-andesites from Hakone. Beyond these few examples, no alkali feldspar has yet been definitely identified in the course of the present study, although some of the rocks with high crystallinity from Amagi and Asitaka might carry certain kinds of alkali feldspar in their groundmass.

Olivine. Olivine is naturally found much more in the basalts and basic andesites than in the other rock-types, although small amounts of it occur in the trachyandesite from Io-sima and in the dacites from Amagi. In many basalts the mineral is usually present in relatively small and accessory amounts, especially in rocks the norms of which do not show olivine. Indeed, some basalts from O-sima, Miyake-sima, Hatizyo-sima, as elsewhere in the Idu peninsula, are entirely devoid of this mineral. In a few basalts, however, such as those from Kita Io-sima, Tori-sima, Amagi, Huzi, and from the other volcanoes, the mineral is very conspicuous and so great in amount that their norms yield but scanty quartz (residual silica) or a little olivine instead of the quartz. In most olivine-bearing rocks, such as those from Huzi, Amagi, and Kita Io-sima, it occurs, besides the phenocrysts in the same rock, as a groundmass constituent.

Although the olivine sometimes shows a euhedral outline with the usual habit, more often it forms either rounded or indented individuals surrounded with or without a corona of some other minerals. The corona, when present, usually consists of aggregates of monoclinic pyroxene, either augite or pigeonite. But in some rocks, in which olivine and hypersthene occur together in addition to monoclinic pyroxene, the olivine is often enclosed by a shell of hypersthene, which in turn is surrounded by grains of monoclinic pyroxene. In a few cases the olivine, on the contrary, encloses a core of hypersthene.

The composition of the olivine as determined by measuring the optic angle and the indices of refraction, ranges from nearly $Fo_{80}Fa_{20}$ to $Fo_{60}Fa_{40}$ (wt. %). On the whole, zoning due to chemical difference does not seem very common, although sometimes it is noticed through variations in the optic angle in different parts of the same crystal, the variation recognized being about 3° to 10°. In most zoned olivines, the core is richer in the forsterite molecule than in the margin, while reversed zoning is also met with. No definite paragenic relation could be detected between the composition of the olivines and that of the associated feldspars (see Fig. 13).

In most of the olivine-bearing rocks from the Quaternary volcanoes, the mineral is usually fresh or only slightly altered, which if altered, it gives rise sometimes, marginally, to iron-oxide, and sometimes both marginally and along cracks in the crystal to a reddish-brown iddingsite or to a greenish chlorite. In similar rocks among the Tertiary volcanics, especially those of lower Miocene (Idu) and older (Haha-sima, Bonin Islands), the mineral is more or less completely pseudomorphed by some other mineral, usually a greenish chlorite or calcite, or both.

Pyroxene. Pyroxene is the commonest mafic mineral found in the rocks under investigation, it being met with in one form or another in almost every rocks, although in varying amounts. They are mostly in the form of either augite, hypersthene, or pigeonite.

Augite occurs in all rock-types from basalt to liparite, usually as porphyritic individuals, although in some rocks, such as the basalts from

Huzi, Amagi, and Kita Io-sima, as well as in the andesites from Hakone, Usami, and Amagi, it occurs, besides the phenocrysts, as a constituent of the groundmass. In some cases the mineral may be present to the exclusion of other mafic minerals, but in many others it is accompanied by one or more of these. When augite occurs together with olivine in the same rock, the former often encloses the latter, besides forming isolated individuals. In many rocks, in which augite and hypersthene occur together, the two pyroxenes, in addition to forming their own individuals, are intergrown with each other, either lamellarly or zonally, the augite as a rule forming the exterior of the intergrown crystal.

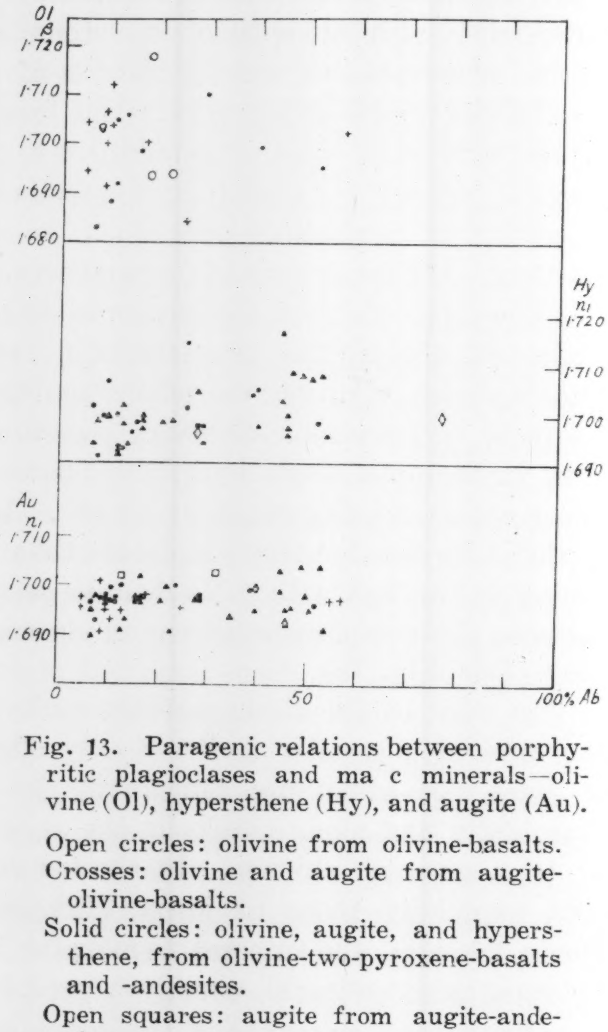

Fig. 13. Paragenic relations between porphyritic plagioclases and mafic minerals—olivine (Ol), hypersthene (Hy), and augite (Au).

Open circles: olivine from olivine-basalts.
Crosses: olivine and augite from augite-olivine-basalts.
Solid circles: olivine, augite, and hypersthene, from olivine-two-pyroxene-basalts and -andesites.
Open squares: augite from augite-andesites.
Open diamonds: hypersthene from hypersthene-andesite.
Solid triangles: hypersthene and augite from two-pyroxene-basalts and -andesites.

The augite is generally euhedral with the usual habits. Lamellar twinning is very often met with. Zoning due to chemical difference is very frequently recognized by measuring the optic angle in different parts of the same crystal; although if zoned, the angle is usually larger in the core than in the margin, reversed and recurrent zonings are also met with. The range of the optic angle is nearly 2V=57° to 45°, while tne extreme margin of zoned augite may become more pigeonitic—that is, 2V=40° or smaller. When the augite is bordered by pigeonite having a small optic angle, as observed in many basalts, the boundary separating them is usually very sharp,

Hypersthene also, though in varying amounts, is found in all the rock-types from basalt to liparite, usually as a porphyritic ingredient. In some rocks, such as those from Asitaka, Hakone, Usami, and Amagi, however, the mineral occurs, together with augite or pigeonite or both, as microphenocrysts in the groundmass besides occurring as phenocrysts. Although in most olivine-rich basalts the hypersthene may be entirely absent or merely accessory, in many olivine-poor and olivine-free rocks it occurs as an essential constituent, together with augite, taking in a sense the place of olivine. In these rocks the quantity of hypersthene often exceeds that of augite, while in some exceptional rocks, as those from Asitaka, the former make up the bulk of the porphyritic mafic constituents, with or without negligible olivine or augite or both. Besides occurring as isolated individuals, hypersthene is very often intergrown with augite or groundmass pigeonite, while the former is surrounded by granular aggregates of one of the two last-named. A lamellar intergrowth of porphyritic pigeonite and hypersthene has been described from Hakone. Sometimes, porphyritic hypersthene encloses a core of augite with random crystallographic relations, while more often, the reverse is the case. Reference has already been made to the fact that a similar relation holds between hypersthene and olivine. In certain liparites from Nii-sima and Kodu-sima, hypersthene is present, either to the exclusion of or in company with one or more of either augite, hornblende, or biotite.

In most cases, hypersthene is well-shaped with the usual habits and normal optic orientation (optic plane parallel to c-axis), although a clinohypersthene has been described from the miharaite of O-sima. Pleochroism is moderately exhibited; usually, X—yellowish brown, Y—greenish brown, and Z—green. Zoning due to chemical difference is frequently met with. In zoned crystals, the optic angle about X usually decreases from core to margin of the same crystal either continuously or stepwise. Reversed and recurrent zonings are more often met with in hypersthene than in augite. The range of the optic angle is nearly $2V(-)=79°$ to $2V(-)=61°$, although a much smaller angle has been measured in a hypersthene from Hakone with the minimum $2V(-)=47$.

A bronzite in a tuff from Titi-sima, Bonin Islands, has been described independently by both Y. Kikuchi[82] and S. Kozu[83]. In the andesites from the same island, rhombic pyroxene occurs, besides as porphyritic individuals, together with monoclinic pyroxene as incipient crystals with various habits in the glassy groundmass. Since, optically, the rhombic pyroxene is much like the hypersthene in the andesites from the adjoining shores, there is no need for special comment.

---

[82] Y. KIKUCHI, *Jour. Col. Sci., Tokyo Imp. Univ.*, **3** (1889), 81.

[83] S. KOZU, *Jour. Jap. Assoc. Min. Petr. Econ. Geol.*, **6** (1931), 275.

Pigeonite occurs frequently in the form of a rim surrounding olivine, augite, and hypersthene of the phenocrysts, as well as in the groundmass of basalts and andesites. The porphyritic pigeonite in some andesites from Hakone has been studied by its discoverer, Kuno, with valuable results concerning the crystallization of pyroxenic components from magma. Pigeonite, which usually occurs as prisms with occasional lamellar twinning on (100), is characterized by its smaller optic angle than that of common augite. Although, in some instances, the optic angle 2V is as large as 40° or more, in many others it is usually smaller than 30°, while nearly-uniaxial pigeonite is not infrequently met with. Zoning due to chemical difference is sometimes recognizable through variations in the optic angle in different parts of the same crystal. If zoned, however, the margin is usually smaller in the optic angle than in the core.

Alkali-pyroxene is all but absent. In its solitary occurrence in the trachyandesite from Io-sima it is restricted to the groundmass, in which it occurs as a rim enclosing a core of colorless or pale-green augite (diopsidic), besides occurring as isolated prismatic individuals. To judge from its optic angle about X, its pleochroism, and its indices of refraction, this alkali-pyroxene has an acmitic composition.

The paragenic relations between the porphyritic pyroxenes and the porphyritic plagioclases are shown in the diagrams, Fig. 13, where the indices of refraction of the pyroxenes and the compositions of the plagioclases are taken as ordinates and abscissae respectively. No systematic paragenic relation can be recognized on these diagrams. But, as has been pointed out in previous papers[84] on the basis of similar diagrams, the well-differentiated Amagi rocks belong exclusively to one and the same genetical lineage, and the basaltic rocks from the Seven Idu Islands to another genetical lineage. It is thus inferred that, although all the rocks from the region studied may belong to a common magmatic suite (a regional mother magma), they are probably divided into several local groups, each of which belongs to a particular genetical lineage, possibly due to different rate of cooling and different crystallization history of local magmas.

The compositions of the pyroxenes, so far determined by measuring the optic angles and the indices of refraction, are plotted in the diagram, Fig. 14. Another similar diagram, Fig. 15, shows the compositions of the pyroxenes from Hakone andesites studied by Kuno. As will be seen from these diagrams, the plots of the porphyritic augite fall exclusively

---

84) H. TSUYA, *Bull. Earthq. Res. Inst.*, **7** (1929), 329; *Proc. Third Pan-Pacific Sci. Congr.*, Tokyo, **1** (1926), 2393.

within Kuno's *two-pyroxene field*[85] of the $CaSiO_3$-$MgSiO_3$-$FeSiO_3$ diagram.

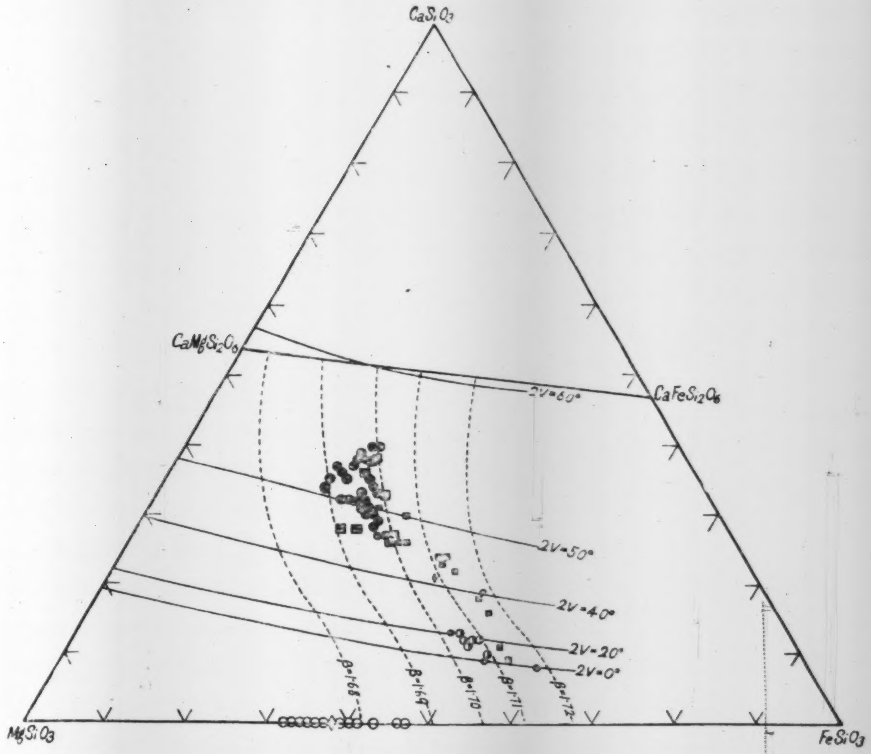

Fig. 14. Compositions of pyroxenes in the volcanic rocks from Idu and the Southern Islands.

Large solid circles: Porphyritic augite from two-pyroxene (±olivine)-bearing rocks.
Large open circles: Porphyritic hypersthene from two-pyroxene (±olivine)-bearing rocks.
Large solid squares: Porphyritic augite from augite (±olivine)-bearing rocks.
Open diamond: Porphyritic hypersthene from hypersthene-andesite.
Half-solid circles: Groundmass pyroxene from two-pyroxene (±olivine)-bearing rocks.
Small solid squares: Groundmass pyroxene from augite (±olivine)-bearing rocks.

To judge from their average optic angles and mean indices of refraction, the porphyritic augites that are plotted in the diagrams seem to be poorer in lime and richer in iron-oxide than the chemically analyzed, pyrogenic monoclinic pyroxenes from various localities in Japan. Most of them, however, are zonally built in the manner as already mentioned, suggesting that the margin of zoned augite is probably richer in iron-oxide and poorer in lime than its core. The augites from Wadaki, Idu,

---

85) H. KUNO, *Jap. Jour. Geol. Geogr.*, **13** (1936), **141**.

and from Yone-yama, Etigo, both of which were chemically analyzed,

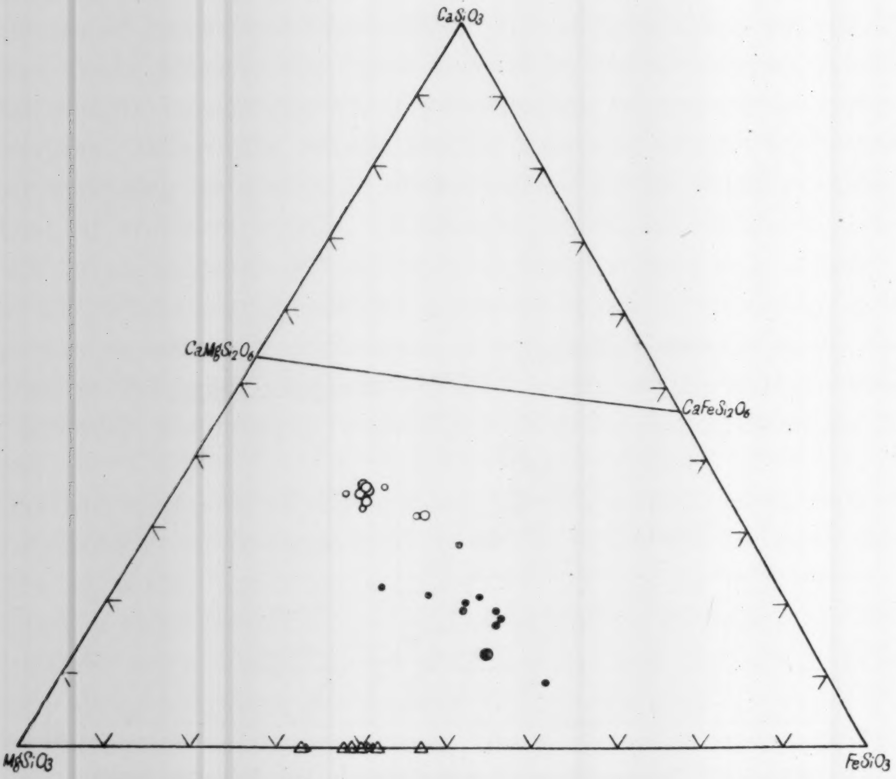

Fig. 15. Compositions of pyroxenes in the andesites from Hakone and in the basalt from Aziro, Idu. (Data given by H. Kuno, *loc. cit.*)

Large open circles: Porphyritic augites.
Large solid circle: Porphyritic pigeonite.
Small open circles: Groundmass augites.
Small solid circles: Groundmass pigeonites.
Large open triangles: Porphyritic hypersthenes.
Small open triangles: Groundmass hypersthenes.

also show a similar zoning.[86] From these facts in view, it is inferred that, although the monoclinic pyroxene that lies within the two-pyroxene field may have a composition-range (a limit of miscibility of the $MgSiO_3$-$FeSiO_3$ series in the $CaMgSi_2O_6$-$CaFeSi_2O_6$ series)[87], the pyroxene within that range becomes richer in iron-oxide and poorer in lime with advancing crystallization.

Like the hypersthenes in the andesites from the Kusatu-Sirane volcano[88], those in the rocks under investigation do not fit well into the curve for the optic angle in Winchell's diagram showing the variations of composition and optic properties in the rhombic pyroxene series, if the curves for the indices of refraction in that diagram be taken as normal. With the corresponding indices of refraction, they are characterized by more or less smaller optic angles as compared with the hypersthenes upon which Winchell's diagram is based. This character thus confirms Tsuboi's note(89) concerning the relation between the optic angles and the indices of refraction of a number of rhombic pyroxenes from various localities in Japan. In the above figures the hypersthenes are plotted on the basis of the curves proposed by Bowen and Schairer for the variations of composition and indices of refraction in the rhombic pyroxene series, which curves seem better for our rhombic pyroxenes than Winchell's. As the chemical analyses of rhombic pyroxenes from various localities in Japan show, the hypersthenes studied also may contain $CaSiO_3$ and other minor constituents, besides the two main components, $MgSiO_3$ and $FeSiO_3$. But, since the actual contents of $CaSiO_3$ and other minor constituents in them cannot be determined from their optical properties alone, the approximate compositions of the hypersthenes as expressed in terms of the two main components, are plotted in the above figures. Thus, they rang from nearly $(MgSiO_3)_{80}(FeSiO_3)_{20}$ to $(MgSiO_3)_{54}(FeSiO_3)_{46}$ (wt. %), all lying within the two-pyroxene field(90). As to the course of crystallization of hypersthene, nothing can be said with certainty at present, although the manner of variation of the optic angle in different parts of zoned hypersthene suggests that with advancing crystallization the mineral becomes, in most cases, richer in ferrosilite molecule.

---

[86] H. Kuno and M. Sawatari, *Jap. Jour. Geol. Geogr.*, **11** (1934), 323.
[87] S. Tsuboi, *ibid.*, **10** (1932), 67.
[88] H. Tsuya, *Bull. Earthq. Res. Inst.*, **12** (1934), 67.

The groundmass pyroxenes, except the augite and hypersthene that occur together as microphenocryst in the groundmass of some two-pyroxene-bearing rocks, are exclusively monoclinic pyroxenes which are usually poorer in lime and richer in iron-oxide than the porphyritic augites, and most of which have compositions lying within Kuno's *pigeonite field* of the $CaSiO_3$-$MgSiO_3$-$FeSiO_3$ diagram.

In most of the Quaternary rocks, pyroxenes are usually quite fresh, while in many Tertiary rocks, especially in some of the lower Miocene rocks from Idu, they are more or less completely replaced by chlorite. Augite is often left almost unaltered even though adjacent to chloritized olivine or hypersthene. The augite of the basalt-xenoliths in the liparites

---

89) S. TSUBOI, *Jap. Jour. Geol. Geogr.*, **12** (1935), 109.

90) The hypersthene in the almost aphyric olivine-bearing two-pyroxene-andesite (No. 76) from Aoga-sima has exceptionally high indices of refraction ($n_1 = 1{\cdot}715$), and its composition, so far judged from the indices of refraction, is $(MgSiO_3)_{47}$ $FeSiO_3)_{53}$.

from Nii-sima and Kodu-sima is converted partly to a green hornblende. Being a phenomenon similar to that observed in the Omogo acidic rocks[91], this seems to be an example confirming Bowen's view regarding the effect of acid magma upon inclusions of less acid igneous rocks.

Hornblende. Hornblende is found in liparites as well as in dacites and also in some few andesites. In most of these cases, the mineral occurs as porphyritic individuals either in association with the other mafic minerals—usually pyroxene or biotite or both—or to the exclusion of these, but in a few rocks, such as the dacites from Amagi, it is found, besides as phenocrysts, as microphenocrystic flakes in the glassy groundmass. The trachyandesite from Io-sima also carries hornblende in the groundmass. Most of the pyroxene-andesites from Amagi might carry hornblende, which however has been completely converted to a granular aggregate of magnetite, plagioclase, and pyroxene. A similar conversion of hornblende has been described from the pigeonite (porphyritic)-bearing andesites of Hakone. Hornblende occurs as rare phenocrysts in some liparites from Nii-sima and Kodu-sima, in most of which the mineral is found associated with minute biotite flakes. The hornblende in some of the Tertiary rocks from Idu is sometimes quite fresh or only slightly altered, but more often it is completely altered in the same way as that from Amagi or pseudomorphed by secondary material, usually chlorite.

When fresh, hornblende is greenish-brown with moderate pleochroism and usual habits: neither basaltic nor alkaline hornblende is presented. Zoning due to chemical difference in different parts of the same crystal is rarely met with: if zoned, the optic angle is usually larger in the core than in the margin.

Biotite. Biotite is distributed less extensively than hornblende, its occurrence being virtually restricted to certain liparites and to a few dacites. Greenish-brown biotite in the form of very minute flakes is found in most of the liparites from Nii-sima and Kodu-sima. Accompanying this biotite, which has usually $\gamma = 1{\cdot}656 \sim 1{\cdot}665$ and $2E = 38°$ or smaller, there often occurs biotite of another type in flakes of a deep reddish-brown color, with much higher indices of refraction and larger optic angle. From a thermal study of biotite flakes from the Tenzyo-san lava of Kodu-sima, it was proved that this reddish-brown biotite is a thermally-decomposed product of the other greenish-brown biotite in the same rock[92].

Silica mineral. Most of the basalts and andesites carry silica mineral in their groundmass, but in such amounts sufficient to account for

---

91) H. TSUYA, *Bull. Earthq. Res. Inst.*, **13** (1936), 910.
92) H. TSUYA, *Bull. Earthq. Res. Inst.*, **7** (1929), 306.

the normative quartz (residual silica) that we find in their analyses. The silica mineral occurs in three different forms: cristobalite, tridymite, and quartz. A reference to the occurrence of these minerals has been specially made by Kuno in connection with the petrography of a basalt from Aziro, north Idu[93].

Cristobalite and tridymite occur either together or by themselves, interstitially as well as in shapeless patches, and/or as well-shaped plates and prismoides in the groundmass. They can be verified rather easily in rocks with a coarse-grained groundmass, whereas in a fine-textured groundmass certain areas of patchy polarization indicate the presence of one or more of these minerals. In some rocks with microscopic vesicles, besides as interstice-fillings, they are found in the form of a lining to the vesicles.

Quartz also may sometimes be detected in the interstices of a less glassy, coarser-grained groundmass. Porphyritic quartz is met with in most of the liparites and dacites, though in varying amounts, in which it usually occurs with rounded or irregularly broken outlines, and although exceptionally, in the bipyramidal form. The potash-liparite from Manzo-yama, Simoda, carries locally bipyramidal quartz of large size (up to 8 mm dia.), although by far the greater part of the mass is destitute of that mineral. In some andesites from Amagi and Hakone accessory quartz occurs in the form of rounded grains. Most of the olivine-basalts from the Omuro-yama volcano group carry porphyritic crystals of quartz, often rimmed by grains of pigeonitic augite, as in the case of quartz in many of the quartz-basalts from other regions. Like the porphyritic crystals of andesine that occur in the same rocks, the quartz is xenocrysts, the apparent source of which is the dacite agglomerate underlying the basalts of the group. An exposure of this dacitic agglomerate is seen at Yosida on the southwest foot of the Komuro-yama volcano, where it carries abundant well-shaped crystals of quartz (up to 1 cm dia.).

Magnetite. Almost all the rocks contain, though in varying amounts, an opaque mineral of the iron-ore group, usually magnetite: in basalts and basaltic andesites the mineral usually occurs in the groundmass only, whereas in some andesites and more acid rocks it is found, besides in the groundmass, as a rare accessory of the phenocrysts. The magnetite is usually in distinct crystals, sharply bounded or with rounded edges and angles. Sometimes, and especially in coarser-grained basalts, it occurs in shapeless patches, tending to enwrap the other minerals of the groundmass. Porphyritic magnetite is found intimately associated with

---

93) H. KUNO, *Bull. Earthq. Res. Inst.*, **11** (1933), 400.

the other mafic minerals in the same rock. Ilmente has been reported from the andesites of Hakone.

Apatite. This mineral is observed more frequently in andesites and the more acid rocks than in basalts: it is almost constantly met with in the andesites from Amagi, Usami, and Hakone. The trachyandesite from Io-sima contains slender needles of almost-colorless apatite as inclusions in the porphyritic minerals and as isolated individuals dispersed through the rock.

B. *Chemical Characters.*

The chemical analyses accompanying descriptions of rocks in this paper total 106 exclusive of those from the Marianas Islands, and these may be itemized as shown in Table XLIV, according to their locality and silica content. In the table, the numerals in brackets indicate the number of analyses that were published before 1925, while the others are those that were made later. Besides these, there are some 40 older analyses that have not been quoted in this paper. Of the 95 analyses made during recent years, since 1925, 76 were made by Tanaka for the writer, including 59 hitherto unpublished results. The 6 analyses for Hakone, 5 for Taga, and 2 for local masses near Aziro, north Idu, were made by the same analyst for H. Kuno. The following discussion concerns the analyses given in this paper, excluding however those in the columns that are headed by capital letters in the tables of chemical analyses.

The general chemical characters of a series of volcanic rocks are usually discussed with the aid of variation diagrams, that is, by plotting the chemical analyses of the rocks on rectangular co-ordinates with silica as abscissae and the other oxides as ordinates. It should be emphasized, however, that a variation diagram, in which many analyses of porphyritic rocks with large phenocrysts are incorporated, may not be a "magma variation diagram", for the reason that the bulk analyses of porphyritic rocks may depart more or less from the composition of any past magmatic liquid, unless the phenocrysts in such a rock include all the material that separated from some other liquid while it was changing to that liquid in which they are now suspended[94]. It follows, therefore, that magma variation diagrams should be drawn only for rocks that either virtually represent or closely approach the composition of magmatic liquids. The rocks that come within this category are the

---

[94] S. TSUBOI, *Jour. Fac. Sci., Imp. Univ., Tokyo,* **1** (1925), 77.
N. L. BOWEN, The Evolution of the Igneous Rocks. Princeton (1928), 92.

Table XLIV. Number of the Chemical Analyses accompanying Descriptions of Rocks in this Paper.

Localities			SiO$_2$ contents <50%	>50% <55%	>55% <60%	>60% <65%	>65% <70%	>70%	Total
Tertiary	Ogasawara Islands	Haha-sima	—	—	**1**	—	—	—	**1**
		Titi-sima	—	(3)**	(1)	**1**	—	—	(4) **1**
	Idu Peninsula		**1**	**5**	**5**	**6**	**3**	**1**	**24**
Quaternary	Idu Peninsula and its northern outskirt	Local masses near Aziro	—	1	1	—	—	1	3
		Tensi-yama	—	—	**1**	—	—	—	**1**
		Usami Volcano	—	**4**	**3**	**1**	—	—	**8**
		Taga Volcano	—	5 **5**	1	—	—	—	6 **5**
		Asitaka-yama	—	**1**	—	—	—	—	**1**
		Hakone-yama	—	—	5	1	—	—	6
		Amagi-san	**1**	**2**	**1**	**2**	**1**	**1**	**8**
		Omuro-yama Group	—	**1**	**1**	—	—	—	**2**
		Huzi-san	**2**	5	—	**1**	—	—	5 **3**
	Seven Idu Islands	Utone-sima	—	(1)	—	—	—	—	(1)
		To-sima	(1)	—	—	—	—	—	(1)
		Mikura-sima	—	**1**	—	—	—	—	**1**
		Nii-sima	—	—	—	—	—	1	1
		Kodu-sima	—	1	—	—	—	5	6
		Hatizyo-sima	—	**1**	—	—	—	—	**1**
		Miyake-sima	—	(2) **2**	—	—	—	—	(2) **2**
		O-sima	1	(2)4	—	—	—	—	(2)5
	Southern Islands	Kita Io-sima	1	—	—	—	—	—	1
		Io-sima	—	—	2	(1)*	—	—	(1)2
		Tori-sima	**1**	—	—	—	—	—	**1**
		Aoga-sima	—	—	—	**1**	—	—	**1**
Total			(1) 2 **8**	(8) 16 **22**	(1) 9 **12**	(1) 1 **12**	**4**	7 **2**	$\underbrace{(11)\ 35\ \mathbf{60}}_{106}$

* Analysis of 1914 pumice from the submarine volcano ("Sin Io-sima" volcano) near Minami Io-sima. ** Includes one from Ototo-sima.

The number of hitherto unpublished analyses are distinguished by gothic letters from those already published.

aphyric, or aphanitic rocks, since they were formed by direct consolidation of magmatic liquids. The groundmass of porphyritic rocks also is expected to come in the same category, provided its composition is known either micrometrically or chemically. With this in view, the ordinary variation diagram for rocks with various porphyricity may be called either a "rock variation diagram" or a "rock comparison diagram". Although a diagram of this kind may be of little use in petrogenesis, comparison of the general chemical characters of a series of rocks with another is facilitated by constructing such diagrams for both series and observing the similarities and differences between them.

Magma variation diagram. Of all the analyses given, those shown in Table XLV (each reduced to 100% as water-free) are the most suitable for fixing a magma variation diagram. They are of aphyric, or aphanitic rocks, entirely free from phenocrysts or with but a very small proportion of phenocrysts. Fig. 16 is a magma variation diagram for the 10 analyses so chosen. As will be seen from the figure, all the points representing these rocks lie close to smooth curves for the oxides.

Table XLV. Analyses of Aphyric, or Aphanitic, Rocks from Idu and Southern Islands (calculated to 100% as water-free).

	1	2	3	4	5	6	7	8	9	10
SiO_2	50·97	52·62	52·79	54·28	54·91	57·27	60·21	62·27	64·36	75·41
Al_2O_3	14·65	15·68	15·88	15·29	14·53	15·67	15·57	14·73	14·29	13·61
Fe_2O_3	3·80	5·62	4·42	2·88	1·87	4·63	4·69	1·77	1·79	0·77
FeO	10·16	8·22	9·94	10·41	12·35	7·17	6·02	7·77	6·77	0·72
MgO	5·44	6·14	4·13	3·64	3·04	3·03	2·19	1·84	2·14	0·32
CaO	11·67	8·09	8·98	8·41	8·07	7·41	6·49	6·12	6·73	0·94
Na_2O	1·84	2·02	2·47	2·87	2·60	2·98	2·89	3·55	2·79	4·53
K_2O	0·26	0·26	0·32	0·49	0·50	0·56	0·59	0·47	0·67	3·41
TiO_2	0·80	1·15	0·75	1·39	1·65	0·98	1·06	1·06	0·25	0·13
P_2O_5	0·13	0·06	tr.	0·11	0·16	0·08	0·11	0·20	tr.	0·08
MnO	0·28	0·14	0·32	0·23	0·32	0·22	0·18	0·22	0·21	0·08

1. Basalt (No. 91, Table XXXIII), O-sima.
2. Basalt (No. 24, Table IX), Kadono, Kita Kanomura, north Idu.
3. Basalt (No. 60, Table XXIV), Taga volcano.
4. Basalt (No. 88, Table XXXI), Miyake-sima.
5. Basalt (No. 83, Table XXX), Hatizyo-sima.
6. Andesite (No. 32, Table XIII), Aziro, north Idu.
7. Andesite (No. 54, Table XXII), Usami volcano.
8. Andesite (No. 76, Table XXIX), Aoga-sima.
9. Andesite (No. 5, Table II), Titi-sima.
10. Liparite (No. 111, Table XL), Ombasi-zima.

The groundmass compositions of some porphyritic rocks from Hakone, Taga, and O-sima were calculated by Kuno[95], with results as shown in Table XLVI, in which the average groundmass composition of four

---

[95] Kuno has drawn a magma variation diagram for 19 analyses (including 10 of the calculated groundmass of porphyritic rocks) from Hakone, Taga, and O-sima. The left half of the writer's diagram naturally resembles Kuno's diagram though it was drawn independently before the latter was published. H. KUNO, *Bull. Volc. Soc., Japan*, **3** (1936), 53

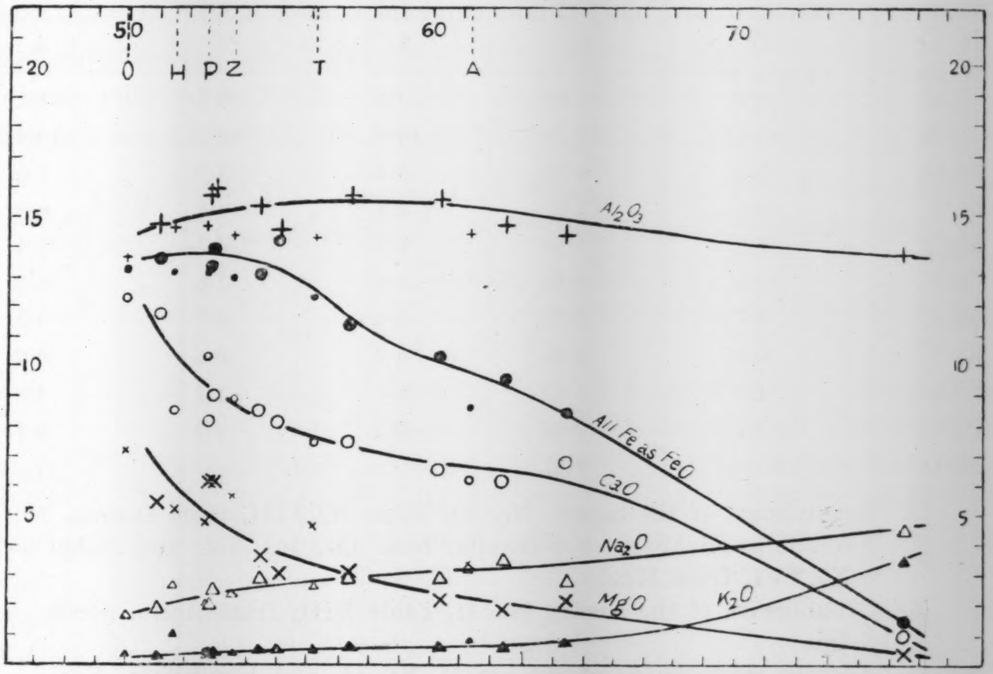

Fig. 16. Magma variation diagram of Idu and the Southern Islands.

The plots of the 10 analyses given in Table XLV are distinguished by larger symbols from the plots of the calculated groundmass compositions given in Table XLVI. P is the average of 4 O-sima basalts (Nos. 9?, 93, 94, 96, Table XXXIII), each of which has a small proportion of phenocrysts.

Huzi basalts is also quoted[96]. They are plotted, together with the average of 4 slightly porphyritic basalts from O-sima, on the magma variation diagram, Fig. 16. As will be seen from the diagram, their indicative points, except those of Huzi basalts, lie fairly close to the curves of the diagram, although most of the points for magnesia deviate rather notably from the curve for that oxide. Since the analyses plotted on the diagram are of rocks that have been collected from widely separated points and horizons (Tertiary and Quaternary) within the region studied they suggest that the magmas that generated in the region during the whole course of volcanism from Tertiary to Recent belong to a common suite. According to the fourfold division of igneous rocks suggested by Peacock, the magma suite belongs to a calcic series, the alkali-lime index—that is, the silica value on the variation diagram at which the curves for total alkalies and lime intersect—being about 67[97]. The magma suite

---

[96] H. TSUYA, *Bull. Earthq. Res. Inst.*, **13** (1935), 655.

[97] The alkali-lime index calculated from the curves of Kuno's diagram is about 66·3.

Table XLVI. Groundmass Composition of the Porphyritic Rocks from O-sima, Huzi, Taga, and Hakone.

	O	H	Z	T	A
SiO_2	49·9	51·46	53·4	56·1	61·2
Al_2O_3	13·7	14·70	14·4	14·3	14·4
Fe_2O_3	3·2	4·52	5·1	3·3	2·6
FeO	10·4	9·07	8·4	9·3	6·3
MgO	7·2	5·10	5·7	4·7	3·4
CaO	12·3	8·51	8·9	7·6	6·2
Na_2O	1·7	2·73	2·4	2·7	3·3
K_2O	0·4	1·06	0·4	0·6	0·9
TiO_2	1·2	1·97	1·1	1·4	1·3
P_2O_5	tr.	0·34	0·2	0·2	0·1
MnO	——	0·27	——	——	——

O. Groundmass of the basalt, No. 90, Table XXXIII, from O-sima.

H. Average groundmass of 4 basalts, Nos. 101, 103, 104, 106, Table XXXVI, from Huzi.

Z. Groundmass of the basalt, No. 31, Table XIII, from Aziro, north Idu.

T. Average groundmass of one basalt, No. 62, and 3 andesites, Nos. 63, 64, 66, Table XXIV, from Taga.

A. Average groundmass of 4 andesites, Nos. 41, 43, 44, 45, Table XIX, from Hokone.

of the present region is thus the most calcic so far known in the world. In the shape of the curve for each oxide, excepting certain differences in the heights of the curve, the magma variation diagram resembles the variation diagram of the world's type-average (average basalt, andesite, dacite, and rhyolite) as calculated by Daly[98], the alkali-lime index for the latter being about 60.

The groundmass of the Huzi basalts is distinctly richer in alkalies and poorer in lime than the aphyric basalts (or the groundmass of the porphyritic basalts) from Idu[99]. So also does the aphanitic andesite from Huzi (No. 107, Table XXXVI, not plotted on the diagram, Fig. 16) compared with the aphyric andesites (or the groundmass of the porphyritic andesites) from Idu. The bulk compositions of the Huzi rocks differ in the same way from those of the Idu rocks. No explanation can be offered at present for these differences between the rocks of Huzi and Idu. It is worth noting, however, that the Huzi rocks bear a closer

---

98) N. L. BOWEN, *loc. cit.*, 123.

99) The affinities of the Huzi basalts with the "plateau basalt" and their differences from the O-sima basalts have already been pointed out in the previous paper of mine. H. TSUYA, *Bull. Volc. Soc. Japan*, **2** (1934), 149.

resemblance in chemical composition to rocks from the volcanoes Kayagatake-Kurohuzi[100] and Iidunayama-Kurohimeyama[101] than to the Idu rocks. Thus, these two volcanoes have yielded basaltic and andesitic rocks which, like the Huzi rocks, are distinctly high in alkalies and low in lime compared with the Idu rocks (Tables XLVII and XLVIII). They lie independently in the northern part of the Huzi volcanic zone—namely Kayagatake-Kurohuzi about 50 km NNW. of Huzi and Iiduna-Kurohimeyama about 170 km NNW. of Huzi—but beyond the region that we concern in this paper. It is inferred, therefore, that the Huzi volcanic zone in a wide sense may be divided petrologically into two parts —the northern part (inland part) including the inland volcanoes Huzi-

Table XLVII. Analyses of Rocks from the Volcanoes
Kayagatake-Kurohuzi and Iidunayama-Korohimeyama.
S. Tanaka, analyst.

	1	2	3	4	5	6	7	8
SiO_2	52·35	64·41	48·70	55·06	55·32	55·91	58·05	59·44
Al_2O_3	18·86	17·11	20·07	21·13	19·04	19·49	17·90	19·00
Fe_2O_3	3·68	2·57	3·62	2·28	2·25	2·33	3·50	5·24
FeO	5·29	2·62	7·16	5·61	5·93	5·70	2·64	1·42
MgO	4·42	2·02	3·95	2·15	3·92	3·56	2·56	2·15
CaO	8·32	5·80	10·56	7·55	8·22	8·08	7·05	6·85
Na_2O	3·62	3·57	2·73	2·27	3·26	2·56	3·01	2·58
K_2O	0·97	1·23	0·92	0·99	1·15	1·19	0·91	1·25
H_2O +	1·03	0·45	0·50	1·15	0·36	0·28	1·32	0·78
H_2O −	0·75	0·11	0·92	0·74	0·12	0·14	1·65	0·57
TiO_2	1·05	0·56	0·88	0·70	0·60	0·67	0·45	0·50
P_2O_5	0·27	0·13	0·14	0·24	0·20	0·24	0·16	0·20
MnO	0·10	0·07	0·16	0·15	0·14	0·15	0·10	0·18
Total	100·71	100·65	100·31	100·02	100·51	100·30	100·50*	100·16

* includes S 1·20.

1. Olivine-bearing augite-labradorite-andesite. Kayagatake.
2. Green-hornblende-andesine-dacite. Kurohuzi.
3. Augite-olivine-basic-bytownite-basalt. Iidunayama.
4. Olivine-bearing two-pyroxene-bytownite-andesite. Iidunayama.
5. Augite-bearing brown-hornblende-hypersthene-bytownite-andesite. Kurohimeyama.
6. Two-pyroxene-bytownite-andesite. Kurohimeyama.
7. Brown-hornblende-two-pyroxene-dacite. Kurohimeyama.
8. Basaltic-hornblende-labradorite-andesite. Iidunayama.

---

100) M. Ichiki, *Bull. Earthq. Res. Inst.*, **7** (1929), 335.
101) S. Yamada, *ibid.*, **12** (1933), 96.

Table XLVIII. Comparison of Lime and Alakli Contents of Rocks from Huzi, O-sima, Kayagatake and Iidunayama.

	Huzi		Iiduna	Kayagatake	O-sima	
	No. 99	No. 106	3	1	No. 90	No. 95
SiO_2	49·60	51·30	48·70	52·35	48·02	51·45
CaO	8·80	9·76	10·56	8·32	14·14	10·71
Na_2O	2·90	2·55	2·73	3·62	1·28	1·23
K_2O	0·93	0·71	0·92	0·97	0·30	0·37

san, Kayaga-take, Yatuga-take, Iiduna-yama, Kurohime-yama, Myoko-zan, etc., in the central Japan, and the southern part (oceanic part) including, in addition to the volcanoes in the Idu peninsula, the insular and submarine volcanoes of the Seven Idu Islands and the Southern Islands. These two parts—northern and southern—of the so-called Huzi volcanic zone may be referred to respectively as the *Huzi Volcanic Zone proper* and the *O-sima Volcanic Zone*, after the most celebrated volcanoes in the respective parts. So far as data now available are concerned, *the rocks from the Huzi volcanic zone proper are relatively high in alkalies and low in lime, while those from the O-sima volcanic zone, with a few exceptions of local masses of alkaline rocks, are relatively low in alkalies and high in lime.* Asitaka and Hakone, which may be included respectively in the Huzi volcanic zone proper and the O-sima volcanic zone, lie near the possible boundary separating the two zones. Whether or not the petrological differences of these two zones are in any way connected with some differences in the geotectonic structure of them is a matter of pure speculation.

Rock variation diagrams. When the analyses of a series of rocks with various porphyricity have been plotted on a variation diagram, it is usually seen that the points for each oxide scatter considerably from any smooth curve, so that a better understanding of the general chemical characters of a number of such rocks can be had from type-averages of the analyses than from individual analyses, Although, in the case of the silica content, the analyses now under investigation may be divided broadly into four groups corresponding respectively to four petrographic types—basalt, andesite, dacite, and liparite—, the silica range of each group so divided is wide and consequently overlaps that of its neighbour. In calculating the type-averages, therefore, the analyses (each reduced to 100% as water-free) were divided from the purely chemical point of view into seven types, as follows:

Chemical type	Silica range in %	Rock type
I	<50	Basalt
II	$50< \ <55$	Andesite-basalt
III	$55< \ <60$	Andesite
IV	$60< \ <65$	Dacite-andesite
V	$65< \ <70$	Dacite
VI	$70< \ <75$	Liparite-dacite
VII	$75<$	Liparite

The analyses for each chemical type were then averaged.

In according with the foregoing plan, the type averages for the Tertiary and the Quaternary rocks were calculated separately with

Table XLIX. Type Averages of the Tertiary Porphyritic Rocks from Idu and Bonin.

	I	II	III	IV	V	VI*
SiO_2	49·28	51·38	57·49	62·30	66·72	73·31
Al_2O_3	19·53	19·86	17·67	16·60	15·99	13·94
Fe_2O_3	2·60	3·35	3·15	3·25	3·30	1·26
FeO	7·81	6·35	5·25	3·53	1·83	1·64
MgO	6·47	4·59	4·03	2·86	1·93	0·51
CaO	11·38	10·96	8·12	6·05	4·33	2·64
Na_2O	1·76	2·13	2·60	3·39	3·56	3·96
K_2O	0·16	0·27	0·65	1·08	1·59	2·23
TiO_2	0·76	0·85	0·79	0·69	0·59	0·36
P_2O_5	0·10	0·07	0·09	0·13	0·08	0·07
MnO	0·15	0·19	0·15	0·12	0·08	0·08

* Two analyses with $SiO_2>70\%$ were averaged as one type.

Table L. Type Averages of the Quaternary Porphyritic Rocks from Idu and the Southern Islands.

	I	II	III	IV	V	VI	VII
SiO_2	49·21	51·93	56·80	61·83	68·39	71·06	77·29
Al_2O_3	18·51	18·64	17·56	16·67	15·09	14·70	13·31
Fe_2O_3	3·12	3·27	2·44	3·00	1·20	1·12	0·78
FeO	7·97	7·33	6·07	4·01	3·10	2·15	0·46
MgO	5·74	4.54	4·14	2·71	1·41	1·30	0·22
CaO	11·46	10·19	8·29	6·25	4·30	3·49	1·28
Na_2O	2·13	2·33	2·94	3·28	4·22	3·60	4·35
K_2O	0·47	0·44	0·67	1·22	1·46	2·06	2·12
TiO_2	1·04	1·05	0·81	0·75	0·56	0·36	0·10
P_2O_5	0·12	0·12	0·13	0 16	0·13	0·08	tr.
MnO	0·23	0·16	0·15	0·12	0·14	0·08	0·09

results as given in Tables XLIX and L respectively, the averages being

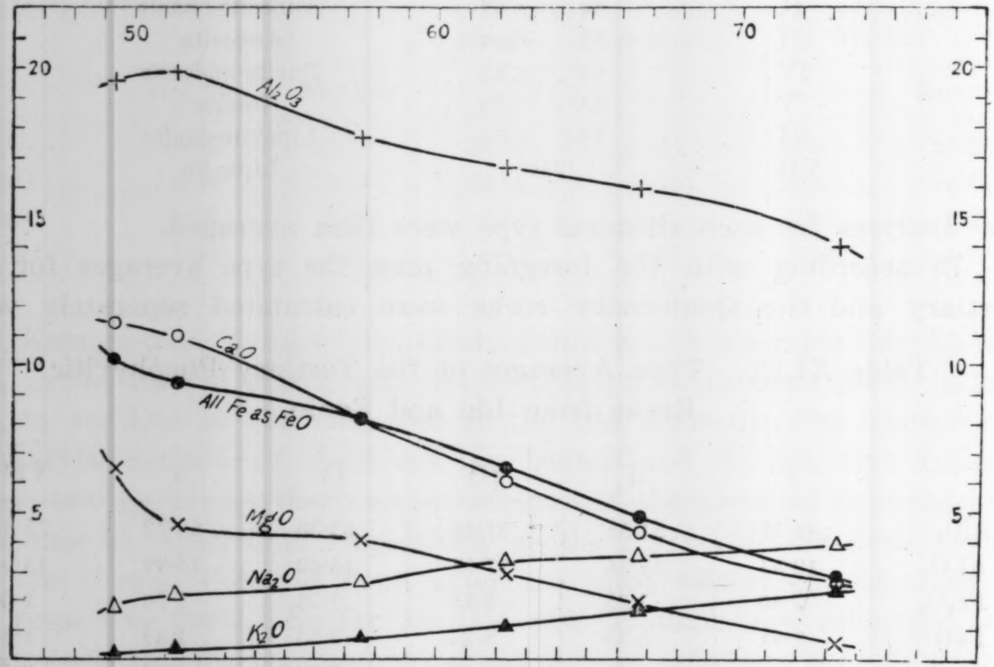

Fig. 17. Variation diagram of the Tertiary porphyritic rocks from Idu and Bonin.

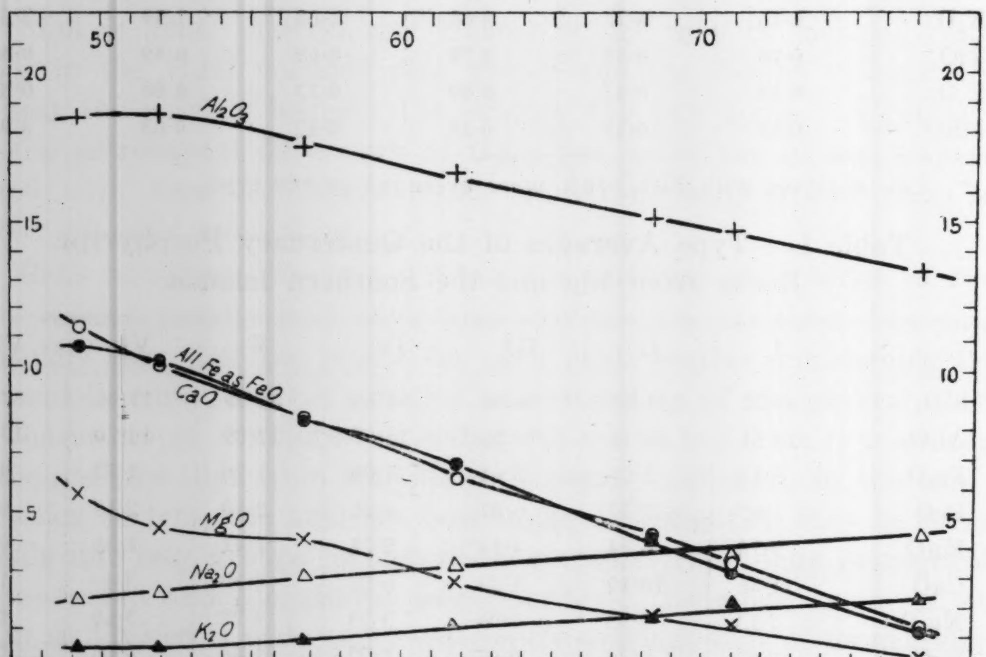

Fig. 18. Variation diagram of the Quaternary porphyritic rocks from Ídu and the Southern Islands.

based on the porphyritic rocks only, the alkaline rocks (potash-liparite and trachyandesite) calling for separate treatment. Had the type averages been based on both the porphyritic and non-porphyritic rocks, they would have showed slightly lower alumina and slightly higher iron-oxides than the results given in the above tables.

In Figs. 16, 17, the type averages are plotted of the Tertiary and the Quaternary rocks respectively. The figures for the two are much alike, the corresponding curve in one being almost a duplicate of the other. The alkali-lime index is 65·2 for the Tertiary series and 65·7 for the Quaternary series.

The lavas of the Amagi volcano form a graded series extending from basalt, through andesite, to dacite. The serial relations are admirably shown by the analyses (Table XVII) of the eight representative rocks that have been plotted as a variation diagram, Fig. 19. The alkali-lime index for the Amagi series is 65·2. A comparison of the diagram with either of the previous two diagrams, Figs. 17, 18, shows that both are much alike without any systematic difference between them, thus supporting the view that all the rocks from the region, with the rare exception of the alkaline rocks, belong to a common suite, and that their variation is represented by that of the well-differentiated series of the Amagi volcano.

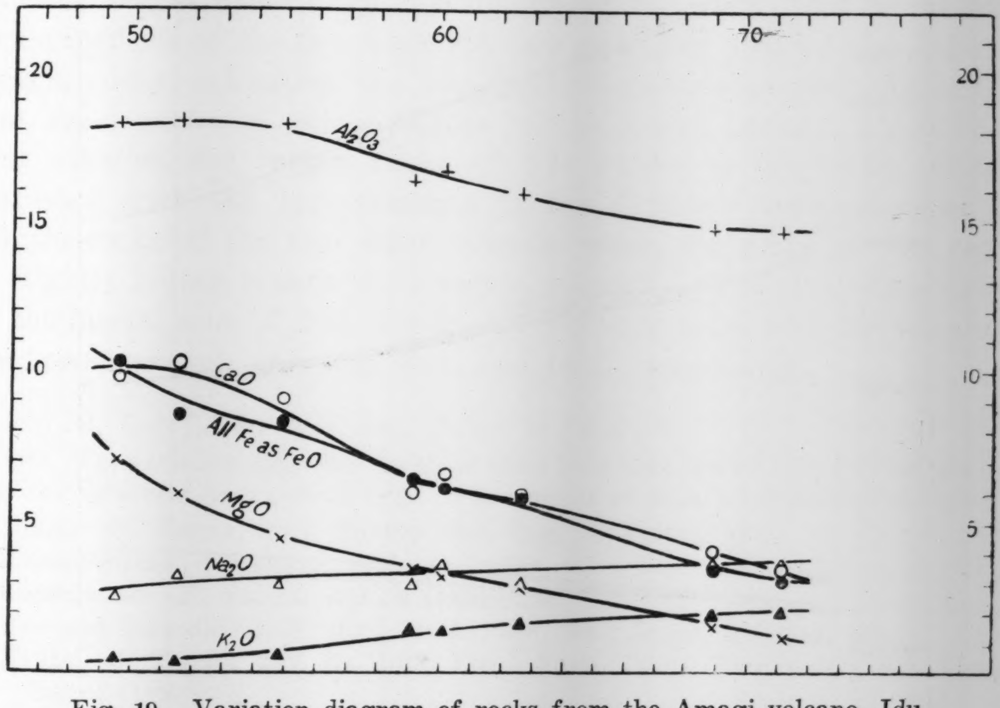

Fig. 19. Variation diagram of rocks from the Amagi volcano, Idu.

Upon comparing any one of the rock variation diagrams of Figs. 17, 18, 19 with the magma variation diagram, Fig. 16, the former will be found to show a decidedly higher alumina curve and lower iron-oxides curve. The deviation is more marked in the low silica side of these diagrams that in the opposite side. This accords with the fact that

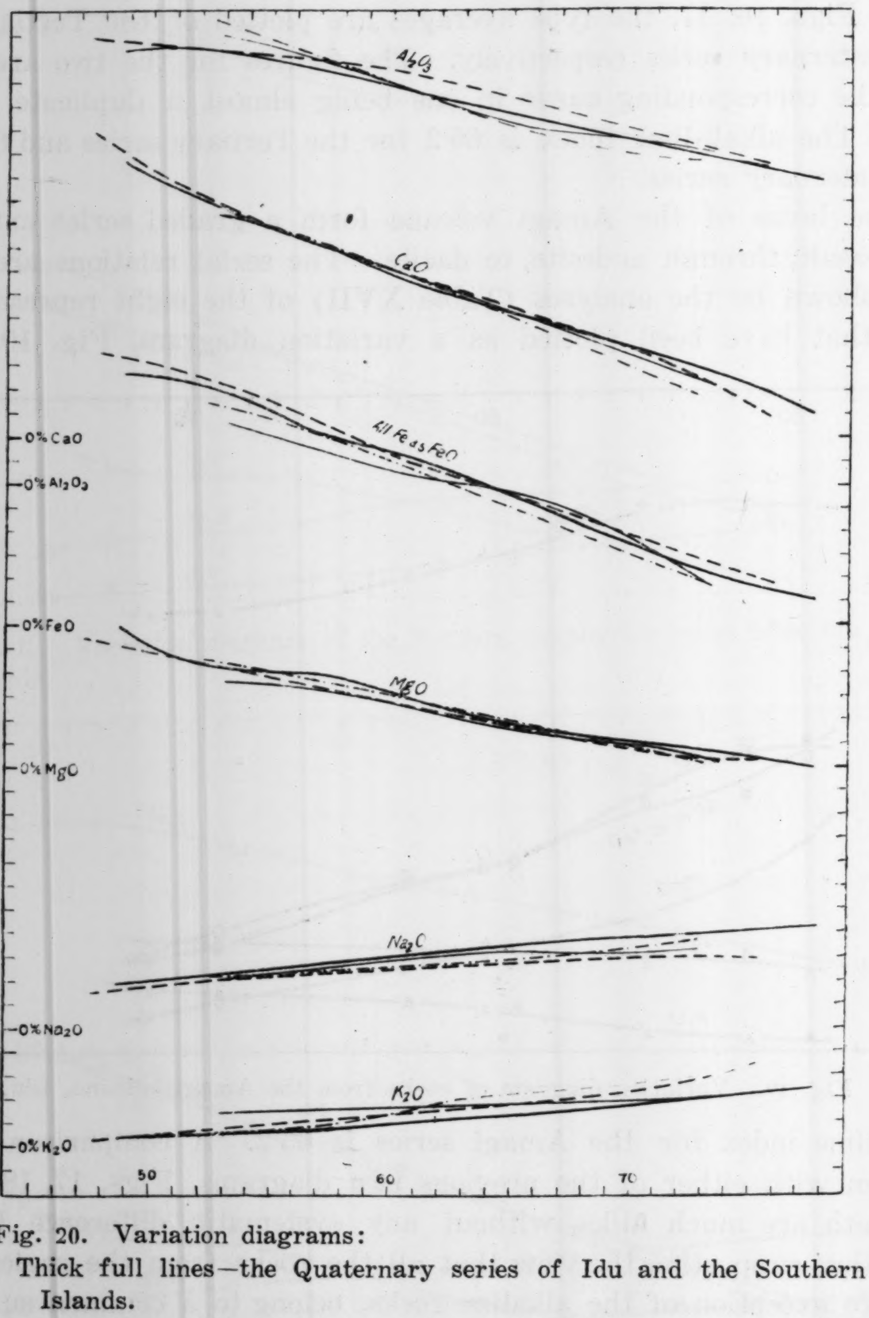

Fig. 20. Variation diagrams:
Thick full lines—the Quaternary series of Idu and the Southern Islands.
Broken lines—Yamada's type-averages of the Japanese volcanic rocks.
Thin full lines—Ryukyu Volcanic Zone.
Broken lines with dots – Medial Volcanic zone of NE. Japan.

basic rocks are generally more porphyritic with phenocrysts of calcic plagioclase and earlier members of mafic minerals, hence diverge more from possible magma liquid than acid rocks.

Assuming that the variation diagram, Fig. 18, for the Quaternary series represents the general chemical variation in the rocks from the region under discussion, it is compared in Fig. 20 with similar diagrams for rocks from two other volcanic zones in Japan, namely, Koto's Medial Volcanic Zone of NE. Japan[102], which includes the volcanoes Asama, Kusatu-Sirane, Nikko-Sirane, Nantai, Bandai, Iwate, Komagatake (Hokkaido), Usu, Tarumai, etc.; and the Ryukyu Volcanic Zone, which includes the volcanoes Aso, Kirisima, Sakura-sima, Io-sima (Osumi), etc.[103] In the figure they are also compared with the variation diagram of the type averages of the Japanese volcanic rocks[104].

As will be seen from the above figure, the variation in the rocks from the region under discussion follows, on the whole, that of the rocks from either one of the two other volcanic zones and that of the Japanese volcanic rocks, exhibiting the common characteristics that distinguish them from rocks of other regions of the world, namely, higher lime, lower alkalies, and larger ratios of iron oxides to magnesia. But, as contrasted with the type-averages of the Japanese volcanic rocks and with the rocks of the two other volcanic zones, the rocks of this region are slightly higher in soda but lower in potash[105]. The alkali-lime indices for the medial zone of NE. Japan, the Ryukyu zone, and for the Japanese type-averages, are 65·0, 65·7, and 66·2, respectively.

---

102) B. Koto, *Jour. Geol. Soc., Tokyo,* **23** (1916), 1.

103) The variation diagrams for these zones have been drawn only for the analyses made during recent years, since 1925. The sources of these analyses are as follows:

Asama—H. Tsuya, *Bull. Earthq. Res. Inst.,* **11** (1933), 575.
Kusatu-Sirane—H. Tsuya, *ibid.,* **12** (1933), 52.
Komagatake—H. Tsuya, *ibid.,* **8** (1930), 238.
Usu and Tarumai—J. Suzuki, *Bull. Volc. Soc., Japan,* **2** (1935), 123.
Nantai—S. Tsuboi and K. Sugi, *Guide-Book, Third Pan-Pacific Sci. Congr.,* Tokyo, (1926).
Nikko-Sirane—two new analyses, yet unpublished.
Aso—H. Tsuya, *Jour. Geol. Soc., Tokyo,* **36** (1929), 17.
Sakura-sima—K. Yamaguchi, *ibid.,* **35** (1928), 195, 241.
Io-zima—H. Tanakadate, *Proc. Imp. Acad.,* **11** (1935), 371.

104) S. Yamada, *Jour. Geol. Soc., Tokyo,* **37** (1930), 1.

105) Kuno has remarked that the basalts from the Huzi Volcanic Zone in general are poorer in alkalies, especially potash, than the basalts from the volcano Alaid and its new adjunct Taketomi-sima—a volcano in the NE. part of the Tisima (Kurile) Volcanic Zone. H. Kuno, *Jap. Jour. Geol. Geogr.,* **12** (1835), 153. The basaltic andesites from Tokati-dake, another volcano in the SW. part of that zone, are also high in alkalies compared with the former. H. Tsuya and F. Tada, *Bull. Earthq. Res. Inst.,* **2** (1927), 49.

Variation in the norm composition. The Q:F:M, Or:Ab:An, and Wo:En:Fs: ratios in the norms of the rocks from the region under discussion are plotted respectively in Figs. 21, 22, 23, in each of which they are compared with similar ratios for the type-averages of the Japanese volcanic rocks.

As will be seen from Fig. 21, the Q:F:M ratios of the aphyric rocks differ from those of the phyric rocks, the difference being more marked in the basic rocks (basalts and basaltic andesites) than in the more

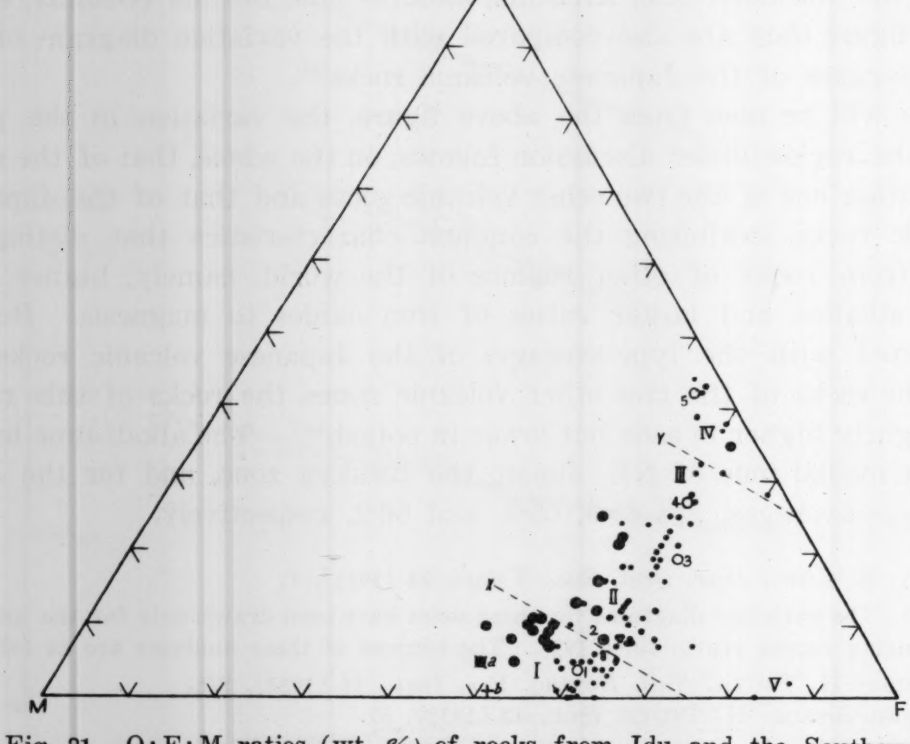

Fig. 21. Q:F:M ratios (wt. %) of rocks from Idu and the Southern Island. Q—normative quartz, F—normative feldspar, M—normative mafic minerals.

Large solid circles: Aphyric rocks.
Small solid circles: Phyric rocks.
Open circles: Yamada's type-averages of the Japanese volcanic rocks.
Crosses: a—average of 14 Deccan basalts.
b—Daly's average of 43 plateau basalts.

I. Basalt field. II. Andesite field. III. Dacite field. IV. Liparite field. V. Trachyandesite field. The lines X, Y, on which the ratios (Q+F)/(M+F) equal respectively to 0·75 (or 3/4) and 1·33 (or 4/3), are the most suitable boundaries that separate the andesite field from the basalt field and the liparite field respectively.

acid rocks. The aphyric basalts are poorer in F and richer in Q and M than the phyric basalts. This accords with the fact that the phyric basalts of the present region contain usually large quantities of plagioclase phenocrysts. The line X, every point on which has $(Q+F)/(M+F)=0{\cdot}75$ (or 3/4), is the most suitable boundary that separates the basalt field (I) from the andesite field (II). The other line Y, every point on which has $(Q+F)/(M+F)=1{\cdot}33$ (or 4/3), is the most suitable boundary that separates the liparite field (IV) from the dacite field (III) (cf. the introduction of this paper). The points for the aphyric basalts

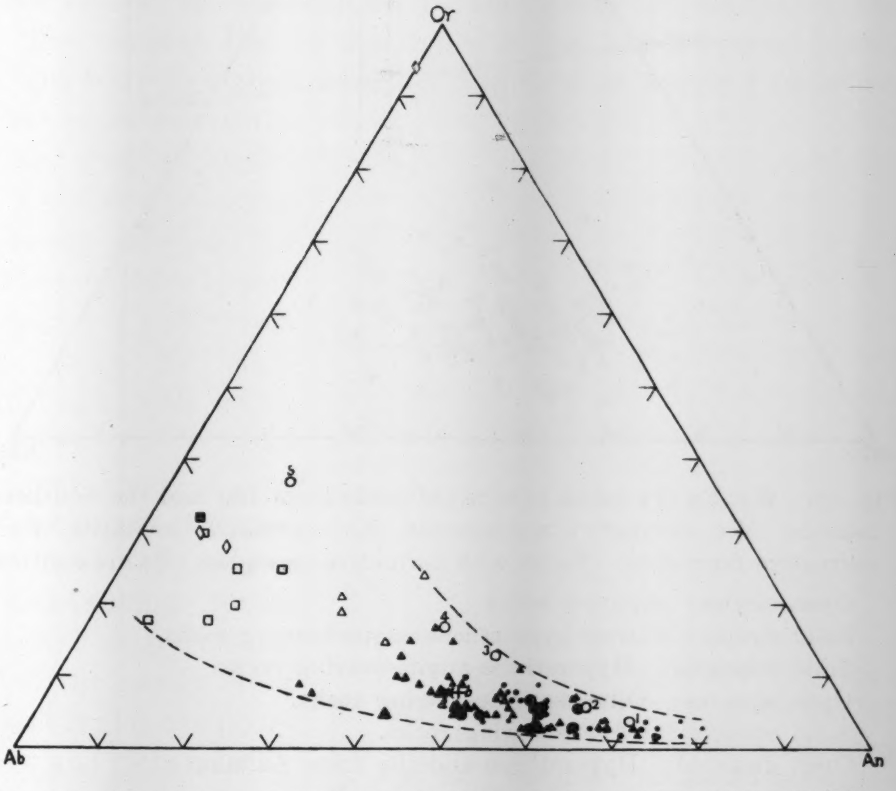

Fig. 22. Or : Ab : An ratio (wt. %) of rocks from Idu and the Southern Islands. Or—normative orthoclase, Ab—normative albite, An—normative anorthite.

Large solid circles: Aphyric basalts.
Small solid circles: Phyric basalts.
Large solid triangles: Aphyric andesites.
Small solid triangles: Phyric andesites.
Open triangles: Dacites.
Open squares: Phyric plagioliparites.
Solid square: Aphanitic liparite.
Open diamonds: Trachyandesites:
Solid diamond: Potash-liparite.
Open circles: Type-averages of the Japanese volcanic rocks.

lie more close to the plot of the average of 14 Deccan basalts106) than to the plot of Daly's average of 43 basalts in the world107).

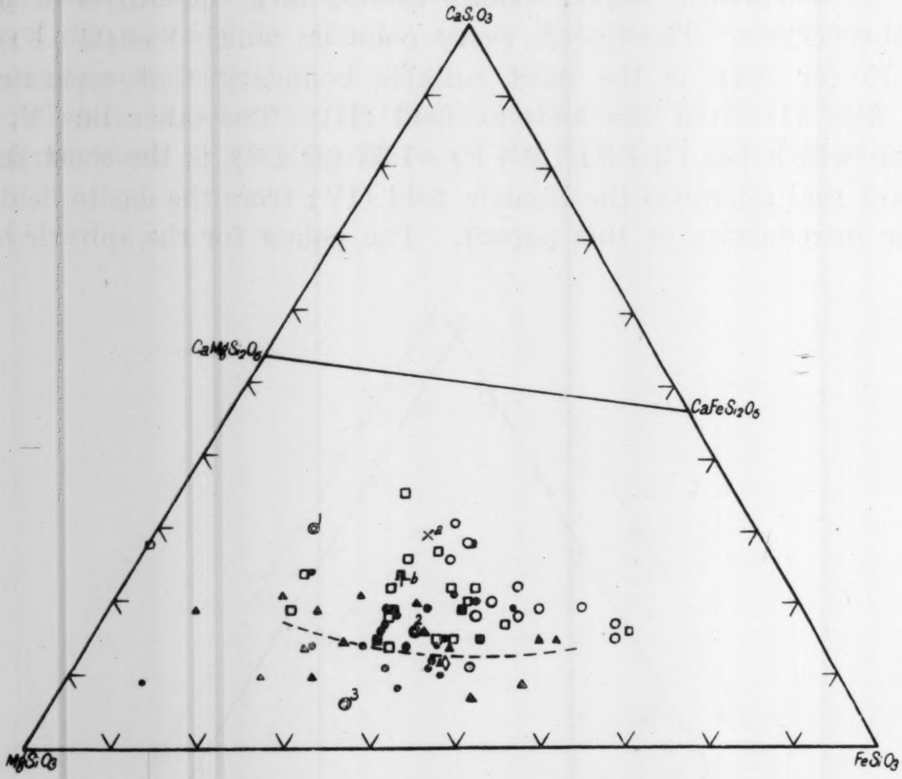

Fig. 23. Wo : En : Fs ratios (wt. %) of rocks from Idu and the Southern Islands. Wo—normative wollastonite, En—normative enstatite, Fs—normative ferrosilite. Rocks with normative corundum (C) are omitted.

Open circles: Aphyric rocks.
Solid circles: Olivine-hypersthene-augite-bearing rocks.
Solid triangles: Hypersthene-augite-bearing rocks.
Open squares: Olivine-augite-bearing rocks.
Solid squares: Olivine-bearing rocks.
Open diamond: Hypersthene-andesite from Asitaka.
Crosses: a—average of 14 Deccan basalts.
b—average of 43 world's plateau basalts.
Double circles: Type-averages of the Japanese volcanic rocks. 1—type basalt, 2—type basalt-andesite, 3—type andesite.

Fig. 22 shows that the normative feldspars of rocks from the region under discussion are, as a whole, poorer in Or than the type averages of the Japanese volcanic rocks. The normative feldspars of the aphyric basalts are poorer in An and richer in Ab and Or than those of most of the phyric basalts, but compared with the normative feldspar of the

---

106) L. L. FERMOR, *Rec. Geol. Surv., India,* 48 (1935), 344.

107) R. DALY, Igneous Rocks and the Depths of the Earth. New York (1933), 17.

average of Deccan basalts, the former are richer in An[108].

The normative pyroxenes, Fig. 23, of most of the aphyric rocks are richer in Fs than those of most of the phyric rocks, the Fs-richest pyroxenes being shown by the norms of the aphyric basalt (No. 83) from Hatizyo-sima, the almost-aphyric andesite (No. 76) from Aoga-sima, and of the vitrophyric trachyandesite (No. 118) from Io-sima. Comparing Figs. 23 and 14, we find that the normative pyroxenes of most of the phyric rocks correspond in composition to the mixtures of the modal pyroxenes (augite, hypersthene, and groundmass pigeonite) of the same rocks, whereas the normative pyroxenes of most of the aphyric rocks correspond in composition to the modal pigeonites of the same rocks. The brocken line in the figure is the two-pyroxene boundary[109], namely, the boundary that separates the field of augite (±olivine)-bearing rocks (upper side of the line) from that of hypersthene (±olivine)-bearing rocks (lower side of the line). The points for hypersthene-augite (±olivine)-bearing rocks lie scattered through both fields, while those for olivine-basalts and most of the aphyric rocks are included in the field of augite (±olivine)-bearing rocks. The normative pyroxenes of most of the basalts from the present region are poorer in Wo and richer in Fs than the normative pyroxenes of the plateau basalts (average Deccan basalt and Daly's average of world's plateau basalts).

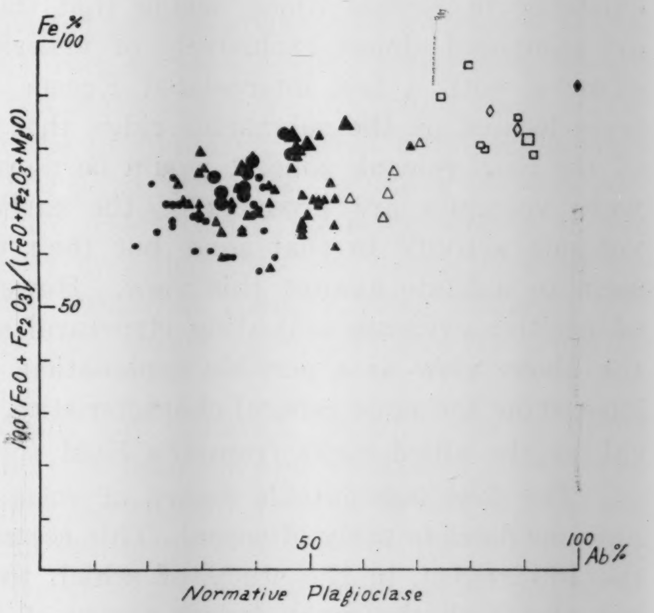

Fig. 24. Variation in the Fe-values, $100\times(FeO+Fe_2O_3)/(FeO+Fe_2O_3+MgO)$, in relation to the compositions of the normative plagioclases of rocks from Idu and the Southern Islands. The symbols are the same as those in Fig. 22.

Variation in the Fe-values. The variation in the Fe-values—ratios of iron-oxides to iron-oxides plus magnesia in the analyses of rocks—is shown in Fig. 24, in which the Fe-values (in per cent) are plotted with the compositions of normative plagioclases as abscissae. Although this values inclease as a whole as the normative plagioclases become richer in Ab, the increase is not marked. It has been pointed out elsewhere[110] that, as in the case of the actual paragenic relations between modal pyroxenes and modal plagioclases, the relations between the Fe-values and the compositions of normative plagioclases differ according to the particular genetical lineages of rocks (cf. Fig. 13 and the discussion thereof).

---

[108] The normative feldspars of Huzi basalts lie in composition more close to those of Deccan basalts compared with the normative feldspars of basalts from Idu and the Southern Islands.

[109] S. TSUBOI, *Jap. Jour. Geol. Geogr.*, **10** (1932~33), 77.

IV. SUMMARY AND CONCLUSIONS.

When volcanic activity began in the region studied is a matter of conjecture. There is no doubt, however, that volcanoes were already in existence in Eocene times, seeing that the Ogasawara (Bonin) Islands are composed almost exclusively of andesitic rocks, both explosive and effusive, with a few intercalated Eocene limestones. If these islands were located on the submarine ridge that underlies the insular volcanoes of the Huzi volcanic zone, it would be more than likely that the Ogasawara volcanics are products of the earliest recognized forerunner of volcanic activity in that zone, but their more or less outlying position seem to militate against this view. However, notwithstanding the lack of positive evidence indicating structural similarity, the writer presents the above view as a possible explanation, because the Ogasawara andesites show the same general characteristics, both microscopical and chemical, as the allied rocks from the Huzi volcanic zone.

The first indisputable record of volcanic activity in the Huzi volcanic zone dates to early Miocene. This seems to be the case not only with the Idu region, in the study of which the writer is chiefly concerned, but also with the much larger region of the "fossa magna", of which Idu forms but a small part. Through the whole of the period that succeeded it, the same general sequence of volcanic activity has beeu maintained in most parts of the fossa magna with certain local differences. It is therefore highly probable that, although local volcanic activity had already manifested itself in Eocene times in the Ogasawara Islands, more active and more regional activity had started contemporaneously with the tectonic disturbances, the result of all which is the fossa magna, which severed the geologic continuation between southwestern and northeastern Japan. As to whether or not the Ogasawara Islands were subjected to the same disturbances, the writer is unable to say.

---

[110] H. TSUYA, *Bull. Earthq. Res. Inst.*, 7 (1929), 332; *Proc. Third Pan-Pacific Sci. Congr.*, Tokyo, **1** (1926), 2396.

The lower Miocene volcanism in Idu, which occurred beneath the sea of that time, is represented by a thick series of highly altered volcanics (lavas and pyroclastics), referred to as the Yugasima beds (or the propylite series). This series consists for the most part of basaltic and andesitic rocks, although dacites and liparites are also represented, especially in the upper horizons of the series. The succession of these rocks implies considerable time, during which certain structural deformations might possibly have recurred, resulting in several periods of volcanic accumulation. But its actual duration is a question we have no means of answering at present, the only precise datum being the faunal evidence (*Lepidocyclina* limestone from Simo-Siroiwa and *Miogypsina* limestone from Nasimoto), which assigns certain dacitic volcanics lying some distance above the base of the series to lower Miocene.

The propylite series is invaded by numerous minor intrusives (dikes, sheets, and necks) of various rock-types—diabase, porphyrite, basalt, andesite, dacite, and liparite (quartz-porphyry). Although these intrusives are evidently later than the propylite series, not all of them were formed contemporaneously. The basic intrusives (including diabase, porphyrite, basalt, and andesite) are mostly older, all being altered in the same way as the propylite series in which they are found, whereas the more acid intrusives are mostly somewhat younger, being probably correlated with the acid volcanics that overlie unconformably the propylite series.

The lower Miocene volcanism was followed, probably during upper Miocene, by submarine eruptions of liparites and dacites, with subordinate andesites, all of which are distributed mostly in south Idu and rather locally in north Idu. As just mentioned, some of the minor intrusives in the propylite series, especially those of acid rocks, might be the feeders of the upper Miocene volcanics. In contrast with the propylite series, these upper Miocene volcanics are either quite fresh or are but little altered.

The foregoing phase of volcanism was succeeded, most probably during lower Pliocene, by a subordinate phase of activity characterized by minor intrusions (dikes) and extrusions of andesites. Regarding volcanism during this period, however, we are largely in the dark as only a few rocks in Idu have been identified with that period.

In the uppermost Pliocene, eruptions of basalts, dacites, and andesites, occurred only locally in Idu, and these were again exclusively submarine.

At the close of the Tertiary or the beginning of the Pleistocene, Idu peninsula was subjected like the other regions in the fossa magma to crustal movement, generally in the sense of uplift, and it was not until some time after this movement, which raised so much of the Tertiary sea-floor into land, that Pleistocene volcanism became vigorous. This volcanism was concentrated mainly in the northern part of the peninsula, while in the southern part, Tertiary volcanism was succeeded by that relative quiescence which marked the Pleistocene aud Recent epochs.

The first phase of lower Pleistocene volcanism is thus represented by eruptions of basalts, andesites, and dacites, all occurring in the forms of tuff and tuff-breccia that now occupy the bulk of the lacustrine deposits (Ono beds, Simo-Hata beds, and Simo-Tanna beds) accumulated during that period on the erosion reliefs of the Tertiary formations. It was followed at the end of lower Pleistocene and in the upper Pleistocene, when the lower Pleistocene deposits had been more or less deformed, by eruptions of central volcanoes. The volcanoes Tensi, Usami, Taga, Yugawara, Asitaka, Amagi, Hakone, and others in the northwestern part of the Idu peninsula yet unstudied, as also the dacitic masses in the vicinity of Atami, are all products of this phase of activity, with however certain differences in the times when the activities began and in the period for which they lasted. The basaltic Omuro-yama group represents the last volcanism in the peninsula, which probably occurred some time later when the older volcanoes Tensi, Usami, Taga, etc., were subjected to more or less dislocation and dissection; while the numerous hot-springs there represent a stage of post-volcanic thermal activity. So far as its visible part is concerned, Huzi may date from a much later age, probably Recent. That one of the earliest lava-flows from the volcano is younger than the older somma of Hakone has been definitely proved by field evidence.

All the insular volcanoes of the Seven Idu Islands and the Southern Islands are undoubtedly products of Quaternary volcanism, whatever may be the history of their foundation. Of these, the dissected basaltic volcanoes Utone-sima, To-sima, Mikura-sima, Higasi-yama (Hatizyo-sima), Tori-sima, and Kita Io-sima probably date to Pleistocene. With the exception of Tori-sima[111], we have no record of eruption of any of them. The basaltic volcanoes O-sima, Miyake-sima, Nisi-yama (Hatizyo-sima), and Aoga-sima have been active in Recent times, all displaying lava out-flows in historic times. The liparitic volcanoes Nii-sima and

---

[111] The only recorded activity of this island is a mere paroxismal explosion of phreatic origin that occurred in 1902.

Kodu-sima, according to records, also have had one eruption each.

With the exception of the rarer alkaline rocks (potash-liparite and trachyandesite), the rocks that erupted in the course of the volcanism just outlined above have all several characteristics in common, mineralogical as well as chemical, with however certain differences due to local peculiarities. Whether chemically or mineralogically, there seems to be no systematic difference between the Tertiary and Quaternary series, excepting that the former usually has a higher water-content than the latter. A petropraphic similarity in the Ogasawara rocks to allied rocks from Idu is quite apparent.

Of the various rock-types represented, the basalts and basaltic andesites are most predominant besides being regional in distribution, while the others are rather local. These regional rock-types are usually characterized by phenocrysts of calcic plagioclase (anorthite to calcic labradorite) and pyroxenes (augite or hypersthene or both), with or without olivine, in a groundmass containing less calcic plagioclase (bytownite to sodic labradorite), pigeonite, magnetite, and one or more of silica minerals (cristobalite, tridymite, and quartz). It is notable that most of the young lavas from Miyake-sima, Hatizyo-sima, Aoga-sima, etc., are poor in phenocrysts or almost aphyric, while the old lavas from these volcanoes are sometimes strongly porphyritic with large phenocrysts of anorthite. Like the latter, most of the lavas from the Pleistocene basaltic volcanoes (Kita Io-sima, Tori-sima, Mikura-sima, etc.), as also the basalts in the Tertiary series, are strongly porphyritic, sometimes with large phenocrysts of anorthite, the less porphyritic or almost-aphyric rocks being rarely met with.

The variation diagram of the aphyric and aphanitic rocks (magma variation diagram) from both the Tertiary series and the Quaternary volcanoes shows smooth curves for all oxides, showing the probable variations in the magmatic liquids from which most of the volcanic rocks of the present region seem to have been derived.

The variation diagram of type-averages of the Tertiary porphyritic rocks is identical with the same diagram of the Quaternary porphyritic rocks. The two are again similar to the variation diagram of the well-differentiated rocks of one volcano, namely, Amagi, with the result that either of these two diagrams will represent the chemical variation for rocks of the entire region. The variation on the whole follows that of type-averages of the Japanese volcanic rocks, thus showing the common characteristics that distinguish them from corresponding type-averages of the world's igneous rocks: namely, in containing higher lime, lower alkalies, and larger ratios of iron-oxides to magnesia. But, as compared with type-averages of the Japanese volcanic rocks, the corresponding type-averages of the present region are usually a little higher in soda but lower in potash. So also do the latter as compared with the rocks from the two other volcanic zones in Japan, namely, the medial volcanic zone of NE. Japan and the Ryukyu volcanic zone.

The rocks of the region studied, except a few alkaline rocks, may be treated as a connected suite, all belonging to what Peacock calls the "calcic series", with high alkali-lime index, 62·5 for the Tertiary series and 65·7 for the Quaternary series. If the entire suite has originated from a common magma, we would have to admit that acid rocks such as liparites were derived by processes of differentiation from a basaltic magma. During the whole period since the Tertiary, however, volcanism in the present region has been alternately basaltic (or andesitic) and liparitic (or dacitic). This recurrence of similar rock-types points to one of two explanations: (1) either a body of acid magna that had separated out during early Tertiary or before it had remained throughout succeeding ages as an available source of the acid rocks that erupted during several distinct epochs, or (2) that differentiation to an advanced stage had proceeded repeatedly along definite lines at wide intervals of time. Although, of these two alternatives, the former is the more simple, the latter process also must have operated at certain local centres in the region, seeing that well-differentiated rocks intimately related, structurally as well as petrologically, occur in certain central volcanoes such as Amagi.

Although the rocks of the so-called Huzi volcanic zone may be treated on the whole as a connected magmatic suite, we find certain differences among them due to local peculiarities, mineralogical as well as chemical. Thus the Huzi rocks differ from the allied rocks of Idu and the Southern Islands in that the former are distinctly higher in alkalies, especially potash, and lower in lime than the latter. So also do the rocks from the volcanoes Kayaga-take and Iiduna-yama compared with the allied rocks of Idu and the Southern Islands. Although these two volcanoes lie farther north of Huzi, they belong in a wide sense to the Huzi volcanic zone. From these facts in view, the writer believes that the Huzi volcanic zone may be divided petrologically into two subzones, namely, the northern inland zone referred to as the *Huzi Volcanic Zone proper*, and the southern oceanic zone referred to as the *O-sima Volcanic Zone*. The Huzi volcanic zone proper includes the inland volcanoes Huzi, Kayaga-take, Iiduna-yama Kurohime-yama, and many others (Myoko-zan, Yatuga-take volcano group, etc.) yet unstudied, all of which are linearly arranged in a NNW.-SSE. direction on the fossa magna, while the O-sima volcanic zone includes, in addition to the volcanoes of the Idu peninsula, the insular and submarine volcanoes of the Pacific—the Seven Idu Islands and the Southern Islands. To generalize, *although the rocks of the so-called Huzi volcanic zone, with the exception of a few alkaline rocks, belong on the whole to a calcic series, the rocks from its northern inland part—the Huzi volcanic zone proper—are higher in alkalies and lower in lime than those from the southern oceanic part—the O-sima volcanic zone.* Whether or not the chemical differences of these two sub-zones are in any way connected with some differences in the geotectonic structure and in the nature of rocks of their foundation is a question we have no means of answering at present.

The O-sima volcanic zone just proposed has two kinds of alkaline rocks, namely, potash-liparite (Manzo-yama and Kodu-sima) and trachyandesite (Io-sima). As to the genesis of the potash-liparite, a possible explanation was offered in an earlier paper[112]. As to the genesis of the trachyandesite, little can be said with certainty at present except that its local distribution in the Volcano Islands group and the occcurrence in it of porphyritic olivine and augite, both of which are similar in microscopic characters to the respective minerals in the basalts from the same group, make it possible that it is genetically related to these basalts. In this connection the distribution of the sites of volcanic vents in the Volcano Islands group calls for notice. Although the general trend of this group is from NNW. to SSE.—that is, the trend of the so-called Huzi volcanic zone—, Io-sima, besides being elongated in outline from NE. to SW., has numerous solfataras which are aligned on fissures running in the same direction. The trachyandesitic submarine volcano, "Sin-to Volcano", also lies on a line running NE.-SW. through the basaltic volcano, Minami Io-sima. Similar relation holds between the basaltic and liparitic volcanoes of the Seven Idu Islands[113]. Therefore, if the sites of volcanic vents were fixed by dislocation or lines of weakness in the earth's crust, these two trends—the NNW.-SSE. trend of the basaltic (or andesitic) volcanoes and the NE.-SW. trend of the liparitic (or dacitic) and trachyandesitic volcanoes—may be a surface manifestation of the underground structure of the region, the former representing a principal fracture (Daly's "abyssal fissure")[114] connected with deep-seated reservoirs of a regional basaltic magma, and

---

112) H. TSUYA, *Bull. Earthq. Res. Inst.*, **7** (1929), 313.

113) H. TSUYA, *Bull. Earthq. Res. Inst.*, **10** (1932), 255; *Proc. Third. Pan-Pacific Sci. Congr.*, Tokyo, **1** (1926), 2399.

114) R. DALY, Igneous Rocks and the Depths of the Earth. New York (1933), 242.

the latter a subsidiary fracture connected with shallow-seated reservoirs of local differentiates, either liparitic or trachyandesitic, from the basaltic magma.

In conclusion, a few remarks should be added here regarding the alteration through secondary changes of the Tertiary volcanics in Idu, although on this point the writer has not yet been able to gather much information. As already noted, the only rocks that are altered to any important extent are these of the propylite series and the minor intrusives in that series. The common secondary minerals in them are chlorite, calcite, sericite, epidote, limonite, haematite, pyrite, zeolite, albite, and quartz, with amorphous silica, two or more of these minerals always occurring together. The alteration, however, has not advanced to the same degree and in the same way throughout the series. In some parts of the series, most of the rocks are almost unchanged, although, as a rule, incipient alteration of the constituent minerals is found only to a very slight extent, while in many others the alteration is considerable, resulting in virtual disappearance of the original structure of the rock, whether viewed microscopically or in the field. We often find that complete recrystallization has occurred, showing a mosaic of quartz and feldspar, with occasional flakes of sericite and chlorite.

Since the alteration of the propylite series has advanced farther not only at and near the contacts with minor intrusives in the series, but also in the intrusives themselves than at distances away from the contacts, it could only have been caused by local and chemical effects, that is to say, by chemical reactions between the original rocks of the series and some hydrothermal solutions[115] that possibly generated in a post-magmatic stage subsequent to the minor intrusions rather than by regional and dynamic agencies. The metamorphic changes justifying the name, propylite, were probably caused by a sodiferous hydrothermal solution, possibly related to the basic intrusives (diabase, porphyrite, basalt, and andesite). The product of this intense mineralization which is so economically important and which has been worked in several parts of the propylite series in the region, was generated probably by a hydrothermal solution rich in silica generally related to the acid intrusives (dacite and liparite or quartz-porphyry). K. Sugi divided the metamorphism of the Misaka series of the Nakagawa district adjoining the northern part of Hakone, which is intruded by a large quartz-diorite mass, and which is a lower Miocene series correlated with the propylite series of Idu, into two stages: dynamic metamorphism caused by a mountain-building movement generated within a geosynclinal area before the intrusion of the quartz-diorite and contact metamorphism at the time of that intrusion[116]. The writer is of the opinion that the dynamic metamorphism, if it did occur, must have been due merely to local stresses that generated outside the boundary of the quartz-diorite mass at the beginning of the intrusion of that mass, seeing that the metamorphism is quite local in the Misaka series both at and near the contacts with the intrusive, and that such metamorphism is never met with in the propylite series of Idu, which belongs to the same geotectonic unit as the Misaka series.

---

[115] T. KATO, *Jap. Jour. Geol. Geogr.*, **6** (1928), 31.

20. 富士火山帯の火山作用，特に伊豆及び南方諸島の地質及び岩石に就いて

地震研究所　津屋弘逵

此論文では富士火山，伊豆半島，南方諸島等の地質及び岩石に就いて，筆者が既に發表した研究に其後の研究結果を加へ，所謂富士火山帶特に其富士火山以南小笠原火山列島に至る地域に於ける第三紀及び其後の火山作用を地質學的並びに岩石學的見地より考察した．即ち，先づ同地域に行はれた火山作用を古第三紀火山作用，新第三紀火山作用，及び第四紀火山作用に分ち，各期の代表的火山岩類を噴出順序及び種類に依りて細別記述し，次に全岩類の主要造岩鑛物の顯微鏡的性質を總括し，最後に其化學成分上の特質な說明し，所謂富士火山帶は岩石學的に見て第三紀及び第四紀の噴出物を通じて他の火山帶とは異なつた全般的特質を有するが，少くとも第四紀の火山のみに就いて見たる富士火山帶は富士火山及び以北の內陸火山を含む支帶と伊豆半島及び以南の海洋火山を含む支帶とに分たれ，各支帶は夫々岩石學的(特に化學成分上の)特質を示し，前者を狹義の富士火山帶，後者を大島火山帶と稱する事の至當なるを論じた．

---

[116] K. SUGI, *Jap. Jour. Geol. Geogr.*, **9** (1931), 87.

21. *On the Elastic Deformation of a Stratified Body Subjected to Vertical Surface Loads.*

By Katsutada SEZAWA and Kiyoshi KANAI,

Earthquake Research Institute.

(Read Feb. 16, 1937.—Received March 20, 1937.)

1. *Introduction.*

The elastic deformation of a semi-infinite body subjected to vertical loads on its surface was discussed some years ago by Boussinesq,[1] Nagaoka,[2] Terazawa,[3] etc. Terazawa[4] furthermore gave a criterion such that the vertical component of surface displacement under vertical loads should invariably be directed downward. On the other hand, some of the results in both Matumura's paper[5] and Anzo's[6] in connexion with the deformation of an elastic foundation seemed to show that in the case of a stratified body the surface deformation may be partly upward. Although Nishimura[7] solved a similar problem more exactly, and obtained a result agreeing with Terazawa's criterion, owing to his case being restricted to a very thin surface layer there is still some doubt whether or not the surface deformation in a body, having a layer of a thickness that is comparable to the width of the load distribution, may still always be in the downward sense. With a view to ascertaining the nature of the problem, we solved it from a different point of view for a wide range of ratio of thickness of layer to width of load distribution, the problem in the present paper, however, being restricted to a two-dimensional case.

2. *Solution of the problem.*

Let ρ, λ, μ, ρ', λ', μ' be the densities and the elastic constants of the surface layer (of thickness H) and the subjacent medium, the axes of x, y being taken as shown in Fig. 1. If χ, χ' be Airy's functions, the solutions of the elastic equilibrium of both media can be deduced from the differential equations

---

[1] J. BOUSSINESQ, *Application des Potentials . . . .*, (Paris, 1885).

[2] H. NAGAOKA, *Proc. Phys.-Math. Soc., Tokyo*, **6** (1912), 208.

[3] K. TERAZAWA, *Journ. Coll. Sci., Tokyo Imp. Univ.*, **37** (1916), 1~64; *Phil. Trans. Roy. Soc.*, **217** (1916), 35.

[4] Ditto, *Journ. Phys.-Math. Soc., Japan.* **1** (1927), 141~143.

[5] M. MATUMURA, *Journ. Civil Eng., Japan*, **17** (1931), 813~869.

[6] Z. ANZÔ, *Bull. Fac. Eng., Kyûsyu Imp. Univ.*, **8** (1933), 232~247.

[7] G. NISHIMURA, *Bull. Earthq. Res. Inst.*, **10** (1932), 23~28.

$$\nabla^4\chi=0\,, \qquad \nabla^4\chi'=0\,, \tag{1}$$

so that the stresses in both media are such that

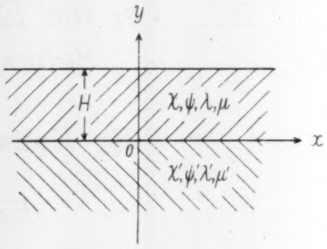

Fig. 1.

$$\left.\begin{aligned} \sigma_x&=\frac{\partial^2\chi}{\partial y^2}\,, & \sigma &=\frac{\partial^2\chi}{\partial x^2}\,, & \tau_{xy}&=-\frac{\partial^2\chi}{\partial x\partial y}\,, \\ \sigma'_x&=\frac{\partial^2\chi'}{\partial y^2}\,, & \sigma'_y&=\frac{\partial^2\chi'}{\partial x^2}\,, & \tau'_{xy}&=-\frac{\partial^2\chi'}{\partial x\partial y}\,. \end{aligned}\right\} \tag{2}$$

If complementary functions ψ, ψ' satisfy the conditions

$$\frac{\partial^2\psi}{\partial x\partial y}=\nabla^2\chi\,, \qquad \frac{\partial^2\psi'}{\partial x\partial y}=\nabla^2\chi'\,, \tag{3}$$

$$\nabla^2\psi=0\,, \qquad \nabla^2\psi'=0\,, \tag{4}$$

then the displacements (u, v), (u', v') in both media are

$$\left.\begin{aligned} 2\,\mu u&=-\frac{\partial\chi}{\partial x}+(1-\sigma)\frac{\partial\psi}{\partial y}\,, & 2\,\mu v&=-\frac{\partial\chi}{\partial y}+(1-\sigma)\frac{\partial\psi}{\partial x}\,, \\ 2\mu' u'&=-\frac{\partial\chi'}{\partial x}+(1-\sigma')\frac{\partial\psi'}{\partial y}\,, & 2\mu' v'&=-\frac{\partial\chi'}{\partial y}+(1-\sigma')\frac{\partial\psi'}{\partial x}\,, \end{aligned}\right\} \tag{5}$$

where σ, σ' are the respective Poisson's ratios, namely $\sigma=\lambda/2(\lambda+\mu)$, $\sigma'=\lambda'/2(\lambda'+\mu')$.

The elementary solutions of χ, χ', ψ, ψ' satisfying (1), (4) are such that

$$\left.\begin{aligned} \chi&=\cos mx\,(Ay\,\mathrm{sh}\,my+B\mathrm{ch}my+Cy\,\mathrm{ch}\,my+D\,\mathrm{sh}\,my)\,, \\ \chi'&=\cos mx\,(\mathrm{E}ye^{my}+Fe^{my})\,, \end{aligned}\right\} \tag{6}$$

$$\psi=\sin mx\,(\alpha\,\mathrm{ch}\,my+\beta\,\mathrm{sh}\,my)\,, \qquad \psi'=\sin mx\gamma e^{my}\,. \tag{7}$$

Substituting (6), (7) in (3), we get

$$\alpha=\frac{2}{m}C\,, \qquad \beta=\frac{2}{m}A\,, \qquad \gamma=\frac{2}{m}E\,. \qquad (8), (9), (10)$$

The boundary conditions are

$$y=0; \qquad u=u', \quad v=v', \quad \sigma_y=\sigma'_y, \quad \tau_{xy}=\tau'_{xy}, \qquad (11), (12), (13), (14)$$

$$y=H; \qquad \tau_{xy}=0, \quad \sigma_y=\varphi(x). \qquad (15), (16)$$

Substituting (6) ~ (10) in (11) ~ (16) and using (2), we get

$$\left.\begin{aligned}
\frac{C\Phi}{A}&=\Big[4\mu\mu'(1-\sigma)(1-\sigma')+mH(\mu-\mu')\Big\{(3-4\sigma')\mu+\mu'\Big\}\Big]\operatorname{ch}mH\\
&\qquad+\Big\{\mu^2(3-4\sigma')-2\mu\mu'\sigma(1-2\sigma')+\mu'^2(1-2\sigma)\Big\}\operatorname{sh}mH,\\
\frac{D\Phi}{A}&=\frac{-1}{m}\Bigg\{\Big[4\mu\mu'(1-\sigma)(1-\sigma')+mH\Big\{\mu^2(3-4\sigma')-2\mu\mu'\sigma(1-2\sigma')\\
&\qquad+\mu'^2(1-2\sigma)\Big\}\Big]\operatorname{ch}mH+\Big[\Big\{\mu+\mu'(1-2\sigma)\Big\}\Big\{\mu(3-4\sigma')\\
&\qquad-\mu'(1-2\sigma)\Big\}+4mH\mu\mu'(1-\sigma)(1-\sigma')\Big]\operatorname{sh}mH\Bigg\},\\
\frac{E\Phi}{A}&=\Big\{4\mu'^2(1-\sigma)^2+2mH\mu'(\mu-\mu')(1-\sigma)\Big\}\operatorname{ch}mH\\
&\qquad+2\mu'(1-\sigma)\Big[\Big\{\mu+\mu'(1-2\sigma)\Big\}-mH(\mu-\mu')\Big]\operatorname{sh}mH,\\
\frac{F\Phi}{A}&=\frac{-2\mu'(1-\sigma)}{m}\Bigg\{2\Big\{\mu'(1-\sigma)+mH\mu(1-\sigma')\Big\}\operatorname{ch}mH\\
&\qquad+\Big[2\mu(1-\sigma')+mH\Big\{\mu(1-2\sigma')+\mu'\Big\}\Big]\operatorname{sh}mH\Bigg\},\\
&B=F, \quad \alpha=\frac{2}{m}C, \quad \beta=\frac{2}{m}A, \quad \gamma=\frac{2}{m}E,
\end{aligned}\right\}\quad(17)$$

where

$$\Phi=2\mu'(1-\sigma)\Big\{\mu(1-2\sigma')+\mu'\Big\}\operatorname{ch}mH$$
$$+\Big[4\mu\mu'(1-\sigma)(1-\sigma')-mH(\mu-\mu')\Big\{(3-4\sigma')\mu+\mu'\Big\}\Big]\operatorname{sh}mH. \qquad (18)$$

The elementary value of σ_y at $y=H$ is

$$\sigma_y=-m^2\cos mx(AH\operatorname{sh}mH+B\operatorname{ch}mH+CH\operatorname{ch}mH+D\operatorname{sh}mH). \qquad (19)$$

Hence in the special case

$$y=H; \qquad \sigma_y=P\cos mx, \qquad (20)$$

the solution of the corresponding vertical component of displacement at the surface assumes the form

$$v_{y=H}=\frac{PH\cos mx\,(1-\sigma)}{\mu\qquad mH}\left[\frac{1+2R(mH)e^{-2mH}-Ne^{-4mH}}{1-2\{R(mH)^2+S\}e^{-2mH}+Ne^{-4mH}}\right], \tag{21}$$

where

$$\left.\begin{aligned}&N=N'/M', \qquad R=R'/M', \qquad S=S'/M',\\ M'&=\mu^2(3-4\sigma')+2\mu\mu'(5-6\sigma'-6\sigma+8\sigma\sigma')+\mu'^2(3-4\sigma),\\ N'&=\mu^2(3-4\sigma')+2\mu\mu'(-3+2\sigma'+2\sigma)+\mu'^2(3-4\sigma),\\ R'&=2(\mu-\mu')\{\mu(3-4\sigma')+\mu'\},\\ S'&=\mu^2(3-4\sigma')+2\mu\mu'(1-2\sigma)(1-2\sigma')+\mu'^2(-5+12\sigma-8\sigma^2).\end{aligned}\right\} \tag{22}$$

The maximum value of the displacement $v_{y=H}$, which is distributed sinusoidally, for different ratios of the thickness H to the wave length $2\pi/m$ as well as for different values of μ/μ' are shown in Fig. 2. It should be borne in mind that the broken line specially shows the maximum vertical displacement at $y=0$, namely, the bottom boundary of the layer, for the case $\mu/\mu'=1/2$.

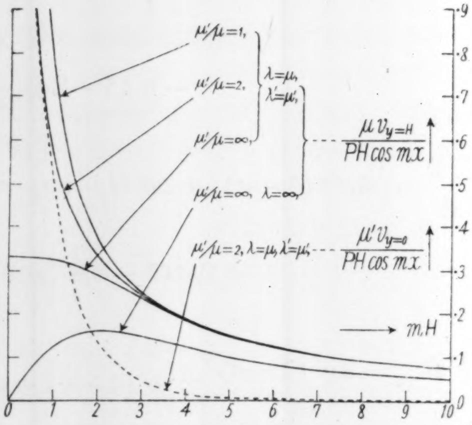

Fig. 2. Maximum values of v for sinusoidally distributed loads.

We shall now generalize the solution in (19) in the form

$$\sigma_y(\text{at } y=H)=\int_0^\infty -m^2\cos mxA\phi(H,m)\,dm\,, \tag{23}$$

where

$$\phi(H,m)=H\,\mathrm{sh}\,mH+\frac{B}{A}\mathrm{ch}\,mH+\frac{C}{A}H\,\mathrm{ch}\,mH+\frac{D}{A}\mathrm{sh}\,mH. \tag{24}$$

Comparing (23) with Fourier's integral (for an even function)

$$\sigma_y(\text{at } y=H)=\varphi(x)=\frac{2}{\pi}\int_0^\infty\cos mx\,dm\int_0^\infty\varphi(\lambda)\cos m\lambda\,d\lambda\,,$$

we get

$$A=\frac{-2}{\pi m^2\phi(H,m)}\int_0^\infty\varphi(\lambda)\,\mathrm{ccs}\,m\lambda\,d\lambda\,. \tag{25}$$

The corresponding vertical component of displacement in the layer is then

$$v = \frac{2}{\pi}\int_0^\infty \frac{\cos mx}{2\mu}\,\frac{\Phi(y,m)}{m^2\varphi(H,m)}\,dm\int_0^\infty \varphi(\lambda)\cos m\lambda d\lambda\,, \tag{26}$$

where

$$\begin{aligned}\Phi(y,m) = &\left\{my\,\mathrm{ch}\,my-(1-\sigma)\,\mathrm{sh}\,my\right\}+\frac{B}{A}m\,\mathrm{sh}\,my\\ &-\frac{C}{A}\left\{(1-2\sigma)\,\mathrm{ch}\,my-my\,\mathrm{sh}\,my\right\}+\frac{D}{A}m\,\mathrm{ch}\,my\,.\end{aligned} \tag{27}$$

It is possible to write the horizontal component of displacement in the same way as in the foregoing.

3. *Distribution of surface displacements and inclinations in a general case.*

The surface vertical displacement is now clearly of the form

$$\begin{aligned}v_{y=H} = \int_0^\infty \frac{2\cos mx}{\pi\mu m}(1-\sigma)&\left[\frac{1+2R(mH)e^{-2mH}-Ne^{-4mH}}{1-2\{R(mH)^2+S\}e^{-2mH}+Ne^{-4mH}}\right]\\ &\cdot dm\int_0^\infty \varphi(\lambda)\cos m\lambda d\lambda\,,\end{aligned} \tag{28}$$

R, S, N being shown in (22).

In the special case, $\mu=\mu'$, $\sigma=\sigma'$, that is, in the case of a semi-infinite body, there exist the relations $R=0$, $S=0$, $N=0$, so that the integral (28) can be evaluated very readily for any form of $\varphi(\lambda)$.

Let

$$\varphi(x) = \frac{Pa^2}{a^2+x^2}\,, \tag{29}$$

the maximum and the resultant of the pressure being P and πPa respectively. Since the integral (28) is somewhat difficult to evaluate even in the case of pressure distribution (29), we shall for simplicity calculate the surface inclination of the body. The surface inclination in the case of pressure distribution of type (29) assumes the form

$$\frac{\partial v_{y=H}}{\partial x} = -\int_0^\infty \frac{Pa\sin mx e^{-ma}}{\mu}(1-\sigma)\left[\frac{1+2R(mH)e^{-2mH}-Ne^{-4mH}}{1-2\{R(mH)^2+S\}e^{-2mH}+Ne^{-4mH}}\right]dm\,. \tag{30}$$

As already mentioned, in the special case where $\mu=\mu'$, $\sigma=\sigma'$, namely, that of a semi-infinite body, the expression within the pair of brackets in (30) tends to unity, the evalution being consequently very simple.

Unless μ'/μ is as large as $\mu'/\mu \gg 2$, the integral (30) can be evaluated by expanding in series the expression within the pair of brackets, the expression of the surface inclination accordingly being

$$\frac{\partial v_{y=H}}{\partial x}=-\int_0^\infty \frac{2Pa(1-\sigma)}{\mu}\sin mx\left\{\frac{1}{2}e^{-ma}+\eta_1 e^{-m(a+2H)}+\eta_2 e^{-m(a+4H)}\right.$$
$$\left.+\eta_3 e^{-m(a+6H)}+\;.\;.\;.\;.\right\}dm\,, \qquad (31)$$

where

$$\eta_1=S+RHm+RH^2m^2\,,$$

$$\eta_2=(2S^2-N)+2RSHm+4RSH^2m^2+2R^2H^3m^3+2R^2H^4m^4\,,$$

$$\eta_3=S(4S^2-3N)+(4S^2-N)RHm+3(4S^2-N)RH^2m^2+8R^2SH^3m^3$$
$$+12R^2SH^4m^4+4R^3H^5m^5+4R^3H^6m^6\,,$$

$$\eta_4=(8S^4-8NS^2+N^2)+4(2S^2-N)RSHm$$
$$+16(2S^2-N)RSH^2m^2+\;.\;.\;.\;.+8R^4H^8m^8\,,$$

$$\eta_5=S(16S^4-20NS^2+5N^2)+(16S^4-12NS^2+N^2)RHm$$
$$+5(16S^4-12NS^2+N^2)RH^2m^2+\;.\;.\;.\;.+16R^5H^{10}m^{10}\,,$$

$$\eta_6=(32S^6-48NS^4+16N^2S^2-N^3)+2(16S^4-16NS^2+3N^2)RSHm$$
$$+12(16S^4-16NS^2+3N^2)RSH^2m^2+\;.\;.\;.\;.\,,$$

$$\eta_7=S(64S^6-112NS^4+56N^2S^2-7N^3)$$
$$+(64S^6-80NS^4+24N^2S^2-N^3)RHm$$
$$+7(64S^6-80NS^4+24N^2S^2-N^3)RH^2m^2+\;.\;.\;.\;.\;.\;.\,,$$

$$\eta_8=(128S^8-256NS^6+160N^2S^4-32N^3S^2+N^4)$$
$$+8(16S^6-24NS^4+10N^2S^2-N^3)RSHm$$
$$+64(16S^6-24NS^4+10N^2S^2-N^3)RSH^2m^2+\;.\;.\;.\;.\;.\,,$$

$$\eta_9=S(256S^8-576NS^6+432N^2S^4-120N^3S^2+9N^4)$$
$$+(256S^8-448NS^6+240N^2S^4-40N^3S^2+N^4)RHm$$

$$+9(256S^8-448NS^6+240N^2S^4-40N^3S^2+N^4)RH^2m^2$$

$$+\cdot\cdot\cdot\cdot\cdot,$$

$$\cdots\cdots\cdots\cdots\cdots\cdots\cdots \qquad (32)$$

In the case where μ'/μ is fairly large, including the case $\mu'/\mu=\infty$, the expanded form shown in (31) diverges. Here we shall alternatively assume that the expression (28) is equivalent to the form

$$v_{y=H}=\frac{H}{\mu\pi}\int_0^\infty \frac{1}{mH}\sum_n A_n e^{-c_n m}dm\int_{-\infty}^{\infty}\varphi(\lambda)\cos m(x-\lambda)\,d\lambda\,, \qquad (33)$$

from which it follows that

$$\frac{1}{mH}\sum_n A_n e^{-c_n m}=\frac{(1-\sigma)}{mH}\left[\frac{1+2R(mH)e^{-2mH}-Ne^{-4mH}}{1-2\{R(mH)^2+S\}e^{-2mH}+Ne^{-4mH}}\right], \qquad (34)$$

the pressure distribution being restricted to even type about the plane $x=0$. Since the right-hand side of (34) exactly corresponds to the ordinates of the curves in Fig. 2, the expansion shown on the left-hand side of the same expression is tantamount to analysing the curves under consideration in a series of exponential functions, the values of A_n and c_n being thereby determined. The present method is available for a wide range of cases.

Now, the inclination of the surface corresponding to (33) is written

$$\frac{\partial v_{y=H}}{\partial x}=-\frac{2}{\mu\pi}\int_0^\infty \sum_n A_n e^{-c_n m}\sin mx\,dm\int_0^\infty \varphi(\lambda)\cos m\lambda\,d\lambda\,, \qquad (35)$$

hence assuming the same form of $\varphi(\lambda)$ as that in (29), we get

$$\frac{\partial v_{y=H}}{\partial x}=-\frac{Pa}{\mu}\sum_n\frac{A_n x}{(c_n+a)^2+x^2}\,. \qquad (36)$$

It may be noted moreover that it is the integral of (36) that gives rise to the displacement distribution, namely,

$$v_{y=H}=-\frac{Pa}{\mu}\sum_n\frac{A_n}{2}\log_e\frac{\left(\frac{c_n}{H}+\frac{a}{H}\right)^2+\left(\frac{x}{H}\right)^2}{\left(\frac{c_n}{H}+\frac{a}{H}\right)^2+\left(\frac{\infty}{H}\right)^2}, \qquad (37)$$

provided the displacement $v_{y=H}$ at $x=\infty$ is zero.

It was found empirically that, for $x>0$, the inclination determined by means of (36) always assumes a positive value for any condition of the elastic constants. This matter will be dealt with more fully in the next section. Using the mathematical results above given, we calculated the distribution of the inclination on the surface for three cases, (i) $\mu'=\mu$, (ii) $\mu'/\mu=2$, (iii) $\mu'/\mu=\infty$, and for different values of a/H for these three cases, σ being assumed to be $1/4$; the results are shown in Figs. 3, 4, 5. From the form of $\varphi(x)$ in (29), it is shown that the smaller the value of μ/μ' or that of a/H, the greater the concentration of the vertical displacement in the neighbourhood of line $x=0$. It also appears from Figs. 3, 4, 5 that the displacements are invariably directed downward like that due to Terazawa's criterion for the case of a semi-infinite body. From tentative calculations it was found that the present conclusion is also valid for the case of an incompressible body.

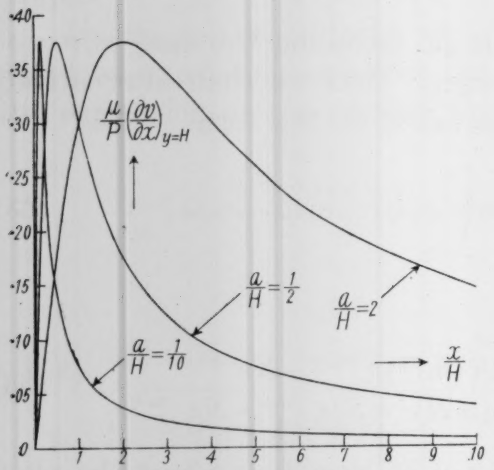

Fig. 3. Distribution of surface displacements. $\mu'=\mu$.

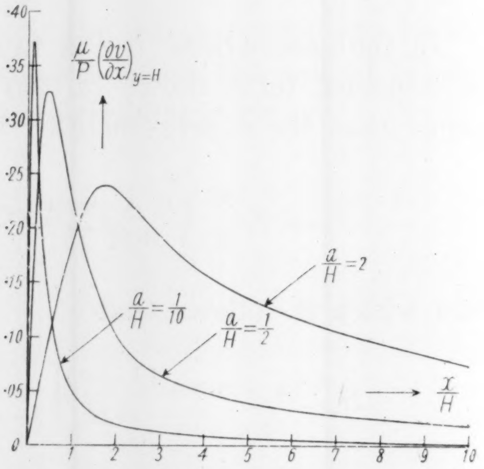

Fig. 4. Distribution of surface displacements. $\mu'/\mu=2$.

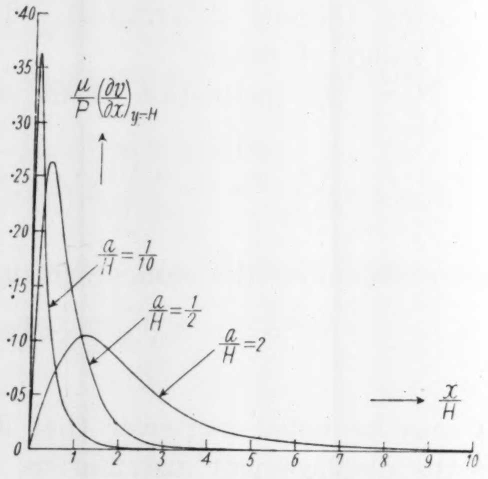

Fig. 5. Distribution of surface displacements. $\mu'/\mu=\infty$.

4. *A more general criterion of the sense of the vertical displacement on the surface.*

Although we have shown some examples of the general deformation of the surface in a stratified body, we have yet given no accurate criterion with regard to the sense of the vertical displacement on the surface.

Now, it is generally possible to write

$$\frac{\partial v_{y=H}}{\partial x}=\frac{-1}{\mu\pi}\int_0^\infty \sum_n A_n e^{-c_n m}\sin mx\,dm\int_{-\infty}^\infty \varphi(\lambda)\cos m\lambda\,d\lambda \tag{35$'$}$$

for an even distribution of the surface pressure with respect to x, provided expansion

$$\sum_n A_n e^{-c_n m}=(1-\sigma)\left[\frac{1+2R(mH)e^{-2mH}-Ne^{-4mH}}{1-2\{R(mH)^2+S\}e^{-2mH}+Ne^{-4mH}}\right] \tag{34$'$}$$

in (34) is possible. Rearranging (35′) in the form

$$\frac{\partial v_{y=H}}{\partial x}=\frac{-1}{\mu\pi}\int_{-\infty}^\infty \varphi(\lambda)\,d\lambda\int_0^\infty \sum_n A_n e^{-c_n m}\sin m(x-\lambda)\,d\lambda\,, \tag{38}$$

and using the integral

$$\int_0^\infty \sum_n A_n e^{-c_n m}\sin m(x-\lambda)\,d\lambda=\sum_n\frac{A_n(x-\lambda)}{c_n^2+(x-\lambda)^2}\,, \tag{39}$$

we have

$$\frac{\partial v_{y=H}}{\partial x}=\frac{-1}{\mu\pi}\int_{-\infty}^\infty \sum_n\frac{A_n(x-\lambda)}{c_n^2+(x-\lambda)^2}\varphi(\lambda)\,d\lambda\,, \tag{40}$$

the integral of which is

$$v_{y=H}=\frac{-1}{\mu\pi}\int_{-\infty}^\infty \frac{A_n}{2}\log_e\frac{c_n^2+(x-\lambda)^2}{c_n^2+(\infty-\lambda)^2}\varphi(\lambda)\,d\lambda\,, \tag{41}$$

under the condition that $v_{y=H}$ at $x=\pm\infty$ is zero. Putting $x-\lambda=-X$, we get

$$v_{y=H}=\frac{-1}{\mu\pi}\int_{-\infty}^\infty \sum_n\frac{A_n}{2}\log_e\frac{\left(\frac{c_n}{H}\right)^2+\left(\frac{X}{H}\right)^2}{\left(\frac{c_n}{H}\right)^2+\left(\frac{\infty_1}{H}\right)^2}\varphi(x+X)\,dX\,, \tag{42}$$

where ∞_1 denotes the condition that X tends to $\mp\infty$.

On the other hand, we find that the displacement distribution for the special type of $\varphi(x)$, namely

$$\varphi(x)=\frac{Pa^2}{a^2+x^2}\,, \tag{29$'$}$$

is given by

$$v_{y=H}=-\frac{Pa}{\mu}\sum_n\frac{A_n}{2}\log_e\frac{\left(\frac{c_n}{H}+\frac{a}{H}\right)^2+\left(\frac{x}{H}\right)^2}{\left(\frac{c_n}{H}+\frac{a}{H}\right)^2+\left(\frac{\infty}{H}\right)^2}, \tag{37'}$$

where A_n's and c_n's are invariably the same as those in (34'), namely, those in (42). In the special case where the pressure of type $\varphi(x)$ is concentrated quite close to $x=0$, it is possible to put $a/H\to 0$, so that the expression of (37') may assume the form

$$v_{y=H}=-\frac{Pa}{\mu}\sum_n\frac{A_n}{2}\log_e\frac{\left(\frac{c_n}{H}\right)^2+\left(\frac{x}{H}\right)^2}{\left(\frac{c_n}{H}\right)^2+\left(\frac{\infty}{H}\right)^2}, \tag{43}$$

regardless of whether c_n/H is large or small. The assumed condition $a/H\to 0$ is virtually equivalent to treatment of the case of a semi-infinite body. From Terazawa's criterion,[8] therefore, the expression of $v_{y=H}$ in (43) always assumes a negative value for any value of $x(\lessgtr 0)$. Thus x in (43) may be replaced by X, whence it follows that the first factor in the integrand in (42), is greater than zero, that is

$$\sum_n\frac{A_n}{2}\log_e\frac{\left(\frac{c_n}{H}\right)^2+\left(\frac{X}{H}\right)^2}{\left(\frac{c_n}{H}\right)^2+\left(\frac{\infty_1}{H}\right)^2}>0 \tag{44}$$

for any $X(\lessgtr 0)$.

From the condition that the pressure is always directed in the sense of gravity, the second factor in the integrand in (42) is also greater than zero, namely,

$$\varphi(x+X)>0 \tag{45}$$

for any $x+X(x\lessgtr 0,\ X\gtrless 0)$.

From (44), (45) we conclude that the expression in (42) is always negative, that is,

$$v_{y=H}<0\,, \tag{46}$$

the problem thus being proved from general considerations. Whether the material of the solid is compressible or incompressible does not matter.

It is easy, though not rigorous, to prove alternatively from common sense reasoning that $v_{y=H}<0$. The deformation of a stratified body under vertical loads, distributed in whatever way, is virtually the same as the resultant in the superposition of different deformations, every one of which is caused by a point load. Since the problem of the deformation of a body of any stratification that is subjected to a point load, is invariably the same as that of a semi-infinite body, the deformation due to every point load is always directed downward. The superposition of the deformations of downward displacements gives a resultant displacement of the same downward sense, the proof of the problem being thus very simply obtained. It thus appears, at all events, that all problems, whether of a semi-infinite body, or even of a multi-layered body, can be reduced to that of the case of a point load. It should however be borne in mind that although this final discussion has resulted also from a special case of Terazawa's criterion, the explanation shown in the beginning of this section, in which the general case of Terazawa's condition was partly availed of, is a more exact one.

---

[8] K. TERAZAWA, *loc. cit.* 4).

21. 地表層が鉛直荷重を受ける場合の彈性的變形分布に就て

地震研究所 {妹澤克惟
金井清

半無限體が鉛直荷重を受ける場合の彈性的變形の問題は幾多の學者によつて研究し盡され，その場合に表面變形が必ず下向になるといふ規範を寺澤教授などが態々出した程にもなつてをるのである．然るに表面層のある場合は計算が遙かに困難になる爲に，ある計算の結果では必しも寺澤教授の規範の如くならぬ場合さへも現れてをるのである．しかし之の正確な決定は普通の數學的運算法では寧ろ定らぬのが當然のやうにも見える．

之を正確に決定する爲にこの論文を作つたのであつて，その理論的證明は半無限體のとき程簡單には行かぬけれども，兎も角も特別の應用數學的方法を問題の一般性が失はれぬやうに採用し且つ寺澤教授の規範も部分的に利用することにより，結局半無限體の場合と同じ結論に到達したのである．卽ち層のある場合でも表面變位はやはり下向にしかならぬといふことである．

尙，後で氣のついたことは，層のある場合でもない場合でも問題は表面に點の荷重の働く場合のよせ集めであるといふことである．點の場合には表面層が無限に薄い場合以外はすべて半無限體の場合に持つて行くことができる．從てあらゆる場合の問題は點の荷重の場合の規則さへわかつてをればよいといふことになり，卽ちこの論文の問題に常識的の證明を與へ得ることもわかるのである，但し之は寺澤規範の極く特別の場合を應用したのに過ぎず前の一般的の說明の方が理論的に正確である．

22. *The Same Stationary Vibration of an Origin Accompanying Different Types of Disturbances Therefrom.*

By Katsutada SEZAWA and Kiyoshi KANAI,

Earthquake Research Institute.

(Read Jan. 19, 1937.—Received March 20, 1937.)

1. In a previous paper[1] we discussed the probability of resonance phenomena in the stationary vibration of the surface of a spherical cavity, and concluded that, owing to the vibrational energy being dissipated towards infinity, even under resonance conditions, the vibration of the cavity scarcely assumes an infinitely large amplitude for a finite value of n. In the case of smaller values of n the amplitudes of the stationary vibration as well as of the dissipation waves were not sensibly large even under resonance conditions. With a view to ascertaining the most probable resonance frequencies in such a case, we assumed a disturbance at the origin of a type differing entirely from that of the previous case. Since in the case without dissipation, the vibration type of a body under resonance could be uniquely determined provided its vibrational mode were specified, the investigation of the separate cases in which the same mode of vibration are excited under disturbances assumed to be different would give a better answer to the determination of the true resonance conditions just mentioned. In contrast to the previously assumed normal force at the surface of the cavity, we shall now consider the case in which the surface at the spherical cavity is subjected to a periodically changing shearing force.

2. The solutions of the problem being the same as those in the previous paper,[2] the boundary conditions are such that

$$\widehat{rr}=0, \quad \widehat{r\theta}=p_s\frac{dP_n(\cos\theta)}{d\theta}e^{ipt} \tag{1}$$

at $r=a$. In virtue of the relations

---

[1] K. SEZAWA and K. KANAI, "Resonance Phenomena and Dissipation Waves in the Stationary Vibration of the Surface of a Spherical Cavity," *Bull. Earthq. Res. Inst.*, **15** (1937), 13~20.

[2] *loc. cit.* 1).

$$\widehat{rr}=\lambda\Delta+2\mu\frac{\partial u}{\partial r}, \quad \widehat{r\theta}=\mu\left(\frac{\partial v}{\partial r}-\frac{v}{r}+\frac{1}{r}\frac{\partial u}{\partial \theta}\right), \tag{2}$$

where $u=u_1+u_2$, $v=v_1+v_2$, we find

$$\left.\begin{aligned}
&2A_n\left\{-\frac{(n-1)}{h^2r^2}H^{(2)}_{n+\frac{1}{2}}(hr)+\frac{1}{hr}H^{(2)}_{n+\frac{3}{2}}(hr)\right\}\\
&\quad+B_n\left\{-\frac{2(n^2-1)}{j^2r^2}H^{(2)}_{n+\frac{1}{2}}(jr)+\frac{2n+1}{jr}H^{(2)}_{n+\frac{3}{2}}(jr)-H^{(2)}_{n+\frac{5}{2}}(jr)\right\}=\frac{p_s\sqrt{r}}{\mu},\\
&A_n\left[\left\{\left(\frac{\lambda}{\mu}-\frac{2n(n-1)}{h^2r^2}\right)H^{(2)}_{n+\frac{1}{2}}(hr)+2\left\{\frac{2n+1}{hr}H^{(2)}_{n+\frac{3}{2}}(hr)-H^{(2)}_{n+\frac{5}{2}}(hr)\right\}\right]\right.\\
&\qquad\qquad+2B_n n(n+1)\left\{-\frac{n-1}{j^2r^2}H^{(2)}_{n+\frac{1}{2}}(jr)+\frac{1}{jr}H^{(2)}_{n+\frac{3}{2}}(jr)\right\}=0
\end{aligned}\right\} \tag{3}$$

at $r=a$. When $\lambda=\mu$, we have

$$\left.\begin{aligned}
&A_n\Phi=\frac{p_s\sqrt{a}}{\mu}\frac{2n(n+1)}{ja}\left\{\frac{n-1}{ja}H^{(2)}_{n+\frac{1}{2}}(ja)-H^{(2)}_{n+\frac{3}{2}}(ja)\right\},\\
&B_n\Phi=\frac{p_s\sqrt{a}}{\mu}\left[\left\{1-\frac{2n(n-1)}{h\,a^2}\right\}H^{(2)}_{n+\frac{1}{2}}(ha)\right.\\
&\qquad\qquad\qquad\left.+2\left\{\frac{2n+1}{ha}H^{(2)}_{n+\frac{3}{2}}(ha)-H^{(2)}_{n+\frac{5}{2}}(ha)\right\}\right],\\
&\Phi=\left[\left\{1-\frac{2n(n-1)}{h^2a^2}\right\}H^{(2)}_{n+\frac{1}{2}}(ha)+2\left\{\frac{2n+1}{ha}H^{(2)}_{n+\frac{3}{2}}(ha)-H^{(2)}_{n+\frac{5}{2}}(ha)\right\}\right]\\
&\qquad\cdot\left\{-\frac{2(n+1)(n-1)}{j^2a^2}H^{(2)}_{n+\frac{1}{2}}(ja)+\frac{2n+1}{ja}H^{(2)}_{n+\frac{3}{2}}(ja)-H^{(2)}_{n+\frac{5}{2}}(ja)\right\}\\
&\qquad+\frac{4n(n+1)}{hja^2}\left\{\frac{n-1}{ja}H^{(2)}_{n+\frac{1}{2}}(ja)-H^{(2)}_{n+\frac{3}{2}}(ja)\right\}\\
&\qquad\qquad\qquad\cdot\left\{-\frac{n-1}{ha}H^{(2)}_{n+\frac{1}{2}}(ha)+H^{(2)}_{n+\frac{3}{2}}(ha)\right\}.
\end{aligned}\right\} \tag{4}$$

The final solutions are such that

$$u_1=\frac{A_n\sqrt{r}}{hr}\left\{-\frac{n}{hr}H^{(2)}_{n+\frac{1}{2}}(hr)+H^{(2)}_{n+\frac{3}{2}}(hr)\right\}P_n(\cos\theta)e^{ipt},$$

$$
\left.
\begin{aligned}
v_1 &= -\frac{A_n\sqrt{r}}{h^2r^2} H^{(2)}_{n+\frac{1}{2}}(hr)\frac{dP_n(\cos\theta)}{d\theta} e^{ipt},\\
u_2 &= -\frac{B_n\sqrt{r}}{j^2r^2}\, n(n+1) H^{(2)}_{n+\frac{1}{2}}(jr) P_n(\cos\theta) e^{ipt},\\
v_2 &= \frac{B_n\sqrt{r}}{jr}\left\{-\frac{n+1}{jr}H^{(2)}_{n+\frac{1}{2}}(jr) + H^{(2)}_{n+\frac{3}{2}}(jr)\right\}\frac{dP_n(\cos\theta)}{d\theta}\, e^{ipt},
\end{aligned}
\right\}
\tag{5}
$$

the values of the constants A_n, B_n being shown in (4). Using these equations we shall calculate the displacements u, v at the surface $r=a$ as well as those of dissipation waves u_1, v_2 at $r=\infty$ for three cases of n, namely $n=1$, 2, 4; u_1, v_2 being radial displacement of dilatational waves and transverse displacement of distortional waves respectively. The results for the three cases are shown in Figs. 1~6.

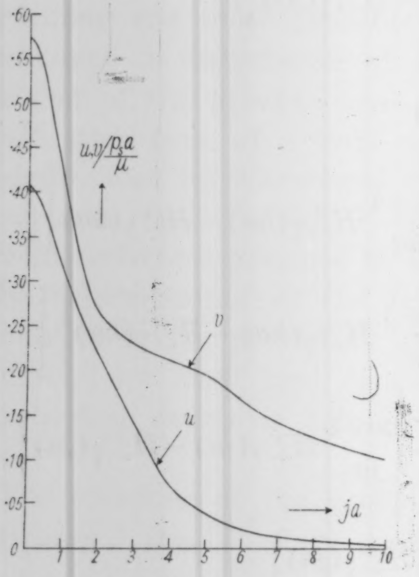

Fig. 1. Displacements at $r=a$; $n=1$.

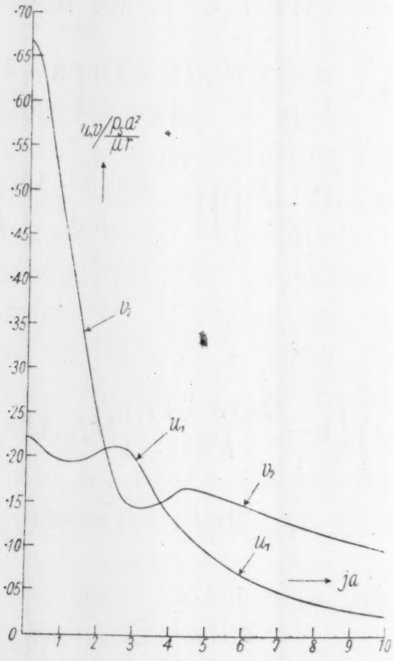

Fig. 2. Amplitudes of dissipation waves; $n=1$.

In the present results, $P_n(\cos\theta)$ in u or $dP_n(\cos\theta)/d\theta$ in v was again conventionally replaced by unity.

The solutions of the case $n=\infty$ are easily obtained in the same manner as those described in the previous paper, which however are omitted here.

3. Figs. 1, 3, 5 show that the value of u/v, namely, the ratio of the radial to transverse displacements at the origin invariably tends to zero for infinitely large values of ja, that is to say, the movement of the surface at the origin is purely transverse for extremely high vibrational frequencies. Figs. 3, 5 also show that both u and v assume maximum values at $ja=1{\cdot}15$, $1{\cdot}5$, $0{\cdot}9194\,n$ for $n=2$, $n=4$, $n=\infty$

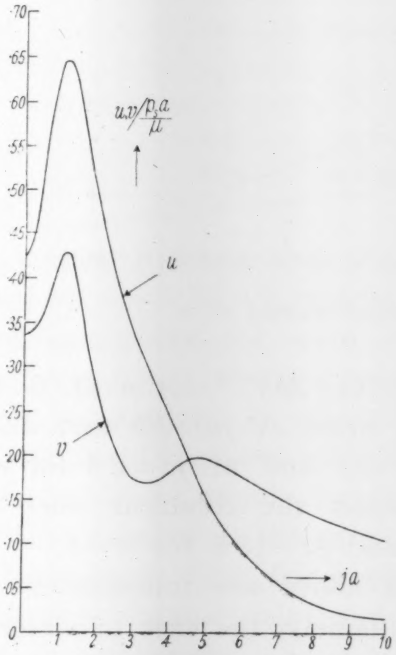

Fig. 3. Displacement at $r=a$; $n=2$.

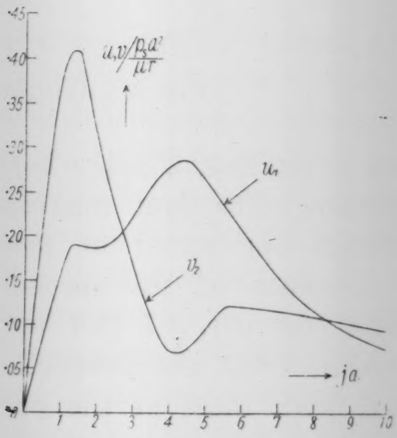

Fig. 4. Amplitutes of dissipation waves; $n=2$.

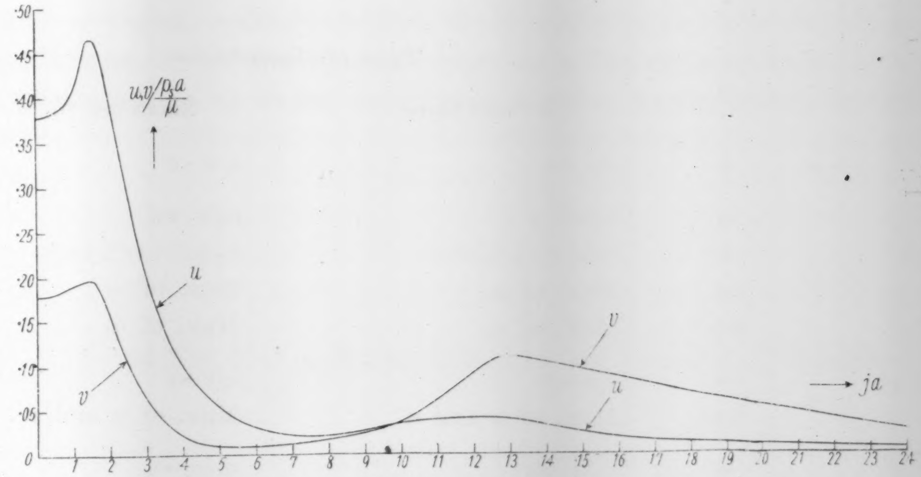

Fig. 5. Displacement at $r=a$; $n=4$.

respectively.

From Figs. 2, 4, 6 it will be seen that, while the relation that $u_1/v_2 \to 0$ for $ja \to \infty$ also holds, the same ratio at $ja \to 0$ assumes the values $\mu/(\lambda+2\mu)$, $2\{\mu/(\lambda+2\mu)\}^{3/2}$, $(3/10)\{\mu/(\lambda+2\mu)\}^{3/2}$ for $n=1, 2, 4$ respectively. The first maxima of u_1, v_2 arise at $ja=2{\cdot}5$ and $4{\cdot}5$ respectively for $n=1$; at $ja=1{\cdot}4$ for $n=2$; and at $ja=2{\cdot}5$ for $n=4$. The presence of the second maxima obeys the condition such that $ja=4{\cdot}4$ (for u_1), $5{\cdot}7$ (for v_2) for $n=2$, and $ja=13{\cdot}5$ for $n=4$.

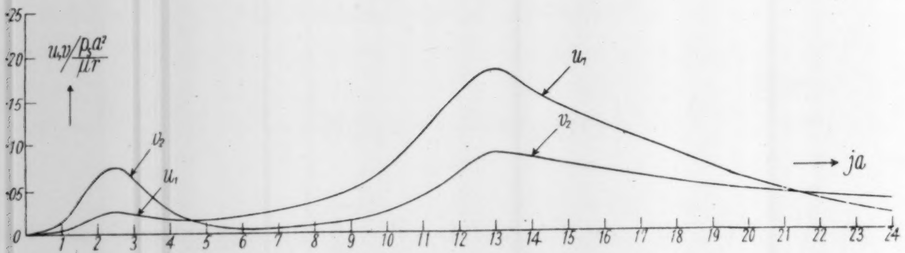

Fig. 6. Amplitudes of dissipation waves; $n=4$

Almost all the properties mentioned above are immediately connected with those of the previous case, namely, the case in which the spherical origin is subjected to disturbance of normal pressure type, both the results being arranged in Table I for comparison.

Table I.

Source	r	ja	Type of disturbance	
			Normal force	Shearing force
$n=1$	$r=a$	∞	$v/u \to 0$	$u/v \to 0$
	$r=\infty$	∞	$v_2/u_1 \to 0$	$u_1/v_2 \to 0$
		0	$v_2/u_1 = (\lambda+2\mu)/\mu$	$v_2/u_1 = (\lambda+2\mu)/\mu$
		4·5	Max. of u_1	Max. of v_2
		2·5	Max. of v_2	Max. of u_1
$n=2$	$r=a$	∞	$v/u \to 0$	$u/v \to 0$
		1·15	Max. of u and v	Max. of u and v
	$r=\infty$	∞	$v_2/u_1 \to 0$	$u_1/v_2 \to 0$
		0	$v_2/u_1 = \frac{1}{2}\left(\frac{\lambda+2\mu}{\mu}\right)^{\frac{3}{2}}$	$v_2/u_1 = \frac{1}{2}\left(\frac{\lambda+2\mu}{\mu}\right)^{\frac{3}{2}}$
		1·4	1st max. of u_1 and v_2	1st max. of u_1 and v_2 (sub.)
		5·7	2nd max. of u_1	2nd max. of v_2
		4·4	2nd max. of v_2 (sub.)	2nd max. of u_1

(to be continued.)

Table I. (*Continued*)

$n=4$	$r=a$	∞	$v/u \to 0$	$u/v \to 0$
		1·5	Max. of u and v	Max. of u and v
	$r=\infty$	∞	$v_2/u_1 \to 0$	$u_1/v_2 \to 0$
		0	$v_2/u_1=\frac{10}{3}\left(\frac{\lambda+2\mu}{\mu}\right)^{\frac{3}{2}}$	$v_2/u_1=\frac{10}{3}\left(\frac{\lambda+2\mu}{\mu}\right)^{\frac{3}{2}}$
		2·5	1st max. of u_1 and v_2	1st max. of u_1 and v_2
		13·5	2nd max. of u_1 and v_2	2nd max. of u_1 and v_2

It now appears that the resonances for $n=2$ and $n=4$ are conditioned by $ja=1{\cdot}15, 1{\cdot}5$ respectively. The resonance condition of a solid vibrating sphere for $n=2$ is $ja=2{\cdot}64$, which obviously differs from that for a body having a spherical cavity of the same radius.

4. It is possible, at all events, to conclude that since the ratio of v_2/u_1 tends to increase with increase in n, the amplitudes of transverse waves would be unduly large conformably with the extent of the complexity presented at the origin by the distribution of the disturbances. It also appears that, for a given type of disturbance at the origin, the amplitudes assume relatively large values for a certain range of vibrational frequencies. That it is hardly possible for transverse waves of very high frequency to exist is also obvious.

Finally, it should be borne in mind that, since the present examples are here given as idealized models for explaining the nature of a fairly complex seismic origin, it is immaterial whether the actual seismic origin be of the doublet type, or a quadruplet type, or even of such diverse type as to be free from regular geometrical conditions.

---

22. 震源に於ける異型の發振に伴ふその同型の定常振動

地震研究所 妹澤克惟
金井清

この前の報告で，球窩面が强制共振をなしても逸散波がある爲に無限大の振幅になり得ぬことを述べて置いた．而して何れの振動數が尤もらしい共振振動數であるかを正確にきめられぬことをも附加へて置いた．一體，逸散波さへなければ，强制力が如何に働いてもある定まつた型の振動は共振に於て一定の變位分布をなし，且つその共振週期も變る筈がないものである．然るに只

今の場合には逸散波があるからこの規則も完全には行はれ難い．しかし振動數の點では近似的に成立つであらうといふ考のもとにこの研究を試みたのである．

前回では球型源に壓力型の振動力を與へた代りに，今回は剪力型の振動力を與へて前と同じ型の振動を誘起さして見ることにした．計算の方法は前回と似たものである．

計算の結果によると前回の方法でも今回の方法でも，定常振動は定常振動同志に於て，逸散波は逸散波同志に於て，それぞれ一定の振動週期になると極大振動が現れ，それは原振動力の型には無關係といふことがわかつたのである．このやうにして所謂共振週期を見出した譯である．勿論之等は固形球の自由振動週期とは非常に違つてをる．

尙，振動週期の極めて長い場合には逸散波の傳播方向の變位と直角の方向の變位との比が振動力の型に無關係に一定値を取る．

振動週期の極く短い場合には，前回の振動型では半徑方向の變位が直角方向のそれよりも遙かに大きくなり，今回の振動型では逆になる．即ち原點を核として計算すると特別の場合しか出ないことがわかる．

この論文の計算はその儘實際にあてはまるとは考へないけれども，一つの理想的模型として取つたのに過ぎぬものである．

23. *On the Free Vibrations of a Surface Layer due to an Obliquely Incident Disturbance.*

By Katsutada SEZAWA and Kiyoshi KANAI,

Earthquake Research Institute.

(Read March 16, 1937.—Received March 20, 1937.)

1. It has been established that if the primary waves were directed vertically upwards, the damping constant of the vibration would invariably be the same whatever the type of wave form of the initial disturbance.[1] If $V_1=\sqrt{(\lambda'+2\mu')/\rho'}$, $V_2=\sqrt{\mu'/\rho'}$, $\alpha_2=\sqrt{\rho'\mu'/\rho\mu}$, $\alpha_1=\sqrt{\rho'(\lambda'+2\mu)/\rho(\lambda+2\mu)}$, the coefficients of damping are

$$k_1=\frac{V_1}{2H}\log_e\left|\frac{1+\alpha_1}{1-\alpha_1}\right|,\quad k_2=\frac{V_2}{2H}\log_e\left|\frac{1+\alpha_2}{1-\alpha_2}\right| \tag{1}$$

for dilatational and distortional disturbances respectively. Although the problem is greatly complicated, if the disturbance is directed obliquely to the layer, the special case in which the obliquely incident primary disturbance consists of transverse waves with movements orientated horizontally, is particularly simple, the damping coefficient then being uniquely determined as a certain function of the incident angle,[2] namely,

$$k_2=\frac{V_2}{2H\cos e'}\log_e\left|\frac{1+\nu}{1-\nu}\right|, \tag{2}$$

where $\nu=\sqrt{\rho\mu'/\rho\mu}(\cos e'/\cos e)$.

The nature of damping of free vibration due to obliquely incident longitudinal waves or to obliquely incident transverse waves with movements orientated in a vertical plane, however, is not simple. This is because no point along the layer is ever subjected to the initial disturbance simultaneously, and also because, after every free vibration, whether of longitudinal or transverse type, both longitudinal and transverse vibrations are excited. Discussion of this problem from the elementary stage of the solutions is however extremely difficult. It appears however that Nishimura's result[3] in connection with the forced vibration of a layer due to an obliquely incident disturbance renders it possible to examine the problem without encountering serious difficulties. Although we studied previously also a case[4] included in Nishimura's solutions, owing to its being a rather limited case, the result is of little avail for the present discussion.

---

[1] K. SEZAWA and K. KANAI, "Decay Constants of Seismic Vibrations of a Surface Layer," *Bull. Earthq. Res. Inst.*, **13** (1935), 255.

[2] Ditto, "Damping in Seismic Vibrations of a Surface Layer due to an Obliquely Incident Disturbance," *Bull. Earthq. Res. Inst.*, **14** (1936), 357.

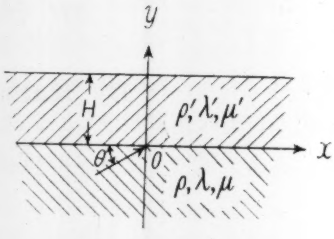

Fig. 1.

2. The elementary solutions are such that

$$\left.\begin{array}{c}
\phi_0 = e^{i(fx-ry-pt)}, \\
\phi = Ae^{i(fx+ry-pt)}, \quad \psi = Be^{i(fx+sy-pt)}, \\
\phi' = Ce^{i(fx-r'y-pt)} + De^{i(fx+r'y-pt)}, \quad \psi' = Ee^{i(fx-s'y-pt)} + Fe^{i(fx+s'y-pt)}, \\
r^2 = \dfrac{\rho p^2}{\lambda+2\mu} - f^2, \; s^2 = \dfrac{\rho p^2}{\mu} - f^2, \; r'^2 = \dfrac{\rho' p^2}{\lambda'+2\mu'} - f^2, \; s'^2 = \dfrac{\rho' p^2}{\mu'} - f^2.
\end{array}\right\} \quad (3)$$

From the boundary conditions at $y=0$ and $y=H$ it is possible to determine A, B, C, D, E, F, namely,

$$\left.\begin{array}{l}
A = \Delta^{-1}\{\alpha_A + \beta_A e^{i(a'+b')fH} + \gamma_A e^{i(a'-b')fH} + \delta_A e^{-i(a'+b')fH} + \varepsilon_A e^{-i(a'-b')fH}\}, \\
B = \Delta^{-1}\{\alpha_B + \beta_B e^{i(a'+b')fH} + \gamma_B e^{i(a'-b')fH} + \delta_B e^{-i(a'+b')fH} + \varepsilon_B e^{-i(a'-b')fH}\}, \\
C = \Delta^{-1}\{\alpha_C + \delta_C e^{-i(a'+b')fH} + \varepsilon_C e^{-i(a'-b')fH}\}, \\
D = \Delta^{-1}\{\alpha_D + \beta_D e^{i(a'+b')fH} + \gamma_D e^{i(a'-b')fH}\}, \\
E = \Delta^{-1}\{\alpha_E + \gamma_E e^{i(a'-b')fH} + \delta_E e^{-i(a'+b')fH}\}, \\
F = \Delta^{-1}\{\alpha_F + \beta_F e^{i(a'+b')fH} + \varepsilon_F e^{-i(a'-b')fH}\},
\end{array}\right\} \quad (4)$$

where

$$\Delta^{-1} = Me^{ifH[a'(m-2p)+b'(m-2n+2q)]}, \text{ [5]} \quad (5)$$

$$M = \sum_{m=0}^{\infty} (-1)^m \sum_{n=0}^{m} \frac{m!}{n!(m-n)!} \sum_{p=0}^{n} \frac{n!}{p!(n-p)!}$$

$$\cdot \sum_{q=0}^{p} \frac{p!}{q!(p-q)!} \alpha_\Delta^{-(m+1)} \beta_\Delta^{m-n} \gamma_\Delta^{n-p} \delta_\Delta^{p-q} \varepsilon_\Delta^{q}. \quad (6)$$

---

3) G. NISHIMURA, "On the Effect of Discontinuity Surface on the Propagation of Elastic Waves (VII)," *Bull. Earthq. Res. Inst.*, **13** (1935), 540~554.

4) K. SEZAWA and K. KANAI, "Reflection and Refraction of Seismic Waves in a Stratified Body," *Bull. Earthq. Res. Inst.*, **10** (1932), 805~816; **12** (1934), 269~276.

5) G. NISHIMURA also expanded Δ^{-1} in a somewhat similar form for evaluating the integral for free waves but not for obtaining the modulus of damping.

M may be named as *decay modulus* of vibrations. The terms α_Δ, β_Δ, ……; α_A, β_A, ……; α_B, β_b, ……; ……; α_F, β_F, …… in (2), (3), (4) correspond to the respective coefficients of e^o, $e^{i(r'+s')H}$, $e^{i(r'-s')H}$, $e^{-i(r'+s')H}$, $e^{-i(r'-s')H}$, in $\varDelta$, $\varDelta_A$, $\varDelta_E$, $\varDelta_C$, $\varDelta_L$, $\varDelta_E$, $\varDelta_F$, in Nishimura's paper[6]; the same notations being arranged in Table I.

Table I.

Coeffient of	in $\varDelta$	in $\varDelta_A$	in $\varDelta_B$	in $\varDelta_C$	in $\varDelta_D$	in $\varDelta_E$	in $\varDelta_F$
e^o	α_Δ	α_A	α_B	α_C	α_D	α_E	α_F
$e^{i(r'+s')H}$	β_Δ	β_A	β_B	β_C	β_D	β_E	β_F
$e^{i(r'-s')H}$	γ_Δ	γ_A	γ_B	γ_C	γ_D	γ_E	γ_F
$e^{-(ir'+s')H}$	δ_Δ	δ_A	δ_B	δ_C	δ_D	δ_E	δ_F
$e^{-i(r'-s')H}$	ε_Δ	ε_A	ε_B	ε_C	ε_D	ε_E	ε_F

3. Fourier's integral for a two-dimensional case is

$$\chi(x,\ y)=\frac{1}{4\pi^2}\int_{-\infty}^{\infty}df\int_{-\infty}^{\infty}dr\int_{-\infty}^{\infty}d\xi\int_{-\infty}^{\infty}\chi(\xi,\ \eta)e^{if(x-\xi)-ir(y-\eta)}d\eta, \tag{7}$$

from which we may write

$$\phi_o=\Phi\{fx-ry-pt\}, \tag{8}$$

Φ being the type of initial disturbance, and

$$\begin{aligned}\phi=M\Big\{&\alpha_A\Phi\Big[f\{x+(m-2p)a'H+(m-2n+2q)b'H\}+ry-pt\Big]\\&+\beta_A\Phi\Big[f\{x+(m-2p+1)a'H+(m-2n+2q+1)b'H\}+ry-pt\Big]\\&+\gamma_A\Phi\Big[f\{x+(m-2p+1)a'H+(m-2n+2q-1)b'H\}+ry-pt\Big]\\&+\delta_A\Phi\Big[f\{x+(m-2p-1)a'H+(m-2n+2q-1)b'H\}+ry-pt\Big]\\&+\varepsilon_A\Phi\Big[f\{x+(m-2p-1)a'H+(m-2n+2q+1)b'H\}+ry-pt\Big]\Big\},\end{aligned} \tag{9}$$

---

[6] G. **Nishimura**, *loc. cit.* 3).

$$\begin{aligned}\psi=M\Big\{&\alpha_B\Phi\Big[f\{x+(m-2p)a'H+(m-2n+2q)b'H\}+sy-pt\Big]\\&+\beta_B\Phi\Big[f\{x+(m-2p+1)a'H+(m-2n+2q+1)b'H\}+sy-pt\Big]\\&+\gamma_B\Phi\Big[f\{x+(m-2p+1)a'H+(m-2n+2q-1)b'H\}+sy-pt\Big]\\&+\delta_B\Phi\Big[f\{x+(m-2p-1)a'H+(m-2n+2q-1)b'H\}+sy-pt\Big]\\&+\varepsilon_B\Phi\Big[f\{x+(m-2p-1)a'H+(m-2n+2q+1)b'H\}+sy-pt\Big]\Big\},\end{aligned}\tag{10}$$

$$\begin{aligned}\phi'=M\Big\{&\alpha_C\Phi\Big[f\{x+(m-2p)a'H+(m-2n+2q)b'H\}-r'y-pt\Big]\\&+\delta_C\Phi\Big[f\{x+(m-2p-1)a'H+(m-2n+2q-1)b'H\}-r'y-pt\Big]\\&+\varepsilon_C\Phi\Big[f\{x+(m-2p-1)a'H+(m-2n+2q+1)b'H\}-r'y-pt\Big]\\&+\alpha_D\Phi\Big[f\{x+(m-2p)a'H+(m-2n+2q)b'H\}+r'y-pt\Big]\\&+\beta_D\Phi\Big[f\{x+(m-2p+1)a'H+(m-2n+2q+1)b'H\}+r'y-pt\Big]\\&+\gamma_D\Phi\Big[f\{x+(m-2p+1)a'H+(m-2n+2q-1)b'H\}+r'y-pt\Big]\Big\},\end{aligned}\tag{11}$$

$$\begin{aligned}\psi'=M\Big\{&\alpha_E\Phi\Big[f\{x+(m-2p)a'H+(m-2n+2q)b'H\}-s'y-pt\Big]\\&+\gamma_E\Phi\Big[f\{x+(m-2p+1)a'H+(m-2n+2q-1)b'H\}-s'y-pt\Big]\\&+\delta_E\Phi\Big[f\{x+(m-2p-1)a'H+(m-2n+2q-1)b'H\}-s'y-pt\Big]\\&+\alpha_F\Phi\Big[f\{x+(m-2p)a'H+(m-2n+2q)b'H\}+s'y-pt\Big]\\&+\beta_F\Phi\Big[f\{x+(m-2p+1)a'H+(m-2n+2q+1)b'H\}+s'y-pt\Big]\\&+\varepsilon_F\Phi\Big[f\{x+(m-2p-1)a'H+(m-2n+2q+1)b'H\}+s'y-pt\Big]\Big\}.\end{aligned}\tag{12}$$

Since the form of decay modulus M in (6) is independent of the type of original disturbance, Φ, the behaviour of the free vibration of the layer is invariably the same, though it is not so simple as that in exponential damping.

In equations (9) ~ (12), α_A, β_A, ...; α_B, β_B, ...; ...... are functions of densities as well as of elastic constants in the layer and the subjacent medium, besides of the incidence angle of the primary waves. Since, on the other hand, ϕ, ψ, ϕ', ψ' have the same and invariable damping modulus M (shown in (6)), the respective vibrational modes, namely dilatational and distortional, including both types of dissipation waves, decay quite in the same way. The only difference between ϕ, ψ, ϕ', ψ' is in the ratios of the general amplitudes, which differ with the differences in α_A, β_A, ...; α_B, β_B, ...; ......, r, s, r', s', so that it is not possible for even one out of ϕ, ψ, ϕ', ψ' to prevail even with lapse of time.

It may seem odd that the vibrations are not separated into two kinds, dilatational and distortional. Such separation however would be hardly possible unless the primary disturbance were composed of dilatational and distortional waves even in the case of simultaneous application of the disturbance at all points on the boundary surface of the layer.

4. It has already been remarked that from the decay modulus shown in (6), namely,

$$M=\sum_{m=0}^{\infty}(-1)^m\sum_{n=0}^{m}\frac{m\,!}{n\,!(m-n)\,!}\sum_{p=0}^{n}\frac{n\,!}{p\,!(n-p)\,!}$$

$$\cdot\sum_{q=0}^{p}\frac{p\,!}{q\,!(p-q)\,!}\alpha_\Delta^{-(m+1)}\beta_\Delta^{m-n}\gamma_\Delta^{n-p}\delta_\Delta^{p-q}\varepsilon_\Delta^{q}, \tag{6'}$$

no such simple decay constant as the coefficient of exponential function is deduced. Were the disturbance, however, to be applied simultaneously at all points on the boundary surface of the layer just mentioned, the modulus under consideration would immediately give the damping constant. In that case the direction of propagation of the disturbance should be in the vertical sense, from which results the condition that f tends to zero, while r, s, r', s' remain as finite values. It follows then that Nishimura's values Δ, Δ_A, Δ_B, ..., Δ_F[7] tend to assume the forms

$$\Delta=\frac{ss'^5}{f^{10}}\chi\{(\mu s^2r'-\mu'rs'^2)e^{ir'H}+(\mu s^2r'+\mu'rs'^2)e^{-ir'H}\},$$

---

[7] G. NISHIMURA, *loc. cit.* 3).

$$\left.\begin{aligned}
&\varDelta_A=\frac{-ss'^5}{f^{10}}\chi\{(\mu r's^2+\mu' rs'^2)e^{ir'H}+(\mu r's^2-\mu' rs'^2)e^{-ir'H}\},\\
&\varDelta_B\to 0,\qquad \varDelta_C=\frac{2}{f^{10}}rs^3s'^5\mu e^{-ir'H}\chi,\\
&\varDelta_D=\frac{-2}{f^{10}}rs^3s'^5e^{ir'H}\chi,\qquad \varDelta_E\to 0,\qquad \varDelta_F\to 0,\\
&\chi=(\mu s-\mu' s')e^{is'H}+(\mu s+\mu' s')e^{-is'H}.
\end{aligned}\right\}\tag{13}$$

Whence

$$\left.\begin{aligned}
A&=\frac{-\{(1+\alpha)e^{2ir'H}+(1-\alpha)\}}{(1-\alpha)e^{2ir'H}+(1+\alpha)},\\
C&=\frac{2\beta}{(1-\alpha)e^{2ir'H}+(1+\alpha)},\\
D&=\frac{-2\beta e^{2ir'H}}{(1-\alpha)e^{2ir'H}+(1+\alpha)},
\end{aligned}\right\}\tag{14}$$

where $\alpha=\sqrt{\rho'(\lambda'+2\mu')/\rho(\lambda+2\mu)}$, $\beta=\sqrt{\rho(\lambda'+2\mu')/\rho'(\lambda+2\mu)}$.

If the primary waves

$$\phi_0=\Phi(-ry-pt)\tag{15}$$

are incident on the bottom surface of the layer, free oscillation of the layer of the type

$$\begin{aligned}
\phi'=2\beta\sum_{m=0}^{\infty}(-1)^m\frac{(1-\alpha)^m}{(1+\alpha)^{m+1}}\Phi(-r'y-pt+2mr'H)\\
-2\beta\sum_{m=0}^{\infty}(-1)^m\frac{(1-\alpha)^m}{(1+\alpha)^{m+1}}\Phi\{r'y-pt+2(1+m)r'H\},
\end{aligned}\tag{16}$$

and the dissipation waves

$$\begin{aligned}
\phi=-\sum_{m=0}^{\infty}(-1)^m\frac{(1-\alpha)^{m+1}}{(1+\alpha)^{m+1}}\Phi(ry-pt+2mr'H)\\
-\sum_{m=0}^{\infty}(-1)^m\frac{(1-\alpha)^m}{(1+\alpha)^m}\Phi\{ry-pt+2(1+m)r'H\}
\end{aligned}\tag{17}$$

are excited, whence the vibration of the layer are of the purely exponential type

$$e^{-kt}$$

with the coefficient of damping

$$k=\frac{V'}{2H}\log_e\frac{1+\alpha}{1-\alpha}. \tag{18}$$

It should be borne in mind that, even should the initial disturbance Φ be of a very sharp type, the functions Φ in ϕ' or ϕ would be deformed to a fairly gradual type after every successive oscillation due to inner resistance,8) etc., so that it would then be possible for the vibration to assume almost sinusoidal and damped forms.

At all events, the special point in our ideas that differs from the classical theory of free vibration is that in the present case, the vibrations of higher orders are unlikely to occur. From results of vibration experiment, however, it would be rather improbable for the natural vibrations of higher orders in a body to exist under the action of a single shock of very short duration (compared with its first natural period) and of localized type, even though such vibrations might be damped by other causes such as viscous friction, etc. The only possible case of exciting vibrations of higher orders due to apparent short duration is that in which the sources of disturbance are initially so distributed in a body as in the case of statical deformation of the same body that is to be released simultaneously.

23. 斜のディスターバンスによつて誘起する表面層の自由振動に就て

地震研究所 妹澤克惟
金井清

縱波が來ても橫波が來てもそれが地中の眞下から來る場合には，それによつて誘起する表面層の自由振動は逸散性によつて減衰するとしても，その減衰性が簡單な指數函數的性質即ち粘性によつて減衰する場合の性質と變らぬことがわかつた．又斜に波動が來る場合でも，振動方向が水平の橫波の場合には特に同じ性質のあることがわかつたのである．然るにそれ以外の振動方向の橫波や一般的の縱波が斜から來る場合は，減衰性が非常に複雜になるものである．この場合の計

---

8) K. Sezawa, "Decay of Waves in a Visco-elastic Solid Bodies," *Bull. Earthq. Res. Inst.*, **3** (1927), 43.

算を根本からやることは可なり面倒であるが，幸にも西村技師により同じやうな場合の强制振動の研究結果が出してあるからその結果を借用して計算を試みた．勿論，西村技師の計算の特別の場合はそれよりも前に筆者等が出したけれども西村技師のもの程に一般的には役に立たぬ．

只今の研究の結果，表面層の振動の減衰性には相當複雜な性質があり，指數函數などでは規定できぬけれども兎も角も一定の方則のある Decay modulus に從て減衰し，それは最初のディスターバンスの型によらぬことがわかつたのである．又その振動は縱波の種類と橫波の種類とから成立つてをるけれども，その何れかの型が時間と共に後迄殘るといふやうなことはなく同じ割合で減衰することが知られた．

又，問題を特別の場合，卽ち入射角が鉛直の場合にもつて行くと複雜な計算の後に初め述べたやうな簡單な場合になることがわかるのである．一寸考へると，斜のディスターバンスによつて表面層の縱振動と橫振動とが誘起されその一方がより速に減衰するやうに見えるけれども，計算の結果は寧ろ鉛直方向に縱橫2種のディスターバンスが同時に働く場合にそのやうな性質の存在し得ることを示すものである．

斜のディスターバンスの働くのは極く近距離に震源のある場合であらうから，實際問題としても現象の分析が稍困難な場合に當つてをる譯である．しかし遠方の震源の場合にはディスターバンスが衝擊型でなく週期的振動の方が勝つてをるから，その方から別の困難が生ずるのである．何れにしても表面層の自由振動といふ問題は餘り簡單でなく寧ろ不明瞭な事柄に近い譯である．尙，この論文等の計算に於て始めの衝擊の型が繰返されるやうに見えるかも知れぬけれども，實際問題としては固體內の粘性等の爲に繰返しの振動が減衰性正弦波に近くなるのは當然といはればならぬ．

只今のやうな新しい問題と古典的な自由振動の考卽ち節平面が不動であるといふ問題との間の非常な相違は，只今の問題では衝擊によつて高次の自由振動が現れ難いことである．しかしディスターバンスが衝擊型であるにしても適當の間隔で二度與へられれば第2次の減衰自由振動が現れ得るものである．この場合に節平面が振動性になるのはいふまでもない．但し單なる衝擊で高次の自由振動が現れ難いことは古典的考から得られた實驗卽ち固體の第1次振動週期よりも短い時間で働く衝擊の場合の結果から見ると同樣ではある．之等に關する概念は週期的强制振動のある場合の共振に於ける節面が逸散のないときの自由振動の場合の節面と同じになることから容易に得られる譯である．別に注意すべき事は，短い時間中に衝擊が働くやうに見えても最初の時間に應力が固體全體に適當に分布せる場合，卽ち始めは靜力學的に力が働く場合には，ディスターバンスの原點が固體中到る所にあるから，このときには高次振動があつても差支がない譯である．

24. *Energy Dissipation in the Vibrations of a Bridge. I.*

By Katsutada SEZAWA and Kiyoshi KANAI,

Earthquake Research Institute.

(Read March 16, 1937.—Received March 20, 1937.)

1. *Introduction.*

As the result of a number of investigations[1] made during the last two years, it was found that in the seismic vibration of a structure, the dissipation of vibrational energy into the ground takes up the largest part of its damping. We shall now show that it is also possible for a like property to exist in the vibrations of a bridge under periodic forces. Although the vibration problem of a bridge under fixed or moving excitation for the case without dissipation was solved by Zimmermann,[2] Radakovic,[3] Timoshenko,[4] Mononobe,[5] Inglis,[6] Jeffcott,[7] Schmidt,[8] Steuding,[9] Lowan,[10] etc., no attempt seems yet to have been made to ascertain the conditions attending the dissipation of vibrational energy of a bridge span into its piers and adjacent spans.

In the problem of dissipation of vibrational energy, if the conditions were such that the velocity of transmission of the vibrational waves along the bridge spans is much higher than that of the moving excitation, this fact would be more important than any of the other conditions. The velocity of flexural waves along a bridge is $v=(ELp^2/\rho a)^{\frac{1}{4}}$ where EI, ρa are the flexural stiffness of the bridge and mass per unit length of its span respectively, and $p/2\pi$ the number of forced

---

1) K. SEZAWA and K. KANAI, *Bull. Earthq. Res. Inst.*, **13** (1935); **14** (1936).

2) H. ZIMMERMANN, *Schwingungen eines Traegers mit bewegter Last* (Berlin, 1896).

3) M. RADAKOVIC, *Sitzungsber. Akad. Wiss., Wien*, **108** (1899), 577~612.

4) TIMOSHENKO, *Phil. Mag.*, **43** (1922), 1018~1019.

5) N. MONONOBE, *Journ. Civil. Eng., Japan*, **7** (1921), 561~604; **10** (1924), 79~122.

6) C. E. INGLIS, *Proc. Inst. Civil. Eng.*, **218** (1924), 499~504; *Proc. Roy. Soc.*, **118** (1928), 60~96.

7) H. H. JEFFCOTT, *Phil. Mag.*, **8** (1929), 66~97.

8) H. SCHMIDT, *Verh. 3-int. Kongr. techn. Mech.* (1930), 138~142.

9) H. STEUDING, *Ing. Arch.*, **5** (1934), 275~305.

10) A. N. LOWAN, *Phil. Mag.*, **19** (1935), 708~719.

excitations per sec. While in the example shown in this paper it is plausible that $v=160$ m/s for $p/2\pi=3$, a locomotive imparting an excitation of such frequency may, for example, run at a speed of 14 m/s (50 km/h), in which case the difference in values between v and V will be enormous.

In the present paper we shall consider the simple case in which the position of the exciting force is fixed, besides which the position under consideration is exactly at the middle point of a bridge span, by means of which it is still possible to ascertain the qualitative nature of the energy dissipation in question.

2. *Mathematical theory.*

Let E_1I_1, ρ_1a_1, E_2I_2, ρ_2a_2 be the flexural stiffness and mass per unit length of a span under the disturbing force and those of each adjacent span respectively, and let also $E'a'$, $\rho'a'$ be the longitudinal stiffness and mass per unit length of each pier respectively, the periodic force being of the type Fe^{ipt}. Let it also be assumed that each bridge span rests on a pair of piers without moment of force at its ends. The differential equations of the vibrational movements of the respective parts under consideration are

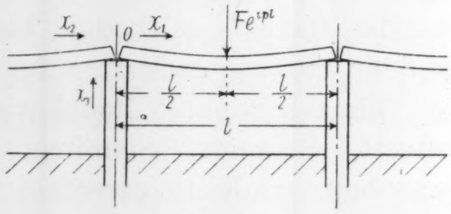

Fig. 1.

$$\rho_1a_1\frac{\partial^2 y_1}{\partial t^2}+E_1I_1\frac{\partial^4 y_1}{\partial x_1^4}=0,\ \rho_2a_2\frac{\partial^2 y_2}{\partial t^2}+E_2I_2\frac{\partial^4 y_2}{\partial x_2^4}=0,\ \rho'a'\frac{\partial^2 u}{\partial t^2}=E'a'\frac{\partial^2 u}{\partial x_3^2}. \tag{1}$$

The appropriate solutions of these equations are such that

$$y_1=e^{ipt}\{Ae^{i\sqrt{p}\,c_1x_1}+Be^{-i\sqrt{p}\,c_1x_1}+Ce^{\sqrt{p}\,c_1x_1}+De^{-\sqrt{p}\,c_1x_1}\}, \tag{2}$$

$$y_2=e^{ipt}\{Ge^{i\sqrt{p}\,c_2x_2}+He^{\sqrt{p}\,c_2x_2}\}, \tag{3}$$

$$u=\alpha e^{i(pt+hx_3)}, \tag{4}$$

where

$$\frac{p}{h}=\sqrt{\frac{E'}{\rho'}},\ c_1=\left(\frac{\rho_1a_1}{E_1I_1}\right)^{\frac{1}{4}},\ c_2=\left(\frac{\rho_2a_2}{E_2I_2}\right)^{\frac{1}{4}}. \tag{5}$$

If, as already mentioned, the two ends of every span of the bridge are supported without moment of force, and the middle point of a one span is sujected to a periodic force without moment of force, the boundary conditions would be represented by

$$x_1=o,\ x_2=o,\ x_3=o;\qquad y_1=y_2,\quad y_2=u,\quad E_1I_1\frac{\partial^2 y_1}{\partial x_1^2}=0,\qquad (6),\ (7),\ (8)$$

$$E_2I_2\frac{\partial^2 y_2}{\partial x_2^2}=0,\quad -E_1I_1\frac{\partial^3 y_1}{\partial x_1^3}+E_2I_2\frac{\partial^3 y_2}{\partial x_2^3}=E'a'\frac{\partial u}{\partial x_3},\qquad (9),\ (10)$$

$$x_1=\frac{l}{2};\qquad \frac{\partial y_1}{\partial x_1}=0,\quad -E_1I_1\frac{\partial^3 y_1}{\partial x_1^3}=\frac{F}{2}e^{ipt}.\qquad (11),\ (12)$$

Substituting (2), (3), (4) in (6) ~ (12), we get

$$\begin{aligned}
A\Phi&=\{\nu_2(\gamma_1\cos\gamma_1+\overline{\nu_1+\gamma_1}\mathrm{ch}\,\gamma_1)+\nu_1\gamma_2\mathrm{ch}\,\gamma_1\}+i\{\nu_2\gamma_1(\mathrm{sh}\,\gamma_1-\sin\gamma_1)+\nu_1\gamma_2\mathrm{ch}\,\gamma_1\},\\
B\Phi&=\{\nu_2(\gamma_1\cos\gamma_1-\nu_1-\gamma_1\mathrm{ch}\,\gamma_1)-\nu_1\gamma_2\mathrm{ch}\,\gamma_1\}+i\{\nu_2\gamma_1(\sin\gamma_1-\mathrm{sh}\,\gamma_1)-\nu_1\gamma_2\mathrm{ch}\,\gamma_1\},\\
C\Phi&=\{\nu_2\gamma_1(\cos\gamma_1+\sin\gamma_1+\mathrm{ch}\,\gamma_1-\mathrm{sh}\,\gamma_1)+\nu_1\gamma_2\cos\gamma_1\}-i\nu_1(\nu_2+\gamma_2)\cos\gamma_1,\\
D\Phi&=\{\nu_2\gamma_1(\cos\gamma_1-\sin\gamma_1+\mathrm{ch}\,\gamma_1+\mathrm{sh}\,\gamma_1)-\nu_1\gamma_2\cos\gamma_1\}+i\nu_1(\nu_2+\gamma_2)\cos\gamma\ ,\\
H\Phi&=2\nu_2\gamma_1(\cos\gamma_1+\mathrm{ch}\,\gamma_1),\quad G=H,\quad \alpha=2H,
\end{aligned}\qquad (13)$$

$$\Phi=\frac{32\gamma_1^3}{\eta}\Big[-\{\nu_2\gamma_1(\cos\gamma_1\mathrm{sh}\,\gamma_1+\sin\gamma_1\mathrm{ch}\,\gamma_1)+\nu_1\gamma_2\cos\gamma_1\mathrm{ch}\,\gamma_1\}$$
$$+i\nu_1(\nu_2+\gamma_2)\cos\gamma_1\mathrm{ch}\,\gamma_1\Big],\qquad (14)$$

where

$$\nu_1=\sqrt{\frac{E'\rho'a'\,l^2}{E_1\rho_1a_1I_1}},\quad \nu_2=\sqrt{\frac{E'\rho'a'^2l^2}{E_2\rho_2a_2I_2}},\quad \gamma_1=\frac{\sqrt{p}\ c_1l}{2}=\frac{1}{2}\left(\frac{\rho_1a_1l'p^2}{E_1I_1}\right)^{\frac{1}{4}},$$

$$\gamma_2=\frac{\sqrt{p}\ c_2l}{2}=\frac{1}{2}\left(\frac{\rho_2a_2l^4p^2}{E_2I_2}\right)^{\frac{1}{4}},\quad \eta=\frac{Fl^3}{2E_1I_1}\ .\qquad (15)$$

(i) In the special case in which both ends of a given span rest on a pair of piers and no adjacent span exists, ν_2 assumes an infinitely large value, so that we have

$$\left.\begin{aligned}
A\Phi'&=\{\gamma_1\cos\gamma_1+(\nu_1+\gamma_1)\mathrm{ch}\,\gamma_1\}+i\gamma_1(-\sin\gamma_1+\mathrm{sh}\,\gamma_1),\\
B\Phi'&=\{\gamma_1\cos\gamma_1-(\nu_1-\gamma_1)\mathrm{ch}\,\gamma_1\}+i\gamma_1(\sin\gamma_1-\mathrm{sh}\,\gamma_1),\\
C\Phi'&=\gamma_1(\cos\gamma_1+\sin\gamma_1+\mathrm{ch}\,\gamma_1-\mathrm{sh}\,\gamma_1)-i\nu_1\cos\gamma_1,
\end{aligned}\right\}\qquad (13')$$

$$\left.\begin{aligned} D\Phi' &= \gamma_1(\cos\gamma_1 - \sin\gamma_1 + \operatorname{ch}\gamma_1 + \operatorname{sh}\gamma_1) + i\nu_1\cos\gamma_1, \\ \alpha\Phi' &= 4\gamma_1(\cos\gamma_1 + \operatorname{ch}\gamma_1), \end{aligned}\right\}$$

$$\Phi' = \frac{32\gamma_1^3}{\eta}\Big[-\gamma_1(\cos\gamma_1\operatorname{sh}\gamma_1 + \sin\gamma_1\operatorname{ch}\gamma_1) + i\nu_1\cos\gamma_1\operatorname{ch}\gamma_1\Big]. \qquad (14')$$

These forms resemble those of the dissipation problem in the case of a building structure.

(ii) For the case in which there are neighbouring spans of the same type, we may put $\nu_1 = \nu_2 = \nu$, $\gamma_1 = \gamma_2 = \gamma$, so that (13), (14) reduce to

$$\left.\begin{aligned} A\Phi &= \{\gamma(\cos\gamma + 2\operatorname{ch}\gamma) + \nu\operatorname{ch}\gamma\} + i\gamma(-\sin\gamma + \operatorname{ch}\gamma + \operatorname{sh}\gamma), \\ B\Phi &= (\gamma\cos\gamma - \nu\operatorname{ch}\gamma) + i\gamma(\sin\gamma - \operatorname{ch}\gamma - \operatorname{sh}\gamma), \\ C\Phi &= \gamma(2\cos\gamma + \sin\gamma + \operatorname{ch}\gamma - \operatorname{sh}\gamma) - i(\nu+\gamma)\cos\gamma, \\ D\Phi &= \gamma(-\sin\gamma + \operatorname{ch}\gamma + \operatorname{sh}\gamma) + i(\nu+\gamma)\cos\gamma, \\ H\Phi &= 2\gamma(\cos\gamma + \operatorname{ch}\gamma), \quad G = H, \quad \alpha = 2H, \end{aligned}\right\} \qquad (16)$$

$$\Phi = \frac{32\gamma^3}{\eta}\Big[-\gamma(\cos\gamma\operatorname{ch}\gamma + \cos\gamma\operatorname{sh}\gamma + \sin\gamma\operatorname{ch}\gamma) + i(\nu+\gamma)\cos\gamma\operatorname{ch}\gamma\Big]. \qquad (17)$$

We shall write the solutions of the present case in their real forms. Thus, corresponding to the disturbance

$$F\cos pt \qquad (18)$$

at $x_1 = l/2$, we have

$$y_{1_{x_1=\frac{l}{2}}} = \frac{-\eta}{32\gamma^3}\sqrt{\frac{R^2+S^2}{P^2+Q^2}}\cos\left(pt - tan^{-1}\frac{S}{R} + tan^{-1}\frac{Q}{P}\right), \qquad (19)$$

$$y_2 = \frac{-\eta}{32\gamma^2}\frac{(\cos\gamma + \operatorname{ch}\gamma)}{\sqrt{P^2+Q^2}}\cos\left(pt + \sqrt{p}\,cx_2 + tan^{-1}\frac{Q}{P}\right), \qquad (20)$$

$$u = \frac{-\eta}{16\gamma^2}\frac{(\cos\gamma + \operatorname{ch}\gamma)}{\sqrt{P^2+Q^2}}\cos\left(pt + hx_3 + tan^{-1}\frac{Q}{P}\right), \qquad (21)$$

where

$$\left.\begin{aligned} P &= \gamma(\cos\gamma\operatorname{ch}\gamma + \cos\gamma\operatorname{sh}\gamma + \sin\gamma\operatorname{ch}\gamma), \\ Q &= (\nu+\gamma)\cos\gamma\operatorname{ch}\gamma, \\ R &= \gamma(2 + 2\cos\gamma\operatorname{ch}\gamma - \sin\gamma\operatorname{ch}\gamma + \cos\gamma\operatorname{sh}\gamma), \\ S &= (\nu+\gamma)(\cos\gamma\operatorname{sh}\gamma - \sin\gamma\operatorname{ch}\gamma). \end{aligned}\right\} \qquad (22)$$

In the same way it is possible to write the expression of the bending moments at $x_1=l/2$, namely,

$$\frac{l^2}{\eta}\frac{\partial^2 y_1}{\partial x_1^2}_{x_1=l/2}=\frac{1}{4\gamma^2}\sqrt{\frac{R'^2+S'^2}{P^2+Q^2}}\cos\left(pt-tan^{-1}\frac{S'}{R'}+tan^{-1}\frac{Q}{P}\right), \tag{23}$$

where

$$\left.\begin{aligned} R'&=\gamma(\cos\gamma\,\mathrm{sh}\,\gamma+\sin\gamma\,\mathrm{ch}\,\gamma+2\sin\gamma\,\mathrm{sh}\,\gamma),\\ S'&=(\nu+\gamma)(\cos\gamma\,\mathrm{sh}\,\gamma+\sin\gamma\,\mathrm{ch}\,\gamma).\end{aligned}\right\} \tag{24}$$

The approximate resonance condition of case (i) as well as case (ii) is

$$\text{(i), (ii)} \qquad \cos\gamma_1=0. \tag{25}$$

In either case of (i) or (ii), even should no damping force exist, the amplitude of vibrations would not assume an infinitely large value owing to the condition that the denominators of the expressions for amplitudes in both cases are

$$\left.\begin{aligned} &\text{(i)} && \sqrt{\gamma_1^2(\cos\gamma_1\mathrm{sh}\,\gamma_1+\sin\gamma_1\mathrm{ch}\,\gamma_1)^2+\nu_1^2(\cos\gamma_1\mathrm{ch}\,\gamma_1)^2},\\ &\text{(ii)} && \sqrt{\gamma^2(\cos\gamma\,\mathrm{ch}\,\gamma+\cos\gamma\,\mathrm{sh}\,\gamma+\sin\gamma\,\mathrm{ch}\,\gamma)^2+(\nu+\gamma)^2(\cos\gamma\,\mathrm{ch}\,\gamma)^2}\end{aligned}\right\} \tag{26}$$

respectively.

3. *A numerical example and its interpretation.*

We shall take the case of a deck girder bridge, one span of which is 25 m long (l) and weighing 33 tons. We shall suppose that a locomotive weighing three times that of the bridge rests on that span (weights of the same mass density as that of the locomotive being distributed in the neighbouring spans). If the stiffness of the bridge were so designed that its central deflection δ due to loading as well as its own weights (ρal) should be 1/1000 that of the span length, we would have

$$\rho a=4.33.10^3/25=5\cdot 28.10^3 \text{ kg mass/m},$$

$$EI=\frac{5(\rho alg)l^3}{384\,\delta}=\frac{5(4.33.10^3.9\cdot 8)25^3}{484.0\cdot 025}=10\cdot 525.10^9 \text{ kg mass m}^3/\text{s}^2.$$

If for the piers we assume

$$a'=1.5=5 \text{ m}^2,\ E'=2\cdot 1.10^9.9\cdot 8 \text{ kg mass/m.s}^2,\ \rho'=3.10^3 \text{ kg mass/m}^3,$$

we get for case (ii)

$$\nu=\sqrt{\frac{2\cdot 1.9\cdot 8.10^9.3.10^3.5^2.25^2}{10\cdot 525.10^9.5\cdot 28.10^3}}=76\cdot 1.$$

Using this relation we calculated $y_{1x_1=l/2}$, $y_{2\,\max}$, $u_{\max}$ for different values of γ, namely $(\rho a l^4 p^2/EI)^{\frac{1}{4}}$, the results being shown in Fig. 2. Every ordinate of this figure may be assumed to indicate the relative value of any one of $y_{1x_1=l/2}$, $y_{2\,\max}$, $u_{\max}$ for the disturbing force Fe^{ipt} of like intensity but of different vibrational frequencies.

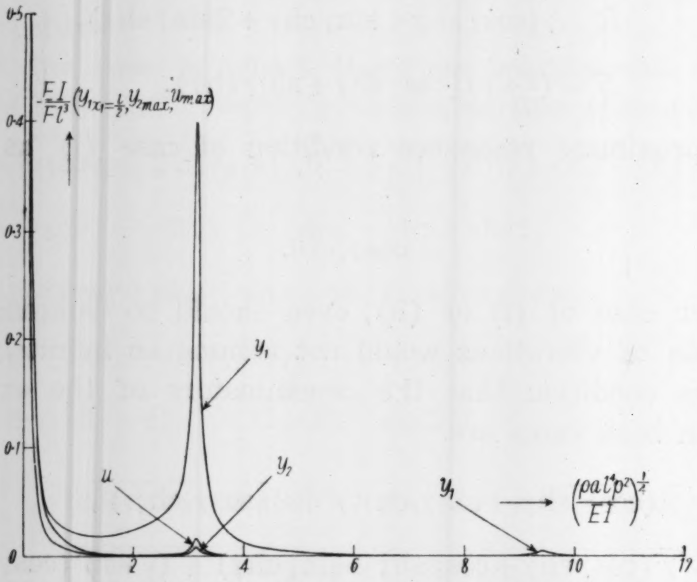

Fig. 2. Resonance curve. F=constant.

The amplitude of vibration assumes an infinitely large value at zero frequency and a minimum value between the zero frequency under consideration and the first resonance condition $(\rho a l^4 p^2/EI)^{\frac{1}{4}}\approx\pi$. It will be seen that although the amplitude in the first resonance is about twenty times that at the condition of minimum amplitude above mentioned, the amplitude under the third resonance $(\rho a l^4 p^2/EI)^{\frac{1}{4}}\approx 3\pi$ is comparable to that at the same condition. Under the second resonance in the present case we have little amplitude owing to the disturbing force working at the node of its free vibration. Generally speaking, the higher the order of resonance, the greater the diminution in the vibration amplitude, the resulting phenomena closely resembling those in damping due to viscous resistance.

The American Railway Engineering Association[11] has recently reported from experimental results that, in the curves of *dynamic*

---

[11] *Bull. American Railway Eng. Assoc.*, **37** (1935), No. 380.

magnifiers, namely, in the resonance curves for the vibrations of a bridge under disturbance of a given intensity, the amplitude under resonance condition is about five or six times that at very low vibrational frequency. Although no investigation seems to have been made, judging from the paper, into the probable source of the damping in vibration, it is obvious that the damping in the experiments resulted from all possible sources. Since in our paper we discuss the damping due to only one of the probable causes, there is reason for the damping in the report under consideration being somewhat greater than our theoretical value.

The maximum amplitude $y_{2\,\max}$, of waves in the adjacent spans are one-half that of $u_{\max}$ in the piers for any vibrational frequency. Since, as shown in Fig. 2, the amplitudes of both kinds of waves, $y_{2\,\max}$ and $u_{\max}$, are usually very small compared with that of $y_{1\,\max}$ excepting near zero frequency, and since furthermore the waves once transmitted outwards are damped by friction, etc., the effect of the reflected waves in y_2 and u, even if existent, on y_1 would virtually be very small.

It is rather difficult, in actual experiments, to keep F constant for any vibrational frequency. In the case of a locomotive or an exciting machine, the condition

$$F = f\gamma^4\left(=f\frac{\rho a l^4 p^2}{16EI}\right), \tag{27}$$

where f is a constant, probably exists. From this consideration the result in Fig. 2 is reproduced in the form shown in Fig. 3. This

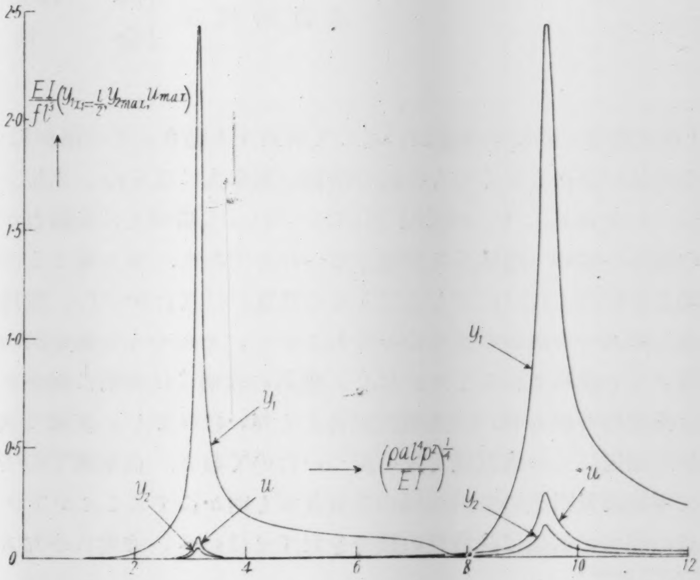

Fig. 3. Resonance curve. $f=$ constant $\left(F=f\,\frac{\rho a l^4 p^2}{16EI}\right)$.

figure shows that the vibration amplitudes, even in non-resonance condition, tend to increase with increase in the vibrational frequency. In their meaning, the oscillation curves given in the report of the American Railway Association[12] correspond exactly to our curves in Fig. 3. It will be seen that the steepness of the curves near resonance conditions is more marked in our case, the reason for which is apparent from the preceding discussion.

The question may arise whether or not it is possible for the present results to apply immediately to the case of such a quickly moving disturbance as passing the bridge span within five or six repetitions of its pulsations. In that case the problem could be solved by expanding the expression of the force Fe^{ipt} in harmonic series as done by Inglis,[13] a detailed method for which is now under investigation.

In conclusion we wish to express our thanks to Professor Tanaka, who supplied us with much valuable information on bridge construction and data respecting its vibrations.

---

24. 橋梁の振動に於ける勢力の逸散性（第1報）

地震研究所 妹澤克惟
金井清

これまで，地上構造物特に建物が地震動によつて振動する場合にその振動勢力が地中に逸散し，從て構造物の內部抵抗が存在しなくても共振の振幅は無限大にならぬこと及びそれに伴ふ現象を研究した．今回はそれを延長して，地震動ではないけれども橋梁上に振動力が働く場合に橋桁の振動勢力が隣りの橋桁や橋脚へ逸散する問題を考へたのである．第1報として振動力が橋桁に沿うて移動しない場合を研究したけれども之でもその性質だけはわかつた．尙地上の場合のやうに半無限體が下に無く寧ろ一方向的の連りのみであるから，そのやうな部分的の計算上の略算の爲に逸散理論の本質までも誤解されることがなく，逸散の說明には非常に都合がよいのである．

計算の結果地上構造物の場合程には逸散性が甚しくないけれども，米國で試みられた橋梁振動の減衰性の大部分の原因はこの逸散性で說明がついたのである．尙米國での研究の場合には明瞭に出ぬ部分例へば零振動數附近の振動振幅の性質なども明かにすることができたのである．

橋脚や隣り合せの橋桁の振幅は逸散性の媒介をなすとはいへ，非常に小なる振幅であることは

---

[12] *loc. cit.* 11).

[13] C. E. INGLIS, *loc. cit.* 6).

注意を要する．又同轉體の遠心力によつて起るやうな振動の場合に，共振を越した高い振動數でもその振幅が必しも小さくはならぬこともわかるのである．

振動力が橋桁に沿うて移動する問題も考慮中であるが，それよりも只今の問題に大切な事は，その移動速度が橋桁に沿うて傳はる撓み波動の速度よりも遙かに低いことであつて，之は只今の問題でも充分に滿足してをる．

25. *The Vibration due to Obliquely Incident Waves of a Surface Stratum Adhering Closely to the Subjacent Medium, and the Properties of its Resonance Condition.*

By Genrokuro NISHIMURA and Takeo TAKAYAMA,

Earthquake Research Institute.

(Read Oct. 20, 1936—Received March 20, 1937.)

Introduction

In the previous paper[1] (in Japanese) one of the present writers discussed the vibratory motions of a surface layer and a subjacent semi-infinite elastic body when a dilatational wave is obliquely incident on the common boundary where the two solids adhere closely. The first chapter of that paper discussed the general properties of forced waves propagated in the two solids, namely, in the surface layer and in the subjacent solid when a dilatational wave of harmonic wave-type of infinite extent is obliquely incident on the bottom surface of the surface layer. In the second chapter were explained, analytically, the general phenomena of free wave-motions in the two solids when a dilatational wave of finite extent is obliquely incident on the common boundary.

The present paper, which is a continuation of the previous one, deals numerically, aided with numerous figures, with the case when a dilatational wave of harmonic type of infinite extent is obliquely incident on the bottom surface of the surface layer and the angle of incidence of this wave becomes 45°. From the mathematical results in the present paper, we obtained a number of facts helpful in studying the forced stationary vibrations of a particle in the surface layer of the earth's crust. We stated in the previous paper[2] that K. Sezawa[3] and K. Kanai have studied the forced wave-motions in the surface layer when a dilatational harmonic wave of infinite extent is obliquely incident upon the bottom surface of a surface layer and the angle of incidence of that wave becomes 45° as in the present paper. The elasticity conditions dealt with in their paper, however, differ somewhat from those

---

1) G. NISHIMURA, *Bull. Earthq. Res. Inst.*, **13** (1935), 540~554.

2) G. NISHIMURA, *loc. cit.*

3) K. SEZAWA and K. KANAI, *Bull. Earthq. Res. Inst.*, **10** (1932), 806; **12** (1934), 269.

treated in the present paper, namely, that whereas the ratio of rigidity of the surface stratum to that of the subjacent medium is 1/2 in Sezawa's case, in the present paper it is 1/10 for the purpose of theoretically investigating the seismal oscillation of the ground at Marunouti, a ground typifying the down-town of Tokyo.

In recent years the predominating periods of seismic oscillations of various grounds have been studied experimentally by M. Ishimoto[4], T. Saita[5], and W. Inouye[6]. Their views of the seismal oscillations of a surface layer of the earth's crust involve the assumption that the surface layer may be treated as an isolated elastic pendulum, the subjacent medium having no relation to the vibration in the surface layer. This theory seems to be supported in particular by the results[7] of analysis of the seismic acceleration of the ground at Marunouti. Sezawa[8], who has mathematically studied the vibrations of a surface stratum when elastic waves of infinite and finite extent are incident vertically upward on the bottom surface of the surface layer, shows that it is not satisfactory, in dealing with the seismal vibrations of the surface stratum, to assume that the stratum is an isolated body, as we do in the case of an elastic pendulum. He also extended his theory to enable comparison of his mathematical results with the actual facts[9] as learned from the seismometrical observations at Marunouti.

As already mentioned, we shall study in the present paper the forced stationary oscillations of the surface layer when harmonic waves of infinite extent are obliquely incident on the bottom surface of the surface layer. For this reason it will not be possible for us to explain from the results in the present paper the existence of predominating periods of seismal oscillations in the surface layer, which may result from the seismal vibrations of the surface layer due to free seismic waves propagated in the surface layer, although we shall be able to explain satisfactorily the existence of resonance periods of vibration in the surface layer. The former we shall no doubt be able to explain upon carefully studying the mathematical results contained in the second chapter[10] of the preceding paper.

---

4) M. ISHIMOTO, *Bull. Earthq. Res. Inst.*, **9** (1931), 316; **9** (1931), 473; **10** (1932), 171; **12** (1934), 234.

5) T. SAITA and M. SUZUKI, *Bull. Earthq. Res. Inst.*, **12** (1934), 517.

6) W. INOUYE, *Bull. Earthq. Res. Inst.*, **12** (1934), 712.

7) T. SAITA and M. SUZUKI, *loc. cit.*

8) K. SEZAWA, *Bull. Earthq. Inst.*, **8** (1930), 1.
K. SEZAWA and K. KANAI, *Bull. Earthq. Res. Inst.*, **13** (1635), 251.

9) T. SAITA and M. SUZUKI, *loc. cit.*

10) G. NISHIMURA, *loc. cit.*

Chapter I. Bodily Waves in a Semi-infinite Solid having a Surface Layer When a Dilatational Harmonic Wave of Infinite Extent is Obliquely Incident on the Common Boundary of These Two Solids where They Adhere Closely.

1. *General Solutions.*

Let the horizontal boundary of a surface layer of thickness H and a subjacent medium be $y=0$, and let the axis of x be on this common boundary, the axis of y being drawn vertically downward and positive, as shown in Fig. 1. Again let ρ and λ, μ be the density and Lame's elastic constants of the subjacent medium $y \geqq 0$ and ρ', and λ', μ' those of the surface layer.

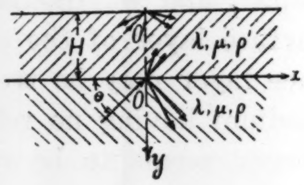

Fig. 1.

If the primary incident wave in the subjacent medium $y \geqq 0$ be of the type

$$\phi_0 = a e^{i(fx-ry-pt)}, \tag{1}$$

where a is a constant representing the intensity of this wave; and $p=2\pi/T$, where T is the period of this incident harmonic wave; and $r^2=\{\rho p^2/(\lambda+2\mu)\}-f^2$, obviously, f will depend on the wave-length L and the emergent angle θ of this wave. When the primary wave expressed by (1) is incident on the bottom surface of the surface layer, the following two waves are reflected at the common boundary in the subjacent medium $y \geqq 0$,

$$\phi = A e^{i(fx+ry-pt)}, \tag{2}$$

$$\psi = B e^{i(fx+sy-pt)}, \tag{3}$$

where ϕ is the reflected dilatational wave and ψ the reflected distortional wave, both of which respectively satisfy the wave equations

$$\frac{\partial^2 \phi}{\partial t^2} = \frac{\lambda+2\mu}{\rho} \nabla^2 \phi, \tag{4}$$

$$\frac{\partial^2 \psi}{\partial t^2} = \frac{\mu}{\rho} \nabla^2 \psi. \tag{5}$$

In expressions (2), (3), A and B are arbitrary constants to be determined from the boundary conditions at $y=0$ and $y=-H$, and $s^2=\rho p^2/\mu - f^2$. Naturally wave expression (1) satisfies wave equation (4).

Let the refracted and reflected waves in the surface layer due to the incidence of the primary wave (1) be expressed by

$$\phi' = Ce^{i(fx-r'y-pt)} + De^{i(fx+r'y-pt)}, \tag{6}$$

$$\psi' = Ee^{i(fx-s'y-pt)} + Fe^{i(fx+s'y-pt)}, \tag{7}$$

where C and E are respectively intensities of the refracted dilatational and distortional waves to be determined, and also D, F those of the dilatational and distortional waves reflected at the free surface of the layer $y=-H$; and let $r'^2=\rho'p^2/(\lambda'+2\mu')-f^2$, $s^2=\rho'p^2/\mu'-f^2$ respectively. Obviously, ϕ' and ψ' satisfy the following wave equations in the surface layer:

$$\frac{\partial^2\phi'}{\partial t^2}=\frac{\lambda'+2\mu'}{\rho'}\Gamma^2\phi', \tag{8}$$

$$\frac{\partial^2\psi'}{\partial t^2}=\frac{\mu'}{\rho'}\Gamma^2\psi'. \tag{9}$$

Let U' and V' be the horizontal and vertical movements of the particle in the surface layer respectively, and U and V be those in the subjacent medium, when we shall then be able to obtain these movements from (6), (7) and (1), (2), (3) respectively. Now we can easily obtain the horizontal and the vertical displacements $(u_0,\ v_0)$ of a particle due to the incident primary wave (1) as follows:

$$\left.\begin{aligned} u_0&=if\alpha e^{i(fx-ry-pt)},\\ v_0&=-ir\alpha e^{i(fx-ry-pt)}.\end{aligned}\right\} \tag{10}$$

The horizontal and vertical movements in the lower medium $y \geqq 0$ due to waves ϕ and ψ are respectively given by

$$\left.\begin{aligned} u_1&=ifAe^{i(fx+ry-pt)},\\ v_1&=irAe^{i(fx+ry-pt)},\end{aligned}\right\} \tag{11}$$

$$\left.\begin{aligned} u_2&=isBe^{i(fx+sy-pt)},\\ u_2&=-ifBe^{i(fx+sy-pt)},\end{aligned}\right\} \tag{12}$$

those in the surface layer due to waves ϕ' and ψ' being expressed by

$$\left.\begin{aligned} u_1'&=ifCe^{i(fx-r'y-pt)}+ifDe^{i(fx+r'y-pt)},\\ v_1'&=-ir'Ce^{i(fx-r'y-pt)}+ir'De^{i(fx+r'y-pt)},\end{aligned}\right\} \tag{13}$$

$$\left.\begin{aligned} u_2' &= -is'Ee^{i(fx-s'y-pt)}+is'Fe^{i(fx+s'y-pt)}\,, \\ v_2' &= -ifEe^{i(fx-s'y-pt)}-ifFe^{i(fx+s'y-pt)}\,. \end{aligned}\right\} \tag{14}$$

We then get the expressions

$$U=u_0+u_1+u_2\,, \qquad V=v_0+v_1+v_2\,,$$

$$U'=u_1'+u_2'\,, \qquad V'=v_1'+v_2'\,,$$

or

$$U=if\mathfrak{a}^{i(fx-ry-pt)}+ifAe^{i(fx+ry-pt)}+isBe^{i(fx+sy-pt)}\,, \tag{15}$$

$$V=-ir\mathfrak{a}e^{i(fx-ry-pt)}+irAe^{i(fx+ry-pt}-ifBe^{i(fx+sy-pt)}\,, \tag{16}$$

$$U'=ifCe^{i(fx-r'y-pt)}+ifDe^{i(fx+r'y-pt)}-is'Ee^{i(fx-s'y-pt)}+is'Fe^{i(fx+s'y-pt)}\,, \tag{17}$$

$$V'=-ir'Ce^{i(fx-r'y-pt)}+ir'De^{i(fx+r'y-pt)}-ifEe^{i(fx-s'y-pt)}-ifFe^{i(fx+s'y-pt)}\,. \tag{18}$$

The conditions in which the displacements and the stresses of both solids are continuous at the common boundary $y=0$ are analytically expressed by

$$\left.\begin{aligned} U=U'\,, \qquad V=V'\,, \\ \lambda\left(\frac{\partial U}{x}+\frac{\partial V}{\partial y}\right)+2\mu\frac{\partial V}{\partial y} &= \lambda'\left(\frac{\partial U'}{\partial x}+\frac{\partial V'}{\partial y}\right)+2\mu'\frac{\partial V'}{\partial y}\,, \\ \mu\left(\frac{\partial V}{\partial x}+\frac{\partial U}{\partial y}\right) &= \mu'\left(\frac{\partial V'}{\partial x}+\frac{\partial U'}{\partial y}\right), \end{aligned}\right\} \tag{19}$$

and the conditions in which the top surface of the surface layer $y=-H$ is a free surface are also expressed by

$$\left.\begin{aligned} \lambda'\left(\frac{\partial U'}{\partial x}+\frac{\partial V'}{\partial y}\right)+2\mu'\frac{\partial V'}{\partial y} &= 0\,, \\ \mu'\left(\frac{\partial V'}{\partial x}+\frac{\partial U'}{\partial y}\right) &= 0\,. \end{aligned}\right\} \tag{20}$$

We obtain the following values of A, B, C, D, E, and F thus determined from conditions (19), (20)

$$\left.\begin{aligned} A=\frac{\Delta_A}{\Delta}\mathfrak{a}\,, \qquad B=\frac{\Delta_B}{\Delta}\mathfrak{a}\,, \qquad C=\frac{\Delta_C}{\Delta}\mathfrak{a}\,, \\ D=\frac{\Delta_D}{\Delta}\mathfrak{a}\,, \qquad E=\frac{\Delta_E}{\Delta}\mathfrak{a}\,, \qquad F=\frac{\Delta_F}{\Delta}\mathfrak{a}\,, \end{aligned}\right\} \tag{21}$$

where

$$
\begin{aligned}
J=16\frac{r's'}{f^2}\left(1-\frac{s'^2}{f^2}\right)\Bigg[&-\mu^2\left\{\left(1-\frac{s^2}{f^2}\right)^2+4\frac{rs}{f^2}\right\}+\mu\mu'\left(1-\frac{s^2}{f^2}+2\frac{rs}{f^2}\right)\left(3-\frac{s'^2}{f^2}\right)\\
&-2\mu'^2\left(1+\frac{rs}{f^2}\right)\left(1-\frac{s'^2}{f^2}\right)\Bigg]\\
+e^{i(r'+s')H}\left\{\left(1-\frac{s'^2}{f^2}\right)^2+4\frac{r's'}{f^2}\right\}\Bigg[&\mu^2\left(1+\frac{r's'}{f^2}\right)\left\{\left(1-\frac{s^2}{f^2}\right)^2+4\frac{rs}{f^2}\right\}\\
&-\mu\mu'\left\{\left(1+\frac{s^2}{f^2}\right)\left(1+\frac{s'^2}{f^2}\right)\left(\frac{sr'}{f^2}+\frac{rs'}{f^2}\right)+2\left(1-\frac{s^2}{f^2}+2\frac{rs}{f^2}\right)\left(1-\frac{s'^2}{f^2}+2\frac{r's'}{f^2}\right)\right\}\\
&+\mu'^2\left(1+\frac{rs}{f^2}\right)\left\{\left(1-\frac{s'^2}{f^2}\right)^2+4\frac{r's'}{f^2}\right\}\Bigg]\\
+e^{i(r'-s')H}\left\{\left(1-\frac{s'^2}{f^2}\right)^2-4\frac{r's'}{f^2}\right\}\Bigg[&-\mu^2\left(1-\frac{r's'}{f^2}\right)\left\{\left(1-\frac{s^2}{f^2}\right)^2+4\frac{rs}{f^2}\right\}\\
&+\mu\mu'\left\{\left(1+\frac{s^2}{f^2}\right)\left(1+\frac{s'^2}{f^2}\right)\left(\frac{sr'}{f^2}-\frac{rs'}{f^2}\right)+2\left(1-\frac{s^2}{f^2}+2\frac{rs}{f^2}\right)\left(1-\frac{s'^2}{f^2}-2\frac{r's'}{f^2}\right)\right\}\\
&-\mu'^2\left(1+\frac{rs}{f^2}\right)\left\{\left(1-\frac{s'^2}{f^2}\right)^2-4\frac{r's'}{f^2}\right\}\Bigg]\\
+e^{-i(r'-s')H}\left\{\left(1-\frac{s'^2}{f^2}\right)^2-4\frac{r's'}{f^2}\right\}\Bigg[&-\mu^2\left(1-\frac{r's'}{f^2}\right)\left\{\left(1-\frac{s^2}{f^2}\right)^2+4\frac{rs}{f^2}\right\}\\
&+\mu\mu'\left\{2\left(-\frac{s^2}{f^2}+2\frac{rs}{f^2}\right)\left(1-\frac{s'^2}{f^2}-2\frac{r's'}{f^2}\right)+\left(1+\frac{s^2}{f^2}\right)\left(1+\frac{s'^2}{f^2}\right)\left(\frac{rs'}{f^2}-\frac{r's}{f^2}\right)\right\}\\
&-\mu'^2\left(1+\frac{rs}{f^2}\right)\left\{\left(1-\frac{s'^2}{f^2}\right)^2-4\frac{r's'}{f^2}\right\}\Bigg]\\
+e^{-i(r'+s')H}\left\{\left(1-\frac{s'^2}{f^2}\right)^2+4\frac{r's'}{f^2}\right\}\Bigg[&\mu^2\left(1+\frac{r's'}{f^2}\right)\left\{\left(1-\frac{s^2}{f^2}\right)^2+4\frac{rs}{f^2}\right\}\\
&+\mu\mu'\left\{\left(1+\frac{s^2}{f^2}\right)\left(1+\frac{s'^2}{f^2}\right)\left(\frac{rs'}{f^2}+\frac{sr'}{f^2}\right)-2\left(1-\frac{s^2}{f^2}+2\frac{rs}{f^2}\right)\left(1-\frac{s'^2}{f^2}+2\frac{r's'}{f^2}\right)\right\}\\
&+\mu'^2\left(1+\frac{rs}{f^2}\right)\left\{\left(1-\frac{s'^2}{f^2}\right)^2+4\frac{r's'}{f^2}\right\}\Bigg],
\end{aligned}
\tag{22}
$$

$$
\begin{aligned}
\Delta_A = 16\frac{r's'}{f^2}\left(1-\frac{s'^2}{f^2}\right)\Bigg[&\mu^2\left\{1\left(-\frac{s^2}{f^2}\right)^2-4\frac{rs}{f^2}\right\}-\mu\mu'\left(1-\frac{s^2}{f^2}-2\frac{rs}{f^2}\right)\left(3-\frac{s'^2}{f^2}\right)\\
&+2\mu'^2\left(1-\frac{rs}{f^2}\right)\left(1-\frac{s'^2}{f^2}\right)\Bigg]\\
+e^{i(r'+s')H}\left\{\left(1-\frac{s'^2}{f^2}\right)^2+4\frac{r's'}{f^2}\right\}\Bigg[&-\mu^2\left(1+\frac{r's'}{f^2}\right)\left\{\left(1-\frac{s^2}{f^2}\right)^2-4\frac{rs}{f^2}\right\}\\
&+\mu\mu'\left\{\left(1+\frac{s^2}{f^2}\right)\left(1+\frac{s'^2}{f^2}\right)\left(\frac{r's}{f^2}-\frac{rs'}{f^2}\right)+2\left(1-\frac{s^2}{f^2}-2\frac{rs}{f^2}\right)\left(1-\frac{s'^2}{f^2}+2\frac{r's'}{f^2}\right)\right\}\\
&-\mu'^2\left(1-\frac{rs}{f^2}\right)\left\{\left(1-\frac{s'^2}{f^2}\right)^2+4\frac{r's'}{f^2}\right\}\Bigg]\\
+e^{i(r'-s')H}\left\{\left(1-\frac{s'^2}{f^2}\right)^2-4\frac{r's'}{f^2}\right\}\Bigg[&\mu^2\left(1-\frac{r's'}{f^2}\right)\left\{\left(1-\frac{s^2}{f^2}\right)^2-4\frac{rs}{f^2}\right\}\\
&-\mu\mu'\left\{\left(1+\frac{s^2}{f^2}\right)\left(1+\frac{s'^2}{f^2}\right)\left(\frac{sr'}{f^2}+\frac{rs'}{f^2}\right)+2\left(1-\frac{s^2}{f^2}-2\frac{rs}{f^2}\right)\left(1-\frac{s'^2}{f^2}-2\frac{r's'}{f^2}\right)\right\}\\
&+\mu'^2\left(1-\frac{rs}{f^2}\right)\left\{\left(1-\frac{s'^2}{f^2}\right)^2-4\frac{r's'}{f^2}\right\}\Bigg]\\
+e^{-i(r'+s')H}\left\{\left(1-\frac{s'^2}{f^2}\right)^2+4\frac{r's'}{f^2}\right\}\Bigg[&-\mu^2\left(1+\frac{r's'}{f^2}\right)\left\{\left(1-\frac{s^2}{f^2}\right)^2-4\frac{rs}{f^2}\right\}\\
&+\mu\mu'\left\{\left(1+\frac{s^2}{f^2}\right)\left(1+\frac{s'^2}{f^2}\right)\left(\frac{rs'}{f^2}-\frac{r's}{f^2}\right)+2\left(1-\frac{s^2}{f^2}-2\frac{rs}{f^2}\right)\left(1-\frac{s'^2}{f^2}+2\frac{r's'}{f^2}\right)\right\}\\
&-\mu'^2\left(1-\frac{rs}{f^2}\right)\left\{\left(1-\frac{s'^2}{f^2}\right)^2+4\frac{r's'}{f^2}\right\}\Bigg]\\
+e^{-i(r'-s')H}\left\{\left(1-\frac{s'^2}{f^2}\right)^2-4\frac{r's'}{f^2}\right\}\Bigg[&\mu^2\left(1-\frac{r's'}{f^2}\right)\left\{\left(1-\frac{s^2}{f^2}\right)^2-4\frac{rs}{f^2}\right\}\\
&+\mu\mu'\left\{\left(1+\frac{s^2}{f^2}\right)\left(1+\frac{s'^2}{f^2}\right)\left(\frac{r's}{f^2}+\frac{rs'}{f^2}\right)-2\left(1-\frac{s^2}{f^2}-2\frac{rs}{f^2}\right)\left(1-\frac{s'^2}{f^2}-2\frac{r's'}{f^2}\right)\right\}\\
&+\mu'^2\left(1-\frac{rs}{f^2}\right)\left\{\left(1-\frac{s'^2}{f^2}\right)^2-4\frac{r's'}{f^2}\right\}\Bigg],
\end{aligned}
\tag{23}
$$

$$\begin{aligned}
\Delta_B=16\frac{rr's'}{f^3}\left(1-\frac{s'^2}{f^2}\right)&\left[4\mu^2\left(1-\frac{s^2}{f^2}\right)-\mu\mu'\left(3-\frac{s^2}{f^2}\right)\left(3-\frac{s'^2}{f^2}\right)+4\mu'^2\left(1-\frac{s'^2}{f^2}\right)\right]\\
&+2e^{i(r'+s')H}\frac{r}{f}\left\{\left(1-\frac{s'^2}{f^2}\right)^2+4\frac{r's'}{f^2}\right\}\Bigg[-2\mu^2\left(1-\frac{s^2}{f^2}\right)\left(1+\frac{r's'}{f^2}\right)\\
&\qquad+\mu\mu'\left(3-\frac{s^2}{f^2}\right)\left(1-\frac{s'^2}{f^2}+2\frac{r's'}{f^2}\right)-\mu'^2\left\{\left(1-\frac{s'^2}{f^2}\right)^2+4\frac{r's'}{f^2}\right\}\Bigg]\\
&+2e^{i(r'-s')H}\frac{r}{f}\left\{\left(1-\frac{s'^2}{f^2}\right)^2-4\frac{r's'}{f^2}\right\}\Bigg[2\mu^2\left(1-\frac{s^2}{f^2}\right)\left(1-\frac{r's'}{f^2}\right)\\
&\qquad-\mu\mu'\left(3-\frac{s^2}{f^2}\right)\left(1-\frac{s'^2}{f^2}-2\frac{r's'}{f^2}\right)+\mu'^2\left\{\left(1-\frac{s'^2}{f^2}\right)^2-4\frac{r's'}{f^2}\right\}\Bigg]\\
&+2e^{-i(r'+s')H}\frac{r}{f}\left\{\left(1-\frac{s'^2}{f^2}\right)^2+4\frac{r's'}{f^2}\right\}\Bigg[-2\mu^2\left(1-\frac{s^2}{f^2}\right)\left(1+\frac{r's'}{f^2}\right)\\
&\qquad+\mu\mu'\left(3-\frac{s^2}{f^2}\right)\left(1-\frac{s'^2}{f^2}+2\frac{r's'}{f^2}\right)-\mu'^2\left\{\left(1-\frac{s'^2}{f^2}\right)^2+4\frac{r's'}{f^2}\right\}\Bigg]\\
&+2e^{-i(r'-s')H}\frac{r}{f}\left\{\left(1-\frac{s'^2}{f^2}\right)^2-4\frac{r's'}{f^2}\right\}\Bigg[2\mu^2\left(1-\frac{s^2}{f^2}\right)\left(1-\frac{r's'}{f^2}\right)\\
&\qquad-\mu\mu'\left(3-\frac{s^2}{f^2}\right)\left(1-\frac{s'^2}{f^2}-2\frac{r's'}{f^2}\right)+\mu'^2\left\{\left(1-\frac{s'^2}{f^2}\right)^2-4\frac{r's'}{f^2}\right\}\Bigg],
\end{aligned}\tag{24}$$

$$\begin{aligned}
\Delta_C=8\frac{rs'}{f^2}\left(1+\frac{s^2}{f^2}\right)\left(1-\frac{s'^2}{f^2}\right)&\left[-\mu^2\left(2\frac{r's}{f^2}-1+\frac{s^2}{f^2}\right)+\mu\mu'\left(2\frac{r's}{f^2}-1+\frac{s'^2}{f^2}\right)\right]\\
&+2e^{-i(r'-s')H}\frac{r}{f}\left(1+\frac{s^2}{f^2}\right)\left\{\left(1-\frac{s'^2}{f^2}\right)^2-4\frac{r's'}{f^2}\right\}\\
&\qquad\cdot\left[\mu\mu'\left\{\frac{s}{f}\left(1-\frac{s'^2}{f^2}\right)+2\frac{s'}{f}\right\}-\mu^2\left\{\frac{s'}{f}\left(1-\frac{s^2}{f^2}\right)+2\frac{s}{f}\right\}\right]\\
&+2e^{-i(r'+s')H}\frac{r}{f}\left(1+\frac{s^2}{f^2}\right)\left\{\left(1-\frac{s'^2}{f^2}\right)^2+4\frac{r's'}{f^2}\right\}\\
&\qquad\cdot\left[\mu\mu'\left\{-\frac{s}{f}\left(1-\frac{s'^2}{f^2}\right)+2\frac{s'}{f}\right\}+\mu^2\left\{-\frac{s'}{f}\left(1-\frac{s^2}{f^2}\right)+2\frac{s}{f}\right\}\right],
\end{aligned}\tag{25}$$

$$\begin{aligned}
J_D=8\frac{rs'}{f^2}\left(1+\frac{s^2}{f^2}\right)\left(1-\frac{s'^2}{f^2}\right)&\left[-\mu^2\left\{2\frac{r's}{f^2}+1-\frac{s^2}{f^2}\right\}+\mu\mu'\left\{2\frac{r's}{f^2}+1-\frac{s'^2}{f^2}\right\}\right]\\
&+2e^{i(r'+s')H}\frac{r}{f}\left(1+\frac{s^2}{f^2}\right)\left\{\left(1-\frac{s'^2}{f^2}\right)^2+4\frac{r's'}{f^2}\right\}\\
&\cdot\left[-\mu\mu'\left\{\frac{s}{f}\left(1-\frac{s'^2}{f^2}\right)+2\frac{s'}{f}\right\}+\mu^2\left\{\frac{s'}{f}\left(1-\frac{s^2}{f^2}\right)+2\frac{s}{f}\right\}\right]\\
&+2e^{i(r'-s')H}\frac{r}{f}\left(1+\frac{s^2}{f^2}\right)\left\{\left(1-\frac{s'^2}{f^2}\right)^2-4\frac{r's'}{f^2}\right\}\\
&\cdot\left[\mu\mu'\left\{\frac{s}{f}\left(1-\frac{s'^2}{f^2}\right)-2\frac{s'}{f}\right\}+\mu^2\left\{\frac{s'}{f}\left(1-\frac{s^2}{f^2}\right)-2\frac{s}{f}\right\}\right],
\end{aligned}\tag{26}$$

$$\begin{aligned}
J_E=8\frac{rr'}{f^2}\left(1+\frac{s^2}{f^2}\right)\left(1-\frac{s'^2}{f^2}\right)&\left[\mu^2\left\{\frac{s'}{f}\left(1-\frac{s^2}{f^2}\right)+2\frac{s}{f}\right\}-\mu\mu'\left\{\frac{s}{f}\left(1-\frac{s'^2}{f^2}\right)+2\frac{s'}{f^2}\right)\right]\\
&+2e^{-i(r'+s')H}\frac{r}{f}\left(1+\frac{s^2}{f^2}\right)\left\{\left(1-\frac{s'^2}{f^2}\right)^2+4\frac{r's'}{f^2}\right\}\\
&\cdot\left[\mu\mu'\left(1-\frac{s'^2}{f^2}+2\frac{r's}{f^2}\right)-\mu^2\left(1-\frac{s^2}{f^2}+2\frac{r's}{f^2}\right)\right]\\
&+2e^{i(r'-s')H}\frac{r}{f}\left(1+\frac{s^2}{f^2}\right)\left\{\left(1-\frac{s'^2}{f^2}\right)^2-4\frac{r's'}{f^2}\right\}\\
&\cdot\left[-\mu\mu'\left(1-\frac{s'^2}{f^2}-2\frac{r's}{f^2}\right)+\mu^2\left(1-\frac{s^2}{f^2}-2\frac{r's}{f^2}\right)\right],
\end{aligned}\tag{27}$$

$$\begin{aligned}
J_F=8\frac{rr'}{f^2}\left(1+\frac{s^2}{f^2}\right)\left(1-\frac{s'^2}{f^2}\right)&\left[\mu^2\left\{\frac{s'}{f}\left(1-\frac{s^2}{f^2}\right)-2\frac{s}{f}\right\}+\mu\mu'\left\{\frac{s}{f}\left(1-\frac{s'^2}{f^2}\right)-2\frac{s'}{f}\right\}\right]\\
&+2e^{i(r'+s')H}\frac{r}{f}\left(1+\frac{s^2}{f^2}\right)\left\{\left(1-\frac{s^2}{f^2}\right)^2+4\frac{r's'}{f^2}\right\}\\
&\cdot\left[\mu\mu'\left(1-\frac{s'^2}{f^2}-2\frac{r's}{f^2}\right)-\mu^2\left(1-\frac{s^2}{f^2}-2\frac{r's}{f^2}\right)\right]\\
&+2e^{-i(r'-s')H}\frac{r}{f}\left(1+\frac{s^2}{f^2}\right)\left\{\left(1-\frac{s'^2}{f^2}\right)^2-4\frac{r's'}{f^2}\right\}\\
&\cdot\left[-\mu\mu'\left(1-\frac{s'^2}{f^2}+2\frac{r's}{f^2}\right)+\mu^2\left(1-\frac{s^2}{f^2}+2\frac{r's}{f}\right)\right],
\end{aligned}\tag{28}$$

It will be seen that the constants A, B, C, D, E, F thus determined usually become complex values, being transcendental functions, the variables of which are composed of the emergent angle θ and the wavelength L of the primary wave (1), and also the densities, the elastic constants of both media, and naturally the thickness of the surface layer H. Now each orbital motion of a particle in both media due to the seven waves expressed by (1), (2), (3), (6), and (7) is simple-harmonic, the orbit of which becomes a straight line. The amplitude and phase-differance of this simple-harmonic motion are transcendental functions having the same variables as the six constants A, B, C, D, E, and F. For these reasons every particle in both media (the surface layer and the subjacent medium) generally pursue elliptic orbital motions. The major and minor axes of the elliptic orbits and the inclination angle which the major axis makes with the horizontal surface are also transcendental functions, the variables of which are composed of θ, L, H, ρ, ρ', λ, μ, λ', μ'. We shall now study an example in which $\rho=\rho'$, $\lambda=\mu$, $\lambda'=\mu'$, $\mu'/\mu=1/10$[11] and the emergent angle of the primary wave $\theta=45°$. We then get the following expressions of Δ, Δ_A, Δ_B, Δ_C, Δ_D, Δ_E, and Δ_F in order to determine A, B, C, D, E, F:

$$\begin{aligned}\Delta=&\,740496+6802609\cos(r'+s')H+4482215\cos(r'-s')H\\&-i4388760\sin(r'+s')H+i480220\sin(r'-s')H\,,\end{aligned}\tag{29}$$

$$\begin{aligned}\Delta_A=&\,1210195-1505732\cos(r'+s')H-3106149\cos(r'-s')H\\&+i520046\sin(r'+s')H-i4052695\sin(r'-s')H\,,\end{aligned}\tag{30}$$

$$\Delta_B=917154+3344876\cos(r'+s')H+3451535\cos(r'-s')H\,,\tag{31}$$

$$\begin{aligned}\Delta_C=&\,336645+2086088\cos(r'+s')H+574416\cos(r'-s')H\\&-i2086088\sin(r'+s')H-i574416\sin(r'-s')H\,,\end{aligned}\tag{32}$$

$$\begin{aligned}\Delta_D=&\,413626-622049\cos(r'+s')H-1926347\cos(r'-s')H\\&-i622049\sin(r'+s')H-i1926347\sin(r'-s')H\,,\end{aligned}\tag{33}$$

$$\begin{aligned}\Delta_E=&\,179836-811769\cos(r'+s')H-610075\cos(r'-s')H\\&+i811769\sin(r'+s')H-i610075\sin(r'-s')H\,,\end{aligned}\tag{34}$$

$$\begin{aligned}\Delta_F=&\,603094+660665\cos(r'+s')H+749609\cos(r'-s')H\\&+i660665\sin(r'+s')H-i749609\sin(r'-s')H\,,\end{aligned}\tag{35}$$

---

[11] K. Sezawa has already studied the orbital motion of the top surface particle in the surface layer when $\rho=\rho'$, $\lambda=\lambda'$, $\mu=\mu'$, $\theta=45°$ and $\mu'/\mu=1/2$. K. SEZAWA and K. KANAI, *Bull. Earthq. Res. Inst.*, **10** (1932), 806; **12** (1934), 269.

where

$$r'H=19{\cdot}3657\left(\frac{H}{L}\right), \qquad s\,H=34{\cdot}1264\left(\frac{H}{L}\right). \tag{36}$$

The values A, B, C, D, E, and F, therefore, become complex values which are transcendental functions, only H/L being variable.

We have calculated the values of A, B, C, D, E, and F for various values of H/L as shown in Table I.

Table I.

$\frac{H}{L}$	A	B	C	D	E	F
0·01	−0·2900 +*i*0·01738	0·6263 +*i*0·1311	0·2524 −*i*0·03596	−0·1755 −*i*0·03980	−0·1066 +*i*0·02334	0·1581 +*i*0·07362
0·02	−0·3203 +*i*0·04315	0·5704 +*i*0·2743	0·2631 −*i*0·07389	−0·1699 −*i*0·07989	−0·1196 +*i*0·04972	0·1228 +*i*0·1552
0·03	−0·457 +*i*0·07623	0·4270 +*i*0·4301	0·2871 −*i*0·1142	−0·1645 −*i*0·1210	−0·1551 +*i*0·07910	0·02932 +*i*0·2448
0·04	−0·6803 −*i*0·003673	0·09698 +*i*0·4805	0·3333 −*i*0·1454	−0·1745 −*i*0·1795	−0·2426 +*i*0·07678	−0·1935 +*i*0·2585
0·048	−0·8279 −*i*0·4387	−0·1176 +*i*0·2021	0·3682 −*i*0.1489	−0·1689 −*i*0·2937	−0·2964 −*i*0·02473	−0·3342 +*i*0·03464
0·05	−0·7827 −*i*0·5753	−0·1043 +*i*0·1188	0·3733 −*i*0·1513	−0·1512 −*i*0·3311	−0·2884 −*i*0·05594	−0·3194 −*i*0·03344
0·06	−0·2547 −*i*0·9607	0·07335 −*i*0·001686	0·4259 −*i*0·1925	0·04561 −*i*0·4789	−0·1910 −*i*0·1256	−0·1341 −*i*0·1638
0·07	0·4040 −*i*0·9141	0·01668 +*i*0·01349	0·5753 −*i*0·1877	0·3963 −*i*0·4612	−0·1141 −*i*0·1171	−0·0530 −*i*0·1477
0·08	0·8919 −*i*0·02904	−0·02670 −*i*0·2301	0·6863 +*i*0·01089	0·6559 −*i*0·05989	−0·05745 −*i*0·07488	0·006337 −*i*0·1733
0·09	0·6612 +*i*0·3374	0·2404 −*i*0·3772	0·5596 +*i*0·1813	0·4420 +*i*0·3079	−0·04461 −*i*0·01663	0·1112 −*i*0·1462
0·10	0·3057 +*i*0·5152	0·4620 −*i*0·2706	0·4215 +*i*0·1850	0·1826 +*i*0·3572	−0·05534 +*i*0·02369	0·1705 −*i*0·05858
0·11	0·1014 +*i*0·5494	0·5458 −*i*0·09880	0·3545 +*i*0·1403	0·04778 +*i*0·3111	−0·06902 +*i*0·05588	0·1804 +*i*0·03998
0·12	−0·04678 +*i*0·6060	0·5243 +*i*0·08470	0·3319 +*i*0·09623	−0·01636 +*i*0·2711	−0·09132 +*i*0·09267	0·1443 +*i*0·1484
0·13	−0·2665 +*i*0·7236	0·3488 +*i*0·2442	0·3406 +*i*0·07184	−0·06111 −*i*0·2708	−0·1482 +*i*0·13337	0·01243 +*i*0·2543
0·14	−0·7474 +*i*0·6470	0·02267 +*i*0·09876	0·3422 +*i*0·1002	−0·1805 +*i*0·2864	−0·2634 +*i*0·1003	−0·2449 +*i*0·1629
0·146	−0·9121 +*i*0·3243	0·04810 −*i*0·1609	0·3014 +*i*0·1136	−0·2721 +*i*0·2213	−0·2808 +*i*0·01645	−0·2591 −*i*0·03174
0·15	−0·8805 +*i*0·1346	0·1503 −*i*0·2425	0·2770 +*i*0·1000	−0·2942 +*i*0·1569	−0·2602 −*i*0·02140	−0·1987 −*i*0·1079

(to be continued.)

Table I. (*continued*)

$\frac{H}{L}$	*A*	*B*	*C*	*D*	*E*	*F*
0·16	−0·6951 −*i*0·1003	0·4194 −*i*0·2253	0·2333 +*i*0·04766	−0·3012 +*i*0·03325	−0·1927 −*i*0·04930	−0·02214 −*i*0·1384
0·17	−0·5831 −*i*0·1681	0·5227 −*i*0·09612	0·2246 −*i*0·004865	−0·2835 −*i*0·04843	−0·1615 −*i*0·03740	0·05252 −*i*0·08033
0·18	−0·5350 −*i*0·2163	0·5449 +*i*0·03658	0·2276 −*i*0·05445	−0·2677 −*i*0·1215	−0·1517 −*i*0·02233	0·07266 −*i*0·01694
0·19	−0·5274 −*i*0·2876	0·5101 +*i*0·1574	0·2407 −*i*0·1082	−0·2485 −*i*0·2055	−0·1557 −*i*0·01061	0·05598 +*i*0·04148
0·20	−0·5221 −*i*0·4262	0·3998 +*i*0·2903	0·2739 −*i*0·1730	−0·2076 −*i*0·3201	−0·1733 −*i*0·00893	−0·003397 +*i*0·08425
0·21	−0·4378 −*i*0·7121	0·1650 +*i*0·3278	0·3615 −*i*0·2417	−0·07867 −*i*0·4766	−0·2001 −*i*0·04021	−0·1157 +0·05599
0·22	0·07050 −*i*0·9944	−0·01654 +*i*0·05123	0·5182 −*i*0·2151	0·2422 −*i*0·5153	−0·1629 −*i*0·1215	−0·1274 −*i*0·1409
0·23	0·6484 −*i*0·6635	0·2296 −*i*0.09769	0·5603 −*i*0·1039	0·4396 −*i*0·2950	−0·04799 −*i*0·1023	0·1033 −*i*0·01651
0·24	0·8830 −*i*0·1794	0·2767 +*i*0·08641	0·5932 −*i*0·06207	0·5393 −*i*0·1215	−0·009823 −*i*0·009514	0·1684 +*i*0·01617
0·25	0·8653 +*i*0·4845	0·04180 +*i*0·07509	0·6603 +*i*0·07471	0·6173 +*i*0·2140	−0·04990 +0·07528	0·03877 +*i*0·1226
0·26	0·2670 +*i*0·8976	0·6557 −*i*0·2258	0·5331 +*i*0·2482	0·3099 +*i*0·5315	−0·1241 +*i*0·08080	−0·04985 +*i*0·03045
0·27	−0·1903 +*i*0·7610	0·3093 −*i*0·2763	0·3678 +*i*0·2360	−0·00847 +*i*0·4820	−0·1446 +*i*0·05485	0·00403 −*i*0·01997
0·28	−0·3754 +*i*0·5888	0·4486 −*i*0·1672	0·2887 +*i*0·1686	−0·1524 +*i*0·3557	−0·1464 +*i*0·04993	0·04777 +*i*0·009689
0·29	−0·4848 +*i*0·4843	0·4864 −*i*0·02598	0·2554 +*i*0·1053	−0·2210 +*i*0·2513	−0·1546 +*i*0·0590	0·04958 +*i*0·06809
0·30	−0·6200 +*i*0·4142	0·4294 +*i*0·1191	0·2453 +*i*0·04930	−0·2674 +*i*0·1627	−0·1814 +*i*0·07318	−0·004081 +*i*0·1344
0·31	−0·8554 +*i*0·2662	0·2201 +*i*0·1997	0·2611 −*i*0·00664	−0·3075 +*i*0·05902	−0·2457 +*i*0·06682	−0·1568 +*i*0·1528
0·32	−0·9637 −*i*0·2337	−0·00547 −*i*0·08623	0·3072 −*i*0·02099	−0·2781 −*i*0·08476	−0·2961 −*i*0·04435	−0·2968 −*i*0·08612
0·33	−0·5461 −*i*0·5079	0·2907 −*i*0·3375	0·3019 −*i*0·00043	−0·1792 −*i*0·1287	−0·1940 −*i*0·1206	−0·06628 −*i*0·2681
0·34	−0·3070 −*i*0·4319	0·5226 −*i*0·2214	0·2805 −*i*0·02013	−0·1448 −*i*0·1337	−0·1253 −*i*0·09193	0·09951 −*i*0·1926
0·35	−0·2129 −*i*0·3700	0·6014 −*i*0·06320	0·2753 −*i*0·05531	−0·1278 −*i*0·1613	−0·1006 −*i*0·05843	0·1577 −*i*0·09680

(*to be continued.*)

Table I. (*continued.*)

$\frac{H}{L}$	*A*	*B*	*C*	*D*	*E*	*F*
0·36	−0·1532 −*i*0·3509	0·6117 +*i*0·08624	0·2842 −*i*0·09645	−0·1018 −*i*0·2065	−0·09114 −*i*0·03191	0·1734 −*i*0·01299
0·37	−0·08177 −*i*0·3605	0·5749 +*i*0·2359	0·3097 −*i*0·1434	−0·05252 −*i*0·2672	−0·08775 −*i*0·00910	0·1656 +*i*0·06609
0·38	0·03885 −*i*0·3800	0·4746 +*i*0·3959	0·3641 −*i*0·1955	0·04477 −*i*0·3361	−0·08814 +*i*0·01407	0·1320 +*i*0·1490
0·39	0·2626 −*i*0·3438	0·2515 +*i*0·5480	0·4762 −*i*0·2340	0·2389 −*i*0·3742	−0·09481 +*i*0·04326	0·04968 +*i*0·2372
0·40	0·5351 −*i*0·01646	−0·1723 +*i*0·5382	0·6585 −*i*0·1653	0·5317 −*i*0·2072	−0·1274 +*i*0·08438	−0·1327 +*i*0·2874
0·41	0·2302 +*i*0.5118	−0·5512 +*i*0·05002	0·7112 +*i*0·08777	0·5195 +*i*0·2370	−0·2281 +*i*0·0,481	−0·3887 +*i*0·1137
0·42	−0·1461 +*i*0·3267	−0·2375 −*i*0·5773	0·5413 +*i*0·2394	0·2158 +*i*0·3765	−0·2268 −*i*0·05021	−0·2833 −*i*0·2559
0·43	−0·1493 +*i*0·2308	0·2554 −*i*0·5901	0·3923 +*i*0·2240	0·03189 +*i*0·3334	−0·1479 −*i*0·06478	−0·01803 −*i*0·2791
0·44	−0·1734 +*i*0·2169	0·4856 −*i*0·4207	0·3181 +*i*0·1702	−0·06523 +*i*0·2639	−0·1141 −*i*0·03934	0·1019 −*i*0·1900
0·45	−0·2026 +*i*0·2074	0·5850 −*i*0·2597	0·2824 +*i*0·1198	−0·1166 +*i*0·1996	−0·1019 −*i*0·01469	0·1506 −*i*0·1048
0·46	−0·2281 +*i*0·2045	0·6257 −*i*0·1172	0·2650 +*i*0·07635	−0·1444 +*i*0·1454	−0·09866 +*i*0·007830	0·1682 −*i*0·02853
0·47	−0·2550 +*i*0·2150	0·6302 +*i*0·01860	0·2582 +*i*0·03760	−0·1595 +*i*0·1002	−0·1015 +*i*0·03104	0·1661 +*i*0·04647
0·48	−0·2982 +*i*0·2181	0·5951 +*i*0·1601	0·2601 +*i*0·001499	−0·1680 +*i*0·06445	−0·1127 +*i*0·05819	0·1398 +*i*0·1286
0·49	−0·4013 +*i*0·3112	0·4835 +*i*0·3133	0·2730 −*i*0·03177	−0·1782 +*i*0·03949	−0·1441 +*i*0·09097	0·06220 +*i*0·2217
0·50	−0·6874 +*i*0·3272	0·1999 +*i*0·3848	0·3008 −*i*0·05010	−0·2161 +*i*0·02101	−0·2270 +*i*0·1046	−0·1392 +*i*0·2629
0·51	−0·9911 −*i*0·1167	−0·01575 +*i*0·04249	0·3048 −*i*0·03623	−0·2880 −*i*0·07397	−0·3013 −*i*0·00839	−0·3069 +*i*0·003146
0·52	−0·7262 −*i*0·5399	0·2513 −*i*0·1332	0·2776 −*i*0·06838	−0·2546 −*i*0·2202	−0·2239 −*i*0·09184	−0·1181 −*i*0·1633
0·53	−0·4597 −*i*0·6680	0·3912 −*i*0·00976	0·2890 −*i*0·1313	−0·1732 −*i*0·3298	−0·1666 −*i*0·08871	0·00253 −*i*0·1185
0·54	−0·2259 −*i*0·7822	0·3628 +*i*0·1383	0·3446 −*i*0·1988	−0·04603 −*i*0·4416	−0·1406 −*i*0·07982	0·02685 −*i*0·05806
0·55	0·1573 −*i*0·8913	0·1920 +*i*0·2099	0·4729 −*i*0·2422	0·2084 −*i*0·5225	−0·1181 −*i*0·08254	−0·00028 −*i*0·03795

(*to be continued.*)

Table I. (*continued.*)

$\frac{H}{L}$	*A*	*B*	*C*	*D*	*E*	*F*
0·56	0·8097 −*i*0·5435	−0·000271 −*i*0·02810	0·6619 −*i*0·1007	0·6051 −*i*0·2609	−0·06393 −*i*0·07543	0·00665 −*i*0·1073
0·57	0·9062 +*i*0·08601	0·1720 −*i*0·2176	0·6294 +*i*0·08278	0·5896 +*i*0·1234	−0·02364 −*i*0·02377	0·1159 −*i*0·1027
0·58	0·6069 +*i*0·5071	0·3899 −*i*0·1238	0·5037 +*i*0·1392	0·3596 +*i*0·2989	−0·02765 +*i*0·04625	0·1826 +*i*0·01920
0·59	0·3322 +*i*0·7449	0·3768 +*i*0·08694	0·4524 +*i*0·1235	0·2273 +*i*0·3397	−0·06557 +*i*0·1112	0·1290 +*i*0·1732
0·60	−0·1102 +*i*0·9639	0·09750 +*i*0·1301	0·4476 +*i*0·1544	0·1098 +*i*0·4330	−0·1682 +*i*0·1467	−0·09655 +*i*0·2335
0·62	−0·6685 +*i*0·2862	0·3361 −*i*0·3129	0·2637 +*i*0·1517	−0·2571 +*i*0·2586	−0·2027 −*i*0·01298	−0·06259 −*i*0·1202
0·885	0·3189 −*i*0·8110	−0·3082 −*i*0·1115	0·6559 −*i*0·1294	−0·4740 −*i*0·3636	−0·1775 −*i*0·1237	−0·2426 −*i*0·1976
1·205	0·5145 −*i*0·3859	0·2771 +*i*0·4306	0·5191 −*i*0·2071	0·3552 −*i*0·3519	−0·05784 +*i*0·01889	0·1062 +*i*0·1668
1·525	0·5316 −*i*0·6787	0·3314 −*i*0·06654	0·5061 −*i*0·1163	0·3436 −*i*0·3141	−0·04688 −*i*0·09924	0·1383 −*i*0·1509
1·845	0·03301 −*i*0·8618	0·2226 +*i*0·25503	0·4387 −*i*0·2499	0·1350 −*i*0·5245	−0·1294 −*i*0·07142	−0·00484 −*i*0·00860
2·165	−0·6765 −*i*0·5605	−0·1947 +*i*0·2536	0·4218 −*i*0·1889	−0·06479 −*i*0·3735	−0·2891 −*i*0·03234	−0·3501 +*i*0·04173
2·485	0·01920 −*i*0·4298	0·5465 +*i*0·2565	0·3385 −*i*0·1635	0·00835 −*i*0·3094	−0·07914 −*i*0·01483	0·1674 +*i*0·06543
2·805	−0·2088 −*i*0·9627	0·05807 −*i*0·09933	0·4397 −*i*0·1635	0·07520 −*i*0·4438	−0·1874 −*i*0·1416	−0·1345 −*i*0·2168

2. *The Orbital motion of a Surface Particle in the Surface Layer.*

Now, taking the real parts only, we get the following horizontal and vertical oscillations U' and V' on the top surface of the surface layer.

$$\left.\frac{LU'}{2\pi\alpha}\right]_{x=0}=\cos\theta\cos z\Big[(C'-D')\sin a-(C''+D'')\cos a$$

$$+\frac{s'}{f}\Big\{-(E'+F')\sin b+(E''-F'')\cos b\Big\}\Big]$$

$$+\cos\theta\sin z\Big[(C'-D'')\sin b+(C'+D')\cos a$$

$$+\frac{s'}{f}\Big\{-(E''+F')\sin b+(-E'+F')\cos b\Big], \tag{37}$$

$$\left.\frac{LV'}{2\pi a}\right]_{z=0}=\cos\theta\cos z\left[\frac{r'}{f}\left\{-(C'+D')\sin a+(C''-D'')\cos a\right\}\right.$$

$$\left.-(E'-F')\sin b+(E''+F'')\cos b\right]$$

$$+\cos\theta\sin z\left[\frac{r'}{f}\left\{-(C''+D'')\sin a+(-C'+D')\cos a\right\}\right.$$

$$\left.-(E''-F'')\sin b-(E'+F')\cos b\right], \qquad (38)$$

where $z=\frac{2\pi}{T}t$, $\frac{r'}{f}=4{\cdot}3588$, $\frac{s'}{f}=7{\cdot}6811$, $a=19{\cdot}3657\left(\frac{H}{L}\right)$ and $b=34{\cdot}1264\left(\frac{H}{L}\right)$. As will be seen from the following expressions (39), C', D', E', and F' are real parts of C, D, E, and F respectively, while C'', D'', E'', and F'' correspond to imaginary parts of them:

$$\left.\begin{array}{ll} C=C'+iC'', & D=D'+iD'', \\ E=E'+iE'', & F=F'+iF''. \end{array}\right\} \qquad (39)$$

Expressions (37), (38) are next rewritten:

$$\left.\frac{LU'}{2\pi a}\right]_{z=0}=\sqrt{\alpha^2+\beta^2}\,\sin\left\{z+\tan^{-1}\frac{\beta}{\alpha}\right\}, \qquad (40)$$

$$\left.\frac{LV'}{2\pi a}\right]_{z=0}=\sqrt{\alpha'^2+\beta'^2}\,\sin\left\{z+\tan^{-1}\frac{\beta'}{\alpha'}\right\}, \qquad (41)$$

where

$$\alpha=\left\{(C''-D'')\sin b+(C'+D')\cos a\right\}$$

$$+\frac{s'}{f}\left\{-(E''+F'')\sin b+(-E'+F')\cos b\right\}, \qquad (42)$$

$$\beta=\left\{(C'-D')\sin a-(C''+D'')\cos a\right\}$$

$$+\frac{s'}{f}\left\{-(E'+F')\sin b+(E''-F'')\cos b\right\}, \qquad (43)$$

$$\alpha'=\frac{r'}{f}\left\{-(C''+D'')\sin a+(-C'+D')\cos a\right\}$$

$$+\left\{-(E''-F'')\sin b-(E'+F')\cos b\right\}, \qquad (44)$$

$$\beta' = \frac{r'}{f}\left\{-(C'+D')\sin a + (C''-D'')\cos a\right\}$$
$$+\left\{-(\mathrm{E}'-F')\sin b + (E''+F'')\cos b\right\}, \tag{45}$$

and the values α, β, α', β' become circular functions, $H\ L$ alone being variable. $\tan^{-1}(\beta\ \alpha)$ and $\tan^{-1}(\beta'/\alpha')$ should be taken satisfying the conditions that

$$\left.\begin{aligned} \sqrt{\alpha^2+\beta^2}\sin\gamma &= \alpha\,, \\ \sqrt{\alpha^2+\beta^2}\cos\gamma &= \beta\,, \\ \gamma &= \tan^{-1}\frac{\beta}{\alpha}\,, \end{aligned}\right\}$$

$$\left.\begin{aligned} \sqrt{\alpha'^2+\beta'^2}\sin\gamma' &= \alpha'\,, \\ \sqrt{\alpha'^2+\beta'^2}\cos\gamma' &= \beta'\,, \\ \gamma' &= \tan^{-1}\frac{\beta'}{\alpha'}\,. \end{aligned}\right\}$$

It will be seen from expressions (40), (41) that forced stationary harmonic vibrations (horizontal and vertical) are caused in the stratum by the periodic incident wave (1). The amplitudes of the same vibrations (vertical and horizontal) and the phase-differences are both transcendental functions, only H/L being variable. The phases of the vibrations on the free surface of the layer usually differ from those of vibrations (horizontal and vertical respectively) at the bottom surface. We shall return to the horizontal and vertical stationary oscillations (40) and (41) in the next chapter.

Now we can easily get from expressions (40) and (41) the orbit of the particle in the surface layer as follows:

$$\frac{U'^2}{(\alpha^2+\beta^2)} + \frac{V'^2}{(\alpha'+\beta'^2)} - \frac{2\cos\varepsilon}{\sqrt{\alpha^2+\beta^2}\sqrt{\alpha'^2+\beta'^2}}U'V' = \frac{4\pi^2\mathfrak{a}^2}{L^2}\sin^2\varepsilon\,, \tag{46}$$

where

$$\varepsilon = \tan^{-1}\frac{\beta'}{\alpha'} - \tan^{-1}\frac{\beta}{\alpha}\,. \tag{47}$$

It will be seen from expression (46) that the orbit of the particle in the surface layer is usually an ellipse, whose major and minor axes ξ, η are respectively given by

$$\left.\begin{aligned} \xi &= \frac{\sin\varepsilon}{\sqrt{\gamma}}\,, \\ \eta &= \frac{\sin\varepsilon}{\sqrt{\delta}}\,, \end{aligned}\right\} \tag{48}$$

where γ, δ are the roots of the equation

$$\zeta^2 - \frac{(\alpha^2+\beta^2+\alpha'^2+\beta'^2)}{(\alpha^2+\beta^2)(\alpha'^2+\beta'^2)}\zeta + \frac{\sin^2\varepsilon}{(\alpha^2+\beta^2)(\alpha'^2+\beta'^2)} = 0\,, \tag{48'}$$

the inclination angle τ which the major axis makes with the horizontal surface being

$$\tan 2\tau = -\frac{2\cos\varepsilon\sqrt{(\alpha^2+\beta^2)(\alpha'^2+\beta'^2)}}{(\alpha'^2+\beta'^2)-(\alpha^2+\beta^2)}\,. \tag{49}$$

We calculated the major and minor axes of the elliptic orbit of the particles on the top and the bottom surfaces of the surface layer, the ratio of the minor to the major axes, and the inclination angle of the same elliptic orbit for several cases of $H L$, the results being given in Table II and Table III, and shown in Figs. 2~7.

Table II. Major and Minor Axes of Elliptic Orbit of Particle on Top Surface.

$\frac{H}{L}$	ξ (Major axis)	η (Minor axis)	η/ξ	τ (Inclination of major axis in degrees)
0·01	2·08	0·10	0·048	41°
0·02	2·32	0·20	0·086	38°
0·03	2·80	0·45	0·160	35°
0·04	3·55	1·12	0·316	28°
0·05	3·90	2·25	0·577	35°
0·06	3·00	2·30	0·767	99°
0·07	3·85	1·46	0·376	90°
0·08	4·54	1·05	0·231	86°
0·09	3·73	0·50	0·134	73°
0·10	2·95	0·40	0·135	66°
0·11	2·60	0·46	0·203	57°
0·12	2·50	0·75	0·30	46°
0·13	2·85	1·36	0·477	34°
0·14	3·10	2·14	0·691	10°
0·15	2·85	1·70	0·596	154°

(*to be continued.*)

Table II. (*continued.*)

$\frac{H}{L}$	ξ (Major axis)	η (Minor axis)	η/ξ	τ (Inclination of major axis)
0·16	2·46	1·03	0·429	136°
0·17	2·15	0·44	0·205	130°
0·18	2·08	0·14	0·0673	128°
0·19	2·17	0·20	0·0922	125°
0·20	2·57	0·64	0·249	121°
0·21	3·22	1·30	0·4035	113°
0·22	3·55	1·94	0·546	98°
0·23	3·88	1·25	0·322	76°
0·24	3·75	0·14	0·0373	76°
0·25	4·17	0·55	0·1318	92°
0·26	3·84	0·50	0·132	99°
0·27	3·05	0·145	0·0492	108°
0·28	2·54	0·15	0·0590	116°
0·29	2·34	0·50	0·214	125°
0·30	2·40	0·900	0·375	137°
0·31	2·78	1·50	0·540	157°
0·32	3·40	1·77	0·521	5°
0·33	3·03	1·20	0·364	25°
0·34	2·84	0·65	0·230	44°
0·35	2·24	0·40	0·1785	43°
0·36	2·20	0·34	0·154	50°
0·37	2·43	0·25	0·1028	53°
0·38	2·90	0·30	0·1034	57°
0·39	3·59	0·54	0·1504	58°
0·40	4·55	1·02	0·224	58°
0·41	5·45	0	0	49°
0·42	4·70	0·50	0·1063	44°
0·43	3·50	0·10	0·0286	46°
0·44	2·68	0·07	0·0161	47°
0·45	2·34	0·10	0·0428	47°
0·46	2·10	0·15	0·0714	45°
0·47	2·05	0·20	0·098	45°
0·48	2·20	0·32	0·1454	38°
0·49	2·63	0·61	0·232	31°
0·50	3·23	1·18	0·365	21°
0·51	3·35	1·89	0·564	179°
0·52	2·67	1·60	0·60	150°
0·53	2·57	1·04	0·405	125°
0·54	2·85	0·64	0·2245	111°
0·55	3·51	0·31	0·088	102°
0·56	4·20	0·28	0·0667	90°
0·57	3·95	0·65	0·1645	86°
0·58	3·30	0·45	0·1363	68°
0·59	3·14	1·25	0·398	60°
0·60	3·10	2·37	0·764	55°

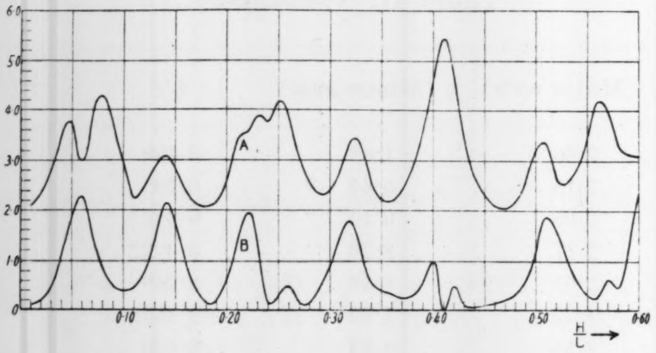

Fig. 2. Major and minor axes of the elliptic orbits of a particle on the top surface of the surface layer. A: Major axis, B: Minor axis.

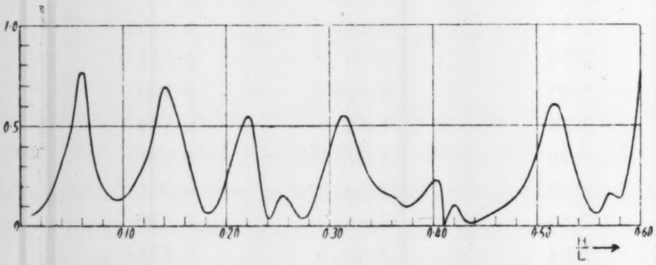

Fig. 3. Ratio of the minor to the major axes of the elliptic orbits of the particle on the top surface of the surface layer.

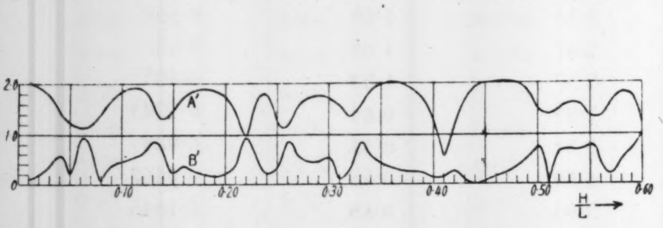

Fig. 4. Inclinatlon angle of the elliptic orbit of the particle on the top surface of the surface layer.

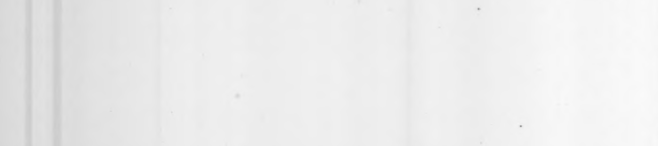

Fig. 5. Major and minor axes of the elliptic orbit of the particle on the bottom surface of the surface layer. A′: Major axis, B′: Minor axis.

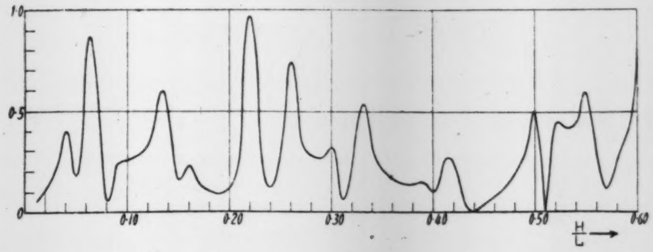

Fig. 6. Ratio of the minor to the major axes of the elliptic orbits of the particles on the bottom surface of the surface layer.

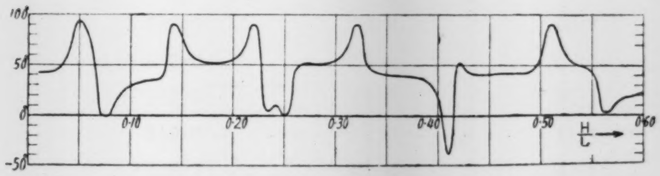

Fig. 7. Inclination angle of the elliptic orbit of the particle on the bottom surface of the surface layer.

Table III. Major and Minor Axes of Elliptic Orbit of Particle on Bottom Surface.

$\frac{H}{L}$	ξ' (Major axis)	η' (Minor axis)	η'/ξ'	τ' (Inclination of major axis)
0·01	2·03	0·10	0·0493	42°
0·02	1·95	0·20	0·1025	43°
0·03	1·79	0·36	0·201	45°
0·04	1·45	0·58	0·400	62°
0·05	1·25	0·22	0·176	94°
0·06	1·16	0·90	0·776	77°
0·07	1·18	0·80	0·678	2°
0·08	1·43	0·08	0·056	1°
0·09	1·67	0·38	0·2275	20°
0·10	1·85	0·46	0·2485	29°
0·11	1·92	0·52	0·271	32°
0·12	1·90	0·61	0·321	34°
0·13	1·61	0·87	0·540	36°
0·14	1·31	0·65	0·496	89°·5
0·15	1·50	0·23	0·1533	75°
0·16	1·75	0·38	0·217	57°
0·17	1·85	0·25	0·135	54°
0·18	1·90	0·20	0·1052	52°
0·19	1·85	0·15	0·0811	52°
0·20	1·75	0·20	0·1143	55°

(*to be continued.*)

Table III. (*continued.*)

$\frac{H}{L}$	ξ' (Major axis)	η' (Minor axis)	η'/ξ'	τ' (Inclination of major axis)
0·21	1·45	0·36	0·2481	66°
0·22	0·99	0·97	0·970	90°
0·23	1·68	0·52	0·3095	8°
0·24	1·79	0·21	0·1173	9°
0·25	1·25	0·32	0·256	0°
0·26	1·18	0·87	0·737	43°
0·27	1·58	0·57	0·361	52°
0·28	1·72	0·47	0·273	51°
0·29	1·76	0·45	0·256	52°
0·30	1·71	0·53	0·310	55°
0·31	1·60	0·10	0·0625	65°
0·32	1·36	0·30	0·2205	90°·5
0·33	1·57	0·83	0·529	51°
0·34	1·85	0·58	0·3135	41°·5
0·35	1·95	0·41	0·210	40°
0·36	2·00	0·33	0·165	39°
0·37	1·98	0·27	0·1363	38°
0·38	1·86	0·25	0·1344	37°
0·39	1·70	0·24	0·1412	33°
0·40	1·25	0·125		21°
0·41	0·55	0·13	0·2363	141°
0·42	1·15	0·27	0·2347	52°
0·43	1·70	0·110	0·0588	42°
0·44	1·93	0	0	41°
0·45	2·00	0·08	0·040	41°
0·46	2·04	0·15	0·0736	40°·5
0·47	2·04	0·23	0·1128	41°
0·48	2·00	0·35	0·175	42°
0·49	1·85	0·51	0·276	43°
0·50	1·50	0·75	0·500	59°
0·51	1·40	0	0	90°
0·52	1·50	0·66	0·440	69°
0·53	1·62	0·68	0·4195	53°
0·54	1·60	0·70	0·438	49°
0·55	1·35	0·80	0·593	42°
0·56	1·35	0·40	0·2963	4°
0·57	1·63	0·18	0·1105	8°
0·58	1·82	0·48	0·2637	18°
0·59	1·78	0·69	0·388	19°
0·60	1·23	1·00	0·8130	23°

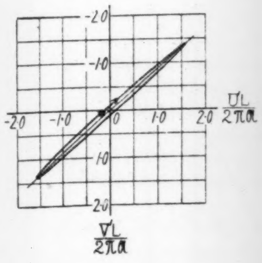

Fig. 8. $\frac{H}{L}=0{\cdot}01$,

$x=0$, $y=-H$.

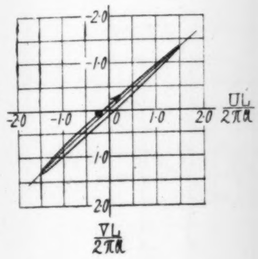

Fig. 9. $\frac{H}{L}=0{\cdot}01$,

$x=0$, $y=0$.

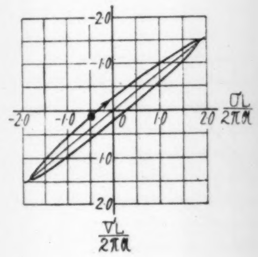

Fig. 10. $\frac{H}{L}=0{\cdot}02$,

$x=0$, $y=-H$.

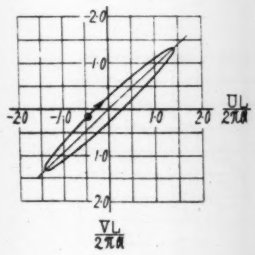

Fig. 11. $\frac{H}{L}=0{\cdot}02$,

$x=0$, $y=0$.

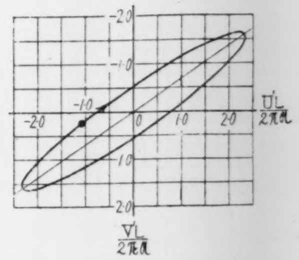

Fig. 12. $\frac{H}{L}=0{\cdot}03$,

$x=0$, $y=-H$.

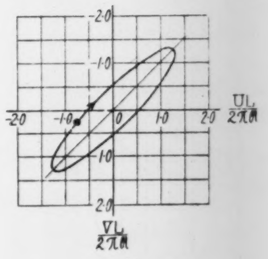

Fig. 13. $\frac{H}{L}=0{\cdot}03$,

$x=0$, $y=0$.

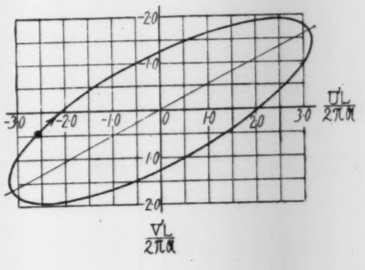

Fig. 14. $\frac{H}{L}=0{\cdot}04$,

$x=0$, $y=-H$.

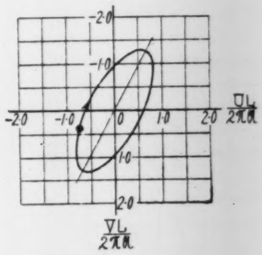

Fig. 15. $\frac{H}{L}=0{\cdot}04$,

$x=0$, $y=0$.

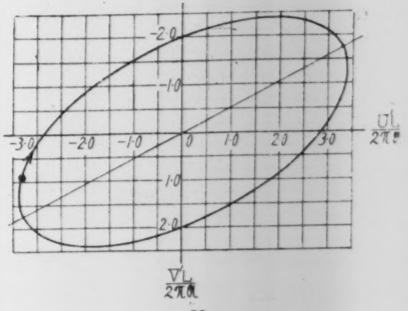

Fig. 16. $\frac{H}{L}=0{\cdot}05$,

$x=0$, $y=-H$.

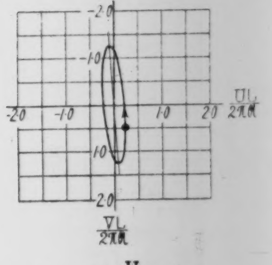

Fig. 17. $\frac{H}{L}=0{\cdot}05$,

$x=0$, $y=0$.

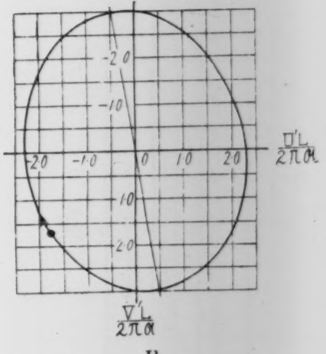

Fig. 18. $\frac{H}{L}=0{\cdot}06$,

$x=0$, $y=-H$.

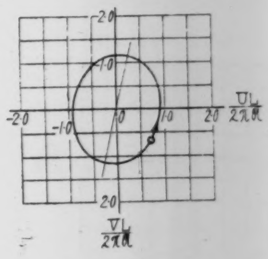

Fig. 19. $\frac{H}{L}=0{\cdot}06$,

$x=0$, $y=0$.

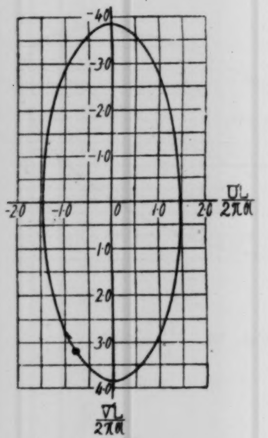

Fig. 20. $\frac{H}{L}=0{\cdot}07$,

x=0, y=−H.

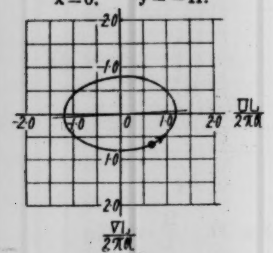

Fig. 21. $\frac{H}{L}=0{\cdot}07$,

x=0, y=0.

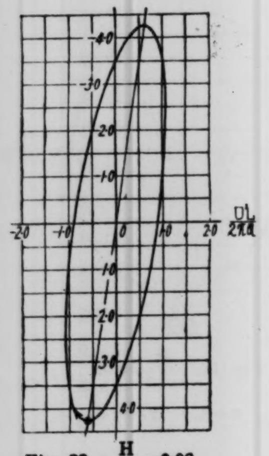

Fig. 22. $\frac{H}{L}=0{\cdot}08$,

x=0, y=−H.

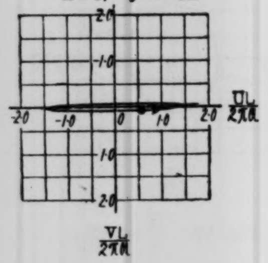

Fig. 23. $\frac{H}{L}=0{\cdot}08$,

x=0, y=0.

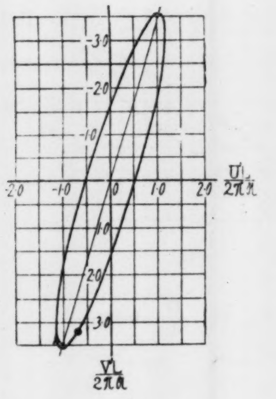

Fig. 24. $\frac{H}{L}=0{\cdot}09$,

x=0, y=−H.

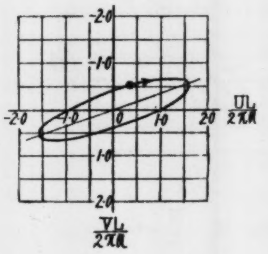

Fig. 25. $\frac{H}{L}=0{\cdot}09$,

x=0, y=0.

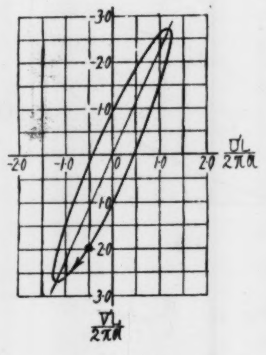

Fig. 26. $\frac{H}{L}=0{\cdot}10$,

x=0, y=−H.

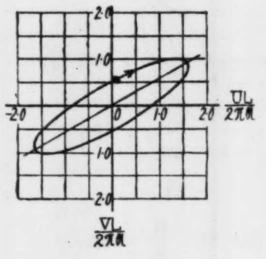

Fig. 27. $\frac{H}{L}=0{\cdot}10$,

x=0, y=0.

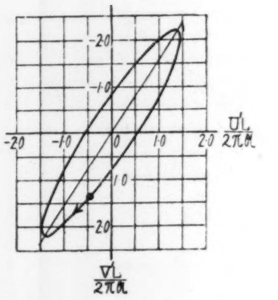

Fig. 28. $\frac{H}{L}=0{\cdot}11$,

x=0, y=−H.

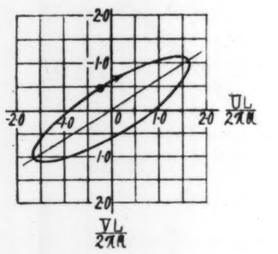

Fig. 29. $\frac{H}{L}=0{\cdot}11$,

x=0, y=0.

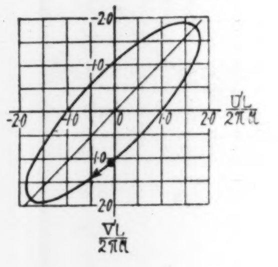

Fig. 30. $\frac{H}{L}=0{\cdot}12$,

x=0, y=−H.

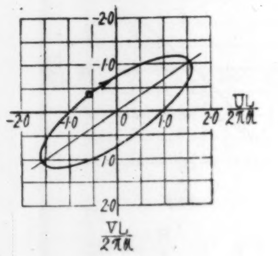

Fig. 31. $\frac{H}{L}=0{\cdot}12$,

x=0, y=0.

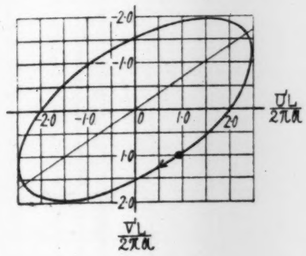

Fig. 32. $\frac{H}{L}=0{\cdot}13$,

$x=0$, $y=-H$.

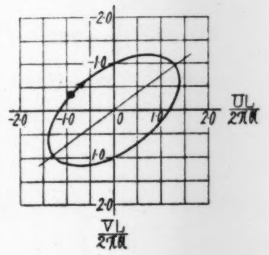

Fig. 33. $\frac{H}{L}=0{\cdot}13$,

$x=0$, $y=0$.

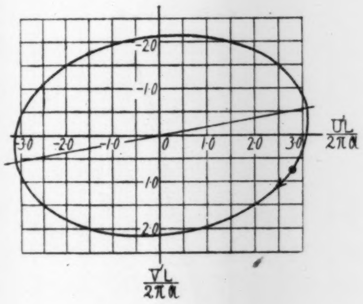

Fig. 34. $\frac{H}{L}=0{\cdot}14$,

$x=0$, $y=-H$.

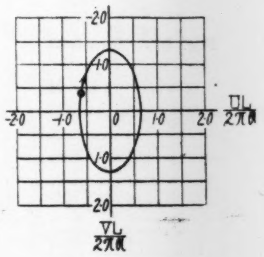

Fig. 35. $\frac{H}{L}=0{\cdot}14$,

$x=0$, $y=0$.

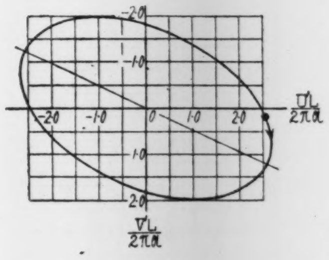

Fig. 36. $\frac{H}{L}=0{\cdot}15$,

$x=0$, $y=-H$.

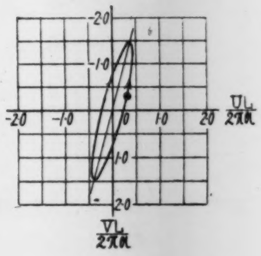

Fig. 37. $\frac{H}{L}=0{\cdot}15$,

$x=0$, $y=0$.

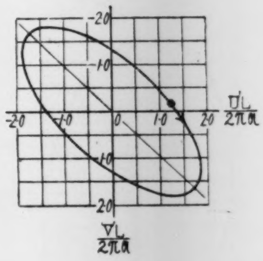

Fig. 38. $\frac{H}{L}=0{\cdot}16$,

$x=0$, $y=-H$.

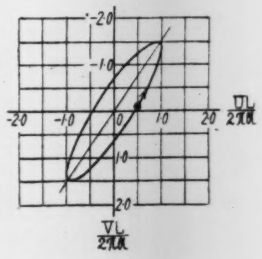

Fig. 39. $\frac{H}{L}=0{\cdot}16$,

$x=0$, $y=0$.

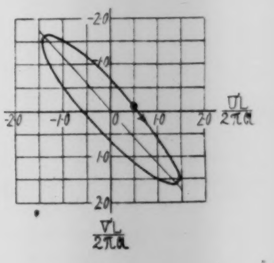

Fig. 40. $\frac{H}{L}=0{\cdot}17$,

$x=0$, $y=-H$.

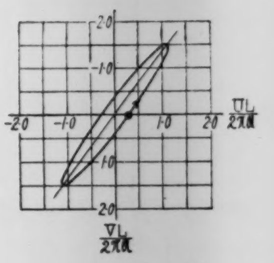

Fig. 41. $\frac{H}{L}=0{\cdot}17$,

$x=0$, $y=0$.

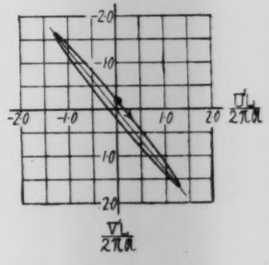

Fig. 42. $\frac{H}{L}=0{\cdot}18$,

$x=0$, $y=-H$.

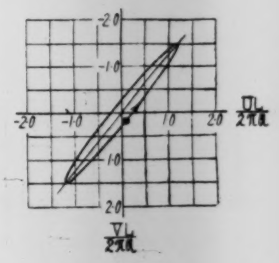

Fig. 43. $\frac{H}{L}=0{\cdot}18$,

$x=0$, $y=0$.

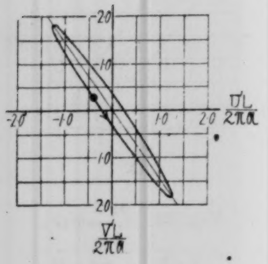

Fig. 44. $\frac{H}{L}=0{\cdot}19$,

x=0, y=−H.

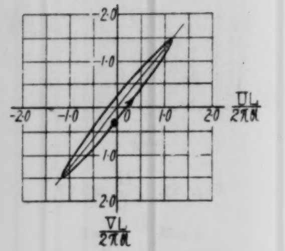

Fig. 45. $\frac{H}{L}=0{\cdot}19$,

x=0, y=(

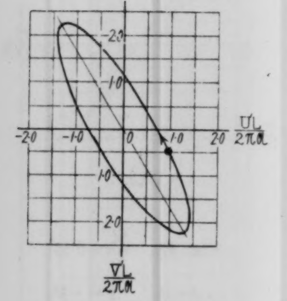

Fig. 46. $\frac{H}{L}=0{\cdot}20$,

x=0, y=−H.

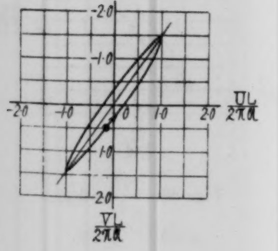

Fig. 47. $\frac{H}{L}=0{\cdot}20$,

x=0, y=0.

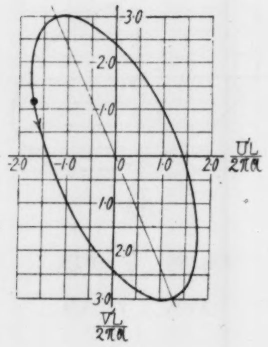

Fig. 48. $\frac{H}{L}=0{\cdot}21$,

x=0, y=−H.

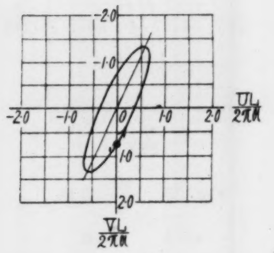

Fig. 49. $\frac{H}{L}=0{\cdot}21$,

x=0, y=0.

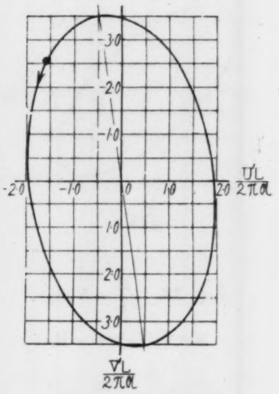

Fig. 50. $\frac{H}{L}=0{\cdot}22$,

x=0, y=−H.

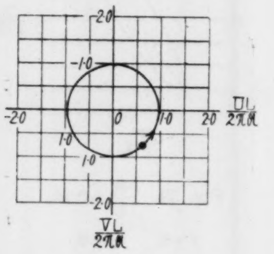

Fig. 51. $\frac{H}{L}=0{\cdot}22$,

x=0, y=0.

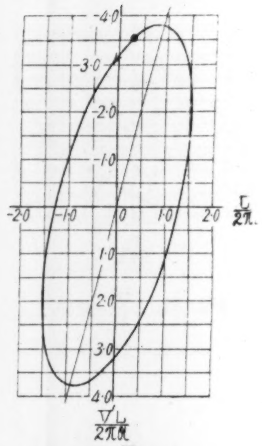

Fig. 52. $\frac{H}{L}=0{\cdot}23$,

x=0, y=−H.

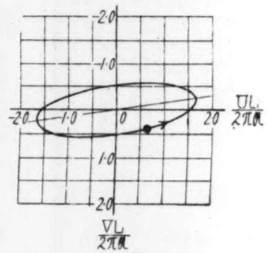

Fig. 53. $\frac{H}{L}$ 0.23,

x=0, y=0.

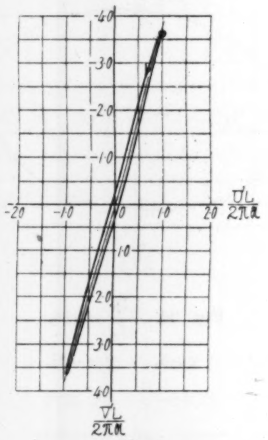

Fig. 54. $\frac{H}{L}=0{\cdot}24$,

x=0, y=−H.

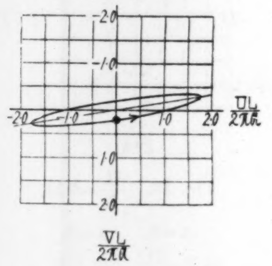

Fig. 55. $\frac{H}{L}=0{\cdot}24$,

x=0. y=0.

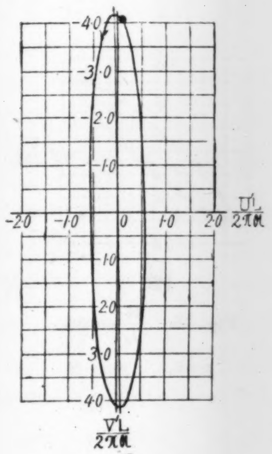

Fig. 56. $\frac{H}{L}=0{\cdot}25$,

x=0, y=−H.

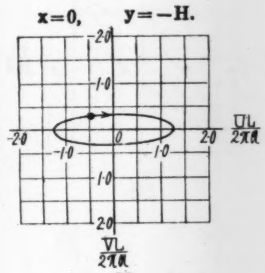

Fig. 57. $\frac{H}{L}=0{\cdot}25$,

x=0, y=0.

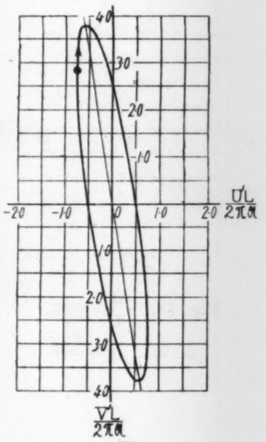

Fig. 58. $\frac{H}{L}=0{\cdot}26$,

x=0, y=−H.

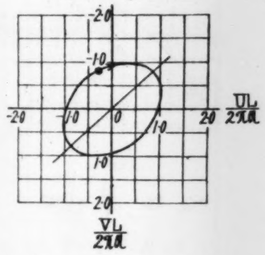

Fig. 59. $\frac{H}{L}=0{\cdot}26$,

x=0, y=0.

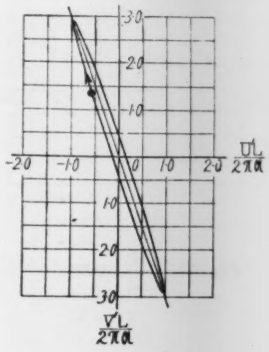

Fig. 60. $\frac{H}{L}=0{\cdot}27$,

x=0, y=−H.

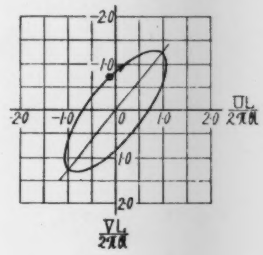

Fig. 61. $\frac{H}{L}=0{\cdot}27$,

x=0, y=0.

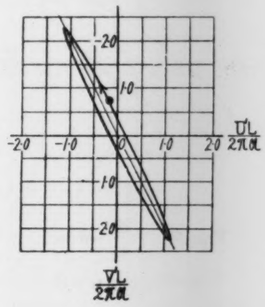

Fig. 62. $\frac{H}{L}=0{\cdot}28$,

x=0, y=−H.

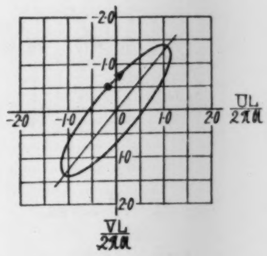

Fig. 63. $\frac{H}{L}=0.28$,

x=0, y=0.

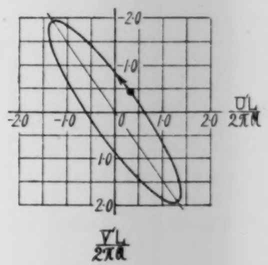

Fig. 64. $\frac{H}{L}=0{\cdot}29$,

x=0, y=−H.

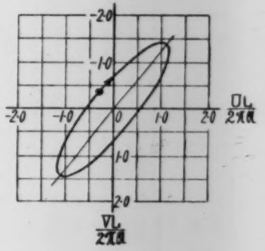

Fig. 65. $\frac{H}{L}=0{\cdot}29$,

x=0, y=0,

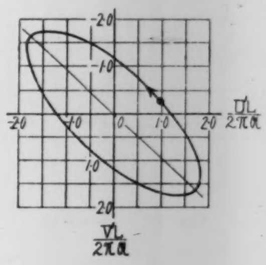

Fig. 66. $\frac{H}{L}=0{\cdot}30$,

x=0, y=−H.

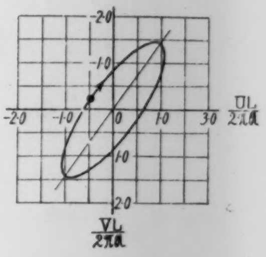

Fig. 67. $\frac{H}{L}=0{\cdot}30$,

x=0, y=0.

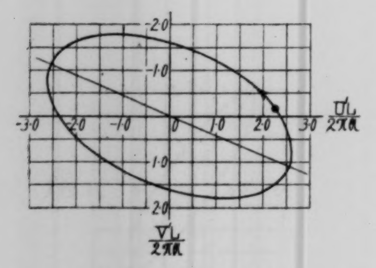

Fig. 68. $\frac{H}{L}=0{\cdot}31$,

$x=0$, $y=-H$.

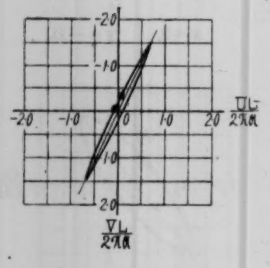

Fig. 69. $\frac{H}{L}=0{\cdot}31$,

$x=0$, $y=0$.

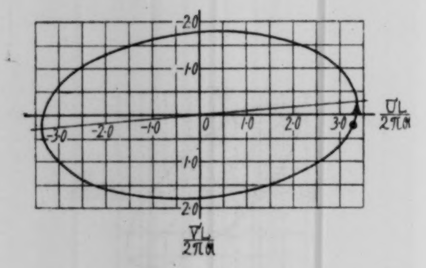

Fig. 70. $\frac{H}{L}=0{\cdot}32$,

$x=0$, $y=-H$.

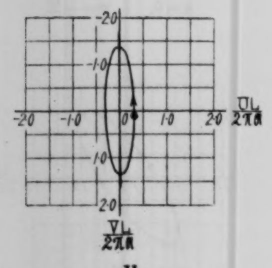

Fig. 71. $\frac{H}{L}=0{\cdot}32$,

$x=0$, $y=0$.

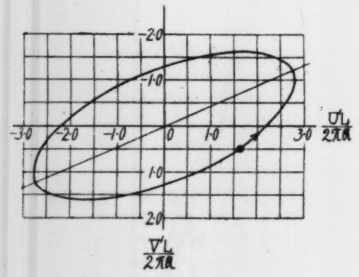

Fig. 72. $\frac{H}{L}=0{\cdot}33$,

$x=0$, $y=-H$.

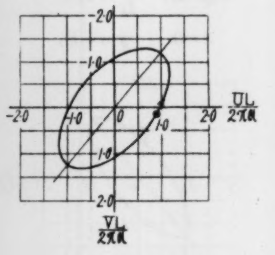

Fig. 73. $\frac{H}{L}=0{\cdot}33$,

$x=0$, $y=0$.

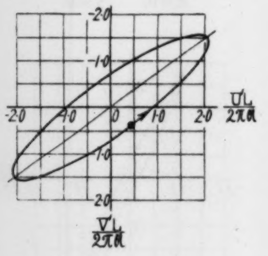

Fig. 74. $\frac{H}{L}=0{\cdot}34$,

$x=0$, $y=-H$.

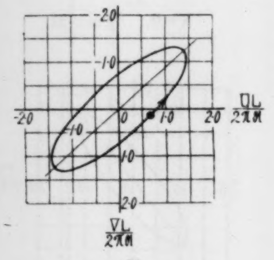

Fig. 75. $\frac{H}{L}=0{\cdot}34$,

$x=0$, $y=0$.

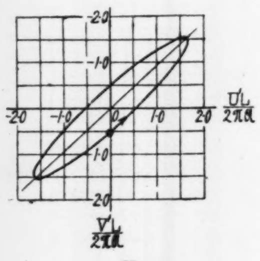

Fig. 76. $\frac{H}{L}=0{\cdot}35$,

$x=0$, $y=-H$.

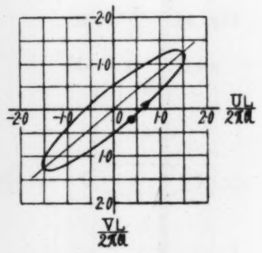

Fig. 77. $\frac{H}{L}=0{\cdot}35$,

$x=0$, $y=0$.

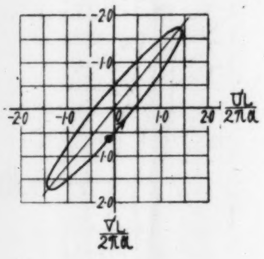

Fig. 78. $\frac{H}{L}=0{\cdot}36$,

$x=0$, $y=-H$.

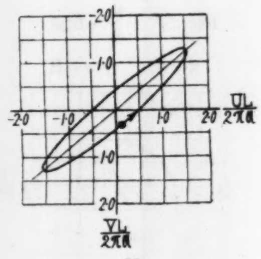

Fig. 79. $\frac{H}{L}=0{\cdot}36$,

$x=0$, $y=0$.

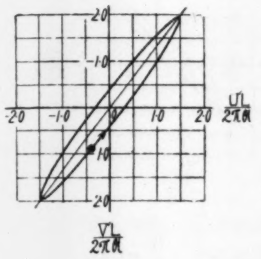

Fig. 80. $\frac{H}{L}=0{\cdot}37$,

$x=0, \quad y=-H$.

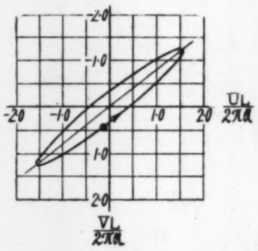

Fig. 81. $\frac{H}{L}=0{\cdot}37$,

$x=0, \quad y=0$.

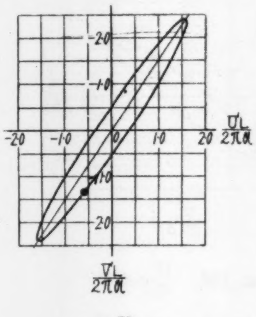

Fig. 82. $\frac{H}{L}=0{\cdot}38$,

$x=0, \quad y=-H$.

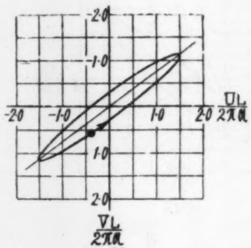

Fig. 83. $\frac{H}{L}=0{\cdot}38$,

$x=0, \quad y=0$.

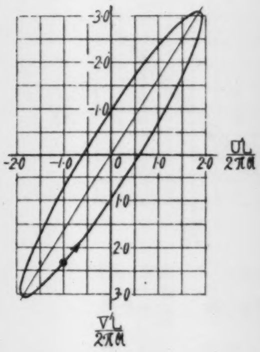

Fig. 84. $\frac{H}{L}=0{\cdot}39$,

$x=0, \quad y=-H$.

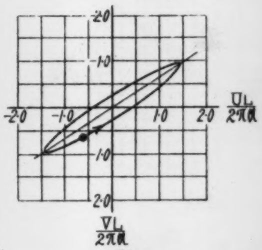

Fig. 85. $\frac{H}{L}=0.39$,

$x=0, \quad y=0$.

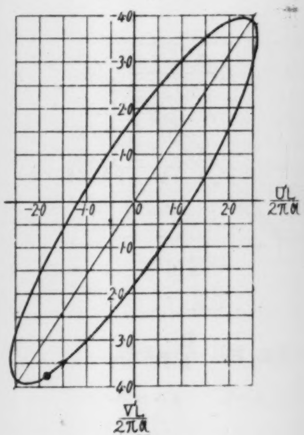

Fig. 86. $\frac{H}{L}=0{\cdot}40$,

$x=0, \quad y=-H$.

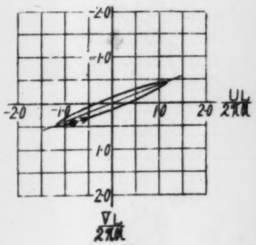

Fig. 87. $\frac{H}{L}=0{\cdot}40$,

$x=0, \quad y=0$.

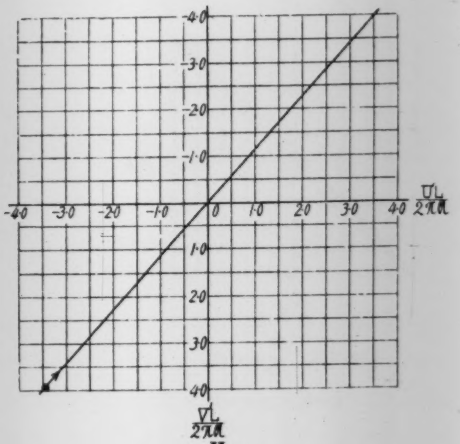

Fig. 88. $\frac{H}{L}=0{\cdot}41$,

$x=0, \quad y=-H$.

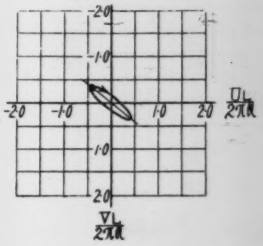

Fig. 89. $\frac{H}{L}=0{\cdot}41$,

$x=0, \quad y=0$.

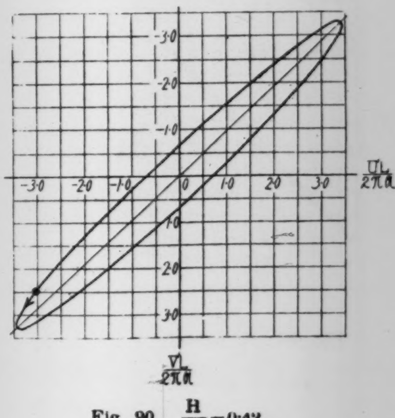

Fig. 90. $\frac{H}{L}=0{\cdot}42$,

$x=0, \quad y=-H$.

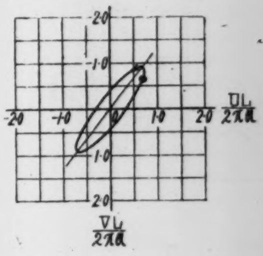

Fig. 91. $\frac{H}{L}=0{\cdot}42$,

$x=0, \quad y=0$.

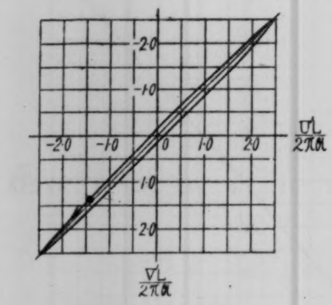

Fig. 92. $\frac{H}{L}=0{\cdot}43$,

$x=0, \quad y=-H$.

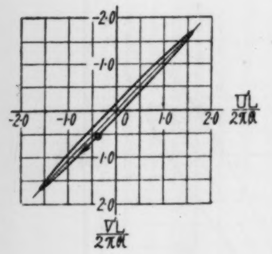

Fig. 96. $\frac{H}{L}=0{\cdot}45$,

$x=0, \quad y=-H$.

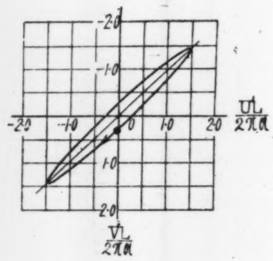

Fig. 100. $\frac{H}{L}=0{\cdot}47$,

$x=0, \quad y=-H$.

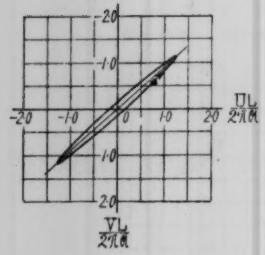

Fig. 93. $\frac{H}{L}=0{\cdot}43$,

$x=0, \quad y=0$.

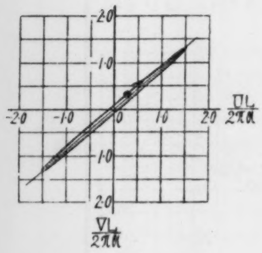

Fig. 97. $\frac{H}{L}=0{\cdot}45$,

$x=0, \quad y=0$.

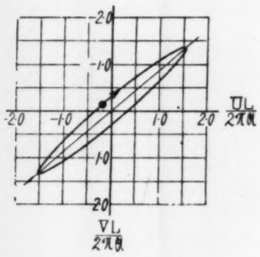

Fig. 101. $\frac{H}{L}=0{\cdot}47$,

$x=0, \quad y=0$.

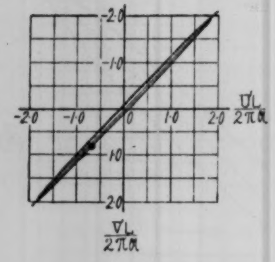

Fig. 94. $\frac{H}{L}=0{\cdot}44$,

$x=0, \quad y=-H$.

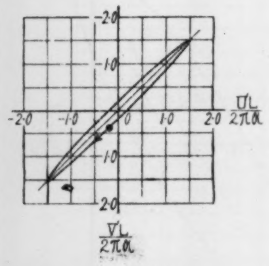

Fig. 98. $\frac{H}{L}=0{\cdot}46$,

$x=0, \quad y=-H$.

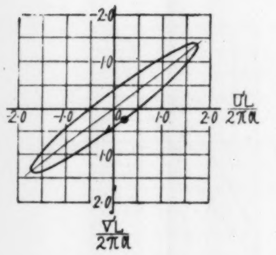

Fig. 102. $\frac{H}{L}=0{\cdot}48$,

$x=0, \quad y=-H$.

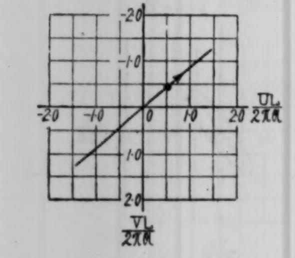

Fig. 95. $\frac{H}{L}=0{\cdot}44$,

$x=0, \quad y=0$.

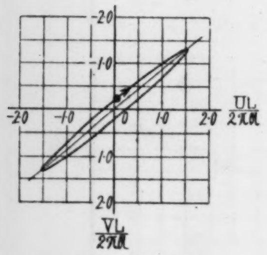

Fig. 99. $\frac{H}{L}=0{\cdot}46$,

$x=0, \quad y=0$.

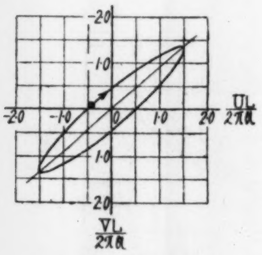

Fig. 103. $\frac{H}{L}=0{\cdot}48$,

$x=0, \quad y=0$.

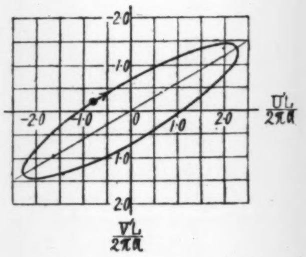

Fig. 104. $\frac{H}{L}=0{\cdot}49$,

$x=0$, $y=-H$.

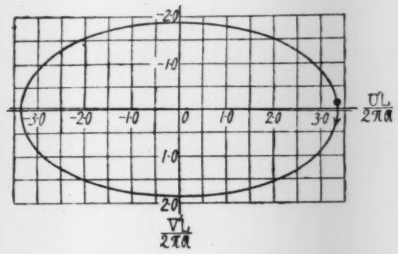

Fig. 108. $\frac{H}{L}=0{\cdot}51$,

$x=0$. $y=-H$.

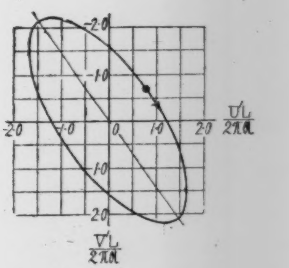

Fig. 112. $\frac{H}{L}=0{\cdot}53$,

$x=0$, $y=-H$.

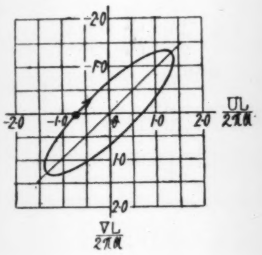

Fig. 105. $\frac{H}{L}=0{\cdot}49$,

$x=0$, $y=0$.

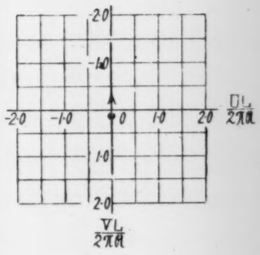

Fig. 109. $\frac{H}{L}=0{\cdot}51$,

$x=0$, $y=0$

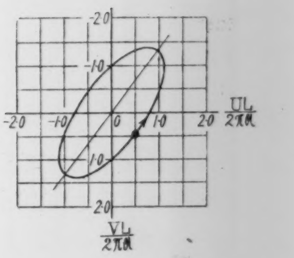

Fig. 113. $\frac{H}{L}=0{\cdot}53$,

$x=0$, $y=0$.

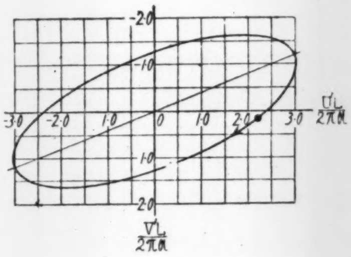

Fig. 106. $\frac{H}{L}=0{\cdot}50$,

$x=0$, $y=-H$.

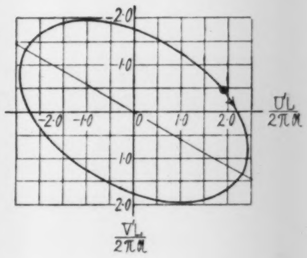

Fig. 110. $\frac{H}{L}=0{\cdot}52$,

$x=0$, $y=-H$.

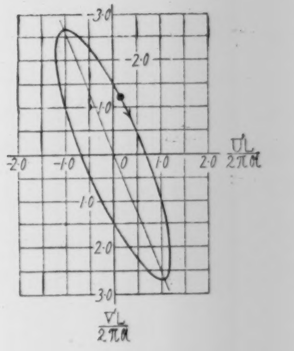

Fig. 114. $\frac{H}{L}=0{\cdot}54$,

$x=0$, $y=-H$.

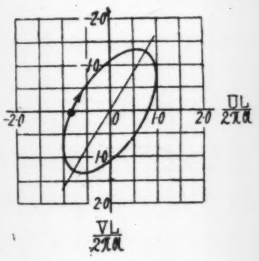

Fig. 107. $\frac{H}{L}=0{\cdot}50$,

$x=0$, $y=0$.

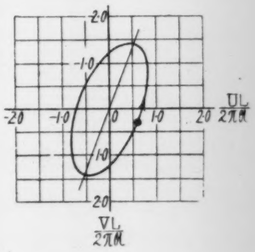

Fig. 111. $\frac{H}{L}=0{\cdot}52$,

$x=0$, $y=0$.

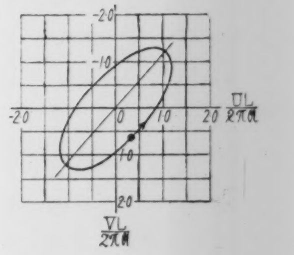

Fig. 115. $\frac{H}{L}=0{\cdot}54$,

$x=0$, $y=0$.

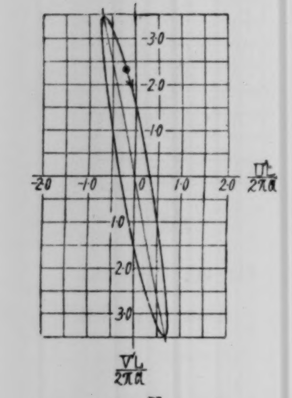

Fig. 116. $\frac{H}{L}=0{\cdot}55$,

x=0, y=−H.

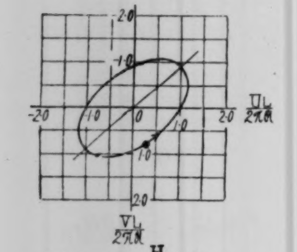

Fig. 117. $\frac{H}{L}=0{\cdot}55$,

x=0, y=0.

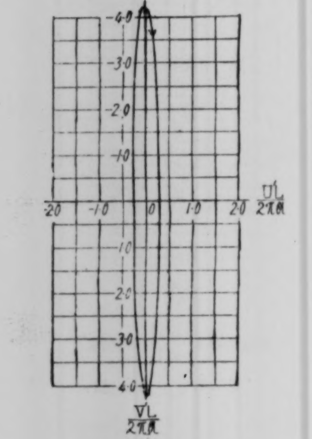

Fig. 118. $\frac{H}{L}=0{\cdot}56$,

x=0, y=−H.

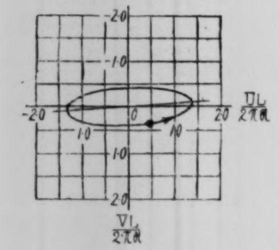

Fig. 119. $\frac{H}{L}=0{\cdot}56$,

x=0, y=0.

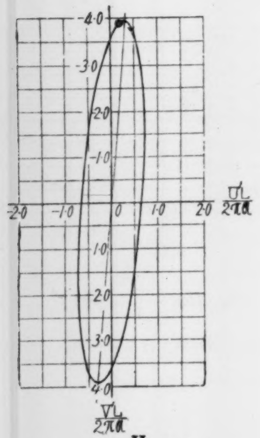

Fig. 120. $\frac{H}{L}=0{\cdot}57$,

x=0, y=−H.

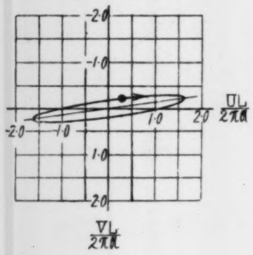

Fig. 121. $\frac{H}{L}=0{\cdot}57$,

x=0, y=0.

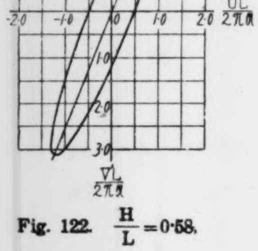

Fig. 122. $\frac{H}{L}=0{\cdot}58$,

x=0, y=−H.

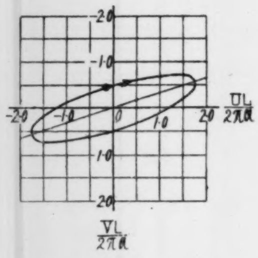

Fig. 123. $\frac{H}{L}=0{\cdot}58$,

x=0, y=0.

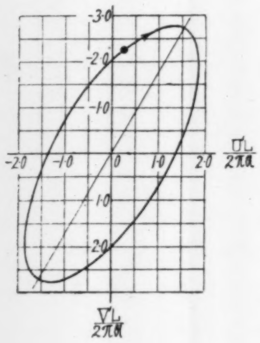

Fig. 124. $\frac{H}{L}=0{\cdot}59$,

x=0, y=−H.

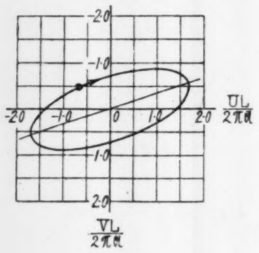

Fig. 125. $\frac{H}{L}=0{\cdot}59$,

x=0, y=0.

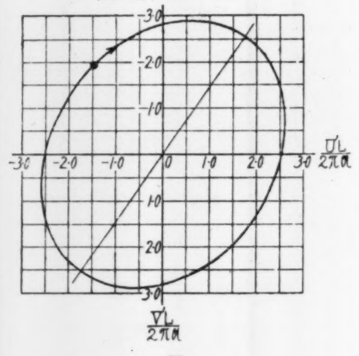

Fig. 126. $\frac{H}{L}=0{\cdot}60$,

x=0, y=−H.

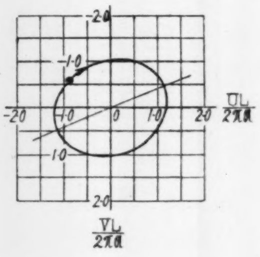

Fig. 127. $\frac{H}{L}=0{\cdot}60$,

x=0, y=0.

Upon comparing these figures with those obtained by K. Sezawa[12], it will be seen that the minor and major axes, their ratio, and the inclination angle of the elliptic orbit of the top surface particle in the surface layer in the present case of $\mu'/\mu=1/10$ have markedly larger fluctuations with respect to the variation in H/L than those in the case of $\mu'/\mu=1/2$. As already pointed out by Sezawa[13], these fluctuations of ξ, η and η/ξ or ε may be caused by interference effects of the reflected and refracted waves in the surface layer, while the fact that fluctuations in the case of $\mu'/\mu=1/10$ become larger than those in the case of $\mu'/\mu=1/2$ may mainly be caused by the fact that the selective resonance in the surface layer in the former case becomes markedly more effective than in the latter. The resonance phenomena in the surface layer will be discussed in the next chapter.

We calculated the types of orbital motions on the free and the bottom surfaces of the surface layer for the respective cases of H/L in the present example, the results being shown in Fig. 8~127. In these figures, the emergent angle of the primary wave in the subjacent medium is always 45° at the lower boundary of the surface layer. It will be seen on comparing these figures, that the minor and major axes, their ratio, and the inclination angle which the major axis makes with the horizontal surface fluctuate markedly with respect to the variation in H/L.

Chapter II. Resonance Phenomenon in the Surface Layer.

We have already calculated the forced stationary vibrations (horizontal and vertical) on the free surface of the surface layer when a dilatational harmonic wave of infinite extent is obliquely incident on the bottom surface of the stratum, being expressed by (40) and (41), namely,

$$\left.\frac{LU'}{2\pi a}\right]_{\substack{y=-H\\x=0}}=\sqrt{\alpha^2+\beta^2}\,\sin\left\{z+\tan^{-1}\frac{\beta}{\alpha}\right\}, \tag{40'}$$

$$\left.\frac{LV'}{2\pi a}\right]_{\substack{y=-H\\x=0}}=\sqrt{\alpha'^2+\beta'^2}\,\sin\left\{z+\tan^{-1}\frac{\beta'}{\alpha'}\right\}, \tag{41'}$$

in which a and b become $19{\cdot}3657\,H/L$ and $34{\cdot}1264\,H/L$ respectively. If we numerically calculate the amplitudes of the forced vibrations expressed by (40) and (41) with the respective values of H/L, we get Table IV, the results being shown in Figs. 128, 129. Phase-differences $\tan^{-1}\beta/\alpha$

---

[12] K. SEZAWA and K. KANAI, *Bull. Earthq. Res. Inst.*, **12** (1934), 269.

[13] K. SEZAWA and K. KANAI, *loc. cit.*

and $\tan^{-1}\beta'/\alpha'$ are also shown in Table IV.

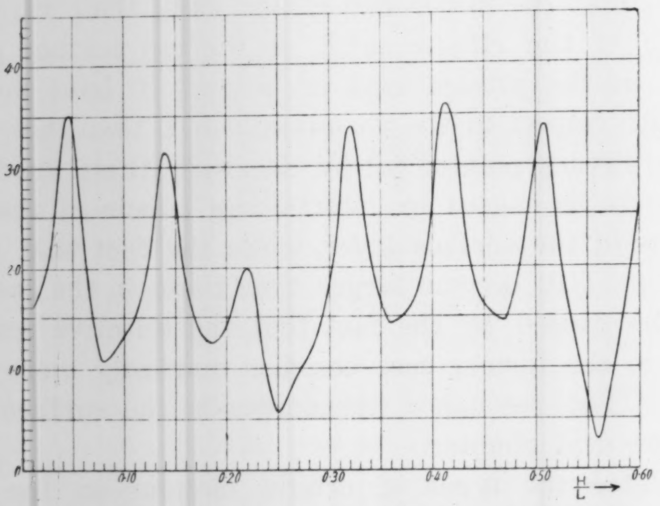

Fig. 128. Resonance curve of horizontal vibration. (Horizontal displacement amplitude of the particle on the top surface of the surface layer.)

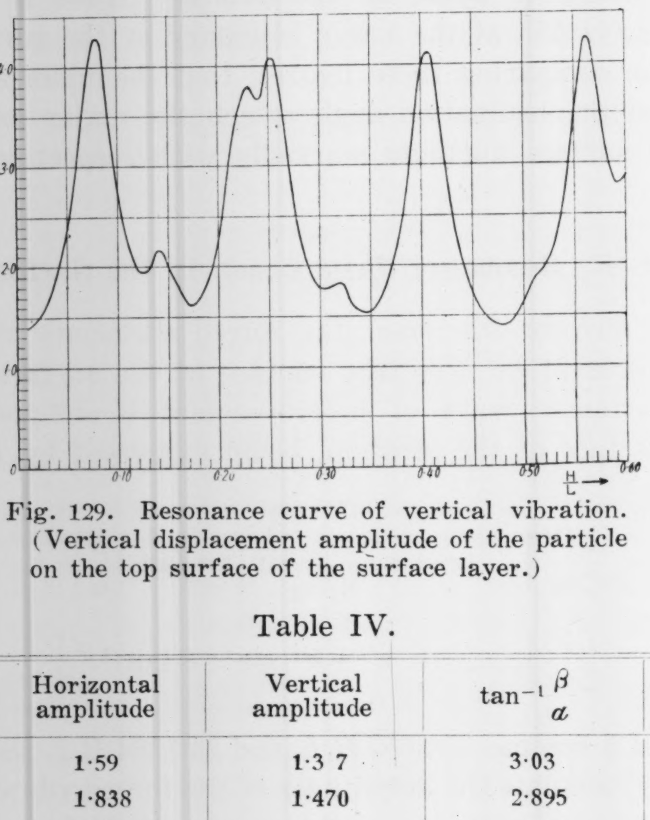

Fig. 129. Resonance curve of vertical vibration. (Vertical displacement amplitude of the particle on the top surface of the surface layer.)

Table IV.

$\frac{H}{L}$	Horizontal amplitude	Vertical amplitude	$\tan^{-1}\frac{\beta}{\alpha}$	$\tan^{-1}\frac{\beta'}{\alpha'}$
0·01	1·59	1·3 7	3·03	3·09
0·02	1·838	1·470	2·895	3·05
0·03	2·356	1·632	2·662	2·914
0·04	3·227	1·93	2·201	2·914
0·05	3·410	2·88	1·431	2·821

(to be continued.)

Table IV. (*continued.*)

$\frac{H}{L}$	Horizontal amplitude	Vertical amplitude	$\tan^{-1}\frac{\beta}{\alpha}$	$\tan^{-1}\frac{\beta'}{\alpha'}$
0·06	2·340	3·004	0·825	2·522
0·07	1·482	3·86	0·544	2·160
0·08	1·080	4·552	0·614	1·915
0·09	1·169	3·59	0·641	1·102
0·10	1·248	2·743	0·489	0·813
0·11	1·474	2·220	0·298	0·670
0·12	1·873	1·957	0·0327	0·605
0·13	3·517	1·957	2·767	0·555
0·14	5·145	2·162	2·05	0·356
0·15	2·680	1·975	1·269	0·0819
0·16	1·880	1·81	0·717	3·06
0·17	1·456	1·633	0·350	3·0
0·18	1·279	1·682	0·0254	3·04
0·19	1·265	1·866	2·821	3·00
0·20	1·414	2·247	2·393	2·937
0·21	1·750	3·012	1·780	2·743
0·22	1·994	3·55	0·930	2·344
0·23	1·531	3·78	2·936	1·929
0·24	0·938	3·660	1·893	1·734
0·25	0·567	4·174	0·209	1·346
0·26	0·753	3·832	1·541	0·832
0·27	0·966	2·927	0·638	0·492
0·28	1·124	2·300	0·134	0·322
0·29	1·380	1·943	2·913	0·225
0·30	1·824	1·78	2·567	0·163
0·31	2·620	1·794	2·103	0·0894
0·32	3·38	1·830	1·350	3·03
0·33	2·812	1·630	0·617	2·863
0·34	2·08	2·02	0·213	2·905
0·35	1·682	1·542	3·130	2·797
0·36	1·44	1·690	3·060	2·753
0·37	1·492	1·950	2·874	2·677
0·38	1·61	2·403	2·759	2·539
0·39	1·925	3·103	2·611	2·301
0·40	2·59	3·97	2·358	1·883
0·41	3·580	4·09	1·830	1·303
0·42	3·400	3·27	1·079	0·840
0·43	2·473	2·503	0·610	0·574
0·44	1·88	2·015	0·372	0·418

(*to be continued.*)

Table IV. *(continued)*

$\frac{H}{L}$	Horizontal amplitude	Vertical amplitude	$\tan^{-1}\frac{\beta}{\alpha}$	$\tan^{-1}\frac{\beta'}{\alpha'}$
0·45	1·605	1·710	0·239	0·314
0·46	1·52	1·534	0·132	0·252
0·47	1·455	1·431	0·0249	0·203
0·48	1·77	1·40	3·02	0·173
0·49	2·297	1·449	0·787	0·144
0·59	3·054	1·626	2·339	0·0928
0·51	3·380	1·873	1·496	3·070
0·52	2·453	1·958	0·890	2·918
0·53	1·670	2·190	0·470	2·817
0·54	1·180	2·680	0·126	2·671
0·55	0·738	3·480	0·867	2·404
0·56	0·292	4·237	0·677	1·852
0·57	0·701	3·950	0·134	1·402
0·58	1·268	3·145	2·546	1·088
0·59	1·854	2·788		0·943
0·60	2·60	2·90		0·740
0·62	1·855	2·120	——	0·142

Taking next the real parts only, we easily get the stationary vibrations of the bottom surface of the surface layer from expressions (15) and (16) as follows:

$$\left.\frac{UL}{2\pi a}\right]_{\substack{y=0\\x=0}}=\cos\theta\sqrt{\left(1+A'+B'\right)^2+\left(A''+\frac{s}{f}B''\right)^2}\sin(z+\alpha)\,, \tag{50}$$

$$\left.\frac{VL}{2\pi a}\right]_{\substack{y=0\\x=0}}=\cos\theta\sqrt{\left(-\frac{r}{f}+\frac{r}{f}A'-B'\right)^2+\left(B''-\frac{r}{f}A''\right)^2}\sin(z+\alpha')\,, \tag{51}$$

where

$$\alpha=\tan^{-1}\left\{\frac{-\left(A''+\frac{s}{f}B''\right)}{\left(1+A'+\frac{s}{f}B'\right)}\right\}, \tag{52}$$

$$\alpha'=\tan^{-1}\left\{\frac{\left(B''-\frac{r}{f}A''\right)}{\left(-\frac{r}{f}+\frac{r}{f}A'-B'\right)}\right\}, \tag{53}$$

and $\cos\theta=0{\cdot}7071$. Obviously α and α' should be taken satisfying

$$\left.\begin{aligned}\sqrt{\left(1+A'+\frac{s}{f}B'\right)^2+\left(A''+\frac{s}{f}B''\right)^2}\,\sin\alpha&=-\left(A''+\frac{s}{f}B''\right),\\ \sqrt{\left(1+A'+\frac{s}{f}B'\right)^2+\left(A''+\frac{s}{f}B''\right)^2}\,\cos\alpha&=1+A'+\frac{s}{f}B',\end{aligned}\right\}$$

$$\left.\begin{aligned}\sqrt{\left(-\frac{r}{f}+\frac{r}{f}A'-B'\right)^2+\left(B''-\frac{r}{f}A''\right)^2}\,\sin\alpha'&=\left(B''-\frac{r}{f}A''\right),\\ \sqrt{\left(-\frac{r}{f}+\frac{r}{f}A'-B'\right)^2+\left(B''-\frac{r}{f}A''\right)^2}\,\cos\alpha'&=\left(-\frac{r}{f}+\frac{r}{f}A'-B'\right).\end{aligned}\right\}$$

In these expressions, A', A'' and B', B'' are the real and the imaginary parts of A and B such that

$$A=A'+iA'', \qquad B=B'+iB'', \tag{54}$$

the values of which are given in Table I with the respective values of H/L when $\rho=\rho'$, $\lambda=\mu$, $\lambda'=\mu'$, $\theta=45°$, $\mu'/\mu=1/10$. In the present actual case, we calculated the amplitudes of the forced stationary vibrations (horizontal and vertical) at the bottom surface of the surface layer (shown in Table V), the phase-differences α and α' being also calculated. Figs. 130, 131 show the amplitudes (horizontal and vertical) of the bottom surface of the surface layer.

Table V.

$\frac{H}{L}$	Horizontal amplitude	Vertical amplitude	α	α'
0·01	1·491	1·358	2·996	3·080
0·02	1·457	1·347	2·817	3·020
0·03	1·330	1·327	2·548	2·952
0·04	0·847	1·302	2·035	2·875
0·05	0·219	1·271	1·623	2·749
0·06	0·937	1·157	0·815	2·516
0·07	1·195	0·785	0·550	2·155
0·08	1·415	0·0714	0·414	2·504
0·09	1·594	0·650	0·227	0·890
0·10	1·654	0·989	0·0385	0·597
0·11	1·647	1·120	2·185	0·422
0·12	1·605	1·170	2·784	0·320
0·13	1·398	1·191	2·444	0·288
0·14	0·652	1·310	1·906	0·300
0·15	0·433	1·460	0·730	0·183

(*to be continued.*)

Table V. (*continued*)

$\frac{H}{L}$	Horizontal amplitude	Vertical amplitude	a	a'
0·16	0·978	1·493	0·453	0·0591
0·17	1·154	1·490	0·237	3·10
0·18	1·194	1·481	0·0798	3·02
0·19	1·1425	1·476	3·075	2·922
0·20	0·983	1·450	2·982	2·785
0·21	0·659	1·350	0·706	2·288
0·22	0·960	0·982	3·135	2·548
0·23	1·672	0·573		
0·24	1·770	0·336		
0·25	1·460	0·315		
0·26	1·037	0·975	2·871	0·953
0·27	1·065	1·289	3·01	0·393
0·28	1·160	1·395		
0·30	1·064	1·464	2·671	0·143
0·31	0·676	1·455	3·03	0·0321
0·32	0·302	1·388	1·514	3·065
0·33	1·185	1·305	0·852	3·05
0·34	1·470	1·30	0·462	3·025
0·35	1·550	1·30	0·235	2·974
0·36	1·570	1·285	0·0713	2·899
0·37	1·562	1·245	3·06	2·796
0·38	1·510	1·146	2·904	2·647
0·39	1·434	0·941	2·692	2·408
0·40	1·168	0·443	2·339	2·056
0·41	0·441	0·362	1·567	1·127
0·42	0·719	0·906	1·248	0·783
0·43	1·267	1·150	0·654	0·529
0·44	1·445	1·255	0·362	0·366
0·45	1·513	1·310	0·175	0·256
0·46	1·535	1·330	0·0264	0·172
0·47	1·530	1·340	3·03	0·103
0·48	1·498	1·340	2·851	0·0462
0·49	1·387	1·332	2·599	3·130
0·50	0·997	1·335	2·139	3·116
0·51	0·0240	1·402	2·452	3·06
0·52	0·837	1·427	0·787	2·939
0·53	1·110	1·388	0·449	2·80
0·54	0·714	1·297	0·487	2·616
0·55	1·160	1·067	0·260	2·326

(*to be continued.*)

Table V. (*continued*)

$\frac{H}{L}$	Horizontal amplitude	Vertical amplitude	a	a'
0·56	1·3475	0·3885	0·323	1·608
0·57	1·644	0·2852	0·173	0·851
0·58	1·760	0·710	3·05	0·679
0·59	1·690	0·874	2·734	0·562
0·60	1·184	1·037	2·294	0·604

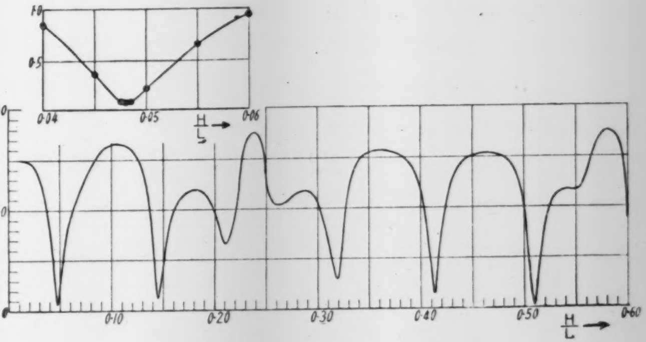

Fig. 130. Horizontal displacement amplitude of the particle on the bottom surface of the surface layer.

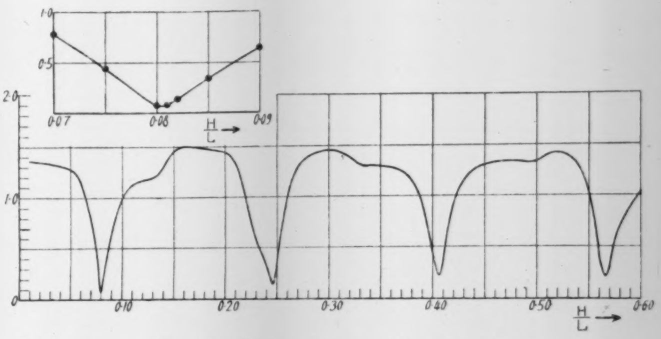

Fig. 131. Vertical displacement amplitude of the particle on the bottom surface of the surface layer.

It will be seen from Figs. 128, 129, 130, and 131 that the horizontal and the vertical vibration amplitudes on the top surface are usually larger than the respective amplitudes on the bottom surface of the surface stratum. It will be seen, moreover, that the respective positions of the maxima and minima of the horizontal (or vertical) vibration amplitudes with respect to the same values of H/L are completely changed in both amplitudes on the top surface and those on the bottom surface of the surface stratum. Generally speaking, the amplitude at the bottom surface of the surface layer becomes minimum and very small for the values of H/L, for which the amplitude on the top surface of the surface layer becomes maximum and very large. It is clear that the curves shown in Figs. 128, 129 are *resonance curves* of the vibrations (horizontal and vertical) of the surface stratum. And it will be seen from Figs. 128, 129 that the amplitudes of the forced oscillation at the top surface of the surface layer become relatively large at such periods as are synchronous successively with the resonance periods of vibration of the surface stratum. These resonance periods of oscil-

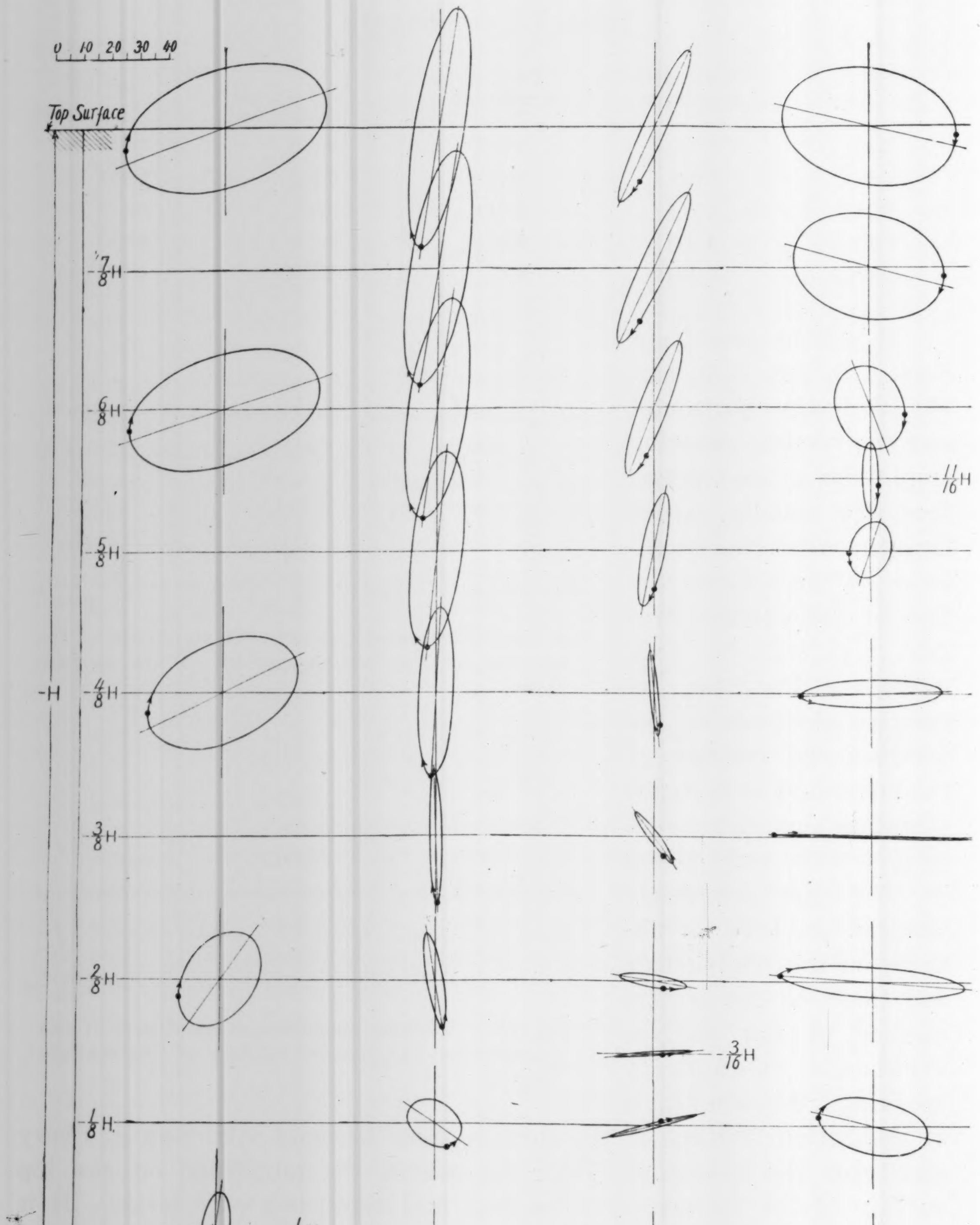
0 10 20 30 40
Top Surface
7/8 H
6/8 H
5/8 H
H
4/8 H
3/8 H
2/8 H
1/8 H
1/32 H
0
Bottom Surface
11/16 H
3/16 H
H/L = 0·048
H/L = 0·08
H/L = 0·10
H/L = 0·146

Fig. 132.

lation of the surface stratum usually differ in their horizontal and vertical vibrations as may be seen in Figs. 128, 129. The curves shown in Figs. 128, 129 are not regular as in the resonance curves when the primary waves are vertically upward incident on the bottom surface of the surface layer[14].

When the primary wave is vertically upward and incident on the bottom surface of the surface layer, and the periods of the primary incident wave become synchronous with the resonance periods of oscillation of the surface stratum, the bottom surface of the surface layer should become a nodal plane[15], that is, the displacements of particles on the bottom surface of the surface layer become zero. This fact, however, may not necessarily obtain when the primary wave is obliquely incident on the bottom surface of the surface layer, as may be seen from Figs. 130 and 131. It is noteworthy, moreover, that the fundamental resonance period of oscillation of the horizontal seismal vibration becomes longer than that of the vertical seismal vibration, and that in the case of horizontal vibration the ratio of the resonance period of higher order to the fundamental one tends to become larger than the ratio of the resonance period of the same higher order to the fundamental one in the case of vertical vibration, as may also be seen from Figs. 130 and 131. The resonance curves in Figs. 130 and 131 show that the amplitudes of the horizontal vibration usually become smaller than those of the vertical one, as may conspicuously be seen in resonance conditions.

Calculating from expressions (40) and (41) the vibrational movements of particles in the surface stratum, we obtain Fig. 132 which shows the elliptic orbits of particles on surfaces $y=0$, $y=\frac{1}{8}H$, $y=-\frac{2}{8}H$, $y=-\frac{3}{8}H$, $y=-\frac{4}{8}H$, $y=-\frac{5}{8}H$, $y=-\frac{6}{8}H$, $y=-\frac{7}{8}H$, and $y=-H$ when $H/L=0{\cdot}048$, $0{\cdot}080$, $0{\cdot}100$ and $0{\cdot}145$ respectively. Of course, in Fig. 132, the cases of $H/L=0{\cdot}048$ and $H/L=0{\cdot}145$ correspond to the movements of particles in the surface layer when the periods of the primary incident wave become equal to the fundamental and the second resonance periods of horizontal vibrations in the surface layer respectively, and the case of $H/L=0{\cdot}080$ corresponds to the movement of particles in the surface stratum when the period of the primary incident wave becomes equal to the fundamental resonance period of vertical vibration of the surface stratum. The horizontal movements of particles in the surface layer when $H/L=0{\cdot}048$, $0{\cdot}080$, $0{\cdot}100$ and $0{\cdot}145$ are shown in Figs. 133, 134, 135 and 136 respectively[16]. It will be seen from Figs. 132~136 that even if the period of the primary incident wave becomes synchronous with the resonance periods (of horizontal and vertical vibrations) of the surface layer, the amplitudes of displacement (of horizontal and vertical vibrations) do not become infinite as in the case of an isolated elastic pendulum. It will be seen, moreover, that the vibration modes

---

[14] K. SEZAWA and K. KANAI, *loc. cit.*

[15] K. SEZAWA and K. KANAI, *loc. cit.*

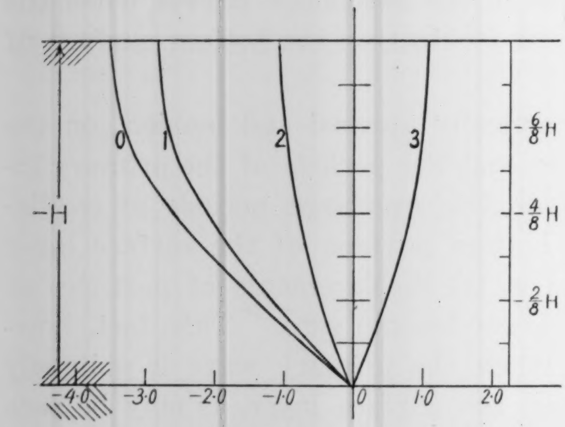

Fig. 133. Horizontal displacement in the surface layer when $H/L=0{\cdot}048$.

0: $\frac{t}{T}=0$, 1: $\frac{t}{T}=2{\cdot}2$, 2: $\frac{t}{T}=0{\cdot}4$,

3: $\frac{t}{T}=0{\cdot}7$.

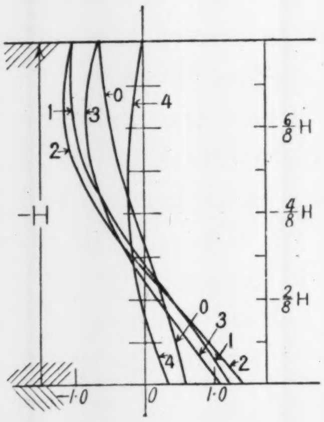

Fig. 134. Horizontal displacement in the surface layer when $H/L=0{\cdot}08$.

0: $\frac{t}{T}=0$, 1: $\frac{t}{T}=0{\cdot}2$, 2: $\frac{t}{T}=0{\cdot}3$,

3: $\frac{t}{T}=0{\cdot}4$, 4: $\frac{t}{T}=0{\cdot}5$.

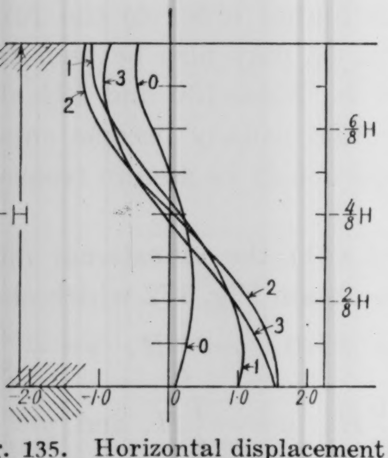

Fig. 135. Horizontal displacement in the surface layer when $H/L=0{\cdot}100$.

0: $\frac{t}{T}=0$, 1: $\frac{t}{T}=0{\cdot}2$, 2: $\frac{t}{T}=0{\cdot}3$,

3: $\frac{t}{T}=0{\cdot}4$.

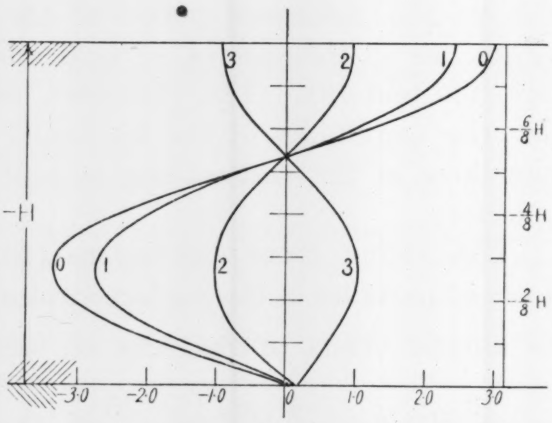

Fig. 136. Horizontal displacement in the surface layer when $H/L=0{\cdot}145$.

0: $\frac{t}{T}=0$, 1: $\frac{t}{T}=0{\cdot}2$, 2: $\frac{t}{T}=0{\cdot}3$,

3: $\frac{t}{T}=0{\cdot}4$.

---

[16] To obtain the results shown in Figs. 132~136, we used expressions (44) and (45).

(of horizontal and vertical vibrations) in the resonance conditions do not necessarily become equal to the free vibration modes that may be excited in the surface layer when it may be assumed as an isolated elastic pendulum. It may be worth noticing, furthermore, that the resonance periods of the vibrations (horizontal and vertical) of the surface stratum are not constant, but depend upon the angle of incidence of the primary wave at the bottom surface of the surface layer. From Figs. 130 and 131, we can get the resonance periods of vibration when the incidence angle of the primary dilatational wave becomes 45°, as shown in Table VI. If then the wave velocity V_1 of the dilatational wave in the subjacent medium and also the period T of the primary incident dilatational wave are known, the resonance periods of vibration of the surface stratum in an actual case can easily be determined by the values shown in Table V and by the relation $L = V_1 T$, when the angle of incidence of the primary wave becomes 45°.

Table VIa. Resonance Periods of Horizontal Vibration.

1st	2nd
$0{\cdot}048\,H/L$	$0{\cdot}145\,H/L$

Table VIb. Resonance Periods of Vertical Vibration.

1st	2nd
$0{\cdot}08\,H/L$	$0{\cdot}245\,H/L$

Recently T. Saita[17] and M. Suzuki studied the seismal vibrations at Marunouti, Tokyo, Japan. The English abstract of their paper in Japanese reads as follows:

> Lately the authors have observed seismic disturbances at Marunouchi where is the representative ground of the down town in Tokyo. These observations were held at the same time in three places; which are surface ground, 30 feet and 68 feet deep underground respectively. The 68 feet deep underground level is exactly the boundary of alluvium and diluvium. The diluvium is made of compact materials and its bearing power is greater than 20 tons per square foot, while the alluvium is made of soft materials and its bearing power is less than 1 ton per square foot. Therefore, these observations have determined how 68 feet thick soft alluvial layer vibrates by seismic disturbances. The instruments were Ishimoto's seismic accelerometers. The authors have found that, in alluvial layer, there are numerous waves having about 0·2 sec. and 0·7 sec. periods; in diluvial formation, 0·25 sec. and 0·45 sec. respectively. In consequence of drawing the resonance curve for vibrations in the alluvium, the author are able to ascertain that 0·25 sec. and 0·75 sec. are the proper periods of the alluvial layer. Moreover, the acceleration in 68 feet deep undreground was about 1/3 to 1/5 of the surface ground. These data will be available to engineering seismology and prevention of earthquake disaster.

The amplitude ratio curve obtained by them is shown in Fig. 137, in which the abscissa corresponds to the vibration period of the alluvium surface layer and the ordinate shows the ratio of the horizontal accerelation amplitudes at the top surface to those 68 feet underground. We do not know, however, the angle of incidence of the seismic waves at the bottom surface of the alluvium surface layer or the particular kind of incident seismic wave referred to in Saita's data of observations, so that our mathematical results may not be theoretically applicable to Saita's observation. But if we assume that the acceleration in Saita's data is of harmonic type, it is possible to say that the ratios of the maximum horizontal displacement amplitudes at the top surface to those at the bottom surface, which are shown respectively in Figs. 128 and 130, become approximately the same as the actual ratios of the large horizontal accelerations at the top surface to those at the bottom surface of the alluvium layer in Saita's data. The values of the actual ratios obtained by Saita are from about 1/3 to 1/5 as mentioned in his paper. By calculating the ratio of the displacement amplitudes on the top to those on the bottom surfaces with the respective values of H/L from Table III and IV, we get Table VII in which the ratios are given, the results being shown in Figs. 138 and 139. Fig. 138 corresponds to the horizontal displacement amplitude ratio and Fig. 139 shows the vertical displacement amplitude ratio. If we compare next the amplitude ratio curve in Fig. 138 with

---

[17] T. SAITA and M. SUZUKI, "On the Upper Surface and Underground Seismic Disturbances at the Down Town in Tokyo," *Bull. Earthq. Res. Inst.*, **12** (1934), 517.

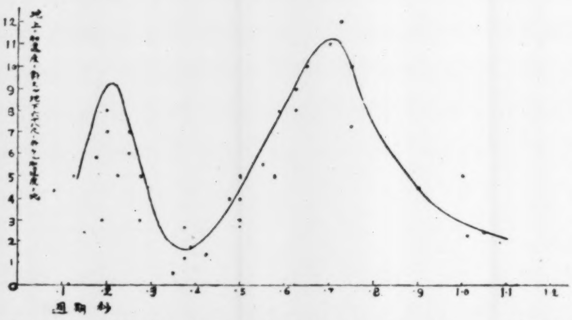

Fig. 137. Horizontal acceleration amplitude ratio obtained by T. Saita and M. Suzuki.

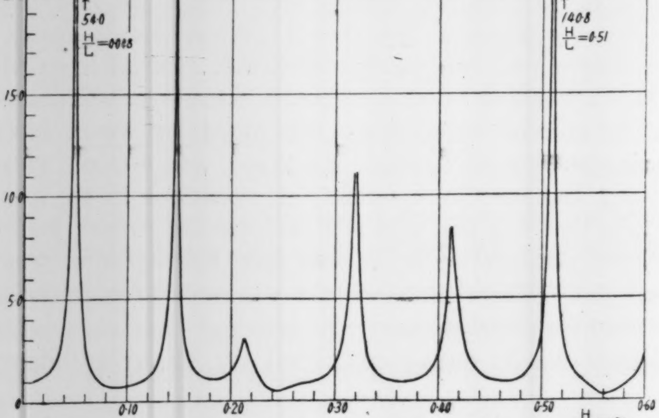

Fig. 138. Horizontal displacement amplitude ratio.

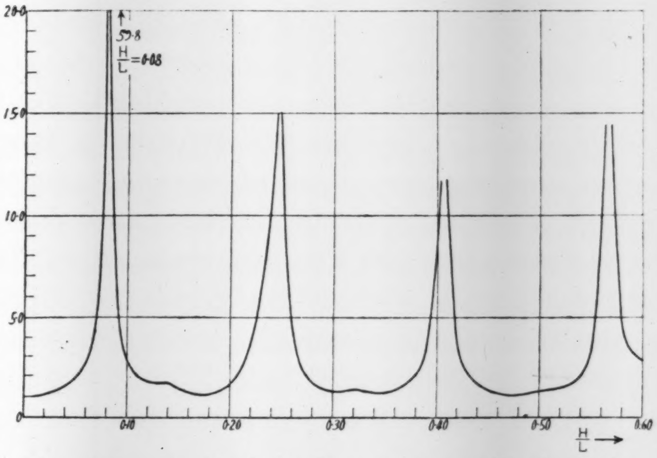

Fig. 139. Vertical displacement amplitude ratio.

Table VII.

$\frac{H}{L}$	Horizontal displacement amplitude ratio	Vertical displacement amplitude ratio	$\frac{H}{L}$	Horizontal displacement amplitude ratio	Vertical displacement amplitude ratio
0·01	1·066	1·022	0·32	11·20	1·318
0·02	1·1675	1·091	0·33	2·373	1·250
0·03	1·771	1·230	0·34	1·415	1·554
0·04	3·810	1·482	0·35	1·085	1·186
0·05	15·552	2·265	0·36	0·917	1·315
0·06	2·498	2·597	0·37	0·956	1·566
0·07	1·240	4·918	0·38	1·066	2·096
0·08	0·764	3·754	0·39	1·342	3 295
0·09	0·734	5·511	0·40	2·22	8·96
0·10	0·755	2·775	0·41	8·120	11·28
0·11	0·895	1·982	0·42	4·786	3·610
0·12	1·167	1·672	0·43	1·952	2·173
0·13	1·799	1·642	0·44	1·301	1·605
0·14	4·825	1·650	0·45	1·061	1·305
0·15	6·200	1·352	0·46	0·990	1·154
0·16	1·923	1·212	0·47	0·951	1·067
0·17	1·262	1·096	0·48	1·181	1·045
0·18	1·071	1·135	0·49	1·655	1·137
0·19	1·1075	1·264	0·50	3·064	1·219
0·20	1·438	1·550	0·51	1·408	1·336
0·21	2·655	2·231	0·52	2·930	1·373
0·22	2·076	3·616	0·53	1·550	1·577
0·23	0·917	6·600	0·54	1·652	2·065
0·24	0·529	10·90	0·55	0·636	3·262
0·25	0·479	13·25	0·56	0·217	10·90
0·26	0·726	3·932	0·57	0·427	13·85
0·28	0·969	1·649	0·58	0·721	4·430
0·30	1·715	1·215	0·59	1·097	3·190
0·31	3·861	1·232	0·60	2·195	2·798

that in Fig. 137, it will be seen that the first and second resonances in Fig. 138 correspond very roughly to the maxima at 0·7 sec. and 0·2 sec. respectively in Fig. 137. Since Saita has obtained only the amplitude ratio curve shown in Fig. 137, and has not shown the resonance curve[18] such as that shown in Fig. 138. It is impossible theoretically to compare Fig. 138, which is obtained from the resonance curve in Fig. 128, with the amplitude ratio curve in Fig. 137 obtained by Saita, with the result that we assume here that when the resonance curve is constructed from Saita's actual data, the resonance periods of Marunouti ground will work out to about 0·7 sec. and 0·2 sec. The magnitudes of these amplitude ratios at the respective resonances are then not strictly the same in Figs. 137 and 138. The ratio of the abscissa, at which the first maximum occurs, to that which gives the second maximum in Fig. 138, is about 3, the same ratio in Fig. 137 being about 3·5. These two values are also approximately equal in the two cases, that is, our mathematical results and Saita's experimental results.

From the foregoing discussion, it may be said that it will be in order to use the mathematical results in the present paper for obtaining the wave velocity of the dilatational wave in the diluvium lying under a top surface 20 m. thick at Marunouti. Therefore, using the value of the abscissa which gives the first maximum of the amplitude ratio in Fig. 138, such that

$$\frac{H}{L}=\frac{H}{V_1T}=0{\cdot}048\,,$$

and the assumed resonance period of 0·7 sec. in Fig. 138, we get

$$\frac{H}{V_1\times 0{\cdot}7}=0{\cdot}048\,,\quad \text{or}\quad V_1\doteqdot 570\text{ m/s}\,,$$

assuming that the thickness of the alluvium at Marunouti is 20 meters, and the densities of the alluvium and diluvium are the same there.

Conclusion.

The present paper is a study of the forced stationary vibration of a surface stratum when a dilatational wave of harmonic type of infinite extent is obliquely incident on the bottom surface of the surface layer, therefore showing that there are resonance periods of oscillation in the surface layer. The amplitudes (horizontal and vertical) of the forced oscillations at the top surface of the surface layer become of course relatively large at such periods as are synchronous successively with the resonance periods of vibration of the surface layer. These resonance periods of oscillation of the surface stratum usually differ in their horizontal and vertical vibrations, and the fundamental resonance period of oscillation of the horizontal vibration becomes longer than that of the vertical vibration. When the primary wave is obliquely incident on the bottom surface of the surface layer, and the periods of the primary incident wave become synchronous with the resonance periods of oscillation of the surface layer, the bottom surface of the surface layer does not become necessarily a nodal plane of oscillation, as in the case when the primary wave is vertically upward and incident on the bottom surface of the surface layer. The forced vibration modes of horizontal and vertical vibrations of the surface layer in resonance condition do not necessarily become equal to the free vibration modes that may be excited in the surface layer, when it may be assumed to be an isolated elastic pendulum. Even if the period of the primary incident wave becomes synchronous with the resonance periods (of horizontal and vertical oscillations) of the surface layer, the displacement amplitudes (of horizontal and vertical vibrations) do not become infinite as in the case of the isolated elastic pendulum. It is noteworthy, moreover, that the resonance periods of vibrations (horizontal and vertical) of the surface layer are not constant, but depend upon the angle of incidence of the primary wave at the bottom surface of the surface layer.

---

[18] Saita has not shown in his paper the resonance curve of the horizontal seismal vibration of the surface stratum of alluvium, but he informed the present authors that he had also obtained it.

We are yet unable theoretically to deal with the predominating periods in the surface layer in the seismal disturbance, which have an important connection with the prevention of earthquake disasters. It is our intention, on the next occasion, to study the predominating periods in the surface layer in a seismal disturbance by using the mathematical results given in the second chapter[19] of the previous paper. The wave phenomena in the surface layer when distortional waves of both finite and infinite extents are obliquely incident on the bottom of the surface layer having now been brought under mathematical treatment, the full results will be made available in the near future.

---

19) G. NISHIMURA, *loc. cit.*

The present authors wish to express their sincere thanks to Professor K. Sezawa for his interest and kind guidance in the course of the present study.

25. 斜めの入射波による表面層の振動とその共振れ性質

地震研究所 西村源六郎
地震研究所 高山威雄

前論文1)の續報である本論文では具體的の例に就て數計算を行ひ，地表層に共振れ振動週期のある事を知つた．この週期は地表層の所謂固有週期と言つてよいかも知れないが，表面層に入射する强制波の入射角によつて異つた値をとるものである．この共振れ週期で表面層の振動を起しても表面層の振幅は無限大にならない事は勿論であるが，その振動の Mode は必ずしも表面層だけを彈性振子と考へた場合の自己振動の mode と一致しない事は注意を要す．齋田氏等2)の求めた丸ノ内での水平加速度振幅の觀測結果に對する解釋に就ては彈性振子的な考の基でこれを處理してゐる樣であるが，著者達は次に發表する事にしてゐる表面層内に於ける free waves の問題を解決し，以つて forced waves に關する本論文より得た結果とを適當に組合せて，表面層の振動問題を解決してみたいと考へてゐる．

---

1) 西村源六郎　地震研究所彙報 **13** (1935), 540〜554.
2) 齋田時太郎，鈴木正治　地震研究所彙報 **12** (1934). 517.

26. *Geophysical Studies of Volcano Mihara, Oosima Island; Topographic Survey of the Crater of Mihara and the Magnetic Survey of Oosima.*

By Ryutaro TAKAHASI and Takesi NAGATA,

Earthquake Research Institute.

(Read Oct. 20, 1936 and Jan. 19, 1937.—Recieved Mar. 20, 1937.)

Introduction.

The typically double-coned volcano Mihara in Oosima, one of the seven volcanic islands of Idu, and one of the most active volcanoes in Japan, is very interesting, whether regarded geologically or geophysically.

The geology of this volcano has been studied by O. E. Naumann,[1] T. Wada,[2] J. Milne,[3] N. Yamazaki,[4] N. Fukuchi,[5] very thoroughly by S. Tsuboi[6] in 1900; and, recently, petrographically by H. Tsuya[7] in his study of the Huzi volcanic chain.

S. Nakamura[8] and others have studied it from the geophysical standpoint. F. Omori,[9] who made a thorough, detailed investigation, seismologically and geophysically, during the active period of 1911∼14, reported in detail the complete process of this eruption of the Hawaiian type.

One of the present writers, in the course of geophysical studies of volcano Asama, found, in collaboration with T. Minakami,[10] that it is possible to predict the explosive Vulcan type eruption of the volcano.

---

[1] O. E. NAUMANN, *Zeitschr. d. Deutschen. Geol. Gesell.*, **29** (1877), 364.

[2] T. WADA, "*Gakugei Sirin.*", **1**, No. 1, 1877.

[3] J. MILNE, *Geological Magazine*, Series II. Vol. 1. No. 5. 1877; *Transact. seism. soc. Japan.*, IX, Part II. 1887.

[4] N. YAMAZAKI, *Rep. Earthq. Inv. Comm.*, No. 9 (1899), 33.

[5] N. FUKUCHI, *Journ. Geogr. Tokyo*, **14** (1902), No. 161 and 162; *Rep. Earthq. Inv. Comm.*, (1906), No. 53, p. 87.

[6] S. TSUBOI, *Journ. Coll. Sci. Imp. Univ. Tokyo.*, **43** (1936), Art. 6.

[7] H. TSUYA, *Bull. Earthq. Res. Inst.*, **15** (1937), 1.

[8] S. NAKAMURA, and others. *Proc. Tokyo. Math. Soc.*, **4** (1908), p. 293.
Journ. Geogr. Soc. Tokyo, **20** Nos. 238∼239 pp. 682 and 786 (1908).

[9] OMORI, *Rep. Earthq. Inv. Comm.*, No. 81, (1915).

[10] T. MINAKAMI, *Bull. Earthq. Res. Inst.*, **13** (1935), 318; 629; 790.
R. TAKAHASI, *Bull. Earthq. Res. Inst.*, **11** (1933), 25.

The main object of the present study of volcano Mihara is to enable comparisons of these two volcanoes of different types, and obtain data on which to base future studies of the volcano.

Past activities of volcano Mihara have been reported in detail by S. Nakamura,[11] but they are never frequent. The most recent was that during the epoch 1911～14, when molten lava, now called Taisyô Lava, filled the crater almost to the lowest brim and solidified there, so that the topography of the crater changed completely.

After this eruption, there has been no marked activity; only incessant rumblings, vapour emissions, occasional volcanic earthquakes, and ash precipitation, besides the gradual changes in the topography of the crater. Since it is consequently impossible to make observations of phenomena directly related to the eruption, such as we do at the Asama Volcano Observatory, we must be content with studies of the phenomena just mentioned as well as with the various geophysical surveys as data for the study of future eruptions.

In these respects we have so far made the following surveys. Since it is obvious that marked magnetic disturbances occur at the time of eruption of a volcano, as was reported by S. T. Nakamura and Y. Kato,[12] measurements have been made of the three elements of terrestrial magnetism at 12 stations widely separated in Oosima, with the object of seeking some clue to the relation between volcanic activity and magnetism. This is one of the surveys. So far, the topography of the crater has been surveyed by a number of investigators,[13] the most recent being that made by S. Nakamura in 1924, since when, however, the crater pit has grown very large owing to parts of its wall falling from time to time.

In Asama, the crater floor rises considerably before an eruption—a phenomenon that is doubtless very conspicuous in volcanoes with basic lava like Mihara. Indeed, in the eruption of 1914, the molten lava poured out of the crater pit and filled the crater.[14] The depth of the present crater pit is therefore a measure of the activity of this volcano.

In these circumstances topographic surveys of the interior of the

---

11) *Rep. Earthq. Inv. Comm.*, No. 79, (1915), 38.

12) *Jap. Journ. Astr. Geophys.*, **12** (1934), 19.

13) S. NAKAMURA and others. *Rep. Earthq. Inv. Comm.*, No. 81.
J. OKAMURA, *Rep. Jap. Geol. Survey.*, **48**.
S. TSUBOI, *loc. cit.*
J. KONDO, *Rep. Earthq. Inv. Comm.*, No. 81.

14) F. OMORI, *loc. cit.*

crater pit as well as the interior of the old crater were made. By repeating these measurements, it is hoped to obtain some clue to the relation of the topographic changes in the crater to other volcanic phenomena.

Magnetic Survey of Oosima.

In the case of the Nôbi earthquake of 1891, A. Tanakadate and H. Nagaoka[15] measured terrestrial magnetism with a view to detecting variations due to the earthquake. Since then, investigations in this direction have been neglected by seismologists, although magnetic surveys have regularly been made.

Recently S. T. Nakamura and Y. Kato,[16] with the aid of the Barrow type dip circle, observed in the eruption in 1929 of Komagatake, Hokkaido, abnormal variations in the inclination. In the eruption of Asama in July, 1935, T. Minakami,[17] at the Asama Volcano Observatory, observed marked variations in declination.

It is most probable therefore that similar variations in terrestrial magnetism will accompany future eruptions of Mihara. The magnetic elements may again vary with the volcanicity during ordinary times. In order to verify these assumptions, and also as data for future eruptions, terrestrial magnetism was measured at twelve stations, four of which

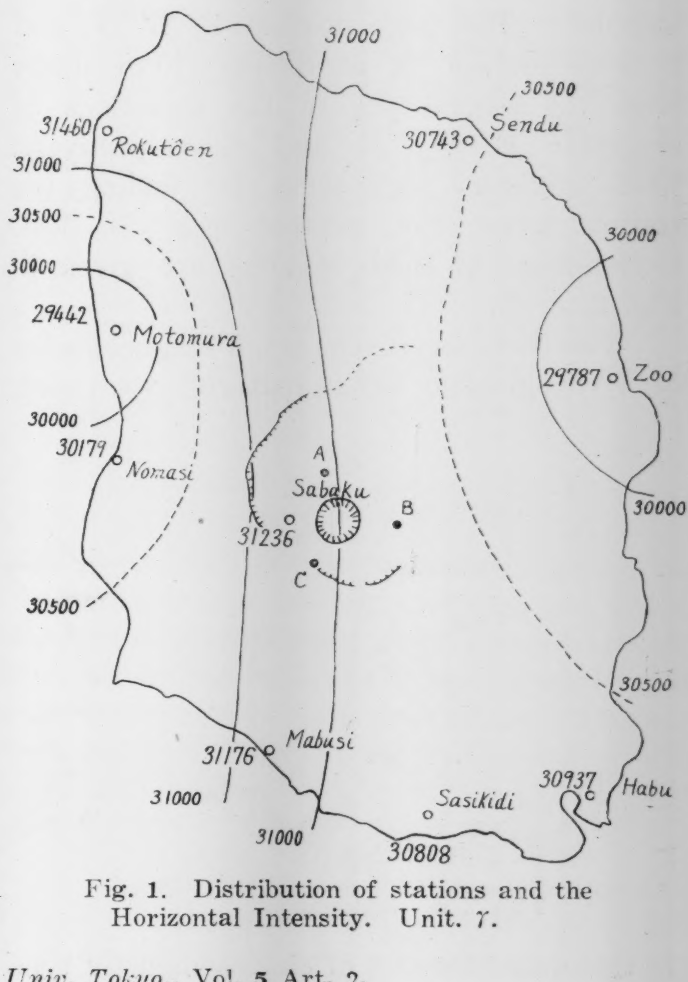
31000
30500
Sendu
30743
31460
Rokutôen
31000
30500
30000
29442
Motomura
30000
30179
Nomasi
30500
A
Sabaku
B
31236
C
29787
Zoo
30000
30000
30500
Mabusi
31176
31000
31000
Sasikidi
30808
30937
Habu

Fig. 1. Distribution of stations and the Horizontal Intensity. Unit. γ.

---

[15] *Journ. Coll. Sci. Imp. Univ. Tokyo.*, Vol. 5 Art. 2.

[16] Y. Kato, *loc. cit.*

[17] T. Minakami, *loc. cit.*

were within the somma, the remaining eight around the volcano.

The stations were distributed as shown in Fig. 1. Eight stations were distributed almost equidistantly along the coast of Oosima, except for the S.E. side of the island, where the coast is very rugged. At Motomura and Mabusi, the points occupied by the Hydrographic Office of the Japanese Navy were reoccupied. The middle of the playground of the primary school, which is about 50 m north of the Habu station of the Hydrographic Office, was selected for our Habu station. As the Hydrographic Office station at Sendu was inconvenient for transporting the magnetometer, our measurements at Sendu were carried out at the Sendu Primary School, 1 km north of the former point. At stations A, B, C within the somma, only the inclination was observed.

Each station was marked by five pegs as shown schematically in Fig. 2. The central peg was driven into the ground on which the magnetometer was installed. The pegs marked E, W, N, and S were driven in at points 10 m apart from the central peg in the directions of magnetic E, W, N and S respectively. These auxiliary pegs serve for finding the station when the central peg is lost. Sketch-maps of these stations are given in Fig. 3, a—h.

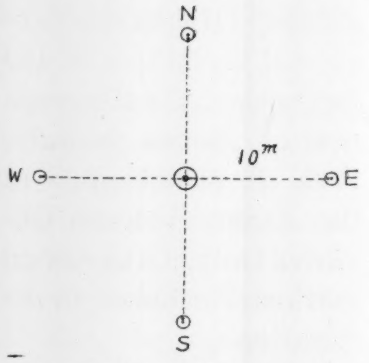

Fig. 2. The station mark.

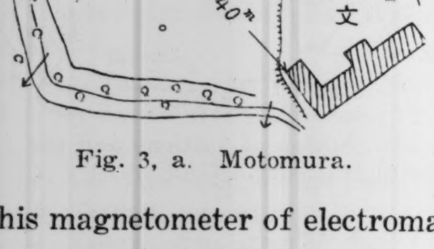

Fig. 3, a. Motomura.

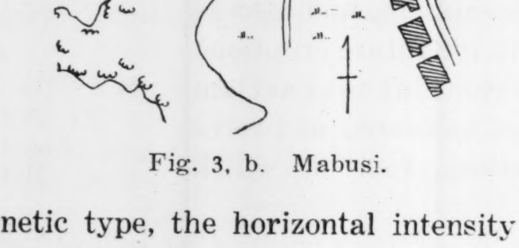

Fig. 3, b. Mabusi.

For these measurements, a magnetometer of Hydrographic Office pattern[18] was used. In this magnetometer of electromagnetic type, the horizontal intensity is measured by the improved sine-method devised by A. Tanakadate, and the declination by making the axis of the Helmholtz coil of the

---

[18] *Bull. Hydro. Office*, Vol. **8** (1937).

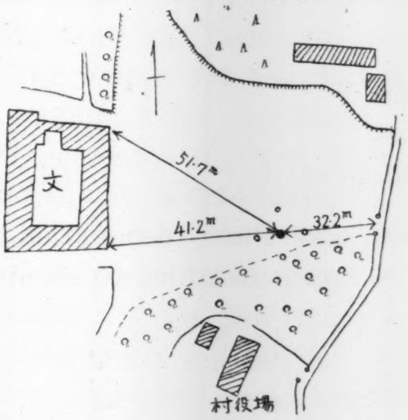
文
51·7m
41·2m
32·2m
村役場

Fig. 3, c. Sasikidi.

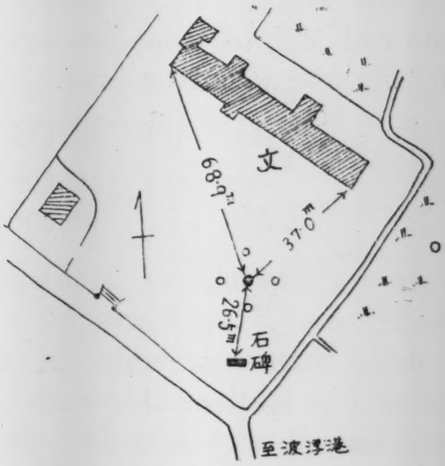
文
68·9m
37·0m
26·5m
石碑
至波浮港

Fig. 3, d Habu.

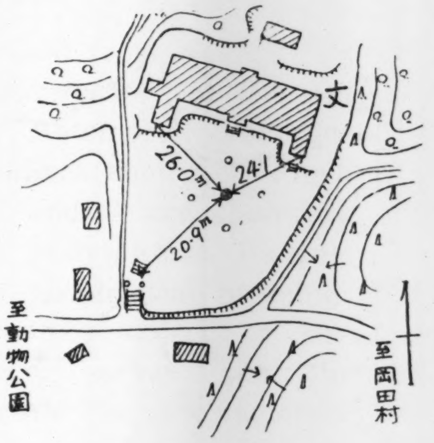
文
26·0m
24·1
20·9m
至動物公園
至岡田村

Fig. 3, e. Sendu.

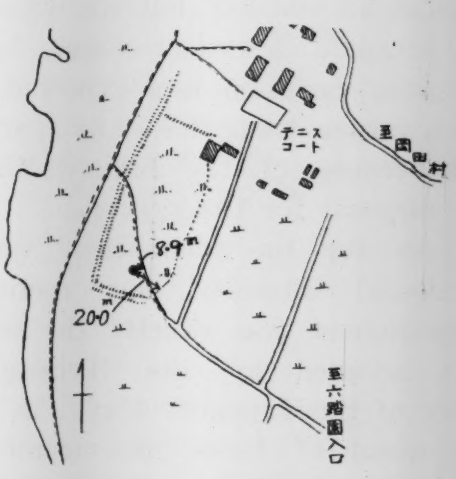
テニスコート
至岡田村
8·9m
20·0m
至六踏園入口

Fig. 3, f. Rokutôen.

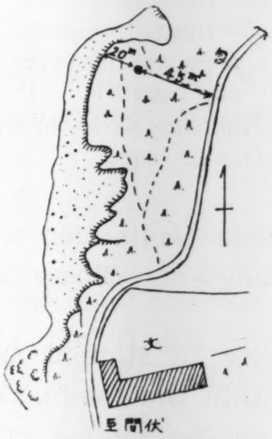
20m
45m
文
至間伏

Fig. 3, g. Nomasi.

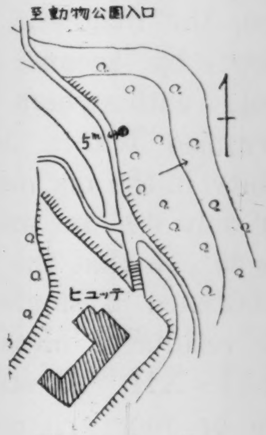
至動物公園入口
5m
ヒュッテ

Fig. 3, h. Zoo.

magnetometer coincident with the direction of the field. Coincidence is established when a small magnet suspended at the center of the Helmholtz coil does not move even when the direction of the current in the coil is reversed. The accuracy of measurements obtained by us with this magnetometer was

$\varDelta\delta = \pm 0{\cdot}1'$ in the declination,
$\varDelta\theta = \pm 0{\cdot}1'$ in the inclination,
$\varDelta H = \pm 1\gamma$ in the horizontal intensity.

At the stations of Motomura, Mabusi, and Habu, declination was measured every two hours for a day of 24 hours in order to eliminate the daily variation, while at the remaining five stations the mean of three measurements was adopted. It is obviously better to make 24-hour observations at all stations, but we decided on the schedule described above, because the time variation was expected to be much larger than the daily variation, and because of the limited time at our disposal for the survey.

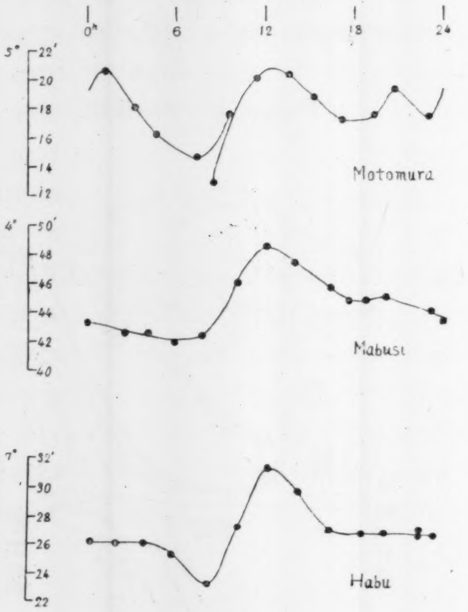

Fig. 4. The daily variations in declination.
Motomura: a small disturbance was observed at Kakioka betw. $16^h - 1^h$.
Mabusi: slow variations.
Habu: calm.

As for the inclination and the horizontal intensity, our method of measurement was exactly the same as that adopted by the Hydrographic Office of the Japanese Navy, in which the mean of three measurements is taken for the value of the station in question. When inclination alone was measured, the magnetic meridian was determined by means of a striding declinator, with which the meridian is determined within 30′, while the uncertainty in the declination causes an error of only 0·1′ in the determined value of the inclination when the latter is 45°, so that the accuracy was quite sufficient. These measurements consisted of single observations.

The results of measurements taken at these 12 stations are given in Tables I∼XII. At stations A, B, and C within the somma, bearings of three or four triangulation points either on the somma or on the parasitic cones were taken for determining the position of each station, from which measurements the astronomical meridian was also calculated, so that the magnetic declination was determined within an error of 20′. Although this is not sufficiently small for finding the variation in magnetism by repeated observations, it is good enough for determining the distribution of local anomaly in this volcanic island.

The values for the declination, inclination, and horizontal intensity thus obtained are graphically represented in Figs. 1, 5, and 6. It is interesting to note that the declination is very anomalous near the crater. Since, however, Oosima consists entirely of basaltic lava and ashes, the distribution of terrestrial magnetism may be very complicated, as is easily surmised from Nakamura's measurements[19] of the dip near Motomura. The contour lines shown in Figs. 1, 5 and 6 are therefore only provisional, having little geophysical meaning. Since the object of the present survey was to ascertain the time variation and not local anomalies, no increase was made in the number of stations. In case of necessity, the whole island could be covered with measurements, although of rather low accuracy, using the present stations as standards.

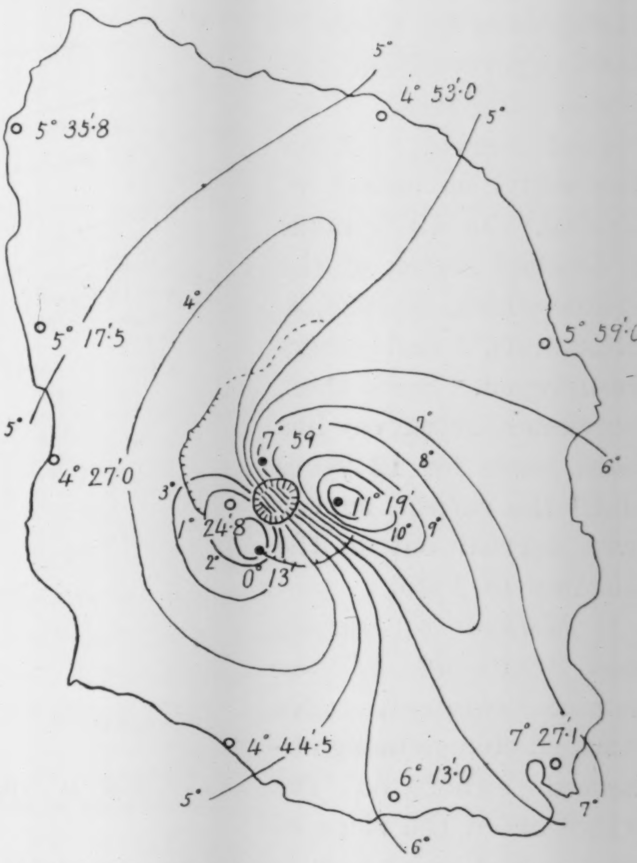

Fgi. 5. Distribution of the westerly declination.

Topographic Survey of the Crater.

Surveys and sketches made in the past. In 1907, S. Nakamura, T. Terada, and D. Ishitani,[20] and others surveyed for the first time the topography of the crater of Mihara. Since 1911, owing to the activities of the volcano, the appearance of the crater underwent rapid changes. These changes were sketched from time to time by Mr. Sato,[21] the village master of Motomura at that time. Another survey of the crater was made in 1913 by Okamura,[22] and a sketch map by Kondo,[23] both experts of the Imperial Japanese Geological Survey. After the activities ceased, S. Tsuboi,[24] in 1916, made a detailed sketch of the crater which, in 1924, S. Nakamura[25] and others resurveyed. Since then, no sketch or survey has been made for 12 years until the present survey was carried out in the autumn of 1936.

---

[19] S. Nakamura, "*Zisin*", **6** (1934), 637.

[20] *loc. cit.*

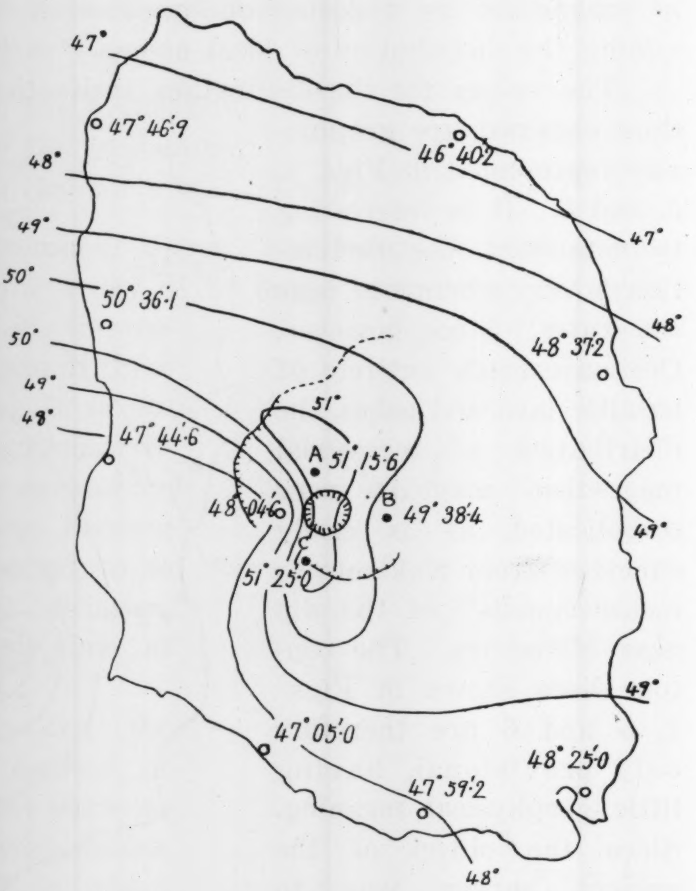

Fig. 6. Distribution of the inclination.

Method of survey and treatment of the results obtained. No marked change being observed either on the ridge or on the slope of the central cone, our survey was restricted to the bottom of the old crater and the interior of the present crater pit. The survey was accordingly divided into two parts; the one a topographic survey of the crater bottom by means of a plane table and a photographic theodolite, and the other a survey of the interior of the pit mainly by means of a sextant.

a) Topography of the old crater bottom. For various reasons, absolute determinations of the position, azimuth, and the height of the

---

21) SATO, *loc. cit.*
22) OKAMURA, *loc. cit.*
23) KONDO, *loc. cit.*
24) S. TSUOBI, *loc. cit.*
25) not yet published.

area in question as referred to triangulation points were not made, only relative values having been determined. Seeing that our survey is for changes in topography in the crater, absolute determinations could be dispensed with. All the heights were obtained on the assumption that the highest point of the central cone is 155·25 m above mean sea level.

The position of the base-line and its expansion net is shown in Fig. 7. The form of the expansion net is not as we could have wished, but the topography prevented anything better. The length of base-line was measured with a stadia bar 1 m long and a micrometer theodolite included in the Zeiss photographic survey instrument. The expansion of the base-line and other trigonometric measurements were executed with the Wild theodolite. The trigonometric points for the plane table work were selected as shown in the same figure, namely 10 points on the ridge of the central cone, and 4 on the edge of the present crater pit.

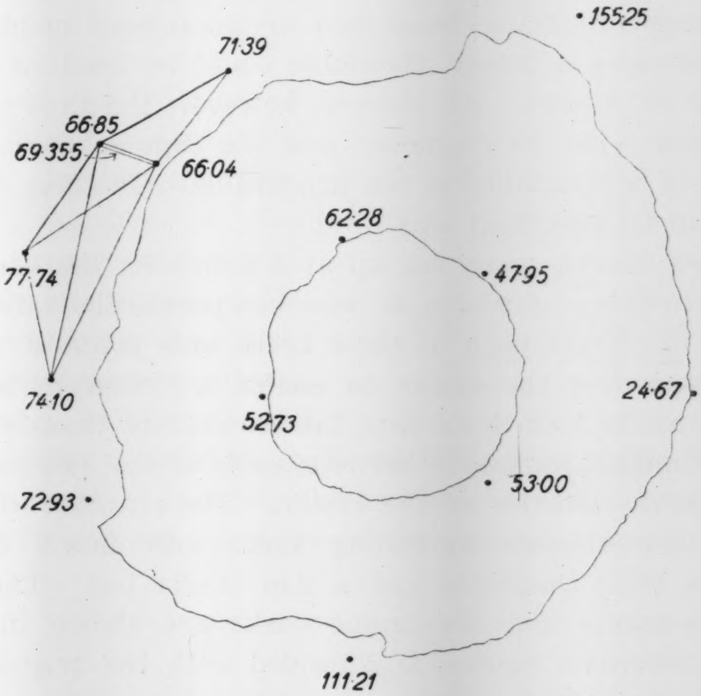

Fig. 7. The base-line, its expansion net, and the numerals show relative heights in meter.

Details of the topography were plotted on three field sheets in scale 1:1500. Owing to poor weather conditions, the cracks and fumaroles in the crater, and details of the wall of the old crater were not fully sketched but all other features on the bottom of the old crater were plotted within an error of 2 m. The results of the survey are shown in Fig. 8, Pl. XX.

b) Besides this plane table survey, a photographic survey was executed in parallel. Features of the crater were photographed from the ends of 3 base-lines with the Zeiss photographic survey camera. As plotting of the topography from the plates obtained is not yet completed, only a few of the photographs thus obtained are shown here (Figs. 9~12, Pl. XXI and XXII).

Survey of the interior of the present crater pit. The depth and other features of the interior of the present crater could be determined from measurements made from two or three fixed points on its edge. In favourable cases a transit theodolite could be used as was done by T. Minakami at Asama. At Mihara, however, the present crater is so deep compared with its diameter, and the edge so liable to give way, that the use of a theodolite is not practicable. In these circumstances, the method to be described was used.

Reference marks were set up at 4 points on the edge of the present crater, in three of which it was comparatively safe to approach the edge of it. From each of these three safe points a wooden frame-work projected over the crater to enable an observer at the end of the frame-work to look down into the crater, and thus, with a sextant, measure the angles subtended between each of the two reference points and a point in the interior of the crater. The positions of the reference marks, and the distance separating them were newly determined by means of the Wild theodolite and a 2 m stadia bar. The positions of the reference marks and the frame-works are shown in Figs. 13 and 14. Of the reference marks, D coincided with the trigonometric point used in the plane table work. Since each frame-work is from 5 to 6 m distant from its reference mark, the usual reduction for this eccentricity was made.

From the angle thus observed, the positions of the marked points in the interior of the present crater were determined by the method of least squares. These points are referred to rectangular coordinates x, y, z, with the origin at A and the x axis towards AB.

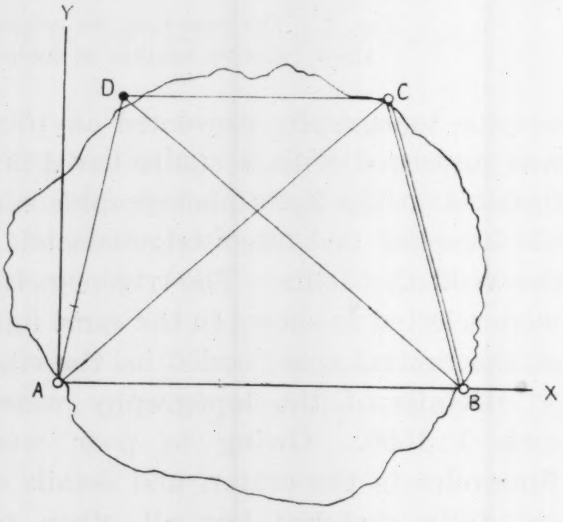

Fig. 13. Positions of reference marks.

At present, molten incandescent lava is seen in two openings in the bottom of the present crater. Although the shape of these openings vary from time to time, their mean positions remain unchanged. The coordinates of these openings in Nov., 1936, were as follows:

	Larger one	Smaller one
	m m	m m
x	104·6 ± 1·7	95·1 ± 1·4
y	91·7 ± 1·8	81.3 ± 1·3
z	−267·7 ± 3·4	−289·4 ± 2·7

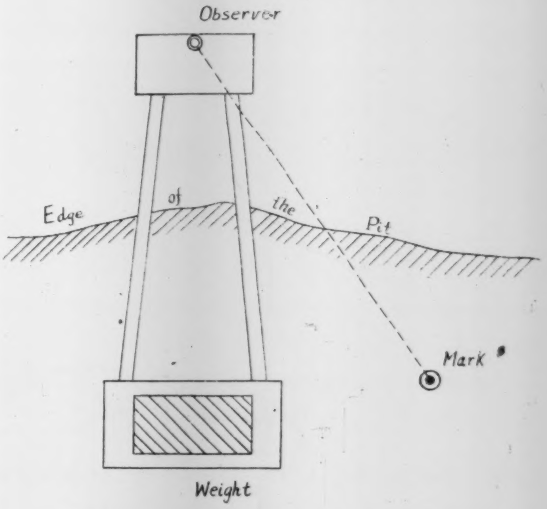

Fig. 14. Relative position of a reference mark and a framework.

The map of the interior of the pit in Fig. 8, is based on these determinations. In mapping, photographs and sketches of the interior of the present crater that were made simultaneously with the sextant work were consulted. According to these determinations, the present crater is almost conical in shape, with a vertex angle of 30°. Except in the northern part, its wall has a shelf showing the incessant breaking away of the pit wall. In Fig. 15 a, b, the sections of the present crater are shown.

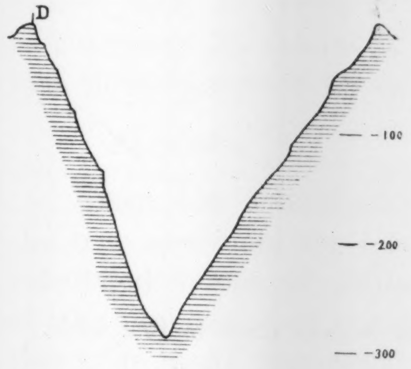

Fig. 15, a. Vertical section of the present crater. Unit: meter.

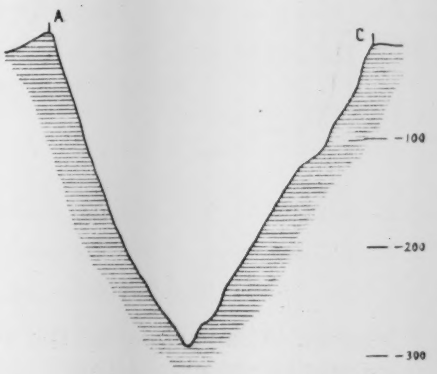

Fig. 15. b. Vertical section of the present crater. Unit: meter.

Changes in the topography of the crater up to the present. Upon comparing the results of the present survey with those of S. Nakamura made in 1924, we find that although there is no remarkable change in the central cone, except for small falls of the crater wall, the diameter of the present crater has greatly increased during the interval between 1924 and 1936, it being now 3 times larger in diameter and 10 times larger in area than when last surveyed. These features are shown in Fig. 16. Fig. 17, a, b show the sections of the pit in vertical planes, one of which passes through the highest point of the central cone and the center of the present crater in 1923, and the other per-

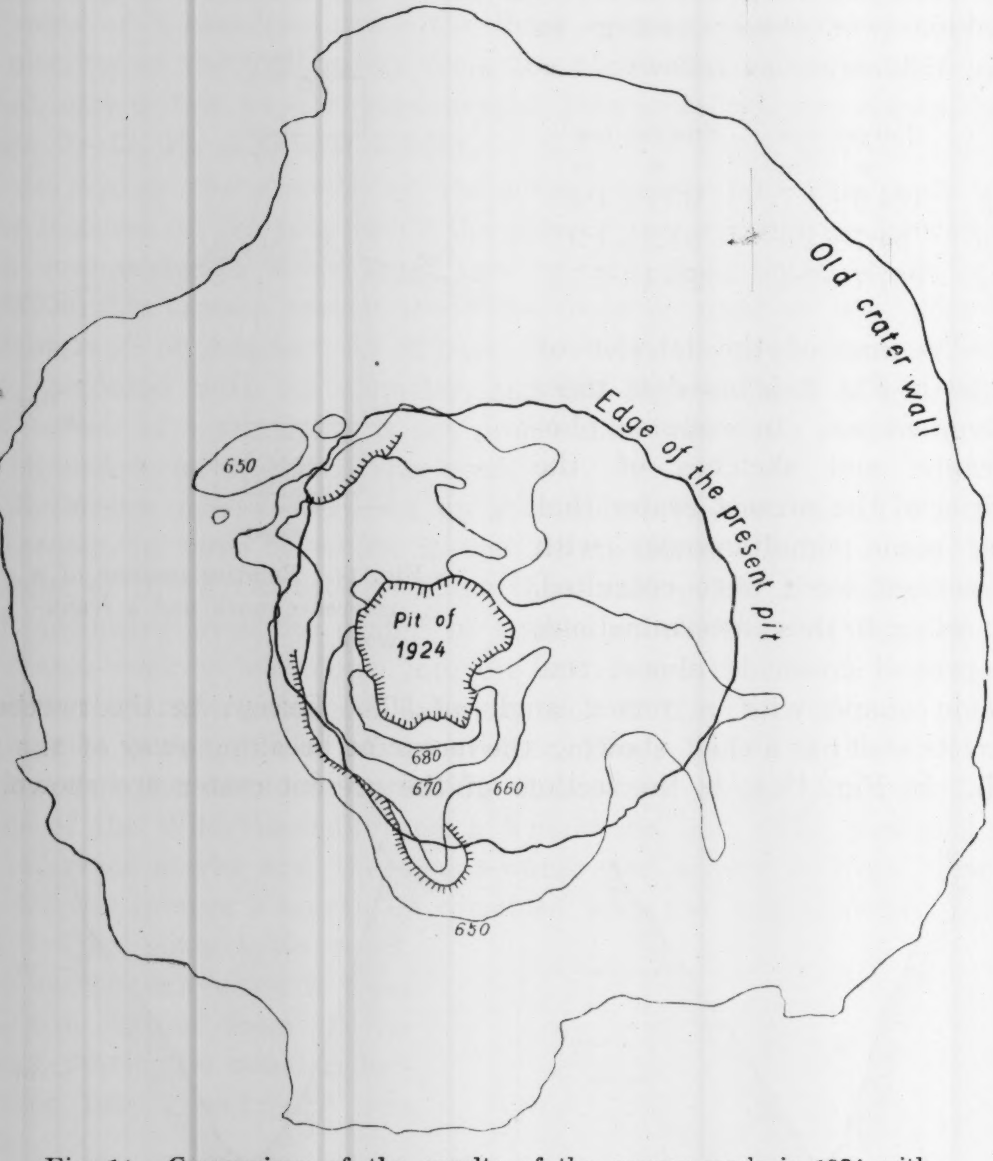
Old crater wall
Edge of the present pit
Pit of 1924
650
680
670
660
650

Fig. 16. Comparison of the results of the survey made in 1924 with those of the presnt one.

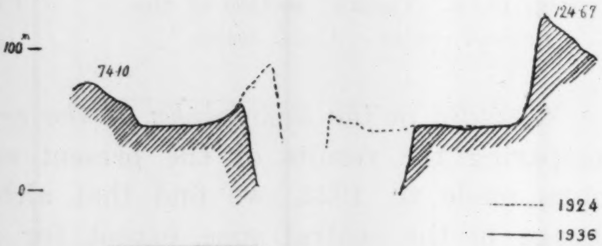
100m
0
74·10
124·67
1924
1936
0
200m

Fig. 17, a. Vertical section of the pit. Unit: meter.

pendicular to the former plane. As will be seen from this figure and Fig. 16, the collapse of the crater wall is much more marked on the east side than on the west.

As to the depth of the present crater, in the absence of any old data, it is not possible to make any observations regarding changes in it. It is reported however that, Mr. Iwata of the Yomiuri Newspaper staff succeeded in 1933 in descending to a depth of 1250 syaku (379 m) from which data it is possible to estimate that the present crater, which was more than 400 m deep at that time, has become shallower by more than 100 m in four years.

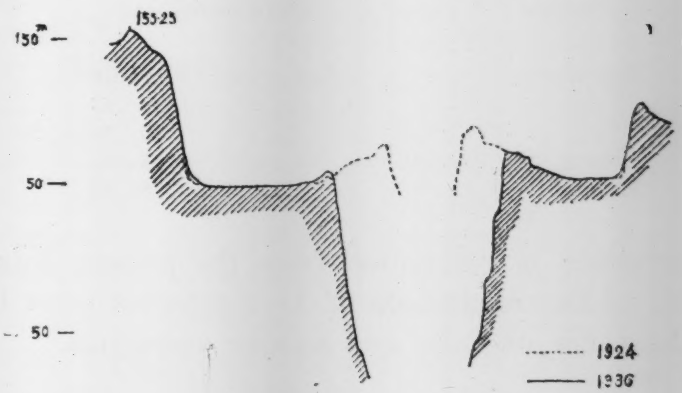

Fig. 17, b. Vertical section of the pit.
Unit: meter.

In conclusion, we wish to express our hearty thanks to the Hattori Hôkôkai, with the aid of whose grant the present surveys were made; and to the Hydrographic Office of the Japanese Navy who kindly placed their magnetometer at our disposal. Our thanks are also due to Professor M. Ishimoto, the director of our Institute, for his interest and encouragements thoughout the present work.

Appendix 1.

From the astronomical observation made for the determination of the true meridian, the latitudes of stations were also calculated. These calculated values of latitude seem to show that there are deviations of the plumb-line of the order of 30″ at all our stations, though the theodolite used was very inadequate for such accurate measurements, the smallest division of its vertical circle being 1′.

Appendix 2.

On Dec. 27, 1936, a strong earthquake occurred in the neighbourhood of Niizima, an volcanic island at 50 km SW of Oosima. In connection with the study of this earthquake, dip measurements were repeated at our stations of Motomura, Nomasi, and Mabusi, with the same instrument. The observed values are shown in Table XIII. Compared with the results of the former observation, no anomalous

Table XIII.

Station	Date and Time		Dip
		h m	° ′
Motomura	Jan. 24.	9 18	50 38·9
,,	,,	9 48	50 37·8
,,	,,	10 10	50 37·9
Nomasi	,,	13 46	47 44·5
Mabusi	,,	15 04	47 05·4

variation is recognized from the present data, because the variation in dip of the magnitude of 1∼2 minutes must be considered to be within the range of daily and secular variations.

LISTS OF MAGNETIC OBSERVATIONS.

Table I. Station, Motomura.

Lat. = 34° 45·′1 Long. = 139° 21·′3 Sept., 1936.

Declination.

Date	Time	δ	Date	Time	δ
	h m	° ′		h m	° ′
9	8 36	5 12·8 W	9	20 45	5 19·3 W
9	8 57	5 18·1	9	23 02	5 17·4
9	11 24	5 20·1	10	1 06	5 17·0
9	13 41	5 20·2	10	3 06	5 18·0
9	15 21	5 18·7	10	4 52	5 16·3
9	17 07	5 17·1	10	7 40	5 14·7
9	19 20	5 17·5	10	9 34	5 17·6

Mean = 5° 17·′5 W

Dip.

Date	Time	θ
	h m	° ′
9	9 46	50 36·2
9	10 00	50 36·8
9	16 08	50 35·3
10	9 48	50 36·3

Mean = 50° 36·′1

Horizontal Intensity.

Date	Time	H
	h m	γ
9	9 28	29435
9	15 49	29457
10	8 11	29435

Mean = 29442 γ

Table II. Station, Nomasi.

Lat. = 34° 34·′ Long. = 139° 21·′4 Sept., 1936.

Declination.

Date	Time	δ
11	$6^{h}\ 56^{m}$	$4^{\circ}\ 26{\cdot}5'$ W
11	8 54	4 27·4

Mean = 4° 27·′0 W

Dip.

Date	Time	θ
11	$9^{h}\ 58^{m}$	$47^{\circ}\ 44{\cdot}6'$

Horizontal Intensity.

Date	Time	H
11	$7^{h}\ 32^{m}$	30125^{γ}
11	9 20	30206
11	9 42	30206

Mean = 30179 γ

Table III. Station, Mabusi.

Lat. = 34° 41·′4 Long. = 139° 23·′1 Sept., 1936.

Declination.

Date	Time	δ	Date	Time	δ
11	$17^{h}\ 44^{m}$	$4^{\circ}\ 44{\cdot}7'$ W	12	$7^{h}\ 52^{m}$	$4^{\circ}\ 42{\cdot}3'$ W
11	20 03	4 45·0	12	10 08	4 46·0
11	22 16	4 44·0	12	12 08	4 48·5
12	0 00	4 43·2	12	13 54	4 47·4
12	2 25	4 42·5	12	16 07	4 45·6
12	4 05	4 42·5	12	18 36	4 44·8
12	5 55	4 41·8			

Mean = 4° 44·′5 W

(*to be continued*)

Table III. (*continued*)

Dip.

Date	Time	θ
	h m	° ′
11	20 39	47 05·5
12	10 50	47 05·4
12	17 13	47 04·2

Mean = 47° 05·′0

Horizontal Intensity.

Date	Time	H
	h m	γ
11	18 36	31200
12	8 30	31162
12	9 20	31164
12	16 42	31189

Mean = 31176 γ

Table IV. Station, Sasikidi.

Lat. = 34° 40·′9 Long. = 139° 24·′8 Sept., 1936.

Declination.

Date	Time	δ
	h m	° ′
13	15 05	6 13·8 W
13	16 59	6 12·3

Mean = 6° 13·′0 W

Dip.

Date	Time	θ
	h m	° ′
13	15 54	47 58·8
13	16 34	47 59·6

Mean = 47° 59·′2

Horizontal Intensity.

Date	Time	H
	h m	γ
13	15 30	30808
13	17 22	30808

Mean = 30808 γ

Table V. Station, Habu.

Lat. = 34° 41′·1 Long. = 139° 25·′4 Sept., 1936.

Declination.

Date	Time	δ	Date	Time	δ
	h m	° ′		h m	° ′
16	22 26	7 26·9 W	17	8 16	7 23·6 W
16	23 33	7 26·9	17	10 07	7 27·6
17	0 15	7 26·6	17	12 13	7 31·6
17	2 00	7 26·4	17	14 08	7 29·7
17	3 59	7 26·4	17	16 28	7 26·9
17	5 50	7 25·7	17	20 05	7 26·8

Mean = 7° 27·′1 W

Dip.

Date	Time	θ
	h m	° ′
17	9 23	48 25·0
17	15 24	48 24·4
17	19 30	48 25·6

Mean = 48° 25·′0

Horizontal Intensity.

Date	Time	θ
	h m	γ
16	23 06	30944
17	8 43	30913
17	15 00	30961
17	19 03	30939

Mean = 30937 γ

Table VI. Station, Zoo.

Lat. = 34° 45·′5 Long. = 139° 26·′2 Sept., 1936.

Declination.

Date	Time	δ
	h m	° ′
18	17 20	5 59·0 W

(to be continued)

Table VI. (*continued*)

Dip.

Date	Time	θ
18	18ʰ 13ᵐ	48° 37′·2

Horizontal Intensity.

Date	Time	H
18	17ʰ 48ᵐ	29787γ

Table VII. Station, Sendu.

Lat.=34° 47·′0 Long.=139° 24·′9 Sept., 1936.

Declination.

Date	Time	δ
19	19ʰ 08ᵐ	4° 53′·0 W
19	19 50	4 53·2
22	23 04	4 52·8

Mean=4° 53·′0 W

Dip.

Date	Time	θ
19	16ʰ 52ᵐ	46° 39′·4
19	21 39	46 40·6
22	23 56	46 40·6

Mean=46° 40·′2

Horizontal Intensity.

Date	Time	H
19	16ʰ 30ᵐ	30753γ
19	20 18	30738
19	20 31	30739
22	23 29	30741

Mean=30743 γ

Table VIII. Station, Rokutôen.

Lat. = 34° 46·′7 Long. = 139° 23·′1 Sept., 1936.

Declination.

Date	Time	δ
23	$17^{\mathrm{h}}\ 38^{\mathrm{m}}$	$5^{\circ}\ 36'{\cdot}5$ W
23	19 38	5 35·2

Mean = 5° 35·′8 W

Dip.

Date	Time	θ
23	$20^{\mathrm{h}}\ 04^{\mathrm{m}}$	$47^{\circ}\ 46'{\cdot}4$
23	23 00	47 47·4

Mean = 47° 46·′9

Horizontal Intensity.

Date	Time	H
23	$18^{\mathrm{h}}\ 14^{\mathrm{m}}$	31469
23	23 31	31452

Mean = 31460 γ

Table IX. Station, Sabaku.

Lat. = 34° 43·′5 Long. = 139° 23·′1 Sept., 1936.

Declination.

Date	Time	δ
24	$21^{\mathrm{h}}\ 54^{\mathrm{m}}$	$1^{\circ}\ 24'{\cdot}8$ W

Dip.

Date	Time	θ
24	$21^{\mathrm{h}}\ 58^{\mathrm{m}}$	$48^{\circ}\ 04'{\cdot}6$

(to be continued)

Table IX. (*continued*)

Horizontal Intensity.

Date	Time	H
24	21h 26m	31236γ

Bearing.

Mark	V.C.	R	V.C.	L
Gosinkatyaya. Flag-pole	330°	23·3′	150°	21·6′
Kagamihata △ (Highest pt.)	345	55·1	165	54·8
Kakotyaya. Sign-post	61	44·1	241	41·8
Mihara shrine. N. edge of roof	94	34·9	274	30·3
Kasso-dai. Flag-pole	163	06·3	343	03·7

Table X. Station A, (Kawadiri).

Sept. 1936.

Bearing.

Mark	V.C.	R	V.C.	L
Gosinkatyaya monument	298°	16·0′	118°	13·8′
Kagamihata △	316	30·8	136	28·0
N. end of somma	27	42.0	202	40·6
Highest pt. of central cone	140	14·2	320	11·0

Magnetic Observation.

Date	Time	Read. of Magnetic Meridian	θ	δ
25	14h 45m	176° 58·0′	51° 15·6′	7° 59′ W

Table XI. Station B, (Tutuisi).

Sept. 1936.

Bearing.

Mark	V.C.	R	V.C.	L
N. end of somma	350°	55·2′	170°	59·8′
Itonasi △	8	26·2	188	24·4
Siroisi △	168	27·4	348	25·4

(*to be continued*)

Table XI. (*continued*)

Magnetic Observation.

Date	Time	Read of Magnetic Meridian	θ	δ
	h m	° ′	° ′	° ′
25	15 42	165 38·0	49 38·4	11 19 W

Table XII. Station C, (Akazawa).

Sept. 1936.

Bearing.

Mark	V.C.	R	V.C.	L
	°	′	°	′
Siroisi △	155	21·8	335	20·0
Hutatune pt.	234	34·8	54	33·4
Kassodai. Flag-pole	347	23·8	167	21·6
Mihara △	358	59·6	178	57·4

Magnetic Observation.

Date	Time	Read. of Magnetic Meridian	θ	δ
	h m	° ′	° ′	° ′
25	16 45	234 14·0	51 25·0	0 13 W

26. 伊豆大島三原火山の地球物理學的研究
火口の地形測量及大島磁氣測定

地震研究所 {高橋龍太郎
永田武

伊豆大島三原火山は我國の活火山の一つであつて，その地質學的，地球物理學的研究は多くの人々によつて行はれて來た．筆者等は三原火山の研究の一部として，先づ火口附近の地形測量，火口底の深度測定等を行ひ，現在迄の火口の變化を知ると同時に，今後の變化の記錄を容易ならしめた．次に大島全島にわたる地磁氣測定を行ひ，この測定を繰返す事により將來火山活動に伴ふ地磁氣の變動を見出さんとするものである．三原火山は淺間火山に比べて，やゝ性質を異にする火山であるから，兩火山の地球物理學的特性の對比は興味深く，その爲に現在，三原山にても火山微動，地電流等の常時觀測が行はれてゐる．

之等の研究は凡て，服部報公會の補助によつて施行されたものであつて，同會に對して深く感謝の意を表す．

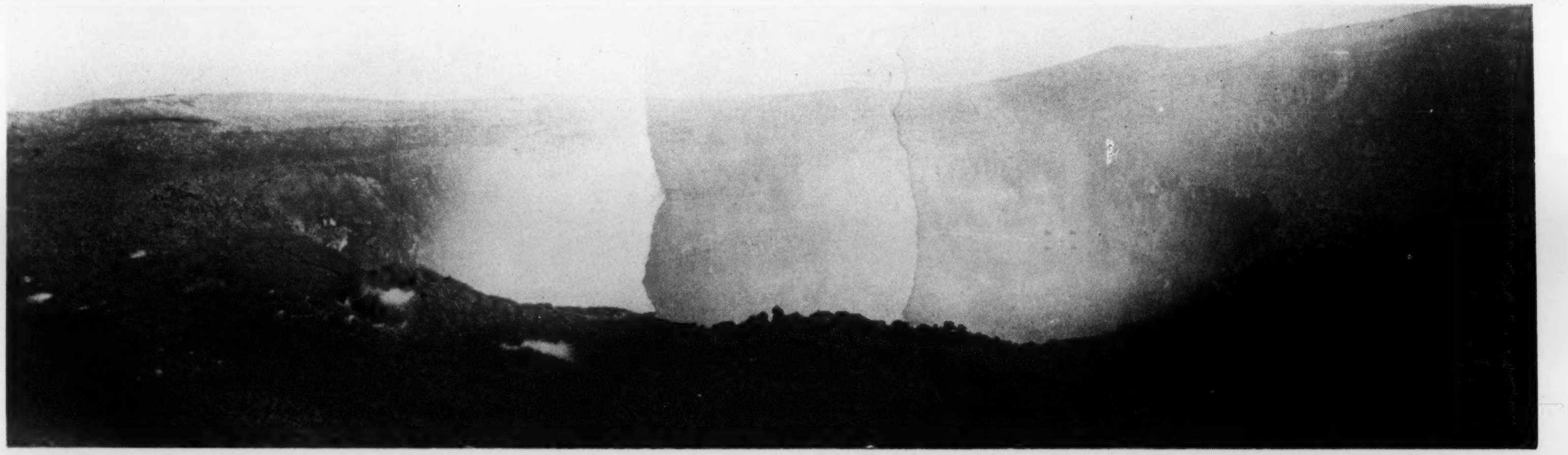

Fig. 9. General View of the Crater as seen from the SSW Ridge of the Old Crater Wall.

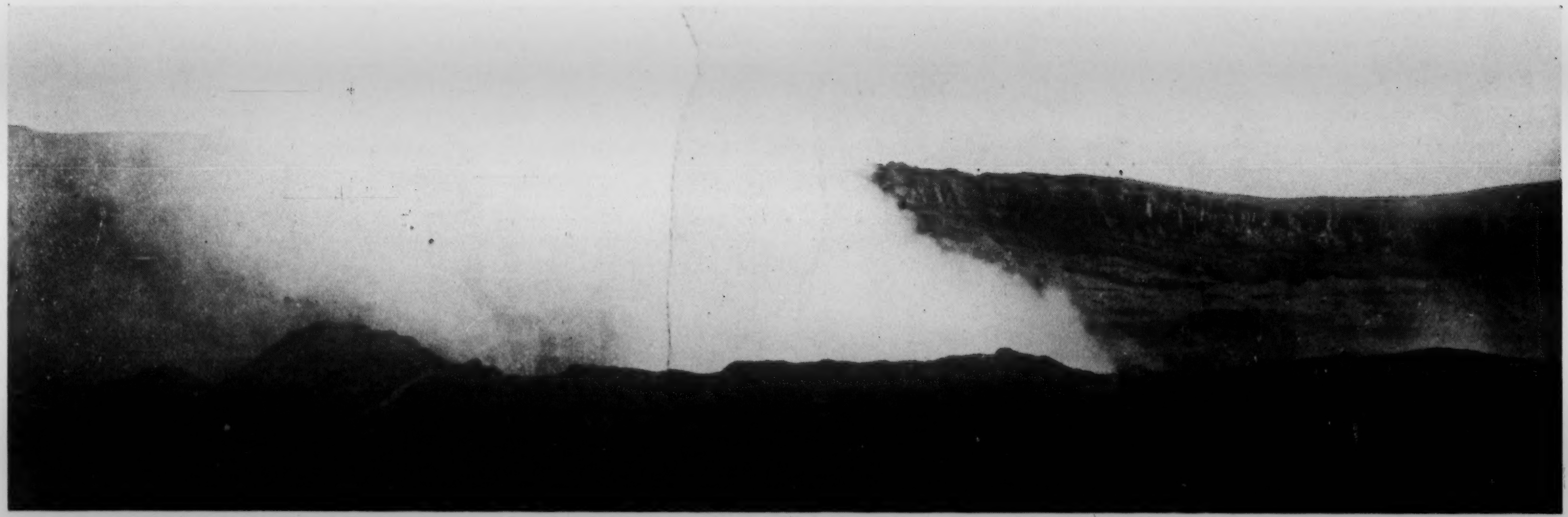

Fig. 10. The same as seen from Kakô-tyaya (crater cottage) on the NW Ridge of the Old Crater Wall.

（震研彙報 第十五號 圖版 高橋・永田）

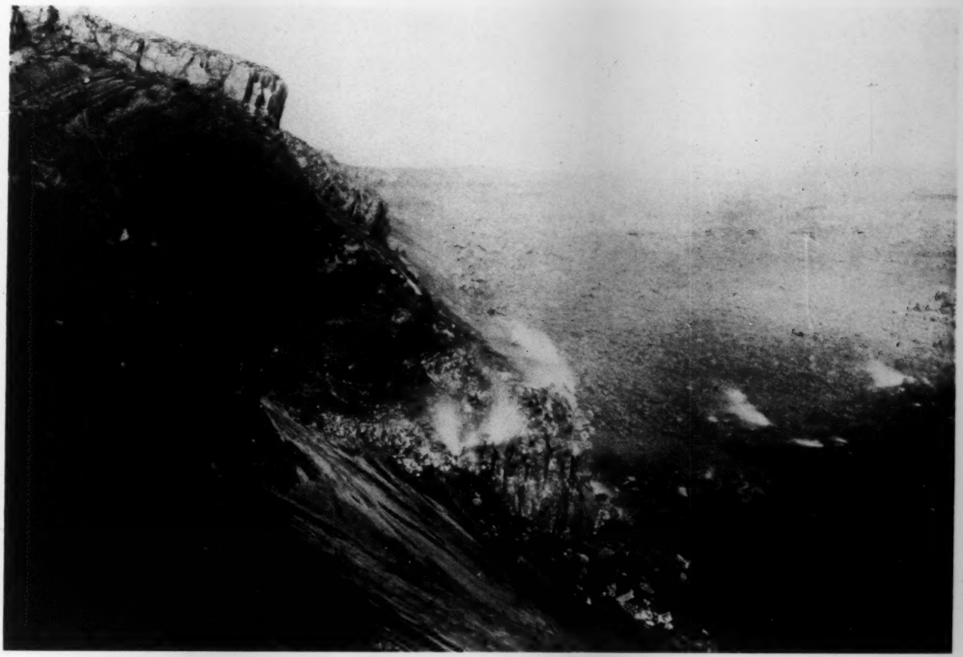

Fig. 11. A Part of the Old Crater Wall.

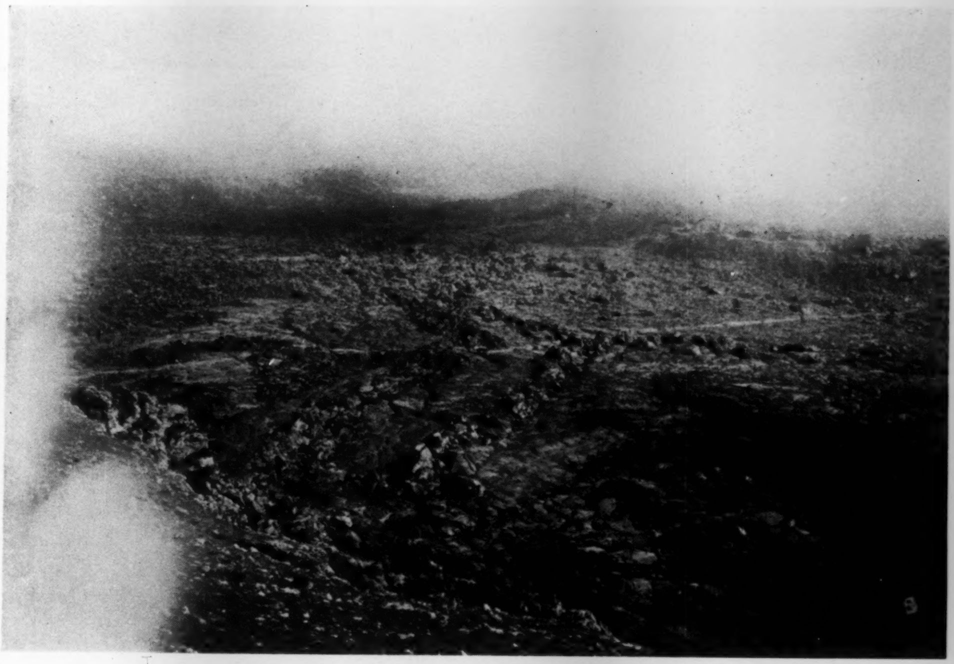

Fig. 12. General Features of the Old Crater Bottom.

Fig. 18, a. Motomura.

Fig. 18, b. Sendu.

Fig. 18, c. Mabusi.

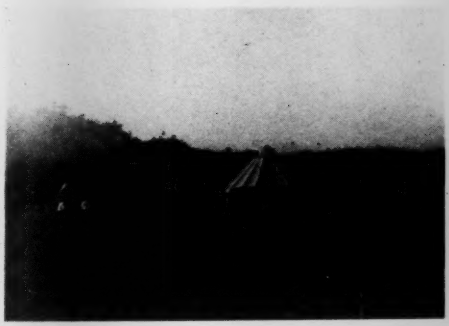
Fig. 18, d. Rokutôen.

Fig. 18, e. Sasikidi.

Fig. 18, f. Sabaku.

Fig. 18. Magnetic survey stations.

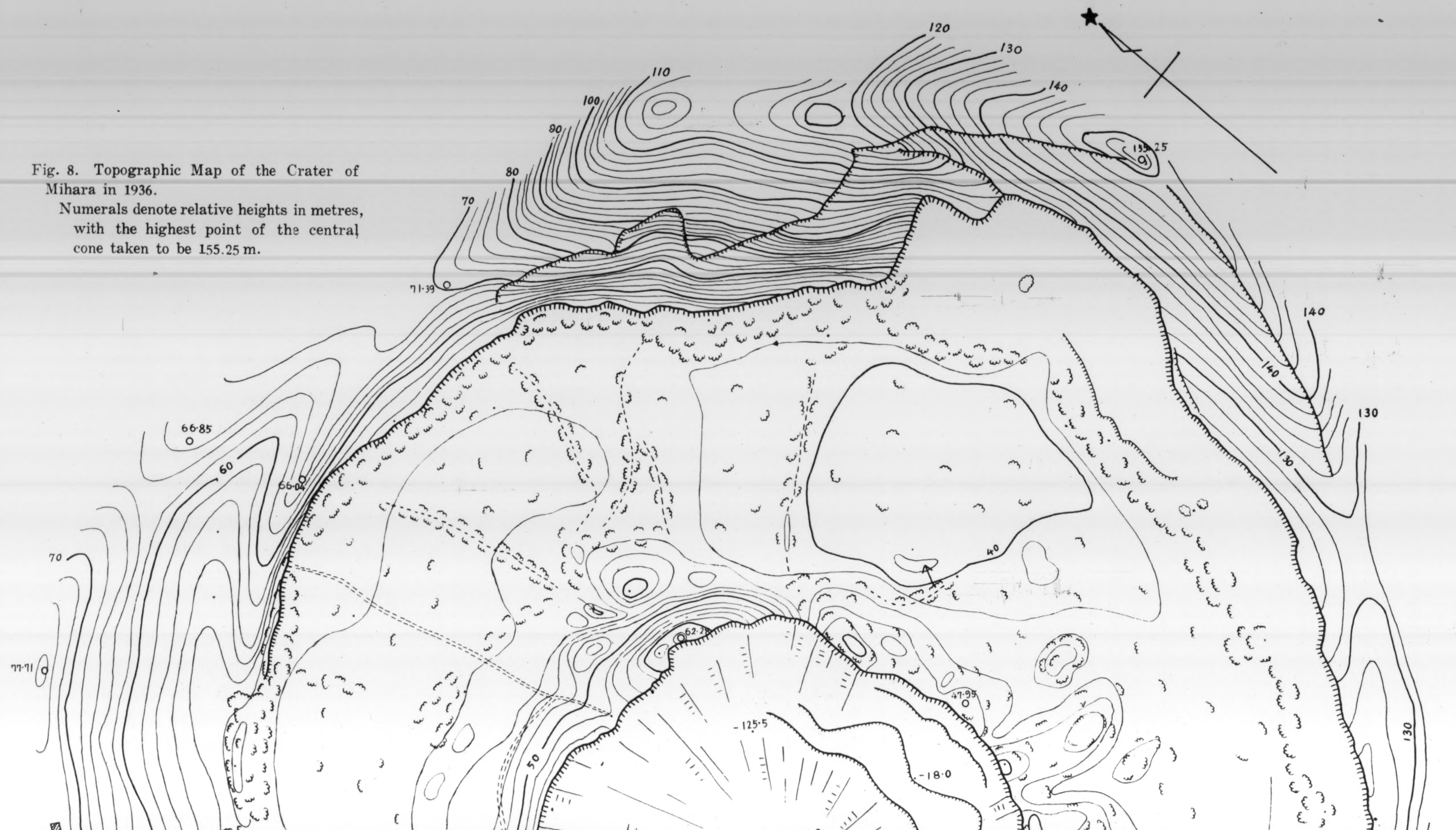
120
130
140
110
100
90
80
70
155.25
71·39
140
140
130
130
66·85
60
66·04
70
77·71
40
62·28
47·95
-125·5
-18·0
50
130

Fig. 8. Topographic Map of the Crater of Mihara in 1936.
Numerals denote relative heights in metres, with the highest point of the central cone taken to be 155.25 m.

（震研彙報 第十五號 圖版 高橋・永田）

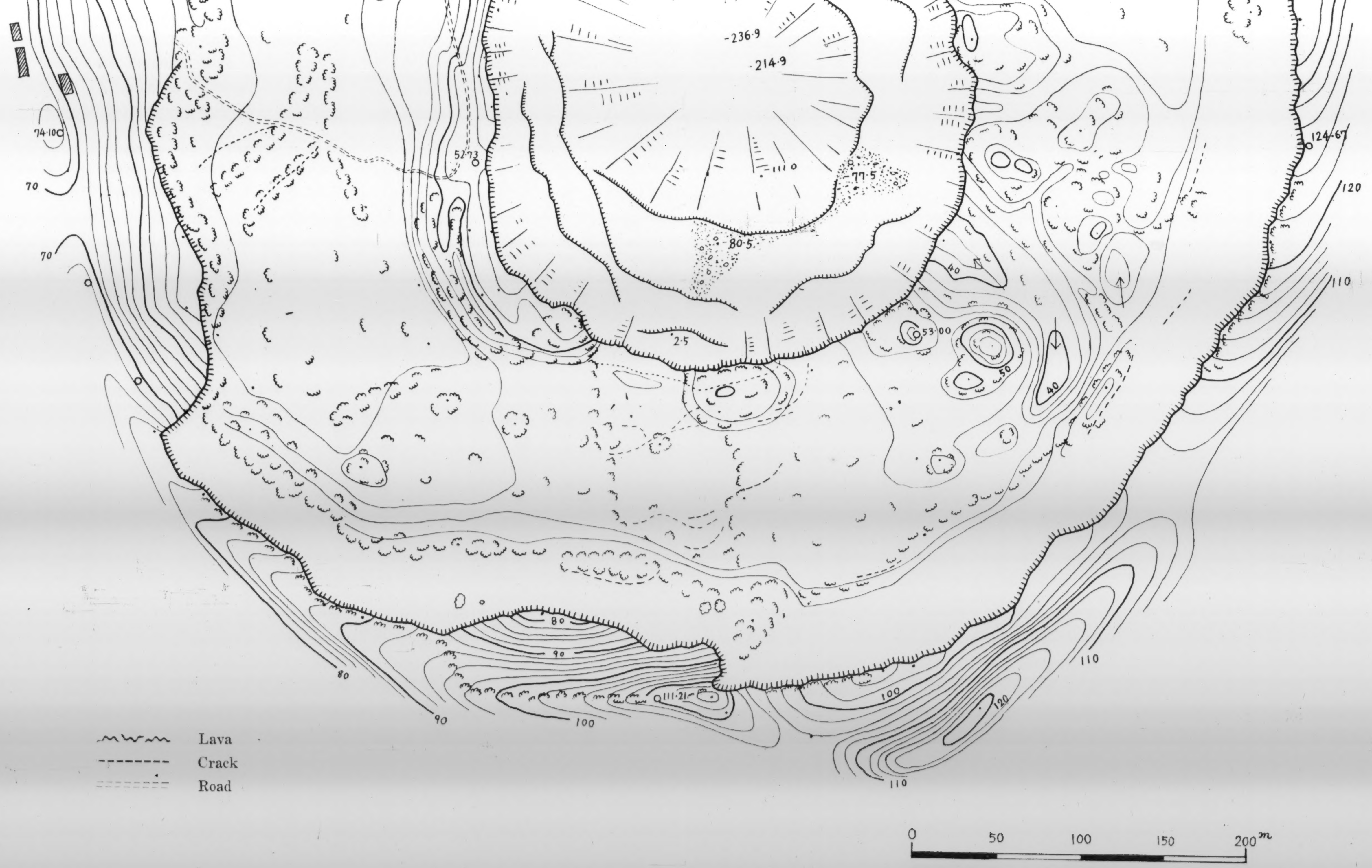
-236·9
-214·9
·111
77·5
80·5
2·5
53·00
50
40
40
124·67
120
110
74·10
70
70
52·73
80
90
100
111·21
80
90
100
110
120
110
Lava
Crack
Road
0
50
100
150
200m

27. *Tilt Observations during the Recent Activities of Volcano Asama.*

By Ryûtarô TAKAHASI and Takeshi MINAKAMI,

Earthquake Research Institute.

(Read May 18, 1937.—Received Mar. 20, 1937.)

1. *Introduction.* It has become evident from tilt observations made at Kilauea[1] and Asama that a volcano eruption is usually preceded by tilts of its flanks. We have already reported in this Bulletin[2] the remarkable tilts of the ground observed in the case of Asama's activities in 1932 and 1935.

After the activities in 1935 had stopped, we established a new tiltmeter station in the "Oni no Osidasi", the lava stream of 1783, the new station being thus 5 km north of the crater. Since then tilt observations have been continued at three stations, namely Komoro, the Asama Volcano Observatory, and Osidasi. Komoro is 12 km SW of the crater, and the Asama Volcano Observatory 4 km E of the crater. At Osidasi and the Volcano Observatory the tiltmeter is installed in a deep cave excavated in the natural rock, which seems most suitable for this sort of observation, particularly as the air temperature in the cave is quite free from annual variations, being below 0°C even in summer.

As to the activities of the volcano. those of 1935, which began in April, ended in November, after which the volcano, which was very quiet until the end of February, 1936, became active again, resulting in a number of explosions of varying severity during July and August of that year. The present report describes these explosions and the tilts of the ground observed at the stations just mentioned during these active periods.

2. *The eruptions in 1936.* In the following table are given the dates and the severity of all the eruptions that occurred in 1936, classified, as in previous reports, into four groups, A, B, C, D, according to magnitude. A denotes a violent explosion with strong detonation and projection of numerous volcanic bombs, small fragmental lavas, and ashes, the earth-shaking and air vibrations being sensible as far as 100 km from the crater. B denotes an explosion with strong detonation, also with projection of volcanic bombs and ashes, but to a smaller degree than A. The earth-shaking and air vibrations are felt up to 50 km of the volcano. C is an explosion, with or without detonation, with projection of small bombs, fragmental material and ashes; the earth-shaking being sensible only to seismographs and there is no air

---

[1] T. A. JAGGAR and R. H. FINCH, *Bull. Seis. Soc. Amer.*, **19** (1929), 38.

[2] R. TAKAHASI, *Bull. Earthq. Res. Inst.*, **11** (1933), 25.
T. MINAKAMI, *ibid.*, **13** (1935), 629.

Table I.

No.	Class	Date	Time of Occurence	No.	Class	Date	Time of Occurence
			h m				h m
1	A	Feb. 7	1 47 p.m.	31	D	July 19	2 40 a.m.
2	D	8	8 15 a.m.	32	D	19	5 40 a.m.
3	D	8	9 37 a.m.	33	D	20	8 05 a.m.
4	D	9	6 55 p.m.	34	D	20	8 15 a.m.
5	C	10	10 03 a.m.	35	C	20	9 40 a.m.
6	D	11	11 54 a.m.	36	C	20	10 10 a.m.
7	D	12	1 44 p.m.	37	D	21	6 40 a.m.
8	C	12	2 p.m.	38	C	21	9 50 a.m.
9	D	13	6 45 p.m.	39	C	22	9 24 p.m.
10	A	15	3 55 p.m.	40	A	23	1 30 a.m.
11	D	16	0 35 p.m.	41	D	23	6 10 a.m.
12	D	17	3 22 p.m.	42	C	24	1 40 p.m.
13	D	22	0 55 p.m.	43	D	25	5 45 a.m.
14	D	Mar. 3	9 22 a.m.	44	D	25	8 05 a.m.
15	B	6	4 10 p.m.	45	D	25	9 25 a.m.
16	A	7	10 30 a.m.	46	D	25	2 44 p.m.
17	C	7	0 41 p.m.	47	D	25	4 42 p.m.
18	D	23	0 15 p.m.	48	D	26	8 20 a.m.
19	C	Apr. 20	1 21 a.m.	49	D	26	9 00 a.m.
20	C	23	8 16 a.m.	50	D	26	4 36 p.m.
21	D	24	11 23 a.m.	51	C	27	1 00 a.m.
22	D	24	1 32 p.m.	52	C	27	5 26 a.m.
23	D	June 23	4 p.m.	53	D	27	10 30 a.m.
24	D	July 1	5 a.m.	54	D	28	0 20 p.m.
25	D	4	4 20 p.m.	55	D	28	2 10 p.m.
26	D	10	7 a.m.	56	B	29	9 12 a.m.
27	D	10	7 30 a.m.	57	D	29	9 29 a.m.
28	D	14	10 a.m.	58	D	29	11 00 a.m.
29	D	15	8 30 a.m.	59	B	Aug. 4	4 18 a.m.
30	D	17	4 30 a.m.	60	D	4	5 23 a.m.

(*to be continued.*)

Table I. (*Continued.*)

No.	Class	Date	Time of Occurence h m	No.	Class	Date	Time of Occurence h m
61	D	Aug. 11	9 55 a.m.	68	D	Oct. 6	7 10 p.m.
62	D	16	5 37 p.m.	69	D	7	3 40 p.m.
63	D	16	5 56 a.m.	70	D	10	5 55 p.m.
64	C	Sept. 19	6 16 p.m.	71	C	15	7 28 a.m.
65	C	20	7 30 p.m.	72	B	17	9 34 a.m.
66	D	21	8 00 a.m.	73	C	Nov. 4	2 20 p.m.
67	C	Oct. 1	10 30 a.m.	74	C	5	4 17 p.m.

vibration. D is a small non-detonating eruption with projection of only volcanic gravels and ashes, with or without volcanic tremors.

3. *Tilt observations.* The readings of the tiltmeter records obtained at the three stations are given in Table II. These readings were taken from continuous photographic records for times corresponding to 0^h, 6^h, 12^h, and 18^h each day. In the table will also be found the air temperature at noon each day as observed at the Volcano Observatory.

Although owing to many difficulties, the observation at Osidasi often had to be dispensed with in the winter months, the general tendency of the tilts could still be known.

Table II. A–a.

E–W Component of Tilting at the Volcano Observatory.

Unit = $0''\cdot05$

The increases in readings indicate tilt of the ground in the sense of E downward.

Date \ Time	0^h	6^h	12^h	18^h	Date \ Time	0^h	6^h	12^h	18^h
Jan. 1	−36·0	−33·0	−30·0	−31·0	Jan. 14	−47·0	−44·0	−31·5	−25·0
2	−36·0	−35·5	−34·0	−34·0	15	−26·0	−31·0	−21·0	−16·0
3	−39·0	−41·5	−42·5	−43·0	16	−15·0	−20·0	− 6·0	+ 7·0
4	−42·0				17	+17·0	+11·0	+21·5	
5	−40·0	−32·5	−28·0	−31·5	18		+45·0	+49·5	+58·0
6	−39·0	−40·0	−40·5	−44·5	19	+62·0	+51·0	+63·0	+69·0
7	−51·0	−55·0	−62·0	−68·0	20	+62·0	+49·0	+51·0	+58·0
8	−78·0				21	+69·0			
9					22				
10					23		+17·0	+23·0	+33·5
11	−30·0	−27·0	−24·5	−22·0	24	+25·0	+ 9·0	+11·5	+21·5
12	−26·0	−36·0	−32·0	−29·0	25	+24·0	+ 7·5	+ 7·0	+ 3·0
13	−37·0	−48·0	−48·0	−47·0	26	− 5·0	−28·0	−46·0	−54·0

(*to be continued.*)

Table II. (*Continued.*)

Date \ Time		0^h	6^h	12^h	18^h	Date \ Time		0^h	6^h	12^h	18^h
Jan.	27	−54·0			−54·0	Mar.	8	+10·5	0	0	+ 1·0
	28	−52·0	−44·0	−26·0	− 8·0		9	− 5·0	−12·0	−19·0	−19·0
	29	− 9·0	−31·0	−40·0	−47·0		10	−22·0	−23·5	−14·0	− 8·0
	30	−54·0	−64·0	−69·0	−62·0		11	− 8·0	−10·0	+ 2·0	+11·0
	31	−56·5	−50·0	−31·0	− 9·0		12	+ 7·0	− 3·0	− 8·0	− 8·0
Feb.	1		+22·5	+26·0	+28·5		13	−17·0	−25·0	−33·0	−42·0
	2	+32·5	+37·5	+47·0	+46·0		14	−49·0	−54·5		
	3	+47·0	+38·0	+42·5	+42·0		15	−14·0	−18·0	−22·5	−26·0
	4	+41·0	+30·0	+30·0	+34·0		16	−27·0	−30·0	−27·0	−22·5
	5	+31·0	+15·0	+ 5·0	+ 4·0		17	−17·0	−24·0	−26·0	−27·0
	6	+ 2·0	− 5·5	− 3·0	+ 1·5		18	−27·0	−29·0	−32·0	−35·0
	7	+ 3·0	− 6·5	− 8·0	− 6·5		19	−36·5	−40·0	−39·0	−35·0
	8	− 5·0	−13·0	−20·5	−24·5		20	−28·0	−32·0	−28·0	−20·0
	9	−28·0	−36·0				21	−25·0	−28·5	−32·0	−34·0
	10		−25·0	−22·0	−18·0		22	−36·0	−39·5	−40·0	−36·0
	11	−22·0	−27·0	−26·0	−19·0		23	−34·0	−41·0	−43·0	−42·0
	12	−22·0	−25·0	−17·5	−13·0		24	−41·5	−46·0	−46·0	−47·0
	13	−14·0	−15·5	− 1·5	+12·0		25	−48·0	−49·0	−51·0	−50·5
	14	+ 4·0	− 4·0	− 1·5	− 1·5		26	−48·5	−49·0	−45·5	−42·0
	15	− 9·0	−20·0	−16·0	−11·0		27	−36·0	−40·0	−37·5	−33·5
	16	−11·0	−20·0	−17·0	−14·0		28	−38·0	−40·5	−44·0	−47·0
	17	−14·0	−26·0	−28·0	−31·0		29	−48·0	−50·0	−51·0	−52·0
	18	−36·0	−42·0	−49·0	−54·5		30	−52·0	−54·0	−55·0	−52·5
	19	−58·0	−63·0	−63·0	−59·0		31	−46·0	−44·0	−35·0	−28·0
	20	−55·0	−62·0	−56·0	−48·0	Apr.	1	−34·0	−37·0	−33·0	−27·0
	21	−45·0	−54·0	−45·0	−36·0		2	−28·0	−36·0	−36·0	−31·5
	22	−30·0	−29·0	−17·5	− 7·0		3	−34·0	−41·0	−43·0	−47·0
	23	−13·5	−18·0	−13·0	−16·0		4	−49·0	−51·5	−54·0	−53·0
	24	−22·0	−31·0	−32·0	−25·5		5	−50·0	−53·0	−47·0	−41·5
	25	−31·5	−38·0	−39·0	−31·5		6	−45·0	−50·5	−52·5	−54·5
	26	−31·5	−29·0	−18·5	−13·0		7	−50·5	−55·0	−57·0	−59·0
	27	−14·0	−23·0	−20·0	−11·0		8	−60·0	−61·0	−63·5	−64·0
	28	−22·0					9	−65·0	−66·0	−67·0	−68·5
	29						10	−69·0	−67·0	−68·0	−69·0
							11	−70·0	−70·0	−70·0	−69·0
							12	−68·0	−69·0	−70·5	−70·0
							13	−70·0	−71·0	−72·0	−72·5
Mar.	6		+10·0	+10·5	+25·0		14	−73·0	−74·0	−75·0	−76·0
	7	+17·0	+ 7·0	+12·0	+17·0		15	−75·0	−75·5	−76·0	−75·0

(*to be continued.*)

Table II. (*Continued.*)

Time / Date	0^h	6^h	12^h	18^h	Time / Date	0^h	6^h	12^h	18^h
Apr. 16	−75·5	−75·5	−76·0	−77·0	May 25		+13·5	+16·0	+18·5
17	−77·5	−78·0	−78·0	−78·0	26	+21·0	+25·0	+30·0	+34·0
18	−77·0	−77·0	−77·5	−78·0	27				
19	−77·0	−77·0	−77·0	−78·0	28	+28·0	+27·0	+27·5	+27·5
20	−78·0	−78·0	−78·0	−77·0	29	+27·5	+29·5	+29·0	+27·5
21	−77·0	−77·0	−76·5	−76·5	30	+31·0	+30·5	+29·0	+27·5
22	−76·0	−76·0	−77·0	−78·0	31	+25·5	+24·5	+24·5	+24·0
23	−78·0	−77·5	−75·5	−79·5	Jnne 1	+22·0	+14·0	+13·0	+10·5
24	−79·0	−78·0	−76·0	−75·5	2	+ 7·5	+ 2·5	− 2·5	− 4·5
25	−76·0	−77·0	−78·5	−79·0	3	− 8·0			
26	−79·0	−80·0	−80·5	−80·0	4				
27	−81·0	−82·0	−82·0	−81·0	5				
28	−80·0	−80·0	−80·0	−80·0	6				−14·0
29	−81·0	−82·0	−83·0	−83·0	7	−13·5	−12·5	−15·0	−16·0
30	−82·5	−83·5	−83·5	−84·0	8	−15·0	−12·5	−11·5	−11·0
May 1	−84·0	−84·0	−85·0	−85·0	9	−10·0	− 8·0	− 7·0	− 6·0
2	−86·0	−86·0	−85·0	−83·5	10	− 5·0	− 4·5	− 4·5	− 4·5
3	−83·0	−83·0	−83·0	−84·0	11	− 4·0	− 5·0	− 8·5	−11·0
4	−83·0	−82·0	−83·0	−83·0	12	−11·0	−10·0	−10·5	− 8·5
5	−82·0	−82·0	−82·5	−82·5	13	− 7·0	− 7·0	− 5·0	
6	−82·0	−81·0	−82·0	−83·0	14			− 4·0	− 3·5
7	−82·0	−82·0	−83·0	−84·0	15	− 3·0	− 2·5	− 2·5	− 2·0
8	−84·0	−86·0	−85·0	−83·0	16	− 2·0	− 1·0	0·0	0·0
9	−82·0	−82·0	−83·0	−83·0	17	+ 0·5	+ 1·0	+ 1·5	+ 2·0
10	−82·0	−81·5	−82·0	−82·5	18	+ 2·0	+ 3·5	+ 4·0	+ 4·0
11	−81·5	−79·0	−79·0	−78·5	19	+ 4·5	+ 4·0	+ 4·0	+ 5·0
12	−77·0	−76·0	−75·0	−72·0	20	+ 6·5	+ 7·5	+ 7·0	+ 7·0
13	−71·0	−70·5	−70·0	−68·5	21	+ 8·0	+ 8·5	+10·0	+11·0
14	−67·0	−67·0	−66·0	−65·0	22	+11·0	+11·5	+12·0	+12·0
15	−64·0	−62·0	−61·0	−60·0	23	+12·0	+13·0	+13·0	+14·0
16	−58·5	−56·5	−55·0	−53·0	24	+14·0	+15·0	+15·5	+15·5
17	−52·0	−50·0	−49·0	−47·0	25	+16·5	+17·0	+18·0	+18·0
18	−44·0	−44·5	−45·0	−43·0	26	+18·0	+18·5	+19·0	+19·5
19	−39·0	−36·0	−33·0	−31·0	27	+20·5	+21·0	+21·0	+21·0
20	−29·0	−26·5	−25·0	−22·0	28	+20·5	+20·5	+21·5	+22·0
21	−19·0	−18·0	−18·0	−16·0	29	+22·0	+22·0	+22·0	+22·0
22	−12·0	−10·0	− 8·0	− 6·0	30	+23·0	+19·0	+19·0	+18·5
23	− 3·0				July 1	+19·0	+18·5	+18·5	+18·5
24					2	+18·0	+18·0	+22·0	+22·0

(*to be continued.*)

Table II. (*Continued.*)

Time Date	0^h	6^h	12^h	18^h	Time Date	0^h	6^h	12^h	18^h
July 3	+22·0	+21·0	+21·0	+21·0	Aug, 11	+80·5	+80·5	+81·0	+83·0
4	+21·0	+21·0	+20·5	+20·0	12	+83·5	+83·5	+85·0	+87·0
5	+20·0	+22·0	+23·0	+24·0	13	+87·0	+88·0	+88·0	+88·5
6	+24·5	+25·5	+24·5	+24·5	14	+89·0	+89·0	+90 0	+89·0
7	+24·5	+25·0	+25·5	+25·5	15	+88·5	+89·0	+89·0	+89·0
8	+25·5	+26·0	+27·0	+28·0	16	+89·5	+91·0	+92·0	+92·0
9	+28·0	+28·0	+28·5	+29·0	17	+92·0	+91·0	+91·0	+91·5
10	+29·0	+29·0	+30·0	+32·0	18	+91·5	+91·0	+90·0	+90·0
11	+32·5	+32·5	+33·5	+35·0	19	+90·0	+90·0	+89·5	+89·0
12	+37·0	+38·0	+38·0	+38·5	20	+89·0	+89·5	+90·0	+90·0
13	+38·5	+38 0	+38·5	+40·0	21	+89·5	+89·0	+89·0	+89·5
14	+41·0	+41·0	+41·5		22	+90·0	+89·5	+90·0	+90·0
15					23	+89·5	+89·0	+89·0	+88·5
16				+52·0	24	+89·0			
17	+52·0	+53·0	+53·0	+53·0	25				
18	+53·0	+52·0	+52·0	+53·0	26				
19	+52·0	+52·0	+52·0	+52·5	27				
20	+52·0	+51·0	+50·5	+50·0	28				
21	+51·0	+51·0	+50·5	+50·5	29	+92·5	+92·5	+92·0	+92·0
22	+51·0	+52·0	+52·0	+51·5	30	+92·0	+92·0	+93·0	+93·0
23	+52·0	+52·0	+52·0	+52·0	31	+93·0	+92·0	+92·0	+93·0
24	+52·0	+51·5	+51·0	+50·0	Sept. 1	+92·0	+92·0	+92·0	+92·0
25	+50·0	+50·5	+52·0	+52·0	2	+92·0	+91·5	+92·0	+92·0
26	+50·0	+51·0	+51·0	+52·0	3	+92·0	+92·0	+92·0	+92·0
27	+52·0	+53·0	+51·0	+53·0	4	+92·0	+91·0	+91·0	+90·5
28	+53·0	+54·0	+55·0	+56·0	5	+91·0	+90·0	+90·0	+90·0
29	+57·0	+57·0	+57·0	+58·0	6	+90·0	+90·5	+91·0	+91·0
30	+58·0	+58·0	+58·0	+59·0	7	+91·0	+90·5	+90·0	
31	+60·0	+60 0	+61·0	+62·0	8			+88·0	+88·0
Aug. 1	+62·0	+63·0	+63·0	+64·0	9	+89·0	+91·0	+90·5	+91·0
2	+59·0	+59·0	+58·0	+60·0	10	+91·5	+91·0	+91·0	+91·0
3	+61·0	+63·0	+64·0	+63·5	11	+91·0	+91·0	+90·5	+91·0
4	+64·5	+65·0	+64·0	+65·0	12	+91·0	+91·0	+90·5	+90·5
5	+66·5	+68·0	+68·0	+68·0	13	+91·0	+91·0	+91·0	+90·0
6	+69·0	+70·5	+71·5	+72·0	14	+90·0	+90·0	+90·0	+90·0
7	+72·5	+72·5	+72·5	+72·5	15	+90·5	+90·5	+90·0	+90·0
8	+73·0	+73.0	+74·5	+75·0	16	+89·5	+89·0	+89·0	+89·0
9	+77·0	+77·0	+77·0	+78·0	17	+89·0	+89·0	+89·0	+88·0
10	+78·0	+78·5	+79·5	+80·0	18	+87·0	+86·5	+86·5	+87·0

(*to be continued.*)

Table II. (*Continued.*)

Time / Date	0h	6h	12h	18h	Time / Date	0h	6h	12h	18h
Sept. 19	+87·0	+86·5	+85·0	+86·0	Oct. 11	+78·0	+78·0	+77·0	+78·0
20	+86·0	+86·0	+85·0	+85·0	12	+78·0	+76·5	+76·0	+76·5
21	+85·0	+85·0	+84·0	+84·0	13	+77·0	+77·0	+77·0	+79·0
22	+84·0	+84·0	+84·0	+84·0	14	+80·5	+81·0	+78·0	+76·5
23	+84·0	+84·0	+84·0	+84·0	15	+76·5	+75·5		
24	+83·5	+82·0	+82·0	+85·0	16				
25	+84·0	+84·0	+84·0	+84·0	17			+77·5	+78·5
26	+83·5	+83·5	+82·5	+82·0	18	+79·0	+79·0	+79·0	+78·0
27	+82·0	+82·0	+82·5	+82·5	19	+76·5	+76·0	+76·0	+76·0
28	+83·0	+83·0	+83·0	+83·5	20	+77·0	+77·5	+77·0	+76·5
29	+83·0	+82·5	+83·0	+83·0	21	+75·0	+76·5	+78·0	+78·5
30	+83·0	+82·0	+82·0	+82·0	22	+78·0	+77·0	+76·5	+77·0
Oct. 1	+81·0	+80·0	+80·0	+80·0	23	+79·0	+84·0	+87·0	+88·0
2	+79·5	+78·5	+78·5	+78·5	24	+87·0	+88·5	+89·0	+85·5
3	+77·0	+77·5	+78·0	+79·0	25	+85·0	+85·0	+84·0	+83·0
4	+79·0	+79·5	+81·0	+82·5	26	+80·0	+78·0	+78·0	+77·0
5	+83·0	+83·0	+81·5	+82·0	27	+76·0	+76·0	+78·0	+77·5
6	+83·0	+82·0	+81·0	+81·0	28	+81·0	+85·0	+85·0	+84·0
7	+81·5	+81·5	+81·0	+82·0	29	+82·0	+81·0	+80·5	+80·5
8	+82·0	+81·0	+79·0	+78·0	30	+79·0	+78·0	+77·5	+78·0
9	+80·0	+79·0	+76·0	+77·0	31	+77·0	+76·0	+76·5	+77·0
10	+78·0	+77·0	+77·0	+77·0					

Table II. A-b.

N-S Component of Tilting at the Volcano Observatory.

Unit=0″·05

The increases in readings indicate tilt of the ground in the sense of S downward.

Time / Date	0h	6h	12h	18h	Time / Date	0h	6h	12h	18h
Jan. 1	−11·0	−10·5	− 6·0	−12·0	Jan. 9				
2	−14·0	− 8·0	− 2·0	− 3·5	10				
3	− 4·5	− 1·0	+ 1·0	+ 1·0	11				
4	+ 1·0	+ 1·0			12			−31·5	−40·5
5		0·0	−14·0	−20·0	13	−52·0	−43·0	−52·5	−61·5
6	−15·0	+ 4·0	−11·0	−22·0	14		−30·0	−45·0	−49·0
7	−30·0	−36·0	−50·0	−54·0	15	−40·0	−10·0	−18·0	−26·0
8	−52·5	−50·0			16	−26·0	−16·0	−28·0	−19·0

(*to be continued.*)

Table II. (*Continued.*)

Time Date	0ʰ	6ʰ	12ʰ	18ʰ	Time Date	0ʰ	6ʰ	12ʰ	18ʰ
Jan. 17	− 8·0	+ 2·5	+ 3·0	+ 8·0	Feb. 25	+ 1·0	− 2·5	− 5·0	− 9·0
18	+17·0	+10·0	+18·0		26	−19·0	−10·0	+ 5·0	+14·0
19			+26·0	+26·0	27	+12·0	+16·0	+16·0	+ 6·0
20	+28·5	+41·5	+42·0	+41·0	28	0·0	+ 5·0	+ 9·0	+ 8·0
21	+33·0	+35·0	+27·0	+29·0	29	− 1·0	−14·0	−13·5	−10·5
22	+37·0	+51·0	+47·0	+39·0	Mar. 1	−20·0	−11·0	− 8·5	+ 7·0
23	+37·0	+48·0	+49·0	+41·0	2	+ 5·0	+15·0	+15·0	+11·0
24	+41·0	+54·0	+54·0	+47·0	3	+ 4·5	+16·0	+17·0	+15·0
25	+44·0	+55·0	+53·5	+56·0	4	+ 2·5	+10·0	+10·0	+ 6·5
26	+57·0	+43·5	+22·0	+11·0	5	+ 1·0	+10·0	− 2·0	+ 7·0
27	+ 4·0	−13·0	− 7·0	− 6·0	6	+12·0	+23·0	+18·0	+17·0
28	+ 3·0	+10·0	+20·0	+31·0	7	+23·0	+26·0	+21·0	+16·0
29	+40·0			+36·0	8	+18·0	+22·0	+22·0	+19·5
30	+23·5	+ 7·5	+ 5·0	+ 9·0	9	+ 9·5	− 3·0	− 9·5	− 9·5
31	+ 8·5	+ 8·0	+34·0		10	−18·0	−13·0	−18·0	− 9·0
Feb. 1		+22·0	+35·0		11	−13·0	− 2·0	+ 2·0	+ 8·0
2		+33·5	+29·0	+35·0	12	+ 6·5	− 2·0	− 4·0	− 8·0
3	+37·0	+47·5	+44·5	+48·0	13	−20·0	−31·0	−45·0	−55·0
4	+45·0	+53·0	+57·0	+61·0	14	−60·5			
5	+55·0	+52·0	+48·0	+44·0	15	0·0	− 7·0	−15·0	−21·5
6	+25·0	+20·5	+22·0	+23·0	16	−23·0	−27·0	−25·5	−23·5
7	+16·0	+18·0	+24·0	+27·0	17	−18·0	−20·0	−20·0	−19·0
8	+18·0	+11·0	+ 6·5	+ 3·0	18				
9	− 2·0				19	−43·0	−51·0	−60·0	−50·0
10		−15·0	−17·0	−12·0	20	−42·0	−33·0	−23·0	−23·0
11	−18·0	−18·0	−15·5	−12·5	21	−21·0	−15·5	−18·0	−22·0
12	−16·0	− 8·0	− 7·0	+10·5	22	−28·0	−34·5	−37·0	−41·0
13	+12·0	+17·0	+11·0	+25·0	23	−46·0	−46·0	−47·0	−47·5
14	+21·0	+27·0	+27·0	+27·0	24	−51·5	−53·0	−58·0	−62·0
15	+21·0	+12·0	+16·5	+15·0	25	−64·0	−70·5	−77·0	−80·0
16	+ 5·5	+11·0	+14·0	+13·0	26	−81·5	−74·0	−73·0	−61·0
17	− 1·0	− 1·5	− 4·5	− 8·0	27	−53·0	−42·0	−34·0	−29·0
18	− 4·0	−10·0	−20·5	−33·5	28	−28·0	−30·0	−34·0	−39·0
19					29	−44·0	−50·5	−57·0	−60·0
20	−13·0	− 1·5	+ 1·5	+11·0	30	−62·0	−66·0	−69·5	−78·0
21	+14·0	+26·0	+38·0		31	−76·0	−69·0	−41·0	−26·0
22		+28·5	+47·0	+62·0	Apr. 1	−16·0	−15·0	−11·0	−10·5
23		+37·0	+37·0	+35·0	2	−10·5	− 8·0	− 7·0	− 6·0
24	+25·0	+15·5	+13·5	+ 7·5	3	− 2·0	−23·5	−33·0	−39·0

(*to be continued.*)

Table II. (*Continued.*)

Time Date	0^h	6^h	12^h	18^h	Time Date	0^h	6^h	12^h	18^h
Apr. 4	−48·0	−54·0	−54·0	−44·0	May 13	−199·0	−197·0	−195·5	−194·0
5	−33·0	−21·0	−27·0	−15·0	14	−194·0	−193·0	−190·0	−190·0
6	−10·0	−11·5	−15·0	−14·0	15	−189·0	−187·0	−186.0	−183·0
7	−19·5	−26·0	−28·0	−32·0	16	−182·0	−181·0	−178·0	−176·5
8	− 37·0	− 41·0	− 41·0	− 45·0	17	−175·0	−173·0	−171·0	−170·0
9	− 48·0	− 54·0	− 58·0	− 62·0	18	−167·0	−163·0	−159·0	−156·0
10	− 67·0	− 69·0	− 68·0	− 71·5	19	−157·0	−156·5	−156·0	−155·0
11	− 77·0	− 78·0	− 83·0	− 89·0	20	−153·0	−152·0	−152·0	−152·0
12	− 94·0	− 86·0	− 84·0	− 86·0	21	−150·0	−145·0	−142·0	−140·0
13	− 88·0	− 89·0	− 91·5	− 92·0	22	−140·0	−140·0	−140·0	−140·0
14	− 92·0	− 92·5	− 92·0	− 95·0	23	−140·0	−139·0	−137·5	−137·0
15	− 97·0	− 96·0	− 97·0	−100·0	24	−137·0	−135·0	−133·5	−132·0
16	−102·0	−103·0	−104·0	−107·0					
17	−106·0	−110·0	−114·0	−115·0					
18	−113·0	−115·0	−116·0	−119·0					
19	−121·5	−122·0	−124·0	−127·0	June 7		− 42·0	− 42·0	− 24·0
20	−131·0	−133·0	−135·0	−139·0	8	− 35·0	− 29·0	− 29·0	− 33·0
21	−142·5	−142·0	−145·0	−148·0	9	− 33·0	− 34·0	− 36·0	− 34·0
22	−149·0	−150·0	−153·0	−157·0	10	− 34·5	− 34·0	− 35·0	− 36·0
23	−159·0	−160·0	−161·0	−160·0	11	− 35·5	− 35·0	− 36·0	− 36·0
24	−159·0	−164·0	−171·0	−174·0	12	− 36·0	− 36·0	− 36·0	− 37·0
25	−173·0	−173·0	−173·0	−173·0	13	− 37·0			
26	−179·0	−179·0	−176·0	−181·0	14		− 29·0	− 27·0	− 28·0
27	−178·0	−177·0	−180·0	−182·0	15	− 28·5	− 28·5	− 28·0	− 28·0
28	−186·0	−189·0	−189·0	−188·0	16	− 27·0	− 27·0	− 26·0	− 26·0
29	−190·0	−188·5	−188·0	−189·0	17	− 26·0	− 25·0	− 25·0	− 24·0
30	−191·0	−191·0	−193·0	−195·0	18	− 24·0	− 23·5	− 22·5	− 21·0
May 1	−198·0	−198·0	−197·0	−199·0	19	− 20·5	− 20·0	− 19·5	− 18·0
2	−197·0	−197·5	−200·0	−204·0	20	− 17·0	− 14·5	− 14·0	− 13·5
3	−206·0	−206·0	−206·0	−206·0	21	− 12·0	− 12·0	− 11·0	− 11·0
4	−207·0	−206·5	−205·5	−206·5	22	− 10·5	− 10·5	− 8·0	− 8·0
5	−208·0	−205·5	−206·0	−207·0	23	− 8·0	− 7·0	− 6·0	− 5·0
6	−211·0	−209·0	−209·0	−210·0	24	− 5·0	− 4·0	− 3·0	− 2·0
7	−224·0	−210·0	−209·0	−207·5	25	+ 1·0	+ 3·0	+ 5·5	+ 5·5
8	−206·5	−215·0	−206·5	−209·0	26	+ 6·0	+ 7·0	+ 8·0	+ 8·5
9	−209·0	−205·5	−204·0	−206·0	27	+ 10·0	+ 11·0	+ 11·5	+ 13·0
10	−206·0	−204·0	−201·0	−202·0	28	+ 15·0	+ 20·0	+ 21·0	+ 23·0
11	−203·0	−203·0	−202·0	−203·0	29	+ 24·0	+ 25·5	+ 25·5	+ 26·0
12	−204·0	−201·0	−198·0	−198·0	30	+ 27·0	+ 28·0	+ 29·5	+ 29·5

(*to be continued.*)

Table II. (*Continued.*)

Time / Date	0^h	6^h	12^h	18^h	Time / Date	0^h	6^h	12^h	18^h
July 1	+ 30·0	+ 30·5	+ 31·0	+ 31·0	Aug. 24	+13·5	+13·0	+12·5	+13·0
2	+ 32·0	+ 32·5	+ 33·5	+ 35·0	25	+14·0	+14·5	+14·0	+14·0
3	+ 38·0	+ 40·0	+ 41·0	+ 40·0	26	+13·0	+13·0	+12·0	+12·0
4	+ 39·0	+ 42·0	+ 42·0	+ 42·0	27	+12·0	+12·0	+12·0	+13·0
5	+42·0	+44·0	+48·0	+49·0	28				
6	+48·0	+51·0	+52·0	+52·0	29		+11·0	+12·0	+11·0
7	+53·0	+54·0	+55·0	+55·0	30	+12·0	+11·0	+10·5	+10·5
8	+57·0	+56·0	+57·0	+56·0	31	+ 9·5	+11·0	+11.0	+12·0
9	+56·0	+57·0	+57·5	+57·5	Sept. 1	+11·0	+11·0	+11·5	+12·0
10	+58·0	+59·0	+61·0	+59·0	2	+12·0	+14·0	+15·0	+15·5
11	+58·0				3	+15·5	+16·0	+17·0	+17·0
					4	+16·0	+15·0	+16·0	+16·0
					5	+15·5	+15·5	+15·0	+15·0
					6	+14·5	+12·0	+12·0	+12·0
30		+35·0	+35·0	+31·0	7	+12·0	+12·0	+11·5	+11·0
31	+32·0	+32·0	+30·5	+30·0	8	+12·0	+10·5	+10·5	+11·0
Aug. 1	+31·5	+31·0	+30·0	+28·0	9	+10·5	+ 9·0	+11·5	+11·5
2	+27·0	+25·0	+23·0	+22·0	10	+12·0	+11·5	+11·0	+10·0
3	+21·0	+23·0	+23·0	+24·0	11	+10·0	+10·0	+ 9·0	+ 8·0
4	+24·5	+24·5	+26·5	+25·0	12	+ 7·5	+ 8·5	+ 8·0	+ 7·5
5	+24·0	+24·0	+24·0	+23·0	13	+ 8·0	+ 8·0	+ 9·0	+ 8·0
6	+23·0	+23·0	+22·0	+21·0	14	+ 7·5	+ 7·0	+ 8·0	+ 8·0
7	+21·0	+20·0	+20·0	+18·0	15	+ 7·5	+ 7·5	+ 7·5	+ 7·0
8	+17·0	+17·0	+16·0	+15·0	16	+ 7·5	+ 8·0	+ 8·0	+ 8·0
9	+17·0	+20·0	+18·0	+17·0	17	+ 8·0	+ 9·0	+ 6·0	+ 5·0
10	+15·0	+16·0	+16·0	+15·5	18	+ 5·0	+ 5·0	+ 6·5	+ 6·0
11	+15·0	+18·0	+18·0	+18·5	19	+ 5·0	+ 4·0	+ 5·0	+ 5·0
12	+17·0	+16·0	+16·0	+16·0	20	+ 7·0	+ 7·0	+ 8·0	+ 7·0
13	+16·0	+17·0	+16·5	+16·5	21	+ 9·0	+ 7·5	+ 7·5	+ 7·0
14	+15·5	+15·5	+15·0	+13·0	22	+ 7·0	+ 9·0	+ 9·0	+10·0
15	+12·5	+13·0	+14·0	+14·0	23	+10·0	+10·0	+10·0	+10·0
16	+11·5	+13·0	+12·0	+11·0	24	+11·0	+10·0	+ 9·5	+ 9·0
17	+10·0	+11·0	+12·0	+12·0	25	+ 9·5	+10·0	+ 9·0	+ 8·5
18	+14·0	+15·0	+15·0	+15·0	26	+ 8·0	+ 8·0	+ 8·0	+ 9·5
19	+14·5	+14·0	+14·0	+14·0	27	+ 9·5	+ 9·5	+10·0	+11·0
20	+14·5	+14·5			28	+12·0	+14·0	+14·0	+13·0
21					29	+12·0	+11·0	+10·0	+10·0
22		+19·0	+18·0	+17·0	30	+ 9·5	+ 9·0	+ 9·0	+ 8·5
23	+17·0	+16·5	+16·0	+15·0	Oct. 1	+10·0	+ 8·0	+ 8·0	+ 7·0

(*to be continued.*)

Table II. (*Continued.*)

Time Date	0^h	6^h	12^h	18^h	Time Date	0^h	6^h	12^h	18^h
Oct. 2	+ 9·0	+ 7·5	+ 7·5	+ 7·0	Oct. 17				
3	+ 8·0	+ 8·0	+ 8·0	+ 9·0	18	+ 8·0	+ 8·0	+ 8·0	+ 8·0
4	+ 9·0	+ 9·0	+ 8·0	+ 6·0	19	+ 8·0	+ 8·0	+10·5	+11·5
5	+ 2·0	+ 6·0	+ 3·5	+ 1·0	20	+15·0	+12·0	+12·0	+11·0
6	0·0	− 0·5	− 0·5	− 1·0	21	+ 8·0	+11·0	+10·0	+ 7·0
7	− 2·0	− 2·5	− 2 5	− 2·0	22	+ 6·0	+ 7·0	+11·0	+12·0
8	− 2·0	− 1·0	0·0	+ 2·0	23	+12·5	+17·0	+16·0	+ 7·0
9	+ 3·0	+ 5·0	+ 5·0	+ 8·0	24	−10·0	− 9·0	−14 0	−15·0
10	+10·0	+10·0	+ 8·5	+ 9·0	25	−13·0	−10·0	− 6·5	− 6·5
11	+ 8·0	+ 7·0	+ 7·0	+ 7·0	26	− 4·5	− 4·0	+ 1·0	+ 5·0
12	+ 7·0	+ 6·0	+ 6·0	+ 8·0	27	+ 8·0	+11·0	+13·0	+14·5
13	+11·0	+ 9·0	+ 7·0		28	+21·0	+24·0	+20·0	+17·0
14					29	+ 5·0	+ 9·0		
15					30				+18·0
16					31	+18·0	+21·0	+22 0	+24·0

Table II. B-a.

E-W Component of Tilting at Oni-no-osidasi.

Unit$=0''\cdot1$

The increases in readings indicate tilt of the ground in the sense of E downward.

Time Date	0^h	6^h	12^h	18^h	Time Date	0^h	6^h	12^h	18^h
Jan. 1					Jan. 16	+ 6·5	+ 6·0	+ 6·0	+ 6·0
2					17	+ 5·5	+ 5·0	+ 5·0	+ 4·0
3					18	+ 3·0	+ 3·0	+ 3·0	+ 3·0
4					19	+ 1·5	+ 2·0	+ 1·0	− 1·5
5				+14·0	20	− 1·0	+ 0·5	+ 1·0	− 1·0
6	+13·0	+ 9·0	+ 4·5	+ 1·0	21	− 3·0	− 2·0	− 2·0	− 1·5
7	+ 1·0	+ 1·5	+ 4·5	+ 5·5	22	− 2·0	− 2·0	− 2 0	− 2·0
8	+ 8·0	+10·0	+10·0	+ 9·5	23	− 1·5	− 2·5	− 3·5	− 5·0
9	+10·0	+ 9·0	+ 9·0	+ 8·5	24	− 7·0	− 8·0	− 9·0	−10·0
10	+ 8·0	+ 7·0	+ 6·0	+6 ·0	25	−10·0	− 4·5	− 4·0	− 4·0
11	+ 9·0	+ 9·0	+ 8·0	+ 7·5	26	− 5·0	0·0	+ 4·0	+ 4·0
12	+ 7·5	+ 8·0	+ 7·0	+ 7·0	27	+ 5·0	+ 8·0	+ 7·0	+ 6·0
13	+ 8·0	+10·5	+12·0	+12·5	28	+ 4·5	+ 3·0	+ 3·0	+ 3·0
14	+10·0	+ 7·0	+ 4·0	+ 4·0	29	+ 4·0	+ 6·5	+10·5	+13·5
15	+ 6·0	+ 7·0	+ 6·0	+ 6·5	30	+15·0	+16·0	+17·0	+18·0

(*to be continued.*)

Table II. (*Continued.*)

Time Date	0^{h}	6^{h}	12^{h}	18^{h}	Time Date	0^{h}	6^{h}	12^{h}	18^{h}
31	+17·5	+16·5	+13·5	+12·0					
Feb. 1	+ 9·0	+ 9·0	+10·0	+10·0					
2									
3					May 29				−36·0
4	+ 5·0	+ 6·0	+ 7·0	+ 7·0	30	−35·0	−34·0	−33·0	−31·5
5	+ 7·0	+ 5·5	+ 5·5	+ 3·0	31	−30·0	−30·0	−29·5	−26·5
6	+ 1·0	+ 2·0	+ 3·0	+ 3·5	June 1	−24·5	−22·0	−21·0	−21·0
7	+ 4·5	+ 8·0	+12·0	+15·5	2	−26·0	−27·0		
8	+18·5	+19·0	+20·0	+21·0					
9	+22·0	+24·5	+26·0	+28·0					
10	+28·0	+28·0	+28·0	+28·0					
11	+28·0				July 13	−19·5	−16·5	−14·0	−14·0
12					14	−14·0	−13·0	−13·5	−15·0
13					15	−15·0	−13·0	−13·0	−13·0
14					16	−13·0	−13·0	−13·0	−13·0
15					17	−15·0	−15·0	−15·0	−15·5
16					18	−15·5	−15·0	−15·0	−15·0
17					19	−15·5	−15·0	−15·0	−16·0
18					20	−16·0	−16·5	−16·5	−16·5
19	+14·0	+15·0	+16·0	+16·0	21	−16·5	−16·5	−17·0	−17·0
20	+16·5	+16·5	+16·0	+16·5	22	−17·0	−17·0	−17·5	−17·0
21	+15·5	+16·0	+15·5	+14·0	23	−17·0	−17·5	−19·0	−19·0
22	+13·0	+11·5	+10·0	+ 8·5	24	−19·0	−18·0	−18·0	−18·0
23	+ 7·5	+ 6·0	+ 6·0	+ 6·0	25	−18·0	−19·0	−19·0	−19·5
24	+ 6·0	+ 6·0	+ 6·0	+ 6·0	26	−19·5	−20·0		
25	+ 6·0	+ 6·5	+ 7·0	+ 7·5	27				
Mar. 2			+ 5·0	+ 7·0	Aug. 2	−17·0	−17·5	−18·0	−17·0
3	+ 7·0	+ 8·0	+ 8·0	+ 7·0	3	−16·0	−16·0	−16·0	−16·0
4	+ 6·0	+ 6·5	+ 8·0	+10·0	4	−16·0	−16·0	−16·0	−15·5
5	+11·0	+12·0	+12·0	+11·0	5	−15·0	−15·0	−15·0	−15·0
6	+11·0	+11·0	+10·5	+11·0	6	−14·5	−14·0	−14·0	−14·0
7	+10·0	+ 9·0	+ 8·0	+ 8·5	7	−14·5	−14·0	−14·5	−15·0
8	+ 9·0	+ 8·5	+ 7·0	+ 5·0	8	−14·0	−14·5	−14·0	−14·0
9	+ 5·0	+ 5·0	+ 5·0	+ 5·0	9	−14·0	−14·0	−14·0	−14·5
10	+ 5·0	+ 5·0	+ 5·0	+ 5·5	10	−14·0	−14·0	−14·0	−14·0
11	+ 6·0	+ 6·5	+ 7·0	+ 8·0	11	−14·0	−13·0	−14·0	−15·0

(*to be continued.*)

Table II. (*Continued.*)

Date \ Time	0^h	6^h	12^h	18^h	Date \ Time	0^h	6^h	12^h	18^h
Aug. 12	−15·0	−15·0	−16·0	−16·0	Sept. 16	+ 1·5	+ 2·0	+ 2·0	+ 3·0
13	−16·0	−15·0	−15·5	−16·0	17	+ 3·0	+ 4·5	+ 6·0	+ 7·0
14	−16·0	−15·0	−15·0	−15·0	18	+ 7·0	+ 7·0	+ 8·0	+ 8·0
15	−14·5	−13·0	−13·0	−12·5	19				+ 7·0
16	−12·0	−11·0	−12·0	−12·5	20	+ 7·0	+ 7·0	+ 8·0	+ 8·0
17	−12·0	−11·0	−11·5	−11·5	21	+ 8·0	+ 8·5	+ 8·0	+ 8·0
18	−11·0	−10·0	− 9·0	− 9·0	22	+ 7·5	+ 6·0	+ 6·0	+ 5·5
19	− 9·0	− 9·5	− 9·0	− 9·0	23	+ 5·0	+ 5·0	+ 5·0	+ 6·0
20	− 8·0	− 8·5	− 9·0	− 9·0	24	+ 6·0	+ 6·0	+ 6·0	+ 6·0
21	− 9·0	− 9·5	− 9·5	− 9·5	25	+ 5·5	+ 6·0	+ 6·0	+ 6·0
22	−10·0	−10·0	−10·0	−10·0	26	+ 6·0	+ 6·5	+ 6·0	+ 6·5
23	−11·0	−12·0	−13·0	−14·0	27	+ 7·0	+ 8·0	+ 7·0	+ 7·0
24	−14·0	−13·5	−14·0	−13·0	28	+ 6·0	+ 6·0	+ 7·0	+11·0
25	−13·0	−13·0	−13·0	−12·5					
26	−12·0	−12·0	−11·0	− 9·0					
27	− 8·5	− 9·0	− 9·0	− 9·0					
28	− 9·0	− 9·5	− 8·0	− 9·0	Oct. 3			+12·5	+13·5
29	− 8·0	− 7·0	− 6·5	− 6·5	4	+13·0	+12·0	+12·0	
30	− 6·0	− 5·0	− 5·0	− 5·5	5				
31	− 5·5	− 5·0	− 5·0	− 4·0	6				
Sept. 1	− 3·0	− 3·0	− 3·0	− 3·0					
2	− 2·0	− 2·0	− 2·5	− 3·0	18				
3	− 3·0	− 3·5	− 3·5	− 4·5	19			+ 7·0	+ 7·0
4	− 5·0	− 5·0	− 5·0	− 5·0	20	+ 7·0	+ 7·0	+ 8·0	+ 8·0
5	− 5·0	− 4·0	− 4·0	− 4·0	21	+ 8·0	+ 8·0	+ 9·0	+ 9·0
6	− 3·0	− 3·0	− 4·0	− 4·5	22	+ 9·0	+ 9·0	+ 9·0	+10·0
7	− 4·0	− 3·5	− 3·5	− 3·0	23	+ 8·0	+ 8·0	+ 8·0	+ 8·0
8	− 3·0	− 2·5	− 2·0	− 1·0	24	+ 7·0	+ 7·0	+ 7·0	
9	− 1·0	− 1·0			25			+ 8·0	+ 8·0
10					26	+ 8·0	+ 8·5	+ 8·5	+ 8·0
11					27	+ 8·0	+ 7·5	+ 7·0	+ 7·5
12			+ 1·0	0·0	28	+ 8·0	+ 8·5	+ 8·0	+ 8·0
13	+ 1·0	+ 1·0	+ 1·0	+ 1·0	29	+ 8·0	+ 7·0	+ 7·0	+ 7·0
14	+ 1·5	+ 2·0	+ 2·5	+ 1·5	30	+ 8·0			
15	0·0	+ 0·5	+ 1·0	+ 0·5	31				

(*to be continued.*)

Table II. B-b.

N-S Component of Tilting at Oni-no-osidasi.

Unit=0″·1

The increases in readings indicate tilt of the ground in the sense of S downward.

Date \ Time		0h	6h	12h	18h	Date \ Time		0h	6h	12h	18h
						Feb.	21	+43·0	+54·0	+56·0	+58·0
							22	+60·0	+60·0	+60·0	+61·0
Jan.	18				+ 9·0		23	+60·0	+59·0	+60·5	+61·0
	19	+10·0	+12·0	+11·0	+ 8·0		24	+61·0	+60·0	+59·0	+59·5
	20	+ 8·0	+ 9·0	+11·0	+10·5		25	+59·0	+58·0	+58·5	+58·5
	21	+13·0	+15·0	+16·0	+15·0		26	+58·5	+58·0	+57·0	+57·0
	22	+15·5	+16·0	+16·0	+15·5		27	+57·0	+59·0	+58·5	+58·5
	23	+19·0	+24·0	+26·5	+26·0		28	+59·0	+59·5	+59·0	+58·0
	24	+27·0	+30·0	+31·5	+3·00		29	+58·0	+58·5	+58·5	+59·0
	25	+30·5	+31·5	+31·0	+27·0	Mar.	1	+60·0	+60·5	+62·0	+62·5
	26	+28·5	+27·5	+26·0	+26·5		2	+63·0	+63·5	+63·5	+60·0
	27	+27·0	+29·0	+31·0	+31·5		3	+58·5	+58·5	+58·5	+57·0
	28	+34·0	+35·0	+33·0	+32·0		4	+56·0	+56·5	+56·5	+57·0
	29	+32·0	+32·0	+30·0	+28·0		5	+55·0	+53·0	+51·0	+50·0
	30	+28·0	+30·0	+31·0	+33·0		6	+51·0	+51·5	+52·0	+52·0
	31	+38·0	+39·5	+36·0	+36·0		7	+53·0	+57·5	+58·5	+58·5
Feb.	1	+37·5	+40·0	+43·0	+45·0		8	+58·0	+58·0	+57·5	+58·5
	2	+48·0	+51·5	+53·0	+53·0		9	+59·0	+58·5	+57·0	+56·5
	3	+53·0	+54·0	+54·0	+53·0		10	+57·0	+57·0	+57·0	+56·5
	4	+53·0	+53·5	+53·5	+53·5		11	+55·0	+54·0	+52·5	+53·0
	5	+52·5	+50·5	+50·0	+49·0		12	+54·0	+55·0	+55·0	+53·5
	6	+50·0	+50·5	+49·0	+49·0		13	+53·5	+53·5	+54·0	+52·5
	7	+51·0	+52·5	+53·0	+52·5		14	+51·0	+47·0	+43·0	
	8	+54·0	+55·0	+55·0	+54·0						
	9	+54·0	+55·0	+54·5	+53·5						
	10	+53·5	+55·0	+56·0	+56·5						
	11	+55·0	+54·0	+55·0	+57·0	July	13	+ 6·0	+ 6·0	+ 6·5	+ 7·0
	12	+57·0	+56·0	+55·0	+55·0		14	+ 7·0	+ 7·0	+ 6·5	+ 6·0
	13	+56·0	+57·0	+56·5	+58·5		15	+ 6·0	+ 6·0	+ 6·0	+ 6·0
	14	+59·5	+60·0	+58·0	+60·0		16	+ 5·5	+ 4·5	+ 4·0	+ 3·0
	15	+60·0	+59·5	+58·5	+58·5		17	+ 2·0	+ 1·0	+ 1·0	+ 1·0
	16	+59·5	+58·5	+60·0	+62·0		18	− 1·5	− 3·0	− 4·0	− 4·0
	17	+62·0	+63·0	+62·0	+63·0		19	− 3·5	− 4·5	− 6·5	− 8·0
	18	+63·0	+60·0	+57·0	+53·0		25	− 9·0	−11·0	−12·0	−12·0
	19	+51·0	+50·0	+50·0	+50·0		21	−11·0	−11·0	−12·0	−13·0
	20	+51·0	+53·0	+54·0	+54·0		22	−13·0	−14·0	−13·0	−13·0

(*to be continued.*)

Table II. (*Continued.*)

Time / Date	0^h	6^h	12^h	18^h	Time / Date	0^h	6^h	12^h	18^h
July 23	−13·0	−13·0	−13·0	−13·0	Sept. 12				
24	−13·0	−13·0	−13·0	−12·0	13				
25	−13·5	−14·0	−13·0	−13·0	14				
26	−14·0	−14·0			15				
					16				
					17				
					18			−3·5	−3·0
Aug. 10	−12·5	−12·0	−13·0	−15·0	19	−3·0	−5·5	−7·0	−8·5
11	−16·0	−16·0	−16·0	−17·0	20	−8·5	−11·0	−11·5	−12·0
12	−20·0	−20·5	−20·0	−23·0	21	−10·0	−9·0	−10·0	−11·5
13	−25·0	−26·0	−25·5	−25·5	22	−13·5	−17·0	−22·5	−25·0
14	−27·0	−25·5	−24·5	−23·0	23	−27·0	−29·0	−27·0	−24·0
15	−21·5	−22·5	−23·5	−23·5	24	−23·0	−23·5	−24·5	−27·0
16	−22·5	−23·0	−26·0	−26·0	25	−28·0	−27·0	−28·0	−29·0
17	−26·0	−27·0	−28·0	−26·0	26	−29·0	−28·5	−29·0	−29·0
18	−26·0	−26·0	−26·5	−23·5	27	−28·0	−26·0	−24·0	−24·0
19	−22·0	−20·0	−20·0	−22·5	28	−25·0	−27·0	−28·0	−28·0
20	−21·0	−21·0	−24·0	−25·0					
21	−25·0	−24·5	−25·0	−27·0					
22	−30·0	−31·0	−31·5	−31·0					
23	−33·0	−34·0	−36·0	−39·0	Oct. 6	+10·0	+10·5	+11·0	+10·5
24					7	+7·5	+7·5	+7·0	+6·5
25					8	+4·5	+3·5	+2·5	+2·0
26					9	+2·5	+3·5	+4·5	+4·0
27					10	+3·5	+3·0	+2·0	0·0
28		−11·0	−11·0	−11·0	11	−1·0	−2·0	−2·0	−1·5
29	−12·5	−14·5	−16·0	−13·0	12	−3·0	−3·0	−1·0	−1·0
30	−12·0	−15·0	−18·0	−18·5	13	−2·0	−2·0	−2·0	−2·5
31	−20·5				14	−2·5	−3·0	−2·5	−0·5
					15	+0·5	+1·5	+2·0	+2·0
					16	+2·0	+2·0	+2·0	+1·0
					17	0·0	+2·0	+4·0	+3·5
Sept. 5			+31·0	+30·0	18	+1·5	−1·0	−0·5	0·0
6	+26·0	+25·0	+25·5	+26·5	19	−1·0	−1·5	0·0	+2·0
7	+24·0	+24·0	+24·5	+24·0	20	+3·0	+5·0	+7·0	+8·5
8	+20·0	+17·0	+17·5	+17·5	21	+10·0	+12·0	+14·0	+14·0
9	+16·0	+12·0	+13·5	+13·0	22	+12·0	+8·0	+9·0	+9·0
10	+11·0	+6·5	+5·0		23	+8·0	+7·0	+7·0	
11					24				

(*to be continued.*)

Table II. C-a.

E-W Component of tilting at Komoro.

Unit = $0''\cdot05$

The increases in readings indicate tilt of the ground in the sense of W downward.

Time / Date	0^h	6^h	16^h	18^h	Time / Date	0^h	6^h	12^h	18^h
Jan. 1	+ 33·0	+ 34·0	+ 35·0	+ 33·5	Mar. 4	+129·5	+130·0	+131·0	+136·0
2	+ 33·0	+ 30·0	+ 27·5	+ 26·5	5	+139·0	+135·0	+137·0	+137·0
3	+ 22·5	+ 19·0	+ 16·5	+ 13·0	6	+139·0	+137·0	+140·0	+149·0
4	+ 10·0	+ 10·5	+ 12·0	+ 13·0	7	+144·5	+143·5	+148·0	+147·0
5	+ 14·5	+ 16·0	+ 20·0	+ 27·5	8	+143·0	+138·0	+138·0	+135·0
6	+ 32·5	+ 37·5	+ 43·0	+ 53·5	9	+130·5	+127·5	+130·5	+127·0
7	+ 60·0	+ 63·5	+ 63·0	+ 67·0	10	+124·0	+124·0	+126·0	+127·0
8	+ 71·5	+ 74·0	+ 73·0	+ 75·0	11	+125·0	+123·0	+124·0	+124·0
9	+ 76·0	+ 76·5	+ 80·0		12	+123·0	+121·5	+120·0	+115·0
					13	+108·5	+104·5	+100·0	+ 96·0
					14	+ 96·0	+ 92·0	+ 88·0	+ 84·0
Feb. 8				+ 34·0	15	+ 80·0	+ 77·0	+ 72·0	+ 67·5
9	+ 28·0	+ 26·0	+ 22·0	+ 17·5	16	+ 67·5	+ 70·0	+ 75·0	+ 78·0
10	+ 13·0	+ 10·0	+ 9·5	+ 9·5	17	+ 78·0	+ 77·0	+ 76·0	+ 70·0
11	+ 9·0	+ 6·0	+ 7·0	+ 10·0	18	+ 67·0	+ 66·0	+ 64·0	+ 63·0
12	+ 11·0	+ 11·0	+ 10·0	+ 11·0	19	+ 68·0	+ 77·0	+ 83·0	+ 85·0
13	+ 11·0	+ 11·0	+ 13·0	+ 15·0	20	+ 88·5	+ 87·5	+ 89·0	+ 89·0
14	+ 14·5	+ 13·0	+ 14·5	+ 15·0	21	+ 87·5	+ 85·0	+ 80·0	+ 76·5
15	+ 15·0	+ 16·0	+ 17·0	+ 18·0	22	+ 75·0	+ 75·0	+ 76·5	+ 75·0
16	+ 19·0	+ 18·0	+ 18·0	+ 16·0	23	+ 68·5	+ 66·5	+ 66·5	+ 66·5
17	+ 16·0	+ 15·0	+ 13·0	+ 10.0	24	+ 66·5	+ 65·0	+ 65·0	+ 62·0
18	+ 5·0	+ 5·0	+ 1·0	+ 1·0	25	+ 61·0	+ 61·5	+ 65·0	+ 69·0
19	+ 1·0	+ 4·0	+ 4·0	+ 4·0	26	+ 78·5	+ 81·0	+ 98·0	+104·5
20	+ 5·0	+ 7·0	+ 7·0	+ 8·0	27	+110·5	+115·0	+108·0	+105·0
21	+ 15·0	+ 17·0	+ 23·5	+ 31.0	28	+ 99·0	+ 90·0	+ 80·0	+ 72·0
22	+ 36·0	+ 35·0	+ 37·5	+ 35·0	29	+ 69·0	+ 66·0	+ 63·0	+ 60·0
23	+ 33·0	+ 31·0	+ 29·0	+ 28·0	30	+ 60·0	+ 61·5	+ 66·5	+ 74·0
24	+ 29·0	+ 30·0	+ 30·0	+ 28·0	31	+ 82·0	+ 87·0	+ 90·0	+ 92·0
25	+ 25·0	+ 24·0	+ 23·0	+ 26·5	Apr. 1	+ 92·0	+ 89·0	+ 87·0	+ 87·0
26	+ 29·5	+ 28·0	+ 25·0	+ 24·5	2	+ 86·0	+ 85·0	+ 82·0	+ 76·0
27	+ 23·0	+ 22·0	+ 21·0	+ 22·0	3	+ 68·5	+ 60·0	+ 52·5	+ 50·0
28	+ 24·0	+ 24·0	+ 30·0	+ 48·0	4	+ 52·0	+ 53·0	+ 55·0	+ 55·5
29	+ 64·0	+ 76·0	+ 85·0	+ 97·0	5	+ 57·0	+ 59·0	+ 59·5	+ 59·0
Mar. 1	+104·0	+107·0	+111·0	+124·0	6	+ 58·5	+ 57·0	+ 56·5	+ 56·5
2	+127·0	+125·0	+126·5	+131·0	7	+ 56·5	+ 53·5	+ 49·5	+ 48·5
3	+130·0	+128·0	+127·0	+128·5	8	+ 48·5	+ 47·0	+ 46·5	+ 46·0

(to be continued.)

Table II. (*Continued.*)

Time / Date	0h	6h	12h	18h	Time / Date	0h	6h	12h	18h
Apr. 9	+ 46·0	+43·0	+41·0	+42·0	May 18	+47·0	+46·5	+45·0	+42·0
10	+ 44·0	+45·5	+45·0	+48·0	19	+42·0	+40·0	+39·5	+41·5
11	+ 49·0	+55·0	+60·0	+60·0	20	+41·0	+40·5	+40·0	+39·0
12	+ 60·0	+60·0	+59·0	+60·0	21	+40·0	+40·0	+38·5	+38·0
13	+61·0	+61·0	+63·0	+69·0	22	+37·5	+37·5	+36·0	+35·0
14	+73·0	+76·5	+78·0	+79·0	23	+34·0	+36·0	+35·0	+35·0
15	+79·0	+80·0	+79·0	+77·0	24	+35·0	+33·0	+31·0	+31·0
16	+74·0	+67·5	+64·0	+60·5	25	+30·0	+28·0	+25·0	+24·0
17	+61·0	+60·0	+59·0	+56·5	26	+23·5	+20·0	+17·5	+18·0
18	+56·0	+54·0	+52·0	+46·0	27	+18·5	+19·0	+21·5	+21·0
19	+42·0	+42·0	+44·0	+46·0	28	+17·0	+13·0	+ 8·0	+ 6·0
20	+48·0	+47·0	+45·0	+43·0	29	+ 3·0	0	− 2·0	− 2·0
21	+42·0	+40·0	+37·0	+37·0	30	+ 1·5	− 3·0	− 3·5	− 2·0
22	+37·0	+38·5	+40·0	+41·0	31	0	− 5·0	−10·0	−13·0
23	+42·0	+44·0	+46·0	+44·0	June 1	−13·0	−15·5	−18·0	−20·0
24	+45·0	+45·0	+44·0	+41·0	2	−20·0	−20·0	−22·5	−20·0
25	+39·0	+38·5	+35·5	+34·0	3	−20·0	−22·0	−19·0	−15·0
26	+31·0	+33·0	+32·0	+32·5	4	−15·0	−15·0	−11·0	− 7·0
27	+33·0	+33·0	+32·5	+33·0	5	− 5·0	− 4·0	− 4·0	− 3·0
28	+35·0	+36·0	+36·5	+37·0	6	− 1·5	− 1·0	0	+ 2·0
29	+39·5	+41·0	+44·0	+45·0	7	+ 2·5	+ 2·0	+ 3·5	+ 5·5
30	+46·0	+48·0			8	+ 6·0	+ 4·0	+ 4·5	+ 6·0
					9	+ 6·0	+ 6·5	+ 6·5	+ 6·5
					10	+ 6·5	+ 6·0	+ 3·0	+ 4·5
May 3			+50·0	+47·5	11	+ 4·5	+ 4·0	+ 2·0	+ 0·5
4	+49·0	+50·0	+48·5	+48·0	12	+ 0·5	0	− 0·5	0
5	+49·0	+49·0	+47·0	+47·5	13	0	0	0	+ 1·5
6	+47·5	+47·0	+45·5	+49·0	14	+ 2·5	+ 3·5	+ 3·0	+ 4·5
7	+49·0	+47·0	+46·0	+44·0	15	+ 6·0	+ 6·0	+ 6·5	+ 7·0
8	+44·0	+44·0	+42·0	+42·0	16	+ 7·5	+ 7·0	+ 6·5	+ 6·5
9	+42·0	+43·0	+41·0	+40·0	17	+ 7·5	+ 8·0	+ 8·0	+ 9·0
10	+40·0	+39·0	+37·0	+37·5	18	+10·0	+11·0	+11·0	+11·0
11	+37·5	+37·5	+35·0	+34·0	19	+11·0	+10·5	+11·5	+13·0
12	+36·0	+37·0	+36·0	+36·0	20	+12·0	+12·0	+11·0	+12·0
13	+37·0	+37·5	+37·0	+38·0	21	+12·0	+10·0	+ 9·0	+ 8·0
14	+39·0	+39·0	+37·0	+38·0	22	+ 7·0	+ 6·5	+ 5·0	+ 5·0
15	+39·0	+39·5	+37·5	+38·0	23	+ 5·0	+ 4·5	+ 2·0	+ 3·0
16	+40·0	+40·0	+39·0	+41·0	24	+ 2·5	+ 2·0	+ 0·5	+ 2·0
17	+46·5	+46·5	+45·0	+45·0	25	+ 2·5	+ 1·5	0	− 1·0

(*to be continued.*)

Table II. (*Continued.*)

Time / Date	0^h	6^h	12^h	18^h	Time / Date	0^h	6^h	12^h	18^h
June 26	−1·0	−2·0	−3·5	−2·5	Aug. 22	+25·0	+25·0	+26·5	+28·0
27	−1·0	+1·5	+2·0	+6·0	23	+30·0	+30·0	+31·0	+34·5
28	+6·0	+6·0	+5·5	+5·5	24	+35·0	+37·0	+40·0	+42·5
					25	+44·0	+43·0	+40·0	+39·0
					26	+37·5	+36·0	+36·0	+36·0
					27	+35·0	+33·0	+35·0	+37·0
July 20	−11·0	−13·5	−14·0	−13·0	28	+36·5	+36·5	+39·0	+41·0
21	−9·0	−7·5	−4·0	−5·0	29	+41·0	+42·0	+42·0	+41·5
22	−4·0	−8·5	−13·5	−16·5	30	+40·0	+40·0	+40·0	+40·0
23	−13·5	−16·0	−18·0	−17·5	31	+41·0	+40·5	+41·0	+41·5
24	−17·0	−15·0	−12·0	−9·0	Sept. 1	+41·5	+40·5	+40·0	+40·0
25	−5·0	−4·5	−5·0	−4·0	2	+32·0	+38·0	+37·0	+33·0
26	−2·0	−1·0	−1·0	+2·0	3	+30·0	+27·0	+23·0	+23·0
27	+6·5	+9·0	+14·0	+16·0	4	+23·5	+23·5	+23·5	+24·0
28	+18·0	+18·0	+17·0	+17·5	5	+24·5	+25·0	+23·5	+25·0
29	+20·0	+20·0	+20·0	+22·0	6	+27·5	+29·0	+28·5	+28·5
30	+23·0	+24·0	+22·5	+24·0	7	+32·0	+33·5	+34·5	+34·0
31	+29·0	+31·5	+32·5	+34·0	8	+37·5	+37·5	+36·0	+36·5
Aug. 1	+36·0	+35·5	+35·0	+36·0	9	+39·0	+38·5	+37·5	+43·0
2	+37·0	+36·0	+37·5	+40·0	10	+44·5	+43·0	+43·0	+45·0
3	+41·0	+40·5	+40·5	+42·0	11	+45·0	+48·5	+52·0	+55·0
4	+44·0	+46·0	+46·5	+45·5	12	+53·0	+52·0	+53·5	+55·5
5	+44·5	+43·0	+43·0	+43·0	13	+56·0	+56·5	+56·5	+58·0
6	+42·5	+42·5	+42·0	+41·5	14	+59·0	+58·5	+58·0	+59·0
7	+41·5	+41·0	+40·0	+40·0	15	+57·0	+54·5	+54·0	+55·0
8	+40·0	+39·5	+39·5	+40·0	16	+54·0	+53·5	+54·0	+58·0
9	+39·0	+38·0	+37·5	+38·0	17	+57·0	+50·0	+51·0	+50·0
10	+37·0	+37·0	+39·0	+40·0	18	+49·0	+43·5	+44·0	+45·5
11	+40·0	+40·0	+39·5	+39·5	19	+45·5	+45·0	+46·0	+48·0
12	+38·0	+36·0	+36·5	+35·5	20	+46·0	+44·0		
13	+35·5	+35·0	+35·0	+35·5	21				
14	+36·0	+35·5	+36·0	+36·0	22				
15	+35·0	+35·0	+35·0	+35·0	23				
16	+35·5	+35·0	+36·0	+38·0	24				+17·0
17	+40·0	+41·0	+39·5	+39·0	25	+11·0	+5·0	+7·0	+9·5
18	+40·0	+38·5	+38·0	+38·0	26	+11·5	+12·5		
19	+33·0	+28·0	+27·0	+29·0	27			+20·0	+14·0
20	+29·0	+27·5	+26·5	+27·0	28	+10·0	+9·0	+9·0	+8·0
21	+26·5	+26·0	+23·5	+24·0	29			+7·0	+6·5

(*to be continued.*)

Table II. (*Continued.*)

Time Date	0^h	6^h	12^h	18^h	Time Date	0^h	6^h	12^h	18^h
Sept. 30	+ 6·5	+ 6·0	+ 5·5	+ 5·0	Dec. 14	−21·0	−21·0	−19·0	−18·0
Oct. 1	+ 4·0	0	− 1·0	0	15	−18·0	−17·5	−13·0	
2	+ 1·0	+ 4·0	+ 7·0	+11·0	16				
					17				− 7·0
					18	−15·0	−16·0	−17·0	−15·0
					19	−17·0	−21·0	−23·5	−24·0
Dec. 2				+ 4·0	20	−24·5	−24·5	−24·0	−23·0
3	+ 3·0	+ 1·0	+ 0·5	+ 3·5	21	−20·0	− 6·0	− 2·0	− 4·5
4	+ 1·0	+ 0·5	+ 1·0	+ 3·0	22	− 5·0	0	− 2·5	− 1·0
5	− 3·0	− 5·5	− 5·5	− 3·5	23	− 3·0	− 6·5	− 6·5	− 6·5
6	0	+ 4·5	+ 0·5	+ 7·0	24	− 8·0	− 8·5	− 8·5	− 6·5
7	+11·0	+11·0	+ 9·0	+11·5	25	− 5·0	− 7·0	− 7·0	− 5·5
8	+10·0	+ 7·5	+ 5·0	+ 6·0	26				
9	+ 6·0	+ 2·0	+ 1·5	+ 5·0	27			−10·0	−15·0
10	+ 7·0	+ 9·0	+ 9·5	+11·0	28	−21·0	−20·0	−21·0	−22·5
11	+12·0	+12·0	+10·0	− 2·0	29	−27·5	−28·0	−28·0	−28·5
12	−13·0	−15·0	−15·5	−15·5	30	−30·0	−31·0	−29·0	−29·0
13	−19·0	−20·0	−21·5	−21·0	31	−29·0	−22·5	−16·5	−15·5

Table II. C-b.

N-S Component of tilting at Komoro.

Unit=0″·05

The increases in readings indicate tilt of the ground in the sense of N downward.

Time Date	0^h	6^h	12^h	18^h	Time Date	0^h	6^h	12^h	18^h
Jan. 1	−24·0	−27·0	−28·0	−29·0	Jan. 13	−25·5	−24·5	−26·5	−26·0
2	−28·5	−29·0	−30·0	−29·0	14	−24·5	−23·5		
3	−27·5	−28·5	−28·5	−27·0					
4	−25·0	−25·5	−28·0	−27·5					
5	−27·0	−28·0	−31·5	−32·0	25			−23·0	−21·5
6	−33·0	−34·0	−33·0	−30·5	26	−20·0	−19·0	−18·0	−16·0
7	−30·5	−33·5	−38·5	−37·5	27	−13·5	−10·0	− 8·5	−10·0
8	−38·0	−41·0	−41·0	−38·0	28	−13·0	−12·5	−13·0	−12·5
9	−36·0	−35·5	−37·0	−35·0	29	−13·0	−12·5	−11·0	− 9·0
10	−34·0	−33·0	−33·5	−33·0	30	− 7·5	− 6·0	− 3·5	− 5·0
11	−32·5	−32·5	−35·0	−32·0	31	− 7·5	− 8·0	− 9·0	−11·0
12	−30·0	−30·0	−30·5	−29·0	Feb. 1	−11·0	−12·0	−15·0	−16·0

(to be continued.)

Table II. (*Continued.*)

Time / Date	0^h	6^h	12^h	18^h	Time / Date	0^h	6^h	12^h	18^h
Feb. 2	−16·5	−18·0	−18·0	−18·0	Mar. 12	+18·5	+21·5	+20·0	+18·5
3	−17·5	−17·5	−17·5	−16·5	13	+15·5	+13·5	+10·0	+11·0
4	−16·5	−18·0	−17·0	−15·0	14	+11·5	+14·0	+17·0	+20·0
5	−15·0	−15·0	−17·0	−16·5	15	+22·0	+23·5	+24·0	+23·5
6	−13·0	−11·0	− 9·0	− 7·5	16	+24·5	+23·0	+20·5	+19·5
7	− 6·5	− 6·5	− 6·5	− 4·0	17	+20·5	+23·0	+23·0	+24·5
8	− 4·0	− 4·5	− 5·0	− 4·0	18	+27·0	+30·0	+30·0	+34·5
9	− 4·0	− 4·0	− 4·0	− 4·0	19	+35·0	+31·5	+25·0	+21·5
10	− 2·0	− 1·5	0	0	20	+21·0	+20·5	+19·5	+21·0
11	0	0	− 1·0	− 2·0	21	+21·5	+24·0	+27·0	+30·0
12	− 3·0	− 2·5	− 3·0	− 5·0	22	+32·0	+34·0	+33·0	+32·0
13	− 5·0	− 5·0	− 6·5	− 7·0	23	+23·5	+32·5	+33·0	+34·5
14	− 6·5	− 6·0	− 6·0	− 5·0	24	+37·0	+37·0	+37·0	+44·0
15	− 5·0	− 2·0	− 3·5	− 3·0	25	+42·0	+43·0	+41·5	+39·0
16	− 1·0	+ 1·0	+ 2·0	+ 3·0	26	+33·5	+33·0	+29·0	+24·5
17	+ 3·5	+ 4·5	+ 6·0	+ 6·0	27	+23·5	+19·5	+19·5	+21·0
18	+ 8·5	+11·5	+10·5	+ 9·0	28	+23·5	+26·0	+26·5	+26·5
19	+13·0	+17·0	+20·0	+21·5	29	+26·5	+26·5	+26·0	+27·5
20	+23·0	+25·0	+27·0	+27·0	30	+29·5	+32·0	+27·0	+22·0
21	+25·5	+22·0	+20·0	+20·0	31	+17·0	+13·5	+12·0	+11·0
22	+18·5	+15·0	+13·0	+13·0	Apr. 1	+10·0	+11·0	+12·0	+12·5
23	+16·0	+17·0	+18·5	+20·5	2	+16·0	+17·5	+17·5	+19·0
24	+21·0	+20·5	+21·0	+22·0	3	+20·0	+19·0	+18·0	+18·0
25	+24.0	+26·0	+25·5	+25·0	4	+20·0	+22·5	+25·0	+25·5
26	+25·0	+27·0	+27·0	+27·5	5	+23·5	+20·5	+16·5	+14·5
27	+27·5	+27·5	+27·0	+27·5	6	+17·0	+20·0	+23·0	+24·0
28	+28·5	+29·5	+30·0	+30·5	7	+25·0	+26·0	+25·5	+26·5
29	+30·5	+30·0	+27·0	+26·0	8	+28·0	+29·0	+29·0	+30·0
Mar. 1	+26·5	+23·0	+20·0	+20·0	9	+31·0	+31·5	+34·0	+37·0
2	+20·0	+19·0	+18·5	+18·5	10	+40·0	+43·0	+45·5	+42·5
3	+20·5	+21·5	+20·0	+22·5	11	+39·5	+36·0	+33·5	+32·0
4	+25·5	+25·0	+23·0	+22·0	12	+32·5	+32·5	+32·5	+33·0
5	+23·0	+22·0	+21·0	+22·0	13	+35·0	+36·0	+36·5	+38·0
6	+24·0	+23·5	+22·0	+18·5	14	+35·5	+30·0	+28·0	+27·5
7	+17·5	+19·0	+18·5	+17·5	15	+27·0	+25·0	+21·0	+20·5
8	+19·0	+20·0	+21·0	+21·5	16	+21·0	+22·0	+23·0	+25·5
9	+22·5	+22·5	+22·0	+23·5	17	+28·5	+30·0	+31·0	+31·5
10	+25·5	+25·0	+23·0	+20·5	18	+32·0	+31·5	+27·5	+25·0
11	+23·5	+23·5	+22·0	+18·5	19	+23·0	+22·0	+23·0	+23·0

(*to be continued.*)

Table II. (*Continued.*)

Time Date	0^h	6^h	12^h	18^h	Time Date	0^h	6^h	12^h	18^h
Apr. 20	+26·0	+26·0	+26·0	+27·0	May 29	−13·0	−13·0	−12·0	−7·0
21	+29·5	+31·0	+30·0	+34·5	30	−3·5	0	+3·5	+7·0
22	+33·0	+31·0	+27·5	+23·5	31	+10·0	+2·0	−11·0	−22·0
23	+20·5	+19·5	+20·0	+20·5	June 1	−27·0	−29·0	−30·0	−28·5
24	+24·5	+30·0	+26·0	+22·5	2	−23·5	−21·0	−19·5	−15·0
25	+20·0	+20·0	+18·5	+15·0	3	−10·0	−7·0	−4·5	+1·5
26	+9·5	+6·0	+5·0	+5·5	4	+3·5	+6·5	+11·0	+15·5
27	+7·0	+10·0	+8·5	+11·0					
28	+14·5	+14·0	+10·5	+10·5					
29	+12·0	+14·0	+18·0	+21·5					
30	+25·5	+28·0	+29·0	+31·5	10				+9·5
May 1	+33·5	+35·0	+35·0	+36·5	11	+9·0	+9·0	+8·5	+10·5
2	+40·5	+42·5	+37·0	+34·0	12	+12·5	+12·0	+10·0	+11·0
3	+33·0	+33·0	+32·5	+34·0	13	+13·0	+11·0	+8·5	+9·0
4	+35·5	+36·5	+36·5	+38·5	14	+12·5	+14·5	+14·0	+15·0
5	+39·5	+39·5	+37·5	+39·5	15	+16·5	+17·5	+18·0	+19·5
6	+41·0	+41·0	+40·5	+40·5	16	+20·5	+21·0	+21·0	+22·0
7	+39·5	+37·5	+35·0	+33·5	17	+24·5	+24·5	+24·0	+27·5
8	+35·0	+34·0	+33·5	+33·0	18	+29·0	+30·0	+29·0	+30·5
9	+35·0	+32·5	+34·0	+35·0	19	+31·5	+30·0	+30·5	+31·5
10	+36·5	+33·5	+32·5	+33·0	20	+31·0	+31·0	+32·0	+33·0
11	+33·5	+32·0	+32·0	+34·0	21	+34·0	+34·0	+33·5	+33·5
12	+36·0	+35·5	+37·0	+39·5	22	+32·5	+30·0	+28·5	+30·0
13	+41·5	+41·0	+42·0	+45·0	23	+30·0	+28·0	+24·5	+24·5
14	+46·0	+45·5	+45·0	+45·0	24	+25·0	+24·0	+20·0	+20·0
15	+45·5	+45·5	+46·0	+49·5	25	+20·5	+21·0	+18·5	+18·5
16	+51·5	+51·5	+51·5	+53·0	26	+19·0	+18·5	+16·5	+17·0
17	+54·0	+54·0	+54·0	+57·0	27	+18·5	+19·0	+17·0	+17·0
18	+56·5	+54·5	+54·5	+55·5	28	+19·0	+18·0	+16·0	+12·0
19	+55·5	+55·5	+55·5	+54·0					
20	+53·0	+51·5	+52·0	+55·0					
21	+58·0	+59·0	+60·0	+61·0					
22	+61·0	+58·5	+59·0	+59·0	July 12				−18·0
23	+58·5	+57·0	+54·0	+52·5	13	−4·0	+5·5	+1·0	−9·0
24	+48·5	+45·5	+42·5	+36·5	14	−15·0	−23·0	−25·5	−24·5
25	+31·0	+26·5	+25·5	+25·0	15	−16·5	−13·5	−12·0	−10·0
26	+25·0	+25·0	+25·0	+25·5	16	−5·0	−5·0	−4·5	−2·0
27	+26·0	+26·5	+26·5	+23·0	17	+3·5	+10·0	+9·5	+17·0
28	+15·0	+3·0	−6·0	−10·0	18	+19·0	+17·5	+18·5	+16·5

(*to be continued.*)

Table II. (*Continued.*)

Time / Date		0^h	6^h	12^h	18^h	Time / Date		0^h	6^h	12^h	18^h
July	19	+ 16·5	+ 17·0	+ 18·0	+ 19·5	Aug.	27	+103·5	+103·0	+100·0	+ 99·0
	20	+ 23·0	+ 27·5	+ 27·5	+ 27·5		28	+100·0	+100·5	+101·0	+103·0
	21	+ 32·0	+ 33·5	+ 36·0	+ 41·0		29	+105·0	+106·5	+106·5	+109·5
	22	+ 48·5	+ 43·0	+ 38·5	+ 40·5		30	+111·5	+112·5	+110·5	+114·0
	23	+ 41·0	+ 36·5	+ 37·5	+ 38·5		31	+115·5	+115·0	+111·5	+111·0
	24	+ 37·5	+ 36·0	+ 37·5	+ 45·0	Sept.	1	+112·0	+111·0	+107·5	+107·0
	25	+ 53·0	+ 58·5	+ 60·0	+ 64·5		2	+ 92·0	+ 65·0	+ 52·0	+ 47·0
	26	+ 73·0	+ 76·5	+ 78·5	+ 83·0		3	+ 46·0	+ 47·0	+ 48·0	+ 53·0
	27	+ 82·0	+ 81·0	+ 80·0	+ 81·0		4	+ 60·0	+ 63·5	+ 65·0	+ 70·0
	28	+ 81·5	+ 81·0	+ 79·0	+ 81·0		5	+ 74·0	+ 76·0	+ 76·0	+ 79·0
	29	+ 83·0	+ 83·0	+ 82·5	+ 85·0		6	+ 80·0	+ 81·0	+ 79·5	+ 82·0
	30	+ 91·5	+ 94·0	+ 94·0	+ 96·0		7	+ 84·5	+ 87·5	+ 88·0	+ 87·5
	31	+102·0	+103·5	+102·5	+105·0		8	+ 88·0	+ 88·5	+ 87·5	+ 87·5
Aug.	1	+108·5	+109·0	+106·5	+107·0		9	+ 90·0	+ 92·5	+ 93·5	+ 94·0
	2	+108·5	+110·5	+111·0	+113·0		10	+ 96·0	+ 98·0	+ 97·0	+ 95·0
	3	+114·5	+115·5	+116·5	+117·5		11	+ 96·0	+ 98·0	+ 98·0	+ 99·0
	4	+117·0	+115·5	+114·5	+116·0		12	+101·0	+103·0	+103·0	+101·0
	5	+116·0	+114·5	+113·5	+111·5		13	+101·5	+103·0	+103·0	+104·0
	6	+111·5	+112·0	+110·0	+107·5		14	+106·0	+103·5	+102·5	+103·0
	7	+107·5	+106·5	+103·5	+102·0		15	+101·5	+ 99·0	+ 98·0	+ 99·0
	8	+100·5	+100·5	+ 99·5	+ 98·5		16	+ 99·0	+ 98·0	+ 97·0	+ 95·0
	9	+100·5	+101·0	+ 99·0	+ 95·0		17	+ 99·5	+ 98·5	+ 99·0	+ 99·5
	10	+ 96·0	+ 97·0	+ 97·0	+ 97·0		18	+ 98·0	+ 95·5	+ 94·5	+ 95·5
	11	+ 96·0	+ 95·0	+ 93·0	+ 89·5		19	+ 95·5	+ 96·5	+ 97·5	+100·5
	12	+ 88·5	+ 89·5	+ 88·0	+ 85·5		20	+100·5	+ 99·5	+ 98·5	+100·0
	13	+ 87·5	+ 89·0	+ 88·5	+ 87·5		21	+100·0	+ 98·5	+ 98·0	+ 96·0
	14	+ 91·0	+ 92·0	+ 93·0	+ 93·5		22	+ 92·0	+ 90·0	+ 89·0	+ 89·0
	15	+ 96·5	+ 97·0	+ 97·0	+ 95·0		23	+ 91·5	+ 93·5	+ 94·5	+ 95·5
	16	+ 96·0	+ 96·5	+ 96·5	+ 94·0		24	+ 90·0	+ 80·0	+ 80·0	+ 83·0
	17	+ 92·0	+ 89·0	+ 87·0	+ 87·0		25	+ 82·5	+ 68·0	+ 59·0	+ 63·0
	18	+ 88·5	+ 89·0	+ 89·5	+ 89·5		26	+ 65·0	+ 49·0	+ 52·0	+ 58·5
	19	+ 90·0	+ 90·0	+ 89·0	+ 99·0		27	+ 59·5	+ 60·0	+ 55·0	+ 47·5
	20	+ 93·0	+ 93·0	+ 86·0	+ 81·0		28	+ 40·5	+ 35·0	+ 33·0	+ 34·0
	21	+ 78·0	+ 75·5	+ 69·0	+ 69·0		29	+ 36·5	+ 40·0	+ 45·0	+ 49·5
	22	+ 76·0	+ 78·5	+ 77·5	+ 83·0		30	+ 52·5	+ 53·0	+ 52·0	+ 52·5
	23	+ 88·0	+ 89·0	+ 92·0	+ 96·5	Oct.	1	+ 54·5	+ 54·5	+ 53·5	+ 53·0
	24	+ 99·0	+ 89·0	+ 99·5	+102·0		2	+ 55·5	+ 60·0	+ 62·5	+ 62·5
	25	+104·0	+104·5	+102·0	+103·5		3	+ 63·5	+ 63·0	+ 59·0	+ 50·0
	26	+103·5	+103·0	+101·5	+102·0		4	+ 31·0	+ 18·0	+ 13·5	+ 17·0

(*to be continued.*)

Table II. (*Continued.*)

Time Date	0^h	6^h	12^h	18^h	Time Date	0^h	6^h	12^h	18^h
Oct. 5	+17·5	+ 8·0	+ 0·5	+ 2·5	Nov. 25	−53·0	−54·5	−55·5	−53·5
6	− 5·0	−24·0	−20·0	− 7·0	26	−57·0	−68·0	−85·0	−78·5
7	+ 1·0	− 4·0	0	+ 8·0	27	−71·5	−67·5	−62·5	−55·5
8	+12·0	+ 2·0	− 6·0	+ 1·0	28	−47·5	−38·5	−30·0	−24·0
9	− 4·0	−22·0	−29·0	−21·0	29	−20·0	−17·5	−20·0	−25·0
10	−11·0	− 5·0	0	+ 8·0	30	−25·0	−27·5	−33·0	−38·5
11	+15·0	+18·0	+21·0	+23·5	Dec. 1	−31·5	−28·0	−26·0	
12	+22·5	+18·0	+17·5	+21·5	2				− 2·5
13	+25·5	+29·5	+33·0	+36·0	3	− 7·0	− 8·5	− 7·5	− 4·5
14	+39·5	+41·5	+42·5	+45·0	4	− 2·0	− 1·0	+ 2·5	+ 3·5
15	+48·0	+37·5	+22·0	+21·0	5	+ 5·0	+ 2·0	+ 2·0	+ 3·0
16	− 3·0	−17 0	−17·0	−12·0	6	+13·0	+ 8·5	+ 7·0	+16·0
17	+ 2·0	+15·0	+24·0	+33·5	7	+24·0	+11·0	+12·5	+11·5
18	+42·0	+48·0			8	+ 9·0	+ 6·5	+ 5·5	+ 4·5
					9	+ 3·0	+ 3·5	+ 5·0	+ 4·5
					10	+ 4·0	+ 5·0	+ 4·5	+ 0·5
					11	+10·0	+15·0	+ 9·0	− 6·5
Nov. 5			− 7·0	− 2·0	12	−11·0	−16·0	−21·5	−22·5
6	− 4·0	−13·0	−17·0	−12·5	13	−26·0	−29·0	−33·5	−35·0
7	−15·0	−15·5	−11·0	− 5·0	14	−37·5	−39·0	−35 5	−33·5
8	0	+ 4·0	+ 9 0	+17·0	15	−29·5	−21·5	−15·0	−13·5
9	+ 4·0	−31·0	−41·0	−32·5	16	−13·0	−11·0	+ 2·0	+13·0
10	−38·0	−49·0	−54·0	−53·5	17	+16·0	+16·0	+ 7·5	− 3·5
11	−53·5	−53·5	−45·0	−35·0	18	− 8·0	−13·0	−17·0	−19 0
12	−30·0	−26·0	−17·5	− 7·0	19	−21·5	−27·0	−32·0	−34·5
13	−21·0	−44·0	−50·5	−42·5	20	−41·0	−39·0	−36·0	−34·5
14	−34·0	−36·0	−33·5	−24·0	21	−24·5	−10·0	− 3·0	+ 1·0
15	−16·5	−12·5	−10·0	− 3·5	22	+ 5·0	+11·5	+13·5	+19·5
16	+ 2·0	+ 6·0	+ 8·5	+13·0	23	+20·5	+14·5	+13·5	+16·5
17	+15·5	+15·5	+11·0	+13·5	24	+12·0	+ 9·0	+10·0	+11·0
18	+13·5	+ 7·0	+ 1·0	+ 4·0	25	+12·0	+ 9·5	+ 8·5	+10·0
19	+ 8·0	+ 9·0	+10·5	+14·0	26	+ 5·5	+ 4·5	+ 8·5	+15·5
20	+12·5	+ 9·0	+ 5·0	+ 1·0	27	+15·0	+ 9·5	+10·0	+10·0
21	0	− 2·0	− 4·5	− 3·5	82	+ 7·5	+ 4·5	+ 4·5	+ 2·0
22	− 3·5	− 3·5	− 9·5	−10·5	29	− 1·0	− 1·5	− 2·5	− 2·5
23	−11·5	−16·5	−23·0	−28·0	30	− 2·5	− 4·0	− 3·5	− 4 5
24	−37·5	−53·5	−67·0	−59 0	31	− 5·5	+ 5·5	+ 4·0	+ 4·5

(*to be continued.*)

Table III.

Air temperature at noon. (Asama Volcano Observatory)

Date	1936											
	Jan.	Feb.	Mar.	Apr.	May	June	July	Aug.	Sept.	Oct.	Nov.	Dec.
	°C	°C	°C	°C	°C	°C	°C	°C	°C	°C	°C	°C
1	+ 0·5	− 5·5	− 3·0	+ 1·4	+11·5	+14·0	+17·4	+27·0	+22.0	—	+ 9·0	—
2	− 1·3	− 6·5	− 3·2	+ 2·0	+11·0	+17·0	+14·5	+23·8	+24·2	+13·0	+ 5·8	+ 6·8
3	+ 2·0	− 4·7	− 2·0	+ 0·8	+13·0	+16·0	+18·5	+20·6	+23·5	+14·0	+ 7·8	+ 3·2
4	− 1·0	− 7·5	− 3·0	+ 3·6	+14·8	+13·0	+18·8	+22·5	+23·0	+14·0	+10·8	—
5	− 1·0	− 5·0	− 3·4	+ 2·0	+15·0	+16·5	+17·2	+22·8	+23·5	+14·5	+ 9·5	− 1·2
6	− 3·0	− 5·5	− 2·5	+ 6·5	+17·0	+15·0	+13·5	+23·3	+25·0	+14·5	+ 6·8	− 1·0
7	− 4·0	− 4·1	− 0·3	+ 9·5	+12·0	+14·5	+13·5	+25·5	+25·0	+13·0	+ 5·1	− 2·3
8	− 3·0	− 5·1	− 4·5	+ 8·7	+10·5	+15·5	+17·2	+21·0	+25·0	+12·5	+ 7·4	− 2·0
9	− 2·5	− 1·0	− 5·5	+ 9·0	+12·0	+13·0	+15·7	+21·5	+24·0	+11·3	+ 5·0	—
10	− 3·5	− 0·1	− 4·5	+ 5·7	+13·0	+13·4	+17·0	+21·5	+24·0	+12·8	+ 1·8	− 2·2
11	− 7·0	− 2·0	− 2·0	+ 4·5	+16·0	+17·5	+18·2	+21·0	+21·8	+14·0	+ 3·5	—
12	− 3·5	− 3·0	− 1·0	+ 1·6	+20·5	+16·5	+20·5	+25·0	+25·0	+10·5	+ 5·4	+ 6·0
13	− 2·0	− 3·2	+ 2·0	+ 0·5	+ 9·0	+19·0	+16·5	+25·3	+21·0	+10·8	+ 5·0	+ 6·0
14	− 2·5	− 1·4	+ 4·8	+ 5·0	+18·0	+19·5	+19·5	+23·5	+23·2	+12·4	+ 5·8	± 0·0
15	− 5·0	− 1·0	+ 1·5	+ 4·1	+17·5	+19·0	+23·0	+22·5	+21·0	+11·3	+10·0	− 3·0
16	− 6·0	− 0·8	− 0·2	+ 5·5	+13·6	+21·5	+25·6	+13·0	+18·0	+13·5	+ 6·2	− 0·5
17	− 8·5	+ 0·5	− 0·3	+ 4·8	+13·0	+23·0	+26·0	+19·0	+14·0	+12·0	+ 6·6	+ 2·7
18	− 6·0	+ 3·2	+ 4·5	+ 6·0	+15·0	+21·5	+21·2	+14·5	+18·0	+11·0	+ 6·6	+ 7·3
19	− 5·0	− 2·0	+ 4·5	+ 9·6	+11·0	+18·0	+26·0	+21·0	+15·5	+ 9·5	+ 5·8	+ 6·5
20	− 5·7	− 2·4	+ 1·0	+10·3	+16·5	+20·9	+23·5	+19·7	+15·0	+ 8·0	+ 2·5	+ 1·0
21	− 5·0	− 5·6	+ 0·6	+12·2	+11·9	+20·0	+23·0	+21·8	+14·5	+11·0	+ 2·5	± 0·0
22	− 5·5	− 5·8	+ 3·0	+ 9·7	+17·0	+25·5	+24·5	+20·2	+18·0	+11·0	+ 2·0	+ 0·8
23	− 5·5	− 6·7	− 2·0	+ 9·8	+14·0	+24·5	+23·6	+21·0	+18·5	+ 6·0	+ 2·0	− 1·0
24	− 6·3	− 3·0	− 4·0	+10·5	+11·0	+21·5	+23·0	+22·2	+18·0	+ 7·2	+ 3·5	− 1·0
25	− 7·7	− 3·0	+ 0·4	+ 7·0	+ 9·0	+23·0	+25·2	+22·8	+19·5	+ 9·3	+ 2·0	+ 0·8
26	− 3·3	− 6·8	− 1·5	+ 9·0	+12·0	+21·9	+26·0	+21·5	+14·0	+ 8·0	+ 1·0	− 2·0
27	− 3·6	− 5·0	+ 4·0	+12·6	+ 8·0	+19·5	+25·0	+23·2	+15·0	+ 9·9	+ 3·8	− 0·5
28	− 3·0	− 5·0	+ 3·0	+10·4	+ 9·0	+16·2	+27·5	+24·0	+21·0	+10·0	—	± 0·0
29	− 1·0	− 3·0	+ 5·8	+ 7·5	+13·0	+18·5	+27·8	+25·0	+13·0	+11·0	—	± 0·0
30	− 4·1	—	+ 1·7	+ 7·5	+11·0	+17·0	+27·2	+26·2	+17·5	+11·0	—	− 1·0
31	− 7·3	—	− 0·2	—	+ 6·5	—	+25·4	+26·0	—	+12·0	—	− 1·5

In Fig. 1 are given the curves for the eruptions, the air temperature at the Volcano Observatory, and the tilts at all three stations, from which it will be seen that the extent to which the tilts varied was very pronounced in February and March, when the eruptions were also frequent. It is worthy of note that the amount of tilt is larger at the Observatory than at the other two stations. The tilts at the Observatory appeared as early as the beginning of January, that is, a month before the explosion group began its activities

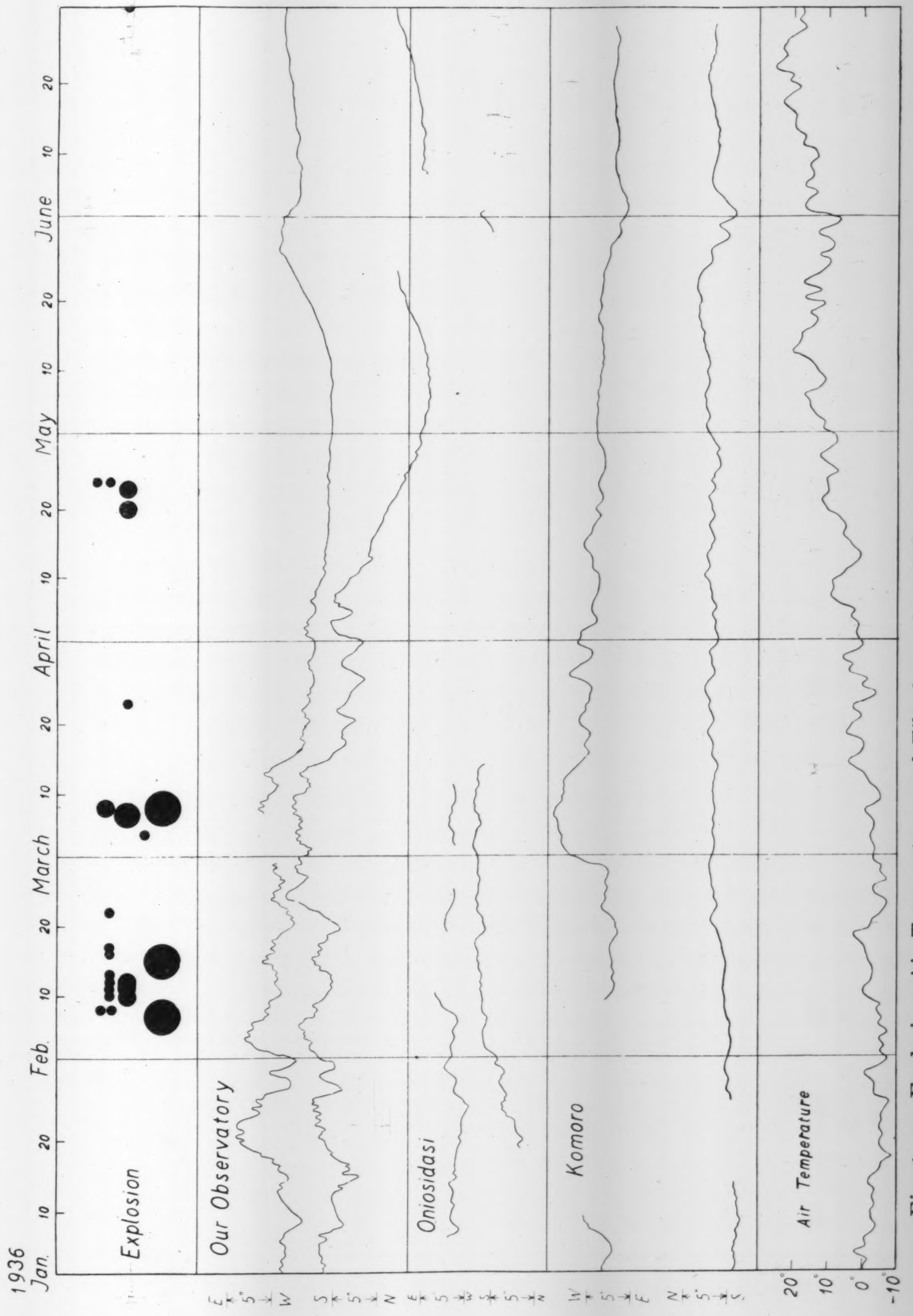

Fig. 1, a. Explosion, Air Temperature, and Tilt observed at Different Stations around the Volcano Asama.

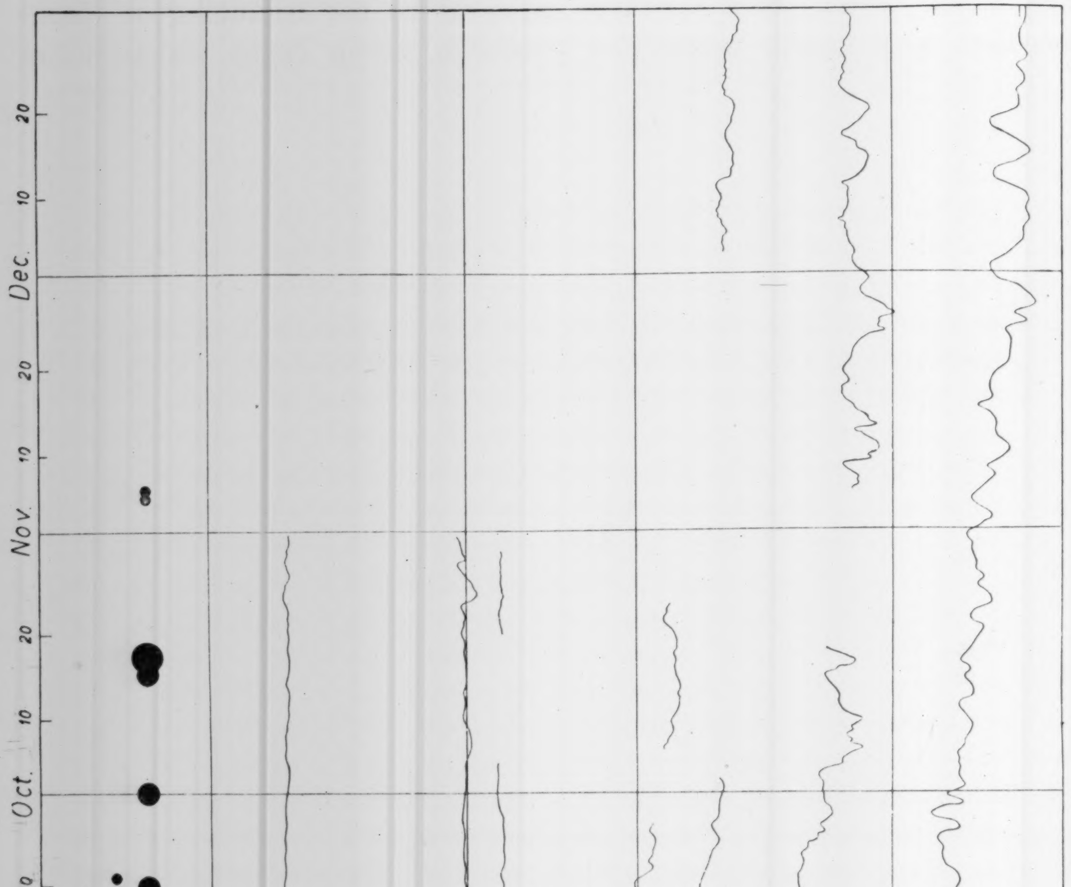

Fig. 1, b. Explosion, Air Temperature, and Tilt observed at Different Stations around the Volcano Asama.

on Feb. 7, while those at Komoro made no marked appearance in connexion with this explosion group, although there was a conspicuous variation amounting to 7″ before the explosion group began activities on March 7.

As to the depth of the crater, the rise of new lava had been noticed since October 1935, causing tilts in the ground flanking the volcano, and finally resulting in the explosion groups of February and March the following year.

After these explosions, the tilts gradually calmed down, and in May and June, became very quiet. The activity of the volcano was correspondingly calm in May and June, except for a number of April.

Since the middle of May, however, a gradual but uni-directional tilt kept up till July, pointing to increasing volcanic energy, when violent explosions then came in succession, the first on July 20.

After these activities, the volcano became very quiet again, and remained so till the end of 1936. The tilts were also gentle, merely repeating small variations within restricted limits.

Since, as will be seen from Fig. 1, the observed tilts are quite independent of the air temperature, the tilts described above may all be regarded as being related to the activities of the volcano.

It may be concluded from the present observations that the following relation hold between tilting and volcanic activity. Preceding a volcanic explosion group by from 7 to 30 days, a marked variation occurs in the tilts, which, as the explosions begin, gradually diminish.

Usually the variation in tilt appears simultaneously at the three stations, but is largest in amount at the Volcano Observatory and smallest at Osidasi, which probably is due to the underground structure of the volcano and to the topography of the respective stations. The fact that the tiltmeter room at the Volcano Observatory is an excavation in the huge lava mass, while, in contrast to it, that at Osidasi was originally a natural cave formed by the accumulation of small lava fragments from the lava stream of 1783 may be a cause of this phenomenon.

Generally speaking, Asama is active for 3 years, after which it stays quiet for 3 years, and then gets active again for another 3 years, the cycle being repeated. The explosions that occur in an active period may also be divided into groups, each group consisting of from 5 to 19 successive explosions. Usually, the earlier group consists of severer explosions than those in the later group. In the same way, the tilts connected with the earlier explosion group are larger than those con-

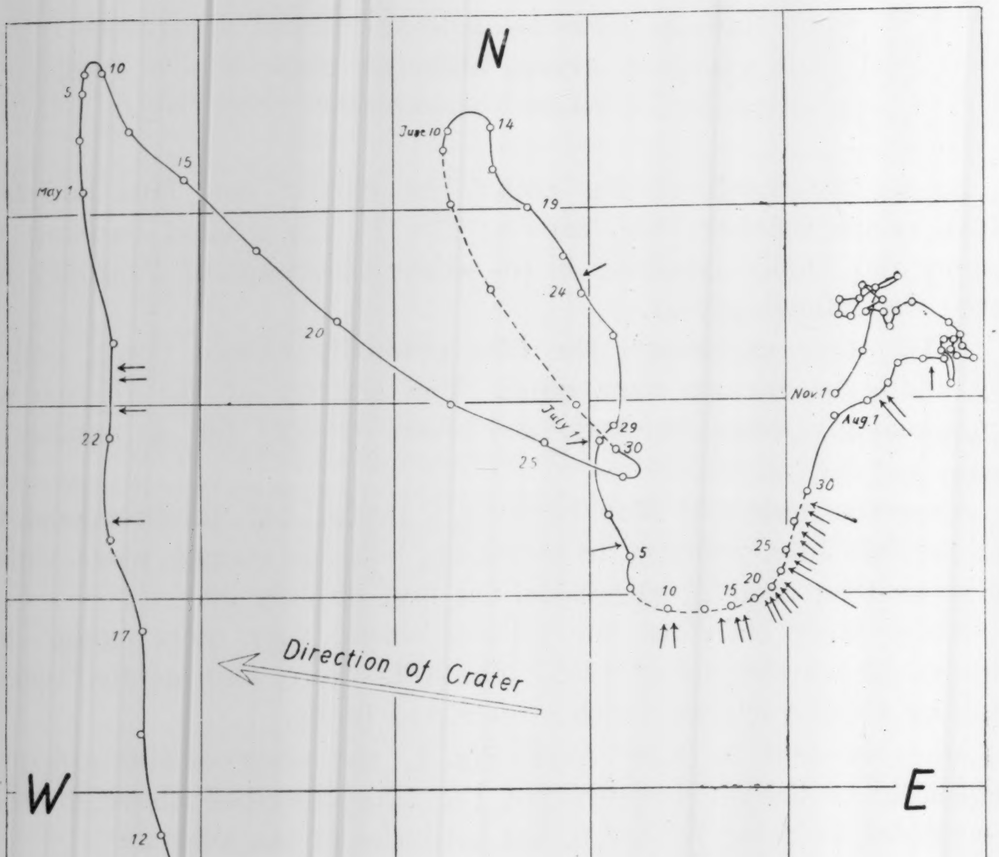

Fig 2. Vector diagram of the tilt variation of the ground as observed at the Asama Observatory. The curve progresses towards the same direction as water on the ground flows 5.

（震研彙報 第十五號 圖版 高橋・水上）

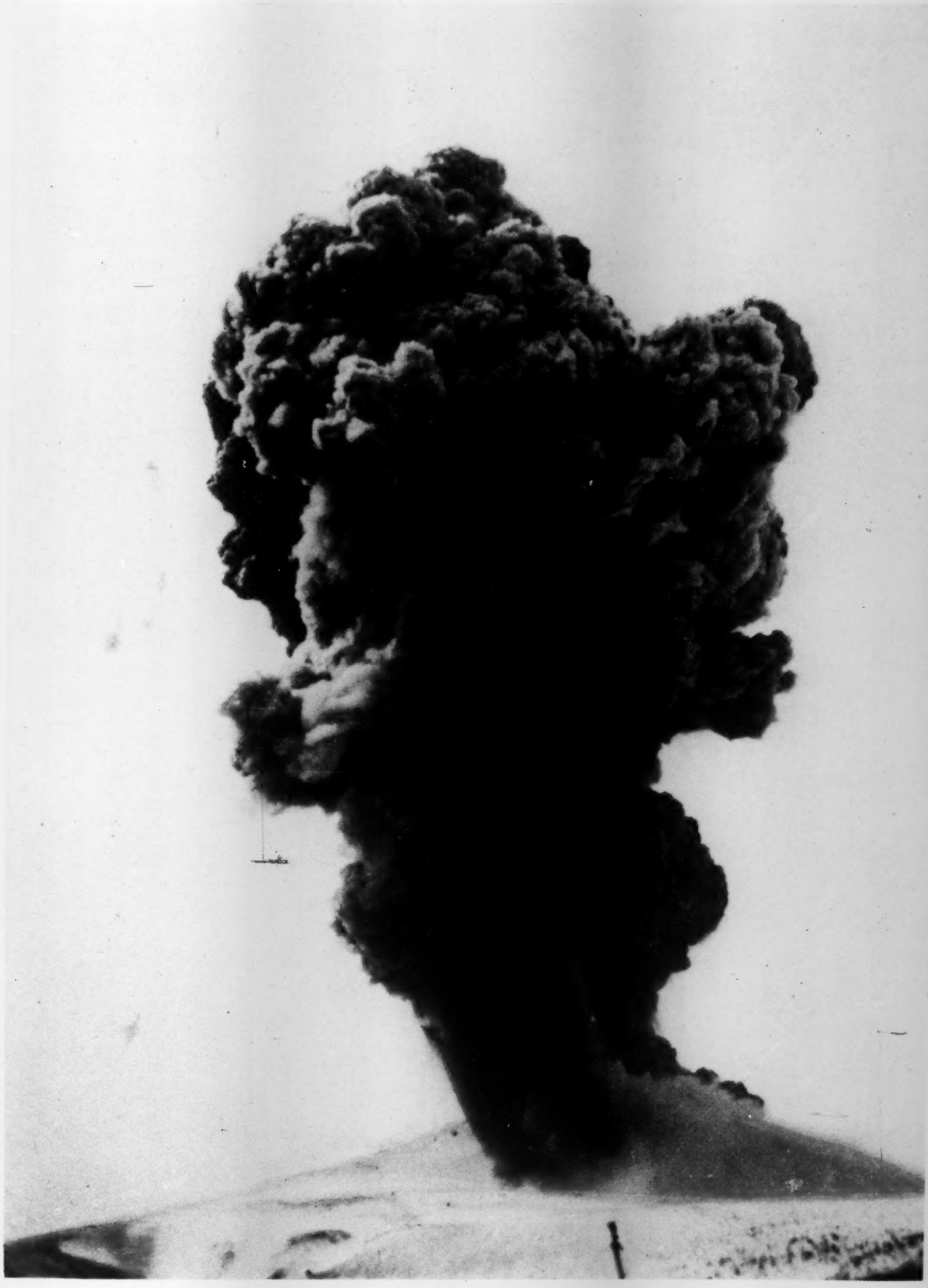

Fig. 3. The Explosion on March 12, 1937.

nected with the later groups. In fact, the tilt that preceded the explosion group of April, 1935, amounted to as much as 40″, while those that preceded the explosions of 1936 were not so large as this although they were about 5 times larger than the variations observed during periods of quiescence.

It is also notable that the crater bottom begins to rise at the same time as the variations in tilt.

In conclusion the writers wish to express their hearty thanks to the Council of the Foundation for the Promotion of Science and Industrial Research of Japan, with the aid of whose grant the studies at Asama are being maintained.

27. 最近の淺間火山の活動と地表傾斜變化

地震研究所 高橋龍太郎
水上武

淺間火山の活動に著しい地表傾斜變化の伴ふ事は既に報告した事がある.

本報告は火山の周圍 3 ケ所に傾斜計を設置し，昭和 11 年の火山活動と傾斜變化とに就いて比較研究したものである.

尙この觀測を施行するに當り. 日本學術振興會より研究費を支給された事を厚く感謝する次第である.

28. Changes in the Depth of the Crater Floor of Volcano Asama in the Recent Activities.

By Takeshi MINAKAMI,

Earthquake Research Institute.

(Read Feb. 16, 1937.—Received March 20, 1937.)

The auther, since the summer of 1934, has been making repeated measurements of the depth of the crater floor in order to study the vertical changes in the lava surface in the crater. As already reported in the previous paper[1], during the inactive period of the volcano in 1934, the floor level slowly rose and fell through the small range of about 1 meter a month. Since the violent outburst of April, 1935, about two hundred explosions occurred during the rest of that year and 1936. His main object was to ascertain the changes brought about in the crater floor with the progress and decline of explosive activitiy, particularly immediatly preceding and following an explosion; for with the elucidation of this phenomenon we should be in possession of an important clue to the mechanism of explosions.

First the depths of two or three points on the crater floor were acurately measured by triangulation, and the form of the crater floor determined by means of photographs taken from several points on the edge of the crater wall. The methods of triangulation and photographic survey are however available only when a very small quantity of vapour and gases is issuing from the crater, and because the crater of Volcano Asama is usually enveloped in these vapours, the methods just described can be employed only on the rarest of occasions. The upper part of the crater wall for a distance of 20∼50 m retains a constant slope, beyond which the slope down to the floor gets much steeper. These inclinations of the slopes remainded intact despite the recent activities, as the result of which the inclinations of various points on the upper crater wall were utilized as scale for reference in measuring the depth. Although the values for the depth of the crater wall by means of this method are generally subject to errors of ±4 m, they can be availed of without serious results during the active period of the volcano, seeing that the crater floor rises and falls within a range of 200 m in the short interval of a few days, when there is also a large quantity of vapour in the crater.

---

[1] T. MINAKAMI, *Bull. Earthq. Res. Inst.*, **13** (1935), 318.

2. Vertical Changes in the Depth of the Crater Floor.

Generally speaking, the depth changes in the crater floor of Volcano Asama may be classified into two kinds according to their characters. In the one the crater floor rises or falls as a whole, which is caused probably by increase or decrease in the pressure under the floor, while in the other, explosions eject a part of the floor from the crater in the form of volcanic bombs and ash, although when such material falls back again into the crater after ejection and accumulates there the crater floor changes in depth. These two kinds of changes therefore differ greatly in character.

This paper is a study of these two kinds of changes in the crater floor that were observed in both quiet and active periods of 1934, 1935, and 1936.

As will be seen from Figs. 1, 2, 3, and 4, the outline of the vertical change in the crater floor as the result of the recent activities is represented by means of E–W profiles through the center of the crater.

Fig. 1. This shows the changes in the crater floor at the time of transition from the inactive period since 1931 to the recent activity.

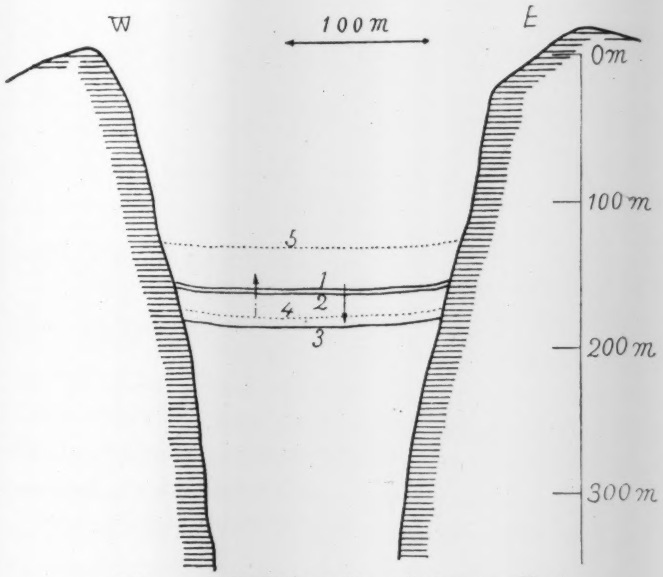

The crater floor on
1, July 9, 1934.
2, Aug. 8, 1934.
3, Sept. 7, 1934.
4, Oct. 26, 1934.
5, April 20, 1935.

Fig. 1. E-W profile of the crater.

The crater floor, which was sinking from July to October 1934 and began to rise after October, the same year, showed a net rise of about 70 m at the time of the violent explosions on April 20, 1935.

Fig. 2. A mass of lava from the floor measuring 150 m E-W, 150 m N-S, and 100 m in depth, was ejected by the violent explosion on April 20, followed by swarms of explosions in May and June.

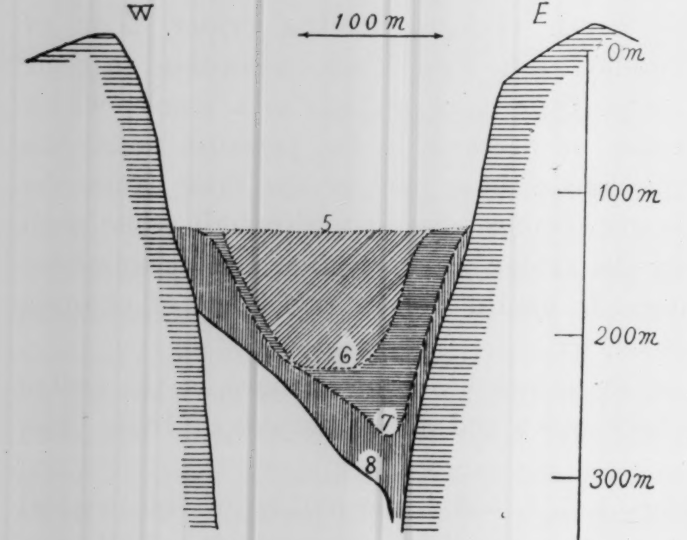

Fig. 2. F-W profile of the crater.

5, the crater floor on April 1935. (before the explosion on April 20, 1935.)
6, the crater floor on April 20, 1935. (after the explosion on April 20, 1935.)
7, the crater floor on June 10, 1935.
8, the crater floor on July 15, 19 5.
▨ the lava ejected by the violent explosion of April 20, 1935.
▤ the lava ejected by the explosions occurred during April, May and June, 1935.
▥ the lava ejected by the explosions occurred during June and July, 1935.

Owing to ejections of the lava that had formed the NE part of the floor, the depth of that part of the floor showed marked increase. Naturally, in these activities, the NE part of the floor appeared to be connected with the center of explosions.

Fig. 3. A part of the lava fragements from the NE part of the

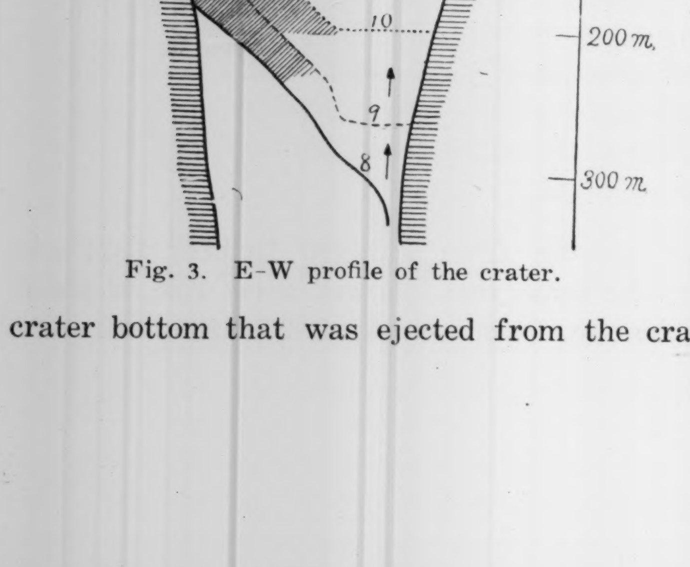

Fig. 3. E-W profile of the crater.

8, the crater floor on July 15, 1935.
9, the crater floor on Aug. 2, 1935.
10, the crater floor on Oct. 23, 1935.
▨ volcanic bombs and ash accumulated on the floor.
↑ elevation of new lava.

crater bottom that was ejected from the crater fell back again on the

SW part of the floor, as the result of which the accumulation of volcanic bombs and ash on the floor formed a slope from SW to NE.

In August, however, from the hollowed NE part of the floor, new lava that appeared to be fairly fluid began to rise. From a survey made, the new lava increased in height, its surface as seen in Fig. 11 being very flat.

Fig. 4. On November 7, 1935, violent explosions began at 11h 50m a.m. and continued for three hours, as the result of which most of the ejected lava fragement accumulated on the SW part of the floor. Part of these fragmental lava fell as volcanic ash in the Kwanto district and on the streets of Tokyo. The amount of this fragmental material is estimated to have been about 10^6 tons.

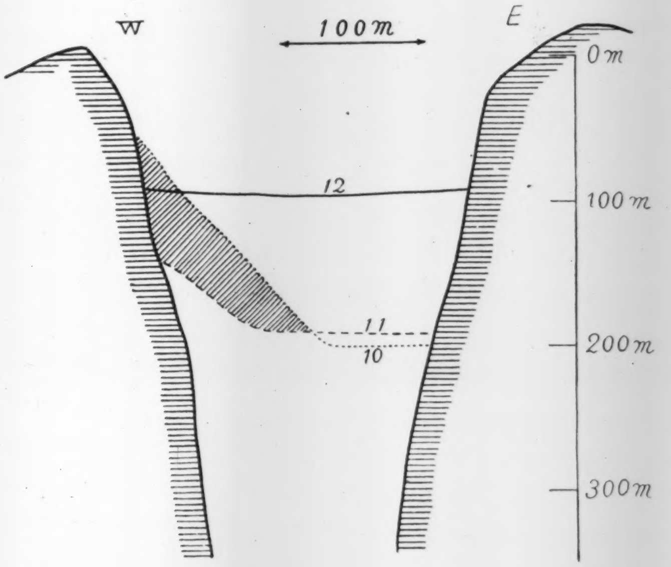

10, the crater floor on Oct. 23, 1935.

11, the crater floor on Nov. 15, 1935.

12, the crater floor on Aug. 13, 1936.

▨ volcanic bombs and ash ejected by the violent explosion on Nov. 7, 1935.

Fig. 4. E-W profile of the crater.

The new lava that had risen during August, 1935, was ejected by the explosions in February and March, 1936, resulting in marked changes in the crater floor. Since then, the floor continued to rise, its depth according to the triangulation of August 13, 1936, being only 70 m, but the explosions of September, October, November again markedly changed the form of the floor.

According to tilting records obtained with Ishimoto clinographs set at three stations at the foot of Asama, floor elevations of the first kind that were observed during the periods from October 1934 to April 1935, and from November 1935 to March 1936, were accompanied with remarkable tiltings of the ground.

These ground tilts at Volcano Asama however will be dealt with separately in a forthcoming paper.

From these ground tilts and the vertical changes in the crater floor, it may be concluded that the former was the result of recent activities of the volcano and the elevations of the floors the result of the same cause, namely, increase of pressure underground. It might be added that tiltings of the ground and upheavals of the crater floor were usually preceded by swarms of explosions. Seeing that the main explosion of a swarm is usually very violent, it is probable that once the crater floor has been broken by the main explosion the floor crushes in through lessened weaker pressure, thus permitting a number of other explosions.

In conclusion, the auther wishes to express his cordial thanks to Professor Mishio Ishimoto for his interest and encouragement in this study.

---

28. 最近の活動に伴へる淺間火山の火口底深さの變化

地震研究所 水上 武

最近の活動に於いて現はれた火口底深さの變遷を見ると，次の二つに分けられる．

第1は火口底そのものが全體として上昇或は沈下する現象である．第2は火山爆發に依つて火口底熔岩が噴出して火口底の深さを深め，或は，一度噴出した熔岩が再び火口底の一部に堆積して火口底の深さを減ずる爲めに生ずる火口底の變化である．

（震研彙報 第十五號 圖版 水上）

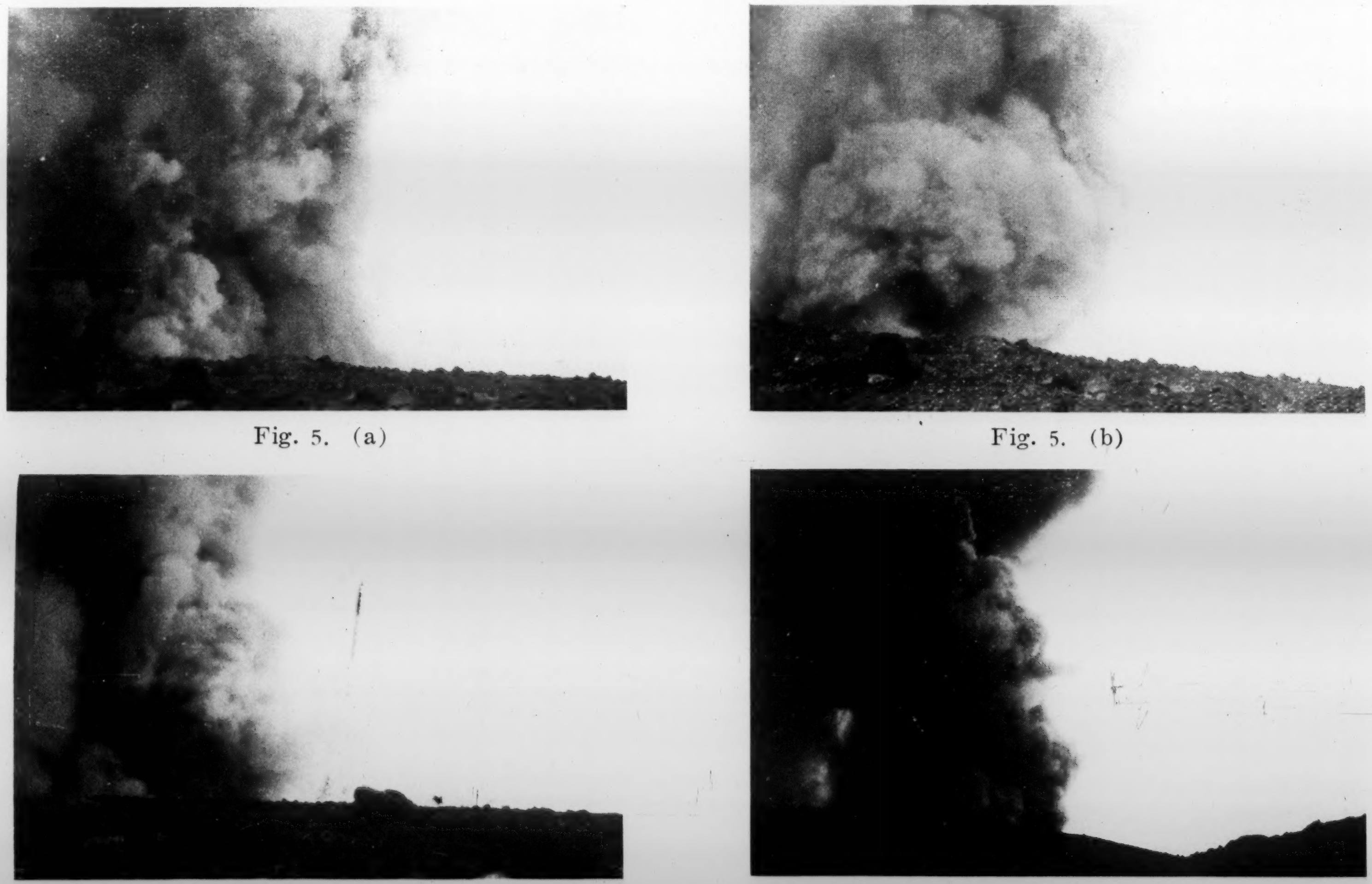

Fig. 5. (a)

Fig. 5. (b)

Fig. 5. (c)

Fig. 5. (d)

The small explosion on Aug. 1935, as seen at a distance of 100 m from the crater.

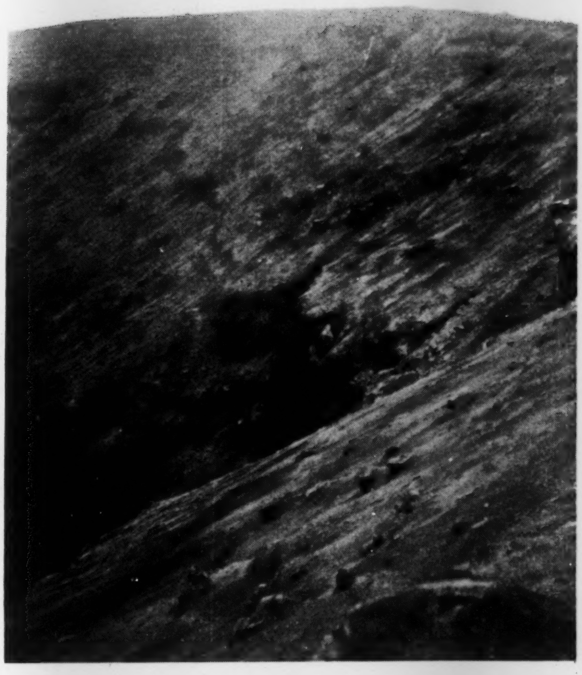

Fig. 6 (a)

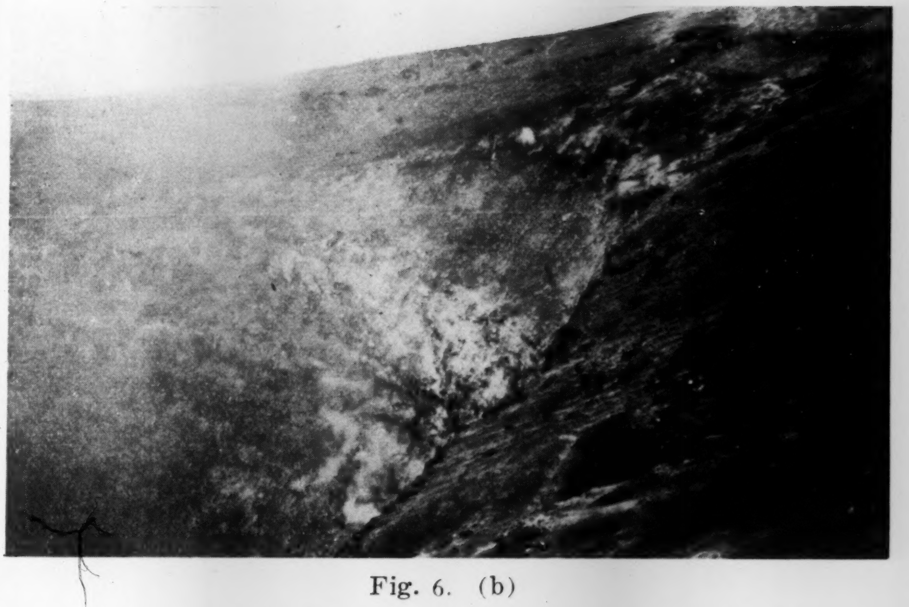

Fig. 6. (b)
The upper part of the crater wall.

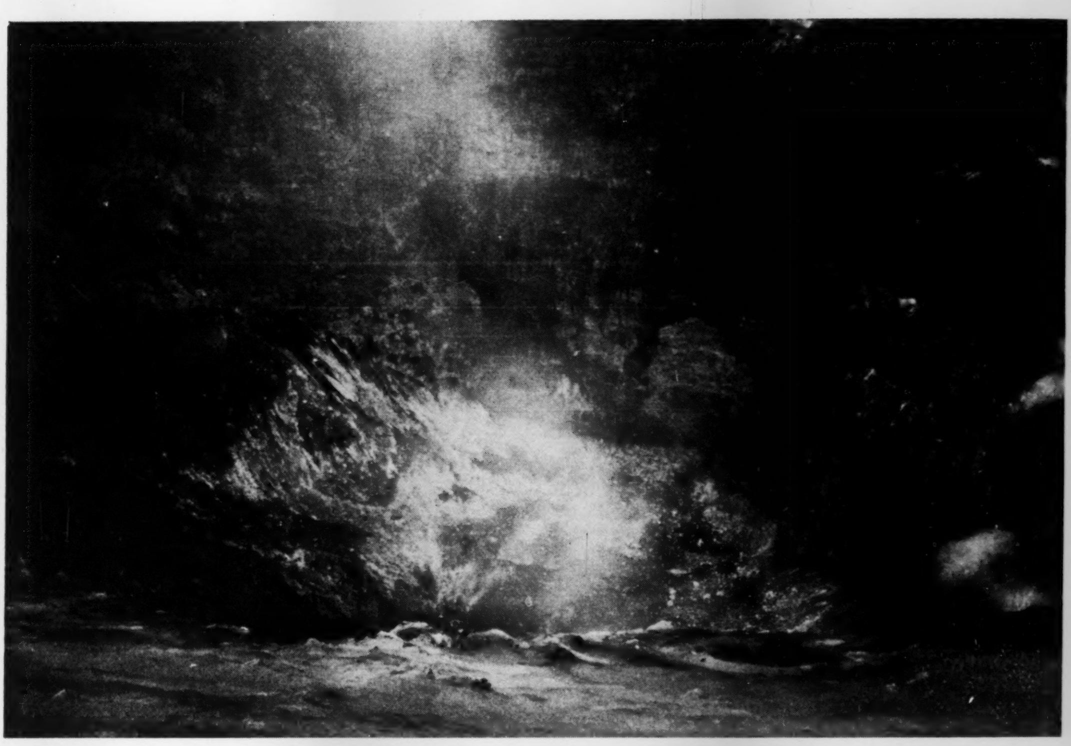

Fig. 7. The crater floor on July 10 1935.

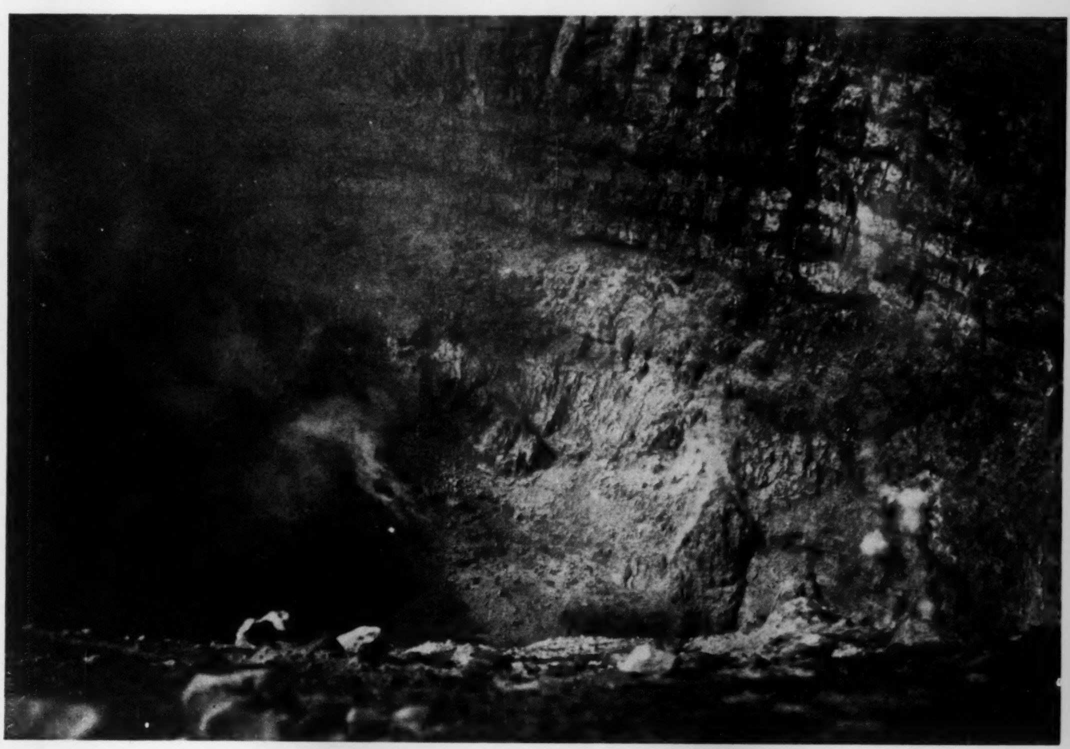

Fig. 8. The crater floor on Aug. 1935.

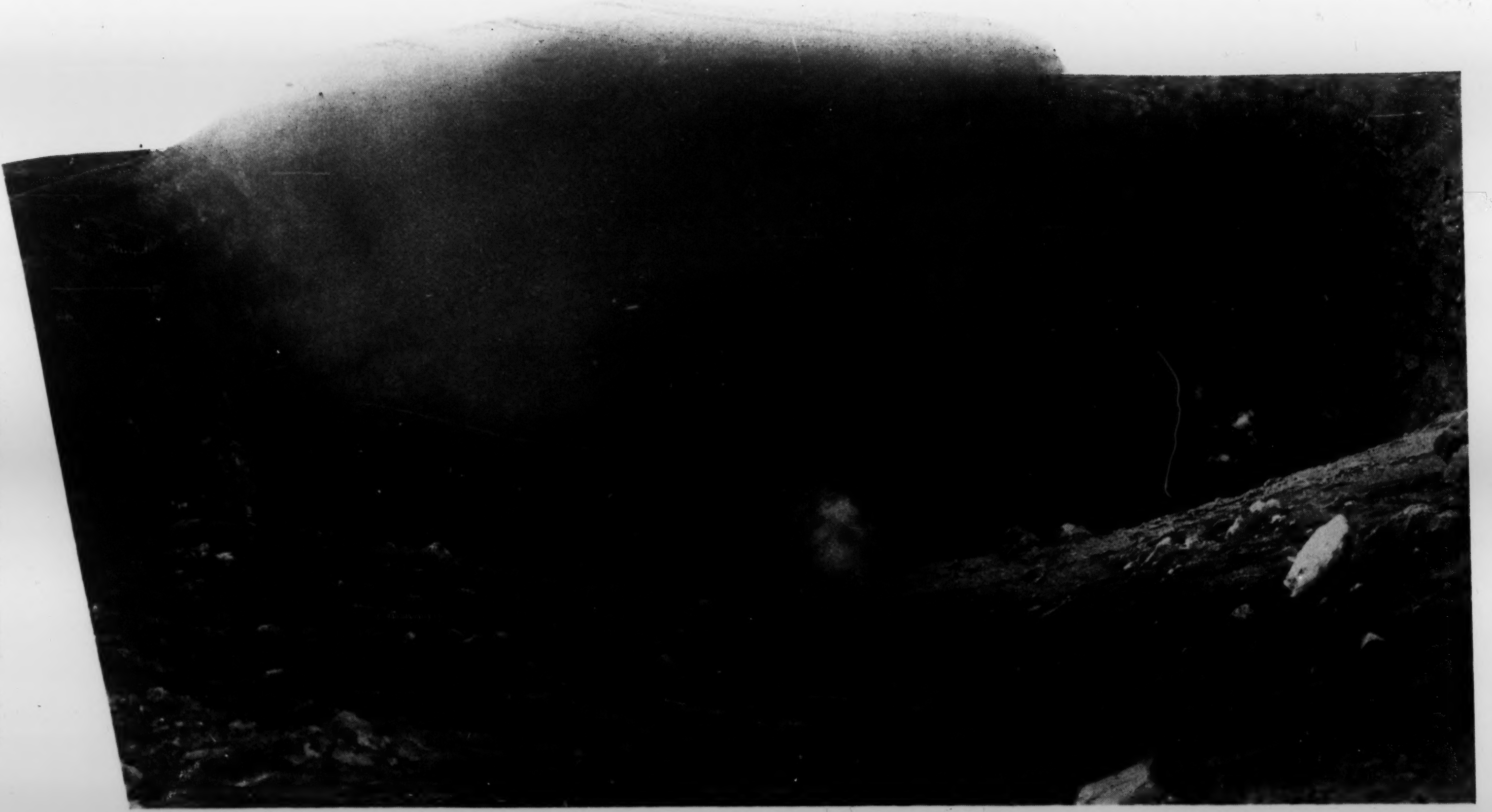

Fig. 9. The crater as seen from the south edge of the crater wall. (Sept. 1935.)

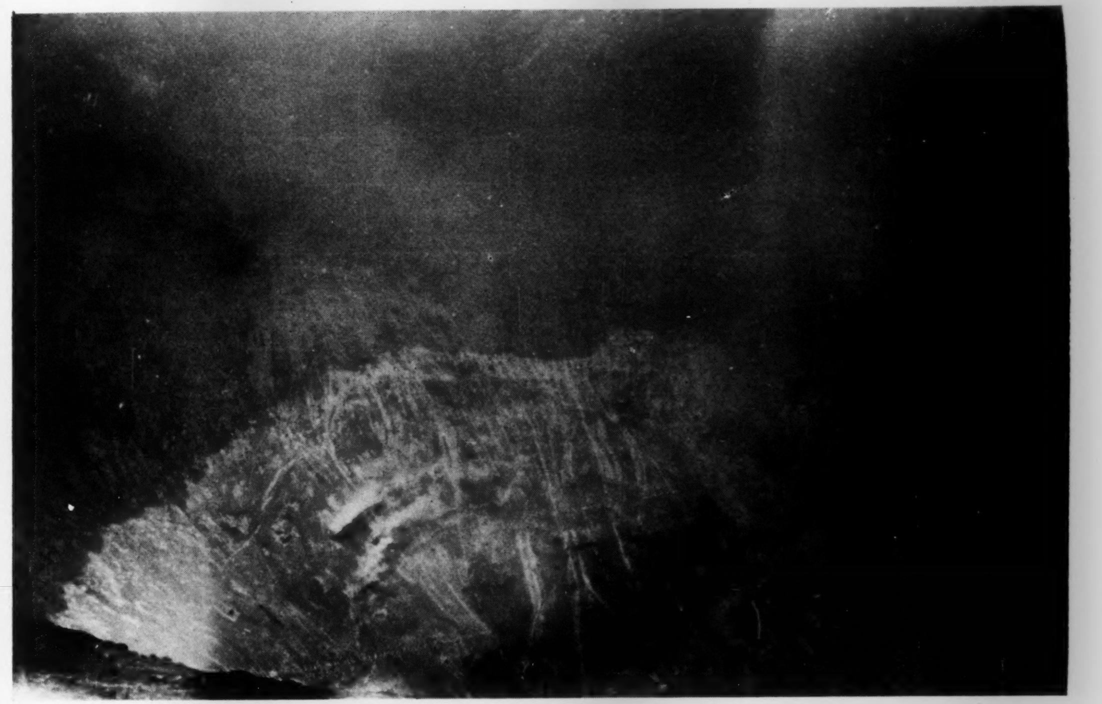

Fig. 10. (a)

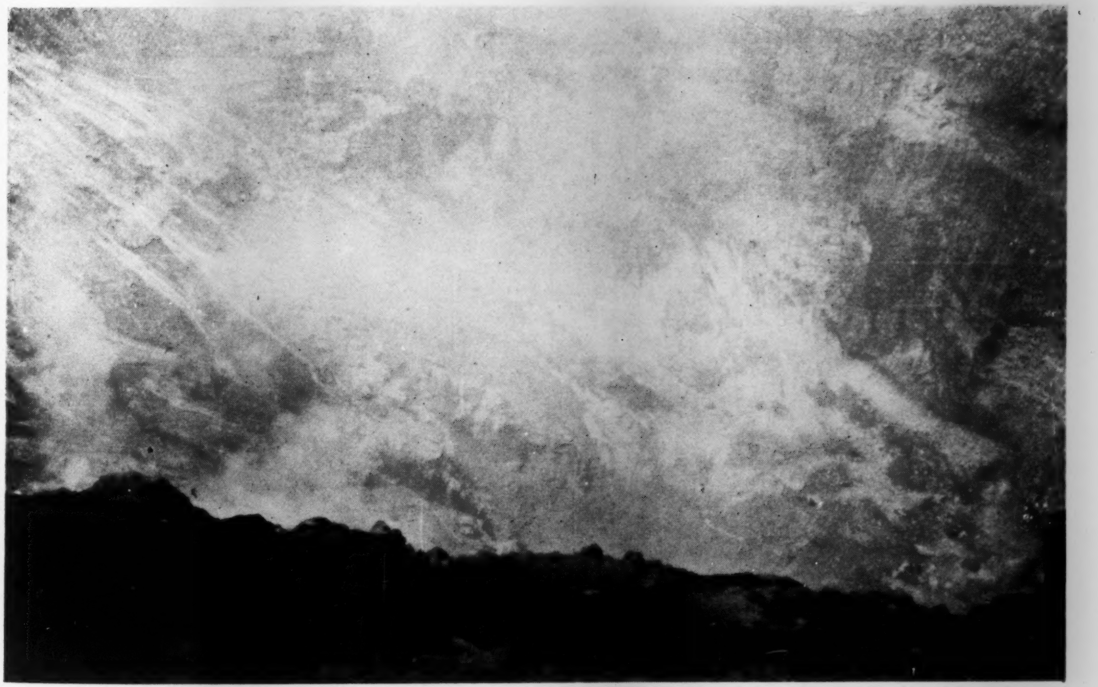

Fig. 10. (b)

Bombs and ash accumulated on the west part of the crater floor.

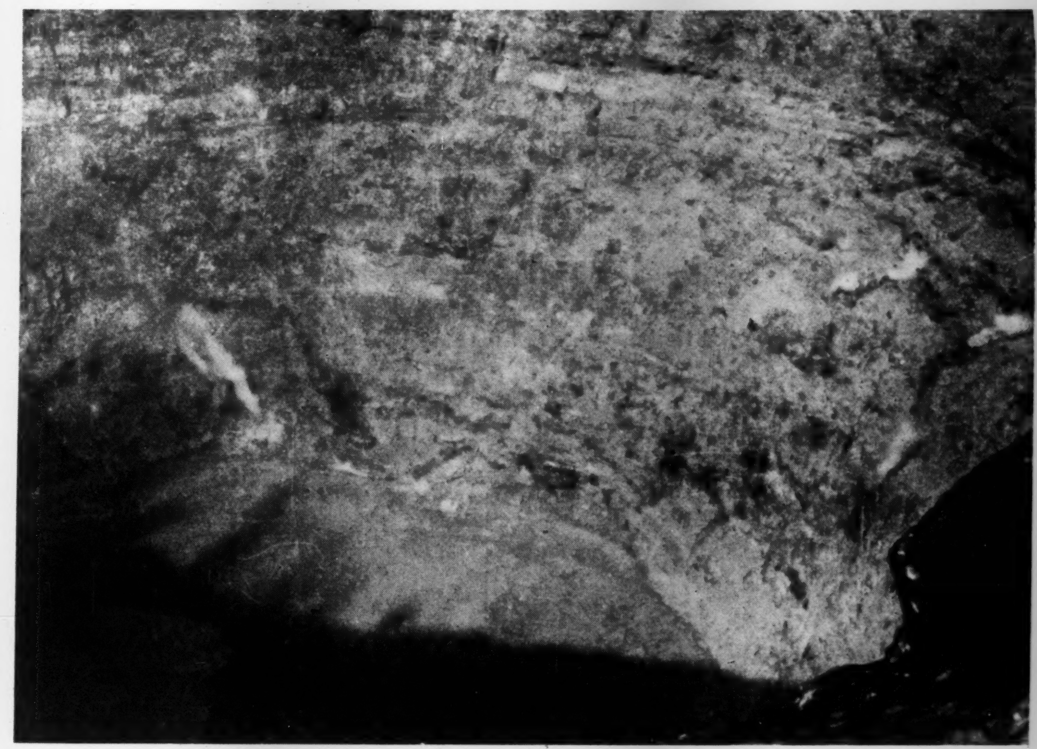

Fig. 11. (a)

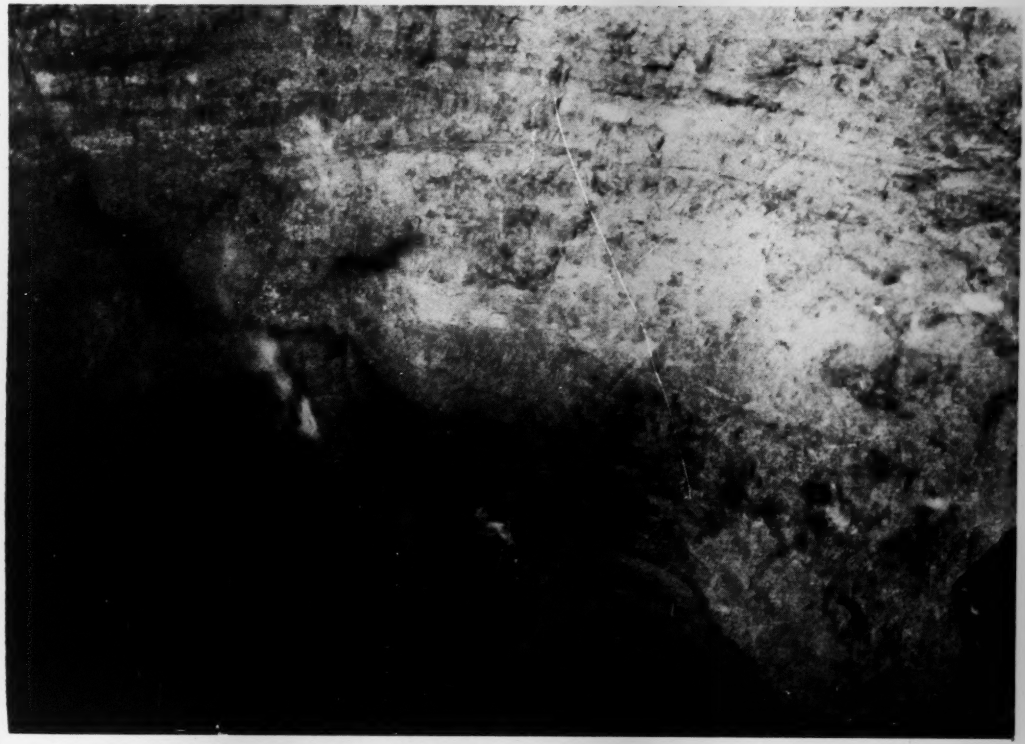

Fig. 11. (b)

The crater floor on Sept. 1935 (elevation of new lava.)

（震研彙報 第十五號 圖版 水上）

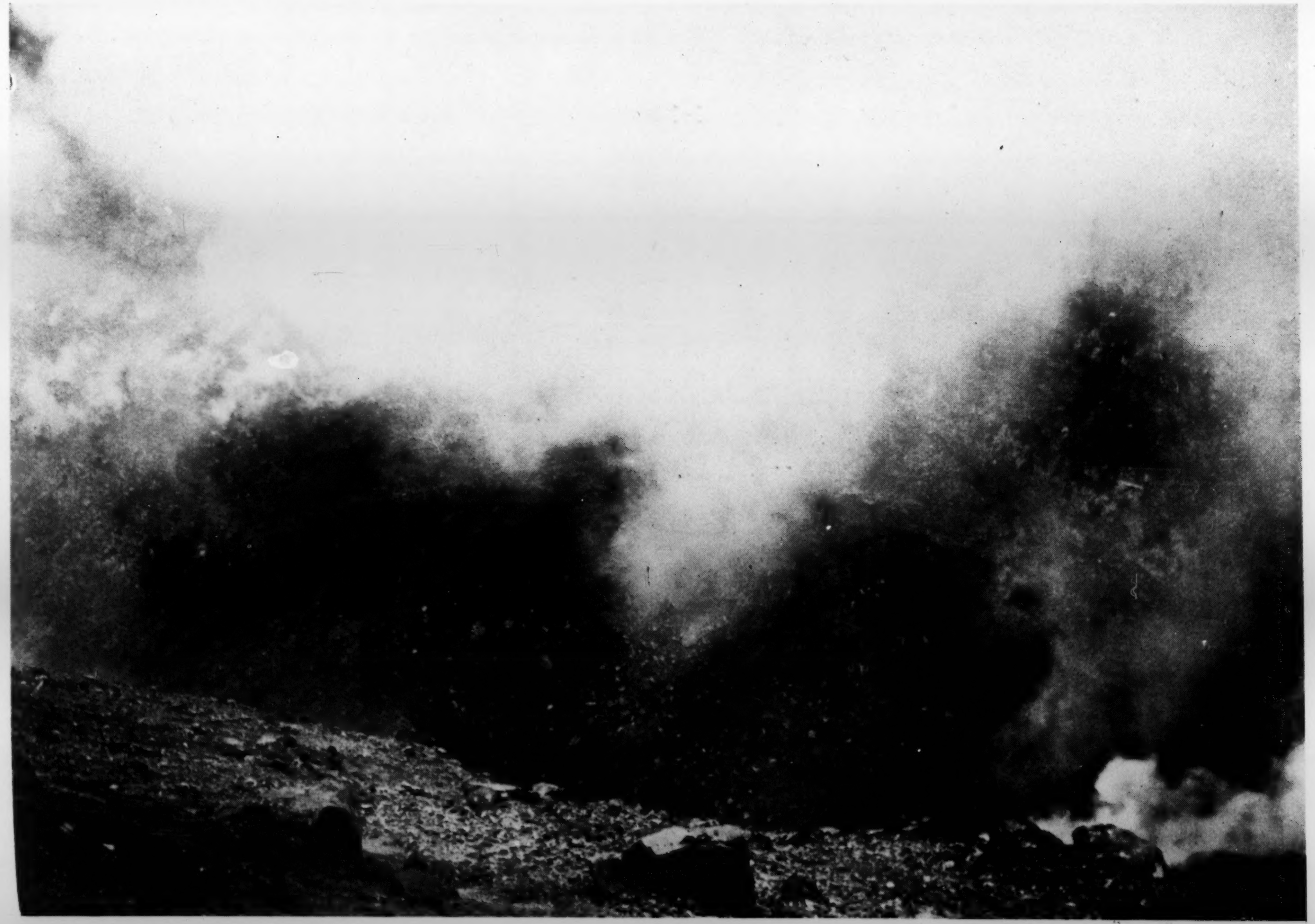

Fig. 12. The crater floor of small depth on Aug. 1936. (seen from east edge of crater wall.)

29. 新島地震前後に於ける同地方地磁氣伏角測定値の比較*

地震研究所　永田　武

（昭和12年2月16日發表—昭和12年3月22日受理）

1. 緒　言

1936年12月27日に伊豆新島附近にかなり顯著な地震が發生し，新島及び式根島等に於いては，人畜及家屋に若干の損害を受け山崩，地割れ等をも生じた[1]．數年前から中村左衛門太郎博士，及加藤理學士[2]によつて，地震に伴つて，その震源地方の地磁氣要素に異常變化の生ずる事が屢々報告されてゐるのであるが，幸ひにも新島に於いては1928年8月，中村清二博士[3]によつて，同島中央部の8點に於ける伏角の測定を行はれたものがある．筆者は地震後同地方調査の機會を得たので，前記中村博士による測點を再測して變化を知ると同時に，將來に供へて出來るだけ多く新測點の設置を行つた．

2. 測定裝置及測定誤差

中村博士による前測定は Dover 製の Dip-Circle によつて行はれてゐるのであるが Dip-Circle は，筆者の經驗によれば使用に相當の熟練と注意をもつてしても猶且2′～3′の誤差は免れず些細の不注意によつてそれ以上の誤差を生ずる惧れもあるので，筆者の場合は運搬上の若干の不便を犧牲にして，海軍水路部型 Earth Inductor を使用した．勿論前測定が±1′又はそれ以上の誤差を有する場合に，それ以上の精度は，前測點再測に關する限り無意味になるのであるが，將來再び測定する場合の事を考慮に入れて測定精度を高めた次第である．

水路部型磁氣儀 Earth Inductor は高橋助教授及筆者[4]が伊豆大島の磁氣測定に使用した物と同一である．然し今回の測定に於ては地磁氣子午線の決定は總て磁針を用ひ

---

* 高橋所員紹介．

1） 萩原尊禮，表俊一郎　地震研究所彙報 **15** (1937)．559．

2） 例へば Y. KATO, *Jap. Journ. Astro. Geophys*, **10** (1933) 249; **12** (1934) 1; **12** (1934) 237.

3） 中村清二　地震 **6** (1934) 637．

4） R. TAKAHASI and T. NAGATA, *Bull. Earth. Res. Inst.*, **15** (1937). 441

て行つた．磁針による地磁氣子午線の決定誤差について豫じめ實驗の結果，筆者の場合には大體 ±15′ 以內である事が分つた．伏角 θ の附近に於いて地磁氣子午線の決定に δ の誤差のある場合の伏角の測定誤差を $\varDelta\theta$ とすれば

$$\tan \varDelta\theta \simeq \frac{\delta^2}{4} \sin 2\theta.$$

$\theta = 45°$，$\delta = 30'$ としても $\varDelta\theta \sim 0{\cdot}1'$ にすぎない．卽ちこの理由による誤差を ε_1 とすれば

$$\varepsilon_1 \gtrsim \pm 0{\cdot}1'$$

次に電流計の感度を充分高めれば，伏角の測定精度を ±0·1′ に迄する事が出來るのであるが，今回の測定に於いては，測定者が筆者一人である爲と，多少一測定を迅速に行ふ必要があつたので，やゝ精度を下げたのでその結果として生ずる誤差は，

$$\varepsilon_2 = \pm 0{\cdot}3'.$$

從つて全體の誤差 ε は，

$$\varepsilon \leqq \pm\sqrt{\varepsilon_1^{\,2} + \varepsilon_2^{\,2}} = \pm 0{\cdot}33'. \qquad (1)$$

3. 測定及測定結果

中村博士による 1928 年度の測定は第 1 圖に示す如く，新島中央部の麥畑道路上の8 點であつて，其の分布區域は，南北共約 2 km の極めて狹い地域である．筆者の測定は地震後丁度一ケ月目の 1937 年 1 月 29，30 兩日にわたつて行はれ，更に 2 月 3 日に再測を行つたのである．その測定値及測定時刻は第 1 表に示す如くである．測定

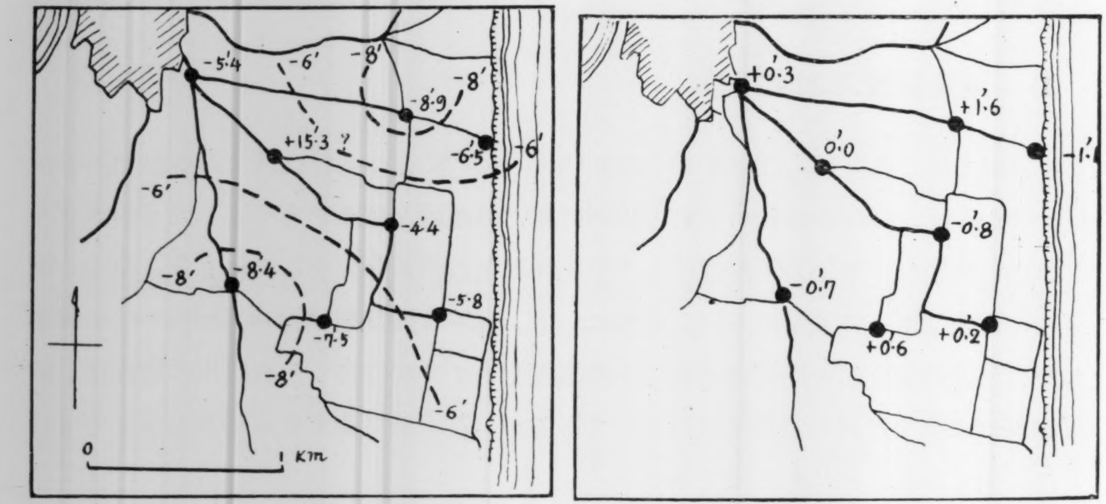

(a) Jan. 1937—Feb. 1937.

(b) Aug. 1928—Jan. 1937.

第 1 圖 伏角の局部變化
Local variations in dip in Niisima.

結果の整理を行ふに當り，筆者の場合は柿岡地磁氣觀測所の値をその標準として採用した．即ち柿岡に於ける値に對して新島の磁氣伏角が相對的に變化した値を求めるのである．

第 I 表 新島に於ける伏角測定値

測點	年月日	時刻		伏角測定値	年月日	時刻		伏角測定値	年月日	時刻		伏角測定値
	1928	h	m	° ′	1937	h	m	° ′	1937	h	m	° ′
No. 1	Aug. 26	16	35	46 55·6	Jan. 29	9	20	46 54·0	Feb. 3	9	10	46 51·0
2	〃	17	36	47 18·7	〃	10	45	47 12·6	〃	10	05	47 13·0
3	〃	18	29	47 16·6	〃	13	40	47 12·0	〃	10	44	47 10·1
4	Aug. 27	8	27	46 59·1	Jan. 30	11	04	47 19·2	〃	13	06	47 17·9
5	〃	9	33	47 23·1	〃	10	01	47 24·0	〃	11	38	47 25·4
6	〃	10	16	47 01·0	〃	12	03	47 05·3	〃	13	53	47 06·2
7	〃	11	40	47 01·0	〃	14	24	46 57·7	〃	14	40	47 00·2
8	〃	12	25	47 04·5	〃	15	30	47 00·2	〃	15	14	47 01·2

さてかゝる測定に於いて最も注意すべき事は，測定中に起つた地球表面上廣範圍にわたる一般的な磁氣擾亂を測定値より除去する事であるが，例へば伏角について柿岡，豐原，青島三觀測所の一日平均値を圖示すれば第2圖に示す如く，非常に良く三者の平行性を示し，その振幅に於いても 1′ 以内にては一致してゐると云へる.5) 又每時測定値による比較を行つて見ても更に良い精度で各觀測量の變化量が一致してゐる事が分つた．

さて中村博士の測定の場合に於て 1928 年 8 月 26～27 の兩日にわたり，著しい磁氣擾亂が生じて居り6)，その最大振幅は伏角に於て 7′ に達する．又筆者の第2回の測定即ち2月3日にも亦稍著しい磁氣嵐があり，7) 伏角に於いてその最大變化量は5′に達する．從つて，各測定値から一般的な磁氣擾亂を除去する爲には，その測定時刻を分位迄精確に考慮に入れて行はれねばならない．觀測點 i に於ける時刻 t の伏角の測定値を $\theta_i(t)$ で表はし，その同時刻に於ける柿岡の伏角を $\theta_k(t)$ で表はす事にする．中村博士の測定，筆者の第一及第二回の測定について，それぞれ $\theta_i(t_2)-\theta_i(t_1)$，$\theta_k(t_2)-\theta_k(t_1)$，$\theta_i(t_3)-\theta_i(t_2)$，$\theta_k(t_3)-\theta_k(t_2)$ を作る．但し t_1，t_2，t_3 等の指數は，前記

---

5) 此の値は氣象要覽に發表せられた，水平及垂直各分力の一日平均値 $\overline{H}$，$\overline{V}$ から $\tan\theta=\overline{V}/\overline{H}$ として計算したものであるから，嚴密に云へば伏角の一日平均値とは異る．然し $\overline{\tan\theta}=\dfrac{\overline{V}}{\overline{H}}+\mu$，$\mu\simeq\dfrac{\overline{V}}{\overline{H}}\left(\dfrac{\overline{(\Delta H)^2}}{\overline{H}^2}-\dfrac{\overline{\Delta H\cdot\Delta V}}{\overline{H}\cdot\overline{V}}\right)$ であるから，$\overline{H}=35000\gamma\cdot\Delta H=100\gamma$ としても $\mu=10^{-5}$. 之は考へる精度に於いては省略出來る微小項である．

6) 柿岡地磁氣觀測所報告昭和3年度．

7) この柿岡の測定値は中央氣象臺岡田臺長，柿岡觀測所今道技師の御好意によるものである，此處に厚く感謝の意を表する．

の 1928 年 8 月，1937 年 1 月，1937 年 2 月の各觀測群を表はすものとする．之等の値は第 II 表及第 III 表に示す如くであり，之から$\theta_i(t_{j+1})-\theta_i(t_j)$と $\theta_k(t_{j+1})-\theta_k(t_j)$ ($j=1,\ 2$) の關係圖を作れば第 3 圖になる．若し新島の測定區域に於て測定された伏角の變化が，局部的のものではなく一般的な磁氣擾亂ならば，第 2 圖に於ける各點は，O 點を通る直線上に乘る筈である．又若し，その區域全體そして一樣な局部的に變化してゐる上に一般的な磁氣擾亂が重疊してゐるならば O 點を通らざる直線になる．

第 II 表

測點 No	$\theta_i(t_2)-\theta_i(t_1)$	$\theta_k(t_2)-\theta_k(t_1)$	$\Delta\theta_i$
	′	′	′
1	− 1·6	+3·8	− 5·4
2	− 6·1	+2·8	− 8·9
3	− 4·6	+1·9	− 6·5
4	+20·1	+4·8	+15·3
5	+ 1·1	+5·5	− 4·4
6	− 0·1	+5·1	− 5·8
7	− 3·3	+4·2	− 7·5
8	− 4·3	+4·1	− 8·5

第 III 表

測 點	$\theta_i(t_3)-\theta_i(t_2)$	$\theta_k(t_3)-\theta_k(t_2)$	$\Delta\theta_i$
	′	′	′
1	−3·0	−2·7	+0·3
2	+0·6	−1·0	+1·6
3	−0·9	+0·2	−1·1
4	+1·0	+1·0	0·0
5	−1·3	−0·5	−0·8
6	+1·0	+0·8	+0·2
7	+2·3	+1·7	+0·6
8	+1·0	+1·7	−0·7

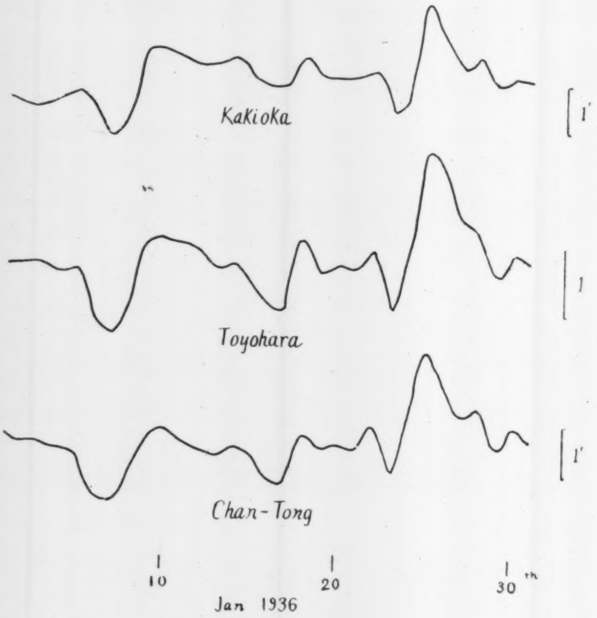

第 2 圖 伏角の時間變化の一例

General time variations of dip in the Far East.

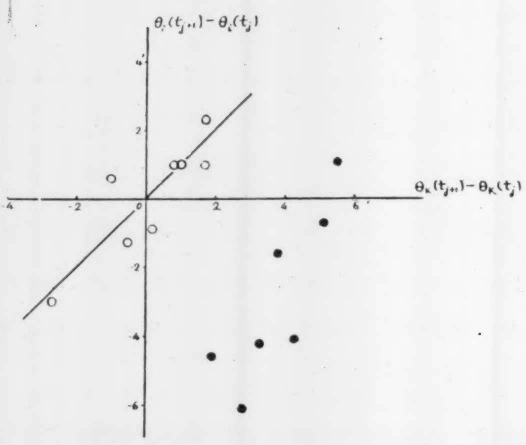

第 3 圖 測定變化量と柿岡に於ける標準値との比較

Comparison of observed variations with general magnetic disturbances.

● Aug. 1928～Jan. 1937

○ Jan. 1937～Feb. 1937

さて筆者の場合に於いて，$t_3\sim t_2$ の場合は若干の誤差を宥せば，殆ど O 點を過ぎる直線上にあつて然もその傾斜はほゞ 45° である．卽ち見かけ上最大 5·1′ に達する磁氣

の局部的異常變化と見られたものは實は一般的な磁氣嵐に他ならないといふ結論に達する．且この場合に於いては柿岡，新島兩地方の磁氣變動の大きさはほゞ等しい事が分る．次に $t_2 \sim t_1$ の場合であるが，之は第2圖に於いて O 點をはるかに外れて居り且つ又直線的關係も成立しない樣である．即ちこの場合は局部的異常變化があつたと考へられる．$t_3 \sim t_2$ の場合の結果を考慮すれば，一般的な磁氣擾亂を取除く爲に次式を採用する事が宥される．即ち測點 i に於ける，求める異常變化量を $\varDelta\theta_i$ とすれば，

$$\varDelta\theta_i = [\theta_i(t_{j+1}) - \theta_i(t_j)] - \lambda[\theta_k(t_{j+1}) - \theta_k(t_j)]$$

$$(j=1,\ 2)$$

λ は時間の函數である場合も考へられるが，今の場合之を判別する材料は無いので，時間にはよらないものとし，且前の結果から $\lambda=1$ とおいて差支へない．斯くして得られた $\varDelta\theta_i$ の値は第 II 表及第 III 表に示されて居り，之を地圖上に圖示したものが第1圖である．同圖(b)に於いては前述の如く，1 月 29，30 日から 2 月 3 日迄の短期間には局部的變化は無かつたと考へて良いであらう．測定誤差 0·4′ をはるかに越える 1′ 以上の偏倚があるけれども，この程度の誤差は測定位置附近の極く僅かな狀態の變化によつても起り得るので，特に取上げて論ずる事は出來ないと思ふ．次に 1928 年 8 月より 1937 年 1 月迄の變化（第 1 圖 (a)）であるが，全體として伏角の減少してゐる傾向のあるのは明瞭である．但 No. 4 測點に於て著しい增加を示してゐるが，その周圍の變化に比して，この點のみ著しく異常變化を起す爲には，其の原因が極めて淺い所になければならない[8]．從つて之は地表の人爲的な變動によるものと考へた方が妥當である故，この測點は取除いて考へる事にする．然る時には第 3 圖 (a) に示す如き等伏角變化線を引く事が出來よう．即ち南，北にそれぞれ變化の極大區域を有する比較的簡單な曲面になる．かゝる變化を生ずる爲の地下構造の變化はポテンシャル論から容易に推察出來るけれども，測定値が伏角のみの場合では，一義的にそれを決定する事は出來ない．

以上の考察から新島地震前後 9 年間に新島地方には地磁氣伏角の異常變化のあつた事は認められる．然し乍ら，之等の變化が 9 年間に徐々に起つたものであるか，又は地震によつて急激に變化したのであるかの判別は出來ない．又今度の測定地は海中の孤島であるので，標準點柿岡からの途中の測定網が缺除してゐる故に，地震との對應

---

8) 第 3 圖に示す如く No. 4 の周圍の測點迄は約 500 m である．この範圍にて No. 4 のみ異常變化がある爲には，假に No. 4 測點直下に N 方向に 45° の伏角を以て傾斜せる磁氣双極子の存在を假定すれば，その深さはおよそ 300 m 以下の値でなければならない．

について充分結論づける事が出來ない．更に極言すれば，若し地震現象が地磁氣異常變化を起し得るものならば，常に有感覺程度の地震を發生する地方にある，柿岡の觀測値自身が，標準値として不充分である事が考へられよう．之等は將來に殘る問題であつて，機會ある毎に解決に努力したいと思ふ．

4. 新測點の測定値

前述8點の測點の他に，新たに No. 9〜No. 24 の新測點を設け，それぞれ伏角の測定を行つた．測點は出來る限り一樣に分布し，なるべく廣範圍に擴げるのが理想的であるが，山岳地方は機械運搬不能の爲，止むなく新島平坦部を測定網で蔽ふに止まつた．測定時及測定値は第IV表に示す如くであり，第4圖にその分布を示す．將來の測定者の便宜の爲に，前の8點と共に之等測點附近の地形圖を第5圖以下に挿入する．

第　IV　表

測定點	測定年月日	時刻	伏角測定値
No. 9	1937, Jan. 31	9 h 04 m	47° 05′·0
10	〃	10 32	46 56·8
11	〃	11 35	46 49·6
12	〃	13 40	47 06·0
13	〃	14 43	47 08·2
14	〃	15 48	47 07·2
15	〃	16 52	47 10·6
16	〃 Feb. 1	8 40	47 33·8
17	〃	11 05	47 07·2
18	〃	13 20	48 08·2
19	〃	13 50	48 16·8
20	〃	14 38	47 52·5
21	〃	16 30	47 50·1
22	〃 Feb. 3	16 08	47 17·0
23	〃 Feb. 4	9 30	46 52·0
24	〃	11 15	47 15·5

5. 結　語

今回の測定に於いては，新島地方に磁氣の異常變化の存在する事は認められたけれども，その地震との關係に就いて充分斷言し得る程の結論には至らなかつた．即ちこの磁氣異常變化の原因に地震を持來る必然性を認める迄には達しなかつた．この問題は地磁氣の局部的異常變化についての一般的考察の結果にまつべきであらう．この報告に於いては磁氣嵐の有無に關せず，野外に於ける測定値から，一般的變化を取除く

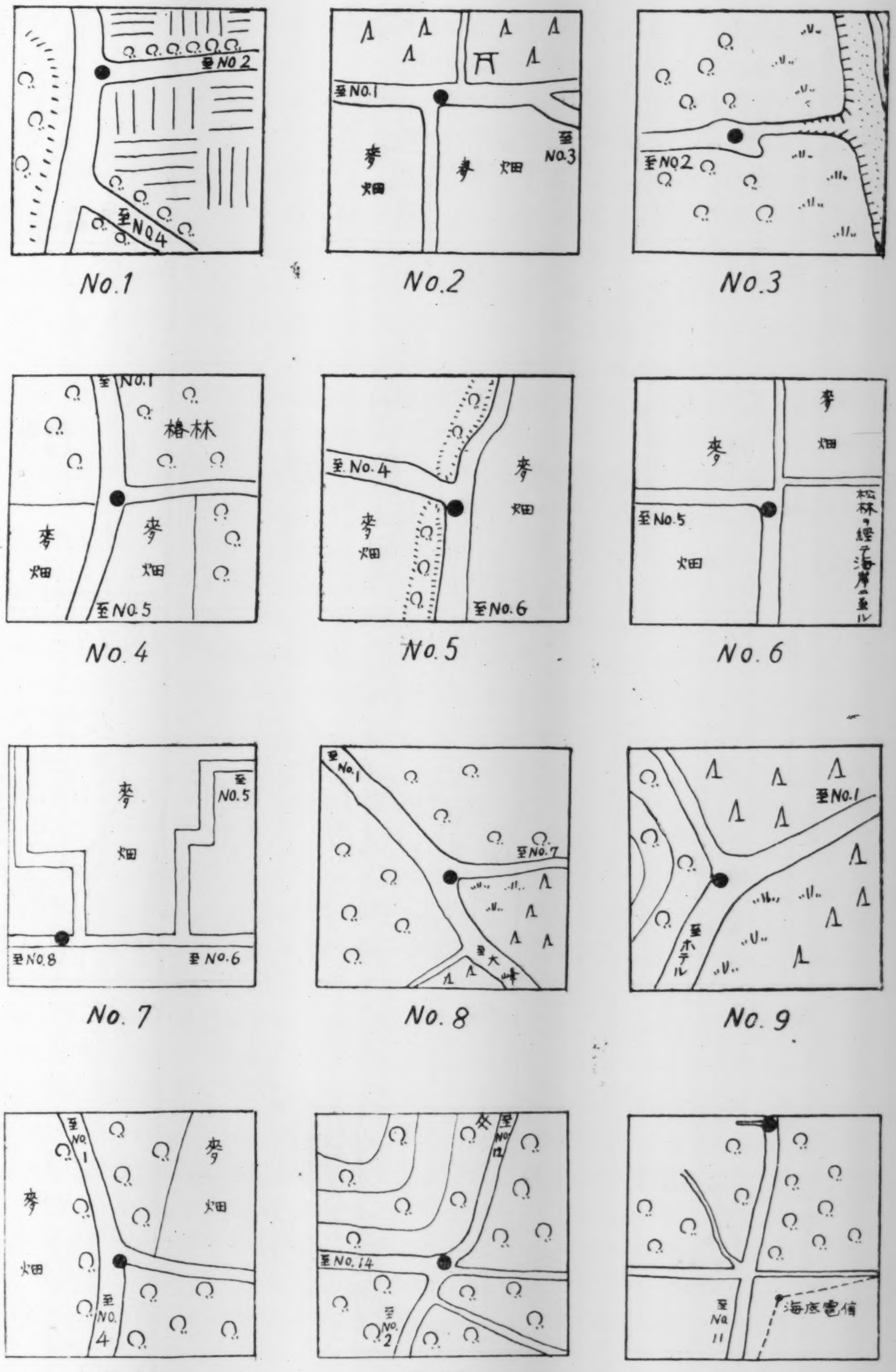
至NO.2
至NO.4
至NO.1
麥畑
麥畑
至NO.3
至NO.2
至NO.1
椿林
麥畑
麥畑
至NO.5
至No.4
麥畑
麥畑
至No.6
麥畑
麥畑
至No.5
畑
松林ヲ經テ海岸ニ至ル
麥畑
至NO.5
至NO.8
至NO.6
至No.1
至No.7
至No.1
至ホテル
至No.1
麥畑
麥畑
至NO.4
至No.12
至No.14
至No.2
至No.11
海底電信

No.1 No.2 No.3

No.4 No.5 No.6

No.7 No.8 No.9

No.10 No.11 No.12

第5圖 地磁氣測點地形圖（續く）

Topographies of the Magnetic Stations.

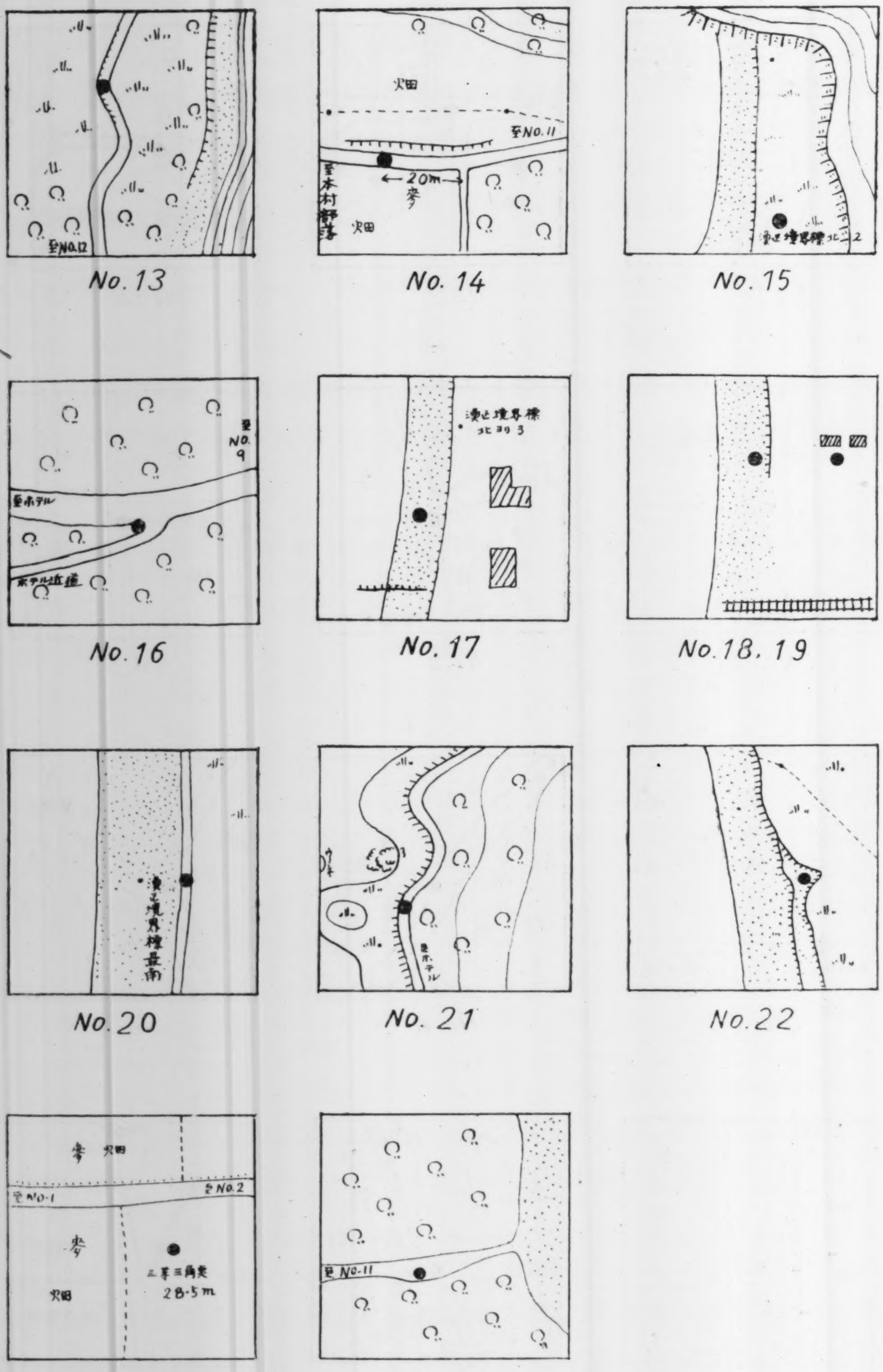
至NO.12
火田
至NO.11
至本村部落
20m
麥
火田
濱辺境界標北 2
至NO.9
至ホテル
ホテル近道
濱辺境界標
北ヨリ 3
濱辺境界標最南
至ホテル
麥　火田
至NO.1
至NO.2
麥
火田
三等三角點
28.5m
至NO.11

No. 13　No. 14　No. 15

No. 16　No. 17　No. 18, 19

No. 20　No. 21　No. 22

No. 23　No. 24

第 5 圖　地磁氣測點地形圖（續き）
Topographies of the Magnetic Stations.

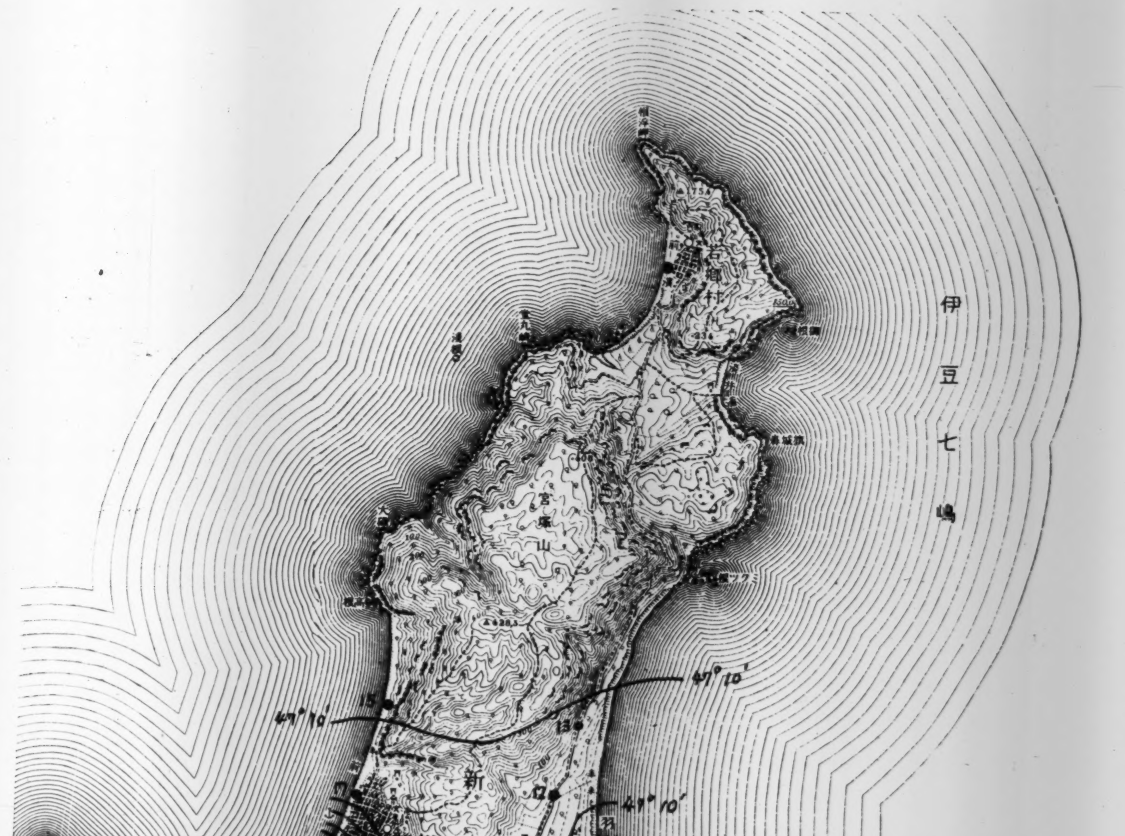
伊豆七島
伊豆七島
新島
宮塚山
本村
47°10′
47°10′
47°10′
47°10′
47°0′
15
13
17
24
11
22
2
3
4
5
6
7
8
9
10
16
21
23

第 4 圖　新島に於ける伏角分布圖

The general Index Map with Isoclinic Lines.

a) 測點 No. 3.

b) 測定 No. 4.

c) 測定 No. 6.

d) 測點 No. 17.

（震研彙報 第十五號 圖版 永田）

a) 測定に使用せる水路部型磁氣儀
Earth Inductor and Striding Declinator.

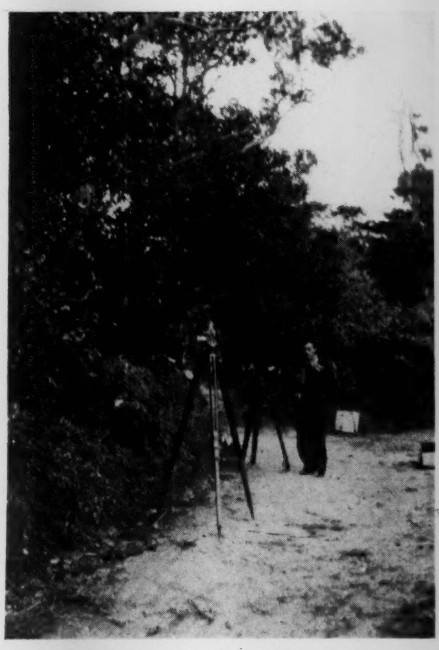

b) 測 點 No. 5.

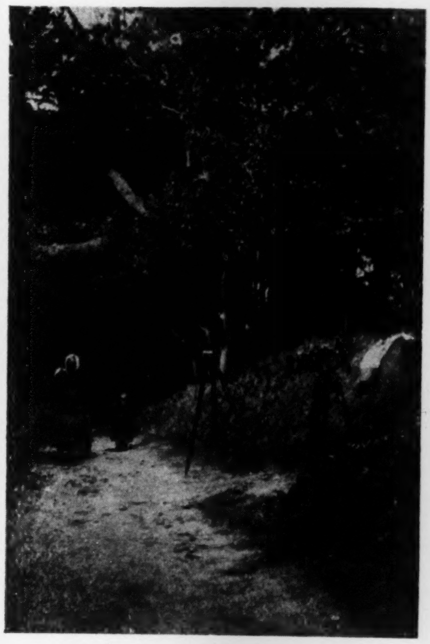

c) 測 點 No. 10.

d) 測 點 No. 13.

（震研彙報 第十五號 圖版 永田）

爲に各測定時について，充分その吟味を必要とする事を注意し，詳細は今後の研究に俟つ事にする．猶この目的の爲に，今後の測定に於いては例へば筆者8) の Dip Variometer を携帶用として製作し，野外測定期間中の時間變化を記錄せしめたいと思つてゐる．

擱筆するに當り，此の調査に際し終始御懇切な御指導と御督勵を賜つた石本先生及高橋先生に衷心より御禮申上げる．同時にこの調査に興味を持たれて，種々御督勵を賜つた中村淸二先生，及び測定機の使用に關し多大の御援助を蒙つた海軍水路部各位に厚く御禮申上げる．

29. *A Comparison of the Results of Magnetic Surveys Before and After the Earthquake in Niisima, December 27, 1936.*

By Takesi NAGATA,

(Earthquake Research Institute.)

After the earthquake of Niisima, one of Idu islands, on Dec. 27th, 1936, magnetic dip angles were observed at 8 points in the island, and the results were compared with the values obtained by S. Nakamura in Aug. 1928.

In this comparison, the dip angles were compared with those at the same instant of Kakioka, the central magnetic observatory of Japan, in order to eliminate the general terrestrial magnetic disturbances from the observed values. The reduced results show that there is a certain anomalous variation of 9 minutes in its maximum value, as shown in Fig. 1.

The method of reduction is discussed for general cases. Finally, the observations of dip angles at the 16 new stations are given.

---

8) T. NAGATA, *Bull. Earthq. Res. Inst.*, **15** (1937), 185.

30. 伊豆伊東溫泉に就て

靜岡縣賀茂郡濱崎村須崎
三井地球物理研究所
福富孝治
藤井次郎

（昭和12年1月16日發表—昭和12年3月20日受理）

I. 緒言

伊東溫泉は伊豆半島の東岸なる伊東沖積平地に湧出し，熱海と共に古來著名であつて伊豆半島に介在する溫泉中其總溫泉穿井數と湧出量の大なる事に於て第一である．昭和11年10月末に於ける伊東溫泉組合の調査[1]に依れば，溫泉井の總數658に達し現に溫泉の湧出を爲しつゝあるもの 386，其一晝夜間湧出量の總計は $2{\cdot}16\times10^5$ hl. に昇ると云ふ．

筆者等は昭和11年8月25日—30日の6日間伊東溫泉中207個の溫泉，7個の普通井戶に就て其湧出溫度，湧出量の測定を行ひ，採水を行つて其含有せる主要化學成分の分析を行ひ，同年12月1—4日の4日間に於て其靜止水頭高の測定並に湧出量の再測を行つた．本論文は之等の測定結果に就ての研究報告である．

II. 測定の方法及結果

今日の伊東溫泉に於ける溫泉の湧出の狀態は 40～270 m 深の穿井の口より自然に湧出を爲しつゝあり，ポンプを使用して溫泉を汲上げるものも一旦自然湧出をなし，貯溜したるものに就て行ふ樣になつて居るので，此研究にも甚だ好都合であつた．湧出溫度は$\frac{1}{2}$度目盛最高寒暖計を用ひて溫泉穿井口に於て測定した．湧出量の測定も穿井口で行つたが，多くの場合容器を用ひる測定が困難であつたので，湧出量測定器を製作使用した．使用した湧出量測定器は谷津溫泉の調査[2]の場合に詳報したから此處には其詳細は述べないが，第1圖(甲)に其寫眞を示した．流入口(E)を湧出口にあてがつて湧出する全溫泉が流入口より入つて排水口(F)より溢出する樣にし，その水の運動に依つて(EF)の圓筒內に裝置されたプロペラを廻轉せしめ，プロペラが10回廻轉する毎に，小重錘の附いたバネを歪ませては離し，これが金屬性の薄膜を叩いて音を發しこれが管H內部の空氣に振動を傳へて耳に聽ける樣にした．第2圖は水

---

1) 伊東溫泉組合，昭和11年度 秋季溫泉調査表．

2) 福富孝治，地震 8 (1936) 457—468.

道を用ひて檢定した結果であつて，此音が 10 回卽ちプロペラが 100 回廻るに要する時間 T（秒）と湧出量 V（立/分）との關係を圖示したものである．卽ち湧出量 V は

$$V=\frac{642{\cdot}46}{T(1-0{\cdot}355\times10^{-2}T)}$$

但し（$T<120$ 秒）　(1)

なる實驗式で可成りよく表されるのである．第1圖（乙）は此湧出量測定器を用ひて實測中の模様を示して居る．靜止水頭高の測定には第3圖に示す如き装置を用ひた．卽ち直徑 10 cm の眞鍮製の圓板の下にフエルトを貼布したものにて穿井の湧出口を封鎖し，圓板の中央に延直上方に向けて取り付けられた內徑 0·8 cm の中空の目盛硝子管中に上昇した水柱の高さを測定した．

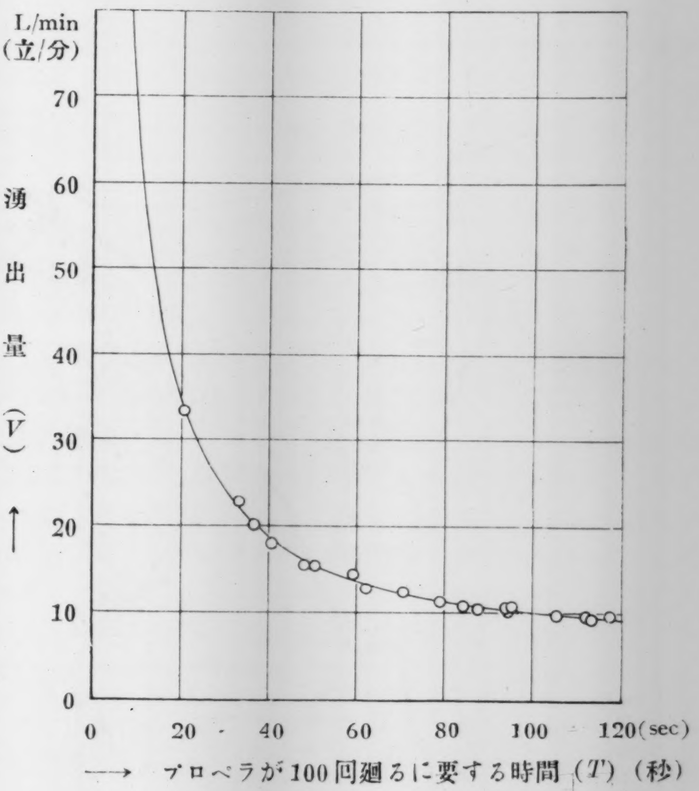

第2圖　湧出量測定器の檢定曲線

(Fig. 2. Calibration curve of the volume output mesuring device.)

採水した資料に就ては Cl′, SO_4'', Ca¨, SiO_2 及 Alkalinity（$CaCO_3$ で便宜上表した）の分析を行つた．（伊東の 2, 3 の溫泉に就ての內務省東京衞生試驗所の分析結果に依れば第II表の如く NaCl, Na_2SO_4, $CaSO_4$ が其主成分である故である）．分析の方法に就ては熱海溫泉調査[3] の際に述べた通りであるから，此處には省略した．之等の結果は第 I 表に示してある．第4圖中黑丸は今度調査を行つた溫泉の位置を示す．黑丸に附けてある番號は第 I 表中の溫泉番號である．

---

[3] T. Fukutomi, *Bull. Earthq. Res. Inst.*, **15** (1937), 113～128.

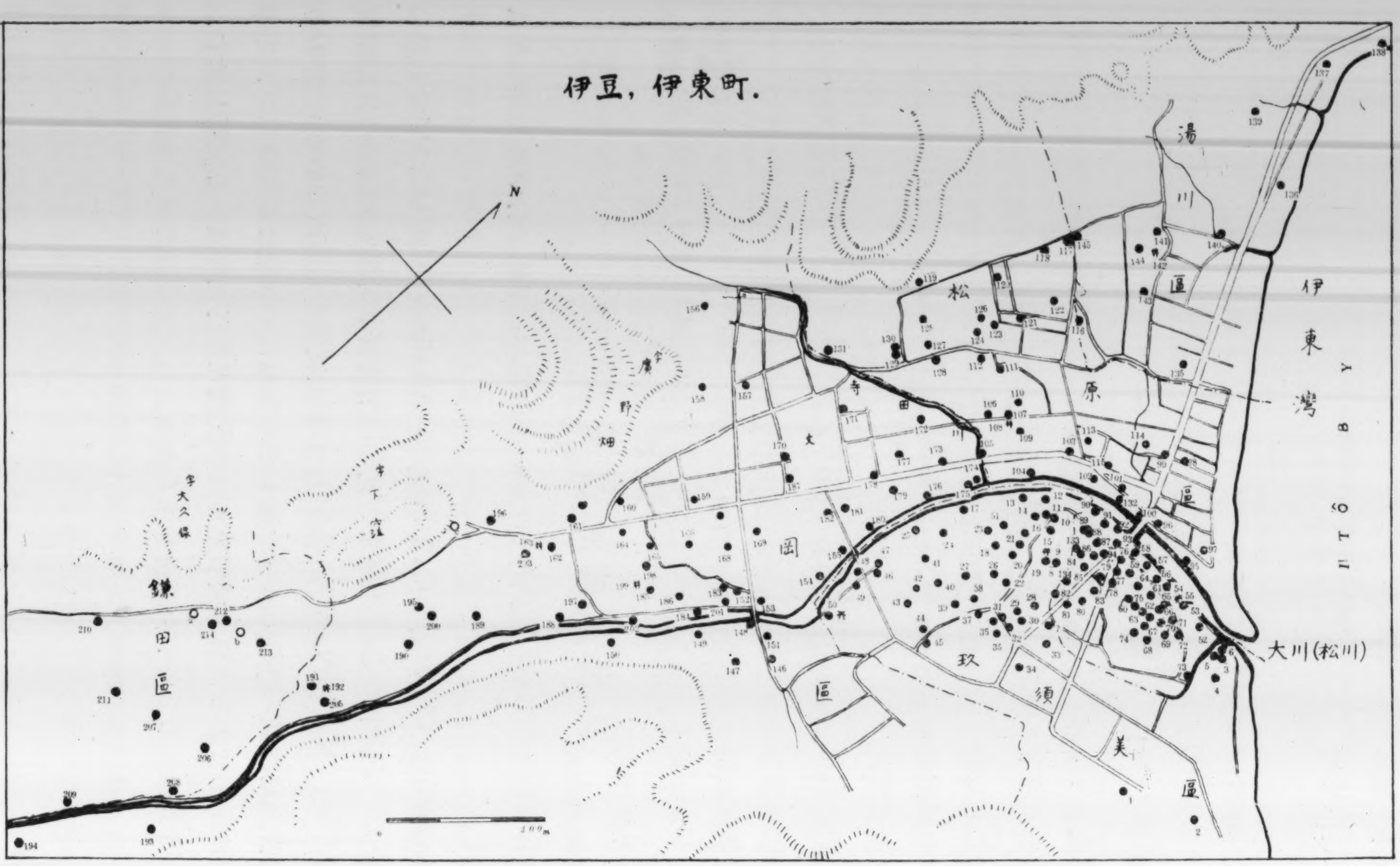
伊豆，伊東町.
N
伊東灣
ITO BAY
大川(松川)
湯川區
松原區
寺田
文
岡
玖須美區
鎌田區
字大久保
字下宿
400m

第4圖 伊東に於る溫泉井の分布 (Fig. 4. Distribution of the Itô thermal springs.)

● 測定せる溫泉の位置 (Site of the studied thermal spring.)

♯ 測定せる普通井戸の位置 (Site of the observed ordinary well.)

黑丸に附したる番號は第1表中の溫泉番號なり. (Numeral attached to black circle denotes thermal spring number in Table I.)

第 I 表 Table I.

No.	溫泉組合番號	穿井の深 Depth of hot spring	湧出溫度 Orifice temperature	湧出量 Volume output Aug. 25—30		靜止水頭（湧出口上高） Height of statical head above the orifice	口徑 Diameter of orifice	湧出口海面上高 Height of orifice above mean sea-level	靜止水頭海面上高 Height of statical head above mean sea-level	化學成分 Chemical Constituents Cl					l : m : n
				Aug. 25—30	Dec. 1—4					Cl	SO$_4$	SiO$_2$	Alkalinity as CaCO$_3$	Ca	
		m	°C	l/m	l/m	cm	cm	m	cm	mg/l	mg/l	mg/l	mg/l	mg/l	
1	玖須美—155	167	41·3	50·0	57·7	154	5 08	2·67	421	809	371	70·7	46	37	13 : 40 : 47
2	〃 —111	145	40·5	(10·8)	——	——		2·11	——	4210	974	48·8	28	169	64 : 0 : 36
3	〃 —123	91	42·7	12·3	11·1	50	〃	1·45	195	2800	738	34·7	73	191	42 : 25 : 33
4	〃 —124	91	41·2	16·3	20·5	——	〃	1·16	——	2300	640	54·8	31	92	34 : 23 : 42
5	〃 —122	91	39·0	12·6	——	——		0·99	——	1470	447	45·8	52	77	22 : 25 : 53
6	〃 —121	91	40·0	13·7	23·0	72	〃	1·28	200	1420	405	43·0	54	88	21 : 30 : 50
7	〃 — 48	117	39·0	(5?)	——	——		2·01	——	1247	482	51·7	44	104	18 : 28 : 54
8	〃 — 46	82	44·8	(15·5)	——	——		1·95	——	2668	632	69·6	55	163	40 : 34 : 26
9	〃 —46井戸	—	26·0	——	——	——		——	——	229	111	38·0	29	164	——
10	〃 — 3	60	47·0	30·8	——	——		2·21	——	1150	396	58·5	35	74	17 : 59 : 25
11	〃 — 4	72	48·5	9·7	——	——		2·57	——	1250	488	35·3	35	62	18 : 64 : 18
12	〃 — 5	60	45·0	14·8	22·2	57	〃	2·06	263	1540	480	42·7	39	108	23 : 47 : 30
13	〃 — 6	72	47·0	9·0	——	60	〃	2·32	292	1630	555	44·5	41	90	24 : 54 : 23
14	〃 — 16	63	44·8	[21·6]	——	——		2·26	——	1815	495	54·3	47	126	27 : 43 : 30
15	〃 — 18	67	44·7	18·0*	21·7	24·5	〃	2·28	252	1119	401	54·2	40	81	16 : 51 : 33
16	〃 — 15	61	47·0	18·0	16·7	30	〃	2·46	276	1271	450	52·7	28	99	18 : 58 : 24
17	〃 — 10	90	50·0	24·0	26·0	38	〃	1·49	187	1203	488	59·4	34	116	17 : 70 : 13
18	〃 — 8	54	46·0	23·0	22·0	24	〃	2·55	279	3330	903	54·0	62	196	50 : 31 : 19
19	〃 — 24	81	45·0	35·8	40·4	67	〃	1·60	227	2240	603	36·1	59	193	33 : 39 : 27
20	〃 — 23	71	47·0	19·5	13·3	30	〃	2·32	262	1137	588	58·2	41	119	26 : 52 : 22
21	〃 — 22	81	44·3	27·1	30·8	39	〃	2·11	250	2790	697	44·3	57	156	42 : 31 : 28
22	〃 — 32	68	44·8	25·5	24·7	52	〃	1·33	185	892	447	61·1	37	58	13 : 53 : 34
23	〃 — 33	72	47·7	13·3	17·1	30	〃	2·03	233	2620	732	60·9	45	137	39 : 45 : 16
24	〃 — 36	—	49·5	13·9	——	——	〃	3·33	——	1063	480	58·0	31	86	15 : 69 : 16
25	〃 — 39	51	50·5	26·8	29·0	35	〃	3·74	409	871	428	60·0	49	59	12 : 75 : 13

(次頁へ續く)

第 I 表 (續)

No.	溫泉組合番號	穿井の深 Depth of hot spring	湧出溫度 Orifice temperature	湧出量 Volume output Aug. 25—30		靜止水頭（湧出口上高） Height of statical head above the orifice	口徑 Diameter of orifice	湧出口海面上高 Height of orifice above mean sea-level	靜止水頭海面上高 Height of statical head above mean sea-level	化學成分 Chemical constituents Cl					l : m : n
				Aug. 25 —30	Dec. 1 — 4					Cl	SO_4	SiO_2	Alkalinity as $CaCO_3$	Ca	
		m	°C	l/m	l/m	cm	cm	m	cm	mg/l	mg/l	mg/l	mg/l	mg/l	
26	玖須美— 41	64	48·4	25·5	23·7	61	5·08	2·44	305	865	413	52·1	31	71	12 : 67 : 21
27	〃 — 42	67	45·6	13·0	15·3	42	〃	3·09	351	1001	404	55·4	36	49	14 : 55 : 30
28	〃 — 49	55	42·8	11·0	13·5	40	〃	2·20	260	757	361	57·0	32	65	11 : 48 : 42
29	〃 — 53	46	49·0	27·7	29·0	28	〃	3·27	355	712	424	65·0	29	70	10 : 71 : 19
30	〃 — 52	64	46·8	17·3	13·6	25	〃	3·16	341	585	382	47·2	30	62	8 : 64 : 28
31	〃 — 71	56	49·0	14·8	22·7	23	〃	2·62	285	751	409	67·0	27	73	10 : 71 : 19
32	〃 — 59	60	36·2	[5·4]	——	——		2·62	——	515	367	65·7	34	51	7 : 25 : 67
33	〃 —150	71	38·5	30·8	28·8	57	〃	2·33	290	407	225	59·7	29	16	6 : 35 : 59
34	〃 — 99	73	41·2	12·4	10·8	77	〃	2·39	316	608	342	58·7	61	34	9 : 43 : 48
35	〃 — 61	101	39·0	25·5	27·2	155	〃	2·68	423	429	287	53·9	41	18	6 : 37 : 57
36	〃 — 69	45	49·3	15·2	16·7	19	〃	2·73	292	465	427	64·0	30	65	6 : 75 : 19
37	〃 — 75	61	48·0	26·7	20·2	16	6·35	2·84	300	387	331	54·2	34	46	5 : 71 : 24
38	〃 — 78	84	42·5	[18]	——	——		2·91	——	749	354	34·6	43	23	11 : 47 : 43
39	〃 — 79	73	42·5	(13)	——	——		3·32	——	688	340	58·5	36	35	10 : 47 : 43
40	〃 — 81	91	49·8	30·2	34·7	57	5·08	3·02	359	617	386	59·5	27	62	8 : 75 : 16
41	〃 — 87	64	50·1	45·8	38·3	58	〃	3·60	418	1377	483	63·9	32	105	20 : 68 : 12
42	〃 — 90	63	50·2	26·4	——	——		3·35	——	839	418	61·2	26	100	12 : 75 : 14
43	〃 — 93	118	45·2	(3·6)	——	——		3·93	——	3202	700	54·8	45	180	48 : 30 : 23
44	〃 — 83	73	41·2	[5·4]	——	——		3·68	——	672	382	62·8	37	26	10 : 43 : 48
45	〃 —151	83	44·0	[9]	——	——		2·24	——	1253	493	55·2	39	94	18 : 47 : 35
46	〃 — 98	67	51·0	61·5	57·5	57	〃	4·38	495	615	318	65·8	31	78	8 : 80 : 12
47	〃 —103	56	51·0	17·0	18·8	11	〃	4·74	485	615	366	53·4		77	8 : 80 : 12
48	〃 —102	55	51·7	32·6	——	——		4·67	——	240	350	59·3	26	79	3 : 87 : 11
49	〃 — 00	77	50·0	39·5	32·6	56	〃	4·84	540	708	407	65·7	25	71	10 : 75 : 15
50	〃 —153	100	47·0	47·7	40·9	37	〃	3·44	380	421	400	52·4	24	81	6 : 67 : 27

(次頁へ續く)

第 I 表 (續)

No.	溫泉組合番號	穿井の深 Depth of hot spring	湧出溫度 Orifice temperature	湧出量 Volume output Aug. 25—25	湧出量 Volume output Dec. 1—4	靜止水頭（湧出口上高） Height of statical head above the orifice	口徑 Diameter of orifice	湧出口海面上高 Height of orifice above mean sea-level	靜止水頭海面上高 Height of statical head above mean sea-level	化學成分 Chemical constituents Cl	SO$_4$	SiO$_2$	Alkalinity as CaCO$_3$	Ca	l : m : n
		m	°C	l/m	l/m	cm	cm	m	cm	mg/l	mg/l	mg/l	mg/l	mg/l	
51	玖須美— 9	45	——	——	12·5	22	5·08	2·99	123	——	——	——	——	——	—— ——
52	松 原—285	91	41·2	15·6	12·7	93	〃	0·79	172	2180	561	48·7	70	141	33 : 26 : 42
53	〃 —222	120	44·1	(20·8)	14·2	85	〃	1·13	198	3400	702	49·0	64	158	51 : 23 : 26
54	〃 —221	73	43·0	9·2	——	——		1·77	——	1180	342	43·6	56	113	17 : 44 : 39
55	〃221附近井戸	——	26·3	——	——	——		——	——	274	132	40·5	79	89	—— ——
56	〃 —220	64	40·0	11·1	9·5	21	〃	1·99	220	389	231	47·8	48	22	5 : 41 : 54
57	〃 —219	73	43·3	11·2	——	——		1·13	——	1960	598	45·7	55	144	29 : 36 : 35
58	〃 —218	73	39·2	31·7	10·8	59	〃	1·46	205	710	294	45·3	46	38	10 : 35 : 55
59	〃 —216	64	43·2	(5·4)	——	——		1·97	——	1176	384	50·2	54	55	17 : 44 : 39
60	〃 —215	55	32·2	22·1	26·5	——		1·59	——	402	204	33·4	41	25	6 : 12 : 83
61	〃 —224	55	37·3	18·7	20·6	45	〃	1·58	203	351	213	47·3	64	26	5 : 31 : 64
62	〃 — 06	91	39·8	28·0	29·0	93	〃	1·96	289	971	352	49·0	52	45	14 : 34 : 52
63	〃 —207	84	41·0	17·8	——	——		1·56	——	984	371	42·6	52	30	14 : 38 : 48
64	〃 —2 3	73	41·2	10·8	——	——		1·80	——	637	277	49·1	46	20	9 : 43 : 48
65	〃 —225	91	33·4	14·3	——	——		1·65	——	355	147	41·2	44	17	5 : 17 : 79
66	〃 —226	78	40·5	(6·3)	——	——		1·66	——	1293	377	45·7	50	126	19 : 33 : 48
67	〃 —209	——	28·5	(4·2)	——	——		1·98	——	139	72	32·8	43	31	2 : 0 : 98
68	〃 —210	——	36·0	——	——	——		1·14	——	134	101	29·6	40	23	1 : 29 : 70
69	〃 —212	73	39·6	[5]	——	——		2·43	——	1881	454	45·6	59	113	28 : 23 : 49
70	〃 —213	82	37·5	——	——	——		1·32	——	1514	477	43·6	58	73	23 : 19 : 58
71	〃 —227	91	37·4	19·3	——	——		2·00	——	1259	379	27·2	56	79	19 : 22 : 60
72	〃 —228	127	43·6	19·7	19·7	153<	〃	1·26	279<	2973	763	72·2	64	138	45 : 26 : 30
73	〃 —232	73	38·0	12·0	10·3	95	〃	0·78	173	1485	485	37·4	68	73	22 : 21 : 57
74	〃 —202	84	42·0	[10]	10·7	70	〃	1·25	195	1174	502	45·8	59	72	17 : 39 : 45
75	〃 —205	91	41·7	(65·7)	——	——		1·24	——	752	330	64·5	45	25	11 : 43 : 46

(次頁へ續く)

第 I 表 (續)

No.	溫泉組合番號	穿井の深 Depth of hot spring	湧出溫度 Orifice temperature	湧出量 Volume output Aug. 25—30	Dec. 1—4	靜止水頭 湧出口上高 Height of statical head above the orifice	口徑 Diameter of orifice	湧出口海面上高 Height of orifice above mean sea-level	靜止水頭海面上高 Height of statical head above mean sea-level	化學成分 Chemical constituents Cl	SO$_4$	SiO$_2$	Alkalinity as CaCO$_3$	Ca	l : m : n
		m	°C	l/m	l/m	cm	cm	m	cm	mg/l	mg/l	mg/l	mg/l	mg/l	
76	松 原—217	73	43·2	(25·8)	—	—		1·23	—	985	331	51·3	53	50	14 : 47 : 39
77	〃 —173	64	43·3	23·7	20·6	87	5·08	1·33	220	995	440	50·7	41	63	14 : 47 : 39
78	〃 —174	45	41·8	[84]	61·2	91	〃	1·16	207	774	377	51·2	41	51	11 : 44 : 45
79	〃 —176	55	44·8	(10·8)	—	—		1·93	—	964	471	47·8	35	65	14 : 53 : 34
80	〃 —184	144	43·2	(63·2)	70·0	150<		1·01	256<	2872	712	58·1	62	114	43 : 40 : 17
81	〃 —191	75	44·0	19·1	—	—		1·35	—	1054	434	52·8	48	62	15 : 42 : 43
82	〃 —194	73	43·0	28·1	27·6	51	〃	2·16	267	1125	483	51·0	47	50	16 : 40 : 44
83	〃 —182	71	46·5	16·2	—	—		1·42	—	1843	550	48·2	54	128	27 : 49 : 24
84	〃 —178	73	47·0	25·7	24·5	—	〃	1·32	—	2782	710	50·4	54	233	42 : 50 : 8
85	〃 —179	45	43·3	[18]	—	—		2·01	—	948	474	51·6	36	75	14 : 47 : 39
86	〃 —181	55	45·3	13·8	—	—	〃	1·45	—	1091	394	51·3	66	135	16 : 46 : 38
87	〃 —238	48	46·3	26·4	24·0	96		1·02	198	1205	560	56·0	35	64	18 : 48 : 34
88	〃 —170	64	45·5	30·0	—	—		1·66	—	1219	415	80·7	45	73	18 : 46 : 36
89	〃 —169	64	44·8	31·0	16·2	74	〃	1·86	260	1236	416	52·3	45	86	18 : 50 : 32
90	〃 —168	63	45·0	[7]	—	—		2·89	—	3193	615	53·3	61	247	48 : 29 : 23
91	〃 —167	65	43·5	28·2	32·7	38	〃	2·04	242	760	362	53·2	39	49	11 : 50 : 39
92	〃 —165	93	45·7	[54]	—	—		2·93	—	3436	878	51·0	59	332	52 : 29 : 20
93	〃 —166	73	43·7	24·7	—	—		1·74	—	1696	564	43·2	53	135	25 : 41 : 34
94	〃 —171	45	34·8	8以下	—	—		2·18	—	144	168	34·4	97	22	2 : 24 : 74
95	〃 — 6	82	37·6	(13·5)	13·2	18	〃	1·89	207	404	173	46·6	50	64	6 : 32 : 63
96	〃 — 3	82	43·7	32·2	28·6	85	〃	1·44	229	2190	447	43·3	36	216	33 : 35 : 32
97	〃 — 10	82	43·0	21·8	15·2	31	〃	1·70	201	1730	437	51·4	35	1140	26 : 38 : 37
98	〃 — 40	129	42·5	(18·0)	—	—		1·17	—	2360	574	47·0	34	796	35 : 29 : 36
99	〃 —武智茂	—	(43·3)	—	—	—		—	—	3260	690	48·0	40	493	49 : 22 : 29
100	〃 — 17	113	45.0	[30]	25·7	52	〃	1 44	196	2730	724	44·0	48	280	41 : 34 : 25

(次頁へ續く)

第 I 表 (續)

No.	温泉組合番號	穿井の深 Depth of hot spring	湧出温度 Orifice temperature	湧出量 Volume output Aug. 25 —30	Dec. 1 — 4	靜止水頭（湧出口上高） Height o statical head above he orifice	口徑 Diameter of orifice	湧出口海面上高 Height of orifice above mean sea-level	靜止水頭海面上高 Height of statical head above mean sea-level	化學成分 Chemical constituents Cl	SO_4	SiO_2	Alkalinity as $CaCO_3$	Ca	l : m : n
		m	°C	l/m	l/m	cm	cm	m	cm	mg/l	mg/l	mg/l	mg/l	mg/l	
101	松 原— 23	78	44·0	10·0	12·6	22	5·08	1·77	199	3000	718	44·2	51	217	45 : 27 : 28
102	〃 — 27	78	44·0	33·7	22·6	45	〃	1·65	210	2950	711	47·0	50	201	44 : 28 : 28
103	〃 —274	91	38·2	11·2	——	——		1·29	——	1470	418	38·8	50	120	22 : 22 : 56
104	〃 — 39	136	47·5	26·5	24·0	55	〃	2·59	314	6340	1054	52·5	81	549	96 : 3 : 6
105	〃 —150	100	49·7	55·0	52·0	83	〃	——	——	4530	698	47·9	60	459	68 : 32 : 0
106	〃 —109	122	47·0	26·9	23·5	100	〃	3·04	404	2370	579	48·2	36	321	35 : 45 : 19
107	〃 — 66	127	49·0	33·5	34·6	75	〃	3·16	391	3960	851	43·8	48	358	60 : 35 : 5
108	〃—153附近井戸	——	20·8	——	——	——		——	——	40	28	35·6	42	32	—— ——
109	〃 —153	55	49·0	69·2	——			2·90	——	3950	724	30·0	47	464	59 : 35 : 5
110	〃 —103	136	49·2	58·5	55·9	53	〃	2·88	341	5050	916	42·7	55	493	76 : 24 : 0
111	〃 — 99	109	47·3	44·7	39·6	73	〃	3·56	429	947	402	40·8	36	147	14 : 62 : 24
112	〃 — 79	117	48·3	21·7	28·5	44	〃	3·73	417	2990	610	44·8	44	289	45 : 43 : 12
113	〃 —154	91	37·5	8以下	——	47	〃	1·65	212	2200	515	41·3	45	250	33 : 12 : 56
114	〃 — 46	140	44·0	19·3	12·9	69	〃	2·54	323	3930	777	66·2	45	674	59 : 17 : 24
115	〃 —284	73	42·0	23·2	22·1	51	〃	1·61	212	1890	524	46·2	45	124	28 : 32 : 40
116	〃 —119	120	45·2	[18]	——			3·24	——	917	380	55·6	46	180	13 : 55 : 32
117	〃 —136	64	43·5	[360]	——			3·49	——	395	275	34·9	46	96	5 : 54 : 41
118	〃 —160	51	44·7	(36)	——			3·94	——	446	308	47·9	35	77	6 : 58 : 36
119	〃 —243	118	47·5	29·0	17·2			——	——	518	343	49·0	43	69	7 : 68 : 25
120	〃 —120	100	47·3	13·8	——	20	〃	4·55	475	766	364	52·4	38	118	11 : 64 : 25
121	〃 —125	145	47·8	47·7	44·5	82	〃	3·60	442	1143	371	59·2	67	148	17 : 62 : 22
122	〃 —132	145	43·3	(3·6)	9立以下	28	〃	3·68	396	1792	479	42·2	40	280	27 : 38 : 36
123	〃 — 55	110	40·5	54·5	54·7	60	〃	3·59	419	816	326	55·5	38	131	12 : 38 : 50
124	〃 — 77	198	48·0	33·3	——	——		3·81	——	875	362	56·2	35	129	12 : 60 : 28
125	〃 — 88	91	50·3	[56]	17·2	25	〃	4·70	495	935	366	47·0	45	133	13 : 74 : 13

(次頁へ續く)

第 I 表 (續)

No.	溫泉組合番號	穿井の深 Depth of hot spring	湧出溫度 Orifice temperature	湧出量 Volume output		靜止水頭湧出口上高 Height of statical head above the orifice	口徑 Diameter of orifice	湧出口海面上高 Height of orifice above mean sea-level	靜止水頭海面上高 Height of statical head above mean sea-level	化學成分 Chemical constituents					l : m : n
				Aug. 25 —30	Dec. 1 — 4					Cl	SO_4	SiO_2	Alkalinity as $CaCO_3$	Ca	
		m	°C	l/m	l/m	cm	cm	m	cm	mg/l	mg/l	mg/l	mg/l	mg/l	
126	松原— 76	127	51·0	21·3	30·6	68	5·08	3·85	453	1479	437	44·8	39	196	22 : 70 : 6
127	〃 — 83	164	50·5	16·6	——	——		4·22	——	2614	653	50·7	45	216	39 : 56 : 5
128	〃 — 82	63	48·0	(21·6)	——	——		3·23	——	906	438	37·4	41	166	13 : 65 : 22
129	〃 — 69	91	52·2	28·7	25·3	27	〃	4·74	501	268	364	55·0	29	105	3 : 63 : 34
130	〃 — 70	109	51·0	18·4	16·0	20	〃	4·72	492	1164	425	51·0	31	161	17 : 74 : 10
131	〃 —248	103	48·0	35·0	——	——		5·01	——	86	282	42·2	21	56	0 : 74 : 25
132	〃 — 22	91	47·0	——	——	50	〃	1·37	212	4150	——	——	——	——	63 : 26 : 12
133	〃 —177	76	——	——	30·8	70	〃	1·30	200	——	——	——	——	——	——
134	〃 —187	82	——	——	18·1	63	〃	1·47	210	——	——	——	——	——	——
135	湯川— 25	178	44·0	22·3	21·5	69	〃	2·61	321	5434	1031	42·2	53	794	82 : 0 : 18
136	〃 — 28	200	42·0	40·0	41·2	145	〃	2·56	401	1 55	548	35·2	13	522	28 : 32 : 40
137	〃 — 31	236	43·5	(108)	——	——		4·33	——	2450	570	32·8	24	574	37 : 31 : 32
138	〃 — 33	236	44·0	72·0	——	——		2·29	——	187	374	35·5	16	87	2 : 58 : 40
139	〃 — 13	218	42·0	43·5	54·7	63	7·62	3·31	394	1800	533	42·6	13	531	27 : 33 : 40
140	〃 — 27	145	42·3	40·5	36·0	128	5·08	3·44	472	309	343	41·0	79	126	4 : 51 : 45
141	〃 — 15	270	43·0	32·5	45·5	53	〃	——	384	2982	628	34·7	41	323	45 : 24 : 32
142	〃 —15附近井戸	——	16·4	——	——	——		——	——	22	47	44·2	42	18	——
143	〃 — 16	158	44·0	28·2	30·0	30	〃	3·00	330	863	381	62·9	37	161	12 : 51 : 37
144	〃 — 17	171	42·5	80·0	——	——		3·04	——	430	344	45·9	28	102	6 : 50 : 44
145	〃 — 1	73	44·7	43·0	31·5	29	〃	3·90	419	435	314	36·3	35	72	6 : 58 : 35
146	岡 —116	121	45·0	[40]	—	——		3·31	——	555	382	85·4	31	54	6 : 58 : 34
147	〃 —112	118	45·0	(3·1)	——	——		5·51	——	596	503	71·5	23	128	8 : 57 : 34
148	〃 —115	——	48·5	(18·4)	——	——		——	——	517	440	161·0	32	32	7 : 72 : 22
149	〃 —107	109	45·0	23·1	22·1	84	〃	5·18	602	258	306	88·7	28	26	3 : 61 : 36
150	〃 —202	111	41·5	18·7	——	——		5·44	——	114	247	99·5	24	29	0 : 50 : 49

(次頁へ續く)

第 I 表 (續)

No.	溫泉組合番號	穿井の深 Depth of hot spring	湧出溫度 Orifice temperature	湧出量 Volume output Aug. 25 —30	Dec. 1 — 4	靜止水頭（湧出口上高） Height of statical head above the orifice	口徑 Diameter of orifice	湧出口海面上高 Height of orifice above mean sea-level	靜止水頭海面上高 Height of statical head above mean sea-level	化學成分 Chemical constituents Cl	SO$_4$	SiO$_2$	Alkalinity as CaCO$_3$	Ca	l : m : n
		m	°C	l/m	l/m	cm	cm	m	cm	mg/l	mg/l	mg/l	mg/l	mg/l	
151	岡 —102	120	48·0	33·7	34·5	66	5·08	4·65	531	749	412	73·8	35	65	10 : 68 : 22
152	〃 — 59	140	51·0	15·0	15·3	65	〃	5·45	610	748	419	87·5	21	82	10 : 78 : 12
153	〃 — 75	91	45·4	15·0	——	——		5·21	——	285	338	65·0	33	38	3 : 63 : 34
154	〃 — 34	82	49·5	20·5	11·5	80	〃	4·71	551	153	318	67·0	21	59	1 : 79 : 20
155	〃 — 32	82	52·2	70·0	79·5	——		4·50	——	450	389	79·8	108	22	6 : 86 : 8
156	〃 —192	220	54·6	[140]	——	——		——	——	88	353	44·7	21	70	0 :100 : 0
157	〃 —148	127	54·5	56·0	49·0	125	〃	5·65	690	87	348	51·0	18	63	0 :100 : 1
158	〃 —191	190	49·0	——	——	——		7·07	——	88	350	52·5	25	71	0 : 78 : 22
159	〃 — 82	91	53·5	47·0	39·7	72	7·62	5·81	653	95	341	54·8	21	63	0 : 95 : 5
160	〃 —187	133	54·7	23·1	40·6	106	5·08.	5·74	680	87	370	43·3	22	56	0 :100 : 0
161	〃 —188	127	51·2	(59·6)	——	——		5·69	——	92	340	36·8	20	67	0 : 49 : 51
162	〃 —189	150	51·8	(27·2)	——	——		6·03	——	73	261	51·3	24	112	0 : 51 : 48
163	〃—70附近井戸	——	19·3	——	——	——		——	——	47	85	42·6	62	44	——
164	〃 — 70	91	53·0	64·0	47·5	58	〃	6·09	667	88	316	54·3	23	55	0 : 93 : 7
165	〃 — 68	91	52·0	52·0	43·3	46	〃	6·15	661	86	287	56·5	23	50	0 : 89 : 11
166	〃 — 63	91	44·5	15·2	——	——		5·34	——	695	200	52·5	29	35	0 : 61 : 39
167	〃 — 62	100	52 0	52·0	41·0	58	〃	5·78	636	99	318	62·2	24	49	0 : 89 : 11
168	〃 — 55	91	44·5	12·3	9立以下	56	〃	4·87	543	84	290	50·2	——	6	0 : 99 : 1
169	〃 — 52	191	51·0	(10·1)	——	——		5·91	——	83	326	54·2	——	6	0 : 86 : 14
170	〃 —185	146	53·5	49·3	47·5	93	〃	5·47	640	85	327	51·3	24	70	0 : 95 : 5
171	〃 —181	124	54·5	53·5	62·0	110	〃	5·60	670	124	362	28·9	25	72	0 : 98 : 1
172	〃 —180	127	51·0	16·4	46·1	12	6·35	4·76	488	2005	524	51·7	37	88	30 : 64 : 6
173	〃 — 11	127	50·0	23·7	19·6	29	5·08	——	451	2567	576	48·0	48	218	38 : 55 : 7
174	〃 — 35	80	43·0	24·7	——	50	〃	2·66	316	763	321	42·2	33	52	10 : 49 : 41
175	〃 — 1	55	48·4	43·5	——	——		4·62	——	918	360	46·5	30	73	13 : 67 : 20

(次頁へ續く)

第 I 表 （續）

No.	溫泉組合番號	穿井の深 Depth of hot spring	湧出溫度 Orifice temperature	湧出量 Volume output Aug. 25—30	 Dec. 1—4	靜止水頭（湧出口上高） Height of statical head above the orifice	口徑 Diameter of orifice	湧出口海面上高 Height of orifice above mean sea-level	靜止水頭海面上高 Height of statical head above mean sea-level	化學成分 Chemical constituents Cl	 SO$_4$	 SiO$_2$	 Alkalinity as CaCO$_3$	 Ca	l : m : n
		m	°C	l/m	l/m	cm	cm	m	cm	mg/l	mg/l	mg/l	mg/l	mg/l	
176	岡 — 19	91	48·7	19·0	——	49	5·08	3·16	365	767	349	50·0	33	82	11 : 70 : 20
177	〃 — 26	155	49·5	43·0	34·3	103	〃	3·44	447	2538	553	63·7	11	160	38 : 53 : 9
178	〃 — 25	109	52·3	54·5	38·4	65	〃	4·92	557	195	324	49·5	26	54	2 : 90 : 9
179	〃 — 21	40	35·5	(15·5)	——	——		3·52	——	132	149	52·4	40	20	1 : 27 : 72
180	〃 — 47	37	39·5	(5·4)	——	——		3·91	——	213	247	48·0	28	32	3 : 41 : 56
181	〃 — 41	145	48·0	16·7	10立位	130	〃	4·78	608	310	309	50·9	30	43	4 : 72 : 24
182	〃 — 27	91	52·5	54·0	30·0	42	〃	5·52	594	99	321	56·4	22	61	0 : 91 : 9
183	〃 —145	140	52·2	31·8	——	——		5·67	——	505	374	91·0	22	66	7 : 86 : 8
184	〃 —199	109	45·9	10·4	12·2	88	〃	5·22	610	269	296	66·9	24	53	3 : 65 : 32
185	〃 — 88	91	48·0	28·5	25·5	31	〃	6·17	648	115	293	85·5	31	31	0 : 72 : 25
186	〃 — 78	91	51·0	(16·7)	——	——		6·20	——	219	299	78·5	25	33	2 : 84 : 14
187	〃 —183	136	50·5	40·5	50·0	67	〃	5·75	642	113	263	75·8	38	40	0 : 84 : 16
188	〃 —206	111	44·0	34·8	——	——		5·79	——	68	204	70·5	39	36	0 : 60 : 40
189	〃 —210	73	40·5	47·5	31·2	70	〃	6·44	714	56	198	47·8	30	29	0 : 47 : 53
190	〃 —211	180	44·9	32·5	29·7	101	〃	7·52	853	77	240	64·8	23	52	0 : 63 : 37
191	〃 —216	160	46·0	18·5	——	49	〃	10·10	1059	68	218	37·6	24	59	0 : 67 : 33
192	〃 -216附近井戸	——	20·7	——	——	——		——	——	22	32	19·0	43	27	——
193	〃 —217	200	45·0	14·8	——	——		14·97	——	84	280	30·3	18	74	0 : 63 : 36
194	〃 —219	173	37·8	[25]	——	——		16·03	——	73	221	24·9	16	53	0 : 36 : 63
195	〃 —129	78	46·2	47·6	41·0	81	〃	7·50	831	74	272	59·3	28	26	0 : 68 : 32
196	〃 —140	127	53·8	47·7	——	38	〃	10·88	1126	83	332	60·2	28	72	0 : 96 : 4
197	〃 — 91	130	48·5	20·5	19·1	59	〃	5·83	642	75	262	65·0	25	74	0 : 77 : 23
198	〃 — 87	125	49·0	10·8	——	——		5·93	——	86	293	63·3	27	77	0 : 78 : 22
199	〃 —87附近井戸	——	22·0	——	——	——		——	——	25	43	40·3	46	21	——
200	〃 —220	95	——	——	25·5	79	〃	6 82	761	——	——	——	——	——	——

（次頁へ續く）

第 I 表 （續）

No.	溫泉組合番號	穿井の深 Depth of hot spring	湧出溫度 Orifice temperature	湧出量 Volume output Aug. 25 —30	湧出量 Volume output Dec. 1 — 4	靜止水頭（湧出口上高） Height of statical head above the orifice	口徑 Diameter of orifice	湧出口海面上高 Height of orifice above mean sea-level	靜止水頭海面上高 Height of statical head above mean sea-level	化學成分 Chemical constituents Cl	SO$_4$	SiO$_2$	Alkalinity as CaCO$_3$	Ca	1 : m : n
		m	°C	l/m	l/m	cm	cm	m	cm	mg/l	mg/l	mg/l	mg/l	mg/l	
201	岡 — 72	109	—	—	9立以下	43	5·08	5·40	583	—	—	—	—	—	—
202	〃 — 80	110	—	—	18·3	50	〃	6·12	662	—	—	—	—	—	—
203	〃 —204	143	—	—	—	88	〃	5·62	650	—	—	—	—	—	—
204	〃 —156	—	—	—	—	47	〃	—	—	—	—	—	—	—	—
205	〃 —216附近新溫泉	—	—	—	—	65	〃	—	—	—	—	—	—	—	—
206	鎌 田— 20	124	44·9	37·7	32·6	120	〃	12·42	1362	79	282	33·0	17	57	0 : 63 : 37
207	〃 — 12	120	49·0	17·7	—	—	〃	13·95	—	85	321	25·4	19	63	0 : 78 : 22
208	〃 — 23	145	47·0	(12·3)	9立以下	34	〃	13·99	1433	69	223	30·6	23	47	0 : 71 : 29
209	〃 — 16	178	35·5	(2·7)	—	—	〃	13·57	—	71	255	30·4	24	62	0 : 28 : 72
210	〃 — 2	170	48·4	37·0	—	154<	〃	—	—	90	349	49·1	30	75	0 : 76 : 24
211	〃 — 22	113	45·2	22·7	—	54	〃	14·01	1455	68	258	29·5	22	46	0 : 64 : 36
212	〃 — 8	180	51·7	19·2	—	77	〃	13·65	1443	85	297	41·8	22	77	0 : 88 : 12
213	〃 — 3	164	52·2	18·8	—	102	〃	10·07	1109	85	337	54·7	27	70	0 : 90 : 10
214	〃 — 13	160	—	—	—	9	〃	13·82	1391	—	—	—	—	—	—

湧出量の欄に（　）［　］を附したるものは夫々容器に依る測定並溫泉組合に依つて昨年度行はれたる測定の値なり．何等の印なきものは前述の湧出量測定器に依り測定したる値なり．

III. 論　　議

1. 伊東町附近の地質と溫泉穿井の深さの分布.

伊東附近の地質は津屋博士の研究[4]に依れば伊豆半島の基底をなすと考へられて居る所謂 Propylite（第三紀）が南方山地の一部に露出し，其上に所謂熱海火山に屬する輝石安山岩の集塊岩と熔岩層（以下第四紀）が介在して伊東低地の北西南の三方を圍繞して山地の基骨をなして居り，南部山地の一部には其上に所謂梅の木平火山及城星火山に屬する橄欖石輝石安山岩及橄欖石玄武岩が存在し，其上に伊東町附近一帶に厚い所では數十米の厚層をなして居る玄武岩質火山荒砂層が堆積して居る．然して之等の地層は伊東低地の兩崖に於て南南西—北北東の2平行斷層に依り切斷され，中央の部は陷沒して低地を作り，其間を松川が流下してそこに松川沖積平地を形成して居る．溫泉は何れも松川沖積平地の部分に湧出して居るのである．

靜岡縣警察部衞生課の調査[5]に依れば各溫泉井の深さは第I表に示した通りであつて，其深さは最淺 40 m 位から最深 270 m までである．其深さの地理的分布を吟味するために，熱海溫泉の研究の場合と同樣に全區域を 100 m×100 m の mesh に分け，相隣接する9の mesh に就き，その中央の mesh の値に2を乘じ，他の mesh の値に1を乘じて加重平均を作り，之を以て中央の mesh に於ける深さとし，この操作を全 mesh に就き行つてこの得られた深さの値の地理的分布を調べた（第5圖）.

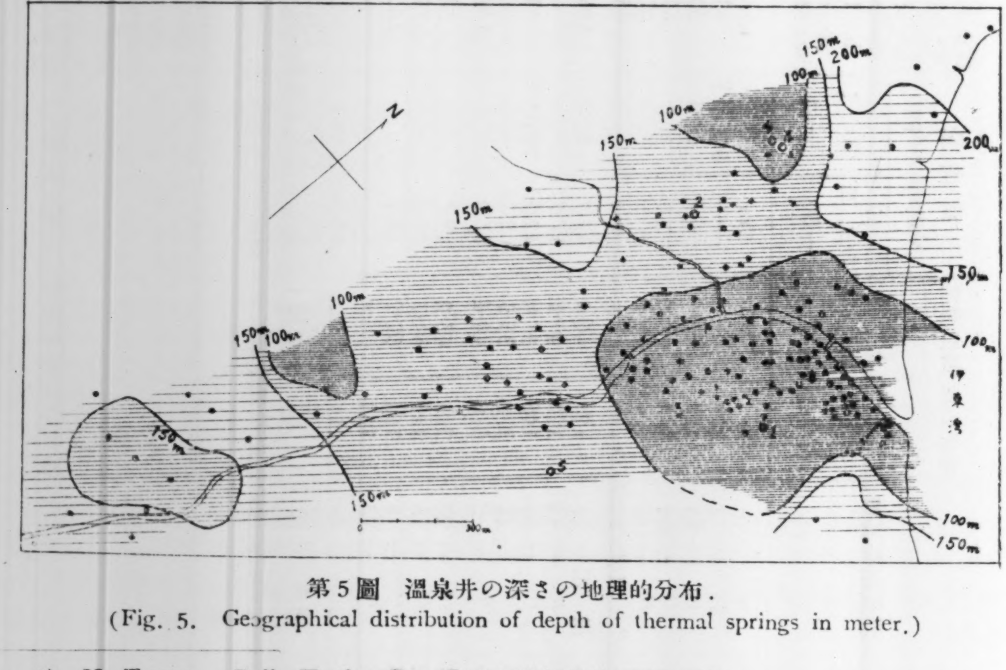

第5圖　溫泉井の深さの地理的分布.
(Fig. 5. Geographical distribution of depth of thermal springs in meter.)

---

[4] H. TSUYA, *Bull. Earthq. Res. Inst.*, **8** (1930), 409～426.

[5] 靜岡縣警察部衞生課, 伊東溫泉調査圖（昭和3年）.

斯くして得られた溫泉井の深度分布は，熱海溫泉の場合の如くには深さの變化が激しい所が見られない．然し乍ら溫泉が比較的淺く湧出する個所は圖に見られる通り3ケ所あつて，古來天然溫泉として知られて居る和田湯[6]（第5圖中1），出來湯[7]（第5圖中3），猪戸元湯[8]（第5圖中2），馬の湯（第5圖中5）及大正12年關東大地震當時，家の床板を破つて噴出したと云ふ場所（第5圖中4）が何れも溫泉が比較的淺く湧出する場所であるのは興味ある一致と云はねばならない．之等穿井の底の部，即ち溫泉の湧出する地層が上記地層の何であつたかは，ボーリングの土質の調査に俟たなければならないが，後述する如く之等の地層の部分では源溫泉及地下水が略水平に流動し混合を行つて居る舞臺に過ぎず，A，B 2 溫泉源の起源は尙深い所にあるか，若しくは他の地區から流れ來つたものと考へられるのである．

2. 溫泉の溫度.

伊東溫泉の湧出溫度は測定數 197 の中，50～55°C のもの 36，45～50°C のもの 64，40～45°C のもの 72，35～40°C のもの 21，30～35°C のもの 3，25～30°C のもの 1 であつて，40～50°C 間の溫泉が全數の約7割を占めて居る．第6圖は伊東溫泉に於ける湧出溫度と，湧出量との關係を示す．その關係は決して簡單ではないが，湧出量の少ない溫泉では溫度が多少低下して居る事が判る．之等は明に溫泉の熱の一部が地表の近くで周圍の土地或は空氣中に逃去る影響であつて，一溫泉に就ては湧出量の少ない時程，氣溫の影響を蒙つて溫度が低い事が知られて居るが，第6圖の如く

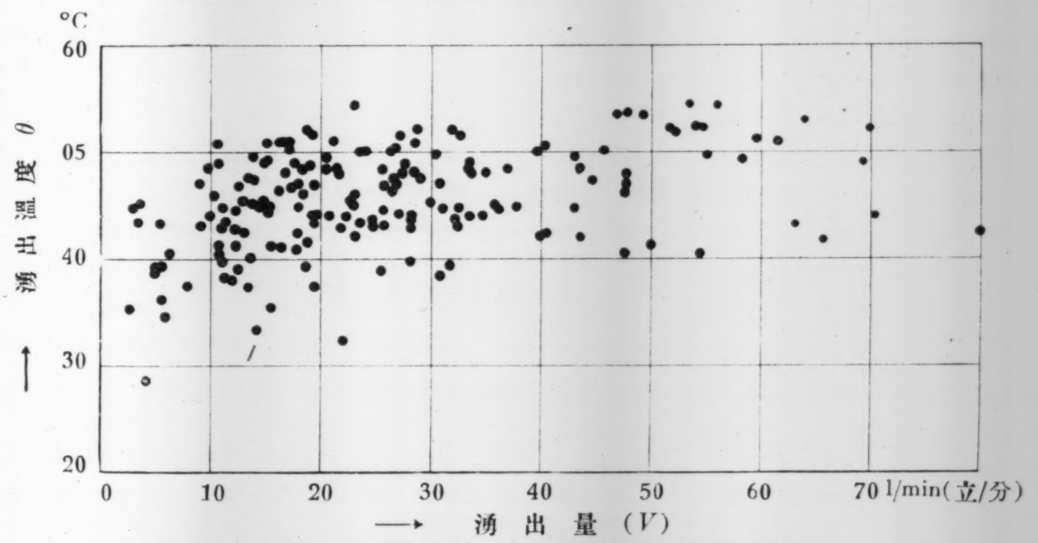

第6圖　伊東溫泉に於る湧出溫度と湧出量との關係.

(Fig. 6. Relation between orifice temperatures θ and volume outputs V of Itô thermal springs.)

---

[6] 慶長3年始めて浴場を構ふと云ふ．（增訂豆州志稿卷 6，38～39.）

[7] 寛永中始めて湧出すと云ふ．（　〃　〃）.

[8] 天保11年始めて浴湯を構ふと云ふ．（　〃　〃）.

一地方の多數の溫泉に就てはあまり簡單な關係が見られないのが普通である．之等の特種の場合9)に就ては旣に論じた所である．今之等土地上層に於ける熱逃避の影響を除去して地下に於ける泉溫の地理的分布を近似的に吟味するために，溫泉の湧出する全面積を 100 m×100 m の mesh に分け，その各々の mesh 中に於ける湧出溫度の最高を以てその mesh の地下に於ける泉溫と見做して之等の溫度の地理的分布を吟味したのが第7圖である．卽ち地下に於ける泉溫の分布は，伊東平地の西邊地區に高く 50°C 以上を示し，其部分を遠ざかると段々低く南方では 40°C 以下の所もある．

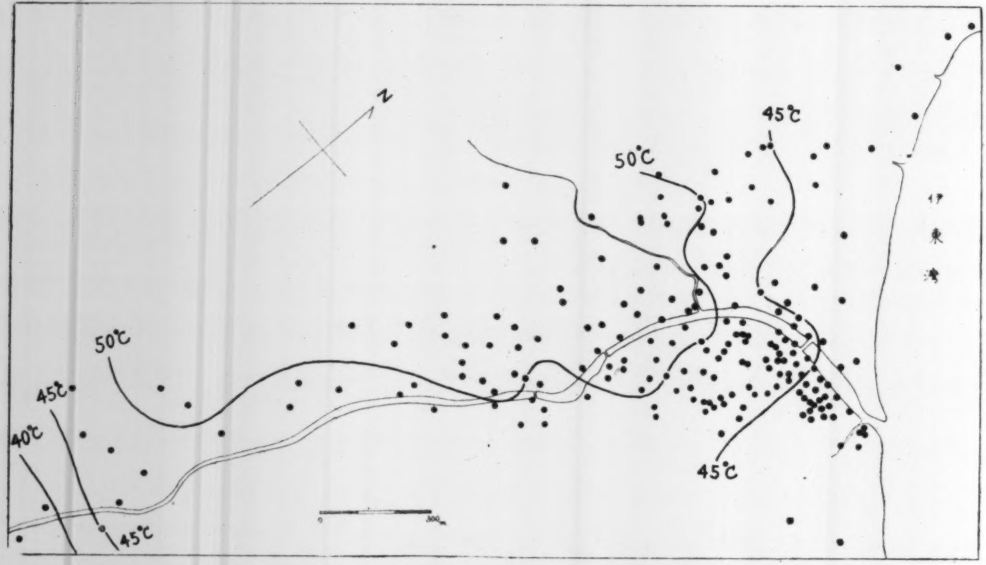

第7圖　地下泉溫の地理的分布

(Fig. 7. Geographical distribution of underground temperature of Itô hot spring.)

3. 鹽分，硫酸鹽，石灰分，珪酸鹽等の地理的分布．

Cl 含有量の地理的分布は第8圖に示す如く，伊東町の海岸寄りで大きく No. 104 では最高で 6·34 g/l に達し，谷の上方岡，鎌田方面では小で 0·01 g/l 以下である．硫酸鹽の含有量も鹽分の分布と全く相似な關係を示し，No. 104 に於て最高 1·054 g/l である．Ca の含有量の地理的分布も第9圖に示す如く略同様な分布を示すが，特に松川以北寺田川以東の地域の溫泉に多く含まれ，No. 97 で最高で 1·14 g/l に達する．SiO_2 の分布は第10圖の如く Cl 含有量，SO_4 含有量，Ca 含有量の分布とは全く異つた様子を示し，岡區松川以南の地區の溫泉に多く含まれ，海岸寄りや鎌田方面の溫泉には殆んど含まれない．

上記の中 Cl, SO_4, Ca 等は主として A なる松原源溫泉に含有され，SiO_2 は岡區松川以南の地域に湧出する冷地下水に含有されて居る事後述の通りである．

---

9) T. Fukutomi, *Bull. Earthq. Res. Inst.*, **14** (1936), 259～270.

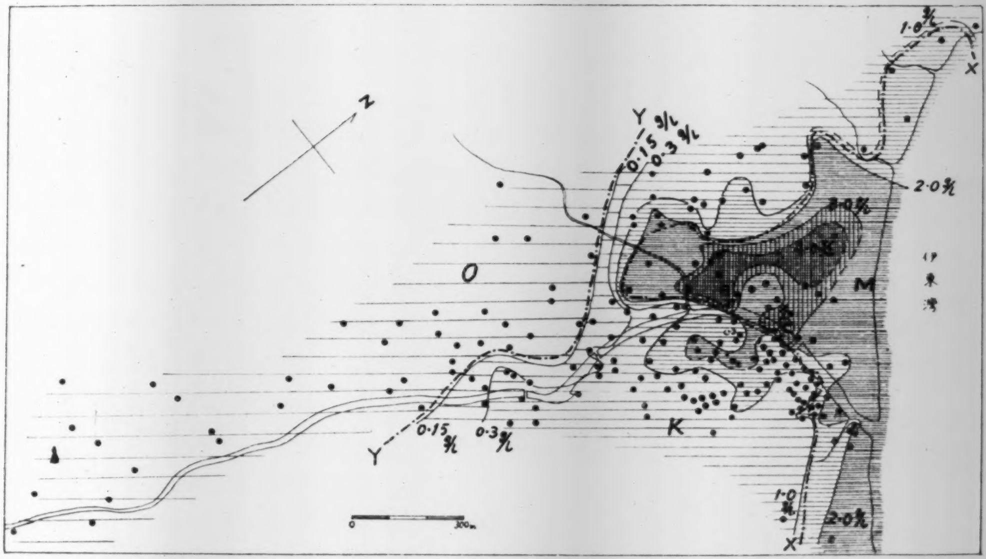
N
Y g/l
0.15 g/l
0.3 g/l
1.0 g/l
X
2.0 g/l
3.0 g/l
O
M
K
伊東灣
0.15 g/l
0.3 g/l
Y
1.0 g/l
2.0 g/l
X
0
300m

第8圖 鹽分含有量の地理的分布

(Fig. 8. Geographical distribution of amount of Cl in g/l.)

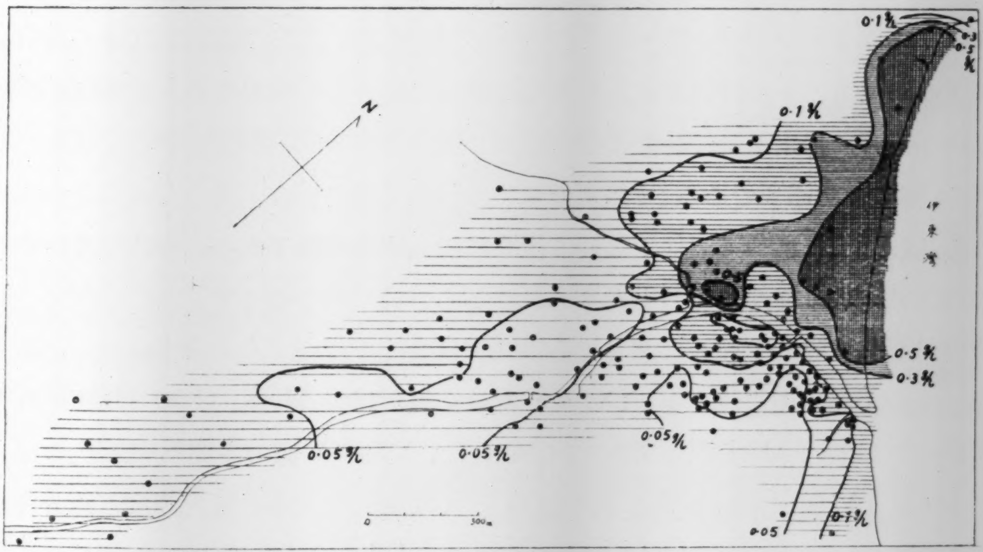
0.1 g/l
0.3
0.5 g/l
N
0.1 g/l
伊東灣
0.5 g/l
0.3 g/l
0.05 g/l
0.05 g/l
0.05 g/l
0.05
0.1 g/l
0
300m

第9圖 Ca含有量の地理的分布

(Fig. 9. Geographical distribution of amount of Ca in g/l.)

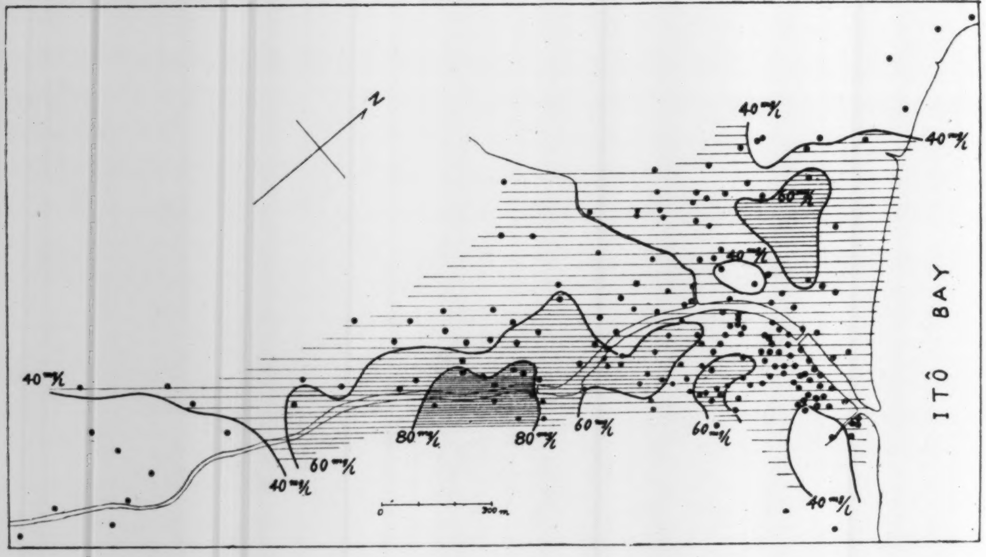

第10圖 珪酸鹽含有量の地理的分布
(Fig. 10. Geographical distribution of amount of SiO_2 in mg/l.)

4. 湧出溫度と鹽分含有量との關係，並に溫泉の系統.

今日までに行つた調査に依れば，一地方の溫泉に就ては溫泉溫度と Cl 含有量との間に簡單な關係が存在し，例へば南伊豆の蓮臺寺，下賀茂，下河津の諸溫泉の各々に於ては湧出溫度と鹽分含有量との間には linear な關係があり，熱海溫泉に於ても之等の間の關係は 2 本の直線で略々表される事が判つたが，之等の直線的關係の說明としては 1 の源溫泉と 1 の冷地下水とが種々の割合で混合した結果であると解釋したのであつた．然るに伊東溫泉に於ては湧出溫度，鹽分含有量間の關係は極めて複雜であつて第 11 圖に示す通りである．(伊東溫泉では熱海溫泉の場合と異つて溫泉井の深さが何れも比較的大であつて，地下に於て溫泉に混入する冷地下水と，極めて淺い普通井戸の水とは可成り異つて居ると考へられるから，此の場合には普通井戸の測定の値は溫泉の値からは除外した)．然し乍ら其關係は全く不規則であるのではなく，第 8 圖に示した如く伊東溫泉地方を XX, YY なる 2 線を以て M, K, O の 3 地區に分ち，XX 線より以北の M 地區内の溫泉を○で表し，XX, YY 線の中間 K 地區内の溫泉を●で表し，YY 線以南の O 地區内の溫泉を × で表して夫等の湧出溫度と鹽分含有量間の關係を圖示すれば第 11 圖の如くであつて，之等の 3 小地區内の各溫泉群に就ては之等の量の間には略々正の相關關係が存在する事を認知する事が出來る．尙之等の點の分布は圖に見られる如く，略々三角形の形を爲して居るのであつて，之等の說明としては從來の考への如く此三角形の 1 つの頂點 A ($\theta_1 = 47{\cdot}4°\mathrm{C}$, $x_1 = 6{\cdot}6$ g/l) で表される樣な溫度は今 1 つの溫泉に比較しては低いが，鹽分の含有量は非常に大きい源溫

泉と，他の頂點 B（$\theta_2=54{\cdot}8$°C, $x_2=0{\cdot}085$ g/l）で表される溫度は可成り高いが，殆んど鹽分を含まない源溫泉と，殘りの頂點 C（$\theta_3=28$°C, $x_3=0{\cdot}02$ g/l）で表される溫度

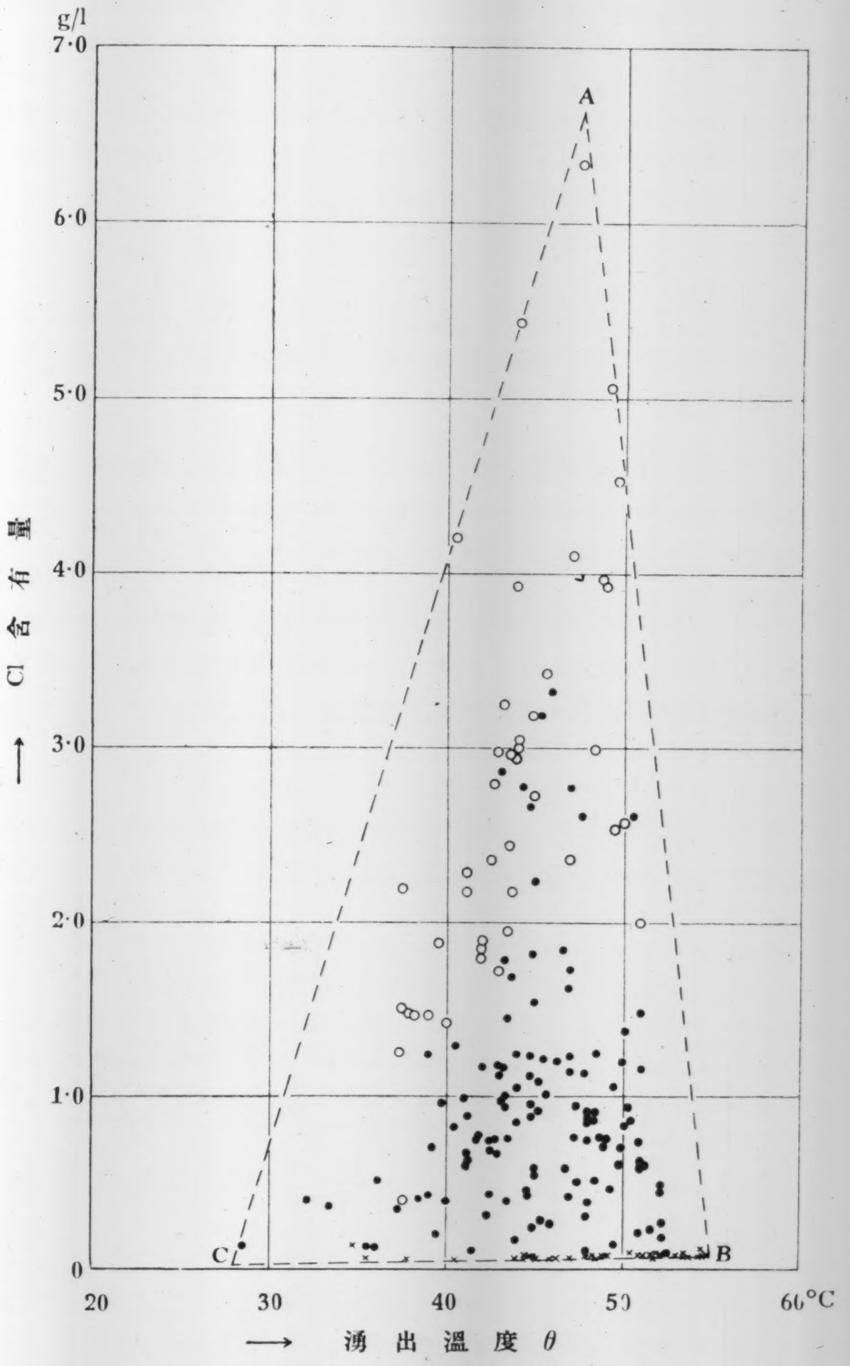

第11圖　Cl 含有量と湧出溫度との關係

(Fig. 11. Relation between Cl-content and orifice temperature θ of Itō thermal spring)

○ 第8圖中 M 地域の溫泉 (thermal spring of M region in Fig. 8.)
● 第8圖中 K 地域の溫泉 (thermal spring of K region in Fig. 8.)
× 第8圖中 O 地域の溫泉 (thermal spring of O region in Fig. 8.)

低く鹽分も殆ど含まない冷地下水との3系統の水が任意に種々の割合で混入した結果と考へれば都合よく説明されるのである．

今 A (θ_1, x_1), B (θ_2, x_2), C (θ_3, x_3) なる3源泉の混入の百分率を l, m, n とすれば，その結果生じた溫泉を (θ, x) とし，溫泉溫度が地表附近に於て低下する影響を度外視すれば（此影響は湧出量が極めて小でなければ度外視しても近似的には先づ差支へないと考へられる.）

$$\frac{l}{(\theta-\theta_3)(x_2-x_3)-(\theta_2-\theta_3)(x-x_3)}=\frac{m}{(\theta_1-\theta_3)(x-x_3)-(\theta-\theta_3(x_1-x_3)}$$

$$=\frac{100}{(\theta_1-\theta_2)(x_2-x_3)-(\theta_2-\theta_3)(x_1-x_2)} \qquad (2)$$

$$l+m+n=100$$

なる關係[10]がある．伊東の各溫泉に於て之等3源泉 A, B, C の混合の百分率 l, m, n を近似的に計算すれば第I表の通りである．之等の値から $r_1=\frac{l}{l+m}$ の値，即ち1溫泉中に混入して居る2源溫泉の混入量の和に對するA源溫泉の混入量の割合を計算して第12圖に其地理的分布を吟味した．r_1 の値はA溫泉のみが含まれる時 $r_1=1$, B溫泉のみが含まれる時は $r_1=0$ となり，A, B が等量に混ずる時 $r_1=\frac{1}{2}$ である．第12圖を見るに r_1 は海岸方面に大きく，特に松原方面では內陸深く入りこんで居り，此方面にA溫泉源が存在するらしい事を暗示する．又 r_1 は岡，鎌田方面に著しく小であ

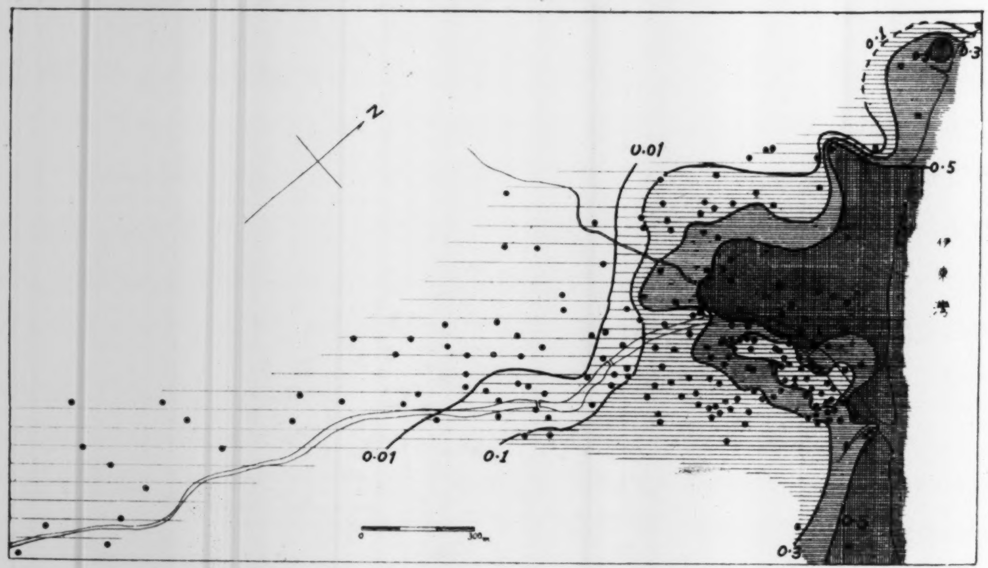

第12圖　溫泉系統分布圖（$r_1=\frac{l}{l+m}$ の地理的分布）

(Fig. 12.　Geographical distribution of $r_1=\frac{l}{l+m}$.)

---

[10] 吉村信吉，地理學評論 8 (1932) 482.

り，B溫泉源が伊東低地の西邊に存在する事を示す．こゝに注意すべきは $r_1<\frac{1}{2}$ なる溫泉分布の面積が$r_1>\frac{1}{2}$ なる溫泉分布の面積に比較して著しく大なる事であつて，之は後述したる如くB源溫泉の壓力がA源溫泉の夫に比較して可成り大なる事とよく一致して居るのである．

斯くの如く伊東溫泉に於ける湧出溫度と鹽分含有量との關係は伊豆に於る他の溫泉例へば熱海溫泉等に比較して可成り複雜であつた．即ち熱海溫泉に於ては各々1個の源溫泉と一つの冷地下水との混合結果と見做し得る異なれる溫泉の系統が二つ獨立に存在し，其中間と見做し得べきものがなかつたのに反し，伊東の溫泉に於てはAなる源溫泉とCなる地下水との混合に依り生じた溫泉系統と，Bなる源溫泉とCなる地下水との混合に依り生じた溫泉系統とが只獨立に存在せずして相互に干渉して其中間性の溫泉を多數に生じたる點に於て著しく異なるのである．之を要するに，之等の差異は恐くは其地下構造上の差異に歸すべきであつて，熱海の場合に於ては第2系統の溫泉は深き部分に層狀をなして可成りの廣範圍に於て存在して居たのに對し，第1系統の溫泉は構造線に沿ひ地下深所より上昇し來り，町中央の極限された小區域に於てのみ湧出するも，其區域內にては極めて淺く堀れば得られたと云ふが如く，兩溫泉系統は地下に於ける其構成を著しく異にしたのに反し，伊東の場合に於ては既に述べたるが如く，其兩系統の溫泉には地下構造上に著しき差異を認め得ざるに依ると考へられるのである．

最後に混入せる冷地下水の百分率の地理的分布を吟味すれば，第13圖の如くであ

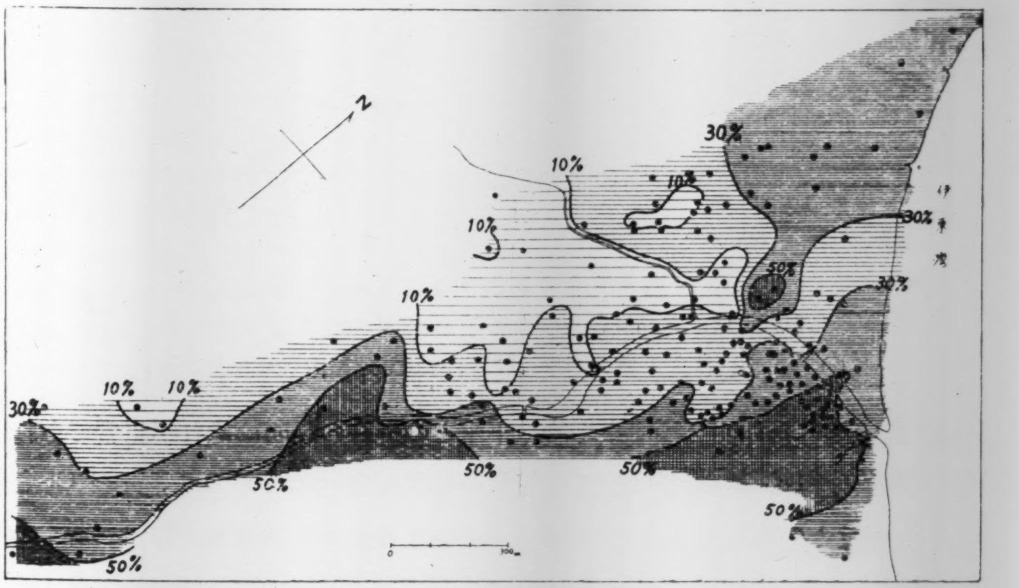

第13圖　混入せる冷地下水の百分率 (n) の分布
(Fig. 13. Geographical distribution of percentage ratio n of mixed underground water.)

る．即ち地下水混入は伊東平地の南東方面及東方に著しく湧出量の5割以上を占める區域も可成り廣く，北西方向に於ては冷地下水の混入は極めて少ないのである．

5. 諸化學成分相互間の關係．

第14圖は Cl-含有量と SO_4-含有量との關係を示すが，この關係を見るに硫酸鹽の含有量と Cl-含有量との間には略々直線的關係が窺はれ，硫酸含有量は Cl-含有量の大なるもの程大である．伊東溫泉に於ては主要成分として NaCl, $CaSO_4$, Na_2SO_4 を含有するから上記の關係から NaCl の分量と（$CaSO_4+Na_2SO_4$）の分量の間には直線的關係がが存在する事が判つたのである．

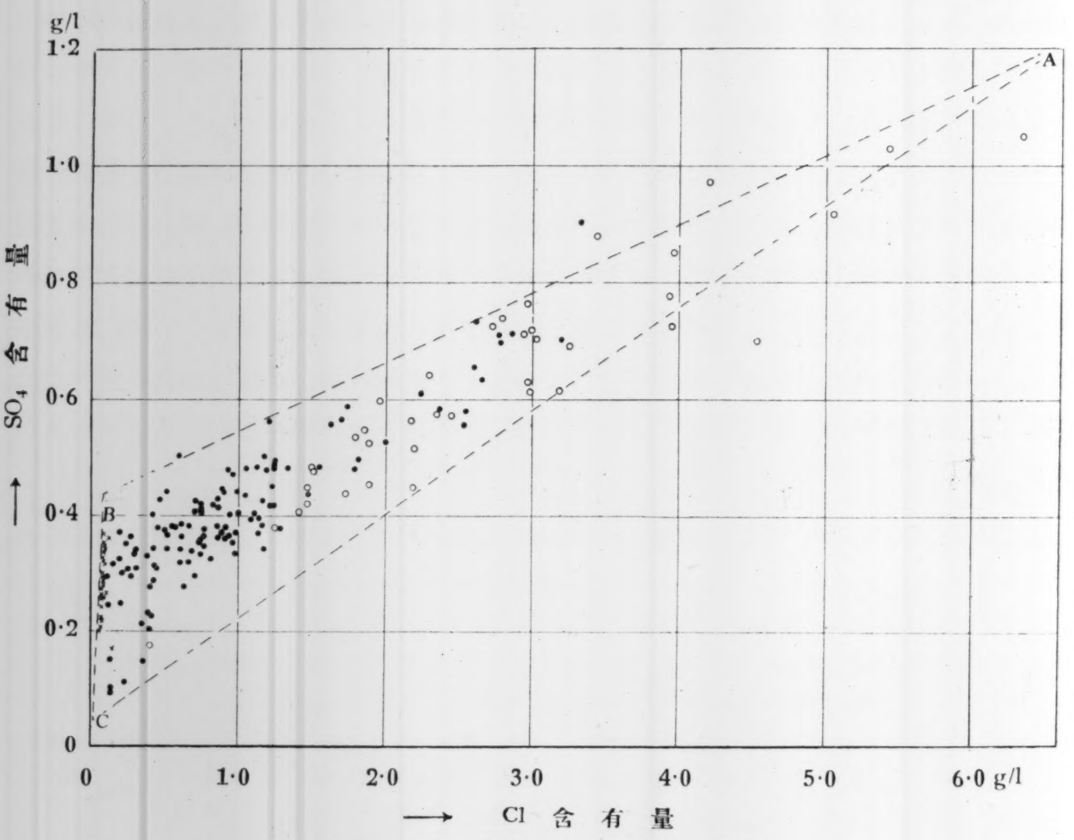

第14圖 Cl 含有量と SO_4 含有量との關係

(Fig. 14. Relation between Cl-content and SO_4-content.)

○, ●, × は夫々第8圖中 M, K, O の 地域内の溫泉を示す。

前節に於て述べた如く2源溫泉と冷地下水との混合の説明はそれが正當であれば，當然諸化學成分相互間の關係に於ても相似の結果を得べきであつて，實際 Cl-含有量と SO_4-含有量との關係及 SO_4-含有量と SiO_2-含有量との關係等に就て，斯くの如き關係が存在する事か判つたのである．之は第14圖に示した如く三角形 A, B, C のBで代表される源溫泉とCで代表される地下水とは，共鹽分含有量及硫酸鹽含有量の少

なき點に於ては類似せるに反し，A なる源溫泉は Cl-含有量大なると共に SO_4-含有量も著しく大であつて，從つて上述の如き直線的關係を生じたるものと考ふる事が出來る．今數量的に之を確めるために前節に於て溫度と Cl-含有量との關係から求めた A,B,C 3 源泉の混合の百分率，l, m, n を今 Cl-含有量–SO_4 含有量の關係から同樣の方法に依つて計算して $r_2=\frac{l}{l+m}$ を求め，横軸に溫度–Cl-含有量の關係より求めた r_1 を縱軸には Cl-含有量–SO_4 含有量から求めた r_2 をとつて點を plot すれば第 15 圖を得る．卽ち點の分布は原點を通り，横軸と 45° の傾きの直線を中心に分布して居て一つ一つの溫泉の場合に於ては可成り異つた値も存在するが，全般の傾向は之等兩方法に依つて求めた値は互に一致して居ると見る事が出來よう．

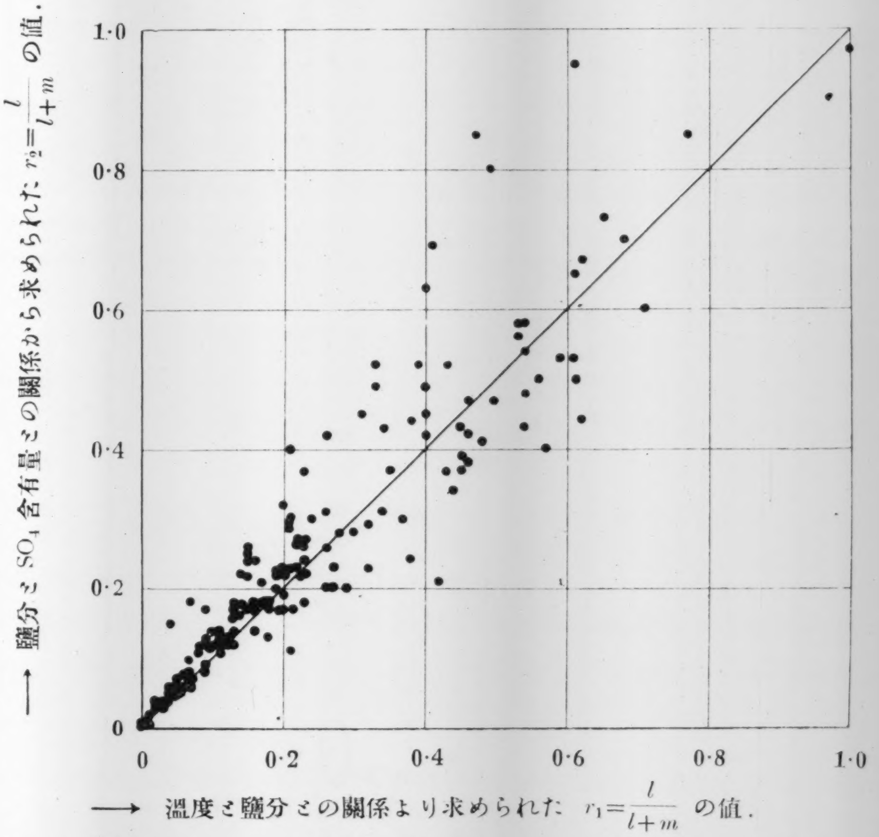

第 15 圖　r_1 と r_2 との比較．（Fig. 15.　Comparison of r_1 with r_2.）

又第 16 圖は SO_4-含有量と SiO_2-含有量との關係を示して居るが，之に於ても點の分布は圖に見られる如く，三角形 ACD で大體表す事が出來る樣である．

Ca-含有量と SO_4-含有量との關係（第 17 圖）は上の場合に比べては簡單ではない．卽ちこの場合には $CaSO_4$ の如き化合物が考へられるからである．今大川以北，支流寺田川以東の溫泉（圖中白丸で示し，他の溫泉は黑丸で表はす）を除けば他の溫泉に

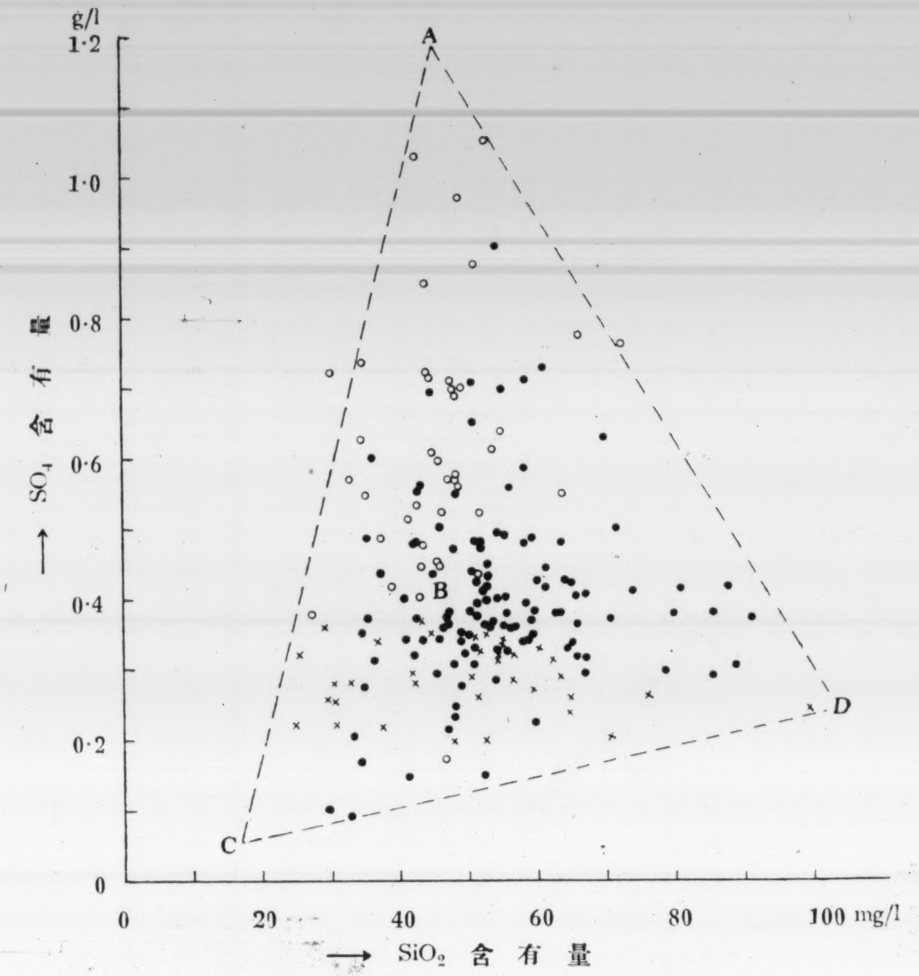

第16圖 SO_4-含有量と SiO_2 含有量との關係.
(Fig. 16. Relation between amount of SO_4 and that of SiO_2.)

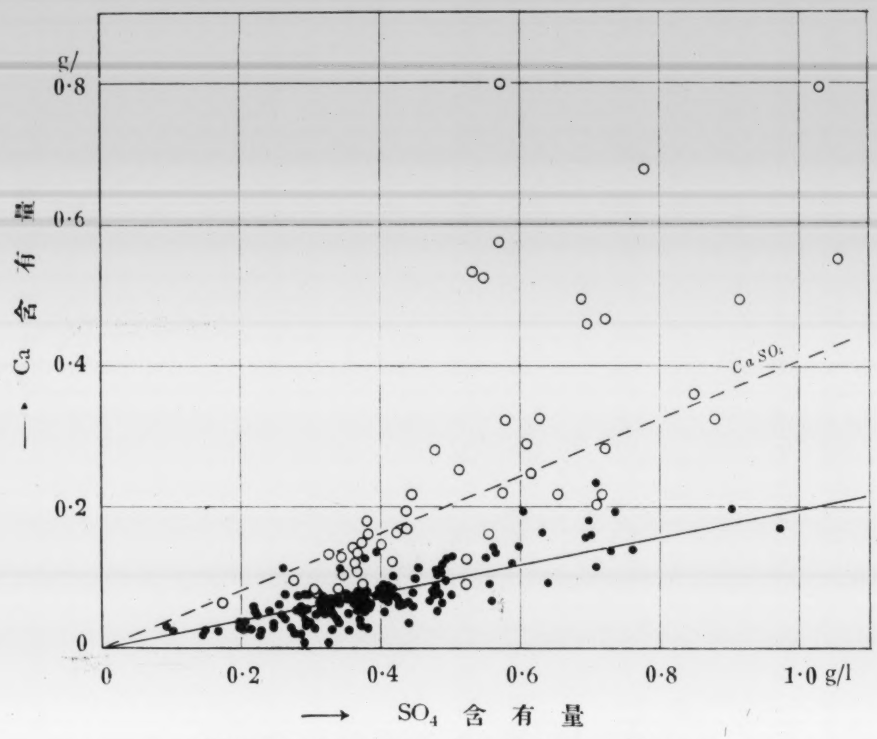

第17圖 Ca-含有量と SO_4-含有量との關係.
(Fig. 17. Relation between amount of Ca and that of SO_4.)

○ 大川及其支流寺田川に依つて限られる北方地區の溫泉
(hot spring of the nothern region which is limited by the River Matu and its tributary Terada.)

● 其他の溫泉 (hot spring of the other region.)

就ては，大約 Ca-含有量と SO_4-含有量との間には linear な關係が見られる．これは第 II 表に示したる如く，伊東溫泉に於ては SO_4-化合物としては $CaSO_4$ と Na_2SO_4 が多く含まれ，他は度外視出來る程度であるから，溫泉中に含まれる $CaSO_4$ と Na_2SO_4 との分量の間に linear な關係があると云ふ事に外ならない．即ち大體に於て伊東溫泉に於ても其中に含有する主成分 NaCl, $CaSO_4$, Na_2SO_4 の含有量の間には直線的關係が存在する事が判つたのであつて，之等の事實も源溫泉と冷地下水との混合に依つて生じたと考へると好都合である事は既に注意した所[12]である．大川以北，支流寺田川以東の溫泉即ち主としてA源溫泉を含む溫泉に於ては Ca-化合物の量は極めて多量に含まれて居る事が判つた．

第 II 表

Table II.

伊東溫泉の主要含有成分

（內務省東京衞生試驗所の分析結果に依る）

含有成分 (Mineral constituents)	松原溫泉[11]	荒木溫泉 （玖須美）	玖須美區溫泉	齊藤氏方溫泉 （岡）
	g/l	g/l	g/l	g/l
NaCl	0·4281	1·3195	0·7628	0·0559
$CaSO_4$	0·1379	0·2436	0·1750	0·0546
Na_2SO_4	0·2771	0·1790	0·2557	0·3209
K_2SO_4	0·0335	——	——	——
$MgCl_2$	0·0221	——	——	——
H_2SiO_3	0·0653	0·0740	0·0688	0·0364
KCl	——	0·0320	——	0·0122
$MgSO_4$	——	0·1653	0·0917	——
$Mg(HCO_3)_2$	——	0·0608	0·0410	——
$CaCl_2$	——	——	0·0228	——
$Ca(HCO_3)_2$	——	——	——	0·0619
第 I 表中の No.	——	——	No. 50(？)	No. 200
溫泉分類	單純溫泉	食鹽泉	食鹽泉	單純溫泉

6. 靜止水頭海面上高の分布．

こゝに靜止水頭とは溫泉井から湧出して居る溫泉の管を繼ぎ足した時，湧出の止つた高さを便宜上呼んだのである．測定可能の溫泉に就て靜止水頭の湧出口よりの高さを第3圖に示した裝置を用ひて測定したが，幸にして靜岡縣警察部衞生課に依つて最

---

[11] R. Ishizu, *The Mineral springs of Japan.*, (1916).

[12] T. Fukutomi, *Bull. Earthq. Res. Inst.*, **14** (1936), 259～270.

近湧出口の海面上高の測定[13]が行はれたので，第I表に示した如く靜止水頭の海面上高を求むる事が出來た．其地理的分布を第18圖に示した．靜止水頭の海面上高の分布は伊東沖積平地の奥，鎌田方面に於て高く，海岸に近づくにつれて概して低いが，特に鎌田，岡の北西部字大久保，下窪方面に於て靜止水頭の高さが可成り高い．此部分では第I表に示した測定を行つた溫泉の外にも第4圖又は第18圖中に a, b, cで示した點では最近掘穿により地上約2 mの高さに噴湯する溫泉が得られたと云ふ事であつて，その海面上の高さも大體第18圖中に記入した．尚，鎌田源溫泉の湧出地點は溫泉の地下溫度の分布や，溫泉の系統分布をも考慮すれば，この附近に存在するらしい事が推察される．

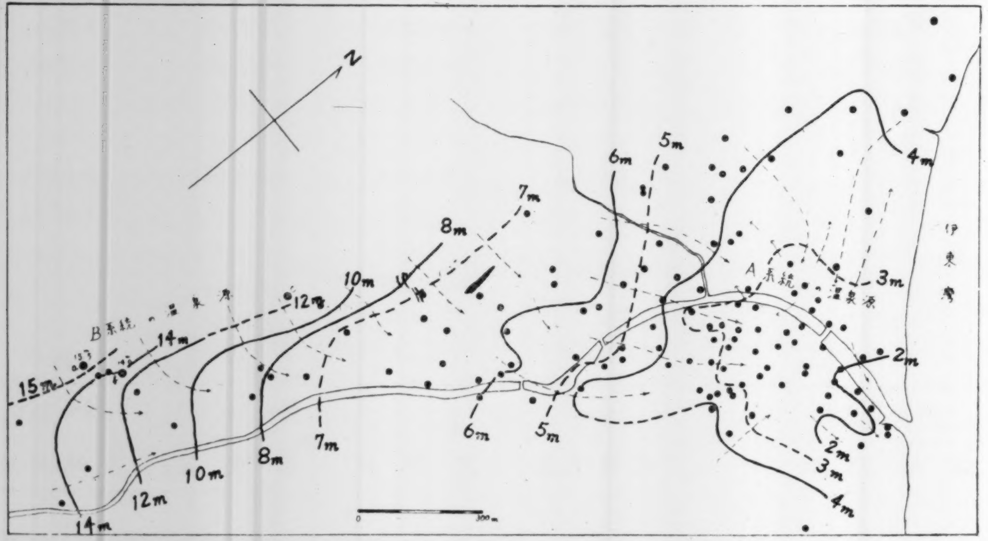

第18圖　靜止水頭海面上高の地理的分布．
(Fig. 15. Geographical distribution of height of statical head above mean sea-level in meter.)

靜止水頭の海面上高は所謂 pressure head に或る常數を加へたものと考へられ，地下に於ける水の水平移動の方向は蓮臺寺溫泉の調査[14]の場合に述べたるが如く，この等高線に直角な方向であるべき筈であり，多少の例外はあるが全體としては，圖中矢印の方向に地下に於て流動が行はれて居ると考へられるのである．

既に述べたるが如く伊東溫泉は3種の水系の混合の結果と考へられるから，上に述べた靜止水頭海面上高の分布は之等の混入後の合成溫泉に就ての結果であるが，3種の水系の相互間の關係は，これに依つては判らない．此關係を明に知る一手段として第19圖に示した如く三成分系を用ひ正三角形内の1點から各邊に下した垂線の長さ

---

13) 靜岡縣警察部衛生課，伊東溫泉調査圖（昭和3年）．

14) T. Fukutomi, *Bull. Earthq. Res. Inst.*, **13** (1935), 616～628．

を以て A, B, C 3水系の混入容積の百分率 l, m, n を表さしめる． この點に靜止水頭の海面上高を記入してその等高線を畫いた．圖から pressure head の最も高きもの

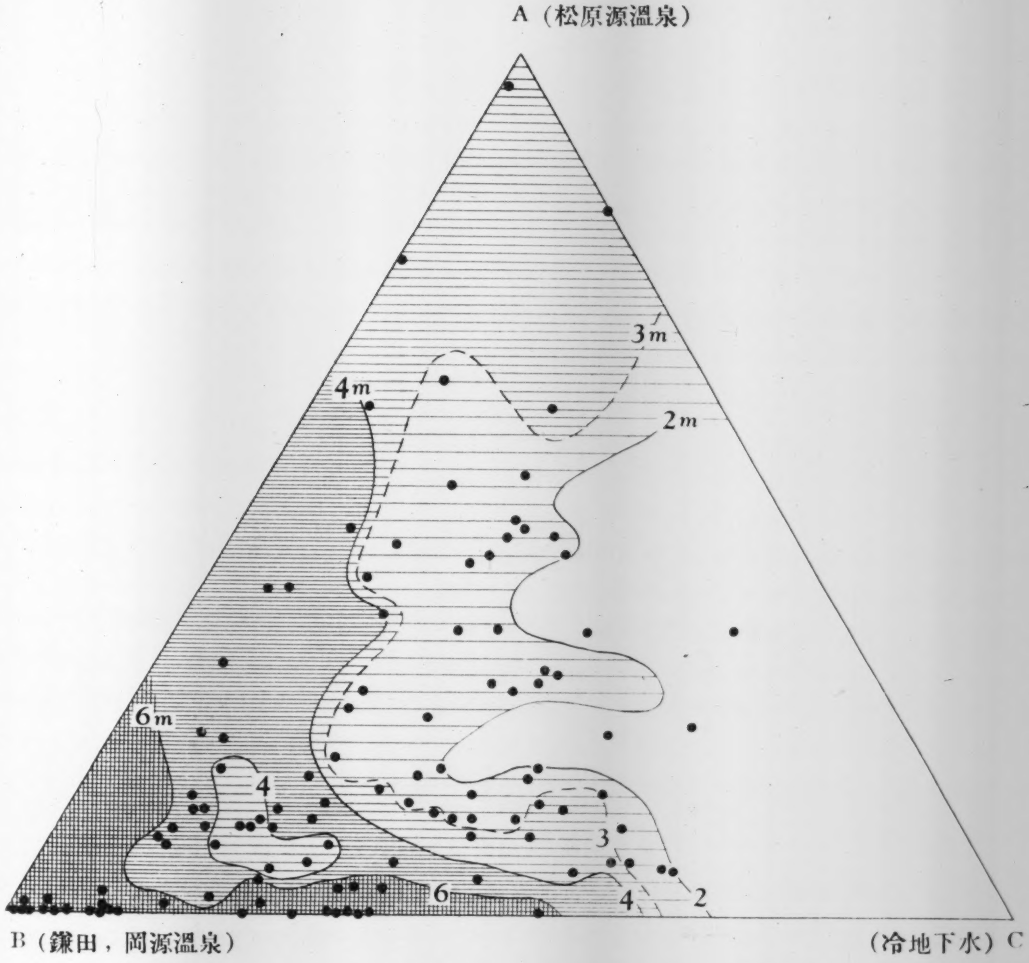

第19圖　三源泉の混入比と pressure head との關係.
(Fig. 19. Relation between the percentage ratio of mixing of 3 source of springs and the pressure head.)

は明に B 卽岡，鎌田源溫泉の多く含まれて居るものであり，A 卽松原源溫泉の多く含まれるもの之に次ぎ，C 卽地下水の多く含まれるものは最も低い．換言すれば岡，鎌田源溫泉は最も其勢大にして，松原源溫泉之に次ぎ，冷地下水は最も弱勢なる事が判つたのである．之は既に溫泉の系統分布の際に述べたる如く，A・B 兩系の溫泉混入の割合 r に就て $r<\frac{1}{2}$ なる溫泉の占める面積が $r>\frac{1}{2}$ なる溫泉の占める面積に比較して著しく大であつた事とよく一致して居り，伊東溫泉に於ては岡，鎌田源溫泉が最も重要な役割をなして居る事が判つたのである．

7. 靜止水頭の湧出口上の高さと湧出量.

次に伊東溫泉に於ては第 I 表に示す如く湧出口の斷面積は多くは一定であつたので

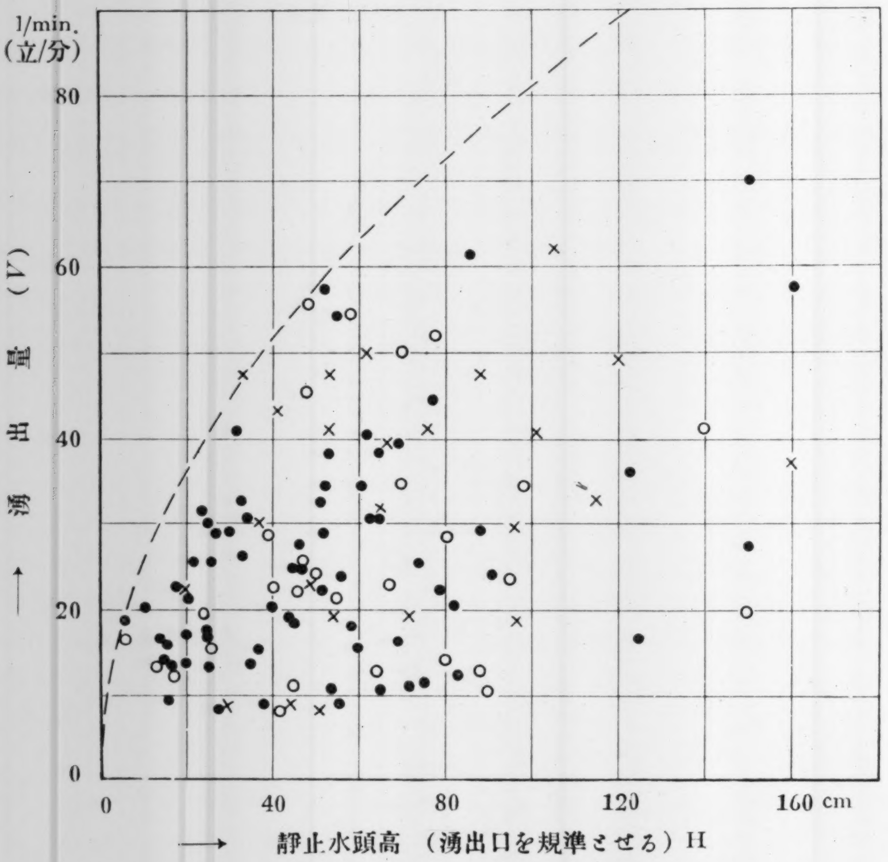

第20圖　伊東溫泉に於ける湧出量と靜止水頭湧出口上高さの關係

(Fig. 20. Relation between volume output and height of statical head above mean sea-level.)

湧出量と靜止水頭の湧出口上の高さとの關係を第20圖に示す如く調べた．圖中○は第8圖中M地區の溫泉，●はK地區内の溫泉，×はO地區内の溫泉を示す．其關係は極めて複雜であつて，上の様な小地區に分けても夫等の間には簡單な關係は見られない．只一つの溫泉に就ては野滿博士の別府溫泉に於ける研究[15]に依れば湧出量Vと靜止水頭の湧出口上の高さHとの間にはCを常數とすれば

$$V=CH \qquad (3)$$

なる簡單な關係がある事が確められたが，此伊東溫泉の場合に於ても斯くの如き關係あるものと假定すれば，第20圖の關係からこのCなる溫泉水路中の摩擦の狀態を示す常數は其溫泉毎に著しく異なり，然かも近接した溫泉でも可成り異つた値を持つ事が判る．こゝに注意すべきは今靜止水頭の湧出口上の高さHと等しい水深を持つ大きな水槽を考へ，その底に湧出口と等しい面積Sなる穴を穿つた時の湧出量V_0

---

15) 野滿隆治，日本數學物理學會誌第10卷第2號別册

は Bernoulli の法則に從つて $V_0=A\sqrt{2gH}$（但し g は地球表面に於ける地球引力の加速度である）であるが，この伊東溫泉の場合では第20圖に示される如く同一 H に對する湧出量 V は決して 0·15 V_0（圖中點線）を超過する事は無かつたのである．

IV. 結　　語

以上に於て伊東溫泉の物理的，化學的諸性質に就て研究した結果，伊東溫泉は二つの性質の異つた源溫泉と一つの冷地下水との混合によりて構成されて居る事，然して其溫泉源の一は伊東町の西方大久保，下窪方面の地下より湧出し，溫度は比較的高く 55°C 以上の溫度を有するが，其化學成分の含有量は極めて少なく勿論單純溫泉に屬する．又其湧出は極めて優勢であつて最も高い pressure head を有する．伊東町附近一帶に堆積する玄武岩質荒砂層の噴出中心は津屋博士の研究に依れば，此溫泉源とはあまり遠くない地點に存在する如くであつて，溫泉現象が火山活動の末期の現象に外ならぬ事を思へば，興味深い事と考へられるのである．今一つの溫泉源は確かな位置は不明であるが，恐らくは松原に於て第4圖中 No. 104, No. 105 の溫泉附近の地下に存在するものの如く，溫度は 47·5°C 以上を有し，其含有する化學成分の量として Cl, SO_4, Ca は極めて大きく夫々 6·6 g/l, 1·2 g/l, 1·1 g/l 以上に達し食鹽泉に屬する．この源溫泉が多量に混入する溫泉が海岸線に沿つて存在する事は，この溫泉と海水との間に多少の關係ある事を暗示する樣に見える．又海岸近くの溫泉では其湧出量は潮汐の滿干に伴つて增減し，例へば潮位 1 m の變化に對し第4圖中 No. 132 の溫泉では平均湧出量 50立/分であつたが其1割，尙海岸に近い No. 6 では平均湧出量は 19立/分位であつたが，其4割の變化を行つた．然し乍ら湧出溫度や鹽分含有量は測定の誤差の範圍では殆んど變化が認められなかつたのは，南伊豆谷津溫泉の場合[16]と同樣であつた．尙之等の問題に就ては今日の所俄に其因つて來る所の推測を許さないのであつて將來の綿密なる調査に讓り度いと思ふ．最後に混入する冷地下水は略 28°C の溫度を有し，含有する化學成分は槪して極めて少なく第13圖に示す如く，伊東平野の南東部の地下に主として湧出するが，嚴密には旣に注意した如く2種類の冷地下水があつて外の點では略々同性質であるが，岡區大川以南の地區に湧出するものは他のものに比較して可成り多量の SiO_2 を含有する點に於て異なるのである．

終りに臨み伊東に於ける2回の測定に際し，種々御後援を辱ふしたる伊東溫泉組合に對し，特に觀測中終始同行され御懇切なる御援助を賜つた伊東溫泉組合片岡熊之助氏に對し厚く感謝の意を表する次第である．又本研究に關し種々御批評並御助言を賜つた坪井忠二先生に對し厚く御禮申上げる次第である．　（昭和12年3月20日）

---

[16] 福富孝治，地震 8 (1936), 457〜468.

30. *On the Thermal Springs of Itô, Izu Peninsula.*

By Takaharu FUKUTOMI and Zirô HUZII.

(Mitsui Geophysical Obeservatory.)

Itô, situated at the eastern coast of Izu Peninsula, is one of the most famous hot spring resorts in Central Japan. At present, there are about 400 thermal springs of which volume output in total amount attains to so great amount as $2{\cdot}16\times10^5$ hectolitres per day. The writers recently had an opportunity of observing the orifice temperatures, the volume outputs (see Fig. 1 and 2), the heights of the statical head (see Fig. 3) beside analysing some of the chief chemical constituents of the water of 207 of these thermal springs. (see Fig. 4 and Table I). The results of this investigation are briefly summarized as follows:

(1) It seems that the depths of hot springs indicate approximately the depth of the source of the hot water, their geographical distribution was investigated as shown in Fig. 5. The depth change from 40 to 270 m, and there are no such rapid changes of depth which were seen in case of the Atami hot springs. An interesting coincidence is that the natural springs from ancient time are in regions where the wells are comparatively shallow.

(2) Fig. 6 shows the relation between orifice temperatures and volume outputs of the thermal springs of Itô. The distribution of the underground temperature of the hot springs was also investigated as shown in Fig. 7.

(3) The geographical distribution of the amounts of Cl, SO_4, Ca and SiO_2 were found to be as shown in Fig. 8, 9 and 10. The first three of them, except SiO_2, show rather similar distribution, being the large concentration found in the coastal region of Itô where the source of hot springs of A type exist. SiO_2 was contained chiefly in the cold underground water originated from the underground of eastern parts of Itô basin.

(4) Fig. 11 shows the relation between orifice temperatures and amounts of Cl. From the figure, being estimated that Itô thermal spring were the mixture of two primary hot springs A (47·4°C, 6·6 g/l), B (54·8°C, 0·085 g/l), and one cold underground water C (28°C, 0·02 g/l), we calculated the percentage ratio l : m : n of mixing respectively. Fig. 12 indicate the geographical distribution of the value of $r_1=\dfrac{l}{l+m}$ which is the percentage ratio of A primary spring to the total volume outputs of two primary hot springs. From the figure, we can see that the A or B primary hot spring exists in the underground of the coastal region or south-western suburb of Itô town. Fig. 13. shows the geographical distribution of the percentage ratio of the cold underground water.

(5) Fig. 14 shows the relation between Cl-contents and SO_4-contents. From the figure, calculating again the percentage ratio $r_2=\dfrac{l}{l+m}$ of mixing of the primary spring A and B, the relation between r_1 and r_2 was investigated in Fig. 15. Fig. 16 shows the relation between the amounts of SO_4 and those of SiO_2. Relation between amounts of Ca and amounts of SO_4 was shown in Fig. 17. From the figure, we can see that there are linear relation between the amount of $CaSO_4$ and Na_2SO_4 contained in the thermal springs of Itô, excepting the hot springs exist in the northern region limited by the River Matu and its tributary Terada, where the Ca-contents are very large.

(6) Fig. 18 shows the geographical distribution of the statical head above mean sea-level. Fig. 19 shows the relation between the pressure head of the hot springs and the percentage ratio l : m : n of mixing of 3 primary springs A, B and C. From the figure we can conclude that the primary hot spring B has the greatest pressure, and the underground water C has the smallest

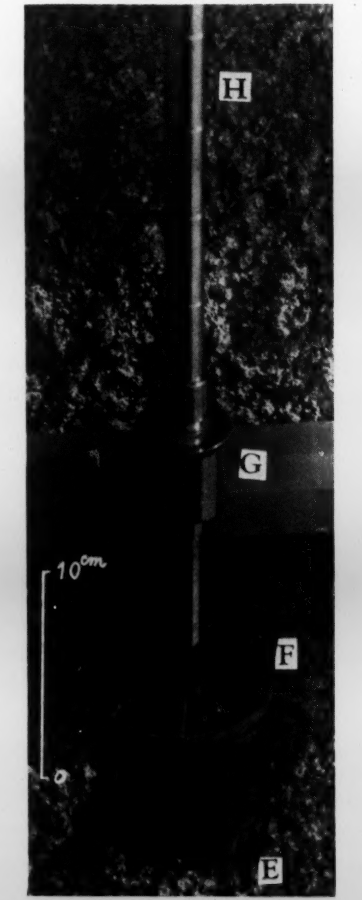

第1圖（甲） 湧出量測定器

(Fig. 1 (a) Volume output measuring device).

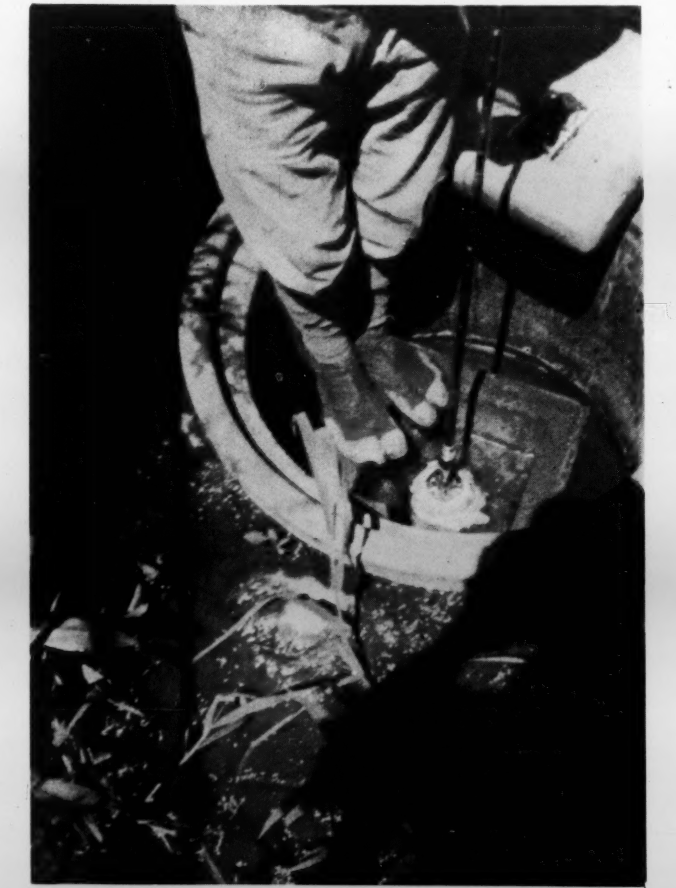

第1圖（乙） 伊東町鎌田區鎌田共同湯（No. 212）に於る湧出量測定の實況.

(Fig. 1 (b) Measurement of volume output of a hot spring of Itô.)

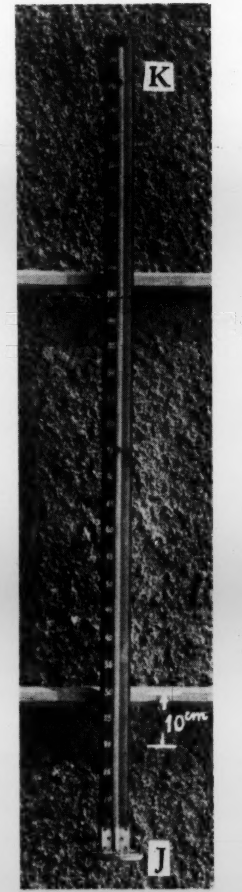

第3圖 靜止水頭測定裝置（全長160糎）

(Fig. 3. Statical head measuring device.)

pressure.

(7) Fig. 20 shows the relation between the volume outputs and the heights of statical head above the orifices of the Itô thermal springs. The relation is not so simple as referred to one hot spring.

(8) There is no doubt of the existence in the town of Itô and neighbourhood of 3 primary springs of entirely different character–the one (B) characterized by high temperature, small amounts of chemical constituents, and the other (A), differing from the preceding in its relatively low temperature, moderate quantity of chloride, sulphate, Ca, and the last one (C), the cold underground water.

31. 震央距離の比較的大なる地震による東京近傍卓越振動周期

地震研究所 石本巳四雄

（昭和12年3月16日發表―昭和12年3月20日受理）

緒　　言

著者は數回に亘つて加速度地震計觀測結果より地震動の1特徴と見られる，各地に固有的に發生する震動の卓越周期を問題となし，所謂地盤の良否と密接の關係ある事を述べた[1]．此の事實は實際の大地震の際特に木造建築物の破損，倒壞に至る實狀に照し，良く一致する事は勿論である．然し乍ら，震央距離の大小によつて地震動中に卓越する振動周期に差異あるのではないかと云ふ疑問を抱く人々も尠くない事を思ひ，此の點を充分確めて置く必要を痛感した次第である．從つて今回は特に震央距離の比較的大なる地震を選び，東京附近にて觀測した地震動に就き卓越震動周期を調べる事とした．勿論前論文中にも已に報告したものもあるが，其等も再錄して論ずる事とした．

今回の觀測に使用した加速度地震計の常數等に關しては總て前回と同樣であるから此所には述べない．又觀測點の位置も前回と同樣であるが，2～3改廢の行はれたのは止むを得ない．而して今回問題となした6個の地震は次の如くである．

A	昭和 8年3月 3日	三陸沖合地震
B	昭和 8年6月19日	金華山沖合地震
C	昭和 9年4月 7日	鹿島沖合地震
D	昭和 9年8月18日	岐阜八幡附近地震
E	昭和10年3月31日	鹽屋崎沖合地震
F	昭和10年7月11日	靜岡附近地震

以上の地震につき震央距離，各觀測點における最大加速度等は次の如くである．

---

[1] 石本巳四雄　震研彙報 **10** (1932), 171; **12** (1934), 234; **13** (1935), 592; **14** (1936), 240.

發震時	震度		各地最大加速度 (gal)											初期微動繼續時間（本鄉）	震央	震央距離（本鄉）
			本鄉	丸ノ內	神田	青山	濱松町	駒場	向島	深川	赤羽	野毛山	橫濱公園	高島町		
昭和 8 年 月,日 時 分 3 3 2 32	III	S	18·7	26·0	33·5	27·3			27·0	27·7		22·7		20·7	sec 66·0	三陸沖	km 568
		N	24·5	23·5	37·8	29·2			29·2	32·7		26·3		16·4			
		W	21·3	26·6	26·2	36·4			20·4	44·3	27·9	21·2		20·7			
		E	25·1	30·8	23·3	26·5			18·5	36·6	33·3	18·7		19·2			
		平均	**22·4**	**26·7**	**30·2**	**29·9**			**23·8**	**35·3**	**30·6**	**22·2**		**19·3**			
6 19 6 38	II	S	3·8	9·6	7·0	8·4			8·6	12·9	5·9	6·2	9·5	7·2	43·1	金華山沖	377
		N	3·7	10·6	6·0	6·8			6·5	9·8	6·8	6·2	8·6	7·6			
		W	4·4	8·0	6·0	6·1			7·5	9·4	7·2	7·0	10·8	6·5			
		E	3·9	8·3	6·9	7·0			7·0	10·5	5·9	7·8	13·0	7·8			
		平均	**3·9**	**9·1**	**6·5**	**7·1**			**7·4**	**0·7**	**6·5**	**6·8**	**10·5**	**7·3**			
昭和 9 年 4 7 4 10	II	S	7·0	8·0	8·8	6·2			6·8			8·2	4·5	2·7	26·2	鹿島灘	227
		N	7·0	8·7	9·7	7·4			7·2			6·3	4·0	2·2			
		W	6·5	8·2	7·1	10·4			7·4			5·8	4·7	1·6			
		E	5·8	9·1	8·0	8·7			6·2			9·4	4·8	1·3			
		平均	**6·6**	**8·5**	**8·4**	**8·2**			**6·9**			**7·4**	**4·5**	**2·0**			
8 18 11 40	I	S	1·9	3·2	2·6	2·0			2·4		1·9		5·2	2·3	30·2	岐阜八幡附近	243
		N	1·6	3·0	3·9	1·8			1·3		2·3		6·0	2·5			
		W	1·5	4·0	2·7	1·7			1·1		2·3		4·2	3·2			
		E	1·4	3·6	2·5	1·6			1·1		2·5		4·8	2·4			
		平均	**1·6**	**3·5**	**2·9**	**1·8**			**1·5**		**2·3**		**5·1**	**2·6**			
昭和 10 年 3 31 6 20	II	S	4·1	8·0							4·4			2·7	27·2	鹽屋崎沖	247
		N	5·0	8·3							3·8			2·9			
		W	5·1	10·1				6·0			5·8			3·2			
		E	5·1	9·2				6·8			7·9			3·5			
		平均	**4·8**	**8·9**				**6·4**			**5·5**			**3·1**			
7 11 17 25	II	S	5·1	9·7			6·0				4·7			9·2	18·2	靜岡附近	146
		N	4·1	11·8			7·1				5·1			9·7			
		W	3·8	11·0			4·9				4·7			12·5			
		E	3·4	12·1			7·1				5·2			12·1			
		平均	**4·1**	**11·2**			**6·3**				**4·9**			**10·9**			

以上の表に見る如く，最大加速度は一般に下町の方が大であるのは，何れも震央距離の大なる地震を問題として居るからである．此の事實は已に述べた事であるが，今回も同樣に證明された譯である．

各論

A. 昭和 8 年 3 月 3 日三陸沖合地震（第1圖）

此の地震は三陸沖合，釜石東方 200 粁附近に震央のあつた地震であり，地震動は各地において災害を齎す程度とはならず，釜石においても不良構造住宅が，小破したのみであつた．此の地震は反つて津浪を伴つた點に於て注目されたもので，其れに關する報告は多い2)．

此の地震に就て東京附近の觀測は 9 個所において加速度地震計により觀測され，卓越周期は已に報告されたのであるが，比較のため今一度掲載する．地震動は東京に於ても比較的强く感ぜられ，本鄕，青山，野毛山(横濱)の如き山ノ手にては 0.3 秒附近に卓越周期が認められる事は一般の地震と同樣である．又丸ノ内は 0·6 秒，神田は 0.7 秒に明瞭の固有振動周期が認められて居るが，深川，向島，赤羽，高島町の如きは比較的廣い範圍の周期に分布して居る事が判る．以上の中後者は何れも表面土層の厚い地域であり其の基本周期，倍音周期の發生に相當して震動の發生が行はれて居る如く見られる．一般に云へば遠い地震に關しては基本周期の震動多く，三次振動の發生は少ないのが原則と思はれる．即ち遠い地震によつ

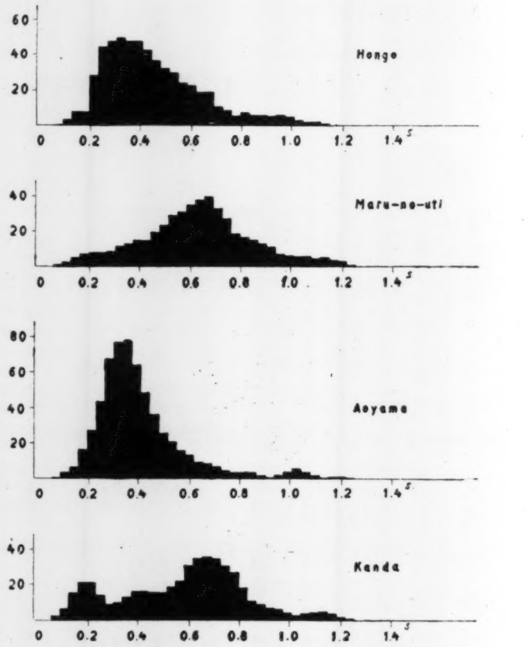

第 1 圖　昭和8年3月3日 三陸沖合地震による各地震動卓越周期

---

2) 震研彙報 別冊第1號，氣象要覽，驗震時報．

て地盤の悪しき所が益々其の特長を發揮する事となる.

B. 昭和8年6月19日金華山沖合地震（第2圖）

此の地震は3月3日の津浪を伴つた地震の餘震とも考へられる. 相當著しい震動を與へたもので，當時津浪の來襲が懸念されたが，其の來襲は無かつた. 因に此の地震に伴つた餘震の發生は見なかつたもので，其の關係に就ては別に論及してある[3].

第2圖を見るに，本郷に於ては0·4秒，0·9秒，青山においては0·4秒，0·8秒，1·2秒の卓越周期が見られ，横濱野毛山にては0·3秒，0·5秒，0·7秒の卓越周期が認められる. 此の現象は已に論じた事もあるが，從來の例に徴して特別の考へ方が行はれて居る[4]. 卽ち此れは恐らく其の土地固有のもののみならず，他地域から擴散し來つた波動が重疊して居ると見る事が出來やう. 又丸ノ内は0·6秒，神田は0·7秒附近に極大のあるのは通例の場合と一致する. 赤羽，向島及び深川は互に類似性を示して居り，夫れ夫れ0·8秒，0·7秒及び0·9秒が各地の基本振動周期の如くに考へられる. 何れにも0·3秒附近のものが見えるが，此れは三次振動周期或ひは山手より擴散し來つた

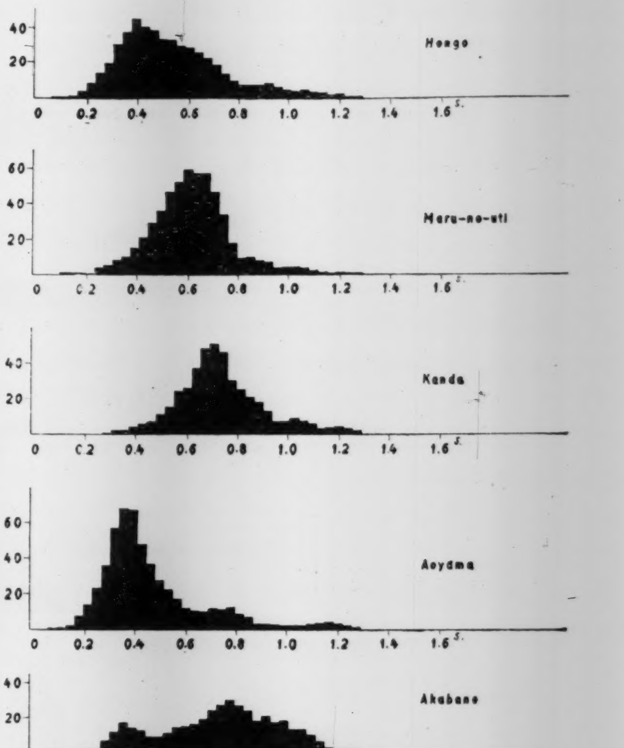

第2圖 昭和8年6月19日 金華山沖合地震による各地震動卓越周期

---

3) 石本巳四雄 地震 9 (1937), 108.

4) 昭和6年10月3日 秩父地方に起つた地震は此の樣式を最もよく示した. （前掲）

波動とも考へられる．横濱公園の特性は非常に偏平にて 0·5 秒及び 1 3 秒附近に極大が見られる．此の地域には 1·3 秒程度の周期の震動が著しく發生する事は且て注意した事である．高島町に於ては 0·8～1·1 秒に頻度の大なる所が見えるが，此れは今回問題とした他の何れの地震に對しても同樣の現象が見られる．卽ち此れは此の土地の震動習性として見る事が出來やう．

C. 昭和9年4月7日鹿島沖合地震（第3圖）

此の地震は東京附近に於ては些して大なる地震ではなかつた．本郷，青山，駒場の山手におけるものは例によつて 0·3 秒附近の卓越振動周期を示したが，丸ノ內は 0·6秒，神田は 0·2 秒及び 0·6 秒であり，向島に於ては 0·2 秒と 0·9 秒附近，横濱公園にては 0·6 秒，1·3秒，高島町にて 0·9～1·2 秒の卓越周期が觀測された．下町におけるものは一般に各周期に一樣の發生を與へ，一見平坦なる狀況を示して居る．

D. 昭和9年8月18日岐阜八幡附近の地震（第4圖）

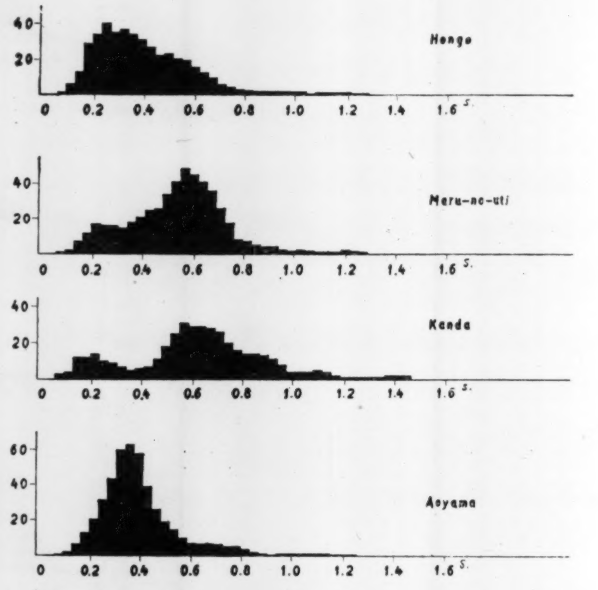

第3圖 昭和9年4月7日 鹿島灘地震による各地震動卓越周期

氣象要覽によれば此の地震の震央附近に於ては，木造家屋の大破．石塔の顚倒等もあつたと報告されて居るが，東京附近に於ては漸く有感覺の程度であつた．共の震動中卓越せるものは，第4圖に示すもので，此の場合震央が觀測點の西方にあり，且つ陸上に存在した事が以上3例と異るものである．

本郷においては珍らしく 0·45 秒及び 0·7 秒に卓越振動があつた．斯様の類似例は昭和 6 年 8 月 10 日の大井川附近に就て其の例を見た．震央方向が同じく西方にあつた關係であらう．青山も極大が二つあり本郷の例とよく似て居る．丸ノ内は 0·6 秒，神田は 0·7 秒にて一般の場合と一致して居る．向島，赤羽は何れも 0·7 秒及び 1·0 秒に卓越周期あるが，曲線は寧ろ平坦である．横濱公園は特に 1·4～1·8 秒に波の多いのが著しく，高島町に於ては 1·1 秒に極大が認められる．

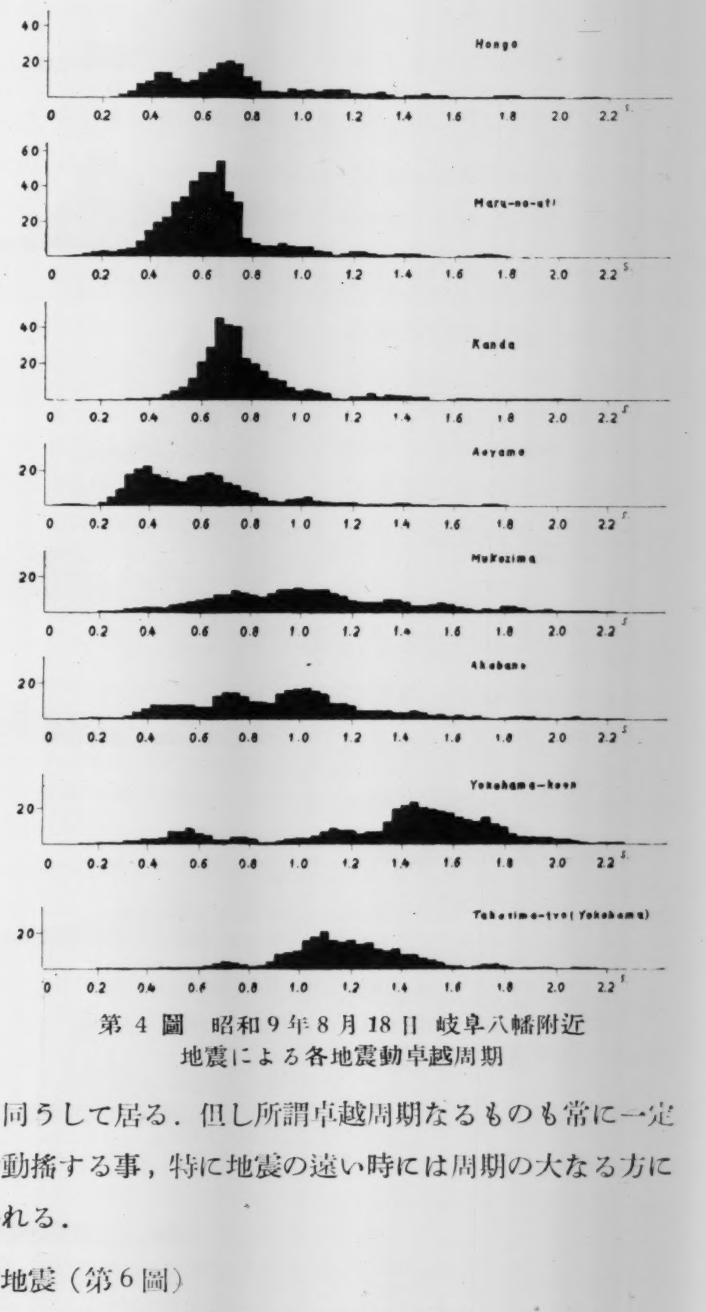

第 4 圖　昭和 9 年 8 月 18 日 岐阜八幡附近地震による各地震動卓越周期

E.　昭和 10 年 3 月 31 日鹽屋崎北東沖地震（第 5 圖）

本郷 0·4 秒，丸ノ内 0·7 秒，赤羽 0·4 秒及び 0·8 秒，高島町 0·4 秒及び 1·1 秒に何れも極大が認められた．何れの曲線を見ても一般の場合と傾向を同うして居る．但し所謂卓越周期なるものも常に一定でなく，震央距離に從つて多少動搖する事，特に地震の遠い時には周期の大なる方に片寄る事が一般特長として見られる．

F.　昭和 10 年 7 月 11 日靜岡地震（第 6 圖）

此の地震は靜岡市附近に起つたもので，家屋大破，石燈籠倒壞等の起つたものである．東京に於ては震度 II の程度であつた．本郷は 0·3 秒，丸ノ内 0·7 秒，濱松町 0·3 及び 1·1 秒附近，赤羽 0·4 秒，0·7～1·1 秒，高島町 0·3，0·7，1·0 秒等である．

結　　論

以上の如く震央の比較的遠方にあつた地震の東京附近に與へた地震動は其の土地固

有の振動の誘起されたものが，卓越周期となつて現はれる事は從來述べた事と同樣であるが，山手におけるものは多少其の周期の大となる事が認められる．又下町に於ては其の地域の表面土層の厚さと密接の關係にあるものとして，此の場合其の基本振動周期が多く出現する如くである．此れに反して近い地震においては三次振動と思はれるものが多く誘發されるのである．

以上を要するに，地震の遠近によつて地震動中に卓越する震動中，加速度の大なる震動の振期は大差なく，其の地域の固有振動と信ずべきものが發生し，所謂地盤惡しき所に於て，木造家屋の倒壞する事實は以上の觀測と一致するものである．卽ち山手においては特にある限られた周期（0·3秒附近）のみが加速度の大なる震動として卓越する關係上，其の最大加速度は比較的大であつても，周期の大なる建物，例へば五重塔の如きは倒壞に至らぬと思はれる．此の事實は家屋の

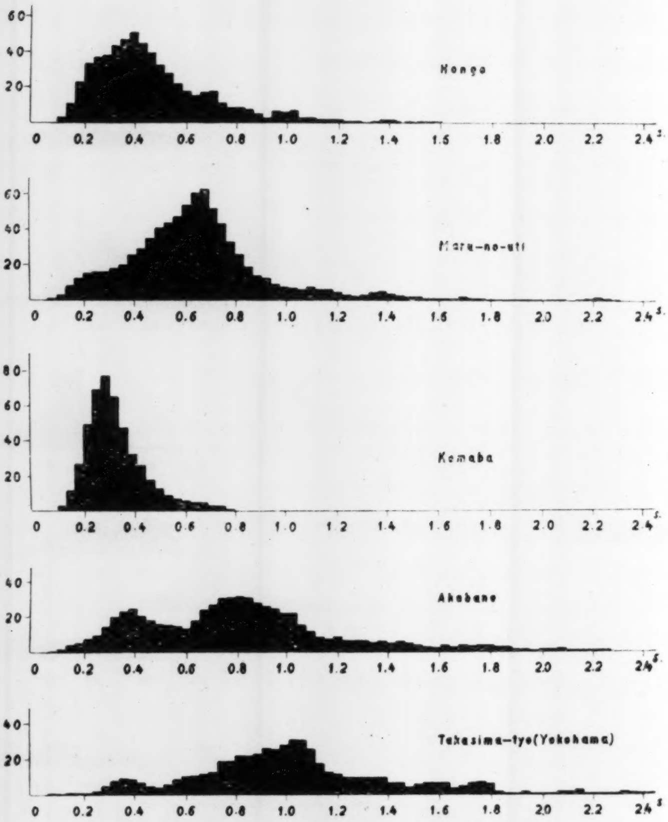

第 5 圖　昭地10年3月31日 鹽屋崎沖合
地震による各地震動卓越周期

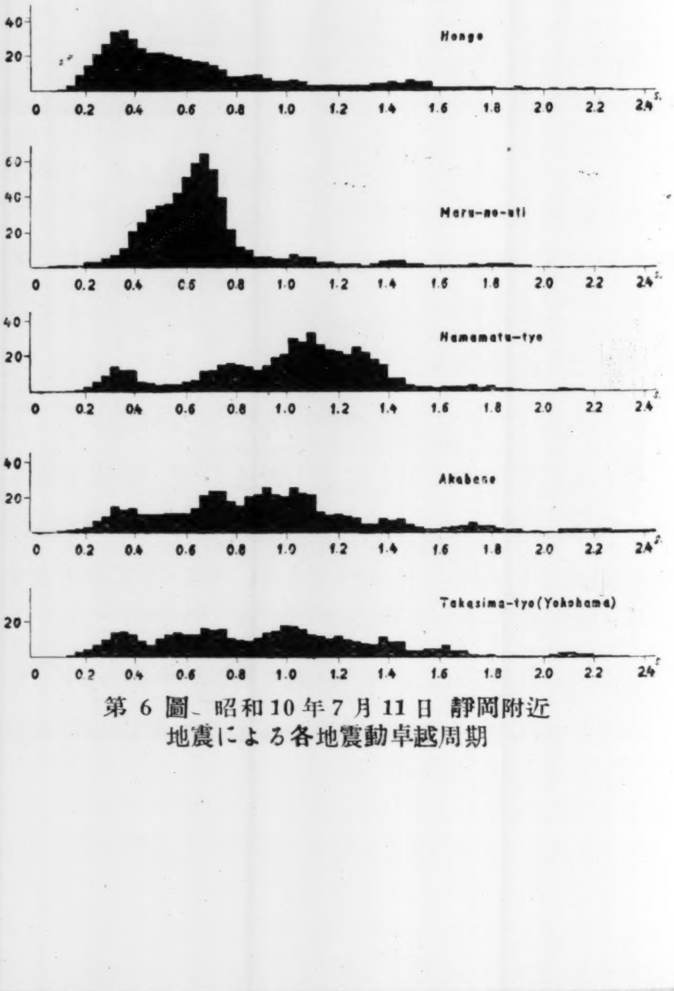

第 6 圖　昭和10年7月11日 靜岡附近
地震による各地震動卓越周期

構造上特に注意すべき性質にて，先づ山手と下町とにては地震動中卓越振動周期の異る事實及び最大加速度の異る點を充分參酌して，耐震上萬全を期する事を努力すべき性質のものと信ずる.

終りに臨み此等の觀測は服部報公會及び日本學術振興會の援助の下に行はれたるものにつき，深甚の謝意を表する次第である.

附記： 因に震央距離の大なる地震に對しては，寧ろ下町の地震動の最大加速度が優れて居るが，今此れを何處も一定と假定する．然る時，震動の變位振幅を考へると，其れは振動周期の二乘に比例する．卽ち加速度の大なる震動の振幅は下町に於て4～10倍となるのは當然の事となる．而して此の振幅の大となる事は木造家屋の如き變形性ある物體に對しては，充分破壞を齎すべき要素として考へられるものであるが，單に震動振幅と云へば變位地震計によつて得られる加速度の小なる震動の振幅を採用する虞れが充分ある爲め，筆者は加速度の大きさと共の振動周期とに注目して地震動を解釋し，震害の如何を論ぜんとするものである．振幅を問題とすべしと云ふ棚橋博士の所說[5] に關し，以上の意味に於て全くの贊意を表するものである.

31. *Observations des périodes prédominates dans les secousses séismiques dont la distance épicentrale est assez grande*

par Mishio ISHIMOTO,

Institut de Recherches sur les Tremblements de terre.

Nous avons étudié les secousses séismiques dont la distance épicentrale est assez grande. Nous constatons en tout cas que les secousses observées à chaque station ont une relation serrée avec la couche superficielle et la période n'est que celle de son oscillation propre. Quand la distance épicentrale deviend assez grande, il y fréquente l'oscillation fondamentale de couche surtout dans la partie basse de la ville de Tôkyô.

5） 棚橋諒： 建築雑誌 **49** (1935), 578.

32. 土の收縮に關する二三の實驗

地震研究所　飯田汲事

（昭和12年3月16日發表――昭和12年3月22日受理）

1. 緒　言

東京近傍特に江東地帶[1]或ひは丸の內地帶[2]等の地盤沈下に關する最近の研究によると，共の原因の大部分は地表面にある軟弱地層の收縮に在る樣である．從つて此の地表面の軟弱地層の收縮を生ぜしむ可き原因を調査研究する一手段として，土の種々なる物理的，力學的諸性質の研究が必要となる．從來此の方面の土の性質の研究特に表面荷重或ひは自重による土の壓縮沈下[3]，水分減少による土の收縮[4]等の實驗的研究は澤山あるが，振動による土の收縮沈下を取扱つたものが尠い樣である．

吾々は自動車，電車等の交通機關或ひは工場の電動機等共の他のものが地面に與へる振動の相當大なる事を日常經驗する所であるが，石本博士[5]の最近の研究によれば，地面微動に消長があり1日中に於て共の微動振幅の最大は日中に於てであり，或る場合には共の値が相當大なる値に達する事もある．又夜中に於て共の微動振幅が最小となり微動も休息した樣な狀態となる．斯くの如く晝夜の間に於て微動に消長のあるのは，共の原因の大部分は交通機關等に因るものであらうと思はれる．

本實驗の目的は此等の問題と關聯して行はれたもので，自然の堆積狀態の土に於てその含水量減少による收縮と振動の影響による收縮とを比較研究し，又一方土の含水量減少による土の密度及び高さの變化は土の種類及び狀態によつて差異ある事を前論文[6]に於て指摘したが，今回は更に詳細に此等の關係を實驗的に求めたのである．猶最後に此等の實驗結果より土の構造に關し二三の考察を試みる事とした．

試驗土の種類は本鄕大學構內に於て地表面下2mの表面層中より採取せる赤土及び

1）宮部直巳　地震研究所彙報 **10**（1932），884；**13**（1935），587；**13**（1935），763；**15**（1937），102；基礎研究 **1**（1937），16.
渡邊貫　地質學雜誌 **42**（1935），634；鐵道省土質調查委員會報告 **4**（1936），63.

2）北澤五郎　基礎研究 **1**（1937），11.

3）鐵道省土質調查委員會報告；基礎研究；內務省土木試驗所報告等參照.

4）宮部直巳　地震研究所彙報 **13**（1935），763.
高田昭　內務省土木試驗所報告 **20**（1931），1.

5）石本巳四雄　地震研究所談話會發表.

6）石本巳四雄，飯田汲事　地震研究所彙報 **15**（1937），67～86.

丸の內第一生命保險相互株式會社建築敷地の地表面下約 8 m の表面層中より採取せる沈泥質粘土にして，前回[7]採用したものと全く同種類のものである.

2. 實　　驗

(1) 靜力學的實驗及び結果

此の實驗は要するに試驗土の含水量を減少せしめ，含水量と體積減少或ひは密度の變化を測定したものである.

先づ最初採取せる自然狀態に近い土塊より切斷面積は何れも 4·5 cm×4·5 cm，高さは本鄉の赤土に於て約 30 cm，20 cm，15 cm 等，丸の內の沈泥質粘土に於て約25 cm，15 cm，10 cm 等の試驗土柱を切り取り其の重量及び體積を測定し，次に此等を略々溫度一定の室に放置し極めて徐々に水分を蒸發せしめ，約1ヶ月に亘り1日に1回乃至2回宛其の重量及び體積，高さの變化等を測定した．又同時に含水量をも測定したが，最初の含水率は本鄉の赤土では 55·2%，丸の內の沈泥質粘土では 50·0% であつた．體積の測定には物指にて縱，橫，高さを量りそれより求める方法及び水銀を充した壺の中に土柱を押し込み，土柱の體積により流出した水銀の重量を測定し，此の時の溫度に相當する密度を用ひて土柱の體積を知る方法の兩方法を同時に採用したが，兩者は測定の誤差の範圍內に於て一致した．斯くして體積と重量との關係より土の密度を測定した．その密度と含水率との關係は第1圖，第I表に示してある．第1圖に示す如く，本鄉の赤土は丸の內の沈泥質粘土に比較して密度が小さく又含水率に對する變化も異つてゐる．卽ち含水量に對する其

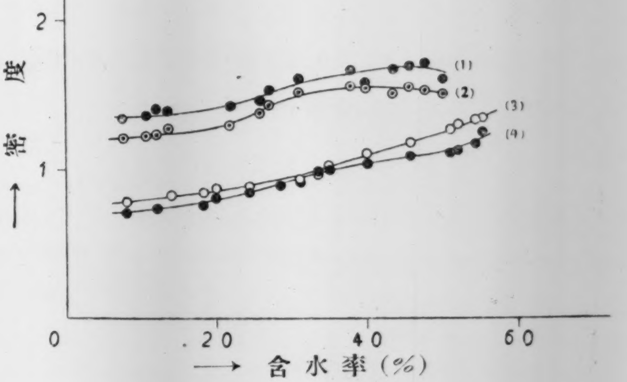

第1圖　含水率と密度との關係

縱軸：密度　橫軸：含水率（%）

(1)，(2) は丸の內の沈泥質粘土

(3)，(4) は本鄉の赤土

(1)，(3) は最初 20 分間振動を與へ後水分を減少させた場合である.

Fig. 1. Diagram showing the relation between moisture content and density of soil in the natural state.

Abscissa: moisture content (%). Ordinate: density.

(1), (2): the silty-clay at Maru-no-uti.

(3), (4): the loam at Hongô.

(1), (3): showing the effect of vibration for 20 min at initial state.

---

[7] 石本巳四雄，飯田汲事　地震研究所彙報 **14** (1936)，632.　機械的分析の結果は同論文中の第1表に示してある.

第 I 表 含水率及び密度

沈泥質粘土 （丸の内）			赤土 （本郷）		
含水率	密度 (No. 1)	密度 (No. 2)	含水率	密度 (No. 1)	密度 (No. 2)
50·0	1·60	1·49	55·2	1·34	1·25
47·6	1·72	1·56	54·3	1·33	1·18
45·6	1·70	1·54	52·0	1·30	1·13
43·4	1·67	1·59	51·0	1·27	1·11
39·8	1·60	1·68	45·7	1·18	1·09
37·8	1·67	1·63	40·0	1·11	1·04
30·9	1·61	1·53	35·0	1·03	1·00
27·0	1·53	1·48	33·6	0·97	0·99
25·9	1·45	1·39	31·1	0·94	0·93
21·9	1·42	1·33	28·6	0·90	0·89
13·6	1·39	1·29	22·2	0·38	0·84
12·1	1·38	1·26	20·0	0·86	0·80
10·8	1·36	1·21	18·2	0·84	0·75
8·0	1·34	1·20	8·0	0·78	0·73

の密度の變化は本郷の赤土に於ては殆ど直線的關係を保つて變化するが，丸の內の沈泥質粘土は含水量の減少に對し最初はその密度を增加する傾向にあるが，含水率30%以下となるに及び密度は減少し其の變化は本郷の赤土の如き傾向を示す事が判明した．圖中番號を附してあるのは土に一定時間約20分間共鳴の狀態に於て振動を與へた場合と然らざる場合とを比較對照したものであつて，番號(1)，(3)は何れも振動による場合で，振動の影響により體積の減少を生じ密度が大となつてゐる．

含水率に對する體積變化，高さの變化，橫幅の變化等は第2圖，第3圖，第4圖に示してある．又縱幅の變化もあるが此れは橫幅の變化と同程度のため其の圖は省略した．

含水量の減少に伴ひ體積，高さ，橫幅等は何れも減少するが，本郷の赤土と丸の內の沈泥質粘土とでは其の減少狀態が異り，丸の內の土は 50% より 30% 迄

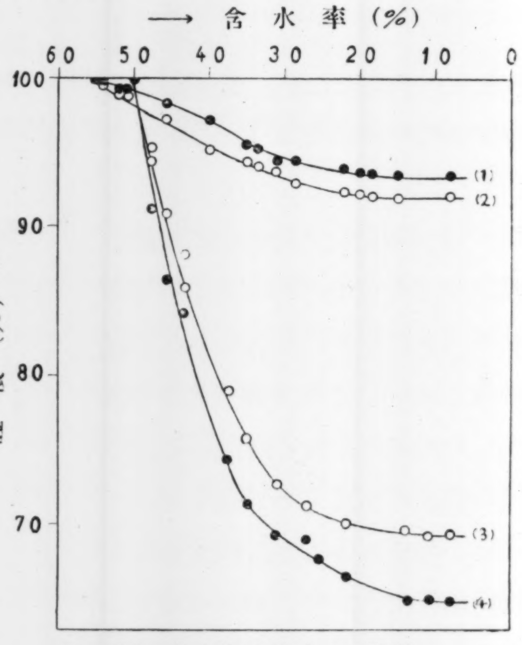

第 2 圖 含水率さ體積さの關係

(1)，(2) は本郷の赤土

(3)，(4) は丸の內の沈泥質粘土

(1)，(3) は最初 20 分間振動を與へ後水分を減少させた場合である

Fig. 2. Diagram showing the relation between volume and moisture content.

Abscissa: moisture content (%).

Ordinate: volume (%).

(1), (2): the loam at Hongô. (3), (4): the silty-clay at Maru-no-uti. (1), (3): showing the effect of vibration for 20 min at initial state.

の含水率の變化に對し體積，高さ，横幅等の諸量は急激に減少する．本郷の赤土[8]に於

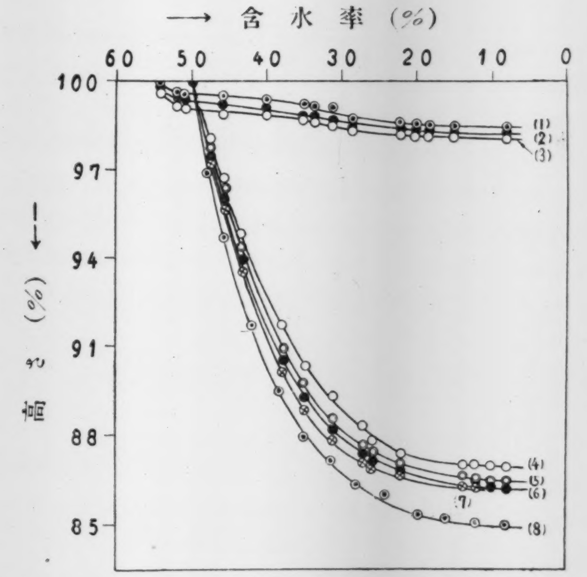

第 3 圖　含水率と高さとの關係
縱軸：高さ (%)　横軸：含水率 (%)

(1), (2), (3)　は本郷の赤土
(1)　初めの高さ $h_0=21{\cdot}2$ cm　振動を與へずに水分を取つた場合
(2)　$h_0=36{\cdot}6$ cm　″
(3)　$h_0=23{\cdot}1$ cm　最初 20 時間振動を與へ後水分を取つた場合
(4), (5), (6), (7), (8)　は丸の内の沈泥質粘土
(4)　$h_0=15{\cdot}1$ cm　振動を與へずに水分を取つた場合
(5)　$h_0=15{\cdot}1$ cm　最初 20 分間振動を與へ後水分を取つた場合
(6)　$h_0=24{\cdot}9$ cm　振動を與へずに水分を取つた場合
(7)　$h_0=24{\cdot}9$ cm　最初 20 分間振動を與へ後水分を取つた場合
(8)　$h_0=14{\cdot}8$ cm　最初 20 時間振動を與へ後水分を取つた場合

Fig. 3. Diagram showing the relation between height and moisture content.
Ordinate: height (%). Abscissa: moisture content (%).
(1), (2), (3): the loam at Hongô.
(1) Initial height $h_0=21{\cdot}2$ cm. No vibration. (2) $h_0=36{\cdot}6$ cm. No vibration.
(3) $h_0=23{\cdot}1$ cm. Vibration for 20 hours at initial state.
(4), (5), (6), (7), (8): the silty-clay at Maru-no-uti.
(4) $h_0=15.1$ cm. No vibration. (5) $h_0=15{\cdot}1$ cm. Vibration for 20 min at initial state. (6) $h_0=24{\cdot}9$ cm. No vibration. (7) $h_0=24{\cdot}9$ cm. Vibration for 20 min at initial state. (8) $h_0=14{\cdot}8$ cm. Vibration for 20 hours at initial state.

ても含水率が約 30% に迄減少する間は以上の諸量は略々直線的關係をなして減少し，

---

[8] 高田氏の研究によれば含水率 w と收縮率 ε_s との間に $\frac{\varepsilon_s}{w}=R$ なる關係があり，即ち直線的關係が存在する．一般には體積減少の始まる時の含水率を W とすれば $(W-w)R=\varepsilon_s$ $W>w$ なる關係がある．土木試驗所内地表下約 3 m の箇所より採取せる赤土の收縮は 100% 以上より約 40% 迄の含水率の變化に對し體積減少率は 10% 程度であるが，40% 以下の含水率減少に對し 18% 程度の減少率を生ずる．高田昭 前掲

終局に於ける減少は最初の値に比して體積に於て約 8%，高さに於て約 2%，横幅に於て同じく 2% である．此等の減少の割合は丸の内の沈泥質粘土の終局の値即ち體積に於て約 36%，高さに於て約 15%，横幅に於て約 13% の減少等の値に比して何れも小なる値を示してゐる．

今高さの收縮を一例にとりその收縮の割合と含水率との關係を求めれば次の如くになる．最初の高さを h_0，收縮量を δh，含水率を w（%），最初の含水率を W（%）とすれば

$$\frac{\delta h}{h_0}=A(1-e^{-B(W-w)})$$

なる實驗公式が得られる．勿論 $\delta h/h_0$ は百分率で與へてある．A，B は常數であつて

$$\text{本郷の赤土}\begin{cases}A=2\%\\B=0{\cdot}0672\end{cases}\qquad\text{丸の内の沈泥質粘土}\begin{cases}A=15\%\\B=0{\cdot}0873\end{cases}$$

である．此の關係から見ると土の種類により此等の常數が異り，從つて此等常數の差異から土の性質も判別出來るやうに思はれる．なほ此等の圖から知られる如く最初與へし振動の影響が大である．第3圖中（5），（7）は最初 20 分間振動を與へた場合であり（3），（8）は振動によつて收縮する所迄收縮せしめ其の後水分を減少させた場合であつて，他の場合に比して何れも大なる收縮を示し丸の内の沈泥質粘土に於ては 1% 以上の差を示してゐる．此れに反し本郷の赤土に於ては餘り變化はない．又始めの土の高さの異ひによつてその變化に如何なる差異を生ずるかを示す一例として第3圖中（1），（2）及び（4），（6）に示したが高さの大なる方の收縮は稍々大なる値を示す様である．（5），（7）は（4），（5）に相當した高さの土に最初振動を與へ後水分を蒸發させて乾かした場合であつて，何れも振動が土の收縮を増加せしめる事が判る．

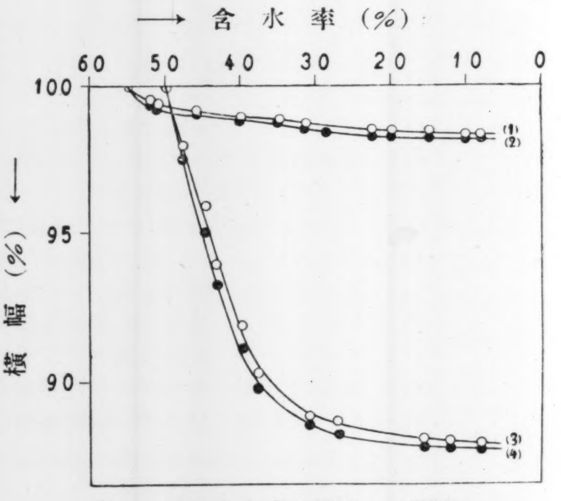

第 4 圖　含水率と横幅との關係

（1），（2）は本郷の赤土
（3），（4）は丸の内の沈泥質粘土
（1），（3）は最初 20 分間振動を與へ後水分を減少させた場合である

Fig. 4. Diagram showing the relation between width and moisture content.
Ordinate: width (%).
Abscissa: moisture content (%).
(1), (2) The loam of Hongô. (3), (4) The silty-clay of Maru-no-uti. (1), (3) Showing the effect of vibration for 20 min at initial state.

土の乾燥中本郷の赤土に於ては重量の減少は體積の減少に比して大であり，丸の内の沈泥質粘土に於ては重量の減少と體積の減少とは含水率 30% 迄の變化範圍では殆ど直線的關係を保持して變化する．從つて此の關係から兩者は各々その土の密度の含水率に對する變化を異にしてゐる事が判る．

次に含水量の變化に對する土の體積膨張率の變化を求めたのが第5圖である．此の圖は試驗土を含水量零の狀態に迄乾燥させ次に此の土に徐々に水分を吸收せしめ，水銀を用ひ土の密度測定の際使用したと同一方法に因りその體積及び重量，含水率等を測定したものである．此の場合の土の乾燥前の寸法は何れも約 5 cm×4 cm×4 cm である．其の結果は丸の內の沈泥質粘土の膨脹率は含水率 10% を越えると增大するが，本郷の赤土は左程變化しない．但し丸の內の土に於ては含水率 34～35% 以上になると龜裂を生じ測定不能になつた．又本郷の土に於ても同様に含水率約 30% に於て破壞された．何れにしても乾燥前の狀態に戻らず，龜裂を生ぜしめない様にしながら始めの含水率 50% 以上に水分を吸收せしめる事は不可能であつた．

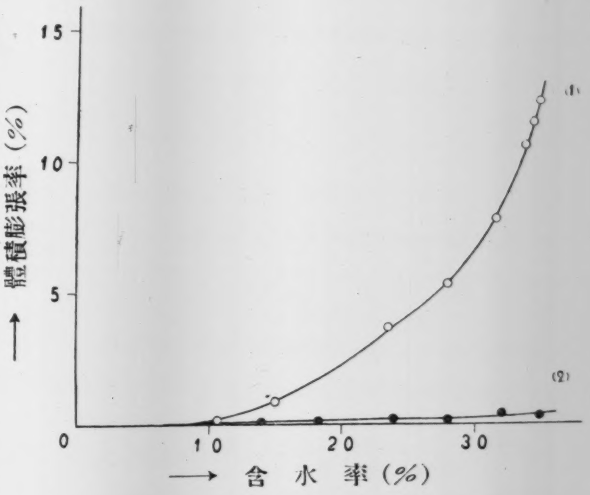

第 5 圖　含水率さ體積膨張率さの關係

(1)　丸の内の沈泥質粘土

(2)　本郷の赤土

Fig. 5. Diagram showing the relation between expansion of volume and moisture content.

(1) The silty-clay of Maru-no-uti. (2) The loam of Hongō.

Ordinate: expansion of volume.
Abscissa: moisture content.

(2) 動力學的實驗及び結果

此の實驗は土の振動による收縮を取扱つたもので其の裝置の略圖は第6圖に示す如くである．此の實驗裝置の主要部分は已に前論文[9]に示したものと全く同様なるものであるが今回の目的に添ふ様適當な工夫をなした．卽ち今回は電磁石のコイル(E.M.)の回路に 50 サイクル/秒の一定の振動電流を通し，振動鐵盤（D）の厚さを 1 mm となし，振動振幅を變化せしめる爲に電磁石のコイルを通る電流を加減し電磁石の強さを適當にかへ或ひは鐵盤上の重量を加減した．

---

[9] 石本巳四雄，飯田汲事　前揭.

斯様にして毎秒100振動をなす振動鐵盤（V）を採用し，其の上に土柱（S）を乘せ土柱を振動せしめ その收縮沈下狀態を觀測した．今その收縮の時間的變化を擴大して連續的に記錄するために圖の如き工夫をなした．即ち土の上部に細き棒をさし込み其の一端から凸起を出し，その凸起の尖端を一定廻轉軸を有する槓杆Kの劣腕（K_2）と接觸せしめ，優腕（K_1）にはその一部から腕を出し，描針（N）が附してある．この描針の先端が時計仕掛回轉ドラム上に巻いた煤煙紙上に接觸してゐるので時の經過に從つて槓杆の偏りを記錄する事となる．槓杆の偏り運動は土の沈下によつて行はれるものである．猶時計仕掛回轉ドラムは1時間1回轉1日1回轉等適當のものを隨時使用した．幾何倍率は約7倍から10倍迄變化せしめられるやうになつてゐる．

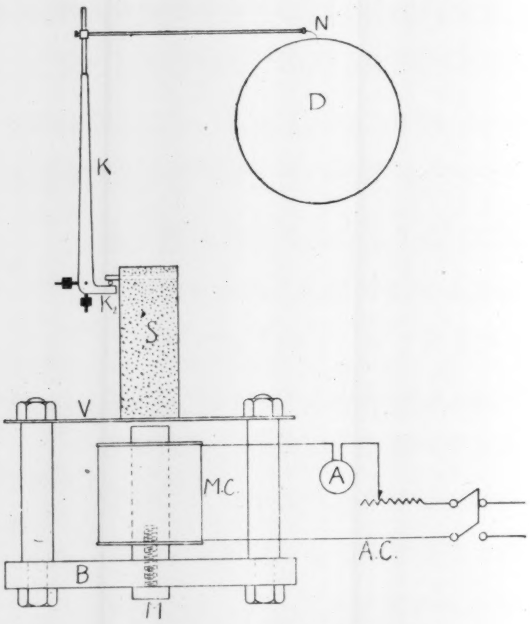

第6圖 土の振動實驗裝置
A 電流計 A.C 交流 B 鐵盤 D 時計仕掛回轉ドラム K_1 槓杆の優腕 K_2 槓杆の劣腕 M 電滋石 N 描針 M.C 電磁石コイル S 試驗土 V 振動鐵盤

Fig. 6. Experimental arrangement of vibration.

A: ammeter. A.C.: alternating current. B: steel plate. D: drum. K_1: long arm. K_2: short arm. M: electromagnet. N: needle. M.C.: A.C. coil. S: specimen. V: vibrating plate.

振動實驗中土の含水量及び溫度の變化を成る可く防ぐために地面下3mの略々恒溫恒濕の土中室を選び更に土の外側には土にふれない程度に濕布を巡らして置いた．室內の溫度は實驗が一週間以上に亙る場合にも15°Cの恒溫を保ち得，濕度は100%であつた．なほ振動中土の踊りを防ぐため油粘土を用ひ土柱の底面を振動鐵盤に固着させた．實驗は次の順序で行つた．(i) 振動のみの影響，(ii) 振動と含水減少との兩方の影響，(iii) 含水率の變化のみの影響，(iv) 振動及び含水率の變化のない場合等である．實驗前後に於て重量の測定を行ひその變化の有無を檢したが，振動のみの影響を觀測する場合に於ても長時間に亙るも多くの場合 含水率の變化は0·2%以下であつた．又自然狀態の土を一度ねり直し，これを元と同じ狀態と思はれる程度迄壓縮して土柱を作り，此れを用ひて同じ實驗を繰り返した．

以上の結果を全部網羅して圖に示したのが第7圖である．圖から知られる如く本郷の赤土は殆ど變化なく，丸の內の沈泥質粘土は大なる變化をなす事が判明した次第で

ある．何れの場合も振動による影響は顯著で振動を與へた場合は成し得た實驗範圍內

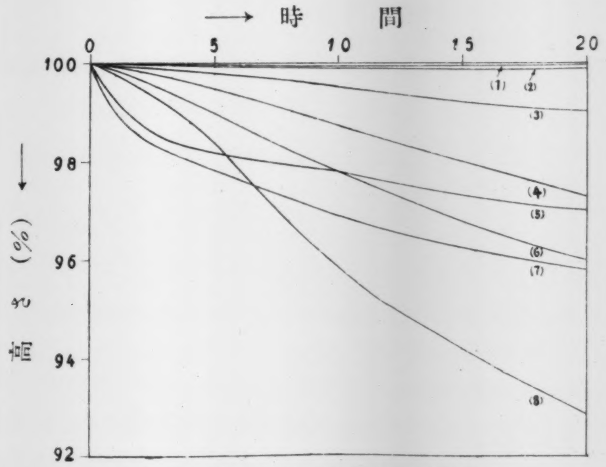

第 7 圖　高さと時間との關係

本鄉の赤土
　(1) 振動を與へない場合（含水率一定）(2) 振動を與へた場合（含水率一定）
丸の內の沈泥質粘土
　振動を與へない場合：(3) 含水率一定　(4) 含水率3%減少　(5) 含水率一定，ねり直しの土
振動を與へた場合：(6) 含水率一定　(7) 含水率一定，ねり直しの土　(8) 含水率 3% 減少

Fig. 7. Diagram showing the relation between height and time.

The loam of Hongô: (1) Case of no vibration (moisture content, constant). (2) Case of vibration (moisture content, constant).
The silty-clay of Maru-no-uti: Case of no vibration [(3) moisture content, constant. (4) decrease in moisture content, 3%. (5) mois. cont., constant. soil in recomposed state.] Case of vibration [(6) mois. cont., constant. (7) mois. cont., constant. soil in recomposed state. (8) decrease in moisture content, 3%.]

に於ては自量により沈下する場合の 4 倍も大であり，同じ時間內で含水率を 3% 變化させた場合と比較して 1·5 倍も大である．又振動させながら水分を減少させた場合は最も大なる收縮を生ずる事が判明した．結局此の場合は (4) (6) 兩曲線を加へ合せたやうな變化を示し 46 時間後に於て 10% の高さの收縮を生じてゐる（但し圖に示してない）．又ねり直した土に於ては最初の時に於ける收縮は相當大であるが，時間の經過するに從つて其の收縮曲線は自然土の場合の曲線に追從して行くやうな傾向が見られる．何れにしても土の緻密になり行く有樣が窺はれる．

又振動振幅を變へた場合は第 8 圖に示す如くであつて，振幅の大なる程土の收縮が大となる．

以上何れの場合に於ても本鄉の赤土は丸の內の沈泥質粘土に比して極めて收縮の小なる事が判明した次第である．又土を振動せしめる場合其の振動周期が土の共鳴振動周期であるか否かについても考慮を要する事であり，實際共鳴振動の場合は大なる收

縮を生ずるのである．第7圖(8)は殆ど共鳴狀態の振動の場合を取扱つたのであり，如何によく收縮10)を生ずるかが知れるであらう．

今試驗土の最初の高さと共鳴に於ける1秒間の振動數との關係を表示すれば，次の如くである．

高さ 種類	30 cm	25 cm	20 cm	15 cm	10 cm	縱波の速度
赤土 （本鄉）	170	200	250	330	500	200 m/sec
沈泥質粘土 （丸の內）	58	70	88	116	175	70 m/sec

斯樣な關係より知られる如く，本鄉の赤土の共鳴振動數は實驗の振動數 100 に比して可成り大である．然しながら靜力學的實驗の所に於て述べた如く共鳴振動で振動させた場合もあるが，その變化の有樣は丸の內の沈泥質粘土の場合に比して左程大ではない．

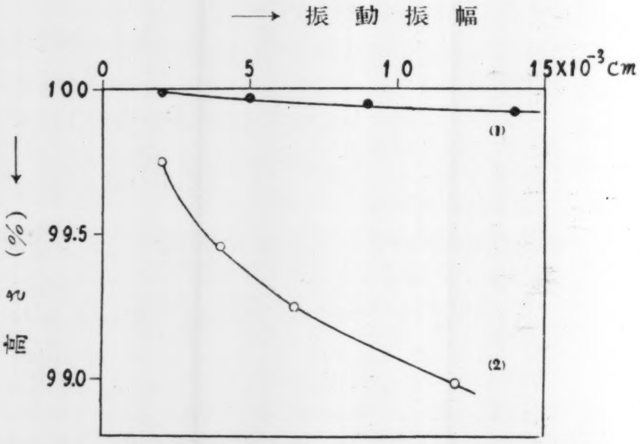

第 8 圖 振動振幅と高さの減少の割合との關係
縱軸：高さ（%） 橫軸：振動振幅
（1） 本鄉の赤土 （2）丸の內の沈泥質粘土
最初の高さ 20 cm, 5 時間後の高さの變化を示す．

Fig. 8. Relation between the height of soil and the amplitude of vibration after the elapse of 5 hours. Initial height 20 cm.
Ordinate: height (%).
Abscissa: amplitude of vibration.
(1) The loam of Hongō. (2) The silty-clay of Maru-no-uti.

3. 實驗結果に對する考察

以上述べた實驗結果より考察すれば，水分減少或ひは振動に因る土の收縮は，其の何れの場合に於ても丸の內の沈泥質粘土は本鄉の赤土に比して大なる收縮を示し，本鄉の赤土の場合には殆ど收縮を見ないとも云へよう．今振動に因る收縮と乾燥による收縮との關係を模型的に圖示すれば第9圖の如くであつて，乾燥させた場合は高さと同程度の橫の收縮を生ずるが，振動の場合には實驗の範圍內に於て橫の變化は殆どなく高さの減少のみを生ずる．此れは土の粒子の移

10） 振動により收縮を來す場合には土の狀態も異りその結果勿論彈性も變ずる事が豫想される．但し前論文（石本巳四雄，飯田汲事 前揭）に示した實驗の如くその振動振幅は極めて小さく，實驗時間も1分間程度であり收縮も約2000倍の擴大に於て 5 mm～10 mm 程度ならば，實驗の前後に於て其の彈性が大體一樣であると見做しても差支へなからうと思はれる．

動や空隙の減少等の影響と考へられ結局緻密度に關した問題に歸せられる．今上述の2原因による土の收縮を高さの變化を標準にとり此れを比較する事にすれば，丸の内の沈泥質粘土では20時間後に於ては含水率6%の減少による收縮と6×10^{-3} cmの振幅（每秒100振動）の振動による收縮とは同程度である．又自重のみにて含水率の變化なき場合の收縮と比較すれば振動による場合はその4倍も大なる收縮を生ずる．本郷の赤土に於ては左程の變化が認められない．振動中は横の縮みは少いが振動停止後此れを乾燥せしめれば收縮を伴ひ，結局丸の内の土に於ては體積に於て約36%，高さに於て約15%，横に於て約13%の減少本郷の土は體積に於て約8%，その他横及び高さに於ては2%程度の減少を生ずるのである．

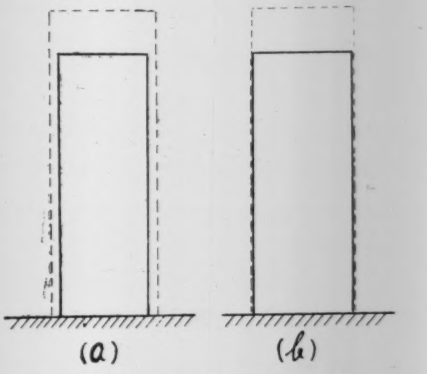

第9圖　土の收縮の有様を示す
(a)　乾燥させた場合
(b)　振動させた場合

Fig. 9.　Schematic diagram showing the shrinkage of soil.
(a)　Case of decrease in moisture content.
(b)　Case of vibration.

此等の事實より思考すれば兩者の土はその構造に相異が存すると考へられる．今其の構造を模型的に示したのが第10圖である．卽ち土の粒子間の連絡が單なる粘性液體，コロイド物質及び空隙等で行はれてゐるものと更にそれ以外の他の彈性體によつて連結されてゐるものとの2種類である．前者を粒子狀構造後者を海綿狀構造或は骨骼構造と名づけるならば，丸の内の沈泥質粘土は前者に屬し本郷の赤土は後者に屬すると考へるのが至當である．斯様に考へる事によつて，土が水分を失ひ收縮する場合に於ても振動に因つて收縮する場合に於ても，粒子狀構造をなしたものは最も緻密な狀態に近づく爲によく收縮するが，海綿狀構造のものは各粒子間の連結物の爲めに多少の收縮を生ずるも，それ自體が已に一種の緻密度の最後の狀態になつてゐると考へる事が出來從つて餘り收縮が行はれないのであらう．今粒子狀構造の場合に水分減少或ひは振動に因る收縮を模型的に考へるならば第11圖（簡單のために此處では土粒子の3種類の配列を考へてゐる）に示す如く，水分を含んでゐる最初の狀態が例へば

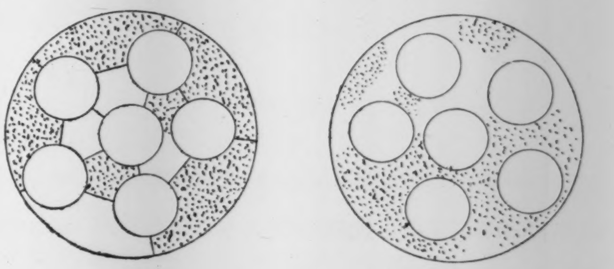
(a)　(b)

第10圖　土の構造を示す模型圖
(a)　本郷の赤土　(b)　丸の内の沈泥質粘土

Fig. 10.　Schematic diagram showing the structure of soil.
(a)　The loam of Hongô
(b)　The silty-clay of Maru-no-uti.

A であり最後に水分を失ひたる時の狀態が a′ であると假定すれば，此れは最も間隙の多い粒子の並び方であり，B→b′，C→c′ に移るにつれて間隙が小となる．含水を減少し或ひは振動を與へて收縮を生ぜしめる場合，間隙率の減少を生ずるならばそれは A→a′ 或ひは B→b′ C→c′ になり得た丈でも說明されるが，含水減少に因る收縮と振動による收縮とは終局に於ては勿論振動中に於ても含水の減少を生ぜずしてその高さの減少或は間隙率を異にするならば，振動中に於て粒子の移動が A→B 或ひは B→C になりそれが最後に水分を失つて B→b′ 或ひは C→c′ に成り得たと假定すれば大體の說明がされるやうにも思はれる．

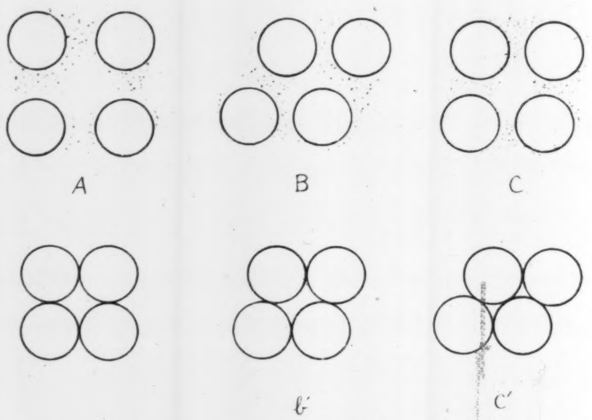

第 11 圖　土粒子の配列の模型圖

Fig. 11. Schematic diagram of arrangement of soil particles.

今間隙率と含水率との關係を最初の狀態のまゝ乾燥せしめた場合と，振動を與へて後乾燥させた場合とに付本郷及び丸の內の試驗土について求めれば第 12 圖の如くになる．此の圖に於ける間隙率 P は

$$P=100-\frac{G}{G_s}(1-w)$$

なる關係から計算出來る．玆に G は含水率 w に對する比重であり，G_s は眞の比重である．G_s の測定は比重壜を用ひたのであつてその結果は本郷の赤土では $G_s=2{\cdot}632$，丸の內の沈泥質粘土では $G_s=2{\cdot}660$ である．

第 12 圖に於て示す如く本郷の赤土に於ては最初の間隙率 78·6% のものが最後に 75·2% となりその減少率は 4·3% となる．又振動による影響を求めると最初の間隙率 77·4% のものが最後に 72·8% となり 5·95% の減少を生ずる事が判明した．又丸の內の沈泥質粘土について求めれば最初 73·0% の

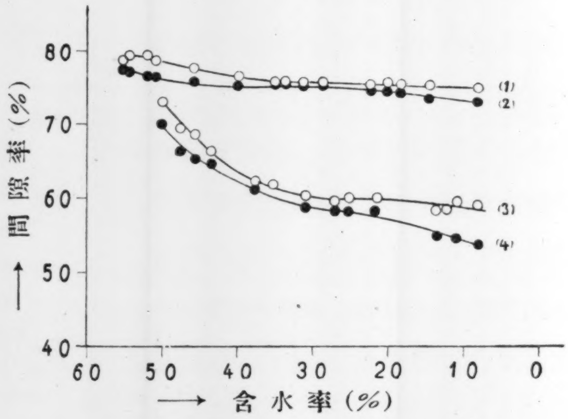

第 12 圖　含水率と間隙率との關係
(1)，(2) は本郷の赤土　(3)，(4) は丸の內の沈泥質粘土　(2)，(4) は振動の影響によりその變化の大なるを示す．

Fig. 12. Relation between porosity and moisture content.
(1), (2): the loam of Hongô. (3), (4): the silty-clay of Maru-no-uti. (2), (4): showing the effect of vibration. Ordinate: porosity (%). Abscissa: moisture content (%).

ものが最後に 58·3% に減じて居りその減少率は 20·2% となる．又振動の影響による場合の最初の間隙率 69·9% のものが最後に 53·6% となり 23·4% の減少を生じた．かくの如くにして吾々は土の種類により又土の狀態によつて著しくその性質を異にする事を知り得た次第である．本郷の赤土は丸の内の沈泥質粘土に比して間隙率の變化の少いのは前述の如き土の構造的差異を考へる事によつても説明される．

土の粒子を一樣な大さと假定するがその並び方或ひは緻密度に關する Graton 及び Fraser 兩氏の研究[11]の結果を綜合して見るに，此の結果を第 II 表に於て示したが，

第　II　表

	Case 1	Case 2	Case 3	Case 4	Case 5	Case 6
Name	Cubic	Orthorhombic	Rohmbo-hedral	Orthorhombic	Tetragonal-sphenoidal	Rhombo-hedral
Tangent neighbours	6	8	12	8	10	12
Face angle	90°	90°, 60° ~120°	90°, 60° ~120°	90°, 60° ~120°	60°~120° 75°31′ ~104°29′	60°~120°
Spacing of layers	$R\sqrt{4}$	$R\sqrt{3}$	$R\sqrt{2}$	$R\sqrt{4}$	$R\sqrt{3}$	$2R\sqrt{2\;3}$
Volume of unit cell	$8{\cdot}00R^3$	$6{\cdot}93R^3$	$5{\cdot}66R^3$	$6{\cdot}93R^3$	$6{\cdot}00R^3$	$5{\cdot}66R^3$
Volume of unit void	$3{\cdot}81R^3$	$2{\cdot}74R^3$	$1{\cdot}47R^3$	$2{\cdot}74R^3$	$1{\cdot}81R^3$	$1{\cdot}47R^3$
Porosity	47·64%	39·54%	25·95%	39·54%	30·19%	25·95%

粒子の並び方によつて或る列の粒子の中心を通る平面から次の列の粒子の中心を通る平面迄の距離が $2R$（R は粒子の半徑）から最小 $\sqrt{2}\,R$ に迄變る．又間隙率も最大 47·64% から最小 25·95% に迄變化する．今粒子と粒子との接觸が Case 1 である場合に，此等が並び方をかへて Case 2 或ひは Case 3 に變化したとすればその高さの變化率は第 III 表に示す如くになる．

第 III 表から知られる如く，何等かの擾亂によつて粒子の配列が Case 1 から Case 2 或ひは Case 1 から Case 3 等に移動したとすれば其の影響のみに因る高さの減少變化率は夫々 13·5%，29·5% 等となる．從つて此の結果よりすれば丸の内の沈泥質粘土の粒子が振動によつて Case 1 から Case 2 或ひは Case 2 から Case 3 となる樣な配列狀態の場合に相當した移動を行つたとも考へられる．

---

11) L. C. GRATON and H. J. FRASER, *Journ. Geol.*, **43** (1935), 785.

斯くの如く振動が土の收縮に及す影響は相當大なるもので，埋め立て地の如きは最初の狀態に於ては振動の影響は水分減少或ひは自重による影響以上に大である事が判明した次第である．從つて東京近傍其の他の地方の軟地盤の沈下も振動と密接な關係がある樣に考へられるので，今假りに地面に振動を與へるものの例として自動車の數をとり此の數が地面に振動を與へる量に比例すると假定しその自動車數の年變化を圖示すれば第 13 圖の如くになる．[12] 同圖中に電車及び小型自動車の數をも同時に示したが電車の數は殆ど增減しないに反し，自動車の數は關東震災以後急激に增加してゐる．最近に於ては小型自動車の增加も亦著しい．今一例として茅場町所在の水準點の沈下圖[13]（第 14 圖）を取りその沈下狀況と上述の振動量とを比較すれば，大體類似な形を示してゐる．震災以後沈下速度を急激に增加してゐるが，一方自動車による振動も急激に大となり，此等が沈下の原因に相當な役割をなしてゐるやうにも思はれる．

第 III 表

Case の移動	高さの變化率	間隙率の變化
Case 1→Case 2	13·5%	17·7%
Case 1→Case 3	29·5%	45·5%
Case 1→Case 6	20·0%	
Case 6→Case 3	11·9%	
Case 2→Case 3	18·5%	25·3%
Case 2→Case 6	7·5%	
Case 1→Case 5		36·5%
Case 2→Case 5		23·6%
Case 5→Case 6		14·1%

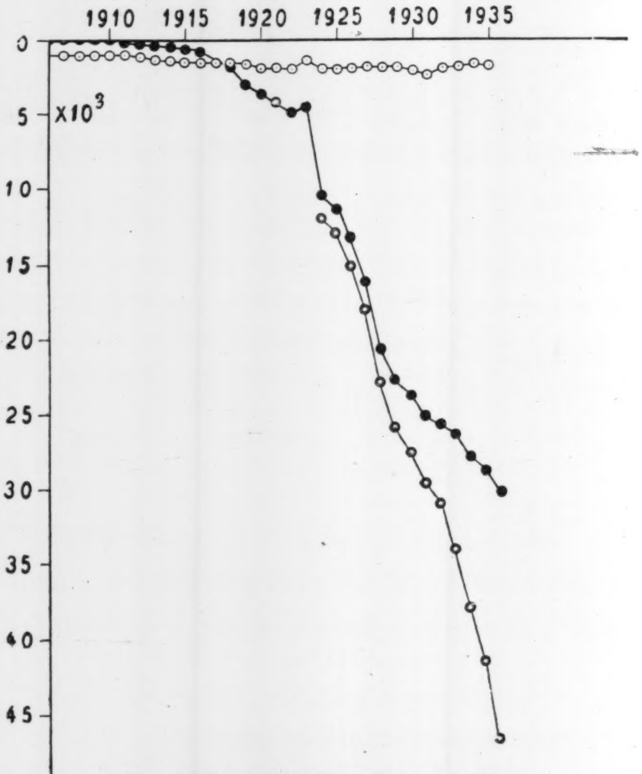

第 13 圖　自動車及び電車の年變化
縱軸：車臺數　橫軸：年
● 自動車 (motor-car) ○電車 (electric-car) ⊙ 自動車
（小型自動車，自動車，自動自轉車全部を含む）
Fig. 13. Number of motor-cars and electric-cars.
Ordinate: number. Abscissa: year.

勿論現在の沈下は種々なる原

---

[12] 此の資料は警視廳交通課統計掛の御好意により調査し得たもので玆に謝意を表する．

[13] 同圖は宮部直巳博士の論文中より拜借したものである．宮部直巳 地震研究所彙報別冊 2 (1935), 215.

因により行はれてゐる事は勿論であるが，終局の所は上述の實驗の如く大體 15% 程度の收縮を生ずるものであるとすれば表面粘土層 30 m の所は約 5 m 程の沈下を生じて落付くものと思はれる．尤もこの量は絶對的のものではなく表面荷重其の他の影響により增減を生ずる事は勿論である．

表面土壤層の性質と沈下とは密接な關係を有し，或る地帶に沈下增大が認められるに拘はらず他の地方に於ては殆ど沈下を生じないと云ふが如き事實は，此等の地方を形成する表面土の性質の差異に基くものと思はれる．例へば本郷と丸の內とに於てその地盤沈下に差異の存するのは，本實驗結果の如き土の性質に差異の存する事から豫期され得る事であり，又丸の內の沈泥質粘土は本郷の赤土に比して彈性係數が小であり[14]，丸の內の土の如きは自動車の如き振動によつて共鳴振動が起され易いやうに思はれる點も沈下に差異の存する一つの原因であらう．

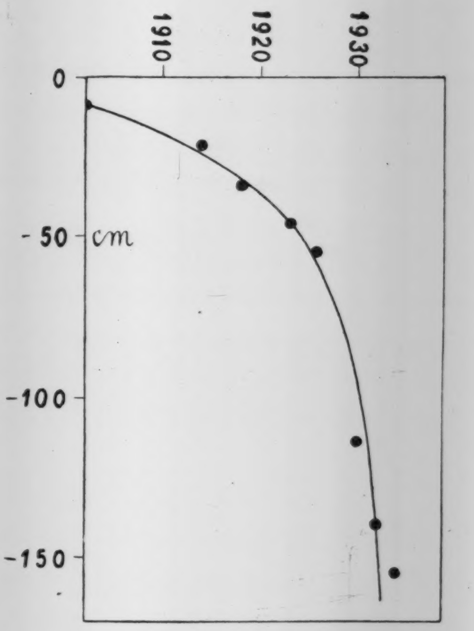

第 14 圖　B. M. 3378 の沈下
縦軸：沈下量　横軸：年
Fig. 14. Subsidence of B.M. 3378.
Ordinate: amount of subsidence.
Abscissa: year.

4. 結語

本實驗に於ては自然の堆積狀態の土の收縮現象を振動及び水分減少との 2 方面から觀察した．振動による土の收縮は水分減少率 6% 程度と同程度であり，水分減少なき自量により收縮する場合の約 4 倍大であるが，此等の收縮現象は土の採取當時の含水率 50% 以上に於ける初めの狀態に於てであり，振動周期は 0·01 秒，振幅 80μ なる條件の下に於てである．又土の收縮は振動振幅（或ひは共鳴狀態の周期）の增大と共に增加する．土の種類により土の狀態によつて其の收縮に差異の存する事も判明した．卽ち本郷の赤土は殆ど收縮變化なきも，丸の內の沈泥質粘土の收縮變化は顯著である．此等の事實から各地の土の性質の差異が地盤沈下と密接な關係にあると考へられる．

含水量の減少と共に土の密度も變化し，丸の內の沈泥質粘土は含水率 50% から 30 %迄の變化範圍に於て寧ろ稍增加の傾向を示すが，含水率のそれ以下の値に對して密

---

14)　石本巳四雄，飯田汲事　前掲.

度も小さくなる．此れに反し本鄉の赤土は初めから含水量の減少と共に密度を減少する．又間隙率の變化は本鄉の赤土は左程なきも，丸の內の沈泥質粘土は 20% 以上の變化を生じ含水量の減少と共に小さくなる．

以上の結果から土の構造を推察すれば本鄉の赤土に對しては海綿構造，丸の內の沈泥質粘土に對しては粒子狀構造を考へるのが至當と思はれる．勿論此等土の粒子間は一般に粘性液體（水，コロイド物質をも含む）にて充されてゐると考へられる．

終りに臨み種々御懇篤なる御指導を賜つた石本先生並びに丸の內の實驗土を戴いた鐵道省土質調査委員會の渡邊貫博士に厚く御禮申し上げる．猶色々御注言を戴いた宮部博士に感謝の意を表する次第である．

---

32. *Some Experiments on the Shrinkage of Soil.*

By Kumizi IIDA,

Earthquake Research Institute.

This paper describes experiments made in connexion with shrinkage of soil in the natural state caused by vibration and decrease in moisture content of the soil. These experiments concerned with the problem of subsidence of the upper superficial layer of the earth's crust. Variation in soil density with moisture content was also investigated. Finally the structure of the soil was assumed from these experiments. In the present experiment, the same kinds of soil from Hongô and Maru-no-uti in Tôkyô were used as those in our preceding studies.

The results of the experiments are summarised as follows:

1) The density of the loam at Hongô diminishes with increase of moisture content, while that of the silty-clay at Maru-no-uti increases somewhat with moisture content ranging from about **50%~30%,** and then diminishes with decrease in moisture content below 30%. In the case of the silty-clay at Maru-no-uti the variation in porosity of soil with moisture content is greater than in that of the loam at Hongô.

2) The extent of shrinkage differs with the kind and the condition of the soil. The contraction in volume of the silty clay at Maru-no-uti increases with decrease of moisture content, while that of the loam at Hongô is not so conspicuous. The shrinkage in height of the silty-clay at Maru-no-uti and of the loam at Hongô finally reach about 15% and 2% respectively.

3) The shrinkage of these kinds of soil caused by vibration is greater than that caused by decrease in moisture content. The rate of shrinkage of soil increases with increase in vibration amplitude. These relations are shown in Figs. 8 and 9.

4) From these experiments, it may be assumed that the structure of the loam at Hongô is somewhat spongy, the cavities of the elastic skeleton of which are filled with viscous liquid, while that of the silty-clay at Maru-no uti is similar to that in which soil particles are suspended in a viscous liquid.

33.　昭和11年12月27日伊豆新島地震餘震觀測並に踏査報告

地震研究所 ｛萩原尊禮
　　　　　　表俊一郎

(昭和12年1月19日發表——昭和12年3月20日受理)

緒言　昭和11年12月27日9時14分伊豆新島附近に發生した地震は新島及式根島に相當の震害を與へ，數十戸の全壞家屋と死者3名を出した．此の地震は本震の發生する以前に既に地震活動が認められたのであつて，新島には本震の發生する數日前より日に數回地鳴を伴ふ地震が感じられた．是等の前震と本震との時間的關係及び本震の震央位置の決定に關しては福富理學士の報文[1]がある筈であるから之に讓ることとし，本報告に於ては專ら筆者等の行つた餘震の出張觀測と實地踏査の結果に就いて述べる．

餘震觀測　本震直後に於ける餘震の回數は極めて大であつたらしく．27日の夜徹宵警戒に當つた新島本村消防組の談に依れば27日18時より翌28日6時迄に約300回の地震を數へたと云ふ．然し餘震は其の後急速に減少に向つた．筆者等は先づ本村の小學校校舍に携帶用加速度地震計を据付け28日13時30分より觀測を開始した．元來此の種の地震の震源位置決定には4點觀測が望ましいのであるが，地震計の設置に適當な場所は上記の本村の外に若鄉村及び式根島の3ケ所に限られ，然も此の3點は互に一直線に近い位置にあるため觀測點として好適とは云へない．これがため本村及び式根島の2點に夫々地震計水平兩成分を設置し，2點に於ける初期微動繼續時間と地震動の初動方向とより震源位置を決定する方法を試みたのであつたが，既に地震活動は衰へ明確な初動の記象を與へる程度の大きい餘震の發生は見られなくなつた．從つて方針を變更し本村，若鄉村，式根島足附の3點に地震計を据付けることになり，結局3點觀測が開始されたのは12月31日19時であつて翌年1月3日15時迄繼續された．使用した地震計は次に示す通りである．

---

1) 地震研究所彙報に發表の豫定

設置場所	地震計	方向	感度（又は倍率）
新島本村小學校	携帶用加速度地震計 No. 1	NE–SW	1 mm＝2·2 gal
新島若鄉村役場	携帶用加速度地震計 No. 2	NE–SW	1 mm＝2·2 gal
式根島足附溫泉ホテル附近の民家	携帶用加速度地震計 No. 3	N–S	1 mm＝2·2 gal
	携帶用變位地震計	E–W	×30

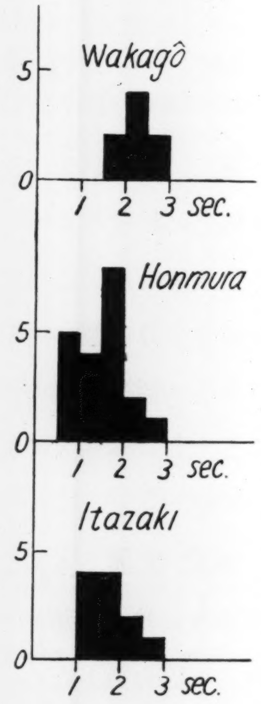

第1圖 橫軸：餘震の初期微動繼續時間
縱軸：頻度

第1圖は3點觀測を行つた期間に於ける地震に就き，橫軸に初期微動繼續時間を，縱軸に其の頻度を取つたものである．此の圖から次の樣なことが云はれる．

（1） 本村は若鄉村及式根島に比較して地震回數が甚だ多い．

（2） 本村に於ては初期微動繼續時間は2秒附近のものが最も多い．

（3） 本村に於ては初期微動繼續時間が1秒以下のものが存在するが，若鄉村及び式根島にそれが無い．

（4） 若鄉村の初期微動繼續時間は比較的長い．

而して各觀測點に於け記象を對照するに，3點に於て共に記錄された地震の數は極めて少く，何れも1點又は2點のみに記錄され他の觀測點には全く記錄されないものが多い．卽ち地震動の起る範圍は極めて局部的なのである．從つて個々の地震に就いて震源位置を決定することは出來ないのであつて震源を決定出來た地震は次の3箇の地震に過ぎない．

發震時				初期の微動繼續時間		
				本村	若鄉	式根
月	日	時	分	秒	秒	秒
12	31	21	54	1·65	2·35	1·70
1	1	17	01	1·90	2·45	2·00
1	2	12	16	1·80	2·40	2·05

3點に於て觀測せられた初期微動繼續時間を利用して震央を決定するには大森公式 $D=kT$〔D は震源距離（粁），T は初期微動繼續時間（秒）〕に於ける常數 k の値を假定する必要がある．

今回は k の値としては，曾て那須博士が伊東及伊豆地震に際して求められた初期微動繼續時間2秒前後の地震に對する k の値5を採用することゝした．斯樣にして

決定された震央の位置は第2圖に示す通りである．震源の深さは何れも約8 km であ

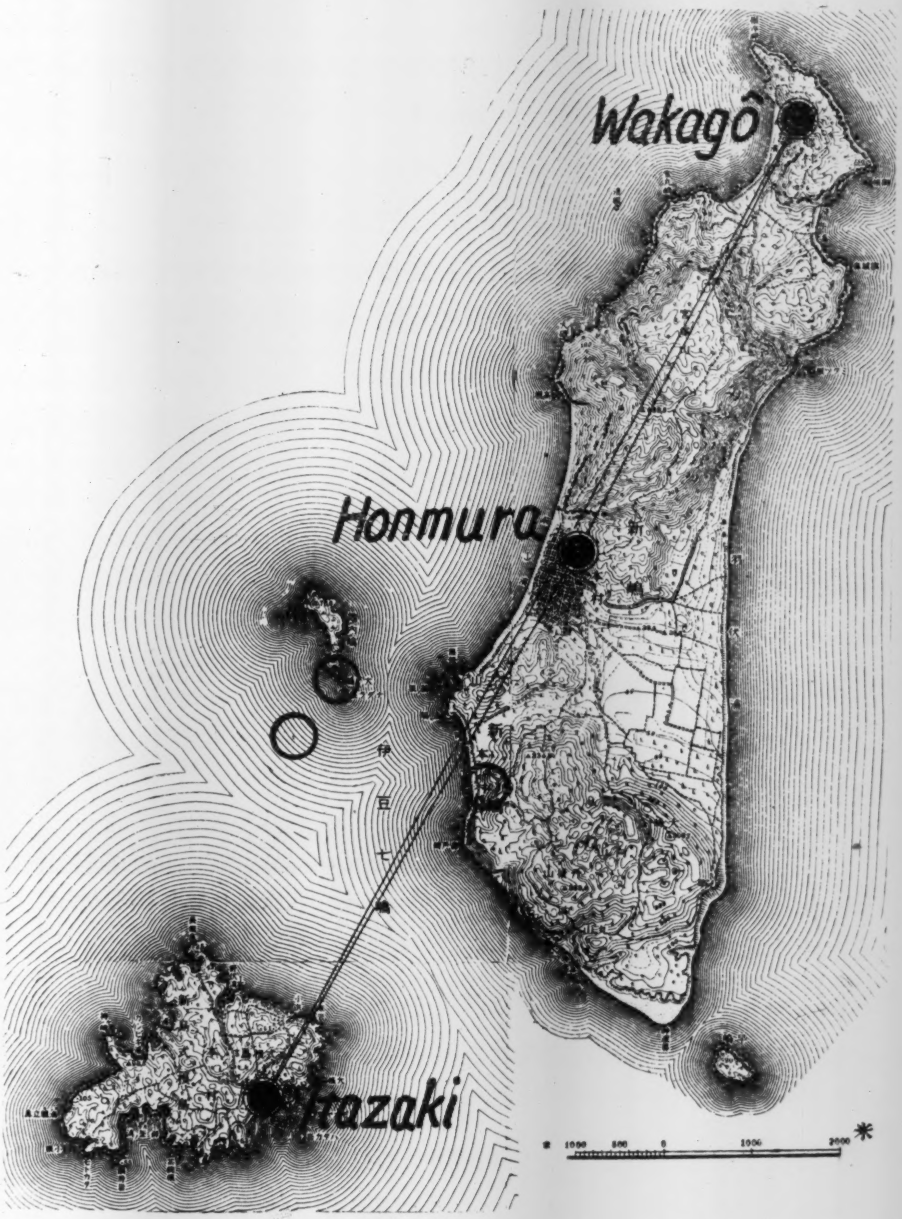

第　2　圖　新嶋地形圖　◉　觀測點　○　餘震の震央

る．此處に震源位置の決定された地震は前に述べた通り若鄉村，本村，式根島の3箇所の地震計に記錄されたものであり，他の多くの餘震は3點全部に於ては記錄が得られなかつたことから，實際は此處に決定された震央の位置より比較的廣範圍の場所に，然も比較的淺所に數多くの地震が發生してゐることが推定されるのである．卽ち餘震の中でも比較的震源の深いものが此處に撰ばれて震源位置が決定されたと見做せよう．而して本村には餘震回數が多いこと及び初期微動繼續時間が比較的短いこと等

前に箇條書きにした事實から，餘震の活動の中心はやはり本村から餘り遠からざる所に存在したことが想像されるのである．

震　害　今回の地震に依り震害を受けた場所は新島及び式根島に限られて居るのであつて，破壞的地震としては左程大規模なものではない．大島，利島，神津島等には全く震害はない．新島，式根島の被害を記するに當つて先づ同島の建築物に就いて述べる必要がある．同島には所謂抗火石に依る石造構造物が極めて多い．抗火石は浮石質の流紋岩であつて向山から盛に切出され比重は1に近く，加工も極めて容易であることから同島の住民にとつては經濟的にも極めて優良な建築材料であり，又同島に於ては耐風建築と云ふことが重要であるが此の點にも亦石造は適してゐるから，これがため廣く抗火石材が使用せられてゐる．同島に於ける石と云ふ石は皆抗火石と思へば間違ひはなく，石造家屋，石造倉庫は勿論，壁，墓石，門柱，鳥居，何れも抗火石より成つてゐる．第3圖は石造倉庫の代表的なるものを示す．其の構造は多く第4圖に示す如く先づ壁を築き，石材を合掌せしめてその上へ石材の家根を葺くのであつて，棟木に相當するものがないのが我々の注意を惹く．斯様な純石造の他に屋根のみ普通の木造家屋式に木材を使用して瓦葺としたもの，又一部を木造一部を石造とした半木半石の折衷的の建物もある．木造家屋も勿論多數あつて之は多く平家であり，二階建は二三の旅館風の建物，小學校校舍等に限られ其の數は極めて少い．

第 3 圖　代表的な杭火石造建築物（本村）
震害を受けず

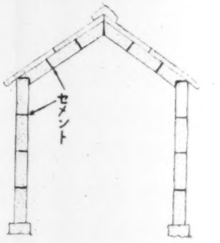

第4圖　抗火石造建築の施工を示す

今回の地震に由る被害は概して云へば純粹の石造家屋及び木造家屋は比較的損傷少く，半石造半木造のものが多く損害を蒙つた様である．又石造建築物の破壞も地震動に由る直接の破壞ではなく，村落は多く砂地にある關係上，地盤の沈下，龜裂等に由り構造物が破壞に至つた場合が相當に多い．

次表は村役場の調査に依る家屋の被害統計である．全戸數は本村570戸，若郷村65戸である．多くの家が納屋，便所，湯殿等を別棟として持つて居る關係上戸數の割合に棟數は甚だ多い．

村名	村營家屋		民家		
	半壞（棟）	破損（棟）	全壞（棟）	半壞（棟）	破損（棟）
本村	5	11	18	430	512
若郷村	6	3	20	40	63

死者は新島に於て2名，式根島に於て1名を出したが何れも岩石の崩落に由るものである．

本村に於ける被害家屋の分布に就いては少しく詳細に調査したので次に其の概略を述べる．第5圖乃至第6圖は構造別に依る家屋の無被害，被害の分布圖である．圖中何れも○は損傷少きもの，●は損傷多きものである．

a. 石造家屋（屋根石葺き）（第5圖）及び石造家屋（屋根トタン葺き）（第6圖）此種の家屋は損傷を被つたものが非常に少いが，損傷を受けたものは東部に集つてゐる傾向がある．圖は家屋全體を損傷少きもの及び損傷多きものの二種類に分類して記入したものである．

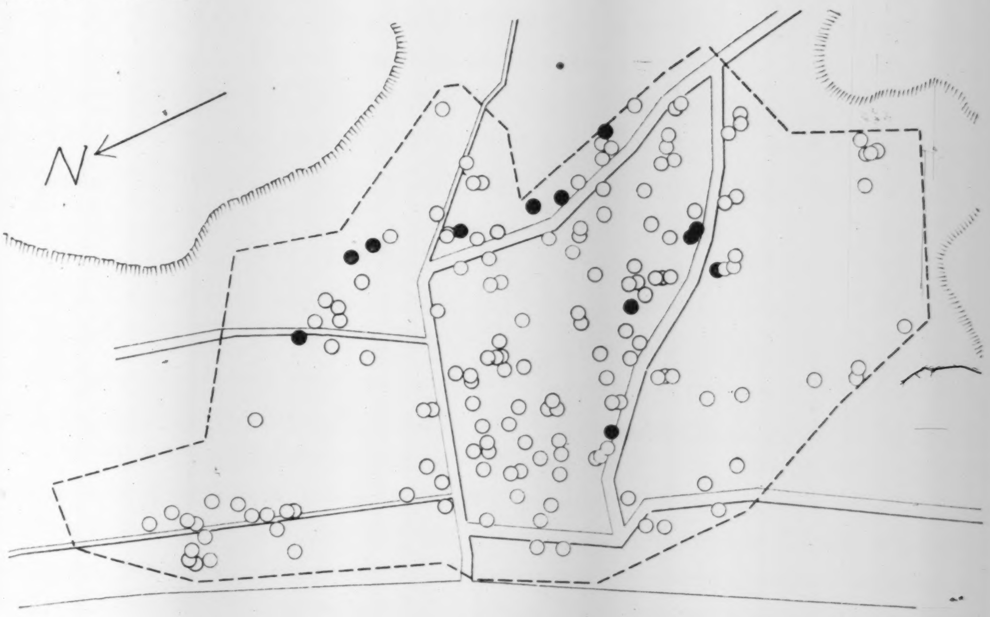

第5圖　石造（石屋根）建築物分布圖（本村）

○　損傷少きもの

●　損傷多きもの

b. 石造家屋（屋根瓦葺き）（第7圖）之は壁を抗火石にて作り屋根は木材にて組み瓦を葺いたものであるが，石造石屋根の場合に比較して被害家屋の率は稍々多い．

c. 木骨石造（屋根瓦葺き）（第8圖），此の種の家屋は被害多く，約半數が多大の

損傷を受けてゐる．

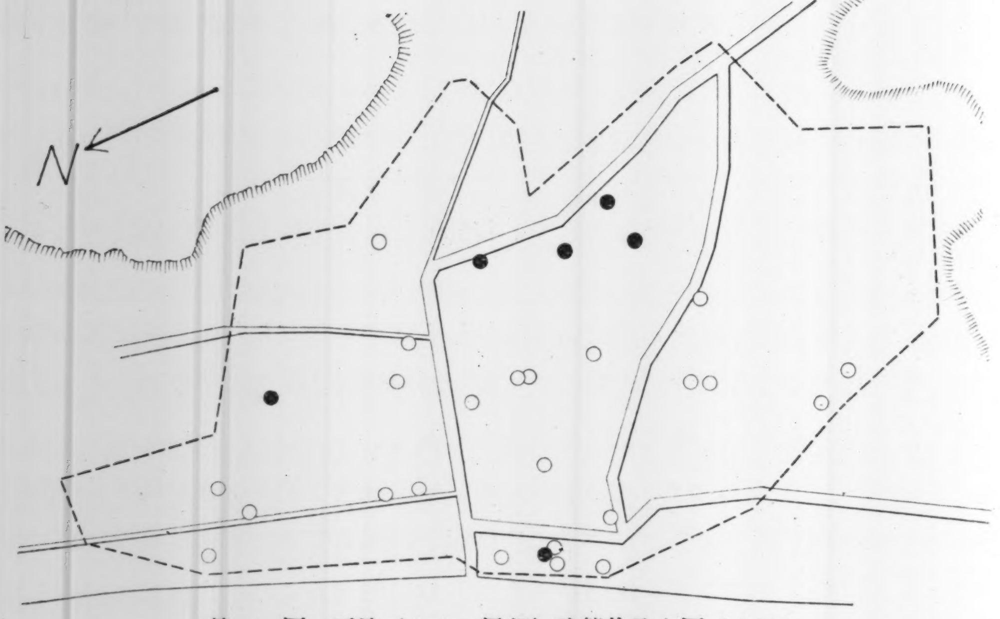

第 6 圖　石造（トタン屋根）建築物分布圖（本村）

○　損傷少きもの

●　損傷多きもの

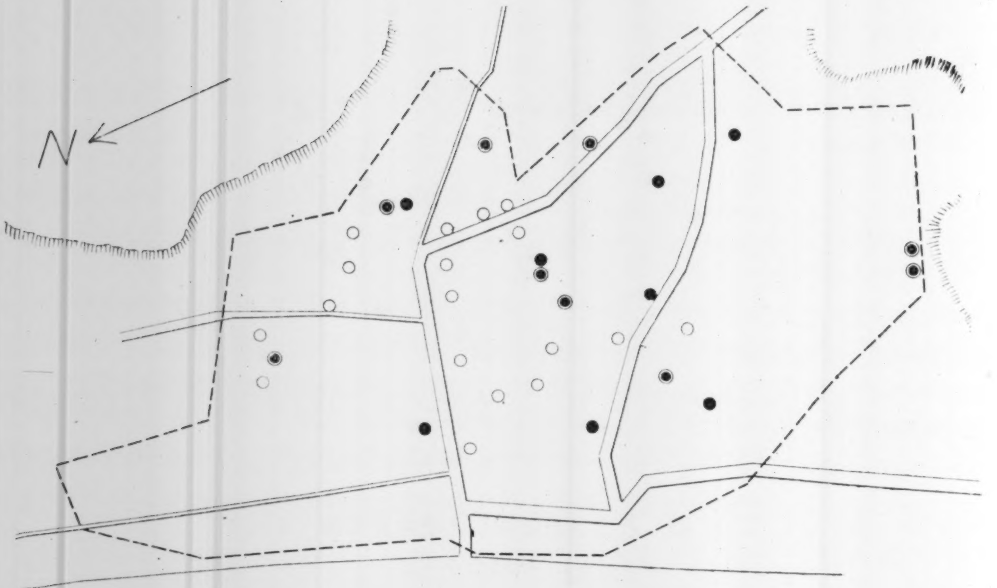

第 7 圖　石造（瓦屋根）建築物分布圖（本村）

○　損傷少きもの

●　損傷多きもの

◉　損傷特に甚しきもの

d.　木骨石造（屋根トタン葺き）（第9圖）此の種の家屋は家根が瓦葺きのものに

比較しては損傷が少い．

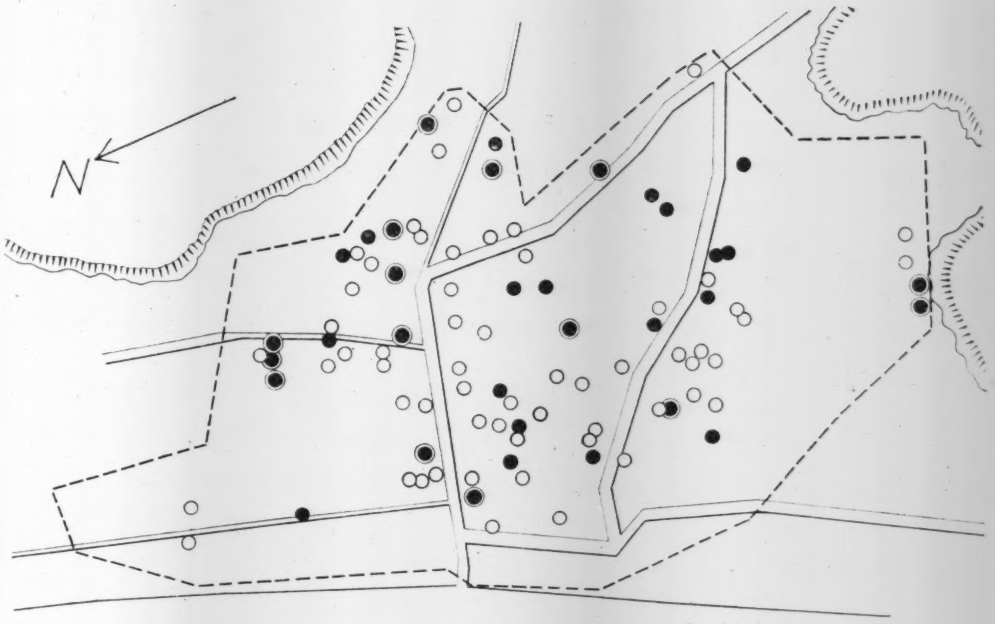

第 8 圖　木骨石造（瓦屋根）建築物分布圖（本村）

○ 損傷少きもの
● 損傷多きもの
◉ 損傷特に甚しきもの

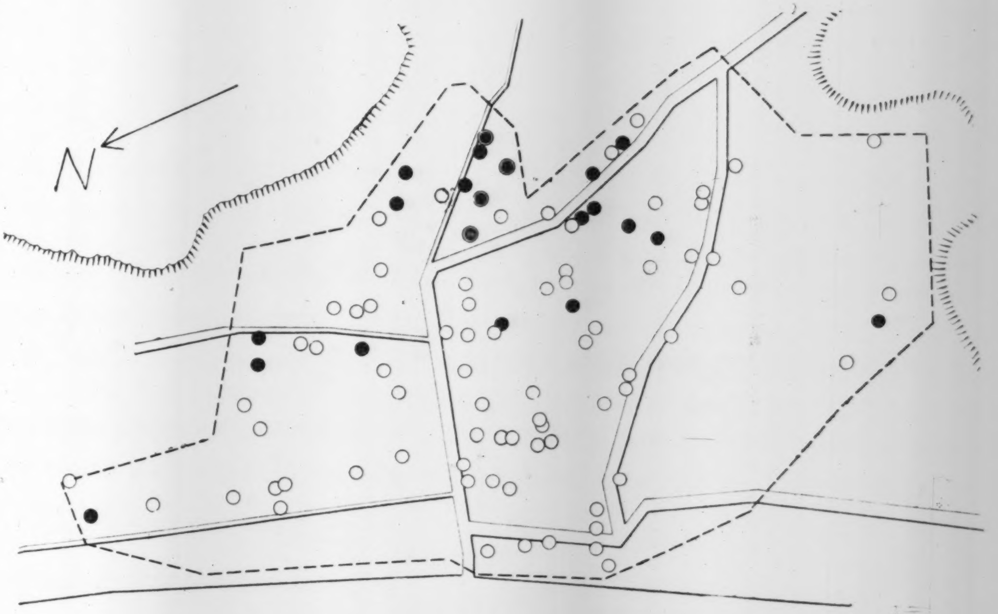

第 9 圖　木骨石造（トタン屋根）建築物分布圖（本村）

○ 損傷少きもの
● 損傷多きもの
◉ 損傷特に甚しきもの

e. 屋根瓦のみに就いて被害を云へば第 10 圖に見る如くである．石造家屋に比較

して非常な相違である．

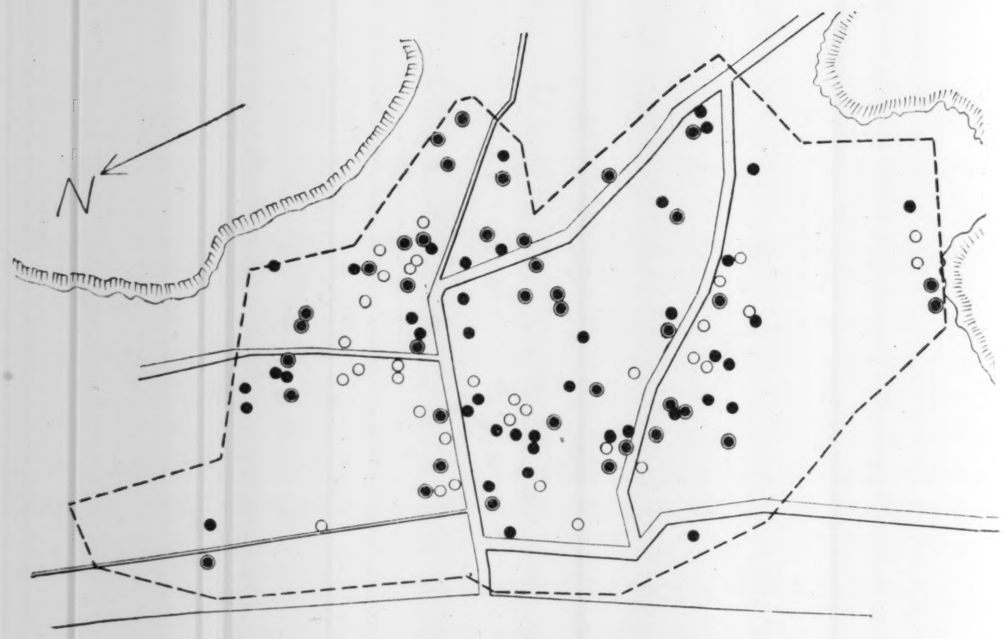

第 10 圖　瓦屋根建築物分布圖（本村）
○　損傷少きもの
●　損傷多きもの
◉　損傷特に甚しきもの

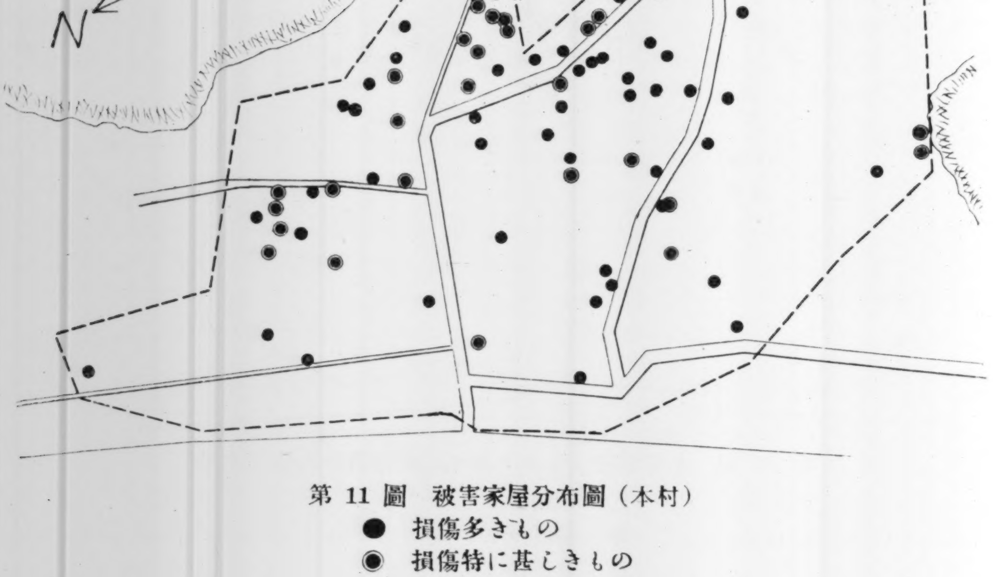

第 11 圖　被害家屋分布圖（本村）
●　損傷多きもの
◉　損傷特に甚しきもの

f.　第 11 圖は以上述べた被害家屋のみを全部地圖上に記入したものであるが，被

害家屋は東部の地域に密集してゐる傾向が見られるのである．

本村に於ける地質は表面に砂層があり，其の下部に白ママと稱する流紋岩質碎片の累層が厚く存在する．砂層の厚さは場所に依り一定せず，1m 以下の所もあり 10m 程度の所もある．砂層の厚さの分布に關しては精細な材料を缺くが，之と被害分布との間には明瞭な關係は見られない樣である．今回は唯，本村の東部に於て比較的被害が大であつたと云ふ事實を擧げて將來の研究の資とするに止めて置く．

若鄕村に於ける被害は本村と大差はない．若鄕村は流紋岩の絶壁に圍まれた僅かの砂地に發達した村落であり，砂層の厚さは海岸附近に於て約 15m，海岸を離れるに從つて次第に淺くなつてゐる．此の村落に於ては地盤，特に路面の龜裂が著しかつた（第49圖參照）．家屋の被害は槪して海岸寄り及び村落の南端に於て比較的多い．

式根島に於ける震害は新島に比較すれば輕少である．被害家屋の主なるものの寫眞を第61圖乃至第64圖に示してある．

木造家屋の水平移動　この現象の目立つたのは若鄕村である．第12圖は若鄕村役場にて調査した家屋の移動量と方向である．便宜上，村道の方向を南北に取つて居るので圖に於ては之を N′, S′ にて示してある．移動量は一つの家屋の部分で最も移動した所を測定してあるが，實際は家屋の重心の移動量は，住家に於ては，最大のもので 10cm 程度である．圖に於て東寄りの北の方向に多く移動が起つてゐるのが見られるのである．本村に於ては木造家屋の水平移動を行つたものは殆ど無く，十三社に於ける拜殿が N 30° E の方向へ約 7cm 移動してゐるのが目立つた程度である．式根島にはこの現象は起つてゐない．

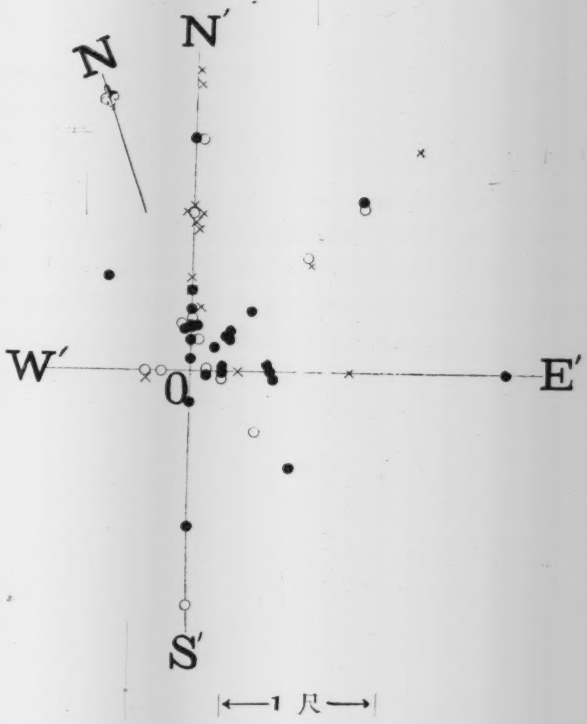

第12圖　家屋の水平移動量（若鄕村）
○ 住家　● 非住家　× 便所

地變　新島の地形は斷崖が多いので，至る所斷崖の崩落が起つた．本村から若鄕村へ通ずる村道は之がため全く不通となつた．式根島に於ては地奈多溫泉附近の崖崩れが著しい．

地割れは前記若鄕村に於けるものの他，本村より羽伏浦（新島東海岸）へ至る村道中 2，3 箇所に著しいものが見られた（第56圖）．地內島（無人島）も海岸の斷崖は至る所崩壞を見た．山崩れ又は斷層の如き大規模の地變は一切見られなかつた．

終りに臨み，今回の調査に際して多大の御便宜を與へられた東京市廳出張所，本村役場，本村小學校，並に若鄕村役場の方々に對して深甚なる感謝の辭を呈する次第である．

---

33. *The Niizima Earthquake of December 27, 1936.*

By Takahiro HAGIWARA and Syun'itirô OMOTE,

Earthquake Research Institute.

A strong earthquake occurred in the neighbourhood of Niizima, a small island of the Idu (Idu Sititô) group, at 9 h 14 m, December 27, 1936. Several tens of dwelling houses in the island were demorished and 3 persons killed by falling of the cliffwalls. Aftershocks, orignating from a depth of less than 10 km, were recorded in the neighbourhood of Honmura, a village in the middle part of the island, by means of the network of seismological stations temporarily established at three places in the island after the earthquake.

（震研彙報　第十五號　圖版　萩原・表）

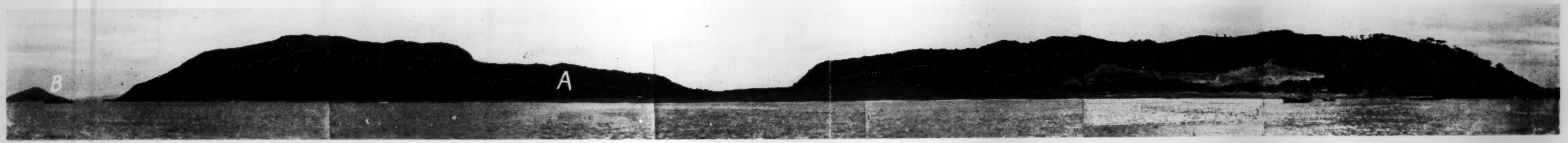

第 13 圖　新嶋全景（本村沖より撮影）A 本村　B 利嶋

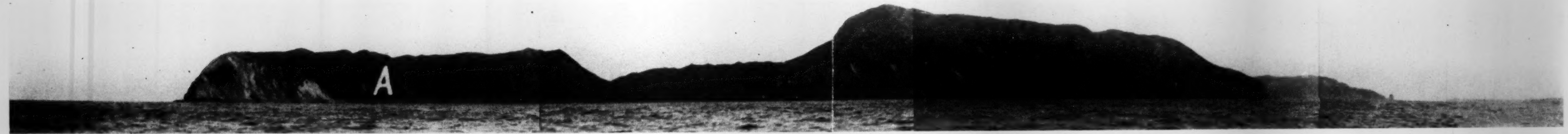

第 14 圖　新嶋全景（若郷村沖より撮影）A 若郷村

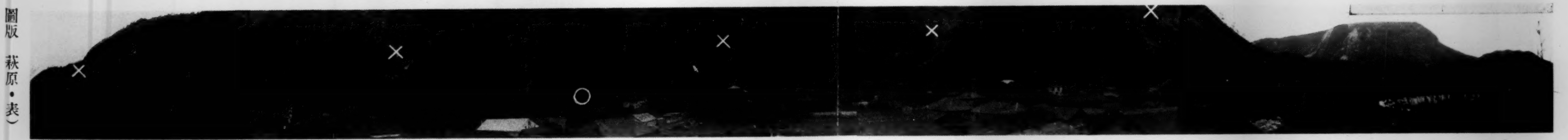

第 15 圖　若郷村全景（海岸砂丘上より撮影）○ 村役場（地震計設置場所）× 崖崩れ

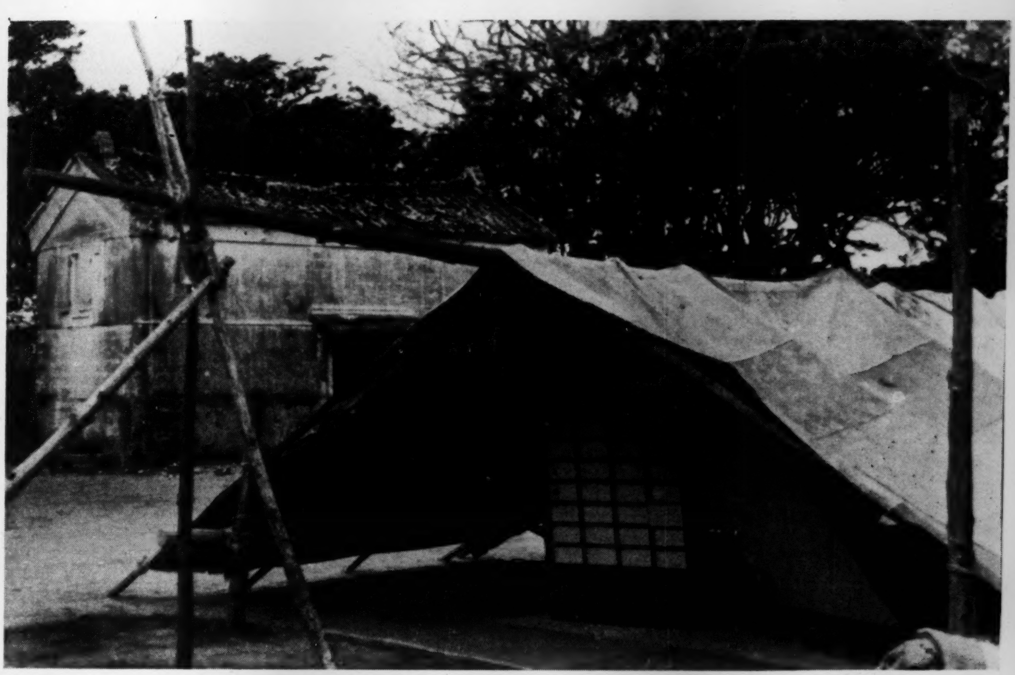

第 16 圖　本村役場倉庫の破損（本村）

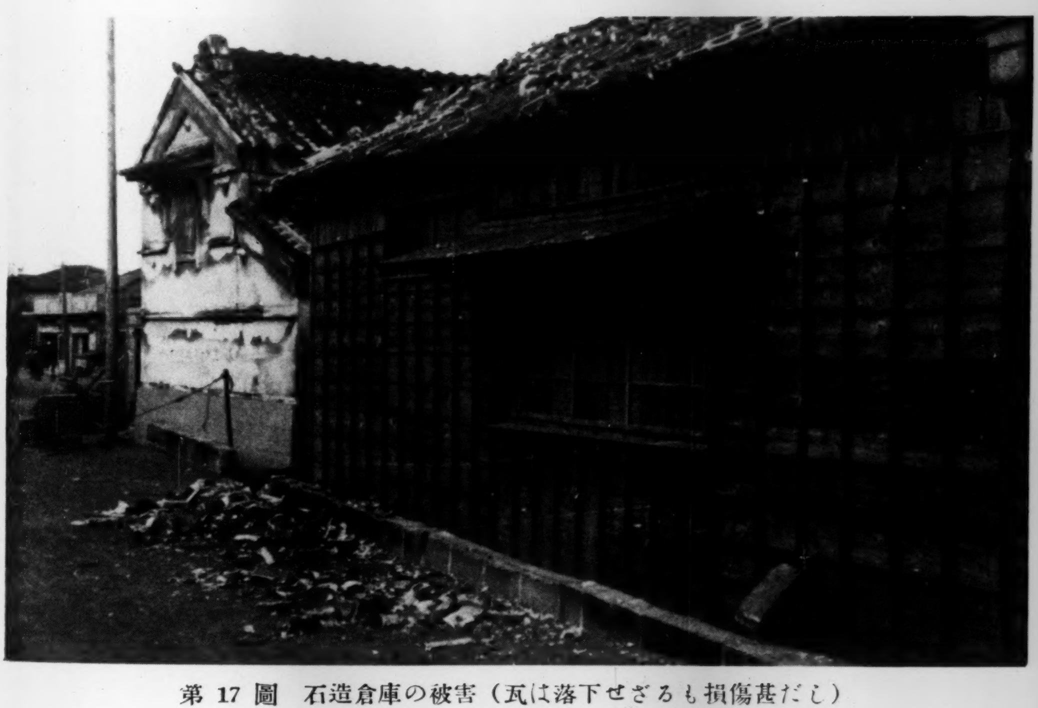

第 17 圖　石造倉庫の破害（瓦は落下せざるも損傷甚だし）
及び木造瓦葺屋根の破損（本村）

（震研彙報　第十五號　圖版　萩原・表）

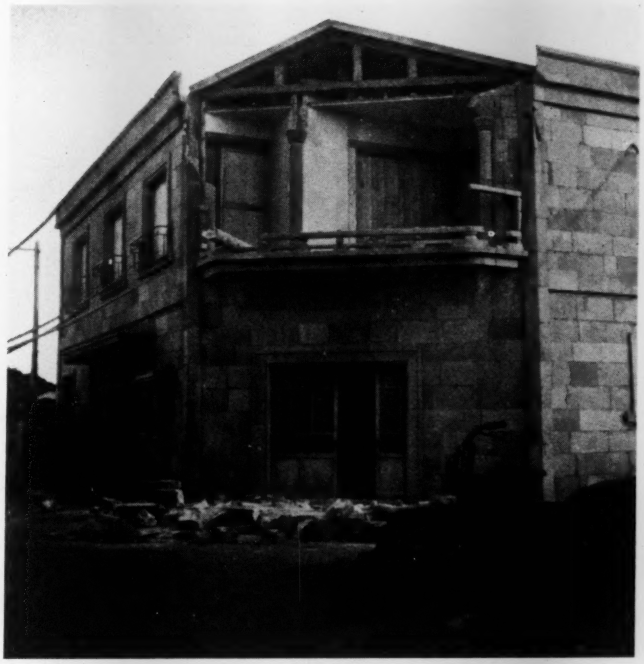

第 18 圖　木骨石造葺家屋の破損（本村）

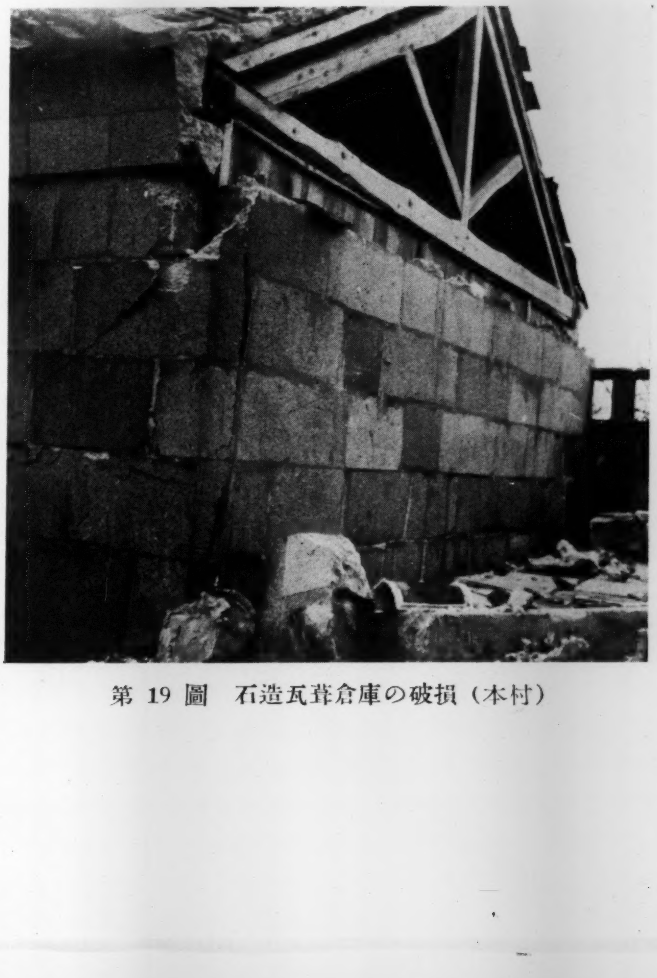

第 19 圖　石造瓦葺倉庫の破損（本村）

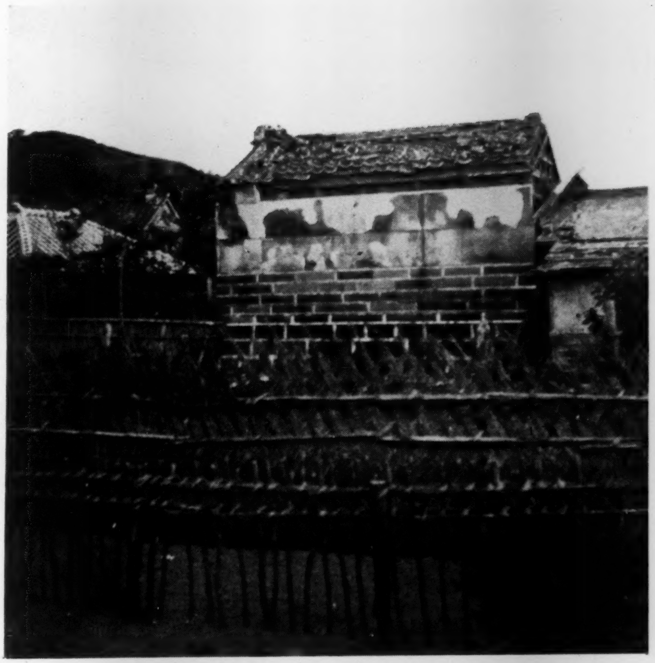

第 20 圖　石造瓦葺倉庫の破損（本村）

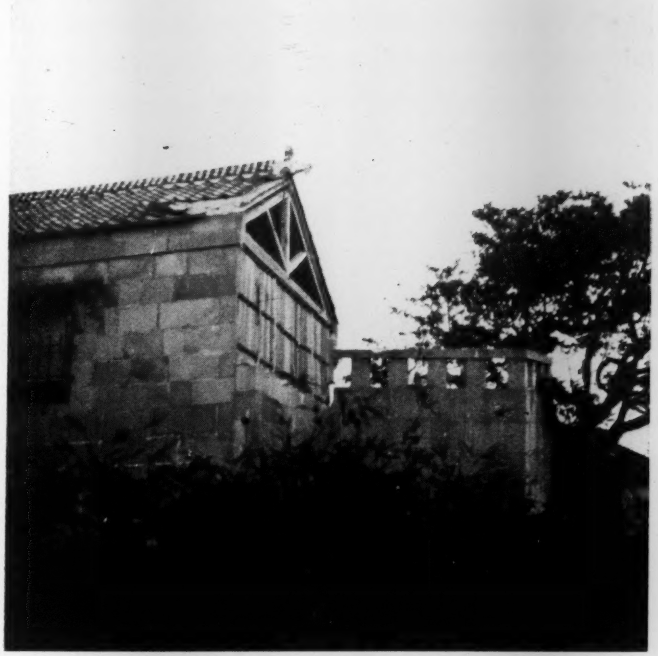

第 21 圖　石造倉庫の破損（本村）

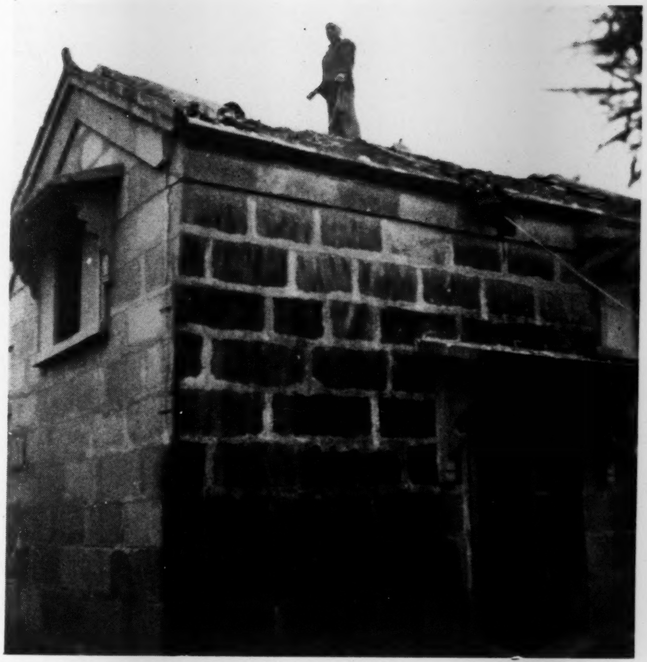

第 22 圖　石造瓦葺倉庫の破損（本村）

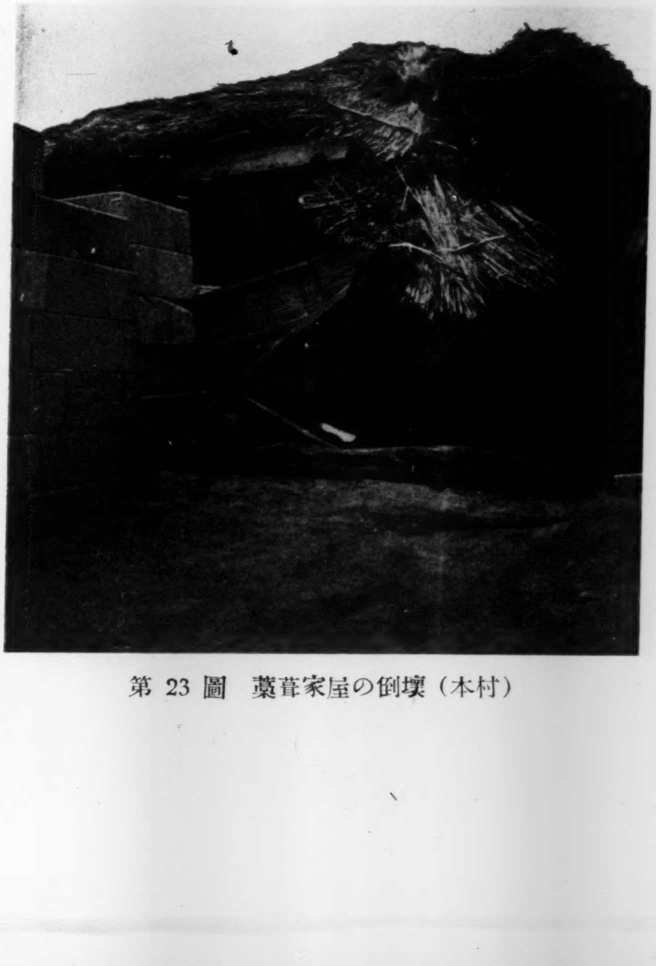

第 23 圖　藁葺家屋の倒壞（本村）

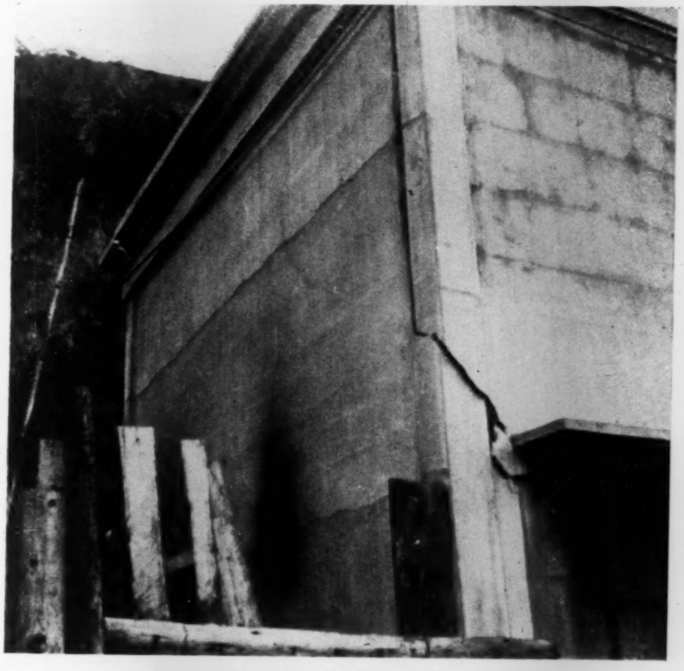

第 24 圖 石造倉庫の破損（本村）

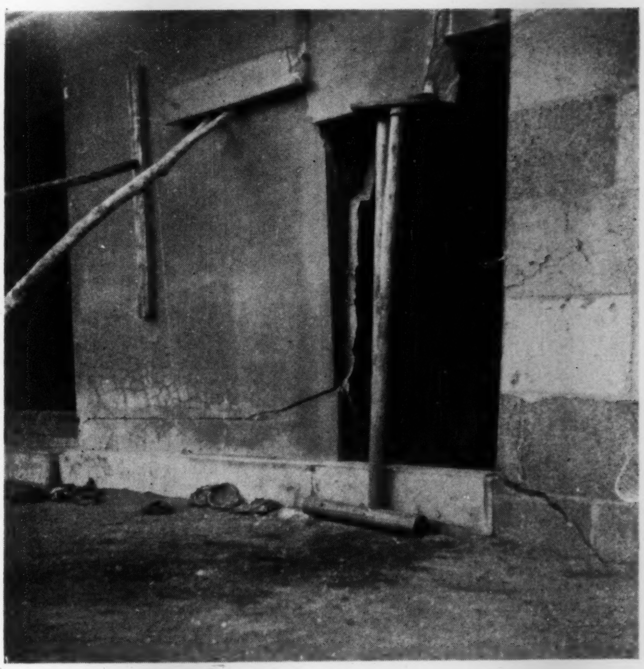

第 25 圖 石造家屋の破損（本村）

（震研彙報 第十五號 圖版 萩原・表）

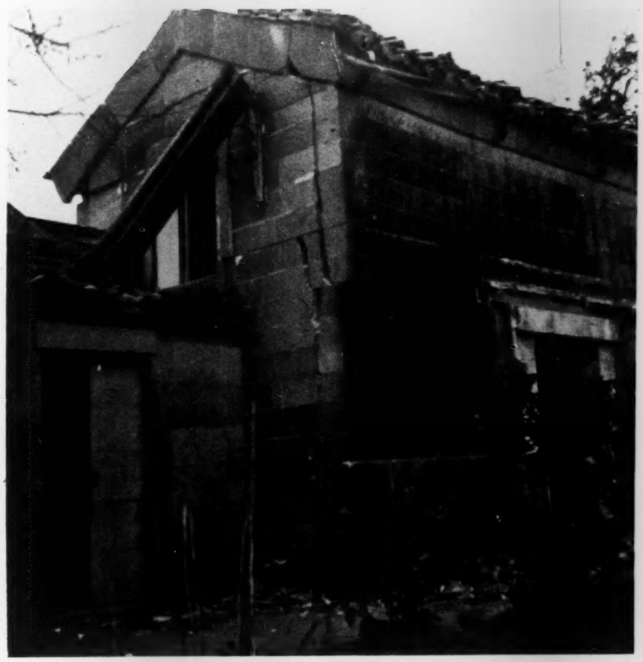

第 26 圖 石造瓦葺倉庫の破損（本村）

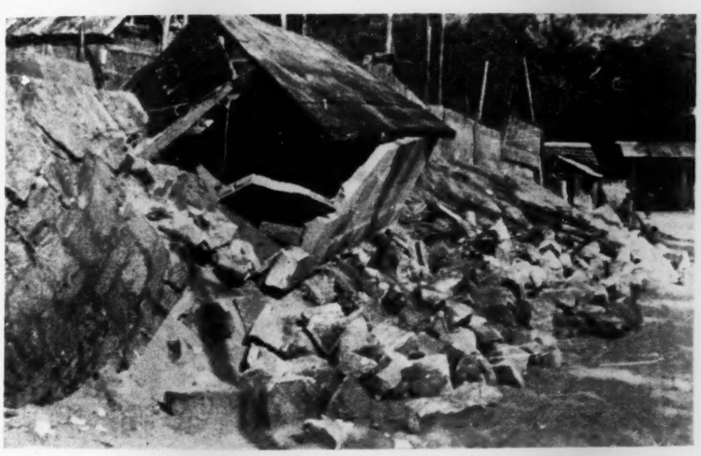

第 27 圖 石造納屋の倒壞（本村）

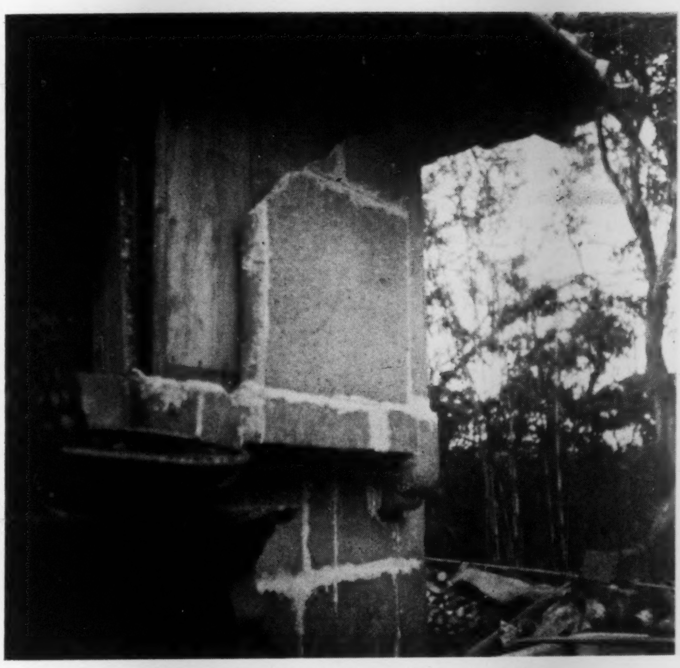

第 28 圖　石造家屋の破損（本村）

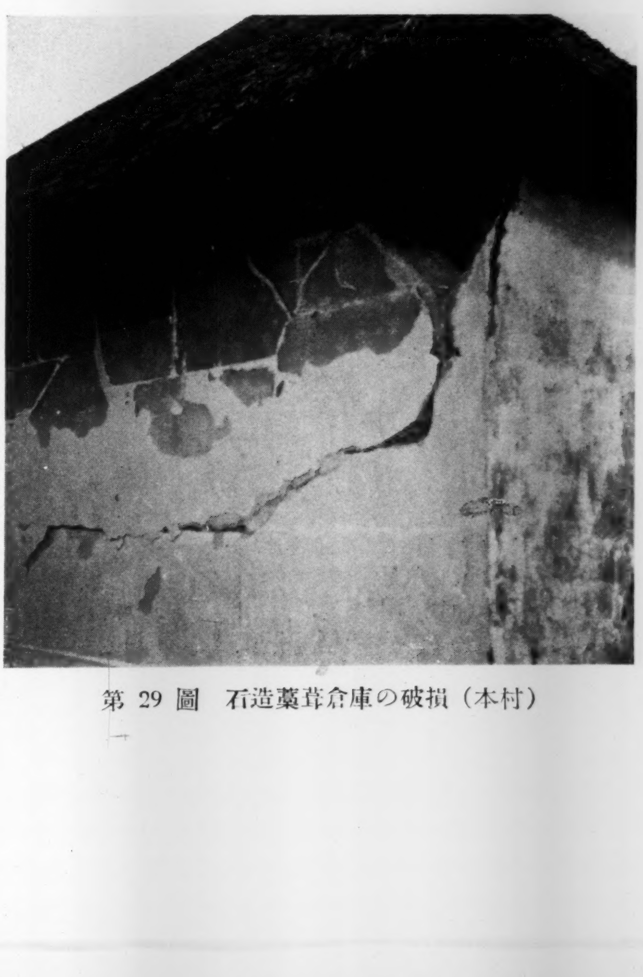

第 29 圖　石造藁葺倉庫の破損（本村）

（震研彙報　第十五號　圖版　萩原・表）

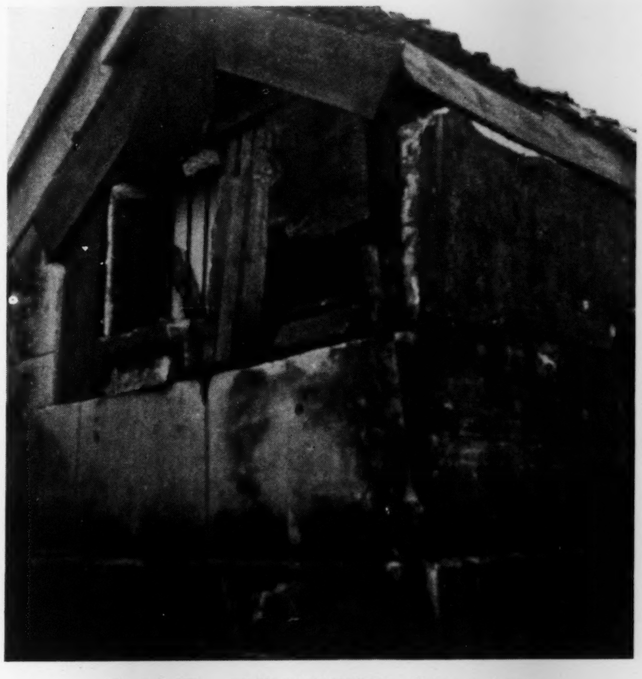

第 30 圖 石造瓦葺家屋の破損（本村）

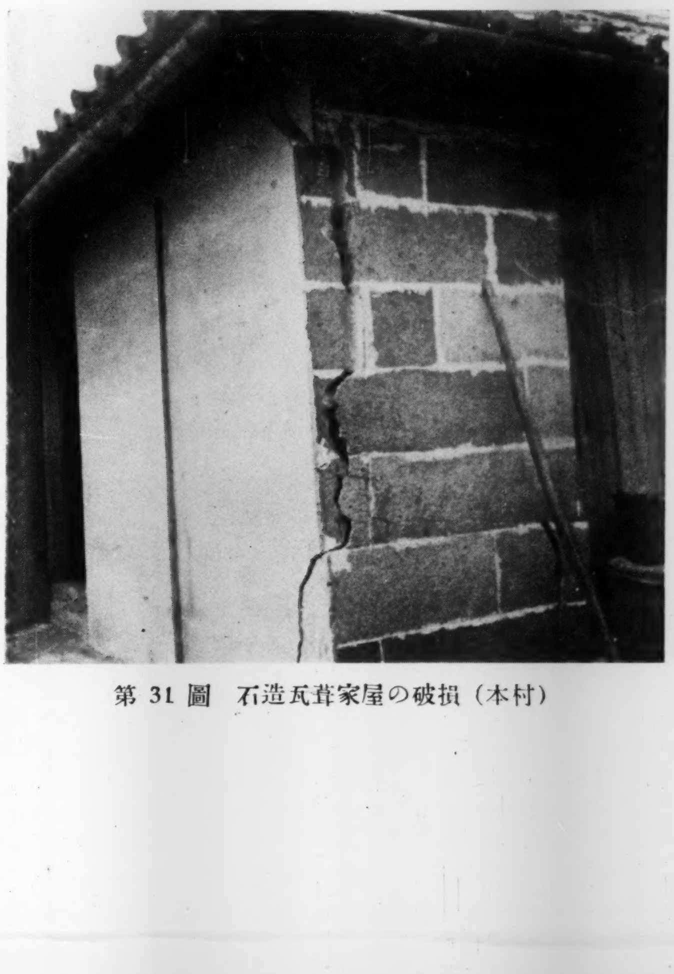

第 31 圖 石造瓦葺家屋の破損（本村）

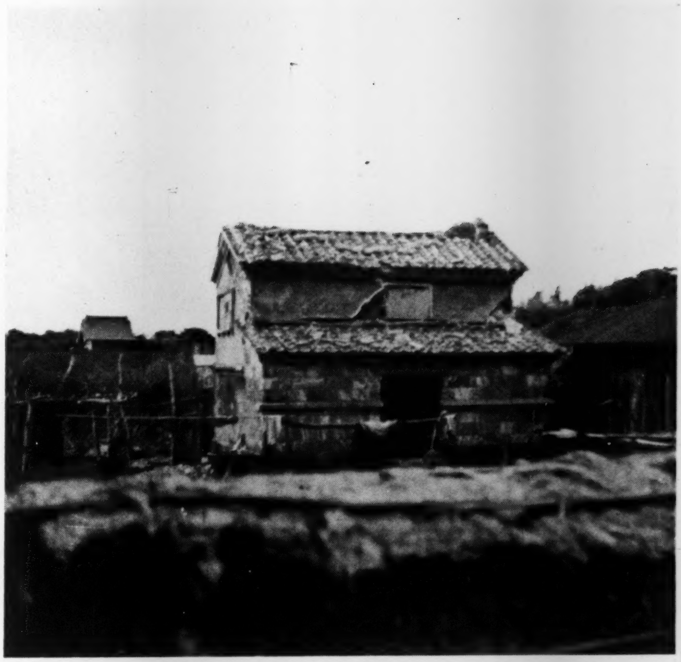

第 32 圖　石造瓦葺倉庫の破損（本村）

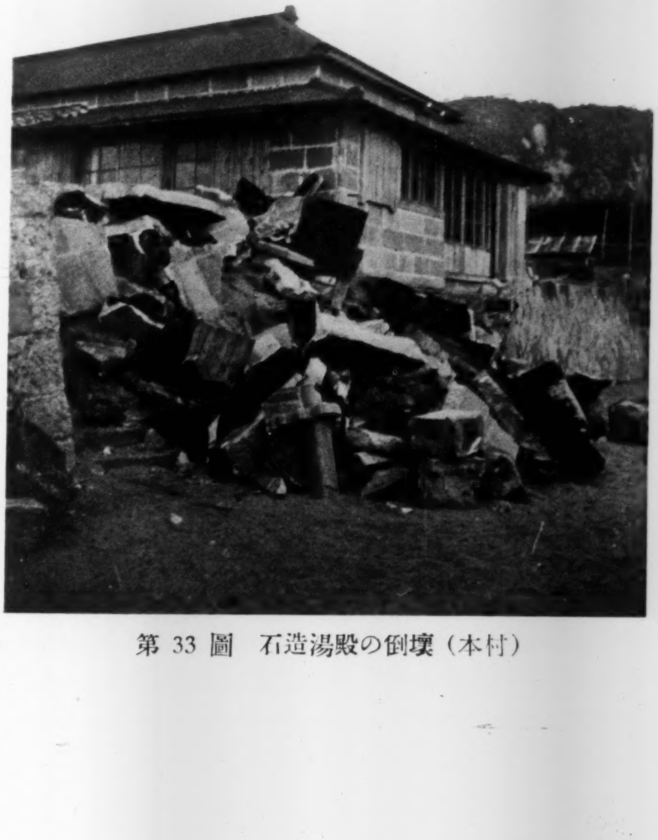

第 33 圖　石造湯殿の倒壊（本村）

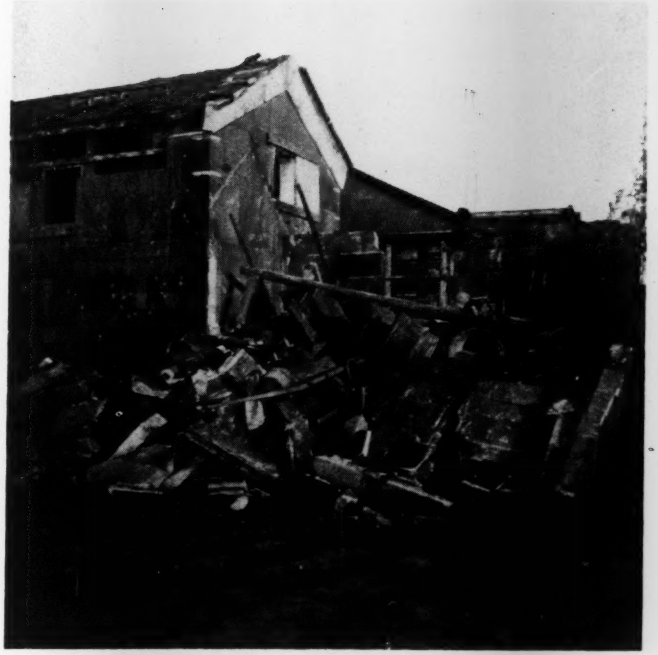

第 34 圖　石造納屋の倒壞（本村）

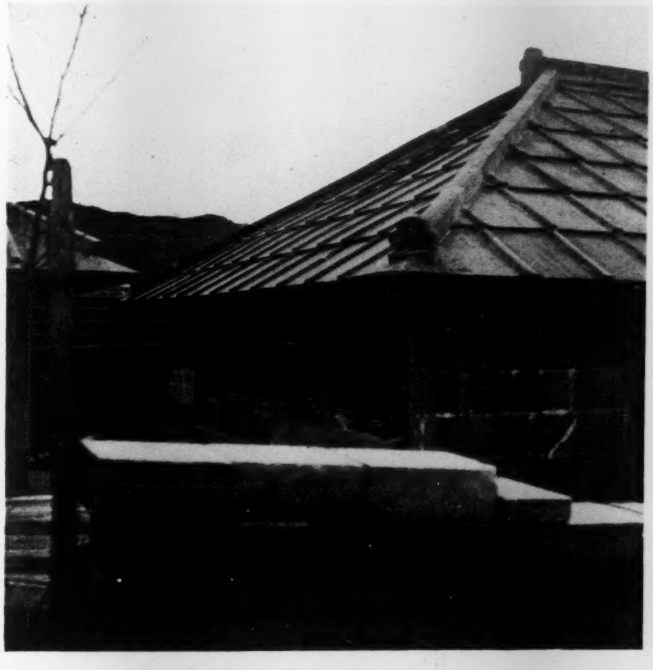

第 35 圖　石造家屋の破損（本村）

第 36 圖 石造瓦葺工場の破損（本村）

第 37 圖 石造工場の破損（本村）

（震研彙報 第十五號 圖版 萩原・表）

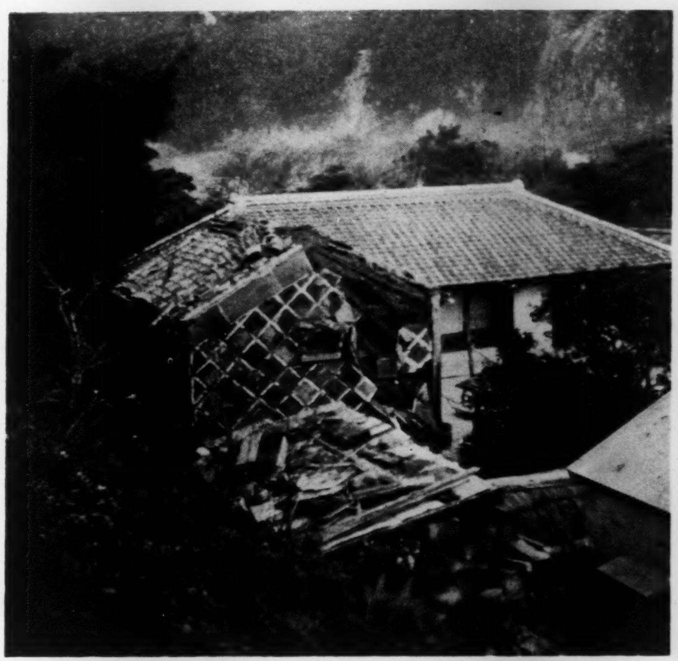

第 38 圖　石造瓦葺倉庫の破損（本村）

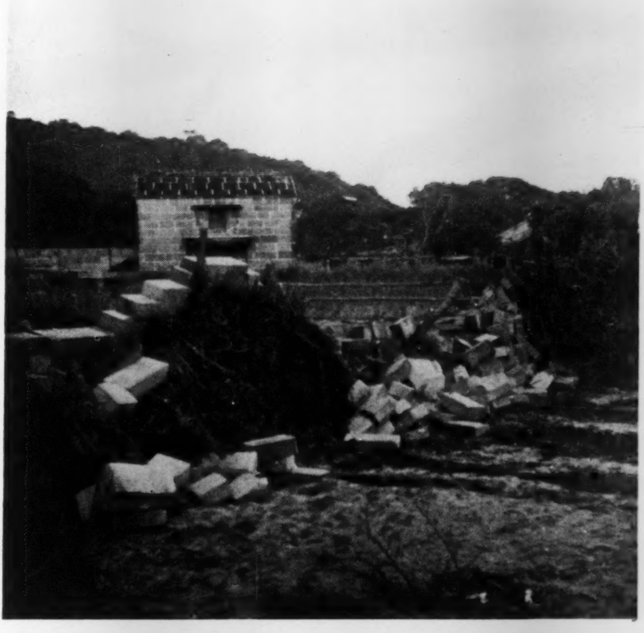

第 39 圖　石垣の倒壊（本村）

（震研彙報　第十五號　圖版　萩原・表）

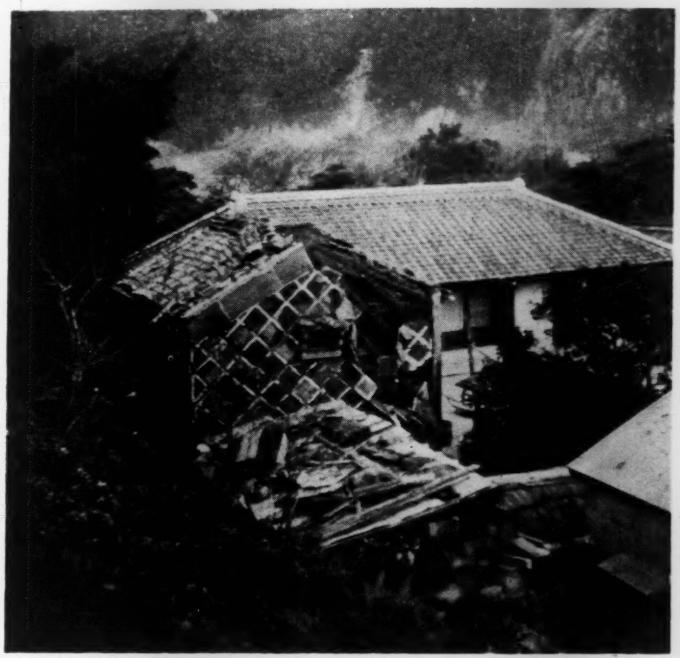

第 38 圖　石造瓦葺倉庫の破損（本村）

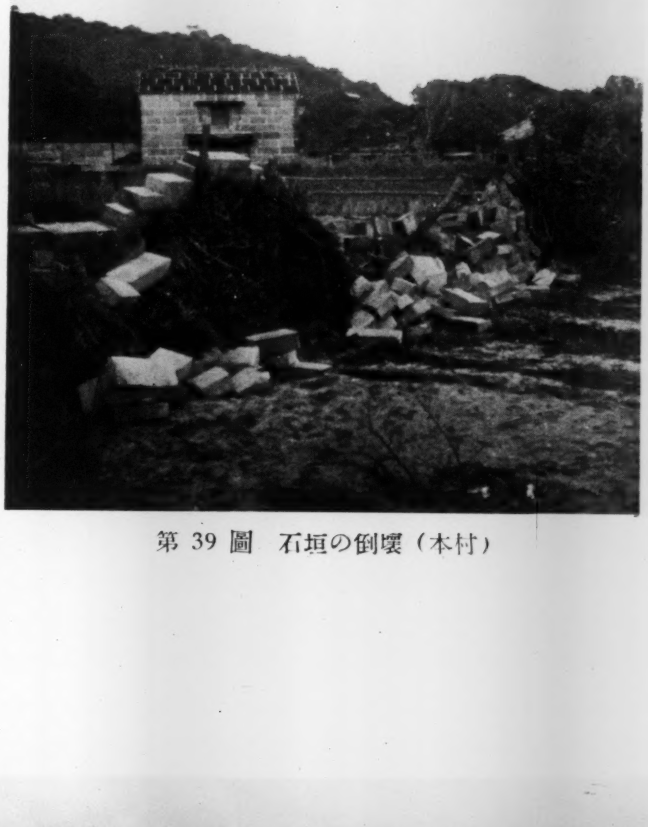

第 39 圖　石垣の倒壞（本村）

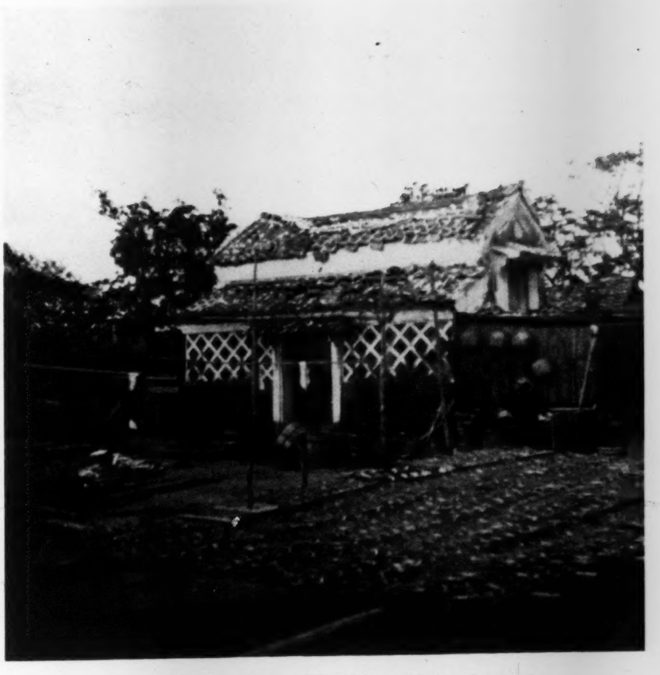

第 40 圖　石造瓦葺倉庫の破害（本村）

第 41 圖　石造瓦葺倉庫の破損（本村）

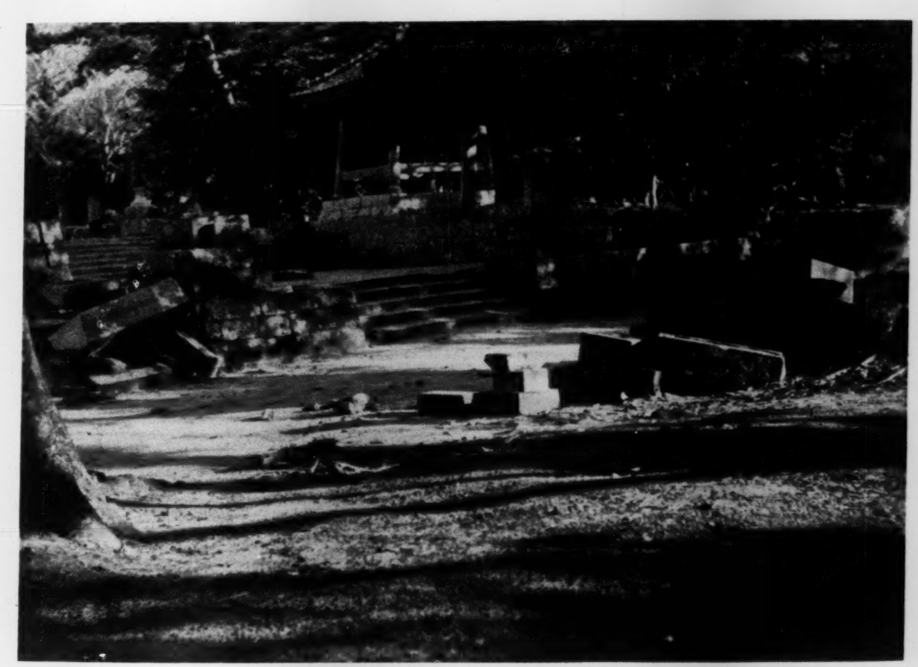

第 42 圖　長榮寺の門柱及び石碑の倒壞（本村）
（本村役場前田長八氏撮影）

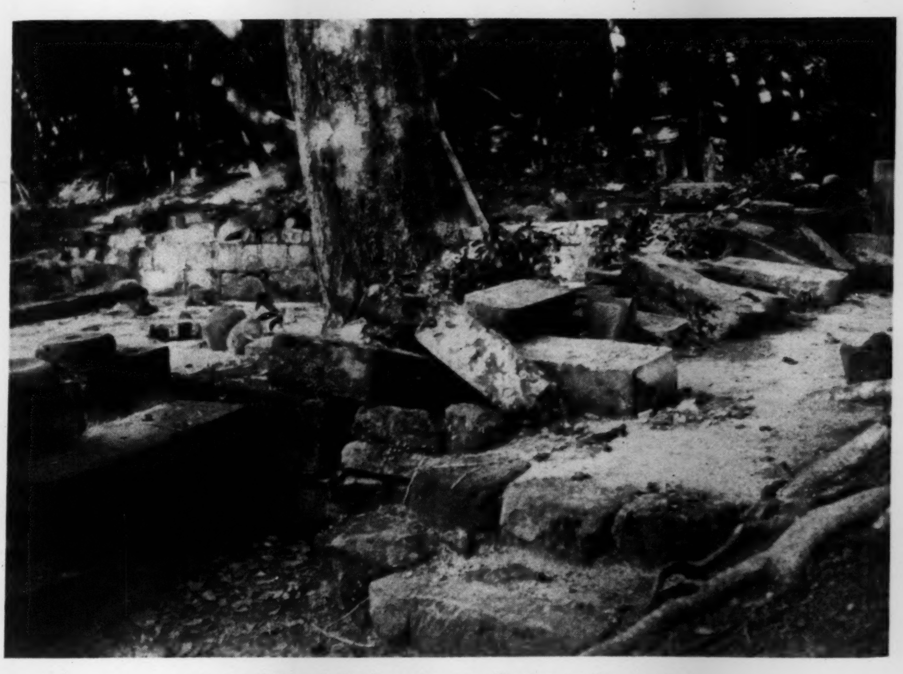

第 43 圖　長榮寺に於ける墓石の倒壞（本村）
（本村役場前田長八氏撮影）

（震研彙報　第十五號　圖版　萩原・表）

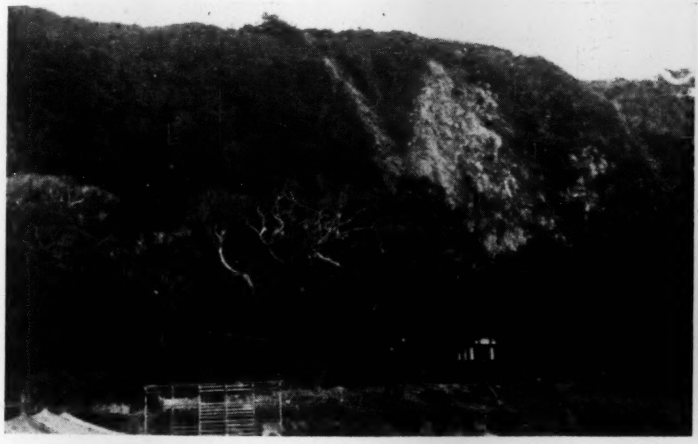

第 44 圖　本村小學校裏手の山崩（本村）

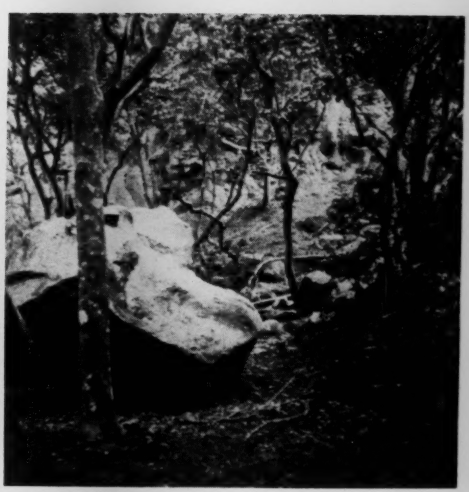

第 45 圖　小學校裏手に顚落せる巨石（本村）

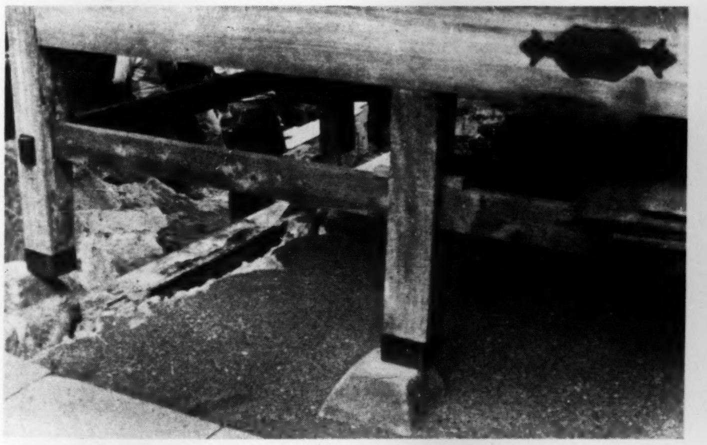

第 46 圖　十三社神社の柱の水平移動約 7 cm（本村）

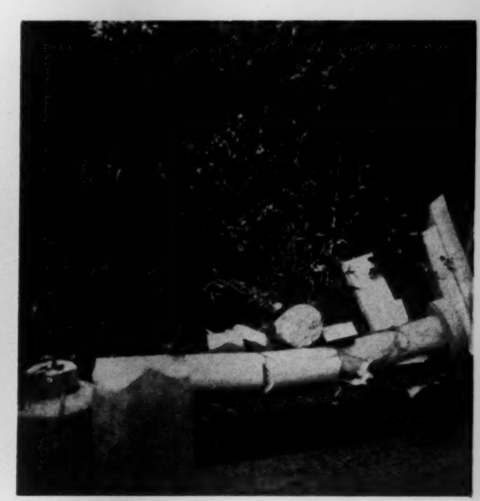

第 47 圖　神社鳥居の倒壞（本村）

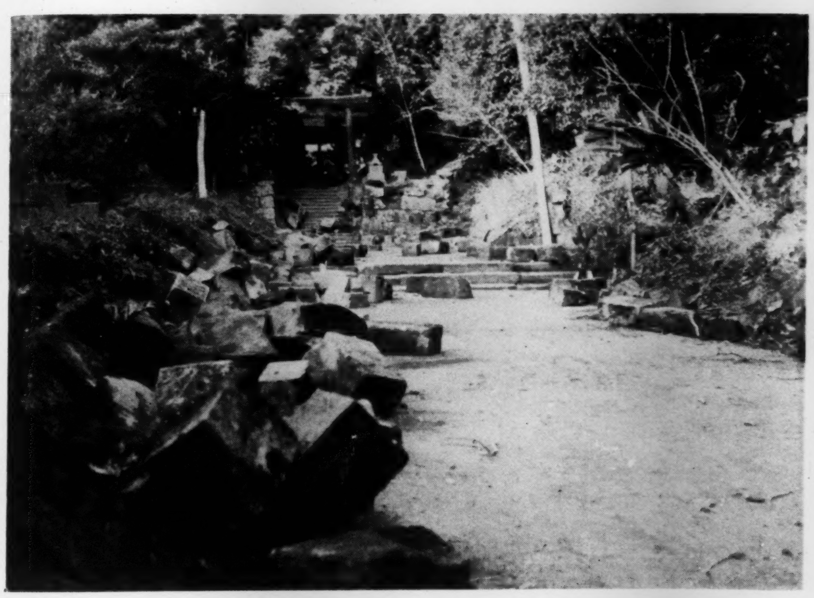

第 48 圖 十三社神社石垣の倒壞（本村）

（本村役場前田長八氏撮影）

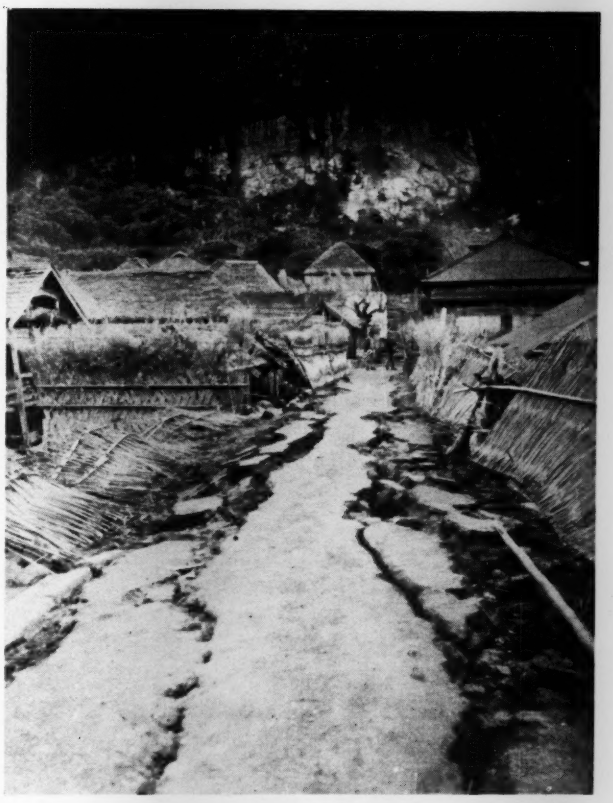

第 49 圖 村道の龜裂（若鄉村）

（本村役場前田長八氏撮影）

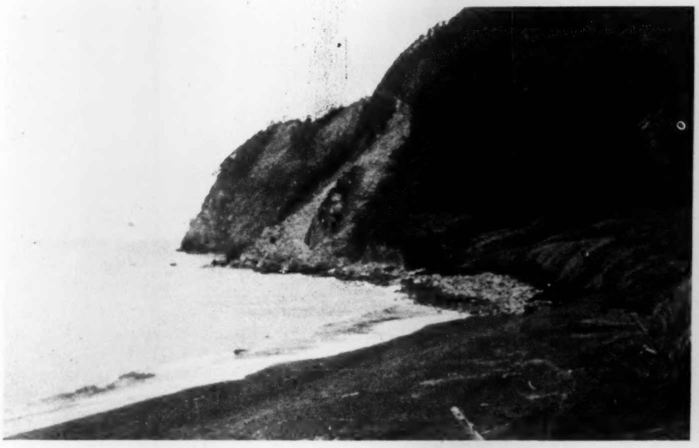

第 50 圖　若郷村北方海岸に於ける崖崩れ（一名埋死す）

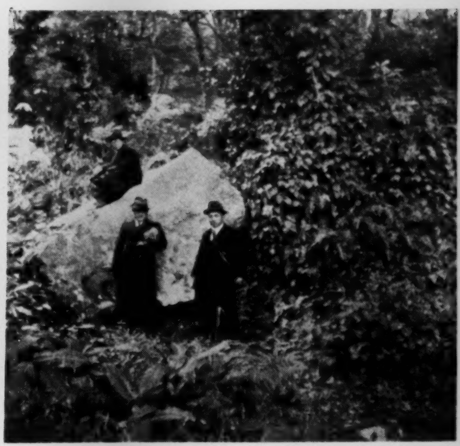

第 51 圖　若郷小學校裏手に顚落せる巨石（若郷村）

（震研彙報　第十五號　圖版　萩原・表）

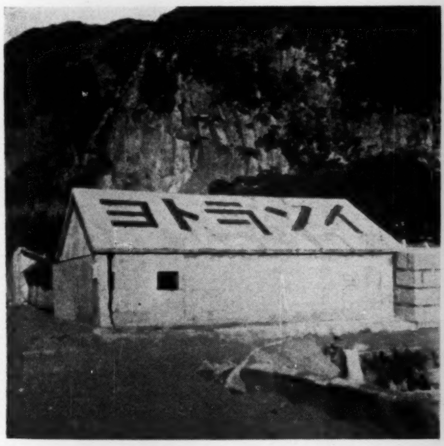

第 52 圖　石造倉庫の被害（若郷村）

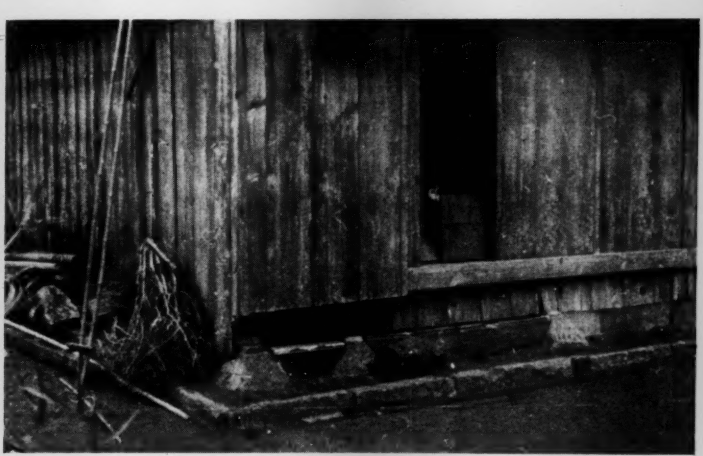

第 53 圖　木造家屋の水平移動（若郷村）

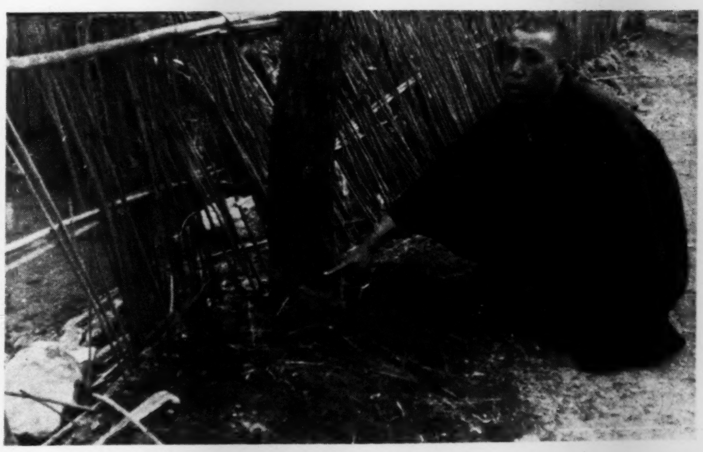

第 54 圖　砂地の沈下に由り松樹の根元約 5 cm 浮出る（若郷村）

（震研彙報　第十五號　圖版　萩・原表）

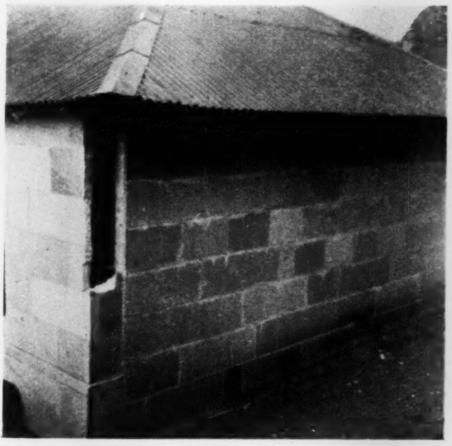

第 55 圖　石造倉庫の被害（若郷村）

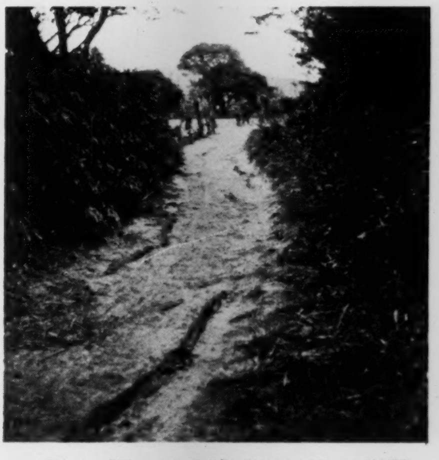

第 56 圖　羽伏浦附近村道の亀裂

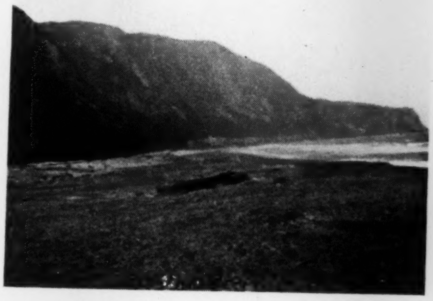
第 57 圖　羽伏浦より宮塚山東部の崖崩れを遠望す

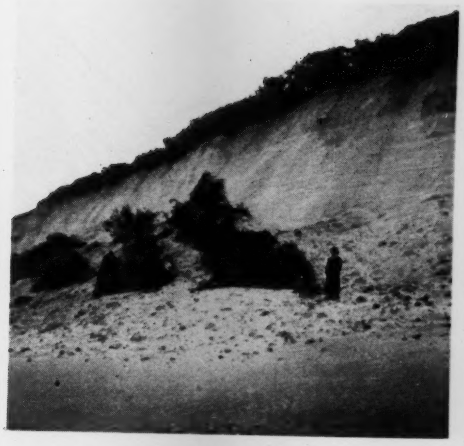
第 58 圖　羽伏浦海岸の崖崩れ

（震研彙報　第十五號　圖版　萩原・表）

第 59 圖　羽伏浦附近の崖崩れ

第 60 圖　羽伏浦より若郷村に至る村道の被害

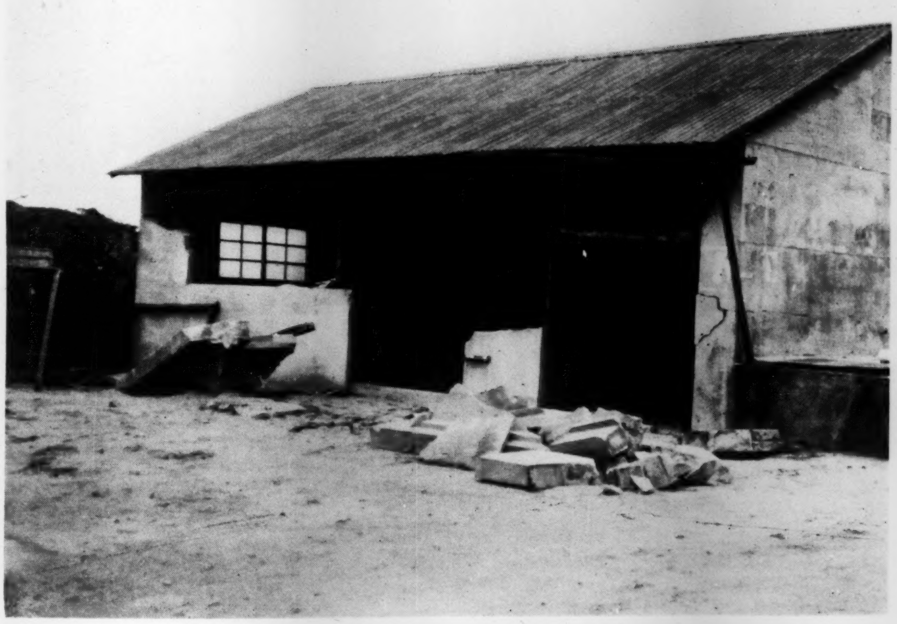

第61圖 消防ポンプ置場の破壞（式根島）

第62圖 同上（裏手より撮影）（式根島）

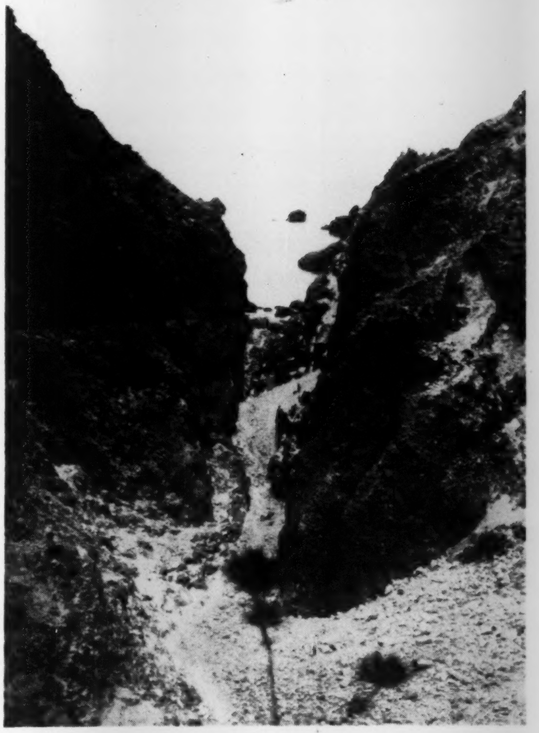

第 63 圖 地奈多溫泉通路の埋沒（式根島）

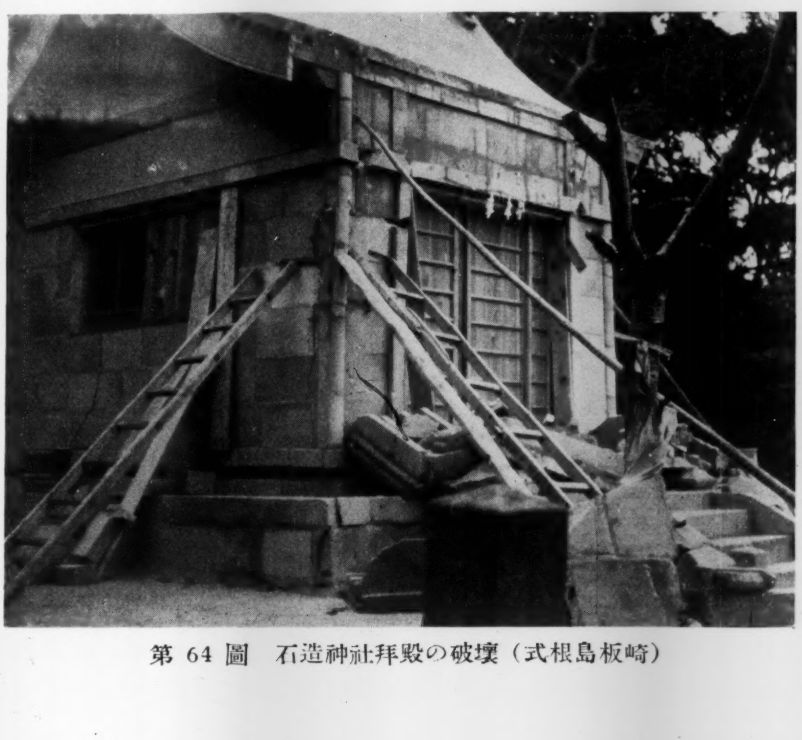

第 64 圖 石造神社拜殿の破壞（式根島板崎）

34. 大分縣坂の市—鹿兒島縣伊集院村間並に宮崎縣細島町－熊本縣熊本市間の水準改測結果

本所に於ては昭和 11 年に於いて，九州地方に於ける水準改測を陸地測量部に委託して此れを行ひ，同地方の高低變化の狀況を審かにする事を得たり．玆に揭げて，研究に資せむとす．

水準改測を施行したる水準線及びその測量時期は次表に示す．

水準線區間	舊測量	新測量
坂の市——大分	明治29年12月	昭和11年 5月
大分——小倉	明治25年 9~10月	〃 5~7 月
小倉——福岡	明治23年 5~7 月	〃 5~6 月
福岡——久留米	明治23年 5~7 月	〃 6~7 月
久留米——熊本——佐數	明治24年10~12月	〃 7~11月
佐數——下伊集院	I 明治24年11月～明治25年2月	
	II 大正4年 2~4 月	〃 9~11月
細島—— 延岡	I 明治29年8月	
	II 昭和7年11月	〃 11月
延岡——高千穗村(B.M. 2672)	明治28年10~11月	〃 5~8 月
高千穗村——七瀧村(B.M. 2695)	明治29年 7~9 月	〃 8~10月
七瀧村——熊本	明治29年 2~3 月	〃 9~10月

附圖は，上表の各區間及びその區間に在る水準點の垂直變動を示したるものにして其等の垂直變動は，坂の市—小倉—熊本—下伊集院の線に就いては，坂の市に在る B. M. 2633 の變動量を 81·7 mm とし，延岡—熊本の線に就いては，延岡に在る B. M. 2635 の變動量を 31·8 mm として計算せるものなり．

上述の水準改測は，原田積善會より本所に寄附せられたる研究資金によりて遂行せられたるものにして，玆に附記して深謝の意を表す．

以上

昭和 12 年 6 月

地震研究所

34. *The Results of Precise Levelling along the Line between Sakanoiti and Izyûin, via Kokura, Hukuoka, and Kumamoto, and the Line between Hosozima and Kumamoto, via Nobeoka.*

The line of levels from Sakanoiti to Izyûin, via Kokura, Hukuoka and Kumamoto, and the line from Hosozima to Kumamoto, via Nobeoka were recently relevelled by the Military Land Survey at our request.

The lines of levels in question are shown in the annexed Figs. 1—5, together with the relative vertical displacements of bench-marks obtained by comparing the results of recent measurements with those made previously.

The dates of the surveys are as follows:

Lines of Levels	Earlier Survey	Recent Survey
Sakanoiti—Oita	Dec., 1896	May, 1636
Oita—Kokura	Sept.,—Nov., 1892	May—July, 1936
Kokura—Hukuoka	May—July, 1890	May—June, 1936
Hukuoka—Kurume	May—July, 1892	June—July, 1936
Kurume—Kumamoto—Sasiki	Oct.—Dec., 1891	July—Nov., 1936
Sasiki—Izyûin	I Nov., 1891—Feb., 1892	Sept.—Nov., 1936
	II Feb.—Apr., 1915	
Hosozima—Nobeoka	I Aug., 1896	Nov., 1936
	II Nov., 1932	
Nobeoka—Takatiho (B.M. 2672)	Oct.—Nov., 1895	May—Aug., 1936
Takatiho—Nanataki (B.M. 2672) (B.M. 2695)	July—Sept., 1896	Aug.—Oct., 1936
Nanataki—Kumamoto	Feb.—March, 1896	Sept.—Oct., 1936

The vertical diaplacements of the bench-marks along the line from Sakanoiti to Izyûin, via Kokura, Hukuoka and Kumamoto, are referred to B.M. 2633, situated at Sakanoiti, the height of which had changed by 81·7 mm. The vertical displacements of the bench-marks on the line from Hosozima to Nobeoka are referred to the mareograph station, the height of which is regarded as unchanged, while those of the bench-marks distributed between Nobeoka and Kumamoto are referred to B.M. 2635, the vertical displacement of which was assumed to be 31·8 mm.

The recent relevelling was made possible with the aid of research fund granted by the Harada Sekizenkwai, to the council of which are due our sincere thanks.

April, 1937

The Earthquake Research Institute.

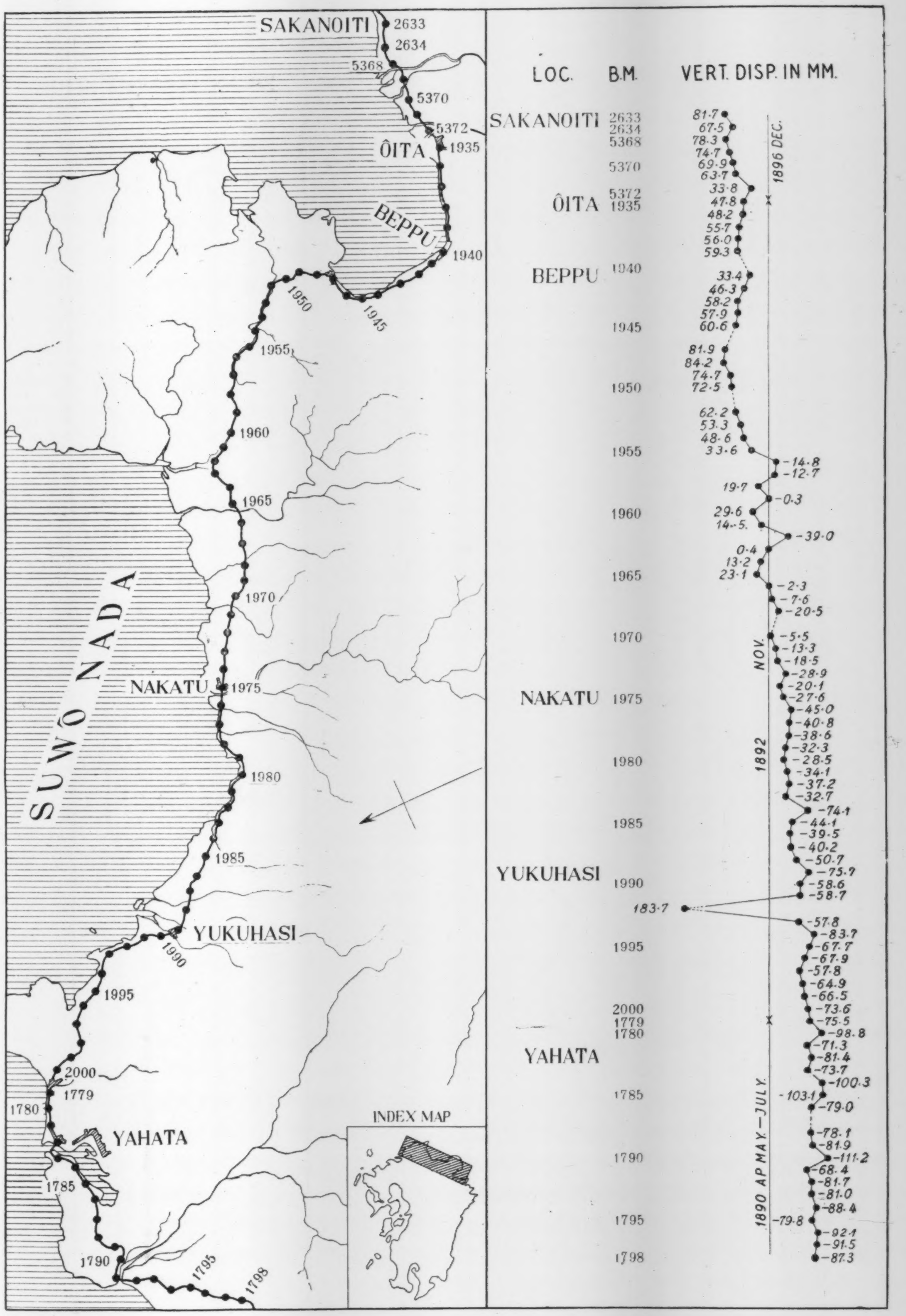
SAKANOITI
2633
2634
5368
5370
5372
ÔITA
1935
BEPPU
1940
1945
1950
1955
1960
1965
1970
SUWŌ NADA
NAKATU
1975
1980
1985
YUKUHASI
1990
1995
2000
1779
1780
YAHATA
1785
1790
1795
1798
INDEX MAP
LOC.
B.M.
VERT. DISP. IN MM.
SAKANOITI 2633 2634 5368 5370
ÔITA 5372 1935
BEPPU 1940
1945
1950
1955
1960
1965
1970
NAKATU 1975
1980
1985
YUKUHASI 1990
1995
2000 1779 1780
YAHATA
1785
1790
1795
1798
81·7
67·5
78·3
74·7
69·9
63·7
33·8
47·8
48·2
55·7
56·0
59·3
33·4
46·3
58·2
57·9
60·6
81·9
84·2
74·7
72·5
62·2
53·3
48·6
33·6
-14·8
-12·7
19·7
-0·3
29·6
14·5.
-39·0
0·4
13·2
23·1
-2·3
-7·6
-20·5
-5·5
-13·3
-18·5
-28·9
-20·1
-27·6
-45·0
-40·8
-38·6
-32·3
-28·5
-34·1
-37·2
-32·7
-74·1
-44·1
-39·5
-40·2
-50·7
-75·7
-58·6
-58·7
183·7
-57·8
-83·7
-67·7
-67·9
-57·8
-64·9
-66·5
-73·6
-75·5
-98·8
-71·3
-81·4
-73·7
-100·3
-103·1
-79·0
-78·1
-81·9
-111·2
-68·4
-81·7
-81·0
-88·4
-79·8
-92·1
-91·5
-87·3
1896 DEC.
NOV. 1892
1890 AP MAY.—JULY.

Fig. 1.

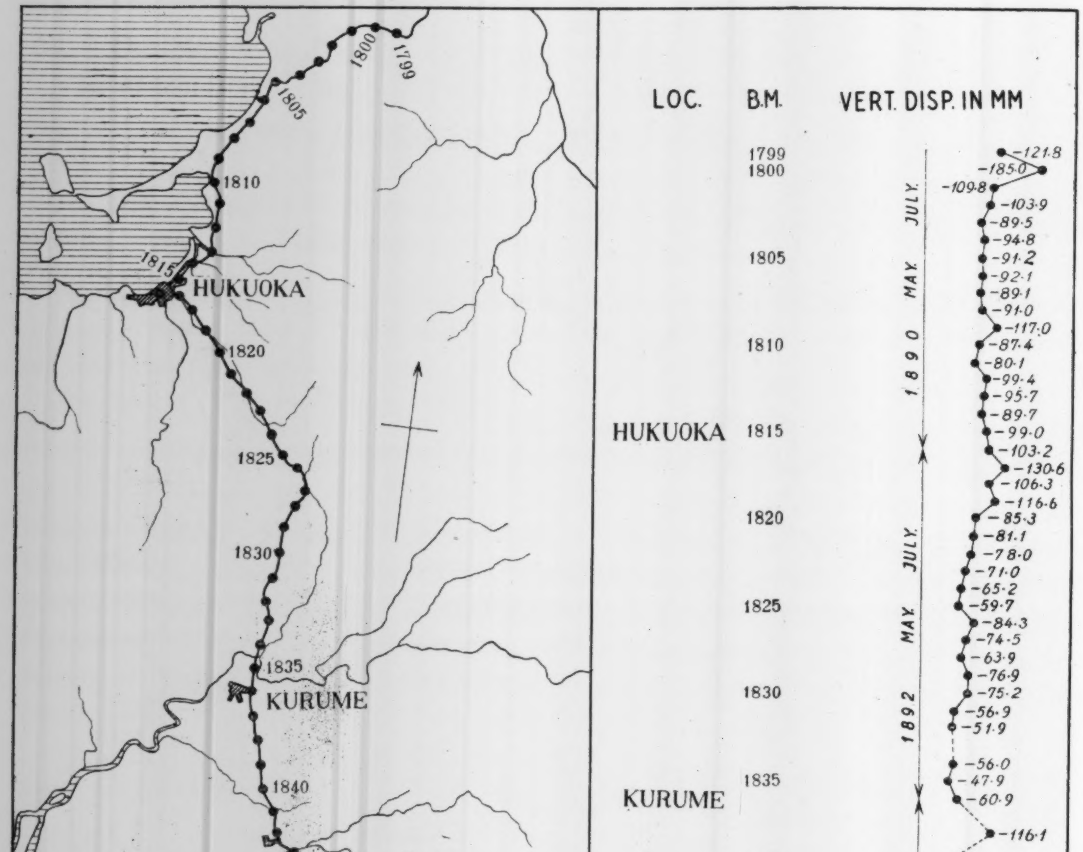
1799
1800
1805
1810
1815
HUKUOKA
1820
1825
1830
1835
KURUME
1840
1845
1850
1855
1860
1865
1870
2365
KUMAMOTO
1873
INDEX MAP
LOC.
B.M.
VERT. DISP. IN MM
HUKUOKA
KURUME
KUMAMOTO
1799
1800
1805
1810
1815
1820
1825
1830
1835
1840
1845
1850
1855
1860
1865
1870
1873
2365
JULY.
MAY.
1890
JULY.
MAY.
1892
NOV.
OCT.
1891
-121.8
-185.0
-109.8
-103.9
-89.5
-94.8
-91.2
-92.1
-89.1
-91.0
-117.0
-87.4
-80.1
-99.4
-95.7
-89.7
-99.0
-103.2
-130.6
-106.3
-116.6
-85.3
-81.1
-78.0
-71.0
-65.2
-59.7
-84.3
-74.5
-63.9
-76.9
-75.2
-56.9
-51.9
-56.0
-47.9
-60.9
-116.1
-29.4
-52.1
-36.9
-41.8
-8.4
-7.9
-1.5
15.0
7.0
11.9
-2.8
24.8
-8.5
18.1
8.3
16.8
19.2
40.4
45.6
55.6
53.2
68.8
56.3
55.6
-8.7
16.5

Fig. 2.

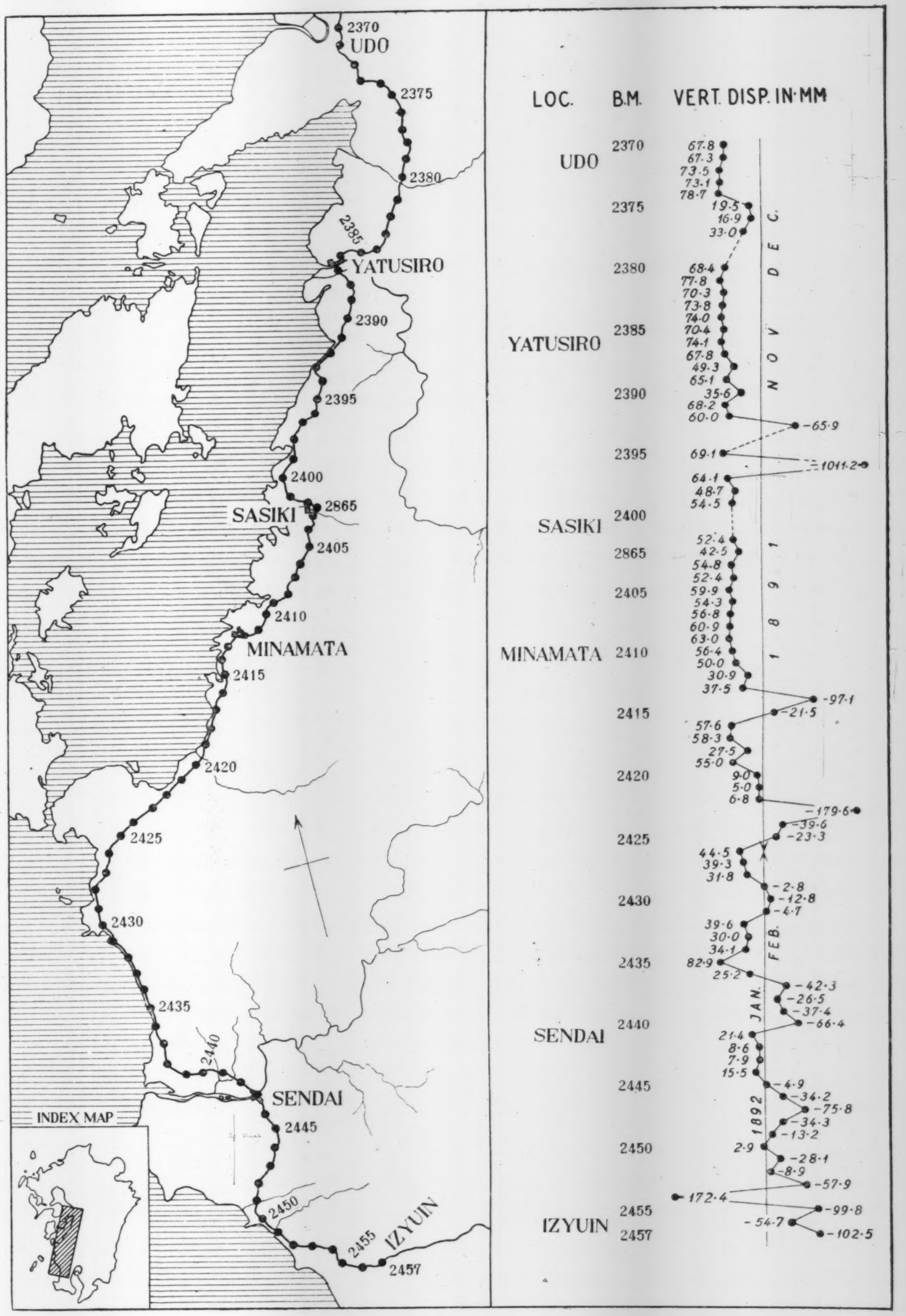
2370
UDO
2375
2380
2385
YATUSIRO
2390
2395
2400
SASIKI
2865
2405
2410
MINAMATA
2415
2420
2425
2430
2435
2440
SENDAI
2445
2450
2455
IZYUIN
2457
INDEX MAP
LOC.
B.M.
VERT. DISP. IN·MM
UDO
YATUSIRO
SASIKI
MINAMATA
SENDAI
IZYUIN
2370
2375
2380
2385
2390
2395
2400
2865
2405
2410
2415
2420
2425
2430
2435
2440
2445
2450
2455
2457
67·8
67·3
73·5
73·1
78·7
19·5
16·9
33·0
68·4
77·8
70·3
73·8
74·0
70·4
74·1
67·8
49·3
65·1
35·6
68·2
60·0
-65·9
69·1
1011·2
64·1
48·7
54·5
52·4
42·5
54·8
52·4
59·9
54·3
56·8
60·9
63·0
56·4
50·0
30·9
37·5
-97·1
-21·5
57·6
58·3
27·5
55·0
9·0
5·0
6·8
-179·6
-39·6
-23·3
44·5
39·3
31·8
-2·8
-12·8
-4·7
39·6
30·0
34·1
82·9
25·2
-42·3
-26·5
-37·4
-66·4
21·4
8·6
7·9
15·5
-4·9
-34·2
-75·8
-34·3
-13·2
2·9
-28·1
-8·9
-57·9
172·4
-99·8
-54·7
-102·5
NOV DEC.
1891
JAN.
FEB.
1892

Fig. 3.

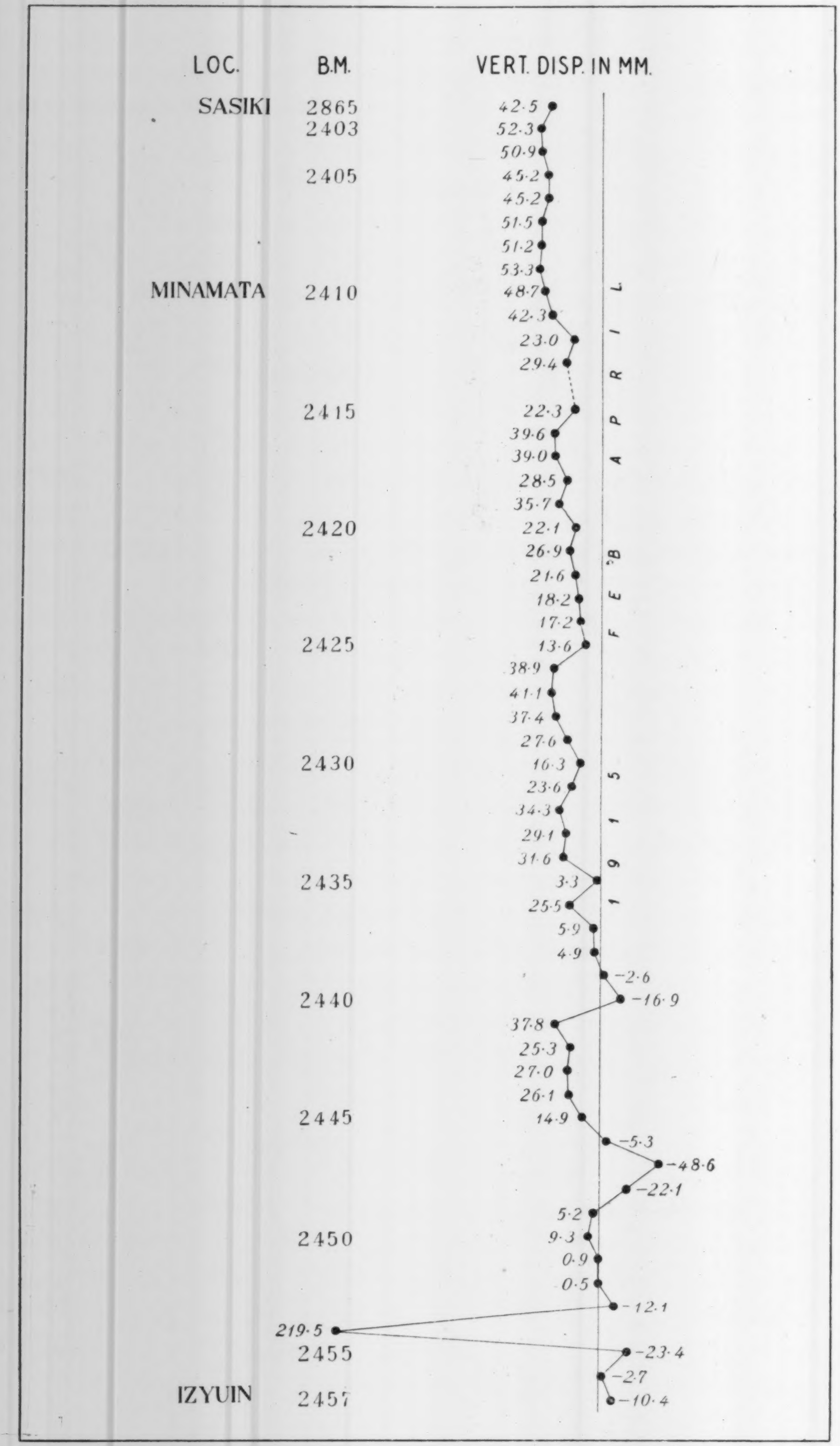
LOC.
B.M.
VERT. DISP. IN MM.
SASIKI
MINAMATA
IZYUIN
2865
2403
2405
2410
2415
2420
2425
2430
2435
2440
2445
2450
2455
2457
42·5
52·3
50·9
45·2
45·2
51·5
51·2
53·3
48·7
42·3
23·0
29·4
22·3
39·6
39·0
28·5
35·7
22·1
26·9
21·6
18·2
17·2
13·6
38·9
41·1
37·4
27·6
16·3
23·6
34·3
29·1
31·6
3·3
25·5
5·9
4·9
−2·6
−16·9
37·8
25·3
27·0
26·1
14·9
−5·3
−48·6
−22·1
5·2
9·3
0·9
0·5
−12·1
219·5
−23·4
−2·7
−10·4
APRIL
FEB
1915

Fig. 4.

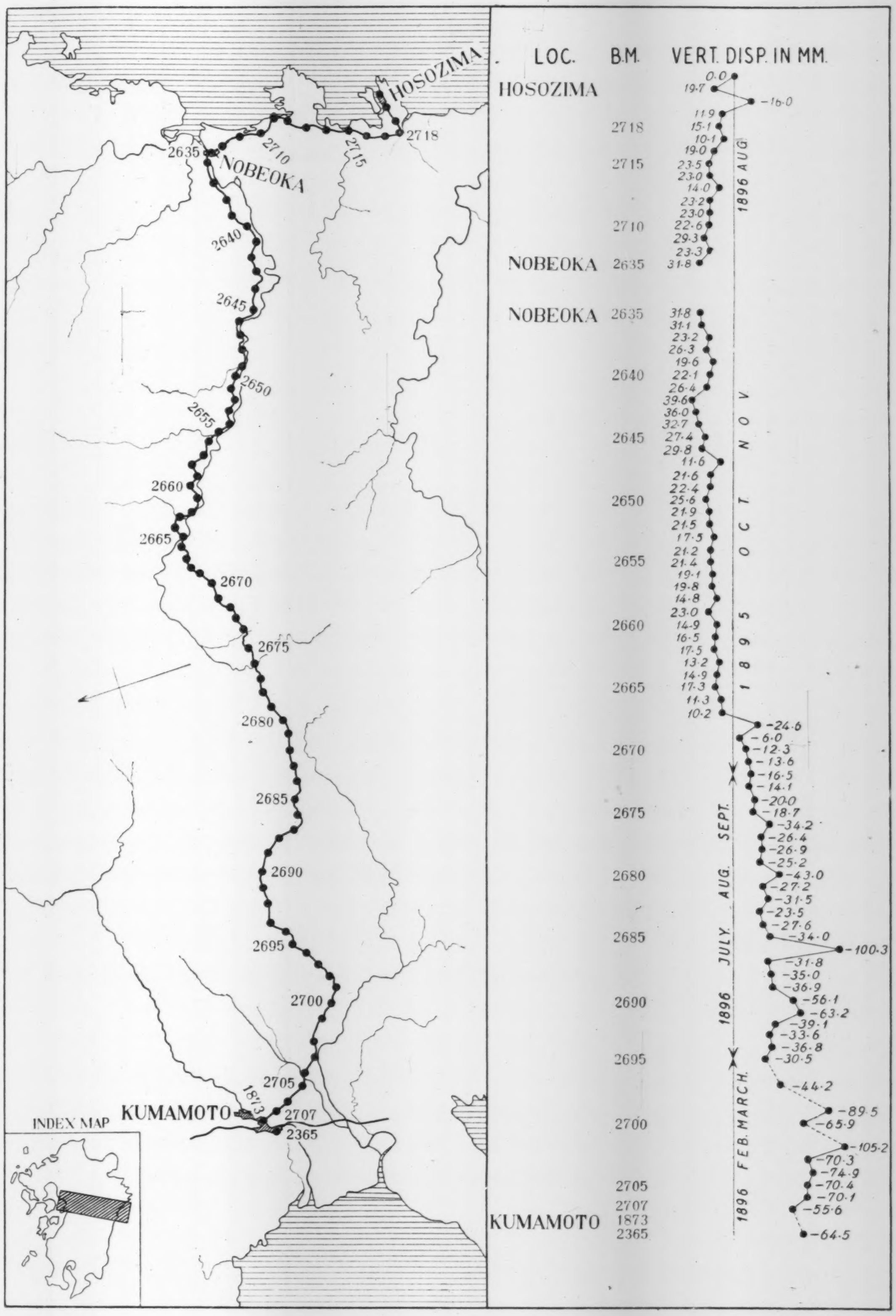
HOSOZIMA
NOBEOKA
KUMAMOTO
INDEX MAP
2635
2640
2645
2650
2655
2660
2665
2670
2675
2680
2685
2690
2695
2700
2705
2707
2710
2715
2718
1873
2365
LOC.
B.M.
VERT. DISP. IN MM.
HOSOZIMA
2718
2715
2710
NOBEOKA 2635
0.0
19.7
-16.0
11.9
15.1
10.1
19.0
23.5
23.0
14.0
23.2
23.0
22.6
29.3
23.3
31.8
1896 AUG.
NOBEOKA 2635
2640
2645
2650
2655
2660
2665
31.8
31.1
23.2
26.3
19.6
22.1
26.4
39.6
36.0
32.7
27.4
29.8
11.6
21.6
22.4
25.6
21.9
21.5
17.5
21.2
21.4
19.1
19.8
14.8
23.0
14.9
16.5
17.5
13.2
14.9
17.3
11.3
10.2
1895 OCT NOV
2670
2675
2680
2685
2690
2695
2700
2705
2707
KUMAMOTO 1873
2365
-24.6
-6.0
-12.3
-13.6
-16.5
-14.1
-20.0
-18.7
-34.2
-26.4
-26.9
-25.2
-43.0
-27.2
-31.5
-23.5
-27.6
-34.0
-100.3
-31.8
-35.0
-36.9
-56.1
-63.2
-39.1
-33.6
-36.8
-30.5
-44.2
-89.5
-65.9
-105.2
-70.3
-74.9
-70.4
-70.1
-55.6
-64.5
1896 JULY. AUG. SEPT.
1896 FEB. MARCH.

Fig. 5.

正　　誤

頁 585, 587, 589 及 49 論文の各奇數頁の柱の Part 2. は Part 3. の誤植

Erratum

Page 585, 587, 589 and 785~827: read "Part 3." for "Part 2."

---

er

By Katsutada SEZAWA and Kiyoshi KANAI,

Earthquake Research Institute.

(Read May 17, 1937.—Received June 21, 1937.)

1. *Introduction.*

A few years ago we had occasion to conclude in a paper[1] that if the whole energy of seismic waves were transmitted along a surface-layer in the form of Love-waves, their amplitudes would diminish with increase in the thickness of that layer, the discussion being however of an approximate character. Stoneley[2] recently found that, as expected from the approximate theory of waves, Love-waves of minimum group velocity are likely to predominate in seismograms and analysing such results, confirmed the existence of Jeffrey's discontinuity of about 480 km depth. Our previous conclusion just referred to therefore appears to differ somewhat from Stoneley's. On the other hand, one of us[3] had obtained mathematical formulae showing amplitude differences in Love-waves of different wave lengths that are generated from an internal source, by means of which it is now possible to know that the nature of the propagation is more in harmony with Stoneley's conclusion than with ours just mentioned.

2. *Love-waves generated from a source in the layer.*

We shall now deal with a three-dimensional problem. Let the thickness of the stratum and the depth of the seismic origin from the free surface be η and $\eta-\xi$ respectively, and let the densities and rigidities of the stratum and those of the subjacent medium be ρ, μ, ρ', μ', the axes of r, z being taken as shown in the sketch.

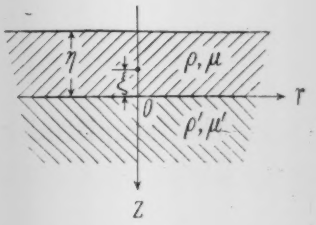

Fig. 1.

---

[1] K. SEZAWA and K. KANAI, "Periods and Amplitudes of Oscillations in L- and M-phases," *Bull. Earthq. Res. Inst.*, **13** (1935), 18~38.

[2] R. STONELEY, "Surface-waves associated with 20° Discontinuity," *M. N. R.A.S., Geophys. Suppl.*, **4** (1937), 39~43.

[3] K. SEZAWA, "Love-waves Generated from a Source of a certain Depth," *Bull. Earthq. Res. Inst.*, **13** (1935), 1~17.

35. Relation between the Thickness of a Surface Layer and the Amplitudes of Love-waves.

By Katsutada SEZAWA and Kiyoshi KANAI,

Earthquake Research Institute.

(Read May 17, 1937.—Received June 21, 1937.)

1. *Introduction.*

A few years ago we had occasion to conclude in a paper[1] that if the whole energy of seismic waves were transmitted along a surface layer in the form of Love-waves, their amplitudes would diminish with increase in the thickness of that layer, the discussion being however of an approximate character. Stoneley[2] recently found that, as expected from the approximate theory of waves, Love-waves of minimum group velocity are likely to predominate in seismograms and analysing such results, confirmed the existence of Jeffrey's discontinuity of about 480 km depth. Our previous conclusion just referred to therefore appears to differ somewhat from Stoneley's. On the other hand, one of us[3] had obtained mathematical formulae showing amplitude differences in Love-waves of different wave lengths that are generated from an internal source, by means of which it is now possible to know that the nature of the propagation is more in harmony with Stoneley's conclusion than with ours just mentioned.

2. *Love-waves generated from a source in the layer.*

We shall now deal with a three-dimensional problem. Let the thickness of the stratum and the depth of the seismic origin from the free surface be η and $\eta-\xi$ respectively, and let the densities and rigidities of the stratum and those of the subjacent medium be ρ, μ, ρ', μ', the axes of r, z being taken as shown in the sketch.

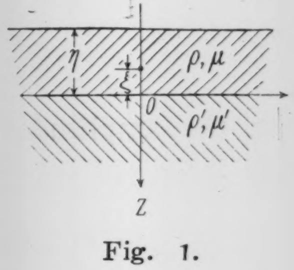

Fig. 1.

---

[1] K. SEZAWA and K. KANAI, "Periods and Amplitudes of Oscillations in L- and M-phases," *Bull. Earthq. Res. Inst.*, **13** (1935), 18∼38.

[2] R. STONELEY, "Surface-waves associated with 20° Discontinuity," *M. N. R.A.S., Geophys. Suppl.*, **4** (1937), 39∼43.

[3] K. SEZAWA, "Love-waves Generated from a Source of a certain Depth," *Bull. Earthq. Res. Inst.*, **13** (1935), 1∼17.

The solutions differ according as the source of disturbance is in the layer or in the subjacent medium. In the former case the displacement of waves generated from the origin is written in the form

$$v_o=e^{-ipt}\frac{\partial}{\partial(kr)}\frac{e^{ikR}}{kR}, \tag{1}$$

where $R^2=r^2+(z+\xi)^2$ and $k^2=\rho p^2/\mu$, $2\pi/k$ being the wave length within the layer. The amplitudes of waves at a relatively large distance is then

$$v=\frac{4\pi\kappa}{k^2}\frac{\partial H_o^{1)}(\kappa r)}{\partial(\kappa r)}e^{-i\left(pt-\frac{\pi}{2}\right)}$$

$$\cdot\frac{\left\{\mu\sqrt{k^2-\kappa^2}\cos\sqrt{k^2-\kappa^2}\xi+\mu'\sqrt{\kappa^2-k'^2}\sin\sqrt{k^2-\kappa^2}\xi\right\}\cos\sqrt{k^2-\kappa^2}(\eta+z)}{\sqrt{k^2-\kappa^2}F'(\kappa)}$$

$$+\left(\frac{k'}{k}\right)^2 e^{i\left(k'r-pt+\frac{\pi}{2}\right)}\frac{\mu'}{\mu}\frac{\cos\sqrt{k^2-k'^2}(\eta-\xi)\cos\sqrt{k^2-k'^2}(\eta+z)}{(k^2-k'^2)\sin^2\sqrt{k^2-k'^2}\eta}\frac{1}{r^2}+\cdots, \tag{2}$$

where $k'^2=\rho' p^2/\mu'$, $2\pi/k'$ being the wave length of the same period in the subjacent medium, and κ is the first real root of

$$F(\kappa)=2\left\{\mu'\sqrt{\kappa^2-k'^2}\cos\sqrt{k^2-\kappa^2}\eta-\mu\sqrt{k^2-\kappa^2}\sin\sqrt{k^2-\kappa^2}\eta\right\}=0. \tag{3}$$

The first term in (2) gives Love-waves and the second the disturbance that is transmitted with the velocity of transverse waves in the layer.

The form of $F'(\kappa)$ is as follows

$$F\ (\kappa)=2\left\{\left(\mu\kappa\eta+\frac{\mu'\kappa}{\sqrt{\kappa^2-k'^2}}\right)\cos\sqrt{k^2-\kappa^2}\eta\right.$$

$$\left.+\left(\mu\kappa+\mu'\kappa\eta\sqrt{\kappa^2-k'^2}\right)\frac{\sin\sqrt{k^2-\kappa^2}\eta}{\sqrt{k^2-\kappa^2}}\right\}. \tag{4}$$

Thus, the amplitudes of waves on the free surface $z=-\eta$ at a relatively large epicentral distance are

$$v=\left\{2\pi\frac{\partial H_o^{1)}(\kappa r)}{\partial(\kappa r)}e^{-i\left(pt-\frac{\pi}{2}\right)}\right\}$$

$$\cdot\left[\frac{\left(\frac{\kappa}{k}\right)^2\mu\cos\sqrt{k^2-\kappa^2}\xi+\mu'\sqrt{\frac{\kappa^2-k'^2}{k^2-\kappa^2}}\sin\sqrt{k^2-\kappa^2}\xi}{\left(\mu\kappa\eta+\frac{\mu'\kappa}{\sqrt{\kappa^2-k'^2}}\right)\cos\sqrt{k^2-\kappa^2}\eta+\left(\mu'\kappa\eta\sqrt{\frac{\kappa^2-k'^2}{k^2-\kappa^2}}+\frac{\mu\kappa}{\sqrt{k^2-\kappa^2}}\right)\sin\sqrt{k^2-\kappa^2}\eta}\right]$$

$$+\left(\frac{k'}{k}\right)^2 e^{i\left(k'r-pt+\frac{\pi}{2}\right)}\frac{\mu'}{\mu}\frac{\cos\sqrt{k^2-k'^2}(\eta-\xi)}{(k^2-k'^2)\sin\sqrt{k^2-k'^2}\eta}\frac{1}{r^2}+\cdots. \quad (5)$$

3. *Love-waves generated from a source in the subjacent medium.*

In this case the depth of the seismic origin from the free surface is $\eta+\xi$, so that $R^2=r^2+(z-\xi)^2$. The primary waves in this case are written in the form

$$v_o=e^{-ipt}\frac{\partial}{\partial(k'r)}\frac{e^{ik'R}}{k'R}. \quad (6)$$

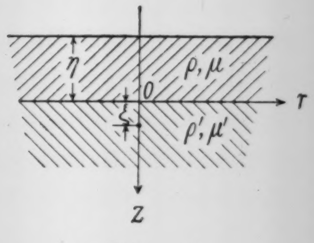

Fig. 2.

Since it has been specified that the amplitudes of the primary waves are invariably the same for both cases in the position of the source, Love-waves generated from the origin in the subjacent medium have unduly large amplitudes.

The amplitudes of waves on the free surface due to the disturbance (6) are expressed by

$$v=\left\{\frac{2\pi k^2}{k'^2}\frac{\partial H_o^{(1)}(\kappa r)}{\partial(\kappa r)}e^{-i\left(pt-\frac{\pi}{2}\right)}\right\}$$

$$\cdot\frac{\left(\frac{\kappa}{k}\right)^2\mu' e^{-\sqrt{\kappa^2-k'^2}\xi}}{\left(\mu\kappa\eta+\frac{\mu'\kappa}{\sqrt{\kappa^2-k'^2}}\right)\cos\sqrt{k^2-\kappa^2}\eta+\left(\mu'\kappa\eta\sqrt{\frac{\kappa^2-k'^2}{k^2-\kappa^2}}+\frac{\mu\kappa}{\sqrt{k^2-\kappa^2}}\right)\sin\sqrt{k^2-\kappa^2}\eta}$$

$$+e^{-i\left(k'r-pt+\frac{\pi}{2}\right)}\frac{\mu'}{\mu}\frac{\mu'\cos\sqrt{k^2-k'^2}\eta-\mu\sqrt{k^2-k'^2}\xi\sin\sqrt{k^2-k'^2}\eta}{\mu(k^2-k'^2)\sin^2\sqrt{k^2-k'^2}\eta}\frac{1}{r^2}+\cdots. \quad (7)$$

The solutions shown in the preceding section and in this were obtained in our previous paper.[4]

4. *Application of the solutions to a layer of 480 km thickness.*

The layer discussed by Stoneley[5] is 480 km thick and the constants assumed by him relating to that layer are such that

$$\rho=3{\cdot}5,\quad \rho'=4{\cdot}11,\quad \sqrt{\mu/\rho}=4{\cdot}7\text{ km/s},\quad \sqrt{\mu'/\rho'}=5{\cdot}66\text{ km/s},$$

$$\mu=7{\cdot}73.10^{11},\quad \mu'=13{\cdot}2.10^{11}.$$

---

[4] K. SEZAWA, *loc. cit.* 3).

[5] R. STONELEY, *loc. cit.* 2).

The relations between k/κ and $\kappa\eta$ as shown in Stoneley's paper, are

$k/\kappa=$	1·00	1·02	1·04	1·05	1·06	1·08	1·10	1·12	1·14	1·16	1·18	1·1866
$\kappa\eta=$	∞	6·7280	4·3745	3·6	3·3009	2·6342	2·1530	1·7693	1·4374	1·1248	0·7940	0

Substituting these values in (5) and (7), we have obtained the relation between $\kappa\eta$ and v for Love-waves for various cases of ξ/η, namely, (i) $\xi/\eta=0·9$, (ii) $\xi/\eta=0·5$, (iii) $\xi/\eta=0·1$, (iv) $\xi/\eta=-0·1$ (v) $\xi/\eta=-1$, (vi) $\xi/\eta=-2$, the results being shown in Figs. 3, 4. The symbols K_1, K_2 in Figs. 3, 4 are written in place of the first factors of the respective first terms on the right-hand side of the equations (5), (7). For the reason given in the last section, the amplitudes of radiated Love-waves in the cases (iv), (v), (vi) are unnaturally large.

5. *Interpretation of the result.*

Figs. 3, 4 show that, generally speaking, the greater the depth of the origin, the greater the increase in the amplitudes of Love-waves for every vibrational frequency. The most important fact gleaned from the present study is that the amplitude of Love-waves of a given wave length assumes a maximum value for a certain thickness η of the layer. The amplitude of the same waves diminishes in the layer of a thickness that is either larger or smaller than the one just mentioned. The value of $\kappa\eta$ at which the amplitude of Love-waves is maximum, tends to increase with decrease in the depth of the seismic origin. It ap-

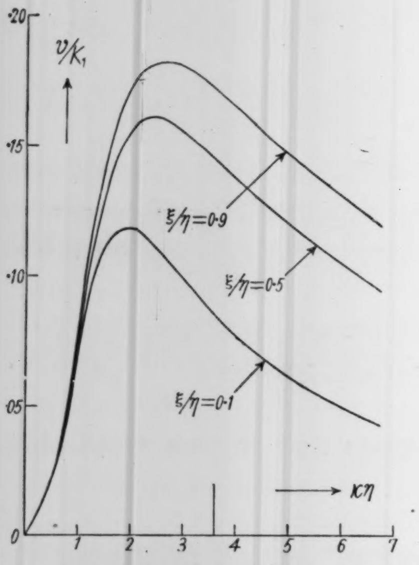

Fig. 3. Amplitudes of Love-waves.

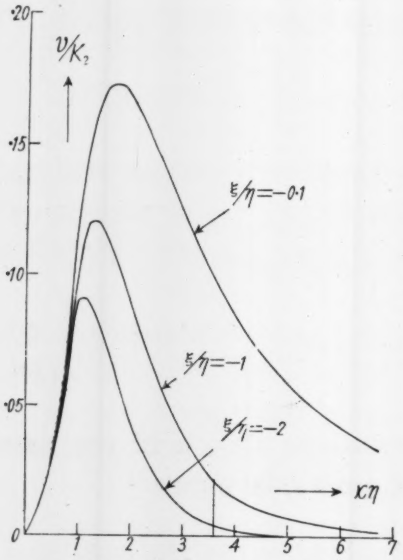

Fig. 4. Amplitudes of Love-waves.

pears that $\kappa\eta=3{\cdot}6$ (shown by vertical strips in Fig. 3, 4), which defines the minimum group velocity of Love-waves, is likely to agree with the $\kappa\eta$ that corresponds to the maximum amplitude merely in the case of an extremely shallow seismic origin. Thus, the predominant period of the L-phase in seismograms is liable to augment with increase in the thickness of the layer—a fact virtually agreeing with that which naturally results from the idea of minimum group velocity.

The physical interpretation of the question why the amplitudes of Love-waves tend to diminish for any $\kappa\eta$, that is larger or smaller than its special one, is not difficult. For a larger value of $\kappa\eta$, the wave energy distributed in unit area of the layer becomes less in intensity, whereas for a smaller value of $\kappa\eta$, the major part of the same energy is scattered in the subjacent medium.

It is also possible to understand why surface waves, under damping resistance, hardly die away even with increase in epicentral distance.

---

35. 地表層の厚さとラブ波の振幅との關係

地震研究所 {妹澤克惟
金井清

ラブ波の地表層中に於ける振動勢力はレーレー波と異なり，大體に於てその全體の厚さにわたつて分布してをるから，原勢力が一定であれば地表層の厚さが厚くなるに從てその振幅が減少するやうに考へ易いのである．著者の一人が以前に出して置いたところのその振幅に關する正確な公式を應用して計算して見ると，その結果は必しも前述の性質と一致しない事がわかつた．卽ち地表層の厚さが原波長のある割合の場合にラブ波の振幅が極大になり，それよりも厚くても薄くても振幅が減少するのである．その極大になる所は實驗的に波動の群速度が極少になるやうな場合であることが歐洲の地震學者によつて述べられてをるが，計算の結果によると少し違つた場合に極大値を取る．しかし傾向としては割合によく一致してをるやうに見える．

常識的には振幅が極大になる波長よりも短い波長のときには地表層の單位面積中の勢力が少くなる事であり，それよりも長い波長のときには地震勢力が固體波として主として下層中へ傳播する事を意味するものである．之については原點が地表層中にあつても下層中にあつても同じ事がいひ得るのである．

尙，震央距離が遠くなる程ラブ波の波長が長くなるのは分散性と減衰性に基づくとした所の我々の以前の考は少しく訂正する必要がある．卽ち實際の地表層は無數の層から成立つてをり，それぞれの層に特有なラブ波が傳はると考へて置き，遠方になるに從つて短い波長のものが減衰するとすればよいのである．卽ち單に一つの層とすると波動の減衰性があまりにも小さ過ぎる事が我々によつて研究してあつたが，その難點は之によつても解決できる譯である．又，英國の人が言つてをるやうに480粁もある表面層にもそれに特有なラブ波が有限振幅を以て傳播し得る事も了解できるのである．

36. *On the Plastic Properties of the Earth's Core.*

By Katsutada SEZAWA,

Earthquake Research Institute.

(Read June 15, 1937.—Received June 21, 1937.)

1. *Introduction.*

It seems that the Earth's core transmits only longitudinal waves, not transverse waves. It is however uncertain whether this results from the extremely small torsion modulus of the material within the core or from particularly high viscous resistance of the same material against distortional movement. Since, as a matter of fact, the Earth's core is subjected to enormously high pressure, the material in that core is probably in a certain plastic state. The special features of a general plastic body are its increased viscous resistance against distortional force (for any quickness) and its almost incompressible condition in any (statical) deformation, whence it follows from either one of these features of the plastic body that, were the Earth's core a plastic body, transmission of transverse waves (relatively long waves) through the same core would be improbable.

Now it is well known that the velocity of the core waves is about $1/\sqrt{3}$ of that of the longitudinal waves transmitted through the rocky shell immediately next to the core. If the material within the core were in a plastic state, and that in the rocky shell is in an elastic state, both being of the same density, the relation cited above would then be a most likely one, regardless of the denser character of the Earth's core. Whether or not the material forming the core is as dense as iron or nickel is another problem calling for different treatment.

As already mentioned, we shall assume that, although the Earth's central core is in a plastic condition, the outer shell is in a purely elastic state, the density of the material being assumed uniform throughout the Earth. Gravity is taken as a body force, but the effect of the Earth's rotation is neglected. Although there are a number of theories defining the plastic state of materials, yet in accordance with the present vogue among investigators of plastic bodies, we shall take the maximum shear stress theory, which was originated by Saint Venant[1] and developed by certain mathematicians eminent in applied mechanics[2]. Although the criterea of the plastic state differ with authors, as the quantitative difference between them is not very marked, we shall use the maximum shear stress theory throughout this paper.

---

[1] St. VENANT, *C. R.*, **70** (1870), **73** (1871).

2. *Equilibrium of the elastic shell.*

Assuming that the material displacement is invariably symmetrical with respect to the Earth's centre, that is, that displacement u is perfectly radial, the strain and stress components are then expressed by

$$\left.\begin{aligned}
&e_{rr}=\frac{\partial u}{\partial r}\,, \quad e_{\theta\theta}=e_{\phi\phi}=\frac{u}{r}\,, \quad \Delta=\frac{\partial u}{\partial r}+\frac{2u}{r}\,,\\
&\widehat{rr}=\lambda\Delta+2\mu\frac{\partial u}{\partial r}=\lambda\left(\frac{\partial u}{\partial r}+\frac{2u}{r}\right)+2\mu\frac{\partial u}{\partial r}\,,\\
&\widehat{\theta\theta}=\widehat{\phi\phi}=\lambda\Delta+2\mu\frac{u}{r}=\lambda\left(\frac{\partial u}{\partial r}+\frac{2u}{r}\right)+2\mu\frac{u}{r}\,,
\end{aligned}\right\} \tag{1}$$

where λ, μ are Lamé's elastic constants. The gravitational potential V and the resulting radial pressure p are connected by the formulae

$$\left.\begin{aligned}
&V=\frac{2}{3}\pi\gamma\rho(3a^2-r^2)\,, && -\frac{1}{\rho}\frac{\partial p}{\partial r}+\frac{\partial V}{\partial r}=0\,,\\
&\frac{\partial p}{\partial r}=-\frac{4}{3}\pi\gamma\rho^2 r\,, && p=\frac{2}{3}\pi\gamma\rho^2(a^2-r^2)\,,
\end{aligned}\right\} \tag{2}$$

where a is the Earth's radius, ρ the Earth's mean density (assmed almost uniform), and γ the gravitational constant. The equation of equilibrium of the elastic shell is

$$\rho\frac{\partial V}{\partial r}+\frac{\partial\widehat{rr}}{\partial r}+\frac{1}{r}(2\widehat{rr}-\widehat{\theta\theta}-\widehat{\phi\phi})=0\,, \tag{3}$$

the effect of pressure on the change of density being neglected. Substituting from (1), (2) in (3), we obtain

$$-\frac{4}{3}\pi\gamma\rho^2 r+(\lambda+2\mu)\left(\frac{\partial^2 u}{\partial r^2}+\frac{2}{r}\frac{\partial u}{\partial r}-\frac{2u}{r^2}\right)=0\,. \tag{4}$$

The solution for the present statical problem is then

$$u=\frac{2}{15}\frac{\pi\gamma\rho^2}{\lambda+2\mu}r^3+Br+\frac{C}{r^2}\,, \tag{5}$$

---

[2] A. Nadai, *Der bildsame Zustand der Werkstoffe* (Berlin, 1927), *Handbuch d. Physik*, **6**, Plastizität u. Erddruck. Nadai's problem and various plastic theories dealt by other people are involved in these books.

where B, C are determined by boundary conditions. The stress components are

$$\left.\begin{aligned}\widehat{rr}&=\frac{\pi\gamma\rho^2(10\lambda+12\mu)}{15(\lambda+2\mu)}r^2+(3\lambda+2\mu)B-\frac{4\mu C}{r^3},\\ \widehat{\theta\theta}=\widehat{\phi\phi}&=\frac{\pi\gamma\rho^2(10\lambda+4\mu)}{15(\lambda+2\mu)}r^2+(3\lambda+2\mu)B+\frac{2\mu C}{r^3}.\end{aligned}\right\} \tag{6}$$

The boundary conditions are such that the normal stress is zero at the free surface, while the maximum shear stress at the boundary between the shell and the core assumes a definite value k. Mathematically these conditions are expressed by

$$\left.\begin{aligned}&r=a; \quad \widehat{rr}=0,\\ &r=b; \quad \widehat{rr}-\widehat{\theta\theta}=\pm 2k, \qquad \widehat{rr}-\widehat{\phi\phi}=\pm 2k,\end{aligned}\right\} \tag{7}$$

where b is the radius of the Earth's core. An additional condition is

$$r=c(a>c>b); \quad |\widehat{rr}-\widehat{\theta\theta}|\not> 2k, \quad |\widehat{rr}-\widehat{\phi\phi}|\not> 2k. \tag{8}$$

After reading this paper, these conditions were found to be rather needless.

Substituting (6) in (7) we obtain

$$\left.\begin{aligned}\frac{6\mu C}{b^3}&=\frac{8}{15}\pi\gamma\rho^2\frac{\mu}{\lambda+2\mu}b^2\pm 2k,\\ (3\lambda+2\mu)B&=\frac{-\pi\gamma\rho^2a^2}{15(\lambda+2\mu)}\left\{(10\lambda+12\mu)-\frac{16\mu}{3}\frac{b^5}{a^5}\right\}\pm\frac{4}{3}k\frac{b^3}{a^3}.\end{aligned}\right\} \tag{9}$$

The stress components are therefore

$$\left.\begin{aligned}\widehat{rr}&=\frac{-\pi\gamma\rho^2(10\lambda+12\mu)}{15(\lambda+2\mu)}(a^2-r^2)+\frac{2}{3}b^3\left(\frac{1}{a^3}-\frac{1}{r^3}\right)\left\{\frac{8\pi\gamma\rho^2\mu}{15(\lambda+2\mu)}b^2\pm 2k\right\},\\ \widehat{\theta\theta}=\widehat{\phi\phi}&=\frac{-\pi\gamma\rho^2(10\lambda+12\mu)}{15(\lambda+2\mu)}a^2+\frac{\pi\gamma\rho^2(10\lambda+4\mu)}{15(\lambda+2\mu)}r^2\\ &\quad+\left(\frac{2}{3}\frac{b^3}{a^3}+\frac{b^3}{3r^3}\right)\left\{\frac{8\pi\gamma\rho^2\mu}{15(\lambda+2\mu)}b^2\pm 2k\right\}.\end{aligned}\right\} \tag{10}$$

It is to be borne in mind that the stresses in (10) should satisfy the condition (8).

In the special case $\mu/\lambda\to 0$, equations in (10) reduce to

$$\left.\begin{aligned}\widehat{rr}&=\frac{-2\pi\gamma\rho^2}{3}(a^2-r^2)\pm\frac{4}{3}kb^3\left(\frac{1}{a^3}-\frac{1}{r^3}\right),\\ \widehat{\theta\theta}=\widehat{\phi\phi}&=\frac{-2\pi\gamma\rho^2}{3}(a^2-r^2)\pm\frac{4}{3}kb^3\left(\frac{1}{a^3}+\frac{1}{2r^3}\right).\end{aligned}\right\} \tag{11}$$

3. *The equilibrium of the plastic core.*

The equation of the equilibrium of the plastic core is the same as (3), namely,

$$-\frac{4}{3}\pi\gamma\rho^2 r+\frac{\partial\widehat{rr}}{\partial r}+\frac{1}{r}(2\widehat{rr}-\widehat{\theta\theta}-\widehat{\phi\phi})=0\,, \tag{3'}$$

where $\widehat{\theta\theta}=\widehat{\phi\phi}$, and the equation of the plastic condition is

$$\widehat{rr}-\widehat{\theta\theta}=\mp 2k \tag{12}$$

for any $r(r<b)$. From (3′), (12) we obtain

$$-\frac{4}{3}\pi\gamma\rho^2 r+\frac{\partial\widehat{rr}}{\partial r}\mp\frac{4k}{r}=0\,. \tag{13}$$

Integrating this we get

$$\widehat{rr}\mp 4k\log_e r-\frac{2}{3}\pi\gamma\rho^2 r^2+I=0\,, \tag{14}$$

where I is the integration constant. From (10) the boundary condition is

$$r=b\,;\qquad \widehat{rr}=\frac{-\pi\gamma\rho^2(10\lambda+12\mu)}{15(\lambda+2\mu)}(a^2-b^2)\\+\frac{2}{3}b^3\left(\frac{1}{a^3}+\frac{1}{b^3}\right)\left(\frac{8}{15}\pi\gamma\rho^2\frac{\mu}{\lambda+2\mu}b^2\pm 2k\right). \tag{15}$$

Determining I in (14) by means of (15), we obtain

$$\left.\begin{aligned}\widehat{rr}&=\pm 4k\log_e\frac{r}{b}-\frac{2}{3}\pi\gamma\rho^2(b^2-r^2)-\pi\gamma\rho^2\frac{10\lambda+12\mu}{15(\lambda+2\mu)}(a^2-b^2)\\&\qquad+\frac{2}{3}\left(\frac{b^3}{a^3}+1\right)\left(\frac{8}{15}\pi\gamma\rho^2\frac{\mu}{\lambda+2\mu}b^2\pm 2k\right).\\\widehat{\theta\theta}&=\widehat{\phi\phi}=\pm 2k+\widehat{rr}\,.\end{aligned}\right\} \tag{16}$$

When $\mu/\lambda\rightarrow 0$, these equations reduce to

$$\left.\begin{aligned}\widehat{rr}&=\pm 4k\log_e\frac{r}{b}-\frac{2}{3}\pi\gamma\rho^2(a^2-r^2)\pm\frac{4}{3}k\left(\frac{b^3}{a^3}+1\right),\\\widehat{\theta\theta}&=\widehat{\phi\phi}=\pm 2k+\widehat{rr}\,.\end{aligned}\right\} \tag{17}$$

In the case of the Earth's core the upper signs in these solutions should always be used.

By comparing (11) and (17), we find that when $\mu/\lambda\rightarrow 0$, the additional stresses in the core are

$$\pm 4k \log_e \frac{r}{b} \pm \frac{4}{3}k\left(1+\frac{b^3}{r}\right), \quad \pm 4k \log_e \frac{r}{b} \pm \frac{4}{3}k\left(1-\frac{b^3}{2r^3}\right)$$

for $\widehat{rr}$ and $\widehat{\theta\theta}(=\widehat{\phi\phi})$ respectively.

4. *Possible slip planes in the plastic core.*

The angle β which the slip surfaces in the plastic core make with any radius of the Earth is obtained by the formula

$$\tan 2\beta = \frac{\widehat{rr}-\widehat{\theta\theta}}{2\widehat{r\theta}} = \frac{\widehat{rr}-\widehat{\phi\phi}}{2\widehat{r\phi}}, \tag{19}$$

where $\widehat{r\theta}$ is the shear stress between r and θ, and $\widehat{r\phi}$ that between r and ϕ.

Since $\widehat{r\theta}=0(\widehat{r\phi}=0)$ in the present case, we get $2\beta=\pi/2$, so that

$$\beta=\pi/4, \tag{20}$$

namely $\tan\beta=1$. The equation of the slip surfaces is such that

$$\frac{rd\theta}{dr}\left(=\frac{rd\phi}{dr}\right)=\tan\beta, \tag{21}$$

from which we have

$$\theta=A \log_e r, \qquad \phi=B \log_e r. \tag{22}$$

The surfaces are therefore of the type of logarithmic spiral. It is immaterial whether the sections of the surfaces are directed in the sense of θ or ϕ or in that of a certain azimuth between θ and ϕ.

5. *The numerical solution and its interpretation.*

The approximate values of the radii of the Earth and its core are given by $a=6370$ km, $a-b=2900$ km, so that $b/a=0{\cdot}545$. It is possible to assume $\gamma\rho^2a^2=8.10^{11}$ in C. G. S. units. The value of the plastic constant k of the Earth's core is not known. According to Griggs's tests(3) of solenhofen limestone and marble under high hydrostatic pressure, the yield points due to a longitudinal force do not differ markedly, though increasing somewhat, in the hydrostatic pressure applied.

(i) If we assume that the materials in the core and in the shell immediately next to it have plastic constants of the same value as their respective plastic constants under atmospheric pressure (the actual temperature and melting point being both raised), we may then approximately put

---

3) D. T. GRIGGS, *Journ. Geol.*, **44** (1936), 541~577.

$$2k=5.10^{9}\ \text{(C. G. S.)}\,. \tag{23}$$

Thus, from (9)

$$\left.\begin{aligned} \frac{6\mu C}{b^{3}} &= 5.10^{9}+4.10^{11}\frac{\mu}{\lambda}\,, \\ (3\lambda+2\mu)B &= 0{\cdot}436.10^{11}\frac{\mu}{\lambda}-16{\cdot}8.10^{11}, \end{aligned}\right\} \tag{24}$$

from which μC and $(3\lambda+2\mu)$ B are determined as functions of μ/λ. In both equations of (24), μ/λ is assumed to be relatively small. Comparing these results with the condition (8), we get

$$\mu/\lambda < 1{\cdot}36.10^{-2}\,. \tag{25}$$

The result in (24) is therefore

$$\left.\begin{aligned} \frac{6\mu C}{b^{3}} &< 10{\cdot}4.10^{9}\,, & (C>0) \\ (3\lambda+2\mu)B &> -16{\cdot}8.10^{11}. & (B<0) \end{aligned}\right\} \tag{26}$$

The condition for the Poisson's ratio is

$$\frac{1}{2}>\sigma>0{\cdot}493\,. \tag{27}$$

The last condition has resulted from the assumption (23). Although in the present calculation the value of $2k$ has been given, no assumption regarding the absolute values of λ and μ has been made. Although the result well conforms with the properties of a general plastic body and also with the nature of seismic core waves, since the radius of the Earth and that of its core are of comparable order and not so much different as in the case of Mars⁽⁴⁾, there still remains some question as to whether the Earth's state shall change from elastic to plastic just on its core's boundary.

(ii) The analysis of seismic waves shows that $\sigma=1/4$ even at such a deep part of the Earth's shell as immediately next to the core. Thus, if we assume that Poisson's ratio σ is 1/4, namely $\lambda=\mu$, in the rocky shell as well as in the core, we then have

$$\left.\begin{aligned} \frac{6\mu C}{b^{3}} &= 1{\cdot}33.10^{11}+2k\,, \\ (3\lambda+2\mu)\beta &= -12{\cdot}3.10^{11}+0{\cdot}213\,k, \end{aligned}\right\} \tag{28}$$

from which μC and $(3\lambda+2\mu)B$ are determined as functions of k. Re-

---

4) H. JEFFREYS, "The Density Distributions in the Inner Planets," M. N. R. A. S. *Geophys. Suppl.*, **4** (1937), 62—71.

ferring to the condition (8), we get

$$2k > 1{\cdot}22.10^{11}\,. \tag{29}$$

The result in (28) is therefore

$$\left.\begin{aligned} \frac{6\mu C}{b^3} &> 2{\cdot}55.10^{11}\,, \\ (3\lambda+2\mu)B &> -12{\cdot}1.10^{11}\,. \end{aligned}\right\} \tag{30}$$

From the first hypothesis it follows that the material in the rocky shell, owing to some transformation of that material, changes its state from compressible to incompressible in the immediate vicinity of the boundary of the core, that is, σ changes from 1/4 to 1/2, the other properties of the same material changing from elastic to plastic also in the same vicinity. An alternative explanation resulting from the second hypothesis, though impossible to confirm it even with the data of high pressure experiments that have been made, would be such that while the plastic constant k in a fairly deep part in the Earth is as large as $2k=10^{11}$ (C. G. S.), the Poisson's ratio remains nearly $\sigma=1/4$ even within the same core. It is now possible to assume that the actual condition of the Earth's core (and the shell next to it) is probably intermediating between that in (i) and that in (ii).

Added July. 7, 1937.—From our continued study (the paper read July 6, 1937), it was found that the condition (8) is rather needless. The plastic state of the core is naturally accompanied by the plastic state of the Earth's surface staratum of thickness of a few hundred kilometers, the layer intermediating between the surface stratum in question and the core being possibly elastic. The full explanation will be shown in next Bulletin.

36. 地球の核のプラスチック性に就て

地震研究所 妹澤克惟

地球の核には縦波のみが通つて横波が通らぬやうである．しかし之は核の物質の剛性が極めて小さい爲であるか，或は捩り振動に對して粘性が特にきく爲であるかは明瞭でない．地球の核が高壓を受けてをる爲にプラスチックの状態にある事は明かである．一般のプラスチック體の特性の一つは捩りの力に對して粘性が強く働く事であり，他の一つは非壓縮性である．從つて地球の核がプラスチックであるとすれば横波が通り難い事は當然なやうにも思はれる．殊に核のみがプラスチック性であり從つて非壓縮性であるとすると，核の內部とその外部との縦波の速度の差も說明できるやうである．

今，地球の核のみがプラスチック性であり，外殼は彈性であるとし，重力を正確に考へて理論的計算を試みて見る．プラスチックの理論は最も多く用ひられてをる所の極大剪應力の說に從つて試みる．他の理論でも數値の程度はそれ程には違はない．核の中ではすべての狀況が對數函數的の性質を具備する事は容易に證明される．

理論に計算をあてはめて見る場合に，米國のある實驗結果に從ひ，プラスチックの常數が地球の核の附近でも地表面附近のそれと同じであると假定して見ると（溫度の方は，融點が壓力とともに增加するから態と見逃して置いた)，核の性質は非壓縮性でなければならぬ事がわかるのである．之は一般のプラスチック體と共通の性質であり，且つ地球の核を通る地震波の性質とも一致してをり，一寸面白いともいひ得る譯である．しかしプラスチック論からいふと，彈性からプラスチック性に變る事が，必ずしも實際の核の表面でなくてもよいといふ事の自由さが殘されをるものである．之は地球の半徑とその核の半徑が同じ程度の値を持つて居り，火星のそれ等のやうな相違がないからである．それで別の考として Poisson 比が核の中までも 1/4 であるとして問題を取扱ふ事もやつて見たのである．

そのやうにして出發して見ると，地球の核の面が恰度彈性からプラスチックに變る面であるとするときに，プラスチックの常數が前に假定した地表面での値よりも 100倍も大きくなければならぬ事が知られるのである．米國のあまり高くない壓力での實驗でも常數が增加する傾向にはあるが，そのやうな高壓のもとでの實驗結果は未だないから，斯る大きなプラスチック性がおかしいとは斷言できない．しかし如何にも大き過ぎるやうに見える事は事實である．

實際問題としては，地球の核及びその附近では Poisson 比が 1/4 と 1/2 との間にあり，プラスチックの常數は地表面で測定したそれの何倍か又は何十倍かのものであると考へる方がよいのではなからうか．

1937 年 7 月 7 日追記――この研究を進めた結果（7 月 6 日發表)，核のプラスチック性を前記のやうに大きく取らず，普通の値にすると，地球の表面に數百粁の厚さのプラスチック性の層があり，この層と地球の核との間は彈性であればよい事がわかつた。この方が反て種種の事柄をよく說明するやうである。委しい事は次の報告で述べる。

37. *Energy Dissipation in the Vibrations of a Bridge. II.*

By Katsutada SEZAWA and Kiyoshi KANAI,

Earthquake Research Institute.

(Read April 19, 1937.—Received June 21, 1937.)

1. *Introduction.*

In the previous paper[1] we discussed the decay of the vibrations of a bridge through dissipation of its vibrational energy into its piers and adjacent spans. Whereas in the previous case the exciting force was at the middle point of a bridge span, we shall now consider the case in which the position of the exciting force remains fixed at any point in the same span.

2. *Mathematical treatments.*

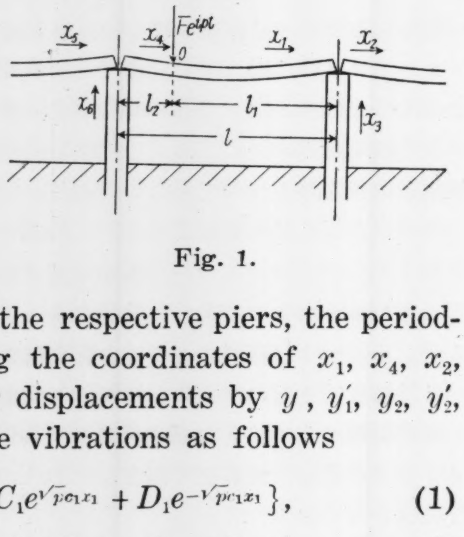

Fig. 1.

The distances of the position of the exciting force from both ends of a given span are l_1, l_2 respectively, so that $l_1+l_2=l$. Let E_1I_1, ρ_1a_1, E_2I_2, ρ_2a_2, E_3I_3, ρ_3a_3 be the flexural stiffness and mass per unit length of the span in which the disturbing force is applied and those of the respective adjacent spans, and let also E_4a_4, ρ_4a_4, E_5a_5, ρ_5a_5 be the longitudinal stiffnesses and masses per unit length of the respective piers, the periodic force being of the type Fe^{ipt}. Taking the coordinates of x_1, x_4, x_2, x_5, x_3, x_6, and writing the corresponding displacements by y, y_1', y_2, y_2', u, u', we get the general solutions of the vibrations as follows

$$y_1=e^{ipt}\{A_1e^{i\sqrt{p}c_1x_1}+B_1e^{-i\sqrt{p}c_1x_1}+C_1e^{\sqrt{p}c_1x_1}+D_1e^{-\sqrt{p}c_1x_1}\}, \tag{1}$$

$$y_1'=e^{ipt}\{A_2e^{i\sqrt{p}c_1x_4}+B_2e^{-i\sqrt{p}c_1x_4}+C_2e^{\sqrt{p}c_1x_4}+D_2e^{-\sqrt{p}c_1x_4}\}, \tag{2}$$

$$y_2=e^{ipt}\{G_1e^{-i\sqrt{p}c_2x_2}+H_1e^{-\sqrt{p}c_2x_2}\}, \tag{3}$$

$$y_2'=e^{ipt}\{G_2e^{i\sqrt{p}c_3x_5}+H_2e^{\sqrt{p}c_2x_5}\}, \tag{4}$$

$$u=e^{ipt}\alpha_1e^{if_1x_3}, \tag{5}$$

$$u'=e^{ipt}\alpha_2e^{if_2x_6}, \tag{6}$$

---

[1] K. SEZAWA and K. KANAI, *Bull. Earthq. Res. Inst.*, **15** (1937). 385~393.

where

$$\left.\begin{aligned} &c_1=\left(\frac{\rho_1 a_1}{E_1 I_1}\right)^{\frac{1}{4}}, \qquad c_2=\left(\frac{\rho_2 a_2}{E_2 I_2}\right)^{\frac{1}{4}}, \qquad c_3=\left(\frac{\rho_3 a_3}{E_3 I_3}\right)^{\frac{1}{4}}, \\ &p/f_1=\sqrt{E_4/\rho_4}, \qquad p/f_2=\sqrt{E_5/\rho_5}. \end{aligned}\right\}$$

The two ends of every span of the bridge are supported without moment of force, and any point of the middle span is subjected to a periodic force without moment of force. The boundary conditions are then expressed by

$$x_1=0, \quad x_4=0; \qquad y_1=y_1', \quad \frac{\partial y_1}{\partial x_1}=\frac{\partial y_1'}{\partial x_4}, \quad \frac{\partial^2 y_1}{\partial x_1^2}=\frac{\partial^2 y_1'}{\partial x_4^2}, \qquad (7), (8), (9)$$

$$E_1 I_1\left(\frac{\partial^3 y_1}{\partial x_1^3}-\frac{\partial^3 y_1'}{\partial x_4^3}\right)=Fe^{ipt}, \qquad (10)$$

$$x_1=l_1, \quad x_2=0, \quad x_3=0; \qquad y_1=u, \quad y_2=u, \quad \frac{\partial^2 y_1}{\partial x_1^2}=0, \quad \frac{\partial^2 y_2}{\partial x_2^2}=0,$$
$$(11), (12), (13), (14)$$

$$E_1 I_1\frac{\partial^3 y_1}{\partial x_1^3}-E_2 I_2\frac{\partial^3 y_2}{\partial x_2^3}=E_4 a_4\frac{\partial u}{\partial x_3}, \qquad (15)$$

$$x_4=-l_2, \quad x_5=0, \quad x_6=0; \quad y_1'=u', \quad y_2'=u', \quad \frac{\partial^2 y_1'}{\partial x_4^2}=0, \quad \frac{\partial^2 y_2'}{\partial x_5^2}=0,$$
$$(16), (17), (18), (19)$$

$$E_3 I_3\frac{\partial^3 y_2'}{\partial x_5^3}-E_1 I_1\frac{\partial^2 y_1'}{\partial x_4^3}=E_5 a_5\frac{\partial u'}{\partial x_6}. \qquad (20)$$

We now write

$$\left.\begin{aligned} &\sqrt{p}c_1 l_1=\gamma_1, \quad \sqrt{p}c_2 l_2=\gamma_2, \quad \frac{F}{(\sqrt{p}c_1)^3 E_1 I_1}=2\eta, \quad \frac{E_2 I_2 c_2^3}{E_1 I_1 c_1^3}=\xi_1, \\ &\frac{E_3 I_3 c_3^3}{E_1 I_1 c_1^3}=\xi_2, \quad \frac{E_4 a_4 f_1}{E_1 I_1(\sqrt{p}c_1)^3}=\frac{\nu_1}{\gamma_1}, \quad \frac{E_5 a_5 f_2}{E_1 I_1(\sqrt{p}c_1)^3}=\frac{\nu_2}{\gamma_1}, \end{aligned}\right\} \qquad (21)$$

and take a special case such that

$$\left.\begin{aligned} &E_1 I_1=E_2 I_2=E_3 I_3=EI, \qquad \rho_1 a_1=\rho_2 a_2=\rho_3 a_3=\rho a, \\ &E_4 a_4=E_5 a_5=E'a', \qquad \rho_4 a_4=\rho_5 a_5=\rho' a', \\ &\xi_1=\xi_2=\xi, \qquad \nu_1=\nu_2=\nu. \end{aligned}\right\} \qquad (22)$$

Substituting the solutions of (1) ~ (6) in the boundary conditions (7) ~ (20) for the special case cited above, we get

$$\begin{aligned}
A_1\Phi=\gamma_1 e^{i\gamma_2}&\Big[-\gamma_1\Big\{(\cos\gamma_2+\operatorname{ch}\gamma_2)+\operatorname{sh}\gamma_2\Big\}+i\Big\{\gamma_1\sin\gamma_2+2(\gamma_1+\nu)\operatorname{sh}\gamma_2\Big\}\Big]\\
&+\gamma_1 e^{-i\gamma_1}\operatorname{ch}\gamma_0\Big[\gamma_1\Big\{\cos\gamma_2+\operatorname{ch}\gamma_2\Big\}-2\sin\gamma_2-\operatorname{sh}\gamma_2\Big\}\\
&\qquad+i\Big\{(\gamma_1+4\nu)\sin\gamma_2+2\nu\operatorname{sh}\gamma_2\Big\}\Big]\\
&+e^{-i\gamma_1}\operatorname{sh}\gamma_0\Big[\Big\{\gamma_1^2(\cos\gamma_2+\operatorname{ch}\gamma_2)+2(-\gamma_1^2+\nu\gamma_1+2\nu^2)\sin\gamma_2-\gamma_1^2\operatorname{sh}\gamma_2\Big\}\\
&\qquad\qquad+i\gamma_1\Big\{-2\nu(\cos\gamma_2+\operatorname{ch}\gamma_2)+(\gamma_1+4\nu)\sin\gamma_2\Big\}\Big],
\end{aligned}\tag{23}$$

$$\begin{aligned}
B_1\Phi=\gamma_1 e^{-i\gamma_2}&\Big[\gamma_1\Big\{(\cos\gamma_2+\operatorname{ch}\gamma_2)+\operatorname{sh}\gamma_2\Big\}+i(\gamma_1\sin\gamma_2-2\nu\operatorname{sh}\gamma_2)\Big]\\
&+\gamma_1 e^{i\gamma_1}\operatorname{ch}\gamma_0\Big[\gamma_1\Big\{-(\cos\gamma_2+\operatorname{ch}\gamma_2)+2\sin\gamma_2+\operatorname{sh}\gamma_2\Big\}\\
&\qquad-i\Big\{(3\gamma_1+4\nu)\sin\gamma_2+2(\gamma_1+\nu)\operatorname{sh}\gamma_2\Big\}\Big]\\
&+e^{i\gamma_1}\operatorname{sh}\gamma_0\Big[\Big\{-\gamma_1^2(\cos\gamma_2+\operatorname{ch}\gamma_2)-2\nu(3\gamma_1+2\nu)\sin\gamma_2+\gamma_1^2\operatorname{sh}\gamma_2\Big\}\\
&\qquad\qquad-i\gamma_1\Big\{2(\gamma_1+\nu)(\cos\gamma_2+\operatorname{ch}\gamma_2)-(3\gamma_1+4\nu)\sin\gamma_2\Big\}\Big],
\end{aligned}\tag{24}$$

$$\begin{aligned}
C_1\Phi=\gamma_1 e^{\gamma_2}&\Big[-(\gamma_1+2\nu)\sin\gamma_2+i\gamma_1\Big\{(\cos\gamma_2+\operatorname{ch}\gamma_2)-2\sin\gamma_2-\operatorname{sh}\gamma_2\Big\}\Big]\\
&+\gamma_1 e^{-\gamma_1}\cos\gamma_0\Big[-(\gamma_1+2\nu)(\sin\gamma_2+2\operatorname{sh}\gamma_2)\\
&\qquad-i\gamma_1\Big\{(\cos\gamma_2+\operatorname{ch}\gamma_2)+\operatorname{sh}\gamma_2\Big\}\Big]\\
&+e^{-\gamma_1}\sin\gamma_0\Big[\gamma_1(\gamma_1+2\nu)\Big\{(\cos\gamma_2+\operatorname{ch}\gamma_2)+\operatorname{sh}\gamma_2\Big\}\\
&\qquad\qquad-i\Big\{\gamma_1^2\sin\gamma_2+2(\gamma_1^2+2\nu\gamma_1+2\nu^2)\operatorname{sh}\gamma_2\Big\}\Big],
\end{aligned}\tag{25}$$

$$\begin{aligned}
D_1\Phi=\gamma_1 e^{-\gamma_2}&\Big[(\gamma_1+2\nu)\sin\gamma_2-i\gamma_1\Big\{(\cos\gamma_2+\operatorname{ch}\gamma_2)+\operatorname{sh}\gamma_2\Big\}\Big]\\
&+\gamma_1 e^{\gamma_1}\cos\gamma_0\Big[(\gamma_1+2\nu)(\sin\gamma_2+2\operatorname{sh}\gamma_2)\\
&\qquad+i\gamma_1\Big\{(\cos\gamma_2+\operatorname{ch}\gamma_2)+2\sin\gamma_2+3\operatorname{sh}\gamma_2\Big\}\Big]
\end{aligned}$$

$$+e^{\gamma_1}\sin\gamma_0\Big[-\gamma_1(\gamma_1+2\nu)\Big\{(\cos\gamma_2+\operatorname{ch}\gamma_2)+3\operatorname{sh}\gamma_2\Big\}$$

$$+i\Big\{-2\gamma_1^2(\cos\gamma_2+\operatorname{ch}\gamma_2)+\gamma_1^2\sin\gamma_2+4\nu(\gamma_1+\nu)\operatorname{sh}\gamma_2\Big\}\Big], \quad (26)$$

$$\frac{\eta\Phi}{4}=\gamma_1(\gamma_1+2\nu)(-\cos\gamma_0\operatorname{sh}\gamma_0+\sin\gamma_0\operatorname{ch}\gamma_0+\sin\gamma_0\operatorname{sh}\gamma_0)$$

$$+i\Big[\gamma_1^2-\gamma_1^2\cos\gamma_0(\operatorname{ch}\gamma_0+\operatorname{sh}\gamma_0)+\sin\gamma_0\Big\{\gamma_1^2\operatorname{ch}\gamma_0-2\nu(\gamma_1+\nu)\operatorname{sh}\gamma_0\Big\}\Big], \quad (27)$$

$$H_1\Phi=2\gamma_1\Big[\Big\{-(\gamma_1+2\nu)(\sin\gamma_0\operatorname{sh}\gamma_2+\operatorname{sh}\gamma_0\sin\gamma_2)+i\gamma_1\Big\{(\cos\gamma_0-\operatorname{ch}\gamma_0)(\sin\gamma_2+\operatorname{sh}\gamma_2)$$

$$-(\sin\gamma_0-\operatorname{sh}\gamma_0)(\cos\gamma_2+\operatorname{ch}\gamma_2)-(\sin\gamma_0\operatorname{sh}\gamma_2+\operatorname{sh}\gamma_0\sin\gamma_2)\Big\}\Big], \quad (28)$$

$G_1=H_1$, $G_2=H_2=R''+iS''$ (which appears presently), (29), (30)

where

$$\gamma_1=\sqrt{pc_1}\,l_1, \quad \gamma_2=\sqrt{pc_2}\,l_2, \quad \gamma_0=\gamma_1+\gamma_2=\sqrt{pc}\,l,$$

$$\nu=\nu_1=\nu_2=\sqrt{\frac{E'\rho'a'^2l_1^2}{EI\rho a}}, \quad \eta=\frac{Fl_1^3}{2\gamma_1^3EI}. \quad (31)$$

Although not given here, similar results were obtained for the general case.

We shall now write the solutions of the present case in their real forms. Thus, corresponding to the disturbance

$$F\cos pt \quad (32)$$

at $x_1=0$ $(x_4=l_2)$, we have

$$y_1=\left(\frac{Fl^3}{EI}\right)\left(\frac{l_1}{l}\right)^3\frac{1}{4\gamma_1^3}\sqrt{\frac{R^2+S^2}{P^2+Q_2}}\cos\left(pt-\tan^{-1}\frac{Q}{P}+\tan^{-1}\frac{S}{R}\right), \quad (33)$$

where

$$P=\gamma_1(\gamma_1+2\nu_1)(-\cos\gamma_0\operatorname{sh}\gamma_0+\sin\gamma_0\operatorname{ch}\gamma_0+\sin\gamma_0\operatorname{sh}\gamma_0), \quad (34)$$

$$Q=\gamma_1^2-\gamma_1^2\cos\gamma_0(\operatorname{ch}\gamma_0+\operatorname{sh}\gamma_0)+\sin\gamma_0\Big\{\gamma_1^2\operatorname{ch}\gamma_0-2\nu_1(\gamma_1+\nu_1)\operatorname{sh}\gamma_0\Big\}, \quad (35)$$

$$R=\gamma_1(\gamma_1+2\nu_1)\Big[-2\sin\gamma_0\,\mathrm{sh}\,\gamma_0-2\sin\gamma_2\,\mathrm{sh}\,\gamma_2$$
$$+\mathrm{sh}\,\gamma_1\Big\{\cos\gamma_0(\sin\gamma_2+2\,\mathrm{sh}\,\gamma_2)-\sin\gamma_0(\cos\gamma_2+2\,\mathrm{sh}\,\gamma_2)\Big\}$$
$$+\sin\gamma_1\Big\{\mathrm{ch}\,\gamma_0(2\sin\gamma_2+\mathrm{sh}\,\gamma_2)+\mathrm{sh}\,\gamma_0(2\sin\gamma_2-\mathrm{ch}\,\gamma_2)\Big\}\Big], \tag{36}$$

$$S=4\nu_1(\gamma_1+\nu_1)(\sin\gamma_0\,\mathrm{sh}\,\gamma_1\,\mathrm{sh}\,\gamma_2-\mathrm{sh}\,\gamma_0\sin\gamma_1\sin\gamma_2)$$
$$+\gamma_1^2\Big[2(\cos\gamma_2\,\mathrm{sh}\,\gamma_2-\sin\gamma_2\,\mathrm{ch}\,\gamma_2-\sin\gamma_2\,\mathrm{sh}\,\gamma_2)$$
$$-2\sin\gamma_0\,\mathrm{sh}\,\gamma_0-\sin\gamma_0\,\mathrm{ch}\,\gamma_0+\cos\gamma_0\,\mathrm{sh}\,\gamma_0$$
$$+\cos\gamma_0\Big\{\mathrm{sh}\,\gamma_1(\cos\gamma_2+\sin\gamma_2+2\,\mathrm{sh}\,\gamma_2)+\mathrm{ch}\,\gamma_1\sin\gamma_2\Big\}$$
$$+\sin\gamma_0\Big\{\mathrm{sh}\,\gamma_1(-\cos\gamma_2+\sin\gamma_2+\mathrm{sh}\,\gamma_2)-\mathrm{ch}\,\gamma_1(\cos\gamma_2+\mathrm{ch}\,\gamma_2)\Big\}$$
$$+\mathrm{ch}\,\gamma_0\Big\{\sin\gamma_1(2\sin\gamma_2-\mathrm{ch}\,\gamma_2+\mathrm{sh}\,\gamma_2)-\cos\gamma_1\,\mathrm{sh}\,\gamma_2\Big\}$$
$$+\mathrm{sh}\,\gamma_0\Big\{\sin\gamma_1(\sin\gamma_2-\mathrm{ch}\,\gamma_2+\mathrm{sh}\,\gamma_2)+\cos\gamma_1(\cos\gamma_2+\mathrm{ch}\,\gamma_2)\Big\}\Big]. \tag{37}$$

The displacements of waves in adjacent spans and in the piers are

$$y_2(\text{waves})=-\left(\frac{Fl^3}{EI}\right)\left(\frac{l_1}{l}\right)^3\frac{1}{4\gamma_1^2}\sqrt{\frac{R'^2+S'^2}{P^2+Q^2}}\cos\left(pt-\tan^{-1}\frac{Q}{P}+\tan^{-1}\frac{R'}{S'}\right), \tag{38}$$

$$y_2'(\text{waves})=\left(\frac{Fl^3}{EI}\right)\left(\frac{l_1}{l}\right)^3\frac{1}{4\gamma_1^2}\sqrt{\frac{R''^2+S''^2}{P^2+Q^2}}\cos\left(pt-\tan^{-1}\frac{Q}{P}+\tan^{-1}\frac{R''}{S''}\right), \tag{39}$$

$$u=2y_2,\qquad u'=2y_2', \tag{40}$$

where

$$R'=(\gamma_1+2\nu)(\sin\gamma_0\,\mathrm{sh}\,\gamma_2+\mathrm{sh}\,\gamma_0\sin\gamma_2), \tag{42}$$

$$S'=\gamma_1\Big\{-(\cos\gamma_0-\mathrm{ch}\,\gamma_0)(\sin\gamma_2+\mathrm{sh}\,\gamma_2)+(\sin\gamma_0-\mathrm{sh}\,\gamma_0)(\cos\gamma_2+\mathrm{ch}\,\gamma_2)$$
$$+(\sin\gamma_0\,\mathrm{sh}\,\gamma_2+\mathrm{sh}\,\gamma_0\sin\gamma_2)\Big\}, \tag{43}$$

$$R''=(\gamma_1+2\nu)\Big\{\cos\gamma_0\,\mathrm{sh}\,\gamma_0\sin\gamma_2+\sin\gamma_0\,\mathrm{ch}\,\gamma_0\,\mathrm{sh}\,\gamma_2-\sin\gamma_0\,\mathrm{sh}\,\gamma_0(\cos\gamma_2+\mathrm{ch}\,\gamma_2)\Big\}, \tag{44}$$

$$
\begin{aligned}
S'' = \gamma_1 \Big\{ & (\cos\gamma_0 \operatorname{ch}\gamma_0 - 1)(\sin\gamma_2 - \operatorname{sh}\gamma_2) + \cos\gamma_0 \operatorname{sh}\gamma_0 (\cos\gamma_2 + \sin\gamma_2 + \operatorname{ch}\gamma_2) \\
& + \sin\gamma_0 \operatorname{ch}\gamma_0 (-\cos\gamma_2 - \operatorname{ch}\gamma_2 + \operatorname{sh}\gamma_2) \\
& \qquad + \sin\gamma_0 \operatorname{sh}\gamma_0 (-\cos\gamma_2 + \sin\gamma_2 - \operatorname{ch}\gamma_2 + \operatorname{sh}\gamma_2) \Big\}.
\end{aligned}
\tag{45}
$$

When ν_1 is fairly large, $\sqrt{P^2+Q^2} \rightarrow 2\nu_1^2 \sin\gamma_0 \operatorname{sh}\gamma_0$, so that the approximate resonance conditions are expressed by

$$
\sin\gamma_0 = 0, \qquad \left\{ \sin(\rho a l^4 p^2/EI)^{\frac{1}{4}} = 0 \right\}. \tag{46}
$$

In our example which will appear in the next section, $\nu_1 = 19{\cdot}025$. However, in resonance conditions, even should no damping force exist in the structure of the span, the amplitude of the vibrations will not assume an infinitely large value because of the condition that the denominator of the actual expression for the amplitude is

$$
\sqrt{P^2+Q^2}\,, \tag{47}
$$

each of P and Q being of a certain finite value.

3. *A numerical example and its interpretation.*

We shall take the case of a deck girder bridge of the same size and weight as those shown in the preceding paper, but with the difference that the exciting force is at $l/4$ from one end ($\nu_1 = 19{\cdot}025$).

Using the relations already obtained, we calculated $y_{1x_1=0}$, $y_{2\max}$, $y'_{2\max}$, $u_{\max}$, $u'_{\max}$, for different values of γ_0, namely $(\rho a l^4 p^2/EI)^{\frac{1}{4}}$, the result being shown in Fig. 2. The ordinates corresponding to $y_{2\max}$, $y'_{2\max}$ are shown on a magnified scale in Fig. 3. Every ordinate of these figures may be assumed to indicate the relative value of any one of $y_{1x_1=0}$, $y_{2\max}$, or $y'_{2\max}$ for a given intensity of f in the disturbing force

$$
F = f\gamma_0^4 \left(= f\frac{\rho a l^4 p^2}{EI} \right), \tag{48}
$$

but for different vibrational frequencies. It is evident that, in the case of a locomotive or of an exciting machine, the condition that f is a constant, must exist.

The values of $u_{\max}$, $u'_{\max}$ are always twice those of $y_{2\max}$, $y'_{2\max}$ for any vibrational frequency. The reason why we may neglect the reflectional waves in the adjacent spans and in piers was explained in the last paper.

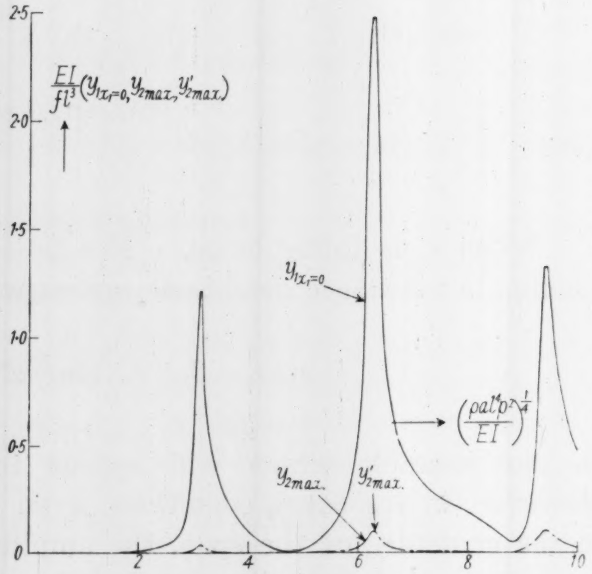

Fig. 2. Resonance curves of bridge vibrations.

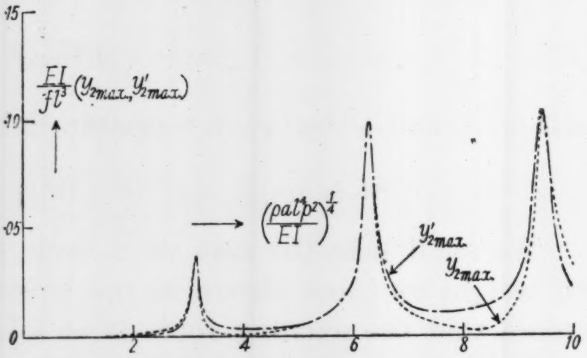

Fig. 3. Resonance curves of bridge vibrations. $y_{2\max}$, $y'_{2\max}$ on a magnified scale.

It will be seen from Figs. 2, 3 that, under the second resonance $(\rho a l^4 p^2/EI)^{\frac{1}{4}} \approx 2\pi$, the amplitude of vibration is about twice that of first resonance $(\rho a l^4 p^2/EI)^{\frac{1}{4}} \approx \pi$ or even that of the third resonance $(\rho a l^4 p^2/EI)^{\frac{1}{4}} \approx 3\pi$. This results from the condition that the disturbance imparts its force at the loop $l/4$ from one end of the span for the second vibrational mode of the bridge span.

From the vibrational nature of a bridge span, it is known that the most dangerous condition, if it be the case, among those in which velocities of moving disturbance on a bridge differ, is covered in the results of the present paper and the preceding one. While, generally speaking, the effect of the disturbance imparted by a locomotive upon a bridge of a finite span dies away before the application of a finite number of impacts, the cases which we discussed here, on the other hand, are such that vibrational disturbance continues to be effective for an infinitely long time.

It should be borne in mind that, since in our papers, we have discussed the damping from only one out of the numerous likely causes, such as viscous damping in the structure, energy dissipation in the form of elastic waves through neighbouring structural members, solid friction at the ends of every span, etc., the resonance curves in our calculation should be rather sharp compared with those obtained from vibration experiments on actual bridges.

37. 橋梁の振動に於ける勢力の逸散性（第2報）

地震研究所 {妹澤克惟
金井清

同じ題名の前回の報告では，橋梁の橋桁上に振動力が働く場合にその振動勢力が彈性波さして隣の橋桁や橋脚に傳播する爲にこの橋桁の振動か減衰する事を示して置いた．實際に於て橋梁の振動減衰性の相當に大きな部分はこの逸散性が受持つてをるやうである．前回のものは振動力が橋桁の中央に働く場合であつたが，今回は任意の點にそれが働く場合を研究したのである．

普通の場合に振動力が振動體の節點に働くか，腹に働くかさいふ事の結果さしての傾向もこの研究結果に大いに現れてをるやうであるが，逸散性のためにその性質が少しく訂正される．しかし最も著しい特性は共振の振幅が相當に少くなり實際の觀測の數倍位になる事を示すこさである．但しこの數倍さいふ事は多くの減衰力の一つのみを取つてをるからである．

機關車が橋梁上を動くにしても，橋に最惡の影響を與へるのはその位置が動かずに靜止する場合である事は共振の力學から明かである．只今の論文はそのやうな場合を論じたさいふ事によつて實際問題さ結びつけ得るのである．しかしこの論文の別の目的は，地上にある建物の場合にその震動勢力の逸散性について誰にもわかるやうな解釋を與へにくかつたものが，今回の論文によつてその性質を容易に示し得たさいふ點にある．

---

38. *Model Experiment Confirmations of a Dynamic Method of Minimizing the Seismic Vibrations of a Structure.*

By Katsutada SEZAWA and Kiyoshi KANAI,

Earthquake Research Institute.

(Read June 15, 1937.—Received June 21, 1937.)

1. *Introduction.*

In the previous paper[1] we made a suggestion based on theory regarding a dynamic method of minimizing the seismic vibrations of a structure. It was theoretically ascertained that if an inertia mass with suitably selected elastic and viscous resistances were placed within the structure, the amplitudes or stresses in the same structure would be minimized to or below a certain critical for any vibrational frequency of seismic vibrations. The present paper confirms the theory just mentioned by means of model experiments. Since, as already stated, the amplitude of seismic vibrations is particularly large in the horizontal sense, and since moreover the vibration of a structure is most sensible to the same horizontal movement of the ground, the experiments were made specially for the case of horizontal motion.

Although the vibrational forces from the exciter in the present experiments were all of sinusoidal type, yet, owing to the condition that oscillation of an irregular type is nothing more than a combined form of different sinusoidal oscillations, it is possible that the present results apply to the general case to a considerable extent.

2. *The method of experiment.*

The vibration table used in the experiments was the same as that used by Saita (the original one being probably designed by Ishimoto and Takahasi). A hanging table oscillated to and fro by means of periodic forces supplied by a $^1/_4$ H.P. motor through gear arrangement, oil resistances being applied to both sides of the table for flattening the peak of the resonance condition, $T=1{\cdot}175$ sec, of the table vibration.

---

[1] K. SEZAWA and K. KANAI, "A Method of Minimizing the Seismic Vibrations of a Structure," *Bull. Earthq. Res. Inst.*, **15** (1937), 21～32.

Inasmuch as the periods of vibrations available in our experiments were of the range 0·1 sec to 0·5 sec (though tests were made even for $T=1{\cdot}175$ sec), resonances of such long periods as 1·175 sec were quite immaterial. Since, however, the motor power was not sufficiently high, it was rather difficult to avoid conspicuous changes in the vibration amplitudes of the table for different vibrational frequencies. If, on the other hand, the ratio of the amplitude of the vibration table to that of the structure were taken as we did in our analysis, the difference in the amplitudes of the table for different frequencies would not greatly vitiate the solution of the problem under consideration.

The model for our experiments was a two-storied structure with rigid wooden floors and elastic steel columns. The height below the first floor and that between the first and the second floors were both $l=20$ cm (total height of the structure being 46 cm), whereas the length and width of each floor were 84 cm and 16 cm respectively. The mass to be concentrated on each floor was 4787 gm., the total mass of the structure excepting that of the damper being therefore 9574 gm. The columns in the respective floors consisted of four plate walls, 0·8 mm thick and 12 cm wide with both their ends in approximately clamped condition. The stiffness of the wall columns was found by free vibration tests of the upper floor, using the formula

$$ml^3p^2/EI=12, \tag{1}$$

where EI is the resultant stiffness of the columns in every floor and p the vibrational frequency. The result of the experiment showed that $EI=6{\cdot}587$ $kg.$ m^3/sec^2. The period of free vibration of the whole structure was found to be 0·238 sec. A general view of the structure together with that of the vibration table is shown in Fig. 1.[2]

The dynamic vibration dampers were of piston type, one of them being made of wood and the other of metal. Although the wooden damper was quite satsfactory, yet owing to its tendency to shrink with time, we used the metal damper for the main experiments. The chamber on the second floor, Fig. 1, is the metal damper and that underneath the same floor the wooden damper. As to the metal damper, the piston that imparts the damping resistance μ' has a mass M supported by the plate spring c. The piston part was reconstructed from a usual static piston damper (probably in Ishimoto's seismograph), but a large sectorial aperture (μ' in Fig. 1) was perforated in the cylinder end in order to obtain the condition of an exceedingly weak

---

[2] T. TAKAYAMA and others kindly assisted us in photographing these and some other data.

Table I.

Case	A	B	C	D	E	F	G
M in gm	722	942	1272	1652	2607	3562	5472
$M/(2m)$	0·0755	0·0996	0·133	0·173	0·272	0·372	0·571

viscous resistance in the damper, which proved to be rather efficient as a dynamic damper. The mass M of the damper was of seven kinds, as shown in Table I. The period of free vibration of the damper alone in Case D was roughly 0·26 sec. The aperture at the cylinder end was of five kinds (excepting an auxiliary one 3′) as shown in Table II, the area of the cylinder section being 54·19 cm^2. Since, strictly speaking, the width of gap between the piston and the cylinder was 0·15 mm, the area of the aperture in Case 1 was not exactly zero.

Table II.

Case	1	2	3	3′	4	5
Area of aperture in cm^2	0	0·1469	0·578	1·071	3·106	8·96
Area ratio of aperture-cylinder	0	0·00271	0·01067	0·1976	0·05732	0·1653

The amplitudes and vibrational frequencies were observed with the aid of a smoke cylinder driven by a synchronous motor, the whole contrivance being firmly fixed to the vibration table. The disturbing effects of this motor on the vibration table was found to be negligible.

In the case of forced vibrations, the displacements of the first and second floors and the damper, all relative to the table, besides the displacement of the table itself relative to the room floor, were recorded without magnification on the cylinder revolving once in two minutes. In the case of free vibration, the displacements of both floors in the structure were magnified ten times.

3. *The experiments and their results.*

Although the vibration experiments were made for various combinations of damper mass and aperture of the piston, the elastic resistance of the damper was kept constant throughout the experiments. The cases with which we experimented were

A1, A5, B1, B3, B4, B5, C1, C2, C3, C4, C5, D1, D2, D3,
D4, D5, E1, E2, E3, E4, E5, F1, F2, F3, F4, F5, G1, G2.

The original data recorded on smoked papers were generally of the type shown in Figs. 2a, 2b which exactly correspond to Cases

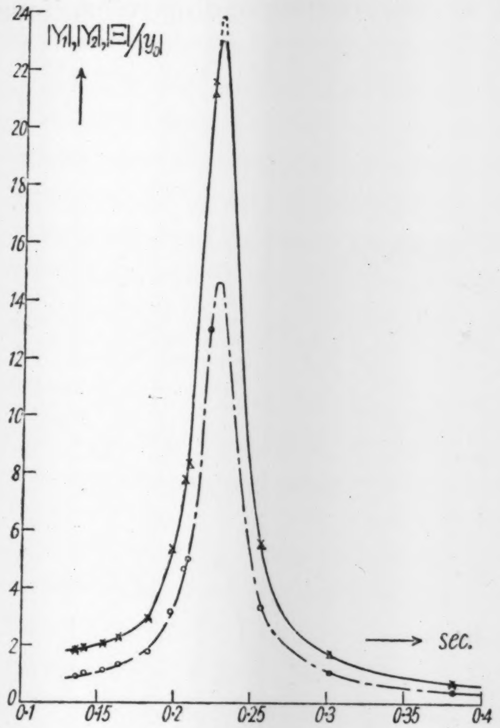

Fig. 3. A1.

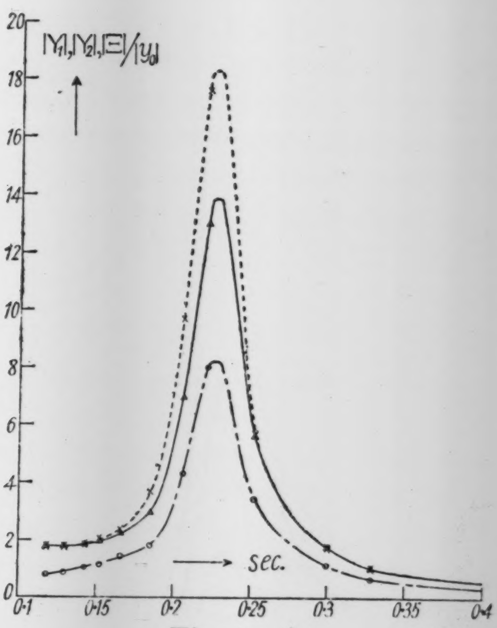

Fig. 4. A5.

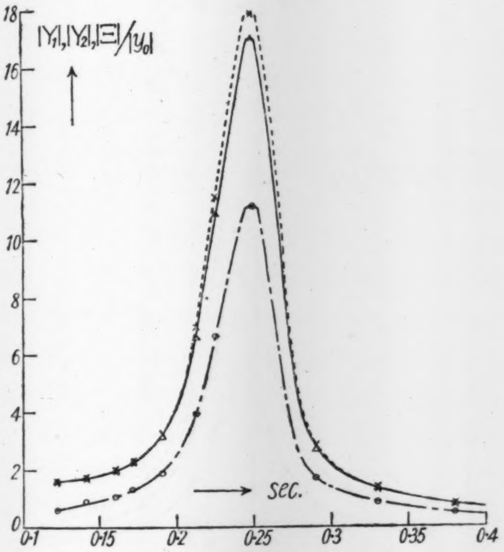

Fig. 5. B1.

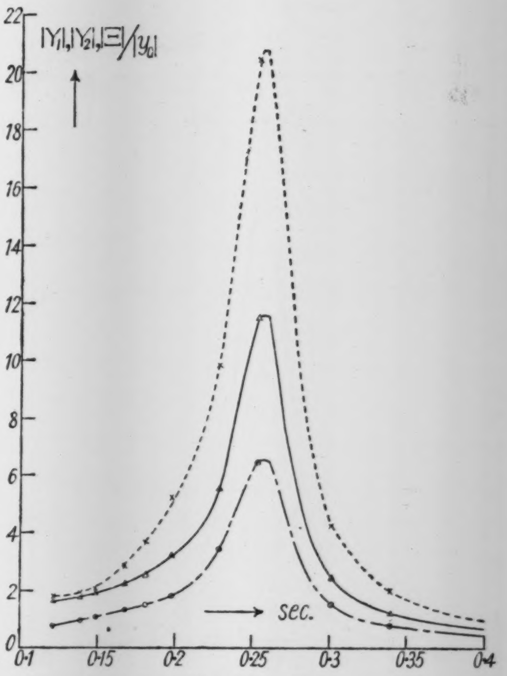

Fig. 6. B3.

A1 ahd D3 respectively. (As will be shown later, Case A1 represents an undamped condition and Case D3 an extremely damped condition.)

All the amplitudes of the respective floors and the damper relative to that of the vibration table as well as the corresponding vibrational

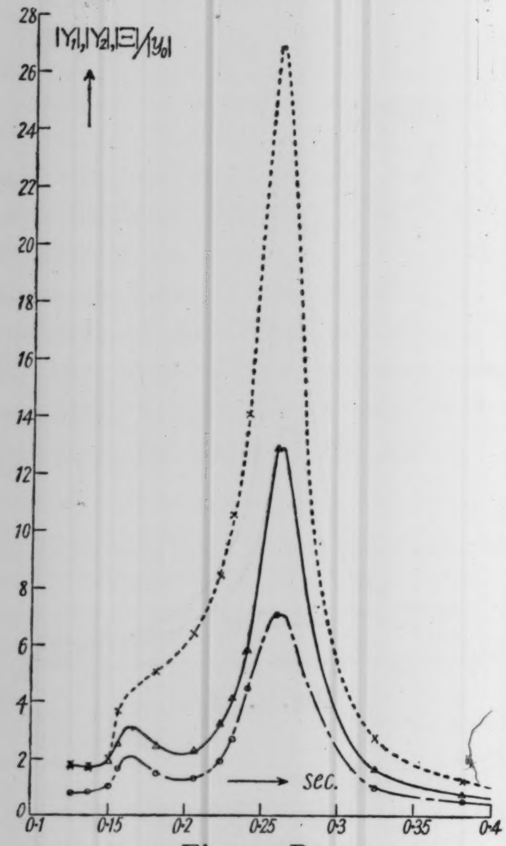

Fig. 7. B4.

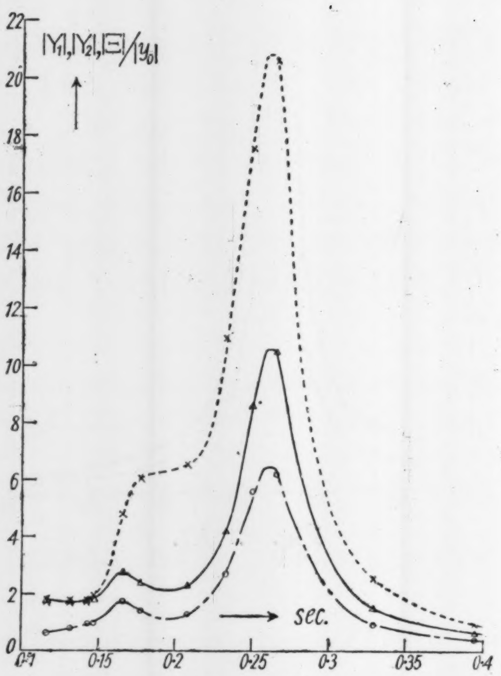

Fig. 8. B5.

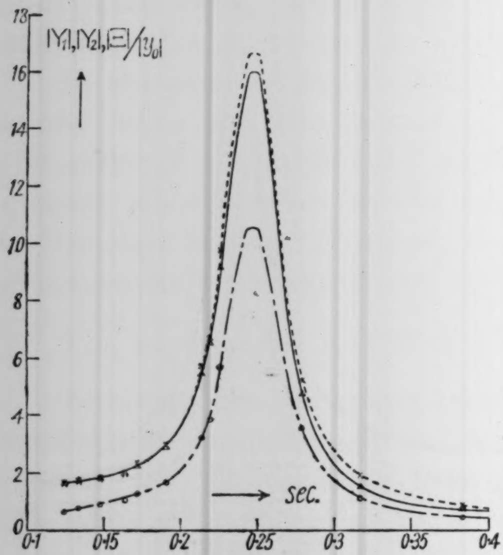

Fig. 9. C1.

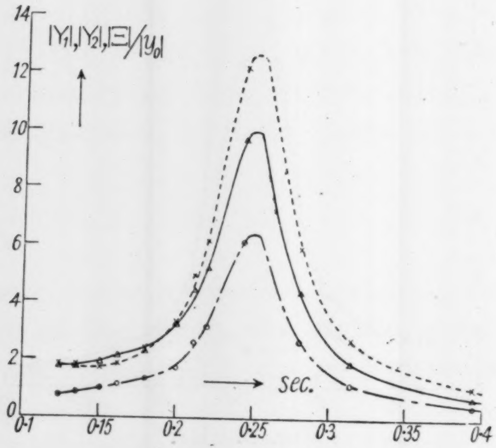

Fig. 10. C2.

frequencies, were read off from records of the type shown in Figs. 2a,

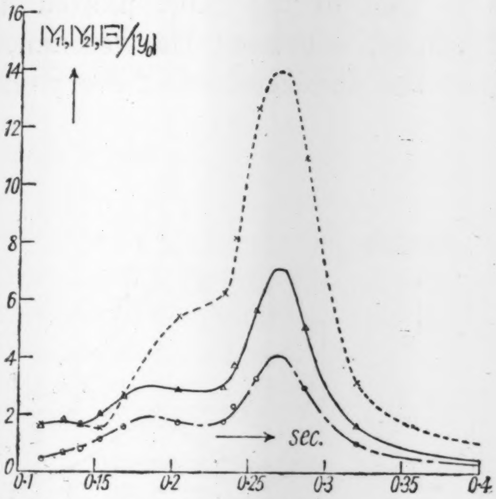

Fig. 11. C3.

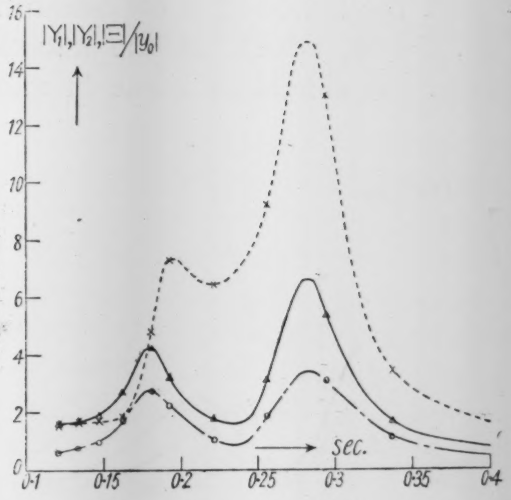

Fig. 12. C4.

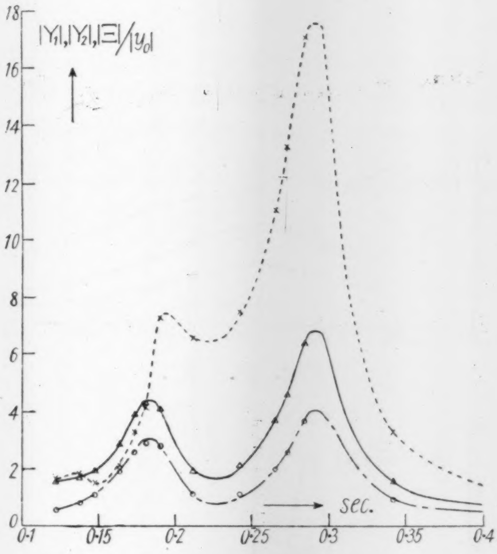

Fig. 13. C5.

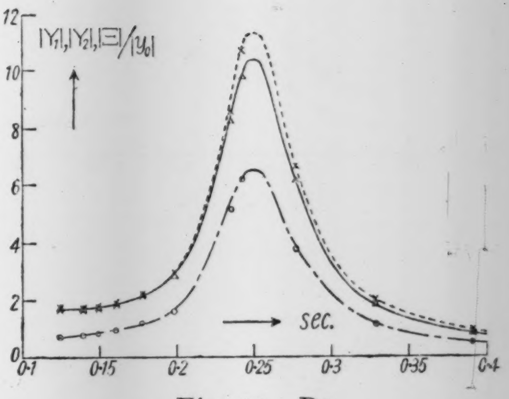

Fig. 14. D1.

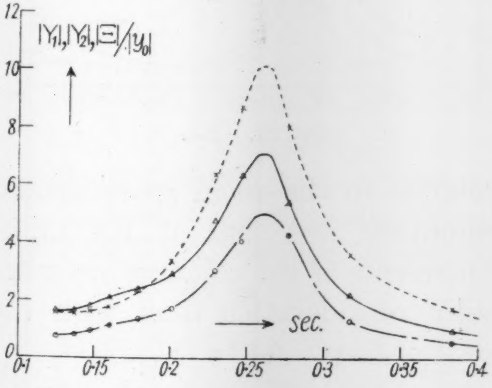

Fig. 15. D2.

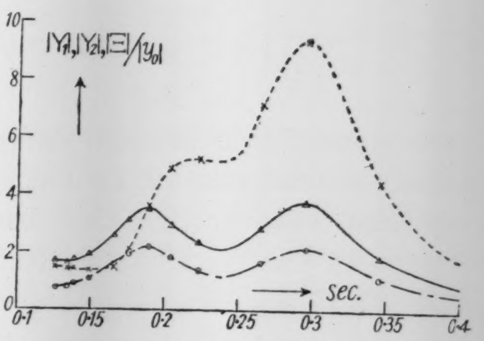

Fig. 16. D3.

2b and the ratios of these amplitudes to that of the table plotted in Figs. 3∼30, which, in the nature of things, represent the resonance curves. It should be borne in mind that the displacement of every one

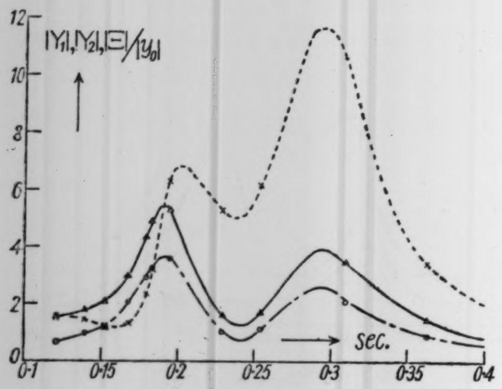

Fig. 17. D4.

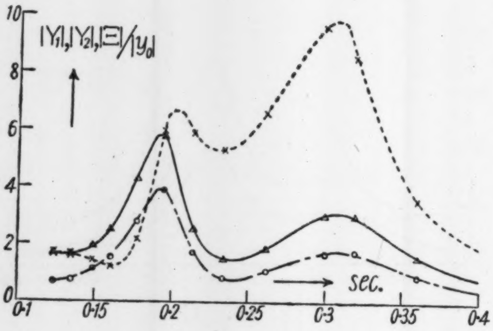

Fig. 18. D5.

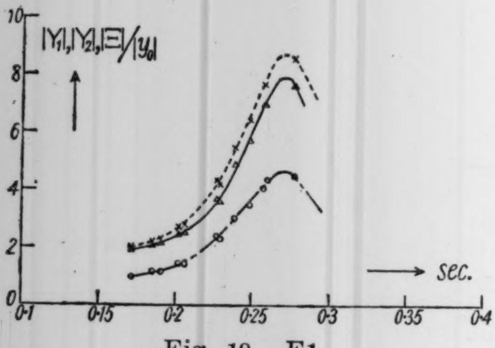

Fig. 19. E1.

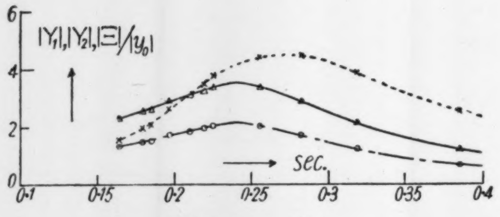

Fig. 20. E2.

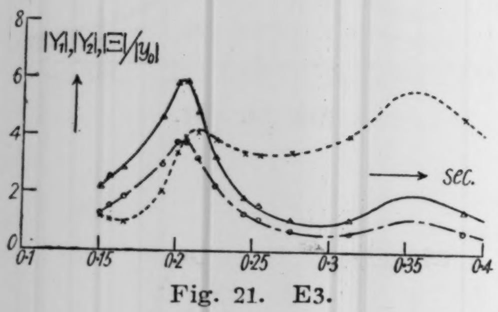

Fig. 21. E3.

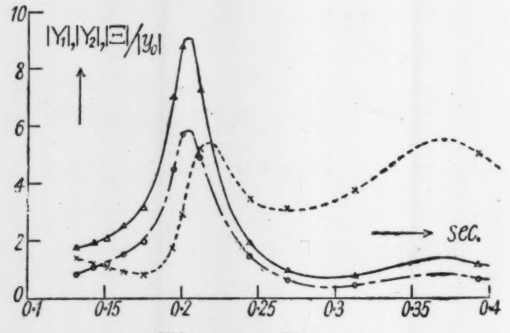

Fig. 22. E4.

of the respective floors and dampers relative to the room space should be the vectorial sum of its recorded amplitude and that of the table. It appears however that the bending moments of the columns are more in line with the relative amplitudes under consideration than with the actual amplitudes. The ratios $|y_1-y_0|/|y_0|$ $(=|Y_1|/|y_0|)$, $|y_2-y_0|/|y_0|$ $(=|Y_2|/|y_0|)$, $|\xi+y_2-y_0|/|y_0|$ $(=|\Xi|/|y_0|)$; namely, the ratios of the relative vectorial amplitudes of the first and second floors and the damper to that of the table, are shown by chain, full, and broken lines in the figures just mentioned.

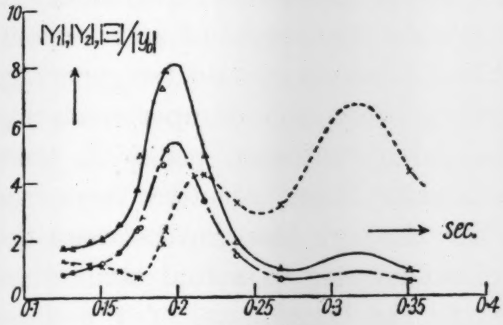

Fig. 23. E5.

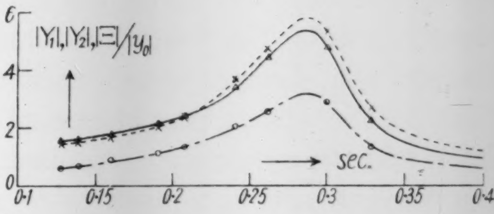

Fig. 24. F1.

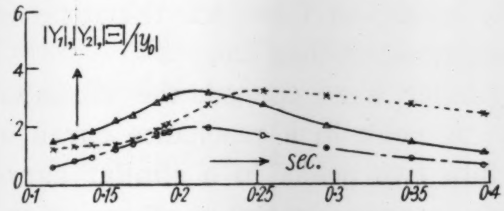

Fig. 25. F2.

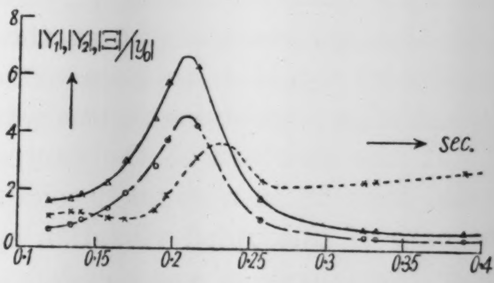

Fig. 26. F3.

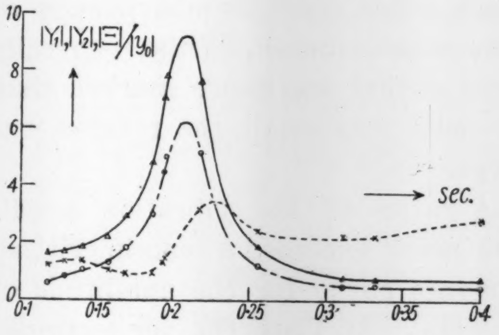

Fig. 27. F4.

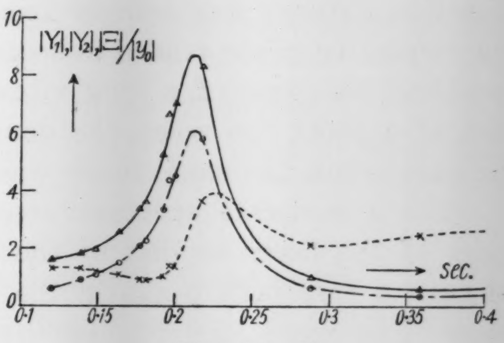

Fig. 28. F5.

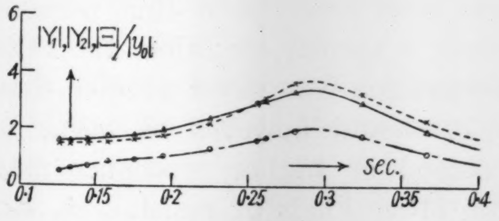

Fig. 29. G1.

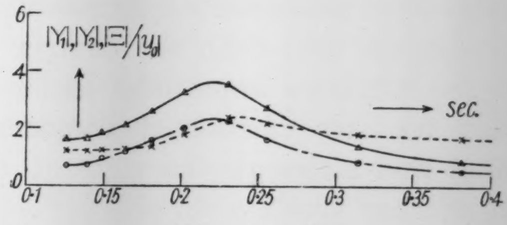

Fig. 30. G2.

Since in Cases A1, B1, C1, D1, E1, F1, G1, the aperture of the damper cylinder was closed, the movement of the damper, particularly in the case of the smaller damper mass, was in such a condition that it was almost fixed to the second floor; see Figs. 3, 5, 9, 14, 19, 24, 29. The data given in these figures represent the resonance curves in the case of an uncoupled vibration. As to resonance conditions of higher frequencies, the problem lies outside the scope of our experiments. The peaks in resonance conditions, however, would be generally pronounced for any area of the aperture were the damper mass extremely small. On the other hand, the fairly flattened peaks in cases wherein the damper mass was exceptionally large, resulted from the effect of the viscous resistance of the air through the gap between the piston and the cylinder. Application of such cases to actual structures, nevertheless, are not practicable owing to the large mass of the damper. The resonance frequency of the approximately uncoupled vibration, as a matter of fact, increased with increase in the damper mass. It is also obvious that unless the damper was effective, the vibration amplitudes would have been extremely large; in Case A1, the ratio of $|y_2-y_0|/|y_0|$ under resonance was even greater than 20.

If the aperture of the damper cylinder were opened, the vibration would then be in a coupled condition. A peak in a resonance curve in the case of uncoupled vibration split into two peaks in a similar curve when the vibration was coupled. With increase in the aperture of the cylinder, the vibrational frequencies of both resonances in coupled vibration differed increasingly from each other, and the sharpnesses of the respective peaks tended to become more pronounced. While, generally speaking, the peak of a long vibrational period was more marked than that of a short one when the damper mass was small, the reverse was the case when the same mass was large.

For a moderate aperture area, the ratios of the vibration amplitudes of the floors to that of the table never exceeded a certain critical. In such a case both peaks in the resonance curve for the amplitude of every floor were likely to be nearly equal. In Case D3, for example, the ratio of the amplitude of the second floor to that of the table under both resonance conditions was less than four. It is thus possible to conclude that with the damper in such a special condition, the ratio of the vibration amplitudes under consideration was never greater than four for any vibrational frequency. It should however be borne in mind that although the state of the second or higher resonance may be another problem for discussion, since other kinds of resistances, say, solid viscosity, etc., took up the largest part of the damping in vibration, there is no need for further comment.

It appears probable that, were the damper of the present type effective in the case of the forced vibration, the free vibration of a structure with the same damper would also be damped very rapidly. With a view to obtaining a thorough insight of this question, free vibration experiments of the model structure were conducted in such a state of the model that the vibration table is fixed to the room floor and the damper pertakes of the vibrational resistance, nearly every case in experiment under forced vibration having been tested in this way. It was shown that damping condition under free vibration fairly conforms with that under forced vibration, that is to say, an effective damper under forced vibration of a structure is also effective in damping its free vibration—a satisfactory condition in an actual case where the seismic vibration of a structure is composed usually of both forced and free vibrations. The results of free vibration tests for Cases A1 and D3′ (nearly equal to condition D3) are shown as examples in Figs. 31a, 31b. It will be seen that although the free vibration in A1 was hardly damped, that in D3′ died away very rapidly (unceasing vibratory tail in Fig. 31b being caused by the small structural movements of the model).

4. *Mathematical theory.*

No mathematical equation corresponding exactly to the present case has yet been formulated. We shall use the mathematical symbols.

l_1, l_2 = height of column between the vibration table and the first floor and that between the first and second floors,

E_1I_1, E_2I_2 = stiffnesses of the columns above mentioned,

x_1, x_2 = coordinates taken along both kinds of columns from their respective lower ends,

y_1, y_2 = deflection of columns at x_1, x_2,

m_1, m_2 = mass concentrated on the first and second floors,

M, c, μ' = mass, stiffness, and damping constant of the vibration damper,

ξ = horizontal displacement of the mass of the damper relative to the second floor,

$y_0 = be^{ipt}$ = horizontal displacement of the table.

The solutions of the column deflections are written

$$\left.\begin{aligned} y_1 &= (A_1 + B_1x_1 + C_1x_1^2 + D_1x_1^3)\,e^{ip}\,, \\ y_2 &= (A_2 + B_2x_2 + C_2x_2^2 + D_2x_2^3)\,e^{ipt}. \end{aligned}\right\} \qquad (1)$$

The boundary conditions are such that

$$x_1=0\,; \qquad y_1=be^{ipt}, \quad \frac{\partial y_1}{\partial x_1}=0, \tag*{(2), (3)}$$

$$x_1=l_1, \quad x_2=0\,; \qquad \frac{\partial y_1}{\partial x_1}=0, \quad \frac{\partial y_2}{\partial x_2}=0, \tag*{(4), (5)}$$

$$y_1=y_2, \quad -E_2I_2\frac{\partial^3 y_2}{\partial x_2^3}=-E_1I_1\frac{\partial^3 y_1}{\partial x_1^3}+m_1\frac{\partial^2 y_1}{\partial t^2}, \tag*{(6), (7)}$$

$$x_2=l_2\,; \qquad \frac{\partial y_2}{\partial x_2}=0, \quad -E_2I_2\frac{\partial^3 y_2}{\partial x_2^3}+m_2\frac{\partial^2 y_2}{\partial t^2}-c\xi-\mu'\frac{\partial \xi}{\partial t}=0, \tag*{(8), (9)}$$

$$M\left(\frac{\partial^2 \xi}{\partial t^2}+\frac{\partial^2 y_2}{\partial t^2}\right)+c\xi+\mu'\frac{\partial \xi}{\partial t}=0. \tag*{(10)}$$

Writing

$$\gamma_1=\frac{m_1l_1^3p^2}{E_1I_1}, \quad \gamma_2=\frac{m_2l_2^3p^2}{E_2I_2}, \quad \gamma_3=\frac{(m_2+M)l_2^3p^2}{E_2I_2}, \quad \eta=\frac{E_2I_2l_1^3}{E_1I_1l_2^3}, \tag*{(11)}$$

and solving (1) ~ (10) we get

$$A_1=b, \quad B_1=0, \quad C_1=-\frac{3}{2}l_1D_1, \quad B_2=0 \quad C_2=-\frac{3}{2}l_2D_2, \tag*{(12) ~ (16)}$$

$$\frac{D_1l_1^3\Phi}{2b}=\left[12\eta\left(\gamma_3-\frac{Mp^2}{c}\gamma_2\right)+\gamma_1\left\{(12-\gamma_3)-\frac{Mp^2}{c}(12-\gamma_2)\right\}\right]$$

$$+i\left\{12\eta\frac{\mu'p}{c}\gamma_3+\gamma_1\frac{\mu'p}{c}(12-\gamma_3)\right\}, \tag*{(17)}$$

$$\frac{A_2\Phi}{b}=-12\left[\left\{(12-\gamma_3)-\frac{Mp^2}{c}(12-\gamma_2)\right\}+i\frac{\mu'p}{c}(12-\gamma_3)\right], \tag*{(18)}$$

$$\frac{D_2l_2^3\Phi}{2b}=12\left\{\left(\gamma_3-\frac{Mp^2}{c}\gamma_2\right)+i\frac{\mu'p}{c}\gamma_3\right\}, \tag*{(19)}$$

$$\Phi=\left[12\eta\left(\gamma_3-\frac{Mp^2}{c}\gamma_2\right)-(12-\gamma_1)\left\{(12-\gamma_3)-\frac{Mp^2}{c}(12-\gamma_2)\right\}\right]$$

$$+i\left\{12\eta\frac{\mu'p}{c}\gamma_3-(12-\gamma_1)\frac{\mu'p}{c}(11-\gamma_3)\right\}, \tag*{(20)}$$

from which we get

$$y_{1x_1=l_1} = -\frac{12}{\Phi}\left[\left\{(12-\gamma_3) - \frac{Mp^2}{c}(12-\gamma_2)\right\} + i\frac{\mu' p}{c}(12-\gamma_3)\right], \tag{21}$$

$$y_{2x_2=l_2} = -\frac{12^2 b}{\Phi}\left\{\left(1-\frac{Mp^2}{c}\right) + i\frac{\mu' p}{c}\right\}. \tag{22}$$

Taking the real parts, we have

$$y_0(=y_{1x_1=0}) = b\cos pt, \tag{23}$$

$$y_{1x_1=l_1} = -12b\sqrt{\frac{R^2+S^2}{P^2+Q^2}}\cos\left(pt-\tan^{-1}\frac{Q}{P}+\tan^{-1}\frac{S}{R}\right), \tag{24}$$

$$y_{2x_2=l_2} = -12^2 b\sqrt{\frac{R'^2+S'^2}{P^2+Q^2}}\cos\left(pt-\tan^{-1}\frac{Q}{P}+\tan^{-1}\frac{S'}{R'}\right), \tag{25}$$

$$\xi_0 = -12^2 b\frac{\frac{Mp^2}{c}}{\sqrt{P^2+Q^2}}\cos\left(pt-\tan^{-1}\frac{Q}{P}\right), \tag{26}$$

where

$$\left.\begin{aligned}
&P = 12\eta\left(\gamma_3-\frac{Mp^2}{c}\gamma_2\right) - (12-\gamma_1)\left\{(12-\gamma_3)-\frac{Mp^2}{c}(12-\gamma_2)\right\},\\
&Q = \frac{\mu' p}{c}\left\{12\eta\gamma_3 - (12-\gamma_1)(12-\gamma_3)\right\},\\
&R = (12-\gamma_3) - \frac{Mp^2}{c}(12-\gamma_2), \qquad S = \frac{\mu' p}{c}(12-\gamma_3),\\
&R' = \left(1-\frac{Mp^2}{c}\right), \qquad\qquad\qquad\quad S' = \frac{\mu' p}{c}.
\end{aligned}\right\} \tag{27}$$

In the special case wherein the stiffness of the columns below the first floor, $E_1 I_1$, is extremely large, the above solutions reduce to those of a one-storied structure as shown in the previous paper[3].

Applying the equations just obtained to such a special case as corresponds to D3 in the experiments, some of numerical data being shown in Secion 2, we obtained the resonance curves as shown in Fig. 32a. In the present case the numerical values obtained in Sections 2 and 3 are such that

---

3) *loc. cit.* 1).

$$\gamma_1=\gamma_2=0{\cdot}0063\left(\frac{2\pi}{T}\right)^2,\quad \gamma_3=0{\cdot}00811\left(\frac{2\pi}{T}\right)^2,\quad \frac{Mp^2}{c}=\left(\frac{0{\cdot}262}{T}\right)^2,$$

$$\eta=1,\ \frac{\mu' p}{c}=\frac{0{\cdot}065}{T}\ \left(\text{obtained by free vibration tests of the damper}\right),$$

T being the period of forced vibration in sec. The results obtained in the experiments are plotted in Fig. 32b

In the present case, too, the ratios, $|Y_1|/|y_0|$, $|Y_2|/|y_0|$, $|\Xi|/|y_0|$, namely, the relative vectorial amplitudes of the first and second floors and the damper are shown by chain, full, and broken lines respectively. It will be seen that both the results, mathematical and experimental, fairly agree (excepting the large displacement of the damper in mathematical result).

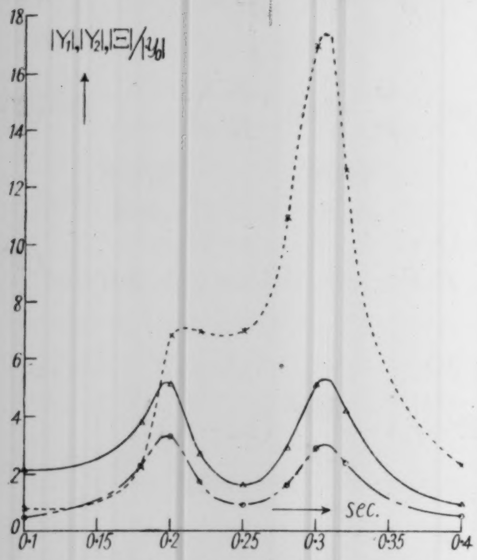

Fig. 32a. D3. Mathematical.

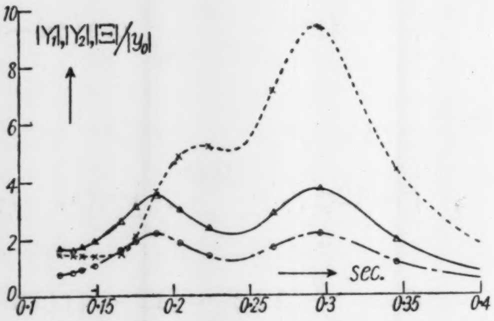

Fig. 32b. D3. Experimental.

Since there are some damping resistances still in the models arising from other causes, such as material damping within the models, etc., perhaps perfect agreement would be rather unreasonable.

5. *Application of the mathematical and experimental results to a full-scale structure and damper.*

It is obvious that any accurate mathematical result should apply to an actual case provided the values of all the numerical constants for both sides are the same. The question may arise whether or not the results of model experiments may be used forthwith in an actual case. A well established law of similitude would eliminate any difficulties in the problem.

As already shown in the theoretical discussion, the parameters required for defining the results are such that

$$\text{(i)}\quad \frac{m_1 l_1^3 p^2}{E_1 I_1},\quad \frac{m_2 l_2^3 p^2}{E_2 I_2},\quad \cdots\cdots\cdots,\quad \frac{E_2 I_2 l_1^3}{E_1 I_1 l_2^3},\quad \cdots\cdots\cdots. \tag{28}$$

$$\text{(ii)}\quad \frac{M}{m},\quad \frac{E_1 I_1}{m_1 l_1^3}\cdot\frac{M}{c},\quad \frac{\mu'^2}{Mc}, \tag{29}$$

m being the total mass of the structure. Thus, if these quantities were respectively the same both for the model and the full-scale structure, the results from the model experiments would straightway apply to the full-scale structure.

The conditions in (28) are nothing more than those for the case without damper. Barring structural failures, it is an easy matter, at all events, to obtain such a condition.

The conditions in (29), which are additive, are required in the case with damper. In the case of a (circular) piston type damper, condition (29) may be replaced by

$$\frac{M}{m},\quad \frac{E_1 I_1}{m_1 l_1^3}\,\frac{M}{c},\quad \frac{4\pi Sl}{a}\,\frac{\mu}{Mp}, \tag{29$'$}$$

S, a, l, μ being piston area, orifice area, orifice length, eddy viscosity of the air respectively. The second item in (29′) is the ratio of the vibration period of the structure to that of the damper.

Our mathematical and experimental results show that the condition of the efficient damper is such that M/m is of the order of 1/10 and the natural vibration period of the damper must be nearly equal to that of the structure, whereas condition, $\mu'^2/Mc=$ a constant, is somewhat complex. It is possible to assume that, if p were the same both for the model as well as for the actual structure, $m_1 l_1^3/E_1 I_1$ being the same, $Sl\mu/ap$ should be increased linearly with M, which is not a difficult matter in an actual case.

6. *Concluding remarks.*

From experimental as well as mathematical investigations it has been ascertained that, by a suitable choice of the mass, elastic and damping resistances of the damper, the amplitudes of the seismic vibrations are strongly damped for any vibrational frequency, including those under resonance conditions. The ratio of the damper mass to that of the structure should be of the order of 1/10, which is not too small. But as the viscous resistance required in the dynamic damper of a structure is rather less than what may be expected from the case of a static damper, there is every possibility of applying the present method to the actual case without much difficulty. A practicable method would be to construct a double-walled chamber in the structure, the inner wall of which is supported by some elastic springs so that it will act as a pendulum of nearly the same vibration period as that of the structure. The action of the wooden damper in our model experiments gave us this hint. However, the viscous resistance of the air between the walls would be quite enough for dampening the motion of the structure.

For convenience and in order to expedite our work, in our model for the experiments a number of parts (although with modifications) were adapted from other instruments that were designed by some members of staff in our Institute.

In conclusion we wish to express here our thanks to the Council of the Japan Society of the Promotion of Scientific Research for aid received for conducting these experiments.

---

38. 構造物震動の力學的制振法の模型實驗的確め

地震研究所 {妹澤克惟
{金井清

前の論文で構造物に力學的制振器を取付ける事によつてその構造物が如何なる振動週期の地震動にも其れの屈曲モーメントや振幅か大きくならずに濟む方法を示して置いた. 只今の論文では之を模型實驗によつて確めたのであるが，その場合に用ひたのは 2 階建の構造物の模型であり，その理論も未だ出してなかつたから，數式を新に作り，實驗と比較して見たのである.

振動臺は簡單の爲に地震研究所の方々が試みたやうな吊臺を用ひ，その自己振動週期を避けるやうにした. 制振器も簡單の爲に石本博士の地震計等に用ひたピストン式を借用したが，力學的制振器では結局はピストンの粘性力が强過ぎる爲にそれにピストンの直徑の1/10位の大きな穴を作つて初めて効果が現れた. 制振器の質量と上記の穴を種々變化して見たが，數式でも出るやうに，制振器に適當の質量，彈性，粘性力を用ひれば，振動臺の如何なる週期の動きに對しても，屋根の振幅が振動臺のそれの四五倍を出ぬ事がわかつたのである. 不規則な地震も結局は種々の週期の振動の組合せであるから，之は甚だ好都合な事柄といはねばならぬ.

あまり効果のないやうな制振器の組合せに於ける性質も大體に於て數理の結果と一致してをることがわかつた. 又，更に大切な事は，制振器か强制振動に對して特に有効な狀態になつてをる場合には，その狀態の制振器を取付けた構造物模型の自由振動も特に著しく制振される事が明か

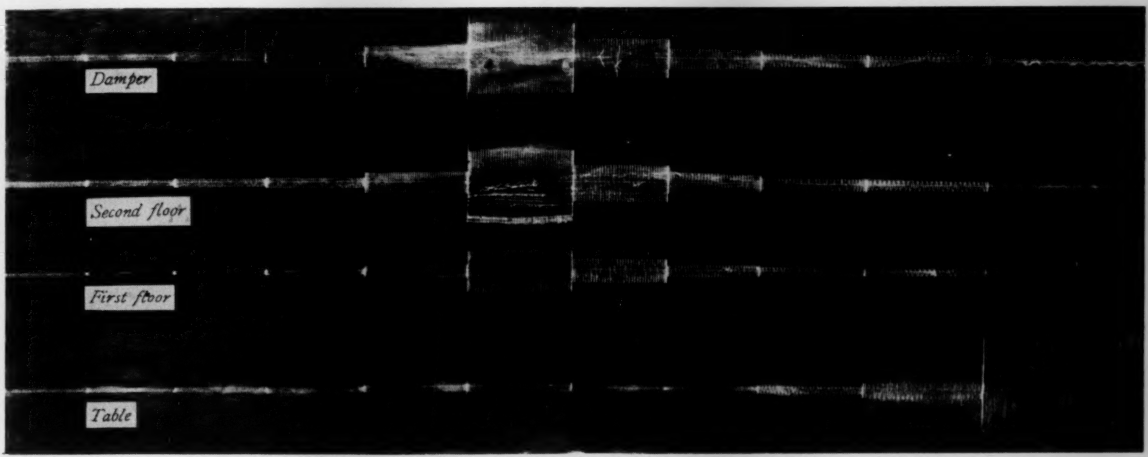

Fig. 2a. Forced vibrations of Case A1. Not well damped. Damper and the second floor vibrate with the same amplitude for any frequency. (Contraction: 1/2)

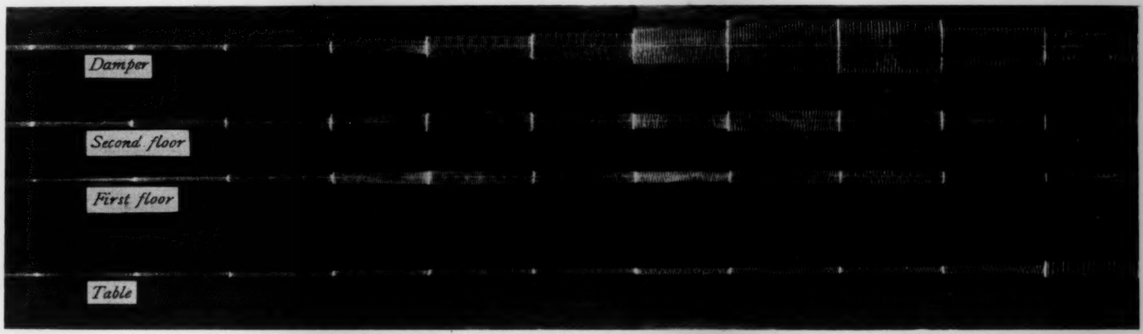

Fig. 2b. Forced vibrations of Case D3. Floor vibrations are well damped for any frequency. (Contraction: 1/2)

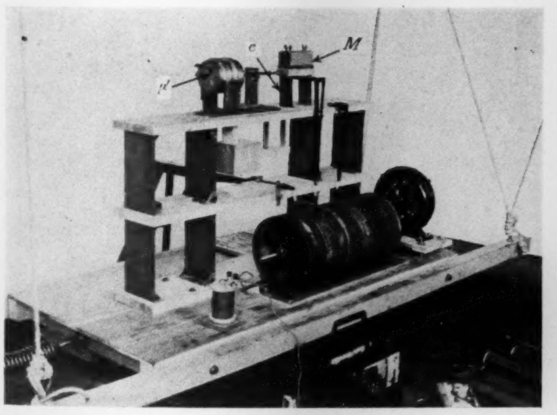

Fig. 1. Model arrangements.

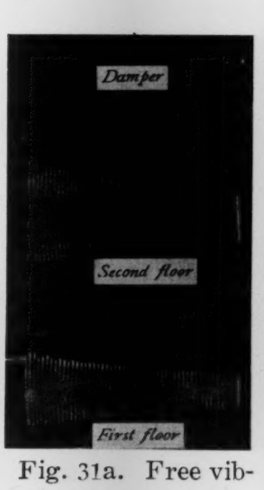

Fig. 31a. Free vibration; A1. Not damped. (Magnif.: 1/2 for damper, 5 for floors.)

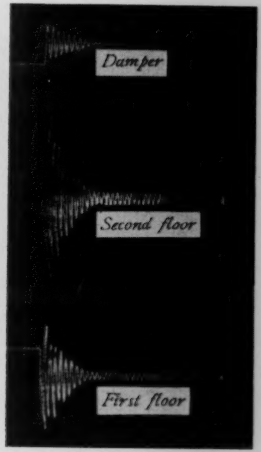

Fig. 31b. Free vibration; D3′. Well damped. (Magnif.: 1/2 for damper, 5 for floors.)

（震研彙報 第十五號 圖版 妹澤・金井）

になつたのである．構造物の地震時に於ける振動は強制振動さ思はれるものさその自由振動さ考へられるものさの組合せであるから，如何なる場合にもその効果を表し得る事が考へられる．

理論さ模型實驗さが甚だよく合ふ事は既に述べた通りである．條件さへ同じであれば理論がそのまゝ實物へ應用できる事も當然である．模型實驗を實物にあてはめるには相似の條件が必要である．しかし，構造物の破壞を考へずにその振動性のみを論ずる場合には之亦極く簡單である．制振器がないさきには

$$\frac{m_1 l_1^3 p^2}{E_1 I_1},\qquad \frac{m_2 l_2^3 p^2}{E_2 I_2},\qquad \cdots\cdots,\qquad \frac{E_2 I_2 l_1^3}{E_1 I_1 l_2^3},\qquad \cdots\cdots,$$

なる値が模型にも實物にも同じであれば充分であり，且つ之は容易に滿足し得る條件である．制振器があるさ上記のものゝ外に

$$\frac{M}{m}\left(=\frac{\text{制振器の質量}}{\text{構造物の質量}}\right),\qquad \frac{T_1}{T}\left(=\frac{\text{制振器の週期}}{\text{構造物の週期}}\right),\qquad \frac{\mu l^2}{Mc}$$

がそれぞれ一定であるさいふ條件が加はればよいのである．

模型實驗によるさ，最も効果的の場合は M/m が 1/10 位であり，$T_1/T=1$ である．第3の條件による粘性も可なり小さなものでよい事がわかる．尙，木製の制振器を作つて氣のついた事であるが，實際の制振器の問題さしては物置か何かを二重の壁にし，內側のそれに多少の彈性的支へを作ればよい．壁さ壁さの間の隙間や窓などもそれ程狹くする必要のなさそうなこさもわかつたのである．

39. *On the Elastic Waves due to Pressure Variation on the Inner Surface of a Spherical Cavity in an Elastic Solid.*

By Genrokuro NISHIMURA,

Earthquake Research Institute.

(Read Feb. 16, 1937.—Received June 20, 1937.)

1. As is well known, when a great earthquake occurs, the epicentral region of the earth's crust is subjected to severe seismal vibrations due mainly to seismic wave-energy propagated from the earthquake origin, in addition to which permanent crustal deformations occur in the region, accompanied sometimes with considerable dislocation. This paper is one of two preliminary studies of the dynamical nature of earthquakes. The other preliminary study[1] (already published) discussed the statical deformations of the surface of a semi-infinite gravitating elastic solid when a force acts on the surface of its spherical cavity.

2. Using the solutions obtained by K. Sezawa[2] of equations of motion of homogeneous isotropic solid in the case of steady state of simple-harmonic motion, H. Kawasumi[3] and R. Yoshiyama obtained formulae of displacements expressing the diverging bodily waves (longitudinal and transverse) that emanate from a spherical cavity. The boundary-conditions of stresses assumed by them for the inner surface of a spherical cavity of radius a are

$$\left.\begin{aligned}
\widehat{rr}_{r=a} &= Nf(t)P_n^m(\cos\theta)\begin{matrix}\cos\\-\sin\end{matrix}\Big\} m\phi,\\
\widehat{r\theta}_{r=a} &= Tf(t)\,\frac{dP_n^m(\cos\theta)}{d\theta}\;\begin{matrix}\cos\\-\sin\end{matrix}\Big\} m\phi,\\
\widehat{r\phi}_{r=a} &= -mTf(t)\,\frac{P_n^m(\cos\theta)}{\sin\theta}\begin{matrix}\sin\\\cos\end{matrix}\Big\} m\phi.
\end{aligned}\right\}$$

Needless to say, the origin of the spherical polar co-ordinates $(r,\ \theta,\ \phi)$

---

[1] G. NISHIMURA, *Bull. Earthq. Res. Inst.*, **12** (1934), 368∼401.

[2] K. SEZAWA, *Bull. Earthq. Res. Inst.*, **10** (1932), 299∼334.

[3] H. KAWASUMI and R. YOSHIYAMA, *Disin*, **7** (1935), 367.

is the centre of the spherical cavity. K. Sezawa[4] and W. Inouye[5] have also studied the elastic waves radiated from a spherical cavity in an elastic solid for the case when a variable pressure acts on the inner surface of the cavity. The form $f(t)$ of the time-variation of pressure assumed by them are such that

$$\left.\begin{aligned} &f(t)=0, \quad t<0 \\ &f(t)=N(1-e^{-qt}), \quad t>0 \end{aligned}\right\} \qquad \text{(a)}$$

$$\left.\begin{aligned} &f(t)=0, \quad t\lesseqgtr\tau \\ &f(t)=N, \quad -\tau<t<\tau \end{aligned}\right\} \qquad \text{(b)}$$

where t indicates time. The form (a) is assumed by K. Sezawa and W. Inouye, while expession (b) corresponds to the form assumed by H. Kawasumi and R. Yoshiyama.

3. When the boundary-conditions on the inner surface of the spherical cavity are expressed by

$$\left.\begin{aligned} &\widehat{rr}_{r=a}=-f(t), \\ &\widehat{r\theta}_{r=a}=\widehat{r\phi}_{r=a}=0, \end{aligned}\right\} \qquad (1)$$

the diverging wave[6] radiated from the cavity becomes merely a longitudinal wave, which causes only radial vibrations of particles in the medium, as

$$u=\frac{\partial\phi}{\partial r}, \qquad (2)$$

where

$$\phi=-\frac{a}{2\pi\rho}\frac{1}{r}\int_{-\infty}^{\infty}\frac{\varphi(p)e^{-ip\left(t-\frac{r-a}{v}\right)}}{(p-\alpha)(p-\beta)}dp, \qquad (3)$$

$$\varphi(p)=\int_{-\infty}^{\infty}f(\lambda)e^{-ip\lambda}d\lambda, \qquad (4)$$

$$\alpha=\frac{2V}{a}\sqrt{1-\left(\frac{V}{v}\right)^2}+i\frac{2V^2}{av}, \quad \beta=-\frac{2V}{a}\sqrt{1-\left(\frac{V}{v}\right)^2}+i\frac{2V^2}{av}, \qquad (5)$$

---

[4] K. SEZAWA, *Bull. Earthq. Res. Inst.*, **13** (1935), 740.
K. SEZAWA and K. KANAI, *Bull. Earthq. Res. Inst.*, **14** (1936), 10~17.

[5] W. INOUYE, *Bull. Earthq. Res. Inst.*, **15** (1937), 90.

[6] H. KAWASUMI and R. YOSHIYAMA, *loc. cit.*

and v and V are the respective velocities of the longitudinal and transverse waves in the medium, such as $\sqrt{\frac{\lambda+2\mu}{\rho}}$, $\sqrt{\frac{\mu}{\rho}}$.

Now let the normal stress $\widehat{rr}$ on the inner surface of the cavity be zero until the time becomes t_0, when we shall express it by

$$\widehat{rr}_{r=a}=-P\frac{t+t_0}{t_m}e^{1-\frac{t_0+t}{t_m}}, \tag{6}$$

where P denotes the maximum intensity of pressure when the time becomes t_m. Expression (3) then becomes

$$\phi=\frac{aP}{2\pi\rho}\frac{t_0}{rt_m}e^{1-\frac{t_0}{t_m}}K\left(t-\frac{r-a}{v}\right)+\frac{aP}{2\pi\rho r}\frac{e^{1-\frac{r-a}{t_m}}}{t_m}K'\left(t-\frac{r-a}{v}\right), \tag{7}$$

where

$$\left.\begin{aligned}K\left(t-\frac{r-a}{v}\right)&=\int_{-\infty}^{\infty}\frac{e^{ip\left(t-\frac{r-a}{v}\right)}}{(p-\alpha)(p-\beta)\left(p-i\frac{1}{t_m}\right)}dp,\\K'\left(t-\frac{r-a}{v}\right)&=\int_{-\infty}^{\infty}\frac{e^{ip\left(t-\frac{r-a}{v}\right)}}{(p-\alpha)(p-\beta)\left(p-i\frac{1}{t_m}\right)^2}dp.\end{aligned}\right\} \tag{8}$$

Now using Cauchy's theorem of residues, we find that when $t\leq\frac{r-a}{v}$,

$$K\left(t-\frac{r-a}{v}\right)=0,\quad K'\left(t-\frac{r-a}{v}\right)=0, \tag{9}$$

and when $t\geq\frac{r-a}{v}$, the evaluated integrals become

$$\begin{aligned}K\left(t-\frac{r-a}{v}\right)=&\frac{2\pi i}{(a-\beta)\left\{\alpha\beta-\frac{1}{t_m^2}-\frac{i(\alpha+\beta)}{t_m}\right\}}\left[\left(\beta-i\frac{1}{t_m}\right)e^{i\alpha\left(t-\frac{r-a}{v}\right)}\right.\\&\left.-\left(\alpha-i\frac{1}{t_m}\right)e^{i\beta\left(t-\frac{r-a}{v}\right)}+(\alpha-\beta)e^{-\frac{1}{t_m}\left(t-\frac{r-a}{v}\right)}\right],\end{aligned} \tag{10}$$

$$K'\left(t-\frac{r-a}{v}\right)=-\frac{2\pi i}{(\beta-\alpha)\left(\dfrac{1}{t_m^{\,2}}-\alpha^2+i\dfrac{2\alpha}{t_m}\right)}\Bigg[e^{i\alpha\left(t-\frac{r-a}{v}\right)}$$

$$+i\left(\alpha-i\frac{1}{t_m}\right)\left(t-\frac{r-a}{v}\right)e^{-\frac{1}{t_m}\left(t-\frac{r-a}{v}\right)}-e^{-\frac{1}{t_m}\left(t-\frac{r-a}{v}\right)}\Bigg]$$

$$+\frac{2\pi i}{(\beta-\alpha)\left(\dfrac{1}{t_m^{\,2}}-\beta^2+i\dfrac{2\beta}{t_m}\right)}\Bigg[e^{i\beta\left(t-\frac{r-a}{v}\right)}$$

$$-i\left(\beta-i\frac{1}{t_m}\right)\left(t-\frac{r-a}{v}\right)e^{-\frac{1}{t_m}\left(t-\frac{r-a}{v}\right)}+e^{-\frac{1}{t_m}\left(t-\frac{r-a}{v}\right)}\Bigg]. \qquad (11)$$

Therefore the diverging wave radiated from the cavity is expressed by

$$u=\frac{aP}{\rho}\frac{t_m}{v}e^{1-\frac{t_0}{t_m}}\frac{1}{r}\Bigg[\frac{e^{-(1+\eta)\tau}}{\zeta(\eta^2+\zeta^2)}\left\{(\zeta^2+\eta^2+\eta)\left(\frac{t_0}{t_m}\right)+\frac{\zeta^2(1-\eta)-\eta^2(1+\eta)}{(\eta^2+\zeta^2)}\right\}\sin\zeta\tau$$

$$+\frac{e^{-(1+\eta)\tau}}{\zeta(\eta^2+\zeta^2)}\left\{\zeta\frac{t_0}{t_m}-\frac{\zeta(\eta^2+\zeta^2+2\eta)}{(\eta^2+\zeta^2)}\right\}\cos\zeta\tau$$

$$+\left\{\frac{1-\dfrac{t_0}{t_m}}{({}^2\eta+\zeta^2)}+\frac{2\eta}{(\eta^2+\zeta^2)^2}\right\}e^{-\tau}-\frac{1}{(\eta^2+\zeta^2)}\tau e^{-\tau}\Bigg]$$

$$-\frac{aP}{\rho}\frac{t_m^2}{r^2}e^{1-\frac{t_0}{t_m}}\Bigg[\frac{e^{-(1+\eta)\tau}}{\zeta(\eta^2+\zeta^2)}\left\{\eta\left(\frac{t_0}{t_m}\right)+\frac{\zeta^2-\eta^2}{\eta^2+\zeta^2}\right\}\sin\zeta\tau$$

$$+\frac{e^{-(1+\eta)\tau}}{\zeta(\eta^2+\zeta^2)}\left\{\zeta\left(\frac{t_0}{t_m}\right)-\frac{2\eta\zeta}{(\eta^2+\zeta^2)}\right\}\cos\zeta\tau$$

$$+\left\{\frac{2\eta}{(\eta^2+\zeta^2)^2}-\frac{\dfrac{t_0}{t_m}}{(\eta^2+\zeta^2)}\right\}e^{-\tau}-\frac{1}{(\eta^2+\zeta^2)}\tau e^{-\tau}\Bigg], \qquad (12)$$

where

$$\tau=\frac{1}{t_m}\left(t-\frac{r-a}{v}\right),\quad \eta=\frac{2t_mV^2}{av}-1,\quad \zeta=2\frac{t_mV}{a}\sqrt{1-\frac{V^2}{v^2}}. \qquad (13)$$

It will be seen from expression (12) that there are two kinds of radial vibrations, one of which has its amplitude proportional to the inverse ratio of the distance of the particle from the center of the cavity and the other proportional to the square of the inverse ratio of the distance; whence it follows that the vibrations of a particle near the cavity are more complicated than those some distance away from it. The longitudinal vibrations of a particle in the medium far from the cavity are expressed approximately by

$$u \approx \frac{aP_0}{\mu}\left(\frac{a}{r}\right)e^{1-\frac{t_0}{t_m}}\left[\frac{e^{-(1+\eta)\tau}}{\zeta(\eta^2+\zeta^2)}\left\{(\zeta^2+\eta^2+\eta)\frac{t_0}{t_m}+\frac{\zeta^2(1-\eta)-\eta^2(1+\eta)}{(\eta^2+\zeta^2)}\right\}\sin\zeta\tau\right.$$
$$+\frac{e^{-(1+\eta)\tau}}{\zeta(\eta^2+\zeta^2)}\left\{\zeta\left(\frac{t_0}{t_m}\right)-\frac{\zeta({}^2+\eta^2+2\eta)}{(\eta^2+\zeta^2)}\right\}\cos\zeta\tau$$
$$\left.+\left\{\frac{1-\dfrac{t_0}{t_m}}{(\eta^2+\zeta^2)}+\frac{2\eta}{(\eta^2+\zeta^2)^2}\right\}e^{-\tau}-\frac{1}{(\eta^2+\zeta^2)}\tau e^{-\tau}\right], \quad (14)$$

which are derived from expression (12).

To ascertain the nature of the radial vibrations of a particle, we obtained Figs. 1∼3 from expression (14) when the Poisson ratio of the medium is 1/4, $a/t_m v$ being tentatively put as 1. Fig. 4 shows the time-variations in the pressure on the surface of the cavity corresponding to $\frac{t_0}{t_m}=0$, 0·50, and 1·50 respectively. It will be seen from Figs. 1∼4 that the particles in the medium that is far from the spherical cavity become damped radial vibrations and their amplitudes reach maximum when $\frac{t_0}{t_m}=0$, in which case their apparent periods of vibrations in the initial state become also the longest. The apparent

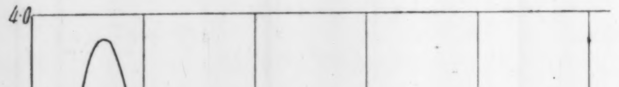

Fig. 1. The radial vibration of a particle in the medium of Poisson's ratio $\frac{1}{4}$, when $\frac{a}{t_m v}=1$ and $\frac{t_0}{t_m}=0$. Unit of ordinate $=\frac{Pa}{27\mu}\left(\frac{a}{r}\right)$, abscissa $\tau=\frac{v}{a}\left\{t-\frac{1}{v}(r-a)\right\}$.

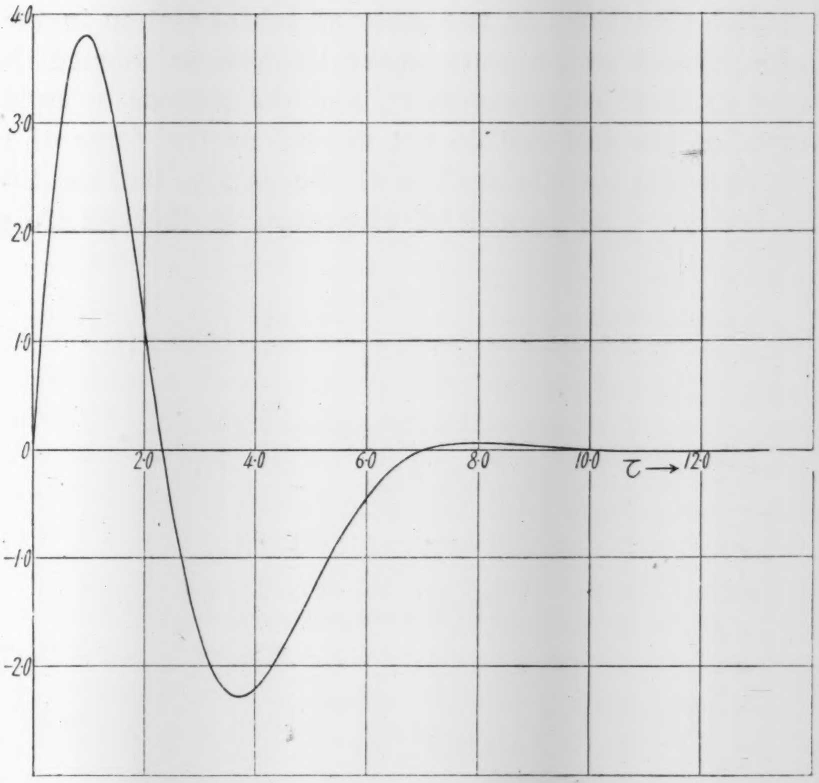

Fig. 2. The radial vibration of a particle when Poisson's ratio $=\frac{1}{4}$, $\frac{a}{t_m v}=1$ and $\frac{t_0}{t_n}=0{\cdot}5$. Unit of ordinate $=\frac{Pa}{27\mu}\left(\frac{a}{r}\right)$, abscissa $\tau=\frac{v}{a}\left\{t-\frac{1}{v}(r-a)\right\}$.

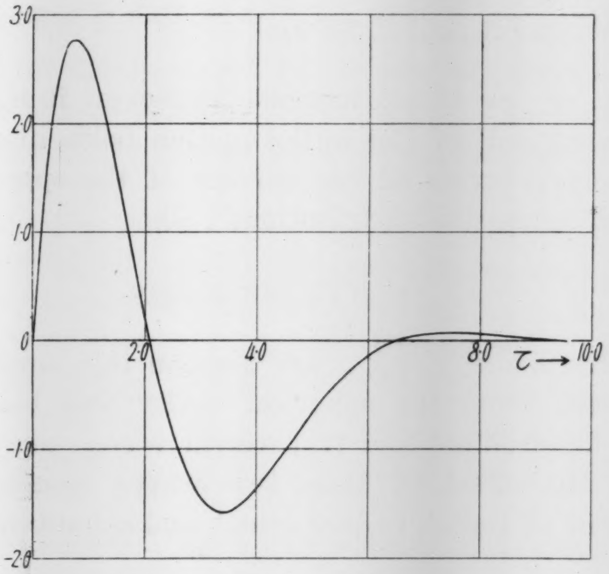

Fig. 3. The radial vibration of a particle when Poisson's ratio $=\frac{1}{4}$, $\frac{a}{t_m v}=1$ and $\frac{t_0}{t_m}=1{\cdot}5$. Unit of ordinate $=\frac{Pa}{27\mu}\left(\frac{a}{r}\right)$, abscissa $\tau=\frac{v}{a}\left\{t-\frac{1}{v}\left(r-a\right)\right\}$.

periods of radial vibrations in the state of initial motion in the case of sudden commencement of pressure generally become shorter than those in the case of gradual commencement, and the periods of radial vibrations, however, of the tail end do not depend on the form of the time-variations in pressure on the surface of the cavity, but on the dimensions of the cavity. The periods of vibrations in the tail are generally longer than those of the initial motion. Moreover, it may be seen that Shida's law of push-pull of the initial motion holds also in this case.

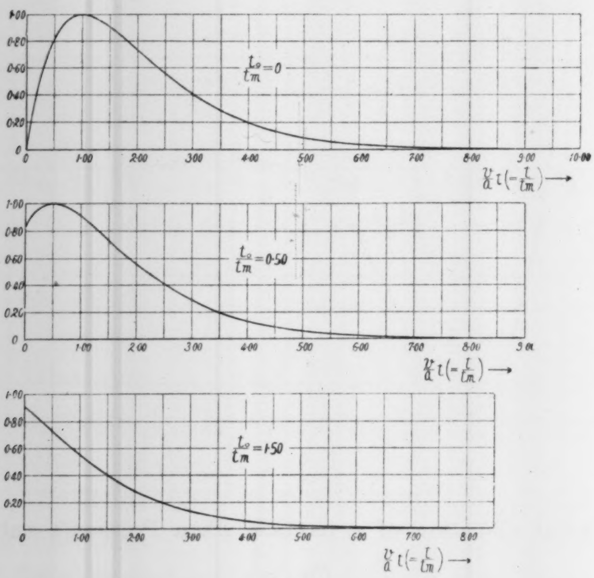

Fig. 4. Time-variations in pressure on the surface of the spherical cavity when $\frac{t_0}{t_m}=0$, $\frac{t_0}{t_m}=0{\cdot}50$ and $\frac{t_0}{t_m}=1{\cdot}50$. Unit of ordinate $=-P$.

4. When the normal stress on the surface of the spherical cavity has co-latitudinal and azimuthal distributions[7], like

$$\widehat{rr}_{r=a}=-Pf(t)\sin 2\theta\cos\phi, \tag{15}$$

and the shear stresses $\widehat{r\theta}_{r=a}$, $\widehat{r\phi}_{r=a}$ are zero on this surface, the diverging waves radiated from the spherical cavity then become two bodily waves, like the longitudinal and transversal waves, and the particles in the medium as the effect of these two waves assume the following vibrational motions of radial, co-latitudinal, and azimuthal displacements:

---

[7] Honda has already studied the wave-motions when the pressure distribution on the surface of a spherical cavity has the same distribution as in Section 4, but the time-factor in his paper is simple-harmonic, like e^{ipt}.

H. HONDA, *Geophy. Mag.*, **8** (1934), 153~164.

$$\left.\begin{aligned}
u_1&=\frac{1}{2\pi}\frac{a^3}{r^4}\int_{-\infty}^{\infty}K(p)\frac{P(p)e^{ip\left\{t-\frac{1}{v}(r-a)\right\}}}{p^2\psi(p)}\sin 2\theta\cos\phi\,dp,\\
v_1&=\frac{1}{\pi}\frac{a^3}{r^4}\int_{-\infty}^{\infty}K(p)\frac{Q(p)e^{ip\left\{t-\frac{1}{v}(r-a)\right\}}}{p^2\psi(p)}\cos 2\theta\cos\phi\,dp,\\
w_1&=-\frac{1}{\pi}\frac{a^3}{r^4}\int_{-\infty}^{\infty}K(p)\frac{Q(p)e^{ip\left\{t-\frac{1}{v}(r-a)\right\}}}{p^2\psi(p)}\cos\theta\cos\phi\,dp,
\end{aligned}\right\}\qquad(16)$$

$$\left.\begin{aligned}
u_3&=-\frac{3}{\pi}\frac{a^3}{r^4}\int_{-\infty}^{\infty}K(p)\frac{S(p)e^{ip\left\{t-\frac{1}{V}(r-a)\right\}}}{p^2\psi(p)}\sin 2\theta\cos\phi\,dp,\\
v_3&=-\frac{1}{\pi}\frac{a^3}{r^4}\int_{-\infty}^{\infty}K(p)\frac{T(p)e^{ip\left\{t-\frac{1}{V}(r-a)\right\}}}{p^2\psi(p)}\cos 2\theta\cos\phi\,dp,\\
w_3&=\frac{1}{\pi}\frac{a^3}{r^4}\int_{-\infty}^{\infty}K(p)\frac{T(p)e^{ip\left\{t-\frac{1}{V}(r-a)\right\}}}{p^2\psi(p)}\cos\theta\sin\phi\,dp,
\end{aligned}\right\}\qquad(17)$$

where

$$K(p)=\int_{-\infty}^{\infty}f(\lambda)e^{-ip\lambda}\,d\lambda. \qquad (18)$$

In these expressions, u_1, v_1, w_1 are the radial, co-latitudinal, and azimuthal components of displacement due to the longitudinal wave, and u_3, v_3, w_3 are those due to the transverse wave. The functions of p, such as $\psi(p)$, $P(p)$, $Q(p)$, $S(p)$, and $T(p)$ in expressions (16) and (17) are

$$\begin{aligned}
\psi(p)=\Bigg[\left(\frac{ap}{v}\right)^6&-i\left\{\frac{3\lambda+10\mu}{(\lambda+2\mu)}+5\frac{V}{v}\right\}\left(\frac{ap}{v}\right)^5\\
&-\left\{\frac{(15\lambda+26\mu)}{(\lambda+2\mu)}\frac{V}{v}+21\left(\frac{V}{v}\right)^2+\frac{(3\lambda+34\mu)}{(\lambda+2\mu)}\right\}\left(\frac{ap}{v}\right)^4\\
&+i\left\{72\frac{\mu}{\lambda+2\mu}+9\frac{(7\lambda+10\mu)}{(\lambda+2\mu)}\left(\frac{V}{v}\right)^2+5\frac{(3\lambda+10\mu)}{(\lambda+2\mu)}\frac{V}{v}+48\left(\frac{V}{v}\right)^3\right\}\left(\frac{ap}{v}\right)^3\\
&+\left\{72\frac{\mu}{(\lambda+2\mu)}\frac{V}{v}+48\frac{(3\lambda+4\mu)}{(\lambda+2\mu)}\left(\frac{V}{v}\right)^3+3\frac{(3\lambda+10\mu)}{(\lambda+2\mu)}\left(\frac{V}{v}\right)^2\right.\\
&\qquad\left.+48\left(\frac{V}{v}\right)^4+72\frac{\mu}{(\lambda+2\mu)}\right\}\left(\frac{ap}{v}\right)^2
\end{aligned}$$

$$-i\left\{72\frac{\mu}{(\lambda+2\mu)}\left(\frac{V}{v}\right)^2+48\frac{(3\lambda+4\mu)}{(\lambda+2\mu)}\left(\frac{V}{v}\right)^4+72\frac{\mu}{(\lambda+2\mu)}\frac{V}{v}\right.$$

$$\left.+48\frac{(3\lambda+4\mu)}{(\lambda+2\mu)}\left(\frac{V}{v}\right)^3\right\}\left(\frac{ap}{v}\right)$$

$$-\left\{72\frac{\mu}{(\lambda+2\mu)}\left(\frac{V}{v}\right)^2+48\frac{(3\lambda+4\mu)}{(\lambda+2\mu)}\left(\frac{V}{v}\right)^4\right\}\Bigg], \qquad (19)$$

$$P(p)=-i\left(\frac{1}{V}\right)^4\left(\frac{1}{v}\right)^3a^4r^3p^7-\left\{5\left(\frac{1}{V}\right)^3\left(\frac{1}{v}\right)^3(ar)^3+4\left(\frac{1}{V}\right)^4\left(\frac{1}{v}\right)^2a^4r^5\right\}p^6$$

$$+i\left\{21\left(\frac{1}{V}\right)^2\left(\frac{1}{v}\right)^3a^2r^3+20\left(\frac{1}{V}\right)^3\left(\frac{1}{v}\right)^2a^3r^2+9\left(\frac{1}{V}\right)^4\left(\frac{1}{v}\right)a^4r\right\}p^5$$

$$+\left\{48\left(\frac{1}{V}\right)\left(\frac{1}{v}\right)^3ar^3+84\left(\frac{1}{V}\right)^2\left(\frac{1}{v}\right)^2a^2r^2\right.$$

$$\left.+45\left(\frac{1}{V}\right)^3\left(\frac{1}{v}\right)a^3r+9\left(\frac{1}{V}\right)^4a^4\right\}p^4$$

$$-i\left\{48\left(\frac{1}{v}\right)^3r^3+192\left(\frac{1}{V}\right)\left(\frac{1}{v}\right)^2ar^2+189\left(\frac{1}{V}\right)^2\left(\frac{1}{v}\right)a^2r+45\left(\frac{1}{V}\right)^3a^3\right\}p^3$$

$$-\left\{192\left(\frac{1}{v}\right)^2r^2+432\left(\frac{1}{v}\right)\left(\frac{1}{V}\right)ar+189\left(\frac{1}{V}\right)^2a^2\right\}p^2$$

$$+i\left\{432\left(\frac{1}{v}\right)r+432\left(\frac{1}{V}\right)a\right\}p+432, \qquad (20)$$

$$Q(p)=\left(\frac{1}{V}\right)^4\left(\frac{1}{v}\right)^2a^4r^2p^6-i\left\{5\left(\frac{1}{V}\right)^3\left(\frac{1}{v}\right)^2a^3r^2+3\left(\frac{1}{V}\right)^4\left(\frac{1}{v}\right)a^4r\right\}p^5$$

$$-\left\{21\left(\frac{1}{V}\right)^2\left(\frac{1}{v}\right)^2a^2r^2+15\left(\frac{1}{V}\right)^3\left(\frac{1}{v}\right)a^3r+3\left(\frac{1}{V}\right)^4a^4\right\}p^4$$

$$+i\left\{48\left(\frac{1}{V}\right)\left(\frac{1}{v}\right)^2ar^2+63\left(\frac{1}{V}\right)^2\left(\frac{1}{v}\right)a^2r+15\left(\frac{1}{V}\right)^3a^3\right\}p^3$$

$$+\left\{48\left(\frac{1}{v}\right)^2r^2+144\left(\frac{1}{V}\right)\left(\frac{1}{v}\right)ar+63\left(\frac{1}{V}\right)^2a^2\right\}p^2$$

$$-i\left\{144\left(\frac{1}{v}\right)r+144\left(\frac{1}{V}\right)a\right\}p-144, \qquad (21)$$

$$S(p)=i\left\{2\left(\frac{1}{v}\right)^3\left(\frac{1}{V}\right)^2a^3r^2\right\}p^5$$

$$
\begin{aligned}
&+\left\{10\left(\frac{1}{v}\right)^2\left(\frac{1}{V}\right)^2 a^2r^2+6\left(\frac{1}{v}\right)^3\left(\frac{1}{V}\right)a^3r\right\}p^4\\
&-i\left\{24\left(\frac{1}{v}\right)\left(\frac{1}{V}\right)^2 ar^2+30\left(\frac{1}{v}\right)^2\left(\frac{1}{V}\right)a^2r+6\left(\frac{1}{v}\right)^3a^3\right\}p^3\\
&-\left\{24\left(\frac{1}{V}\right)^2r^2+72\left(\frac{1}{v}\right)\left(\frac{1}{V}\right)ar+30\left(\frac{1}{v}\right)^2a^2\right\}p^2\\
&+i\left\{72\left(\frac{1}{V}\right)r+72\left(\frac{1}{v}\right)a\right\}p+72\,,
\end{aligned}
\tag{22}
$$

$$
\begin{aligned}
T(p)=&\,2\left(\frac{1}{v}\right)^3\left(\frac{1}{V}\right)^3a^3r^3p^6-i\left\{10\left(\frac{1}{v}\right)^2\left(\frac{1}{V}\right)^3a^2r^3+6\left(\frac{1}{v}\right)^3\left(\frac{1}{V}\right)^2a^3r^2\right\}p^5\\
&-\left\{24\left(\frac{1}{v}\right)\left(\frac{1}{V}\right)^3ar^3+30\left(\frac{1}{v}\right)^2\left(\frac{1}{V}\right)^2a^2r^2+12\left(\frac{1}{v}\right)^3\left(\frac{1}{V}\right)a^3r\right\}p^4\\
&+i\left\{24\left(\frac{1}{V}\right)^3r^3+72\left(\frac{1}{v}\right)\left(\frac{1}{V}\right)^2ar^2+60\left(\frac{1}{v}\right)^2\left(\frac{1}{V}\right)a^2r+12\left(\frac{1}{v}\right)^3a^3\right\}p^3\\
&+\left\{72\left(\frac{1}{V}\right)^2r^2+144\left(\frac{1}{v}\right)\left(\frac{1}{V}\right)ar+60\left(\frac{1}{v}\right)^2a^2\right\}p^2\\
&-i\left\{144\left(\frac{1}{V}\right)r+144\left(\frac{1}{v}\right)a\right\}p-144\,.
\end{aligned}
\tag{23}
$$

Now let the time-factor $f(t)$ in expression (15) be

$$f(t)=\frac{t+t_0}{t_m}e^{1-\frac{t_0+t}{t_m}}\,, \tag{24}$$

when $t \geq 0$, and

$$f(t)=0, \tag{25}$$

when $t \leq 0$ as in the case of Section 3. But since the integral expressions in (16) and (17) have singular points of higher order, evaluation of the contour-integrals becomes impossible, with the result that it may be impossible to study the wave-motions of particles on and near the surface of the spherical cavity with the present method[8]. We shall therefore study the vibrational motions of particles far from the cavity when the pressure distributions on the surface of it are expressed by (15). To simplify the mathematical treatment, let the Poisson ratio be 1/4, as in the preceding section, when the radial vibration u_1 due to the longitudinal wave, and the co-latitudinal and azimuthal vibrations v_3, w_3 due to the transverse wave become

---

[8] If we calculate afresh the displacement-potentials consistent with the boundary-conditions of stresses on the inner surface of the spherical cavity, it is possible to investigate the vibrational motions of the particles on and near the surface of the spherical cavity.

$$u_1 \approx \frac{V^2 v}{6\pi\mu a^3} \frac{1}{r} \int_{-\infty}^{\infty} K(p) \frac{P'(p) e^{ip\left\{t-\frac{1}{v}(r-a)\right\}}}{\psi'(p)} \sin 2\theta \cos\phi dp, \tag{26}$$

$$v_3 \approx -\frac{v^4}{3\pi\mu V a^3} \frac{1}{r} \int_{-\infty}^{\infty} K(p) \frac{T'(p) e^{ip\left\{t-\frac{1}{V}(r-a)\right\}}}{\psi'(p)} \cos 2\theta \cos\phi dp, \tag{27}$$

$$w_3 \approx \frac{v^4}{3\pi\mu V a^3} \frac{1}{r} \int_{-\infty}^{\infty} K(p) \frac{T'(p) e^{ip\left\{t-\frac{1}{V}(r-a)\right\}}}{\psi'(p)} \cos\theta \sin\phi dp, \tag{28}$$

where

$$P'(p) = -i\left(\frac{1}{V}\right)^4 a^4 p^5 - 5\left(\frac{1}{V}\right)^3 a^3 p^4 - i21\left(\frac{1}{V}\right) a^2 p^3 + 48\left(\frac{1}{V}\right) a p^2 - i48p, \tag{29}$$

$$T'(p) = 2\left(\frac{1}{v}\right)^3 a^3 p^4 - i10\left(\frac{1}{v}\right)^2 a^2 p^3 - 24\left(\frac{1}{v}\right) a p^2 + i24p, \tag{30}$$

$$\psi'(p) = (p+a_1)(p+a_2)(p+a_3)(p+a_4)(p+a_5)(p+a_6), \tag{31}$$

and

$$\left.\begin{array}{lll} a_1 = (\alpha_1 - i\beta_1)\dfrac{v}{a}, & a_2 = -(\alpha_1 + i\beta_1)\dfrac{v}{a}, & a_3 = (\alpha_2 - i\beta_2)\dfrac{v}{a}, \\[2ex] a_4 = -(\alpha_2 + i\beta_2)\dfrac{v}{a}, & a_5 = (\alpha_3 - i\beta_3)\dfrac{v}{a}, & a_6 = -(\alpha_3 + i\beta_3)\dfrac{v}{a}, \\[2ex] \left.\begin{array}{l}\alpha_1 = 0\cdot83199, \\ \beta_1 = 2\cdot10618,\end{array}\right\} & \left.\begin{array}{l}\alpha_2 = 2\cdot416332, \\ \beta_2 = 1\cdot040118,\end{array}\right\} & \left.\begin{array}{l}\alpha_3 = 0\cdot600844, \\ \beta_3 = 0\cdot463744.\end{array}\right\} \end{array}\right\} \tag{32}$$

$\psi'(p)$ expressed by (31) may be obtained from expression (19), and is due to H. Kawasumi[9]. In this case, the respective amplitudes of the co-latitudinal and the azimuthal components of displacements of the longitudinal wave are less than the radial displacement of the wave, and those of the radial component of displacement due to the transverse wave are also less than those of the co-latitudinal and the azimuthal components of displacement. We therefore omit these displacements in studying vibrations far from the cavity.

By letting the time-factor $f(t)$ be (24) and (25), the expressions (26), (27), (28) become

---

[9] H. KAWASUMI and R. YOSHIYAMA, *loc. cit.*

$$u_1 \approx -\frac{V^2 vP}{6\mu\pi a^3}\frac{1}{r}e^{1-\frac{t_0}{t_m}}\sin 2\theta\cos\phi\, X\left(t-\frac{1}{v}(r-a)\right), \tag{33}$$

$$v_3 \approx \frac{1}{3\pi}\frac{v^4 P}{\mu V a^3}\frac{1}{r}e^{1-\frac{t_0}{t_m}}\cos 2\theta\cos\phi\, Y\left(t-\frac{1}{V}(r-a)\right), \tag{34}$$

$$w_3 \approx -\frac{1}{3\pi}\frac{v^4 P}{\mu V a^3}\frac{1}{r}e^{1-\frac{t_0}{t_m}}\cos\theta\sin\phi\, Y\left(t-\frac{1}{V}(r-a)\right), \tag{35}$$

where

$$X\left(t-\frac{1}{v}(r-a)\right)=\int_{-\infty}^{\infty}\frac{P'(p)}{\psi'(p)}\left\{\frac{t_0}{t_m}\frac{i}{\left(p-i\frac{1}{t_m}\right)}+\frac{1}{t_m}\frac{1}{\left(p-i\frac{1}{t_m}\right)^2}\right\}e^{ip\left\{t-\frac{1}{v}(r-a)\right\}}dp, \tag{36}$$

$$Y\left(t-\frac{1}{V}(r-a)\right)=\int_{-\infty}^{\infty}\frac{T'(p)}{\psi'(p)}\left\{\frac{t_0}{t_m}\frac{i}{\left(p-i\frac{1}{t_m}\right)}+\frac{1}{t_m}\frac{1}{\left(p-i\frac{1}{t_m}\right)^2}\right\}e^{ip\left\{t-\frac{1}{V}(r-a)\right\}}dp. \tag{37}$$

For evaluating the integrals of expressions (36) and (37), we found, after laborious mathematical work, the following relations when $\frac{a}{t_m v}=1$[10]:

$$\begin{aligned}\frac{P'(p)}{\psi'(p)\left(p-i\frac{1}{t_m}\right)^2}=&\frac{(\gamma_1-i\delta)\frac{a^6}{v^6}}{\left\{p-(-\alpha_1+i\beta_1)\frac{v}{a}\right\}}+\frac{(-\gamma_1-i\delta)\frac{a^6}{v^6}}{\left\{p-(\alpha_1+i\beta_1)\frac{v}{a}\right\}}\\&+\frac{(-\gamma_2+i\delta_2)\frac{a^6}{v^6}}{\left\{p-(-\alpha_2+i\beta_2)\frac{v}{a}\right\}}+\frac{(\gamma_2+i\delta_2)\frac{a^6}{v^6}}{\left\{p-(\alpha_2+i\beta_2)\frac{v}{a}\right\}}\\&+\frac{(-\gamma_3+i\delta_3)\frac{a^6}{v^6}}{\left\{p-(-\alpha_3+i\beta_3)\frac{v}{a}\right\}}+\frac{(\gamma_3+i\delta_3)\frac{a^6}{v^6}}{\left\{p-(\alpha_3+i\beta_3)\frac{v}{a}\right\}}\\&-\frac{\gamma_4\frac{a^5}{v^5}}{\left(p-i\frac{v}{a}\right)^2}+\frac{i\delta_4\frac{a^6}{v^6}}{\left(p-i\frac{v}{a}\right)},\end{aligned} \tag{38}$$

---

[10] The vibrations of particles for the cases when $\frac{a}{t_m v}>1$ and <1 will be the next object of our study.

$$\frac{P'(p)}{\psi'(p)\left(p-i\frac{1}{t_m}\right)}=\frac{(-\xi_1+i\eta_1)\frac{a^5}{v^5}}{\left\{p-(-\alpha_1+i\beta_1)\frac{v}{v^5}\right\}}+\frac{(-\xi_1-i\eta'_1)\frac{a^5}{v^5}}{\left\{p-(\alpha_1+i\beta_1)\frac{v}{a}\right\}}$$
$$+\frac{(\xi_2-i\eta_1)\frac{a^5}{v^5}}{\left\{p-(-\alpha_2+i\beta_2)\frac{v}{a}\right\}}+\frac{(\xi_3+i\eta_3)\frac{a^5}{v^5}}{\left\{p-(\alpha_2+i\beta_2)\frac{v}{a}\right\}}$$
$$+\frac{(\xi_3-i\eta_3)\frac{a^5}{v^5}}{\left\{p-(-\alpha_3+i\beta_3)\frac{v}{a}\right\}}+\frac{(\xi_3+i\eta_3)\frac{a^5}{v_5}}{\left\{p-(\alpha_3+i\beta_3)\frac{v}{a}\right\}}$$
$$+\frac{\xi_4\frac{a^5}{v^5}}{\left(p-i\frac{v}{a}\right)}, \tag{39}$$

$$\frac{T'(p)}{\psi'(p)\left(p-i\frac{1}{t_m}\right)^2}=\frac{(\gamma'_1-i\delta'_1)\frac{a^6}{v^6}}{\left\{p-(-\alpha_1+i\beta_1)\frac{v}{a}\right\}}+\frac{(-\gamma'_1-i\delta'_1)\frac{a^6}{v^6}}{\left\{p-(\alpha_1+i\beta_1)\frac{v}{a}\right\}}$$
$$+\frac{(-\gamma'_2-i\delta'_2)\frac{a^6}{v^6}}{\left\{p-(-\alpha_2+i\beta_2)\frac{v}{a}\right\}}+\frac{(\gamma'_2-i\delta'_2)\frac{a^6}{v^6}}{\left\{p-(\alpha_2+i\beta_2)\frac{v}{a}\right\}}$$
$$+\frac{(\gamma'_3-i\delta'_3)\frac{a^6}{v^6}}{\left\{p-(-\alpha_3+i\beta_3)\frac{v}{a}\right\}}+\frac{(-\gamma'_3-i\delta'_3)\frac{a^6}{v^6}}{\left\{p-(\alpha_3+i\beta_3)\frac{v}{a}\right\}}$$
$$+\frac{\gamma'_4\frac{a^5}{v^5}}{\left(p-i\frac{v}{a}\right)^2}+\frac{i\delta'_4\frac{a^6}{v^6}}{\left(p-i\frac{v}{a}\right)}, \tag{40}$$

$$\frac{T'(p)}{\psi'(p)\left(p-i\frac{1}{t_m}\right)}=\frac{(-\xi'_1+i\eta'_1)\frac{a^5}{v^5}}{\left\{p-(-a_1+i\beta_1)\frac{v}{a}\right\}}+\frac{(-\xi'_1-i\eta'_1)\frac{a^5}{v^5}}{\left\{p-(a_1+i\beta_1)\frac{v}{a}\right\}}$$
$$+\frac{(\xi'_2+i\eta'_2)\frac{a^5}{v^5}}{\left\{p-(-\alpha_2+i\beta_2)\frac{v}{a}\right\}}+\frac{(\xi'_2-i\eta'_2)\frac{a^5}{v^5}}{\left\{p-(\alpha_2+i\beta_2)\frac{v}{a}\right\}}$$

$$+\frac{(-\xi_3'-i\eta_3')\frac{a^5}{v^5}}{\left\{p-(-\alpha_3+i\beta_3)\frac{v}{a}\right\}}+\frac{(-\xi_3'+i\eta_3')\frac{a^5}{v^5}}{\left\{p-(\alpha_3+i\beta_3)\frac{v}{a}\right\}}$$

$$+\frac{\xi_4'\frac{a^5}{v^5}}{\left(p-i\frac{v}{a}\right)},$$

where

$$\left.\begin{array}{llll}\gamma_1=3\cdot144601, & \gamma_2=0\cdot403808, & \gamma_3=0\cdot513517, & \gamma_3=1\cdot49546, \\ \delta_1=1\cdot453949, & \delta_2=0\cdot120422, & \delta_3=0\cdot888087, & \delta_4=0\cdot89088.\end{array}\right\}\quad(42)$$

$$\left.\begin{array}{llll}\xi_1=3\cdot9083103, & \xi_2=2\cdot029293, & \xi_3=1\cdot427375, & \xi_4=0\cdot903283, \\ \eta_1=0\cdot468814, & \eta_2=0\cdot307162, & \eta_3=0\cdot258230, & \end{array}\right\}\quad(43)$$

$$\left.\begin{array}{llll}\gamma_1'=0\cdot171372, & \gamma_2'=0\cdot033059, & \gamma_3'=0\cdot620073. & \gamma_4'=1\cdot102391, \\ \delta_1'=0\cdot055933, & \delta_2'=0\cdot016417, & \delta_3'=0\cdot332791, & \delta_4'=0\cdot810283,\end{array}\right\}\quad(44)$$

$$\left.\begin{array}{llll}\xi_1'=0\cdot080683, & \xi_2'=0\cdot080538, & \xi_3'=0\cdot551045, & \xi_4'=1\cdot102381, \\ \eta_1'=0\cdot236124, & \eta_2'=0\cdot038354, & \eta_3'=0\cdot132560, & \end{array}\right\}\quad(45)$$

By using these relations, we may be able to evaluate the integrals in (36) and (37) by Cauchy's residue methods, the diverging waves far from the cavity being determined as follows:

$$u_1\approx-\frac{Pa}{27\mu}\left(\frac{a}{r}\right)e^{1-\frac{t_0}{t_m}}\sin2\theta\cos\phi\cdot$$

$$\cdot\left[2\sqrt{\left(-\gamma_1+\frac{t_0}{t_m}\eta_1\right)^2+\left(-\delta_1-\frac{t_0}{t_m}\xi_1\right)^2}\,e^{-\beta_1\tau}\sin\left\{\alpha_1\tau+\tan^{-1}\left(\frac{-\delta_1-\frac{t_0}{t_m}\xi_1}{-\gamma_1+\frac{t_0}{t_m}\eta_1}\right)\right\}\right.$$

$$+2\sqrt{\left(\gamma_2-\frac{t_0}{t_m}\eta_2\right)^2+\left(\delta_2+\frac{t_0}{t_m}\xi_2\right)^2}\,e^{-\beta_2\tau}\sin\left\{\alpha_2\tau+\tan^{-1}\left(\frac{\delta_2+\frac{t_0}{t_m}\xi_2}{\gamma_2-\frac{t_0}{t_m}\eta_2}\right)\right\}$$

$$+2\sqrt{\left(\gamma_3-\frac{t_0}{t_m}\eta_3\right)^2+\left(\delta_3+\frac{t_0}{t_m}\xi_3\right)^2}\,e^{-\beta_3\tau}\sin\left\{\alpha_3\tau+\tan^{-1}\left(\frac{\delta_3+\frac{t_0}{t_m}\xi_3}{\gamma_3-\frac{t^0}{t_m}\eta_3}\right)\right\}$$

$$\left.-\gamma_4\tau e^{-\tau}+\left(\delta_4+\frac{t_0}{t_m}\xi_4\right)e^{-\tau}\right],\qquad(46)$$

$$v_3 \approx \frac{Pa}{27\mu}\left(\frac{a}{r}\right)e^{1-\frac{t_0}{t_m}}\cos 2\theta\cos\phi\left(\frac{18}{1{\cdot}7325}\right)\cdot$$

$$\cdot\left[2\sqrt{\left(-\gamma'_1+\frac{t_0}{t_m}\eta'_1\right)^2+\left(-\delta'_1-\frac{t_0}{t_m}\xi'_1\right)^2}\, e^{-\beta_1\tau'}\sin\left\{\alpha_1\tau'+\tan^{-1}\left(\frac{-\delta'_1-\frac{t_0}{t_m}\xi'_1}{-\gamma'_1+\frac{t_0}{t_m}\eta'_1}\right)\right\}\right.$$

$$+2\sqrt{\left(\gamma'_2+\frac{t_0}{t_m}\eta'_2\right)^2+\left(-\delta'_2+\frac{t_0}{t_m}\xi'_2\right)^2}\, e^{-\beta_2\tau'}\sin\left\{\alpha_2\tau'+\tan^{-1}\left(\frac{-\delta'_2+\frac{t_0}{t_m}\xi'_2}{\gamma'_2+\frac{t_0}{t_m}\eta'_2}\right)\right\}$$

$$+2\sqrt{\left(-\delta'_3-\frac{t_0}{t_m}\xi'_3\right)^2+\left(-\gamma'_3-\frac{t_0}{t_m}\eta'_3\right)^2}\, e^{-\beta_3\tau'}\sin\left\{\alpha_3\tau'+\tan^{-1}\left(\frac{-\delta'_3-\frac{t_0}{t_m}\xi'_3}{-\gamma'_3-\frac{t_0}{t_m}\eta'_3}\right)\right\}$$

$$\left.+\gamma'_4\tau' e^{-\tau'}+\left(\delta'_4+\frac{t_0}{t_m}\xi'_4\right)e^{-\tau'}\right], \tag{47}$$

$$w_3 \approx -\frac{Pa}{27\mu}\left(\frac{a}{r}\right)e^{1-\frac{t_0}{t_m}}\cos\theta\sin\phi\left(\frac{18}{1{\cdot}7325}\right)\cdot$$

$$\cdot\left[2\sqrt{\left(-\gamma'_1+\frac{t_0}{t_m}\eta'_1\right)^2+\left(-\delta'_1-\frac{t_0}{t_m}\xi'_1\right)^2}\, e^{-\beta_1\tau'}\sin\left\{\alpha_1\tau'+\tan^{-1}\left(\frac{-\delta'_1-\frac{t_0}{t_m}\xi'_1}{-\gamma'_1+\frac{t_0}{t_m}\eta'_1}\right)\right\}\right.$$

$$+2\sqrt{\left(\gamma'_2+\frac{t_0}{t_m}\xi'_2\right)^2+\left(-\delta'_2+\frac{t_0}{t_m}\xi'_2\right)^2}\, e^{-\beta_2\tau'}\sin\left\{\alpha_2\tau'+\tan^{-1}\left(\frac{-\delta'_2+\frac{t_0}{t_m}\xi'_2}{\gamma'_2+\frac{t_0}{t_m}\eta'_2}\right)\right\}$$

$$+2\sqrt{\left(-\gamma'_3-\frac{t_0}{t_m}\eta'_3\right)^2+\left(-\delta'_3-\frac{t_0}{t_m}\xi'_3\right)^2}\, e^{-\beta_3\tau'}\sin\left\{\alpha_3\tau'+\tan^{-1}\left(\frac{-\delta'_3-\frac{t_0}{t_m}\xi'_3}{-\gamma'_3-\frac{t_0}{t_m}\eta'_3}\right)\right\}$$

$$\left.+\gamma'_4\tau' e^{-\tau'}+\left(\delta'_4+\frac{t_0}{t_m}\xi'_4\right)e^{-\tau'}\right], \tag{48}$$

where

$$\tau=\frac{v}{a}\left\{t-\frac{1}{v}(r-a)\right\},\quad \tau'=\frac{v}{a}\left\{t-\frac{1}{V}(r-a)\right\}. \tag{49}$$

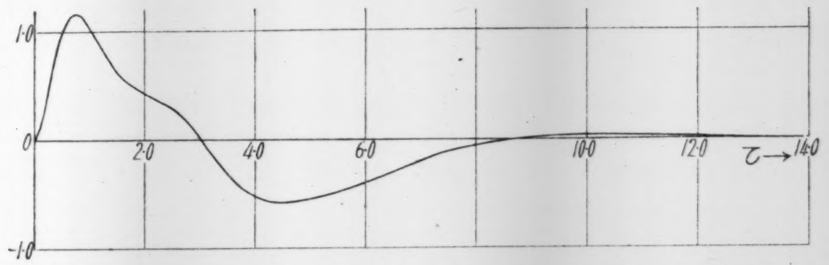

Fig. 5a. The radial vibration of a particle due to the longitudinal wave when $\frac{a}{t_m v}=1$, $\frac{t_0}{t_m}=0$. Unit of ordinate $=\frac{Pa}{27\mu}\left(\frac{a}{r}\right)\sin 2\theta\cos\phi$, abscissa $\tau=\frac{v}{a}\left\{t-\frac{1}{v}(r-a)\right\}$.

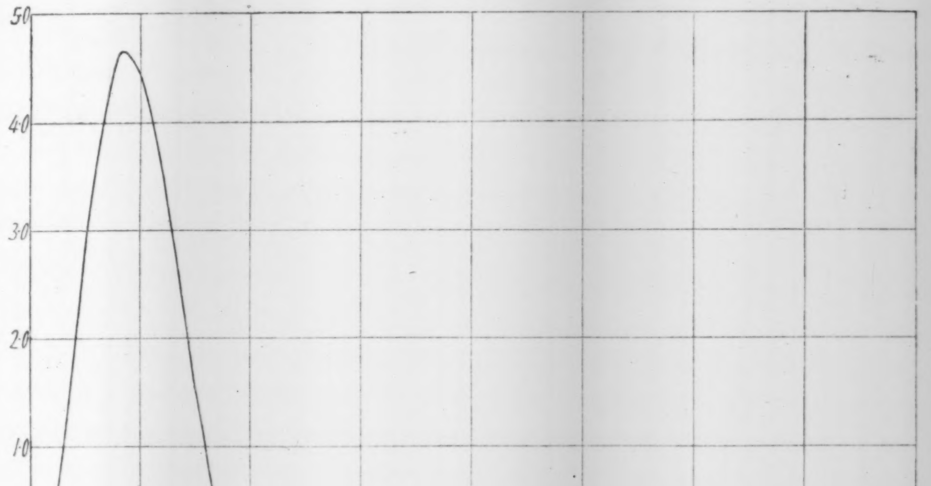

Fig. 5b. The azimuthal or the co-latitudinal vibrations of a particle due to the transverse wave when $\frac{a}{t_m v}=1$, $\frac{t_0}{t_m}=0$. Units of ordinate are $\frac{Pa}{27\mu}\left(\frac{a}{r}\right)$. $\cdot\cos 2\theta\cos\phi$ and $\frac{Pa}{27\mu}\left(\frac{a}{r}\right)\cos\theta\sin\phi$ for the azimuthal and the co-latitudinal vibrations respectively. Abscissa $\tau'=\frac{v}{a}\left\{t-\frac{1}{V}(r-a)\right\}$.

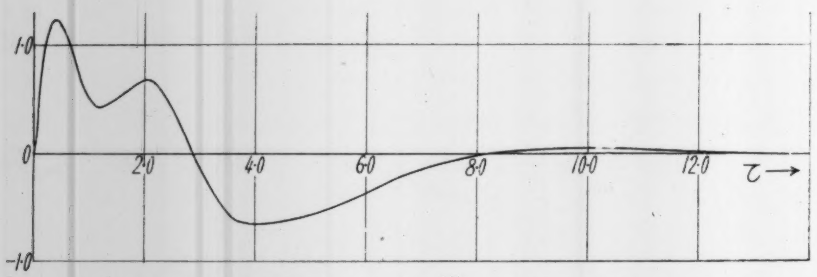

Fig. 6a. The radial vibration of a particle due to the longitudinal wave when $\frac{a}{t_m v}=1$, $\frac{t_0}{t_m}=0{\cdot}50$. Unit of ordinate $=\frac{Pa}{27\mu}\left(\frac{a}{r}\right)\sin 2\theta\cos\phi$, abscissa $\tau=\frac{v}{a}\left\{t-\frac{1}{v}(r-a)\right\}$.

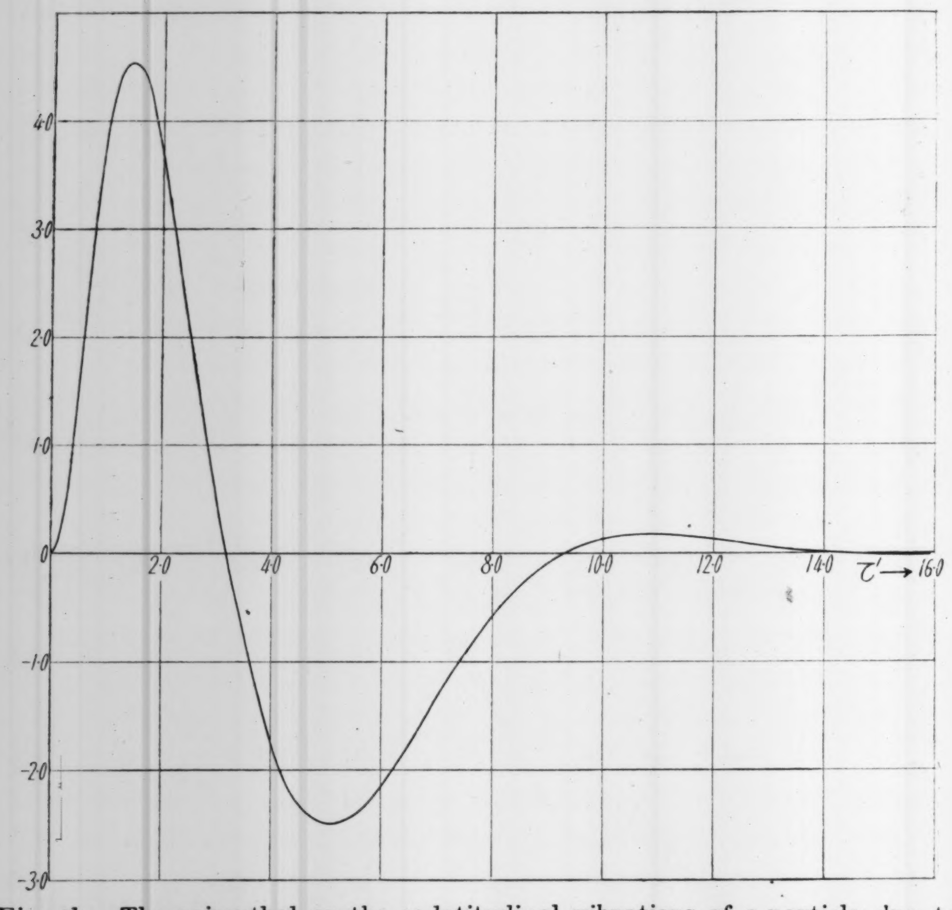

Fig. 6b. The azimuthal or the co-latitudinal vibrations of a particle due to the transverse wave when $\frac{a}{t_m v}=1$, $\frac{t_0}{t_m}=0{\cdot}50$. Unit of ordinate are $\frac{Pa}{27\mu}\left(\frac{a}{r}\right)\cdot\cos 2\theta\cos\phi$ and $\frac{Pa}{27\mu}\left(\frac{a}{r}\right)\cos\theta\sin\phi$ for the azimuthal and the co-latitudinal vibrations respectively. Abscissa $\tau'=\frac{v}{a}\left\{t-\frac{1}{V}(r-a)\right\}$.

To get the vibrations of particles which are some distance away from the origin of disturbance, we calculate numerically the expressions (46), (47), and (48) for the cases when $\frac{t_0}{t_m}=0$, 0·50, and 1·50, the results being shown in Figs. 5a, 5b, 6a, 6b, and 7a, 7b respectively. The time-variations in the normal stresses on the surface of the spherical cavity for the cases when $\frac{t_0}{t_m}=0$, 0·50, and 1·50 are shown in Fig. 4. In Figs.

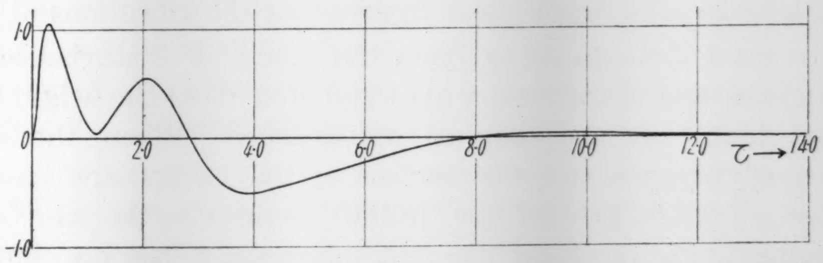

Fig. 7a. The radial vibration of a particle due to the longitudinal wave when $\frac{a}{t_m v}=1$, $\frac{t_0}{t_m}=1·50$. Unit of ordinate $=\frac{Pa}{27\mu}\left(\frac{a}{r}\right)\sin 2\theta\cos\phi$, abscissa $\tau=\frac{v}{a}\left\{t-\frac{1}{v}(r-a)\right\}$.

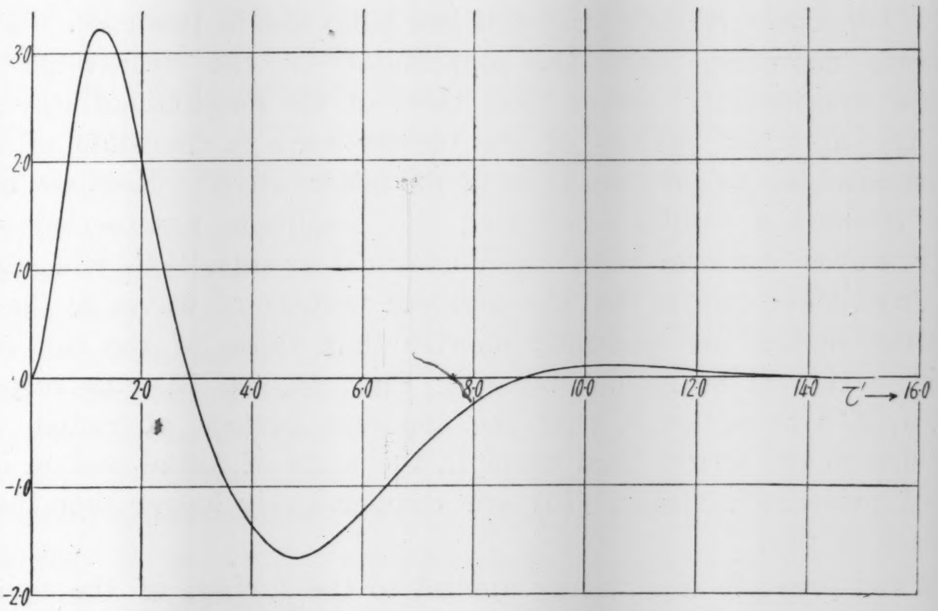

Fig. 7b. The azimuthal or the co-latitudinal vibration of a particle due to the transverse wave when $\frac{a}{t_m v}=1$, $\frac{t_0}{t_m}=1·50$. Units of ordinate are $\frac{Pa}{27\mu}\cdot\left(\frac{a}{r}\right)\cos 2\theta\cos\phi$, and $\frac{Pa}{27\mu}\left(\frac{a}{r}\right)\cos\theta\sin\phi$ for the azimuthal and the co-latitudinal vibrations respectively. Abscissa $\tau'=\frac{v}{a}\left\{t-\frac{1}{V}(r-a)\right\}$.

5a, 6a, 7a are shown the radial vibrations of particles due to the longitudinal wave for the cases when $\frac{t_0}{t_m}=0$, 0·50, and 1·50 respectively. Figs. 5b, 6b, 7b show the co-latitudinal or the azimuthal vibrations due to the transverse wave for the respective cases when $\frac{t_0}{t_m}=0$, 0·50 and 1·50. It will be seen from these figures that the vibrations of particles, which are some distance away from the origin of disturbance, are due to longitudinal and transverse waves radiated from the origin of disturbance and that they are damped oscillations. When the maximum intensities of pressure on the surface of the cavity are constant, the amplitudes of vibrations of the initial motions in the case of sudden commencement of pressure, do not necessarily become larger than those in the case of gradual commencement. It will also be seen from these figures that the apparent periods of vibrations in the state of initial motion in the case of sudden commencement of pressure generally become shorter than those in the case of gradual commencement. Obviously, Shida's push-pull law holds also in this case. It will be seen, moreover, that the amplitudes of the transverse wave become considerably larger than those of the longitudinal wave, and that the apparent periods of the former wave in the state of initial motion are also longer than those of the latter wave.[11] Needless to say, these theoretical results concerning the amplitude and period of the bodily waves conform with seismometrical results. It will also be seen from these figures that the apparent periods of waves in the state of initial motion are generally shorter than those of the tail of the waves. It will be seen, comparing Figs. 5a, 6a, 7a with respective Figs. 1, 2, 3 in section 3, that the apparent periods of radial vibrations due to the longitudinal wave in the state of initial motion in the case of pressure variation (15) are comparatively longer than those in the case of (1).

5. When pressure is suddenly applied to the surface of the cavity in the elastic medium, and its intensity exceeds the breaking stress of the material, cracks may suddenly appear in the material near the cavity, when the intensity of pressure in the cavity may vary discontinuously. Using agar-agar as the material, S. Yamaguti[12] has shown by his model experiment on the mechanism of the occurrence of earthquakes that the pressure in the cavity varies discontinuously at the moment the agar-agar begins to break. We shall now consider the wave-motions when the pressure in the cavity suddenly increases and a discontinuity appears in the timevariation in pressure.

---

[11] Concerning the longitudinal and transverse waves of shock wave-type, W. Inouye has also shown that the duration of time of the former wave becomes comparatively shorter than that of the latter wave.

W. INOUYE, *Bull. Earthq. Res. Inst.*, *loc. cit.*

[12] S. YAMAGUTI, *Bull. Earthq. Res. Inst.*, **13** (1935), 772.

(a) When the normal stress acts uniformly on the surface of the spherical cavity in the material, and it shows discontinuous time-variations like *A*, *B*, *C*, *D* in Fig. 8, the diverging waves radiated from the spherical cavity are respectively obtained by suitably superposing the waves shown in Figs. 1~3 in Section 3. The results are shown in Fig. 9, in which the respective waves are the diverging longitudinal waves radiated from the cavity. The waves with letters *A*, *B*, *C*, *D* correspond of course to the respective normal stresses *A*, *B*, *C*, *D*, the time-variations of which are shown in Fig. 8.

(b) When the pressure acting on the surface of the spherical cavity has the distribution $\sin 2\theta \cos\phi$, and it shows discontinuous time-variations, such as *A*, *B*, *C*, *D* in Fig. 8, the diverging longitudinal and transverse waves radiated from the

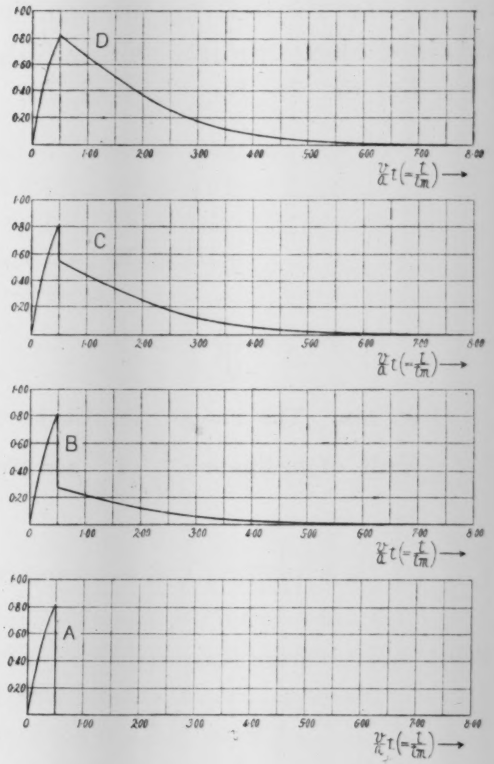

Fig. 8. The time-variations in pressure on the surface of a spherical cavity. Unit of ordinate $=-P$.

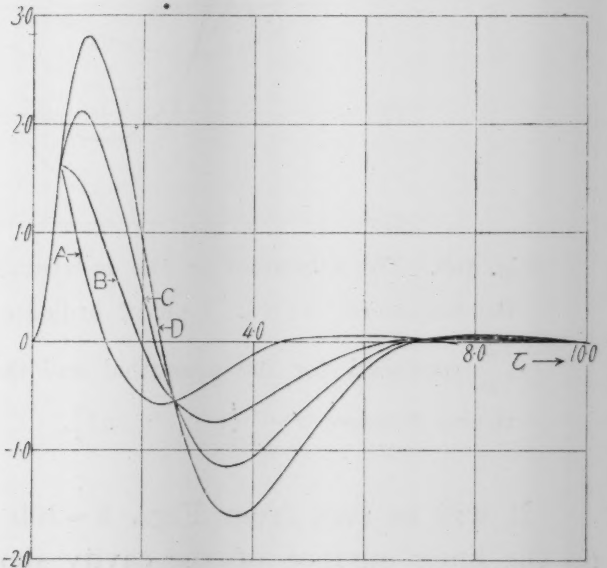

Fig. 9. The radial vibrations of particle due to the longitudinal wave. Unit of ordinate $=\dfrac{Pa}{27\mu}\left(\dfrac{a}{r}\right)$, abscissa $\tau=\dfrac{v}{a}\left\{t-\dfrac{1}{v}(r-a)\right\}$.

cavity are respectively shown in Figs. 10a and 10b. Of course we obtained these figures by suitably superposing the waves shown in Fgs. 5a, 6a, 7a, 5b, 6b, and 7b.

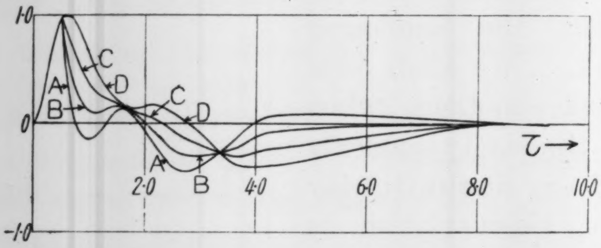

Fig. 10a. The radial vibrations of particle due to the longitudinal waves. Unit of ordinate$=\frac{Pa}{27\mu}\left(\frac{a}{r}\right)\sin 2\theta\cos\phi$, abscissa $\tau=\frac{v}{a}\left\{t-\frac{1}{v}(r-a)\right\}$.

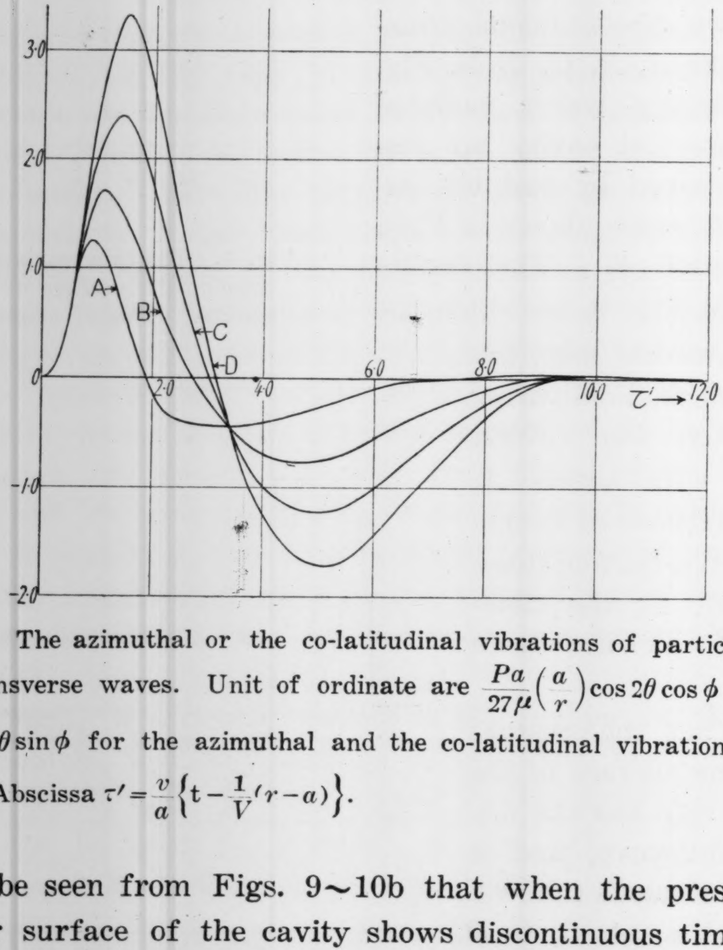

Fig. 10b. The azimuthal or the co-latitudinal vibrations of particle due to the transverse waves. Unit of ordinate are $\frac{Pa}{27\mu}\left(\frac{a}{r}\right)\cos 2\theta\cos\phi$ and $\frac{Pa}{27\mu}\cdot\left(\frac{r}{a}\right)\cos\theta\sin\phi$ for the azimuthal and the co-latitudinal vibrations respectively. Abscissa $\tau'=\frac{v}{a}\left\{t-\frac{1}{V}(r-a)\right\}$.

It will be seen from Figs. 9∼10b that when the pressure acting on the inner surface of the cavity shows discontinuous time-variations as shown in Fig. 8, the apparent periods of the waves generally become short.

In conclusion the author expresses his sincere thanks to Professor

K. Sezawa for his kind guidance in the course of the study, and he also expresses his best thanks to Mr. T. Takayama for his assistance in preparing this paper.

39. 彈性體內に在る球狀空窩の內面に作用する壓力變化によつて生ずる彈性波

地震研究所 西村源六郎

大地震の際，震央附近は主として震源より來た波動勢力による烈しい地震動に見舞はれる．それと同時に，そこには永久變位性の地殼變形が見られる．時には斷層が出現する事もある．

本論文は此れ等の事實に撞着しない様な震源を假想してその力學的性質を研究する爲めの準備研究の一つである．本論文では表題の様に彈性體內に球状空窩を假想して，その內面に作用する壓力の分布及びその時間的變化を種々與へた場合に生ずる彈性波の性質を明かにした．

40. *Relations between Gravity Values and Corresponding Subterranean Mass Distribution.*

By Chûji TSUBOI and Takato FUCHIDA.

Earthquake Research Institute.

(Read March 16 and April 20, 1937.—Received July 20, 1937.)

Let *AA* in Fig. 1 be the plane of the earth's surface along which the gravity values are known from point to point, and *BB* another plane which is at a depth d from the surface and on which are distributed surface densities responsible for these gravity values. Assume further that the surface densities along *BB* and, consequently the gravity values along *AA*, do not change in the direction that extends from $+\infty$ to $-\infty$ perpendicularly to the plane of this paper, so that they can be expressed by $\rho(y)$ and $g(x)$ respectively, x and y being the abscissae along *AA* and *BB*, with line *OO* as the common origin. The gravity $g(x)$ at $x=x$ due to $\rho(y)$ is then given by

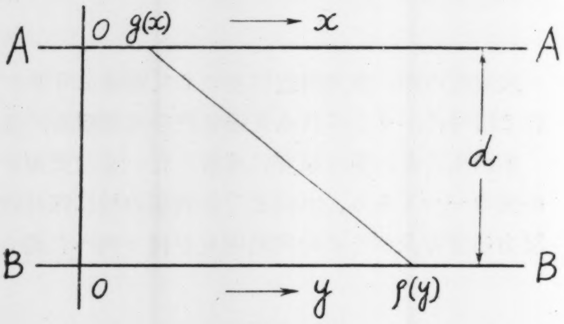

Fig. 1.

$$g(x)=2k^2d\int_{-\infty}^{+\infty}\frac{\rho(y)}{(y-x)^2+d^2}dy.$$

The direct analytical solution of this integral equation for an actually observed $g(x)$ is usually not possible, and it has been for this reason that problems of this kind have been studied in the other direction, viz., by searching such $\rho(y)$ by trial and error method that will give gravity values which agree best with the observed. The numerical solution of the equation, though theoretically simple, becomes almost insuperably complex, were more or less accurate results required.

If $\rho(y)$ were a harmonic function of y, then matters would be greatly simplified.¹⁾

Thus, if

---

1) It has been informed that a similar idea was proposed by H. RAINBOW.

$$\rho(y)=\rho_n \cos ny, \tag{1a}$$

then

$$g(x)=2k^2d\rho_n\int_{-\infty}^{+\infty}\frac{\cos ny}{(y-x)^2+d^2}dy.$$

Putting

$$p=y-x,$$

we get

$$\begin{aligned}g(x)&=2k^2d\rho_n\int_{-\infty}^{+\infty}\frac{\cos n(p+x)}{p^2+d^2}dp\\&=2k^2d\rho_n\left\{\cos nx\int_{-\infty}^{+\infty}\frac{\cos np}{p^2+d^2}dp-\sin nx\int_{-\infty}^{+\infty}\frac{\sin np}{p^2+d^2}dp\right\}\\&=2\pi k^2\rho_n e^{-nd}\cos nx,\end{aligned} \tag{1b}$$

making use of the integrals

$$\int_{-\infty}^{+\infty}\frac{\cos np}{p^2+d^2}dp=\frac{\pi}{d}e^{-nd}$$

and

$$\int_{-\infty}^{+\infty}\frac{\sin np}{p^2+d^2}dp=0.$$

Conversely if

$$g(x)=g_n\cos nx, \tag{2a}$$

then

$$\rho(y)=\frac{g_n}{2\pi k^2}e^{nd}\cos ny. \tag{2b}$$

That there is no other density distribution at depth d that produces the same gravity values as $\rho(y)$ can be proved in the following way. If $\rho'(y)$ be any one of such distributions, then the gravity values on the earth's surface due to $\{\rho'(y)-\rho(y)\}$ must be zero from point to point. Therefore $\{\rho'(y)-\rho(y)\}$ cannot be other than zero, in other words $\rho'(y)$ and $\rho(y)$ are equal everywhere.

From the relations (1) and (2), we see that

(1) $g(x)$ and $\rho(y)$ are harmonic functions which are in phase with each other, and the ratio of amplitudes is given by $2\pi k^2e^{-nd}$,

(2) for given ρ_n and d, g_n decreases if n increases,

(3) for given ρ_n and n, g_n decreases if d increases,

(4) for given g_n and d, ρ_n increases if n increases,
(5) for given g_n and n, ρ_n increases if d increases.

While the relations (1) and (2) hold for the simple case with a single value of n, those for different n's may be superposed by mere addition in order to get corresponding relations which hold for more general and complicated cases. Thus, if

$$\rho(y)=\sum_n A_n \cos ny+\sum_n B_n \sin ny,$$

then

$$g(x)=2\pi k^2\left\{\sum A_n e^{-nd}\cos nx+\sum_n B_n e^{-nd}\sin nx\right\},$$

and conversely if

$$g(x)=\sum_n \alpha_n \cos nx+\sum_n \beta_n \sin nx,$$

then

$$\rho(y)=\frac{1}{2\pi k^2}\left\{\sum_n \alpha_n e^{nd}\cos ny+\sum_n \beta_n e^{nd}\sin ny\right\}.$$

Although the summations in the above expressions do not necessarily imply that the n's are successive integers as in the case of Fourier series, this constitutes the most important field for application of the above relations to actual problems.

If a distribution of gravity gradients along the earth's surface is given instead of that of gravity values, there is a similar method for finding the subterranean density distribution that is responsible for these gradient values. Thus, if

$$\frac{\partial g}{\partial x}=\sum_n A_n \cos nx+\sum B_n \sin nx,$$

then

$$g(x)=\sum_n \frac{A_n}{n}\sin nx-\sum_n \frac{B_n}{n}\cos nx+G,$$

so that

$$\rho(y)=\frac{1}{2\pi k^2}\left\{\sum_n \frac{A_n}{n}e^{nd}\sin ny-\sum_n \frac{B_n}{n}e^{nd}\cos ny\right\}+P.$$

Before proceeding to apply the present method to practical problems, investigations will be made of the range of its applicability and of the errors that may arise therefrom. In the above theories, each elementary strip of the subterranean plane has been assumed to extend from $+\infty$ to $-\infty$ and to be of uniform density in the direction perpendicular to the paper, which condition, however, is never met with in practice. Errors would therefore arise in the values of the gravity if an elementary strip of a subterranean plane that is actually of a finite length were regarded as infinitely long. Let the length of the strip be $2l$ and the linear density ρ, then the gravity at point P, which is at a vertical distance d and a horizontal distance s from the middle point of the strip, is given by

$$g=\frac{2k^2\rho d}{d^2+s^2}\left(1+\frac{d^2+s^2}{l^2}\right)^{-\frac{1}{2}}$$

$$=g_\infty\left(1+\frac{d^2+s^2}{l^2}\right)^{-\frac{1}{2}}.$$

The value of l which gives the same ratio, $\frac{g}{g_\infty}$, varies with the values of s as shown by the curves in Fig. 2. If both l and s are several times d, then the ratio is greater than 0·90, so that in these cases the errors in question are less than 10%.

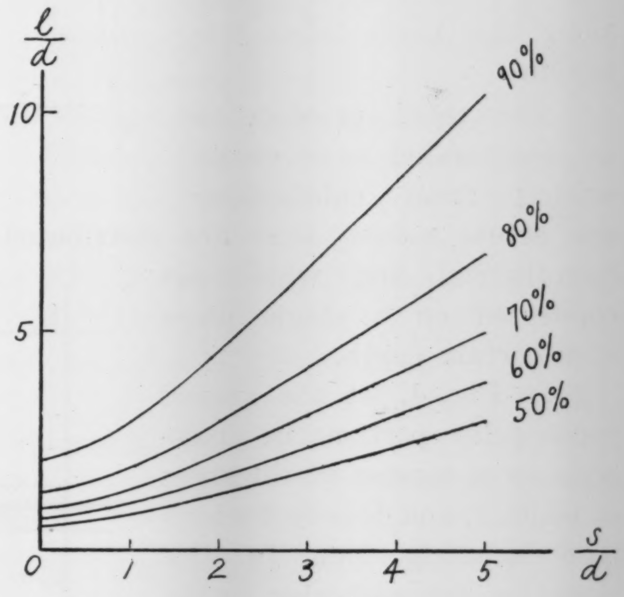

Fig. 2.

In the second place, the plane on which the densities are distributed has been assumed to extend from $+\infty$ to $-\infty$ in y-direction also. If the width of this plane is finite, say $2y$, the gravity due to it at the point above its centre is given by

$$g=4k^2\rho\tan^{-1}\frac{y}{d}$$

which tends to

$$g_\infty=2\pi k^2\rho$$

if y tends to infinity. The ratio $\frac{g}{g_\infty}$ is therefore given by

$$\frac{g}{g_\infty}=\frac{2}{\pi}\tan^{-1}\frac{y}{d}$$

the values of which are plotted in Fig. 3. If $\frac{y}{d}$ is greater than 6, errors arising from regarding the plane as of infinite width will be less than 10%.

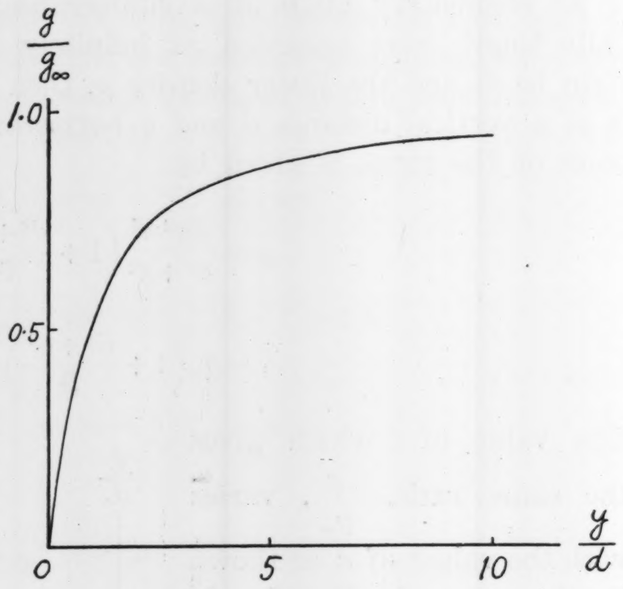

Fig. 3.

Since in both the above calculations, the surface density on the subterranean plane has been assumed to be uniform throughout, estimations of errors are subject to certain changes, were the variation in density along this plane taken into account.

The third problem to be investigated is on errors arising from substituting the actual masses that are distributed in space by those that are hypothetical and which are condensed on a single plane at a certain depth.

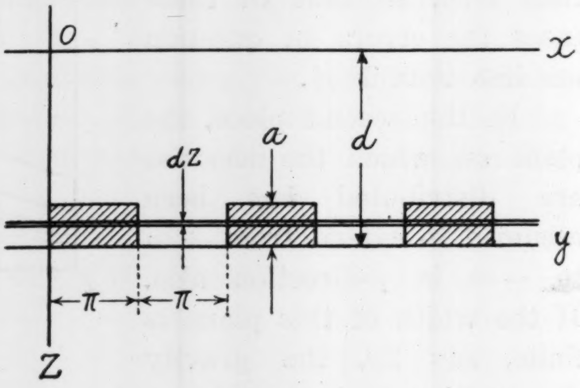

Fig. 4.

In Fig. 4, let the shaded rectangular portions be cross-sections of masses of thickness a, width π, and density 1 which are infinitely long in the direction perpendicular to the paper and which are distributed at a regular periodic interval π. The density distribution in y-direction along a layer at depth z and of thickness dz is

$$\begin{aligned}\rho(y) &= dz \qquad 0<y<\pi \\ &= 0 \qquad \pi<y<2\pi.\end{aligned}$$

As the Fourier expression for $\rho(y)$ is

$$\rho(y)=\left\{\frac{1}{2}+\frac{2}{\pi}\sum\frac{1}{2n+1}\sin\,(2n+1)y\right\}dz,$$

the corresponding surface gravity is given by

$$dg(x)=2\pi k^2\left\{\frac{1}{2}+\frac{2}{\pi}\sum\frac{e^{-(2n+1)z}}{2n+1}\sin(2n+1)x\right\}dz.$$

Integrating this throughout the whole thickness of the masses from $(d-a)$ to d, we have finally

$$g(x)=2\pi k^2\left[\frac{a}{2}+\frac{2}{\pi}\sum\frac{1}{(2n+1)^2}\left\{e^{-(2n+1)(d-a)}-e^{-(2n+1)d}\right\}\sin(2n+1)x\right].$$

On the other hand, the surface gravities due to the same masses if they were respectively condensed at depths d, $\left(d-\frac{a}{2}\right)$ and $(d-a)$ would be

$$g_d(x)=2\pi k^2\left\{\frac{a}{2}+\frac{2a}{\pi}\sum\frac{1}{2n+1}e^{-(2n+1)d}\sin(2n+1)x\right\},$$

$$g_{d-\frac{a}{2}}(x)=2\pi k^2\left\{\frac{a}{2}+\frac{2a}{\pi}\sum\frac{1}{2n+1}e^{-(2n+1)\left(d-\frac{a}{2}\right)}\sin(2n+1)x\right\}$$

and

$$g_{d-a}(x)=2\pi k^2\left\{\frac{a}{2}+\frac{2a}{\pi}\sum\frac{1}{2n+1}e^{-(2n+1)(d-a)}\sin(2n+1)x\right\}.$$

These values of gravity are compared in Tables I, II.

TABLE I.

$2\pi=40$ km. $d=\frac{\pi}{2}=10$ km.

$a=\frac{\pi}{4}=5$ km. unit=milligal.

x	g	g_d	$g_{d-\frac{a}{2}}$	g_{d-a}	g_d-g	$g_{d-\frac{a}{2}}-g$	$g_{d-a}-g$
90°	290	264	288	324	−26	−2	+34
120°	284	258	280	314	−26	−4	+30
150°	255	237	253	279	−18	−2	+24
180°	209	209	209	209	0	0	0
210°	163	180	166	140	+17	+3	−23
240°	135	161	138	105	+26	+3	−30
270°	128	154	130	95	+26	+2	−33

TABLE II.

$2\pi = 40$ km. $d = \frac{\pi}{2} = 10$ km.

$a = \frac{\pi}{4} = 2{\cdot}5$ km. unit = milligal.

x	g	g_d	$g_{d-\frac{a}{2}}$	g_{d-a}	$g_d - g$	$g_{d-\frac{a}{2}} - g$	$g_{d-a} - g$
90°	138	132	137	145	−6	−1	+7
120°	134	128	134	140	−6	0	+6
150°	123	119	122	126	−4	−1	+3
180°	104	104	104	104	0	0	0
210°	87	90	87	82	+3	0	−5
240°	75	80	75	69	+5	0	−6
270°	71	77	71	64	+6	0	−7

It will be seen from the tables that the errors are very small if the masses are condensed on their middle plane at depth $\left(d - \frac{a}{2}\right)$.

Consider in the second place the case in which two layers of different densities are bounded by a sinusoidal cylindrical surface of amplitude a. If the difference in density is 1, to find the gravity values due to this mass distribution is equivalent to finding the same due to the mass distribution shown in Fig. 5.

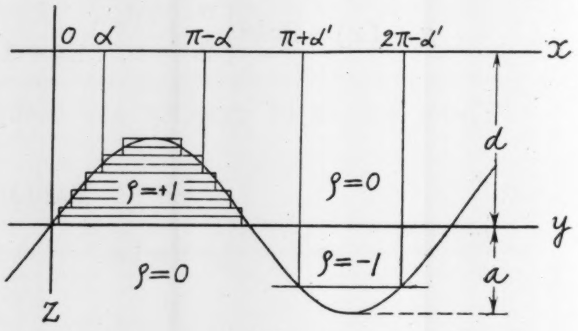

Fig. 5.

As in the preceding example, consider a layer at depth z and of thickness dz. The density distribution in y-direction along this layer is,

for the upper half,

$$\rho(y) = 0 \qquad 0 < x < \alpha, \quad \pi - \alpha < x < 2\pi$$

$$\rho(y) = dz \qquad \alpha < x < \pi - \alpha,$$

and for the lower half,

$$\rho(y) = 0 \qquad 0 < x < \pi + \alpha', \quad 2\pi - \alpha' < 2\pi$$

$$\rho(y) = -dz \qquad \pi + \alpha' < x < 2\pi - \alpha'.$$

The Fourier expressions for $\rho(y)$ is,

for the upper half,

$$\rho(y)=\left\{\frac{\pi-2\alpha}{2\pi}-\frac{2}{\pi}\sum\frac{\sin 2n\alpha}{2n}\cos 2ny\right.$$

$$\left.+\frac{2}{\pi}\sum\frac{\cos(2m+1)\alpha}{2m+1}\sin(2m+1)y\right\}dz$$

and for the lower half,

$$\rho(y)=\left\{-\frac{\pi-2\alpha'}{2\pi}+\frac{2}{\pi}\sum\frac{\sin 2n\alpha'}{2n}\cos 2ny\right.$$

$$\left.+\frac{2}{\pi}\sum\frac{\cos(2m+1)\alpha'}{2m+1}\sin(2m+1)y\right\}dz.$$

The surface gravity which corresponds to this elementary layer is, for the upper half,

$$dg(x)=2\pi k^2\left\{\frac{\pi-2\alpha}{2\pi}-\frac{2}{\pi}\sum\frac{\sin 2n\alpha}{2\pi}e^{-2nz}\cos 2nx\right.$$

$$\left.+\frac{2}{\pi}\sum\frac{\cos(2m+1)\alpha}{2m+1}e^{-(2m+1)z}\sin(2m+1)x\right\}dz$$

and for the lower half,

$$dg(x)=2\pi k^2\left\{-\frac{\pi-2\alpha'}{2\pi}+\frac{2}{\pi}\sum\frac{\sin 2n\alpha'}{2n}e^{-2nz}\cos 2nx\right.$$

$$\left.+\frac{2}{\pi}\sum\frac{\cos(2m+1)\alpha'}{2m+1}e^{-(2m+1)z}\sin(2m+1)x\right\}dz.$$

To find the gravity values due to the whole mass, these expressions must be integrated with respect to z throughout the full range of amplitude of the sinusoidal wave, but this is unfortunately not possible and a numerical integration has to be resorted to. Dividing the mass into ten elementary layers as in Fig. 5, the mass in each layer which is regarded as being rectangular in shape, is condensed on its respective middle plane and the gravity values due to all these are summed up. On the other hand, if the whole mass is condensed on the middle plane of the sinusoidal curve, the density distribution along this plane is given by

$$\rho(y)=a\cos y$$

and the corresponding gravity values by

$$g(x)=2\pi k^2 a e^{-d}\cos x.$$

The gravity values due to these two different mass distributions are compared in Table III. From these results, we see that if the amplitude of the sinusoidal curve is less than one-fourth its mean depth, the errors arising from condensing the masses on the middle plane are negligible.

TABLE III.

x	$d=\frac{\pi}{2}=10$ km. $\lambda=2\pi=40$ km. $a=\frac{\pi}{8}=2{\cdot}5$ km.			$d=\frac{\pi}{2}=10$ km. $\lambda=2\pi=40$ km. $a=\frac{\pi}{8}=5{\cdot}0$ km.			$d=\frac{\pi}{2}=15$ km. $\lambda=2\pi=40$ km. $a=\frac{\pi}{8}=2{\cdot}5$ km.			$d=\frac{\pi}{2}=15$ km. $\lambda=2\pi=40$ km. $a=\frac{\pi}{8}=1{\cdot}25$ km.		
	Actual	Cond.	Diff.	Actual	Cond.	Diff.	Actual	Cond.	Diff.	Actual	Cond.	Diff.
90°	48	44	− 4	106	87	− 19	110	96	− 14	51	48	− 3
120°	40	38	− 2	86	76	− 10	90	83	− 7	43	41	− 2
150°	22	22	0	45	44	− 1	43	48	+ 5	23	24	+ 1
180°	− 2	0	+ 2	− 9	0	+ 9	− 9	0	+ 9	− 2	0	+ 2
210°	− 24	− 22	+ 2	− 47	− 44	+ 3	− 53	− 48	+ 5	− 25	− 24	+ 1
240°	− 38	− 38	0	− 77	− 76	+ 1	− 81	− 83	− 2	− 41	− 41	0
270°	− 44	− 44	0	− 87	− 87	0	− 91	− 96	− 5	− 46	− 48	− 2

The fourth problem to be investigated is on the convergency of the Fourier series used. The differentiation of a convergent Fourier series, term by term, does not always give another convergent series. Since in practical problems, it will suffice to treat them with a Fourier series of finite term number, convergency of the series is out of question. It has been shown that if

$$g(x)=\sum\alpha_n \cos nx+\sum\beta_n \sin nx$$

then

$$\rho(y)=\frac{1}{2\pi k^2}\left\{\sum\alpha_n e^{nd}\cos ny+\sum\beta_n e^{nd}\sin ny\right\}.$$

If $g(x)$ is convergent, $\rho(y)$ is not necessarily also convergent, because the factor e^{nd}, which is increasing with increasing n, is multiplied to the α's and β's. If $\rho(y)$ thus obtained is found to be divergent, the physical interpretation is that this particular gravity distribution cannot be produced by a condensed density distribution at depths greater than d, and d must be less than that threshold value for which the series becomes convergent.

Applications of Fourier series as just described imply that the same distributions of gravity together with distributions of subterranean density are repeated periodically also beyond the range in which they are expressed in those series. Although this is evidently not actually the case, results obtained on this assumption will not greatly differ from the actual, because the mass distribution corresponding to the difference of the actual and the hypothetical Fourier density distributions beyond this range will produce no large gravity in the range in question.

What will now be given are some of the many examples of the applications of the present method.

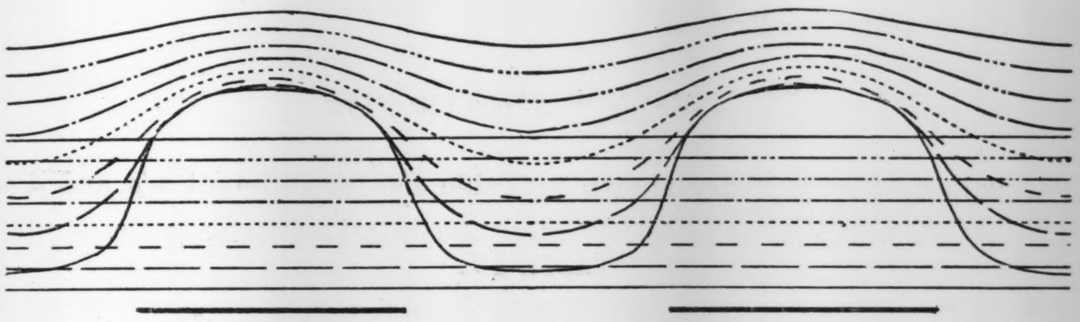

Fig. 6.

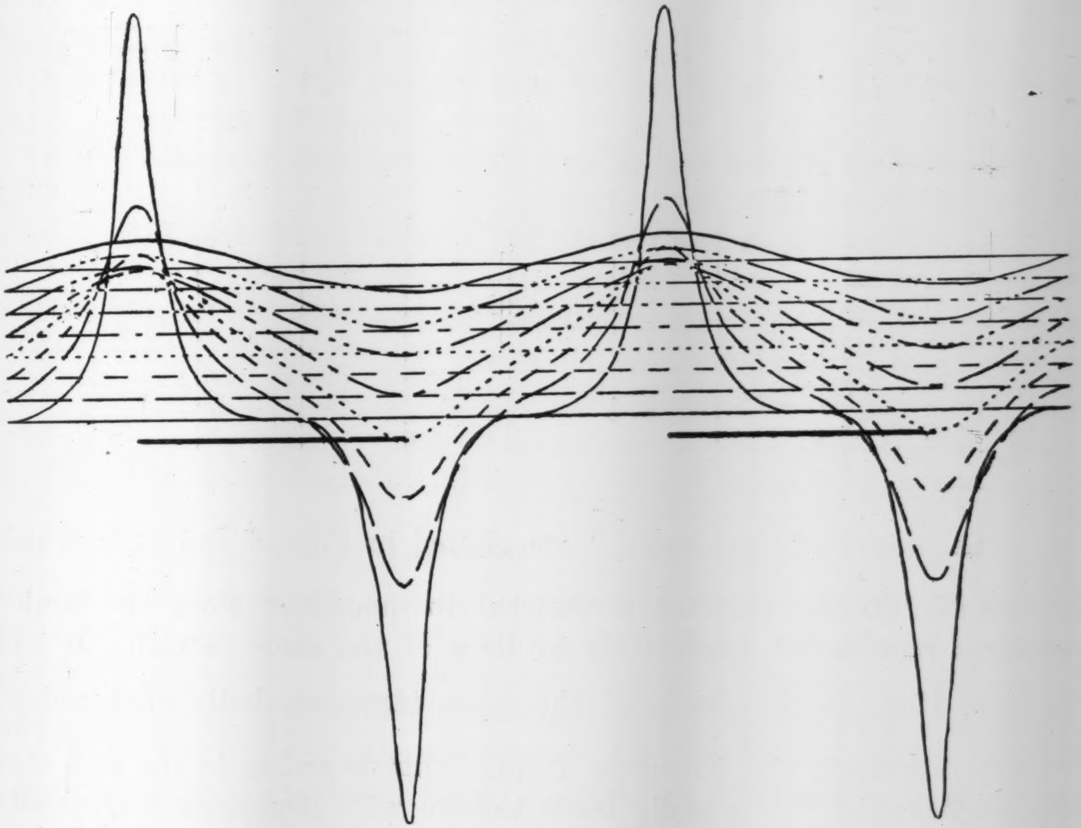

Fig. 7.

(1) In Figs. 6 and 7, let the thick lines represent sections of

strips of planes at depth d, with width π, and surface density 1. The density distribution along y-direction is

$$\rho(y)=\frac{1}{2}-\frac{2}{\pi}\sum_{0}^{\infty}\frac{1}{2n+1}\sin(2n+1)y$$

so that the surface gravity is

$$g(x)=2\pi k^2\left[\frac{1}{2}-\frac{2}{\pi}\sum\frac{1}{2n+1}e^{-(2n+1)d}\sin(2n+1)x\right]$$

and the gravity gradient is

$$\frac{\partial g}{\partial x}=-4k^2\sum e^{-(2n+1)d}\cos(2n+1)x.$$

The values of $e^{-(2n+1)d}$ are shown in Table IV for different n's and d's.

TABLE IV.

n \ d	$\frac{\pi}{12}$	$2\times\frac{\pi}{12}$	$3\times\frac{\pi}{12}$	$4\times\frac{\pi}{12}$	$5\times\frac{\pi}{12}$	$6\times\frac{\pi}{12}$	$7\times\frac{\pi}{12}$	$8\times\frac{\pi}{12}$	$9\times\frac{\pi}{12}$
0	0·770	0·592	0·456	0·351	0·270	0·201	0·160	0·123	0·095
1	456	201	95	43	20	9	4	1	
2	270	73	20	5					
3	160	25	4						
4	95	9							
5	56	3							
6	33								
7	20								
8	12								
9	7								
10	4								
11	2								

The values of $g(x)$ and $\frac{\partial g}{\partial x}$ are plotted in Figs. 6 and 7, in which curves of different patterns correspond to quantities along the earth's surfaces represented respectively by lines of the same pattern. It will be seen that, as the depth of the mass increases, both $g(x)$ and $\frac{\partial g}{\partial x}$ rapidly approach the harmonic form. This is owing to the fact that the coefficient $e^{-(2n+1)d}$ rapidly tends to zero with increasing d, especially for larger values of n.

(2) The next problem is to find the subterranean mass distribu-

tion that will produce surface gravity of the form

$$g(x)=g_0e^{-x^2}.$$

If we use in this case Fourier integral instead of Fourier series, we have

$$g(x)=\frac{2g_0}{\pi}\int_0^\infty\int_0^\infty e^{-\lambda^2}\cos nx\cos n\lambda d\lambda dn,$$

and because

$$\int_0^\infty e^{-\lambda^2}\cos n\lambda d\lambda=\frac{\sqrt{\pi}}{2}e^{-\frac{n^2}{4}},$$

we have

$$g(x)=\frac{g_0}{\sqrt{\pi}}\int_0^\infty e^{-\frac{n^2}{4}}\cos nxdn.$$

The corresponding subterranean mass distribution is therefore

$$\rho(y)=\frac{g_0}{2k^2\pi^{\frac{3}{2}}}\int_0^\infty e^{nd-\frac{n^2}{4}}\cos nydn.$$

Because the coefficients $e^{nd-\frac{n^2}{4}}$ rapidly tends to zero as n increases, as shown in Table V, this integral may be substituted by a summation of finite terms with sufficient accuracy.

The values of $\rho(y)$ are plotted in Fig. 8. It is remarkable that in order to have surface gravity values of the type of a probability curve it is necessary to have a certain negative density.

TABLE V.

d n	0·5	1·0	1·5
0·5	1·206	1·548	1·988
1·5	1·206	2·552	5·403
2·5	731	2·552	8 908
3·5	269	1·548	8·905
4·5	60	569	5·403
5·5	18	127	1·988
6·5	1	17	444
7·5		1	60
8·5			5

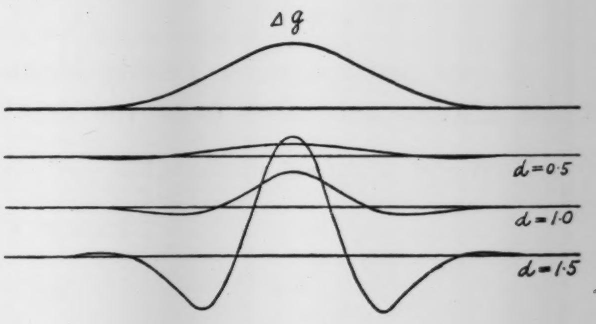

Fig. 8.

(3) The final example concerns the results of actual gravity measurements made by Vening Meinesz2) in the Dutch East Indies.

---

2) VENING MEINESZ, *Gravity Expeditions at Sea* 1923~1932., Vol II. (1934), Delft.

The regional isostatic anomalies along his profile No. 21, as shown by him are given in Table VI. Plotting these values according to distance as in Fig. 9, and connecting them by a smooth curve, the values for every 25 km were read off from the curve, of which there are 36 in all. As the curve seems to tend to 40 milligals toward both ends, this value was subtracted from all the observed values so as to get the very local gravity anomalies alone. With these 36 values, the gravity anomalies were subjected to harmonic analysis. The coefficients of the Fourier terms found were :

TABLE VI.

Point	Reg. Isos. An.
No. 394	+ 22
395	+ 1
396	− 23
397	− 47
398	−104
29	+ 12
399	+ 33
400	+ 7

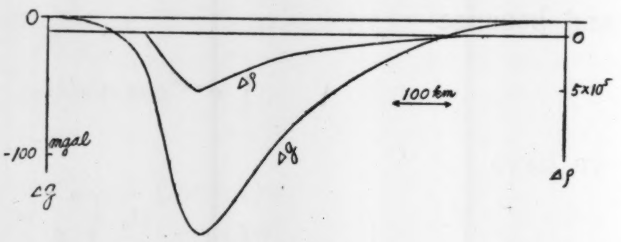

Fig. 9.

TABLE. VII.

n	sin	cos	n	sin	cos	n	sin	cos
0	—	46·1	7	1·0	1·3	14	− 0·2	0
1	−42·6	−44·6	8	− 0·7	0·7	15	− 0·1	− 0·2
2	22·9	−14·5	9	− 0·4	− 0·2	16	0	− 0·1
3	6·8	13·4	10	− 0·1	− 0·3	17	+ 0·2	− 0·3
4	− 7·5	4·1	11	0·2	− 0·2	18	—	0·1
5	− 2·0	− 4·4	12	0·4	0			
6	2·4	− 1·5	13	− 0·1	0·2			

If we assume with Vening Meinesz that the mass responsible for these gravity anomalies is at the depth of 25 km, which corresponds to $\frac{\pi}{18}$, then the Fourier coefficients for $2k^2\pi\rho(y)$ become :

TABLE VIII.

n	sin	cos	n	sin	cos	n	sin	cos
0	—	46·1	7	3·4	4·4	14	− 2·3	0
1	−50·7	−53·1	8	− 2·8	2·8	15	− 1·4	− 2·7
2	32·5	−20·6	9	− 1·9	− 1·0	16	0	− 1·6
3	11·5	22·6	10	− 0·6	− 1·7	17	4·2	− 6·2
4	−15·1	8·2	11	1·4	− 1·4	18	—	2·3
5	− 4·8	−10·5	12	3·2	0			
6	6·8	− 4·3	13	− 1·0	1·9			

This density distribution is also shown in Fig. 9. At the negative maximum

$$2\pi k^2\rho=0.200,$$

therefore

$$\rho=\frac{0{\cdot}200}{2\times 3{\cdot}1\times 6{\cdot}7\times 10^{-8}}=5\times 10^5.$$

This is equivalent to a mass of density 0·6 and thickness 8 km, which result is in exact agreement with Meinesz's assumption.

40. 重力と地下構造との關係

地震研究所 ｛坪井忠二
　　　　　　｛淵田隆門

第1圖に於いて AA を地表面，BB を深さ d の面とし，BB の上に表面密度が分布して居るとする。AA 面上の重力及び BB 面上の密度は紙に垂直な方向には變化なく無限に延びて居て，夫々 $g(x)$ 及び $\rho(y)$で表し得るとする。若し

$$\rho(y)=\rho_n\cos ny$$

であるならば

$$g(x)=2\pi k^2\rho_n e^{-nd}\cos nx$$

である。逆に

$$g(x)=g_n\cos nx$$

ならば

$$\rho(y)=\frac{g_n}{2\pi k^2}e^{nd}\cos ny$$

でなければならない。此の關係を一般化すれば次の通りになる。即ち

$$\rho(y)=\sum A_n\cos ny+\sum B_n\sin ny$$

ならば

$$g(x)=2\pi k^2\{\sum A_n e^{-nd}\cos nx+\sum B_n e^{-nd}\sin nx\}$$

である。逆に

$$g(x)=\sum\alpha_n\cos nx+\sum\beta_n\sin nx$$

ならば

$$\rho(y)=\frac{1}{2\pi k^2}\left\{\sum\alpha_n e^{nd}\cos ny+\sum\beta_n e^{nd}\sin ny\right\}$$

である。是等の關係を利用すれば與へられた $\rho(y)$ から $g(x)$ を求めること，又逆に與へられた $g(x)$ から $\rho(y)$ を求めることが出來る。後の場合には d を假定しなければならないのは勿論の事である。

本文には上記の關係の導き方，その應用例數個と，此の方法がどの位の精度で適用されるかと云ふ吟味が述べてある。

41. *The Deflections of the Vertical, the Undulation of the Geoid, and Gravity Anomalies.*

By Chûji TSUBOI,

Earthquake Research Institute.

(Read June 15, 1937.—Received June 20, 1937.)

Let *AA* in Fig. 1 be the plane of the earth's surface, the gravity anomalies along which are known from point to point, and *BB* another plane which is at a depth d from the surface, and on which are distributed the surface densities responsible for these gravity anomalies. Assume further that the surface densities along *BB*, and consequently the gravity anomalies along *AA*, do not change in the direction that extends from $+\infty$ to $-\infty$ perpendicularly to the plane of this paper, so that they can be expressed by $\rho(y)$ and $\Delta g(x)$ respectively, x and y being the abscissae along *AA* and *BB*, with line *OO* as the common origin. It was shown in the preceding paper[1] that if

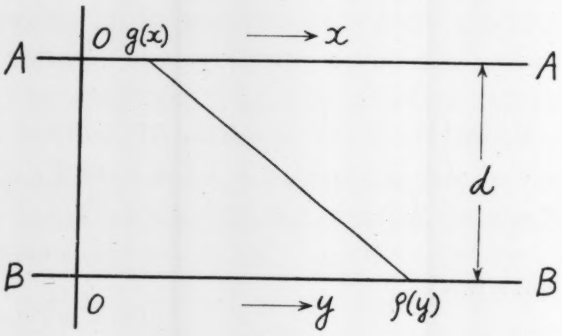

Fig. 1.

$$\rho(y) = \rho_n \cos ny\,,$$

then

$$\Delta g(x) = 2\pi k^2 \rho_n e^{-nd} \cos nx\,.$$

The horizontal component of attraction due to the same mass is given by

$$\frac{\partial V}{\partial x} = 2k^2\rho_n \int_{-\infty}^{+\infty} \frac{(y-x)\cos ny}{(y-x)^2+d^2}\,dy\,.$$

Putting
$$p = y - x\,,$$

we get
$$\frac{\partial V}{\partial x} = 2k^2\rho_n \int_{-\infty}^{+\infty} \frac{p\cos n(p+x)}{p^2+d^2}\,dp$$

---

[1] C. TSUBOI and T. FUCHIDA, *Bull. Earthq. Res. Inst.*, **15** (1937), 636.

$$=2k^2\rho_n\left\{\cos nx\int_{-\infty}^{+\infty}\frac{p\cos np}{p^2+d^2}dp-\sin nx\int_{-\infty}^{+\infty}\frac{p\sin np}{p^2+d^2}\,dp\right\}$$

$$=-2\pi k^2\rho_n e^{-nd}\sin nx\,,$$

making use of the integrals

$$\int_{-\infty}^{+\infty}\frac{p\cos np}{p^2+d^2}\,dp=0$$

and

$$\int_{-\infty}^{+\infty}\frac{p\sin np}{p^2+d^2}\,dp=\pi e^{-nd}.$$

The deflection of the vertical $\varDelta\theta$ at $x=x$ is given by

$$\varDelta\theta=\frac{1}{g}\frac{\partial V}{\partial x}$$

$$=-\frac{2\pi k^2\rho_n}{g}e^{-nd}\sin nx\,.$$

The height of the geoid h at $x=x$ relative to that at $x=x_0$ is obtained by integrating the above expression with respect to x from x_0 to x, thus

$$h=\int_{x_0}^{x}\varDelta\theta dx$$

$$=\frac{2\pi k^2\rho_n}{ng}e^{-nd}\cos nx-h_0\,.$$

Comparing this expression with that for $\varDelta g$, we see that h and $\varDelta g$ are in phase with each other, a positive gravity anomaly being associated with up-warping of the geoid and a negative anomaly with down-warping.

If we omit the h_0 in the expression for h, which is a constant and combine it with that for $\varDelta g$, we get

$$h=\frac{\varDelta g}{ng}\,.$$

It is to be noted that h can be calculated from $\varDelta g$ with the aid of this expression without any previous knowledge of the depth of the subterranean mass $\rho(y)$.

Since

$$n = \frac{2\pi}{\lambda_n},$$

we have

$$h = \frac{\lambda_n}{2\pi}\frac{\Delta g}{g}.$$

If, for instance, we put

$$\lambda_n = 100\ \text{km},$$

$$|\Delta g| = 0.100\ \text{gal},$$

then we get

$$|h| = \frac{10^7 \times 0.1}{2\pi \times 10^3} \doteqdot 170\ \text{cm}.$$

The above relation between h and Δg can be extended to more general and complicated cases in which there is more than one harmonic component. Thus, if

$$\Delta g(x) = \sum A_n \cos nx + \sum B_n \sin nx,$$

then

$$h = \frac{a}{2\pi g}\left\{\sum \frac{A_n}{n}\cos nx + \sum \frac{B_n}{n}\sin nx\right\},$$

where a is the extent of the range in which Δg is expressed in the Fourier series. It is not necessary that all the harmonic components of Δg should be due to the mass at one and the same depth, the only requirement being that each component shall be due to the mass that is respectively horizontal.

Because each of the Fourier coefficients for h is n times smaller than the corresponding one for Δg, the relative variation in the height of the geoid will be much smaller than that in Δg.

The gravity anomalies found by Vening Meinesz along his profile No. 21 have already been discussed in the preceding paper. Utilizing the Fourier coefficients for Δg calculated in that paper, those for h were found to be as follows:

n	sin	cos	n	sin	cos	n	sin	cos
1	42·6	44·6	4	1·9	−1·0	7	−0·1	−0·2
2	−11·5	7·3	5	0·4	0·9	8	0·1	0·1
3	− 2·3	−4·5	6	−0·4	0·3			

The form of the geoid along this profile, which was obtained by synthesis of the harmonic components given in the table, is shown in Fig. 2.

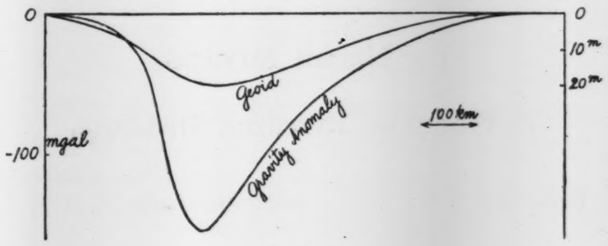

Fig. 2.

It is hoped that the method here proposed, which corresponds to that of Stokes, except that the latter applies to spherical surfaces, will find many applications in practical problems.

---

41. 鉛直線偏倚，ジオイドの凹凸と重力異常

地震研究所　坪井忠二

適當な假定を設けると，表題の三者の間に簡單な關係がある事を示す．特に重力異常が與へられればジオイドの凹凸が解ると云ふ事は應用が廣いと考へられる．本文中には蘭領印度諸島附近に於けるマイネスの測定について應用例が示してある．

42. *Supplementary notes to the Study of Crustal Deformation in the Tango District.*

By Naomi MIYABE,

Earthquake Research Institute.

(Read April 17, 1937.—Received June 21, 1937.)

1. In studying the crustal deformation in the Tango district with the aid of an analysis of the data of horizontal displacements of triangulation points, the existence of the Gô-mura fault and the Yamada fault, both of which appeared at the time of the destructive earthquake of 1927, was ignored, i.e., the crustal deformation was believed to be continuous over the zone traversed by active faults[1]. This, of course, is one hypothesis on the basis of which a study of crustal deformation in this district may be extended. There is however another hypothesis for reference in studying the crustal deformation, namely, that in which the crustal deformation is believed to be discontinuous in the zone traversed by active faults. Yamaguti, who recently studied the modes of crustal deformation in the Idu district based on such an hypothesis, obtained some interesting results[2].

On the basis of the above mentioned hypothesis, the study of the mode of crustal deformation in the Tango district was revised, the result being as follows:

2. In order to show clearly the mode of deformation of the earth's crust, the horizontal divergence, rotation, etc. were calculated as before[3] by using the data of horizontal displacements of the triangulation points distributed in this region[4].

Calculations of the amounts of

horizontal divergence $\Delta=\frac{\partial u}{\partial x}+\frac{\partial v}{\partial y}$

and horizontal rotation $\zeta=\frac{1}{2}\left(\frac{\partial v}{\partial x}-\frac{\partial u}{\partial y}\right)$

---

[1] T. TERADA and N. MIYABE, *Bull. Earthq. Res. Inst.*, **7** (1929), 223—239. C. TSUBOI, *Ibid.* **8** (1930). 153—221.

[2] S. YAMAGUTI, not yet published.

[3] C. TSUBOI, loc. cit. 1).

[4] Rikuti Sokuryôbu (Military Land Survey), Report issued in 1930.

were made for regions I, II, III, separately, divided by the lines *AB* and *CD* representing the general trend of the Gô-mura fault and the Yamada fault, as shown in Fig. 1.

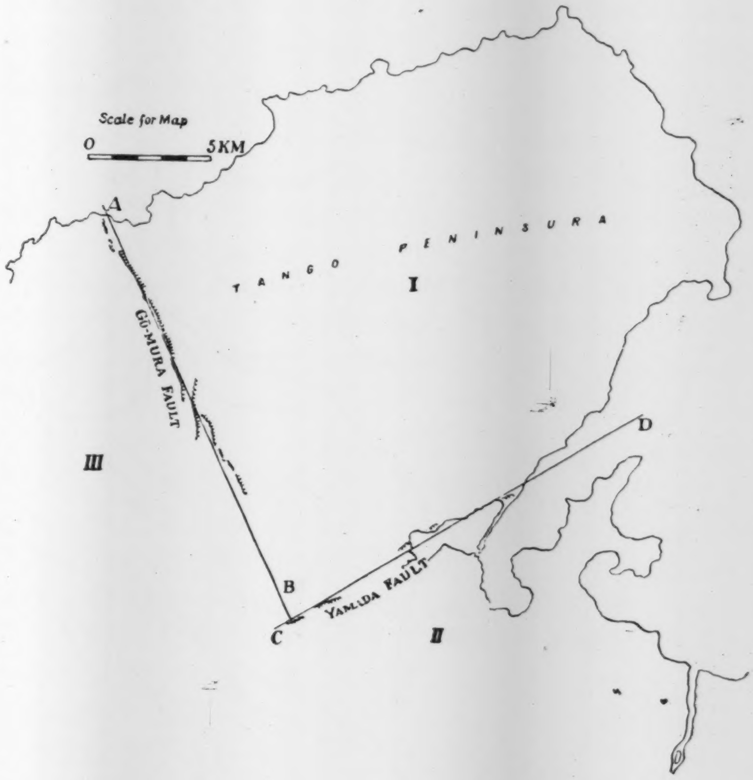

Fig. 1. Regions I, II, III in Tango district.

It is possibly a question whether the westward elongation of the line *CD* (the Yamada fault) ever really existed or not. However, in the zone into which the Yamada fault prolongs itself, the amounts of horizontal displacements are generally smaller and no trace of the active fault was apparent. Therefore, the horizontal deformation of the earth's crust was tentatively regarded as continuous over this zone. The distribution of the horizontal divergcnce Δ and rotation ζ thus calculated are shown in Figs. 2~3 respectively.

Except in certain respects, the mode of distribution of these quantities i.e., the mode of horizontal crustal deformation, is very similar to those obtained in the previous investigations[5].

The values of Δ in region I are generally positive, especially in the part close to the Gô-mura fault, while, in region III, contiguous to the west of region I, the values of Δ are negative. In previous investigations, the configuration of equal contour lines was greatly deformed by the greater amount of negative divergence in the zone along the Gô-mura fault, which however is not observed in the results of the recent study.

---

[5] C. TSUBOI, *loc. cit.* 1)

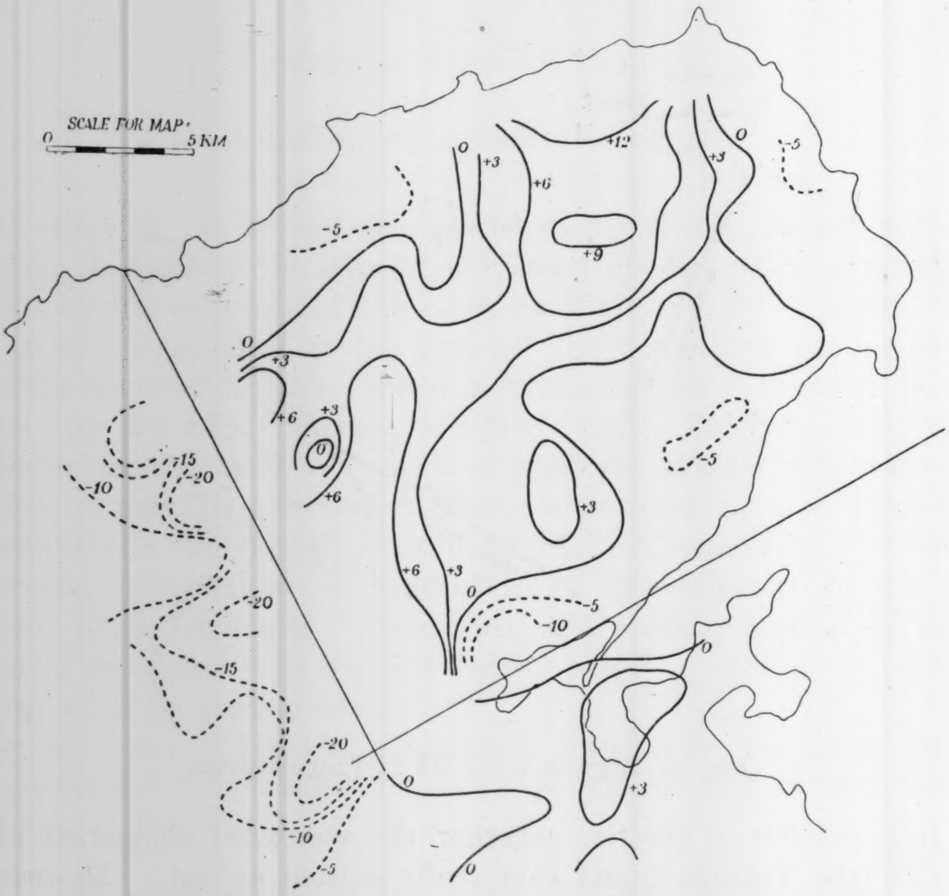

Fig. 2. Distribution of horizontal divergence. (Numerals against contour lines designate amounts of divergence in 10^{-5})

In constructing Figs. $2\sim3$, the values of the horizontal deformation were calculated for every 2^2 km. The modes of crustal deformations studied here are therefore those obtained through a mesh of only 2×2 km, so that it is not possible to go into greater detail regarding the mode of crustal deformation from the present result of analysis.

In Fig. 4, the frequency of squares of 2×2 km is plotted against the values of $\varDelta$. Frequency curves I and III correspond to regions I and III respectively.

From the curves in Fig. 4, we notice (i) that squares whose values of $\varDelta$ are small are generally speaking more frequent than those whose values of $\varDelta$ are large, and (ii) that in curve I showing the frequency of squares with regard to Δ in region I, a maximum occurs at $\Delta = 7 \times 10^{-5}$.

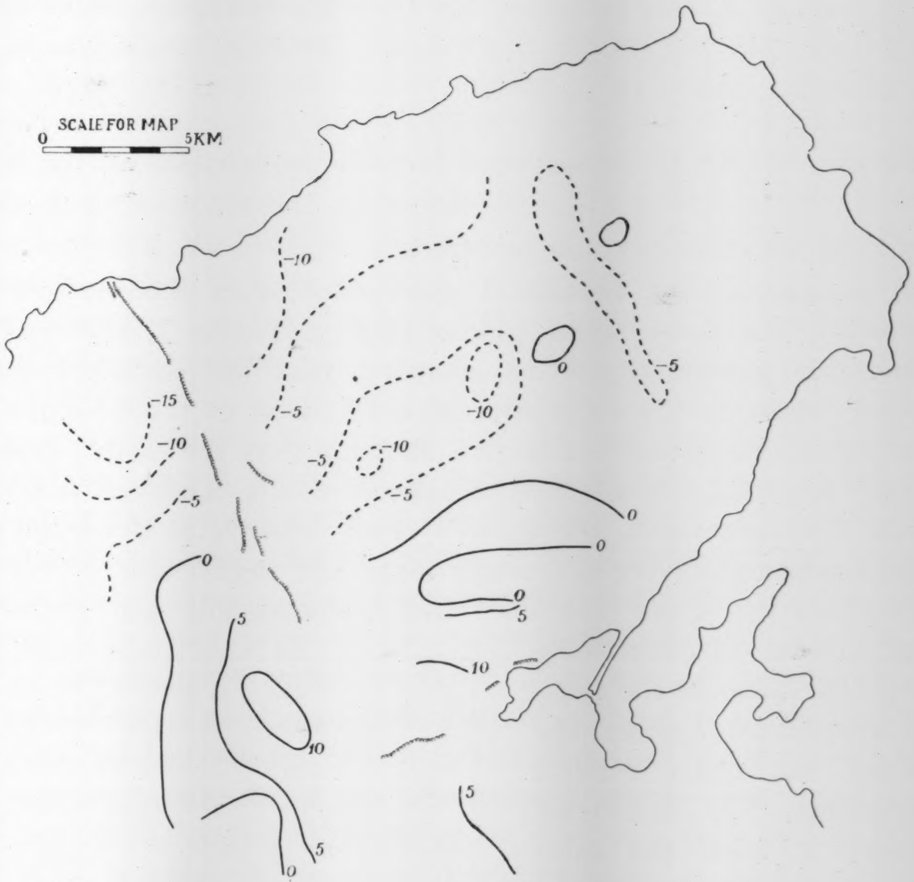
SCALE FOR MAP
0
5KM
-10
-5
0
-15
-10
-5
-10
-10
-5
-5
-5
0
0
0
0
5
5
10
10
10
5
5
0

Fig. 3. Distribution of rotation. (Numerals against contour lines designate amounts of rotation in 10^{-5})

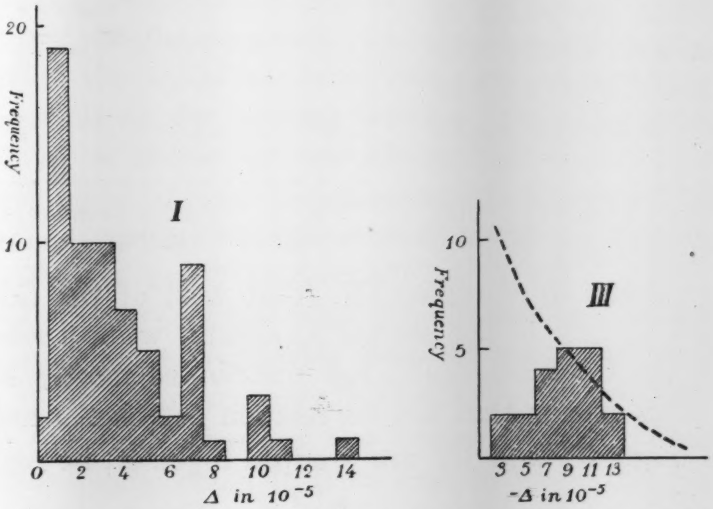

Fig. 4. Frequency distribution of Δ in regions I and III.

The former corresponds to the fact that the crustal deformation associated with this earthquake is localized within a relatively limited area, in fact, in a zone including the Gô-mura fault, the latter probably indicating that the earth's crust in the Tango peninsula was in general deformed as much as 7×10^{-5}.

3. We may expect to obtain some hints in explanation of the mechanism of crustal deformation by comparing the amounts of horizontal deformation with the vertical movements.

In comparing the horizontal divergence with the vertical earth movements[6], we notice at a glance that in region I, the horizontal divergence is generally positive, showing that the earth's crust was depressed, while, in the adjacent region III, west of the Gô-mura fault, the horizontal divergence is negative, showing that the earth's crust was elevated. Especially in the neighbourhood of the southern end of the apparent Gô-mura fault, the earth's crust was elevated conspicuously and the horizontal divergence fairly large and negative.

To study the above mentioned fact systematically and statistically, a diagram was constructed by plotting the values of the horizontal divergence against the values of the mean vertical displacements, δh, calculated for every 2×2 km the same squares as those for which the horizontal divergence was calculated. The result is shown in Fig. 5. Since the points in this diagram are widely dispersed, the linear relation between Δ and δh cannot be readily seen.

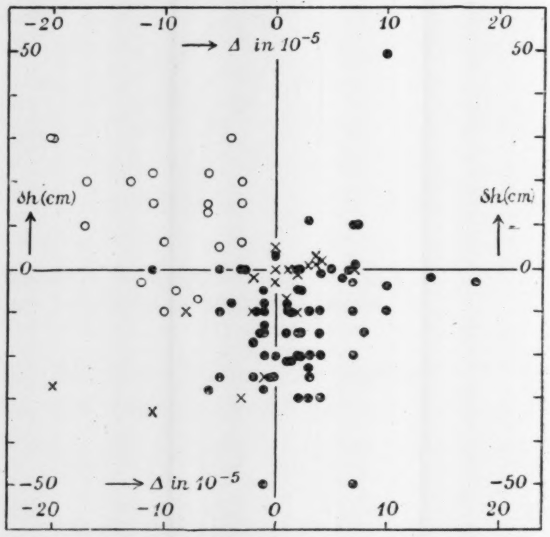

Fig. 5. Relation between Δ and δh in regions I (●), II (×), III (○).

We notice however that the points representing the relation between Δ and δh of region III, (that west of the Gô-mura fault) are distributed mainly in the second quadrant, while those of region I (that east of the Gô-mura fault) are distributed mostly in the fourth quadrant. This means that the correlation between Δ and δh may, if the points of region I and III are grouped together, be regarded on the whole as negative, i.e., that part of the region where the earth's crust was contracted horizontally has been elevated and the depressed part of the region has elongated horizontally.

---

[6] Rikuti Sokuryôbu (Military Land Survey), Report issued in 1930.

The points representing the relation between Δ and δh of region II are mostly concentrated in the neighbourhood of the origin of the coordinates, showing that crustal deformation in this region was not so marked as in other regions, either in horizontal or vertical direction.

If, however, a number of points distributed in the third quadrant, and representing the relation between Δ and δh of a part of region III adjacent to region II were grouped together with those concentrated in the neighbourhood of the origin of the coordinates, the correlation of Δ with δh will be positive.

4. From the distribution of rotational deformations, as shown in Fig. 3, it will be noticed in rather a conspicuous way that, in the neighbourhood of the southern end of the Gô-mura fault, the earth's crust was rotated counter-clockwise, while in the neighbourhood of Amino, i.e., near the northern end of the active Gô-mura fault, it was rotated clockwise. In other parts of the region under consideration, the difference in the modes of rotational deformation was not conspicuous.

The enormous rotational deformation in the zone including the active faults, as just shown, is due to the fact that the direction of the horizontal displacemants of the triangulation points distributed in different parts of the region through which Gô-mura fault passes, are opposite to each other, the amounts displaced being as large as 1 metre or more.

5. Next the horizontal displacements of each of triangulation point was reduced into two components, i.e., the component parallel to the general trend of the Gô-mura fault and the component perpendicular to it, the direction of the general trend of the Gô-mura fault being taken as N24°W, as shown by line *AB* in Fig. 1.

The distribution of the components of horizontal displacements perpendicular and parallel to the general trend of the Gô-mura fault are shown in Figs. 6 and 7 respectively.

From Fig. 6, the perpendicular components of the horizontal displacements appear to be continuous over the area that is traversed by the Gô-mura fault, their amounts generally being smaller in the eastern part of the fault than in the western part. As the sense of direction of these components is from east to west, the Gô-mura fault is thought as being made apparent by the crustal deformation to widen the crack of the fault, so far as the distribution of the perpendicular components of the horizontal displacements shows.

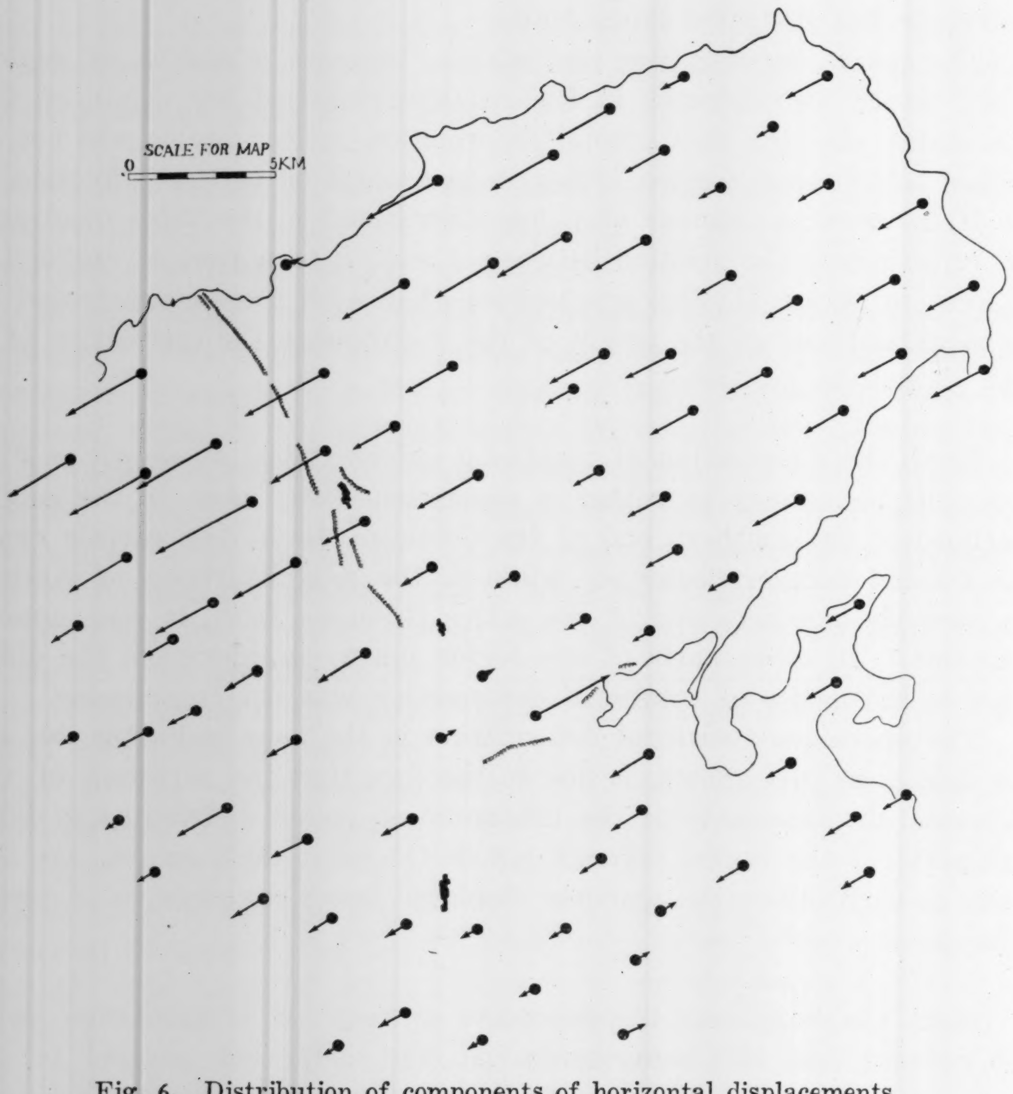

Fig. 6. Distribution of components of horizontal displacements, perpendicular to the trend of the Gô-mura fault.

A similar feature is also noticed in the parallel components, i.e., the components approximately perpendicular to the trend of the Yamada fault, as shown in Fig. 7.

It will also be noted that on different sides of the fault lines, the directions of the components of horizontal displacements parallel to their trends are reversed.

In the zone on the westward elongation of the Yamada fault, which elongation was not apparent at the time of the destructive earthquake, the components perpendicular to its trend show a contraction of the earth's crust while the components parallel to its trend do not show any signs of shearing deformation, having a burried fault-plane as a shear plane, so far as observed in zones where the fault lines are readily apparent.

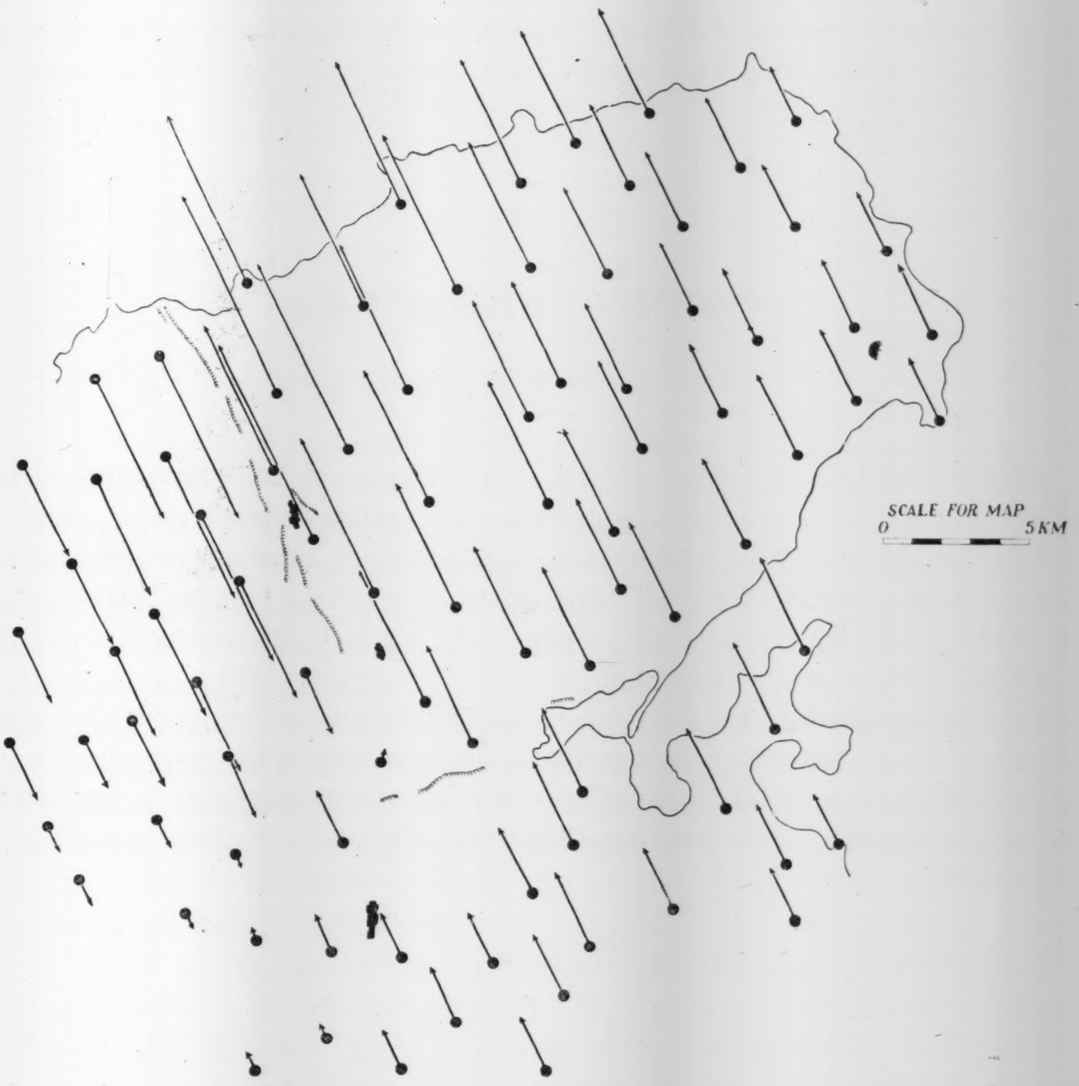

Fig. 7. Distribution of components of horizontal displacements, parallel to the trend of the Gô-mura fault.

Lastly, it should be remarked that the method of investigation described above is one way of studying the crustal deformation associated with the destructive Tango earthquake.

As the mechanism responsible for the appearance of faults on the surface of the earth, there may possibly be explanations, the results of analysis based on which may differ in several respects from the present

results described in this paper. The question then arises, what is the most probable explanation of the mechanism that brings about crustal deformation? We cannot, at present, answar the question, for we are not aware of any fact that would be a criterion of the question asked.

42. 丹後地方の地殼變形研究補遺

地震研究所 宮部直巳

丹後地方の地殼變形に關する坪井氏の研究並に筆者等の前報文に於いては，郷村斷層及び山田斷層の存在を無視し，これ等の斷層の過る地帶を通しても，地殼變形が連續的であつたと假定してある．これ等の斷層を境界とする兩側の地域での地殼變形は，この斷層地帶で不連續的であるとすることも亦一つの考へ方であるから，本文に於いては，さういふ見方で問題を取扱つてみた．その結果は，大體の變形の分布方式は以前に報告した所と大差なく，斷層地帶に於ける大なる變形の影響は豫期される通りなくなつてゐる．

又，水平移動を郷村斷層に略直角なる方向と，之に平行する方向との2成分に分析してその分布を調べてみると．斷層の新らしい割目の出顯した地域では，斷層に直角の方向には何れものびたやうな變形をなし，平行の方向に著しい *shear* のあつたことが認められた．併し，出顯した斷層の延長上の地帶では，この假想的斷層線に直角の方向には押し合び，之に平行なる方向に於ける *shear* は著しくない．

43. *Some Physical Properties of the Lava of Volcanoes Asama and Mihara.*

I. Electric Conductivity and Its Temperature-Coefficient.

By Takesi NAGATA.

Earthquake Research Institute

(Read May 18, 1937.—Received June 21, 1937.)

1. Introduction.

Recently a number of reports[1] have been published of studies of electric and magnetic disturbances accompanying activities of volcanoes, such, for example, as sudden variations in terrestrial magnetism and earth-current. Obviously, continuous and systematic observations of the phenomena, especially of their characteristics in detail, are most important in the present study, as also experimental investigations of the electric and magnetic properties of lava,[2] which may be related directly or indirectly to electric and magnetic disturbances. The writer, therefore, endeavoured to measure the magnetic susceptibility, coercive force, electric conductivity, and the ionization of volcanic lava, and their temperature-coefficients.

First, we measured the electric conductivity and the temperature-coefficient of a number of volcanic rocks ejected from the volcanoes Asama and Mihara. It is well known that conspicuous earth-current disturbances occur in connection with eruptions of volcanoes in the neighbourhood of craters. As possible causes of this phenomenon, there are several facts to be considered in connection with volcanic eruptions, such as electro-motive force due to inequalities in the extent of ionization of the lava in the crater, thermo-electric current produced by inequalities in its neighbourhood, and disturbances in the electric field around the crater due to anomalous variation in electric conductivity of lava in the volcano. Although we cannot at present say which of these is the most potent cause of the disturbances, a knowledge of the magnitude of the conductivity, it is believed, might furnish a clue to this problem.

---

[1] For example, Y. KATO, *Jap. Jour. Astr. Geophys.*, **12** (1934), 19.
T. MINAKAMI, *Bull. Earthq. Res. Inst.*, **13** (1935), 629 ; 790.

[2] Following reports have been published of studies on these characteristics of Mihara lava :—" Permanent magnetism of volcanic bombs " by S. NAKAMURA and S. KIKUCHI, *Proc. Tokyo. Math. Phys. Soc.*, **6** (1912), 268; " Measurement of electric conductivity etc. " by K. FUZI and T. MIZOGUCHI, *Proc. Tokyo. Math. Phys. Soc.*, **7** (1914), 243.

The variation in electric conductivity with temperature is expected to be closely related to that of the viscosity of the lava, as in the case of viscous glass, in which, as is known empirically, the reciprocal of the ionic conductivity varies linearly with the coefficient of viscosity. If this assumption holds in the case of volcanic lava, we can easily obtain the value of the temperature-coefficient of viscosity by measuring its electric conductivity, the absolute value of which, however, must be measured dynamically.

2. Method of Experiments.

The specimens were crushed fine, the diameter of the particles being about 0·1 mm. A portion of the crushed lava and a pair of electrodes were placed together with a thermo-junction in a Tammun-tube, 10 cm long and 1·8 cm in diameter, arranged as shown in Fig. 1. The electrodes, which were small platinum spheres of 1·7 mm diameter, were connected to the ends of platinum lead-wires 0·5 mm in diameter, inserted in porcelain tubes, except that part of the wires 1 mm from the centre of each sphere. The distance between these two electrodes was 11·5 mm, and the constant for reducing the apparent conductivity into specific conductivity was determined by using fused NaCl and dilute solution of H_2SO_4. In the beginning of this experiment, the conductivity was measured by the so-called Kohlrausch bridge method. Provided a higher order of accuracy is not required, the method of directly measuring the resistance is also applicable, experiment by this method being easier. Consequently in most of the experiments, the conductivity was measured directly. To render the polarization effect as small as possible, alternating-current of 50-cycles was used throughout this experiment. The procedures in these two methods are shown in Figs. 2, and 3.

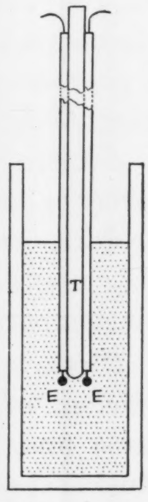

Fig. 1. Arrangement of electrode with specimen.
E; Electrode.
T; Thermo-junction.

3. Results of Experiment.

The electric conductivity of Miharaite (basic molten lava of Volcano Mihara) ejected in 1913, and that of olivine-bearing-hypersthene-augite-andesite (the bread-crust bomb) of Volcano Asama ejected in September, 1929, were measured at various temperature ranging from 400°C to 1250°C. The chemical composition of these two rocks are reproduced in Table I from the papers by S. Tsuboi[3] (for Mihara) and by H. Tsuya[4] (for Asama).

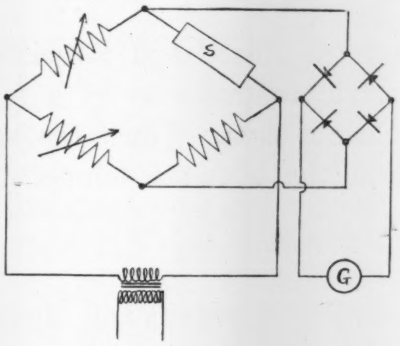

Fig. 2. Electric connection in bridge method.
S; Specimen.
G; Galvanometer.

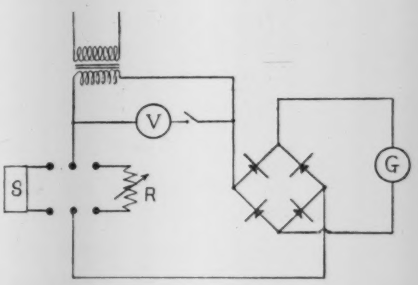

Fig. 3. Electric connection in direct measurement method.
S; Specimen.
R; Standard variable resistance.

Table I. Bulk Compositions of Specimens.

	Mihara	Asama
SiO_2	51·45	60·24
Al_2O_3	16·84	16·43
Fe_2O_3	1·49	1·54
FeO	10·95	5·26
MgO	4·48	3·92
CaO	10·71	7·02
Na_2O	—	3·00
Mg_2O_3	1·23	—
K_2O	0·37	1·16
H_2O+	0·72	1·17
H_2O-		0·06
TiO_2	1·27	0·70
P_2O_5	0·26	0·13
M_n O	0·19	0·11

---

3) Y. Okamura, *Rep. Geol. Surv.*, **48** (1914),

4) H. Tsuya, *Bull. Earthq. Res. Inst.*, **11** (1933), 575.

The heating and cooling velocities were nearly uniform, and times required for raising the temperature from 300°C to 1250°C and that for lowering from 1200°C to 300°C were about three hours. The relation between the reciprocal of the absolute temperature and the logarithm of the specific electric conductivity was shown in Figs. 4, and 5.

From these figures, it will be seen that the Rasch and Hinrichsen formula⁵⁾ for temperature effect on the electric conductivity of a fused salt in amorphous state is applicable to volcanic lava. Thus, the relation between the specific conductivity σ and the absolute temperature T of lava is expressed by the formula,

$$\log \sigma = A - B/T, \tag{1}$$

where A and B are constants, each of which is significant thermodynamically. Differentiating both sides of equation (1) with respect to T, we have

$$\frac{d \log \sigma}{dT} = \frac{C}{RT^2}. \tag{2}$$

This equation is a modified form of van't Hoff's equation reffered to by Rasch and Hinrichsen.⁶⁾

In the case of Miharaite, the formula is not so exact as in Asama

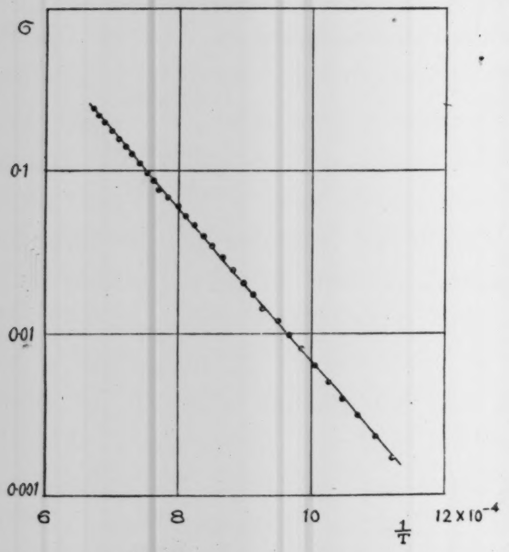

Fig. 4. Relation between temperature and specific electric conductivity of Asama lava in amorphous state.

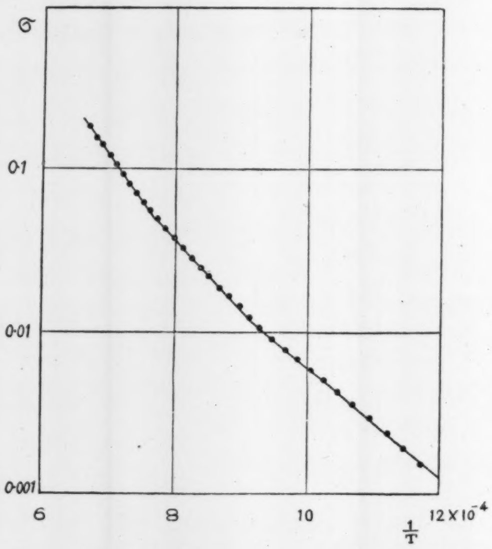

Fig. 5. Relation between temperature and specific electric conductivity of Mihara lava in amorphous state.

---

5) E. RASCH and F. W. HINRICHSEN, *Z. S. f. Elektroch.*, **14** (1908), 41.

6) loc. cit.

lava. In a similar case of glass, L. L. Holladay[7] proposed theoretically another formula of the form

$$\log\sigma = A - \frac{1}{2}\log T - B/T, \tag{3}$$

although there seems to be some arbitrariness in his theoretical considerations. In opposition to Holladay's theory, H. Schönborn[8] explained the deviation from the linear relation between $\log\sigma$ and $1/T$ by pointing out the existence of a critical point where the chemical state of the glass changed discontinuously and the temperature-coefficient in equation (1) also changed discontinuously at this point. Although the writer will not attempt here to criticize this problem, his further studies are expected to provide an explanation of the foregoing deviation from the linear relation.

The curves in Fig. 6 show the variations in intensity of the current that flows through the specimen when the alternating-voltage applied in each case was 10·5, 6·3, and 4·2 volts respectively. Supposing that I is the current-flow, σ the specific conductivity, V the applied voltage, and C a constant depending on the dimensions of the specimen, the following relation is established when the conductivity is measured directly,

$$I = C\sigma V.$$

From the curves shown in Fig. 6, there is no change in the relation between $\log\sigma$ and $1/T$, even if the magnitude of the applied voltage is changed. For the purpose of ascertaining whether the relation does not depend on applied voltage, the conductivity was measured at temperatures of 820°, 960°, 1050°, and 1190°C, at various voltages ranging from 0·01 to 10·0 volts. The results are shown in Fig. 7. The curves in the figure show that current and field intensity are in linear relation, that is, the conductivity is independent of the applied voltage.

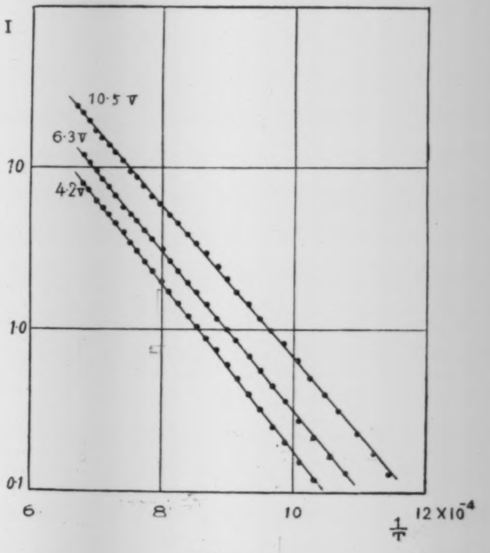

Fig. 6.

---

[7] L. L. HOLLADAY, *Journ. Frank. Inst.*, **229** (1923), 195.

[8] H. SCHÖNBORN, *Z. S. f. Phys.*. **22** (1924), 305.

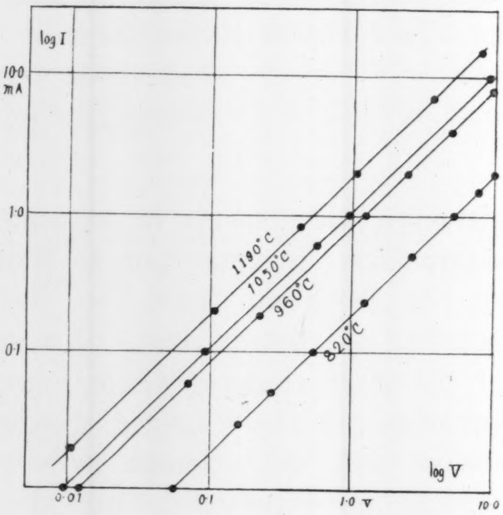

Fig. 7.

In heating the specimens, the existence of a critical point was noticed at 1130°C, as shown in Fig. 8. The equation $\log\sigma = A - B/T$ is applicable within the range of temperature from 400°C to 900°C, whereas at temperature higher than 960°C, coefficient B gradually diminishing, which however increases discontinuously at 1130°C. The existence of this critical point at 1130°C is a common feature of igneous rocks ejected from Asama and from Mihara. At this critical point some portion of the rocks may begin to melt. Upon heating powdered specimen at room temperature, which will hereafter be called "initial heating," the curve showing the relation of conductivity to temperature breaks at 1130°C, as shown in Figs. 9, and 10. In these two different states, i.e., the one lower than and the other higher than 1130°C, the decomposition-voltages differ. It was found to be 1·60 volts in the former and 0·95 volts in the latter states respectively, which shows that the ionized molecules govering electric conduction differ in these two states. From these results, the temperature of 1130°C may be regard-

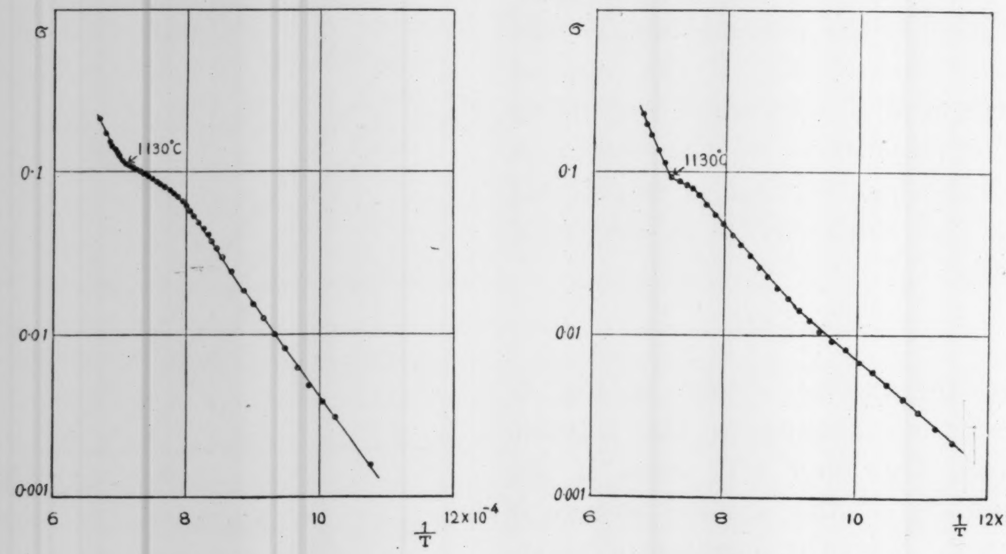

Fig. 8. (a) Fig. 8. (b)

Relation between σ and T in heating process.

(a) Asama lava. (b) Mihara lava.

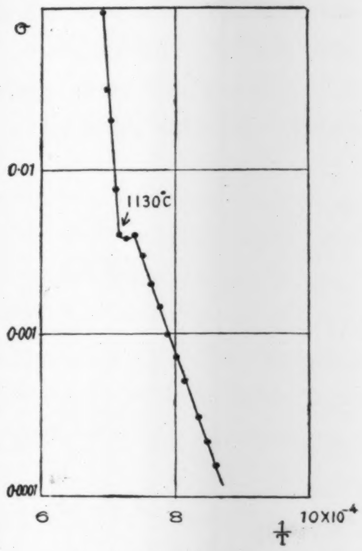

Fig. 9. Relation between σ and T in initial heating process. (Mihara lava)

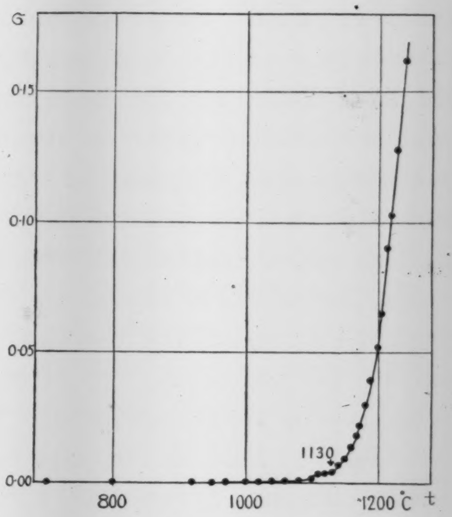

Fig. 10. Relation between σ and t in initial heating process. (Asama lava)

ed as the beginning of the apparent melting of these two rocks, though they are partly ionized at lower temperature than 1130°C. It may be regarded as rather natural that, in cooling, they assume the over-cooled state just as in the case of ordinary glass, with slight recrystallization or transition, the rock being, as a whole, in the amorphous state. The conductivity obtained at the temperature of our experiment may not be exactly the same as that in the final chemical state of the rocks at the same temperature, seeing that the extraordinary slowness in the velocity of chemical reaction in these rocks should be taken into the consideration. In other words, each state in the heating or cooling process in our experiments is not in heterogeneous equilibrium. Notwithstanding this defect, petrologically, the results of our experiments are satisfactory for our purpose of estimating the order of magnitude of earth-current disturbances due to anomalies in the conductivity of heated lava, or of securing a general idea of viscosity-variation due to temperature.

4. Earth-Current and Electric Conductivity of Lava.

As mentioned in § 1, the earth-current varies when the electric conductivity of a part of the earth's crust undergoes marked changes. From our experiments, at temperatures higher than 1200°C[9] the specific resistivity of andesite and basalt is smaller than 5 ohm cm, while at room temperature, that of igneous rocks, sand-stones, and other soils is of the order of $10^3 \sim 10^5$ ohm/cm.[10] We shall now estimate the magnitude of the anomaly just mentioned. In the case of a volcano, we could consider a simple model like the following: for the sake of simplicity, we shall deal with a two-dimensional problem. In Fig. 11, the circle represents the boundary of the crater, in the outer region of which the electric conductivity σ_2 of the medium is homogeneous, and in the inner region of which the conductivity σ_1 is also uniform. We assume that the electric field E is constant at points infinitely distant from the circle. With these assumptions, we get for the field of the stationary current,

---

[9] Approximate values of temperature of the heated lava in craters have been reported as follows. 1000°C (Mihara), 1000°C (Asama), 1100~1300°C (Kilauea), 1150~1180°C (Vesuvius), 1100~1150°C (Storomboli).

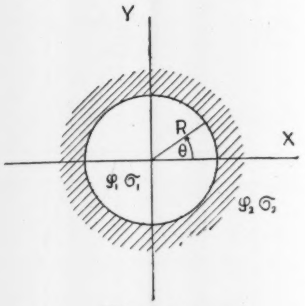

Fig. 11.

$$\left.\begin{aligned} \mathbf{i} &= -\sigma \operatorname{grad} \varphi \\ \sigma_1 \nabla^2 \varphi_1 &= 0 \\ \sigma_2 \nabla^2 \varphi_2 &= 0 \end{aligned}\right\}, \tag{1}$$

where φ_1 and φ_2 are the potentials in the inner and outer regions of the boundary-circle of radius R.

The boundary-conditions (contact electro-motive force at the boundary not taken into consideration) are

$$\left.\begin{aligned} &(\varphi_1)_{r=R} - (\varphi_2)_{r=R} = 0 \\ &\sigma_1 \left(\frac{\partial \varphi_1}{\partial r}\right)_{r=R} - \sigma_2 \left(\frac{\partial \varphi_2}{\partial r}\right)_{r=R} = 0 \\ &\left(\frac{\partial \varphi_2}{\partial x}\right)_{r=\infty} = -E, \ \left(\frac{\partial \varphi_2}{\partial y}\right)_{r=\infty} = 0 \end{aligned}\right\}. \tag{2}$$

From these equations and boundary-conditions, we get the following solutions in polar-coordinate, the origin of which has been taken at the centre of the circle, and azimuth θ is measured with reference to the X-axis,

$$\left.\begin{aligned} \varphi_1 &= C - \frac{2E\sigma_2}{\sigma_1 + \sigma_2} \, r \cos\theta \\ \varphi_2 &= C - Er\cos\theta + \frac{\sigma_1 - \sigma_2}{\sigma_1 + \sigma_2} E \ \ r^2 \cos\theta \end{aligned}\right\}. \tag{3}$$

---

[10] *Handb. d. Exp. Phys.*, XXV, 3. Teil p.p. 464~471.
T. HATTORI and R. OGIMURA, *Bull. Geotech. Comm. Gov. Railways Japan*, **3** (1934), 192.

Outside the circle, the intensity of the electric field is expressed by

$$\left.\begin{aligned} E_x &= -\frac{\partial\varphi_2}{\partial x} = E\left\{1+\frac{\sigma_1-\sigma_2}{\sigma_1+\sigma_2}\left(\frac{R}{r}\right)^2\cos 2\theta\right\} \\ E_y &= -\frac{\partial\varphi_2}{\partial y} = E\frac{\sigma_1-\sigma_2}{\sigma_1+\sigma_2}\left(\frac{R}{r}\right)^2\sin 2\theta \end{aligned}\right\}. \tag{4}$$

If the results of this calculation can be applied to the problem of disturbances in the earth-current in the vicinity of the crater, the magnitude of the disturbances in the electric field due to anomalies in the conductivity of lava in the crater, is given by the formula,

$$\varDelta E = E\frac{\sigma_1-\sigma_2}{\sigma_1+\sigma_2}\left(\frac{R}{r}\right)^2. \tag{5}$$

As we have dealt with a stationary state in the foregoing considerations, the results cannot be used in explaining the case of a sudden commencement of disturbances due to abrupt change in conductivity. It can be used only in explaining a gradual change in the electric field.

When the lava in the crater is in the molten state, the ratio σ_1/σ_2 amounts to $10^3 \sim 10^5$ and $\varDelta E \simeq +E(R/r)^2$, whereas if the interior of the crater were approximately hollow, $\varDelta E = -E(R/r)^2$. It is possible for the electric field actually to vary between these two extreme cases. Further detailed discussion must be withheld until the survey of the electric field in the vicinity of the volcano is completed.

5. Viscosity and Electric Conductivity of Lava.

In our experiment, the electric conductivity of lava in the amorphous state satisfies approximately the equation

$$\log\sigma = A - B/T, \quad \therefore\ \sigma = ae^{-\frac{B}{T}}.$$

This means that the velocity of the ions in electric conduction are distributed microscopically after Maxwell's law. As in the fluid state, Stokes' law may be invoked in considering the effect of viscosity on the motion of these ions, provided Maxwell's distribution is assumed. Then

$$u = \frac{k}{6\pi r\eta}, \tag{1}$$

where u is the velocity of the ions, η the coefficient of viscosity, K the intensity of the electric field, and r the radius of an ion. On the other hand, the specific conductivity σ is given by

$$\sigma = NuzF, \tag{2}$$

where N is the number of ions in unit volume, z the electric charge of an ion, and F Faraday's constant. From equations (1) and (2), we get

$$\sigma = \frac{NzFK}{6\pi r} \cdot \frac{1}{\eta}. \tag{3}$$

Taking $(NzFK)/(6\pi r) = \text{constant} = C$, and $1/\sigma = \text{specific resistivity} = w$, we have

$$w = C\eta. \tag{4}$$

Although this relation does not exactly hold in the case of vitreous substances, it may be used in estimating the values of the coefficient of viscosity, as measurement of conductivity is not so difficult compared with measurement of viscosity by dynamical methods.

In glass engineering, F. F. S. Bryson[11] showed that an approximate parallelism between w and η holds in the case of ordinary glass. Seeing that both glass and volcanic lava are silicates, it would seem that in the case of volcanic lava, it would also be practicable to estimate the variation in viscosity by measuring its electric conductivity. This problem is now receiving the attention of the writer.

6. Conclusion.

This report is a preliminary study on the electric and magnetic properties of volcanic lava, in which the general aspects of the relation between electric conductivity and temperature is discussed, details of which appear in a following paper.

In couclusion, the writer wishes to express here his sincere thanks to Prof. M. Ishimoto and Dr. R. Takahasi for their encouragement in this study. His cordial thanks are also due to Dr. H. Tsuya for his interest in the present work.

---

[11] F. F. S. BRYSON, *Journ. Soc. Glass Tech.*, **11** (1927), 331.

5

43. 淺間及三原火山熔岩の物理的性質

I. 電氣傳導度及び其の溫度變化

地震研究所 永田 武

最近火山活動に伴ふ，地殼の電磁氣的要素の變化の研究が盛んになつたが，一方に於いては火山熔岩の電磁氣的性質を實驗的に調べる事も，此の問題に關連して興味ある事さ思ふ．

從來此の種の實驗的研究は，二，三斷片的に報告されたものがあるが，筆者はいま少しく組織的に淺間及三原兩火山の代表的噴出熔岩に就いて，其の電磁氣的性質を調べる事にした．

本報告では，先づ熔岩の電氣傳導度の溫度による變化を調べ，1130°C 附近に變異點が存在して，之以上の溫度に於いては，電氣傳導度が急激に增加よる事，又玻璃狀態を保たしめて冷却する時には，$\log \sigma = A - B/T$（σ は比電氣傳導度，T は絕對溫度，A, B は常數）の關係が適用される事が分つた．

この實驗結果の應用さして，地電流の變化，赤熱熔岩の粘度の溫度變化等に對して，若干の議論を行つた．

44. *Notes on the Origin of Earthquakes.* (*Third paper.*)

By Win INOUYE,

Earthquake Research Institute.

(Read April 20, 1937.—Received June 21, 1937.)

1. *Introduction*

In his previous papers,[1] the writer, under the same title as above, discussed theoretically the mechanisms of radiations of earthquake waves from a seismic origin, assuming their shape to be spherical. Should the pressure in the volcanic vent change, or should faults be newly formed or activated by certain endogenic forces, earthquake waves would emanate from these origins. In these cases, it is preferable to regard these waves as having originated from line sources than that they did so from spherical origins. Moreover, if, generally speaking, we regard the elastic waves as having originated from fissures opened in the earth's crust by the action of certain forces, it would seem to the author that all that is sufficient as a first step is to assume that they originated as the result of certain changes in the normal and tangential stresses at the boundaries of the line sources.

In the following paragraphs, the writer discusses the foregoing problem in two dimensions only, leaving the cases for three dimensions to a future opportunity.

2. *Elliptic Origin*

The equations of motion in an isotropic homogeneous elastic body in elliptic coordinates are given by

$$\left.\begin{aligned} \rho\frac{\partial^2\Delta}{\partial t^2} &= \frac{\lambda+2\mu}{c^2(\cosh^2\xi-\cos^2\eta)}\left(\frac{\partial^2\Delta}{\partial\xi^2}+\frac{\partial^2\Delta}{\partial\eta^2}\right) \\ \rho\frac{\partial^2\varpi}{\partial t^2} &= \frac{\mu}{c^2(\cosh^2\xi-\cos^2\eta)}\left(\frac{\partial^2\varpi}{\partial\xi^2}+\frac{\partial^2\varpi}{\partial\eta^2}\right) \end{aligned}\right\},$$

where

ξ, η=curvilinear coordinates related to Cartesian coordinates (x, y) in the form,

---

[1] W. INOUYE, *Bull. Earthq. Res. Inst.*, **14** (1936), 582; **15** (1937), 90.

$$\left.\begin{array}{l} x = c\cosh\xi\cos\eta \\ y = c\sinh\xi\sin\eta \end{array}\right\},$$

$$\left.\begin{array}{l} \Delta = h_1^2\left\{\dfrac{\partial}{\partial\xi}\left(\dfrac{u}{h_1}\right)+\dfrac{\partial}{\partial\eta}\left(\dfrac{v}{h_1}\right)\right\} \\[2ex] 2\varpi = h_1^2\left\{\dfrac{\partial}{\partial\xi}\left(\dfrac{v}{h_1}\right)+\dfrac{\partial}{\partial\eta}\left(\dfrac{u}{h_1}\right)\right\} \\[2ex] \dfrac{1}{h_1^2} = c^2(\cosh^2\xi-\cos^2\eta) \end{array}\right\},$$

where

u, v = components of displacement referred to curvilinear coordinates, ξ and η, respectively,

ρ = density of isotropic solid,

λ, μ = Lame's elastic constants.

According to Prof. K. Sezawa[2] the solutions of these equations are expressed by

$$\left.\begin{array}{l} \Delta = \sum\limits_{n=0}^{\infty} B_n H_n(\xi,\ q)\begin{Bmatrix} ce_n(\eta,\ q) \\ se_n(\eta,\ q)\end{Bmatrix}e^{ipt} \\[2ex] 2\varpi = \sum\limits_{n=0}^{\infty} C_n H_n(\xi,\ q')\begin{Bmatrix} ce_n(\eta,\ q') \\ se_n(\eta,\ q')\end{Bmatrix}e^{ipt} \end{array}\right\}, \tag{1}$$

where $q=\dfrac{h^2c^2}{32}$, $q'=\dfrac{k^2c^2}{32}$, $\dfrac{\rho p^2}{\lambda+2\mu}=h^2$, $\dfrac{\rho p^2}{\mu}=k^2$,

$H_n(\xi,\ q)$, $H_n(\xi,\ q')$ are the solutions of the following equations,

$$\left.\begin{array}{l} \dfrac{d^2H_n(\xi,\ q)}{d\xi^2}+(h^2c^2\cosh^2\xi-n^2)H_n(\xi,\ q)=0 \\[2ex] \dfrac{d^2H_n(\xi,\ q')}{d\xi^2}+(k^2c^2\cosh^2\xi-n^2)H_n(\xi,\ q')=0 \end{array}\right\}. \tag{2}$$

Whence the components of displacement of the dilatational wave that answers to Δ and satisfies $\varpi=0$ in (1) are given by

$$u_1 = -\sum_{n=0}^{\infty}\frac{B_n}{h^2c\sqrt{\cosh^2\xi-\cos^2\eta}}\frac{\partial H_n(\xi,q)}{\partial\xi}\begin{Bmatrix} ce_n(\eta,q) \\ se_n(\eta,q)\end{Bmatrix}e^{ipt}$$

---

[2] K. SEZAWA, *Bull. Earthq. Res. Inst.*, **5** (1928), 59.

$$\left. v_1 = -\sum_{n=1}^{\infty} \frac{B_n}{h^2 c\sqrt{\cosh^2 \xi - \cos^2 \eta}} H_n(\xi, q) \left\{ \begin{matrix} \dfrac{\partial ce_n(\eta, q)}{\partial \eta} \\ \dfrac{\partial se_n(\eta, q)}{\partial \eta} \end{matrix} \right\} e^{ipt} \quad \right\}.$$

The components of displacement of the distortional wave that satisfies $\Delta = 0$ are given by

$$\left. \begin{aligned} u_2 &= -\sum_{n=1}^{\infty} \frac{C_n}{k^2 c\sqrt{\cosh^2 \xi - \cos^2 \eta}} H_n(\xi, q') \left\{ \begin{matrix} \dfrac{\partial ce_n(\eta, q')}{\partial \eta} \\ \dfrac{\partial se_n(\eta, q')}{\partial \eta} \end{matrix} \right\} e^{ipt} \\ v_2 &= -\sum_{n=1}^{\infty} \frac{C_n}{k^2 c\sqrt{\cosh^2 \xi - \cos^2 \eta}} \frac{\partial H_n(\xi, q')}{\partial \xi} \left\{ \begin{matrix} ce_n(\eta, q') \\ se_n(\eta, q') \end{matrix} \right\} e^{ipt} \end{aligned} \right\}.$$

Since on the surface, $\xi = \xi_0$, the two equations

$$\lambda \Big[\Delta \Big]_{\xi=\xi_0} + 2\mu \left[\frac{1}{c\sqrt{\cosh^2 \xi - \cos^2 \eta}} \frac{\partial (u_1 + u_2)}{\partial \xi} \right.$$

$$\left. + \frac{v_1 + v_2}{c^2(\cosh^2 \xi - \cos^2 \eta)} \frac{\partial}{\partial \eta} \left(c\sqrt{\cosh^2 \xi - \cos^2 \eta} \right) \right]_{\xi=\xi_0} = \text{normal stress},$$

$$\mu \left[\frac{\partial}{\partial \xi} \left(\frac{v_1 + v_2}{c\sqrt{\cosh^2 \xi - \cos^2 \eta}} \right) + \frac{\partial}{\partial \eta} \left(\frac{u_1 + u_2}{c\sqrt{\cosh^2 \xi - \cos^2 \eta}} \right) \right]_{\xi=\xi_0}$$

$$= \text{tangential stress}$$

must hold.

3. *Line Origin*

If now we consider a line origin, we may put $\xi_0 = 0$, and for simplicity, put $\lambda = \mu$.

The normal stress at the origin is then given by
normal stress $(\equiv \Phi(\eta)\, e^{ipt})$

$$= \mu e^{ipt} \left[\sum_{n=0}^{\infty} B_n H_n(\xi, q)\, ce_n(\eta, q) \right.$$

$$+ 2 \left[\frac{1}{c\sqrt{\cosh^2 \xi - \cos^2 \eta}} \left\{ - \sum_{n=0}^{\infty} \frac{-B_n \cosh \xi \sinh \xi}{h^2 c(\cosh^2 \xi - \cos^2 \eta)^{\frac{3}{2}}} \frac{\partial H_n(\xi, q)}{\partial \xi} ce_n(\eta, q) \right. \right.$$

$$- \sum_{n=0}^{\infty} \frac{B_n}{h^2 c\sqrt{\cosh^2 \xi - \cos^2 \eta}} \frac{\partial^2 H_n(\xi, q)}{\partial \xi^2} ce_n(\eta, q)$$

$$+\sum_{n=1}^{\infty}\frac{-C_n\cosh\xi\sinh\xi}{k^2c(\cosh^2\xi-\cos^2\eta)^{\frac{3}{2}}}H_n(\xi,q')\frac{\partial se_n(\eta,q')}{\partial\eta}$$

$$+\sum_{n=1}^{\infty}\frac{C_n}{k^2c\sqrt{\cosh^2\xi-\cos^2\eta}}\frac{\partial H_n(\xi,q')}{\partial\xi}\frac{\partial se_n(\eta,q')}{\partial\eta}\Bigg\}$$

$$+\Bigg\{-\sum_{n=1}^{\infty}\frac{B_n}{h^2c^3(\cosh^2\xi-\cos^2\eta)^{\frac{3}{2}}}H_n(\xi,q)\frac{\partial ce_n(\eta,q)}{\partial\eta}$$

$$-\sum_{n=1}^{\infty}\frac{C_n}{k^2c^3(\cosh^2\xi-\cos^2\eta)^{\frac{3}{2}}}\frac{\partial H_n(\xi,q')}{\partial\xi}se_n(\eta,q')\Bigg\}$$

$$\times c(\cosh^2\xi-\cos^2\eta)^{-\frac{1}{2}}\cos\eta\sin\eta\Bigg]\Bigg]_{\xi=0}.$$

The upper equation of (2) for a small value of ξ may be written in the form,[3]

$$\frac{d^2H_n(\xi,q)}{d\xi^2}+\left[(h^2c^2-n^2)+h^2c^2\left(\xi^2+\frac{\xi^4}{3}+\cdots\right)\right]H_n(\xi,q)=0.$$

Putting $H_n(\xi,q)$ in the expanded form,

$$H_n(\xi,q)=a_0+a_1\xi+a_2\xi^2+\cdots$$

and neglecting small quantities of the second order, we obtain,

$$H_n(\xi,q)=e^{-i\sqrt{h^2c^2-n^2}\,\xi}.$$

In the same manner we obtain,

$$H_n(\xi,q')=e^{-i\sqrt{k^2c^2-n^2}\,\xi}.$$

Thus the normal stress at the boundary reduces to

$$\Phi(\eta)e^{ipt}=\mu e^{ipt}\Bigg[\sum_{n=0}^{\infty}B_nce_n(\eta,q)$$

$$+\frac{1}{\sin^2\eta}\Bigg\{-\sum_{n=0}^{\infty}\alpha_nB_nce_n(\eta,q)+\sum_{n=1}^{\infty}\beta_nC_n\frac{\partial se_n(\eta,q')}{\partial\eta}\Bigg\}$$

$$+\frac{\cos\eta}{\sin^3\eta}\Bigg\{-\sum_{n=1}^{\infty}\gamma B_n\frac{\partial ce_n(\eta,q)}{\partial\eta}-\sum_{n=1}^{\infty}\beta_nC_nse_n(\eta,q')\Bigg\}\Bigg],$$

---

3) K. SEZAWA, *Bull. Earthq. Res. Inst.*, **2** (1927), 29.

where

$$\left.\begin{aligned}\alpha_n &= -2\left(1-\frac{n^2}{k^2c^2}\right)\\ \beta_n &= \frac{-2i\sqrt{k^2c^2-n^2}}{k^2c^2}\\ \gamma &= \frac{2}{h^2c^2}\end{aligned}\right\}.$$

The tangential stress at the origin is given by tangential stress $(\equiv\Phi'(\eta)e^{ipt})$

$$\begin{aligned}&=\mu e^{ipt}\Bigg[\frac{\partial}{\partial\xi}\left[-\sum_{n=1}^{\infty}\frac{B_n}{h^2c^2(\cosh^2\xi-\cos^2\eta)}H_n(\xi,q)\frac{\partial ce_n(\eta,q)}{\partial\eta}\right]\\
&+\frac{\partial}{\partial\xi}\left[-\sum_{n=1}^{\infty}\frac{C_n}{k^2c^2(\cosh^2\xi-\cos^2\eta)}\frac{\partial H_n(\xi,q')}{\partial\xi}se_n(\eta,q')\right]\\
&+\frac{\partial}{\partial\eta}\left[-\sum_{n=0}^{\infty}\frac{B_n}{h^2c^2(\cosh^2\xi-\cos^2\eta)}\frac{\partial H_n(\xi,q)}{\partial\xi}ce_n(\eta,q)\right]\\
&+\frac{\partial}{\partial\eta}\left[\sum_{n=1}^{\infty}\frac{C_n}{k^2c^2(\cosh^2\xi-\cos^2\eta)}H_n(\xi,q')\frac{\partial se_n(\eta,q')}{\partial\eta}\right]\Bigg]_{\xi=0}\\
&=\mu e^{ipt}\Bigg[-\frac{\alpha'_0B_0}{\sin^2\eta}\frac{\partial ce_0(\eta,q)}{\partial\eta}-2\sum_{n=1}^{\infty}\frac{\alpha'_nB_n}{\sin^2\eta}\frac{\partial ce_n(\eta,q)}{\partial\eta}\\
&-\sum_{n=0}^{\infty}\frac{-\alpha'_nB_n\sin2\eta}{\sin^4\eta}ce_n(\eta,q)-\sum_{n=1}^{\infty}\frac{\beta'_nC_n}{\sin^2\eta}se_n(\eta,q')\\
&+\sum_{n=1}^{\infty}\left\{\frac{-\gamma'C_n\sin2\eta}{\sin^4\eta}\frac{\partial se_n(\eta,q')}{\partial\eta}+\frac{\gamma'C_n}{\sin^2\eta}\frac{\partial^2se_n(\eta,q')}{\partial\eta^2}\right\}\Bigg],\end{aligned}$$

where

$$\left.\begin{aligned}\alpha'_n &= \frac{-i\sqrt{h^2c^2-n^2}}{h^2c^2}\\ \beta'_n &= \frac{-(k^2c^2-n^2)}{k^2c^2}\end{aligned}\right\}.$$

$$\gamma' = \frac{1}{k^2c^2} \quad \Bigg\}$$

Since we cannot proceed further in the general manner, we must content ourselves by solving the problem approximately. We accordingly use Mathieu functions of the 0th to 6th orders, and, neglect the higher terms in q.

The Mathieu functions[4] are then given by

$$\left.\begin{aligned}
ce_0 &= 1+4q\cos 2\eta \\
ce_1 &= \cos\eta + q\cos 3\eta \\
ce_2 &= \cos 2\eta + q\left(\frac{2}{3}\cos 4\eta - 2\right) \\
ce_3 &= \cos 3\eta + q\left(-\cos\eta + \frac{1}{2}\cos 5\eta\right) \\
ce_4 &= \cos 4\eta + q\left(-\frac{2}{3}\cos 2\eta + \frac{2}{5}\cos 6\eta\right) \\
ce_5 &= \cos 5\eta + q\left(-\frac{1}{2}\cos 3\eta + \frac{1}{3}\cos 7\eta\right) \\
ce_6 &= \cos 6\eta + q\left(-\frac{2}{5}\cos 4\eta + \frac{2}{7}\cos 8\eta\right)
\end{aligned}\right\},$$

$$\left.\begin{aligned}
se_1 &= \sin\eta + q\sin 3\eta \\
se_2 &= \sin 2\eta + \frac{2}{3}q\sin 4\eta \\
se_3 &= \sin 3\eta + q\left(-\sin\eta + \frac{1}{2}\sin 5\eta\right) \\
se_4 &= \sin 4\eta + q\left(-\frac{2}{3}\sin 2\eta + \frac{2}{5}\sin 6\eta\right) \\
se_5 &= \sin 5\eta + q\left(-\frac{1}{2}\sin 3\eta + \frac{1}{3}\sin 7\eta\right) \\
se_6 &= \sin 6\eta + q\left(-\frac{2}{5}\sin 4\eta + \frac{2}{7}\sin 8\eta\right)
\end{aligned}\right\}.$$

---

4) B van der Pol and M.J.O. Strutt, *Phil. Mag.*, **5** (1928), 18; M.J.O. Strutt, *Ann. d. Phys.*, **84** (1927), 485.

Introducing these equations into the boundary conditions given above, the normal and tangential stresses at the origin are expressed by

normal stress $\left(\equiv a_o+\sum_{n=1}^{\infty} a_n \cos n\eta\right)$

$$\begin{aligned}
&=\mu\Big[\{\varepsilon_{1,0}B_0+\varepsilon_{1,2}B_2+\varepsilon_{1,4}B_4+\varepsilon_{1,6}B_6+\nu_{1,2}C_2+\nu_{1,4}C_4+\nu_{1,6}C_6\}\\
&+(B_1, B_3, B_5, C_1, C_3, C_5,)\cos\eta\\
&+\{\varepsilon_{2,0}B_0+\varepsilon_{2,2}B_2+\varepsilon_{2,4}B_4+\varepsilon_{2,6}B_6+\nu_{2,2}C_2+\nu_{2,4}C_4+\nu_{2,6}C_6\}\cos 2\eta\\
&+(B_1, B_3, B_5, C_1, C_3, C_5)\cos 3\eta\\
&+\{\varepsilon_{3,2}B_2+\varepsilon_{3,4}B_4+\varepsilon_{3,6}B_6+\nu_{3,4}C_4+\nu_{3,6}C_6\}\cos 4\eta\\
&+(B_1, B_3, B_5, C_1, C_3, C_5)\cos 5\eta\\
&+\{\varepsilon_{4,0}B_0+\varepsilon_{4,2}B_2+\varepsilon_{4,4}B_4+\varepsilon_{4,6}B_6\}\frac{1}{\sin^2\eta}\\
&+(B_1, B_3, B_5, C_1, C_3, C_5)\frac{\cos\eta}{\sin^2\eta}+\cdots\cdots\cdots\Big],
\end{aligned}$$

tangential stress $\left(\equiv\sum_{n=1}^{\infty} b_n \sin n\eta\right)$

$$\begin{aligned}
&=\mu\Big[(B_1, B_3, B_5, C_1, C_3, C_5)\sin\eta\\
&+\{\varepsilon'_{1,2}B_2+\varepsilon'_{1,4}B_4+\varepsilon'_{1,6}B_6+\nu'_{1,2}C_2+\nu'_{1,4}C_4+\nu'_{1,6}C_6\}\sin 2\eta\\
&+(B_1, B_3, B_5, C_1, C_3, C_5)\sin 3\eta\\
&+\{\varepsilon'_{2,2}B_2+\varepsilon'_{2,4}B_4+\varepsilon'_{2,6}B_6+\nu'_{2,2}C_2+\nu'_{2,4}C_4+\nu'_{2,6}C_6\}\frac{\cos\eta}{\sin\eta}\\
&+\{\varepsilon'_{3,0}B_0+\varepsilon'_{3,2}B_2+\varepsilon'_{3,4}B_4+\varepsilon'_{3,6}B_6+\nu'_{3,2}C_2+\nu'_{3,4}C_4+\nu'_{3,6}C_6\}\frac{\cos\eta}{\sin^3\eta}\\
&+\cdots\cdots\cdots\cdots\cdots\cdots\Big],
\end{aligned}$$

where

$$\left.\begin{aligned}
&\varepsilon_{1,0}=1+8q\alpha_0\\
&\varepsilon_{1,2}=-2q+2\alpha_2+\frac{8}{3}q\alpha_2-4\gamma-\frac{64}{3}q\gamma
\end{aligned}\right|$$

$$\left.\begin{aligned}
\varepsilon_{1,4}&=\frac{16}{15}q\alpha_4+4\alpha_4-32\gamma-\frac{31}{3}q\gamma\\
\varepsilon_{1,6}&=\frac{24}{35}q\alpha_6+6\alpha_6-108\gamma-\frac{2112}{35}q\gamma\\
\nu_{1,2}&=-2\beta_2-\frac{16}{3}q'\beta_2\\
\nu_{1,4}&=-8\beta_4-\frac{88}{15}q'\beta_4\\
\nu_{1,6}&=-\frac{208}{35}q'\beta_6-18\beta_6
\end{aligned}\right\},$$

$$\left.\begin{aligned}
\varepsilon_{2,0}&=4q\\
\varepsilon_{2,2}&=1+\frac{8}{3}q\alpha_2-\frac{32}{3}q\gamma\\
\varepsilon_{2,4}&=-\frac{2}{3}q+4\alpha_4+\frac{16}{5}q\alpha_4-16\gamma-\frac{192}{5}q\gamma\\
\varepsilon_{2,6}&=8\alpha_6-96\gamma+\frac{64}{35}q\alpha_6-\frac{2656}{35}q\gamma\\
\nu_{2,2}&=-8q'\beta_2\\
\nu_{2,4}&=-12\beta_4-\frac{64}{5}q'\beta_4\\
\nu_{2,6}&=-32\beta_6-\frac{432}{35}q'\beta_6
\end{aligned}\right\},$$

$$\left.\begin{aligned}
\varepsilon_{3,2}&=\frac{2}{3}q\\
\varepsilon_{3,4}&=1+\frac{8}{5}q\alpha_4-\frac{48}{5}q\gamma\\
\varepsilon_{3,6}&=-\frac{2}{5}q+4\alpha_6+\frac{16}{7}q\alpha_6-24\gamma-\frac{256}{7}q\gamma\\
\nu_{3,4}&=-8q'\beta_4\\
\nu_{3,6}&=-20\beta_6-\frac{96}{7}q'\beta_6
\end{aligned}\right\},$$

$$\left.\begin{aligned}
\varepsilon_{4,0} &= -\alpha_0 - 4q\alpha_0 \\
\varepsilon_{4,2} &= -\alpha_2 - \frac{2}{3}q\alpha_2 + 4\gamma + \frac{32}{3}q\gamma \\
\varepsilon_{4,4} &= -\alpha_4 + 16\gamma + \frac{4}{15}q\alpha_4 + \frac{176}{15}q\gamma \\
\varepsilon_{4,6} &= -\alpha_6 + 36\gamma + \frac{4}{35}q\alpha_6 + \frac{416}{35}q\gamma
\end{aligned}\right\},$$

$$\left.\begin{aligned}
\varepsilon'_{1,2} &= -16q\alpha'_2 \\
\varepsilon'_{1,4} &= -24\alpha'_4 - \frac{128}{5}q\alpha'_4 \\
\varepsilon'_{1,6} &= -64\alpha'_6 - \frac{1536}{35}q\alpha'_6 \\
\nu'_{1,2} &= \frac{64}{3}q'\gamma' + \frac{8}{3}q'\beta'_2 \\
\nu'_{1,4} &= 32\gamma' + 4\beta'_4 + \frac{16}{5}q'\beta'_4 + \frac{192}{5}q'\gamma' \\
\nu'_{1,6} &= 8\beta'_6 + 96\gamma' + \frac{64}{35}q'\beta'_6 + \frac{1472}{35}q'\gamma'
\end{aligned}\right\},$$

$$\left.\begin{aligned}
\varepsilon'_{2,2} &= 4\alpha'_2 + \frac{32}{3}q\alpha'_2 \\
\varepsilon'_{2,4} &= 16\alpha'_4 + \frac{176}{15}q\alpha'_4 \\
\varepsilon'_{2,6} &= 36\alpha'_6 + \frac{416}{35}q\alpha'_6 \\
\nu'_{2,2} &= -2\beta'_2 - \frac{8}{3}q'\beta'_2 \\
\nu'_{2,4} &= -4\beta'_4 - \frac{16}{15}q'\beta'_4 \\
\nu'_{2,6} &= -6\beta'_6 - \frac{24}{35}q'\beta'_6
\end{aligned}\right\},$$

$$\left.\begin{aligned}
\varepsilon'_{3,0}&=2\alpha'_0+8q\alpha'_0\\
\varepsilon'_{3,2}&=2\alpha'_2-\frac{8}{3}q\alpha'_2\\
\varepsilon'_{3,4}&=2\alpha'_4-\frac{8}{15}q\alpha'_4\\
\varepsilon'_{3,6}&=2\alpha'_6-\frac{8}{35}q\alpha'_6\\
\nu'_{3,2}&=-4\gamma'-\frac{16}{3}q'\gamma'\\
\nu'_{3,4}&=-8\gamma'-\frac{32}{15}q'\gamma'\\
\nu'_{3,6}&=-12\gamma'-\frac{48}{35}q'\gamma'
\end{aligned}\right\}.$$

If now we consider the case in which uniform pressure changes periodically with time within the line origin, we may put the normal stress at the boundary of the origin as a_0e^{ipt} and the tangential stress as zero. Moreover we may put for symmetry,

$$B_1\equiv B_3\equiv B_5\equiv C_1\equiv C_3\equiv C_5\equiv 0.$$

We thus obtain the following simultaneous equations:

$$\left.\begin{aligned}
&\varepsilon_{1,0}B_0+\varepsilon_{1,2}B_2+\varepsilon_{1,4}B_4+\varepsilon_{1,6}B_6+\nu_{1,2}C_2+\nu_{1,4}C_4+\nu_{1,6}C_6=\frac{a_0}{\mu}\\
&\varepsilon_{2,0}B_0+\varepsilon_{2,2}B_2+\varepsilon_{2,4}B_4+\varepsilon_{2,6}B_6+\nu_{2,2}C_2+\nu_{2,4}C_4+\nu_{2,6}C_6=0\\
&0B_0+\varepsilon_{3,2}B_2+\varepsilon_{3,4}B_4+\varepsilon_{3,6}B_6+0C_2+\nu_{3,4}C_4+\nu_{3,6}C_6=0\\
&\varepsilon_{4,0}B_0+\varepsilon_{4,2}B_2+\varepsilon_{4,4}B_4+\varepsilon_{4,6}B_6+0C_2+0C_4+0C_6=0\\
&0B_0+\varepsilon'_{1,2}B_2+\varepsilon'_{1,4}B_4+\varepsilon'_{1,6}B_6+\nu'_{1,2}C_2+\nu'_{1,4}C_4+\nu'_{1,6}C_6=0\\
&0B_0+\varepsilon'_{2,2}B_2+\varepsilon'_{2,4}B_4+\varepsilon'_{2,6}B_6+\nu'_{2,2}C_2+\nu'_{2,4}C_4+\nu'_{2,6}C_6=0\\
&\varepsilon'_{3,0}B_0+\varepsilon'_{3,2}B_2+\varepsilon'_{3,4}B_4+\varepsilon'_{3,6}B_6+\nu'_{3,2}C_2+\nu'_{3,4}C_4+\nu'_{3,6}C_6=0
\end{aligned}\right\} \qquad (3)$$

We obtain B_0, B_2, B_4, B_6, C_2, C_4, and C_6 from these equations.

Now when ξ is large, the asymptotic solution of Mathieu's equation (2) is obtained in the form5).

---

5) K. SEZAWA, *loc. cit.*

$$H_n(\xi, q) \doteq \frac{e^{-i\xi_1}u}{\sqrt{\xi_1}},$$

where

$$\xi_1 = hc \sinh \xi, \quad u = 1 + \frac{a_1}{\xi_1} + \frac{a_2}{\xi_1^2} + \cdots\cdots\cdots\cdots,$$

$$\left.\begin{aligned}
&a_1 = \frac{i}{2}(j^2 - M^2 + 1) \\
&a_2 = -\frac{j^2}{2} + \frac{1}{8}(j^2 - M^2 + 1)(2 - j^2 + M^2) \\
&\cdots\cdots\cdots\cdots\cdots\cdots \\
&j = hc, \quad M^2 = a + \frac{j^2}{2}, \quad a = \frac{h^2c^2}{2} - n^2
\end{aligned}\right\}.$$

Hence the radial component of the dilatational wave at a distant point is given by

$$\begin{aligned}
u_1 &= -\sum_{n=0}^{\infty} \frac{B_n}{h^2c\sqrt{\cosh^2\xi - \cos^2\eta}} \frac{\partial H_n(\xi, q)}{\partial \xi} ce_n(\eta, q)e^{ipt} \\
&= -\sum_{n=0}^{\infty} \frac{B_n}{h^2c\cosh\xi} \frac{\partial}{\partial\xi}\left(\frac{e^{-ihc\sinh\xi}}{\sqrt{hc\sinh\xi}}\right) ce_n(\eta, q)e^{ipt} \\
&= \sum_{n=0}^{\infty} \frac{iB_n}{h\sqrt{hc\sinh\xi}} ce_n(\eta, q)e^{i(pt - hc\sinh\xi)} \\
&= \sum_{n=0}^{\infty} \frac{iB_n}{h^{\frac{3}{2}} R^{\frac{1}{2}}} ce_n(\eta, q)e^{i(pt - hR)} \\
&= -\sum_{n=0}^{\infty} \frac{1}{h^{\frac{3}{2}} R^{\frac{1}{2}}} \Big\{A_n' ce_n(\eta, q)\sin(pt - hR) \\
&\qquad\qquad + B_n' ce_n(\eta, q)\cos(pt - hR)\Big\},
\end{aligned}$$

where $A_n' + iB_n' = B_n$ and R stand for the distance from the origin.

As an example, we put

$$q = 0{\cdot}003333, \quad q' = 0{\cdot}01,$$

whence we have $$h^2c^2 = 0{\cdot}1066, \quad k^2c^2 = 0{\cdot}32.$$

We thus obtain from the equations (3),

$$\left.\begin{aligned}\mu A'_0&=-0{\cdot}01065a_0, & \mu B'_0&=-0{\cdot}0001858a_0\\ \mu A'_2&=+0{\cdot}007775a_0, & \mu B'_2&=+0{\cdot}003823a_0\\ \mu A'_4&=+0{\cdot}001666a_0, & \mu B'_4&=-0{\cdot}004619a_0\\ \mu A'_6&=-0{\cdot}0009628a_0, & \mu B'_6&=+0{\cdot}001551a_0\end{aligned}\right\}.$$

The azimuthal distribution of the radial component (at a distant point) of the dilatational wave in this case is shown in Fig. 1. As will be seen from the figure, at the same epoch only one kind of wave, namely, either pull or push wave, may be observed throughout the azimuth at places equally distant from the origin.

We may here mention that in the case under consideration, the wave length of the dilatational wave is 9·64 times greater than the linear dimension of the origin, that is 2c. If we change the wave length, we may obtain different distributions of the displacement of the radial component of the dilatational wave in azimuth.

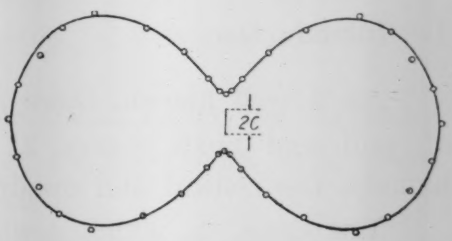

Fig. 1. The azimuthal distribution, at a distant point, of the radial component of displacement of the dilatational wave, the wave length of which is 9·64 times greater than 2c.

The case in which the tangential stress at the boundary of the origin undergoes periodic changes will be treated in a future paper.

In conclusion, the writer's cordial thanks are due to Prof. M. Ishimoto, Prof. Ch. Tsuboi, Prof. R. Takahasi and Prof. F. Kishinouye for their kind advices.

---

44. 發震機構に就いて（第3報）

地震研究所 井上宇胤

第一報及び第二報に於ては震源を球形と考へ其の表面に働く垂直應力の變化によつて生ずる彈性波に就いて數理的研究を行つた．此處では火山の管形の火口内部に於ける壓力の變化によつて生ずる地震波の場合及び斷層運動によつて生ずる地震波の場合等を論ずる爲に球形震源の代りに線形震源を考へ其の表面に働く應力の變化によつて生ずる彈性波の方位的特性を調査した．未だ極めて豫備的な研究であるが一般に割目の生成に伴つて生ずる彈性波の研究にも役立つものと思はれる．

45. *Notes on the Origin of Earthquakes.* (*Fourth paper.*)

By Win INOUYE,

Earthqauke Research Institute.

(Read June 15, 1937.—Received June 21, 1937.)

1. Introduction.

As is well known, there are two types of geographical distribution of pull and push waves at the initial phase of earthquake waves, namely, the conical and quadrant types.

The cases in which conical types were observed have been fully examined by Prof. M. Ishimoto[1] and Dr. T. Minakami,[2] while the cases in which the quadrant types were observed have been thoroughly treated by Dr. K. Honda.[3] According to these investigators, it seems to the writer that these cases could be satisfactorily explained by assuming certain simple forms of azimuthal differences in the stresses at a spherical surface taken at the seismic focus, such as $P_2(\cos\theta)$ for the conical type and $P_2^1(\cos\theta)$ for the quadrant type, these stresses undergo rapid changes.

The writer,[4] with the assistance of Mr. H. Kimura, tried to reproduce these types of distributions of initial motions by means of artificial earthquakes, but the results were negative.

The only representation available is the sound emitted by a tuning fork. In this case the compressional wave and the rarefactional wave are separated by two surfaces parabolic to each other. The solid angle of each of these paraboloides is about 120°. The true mechanism of the emission of sound waves in this case is not yet known. In practise, to comprehend the phenomena it is sufficient to consider a couple of doublets acting along a line in opposite phase and a sink when the two prongs of the tuning fork move outward, and a source when they move inward alternately between the two prongs.

When the writer fired an explosive placed in a short metal tube

---

1) M. ISHIMOTO, *Bull. Earthq. Res. Inst.*, **10** (1932), 449; *Proc. Imp. Acad. Tokyo*, **8** (1932), 36.

2) T. MINAKAMI, *Bull. Earthq. Res. Inst.*, **13** (1935), 114.

3) H. HONDA, *Geophys. Mag.*, **8** (1934), 153; **8** (1935), 327.

4) W. INOUYE and H. KIMURA, *Bull. Earthq. Res. Inst.*, **13** (1935), 194.

open at one end and closed and flanged at the other end, which telescoped into another similar tube (the whole placed under the ground), in all azimuths nothing but push waves was observed.[5] It seems, however, that if the lengths of the tubes are long enough to be comparable with the wave length (5～10 meters in our experiments), we should expect pull waves in some of the directions, seeing that this case may be regarded as corresponding to a couple of doublets acting along a line in opposite phase.

As just said, there are, in earthquakes, two types of distribution of push and pull waves, and in the majority of cases only these two types are observed.

These facts suggest that in the seismic focus, under the enormous hydrostatic pressure due to the weight of the overlying rock mass, certain special conditions of things must exist.

In the following paragraphs, the writer attempts to make clear the conditions prevailing within the seismic focus based on facts so far observed in connexion with seismic waves as already stated.

He is of the opinion that there are several ways of ascertaining these conditions. For example, we may be able to solve the problem by assuming that the material at the seismic focus is in a liquid state, that is, liquid magma, or by assuming that it is in a plastic state. In this study the writer avails himself of the ordinary elastic theory.

2. The Conical Type.

A spherical mass is taken for the seismic focus, and it is assumed that the elastic theory is applicable to this mass so long as the stresses are under the limit of the strength of the material.

We shall now consider the equilibrium of a spherical body.

The equations of equilibrium of elastic bodies in spherical coordinates, where the azimuthal component of the displacement is omitted, are expressed by

$$\left.\begin{aligned} &(\lambda+2\mu)\frac{\partial\Delta}{\partial r}-\frac{2\mu}{r}\frac{\partial\varpi}{\partial\theta}-\frac{2\mu}{r}\varpi\cot\theta=0 \\ &\frac{\lambda+2\mu}{r}\frac{\partial\Delta}{\partial\theta}+2\mu\frac{\partial\varpi}{\partial r}+2\mu\frac{\varpi}{r}=0 \end{aligned}\right\}, \qquad (1)$$

where u, v are radial and colatitudinal components of displacement, and

---

[5] W. INOUYE, *Bull. Earthq. Res. Inst.*, **14** (1936), 582.

$$\left.\begin{aligned} \Delta &= \frac{\partial u}{\partial r}+\frac{2u}{r}-\frac{1}{r}\frac{\partial v}{\partial \theta}+\frac{v}{r}\cot\theta \\ 2\varpi &= \frac{\partial v}{\partial r}+\frac{v}{r}-\frac{1}{r}\frac{\partial u}{\partial \theta} \end{aligned}\right\} . \tag{2}$$

Eliminating u and v in (1) by means of (2), we get

$$\frac{\partial^2 \Delta}{\partial r^2}+\frac{2}{r}\frac{\partial \Delta}{\partial r}+\frac{1}{r^2}\frac{\partial^2 \Delta}{\partial \theta^2}+\frac{1}{r^2}\frac{\partial \Delta}{\partial \theta}\cot\theta=0,$$

$$\frac{\partial^2 \varpi}{\partial r^2}+\frac{2}{r}\frac{\partial \varpi}{\partial r}+\frac{1}{r^2}\frac{\partial^2 \varpi}{\partial \theta^2}+\frac{1}{r^2}\frac{\partial \varpi}{\partial \theta}\cot\theta-\frac{\varpi}{r^2}(1+\cot^2\theta)=0 .$$

Solving these equations we get

$$\left.\begin{aligned} \Delta &= \left(A_n r^n+\frac{B_n}{r^{n+1}}\right)P_n(\cos\theta) \\ 2\varpi &= \left(A'_n r^n+\frac{B'_n}{r^{n+1}}\right)\frac{dP_n(\cos\theta)}{d\theta} \end{aligned}\right\} . \tag{3}$$

According to Prof. K. Sezawa and Dr. G. Nishimura,[6] the displacement (u_1, v_1) that answers to Δ in (3) and satisfies $\varpi=0$ is given by

$$\left.\begin{aligned} u_1 &= \left[\frac{A_n(n+2)}{2(2n+3)}r^{n+1}+\frac{B_n(n-1)}{2(2n-1)r^n}\right]P_n(\cos\theta) \\ v_1 &= \left[\frac{A_n}{2(2n+3)}r^{n+1}-\frac{B_n}{2(2n-1)r^n}\right]\frac{dP_n(\cos\theta)}{d\theta} \end{aligned}\right\} ,$$

in which $n=0, 1, 2, \ldots\ldots$ for A_n and $n=1, 2, 3, \ldots\ldots$ for B_n.

The displacement (u_2, v_2) derived from the value of ϖ in (3) under the condition, $\Delta=0$, is expressed by

$$\left.\begin{aligned} u_2 &= \left[\frac{A'_n n(n+1)}{2(2n+3)}r^{n+1}-B'_n\frac{n(n+1)}{2(2n-1)r^n}\right]P_n(\cos\theta) \\ v_2 &= \left[\frac{A'_n(n+2)}{2(2n+3)}r^{n+1}+\frac{B'_n(n-2)}{2(2n-1)r^n}\right]\frac{dP_n(\cos\theta)}{d\theta} \end{aligned}\right\} ,$$

in which $n=1, 2, \ldots\ldots$

The displacement (u_3, v_3) which satisfies $\Delta=0$, $\varpi=0$ is expressed by

---

[6] K. SEZAWA and G. NISHIMURA, *Bull. Earthq. Res. Inst.*, **7** (1929), 389.

$$\left.\begin{aligned} u_3 &= \left[A''_n n r^{n-1} - \frac{B''_n (n+1)}{r^{n+2}} \right] P_n(\cos\theta) \\ v_3 &= \left[A''_n r^{n-1} + \frac{B''_n}{r^{n+2}} \right] \frac{dP_n(\cos\theta)}{d\theta} \end{aligned}\right\},$$

where $n=0,\ 1,\ 2, \ldots\ldots$

Here we assume that just before the equilibrium is destroyed, resulting in an earthquake, the maximum shear stresses in the entire space within the spherical mass reach the limit of strength of the material, which means that the maximum shear stress is constant throughout the spherical body, and independent of the coordinates r, θ.

The condition of the maximum shear stress in the case with axial symmetry is expressed by

$$\widehat{r\theta}^2 + \left(\frac{\widehat{rr} - \widehat{\theta\theta}}{2} \right)^2 = K^2 ,$$

where

$$\widehat{rr} = \lambda\Delta + 2\mu \frac{\partial u}{\partial r} ,$$

$$\widehat{\theta\theta} = \lambda\Delta + 2\mu \left(\frac{1}{r} \frac{\partial v}{\partial \theta} + \frac{u}{r} \right),$$

$$\widehat{r\theta} = \mu \left(\frac{\partial v}{\partial r} - \frac{v}{r} + \frac{1}{r} \frac{\partial u}{\partial \theta} \right).$$

The displacement that satisfies this condition is limited to u_3, v_3, namely, the displacements independent of dilatation and rotation, which, moreover, is limited to terms containing A''_n.

In this case, the displacement $(u_3,\ v_3)$ is expressed by

$$\left.\begin{aligned} u_3 &= A''_n n r^{n-1} P_n(\cos\theta) \\ v_3 &= A''_n r^{n-1} \frac{dP_n(\cos\theta)}{d\theta} \end{aligned}\right\}.$$

The condition of the maximum shear stress at a point $(r,\ \theta)$ is then given by

$$\mu^2 A''^2_n r^{2n-4} \left[4(n-1)^2 \left(\frac{dP_n(\cos\theta)}{d\theta} \right)^2 + \left\{ \frac{d^2 P_n(\cos\theta)}{d\theta^2} - n(n-2) P_n(\cos\theta) \right\}^2 \right] = K^2 .$$

This condition is satisfied throughout the spherical body only when $n=2$.

In this case, the equation becomes

$$9\mu^2 A_n'^2 = K^2 ,$$

which contains no term involving the coordinates, so that the displacement is given by

$$\left.\begin{aligned} u_3 &= \frac{2K}{3\mu} r P_2(\cos\theta) \\ v_3 &= \frac{K}{3\mu} r \frac{dP_2(\cos\theta)}{d\theta} \end{aligned}\right\} .$$

The normal stress due to the displacement at the boundary of the sphere independent of its radius is given by

$$\widehat{rr} = \frac{4}{3} K P_2(\cos\theta) ,$$

and the tangential stress by

$$\widehat{r\theta} = \frac{2K}{3} \frac{dP_2(\cos\theta)}{d\theta} .$$

Seismic waves may be generated by certain rapid changes in these stresses caused by destruction of the equilibrium within the seismic focus by some causes.

The initial motions of the seismic waves in this case correspond to the conical type.

3. Quadrant Type.

We shall next take the general case of the equilibrium of a spherical body.

Let r, θ, ϕ be spherical polar coordinates, and let u, v, w stand for the components of the displacement in the direction of the radius, colatitude, and azimuth, when the equations of equilibrium of the body may be expressed by

$$\left.\begin{aligned} (\lambda+2\mu)\frac{\partial \Delta}{\partial r} - \frac{2\mu}{r\sin\theta}\frac{\partial(\varpi_\phi \sin\theta)}{\partial\theta} + \frac{2\mu}{r\sin\theta}\frac{\partial \varpi_\theta}{\partial\phi} &= 0 \\ (\lambda+2\mu)\frac{1}{r}\frac{\partial \Delta}{\partial\theta} - \frac{2\mu}{r\sin\theta}\frac{\partial \varpi_r}{\partial\phi} + \frac{2\mu}{r}\frac{\partial(\varpi_\phi r)}{\partial r} &= 0 \\ (\lambda+2\mu)\frac{1}{r\sin\theta}\frac{\partial \Delta}{\partial\phi} - \frac{2\mu}{r}\frac{\partial(\varpi_\theta r)}{\partial r} + \frac{2\mu}{r}\frac{\partial \varpi_r}{\partial\theta} &= 0 \end{aligned}\right\} , \qquad (7)$$

where

$$\left.\begin{aligned}
\Delta &= \frac{1}{r^2\sin\theta}\left[\frac{\partial(ur^2\sin\theta)}{\partial r}+\frac{\partial(vr\sin\theta)}{\partial\theta}+\frac{\partial(wr)}{\partial\phi}\right]\\
2\varpi_r &= \frac{1}{r^2\sin\theta}\left[\frac{\partial}{\partial\theta}(wr\sin\theta)-\frac{\partial}{\partial\phi}(vr)\right]\\
2\varpi_\theta &= \frac{1}{r\sin\theta}\left[\frac{\partial u}{\partial\phi}-\frac{\partial(wr\sin\theta)}{\partial r}\right]\\
2\varpi_\phi &= \frac{1}{r}\left[\frac{\partial(vr)}{\partial r}-\frac{\partial u}{\partial\theta}\right]
\end{aligned}\right\}. \qquad (8)$$

Eliminating u, v, w in (7) by means of (8), we get

$$\left.\begin{aligned}
&\frac{1}{r^2}\frac{\partial}{\partial r}\left(r^2\frac{\partial\Delta}{\partial r}\right)+\frac{1}{r^2\sin\theta}\frac{\partial}{\partial\theta}\left(\sin\theta\frac{\partial\Delta}{\partial\theta}\right)+\frac{1}{r^2\sin^2\theta}\frac{\partial^2\Delta}{\partial\phi^2}=0\\
&\frac{\partial^2\varpi_r}{\partial r^2}+\frac{4}{r}\frac{\partial\varpi_r}{\partial r}+\frac{2}{r^2}\varpi_r+\frac{1}{r^2\sin\theta}\frac{\partial}{\partial\theta}\left(\sin\theta\frac{\partial\varpi_r}{\partial\theta}\right)+\frac{1}{r^2\sin^2\theta}\frac{\partial^2\varpi_r}{\partial\phi^2}=0\\
&\frac{1}{r}\frac{\partial^2(\varpi_\theta r)}{\partial r^2}+\frac{1}{r^2\sin^2\theta}\frac{\partial^2\varpi_\theta}{\partial\phi^2}-\frac{1}{r^2\sin^2\theta}\frac{\partial^2(\varpi_\phi\sin\theta)}{\partial\phi\partial\theta}-\frac{1}{r}\frac{\partial^2\varpi_r}{\partial r\partial\theta}=0\\
&\frac{1}{r}\frac{\partial^2(\varpi_\phi r)}{\partial r^2}+\frac{1}{r^2}\frac{\partial}{\partial\theta}\frac{1}{\sin\theta}\frac{\partial(\varpi_\phi\sin\theta)}{\partial\theta}-\frac{1}{r^2}\frac{\partial}{\partial\theta}\frac{1}{\sin\theta}\frac{\partial\varpi_\theta}{\partial\phi}-\frac{1}{r\sin\theta}\frac{\partial^2\varpi_r}{\partial r\partial\phi}=0
\end{aligned}\right\}.$$

Solving these equations we obtain

$$\left.\begin{aligned}
\Delta &= \left(A_{mn}r^n+\frac{A'_{mn}}{r^{n+1}}\right)P_n^m(\cos\theta)\left.\begin{matrix}\cos\\ \sin\end{matrix}\right\}m\phi\\
2\varpi_r &= \left(B_{mn}r^{n-1}+\frac{B'_{mn}}{r^{n+2}}\right)P_n^m(\cos\theta)\left.\begin{matrix}\sin\\ -\cos\end{matrix}\right\}m\phi\\
2\varpi_\theta &= \left[\left(D_{mn}r^n+\frac{D'_{mn}m}{r^{n+1}}\right)\frac{P_n^m(\cos\theta)}{\sin\theta}\right.\\
&\qquad\left.+\left(\frac{B_{mn}}{n}r^{n-1}-\frac{B'_{mn}}{(n+1)r^{n+2}}\right)\frac{dP_n^m(\cos\theta)}{d\theta}\right]\left.\begin{matrix}\sin\\ -\cos\end{matrix}\right\}m\phi\\
2\varpi_\phi &= \left[\left(D_{mn}r^n+\frac{D'_{mn}}{r^{n+1}}\right)\frac{dP_n^m(\cos\theta)}{d\theta}\right.\\
&\qquad\left.+\left(\frac{B_{mn}}{n}r^{n-1}-\frac{B'_{mn}}{(n+1)r^{n+2}}\right)\frac{P_n^m(\cos\theta)}{\sin\theta}\right]\left.\begin{matrix}\cos\\ \sin\end{matrix}\right\}m\phi
\end{aligned}\right\}, \qquad (9)$$

in which A_{mn}, A'_{mn}, B_{mn}, B'_{mn}, D_{mn}, D'_{mn} are arbitrary constants.

The displacement (u_1, v_1, w_1) answering to Δ in (9) and satisfying $\varpi_r=\varpi_\theta=\varpi_\phi=0$ is expressed by⁷⁾

---

7) K. SEZAWA and G. NISHIMURA, *loc. cit.*

$$\left.\begin{aligned}
u_1&=\left[\frac{A_{mn}(n+2)}{2(2n+3)}r^{n+1}+\frac{A'_{mn}(n-1)}{2(2n-1)r^n}\right]P_n^m(\cos\theta)\left.\begin{matrix}\cos\\ \sin\end{matrix}\right\}m\phi\\
v_1&=\left[\frac{A_{mn}}{2(2n+3)}r^{n+1}-\frac{A'_{mn}}{2(2n-1)r^n}\right]\frac{dP_n^m(\cos\theta)}{d\theta}\left.\begin{matrix}\cos\\ \sin\end{matrix}\right\}m\phi\\
w_1&=-\left[\frac{A_{mn}m}{2(2n+3)}r^{n+1}-\frac{A'_{mn}}{2(2n-1)r^n}\right]\frac{P_n^m(\cos\theta)}{\sin\theta}\left.\begin{matrix}\sin\\ -\cos\end{matrix}\right\}m\phi
\end{aligned}\right\}.$$

The displacement $(u_2,\ v_2,\ w_2)$ that answers to ϖ_r together with the second terms in the expression of ϖ_θ, ϖ_ϕ given in (9) under the condition that $\Delta=0$, is expressed by

$$\left.\begin{aligned}
u_2&=0\\
v_2&=\left[\frac{mB_{mn}}{n(n+1)}r^n+\frac{mB'_{mn}}{n(n+1)r^{n+1}}\right]\frac{P_n^m(\cos\theta)}{\sin\theta}\left.\begin{matrix}\cos\\ \sin\end{matrix}\right\}m\phi\\
w_3&=-\left[\frac{B_{mn}}{n(n+1)}r^n+\frac{B'_{mn}}{n(n+1)r^{n+1}}\right]\frac{dP_n^m(\cos\theta)}{d\theta}\left.\begin{matrix}\sin\\ -\cos\end{matrix}\right\}m\phi
\end{aligned}\right\}.$$

The displacement $(u_4,\ v_4,\ w_4)$ derived from the values of the first terms of ϖ_θ, ϖ_ϕ in (9) fulfilling the conditions, $\Delta=\varpi_r=0$, is written

$$\left.\begin{aligned}
u_4&=\left[\frac{D_{mn}n(n+1)}{2(2n+3)}r^{n+1}+\frac{D'_{mn}n(n+1)}{2(2n-1)r^n}\right]P_n^m(\cos\theta)\left.\begin{matrix}\cos\\ \sin\end{matrix}\right\}m\phi\\
v_4&=\left[\frac{D_{mn}(n+3)}{2(2n+3)}r^{n+1}+\frac{D'_{mn}(n-2)}{2(2n-1)r^n}\right]\frac{1}{m}\frac{dP_n^m(\cos\theta)}{d\theta}\left.\begin{matrix}\cos\\ \sin\end{matrix}\right\}m\phi\\
w_4&=-\left[\frac{D_{mn}m(n+3)}{2(2n+3)}r^{n+1}+\frac{D'_{mn}m(n-2)}{2(2n-1)r^n}\right]\frac{P_n^m(\cos\theta)}{\sin\theta}\left.\begin{matrix}\sin\\ -\cos\end{matrix}\right\}m\phi
\end{aligned}\right\}.$$

The displacement $(u_3,\ v_3,\ w_3)$ that satisfies $\Delta=\varpi_r=\varpi_\theta=\varpi_\phi=0$, is expressed by

$$\left.\begin{aligned}
u_3&=\left[C_{mn}nr^{n-1}-\frac{C'_{mn}(n+1)}{r^{n+2}}\right]P_n^m(\cos\theta)\left.\begin{matrix}\cos\\ \sin\end{matrix}\right\}m\phi\\
v_3&=\left[C_{mn}r^{n-1}+\frac{C'_{mn}}{r^{n+2}}\right]\frac{dP_n^m(\cos\theta)}{d\theta}\left.\begin{matrix}\cos\\ \sin\end{matrix}\right\}m\phi\\
w_3&=-m\left[C_{mn}r^{n-1}+\frac{C'_{mn}}{r^{n+2}}\right]\frac{P_n^m(\cos\theta)}{\sin\theta}\left.\begin{matrix}\sin\\ -\cos\end{matrix}\right\}m\phi
\end{aligned}\right\}.$$

Here we assume, as in the previous case, that the maximum shear stresses are constant throughout the spherical body attaining the limit of ultimate strength of the material against breaking down of the resistance immediately preceding an earthquake.

The condition of maximum shear stress is expressed by[8]

$$\frac{1}{2}\left[\left(\frac{\widehat{rr}-\widehat{\theta\theta}}{2}\right)^2+\left(\frac{\widehat{\theta\theta}-\widehat{\phi\phi}}{2}\right)^2+\left(\frac{\widehat{\phi\phi}-\widehat{rr}}{2}\right)^2\right]+\frac{3}{4}\left(\widehat{r\theta}^2+\widehat{\theta\phi}^2+\widehat{\phi r}^2\right)=K^2\,,$$

where

$$\left.\begin{aligned}
\widehat{rr}&=\lambda\Delta+2\mu\frac{\partial u}{\partial r}\\
\widehat{\theta\theta}&=\lambda\Delta+2\mu\left(\frac{1}{r}\frac{\partial v}{\partial\theta}+\frac{u}{r}\right)\\
\widehat{\phi\phi}&=\lambda\Delta+2\mu\left(\frac{1}{r\sin\theta}\frac{\partial w}{\partial\phi}+\frac{v}{r}\cot\theta+\frac{u}{r}\right)\\
\widehat{r\theta}&=\mu\left(\frac{\partial v}{\partial r}-\frac{v}{r}+\frac{1}{r}\frac{\partial u}{\partial\theta}\right)\\
\widehat{\theta\phi}&=\mu\left\{\frac{1}{r}\left(\frac{\partial w}{\partial\theta}-w\cot\theta\right)+\frac{1}{r\sin\theta}\frac{\partial v}{\partial\phi}\right\}\\
\widehat{\phi r}&=\mu\left(\frac{1}{r\sin\theta}\frac{\partial u}{\partial\phi}+\frac{\partial w}{\partial r}-\frac{w}{r}\right)
\end{aligned}\right\}.$$

The displacements that satisfy this condition are restricted to u_3, v_3, w_3 (taking only the first terms containing C_{mn}), that is displacements independent of dilatation and rotation.

In this case, the displacement (u_3, v_3, w_3) is given by

$$\left.\begin{aligned}
u_3&=C_{mn}nr^{n-1}P_n^m(\cos\theta)\cos m\phi\\
v_3&=C_{mn}r^{n-1}\frac{dP_n^m(\cos\theta)}{d\theta}\cos m\phi\\
w_3&=-mC_{mn}r^{n-1}\frac{P_n^n(\cos\theta)}{\sin\theta}\sin m\phi
\end{aligned}\right\}.$$

The condition of maximum shear stress at any point (r, θ, ϕ) is then given by

$$\begin{aligned}
\mu^2C_{mn}^2r^{2n-4}\Bigg[\frac{1}{2}\cos^2 m\phi\Bigg[&\left\{n(n-2)P_n^n(\cos\theta)-\frac{d^2P_n^n(\cos\theta)}{d\theta^2}\right\}^2\\
&+\left\{\frac{d^2P_n^m(\cos\theta)}{d\theta^2}+\frac{m^2}{\sin^2\theta}P_n^n(\cos\theta)-\cot\theta\frac{dP_n^n(\cos\theta)}{d\theta}\right\}^2\\
&+\left\{-m^2\frac{P_n^m(\cos\theta)}{\sin^2\theta}+\frac{dP_n^n(\cos\theta)}{d\theta}\cot\theta-n(n-2)P_n^m(\cos\theta)\right\}^2\Bigg]
\end{aligned}$$

---

[8] HENCKY, *Zeits. f. A. M. M.*, **4** (1924), 323.

$$+3\cos^2 m\phi\,(n-1)^2\left(\frac{dP_n^m(\cos\theta)}{d\theta}\right)^2$$

$$+3\frac{\sin^2 m\phi}{\sin^2\theta}m^2\left[\left[\left\{\cot\theta P_n^m(\cos\theta)-\frac{dP_n^m(\cos\theta)}{d\theta}\right\}^2\right.\right.$$

$$\left.\left.+(n-1)^2(P_n^m(\cos\theta))^2\right]\right]=K^2\,.$$

The condition that this equation shall hold throughout the spherical body is fulfilled in cases in which $n=2$, $m=1$ and $n=2$, $m=2$.

In the former case the equation becomes

$$27\mu^2C_{1,2}^2=K^2\,,$$

and in the latter

$$108\mu^2C_{2,2}^2=K^2\,.$$

In the case in which $n=2$, $m=1$, the displacement is given by

$$\left.\begin{aligned} u_3&=\frac{3}{\sqrt{27}}\frac{K}{\mu}r\sin 2\theta\cos\phi \\ v_3&=\frac{3}{\sqrt{27}}\frac{K}{\mu}r\cos 2\theta\cos\phi \\ w_3&=-\frac{3}{\sqrt{27}}\frac{K}{\mu}r\cos\theta\sin\phi \end{aligned}\right\}.$$

The normal stress at the boundary of the sphere due to the displacement is given by

$$\widehat{rr}=\frac{6}{\sqrt{27}}K\sin 2\theta\cos\phi\,,$$

and the tangential stresses by

$$\left.\begin{aligned} \widehat{r\theta}&=\frac{6}{\sqrt{27}}K\cos 2\theta\cos\phi \\ \widehat{r\phi}&=-\frac{6}{\sqrt{27}}K\cos\theta\sin\phi \end{aligned}\right\}.$$

In the case in which $n=2$, $m=2$, the displacement is given by

$$\left.\begin{aligned} u_3&=\frac{6}{\sqrt{108}}\frac{K}{\mu}r\sin^2\theta\cos 2\phi \\ v_3&=\frac{3}{\sqrt{108}}\frac{K}{\mu}r\sin 2\theta\cos 2\phi \\ w_3&=-\frac{6}{\sqrt{108}}\frac{K}{\mu}r\sin\theta\sin 2\phi \end{aligned}\right\}.$$

The normal stress at the boundary of the sphere is given by

$$\widehat{rr}=\frac{12}{\sqrt{108}}K\sin^2\theta\cos2\phi\,,$$

and the tangential stresses by

$$\left.\begin{aligned}\widehat{r\theta}&=\frac{6}{\sqrt{108}}K\sin2\theta\cos2\phi\\ \widehat{r\phi}&=-\frac{24}{\sqrt{108}}K\sin\theta\sin2\phi\end{aligned}\right\}.$$

As in the former case, seismic waves may be generated by some rapid changes undergone in these stresses.

The initial motions of the seismic waves in these cases belong in the quadrant type category.

4. Remarks.

In the preceeding two articles, the writer treated the problem without taking into consideration the outer medium of the spherical mass, assuming that the elasticity of the outer medium differs from that of the spherical mass, a conception that may be permissible if we assume that the spherical portion in the medium is locally weakened by certain causes, such as local heating, etc.

If we assume that the elasticity of the outer medium differs from that within the spherical mass, we can satisfy the boundary conditions at the spherical surface, that is the displacements and the stresses are continuous at the spherical surface $r=a$, by using all the various displacements in the outer medium in contrast with displacement u_3, v_3, w_3, that is, the displacement independent of dilatation and rotation, within the spherical mass. It must be remembered, moreover, that we are considering only the state of things within the seismic focus, leaving out of consideration both the external and internal forces that bring about the earthquake.

If we assume that the material within the sphere to be of plastic nature, the case in which the stresses are independent of the azimuth, namely the case $P_0(\cos\theta)$, is also possible to exist.[9]

5. Summary.

In the majority of earthquakes, we observe two types of distributions of push and pull waves at the initial phase of earthquake waves, namely, conical and quadrant, although we cannot yet represent any one of these types by means of artificial earthquakes.

---

[9] K. SEZAWA, *Bull, Earthq. Res. Inst.*, **9** (1931), 398.

These facts suggest the existence of certain special conditions in the seismic focus.

The writer investigated the conditions prevailing within the seismic focus with the above stated facts as basis, and arrived at the conclusion that the maximum shear stresses might be constant within the seismic focus reaching the limit of ultimate strength of the material immediately preceding an earthquake.

In conclusion, the writer's cordial thanks are due to Prof. M. Ishimoto, Prof. K. Sezawa, Prof. Ch. Tsuboi, and Prof. N. Miyabe for their kind advices.

---

45. 發震機構に就いて（第4報）

地震研究所　井上宇胤

初動の“壓し波”“引き波”の地理的分布に就いては多數の研究がなされてゐる．此等の研究によつて初動の地理的分布には二種類ある事が分つた．卽ち在來から知られてゐた四象限型と石本所長の研究されたコニカル型とである．

然るに理論的には他の多くの型を考へる事が可能であると共に他方今日迄の人工地震によつては以上の二つの型の孰れをも表現し得ないのである．

此等の事實から筆者は震源に於ては何事か特殊な事情が存在するのではなからうかとの考へを以て以上の二つの型のみ生起する樣な震源に於ける狀態を考察してみたのである．

其の結果震源に於ける物質を彈性體と考へるならば，地震の發生する直前に於ては震源の全域に亘り，一樣に最大剪應力が其の彈性體の破壞限度に達してゐると云ふ事になつた．

勿論此の樣な狀態から如何にして地震波が發生するか或は又，如何なる力によつて斯の如き狀態を引き起したかは今は問題としてゐない．

只單に此の樣な狀態に於ける應力が或る早さをもつて消失或は單に變化したならば以上の二つの型に相當する初動が觀測されるであらうと云ふのである．

46. *Observations sur des secousses d'une petite amplitude*

par Mishio ISHIMOTO,

Institut de Recherches sur les Tremblements de terre.

(Lu le 16 Février 1937; reçu le 20 Juin 1937.)

Introduction.

On sait d'une part qu'il y a des secousses de petite amplitude fréquentes spécialement dans la partie haute de Tôkyô (Hongô), secousses dont la période est de 0,3 seconde. D'autre part des secousses d'une telle période apparaissent aussi dans les enregistrements sismiques obtenus par les sismographes et les savants[1] ont imaginé que cette sorte de secousses est analogue aux rides qui se superposent à une grande vague de la mer.

D'après les résultats obtenus avec un appareil analyseur construit par Suyehiro[2], on a constaté qu'il y a toujours des secousses d'une telle période parmi les secousses sismiques observées surtout dans la ville de Tôkyô. Peu après, l'auteur[3] a réussi à enregistrer cette sorte de secousses au moyen d'un seismographe accélérométrique et il a constaté qu'elles composent la plus grande partie des secousses sismiques possedant les plus grandes valeurs d'accélération. Pour expliquer l'origine de ces secousses, nous avons considéré une couche de sol qui se trouve à la surface d'un terrain ayant un degré d'élasticité comparativement plus petit que celle de la roche souterraine. Il est nécessaire de tenir compte de ces secousses quand on veut connaitre quelques propriétés de la couche superficielle ainsi que la nature de secousses sismiques. De plus on peut imaginer qu'il y aura des cas où l'on trouvera quelques variations dans l'amplitude des secousses juste avant l'apparition d'un tremblement de terre.

Voici un exemple d'enregistrement (Fig. 1) obtenu à Hongô avec un micro-séismographe[4] que nous avons dernierèment construit. A l'aide de cet enregistrement, on comprendra la variation générale de

---

[1] S. SEKIYA & F. OMORI, *Trans. Seism. Soc. Jap.*, **16** (1892), 44.

[2] K. SUYEHIRO, *Bull. Earthq. Res. Inst.*, **1** (1926), 59.

[3] M. ISHIMOTO, *Bull. Earthq. Res. Inst.*, **9** (1931), 316; **9** (1931), 473; **10** (1932), 171.

[4] M. ISHIMOTO, *Bull. Earthq. Res. Inst.*, **14** (1936), 248.

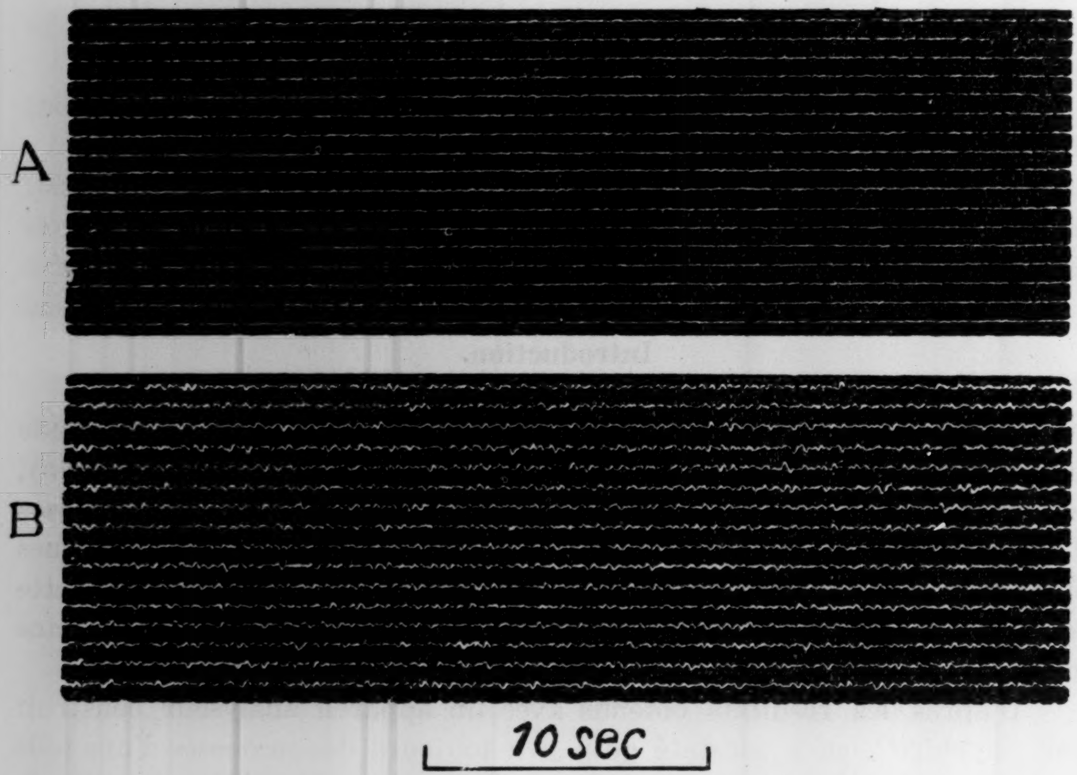

Fig. 1. Enregistrement obtenu par le micro-séismographe.

Le 13 Décembre, 1934. A: 1 h ~ 3 h 50 m.
B: 12 h ~ 14 h 40 m.

l'amplitude des secousses. Leur amplitude arrive à 2~3 μ pendant la journée tandis qu'elle diminue jusqu'à la limite d'enregistrement pendant la nuit. Evidemment, la période des secousses demeure toujours de 0,3 seconde environ. Le fait qu'il y a une période diurne dans les variations de l'amplitude, nous amène à considérer qu'il y a là un effet de communication: c'est-à-dire qu'il y a une production des secousses par les automobiles, par les camions, par les tamways etc. Nous avons voulu, en tout cas, étudier surtout les secousses de petite amplitude observées à notre Institut.

Nous avons construit un pendule d'après le type de Wood-Anderson. Ses dimensions élémentaires sont les suivantes,

Longueur du fil de cuivre	8,8 cm
Diamètre du fil	0,061 mm
Longueur de la masse	3,6 cm
Diamètre de la masse	0,425 cm

Pour déterminer la caractéristique du pendule, nous avons exécuté une expérience en donnant une inclinaison au pendule et en déterminant sa période propre d'oscillation. La Fig. 2 représente la relation entre les deux valeurs: l'angle d'inclinaison (θ) est à l'abscisse et la période (T_0)

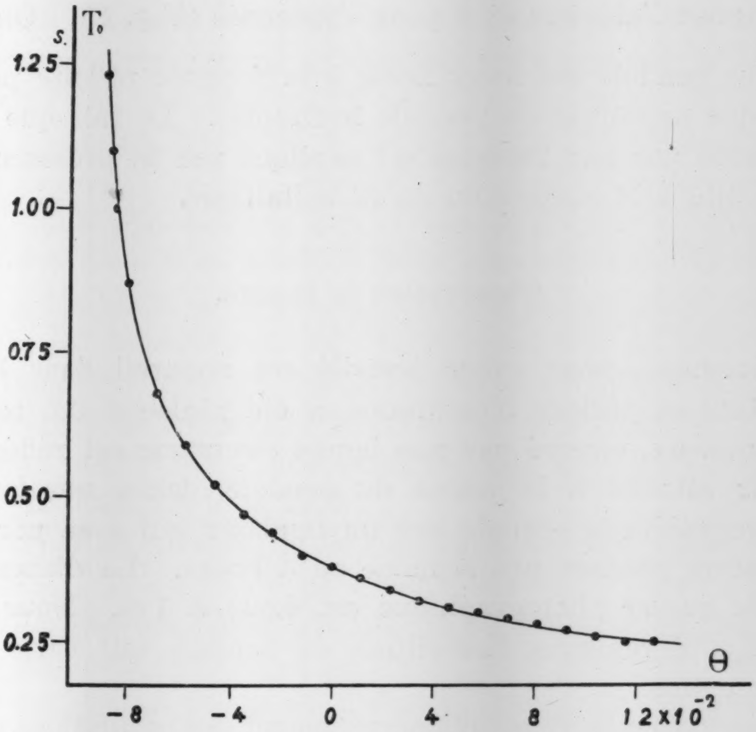

Fig. 2. Variation de la période propre de pendule (T_0) avec l'inclinaison (θ).

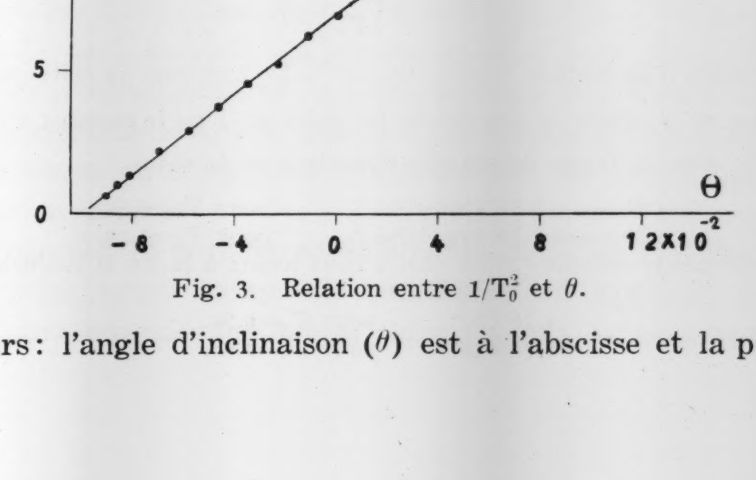

Fig. 3. Relation entre $1/T_0^2$ et θ.

est à l'ordonnée. On comprendra tout de suite que la période du pendule varie dans l'intervalle de 0,25~1,25 sec. Pour comprendre facilement la caractéristique du pendule, nous avons tracé une autre courbe prenant $\frac{1}{T_0^2}$ pour l'abscisse et θ pour l'ordonnée (Fig. 3). On peut constater que ce pendule est assez fidèle à la formule réduite par la théorie dynamique appliquée au pendule horizontal. Le fait que cette ligne droite ne passe pas par l'origine est expliqué par la présence d'un module de rigidité à la suspension du fil métallique.

Observation à Hongô.

Premièrement, nous avons installé cet appareil dans la cave de notre Institut: sa période d'oscillation a été réglée à 0,3 seconde. Le faisceau lumineux, envoyé par une lampe électrique est réfléchi par un petit miroir attaché à la masse du pendule, donne une image sur le papier photographique enroulé sur un tambour qui a sa période complete de rotation pendant une semaine ou 4 hours. La distance entre le miroir et le papier photographique est égale à 1 m. Nous avons, en effet, réussi à enregistrer l'amplitude du pendule qui varie suivant le passage du temps.

Pour exprimer le degré d'amortissement des oscillations du pendule, nous avons adopté l'intervalle de temps (τ) où l'amplitude initiale du pendule diminue jusqu'à la moitié de sa valeur. Cet intervalle a été déterminé comme 1 m 30 sec environ pour toutes les périodes d'oscillation. Si les secousses sont représentées par une oscillation sinusoïdale, l'amplitude de l'image sur le papier photographique aura une valeur[5]

---

5) D'après la formule d'oscillation d'un pendule libre, nous obtenons $x=ce^{-\lambda t}\cos(\sqrt{n^2-\lambda^2}t+\alpha)$ où $\lambda=\log_e 2/\tau$. Nous avons, donc, $\lambda=0,00769$ pour $\tau=Im$ 30s. D'autre coté nous avons

$$(\theta h)_{\max}=\frac{Mh^2}{I}\frac{a}{\sqrt{\left(\frac{T^2}{T_0^2}-1\right)^2+4s^2\frac{T^2}{T_0^2}}}$$

d'après la formule d'oscillation forcée, où $s=\frac{\lambda}{n}$, h=2.125 mm (la distance entre le centre d'oscillation et le centre de gravité de pendule) et I est le moment d'inertie. Nous avons $\frac{Mh^2}{I}=\frac{2}{3}$ avec la forme de masse cylindrique et de suite

$$(\theta h)_{\max}=2/3\times 1360=906,7 \qquad \text{pour } T_0=0,3\text{s.}$$
$$(\theta h)_{\max}=2/3\times 400 \;=266,7 \qquad \text{pour } T_0=1,0\text{s.}$$

Comme l'amplification optique $=200/h$ (cm), nous avons à la fin le coefficient d'amplification

$$4,26\times 10^5 \qquad \text{pour } T_0=0,3\text{s.}$$
$$1,25\times 10^5 \qquad \text{pour } T_0=1,0\text{s.}$$

$4{,}26 \times 10^5$ fois plus grande que celle des secousses de la terre.

La figure 4 représente un des exemples obtenus par l'installation décrite ci-dessus: on verra à (a) que l'amplitude manifeste une forme en zig-zag au passage du temps, tandis que son maximum ne dépasse pas une certaine valeur. Ce fait nous suggère qu'il y a des origines nombreuses aux perturbations qui agitent incessamment la terre autour de la station. On voit clairement une période diurne dans la Fig. 4 (b), qui se répète toujoures de la même façon. Des 6 heures du matin l'amplitude augmente progressivement et elle est presque constante dans la journée. Mais elle diminue des 11 heures du soir et elle arrive au minimum entre 2∼4 *h* du matin. Nous pouvons, donc, en tirer la conclusion que cette sorte de secousses provient entièrement des secousses produites par les communications. Cette conclusion se trouve confirmée quand on remarque que les enregistrements obtenus à Mitika par la même installation de l'appareil: Mitaka, lieu très calme où l'on ne peut noter presque aucun effet des perturbations de communication. On verra cette circonstance plus tard.

Considérons, maintenant, le lieu de naissance des secousses par les communications. Nous comptons d'abord la rue de Hongô qui se trouve à 300 m de distance de notre Institut, où les automobiles, les tramways roulent incessamment pendant la journée. Nous comptons deuxièmement la rue de Yayoi-tyô, à 150 m de distance: rue moin mouvementée que la rue de Hongô. Il nous semble que les secousses se propagent principalement de ces deux rues. Mais quand nous réfléchissons au sujet de cette perturbation de la terre, nous sommes tentés de la considérer comme l'effet total de toutes les communications dans la ville de Tôkyô. Conséquement, cette sorte de vibration n'a aucune relation avec les éléments météorologiques. La terre répète toujours de la même façon sa variation diurne. Cela a été prouvé par les observations exécutées du 13 Septembre 1935 au 20 Avril 1936.

Nous avons exécuté une autre observation avec le pendule dont la période propre demeure 1 seconde (Fig. 4c). Cette fois-ci, nous n'avons pas pu constater l'existence de la variation diurne. On peut conclure que la période de 1 seconde n'a aucune relation avec les vibrations produites par les communications. Cette période de vibration doit avoir une certaine relation avec les éléments météorologiques; parce que l'on constate de temps en temps une augmentation de l'amplitude dans les enregistrements obtenus.

Pour chercher la période prédominante dans les secousses de petite amplitude, nous avons essayé de construire un appareil enregistreur comportant un pendule du même type. Cette fois-ci, cependant, sa période a été modifiée lentement par l'inclinaison d'une estrade sur laquelle le pendule est posé.

Nous avons déjà écrit que la période d'oscillation du pendule varie entre 0,25∼1,25 seconde avec la variation de l'inclinaison: cette propriété joue un rôle important dans l'exécution de l'expérience ci-jointe. L'aspect général de cette installation est représenté schématiquement dans la Fig. 5. La période d'inclinaison de l'estraide ainsi que celle de la rotation du tambeur se trouve être une heure: naturellement, ces mouvements sont produits par deux moteurs synchrones qui marchent avec le courant électrique alternatif de la ville. Un des enregistrements obtenus par cet appareil est montré dans la Fig. 6. Nous pouvons remarquer que ce diagramme représent un spectre, analogue à celui de l'optique. Quand la période du pendule approche de son maximum, on ne peut éviter d'avoir une image puisse déplacer suivant l'existence de la composante perpendiculaire d'inclinaison à celle qui est produite; mais cela n'est pas d'une grande importance pour notre expérience. Nous constatons, certainement, d'un coup d'oeil que l'amplitude des secousses

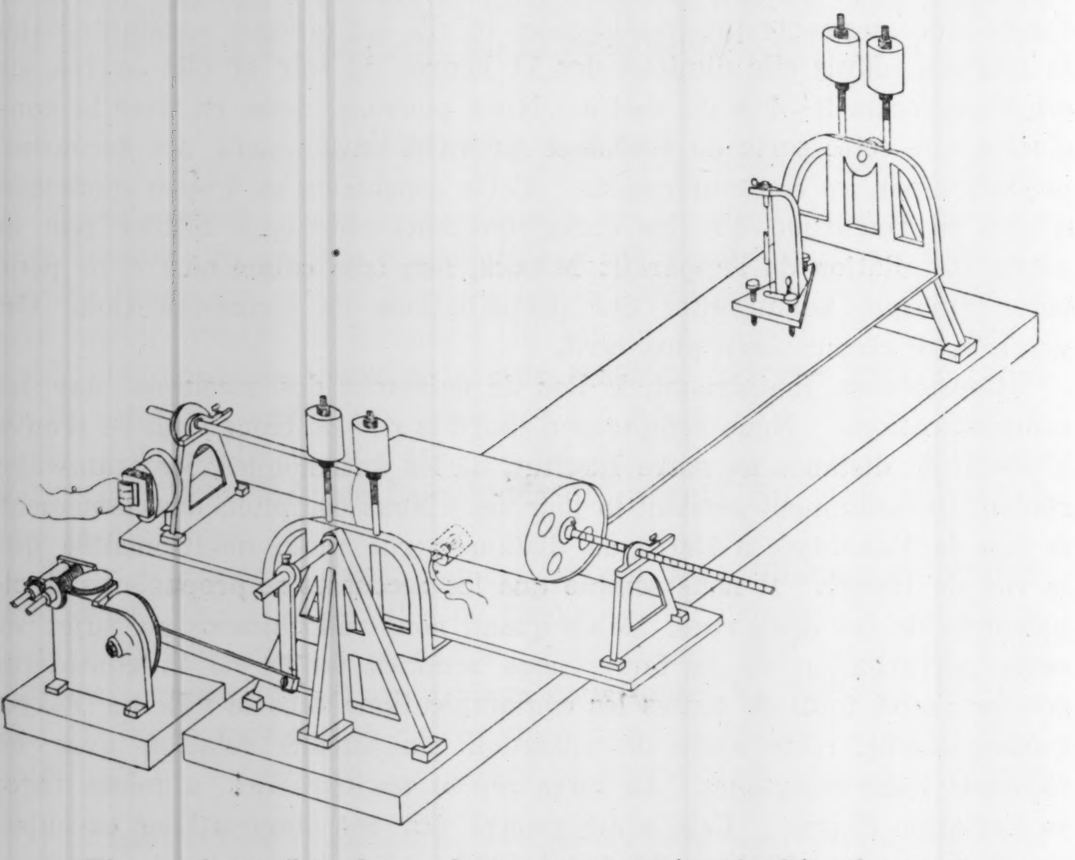

Fig. 5. Appareil analyseur des secousses représenté schématiquement.

demeur petite pendant la nuit: de plus les secousses se distribuent dans un certain domaine autour de la période de 0,3 sec.

Pour trouver le domaine de la période prédominante encore plus nettement, nous avons retracé cet enregistrement: nous avons transformé l'abscisse en valeur de période de pendule au lieu de sin θ: période qui est proportionelle à $\sqrt{\frac{1}{\theta}}$. La Fig. 7 est le diagramme obtenu à la fin. Nous constatons qu'il y a une certaine variation d'amplitude discontinue dans le domaine de la période de 0,3 seconde, tandis que l'amplitude est assez petite dans le domaine de 1,0 seconde.

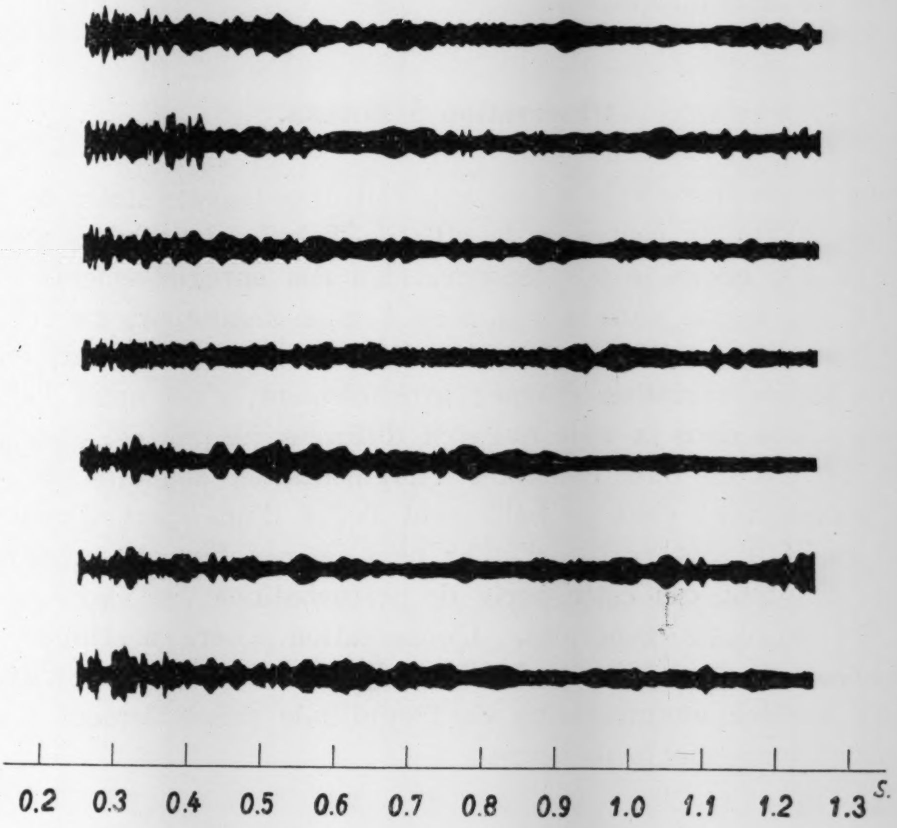

Fig. 7. Diagramme retracé d'après la Fig. 6.

Observation à Maru-no-uti.

Avec le même pendule, nous avons exécuté une autre observation à Maru-no-uti, au même lieu où nous avons installé notre séismographe aceélérométrique. Naturellement, la période propre du pendule était réglée à 0,6 seconde. Comme cet endroit est situé juste en face de la gare de Tôkyô, il y a un certain nombre de perturbations causées par toutes les sortes de communications. Conséquemment, nous sommes obligés de diminuer la sensibilité de notre appareil; la distance entre le pendule et le papier photographique a été ramenée à en 50 cm. La Fig. 8 représente un des enregistrements obtenus: on remarque tout de suite qu'il manifeste la même caractéristique que celui obtenu à Hongô. Certainement, les secousses sont considérables pendant la journée, tandis qu'elles deviennent tout à fait nulles pendant la nuit (entre 2~4 h). Nous pouvons conclure que ces perturbations ont pour unique origine des effets de communications.

Observation à Mitaka.

Nous avons installé le même appareil dans l'observatoire de Mitaka éloigné de 20 km du centre de la ville de Tôkyô. La période propre du pendule a été réglée à 0,3 seconde. Un des enregistrements obtenus là-bas est représenté dans la Fig. 9 où l'on ne distinguera aucune variation de l'amplitude. Mais, quand on l'étudie minutieusement, on trouvera une légère variation diurne; probablement, c'est aussi l'effet des communications dans la ville qui sont diffusées jusqu'à cet endroit.

On pourra de plus constater l'augmentation soudaine de perturbation successives: c'est probablement l'effet d'une part d'une pompe puisant de l'eau souterraine, d'auter part des pas d'un observateur quelconque. En tout cas cette sorte de perturbations est clairement distincte des secousses générales. L'observation a été continuée du 11 Novembre 1936 au 9 Février 1937: malheureusement, nous n'avons pu constater aucune augmentation de l'amplitude préalablement à l'apparition des tremblements de terre.

Conclusion.

D'après les résultats obtenus par nos observations, nous pouvons conclure que les secousses de petite amplitude qui se manifestent dans la ville de Tôkyô ont pour origine des vibrations produites par des comminications, c'est-à-dire qu'elles sont d'origine artificielle. La variation diurne des secousses se répète toujours de la même façon bien que ne soit pas la meme aux différents endroits. Leur période a une relation étroite avec l'épaisseur et les constantes élastiques de la couche qui se trouve à la surface terrestre. Nous pouvons dire autrement qu'il y a toujours une période propre des secousses qui correspond à la nature particulière du sol superficiel aux divers lieux. Certainement, cette

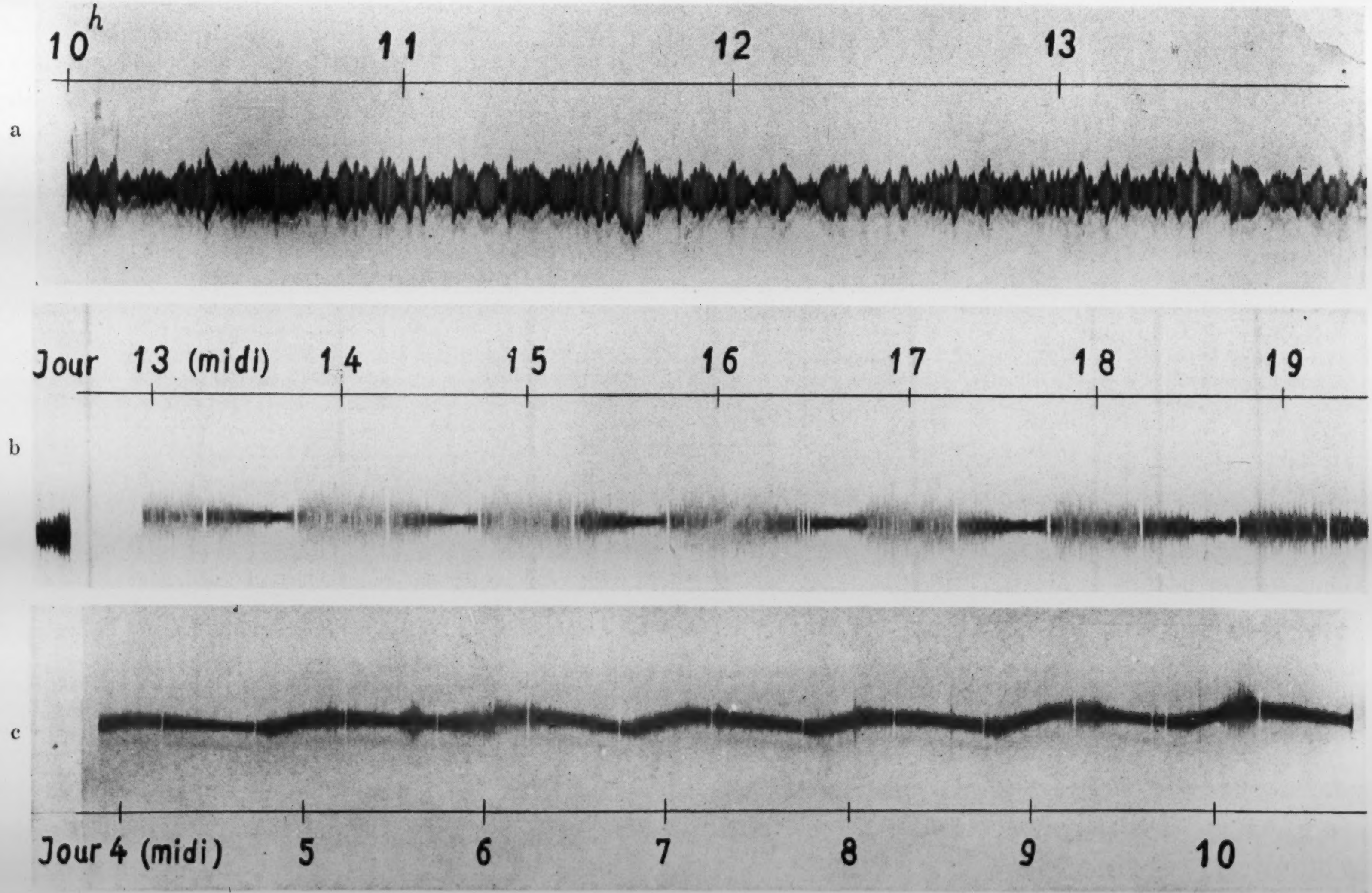

Fig. 4. Enregistrements obtenus par le pendule.
a) $T_0=0{,}3$ s. b) $T_0=0{,}3$ s. c) $T_0=1{,}0$ s.

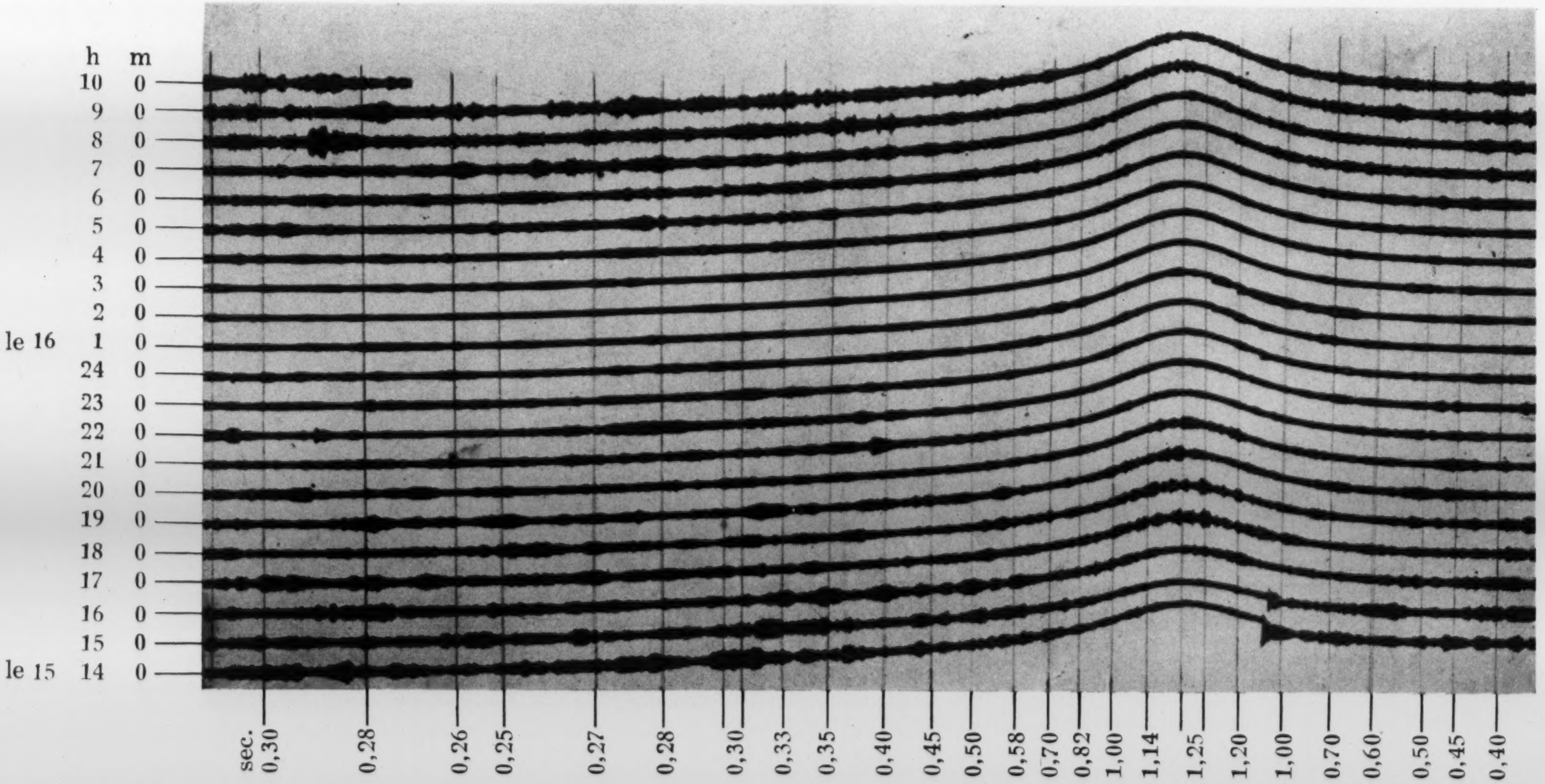

Fig. 6. Enregistrement obtenu par l'appareil analyseur des secousses.
(de 15 au 16, 1936.)

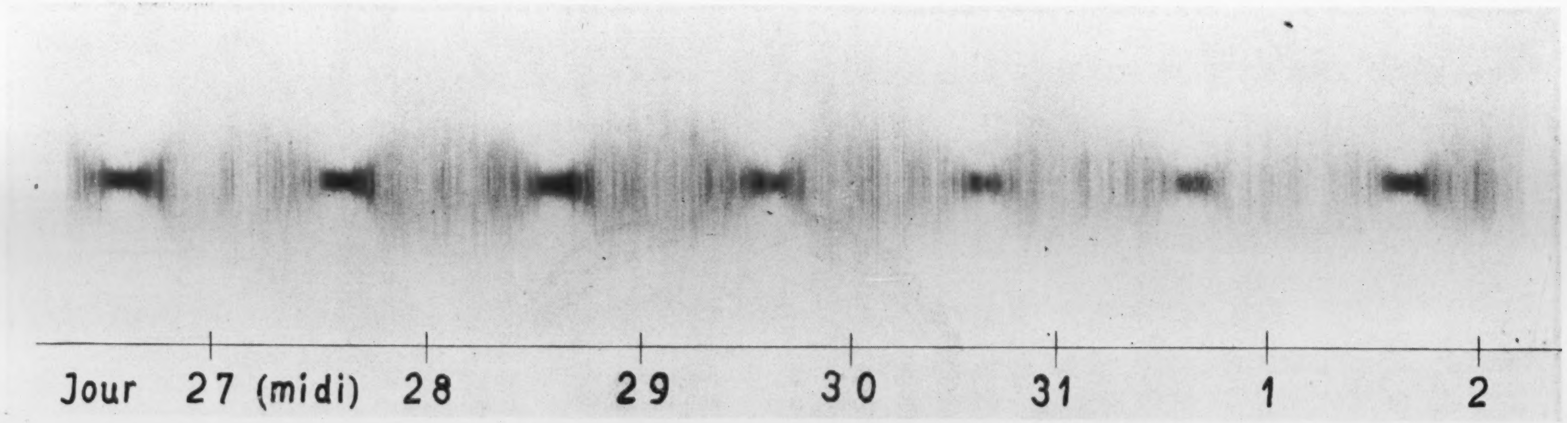

Fig. 8. Enregistrement obtenu à Maru-no-uti.

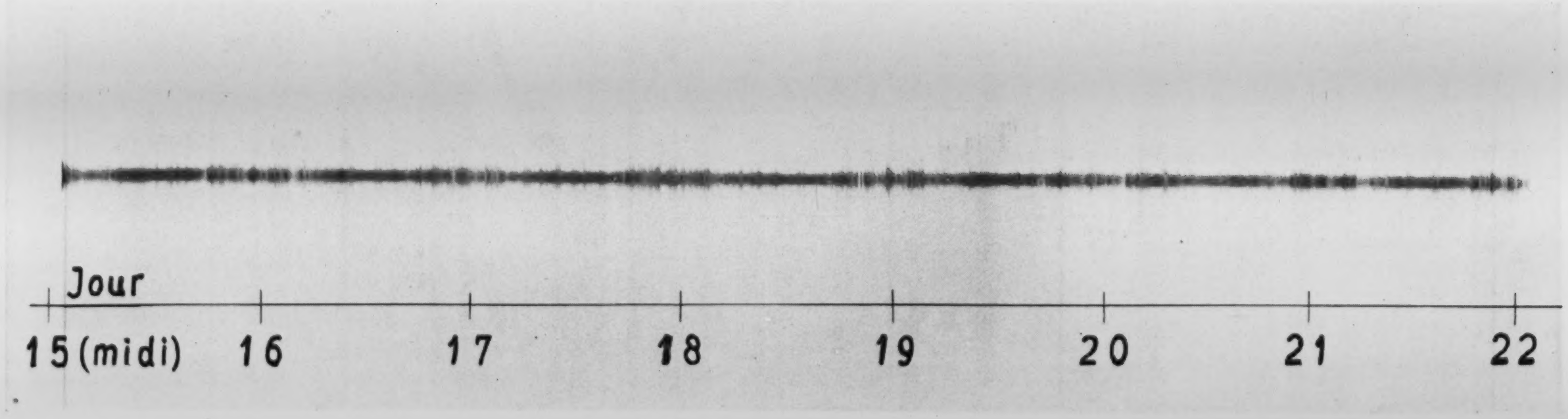

Fig. 9. Enregistrement obtenu à Mitaka.

（震研彙報　第十五號　圖版　石本）

période propre du sol se manifeste au moment de l'apparition des tremblement de terre.

Nous avons l'intention de réaliser à l'avenir, observations avec des pendules ayant les périodes propres de 4 et 8 sec correspondant aux périodes spéciales des secousses pulsatoires.

46. 東京地方微動の觀測

地震研究所　石本巳四雄

1. 東京山ノ手方面で微動計を設置して觀測を行つて見ると，0·3 秒程度の微動が常に存する事が知られて居る．此の周期の振動は地震動の中にも加速度の大なるものとして卓越するものであるから，此の微動を特に研究しやうと企てた．卽ち Wood-Anderson 型の振子を製作して其の特性の中，其の自己周期を傾斜角によつて變化せしめると，0·25～1·25 秒に變化する事が判明した．

2. 以上の振子を研究所地下室に設置し，周期を 0·3 秒或ひは 1 秒に保つて觀測して得られた結果が第 4 圖 a, b, c である．此の圖から見られる如く，微動の消長には日變化があり，其の原因は全く交通機關によるものであると考へられる．なほ以上の 0·3 秒周期の微動は氣象要素に無關係である事も判つた．又振子の周期を緩漫に變化せしめる裝置を製作して觀測を行つて見ると，0·3 秒附近に微動が卓越する事も認められた．

3. 丸ノ內における觀測では，此所は微動が激しく，約 1/2 の感度となし，振子の周期も 0·6 秒に保つた．其の得られた結果から見れば微動の特性は本鄕におけるものと酷似するものである．（第 8 圖）

4. 三鷹における觀測では此所は致つて平穩である事が判り，日變化は殆ど認められぬ狀況である．長期に亘つて特に地震前に微動の振幅が大となる疑があつたが，此れは認められなかつた．

5. 要するに從來屢々問題となつて居た山ノ手方面に存在する 0·3 秒の周期の振動は全く交通機關に原因するものであり，地表層の彈性と其の厚さとに密接の關係をもつものと考へられる．從つて地震の場合にも此の周期の振動が誘導され易いのも當然の事であらう．

47. On the So-called Mukuhira's Arc as the Foreshadow of an Earthquake.

By S. FUJIWHARA,

The Central Meteorological Observatory, Tokyo.

(Received Jan. 19, 1937.)

§1. *North Izu Earthquake.* At 12h 50m on November 25. 1930, Prof. M. Ishino[1], dean of the Science Faculty of the Imperial University of Kyoto, received a telegram from an unknown young man, Mr. Hirokiti Mukuhira, of Eziri, near Miyazu, Kyoto Prefecture, reading:

"At about 4h tomorrow morning there will occur an earthquake in Izu province". The telegram was handed in for despatch at the Hasidate telegraph office at 12h 35m of the same day. As predicted, an earthquake occurred the next morning at 4h 03m in the north Izu district, killing 259 persons and demolishing 2,142 houses[2]. Immediately afterward the story of Mukuhira's telegram was reported by the "Osaka-Mainiti", and the "Tokyo Nitiniti" two well known newspapers in Japan. Prof. T. Shida of Kyoto University" proceeded to Eziri to ascertain how the young man succeeded in forecasting the earthquake, but on his return to Kyoto he published nothing in regard to the matter. As gathered from descriptions in the newspapers, Mukuhira observed an optical phenomenon in the sky resembling a rainbow arc, and upon the basis of certain observed facts, made some sort of calculation and hit the time and place of the earthquake.

§2. *Mukuhira's Arc.* It is said that Mukuhira had been studying, rather in secret, this phenomenon since 1919, and was engaged on it all through the times of the great Kwanto earthquake of Sept. 1, 1913, of the Tazima earthquake of May 23, 1925, and of the Tango earthquake of March 7, 1927, etc.

Since then (1930) he published his earthquake forecasts, but as some of them were failures, the police forbad these forecasts. During this time his laboratory was closed to visitors, while his method of forecasting was strictly guarded as secrets from inquisitive people. In 1933, he removed to Tanabe, Wakayama prefecture, and there continued his studies. Finally in August 1935, he published a small pamphlet in Japanese entitled "On the Precursors of Earthquakes and the Phenomenon of Mukuhira's Arc." According to this brochure, the number of arcs observed by him since 1919 totaled 449, of which the outstanding ones are shown in Fig. 1. The arc differs from the rainbow, or any kind of halo or corona or iridescent cloud. It is never the less dimly coloured. It appears, according to him, in a clear sky for a few minutes at sun-rise, sun-set, midday and midnight. From its duration he calculates the time of occurrence, and from its shape and orientation, the direction and distance of the earthquake focus. He has not yet published his method of calculation in detail, but declares he is willing to so some time in the future.

---

[1] The present writer wrote to Dean Ishino and received an answer afirming the time he received the telegram, and its contents.

[2] There are many reports on this earthquake e.g. *Seismological Bulettin Cent. Met. Obs. Japan.*, 1930, Bull. of the *Earthq. Research Inst. Japan*, Vol. 9, dtc.

§3. *Kawati-Yamato Earthquake.* According to Mukuhira, many have observed similar phenomena, but it was since the Kawati-Yamato Earthquake that the phenomenon has been noticed by authorised meteorological observers. The Kitugawa meteorological station reported[3] as follows:–

"About sunset on Feb. 20, 1936, an optical phenomenon was observed by the Kitugawa Meteorological Station, Osaka, belonging to the Central Meteorological

Fig. 1

Mukuhira's arc (after Mukuhira)

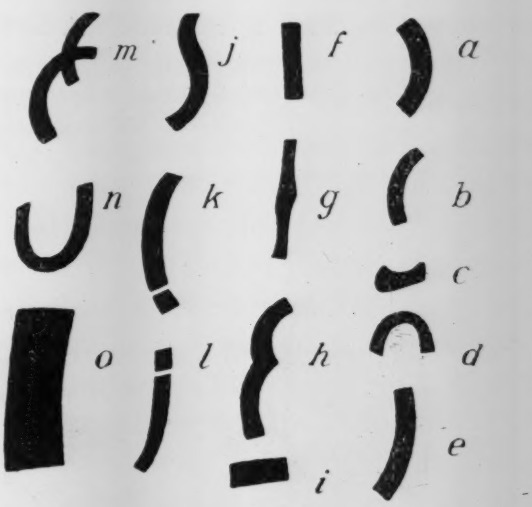

These Arcs appeared preceding respectively

a The great Kwanto earthquake on Sept. 1, 1923.
b The strong Sagami earthquke on Jan. 15, 1924.
c The strong Tyûgoku earthquake on Jan. 9, 1934.
d The great Izu earthquake on Nov. 26, 1930.
e The violent Tango earthquake on Mar. 7, 1927.
f The strong Sagami earthquake on June 17, 1931.
g The violent Tazima earthquake on May 23, 1925.
h The great Sanriku earthquake on March 3, 1933.
i The strong Saitama earthquake on Sept. 21, 1931.
j The greatT aiwan earthquake on April 21, 1935.
k The strong Kii earthquake on July 4, 1929.
l The strong Sendai earthquake on Aug. 6, 1927.
n The strong Hyûganada earthquake on Nov. 2, 1931.
and m is the double arcs and O is the post arc.

---

[3] Kisyoyoran (Monthly Geophysical Summary in Japanese issued by the Central Meteoroiogical Observatory) 1936, Feb. p. 187.

Observatory of Japan. Ten minutes before sunset, an observer noticed nothing but an ordinary calmness around the sun with some evening red sky tinted on patches of stratocumulus. He then went into his room, but 4 minutes before sunset (17h 45m, 135° M.T.) he noticed through the window the peculiar bright spots above the western horizon, as shown in Fig. 2, in which A is the visible sun veiled by a thin bank

Fig. 2. New Optical phenomenon Observed at Kitugawa Meteorological Station, Osaka $17^h 45^m$ Feb. 20, 1936.

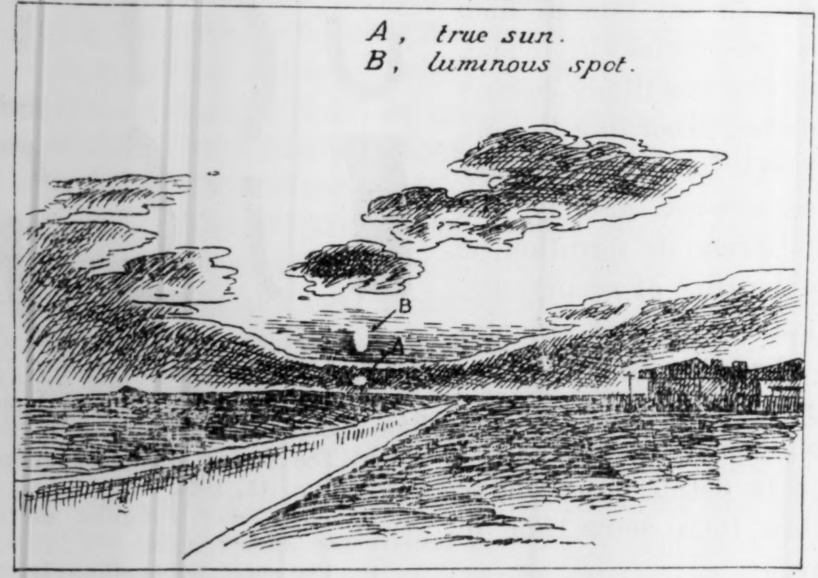
A, true sun.
B, luminous spot.
B
A

of cloud, and B a bright golden spot somewhat diffused at the upper edge. The observer rushed out doors at once and observed it carefully. The spot disappeared after 1 minute. At that time a moderate north wind 4·9 m/s, was blowing; the air temperature was 3·1°C; humidity 61%; sky clear, Stcu. vesperalis amount 1, with a thin haze hanging low over the bay. At 10h 8m the next morning (i.e. Feb. 21) there occurred a strong earthquake in the southeastern part of Oosaka prefecture a-

Fig. 3. New Optical arc observed at Hatinohe Meteorological Station. $6^h 15^m$, Nov. 1, 1936.

A, Point of Sun rise.
BC, Luminous Arc.

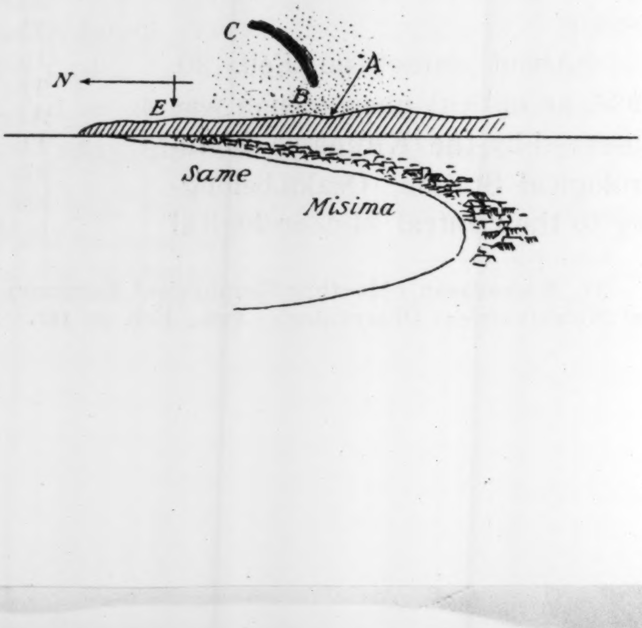

round Mt. Nizyosan, as a result of which 9 persons were killed and 20 houses demolished.

§4. *Sanriku Earthquake.* The Hatinohe Meteorological Station reported: "About a quarter past 6 in the morning of Nov. 1, 1936, an optical phenomenon was observed east of the Hatinohe Meteorological Station (N 40°32′, E 141°32′). As shown in Fig. 3, it hung from about 6° to about 10° above the horizon with a horizontal dimension of about 8°. It curved northward and resembled a rainbow, but it was not. The curve was rather parabolic with its width a little smaller than an ordinary rainbow. The principal colours were thin yellow and red with some tints of purple. It was very thin in the sunrise sky and only a very careful observer could accurately observe it. It lacked lustre. It lasted about 4 or 5 minutes. The sky was clear with spotted Cu. here and there and St. above the western horizon amounting to 1 as a whole. There was no cloud in the vicinity of sunrise. The wind was WSW 7·7 m/s; swell 3; wind-wave 3; air temperature 6·1°C, humidity 73%. The night preceding there was a thunder storm. The next morning but one, Nov. 3, an earthquake occurred at 5h 45m shaking the region over an area of 1,800 km diameter. The epicenter was located by the Central Meteorological Observatory at E long. 142·0°, N lat. 38·4°.

Since these two examples are quite authentic, it is certain that there is a new optical phenomenon which was hitherto unknown to us. It is, however, not yet certain whether the phenomenon is really correlated with earthquakes or not, nor do we know anything about its physical cause. Still there is some hope of finding the true nature of the phenomenon, which may serve as one of the means of forecasting earthquakes. At all event's, it behoves us to endeavour to search for more scientific data before drawing any hasty conclusions from it.

A similar example was reported by Mr. Tutui, lighthouse keeper at Himezima Island[4]. At sunrise on Feb. 12, 1933, for 7 minutes he observed a mock sun, at first above the rising sun, and later below it for 3 munutes. On the 13th, about 6h am, two shocks occurred in the Volcano district of Mt. Aso, while on the 14th an earthquake was felt at Wakayama about noon.

Another example was reported by Mr. Y. Nakata[5], director of the Miyako meterological station, with respect to the report of the director of the Fishery Institute of Iwate Prefecture at Kamaisi. On the morning of July 9 or 10, 1935, he observed from his boat at sea in the Pacific a golden mock sun above the true sun at sunrise. Never having witnessed such a phenomenon before, he mentioned it to Mr. Nakata upon his reaching shore. On the 11th, at 17h, 24m, an earthquake occurred in the vicinity of Sizuoka, where 9 persons were killed and 363 houses thrown down.

---

[4] *Kisyo yoran*, Feb. 1933.

[5] In a private communication to the writer Mr. Nakata inquired about the optical nature of the phenomenon, without any mention whatsoever of earthquakes.

There are of course many examples of similar phenomena in Mukuhira's field notes, which he may publish in the future. The foregoing instances are those that were observed by reliable witnesses other than and independent of Mukuhira.

There are some who are inclined to look upon the phenomenon as one of electric nature, among whom is Mukuhira himself. In the present stage of our knowledge of the phenomenon, however, practically any hypothesis could invoked to explain it, so that the real explanation must be left to future research.

47. 所謂椋平虹に就て

藤原咲平

概要 椋平虹の由來，形象及椋平氏以外の觀測を紹介す.

48. *Über die Jahresschwankung der Erdbebenhäufigkeit in Japan.*

Takeo MATUZAWA, Hirosi NAKAMATI, Yosio NISIKAWA
und Yosimaru YOSIMURA,

Institut für Erdbebenforschung.

(Vorgelegt 18. Mai 1937—Eingegangen 19. Juni 1937.)

1. Einleitung. Das Problem der Jahresperiodizität der Erdbebenhäufigkeit ist ganz übersichtlich von V. Conrad(1) zusammengefasst. Früher untersuchte F. Omori(2) die jährliche Bebenhäufigkeitsschwankung in Japan. Nach ihm wurde Japan in zwei Gruppen Gebiete geteilt, nämlich in der einen fällt das Häufigkeitsmaximum im Winter und in der anderen im Sommer. Wir wollen hier ähnliche Untersuchung wiederholen wegen den folgenden Gründen; erstens war das Beobachtungsmaterial zu seiner Zeit sicher mangelhafter als heute, zweitens lief seine Statistik über die Zahl der gefühlten Beben in dem betreffenden Ort und nicht die Zahl der Epizentren, nämlich wurde ein und dasselbe Beben manchmal mehrmals gezählt, drittens wollen wir die verfeinertere Methode der Statistik anwenden, um etwas sicheres sehen zu können.

2. Zusammenordnung der Beobachtungsmaterialien. Seit 1926 sind alle instrumentell bestimmten Epizentren in Japan in "Kisyô Yôran" publiziert. Hier ist ganzes Japan in viereckige Gebiete von ein gradigen Längen und Breiten eingeteilt und die Zahl der Epizentren in jedem Gebiete ist monatlich zusammengefasst. Die Statistik läuft vom Anfang 1926 bis zum Ende 1935 also 10 Jahre. Die zehnjährige Bebenhäufigkeit in jedem viereckigen Gebiet ist in Fig. 1 gezeigt.

Die Methode der Analyse ist ganz ähnlich wie der, die einer(3) von uns zur Analyse einiger Nachbeben einmal angewandt hat. Nämlich ist die Bebenzahl jährlich harmonisch analysiert und die Vektoren in der harmonischen Uhr sind mit Hilfe der Theorie von "Random Walk" diskutiert.

---

1) V. CONRAD, *Handbuch d. Geophys.*, **4** (1932) 1047~1082.

2) F. OMORI, *Rep Imp. Earthq. Invest. Commit.*, **30** (1900); *Publ. Earthq. Invest. Commit.*, **8** (1902); *Bull. Earthq. Invest. Commit.*, **2** (1903) No. 1; *Journ. Coll. Sci. Tôkyô*, **11** (1899).

3) T. MATUZAWA, *Bull. Earthq. Res. Inst.*, **4** (1936), 38~67.

Das ganze Verfahren ist in den folgenden Tabellen (Tabelle 1～69) ersichtlich.

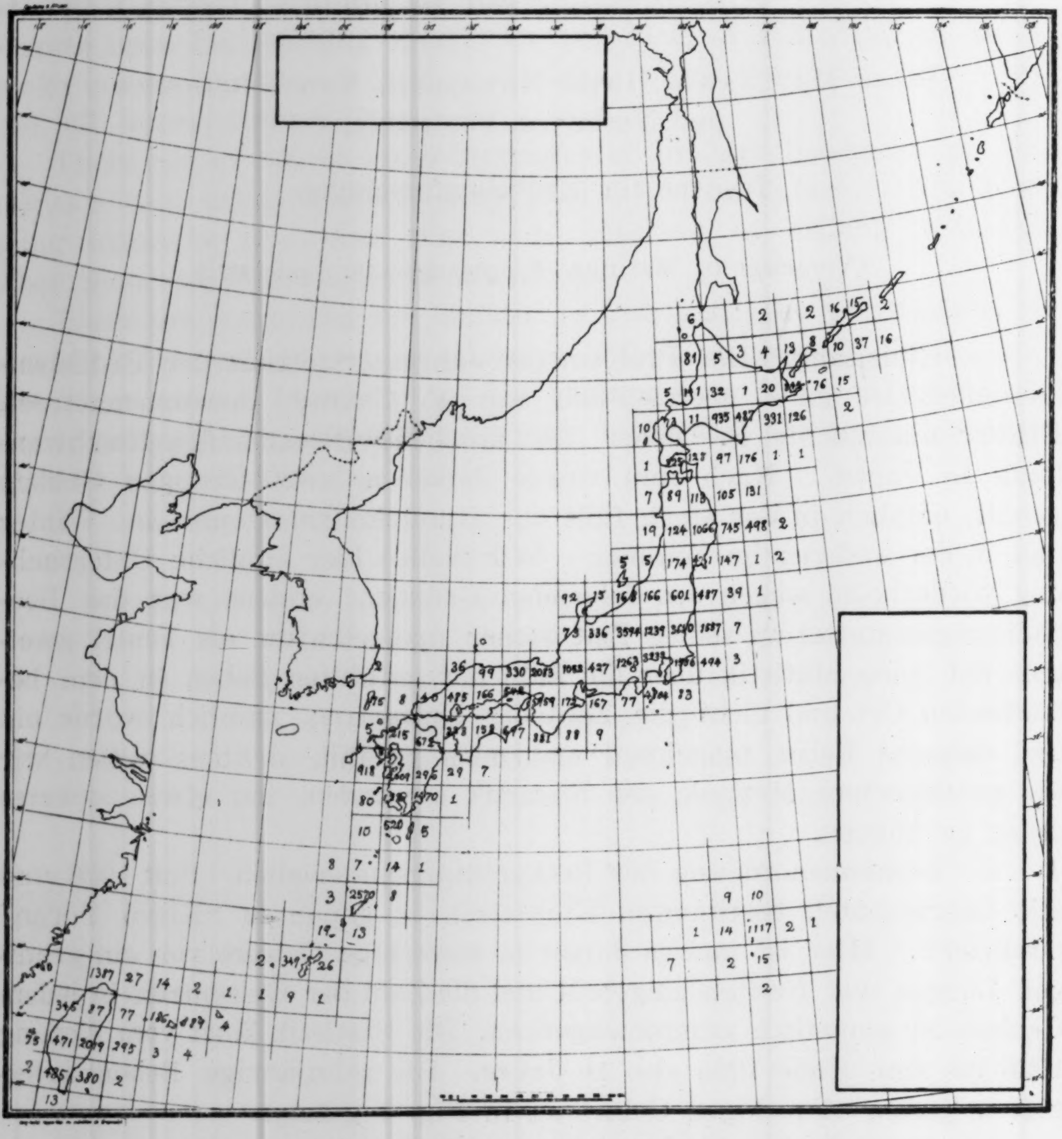

Fig. 1. Zehnjährige Bebenzahl.

3. Zusammenfassende Bemerkungen. Fig. 2 zeigt die Verteilung der gemittelten Vektoren, deren zugefügte Ziffer die Wahrscheinlichkeit $(1-W_1)$ als Realität bedeutet.

Es gibt 6 Gebiete, die sich durch den 0·94 überschreitenden Wert der Wahrscheinlichkeit $(1-W_1)$ auszeichnen, nämlich (24° N, 120° E) mit 0,953, (28° N, 129° E) mit 0,999, (30° N, 130° E) mit 0,982, (32° N, 130° E) mit 0,942, (35° N, 133° E) mit 0,991 und (42° N, 144° E) mit 0,964.

Es ist eine ganz merkwürdige Tatsache, dass meistens in diesen Gebieten es sich um die Menge lokale Beben aus einem räumlich ganz beschränkten Herdgebiet handelt.

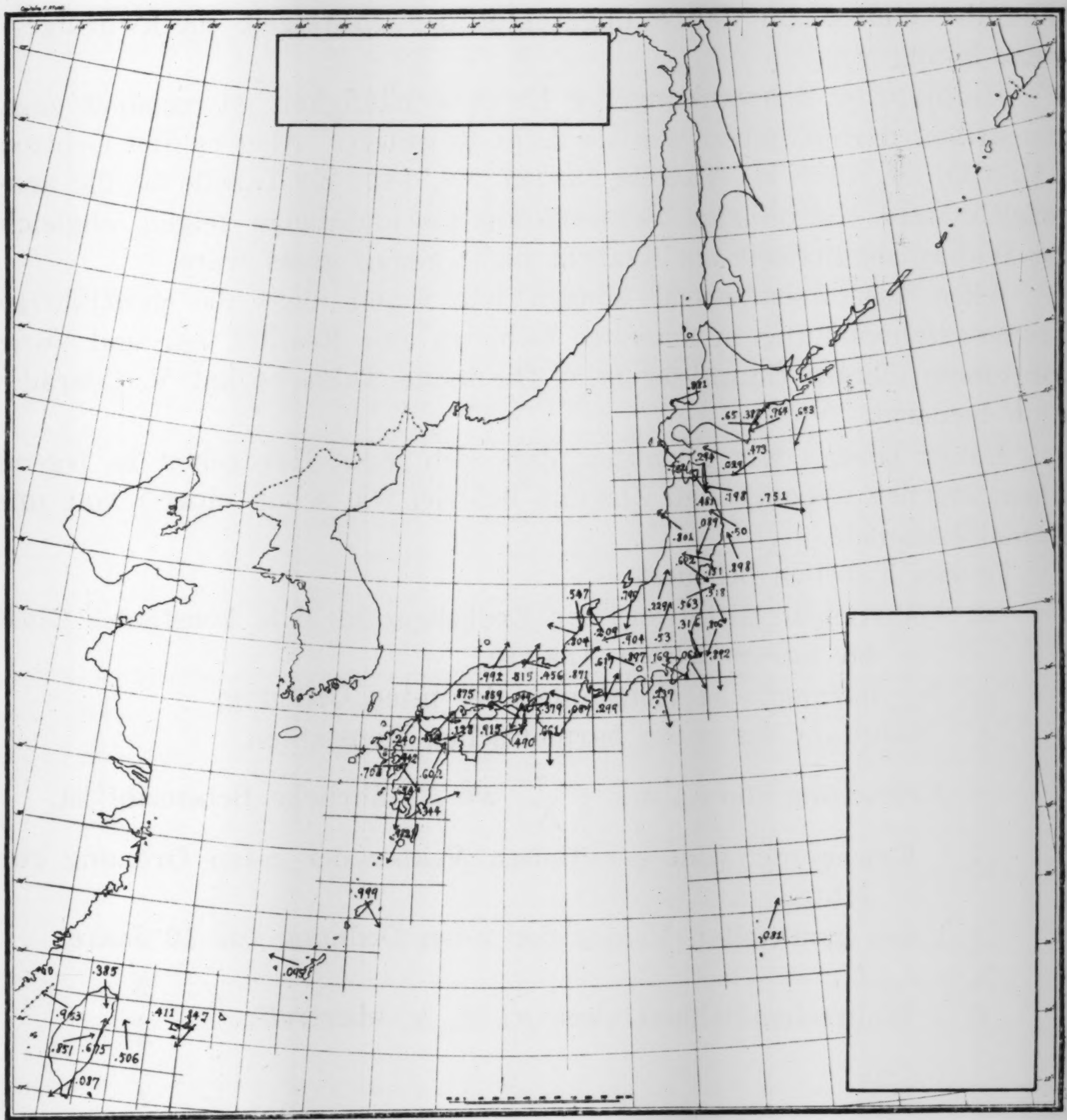
.65
.751
.198
.473
.029
.301
.50
.898
.547
.790
.563
.318
.53
.904
.209
.304
.892
.992
.815
.456
.871
.875
.379
.299
.915
.490
.240
.708
.602
.344
.999
.385
.953
.851
.506
.087
.411
.081

Fig. 2. Richtung der gemittelten Vektoren der jährlichen Häufigkeitsschwankung. Richtung Ost entspricht Januar-maximum, dann läuft in die entgegengesetzte Uhrzeigerbewegung.

Die jahreszeitliche Bebenhäufigkeitsschwankung ändert sich von Ort zu Ort; folglich je weiteres Gebiet wir in Rechnung zusammenhaben, desto undeutlicher wird die Charakteristik der Jahresperiodizität.

Es gibt auch manche Gebiete mit grossem jährlichem Wert von *k*, trotzdem der gemittelte Vektor für 10 Jahre nur kleine Wahrscheinlichkeit als Realität hat, z. B. Tabelle 14, Tabelle 26, Tabelle 28, Tabelle

33, Tabelle 43 u. s. w. nämlich in diesen Gebieten kommen die Erdbeben ungefähr einmal im Jahre ungeachtet der Jahreszeit merkwürdigerweise häufig vor.

Halbjährige Schwankung der Erdbebenhäufigkeit ist meistens ganz undeutlich, darum haben wir sie nicht tabelliert. Aber es gibt Gebiete, z. B. (35° N, 139° E) Tabelle 33, (27° N, 142° E) Tabelle 60, die ausgezeichnetere Halbjährige Schwankung als einjährige zeigen, obgleich die Wahrscheinlichkeit als Realität nicht genug gross wäre.

Alles zusammenfassend können wir sagen, dass die ganzjährige Frequenzschwankung in manchen Gebieten eine Realität ist, und zwar von einem lokalen Charakter ist. Die letzte Tatsache hat V. Conrad(4) auch bemerkt.

Daher können wir vermuten, dass sich jedes Herdgebiet in irgend einem eigenen dynamischen Zustand befinde, wie schon einer(5) von uns einmal bemerkte.

In den Tabellen bedeutet

a_0: jährlichen Mittelwert der Erdbebenzahl, d. h. konstantes Glied in der harmonischen Analyse,

a_n, b_n: harmonische Konstanten der n-ten Ordnung,

c_n: Resultant der n-ten harmonischen Konstanten,

ε: Erwartung von c_n, d. i. $\sqrt{\frac{\pi}{N}}$, wo N jährliche Bebenzahl ist,

${}_nl_m$: Erwartung vom gemittelten Vektor der n-ten Ordnung für 10 Jahre.

${}_nc_m$: den gemittelten Vektor der n-ten Ordnung für 10 Jahre.

k_n: ${}_nc_m/{}_nl_m$,

W_n: Wahrscheinlichkeit, dass ${}_nc_m/{}_nl_m$ k_n übertreffe.

---

(4) V. CONRAD, *Handbuch d. Geophys.*, **4** (1932), 1052.

(5) T. MATUZAWA, *Bull Earthq. Res. Inst.*, **14** (1936), 38~67.

Tabelle I.

Gebiet 43° N∼44° N, 145° E∼146° E.

Jahr	Monatliche Bebenzahl												Σ	a_0	$\frac{a_1}{a_0}$	$\frac{b_1}{a_0}$	c_1^2	ε	c_1/ε
	Jan.	Feb.	März	April	Mai	Juni	Juli	Aug.	Sept.	Oct.	Nov.	Dez.							
1926	17	10	9	1	3	0	4	2	0	2	7	4	59	4·91	1·02	0·17	1·239	0·23	4·85
27	2	19	8	1	9	10	5	2	4	4	3	12	79	6·58	0·32	0·33	0·211	0·199	2·31
28	5	9	12	6	13	9	1	10	2	4	3	3	77	6·41	−0·05	0·57	0·327	0·202	2·83
29	6	4	10	7	5	6	3	2	4	5	3	3	58	4·83	0·14	0·39	0·172	0·233	1·78
30	8	2	4	4	1	3	1	7	5	5	5	4	49	4·08	0.25	−0·34	0·178	0·24	1·66
31	5	3	8	15	12	7	3	3	8	5	4	9	82	6·83	−0·01	0·39	0·152	0·16	1·99
32	8	8	10	10	9	6	10	6	5	6	10	5	93	7·75	0·04	0·19	0·038	0·17	1·04
33	4	6	6	9	9	7	7	11	14	5	5	11	94	7·83	−0·21	−0·08	0·551	0·13	1·23
34	6	6	3	9	8	10	5	19	10	8	9	9	102	8·50	−0·30	−0·24	0·148	0·11	2·25
35	1	5	5	2	3	1	9	13	77	15	9	13	151	12·58	−0·52	−1·21	1·735	0·14	9·15
Σ	62	70	75	64	72	59	48	75	129	59	58	73	844		0·68	0·17	4·251		

${}_1l_m=0·206$ ${}_1c_m=0·701$ $k_1=0·34$ $W_1=0·891$

Tabelle II.

Gebiet 43° N~44° N, 141° E~142° E.

Jahr	Monatliche Bebenzahl												Σ	a_0	$\frac{a_1}{a_0}$	$\frac{b_1}{a_0}$	c_1^2	ε	c_1/ε
	Jan.	Feb.	März	April	Mai	Juni	Juli	Aug.	Sept.	Oct.	Nov.	Dez.							
1926	1	0	0	0	3	0	1	1	0	2	1	0	9	·75	− ·41	− ·17	·197	·59	·75
27	0	0	1	0	2	0	0	2	1	2	4	0	12	1·00	− ·12	− ·79	·639	·512	1·56
28	2	1	4	1	2	3	2	1	0	2	1	0	19	1·58	·85	−1·32	2·452	·370	4·23
29	1	2	1	0	2	5	0	3	0	0	0	0	14	1·17	− ·67	·66	·835	·473	1·99
30	0	0	0	2	1	1	0	4	0	0	0	0	8	·67	−1·19	·34	1·532	·626	1·98
31	1	0	0	1	2	2	4	0	3	0	1	0	14	1·17	− ·66	·04	·923	·473	2·03
32	1	1	0	0	1	0	3	0	4	0	0	0	10	·83	− ·73	− ·42	·709	·560	1·50
33	1	0	5	4	1	0	3	2	3	0	0	2	21	1·75	− ·14	·44	·213	·386	1·20
34	1	3	0	1	5	1	2	2	1	0	2	1	19	1·58	− ·44	·34	·309	·406	1·37
35	1	2	0	2	0	1	0	2	5	0	1	1	15	1·25	− ·14	− ·42	·196	·456	·97
Σ	9	9	11	11	19	13	15	17	17	6	10	4	141		−3·95	−1·30	8·061		

${}_1l_m = \cdot 284$ ${}_1c_m = \cdot 416$ $k_1 = 1\cdot 46$ $W_1 = \cdot 119$

Tabelle III.

Gebiet 42° N ~ 43° N, 145° E ~ 146° E.

Jahr	Monatliche Bebenzahl												Σ	a_0	$\frac{a_2}{a_0}$	$\frac{b_1}{a_0}$	c_1^2	ε	c_1/ε
	Jan.	Feb.	März	April	Mai	Juni	Juli	Aug.	Sept.	Okt.	Nov.	Dez.							
1926	0	1	0	0	0	0	0	1	1	0	1	5	9	·75	·96	− ·93	1·786	·590	2·27
27	2	4	1	0	1	0	1	1	1	7	1	1	20	1·67	·44	− ·60	·553	·396	1·88
28	1	1	9	2	2	3	1	0	1	2	2	2	26	2·17	·29	·61	·456	·348	1·94
29	1	2	2	0	0	2	0	0	3	1	0	0	11	·92	·09	·02	·008	·534	·17
30	0	1	0	0	0	1	0	2	0	1	0	2	7	·58	·00	− ·57	·324	·670	·85
31	1	1	2	2	2	2	1	2	0	1	1	0	15	1·25	− ·28	·54	·370	·457	1·33
32	0	0	2	0	1	1	1	3	0	1	0	1	10	·83	− ·63	·02	·397	·561	1·12
33	2	0	0	0	3	0	0	2	0	2	1	1	11	·92	·02	− ·33	·109	·534	·62
34	0	0	1	0	0	1	3	1	2	0	0	0	8	·67	−1·30	− ·21	1·734	·627	2·10
35	0	0	0	0	1	0	1	0	3	2	2	0	9	·75	− ·44	−1·21	1·657	·590	2·18
Σ	7	10	17	4	10	10	8	12	11	17	8	12	126		− ·85	−2·66	7·394		

$_1l_m = ·272$ $_1c_m = ·279$ $k_1 = 1·03$ $W_1 = ·347$

Tabelle IV.

Gebiet 42° N~43° N, 144° E~145° E.

Jahr	Monatliche Bebenzahl												Σ	a_0	$\frac{a_1}{a_0}$	$\frac{b_1}{a_0}$	c_1^2	ε	c_1/ε
	Jan.	Feb.	März	April	Mai	Juni	Juli	Aug.	Sept.	Okt.	Nov.	Dez,							
1926	5	2	4	5	7	4	4	5	4	1	3	2	46	3·83	− ·23	·30	·143	·261	1·45
27	3	3	1	5	0	1	0	5	3	0	2	0	23	1·92	·04	·09	·010	·370	·27
28	3	1	2	1	2	3	1	10	3	1	4	3	34	2·83	− ·31	− ·42	·273	·304	1·37
29	2	1	3	3	1	2	2	11	6	4	6	4	45	3·75	− ·26	− ·62	·452	·264	2·55
30	1	1	5	5	5	1	2	0	2	1	0	0	23	1·92	− ·17	1·04	1·111	·370	2·85
31	0	0	4	2	3	4	5	6	4	7	4	2	41	3·58	− ·53	− ·37	·418	·277	2·34
32	4	0	1	3	3	8	3	8	3	0	5	1	39	3·25	− ·62	− ·05	·387	·284	2·19
33	1	0	2	1	2	0	4	5	4	3	2	0	24	2·00	− ·70	− ·61	·862	·362	2·57
34	0	1	2	4	2	1	1	4	5	3	0	3	26	2·17	− ·34	− ·18	·148	·348	1·10
35	4	1	2	2	0	1	7	3	4	2	0	2	28	2·33	− ·32	− ·23	·155	·325	1·21
Σ	23	10	26	31	25	25	29	57	38	22	26	17	329		−3·44	−1·05	3·96		

${}_1l_m = ·198$ ${}_1c_m = ·360$ $k_1 = 1·82$ $W_1 = ·0365$

Tabelle V.

Gebiet 42° N~43° N, 143° E~144° E.

Jahr	Monatliche Bebenzahl												Σ	a_0	$\frac{a_1}{a_0}$	$\frac{b_1}{a_0}$	$\overline{c_1^2}$	ε	c_1/ε
	Jan.	Feb.	März	April	Mai	Juni	Juli	Aug.	Sept.	Okt.	Nov.	Dez.							
1926	2	1	2	0	1	0	2	2	1	4	7	7	29	2·42	·60	−·85	1·082	·328	3·17
27	4	5	1	5	2	1	0	0	4	4	0	1	27	2·25	·43	·20	·224	·341	1·39
28	0	3	3	3	6	3	3	3	2	5	1	3	35	2·92	−·28	·18	·220	·299	1·57
29	1	2	3	0	3	2	0	1	0	1	1	0	14	1·17	·09	·68	·470	·473	1·45
30	1	1	1	1	0	5	1	1	0	1	3	3	18	1·50	·03	−·08	·007	·418	·20
31	6	3	7	2	3	3	1	4	4	0	0	7	40	3·33	·38	·19	·180	·280	1·52
32	8	7	5	7	8	13	12	8	7	6	6	6	93	7·75	−·28	·09	·086	·184	1·59
33	19	10	14	4	9	9	14	7	14	14	5	5	124	11·16	·12	−·05	·016	·159	·80
34	9	7	4	8	10	11	6	12	4	0	4	4	79	6·58	−·26	·36	·197	·199	2·22
35	1	2	3	0	2	2	0	3	2	1	1	1	18	1·50	−·08	·08	·012	·418	·26
Σ	51	41	43	30	44	49	39	41	38	36	28	37	477		·75	·80	2·494		

${}_1l_m = {\cdot}158$ ${}_1c_m = {\cdot}110$ $k_1 = {\cdot}70$ $W_1 = {\cdot}613$

Tabelle VI.

Gebiet 42° N~43° N, 142° E~143° E.

Jahr	Monatliche Bebenzahl												Σ	a_0	$\frac{a_1}{a_0}$	$\frac{b_1}{a_0}$	c_1^2	ε	c_1/ε
	Jan.	Feb.	März	April	Mai	Juni	Juli	Aug.	Sept.	Okt.	Nov.	Dez.							
1926	0	0	0	0	0	0	0	0	0	0	0	0	0	0	0	0	0		
27	0	0	3	0	0	0	0	0	0	0	0	0	3	·250	·96	1·68	3·74	1·021	1·89
28	0	0	0	1	0	0	0	0	0	1	0	0	2	·167	0	0	0	1·25	0
29	0	1	0	0	0	0	0	0	0	0	0	0	1	·083	1·734	0·96	3·91	1·77	1·12
30	0	0	0	0	0	1	3	7	6	3	2	4	26	2·167	− ·65	− ·89	1·21	·35	3·15
31	4	255	65	25	20	7	20	13	9	7	4	9	438	36·5	·98	·92	1·81	·084	16·0
32	0	0	2	1	1	0	0	0	0	0	159	70	233	19·4	1·21	−1·45	3·57	·12	15·8
33	2	0	4	2	1	2	0	4	1	1	1	1	19	1·584	− ·09	·23	·06	·41	·59
34	2	0	0	0	0	1	0	1	0	2	1	0	7	·583	·24	− ·83	·75	·67	1·30
35	3	12	13	7	5	2	4	6	108	22	6	18	206	17·18	− ·28	−1·07	1·22	·12	9·17
Σ	11	268	87	36	27	13	27	31	124	36	173	102	935		4·10	− ·45	16·22		

${}_1l_m = ·403$ ${}_1c_m = ·413$ $k_1 = 1·025$ $W_1 = ·35$

Tabelle VII.

Gebiet 41° N~42° N, 143° E~144° E.

Jahr	Monatliche Bebenzahl												Σ	a_0	$\frac{a_1}{a_0}$	$\frac{b_1}{a_0}$	c_1^2	ε	c_1/ε
	Jan.	Feb.	März	April	Mai	Juni	Juli	Aug.	Sept.	Okt.	Nov.	Dez.							
1926	0	0	3	2	2	3	0	0	1	0	1	3	15	1·25	·06	·62	·388	·457	1·36
27	0	3	1	0	3	0	2	7	2	1	2	0	21	1·75	− ·62	− ·29	·468	·387	1·77
28	1	0	4	0	0	3	3	0	1	1	2	2	17	1·42	− ·04	·04	·003	·430	·13
29	2	0	4	1	4	2	1	3	0	1	1	0	19	1·58	− ·30	·59	·438	·406	1·63
30	1	3	1	1	1	1	1	4	0	0	1	2	16	1·33	·06	·17	·032	·443	·40
31	0	4	3	1	3	2	2	1	1	0	1	1	19	1·58	− ·03	·68	·463	·406	1·68
32	1	1	0	2	0	0	0	2	11	0	0	2	19	1·58	− ·39	− ·95	1·054	·406	2·60
33	0	0	0	0	0	0	5	2	0	2	3	0	12	1·00	− ·71	− ·93	1·369	·512	2·29
34	1	0	2	0	3	1	0	1	3	4	3	3	21	1·75	·13	− ·61	·389	·387	1·61
35	1	3	0	3	0	0	1	1	1	4	1	2	17	1·42	0·40	− ·32	·262	·430	1·19
Σ	7	14	18	10	16	12	15	21	20	13	15	15	176		−1·44	−1·00	4·866		

${}_1l_m=\cdot220$ ${}_1c_m=\cdot175$ $k_1=\cdot80$ $W_1=\cdot527$

Tabelle VIII.

Gebiet 41° N~42° N, 142° E~143° E.

Jahr	Monatliche Bebenzahl												Σ	a_0	$\frac{a_1}{a_0}$	$\frac{b_1}{a_0}$	c_1^2	ε	c_1/ε
	Jan.	Feb.	März	April	Mai	Juni	Juli	Aug.	Sept.	Okt.	Nov.	Dez.							
1926	0	0	0	0	1	0	0	0	1	1	1	1	5	·42	·14	− ·93	·88	·793	1·18
27	0	0	1	0	1	0	0	0	0	0	0	0	2	·167	0	1·71	2·92	1·252	1·37
28	0	0	0	0	1	0	0	0	0	1	0	0	2	·167	− ·48	−·120	·244	1·252	·39
29	1	1	1	0	1	5	2	0	0	0	0	1	12	1·00	− ·60	·70	·85	·512	1·80
30	0	1	0	0	0	0	2	0	0	3	1	2	9	·75	·24	− ·97	·99	·590	1·69
31	0	0	0	3	4	4	1	0	0	0	0	0	12	1·00	−1·08	1·41	3·15	·512	3·47
32	1	1	0	3	1	0	1	0	15	2	1	4	29	2·42	− ·22	− ·93	·91	·329	2·76
33	1	0	2	0	0	0	1	0	0	2	2	0	8	·67	·49	− ·49	·48	·625	1·11
34	0	0	4	2	1	0	1	0	1	2	1	1	13	1·03	·21	·59	·39	·492	1·27
35	0	1	1	0	0	0	1	0	2	0	0	0	5	·42	− ·26	− ·14	·09	·793	·38
Σ	3	4	9	8	10	9	9	0	19	11	6	9	97		−1·56	·83	10·90		

${}_1l_m=1{\cdot}04$ ${}_1c_m=\cdot177$ $k_1=\cdot169$ $W_1=\cdot971$

Tabelle IX.

Gebiet 41° N~42° N, 141° E~142° E.

Jahr	Monatliche Bebenzahl												Σ	a_0	$\frac{a_1}{a_0}$	$\frac{b_1}{a_0}$	c_1^2	ε	c_1/ε
	Jan.	Feb.	März	April	Mai	Juni	Juli	Aug.	Sept.	Okt.	Nov.	Dez.							
1926	0	0	0	0	0	0	0	0	0	0	0	1	1	·08	1·75	1·00	4·062	1·77	1·14
27	0	0	1	1	0	0	2	3	2	1	2	2	14	1·17	− ·33	− ·73	·641	·474	1·69
28	1	2	1	2	3	1	1	2	3	1	2	1	20	1·42	·25	·06	·066	·396	·65
29	3	3	1	0	0	3	2	2	0	1	1	1	17	1·92	·10	− ·06	·013	·430	·27
30	1	3	1	3	1	0	5	0	2	2	2	3	23	1·67	− ·15	·01	·022	·369	·40
31	1	0	0	0	0	3	1	0	0	1	3	1	10	·83	− ·05	− ·52	·272	·561	·93
32	0	1	1	1	2	2	1	2	2	1	1	1	15	1·25	− ·50	·00	·250	·458	1·09
33	1	0	0	1	0	1	1	0	2	0	2	0	8	·67	− ·21	− ·49	·284	·626	·685
34	0	0	0	0	3	0	0	1	0	0	3	0	7	·58	− ·24	− ·14	·077	·670	·41
35	0	1	1	0	1	0	3	1	2	4	0	0	13	1·08	− ·62	− ·62	·768	·480	1·83
Σ	7	10	6	8	10	10	16	11	13	11	16	10	128		·00	−1·49	6·455		

${}_1l_m = \cdot 254 \quad {}_1c_m = \cdot 149 \quad k_1 = \cdot 59 \quad W_1 = \cdot 706$

Tabelle X.

Gebiet 41° N~42° N, 140° E~141° E.

Jahr	Monatliche Bebenzahl												Σ	a_0	$\frac{a_1}{a_0}$	$\frac{b_1}{a_0}$	c_1^2	ε	c_1/ε
	Jan.	Feb.	März	April	Mai	Juni	Juli	Aug.	Sept.	Okt.	Nov.	Dez.							
1926	1	1	2	2	0	2	0	2	0	0	1	1	12	1·00	− ·13	·48	·247	·512	·97
27	1	0	1	0	0	1	1	1	0	0	1	0	6	·50	− ·24	·00	·057	·723	·33
28	0	0	0	0	1	2	0	0	0	0	0	2	5	·42	− ·19	·33	·145	·792	·481
29	2	1	0	0	1	22	19	11	3	5	6	2	72	6·00	−1·17	− ·19	1·405	·209	5·68
30	15	1	0	5	2	0	0	0	0	0	2	0	25	2·08	1·27	·44	1·806	·354	3·85
31	0	0	3	1	1	1	0	1	0	1	4	0	12	1·00	·21	·00	·044	·512	·41
32	0	1	0	7	1	0	1	1	0	1	0	2	14	1·12	·04	·87	·758	·473	1·84
33	0	0	3	0	3	1	0	2	0	0	0	1	10	·83	− ·35	·84	·828	·560	1·63
34	0	0	0	4	3	2	4	0	0	3	2	0	18	1·50	− ·69	·32	·578	·418	1·82
35	0	0	5	0	1	1	12	15	8	9	1	1	51	4·25	−1·08	− ·82	1·838	·248	5·47
Σ	19	4	12	19	13	32	37	33	11	19	17	9	225		−2·07	2·27	7·706		

${}_1l_m = \cdot 278$ ${}_1c_m = \cdot 307$ $k_1 = 1\cdot 10$ $W_1 = \cdot 298$

Tabelle XI.

Gebiet 40° N～41° N, 142° E～143° E.

Jahr	Monatliche Bebenzahl												Σ	a_0	$\frac{a_1}{a_0}$	$\frac{b_1}{a_0}$	c_1^2	ε	c_1/ε
	Jan.	Feb.	März	April	Mai	Juni	Juli	Aug.	Sept.	Okt.	Nov.	Dez.							
1926	0	0	0	0	0	0	0	0	0	0	0	2	2	·17	1·71	−1·00	3·924	1·25	1·58
27	3	0	1	0	0	0	0	0	0	0	0	0	4	·33	1·74	·42	3·204	·89	2·01
28	0	0	0	0	3	2	0	0	2	1	1	1	10	·83	− ·58	− ·10	·346	·55	1·07
29	0	0	0	0	0	1	0	0	0	0	0	0	1	·08	−1·75	1·00	4·062	1·77	1·22
30	0	0	0	0	0	0	0	1	1	1	0	0	3	·25	− ·92	−1·56	3·280	1·02	1·76
31	1	0	3	6	1	3	0	0	1	2	0	1	18	1·50	− ·03	·85	·723	·418	2·02
32	2	1	0	1	1	13	5	2	5	0	0	0	30	2·50	−1·21	·24	1·521	·324	3·81
33	0	2	0	0	3	1	4	0	2	0	0	0	12	1·00	− ·94	·39	1·035	·512	1·99
34	2	0	1	1	0	2	3	4	0	1	0	1	15	1·25	− ·65	− ·09	·430	·458	1·43
35	1	1	3	0	1	0	1	0	0	1	1	1	10	·83	·65	·33	·531	·55	1·32
Σ	9	4	8	8	9	22	13	7	11	6	2	6	105		−1·98	·48	19·08		

$_1l_m = ·437$　$_1c_m = ·204$　$k_1 = ·47$　$W_1 = ·802$

Tabelle XII.

Gebiet 40° N~41° N, 141° E~142° E.

Jahr	Monatliche Bebenzahl												Σ	a_0	$\frac{a_1}{a_0}$	$\frac{b_1}{a_0}$	c_1^2	ε	c_1/ε
	Jan.	Feb.	März	April	Mai	Juni	Juli	Aug.	Sept.	Okt.	Nov.	Dez.							
1926	0	0	0	0	0	0	0	0	0	0	0	0	0	0	0	0	0		
27	0	0	0	0	2	0	1	0	0	0	0	1	4	·33	− ·57	·63	·721	·887	·96
28	0	0	0	0	0	0	0	0	0	0	0	0	0	0	0	0	0		
29	0	0	1	0	0	1	0	0	0	1	0	1	4	·33	·24	− ·06	·061	·887	·28
30	1	0	0	1	0	0	0	0	2	1	1	0	6	·50	·16	− ·86	·765	·724	1·21
31	1	0	42	0	0	0	0	1	0	0	0	2	46	3·83	·99	1·52	3·290	·261	6·95
32	1	0	0	1	0	4	2	4	2	0	2	0	16	1·33	− ·99	− ·31	1·076	·443	2·34
33	0	0	3	0	3	1	1	1	3	0	0	3	15	1.25	− ·22	·14	·068	·457	·57
34	1	1	2	2	1	2	1	0	1	1	2	0	14	1·17	·02	·36	·130	·473	·76
35	1	0	2	0	0	2	1	2	0	0	0	0	8	·67	− ·61	·43	·557	·626	1·19
Σ	5	1	50	4	6	10	6	8	8	3	5	7	113		− ·98	1·85	6·67		

${}_1l_m = ·258$ ${}_1c_m = ·209$ $k_1 = ·81$ $W_1 = ·519$

Tabelle XIII.

Gebiet 39° N ~ 41° N, 143° E ~ 145° E.

Jahr	Monatliche Bebenzahl												Σ	a_0	$\frac{a_1}{a_0}$	$\frac{b_1}{a_0}$	c_1^2	ε	c_1/ε
	Jan.	Feb.	März	April	Mai	Juni	Juli	Aug.	Sept.	Okt.	Nov.	Dez.							
1926	0	0	0	0	0	0	0	0	1	0	0	2	3	·25	·80	−1·20	2·08	1·02	1·41
27	0	0	1	0	0	0	0	0	0	0	0	0	1	·083	·96	−1·69	3·78	1·72	1·13
28	0	1	0	0	0	0	0	0	0	1	2	0	4	·33	3·39	−1·09	12·68	·886	4·02
29	0	0	1	0	0	0	0	0	0	0	0	0	1	·083	·96	−1·69	3·78	1·72	1·13
30	0	0	0	0	1	0	0	0	0	0	0	0	1	·083	− ·96	1·69	3·78	1·72	1·13
31	2	0	0	0	0	1	0	0	2	0	4	1	10	·83	·60	−1·04	1·422	·56	2·15
32	2	3	4	7	0	0	2	0	0	1	1	0	20	1·66	·51	1·01	1·28	·396	2·86
33	125	3	1038	267	96	7	31	3	25	10	14	2	1621	135·1	·68	1·49	2·683	·04	41
34	1	0	1	2	3	0	1	0	0	0	0	0	8	·67	− ·24	1·34	1·853	·626	2·17
35	0	0	0	0	0	0	0	0	0	0	0	0	0	0	0	0	0		
Σ	130	7	1045	276	100	8	34	3	28	12	21	5	1669		6·70	−1·18	33·35		

${}_1l_m = \cdot 577$ ${}_1c_m = \cdot 6803$ $k_1 = 1\cdot 18$ $W_1 = \cdot 249$

Tabelle XIV.

Gebiet 39° N~40° N, 142° E~143° E.

Jahr	Monatliche Bebenzahl												Σ	a_0	$\frac{a_1}{a_0}$	$\frac{b_1}{a_0}$	c_1^2	ε	c_1/ε
	Jan.	Feb.	März	April	Mai	Juni	Juli	Aug.	Sept.	Okt.	Nov.	Dez.							
1926	5	5	1	0	8	7	9	5	8	1	4	7	60	5·00	− ·32	− ·12	·116	·229	1·49
27	3	2	9	8	5	0	0	6	4	4	4	1	46	3·83	1·04	·29	1·165	·261	4·14
28	1	2	0	1	71	61	5	11	10	2	1	2	167	13·92	−1·23	·91	2·341	·137	11·2
29	2	0	7	3	11	6	7	16	8	10	6	2	78	6·50	− ·65	− ·24	·480	·201	3·45
30	4	9	11	1	9	2	0	1	1	5	1	1	45	3·75	·49	·71	·744	·264	3·27
31	0	0	6	1	5	6	0	4	0	0	1	0	23	1·92	− ·67	·93	1·313	·369	3·11
32	0	0	0	3	0	2	0	0	2	0	1	1	9	·75	− ·35	·20	·162	·591	·68
33	2	7	0	0	1	36	0	1	0	1	0	0	48	4·00	−1·02	·87	1·797	·256	5·24
34	9	12	14	3	3	0	6	4	10	2	9	6	78	5·67	·44	− ·25	·256	·201	2·52
35	6	4	4	2	0	2	1	10	5	133	18	8	193	16·08	·14	−1·59	2·547	·127	12·6
Σ	32	41	52	22	113	122	28	58	48	158	45	28	747		−2·13	1·71	10·921		

${}_1l_m = {\cdot}330$ ${}_1c_m = {\cdot}273$ $k_1 = 83$ $W_1 = {\cdot}501$

Tabelle XV.

Gebiet 39° N~40° N, 141° F~142° E.

Jahr	Monatliche Bebenzahl												Σ	a_0	$\frac{a_1}{a_0}$	$\frac{b_1}{a_0}$	c_1^2	ε	c_1/ε
	Jan.	Feb.	März	April	Mai	Juni	Juli	Aug.	Sept.	Okt.	Nov.	Dez.							
1926	10	7	6	8	5	20	14	0	6	5	3	12	96	8·00	−·122	·255	·0799	·181	1·56
27	3	2	1	1	5	3	1	2	3	3	4	1	29	2·42	−·036	−·13	·024	·329	·47
28	3	1	3	1	2	5	4	3	2	1	1	0	26	2·17	−·54	·25	·354	·348	1·71
29	1	2	2	4	1	3	1	0	1	5	4	4	28	2·33	·33	−·16	·135	·335	1·09
30	10	2	10	6	9	5	6	7	5	1	6	1	68	5·67	−·083	·34	·122	·215	1·62
31	5	3	12	14	6	5	11	10	13	15	92	16	212	17·25	·36	−·74	·677	·122	6·75
32	34	17	20	14	13	18	9	8	9	5	8	11	166	13·93	·36	·37	·267	·137	3·87
33	13	9	4	6	35	19	25	17	16	9	8	7	168	14·00	−·58	·14	·356	·137	4·36
34	15	5	11	5	4	7	4	15	15	10	13	14	128	10·67	·17	−·39	·181	·156	2·73
35	11	6	11	8	14	8	6	13	13	29	12	14	145	11·92	·030	−·38	·145	·147	2·59
Σ	105	54	80	67	104	93	91	75	83	83	151	80	1066		−·161	−·44	2·368		

${}_1l_m=\cdot154$ ${}_1c_n=\cdot047$ $k_1=\cdot305$ $W_1=\cdot911$

Tabelle XVI.

Gebiet 39° N~40° N, 140° E~141° E.

Jahr	Monatliche Bebenzahl												Σ	a_0	$\frac{a_1}{a_0}$	$\frac{b_1}{a_0}$	c_1^2	ε	c_1/ε
	Jan.	Feb.	März	April	Mai	Juni	Juli	Aug.	Sept.	Okt.	Nov.	Dez.							
1926	0	0	0	0	1	1	0	0	0	0	1	2	5	·42	·33	− ·19	·145	·793	·480
27	0	0	1	3	1	4	2	1	0	1	0	0	13	1·08	− ·97	·81	1·597	·492	2·57
28	2	1	2	1	3	3	0	0	2	3	1	0	18	1·50	− ·08	·19	·042	·417	·49
29	2	0	2	1	1	3	1	1	1	3	3	6	24	2·00	·36	− ·41	·247	·363	1·50
30	0	2	1	2	1	1	0	1	2	0	1	3	14	1·17	·30	·09	·098	·473	·66
31	1	2	1	4	1	1	1	0	0	0	0	0	11	·92	·15	1·30	1·712	·534	2·45
32	0	0	0	0	2	1	2	1	0	0	0	0	6	·50	−1·58	·58	2·832	·723	2·33
33	0	0	4	2	0	3	1	3	2	2	1	0	18	1·50	−1·02	·10	1·05	·417	2·46
34	2	1	0	0	1	0	0	2	0	2	1	0	9	·75	·25	− ·11	·474	·590	·46
35	0	0	0	1	1	1	0	1	0	0	1	1	6	·50	− ·28	·16	·104	·723	·45
Σ	7	6	11	14	12	18	7	10	7	11	9	12	124		−2·54	2·52	7·951		

${}_1l_m = \cdot 282 \quad {}_1c_m = \cdot 358 \quad k_1 = 1\cdot 27 \quad W_1 = \cdot 199$

Tabelle XVII.

Gebiet 38° N~39° N, 142° E~143° E.

Jahr	Monatliche Bebenzahl												Σ	a_0	$\frac{a_1}{a_0}$	$\frac{b_1}{a_0}$	c_1^2	ε	c_1/ε
	Jan.	Feb.	März	April	Mai	Juni	Juli	Aug.	Sept.	Okt.	Nov.	Dez.							
1926	0	0	0	0	5	0	0	0	0	0	2	0	7	·58	− ·43	·74	·732	·67	1·28
27	0	2	0	1	0	3	2	4	3	0	0	0	15	1·25	− ·51	− ·14	·279	·457	1·15
28	1	3	0	0	6	0	2	0	0	0	3	1	16	1·33	·62	·45	·586	·443	1·73
29	0	1	5	0	0	0	1	3	0	1	0	0	11	·92	·33	·42	·285	·535	·998
30	0	0	4	0	5	2	0	0	0	0	0	0	11	·92	− ·40	1·60	2·72	·535	3·09
31	1	0	0	0	0	1	1	0	1	0	0	0	4	·33	− ·70	− ·18	·522	·887	·815
32	0	2	3	3	2	4	0	0	1	0	0	0	15	1·25	− ·23	1·26	1·640	·457	2·80
33	0	0	0	0	0	1	11	4	7	4	1	4	32	2·67	− ·93	− ·90	1·674	·313	4·03
34	0	1	3	1	1	0	1	0	0	0	0	0	7	·58	·24	1·43	2·102	·67	2·17
53	8	0	2	0	2	0	1	0	3	0	3	0	19	1·58	·74	·18	·580	·406	1·87
Σ	10	9	17	5	21	11	19	11	15	5	9	5	137		−1·27	4·86	11·12		

${}_1l_m = {\cdot}333 \qquad {}_1c_m = {\cdot}502 \qquad k_1 = 1{\cdot}51 \qquad W_1 = 102$

Tabelle XVIII.

Gebiet 38° N~39° N, 141° E~142° E.

Jahr	Monatliche Bebenzahl												Σ	a_0	$\frac{a_1}{a_0}$	$\frac{b_1}{a_0}$	c_1^2	ε	c_1/ε
	Jan.	Feb.	März	April	Mai	Juni	Juli	Aug.	Sept.	Okt.	Nov.	Dez.							
1926	3	3	4	2	1	5	3	2	3	5	2	12	45	3·75	·35	−·27	·195	·264	1·67
27	19	5	1	2	3	2	3	31	4	5	6	5	86	7·03	−·09	−·53	·289	·191	2·81
28	6	4	3	4	1	5	3	1	4	1	0	3	35	2·92	·16	·31	·121	·296	1·17
29	3	10	5	7	6	9	0	2	2	0	0	2	46	3·83	·10	·97	·950	·261	3·74
30	4	1	0	3	2	0	2	3	6	2	1	8	32	2·67	·23	−·52	·327	·313	1·81
31	7	2	5	4	1	3	3	8	6	1	4	2	46	3·83	−·05	−·13	·019	·261	·53
32	4	2	3	2	3	4	4	4	3	0	5	2	36	3·00	−·14	·01	·019	·295	·47
33	4	2	2	0	11	30	8	2	2	1	1	3	66	5·50	−·98	·64	1·370	·218	5·37
34	5	1	2	0	3	5	9	2	5	4	7	5	48	4·00	−·18	−·44	·226	·256	1·86
35	2	2	5	2	3	2	0	9	1	1	1	3	31	2·58	−·14	·14	·039	·318	·62
Σ	57	32	30	26	34	65	35	64	36	20	27	45	471		−·74	·18	3·551		

${}_1l_m=\cdot188$ ${}_1c_m\cdot076$ $k_1=\cdot404$ $W_1=\cdot849$

Tabelle XIX.

Gebiet 38° N~39° N, 140° E~141° E.

Jahr	Monatliche Bebenzahl												Σ	a_0	$\frac{a_1}{a_0}$	$\frac{b_1}{a_0}$	c_1^2	ε	c_1/ε
	Jan.	Feb.	März	April	Mai	Juni	Juli	Aug.	Sept.	Okt.	Nov.	Dez.							
1626	0	0	0	0	0	0	0	0	0	3	0	6	9	·75	1·16	−1·33	3·114	·59	2·99
27	0	6	2	0	2	4	2	2	0	2	0	1	21	1·75	−·11	·47	·233	·387	1·25
28	0	5	1	0	0	0	3	3	0	1	1	2	16	1·33	·19	−·25	·098	·443	·706
29	1	0	2	0	0	1	0	0	2	4	0	0	10	·83	·28	−·70	·568	·561	1·34
30	1	4	0	0	2	0	5	0	2	0	2	3	19	1·58	·11	−·13	·029	·406	·42
31	2	5	0	1	6	3	1	3	4	2	1	1	29	2·42	−·24	·13	·074	·329	·83
32	0	1	5	0	1	2	1	1	2	3	0	2	18	1·50	·00	·05	·002	·417	·03
33	3	0	9	4	2	2	9	1	1	2	0	1	34	2·83	−·28	·63	·475	·304	2·27
34	3	1	1	1	0	1	2	0	0	0	0	0	9	·75	·33	·64	·518	·59	1·22
35	1	0	0	0	1	0	0	0	2	1	3	1	9	·75	·41	−1·11	1·390	·59	2·07
Σ	11	22	20	6	14	13	23	10	13	18	7	17	174		1·85	−1·60	6·501		

${}_1l_m = {\cdot}255$ ${}_1c_m = {\cdot}245$ $k_1 = {\cdot}96$ $W_1 = {\cdot}398$

Tabelle XX.

Gebiet 37° N ~ 38° N, 141° E ~ 142° E.

Jahr	Monatliche Bebenzahl												Σ	a_0	$\frac{a_1}{a_0}$	$\frac{b_1}{a_0}$	c_1^2	ε	c_1/ε
	Jan.	Feb.	März	April	Mai	Juni	Juli	Aug.	Sept.	Okt.	Nov.	Dez.							
1926	0	1	1	0	4	1	1	0	1	9	2	5	25	2·08	·19	− ·70	·52	·355	2·03
27	11	4	2	5	8	1	1	10	3	2	2	5	54	4·50	·18	·09	·04	·241	·83
28	2	7	1	3	2	3	1	3	2	9	6	2	41	3·42	·25	− ·38	·20	·377	1·19
29	2	5	7	7	3	20	9	9	10	3	3	2	80	6·67	−·69	·21	·52	·198	3·64
30	2	3	5	2	4	6	6	2	1	3	3	3	40	3·33	−·21	·27	·11	·280	1·18
31	3	5	4	7	4	3	3	8	4	2	5	3	51	4·25	−·08	·10	·02	·246	·58
32	4	0	5	4	5	0	3	6	9	4	3	2	45	3·75	−·24	− ·25	·12	·264	1·31
33	9	6	1	1	0	1	2	4	3	5	5	6	43	3·58	·68	− ·54	·75	·270	3·21
34	5	0	0	4	2	0	2	1	0	1	6	4	25	2·08	·54	− ·28	·37	·355	1·71
35	3	4	11	14	4	3	10	8	11	5	2	8	83	6·92	−·17	·15	·05	·195	1·15
Σ	41	35	37	47	36	38	38	51	44	43	37	40	487		·46	−1·33	2·70		

${}_1l_m = \cdot164$ ${}_1c_m = \cdot140$ $k_1 = \cdot854$ $W_1 = 482$

Tabelle XXI.

Gebiet 37° N ~ 38° N, 138° E ~ 139° E.

Jahr	Monatliche Bebenzahl												Σ	a_0	$\frac{a_1}{a_0}$	$\frac{b_1}{a_0}$	c_1^2	ε	c_1/ε
	Jan.	Feb.	März	April	Mai	Juni	Juli	Aug.	Sept.	Okt.	Nov.	Dez.							
1926	1	1	1	0	0	1	2	1	0	1	0	0	8	·67	− ·34	·09	·123	·626	·56
27	1	1	2	2	2	0	8	2	0	7	2	0	27	2·25	− ·51	− ·28	·339	·341	1·71
28	4	2	1	0	1	3	3	0	0	0	1	2	17	1·42	·28	·27	·151	·430	·904
29	0	1	1	1	5	0	1	1	0	0	3	0	13	1·08	− ·23	·39	·205	·492	·92
30	0	0	1	0	4	0	1	1	0	0	2	8	17	1·42	·54	− ·23	·345	·430	1·36
31	7	0	0	2	3	0	1	3	5	2	0	0	23	1·92	− ·05	− ·28	·031	·369	·77
32	5	2	0	0	0	2	2	2	2	2	2	0	19	1·58	·13	− ·47	·238	·407	1·20
33	0	1	0	0	1	2	1	2	0	4	4	0	15	1·25	− ·28	− ·82	·751	·468	1·85
34	2	0	0	0	2	2	1	1	0	0	8	2	18	1·50	·35	− ·63	·519	·418	1·73
35	2	0	2	0	0	1	1	4	0	0	1	0	11	·92	− ·33	− ·12	·123	·535	·65
Σ	22	8	8	5	18	11	21	17	7	16	23	12	168		− ·44	− 2·08	2·875		

${}_1l_m = {\cdot}170 \quad {}_1c_m = {\cdot}213 \quad k_1 = 1{\cdot}25 \quad W_1 = 210$

Tabelle XXII.

Gebiet 37° N~38° N, 140° E~141° E.

Jahr	Monatliche Bebenzahl												Σ	a_0	$\frac{a_1}{a_0}$	$\frac{b_1}{a_0}$	c_1^2	ε	c_1/ε
	Jan.	Feb.	März	April	Mai	Juni	Juli	Aug.	Sept.	Okt.	Nov.	Dez.							
1926	2	1	1	0	0	0	1	1	6	5	6	1	24	2·00	·20	−1·25	1·603	·362	3·50
27	4	4	1	2	6	6	0	0	0	4	3	2	32	2·67	·19	·34	·153	·313	1·25
28	4	3	6	3	1	4	1	3	0	1	1	4	31	2·58	·39	·47	·373	·318	1·92
29	1	11	10	8	1	7	0	7	4	3	1	5	58	4·83	·20	·41	·208	·233	1·96
30	7	5	3	1	4	1	3	5	1	5	2	5	42	3·50	·31	− ·12	·111	·273	1·22
31	8	10	15	6	4	6	8	5	11	6	4	2	85	7·08	·07	·19	·041	·192	1·05
32	1	1	4	2	5	7	5	2	2	1	8	10	48	4·00	·01	− ·03	·007	.256	·33
33	1	3	7	9	5	4	2	5	2	0	3	8	49	4·08	·09	·49	·248	·253	1·97
34	4	0	0	9	13	11	18	5	20	19	6	17	122	10·17	− ·44	− ·44	·387	·160	3·89
35	28	15	24	10	5	4	5	7	6	0	2	4	110	9·17	·68	·59	·811	·169	5·33
Σ	60	53	71	50	44	50	43	40	52	44	36	58	601		1·70	·60	3·941		

${}_1l_m = \cdot 1985$ ${}_1c_m = \cdot 1803$ $k_1 = \cdot 91$ $W_1 = \cdot 437$

Tabelle XXIII.

Gebiet 37° N ~ 38° N, 139° E ~ 140° E.

Jahr	Monatliche Bebenzahl												Σ	a_0	$\frac{a_1}{a_0}$	$\frac{b_1}{a_0}$	c_1^2	ε	c_1/ε
	Jan.	Feb.	März	April	Mai	Juni	Juli	Aug.	Sept.	Okt.	Nov.	Dez.							
1926	36	0	14	3	4	2	1	5	2	1	0	0	68	5·67	·96	·42	1·098	·215	4·87
27	1	0	0	0	2	2	6	1	1	3	1	0	17	1·42	−1·01	− ·49	1·260	·429	2·62
28	5	2	1	0	1	1	0	0	0	0	0	2	12	1·00	1·27	0·37	1·749	·512	2·58
29	0	3	1	0	1	0	1	0	0	0	0	1	7	·58	·71	·78	1·112	·670	1·57
30	0	1	0	0	0	0	1	1	1	1	2	1	8	·67	·09	−1·01	1·025	·626	1·62
31	0	0	0	0	0	0	0	1	0	0	0	0	1	·08	−1·75	−1·00	4·062	1·772	1·14
32	0	0	1	5	0	2	0	0	0	1	0	1	10	·83	− ·07	1·07	1·149	·560	1·91
33	1	0	1	0	1	1	1	0	0	1	1	0	7	·58	− ·10	·10	·020	·670	·21
34	0	0	0	1	1	6	0	0	0	0	0	1	9	·75	−1·08	·97	2·107	·590	2·46
35	0	1	15	0	1	1	0	0	1	3	2	3	27	2 25	·75	·57	·887	·341	2·76
Σ	43	7	33	9	11	15	10	8	5	10	6	9	166		·77	1·78	14·42		

${}_1l_m = {\cdot}380$ ${}_1c_m = {\cdot}194$ $k_1 = {\cdot}51$ $W_1 = {\cdot}771$

Tabelle XXIV.

Gebiet 37° N~38° N, 136° E~137° E.

Jahr	Monatliche Bebenzahl												Σ	a_0	$\frac{a_1}{a_0}$	$\frac{b_1}{a_0}$	c_1^2	ε	c_1/ε
	Jan.	Feb.	März	April	Mai	Juni	Juli	Aug.	Sept.	Okt.	Nov.	Dez.							
1926	0	0	0	0	1	0	0	0	0	0	0	0	1	·08	−1·00	1·75	4·062	1·77	1·14
27	0	0	0	0	0	0	0	0	0	1	0	0	1	·08	·00	−2·13	4·536	1·77	1·20
28	1	1	0	0	0	0	0	0	0	0	0	1	3	·25	1·84	·00	3·385	1·02	1·80
29	0	0	0	0	0	0	0	0	0	0	1	0	1	·08	1·00	−1·75	4·062	1·77	1·14
30	2	0	6	1	0	1	2	0	1	1	4	1	19	1·58	·47	·09	·229	·407	1·17
31	0	0	1	1	0	0	0	2	6	0	5	0	15	1·25	− ·23	−1·15	1·375	·458	2·56
32	1	0	1	0	0	5	0	2	2	0	1	0	12	1·00	− ·70	− ·04	·491	·512	1·37
33	1	0	1	2	0	0	0	0	12	1	0	3	20	1·67	− ·19	−1·00	1·036	·396	2·57
34	0	2	1	0	2	0	0	1	0	1	1	1	9	·75	·39	·16	·177	·591	·71
35	0	0	0	1	2	2	2	1	1	1	1	0	11	·92	−1·01	·10	1·030	·535	1·90
Σ	5	3	10	5	5	8	4	6	22	5	13	6	92		·57	−3·97	20·38		

${}_1l_m = {\cdot}451$ ${}_1c_m = {\cdot}401$ $k_1 = {\cdot}89$ $W_1 = {\cdot}453$

Tabelle XXV.

Gebiet 36° N~37° N, 141° E~142° E.

Jahr	Monatliche Bebenzahl												Σ	a_1	$\frac{a_1}{a_0}$	$\frac{b_1}{a_0}$	c_1^2	ε	$c_1'\varepsilon$
	Jan.	Feb.	März	April	Mai	Juni	Juli	Aug.	Sept.	Okt.	Nov.	Dez.							
1926	9	7	5	5	9	4	5	8	15	14	16	8	105	8·75	·13	− ·49	·257	·173	2·93
27	21	9	1	2	2	1	25	16	12	13	16	9	127	10·58	−·026	− ·63	·655	·157	5·16
28	22	10	6	15	21	16	9	11	26	14	11	19	180	15·00	−·002	− ·10	·010	·132	·76
29	33	12	12	19	17	21	12	20	7	14	17	9	193	16·08	·06	·12	·018	·127	1·06
30	12	20	22	8	4	5	17	16	8	15	9	12	148	11·50	·21	− ·15	·067	·146	1·77
31	10	9	7	10	3	29	10	14	25	21	12	14	164	13·67	−·27	− ·36	·203	·138	3·27
32	19	12	6	16	12	18	10	12	10	7	8	12	142	11·83	−·003	·17	·029	·149	1·14
33	9	11	13	15	9	10	15	7	9	20	7	12	137	11·42	−·13	·02	·017	·151	·86
34	15	14	14	7	17	10	11	13	9	14	9	12	145	12·08	·07	·06	·009	·147	·65
35	16	4	6	10	12	15	66	31	13	8	18	17	216	18·00	−·67	− ·22	·497	·120	5·88
Σ	166	108	92	107	106	129	180	148	134	140	123	124	1557		−·631	−1·58	1·762		

${}_1l_n = {\cdot}133$ ${}_1c_n = {\cdot}1701$ $k_1 = 1{\cdot}28$ $W_1 = {\cdot}196$

Tabelle XXVI.

Gebiet 36° N~37°N, 140° E~141° E.

Jahr	Monatliche Bebenzahl												Σ	a_0	$\frac{a_1}{a_0}$	$\frac{b}{a_0}$	c_1^2	ε	c_1/ε
	Jan.	Feb.	März	April	Mai	Juni	Juli	Aug.	Sept.	Okt.	Nov.	Dez.							
1926	2	22	13	13	28	37	18	33	70	32	74	49	391	32·58	− ·11	− ·61	·384	·0897	6·92
27	5	26	21	14	20	6	14	14	64	52	42	41	319	26·58	·13	− ·66	·453	·0991	6·78
28	32	35	39	30	61	28	27	21	29	17	26	24	369	30·75	·01	·33	·109	·0922	3·58
29	13	19	18	23	7	18	13	8	15	9	20	38	201	16·75	·35	·01	·123	·125	2·81
30	30	29	27	23	41	53	39	32	26	18	21	22	361	30·08	− ·27	·21	·117	·0933	3·67
31	10	30	26	33	45	25	22	42	198	66	26	33	556	46·33	− ·40	− ·63	·557	·0752	9·91
32	43	42	53	54	40	36	52	35	30	35	24	26	470	39·17	·62	·29	,469	·0818	8·38
33	27	30	58	39	41	32	23	24	28	23	22	47	394	32·83	·14	·27	·093	·0892	3·42
34	31	21	31	18	18	30	11	18	24	12	28	17	259	21·58	·15	·09	·031	·110	1·60
35	23	8	16	20	19	35	26	30	26	40	16	21	280	23·33	− ·29	− ·21	·128	·106	3·39
Σ	216	262	302	267	320	300	245	257	510	304	299	318	3600		0·33	− ·91	2·414		

${}_1l_m = \cdot157$ ${}_1c_m = \cdot0968$ $k_1 = \cdot616$ $W_1 = \cdot684$

Tabelle XXVII.

Gebiet 36° N ~ 37° N, 139° E ~ 140° E.

Jahr	Monatliche Bebenzahl												Σ	a_0	$\frac{a_1}{a_0}$	$\frac{b_1}{a_0}$	c_1^2	ε	c_1/ε
	Jan.	Feb.	März	April	Mai	Juni	Juli	Aug.	Sept.	Okt.	Nov.	Dez.							
1926	18	10	10	23	17	5	7	8	7	5	11	12	133	11·08	·26	·35	·164	·153	2·64
27	8	7	18	11	17	6	6	4	13	7	7	3	107	8·92	−·008	·37	·137	·171	2·17
28	13	13	10	10	8	7	7	7	2	4	4	8	93	7·75	·30	·41	·258	·184	2·77
29	6	3	15	14	5	7	5	6	6	9	6	3	85	7·08	−·001	·29	·084	·209	1·39
30	5	13	6	12	7	6	12	7	9	7	8	7	99	8·83	−·036	·075	·0069	·178	·47
31	3	4	7	9	7	7	8	10	358	10	7	13	443	36·92	−·82	−1·40	2·632	·099	16·4
32	14	15	14	13	6	6	3	9	7	5	6	5	103	8·85	·35	·33	·231	·174	2·77
33	4	13	7	9	2	3	3	4	5	4	6	8	68	5·67	·47	·16	·247	·215	2·31
34	6	1	1	3	8	5	4	4	2	1	5	5	45	3·75	−·11	·098	·0217	·264	·56
35	3	4	8	8	7	5	5	3	5	6	2	7	63	5·25	−·013	·27	·0730	·223	1·21
Σ	80	83	96	112	84	87	60	62	414	58	62	71	1239		·392	·953	3·855		

${}_1l_m = \cdot1952 \qquad {}_1c_m = \cdot1031 \qquad k_1 = \cdot53$

Tabelle XXVIII.

Gebiet 36° N~37° N, 138° E~139° E.

Jahr	Monatliche Bebenzahl												Σ	a_0	$\frac{a_1}{a_0}$	$\frac{b_1}{a_0}$	c_1^2	ε	c_1/ε
	Jan.	Feb.	März	April	Mai	Juni	Juli	Aug.	Sept.	Okt.	Nov.	Dez.							
1926	0	0	0	1	1	1	1	2	1	2	1	0	10	·83	− ·82	− ·47	·893	·56	1·69
27	11	0	4	0	0	0	2	0	1	8	2	5	33	2·75	·96	− ·59	1·270	·309	3·65
28	1	5	14	3	4	2	7	9	11	3	7	1	67	5·58	− ·22	− ·04	·050	·217	1·03
29	1	3	7	4	4	3	2	5	4	3	0	21	57	4·75	·43	− ·08	·191	·235	1·86
30	12	7	20	5	8	12	69	272	112	48	17	25	607	50·58	−1·04	− ·89	1·874	·0685	20
31	25	19	28	12	28	20	29	713	79	66	16	13	1044	86·67	−1·24	− ·83	2·227	·0548	27·3
32	33	64	126	139	125	160	226	56	75	29	12	18	1063	88·58	− ·64	·62	·794	·0543	16·5
33	21	15	33	18	14	17	24	21	14	4	12	9	202	16·83	−3·37	·05	11·359	·124	27·1
34	14	15	5	20	31	18	45	9	6	11	27	15	216	18·00	− ·29	·15	·107	·120	27·3
35	6	43	8	13	77	4	18	36	14	15	43	18	295	24·58	− ·09	·13	·025	·103	1·54
Σ	124	171	245	215	288	237	423	1123	317	189	137	125	3594		−6·32	−1·95	18·79		

${}_1l_m = ·433$ ${}_1c_m = ·6514$ $k_1 = 1·53$ $W_1 = ·096$

Tabelle XXIX.

Gebiet 36° N~37° N, 137° E~138° E.

Jahr	Monatliche Bebenzahl												Σ	a_0	$\frac{a_1}{a_0}$	$\frac{b_1}{a_0}$	c_1^2	ε	c_1/ε
	Jan.	Feb.	März	April	Mai	Juni	Juli	Aug.	Sept.	Okt.	Nov.	Dez.							
1926	0	0	0	0	3	1	0	1	0	0	0	0	5	·42	−1·29	1·02	2·705	·793	2·07
27	12	4	7	4	0	5	3	0	2	0	0	1	38	3·17	·61	·63	·79	·288	3·09
28	2	3	4	0	0	1	1	0	2	2	10	0	25	2·08	·70	− ·56	·80	·355	2·52
29	4	1	2	0	3	0	0	5	0	0	2	0	17	1·42	·12	·07	·02	·430	·33
30	1	2	4	2	3	0	0	2	3	1	2	2	22	1·83	·25	·16	·09	·378	·79
31	1	0	3	0	0	0	5	0	9	1	2	3	24	2.00	− ·29	− ·79	·71	·362	2·33
32	1	0	2	2	2	2	1	0	1	1	0	4	16	1·33	·16	·32	·13	·443	·81
33	2	2	13	3	9	13	15	3	3	3	2	6	74	6·17	− ·50	·42	·43	·206	3·18
34	1	1	1	2	2	1	0	0	3	4	5	2	22	1·83	·20	− ·58	·38	·378	1·63
35	9	0	5	4	21	16	12	9	3	3	4	7	93	7·75	− ·56	·38	·46	.184	3·69
Σ	33	13	41	17	43	39	37	20	26	15	27	25	336		− ·60	1·09	6.52		

${}_1l_m=·256$ ${}_1c_m=·124$ $k_1=·485$ $W_1=·791$

Tabelle XXX.

Gebiet 36° N~37° N, 136° E~137° E.

Jahr	Monatliche Bebenzahl												Σ	a_0	$\frac{a_1}{a_0}$	$\frac{b_1}{a_0}$	c_1^2	ε	c_0/ε
	Jan.	Feb.	März	April	Mai	Juni	Juli	Aug.	Sept.	Okt.	Nov.	Dez.							
1926	0	0	0	1	0	0	0	1	0	0	0	0	2	·17	− ·82	·47	·893	1·25	·76
27	3	0	0	0	1	1	1	0	0	0	0	0	6	·50	·22	·46	·260	·722	·71
28	0	1	0	0	1	0	0	0	1	0	0	0	3	·25	− ·08	·32	·108	1·02	·32
29	0	0	1	0	3	0	0	1	0	1	0	0	6	·50	− ·62	·66	·820	·722	1·25
30	0	3	2	0	3	0	2	0	0	13	1	1	25	2·08	·12	− ·68	·476	·355	1·94
31	1	0	0	2	0	0	0	4	1	0	0	1	9	·75	− ·47	− ·31	·317	·591	·95
32	0	0	0	0	1	3	0	0	0	6	0	0	10	·83	− ·63	− ·73	·929	·560	1·72
33	0	1	4	5	0	0	1	0	0	0	0	0	11	·92	·34	1·62	2·74	·534	3·10
34	0	0	0	0	0	0	0	1	0	0	0	0	1	·08	−1·75	−1·00	4·062	1·77	1·14
35	1	0	0	0	1	0	1	0	0	0	0	0	3	·25	− ·32	·56	·416	1·02	·63
Σ	5	5	7	8	10	4	5	7	2	20	1	2	76		−4·01	1·37	11·02		

${}_1l_m=·332$ ${}_1c_m=·423$ $k_1=1·28$ $W_1=·194$

Tabelle XXXI.

Gebiet 35° N～36° N, 141° E～142° E.

Jahr	Monatliche Bebenzahl												Σ	a_0	$\frac{a_1}{a_0}$	$\frac{b_1}{a_0}$	c_1^2	ε	c_1/ε
	Jan.	Feb.	März	April	Mai	Juni	Juli	Aug.	Sept.	Okt.	Nov.	Dez.							
1926	22	0	1	0	5	7	23	0	14	5	9	5	91	7·58	−·16	− ·41	·193	·186	2·34
27	4	1	1	3	3	1	6	24	2	4	2	2	53	4·42	−·83	− ·49	·929	·243	3·97
28	2	0	1	1	2	3	0	3	4	0	1	3	20	1·67	−·26	− ·22	·116	·396	·86
29	11	7	20	8	17	8	5	7	4	10	2	9	108	9·00	·14	·45	·222	·171	2·76
30	1	7	6	1	0	0	3	3	2	4	4	8	39	3·25	·64	− ·39	·561	·284	2·64
31	2	1	0	1	1	0	1	0	4	0	3	0	13	1·08	·13	− ·57	·341	·492	1·19
32	5	1	1	3	0	9	1	4	6	17	1	0	48	4·00	−·35	− ·68	·584	·256	2·99
33	1	1	3	1	1	1	24	0	0	8	34	1	75	6·25	−·11	− ·87	·769	·205	4·28
34	3	0	6	1	0	3	1	1	1	0	3	2	21	1·75	·36	·26	·197	·397	1·12
35	6	2	0	4	1	2	1	0	3	3	2	2	26	2·17	·44	− ·11	·205	·347	1·31
Σ	57	20	39	23	30	34	65	42	40	51	61	32	494		·00	−3·03	4·117		

${}_1l_m = {\cdot}203$ ${}_1c_m = {\cdot}303$ $k_1 = 1{\cdot}49$ $W_1 = {\cdot}108$

Tabelle XXXII.

Gebiet 35° N~36° N, 140° E~141° E.

Jahr	Monatliche Bebenzahl												Σ	a_0	$\frac{a_1}{a_0}$	$\frac{b_1}{a_0}$	c_1^2	ε	c_1/ε
	Jan.	Feb.	März	April	Mai	Juni	Juli	Aug.	Sept.	Okt.	Nov.	Dez.							
1926	3	18	13	11	17	7	10	19	5	15	5	10	133	11·08	−·11	·23	·065	·153	1·66
27	5	9	15	16	11	20	7	6	3	7	3	6	108	9·00	−·18	·63	·429	·171	3·83
28	14	2	10	4	9	14	4	14	11	6	4	43	135	12·08	·30	−·26	·158	·152	2·61
29	5	8	10	2	3	5	2	4	5	9	3	13	69	5·75	·46	−·14	·231	·213	2·26
30	11	13	19	8	84	9	5	19	8	16	13	16	221	18·42	−·21	·52	·315	·119	4·72
31	17	14	5	15	12	10	32	10	11	14	18	14	172	14·33	−·094	−·11	·0209	·135	1·07
32	18	18	16	11	5	22	19	10	10	33	21	9	192	16·00	·059	−·21	·0476	·128	1·70
33	14	5	11	8	8	4	21	17	29	18	54	10	199	16·58	·018	−·75	·563	·125	6·01
34	21	5	8	12	9	8	12	13	13	19	18	13	151	12·58	·11	−·34	·128	·144	2·49
35	8	5	12	25	20	26	7	12	14	17	19	13	178	14·83	−·20	·11	·0521	·133	1·72
Σ	116	97	119	112	178	125	119	124	109	154	158	147	1558		·153	−·32	2·01		

${}_1l_m = ·142$ ${}_1c_m = ·035$ $k_1 = ·25$ $W_1 = ·939$

Tabelle XXXIII.

Gebiet 35° N~36° N, 139° E~140° E.

Jahr	Monatliche Bebenzahl												Σ	a_0	$\frac{a_1}{a_0}$	$\frac{b_1}{a_0}$	c_1^2	ε	c_1/ε	$\frac{a_2}{a_0}$	$\frac{b_2}{a_0}$	c_1^2
	Jan.	Feb.	März	April	Mai	Juni	Juli	Aug.	Sept.	Okt.	Nov.	Dez.										
1926	25	25	16	27	23	16	17	48	11	15	7	8	238	19·8	−·203	·189	·0773	·115	2·42	·167	·332	·138
27	15	12	16	18	15	16	30	16	16	14	16	32	216	18·0	−·037	−·063	·0050	·120	·59	·18	−·152	·0554
28	15	28	9	15	38	15	16	7	18	14	13	15	203	16·92	·002	·25	·0625	·124	2·02	−·044	−·161	·0022
29	14	13	18	9	13	15	28	32	22	23	11	30	228	19·0	−·18	−·29	·117	·117	2·92	·20	·12	·0544
30	12	4	7	31	2	19	20	18	16	14	11	21	175	14·58	−·21	−·075	·505	·134	5·31	·00,	−·079	·00621
31	660	214	9	6	10	23	33	15	37	19	10	13	1049	87·42	1·48	·13	2·207	·062	24	1·46	·36	2·26
32	6	11	17	18	11	8	44	18	41	49	18	28	269	22·42	−·26	−·53	·349	·108	5·47	−·30	·14	·1096
33	27	32	35	33	27	38	26	26	34	32	45	40	395	32·92	·088	·059	·0117	·089	1·22	·44	−·10	·203
34	11	13	29	19	23	18	27	17	7	19	12	20	215	17·92	−·11	·24	·0697	·120	2·20	−·014	−·056	·0033
35	48	15	20	9	13	20	21	9	32	24	16	17	244	20·33	·13	−·19	·053	·113	2·04	·21	·071	·0491
Σ	833	367	176	186	175	188	262	206	234	223	159	224	3232		·70	−·40	3·458			2·287	·471	2·880

${}_1l_m=\cdot186$ ${}_1c_n=\cdot0806$ $k_1=\cdot43$ $W_1=\cdot831$ ${}_2c_n=0\cdot234$ ${}_2l_n=\cdot170$ $k_2=1\cdot37$ $W_2=\cdot153$

Tabelle XXXIV.

Gebiet 35° N~36° N, 138° E~139° E.

Jahr	Monatliche Bebenzahl												Σ	a_0	$\frac{a_1}{a_0}$	$\frac{b_1}{b_0}$	c_1^2	ε	c_1/ε
	Jan.	Feb.	März	April	Mai	Juni	Juli	Aug.	Sept.	Okt.	Nov.	Dez.							
1926	4	4	3	2	4	5	4	4	0	5	2	3	40	3·33	− ·06	·37	·141	·280	1·34
27	4	2	5	0	3	8	1	4	8	4	2	1	42	3·5	− ·32	− ·15	·125	·273	1·29
28	0	5	1	10	5	3	4	0	3	0	0	0	31	2·58	− ·37	1·07	1·282	·318	3·57
29	4	1	0	1	2	2	0	1	2	0	1	4	18	1·50	·47	− ·09	·229	.418	1·14
30	0	0	6	7	1	5	9	1	10	6	2	5	52	4·33	− ·44	·15	·216	·246	1·89
31	2	4	178	57	15	42	12	8	50	70	36	10	484	40·33	·13	·39	·169	·0806	5·10
32	10	15	10	14	9	14	7	26	4	7	11	21	148	12·33	·05	·02	·003	·145	·38
33	21	6	35	42	37	34	12	8	5	9	3	5	217	18·08	− ·18	·94	·916	·120	7·97
34	2	6	2	8	5	6	9	26	6	5	1	4	80	6·66	− ·75	− ·15	·585	·222	3·45
35	5	3	7	7	8	14	20	52	24	6	2	3	151	12·58	−1·04	− ·36	1·211	·144	7·65
Σ	52	46	247	148	89	133	78	130	112	112	60	56	1263		−2·51	2·19	4·877		

${}_1l_m = 221$ ${}_1c_n = ·333$ $k_1 = 1·505$ $W_1 = ·103$

Tabelle XXXV.

Gebiet 35° N~36° N, 137° E~138° E.

Jahr	Monatliche Bebenzahl												Σ	a_0	$\frac{a_1}{a_0}$	$\frac{b_1}{a_0}$	c_1^2	ε	c_1/ε
	Jan.	Feb.	März	April	Mai	Juni	Juli	Aug.	Sept.	Okt.	Nov.	Dez.							
1926	1	1	1	4	0	3	1	0	0	0	0	0	11	0·92	− ·23	1·24	1·590	·533	2·37
27	1	0	4	1	0	3	0	0	1	0	3	0	13	1 08	·22	·39	·200	·492	·91
28	4	1	0	0	2	0	0	0	0	0	1	0	8	·67	1·09	·12	1·202	·626	1·75
29	0	0	0	0	0	1	0	1	1	8	2	1	14	1·17	− ·05	−1·58	2·498	·473	3·35
30	2	1	3	0	0	0	0	0	0	0	2	3	11	·92	1·45	− ·02	2·102	·533	2·72
31	0	0	2	0	1	1	0	2	2	6	0	0	14	1·17	− ·44	− ·80	·833	·473	1·93
32	3	0	3	0	0	1	1	4	2	6	0	3	23	1·92	·07	− ·71	·509	·369	1·93
33	1	0	4	0	2	4	1	2	3	4	2	1	24	2·00	− ·32	− ·22	·150	·362	1·07
34	1	0	1	2	2	2	4	77	24	5	9	6	133	11·08	−1·09	−1·05	2·290	·153	·99
35	5	3	3	2	2	1	58	18	36	15	29	4	176	14·67	− ·73	− ·84	1·238	·133	8·38
Σ	18	6	21	9	9	16	65	104	69	44	48	18	427		− ·03	−3·47	12·61		

${}_1l_m = \cdot 355$ ${}_1c_m = \cdot 347$ $k_1 = \cdot 98$ $W_1 = \cdot 383$

Tabelle XXXVI.

Gebiet 35° N∼36° N, 136° E∼137° E.

Jahr	Monatliche Bebenzahl												Σ	a_0	$\frac{a_1}{a_0}$	$\frac{b_1}{a_0}$	c_1^2	ε	c_1/ε
	Jan.	Feb.	März	April	Mai	Juni	Juli	Aug.	Sept.	Okt.	Nov.	Dez.							
1926	12	5	6	8	4	5	5	10	2	11	5	7	80	6·66	·39	− ·10	·162	·198	2·03
27	10	6	61	12	18	22	16	20	13	11	5	19	213	17·75	·03	·45	·203	·113	3 99
28	13	9	8	28	13	7	8	8	12	10	9	10	135	11·25	·07	·25	·067	·152	1·70
29	7	10	8	8	9	6	6	4	2	4	7	0	71	5·92	·08	·48	·237	·210	2·32
30	3	12	23	3	19	4	6	10	12	5	17	15	129	10·75	·20	·07	·045	·156	1·36
31	6	11	6	6	6	3	4	6	6	3	4	9	70	5·83	·30	·12	·104	·212	1·52
32	8	12	3	5	7	7	6	7	5	14	13	8	95	7·92	·19	− ·29	·120	·182	1·90
33	10	4	12	10	15	2	5	9	8	10	6	5	96	8·00	·02	·15	·023	·181	·84
34	3	7	2	6	7	6	13	8	8	5	8	5	78	6·50	− ·36	− ·13	·147	·201	1·91
35	8	8	10	9	10	4	9	3	10	6	8	10	95	7·92	·16	·09	·034	·182	1·01
Σ	80	84	139	95	108	66	78	85	78	79	82	88	1062		1·08	1·09	1·142		

$_1l_n = ·107$ $_1c_m = ·1534$ $k_1 = 1·43$ $W_1 = ·129$

Tabelle XXXVII.

Gebiet 35° N ~ 36° N, 135° E ~ 136° E.

Jahr	Monatliche Bebenzahl												Σ	a_0	$\frac{a_1}{a_0}$	$\frac{b_1}{a_0}$	c_1^2	ε	c_1/ε
	Jan.	Feb.	März	April	Mai	Juni	Juli	Aug.	Sept.	Okt.	Nov.	Dez.							
1926	0	1	0	0	0	0	0	0	0	1	1	0	3	·25	·92	− ·95	1·693	1 02	1·27
27	1	1	900	491	148	61	39	25	26	14	24	17	1747	145·58	·32	1·55	2·505	·042	37·7
28	5	12	8	10	8	3	4	3	4	10	7	8	82	6·83	·41	·15	·191	·196	2·23
29	7	6	2	3	2	5	7	6	4	6	5	8	61	5·08	·10	− ·29	·094	·227	1·35
30	3	5	4	2	4	2	7	2	4	4	1	4	42	3·50	− ·06	·05	·006	·273	·28
31	4	4	1	3	11	5	8	5	5	0	4	3	53	4·42	−3·47	·23	12·09	·243	14·3
32	2	1	4	2	0	2	3	1	1	1	0	6	23	1·92	·34	·14	·135	·369	·996
33	1	2	6	5	4	3	3	2	1	0	0	1	28	2·33	− ·23	·63	·450	·335	2·00
34	1	0	0	1	3	4	3	3	8	2	3	1	29	2·42	− ·77	− ·55	·895	·329	2·88
35	0	1	0	1	2	3	1	1	3	3	0	0	15	1·25	− ·82	− ·18	·705	·467	1·80
Σ	24	33	925	518	182	88	75	48	56	41	45	48	2083		−3·26	− ·81	18·77		

${}_1l_n = \cdot433$ ${}_1c_m = \cdot336$ $k_1 = \cdot78$ $W_1 = \cdot544$

Tabelle XXXVIII.

Gebiet 35° N~36° N, 134° E - 135° E.

Jahr	Monatliche Bebenzahl												Σ	a_0	$\frac{a_1}{a_0}$	$\frac{b_1}{a_0}$	c_1^2	ε	c_1/ε
	Jan.	Feb.	März	April	Mai	Juni	Juli	Aug.	Sept.	Okt.	Nov.	Dez.							
1926	0	4	2	0	0	3	1	1	4	2	5	5	27	2·25	·36	− ·56	·443	·341	1·95
27	3	1	1	1	0	0	1	7	1	2	24	6	47	3·92	1·11	·66	1·667	·259	4·99
28	34	10	18	20	15	27	23	2	0	1	1	2	153	12·75	− ·02	·83	·689	·143	5·80
29	3	6	3	6	2	0	0	0	2	0	1	2	25	2·08	·79	·78	1 232	·355	3·13
30	0	2	3	1	1	1	0	3	2	0	1	3	17	1·42	·16	·04	·027	.430	·38
31	1	0	0	1	0	0	0	0	0	2	2	1	7	·58	·83	− ·93	1·553	·670	1·86
32	2	2	1	1	2	3	0	0	0	0	0	3	14	1 17	·46	·66	·647	·474	1·71
33	0	0	1	1	2	0	0	2	0	0	0	0	6	·50	− ·74	·86	1·287	·724	1·57
34	0	1	1	1	1	0	0	0	4	0	1	0	9	·75	− ·15	− ·24	·080	·591	·48
35	1	0	0	0	0	1	11	0	1	0	0	1	15	1·25	−1·40	− ·11	1·972	·457	3.07
Σ	44	26	30	32	23	35	36	15	14	7	35	23	320		1·40	1·99	9·597		

${}_1l_n = \cdot 310$ ${}_1c_n = \cdot 263$ $k_1 = \cdot 85$ $W_1 = \cdot 485$

Tabelle XXXIX.

Gebiet 35° N~36°, 133° E~134° E.

Jahr	Monatliche Bebenzahl												Σ	a_0	$\frac{a_1}{a_0}$	$\frac{b_1}{a_0}$	c_1^2	ε	c_1/ε
	Jan.	Feb.	März	April	Mai	Juni	Juli	Aug.	Sept.	Okt.	Nov.	Dez.							
1926	1	0	1	0	5	3	1	0	2	0	2	2	17	1·42	− ·34	·26	·18	·430	·99
27	0	0	7	5	1	2	4	5	1	1	1	0	27	2·25	− ·62	·57	·59	·341	2·25
28	1	2	1	3	9	2	0	0	0	1	1	0	20	1·67	− ·25	1·18	1·45	·396	3·04
29	0	0	2	3	2	1	0	1	0	0	0	0	9	·75	− ·39	1·44	2·23	·590	2·53
30	0	1	0	1	1	3	2	2	0	0	1	4	15	1·25	− ·26	0	·07	·458	·58
31	0	2	0	0	0	0	0	0	0	0	0	0	2	·17	1·71	1·00	3·92	1·25	1·58
32	0	2	0	0	0	0	1	0	0	0	0	0	3	·25	1·84	·68	3·85	1·02	1·92
33	0	0	0	2	0	0	1	0	0	0	0	0	3	·25	·68	1·32	2·20	1·02	1·46
34	0	0	0	0	0	0	0	0	0	0	0	1	1	·08	1·75	1·00	4·56	1·77	1·14
35	0	0	0	0	0	0	0	0	0	0	2	0	2	·17	1·00	1·71	3·92	1·25	1·58
Σ	2	7	11	14	18	11	9	8	3	2	7	7	99		5·22	9·16	22·47		

${}_1l_m = {\cdot}474 \quad {}_1c_m = 1{\cdot}054 \quad k_1 = 2{\cdot}22 \quad W_1 = {\cdot}009$

Tabelle IL.

Gebiet 34° N~35° N, 139° E~140° E.

Jahr	Monatliche Bebenzahl												Σ	a_0	$\frac{a_1}{a_0}$	$\frac{b_1}{a_0}$	c_1^2	ε	c_1/ε
	Jan.	Feb.	März	April	Mai	Juni	Juli	Aug.	Sept.	Okt.	Nov.	Dez.							
1926	13	3	2	2	3	3	1	15	9	0	16	2	69	5·75	·11	− ·60	·372	·213	2·86
27	0	1	4	2	5	1	2	1	1	1	2	0	20	1·67	− ·29	·77	·677	·396	2·08
28	0	2	0	3	5	1	0	1	3	1	4	4	24	2·00	·13	− ·06	·021	·362	·40
29	3	2	4	4	4	8	6	3	26	4	5	7	76	6·33	− ·40	− ·52	·430	·203	3·23
30	2	160	612	64	547	13	17	9	4	13	1176	1290	3907	325·58	·94	− ·27	·957	·028	35
31	5	7	21	1	2	6	8	19	6	6	6	15	102	8·50	− ·02	− ·12	·015	·175	·70
32	4	2	6	12	5	6	1	5	3	8	8	25	85	7·08	·47	− ·17	·250	·192	2·60
33	4	9	2	4	8	6	6	2	2	5	6	5	59	4·92	·08	·16	·032	·231	·77
34	4	3	18	9	8	1	4	1	2	3	5	2	60	5·00	·30	·76	·668	·229	3·57
35	2	3	6	1	6	5	9	159	177	22	5	7	402	33.5	−1·13	−1·23	2·790	·0883	18·9
Σ	37	192	675	102	593	50	54	215	233	63	1233	1357	4804		·19	−1·28	6·212		

$_1l_n = \cdot 2492$ $\quad$ $_1c_m = \cdot 1292$ $\quad$ $k_1 = \cdot 52$ $\quad$ $W_1 = \cdot 763$

Tabelle ILI.

Gebiet 34°～35° N, 137° E～138° E.

Jahr	Monatliche Bebenzahl												Σ	a_0	$\frac{a_1}{a_0}$	$\frac{b_1}{a_0}$	c_1^2	ε	c_1/ε
	Jan.	Feb.	März	April	Mai	Juni	Juli	Aug.	Sept.	Okt.	Nov.	Dez.							
1926	2	0	1	2	0	2	1	1	1	0	1	0	11	·92	−·20	·29	·124	·534	·66
27	5	0	1	1	0	4	3	1	0	0	0	2	17	1·42	−·01	·27	·073	·430	·63
28	1	0	2	0	2	3	0	1	1	1	0	2	13	1·08	−·19	·25	·098	·492	·64
29	0	0	0	1	0	0	1	1	3	0	1	1	8	·67	−·49	− ·87	·997	·626	1·59
30	2	1	4	0	0	0	1	1	3	1	3	4	20	1·67	·65	− ·47	·643	·396	2·03
31	0	4	2	0	1	2	1	2	6	6	1	1	26	2·17	−·17	− ·61	·401	·348	1·82
32	3	3	3	0	0	2	0	1	3	4	3	2	24	2·00	·52	− ·47	·492	·362	1·24
33	1	3	1	1	5	1	0	2	2	0	3	1	20	1·67	·04	·24	·059	·396	·61
34	0	0	1	1	3	0	1	0	0	1	2	0	9	·75	−·23	·39	·205	·592	·76
35	5	2	3	2	0	0	2	1	4	0	1	2	22	1·83	·51	− ·02	·260	·378	1·35
Σ	19	13	18	8	11	14	10	11	23	13	15	15	170		·43	−1·00	3·352		

${}_1l_m = ·183$ ${}_1c_m = ·109$ $k_1 = 596$ $W_1 = ·701$

Tabelle ILII.

Gebiet 34° N~35° N, 136° E~137° E.

Jahr	Monatliche Bebenzahl												Σ	a_0	$\frac{a_1}{a_0}$	$\frac{b_1}{a_0}$	c_1^2	ε	c_1/ε
	Jan.	Feb.	März	April	Mai	Juni	Juli	Aug.	Sept.	Okt.	Nov.	Dez.							
1926	1	2	1	1	2	2	5	2	0	0	0	2	18	1·50	−·50	·40	·410	·418	1.53
27	0	0	0	5	1	1	3	0	1	2	0	0	13	1·08	−·75	·54	·854	·492	1·88
28	2	1	1	2	2	1	1	1	1	1	0	1	14	1·17	·00	·39	·152	.473	·825
29	0	1	1	0	0	3	1	0	2	1	0	0	9	·75	−·72	·03	·519	.591	1·22
30	1	2	1	0	1	1	0	1	0	1	3	1	12	1·00	·56	− ·23	·366	·512	1·18
31	1	1	0	0	2	1	2	2	1	1	0	1	12	1·00	−·56	− ·11	·325	·512	1·11
32	4	0	1	1	0	2	1	4	3	6	3	2	27	1·92	·14	·59	·367	·341	1·78
33	2	2	5	1	4	3	0	1	2	0	2	1	23	·75	·75	−1·07	1·707	·369	3·55
34	1	0	0	1	0	0	0	0	1	1	4	1	9	2·92	·39	·58	·488	·591	1·18
35	0	3	2	11	3	2	1	8	2	1	0	2	35	2·25	·00	− ·84	·705	·299	2·81
Σ	12	12	12	22	15	16	14	19	13	14	12	11	172		−·69	·24	5·893		

${}_1l_m=\cdot 243$ ${}_1c_m=\cdot 073$ $k_1=\cdot 30$ $W_1=\cdot 913$

Tabelle ILIII.

Gebiet 34° N ~ 35° N, 135° E ~ 136° E.

Jahr	Monatliche Bebenzahl												Σ	a_0	$\frac{a_1}{a_0}$	$\frac{b_1}{a_0}$	c_1^2	ε	c_1/ε
	Jan.	Feb.	März	April	Mai	Juni	Juli	Aug.	Sept.	Okt.	Nov.	Dez.							
1926	78	58	50	38	46	102	68	113	145	55	50	32	835	69·58	−·34	−·23	·169	·060	6·85
27	21	24	15	42	22	49	49	25	38	42	20	62	409	34·08	−·24	−·12	·0544	·088	2·65
28	67	75	50	38	31	36	23	45	39	14	40	37	495	41·25	·32	·16	·128	·0797	4·49
29	28	25	27	41	38	22	37	25	30	30	22	25	350	29·17	−·09	·12	·023	·0947	1·60
30	26	73	41	13	44	39	48	40	41	47	31	31	474	39·50	−·028	−·009	·00086	·0814	·35
31	40	32	20	46	44	57	49	77	44	48	28	60	545	45·42	−·24	−·12	·072	·0759	3·54
32	58	53	42	19	26	46	30	37	30	42	34	29	446	37·17	·23	−·013	·053	·0839	2·75
33	30	42	67	118	73	78	56	97	86	60	70	96	873	72·75	−·23	·017	·053	·0599	4·59
34	67	36	60	69	63	55	55	61	45	34	47	57	649	54·08	−·025	·15	·0231	·0695	2·18
35	70	70	69	76	69	64	60	90	55	73	92	95	883	73·58	·086	−·068	·012	·0595	1·84
Σ	485	488	441	500	456	548	475	610	553	445	434	524	5959		−·517	−·113	·588		

${}_1l_m = {\cdot}0766$ ${}_1c_m = {\cdot}053$ $k_1 = {\cdot}69$ $W_1 = {\cdot}621$

Tabelle ILIV.

Gebiet 33° N~34° N, 135° E~136° E.

Jahr	Monatliche Bebenzahl												Σ	a_0	$\frac{a_1}{a_0}$	$\frac{b_1}{a_0}$	c_1^2	ε	c_1/ε
	Jan.	Feb.	März	April	Mai	Juni	Juli	Aug.	Sept.	Okt.	Nov.	Dez.							
1926	8	0	5	1	0	6	9	8	2	11	9	2	61	5·08	−·18	−·56	·346	·227	2·59
27	9	12	1	12	13	9	6	5	7	17	7	15	113	9·42	·15	−·08	·029	·165	1·03
28	10	4	10	1	2	5	4	2	2	2	5	4	51	4·25	·48	·19	.267	·245	2·11
29	2	1	12	4	0	3	4	2	4	5	4	1	42	3·50	·07	·14	·025	·273	·58
30	3	4	2	5	6	4	10	13	4	4	5	5	65	5·42	−·48	−·15	·253	·219	2·30
31	3	14	3	7	4	5	6	3	5	4	3	6	63	5·25	·19	·23	·089	·223	1·34
32	3	2	5	4	5	10	2	6	12	2	11	8	70	5·83	−·13	−·29	·101	·212	1·50
33	6	4	10	8	6	8	12	1	13	6	10	10	94	7·83	−.04	−·08	·008	·183	·59
34	6	3	10	14	11	7	6	6	10	12	10	12	107	8·92	·02	−·01	·001	·171	·185
35	10	7	5	11	8	17	11	26	30	36	29	25	215	17·92	−·04	−·73	·547	·121	6·12
Σ	60	51	63	67	55	74	70	72	89	99	93	88	881		−·04	−1·34	1·667		

${}_1l_u = \cdot 129$ ${}_1c_m = \cdot 134$ $k_1 = 1\cdot 04$ $W_1 = \cdot 339$

Tabelle ILV.

Gebiet 34° N~35° N, 134° E~135° E.

Jahr	Monatliche Bebenzahl												Σ	a_0	$\frac{a_1}{a_0}$	$\frac{b_1}{a_0}$	c_1^2	ε	c_1/ε
	Jan.	Feb.	März	April	Mai	Juni	Juli	Aug.	Sept.	Okt.	Nov.	Dez.							
1926	9	8	10	5	13	13	10	4	7	2	4	5	90	7·50	−·06	·43	·188	·187	2·32
27	3	5	11	9	2	3	7	14	5	8	5	7	79	6·58	−·24	−·07	·062	·199	1·25
28	3	3	4	2	4	5	1	2	5	5	0	6	40	3·33	·15	−·02	·022	·280	·53
29	5	0	7	1	0	1	8	16	6	7	2	3	56	4·67	−·46	−·57	·536	·237	3·09
30	5	3	19	5	2	5	4	6	7	9	5	5	75	6·25	·27	·06	·076	·205	1·34
31	1	4	11	6	10	0	1	4	12	4	4	4	61	5·08	·00	·14	·019	·227	·61
32	2	3	2	6	4	6	4	5	5	4	9	4	54	4·50	−·17	−·18	·061	·241	1·02
33	3	9	2	1	0	5	3	2	1	2	1	2	31	2·58	·29	·26	·151	·319	1·22
34	1	2	2	11	3	1	1	3	5	3	1	2	35	2·92	−·14	·35	·142	·299	1·26
35	3	0	0	4	2	0	0	1	5	7	1	5	28	2·33	·25	−·68	·524	·335	2·16
Σ	35	37	68	50	40	39	39	57	58	51	32	43	549		−·11	−·28	1·781		

${}_1l_m=\cdot 134$ ${}_1c_m=\cdot 03$ $k_1=\cdot 224$ $W_1=\cdot 951$

Tabelle ILVI.

Gebiet 34° N~35° N, 133° E~134° E.

Jahr	Monatliche Bebenzahl												Σ	a_0	$\frac{a_1}{a_0}$	$\frac{b_1}{a_0}$	c_1^2	ε	c_1/ε
	Jan.	Feb.	März	April	Mai	Juni	Juli	Aug.	Sept.	Okt	Nov.	Dez.							
1926	2	0	0	0	2	2	1	5	3	0	1	1	17	1·42	− ·73	− ·44	·726	·430	1·98
27	3	4	6	5	5	1	2	4	1	3	0	0	34	2·83	·01	·66	·435	·304	2·17
28	1	2	1	1	0	1	0	0	2	2	4	3	17	1·42	·70	− ·63	·886	·430	2·19
29	0	0	3	3	2	1	1	1	1	1	1	0	14	1·17	− ·32	·66	·538	·473	1·55
30	0	1	6	4	0	1	1	0	1	6	1	8	29	2·42	·62	− ·11	·396	·329	1·92
31	5	1	5	1	1	1	1	2	0	1	1	2	21	1·75	·62	·32	·486	·387	1·80
32	1	3	1	0	0	0	0	0	1	2	3	0	11	·92	·92	− ·57	1·171	·534	2·02
33	0	1	1	0	1	0	1	0	0	2	4	0	10	·83	·37	− ·65	·559	·560	1·33
34	1	1	0	0	1	0	0	0	1	0	1	0	5	·42	·55	− ·14	·322	·793	·715
35	2	0	0	0	1	0	1	1	0	0	2	1	8	·67	·37	− ·46	·348	·626	·94
Σ	15	13	23	14	13	7	8	13	10	17	18	15	166		3·11	−1·36	5·867		

${}_1l_n = \cdot242$ ${}_1c_m = \cdot339$ $k_1 = 1{\cdot}40$ $W_1 = .141$

Tabelle ILVII.

Gebiet 34° N~35° N, 132° E~133° E.

Jahr	Monatliche Bebenzahl												Σ	a_0	$\frac{a_1}{a_0}$	$\frac{b_1}{a_0}$	c_1^2	ε	c_1/ε
	Jan.	Feb.	März	April	Mai	Juni	Juli	Aug.	Sept.	Okt.	Nov.	Dez.							
1926	45	0	0	0	0	5	3	8	10	2	4	9	86	7·17	·83	−·47	·910	·191	5·00
27	0	8	5	1	27	13	7	13	6	3	8	4	95	7·92	−·61	·33	·481	·182	3·81
28	5	8	8	5	5	2	2	1	8	10	3	2	59	4·92	·27	·01	·073	·231	1·17
29	3	1	2	3	4	3	3	3	2	1	3	8	36	3·00	·12	·04	·016	·295	·43
30	0	1	1	4	2	1	0	1	0	7	2	43	62	5·17	1·19	−·75	1·979	·225	6·26
31	7	6	6	2	1	4	0	3	1	0	8	2	40	3·33	·69	·14	·496	·280	2·52
32	2	4	0	4	2	0	0	0	0	3	10	1	26	2·17	·79	−·34	·740	·348	2·47
33	3	2	7	2	5	7	3	0	0	7	1	1	38	3·17	−·10	·45	·213	·287	1·61
34	2	4	1	2	1	1	2	5	1	1	1	1	22	1·83	−·08	·14	·026	·378	·43
35	2	4	1	4	1	0	2	2	3	1	1	0	21	1·75	·07	·12	·029	·387	·44
Σ	69	38	31	27	48	36	22	36	31	35	41	71	485		3·17	−·33	4·953		

${}_1l_n = {\cdot}222$ ${}_1c_n = {\cdot}319$ $k_1 = 1{\cdot}44$ $W_1 = {\cdot}125$

Tabelle ILVIII.

Gebiet 33° N~34° N, 134° E~135° E.

Jahr	Monatliche Bebenzahl												Σ	a_0	$\frac{a_1}{a_0}$	$\frac{b_1}{a_0}$	c_1^2	ε	c_1'/ε
	Jan.	Feb.	März	April	Mai	Juni	Juli	Aug.	Sept.	Okt.	Nov.	Dez.							
1926	10	1	4	0	4	2	3	1	3	0	0	3	31	2·58	·41	·25	·231	·318	1·51
27	1	0	6	4	3	4	4	4	14	4	4	4	52	4·33	−·38	−·30	·234	·245	1·97
28	8	2	10	14	29	8	25	15	5	13	12	20	161	13·42	−·30	·17	·119	·139	2·48
29	35	27	19	25	6	7	19	9	13	15	11	22	208	17·33	·48	·19	·267	·123	4·20
30	6	20	9	11	5	2	5	3	3	4	3	2	73	6·08	·49	·67	·689	·207	4·02
31	1	8	15	4	2	8	6	7	0	3	0	1	55	4·58	−·14	·72	1·227	·239	4·64
32	2	2	2	3	5	2	3	2	3	2	2	6	34	2·83	·03	·04	·003	·304	·18
33	0	0	4	3	0	1	2	3	1	2	1	1	18	1·50	−·29	·14	·104	·418	·77
34	6	4	5	1	4	2	0	2	3	4	3	3	37	3 92	·39	·01	·152	·291	1·34
35	0	3	2	1	2	1	4	4	5	3	3	0	28	2·33	−·48	−·39	·383	·338	1·85
Σ	69	67	76	66	60	37	71	50	50	50	39	62	697		·21	1·50	3·409		

${}_1l_m = \cdot 184$ ${}_1c_m = \cdot 151$ $k_1 = \cdot 82$ $W_1 = 510$

Tabelle ILIX.

Gebiet 33° N~34° N, 133° E~134° E.

Jahr	Monatliche Bebenzahl												Σ	a_0	$\frac{a_1}{a_0}$	$\frac{b_1}{a_0}$	c_1^2	ε	c_1/ε
	Jan.	Feb.	März	April	Mai	Juni	Juli	Aug.	Sept.	Okt.	Nov.	Dez.							
1926	3	0	1	0	0	1	0	0	0	0	0	0	5	·42	1·05	·55	1·405	·79	1·53
27	1	1	3	0	1	2	3	1	2	6	5	0	25	2·08	− ·10	− ·61	·382	·355	1·74
28	3	6	1	3	0	1	1	0	0	0	0	1	16	1·33	·96	·86	1·661	·443	2·91
29	0	0	3	0	1	0	1	0	1	0	1	1	8	·67	·21	·31	·140	·63	·59
30	1	0	1	0	2	1	4	1	0	0	3	5	18	1·50	·07	− ·28	·083	·418	·69
31	1	0	6	1	0	4	2	3	1	1	1	3	23	1·92	− ·13	·21	·061	·370	·67
32	3	2	0	2	1	2	1	0	1	0	0	2	14	1·17	·39	·43	·337	·473	1·22
33	1	2	2	3	0	0	4	0	1	1	0	1	15	1·25	·02	·45	·203	·458	·98
34	3	4	3	5	0	1	0	2	1	0	0	5	24	2·00	·77	·48	·823	·362	2·51
35	1	0	0	0	0	0	0	0	0	3	2	4	10	·83	1·10	−1·35	3·033	·560	3·11
Σ	17	15	20	14	5	12	16	7	7	11	12	22	158		4·34	1·05	8·126		

${}_1l_m = ·285$ ${}_1c_m = ·447$ $k_1 = 1.57$ $W_1 = ·085$

Tabelle L.

Gebiet 33° N~34° N, 132° E~133° E.

Jahr	Monatliche Bebenzahl												Σ	a_0	$\frac{a_1}{a_0}$	$\frac{b_1}{a_0}$	c_1^2	ε	c_1/ε
	Jan.	Feb.	März	April	Mai	Juni	Juli	Aug.	Sept.	Okt.	Nov.	Dez.							
1926	4	0	1	0	3	0	0	4	2	1	7	11	33	2·75	·70	−·78	1·098	·309	3·39
27	0	2	0	0	3	6	1	2	3	6	3	0	26	2·17	−·59	−·43	·533	·348	2·10
28	0	4	0	1	0	1	1	0	2	1	0	1	11	·92	·26	·05	·070	·535	·49
29	4	0	3	1	1	3	1	1	1	0	4	2	21	1·75	·36	.01	·129	·387	·93
30	0	1	3	3	0	1	2	3	0	4	1	1	19	1·58	−·18	−·03	·033	·407	·45
31	1	5	3	1	2	1	1	2	3	1	4	1	25	2·08	·29	−·02	·084	·355	·82
32	0	4	3	1	4	2	3	0	3	2	0	3	25	2·08	−·05	·32	·104	·355	·91
33	1	0	1	1	1	1	0	2	2	0	1	0	10	·83	−·42	−·07	·181	·560	·76
34	0	0	0	3	9	5	3	2	0	1	3	2	28	2·33	−·74	·55	·850	·417	2·21
35	3	2	3	1	2	2	6	2	1	1	1	1	25	2·08	−·27	·25	·135	·354	1·04
Σ	13	18	17	12	25	22	18	18	17	17	24	22	223		−·64	−·15	3·216		

${}_1l_m = \cdot 179$ ${}_1c_m = \cdot 0658$ $k_1 = \cdot 37$ $W_1 = \cdot 862$

Tabelle LI.

Gebiet 33° N~34° N, 131° E~132° E.

Jahr	Monatliche Bebenzahl												Σ	a_0	$\frac{a_1}{a_0}$	$\frac{b_1}{a_0}$	c_1^2	ε	c_1/ε
	Jan.	Feb.	März	April	Mai	Juni	Juli	Aug.	Sept.	Okt.	Nov.	Dez.							
1926	5	17	9	7	17	21	5	3	0	4	20	4	112	9·33	·07	·42	·180	·167	2·54
27	14	5	2	10	3	50	5	0	5	7	2	3	106	8·92	− ·55	·53	·583	·172	4·45
28	12	11	5	0	3	1	0	2	3	1	5	6	49	4·08	1·07	·04	1·146	·253	4·24
29	6	0	8	0	4	3	9	14	0	2	0	2	48	4·00	− ·58	·08	·342	·256	2·29
30	3	2	1	22	3	1	4	2	0	2	9	0	49	4·08	·07	·66	·440	·253	2·62
31	15	6	7	54	3	6	1	3	4	9	1	3	112	9·33	·26	·93	·932	·167	6·00
32	7	11	10	3	1	0	2	1	1	0	9	6	51	4·25	1·07	·21	1·189	·248	4·40
33	5	5	9	3	3	3	6	3	0	2	1	0	41	3·33	·08	·65	·428	·277	2·36
34	3	0	2	4	1	4	0	2	7	7	21	10	61	5·08	·46	− ·94	1·095	·227	4·61
35	4	11	4	3	1	0	0	14	1	3	0	2	43	3·58	·19	·04	·037	·270	·71
Σ	74	68	57	107	39	89	32	44	21	37	68	36	672		2·13	2·62	6·372		

${}_1l_n = \cdot 252$ ${}_1c_m = \cdot 338$ $k_1 = 1\cdot 34$ $W_1 = \cdot 166$

Tabelle LII.

Gebiet 33° N~34° N, 130° E~131° E.

Jahr	Monatliche Bebenzahl												Σ	a_0	$\frac{a_1}{a_0}$	$\frac{b_1}{a_0}$	c_1^2	ε	c_1/ε
	Jan.	Feb.	März	April	Mai	Juni	Juli	Aug.	Sept.	Okt.	Nov.	Dez.							
1926	2	0	0	3	0	8	1	1	1	0	0	2	18	1·50	− ·62	·51	·644	·418	1·92
27	5	5	3	0	0	0	0	0	0	2	0	0	15	1·25	1·45	·42	2·287	.458	3·30
28	0	1	2	1	3	0	1	0	1	5	25	5	44	3·67	·71	− ·87	1·261	·267	4·21
29	2	2	1	0	1	0	1	6	0	0	3	0	16	1·33	− ·24	− ·36	·187	·443	·98
30	1	15	8	1	3	1	1	0	0	2	0	1	33	2·75	·94	·97	1·824	·309	4·38
31	0	0	3	0	0	2	0	4	0	0	3	1	13	1·08	− ·34	− ·23	·168	·492	·83
32	1	1	2	0	1	1	3	2	2	3	0	2	18	1·50	− ·28	− ·35	·200	·418	1·07
33	2	2	2	3	1	4	0	1	3	1	3	0	22	1·83	− ·01	− ·17	·029	·378	·45
34	0	0	0	5	3	1	1	2	0	0	1	0	13	1·08	− ·71	·96	1·243	·492	2.27
35	1	1	6	1	1	4	2	1	2	1	1	2	23	1·92	− ·07	·39	·157	·369	1·05
Σ	14	27	27	14	13	21	10	17	9	14	36	13	215		·83	1·27	7·994		

${}_1l_n = \cdot 283$ ${}_1c_n = \cdot 152$ $k_1 = \cdot 537$ $W_1 = \cdot 750$

Tabelle LIII.

Gebiet 32° N ~ 33° N, 130° E ~ 131° E.

Jahr	Monatliche Bebenzahl												Σ	a_0	$\frac{a_1}{a_0}$	$\frac{b_1}{a_0}$	c_1^2	ε	c_1/ε
	Jan.	Feb.	März	April	Mai	Juni	Juli	Aug.	Sept.	Okt.	Nov.	Dez.							
1926	32	6	7	8	9	6	3	26	12	2	87	3	201	16·75	·49	− ·39	·392	·125	5·01
27	1	0	19	10	12	5	12	9	11	15	10	64	168	14·00	·42	− ·36	·306	·137	4·04
28	8	13	7	13	4	3	8	34	10	10	7	20	137	11·42	− ·11	− ·31	·108	·151	2·18
29	106	34	14	5	8	27	4	2	9	76	23	56	364	30·33	·91	− ·43	1·013	·093	10·8
30	97	44	25	41	18	13	26	15	7	20	17	16	339	28·25	·63	·30	·487	·096	7·28
31	19	12	16	36	21	6	11	12	12	9	22	42	218	18·17	·38	·11	·157	·120	3·30
32	12	6	6	13	5	13	11	8	4	4	13	5	100	8·33	− ·05	·14	·022	·177	·84
33	13	12	16	11	8	7	6	18	20	18	13	6	148	12·17	·02	− ·21	·045	·146	1·45
34	2	5	6	10	7	20	4	7	24	26	7	1	119	9·92	− ·49	− ·39	·392	·162	3·87
35	13	1	7	3	5	4	10	9	131	13	8	11	215	17·83	·01	−1·19	1·416	·121	9·83
Σ	303	133	123	150	97	104	95	140	240	193	207	224	2009		2·21	−2·73	4·338		

${}_1l_m = ·208$ ${}_1c_n = ·351$ $k_1 = 1·686$ $W_1 = ·058$

Tabelle LIV.

Gebiet 32° N∼33° N, 131° E∼132° E.

Jahr	Monatliche Bebenzahl												Σ	a_0	$\frac{a_1}{a_0}$	$\frac{b_1}{a_0}$	c_1^2	ε	c_1/ε
	Jan.	Feb.	März	April	Mai	Juni	Juli	Aug.	Sept.	Okt.	Nov.	Dez.							
1926	0	0	0	0	1	0	0	0	0	0	0	2	3	·25	·84	·24	·763	1·02	·85
27	0	0	0	1	0	0	0	0	3	1	1	0	6	·50	− ·34	−1·16	1·461	·723	1·67
28	0	0	0	1	1	0	0	0	0	0	0	0	2	·17	− ·47	1·82	3·533	1·25	1·50
29	0	0	1	0	2	2	0	0	0	1	0	0	6	·50	− ·74	·86	·961	·723	1 36
30	1	0	1	1	0	0	0	0	0	0	1	0	4	·33	1·00	·51	1·260	·886	1·27
31	0	0	0	0	0	0	1	0	1	0	0	0	2	·17	−1·47	− ·82	2·83	1·25	1·34
32	2	0	0	0	0	2	1	1	0	0	0	1	7	·58	− ·21	·00	·044	·670	·31
33	20	45	29	41	24	10	3	6	1	2	4	2	187	15·58	·51	1·11	1·492	·129	9·48
34	13	1	0	0	0	0	1	0	0	1	0	1	17	1·42	1·71	− ·12	2·939	·429	4·00
35	0	1	51	0	1	0	1	0	2	3	3	0	62	5·17	·82	1·23	2·185	·225	6·56
Σ	36	47	82	44	29	14	7	7	7	8	9	6	296		1·65	3·67	17·47		

${}_1l_m = {\cdot}418$ ${}_1c_m = {\cdot}402$ $k_1 = {\cdot}96$ $W_1 = {\cdot}398$

Tabelle LV.

Gebiet 32° N ~ 33° N, 129° E ~ 130° E.

Jahr	Monatliche Bebenzahl												Σ	a_0	$\frac{a_1}{a_0}$	$\frac{b_1}{a_0}$	c_1^2	ε	c_1/ε
	Jan.	Feb.	März	April	Mai	Juni	Juli	Aug.	Sept.	Okt.	Nov.	Dez.							
1926	0	4	8	2	1	2	0	2	20	91	0	145	275	22·92	·87	−1·23	2·270	·107	14·1
27	121	146	139	0	0	1	1	1	1	14	1	1	426	13·50	3·89	2·19	19 93	·086	52
28	13	1	4	2	3	7	2	3	2	4	2	5	48	4·00	·33	·03	·110	·256	1·30
29	1	3	5	1	6	0	0	1	2	0	1	4	24	2·00	·44	·58	·530	·362	2·01
30	1	3	1	3	0	1	1	2	1	1	0	1	15	1·25	− ·02	·34	·116	·458	·745
31	3	1	0	0	1	0	0	2	4	2	5	1	19	1·58	·41	−1·04	1·250	·406	2·75
32	2	0	2	0	3	0	2	0	0	0	2	2	13	1·08	·34	·25	·178	·492	·86
33	2	1	0	1	1	1	4	1	0	4	0	1	16	1·33	− ·32	− ·27	·175	·443	·95
34	2	2	0	3	5	3	4	2	19	2	4	5	51	4·25	− ·40	− ·61	·532	·246	2·97
35	1	6	1	4	1	5	4	3	4	0	1	1	31	2·58	− ·31	·32	·199	·318	1·40
Σ	146	167	160	16	21	20	18	17	53	118	16	166	918		5·23	·56	23·02		

${}_1l_m = ·480 \quad {}_1c_m = ·526 \quad k_1 = 1·10 \quad W_1 = ·292$

Tabelle LVI.

Gebiet 31° N~32° N, 131° E~132° E.

Jahr	Monatliche Bebenzahl												Σ	a_0	$\frac{a_1}{a_0}$	$\frac{b_1}{a_0}$	c_1^2	ε	c_1/ε
	Jan.	Feb.	März	April	Mai	Juni	Juli	Aug.	Sept.	Okt.	Nov.	Dez.							
1926	3	8	11	10	14	16	13	11	14	9	6	11	126	10·50	− ·36	·10	·140	·158	2·37
27	12	6	27	13	8	7	9	6	13	19	5	9	134	11·17	·15	·12	·037	·153	1·26
28	20	12	13	16	8	16	2	8	6	15	8	13	137	11·42	·68	·15	·485	·151	4·61
29	15	9	2	13	58	21	9	12	6	2	6	9	162	13·50	− ·43	·70	·675	·139	5·91
30	18	19	6	7	5	13	4	7	6	12	10	9	116	9·67	·40	− ·02	·160	·164	2·44
31	6	2	5	4	11	7	6	6	12	9	138	19	225	18·75	·60	−1·15	1·683	·118	11·0
32	32	18	13	19	10	11	10	7	14	7	9	7	157	13·08	·34	·25	·178	·141	2·99
33	19	8	11	17	25	30	14	7	4	13	18	25	191	15 92	·02	·20	·040	·128	1·56
34	11	7	11	7	8	3	1	7	3	9	12	11	90	7·50	·51	− ·06	·264	·187	2·75
35	0	6	9	9	10	15	32	12	3	7	4	12	119	9 92	− ·67	·18	·481	·162	4·28
Σ	136	95	108	115	157	139	100	83	81	102	216	125	1457		1·24	·47	4·14		

${}_1l_m=·204$ ${}_1c_m=·133$ $k_1=·65$ $W_1=·656$

Tabelle LVII.

Gebiet 31° N~32° N, 130° E~131° E.

Jahr	Monatliche Bebenzahl												Σ	a_0	$\frac{a_1}{a_0}$	$\frac{b_1}{a_0}$	c_1^2	ε	$c_1'\varepsilon$
	Jan.	Feb.	März	April	Mai	Juni	Juli	Aug.	Sept.	Okt.	Nov.	Dez.							
1926	0	4	1	0	1	1	2	1	2	0	1	1	14	1·17	·02	·09	·008	·473	·189
27	0	2	0	1	1	2	3	0	0	0	0	0	9	·75	−·77	·85	1·315	·590	1·94
28	5	1	1	1	0	3	3	0	1	3	1	0	19	1·58	·08	−·09	·014	·406	·29
29	0	0	3	2	1	2	0	0	0	1	0	1	10	·83	·02	1·00	1·00	·560	1·78
30	3	0	0	0	2	1	1	0	1	0	0	0	8	·67	−·09	·34	·123	·626	·56
31	0	1	2	8	0	2	0	0	0	1	5	0	19	1·58	·28	·62	·462	·406	1·67
32	7	2	0	1	1	0	2	0	0	1	2	0	16	1·33	·91	·02	·828	·443	2·05
33	0	0	1	0	1	2	0	0	0	0	0	0	4	·33	−·88	1·36	2·624	·886	1·83
34	0	0	0	0	1	0	1	0	0	3	2	3	10	·83	·42	−1·08	1·342	·560	2·07
35	2	0	1	1	0	1	3	1	1	2	0	1	13	1·08	−·29	−·23	·137	·492	·75
Σ	17	10	9	14	8	14	15	2	5	11	11	6	122		−·30	2·88	7·852		

${}_1l_m = \cdot 280 \qquad {}_1c_m = \cdot 289 \qquad k_1 = 1\cdot 03 \qquad W_1 = \cdot 346$

Tabelle LVIII.

Gebiet 30° N~31° N, 130° E~131° E.

Σ	Monatliche Bebenzahl												Σ	a_0	$\frac{a_1}{a_0}$	$\frac{b_1}{a_0}$	c_1^2	ε	c_1/ε
	Jan.	Feb.	März	April	Mai	Juni	Juli	Aug.	Sept.	Okt.	Nov.	Dez.							
1926	0	0	0	0	2	0	0	0	1	1	0	0	4	·33	− ·76	− ·06	5·81	·885	·86
27	0	0	0	0	1	0	1	0	1	1	5	0	9	·75	·11	−1·19	1·428	·591	2·02
28	0	0	0	0	0	0	0	0	0	1	0	0	1	·08	·00	−2·13	4·537	1·77	1·20
29	0	0	1	1	2	0	1	0	5	2	1	0	13	1·08	− ·54	− ·56	·605	·492	1·58
30	3	1	1	1	0	0	3	1	1	0	0	0	11	·92	·00	·18	·032	·534	·335
31	4	1	1	2	0	0	1	1	3	1	2	3	19	1·58	·59	−1·05	1 451	·406	2·97
32	1	4	0	3	1	1	0	2	2	5	1	2	22	1·83	·24	− ·29	·142	·378	1·0
33	1	2	0	1	1	0	5	0	1	2	3	3	19	1·58	·09	− ·33	·117	·406	·84
34	1	3	0	1	4	0	1	0	390	3	3	1	407	33·92	− ·94	−1·66	2·809	·088	19
35	0	3	2	2	1	1	1	4	1	0	0	0	15	1·25	− ·37	37	·274	·458	1·14
Σ	10	14	5	11	12	2	13	8	405	16	15	9	520		−1·58	−6·72	11·976		

${}_1l_m = ·346 \quad {}_1c_m = ·6903 \quad k_1 = 2·00 \quad W_1 = ·018$

Tabelle LIX.

Gebiet 28° N~29° N, 129° E~130° E.

Jahr	Monatliche Bebenzahl												Σ	a_0	$\frac{a_1}{a_0}$	$\frac{b_1}{a_0}$	c_1^2	ε	c_1/ε
	Jan.	Feb.	März	April	Mai	Juni	Juli	Aug.	Sept.	Okt.	Nov.	Dez.							
1926	2	5	3	0	1	6	5	9	3	4	5	5	48	4·00	− ·22	− ·375	·189	·256	1·70
27	4	2	2	6	11	7	15	12	12	25	43	24	163	13·58	·07	− ·84	·711	·139	6·07
28	14	14	14	11	21	8	6	2	9	1	11	12	123	11·00	·29	·41	·252	·160	3·14
29	14	89	18	8	10	11	20	6	7	10	8	40	241	20·08	·79	·30	·635	·114	7·00
30	1	14	19	22	13	11	15	18	11	15	13	26	178	14·83	− ·006	·05	·003	·133	·41
31	6	35	18	7	5	8	6	6	9	72	20	45	237	19·75	·58	− ·63	·733	·115	7·46
32	44	22	21	22	26	21	18	19	23	16	188	36	456	38·00	·53	− ·62	·665	·083	9·83
33	18	21	25	31	25	62	32	33	35	26	133	24	465	39·66	− ·075	− ·38	·150	·082	4·72
34	17	9	16	21	19	40	22	31	111	26	30	22	364	30·33	− ·45	− ·54	·495	·093	7·58
35	22	17	15	45	16	19	13	14	24	20	25	65	295	24·58	·35	− ·08	·129	·103	3·49
Σ	142	228	151	173	147	193	152	150	244	215	476	299	2570		1·67	−2·70	3·962		

$_1l_m = \cdot 114$ $_1c_m = \cdot 317$ $k_1 = 2\cdot 78$ $W_1 = \cdot 00044$

Tabelle LX.

Gebiet 27° N~28° N, 142° E~143° E.

Jahr	Monatliche Bebenzahl												Σ	a_0	$\frac{a_1}{a_0}$	$\frac{b_1}{a_0}$	c_2^1	ε	$\frac{c_2}{\varepsilon}$	$\frac{a_2}{a_0}$	$\frac{b_2}{a_0}$
	Jan.	Feb.	März	April	Mai	Juni	Juli	Aug.	Sept.	Okt.	Nov.	Dez.									
1926	0	1	2	2	1	0	2	0	0	6	1	5	20	1·67	·42	−·43	·361	·396	1·54	−·50	−·35
27	6	6	6	5	13	4	3	8	3	8	3	2	67	5·58	−·12	·17	·043	·216	1·26	−·27	·03
28	4	8	5	0	11	3	11	5	0	7	6	12	72	6·00	·10	−·04	·012	·209	2·20	·31	−·34
29	7	7	2	9	12	11	9	11	7	4	5	14	98	8·17	−·18	·07	·037	·179	2·02	·24	−·27
30	4	0	5	4	8	3	4	11	0	4	3	2	48	4·00	−·43	·15	·207	·256	·31	·08	·001
31	3	3	6	2	3	0	7	15	16	9	27	12	103	8·58	·06	−·94	·887	·174	1·33	−·23	−·03
32	4	8	13	12	11	14	0	0	10	14	12	7	105	8·75	·13	·14	·037	·173	3·57	−·58	−·21
33	17	8	9	18	6	15	18	6	11	10	12	9	139	11·58	−·04	·07	·007	·150	·94	·10	−·10
34	16	5	15	19	245	14	0	8	32	17	17	10	398	33·17	−·57	·93	1·190	·089	1·41	−·78	−·98
35	15	10	14	5	2	1	4	1	3	2	4	7	67	5·58	·88	·37	·911	·216	2·08	·27	·36
Σ	75	56	77	76	312	65	58	65	82	81	90	80	1117		·25	·49	3·692			−1·36	−1·889

$_1l_m = ·192$ $_1c_m = .055$ $k_1 = ·29$ $W_1 = 919$ $_2l_n = ·174$ $_2c_n = ·210$ $k_2 = 1·21$ $W_2 = ·232$

Tabelle LXI.

Gebiet 26° N~27° N, 127° E~129° E.

Jahr	Monatliche Bebenzahl												Σ	a_0	$\frac{a_1}{a_0}$	$\frac{b_1}{a_0}$	c_2^1	ε	c_1/ε
	Jan.	Feb.	März	April	Mai	Juni	Juli	Aug.	Sept.	Okt.	Nov.	Dez.							
1926	0	0	0	5	1	0	2	52	1	2	0	0	63	5 25	−1·53	−·73	2·873	·223	7·62
27	0	2	0	0	0	0	0	0	0	0	0	2	4	·33	1·76	·00	3·097	·886	1·99
28	0	1	1	0	2	1	0	0	0	0	1	1	7	·58	·24	·64	·467	·670	1·02
29	0	0	3	3	1	5	3	0	2	1	0	0	18	1·50	− ·81	·50	·906	·418	2·28
30	5	4	1	1	3	0	1	4	2	6	0	2	29	2 42	·33	−·33	·217	·329	1·42
31	1	2	2	4	7	8	9	2	2	3	5	7	52	4·33	− ·38	·01	·144	·246	1·54
32	1	0	4	2	0	7	7	7	20	9	9	12	78	6·58	− ·28	−·87	·835	·201	4·55
33	10	9	5	6	19	0	0	8	0	0	2	0	59	4·92	·16	·76	·603	·231	3·37
34	4	0	0	8	2	7	27	5	0	4	1	0	58	4·83	−1·17	·06	1·372	·233	5·03
35	1	0	18	2	4	1	3	2	2	4	1	14	52	4·33	·67	·23	·501	·246	2·88
Σ	22	18	34	31	39	29	52	80	29	29	19	38	420		−1·01	·27	11·02		

${}_1l_m = ·332$ ${}_1c_m = ·105$ $k_1 = ·316$ $W_1 = ·905$

Tabelle LXII.

Gebiet 25° N ~ 26° N, 121° E ~ 122° E.

Jahr	Monatliche Bebenzahl												Σ	a_0	$\frac{a_1}{a_0}$	$\frac{b_1}{a_0}$	c_2^1	ε	c_1/ε
	Jan.	Feb.	März	April	Mai	Juni	Juli	Aug.	Sept.	Okt.	Nov.	Dez.							
1926	11	4	10	10	2	11	9	13	10	9	11	11	111	9·25	·32	−·04	·104	·168	1·92
27	6	7	12	9	18	9	10	18	10	10	11	6	126	10·50	−·14	·20	·060	·158	1·55
28	2	5	9	9	8	9	7	12	14	7	18	8	108	9 00	−·05	−·13	·019	·171	·81
29	4	9	11	6	14	8	6	4	13	12	21	23	131	10·91	·27	−·30	·163	·155	2·61
30	5	11	14	13	21	17	12	6	19	8	13	18	157	13·08	−·11	·12	·027	·141	1·17
31	25	11	0	13	1	9	12	5	3	7	4	5	95	7·92	·31	·12	·111	·182	1·83
32	2	8	0	11	4	4	0	0	5	4	22	7	67	5·58	·54	−·31	·388	·216	2·89
33	4	6	7	9	2	13	5	8	2	6	4	7	73	6·08	−·12	·21	·059	·207	1·17
34	6	0	2	3	9	3	4	13	15	7	5	4	71	5·92	−·47	−·23	·502	·210	3·39
35	12	4	12	4	11	10	35	16	11	15	11	12	153	12·75	−·41	−·22	·217	·143	3·26
Σ	77	65	77	87	90	93	100	95	120	85	102	101	1092		·14	−·88	1·650		

${}_1l_m = \cdot128$ ${}_1c_m = \cdot089$ $k_1 = \cdot697$ $W_1 = \cdot615$

Tabelle LXIII.

Gebiet 24° N ~ 25° N, 124° E ~ 125° E.

Jahr	Monatliche Bebenzahl												Σ	a_0	$\frac{a_1}{a_0}$	$\frac{b_1}{a_0}$	c^1_2	ε	c_1/ε
	Jan.	Feb.	März	April	Mai	Juni	Juli	Aug.	Sept.	Okt.	Nov.	Dez.							
1926	0	1	3	2	0	1	4	63	5	13	1	0	93	7·75	−1·27	− ·95	2·54	·184	8·67
27	1	4	7	2	2	3	1	3	0	100	2	2	127	10·58	·05	−1·43	2·05	·157	9·13
28	0	0	2	3	3	9	5	13	14	12	4	3	68	5·67	− ·78	− ·70	1·10	·225	4·67
29	2	9	5	3	6	6	1	9	4	15	5	6	71	5·92	·03	− ·57	·33	·210	2·74
30	11	3	5	7	8	2	10	7	20	9	1	3	86	7·17	− ·29	− ·35	·21	·191	2·40
31	1	4	9	3	14	7	8	12	3	2	9	19	91	7·58	− ·07	− ·01	·01	·186	·54
32	2	20	6	10	6	8	9	8	12	10	8	4	103	8·58	− ·08	·02	·01	·174	·58
33	3	3	10	6	10	20	25	4	5	8	7	8	109	9·08	− ·59	·19	·38	·169	3·65
34	15	7	3	10	7	1	3	4	1	2	6	5	64	5.33	·58	·32	·44	·221	3·00
35	24	2	10	3	12	4	0	4	6	4	1	9	79	6·58	·59	·21	·39	·199	3,14
Σ	59	53	60	49	68	61	66	127	70	175	44	59	891		−1·83	−3·27	7·46		

${}_1l_m = {\cdot}273$ ${}_1c_m = {\cdot}3747$ $k_1 = 1{\cdot}37$ $W_1 = {\cdot}153$

Tabelle LXIV.

Gebiet 24° N~25° N, 123° E~124° E.

Jahr	Monatliche Bebenzahl												Σ	a_0	$\frac{a_1}{a_0}$	$\frac{b_1}{a_0}$	c_2^1	ε	c_1/ε
	Jan.	Feb.	März	April	Mai	Juni	Juli	Aug.	Sept.	Okt.	Nov.	Dez.							
1926	0	0	0	1	0	0	2	0	0	0	0	0	3	·25	−1·32	·68	2·205	1·02	1 45
27	0	0	0	3	0	1	0	0	0	0	0	0	4	·33	− ·42	1·74	3·204	·887	2·02
28	0	0	0	0	1	0	0	0	0	3	2	1	7	·58	·40	−1·26	1·748	·670	1·97
29	0	1	0	0	0	0	2	2	0	0	0	8	13	1·08	·89	− ·54	1·084	·492	2·12
30	0	0	0	0	0	0	1	41	6	1	1	4	54	4·50	1·32	−1·10	2·952	·241	7·13
31	8	2	2	3	0	3	4	3	2	2	3	0	32	2·67	·13	·04	·019	·313	·44
32	1	3	0	2	4	2	2	1	6	3	2	3	29	2·42	− ·17	− ·27	·102	·329	·97
33	3	0	4	3	3	0	2	1	3	0	4	7	30	2·50	·48	·07	·235	·323	1·50
34	0	0	0	3	0	0	1	0	1	2	1	0	8	·67	− ·25	− ·18	·095	·627	·49
35	1	2	1	0	0	0	0	0	0	0	0	2	6	·50	1·66	·28	2·834	·723	2·33
Σ	13	8	7	15	8	6	14	48	18	11	13	25	186		2·72	− ·54	14·48		

${}_1l_m = \cdot 380 \quad {}_1c_m = \cdot 277 \quad k_1 = \cdot 730 \quad W_1 = \cdot 589$

Tabelle LXV.

Gebiet 24° N ~ 25° N, 120° E ~ 121° E.

Jahr	Monatliche Bebenzahl												Σ	a_0	$\frac{a_1}{a_0}$	$\frac{b_1}{a_0}$	c_2^1	ε	c_1/ε
	Jan.	Feb.	März	April	Mai	Juni	Juli	Aug.	Sept.	Okt.	Nov.	Dez.							
1926	1	1	3	0	1	0	0	2	0	3	0	1	12	1·00	·33	− ·09	·117	·512	·67
27	0	1	0	0	0	1	2	0	0	1	0	0	5	·42	− ·79	·00	·624	·79	1·00
28	0	0	0	1	0	2	0	0	0	0	0	0	3	·52	−1·16	1·32	3·088	1·02	1·72
29	0	1	0	1	1	5	0	0	0	0	0	1	9	·75	− ·69	·97	1·233	·590	1·88
30	0	0	0	0	0	0	0	0	1	1	0	1	3	·25	·24	−1·56	2·491	1·02	1·55
31	0	0	2	0	0	0	1	0	0	2	0	0	5	·42	·00	− ·12	·014	·79	·15
32	0	0	0	1	0	0	3	0	0	0	0	0	4	·33	−1·51	·51	2·540	·89	1·79
33	0	0	0	1	0	3	0	1	2	0	0	0	7	·58	−1·28	·09	1·646	·67	1·92
34	1	0	0	0	2	0	1	0	0	0	0	0	4	·33	− ·51	·88	1·074	·89	1·17
35	1	0	0	157	26	19	24	21	13	13	9	10	293	24·42	− ·44	·96	1·115	·083	12·7
Σ	3	3	5	161	30	30	31	24	16	20	9	13	345		−5·81	2·96	13·92		

${}_1l_n = \cdot 373$ ${}_1c_m = \cdot 652$ $k_1 = 1{\cdot}75$ $W_1 = \cdot 047$

Tabelle LXVI.

Gebiet 23° N～24° N, 122° E～123° E.

Jahr	Monatliche Bebenzahl												Σ	a_0	$\frac{a_1}{a_0}$	$\frac{b_1}{a_0}$	c_2^1	ε	c_1/ε
	Jan.	Feb.	März	April	Mai	Juni	Juli	Aug.	Sept.	Okt.	Nov.	Dez.							
1926	0	1	0	0	0	0	0	0	0	0	0	0	1	·08	1·75	1·00	4·06	1·77	1·14
27	0	0	0	0	0	0	1	0	0	0	0	0	1	·08	−2·13	0	4·53	1·77	1·20
28	1	0	3	7	0	1	10	2	4	5	1	1	35	2·92	− ·61	− ·04	·37	·299	2·03
29	10	2	6	6	0	0	4	3	139	6	4	3	183	15·25	− ·62	− ·32	2·13	·131	11·1
30	10	2	6	2	3	5	3	1	1	4	1	1	39	3·25	·28	·34	·19	·284	1·56
31	0	0	0	0	0	0	0	0	0	0	0	0	0	0	0	0	0		
32	0	1	3	4	0	0	0	1	0	0	0	0	9	·75	·33	1·47	2·27	·590	2·56
33	0	0	0	0	1	3	0	1	0	0	0	3	8	·67	− ·34	·09	·12	·627	·55
34	0	0	0	5	0	0	0	0	0	0	0	2	7	·58	·50	1·16	1·59	·670	1·88
35	1	2	2	1	2	1	0	0	1	0	2	0	12	1·00	·23	·56	·37	·512	1·16
Σ	22	8	20	25	6	10	18	8	145	15	8	10	295		− ·61	3·26	15·63		

${}_1l_a = ·396$ ${}_1c_m = 331$ $k_1 = ·84$ $W_1 = ·494$

Tabelle LXVII.

Gebiet 23° N~24° N, 121° E~122° E.

Jahr	Monatliche Bebenzahl												Σ	a_0	$\frac{a_1}{a_0}$	$\frac{b_1}{a_0}$	c_2^1	ε	c_1/ε
	Jan.	Feb.	März	April	Mai	Juni	Juli	Aug.	Sept.	Okt.	Nov.	Dez.							
1926	0	0	0	0	0	0	0	1	0	0	0	0	1	·08	−·02	− ·01	·0005	1·77	·01
27	1	1	2	1	1	1	0	1	0	0	0	0	8	·67	·16	1·01	1·046	·627	1·63
28	1	9	2	0	0	4	6	14	6	4	1	2	49	4·42	−·47	− ·45	·423	·253	2·57
29	0	5	6	10	7	6	3	0	3	70	7	2	119	9·92	−·01	− ·90	·81	·162	5·56
30	9	13	17	16	20	26	20	16	10	15	7	19	188	15·67	−·24	·22	·106	·129	2·53
31	21	9	13	20	11	15	7	12	9	9	10	14	150	12·50	·16	·19	·062	·145	1·72
32	11	20	17	26	11	14	10	13	15	6	26	18	187	15·57	·20	·08	·046	·129	1·66
33	16	8	4	69	78	44	48	29	20	22	24	36	398	33·17	−·46	·37	·349	·089	6·64
34	36	96	316	21	24	18	11	9	6	13	29	14	593	49·42	·86	1·07	1·885	·073	18·85
35	11	71	101	11	42	16	14	18	16	12	10	4	326	27·08	·36	·82	·672	·098	8·38
Σ	106	232	478	174	194	144	119	113	85	151	114	109	2019		·54	2·40	5·40		

$_1l_n = \cdot2324$ $_1c_m = \cdot2460$ $k_1 = 1\cdot06$ $W_1 = \cdot325$

Tabelle LXVIII.

Gebiet 23° N~24° N, 120° E~121° E.

Jahr	Monatliche Bebenzahl												Σ	a_0	$\frac{a_1}{a_0}$	$\frac{b_1}{a_0}$	c_2^1	ε	c_1/ε
	Jan.	Feb.	März	April	Mai	Juni	Juli	Aug.	Sept.	Okt.	Nov.	Dez.							
1926	1	0	1	1	2	1	1	2	0	3	2	1	15	1·25	− ·17	−·29	·11	·457	·73
27	0	1	1	4	0	2	3	0	4	3	4	3	25	2·08	− ·06	−·40	·16	·355	1·13
28	1	0	0	0	1	0	0	0	0	0	1	3	6	·5	·12	−·05	·02	·123	·196
29	2	0	4	2	1	0	1	3	1	0	0	0	14	1·17	− ·09	·56	·32	·473	1·19
30	0	0	0	0	2	1	2	0	0	1	2	109	117	9·75	1·55	−·94	3·28	·164	11·02
31	14	2	2	2	1	1	0	0	0	1	2	0	25	2·08	1·31	·27	1·79	·354	3·78
32	4	1	4	2	3	3	0	3	0	1	4	0	25	2·08	·17	·33	·13	·354	1·02
33	1	0	3	1	0	0	5	3	8	6	10	33	70	5·83	·85	−·14	·74	·212	4·06
34	9	0	11	6	7	3	7	8	11	11	20	2	95	7·92	·02	−·42	·17	·182	2·27
35	6	7	20	8	16	7	5	1	1	5	0	3	79	6·58	·11	·97	·95	·199	4·90
Σ	38	11	46	26	33	18	24	20	25	31	45	154	471		3·81	·11	7·67		

${}_1l_m = ·276$ ${}_1c_m = ·381$ $k_1 = 1·38$ $W_1 = ·149$

Tabelle. LXIX.

Gebiet 22° N~23° N, 120° E~122° E.

Jahr	Monatliche Bebenzahl												Σ	a_0	$\frac{a_1}{a_0}$	$\frac{b_1}{a_0}$	c_2^1	ε	c_1/ε
	Jan.	Feb.	März	April	Mai	Juni	Juli	Aug.	Sept.	Okt.	Nov.	Dez.							
1926	1	1	4	6	6	5	2	12	20	6	0	9	72	6·00	−·50	−·45	·452	·209	3·22
27	9	6	5	12	3	3	7	26	7	6	1	5	90	7·50	−·35	−·11	·587	·187	4 09
28	50	17	4	7	6	1	5	36	6	4	3	1	140	11·67	·37	−·08	·143	·150	2·52
29	7	3	4	10	4	6	2	1	1	4	5	4	51	4·25	·28	·38	·222	·248	1·90
30	6	2	1	6	4	4	0	7	0	3	3	3	39	3·25	·04	·14	·021	·284	·51
31	4	7	3	5	1	13	9	4	5	6	8	7	72	6·00	−·17	−·12	·043	·209	·99
32	3	8	1	5	2	2	3	2	7	4	4	4	45	3·75	·22	−·18	·808	·264	3·41
33	2	4	3	2	2	2	1	1	1	1	0	7	26	2·17	·61	·27	·445	·348	1·92
34	3	1	1	3	4	5	0	4	0	1	0	0	22	1·83	−·50	·67	·698	·378	2·21
35	12	7	11	6	12	16	16	12	144	37	18	20	311	25·92	−·44	−1·50	1·193	·318	3·44
Σ	97	56	37	62	44	57	45	105	191	72	42	60	868		−·44	−·48	4·612		

${}_1l_m = ·215 \quad {}_1c_m = ·065 \quad k_1 = ·302 \quad W_1 = ·913$

48. 日本に於ける地震發生の一年變化

地震研究所
松澤武雄
仲町容
西川與志男
吉村慶丸

日本を緯度及び經度の一度毎の目に分けてそのなかに起つた地震の數を一月毎にまとめて10年間の材料に就て調べた. 方法は一年毎に調和分析にかけそのベクトルを迷ひ步きの理論 (Random Walk) に照して吟味したものである.

其結果によれば確に一年變化を示す所があるがそれは極めて局部的の性質である事が分つた. 所によつては一年變化よりも半年變化の方が著しい様に見える.

季節は選ばないが一年に一度位地震の目立つて多く起る様な所もある.

49. *Frequency-distribution of the Itô Earthquake Swarm of 1930.*

By Fuyuhiko KISHINOUYE,

Seismological Institute, Faculty of Science,
Tokyo Imperial University.

(Read on March 16, 1937.—Received on March 20, 1937.)

Introduction.

1. Itô, a town noted for its many hot springs, lies on the eastern shore of the Idu Peninsula, about 100 km SW of Tôkyô. On Feb. 13, 1930, the townspeople began to feel a number of small quick shocks accompanied with detonating sounds like that of distant gun firing, such as is heard there occasionally through war-ships at target practice some distance out to sea. These shocks daily increased in frequency and strength. The shock felt on March 4, 5 h 11 m was so strong that it was felt in the southern part of Kwantô district, while the one that occurred on March 9, 19 h 54 m was violent enough to be recorded by almost every seismograph in Japan. The observations made at the Seismological Institute, Tokyo Imperial University, of the conspicuous Itô earthquakes are shown in Table I. The worst of these was the one that came on March 22. Although it was "strong" according to the Japanese intensity scale, damage to the town was slight. It merely shock down roof tiles, overturned stone walls, and threw down objects from shelves. The unusual small damage notwithstanding the violence of the shocks felt by the inhabitants, might have been due to the short duration of the principal part of the earthquake motion, or else the principal motion was too short to cause the houses to vibrate with it. The violence felt, however, was because the period of the vibrations was 0·5 second—the period to which man is most sensible.[1]

After April 12 the shocks diminished in frequency, although about thirty days later, on May 8, they became again active. The inhabitants, however, took care to surpress all outward signs of fear and apprehension lest the visitors to the spas upon getting alarmed might forsake the town, which would be detrimental to the town's main business.

---

[1] M. ISHIMOTO et M. OOTUKA, *Bull. Earthq. Res. Inst.*. **11** (1933), 113~121.

Table I.

Arrival-time of P (Tôkyô)					S–P	total duration	Maximum double amplitude			
							NS	EW	Resul.	T
1930		h	m	s	s	m	μ	μ	μ	s
February	21,	8	37	15·4	13·9	11	120	120	170	0·57
	22,	20	21	12·0	13·7	14	143	126	191	0·66
	28,	18	31	13·2	13·7	5	110	135	174	0·7
March	4,	3	50	53·2	13·8	7	64	89	109	0·7
	4,	5	11	17·3	13·8	12	350	360	500	1·1
	9,	4	39	53·0	14·0	7	182	130	224	0·7
	9,	19	54	48·7	13·7	16	400	361	538	0·85
	13,	4	29	44·7	13·5	12	100	79	128	1·1
	14,	14	18	41·3	13·3	7	79	48	93	1·1
	14,	21	05	30·0	12·5	3	30	26	40	0·56
	15,	18	34	3·7	12·6	9	175	130	218	0·7
	19,	10	16	57·1	13·7	8	136	159	207	1·3
	21,	23	4	23·6	13·4	9	148	92	170	1·1
	22,	17	50	51·7	13·8	20	1000	800	1280	1·0
	26,	14	22	58·5	14·0	20	280	316	422	1·5
	27,	1	41	47·1	13·8	20	267	340	433	1·2
	30,	0	5	36·7	13·7	8	55	46	72	1·3
April	1.	23	4	43·8	13·9	12	179	164	248	1·1
May	9,	12	52	49·7	13·3	15	108	113	159	1·1
	12,	21	27	0·2	14·2	18	464	226	535	1·3
	14,	8	57	2·5	13·4	13	172	146	225	0·9
	15,	15	58	19·4	14·2	13	82	100	129	1·0
	17,	5	14	23·6	13·8	30	560	667	871	1·1
August	15,	11	43	24·3	13·0	10	62	40	74	0·5

Since June no earthquake was felt until the one that occurred on Nov. 7 of the same year, excepting the moderate one of Aug. 15, about 10 km south of Itô. On Nov. 7 seismic activity revived, culminating in the Idu earthquake that came in the early morning of Nov. 26. There were many after-shocks, but they diminished until they ceased in March, the following year.

Since the seismic activity varied as just said, the accesory shocks of the Idu earthquake might have had some relation to the Itô earthquake swarm. In the present paper, however, only the frequency-distribution of the earthquake swarm is investigated in detail,[2] the object being to ascertain the characterististics of earthquake swarms.

---

[2] The preliminary investigations were published in the following papers:
A. IMAMURA, N. NASU, F. KISHINOUYE and C. YASUDA, *Proc. Imp. Acad.*, **6** (1930), 190~193; A. IMAMURA and others, *Disin* **2** (1930), 215~220 and 281~300; F. KISHINOUYE, *Disin*, **2** (1930), 502~503.

Idu Earthquakes before 1930.[3]

2. Since the XII century earthquake records were kept in the Province of Idu, but when they are compared with the records of neighbouring provinces, the earthquakes suffered by Idu are surprisingly few. In the "Meterials for the Earthquake History of Japan"[4] only one earthquake is recorded for Idu. This one occurred on July 30, 841, but the position of the epicentre is not definitely known.

3. In September 1882, a local shock occurred at Atami, a famous watering town about 13 km N of Itô, and was reported shortly after by T. Dan,[5] who states that the duration of the shock seemed very short, probably a few seconds. Damage to houses due to the earthquake were slight, but many retaining walls of terraces were thrown down and tombstones overturned or rotated, judging from which the mode of the earth motion might have been like that of the Itô earthquake swarm.

4. Besides these recorded earthquakes, the writer was told by old residents that swarm earthquake occurred in the Meidi Era (1868～1911), but of which no historical records could be traced. According to inquiries made by the late E. Makino, the time of those earthquakes was 1870.

5. In another case, in June 1905, earthquakes were experienced near the Island of Oosima, Idu, about 40 km SE of Itô.[6]

From data, the writer deduced that the epicentre of the earthquakes lay under the sea between Oosima and the Idu peninsula, slightly south of the Itô earthquakes. According to N. Fukuchi[7] the origin of the earthquakes might be under the sea bed NW of Oosima. Seismic activity began on May 28, 1905, and on June 5 more than one hundred earthquakes were felt followed by nearly twenty of them the next day.[8] His opinion is that there were not so many earthquakes, but only ten or twenty of very long duration. These activities ended by the middle of June.

---

[3] On this subject, the writer wrote in detail: F. KISHINOUYE, *Disin*, **8** (1936), 116～120.

[4] *Rep, Earthq. Inv. Comm.*, **46** (1904).

[5] T, DAN, Notes on the Earthquake at Atami, in the Province of Idzu, on September 28, 1882. *Trans. Seism. Soc. Japan*, **5** (1883), 95.

[6] F. OMORI, *Bull, Earthq, Inv, Comm,,* **2** (1908), 39～100 and *Rep, Earthq, Inv. Comm.*, **68** (1910), 31～38.

[7] N, FUKUCHI, On the geological Aspect of the Oosima (Idu) Earthquake of June 1905. *Rep. Imp. Earthq, Inv. Comm.*, **53** (1906), 87～95.

[8] See also "Miscellaneous Reports on the Oosima (Idu) Earthquakes." *Rep. Imp. Earthq. Inv. Comm.* **53** (1906), 96～97.

In the writer's opinion, these earthquakes might have been an earthquake swarm like the one that visited Itô lying NW of it. Seeing that they had the following characteristics of swarm earthquakes: (i) Swarm earthquakes occurred repeatedly in the region as just mentioned.[9] (ii) The earthquakes were crowded into a few hours of the day. (iii) The duration of each shock was very short, and its motion quick. (iv) No earthquake of destructive intensity occurred. (v) The active volcano Miharayama nearby was not affected in the least.

Seismological observation of the Itô swarm earthquakes.

6. The earthquake swarm began as already mentioned on Feb. 13, 1930, and its frequency increased gradually as shown in fig. 1. On March 10, five seiemographs were set up temporarily, one each at Itô, Usami, Aziro, Kawana and Hasima, surrounding the epicentral region under the supervision of Dr. Imamura. The space distribution of the origins of the earthquakes have been reported already by Dr. N. Nasu[10]. As these temporary stations were closed in April the same year, the period of observation might have been too short for investigating the whole course of earthquake activities, which lasted nearly four months. At Misaki and Kamakura, both about 50 km ENE of Itô (Kamakura is about 20 km NNW of Misaki), seismographs have kept working continuously from the records of which the writer studied these seismic activities. The constants of the instruments at the two stations used for this investigation are shown in Table II.

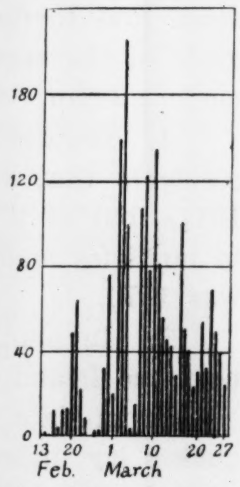

Fig. 1. Frequncy-distribution of earthquakes felt at Itô

Table II.

Station	Seismograph	*M*	*V*	*T*	*v*	Speed of drum
Misaki	Omori-Imamura portable horiz. seismograph	kg 12	120	sec 4	1·5	mm/min ca. 50
Kamakura	Imamura portable horiz. seismograph	7	50	7	1·5	ca. 50

---

[9] The Vogtland swarm earthquakes also occurred repeatedly in 1897, 1900, 1901, 1903 and 1908. E. TAMS, *Zeits. f. angew. Geophys*, **1** (1922~1925), 194.

[10] N. NASU, *Bull. Earthq. Res. Inst.*, **13** (1935), 400~416.

7. Very slight shocks of the earthquake swarm were of course not recorded at these stations as the distance between the stations and the epicentres was about 50 km, and although the epicentral distances of Misaki and Kamakura are nearly equal, the seismograms obtained at Misaki were mainly used for the present investigation, because the magnification of the seismograph there was greater than that of the instrument at Kamakura. (When the observation at Misaki failed to function, those at Kamakura were availed of to fill the deficiency, but when both instruments failed, the data of felt earthquakes at Itô registered by E. Makino11) were adopted.) Most of the earthqakes felt by him (fig. 1) are believed to have been recorded by the seismograph at Misaki, seeing that the daily frequencies reported by him are almost the same as those recorded at Misaki (fig. 2). The lowest limit of sensibility of the earthquakes on seismograms at Misaki was 0·2 mm for double amplitude.

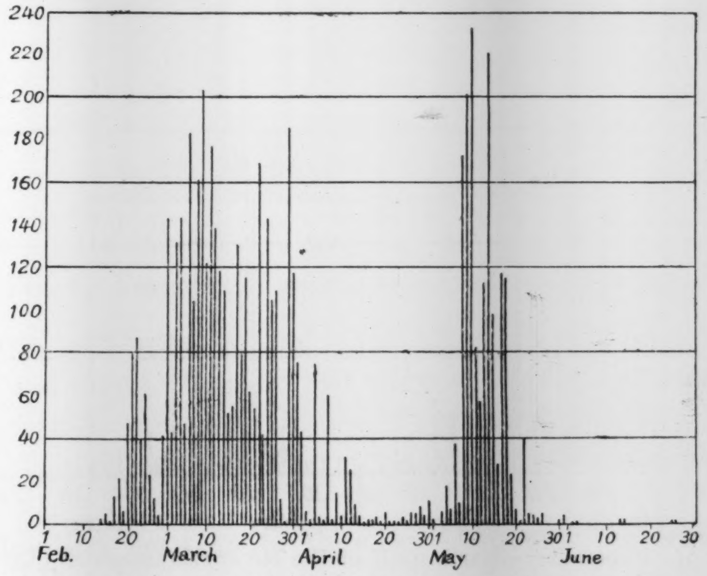

Fig. 2. Frequency-distribution of the Itô earthquakes in 1930 as observed at Misaki.

8. The arrival times of the earthquakes at Misaki are shown in Table III in which the date, hour and minute of arrival are shown, the total number of earthquakes observed being 5735. When a certain minute is repeated in the table, it means that as many number of earthquakes as are repeated occurred in a minute interval. As the clock for the time-marks on the seismograms was not accurate at that time,

---

11) E. Makino zealously undertook the observation of the earthquakes at Itô with an Imamura seismograph since March 1930 untill his untimely death in May 1934.

although the times were checked with those of large earthquakes that were observed at other stations, the range of error in the table may be one minute.

In the next table (IV) the hourly and daily frequencies of the earthquakes are shown. The maximum daily frequency was 233 on May 10, and the maximum of the hourly frequency 74 during 0∼1 h on March 6.

The frequencies at Misaki, compared with the daily frequencies reported in the Kisyô-Yôran, published by the Central Meteorological Observatory of Japan, are shown in fig. 3.

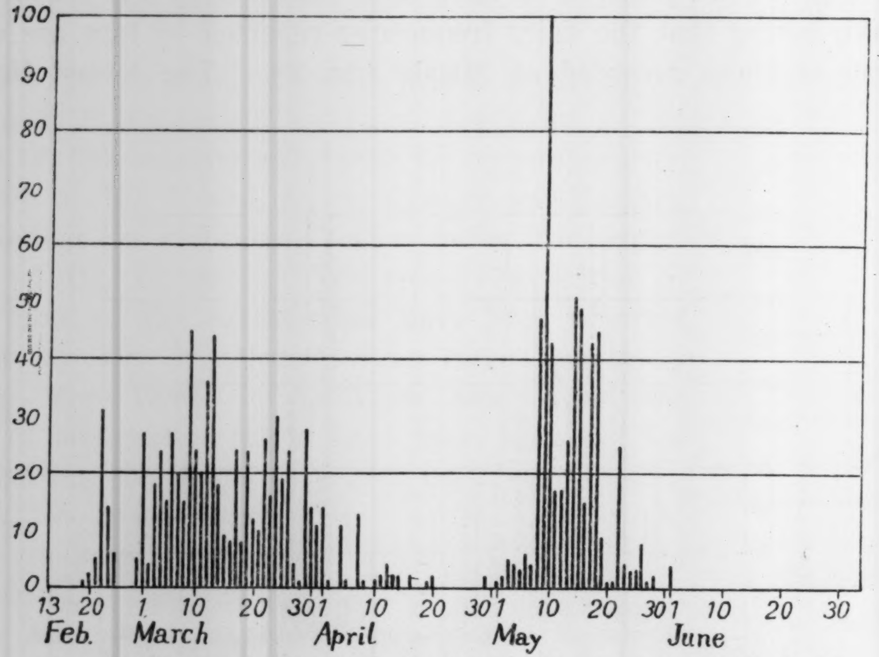

Fig. 3. Frequency-distribution of the Itô earthquakes as observed at local meteorological stations.

Relation between the seismic energy and the frequency of swarm earthquakes.

9. Assuming the energy of an earthquake to be proportional to the square of the amplitude of the seismic wave, the writer summed up the squares of the amplitudes of the first S-wave in the NS component as recorded at Misaki for each day (fig. 4). In this study, the EW component was neglected, because the type of the earthquakes as shown on the seismograms was so similar for every earthquake, (shown in fig. 5, Pl. LVIII) that the relative variation in seismic energy could be obtained by merely measuring one component motion. If fig. 4 were compared with the frequency-distribution in fig. 2, it will be clear that the two diagrams are on the whole similar, whence it may be concluded that the frequency was closely connected with the occurrence of large earthquakes, and that although the number of slight earthquakes was many, they did not play an important role in the time variation in seismic energy. On the other hand, it seems that the large earthquakes occurred when the earthquakes frequency was great.[12]

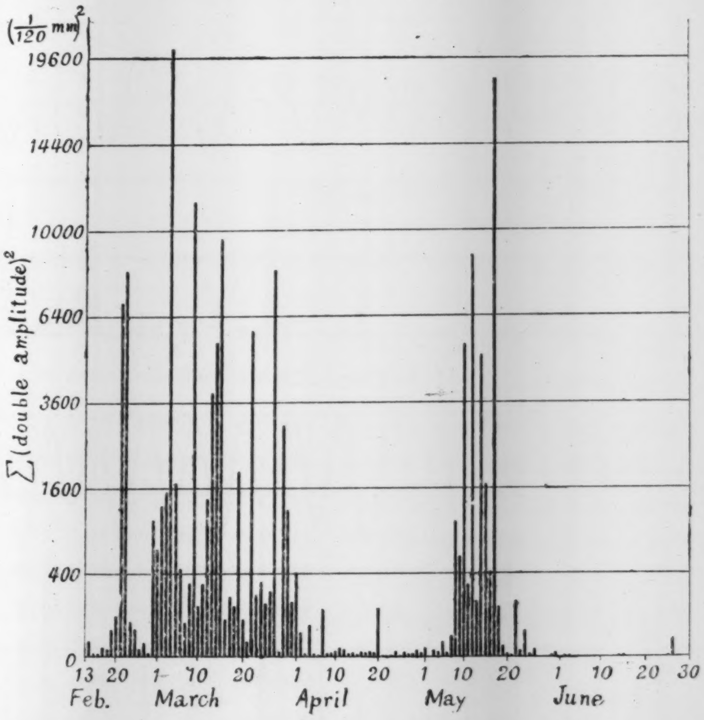

Fig. 4. Variation of seismic energy of Itô earthquakes.

Relation between earthquake frequency and tidal height and the periodicity of frequency.

10. According to the residents of Itô, the earthquakes came mostly at the time of low tide. Fig. 6 seems to show some relation between frequency and tidal height. The lunar periods of the frequency variation were then studied. The investigation was carried out first for frequencies for every 25 solar hours (an average lunar day being about 24 h 51 m) by the method which was described by J. Bartels[13], and recently used by Prof. T. Matuzawa[14] and the writer,[15] in investigat-

---

12) N. Miyabe also noticed the same relation for this earthquake-swarm: N. Miyabe, *Bull. Earthq. Res. Inst.*, **13** (1935), 168.

13) J. Bartels, *Terr. Magn. a. Atm. Elect.*, **40** (1935), 1~60.

14) T. Matuzawa, *Bull. Earthq. Res. Inst.*, **14** (1936), 38~67.

15) F. Kishinouye, *ditto*, **14** (1936), 604~609.

ing the periodicity of earthquake occurrence. The mathematical notations used in the present paper are the same as those used in Prof. Matuzawa's paper, so that an explanation of the method and the notations may be ommitted.

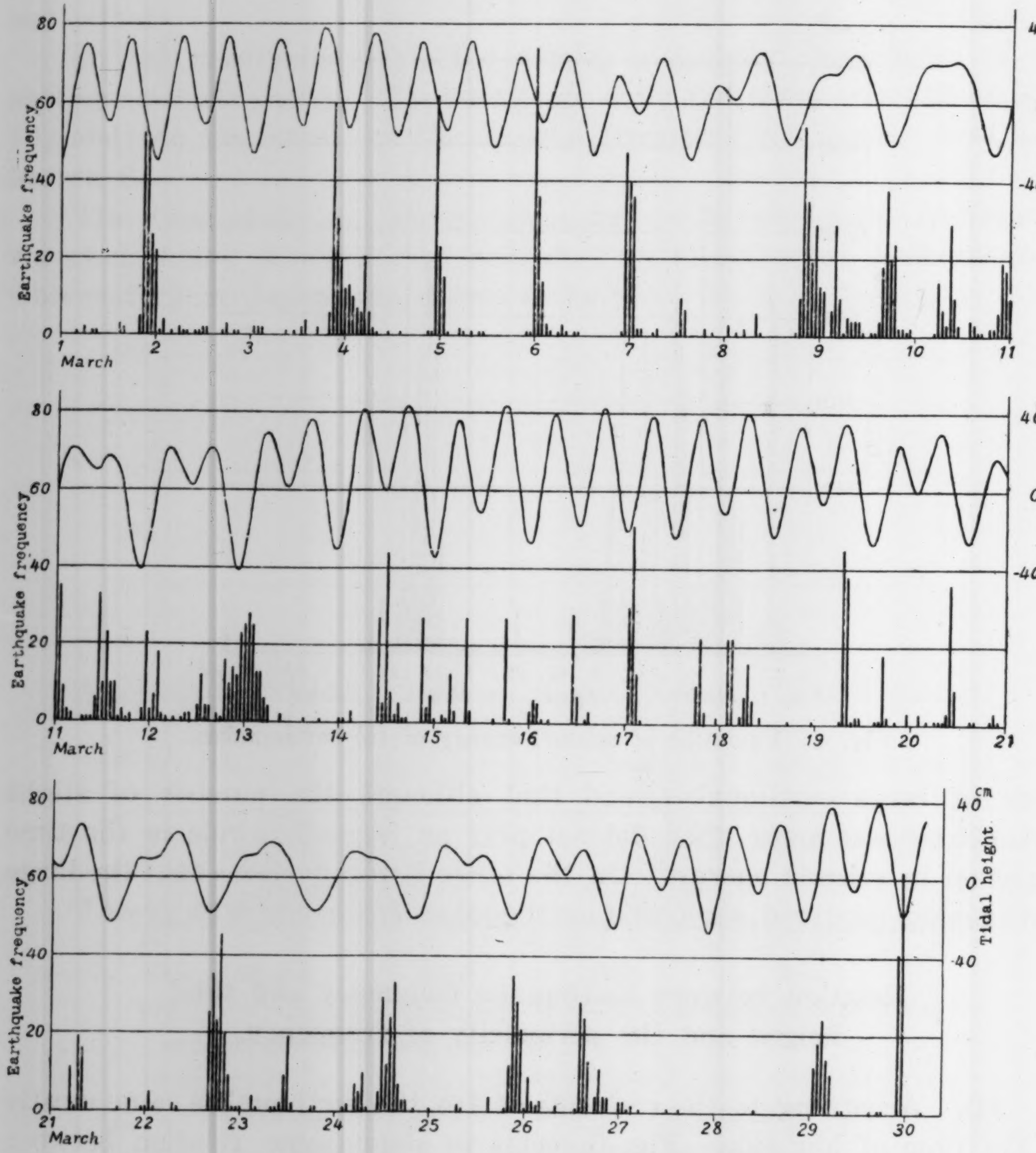

Fig. 6. Tidal height and earthquake frequency observed at Misaki.

11. Tables V and VI give the results of harmonic analysis for about 28 days (ca. 1 lunar month) from 14 h, Feb. 28 to 17 h, March 28 (figs. 7, 8), and from 20 h, April 26 to 23 h, May 24 (figs. 9, 10). In the tables the relative amplitudes c_1 and c_2 for each interval are greater than the corresponding expectancies, but the phase angles have been taken at random, after which the problem of "random walk" was applied to examine the periodicity of the earthquakes. Obtaining the ratio of the average relative amplitude c_m and the expectancy for the average l_m, the probability $w(k)$ that the average amplitude will exceed the expectancy is mentioned at the foot of the tables, where $w(k) = e^{-k^2}$ and $k = c_m/l_m$. For the data in Table V the ratios of the first and second harmonics were obtained as 2·29 and 0·64 respectively,

Table V.

Interval	n	a_0	a_1/a_0	b_1/a_0	a_2/a_0	b_2/a_0	c_1	φ_1'	c_2	φ_2	ε
Feb. 28. 14h ~ March 1, 15h	49	1·96	+0·382	+1·081	−0·983	+0·753	1·146	19°·4	1·238	307°·4	0·253
March 1, 15 ~ 2, 16	173	6·92	−0·380	+1·622	−1·380	−0·633	1·666	346·4	1·518	245·2	0·135
2, 16 ~ 3, 17	19	0·76	+0·257	+0·013	+0·021	−0·709	0·257	87·1	0·709	178·2	0·407
3, 17 ~ 4, 18	197	7·88	−0·045	+1·414	−0·595	+0·444	1·415	358·1	0·742	306·8	0·126
4, 18 ~ 5, 19	109	4·36	+0·234	+1·795	−1·570	+0·653	1·810	7·5	1·700	292·6	0·170
5, 19 ~ 6, 20	137	5·48	+0·228	+1·816	−1·554	+0·616	1·830	7·0	1·672	291·6	0·151
6, 20 ~ 7, 21	151	6·04	+0·799	+1·170	−0·751	+1·489	1·416	34·3	1·668	333·2	0·144
7, 21 ~ 8, 22	114	4·56	+1·493	−0·614	+1·10	−1·320	1·615	112·4	1·718	141·2	0·166
8, 22 ~ 9, 23	249	9·97	+0·585	−0·212	−0·525	−0·022	0·622	109·9	0·525	267·6	0·112
9, 23 ~ 11, 0	124	4·96	−0·158	−0·004	+0·358	−1·190	0·158	268·5	1·243	163·3	0·159
11, 0 ~ 12, 1	180	7·20	−0·203	−0·025	+1·253	−0·148	0·205	263·0	1·262	96·5	0·132
12, 1 ~ 13, 2	189	7·56	+0·770	−0·770	+0·405	−0·775	1·088	135·0	0·874	152·4	0·129
13, 2 ~ 14, 3	67	2·68	+1·651	+0·500	+1·217	+0·754	1·724	73·1	1·432	58·2	0·217
14, 3 ~ 15, 4	111	4·44	−0·694	+0·297	−0·926	−0·860	0·755	293·2	1·263	227·1	0·168
15, 4 ~ 16, 5	63	2·52	−0·042	−0·584	+0·950	+0·284	0·586	184·1	0·992	73·3	0·223
16, 5 ~ 17, 6	135	5·40	+0·670	−0·646	−1·14	−1·191	0·931	133·9	1·648	223·7	0·153
17, 6 ~ 18, 7	90	3·60	−0·160	−1·037	+1·057	−0·828	1·049	188·7	1·343	126·2	0·187
18, 7 ~ 19, 8	72	2·88	+1·840	−0·250	+1·706	−0·490	1·856	97·7	1·774	106·1	0·209
19, 8 ~ 20, 9	76	3·04	+0·720	+0·332	+0·961	−0·454	0·793	65·2	1·064	115·2	0·203
20, 9 ~ 21, 10	104	4·16	+1·45	+0·332	+0·849	−0·125	1·486	103·6	0·858	98·4	0·174
21, 10 ~ 22, 11	15	0·60	−0·99	−0·513	+3·02	+0·085	1·116	242·6	3·02	88·4	0·458
22, 11 ~ 23, 12	178	7·12	+0·101	+1·560	−1·225	+0·006	1·562	3·7	1·225	270·3	0·133
23, 12 ~ 24, 13	83	3·32	+1·150	−0·744	+0·687	−0·233	1·370	122·8	0·725	251·2	0·195
24, 13 ~ 25, 14	87	3·48	+1·616	+0·701	+1·020	+1·159	1·763	66·8	1·544	41·4	0·190
25, 14 ~ 26, 15	150	6·00	−0·217	+1·11	−0·353	−0·934	1·130	349·0	0·998	200·7	0·145
26, 15 ~ 27, 16	72	2·88	+1·12	+0·730	+0·774	+0·427	1·336	57·3	0·884	61·1	0·209
27, 16 ~ 28, 17	1	0·04	−0·375	+1·973	−1·852	−0·725	2·008	349·3	1·988	248·6	1·772
		mean	+0·437	+0·384	+0·094	−0·147					

$$l_1 = 1{\cdot}318,\ l_{1m} = 0{\cdot}254,\ c_{1m} = 0{\cdot}582,\ k_1 = \frac{c_{1m}}{l_{1m}} = 2{\cdot}29,\ w(k_1) = 0{\cdot}005.$$

$$l_2 = 1{\cdot}413,\ l_{2m} = 0{\cdot}272,\ c_{2m} = 0{\cdot}174,\ k_2 = \frac{c_{2m}}{l_{2m}} = 0{\cdot}64,\ w(k_2) = 0{\cdot}66.$$

Table VI.

Interval	n	a_0	a_1/a_0	b_1/a_0	a_2/a_0	b_2/a_0	c_1	φ_1	c_2	φ_2	ε
April 26, 20 h ~27, 21 h	6	0·24	+1·466	−0·791	+0·713	+0·709	1·666	108°·4	1·004	45°·2	0·724
27, 21~28, 22	10	0·40	+0·60	−0·226	−0·522	−0·865	0·641	110·6	1·010	211·1	0·560
28, 22~29, 23	4	0·16	+0·70	−1·56	−0·838	−0·650	1·710	155·9	1·124	232·2	0·886
29, 23~May 1, 0	11	0·44	−1·485	−0·439	+0·889	−0·259	1·548	253·5	0·926	106·3	0·535
May 1, 0~2, 1	2	0·08	+0·375	−1·95	−1·80	−0·725	1·985	169·1	1·940	248.0	1·253
2, 1~3, 2	15	0·60	+0·744	−0·432	+0·12	−1·33	0·860	119·9	1·345	174·7	0·458
3, 2~4, 3	10	0·40	−1·398	+0·45	+1·222	−0·395	1·468	271·9	1·284	108·0	0·561
4, 3~5, 4	8	0·32	+0·388	+0·404	+1·00	+0·238	0·560	40·7	1·028	76·6	0·626
5, 4~6, 5	41	1·64	−0·359	−0·558	+0·366	+0·851	0·663	212·7	0·926	23·2	0·277
6, 5~7, 6	62	2·48	+1·80	−0·571	+1·419	−1·016	1·883	107·6	1·745	125·6	0·225
7, 6~8, 7	246	9·82	+0·762	−0·246	−0·397	−0·613	0·801	108·0	0·730	212·9	0·113
8, 7~9, 8	179	7·16	+0·250	−0·457	−0·511	−0·350	0·521	151·3	0·619	235·6	0·132
9, 8~10, 9	168	6·72	−0·674	+0·112	+0·399	−0·230	0·683	279·5	0·460	120·0	0·137
10, 9~11, 10	74	2·96	+0·253	−0·230	+0·771	+0·645	0·341	132·3	1·005	50·0	0·206
11, 10~12, 11	105	4·20	+0·386	−1·104	−0·397	−0·586	1·170	160·8	0·708	214·1	0·173
12, 11~13, 12	215	8·60	+0·286	−1·30	−0·348	+0·790	1·331	167·6	0·863	336·2	0·121
13, 12~14, 13	93	3·72	−0·270	+0·214	+0·804	−0·678	0·345	306·9	1·051	131·3	0·184
14, 13~15, 14	64	2·56	+0·699	+0·461	−0·566	+0·170	0·837	56·6	0·591	288·3	0·222
15, 14~16, 15	102	4·08	−1·397	+0·058	+0·643	−0·449	1·398	272·4	0·784	138·7	0·174
16, 15~17, 16	134	5·36	+0·143	−0·570	+0·384	−0·386	0·588	166·0	0·544	135·2	0·153
17, 16~18, 17	5	0·20	+0·43	−0·98	+0·35	+4·52	1·070	156·4	4·533	4·4	0·792
18, 17~19, 18	24	0·96	+1·454	+0·735	+0·955	+1·005	1·629	63·2	1·387	43·6	0·362
19, 18~20, 19	4	0·16	+0·40	+1·563	−0·494	+0·888	1·612	14·4	1·015	330·9	0·886
20, 19~21. 20	39	1·56	−1·35	−0·365	+0·369	+0·063	1·399	254·8	0·374	80·3	0·284
21, 20~22, 21	6	0·24	+0·033	−3·97	−0·049	+0·116	3·970	90·5	0·524	337·1	0·724
22, 21~23, 22	4	0·16	−0·813	+1·443	−0·350	−0·713	1·658	330·7	0·794	206·2	0·886
23, 22~24, 23	3	0·12	+0·103	−0·607	−0·748	+1·408	0·616	170·4	1·594	332·1	1·022
	mean		+0·131	−0·272	+0·120	+0·094					

$l_1=1{\cdot}423,\ l_{1m}=0{\cdot}274,\ c_{1m}=0{\cdot}302,\ k_1=1{\cdot}10,\ w(k_1)=0{\cdot}30.$

$l_2=1{\cdot}352,\ l_{2m}=0{\cdot}260,\ c_{2m}=0{\cdot}152,\ k_2=0{\cdot}58,\ w(k_2)=0{\cdot}71.$

while for those in Table VI, the ratios were got as 1·10 and 0·58 respectively. Then, from theory, the lunar periodicity might not be concluded except the first harmonic in the former table. As a whole, when the two cases were combined (the phase difference between the two cases of course taken into account), the ratios for the two harmonics were obtained as 1·55 ($w(k_1)=0{\cdot}09$) and 0·59 ($w(k_2)=0{\cdot}71$) respectively. Had change in sea level any correlation with earthquake frequency, the lunar half-daily period or k_2 must be very great. But since in the above results, the second harmonics were small, the relation between frequency and tidal height might be uncertain for the Itô earthquakes.[16]

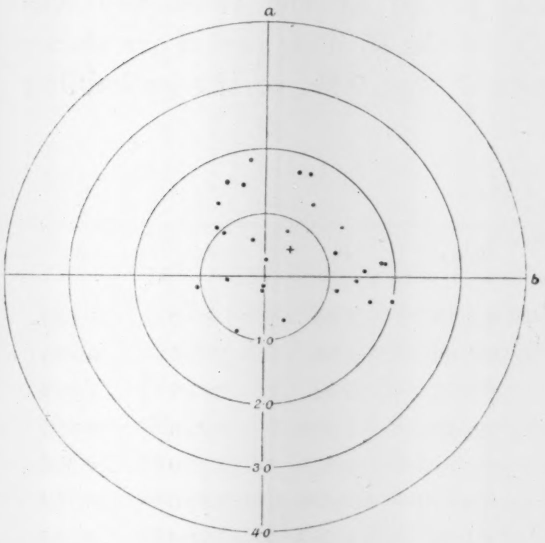

Fig. 7. Harmonic dial of the first harmonic for each of 27 intervals of 25 hours beginning Feb. 28, 14h.

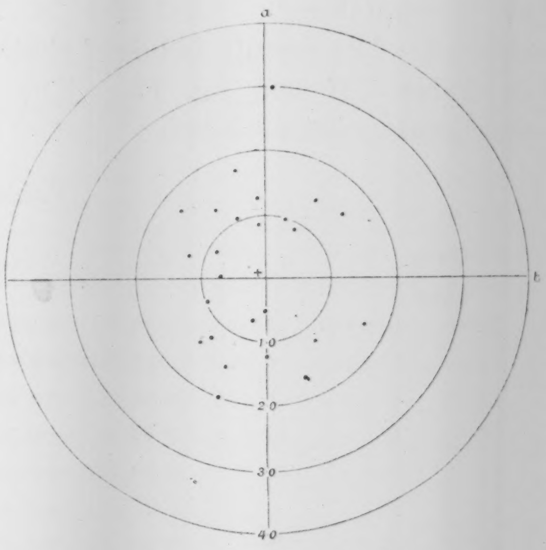

Fig. 8. Harmonic dial of the second harmonic of 25 hours beginning Feb. 28, 14 h.

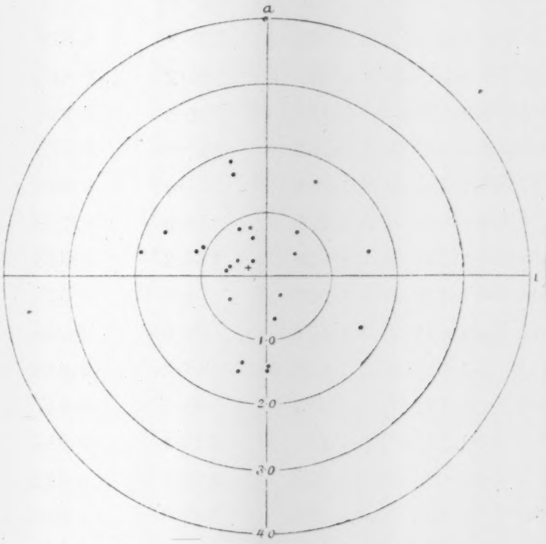

Fig. 9. Harmonic dial of the fiirst harmonic for each of 27 intervals of 25 hours beginning April 26, 20 h.

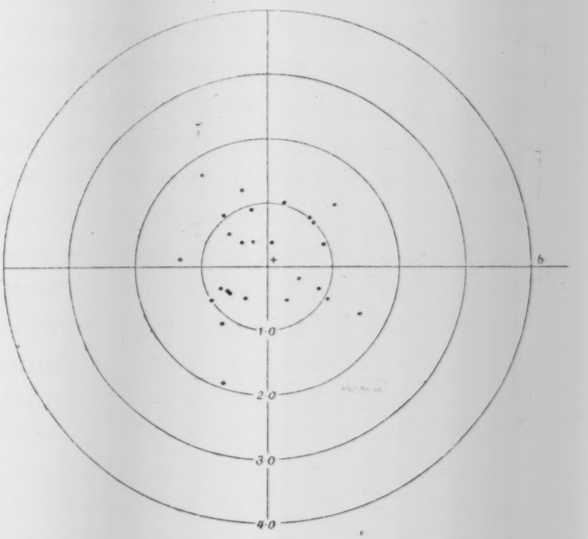

Fig. 10. Harmonic dial of the second harmonic of 25 hours beginning April 26, 20 h.

---

16) To verify these results, correlation coefficients between hourly frequency and tidal height at Misaki, and hourly frequency and hourly change of tidal height were calculated for March 1~28. The coefficients obtained were +0·126±0·025 (prob. error) and +0·010±0·026 respectively.

12. Except in the first series of earthquakes, the frequencies were correlated with the lunar day. The daily period will be seen from fig. 6, while the solar daily period has been found by a number of investigators.[17] Next the 24 hour period of the frequency was studied. The results obtained similarly as the 25 hour period are shown in Table VII and fig. 11. The value k was 0·89, so the probability was great $(w(k)=0{\cdot}45)$.

Table VII.

Date		n	a_0	a_1/a_0	b_1/a_0	c_1	φ_1	ε
1930 Feb.	14	2	0·08	+1·00	+1·19	1·55	48°·2	1·253
	15	4	0·17	+0·750	−1·80	1·95	292·7	0·886
	16	1	0·04	+1·00	−1·74	2·01	299·9	1·770
	17	13	0·54	−0·79	+1·12	1·370	125·0	0·492
	18	21	0·88	+0·834	−1·312	1·554	337·0	0·387
	19	6	0·25	−0·293	+0·830	0·880	109·6	0·724
	20	49	2·04	−0·426	−1·263	1·333	251·4	0·253
	21	79	3·29	+0·098	+0·031	0·103	17·6	0·199
	22	87	3·63	−0·833	+0·062	0·838	175·7	0·190
	23	39	1·63	+1·260	−0·609	1·40	334·2	0·284
	24	61	2·54	−1·290	−0·392	1·348	197·0	0·227
	25	23	0·96	+0·228	−0·665	0·703	288·9	0·370
	26	12	0·50	+1·054	−0·052	1·057	357·2	0·512
	27	4	0·17	−0·022	−0·130	0·132	260·5	0·886
	28	42	1·75	−1·680	+0·592	1·782	160·6	0·273
March	1	143	5·96	−0·995	−1·453	1·760	235·6	0·015
	2	43	1·79	+0 124	+0·995	1·075	83·0	0·270
	3	132	5·50	−0·930	+1·335	1·626	124·8	0·018
	4	143	5·96	+0·408	+1·470	1·523	74·5	0·015
	5	47	1·96	+0·348	+1·635	1·678	78·0	0·258
	6	183	7·63	+0·133	+1·823	1·825	85·8	0·013
	7	104	4·33	+0·114	−1·193	1·199	84·5	0·017
	8	161	6·71	−1·113	+1·231	1·69	132·1	0·014
	9	203	8·46	−0·454	+0·236	0·504	152·5	0·012
	10	122	5·08	+0·375	−0·463	0·596	309·0	0·016
	11	177	7·38	−0·369	−1·963	1·996	259·4	0·013
	12	139	5·79	−0·569	+0·776	0·862	126·2	0·015
	13	118	4·92	+0·844	+1·511	1·734	60·9	0·016
	14	109	4·54	−0·331	−0·659	0·738	243·3	0·017
	15	52	2·17	−0·412	+0·313	0·518	142·8	0·246

(to be continued.)

---

17) See B. GUTENBERG, *Handb. d. Geophys. Bd.*, **4**, §280.

Table VII. (*continued.*)

Date		n	a_0	a_1/a_0	b_1/a_0	c_1	φ_1	ε
1930 March	16	55	2·29	+0·378	−0·835	0·916	294°·3	0·239
	17	132	5·50	+0·136	+1·393	1·400	84·4	0·015
	18	79	3·29	+1·023	+0·683	1·230	33·7	0·200
	19	115	4·79	+0·992	−0·654	1·188	326·6	0·017
	20	62	2·58	+0.728	−1·20	1·407	301·2	0·225
	21	54	2·25	+1·568	−0·344	1·603	347·5	0·241
	22	169	7·04	−1·642	−0·287	1·667	189·9	0·014
	23	42	1·75	+0·291	−1·331	1·363	282·2	0·274
	24	143	5·96	−0·361	−1·29	1·340	254·4	0·015
	25	105	4·38	−1·06	+1·386	1·390	127·4	0·017
	26	109	4·54	−0·990	−0·493	1·106	206·5	0·017
	27	12	0·50	+0·495	+1·123	1·227	66·3	0·512
	28	1	0.04	+1·00	−1·72	2·00	300·2	1·772
	29	186	7·75	+1·45	+1·587	1·588	84·8	0·013
	30	117	4·88	+1·14	+0·672	1·323	30·5	0·016
	31	75	3·13	+0·375	−1·34	1·372	285·6	0·205
April	1	43	1·79	+0·767	−1·474	1·66	297·4	0·270
	2	6	0·25	−0·868	+0·50	1·002	150·0	0·723
	3	2	0·08	+0·714	−1·730	1·871	292·4	1·253
	4	75	3·13	+1·356	+0·844	1·597	31·9	0·204
	5	3	0·13	−0·472	−0·472	0·668	225·0	1·023
	6	2	0·08	+0·712	+0·712	1·004	45·0	1·252
	7	61	2·54	+0·897	−2·51	0·932	70·4	0·227
	8	2	0·08	+0·748	+0·976	1·228	52·6	1·252
	9	15	0·63	+0·315	+1·236	1·276	75·8	0·457
	10	4	0·17	+0·371	−0·485	0·651	305·6	0·885
	11	32	1·33	+1·45	−1·09	1·80	323·0	0·313
	12	26	1·08	+0·866	−1·70	1·94	296·9	0·348
	13	9	0·38	−1·51	−0·032	1·544	181·3	0·591
	14	4	0·17	0	0	0	——	0·886
	15	1	0·04	−2·00	0	2·00	180·0	1·772
	16	2	0·08	−1·725	+0·711	1·866	157·4	1·253
	17	2	0·08	+0·976	+0·748	1·228	37·4	1·253
	18	3	0·13	+1·98	+0·176	2·06	5·1	1·032
	19	1	0·04	+1·00	+1·74	2·00	60·1	1·772
	20	5	0·21	+1·04	−0·202	1·24	349·0	0·792
	21	1	0·04	0	−1·975	1·975	270·0	1·772
	22	1	0·04	−0·524	+1·928	1·998	105·2	1·772
	23	1	0·04	0	−1·975	1·975	270·0	1·772
	24	3	0·13	+0·826	−1·471	0·951	330·2	1·023

(*to be continued.*)

Table VII. (*continued.*)

Date		n	a_0	a_1/a_0	b_1/a_0	c_1	φ_1	ε
1930 April	25	1	0·04	−1·00	+1·74	2·00	119·9°	1·772
	26	5	0·21	−1·042	+0·039	1·044	177·9	0·792
	27	5	0·21	−1·05	−0·337	1·103	197·7	0·792
	28	8	0·33	−0·50	+0·129	0·516	345·5	0·627
	29	4	0·17	−1·68	+0·186	0·249	312·1	0·886
	30	11	0·46	−0·149	−1·487	1·496	264·3	0·534
May	1	2	0·08	−1·84	+0·760	1·994	337·5	1·253
	2	0	0	0	0	0	——	∞
	3	6	0·25	+0·072	−0·729	0·734	275·7	0·723
	4	18	0·75	−0·464	−0·375	0·597	219·0	0·418
	5	7	0·29	+0·373	−0·366	0·523	315·6	0·670
	6	38	1·58	−0·476	+0·490	0·683	134·2	0·287
	7	10	0·42	+1·083	+0·420	1·612	21·2	0·561
	8	173	7·21	+0·655	−0·714	0·991	312·5	0·014
	9	201	8·38	+0·770	+0·214	0·799	15·5	0·013
	10	233	9·71	+0·143	+0·451	0·474	72·4	0·012
	11	82	3·42	+0·618	+0·744	0·967	50·3	0·196
	12	58	2·42	−0·083	+0·619	0·625	97·6	0·233
	13	113	4·71	+0·859	−0·724	1·123	320·0	0·017
	14	221	9·21	+1·094	−0·354	1·150	342·1	0·012
	15	98	4·08	−0·424	+0·350	0·550	140·4	0·179
	16	28	1·17	+0·307	−0·795	0·852	291·1	0·335
	17	117	4·88	+0·607	+0·833	1·029	53·9	0·016
	18	115	4·79	+0·306	−0·777	0·835	291·4	0·017
	19	23	0·96	−1·497	+0·431	1·560	163·9	0·370
	20	7	0·29	+0·013	+0·132	0·135	84·3	0·670
	21	1	0·04	+1·93	+0·523	2·00	15·1	1·772
	22	40	1·67	+0·780	−0·996	1·264	308·0	0·280
	23	5	0·21	0	−0·399	0·399	270·0	0·793
	24	4	0·17	+1·62	−0·012	1·62	355·7	0·887
	25	3	0·13	+0·504	+0·280	0·577	29·1	1·023
	26	5	0·21	−1·08	−0·697	1·285	212·8	0·793
	27	0	0	0	0	0	——	∞
	28	0	0	0	0	0	——	∞
	29	0	0	0	0	0	——	∞
	30	2	0·08	+0·506	−1·88	1·946	285·0	1·253
	31	4	0·17	+1·98	+0·132	1·986	3·8	0·886
			mean	+0·113	−0·005			

$l=1{\cdot}326$, $l_m=0{\cdot}128$, $c_m=0{\cdot}114$, $k=0{\cdot}89$, $w(k)=0{\cdot}46$.

The daily periodicity of the Itô earthquakes however was found questionable from theory.

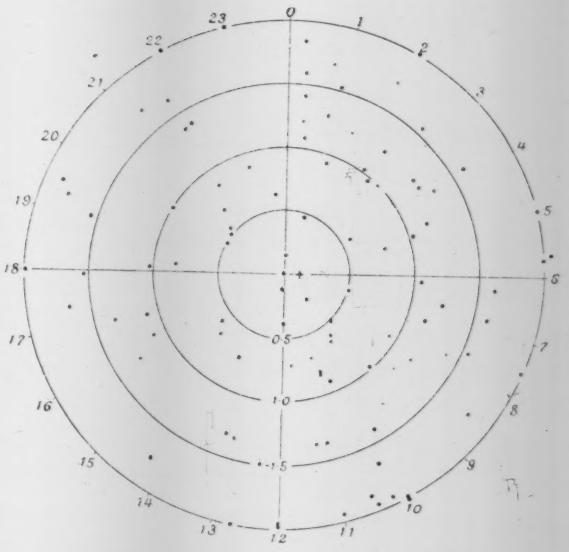

Fig. 11. Harmonic dial of daily variation in earthquake frequency. The numerals in the circumference indicate hours of maximum amplitude.

Frequency variation in short time intervals.

13. As to the conspicuous earthquakes that were felt at Tôkyô (Table I), the frequency variation in slight earthquakes occurred both before and after these moderate ones were investigated. The method of investigation was simple: the frequency for every 20 minutes before and after the principal earthquake was obtained and its time variation studied. In the frequency diagrams (fig. 12), four types of frequency-distribution will be noticed: (i) The frequency in earthquakes, which increases gradually, diminishes when it reaches maximum (shown schematically in fig. 13–a). The diagram indicates the type of earthquake swarm, and in this case the strongest or principal earthquake usually occurrs soon after the culmination of the seismic frequency. (ii) A strong shock occurs alone or accompanying a few earthquakes. (iii) After the strong shock, many small ones occur in succession, and their frequency is maximum at the time of the principal shock, which then diminishes exponentially. (fig. 13–b). The after-shocks of strong earthquakes are generally examples of this case. (iv) Small earthquakes become increasingly frequent, until when near its maximum frequency the principal shock occurrs, after which, virtually no more earthquakes occur (fig. 13–c). To take the case of the frequency of volcanic earthquakes, they increase before the eruption, after which it becomes few.[18]

In fact the type of frequency-distribution cannot be distinctly classified. Frequently the various types merge into one another, although in the present investigation, the type of frequency-distribution was not affected by changes in the time interval of the frequency.

---

[18] F. OMORI, *Rep. Imp. Earthq. Inv. Comm.*, **87** (1918), 58.

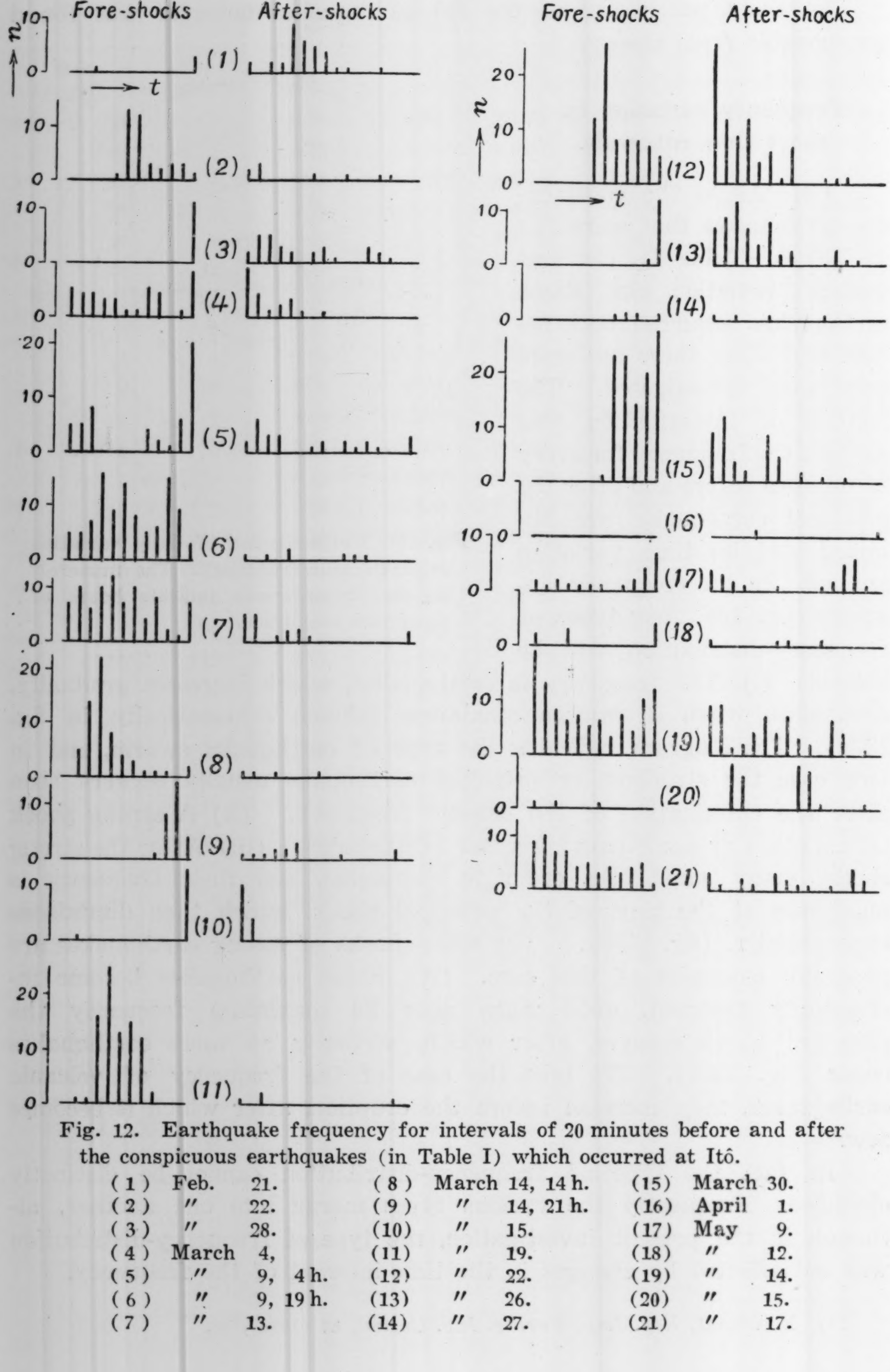

Fig. 12. Earthquake frequency for intervals of 20 minutes before and after the conspicuous earthquakes (in Table I) which occurred at Itô.

(1)	Feb. 21.	(8)	March 14, 14 h.	(15)	March 30.
(2)	″ 22.	(9)	″ 14, 21 h.	(16)	April 1.
(3)	″ 28.	(10)	″ 15.	(17)	May 9.
(4)	March 4,	(11)	″ 19.	(18)	″ 12.
(5)	″ 9, 4 h.	(12)	″ 22.	(19)	″ 14.
(6)	″ 9, 19 h.	(13)	″ 26.	(20)	″ 15.
(7)	″ 13.	(14)	″ 27.	(21)	″ 17.

An experiment in fracture.[19]

14. Generally speaking the causes of these earthquakes are believed to be as follows: A part of the earth's crust is gradually strained by some unknown stress, which when it exceeds the ultimate strength of that part of the earth's crust, an earthquake takes place. A part fracture or a rapid dynamic deformation of the earth's crust follows, at the same time propagating elastic, or seismic waves. Presuming that it is fracturing of the earth's crust that generates an earthquake, the writer carried out a simple experiment in fracture to solve the problem of time distribution of earthquakes.

15. Studies of cracks due to fracture have been made by a number of investigators.[20] The present writer investigated the time process of fracture, by recording the sounds or rapid vibrations of thin wooden boards resulting from fracturing them.

As material for experiment, thin wooden boards ($35 \times 3 \times 0{\cdot}5 \sim 0{\cdot}8$ cm) of regular grains were employed. Wood, being heterogeneous and somewhat brittle, was selected as the most suitable material for studying the fracturing of the earth's crust.

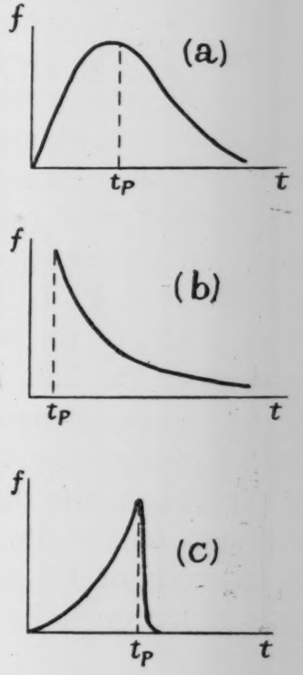

Fig. 13. Schematic diagrams of types of frequency-distribution.
t, time; *tp*, occurrence time of principal shock; *f*, frequency of earthquakes.

16. The apparatus for the expriment was simple as shown in fig. 14. A pick-up *a* of an electric gramophone, divested of its supporting arm, was set on a wooden board *d*, with a steel needle *b*, which was thrust into the upper side of the board. Being supported at *c* and *c'* the board was bent by the weight of a circular cylinder *e*. The cylinder was moved with a wire *f* which was pulled as the screwed rod was rotated by wheel *h*, the wheel being turned by an electric motor. The velocity of pull could be altered by changing the velocity of the motor or gear-ratio.

---

[19] Preliminary report on this experiment was read on Nov. 21, 1933 at the monthly meeting of the Earthquake Research Institute, and published in *Disin*, **6** (1934), 25∼31.

[20] There is considerable literature covering this problem, for example:—
G. NISHIMURA and T. TAKAYAMA, *Bull. Earthq. Res. Inst.*, **10** (1932), 476∼489.

Force was applied to the middle point of the board when fracture occurred at that point. Force of this kind was applied merely for convenience of experiment to record the vibration of the board with the pick-up. When the board cracked, electric current was generated in the coil of the pick-up, the current being amplified with an amplifier, which forms a part of the Haeno radio-seismograph.[21] The current was recorded with an oscillograph on cinematographic films (see middle line, fig. 15. in Pl. LVIII). The displacement every 5 mm of the board at the middle was marked on the film (lower line in fig. 15) by an electric circuit made when metal plate *l* touched the fine copper wires fixed to the bed of the apparatus. Time marks were put on the film (upper line in figure) at intervals of 1/5 second with a synchronous motor made by the writer.[22]

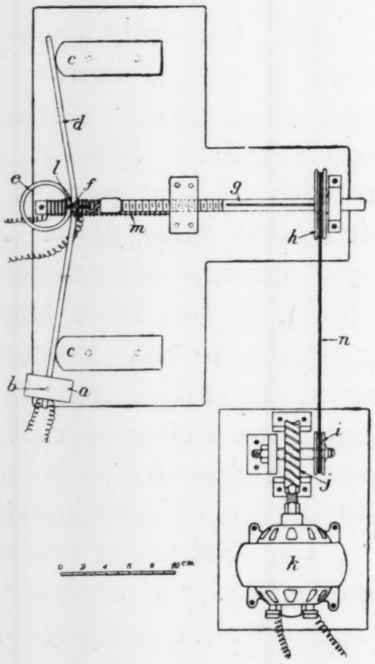

Fig. 14. Apparatus of experiment of fracture.

Results of the experiment.

17. As the bending proceeded, cracking sounds were heard, while the oscillograms recorded many inaudible vibrations. The process of fracture varied with the velocity of bending, the kind of wood, the grain of the board, and the moisture content of the wooden board. As material for the board, cedar, pine, and Japanese cypress were used. (The writer intended also to experiment with rock, instead of the wooden board, but nothing suitable was available.) Fig. 15 in Pl. LVIII is a part of an oscillogram. In the figure are shown many rapid inaudible vibrations and cracking sounds.

When the materials were the same and the velocity of bending equal, the board broke with nearly equal deformation. The velocity was not so great, from about 1 to 2·5 mm per sec at the middle of the board. When deformation proceeded slowly, occasionally loud creaking sounds were heard owing to rupture of the grains, and low silent vibrations were found on the oscillogram. This mode of fracture resembles the mode of occurrence of an earthquake swarm, a group of small

---

21) S. HAENO, *Jap. Journ. Astron. Geophys.*, **8** (1930), 39~50.

22) F. KISHINOUYE, *Bull. Earthq. Res. Inst.*, **10** (1932), 189.

earthquakes and a few larger ones.

When the board was bent quickly, complete fracture occurred with loud cracking sounds following greater deformation than in the case previously mentioned. In this case, sometimes the board broke all at once, but in most cases many small vibrations followed the main breaking. This mode of fracture is believed to be similar to that of after-shocks that follow most great earthquakes.

The Number of vibrations or sounds every 5 sec are shown in fig. 16. They greatly resemble the frequency diagrams in fig. 12.

18. As it is known that the strength of wood in large measure depends on its moisture content, some of the boards were placed in damp situation or immersed in water several days before the experiment. In such cases fracturing occurred slowly, almost without any quick vibrations.

It was found that the process of fracture is affected considerably by the condition of the experimented material and the particular way in which the force acts.

19. On the assumption that the type of frequency-distribution of earthquakes is due to the mode of fracture of the earth's crust, the writer will now attemt to explain the differences in the type of frequency-distribution.

Recently in the epicentral regions of many great earthquakes and swarm earthquakes, the topographical changes that occurred were found by means of precise levellings and triangulations,[23] and most great earthquakes the depths of which are believed to be shallow, are generally accompanied with many after-shocks, whereas small earthquakes and deep-seated earthquakes, the energy of which might be as great as some destructive earthquakes, occur without accessory shocks, and no crustal deformations have been known to follow such earthquakes. From this the writer deduced that the occurrence of many small earthquakes in succession, such as swarm earthquakes (the origins of the Itô earthquakes were also shallow in depth[24]) or after-shocks may be due to fracturing of the upper crust of the earth caused by certain slow deformations. The surface of the earth is free from traction, and the materials that compose the upper layer of the earth may be more brittle than those at depths subjected to high pressure and high temperature, so that upper layer may be liable to be fractured in the manner that a wooden board was broken in the model experiments here

---

[23] See for instance, A. IMAMURA, *Publ. Imp. Earthq. Inv. Comm.*, **25** (1930) and C. TSUBOI, *Jap. Journ. Astron. Geophys.*, **10** (1933), 93~248.

[24] N. NASU, *Bull. Earthq. Res. Inst,*, **13** (1935), 400~416.

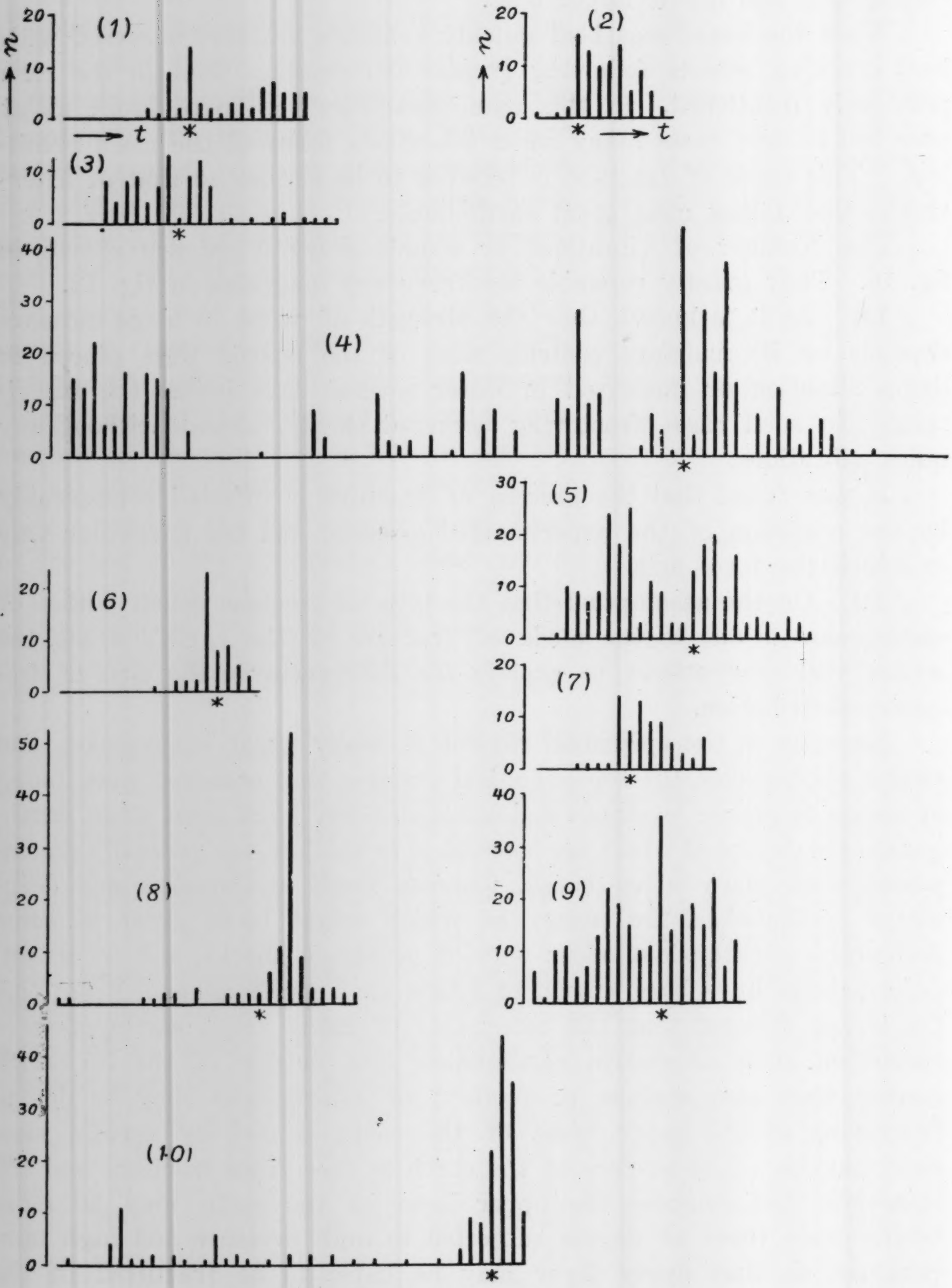

Fig. 16. Experiments in fracture.

n, number of shocks
t, time (5 sec interval)
star, time of shock of maximum amplitude.

described. In other words, since the upper crust is brittle, small cracks may appear in it through crustal deformation, when the vibrations due to the cracking may be regarded as the earthquake motion. It would therefore not be strange if slight earthquakes and deep-seated earthquakes are not followed by accesory shocks, as they do not cause any crustal deformations that could be observed.

20. Small earthquakes that occur near volcanoes may also be caused by crustal deformations resulting from changes in the state of the magma. Moreover, the frequent occurrence of volcanic eathquakes may in some cases be regarded as forerunners of volcanic eruptions, as is generally supposed.

21. Seismic tunamis are believed to be the result of a large deformation of the sea bottom, while the earthquakes caused by tunami usually accompany a large number of after-shocks. If the above mentioned relation between frequent occurrence of earthquakes and crustal deformation is true, tunami may be expected when many earthquakes occur under the sea bed, and one such earthquake is as strong as the earthquakes that generated the tunami. Of course, although the earthquake may be strong the tunami may be small, should the deformation be large in horizontal component and small in vertical, as was the case in the crustal deformation of the Californian earthquake in 1906.

A mathematical expression of frequency-distribution of earthquakes.

22. About fourty years ago, F. Omori[25] obtained a mathematical expression for the frequency-distribution of after-shocks. He assumed frequency f to be proportional to the strain in the earth's crust, say S, namely,

$$f=\alpha S, \tag{1}$$

where α is a positive constant, while the diminishing rate of the strain at a certain time is supposed to be proportional to the earthquake frequency at the time:

$$\frac{dS}{dt}=-\beta f, \tag{2}$$

where β is the other positive constant. Then

$$\frac{df}{dt}=-\alpha\beta f,$$

---

[25] F. Omori, *Rep. Imp. Earthq. Inv. Comm.*, **2** (1894), 103~139.

and we have

$$f=f_0e^{-\lambda t} \qquad (\lambda=\alpha\cdot\beta \text{ and } f_0 \text{ is the value of } f \text{ at } t=0).$$

This formula fairly expresses the frequency-distribution of after-shocks, and is used still at times. M. Enya[26) and S. Kusakabe[27) afterwards extended the above consideration and explained the decrease of frequency.

23. Suppose that an earthquake occurs when a part of the earth's crust has been fractured and the origin of the swarm earthquakes is in a finite region, then the region to be fractured may diminish, or the earthquake-generating power may decrease, while the total number of earthquakes that have occurred untill that time is increased, whence the writer developed the above relation (2) adding two terms to it, namely,

$$\frac{dS}{dt}=-\beta f-\gamma\int_0^t f dt+\delta, \tag{3}$$

where $f=0$ at $t=0$, and γ is a positive constant, and δ another constant to be determined by the initial condition. This equation may be changed to the form,

$$\frac{d^2f}{dt^2}+\beta'\frac{df}{dt}+\gamma' f=0. \tag{4}$$

This is the same as the equation of free-vibration of a pendulum with damper, and is an equation well-known to seismologists.

24. When $\beta^2>4\gamma^2$, the solution may be give as

$$f=f_0'e^{-\mu_1 t}+f_0''e^{-\mu_2 t}, \tag{5}$$

where μ_1, μ_2, f_0' and f_0'' are constants, when the equation (4) may include the result obtained by F. Omori as a special case.

25. When $\beta^2=4\gamma^2$, or in other words γ becomes as great as β, the solution becomes

$$f=\left(\frac{df}{dt}\right)_{t=0} te^{-\nu t}.$$

This expresses the relation between f and t as shown in fig. 13–a, and may explain the frequency-distribution of earthquake swarms in certain cases.

---

26) M. ENYA, *Ditto*, **35** (1901), 35∼56, **57** (1907), 85∼98, and **61** (1908), 63∼70.

27) S. KUSAKABE, *Publ. Imp. Earthq. Inv. Comm.* **17** (1904).

26. Moreover if δ is a function of time the equation (4) is transformed into

$$\frac{d^2f}{dt^2}+\beta'\frac{df}{dt}+\gamma' f=\delta',$$

where δ' is obtained by the initial condition. If δ' be given as the function of t as shown by the dotted line in fig. 17, then the solution may be obtained as the curve in the full line on the same diagram, which may be in better accord with the result of the earthquake swarm described above.[28]

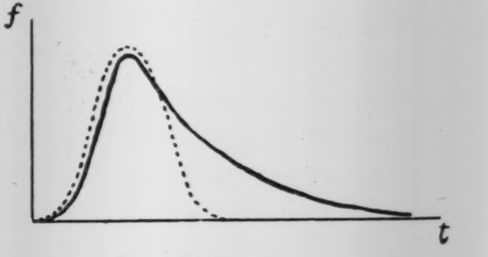

Fig. 17.

At all events, the frequency-distribution of earthquakes may depend upon the plastic property of the earth's upper crust, and the manner in which the earthquake generating force acts. In the writer's opinion, there is no essential difference between the frequency-distributions of after-shocks and earthquake swarms.

---

28) Another explanation of the frequency-distribution in fig. 17 may be obtained, when the conditions $f_0'=-f_0''$ and $\mu_2>\mu_1$ are put in the expression (5). But the consideration in the text may be better in respect of physical meaning than that stated here.

Table III.

Arrival times of the Itô earthquakes at Misaki.

Date	hour	minute	Date	hour	minute	Date	hour	minute
1930 Feb.			20	18	17, 49	22	3	16, 16, 41, 45
14	2	08, 08		19	10		4	32
15	10	50. 51, 51		21	55		5	26, 31, 33, 48
	12	56		22	58		6	02, 04, 20, 21,
16	10	22		23	32, 35, 39, 59			24, 26, 45, 49,
17	10	24, 38	21	0	06			58
	21	16, 18. 43		1	56		7	05
	22	02, 04, 07, 08,		2	14, 15, 32, 33,		8	04, 22, 31, 31,
		08, 09, 26, 35			49			31, 33, 41, 54,
18	0	43		3	06, 36, 40			57
	5	00		5	29		9	10, 12, 18, 36,
	6	18		8	36, 37, 37, 38,			40
	7	09			40		12	49, 49, 51
	8	10, 29, 39		9	29, 37, 55, 56,		14	47, 49
	10	47, 49, 51, 54,			58		17	45
		56, 58		10	00, 03, 03, 05,		18	00, 04, 06, 08,
	11	01, 03, 07, 22,			08. 11, 12, 13,			09. 09, 12, 13,
		23, 50			21, 24, 33, 35,			13, 15, 18, 20,
	15	58			36, 36, 43, 44,			21, 22, 24, 25,
	21	42			50, 50, 55, 55,			25, 26, 28, 30,
19	1	34						32, 33, 33, 35,
	10	48		11	05, 06, 08, 35,			40, 45, 46, 54
	16	46			50		19	09, 25, 32, 33,
	23	15, 25, 55		12	50			49, 52, 59
20	10	37, 59		17	31, 35		20	17, 21. 37, 42
	11	06, 25, 28, 30,		21	03, 06, 07, 08,		21	37, 42, 42
		39, 48, 49			09, 10, 10, 11,		22	30
	12	05, 11, 26, 28,			11, 13, 13, 13,		23	26
		30, 32, 38, 44,			14, 15, 15, 16,		0	41, 51
		44, 45, 49, 50,			18, 18, 21, 29,		6	06
		51, 55			36, 50, 52, 54	23	7	06, 21, 22, 23,
	13	08, 18, 24, 26,		22	10, 10, 10, 10,			23. 26. 27, 29,
		27, 29, 42, 43			20			31, 31, 32, 35,
	14	23, 30, 49		23	53			43, 44, 45, 47,
	15	20, 24, 31. 32,	22	0	38, 54			47, 50, 50, 55,
		33		1	22		8	12, 14, 18, 19,
	17	09		2	02			22, 30

(*to be continued.*)

Table III. (*continued.*)

Date	hour	minute	Date	hour	minute	Date	hour	minute
1930 Feb.			25	19	49	1	21	36, 36, 36, 37,
23	9	57		21	07			38, 38, 38, 38,
	10	21, 28, 28, 29	26	3	14			39, 39, 40, 41,
	14	18, 39		4	41, 42			41, 42, 42, 42,
	17	39, 42		5	22			43, 43, 44, 44,
	21	35		6	34, 49			45, 45, 46, 46,
24	0	41		8	05			47, 47, 47, 48,
	1	48		9	19, 48			48, 49, 50, 50,
	5	00, 12, 13, 54		10	21			50, 52, 53, 54
	10	43, 44		18	55		22	00, 01, 01, 02,
	11	06		20	49			02, 03, 04, 05,
	12	18, 38	27	1	53			05, 06, 07, 08,
	14	58		2	38			08, 08, 08, 09,
	15	04		14	08			10, 10, 11, 14,
	16	26, 28, 28, 30,		15	12			20, 24, 25, 27,
		31, 34, 40, 41,	28	5	15			27, 28, 28, 29,
		41, 44, 49, 50,		18	14, 21, 22, 23,			30, 30, 34, 34.
		53, 54, 56, 56,			23, 26, 28. 28,			34, 35, 37, 38,
		58, 59			29, 30, 31, 32,			38, 38, 40, 41,
	17	03, 03, 06, 07,			38, 49, 56, 56,			41, 43, 46, 47,
		07, 08, 09, 13,			56			48, 50, 52, 53,
		16, 20, 23, 23,		19	08, 11, 19, 20,			57, 59
		29, 30			23, 27, 27, 37,		23	00, 02, 02, 02,
	18	03, 14, 22, 27,			37, 45, 58			03, 03, 04, 05,
		39, 53, 53		20	07, 41, 46. 59			06, 06, 06, 07,
	19	03, 14. 17, 49,		21	10, 12, 16			08, 09, 20, 20,
		49, 50		22	20, 31, 32, 40,			20, 24, 51, 52.
	21	33, 33			52, 59			53, 54, 55, 56,
	23	40	March 1	3	03			58, 58
25	0	17		5	01, 02	2	0	00, 00, 01, 01,
	2	21		7	17			02, 02, 03, 03,
	3	02, 08		8	45			04, 05, 06, 08,
	5	24, 47		14	44, 47, 53			08, 09, 10, 12,
	10	48, 52, 52, 53,		15	03, 25			12, 18, 29, 52,
		56		20	55			53, 55
	11	00, 00, 01, 23,		21	20, 20, 21, 21,		1	09
		54			24, 25, 25, 27,		2	09, 10, 15, 53
	14	44			28, 28, 29, 29,		4	11
	15	08, 40, 56			31, 31, 33, 34,		6	50, 57
	17	17			34, 34, 35, 36,		7	51

(*to be continued.*)

Table III. (*continued.*)

Date	hour	minute	Date	hour	minute	Date	hour	minute
1930 March			3	22	33, 34, 49, 49,	4	23	18, 18, 19, 19,
2	8	35			52, 52, 55, 57,			22, 24, 24, 24,
	10	23			57, 59			26, 28, 28, 29,
	11	23		23	02, 05, 07, 08,			32, 35, 36, 37,
	12	27, 28			13, 15, 18, 18,			37, 38, 39, 40,
	13	37, 38			18, 19, 21, 22,			40, 41, 41, 41,
	17	59			22, 25, 39, 44,			42, 43, 45 47,
	18	59, 59			47, 56, 57, 58			47, 48, 53, 53,
	20	37	4	0	08, 16, 24, 33,			53, 54, 56, 56,
	21	49			34, 34, 35, 37,			56, 56, 57, 57,
3	1	06, 49			38, 40, 44, 58			57, 58
	2	49, 57		1	01, 01, 05, 11,	5	0	01, 02, 03, 05,
	3	00, 17			15, 15, 16, 20,			08, 12, 19, 28,
	9	49			30, 40, 45, 45,			30, 30, 31, 35,
	11	50			59			38, 39, 42, 44,
	13	06, 37		2	00, 00, 00, 10,			44, 50, 53, 53,
	14	43, 43, 43, 47			18, 20, 36, 38,			53, 54, 57
	17	09, 35			43, 54		1	00, 03, 04, 08,
	20	37, 42, 54, 55,		3	14, 30, 44, 44,			08, 08, 11, 11,
		56, 59			45, 47, 49			11, 12, 13, 24,
	21	00, 01, 01. 02,		4	03, 03, 04, 44,			24, 25, 53
		02, 03, 04, 05,			50, 53,		2	40
		05, 06, 06, 08.		5	02, 02, 03, 04,		5	33, 38
		13, 14, 17, 20,			04, 05, 08, 09,		6	10
		20, 22, 22, 22,			09, 10, 10, 11,		8	33
		22, 23, 24, 26,			15, 17, 17, 27,		10	40
		27, 27. 28, 29,			38, 42, 45, 45,		11	47
		29, 30, 30, 30,		6	04, 12, 12, 32,		22	10
		31, 32, 33, 34,			32, 41		23	38
		34, 35, 38, 39,		7	02, 30	6	0	06, 08, 12, 12,
		40, 40, 40, 42,		8	14			13, 18, 19, 21,
		42, 43, 45, 45,		11	50			21, 22, 22, 22,
		46, 49, 51, 51,		14	36			23, 23, 23, 23,
		52, 52, 53, 53,		21	00			24, 25, 25, 25,
		55, 56, 58, 59		22	47			25, 25, 26, 29,
		00, 05, 10, 12,		23	02, 05, 07, 08,			29, 30, 31, 31,
	22	14, 15, 17, 18,			09, 11, 11, 12,			31, 31, 31, 32,
		18, 19, 21, 21,			12, 13, 13, 14,			33, 33, 34, 34,
		25, 27, 28, 28.			14, 14, 15, 15,			34, 35, 36, 36.
		28, 30, 32, 33,			15, 15, 16, 17,			37, 37, 38, 38,

(*to be continued.*)

Table III. (*continued.*)

Date	hour	minute	Date	hour	minute	Date	hour	minute
1930 March			6	23	47. 51, 52, 53,	8	19	48, 49. 50, 52,
6	0	39, 40, 40, 41,			54, 55, 57, 59			53, 56. 57, 57,
		41, 41, 43, 43,	7	0	00, 03, 04, 04,			57, 59
		44, 45, 46, 47,			06, 07, 11, 13,		20	01, 03, 04, 05,
		48, 48, 49, 49,			14, 15, 16, 17,			07, 08, 08. 08,
		50, 50, 51, 51,			18, 19, 20, 20,			10, 11, 11, 12,
		52, 53, 54, 54,			21, 21, 21, 24,			12, 13, 13, 14,
		55, 55, 56, 58,			25, 25, 26, 26,			15, 15, 16, 17,
		58, 59			27, 28, 30, 30,			21, 23, 23, 23,
	1	00, 01, 01, 02,			31, 32, 32, 34,			27, 28, 29, 31,
		05, 05, 07, 09.			35, 36, 37, 37,			31, 32, 32, 33,
		10, 11, 11, 11,			41, 43, 50. 54,			35, 35, 38, 39,
		12, 12, 13, 13,		1	00, 01, 03, 04,			41, 43, 45, 47,
		15, 18, 19, 27,			09, 09, 12, 13,			47, 47, 48, 50,
		27, 30, 32, 33,			21, 21, 22, 23,			51, 51, 51, 52,
		34, 35, 39, 40,			23, 23, 24, 24,			53, 53, 56, 57,
		43, 47, 48, 48.			25, 25, 26, 27,			58, 59
		49, 50, 51, 57			27, 27, 27, 28,		21	01, 01, 05, 07,
	2	03, 03, 09, 14,			28, 28, 30, 30,			07, 08, 14, 19,
		15, 18, 18, 20,			30, 31, 32, 32,			21, 24, 26, 26,
		21, 29, 32, 43,			33, 33, 41, 55			26, 27, 28, 28,
		52, 58		2	01, 15			28, 31, 33, 33,
	3	01, 15, 21		3	24, 52			39, 40, 40, 41,
	4	40		6	42			43, 44, 45, 46,
	6	34		7	38, 45			48, 50. 50, 53,
	7	04, 22, 22		12	03			54, 57. 57
	8	18		13	32, 35, 43, 43,		22	11, 11, 11, 14,
	10	00			44, 45, 46, 48,			15, 15, 17, 17,
	11	48			48, 49			17, 17, 18, 19,
	22	57		14	05, 09, 10. 17,			20, 22, 24, 35,
	23	06, 07, 09, 09,			20, 55, 56			35, 36, 46
		10, 11, 13, 15,		19	39, 40		23	00, 03, 05, 06,
		16, 16, 17, 17,		21	25			06, 06, 08, 11,
		18, 19, 20, 22,	8	1	25, 26, 37			12, 12, 14, 14,
		23, 24, 25, 26,		3	08			15, 16, 16, 16,
		28, 29. 29, 30,		5	45, 46			18, 21, 27, 30,
		33, 34, 34, 36,		8	19, 54, 54, 54,			31, 33, 34, 35.
		37, 38, 39, 39,			55, 55			40, 41, 47, 52,
		40, 41, 42, 42,		9	14	9		59
		42, 44, 46, 47,		18	48		0	02, 12, 13, 27,

(*to be continued.*)

Table III. (*continued.*)

Date	hour	minute	Date	hour	minute	Date	hour	minute
1930 March			9	17	34, 37, 38, 40,	10	14	54, 56, 58, 59
9	0	28, 30, 30, 30,			40, 40, 41, 42,		15	08, 23, 23
		43, 50, 51, 55,			45, 46, 46, 47,		16	36
		56			49, 52, 54, 57,		17	33
	1	01, 01, 03, 08,			58, 59		19	11, 11
		16, 16, 16, 19,		18	04, 06, 12, 13,		20	32, 35
		27, 28, 29, 31			13, 16, 18, 23,		21	51, 51, 51, 52,
	3	05, 06, 06, 17,			32, 34, 35, 38,			52, 53
		37, 39, 59			49, 49, 53, 54,		22	09, 10, 10, 11,
	4	00, 04, 08, 13,			55, 57, 57, 58			12, 12, 12, 13,
		16, 16, 21, 26,		19	00, 01, 02, 03,			15, 15, 20, 21.
		27, 29, 29, 29,			04, 04, 05, 07,			39, 41, 44, 51,
		30, 30, 31, 31,			07, 08, 11, 17,			54, 56, 57
		32, 32, 33, 33,			17, 20, 21, 22,		23	03, 05, 06, 07,
		34, 35, 36, 37,			23, 26, 31, 32,			07, 12, 16, 17,
		38, 38, 39, 47,			36, 40, 44, 54			17, 20, 29, 32,
		48		20	11, 41			34, 40, 43, 44,
	5	00, 05, 08, 16,		21	20, 20			57
		16, 18, 30, 33,		22	55	11	0	44, 46, 48, 51,
		33, 55, 56, 58	10	23	31, 47			54, 54, 54, 57,
	6	56		5	23			57, 58
	7	00, 00, 23, 55,		6	06, 08, 20, 22,		1	01, 03, 04, 10,
		56			37, 41, 43, 44,			10, 12, 14, 15,
	8	12, 21, 21, 51			48. 48, 48. 52,			15, 17, 17, 19,
	9	50, 53, 56, 56			54, 55			25, 27, 31, 33,
	10	03, 04, 18, 41		7	07, 09. 11, 17,			33, 35, 36, 40,
	11	13			36, 42, 48			41, 43. 47, 49,
	13	50		8	47, 51, 58			59
	14	45		9	01, 02, 02, 03,		2	01, 02, 02, 05,
	15	12, 54, 56, 57			03, 04. 04, 04.			05, 12, 14, 17,
	16	10, 10, 22, 24,			04, 0,4 05, 05,			57
		32, 33, 34, 39,			06, 06, 06, 07,		3	11, 14, 22
		39, 41, 47, 48,			08, 08, 09, 11,		4	51, 54
		52, 53, 56, 56,			12, 14, 15, 15,		7	57
		57, 59			16, 21, 25, 49,		8	01
	17	01, 03, 04, 04,			50		9	37
		07, 08, 08, 09,		10	00, 09, 12, 13,		10	18, 35, 53, 56,
		11, 12, 12, 13,			16, 27, 32, 40,			57, 58
		15, 23, 26, 27,			43, 43		11	01, 01, 05, 09,
		31, 31, 32, 33,		11	01, 07, 27			11, 15, 17, 20.

(*to be continued.*)

Table III. (*continued.*)

Date	hour	minute	Date	hour	minute	Date	hour	minute
1930 March			12	2	30, 31, 42, 43,	13	0	31, 33, 39, 41,
11	11	21, 22, 25, 25,			47, 58			42, 53, 57, 57,
		27, 28, 30, 31,		3	13, 30			57, 58
		32, 32, 32, 33,		4	53		1	01, 02, 03, 05,
		34, 35, 37, 37,		6	08			05, 07, 08, 08,
		39, 43, 44, 48,		8	22			11, 14, 23, 25,
		52, 55, 57, 57,		9	32, 37			29, 30, 35, 35,
		59		10	17, 46			39, 40, 41, 42,
	12	00, 01, 08, 10,		12	17, 44, 46, 53			44, 46, 48, 50,
		16, 22, 26, 35,		13	00, 16, 17, 20,			50, 51, 52, 57
		41, 50			23, 24, 27, 31,		2	01, 02, 03, 05,
	13	01, 06, 08, 25,			35, 39, 50			05, 06, 11, 15,
		27, 29, 31. 34,		14	02, 04, 33, 39			15, 22, 24, 24,
		35, 36, 37, 37,		15	00, 02, 02, 04			27, 30, 32, 37,
		38, 39, 40, 41,		17	29, 30			38, 42, 43, 43,
		43, 48, 49, 53,		18	58			45, 46, 47, 54,
		55, 55, 58		19	03, 03, 14, 14,			54
	14	07, 13, 16, 17,			14, 17, 25, 26,		3	02, 04. 10, 10,
		18, 22, 31, 32,			39, 41, 42, 43,			17, 18, 18, 19,
		36, 50			44, 47, 51, 54			20, 21, 28, 46,
	15	07, 12, 25, 26,		20	00, 00, 01. 01,			48
		29, 31, 36, 38,			09, 11, 12, 21,		4	10, 11, 12, 17,
		41, 44			22, 57			20, 23, 25, 27,
	16	59		21	06, 09, 12, 13,			30, 38, 40, 45,
	17	28, 28, 29			14, 20, 29, 29,			45
	18	49			42, 45, 46, 47,		5	00, 04, 17, 17,
	19	45, 56			56, 59			19, 57
	22	42, 43, 59		22	07, 11, 15, 16,		6	13, 18, 33, 34,
	23	14, 15, 15, 18,			22, 29, 31, 32,		9	32, 33
		19, 21, 24, 24,			38, 40, 43, 44		15	39
		28, 30, 30, 34,		23	01, 02, 14, 17,		19	10
		34, 36, 36, 41,			19, 20, 22, 28,		0	31
		43, 43, 44, 46,			29, 30, 33, 34,	14	1	24
		54, 54, 59			35, 35, 36, 39,		3	17, 45, 54
12	0	05, 29, 56			43, 44, 45, 46,		10	41, 41, 44. 54,
	1	09, 25, 29, 35,			48, 54, 54			55
		39, 44, 54		0	02, 02, 09, 10,		11	01, 03, 05, 06,
	2	10, 14, 15, 16,	13		13, 14, 15, 16,			06, 07, 07, 09,
		16, 17, 17, 17.			21, 21, 22, 22,			11, 12, 12, 15,
		20, 25, 26, 29,			25, 26, 28, 29,			15, 16, 19, 19,

(*to be continued.*)

Table III. (*continued.*)

Date	hour	minute	Date	hour	minute	Date	hour	minute
1930 March			15	18	45, 45, 47, 50,	17	2	41, 41, 43, 47,
14	11	21, 21, 21, 21,			55, 57, 57			53, 58, 59
		21, 22, 23, 23,		19	07		3	05, 09, 18, 18,
		23, 24, 24, 25,		0	11, 11, 11			18, 18, 19, 19,
		25, 25, 28, 29,	16	1	37, 40, 43, 49,			19, 20, 23, 32,
		29, 30, 31, 38,			54, 57			36
		39, 40, 40, 43,		2	03, 04, 26, 27,		4	51
		45, 52, 52, 55			27		18	15, 28, 31, 33,
		07, 08, 15, 15,		3	05			34, 46, 46, 46,
	12	22, 23, 37, 53		5	34			46, 58
		00, 33		11	10, 11, 11, 11,		19	01, 07, 07, 08,
	13	06, 16, 18, 35,			12, 15, 15, 15,			10, 10, 11, 12,
	14	51			15, 16, 18, 19,			12, 17, 22, 24,
		21			22. 24, 25, 29,			24, 24, 25, 25,
	15	48			29, 30, 38, 38,			26, 27, 28, 31,
	16	04, 17, 17, 18,			39, 41, 45, 48,			44, 45
	20	19, 21, 22, 22,			48, 52, 53, 59		20	02, 06, 06
		25, 27, 28. 29,		12	02. 03, 28, 32,		23	25, 44
		29, 30, 30, 31,			38, 50, 54		2	32, 36, 36, 37,
		33, 34, 37, 40,		14	21	18		38, 38, 40, 41,
		41, 43, 45, 49,		15	03, 03, 03			42, 42, 42, 48,
		57, 58, 58		1	25, 39, 39, 40,			49, 49, 50, 50,
		05. 23, 39, 47	17		40, 42, 44, 46,			50, 51, 54, 55,
	21	15, 18, 30, 45,			47, 48, 48, 49,			57, 58
	22	59, 59, 59			50, 51, 51, 52,		3	04, 04, 04, 04,
		21			52, 53, 53, 54,			05, 06, 06, 06,
15	0	03, 03			54, 54, 55, 56,			07, 10, 11, 12,
	2	05			56, 57, 57, 57,			13, 15, 16, 17,
	3	01, 01, 02, 04,			58, 58			21, 22, 22, 25,
	4	04, 05, 06, 07,		2	00, 00, 00, 00,			33, 53
		07, 08, 15, 15,			01, 01, 01, 02,		5	32, 57
		22			04, 04, 04, 05,		6	11, 25, 42, 49,
		37, 37, 52			06, 06, 07, 07,			54, 54, 55
	5	01, 10, 21			08, 08, 09, 10,		7	08, 11, 12, 24,
	9	08			11. 11, 12, 12,			26, 28, 29, 33,
	15	17, 23, 24, 25,			13, 13, 14, 14,			35, 36, 43, 46,
	18	26, 26, 28, 30,			14, 14, 15, 16,			47, 47, 50, 50
		31, 33, 33, 33,			17, 18, 20, 20,		8	40, 40, 44, 46,
		34, 34, 39, 40,			20, 21, 23, 23,			47, 48
		41, 41, 43, 44,			24, 25, 26, 41,		10	05, 07

(*to be continued.*)

Table III. (*continued.*)

Date	hour	minute
1930 March 18	17	56
	23	39
19	6	44
	7	00, 22, 28, 29, 29, 30, 31, 31, 32, 32, 32, 32, 33, 33, 33, 34, 35, 36, 36, 37, 39, 39, 40, 42, 43, 43, 44, 45, 45, 46, 46, 47, 48, 49, 49, 49, 50, 50, 51, 51, 52, 55, 56, 56, 57
	8	00, 00, 07, 08, 11, 13, 13, 14, 15, 15, 16, 17, 17, 18, 19, 20, 21. 25, 26, 26, 27, 28, 31, 33, 35, 37, 38, 38, 30, 42, 44, 44, 46, 47, 49, 51, 52, 56
	9	08
	10	15, 21
	11	02, 03
	15	03
	16	35
	17	07, 08, 08, 11, 11, 12, 12, 13, 14, 18, 27, 29, 30, 36, 37, 40, 40, 41
	18	56, 56
	20	03
20	23	54, 55, 55
	2	48, 48. 48
20	4	34
	6	22
	7	45
	8	55
	9	08, 08, 08
	10	03, 04, 05, 05, 05, 07, 08, 10, 10, 12, 14, 16, 16, 17, 17, 18, 18, 18, 19, 20. 20, 21, 22, 22, 23, 23, 25, 28, 28, 28, 30, 30, 31, 32, 37, 51
	11	03, 04, 07, 10, 10, 16, 24, 25, 59
	15	12
	16	46
	20	49
	21	06, 13, 21
	22	58
21	5	17, 25, 26, 28. 32, 33, 34, 39, 40, 42, 47, 47
	6	58
	7	04. 15, 17, 21, 22, 25, 28, 28, 29, 30, 33, 38, 38, 40, 41, 47, 52, 53, 57
	8	02, 02, 03, 05, 12, 13, 16, 16, 18, 21, 34, 34, 36, 46, 51, 51
	9	06, 45
	17	41
	20	06, 16, 17
	23	04
22	0	59
22	1	00, 01, 23, 30, 40
	2	12
	7	06, 08
	8	58
	15	41, 43, 43, 44, 44, 46, 47, 48, 48, 48, 49, 50, 51, 52, 52, 53, 53, 54, 55, 56, 57, 57, 57, 58, 59
	16	02, 04, 05, 05, 06, 06. 07, 07, 08, 09, 09, 10, 10, 11, 13, 14, 14, 16, 16, 18, 18, 31, 32, 35, 38, 39, 40, 46, 46, 54, 55, 55, 56, 57, 59
	17	00, 09, 15 15, 21, 25, 28, 30, 30, 31, 33, 40, 42, 45, 50, 56, 56, 57, 57, 53, 59, 59, 59
	18	00, 01, 02, 02, 03, 03, 03, 04, 05, 05, 06, 06, 08, 09, 09, 09, 10, 10, 13, 15, 16, 19, 20, 21, 24, 24, 26, 26, 28, 29, 32, 33, 37, 39, 40, 40, 45, 46, 50, 51, 51, 53, 53, 56, 57
	19	06, 07, 09, 10,

(*to be continued.*)

Table III. (*continued.*)

Date	hour	minute	Date	hour.	minute	Date	hour	minute
1930 March			24	12	06, 11, 13, 14,	25		17, 20, 20, 21,
22	19	10, 10, 13, 15,			16, 19, 20, 23,			21, 22, 25, 25,
		17, 25, 31, 34,			24, 25, 28, 29,			26, 26, 29, 30,
		35, 38, 50, 50,			30, 33, 34, 35,			30, 32, 33, 35,
		53, 53, 56, 57			39, 43, 43, 45,			37, 37, 38, 42,
	20	05, 28, 33, 35,			45, 45, 54, 54,			52, 54, 54, 57,
		36, 37, 37, 38,			57			58, 59, 59
		49		13	02, 03, 04, 04,		22	01, 01. 03, 04,
	21	32			06, 12, 19, 20,			08, 09, 10, 11,
	22	02			21, 22, 55, 56			15, 15, 16, 20,
23	0	24		14	01, 02, 05, 09,			21, 21, 22, 22,
	3	02, 03, 46, 51			16, 16, 18, 19,			23, 25, 26, 30,
	4	39			28. 30, 33, 35,			30, 39, 40, 42,
	8	53			36, 37, 39, 40,			43, 44, 46, 47
	9	30			43, 46, 47, 49,		23	04, 07, 09, 09,
	10	29, 29			51, 53, 56, 58			10, 11, 11, 11,
	11	32, 34, 35, 37,		15	00, 01, 04, 04,			12, 20, 22, 25,
		54, 55. 56, 58,			05, 08, 09, 10,			26, 29, 31, 31,
		59			10, 14, 15, 15,			33, 35, 39, 46,
	12	00, 02, 03, 06,			17, 18, 19, 19,			59
		10, 13, 13, 14,			20 20, 21, 23,	26	0	51
		16, 17, 17, 18,			24, 25, 27, 27,		1	05, 07, 15, 16,
		20, 22, 27, 28,			30, 34, 34, 39,			26, 28, 31, 43,
		29, 30, 46			44, 46, 49, 51,			45
	13	04, 04			56		2	00, 02, 30
	18	50		16	05, 19. 23, 26,		3	15, 29
	19	56			27, 46, 55		4	41, 51, 58
24	2	29		17	09, 09, 41		8	28, 28
	3	20, 37		18	23, 27, 49		13	59
	5	23, 44, 47, 49,		20	42		14	03, 06. 10, 11,
		49, 55, 59	25	0	04			15, 16, 16, 17,
	6	03, 03, 18, 22,		7	15, 45			18, 19, 19, 20,
		52		8	05			21, 31, 32, 35,
	7	09, 13, 17, 20,		15	23, 24, 35, 56			36, 36, 37, 40,
		24, 25, 25, 26,		19	56			43, 44, 46, 47,
		27, 28		20	00, 02, 06, 15,			52, 54, 57, 58
	8	19			19, 22, 23, 25,		15	00, 04, 05, 08,
	11	48, 52, 56, 56,			26, 30, 32, 45			09, 10, 10, 10,
		59		21	02. 08, 11, 11,			12, 12, 13, 15,
	12	01, 02, 03, 04,			12, 13, 13, 17,			21, 26, 29, 30,

(*to be continued.*)

Table III. (*continued.*)

Date	hour	minute	Date	hour	minute	Date	hour	minute
1930 March			29	5	24, 24, 25, 41,	30	0	38, 41, 44, 51,
26		32, 33, 34, 37,			42, 55			52, 56, 57
		42, 44, 51, 55		7	30		1	06, 25, 46, 46,
	16	02. 03, 06, 08,		8	22			47, 54
		12, 12. 16, 17,		15	52		2	01, 02, 03, 03,
		28, 32, 46, 54,		17	51			03, 06, 06, 07,
		57		18	22			10, 13
	18	14, 15, 19, 34		22	19, 27, 28, 28,		3	10. 11, 52
	19	44, 44, 46, 48.			32, 33, 34, 34,		4	22
		48, 49, 50. 50,			35, 36, 36, 37,		5	30, 40, 45, 46,
		51, 52, 53			37, 38, 39, 39,			54
	20	04. 05, 59, 59			40, 40, 41, 42,		6	04, 07, 07, 08,
	21	00, 03, 05, 10			42, 43, 44, 45,			12, 14, 16, 19,
27	0	14, 34, 52			46, 48, 49, 49,			23, 23, 27, 27,
	1	37, 41, 49			49, 50. 52, 53,			29, 38, 41, 42.
	2	22			53, 53, 54, 54,			44, 46, 46, 47.
	3	30, 31			55, 55, 58. 59,			48, 49, 51, 51,
	5	14			59			52, 53, 54, 54,
	12	11		23	00, 00, 01, 02,			54, 56, 59, 59,
	15	35			03, 04, 06, 06,			59
28	10	15			07, 07, 09. 11,		7	00, 01, 02, 03,
29	1	04, 07, 11, 16,			12, 14, 15, 18,			04, 04, 05, 07,
		21, 33, 33, 36,			19, 22, 23, 23,			07, 11, 12, 13,
		40, 41, 46, 50			29, 30, 30, 30,			17, 17, 18, 20,
	2	05, 16, 17, 28,			33, 34, 34, 35,			21, 26, 26, 30,
		31, 33, 37, 44,			37, 37, 40, 41,			32, 56
		45, 45, 47, 47.			41, 42, 42, 42,		8	21
		49, 53, 54, 56,			43, 44, 45, 45,		13	16
		57, 59			46, 47, 48, 49,		14	17, 17, 32
	3	00, 04, 06, 07,			49, 49, 50, 51,		17	28
		13, 14, 15, 15,			51, 52, 54, 54,	31	4	49
		15, 16, 17, 19,			55, 56, 56, 57,		9	37, 38, 48, 57,
		24, 28, 35, 38.			57, 58, 58, 59,			57, 58, 59
		38, 41, 44. 44,			59, 59		10	02, 03, 04, 04,
		47, 54, 55, 56	30	0	00, 01, 02, 03,			05, 06, 06, 07,
	4	01, 02, 07, 11,			04, 04, 05, 11,			08, 11, 14, 17,
		12, 13, 14, 14,			14, 17, 18, 20,			17, 20, 22, 25,
		15, 17, 17, 19,			23, 23, 23, 25,			26, 31, 33, 36,
		19, 33			26, 26, 27, 27,			36, 37, 41, 43,
	5	04, 10, 10, 12,			31, 34, 35. 36,			45, 45, 54. 56,

(*to be continued.*)

Table III. (*continued.*)

Date	hour	minute	Date	hour	minute	Date	hour	minute
1930			4	3	21, 21, 21, 23,	7	7	36, 38
March 31	10	57, 58, 59			24, 27, 29, 31,		8	31
	11	02, 03, 10, 12,			33, 34, 34, 34,		20	12
		13, 15, 20, 24,			36, 37, 38, 39,	8	6	59
		40, 43, 45, 54			44, 49, 49, 50,		23	38
	12	03, 03, 06, 07,			51, 55	9	0	22, 25, 27, 30,
		11, 11, 17, 20,		4	27, 28, 29, 29,			35, 40, 45, 56,
		22, 25, 29			30, 30, 34, 34,			57, 57
	13	27, 29			35, 36, 37, 38,		6	15, 15
	16	27, 40, 44, 46,			39, 41, 41, 45,		7	40
		53, 57, 57, 59			52		11	00
	17	04, 05		5	00, 02, 11, 12		20	10
	19	21		7	13, 48	10	6	45
April	6	02, 03, 44, 53		11	04, 10, 16, 25,		10	40
1	7	36			28, 32, 38		13	37
	8	08		12	15		22	36
	9	29, 30, 31, 31,		13	57	11	8	13, 19, 24, 25,
		51, 51, 52, 53,		16	56			27, 28, 29, 29,
		55	5	7	06, 07, 07			31, 32, 33, 34,
	10	02, 04, 06, 10,		16	22			36, 39, 40, 41,
		23, 23 27, 46		19	42			41, 43, 43, 45,
	11	04, 19, 33, 34,	6	7	54			50, 52, 52, 53,
		38, 41, 49		23	02			54, 54, 58
	12	05, 08, 13, 15,	7	1	31, 38, 40. 41,		9	00, 05
		17, 39, 47, 47,			42, 42, 43, 43,		14	41, 42
		50			43, 44, 44, 44,		15	39
	13	07, 33			46, 47, 48, 50,	12	9	45, 46, 49, 50
	14	55			51, 51, 56		10	01, 03, 23, 27,
	23	04		2	00, 02, 02, 04,			29, 30, 32, 34,
2	0	28			06, 07, 08, 09,			37, 38, 42, 46,
	4	05			09, 11, 11. 12,			52, 54, 58, 58
	16	29, 59			17, 17, 24. 24,		11	00, 17, 19, 20,
2	20	24. 25			25, 31, 33. 35,			32
3	9	19			35, 39, 39, 40,		16	03
	12	17			41, 42, 43, 45,	13	3	23
4	3	02, 04, 05, 06,			46, 47, 47, 50,		17	41, 46, 52, 57,
		06, 07, 07, 08,			51			58, 59
		08, 09, 11, 12,		3	00, 12, 18		18	14
		13, 14, 14, 17,		4	37		21	27
		18, 19, 20, 20,		5	21	14	6	04

(*to be continued.*)

Table III. (*continued.*)

Date	hour	minute	Date	hour	minute	Date	hour	minute
1930 April			30	11	09, 14, 15, 36,	6	22	09, 46, 46, 51
14	10	19			49, 50		23	38
	18	29		12	40	7	0	06
	22	14		16	04		1	38
15	18	50		18	25, 40		4	39, 51
16	18	51	May 1	19	07		5	30
	21	50		20	02		6	41
17	0	35	3	9	43		7	49
	7	09		10	03, 27		10	45, 47
18	5	51		13	49		22	06
	6	32, 54		19	05	8	5	17, 22, 24, 26,
19	2	23		23	01			32, 33, 34, 34,
20	4	34	4	0	04, 05, 18, 22,			35, 35, 37, 40,
	6	28			27			40, 44, 45, 46,
	8	10*, 37		1	54			52, 54, 55, 56
	18	34		2	14, 22, 24		6	00, 02, 03, 05,
21	12	35		14	27, 31, 41, 43,			08, 11, 13, 14,
22	23	31			44, 46			17, 17, 18, 21,
23	12	19		17	35			24, 25, 26, 27,
24	1	30		18	19			31, 34, 34, 37,
	9	59		19	28			38, 38, 39, 39,
	11	23	5	3	14*			41, 43, 45, 46,
25	22	15		5	06*			47, 49, 49, 50,
26	9	45		7	59			51, 54, 57, 58,
	15	52		8	08			59
	20	15, 31, 31		13	55		7	02, 02, 03, 08,
27	12	49		17	06, 10			09, 14, 18, 20,
	15	06, 18	6	4	54, 56			22, 25, 31, 36,
	21	33		5†	02, 13, 25			43, 44, 48, 56,
	22	49		6†	13, 18, 29, 57			58
28	4	20		7	36		8	07, 07, 08, 11,
	5	09, 09		10	18			12, 13, 16, 20,
	16	12, 27		12	14, 14, 50			22
	18	11, 16		17	47, 59		9	05, 17, 20, 52,
	20	31		19	14, 15, 47, 58			55
29	16	13		20	03, 04, 04, 05,		10	00, 05, 09, 12
	18	28, 28			10, 14, 20, 21,		11	23
	22	39			24, 26, 29, 37		12	35, 40, 52
30	10	54		21	07		13	02, 02, 05, 06,

* Not recorded at Misaki, then Data of Kamakura were adopted.

† Time-keeping was bad.

(*to be continued.*)

Table III. (*continued.*)

Date	hour	minute	Date	hour	minute	Date	hour	minute
1930 May			9	4	52, 53, 54, 55,	9	19	19, 19, 21, 21,
8		07, 07, 08, 08,			56, 57, 57			23, 26, 28, 30,
		11, 12, 12, 14,		5	01, 03, 0,3 04,			34, 41
		14, 15, 15, 16,			05, 09, 10, 11,		20	24, 30
		17, 18, 18, 20,			13, 13, 13, 14.		21	01, 04, 55. 57
		20, 21, 23, 25,			15, 17, 18, 19,		0	15, 17, 28, 30,
		27, 28, 29, 31,			19, 20, 22, 22,			58, 58
		32, 32, 33, 34,			23, 24, 24, 26,	10	1	32, 33
		34, 37, 38, 40,			26, 27, 29, 29,		2	07
		40, 41, 42, 43,			30, 35, 35. 37,		3	21, 23. 26, 26,
		45, 47, 49, 52,			39, 42, 42, 44,			26, 27. 28, 31,
		54			44, 45, 45, 45,			32, 33, 33, 35,
	14	02, 03, 04, 05,			47, 50, 51, 55,			35, 35, 36, 37,
		06, 06, 08, 08.			55, 57, 58			38, 41, 41, 41,
		12, 19, 20, 27,		6	00, 01, 02, 04,			43, 43, 44, 45,
		38, 44			06, 09, 11, 13,			46, 47, 47, 48,
	15	31			17, 19, 22, 26,			49, 51, 52, 52,
	16	59			27, 28, 29, 29,			53, 53, 53, 54,
	17	02, 41. 47			31, 33, 34, 35,			55, 56, 56, 58,
	18	30			37			58, 59, 59
	21	34, 34		7	11		4	01, 01, 02, 03,
	22	30, 47, 48, 49,		9	00, 11, 14, 53,			06, 07, 09, 10,
		53, 55			53			11, 12. 13, 14,
	23	04, 25, 26, 48		10	00, 31, 38**			14, 15, 15, 16,
9	0	37, 40, 41, 42,		11	08, 50			18, 18, 19, 23,
		43, 50, 52		12	01, 04, 17, 18,			25, 27, 30, 30,
	1	00, 01, 04, 07,			18, 19, 34, 36,			31, 34, 42, 50,
		09, 53			36, 37. 41, 51,			59
	2	17, 27, 37			51, 53		5	01
	3	31, 41, 42, 47,		13	02, 09, 10, 13,		6	09
		49, 57			24, 26, 32, 36,		7	32, 48. 54
	4	00, 02, 02, 03,			52		8	09, 13, 16, 16,
		03, 04, 06, 08,		14	00, 59			17, 18, 19, 22,
		11, 11, 13, 14,		16	24, 37, 48			22, 30, 31, 32,
		14, 16, 18, 22,		17	08, 10, 11, 13,			42. 43, 44. 47,
		24, 25, 26, 27,			13, 15, 15, 16**			48, 53, 54, 56,
		30, 33, 35, 36,			18, 23, 30, 38			57, 58
		37, 43, 44, 44,		18	21		9	02, 02, 04, 05,
		45, 48, 51, 52,		19	03, 16. 17, 18.			06, 08, 10, 11,

** 39 earthquakes from May 9, 10 h 38 m to 17 h 16 m were due to Mr. Makino's record.

(*to be continued.*)

Table III. (*continued.*)

Date	hour	minute	Date	hour	minute	Date	hour	minute
1930 May			11	3	21, 21, 24, 25,	12	17	38
10	9	12, 13, 15, 19,			28, 30, 32, 33,		18	30, 39, 41
		20, 22, 39. 54,			33, 34, 35, 37,		21	17, 18, 21, 24.
		54			37, 37, 38, 38,			27, 32
		18, 54			39, 51, 56, 59,		23	45
	10	08, 22. 57, 58,		4	03, 10	13	0	07
	11	08, 13		7	34, 42, 43		1	06
	12	31, 42, 44. 45,		8	05. 21		2	46
	15	45, 45, 46, 47,		10	16, 20, 29, 29,		3	14, 17, 18, 21,
		47, 47, 49, 53,			44, 48			22, 26, 27, 27,
		53, 54, 55, 57		11	03, 03, 04, 05,			30, 34, 44, 44,
		08, 13, 28. 33,			10, 12, 14, 16,			45, 46, 48, 52
	16	41			16, 17, 19, 30,		4	01, 07
		24, 31, 35, 38,			31. 32, 32, 35,		7	33, 37, 39, 41,
	19	40, 41, 43, 43,			36, 43, 44			42, 43, 44, 46,
		45, 47, 50, 58,		12	47			47, 50, 55, 59
		59		14	21, 21, 22, 24		8	02, 03, 04, 05,
		00, 00, 01, 04		18	15, 39			05, 11, 12, 14,
	20	04, 05, 06, 09,		19	46 53, 55			15, 17, 29, 31,
		10, 12, 13, 15,		21	07			34, 37, 39, 40,
		15, 15, 16, 19,		22	27, 38, 40			44, 45, 46, 47,
		22, 24, 29, 35,	12	0	02, 31			49, 50, 52, 53,
		36, 36, 38, 39,		1	13, 15, 18, 19,			55, 59
		40, 44, 45, 45,			25, 26, 27, 27,		9	00, 02, 05, 08,
		46, 46, 46, 47,			29, 29, 30, 36,			09, 11, 17, 26,
		47, 48, 49, 50,			44, 54, 58			50
		50, 51, 53, 53,		2	00, 14, 17, 21,		10	05, 32
		54, 54, 56			44		11	18, 22, 37, 38,
		00, 03, 04, 04,		3	56, 57			39, 41, 50, 53,
	21	06, 44, 45, 46,		4	07, 35			53, 55, 56, 59
		55		5	46		12	03, 04, 09, 25,
	22	07, 08, 37, 37,		8	52			26, 28, 29, 33,
		38, 42. 43. 44,		9	11, 18, 18. 23,			37, 43, 48, 53,
		46, 47			28, 41			54, 55, 59
	23	05, 08, 09, 19		10	10		13	45, 48
11	0	01. 35, 37, 38,		13	46		15	28, 36, 37, 39,
		46, 47, 47		14	29			40, 40, 41. 42
	1	38		16	25, 47		16	04, 06
	3	03, 09, 10, 10,		17	01, 05, 06, 07,		20	54
		14, 14, 17, 19,			14, 19, 20, 33,		22	56

(*to be coontinued.*)

Table III. (*continued.*)

Date	hour	minute	Date	hour	minute	Date	hour	minute
1930 May			14	9	21, 22, 28, 28,	15	12	00, 55
13	23	36, 45			33, 34, 39, 58		14	15
14	1	14		10	14, 25, 26, 28,		15	58
	3	23, 24, 25			29, 47, 51, 52,		16	41, 43, 45, 45,
	4	18, 27, 28, 32.			54, 54, 55, 56			47, 47, 50, 51,
		33, 33, 34, 35,		11	01, 01, 05, 15,			59
		36, 37, 39, 41,			20, 21, 21, 22,		17	02, 03, 05, 08,
		42, 43, 46, 47,			27, 32, 34, 37,			09
		48, 48, 48, 50,			46, 46		18	47, 49, 49, 50,
		51, 53, 54, 55,		12	01, 11, 38, 51,			52, 54, 55, 56,
		57, 57			51, 52, 55, 56.			59
	5	01, 03, 03, 04,			57		19	02, 03, 05, 10,
		06, 07, 07, 08,		13	00, 01, 12, 40			13, 14, 27
		08, 10, 10, 12,		14	25, 30, 39, 40,		20	55
		13, 13, 14, 15,			41, 47, 50, 51		21	55, 59
		16, 17, 18, 18,		15	04, 19, 31, 43		22	02, 26, 28, 35,
		18, 19, 20, 21,		17	59			50
		23, 26, 28, 29,		18	05, 09, 10, 24		23	30, 35
		29, 34, 37, 42,		19	20	16	0	46
		47, 48, 49, 51,		21	42		3	01
		52, 52, 59		22	07, 09, 09, 11,		6	03, 33
	6	00, 00, 04, 06,			13, 14, 14, 15,		8	44
		08, 19, 20, 21,			18, 21, 24, 31,		10	44
		22, 31, 33, 84,			34		11	09, 10, 11, 12,
		42, 43, 48, 52,		23	44			13, 15, 16, 21,
		56	15	0	11. 45, 48, 52,			21, 26, 42
	7	01, 05, 10, 10,			52, 58, 58, 58		19	31, 34
		13, 14, 17, 24,		1	02, 02, 05, 07,		22	29, 29, 34, 47
		27, 40, 44, 45,			12, 15, 15, 16,	17	0	50
		45, 48, 48, 52			17, 18, 18, 19,		1	02, 08, 12, 13,
	8	14, 14, 15, 16,			19, 20, 22, 24,			13, 15, 18, 23,
		21, 25, 26, 27,			29, 31. 33, 45,			24, 24, 25, 25,
		29, 30, 31, 32,			49. 56, 58			26, 28, 35, 37,
		33, 34, 38, 39,		2	00, 02, 06, 58			38, 39, 44, 45,
		40, 41, 42, 43,		6	15			49, 49, 52, 53,
		45, 46, 47, 47,		10	27, 27			55, 59
		50, 51, 56		11	11, 13, 16, 17,		2	02, 05, 08, 08,
	9	02, 02, 05, 06,			19, 27, 28, 29			11, 21, 21, 22,
		08, 09, 09, 13,			29, 44, 45, 47,			25, 28, 29, 33,
		15, 17, 19, 21,			49, 51, 54, 58			43, 51, 52, 52

(*to be continued.*)

Table III. (*continued.*)

Date	hour	minute	Date	hour	minute	Date	hour	minute
1930 May			18	8	03, 05, 05, 06,	22	7	11, 19, 36, 37,
17	3	01, 03, 06, 07,			07, 08, 12, 13,			38, 39, 55
		13, 17, 32, 33,			14, 21, 22, 24,		8	11, 19*, 47
		35, 37, 42, 46			24, 26, 27, 27,		9	05, 10, 11, 12,
	4	05, 07, 10, 19,			45			13, 24, 26
		19, 33, 33, 38,		9	13, 19, 44		11	28
		39, 45, 46, 54		11	27, 45		12	00, 07, 15, 26,
	5	06, 14, 20, 24,		12	09, 13, 57			37, 45, 52
		27, 45		13	10		13	14, 30, 31
	6	20, 21, 35		14	20, 28, 30, 36,		14	22, 35
	7	30, 30, 31, 35,			44, 47, 50		15	08, 24
		53, 57		15	01, 04, 05, 06,		18	50
	8	23, 57			08, 10, 12, 14,		23	24
	9	37, 45, 49, 54,			16, 16, 16, 17,	23	2	01
		55			18, 20, 20, 21,		10	32
	10	09, 26, 34, 37			22, 25, 29, 31,		12	44
	11	24			32, 33, 34, 35,		18	02, 47
	14	27, 51			38, 39, 40, 42,	24	3	18
	16	54			45, 46, 47, 50,		5	22
	17	00			51, 52, 56		8	12
	18	43		16	04, 07, 19		9	19
	19	19, 20, 21, 25,		17	05, 16	25	2	20
		27, 29, 31, 31,	19	8	04		5	32
		34, 35, 38, 41,		10	38		15	22
		44, 48, 53		13	24	26	8	46
	20	32, 47		19	06, 07, 12, 19,		16	22, 27, 34
	23	44			44, 45, 47, 47,		19	18
18	0	17, 17, 47, 48			48, 49, 53, 54,	30	10	07
	2	56, 59			55		12	53
	3	00, 01, 01, 03,		20	00, 02, 03, 06,	31	5	48
		07, 13, 17, 19			15		6	16, 17, 37
	4	04		21	03, 14	June 1	19	10
	5	12	20	0	16	3	11	43
	6	14		1	44	14	2	41
	7	47, 47, 48, 49,		3	17		23	17
		50, 51, 51, 52,		11	52	15	6	07
		53, 53, 53, 54,		23	21, 23, 55		23	30
		54, 54, 55, 56,	21	5	53	25	13	58
		56, 57, 57, 58,	22	2	37*	26	0	10
		59		5	18, 52			
	8	00, 00, 01, 02,		6	06, 23, 31			

Table IV. Hourly frequency of the earthquakes observed at Misaki.

hour day	0~1	1~2	2~3	3~4	4~5	5~6	6~7	7~8	8~9	9~10	10~11	11~12	12~13	13~14	14~15	15~16	16~17	17~18	18~19	19~20	20~21	21~22	22~23	23~24	Total in a day
1930 Feb. 14			2																						2
15											3		1												4
16											1														1
17											2											3	8		13
18	1					1	1	1	3		6	6				1						1			21
19		1									1						1							3	6
20											2	7	14	8	3	5		1	2	1		1	1	4	49
21	1	1	5	3		1			5	5	20	5	1					2				24	5	1	79
22	2	1	1	4	1	4	9	1	9	5			3		2			1	28	7	4	3	1	1	87
23	2						1	20	6	1	4				2			2				1			39
24	1	1				4					2	1	2		1	1	18	14	7	6		2		1	61
25	1		1	2		2					5	5			1	3		1		1		1			23
26				1	2	1	2		1	2	1								1		1				12
27		1	1												1	1									4
28						1													17	11	4	3	6		42
March 1				1		2		1	1						3	2					5	52	50	26	143
2	22	1	4		1		2	1	1		1	1	2	2				1	2		1	1			43
3		2	2	2						1		1		2	4			2			6	60	30	20	132
4	12	13	10	7	6	20	6	2	1			1			1							1	1	62	143
5	23	15	1			2	1		1		1	1											1	1	47
6	74	36	14	3	1		1	3	1		1	1											1	47	183
7	40	36	2	2			1	2					1	10	7					2		1			104
8		3		1		2			6	1									1	10	54	35	19	29	161
9	13	12		7	29	10	1	5	4	4	4	1		1	1	4	18	38	20	24	2	2	1	2	203
10						1	14	7	3	29	10	3			4	3	1	1		2	2	6	19	17	122
11	10	25	9	3	2			1	1	1	6	33	10	23	10	10	1	3	1	2			3	23	177
12	3	7	18	2	1		1		1	2	2		4	12	4	4		2	1	16	10	14	12	23	139
13	25	28	25	13	13	6	4			2						1				1					118
14	1	1		3							5	44	8	2	5	1	1				27	4	7		109
15	1		2	1	13	3				3						1			27	1					52
16	3	6	5	1		1						28	7		1	3									55
17		30	51	13	1														10	22	3			2	132
18			22	22		2	7	16	6		2							1						1	79
19							1	45	38	1	2	2				1	1	18	2		1			3	115
20			3		1		1	1	1	3	36	9				1	1				1	3	1		62
21						11	1	19	16	2								1			3			1	54

(*to be continued.*)

Table IV. (*continued.*)

hour / day	0~1	1~2	2~3	3~4	4~5	5~6	6~7	7~8	8~9	9~10	10~11	11~12	12~13	13~14	14~15	15~16	16~17	17~18	18~19	19~20	20~21	21~22	22~23	23~0	Total in a day
1930 March 22	1	5	1					2	1							25	35	23	45	20	9	1	1		169
23	1			4	1				1	1	2	9	19	2					1	1					42
24			1	2		7	5	10	1			5	29	12	24	33	7	3	3		1				143
25	1							2	1							4				1	12	35	28	21	105
26	1	9	3	2	3				2					1	28	24	13		4	11	4	4			109
27	3	3	1	2		1							1			1									12
28											1														1
29		12	18	24	14	10		1	1							1		1	1				41	62	186
30	31	6	10	3	1	5	33	22	1					1	3			1							117
31					1					7	31	12	11	2			8	2		1					75
April 1							4	1	1	9	8	7	9	2	1									1	43
2	1				1												2				2				6
3										1			1												2
4				42	17	4		2				7	1	1			1								75
5								1								1				1					3
6								1																1	2
7		19	33	3	1	1		2	1												1				61
8							1																	1	2
9	10						2	1				1									1				15
10							1				1			1									1		4
11									27	2					2	1									32
12										4	16	5					1								26
13				1														6	1			1			9
14							1				1								1				1		4
15																			1						1
16																						1			2
17	1							1																	2
18						1	2																		3
19			1																						1
20					1		1		2										1						5
21													1												1
22																								1	1
23													1												1
24		1								1		1													3
25																							1		1
26										1						1					3				5
27													1			2						1	1		5

(*to be continued.*)

Table IV. (*continued.*)

hour / day	0~1	1~2	2~3	3~4	4~5	5~6	6~7	7~8	8~9	9~10	10~11	11~12	12~13	13~14	14~15	15~16	16~17	17~18	18~19	19~20	20~21	21~22	22~23	23~0	Total in a day
1930 April 28					1	2											2		2		1				8
29																	1		2				1		4
30											1	6	1				1		2						11
May 1																				1	1				2
2																									0
3										1	2			1						1				1	6
	5	1	3												6			1	1	1					18
5				1		1		1	1					1				2							7
6					2	3	4	1			1		3					2		4	12	1	4	1	38
7	1	1			2	1	1	1			2												1		10
8						20	37	17	9	5	4	1	3	45	14	1	1	3	1			2	6	4	173
9	7	6	3	6	39	47	21	1		5	3	2	14	9	2		3	12	1	14	2	4			201
10	6	2	1	43	29	1	1	3	22	17	2	4	2			16	5			13	43	9	10	4	233
11	7	1		28	2			3	2		6	19	1		4				2	3		1	3		82
12	2	15	5	2	2	1			1	6	1			1	1		2	9	3			6		1	58
13	1	1	1	16	2			12	26	9	2	12	15	2		8	2				1		1	2	113
14		1		3	26	39	17	16	27	20	12	14	9	4	8	4		1	4	1		1	13	1	221
15	8	23	4				1				2	16	2		1	1	9	5	9	7	1	2	5	2	98
16	1			1			2		1		1	16								2			4		28
17	1	26	16	12	12	6	3	6	2	5	4	1			2		1	1	1	15	2			1	117
18	4		2	8	1	1	1	21	21	3		2	3	1	7	35	3	2							115
19									1		1			1						13	5	2			23
20	1	1		1								1												3	7
21						1																			1
22			1			2	3	7	3	7		1	7	3	2	2			1					1	40
23			1								1		1						2						5
24				1		1			1	1															4
25			1			1										1									3
26									1								3			1					5
27																									0
28																									0
29																									0
30											1		1												2
31						1	3																		4
Total	329	353	284	296	229	231	198	260	262	167	223	291	189	150	155	203	142	162	209	217	225	289	288	375	5727

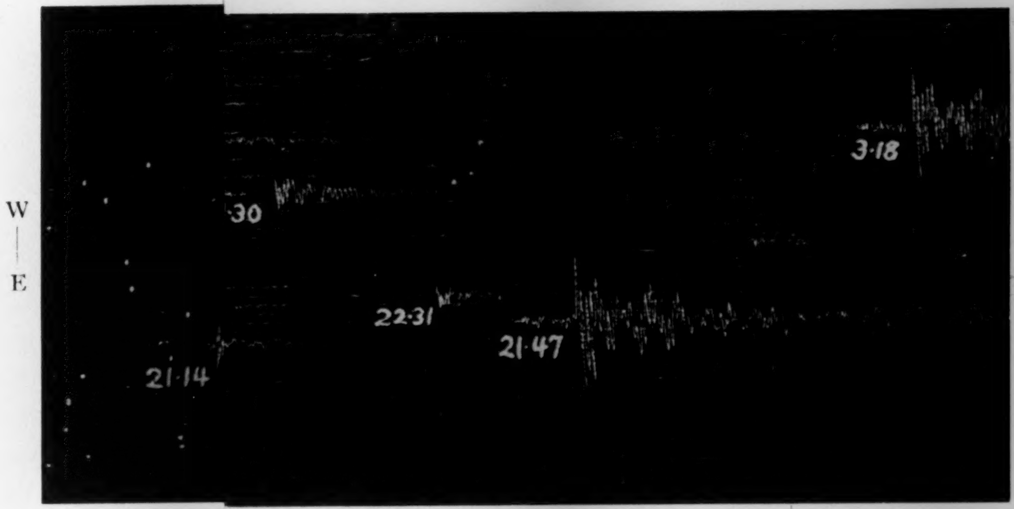

(Full size the actual.)

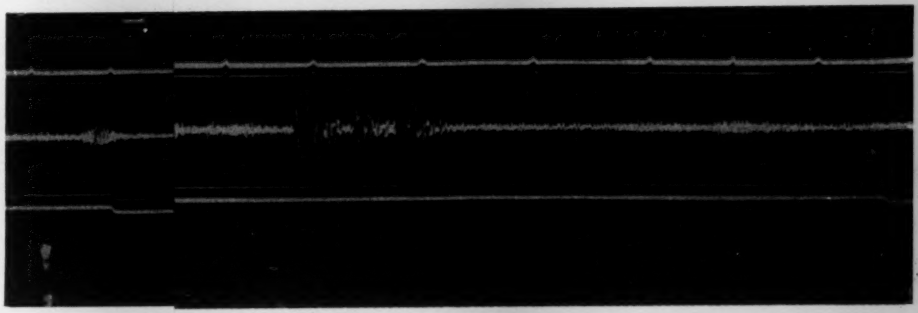

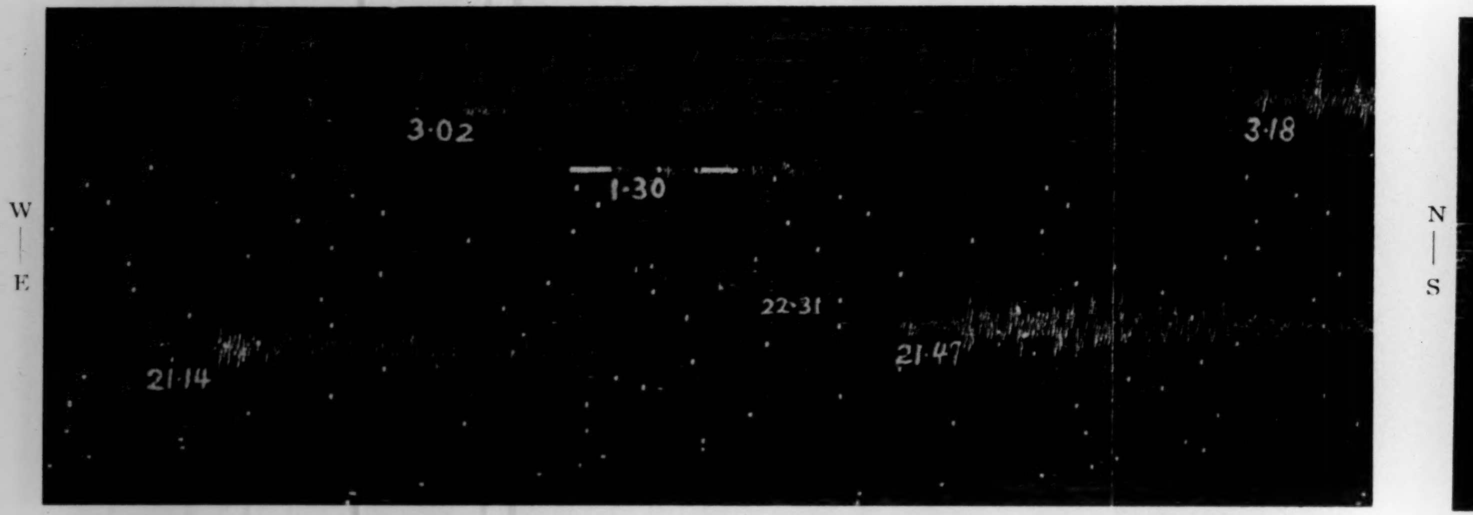

Fig. 5. Parts of seiomogram at Misak

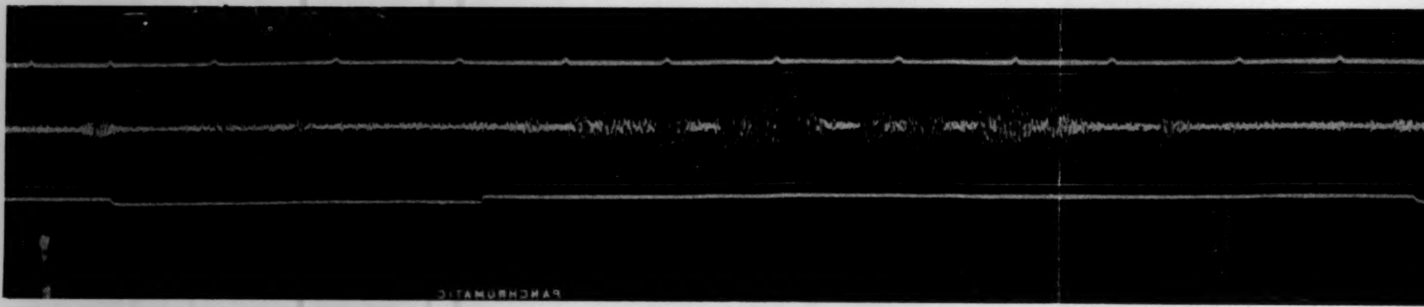

Fig. 15. Part of oscillogram of

（震研彙報 第十五號 圖版 岸上）

[F. KISHINOUYE.]

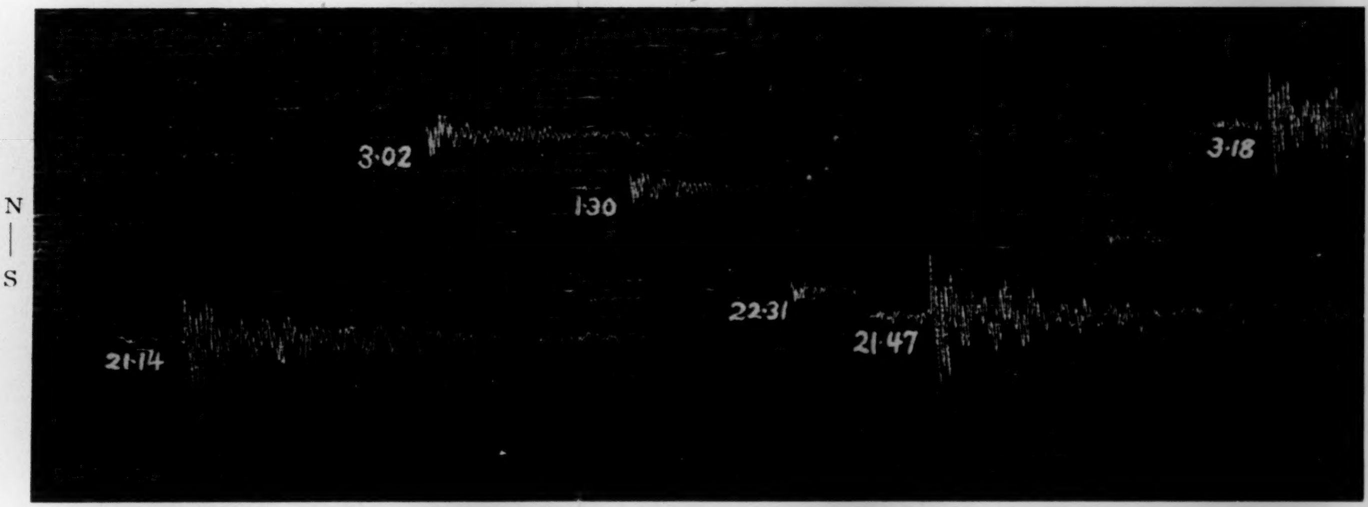

Misaki. March 11~12, 1930.

(Full size the actual.)

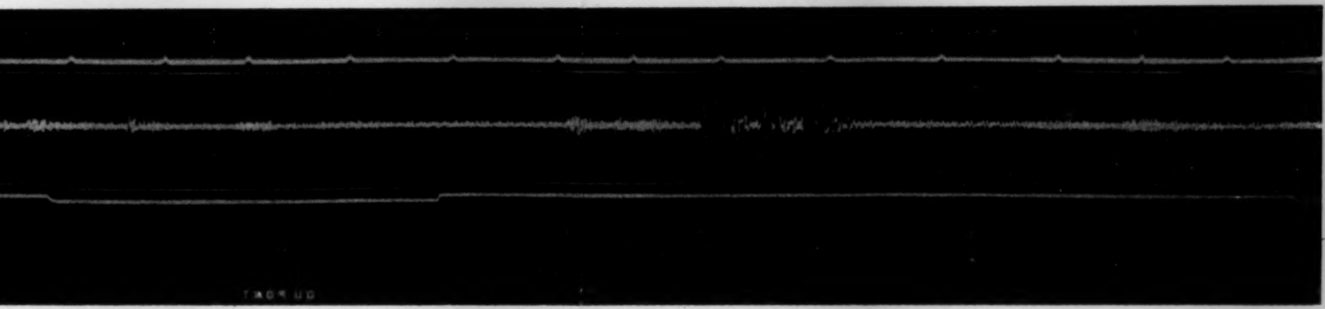

n of fracture experiment.

49. 昭和5年伊東地震群の頻度分布

地震學教室 岸上冬彦

伊東地震群の活動の消長を調べる爲に三崎臨海實驗所内に据付けられてあつた大森・今村式簡單微動計の記象に表はれた伊東地震の發震時を分の桁まで讀みとつて第 3〜4 表を作つた．又其等の地震は各〻記象型が殆ど一定してゐたので南北動のS波の第1動の全振幅の自乘を以て其の地震の勢力を表はすものと假定して，一日毎に各地震の全振幅の自乘の和を求めて第4圖に示した．此は大體に於て毎日の地震頻度を示す第2圖に似てゐるから，強い地震の起つた時は地震の數が多かつたことが判る．或は此から地震の數の多い時は強い地震が起ると云へるかも知れない．又小さな地震は數は多いが地震活動の勢力の變化としては問題にならぬとも考へられる．

次に此の地震は干潮の時に多く起るといはれてゐるので，先づ 25 時間と 12·5 時間との週期を2月 28 日から29日間と3月 28 日から 29 日間とについて調べた．其の結果は前の期間の 25 時間週期の存在することは確率が大きいが，後の期間の 25 時間も兩期間の 12·5 時間週期も偶然の頻度分布としか考へられない．更に兩期間を位相差を考慮して組合はせると，25 時間週期も偶然なことと考へる他は出來なくなつた．若し湖汐と直接關係があれば 12·5 時間週期の方が確率は大きい筈であるのに問題にならぬ程小さいのであるから，湖汐と地震との關係は無かつたと考ふべきであらう．

從來地震群の調査に屢々見出されたことのある 24 時間週期も調べたが，此も確率は小さく，結局此の地震群については1日週期に關しては偶然に起つたこととしか云へない．

地震の頻度分布の期間を 20 分に短くしても分布の型は大體一定してゐて，地震群型，餘震型等3〜4の型に分けられる．地震は地殼の一部の破壞によつて生ずると考へて，此等の頻度分布を說明する爲に木の薄板を曲げて折つてその時に生ずる小振動をオシログラフで記錄して見た．其等の振動の 5 秒間毎の頻度分布を第 16 圖に示した．此と伊東地震群の場合と比べると似てゐる樣に思はれる．

餘震の頻度分布を時に關する函數として表はす數學式は大森·鹽治·日下部の諸氏によつて研究されたが，地震群の場合にも適する樣な式を求めた．大森博士等は地震を起すべき地殼内の歪の大さが地震の數に比例するものと考へ，又歪の減少する割合が地震の頻度に比例するといふ2つの假定から頻度が指數函數によつて減少するといふことを求められた．筆者は地震群の場合には其等の震原が比較的狹い區域に限られてゐるので，その中では地震が起る毎に其の時迄に起つた總數に比例して地震を起すべき區域が減つて行くと考へて (3) 式を假定した．其の樣に考へられば頻度の時に關する式は強い制振器を持つた地震計の運動を示すものと同樣になる．そこで地震群の頻度分布曲線は無週期性の振動曲線と見做され，餘震分布も地震群の特別な場合と考へられ，今求めた式の一つの場合として說明が出來る．

50. 丸の内に於ける表面土と基盤岩との彈性係數測定

地震研究所 飯田汲事

（昭和12年6月15日發表——昭和12年6月21日受理）

緒言

表面層が地震動によつて振動する問題や地震波傳播に關係せる問題等は，地震學上に於て許りでなく，最近土木建築工學上に於ても重要となつて來たので，多くの學者の注意を惹き，或ひは理論的[1]に取扱はれ或ひは實驗的[2]に觀測されてゐる．而して表面層中に於ける振動の卓越周期の存在が明かにされ，地震動中には表面層の性質が多分に含まれてゐる事が判明するやうになつた．

斯くの如く地震動の性質を闡明するに當つては先づ表面層を形成する物質の彈性の研究が重要であるとの見解から，已に前論文[3]に於ては表面土の彈性を研究し報告した次第である．今回の論文は前回の續研究とも見るべきもので，此處に述べた如き表面層の振動問題を取扱ふ場合には，表面層を形成する物質の彈性のみならず，其の表面層下の物質の彈性も必要となる．本研究に於ては特に下層の物質の彈性を取扱つたので，其の結果を報告する次第である．

地動或ひは地震初動入射角等の觀測[4]から地表附近に於ける彈性波の中縱波の速度を求めたのは二三あるが，表面層及び其の下の層の彈性係數の總てに就いて測定した

---

1) 妹澤克惟　地震研究所彙報　8 (1930), 1—11.
妹澤克惟・金井清　地震研究所彙報　13 (1935), 251—265.
妹澤克惟・金井清　同　上 15 (1937), 377—384.
西村源六郎・高山威雄　地震研究所彙報　15 (1937), 394—440.

2) 齊田時太郎・鈴木正治　地震研究所彙報 12 (1934), 517—526.
石本巳四雄　地震研究所彙報 10 (1932), 171; 12 (1934), 234; 13 (1935), 592; 14 (1936), 240.
井上宇胤　地震研究所彙報 12 (1934), 712—740.
那須信治　同　上 9 (1931), 454.

3) 石本巳四雄・飯田汲事　地震研究所彙報 14 (1936), 632—657; 15 (1937), 67—86.

4) 那須信治　地震 1 (1929), 355—364.
鈴木武夫　地震 4 (1932), 479—496; 8 (1936); 72—83.
波江野清藏　日本天文地球物理學輯報 8 (1931), 39—50.

ものは極めて尠ないやうである．最近彈性波探査法によつて求められるやうになつたが[5]，横波の觀測に就いては尙考究の餘地がないでもない．

筆者は丸の内に於て自然狀態のまゝの基盤岩を採取する機會を得る事が出來たので，其の彈性係數を測定し併せて表面土の彈性係數と比較して見た．此處に基盤岩と名づけてあるのは，表面土の如き軟弱な冲積層土が乘つてゐる層の物質を指示したのであつて，表面土とは明確に區別され表面土の所謂基盤をなしてゐる洪積層を形成してゐる硬い砂質粘土の意である．

基盤岩に就て

試驗物體採取場所の位置は丸の内第一生命保險相互會社本館建築敷地（舊警視廳所在地）にして第1圖に於て示す如きA，Bなる2箇所であつて，此の附近に於ては齋田學士鈴木正治氏[6] が嘗て地震動加速度を觀測した．

試驗土及び試驗基盤岩は第2圖に示せる如く，夫々表面下約 8 m 及び約 20·5 m の所より採取せるものである．表面土の機械的分析の結果に就いては已に示した[7]如く沈泥質粘土で可なり軟弱なものであるが，基盤岩は砂質粘土であつて，復興局の所謂第三紀層或ひは東京層の上端部に屬して居り可なり堅牢な物質である．採取箇所附近の地質の略圖は第2圖に示したが，表面層の構造の大略の値を示せば約 3 m 程の煉瓦屑，コンクリート基礎割，粘土などの混合せる表土層，約 14 m の青灰色或ひは暗灰色等の粘土層，約 1·5 m の砂交りの粘土層及び約 1·5 m の砂利層等である．其の下は砂質粘土の所謂基盤岩層である．此の基盤の表面には波紋狀の凹凸があり，更に蟹孔狀の穴が無數にあいてゐる部分もある．基盤岩層のすぐ上部には地下水を含んだ砂利層があるために，基盤岩層の上部は水に浸つて居る．又基盤岩層上部は層狀構造をなして居り，その層と層との境からよく割れる性質がある．從つて大きな試驗體を害さぬ樣に採掘しやうとすると仲々困難であるが，幸ひ石工により厚さ約 25 cm 面積約 60 cm×40 cm の基盤岩を採掘し得る事が出來た．

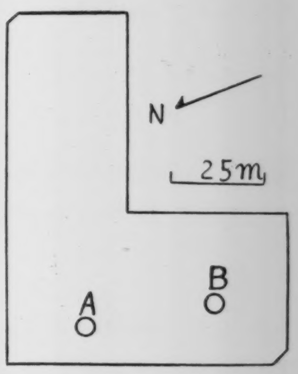

第 1 圖　丸ノ内第一生命相互會社建築敷地内に於ける基盤岩及び表面土採取箇所を示せる略圖

Fig. 1. Diagram showing the places that the specimens are collected.

---

5)　那須信治・萩原尊禮・表俊一郎　地震研究所彙報 **14** (1936)，560—581；**15** (1937)，87—89.

6)　齊田時太郎・鈴木正治　前揭

7)　石本巳四雄・飯田汲事　地震研究所彙報 **14** (1936)，632—657.

扨て試驗物體は上述の基盤岩より鋸を用ひて切りとるのである．此の場合蟹孔のない而も相當均一な層の部分から試驗基盤岩柱を切り取らなければならない關係上，上述の寸法の基盤岩からは高さ 30 cm, 直徑 5 cm の試驗柱を漸く 5，6 本得る事が出來たに過ぎない．從つて試驗柱は相當均一なものであると思はれる．試驗物體は常に水中に保存し實驗のときのみ取り出したのである．然らざれば水分がなくなり乾燥し，基盤岩を形成してゐる砂粒が崩れ落ち自然狀態のものと異つて來るからである．採取當時の含水量を求めると

Aなる場所：　含水率 25·0%

Bなる場所：　　〃　 24·0%

であり，約8ヶ月後水中より取り出して測定した値は夫々 25·5%，24·4% 等にしてその增加は測定の誤差の範圍に入るやうな小さな値を示し，從つて增加してゐないとも云へよう．斯くの如き事實から判斷すれば自然狀態に於ても水は殆ど飽和の狀態にあるものと推察される．

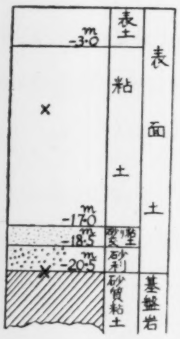

第 2 圖　採取箇所附近に於ける地質及び深度
×印 採取箇所

Fig. 2. Sectional view of the upper superficial layer and the subjacent layer. Mark ×: places that the specimens are collected.

又水分を全部蒸發させ，而して空中及び水中に於て夫々其の重量を測定し，結局基盤岩の眞の比重を求めれば第 I 表の如くになる．第 I 表には此の比重及び見掛けの比重から計算した間隙率の値も同時に揭げてある．第 I 表の如く，採取場所 A 及び B に於ては，其の間隙率及び比重には多小の差異はあるが殆ど同樣な値を示してゐる．

第 I 表　基盤岩の比重及び間隙率

採取場所	比重	間隙率(%)
A	2·74	47·7
B	2·76	47·1

實驗方法及び結果

實驗方法は已に示した方法[8]と全く同樣である．即ち每秒 0〜700 の範圍に連續的に振動數の變化し得る 2 箇の振動盤，一方は縱振動一方は振振動をなすが，其れ等を採用し，而して最初一方に次に他方の上に試驗する基盤岩柱を乘せ，各々其の共鳴する振動數を求めて結局試驗柱に於ける縱波及び橫波の速度を測定したのである．

---

8) 石本巳四雄・飯田汲事　前揭 3)

實驗によつて得られた試驗基盤岩柱の振動曲線の一例を圖示したのが第3圖である．圖の縱軸は振動振幅を，横軸は振動數の變化を示してゐる．第3圖の（a）は縱振動によつて得られたものであり，（b）は捩振動によつて得られたものである．何れの場合にも或る周期に於て，勿論其の周期を異にしてゐるが，振動振幅が最大となつてゐる．振動周期は振動曲線の下に示した1分間の回轉數から計算出來る．振動振幅の最大となる時の振動周期は共鳴周期であるが，此の共鳴周期を縱軸に，試驗基盤岩柱の高さを横軸にとつて圖示すれば第4圖の如くになる．第4圖中（a）は捩振動に就いて求めたものであり，（b）は縱振動に就いて求めたものである．

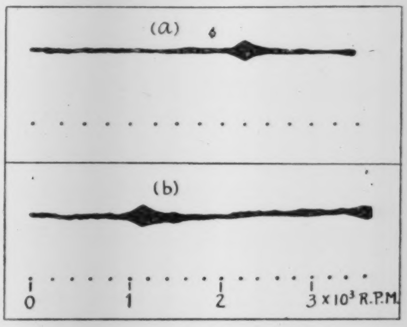

第 3 圖 基盤岩柱（$\rho=1.91$，含水率 $=25.0\%$ $h=28$cm）振動に於ける共鳴曲線圖
（a）縱振動 （b）捩振動

Fig. 3. Resonance curves of the base-rock column.
(a) Longitudinal vibration.
(b) Torsional vibration.
Ordinate: vibration amplitude.
Abscissa: vibration frequency.

今縱振動及び捩振動に於ける共鳴周期を夫々 T_l，T_t とすれば，T_l，T_t は

$$\left.\begin{aligned} T_l &= \frac{4h}{\sqrt{\dfrac{E}{\rho}-\dfrac{\pi^2\gamma_l^2}{16\rho^2h^2}}} \\ T_t &= \frac{4h}{\sqrt{\dfrac{\mu}{\rho}-\dfrac{\pi^2\gamma_t^2}{16\rho^2h^2}}} \end{aligned}\right\} \qquad (1)$$

にて與へられる．玆に h は試驗柱の高さ，ρ は密度，E はヤングの彈性率，μ は剛性率，γ_l は縱振動によつて得られる固體粘性係數，γ_t は捩振動によつて得られる固體粘性係數である．又 T_l，T_t は夫々約 1% の誤差の範圍内で求められる．第3圖の如き關係から試驗體中に於ける縱波の速度或ひは横波の速度を求めるには原點から此の曲線に漸近線を引き，その直線の傾きから求めるのであつて，此の漸近線は（1）の關係によつて

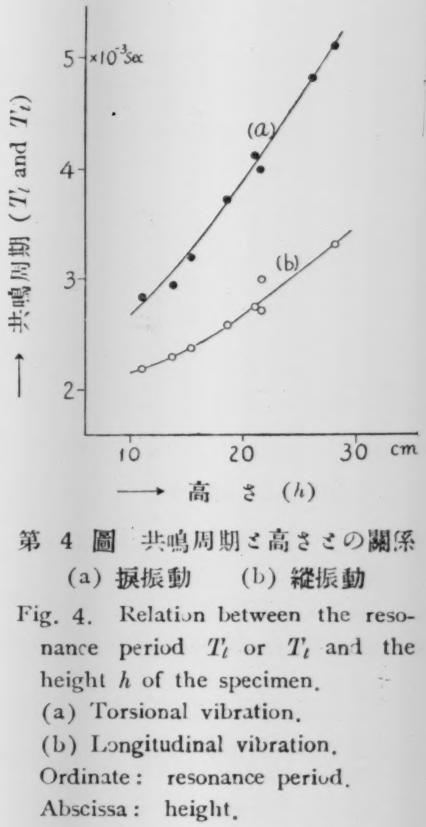

第 4 圖 共鳴周期と高さとの關係
（a）捩振動 （b）縱振動

Fig. 4. Relation between the resonance period T_l or T_t and the height h of the specimen.
(a) Torsional vibration.
(b) Longitudinal vibration.
Ordinate: resonance period.
Abscissa: height.

$$\left.\begin{aligned} T_l &= \frac{4h}{\sqrt{\dfrac{E}{\rho}}} = \frac{4h}{V_l} \\ T_t &= \frac{4h}{\sqrt{\dfrac{\mu}{\rho}}} = \frac{4h}{V_t} \end{aligned}\right\} \qquad (2)$$

で與へられる．玆に V_l，V_t は夫々縦波及び横波の速度である．斯様にして V_l，V_t を測定し，次に

$$\left.\begin{aligned} E &= \rho V_l^2 \\ \mu &= \rho V_t^2 \end{aligned}\right\} \qquad (3)$$

なる關係によつてヤングの彈性率 E 及び剛性率 μ を求める．V_l, V_t，從つて E，μ が求められれば，ポアソン比 σ は

$$\sigma = \frac{1}{2}\left\{\left(\frac{V_l}{V_t}\right)^2 - 2\right\} \quad \text{或ひは} \quad \frac{1}{2}\left\{\frac{E}{\mu} - 2\right\} \qquad (4)$$

なる關係から求められる．斯様にして求めた値を示せば第 II 表の如くになる．

第 II 表　基盤岩の彈性係數

採取場所	密度 ρ	試驗體中の縦波の速度 V_l (m/sec)	試驗體中の横波の速度 V_t (m/sec)	ヤング率 E(C.G.S.)	剛性率 μ(C.G.S.)	ポアソン比 σ	含水率 (%)
A	1·91	380	234	$2{\cdot}76\times10^9$	$1{\cdot}05\times10^9$	0·32	25·0
	1·89	359	220	$2{\cdot}44\times10^9$	$9{\cdot}15\times10^8$	0·33	25·4
B	1·92	404	250	$3{\cdot}13\times10^9$	$1{\cdot}20\times10^9$	0·31	24·0

第 II 表に於ける密度は試驗體の數箇所より切り取れる約 5 cm 立方の立方體の重量及び體積を測定し，それより求めたものの平均の値である．體積の測定には物指にて縦，横，高さを量り，それより求める方法及び水銀を充した壺の中に供試體を押し込み，供試體の體積により流出した水銀の重量を測定し，此の時の溫度に相當する水銀の密度を用ひて供試體の體積を求める方法等を同時に採用して行つた．第 II 表に於ける如く，採取場所 A，B に於て總ての値は多小異つて居り，B の方は A の方に比して稍々大なる値を示してゐる．又 A に 2 種類示してあるのは，採取せる基盤岩に於て極端に異ふと思はれる 2 部分から試驗柱を製作して實驗したからである．此の兩者に於ては彈性の諸係數の値が異つて居るが，小なる値の方は基盤岩層の最上部に屬してゐるものである．

又第 II 表に於ける V_l，V_t の値の測定誤差を求めるために，第 4 圖に於て示した T_l，T_t 等の値を (1) 式に代入し，最小自乘法によつて V_l，V_t（或ひは γ_l，γ_t）等の値を求めた結果第 II 表の値と殆ど一致し，その公算誤差は 2% 程度のものとなつた．從つて上表に於ける測定値には周期に於て 1%，速度に於て 2% 程度の誤差が存在してゐる次第である．

次に基盤岩層が同質等方性の物質から成立してゐると考へ，其の層中に於ける縦波，横波の彈性波傳播速度 V_p，V_s を

$$\left.\begin{aligned} V_p&=\sqrt{\frac{\lambda+2\mu}{\rho}}=\sqrt{\frac{E}{\rho}\frac{1-\sigma}{(1+\sigma)(1-2\sigma)}}=\sqrt{\frac{3}{\rho\beta}\frac{3+E\beta}{9-E\beta}}\\ V_s&=\sqrt{\frac{\mu}{\rho}}=\sqrt{\frac{E}{\rho}\frac{1}{2(1+\sigma)}}=\sqrt{\frac{E}{\rho}\frac{3}{9-E\beta}} \end{aligned}\right\}\qquad(5)$$

なる式から求め，更に β なる壓縮率或ひは體積彈性率 k を

$$\beta=\frac{3(1-2\sigma)}{E}=\frac{1}{k}\qquad(6)$$

なる式から求めれば第 III 表の如くになり，彈性率及び體積彈性率等は 10^9 (C.G.S.) の程度であつて，普通の硬い岩石に比しては可なりに小なる値を示してゐる．

第 III 表　基盤岩層中の彈性波傳播速度

採取場所	V_p (m/sec)	V_s (m/sec)	壓縮率 β (C.G.S.)	體積彈性率 k (C.G.S.)	固體粘性係數	
					γ_l (C.G.S.)	γ_t (C.G.S.)
A	455	234	$3{\cdot}92\times10^{-10}$	$2{\cdot}55\times10^{9}$	$9{\cdot}11\times10^{5}$	$4{\cdot}99\times10^{5}$
	438	220	$4{\cdot}18\times10^{-10}$	$2{\cdot}39\times10^{9}$	$8{\cdot}50\times10^{5}$	$4{\cdot}81\times10^{5}$
B	476	250	$3{\cdot}64\times10^{-10}$	$2{\cdot}75\times10^{9}$	$9{\cdot}98\times10^{5}$	$5{\cdot}03\times10^{5}$

又第 III 表には固體粘性係數 γ_l，γ_t が示してあるが，此等は第 II 表の V_l，V_t の値を (1) 式に代入して求めた値と最小自乘法によつて求めた値との平均の値である．

次に表面土の彈性係數に就いて述べるが，此等の彈性係數に就いては已に研究し報告[9] した次第である．然しながら比較のために再び掲げる事とし，更に前回求めてなかつた表面層中に於ける縦波，横波等の彈性波傳播速度及び壓縮率，體積彈性率等の値をも併せて第 IV 表に示す事にする．此等の値は先に求めたと同樣な假定の下に (5) 式及び (6) 式から計算したものである．第 IV 表に示してある表面土の彈性の

---

[9] 石本巳四雄・飯田汲事　前掲．

第 IV 表 表面土の彈性係數及び彈性波傳播速度

密度 ρ	縱波の速度 V_p (m/sec)	橫波の速度 V_s (m/sec)	ポアソン比 σ	ヤング率 E(C.G.S.)	剛性率 μ(C.G.S.)	壓縮率 β(C.G.S.)	體積彈性率 k (C.G.S.)	含水率 (%)
1·46	121	36·4	0·45	$5{\cdot}61\times10^{7}$	$1{\cdot}93\times10^{7}$	$5{\cdot}35\times10^{-9}$	$1{\cdot}87\times10^{8}$	50·0
1·50	165	58	0·43	$1{\cdot}44\times10^{8}$	$5{\cdot}03\times10^{7}$	$2{\cdot}95\times10^{-9}$	$3{\cdot}39\times10^{8}$	48·7
1·56	214	103	0·35	$4{\cdot}45\times10^{8}$	$1{\cdot}65\times10^{8}$	$2{\cdot}02\times10^{-9}$	$4{\cdot}95\times10^{8}$	42·6
1·56	257	138	0·30	$7{\cdot}69\times10^{8}$	$2{\cdot}97\times10^{8}$	$1{\cdot}56\times10^{-9}$	$6{\cdot}41\times10^{8}$	39·4
1·56	277	160	0·25	$1{\cdot}00\times10^{9}$	$3{\cdot}99\times10^{8}$	$1{\cdot}50\times10^{-9}$	$6{\cdot}67\times10^{8}$	37·6
1·59	381	237	0·19	$2{\cdot}11\times10^{9}$	$8{\cdot}93\times10^{8}$	$8{\cdot}82\times10^{-10}$	$1{\cdot}13\times10^{9}$	31·8

諸係數は種々なる含水率の値に對して求めてあるが，此等は次の如くにして求めたものである．卽ち高さ 25 cm，斷面積 25 cm×25 cm の大さの略々均一な土から，直徑約 4 cm 長さ 25 cm の試驗土柱を多數製作し，始めの含水率は 50% であるが此等を順次に乾燥させ，而して其の乾燥の程度を異にせしめ含水率を變へた次第である．斯樣にして色々異つた含水量を有する同一試驗土の多數の配列を始めに作り，此等に就いて實驗をしたのであつて，例へばある土柱を或る含水率に於て試驗し，次に此の土柱を或る程度迄乾かし更に實驗に用ひ，斯樣な操作を何回も繰返へして實驗すると云ふやうな方法を採用しなかつたのである．それは同一試驗土を何回も使用する事は長い間振動を與へる事と同一結果になり，土の狀態が異つたものとなる恐れをさけた爲である．第 IV 表より知られる如く，試驗土の種類は同一であつても含水量によつてその彈性波の傳播速度或ひは彈性係數が異つてゐる．又表には示さなかつたが固體粘性係數は $10^4\sim10^6$ (C.G.S.) 程度である事は已に報告してある通りである．又壓縮率は 10^{-9} (C.G.S.) 程度のものである事が判つた．

結果に對する考察及び結語

上述の如くにして表面土及び基盤岩の彈性の諸係數を夫々測定し得た次第である．今兩者の彈性係數の比較をして見る事とする．勿論表面土の彈性係數はその含水量によつて異つてゐるから，その變化範圍を示す事とすれば

$$\frac{\rho'}{\rho}\fallingdotseq\frac{1}{1{\cdot}24}=0{\cdot}81$$

$$\frac{E'}{E}\fallingdotseq\frac{1}{43}\sim\frac{1}{1{\cdot}6}\ ;\quad \frac{\mu'}{\mu}\fallingdotseq\frac{1}{47}\sim\frac{1}{1{\cdot}3}$$

$$\frac{V'_p}{V_p}\fallingdotseq\frac{1}{3{\cdot}6}\sim\frac{1}{1{\cdot}2}\ ;\quad \frac{V'_s}{V_s}\fallingdotseq\frac{1}{6}\sim\frac{1}{1{\cdot}1}$$

$$\frac{V'_p}{V'_s} \doteqdot 3{\cdot}3 \sim 1{\cdot}6\,; \quad \frac{V_p}{V_s} \doteqdot 1{\cdot}99 \sim 1{\cdot}91\,.$$

となる．此處に ρ'，E'，μ'，V'_p，V'_s 等は表面土のものを表はし，ρ，E，μ，V_p，V_s 等は基盤岩のものを表はしてゐる．又基盤岩の固體粘性係數は表面土のそれより 1 桁高く $10^5 \sim 10^6$ (C.G.S.) の程度であり，基盤岩の壓縮率は表面土のそれより 1 桁低く 10^{-10}(C.G.S.) の程度である．

上表に於て見る如く，彈性の諸係數の比の變化範圍が可なり大であるが，表面土の實驗に於ては含水率 40% 位迄の値は實際のものに近いと思はれる．含水率 40% 以下のものに對しては試驗土は硬くしまる結果實際のものとは異つたもののやうに思はれる點もあつた．從つてその測定値に多小の誤差があらうと考へられる．又表面土の採取當時の含水率が 50% であつたが，此れを實際の表面層のものに應用する場合には，表面層の上部と地表下 20 m 附近のものとでは可なり含水率や緻密度も異つて居ると考へられるから，表面層全體としては實驗に於ける含水率 40% 程度の彈性係數，卽ちヤング率 $6{\cdot}8 \times 10^8$ (C.G.S.)，剛性率 $2{\cdot}6 \times 10^8$ (C.G.S.) 程度であり，縱波，横波の速度として夫々 250 m/sec，130 m/sec 程度の値を採用すればよいのではなからうかと思はれる．從つて上述の兩者の彈性係數比等も其の變化範圍の平均値を採用すれば，それは表面層と其の下の層との彈性係數比を表はして居ると見る事が出來よう．又此等彈性率の比の變化範圍は工學的に求められた地耐力の比の變化範圍に大體一致してゐる．勿論地表下に於ては壓力等の影響も考へられ，此等のために實際のものは實驗によつて求められたものとは多小異つてゐるであらうが，その値の程度にはそれ程の差があるものとは思はれない．

齋田學士，鈴木氏の兩氏[10] が嘗て丸の內の地表上と地下約 20·5 m の基盤岩上とに於て地震動加速度を觀測し，各場所に於ける卓越周期等を決定されたが，妹澤博士[11] は此の結果を調査して，地表の振幅の大きくなつてゐる所は地下の振幅の大きくなつてゐる所の 3 倍乃至 4 倍である事を指摘され，而して地表の大振幅は同時性の場合に現はれた變位とし，地下の大振幅は他の周期の場合の變位であると假定し，密度一定なる場合に於ける地表層の彈性が地下のそれの 1/9 乃至 1/16 位であるとせられてゐる． 又此の場合地表層中での固體波の速度は下層中に於ける速度の 1/3 乃至 1/4 位である事を必要とし，各層を通じての或る固體波の速度は 200 m/sec 及び 600 ～800 m/sec であらうとせられてゐる． 此の結果と筆者の測定した値とは完全に一致

---

[10] 齊田時太郎・鈴木正治　前揭.

[11] 妹澤克惟・金井淸　前揭.

しない．尤も妹澤博士の得られた上述の値には色々な假定がなされてゐるし，筆者のは直接に實驗によつて得られたものであるから比較すべき性質のものではないかも知れないが，大體の傾向は一致してゐるとも云へよう．此等の點に關しては今後の研究に待つ事にし，此所には唯實驗の結果のみを述べた積りである．要するに實驗結果では基盤岩層の中の縱波及び横波の傳播速度は平均の値として 450 m/sec 及び 235 m/sec 程度のものとなつたのである．

筆を擱くにあたり表面下 20 m 餘の深所から，龜裂し易く採掘困難な基盤岩を害さぬやうに取り出す事を心よく引き受けて下さつた第一生命保險相互會社の名古屋德次學士並びに深礎工業社々長木田保造氏の兩氏に對し深甚の謝意を表する．又彈性係數測定實驗に際し御激勵を賜つた石本先生に厚く感謝の意を表する次第である．

50. *Determination of the Elastic Constants of Superficial Soil and Base-rock at Maru-no-uti, Tôkyô.*

By Kumizi IIDA,

Earthquake Research Institute.

1) The elastic constants of soil in the upper superficial layer and base-rock in the subjacent medium at Maru-no-uti, Tôkyô, were investigated. The superficial soil and base-rock were obtained in their natural state from depths of about 8 m and 20·5 m respectively from the ground surface by means of borings.

2) The transverse wave-velocities as well as the longitudinal wave-velocities in the superficial layer and the subjacent medium were obtained by means of the vibration methods shown in our previous papers12), after which their moduli of rigidity, Young's moduli, Poisson's ratios, bulk moduli, cubic compressibilities and solid viscosity coefficients were computed.

3) The solid viscosity coefficients of the base-rocks are of the order of $10^5 \sim 10^6$ (c.g.s.), their elastic constants of the order of 10^9 (c.g.s.), their cubic compressibilities of the order of 10^{-10} (c.g.s.), their Poisson's ratios are 0·31~0·33, their densities are 1·91, and the longitudinal and transversal wave-velocities in the layer of the base-rocks are about 450 m/sec and 235 m/sec respectively.

4) Let ρ', E', μ', V_p', V_s', ρ, E, μ, V_p, V_s be the densities, elastic constants, longitudinal and transversal wave-velocities of the upper superficial layer and the subjacent medium respectively. The ratios of the elastic constants of the upper superficial layer to those of the subjacent medium are then as follows:

$$\frac{\rho'}{\rho} \doteqdot 0{\cdot}81, \quad \frac{E'}{E} \doteqdot \frac{1}{43} \sim \frac{1}{1{\cdot}6}, \quad \frac{\mu'}{\mu} \doteqdot \frac{1}{47} \sim \frac{1}{1{\cdot}3}, \quad \frac{V_p'}{V_p} \doteqdot \frac{1}{3{\cdot}6} \sim \frac{1}{1{\cdot}2},$$

$$\frac{V_s'}{V_s} \doteqdot \frac{1}{6} \sim \frac{1}{1{\cdot}1}, \quad \frac{V_p'}{V'_s} \doteqdot 3{\cdot}3 \sim 1{\cdot}6, \quad \frac{V_p}{V_s} \doteqdot 1{\cdot}99 \sim 1{\cdot}91\,.$$

---

12) M. ISHIMOTO and K. IIDA *Bull. Earthq. Res. Inst.*, **14** (1936), 632; **15** (1937), 67.

51. Tunami associated with the Sanriku Earthquake that occurred on November 3, 1936.

By Naomi MIYABE,

Earthquake Research Institute.

(Read Jan. 17, 1937.—Received June 21, 1937.)

1. A severe earthquake occurred on November 3, 1936, the epicenter of which was off Kinkwazan. The shock was felt most severely on the Pacific side of northeastern Japan.

On the Pacific side of the prefectures of Hukusima, Miyagi, and Iwate, it was reported that cracks appeared on the walls of warehouses, window panes shattered, and that banks in several places subsided[1].

It was also noticed by a number of people, as already reported by Takayama[2], that, in Siogama Bay, the sea-level was seen to rise abnormally several tens of minutes after the shock was felt. Elsewhere, as also reported by Takayama, the sea-level rose after the earthquake to such an extent that it almost overflowed the banks. Obviously these reports by laymen are subjected more or less to exaggerations so that they cannot be accepted as being entirely correct. It may however be worth while to ascertain whether or not the tunami really occurred in association with this earthquake.

If the tunami was really associated with this earthquake, it should have been recorded by mareographs at several stations on the Pacific coast. The Mareograms were therefore collected from these stations for the purpose of ascertaining the occurrence or otherwise of the tunami through the courtesy of Mr. H. Matuo, a member of the staff of the Doboku Sikenzyo (Department of Domestic Affairs) to whom our best thanks are due.

Through these mareograms, the occurrence of the tunami associated with the earthquake was verified.

2. The epicenter of this earthquake was determined by the authorities of the Central Meteorological Observatory, to be 38.0 N, 142.0 E. The coordinates of the epicenter thus determined may however contain errors of considerable magnitude. These errors may largely be due to the fact that the seismometrical stations are distributed approximately in a line due N–S on the western side of the epicenter, in which case, as just mentioned, it might be difficult to determine the coordinates of the epicenter free of minor errors, as analytically shown in the following:

---

[1] Kisyô-Yôran. No. 447 (1936), 1166

[2] T. TAKAYAMA, *Bull. Earthq. Res. Inst.*, **15** (1937), 179~184

Let the coordinates of the hypocenter of the earthquake be x_0, y_0, z_0 and the durations of the preliminary tremors at i-th station τ_i. We then have

$$(x_i-x_0)^2+(y_i-y_0)^2+z_0^2=(k\tau_i)^3=D_i^2,$$

and similarly for h-th and k-th stations

$$(x_h-x_0)^2+(y_h-y_0)^2+z_0^2=(k\tau_h)^2=D_h^2$$

$$(x_k-x_0)^2+(y_k-y_0)^2+z_0^2=(k\tau_k)^2=D_k^2,$$

where x_i, y_i, x_h, y_h, x_k, y_k are coordinate of i-th, h-th and k-th stations respectively.

The values of x_0 and y_0 can be determined in terms of x_i, y_i, x_h, y_h, x_k, y_k, and D 's. Taking into account the fact that the values of x are relatively small and that their absolute values are approximately equal, we have, for determinining x_0 and y_0, by solving the foregoing simultaneous equations.,

$$x_0=\frac{1}{2}\frac{\{(D_k^2-D_i^2)-(y_h^2-y_i^2)\}(y_k-y_i)-\{(D_k^2-D_i^2)-(y_k^2-y_i^2)\}(y_h-y_i)}{(x_h-x_i)(y_k-y_i)-(x_k-x_i)(y_h-y_i)}$$

$$y_0=\frac{1}{2}\frac{\{(D_h^2-D_i^2)-(y_h^2-y_i^2)\}(x_k-x_i)-\{(D_k^2-D_i^2)-(y_k^2-y_i^2)\}(x_h-x_i)}{(x_k-x_i)(y_h-y_i)-(x_h-x_i)(y_k-y_i)}$$

The fluctuations in the values of x_0 and y_0 may be mainly due to the errors in τ's or D's in the above expressions. On the other hand, the values of the y's may be taken sufficiently large by proper sellection of the seismometrical stations. while the values of x's are in general small, the values of $(x_{h \text{ or } k}-x_i)$ sometimes becoming zero. Hence, for a rough estimation, the fluctuation in the values of x_0 may be regarded as $\frac{y_k-y_i}{x_k-x_i}$ or $\frac{y_h-y_i}{x_h-x_i}$ times that of y_0, the ratio being very large.

In determining the position of the epicenter of the earthquake from the data given in Kisyô-Yôran, the following method was used. Circles of radii $k(t_i-t_0)$ were drawn with their centers at the respective seismometrical stations, where t_i is the time of commencement of the earthquake shock at the i-th station, and t_0 the time of occurrence of the shock at the hypocenter. An envelope of these circles is then drawn, and the approximate center of the envelope is taken as the epicenter. The constant k is the tangent of the slope of a part of the "Laufzeitkurve", in which the curve is straight.

The coordinates of the epicenter thus determined are

$$\lambda=143.0^\circ\mathrm{E}, \qquad \varphi=38.0^\circ\mathrm{N}.$$

The value of λ is larger than that determined by the Central Meteorological Observatory, the departure amounting to about 100 km, which however is within the range of errors that might have been unavoidable in determining the epicenter in the present case.

3. The mareograms from the various stations along the Sanriku coast are reproduced in Figs. 1~7, and the geographical distribution of the stations is shown in Fig. 8.

From a glance at these figures, we clearly notice the sudden occurrence of an upward movement of the sea-level in the mareograms of Tukihama and Isinomaki and also in the mareograms taken at Onahama and Hatinohe, while, in the mareograms of other stations, trace of a tunami or any movement of the sea-level was not noticed as remarkable. This may be due to the smallness of the amplitude of the tunami, on the one hand, and the local disturbances, such as seiches superposing the curves that show the tides, which cannot easily be separated from the disturbance made by the tunami, on the other.

Since the sudden commencements of the upward or downward movement of the sea-level are clearly noticed in the mareograms of Tukihama and Isinomaki, the time of occurrence of these disturbances at these stations can also be determined with considerable accuracy.

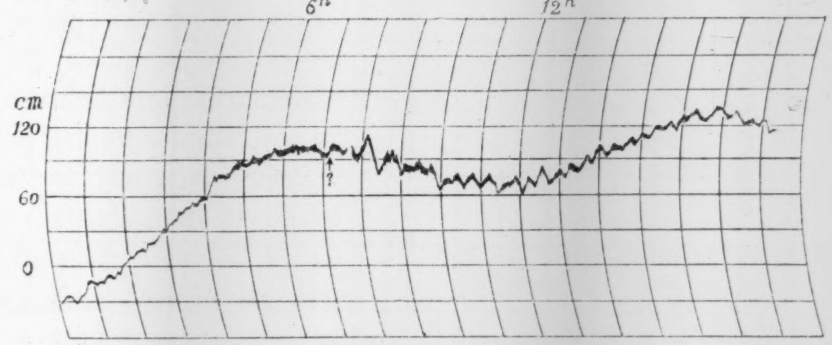

Fig. 1. Mareogram of Hatinohe.

In the mareogram of Onahama, the minor oscillations of the sea-level superpose. The tunami disturbance is however noticeable, its

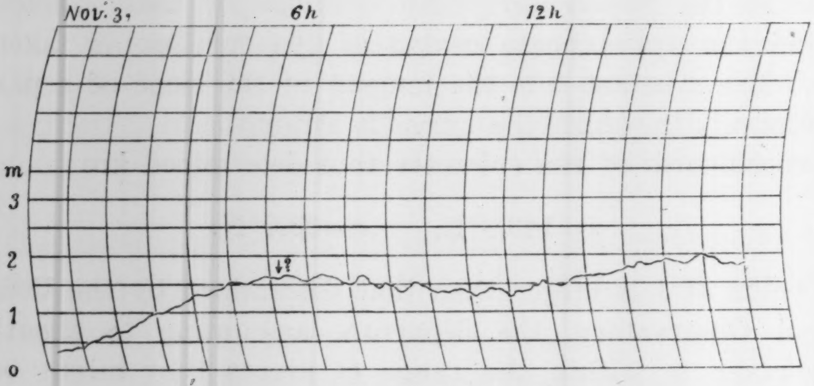

Fig. 2. Mareogram of Kesennuma.

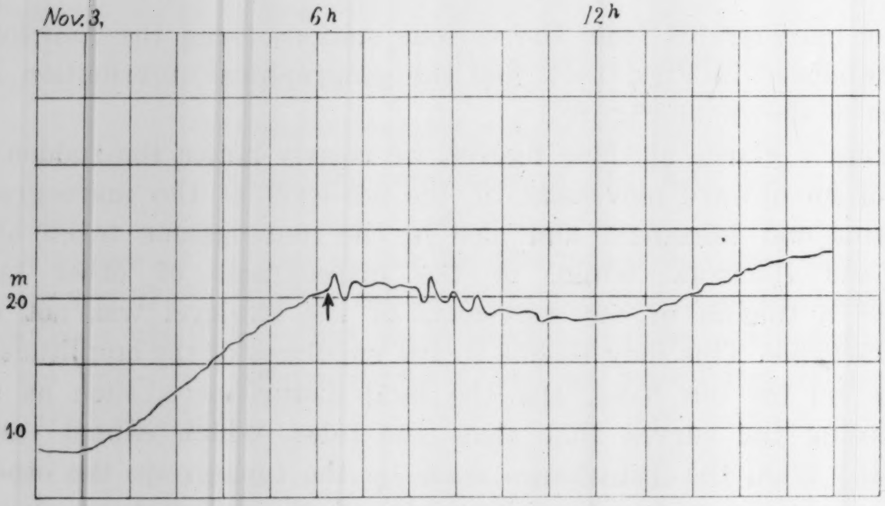

Fig. 3. Mareogram of Tukihama.

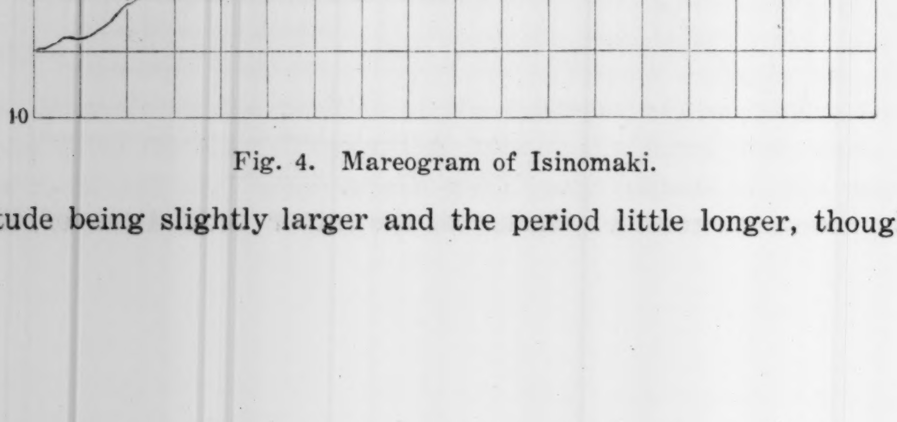

Fig. 4. Mareogram of Isinomaki.

amplitude being slightly larger and the period little longer, though not so markedly as those observed in the mareograms of Tukihama and Isinomaki. In the case of Hatinohe, the determination of the time of commencement of the tunami is more or less difficult. The difficulty lies, on the one hand, in the fact that records of the tide for the interval between 7 h 25 m a.m. and 7 h 40 m a.m. are lacking, on the other hand, to the oscillating motion of the sea-level with periods of about 17∼18 minutes and 30 minutes, which seem to be approximately equal to the period of disturbance of the tunami. Oscillation of the sea-level with such a period as just mentioned may be regarded as the proper oscillation of the water of the shelf sea.

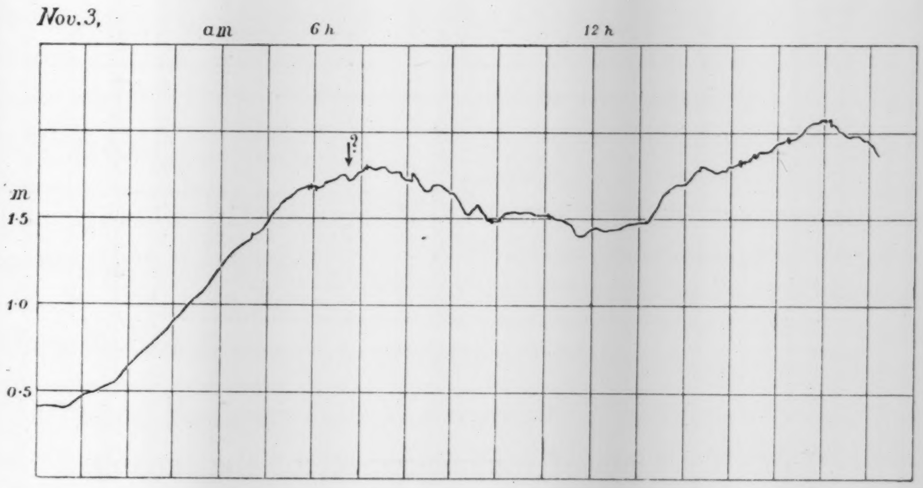

Fig. 5. Mareogram of Siogama.

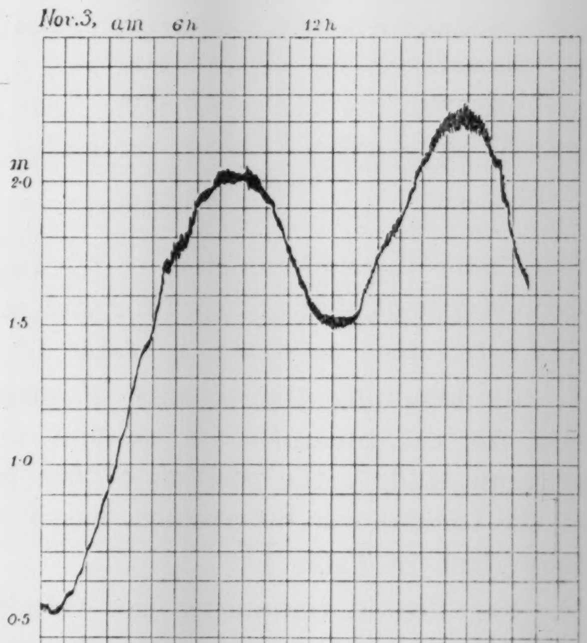

Fig. 6. Mareogram of Hanabutizaki, Siogama.

The disturbances recorded on the mareograms of Hatinohe may therefore be regarded as the oscillation of the water of the shelf sea excited by external disturbances, or tunami. If such is the case, the time of commencement of the tunami should be reduced by several minutes at least, since the amplitude of the oscillation might have increased rather gradually[3].

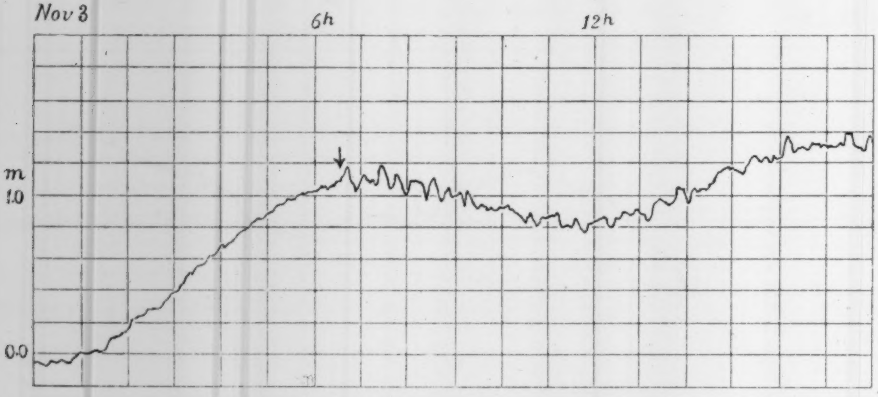

Fig. 7. Mareogram of Onahama.

Table I. Time of commencement of the tunami.

Name of st.	Time of commen't.	Approx. period	Travel time
Hatinohe	7 h 05(25) m	32 m	69(89) m
Kesennuma	6 h 20 m ?		34 m
Tukihama	6 h 14 m	20 m	28 m
Isinomaki	6 h 20 m	40 m	34 m
Siogama	6 h 45 m		59 m
Siogama (Hanabuti-hama)	?		
Onahama	6 h 39 m		53 m

Under these circumstances, the time of commencement of the tunami for each station was determined as shown in Table I.

4. By assuming the velocity of propagation for the tunami $\sqrt{gh}$ as done in the previous study[4], the position of the center of the tunami was determined, based on the data given in Table I.

For use in computing the velocity of propagation of the tunami, the distribution of depths of ocean bed in the region under consideration was reproduced from hydrographic charts issued by the Hydrographic Department of the Imperial Navy, as shown in Fig. 8.

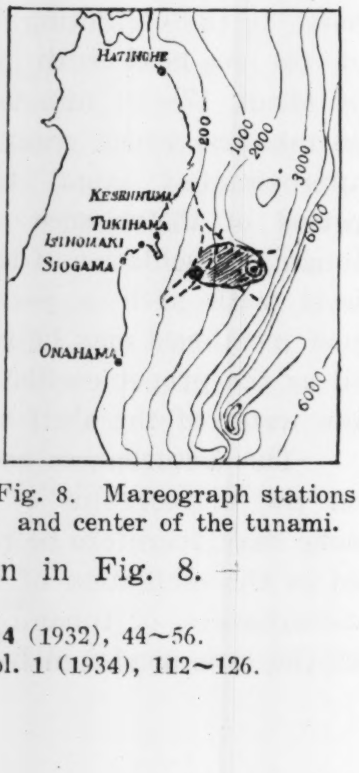

Fig. 8. Mareograph stations and center of the tunami.

---

[3] M. NAKANO, *Proc. Phys. Matsh. Soc., Japan*, **14** (1932), 44~56.

[4] N. MIYABE, *Bull. Earthq. Res. Inst.*, Suppl. Vol. 1 (1934), 112~126.

To determine the center of the tunami, we first tried to take the mareograph stations as temporary centers of the tunami and construct the wave fronts as referred to their respective stations at the time of occurrence of the earthquake. These wave fronts are shown in Fig. 8 by heavy dotted lines. The area within the envelope of these wave fronts may then be regarded as the center or the central region of the tunami.

The epicenter of the earthquake determined in the preceding paragraph and that determined by the Central Meteorological Observatory both lie in the area thus obtained, marked by ● and ⊙ respectively, as shown in Fig. 8.

5. Concluding remarks. In discussing the relation between the crustal deformation and the mechanism of earthquake occurrence, Ishimoto[5] took the earthquake in question as an example of an earthquake that was not accompanied by after shocks, and consequently was not accompanied by either tunami or crustal deformation. According to the writer's opinion, however, it may not be appropriate to take the earthquake referred to even if Ishimoto's hypothesis is probable. The fact that the after-shocks of this earthquake were not felt even by instruments may be due to the great distance of the epicentre and the smallness of the amplitudes of oscillations caused by the after-shocks.

---

5) M. Ishimoto, Disin, **9** (1937), 108~117. (in Japanese)

51. 昭和11年11月3日の三陸地方の地震に伴つた津浪

地震研究所　宮部直巳

昭和11年11月3日三陸附近に强震があつて輕微ながら，福島，宮城，岩手各縣の太平洋岸には被害があつた．

この地震に伴つて津浪らしいものが觀察された報告があつたので，太平洋岸各地の驗潮記錄を蒐めた．それ等の記錄は第1乃至7圖に示してある．津浪といつても，その津浪による被害は勿論なく，又，深く陸上に浸入したといふやうなこともなかつたのであるけれども，驗潮記錄にも見える樣に，津浪らしいものゝあつた事は否定出來ないものゝやうである．併し，若したしかに津浪があつたとしても，その振動の振幅は比較的小さいもののやうに思はれるから，灣の靜振等の重つてゐる2〜3の例では，津浪の始まりが明瞭を缺いてゐる場合がある．それで，驗潮記錄の上で，津浪の到達時刻を充分精密に讀みとることは困難であるが，數分の誤差を許容するとして，各驗潮儀所在地における津浪到達時刻は本文第一表の樣になる．そこで津浪の傳播速度を$\sqrt{gh}$（hは海水の深さ）として，津浪の中心の位置を求めてみると，大體に於いて，震央と思はれる場所に一致する．

是等の事實から考へて，この地震に伴つて津浪があつたとしてもよいやうに思はれる．

最近　石本博士は，餘震に關して興味ある考を述べて居られる．その中に，餘震を伴はない地震は地殼變形，從つて．その地震が海底に起つた場合には津浪を伴はないといふことを述べられた．併し，その1例として，卽ち，餘震を伴はず從つて津浪を伴はなかつた地震の1例として，この昭和11年11月3日の三陸の地震を擧げて居られることについては，筆者は贊意を表し難いのである．石本博士の考察は妥當であつても，少くとも上述の事實を肯定する以上，この地震に津浪が伴はなかつたとすることには同意出來ない．餘震を感じなかつたといふ事實が若しあるとするならば，それは，震央距離が陸地から少くとも200 kmは離れて居ることを想起しつゝ，餘震の震度が充分大でなかつたことを併せて考慮することによつても說明されるであらう．

52. *Relation between the Thickness of a Surface Layer and the Amplitudes of Dispersive Rayleigh-waves.*

By Katsutada SEZAWA and Kiyoshi KANAI,

Earthquake Research Institute.

(Received Sept. 20, 1937.—Read Sept. 21. 1937.)

1. *Introduction.*

Stoneley[1] recently showed that the dispersive Rayleigh-waves of minimum group velocity are likely to predominate in seismograms, the dispersion formula as well as the idea of predominance of waves of certain periods in his case being rather approximate. We shall here attack the same problem from a more appropriate standpoint even though the case in discussion should turn out to be of a rather special kind. As to the dispersion curves for the various conditions, we have already given mathematically accurate results.[2] [3] Although it is possible from these results to determine the amplitudes of waves for any given disturbance, since the numerical calculation is generally extremely difficult, the problem will be restricted here to that case in which the elastic constants of the medium underneath the surface layer are extremely large. The velocity of transmission and the amplitude distribution of the waves in the layer have however already been found.[4] Although the present problem is likely to correspond to that for a thin surface layer of the ground, the result still appears to apply to the case of a thick layer a few hundred kilometer deep, at any rate qualitatively. Our result furthermore shows that the idea of minimum group velocity as applied to the vibrational amplitudes is fairly applicable even in our special case.

Dispersive Rayleigh-waves 'generated from a source.

We shall now deal with a three-dimensional problem. Let the

---

1) R. STONELEY, "Surface-waves associated with 20° Discontinuity," *M. N. R. A. S. Geophys. Suppl.*, **4** (1937), 39∼43.

2) K. SEZAWA, *Bull. Earthq. Res. Inst.*, **3** (1927), 1.

3) K. SEZAWA and K. KANAI, "Discontinuity in Dispersion Curves of Rayleigh-waves," *Bull. Earthq. Res. Inst.*, **13** (1935), 273∼244.

4) K. SEZAWA and K. KANAI, "On the Propagation of Waves along a Surface Stratum of the Earth," *Bull. Earthq. Res. Inst.*, **12** (1934), 263∼268.

thickness of the stratum and the depth of the seismic origin from the free surface be η and $\eta-\xi$ respectively, and let the density and the elastic constants of the layer be ρ, λ, μ, the axes of r, z being taken as shown in the sketch.

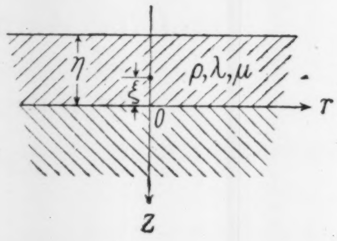

Fig. 1.

If U be the displacement due to the original disturbance, then

$$U=-\frac{1}{h^2}\frac{\partial\Delta_0}{\partial R}=-\frac{1}{h^2}\frac{\partial}{\partial R}\left(e^{-ipt}\frac{he^{ihR}}{R}\right), \tag{1}$$

its horizontal and vertical components being

$$u=-\frac{1}{h^2}\frac{\partial\Delta_0}{\partial r},\quad w=-\frac{1}{h^2}\frac{\partial\Delta_0}{\partial z}, \tag{2}$$

where $h^2=\rho p^2/(\lambda+2\mu)$, $R^2=r^2+z^2$.

The primary disturbance Δ_0 may be written in such forms as

$$\Delta_0=e^{-ipt}h\int_0^\infty\frac{e^{\alpha(z+\xi)}}{\alpha}J_0(fr)fdf, \qquad [z<-\xi] \tag{3}$$

$$\Delta_0=e^{-ipt}h\int_0^\infty\frac{e^{-\alpha(z+\xi)}}{\alpha}J_0(fr)fdf, \qquad [z>-\xi] \tag{4}$$

where $\alpha^2=f^2-h^2$. Adding the reflected waves at the free surface as well as at the boundary $z=0$, we have

$$\Delta_1=e^{-ipt}h\left[\int_0^\infty\frac{e^{\alpha(z+\xi)}}{\alpha}J_0(fr)fdf+\int_0^\infty\frac{e^{-\alpha(z+2\eta-\xi)}}{\alpha}J_0(fr)fdf\right.$$
$$\left.+\int_0^\infty\frac{e^{\alpha(z-2\eta+\xi)}}{\alpha}J_0(fr)fdf+\ldots\ldots\right], \qquad [z<-\xi] \tag{5}$$

$$\Delta_1=e^{-ipt}h\left[\int_0^\infty\frac{e^{-\alpha(z+2\eta-\xi)}}{\alpha}J_0(fr)fdf+\int_0^\infty\frac{e^{\alpha(z-2\eta+\xi)}}{\alpha}J_0(fr)fdf\right.$$
$$\left.+\ldots\ldots\right], \qquad [z>-\xi] \tag{6}$$

corresponding to the primary waves Δ_0 for $z<-\xi$ shown in (3), and

$$\Delta_2=e^{-ipt}h\left[\int_0^\infty\frac{e^{\alpha(z-\xi)}}{\alpha}J_0(fr)fdf+\int_0^\infty\frac{e^{-\alpha(z+2\eta+\xi)}}{\alpha}J_0(fr)fdf+\ldots\ldots\right], \quad [z<-\xi] \tag{7}$$

$$\Delta_2 = e^{-ipt}h\left[\int_0^\infty \frac{e^{-\alpha(z+\xi)}}{\alpha}J_0(fr)fdf + \int_0^\infty \frac{e^{\alpha(z-\xi)}}{\alpha}J_0(fr)fdf \right.$$
$$\left. + \int_0^\infty \frac{e^{-\alpha(z+2\eta+\xi)}}{\alpha}J_0(fr)fdf + \ldots\ldots \right], \quad [z>-\xi] \quad (8)$$

corresponding to the primary waves Δ_0 for $z>-\xi$ shown is (4). Equations (5), (7) satisfy the condition $\partial w_0/\partial r + \partial u_0/\partial z = 0$ at $z=-\eta$ and (6), (8) the condition $w_0=0$ at $z=0$, where u_0, w_0 are displacement components corresponding to Δ.

Superposing (5) and (7),

$$\left.\begin{aligned} \Delta &= 2e^{-ipt}h\int_0^\infty \frac{\mathrm{ch}\,\alpha\xi\,\mathrm{ch}\,\alpha(\eta+z)}{\alpha\,\mathrm{sh}\,\alpha\eta}J_0(fr)fdf, \quad [z<-\xi] \\ \Delta &= 2e^{-ipt}h\int_0^\infty \frac{\mathrm{ch}\,\alpha z\,\mathrm{ch}\,\alpha(\eta-\xi)}{\alpha\,\mathrm{sh}\,\alpha\eta}J_0(fr)fdf. \quad [z>-\xi] \end{aligned}\right\} \quad (9)$$

It is possible to write the displacement components corresponding to Δ in (9), namely,

$$\left.\begin{aligned} u_0 &= \frac{2e^{-ipt}}{h}\int_0^\infty \frac{\mathrm{ch}\,\alpha\xi\,\mathrm{ch}\,\alpha(\eta+z)}{\alpha\,\mathrm{sh}\,\alpha\eta}J_1(fr)f^2df, \quad [z<-\xi] \\ u_0 &= \frac{2e^{-ipt}}{h}\int_0^\infty \frac{\mathrm{ch}\,\alpha z\,\mathrm{ch}\,\alpha(\eta-\xi)}{\alpha\,\mathrm{sh}\,\alpha\eta}J_1(fr)f^2df, \quad [z>-\xi] \end{aligned}\right\} \quad (10)$$

$$\left.\begin{aligned} w_0 &= \frac{-2e^{-ipt}}{h}\int_0^\infty \frac{\mathrm{ch}\,\alpha\xi\,\mathrm{sh}\,\alpha(\eta+z)}{\mathrm{sh}\,\alpha\eta}J_0(fr)fdf, \quad [z<-\xi] \\ w_0 &= \frac{-2e^{-ipt}}{h}\int_0^\infty \frac{\mathrm{sh}\,\alpha z\,\mathrm{ch}\,\alpha(\eta-\xi)}{\mathrm{sh}\,\alpha\eta}J_0(fr)fdf. \quad [z>-\xi] \end{aligned}\right\} \quad (11)$$

Although the condition of no tangential stress at the free surface and no displacement at the boundary $z=0$ are satisfied by Δ, u_0, w_0 in (9), (10), (11), the condition of zero normal stress on the free surface remains unsatisfied. For annulling the normal stress under consideration we take standing vibrations of types

$$\left.\begin{aligned} u_1 &= e^{-ipt}\frac{f}{h^2}(A\,\mathrm{ch}\,\alpha z + B\,\mathrm{sh}\,\alpha z)J_1(fr), \\ w_1 &= -e^{-ipt}\frac{\alpha}{h^2}(A\,\mathrm{sh}\,\alpha z + B\,\mathrm{ch}\,\alpha z)J_0(fr), \end{aligned}\right\} \quad (12)$$

$$\left.\begin{aligned} u_2 &= -e^{-ipt}\frac{\beta}{k^2}(C\,\mathrm{sh}\,\beta z + D\,\mathrm{ch}\,\beta z)J_1(fr), \\ w_2 &= e^{-ipt}\frac{f}{k^2}(C\,\mathrm{ch}\,\beta z + D\,\mathrm{sh}\,\beta z)J_0(fr), \end{aligned}\right\} \tag{13}$$

where $h^2=f^2-\alpha^2$, $k^2=f^2-\beta^2$, and then add u_1 and u_2 to u_0 in (10), w_1 and w_2 to w_0 in (11). The expressions in (12), (13) satisfy the vibratory equations of the layer. The respective superpositions of u_1, u_2, u_0 and w_1, w_2, w_0 do not seriously affect the condition of the original disturbance in (1).

The necessary boundary conditions are such that

$$z=0; \qquad w_1+w_2=0, \quad u_0+u_1+u_2=0, \tag*{(14), (15)}$$

$$z=-\eta; \qquad \frac{\partial}{\partial r}(w_1+w_2)+\frac{\partial}{\partial z}(u_1+u_2)=0, \tag{16}$$

$$\lambda(\Delta+\Delta')+2\mu\frac{\partial}{\partial z}(w_0+w_1+w_2)=0, \tag{17}$$

where $\Delta'=\partial u_1/\partial r+u_1/r+\partial w_1/\partial z$. Substituting (9) ~ (13) in (14) ~ (17), we get

$$\begin{aligned} A\Phi &= -\frac{2fh}{\alpha\,\mathrm{sh}\,\alpha\eta}\Bigg[\left\{1-\frac{2f^2}{f^2+\beta^2}\,\mathrm{ch}\,\alpha\eta\,\mathrm{ch}\,\beta\eta+\frac{f^2+\beta^2}{2\alpha\beta}\,\mathrm{sh}\,\alpha\eta\,\mathrm{sh}\,\beta\eta\right\}\mathrm{ch}\,\alpha(\eta-\xi) \\ &\qquad +\left\{\mathrm{ch}\,\alpha\eta-\frac{f^2+\beta^2}{2f^2}\,\mathrm{ch}\,\beta\eta\right\}\mathrm{ch}\,\alpha\xi\Bigg], \\ B\Phi &= -\frac{2fh}{\alpha\,\mathrm{sh}\,\alpha\eta}\Bigg[\left\{\frac{f^2+\beta^2}{2\alpha\beta}\,\mathrm{ch}\,\alpha\eta\,\mathrm{sh}\,\beta\eta-\frac{2f^2}{f^2+\beta^2}\,\mathrm{sh}\,\alpha\eta\,\mathrm{ch}\,\beta\eta\right\}\mathrm{ch}\,\alpha(\eta-\xi) \\ &\qquad +\left\{\mathrm{sh}\,\alpha\eta-\frac{f^2+\beta^2}{2\alpha\beta}\,\mathrm{sh}\,\beta\eta\right\}\mathrm{ch}\,\alpha\xi\Bigg], \\ C\Phi &= \frac{\alpha k^2}{fh^2}B\Phi, \\ D\Phi &= \frac{2f^2k^2}{\alpha\beta h\,\mathrm{sh}\,\alpha\eta}\Bigg[\left\{1-\frac{f^2+\beta^2}{2f^2}\,\mathrm{ch}\,\alpha\eta\,\mathrm{ch}\,\beta\eta+\frac{2\alpha\beta}{f^2+\beta^2}\,\mathrm{sh}\,\alpha\eta\,\mathrm{sh}\,\beta\eta\right\}\mathrm{ch}\,\alpha(\eta-\xi) \\ &\qquad -\left\{\mathrm{ch}\,\alpha\eta-\frac{f^2+\beta^2}{2f^2}\,\mathrm{ch}\,\beta\eta\right\}\mathrm{ch}\,\alpha\xi\Bigg], \end{aligned} \tag{18}$$

where

$$\Phi=2-\left\{\frac{f^2+\beta^2}{2f^2}+\frac{2f^2}{f^2+\beta^2}\right\}\operatorname{ch}\alpha\eta\operatorname{ch}\beta\eta+\left\{\frac{f^2+\beta^2}{2\alpha\beta}+\frac{2\alpha\beta}{f^2+\beta^2}\right\}\operatorname{sh}\alpha\eta\operatorname{sh}\beta\eta, \tag{19}$$

by means of which the resulting displacements on the free surface $z=-\eta$ are expressed by

$$u_{z=-\eta}=e^{-ipt}\int_0^\infty J_1(fr)\frac{k^2}{\Phi\alpha h\operatorname{sh}\alpha\eta}\left[\left\{1-\frac{2f^2}{f^2+\beta^2}\operatorname{ch}\alpha\eta\operatorname{ch}\beta\eta\right.\right.$$

$$\left.\left.+\frac{2\alpha\beta}{f^2+\beta^2}\operatorname{sh}\alpha\eta\operatorname{sh}\beta\eta\right\}\operatorname{ch}\alpha\xi-\left\{\operatorname{ch}\alpha\eta-\frac{2f^2}{f^2+\beta^2}\operatorname{ch}\beta\eta\right\}\operatorname{ch}\alpha(\eta-\xi)\right]df, \tag{20}$$

$$w_{z=-\eta}=e^{-ipt}\int_0^\infty J_0(fr)\frac{fk^2}{\Phi\alpha\beta h\operatorname{sh}\alpha\eta}\left[\left\{\operatorname{ch}\alpha\eta\operatorname{sh}\beta\eta-\frac{\alpha\beta}{f^2}\operatorname{sh}\alpha\eta\operatorname{ch}\beta\eta\right\}\operatorname{ch}\alpha\xi\right.$$

$$\left.+\left\{\frac{2\alpha\beta}{f^2+\beta^2}\operatorname{sh}\alpha\eta-\operatorname{sh}\beta\eta\right\}\operatorname{ch}\alpha(\eta-\xi)\right]df. \tag{21}$$

The expression of Φ is virtually the same as the dispersion equation shown previously.[5]

In order to evaluate the expressions in (20), (21), we use the relations

$$\left.\begin{aligned}J_0(fr)&=\frac{-i}{\pi}\int_0^\infty\left(e^{ifr\operatorname{ch}j}-e^{-ifr\operatorname{ch}j}\right)dj,\\ J_1(fr)&=\frac{-1}{\pi}\int_0^\infty\left(e^{ifr\operatorname{ch}j}+e^{-ifr\operatorname{ch}j}\right)\operatorname{ch}j\,dj.\end{aligned}\right\} \tag{22}$$

Then

$$u_{z=-\eta}=\frac{-4k^2e^{-ipt}}{\pi h}\int_0^\infty\operatorname{ch}j\,dj\int_0^\infty\frac{1}{\Phi_1(f)}\left(e^{ifr\operatorname{ch}j}+e^{-ifr\operatorname{ch}j}\right)$$

$$\cdot\left[\left\{e^{\xi\sqrt{f^2-h^2}}+e^{-\xi\sqrt{f^2-h^2}}-e^{(2\eta-\xi)\sqrt{f^2-h^2}}-e^{-(2\eta-\xi)\sqrt{f^2-h^2}}\right\}\right.$$

$$+\frac{1}{2f^2-k^2}\left\{\left(f^2+\sqrt{f^2-h^2}\sqrt{f^2-k^2}\right)\left(e^{(\eta-\xi)\sqrt{f^2-h^2}+\eta\sqrt{f^2-k^2}}\right.\right.$$

$$\left.+e^{-(\eta-\xi)\sqrt{f^2-h^2}-\eta\sqrt{f^2-k^2}}-e^{-(\eta+\xi)\sqrt{f^2-h^2}+\eta\sqrt{f^2-k^2}}-e^{(\eta+\xi)\sqrt{f^2-h^2}-\eta\sqrt{f^2-k^2}}\right)$$

---

5) K. SEZAWA and K. KANAI, *loc. cit.* 4).

$$+\,(f^2-\sqrt{f^2-h^2}\sqrt{f^2-k^2})\,(e^{-(\eta_1-\xi)\sqrt{f^2-h^2}+\eta_1\sqrt{f^2-k^2}}$$

$$+\,e^{(\eta-\xi)\sqrt{f^2-h^2}-\eta_1\sqrt{f^2-k^2}}-e^{(\eta+\xi)\sqrt{f^2-h^2}+\eta_1\sqrt{f^2-k^2}}$$

$$\left.\left.-\,e^{-(\eta_1+\xi)\sqrt{f^2-h^2}-\eta_1\sqrt{f^2-k^2}})\right\}\right]f^2\sqrt{f^2-k^2}(2f^2-k^2)\,df, \qquad (23)$$

$$w_{z=-\eta_1}=\frac{-2ik^2e^{-ipt}}{\pi h}\int_0^\infty dj\int_0^\infty\frac{1}{\Phi_1(f)}\,(e^{ifr\,\mathrm{ch}\,j}-e^{-ifr\,\mathrm{ch}\,j})$$

$$\cdot\Big[(f^2+\sqrt{f^2-h^2}\sqrt{f^2-k^2})\,(-e^{(\eta_1+\xi)\sqrt{f^2-h^2}-\eta_1\sqrt{f^2-k^2}}$$

$$+\,e^{-(\eta_1-\xi)\sqrt{f^2-h^2}-\eta_1\sqrt{f^2-k^2}}-e^{(\eta_1-\xi)\sqrt{f^2-h^2}+\eta_1\sqrt{f^2-k^2}}+e^{-(\eta_1+\xi)\sqrt{f^2-h^2}+\eta_1\sqrt{f^2-k^2}})$$

$$+\,(f^2-\sqrt{f^2-h^2}\sqrt{f^2-k^2})\,(e^{(\eta_1+\xi)\sqrt{f^2-h^2}+\eta_1\sqrt{f^2-k^2}}$$

$$-\,e^{-(\eta_1-\xi)\sqrt{f^2-h^2}+\eta_1\sqrt{f^2-k^2}}+e^{(\eta_1-\xi)\sqrt{f^2-h^2}-\eta_1\sqrt{f^2-k^2}}-e^{-(\eta_1+\xi)\sqrt{f^2-h^2}-\eta_1\sqrt{f^2-k^2}})$$

$$+\,\frac{4f^2\sqrt{f^2-h^2}\sqrt{f^2-k^2}}{2f^2-k^2}\,(e^{(2\eta_1-\xi)\sqrt{f^2-h^2}}+e^{\xi\sqrt{f^2-h^2}}-e^{-\xi\sqrt{f^2-k^2}}$$

$$\left.-\,e^{-(2\eta_1-\xi)\sqrt{f^2-h^2}})\right]f(2f^2-k^2)\,df, \qquad (24)$$

where

$$\Phi_1(f)=16f^2\sqrt{f^2-h^2}\sqrt{f^2-k^2}(2f^2-k^2)\left\{e^{\eta_1\sqrt{f^2-h^2}}-e^{-\eta_1\sqrt{f^2-h^2}}\right\}$$

$$+\,(f^2-\sqrt{f^2-h^2}\sqrt{f^2-k^2})\left\{(2f^2-k^2)^2-4f^2\sqrt{f^2-h^2}\sqrt{f^2-k^2}\right\}$$

$$\cdot\left\{e^{\eta_1(2\sqrt{f^2-h^2}+\sqrt{f^2-k^2})}+e^{-\eta_1\sqrt{f^2-k^2}}-e^{\eta_1\sqrt{f^2-k^2}}-e^{-\eta_1(2\sqrt{f^2-h^2}+\sqrt{f^2-k^2})}\right\}. \qquad (25)$$

The expressions in (23), (24) give the displacements at any radial distance on the free surface.

3. *Evaluation of the integrals.*

We shall first evaluate the integrals

$$\int_0^\infty\frac{e^{ifr\,\mathrm{ch}\,j}}{\Phi_1(f)}F_1(f)\,df+\int_0^\infty\frac{e^{-ifr\,\mathrm{ch}\,j}}{\Phi_1(f)}F_1(f)\,df, \qquad (26)$$

$$\int_0^\infty\frac{e^{ifr\,\mathrm{ch}\,j}}{\Phi_1(f)}F_2(f)\,df+\int_0^\infty\frac{e^{-ifr\,\mathrm{ch}\,j}}{\Phi_1(f)}F_2(f)\,df, \qquad (27)$$

contained in (23), (24) respectively, $F_1(f)$ and $F_2(f)$ being the factors within the respective pairs of brackets in (23) and (24). To evaluate the respective first integrals in (26) and (27), we consider the integrals

$$\int_c \frac{e^{iZr\,\mathrm{ch}\,j}}{\Phi_1(Z)}F_1(Z)dZ,\ \int_c \frac{e^{iZr\,\mathrm{ch}\,j}}{\Phi_1(Z)}F_2(Z)dZ \qquad (28),\ (29)$$

taken round the contour in the first quadrant in Fig. 2, and also the integrals

$$\int_c \frac{e^{-iZr\,\mathrm{ch}\,j}}{\Phi_1(Z)}F_1(Z)dZ,\ \int_c \frac{e^{-iZr\,\mathrm{ch}\,j}}{\Phi_1(Z)}F_2(Z)dZ \qquad (30),\ (31)$$

taken round the contours in the fourth quadrant in the same figure.

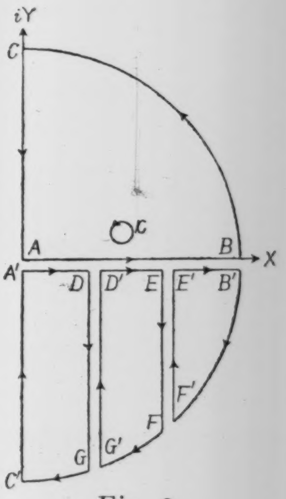

Fig. 2.

Let the roots of $\Phi_1(Z)$ be κ_n, the values of which were found previously.[6] κ_n are thus the singular points in the contours just given. It should however be borne in mind that there are usually a number of roots κ_n. Since, on the other hand, $Z=h$ and $Z=k$ are branch points, we draw the branch lines DG and EF as shown in the figure.

The integrals performed along the circular arcs BC and $B'C'$ vanish when the radii of these arcs are made infinitely large.

The integral of (28) along CA and that of (30) along $C'A'$ cancel each other. Similar conditions exist in (29) as well as in (30).

The integrals worked out along DG, $D'G'$, EF, $E'F'$ are somewhat complex. We write

$$\sqrt{(h+iY)^2-h^2}=\gamma', \qquad \sqrt{(h+iY)^2-k^2}=\delta' \qquad \text{along}\,DG,$$

$$\sqrt{(h+iY)^2-h^2}=-\gamma', \qquad \sqrt{(h+iY)^2-k^2}=\delta' \qquad \text{along}\,G'D',$$

$$\sqrt{(k+iY)^2-h^2}=\gamma'', \qquad \sqrt{(k+iY)^2-k^2}=\delta'' \qquad \text{along}\,EF,$$

$$\sqrt{(k+iY)^2-h^2}=\gamma'', \qquad \sqrt{(k+iY)^2-k^2}=-\delta'' \qquad \text{along}\,F'E'.$$

The integrals of (30) performed along DG and $G'D'$ then cancel each other, similar relations holding in the integrals of (31) with respect to EF and $F'E'$.

Finally the integrals around the pole κ_n for the cases $u_{z=-\eta}$ and $w_{z=-\eta}$ are

---

6) K. SEZAWA and K. KANAI, *loc. cit.* 4).

$$\frac{-2ik^2e^{i\kappa r\,\mathrm{ch}\,j}\mathrm{ch}\,j}{h\gamma\Phi'(\kappa)\,\mathrm{sh}\,\gamma\kappa\eta}\left[\left\{1-\frac{2}{1+\delta^2}\mathrm{ch}\,\gamma\kappa\eta\,\mathrm{ch}\,\delta\kappa\eta+\frac{2\gamma\delta}{1+\delta^2}\mathrm{sh}\,\gamma\kappa\eta\,\mathrm{sh}\,\delta\kappa\eta\right\}\mathrm{ch}\,\gamma\kappa\xi\right.$$
$$\left.+\left\{\frac{2}{1+\delta^2}\mathrm{ch}\,\delta\kappa\eta-\mathrm{ch}\,\gamma\kappa\eta\right\}\mathrm{ch}\,\gamma\kappa(\eta-\xi)\right],\tag{32}$$

$$\frac{2k^2e^{i\kappa r\,\mathrm{ch}\,j}}{h\gamma\delta\Phi'(\kappa)\,\mathrm{sh}\,\gamma\kappa\eta}\left[\left\{\mathrm{ch}\,\gamma\kappa\eta\,\mathrm{sh}\,\delta\kappa\eta-\gamma\delta\,\mathrm{sh}\,\gamma\kappa\eta\,\mathrm{ch}\,\delta\kappa\eta\right\}\mathrm{ch}\,\gamma\kappa\xi\right.$$
$$\left.+\left\{\frac{2\gamma\delta}{1+\delta^2}\mathrm{sh}\,\gamma\kappa\eta-\mathrm{sh}\,\delta\kappa\eta\right\}\mathrm{ch}\,\gamma\kappa(\eta-\xi)\right],\tag{33}$$

where κ is written in lieu of κ_n, and

$$\Phi'(\kappa)=\left(\frac{k}{\kappa}\right)^2\left\{\frac{4}{(1+\delta^2)^2}-1\right\}\mathrm{ch}\,\gamma\kappa\eta\,\mathrm{ch}\,\delta\kappa\eta$$
$$+2\gamma\delta\left\{4-(1+\delta^2)\left(\frac{1}{\gamma^2}+\frac{1}{\delta^2}\right)\right\}\left\{\frac{1}{4\gamma^2\delta^2}-\frac{1}{(1+\delta^2)^2}\right\}\mathrm{sh}\,\gamma\kappa\eta\,\mathrm{sh}\,\delta\kappa\eta$$
$$+\frac{\kappa\eta}{\delta}\left\{\frac{\left(\frac{h}{\kappa}\right)^2(1+\delta^2)}{2\gamma^2}-\frac{2\left(\frac{k}{\kappa}\right)^2}{1+\delta^2}\right\}\mathrm{ch}\,\gamma\kappa\eta\,\mathrm{sh}\,\delta\kappa\eta$$
$$+\frac{\kappa\eta}{\gamma}\left\{\frac{\left(\frac{k}{\kappa}\right)^2(1+\delta^2)}{2\delta^2}-\frac{2\left(\frac{h}{\kappa}\right)^2}{1+\delta^2}\right\}\mathrm{sh}\,\gamma\kappa\eta\,\mathrm{ch}\,\delta\kappa\eta,\tag{34}$$

$$\gamma=\sqrt{1-(h/\kappa)^2},\quad \delta=\sqrt{1-(k/\kappa)^2}.\tag{35}$$

In the present case use has been made of Φ instead of Φ_1.

Since it is known that

$$\left.\begin{aligned}H_0^{(1)}(\kappa r)&=\frac{-2i}{\pi}\int_0^\infty e^{i\kappa r\,\mathrm{ch}\,j}dj,\\ H_1^{(1)}(\kappa r)&=\frac{-2}{\pi}\int_0^\infty e^{i\kappa r\,\mathrm{ch}\,j}\mathrm{ch}\,j\,dj,\end{aligned}\right\}\tag{36}$$

we finally get

$$u_{z=-\eta}=\frac{i\pi}{\eta}e^{-ipt}H_1^{(1)}(\kappa r)\frac{k^2\eta}{h\gamma\Phi'(\kappa)\operatorname{sh}\gamma\kappa\eta}\left[\left\{1-\frac{2}{1+\delta^2}\operatorname{ch}\gamma\kappa\eta\operatorname{ch}\delta\kappa\eta\right.\right.$$

$$\left.\left.+\frac{2\gamma\delta}{1+\delta^2}\operatorname{sh}\gamma\kappa\eta\operatorname{sh}\delta\kappa\eta\right\}\operatorname{ch}\gamma\kappa\xi+\left\{\frac{2}{1+\delta^2}\operatorname{ch}\delta\kappa\eta-\operatorname{ch}\gamma\kappa\eta\right\}\operatorname{ch}\gamma\kappa(\eta-\xi)\right], \quad (37)$$

$$w_{z=-\eta}=\frac{i\pi}{\eta}e^{-ipt}H_0^{(1)}(\kappa r)\frac{k^2\eta}{h\gamma\Phi'(\kappa)\operatorname{sh}\gamma\kappa\eta}\left[\frac{1}{\delta}\left\{\operatorname{ch}\gamma\kappa\eta\operatorname{sh}\delta\kappa\eta\right.\right.$$

$$\left.\left.-\gamma\delta\operatorname{sh}\gamma\kappa\eta\operatorname{ch}\delta\kappa\eta\right\}\operatorname{ch}\gamma\kappa\xi+\frac{1}{\delta}\left\{\frac{2\gamma\delta}{1+\delta^2}\operatorname{sh}\gamma\kappa\eta-\operatorname{sh}\delta\kappa\eta\right\}\operatorname{ch}\gamma\kappa(\eta-\xi)\right]. \quad (38)$$

When there are a number of κ_n, the superposed expressions of the above types (without any further coefficient) are used.

Taking the asymptotic expansions of $H_0^{(1)}(\kappa r)$, $H_1^{(1)}(\kappa r)$ and also simplifying the resulting expressions, we get

$$u_{z=-\eta}=\left[\frac{1}{\sqrt{r\eta}}e^{i(\kappa r-\frac{\pi}{4}-pt)}\right]\frac{1}{\Phi'(\kappa)}\sqrt{\frac{2\pi}{\kappa\eta}}\frac{k^2\eta}{h\gamma}\left[\left\{\frac{2\gamma\delta}{1+\delta^2}\operatorname{sh}\beta\eta-\operatorname{sh}\alpha\eta\right\}\operatorname{ch}\alpha\xi\right.$$

$$\left.+\left\{\operatorname{ch}\alpha\eta-\frac{2}{1+\delta^2}\operatorname{ch}\beta\eta\right\}\operatorname{sh}\alpha\xi\right], \quad (39)$$

$$w_{z=-\eta}=\left[\frac{1}{\sqrt{r\eta}}e^{i(\kappa r+\frac{\pi}{4}-pt)}\right]\frac{1}{\Phi'(\kappa)}\sqrt{\frac{2\pi}{\kappa\eta}}\frac{k^2\eta}{h}\left[\left\{\frac{2}{1+\delta^2}\operatorname{ch}\alpha\eta-\operatorname{ch}\beta\eta\right\}\operatorname{ch}\alpha\xi\right.$$

$$\left.+\left\{\frac{1}{\gamma\delta}\operatorname{sh}\beta\eta-\frac{2}{1+\delta^2}\operatorname{sh}\alpha\eta\right\}\operatorname{sh}\alpha\xi\right]. \quad (40)$$

From (39), (40) it is possible to calculate the horizontal and vertical components of the waves for an assigned displacement at the source such as that shown in (1).

4. *Physical meaning of the integrals.*

As will be seen from (37), (38) or (39), (40), the movement of the ground for any epicentral distance consists only of surface waves. In contrast to this, Rayleigh-waves, in the case of a semi-infinite body, are accompanied by longitudinal and transverse bodily waves of amplitudes both varying as the inverse square of the epicentral distance, and Love-waves in the case of a stratified body by transverse bodily waves of velocity peculiar to the subjacent medium and of amplitudes also varying with the same law as for bodily waves in the case of Rayleigh-waves. The reason why no bodily wave appears in the present case is that, since the subjacent medium is not deformable, the whole vibrational energy in the layer is transmitted in the form of surface waves.

5. *Numerical computation of the mathematical formulae.*

The numerical calculation of the mathematical results in (39), (40) is not simple. For performing the calculation, the expressions within the respective pairs of brackets in (37), (38) will be transformed to

$$\Big[\quad\Big] \text{ for } u_{z=-\eta} = \mathrm{sh}\,\alpha\eta\,\mathrm{ch}\,\alpha\xi\left\{\mathrm{sh}\,\alpha\eta - \frac{2\alpha\beta}{\kappa^2+\beta^2}\,\mathrm{sh}\,\beta\eta\right\} \cdot\left[\frac{\mathrm{ch}\,\alpha\eta - \dfrac{2\kappa^2}{\kappa^2+\beta^2}\,\mathrm{ch}\,\beta\eta}{\mathrm{sh}\,\alpha\eta - \dfrac{2\alpha\beta}{\kappa^2+\beta^2}\,\mathrm{sh}\,\beta\eta}\,\mathrm{th}\,\alpha\xi - 1\right], \quad (41)$$

$$\Big[\quad\Big] \text{ for } w_{z=-\eta} = -\frac{2\alpha\kappa}{\kappa^2+\beta^2}\,\mathrm{sh}\,\alpha\eta\,\mathrm{ch}\,\alpha\xi\left\{\mathrm{ch}\,\alpha\eta - \frac{\kappa^2+\beta^2}{2\kappa^2}\,\mathrm{ch}\,\beta\eta\right\} \cdot\left[\frac{\mathrm{sh}\,\alpha\eta - \dfrac{\kappa^2+\beta^2}{2\alpha\beta}\,\mathrm{sh}\,\beta\eta}{\mathrm{ch}\,\alpha\eta - \dfrac{\kappa^2+\beta^2}{2\kappa^2}\,\mathrm{ch}\,\beta\eta}\,\mathrm{th}\,\alpha\xi - 1\right]. \quad (42)$$

Putting

$$\left.\begin{aligned} &\frac{\mathrm{ch}\,\alpha\eta - \dfrac{2\kappa^2}{\kappa^2+\beta^2}\,\mathrm{ch}\,\beta\eta}{\mathrm{sh}\,\alpha\eta - \dfrac{2\alpha\beta}{\kappa^2+\beta^2}\,\mathrm{sh}\,\beta\eta}\,\mathrm{th}\,\alpha\xi - 1 = \mathrm{I}, \qquad \frac{\mathrm{sh}\,\alpha\eta - \dfrac{\kappa^2+\beta^2}{2\alpha\beta}\,\mathrm{sh}\,\beta\eta}{\mathrm{ch}\,\alpha\eta - \dfrac{\kappa^2+\beta^2}{2\kappa^2}\,\mathrm{ch}\,\beta\eta}\,\mathrm{th}\,\alpha\xi - 1 = \mathrm{I}', \\ &\mathrm{sh}\,\alpha\eta - \frac{2\alpha\beta}{\kappa^2+\beta^2}\,\mathrm{sh}\,\beta\eta = \mathrm{II}, \quad \mathrm{ch}\,\alpha\eta - \frac{\kappa^2+\beta^2}{2\kappa^2}\,\mathrm{ch}\,\beta\eta = \mathrm{III}, \\ &-\frac{2\alpha\kappa}{\kappa^2+\beta^2} = \mathrm{IV}, \quad \alpha\eta = \mathrm{V}, \end{aligned}\right\} \quad (43)$$

then, by means of the volocity equation[7]

$$\frac{\operatorname{ch}\alpha\eta-\dfrac{\kappa^2+\beta^2}{2\kappa^2}\operatorname{ch}\beta\eta}{\operatorname{sh}\alpha\eta-\dfrac{\kappa^2+\beta^2}{2\alpha\beta}\operatorname{sh}\beta\eta}=\frac{\operatorname{sh}\alpha\eta-\dfrac{2\alpha\beta}{\kappa^2+\beta^2}\operatorname{sh}\beta\eta}{\operatorname{ch}\alpha\eta-\dfrac{2\kappa^2}{\kappa^2+\beta^2}\operatorname{ch}\beta\eta}, \qquad (44)$$

we have I=I′. Thus

$$\Big[\quad\Big] \text{ for } u_{z=-\eta}=\text{VI.II.I}, \qquad \Big[\quad\Big] \text{ for } w_{z=-\eta}=\text{IV.VI.III.I}. \qquad (45),\ (46)$$

Calculating I, II, III, IV, V, $\Phi'(\kappa)$, and the coefficients as shown in (39), (40), we get $u_{z=-\eta}$, $w_{z=-\eta}$. It should be remembered that the ratio of $u_{z=-\eta}$ to $w_{z=-\eta}$ is

$$\frac{u}{w}=-\frac{(\kappa^2+\beta^2)}{2\alpha\kappa}\frac{\left\{\operatorname{sh}\alpha\eta-\dfrac{2\alpha\beta}{\kappa^2+\beta^2}\operatorname{sh}\beta\eta\right\}}{\left\{\operatorname{ch}\alpha\eta-\dfrac{\kappa^2+\beta^2}{2\kappa^2}\operatorname{ch}\beta\eta\right\}}, \qquad (47)$$

which is of the same form as obtained previously.[8]

In the present case we shall take $\xi=\eta$, namely, that the source of the disturbance is on the free surface. If we plot I, II, III, IV, V on the base of L/η where $L=2\pi/\kappa$, we get the result as shown in Fig. 3. It will be seen that the variations of the quantities just mentioned for different L/η's are very marked. Although by combining these quantities it is possible to calculate u, w for any L/η, there are still cases of L/η for which the calculation may be performed in some special way.

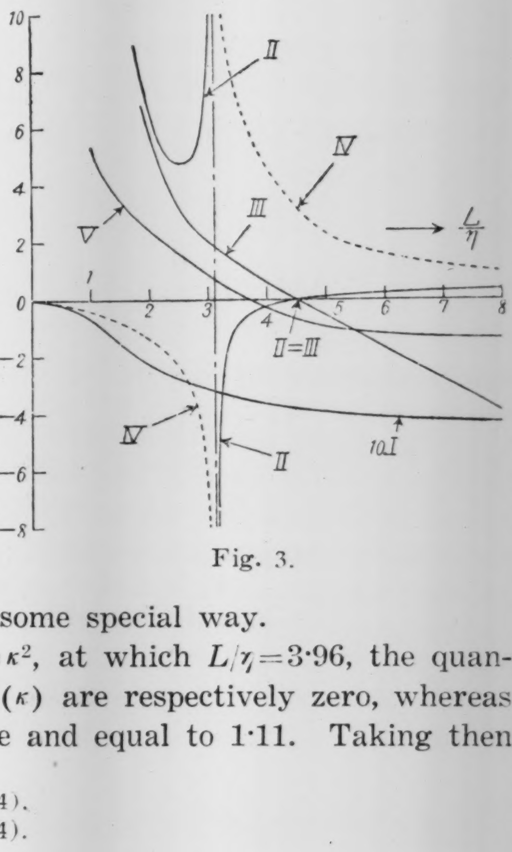

Fig. 3.

(i) In the case $\gamma=0$, namely $h^2=\kappa^2$, at which $L/\eta=3{\cdot}96$, the quantities of the orders $1/\gamma^2$ and $1/\gamma$ in $\Phi'(\kappa)$ are respectively zero, whereas the quantity of the order γ^0 is finite and equal to 1·11. Taking then the numerators of the finite order in u, w we have

---

[7] K. Sezawa and K. Kanai, *loc. cit.* 4).

[8] K. Sezawa and K. Kanai, *loc. cit.* 4).

$$\left.\begin{aligned} u &= \frac{6\sqrt{2\pi\kappa\eta}}{\Phi'(\kappa)}(\sqrt{2}\sin\beta\eta+\kappa\eta\cos\beta\eta)=1{\cdot}964, \\ w &= \frac{3\sqrt{2\pi\kappa\eta}}{\Phi'(\kappa)}\left(-2-\cos\beta\eta+\frac{\kappa\eta}{\sqrt{2}}\sin\beta\eta\right)=-4{\cdot}265. \end{aligned}\right\} \quad (48)$$

(ii) In the case $\delta=0$, namely $k^2=\kappa^2$, at which $L/\eta=1{\cdot}65$, the quantity of the order $1/\delta^2$ in $\Phi'(\kappa)$ vanishes, whereas the quantity of the order δ^0 is

$$\frac{\mathrm{ch}\,\alpha\eta}{12}\left\{151-11(\kappa\eta)^2\right\}-\frac{1}{3}\left\{23+2(\kappa\eta)^2\right\}=-25{\cdot}137,$$

so that

$$\left.\begin{aligned} u &= \frac{-6\sqrt{\pi\kappa\eta}}{\Phi'(\kappa)}\,\mathrm{sh}\,\alpha\eta=9{\cdot}19, \\ w &= \frac{2\sqrt{6\pi\kappa\eta}}{\Phi'(\kappa)}(2\,\mathrm{ch}\,\alpha\eta-1)=-14{\cdot}4. \end{aligned}\right\} \quad (49)$$

(iii) In the case $1+\delta^2=0$, namely $(k/\kappa)^2=2$, at which $L/\eta=3{\cdot}12$, the numerators of u and w have the factors $1/(1+\delta^2)$, whereas $\Phi'(\kappa)$ is of the form

$$\Phi'(\kappa)=\frac{8}{(1+\delta^2)^2}\left(\mathrm{ch}\frac{\kappa\eta}{\sqrt{3}}\cos\kappa\eta+\frac{1}{\sqrt{3}}\,\mathrm{sh}\frac{\kappa\eta}{\sqrt{3}}\sin\kappa\eta\right),$$

the numerator of which, in virtue of the velocity equation, is zero. Since, from the condition of the present case, the denominator is also zero, we take the respective derivatives of the numerator as well as the denominator of $\Phi'(\kappa)$, the result being

$$\begin{aligned} \Phi'(\kappa)=\frac{4}{1+\delta^2}\bigg[&-\frac{1}{\sqrt{3}}\,\mathrm{sh}\frac{\kappa\eta}{\sqrt{3}}\sin\kappa\eta-2{\cdot}014\,\mathrm{ch}\frac{\kappa\eta}{\sqrt{3}}\sin\kappa\eta \\ &-\frac{2{\cdot}014}{\sqrt{3}}\,\mathrm{sh}\frac{\kappa\eta}{\sqrt{3}}\cos\kappa\eta\bigg]=\frac{1}{1+\delta^2}(-4{\cdot}910). \end{aligned}$$

The expressions for u and w consequently become

$$\left.\begin{aligned} u&=\frac{1}{\Phi'(\kappa)}\frac{1}{(1+\delta^2)}\sqrt{6\pi\kappa\eta}\sqrt{6}\\ &\qquad\cdot\left[-\frac{2}{\sqrt{3}}\sin\beta\eta\,\mathrm{ch}\,\alpha\eta-2\cos\beta\eta\,\mathrm{sh}\,\alpha\eta\right]=1{\cdot}826,\\ w&=\frac{1}{\Phi'(\kappa)}\frac{1}{(1+\delta^2)}\sqrt{6\pi\kappa\eta}\sqrt{2}\,(2+0)=-3{\cdot}505. \end{aligned}\right\}\quad(50)$$

6. *Result of calculation and its interpretation.*

After carefully calculating other cases by means of (39), (40), we obtained the result as shown in Fig. 4, K in the same figure denoting the value in every first pair of brackets in (39), (40). The ratio of u/w for every L/η is always the same as that shown previously.[9]

It will be seen from the figure that within the range of calculation, the amplitude of the surface waves assumes its maximum values for two cases of L/η, namely, $L/\eta \approx 2$ and $L/\eta \approx 7$. While the maximum at $L/\eta \approx 2$ is finite, that at $L/\eta \approx 7$ is infinitely large.

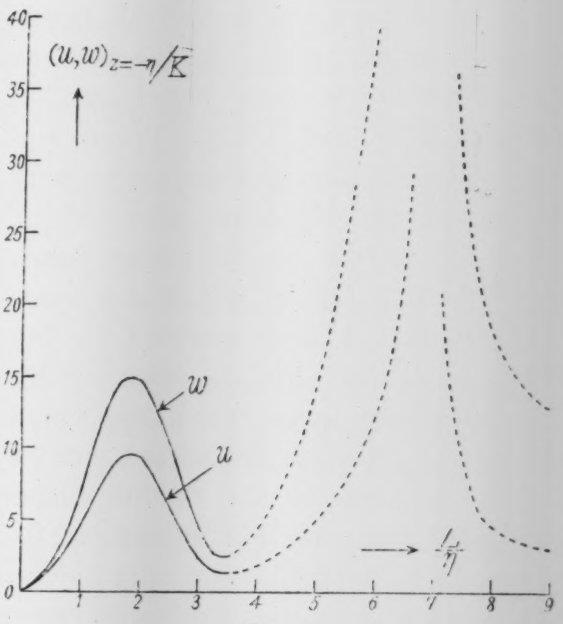

Fig. 4.

$L/\eta \approx 2$, namely $\kappa\eta \approx \pi$, appears to correspond to the case in which the amplitudes of Rayleigh-waves become maximum in the usual sense. Stoneley,[10] using the idea of the minimum group velocity, showed that $\kappa\eta = 3 \sim 2{\cdot}5$ corresponds to the case of maximum amplitude of Rayleigh-waves transmitted through a layer. Although the condition of the subjacent medium in his case differs considerably from ours, the nature of the problem, qualitatively, for the two cases, that is, Stoneley's and ours, seems the same. In the case of Love-waves transmitted over a surface layer as defined by Jeffreys, Stoneley's value[11] for $\kappa\eta$ that corresponds to the maximum amplitude, is 3·6, the value

---

9) K. SEZAWA and K. KANAI, *loc. cit.* 4).

10), 11) R. STONELEY, *loc. cit.* 1).

obtained by us being of the range 2∼3 (for $\xi>0$). It appears therefore that our value $\kappa\eta\approx\pi(L/\eta\approx2)$ for Rayleigh-waves is a plausible one for almost any condition of the subjacent medium. Furthermore, the case treated in the present paper concerns Rayleigh-waves of extremely shallow origin, that is to say, the origin is at the free surface. In the case of Love-waves, the greater the depth of origin, the greater the value of $\kappa\eta$ at which the amplitude of the waves is maximum, tends to increase. Therefore, the value of $\kappa\eta\approx\pi$ in the case of Rayleigh-waves may still be somewhat too small.

To interpret the maximum of u, w at $L/\eta\approx7$ is not a simple matter. Previously,[12] we found the dispersion curves of the case in which the elastic constants of the subjacent medium are extremely large, the curves under consideration being of the type in Fig. 5.

The dispersion curve AOB bends discontinuously at O. In the present case there are actually two dispersion curves, AOB and COD. When $\mu/\mu'=1/\infty$, as in the present case, part AO of curve AB joins part OD of curve CD, while, on the other hand, another part OB of curve AB joins another part CO of curve CD, the value of L/η at point O being 4·619. The infinitely large maximum value at $L/\eta\approx7$ in Fig. 3 belongs, as a matter of fact, to the second dispersion curve COD. No numerical result for the case corresponding to curve OB is given in the present paper. It is probably inadmissible to conceive of waves for such parts as OB and OD in the dispersion curves. The movements of the ground for the case corresponding to OD represent the layer waves with mere transverse (vertical) displacements, and in those for the case corresponding to OB the layer waves of nearly longitudinal (horizontal) displacements, in both of which energy is hardly diffused in the subjacent medium. The infinitely large displacement just mentioned is thus of such a nature as to be but slightly related to the case of ordinary Rayleigh-waves, but are the results of a resonance-like condition of bodily waves.

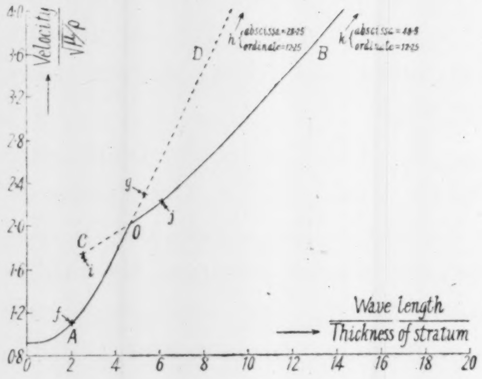

Fig. 5.

Finally, we may conclude that, although in the present paper we have dealt with a very special case of dispersive Rayleigh-waves, the

---

[12] K. SEZAWA and K. KANAI, loc. cit. 3).

result still appears to represent some of the fundamental characters of the general dispersive Rayleigh-waves.

52. 地表層の厚さと分散性レーレー波の振幅との關係

地震研究所 {妹澤克惟
金井清

Stoneley は分散性レーレー波が地表層を傳はるときに卓越せる振動周期のあることを指摘し之は波動の極小群速度に相當するものであるとなした．極小群速度といふことには相當の假定が含まれてをるので，玆に數學的に嚴密な方法で卓越振動周期をしらべて見たのである．

一般の場合はあまりに複雜であるから，ここには下部の層が無限に剛い場合を取つて計算を試みた．この場合には表面波に伴つて傳るや諸固體波が全然存在しないことになる．

今，L を波長，η を地表層の厚さとすると，$L/\eta=2$（$\kappa\eta=\pi$）位のときにレーレー波の振幅が極大値を取り，それよりも長い波長でも短い波長でも振幅が小さくなる傾向をもつものである．但し震原は地表面にあり且つその部分の振幅は一定として考へたものである．Stoneley の考によると下部の層の彈性が表面層の彈性と少しく違ふ場合に $\kappa\eta=3\sim2{\cdot}5$ 位のときにレーレー波の振幅が極大になる．我々の結果は，條件が相當違ふのに拘らず，Stoneley の結果と可なりよく似た傾向をもつことがわかる．同じやうな條件の場合を取扱ふとき，ラブ波の極大振幅が Stoneley によると $\kappa\eta=3{\cdot}6$ となり，我々によると $\kappa\eta=2\sim3$ 位となるのである．尚，只今の場合には震原が地表面にある場合を取扱つてある．然るにラブ波の場合を考へると震原が深くなるにつれて振幅の極大になる $\kappa\eta$ の値が增加する傾向があつたのである．從てレーレー波の場合の $\kappa\eta=\pi$ は未だ寧ろ小さ過ぎるかも知れぬ．

我々の計算によると $L/\eta=7$ 位のところで更に極大になり，且つその場合は無限大の振幅になる．しかし我々が以前に試みた研究と比較するとこの位の波長の波は表面波でなく，且つ無限大の振幅は一種の固體波の共振的現象の結果であることがわかるのである．

只今の研究では分散性レーレー波の特別の場合のみを取扱つたとはいへ，その結果はレーレー波の一般性の傾向だけは表してをるものと思はれる．

53. *The Problem of Elastic Stability of the Earth treated in Polar Coordinates.*

By Katsutada SEZAWA and Kiyoshi KANAI.

Earthquake Research Institute.

(Received Sept. 20, 1937.—Read Sept. 21, 1937.)

1. *Introduction.*

The problem of elastic stability of the Earth under gravitational forces was first solved by Jeans,¹⁾ whose result then attracted the special attention of Lord Rayleigh.²⁾ The assumption made in Jeans's paper and also in Lord Rayleigh's is such that the coordinate position of every material point does not shift, even in the deformed condition of the Earth. Love³⁾ afterwards discussed the problem with some regard to the change of the mean position of the material points. While Love's problem concerns the case of a gravitating uniform sphere, Matuzawa⁴⁾ extended the same problem to the case of a stratified Earth. Almost all these problems were solved by using such Cartesian coordinates as were given by Lamb.⁵⁾ On the other hand, similar vibrational problems in polar coordinates have frequently appeared in our papers.⁶⁾ ⁷⁾ Thus, our previous solutions will now be extended to the case of the elastic stability of the Earth. The treatment of the problem in the condition that will correspond to Love's idea is extremely complex. But, even should the condition of no shift of material points be allowable, the resulting defect or excess of mass on the moving free surface would be fairly effective on the change in gravitational force. From this con-

---

1) J. H. Jeans, "On the Vibrations and Stability of a Gravitational Planet," *Phil. Trans. Roy. Soc.*, **201** (1903), 157~184.

2) LORD RAYLEIGH, "On the Dilatational Stability of the Earth," *Proc. Roy. Soc.*, **77** (1906), 486~499.

3) A. E. H. LOVE, "On the Gravitational Stability of the Earth," *Phil. Trans. Roy. Soc.*, **207** (1908), 171~241; Some Problems of Geodynamics (Cambridge, 1911).

4) T. MATUZAWA, "On the Gravitational Stability of the Earth with a Core," *Proc. Phys.-Math. Soc.*, Japan, [3], **9** (1927), 31~44.

5) H. LAMB, "On the Vibrations of an Elastic Sphere," *Proc. Math. Soc.*, **13** (1882), 192.

6) K. SEZAWA, "Further Studies on Rayleigh-waves having Some Azimuthal Distribution" *Bull. Earthq. Res. Inst.*, **6** (1929), 1~18.

7) K. SEZAWA and K. KANAI, "Amplitudes of P- and S-waves at Different Focal Distances," *Bull. Earthq. Res. Inst.*, **10** (1932), 299~334.

sideration, while dealing with the differential equation in the same sense as that due to Jeans and Lord Rayleigh, we have modified the boundary conditions as follows. The usual conditions at the free boundary of the sphere in polar coordinates are such that

$$\lambda\Delta+2\mu\frac{\partial u}{\partial r}=0,\qquad \frac{\partial v}{\partial r}-\frac{v}{r}+\frac{1}{r}\frac{\partial u}{\partial\theta}=0,\qquad \frac{1}{r\sin\theta}\frac{\partial u}{\partial\phi}+\frac{\partial w}{\partial r}-\frac{w}{r}=0 \tag{1}$$

on $r=a$. Instead of the first of these equations, we have used the equation

$$\lambda\Delta+2\mu\frac{\partial u}{\partial r}=-\rho g u, \tag{2}$$

that is,

$$\frac{4}{3}\pi\gamma\rho^2 u+\lambda\Delta+2\mu\frac{\partial u}{\partial r}=0 \tag{2'}$$

on $r=a$.

2. *Mathematical solutions.*

The general solution of the problem for the case without gravitational force was solved in previous papers.[8] In the present paper we shall reinvestigate the problem from the beginning of its treatment with special regard to the earth's pressure as well as with the gravitational forces in the Earth.

The stress components in polar coordinates are such that

$$\left.\begin{aligned}
\widehat{rr}&=-p_0+\lambda\Delta+2\mu\frac{\partial u}{\partial r},\\
\widehat{\theta\theta}&=-p_0+\lambda\Delta+2\mu\left(\frac{1}{r}\frac{\partial v}{\partial\theta}+\frac{u}{r}\right),\\
\widehat{\phi\phi}&=-p_0+\lambda\Delta+2\mu\left(\frac{1}{r\sin\theta}\frac{\partial w}{\partial\phi}+\frac{v}{r}\cot\theta+\frac{u}{r}\right),\\
\widehat{\theta\phi}&=\mu\left\{\frac{1}{r}\left(\frac{\partial w}{\partial\theta}-w\cot\theta\right)+\frac{1}{r\sin\theta}\frac{\partial v}{\partial\phi}\right\},\\
\widehat{\phi r}&=\mu\left\{\frac{1}{r\sin\theta}\frac{\partial u}{\partial\phi}+\frac{\partial w}{\partial r}-\frac{w}{r}\right\},
\end{aligned}\right\} \tag{3}$$

---

[8] *loc. cit.*, 6), 7).

$$\widehat{r\theta}=\mu\left\{\frac{\partial v}{\partial r}-\frac{v}{r}+\frac{1}{r}\frac{\partial u}{\partial\theta}\right\},$$

where p_0 is the pressure at r, θ, ϕ. The equations of motion are written

$$\left.\begin{aligned}
\rho\frac{\partial^2 u}{\partial t^2}&=\rho\frac{\partial V}{\partial r}+\rho\frac{\partial W}{\partial r}+\frac{\partial\widehat{rr}}{\partial r}+\frac{1}{r}\frac{\partial\widehat{r\theta}}{\partial\theta}+\frac{1}{r\sin\theta}\frac{\partial\widehat{r\phi}}{\partial\phi}\\
&\qquad+\frac{1}{r}(2\widehat{rr}-\widehat{\theta\theta}-\widehat{\phi\phi}+\widehat{r\theta}\cot\theta),\\
\rho\frac{\partial^2 v}{\partial t^2}&=\rho\frac{1}{r}\frac{\partial V}{\partial\theta}+\rho\frac{1}{r}\frac{\partial W}{\partial\theta}+\frac{\partial\widehat{r\theta}}{\partial r}+\frac{1}{r}\frac{\partial\widehat{\theta\theta}}{\partial\theta}+\frac{1}{r\sin\theta}\frac{\partial\widehat{\theta\phi}}{\partial\phi}\\
&\qquad+\frac{1}{r}\left\{(\widehat{\theta\theta}-\widehat{\phi\phi})\cot\theta+3\widehat{r\theta}\right\},\\
\rho\frac{\partial^2 w}{\partial t^2}&=\rho\frac{1}{r\sin\theta}\frac{\partial V}{\partial\phi}+\rho\frac{1}{r\sin\theta}\frac{\partial W}{\partial\phi}+\frac{\partial\widehat{r\phi}}{\partial r}+\frac{1}{r}\frac{\partial\widehat{\theta\phi}}{\partial\theta}\\
&\qquad+\frac{1}{r\sin\theta}\frac{\partial\widehat{\phi\phi}}{\partial\phi}+\frac{1}{r}\left\{3\widehat{r\phi}+2\widehat{\theta\phi}\cot\theta\right\},
\end{aligned}\right\}\tag{4}$$

where u, v, w are components of displacement in r, θ, ϕ directions, V is the gravitational potential due to statical distribution of the mass in the Earth and W that due to increased or decreased mass per unit volume in the vibratory condition of the same Earth. On the other hand, we know that

$$\rho\frac{\partial V}{\partial r}=\frac{\partial p_0}{\partial r},\quad \rho\frac{1}{r}\frac{\partial V}{\partial\theta}=\frac{1}{r}\frac{\partial p_0}{\partial\theta},\quad \rho\frac{1}{r\sin\theta}\frac{\partial V}{\partial\phi}=\frac{1}{r\sin\theta}\frac{\partial p_0}{\partial\phi}.\tag{5}$$

Use the dilatation and rotations

$$\left.\begin{aligned}
\Delta&=\frac{1}{r^2\sin\theta}\left\{\frac{\partial}{\partial r}(r^2u\sin\theta)+\frac{\partial}{\partial\theta}(rv\sin\theta)+\frac{\partial}{\partial\phi}(rw)\right\},\\
2\varpi_r&=\frac{1}{r^2\sin\theta}\left\{\frac{\partial}{\partial\theta}(rw\sin\theta)-\frac{\partial}{\partial\phi}(rv)\right\},
\end{aligned}\right\}\tag{6}$$

$$\left.\begin{aligned}
2\varpi_\theta&=\frac{1}{r\sin\theta}\left\{\frac{\partial u}{\partial\phi}-\frac{\partial}{\partial r}(rw\sin\theta)\right\},\\
2\varpi_\phi&=\frac{1}{r}\left\{\frac{\partial}{\partial r}(rv)-\frac{\partial u}{\partial\theta}\right\},
\end{aligned}\right\}$$

then from (3), (4), (5) we find

$$\left.\begin{aligned}
\rho\frac{\partial^2u}{\partial t^2}&=\rho\frac{\partial W}{\partial r}+(\lambda+2\mu)\frac{\partial\Delta}{\partial r}-2\mu\frac{1}{r\sin\theta}\left\{\frac{\partial}{\partial\theta}(\varpi_\phi\sin\theta)-\frac{\partial\varpi_\theta}{\partial\phi}\right\},\\
\rho\frac{\partial^2v}{\partial t^2}&=\rho\frac{1}{r}\frac{\partial W}{\partial\theta}+(\lambda+2\mu)\frac{1}{r}\frac{\partial\Delta}{\partial\theta}-2\mu\frac{1}{r\sin\theta}\left\{\frac{\partial\varpi_r}{\partial\phi}-\frac{\partial}{\partial r}(r\varpi_\phi\sin\theta)\right\},\\
\rho\frac{\partial^2w}{\partial t^2}&=\rho\frac{1}{r\sin\theta}\frac{\partial W}{\partial\phi}+(\lambda+2\mu)\frac{1}{r\sin\theta}\frac{\partial\Delta}{\partial\phi}-2\mu\frac{1}{r\sin\theta}\left\{\frac{\partial}{\partial r}(r\varpi_\theta)-\frac{\partial\varpi_r}{\partial\theta}\right\}.
\end{aligned}\right\}\quad(7)$$

Eliminating u, v, w in (7) by means of (6) we obtain

$$\left.\begin{aligned}
\rho\frac{\partial^2\Delta}{\partial t^2}&=\rho\Gamma^2W+(\lambda+2\mu)\Gamma^2\Delta,\\
\rho\frac{\partial^2\varpi_r}{\partial t^2}&=\mu\left[\frac{\partial^2\varpi_r}{\partial r^2}+\frac{4}{r}\frac{\partial\varpi_r}{\partial r}+\frac{2}{r^2}\varpi_r\right.\\
&\qquad\left.+\frac{1}{r^2\sin\theta}\frac{\partial}{\partial\theta}\left(\sin\theta\frac{\partial\varpi_r}{\partial\theta}\right)+\frac{1}{r^2\sin^2\theta}\frac{\partial^2\varpi_r}{\partial\phi^2}\right],\\
\rho\frac{\partial^2\varpi_\theta}{\partial t^2}&=\mu\left[\frac{1}{r}\frac{\partial^2(\varpi_\theta r)}{\partial r^2}+\frac{1}{r^2\sin^2\theta}\frac{\partial^2\varpi_\theta}{\partial\phi^2}\right.\\
&\qquad\left.-\frac{1}{r^2\sin^2\theta}\frac{\partial^2(\varpi_\phi\sin\theta)}{\partial\phi\partial\theta}-\frac{1}{r}\frac{\partial^2\varpi_r}{\partial r\partial\theta}\right],\\
\rho\frac{\partial^2\varpi_\phi}{\partial t^2}&=\mu\left[\frac{1}{r}\frac{\partial^2(\varpi_\phi r)}{\partial r^2}+\frac{1}{r^2}\frac{\partial}{\partial\theta}\frac{1}{\sin\theta}\frac{\partial(\varpi_\phi\sin\theta)}{\partial\theta}\right.\\
&\qquad\left.-\frac{1}{r^2}\frac{\partial}{\partial\theta}\frac{1}{\sin\theta}\frac{\partial\varpi_\theta}{\partial\phi}-\frac{1}{r\sin\theta}\frac{\partial^2\varpi_r}{\partial r\partial\phi}\right].
\end{aligned}\right\}\quad(8)$$

It is possible for Poisson's equation to hold for increased or decreased mass per unit volume in the Earth, so that

$$\Gamma^2W=4\pi\gamma\rho\Delta,\qquad(9)$$

where γ is the gravitational constant. The first term of (8) reduces to

$$\rho\frac{\partial^2\Delta}{\partial t^2}-4\pi\gamma\rho\Delta=(\lambda+2\mu)\left[\frac{1}{r^2}\frac{\partial}{\partial r}\left(r^2\frac{\partial\Delta}{\partial r}\right)\right.$$

$$\left.+\frac{1}{r^2\sin\theta}\frac{\partial}{\partial\theta}\left(\sin\theta\frac{\partial\Delta}{\partial\theta}\right)+\frac{1}{r^2\sin^2\theta}\frac{\partial^2\Delta}{\partial\phi^2}\right]. \tag{10}$$

Assuming that

$$\Delta\propto\cos pt, \tag{11}$$

the solutions of (8) become

$$\left.\begin{aligned}
\Delta&=A_{mn}\frac{J_{n+\frac{1}{2}}(hr)}{\sqrt{r}}P_n^m(\cos\theta)\cos m\phi\cos pt,\\
2\varpi_r&=B_{mn}\frac{J_{n+\frac{1}{2}}(kr)}{r^{3/2}}P_n^m(\cos\theta)\sin m\phi\cos pt,\\
2\varpi_\theta&=\left[C_{mn}\frac{J_{n+\frac{1}{2}}(kr)}{\sqrt{r}}\frac{P_n^m(\cos\theta)}{\sin\theta}\right.\\
&\quad\left.+\frac{B_{mn}}{n(n+1)}\frac{1}{r}\frac{d}{dr}\left\{\sqrt{r}\,J_{n+\frac{1}{2}}(kr)\right\}\frac{dP_n^m(\cos\theta)}{d\theta}\right]\sin m\phi\cos pt,\\
2\varpi_\phi&=\left[C_{mn}\frac{J_{n+\frac{1}{2}}(kr)}{m\sqrt{r}}\frac{dP_n^m(\cos\theta)}{d\theta}\right.\\
&\quad\left.+\frac{mB_{mn}}{n(n+1)}\frac{1}{r}\frac{d}{dr}\left\{\sqrt{r}\,J_{n+\frac{1}{2}}(kr)\right\}\frac{P_n^m(\cos\theta)}{\sin\theta}\right]\cos m\phi\cos pt,
\end{aligned}\right\} \tag{12}$$

where

$$h^2=\frac{\rho p^2+4\pi\gamma\rho^2}{\lambda+2\mu},\qquad k^2=\frac{\rho p^2}{\mu}. \tag{13}$$

The solution satisfying $\varpi_r=\varpi=\varpi_\phi=0$ and corresponding to Δ is

$$\left.\begin{aligned}
u_1&=-\frac{A_{mn}}{h^2}\frac{d}{dr}\frac{J_{n+\frac{1}{2}}(hr)}{\sqrt{r}}P_n^m(\cos\theta)\cos m\phi\cos pt,\\
v_1&=-\frac{A_{mn}}{h^2}\frac{J_{n+\frac{1}{2}}(hr)}{r^{3/2}}\frac{dP_n^m(\cos\theta)}{d\theta}\cos m\phi\cos pt,\\
w_1&=\frac{mA_{mn}}{h^2}\frac{J_{n+\frac{1}{2}}(hr)}{r^{3/2}}\frac{P_n^m(\cos\theta)}{\sin\theta}\sin m\phi\cos pt.
\end{aligned}\right\} \tag{14}$$

The solution satisfying $\Delta=\varpi_r=0$ and corresponding to the respective first terms of ϖ_θ, ϖ_ϕ is

$$\left.\begin{aligned} u_3&=-\frac{n(n+1)C_{mn}}{mk^2}\frac{J_{n+\frac{1}{2}}(kr)}{r^{3/2}}P_n^m(\cos\theta)\cos m\phi\cos pt,\\ v_3&=-\frac{C_{mn}}{mk^2}\frac{1}{r}\frac{d}{dr}\left\{\sqrt{r}\;J_{n+\frac{1}{2}}(kr)\right\}\frac{dP_n^m(\cos\theta)}{d\theta}\cos m\phi\cos pt,\\ w_3&=\frac{C_{mn}}{k^2}\frac{1}{r}\frac{d}{dr}\left\{\sqrt{r}\;J_{n+\frac{1}{2}}(kr)\right\}\frac{P_n^m(\cos\theta)}{\sin\theta}\sin m\phi\cos pt. \end{aligned}\right\} \tag{15}$$

The solution satisfying $\Delta=0$ and corresponding to ϖ_r and the respective second terms of ϖ_θ, ϖ_ϕ is

$$\left.\begin{aligned} u_2&=0,\\ v_2&=\frac{mB_{mn}}{n(n+1)}\frac{J_{n+\frac{1}{2}}(kr)}{\sqrt{r}}\frac{P_n^m(\cos\theta)}{\sin\theta}\cos m\phi\cos pt,\\ w_2&=-\frac{B_{mn}}{n(n+1)}\frac{J_{n+\frac{1}{2}}(kr)}{\sqrt{r}}\frac{dP_n^m(\cos\theta)}{d\theta}\sin m\phi\cos pt. \end{aligned}\right\} \tag{16}$$

The solutions u_2, v_2, w_2 are not concerned with the stability problem because of the condition that, besides being independent of γ, it is combined neither with u_1, v_1, w_1 nor u_3, v_3, w_3.

3. *An elastic Earth of uniform density and homogeneous elasticities, the shift of mass position being neglected.*

In this case the boundary conditions are such that

$$\left.\begin{aligned} \widehat{rr}&=\lambda\Delta+2\mu\frac{\partial u}{\partial r}=0,\\ \widehat{r\theta}&=\mu\left\{\frac{\partial v}{\partial r}-\frac{v}{r}+\frac{1}{r}\frac{\partial u}{\partial\theta}\right\}=0,\\ \widehat{r\phi}&=\mu\left\{\frac{1}{r\sin\theta}\frac{\partial u}{\partial\phi}+\frac{\partial w}{\partial r}-\frac{w}{r}\right\}=0 \end{aligned}\right\} \tag{17}$$

at $r=a$. Substituting (14) and (15) in (17) we find

$$\left[\left\{\frac{\lambda}{\mu}(ha)^2-2n(n-1)\right\}J_{n+\frac{1}{2}}(ha)+2(2n+1)haJ_{n+\frac{3}{2}}ha-2(ha)^2J_{n+\frac{5}{2}}(ha)\right]$$
$$\cdot\left[2(n+1)(n-1)J_{n+\frac{1}{2}}(ka)-(2n+1)kaJ_{n+\frac{3}{2}}(ka)+(ka)^2J_{n+\frac{5}{2}}(ka)\right]$$
$$+4n(n+1)\left\{(n-1)J_{n+\frac{1}{2}}(ha)-haJ_{n+\frac{3}{2}}(ha)\right\}\left\{(n-1)J_{n+\frac{1}{2}}(ka)-kaJ_{n+\frac{3}{2}}(ka)\right\}=0, \tag{18}$$

where

$$ha=\sqrt{\frac{\rho p^2+4\pi\gamma\rho^2}{\lambda+2\mu}}a,\qquad ka=\sqrt{\frac{\rho p^2}{\mu}}a. \tag{19}$$

The critical condition under which the free vibration of the Earth becomes unstable may be expressed by $p=0$. In that case (18) reduces to

$$\frac{\lambda}{\mu}haJ_{n+\frac{1}{2}}ha+2(n+1)J_{n+\frac{3}{2}}(ha)-2haJ_{n+\frac{5}{2}}(ha)=0, \tag{20}$$

unless $n=1$. Equation (20) may also be transformed into

$$n=0;\quad \tan ha-\frac{4ha}{4-\left(\frac{\lambda}{\mu}+2\right)(ha)^2}=0, \tag{20'}$$

$$n=2;\quad \tan ha-\frac{ha\left\{120-\left(\frac{3\lambda}{\mu}+14\right)(ha)^2\right\}}{120-3\left(\frac{\lambda}{\mu}+18\right)(ha)^2+\left(\frac{\lambda}{\mu}+2\right)(ha)^4}=0, \tag{20''}$$

$$n=3;\quad \tan ha-\frac{ha\left\{1050-5\left(\frac{3\lambda}{\mu}+26\right)(ha)^2+\left(\frac{\lambda}{\mu}+2\right)(ha)^4\right\}}{1050-15\left(\frac{\lambda}{\mu}+32\right)(ha)^2+2\left(\frac{3\lambda}{\mu}+11\right)(ha)^4}=0. \tag{20'''}$$

In the case $n=1$, we have

$$3\frac{\lambda}{\mu}(ha)^2J_{\frac{3}{2}}(ha)+10haJ_{\frac{5}{2}}(ha)-6(ha)^2J_{\frac{7}{2}}(ha)=0 \tag{21}$$

instead of (20). Equation (21) reduces to

$$\tan ha - \frac{3ha\left\{20-\left(\frac{\lambda}{\mu}+2\right)(ha)^2\right\}}{60-\left(\frac{3\lambda}{\mu}+26\right)(ha)^2}=0. \tag{21'}$$

Although it may appear strange, if the number n were assigned, the critical condition would be the same irrespective of the number m, according to which the deformed figure of the Earth will differ.

Using (20′), (20″), (20‴), (21′), we obtain the critical conditions for various cases of n and λ/μ, the result being shown in Table I. In these treatments we shall assume that $\rho=5{\cdot}5$, $a=6370$ km, $\gamma=648.10^{-10}$ (C. G. S.). The velocities of transmission of longitudinal and transverse waves corresponding to the elasticities given in Table I are shown in Tables II, III.

TABLE I. The value of $\mu/10^{11}$ (C. G. S.)

n	$\lambda/\mu=1$	2	10	200
0	5·10	3·34	0·915	0·0507
1	2·62	1·566	0·441	0·0247
2	1·29	0·892	0·252	0·0152
3	0·848	0·593	0·178	0·0102

TABLE II. The value of $\sqrt{(\lambda+2\mu)/\rho}$ in km.

n	$\lambda/\mu=1$	2	10	200
0	5·28	4·95	4·47	1·370
1	3·78	3·38	3·10	0·952
2	2·65	2·55	2·35	0·748
3	2·15	2·08	1·97	0·612

TABLE III. The value of $\sqrt{\mu/\rho}$ in km.

n	$\lambda/\mu=1$	2	10	200
0	3·05	2·46	1·29	0·0959
1	2·18	1·69	0·896	0·0670
2	1·53	1·27	0·677	0·0526
3	1·24	1·04	0·369	0·0431

It will be seen that the higher the order of n, the more diminishes the value of λ or μ corresponding to the critical condition of stability for any ratio of λ/μ.

4. *An elastic Earth of uniform density and homogeneous elasticities, the shift of position of the material point being taken as a stress condition on the free surface.*

We shall next consider the case in which the condition of normal stress on the free surface is

$$\frac{4}{3}\pi\gamma\rho^2 u+\lambda\Delta+2\mu\frac{\partial u}{\partial r}=0 \tag{2'}$$

on $r=a$, the conditions of shearing stress being the same as those in the previous section. In this case the frequency equation of the vibration assumes the form

$$\begin{aligned}&\Big[\Big\{2n(3n-2)+\frac{\lambda}{\mu}(n-3)(ha)^2\Big\}J_{n+\frac{1}{2}}(ha)-ha\Big\{6(2n+1)\\&\quad+\Big(\frac{\lambda}{\mu}+2\Big)(ha)^2\Big\}J_{n+\frac{3}{2}}(ha)+6(ha)^2J_{n+\frac{5}{2}}(ha)\Big]\Big[2(n^2-1)J_{n+\frac{1}{2}}(ka)\\&\quad-(2n+1)kaJ_{n+\frac{3}{2}}(ka)+(ka)^2J_{n+\frac{5}{2}}(ka)\Big]\\&\quad+2n(n+1)\Big[(n-1)J_{n+\frac{1}{2}}(ha)-haJ_{n+\frac{3}{2}}(ha)\Big]\Big[-\Big\{6(n-1)\\&\qquad\qquad+\Big(\frac{\lambda}{\mu}+2\Big)(ka)^2\Big\}J_{n+\frac{1}{2}}(ka)+6kaJ_{n+\frac{3}{2}}(ka)\Big]=0.\end{aligned} \tag{22}$$

where $4\pi\gamma\rho^2a^2/(\lambda+2\mu)$, arising from the boundary condition, is assumed to be ha under the condition that p is ultimately made zero. In the critical case where $p=0$, (22) finally reduces to

$$n=0;\quad \tanh ha-\frac{ha\Big\{12-\Big(\frac{\lambda}{\mu}+2\Big)(ha)^2\Big\}}{4\Big\{3-\Big(\frac{\lambda}{\mu}+2\Big)(ha)^2\Big\}}=0, \tag{22^{I}}$$

$$n=1;\quad \tanh ha-\frac{3ha}{3-(ha)^2}=0, \tag{22^{II}}$$

$$n=2;\quad \tanh ha-\frac{ha\Big\{372-\Big(24-\frac{6\lambda}{\mu}\Big)(ha)^2-\Big(\frac{\lambda}{\mu}+2\Big)(ha)^4\Big\}}{372-\Big(148-\frac{6\lambda}{\mu}\Big)(ha)^2-\Big(2+\frac{3\lambda}{\mu}\Big)(ha)^4}=0, \tag{23^{III}}$$

$$n=3;\quad \tan ha-\frac{ha\left\{6480+3\left(\frac{5\lambda}{\mu}-254\right)(ha)^2-4\left(\frac{\lambda}{\mu}-1\right)(ha)^4\right\}}{6480+3\left(\frac{5\lambda}{\mu}-974\right)(ha)^2-3\left(\frac{3\lambda}{\mu}-38\right)(ha)^4+\left(\frac{\lambda}{\mu}+2\right)(ha)^6}=0. \tag{22^{\text{IV}}}$$

In this case, too, notwithstanding the differently deformed figure of the Earth, the critical condition for various cases of m is the same, provided the number n is assigned.

The result of calculation of the critical stability for the same numerical conditions as those in the previous case is shown in Table IV.

TABLE IV. The value of $\mu/10^{11}$ (C. G. S.)

n	$\lambda/\mu=1$	200
0	2·358	0·0325
1	1·010	0·0150
2	2·414	0·0333
3	1·082	0·0165

The volocities of transmisston of logitudinal and transverse waves in the media given in Table IV are shown in Table V.

TABLE V. $\sqrt{(\lambda+2\mu)/\rho}$ and $\sqrt{\mu/\rho}$ in km.

n	$\lambda/\mu=1$		$\lambda/\mu=200$	
	$\sqrt{(\lambda+2\mu)/\rho}$	$\sqrt{\mu/\rho}$	$\sqrt{(\lambda+2\mu)/\rho}$	$\sqrt{\mu/\rho}$
0	1·135	0·655	1·093	0·0769
1	0·742	0·429	0·742	0·0522
2	1·148	0·662	1·106	0·0778
3	0·768	0·444	0·779	0·0548

It will be seen from Table IV that in this case, the value of λ or μ is minimum at $n=1$ and maximum at $n=2$ but tends to decrease with further increase of n.

5. *The Earth in a stratified condition in density as well as in elasticities.*

We shall now consider the case wherein the density as well as the elastic constants of the core respectively differ from those of the rocky shell. The expressions of the general solutions for the core are the same as (14), (15), (16), whereas the solutions of the movements of the rocky shell are somewhat complex, as shown in (23) ~ (27). Let the density and elastic constants of the rocky shell be ρ', λ', μ'; then the treatments of the differential equations of elastic vibrations and Poisson's equations of gravity potential give rise to

$$\left.\begin{aligned}
\Delta' &= \left\{A'_{mn}\frac{J_{n+\frac{1}{2}}(h'r)}{r^{3/2}} + A''_{mn}\frac{Y_{n+\frac{1}{2}}(h'r)}{r^{3/2}}\right\}P_n^m(\cos\theta)\cos m\phi\cos pt,\\
2\varpi'_r &= \left\{B'_{mn}\frac{J_{n+\frac{1}{2}}(k'r)}{r^{3/2}} + B''_{mn}\frac{Y_{n+\frac{1}{2}}(k'r)}{r^{3/2}}\right\}P_n^m(\cos\theta)\sin m\phi\cos pt,\\
2\varpi'_\theta &= \Bigg[\left\{C'_{mn}\frac{J_{n+\frac{1}{2}}(k'r)}{\sqrt{r}} + C''_{mn}\frac{Y_{n+\frac{1}{2}}(k'r)}{\sqrt{r}}\right\}\frac{P_n^m(\cos\theta)}{\sin\theta}\\
&\quad + \left\{\frac{B'_{mn}}{n(n+1)}\frac{1}{r}\frac{d}{dr}\left(\sqrt{r}\,J_{n+\frac{1}{2}}(k'r)\right)\right.\\
&\quad \left. + \frac{B''_{mn}}{n(n+1)}\frac{1}{r}\frac{d}{dr}\left(\sqrt{r}\,Y_{n+\frac{1}{2}}(k'r)\right)\right\}\frac{dP_n^m(\cos\theta)}{d\theta}\Bigg]\sin m\phi\cos pt,\\
2\varpi'_\phi &= \Bigg[\left\{C'_{mn}\frac{J_{n+\frac{1}{2}}(k'r)}{m\sqrt{r}} + C''_{mn}\frac{Y_{n+\frac{1}{2}}(k'r)}{m\sqrt{r}}\right\}\frac{dP_n^m(\cos\theta)}{d\theta}\\
&\quad + \left\{\frac{B'_{mn}m}{n(n+1)}\frac{1}{r}\frac{d}{dr}\left(\sqrt{r}\,J_{n+\frac{1}{2}}(k'r)\right)\right.\\
&\quad \left. + \frac{B''_{mn}m}{n(n+1)}\frac{1}{r}\frac{d}{dr}\left(\sqrt{r}\,Y_{n+\frac{1}{2}}(k'r)\right)\right\}\frac{P_n^m(\cos\theta)}{\sin\theta}\Bigg]\cos m\phi\cos pt,
\end{aligned}\right\} \quad (23)$$

where

$$h'^2 = \frac{\rho'p^2 + 4\pi\gamma\rho'^2}{\lambda' + 2\mu'}, \quad k'^2 = \frac{\rho'p^2}{\mu'}. \quad (24)$$

The three kinds of displacement therefore assume the forms

$$\left.\begin{aligned}
u'_1 &= -\left\{\frac{A'_{mn}}{h'^2}\frac{d}{dr}\frac{J_{n+\frac{1}{2}}(h'r)}{\sqrt{r}} + \frac{A''_{mn}}{h'^2}\frac{d}{dr}\frac{Y_{n+\frac{1}{2}}(h'r)}{\sqrt{r}}\right\}P_n^m(\cos\theta)\cos m\phi\cos pt,\\
v'_1 &= -\left\{\frac{A'_{mn}}{h'^2}\frac{J_{n+\frac{1}{2}}(h'r)}{r^{3/2}} + \frac{A''_{mn}}{h'^2}\frac{Y_{n+\frac{1}{2}}(h'r)}{r^{3/2}}\right\}\frac{dP_n^m(\cos\theta)}{d\theta}\cos m\phi\cos pt,\\
w'_1 &= \left\{\frac{mA'_{mn}}{h'^2}\frac{J_{n+\frac{1}{2}}(h'r)}{r^{3/2}} + \frac{mA''_{mn}}{h'^2}\frac{Y_{n+\frac{1}{2}}(h'r)}{r^{3/2}}\right\}\frac{P_n^m(\cos\theta)}{\sin\theta}\sin m\phi\cos pt,
\end{aligned}\right\} \quad (25)$$

$$
\left.\begin{aligned}
u'_3 &= -\left\{ \frac{n(n+1)C'_{mn}}{mk'^2} \frac{J_{n+\frac{1}{2}}(k'r)}{r^{3/2}} \right. \\
&\qquad \left. + \frac{n(n+1)C''_{mn}}{mk'^2} \frac{Y_{n+\frac{1}{2}}(k'r)}{r^{3/2}} \right\} P_n^m(\cos\theta) \cos m\phi \cos pt, \\
v'_3 &= -\left\{ \frac{C'_{mn}}{mk'^2} \frac{1}{r} \frac{d}{dr}\left(\sqrt{r}\, J_{n+\frac{1}{2}}(k'r)\right) \right. \\
&\qquad \left. + \frac{C''_{mn}}{mk'^2} \frac{1}{r} \frac{d}{dr}\left(\sqrt{r}\, Y_{n+\frac{1}{2}}(k'r)\right) \right\} \frac{dP_n^m(\cos\theta)}{d\theta} \cos m\phi \cos pt, \\
w'_3 &= \left\{ \frac{C'_{mn}}{k'^2} \frac{1}{r} \frac{d}{dr}\left(\sqrt{r}\, J_{n+\frac{1}{2}}(k'r)\right) \right. \\
&\qquad \left. + \frac{C''_{mn}}{k'^2} \frac{1}{r} \frac{d}{dr}\left(\sqrt{r}\, Y_{n+\frac{1}{2}}(k'r)\right) \right\} \frac{P_n^m(\cos\theta)}{\sin\theta} \sin m\phi \cos pt,
\end{aligned}\right\} \quad (26)
$$

$$
\left.\begin{aligned}
u'_2 &= 0, \\
v'_2 &= \left\{ \frac{mB'_{mn}}{n(n+1)} \frac{J_{n+\frac{1}{2}}(k'r)}{\sqrt{r}} \right. \\
&\qquad \left. + \frac{mB''_{mn}}{n(n+1)} \frac{Y_{n+\frac{1}{2}}(k'r)}{\sqrt{r}} \right\} \frac{P_n^m(\cos\theta)}{\sin\theta} \cos m\phi \cos pt, \\
w'_2 &= -\left\{ \frac{B'_{mn}}{n(n+1)} \frac{J_{n+\frac{1}{2}}(k'r)}{\sqrt{r}} \right. \\
&\qquad \left. + \frac{B'_{mn}}{n(n+1)} \frac{Y_{n+\frac{1}{2}}(k'r)}{\sqrt{r}} \right\} \frac{dP_n^m(\cos\theta)}{d\theta} \sin m\phi \cos pt.
\end{aligned}\right\} \quad (27)
$$

In this case, too, u'_2, v'_2, w'_2 do not participate in the stability problem.

For simplicity, we shall assume that the rigidity of the core is zero, —a rather probable state of the actual core. We neglect here the effect of mass defect or excess at the free surface of the Earth resulting from the assumption of no shift of material position. The boundary conditions in this case then assume the forms

$$
\left.\begin{aligned}
r=a;\quad \lambda'\Delta' + 2\mu'\frac{\partial u'}{\partial r} = 0, &\qquad \frac{\partial v'}{\partial r} - \frac{v'}{r} + \frac{1}{r}\frac{\partial u'}{\partial \theta} = 0, \\
\frac{1}{r\sin\theta}\frac{\partial u'}{\partial \phi} + \frac{\partial w'}{\partial r} - \frac{w'}{r} = 0, &
\end{aligned}\right\} \quad (28)
$$

$$\left.\begin{aligned} r=b; \quad \lambda'\Delta'+2\mu'\frac{\partial u'}{\partial r}=\lambda\Delta, \quad \mu'\left(\frac{\partial v'}{\partial r}-\frac{v'}{r}+\frac{1}{r}\frac{\partial u'}{\partial\theta}\right)=0, \\ \mu'\left(\frac{1}{r\sin\theta}\frac{\partial u'}{\partial\phi}+\frac{\partial w'}{\partial r}-\frac{w'}{r}\right)=0, \end{aligned}\right\} \tag{29}$$

where *a*, *b* are radius of the Earth and that of its inner core respectively.

Substituting (23), (25), (26) in (28), (29), we have the relations

$$\left\{\frac{A'_{mn}}{h'^2}a'_1+\frac{A''_{mn}}{h'^2}a''_1\right\}-\left\{\frac{C'_{mn}}{k'^2}\frac{2n(n+1)}{m}c'_1+\frac{C''_{mn}}{k'^2}\frac{2n(n+1)}{m}c''_1\right\}=0, \tag{30}$$

$$\left\{\frac{A'_{mn}}{h'^2}2a'_2+\frac{A''_{mn}}{h'^2}2a''_2\right\}+\left\{\frac{C'_{mn}}{k'^2}\frac{1}{m}c'_2+\frac{C''_{mn}}{k'^2}\frac{1}{m}c''_2\right\}=0, \tag{31}$$

$$\begin{aligned} \mu'\left[\left\{\frac{A'_{mn}}{h'^2}\alpha'_1+\frac{A''_{mn}}{h'^2}\alpha''_1\right\}-\left\{\frac{C'_{mn}}{k'^2}\frac{2n(n+1)}{m}\gamma'_1+\frac{C''_{mn}}{k'^2}\frac{2n(n+1)}{m}\gamma''_1\right\}\right] \\ =\mu\left[\frac{A_{mn}}{h^2}\alpha_1-\frac{C_{mn}}{k^2}\frac{2n(n+1)}{m}\gamma_1\right], \end{aligned} \tag{32}$$

$$\begin{aligned} \mu'\left[\left\{\frac{A'_{mn}}{h'^2}2\alpha'_2+\frac{A''_{mn}}{h'^2}2\alpha''_2\right\}+\left\{\frac{C''_{mn}}{k'^2}\frac{1}{m}\gamma'_2+\frac{C''_{mn}}{k'^2}\frac{1}{m}\gamma''_2\right\}\right] \\ =\mu\left[\frac{A_{mn}}{h^2}2\alpha_2+\frac{C_{mn}}{k^2}\frac{1}{m}\gamma_2\right], \end{aligned} \tag{33}$$

$$\begin{aligned} \left\{\frac{A'_{mn}}{h'^2}\alpha'_3+\frac{A''_{mn}}{h'^2}\alpha''_3\right\}+\left\{\frac{C'_{mn}}{k'^2}\frac{n(n+1)}{m}\gamma'_3+\frac{C''_{mn}}{k'^2}\frac{n(n+1)}{m}\gamma''_3\right\} \\ =\frac{A_{mn}}{h^2}\alpha_3+\frac{C_{mn}}{k^2}\frac{n(n+1)}{m}\gamma_3, \end{aligned} \tag{34}$$

$$\left\{\frac{A'_{mn}}{h'^2}\alpha'_4+\frac{A''_{mn}}{h'^2}\alpha''_4\right\}+\left\{\frac{C'_{mn}}{k'^2}\frac{1}{m}\gamma'_4+\frac{C''_{mn}}{k'^2}\frac{1}{m}\gamma''_4\right\}=\frac{A_{mn}}{h^2}\alpha_4+\frac{C_{mn}}{k^2}\frac{1}{m}\gamma_4, \tag{35}$$

where the constants in (30) ~ (35) are as follows:

$$\left.\begin{aligned} a_1 &= \left\{\frac{\lambda}{\mu}(ha)^2-2n(n-1)\right\}J_{n+\frac{1}{2}}(ha) \\ &\qquad +2(2n+1)haJ_{n+\frac{3}{2}}(ha)-2(ha)^2J_{n+\frac{5}{2}}(ha), \end{aligned}\right|$$

$$\left.\begin{aligned}
a_1' &= \left\{\frac{\lambda'}{\mu'}(h'a)^2-2n(n-1)\right\}J_{n+\frac{1}{2}}(h'a)\\
&\qquad +2(2n+1)h'aJ_{n+\frac{3}{2}}(h'a)-2(h'a)^2J_{n+\frac{5}{3}}(h'a),\\
a_1'' &= \left\{\frac{\lambda'}{\mu'}(h'a)^2-2n(n-1)\right\}Y_{n+\frac{1}{2}}(h'a)\\
&\qquad +2(2n+1)h'aY_{n+\frac{3}{2}}(h'a)-2(h'a)^2Y_{n+\frac{5}{2}}(h'a),
\end{aligned}\right\} \tag{36}$$

$$\left.\begin{aligned}
\alpha_1 &= \left\{\frac{\lambda}{\mu}(hb)^2-2n(n-1)\right\}J_{n+\frac{1}{2}}(hb)\\
&\qquad +2(2n+1)hbJ_{n+\frac{3}{2}}(hb)-2(hb)^2J_{n+\frac{5}{2}}(hb),\\
\alpha_1' &= \left\{\frac{\lambda'}{\mu'}(h'b)^2-2n(n-1)\right\}J_{n+\frac{1}{2}}(h'b)\\
&\qquad +2(2n+1)h'bJ_{n+\frac{3}{2}}(h'b)-2(h'b)^2J_{n+\frac{5}{2}}(h'b),\\
\alpha_1'' &= \left\{\frac{\lambda'}{\mu'}(h'b)^2-2n(n-1)\right\}Y_{n+\frac{1}{2}}(h'b)\\
&\qquad +2(2n+1)h'bY_{n+\frac{3}{2}}(h'b)-2(h'b)^2Y_{n+\frac{5}{2}}(h'b),
\end{aligned}\right\} \tag{37}$$

$$\begin{aligned}
c_1,\ c_1',\ c_1'',&=(n-1)\left\{J_{n+\frac{1}{2}}(ka),\ J_{n+\frac{1}{2}}(k'a),\ Y_{n+\frac{1}{2}}(k'a)\right\}\\
&\qquad -a\left\{kJ_{n+\frac{3}{2}}(ka),\ k'J_{n+\frac{3}{2}}(k'a),\ k'Y_{n+\frac{3}{2}}(k'a)\right\},
\end{aligned} \tag{38}$$

$$\begin{aligned}
\gamma_1,\ \gamma_1',\ \gamma_1'',&=(n-1)\left\{J_{n+\frac{1}{2}}(kb),\ J_{n+\frac{1}{2}}(k'b),\ Y_{n+\frac{1}{2}}(k'b)\right\}\\
&\qquad -b\left\{kJ_{n+\frac{3}{2}}(kb),\ k'J_{n+\frac{3}{2}}(k'b),\ k'Y_{n+\frac{3}{2}}(k'b)\right\},
\end{aligned} \tag{39}$$

$$\begin{aligned}
a_2,\ a_2',\ a_2'',&=-(n-1)\left\{J_{n+\frac{1}{2}}(ha),\ J_{n+\frac{1}{2}}(h'a),\ Y_{n+\frac{1}{2}}(h'a)\right\}\\
&\qquad +a\left\{hJ_{n+\frac{3}{2}}(ha),\ h'J_{n+\frac{3}{2}}(h'a),\ h'Y_{n+\frac{3}{2}}(h'a)\right\},
\end{aligned} \tag{40}$$

$$\alpha_2,\ \alpha_2',\ \alpha_2'',=-(n-1)\left\{J_{n+\frac{1}{2}}(hb),\ J_{n+\frac{1}{2}}(h'b),\ Y_{n+\frac{1}{2}}(h'b)\right\}$$

$$+b\left\{hJ_{n+\frac{3}{2}}(hb),\ h'J_{n+\frac{3}{2}}(h'b),\ h'Y_{n+\frac{3}{2}}(h'b)\right\}, \qquad (41)$$

$$c_2,\ c_2',\ c_2'',=-2(n^2-1)\left\{J_{n+\frac{1}{2}}(ka),\ J_{n+\frac{1}{2}}(k'a),\ Y_{n+\frac{1}{2}}(k'a)\right\}$$

$$+(2n+1)a\left\{kJ_{n+\frac{3}{2}}(ka),\ k'J_{n+\frac{3}{2}}(k'a),\ k'Y_{n+\frac{3}{2}}(k'a)\right\}$$

$$-a^2\left\{k^2J_{n+\frac{5}{2}}(ka),\ k'^2J_{n+\frac{5}{2}}(k'a),\ k'^2Y_{n+\frac{5}{2}}(k'a)\right\}, \qquad (42)$$

$$\gamma_2,\ \gamma_2',\ \gamma_2'',=-2(n^2-1)\left\{J_{n+\frac{1}{2}}(kb),\ J_{n+\frac{1}{2}}(k'b),\ Y_{n+\frac{1}{2}}(k'b)\right\}$$

$$+(2n+1)b\left\{kJ_{n+\frac{3}{2}}(kb),\ k'J_{n+\frac{3}{2}}(k'b),\ k'Y_{n+\frac{3}{2}}(k'b)\right\}$$

$$-b^2\left\{k^2J_{n+\frac{5}{2}}(kb),\ k'^2J_{n+\frac{5}{2}}(k'b),\ k'^2Y_{n+\frac{5}{2}}(k'b)\right\}, \qquad (43)$$

$$\alpha_3,\ \alpha_3',\ \alpha_3'',=n\left\{J_{n+\frac{1}{2}}(hb),\ J_{n+\frac{1}{2}}(h'b),\ Y_{n+\frac{1}{2}}(h'b)\right\}$$

$$-b\left\{hJ_{n+\frac{3}{2}}(hb),\ h'J_{n+\frac{3}{2}}(h'b),\ h'Y_{n+\frac{3}{2}}(h'b)\right\}, \qquad (44)$$

$$\gamma_3,\ \gamma_3',\ \gamma_3'',=J_{n+\frac{1}{2}}(kb),\ J_{n+\frac{1}{2}}(k'b),\ Y_{n+\frac{1}{2}}(k'b), \qquad (45)$$

$$\alpha_4,\ \alpha_4',\ \alpha_4'',=J_{n+\frac{1}{2}}(hb),\ J_{n+\frac{1}{2}}(h'b),\ Y_{n+\frac{1}{2}}(h'b), \qquad (46)$$

$$\gamma_4,\ \gamma_4',\ \gamma_4'',=(n+1)\left\{J_{n+\frac{1}{2}}(kb),\ J_{n+\frac{1}{2}}(k'b),\ Y_{n+\frac{1}{2}}(k'b)\right\}$$

$$-b\left\{kJ_{n+\frac{3}{2}}(kb),\ k'J_{n+\frac{3}{2}}(k'b),\ k'Y_{n+\frac{3}{2}}(k'b)\right\}. \qquad (47)$$

Eliminating A'_{mn}, A''_{mn}, ……, C'_{mn} between (30) ~ (35), it is possible to get the frequency equation of the free vibration.

It is an outstanding fact that, were $\mu=0$, the volume elasticity λ as well as density ρ in the core have no place in the problem of elastic stability of the Earth.

Using the equations (30) ~ (47) and assuming that the density of the rocky shell is $\rho'=4{\cdot}5$, we get the values of λ', μ' at which the stability is critical, the result being shown in Table VI. The velocities of transmission of longitudinal and transverse waves in the media shown in Table VI are tabulated in Table VII.

TABLE VI. The values of $\mu'/10^{11}$ in (C. G. S.)

n	$\lambda'/\mu'=1$	2	200
0	5·75	4·58	2·715
1	0·691	——	——
2	0·770	——	——

TABLE VII. $\sqrt{(\lambda'+2\mu')/\rho'}$ and $\sqrt{\mu'/\rho'}$ in km.

n	$\lambda'/\mu'=1$		2		200	
	$\sqrt{(\lambda'+2\mu')/\rho'}$	$\sqrt{\mu'/\rho'}$	$\sqrt{(\lambda'+2\mu')/\rho'}$	$\sqrt{\mu'/\rho'}$	$\sqrt{(\lambda'+2\mu')/\rho'}$	$\sqrt{\mu'/\rho'}$
0	1·959	1·131	2·01	1·0059	11·04	0·779
1	0·680	0·392	——	——	——	——
2	0·716	0·414	——	——	——	——

In this case, provided the ratis of λ'/μ' is not too large, the general properties with respect to the critical condition of stability is fairly similar to those of the condition shown in Section 3 and somewhat similar to those of the condition shown is Section 4. For a large ratio of λ'/μ', say $\lambda'/\mu'=200$, the lowest values of λ', μ' are $\lambda'=5{\cdot}43{\cdot}10^{13}$, $\mu'=2{\cdot}715{\cdot}10^{11}$ respectively. Thus, were the rocky shell incompressible, namely $\mu'/\lambda'\to 0$, the Earth would be gravitationally unstable, even at such a large value of $\lambda'=5{\cdot}43{\cdot}10^{13}$ as hardly obtains in the actual rocks of the Earth's crust.

6. *General discussion of the result.*

Our mathematical solutions show that for the case in which the Earth is entirely uniform in its density as well as elasticities and we neglect the mass defect or excess on the free surface resulting from the assumption that the position of the mass never shifts, the greater the value of n, greater the decrease in the values of λ and μ at which the elastic stability of the Earth is critical, whereas, on the other hand, in the case where the mass effect on the free surface under consideration is taken into account, the value of λ or μ which is minimum at

$n=1$, and maximum at $n=2$, tends to diminish with further increase of n.

It is now possible to imagine that the past condition of the Earth has gradually changed from an extremely deformable state to a more and more rigid one. Thus, if in the past stage of the Earth, its elasticities were less than those of any of the n's in Table IV, the vibrational motion of the Earth for the mode corresponding to every n would have been unstable. We shall assume that the Poisson's ratio is 1/4. Then, the respective vibrational modes $n=0$, 1, 2, 3, ... are unstable, provided $\lambda(=\mu)$ is less than 2·358, 1·010, 2·414, and 1·082 respectively. Similar conditions exist for different Poisson's ratios. Had the elastic constants of the Earth gradually increased, the next stage to be expected would be such that, while the vibrational modes corresponding to $n=1$ is stable, every other mode will be still unstable. With further increase in elastic constants, the modes $n=3$ then becomes stable, and so on. Since, on the other hand, the deformed state is likely to remain unchanged in the condition of higher elastic constants, owing to the probably lower temperature of the solid in that condition, the traces of the unstable state of such a mode as became stable in a relatively later stage will be marked. It follows then that the traces of the past unstable conditions for $n=0$ and $n=2$ would be pronounced. Among other modes traces of instability for the cases $n=3$ as well as $n=1$ would be quite marked. It is impossible for us at present to discuss the cases in which n is greater than 4. But so far as our present investigation is concerned, the conclusion at which we arrive is that traces of the past unstable character of case $n=0$ and $n=2$, that is the cases corresponding to the spherical type and the spheroidal (or particular ellipsoidal) type, will probably be very marked. The particular ellipsoidal type in question indicates such a condition as ($n=2$, $m=1$) or ($n=2$, $m=2$). It should be borne in mind that the above explanation is probable for every case of Poisson's ratio.

From the results in Sections 3, 4, 5 it appears that the problem for the case in which there is a core of no rigidity is likely to assume the character just mentioned, even without regard to the effect of mass defect or excess on the free surface.

Since, furthermore, both cases $n=1$, $n=3$ are also unstable conditions at a stage somewhat earlier than that for $n=0$ or $n=2$, it is impossible to conclude that no trace of the deformation of a pear-shaped type or tetrahedral type can ever remain in the present figure of the Earth.

The question may be raised as to whether or not the condition of

elastic stability might be affected by such a high viscosity of the Earth as is extremely possible at a high-temperature stage of the same Earth. Since, however, the present problem concerns a divergent stability, and not oscillatory stability, the damping effect has virtually very little place in the criteria already given.

53. 極座標上から出した地球の彈性的安定の問題

地震研究所 妹澤克惟
金井清

地球が重力を受けて彈性的に不安定になる問題は Jeans が始めて考へ Lord Rayleigh も之に興味を持つた．しかし物質の點の平均位置が動く事まで考慮に入れて問題を解いたのは Love である．之を核の場合迄延長した松澤博士の計算がある．之等は主として Lamb の考へた直角座標を應用する方法であるが，我々の場合には極座標を用ひて解いた所の似た問題があつたから，之を只今の安定の問題に延長して見たのである．

物理的の考方としてはJeansのやうな場合と，物質點の動く影響を入れたものとの二種を試み，始めの種類では核のある場合をも計算して見たのである．しかし何れの場合にも彈性的變形の結果として現れる重力に關する Poisson の式が大い物を言ふのである．

計算の結果，變形に可なりの違ひを與へる m の如何に拘らず，n が一定でありさへすれば，安定極限が一致することがわかつた．又，層のある場合に核の剛性が零であるとすると核の變容彈性率や，質量（質量の方は近似的）に關係なく安定極限のきまることもわかつたのである．

計算の結果を綜合して見るのに，若し地球が高溫から低溫に向ひ，同時に軟い狀態から剛い狀態に移つたものであるとすると，最も最近に變形の安定の狀態に達した振動狀態は $n=0$ と $n=2$ の場合である．卽ち球形の儘の變形と楕圓體型の變形とであり，且つ之等は殆ど同時であるといつてよい．それより少しく以前の階梯では $n=1$ と $n=3$ とが殆ど同時に安定の狀態に達したのである．卽ち，西洋梨型の變形と四面體型の變形とである．後の階梯程，地球の溫度が低いと考へられ，溫度が低い程一度できた變形が後迄殘ると考へられるから，$n=0$ と $n=2$ との場合が現在の地球の形に最もよく痕跡を殘すものといひ得る．$n=1$ と $n=3$ の場合は上述のもの程ではなくても，他の形から見ると遙かによくその痕跡が殘るといひ得るのである．

地球の歷史的階梯を論ずる位であるから，その高溫時に於ける粘性が彈性的安定を大いに支配するのでないかといふ疑が起るかも知れぬ．しかしここに論ずるのは divergent stability を論ずるのであつて電氣振動にあるやうな oscillatory stability を問題にするのでないから，粘性の影響は自然に消去されるものである．

54. *The Plastic State of the Earth under Gravitational Forces.*

By Katsutada SEZAWA,

Earthquake Research Institute.

(Read July 6, 1937.—Received Sept. 20, 1937.)

1. *The probable plastic condition of the rocky shell.*

In the previous paper[1] I examined the possible plastic condition of the earth's core on the assumption that the rocky shell is almost incompressible, the conclusion pointing to the contingency that were the rocky shell fairly compressible, the material in the same shell would also be plastic. It is well known that the earth's core is in a fluid state, whereas the shell next to it is solid, the reason of which is probably that, although the actual temperature in the core is higher than the melting point of the metals in that core, the same temperature is still lower than the melting point of the rock under hydrostatic pressure corresponding to that of the core. My previous conclusion with respect to the difference in the plastic properties between the earth's core and the shell consequently involves certain ambiguities. From my new calculation it appears that, while the material in the rocky shell may be so compressible that their condition is almost plastic, those in the central part of the earth's core would even be elastic, provided the plastic constants there were the same as that of the shell. But, since the material in the central part, because of the high temperature, will asume extremely low plastic constants, the elastic condition just cited virtually does not exist.

In the present paper we shall assume that the rocky shell next to the core is composed of two layers; namely, the outermost layer 480 km thick that was found by Jeffreys[2] and the next one 2420 km (=2900 km −480 km) thick, every one of the respective layers and the core being of uniform density.

Let a, b, c be the radii of the respective outer boundaries of the outermost layer, the intermediate shell, and the core, their values being

---

[1] K. SEZAWA, "On the Plastic Properties of the Earth's Core," *Bull. Earthq. Res. Inst.*, **15** (1937), 582~589.

[2] H. JEFFREYS, "On the Materials and Density of Earth's Crust," M.N.R.A.S. *Geophys. Suppl.* **4** (1937), *No.* 1, 50~61.

6370 km, 5890 km, and 3470 km respectively. Let also ρ_1, ρ_2, ρ_3 be the densities of the three parts under consideration. Then, from the formula

$$V=\frac{4\pi}{r}\gamma\int_0^r \rho r'^2 dr+4\pi\gamma\int_r^\infty \rho r' dr', \tag{1}$$

the gravitational potentials of the three parts assume the forms

$$\left.\begin{aligned}
V_1&=\frac{4\pi\gamma}{3r}\left\{c^3(\rho_3-\rho_2)+b^3(\rho_2-\rho_1)\right\}+2\pi\gamma\rho_1\left(a^2-\frac{r^2}{3}\right),\\
V_3&=\frac{4\pi\gamma}{3r}c^3(\rho_3-\rho_2)+2\pi r b^2(\rho_2-\rho_1)-\frac{2}{3}\pi\gamma r^2\rho_2+2\pi\gamma a^2\rho_1,\\
V_3&=2\pi\gamma c^2(\rho_3-\rho_2)-\frac{2\pi\gamma}{3}r^2\rho_3+2\pi\gamma b^2(\rho_2-\rho_1)+2\pi\gamma a^2\rho_1,
\end{aligned}\right\} \tag{2}$$

γ, r being the gravitational constant and the radius respectively of any point in the Earth. The rates of pressure change with radius are then

$$\left.\begin{aligned}
\frac{\partial p_1}{\partial r}&=\rho_1\frac{\partial V_1}{\partial r}=\frac{-4\pi\gamma}{3r^2}\left\{c^3\rho_1(\rho_3-\rho_2)+b^3\rho_1(\rho_2-\rho_1)\right\}-\frac{4\pi\gamma\rho_1{}^2 r}{3}\\
&=-\frac{\xi_1}{r^2}-\eta_1 r,\\
\frac{\partial p_2}{\partial r}&=\rho_2\frac{\partial V_2}{\partial r}=-\frac{4\pi\gamma}{3r^2}c^3\rho_2(\rho_3-\rho_2)-\frac{4\pi\gamma\rho_2{}^2 r}{3}=-\frac{\xi_2}{r^2}-\eta_2 r,\\
\frac{\partial p_3}{\partial r}&=\rho_3\frac{\partial V_3}{\partial r}=-\frac{4\pi\gamma\rho_3{}^2 r}{3}=-\eta_3 r.
\end{aligned}\right\} \tag{3}$$

If every medium were in elastic condition, the equations of equilibrium would be of the forms

$$\left.\begin{aligned}
\frac{-\xi_1}{r^2}-\eta_1 r+(\lambda_1+2\mu_1)\left(\frac{\partial^2 u_1}{\partial r^2}+\frac{2}{r}\frac{\partial u_1}{\partial r}-\frac{2u_1}{r^2}\right)&=0,\\
\frac{-\xi_2}{r^2}-\eta_2 r+(\lambda_2+2\mu_2)\left(\frac{\partial^2 u_2}{\partial r^2}+\frac{2}{r}\frac{\partial u_2}{\partial r}-\frac{2u_2}{r^2}\right)&=0,\\
-\eta_3 r+(\lambda_3+2\mu_3)\left(\frac{\partial^2 u_3}{\partial r^2}+\frac{2}{r}\frac{\partial u_3}{\partial r}-\frac{2u_3}{r^2}\right)&=0,
\end{aligned}\right\} \tag{4}$$

where the suffixes 1, 2, 3 refer to the three media under consideration. The solutions of these equations are

$$\left.\begin{aligned} u_1&=\frac{-\xi_1}{2(\lambda_1+2\mu_1)}+\frac{\eta_1 r^3}{10(\lambda_1+2\mu_1)}+B_1 r+\frac{C_1}{r^2},\\ u_2&=\frac{-\xi_2}{2(\lambda_2+2\mu_2)}+\frac{\eta_2 r^3}{10(\lambda_2+2\mu_2)}+B_2 r+\frac{C_2}{r^2},\\ u_3&=\frac{-\eta_3 r^3}{10(\lambda_3+2\mu_3)}+B_3 r. \end{aligned}\right\} \tag{5}$$

The corresponding stresses are such that

$$\begin{aligned} \widehat{rr}_1&=\frac{-\xi_1\lambda_1}{(\lambda_1+2\mu_1)}\frac{1}{r}+\frac{\eta_1(10\lambda_1+12\mu_1)}{20(\lambda_1+2\mu_1)}r_2+(3\lambda_1+2\mu_1)B_1-\frac{4\mu_1 C_1}{r^3},\\ \widehat{\theta\theta}_1=\widehat{\phi\phi}_1&=\frac{-\xi_1(\lambda_1+\mu_1)}{(\lambda_1+2\mu_1)}\frac{1}{r}+\frac{\eta_1(10\lambda_1+4\mu_1)}{20(\lambda_1+2\mu_1)}r^2+(3\lambda_1+2\mu_1)B_1+\frac{2\mu_1 C_1}{r^3},\\ \widehat{rr}_2&=\frac{-\xi_2\lambda_2}{(\lambda_2+2\mu_2)}\frac{1}{r}+\frac{\eta_2(10\lambda_2+12\mu_2)}{20(\lambda_2+2\mu_2)}r^2+(3\lambda_2+2\mu_2)B_2-\frac{4\mu_2 C_2}{r^3},\\ \widehat{\theta\theta}_2=\widehat{\phi\phi}_2&=\frac{-\xi_2(\lambda_2+\mu_2)}{(\lambda_2+2\mu_2)}\frac{1}{r}+\frac{\eta_2(10\lambda_2+4\mu_2)}{20(\lambda_2+2\mu_2)}r^2+(3\lambda_2+2\mu_2)B_2+\frac{2\mu_2 C_2}{r^3},\\ \widehat{rr}_3&=\frac{\eta_3(10\lambda_3+12\mu_3)}{20(\lambda_3+2\mu_3)}r^2+(3\lambda_3+2\mu_3)B_3,\\ \widehat{\theta\theta}_3=\widehat{\phi\phi}_3&=\frac{\eta_3(10\lambda_3+4\mu_3)}{20(\lambda_3+2\mu_3)}r_3+(3\lambda_3+2\mu_3)B_3. \end{aligned} \tag{6}$$

From the boundary conditions that

$$\left.\begin{aligned} &r=a; && \widehat{rr}_1=0, &&\\ &r=b; && \widehat{rr}_1=\widehat{rr}_2, && u_1=u_2,\\ &r=c; && \widehat{rr}_2=\widehat{rr}_3, && u_2=u_3, \end{aligned}\right\} \tag{7}$$

it is possible to determine B_1, C_1. B_2, C_2, B_3, which, however, is somewhat complex. If, however, the differences $\rho_3-\rho_2$, $\rho_2-\rho_1$, $\lambda_1-\lambda_2$, $\lambda_2-\lambda_3$, $\mu_1-\mu_2$, $\mu_2-\mu_3$ are fairly small, we can put $C_1=0$, $C_2=0$, from which we have

$$\left.\begin{aligned} \widehat{rr}_1-\widehat{\theta\theta}_1&=\frac{8\mu_1\pi\gamma\rho_1^2}{15(\lambda_1+2\mu_1)}r^2,\\ \widehat{rr}_2-\widehat{\theta\theta}_2&=\frac{8\mu_2\pi\gamma\rho_2^2}{15(\lambda_2+2\mu_2)}r^2, \end{aligned}\right\} \tag{8}$$

$$\widehat{rr}_3-\widehat{\theta\theta}_3=\frac{8\mu_3\pi\gamma\rho_3^2}{15(\lambda_3+2\mu_3)}r^2. \quad \Bigg)$$

These expressions show that the lateral (horizontal) compression $\widehat{\theta\theta}$ (or $\widehat{\phi\phi}$) is always larger than the radial (vertical) compression $\widehat{rr}$; for example, at $r=a$, $\widehat{rr}_1=0$, $\widehat{\theta\theta}_1=8\mu_1\pi\gamma\rho_1^2r^2/15(\lambda_1+2\mu_1)$. It will be seen that the differences under consideration tend to increase with increase in r. Put $\gamma=648\cdot10^{-10}$, $\rho_1=3\cdot5$, $\rho_2=4\cdot5$, $\rho_3=11$, $\lambda_1=\mu_1$, $\lambda_2=\mu_2$. Then $\widehat{rr}_1-\widehat{\theta\theta}_1$ for different radii assumes the values shown in Table I.

TABLE I.

r (km)	6370	5890	5890	5500	5000	4500	4000	3470	3470	0
$10^{-11}(\widehat{rr}-\widehat{\theta\theta})$ in C. G. S.	1·79	1·53	2·54	2·21	1·92	1·48	1·16	0·88	0	0

Jeffreys conjectured the distribution of tenacity of the earth's crust to be that as shown in Table II. d in Table II denotes the depth beneath the ultrabasic layer. Since tenacity may be taken as $2k$ (k being the plastic constant) at any rate in the order of its value, it is possible to assume that the materials are in a plastic state at almost any depth in the earth, with the exception of the central part of the earth's core.

TABLE II.

d (km)	0	30	300	1000
Tenacity. 10^{-9}	1·5	0·61	0·092	0·009

2. *The plastic equilibrium of the earth.*

With the condition that all the layers of the rocky shell, besides the core, are almost in a plastic state, it is now possible to deal with the earth as a plastic body. The equations of equilibrium assume the forms

$$\left.\begin{aligned}&-\frac{\xi_1}{r^2}-\eta_1 r+\frac{\partial\widehat{rr}_1}{\partial r}+\frac{2}{r}(\widehat{rr}_1-\widehat{\theta\theta}_1)=0,\\&-\frac{\xi_2}{r^2}-\eta_2 r+\frac{\partial\widehat{rr}_2}{\partial r}+\frac{2}{r}(\widehat{rr}_2-\widehat{\theta\theta}_2)=0,\end{aligned}\right\}\qquad(9)$$

---

[3] H. **Jeffreys**, "On the Relation between Fusion and Strength," *Phil. Mag.*, **19** (1935), 840~846.

$$-\eta_3 r+\frac{\partial \widehat{rr}_3}{\partial r}+\frac{2}{r}(\widehat{rr}_3-\widehat{\theta\theta}_3)=0,$$

provided, owing to the conditions of symmetry, the relations $\widehat{\theta\theta}_1=\widehat{\phi\phi}_1$, $\widehat{\theta\theta}_2=\widehat{\phi\phi}_2$, $\widehat{\theta\theta}_3=\widehat{\phi\phi}_3$ exist.

Let k_1, k_2, k_3 be the plastic constants of the successive three layers. Then

$$\widehat{rr}_1-\widehat{\theta\theta}_1=2k_1, \qquad \widehat{rr}_2-\widehat{\theta\theta}_2=2k_2, \qquad \widehat{rr}_3-\widehat{\theta\theta}_3=2k_3. \tag{10}$$

Substituting (10) in (9) and solving the resulting equations, we have

$$\left.\begin{aligned}
&\widehat{rr}_1+4k_1\log r+\frac{\xi_1}{r}-\frac{\eta_1 r^2}{2}+I_1=0,\\
&\widehat{rr}_2+4k_2\log r+\frac{\xi_2}{r}-\frac{\eta_2 r^2}{2}+I_2=0,\\
&\widehat{rr}_3+4k_3\log r+\frac{\xi_3}{r}-\frac{\eta_3 r^2}{2}+I_3=0,
\end{aligned}\right\} \tag{11}$$

where I_1, I_2, I_3 are integration constants. The boundary conditions are

$$\left.\begin{aligned}
&r=a; && \widehat{rr}_1=0,\\
&r=b; && \widehat{rr}_1=\widehat{rr}_2,\\
&r=c; && \widehat{rr}_2=\widehat{rr}_3.
\end{aligned}\right\} \tag{12}$$

Substituting (11) in (12) and determining I_1, I_2, I_3, we obtain

$$\left.\begin{aligned}
\widehat{rr}_1&=\xi_1\Big(\frac{1}{a}-\frac{1}{r}\Big)-\frac{\eta_1}{2}(a^2-r^2)+4k_1\log\frac{a}{r},\\
\widehat{rr}_2&=\Big\{\xi_1\Big(\frac{1}{a}-\frac{1}{b}\Big)+\xi_2\Big(\frac{1}{b}-\frac{1}{r}\Big)\Big\}-\Big\{\frac{\eta_1}{2}(a^2-b^2)+\frac{\eta_2}{2}(b^2-r^2)\Big\}\\
&\qquad +4k_1\log\frac{a}{b}+4k_2\log\frac{b}{r},\\
\widehat{rr}_3&=\Big\{\xi_1\Big(\frac{1}{a}-\frac{1}{b}\Big)+\xi_2\Big(\frac{1}{b}-\frac{1}{c}\Big)\Big\}-\Big\{\frac{\eta_1}{2}(a^2-b^2)+\frac{\eta_2}{2}(b^2-c^2)\\
&\qquad +\frac{\eta_3}{2}(c^2-r^2)\Big\}+4k_1\log\frac{a}{b}+4k_2\log\frac{b}{c}+4k_3\log\frac{c}{r},
\end{aligned}\right\} \tag{13}$$

$$\left.\begin{aligned}\widehat{\theta\theta}_1&=\widehat{\phi\phi}_1=\widehat{rr}_1-2k_1,\\ \widehat{\theta\theta}_2&=\widehat{\phi\phi}_2=\widehat{rr}_2-2k_2,\\ \widehat{\theta\theta}_3&=\widehat{\phi\phi}_3=\widehat{rr}_3-2k_3,\end{aligned}\right\}\tag{14}$$

where

$$\left.\begin{aligned}&\xi_1=\frac{4\pi\gamma}{3}\left\{c^3\rho_1(\rho_3-\rho_2)+b^3\rho_1(\rho_2-\rho_1)\right\}, && && \eta_1=\frac{4\pi\gamma\rho_1^2}{3},\\ &\xi_2=\frac{4\pi\gamma}{3}c^3\rho_2(\rho_3-\rho_2), && \eta_2=\frac{4\pi\gamma\rho_2^2}{3}, && \eta_3=\frac{4\pi\gamma\rho_3^2}{3}.\end{aligned}\right\}\tag{15}$$

On the free surface $r=a$, we have

$$\widehat{rr}_1=0, \qquad \widehat{\theta\theta}_1=\widehat{\phi\phi}_1=-2k_1, \tag{16}$$

which prove that there is lateral (horizontal) compression even on the free surface of the earth.

In the special case $\rho_1=\rho_2=\rho_3(=\rho)$, $k_1=k_2=k_3(=k)$, we get

$$\left.\begin{aligned}\widehat{rr}_1=\widehat{rr}_2=\widehat{rr}_3&=-\frac{\eta}{2}(a^2-r^2)+4k\log\frac{a}{r},\\ \widehat{\theta\theta}_1=\widehat{\theta\theta}_2=\widehat{\theta\theta}_3&=-\frac{\eta}{2}(a^2-r^2)+4k\log\frac{a}{r}-2k.\end{aligned}\right\}\tag{17}$$

The angle β, which the slip surface makes with any radius, is obtained in the same way as that shown previously, namely

$$\tan 2\beta=\frac{\widehat{rr}-\widehat{\theta\theta}}{2\widehat{r\theta}}=\frac{\widehat{rr}-\widehat{\phi\phi}}{2\widehat{r\phi}}, \tag{18}$$

where $\widehat{r\theta}=0$, $\widehat{r\phi}=0$. From the equation of the slip surfaces

$$\frac{rd\theta}{dr}\left(=\frac{rd\phi}{dr}\right)=\tan\beta, \tag{19}$$

we get

$$\theta_n=A_n\log r, \qquad \phi_n=B_n\log r \tag{20}$$

for every layer.

3. *The possible existence of an elastic continent.*

The earth's crust near its surface, as a whole, is subjected to high lateral pressure. If, on the other hand, a continental layer were, owing to its boundary edges or fault surfaces in it, in such a state as to be free from lateral pressure, the condition in some cases would possibly be elastic.

In this case the three strain components

$$\frac{\partial u}{\partial r}, \qquad \frac{u}{r}+\frac{1}{r}\frac{\partial v}{\partial \theta}, \qquad \frac{u}{r}+\frac{v}{r}\cot\theta+\frac{1}{r\sin\theta}\frac{\partial w}{\partial \phi} \tag{21}$$

reduce to

$$\frac{\partial u}{\partial r}, \qquad \frac{u}{r}+\frac{c}{r}, \qquad \frac{u}{r}+\frac{c}{r}, \tag{22}$$

c being a constant, so that

$$\Delta=\frac{\partial(u+c)}{\partial r}+\frac{2(u+c)}{r}. \tag{23}$$

Were u replaced by $u+c$, all the conditions of the problem would be the same as in Section 1. Thus we find that

$$\left.\begin{aligned}\widehat{rr}_1&=\frac{-\xi_1\lambda_1}{\lambda_1+2\mu_1}\frac{1}{r}+\frac{\eta_1(10\lambda_1+12\mu_1)}{20(\lambda_1+2\mu_1)}+(3\lambda_1+2\mu_1)B_1-\frac{4\mu_1C_1}{r^3},\\ \widehat{\theta\theta}_1&=\frac{-\xi_1(\lambda_1+\mu_1)}{(\lambda_1+2\mu_1)}\frac{1}{r}+\frac{\eta_1(10\lambda_1+4\mu_1)}{20(\lambda_1+2\mu_1)}+(3\lambda_1+2\mu_1)B_1+\frac{2\mu_1C_1}{r^3}.\end{aligned}\right\} \tag{25}$$

The boundary conditions are

$$\left.\begin{aligned}&r=a'; \qquad \widehat{rr}_1=0, \qquad \widehat{\theta\theta}_1=0,\\ &r=(a'-t); \qquad \widehat{rr}_1-\widehat{\theta\theta}_1=-2k_1,\end{aligned}\right\} \tag{26}$$

where a' is the radius of the continental surface with respect to the earth's centre and t_1 the depth from the free surface at which the crustal state varies from elastic to plastic. The negative sign $-2k_1$ in (25) was taken because of the condition that, in the present case, the value of the vertical compression exceeds that of the horizontal. Substituting (24) in (25) and eliminating terms higher than the second order in t_1, we get

$$t_1=\frac{\lambda_1+2\mu_1}{\mu_1}\frac{k_1}{(\eta_1a'+\xi_1/a'^2)}. \tag{26}$$

Using the numerical values shown in Section 1 and putting $2k_1=5.10^9$, $\lambda_1=\mu_1$, we get

$$t_1 = 8{\cdot}6\ km.$$

This results from the condition that $\widehat{\theta\theta}_1$ and $\widehat{\phi\phi}_1$ are approximately zero not only at the surface $r=a'$, but almost at any depth near the same surface.

4. *The difference between shallow- and deep-focus earthquakes.*

The actual condition of the crust is such that stresses in the same crust arise from two kinds of statical disturbances, namely, continental loading and the spherical symmetrical central attraction, both being gravitational. Even should the two distubances under consideration be of the same origin, owing to the difference between the respective conditions of their application it would be rather in order to consider the additive effects of the two disturbances thus separated.

The stresses due to continental loading may now be represented by

$$\left.\begin{aligned} r&=a'; & \widehat{rr}_1&=0, \\ r&<a'; & \widehat{rr}_1-\widehat{\theta\theta}_1&=-f(r), \end{aligned}\right\} \tag{27}$$

where $f(r)$ varies increasingly to a certain depth, but diminishes with further increase in depth in consequence of the isostatic support of the continent. $f(r)$ may thus assume the empirical form

$$f(r)=c_1te^{-c_2t}, \tag{28}$$

where t is the depth and c_1, c_2 are constants.

The spherically symmetrical central force gives rise to

$$\widehat{rr}_1-\widehat{\theta\theta}_1=\frac{8\mu_1\pi\gamma\rho_1^2}{15(\lambda_1+2\mu_1)}r^2 \quad (\equiv\varphi(r)), \qquad (r<a) \tag{29}$$

r being nearly equal to a in this case.

It may be assumed that, although not strictly so, the sum of $-f(r)$ and $\varphi(r)$ is the resultant stress condition of the actual crust, the sign of $-f(r)$ being always opposite to that of $\varphi(r)$. Thus, we get

$$\left.\begin{aligned} \sum(\widehat{rr}_1-\widehat{\theta\theta}_1)&=-c_1te^{-c_2t}, & &\Big[t<(a'-a)\Big] \\ \sum(\widehat{rr}_1-\widehat{\theta\theta}_1)&=\frac{8\mu_1\pi\gamma\rho_1^2}{15(\lambda_1+2\mu_1)}a^2-c_1te^{-c_2t}, & &\Big[t>(a'-a)\Big] \end{aligned}\right\} \tag{30}$$

from which it is possible to get the conditions

$$\left.\begin{array}{ll} \sum(\widehat{rr}_1-\widehat{\theta\theta}_1)<2k_1, & (t<t_1) \\ 2k_1<\sum(\widehat{rr}_1-\widehat{\theta\theta}_1), & (t_1<t<t_2) \\ -2k_1<\sum(\widehat{rr}_1-\widehat{\theta\theta}_1)<2k_1, & (t_2<t<t_3) \\ \sum(\widehat{rr}_1-\widehat{\theta\theta}_1)<-2k_1, & (t_3<t) \end{array}\right\} \quad (31)$$

in which, in the majority of cases, $t_1<(a'-a)$, $t_2>(a'-a)$, and $t_3>t_2$.

It appears that $t_1<t<t_2$ gives the depth corresponding to the case of a shallow seismic focus and $t_3<t$ that corresponding to the case of a deep-seated earthquake. In the range $t_1<t<t_2$, the value of the vertical compression exceeds that of the horizontal, whereas in the range $t_3<t$, the horizontal compression is invariably larger than the vertical, the two ranges under consideration being plastic. The intermediate range $t_2<t<t_3$, on the other hand, is elastic in consequence of the condition that the value $|\sum(\widehat{rr}_1-\widehat{\theta\theta}_1)|$ in such a range never exceeds $2k_1$. The reason why an earthquake of intermediate depth, say 100 km, scarcely ever occurs will now be apparent.

The above result suggests that, generally speaking, earthquakes are prone to occur at such depths wherein the condition of the earth's crust varies from elastic to plastic under gravitational forces. Since from the nature of things, the value of $|2(\widehat{rr}_1-\widehat{\theta\theta}_1)|$ in the range of depth $t_1<t<t_2$ does not greatly exceed $2k_1$, $t_1<t<t_2$ may be assumed to be an almost continuous range within which exist shallow-focus earthquakes. On the other hand, deep-focus earthqnakes generally originate within a certain range of depth, say, from 200 km to 400 km. In this range the condition of the crust varies from elastic to plastic. No earthquake occurs at still greater depths because of the perfect plastic condition of the crust at such depths. It should, however, be borne in mind that, for simplicity, we have dealt with the plastic problem of the crust of the outermost layer under the assumption that k_1 is always constant. In the condition of varying k_1 as is actually the case, the problem should be modified to a certain extent.

Added Oct. 20, 1937.—It is possible to know that the folding as well as the reverse fault can be formed by the horizontal compression in excess of the vertical one as a mere result of the central gravitational force, whereas the normal fault arises from the additional action of the continental or mountain loading.

54. 重力を受ける地球のプラスチック釣合

地震研究所 妹澤克惟

この前の論文に於て地球の核だけがプラスチック性であるとすると岩石層までも非壓縮性でなければならぬといふ結論に達した．しかしそれは多少無理であるから更に地球全體を公平に取扱つて見ると殆ど地球全體がプラスチック性となるのである．地球の核は單に金屬性であり高壓に於けるその融解點が内部の溫度よりも低いことに過ぎぬやうである．

地球の表面近くでは橫壓が鉛直壓よりも大きくその結果としてプラスチック性をなすものである．地球の極く中心ではすべての方向の壓力が均一に近づき，從て若しそのプラスチックの常數が表面と同じであれば，その附近のみが彈性體といふことになるが，溫度等の關係から常數が非常に低くその結果やはりプラスチック性をなすものである．

大陸はその自由な周圍の爲に球形體の重力をその儘では受け難く，大陸の極く表面ではある深さまで鉛直壓が橫壓よりも大きくなる．卽ち極く表面は別としてそれ以下の深さではプラスチック體をなすのである．更に少しく深くなると普通の球形體の中心力の作用が大きくなり，その影響である過大橫壓と互に打消してプラスチック體でなくなる傾向がある．一層深くなると橫壓の方が超過して再びプラスチック體となるのである．しかし大陸の表面近くの場合とは過大壓力の方向が違つてをる譯である．

若し地震の源が地殼の彈性體の部分に隣りする部分のプラスチック體の所に存在するものであるとすると，上記の二つのプラスチック層は淺發地震と深發地震の震源層を與へることになる．又二つの層の中間の層は彈性體の性質がある故に震源になり得ないといふ結果にも到達するのである．又，下層のプラスチック體の更に深い所は彈性と隣りしないプラスチック體であり，地震に關係がないことになるのである．

地質學者はしばしば地表附近に橫壓力を假定する．若し自由な周圍の大陸は考へずに單純な地球のみを取つて見ると，重力に起因して橫壓力が當然存在することがわかるのである．卽ち褶曲や Reverse fault の說明がつく．之に反して大陸や山の存在を考へるときに Normal fault の機構がわかる譯である．

55. *Prevalent Periods of Oscillation in Tidal Waves.*

By Katsutada SEZAWA and Kiyoshi KANAI,

Earthquake Research Institute.

(Read July 6, 1937.—Received Sept. 20, 1937.)

1. *Introduction.*

The tidal waves (tunami) that accompanied the earthquake of March 3, 1933, were transmitted through the Pacific Ocean and reached various stations along the coast surrounding that ocean. With respect to these tidal waves, there is, however, some uncertainty as to whether, in the train of waves, it is the beginning phase or the phase of the largest amplitude or any other, that was really transmitted with velocity $\sqrt{g\eta}$, η being the mean depth of the part of the ocean through which the tidal waves were transmitted.

The oscillatory features of sea waves have been discussed by a number of mathematiceans, such as Lord Kelvin,1) Lord Rayleigh,2) Lamb,3) Pidduck,4) and Terazawa,5) but their problems mainly concerned the case wherein the waves are produced by a single impulse. Solutions of such a case are not likely to determine the relation between the amplitudes of surface waves due to periodic forces and the ratio of the length of the generated waves to the depth of the sea. Our last investigation6) with respect to Love-waves suggests that the treatment used therein also applies, in principle, to the present case. It was thus possible for us to find the relation in the case of the tidal waves under consideration.

2. *Tidal waves caused by periodic change of surface pressure.*

Since the nature of tidal waves is almost the same irrespective of whether the disturbance is applied to the sea bed or to the free surface, we shall now consider the case in which a periodic pressure is applied to the free surface.

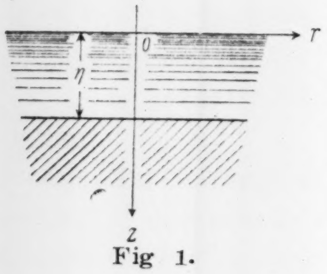

Fig 1.

In the case of a two-dimensional propagation of gravity waves, the differential equa-

---

1) Lord KELVIN, *Proc. Roy. Soc.*, **42** (1887), 80~83.
2) Lord RAYLEIGH, *Phil. Mag.*, (6), **43** (1909), 1~6.
3) H. LAMB, *Proc. Math. Soc.*, (2), **2** (1904), 371~400; *Hydrodynamics*, IX.
4) F. B. PIDDUCK, *Proc. Roy. Soc.*, **83** (1910), 347~356.
5) K. TERAZAWA, *Proc. Roy. Soc.*, **92** (1915), 57~81.
6) K. SEZAWA and K. KANAI, *Bull. Earthq. Res. Inst.*, **15** (1937), 577~581.

tion assumes the form

$$\frac{\partial^2\phi}{\partial r^2}+\frac{1}{r}\frac{\partial\phi}{\partial r}+\frac{\partial^2\phi}{\partial z^2}=0. \tag{1}$$

If the origin of z is on the free surface of the water, the solution of (1) is

$$\phi=Ce^{-ipt}\cosh f(z-\eta)J_0(fr), \tag{2}$$

where η is the depth of the water. Let u, w be the horizontal and vertical displacements of a water particle, then

$$\frac{\partial u}{\partial t}=-\frac{\partial\phi}{\partial r}, \qquad \frac{\partial w}{\partial t}=-\frac{\partial\phi}{\partial z}, \tag{3}$$

whence

$$u=\frac{if}{p}e^{-ipt}C\cosh f(z-\eta)J_1(fr), \tag{4}$$

$$w=-\frac{if}{p}e^{-ipt}C\sinh f(z-\eta)J_0(fr). \tag{5}$$

Since

$$\frac{p_1}{\rho}=\frac{\partial\phi}{\partial t}-gw \tag{6}$$

on the free surface $z=0$, we have

$$p_1=-i\rho Ce^{-ipt}\frac{p^2\cosh f\eta-fg\sinh f\eta}{p}J_0(fr). \tag{7}$$

From Fouriers' integral

$$p_1=e^{-ipt}\int_0^\infty J_0(fr)\,fdf\int_0^\infty F(\alpha)J_0(f\alpha)\,\alpha\,d\alpha, \tag{8}$$

where $F(r)$ is the pressure distribution on the free surface. We shall take the case of a pressure distribution such that

$$e^{-ipt}F(r)=\frac{e^{-ipt}}{\sqrt{c^2+r^2}}, \tag{9}$$

then, since

$$\int_0^\infty\frac{J_0(f\alpha)\,\alpha\,d\alpha}{\sqrt{c^2+\alpha^2}}=\frac{e^{-fc}}{f},^{7)} \tag{10}$$

---

7) K. **Terazawa**, *loc. cit.* 6).

we have

$$p_1 = e^{-ipt}\int_0^\infty e^{-fc} J_0(fr)\,df. \tag{11}$$

From (7) and (11)

$$C = -\frac{p_1}{i\rho}\int_0^\infty \frac{e^{-fc}df}{p^2\cosh f\eta - fg\sinh f\eta}. \tag{12}$$

From (4), (5), (12) we have

$$u = \frac{-e^{-ipt}}{\rho}\int_0^\infty \frac{fe^{-fc}\cosh f(z-\eta)}{p^2\cosh f\eta - fg\sinh f\eta} J_1(fr)\,df, \tag{13}$$

$$w = \frac{e^{-ipt}}{\rho}\int_0^\infty \frac{fe^{-fc}\sinh f(z-\eta)}{p^2\cosh f\eta - fg\sinh f\eta} J_0(fr)\,df. \tag{14}$$

3. *An alternative method of deducing the displacement expression, and additional results.*

The result shown in the preceding section may be obtained alternatively. Let an idealised centre of applied pressure be at $r=0$, $z=-c$. The pressure that diminishes inversely as the radial distance from that centre is then expressed by

$$p_0 = \frac{e^{-ipt}}{\sqrt{r^2+(z+c)^2}}. \tag{15}$$

(i) In the case wherein the pressure is applied to the free surface, we have $c>0$, the expression of the pressure on that surface then being

$$p_0 = \frac{e^{-ipt}}{\sqrt{r^2+c^2}}, \tag{16}$$

which is of the same form as that in (9).

(ii) In the case of a subaqueous disturbance, $0>c>-\eta$. Then, putting $c=-c_1$, we obtain

$$p_0 = \frac{e^{-ipt}}{\sqrt{r^2+(z-c_1)^2}}. \tag{17}$$

(iii) When the pressure is applied to the sea bed, $-\eta>c$ and p_0

is again of the same form as (17).

We shall first consider the case (i). In this case

$$\frac{e^{-ipt}}{\sqrt{r^2+(z+c)^2}}=\frac{e^{-ipt}}{R}=e^{-ipt}\int_0^\infty e^{-f(z+c)}J_0(fr)\,df. \tag{18}$$

The pressure transmission in water is, in idea, nothing more than wave transmission. If (15) or (17) be the initial waves, there are an infinite number of successive reflected waves (namely, the pressure) formed at the free surface as well as on the sea bed. Thus in Case (i) we obtain

$$\begin{aligned} p_0' &= e^{-ipt}\int_0^\infty\Big[e^{-f(z+c)}+e^{f(z-c-2\eta)}-e^{-f(z+c+2\eta)}-e^{f(z-c-4\eta)}+\cdots\Big]J_0(fr)\,df \\ &= e^{-ipt}\int_0^\infty\frac{e^{-f(z+c)}+e^{f(z-c-2\eta)}}{1+e^{-2f\eta}}J_0(fr)\,df=e^{-ipt}\int_0^\infty\frac{e^{-fc}\cosh f\,(z-\eta)}{\cosh f\eta}J_0(fr)\,df. \end{aligned} \tag{19}$$

In case (ii) we have

$$\left.\begin{aligned} p_0' &= \frac{e^{-ipt}}{\sqrt{r^2+(z-c_1)^2}}=e^{-ipt}\int_0^\infty e^{-f(z-c_1)}J_0(fr)\,df, \quad [z-c_1>0] \\ &= e^{-ipt}\int_0^\infty e^{f(z-c_1)}J_0(fr)\,df, \quad [z-c_1<0] \end{aligned}\right\} \tag{20}$$

whence

$$\begin{aligned} p_0' = e^{-ipt}\int_0^\infty\Big[&e^{-f(z-c_1)}+e^{f(z+c_1-2\eta)}-e^{-f(z-c_1+2\eta)}-e^{f(z+c_1-4\eta)}+\cdots \\ &-e^{-f(z+c_1)}-e^{f(z-c_1-2\eta)}+e^{-f(z+c_1+2\eta)}+e^{f(z-c_1-4\eta)}-\cdots\Big]J_0(fr)\,df \\ = e^{-ipt}&\int_0^\infty\frac{2\sinh fc_1\cosh f(\eta-z)}{\cosh f\eta}J_0(fr)\,df, \quad [z-c_1>0] \end{aligned}$$

$$\begin{aligned} p_0' = e^{-ipt}\int_0^\infty\Big[&e^{f(z-c_1)}-e^{-f(z+c_1)}-e^{f(z-c_1-2\eta)}+e^{-f(z+c_1+2\eta)}+e^{f(z-c_1-4\eta)}-\cdots \\ &+e^{f(z+c_1-2\eta)}-e^{-f(z-c_1+2\eta)}-e^{f(z+c_1-4\eta)}+\cdots\Big]J_0(fr)\,df \\ = e^{-ipt}&\int_0^\infty\frac{2\sinh fz\cosh f(\eta-c_1)}{\cosh f\eta}J_0(fr)\,df. \quad [z-c_1<0] \end{aligned} \tag{21}$$

In Case (iii) we have

$$p_0' = e^{-ipt}\int_0^\infty \left[e^{f(z-c_1)} - e^{-f(z+c_1)} - e^{f(z-c_1-2\eta)} + e^{-f(z+c_1+2\eta)} + \cdots \right] J_0(fr)\,df$$

$$= e^{-ipt}\int_0^\infty \frac{e^{-(c_1-\eta)}\sinh fz}{\cosh f\eta} J_0(fr)\,df. \quad (22)$$

We shall particularly consider Case (i). From (6), gravity waves whose surface pressure is not zero, may assume the same forms as (4), (5). The surface pressure in such waves is then

$$p_1 = -i\rho C e^{-ipt} \frac{p^2\cosh f\eta - fg\sinh f\eta}{p} J_0(fr), \quad (7')$$

which must be equal to p_0' in (18), namely,

$$p_1 = p_0', \quad (23)$$

so that

$$C = -\frac{p}{i\rho}\int_0^\infty \frac{e^{-fc}\,df}{p^2\cosh f\eta - fg\sinh f\eta}. \quad (12')$$

Whence it follows that

$$u = -\frac{e^{-ipt}}{\rho}\int_0^\infty \frac{fe^{-fc}\cosh f(z-\eta)}{p^2\cosh f\eta - fg\sinh f\eta} J_1(fr)\,df, \quad (13')$$

$$w = \frac{e^{-ipt}}{\rho}\int_0^\infty \frac{fe^{-fc}\sinh f(z-\eta)}{p^2\cosh f\eta - fg\sinh f\eta} J_0(fr)\,df. \quad (14')$$

(13′), (14′) are thus equivalent to (13), (14) respectively.

For the case in which the disturbance is applied to the sea bed or at any depth beneath the water surface, (4), (5) should be substituted in Bernoulli's equation, the expression of pressure thus formed being equated to that in (21) or (22) for a specified surface, say, $z=\eta$. A more convenient method of obtaining the same solution is, however, the one shown in one[8] of our previous papers.

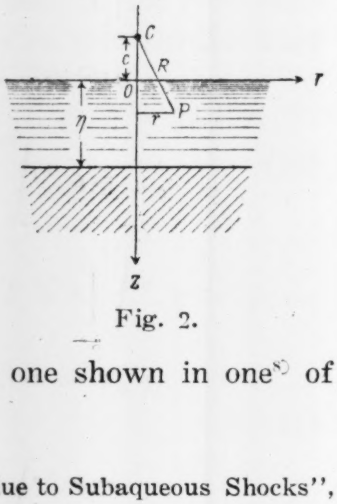

Fig. 2.

---

[8] K. SEZAWA, "Formation of Shallow-water Waves due to Subaqueous Shocks", *Bull. Earthq. Res. Inst.*, **7** (1929), 15∼40.

4. *Evaluation of the integrals for the waves, with results.*

We shall now evaluate (13), (14). Since

$$\left.\begin{aligned} J_0(fr) &= \frac{-i}{\pi}\int_0^\infty (e^{ifr\cosh k} - e^{-ifr\cosh k})\,dk, \\ J_1(fr) &= -\frac{1}{\pi}\int_0^\infty (e^{ifr\cosh k} + e^{-ifr\cosh k})\cosh k\,dk, \end{aligned}\right\} \tag{24}$$

u, w become

$$u = \frac{e^{-ipt}}{\pi\rho}\int_0^\infty \cosh k\,dk\int_0^\infty \frac{e^{-fc}(e^{ifr\cosh k} + e^{-ifr\cosh k})f\cosh f(z-\eta)}{p^2\cosh f\eta - fg\sinh f\eta}\,df, \tag{25}$$

$$w = -\frac{ie^{-ipt}}{\pi\rho}\int_0^\infty dk\int_0^\infty \frac{e^{-fc}(e^{ifr\cosh k} - e^{-ifr\cosh k})f\sinh f(z-\eta)}{p^2\cosh f\eta - fg\sinh f\eta}\,df, \tag{26}$$

so that

$$u_{z=0} = \frac{e^{-ipt}}{\pi\rho}\int_0^\infty \cosh k\,dk\int_0^\infty \frac{e^{-fc}(e^{ifr\cosh k} + e^{-ifr\cosh k})\,f\,df}{p^2 - fg\tanh f\eta}, \tag{27}$$

$$w_{z=0} = \frac{ie^{-ipt}}{\pi\rho}\int_0^\infty dk\int_0^\infty \frac{e^{-fc}(e^{ifr\cosh k} - e^{-ifr\cosh k})\,f\,df}{p^2\coth f\eta - fg}. \tag{28}$$

We must now evaluate the integrals of the following types

$$\int_0^\infty \frac{e^{-ic+ifr\cosh k}f\,df}{p^2 - fg\tanh f\eta},\quad \int_0^\infty \frac{e^{-fc+ifr\cosh k}f\,df}{p^2\coth f\eta - fg}, \qquad \text{(29A), (29B)}$$

$$\int_0^\infty \frac{e^{-fc-ifr\cosh k}f\,df}{p^2 - fg\tanh f\eta},\quad \int_0^\infty \frac{e^{-fc-ifr\cosh k}f\,df}{p^2\coth f\eta - fg}. \qquad \text{(30A), (30B)}$$

The integrals in (29A), (29B) are taken round the upper contour in Fig. 3 and those in (30A), (30B) round the lower contour in the same figure

Let the solutions of $p^2 - fg\tanh f\eta$ be $f=\alpha$, $f=i\beta_1$, $f=i\beta_2, \cdots$, then remembering that

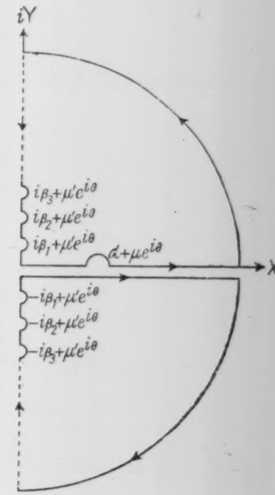

iY
$i\beta_3+\mu' e^{i\theta}$
$i\beta_2+\mu' e^{i\theta}$
$i\beta_1+\mu' e^{i\theta}$
$\alpha+\mu e^{i\theta}$
X
$-i\beta_1+\mu' e^{i\theta}$
$-i\beta_2+\mu' e^{i\theta}$
$-i\beta_3+\mu' e^{i\theta}$

Fig. 3.

$$F(\alpha+\mu e^{i\theta})=F(\alpha)+\frac{F'(\alpha)}{1!}\mu e^{i\theta}+\frac{F''(\alpha)}{2!}(\mu e^{i\theta})^2+\cdots, \tag{31}$$

we obtain

$$\begin{aligned}(29\text{A})+(29\text{B})=&\frac{-2\pi i\alpha e^{-\alpha c+i\alpha r\cosh k}}{g(\tanh\alpha\eta+\alpha\eta\,\mathrm{sech}^2\alpha\eta)}-\int_0^\infty\frac{e^{-fr\cosh k}fdf}{p^2+fg\tan f\eta}2\cos fc\\&+\sum_n\frac{\pi\beta_n e^{-\beta_n r\cosh k}2i\sin\beta_n c}{g(\tan\beta_n\eta+\beta_n\eta\sec^2\beta_n\eta)}.\end{aligned} \tag{32}$$

Although the second term of the right-hand side tends to zero for $r\to\infty$, yet with a view to obtaining its solution in more accurate form, its mathematical evaluation will now be performed.

Put

$$\frac{2\cos fc}{p^2+fg\tan f\eta}=\psi(f), \tag{33}$$

and write

$$\psi(f)=\psi(0)+\frac{\psi'(0)}{1!}f+\frac{\psi''(0)}{2!}f^2+\cdots, \tag{34}$$

where

$$\psi(0)=\frac{1}{p^2},\ \psi'(0)=0,\ \psi''(0)=\frac{-(c^2p^2+2g\eta)}{p^4},\cdots\cdots\cdots\cdots, \tag{35}$$

then

$$\int_0^\infty\psi(f)e^{-fr\cosh k}fdf=\int_0^\infty 2\left\{\frac{1}{p^2}f-\frac{(c^2p^2+2g\eta)}{2p^4}f^3+\cdots\right\}e^{-fr\cosh k}df. \tag{36}$$

By means of the formula⁹⁾

$$\int_0^\infty e^{-fy}f^x df=y^{-(x+1)}\Pi(x), \tag{37}$$

(36) reduces to

$$\int_0^\infty\psi(f)e^{-fr\cosh k}fdf=2\left[\frac{1}{(pr\cosh k)^2}-\frac{3(c^2p^2+2g\eta)}{(pr\cosh k)^4}+\cdots\right]. \tag{38}$$

Now, by means of the integral

---

9) E. JAHNKE u. F. EMDE, *Funktionentafeln*, S. 28.

$$\int_0^\infty \left\{ \frac{1}{(pr\cosh k)^2} - \frac{3(c^2p^2+2g\eta)}{(pr\cosh k)^4} + \cdots \right\} \cosh k dk$$

$$= \int_0^\infty \left\{ \frac{1}{(pr)^2} \frac{d\sinh k}{1+\sinh^2 k} - \frac{3(c^2p^2+2g\eta)}{(pr)^4} \frac{d\sinh k}{(1+\sinh^2 k)^2} + \cdots \right\}$$

$$= \frac{\pi}{2} \left\{ \frac{1}{(pr)^2} - \frac{3(c^2p^2+2g\eta)}{(pr)^4} + \cdots \right\}, \qquad (39)$$

and

$$\left. \begin{aligned} &\int_0^\infty \cosh k e^{i\alpha r \cosh k} dk = -\frac{\pi}{2} H_1^{(1)}(\alpha r), \\ &\int_0^\infty \cosh k e^{-\beta_n r \cosh k} dk = K_1(\beta_n r), \end{aligned} \right\} \qquad (40)^{10)}$$

we get

$$u_{z=0} = \frac{e^{-ipt}}{\rho} \left[\frac{i\pi\alpha e^{-\alpha c} H_1^{(1)}(\alpha r)}{g(\tanh \alpha\eta + \alpha\eta \operatorname{sech}^2 \alpha\eta)} + \frac{2i}{g} \sum_n \frac{\beta_n \sin \beta_n c K_1(\beta_n r)}{\tan \beta_n \eta + \beta_n \eta \sec^2 \beta_n \eta} \right.$$

$$\left. - \left\{ \frac{1}{(pr)^2} - \frac{3(c^2p^2+2g\eta)}{2(pr)^4} + \cdots \right\} \right]. \qquad (41)$$

This is the final solution of $u_{z=0}$.

In the same way it is possible to evaluate the integral for $w_{z=0}$. After performing the contour integrals corresponding to (29B), (30B) and using the relations

$$\left. \begin{aligned} &\int_0^\infty e^{i\alpha r \cosh k} dk = \frac{\pi i}{2} H_0^{(1)}(\alpha r), \\ &\int_0^\infty e^{-\beta_n r \cosh k} dk = K_0(\beta_n r), \end{aligned} \right\} \qquad (42)$$

we get

$$w_{z=0} = \frac{e^{-ipt}}{\rho} \left[\frac{i\pi\alpha e^{-\alpha c} H_0^{(1)}(\alpha r)}{p^2\eta \operatorname{cosech}^2 \alpha\eta + g} - 2i \sum_n \frac{\beta_n \sin \beta_n c K_0(\beta\ r)}{g - p^2\eta \operatorname{cosec}^2 \beta^n \eta} \right.$$

$$\left. + \frac{\eta}{r} \left\{ \frac{1}{(pr)^2} - \frac{9(c^2p^2+2g\eta)}{2(pr)^4} + \cdots \right\} \right]. \qquad (43)$$

---

10) Theory of Bessel Functions, p. 180.

Equations (41), (43) show that the movement of the surface consists of three parts. The first is the one due to gravity waves, whose velocity of transmission is related to the wave length as well as to the depth of the ocean, their amplitudes decaying in agreement with the law of two-dimensional propagation of waves. The second and third parts, on the other hand, lack the features of propagation waves, but represent oscillations like standing waves. While the amplitude corresponding to the second part varies as Bessel's functions of imaginary argument, that corresponding to the third one decays inversely as the second and third powers of the distance from the origin both for the respective u- and w-components of displacement. Strictly speaking, these amplitudes change furthermore with change in the ratio of the length of the generated waves to the depth of the sea, its nature being shown in the next section.

5. *The relation between the length of the tidal waves and sea depth.*

For a relatively large value of r, such asymptotic expansions as

$$H_0^{(1)}(\alpha r)=\sqrt{\frac{2}{\pi\alpha r}}\,e^{i\left(\alpha r-\frac{\pi}{4}\right)},\qquad H_1^{(1)}(\alpha r)=\sqrt{\frac{2}{\pi\alpha r}}\,e^{i\left(\alpha r-\frac{3\pi}{4}\right)} \tag{44}$$

may preferably be used. The part of the tidal waves in the solutions of $u_{z=0}$, $w_{z=0}$ then assumes the forms

$$u_{z=0}=\left\{i\sqrt{\frac{2\pi\eta}{r}}\,\frac{e^{i\left(-pt+\alpha r-\frac{3\pi}{4}\right)}}{\rho g}\right\}\frac{\sqrt{\alpha\eta}\,e^{-\alpha c}}{\tanh\alpha\eta+\alpha\eta\,\mathrm{sech}^2\alpha\eta}, \tag{45}$$

$$w_{z=0}=\left\{i\sqrt{\frac{2\pi\eta}{r}}\,\frac{e^{i\left(-pt+\alpha r-\frac{\pi}{4}\right)}}{\rho g}\right\}\frac{\sqrt{\alpha\eta}\,e^{-\alpha c}}{\frac{p^2\eta}{g}\mathrm{cosech}^2\alpha\eta+1}. \tag{46}$$

From (45), (46) we have obtained the relation between η/λ, (λ being wave length) and the amplitude of tidal waves for three cases of c/η, namely (i) $c/\eta=1/10$, (ii) $c/\eta=1$, (iii) $c/\eta=10$, the results being shown in Fig. 4. The symbol K in Fig. 4 is written in lieu of the respective first factors of the expression $u_{z=0}$, $w_{z=0}$ in (41). The velocity of propagation of the waves (p/f) is also shown by broken lines in the same figure.

It will be seen from Fig. 4 that the vertical displacement of the wave motion assumes its maximum value for a certain ratio of η/λ. With increase of c/ξ, namely, with increase in the area of the applied disturbance, the value of η/λ tends to decrease. In other words, were the area of the applied disturbance large, the vertical amplitude of a relatively longer wave would then be maximum. The horizontal displacement of wave motion tends to decrease with increase in λ in almost every case of c/η, with the exception that c/η is very small, say 0·1, where u, which tends once to decrease with η/λ, again augments for a relatively large value of η/λ, say $\eta/\lambda > 0{\cdot}2$.

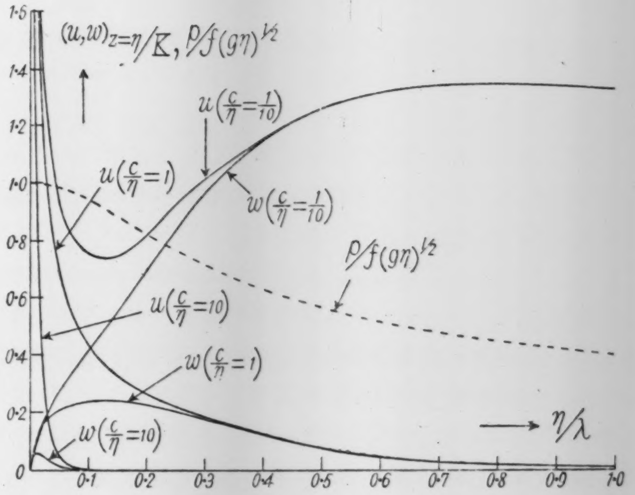

Fig. 4.

It appears that for a fairly large value of η/λ the value of $|u|$ and that of $|w|$ are the same, indicating that the waves are then deep-sea waves, whereas for a smaller value of η/λ the ratio of $|w|/|u|$ becomes negligible, showing the condition that the waves are then long tidal waves.

It appears also that, provided the length of the waves is given, the vertical displacement assumes a relatively large value for a smaller value of c/η, that is to say, the more the pressure concentrated at the very vicinity of the central point of the source, the larger the amplitudes of the generated waves.

In the actual tidal waves (tunami), were the area of the original disturbance given, waves of a certain range of length would be predominant in their train. If, on the other hand, the vibrational frequency were given, the amplitudes of the waves would be more pronounced in the case of a sharp, concentrated original disturbance. It is now possible to conclude that the large amplitudes of tidal waves in the earthquake of 1933 were not the mere effect of a relatively broad area of the seismic origin. Those tidal waves were probably produced by earthquake shocks of certain suddeness occurring in a rather small area, the velocity of transmission of such waves being considerably smaller than $\sqrt{g\eta}$. The conclusion that the beginning phase of a wave train came from the boundary of some large area of the sea bed should now give way to our idea, namely, that the waves were generated from the origin of a relatively small area and transmitted with a velocity much less than $\sqrt{g\eta}$.

55. 振動性津浪の卓越周期

地震研究所 {妹澤克惟
　　　　　 {金井　清

1933 年 3 月の地震に伴つた津浪は太平洋岸にある多くの驗潮儀に記錄された．たとひその津浪が振動性であつても傳播の途中や驗潮儀で減衰力の爲に鈍い振動性となつてしまふから實測の結果を直ちに理論と比較することはむづかしい．しかし單に理論から考へると，原振動力が一定であつてもその振動週期によつて振幅が特に大きくなる場合があるのである．且つその場合の津浪傳播速度は $\sqrt{g\eta}$（η は海の平均深さ）よりも少いものである．

以上の事柄を正確な數理を以てしらべて見たところが，以上の性質は原點に働く力の周期のみでなく，力の働く面積によつて著しく異なることがわかつた．c^2 がこの面積を代表し，λ が波長を示すとすれば，例へば $c/\eta=1/10$ のときには $\eta/\lambda=0{\cdot}5\sim1{\cdot}0$ の範圍で津浪の高さが著しくなり $c/\eta=10$ になると $\eta/\lambda=0{\cdot}01$ 位のところで津浪の高さが高くなり得ることがわかつた．卽ち力の働く面積が大きい程長い波長の津浪が現れ易くなることが知られるのである．

津浪の水平流れは如何なる場合にも η/λ が大きくなる程減少する．但し特別に $c/\eta=1/10$ の如き小なる c の場合には η/λ とともに水平流れが一度減少するけれども $\eta/\lambda=0{\cdot}2$ 以上では再び增加する傾向を持ち，その上で更に減少するものである．

一般に極端に長い λ の場合卽ち $\eta/\lambda\to0$ の場合には水平流れのみ大きく津浪の高さは殆ど無い程度であり，逆に極端に短い波長の場合には津浪の高さとその水平の流れ（表面での）は同じ大きとなり，深海波の性質を備へるに至るものである．

實際の津浪の場合に，原力の働く面積が一定であればある範圍の波長（又は周期）の波が津浪の中に卓越することになる．又振動周期が一定の場合を考へると，原面積が小さなもの程波高が高くなるものである．以上の事から，津浪の高いものが必しも廣い面積から起されるのでなく，場合によつては寧ろ狹い面積のときに高さが高くなり，且つそのときの傳播速度は $\sqrt{g\eta}$ よりも遙かに少いことがわかる．このやうにして出來た鋭い振動のものが傳播の途中で鈍くなり，結果として長波長のものが $\sqrt{g\eta}$ よりも遲い速度で傳つたやうに見えることもあるものであらう．

56. Deformation of the Earth's Crust in Idu Peninsula in Connection with the Destructive Idu Earthquake of Nov. 26, 1930.

By Seiti YAMAGUTI,

Earthquake Research Institute.

(Read March 16, 1937.—Received. Sept. 20, 1937.)

C. Tsuboi[1] has already studied the deformation of the earth's crust in the regions that were severely disturbed by the Idu destructive earthquake of Nov. 26, 1930. Since, at the time of his study, horizontal displacements caused by the earthquake of only 13 second-order trigonometrical points in the regions were available, detailed discussion was impossible. The object of the present paper is to discuss the same problem in greater detail using as data the horizontal and vertical displacements of 71 third-order trigonometrical points in this region which have been measured and placed at our disposal recently by the Military Land Survey. It is hoped to find some physical relationship between the vertical and horizontal displacements of the earth's crust.

The displacements of the trigonometrical points to be discussed were derived from comparisons of their geographical positions after the Idu earthquake and those after the great Kwantô earthquake of 1923. With 71 observed values of eastward (u) and northward (v) components of the displacements, two diagrams indicating u- and v-contours were drawn. On each of these diagrams, two series of parallel lines were drawn with intervals of 2 km., of which the one in EW and the other in NS directions. The values of u anr v at intersections of the lines were estimated by interpolation. In Fig. 1, the displacements of each of the mesh-points are shown by arrows, the heads of which are consecutively connected by straight lines in order that one may visualise the horizontal deformation of the earth's crust. A seismic fault, called the Tanna Fault, appeared at the time of the earthquake of 1930.

Referring to axes x and y, which were taken towards E and N, respectively, the values of $\frac{\partial u}{\partial x}$, $\frac{\partial u}{\partial y}$, $\frac{\partial v}{\partial x}$, and $\frac{\partial v}{\partial y}$ were calculated in the following way. Referring to the square shown in Fig. 2, which is one of a number of squares formed by two series of parallel lines, the

---

[1] C. TSUBOI, *Bull. Earthq. Res. Inst.*, 10 (1932), 435.

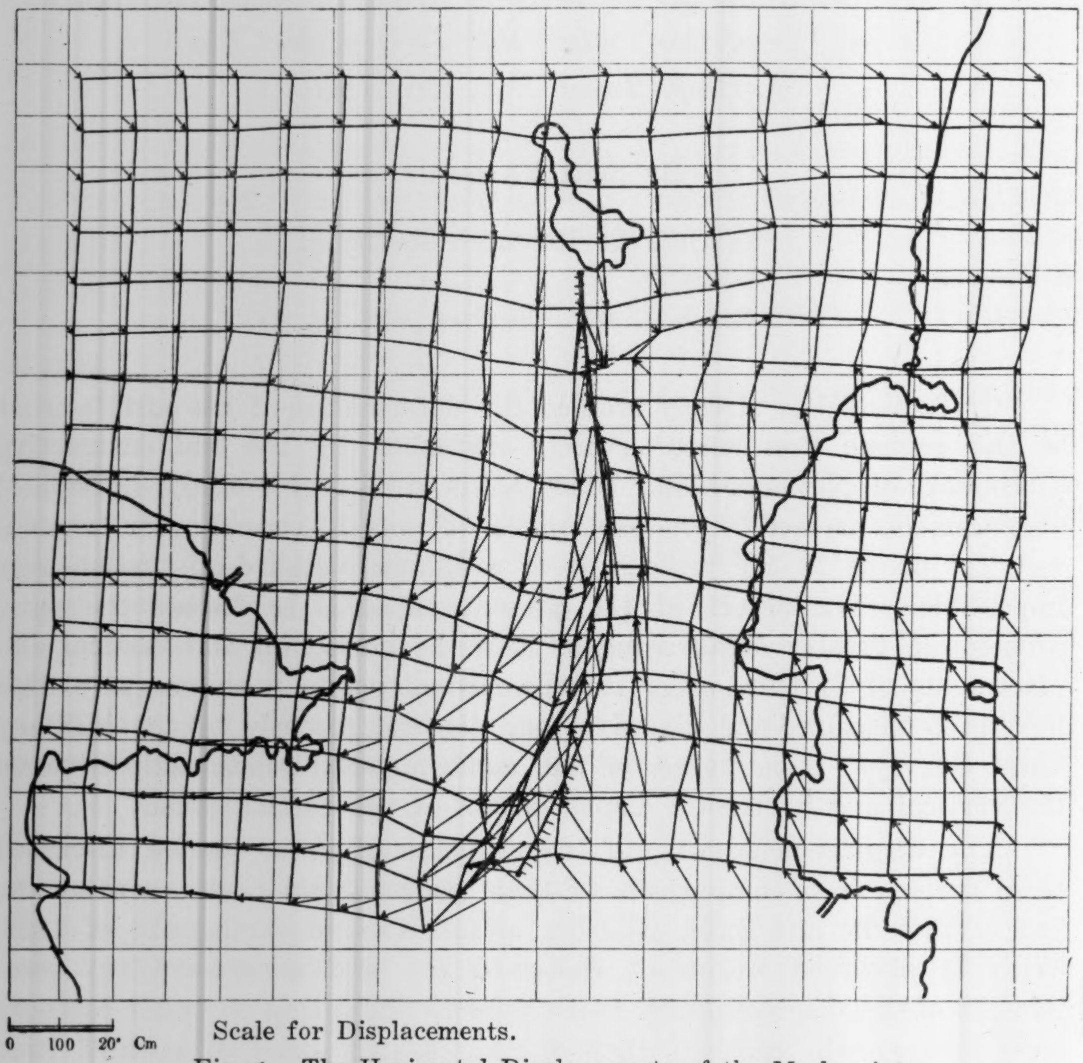

Scale for Displacements.

Fig. 1. The Horizontal Displacements of the Mesh-points.

mean of $\frac{u_2-u_1}{2km}$ and $\frac{u_4-u_3}{2km}$ was taken to be the value of $\frac{\partial u}{\partial x}$ at the centre of the square. From the values of these and other horizontal gradients of horizontal displacements, which were calculated similarly, dilatation $\Delta=\frac{\partial u}{\partial x}+\frac{\partial v}{\partial y}$, shear $\sigma=\frac{1}{2}\left(\frac{\partial u}{\partial y}+\frac{\partial v}{\partial x}\right)$, and rotation $\omega=\frac{1}{2}\left(\frac{\partial u}{\partial y}-\frac{\partial v}{\partial x}\right)$ were obtained. The contour lines of these

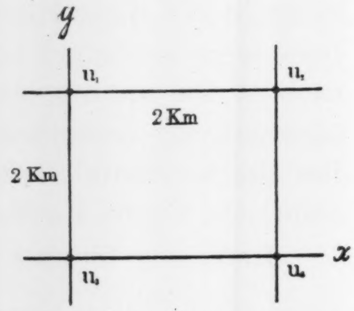

Fig. 2.

quantities are shown in Figs. 3 to 9. In *a* of each figure, the existence of the Tanna Seismic Fault, which is a line of discontinuity of displacement, was taken into consideration, while in *b* it is entirely ignored. The numerals in bracket in Fg. 3, *a*, correspond to the station numbers in Table 1.

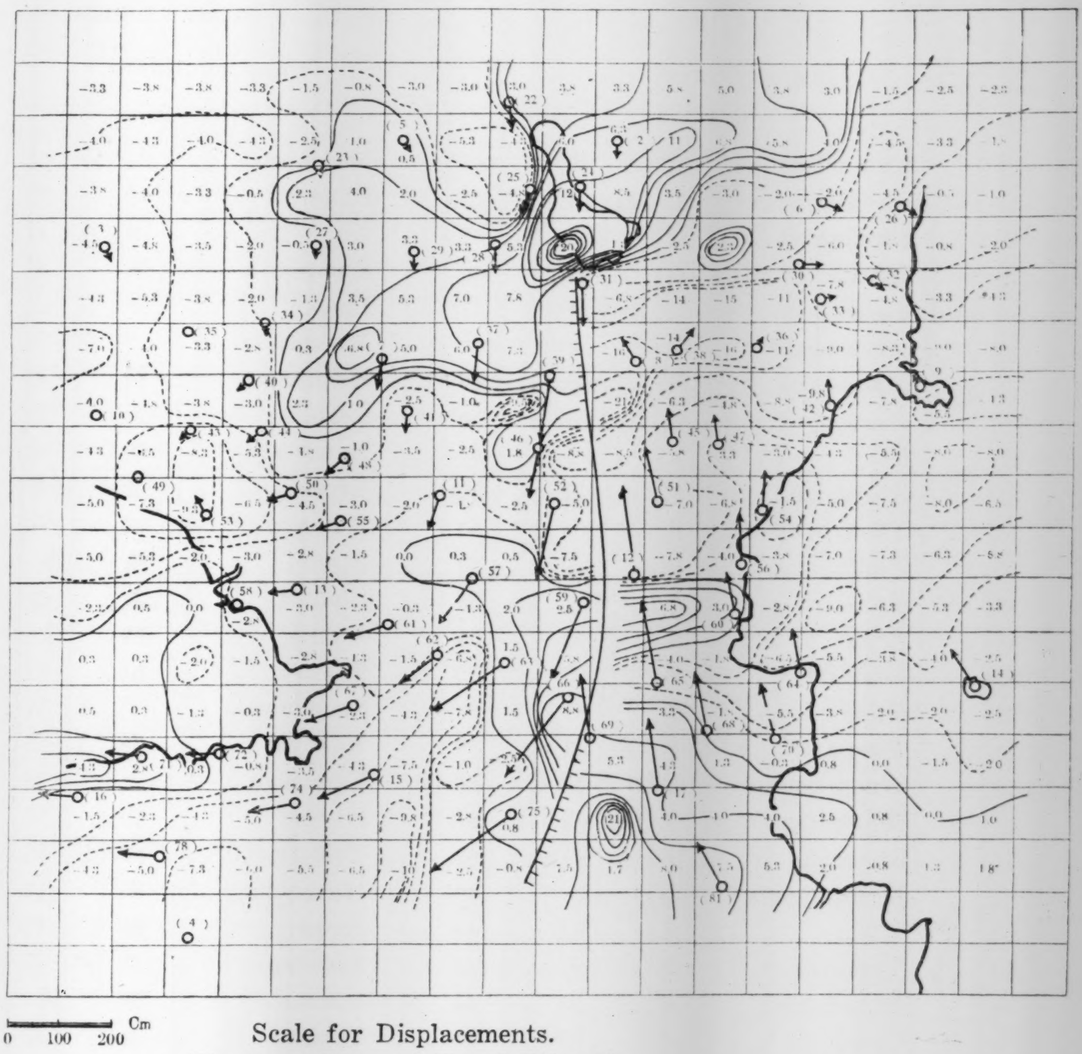

Scale for Displacements.

Fig. 3 *a*. Lines of Equal Dilatation,

$$\varDelta=\frac{\partial u}{\partial x}+\frac{\partial v}{\partial y} \text{ in } 10^{-5}.$$

Arrows show the horizontal displacements of the Triangulation Points.

Comparing the dilatation with vertical displacements, we see that regions of upheaval roughly agree in position with those of contraction, while regions of subsidence agree with those of dilatation. Since it seems from the geological structure of the regions that vertical displacement w may be more closely correlated with u, or $\frac{\partial u}{\partial x}$ than with

Table I.

Station number	Name of Station		Station number	Name of Station	
2	Kamurigatake	冠ヶ岳	43	Nisisawata	西澤田
3	Asitakayama	愛鷹山	44	Okamiya	岡宮
5	Kamiyama	神山	45	Kunimiisi	國見石
6	Isibasi	石橋	46	Kuwabara	桑原
7	Sano	佐野	47	Idusan	伊豆山
8	Miyakami	宮上	48	Misimasiku	三島宿
9	Manaduru	眞鶴	49	Matunaga	松長
10	Negoya	根古屋	50	Ôoka	大岡
11	Ôba	大塲	51	Hatamura	畑村
12	Kurodake	玄岳	52	Hirai	平井
13	Tokukurayama	德倉山	53	Numadu	沼津
14	Hasima	初島	54	Atami$_1$	熱海一
15	Kosaka	小坂	55	Dôniwa	堂庭
16	Enasi	江梨	56	Atami$_2$	熱海二
17	Sukumo	巣雲	57	Kasuya	柏谷
22	Otiai	落合	58	Simokanuki	下香貫
23	Kinesaka	木根坂	59	Nakoya	奈古谷
24	Wadanosumi	和田之角	60	Kamitaga	上多賀
25	Mikunitôge	三國峠	61	Himori	日守
26	Simoaido	下合戸	62	Yokkamati	四日町
27	Minamiyama	南山	63	Nirayama	韮山
28	Mihora	見洞	64	Aziro	網代
29	Yamasitairi	山下入	65	Simotaga	下多賀
30	Ôsawayama	大澤山	66	Ukihasi$_1$	浮橋一
31	Umidaira	海平	67	Tozawa	戸澤
32	Minamiyosiwara	南吉原	68	Usami$_1$	宇佐美一
33	Minamigô	南鄕	69	Ukihasi$_2$	浮橋二
34	Hatibudai	八分臺	70	Usami$_2$	宇佐美二
35	Takayama	高山	71	Kuryô	久料
36	Uyeno	上野	72	Hirasawa	平澤
37	Suwadai	諏訪臺	73	Takyô	田京
38	Karesugi	枯杉	74	Sigesu	重須
39	Siroyama	城山	75	Ôno	大野
40	Nagasakadai	長坂臺	78	Kou	古宇
41	Kamohora	賀茂洞	79	Sizenzi	修善寺
42	Tatigakubo	立ヶ窪	81	Okamura	岡村

the dilatation, the contours of $\dfrac{\partial u}{\partial x}$, were compared with w, the contour of which last was drawn by the Military Land Survey, and shown in Fig. 10, *a*.

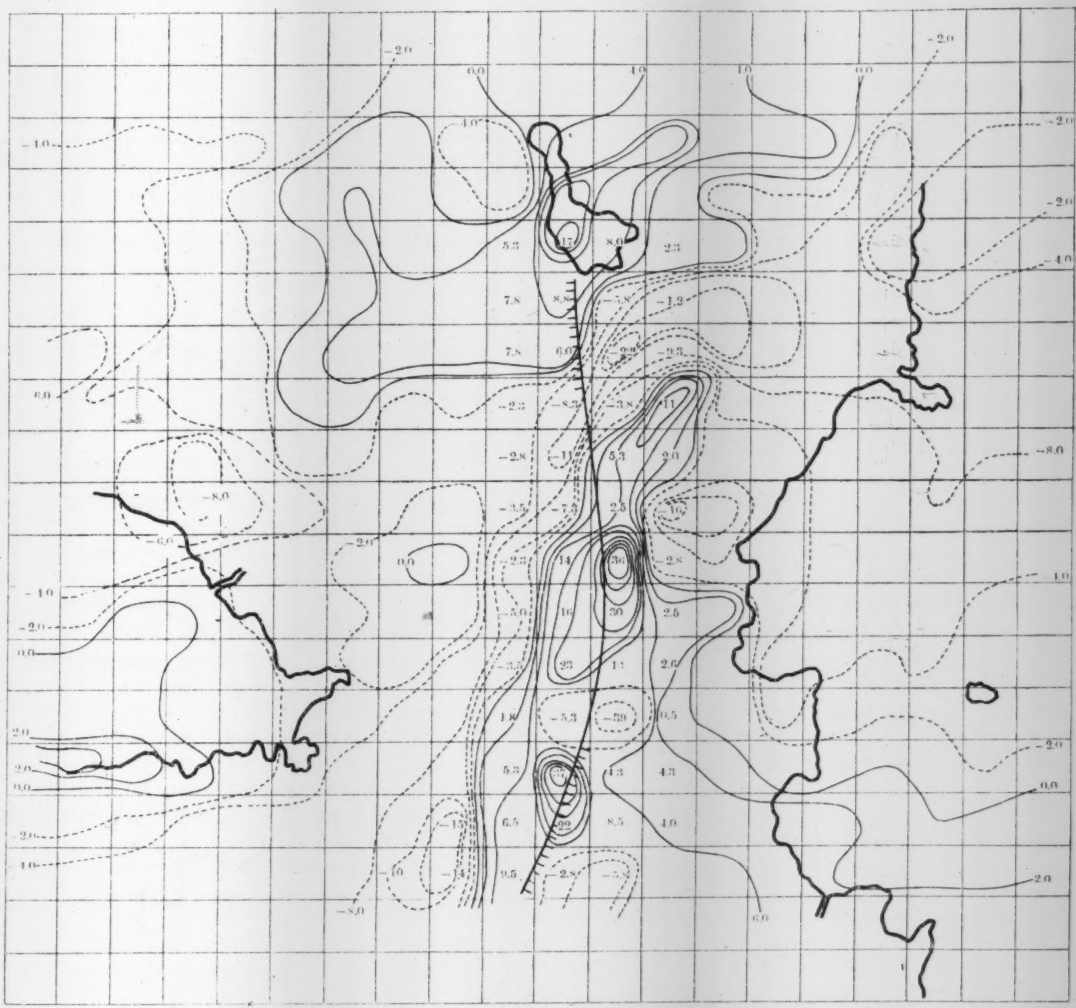
-2.0
-2.0
0.0
4.0
4.0
0.0
-1.0
-4.0
-2.0
-2.0
-4.0
5.3
17
8.0
2.3
7.8
8.8
-5.8
-1.2
6.0
7.8
6.0
-22
-2.3
-2.3
-8.3
-3.8
11
-8.0
-2.8
-11
5.3
2.0
-8.0
-3.5
-7.3
2.5
-16
-6.0
-2.0
0.0
-2.3
14
36
-2.8
1.0
-4.0
-2.0
-5.0
16
30
2.5
0.0
-3.5
23
13
2.6
2.0
1.8
-5.3
-39
0.5
-2.0
2.0
0.0
5.3
4.3
4.3
0.0
-2.0
-15
6.5
22
8.5
4.0
-4.0
-10
-14
9.5
-2.8
-5.8
2.0
-8.0
6.0

Fig. 3 *b*. Lines of Equal Dilatation,

$$\Delta = \frac{\partial u}{\partial x} + \frac{\partial v}{\partial y} \text{ in } 10^{-5}.$$

The existence of the Tanna Fault is entirely ignored.

The relation between u and w is shown in Fig. 10, b, in which the stations situated west of the Tanna Fault are indicated by O. The correlation coefficient between u and w is $-0{\cdot}38 \pm 0{\cdot}10$ if we take all points, and $-0{\cdot}57 \pm 0{\cdot}10$ if we take points only west of the fault. Thus correlation between u and w is especially close for points west of the Tanna Fault. Although nothing definite can be said for the points east of the Tanna Fault, a slight positive correlation seems to exist between u and w. The correlation between u and w may be accounted for by the existence of a system of step-faults, along which parts of the earth's crust had slid as shown in Fig 11.

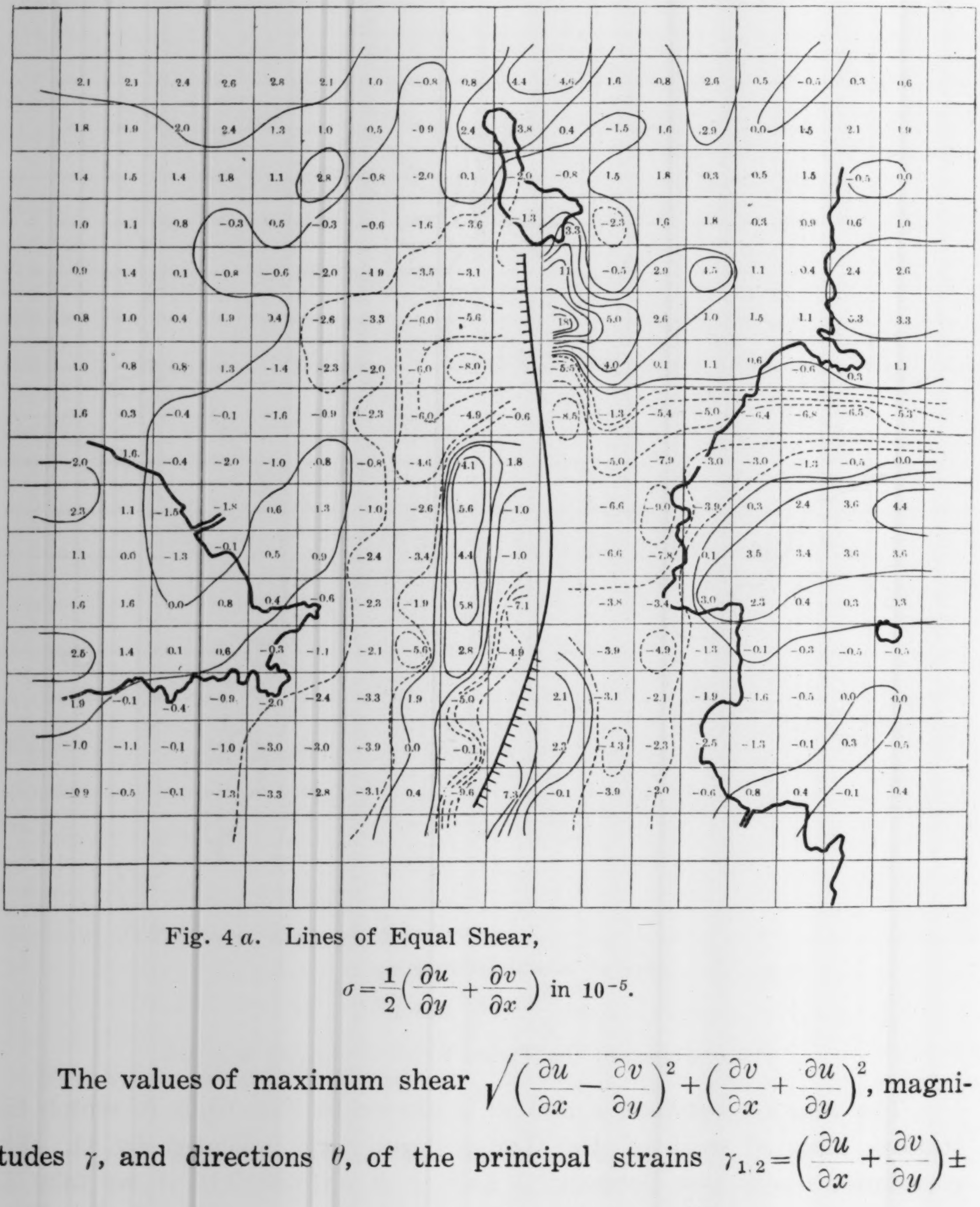

Fig. 4 *a*. Lines of Equal Shear,

$$\sigma=\frac{1}{2}\left(\frac{\partial u}{\partial y}+\frac{\partial v}{\partial x}\right) \text{ in } 10^{-5}.$$

The values of maximum shear $\sqrt{\left(\frac{\partial u}{\partial x}-\frac{\partial v}{\partial y}\right)^2+\left(\frac{\partial v}{\partial x}+\frac{\partial u}{\partial y}\right)^2}$, magnitudes γ, and directions θ, of the principal strains $\gamma_{1.2}=\left(\frac{\partial u}{\partial x}+\frac{\partial v}{\partial y}\right)\pm \sqrt{\left(\frac{\partial u}{\partial x}-\frac{\partial v}{\partial y}\right)^2+\left(\frac{\partial v}{\partial x}+\frac{\partial u}{\partial y}\right)^2}$, and $\theta=\arctan\dfrac{\gamma_1-2\dfrac{\partial u}{\partial x}}{\dfrac{\partial u}{\partial y}+\dfrac{\partial v}{\partial x}}$ were calculated and shown in Figs. 12, 18 respectively.

In order to ascertain the rate at which the magnitudes of the horizontal displacements u and v, and also those of dilatation, shear, rotation, and maximum shear, vary with distance from the Tanna Fault, the mean of their absolute values in zones parallel to the fault, which were taken every 2 km from it, were calculated. The values are plotted in Fig. 14, *a*, *b*, *c*, *d*, *e*, *f*, respectively.

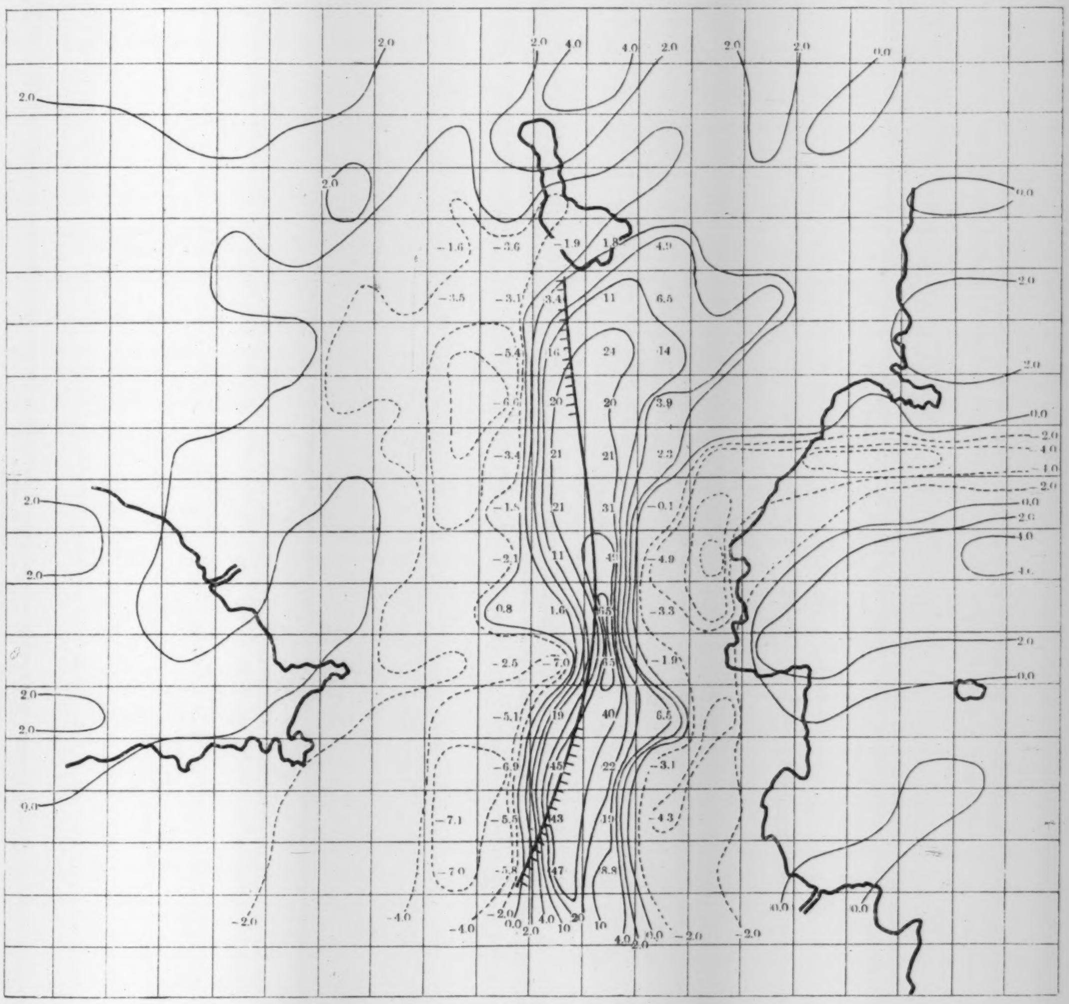
2.0
2.0
4.0
4.0
2.0
2.0
2.0
0.0
2.0
2.0
-1.6
-3.6
-1.9
1.8
4.9
-3.5
-3.1
3.4
11
6.5
-5.4
16
21
14
-6.6
20
20
3.9
-3.4
21
21
2.3
-1.8
21
31
-0.1
-2.1
11
4.9
0.8
1.6
-3.3
-2.5
-7.0
-1.9
-5.1
19
40
6.5
-6.9
45
22
-3.1
-7.1
-5.5
43
19
-4.3
-7.0
-5.8
47
8.8
-2.0
-4.0
-2.0
-4.0
0.0
2.0
4.0
20
10
10
4.0
0.0
-2.0
-2.0
0.0
0.0
2.0
2.0
0.0
2.0
4.0
4.0
2.0
0.0
2.0
4.0
4.0
2.0
0.0
2.0
2.0
2.0
2.0
0.0

Fig. 4 *b*. Lines of Equal Shear,

$$\sigma = \frac{1}{2}\left(\frac{\partial u}{\partial y} + \frac{\partial v}{\partial x}\right) \text{ in } 10^{-5}.$$

The existence of the Tanna Fault is entirely ignored.

All the quantities here calculated are largest near the Tanna Fault, and decrease in magnitudes with distance from the fault, except, however, rotation and shear, which have conspicuous maxima at a distance of 6 km from the fault. As a rule, not only the horisontal displacements u and v, but also dilatation, shear, rotation, and maximum shear too vague are all discontinuous across the fault line, and neither symmetry nor antisymmetry is to be seen east and west of the fault line.

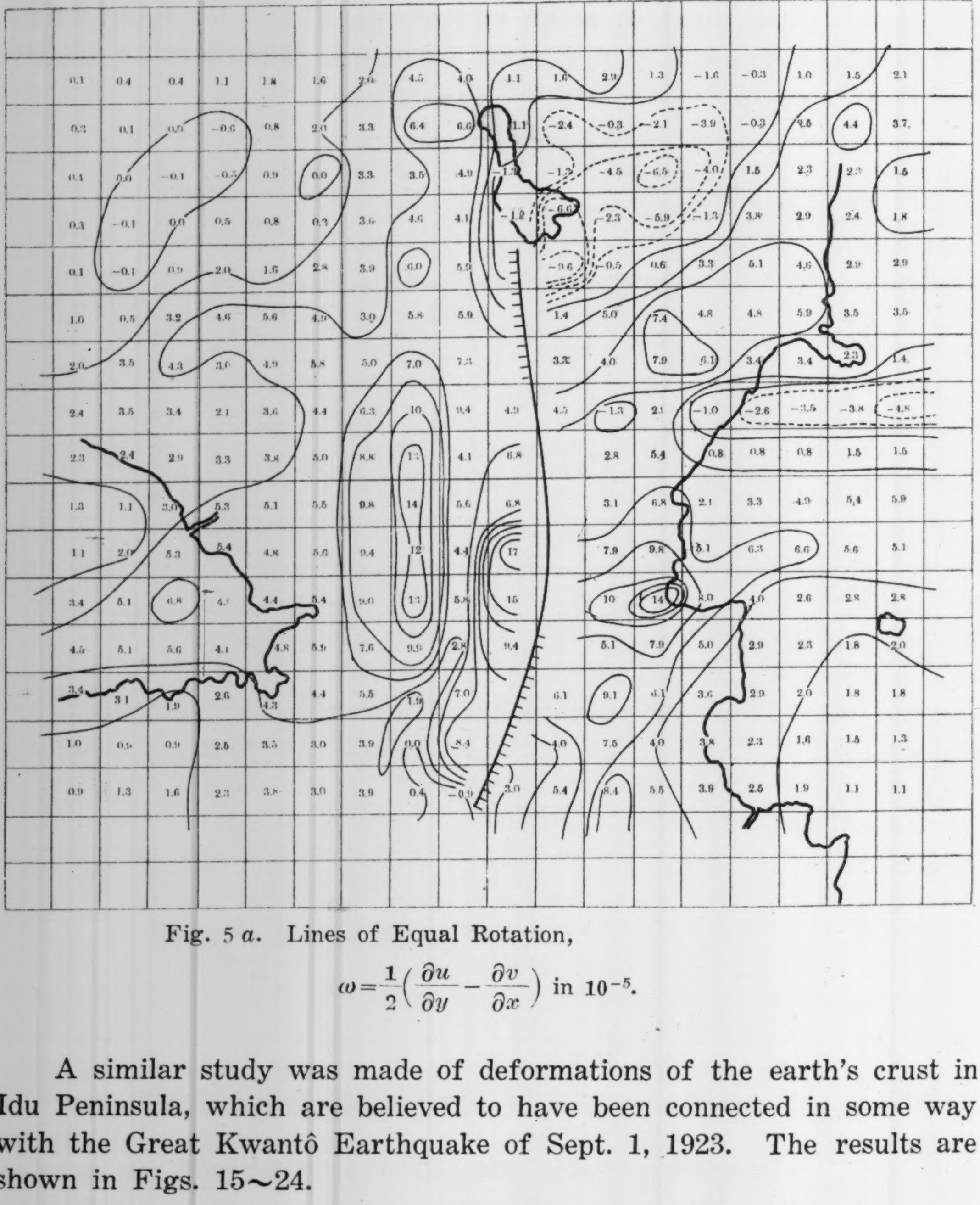

Fig. 5 *a*. Lines of Equal Rotation,

$$\omega=\frac{1}{2}\left(\frac{\partial u}{\partial y}-\frac{\partial v}{\partial x}\right) \text{ in } 10^{-5}.$$

A similar study was made of deformations of the earth's crust in Idu Peninsula, which are believed to have been connected in some way with the Great Kwantô Earthquake of Sept. 1, 1923. The results are shown in Figs. 15~24.

In this case, no distinct indication of the Tanna Fault can be seen, the large deformations of the earth's crust having mostly occurred in the vicinity of the epicentral region, i. e., about the northern coast of Sagami Bay. Thereas in the case of the Idu Destructive Earthquake, the vertical displacement w is negatively correlated with the eastward horizontal displacement u, in that of the Great Kwantô Earthquake we could see no definite correlation between them (the uw—diagram is omitted here).

Comparing the deformations of the earth's crust connected with (*a*) the Great Kwantô Earthquake and (*b*) the Idu Earthquake, we might say that

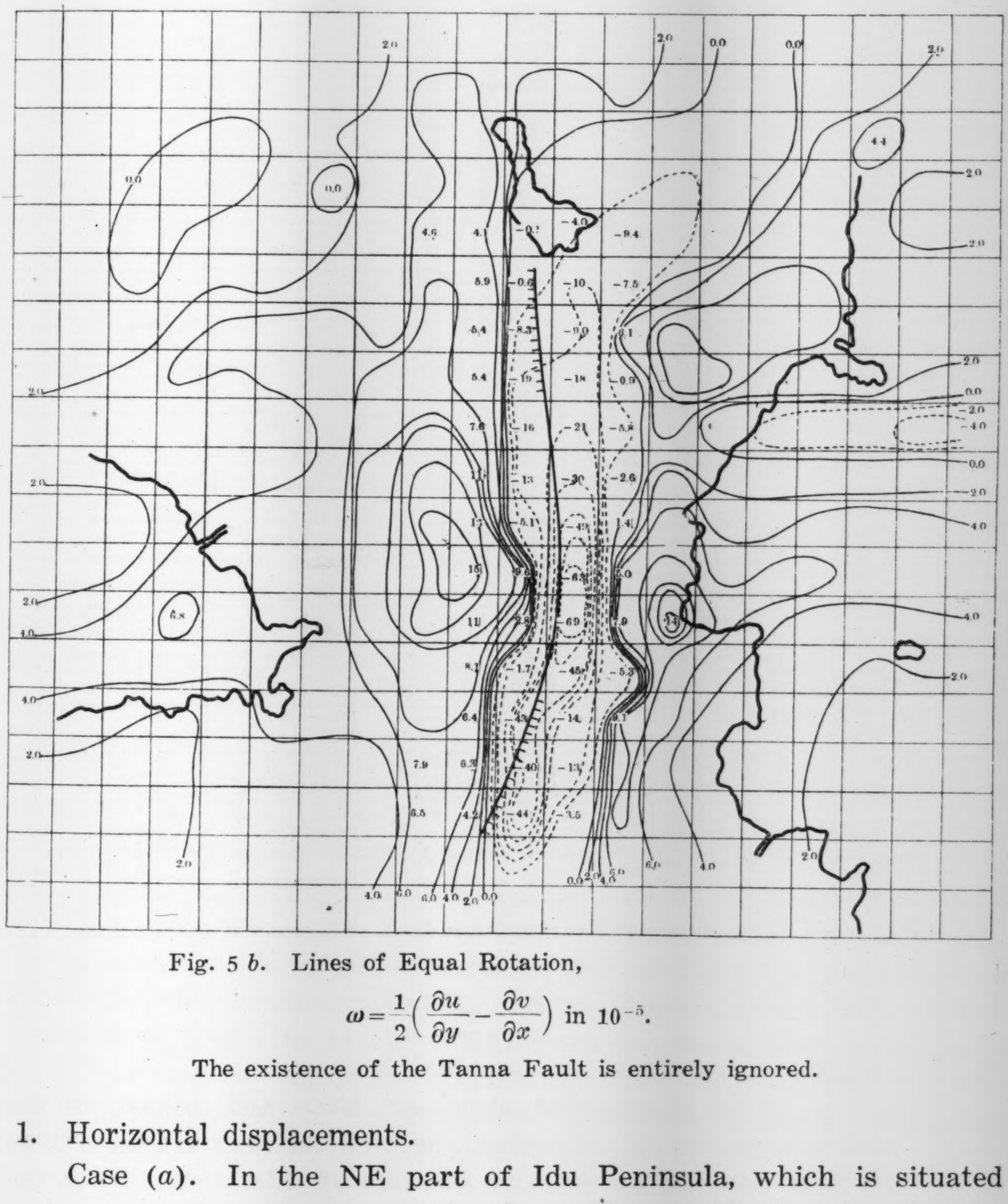
2.0
2.0
0.0
0.0
2.0
0.0
0.0
4.4
2.0
2.0
4.6
4.1
-0.7
-4.0
-9.4
5.9
-0.6
-10
-7.5
5.4
-8.3
-9.0
1.1
2.0
5.4
-19
-18
-0.9
2.0
0.0
-2.0
-4.0
7.6
-16
-21
-5.8
2.0
0.0
-2.0
11
-13
-30
-2.6
4.0
17
-5.1
-49
1.4
18
-63
2.0
2.0
6.8
11
-69
4.0
8.1
-1.7
-45
-5.3
2.0
4.0
6.4
-14
2.0
7.9
6.3
-40
-13
6.5
4.2
-44
-3.5
2.0
6.0
4.0
2.0
4.0
6.0
6.0
4.0
2.0
0.0
0.0
2.0
4.0
6.0

Fig. 5 *b*. Lines of Equal Rotation,

$$\omega=\frac{1}{2}\left(\frac{\partial u}{\partial y}-\frac{\partial v}{\partial x}\right) \text{ in } 10^{-5}.$$

The existence of the Tanna Fault is entirely ignored.

1. Horizontal displacements.

Case (*a*). In the NE part of Idu Peninsula, which is situated near the epicentre of the Great Kwantô Earthquake, the displacements which are fairly large, become small with distance from the NE coast above mentioned towards the western region. (see Fig. 1, 15).

Case (*b*). The horizontal displacements, which are generally large on the wide area of these districts, are extremely large in the neighbourhood of the Tanna Fault.

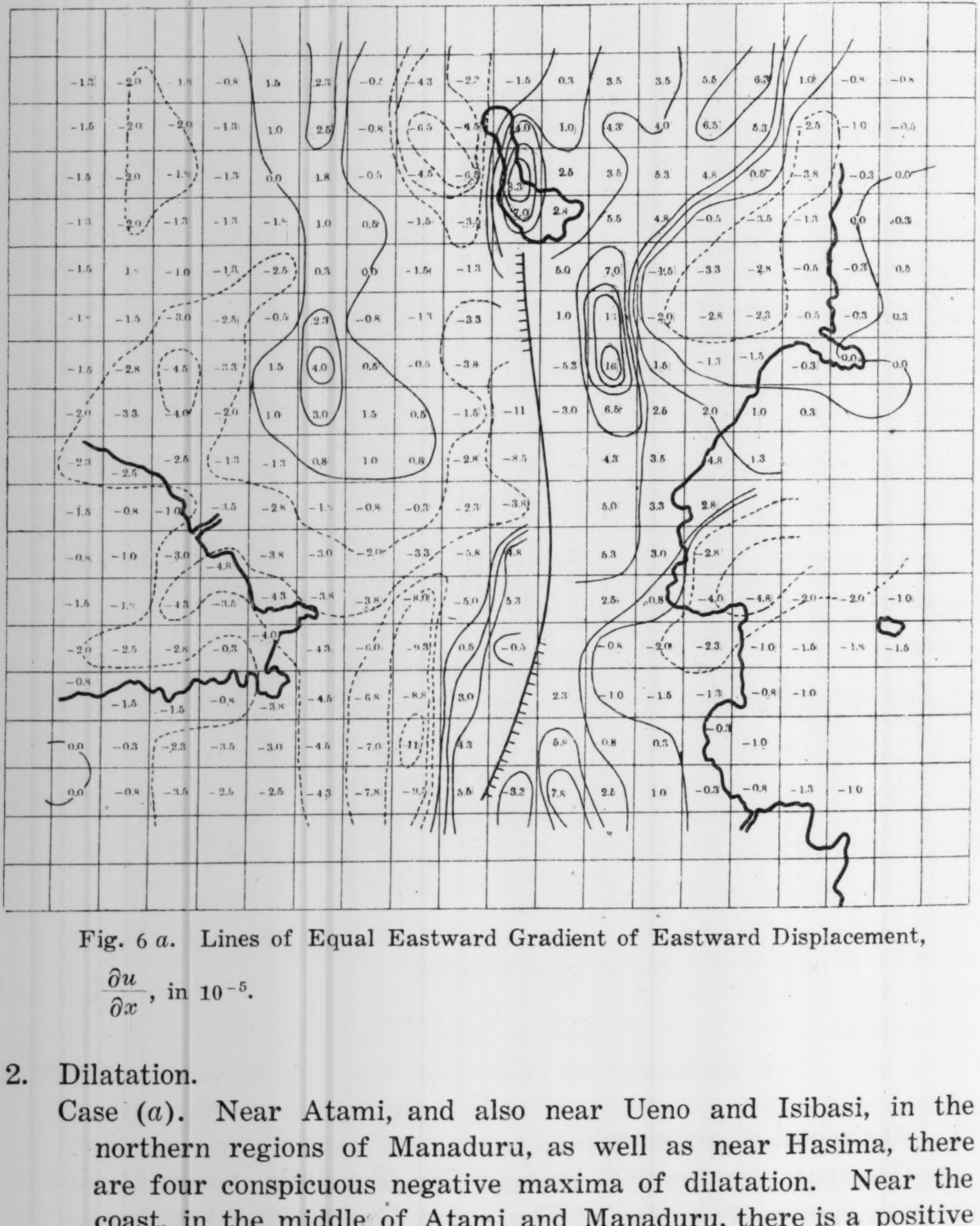

Fig. 6 *a*. Lines of Equal Eastward Gradient of Eastward Displacement, $\dfrac{\partial u}{\partial x}$, in 10^{-5}.

2. Dilatation.

Case (*a*). Near Atami, and also near Ueno and Isibasi, in the northern regions of Manaduru, as well as near Hasima, there are four conspicuous negative maxima of dilatation. Near the coast, in the middle of Atami and Manaduru, there is a positive maximum. Near Suwadai and Kamohara, in the SW region of Asinoko, there is a large positive dilatation (see Fig. 3, 16).

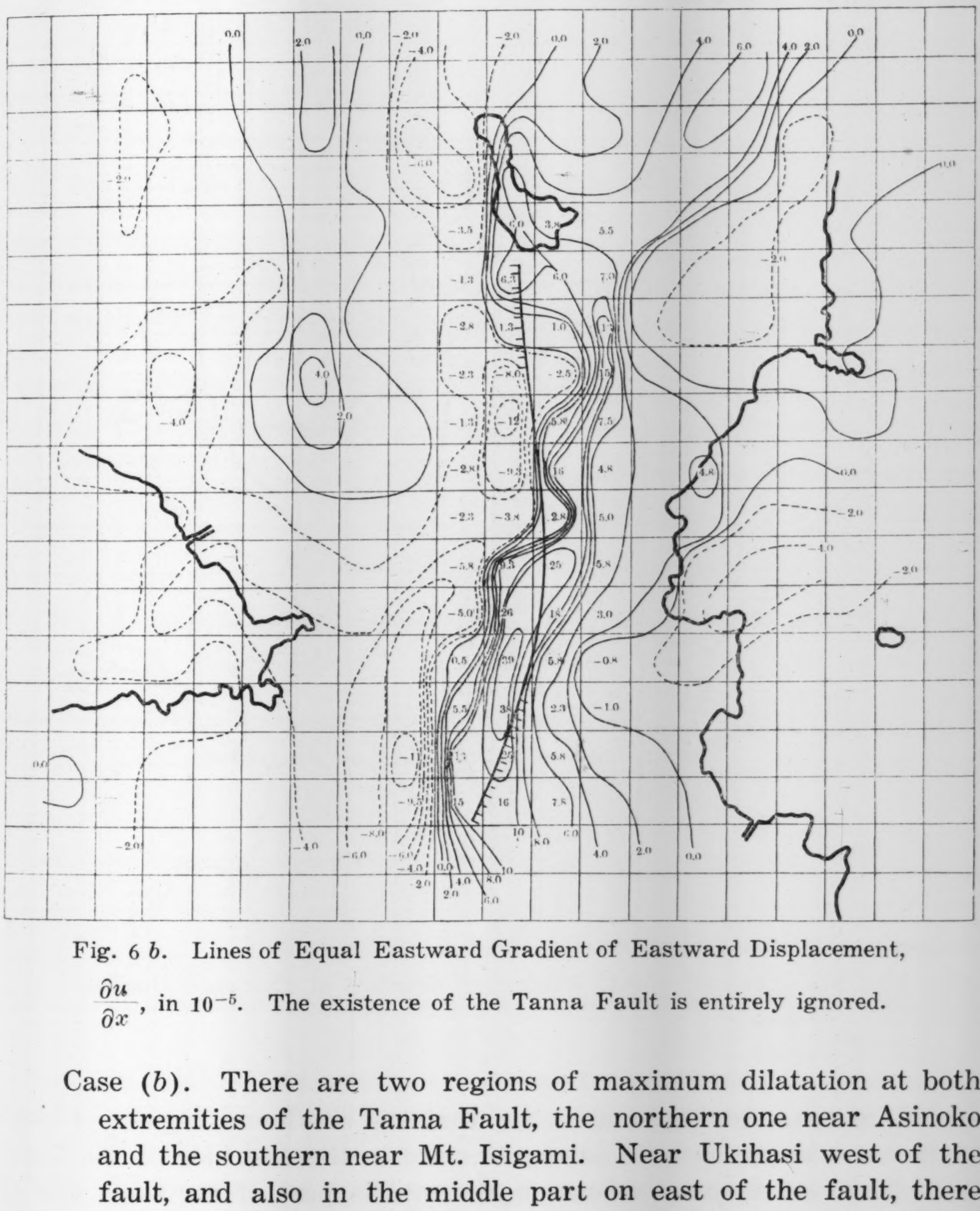

Fig. 6 *b*. Lines of Equal Eastward Gradient of Eastward Displacement, $\frac{\partial u}{\partial x}$, in 10^{-5}. The existence of the Tanna Fault is entirely ignored.

Case (*b*). There are two regions of maximum dilatation at both extremities of the Tanna Fault, the northern one near Asinoko and the southern near Mt. Isigami. Near Ukihasi west of the fault, and also in the middle part on east of the fault, there are *second* maximum dilatations. On the east side of the northern part of the fault, near Miyakami, Karesugi, Minamigô and Ueno, there is a region of negative dilatation.

3. Shear.

Case (*a*). Near Manaduru and in its northern region, there are positive maxima of shear. From the west of this positive region, above cited, to the region near Atami, there is a large value of negative shear (see Fig. 17).

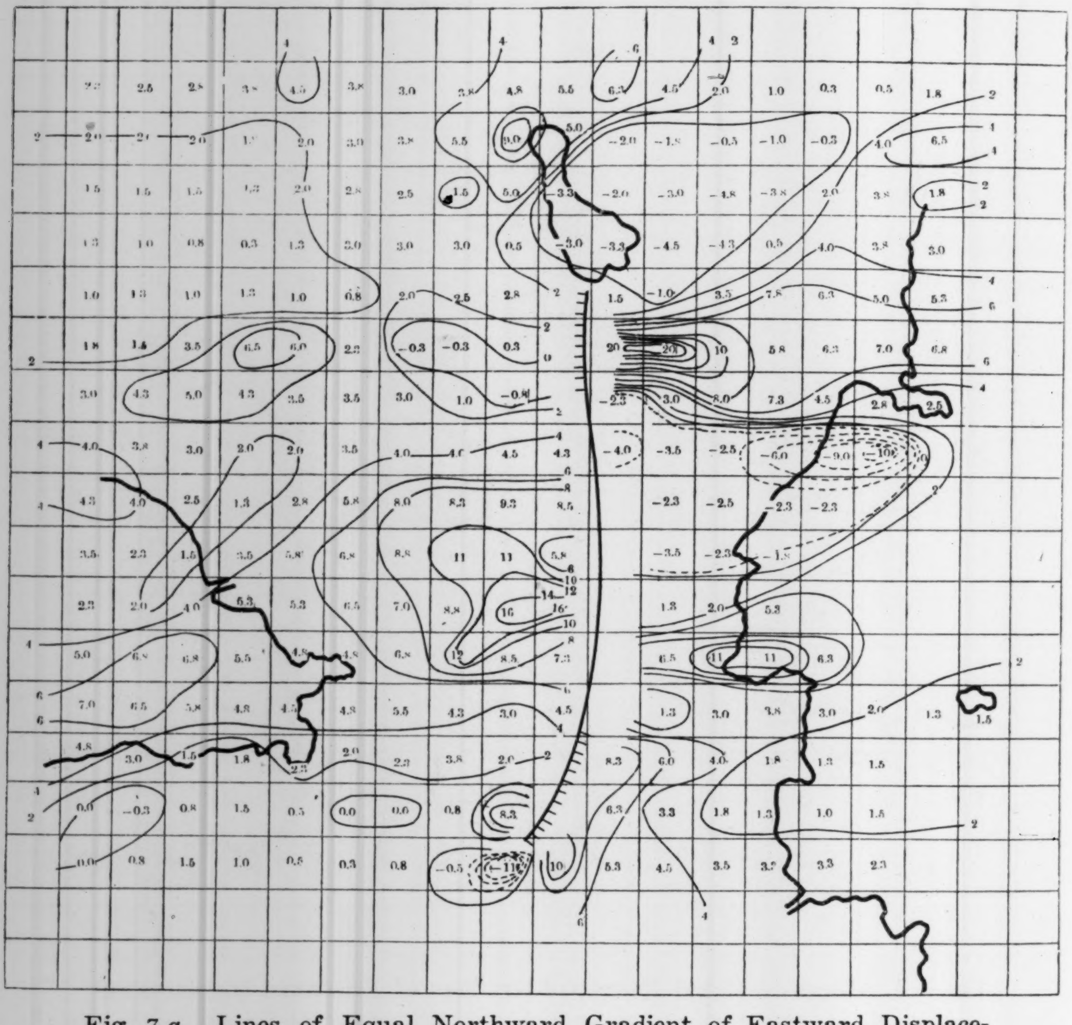
2.5 2.8 3.8 4.5 3.8 3.0 3.8 4.8 5.5 6.3 4.5 2.0 1.0 0.3 0.5 1.8
2.0 2.0 2.0 2.0 3.0 3.8 5.5 9.0 5.0 -2.0 -1.8 -0.5 -1.0 -0.3 4.0 6.5
1.5 1.5 1.5 1.3 2.0 2.8 2.5 1.5 5.0 -3.3 -2.0 -3.0 -4.8 -3.8 2.0 3.8 1.8
1.3 1.0 0.8 0.3 1.3 3.0 3.0 3.0 0.5 -3.0 -3.3 -4.5 -4.3 0.5 4.0 3.8 3.0
1.0 1.3 1.0 1.3 1.0 0.8 2.0 2.5 2.8 1.5 -1.0 3.5 7.8 6.3 5.0 5.3
1.8 1.4 3.5 6.5 6.0 2.3 -0.3 -0.3 0.3 20 20 10 5.8 6.3 7.0 6.8
3.0 4.3 5.0 4.3 3.5 3.5 3.0 1.0 -0.8 -2.3 3.0 8.0 7.3 4.5 2.8 2.5
4.0 3.8 3.0 2.0 2.0 3.5 4.0 4.0 4.5 4.3 -4.0 -3.5 -2.5 -6.0 -9.0 -10
4.3 4.0 2.5 1.3 2.8 5.8 8.0 8.3 9.3 8.5 -2.3 -2.5 -2.3 -2.3
3.5 2.3 1.5 3.5 5.8 6.8 8.8 11 11 5.8 -3.5 -2.3 -1.8
2.3 2.0 4.0 5.3 5.3 6.5 7.0 8.8 16 1.3 2.0 5.3
5.0 6.8 6.8 5.5 4.8 4.8 6.8 12 8.5 7.3 6.5 11 11 6.3
7.0 6.5 5.8 4.8 4.5 4.8 5.5 4.3 3.0 4.5 1.3 3.0 3.8 3.0 2.0 1.3 1.5
4.8 3.0 1.5 1.8 2.3 2.0 2.3 3.8 2.0 8.3 6.0 4.0 1.8 1.3 1.5
0.0 -0.3 0.8 1.5 0.5 0.0 0.0 0.8 8.3 6.3 3.3 1.8 1.3 1.0 1.5
0.0 0.8 1.5 1.0 0.5 0.3 0.8 -0.5 -11 10 5.3 4.5 3.5 3.3 2.3

Fig. 7 *a*. Lines of Equal Northward Gradient of Eastward Displacement, $\frac{\partial u}{\partial y}$ in 10^{-5}.

Case (*b*). In Fig. 4, *a*, we see that the maximum regions of positive shear on both extremities are in the east side of the fault, and of negative shear in the middle part of the same side of the fault. In the west side, the maximum value of positive shear is in the middle region, and those of negative shear, on both extremities of the fault, which are on a quite opposite course compared with the east side of the fault.

From Fig. 4, *b*, we see that the shear has its positive value in the zonal area along the fault, and negative value on both sides of the positive zone. Positively maximum regions exist in the middle and on both extremities of the fault, similar to the preceding case.

4. Rotation.

Case (*a*). Near Atami there exists a positive maximum of rotation, and near Simoaido a negative one. Except this negative maximum region and the negative region of small magnitude near Numatu, the other regions in Idu Peninsula are all of positive rotation (see Fig. 18).

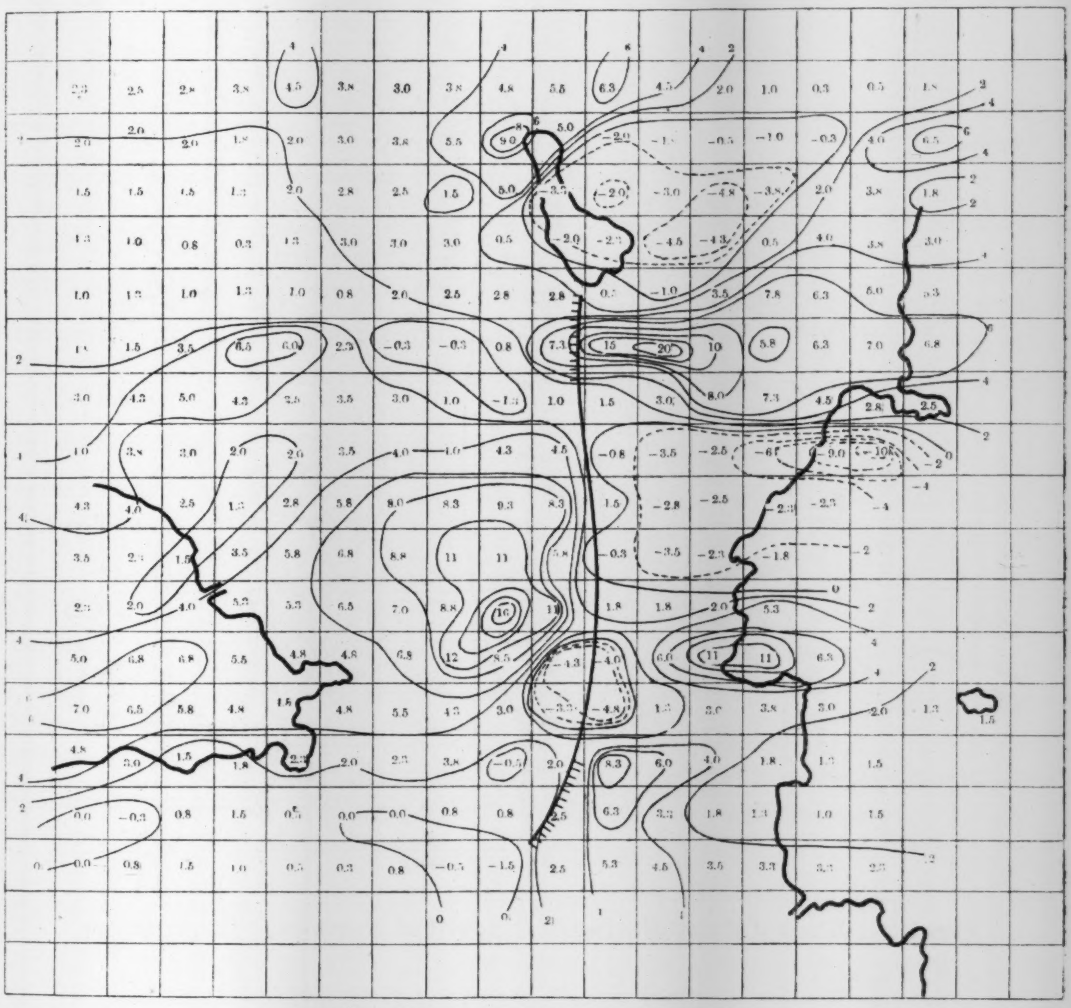

Fig. 7 *b*. Lines of Equal Northward Gradient of Eastward Displacement, $\frac{\partial u}{\partial y}$ in 10^{-5}. The existence of the Tanna Fault is entirely ignored.

Case (*b*). From Fig. 5, *a*, we see that there are two regions of maximum positive rotation on each side at about the middle of the fault, and that the area of Idu Peninsula is mostly of positive rotation, except a small area near the northern extremity of the fault, near Asinoko, Kamurigatake, and Isibasi, all of which are of negative rotation.

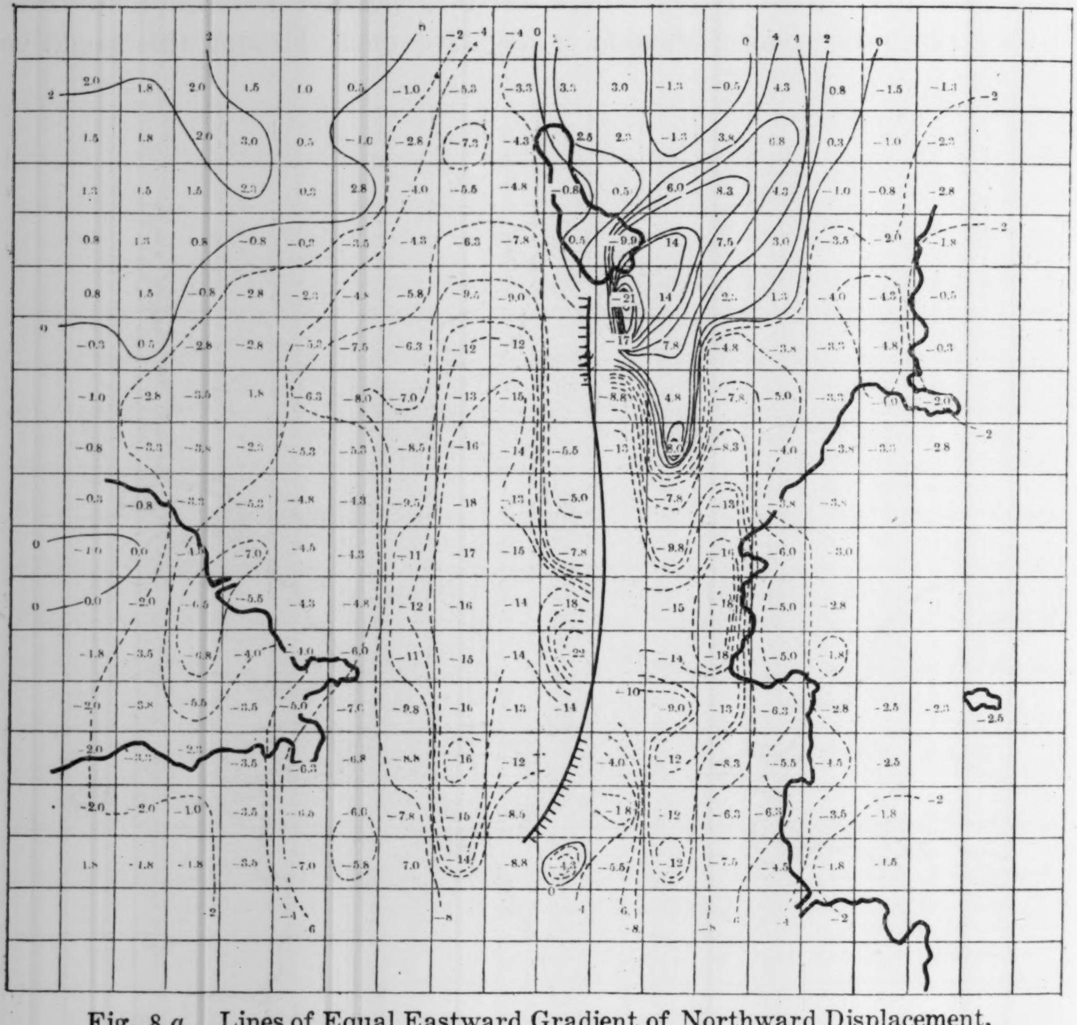

Fig. 8 *a*. Lines of Equal Eastward Gradient of Northward Displacement, $\frac{\partial v}{\partial x}$ in 10^{-5}.

Fig. 5, *b*, shows that the zonal area along the fault is of negative rotation, while on both sides of the zone, we see regions of positive rotation. We also meet with two maximum regions of positive rotation on both sides in the middle part of the fault, similar to the case of Fig. 5, *a*.

5. Maximum Shear.

Case (*a*). Near Minamigô, in the northern region of Manaduru, and near Atami, as well as near Kamiyama and Suwadai, in the western region of Asinoko, there are large values of maximum shear. Near Hasima also, there is a large value of maximum shear. The northern region of Enasi has a rather large value of maximum shear (see Fig. 19).

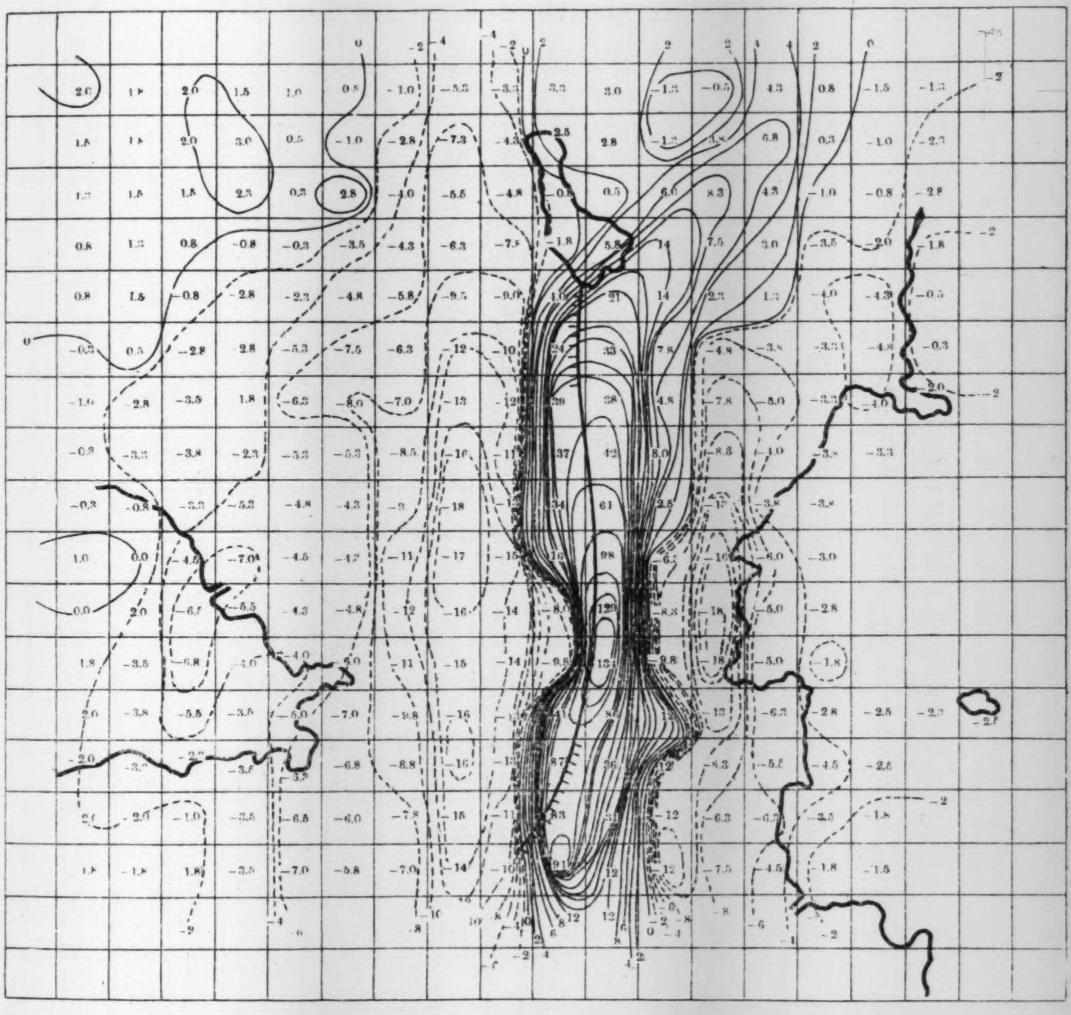

Fig. 8 *b*. Lines of Equal Eastward Gradient of Northward Displacement, $\frac{\partial v}{\partial x}$ in 10^{-5}. The existence of the Tanna Fault is entirely ignored.

Case (*b*). From Fig. 12, *a*, *b*, we see that there are three regions of large values of maximum shear on both extremities, and in the middle part east of the fault, and a region of small value in the middle part west of the fault. These values increase towards the south along the fault.

6. Principal Strain.

Case (*a*). Similar to the case of the horizontal displacements, large values of principal strains exist in the NE region of the Idu Peninsula, their values gradually diminishing with distance from this region towards the west. Most directions of the principal strains along the NE coast of the Idu Peninsula are inclined about 45° to the coast line (see Fig. 20).

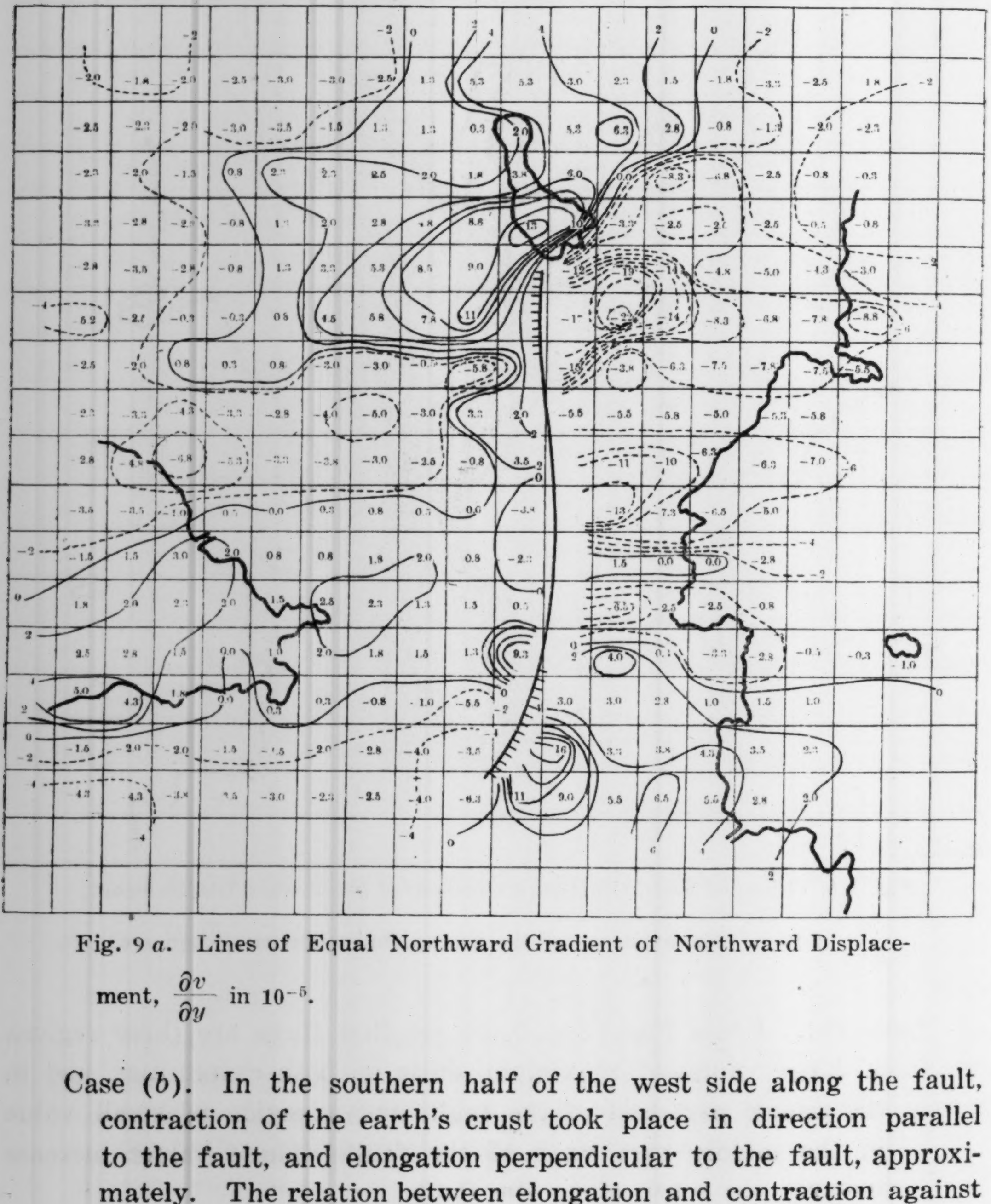

Fig. 9 *a*. Lines of Equal Northward Gradient of Northward Displacement, $\frac{\partial v}{\partial y}$ in 10^{-5}.

Case (*b*). In the southern half of the west side along the fault, contraction of the earth's crust took place in direction parallel to the fault, and elongation perpendicular to the fault, approximately. The relation between elongation and contraction against the fault line is contrary in the northern half of the west side zone compared with the southern half. East of the fault, the principal strains are maximum at both cxtremities of the fault. In the middle part of the fault, a zone with relatively large strains extends from the fault to the coast of Atami. (see Fig. 13, *a*).

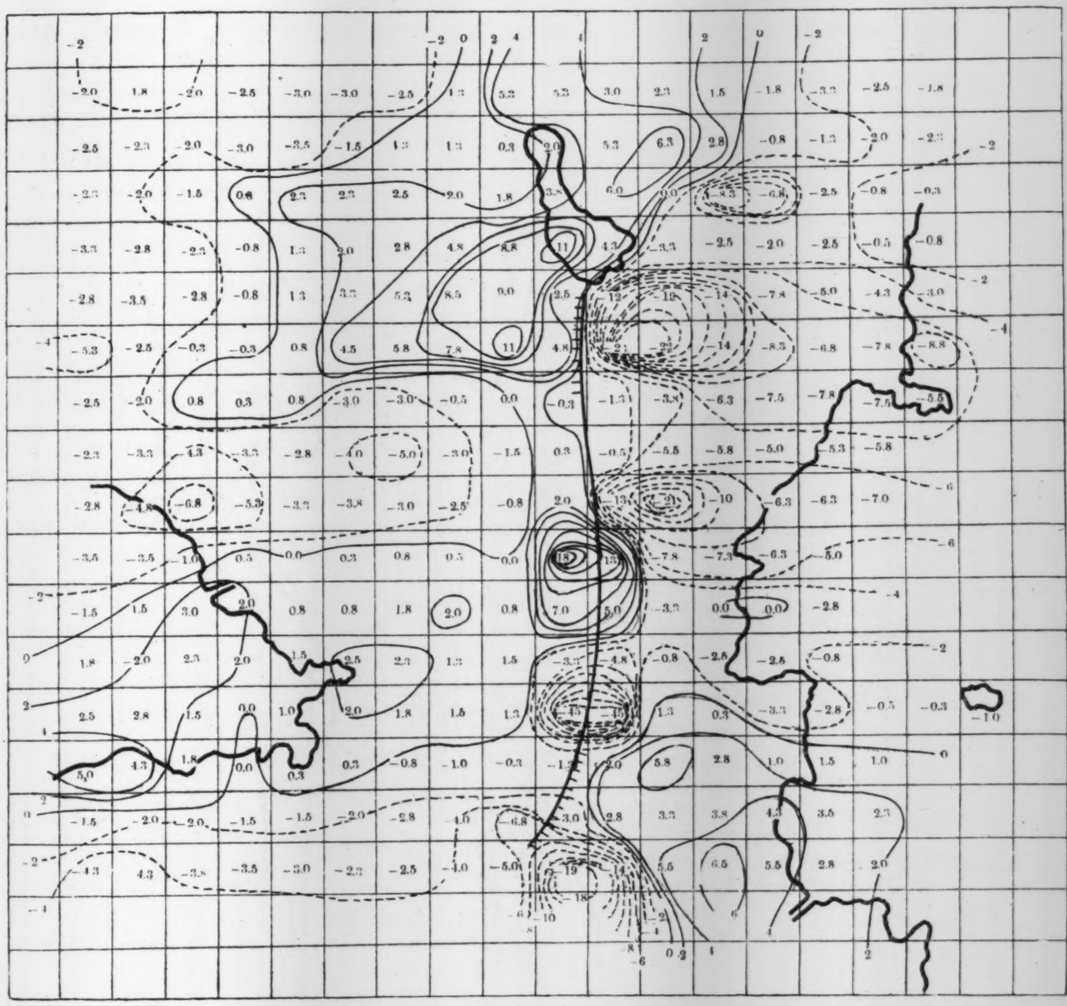

Fig. 9 b. Lines of Equal Northward Gradient of Northward Displacement, $\frac{\partial v}{\partial y}$ in 10^{-5}.

The existence of the Tanna Fault is entirely ignored.

From Fig. 13, *b*, it will be seen that the axes of principal strains are inclined about 45° to the fault line, and that the magnitude of strain increases towards the south from the middle to the southern end of the zone. The amount of strain is usually very small in regions far from the fault.

7. Eastward Gradient of Eastward Displacement $\frac{\partial u}{\partial x}$.

Case (*a*). A positive maximum of $\frac{\partial u}{\partial x}$ exists near Simoaido, situated not very far from the epicentral region of the Great Kwantô Earthquake, and negative maximum near Isibasi in the neighbourhood of Simoaido. A negative maximum of $\frac{\partial u}{\partial x}$ exists also

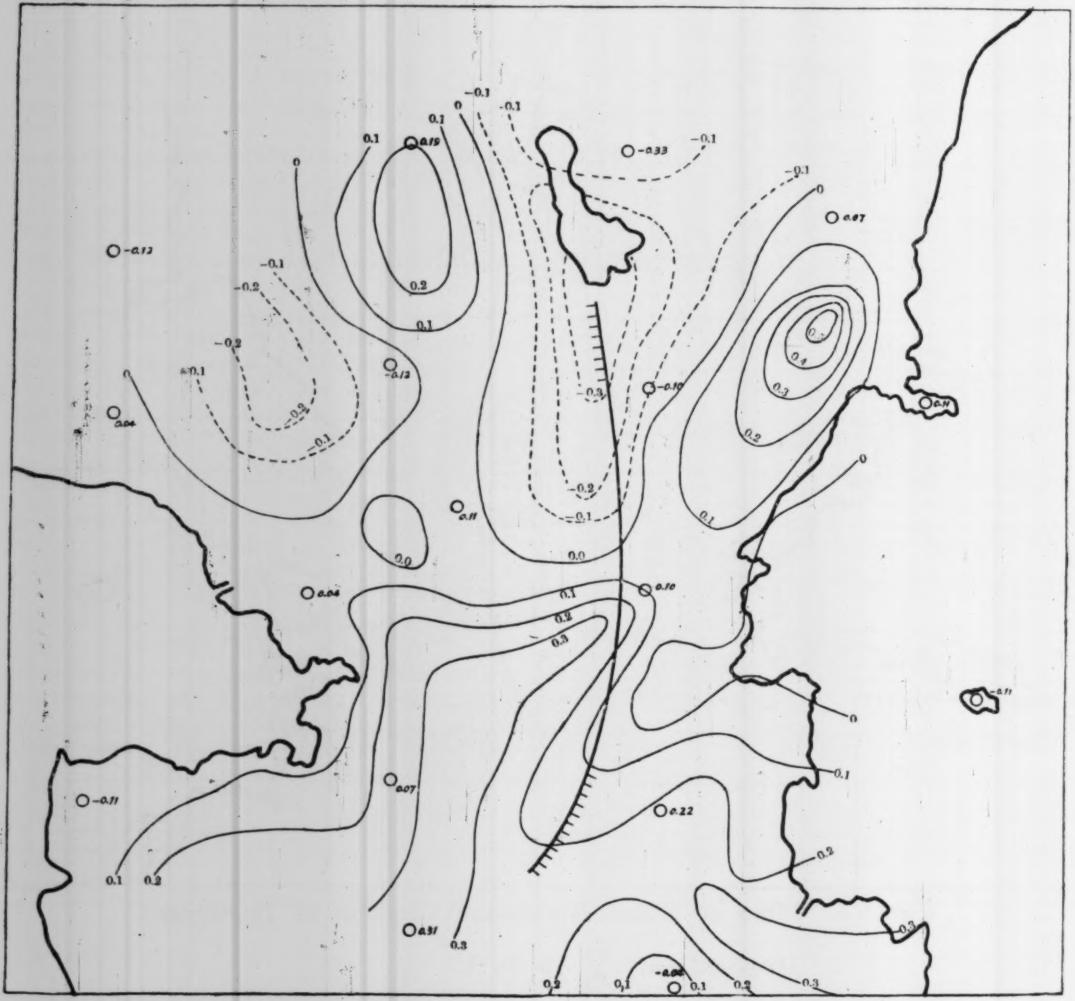
-0.1
0
-0.1
0.1
0.1
0.19
-0.33
-0.1
0
-0.1
0
0.07
-0.13
-0.1
-0.2
0.2
0.1
-0.2
0
-0.1
-0.13
-0.3
-0.10
0.4
0.3
0.04
-0.2
-0.1
0.2
0.11
0
0.11
-0.2
-0.1
0.1
0.0
0.0
0.04
0.10
0.1
0.2
0.3
-0.11
0
0.1
-0.11
0.07
0.22
0.2
0.1
0.2
0.31
0.3
0.3
0.2
0.1
0.1
0.2
0.3

Fig. 10 *a*. Lines of Equal Vertical Displacement, w, in metre, connected with the Idu Destructive Earthquake.

near Atami, facing, near Hatamura, the positive maximum. Generally speaking, large values of $\frac{\partial u}{\partial x}$ exist along the coast line in the N E region of the Idu Peninsula (see Fig. 21).

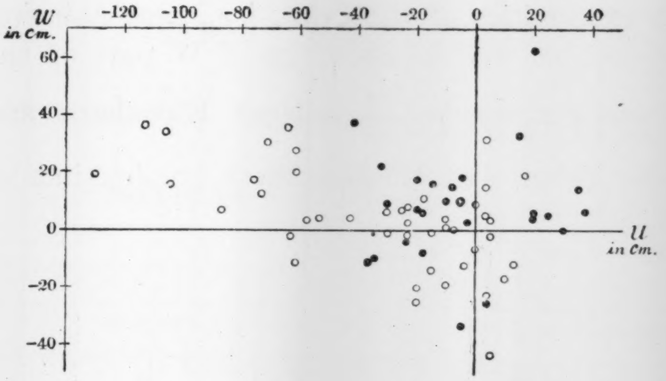

Fig. 10. *b.* $u\ w$ - Diagram. ○ marks the station on the west side of the Tanna Fault.

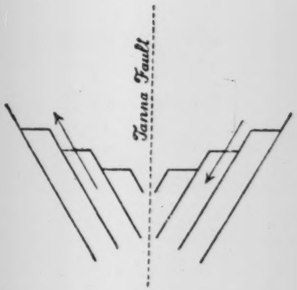

Fig. 11. The Step-Faults.

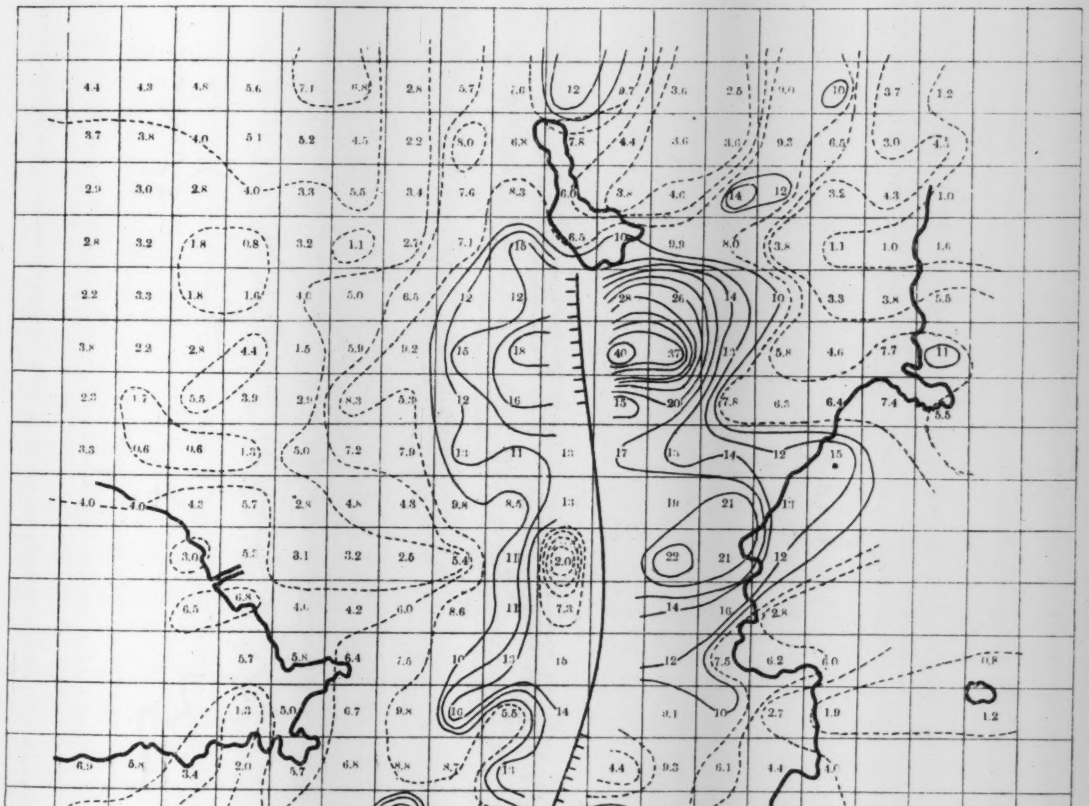

Fig. 12 *a*. Lines of Equal Maximum Shear,

$$\sqrt{\left(\frac{\partial u}{\partial x}-\frac{\partial v}{\partial y}\right)^2+\left(\frac{\partial v}{\partial x}+\frac{\partial u}{\partial y}\right)^2} \text{ in } 10^{-5}.$$

Case (*b*). About both extremities of the fault, i.e., near Asinoko, Karesugi, and Kunimiisi, as well as about the S W part of the Mt. Sukumo, there are maxima of $\frac{\partial u}{\partial x}$. Near Kuwabara and Hirae, and also near Takyô and Kosaka, there are maxima of $\frac{\partial u}{\partial x}$ (see Fig. 6).

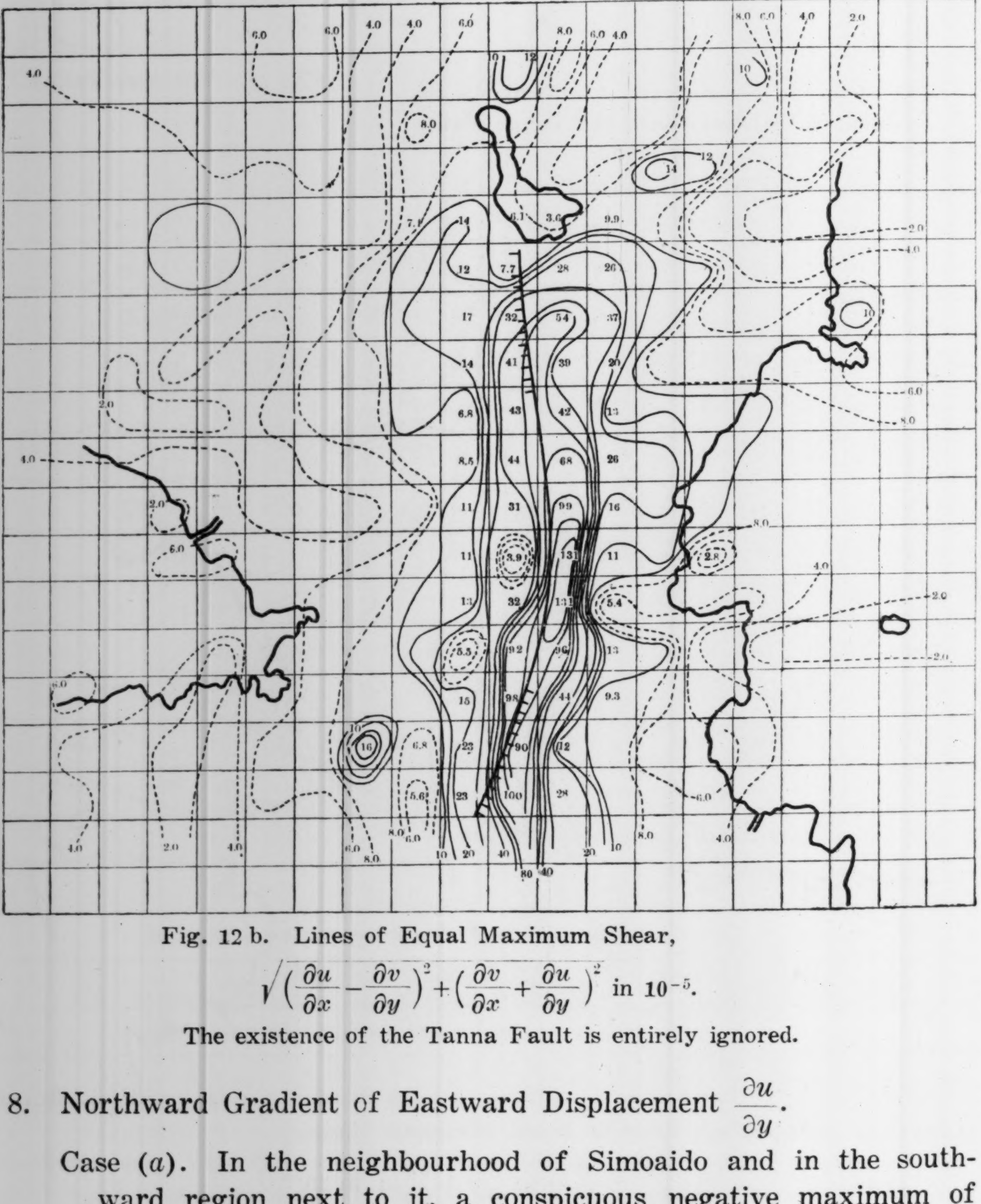
6.0
6.0
4.0
4.0
6.0
8.0
6.0
4.0
8.0
6.0
4.0
2.0
4.0
10
12
10
8.0
12
14
6.1
3.6
9.9
7.1
14
2.0
4.0
12
7.7
28
26
17
32
54
37
10
14
41
39
20
2.0
6.0
6.8
43
42
13
8.0
4.0
8.5
44
68
26
11
31
99
16
8.0
6.0
11
3.9
131
11
2.8
4.0
13
32
131
5.4
2.0
5.5
92
96
13
2.0
6.0
15
98
44
9.3
10
16
6.8
23
90
32
5.6
23
100
28
6.0
4.0
2.0
4.0
6.0
8.0
8.0
6.0
10
20
40
80
40
20
10
8.0
4.0

Fig. 12 b. Lines of Equal Maximum Shear,

$$\sqrt{\left(\frac{\partial u}{\partial x}-\frac{\partial v}{\partial y}\right)^2+\left(\frac{\partial v}{\partial x}+\frac{\partial u}{\partial y}\right)^2} \text{ in } 10^{-5}.$$

The existence of the Tanna Fault is entirely ignored.

8. Northward Gradient of Eastward Displacement $\frac{\partial u}{\partial y}$.

Case (*a*). In the neighbourhood of Simoaido and in the southward region next to it, a conspicuous negative maximum of

$\frac{\partial u}{\partial y}$ exists. In the region near Atami there are positive maxima of $\frac{\partial u}{\partial y}$. In almost the whole of this district we find positive regions of $\frac{\partial u}{\partial y}$.

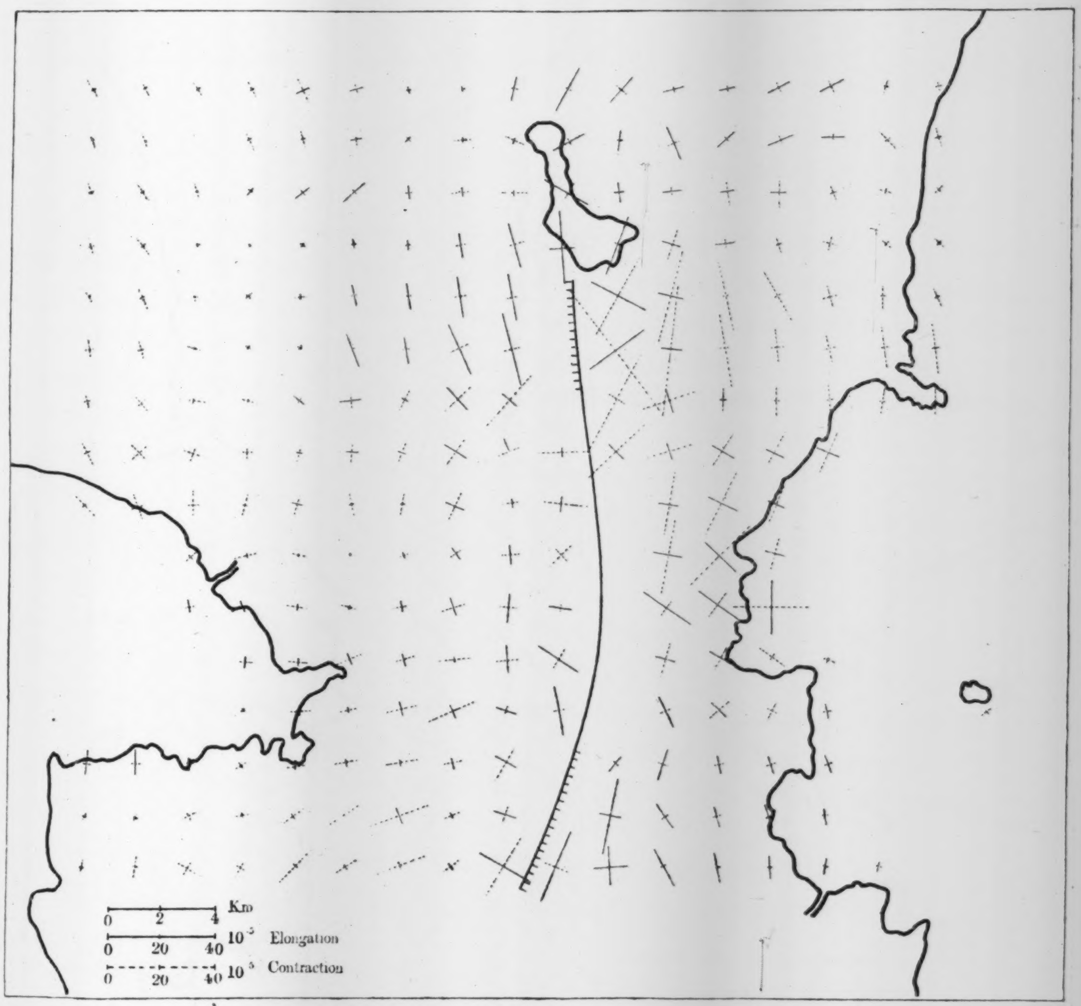

Fig. 13 *a*. Principal Strains,

$$\gamma_{1,2}=\frac{\partial u}{\partial x}+\frac{\partial v}{\partial y}\pm\sqrt{\left(\frac{\partial u}{\partial x}-\frac{\partial v}{\partial y}\right)^2+\left(\frac{\partial v}{\partial x}+\frac{\partial u}{\partial y}\right)^2}.$$

Case (*b*). About the northern extremity of the fault, i. e., near Karesugi, as well as in the middle part west of the fault, near Konaya, there are positive maxima of $\frac{\partial u}{\partial y}$ (see Fig. 7, and 22).

9. Eastward Gradient of Northward Displacement $\frac{\partial v}{\partial x}$.

Case (*a*). Only the regions near Minamiyosiwara, Nirayama, and Takayama have positive values of $\frac{\partial v}{\partial x}$, nearly all the remainder being regions of negative values. There are negative maxima of $\frac{\partial v}{\partial x}$ along the zonal area running from the northern region to the southern, through the coast of Atami.

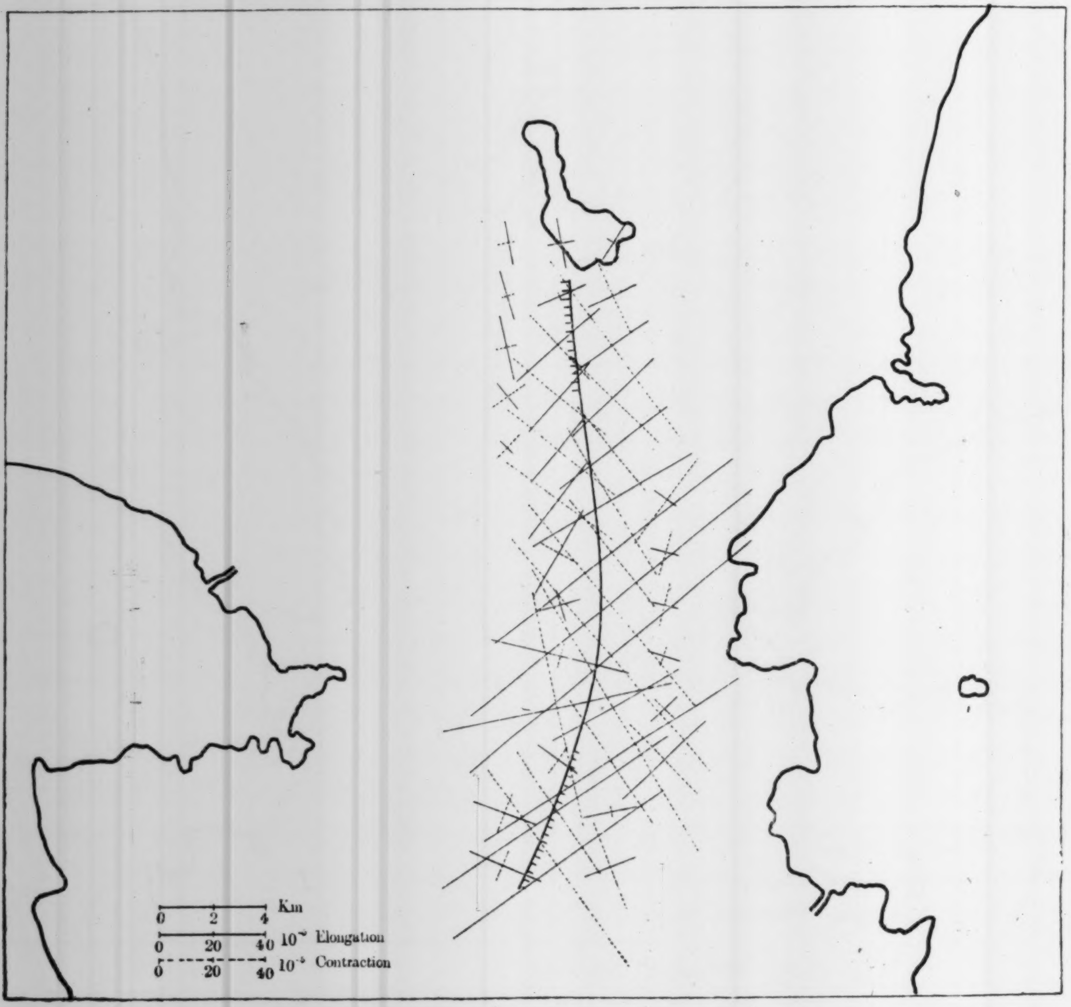

Fig. 13 *b*. Principal Strains,

$$\gamma_{1,\,2}=\frac{\partial u}{\partial x}+\frac{\partial v}{\partial y}\pm\sqrt{\left(\frac{\partial u}{\partial x}-\frac{\partial v}{\partial y}\right)^2+\left(\frac{\partial v}{\partial x}+\frac{\partial u}{\partial y}\right)^2}.$$

The existence of the Tanna Fault is entirely ignored.

Case (*b*). About both extremities of the fault and east of it are conspicuous positive maxima of $\frac{\partial v}{\partial x}$. In the other regions negative values predominate over a wide area, their maxima being along the fault and also in the region near Atami (see Fig. 8, 23).

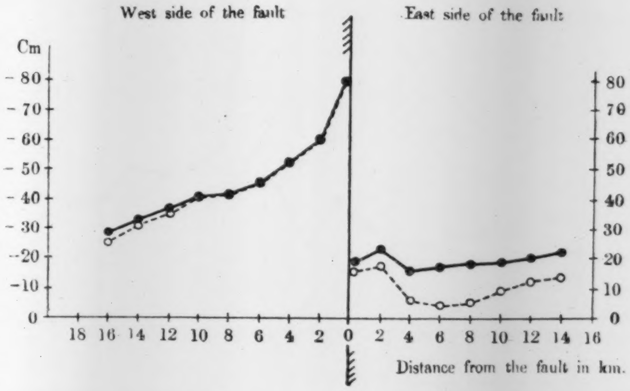

Fig. 14. Absolute (full line), and Algebraic (dotted line) mean of the Quantities.
a. Eastward Displacement, u in cm.

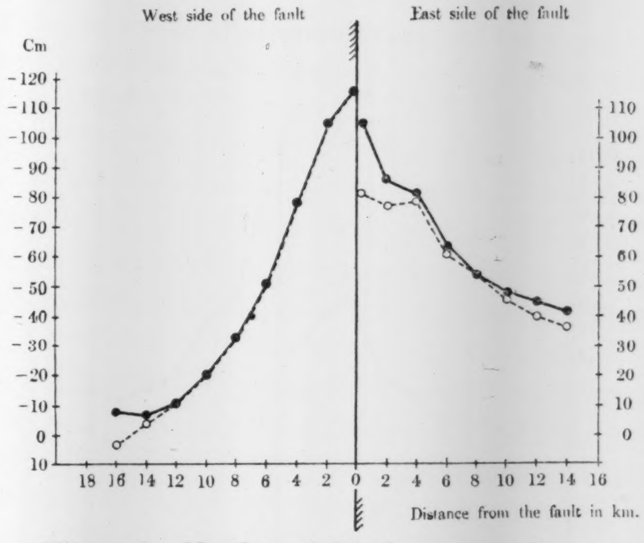

Fig. 14 *b*. Northward Displacement, v in cm.

10. Northward Gradiont of Northward Displacement $\frac{\partial v}{\partial y}$.

Case (*a*). In the N E region of Idu Penidsula, along Sagami Bay, are 3 positive and 3 negative maxima of $\frac{\partial v}{\partial y}$, alternatively. In the western part of Idu Peninsula a positive maximum of $\frac{\partial v}{\partial y}$ exists near Tokukurayama, and near Hasima a negative maximum.

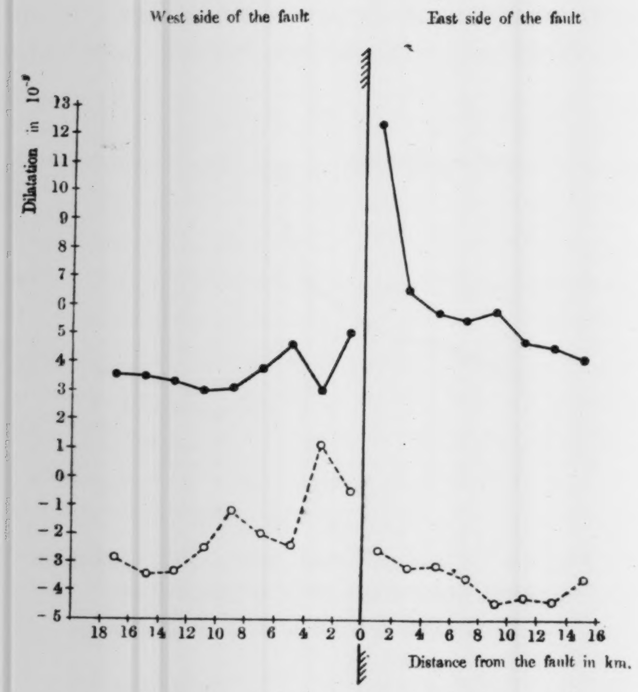

Fig. 14 *c*. Dilatation in 10^{-5}.

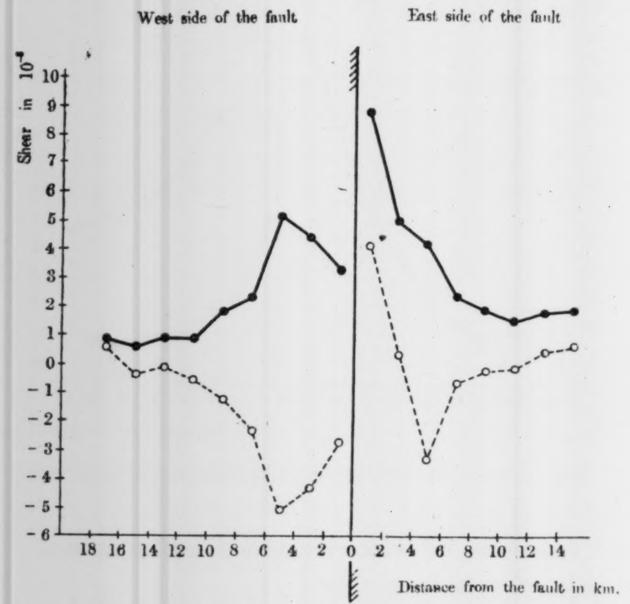

Fig. 14 *d*. Shear in 10^{-5}.

Case (*b*). About the extremities of the fault are positive maxima of $\frac{\partial v}{\partial y}$. On the east side along the fault are some negatively large values of $\frac{\partial v}{\partial y}$ (see Fig. 9, 24).

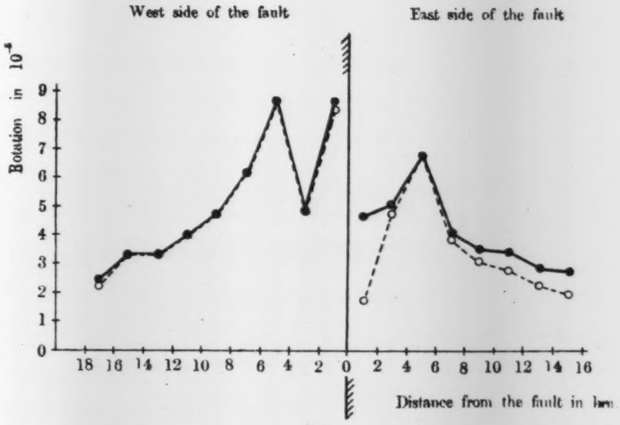

Fig. 14 *c*. Rotation in 10^{-5}.

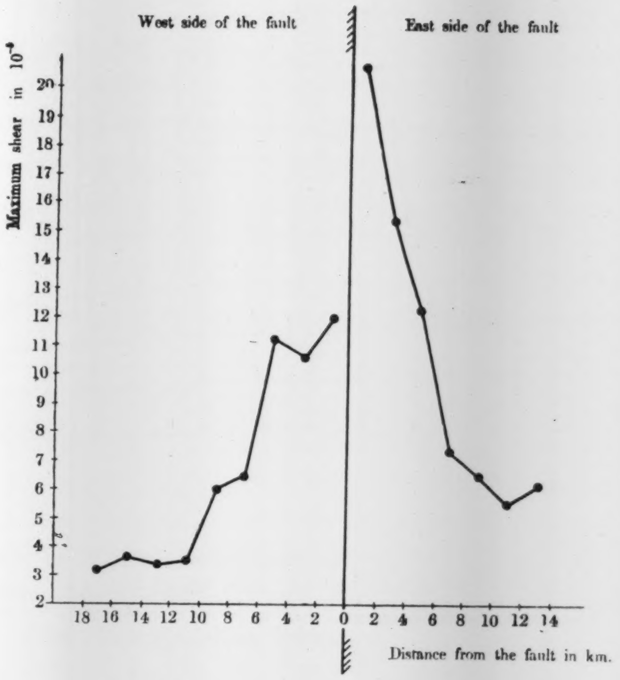

Fig. 14 *f*. Maximum Shear in 10^{-5}.

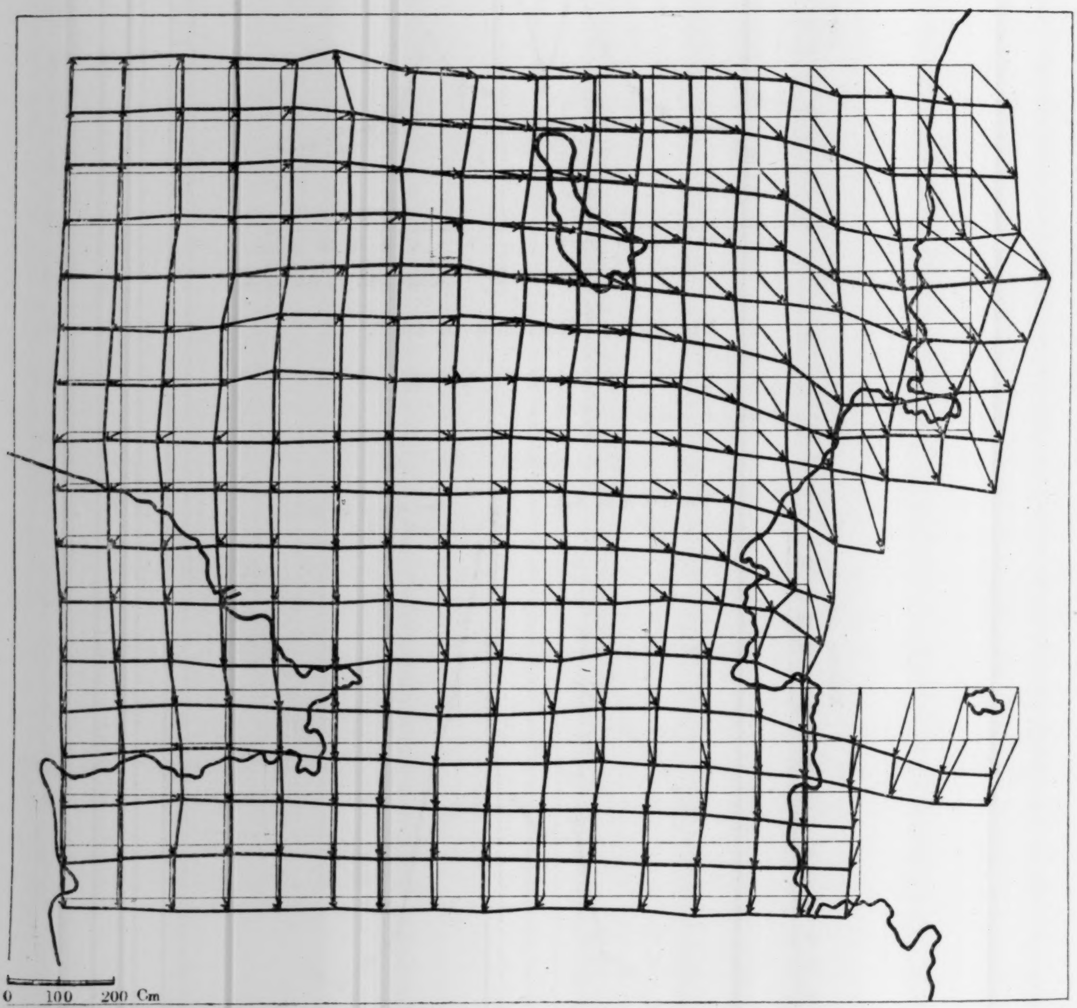

Scale for Displacements.

Fig. 15. Horizontal Displacements of the Mesh-Points, connected with the Great Kwantô Earthquake.

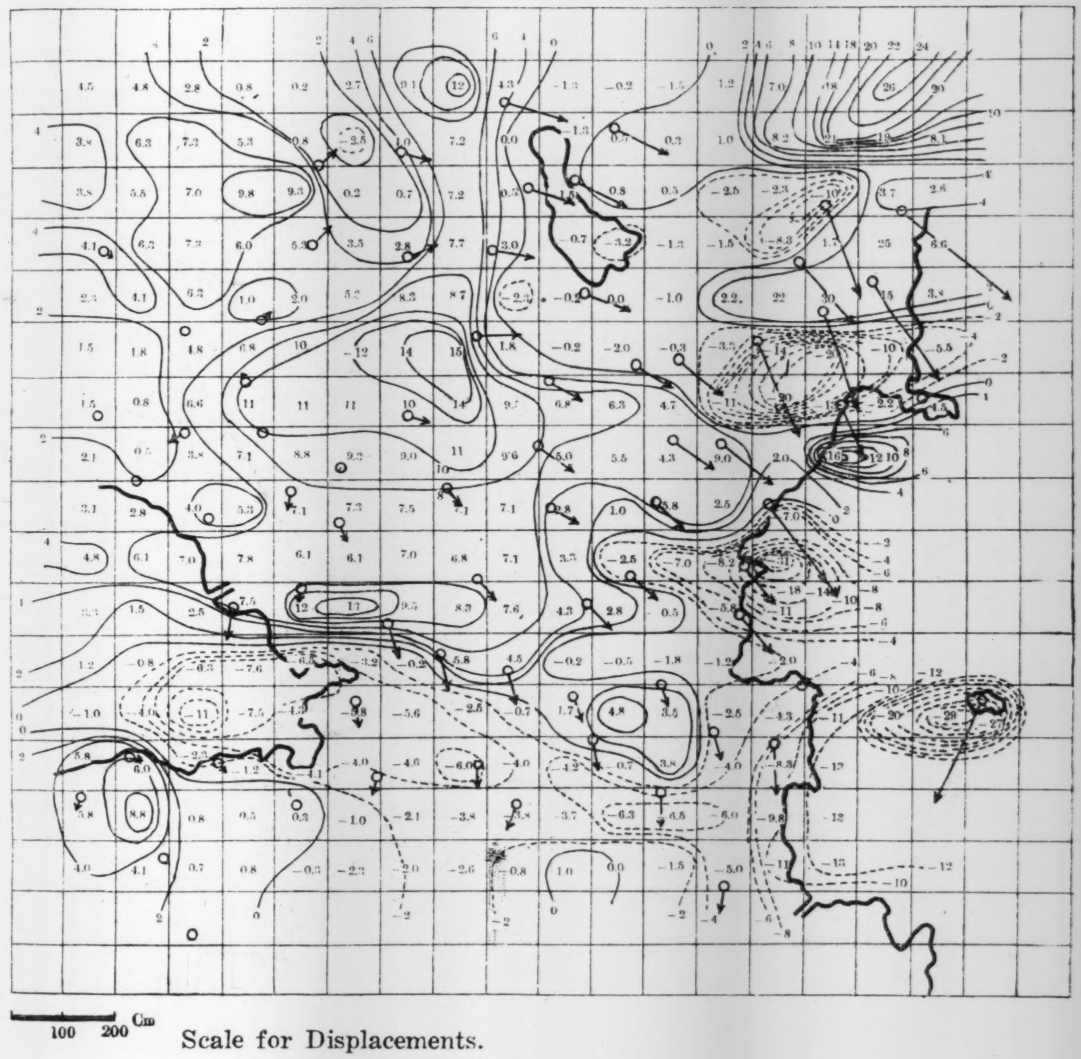

Scale for Displacements.

Fig. 16. Lines of Equal Dilatation, $\Delta = \frac{\partial u}{\partial x} + \frac{\partial v}{\partial y}$ in 10^{-5}, connected with the Great Kwantô Earthquake. Arrows show the horizontal displacements of the Triangulation Points.

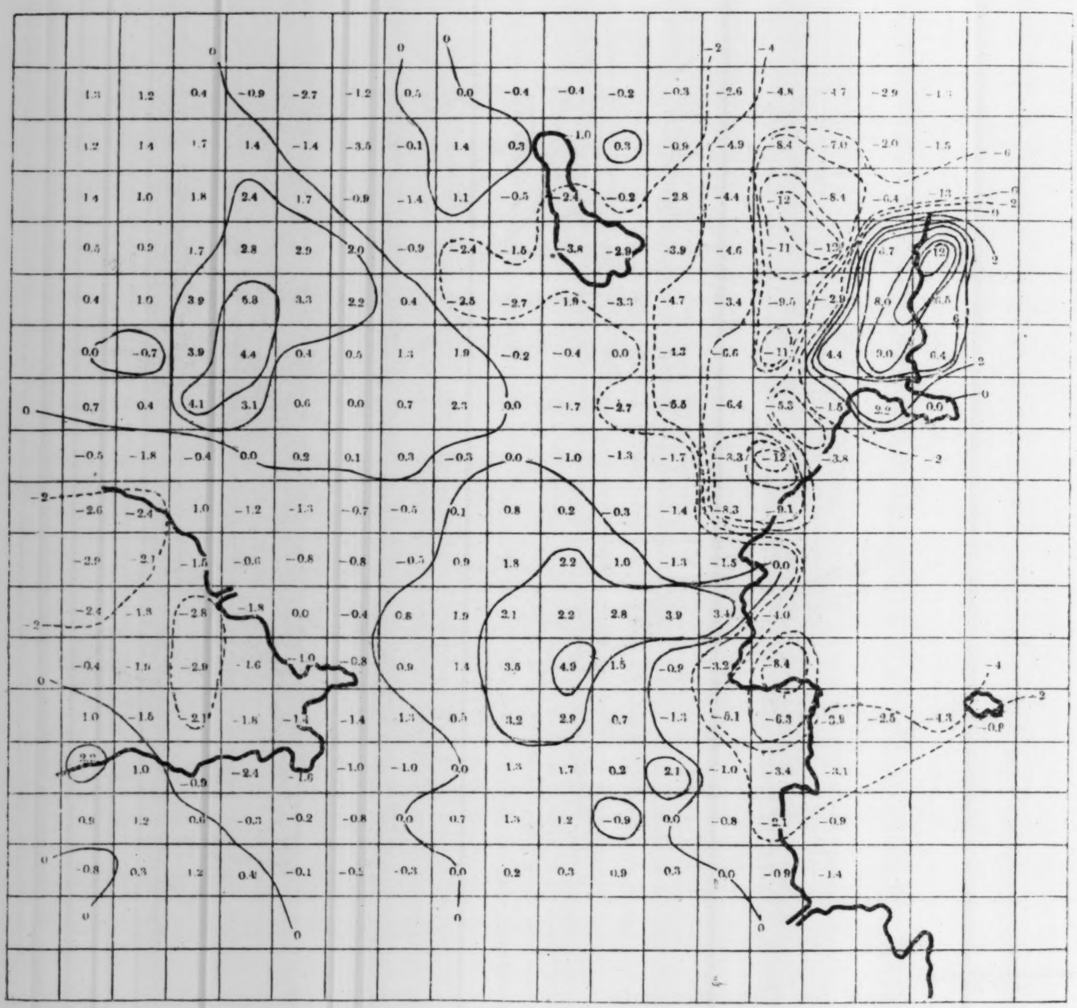

Fig. 17. Lines of Equal Shear, $\sigma=\frac{1}{2}\left(\frac{\partial u}{\partial y}+\frac{\partial v}{\partial x}\right)$ in 10^{-5}, connected with the Great Kwantô Earthquake.

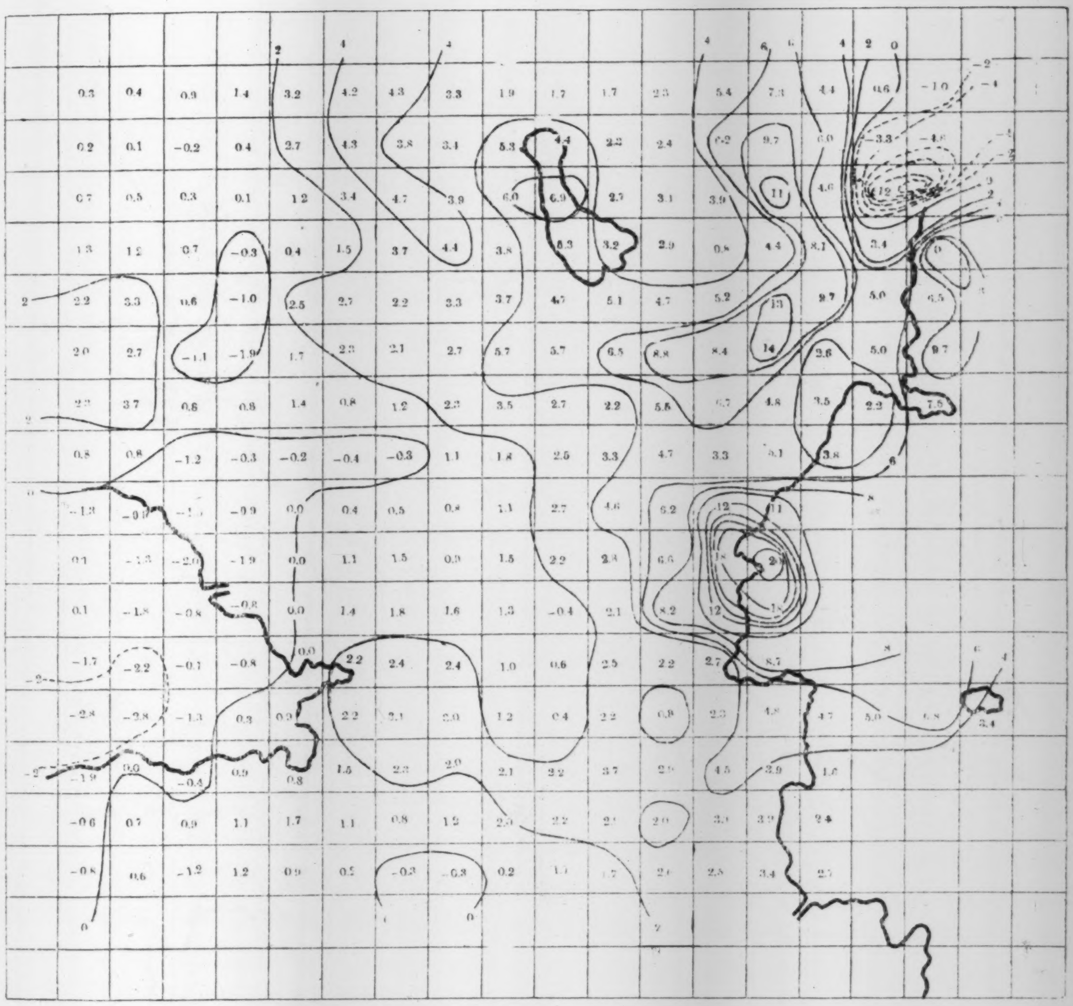
2 4 4 4 6 6 4 2 0
0.3 0.4 0.9 1.4 3.2 4.2 4.3 3.3 1.9 1.7 1.7 2.3 5.4 7.3 4.4 0.6 -1.0 -2 -4
0.2 0.1 -0.2 0.4 2.7 4.3 3.8 3.4 5.3 4.4 2.2 2.4 6.2 9.7 6.0 -3.3 -4.8 -4 -2
0.7 0.5 0.3 0.1 1.2 3.4 4.7 3.9 6.0 6.9 2.7 3.1 3.9 11 4.6 12 0 2 4
1.3 1.2 0.7 -0.3 0.4 1.5 3.7 4.4 3.8 8.3 3.2 2.9 0.8 4.4 8.1 3.4 0
2 2.2 3.3 0.6 -1.0 2.5 2.7 2.2 3.3 3.7 4.7 5.1 4.7 5.2 13 9.7 5.0 6.5 8
2.0 2.7 -1.1 -1.9 1.7 2.3 2.1 2.7 5.7 5.7 6.5 8.8 8.4 14 2.6 5.0 9.7
2 2.3 3.7 0.6 0.8 1.4 0.8 1.2 2.3 3.5 2.7 2.2 5.6 6.7 4.8 3.5 2.2 7.5
0.8 0.8 -1.2 -0.3 -0.2 -0.4 -0.3 1.1 1.8 2.5 3.3 4.7 3.3 5.1 3.8 6
0 -1.3 -0.9 -0.9 0.0 0.4 0.5 0.8 1.1 2.7 4.6 6.2 12 11 8
0.1 -1.3 -2.0 -1.9 0.0 1.1 1.5 0.9 1.5 2.2 2.8 6.6 18 24
0.1 -1.8 -0.8 -0.8 0.0 1.4 1.8 1.6 1.3 -0.4 2.1 8.2 12 18
-2 -1.7 -2.2 -0.1 -0.8 0.0 2.2 2.4 2.4 1.0 0.6 2.5 2.2 2.7 8.7 8 6 4
-2.8 -2.8 -1.3 0.3 0.9 2.2 2.1 2.0 1.2 0.4 2.2 0.9 2.3 4.8 4.7 5.0 6.8 3.4
-2 -1.9 0.0 -0.4 0.9 0.8 1.5 2.3 2.0 2.1 2.2 3.7 2.9 4.5 3.9 1.6
-0.6 0.7 0.9 1.1 1.7 1.1 0.8 1.2 2.3 2.2 2.3 2.0 3.0 3.9 2.4
-0.8 0.6 -1.2 1.2 0.9 0.5 -0.3 -0.3 0.2 1.5 1.7 2.6 2.5 3.4 2.7
0 0 0 2

Fig. 18. Lines of Equal Rotation, $\omega=\frac{1}{2}\left(\frac{\partial u}{\partial y}-\frac{\partial v}{\partial x}\right)$ in 10^{-5}, connected with the Great Kwantô Earthquake.

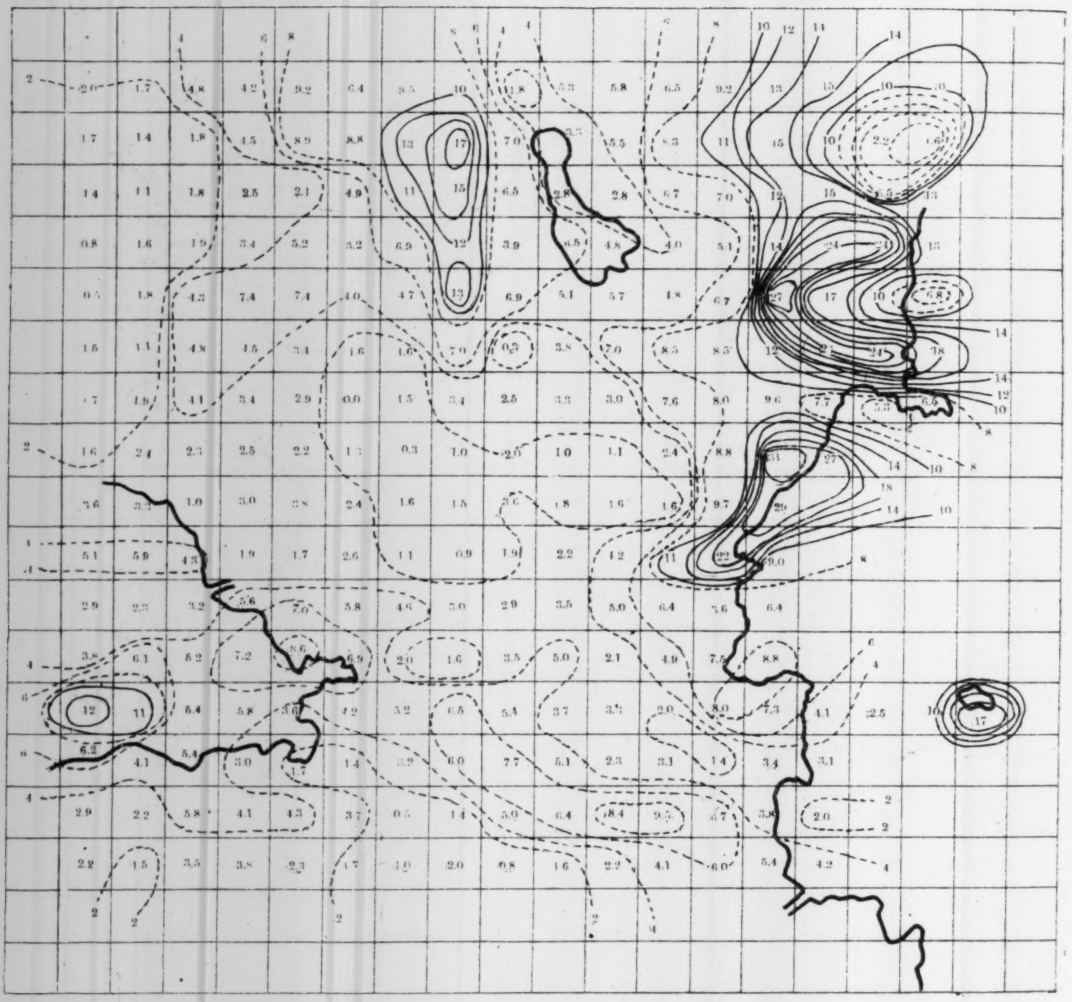

Fig. 19. Lines of Equal Maximum Shear, $\sqrt{\left(\frac{\partial u}{\partial x}-\frac{\partial v}{\partial y}\right)^2+\left(\frac{\partial v}{\partial x}+\frac{\partial u}{\partial y}\right)^2}$ in 10^{-5}, connected with the Great Kwantô Earthquake.

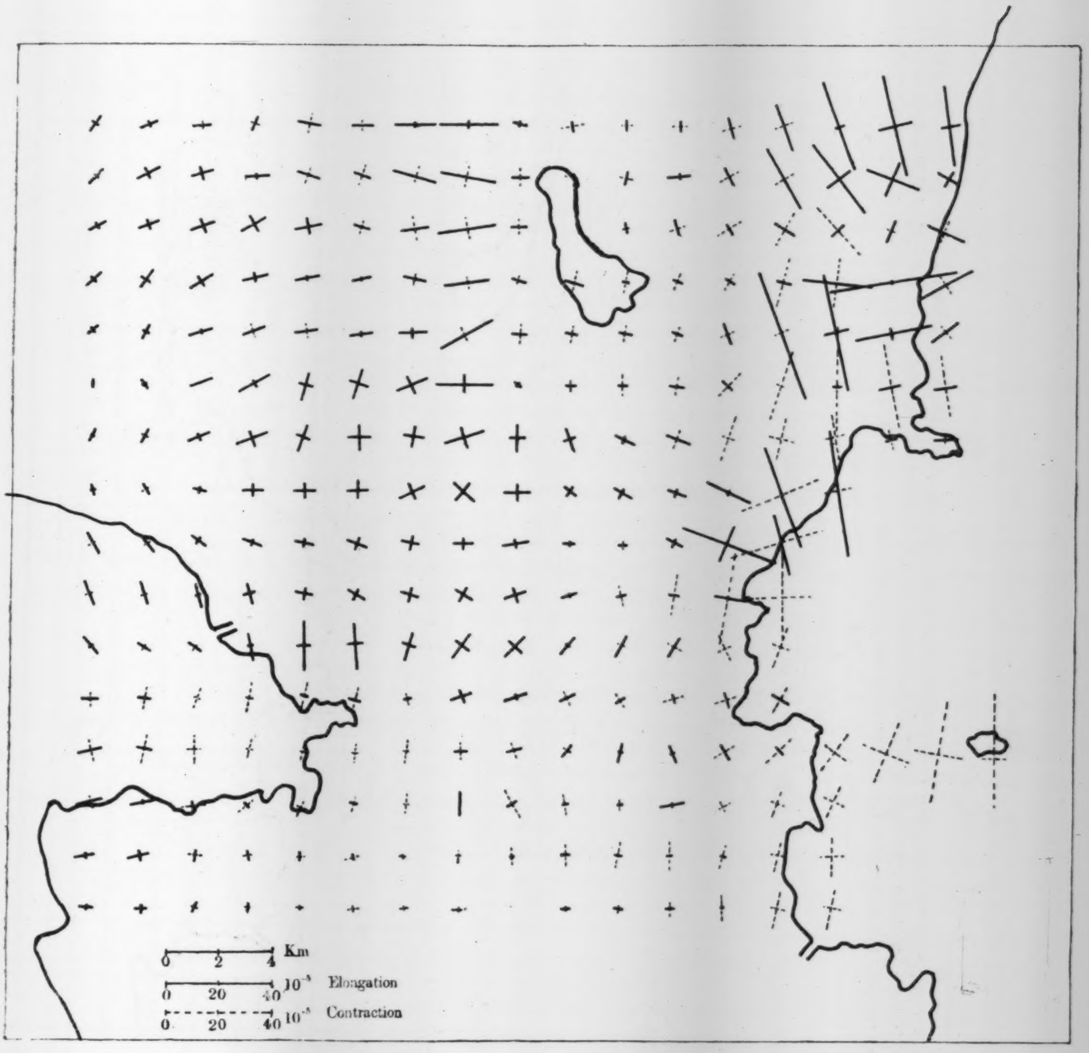
0 2 4 Km
0 20 40 10^{-5} Elongation
0 20 40 10^{-5} Contraction

Fig. 20. Principal Strains, $\gamma_{1,2}=\left(\frac{\partial u}{\partial x}+\frac{\partial v}{\partial y}\right)\pm\sqrt{\left(\frac{\partial u}{\partial x}-\frac{\partial v}{\partial y}\right)^2+\left(\frac{\partial v}{\partial x}+\frac{\partial u}{\partial y}\right)^2}$, connected with the Great Kwantô Earthquake.

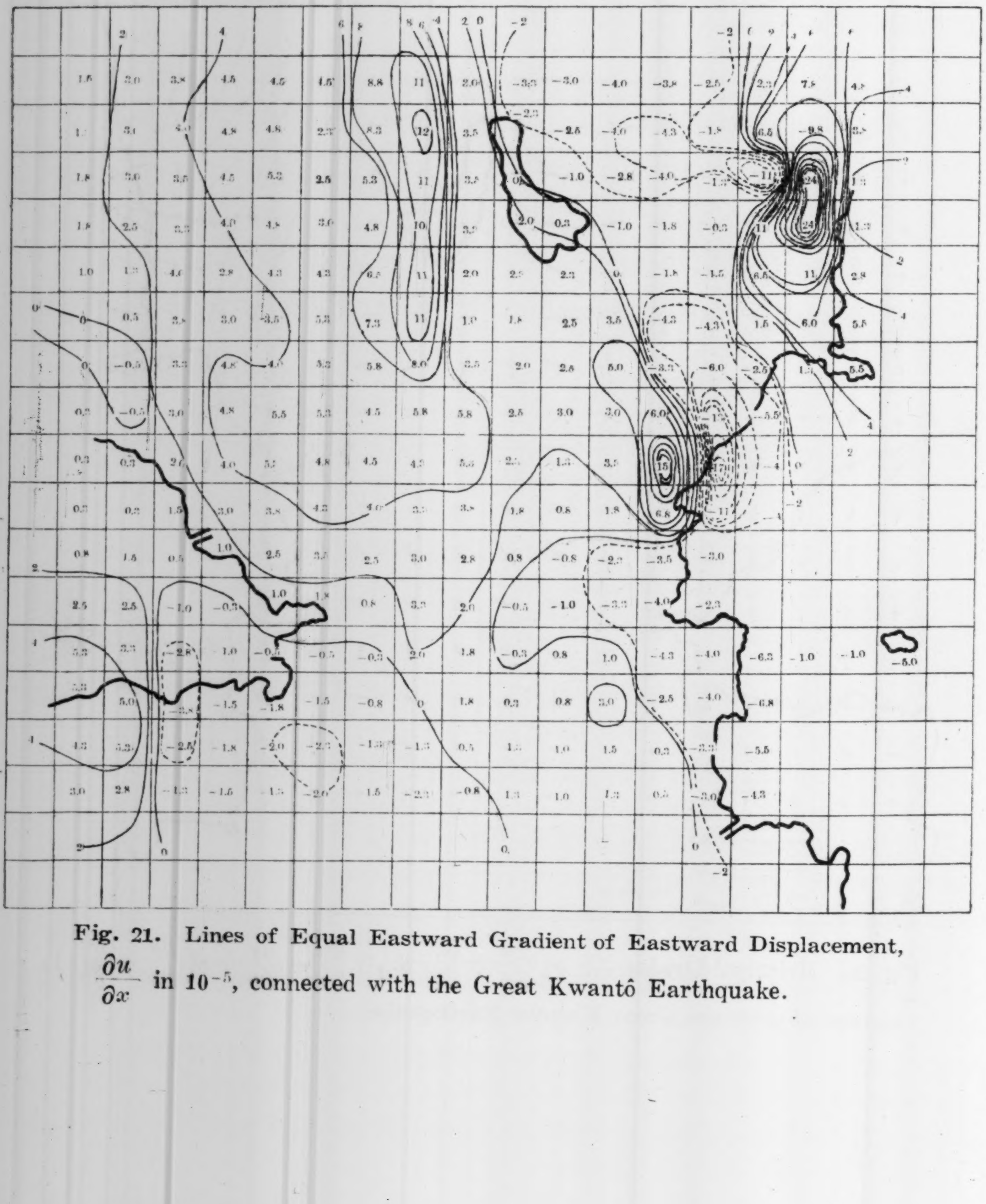
2
4
6
8
2 0
-2
-2
1.5 2.0 3.8 4.5 4.5 4.5 8.8 11 2.0 -3.3 -3.0 -4.0 -3.8 -2.5 2.3 7.5 4.5
-2.3
3.1 4.0 4.8 4.8 2.3 8.3 12 3.5 -2.5 -4.0 -4.3 -1.8 6.5 -9.8 3.5
1.8 3.6 3.5 4.5 5.3 2.5 5.3 11 3.5 0 -1.0 -2.8 -4.0 -1.3 -11 24 1.3
1.8 2.5 3.3 4.0 4.8 3.6 4.8 10 3.5 2.0 0.3 -1.0 -1.8 -0.3 11 24 1.3
1.0 1.3 4.0 2.8 4.3 4.3 6.5 11 2.0 2.5 2.3 0 -1.8 -1.5 6.5 11 2.8
0 0.5 3.8 3.0 3.5 5.3 7.3 11 1.0 1.8 2.5 3.5 -4.3 -4.3 1.5 6.0 5.5
0 -0.5 3.3 4.8 4.0 5.3 5.8 8.0 3.5 2.0 2.5 5.0 -3.3 -6.0 -2.5 1.3 5.5
0.3 -0.5 3.0 4.8 5.5 5.3 4.5 5.8 5.8 2.5 3.0 3.0 6.0 -13 -5.5
0.3 0.3 2.0 4.0 5.3 4.8 4.5 4.3 5.3 2.5 1.5 3.5 15 17 -4 0
0.3 0.3 1.5 3.0 3.8 4.3 4.0 3.3 3.5 1.8 0.8 1.8 6.8 -11 -2
0.8 1.5 0.5 1.0 2.5 3.3 2.5 3.0 2.8 0.8 -0.8 -2.3 -3.5 -3.0
2
2.5 2.5 -1.0 -0.3 1.0 1.8 0.8 3.3 2.0 -0.5 -1.0 -3.3 -4.0 -2.3
4
5.3 3.3 -2.8 1.0 -0.3 -0.5 -0.3 2.0 1.8 -0.3 0.8 1.0 -4.3 -4.0 -6.3 -1.0 -1.0 -5.0
5.3 5.0 -3.8 -1.5 -1.8 -1.5 -0.8 0 1.8 0.3 0.8 3.0 -2.5 -4.0 -6.8
4
4.3 5.3 -2.5 -1.8 -2.0 -2.3 -1.3 -1.3 0.5 1.3 1.0 1.5 0.3 -3.3 -5.5
3.0 2.8 -1.3 -1.5 -1.5 -2.0 1.5 -2.3 -0.8 1.3 1.0 1.3 0.5 -3.0 -4.3
2
0
0
0
-2

Fig. 21. Lines of Equal Eastward Gradient of Eastward Displacement, $\frac{\partial u}{\partial x}$ in 10^{-5}, connected with the Great Kwantô Earthquake.

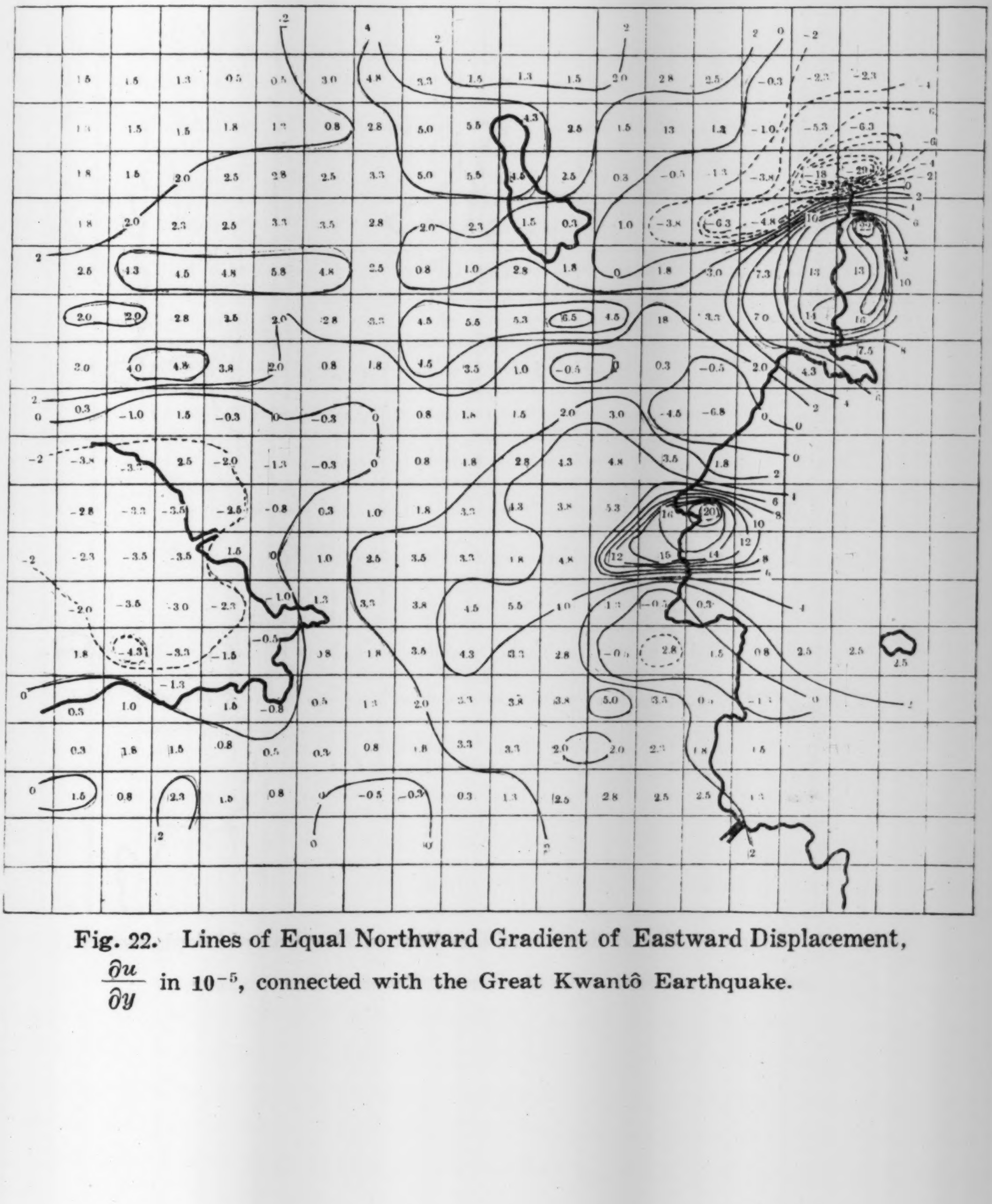

Fig. 22. Lines of Equal Northward Gradient of Eastward Displacement, $\dfrac{\partial u}{\partial y}$ in 10^{-5}, connected with the Great Kwantô Earthquake.

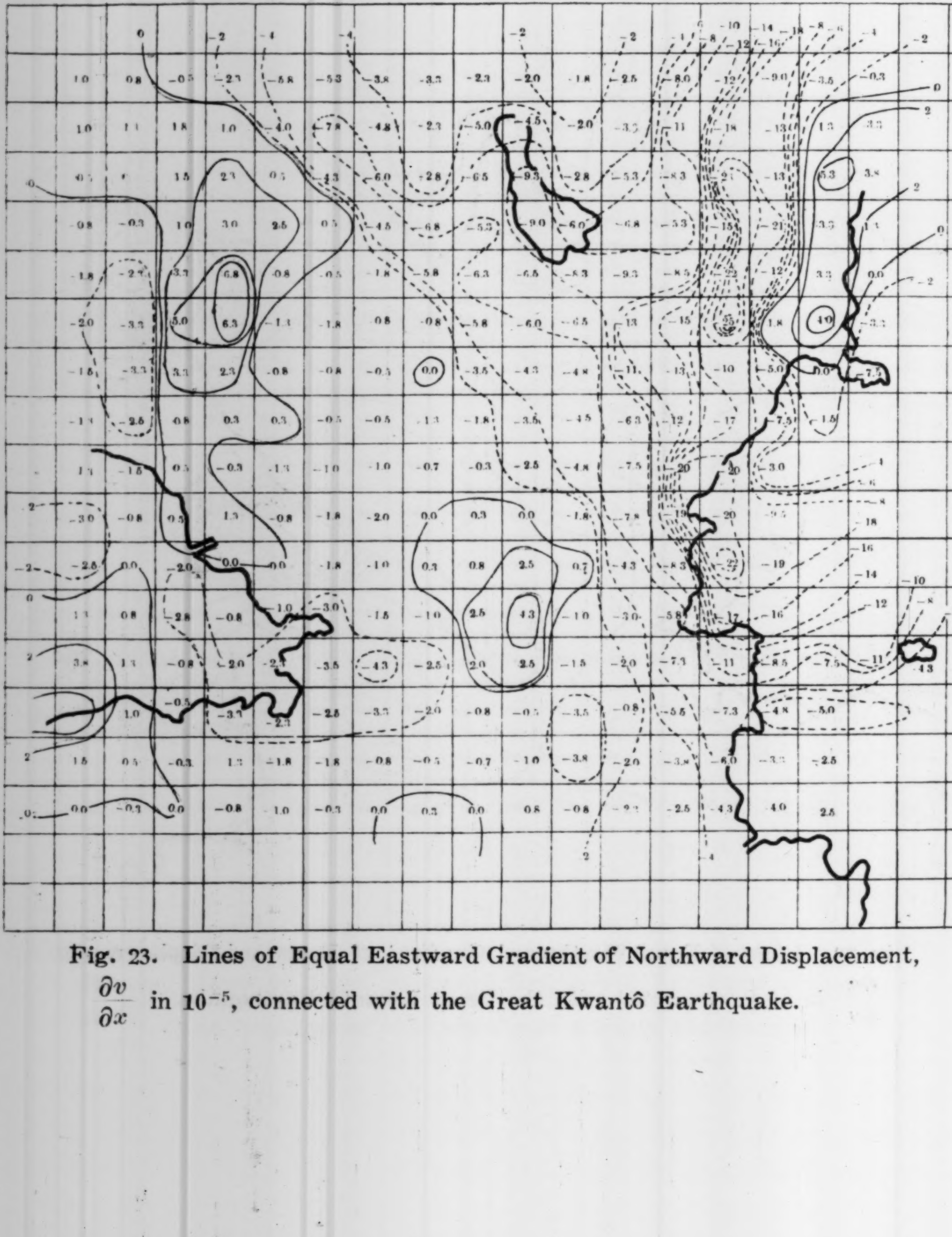

Fig. 23. Lines of Equal Eastward Gradient of Northward Displacement, $\frac{\partial v}{\partial x}$ in 10^{-5}, connected with the Great Kwantô Earthquake.

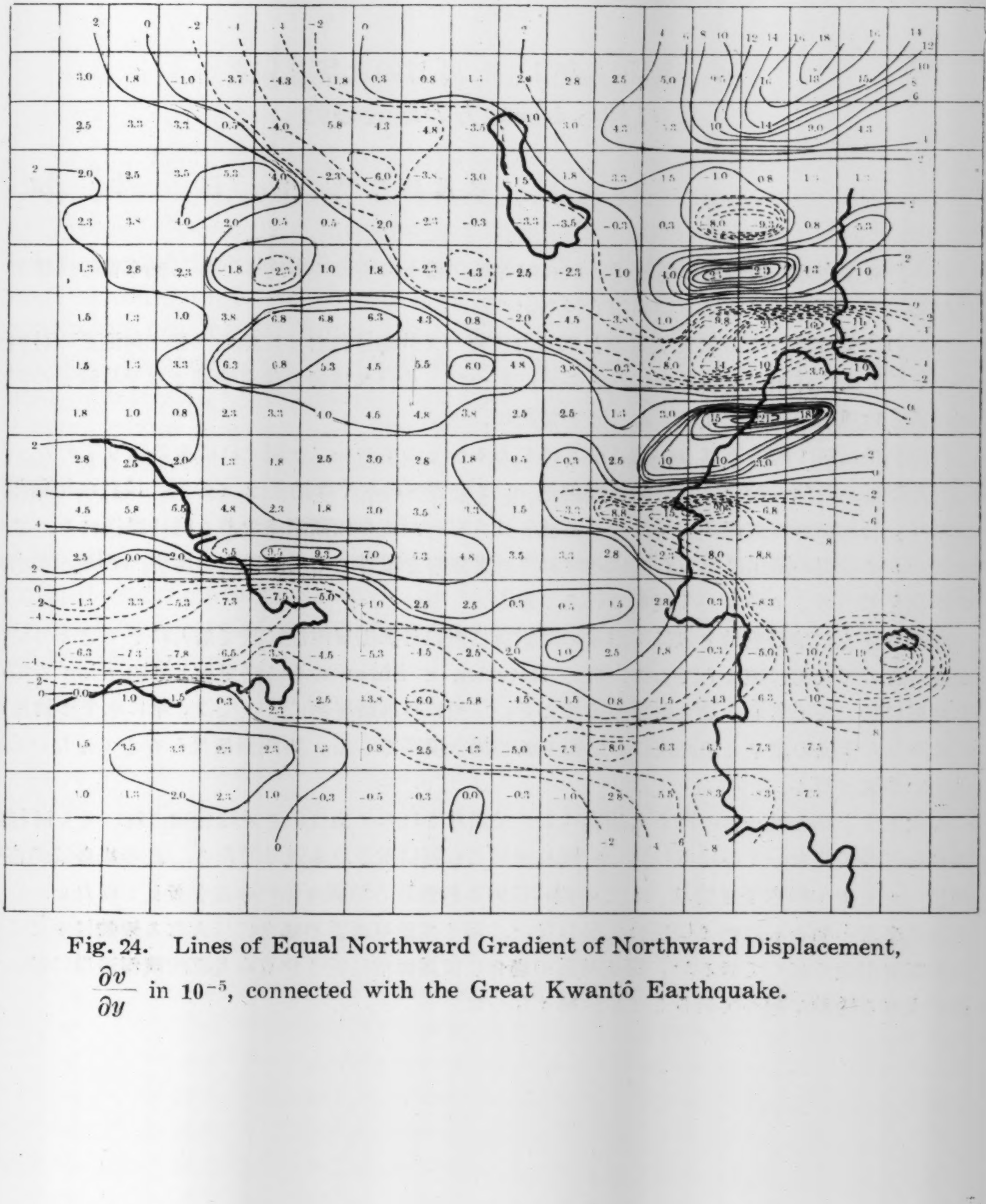
2 0 -2 -4 -4 -2 0 2 4 6 8 10 12 14 16 18 16 14 12 10 8 6
3.0 1.8 -1.0 -3.7 -4.3 -1.8 0.3 0.8 1.3 2.8 2.8 2.5 5.0 9.5 16 13 15
2.5 3.3 3.3 0.5 -4.0 5.8 4.3 4.8 -3.5 10 3.0 4.3 10 14 9.0 4.3
2 2.0 2.5 3.5 5.3 4.0 -2.3 -6.0 -3.8 -3.0 1.5 1.8 3.3 1.5 -1.0 0.8 1.3 1.3
2.3 3.8 4.0 2.0 0.5 0.5 -2.0 -2.3 -0.3 -3.3 -3.5 -0.3 0.3 -8.0 -9.3 0.8 3.3
1.3 2.8 2.3 -1.8 -2.3 1.0 1.8 -2.3 -4.3 -2.5 -2.3 -1.0 4.0 23 23 13 10
1.5 1.3 1.0 3.8 6.8 6.8 6.3 4.3 0.8 -2.0 -4.5 -3.8 1.0 -8.8 -21 -16 -19
1.5 1.3 3.3 6.3 6.8 5.3 4.5 5.5 6.0 4.8 3.8 -0.3 -8.0 -14 -10 -3.5 -19
1.8 1.0 0.8 2.3 3.3 4.0 4.5 4.8 3.8 2.5 2.5 1.3 3.0 15 21 18
2 2.8 2.5 2.0 1.3 1.8 2.5 3.0 2.8 1.8 0.5 -0.3 2.5 10 3.0
4 4.5 5.8 5.5 4.8 2.3 1.8 3.0 3.5 3.3 1.5 -3.3 -8.8 -15 -20 -6.8
4 2.5 -0.0 2.0 6.5 9.5 9.3 7.0 5.3 4.8 3.5 3.3 2.8 -2.3 -8.0 -8.8
2 0 -2 -4 -1.3 3.3 -5.3 -7.3 -7.5 -5.0 -1.0 2.5 2.5 0.3 0.5 1.5 2.8 0.3 -8.3
-4 -6.3 -7.3 -7.8 -6.5 -3.8 -4.5 -5.3 -4.5 -2.5 2.0 1.0 2.5 1.8 -0.3 -5.0 -10 -19
-2 0 0.0 1.0 1.5 0.3 -2.3 -2.5 -3.8 -6.0 -5.8 -4.5 -1.5 0.8 -1.5 -4.3 -6.3 -10
1.5 3.5 3.3 2.3 2.3 1.3 0.8 -2.5 -4.3 -5.0 -7.3 -8.0 -6.3 -6.5 -7.3 -7.5
1.0 1.3 2.0 2.3 1.0 -0.3 -0.5 -0.3 0.0 -0.3 -1.0 2.8 5.8 -8.3 -8.3 -7.5
0 -2 -4 -6 -8

Fig. 24. Lines of Equal Northward Gradient of Northward Displacement, $\frac{\partial v}{\partial y}$ in 10^{-5}, connected with the Great Kwantô Earthquake.

In conclusion, I wish to express may best thanks to Dr. Chûji, Tsuboi, who has given me many useful suggestions in the course of these studies.

56. 昭和5年11月26日の北伊豆裂震に伴へる同地方の地殼變動

地震研究所 **山口生知**

此の伊豆地方の地殼變動の問題は，既に坪井忠二博士に依つて研究された．然し當時は僅かに13點の二等三角測量の結果しか利用し得なかつた．

今回の論文の目的は，其後陸地測量部の力に依つて計測された 71 點の三等三角測量の材料を借用して，更に詳細なる調査を試みることにあつた．尙ほ又地殼の鉛直變動と水平移動との間に何か或る物理學的關係を見出さんことを望んだ．

其の結果は第1圖乃至第 14 圖に示されてゐるがその中の一二を擧ぐれば次の通りである．

丹那斷層の西側に於いては，鉛直變動量 w と東方への水平移動量 u との間には負の相關關係があり，丹那斷層の東側に於ては餘り判然とはしないが正の相關關係がある樣に思はれる．此の u と w との間の關係は第 11 圖に示す如く丹那斷層を境界として階段的地塊層（Step-faults）の存在を考へることによつて說明されると思ふ．

今回計算した地殼變動を表はす諸量の絕對値は概ね丹那斷層附近に於て最大にして之より遠ざかるに從つて次第に減少してゐる．但し Rotation と Shear のみは斷層線より約 6 km を隔てた地域に於いても著しき最大値を有してゐる．一般に丹那斷層線に於いては，單に水平移動量 u, v のみならず他の諸量も不連續にして而も此の線を境界として，東西對稱性を有してゐないのは著しい事實と思ふ．

尙大正十二年九月一日の關東大地震によつて諾起されたと思はれる地殼變動に就いても同樣の調查を行つて見た．その結果は第 15 圖及至第 24 圖に示される通りである．此の場合は鉛直變動量 w と東への水平變動量，u との間には何等判然たる相關々係の存在を發見し得なかつた．又丹那斷層の如きも判然とは現れて居らない．而して伊豆地震の場合には大なる變動は主として丹那斷層附近に起つて居るが，關東地震の場合には震源地に近き伊豆東北部相模灣沿岸に沿ふて最も大なる變動が起つて居ることが分明となつた．

57. *The Water Surface of a Lake as an Indicator of Crustal Deformation.*

By Chûji TSUBOI,

Earthquake Research Institute.

(Read April 20, 1937.—Rec. Sept. 20, 1937.)

Lake Biwa, in Siga Prefecture, with a length of over 60 km in a NNE–SSW direction and an average width of 15 km, is the largest lake in Japan. Along its lute-shaped shore-line (biwa is the Japanese for lute), measuring more than 235 km, are distributed 36 recording or staff water-gauges as shown in Fig. 1, which are in use for civil engineering purposes. Since 1889, when the water-gauges, Nos. 1, 13, 18, 27, and 34 were erected, reading of the height of the lake water have been continued practically without interruption for over 50 years. Through the courtesy of the Siga Prefecture Civil Engineering Section, the writer had access to the monthly means of the height of the lake water as registered by all the gauges up to 1936. The object of the present study is to discuss this wealth of observational material from the geophysical point of view, particularly with reference to the crustal deformations around the lake. This study has been suggested by B. Gutenberg's[1] of crustal deformations in the Great Lakes District of North America.

Table I. Annual Means of the Height of the Lake Water referred to 1897.

Year	Height	Year	Height	Year	Height	Year	Height
	cm		cm		cm		cm
1887	−19·6	1898	−29·9	1909	−57·9	1920	−64·2
88	−22·7	99	− 8·9	1910	−49·6	21	−43·0
89	16·6	1900	−24·6	11	−47·9	22	−81·0
1890	12·2	01	−51·2	12	−45·4	23	−43·1
91	− 7·3	02	−55·7	13	−42·1	24	−88·4
92	6·7	03	−38·8	14	−46·4	25	−63·5
93	− 8·5	04	−55·2	15	−38·7	26	−66·4
94	−42·6	05	−45·9	16	−40·1	27	−60·7
95	−14·3	06	−48·3	17	−38·4	28	−54·6
96	40·3	07	−35·2	18	−46·2	29	−49·9
97	0	08	−54·9	19	−61·7		

---

[1] B. GUTENBERG, *Journ. Geol.*, **41** (1933), 449.

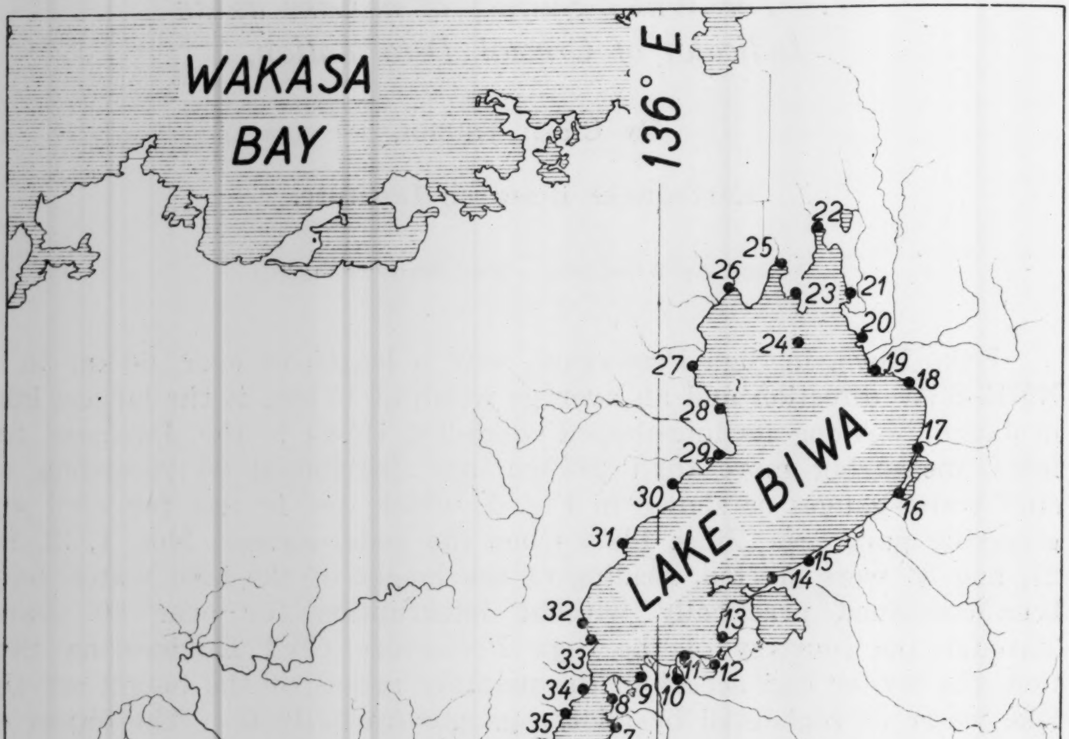
WAKASA BAY
136° E
LAKE BIWA
1
2
3
4
5
6
7
8
9
10
11
12
13
14
15
16
17
18
19
20
21
22
23
24
25
26
27
28
29
30
31
32
33
34
35
36
35° N
35° N
OSAKA BAY
0 10 20 30 KM
136° E

Fig. 1.

From the monthly means of the height of the lake water, the annual means were calculated for each of the 36 gauge stations. Since no determination has been made of the relative heights of the zeros of the gauges at different stations, and since we are here concerned only with the relative rise or fall of the lake water, the arbitrary constant peculiar to each station may be subtracted from the annual means for that station. For convenience, this constant was so taken as to reduce the annual means for 1897 for all the stations to zero.

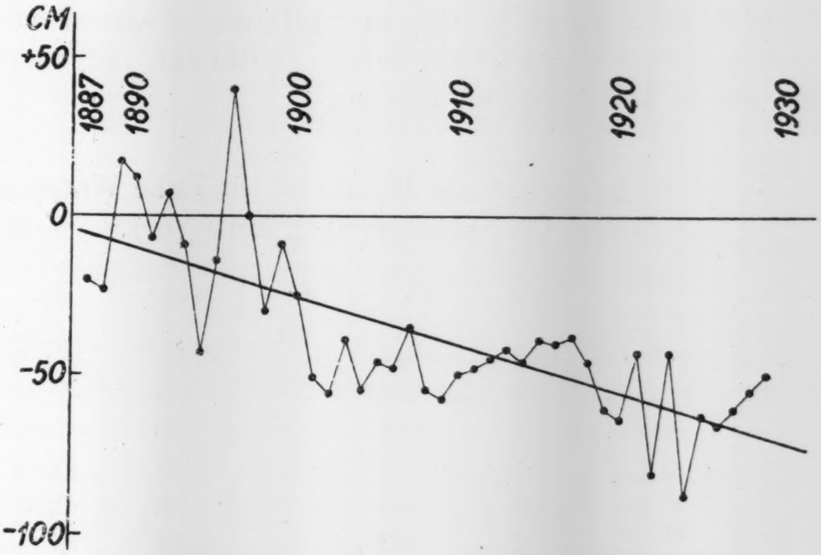

Fig. 2. General Fall of the Level of the Lake Water.

The annual means for the various stations being thus referred to one common datum, the mean of the annual means was calculated for each year with the results given in Table I and plotted in Fig. 2. They clearly indicate the general fall of the water level of the lake.

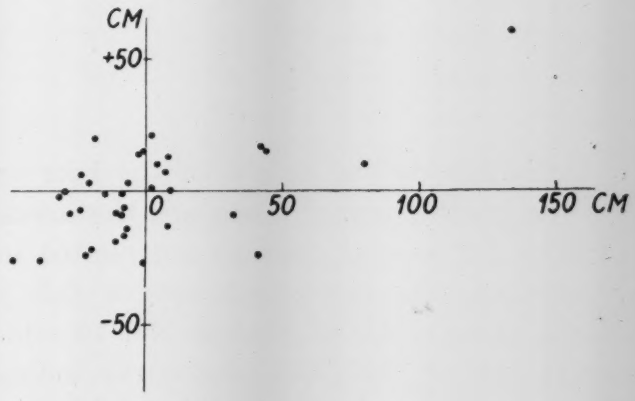

Fig. 3. Correlation Diagram between δh and δr.

If we assume the fall of the water level to be linear with respect to time, the height of the water h in any year was found to be given by

$$h = -1{\cdot}53t - 5{\cdot}5 \text{ (cm)}$$

by the method of least squares, where t is the number of years counted from 1887. The average rate of fall of the water level is thus 1·53 m per century. In this connection, it is interesting to note that around the lake at little more than 200 m above the present lake surface, lake terraces of diluvial age are well developed.

The fluctuations superposed on the general fall of the water level are probably caused by those in the precipitation in and around the lake. Fig. 3 is a diagram correlating the fluctuations in the height of the water level with those in the precipitation observed at Hikone, situated on the eastern coast of the lake. Although not very clearly, the diagram shows the suspected relation.

Table II. Fluctuations in the Height of the Lake Water (δh) and in the Precipitation at Hikone (δr).²⁾

Year	δh	δr	Year	δh	δr	Year	δh	δr
	cm	cm		cm	cm		cm	cm
1894	−26·4	− 49	1906	−13·8	− 7	1918	+ 6·7	+ 7
95	+ 3·4	− 7	7	− 0·9	+ 2	19	− 7·3	−24
96	+59·6	+134	8	−17·3	− 8	20	− 8·2	−28
97	+20·8	+ 2	9	−18·8	−11	21	+14·5	+44
98	− 7·6	− 11	1910	− 8·9	− 9	22	−22·0	−20
99	+14·9	− 1	11	− 5·7	− 8	23	+17·4	+42
1900	+ 0·8	− 15	12	− 1·7	−32	24	−26·3	−39
1	−24·3	− 22	13	+ 3·1	−21	25	0	+ 9
2	−27·3	− 1	14	+ 0·3	−30	26	− 1·3	− 9
3	− 8·8	+ 32	15	+ 9·6	+ 4	27	+ 6·0	−24
4	−23·7	+ 41	16	+ 9·7	+80	28	+13·6	− 3
5	−12·9	+ 8	17	+13·0	+ 8	29	+19·8	−19

Deviations in the height of the lake water at a particular station from the corresponding mean are the anomalies for that station. The anomalies for several stations are plotted in Fig. 4. At Station No. 1, for instance, the curve indicates a fall of water level at a nearly uniform rate, while at Station No. 19 which is situated almost on the opposite side of the lake, the curve indicates a rise of the level with similar amount. Just as by tipping a water-bowl a relative rise of water is caused toward the direction of tipping and a fall in the opposite direction, the rise and fall of the water level just found are to be attributed to tilts of the earth's crust around the lake.

---

2) Taken from Monthly Weather Review of the Central Meteorological Observatory.

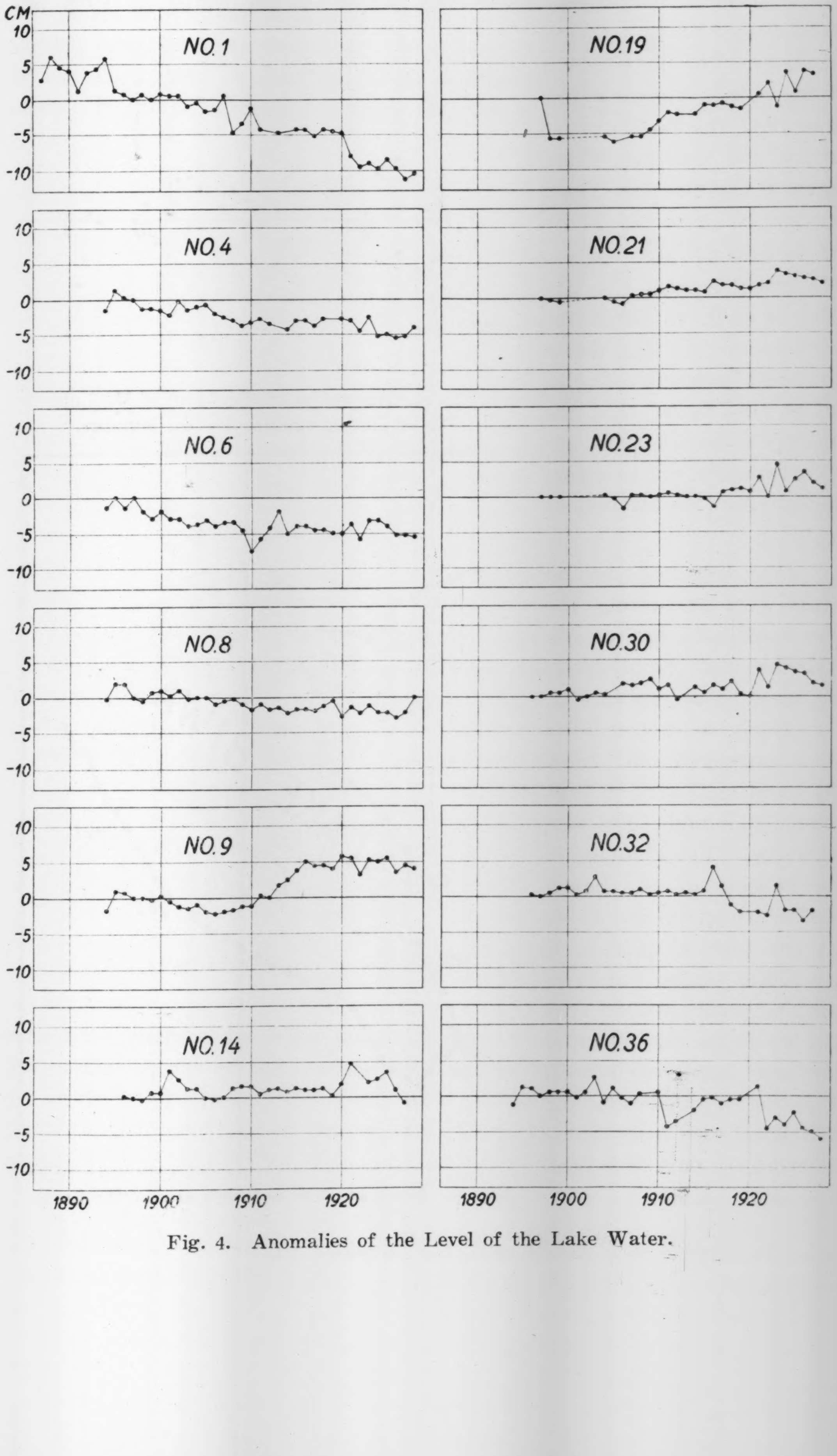

Fig. 4. Anomalies of the Level of the Lake Water.

In Fig. 5, the anomalies in the height of the water in 1928 are plotted against the station numbers. The distribution of the points suggests that since 1887, the earth's crust around the lake has tilted down in the direction from Station No. 1 to No. 20 by 0·7 second of arc. Miyabe's method[3] was also applied in order to determine more accurately the direction and amount of tilt, but it was found that the materials here used are unfortunately not accurate enough for this method of analysis.

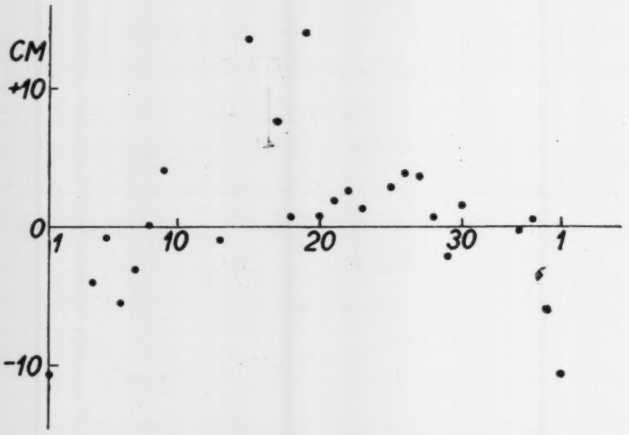

Fig. 5. Anomalies of the Level of the Lake Water plotted against Station Number.

Two lines of precise levels were run along the lake coast, the one on its east side and the other on the west as shown in Fig. 6. Each of these lines were surveyed in 1888, 1918 and 1927, and in 1885 1899, 1917 and 1928 respectively. The changes in the heights of the benchmarks are given in Table III and plotted in Figs. 7, 8. The tilting of the earth's crust around the lake as found by repeated levellings agree well both in direction and amount with what has been deduced from the data of height of the lake water.

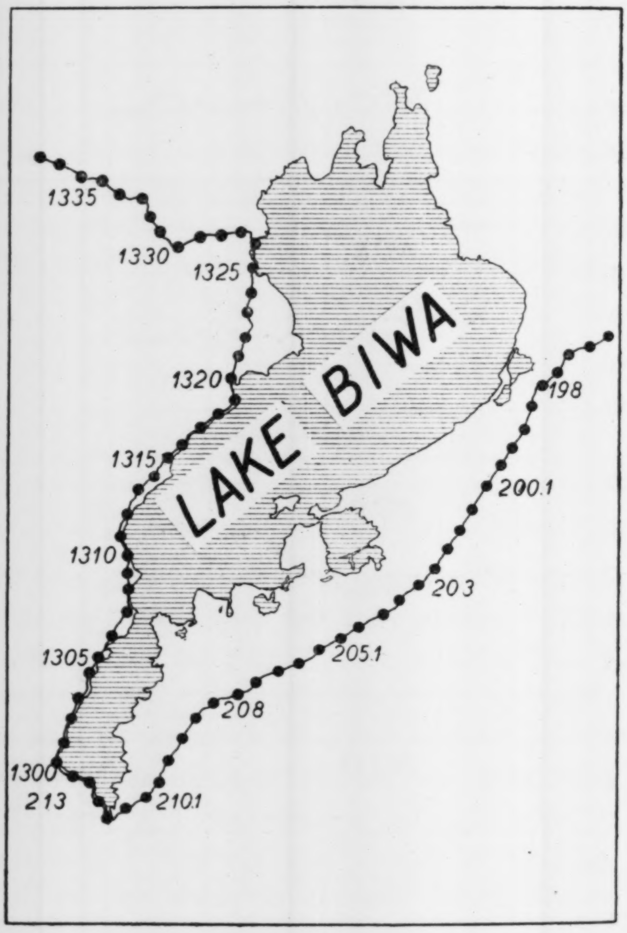

Fig. 6. Lines of Precise Levels around the Lake.

---

[3] N. MIYABE, *Bull. Earthq. Res. Inst.*, **9** (1931), 256.

After all, a lake is a large level by means of which tilts of the earth's crust may be detected. The fact that no great accuracy is to be expected from it does not detract from its usefulness in this respect. If due allowance are made for the effects of meteorological disturbances, such as by wind and rain, both of which bring about changes in the height of the water, the means above-mentiond can be availed of in a protracted and continuous watch for regional tilts of the earth's crust, provided of course that there is a lake in or near that region.

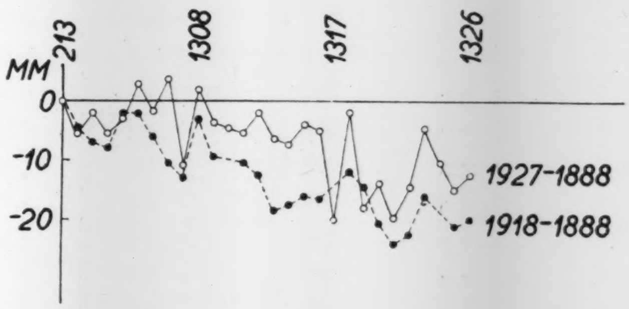

Fig. 7. Changes in the Heights of the Bench Marks.

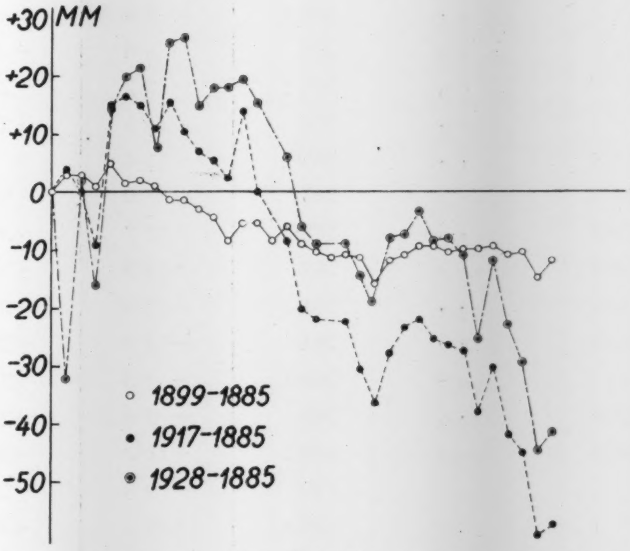

Fig. 8. Changes in the Heights of the Bench Marks.

Table III. Changes in Heights of Bench Marks (mm).

B.M.	1918−1888	1927−1988	B.M.	1899−1885	1917−1885	1928−1885
213	0·0	0·0	213	0·0	0·0	0·0
1300	−4·3	−5·3	212·1	+3·0	+3·8	−31·9
1	−6·9	−2·1	212	+3·0	+0·1	+2·0
2	−7·9	−5·6	211·1	+1·0	−9·2	−16·2
3	−1·9	−2·9	211	+4·9	+15·0	+14·6
4	−1·9	+2·9	210·1	+1·3	+16·3	+19·8
5	−6·1	−1·7	210	+1·9	+14·9	+21·5
6	−10·7	+4·0	209·1	+1·1	+12·1	+10·6
7	−13·1	−10·9	209	−1·6	+15·5	+26·1
8	−3·1	+2·2	208·1	−1·4	+10·7	+21·8
9	−9·8	−3·3	208	−3·0	+7·1	+14·9
1310	——	−4·8	207·1	−4·7	+5·6	+17·8
1	−10·3	−5·4	207	−8·3	+2·5	+17·8
2	−12·7	−2·2	206·1	−5·6	+13·8	+19·6
3	−18·5	−6·5	206	−5·6	+0·3	+15·6
4	−17·3	−7·4	205·1	−8·4	——	——
5	−16·0	−4·2	205	−6·0	−8·5	+6·1
6	−16·7	−5·0	204·1	−9·2	−20·1	−5·8
7	——	−19·8	204	−10·3	−22·2	−8·9
8	−11·8	−1·8	203·1	−11·4	——	——
9	−14·8	−17·9	203	−11·0	−22·4	−9·0
1320	−20·3	−14·2	202·1	−11·7	−30·3	−14·4
1	−24·2	−19·6	202	−15·9	−36·3	−16·7
2	−22·6	−14·3	201·1	−12·0	−28·0	−8·0
3	−16·2	−4·7	201	−11·2	−23·7	−7·5
4	——	−10·5	200·1	−9·3	−21·9	−3·5
5	−21·0	−14·9	200	−9·5	−25·7	−8·7
1326	−20·0	−12·5	199·1	−10·7	−26·3	−7·8
			199	−9·8	−27·6	−11·0
			198·1	−10·2	−38·2	−25·7
			198	−9·7	−30·3	−11·9
			197·1	−11·0	−42·2	−22·9
			197	−10·6	−45·1	−29·6
			196·1	−14·8	−59·3	−44·6
			196	−11·8	−57·3	−41·6

57. 琵琶湖の水位に就いて

地震研究所 坪井忠二

滋賀縣當局の御好意によつて，明治 20 年以降の琵琶湖水位の月別平均の値を入手する事が出來たのでそれを整理した．觀測點の數は 36 の多きに上つてゐる．まづ各點に就き年平均を求めそれを更に各年に就き平均すると琵琶湖水面の一般的昇降が求められる筈である．その結果によると水面は 100 年に 1·53 m の割で低下して來た事が分つた．琵琶湖の周圍には湖岸段丘が發達してゐるとの事であるが，これは以上の事實と對照して面白い事である．此の一般的低下にはかなりの上り下りが伴つてゐるが，これは附近の降水量に支配されるものであらう．

此の一般的低下を差引いた値について見ると，或る點では水位が次第に高まり，又これと湖の反對岸にある點では逆に低まる傾向がある．これは丁度水を入れた茶碗を傾けたのと同じ樣に，附近の地殼が傾斜したことを意味する．明治 20 年以來湖の長軸の方向に北側が凡そ 0·7 秒傾下したことになる．湖岸に沿つて行はれた水準測量の結果もこれと一致する．

58.　車輛，航空機用加速度計の製作

地震研究所　萩原尊禮

（昭和12年9月21日發表――昭和12年9月21日受理）

緒　言　自動車，汽車，飛行機等の交通機關の運行中に於ける機體の振動及び動搖を測定することは，其の操縱法，機體構造，原動機，路面，軌道，或は氣流等の研究に資するところが多い．此の種の目的に使用せられる振動計は本質的には地震計と何等の相違は無いのであるが，目的上其の構造は小型輕量にて且携帶操作に簡便を必要とするため技術的には種々困難な問題を伴ふ．此の場合に於ても一般の地震計の場合と同じく被測定物の變位の記錄を目的とするものと，加速度の記錄を目的とするものとに大別出來るが，車輛，航空機等の如き場合に於ては其の加速度を測定することが最も有意味である．

本文に報告する加速度計は曾て石本教授に由り製作せられた上下成分加速度計を基礎として，更に改造を加へて加速度の上下，前後，左右の3成分を同一記錄紙上に記錄せしむる樣になしたのであつて，航空機に使用し得るため特に小型輕量の點に留意した．

從來の振動計は振子の制振裝置を欠くものが多いが，之は定常狀態に於ける振動を測定するには差支へないが，週期或は振幅が刻々に變化する場合に於ては振子の自已振動の發生に由つて正確な記錄を與へることは出來ない．振子の制振裝置は空氣の粘性を利用するものが溫度に由る影響も少く調節も簡單であるが，加速度計に於ける如く短週期の振子の場合に於ては製作上困難とされて居たが，最近地震計の製作技術が進むに連れて斯樣な短週期の振子の空氣制振裝置も製作が可能となり，此處に報告する加速度計に於ても空氣制振裝置を附することが出來た．

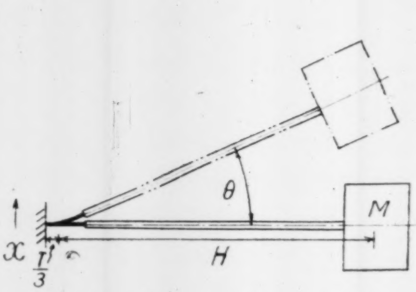

第　1　圖

設計に着手するに當つて豫めの方針として振子の週期は0.05秒，感度は記錄紙上1cmの振れが重力加速度 g（980 gal）（gal は加速度の c.g.s. unit）に相當すること，記錄裝置にはインク式を採用すること等を定めた．

設　計　今，振子を支持して居る盤が振子の軸及び廻轉軸に直角な方向に運動する場合を考へるに，盤の變位を x，振子の廻轉角を θ，振子の重心と廻轉軸との距離を H，振子の質量を M，振子の廻轉能率を I，t を時間とするときは，斯様な場合は振子の重心に $-M\dfrac{d^2x}{dt^2}$ なる力が働いたと同一結果になるから運動方程式は次の如くなる．但し θ は小い量とし，便宜上重力の存在は無視する

$$I\frac{d^2\theta}{dt^2}+\lambda\frac{d\theta}{dt}+k\theta=-MH\frac{d^2x}{dt^2} \qquad (1)$$

或は

$$\frac{d^2\theta}{d^2t}+2\varepsilon\frac{d\theta}{dt}+n^2\theta=-\frac{MH}{I}\frac{d^2x}{dt^2} \qquad (2)$$

此處に $2\varepsilon=\lambda/I$，$n^2=k/I$ である．(1) に於ける $k\theta$ は振子の復元力であつて第1圖の如く振子が板バネを以て支へられるときは，此の板バネの彈性に由り與へられるのであつて，板バネの長さを r とするときは板バネの支點より $r/3$ の距離にある點が振子の廻轉軸に相當する．振動計に於ては振子の運動を槓杆に由り何倍かに擴大して記錄せしむる必要があるが，描針の變位に對する振子の重心の變位卽ち幾何倍率を V_G とし，描針の變位を a とすれば $a=V_GH\theta$ であるから (2) 式より

$$\frac{d^2a}{dt^2}+2\varepsilon\frac{da}{dt}+n^2a=-\frac{MH^2V_G}{I}\frac{d^2x}{dt^2} \qquad (3)$$

今，簡單のため盤が $x=x_m\sin pt$ で表される正弦運動を行ふものとすれば (2) 式の解は

$$\begin{aligned}a=&e^{-\varepsilon t}(C_1\cos n\sqrt{1-h^2}t+C_2\sin n\sqrt{1-h^2}t)\\&+\frac{MH^2V_G}{I}\cdot\frac{1}{n^2}\cdot\frac{1}{\sqrt{\left(1-\frac{1}{a^2}\right)^2+4h^2\frac{1}{u^2}}}\cdot x_mp^2\sin(pt-\delta)\end{aligned} \qquad (4)$$

$$\tan\delta=\frac{2hu}{u^2-1} \qquad (5)$$

但し $u=\dfrac{n}{p}=\dfrac{T_p}{T_n}$，$h=\dfrac{\varepsilon}{n}$，$T_n$ 及び T_p は夫々振子及び盤の振動週期である．(4) 式の右邊の第 1 項は振子の自由振動，第 2 項は振子の强制振動を示す．C_1 及び C_2 は初期條件に由り決定せられる常數であるが，第 1 項は $e^{-\varepsilon t}$ の項に由り時間と共に減少し第2項のみ殘り定常の狀態に達する．今，盤の振動週期に比較して振子の週期

が充分小である場合を考へると，$n \gg p$ 即ち $u \gg 1$ であるから，

$$a \doteqdot \frac{MH^2V_G}{In^2} \cdot x_m p^2 \sin pt = \frac{MH^2V_G}{I} \cdot \frac{T_n^2}{4\pi^2} \cdot x_m p^2 \sin pt = -\frac{MH^2V_G}{I} \cdot \frac{T_n^2}{4\pi^2} \cdot \frac{d^2x}{dt^2}$$

即ち斯の様な條件の下に於ては振子の廻轉角 θ は盤の加速度に比例することになる．此の場合の感度は $\dfrac{V_G MH^2 T_n^2}{4\pi^2 I}$ である．而して $1/\sqrt{\left(1-\dfrac{1}{u^2}\right)^2+4h^2\dfrac{1}{u^2}}$ は u が 1 に對して充分大で無い場合の感度の變化を示すものであるが，第2圖に示す如く適當な制振を與へられた振子に於ては振子の週期に比較して盤の振動週期が少しく大であれば感度は略一定と見做される．即ち適當に減衰を與へられた振子は自己の振動週期より大なる週期を有する振動に對しては加速度計としての條件を滿すことが出來る．今回採用した振子の週期は 0·050 秒であるから，上述の理論から約 0·05 秒より大なる週期の振動に對して加速度計として使用することが出來ると云へる．理想的な加速度計としては振子の週期を限り無く小とす可きであるが，斯樣なことは實際問題としては不可能であり，假令如何に小なる週期に對しても感度の一定である理想的な加速計が存在したと假定しても，週期の小なる振動は變位振幅は小であつても加速度は大となるから，極めて小週期の振動が優越して記錄せられ比較的週期の大きい振動は隱蔽される結果，我々の目的とする振動の記錄が得られるかは疑問である．即ち實際的にはある値より小なる週期を有する振動に對して感度の遞下する方が寧ろ有利の場合が多い．只問題は斯樣な限界を何處に取るかと云ふことであり，之は目的に由り差異があるが，此處に目的とする振動計に於ては 0·05 秒程度より小なる週期に對して感度が遞下しても實際上不都合は起らないと思はれるのである．

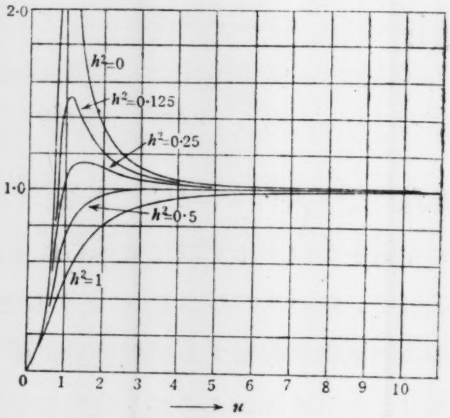

第2圖　縱軸 $1/\sqrt{\left(1-\dfrac{1}{u^2}\right)^2+4h^2\dfrac{1}{u^2}}\Bigr)$

次に槓杆に由り振子の運動を擴大する場合は槓杆の慣性が增加することを考慮する必要がある．現在の場合の如く，可及的小質量の振子を用ひ而もインク式を採用する以上槓杆は相當堅牢なものを使用せざるを得ないので此の現象は無視することは出來ない．今1箇の槓杆に由り擴大し此の槓杆の優腕の先端に描針を附する場合を考へるに槓杆の慣性能率を I_1，優腕の長さを L_1，劣腕の長さを l_1，槓杆の廻轉角を θ_1 とし

槓杆の劣腕と振子の接觸點は振子廻轉軸より L_0 の點にありとすれば，斯様な振動系の運動方程式は（1）式の代りに次の様に書くことが出來る．

$$I\frac{d^2\theta}{dt^2}+\lambda\frac{d\theta}{dt}+k\theta=-FL_0-MH\frac{d^2x}{dt^2}$$

$$I_1\frac{d^2\theta}{dt^2}=Fl_1$$

$$L_0\theta=l_1\theta_1$$

此處に F は振子と槓杆の接觸部に働く力である．上式から θ_1 及び F を消去すれば

$$I'\frac{d^2\theta}{dt^2}+\lambda\frac{d\theta}{dt}+k\theta=-MH\frac{d^2x}{dt^2}$$

$$I'=I+I_1\frac{L_0^2}{l_1^2}$$

即ち振子の慣性は見かけ上増大する．振子の週期 T'_n は $T'_n=2\pi\sqrt{\frac{I'}{k}}$ で與へられるから振子の慣性の増加は見かけ上振子の週期を増大する．此の場合加速度計としての感度は増減しない．何故なれば感度は先に示した通り $\frac{V_G MH^2 T_n^2}{4\pi I}=\frac{V_G MH^2}{k}$ であつて I には無關係な量であるからである．即ち加速度計の場合に於ては振子の慣性能率の見かけ上の増加に由つて感度は直接變化しないが，振子の週期が増大する結果として感度の一定である領域が減少する．

次に問題となることはペン先と記錄紙との間の固體摩擦である．固體摩擦のある場合の振子の運動方程式は

$$I\frac{d^2\theta}{dt^2}+\lambda\frac{d\theta}{dt}+k\theta\pm\rho V_G H=-MH\frac{d^2x}{dt^2}$$

此處に ρ はペン先に働く固體摩擦である．（$\theta>0$ときは正符號，$\theta<0$ のときは負符號）從つて $\rho V_G\geqq M\left|\frac{d^2x}{dt^2}\right|$ のときは振子は運動することは出來ない．即ち振動計の盤が運動しても描針は動き出し得ない．即ち或る値より小なる加速度は記錄し得ないこととなる．此の現象を避けるため振子の質量 M を適當に大とすることが必要となる．

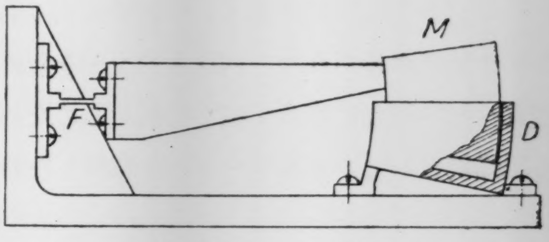

第　3　圖

偖，今回製作した振子は第３圖に示す如き型態を有し，紙面に並行な平面に由る重錘の斷面は廻轉軸の部分を中心とする半徑に由り畫かれた扇狀を成し，一端は微小の間隔を有する壔の中に

挿入され空氣制振裝置を形成して居る．壔の底には小孔を穿ち此處より空氣の一部分を漏洩せしめ，コツクに由り小孔の大さを加減して制振力を適當の値に調節する．重錘の質量は 1 kg，振子の週期 0·050 sec，廻轉軸より重錘の重心に至る距離（H）は 10 cm であり，空氣制振裝置のコツクを閉鎖するときは極限制振（$h=1$）の狀態になすことが出來る．次に感度を記錄紙上の 1 cm が 1000 gal に相當する如くなすには幾何倍率 V_G を幾何になすべきかと云ふに，

$$\frac{V_G MH^2 T_n^2}{4\pi I}=\frac{1}{1000}$$

なる如く V_G を定めれば良い．從つて此の式に $MH^2 \fallingdotseq I$, $T_n=0{\cdot}05$ を代入すれば $V_G=16$ が得られる．即ち斯樣な振子に於ては幾何倍率を約 16 とすれば感度を 1 cm per 1000 gal とすることが出來る．記錄用ペンとしては第 3 圖に見る如きものを採用した廻轉軸の部分に圓壔狀のタンクを有し此處から細い管を通してペン先にインクを供給する．ペン先は簡單に取り外し出來る樣になつて居る．此の記錄用ペンは次の樣な要素を有する．

$$L_1=10\ \text{cm}$$

$$l_1=0{\cdot}62\ \text{cm}$$

慣性能率 I_1 は實驗に由り 150 *c.g.s.* と求められた．今 $L_0\fallingdotseq H$, $I\fallingdotseq MH^2$ として此の慣性の振子に及ぼす影響を調べて見ると $M=1000$ g，$H=10$ cm であるから

$$I\fallingdotseq 1000\times 10^2=10^5\ c.g.s.$$

而して

$$I'=I+I_1\frac{L_0^2}{l_1^2}=1{\cdot}39\times 10^5\ c.g.s.$$

即ち振子の見かけの慣性能率は約 39% 增加し，從つて見かけ上の週期は 0·058 秒となる．目的上振子の質量に制限があるので此の程度の影響は止むを得ない．將來は更に慣性能率の小なる記錄用ペンを製作すべく考究中であるが現在は之を採用とすることとした．

次にペン先の固體摩擦として實驗に由り右表の如き値が求められた．何れもペン先を記錄に差支へない程度に極めて輕く接觸せしめた場合である．現在の場合 $V_G\fallingdotseq 16$ であるから記錄紙としてオイルペーパーを使用した時

記 錄 紙	固體摩擦 ρ)
オイルペーパー	98 dyne
トレーシングペーパー	470 dyne

$$\frac{\rho V_G}{M}=\frac{98\times 16}{10^3}=1{\cdot}6$$

即ち 1·6 gal（gal は加速度の *c.g.s* unit）以下の加速度は記錄し得ないことになる．

現在の場合に於ては記錄紙上 0·1 mm の振れは 10 gal であつて，10 gal 以上の加速度が測定されゝば良いと見られるから此の程度の固體摩擦は無視出來る．固體摩擦は此の他，槓杆の廻轉軸，槓杆と振子との聯結點にも生ずるが之等はペン先の固體摩擦に比較しては省略し得る程度に小さい．

次に考慮せらるべきは被測定物の廻轉運動（或は傾斜運動）の影響である．此の加速度計は盤に垂直及平行の方向の加速度の測定を目的として居るのであるが，此處に採用せる如き振子は廻轉運動の影響を受ける筈である．盤の傾斜は，見かけ上，盤に對して垂直及び水平方向の重力を變化せしむる結果，描針は之に相當して振れるが，之は實際其の方向にそれだけの加速度が實在したと見做さるべきであるから忠實に記錄せられて差支へないものである．只，問題とすべきは廻轉の角加速度である．卽ち廻轉の角加速度は振子に振れを與へ從つて描針を動かす結果，若し其の量が大であれば記錄を困亂せしめることなる．然し實際問題としては角變位は大であつても角加速度の大である場合は稀れであつて，一般の測定に於て角加速度の存在を問題とする場合は極めて少いと思はれる．2)

構　造　第4, 5 及び 7 圖は加速度計の外觀を示し第 6 圖は內部の構造を示す．先に第 3 圖に示した如き振子が主體であつて，斯様な同型の振子 3 箇が夫々上下，前後，左右の 3 成分の加速度計振子としての役割をなす如く適當の向きに配置せられて居る．外形の寸法は 17 cm×23 cm×19 cm であつて之に携帶用の把手を附してある．特殊の部分を除いては成るべく輕金屬を使用し，全體の重量は 15 kg である．圖に於て P は記錄ペンであつて先にも述べた樣に廻轉軸の箇所に圓筒狀のタンク T を有し，此處から優腕に附した細管を通してペン先にインクを供給する．ペン先は口徑 0·1 mm の金屬であつて，優腕の細管とはセルロイド製の管に由り聯結せられて居るから簡單に取外すことが出來る．S は微動螺子であつて，之に由りペン先を上下せしめ適當の壓力で紙面と接觸せしめる．記錄紙は時計裝置に由り R より L に送られる．L は寫

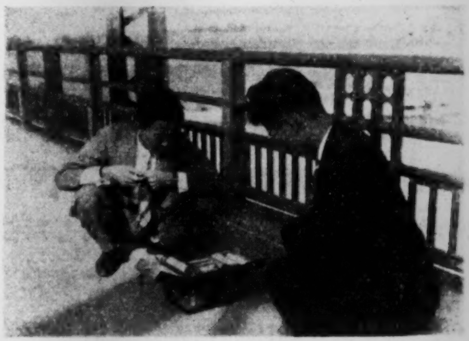

第 7 圖

---

2) 振子の軸を廻轉軸とする角加速度が存在する場合，振子の運動方程式は次の如く書くことが出來る．

$$I\frac{d^2\theta}{dt^2}+\lambda\frac{d\theta}{dt}+k\theta=-I\frac{d^2i}{dt^2}$$

此處に i は廻轉角である．

眞には取外されて居るが自働卷取裝置を附することが出來る．記錄紙の速度は毎秒5 mm 乃至 20 mm に調節出來る．A は記錄紙の進行速度を知るための刻時用ペンであり，電接時計 C に由り乾電池 F を電源とする電流を斷續して電磁石を動作せしめ記錄紙上に凹凸の線を記入する．B は合圖用のペンであつて同じく電磁石に由り動作し必要に應じて押ボタン K を以て記錄紙上に合圖を記入する．D は空氣制振裝置の調節用螺子であつて之に由り振子を適當な減衰狀態に置く．運搬に際しては特に振子をクランプする必要はなく，螺子 S に由りペン先を記錄紙から離して置けば良い．

感度試驗　"statical" の感度試驗は加速度計を平な盤上に戴せ，之を傾斜せしむることに由り簡單に行ふことが出來る．卽ち盤の傾きの角を i とすれば，見かけ上，上下方向には $g(1-\cos i)$，水平方向には $g\sin i$ の一定加速度が働いたと同一結果になる（g は重力加速度）．斯樣にして求められた感度は上下成分は 1 g に對する振れ 0·90 cm，水平成分は 1 g に對して夫々 1·0 cm 及び 9·8 cm である．（第 8 圖）．"dynamical" の感度試驗は振動臺に由り行つた．其結果は第 9 圖に示される通りであつて，振子の自己振動週期 0·05 秒より大なる振動に對しては略々一定の感度を示し理論と良く一致して居る．

實地試驗　實地試驗として次に示す如き測定を行つたが何れも良好な結果を得ることが出來た．測定の結果に對する詳しい論議は本文の目的でないので此處では省略する．

a）人が加速度計を抱へてコンクリートの床上を步行した場合（第 10 圖）．

b）自動車の床面の振動及動搖（第 11 圖）　使用車はナツシユであつて後部座席の前方の床上に器械を置いた．週期小なる振動はエンジンに由る床の振動である．圖に示す記錄は補裝道路上を進行した後停車した場合である．

c）エレベーターの床面の加速度（第 12 圖）　三菱銀行（三菱電機製）16 人乘りエレベーターの床面に加速度計を設置した場合であつて，自動停止の場合と急停止の場合を示す．特定の場所を通過するとき小週期の振動が現はれることがある．

d）橋梁の振動（第 13 圖）荒川新橋の　型鐵橋の中央部の路面上に器械を設置した．圖は積荷滿載の走行トラツクに由る振動である．振動週期が比較的大であるため人體には著しく感じたが加速度は小である．

e）飛行機の機體振動及び動搖　旅客機（スーパーユニバーサル，客席 6）の後部客席の前方の床上に加速度計を置き東京より大阪に至る間測定を行つた．小週期の振動はエンジンに由る振動である．振動及び動搖は車輪が地上から離れると同時に急激に減小する．高空を飛行して居る間は動搖は全く無く，振動も比較的小であつた．

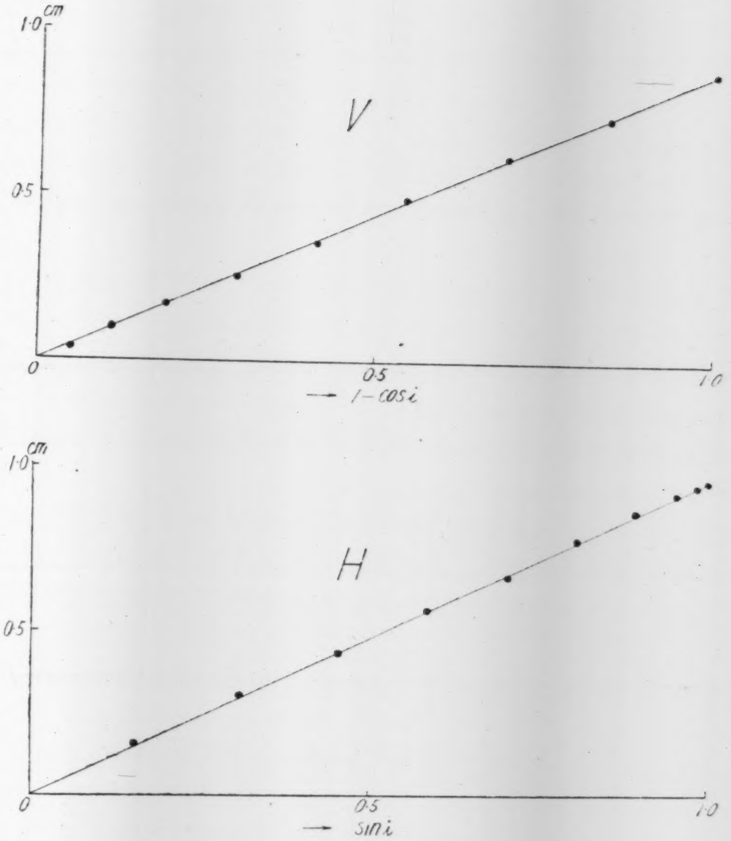

第 8 圖　縱軸 ペン先の振れの量， i 臺の傾斜角．

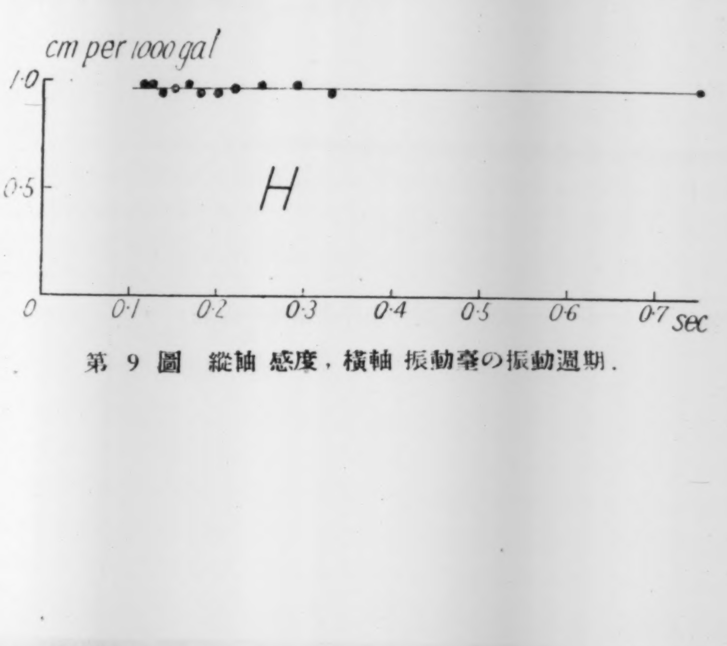

第 9 圖　縱軸 感度，橫軸 振動臺の振動週期．

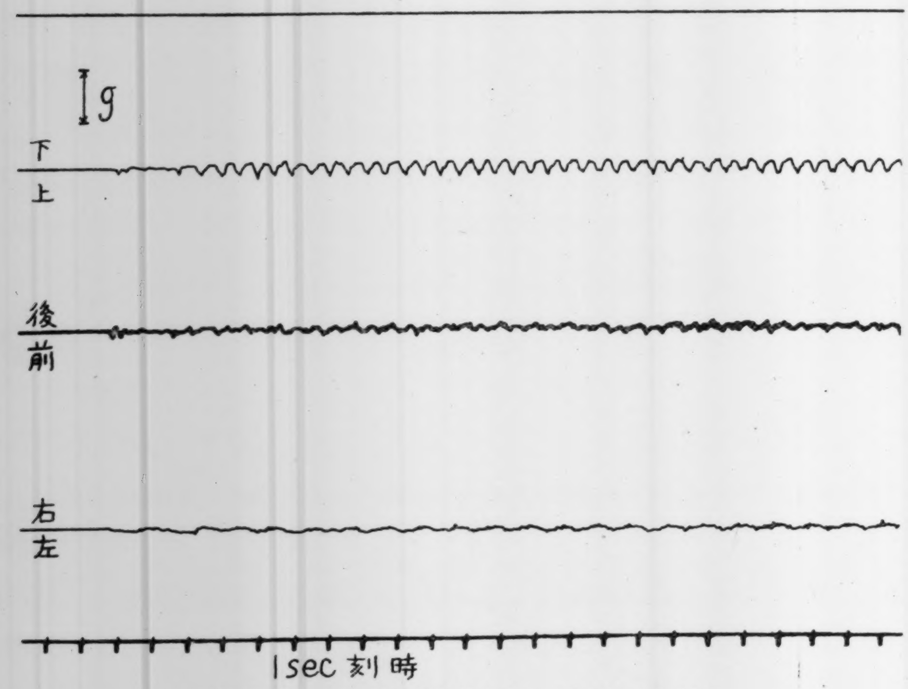

第 10 圖 人が加速度計を抱へて步行した場合

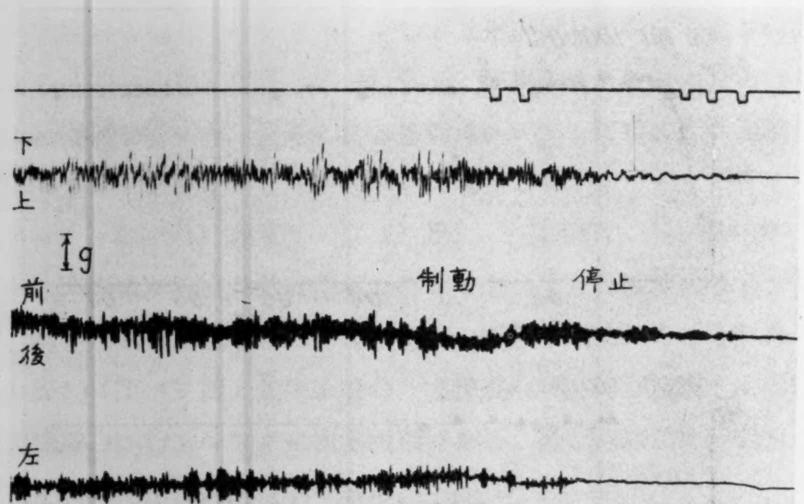

第 11 圖 走行自動車の振動

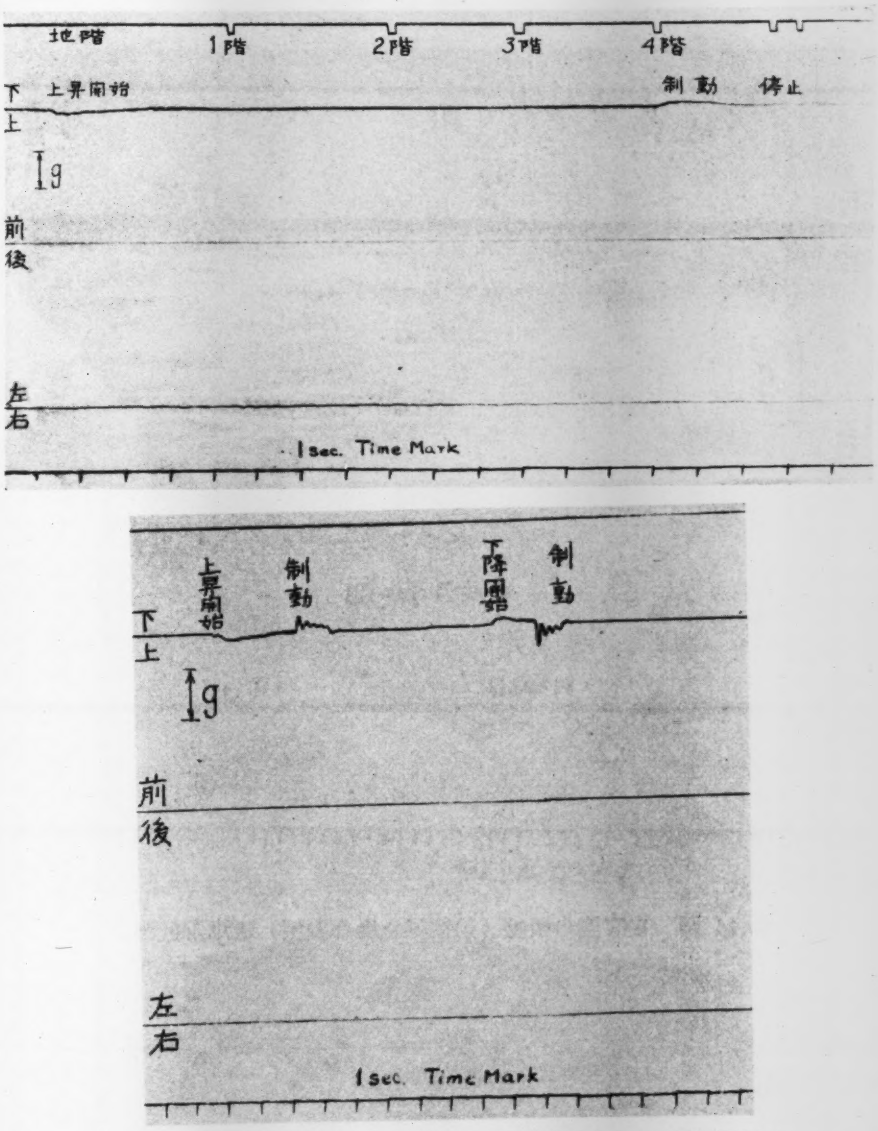

第 12 圖 エレベーターの加速度 上圖 緩制動，下圖 急制動

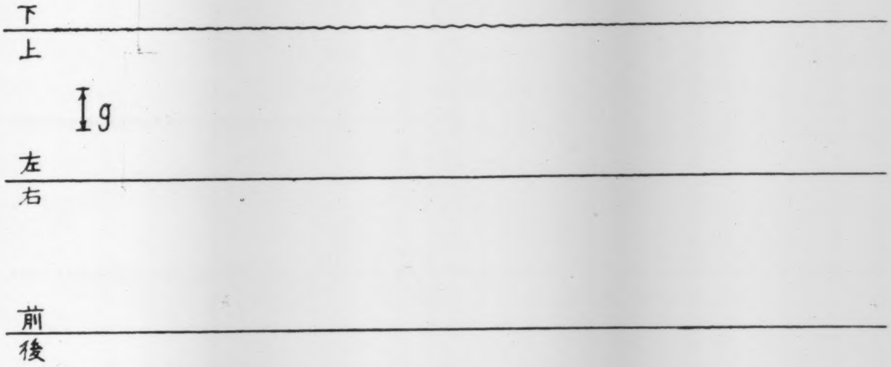

第 13 圖 走行トラックに由る橋梁の振動

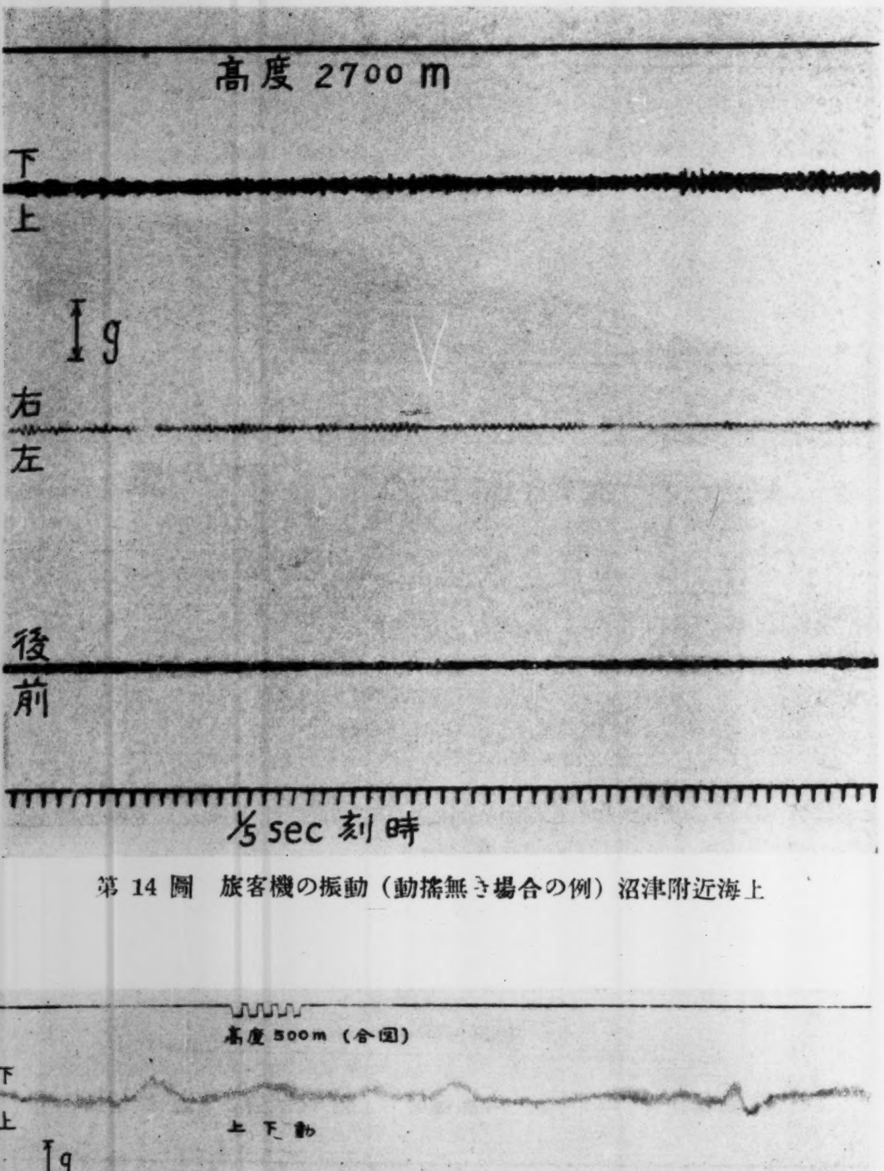

第 14 圖　旅客機の振動（動搖無き場合の例）沼津附近海上

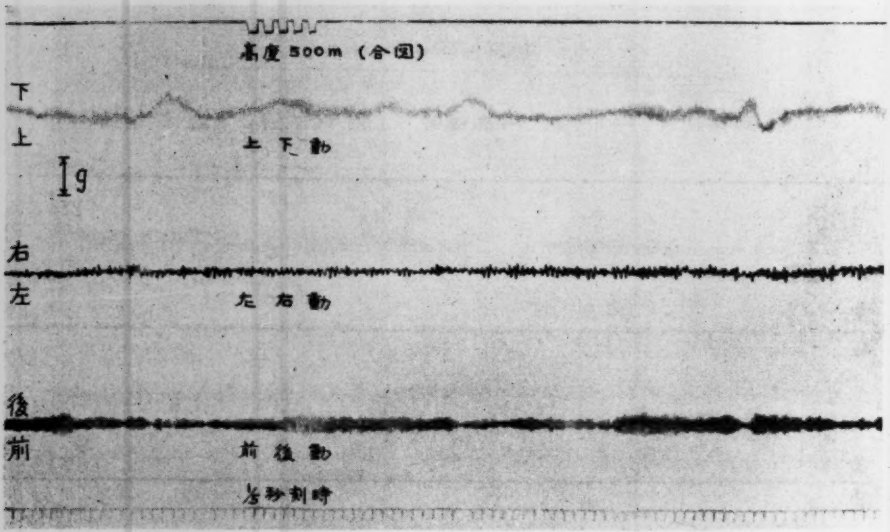

第 15 圖　氣流に由る旅客機の動搖　名古屋附近上空

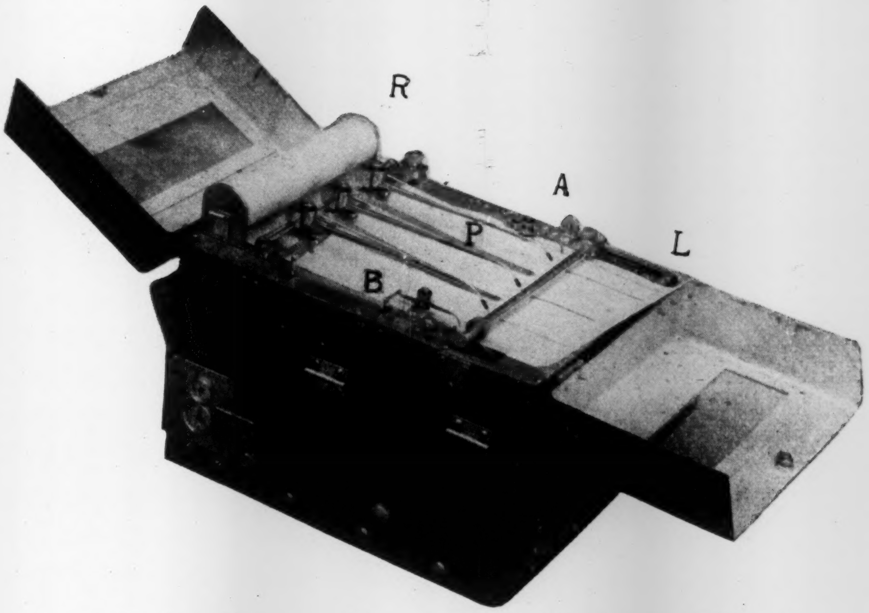

第4圖 R 記錄紙, P 記錄用ペン, A 刻時用ペン, B 合圖用ペン.

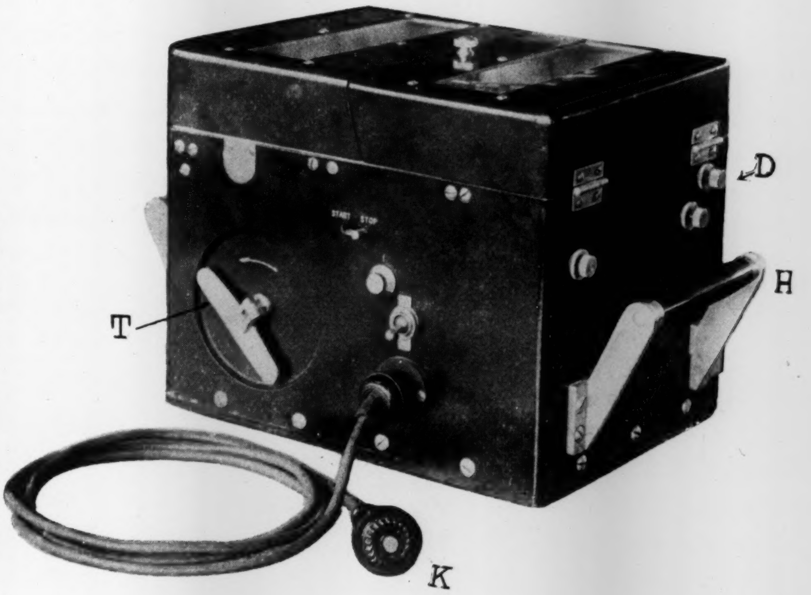
D
START STOP
H
T
K

第5圖 D 減衰器調節用螺子, T 起動機卷螺子, H 把手, K 合圖用押扣鈕.

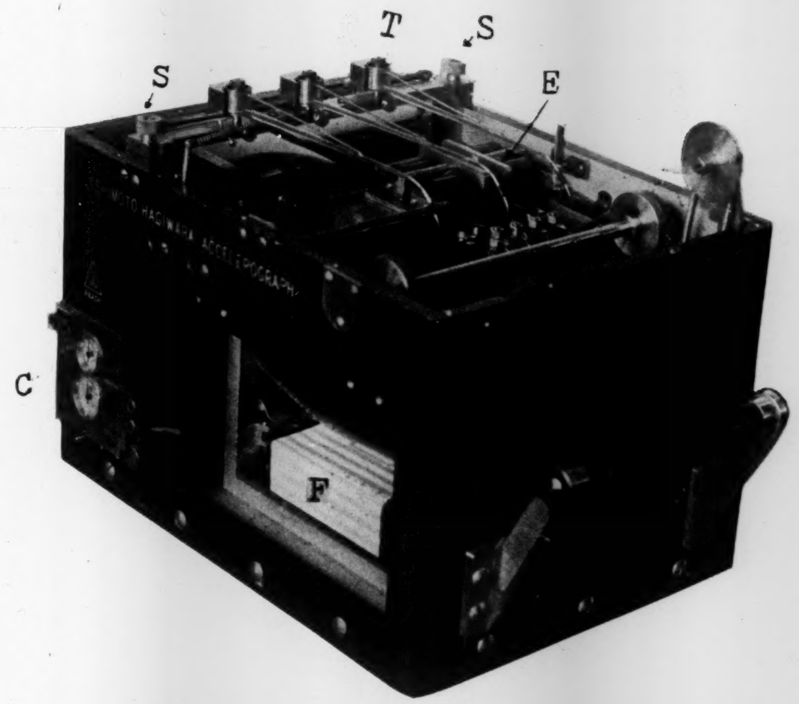

第 6 圖　內部構造を示す．S 微動螺子（ペンの上下位置を調節す），T タンク，E 刻時及合圖用電磁石，C刻時用電接時計，F 乾電池．

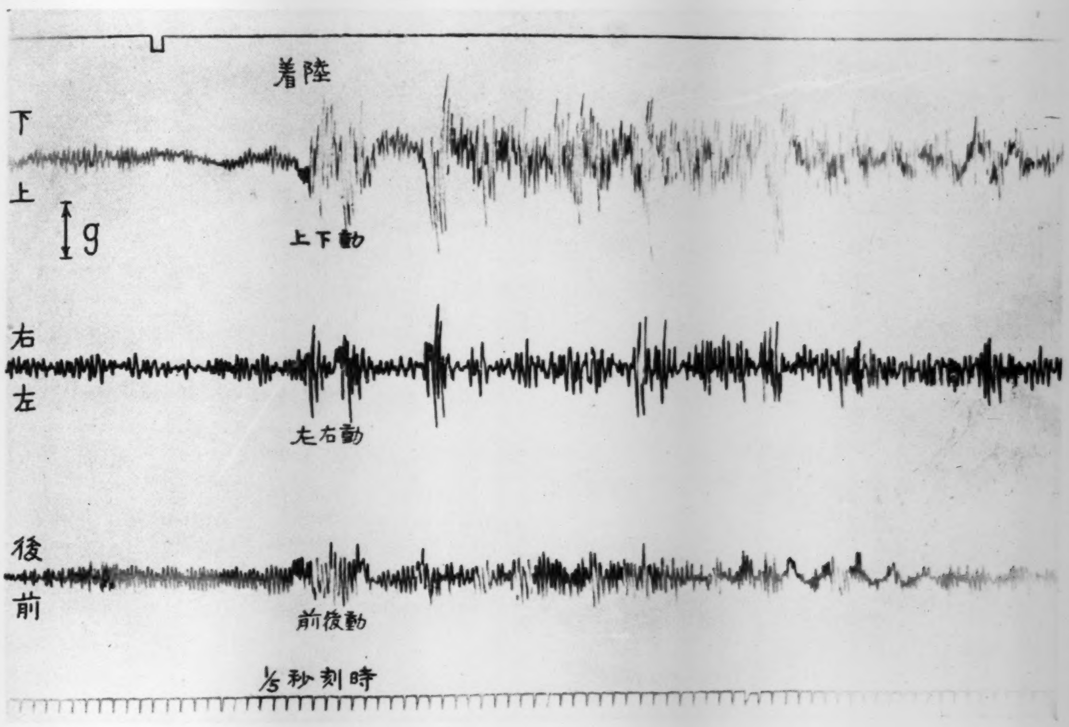

第 16 圖　旅客機の着陸時に於ける振動及び動搖　名古屋飛行場．

（震研彙報　第十五號　圖版　萩原）

（第 14 圖）．比較的低空を飛行する際は上下の動搖が存在した（第 15 圖）．第16圖は着陸時に於ける記錄である．車輪が地に觸れてより振動及び動搖が增大する．上下方向の最大加速度を生ずる時は車輪が地に觸れた瞬間とは限らない．

終りに臨み終始激勵の辭を賜つた石本教授に對し厚く感謝の意を表し，又製作に當つて種々援助の勞を惜まなかつた久田理學士に深く感謝する次第である．尙，實地試驗に際して便宜を與へられた關係官廳會社の各位に對しても此處に深く感謝の辭を呈する．

58. *An Accelerograph for Measuring the Shaking Railroda of Trains, Automobiles, Airoplanes, etc..*

By Takahiro HAGIWARA,

Earthquake Research Institute.

An Accelerograph for measuring the three components, vertical and horizontal, of the shaking of railroad trains, automobiles, airoplanes, etc., was constructed. The elements of the instrument are as follows.

Mass of pendulum	1 kg.
Period of pendulum	0·05 sec.
Geometrical magnification	16
Sensibility	1 cm on the record corresponds to acceleration g.
Damping of pendulum	Critical (air damper).
Dimension of instrument	17 cm × 23 cm × 19 cm.
Total weight of instrument	15 kg.

59. Revisions of my "Notes on the Origins of Earthquakes."

By Win INOUYE,

Earthquake Research Institute.

(Read Sept. 22, 1937.—Received Sept. 21, 1937.)

1. *Introduction*

In the paper[1] entitled "Notes on the Origins of Earthquakes", the writer made a theoretical study of the elastic waves generated from a seismic origin in which the normal pressure on the surface of the spherical cavity could be expressed by the sum of two zonal harmonics $P_0(\cos\theta)$ and $P_2(\cos\theta)$. It was also shown that, assuming the radius of the seismic origin to be constant, the azimuthal distributions of displacement of the dilatational wave at a distant point vary with the wave length.

Since then Prof. K. Sezawa[2], after a thorough study of wave generation from a spherical cavity, called attention to certain errors in the writer's calculations.

With the kind assistance of Dr. G. Nishimura, the writer revised his calculations with results as here shown.

2.

The solution of the equation of motions in spherical coordinates assumes the forms

$$\Delta = A_n \frac{H^{(2)}_{n+\frac{1}{2}}(hr)}{\sqrt{r}} P_n(\cos\theta) e^{ipt},$$

$$\left.\begin{aligned} u_{1,n} &= \frac{-A_n}{h^2}\frac{d}{dr}\frac{H^{(2)}_{n+\frac{1}{2}}(hr)}{\sqrt{r}} P_n(\cos\theta) e^{ipt}, \\ v_{1,n} &= \frac{-A_n}{h^2}\frac{H^{(2)}_{n+\frac{1}{2}}(hr)}{r^{3/2}} \frac{dP_n(\cos\theta)}{d\theta} e^{ipt}, \end{aligned}\right\}$$

---

[1] W. INOUYE, *Bull. Earthq. Res. Inst.*, **14** (1936), 582.

[2] K. SEZAWA, *Bull. Earthq. Res. Inst.*, **14** (1936) 506;
K. SEZAWA and K. KANAI, *Bull. Earthq. Res. Inst.*, **15** (1937), 13.

$$\left.\begin{aligned} u_{2,n}&=\frac{-n(n+1)}{k^2}B_n\frac{H^{(2)}_{n+\frac{1}{2}}(kr)}{r^{3/2}}P_n(\cos\theta)e^{ipt},\\ v_{2,n}&=\frac{-B_n}{k^2}\frac{1}{r}\frac{d}{dr}\left\{\sqrt{r}\,H^{(2)}_{n+\frac{1}{2}}(kr)\right\}\frac{dP_n(\cos\theta)}{d\theta}e^{ipt},\end{aligned}\right\}$$

where $h^2=\dfrac{\rho p^2}{\lambda+2\mu}$, $k^2=\dfrac{\rho p^2}{\mu}$,

u, v = radial and colatitudinal component of displacement respectively.

We shall take a special case in which it is assumed that the surface $r=a$ is free from tangential traction and is under normal pressure $p_nP_n(\cos\theta)e^{ipt}$.

Thus the equations

$$\widehat{rr}=\lambda\Delta+2\mu\frac{\partial u}{dr}=p_nP_n(\cos\theta)e^{ipt},$$

$$\widehat{r\theta}=\mu\left(\frac{\partial v}{\partial r}-\frac{v}{r}+\frac{1}{r}\frac{\partial u}{\partial\theta}\right)=0,$$

where $u=u_{1,n}+u_{2,n}$, $v=v_{1,n}+v_{2,n}$, must hold on that surface.

Satisfying the above conditions, we have

$$2A_n\left\{-\frac{(n-1)}{h^2r^2}H^{(2)}_{n+\frac{1}{2}}(hr)+\frac{1}{hr}H^{(2)}_{n+\frac{3}{2}}(hr)\right\}$$

$$+B_n\left\{-\frac{2(n^2-1)}{k^2r^2}H^{(2)}_{n+\frac{1}{2}}(kr)+\frac{2n+1}{kr}H^{(2)}_{n+\frac{3}{2}}(kr)-H^{(2)}_{n+\frac{5}{2}}(kr)\right\}=0,$$

$$A_n\left\{\left(\frac{\lambda}{\mu}-\frac{2n(n-1)}{h^2r^2}\right)H^{(2)}_{n+\frac{1}{2}}(hr)+2\left(\frac{2n+1}{hr}H^{(2)}_{n+\frac{3}{2}}(hr)-\mathrm{H}^{(2)}_{n+\frac{5}{2}}(hr)\right)\right\}$$

$$+2B_nn(n+1)\left\{-\frac{n-1}{k^2r^2}H^{(2)}_{n+\frac{1}{2}}(kr)+\frac{1}{kr}H^{(2)}_{n+\frac{3}{2}}(kr)\right\}=\frac{p_n\sqrt{r}}{\mu}$$

at $r=a$.

Henceforth, we shall consider only the case $\lambda=\mu$.

(1) The single source, in which the normal pressure at the origin is expressed by $P_0(\cos\theta)e^{ipt}$.

The radial component of the displacement of the dilatational wave is given by

$$u_{1,0}=-\frac{p_0a^2}{\mu r}\frac{1}{x^2}\left[\left(\frac{\alpha_0}{hr}-\beta_0\right)\sin\left\{pt-h(r-a)\right\}\right.$$

$$\left.+\left(\alpha_0+\frac{\beta_0}{hr}\right)\cos\left\{pt-h(r-a)\right\}\right],$$

where
$$\alpha_0+i\beta_0=\left[\frac{3i}{x}+\frac{4}{x^2}-\frac{4i}{x^3}\right]^{-1}$$

and $x=ha$.

And at a distant point from the origin as compared with the wave length, we have

$$u_{1,0}=\frac{-p_0a^2}{\mu r}\frac{x}{\sqrt{9x^4-8x^2+16}}\cos\left\{pt-h(r-a)+\tan^{-1}\left(\frac{1}{x}-\frac{3}{4}x\right)\right\}.$$

(2) The quadruple source in which the normal pressure at the origin is expressed by $P_2(\cos\theta)e^{ipt}$.

The radial component of the displacement of the dilatational wave is given by

$$u_{1,2}=-\frac{p_2a^2}{\mu r}P_2(\cos\theta)\frac{1}{x^2}\left[\left\{\alpha_2\left(\frac{9}{h^2r^2}-1\right)+\beta_2\left(\frac{9}{h^3r^3}-\frac{4}{hr}\right)\right\}\cos\left\{pt-h(r-a)\right\}\right.$$
$$\left.-\left\{\beta_2\left(\frac{9}{h^2r^2}-1\right)-\alpha_2\left(\frac{9}{h^3r^3}-\frac{4}{hr}\right)\right\}\sin\left\{pt-h(r-a)\right\}\right],$$

and at a great focal distance, we have

$$u_{1,2}=-\frac{p_2a^2}{\mu r}P_2(\cos\theta)\frac{1}{x^2}\sqrt{\alpha_2^2+\beta_2^2}\cos\left\{pt-h(r-a)+\tan^{-1}\frac{\beta_2}{\alpha_2}\right\},$$

where

$$\alpha_2+i\beta_2=\left[\left\{\left(\frac{72}{x^4}-\frac{13}{x^2}\right)-i\left(\frac{72}{x^5}-\frac{37}{x^3}+\frac{3}{x}\right)\right\}\right.$$
$$\left.+12(\eta+i\zeta)\left\{-\left(\frac{12}{y^4}-\frac{1}{y^2}\right)+i\left(\frac{12}{y^5}-\frac{5}{y^3}\right)\right\}\right]^{-1},$$

$$\eta+i\zeta=\frac{\left(\frac{24}{x^4}-\frac{2}{x^2}\right)-i\left(\frac{24}{x^5}-\frac{10}{x^3}\right)}{\left(\frac{48}{y^4}-\frac{5}{y^2}\right)-i\left(\frac{48}{y^5}-\frac{21}{y^3}+\frac{1}{y}\right)},$$

and $x=ha$, $y=ka$.

As is well known, at a point distant from the origin, both dilatational and distortional waves have only the radial and the colatitudinal component of displacement, respectively.

The colatitudinal component of the displacement of the distortional wave is given by

$$v_{2,2}=-\frac{p_2a^2}{\mu r}\frac{1}{y^2}(\alpha_2+i\beta_2)(\eta+i\zeta)\left\{i\left(-\frac{6}{k^3r^3}+\frac{3}{kr}\right)+\left(\frac{6}{k^2r^2}-1\right)\right\}$$
$$\times e^{i\{pt-k(r-a)\}}\frac{dP_2(\cos\theta)}{d\theta},$$

and at a great focal distance as compared with the wave length, we have

$$v_{2,2}\doteqdot\frac{p_2a^2}{\mu r}\frac{1}{y^2}\left\{(\alpha_2^2+\beta_2^2)(\eta^2+\zeta^2)\right\}^{\frac{1}{2}}\frac{dP_2(\cos\theta)}{d\theta}$$
$$\times\cos\left\{pt-k(r-a)+\tan^{-1}\frac{\beta_2\eta+\alpha_2\zeta}{\alpha_2\eta-\beta_2\zeta}\right\}.$$

The amplitudes of the radial components of the displacement of the dilatational waves at a distant point generated from the $P_0(\cos\theta)$ and $P_2(\cos\theta)$ origins are plotted against $ha=2\pi\frac{a}{L}$ (where L is the wave length) in Fig. 1. As will be seen from the figure, the curves have maximums at certain ha's, exhibiting spectrum-like features. The amplitudes of the dilational waves in the two cases vanish when $ha=0$, that is the waves are nil when the wave length are very long compared with the dimension of the origin, or in other words, waves do not propagate to a distant point from the point origins.

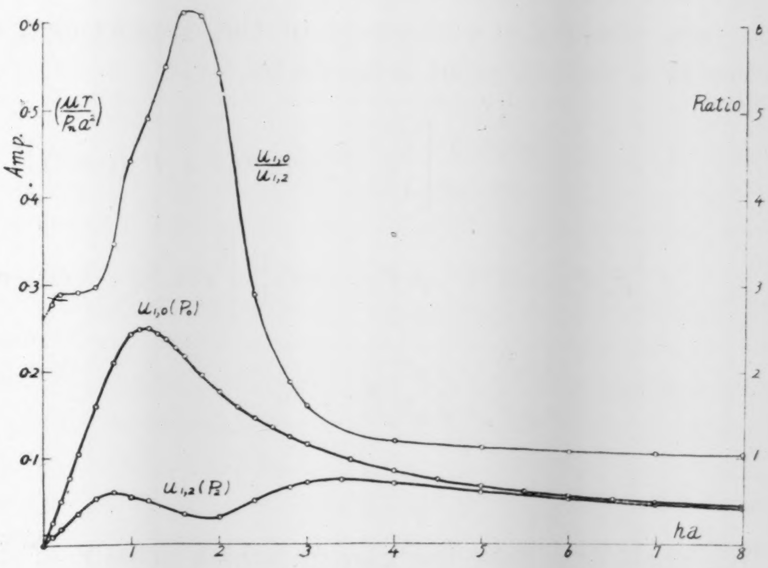

Fig. 1.

The amplitude of the dilatational wave generated from the P_2 origin becomes approximately equal to that from the P_0 origin when $ha>4$, which is due to the fact that the distortional waves appear less and less intensely than the dilatational waves when the wave length diminishes as compared with the size of the seismic origin, so that the dilatational wave is generated mainly from the P_2 origin. (see Fig. 2.)

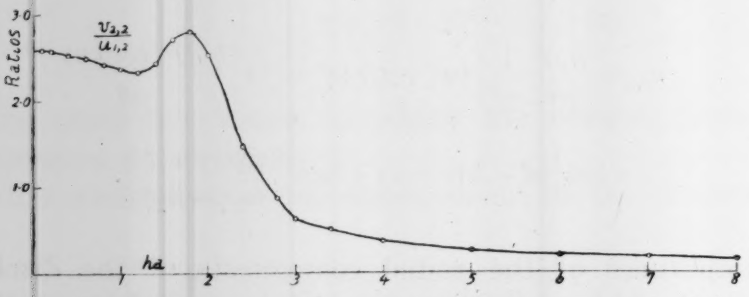

Fig. 2. The proportion of the displacement of the distortional to that of the dilatational wave.

(3) The case in which the normal pressure is expressed by two zonal harmonics $P_0(\cos\theta)$ and $P_2(\cos\theta)$.

In this case, the radial component of the displacement of the dilatational wave at a distant point is given by

$$u_{1,0}+u_{1,2}=-\frac{a^2p'}{\rho r}\frac{1}{x^2}\Bigg[\Big\{\alpha_0\varepsilon P_0(\cos\theta)-\alpha_2P_2(\cos\theta)\Big\}^2$$

$$+\Big\{\beta_0\varepsilon P_0(\cos\theta)-\beta_2P_2(\cos\theta)\Big\}^2\Bigg]^{\frac{1}{2}}\cos\Big\{pt-h(r-a)$$

$$+\tan^{-1}\left(\frac{\beta_0\varepsilon P_0-\beta_2P_2}{\alpha_0\varepsilon P_0-\alpha_2P_2}\right)\Big\},$$

where $p'=+p_2$, $\varepsilon=+\dfrac{p_0}{p_2}$.

(a) We shall first take the case in which a pair of the doublets act along an axis.

Here the normal pressure on the surface of the spherical cavity is given by

$$\Big\{-p'P_2(\cos\theta)-\frac{1}{2}p'P_0(\cos\theta)\Big\}e^{ipt}.$$

The change in the azimuthal distributions of the amplitudes of the dilatational wave as the value of ha varies is shown in Fig. 3. In

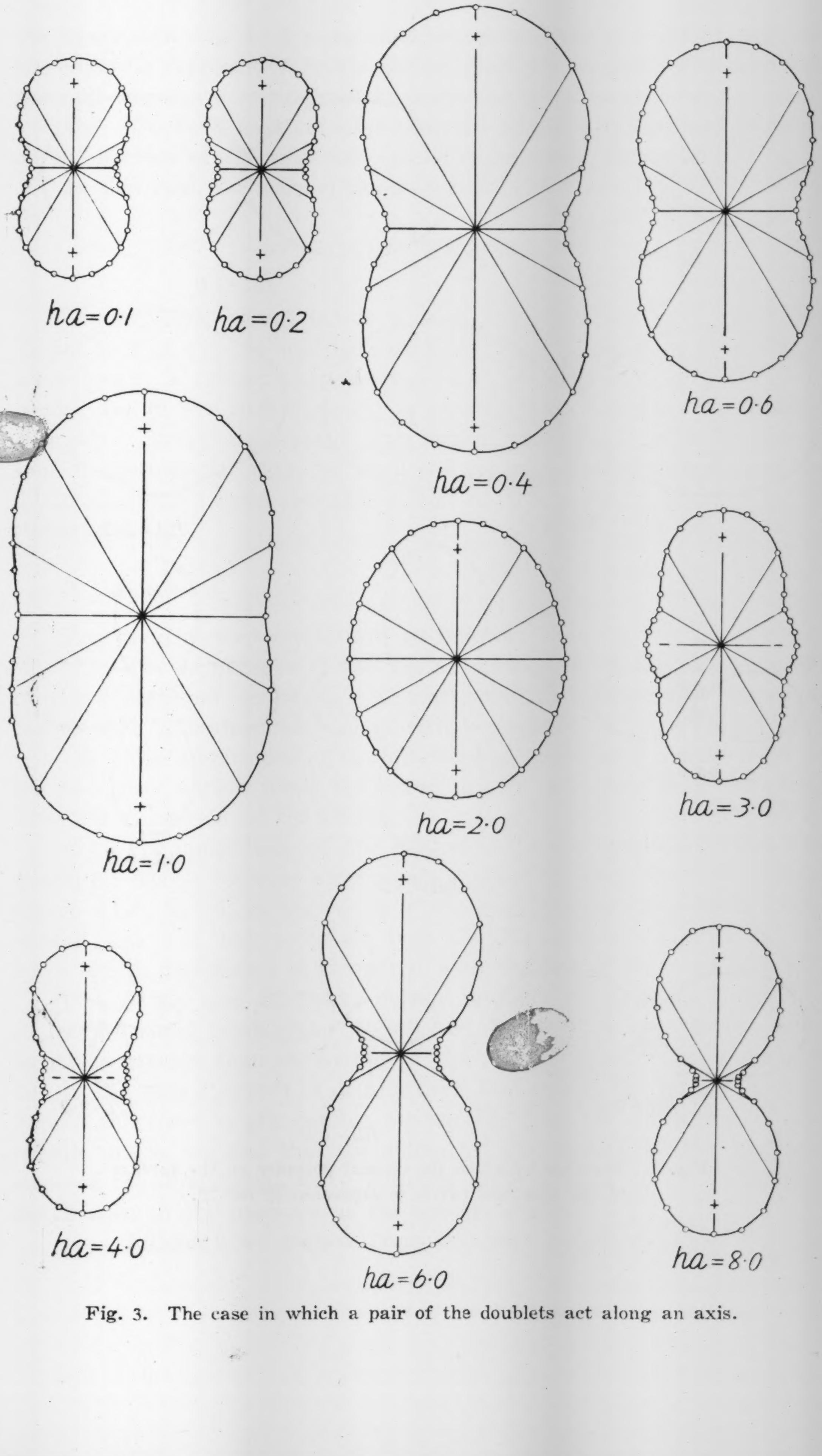
ha=0·1
ha=0·2
ha=0·4
ha=0·6
ha=1·0
ha=2·0
ha=3·0
ha=4·0
ha=6·0
ha=8·0

Fig. 3. The case in which a pair of the doublets act along an axis.

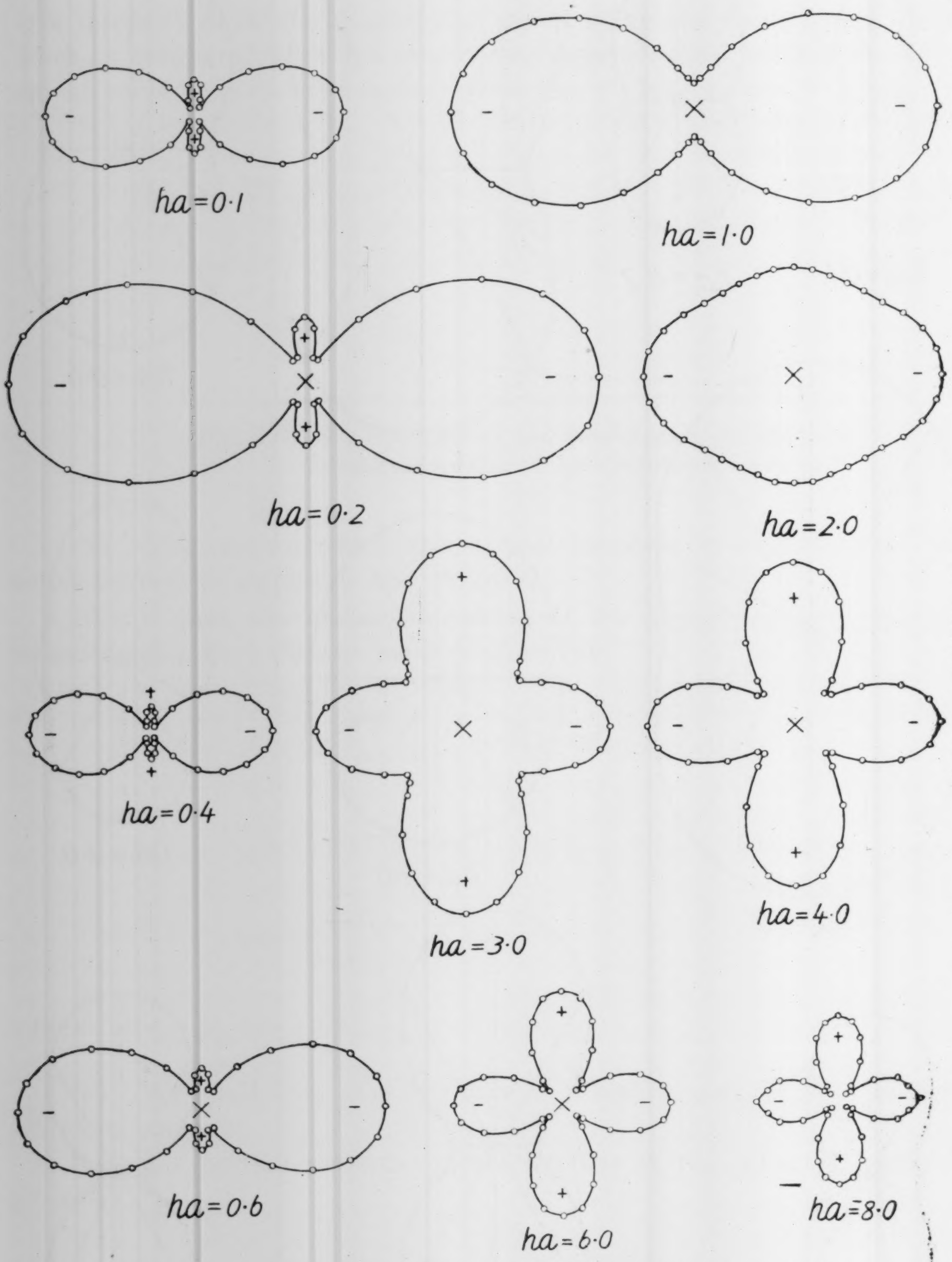

Fig. 4. The case in which the normal pressure on the surface of the spherical cavity is expressed by cos 2θ.

the figure, the axis $\theta=0$ is taken upwards and the amount of the displacement is represented by the vector from the centre. The push and the pull waves are represented by $(+)$ and $(-)$ respectively.

(b) We shall next consider the case in which the normal pressure on the surface of the spherical cavity is expressed by $\cos 2\theta$.

In this case, the normal pressure can be expressed by

$$\left\{-p'P_2(\cos\theta)+\frac{1}{4}p'P_0(\cos\theta)\right\}e^{ipt}.$$

The azimuthal distributions of both the push and pull waves are shown in Fig. 4. As will be seen from Figs. 3 and 4, so long as the wave length is greater than the radius of the seismic origin, the component due to the term $P_0(\cos\theta)$ is greater than that due to the term $P_2(\cos\theta)$. Should the wave length become comparable with the dimension of the seismic origin we shall see the azimuthal distribution of the dilatational wave quite resembling that of the pressure distribution at the origin.

3. *Summary*

The main revised results are as follows:

(1) The amplitudes of the radial component of the displacement of the dilatational waves at a distant point have maximum values at certain *ha*'s in both single and quadruple sources.

(2) The amplitudes of the dilatational waves at a distant point in the two cases vanish when the wave lengths are very long compared with the dimension of the origin.

(3) The amplitude of the dilatational wave generated from the quadruple source becomes appoximately equal to that from the single source when $ha>4$, as the result of the fact that the distortional waves appear less and less intensely than the dilatational waves when the wave length diminishes as compared with the size of the seismic origin.

(4) In the case where the normal pressure at the origin is expressed by two zonal harmonics $P_0(\cos\theta)$ and $P_2(\cos\theta)$, so long as the wave length is greater than the radius of the seismic origin, the component due to the term $P_0(\cos\theta)$ is greater than that due to the term $P_2(\cos\theta)$. Should the wave length become comparable with the dimension of the seismic origin, we find that the azimuthal distribution of the displacement of the dilatational wave becomes quite similar to the azimuthal distribution in the pressure at the seismic origin.

(5) Although we cannot, from the mere results of these calcula-

tions, say anything conclusive regarding the wave length of such waves as might be generated from a seismic origin, the writer considers it preferable to think that waves might be generated having wave lengths comparable with the size of the origin than to think that the wave lengths of the waves are very much longer than the dimension of the seismic origin. (see summary of my "Notes on the Origins of Earthquakes, second paper.")

---

59. 發震機構に就いて（訂正）

地震研究所　井上宇胤

地震研究所彙報第十四卷に掲載した論文中に於て球形震源を考へ其の球面上の壓力變化の方位的分布が $P_0(\cos\theta)$ と $P_2(\cos\theta)$ の重合に依つて現はし得る場合を數理的に取扱つてあるが其の計算中に誤りがあつたのを訂正しておいた.

主なる結果は次の如きものである.

1. 單源から出る縱波も四重源の場合と同樣に波長と震源の大きさとの比率が或る値を取る時に最大の振幅を持つ事が分つた.

2. 單源から出る縱波も四重源から出る縱波も共に震源距離大なる所に於ては震源の大きさに比較して極めて大なる波長を有する波の振幅は零となる.

3. 四重源から出る橫波の振幅は波長が震源の大きさに比して小さく成れば成る程縱波の振幅に比して小となり從つて主として縱波のみ送り出す樣に成る.

4. 震源に於ける壓力變化が單源と四重源の重合に依つて現はし得る場合は波長が震源の大きさに比較して大なる間は單源に依る縱波の方が四重源に依る縱波より卓越して居るが波長が短かく成ると兩方が同程度と成る. 從つて震源に於ける壓力の方位的分布は同一であつても遠方に於て觀測される縱波の振幅の方位的分布は波長に依つて異なるものである.

---

60. *The Arrangement of Layers in the Earth's Crust as deduced from Seismometrical Observations at Hongô, Tokyo (first paper).**

By Zyun'iti Kinosita.

(Read July 7, 1937.—Received Sep. 20, 1937.)

1. The preliminary tremors in the seismograms observed at Hongô, Tôkyô show several phases. Prof. T. Matuzawa and others have frequently investigated the matter, and from the results deduced the structure of the earth's crust, so far as Japan is concerned. Firstly,[1] a distinct phase was found, which was named "1", and whose "P-1" time in every case was about 1·5 sec. The time of phase "2", which was also read in the seismograms, was not so regular as that of "P-1". They found that phase "1" indicated the arrival of the S-wave generated by the incidence of the P-wave on the discontinuous plane in the earth's crust. Assuming the velocity of the seismic wave, the depth of the discontinuous plane was calculated, which value however was corrected later.

After this investigation, Prof. T. Matuzawa studied[2] the time-distance curves of great earthquakes and concluded that the earth's crust in Japan, as in Europe, has two discontinuous planes and calculated the depths of the said planes and the velocity of propagation of seismic waves in each layer (Table I).

In connexion with the Idu earthquakes, Prof. T. Matuzawa[3] and others observed the surface waves, after which the velocities of waves in the shallow parts were found and the depth of the discontinuous plane that generated phase "1" determined to be 4 km. Next,[4] a number of phases that appear after "1" in the preliminary tremor were found and separated into several groups.

The times between P and each groups were 2·5∼3 sec., 4 sec., and about 6 sec. Prof. Matuzawa showed that these phases were arrivals of the secondary wave as phase "1" and that the waves had been generated from deeper discontinuous planes which he determined, as shown in Table I. From "1", the structure of the earth's crust was determined as shown in Table III.

---

* Communicated by M. Ishimoto.

[1] T. Matuzawa, K. Hasegawa and S. Haeno, *Bull. Earthq. Res. Inst.*, **4** (1928), 85.

[2] T. Matuzawa, *Bull. Earthq. Res. Inst.*, **5** (1928), 1, **6** (1929), 177, 205, 213.

[3] T. Matuzawa und T. Fukutomi, *Bull. Earthq. Res. Inst.*, **10** (1932), 499.

[4] T. Matuzawa, K. Yamada and T. Suzuki, *Bull. Earthq. Res. Inst.*, **7** (1929), 241.

Table I. Presumed structure of the earth's crust by T. Matuzawa.

	0 km ~ 20 km	20 km ~ 50 km	50 km ~
Velocity of P-wave	5·0 km/sec.	6·1 km/sec.	7·5 km/sec.
Velocity of S-wave	3·15 km/sec.	3·7 km/sec.	4·5 km/sec.

Table II. The preceding presumption regarding the structure of the earth's crust, corrected by A. Imamura and others.

	0 km ~ 10 km	10 km ~ 20 km	20 km ~ 50 km	50 km ~
Velocity of P-wave	3·68 km/sec.	5·0 km/sec.	6·1 km/sec.	7·5 km/sec.

Table III. The corrected structure by T. Matuzawa and others.

	0 km ~ 4 km	4 km ~ 20 km	20 km ~ 50 km	50 km ~
Velocity of P-wave	1·94 km/sec.	5·0 km/sec.	6·1 km/sec.	7·5 km/sec.
Velocity of S-wave	1·14 km/sec.	3·15 km/sec.	3·7 km/sec.	4·5 km/sec.

After publication of Table I, Prof. A. Imamura[5] and others assumed the structure as shown in Table II, which was based on determinations of the origin of the earthquakes in the Kwantô region.

Recently T. Suzuki[6] studied the angle of incidence of the P-wave at Hongô and Mitaka, and he calculated the velocity of propagation of the P-wave near the earth's surface. This velocity was 500 m/sec.

2. Recently an acceleration seismograph[7] constructed by Prof. M. Ishimoto has been used in almost every branch of seismology with excellent results. As this instrument records very well vibrations of short period, and is very stable, it is well suited for investigating the phases in preliminary tremors. Prof. M. Ishimoto constructed also a tromograph,[8] the magnification of which is about 300 in the vibrating state, with a free oscillation period of 1 sec., and critical damping. Although the constants do not differ much from the old tromographs, the seismograms differ greatly. As this tromograph is very stable, its solid friction is extremely small. The damper and other parts of the seismograph differ from the old instruments.

---

[5] A. IMAMURA, F. KISHINOUYE and T. KODAIRA, *Bull. Earthq. Res. Inst.*, **7** (1931), 471.

[6] T. SUZUKI, *Bull. Earthq. Res. Inst.*, **10** (1932), 517.

[7] M. ISHIMOTO, *Bull. Earthq. Res. Inst.*, **9** (1931), 316.

By means of the phases in the preliminary tremors the writer studied the seismograms obtained by these two new seismographs. Phases "1", "2", etc. which were found by Prof. Matuzawa, were all distinctly seen in these seismograms. In addition to these phases the writer found a new phase, which he calls "E_1", and which appears between P and "1". Phase "1" is called "E_2".

The relations between the times of P-E_1, P-E_2 and the epicentral distances are shown in Fig. 1. The same by the tromograph is Fig. 3. Figs. 2 and 4 show the distribution of the epicentres. Seismograms of the acceleration seismograph for the period from 1932 to 1936 and tromograms for that from Sep. 1934 to Dec. 1936 were studied. According to Figs. 1 and 3, E_1 and E_2 are clearly two groups, and in every case both E_1 and E_2 are seen. The time of P-E_1 is about 0·75 sec. and that of P-E_2 about 1·5 sec. as Prof. Matuzawa's[9] had found.

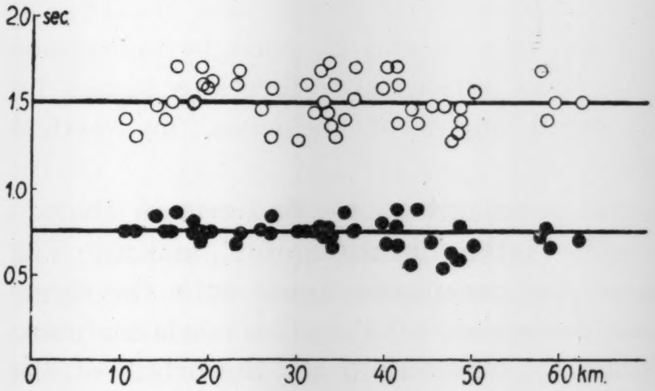

Fig. 1. Relation between the times of appearances of phases from P and the epicentral distances in acceleration seismograms.

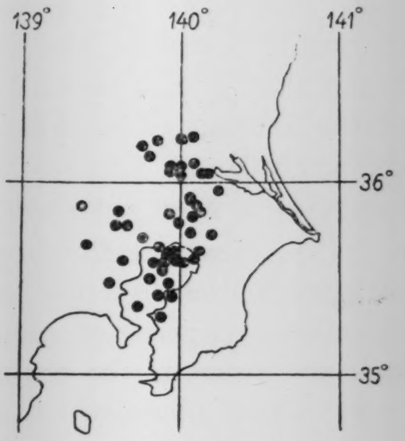

Fig. 2. Distribution of the epicentres of earthquakes studied by acceleration seismograms.

The appearance of E_2 indicated the existence of a discontinuous plane, which had already been calculated to be 4 km deep, from which

---

8) M. Ishimoto, *Bull. Earthq. Res. Inst.*, **14** (1936), 248.

9) T. Matuzaza, K. Hasegawa and S. Haeno, *loc. cit.*

it follows that phase E_1 must have been generated from a shallower discontinuous plane.

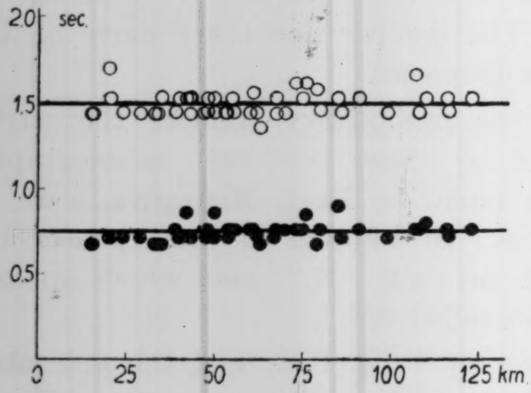

Fig. 3. Relation between the times of appearances of phases from P and the epicentral distances in tromograms.

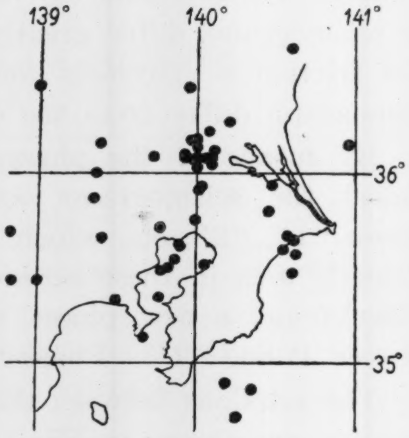

Fig. 4. Distribution of the epicentres of earthquakes studied by tromograms.

3. Phases E_1 and E_2 have certain characteristics in common, which show qualitatively that they indicate the arrivals of secondary S-waves.

(1) E_1 as well as E_2 has considerable amplitude in horizontal components, but in the vertical component they were not observed. In other word E_1 and E_2 are almost horizontal vibrations. Recently T. Suzuki[10] studied the angle of incidence at Hongô and Mitaka and found that it was about 5°. From this, E_1 and E_2 must be indications of the arrivals of S-waves. As these phases are vibrations caused by the arrivals of S-waves with small angles of incidence, its vertical components were not observed.

(2) Next, in the horizontal seismograms we find certain characteristics in the direction and sense of the vibrations of E_1 and E_2. The direction and sense of motion of the two phases agree with the direction and sense of the horizontal component of P. The vibrating plane is a vertical plane which includes the observatory and the origin of the earthquake, with the result that it was made clear that E_1 as well as E_2 was the indications of the arrivals of SV-waves.

(3) Ishimoto's horizontal tromograph being well suited for recording micro-vibrations, E_1 and E_2 are seen distinctly in seismograms of both sensible and insensible earthquakes. The sensibility of the acceleration seismograph at Hongô being suitable for recording the main shock of an earthquake, in the preliminary tremor the sensibility in

---

[10] T. Suzuki, *loc. cit.*

some cases is too low for investigating these phases. In such cases E_1 and E_2 appear in the acceleration seismograms when the amplitudes of P is large. E_1 and E_2 are independent of the magnitude of the earthquake, being dependent only on the amplitudes of the P-waves.

These common characteristics made it clear that the two phases were also the arrivals of secondary S-waves generated at the discontinuous planes by the incidence of the P-wave as Prof. Matuzawa had shown.

4. The next problem is the determination of the depth of the discontinuous plane. The times of P-E_1 as well as of P-E_2, are almost independent of the depth and the epicentral distance. When the time between P and such a phase is short, the variations in the time of appearance cannot be observed. The writer has continued study of the deeper parts, and now roughly estimates the depth of the discontinuous plane. Later an exact calculation will be made, but within the limits of accuracy in these sort of studies, there will be no considerable corrections to make.

Now a case is assumed in which the angle of incidence of the P-wave is 0°. Here, needless to say, the S-wave is not generated from a discontinuous plane. In Fig. 1 and 3, E_1 and E_2 are almost parallel with the abscissa. Assuming then the angle of incidence to be near 0°, we shall make a rough calculation.

τ is the time of P-E_1, that is

$$\tau=\tau_S-\tau_P=\frac{D}{V_S}-\frac{D}{V_P}=\frac{D}{V_P}\left(\frac{V_P}{V_S}-1\right), \qquad (1)$$

where τ_S and τ_P are the respective travel times of the P-wave and S-wave between the discontinuous plane and the earth's surface. D is the thickness of the upper layer; V_P and V_S are the velocities of propagation of the P-wave and the S-wave in the upper layer. To calculate the thickness of D, we need the values of V_P and V_P/V_S. T. Suzuki's value of V_P is 500 m/sec.

Recently K. Iida[11] measured the velocities of elastic waves in the base rock at Marunouti in the laboratory according to which the value of V_P is 0·45 km/sec. and V_S 0·235 km/sec., whence the value of V_P/V_S is 1·9.

Suzuki's value of V_P and Iida's value of V_P are not alike, there being a difference of about 10% between the two. These two values were obtained by different methods. It is in a sense fortunate that the two values differ to such an extent.

---

[11] K. IIDA, *Bull. Earthq. Res. Inst.*, **15** (1937), 828.

If the velocity of the P-wave is 450 m/sec. and V_P/V_S is 1·9, the thickness of D by formula (1) is then 360 m. Next, if V_P is 500 m/sec. and V_P/V_S is 1·9, D is then 420 m. The thickness of the layer is thus about 400 m.

As to the thickness of the lower layer, a rough estimate was made. The time of P-E_2 is about 1·5 sec. By its travel in the upper layer P-E_2 increases about 0·75 sec., making the difference of travel time in the lower layer only 0·75 sec. The V_P and V_P/V_S of this layer were obtained by Prof. Matuzawa.[12] These values were used in the calculation made. The thickness is 2·1 km and the second discontinuous plane about 2·5 km deep.

5. It has already been made clear, qualitatively, that E_1 and E_2 were SV-waves generated from the discontinuous planes. It will next be shown that their amplitudes indicate that they are such kinds of waves.

There are at Hongô acceleration seismographs of three components, but as their sensibilities are somewhat low for quantitative studies of amplitude, we shall here examine, instead of quantitatively, the orders of amplitude. In the tromograms the amplitudes of the phases were exactly measured, but the tromograph has now only one component (E-W). To discuss the amplitudes more fully, observations of three components of the tromographs are desirable. The refraction of the P-wave was calculated by the following formula obtained by H. Kawasumi[13] and T. Suzuki:

$$\left.\begin{aligned} &A_1+\beta B_1-A'+\beta' B'=-A,\\ &\alpha A_1-B_1+\alpha A'+B'=-\alpha A,\\ &-(\beta^2-1)A_1+2\beta B_1+\frac{\mu'}{\mu}(\beta'^2-1)A'+2\frac{\mu'}{\mu}\beta' B'=(\beta^2-1)A,\\ &2\alpha A_1+(\beta^2-1)B_1+2\frac{\mu'}{\mu}\alpha' A'-\frac{\mu'}{\mu}(\beta'^2-1)B'=2\alpha A. \end{aligned}\right\} \qquad (2)$$

Here α, β, α', β' are the direction cosines of the angles of incidence, refraction, and reflection; μ, μ' are the regidities in each layer. The amplitudes are proportional to the values of A_1, B_1, A', B' divided by the velocities of each. To calculate the amplitude of E_1, the ratio of velocities of P-waves in the two layers was assumed to be 1 : 4 and also that $\lambda=2\mu$ in the upper layer and $\lambda=\mu$ in the lower.

---

12) T. MATUZAWA and T. FUKUTOMI, *loc. cit.*

13) H. KAWASUMI and T. SUZUKI, Zisin, 4 (1932).

In Fig. 5, which is a part of the calculation, the ordinate represents the ratio of the amplitude of E_1 to the amplitude of P in the upper layer, and the abscissa the angle of incidence of the P-wave in the upper layer. At Hongô the angle of incidence of the P-wave is about 5°, while here the ratio is about 1/10. The observed E_1 are of this order. An exact study of this problem will be possible when the other components of the tromograph can be included in the observations.

6. Phases E_1 as well as E_2 are the SV-waves generated at the discontinuous planes by the incidence of the P-wave, the depths of these discontinuous planes being 400 m and 2·5 km. As these discontinuous planes clearly exist in the earth's crust, other kinds of waves must also be generated. For example, the writer has already obtained many data which may turn out to be the secondary P-wave generated by the incidence of the S-wave on the discontinuous planes. To determine whether or not these data represent such waves, the orders of amplitudes will now be calculated.

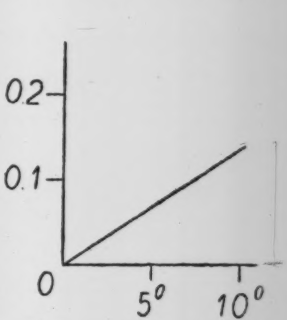

Fig. 5. The ratio of amplitude of E to P.

Further, waves that have arrived at the surface may reflect at that surface and also reflect at the discontinuous plane, then arrive at the surface again. These problems will be treated in a latter paper.

7. The first motion of an earthquake is usually assumed to be of the simple shock-type. Many mathematical studies on the motions of pendulum have been made, assuming the shock in various forms. C. Tsuboi's[14] calculations concern numerous cases of period and damping, they being applicable directly to seismometry. After this calculation, H. Kawasumi[15] attempted to calculate the motion of a pendulum, assuming the shock to be of another form. The forms assumed by the two investigators are

$$f(t) = 2\sin t - \sin 2t, \quad \text{(Tsuboi)}$$

$$f(t) = 3\sin t - \sin 3t. \quad \text{(Kawasumi)}$$

From these two calculations we have the values of the times of first maximum, first zero, second maximum, etc, and also the amplitudes of the first and second maxima, and it was with the aid of these factors that we tried to determine the true values of amplitudes of the first motions from the observed values.

---

[14] C. TSUBOI, *Bull. Earthq. Res. Inst.*, **12** (1934), 426.

[15] H. KAWASUMI, *Bull. Earthq. Res. Inst.*, **14** (1936), 319.

At Hongô, we sometimes get irregular displacement on horizontal seismograms, in which the motions of the pendulum do not show the first zero distinctly. The pendulum, after displacing and making the first maximum, changes in sense and returns to the zero-line. In the irregular cases, the pendulum stops on its return swing and does not make the first zero. Since in these cases, the vertical seismograms distinctly show the first zero, the irregularity of the first motion must only be in a horizontal direction. The time between P and the stop point, which is the point that appears as E_1, is about 0·75 sec.

When the period of first motion is short, P, E_1 and E_2 are clearly separated, but when the period is long and is near 1 sec., these phases are not separated, the seismogram showing only an irregular first motion.

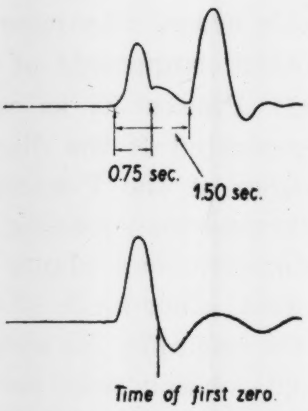

Fig. 6. Irregular form of first motion. Upper curve represents horizontal component and lower curve is vertical component.

8. The problem of irregular propagation of seismic waves has been studied by a number of seismologists in Japan, some of whom maintain that at a considerable depth the structure of the earth's crust is not equal in horizontal direction, while others speak of elastic stresses in the earth's crust. These studies are the results of the observed data direct, the geological structure under the observatory being ignored. K. Iida and K. Kanbara[16] who have studied this problem in connexion with a large number of earthquakes, have considered the inequalities in the geological structure under each observatory and calculated the deviations in the values of the times of occurrences for all the stations in Japan. The writer believes also that the greater part of the deviated values occur near the observatory. From Iida and Kanbara's table the deviated value at Hongô is 1·0 sec.

It takes about 0·8∼0·9 sec. for an elastic wave to pass the upper layer, which is 400 m thick. This almost equals the deviated value. Therefore in discussing the problem of irregular propagation, the geologic structure under every station must be taken into consideration.

Conclusion.

In the preliminary tremors of seismograms observed at Hongô, there are several phases, which Prof. Matuzawa and others have already

---

[16] K. IIDA and K. KANBARA, Zisin, **6** (1934), 310.

（震研彙報　第十五號　圖版　木下）

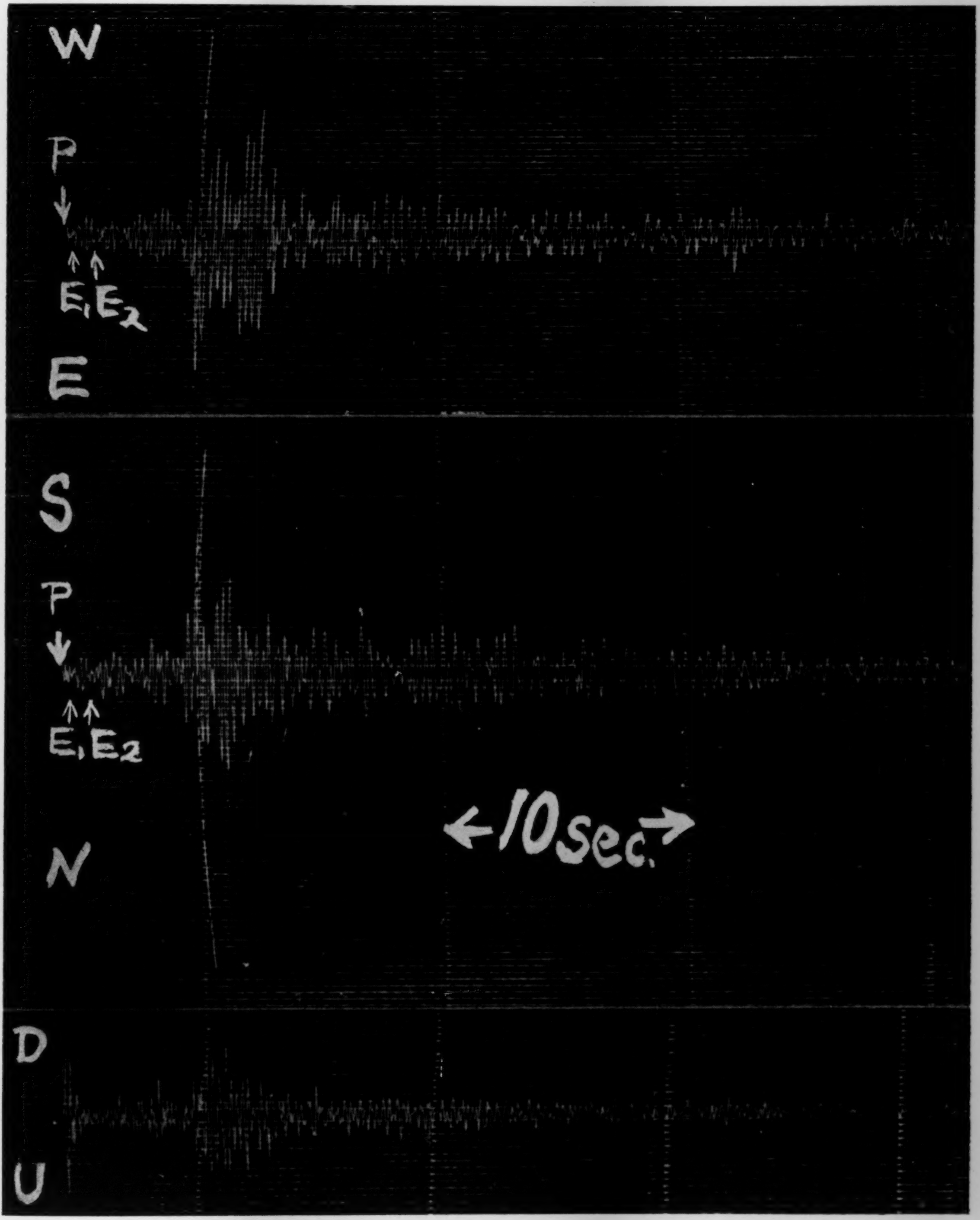

Fig. 7. Acceleration seismogram of the earthquake of March 28, 1937.

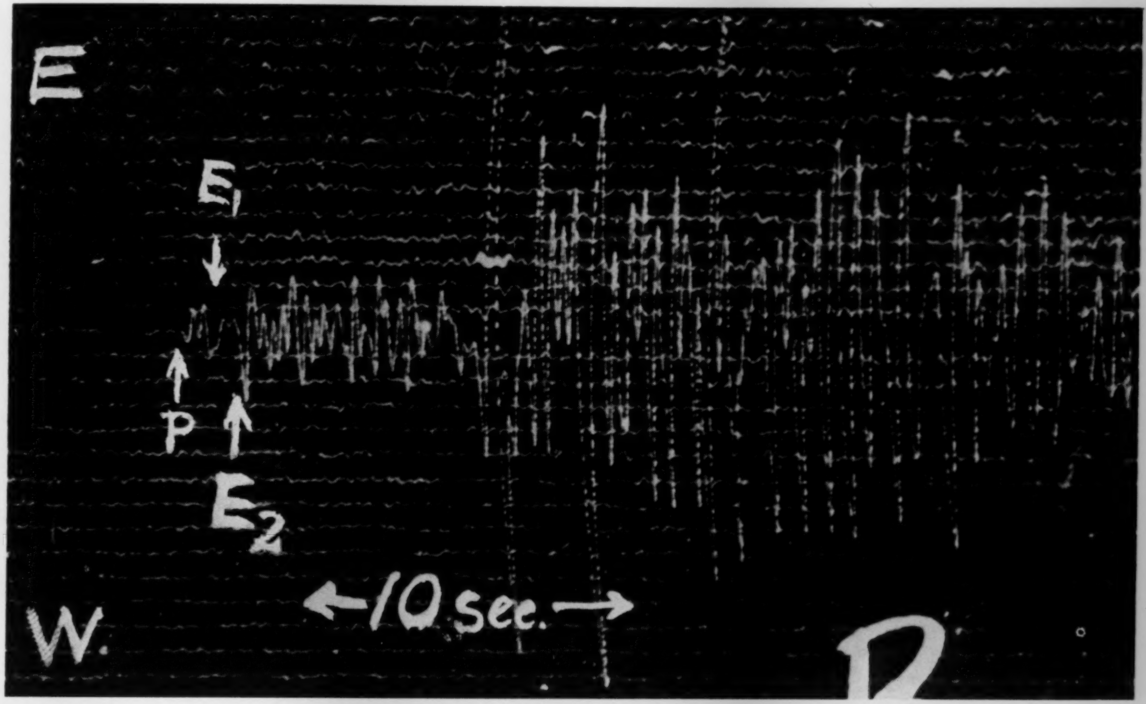

Fig. 9. Tromogram of the earthquake of $7^h\ 27^m$ May 25, 1937.

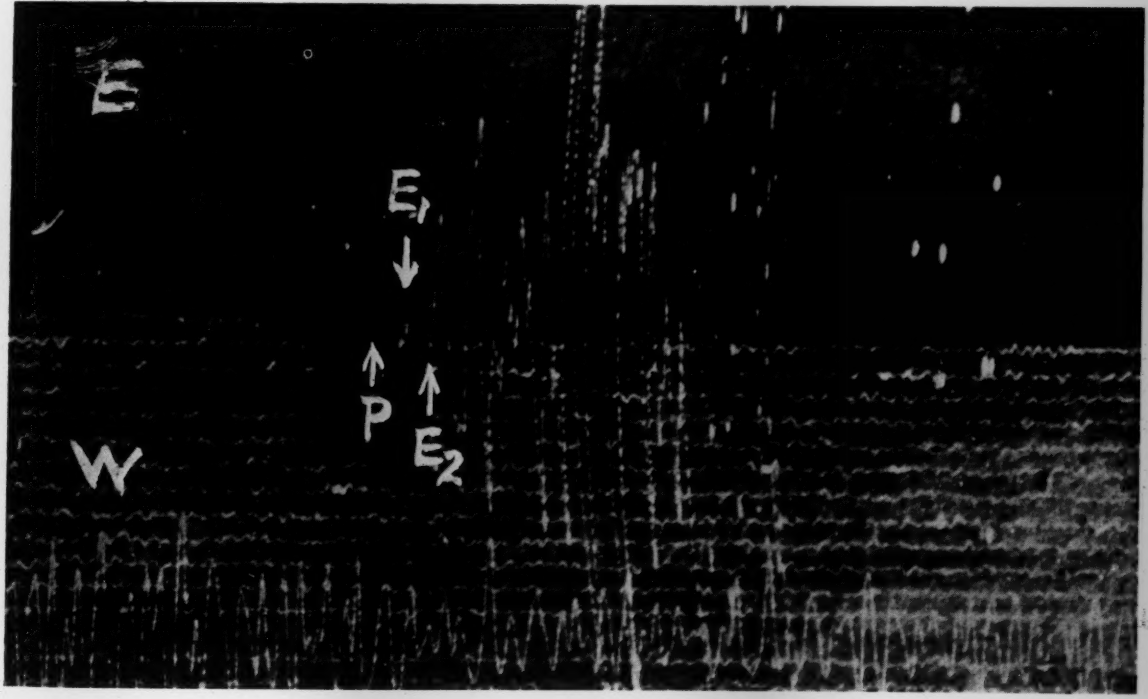

Fig. 10. Tromogram of the earthquake of $9^h\ 38^m$ May 25, 1937.

studied. According to this study another new phase was found, which appears about 0·75 sec. after P, the new phase is named E_1 and the next phase, which was named "1" by Prof. Matuzawa, is named here E_2. With these data, the depths of two discontinuous planes in the earth's crust have been determined.

In conclusion, the writer expresses his best thanks to Professor Mishio Ishimoto and Dr. H. Kawasumi for their kind guidances and instructive discussions.

---

60. 本鄕に於ける地震觀測よる推定し得たる地殼表層の配列（第１報）

木　下　潤　一

本鄕に於ける地震動の初期微動部には數個の位相がある．これに關しては旣に松澤敎授其の他の人々に依つて調査され，其の最も明らかな位相は初動後 1·5 秒位を經て表れるもので，松澤敎授は此の位相は地下４粁に存在する不連續面に P 波が入射し，此の際二次的に生成された S 波であるとした．其の他の位相も旣に知られて居る深い不連續面の影響として說明された．

筆者は石本式加速度地震記象及び石本式微動記象を精査した處，旣に見出されて居る位相は勿論明瞭に見えるが，新らしく初動後 0·75 秒位の處に表れる位相を認めた．この位相と前に松澤敎授によつて見出された初動後 1·5 秒を經て表れる２相は共通な特性を有する．この特性は兩相が何れも前に松澤敎授に依つて考へられた如く二次的な S 波である事を定性的に示したので，二つの不連續面の深さを計算した處，400 米，2·5 粁なる値を得た．振幅も正確な測定が出來ないが大體計算値に近い樣である．

終りにかゝる位相が存在し，かゝる不連續面が存在するため，地震計測學上注意すべき點を二三述べた．

61.　關東地方南部の地質構造

〔橫濱——藤澤間〕

地震研究所　大塚彌之助

（昭和12年7月6日發表－昭和12年9月20日受理）

緒　論
層序概論
層序各說
  沖積統
  洪積統
    關東ロームさ段丘礫層
    下末吉統
  鮮新・洪積統
    長沼統
      長沼層
      田谷層
      屏風浦層
      倉坪層
  鮮新統
    小柴統
      濱　層
      中里層
      小柴層
    金澤統
      大船層
      野島層
      浦郷層
    逗子統
  葉山統（中新統及び古第三系）
地層對比論及び時代推定
地質構造
  斷層構造
  皺曲構造
地殼運動
  造陸運動
  皺曲運動
  斷層成生運動
三浦半島北部地質構造發達史概略
先輩諸說

緒　　論

筆者はさきに「三浦半島北部の層序と神奈川縣南部の最新地質時代に於ける海岸線の變化に就て」の拙論を公にして三浦半島北部の地質に關して簡單な記述を試みたがその後日本學術振興會の補助を得て更にこの附近の調査を繼續することができた．此の調査により前報告中に於ける不備を多數に知ることができたので，之等の不備を補ふためにこゝに稿を改めて再び三浦半島北部の橫濱—藤澤間の層序・構造を述べ，從來の誤謬を訂正し，その地方の地質構造の諸問題を明にせんと思ふ．多少の重複は之を諒とされたい．

この地方は次の様に昔から多數の先輩地質學者の研究があり，その層序學的知識も極めて進んでゐる．

1）　1881 D. BRAUNS：　Mem. Sci. Depart. Tokio Daigaku, 4.

2）　1902 德永重康：　東京以南三浦半島地質論，地質學雜誌，9 卷.

3）　1918 槇山次郎：　神奈川縣下末吉の胡桃化石の產地，地質學雜誌，25卷，296 號.

4) 1920 M. YOKOYAMA: Fossils from the Miura Peninsula and its Immediate North. Jour. Coll. Sci. Imp. Univ. Tokyô, 39, 6.

5) 1923 H. YABE and R. AOKI: Summary of the Stratigraphical and Palaeontological Studies of the Cenozoic of Japan, 1920～1923. Proc. 2nd Pan-Pacific Sci. Congr., pt. 3, pp. 775～796.

6) 1925 青木廉二郎: 三浦半島の海岸，地球，3 卷，1 號.

7) 1925 渡邊久吉: 武藏野系の基底，地學雜誌，37 卷，439 號，pp. 495～500.

8) 1926 矢部長克・青木廉二郎: 大正十二年九月一日の關東大震と地質構造との關係，齋藤報恩會事業年報，第I別刷. pp. 89～92.

9) 1926 Y. OZAWA: Kamakura and Enoshima. Guide Book, Excur. C—5, 3rd Pan-Pacific Sci. Congr.

10) 1927 M. YOKOYAMA: Mollusca from the Upper Musashino of Western Shimôsa and Southern Musashi. Jour. Fac. Sci. Imp. Univ. Tokyo, sec. II, 2, 2.

11) 1929 H. YABE: Geological Age of the Latest Continental Stage of the Japanese Islands. Proc. Imp. Acad., 5, 9, pp. 430～433.

12) 1929 復興局建築部: 東京及び横濱地質調査報告.

13) 1929 槇山次郎: 關東南部の洪積層 小川博士還暦紀念，地學論叢.

14) 1932 鈴木好一: 神奈川縣厚木町北方の鮮新統 1，2，地質學雜誌，39 卷，460～461 號.

15) 1935 清野信雄: 7萬5千分之1東京地質圖幅及び說明書.

之等の上に擧げた論文は何れもこの地方の地質構造の研究をする基礎資料となるものであつて，先輩の尊い記錄である．之から述べることも之等の研究と下記拙論と近頃觀察した事實との綜合結果で，將來の完璧へ向つての一步の前進を示すに過ぎない．

次に三浦半島の地質に關して言及してゐる拙論をこゝに揭げておく．

16) 1930 大磯地塊を中心とする地域の層序に就いて，地質學雜誌，36 卷，433～434 號.

17) 1930 大磯地塊を中心とした地域の最新地質時代の地史，地理學評論，6 卷，1 號.

18) 1930 三浦半島北部の層序と神奈川縣南部の最新地質時代に於ける海岸線の變化に就て，地質學雜誌，37 卷，442 號.

19) 1931 大磯層その他に就いて，地質學雜誌，38 卷，451 號.

20) 1931 第四紀，岩波講座（地質學）.

21）1932 日本群島に見られる沈積輪廻の或るもの，地理學評論，8 卷，12 號．

22）1933 日本の洪積統と鮮新統との境界區分，地質學雜誌．40 卷，483 號．

23）1935 The Quaternary Physiographic History of South-western Kwanto, Proc. Pan-Pacific Sci. Congr. pp. 1589～1592.

24）1935 故山崎博士の三浦半島武山斷層の地質學的考察，地理學評論，11 卷，5 號．

25）1936 Marine Lower Pleistocene of the Central Kwanto Plain (An evidence of basin forming force of the Kwanto plain.) 地震研究所彙報，14 冊，1 號．

この研究は主として日本學術振興會の補助を得て達成したもので，深く同會に謝意を表するものである．

層序概論

この地方に發達してゐる地層は冲積統・洪積統・新第三系であつて，その他に時代未決の地層と蛇紋岩の露出とがある．冲積統は各地の溪谷底に露出し，新第三系上に不整合に横はつてゐる．洪積統は主として横濱附近，藤澤附近，横須賀附近の段丘・丘陵上に分布してゐて，新第三系上に不整合に横はり，その發達區域の地表面は段丘地形の段丘面となつてゐる場合が多い．新第三系は上部から小柴統（濱・中里・小柴各層を含む）・金澤統（大船・野島・浦郷各層を含む）・逗子統の各地質系統に分たれるが，之等は三浦半島北部の大部分を占めて，洪積統以上に對して基盤岩層の役をなしてゐる．逗子統の下に横はる時代未詳の地層は上下二系統に分たれるが共に當分一括して葉山統とした．この上部は中新統であるが，下部は之を貫く蛇紋岩と共に時代未決にしてこゝに論ずる地域の南部に分布してゐる．

上述の地質系統の他にその地質時代を略ぼ鮮新統上部と考へてゐる長沼統が，小柴統・金澤統・逗子統等を不整合に被うて分布してゐる．

以下之等各地層の特徴の詳細を記さう．

層序各說

冲積統

三浦半島北部地方には大きな河流氾濫原がないため，冲積統も廣く分布してゐる處がなく，僅に小溪谷の底に溪谷底の一部を埋めて發達してゐるものしかない．この様な冲積統中主なものは藤澤町附近，大船附近，逗子町，横濱市等に發達してゐるものである．

藤澤町附近の冲積統は相模野臺地の南端から相模灣岸に至る低地帶に發達してゐるもので，この低地の多くの井戸に就いて地質を調べた今村氏によれば，この低地の表面は主として砂層からなり，下に屢々粘土層が横はることが解つてゐる．

この低地の地表面は一定の走向に排列された多くの細長い丘陵列からなる起伏を示してゐる．これらの丘陵列を胴切にした切割面を觀察すると何れも僞層構造を示した砂層が露出してゐて，之等の低い丘陵列が砂丘列であることが推定できる．

この砂丘列は藤澤附近では赤褐色の 3 cm 内外の徑の礫からなる礫層を不整合に被うてゐるし，又一部では新第三系金澤統の侵蝕面上に不整合に横はつてゐる．前者の赤褐色礫層は遊行寺附近で關東ロームの下に横はつてゐるものに類似してゐる．

花井重次學士1) はこの砂丘列の排列に注意されて地殼運動と關係づけて說明せられたが，今村理學士2) は之等の砂丘列を構成する砂粒を物理的に分析して，その分布から砂丘群の風成說を主張してゐる．

相模川河口に近い平塚町附近の深井試錐の標本を，故末廣地震研究所長の御好意で調べたことがあつたが，3) それによると次の如くである．地表から約 84·5 m 附近までは主として砂礫・粘土の互層で，下部程礫質になつてゐる．84·5 m 以下の基盤は黑褐色の凝固した凝灰岩である．地表下 30 m 附近に貝殼交り砂層がある．この貝殼は破片であるが新鮮なもので，その他に *Rotalia compressiuscula* BRADY〔海棲有孔虫〕を多數に含んでゐて少くともこの部分は海成層である．第 1 表はこの層中に含まれる有孔虫である．砂礫層中の砂礫の性質は現在の相模川のものと殆ど區別がつかない．これらの特性と岩層の餘り凝固してゐないこと等から筆者は此の地層全體を冲積統と見做した．

第 I 表　平塚町地表下 30 m の砂層中に含まれる有孔虫

Quinqueloculina seminula LINNAEUS
Triloculina acurieriana D' ORBIGNY
Nonion scapha (FICHTEL et MOLL)
Elphidium crispum (LINNAEUS)
Urigerina pygmaea D' ORBIGNY
Rotalia papilosa compressiuscula BRADY

藤澤町附近の冲積統砂層は後に述べるであらうところの新第三系及び關東ローム層

---

1) 花井重次，地理學評論 2, 9 (1926) に地殼運動によつて濱堤が後退せる事を述べた．
2) 今村學郎，地震研究所談話會にて發表．
3) 地理學評論 5, (1925).

堆積直前の段丘礫層の侵蝕面上に不整合にのるので，沖積統と考へられてゐる．

柏尾川の沿岸は平坦な沖積平野の狀を示してゐる．この平野を構成してゐる物質は主として黑色又は暗青色淤泥で，地表は水田に利用されてゐる．

大船驛の東南深澤村上町屋附近の試錐の結果4)によると地表から3mは粘土質であるが，その下部に砂礫層が約7m程の厚さにあつて，その下に基盤の金澤統が横はつてゐる．金澤統は100m程の厚さで，その下位に逗子統が横はつてゐることも明にされた．大船以西の柏尾川沿岸でも處々基盤が河底に露出してゐる部分があり，沖積統下に埋もれた基盤の起伏が現在の河道と一致してゐないことを示してゐる．この埋もれた起伏決定には試錐か彈性波物理地下探査法の如き方法の助けを必要とする．

大船驛の西北柏尾川河底では海成沖積統の淤泥層が不整合に新第三系の大船層の上に横はり，この不整合面上に横はる淤泥層からはその不整合面に穿孔してゐる *Sanguinolaria* (*Soletellina*) *diphos* (LINNAEUS), *Batillaria zonalis* BRUGUIÈRE, *Ostrea gigas* THUNBERG 等河口半淡水性の泥棲性の軟體動物を採集することができた．この海成層の高度5)は海拔高度約6mに達してゐる．この化石產地以北の柏尾川の沖積統からは未だ海棲動物は見出せなかつた．

この沖積平野の周圍を圍む丘陵は何れも沖積統より古い地層から出來上つてゐる地域なので，沖積統は古い地層から作られてゐるところの開析地形の凹地（溪谷地形）に堆積した地層で，一時海水の侵入した證左も認められた．

鎌倉町附近の沖積統も同樣低地帶を占めてゐる．伊木常誠博士6)は鎌倉町西部低地の井戶に就いて詳しい觀察を報告されてゐるが，之等の材料によると鎌倉町西部（長谷附近）の地表下 3～5m の位置に新第三系逗子統が基盤として横はり，この埋沒してゐる基盤の起伏は溪谷狀を呈し，その上に不整合に砂を主とし，稀に海棲貝殼交り砂を含んだ沖積統が横はつてゐる．然るに由比ケ濱附近では砂層の厚さ 8m 以上に達してゐるらしく，8m 內外の深さの井戶の底は大部分基盤に達しない．

筆者は上の事實から鎌倉町の沖積統も，その基盤である新第三系に作られた侵蝕谷が海に溺れて，入江となり，その入江に砂の堆積が行はれその堆積面が隆起して沖積統からなる低地が作られたと解した．

横濱市の沖積統の諸性質は復興局建築部7)の努力によつて詳細に判明してゐる．復

---

4) 東京帝大工學部三川逸郎學士の御好意でこの貴重な資料を拜見するこさができた．

5) 大船驛の南方鎌倉への縣縣分岐點で海拔 8·5 (1923 年測量)．その附近からこの海成層の露頭まで約 2·5～3m の高度差があらう．

6) 地質要報，明治 36 年，3 號，pp. 109～116.

7) 復興局建築部， 東京及び横濱地質調査報告 (1928).

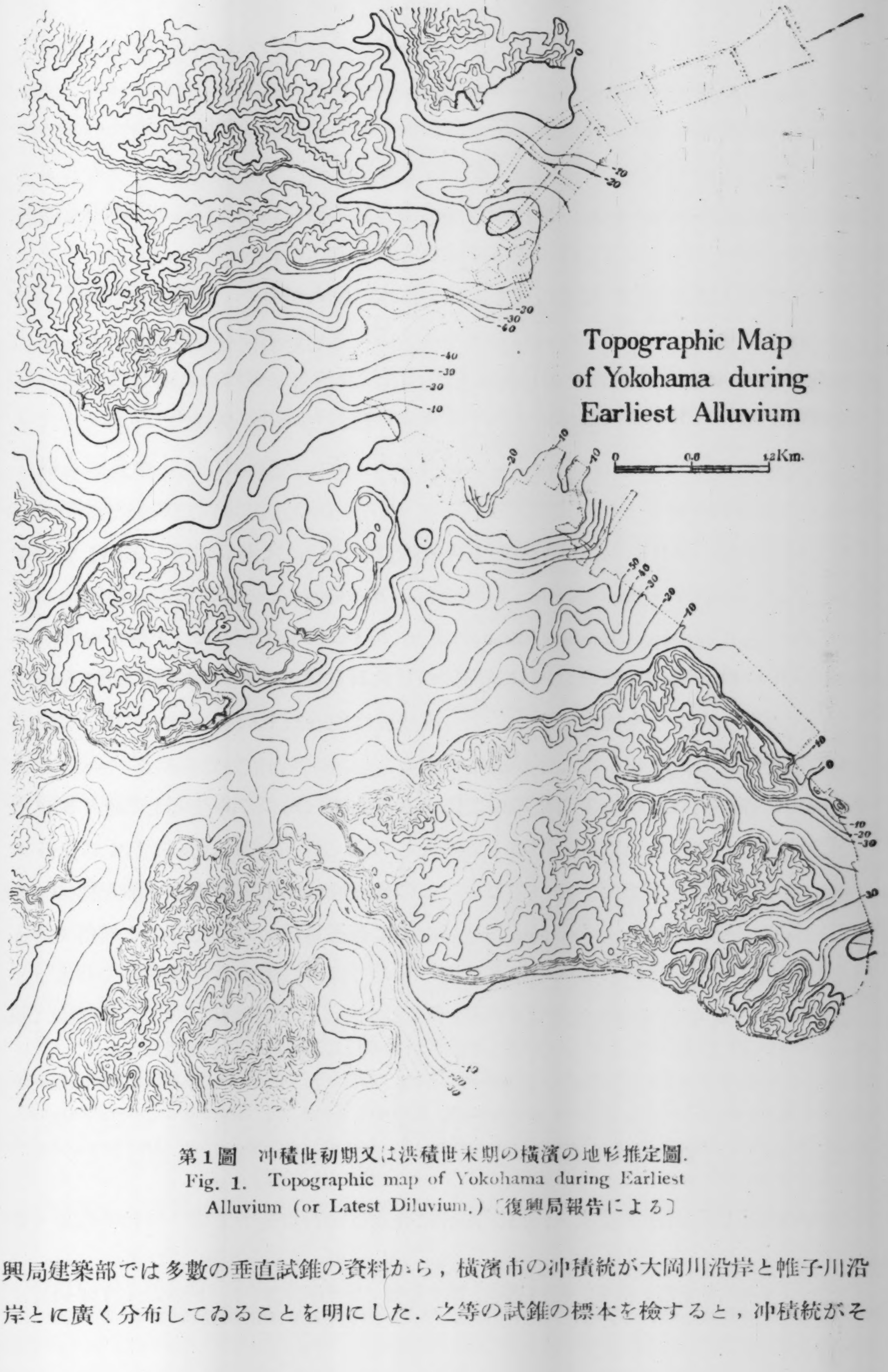
Topographic Map
of Yokohama during
Earliest Alluvium
0
0.6
1.2 Km.
0
-10
-20
-30
-40

第１圖　沖積世初期又は洪積世末期の横濱の地形推定圖.
Fig. 1.　Topographic map of Yokohama during Earliest Alluvium (or Latest Diluvium.)〔復興局報告による〕

興局建築部では多數の垂直試錐の資料から，横濱市の沖積統が大岡川沿岸と帷子川沿岸とに廣く分布してゐることを明にした．之等の試錐の標本を檢すると，沖積統がそ

の堆積前にあつた溪谷を埋めて堆積してゐることをも我々に示した．第1圖は沖積統を假に取除いたと假定した場合にどの様な地形が示されるかを復興局の圖から作圖したもので，沖積統堆積直前の地形概形と見做して差支えあるまい．

横濱市の沖積統は大部分海成層で砂，淤泥からなり基底には礫層が發達してゐる．東木龍七氏[8]は復興局の報告に基いて沖積統下に埋れた河岸段丘の發達してゐることを指摘した．之等の河岸段丘はその地質構造から見て次に述べる様に沖積統堆積前の溪谷地形が開析されてゐる當時に成生されたものと考へられる．

横濱市は第1圖に示した地形に達した後，海水の侵入があり，複雜な海岸線を持つた溺れ谷地形を呈したが，この溺れ谷地形は次第に堆積作用のために埋められ，又一部は合計數 m の隆起運動のために海水を失ひ入江は消失し現地形に達した．

横濱市に關する古文書古圖等によつても舊海岸線が大岡川の溪谷内に入江として入り込んでゐたことが確められてゐるし，之等が人工的に埋められたことも記されてゐる．

上大岡川上流，河口から約 6 km の上大岡附近の河岸には海成泥層が露出してゐて腐木と共に *Batillaria multiformis* (LISCHKE)，*Batillaria zonalis* (BRUGUIÉRE)，*Cyclina sinensis* (GMELIN), *Macoma incongrua*? *v.* MARTENS, *Codakia* (*Pillucina*) *pisidium* (DUNKER) 等の半淡水性河口泥海棲の貝化石を含んでゐる． 故に約 6 km も深く入江のあつたことも推定できる．この海成層は現海面上約 6～7 m の位置にあつて堆積當時に比して隆起したことが推定できる．

大岡川溪谷の出口には山手町臺地の北麓から西北方へ向つて沖積統上部近くに砂礫層が發達してゐて横濱公園近くの地下で消失してゐる．[9] この砂礫層は上流部及び西北部になく溪谷口近くで厚くなつてゐる．この砂礫層は山手町臺地の一部を作つてゐる洪積統砂礫層の崩壞したものが，海流のために運搬堆積せられたものと解釋でき，田中教授も述べた様に灣口砂嘴の如き成因のものではあるまいかと思惟してゐる．

逗子町の溪谷底も一つの廣い沖積面で代表されてゐるが，その堆積物は主として砂•淤泥で現在の海岸から約 2 km の池子からは野村七平氏[10]が次の様な海棲貝化石を報告してゐる．

Lucina bialata PILSBRY, *Paphia undulata* BORN, *Macoma incongrua* v. MARTENS, *Lunella coronata granulata* GMELIN, *Obtortio pupoides* (A. ADAMS), *Diala* sp., *Syncera angustata* PILSBRY, *Batillaria zonalis* BRUGUIÈRE, *Nassarius japonicus* (A. ADAMS), *Astyris varians* (DUNKER), *Astyris martensi* (LISCHKE.)

之等の海棲貝化石は半淡水・淺海淤泥等に普通に棲む貝殼である．堆積狀態は大船

---

8) 東木龍七，地理學評論．3, (1927) 972～978.
9) 復興局建築部，前掲，第14圖版；田中啓爾，地理學評論，1, (1925), pp. 134～137.
10) S. NOMURA, *Sci. Rep. Tohoku Imp. Univ.*, (*Geology*), **15**, (1932) 2.

附近と同様でこの含化石層は野村氏の如く沖積統と考へられる.

上述の各地に於ける沖積統の分布を見て，何れも現在の海岸から數粁の內陸溪谷底地下，或は海拔數 m 內外の位置に海成沖積統が有ることが解つた. 故に我々は上に述べた諸事實から沖積世初期にはこの地方は現在の先志摩半島の海岸地形の如き複雜な入江を持つた海岸地形であつたと推定できる. 沖積統の厚さは埋積谷底の深さから判斷して最大 50〜100 m に垂んとしてゐるから，少くとも三浦半島北部では沖積世に入り 50〜100 m 以上の海面と陸地との運動があつたと考へられる. 第2圖は上述の海面に對する地盤の運動を矢印で表現してみたもので，左向きが隆起，右向きが沈降で三浦半島北部の一般的な造陸運動的地殼運動のみを示した.

沖積統產の海棲貝化石は大部分現在中央日本に普通に生存してゐる種類で西南日本に普通に生存してゐる種類が稀に採集されてゐる. 各地の動物群との類緣關係も嘗て筆者の考案した共通係數によれば，大體三浦半島と同緯度の動物群で代表されてゐる.

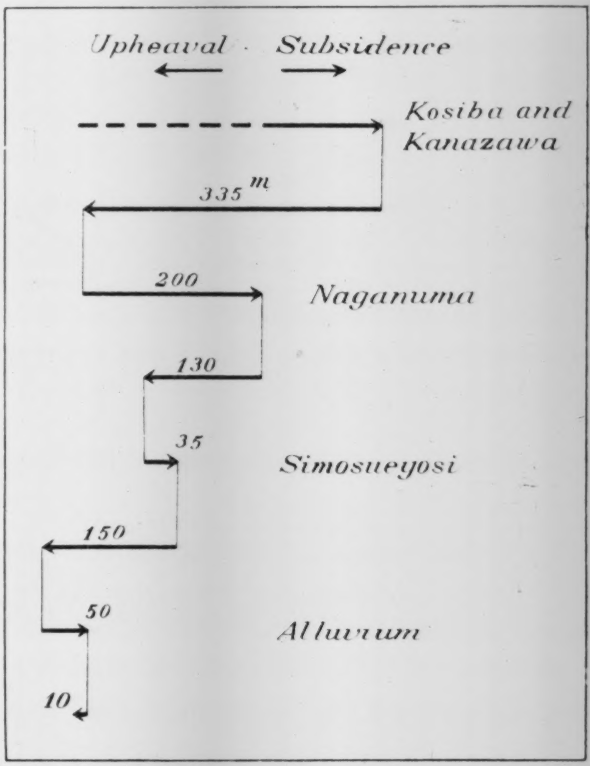

第2圖　三浦半島北部の金澤期以後の造陸運動的地殼變動圖（變動量は概測の量を示す）.
Fig. 2 shows the amount of epeirogenetic displacement since the Kanazawa age.)

横濱の南，金澤八景附近の低地も同様明治初年には六浦莊村大道，川部落附近に迄入江が深く達してゐたが今日では僅に野島附近に入江の面影を認めるのみである.

上述の他，堆積物は極めて小範圍であるが，貝化石を多數に產することと，海岸近く海面上數 m の位置にあることとで知られてゐる海成沖積統が，稲村ケ崎11)，材木座12)，谷津等13)に知られてゐる. 稲村ケ崎の貝層は山川戈止氏，材木座は青木敎授，谷津は野村七平氏によつて夫々報告されたものである. 第3圖は從來報告された海成

---

11) 山川戈登，地質學雜誌，**16.** (1909), 190.
12) 青木廉二郎，地球，**3,** (1925), 1.
13) S. Nomura, *op. cit.*, (1932).

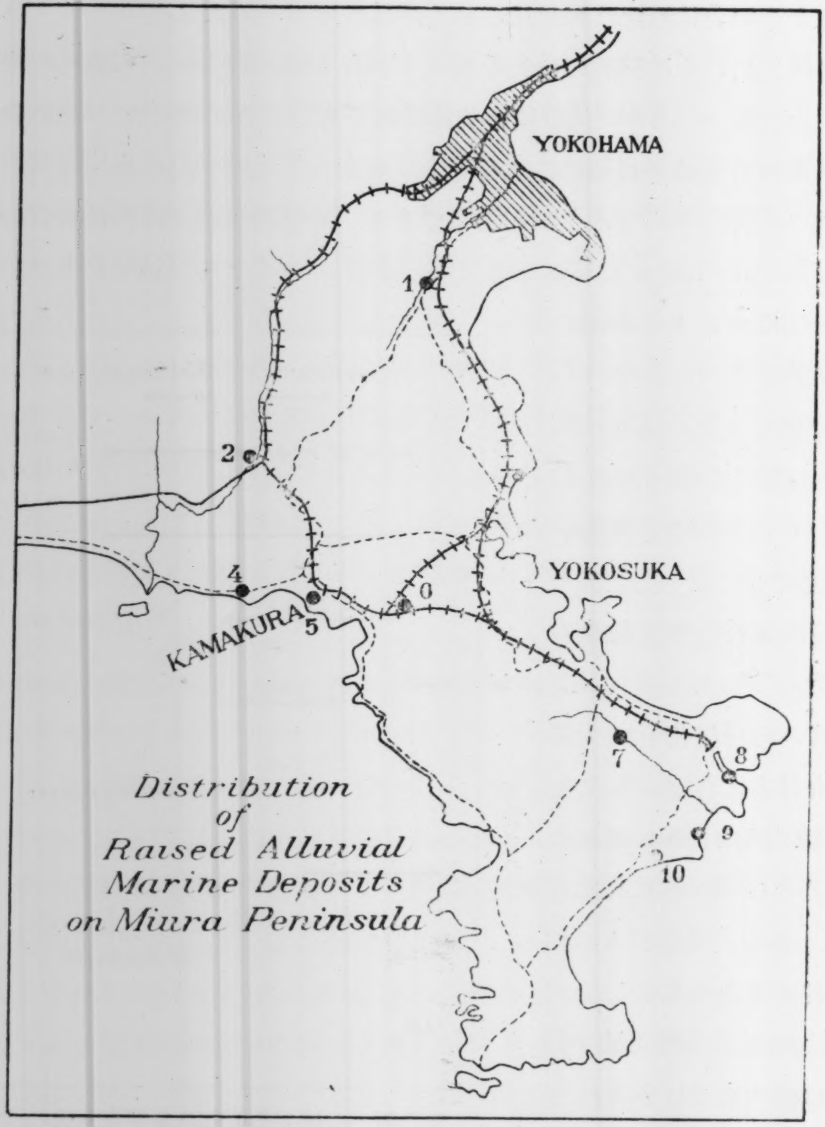
YOKOHAMA
1
2
YOKOSUKA
4
5
6
KAMAKURA
7
8
9
10
Distribution of Raised Alluvial Marine Deposits on Miura Peninsula

第 3 圖　三浦半島隆起海成冲積統の分布圖.〔主さして野村氏による.〕

冲積統の露出地の分布を示す.

附. 葉山町下山口附近に約 15～6 m 前後の段丘が保存されてゐる. この段丘は下山口から日影に至る道路の切割面や下山川の河崖に露出するものから判斷するさ, 最上部に段丘礫層が約 1 m 層の厚さにあり, 次に小さな不整合を隔てゝ約 7 m の砂礫層さ淤泥層さの互層がある. 泥層中にはオニグルミの化石を多數に含んでゐる. このオニグルミの中には德永博士や大石學士やの論議されてゐるやうな孔隙の生じたオニグルミも多數あつた. この地層中からは遂に貝化石は見出すことができなかつた. この段丘層は上表に關東ロームを缺いてゐるこさ, 地形上から判斷して現在の下山川の溪谷底堆積物であるこさ等からして, 洪積世末期のものであるかも知れぬが暫らく冲積統の項に誌して後の研究に俟つこさとする.

洪積統

この地方の洪積統は筆者の前論文に掲げた如く，關東ローム層及び段丘礫層，下末吉層及びdm砂礫層，保土ケ谷礫層及び上部鮮新統とも考へられる長沼層である．

關東ローム層及び後關東ローム段丘礫層．

記述の都合上段丘礫層をもこの項中に含めて述べる．筆者はローム層に他の地層と同様に固有の名稱を與へることの必要を感じてゐたが幸 植田房雄學士[14]によつて關東ロームなる名稱が與へられたので之を利用した．

關東ロームに就いては多數の論文，研究が公にせられたが，最近の久野學士[15]の研究で，大にその層序學的意義が確められたことは喜ぶべき事である．久野氏によれば箱根山，大磯附近の關東ロームは大部分富士火山の成生初期の火山灰からなつてゐると言ふ研究結果を得らるるに至つた．又原田農學士[16]の研究によれば關東ローム中の輕石層（卽ち同氏の浮石土）は關東平野周緣の火山の噴出物であつたらしく，關東平野周緣の火山體に近付く程それを中心としてその粒子が大きく，輕石層は厚くなつてゐることが明にされた．この様な分布事實から知られることは關東ロームが空中から運搬堆積せられたものと解さねばならぬことを示してゐる．尙關東ローム中には未だ陸成・海成の化石が發見されてゐないが，横濱市に露出する關東ロームの基底に近い輕石層中には炭質物が見出されてゐる．

關東ロームは三浦半島北部でも全般に亙つて發達するが，よく發達してゐるところは主として柏尾川以北の丘陵，藤澤町の北部，横濱市附近である．

藤澤町北部では關東ローム層は2枚の黃色輕石粒を含んだ輕石帶を含み，厚さ約6～5mの赤褐色の露頭として示されてゐる．これらの黃白色の輕石帶の內上部のものは原田學士の東京浮石土に該當する様である．之等の輕石帶は箱根の中央圓錐丘の噴出物と考へられてゐる．この露出面は藤澤町遊行寺の北の崖（loc. 1 & 2 in Fig. 4），同じく東の崖（loc. 3 in Fig. 4），諏訪神社裏崖に見られる．この關東ローム層は徑5cm內外の砂礫層を被うてゐる．藤澤附近では黃白色の輕石層は約2枚を數へることができるが，三浦半島宮田附近に分布する關東ロームは約2枚乃至3枚の輕石帶を數へることができる．

横濱市附近の關東ロームは故小澤博士[17]が保土ケ谷驛の南側で示された如く，藤澤附近とは少しく異つてゐるが，輕石帶を2枚介在してゐる點で一致してゐる．

---

[14] 植田房雄，地質學雜誌，**37**，(1930)，441，p. 252.

[15] 久野久，地質學雜誌，**43**，(1936)，511.

[16] 原田，土壤學會雜誌．

[17] Y. Ozawa, *Guide-Book Exc. C-5 Pan-Pacific Sci. Cgr.*, (1926).

保土ケ谷驛の南側の臺地は久保山臺地と普通呼ぶが，細分割して掃部山，野毛山，

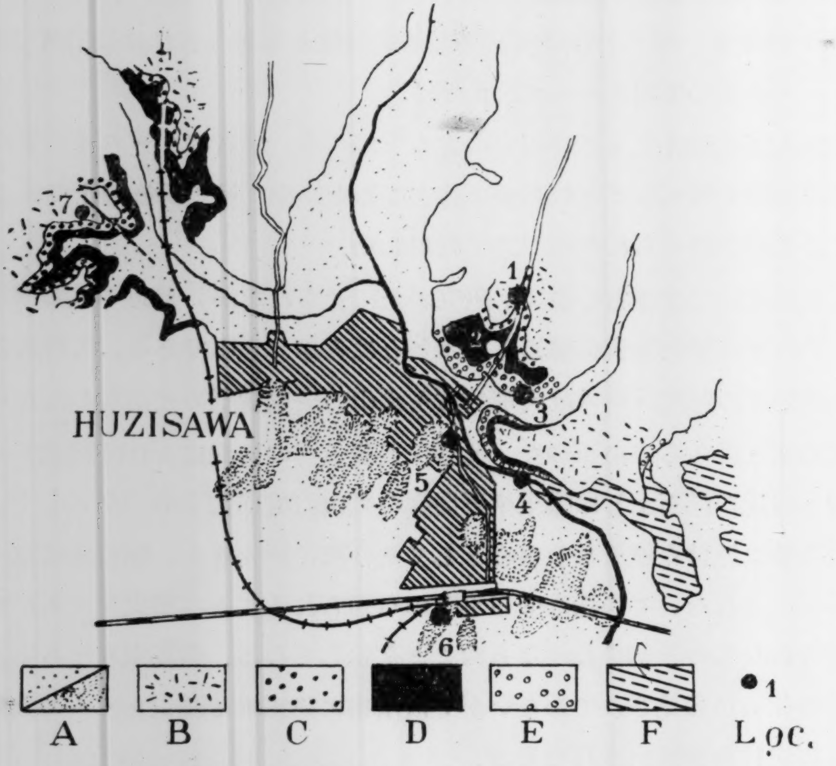

第 4 圖　藤澤附近の地質圖．A＝沖積統及び砂丘，B＝關東ローム，C＝礫，D＝泥，E＝礫，F＝金澤統．

Fig. 4. Geologic map of Huzisawa-mati. A＝Alluvium & sand dune; B＝Kwanto loam; C＝gravel; D＝mud; E＝gravel; F＝Kanazawa series.

久保山，大原山等に分れてゐる．之等は野毛切通，霞橋切通，大丸切通によつて境されてゐる．この臺地の上は多少の起伏はあるが殆ど平坦に近い臺地で，關東ロームの堆積面から形成されたものである．之は筆者[18]の Du 面である．

保土ケ谷驛南側の崖面で觀察すると臺地の上の表面を作つてゐる赤褐色の關東ロームの中部は灰白色・黄白色の厚さ 60 cm の 1 枚の輕石層を含み，下部は二枚以上の輕石層を有してゐる．下部の輕石層間には黑色の粘土を含み，植物の破片を含んでゐることがある．これらの輕石層の下位は灰青色の泥層で約 28 種[19]の半淡水淺海の貝化石を含んでゐる．筆者は關東ローム中に上の赤褐色のローム層から下の輕石層までを含めるが，二次的ロームに於いては各地に上述の如き層序關係なく無層理の事が多い．この二次的ロームは不整合に關東ロームの層理を斜に横切つてゐる．この二次的

---

18) Y. Otuka, *Proc. 5th Pan-Pacific Sci. Cgr.*, (1935) pp. 1589～1592.

19) 地質學雜誌, **37**. (1930), 442, (1935), pp. 325～253.

ローム，關東ローム及びそれに介在する輕石層の層序關係は久保山臺地附近の關東ロームの大部分の露頭に就いて共通に見られるところの關係である．久保山では關東ロームの基底の高さは海拔約 26 m である．

山手町，根岸の兩臺地も關東ロームのよく露出してゐるところである．關東ロームは上部に赤褐色の中部層を横へ下部に黑色の植物破片を含む輕石層が横はつてゐる．

山下町千鳥橋西方 300 m の新山下町の崖に露出してゐる關東ロームは最上部に赤褐色のローム層が横はり，その下に黃褐色の輕石層を横へ，再び赤褐色のローム層となり，その下位に淡黃色，淡黃褐色の輕石層が横はり，その下には海棲貝化石を含む暗灰色の泥層がある．この層序關係は上に述べた樣に根岸，山手町臺地に一般に見られるものである．〔寫眞 2〕

横濱市鶴見區附近に發達する 40～50 m 內外の臺地の上の表面を作る關東ロームは淺野綜合中學校附近，下末吉附近で觀察したところでは中部に 1 枚，下部に一枚以上の淡褐色の輕石帶を含み，全體の厚さ 10 m 內外に及ぶ．二次的ロームは關東ローム層を開析した凹地を埋め，關東ロームとの間に侵蝕間隙を含んでゐる．卽ち關東ローム堆積後侵蝕作用によつて關東ロームの表面に起伏を生じ，その起伏の凹地に二次的ロームが堆積した事が推定出來る．〔寫眞 1 參照〕

横濱市中區本牧池田の西北の崖に露出するローム層も約 2 枚の黃白色の輕石を有しその上表はこの附近の臺地の上表面を作つてゐる．その下位には 3 m の泥層があり整合的に輕石礫又は礫層を伴ふ砂層の上に横はる．この砂礫層の下部は中里泥層で二，三の化石を含んでゐる．

中區天德寺裏，中區箕輪山手警察署裏西の崖，滿坂の西岸，西ノ谷西側の崖等，間門・池袋附近の觀察は何れも上述したやうな層序を確める資料となつた．

上に述べたやうに關東ロームは藤澤，久保山，根岸，横須賀，大津等に於いては平な層理と堆積面 Du を保存し，略ぼ水平な水底堆積物の如き性質を示すに反し，多摩丘陵の延長に當る柏尾川以北の丘陵地，圓海山方面では關東ロームは基盤岩石の凹凸に準じて凸凹な堆積狀態を示し，陸上氣成堆積物としての特徵を示してゐる．

之等の事實は關東ローム堆積直前に多摩丘陵その他に凹凸のある地表の存在したことを示し，武藏野段丘（Du 面）地域には極めて平坦な表面を持つた地表表又は段丘面が保存されてゐて，關東ロームは兩地域に一樣な分布をしたと推定するに都合がよい．卽ち關東ロームの起源に就いて火山灰說が殆ど確定した今日では，多摩丘陵や，圓海山や，柏尾川上流の關東ロームの堆積狀態を以て空中から運搬されたものと見做し，相模野・久保山・根岸・鶴見等に見られるものは元來平坦な堆積面か又はそれに

類似な面の上に堆積したものであらうと解するのがより合理的となつた.

Du 面を作る關東ローム層とその下に續く洪積統との間に往々第5圖の如き侵蝕期の介在したことを暗示する如き不整合の露頭が所々に見出だされることがある. この露頭を仔細に檢すると臺地の表面近くにある二枚の輕石帶は開析溪谷に至るとその凹みに應じて溪谷形より稍々緩く淺く堆積し, 厚さは寧ろ增大し, その程度は上部のもの程淺い. 最上部では殆ど平坦で表面からでは殆どその形態を把握できない程である この様な堆積狀態は流水のために徐々に溪谷底から始めて堆積せられた堆積物の斷面とは全く異る性質の露出面で, 之は寧ろ氣成と解する方が說明し易い. 多摩丘陵その他の Dl 面で觀察推定したやうに, 平坦な武藏野 Du 面の關東ロームも氣成と解した方がこの様な露頭の解釋に都合よくなつた. 故に關東ローム堆積直前の平坦な地表は隆起堆積面に開析作用が僅ばかり開始した程度の臺地の表面であつたと考へられる.

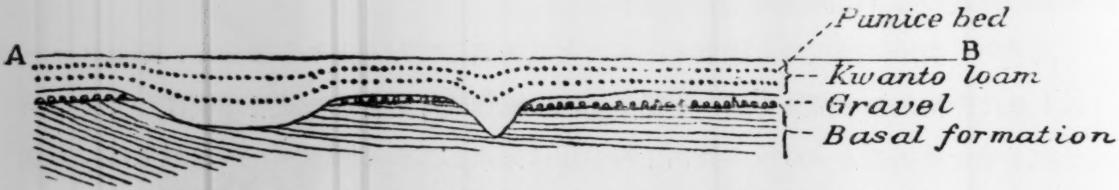

第5圖 關東ローム基底の不整合さ段丘の表面さの關係を示す概念圖.
Fig. 5. A schematic geologic profiles of the Musasino terraces (Du) showing the para-unconformable stratigraphic relation between the Kwanto loam and the underlying formations.

上の様に關東ロームの大部分が氣成のものであつて殆ど水成でないとすれば, 關東ロームの堆積作用は平面的にも高度的にも無關係に分布することとなり, 關東ロームを以て過去に於いて殆ど水平に近く堆積した水成岩の如くに假定して地質構造論をなすのは危險となつた. 關東ロームが氣成であるので, 地形的に時代決定をする事も愼重を要することとなつた. 即ち現在の溪谷底にも段丘上にも一様に關東ロームが分布しても溪谷底では洗ひ流されてしまつたのではあるまいかと言ふ疑が起る. 併し現在の溪谷は多くの場合關東ロームの層理を鋭く切つて形成されてゐるし, 溪谷堆積物中に關東ロームは含まれてゐないから關東ローム堆積以後に形成されたものに違ひあるまい. 矢部博士, 故小澤博士によつて之等の關係は既に明にされてあつた通である.

段丘礫層.

武藏野段丘 Du 面を開析する溪谷に河岸段丘の發達してゐることは既に矢部博士, 東木龍七氏等の研究がある.

横濱市附近の帷子川沿岸にも, 大岡川沿岸にも不明瞭ではあるが數ヶ所にその痕跡を認めることができる.

横濱市神奈川區三ツ澤附近の瀧川南岸には高さ 25 m 内外の高度を持つた河岸段丘が發達してゐる．この段丘上に赤褐色の關東ローム狀の地層が厚く横はつてゐるが，黄色の輕石層の介在を突き止め得なかつた．

帷子川の西南岸には 40 m 前後の段丘地形が見られるが關東ロームは之を被うてゐる．高度 25 m 程の段丘は保土ケ谷ゴルフ場の南岸岡町附近，上星川の東方等に小面積に見られ，この表面に關東ローム狀の地層が被うてゐる．

東木氏は復興局の試錐報告から帷子川沿岸の埋積段丘の存在を指摘されたが，それはこれらの上に述べた段丘より遙に低位のものであつたに違ひない．

柏尾川沿岸にもこの様な段丘が見られる．中川村岡津の北側，下阿久和の附近，戸塚町の東北柏尾，元町附近に見られる．元町・柏尾のものは高度約 25 m で，前に述べた三澤附近のものに類似し，主として僞層砂と關東ロームからなつてゐる．第6圖寫眞3圖はこの段丘とその東側にある丘陵との構造上の關係を示したもので，長沼統の堆積後侵蝕作用により溪谷？が作られ，僞層理砂層の堆積が行はれ，その後關東ロームが降り，堆積してその後の侵蝕作用により現溪谷地形の生じたことを示してゐる．

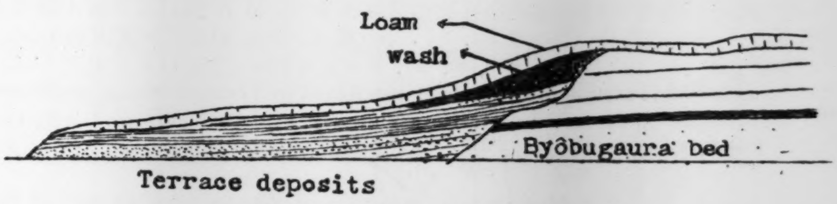

第 6 圖　戸塚競馬場北隅の崖の露出．
Fig. 6 shows the exposure of the bluff, north corner of Totuka race-track.

故に前に筆者が述べておいた如く，關東ローム堆積直前に侵蝕期の存在せることを述べたが，この侵蝕期は上に述べた各段丘の形成せられた時代を含めてゐると解した方がよい．關東ローム堆積直前後にこの地方は隆起の傾向にあつたものと解せられる

即ち上述の事實から此の地方に次の様な地史が推定できる．

關東ローム堆積直前の地形は大體今日と變りなく，低い起伏のある多摩丘陵と平坦な武藏野段丘の表面とは既にあり．隆起の傾向にあつたこれらの地方は共に開析せられ既に段丘が各溪谷に見られた．この初期に當つて關東ロームの堆積があつた．

下末吉統．

横濱市鶴見區の北部下末吉の西の臺地と低地との境界の崖（loc. 1 fig. 8）には次の様な層序が觀察できる．即ち第7圖Gに於いて上部に a, c なる關東ロームがあり一層の厚さ 60 cm ばかりの黄白色の輕石帶 b を含み，その下部は輕石の多い砂岩 d

となり，その下に僞層理の粗砂層 e が 5 m 前後の厚さに横はつてゐる．暗青色の粘土層 f がその下にあり，その粘土層の下部は徐々に砂礫層 g に移過してゐる．この粘土層及砂礫層から多數の貝化石を産してゐる．嘗て横山次郎博士20) の觀察された下末吉の崖は今日では更にその上部が切開かれて，關東ロームとの間の層序が更に明にされた．横山又次郎博士はこの貝化石を研究記載されてゐる．横山博士の採集報告された化石と筆者の採集したものとは筆者の前論文に掲げた．（表略）21)

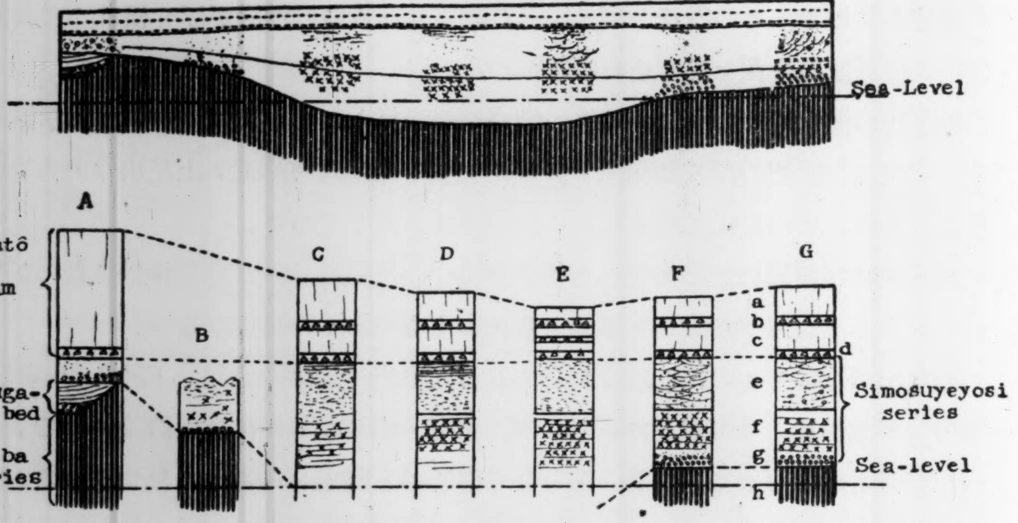

第 7 圖　鶴見—神奈川間の段丘の柱狀地質斷面圖．　第 8 圖にその露出箇所を示してある．A＝高島臺 (loc. 7 fig. 8)，B＝松本 (loc. 6)，C＝栗田谷 (loc. 5)，D＝淺野中學 (loc. 4)，E＝寺谷 (loc. 3)，F＝別所 (loc. 2)，G＝下末吉 (loc. 1.)
〔Columnar geologic section of the terrace distributed in Turumi—Kanagawa districts. The localities of these sections are shown in Fig. 8.　A＝7，B＝6，C＝5，D＝4，E＝3，F＝2，G＝1.〕

この砂礫層の下位は稍々硬化した泥岩層 h で，泥岩層 h と砂礫層 gt の間は不整合關係を示してゐる．

筆者は d，e，f，g を下末吉統と呼ぶ．そして f は下末吉含化石泥層，e を下末吉砂層と呼ぶ．

下末吉統の露頭觀察と同統の分布．

下末吉の南，別所の溪谷出口南側（F in fig. 7；loc. 2 in fig 8）の溪底に半硬化泥岩層 h が露出て，その上に不整合に g 砂礫層が横はる．g 砂礫層は薄く 1 m 以內で直ぐに暗灰色の f 泥層となる．この f 泥層は角礫狀の又は稍々角のとれた輝石・石英安山岩輕石（1 cm 內外）粒を多量に含んでゐて，全體の厚さは 6 m 位である．この泥層の上部は厚さ 30 cm 程の砂泥互層となり，その下に 4 m の褐色の細砂層を横へてゐる．この上部は薄い炭質物を 1 枚挾んだ細粒輕石帶でその上位に泥質な關東ロー

---

20)　横山次郎，地質學雜誌，25，(1918).
21)　大塚彌之助，地質學雜誌，37，(1930)，pp. 352～353.

ム a, c が横はつてゐる．勿論この關東ローム中には黃白色輕石帶 b が挾つてゐて下末吉の露出面の觀察と一致する．

この輝石・石英安山岩・半角礫輕石を含む泥層は寺谷の溪谷出口 (E in fig 7; loc. 3 in fig. 8) には露出するがそれより南では地表の下に隱れて，上部の粗砂層 e が優勢となつてゐる．

鶴見花月園附近では，花月園の東の丘陵に見られるやうに a, b, c, d, e の各層はよく露出してゐる．

花月園入ロ西南側の崖下には含輕石泥層が露出してゐる．同様な層序關係は花月園西南の臺地によく露出してゐて，上部にローム層を横へこゝでは黃白色の輕石帶は 3枚を數へる．最下の輕石層は小さな扁平な輕石粒の集合からなり，次の e 砂層上に横はる．

鷗踊ケ丘住宅地附近 (loc. 4 in fig. 8 の北 500 m) も類似の層序を示すが，e 砂層の下部は暗灰色を呈し，貝化石を產してゐる．第 II 表はその化石表である．之は下末吉含化石泥層より稍々上位の砂層中の貝化石と見做せる．

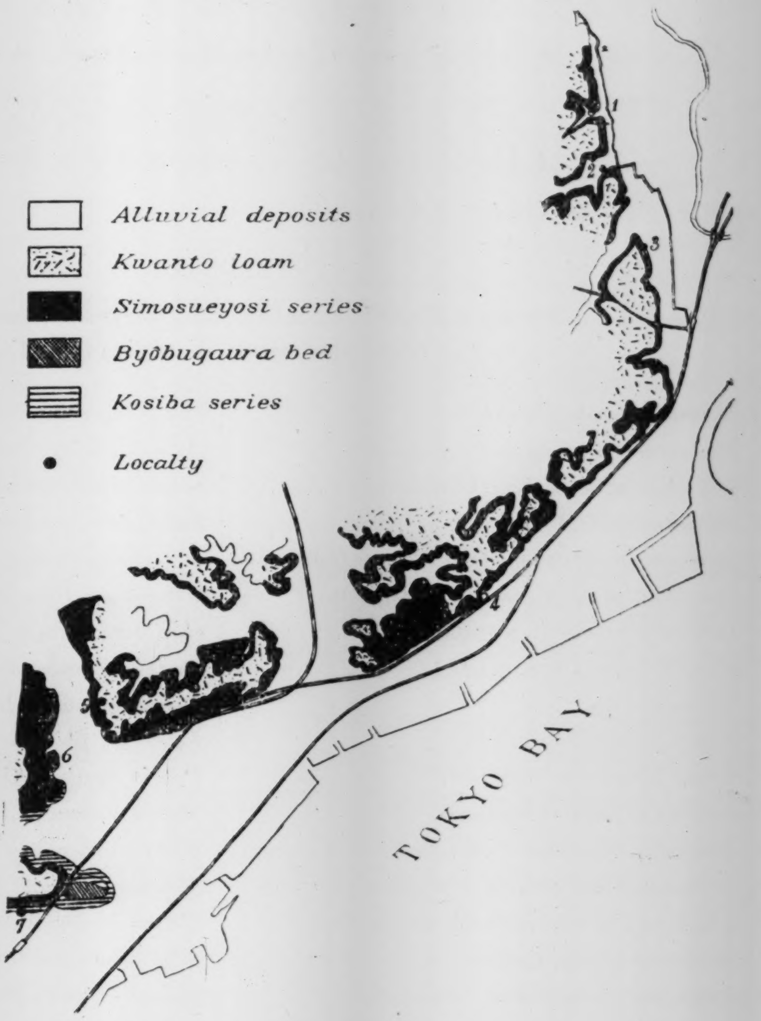
□ Alluvial deposits
▨ Kwanto loam
■ Simosueyosi series
▨ Byôbugaura bed
☰ Kosiba series
● Localty
1
2
3
4
5
6
7
TOKYO BAY

第 8 圖　鶴見—神奈川間の地質圖．番號は第 7 圖の柱狀斷面圖の位置を示す．1＝G 下末吉，2＝F 別所，3＝E 寺谷，4＝D 淺野中學，5＝C 栗田谷，6＝B 松本，7＝A 高島山．
〔Geologic map of Kanagawa-Turumi districts, Yokohama. 1＝Simosueyosi, 2＝Bessyo, 3＝Terayato, 4＝Asano middle school, 5＝Kuritayato, 6＝Matumoto, 7＝Takasimayama.〕

この露出地の南の淺野綜合中學附近(D in fig. 7; loc. 4 in fig. 8)では f 下末吉含化石泥層も運動場の下の鐵道沿線に露出してゐる.

復興局東京・横濱地質調査報告 Pl. 14, k 5 の試錐柱狀斷面圖中，上部層の砂は淺野綜合中學校附近に見られる d 及び e 砂層と考へられる.

東神奈川驛の北，浦島附近の層序も大體前述と同じで，上部は1枚の黄白色輕石帶を含んだ關東ロームがあり，その下位に凝灰質の砂層が厚く發達してゐる. こゝの關東ロームの厚さは 14 m 内外に達し，凝灰質砂層は厚さ 20 m に垂としてゐる. 下位の泥層は地表に露出してゐない.

Table II.

Fossils collected from the Simosueyosi series exposed on the terrace scarp at Tutuzigaoka, Turumi.

Stomatella lyrata PILSBRY
Umbonium moniliferum (LAMARCK)
Homalopoma amussitata (GOULD)
Proclava kochi (PHILIPPI)
Acteopyramis lectissimoides (YOKOYAMA)
Odostomia limpida DALL et BARTSCH
Odostomia dusiensis NOMURA
Syrnola brevis (YOKOYAMA)
Turbonilla sp.
Polynices didyma BOLTEN
Tonna luteostoma (KÜSTER)
Mitrella varians (DUNKER)
Nassarius dominulus (TAPARONE et CANEFRI)
Nassarius fraterculus (DUNKER)
Haedropleura tabatensis (TOKUNAGA)
Ringicula arctata GOULD
Dentalium octangulatum DONOVAN
Dentalium yamakawai YOKOYAMA
Anadara inflata (REEVE)
Pecten laqueatus SOWERBY
Anomia lischkei DAUTZENBERG et FISCHER
Ostrea gigas THUNBERG
Joannisiella cumingii (HANLEY)
Joannisiella lunaris (YOKOYAMA)
Codakia pisidium (DUNKER)
Cardium muticum REEVE
Dosinia japonica REEVE
Dosinia angulosa PHILIPPI
Venerupis philippinarum (ADAMS et REEVE)
Paphia amabilis (PHILIPPI)
Mactra sulcataria REEVE
Racta yokohamensis PILSBRY
Macoma tokyoensis MAKIYAMA
Tellina iridella V. MARTENS
Solen krusensternii SCHRENCK
Panope japonica A. ADAMS
Cryptomya busoensis YOKOYAMA

横濱市神奈川區大口，日本大學第四中學の西 100 m の崖に露出してゐる層序は上部に關東ロームが黄白色の輕石帶を挾んで横はり，その下に褐色の僞層理砂礫層が横はり，この僞層理砂礫層の下に小裂罅の多數に入つた泥層があり，不規則な境界面を以て，角礫輕石を含む泥層が横はつてゐる. 最後の角礫輕石を含む泥層は下末吉含化石泥層と略ぼ同層準のものである.

浦島臺の續きである白樂の東側の臺地は上部に關東ロームが横はり，その下位に褐色の砂層が横はつてゐる.

東京横濱電鐵東白樂驛の西 300 m の臺地（齋藤分）（loc. 6, fig. 8）の麓には灰青色の新第三系が露出してゐて，その上に薄い礫層が横つてゐる．この臺地に沿うて西南へ向つて行くと，旭ケ丘の麓にも新第三系が厚く露頭してゐる．

栗田谷附近で觀察したところでは下部に新第三系が厚く發達し，その上に薄い礫層を横へてゐる．この薄い礫層の上は明褐色の砂層で，その上に關東ローム層が横はつてゐる．新第三系の上限の高さは約 25 m である．(C in fig. 7; loc. 5 in fig. 8).

神奈川區中三ツ澤小學校北側の崖も栗田谷附近と類似である．南三ツ澤から小机方面へ通ずる縣道の坂道には同様な層序關係があり，新第三系上の粗鬆な細砂層中には貝化石が含まれてゐる．筆者は下末吉統と推定した．

横濱驛の北側に聳える高島臺は基盤に新第三系を有し，海拔 25 m 以上には礫層，砂層，關東ローム層が横はつてゐる．

神奈川高等女學校の西南の崖では上から關東ローム層，輕石層，砂礫層，薄い粘土層（化石を含む），砂層，〔不整合〕，途中に砂層を挾む半凝固泥層の順に露出してゐる．筆者は上部砂礫層迄を下末吉統と見做した．この下位は次に述べる屛風浦層に續くものと思はれる．

横濱驛の東北，宮前町洲崎神社附近は基盤は海拔約 20 m 迄新第三系からなつてゐるが，變電所裏手（幸ケ谷幼稚園の下）には不整合があつて，斜に新第三系を截つて圓礫を介在する含化石淤泥層が横つてゐる．この不整合面は前述した下末吉層の基盤の不整合と異るところがあり，化石種及びその堆積狀態は寧ろ次に述べる長沼統の上部の屛風浦泥層の堆積狀態と似るところがある．A in fig. 7 は上の層序關係を柱狀圖で示してゐる．徳永博士[22]の論文にある神奈川驛產化石はこの屛風浦層のものであらう．

上述した各地の露頭から判斷して，關東ローム層基底から新三系上限に至る迄の間に挾まれる厚さ 30 m 内外の砂，淤泥，礫からなる地質系統は槇山博士が下末吉寶泉寺に於いて觀察された含化石淤泥及び礫層の連續と考へることができる．而して下末吉層はその地質系統の下部であり，龍泉寺の化石砂は稍々上位である．

保土ケ谷附近の下末吉統．

保土ケ谷の東南の崖は故小澤博士が汎太平洋學術會議の研究旅行案内書に記されてゐるのでよく知られてゐるが，その後筆者の研究によつて，新第三系上に不整合に横はる礫層（小澤博士論文第3圖 b）とその上の砂泥層（c）とは下末吉統に屬することが明となつた．砂泥層からは多數の半淡水貝化石が採集されて海成層であることも明にされた．（第 III 表）角礫狀の輝石・石英安山岩の輕石 c は砂泥層中に屢々含まれてくる．この海成層は保土ケ谷以西には知られてゐない．

---

22) 徳永重康，地質學雜誌，9.（1902）.

横濱久保山の含化石砂泥層は下末吉統の化石帶としては比較的上部を代表してゐるのであらう．基盤岩石の起伏は第7圖に柱狀斷面圖で示した樣に，保土ケ谷から鶴見北部へ向つて一つの大きな凹地形の存在したことを示してゐる．

横濱市山手町臺地の下末吉統．

横濱市山手町臺地の崖に露出する下末吉統は次圖の如く，中區新山下町の西側の崖に美しい露出面を示してゐる．關東ロームの下位に赤い鐵銹で凝固した含貝化石砂岩層及びその下位に續く泥層がある．兩層の厚さは千鳥橋附近の崖では約 10m に達してゐて，その下位に整合に基底砂礫層が横はつてゐる．この基底砂礫層は西北へ行く程薄く，その基底も海拔 15m 前後に露出するが，この崖の東南では基底層も厚く，基海底は拔 4~5m の位置に低まる．

小港橋の東の小丘の上半部を占める礫もこの下末吉統の基底の砂礫層で，十二天山では關東ローム狀の地層の下に露出してゐる．

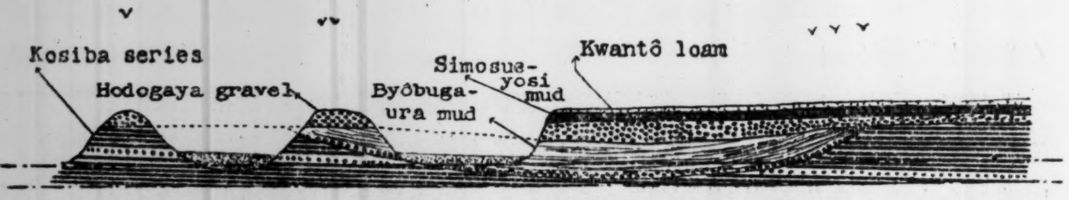

第 9 圖　山手町臺地の地質斷面概念圖（山下町一本牧間）vvv＝山手町，vv＝小港，v＝十二天山．
[Schematic geologic profile of Yamate-tyô terrace (between Yamasita-tyô and Honmoku.) vvv=Yamate-tyô, vv=Kominato, v=Zyûniten.]

Table III.

Fossils collected from the grey silt bed (Simosueyosi series) exposed on the Kuboyama terrace scarp, southeast of Hodogaya station.

Obtortio reticulata (A. ADAMS)
Obtortio perpupoides (YOKOYAMA)
Obtortio septentrionalis (YOKOYAMA)
Diala semistriata (PHILIPPI)
Batillaria multiformis (LISCHKE)
Batillaria zonalis (SOWERBY)
Bedeva birileffi (LISCHKE)
Astyris varians (DUNKER)
Nassarius festivus (POWYS)
Ringicula arctata GOULD
Cylichna yamakawai YOKOYAMA
Retusa cucurbitina YOKOYAMA
Retusa globosa YAMAKAWA
Dentalium octangulatum DONOVAN
Anadara subcrenata (LISCHKE)
Ostrea denselamellosa LISCHKE
Ostrea gigas THUNBERG
Anomia lischkei DAUTZENBERG et FISCHER
Codakia (*Pillucina*) *pisidium* (DUNKER)
Mysella oblongata (YOKOYAMA)
Kellia ojiana YOKOYAMA
Cardium muticum REEVE
Dosinia angulosa PHILIPPI
Tellina diaphana DESHAYES
Theora lubrica GOULD
Raeta elliptica YOKOYAMA

この礫層上の赤褐色の砂泥層からは次の様な貝化石（第IV表）が採集できた．第9圖は新山下町から本牧方面へかけての地質斷面圖である．

Table IV.

Fossils from the brown sand (Simosuyeyosi mud in Fig. 9) exposed on the Yamate-tyô terrace scarp, west of Sin'yamasita-tyô.

Polynices didyma (BOLTEN)
Tonna luteostoma (KÜSTER)
Cancellaria spengleriana DESHAYES
Dentalium sp.
Arca boucardi (JOUSSEAUME)
Anadara inflata (REEVE)
Pecten laqueatus SOWERBY
Lucina sp.
Cardium braunsi TOKUNAGA

Cardium muticum REEVE
Saxidomus purpuratus (SOWERBY)
Dosinia japonica REEVE
Dosinia angulosa (PHILIPPI)
Paphia euglypta (PHILIPPI)
Schizothaerus nuttalei (CONRAD)
Macoma sp. (*tokyoensis*? MAKIYAMA)
Solen sp.
Panope japonica A. ADAMS

橫濱市中區天德寺附近は關東ロームの項でも述べたやうに，輕石圓礫層と含化石粘土質泥層とが基盤の新第三系の上に不整合にのつてゐる．この關係は山手町警察署裏滿坂，西谷，元町の東南側の崖，磯子區方面へと連續してゐる．第 10 圖は之等各地の柱狀斷面圖である．B は西谷，D は滿坂，E は山手町警察署裏，F は天德寺．

中區本牧町池田附近にも美しい露出面がある．關東ロームは臺地の表面から約 12m の厚さにあり，その下位に凝灰質泥層を隔て泥層が 2 m 程ある．その下位には僞層砂が數 m ある．この僞層の基底には極めて薄く砂礫があるが，前述したやうな粗粒褐色砂は見出だされない．この砂礫下は不整合に新第三系の中里層が露出してゐる．砂礫の海拔高度は約 20～25 m 前後である．この砂礫質僞層砂層以上，關東ローム下が層序狀下末吉統に屬せしめられる．第 10 圖の C は池田附近の斷面圖である．

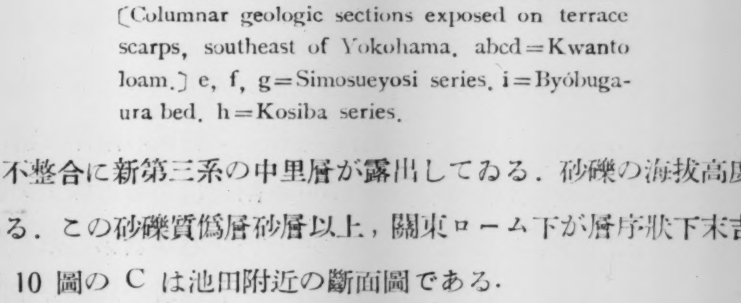

第 10 圖　橫濱東南部段丘の柱狀地質斷面圖．
〔Columnar geologic sections exposed on terrace scarps, southeast of Yokohama. abcd = Kwanto loam.〕 e, f, g = Simosueyosi series. i = Byóbuga-ura bed. h = Kosiba series.

間門池袋では關東ローム下に殆ど上述したやうな下末吉統に相當する地層を見ずに新第三系が露出してゐる（A in fig. 10）．復興局報告の圖に於いてもこの部分から瀧

頭方面へ向つては砂礫層及び泥層の分布は見られない．

磯子區附近は後に述べるやうに長沼統も分布してゐるので，その區別は比較的容易でない．濱磯子町附近から間坂へかけての所謂屛風浦の崖は下部に新第三系，上部に長沼統があり，別に25～30mの高度に段丘礫層が厚く分布してゐる．この段丘礫層と長沼統との層位關係は寫眞4に示す様に前者が後者に不整合でのつてゐて，長沼統とは明な不整合である．この段丘上には厚くローム層が被うてゐて，この段丘礫層がローム堆積以前のものであることを示してゐる．

磯子-屛風浦の崖の西側に岡村町から深く入込んでゐる溪谷壁兩側には，段丘礫層がローム下に露出してゐる．この段丘礫層の基底の高度は上流では50m近くの海拔高度を持つが，岡村町附近では25～30mに達し，中區中村橋方面へ出て，根岸・山手町臺地の崖に露出する下末吉統の礫層に續いてゐる．

屛風浦の崖に於ける段丘礫層もその高度，層序からみて，前に述べたものと略ぼ同時代の礫層と考へられる．

保土ケ谷礫層と呼び，又嘗て筆者が誤つて二俣川礫層と呼んだ礫層は上に述べた下末吉統基底の砂礫層に他ならない．この保土ケ谷礫層は他の關東地方の段丘礫層と異る點は下末吉統と考へられる海成層の基底礫岩層をも一部に於て兼ねてゐることである．この保土ケ谷礫層は第11圖及び地質圖に示す様に都築郡二俣川部落の溪谷底に關東ロームの下に先づ露はれ，西谷，星川，久保山等の臺地の崖に連續露出して，山手・本牧方面へと分布してゐる．その基底の露出高度は二俣川附近で海拔40～50m，西谷村笠部落附近で40～37m，西谷淨水場附近で30～45m，星川町下谷戸で30～40m，保土ケ谷附近で25～30m，新山下町で20～25m，本牧では15～20m位で，この礫層の分布をみるとその高度分布は次第に西北から東南へ向つて低まつてゐる．

この礫層の平面分布をみると西谷附近では，この礫層の西南側は鮮新統が礫層の分布高度より遙に高位に迄分布してゐて，この礫層が次第に薄くなつて消失してゐることを示してゐる．

例へば西谷淨水場の東側の谷を坂本から南方へ上ると，佛向の西方附近までは，關東ロームの下に厚く保土ケ谷礫層が堆積し，谷底の兩岸に露出する新第三系上に不整合にのつてゐるが，溪谷口から約700m附近に至ると保土ケ谷礫層は薄くなつて殆ど新第三系上には礫の痕跡なく，關東ロームが直接新第三系を被うてゐる．此の溪谷を更に上流部へ追跡すると新第三系は保土ケ谷礫層の高度分布限界を遙に超えて，海拔50mに迄も明瞭に露出してゐる．

保土ケ谷驛の北側には海拔50～60mの高度を持つた段丘があり，その周圍の崖に

は保土ケ谷礫層が厚く分布してゐるが，この礫層も西へ行くとその厚さを減じてゐる．種畜場から段丘上へ登る道では約 35 m の高度に關東ロームと新第三系の不整合面がみられるが，保土ケ谷礫層は見られない．

保土ケ谷町の外川神社の西北の小學校附近には海拔 25 m 程の位置に礫層がみられるのに前述の坂路には礫層はなく新第三系は更に高位に露はれてゐる．

久保山臺地の保土ケ谷礫層は保土ケ谷から井土ケ谷への大道路の切割面には露出してゐない．

保土ケ谷礫層の東北の分布も同様に限られてゐて，保土ケ谷礫層の露頭は僅に上星川停車場の東北の崖に露出してゐるのみで，他は高島山附近に露出してゐる．上述の露出以外は長沼統と考へられるものの他は新第三系がその位置を占めてゐて，之等は直接に關東ロームに被はれてゐる．

この礫層の西の分布は關東ロームの下に沒して餘り明でないが，都築郡二俣川村萬騎ケ原の南　須鄉谷海拔附近では 80 m の高度に迄新第三系が露出してゐて，關東ロームは礫層を挾まずに直接に新第三系を被うてゐる．

西谷村市野澤の南約 1 km の尾根でも約 80 m 前後の高度に新第三系の露頭があつて，矢張礫層を伴つてゐない．その他礫層の分布は地質圖及び第 11 圖に示してある様に各地に見出されてゐるが，主として帷子川及びその支流に沿へる段丘部にある．

既に述べた様に保土ケ谷の溪谷，大岡川の溪谷，岡村町の溪こ谷に分布するものもの礫層の連續である．

今この礫層の分布を概念的に示すと第 11 圖の如くで，この分布から判斷して保土ケ谷礫層は帷子川の前身と思はれる古帷子川とも言ふべき河流の氾濫原であつて，横濱港附近に廣い氾濫原を展開してゐたものと考へられる．

古帷子川は二俣川附近から西谷村笠，淨水場附近へ出て，之から放射狀に三角洲砂礫を略ぼ

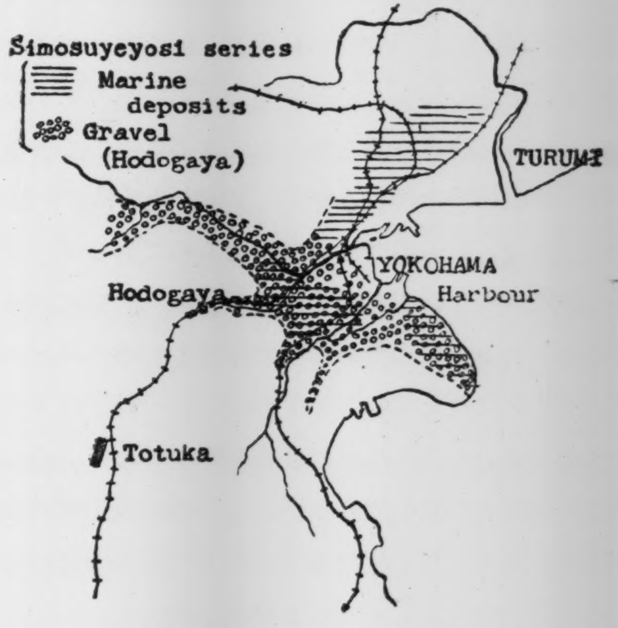

第 11 圖　下末吉統の分布圖
[Map shows the distribution of the Naganuma bed.]

西から東々南へ向けて堆積せしめた．この三角洲礫の末端は下末吉統の海の堆積物で被はれて，下末吉層を堆積せしめた．この三角洲砂礫の扇狀地の要に近い保土ケ谷附近の下末吉層の化石群は第 III 表の様に極めて半淡水性の種類からなつてゐるが，要から遠い新山下町躑躅ケ丘等の化石群（第 II 及び IV 表）はかなり淺海に棲む種類からなつてゐて上の推論に都合がよい．

次に述べる長沼統は後に述べる様に現在の地勢とは全くその分布上の性質を異にしその堆積物の分布も東南から西北へ向つた一つの灣入を想定する様に示されてゐるが下末吉統の分布は極めて現在の地形と密接な關係を持つてゐる．

例へば横濱附近の段丘の表面は新第三系及び長沼統からなる基盤を先づ平に侵蝕して，その上に横はつた保土ケ谷礫層及びその上を被ふ下末吉層と關東ロームの堆積面で表はされてゐることは地質圖から明である．今この段丘面を久保山，根岸等で代表するならば高度は 60～50 m 前後と限定される．この高度の段丘は現在遠望すると何れもその表面が極めて平坦な事に氣付く．寫眞 5 の a はこの平坦な段丘面を示す．この様な段丘は帷子川沿岸に沿うて分布し之と保土ケ谷礫層又は下末吉統の分布とを比べると驚くべき一致をみる．卽ち上述した段丘面の連續は多少高度を高めるが二俣川村附近に迄追跡でき，保土ケ谷礫層の分布と一致する．

この段丘は從來筆者が Du 段丘面としたものに他ならないから，Du 段丘の表面は下末吉統の堆積面と殆ど一致した關東ロームの堆積面である．この段丘面は寫眞 5 にも見られる様に一段高い丘陵面 b と明瞭に境されてゐる．この一段高い丘陵は前に屢々述べた様に保土ケ谷礫層を伴はぬ新第三系が直接に關東ロームに被はれてゐる地方で，多摩丘陵の一部と考へられてゐるものである．筆者は嘗て Dl 面と言ふものを設けて多摩丘陵を代表させて，下末吉統堆積前に既に陸化開析せられてゐたと述べたが，その後 2，3 の學者は倘反對せられてゐるが，少くとも横濱附近に關する限り，筆者の意見の正しい事を示してゐる．卽ち多摩丘陵は下末吉統の堆積直前には既に開析を開始してゐた地表であつた．前述した事から保土ケ谷礫層が下末吉統堆積當時の初の一時代を代表してゐるとすれば，この礫層は多摩丘陵の南部に於いて，西北から東南へ横切る一つの氾濫原の存在を示してゐて，之は現在の地形の研究から推定される結論とかなり一致してゐる[23]．この點は長沼統の分布と段丘地形の分布との間に存する關係と異り，長沼統は多摩丘陵を作る基盤層の一員で，多摩丘陵の表面が作られる前に堆積したものであることが明となつた．

---

[23] 淺井治平，地理學評論，1，(1934)；淺井氏は本論文で帷子川溪谷に就いて類似の意見を述べてゐる．

上記の諸事實から次の様な地史が下末吉時代に推定できる．

多摩丘陵南部は長沼統堆積後陸化し，開析を受けた．少くとも帷子川沿岸では開析谷は西から横濱港方面へと向つて排水された．この排水路に沿うて厚さ約 10 m 前後に保土ケ谷礫層が堆積された．その内 帷子川に沿へる古帷子川の流路が最も大きく，その礫層は西部の丹澤山地地方にそれの礫の源を發してゐたことを示してゐる．次に沈降下末吉海成層が輕石を伴つて堆積した．併し下末吉層は多摩丘陵を被はなかつた次にこの海は後退して，武藏野段丘（Du）面の表面が水面上に露はれた．開析作用は開始する．この初期に當つて關東ロームの降灰があり，多摩丘陵も武藏野段丘も關東ロームに被はれる．開析作用は引續いて行はれ，後關東ローム時代に移る．

Du 面が海成層の堆積面と略ぼ一致してゐることと，その表面が關東ローム堆積後開析されその開析谷は 50 m 前後の厚さの沖積統で埋められてゐることとから下末吉統堆積當時よりのこの地方の垂直地殼運動の量の大體が推定できる．第2圖は之を示した．

鮮新—洪積統

長沼統．

筆者が嘗て長沼層としたものを呼ぶ．長沼統には4つの特色ある化石帶のあることを指摘したことがあつた．併し近頃新らしい露出面が各所に作られたので，更に詳しい層序が可能となつた．次にその層序の概略を記すと

長沼統
- 第一化石帶
  - 踊場砂層
  - 倉坪層泥層
- 〜〜〜〜〜〜〜〜〜〜不整合
- 第二化石帶・第三化石帶
  - 屏風浦砂泥互渋
- 田谷砂礫層
- 〜〜〜〜〜〜〜〜〜〜不整合
- 第四化石帶　長沼層

の如く，第一化石帶と第二化石帶との間には明瞭な侵蝕による不整合，第三化石帶と第四化石帶の間には田谷砂礫層が介在し，第三化石帶は不整合に第四化石帶を被ひ隱してゐる．

從來次の様な諸層名が長沼統の各層に對して先輩によつて提唱されてゐるが，それらの筆者の區分に對する關係は次の通である．

1. 横山博士の長沼帶は第四化石帶長沼層である．
2. 槇山博士の屏風浦層は第二・三化石帶屏風浦砂泥互層．
3. 植田學士の柏尾層大岡層は屏風浦層；富岡層の一部は第四化石帶長沼層である．
4. 筆者の村岡泥層は第四化石帶．

5. 筆者の新山下町層は屛風浦互層である.

6. 松本理學士の片瀬層は長沼統であり，多少の疑問があるが恐らく屛風浦互層であらう.

長沼統の分布.

長沼統の分布は極めて複雜で，加ふるに露頭の不明瞭，層位水平に近きこと等で，不整合面の決定も仲々困難であつた．上に述べた樣に長沼統の層序は統中に尙侵蝕期の介在してゐることを示す不整合もあるが，今之等を一堆積系統と見做して，先づその分布を調べてみた.

先づ戸塚町の南方長沼附近の不整合關係を述べやう．この不整合は槇山博士が最初に發見されたもので，記事としては矢部博士の論文が最初である.

鎌倉郡豐田村附近.（第圖 12 參照）

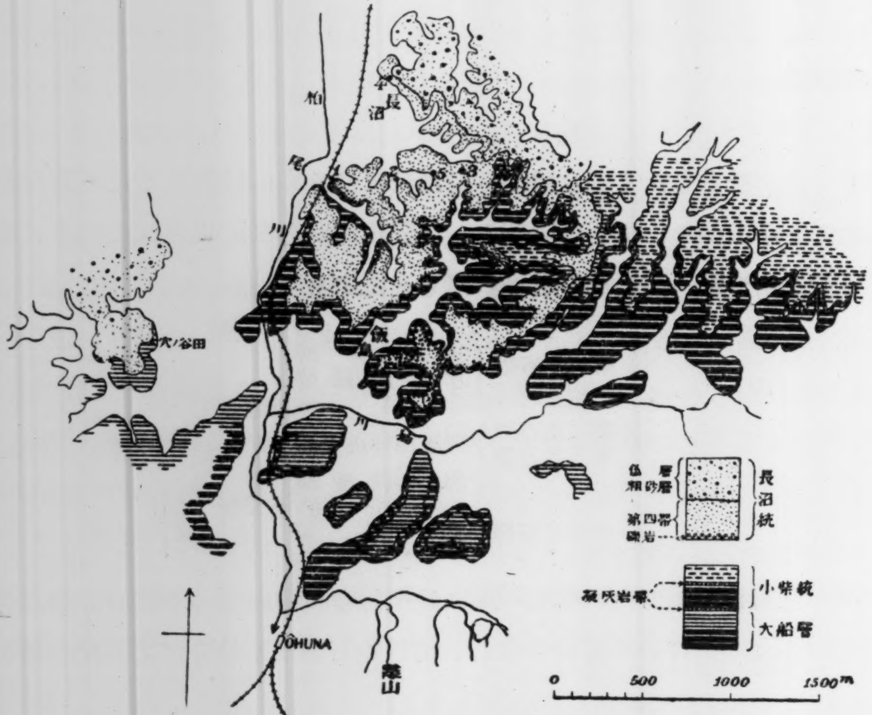

第 12 圖　長沼層標準露出地附近の地質詳圖.
〔A detailed geologic map near the type locality of the Naganuma bed.〕

長沼統の標準露出地及びその基底の不整合はこの豐田村附近で先づ記載されてゐる．豐田村打越谷の西方東海道線の沿線に沿うた久保部落の谷の入口に不整合が見られる．この入口では含化石礫層は不整合に小柴統中の泥層上に載つてゐるのが觀察できる．その不整合は久保の谷に沿うて第 12 圖の如く分布し，loc. 1, 2, 3, 4, 5 か

ら多數の貝化石を産してゐる.

この不整合は飯島，瀧久保，大道の方面へと延長して，大道附近では厚い砂礫層に移化してゐる. 礫は珪質岩が多い.

この不整合は東方へは西谷，小菅谷，日野，横濱共同墓地の方へと續いてゐるが，その露頭は極めて不明瞭である.

西谷から永野谷に至る峠の南斜面に小柴統の上に不整合に先づ 1 m 程の礫層を横へ次に輕石粒と亞炭とを含んだ長沼統が横はつてゐる. この輕石層は谷の亞炭層と同じもので，この附近では第四帶長沼層は屏風浦互層に被ひ隱されてゐる.

この不整合は西方へは田谷の穴を經て，玉繩村關谷，域廻. 村岡村高谷方面へと延長してゐる.

田谷の穴の北，田谷附近では赤褐色の砂礫層が厚く堆積してゐて（之を田谷砂礫層と呼ぶ)，その基底は共後の卍記號附近に見られる. その下位に化石の豐富な第 4 帶長沼層の青灰色砂泥層が露出してゐる. その下位に化石の稀な中里泥層が横はつてゐる.

玉繩村關谷では第四帶長沼層は薄く，田谷砂礫層が被ひ覆してゐるが，玉繩村城山の南斜面では再び，第4帶長沼層が露出し，大船泥層を不整合に被うてゐる. 寫眞6はこの不整合を示してゐる.

植木から藤澤へ達する街道にも長沼層が不整合に大船泥層を被うてゐるのが觀察できる.

村岡村高谷の北の渡內部落へ達する峠にも同樣に上述の不整合が觀察できた. この場所は嘗て筆者が村岡層と呼んだ地層の標準露出地であつたが，今日では第四帶長沼層の一部に屬せしむべきことがわかつた.

磯子區岡村町から大岡川日野方面.

長沼統の東の不整合は上野庭・日野附近に露はれる. 上野庭附近では第四帶長沼層が露出してゐるが，日野の北寺尾附近では田谷砂礫層に被はれて見られない. 日野寺尾附近の丘陵は田谷砂礫層と考へられる厚い黃色砂層からなつてゐる.

大岡町谷戸前・大丸附近は長沼統と新第三系小柴統との不整合の見られるところで不整合の北に小柴統が露出してゐる. この附近では第四帶長沼層は全く見えない. 田谷砂礫層らしいものも薄く不整合面近くに見られるだけである. この不整合を東へ追跡すると岡村町の渓谷笹堀附近に美しい露頭を示してゐる. 寫眞7圖はその露出面である. 前に西谷の澤の上源で見た樣な紫蘇輝石を豐富に含んだ輕石層が亞炭と共に小柴統の中里層上に横はつてゐる. 長沼統は之から以東では磯子區間坂方面へと分布し

てゐる．笹堀では田谷砂礫層は見られなかつた．

磯子區屏風浦附近．

磯子區屏風浦附近では間坂から杉田に至る崖に露出してゐる．基部は輕石質礫を含む僞層砂で，その上に砂泥互層がある．砂泥互層には植物化石葉が屢々含まれてゐるその上部には輕石層があり，この輕石層の上に含化石黑色淤泥層があり數種の貝化石を含んでゐる．そしてこの上に薄い砂層が横はり，更に不整合に關東ロームで被はれてゐる．この地質系統の基底は海拔約 25 m 程の高度に露出し，後に述べる鮮新統中里層を不整合に被うてゐる．

この露出面の海拔 30 m 程の處にある厚さ約 5 m の段丘礫層は前に述べた樣に保土ケ谷礫層と推定した．

長沼統の不整合面は磯子町山王谷の奥でも確められたが，それより東へは分布してゐないやうである．

磯子區山田谷附近では谷の底部は中里層が露出してゐて，丘陵の表面近くに長沼統の泥層が横はつてゐる．

森町附近の丘陵地も約 30 m 以上は淤泥層からなり上大岡から屏風浦に拔ける湘南電鐵の隧道は大部分長沼統の屏風浦砂泥互層からなつてゐる．

東海道線沿線．

長沼統基底の北の不整合は弘明寺の南中里から引越の谷へと露出してゐる．

弘明寺町の山下附近では新第三系の中里層の上に砂礫層が不整合に横はつてゐてその上に含化石泥層が横はつてゐる．この砂礫層は海拔 25 m 前後に在る．この砂礫層は徐々に低下して別所の渓谷では地表下に沒し，泥層が地表に分布してゐる．この砂礫層は田谷砂礫層に該當する．大岡川の最戸の亞炭層はこの砂礫層の上の泥層から産してゐる．この不整合は引越の谷の南側に沿うて兒童遊園地の入口附近から兒童遊園地の方へと延びてゐる．兒童遊園地附近の丘陵上 81 m 附近に發達する僞層理砂層は屏風浦層の上部の砂礫層の砂層と見做した．

井土ケ谷から兒童遊園地に至る道路沿線にもこの屏風浦層上部の砂礫層が見られ，小柴統を不整合に被うてゐる．

保土ケ谷から東海道國道に沿うて南下すると山谷の峠の北斜面には小柴統が露出してゐるが，峠の頂上から南斜面には厚く屏風浦層の砂礫層が見られる．

縣道の山谷の峠は同樣に砂層である．

山谷附近の僞層理砂層は南へ向つて追跡すると平戸附近でその間に含化石泥層が露はれてくるが，その下位に屏風浦層の泥層が横はる．

東海道線鐵道トンネルの附近に露出してゐる長沼統下の不整合は貨物線のトンネルの南口に見られる．卽ち品濃に露出する第二帶の屏風浦層は不整合に小柴統の泥層を被うてゐる．

品濃の溪谷では附圖の地質圖に見られる樣に鐵道線から約700 m の距離附近から新第三系の小柴統の泥層に代つてゐて，不整合がこの附近にあることを示してゐる．この不整合は更に後山田の西から金房谷，中上の方面へと續いてゐる．

戸塚町の北方中川村附近．

鎌倉郡中川村附近では長沼統は含化石泥質砂層を下部に黃茶色の僞層理砂層を上部に橫へてゐる．岡津部落から須鄉谷部落へ至る溪谷で觀察すると，岡津の附近の丘陵の麓には暗靑色の砂質泥層が露はれてゐて，岡津では多數の貝化石を產するが，それらは第 V 表 O の行の如くである

Table V.

Fossils collected from the Naganuma series.

	A	B	C	D	E	F	G	H	I	J	K	L	M	N	O	P	Q	R
Patelloida pygmaea (DUNKER)						F												
Diodora elaborata (SOWERBY)						F												
Emarginula crassicostata SOWERBY						F												
Stomatella lyrata PILSBRY						F								N				
Calliostoma cipangoana YOKOYAMA		B																
Tegula pfeifferi PHILIPPI	A																	
Umbonium costatum KIENER	A					F										P		R
Umbonium moniliferum (LAMARCK)		B			E	F												R
Umbonium decoratum MAKIYAMA											K		M	N				
Umbonium naganumanum OTUKA		B																
Circulus duplicatus (LISCHKE)						F												
Liotia cycloma TOMLIN						F												
Turbo cornutus (SOLANDER)						F												
Turbo coreensis RÉCLUZ											K		M	N				
Astraea haematraga MENKE						F												

（次頁へ續く）

	A	B	C	D	E	F	G	H	I	J	K	L	M	N	O	P	Q	R
Theodoxus tokaidoensis MAKIYAMA [ms.]								H			K			N				
Alvania concinna A. ADAMS			C			F		H	I	J								
Rissoina laevicostulata PILSBRY						F												
Merelina tokunagai (YOKOYAMA)								H	I								Q	R
Syncera paludinoides (YOKOYAMA)		B						H	I	J						P		
Pseudoliotia micans (A. ADAMS)								H										
Turritella naganumensis OTUKA [ms.]		B																
Heliacus dorsuousus (HINDS)						F												
Lemintina imbricata (DUNKER)						F												
Cerithidea katoi OTUKA [ms.]											K			N				
Cerithidea cingulata (GMELIN)										J	K		M	N	O		Q	
Batillaria multiformis yamadensis OTUKA [ms.]								H	I	J	K	L	M	N				
Batillaria multiformis (LISCHKE)		B															Q	R
Batillaria zonalis (BRUGUIÈRE)								H			K	L	M	N			Q	R
Obtortio pupoides (A. ADAMS)								H	I	J						P	Q	R
Obtortio reticulata (A. ADAMS)	A	B				F		H	I	J						P	Q	
Obtortio septentrionalis (TOKUNAGA)								H			K				O	P	Q	R
Scaliola bella A. ADAMS	A							H								P		
Diala picta A. ADAMS										J								
Diala hungerfordi SOWERBY						F		H								P		
Diala semistriata (PHILIPPI)						F		H		J				N			Q	R
Bittium binodulosum YOKOYAMA		B																
Bittium satomii YOKOYAMA						F												
Bittium numamuranum YOKOYAMA									I									
Bittium tamanowensis OTUKA [ms.]				D	E				I									
Cerithium coralium KIENER											K			N				
Gourmya kobelti (DUNKER)						F	G				K					P		
Cerithiopsis matumotoi OTUKA [ms.]						F												
Triphora granulata (DUNKER)						F												
Triphora purpurata (PILSBRY)						F												
Epitonium tokyoensis KURODA		B																
Epitonium tatibanensis OTUKA [ms.]								H										
Epitonium hosohida OTUKA [ms.]								H										
Epitonium densicostata (YOKOYAMA)		B																
Strombiformis kurumana (YOKOYAMA)								H										
Strombiformis ozawai (YOKAYAMA)								H										
Melanella shibana (YOKOYAMA)								H										
Melanella yokoskensis (YOKOYAMA)						F												
Pyramidella pulchella (A. ADAMS)							G	H								P		
Pyramidella pseudopulchella (YOKOYAMA)		B	C															

（次頁へ續く）

	A	B	C	D	E	F	G	H	I	J	K	L	M	N	O	P	Q	R
Mormula rissoina (A. ADAMS)						F												
Pyrgisculus candissimus DALL et BARTSCH								H	I									
Pyrgisculus takinogawensis (TOKUNAGA)		B				F												
Pyrgisculus shigeyasui (YOKOYAMA)																	Q	
Pyrgiscus nihona (OTUKA)		B																
Strioturbonilla pacifica (YOKOYAMA)		B																
Strioturbonilla aurica DALL et BARTSCH								H										
Strioturbonilla mormuloides (NOMURA)						F												
Turbonilla inomatai OTUKA [ms.]																P		
Turbonilla aff, *subaproximata* YOKOYAMA								H		J								
Turbonilla kuratuboensis OTUKA [ms.]								H								P		
Turbonilla kamikuratensis OTUKA [ms.]								H								P		
Turbonilla t-matumotoi OTUKA [ms.]						F												
Turbonilla arayai NOMURA					E													
Turbonilla edoensis YOKOYAMA								H								P		
Turbonilla sp.											K							
Turbonilla sp.						F												
Cingulina adamsi (YOKOYAMA)		B	C															
Syrnola cinctella (A. ADAMS)		B																
Syrnola bicinctella NOMURA								H								P		
Odostomia desimana DALL et BARTSCH								H								P		
Odostomia limpida DALL et BARTSCH						F		H								P		
Odostomia sublimpida YOKOYAMA	A	B	C			F												R
Odostomia fujitanii YOKOYAMA var.								H										
Odostomia yokoyamai NOMURA		B																
Odostomia makiyamai (NOMURA)								H								P		
Odostomia aspera? NOMURA			C															
Odostomia sitiroi NOMURA														N				
Odostomia naganumensis OTUKA [ms.]		B																
Odostomia sp.						F												
Odostomia sp.								H										
Trabecula bicinctella (YOKOYAMA)								H								P		
Babella? sekiyatensis OTUKA [ms.]			C															
Babella caelatior DALL et BARTSCH						F												
Pyrgulina katasensis OTUKA [ms.]						F												
Acteopyramis kitayatensis OTUKA [ms.]			C	D	E													
Acteopyramis lauta NOMURA								H								P		
Trichotropis unicarinata BRODERIP				D														
Crepidula aculeata (GMELIN)						F	G											
Siphopatella walshi (REEVE)		B									K			N				

（次頁へ續く）

	A	B	C	D	E	F	G	H	I	J	K	L	M	N	O	P	Q	R
Strombus luhanus LINNAEUS	A																	
Polynices flemingianus (RÉCLUZ)		B					G									P		
Polynices didyma (BOLTEN)	A	B		D		F	G				K		M					R
Natica janthostoma DESHAYES		B	C	D	E	F		H										R
Sinum javanicum (GRAY)		B																
Erato callosa ADAMS et REEVE		B				F												
Pustularia boivini (KIENER)		B																
Cymatium ozawai OTUKA [ms.]		B			E													
Cymatium subpyrum (YOKOYAMA)		B			E													
Charonia lampas sauliae (REEVE)					E													
Tonna luteostoma (KÜSTER)						F												
Rapana thomasiana (CROSSE)						F	G				K		M				Q	R
Bedeva birileffi (LISCHKE)	A						G	H	I		K			N		P	Q	
Thais bronni (DUNKER)	A					F	G											
Thais clavigera (KÜSTER)						F	G	H			K							
Tritonalia emarginata (SOWERBY)					E													
Tritonalia? crassa (A. ADAMS)					E													
Tritonalia adunca SOWERBY		B																
Latiaxis japonica DUNKER					E													
Pyrene varians (DUNKER)		B	C		E	F	G	H										R
Pyrene siogamensis OTUKA [ms.]																P		
Pyrene bella (REEVE)		B													O	P		
Zafra pumila (DUNKER)		B				F		H									Q	
Microfusus obesiformis (YOKOYAMA)				D	E													
Siphonalia cassidariaeformis declivis (YOKOYAMA)		B		D														
Siphonalia mikado MELVILL var.			C		E													
Siphonalia fuscolineata PEASE		B	C	D	E													
Siphonalia spadicea REEVE		B																
Siphonalia modificata REEVE		B																
Babylonia japonica (REEVE)		B				F										P		R
Nassarius japonicus (A. ADAMS)						F												R
Nassarius festivus (POWYS)		B						H	I	J	K		M	N	O	P	Q	R
Nassarius dominulus (TAPPARONE et CANEFRI)	A	B		D		F	G	H	I	J								
Nassarius gemmulatus (LAMARCK)		B																
Nassarius caelatus (A. ADAMS)		B	C	D	E	F	G	H	I							P		R
Nassarius livescens (PHILIPPI)	A							H			K		M				Q	
Fusinus perplexum (A. ADAMS)		B		D														
Cancellaria spengleriana DESHAYES		B			E	F	G											
Cancellaria noduliformis SOWERBY		B																
Cancellaria ozawai OTUKA [ms.]		B																

（次頁へ續く）

	A	B	C	D	E	F	G	H	I	J	K	L	M	N	O	P	Q	R
Clavus braunsi (YOKOYAMA)		B	C	D														
Clavatula muraokensis OTUKA [ms.]				D	E													
Clavatula consimilis nivalioides (YOKOYAMA)		B																
Clavatula consimilis SMITH																P		
Surcula kamakurana PILSBRY var.		B			E													
Turris leucotropis (ADAMS et REEVE)		B		D														
Brachytoma jeffreysii (SMITH)	A	B	C	D			G											
Brachytoma pseudoprincipalis (YOKOYAMA)	A	B		D														
Tomopleura quantoana (YOKOYAMA)		B																
Lora toyodensis OTUKA [ms.]		B																
Lora yabei OTUKA [ms.]		B																
Lora reticostulata (YOKOYAMA)		B																
Suavodrillia pseudodeclivus OTUKA [ms.]					E													
Cytharella makiyamai OTUKA										J						P		
Cytharella sp.							G											
Mangelia deshayesii (DUNKER)						F				J								
Mangelia gracilenta (REEVE)						F												
Mangelia sp.						F												
Pseudoraphitoma naganumaensis OTUKA		B				F												
Etrema fortilirata (SMITH)		B																
Etrema naganumana OTUKA [ms.]		B																
Ethema subauriformis (SMITH)																P		
Philbertia katasensis OTUKA [ms.]						F												
Philbertia leuckarti (DUNKER)						F				J								
Philbertia ikebei OTUKA [ms.]																P		
Asperdaphne sp.						F												
Terebra edoensis YOKOYAMA																		R
Terebra serotina ADAMS et REEVE		B																
Terebra evoluta DESHAYES		B																
Terebra lischkeana naganumense OTUKA [ms.]		B																
Ringicula oelertiae MORLET						F				J								
Ringicula musashinoensis YOKOYAMA		B	C	D		F	G	H								P	Q	R
Ringicula yokoyamai TAKEYAMA																P		
Ringicula doliaris GOULD						F												
Pyrunculus phiala A. ADAMS																P		
Retusa minima YAMAKAWA	A					F		H	I									
Retusa kamikuratensis OTUKA [ms.]								H										
Retusa truncata YAMAKAWA										J					O	P		
Retusa cucurbitina YOKOYAMA								H								P		R
Tornatina dulcis YOKOYAMA																	Q	R

(次頁へ續く)

	A	B	C	D	E	F	G	H	I	J	K	L	M	N	O	P	Q	R
Acteocina fontinalis (YOKOYAMA)															O			
Cylichna yamakawai YOKOYAMA								H		J					O	P	Q	R
Cylichna shibaensis YAMAKAWA						F												
Rhizorus acuminata BRUGUIÈRE						F												
Solidula strigosa (GOULD)																	Q	
Siphonaria sirius? PILSBRY						F												
Dentalium octangulatum DONOVAN						F	G								O	P		R
Dentalium hexagonum GOULD	A	B		D				H					M					
Dentalium weinkauffi DUNKER	A	B		D	E	F												
Dentalium sp.			C													P		
Nucula tokyoensis YOKOYAMA		B																
Acila divaricata (HINDS)			C		E													
Nuculana gordonis (YOKOYAMA)		B	C		E	F												
Nuculana japonica (ADAMS et REEVE)			C															
Arca ocellata REEVE						F	G											
Arca boucardi JOUSSEAUME						F	G											R
Barbatia reticulata (GMELIN)						F												
Barbatia obtusoides (NYST)						F	G						M					
Barbatia symmetrica REEVE						F	G											
Barbatia yokoyamai (NOMURA)		B		D		F	G											
Anadara granosa (LINNAEUS)		B									K	L	M	N	O		Q	R
Anadara inflata (REEVE)		B	C	D	E	F		H	I									R
Anadara subcrenata (LISCHKE)		B			E			H					M	N	O	P		R
Pseudogrammatodon obliquata (YOKOYAMA)						F												
Glycymeris rotunda (DUNKER)		B																
Crenella diaphana DALL				D	E													
Septifer virgatus (WIEGMAN)						F												
Brachidontes senhausii DUNKER																P		
Volsella barbata (LINNAEUS)						F												
Volsella modiolus (LINNAEUS)		B	C		E													
Chlamys senatoria nobilis (REEVE)		B																
Chlamys nipponensis KURODA		B	C	D	E	F								N				R
Chlamys irregularis (SOWERBY)		B																
Chlamys plica arasudis OTUKA [ms.]		B																
Pecten naganumana YOKOYAMA	A	B			E													
Pecten laqueatus SOWERBY						F	G											R
Pecten tokyoensis TOKUNAGA		B	C	D	E						K							
Spondylus cruentus LINNAEUS	A					F												
Lima basilanica ADAMS et REEVE					E		G											
Lima lischkei LAMY						F												

（次頁へ續く）

	A	B	C	D	E	F	G	H	I	J	K	L	M	N	O	P	Q	R
Lima quantoensis YOKOYAMA						F												
Anomia lischkei DAUTZENBERG et FISCHER		B	C		E	F				J	K			N				
Ostrea gigas THUNBERG					E	F	G		I	J	K	L	M			P	Q	R
Ostrea denselamellosa LISCHKE											K							
Ostrea futamiensis SEKI													M	N				
Ostrea rosacea DESHAYES						F												
Crassatellites nana (ADAMS et REEVE)		B																
Cardita cumingiana DUNKER		B				F					K			N				
Venericardia ferruginosa ADAMS et REEVE		B																
Venericardia ferruginea (CLESSIN)		B																
Trapezium japonicum PILSBRY										J		L		N				
Basterotia gouldi (A. ADAMS)	A					F												
Felaniella usta GOULD							G											
Joannisiella cumingi (HANLEY)		B	C															R
Loripes ictericus (REEVE)		B																
Lucina acutilineata CONRAD					E													
Codakia delicatula PILSBRY						F												
Codakia yamakawai (YOKOYAMA)		B																
Codakia pisidium (DUNKER)	A	B				F		H	I	J						P	Q	R
Kellia ojiana YOKOYAMA								H								P		R
Kellia subelliptica YOKOYAMA																		R
Kellia katasensis OTUKA [ms.]						F												
Kellia naganumensis OTUKA [ms.]		B																
Mysella oblongata (YOKOYAMA)	A															P		
Montacuta subtruncata YOKOYAMA								H										
Montacuta oblongata YOKOYAMA	A																	
Clinocardium braunsi (TOKUNAGA)		B						H										
Clinocardium bulowi (ROLLE)		B				F												
Cardium ebaranum YOKOYAMA						F	G											
Cardium muticum REEVE	A	B			E	F										P	Q	R
Plicatula horrida DUNKER						F												
Plicatula irregularis DUNKER						F												
Pseudochama retroversa (LISCHKE)						F												
Gafrarium yokoyamai OTUKA[24] n. n.	A	B																
Pitar pellucida LAMARCK						F												
Pitar sp.		B																
Callista sinensis (SOWERBY)		B				F												
Saxidomus purpuratus (SOWERBY)	A					F	G											R
Meretrix sp.																		R
Meretrix meretrix (LINNAEUS)		B				F									O			

（次頁へ續く）

---

[24] New name for *Circe scripta* of YOKOYAMA (1920, *Jour. Coll. Sci. Tokyo Imp. Univ.*, **39**, 6, p. 123, pl. 8, figs. 15, 16), not of LINNAEUS 1758.

	A	B	C	D	E	F	G	H	I	J	K	L	M	N	O	P	Q	R
Cyclina sinesis (GMELIN)											K							
Dosinia japonica REEVE	A		C			F		H		J	K					P		
Dosinia angulosa PHILIPPI						F	G											R
Venus sp.							G											
Venus (*Chione*) *minuta* YOKOYAMA	A	B																
Clausinella tiara (DILLWYN)	A	B																
Anomalocardia squamosa (LINNAEUS)											K	L	M	N				
Gomphina aff. *neastartoides* (YOKOYAMA)		B																
Protothaca jedoensis (LISCHKE)		B				F	G				K							
Venerupis mitis (DESHAYES)						F												
Venerupis variegata (HANLEY)						F	G		I	J			M	N				R
Venerupis philippinarum (ADAMS et REEVE)		B				F					K					P		
Protapes irrediviva MAKIYAMA											K		M					
Clementia vatheleti MABILLE			C		E													
Petricola cyclus (PILSBRY)						F												
Petricola divergens (GMELIN)		B				F				J								
Paphia euglypta (PHILIPPI)						F												
Paphia greefei (DUNKER)						F												
Paphia naganumana OTUKA[25] n. n.	A	B																
Paphta amabilis (PHILIPPI)							G											
Paphia undulata (BORN)						F	G	H							O			
Paphia sp.						F												
Mactra imperialis YOKOYAMA																		R
Mactra sulcataria DESHAYES						F												R
Mactra veneriformis REEVE															O			
Standella tokunagai OTUKA [ms.]											K							
Raeta elliptica YOKOYAMA																		R
Raeta yokohamensis PILSBRY						F	G	H								P		
Gari anomala DESHAYES		B																
Zozia abbreviata (GOULD)		B				F												
Semele sinensis A. ADAMS						F	G			J				N		P		
Solecurtus divaricatus (LISCHKE)	A	B				F	G											
Theora lubrica GOULD						F	G									P		R
Gastrana yantaiensis CROSSE et DEBEAUX						F												
Macoma praetexta (MARTENS)																		R
Macoma awajiensis SOWERBY								H										
Macoma incongrua (v. MARTENS)						F			I	J	K	L		N			Q	R
Macoma nipponica TOKUNAGA																P		
Macoma sp.									I									
Tellina venulosa SCHRENCK																		R

(次頁へ續く)

---

[25] n. n. for *Tapes amabilis* of YOKOYAMA (*Jour. Coll. Sci. Tokyo Imp. Univ.*, **39**, 6 (1920), p. 126, pl. 9. fig. 7, (not of PHILIPPI 1847).

	A	B	C	D	E	F	G	H	I	J	K	L	M	N	O	P	Q	R
Tellina pallidula LISCHKE																	Q	
Tellina diaphana DESHAYES												L						R
Tellina gargadia (LINNAEUS)	A	B																
Tellina rutila DUNKER									I									
Tellina jedoensis LISCHKE		B										L			O	P		
Tellina miyatensis YOKOYAMA		B														P		
Tellina nitidula (DUNKER)		B															Q	R
Tellina delta YOKOYAMA																		R
Tellina vestalioides YOKOYAMA	A	B	C			F												R
Solen sp.						F												
Solen krusensternii SCHRENCK																		R
Solen gouldi CONRAD											K			N		P		
Hiatella arctata (LINNAEUS)			C															
Panope japonica A. ADAMS	A	B																
Aloidis venustus (GOULD)		B				F	G							N				
Cryptomya busoensis YOKOYAMA	A	B				F				J								
Mya japonica A. ADAMS		B				F												R
Barnea fragilis SOWERBY							G			J						P		R
Barnea japonica (YOKOYAMA)		B																
Martesia tokyoensis YOKOYAMA																	Q	
Myadora yokoyamai OTUKA	A	B																
Thracia transmontana YOKOYAMA																		R
Thracia papyracea POLLI						F												
Laternula japonica LISCHKE																P		
Pandora bicarinata subsp.						F												
Zirphaea subconstricta YOKOYAMA						F												
Coptothyris grayi (DAVIDSON)				D														

A =Kosugeyato, Hongo-mura. (loc. 39.) Naganuma bed.
B =Naganuma, Toyoda-mura. (loc. 30, 31, 32.) Naganuma bed.
C =Sekiyato, Tamanawa-mura. (loc. 35.) Naganuma bed.
D =Siromeguri, Tamanawa-mura. (loc. 37.) Naganuma bed.
E =Takaya, Muraoka-mura. (loc. 38.) Naganuma bed.
F =Katase and Kosigoe. Byôbugaura bed.
G =Tutumigayato, Toyoda-mura. (loc. 28.) Byôbugaura bed.
H =Kamikurata, Toyoda-mura. (loc. 24.) Byôbugaura bed.
I =Sumerayato, Toyoda-mura. (loc. 26.) Byôbugaura bed.
J =Yamasita-tyo bluff, Yokohama-city. Byôbugaura bed.
K =Totuka-mati (loc. 21, 23.) Byôbugaura bed.
L =Usiroyamada (loc. 10.) Kawakami-mura. Byôbugaura bed.
M =Sinano, Kawakami-mura (loc. 7, 8, 9.) Byôbugaura bed.
N =Inariyato, Nakagama-mura (loc. 12.) Byôbugaura bed.
O =Okatu, Nakagawa-mura, (loc. 6.) Kuratubo bed.
P =Kuratubo, Totuka-mati, (loc. 3.) Kuratubo bed.
Q =Simosuyeyosi, Turumi-ku. Simosueyosi series.
R =Kikuna, Turumi-ku. Simosueyosi series.

この澤に沿うて須郷谷に向ふと，稲荷谷附近に赤褐色砂礫層と含化石砂泥層とが露出してゐるのに氣付く．化石は第V表Nの様なものからなる．赤褐色砂礫層は西側に，含化石砂泥層は東側谷壁に見られる．含化石砂泥層は不整合に新第三系を被うてゐる．稲荷谷の含化石砂泥層と，赤褐色砂礫層と，岡津の砂質泥層との層序關係は現在直接の關係が明でないから暫らく不明であるが，貝化石から判斷したところでは稲荷谷の化石中には屏風浦層のものに普通な化石が見られるのに，岡津の化石中にはそれ等が見られぬので岡津の方が上位と思ふ．戸塚町附近から追跡してきた野外調査の結果は岡津の泥層を上位のものとする方が都合よい結果となつた．

稲荷谷の東の中上附近も同様な關係が見られる．名瀬部落の南200 mの山麓からも貝化石を產してゐる．

金房谷の部落附近も同様な不整合關係が見られる．こゝの不整合の上にくる砂層は貝化石の雌型のみしか採集できなかつたが，*Anadara granosa* (LINNAEUS)の如きものが見られた．

金房谷の南羽根澤の附近には新第三系の半凝固泥岩層が露出してゐて，長沼統に不整合に被はれてゐる．

長沼統の北の不整合は上述した様に阿久和の附近から西方へ延びてゐる様に思へるが，未調査・無露出であるから何も述べられない．

今長沼統の基底の不整合を北から追跡して行くと，阿久和・稲荷谷・後山田・品濃・山谷・兒童遊園地・弘明寺中里・大丸・屏風浦・日野寺尾・長沼・關谷・城廻・村岡と一つの西へ開いた灣入を示してゐることに氣付く．

上記の他に層序・層位上長沼統と考へられるものが，特異な分布をして，即ち本牧附近及び，帷子川沿岸等に知られてゐる．

本牧のものは既に記したことがある新山下町の崖に露出するものである．第9圖及寫眞8圖に示す様に新山下町の崖には下末吉統の保土ケ谷砂礫層と小柴統の中里泥層所謂（ドタン）との間に含海棲貝化石・植物化石を含んだ地質系統が知られてゐる．この軟體動物群は第V表Jの様なものである．この地質系統の基底の不整合面は一つの凹んだ地形を埋めて堆積した地層であることを示してゐる．この凹んだ地形は，山手町臺地の北部僧德院—横濱フェリス高女附近の崖にこの地層の連續が厚く見られることから，この方面へと連續してゐることが確められた．元町裏のこの地層からは次の様な軟體動物が採集されてゐる(第VI表參照)．この地質系統產の海棲貝化石種の大部分は下末吉統とも長沼統とも決定できない様な種からなつてゐるが，之は下末吉統下に不整合に位し，明に異る地質系統からなり，*Batillaria multiformis*の變種，

Table VI. Fossils collected by S. TOKUNAGA from the Byôbugaura bed exposed on the Yamate-tyo terrace scarp, southeast of Moto-mati, Yokohama.

Anadara inflata (REEVE)
Macoma incongrua (v. MARTENS)
Pillucina pisidium (DUNKER)
Acmaea sp.
Turbo coreensis RÉCLUZ
Theodoxus tokaidoensis MAKIYAMA (ms.)
Cerithidea cingulata (GMELIN)
Batillaria multiformis (LISCHKE) (forma *yamadensis* OTUKA) (ms.)
Diala semistriata (PHILIPPI)
Diala sp,
Pyrgisculus candissimus (DALL et BARTSCH)
Crepidula sp.
Natica janthostoma DESHAYES
Polynices flemingianus RÉCLUZ
Rapana thomasiana CROSSE
Astyris varians (DUNKER)
Bedeva birileffi (LISCHKE)
Thais clavigera (KÜSTER)
Nassarius festivus (POWYS)
Nassarius japonicus (A. ADAMS)
Retusa truncata YAMAKAWA
Acteocina exilis (DUNKER)
Cylichna yamakawai YOKOYAMA

Teodoxus tokaidoensis MAKIYAMA 等の屛風ヶ浦層特有の貝化石が含まれてゐるし，植物化石（第 VII 表）は遠藤氏の言の如く稍々古型種をも含んでゐるので，長沼統中の一層とした方がより自然であることを知る.

横濱市帷子川沿岸の長沼統　横濱驛の西方約 1 km 半の淺間臺は，そこに分譲地を作るため臺地の崖に沿うて大きな露出面が作られてゐる．寫眞 9 圖第 13 圖はその一露頭の寫眞及び分布圖である．この寫眞，地質圖で見られるやうに褐色砂と半凝固泥層との互層は殆ど水平に近い層位で，圖の左端に露出するが，この地層は斜な不整合で切られ，不整合上には下部に稀に小礫を介在する細砂層，その上に泥層，亞炭層，

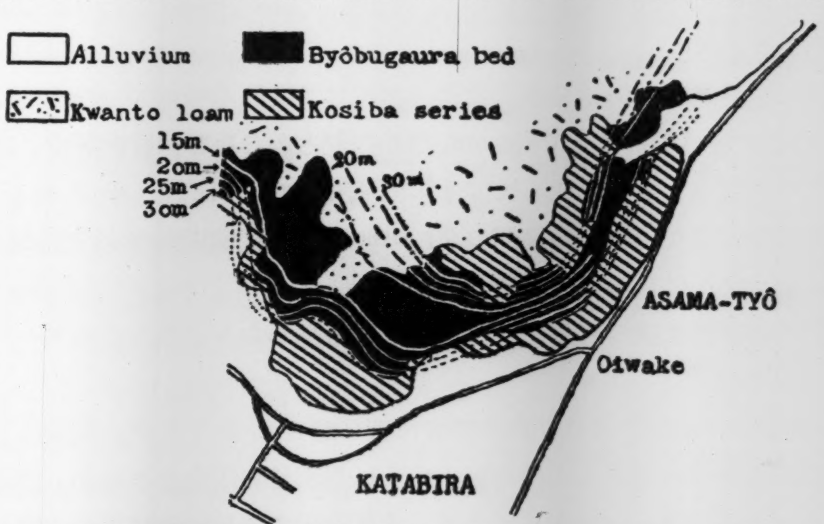

第 13 圖　橫濱市淺間臺附近に於ける屛風浦層さその基底の地形.
〔The map shows the distribution and the basal relief of the Byobugaura bed exposed at Asamadai in Yokohama.〕

泥層の順に重る．泥層中には半淡水性の貝化石が含まれてゐる．

Corbicula orthodonta PILSBRYの多いのは淡水性に近い事を示してゐる．又 *Anadara granosa* (LINNAEUS), *Anadara subcrenata* (LISCHKE) *Ostrea gigas* THUNBERG, *Cyclina sinenses* 等を含んでゐるので海水も勿論含まれてゐたに違ひない． 特に長沼統屛風浦層に普通な *Theodoxus tokaidoensis* MAKIYAMA が數個體採集されてゐる．

この地質系統の平面分布は地質圖又は第 13 圖に示す復舊同高線で解る様に全く新第三系の基盤を刻んだ過去の溪谷を占めてゐて，溺れ谷地形がこの地方に發達してゐたことを示してゐる．この地質系統は上星川附近で保土ケ谷礫層に不整合に被はれてゐる．

横濱驛の東北宮前町背後の崖に露出する地層からは *Anadara granosa* (LINNAEUS), *Ostrea gigas* THUNBERG, *Theodoxus tokaidoensis* MAKIYAMA 等が採集されてゐて，長沼統の一部であることを暗示してゐる．

上述の層序・層位・化石から判斷して此の地質系統を長沼統の一部と考へ得られると信ずる．上星川—山崎の沼ではこの地層はかなり厚く分布してゐる様に見えるが露頭が見られないので後の研究に俟つ．

長沼統の層序．

上に述べた長沼統基底の分布を見ると，長沼統が如何なる層序を示してゐるか大體豫想はつく．次にその詳細を記さう．

第四化石帶長沼層．

標準露出地は鎌倉郡豐田村長沼貝殼坂．主として鼠色 (mineral gray)〔乾いた時〕の0·2 mm 以內の大きさの砂粒と 0·005 mm 內外の泥とからなる泥質砂層で，基底は珪岩質圓礫を含み粗粒となる．貝化石は標準露出地附近で約 112 種（第 V 表 B）を數へ，純海成，黑潮型深度は現在の相模灣の 20 fathoms 內外の深度に普通な種類からなる．

下位は不整合に小柴統の中里泥層と接する．

上位は田谷砂礫層に被はれ，一部覆ひ隱される點からみて整合とは考へられぬ．

厚さ： 長沼附近で約 30 m．

分布： 長沼層の東の分布は田谷砂礫層に覆ひ隱されるため狹い範圍にしか分布しない．長沼から西谷へ超える小徑の頂上近くに長沼層の露出をみるが，之は更にこの尾根に沿うて大道の方へと分布してゐる．大道附近では長沼統は粗砂に變じ，不整合に小柴砂層を被うてゐる．

長沼の東，小菅谷の北の尾根には第 V 表 A の如き化石が採集され，數種の長沼層の特有種を含んでゐるので長沼層がこの尾根上にも分布してゐることがわかつた．

長沼層の西の分布は田谷の穴から關谷の方へと地質圖に示した様な分布をしてゐる．關谷部落の北部で次の様な有孔虫化石と海棲貝化石(第V表C)とを採集した．動物群

の特徴は村岡村高谷產のものと殆ど一致し，長沼產のものとも *Siphonalia* 屬，*Turris* 科の特殊なものは共通してゐる．卽ち *Clavus braunsi* (YOKOYAMA)，*Brachytoma pseudoprincipalis* (YOKOYAMA)の如きはそれらである．有孔虫は *Siphogenerina raphana* (PARKER et JONES) 極めて多く，長沼には却て少い．貝化石でも *Pecten naganumanus* YOKOYAMA，*Anomia lischkei* DAUTZENBERG et FISCHER，*Myadora yokoyamai* OTUKA，*Crassatellites heteroglyptus* PILSBRY 等は關谷では殆ど見當らないか又は稀であつた．

長沼ー關谷間では長沼層は層向 N45°E，NW へ 2° か 3° の緩い dip を持つて排列してゐるが，關谷附近から層向を稍々變じてゐる．玉繩村坂上の南，城廻，村岡村高谷等からは多數の貝化石を產してゐる．第 V 表 D，E にはそれらの貝化石を表示してある．

上に述べた關谷・城廻の貝化石群を見ると *Acila divaricata* (HINDS)，*Siphonalia mikado* (MELVILLE)，*Siphonalia fuscolineata* PEASE，*Chalonia lampas sauliae*，*Clementia vatheleti* MABILLE 等の長沼より稍々深い相を示す貝化石を增加してゐて，長沼で淺い相を示した種類が減少してゐることは極めて面白い事實である．然るにこのより深い相を示す玉繩村附近の長沼層の基底でも植物化石を含む部分があり，興味深き生物群の配置を示してゐる．

長沼層〔第四化石帶〕の地質時代は決定的な動物化石を產せぬので鮮新世末期から洪積世初期へかけての一時期と言へるのみである．*Clavatula dainichiensis muraokensis* OTUKA，*Umbonium giganteum naganumanum* OTUKA，*Cymatium subpyrum* (YOKOYAMA) 等の變異が統計的にみて時代により變異されてゐるから，之等と同型の化石種を含む秋元・二宮等の鮮新世の地層と其の時代に著しい差異があるとは思はれない．

田谷砂礫層．

標準露出地は鎌倉郡豐田村田谷部落．

主として黃褐色の砂層よりなり稀に礫を含む．砂層は屢々僞層構造を示すことあり．砂粒の大きさは標準露出地で 0·5 mm 前後のものが多かつたが採集地の相異により變化があるから一例に過ぎない．後の研究に讓る．

化石類は殆ど稀である．

上位は屛風浦層に略ぼ整合的關係で接してゐる．

下位は前に述べたやうに長沼層に整合ならざる關係で接してゐる．

地層の厚さは不定であるが最も厚く發達してゐる田谷・堤附近で測定したところでは約 50〜45 m 前後の厚さを有してゐる．下部程粗粒となつてゐる．

分布は田谷より西へ向つては小雀方面へ分布し，豐田村金井附近で屛風浦層に被はれる．堤ケ谷の化石層の下部も田谷砂礫層からなり，その層向 N 55° E，NW へ 2°〜3° の程度に傾いてゐる．

田谷から東へ向つては次第にその厚さを減じ，長沼附近の尾根の上，南谷に分布し豊田村下倉田附近で屛風浦層に被はれてゐる．

日野共同墓地附近の砂層は屛風浦層下に殆ど整合的に横はり，新第三系中里層上に横はることからして田谷砂層と考へられる．層向大體 N65°E，NW へ 2°~3° の程度に傾く．

田谷砂礫層の他の分布は大岡川千保附近，弘明寺町附近で屛風浦層下に露出分布してゐるが極めて薄い．併し長沼層第四化石帯を挾まずに直接に中里層の上に横はつてゐることは前に述べた通である．

屛風浦層．

標準露出地は磯子區間坂の南，大岡方面への道路の峠切割面．

主として明鼠色の細砂又は泥からなり，上部は粗粒の落葉色（isabella color）砂層に漸移し，最上部は僞層砂礫層となつてゐる．この上部の砂層中には往々海棲軟體動物を含む淤泥又は泥層が薄く數米以内の厚さで分布してゐることがある．川上村舞岡の奥の淤泥には *Dosinia* 等の雌型の化石印象を産してゐる．

上位は侵蝕による不整合を以て倉坪淤泥層に接するか，又は踊場砂層に被はれる．

化石類は哺乳動物遺骸・植物化石の他多數の海棲貝化石を含んでゐる．第V表 G，H，I，J，K，L，M，N，第 VI 及び VII 表は屛風浦層の化石を示してゐる．

分布は廣く，横濱市内，鎌倉郡下等によく露出してゐる．

新山下町の崖に露出するものは板狀に薄くへげる性質があり，その剝面間に植物化石を含み遠藤誠道學士は第 VII 表の様な種類を報告されてゐる．こゝの地層から筆者は第 V 表 J の様な海棲貝化石を採集した．

Table VII. Fossil plant collected by S. Endô from the Byôbugaura bed which is exposed on the Yamate-tyô terrace scarp, west of Sinyamasita-tyô.

Acer mandshuricum MAXIM?
Acer cfr. *pictum* THUNBERG
Acer cfr. *palmatum* THUNBERG
Carpinus sp. cfr. *yedoensis* MAX.
Cornus submacrophylla NATHORST
Fagus crenata BL.
Hoveniphyllum thunbergi NATHORST
Leguminosites sp,
Ligustrum ibota SIEBOLD
Quercus glandulifera BL.
Quercus sturbergi NATHORST
Quercus angustifolia NATHORST
Quercus sp.
Styrax obassia S. et Z.
Viburnum sp.
Zelkowa keaki SIEBOLD
Phyllites bambusoides NATHORST

淺間臺の露頭と *Theodoxus tokaidoensis* MAKIYAMA の産する半淡水性の地層との分布に就いては既に記した．この貝化石は稻荷谷，元町裏，屛風浦，戸塚町，上倉田等からも産してゐて屛風浦層に普通なものの様に見える．故にこの淺間臺の崖に露出す

る溺れ谷を埋めてゐる地層は，下末吉層と小柴統とに挾まれ，長沼統中の屛風浦層に該當せしめておく．

筆者が嘗て第二帶と呼んだ戶塚・品濃・後山田の化石帶（第V表 K, L, M）は屛風浦層の名稱を以て呼ぶ．品濃・後山田では *Batillaria* 屬，*Cerithium* 屬が多く，この他 *Umbonium decoratum* MAKIYAMA，*Anomalocardia squamosa* (LINNAEUS)，*Protapes irrediviva* MAKIYAMA 等多く，屛風浦層の標準露出地の動物群とは異るが，踊場砂層又は倉坪淤泥層に被はれてゐるので，屛風浦層に含めた．

中川村稲荷谷もこの後山田・品濃・戶塚と類似の動物群を持つことが第V表Nによつて認められる．

田谷砂礫層は上倉田附近の淤泥層で被はれる．上倉田の淤泥層からは第V表Hの樣な貝化石を產し，之等が前述諸地と同樣に屛風浦層の連りである．

この淤泥層は西へ向つて皇谷，堤ケ谷方面へ分布してゐて，皇谷では第V表Iの樣な種類，堤ケ谷では第V表Gの樣な海棲貝化石を採集し得た．堤ケ谷の田谷砂礫層と屛風浦層との境近く，屛風浦層から鹿の趾・肋骨の化石を出した．鹿間學士[20]は *Cervus* cfr. *praenipponicus* SIKAMA を柏尾の類似の層準から報告してゐる．

倉坪淤泥層．

標準露出地： 戶塚町倉坪の西方 200 m の溪谷壁に露出する含化石淤泥層を言ふ．色は鼠色を呈し，輕石粒を混在する．輕石の性質は含紫蘇輝石安山岩の輕石である．

上位は整合的に踊場砂岩で被はれるが，下位は寫眞10圖に示す樣に侵蝕による不整合で屛風浦層に接してゐる．

厚さは不明であるが，標準露出地では10數mに過ぎない．

貝化石は第V表Pの如くで純海成淺海30m以淺の相模灣海底に普通な種類が多い．

分布： 本層と屛風浦層との境界は前記倉坪に見られるのみで，他では兩者の區別は單に些細な岩相上の差異（品濃・後山田のものは稍々粗粒物質を混交してゐる），踊場砂層との境界の性質（之も仲々決定的ではない），及び化石動物群によつた．上記の特徴によつて推定した倉坪層の分布は地質圖の通で，中川村岡津部落に產する海棲貝化石動物群第V表Oも倉坪層に屬せしめた．

踊場砂層．

標準露出地： 戶塚町踊場から谷矢部に至る途中に露出する黃褐色砂層．

厚さは不定であるが 20m 前後．

上位は關東ロームの基底の輕石層又は下末吉統下部の輕石層に類似の無層理陸成輕石層に被はれてゐる．

---

[20] 地質學雜誌，**43**，pp. 170～171，(1937).

下位は整合的に倉坪層を被ふが，更に廣く長沼統發達區域全體に分布してゐる．

化石は殆どない．

谷矢部では倉坪層の貝化石と類似な *Philine sculpta*? A. ADAMS, *Dosinia angulosa* PHILIPPI, *Theora lubrica* DUNKER, *Raeta yokohamensis* PILSBRY, *Ringicula arctata* GOULD 等を含む淤泥層の上に整合に横はつてゐる．（川上村山谷附近では踊場層に似た僞層理黄褐色砂礫層が 30 m 前後の厚さに發達してゐて，平戸附近ではこの砂礫層の中に薄い泥層を介在し，又この砂礫層の下に泥質の部分が露はれてゐる．この下の泥質の部分は南へ行く程厚さを増してゐるが海棲貝化石は *Batillaria* 屬，*Anadara granosa* (LINNAEUS) 等の雌型が得られ，屛風浦層の泥層に移過する．）

筆者は山谷の砂礫層を初め田谷砂礫層と考へたが上記の事實からみれば屛風浦層の砂層とする方がより適切であると思ふ．併し踊場砂層との區別は野外では殆ど不可能なので地質圖には混同して塗色してある．後の研究に俟つ．

長沼統の分布は，第 15 圖に概念的に示した様に，西へ擴がり，東・南・北に不整合を持つ，一つの向斜構造の様に見えるが，この兩翼の傾斜は何れも內側へ向つて 2°～3° の緩傾斜をなし，不整合面近くを除けば殆ど水平に近いので，元來水平に推積した地層が地殼運動によつて向斜構造となつたものではなく，先に存在してゐた凹地に堆積當初から持つ傾斜角によつて示される僞向斜構造であるかも知れぬ．この堆積區域の中心の都會戸塚町をとつてこの凹みを戸塚灣と名付ける．長沼統基底の不整合面の傾斜は南側のものが第 12 圖寫眞 6 圖に示す様な平行不整合的境界面であるのに，北側のものは第 9，第13 圖及び寫眞 7，8，9 圖の様に何れ

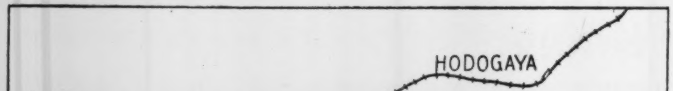

第 15 圖 長沼統各層の分布概念圖
〔Schematic distribution map of subdivisional formations of the Naganuma series.〕

も不整合下の地層の侵蝕急斜面を埋めて生じたと解される樣な不整合からなり，戸塚灣の南北に於ける堆積狀況を異にしてゐる．更にこの統を細分した各層に就いて，それぞれの分布を見ると古い地層程南側を占め，新しい地層は北側で古い層を覆ひ隱してゐる．故に戸塚灣はその堆積初期から末期にかけて，徐々に南が高まり北が低まる運動をし凹地の軸部が北へ移動したと解釋できる．卽ち戸塚灣は次第に南から北へと移動したかの如く見える．

長沼統各層の動物群は最下の長沼層では純海成で，田谷砂礫層を隔て，屏風浦層下部では稍々半淡水成となり，その上部は全く半淡水成となつてゐる．その上に不整合面を隔て橫はる倉坪層では稍々淺海性であるが東京灣奥の動物群に類似するところがあり，分布面積は狹くなり長沼層の動物群に比して淺い相を備へてゐる．そしてこの上に踊場砂層が整合に廣く分布してゐる．故に戸塚町附近は長沼層堆積時代の初に三浦半島方面の隆起運動に伴つて曲窪し，戸塚灣を生じ，長沼統の堆積を開始した．この曲窪地域は三浦半島方面の隆起が尙繼續してゐたためにそれに伴つてその南邊も隆起を續け，戸塚灣底は變形し，ために北側には覆蔽の現象が起つたと解釋できる．この隆起の性質は長沼層下の不整合・田谷砂礫・倉坪層下の不整合・踊場砂層の如く陸化の證を伴ひ一進一退を示し，陸化を繰回す毎に淺い相となつてゐることを示してゐる．

次に東西の動物群の相異を各層に就いて見ると，長沼層は小菅谷化石動物群では數種の汀線附近に棲息する種類を含むが，*Siphonalia* 屬の如き種類は稀であるが，關谷・城廻・村岡等の西部の化石動物群では *Siphonalia* 屬，*Acila divaricata*（HINDS）等を含み深度を增してゐる．故に長沼層堆積當初戸塚灣は西に深かつたと想像するに都合がよい．

屏風浦層も上大岡・屏風浦には *Raeta yokohamensis* PILSBRY，*Laternula japonica* LISCHKE 等を含む他に保存良好の植物化石を多量に含んでゐるのに，西部では堤ケ谷上倉田の化石動物群の如く，純海成種を多數に含んできてゐることは長沼層と特徵を一にしてゐる．

所謂第二帶の特徵を持つた戸塚，品濃，稻荷谷の諸化石動物群は半淡水成であるがその東西の生態學的特質は一樣である．但しこの動物群は東部に迄分布してゐない．

松本理學士の片瀨層はその層準・岩相が屏風浦層に類似してゐる點で筆者は同層にあてたが，その動物群（第 V 表 F）は長沼統の何れのものにも類似しない特性を示してゐるが，その內の數種は長沼層（第四帶）の特徵となる樣な種も含まれてゐる．動物群は主として黑潮（相模灣）の汀線附近の磯近くに棲息するものが多いことは上に述べた戸塚灣の性質からみて都合のよい事實である．

倉坪層に就いては化石動物群が二ヶ所にしか知られぬから何も述べられない．下末吉統の動物群と殆ど區別つかない．

横濱新山下町の屛風浦層・淺間臺の屛風浦層はその特異な堆積狀態から，戸塚灣に注ぐ河谷の沈溺谷か，又は東京方面の長沼時代の海に注ぐ河谷の沈溺谷かの堆積物であらうが，軟體動物は戸塚灣系統であることを暗示してゐる．詳細は鶴見西北方の調査を明にした上でなくては述べ得ない．

鮮新統

小柴統．

濱層．

湘南電鐵湘南富岡驛の東方の崖に露出する粗砂•淤泥の互層は海岸附近の露出面で觀察すると長沼統を除いてこの附近に發達する新第三系中最も上部の層準を代表する地質系統に屬してゐる．濱層はこの粗砂·淤泥の互層を呼ぶ名稱である．

卽ち濱層とは（横濱市）金澤町長濱檢疫所附近の海岸に露出してゐる褐色•淡黄褐色の砂泥互層である．

湘南電鐵湘南富岡驛の北の 100 m 切割面又は同驛の東方の檢疫所への路の中途に露出するものは何れも濱層である．この互層の砂層は屢々粗くなつて礫質に變化することもあるし又泥質部が增加してゐることもある．

杉田の南青砥のトンネル附近では，長濱附近の如く特徵が著しくないが，互層々理は尙よく觀察できる．この地層は中里附近の丘陵上に帽子狀に孤立して殘されてゐるが，保土ヶ谷以北で再び分布範圍を擴げてゐる．

この濱層の上限は今回の調査區域では明でない．下限は整合的に中里泥層と接してゐる．

富岡海岸南部で濱層中里層の整合的境界が海面上數mの位置に露出してゐる．こゝでは境界は緩い傾斜で南へ向つて長濱檢疫所附近の方へと傾き下つて海面下に沒してゐる．長濱檢疫所の南でこの境界は急に海面上に露はれて北斜するに至る．卽ち濱層は長濱檢疫所附近に一つの略ぼ東西の走向の向斜軸を持つた向斜構造をなしてゐる．

湘南富岡驛の南の谷では，この境界が次第に丘陵上へと延び，東へ傾斜し，1 km 位の地點で薄失してしまふ．

湘南電鐵線に沿うて金澤文庫方面へ至ると，粗砂•淤泥の互層は東北へ傾斜し一つの向斜構造を作つて，向斜の南翼には下位の中里層が露はれてくる．

杉田の南の青砥トンネル附近には N20°W 內外の斷層があり，その東側に對して西側が相對的に 20～30 m 內外低下してゐる．筆者はこの地層からは未だ化石を得なかつた．

植田房雄理學士の富岡層は標準露出地の定義がされてないので明なことは述べられないが筆者の濱層は之に該當するのであらう．

長沼統とこの地層とは同時のものではないかとの疑があるが，その疑は確に一應の理由がある．筆者の觀察では濱層は中里層と整合の關係にあるが，長沼統は大抵の場合中里層を侵蝕した急斜面を境として不整合にその上に横はり層位上の特徵を異にしてゐる．濱層は規則正しい互層構造を示してゐるが，長沼統は不規則な層序を示してゐる．上述の樣な理由で筆者は濱層を長沼統とは異る地質系統と推定した．

中里層．

杉田の西南上中里附近に於ける大船泥層に類似した岩層を呼ぶ. 鼠色灰狀の半凝固泥層で厚い層理を示し, 容易に濱層と區別がつく. 筆者が嘗て大船層の露出面として横濱附近に擧げたものは何れもこの地層であつた. 層中に數枚の白色凝灰岩質砂岩層を介在してゐる. 厚さ約 40 m.

鎌倉郡豐田村長沼の長沼層基底の下に露出する泥岩層は外見大船層と類似するが矢張中里層である. この泥層は鍛冶ケ谷の北の鎌倉街道の峠附近から日野方面に露出し峠附近では北へ 2～3° の傾斜をしてゐる. この峠の頂上近く次第に北に向つて低まり地表下に沒してゐるので北斜してゐるのが解る. 日野の附近では稍々粗粒となり, 貝化石を含んでゐる.

鎌倉街道から岐れて上野庭に至る道の途中の崖には日野附近の砂層と類似の砂が露出してゐるが,

Limopsis crenata A. ADAMS, *Pecten tokyoensis* TOKUNAGA, *Turritella fortilirata nipponica* YOKOYAMA, *Clavatula dainichiensis muraokensis* OTUKA 等を採集した.

横濱市中區本牧町池田, 二ツ谷海岸では次の樣な種類を採集した. 卽ち

Yoldia japonica ADAMS et REEVE, *Limopsis tokaiensis* YOKOYAMA, *Dentalium yokoyamai* MAKIYAMA, *Dentalium rhabdotum* PILSBRY, *Natica janthostoma* DESHAYES, *Lora* sp. 等を擧げることができる.

氷取澤の北方では *Turritella fortilirata nipponica* YOKOYAMA を豐富に產する.

帷子川の沿岸和田 (上星川の東南) 附近には *Turritella fortilirata nipponica* YOKOYAMA, *Venericardia ferruginea* AD. & RVE., *Acila divaricata* (HINDS), *Limopsis tokaiensis* YOKOYAMA 等を產してゐる.

小柴砂層.

(横濱市) 金澤町柴部落及びその北の海岸に露出する凝灰質砂層を小柴層と呼ぶ. この砂層は火山碎屑岩質で僞層構造を示し, 東北へ傾き, 下部程粗砂で, 上位は次第に細砂粒となり, 中里層に整合的に接してゐる. 火山碎屑岩中の輕石は主として複輝石石英安山岩の輕石よりなる. 中里層と小柴層との間は漸移的に變化してゐる. 下部は僞層砂部の下位に稍ゝ凝固した凝灰岩, 火山滓等を含む砂岩層がある. この砂岩層の下は次に述べる大船泥層 (又は寺前泥層) である.

小柴層は横山博士が小柴帶とされたもので多數の貝化石を含んでゐる.

湘南電鐵湘南富岡驛の南 900 m 附近に露出する僞層構造を有する含化石凝灰質砂層はこの小柴砂層の延長である. この露出面では層向 NWW: 北へ傾斜する, この砂層はこの層向に沿うて西西北へ延長して, 氷取澤部落に露出してゐる.

氷取澤では圓海山登口より北方氷取澤の部落に達する間に多數の貝化石を產してゐる.

圓海山の北斜面では凝灰質砂層は露出してゐるが, 化石は殆ど含んでゐない. 之等の凝灰質砂岩は主として凝灰岩からなり, 鎌倉郡本鄕村中野の東方から圓海山への登山口附近に露出するものは赤褐色を呈してゐる.

この小柴砂層は更に西の方へ行くと層向を EW に近く變じ, 傾斜も緩くなる. 中野, 鍛冶ケ谷, 和田に露出してゐるが, 凝灰質性分は少くなり, 砂粒も細くなる. これらの部落附近では

最早僞層理砂層は見られない.

小柴砂層の下位の稍々凝固した粗粒凝灰質砂岩は氷取澤の南部，圓海山の南斜面，中野，鍛冶ケ谷，桂等に露出してゐて，中野の東方には *Thyasira nipponica* YABE and NOMURA，*Miltha acutilineata* CONRAD，*Solemya tokunagai* YOKOYAMA 等が產してゐる.

中野では *Anadara kosibensis* OTUKA〔ms.〔, *Limopsis tokaiensis* YOKOYAMA, *Patinopecten yessoensis* (JAY)，*Chlamys yokoyamai* OTUKA〔ms.〕，*Pseudamussium intuscostatum* (YOKOYAMA)，*Brachytoma cosibensis* (YOKOYAMA)，*Brachytoma nakanense* OTUKA〔ms.〕，*Cancellaria kobayasii* OTUKA〔ms.〕 *Erato callosa* ADAMS et REEVE, *Chrysodomus muroi* OTUKA〔ms.〕，*Homalopoma suzukii* OTUKA〔ms.〕，*Astyris varians* (DKR.)，*Cerithidea nakanensis* OTUKA〔ms.〕等を產してゐる.

小柴砂層の下半部には一枚の白色凝灰岩層が介在してゐる．この露出は鍛冶ケ谷の西の崖に露出してゐる白色の凝灰質砂岩で，鍛冶ケ谷凝灰岩層と呼ぶ. この層は大道，中野，氷取澤，柴に續き，小柴層の橫の岩相變化があるに關らずこの凝灰岩層によつて東西の露頭を結び得る.

貝化石群は僞層理を示す砂層中にあるに關らず，腕足貝等を含み，深い相又は寒い相を示してゐる. 第 VIII 表は小柴層產の貝化石を各地に區別表示してある.

Table VIII. Fossils collected from the Kosiba exposed at Kosiba (a) and Hitorisawa (d), and from the Kanazawa series (b & c).

Cylichna musashiensis TOKUNAGA	a			d
Cylichna orientalis YOKOYAMA	a			
Conus sieboldi REEVE	a			
Conus tuberculosus TOMLIN	a			d
Turricula (*Surcula*) *kamakurana* (PILSBRY) var.	a	b	c	
Conus sp. (*cancellatus* HWASS type)				d
Bathytoma mediocarinata (YOKOYAMA)			c	
Brachytoma jeffreysii (SMITH)	a			
Brachytoma cosibensis (YOKOYAMA)	a			d
Clavatula nivalioides (YOKOYAMA)	a			
Clavus benten (YOKOYAMA)				d
Clavus braunsi (YOKOYAMA)	a			d
Clavus tokunagai OTUKA〔ms.〕				d
Mangellia deshayesii (DUNKER)	a			
Asperdaphne sp.				d
Antiplanes? glabra (YOKOYAMA)				d
Lora cancellata OTUKA (*viridula* of YOKOYAMA 1920[27])	a			d
Fulgoraria megaspira (SOWERBY)	a			d
Mitra cosibensis OTUKA (*ebenus* of YOKOYAMA 1920[28])	a			
Mitra sp.				d
Mitra fusiformis (BROCCHI) of YOKOYAMA	a			

(次頁へ續く)

---

27) *Jour. Coll. Sci. Tokyo Imp. Univ.* **39**, 6, p. 45, pl. 2, figs. 5 a, b.

28) *Jour. Coll. Sci. Tokyo Imp. Univ.* **39**, 6, p. 47, pl. 2, figs. 4 a, b.

Mitra plicifera YOKOYAMA	a			
Fusinus makiyamai OTUKA (*niponicus* of YOKOYAMA 1920[29])	a			d
Chrysodomus cosibensis OTUKA n. n.	a		c	
Chrysodomus schrencki YOKOYAMA	a		c	
Buccinum leucostoma LISCHKE			c	
Astyris varians (DUNKER)				d
Cymatium sp. indet.				d
Tritonalia falcata? SOWERBY				d
Trophonopsis nipponicus (YOKOYAMA)	a	b	c	d
Trophon inermis (SOWERBY)	a		c	d
Argobuccinum oregonensis REDFIELD	a		c	d
Ancilla hinomotoensis YOKOYAMA				d
Bittium sp.				d
Bittium binodulosum YOKOYAMA	a			
Trichotropis planicostata YOKOYAMA	a			
Turritella fortilirata nipponica YOKOYAMA	a	b	c	d
Solarium? *lenticulatum* YOKOYAMA	a			
Natica janthostoma DESHAYES	a	b	c	d
Polinices pallidus (BRODERIP et SOWERBY)	a			
Epitonium densicostata YOKOYAMA	a			
Odostomia sp.				d
Homalopoma amussitata GOULD	a			d
Turcicula crumpii (PILSBRY)	a	b	c	
Turcicula convexiuscula (YOKOYAMA)			c	
Margarita umbilicalis BRODERIP et SOWERBY			c	
Diodora yokoyamai cosibensis OTUKA	a			d
Puncturella subconica YOKOYAMA	a			
Emarginula sp.				d
Acmaea kuragiensis YOKOYAMA	a			
Acmaea nojimensis YOKOYAMA			c	
Cellana eucosmia PILSBRY				d
Patelloida pallida (GOULD)	a			d
Dentalium yokoyamai MAKIYAMA	a	b	c	
Dentalium rhabdotum PILSBRY				d
Dentalium weinkauffii DUNKER	a		c	
Aloidis venusta (GOULD) var.	a			d
Nemocardium samarangae MAKIYAMA	a			d
Chama semipurpurata LISCHKE				d
Joannissiella cumingii (HANLEY)	a			
Lucina acutilineata CONRAD	a			d
Venericardia ferruginea A. ADAMS	a		c	d

（次頁へ續く）

---

29) *Jour. Coll. Sci. Tokyo Imp. Univ.* **39**. 6, p. 49, pl, 2, fig. 7.

Venericardia ferruginosa ADAMS et REEVE				d
Astarte hakodatensis YOKOYAMA	a			d
Crassatelits oblongata (YOKOYAMA)	a			d
Myadora reeueana SMITH var.	a			d
Solen grandis				d
Anomia lischkei DAUTZENBERG et FISCHER	a			d
Spisula bernardi (PILSBRY)				d
Tellina salmonea CARPENTER				d
Lima goliath SOWERBY	a			d
Lima japonica A. ADAMS of YOKOYAMA	a		c	d
Lima quantoensis, YOKOYAMA	a			
Chlamys vesiculosus (DUNKER)	a			
Chlamys swiftii etchegoini ANDERRON	a			d
Pseudoamussium intuscostatum (YOKOYAMA)	a			
Pecten tokunagai YOKOYAMA	a			
Pecten yessoensis JAY	a		c	d
Ostrea gigas THUNBERG	a			
Ostrea musashiana YOKOYAMA	a			d
Arca boucardi JOUSSEAUM	a		c	d
Barbatia decussata (SOWERBY)	a			
Barbatia stearnsii (PILSBRY)	a			
Barbatia symmetrica (REEVE)				d
Pseudogrammatodon dalli obliquata (YOKOYAMA)	a			d
Glycimeris nipponicus YOKOYAMA	a			d
Limopsis auritoides (YOKOYAMA)			c	
Limopsis tokaiensis YOKOYAMA	a	b	c	d
Limopsis crenata A. ADAMS	a	b	c	
Limopsis adamsiana YOKOYAMA	a			d
Nuculana yokoyamai KURODA	a			
Nuculana naganumana (YOKOYAMA)		b		
Nucula insignis GOULD	a			
Nucula (*Acila*) *divaricata* (HINDS)			c	
Terebratulina crossei DAVIDSON	a		c	
Terebratulina caputserpentis (LINNAEUS)	a			
Terebratalia gouldii (DALL)	a			
Terebratella nipponensis YOKOYAMA	a			

上に述べたやうに小柴層を最下に中里・濱の諸層を上にし，後二者は主として横濱市附近を占めてゐる．岩相の變化から考察すると濱層と中里＋小柴層とはそれぞれ一つの輪廻を代表する地質系統の様にも見えるが，中里層と濱層とは漸移し，小柴層は次の大船層との間に不整合的關係は確められぬが岩相が急に變化して接してゐるので

暫らく上記三層を小柴統なる一系統中に屬せしめてみた．小柴統の砂に就いては海の深度の變化と言ふ他に，火山碎屑物の沈澱を速ならしめた現象があつた樣に考へられる．中里層と次に述べる大船層とが岩相上類似する如く化石動物群上にも著しい差異が見られぬことは注意する要がある．或は小柴層の砂層は大船層の海が殆と深度を變へずに中里層に迄堆積を續けてゐて，その途中の一時代に火山物質を供給する現象が突發して堆積せられたとも考へられる．後の研究に俟つ．

植田學士分類の小柴層は筆者の小柴層に，富岡層の大部は濱層＋中里層に該當する樣に思はれる．

金澤統．

大船層．

大船泥層は大船驛の周圍の丘陵を構成する稍々凝固した明鼠色の塊狀の層理の厚い泥層の地質系統を呼ぶ．

筆者が嘗て地質學雜誌 第37卷，第 442 號，369 頁，第7行以下，373 頁第 3 行迄に記述した文章は誤である　德永博士が嘗て報ぜられたことのある飯島の鮫の齒を含んでゐる層は大船層ではなくて，中里層であつた．

大船泥層中には數枚の白色凝灰岩層が介在してゐる．大船層はそれらの白色凝灰岩層と細粒均質の泥層とによつて特徵付けられる一地質系統である．筆者の寺前泥層・植田學士の釜利谷層の大部は本層に屬す．

大船層の分布．

大船驛の西方戸部附近の丘陵の下半を構成する泥層は大船泥層の標準露出地である沖積面から 2〜3 m の部分に厚さ 1/3 m 位の戸部白色凝灰岩帶がある．この凝灰岩帶は北へ向つて 2〜3° の傾斜で傾き下つてゐる．岡本・植木等にも同樣大船層が露出してゐるが，戸部凝灰岩帶は傾斜の關係上露出してゐない．城山の南では不整合に長沼統に被はれてゐる．この附近の長沼統は礫層を基底に，その上に薄い「あたん」層を含んでゐる．

大船泥層は城廻の南では野島化石帶（と略ぼ類似の層準に該當する所謂山之內凝灰質砂岩層）に整合してゐる．

城山の東，城廻・關谷附近で長沼統の下に露はれてゐるのは大船泥層で，戸部白色凝灰岩層が僅に露出してゐる．

玉繩村岡本の西の崖から次の樣な貝化石を採集することができた．この附近のこの泥層中には屢々複輝石石英安山岩の輕石が含まれでゐる．

大船驛の南東では大船泥層は小袋谷の西の小山嘴に露出してゐる．　この露頭では大船層は整

合的に野島砂岩層の上に横はつてゐる. この境を東へ追跡すると離山・入谷・本郷村上野の方へ向つて發達してゐる. 岩瀬附近では岩瀬白色凝灰岩層（恐らく戸部のものと同じと思ふ）が厚さ 2m 内外で發達し，よく指準層となつてゐる. この凝灰岩帶は大船層の下半部にある. 之によると大船層は初め大船驛の西では層向 N 80° W〜N 70° W：傾斜 N 2〜5° 程であるが，大船驛の南では層向略ぼ東西，傾斜 N5° 前後に傾き，更に小坂村岩瀬附近では層向 N65°〜70°E，傾斜東北に近く，大船層は更に六浦莊北谷・釜利谷・金澤文庫に達してゐることが明となつた. 岩瀬白色凝灰岩は金澤町附近では金澤文庫の東の海崖・金澤文庫驛の北の大船層中に，赤井・釜利谷の小溪底，本郷村では上野，公田，岩瀬に小坂村では大船（驛の東約 1 km）等に露出してゐる.

筆者がさきに寺前化石帶と呼んだものは大船泥層の東方延長に他ならぬことが明にされた.

大船泥層中の化石は前に述べたものの他東方金澤町からも採集できた.

野島凝灰質砂岩層.

大船層下に整合的に横はる凝灰質砂岩層で貝化石を含んでゐる. 野島層の標準露出地は金澤八景の東方 1 km の野島の丘を造る凝灰質砂岩である. 凝灰岩は主として輝石安山岩質輕石である.

野島凝灰質砂岩層の異相は北鎌倉驛の東北側の崖に露出するもので，筆者はこの部分に對して山ノ内帶なる名稱を與へたことがある. この凝灰岩は火山岩滓角礫の含んだ凝灰質砂岩で，凝固した部分は侵蝕に對する抵抗が强いため切割露頭面では凸出してゐる.

本郷村上野の上流に露出するものは多少粒型小さく泥質砂を含み，美しい互層理を示すことがある.

六浦一三艘附近では白色の凝灰岩帶を含み，*Dentalium yokoyamai* MAKIYAMA，*Turcicula convexiuscula* (YOKOYAMA)，*Limopsis tokaiensis* YOKOYAMA 等を豐富に含む.

浦郷凝灰質砂岩層.

浦郷層は湘南電鐵追濱驛の南に發達する凝灰質角礫岩又は砂礫岩層で野島層の基底礫岩の如きものである. 主として輝石安山岩の角礫凝灰岩よりなる.

湘南電鐵追濱驛の東南階段狀住宅地の崖面にこの平行不整合の露出面がある.

鷹取山・神武寺の凝灰質角礫岩もこの浦郷層である. 神武寺では神武寺表參道の頂上近くに浦郷層の下限をみることができる.

金澤八景驛と神武寺驛との間に浦郷層と逗子統との不整合がよく觀察できる.

浦郷附近では浦郷砂岩層は更に基底粗粒砂礫岩層，灰色又は黃褐色含貝殼砂層（薄い泥灰質砂岩層を介在する），泥灰岩層・砂岩層の互層があり，次に野島層が横はつてゐる. 之等各層間の境界は極めて不明瞭である.

鎌倉町淨明寺附近で浦郷砂礫岩層は不整合に逗子統の上に横はつてゐる. この附近では逗子統も浦郷層も東へ緩く傾斜し，名越から釋迦堂谷へ至る峠の頂上附近には浦郷砂礫岩が露出してゐて，山麓部には逗子統が分布してゐる.

鎌倉驛の西北扇ケ谷，花粧坂附近の含貝化石礫層もこの浦郷層の續きと考へることができる.

鎌倉山附近では浦郷層と野島層との區別がなく，粗粒の凝灰質砂礫岩層は水平に近く，山の上に分布してゐる.

松本理學士の調査によると浦郷層は更に片瀬の東龍口寺山に迄も分布してゐて，この附近で

は傾斜式不整合を示すところさへある．鎌倉山片瀬間の鑽大師停留場（日本自動車）の南方の切割に見られるものは浦郷層との境界と見做した．

江ノ島の北部，棧橋近くに露出する僞層理凝灰質砂層は筆者の觀察では浦郷一野島層のものと思惟する．

逗子統．

逗子統は渡邊久吉博士が逗子頁岩と呼んだもので逗子町の周圍の丘陵を作る地層である．この標準露出地として逗子驛の北側の崖の露出を選定する．渡邊久吉博士によると逗子統は灰色淤泥と火山滓を含む泥質砂岩との互層であり，數枚の白色凝灰岩を含む筆者が嘗て大佛泥岩層として小柴層下に設けたものは逗子統に編入すべきである．

逗子統の上部は多少粗粒となり，含角閃石安山岩質凝灰岩が豐富となるが，下半は比較的均質な互層理を示してゐる．基底部は粗粒砂岩となり，往々黑色の火山滓角礫を含む凝灰岩を含んでゐて，稀に貝化石を含むことがある．

渡邊久吉博士によればこの基底の不整合を發見した地點は逗子の南西海岸鳴鶴崎の北側卽ち田越川河口の西方である，と．

不整合下の地層は此處より葉山町及び西浦村北部の海岸に露出する葉山第三紀層で，鳴鶴崎では頁岩·砂岩の互層からなり，凝灰岩をも交へ頁岩には炭質な部分もあり，厚さ 3～6 cm 程の石炭を挿むことがある．この葉山第三系の露出面の層向は N 20° W：傾斜 NE 60° 或はそれ以上の急角度である．

不整合上の地層は逗子の南方山地の北側に見るもので，基底卽ち前記の地層を不整合に被覆した最下部は厚さ數 m 毎に厚さ數 cm から數 10 cm の軟き細粒砂岩を挿む．田越川口の海岸では基底の砂岩に *Chlamys miurensis* YOKOYAMA，*Lima zushiensis* (YOKOYAMA) 等の貝化石を埋藏してゐる．

渡邊博士によれば不整合上の地層は N 70° W に走り，NE 30° 或は是より緩傾斜するところもある．卽ち著しい傾斜不整合にして，不整合上の地層は逗子頁岩層と命名されたがこの不整合直上の地層から數種の貝化石を採集報告されてゐる．この不整合は更に御幸街道の櫻山トンネルの南口附近に露出してゐる．こゝでは不整合下の地層は直立に近く，層向は N 50° W，傾斜 90～80° 前後である，と．

逗子統の基底は更に東へ向つては二子山·畠山の附近を經て，横須賀市の南から久里濱方面へ達してゐる．千谷技師によれば浦賀附近の逗子統からは海綿·珪藻 (*Coscinodiscus* sp.) 等を產すると．

逗子統の分布．

片瀬附近の逗子統は水平又は 10° 以内の傾斜で分布し，七里ケ濱海岸，腰越町津村附近に露出し，泥灰岩質の結節を持つた地層，又は火山滓角礫岩·凝灰岩等を含んだ地層等を介在してゐる．*Thyasira nipponica* YABE et NOMURA が小動から採集されてゐる．

鎌倉町及び小坪の大部分は逗子統からなつてゐる．長谷の大佛附近では逗子統は層向 N30～40° W：傾斜 NE 30° 前後で泥岩質であるが，小坪附近では N 60°～70° W：N 20°～25° の層位を示してゐる．

小坪の東披露附近には特に目立つ白色凝灰岩層があり，材木座方面へと續いてゐる．

葉山統．（中新統及び古第三系）

先三浦層群·葉山頁岩等と呼ばれた地質系統を一括して，葉山統中に含めた．本統の發達區域の地質構造は極めて複雜であるのに加へて，本地域の性質上詳細な記述は行ひ得ざる事情があ

り，こゝには極めて概略を記し，後世の研究の資としやう.

比較的構造簡單な地域は葉山町鐙摺附近から上山口に至る線の北側で，主として灰色の砂岩層で礫岩層を介在してゐる地質系統が分布してゐる. 一般層向は N 60° W，傾斜は急で南へ70°，80° 垂直に近い値を示し，N 30° W: N60°; N 45°W の急傾斜面を持つた斷層面等があり礫岩層に注目すると東側の地塊程北へ相對的に移動してゐると解し得る. 逗子から葉山へ至る海岸の露頭に就いて觀察すると，堀ノ内森戸海岸に露出する硅質の泥層は層位上上盤に該當する様に見えるが擾亂の程度は大きい. 下山口の海岸には石灰質含化石砂岩があり，不整合に下盤の黑色の泥岩層上に横はつてゐる. 下盤の黑色の泥岩層は葉山町新澤附近で蛇紋岩に貫れてゐる地層に類似してゐる. この不整合上の含化石石灰質砂岩からは次の様な化石が採集でき日本の中下部中新統を暗示するものがある（第9表參照).

Table IX. Fossils collected from the calcareous sandstone exposed on the shore of Simoyamaguti, Hayama-mati.

Ostrea sp.
Glycimeris rotundata (Dunker)
Glycimeris sp.
Ostrea sp.
Crassatellites sp. (very small form)
Trivia hayamensis Otuka 〔ms.〕
Balanus cariosus (Pollas)
Balanus sp.
Astryclypeus integer Tokunaga

故に一般に葉山統と呼ぶものの内に明に不整合によつて二つの地質系統の存在することが明にされる. 渡邊久吉博士が葉山頁岩と呼んだものは恐らく鐙摺—森戸附近に發達する硅質頁岩層・砂岩の地質系統に該當するらしい. 筆者は暫らく上下に二分して上部葉山統を以て不整合上の地質系統葉山頁岩をも含めるとし，蛇紋岩等に貫れる地質系統を下部葉山統とした.

上部葉山統には前述の化石の他含化石石灰岩があり，千谷技師によつて依然から，次の様な有孔虫 *Globigerina* sp., *Rotalia* sp., *Amphistegina* sp.が報告されてゐる.

下部葉山統分布區域の內下山口附近からアルカリ玄武岩質岩石の產出が報告されてゐるが之は從來蛇紋岩と稱せられてゐるものの內にある樣である.

地層對比論（特に房總半島との對比）及び時代推定.

筆者は房總半島に於いて上部より鹿野山層群，秋元層群，高宕畑層群，關層群，豐岡層群なる五つの層群を設けた.

坂倉學士は千葉縣小櫃川流域の詳細な地質圖を製作され，多數の貝化石を採集して多くの有益な層序學的知識を公にされた. 同氏の層序は次の如くである.

鶴舞統.
里見統上部.
里見統中部.

里見統下部．

西畑統．

關　層．

豐岡層．

坂倉氏の言へる如く彼の細分した各層と筆者等の細分した各層とが互に全く同時であることを確めるためには房總半島の地質構造上の配列が西に收斂するため尙多くの研究を要するが大體に於いて房總半島には3つの構造上著しい不整合關係がみられる．即ち（1）天津統基底，（2）秋元層群から佐倉氏の西畑統基底？に續く東から西へ覆蔽される大きな不整合と，（3）三土學士の發見した洪積統基底の不整合である．三浦半島に於ける層位上最も目立つ不整合關係は葉山統と逗子統との間の他，長沼統の基底下末吉統の基底等を擧げることができる．葉山統と逗子統との不整合はその上下の地層の構造上の著しい對照により極めて特異なものである．この不整合に該當するものは房總半島に於いては天津統（筆者の豐岡統）の基底の不整合であらう．この不整合によつて房總・三浦兩半島に劃然と構造上上下の地質系統を區別することが可能の樣に見える．長沼統基底の不整合と下末吉統基底の不整合とは，それらの上下の地層の構造，及び不整合線の分布範圍から判斷して同じ程度の意義を有してゐる．併し各不整合の上下に橫はる地層中の化石動物群を比較すると，長沼統と小柴統との間の相異の方が，長沼統と下末吉統との間の相異より遙に大きいことを示してゐる．秋元層群とその下位の地層又はこの相異は坂倉氏も指摘せる如く西畑層？とその下位との相異に於いても著しいものがある．この大なる相異の原因には海流の影響の差異もあるが，この他に深度，地理的環境の差異も比較的大なる影響を與へた如く認められる．之等の影響は地殼運動にその原因を歸せしめ得るもの多く，房總半島の秋元層群西畑統？基底の不整合に比ぶべきものであらう．

逗子統と金澤統との境界は仔細に檢すると不整合の關係があるが，その關係は平行不整合的なもので，火山碎屑物を堆積する直前に多少の隆起・斷層の形成があつたものと解せられる．この種の不整合關係は房總半島の天津統（豐岡層群）と清澄層（關層）との間の關係を想起せしめる．化石軟體動物の特長と凝灰岩の岩石學的特長とも兩半島に於いて極めて一致してゐる．故に次に房總半島の地層と三浦半島との同時代性の比較に就いて筆者の大體の意見を記して參考に資さう．

下部葉山統は大體に於いて嶺岡附近に分布する蛇紋岩に貫れたる岩層であらう．

上部葉山統は *Lepidocyclina* 類を含む所謂佐久間統であらう．逗子統はその角閃石安山岩質凝灰岩を含む點で大體に於いて豐岡統の下半に近い．豐岡統にも同樣の凝灰

岩を含んでゐる．豐岡統は天津統と略ぼ一致する．

因みに久野學士により天津統天津層上部凝灰岩層の凝灰岩に就いて次の如き岩石學的事實を知つた．こゝに久野氏に厚く謝意を表す．

“ **岩石名** Hypetsthene-augite-hornblende-dacite tuffaceous sandstone. 〔**紫蘇輝石•輝石•角閃石•石英安山岩質凝灰岩砂岩.**〕

角閃石 pleochroism : $Z =$ green, $Y =$ slightly brownish green, $X =$ slightly greenish yellow; absorption : $Z \fallingdotseq Y > X$; $Z \wedge C \fallingdotseq 15^\circ$; $(-)\ 2V = 78$—77° weak; dispersion : $\lambda\rho > v$

紫蘇輝石 pleochroism : weak; $(-)\ 2V = 68^\circ$ distinct; dispersion $\lambda\rho > v$

他に $(-)\ 2V = 89^\circ$—88°; dispersion distinct, $\rho > v$ の無色鑛物あり． その他水成岩なるため microcline, zircon, brown hornblende 等あり”

關層群は金澤統の大部に該當するであらう．その基底の粗粒凝灰岩は金澤統基底の浦郷砂礫岩と一致する．

關統產の化石には *Dentalium yokoyamai* MAKIYAMA, *Turcicula convexeuscula* (YOKOYAMA) *Limopsis tokaiensis* YOKOYAMA 等あり，その岩石學的性質にも類似がある．

高宕畑統の貝化石は小柴化石帶と密接な關係を有してゐる．

長沼統と里見統とはその動物群は完全には一致しないが從來の如く同時代と考へておく．少くとも長沼層は筆者の秋元層群に近きものなることを信じてゐる．*Cymatium subpyrum* (YOK.), *Clavatula dainichiensis* forma *muraokensis* OTUKA, *Umbonium naganumanum* OTUKA が植畑の秋元層群から產してゐるのは都合がよい．

秋元層群は *Parelephas matsumotot* SAHEKI なる象齒を含み松本•槇山•故佐伯・高井等の斯學の先輩の考察した如く恐らく上部鮮新統のものであらう．．

片瀨層は前に述べた如く長沼統に該當し，その動物群・堆積狀態は長沼統中の屛風浦層と考ふる方が自然の樣である．

下末吉統は從來の如く東京層，瀨又階等と略ぼ同時代であらう．

上記の樣に大きな層序間隙に注目して，大體房總・三浦の各層を比較したが，兩地に發達する同時代の地層の厚さは極めて異つてゐる． 之は植田房雄學士•三土學士(未發表)•坂倉學士•鈴木學士(未發表)•等の御努力の東から西へ收斂する樣な地層分布から暗示を受ける樣に，三浦半島地域では地層の層序關係は最も收斂し，房總半島に普通に見られる多數の層が覆ひ隱されるか侵蝕し去られてゐる結果と解することができる．故に三浦半島は各不整合が明瞭に露頭で確認できるが，房總に於いては廣範圍の調査によつて之等が漸く確められるのである．

地質構造．

この地方の地質構造は旣に層序の項の說明によつて大體を覗ひうるが，次にその詳細を記さう．便宜上斷層構造と皺曲構造とに分けて述べる．

斷層構造．

沖積統をも截つて作られてゐるものとして故山崎博士が大岡川溪谷に沿うて走る斷層線を報告されてゐる．1923年の關東大震の際に露はれたものであるが，記事簡單のため詳細は知り得ない．斷層の露はれた地域は沖積統が厚く堆積してゐる．

ローム堆積後の斷層と思はれるものは略ど見出し得なかつた．但し段丘周緣の地辷的機巧によつて斷層の露頭を目撃することがあるが，之等は局部的なもので，大きな地殼運動を推定するには省略してもよい樣に見えるが，地震動により再動する恐れはある．

長沼統を截る斷層は筆者の知る範圍でも 3 ヶ所ある．これらの內 1 つは淺間臺附近のもので，東落ちの正斷層である．

弘明寺のものは略ぼ走向 N 45° E：傾斜 NW 45° 逆斷層東南落ちである．垂直落差約 3 m（第 16 圖參照）．

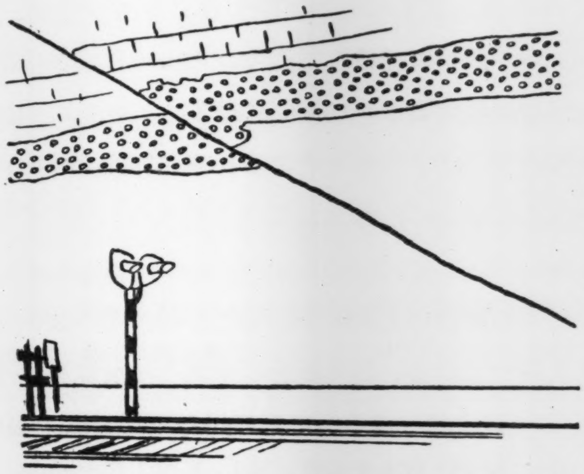

第 16 圖　弘明寺驛に露出する後長沼期逆斷層
〔Post-Naganuma reverse fault exposed at Gumyôzi railroad station.〕

他の一つは大岡火葬場附近のもので，走向略ぼ南北，東へ傾き，逆斷層西落である垂直落差約 1 m 寫眞 11 は之の斷層を示す．

上述した樣に長沼統を截る斷層はその落差數 m で大規模なものではないが，逆斷層の形式を供へてゐることは，この地方が長沼統堆積後も主として西北—東南に收縮する傾向があつたことを示してゐる．この樣な新しい斷層は大地震の際にそのものか又はそれに接近した他地域かに地震斷層を生ずる恐れがある．

上記の樣に長沼統以後の新しい地層に見られる斷層露頭はこの地方では極めて小規模の範圍にしか見られない．併し長沼統堆積前の斷層になると比較的大規模な運動をしてゐる．次に述べるのは之等の大規模な斷層構造に就いての記事である．

杉田斷層．

杉田の南方のトンネル南口に露出する斷層を杉田斷層と呼ぶ．斷層の走向N20°W：傾斜 E 80°，斷層の東側が 10 數 m，西側に對して高まつてゐる．この斷層の南方の延長は不明瞭になる．この斷層によつて東側の中里層は西側の濱互層と接してゐるこ

とがわかつた．

極樂寺斷層．

鎌倉町字極樂寺音無川の溪谷に沿ひ，北鎌倉方面へ延びる比較的大規模の斷層である．

音無川の上源 權現の瀧附近では浦郷砂礫岩狀の岩石が N 50° W : N 15° の走向・傾斜を持つて發達してゐるが，その南方では走向 N 20° E: 傾斜 70° E の小斷層を境として層面は厚さ 1/2 m 位の走向 N 20° E: 傾斜 70°E 位の斷層ネバ帶迄の間で斷層面に平行になる樣に引きづりを示してゐる．この斷層ネバを挾んだ斷層の東では逗子統の岩石が，大體 N20°E 位の走向を持つた小斷層群によつて細裂して相接してゐる．この細裂帶中に露出する薄い砂岩層の分布によつて，上述した斷層系が一つの逆斷層系を呈してゐる．然るに地層の分布は正斷層なることを示してゐる．

この斷層の南の延長は音無川溪谷の西岸の斜面中を走つて七里ケ濱海岸から海中に入る．

この斷層の北の延長は大佛切通のトンネル西口に露はれてゐる．こゝでは西側の金澤統の粗粒砂岩は大きな擾亂を受けた帶を挾んで逗子統に接してゐる．

この斷層は更に佐助稻荷裏山，花粧坂方面へ達するやうであるが明に露頭を確め得られなかつたが，地層の分布及び層向から海藏寺の附近迄は延びてゐるらしい．そして次に述べる扇ケ谷斷層で截られてゐる．

極樂寺斷層に接する兩側の地層は互にこの斷層の走向に平行になる樣にその層向を變へてゐるし，その兩側の層位がかなり異つてゐる．即ち斷層の東側の地層は極樂寺の溪谷では N30°—40°W : E15°—25° を一般走向とするのに音無川の東岸では N50° E : E 70°，NS : E 20°，N 20° E : E 10°，N 20° W : E 15°，NS : E 20° 等で斷層に接する程斷層に平行してゐる．

然るにこの斷層の西側の地層は N 50° W : N 15°，N 60° E : N 15° 等で，東側の一般層向N 30°—40° W に對して東西に近い．

上に述べた樣な特徴から，この極樂寺斷層が鎌倉町附近の地質構造上一つの重要な斷層であることに氣付く．金澤統と逗子統との境界に注目して極樂寺斷層の兩側の落差を見ると相對的に約500 m 程の垂直變位を推定でき，西落である．

扇ケ谷斷層．

扇ケ谷斷層は鎌倉町扇ケ谷から雪の下に至る斷層群で，單なる一斷層面で代表されてゐない．

雪の下窟不動の西で逗子統の層向を測定すると不動附近では N85°E 又は N85°W

で傾斜 N45° 前後の層位を示してゐるが，更に西へ向つて測定して行くと一つの斷層を隔て N45°—30°E，N50°E の層向を有し，N W 55°，30° の傾斜を有する層位に變化する．この斷層の走向は略ぼ南北に近い．次にその北の淨光寺附近を調査するとこの附近に N45°W：SW80° 位の走向・傾斜を持つた數面の斷層面があり，それらの東では層向は東西，南で水平に近く層も一定しない．

淸涼寺谷・及び亀ケ谷切通では N 45° E に近い斷層線さへ見た．併しこの様な斷層線は扇ケ谷から雪の下方面へ至る．

この様に扇ケ谷は多數の斷層の集合からなり略ぼ鐵道線路の西側では金澤統下部の凝灰質砂岩が水平に近く分布してゐるのに東側では逗子統の岩石が露出してゐる．

この斷層の兩側の地層は著しく層位を異にしてゐる．又層向もこの斷層附近で擾亂してゐる．

二階堂斷層．

鎌倉宮から鎌倉天園に至る道路に露出してゐる．二階堂龜ケ淵・獅子舞附近は逗子統が層向 N 40° W：傾斜 N 25°—18° で露出してゐるが，この斷層に接して傾斜を異にし稍々緩く，斷層の東北側の地層は直立し N 60° W の走向をとるが斷層を離れて北するに從つて再び緩く N 7°—10° 前後になる．この斷層の東側の地層は金澤統の特徴を示してゐる．この斷層の東南延長は十二所附近では確め得られなかつた．

池子斷層.

池子町池子附近に發達する斷層構造を池子斷層さ呼ぶ．多數の小斷層の集合した斷層系で，明確な一線では描き得ない．

神武寺・鷹取山は金澤統で構成されてゐるが神武寺驛の東部は逗子統が分布してゐて，兩統の層向・傾斜から推定される分布さ異つてゐる．之は略ぼ東西に近い走向を有つ斷層系が存在し，南落ちのために北へ傾く金澤統が斷層の南側に繰同して露はれてゐるものである．

上に述べた 5 つの斷層は 10 萬分之 1 程度の縮尺の地質圖にも表現し得る程度の斷層で，之等の斷層線を境としてその兩側の層位は異り，斷層線に沿うては地層の擾亂が認められる．之等の斷層はその周圍の或る幅さの帶中の地層が擾亂されてゐることから之に與つた地層（金澤統・逗子統）が今日の様に半硬化せぬ當時の成立に非るかの疑がある．併し之等の斷層の成生の時代を金澤統又は小柴統堆積以後と推定せられるが之等の斷層を被ふ新らしい堆積物がないので時代を限定することは不可能である．唯だ次の諸事實を記して之等の斷層の成生の時代の決定に就いて參考に資さう．

1. 之等の斷層線に沿う地形は必ずしも斷層の兩側の動きの方向と一致してゐないから，斷層線は今日の山背で代表される地形よりは以前に形成されたものであらう．

2. 松本理學士の調査によると，腰越町に露出する金澤統・逗子統中に見られる大

部分の斷層系によつて，長沼統は擾亂されてゐない．之等の點から推して長沼統堆積以前に成生せられ，既に固化したものと考ふることを得る．

上述の斷層系とは別にも一つの斷層系は地層內の割れ目の如き概觀を呈し，複雜に地層を塊裂せしめてゐるものである．逗子町・田浦町・横須賀市附近の逗子統の露出に屢々實見されるもので，その走向 N 30° E 又は N 30° W 位で傾斜は W 60° 又は E 60° のものが多い．この小柴層の兩側では層位は殆ど變更されず層向・傾斜は殆ど一定である．この塊裂構造を造る斷層中には多少それに接した地層の彎曲，マクレ上り又はネバ等を見るが大部分は前述の諸斷層が示した樣な性質がなく，地層は突然斷層によつて切斷され連續を斷たれてゐる．斷層は主として逗子統以下の諸層中によく見られるもので，その分布は接近したものでは數 m の間隔に發達してゐる．

この斷層系の走向は筆者の調査したものでは N 20°—30° E : N 20°—30° W のものが多い．この斷層系は筆者の知る範圍では逗子統の皺曲構造に對して無關係な發達を示してゐる．然るにこの斷層系の分布は逗子統及びそれ以下に著しく觀察でき，金澤統には比較的少いので金澤統堆積初期にこの斷層系が成生せられたのではあるまいかと言ふ疑もあるが，皺曲構造に無關係であることから判ずるとこの斷層系を皺曲構造形成後と考へ得るので，その場合には異る結論を生ずる．

この斷層系はその構造上の特徴から比較的急激に成生された疑があり，逗子統以下に於いて皺曲構造に無關係な分布を示すことが明にされるならば，斷層の時代的解釋に對して新なる解釋が必要とならう．即ち此の斷層系に關する事實は地下數粁の深處に於いて地表に達せぬ斷層構造の成生を見ることの可能性を示し，地震發生機巧に暗示するところ多大となる事を信ずる．

層間異常の問題．

三浦半島南部に於ける層間異常の例は房總半島に於ける程著しくないが，横濱市の西北部の第三紀層中には屢々層間異常をみる．その內井土ケ谷驛より東方の崖に露出するもの，帷子川の沿岸兩側の崖に露出するものは特に著しい．之等の層間異常は特別な或る層準に限られてゐる樣に見える．帷子川の沿岸は地層水平に近いため，層間異常は各地に連續して露出してゐる．帷子川沿岸の層間異常の露頭は次の各地で見られる．横濱市中區井戸ケ谷附近，保土ケ谷區新川島，星川町，和田町等；北鎌倉圓覺寺境內，神武寺北參道，追濱驛附近．

これらの層間異常は水平的分布がかなり廣いので，その說明は種々の假定が行はれ得るが層間異常のある地層は砂層塊と泥層塊との混合でその上下の地層は殆ど擾亂を受けてゐないので層間異常の層に沿うて推し被せ斷層（overthrust）的横辷りが起つ

たか，又は上部の地層の堆積せぬ以前に海底地辷的横辷が起つたかが考へられる．横濱附近の層間異常層とその上に横はる地層との境界は屢々不整合的關係を有するので層間異常を作つた海底地辷があつた後その異常層の上に再び新しく地層が堆積したと解釋でき推し被せ斷層的と考へることは不適當の樣に思ふ．この海底地辷り運動は何時起つたかはこの地層の堆積前後の地史を特に詳査することによつて確められる望がある．幸この層間異常の層は水平分布が廣いから充分に考究してみたいと思つてゐる次に述べる金澤統・小柴統の皺曲構造の成生とこの層間異常の成生との間に何等かの時間的關係の見出だされることも期待出來さうである．

皺曲構造．

この地方の皺曲構造は大岡向斜，濱向斜，極樂寺背斜，釋迦堂口向斜，淨明寺背斜等がある．

横濱市附近．

大岡向斜．

横濱市大岡川溪谷兩岸の臺地の崖に露出する中里層の層位を追跡すると大岡町字大丸の崖に露出してゐる中里層中の白色の凝灰岩層の分布をみると北へ行く程次第にその露頭の高度を增し，遂には仲久保への峠の頂上近くに露出する．

大岡町同潤會住宅地東北の崖面海拔約 15～10 m に露出する白色凝灰岩層も次第に北へ行く程高度を增し，高等工業學校の東側では 30 m 以上の高度に達してゐる．上に述べたものと連續してゐると思はれる白色凝灰岩層は東では岡村天滿宮の登り道で僅に南へ傾斜して露出してゐて，之は更に古泉，腰越磯子方面へと續いてゐる．

蒔田町英和女學校の丘陵を取圍む崖にも白色凝灰岩層の露出があり，同丘陵の西側の崖で地表に露はれ，市營住宅地の北を經て堀內町の南側丘陵の崖に露出してゐる．この附近からこの凝灰岩帶は傾斜殆ど水平に近付き，根岸臺地の崖へと延びてゐる．之は丸山町萬治病院の北側で消失してゐる．

萬治病院の北側でこの白色凝灰岩層は突然消失して，その南數 m の間は地層の層理も明でない．〔この樣な層理不明の露出面は中區宮の前若宮神社附近の崖にも見られ萬治病院の北側と結んで N 60°－70° W の走向の擾亂帶があるのかも知れぬ．〕

上記の樣に中里層の白色凝灰岩は略ぼ N 60° W の層向で南へ 2°～3° に傾斜してゐる．然るに大岡－磯子以南では北へ傾いてゐるので，この部分に一つの向斜が形成されてゐることに氣付くのである．この低角度の向斜を大岡向斜と呼ぶ．

長沼統はこの向斜軸の方向に平行に，凹んだ窪地に堆積した若い地質系統である．

井戸ヶ谷附近の層位觀察も同樣の結果を示してゐる．

濱向斜．

濱向斜に就いては濱層の項で大約説明した．略ぼ長濱檢疫所附近を向斜軸として，南翼は稍々急に 20°～30°，北翼は稍々緩く 4° 前後で，向斜軸は N 60° E 位，東へピツチし下つてゐる．

淨明寺背斜・釋迦堂口向斜．

淨明寺背斜と釋迦堂口向斜とは相並んで鎌倉町東部に發達してゐる．

大塔宮鎌倉宮附近の逗子統の一般層向は N 35°—40° W で，一般傾斜は NE 15° 前後に傾斜してゐる．この層向は鎌倉第二小學校東側山地附近を背斜として，NE に變化し，傾斜もそれと共に E 40° 内外に變る．淨明寺の谷では N 60° E，N 35° E の層向；E 5°～10° の傾斜を示してゐる．この背斜を淨明寺背斜と呼ぶ．

この層向の漸變に從つて金澤統は淨明寺胡桃谷附近から河底に露はれ釋迦堂の丘陵上に這ひ上つてゐる．この釋迦堂の丘陵の南側では層向が逆に N 70° W で N 5° 前後に傾き淨明寺谷との間に一向斜を作つてゐる．之を釋迦堂口向斜と呼んだ．この向斜の軸は略ぼ東西か又は N 70° W で，この軸部の丘陵上に金澤統が發達し，大室山方面へと延びてゐる．

上に述べた樣に三浦半島北部の第三系には斷層及び小皺曲構造が各地に見られるが，一般には單斜構造と考へて差支えない程度の地層分布を示してゐる．之によると小柴統の發達してゐる小柴—氷取澤—圓海山に至る部分は北へ向うて弱い撓曲構造を示してゐるが，その帶の北では殆ど水平に近いし[30]，その南では金澤八景附近までは殆ど水平に近く，その南から北・又は北東へ傾き始め，鷹取山—鎌倉天園—北鎌倉の線の北側に撓曲帶が推定される．

逗子統は鎌倉附近に皺曲構造を認めることができるが，一般には北へ 30° 位に傾く構造を示してゐる．

葉山統中には褶曲・斷層等極めて複雑な構造が見られるが，暫くは不問に附し別の機會に詳細を述べ樣．

地殼運動．

上に述べた層序と地質構造から我々は次の樣な地殼運動がこの地方にあつたことを推定することができる．便宜上，造陸運動，皺曲運動，及び斷層運動に分ける．

造陸運動は第2圖に概念的に示した如く，下部葉山統堆積時代の沈降，上部葉山統堆積時代の沈降，逗子統堆積時代の沈降，金澤統・小柴統の堆積時代の沈降，長沼

30） 德永重康，地質學雜誌 **9**，(1902)，p. 15.

統堆積時代の沈降，下末吉統堆積時代の沈降，沖積統堆積時代の沈降が認められる．之等の沈降時代の間には何れも隆起の時代が介在したことも認められる．第2圖に示す様に沈降と隆起とが交互に地殼を變形させてゐるが，新第三紀以來の總和に於いて隆起が勝つてゐることは注目すべき事實であらう．

皺曲運動．この地方に行はれた皺曲運動は三つの運動時期に區別することができる．

第一は三浦蛇紋岩の迸入を伴つた造構造運動である．下部葉山統はこの地殼變動で著しく變形され，多くの斷層構造を作つた．この造構造運動を“嶺岡”造構造運動と呼ぶ．

第二は大八洲造構造運動で，之は渡邊久吉博士によつて逗子統と葉山統との間の著しい交角不整合（clino-unconformity）から指摘されたものである．この運動によつて上部葉山統は下部葉山統と共に著しく皺曲・斷層構造を作られ，N 45° W の層向を持つ急斜構造に變形された地方もある．

第三は三浦造構造運動で，逗子統・金澤統・小柴統は緩く變形され，大岡・濱・釋迦堂口向斜，極樂寺・淨妙寺背斜を作つた．この運動はその皺曲係數の分布が南に大きく北に小さい事からみて，南北に非對稱的構造を示し，北側の地下に比較的變形され悪い地殼體があり，南の地下に比較的變形され易い地殼體があつて，それらの上を一様に被ふた逗子・金澤・小柴の各統の地層がこれらの地下の兩地殼體の南北方向に收縮するが如き變形によつて變形されたが如き構造を示してゐる．

三浦造構造運動は長沼統堆積時代にも尚完全にその運動を終息せしめず，長沼統中の各層の分布から知れる如く向斜軸は北へ水平移動を起してゐる．

斷層成生運動．

葉山統中には多くの斷層構造があり，それらの或るものは低角度推し被せ斷層*を示すものさへある．之等は何れも嶺岡・大八洲各造構造運動によつて生ぜるものと思惟せられる．斯の如き形式の運動は逗子統以上の地層中には見られぬから三浦造構造運動によつて生成せられたものとは考へられない．

三浦造構造運動によつて生ぜる斷層系中主要なものは次の諸斷層である．即ち衝上斷層には扇ヶ谷・武山斷層があり，何れも斷層面の傾斜は北へ向つてゐる．正斷層は極樂寺・二階堂・池子斷層等でそれらの走向は一定してゐない．

上述した他に逗子統中に屢々見られる無數の斜斷層はその走向略 N30°W，N30°E

---

* 逆斷層中その斷層面の傾斜角 45° 以下のものを推し被せ斷層と呼び，45° 以上のものを衝上斷層と呼ぶ．

のもの多く，金澤統以上ではその分布極めて稀である．金澤統堆積以前の成生としてはその分布に稍々說明困難の點があることは既に述べた如くである．

長沼統堆積後の斷層は衝上斷層の形式で行はれたが，その走向傾斜は一定してゐない．

三浦半島北部地質構造發達史概略

上記の層序と地質構造とから次の様な地質構造發達史が導き出される．

逗子統堆積以前：

葉山統下部の堆積．下部葉山統の構造の複雜化．主として東西の走向を持つ斷層，皺曲軸を形成した．蛇紋岩その他の火成岩の噴出．

之等の地質構造の完成後廣範圍に沍つて侵蝕作用があり，上部葉山統の堆積を見た．上部葉山統の堆積當時の三浦半島北部の狀態は明瞭には述べられない．處々に石灰岩・含化石石灰質砂岩があり，黑潮式動物群を含み，かなり等質の厚層である點から，當時この地域が黑潮式動物群の棲息を許した餘り淺からぬ海底であつたと解しても差支えない．

上部葉山統堆積後斷層の複雜化作用（渡邊久吉博士の大八洲構造運動）によつて，皺曲塊裂して次の逗子統堆積直前迄削剝作用を受けてゐた．皺曲軸はNNE—SSWの方向に收縮したことを示してゐる．

この削剝面に逗子統の堆積が開始された．逗子統堆積後の三浦半島北部は比較的深い陸棚海底となつてゐたものであらう．この堆積期には角閃石安山岩質凝灰岩の火山活動が屢々起つた．

最後に輝石安山岩を主とする火山活動が大規模に起り，金澤統の火山碎屑岩の豐富な地層が厚く堆積した海底地辷的現象がこの過渡期に屢々繰回された．金澤統下に接して露出する逗子統の岩相は常に一定でなく，平行不整合狀をなす．金澤統の基底の浦鄉砂礫岩中には屢々層間異常を見ることもできるし，礫岩中の礫の一部は著しく大形となり，逗子山中の礫を含む様になることもある．この礫岩中には往々海棲貝化石を含んでゐる．

北鎌倉・鎌倉山附近では傾斜不整合の露頭も見出されたので，逗子統堆積後金澤統堆積前に侵蝕の時代があつた様に解される．又その期間迄に逗子統は多少地殼運動により略ぼ現在の構造と類似の構造を作る様な地殼運動の影響を受けた様に思はれる．

逗子統中に見られる層向を斜斷する斷層系は恐らくこの地殼運動繼續中に形成されたものではなからうか．

この地殼運動は傾斜分布から判斷して鎌倉—浦郷の部分と小柴・圓海山の部分とを一撓曲帶として北へ傾斜し下り，その際僅な皺曲構造を各地に形成した．この構造は南へ行く程構造の複雜化が行はれた．逗子統以上の斷層を切る逆斷層・正斷層が殆ど完成された後に削剝期を挾んで大岡向斜の窪みに長沼統が堆積し始めた．

長沼統の堆積以後廣範圍の隆起と削剝とが行はれ，この地方の大部が一進一退を繰回しつゝ陸化した．この運動を多摩隆起運動と呼ぶ．

この陸化面の部は丹澤山地方面から東南へ向つた氾濫原で被はれた．保土ケ谷礫層は卽ちこの氾濫原の礫層で，之に續いて沈降が起り下末吉層が保土ケ谷礫層を堆積した河流の河口を被うた．この時期は筆者の dlII 時代の沈降運動である．Du 面はこの下末吉層及び保土ケ谷礫層の堆積面で略ぼ代表される．

この河底を被うた海は多摩丘陵を覆ひ被せずに現在の Du 段丘面の分布範圍に止つた．この樣な山形は突然隆起して，新しい侵蝕基準に順應しやうとする侵蝕谷の開析が餘り進まぬ內箱根火山中央圓錐丘・富士山火山等の活動となり，關東地方の南部全體に厚い關東ロームの堆積を起した．關東ロームは侵蝕作用の進められぬ程度に速に堆積を行つた．

關東ローム堆積後侵蝕が開始されて，各溪谷は段丘地形を作りながら溪谷底を深められたが，之等は次第に隆起に續く沈降のために沈溺した．そして一時は關東地方南部は複雜な海岸地形を示したが，近年の隆起運動と各河流の埋積作用とは現在の樣な海岸地形に達せしめてゐる．

第2圖に示す如く三浦半島北部は第三紀以來一進一退の沈降・隆起運動を示してゐるが，全體的には隆起の傾向を以て，我國土の面積を擴げる傾向にある．

附．地質構造發達史とは直接關係を有せぬが，こゝに地質と地震災害豫防に關する二三の氣付ける點を述べる． 地震斷層發生の可能性に就いて： 地震斷層の諸特徵より，三浦半島に於ける地震斷層發生の可能性は武山斷層に沿へる地域，横濱市弘明寺•大岡墓地附近，その他の形態的にも明なる斷層線に沿うて有る．崖崩れ發生の可能性に就いて： 横濱市內外に發達する臺地の崖は何れもその危險性がある．卽ち崖高く，基盤岩層と之を被覆する厚き被覆層とはその凝固程度を異にし，加速度大なる基盤層の地震動に對して上部は凝固程度弱く崩壞し易い．横濱——藤澤町以南の崖に露出する逗子統を截る細密なる斜斷層系はそれに沿うて節理を起し易く，この節理に沿うて地震の際崩壞の恐れあり．この山背部は地割・這行の現象を見ることあるべし．地辷發生の可能性に就いて： 武山斷層以北逗子統基底不整合線以南の地域には軟質未凝固の泥層發達し，この地層發達地域は地辷發生の恐れあり． 地割•這行の現象はこの

地域に於いて平時に於いても起り得．地震時に於ける泥砂水噴き・地割發生の可能性に就いて：　この地方の冲積統發達地域は一般に地層凝固せず，且つ渓谷底埋積物なるため水分を多量に含む．故に地震動によつて泥砂水噴き・地割の發生の可能性大なり，特に冲積統と周圍の基盤層との境界線に接して地割の發生の可能性大なり．

横濱市內外の低地・藤澤町以南の低地・鎌倉町の低地等は東京市の下町附近と類似の基盤の性質を有するを以てそれに應ずる施設を必要とす．

先輩諸說

横山又次郎博士．

横山博士はその大著 "Fossils from the Miura peninsula and its immediate north" Jour. Coll. Sci. Tokyo Imp. Univ. 39, 6 に於いて次の點を指摘されてゐる．

卽ち (1) 關東ロームとその下の海成層との間の不整合が存在すること．海成層自身の中にも不整合のあること．(2) 武藏野を作る地層は陸上堆積物 (subaerial series) と海成層との二層からなる．(3) 海成層は厚さ數百米に及び武藏野系と呼び上下二層に分つ．(4) 上層は王子・田端・品川等の武藏野に露はれるもので，*Elephas naumanni* MAKIYAMA (=*Elephas namadicus* of YOKOYAMA) を普通に含んでゐる．(5) 下部は主として三浦半島に露出し，上部から長沼帶・小柴帶・金澤帶・鎌倉帶・横須賀帶・宮田帶とした．地質時代は Pliocene であらうと。

上記の內 (1)(2) は筆者の觀察と一致する．(2) は筆者によつて約7層に細分された．横山博士の下部武藏野系には下限がなかつたが之は後に渡邊久吉博士によつて逗子統の基底と限定された．下部武藏野系の上限は横山博士により横濱市附近とされた如く，上部武藏野系たる下末吉統の下限は横濱市に觀察できそれ以西に見られない．下部武藏野系は更に長沼統下の不整合で二大分できる．横山博士の長沼帶化石產地中杉田・飯島・亀甲山？は小柴統中里泥層產のものと思はれる．(5) 横山博士の小柴帶は小柴產に限り他に杉田・飯島・龜甲山の產地を加へて小柴統の化石產地と見做すことができる．金澤帶の化石產地は金澤統の化石產地であり大船化石產地は恐らく金澤統中に含ましめてよろしいであらう．鎌倉帶は金澤統の下半を代表してゐると考へることができる．横山博士の化石產地中逗子と下宮田產化石は逗子統基底に近い層準の化石である．(6) 下部武藏野系の地質時代は全體として鮮新統であることは異存はあるまい．但し逗子統は上部中新統の疑がある．横須賀化石產地の大津は下末吉統の產地である．

德永博士．

之より先德永博士は此の地方の地質構造の詳細及び數多の化石產地を三浦半島から報告された．同博士の論文 (1902) 中には：

金澤——横須賀間の撓曲構造の存在を既に指摘されてゐる．化石產地中下末吉・子安・象歯を出せる横須賀の產地は下末吉統； 神奈川權現山・川上村・元町裏は屛風浦層； 瀧頭は冲積統に該當する．寺前・野島山は金澤統に屬す．

D. Brauns.

Brauns は三浦半島頸部の化石產地を二三ヶ所擧げてある．それらの內神奈川驛硝壁 (Kanagawa bluff) は一部は屛風浦層の不整合を示してゐる． Brauns は戶塚町附近の長沼統は洪積統と見做してゐる．

青木廉二郎教授.

青木教授は地球第三卷に三浦半島の海岸なる題下にこの地方の新第三系の層序を記され，下部より前三浦層群・三浦層群・及び長沼貝層に區分された．先三浦層群はそれより以前に葉山頁岩の名を以て呼ばれた地層で，筆者の葉山統である．三浦層群は筆者の逗子・金澤・小柴三統を含めたもので，三統を三浦層群の名で呼んでもよい．然し長沼統は明瞭な不整合で下末吉統に境することが分つた．この點で敷島統は更に細分される．横山博士の横須賀帶・宮田帶の一部を東京層と同時代のものであると結ばれたのは重要なる發見であつた．

同教授の第 I 期負の汀線移動は筆者の關東ローム堆積直前の隆起を意味し，第 II 期正の汀線移動は冲積世初期の沈降，第 III 期負の汀線移動は冲積世後期の隆起を意味する．

槇山次郎教授.

槇山教授は關東南部の洪積層を論じ，下部から Kanozanian, Sematian, Naritian, Tatikawan と區分され，屛風浦層を以て Kanozanian とした．筆者の長沼統には以下の數層も含まれる．下末吉統は Sematian に該當してゐる．槇山教授が多摩丘陵を以つて屛風浦附近の Kanozanian stage の堆積から成生せられたるかの如く記されてをられるが，之は筆者の觀察結果と一致してゐる．

青木・田山學士.

青木・田山學士兩先輩は多摩丘陵を以て東京層（又は下末吉統）堆積以後成生されたと論ぜられたが，之は既に槇山博士や筆者が述べた如く，東京層堆積以前に多摩丘陵の表面は開析を開始してゐた．

この他植田學士・池邊學士・鈴木好一學士等の三浦半島の層序に關する記事があるがこれらに就いては本論中にも引用してあるが摘要の型式であるからその詳細を紹介することを遠慮した．

終りに臨み，本研究の達成に當り補助せられたる日本學術振興會・並びに終始御論議・御教示を得たる矢部博士・石本所長・津屋博士・久野學士・鈴木・池邊兩學士に謝意を表す.

（本論文には挿圖 16，寫眞 11，地質圖版 1，を附す.

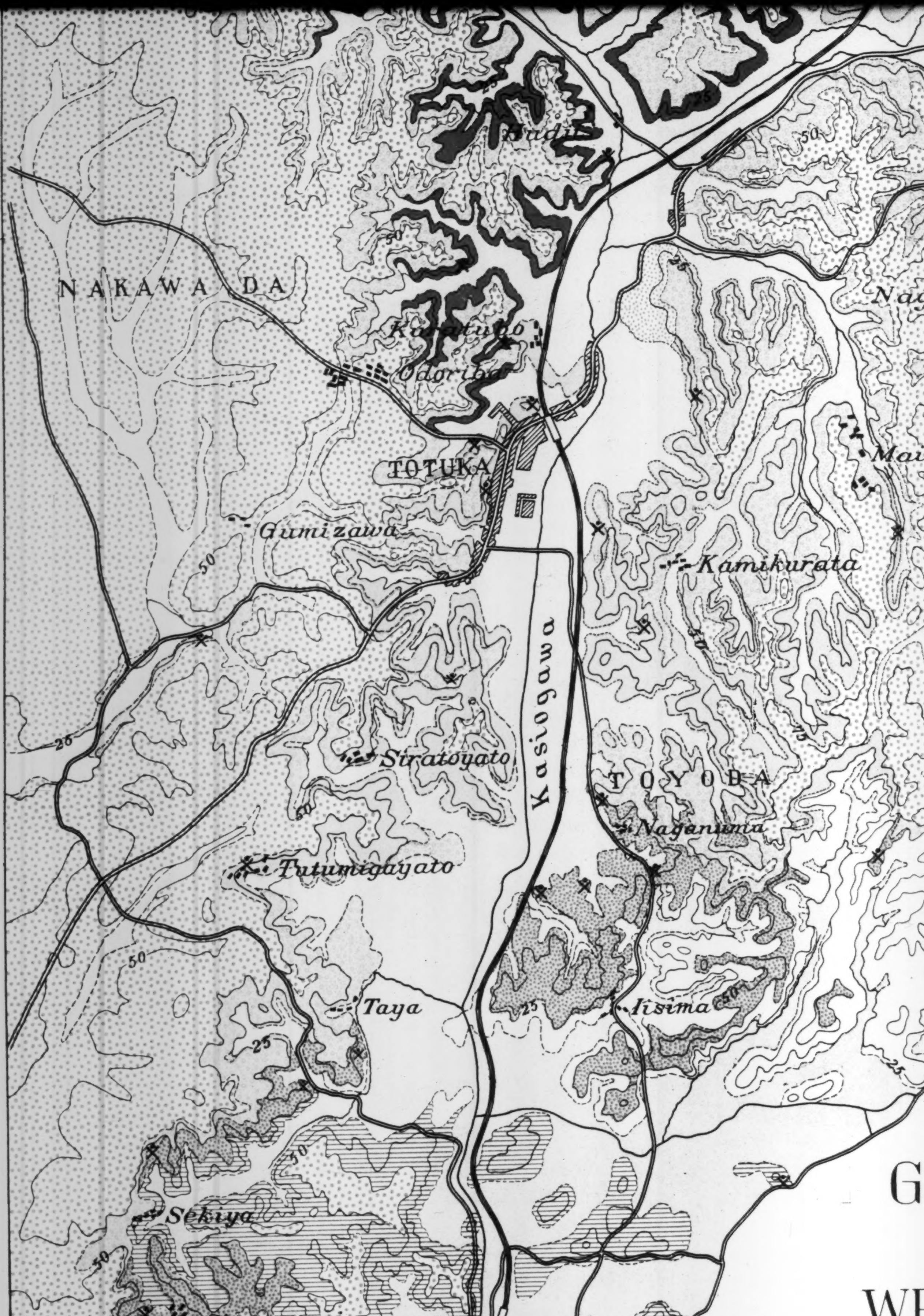
Hadi
NAKAWA DA
Kamatubo
Odoriba
TOTUKA
Gumizawa
Kamikurata
Kasiogawa
Siratoyato
TOYODA
Naganuma
Tutumigayato
Taya
Iisima
Sekiya
Siromeguri
ÔHUNA
MURAOKA
Takaya
Yamazaki
Nag
Mai
G
WE
0
25
50

（震研彙報 第十五號 圖版 大塚）

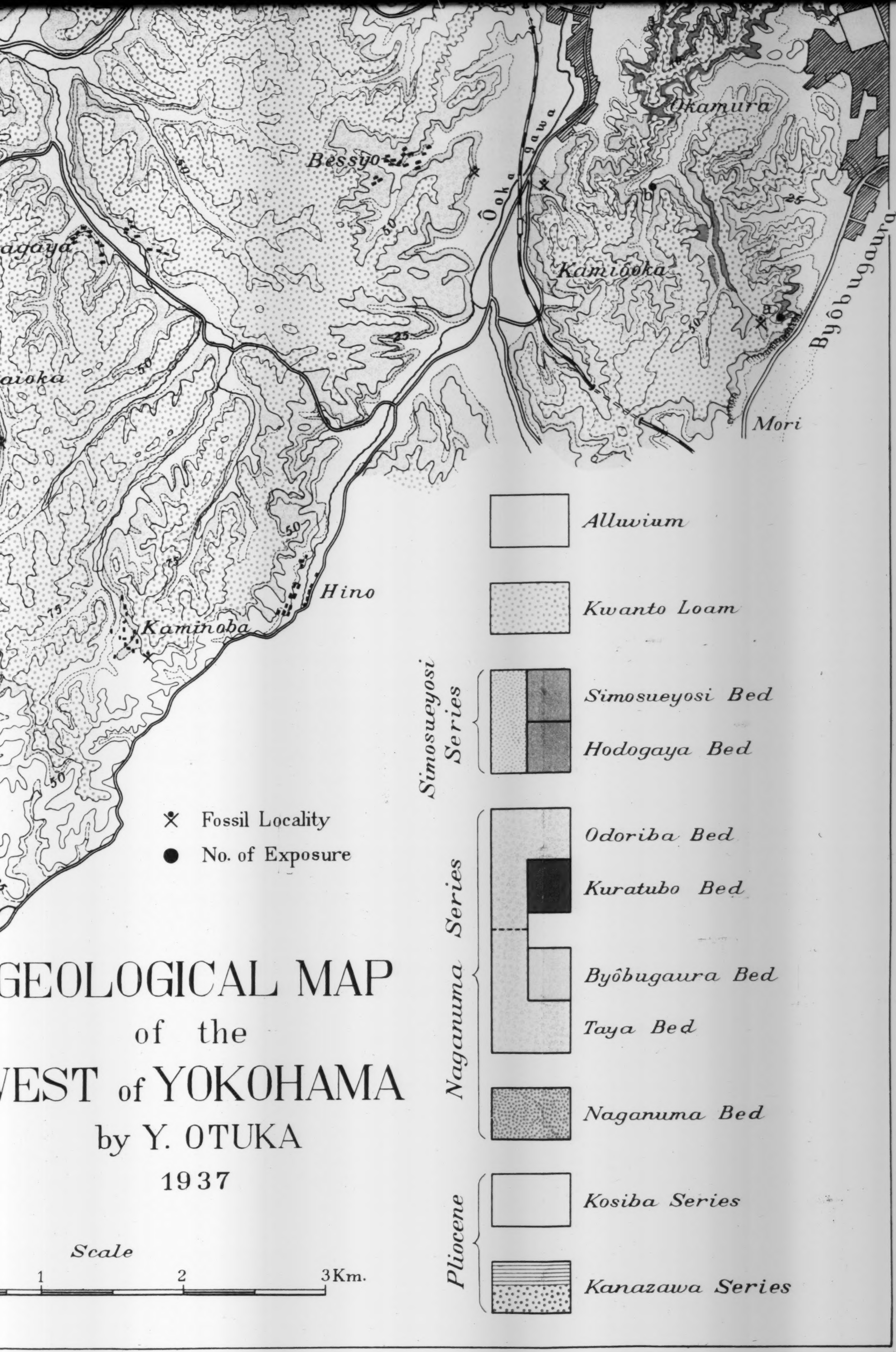

agaya
Bessyo
Ôoka gawa
Okamura
b
25
50
Kamiôoka
a
Byôbugaura
Mori
aioka
50
25
50
Hino
25
75
Kaminoba
50
Fossil Locality
No. of Exposure
Alluvium
Kwanto Loam
Simosueyosi Series
Simosueyosi Bed
Hodogaya Bed
Naganuma Series
Odoriba Bed
Kuratubo Bed
Byôbugaura Bed
Taya Bed
Naganuma Bed
Pliocene
Kosiba Series
Kanazawa Series
Scale
1
2
3Km.

GEOLOGICAL MAP
of the
VEST of YOKOHAMA

by Y. OTUKA

1937

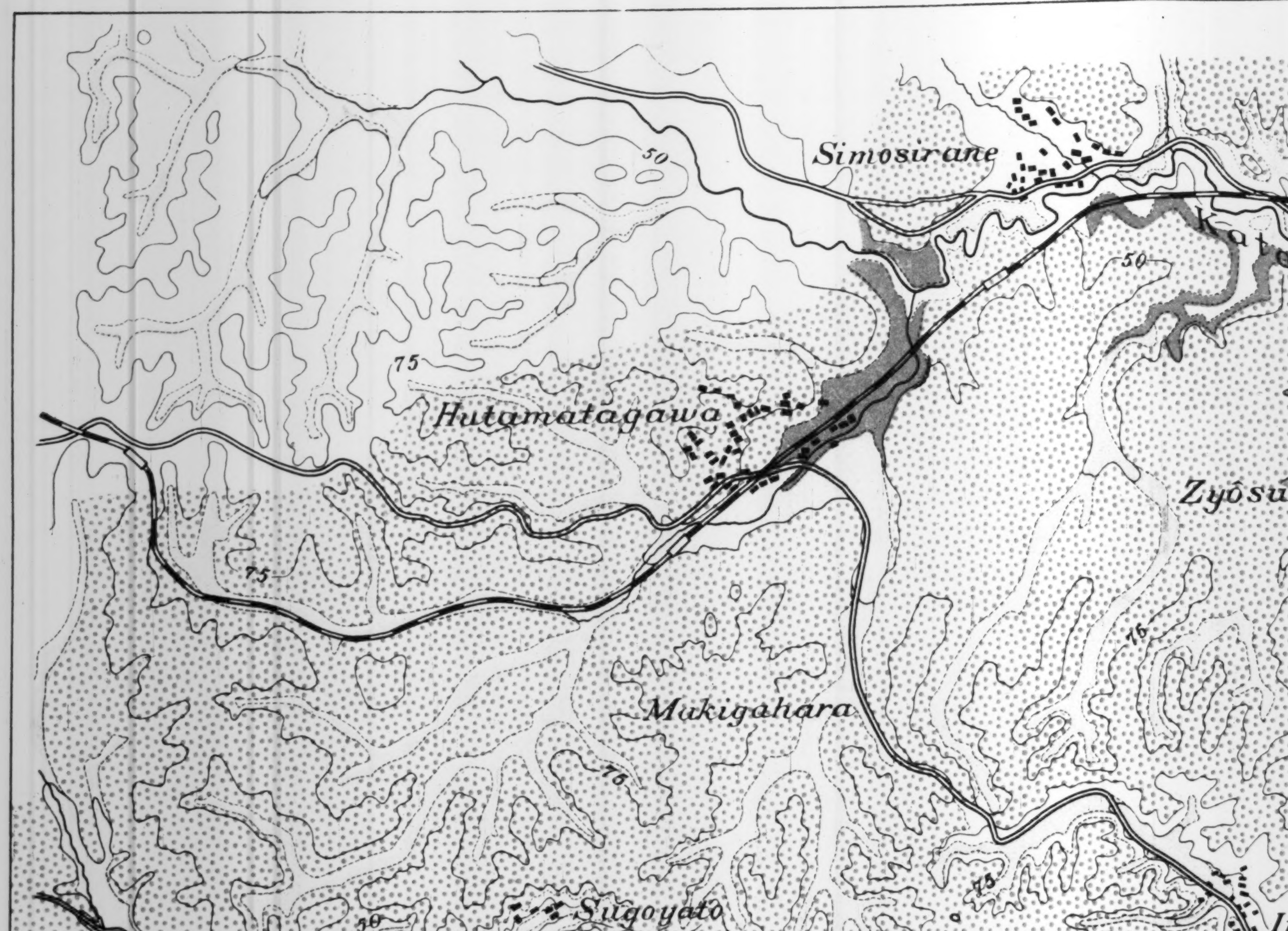
Simosirane
Hutamatagawa
Zyôsu
Mukigahara
Sugoyato
Akuwa
Mozinayato
Kanabusayato
Usiroyamada
Sinano
Inariyato
NAKAGAWA
Hanezawa
Nagaya
NAKAWADA
50
75

[Bull. Earthq. Res. Inst., Vol. XV, Pl. LXVII.]

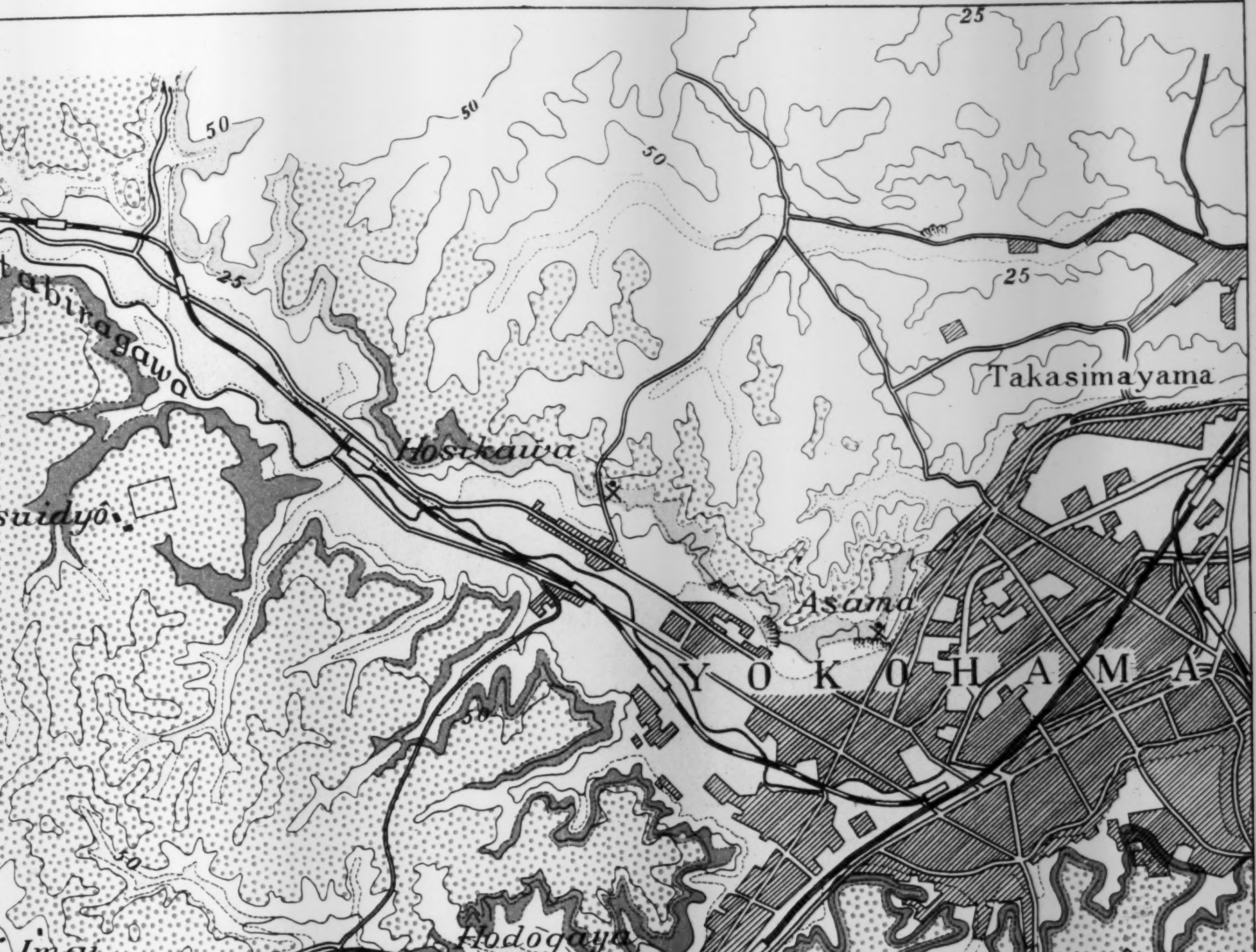
25
50
50
50
25
25
abiragawa
suidyô
Hosikawa
Takasimayama
Asama
YOKOHAMA
50
50
Imai
Hodogaya
Kuboyama
50
50
Zidôyuenti
50
Sanya
50
Gumyozi
25
Okamura
Bessyo
50
Ôokagawa
b
25
50
Kamiôoka

寫眞 1.（右）. 關東ローム (b) と二次的ローム (a). 於橫濱市白樂.

〔Phot. (right) shows an unconformity between the Kwantô loam and the secondary loam, exposed at Hakuraku in Yokohama.〕

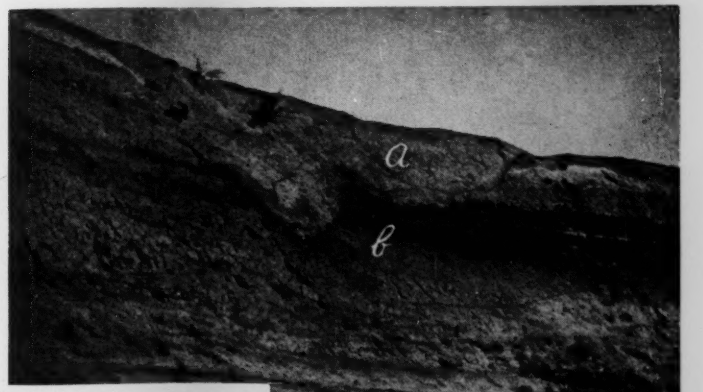

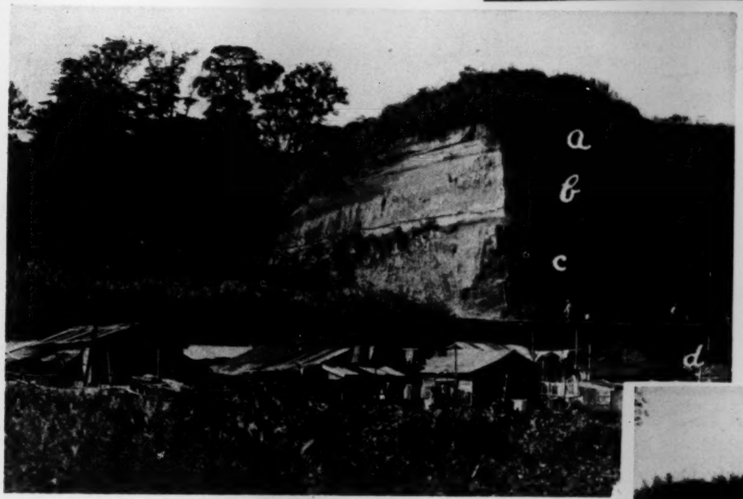

寫眞 2.（左）. 段丘崖，新山下町西南. a＝關東ローム，b＝下末吉層，c＝保土ケ谷礫層，d＝屏風浦層.

Phot. (left). The bluff, sw of Sin'yamasita-tyô, Yokohama. a＝Kwanto loam; b＝Simosueyosi bed; c＝Hodogaya gravel; d＝Byobugaura bed.

寫眞 3.（右）. 戸塚競馬場の東北崖. a＝ローム，b＝段丘層，c＝屏風浦層.

Phot. (right) shows the bluff, northeast corner of Totuka race track. a＝Loam, b＝Terrace sand, c＝Byôbugaura bed.

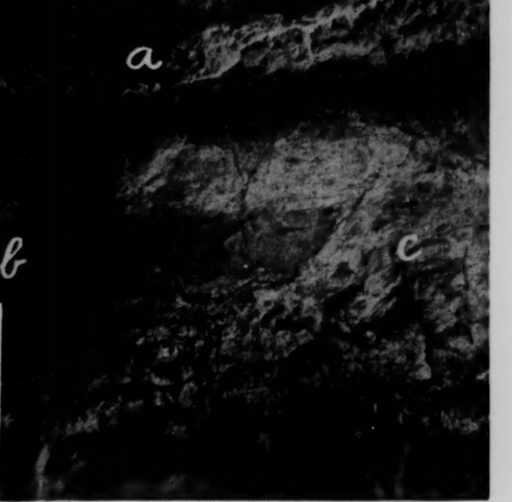

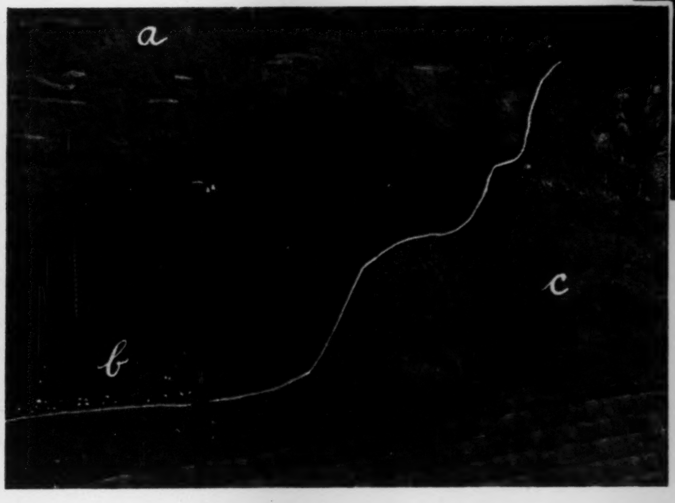

寫眞 4.（左）. 間坂切通南崖. a＝關東ローム；b＝保土ケ谷礫層；c＝屏風浦層.

Phot. (left) shows an unconformity between the Hodogaya gravel (b) and the Byôbugaura bed (c).

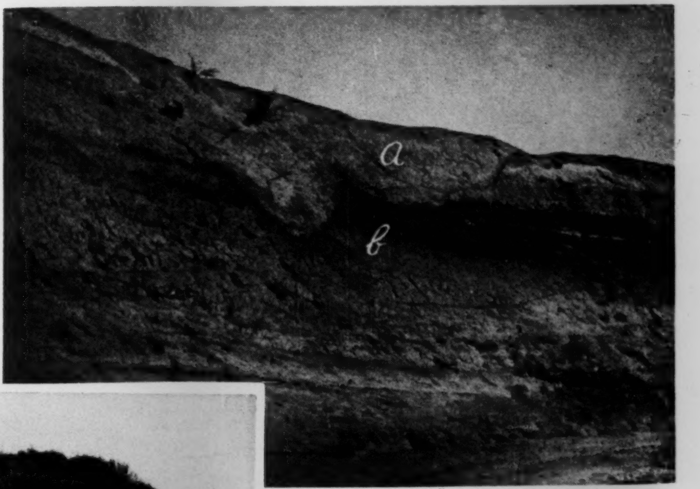

寫眞 1. (右). 關東ローム (b) さ二次的ローム (a). 於橫濱市白樂.

〔Phot. (right) shows an unconformity between the Kwantô loam and the secondary loam, exposed at Hakuraku in Yokohama.〕

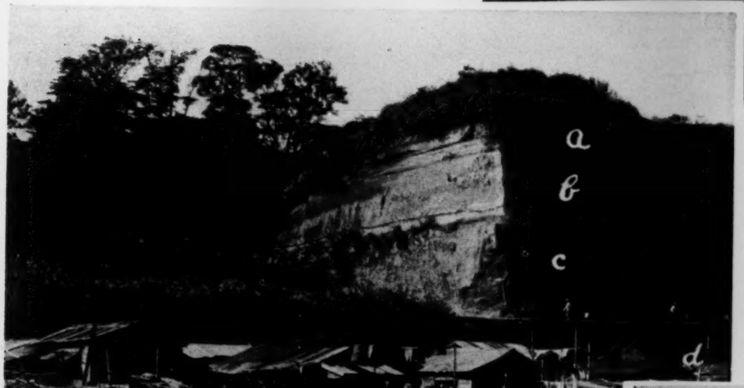

寫眞 2. (左). 段丘崖，新山下町西南. a＝關東ローム，b＝下末吉層，c＝保土ケ谷礫層，d＝屏風浦層.

Phot. (left). The bluff, sw of Sin'yamasita-tyô, Yokohama. a＝Kwanto loam; b＝Simosueyosi bed; c＝Hodogaya gravel; d＝Byobugaura bed.

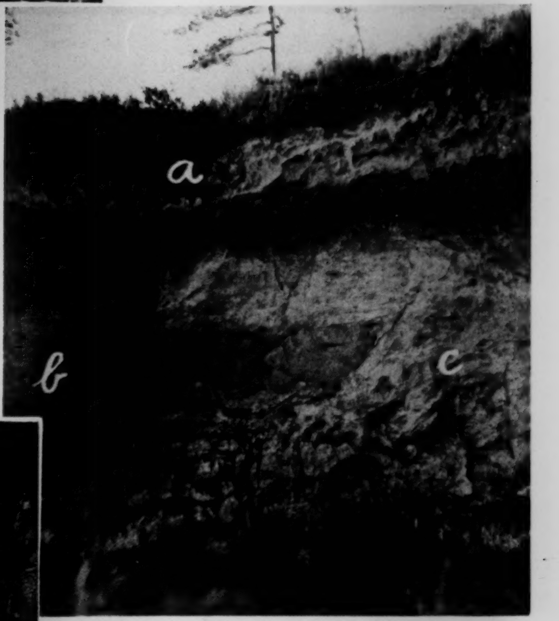

寫眞 3. (右). 戸塚競馬場の東北崖. a＝ローム，b＝段丘層，c＝屏風浦層.

Phot. (right) shows the bluff, northeast corner of Totuka race track. a＝Loam, b＝Terrace sand, c＝Byôbugaura bed.

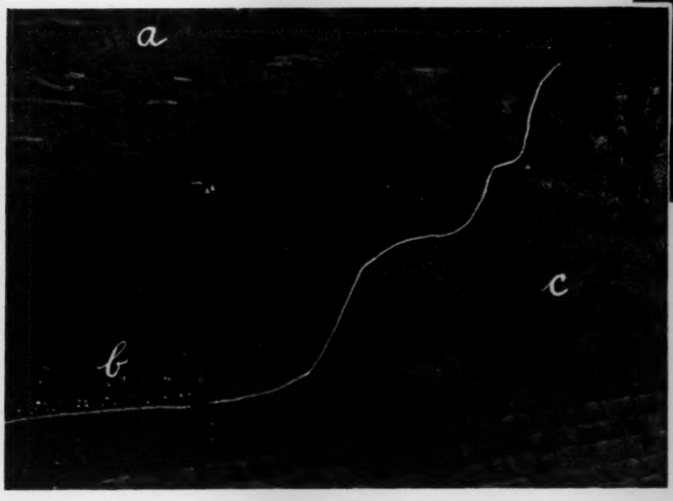

寫眞 4. (左). 間坂切通南崖. a＝關東ローム; b＝保土ケ谷礫層; c＝屏風浦層.

Phot. (left) shows an unconformity between the Hodogaya gravel (b) and the Byôbugaura bed (c).

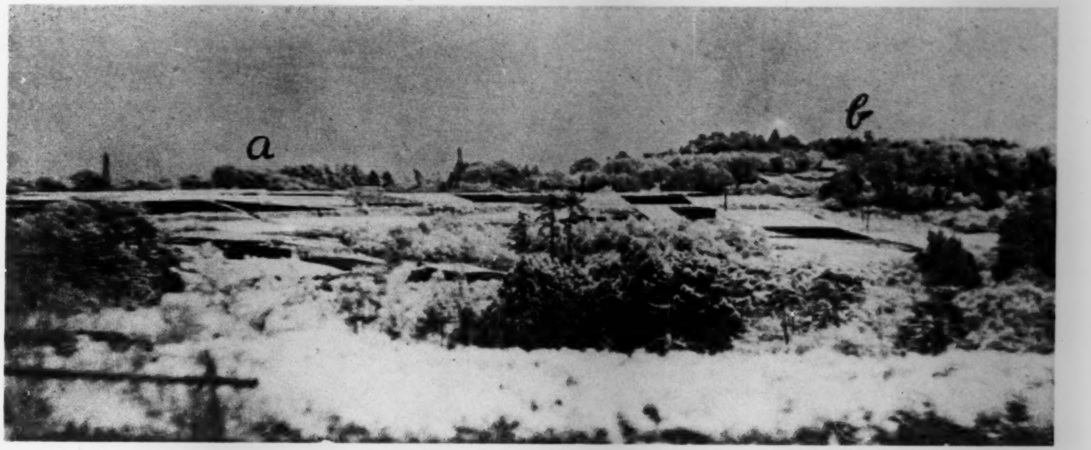

寫眞　5.（上）.帷子川沿岸に於ける武藏野段丘（a）と多摩丘陵（b）とを示す.

Phot. (above) shows the topographic relation of the Musasino terrace (a) to the Tama hill (b) "a" is the surface of the river terrace of the Katabira.

寫眞　6.（左）.長沼統（a）と大船層（b）との不整合を示す.於玉縄村坂下.

Phot. (left) shows an unconformity between the Naganuma bed and the Oohuna bed, exposed at west of Sakasita in Tamanawa-mura.

寫眞　7.（右）.長沼統（a）と中里層（b）との不整合.横濱市中區岡村町笹堀.

Phot. (right) shows an unconformity between the Naganuma series (a) and the Nakazato series (b).

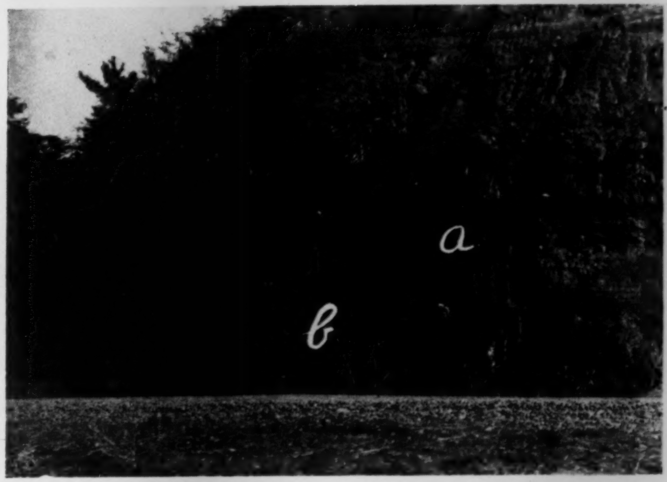

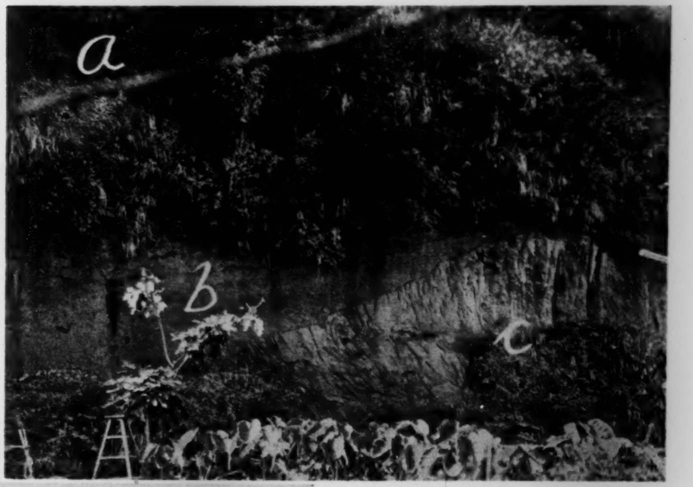

寫眞 8.（右）下末吉統と屏風浦層と中里層との不整合，於新山下町の西の崖.

Phot. (right) shows an unconformity between the Simosueyosi series, the Byobugaura bed, and the Nakazato bed exposed on the bluff of Sinyamasita-tyô.

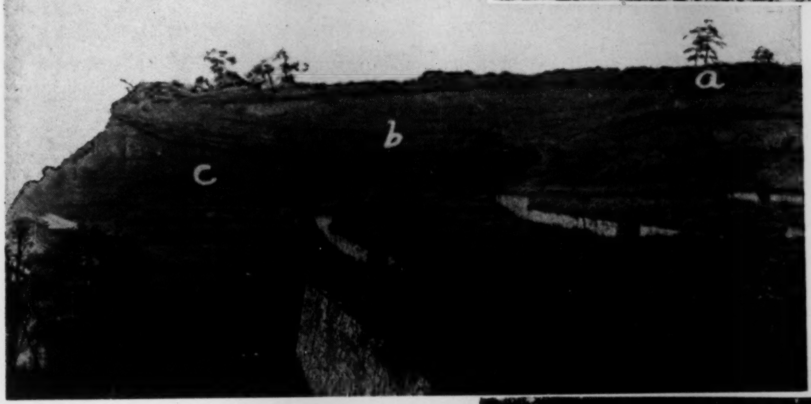

寫眞 9.（左）屏風浦層 (b) と小柴統 (c) との不整合を示す．於淺間臺.

Phot. (left) shows an unconformity between the Byobugaura bed (b) and the Kosiba series (c) exposed at Asamadai, west of Yokohama railroad station.

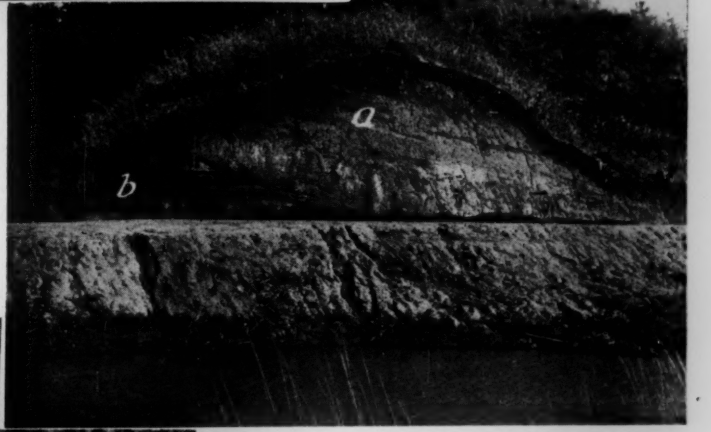

寫眞 10.（右）倉坪層 (a) と屏風浦層 (b) との間の不整合を示す.

Phot. (right) shows an unconformity between the Kuratubo bed (a) and the Byobugaura bed (b) exposed at Kuratubo, N. of totuka.

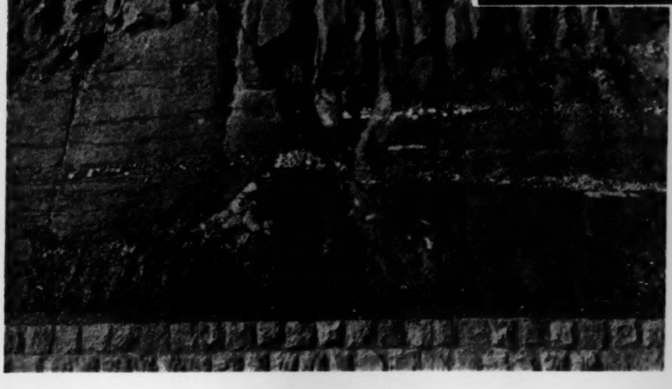

寫眞（左）屏風浦層を切る逆斷層，於大岡墓地，橫濱.

Phot. (left) shows a reverse fault displaced the Byôbugaura bed exposed at Ookaboti in Yokohama.

61. *Geologic Structure of the South Kwantô Region, Japan.* (1)

(*Yokohama—Huzisawa district.*)

Yanosuke OTUKA,

Earthquake Research Institute, Tôkyô Imperial University.

In this paper, the writer describes the stratigraphy, the chronology of the formations, and the tectonics of the district immediately north of the Miura peninsula.

Stratigraphy.

Stratigraphically, this district consists, in descending order, of Alluvial deposits, Post-Kwantô loam terrace deposits, Kwanto loam, Simosueyosi series, Naganuma series, Kosiba series, Kanazawa series, Dusi series, and Hayama series.

The Alluvial deposits mainly consist of unconsolidated marine mud and silt containing marine mollusca. These marine deposits burried some valleys that had formed and submerged after the deposition of the Kwantô loam. As some of these marine deposits are now exposed at 10 meter or so above sea-level, the earth's crust must have upheaved that much after the deposition of these marine deposits.

The Post-Kwantô loam terrace deposits are those that formed after the deposition of the Kwantô loam. The river terraces are distributed along the river courses that disect the depositional surface of the Kwantô loam. These river terraces consist of thin raw sienna coloured gravel beds that rest on the Kwantô loam and other older rocks. These terrace deposits, which are called post-Kwantô loam deposits, are bare in fossils.

The Kwantô loam, which is a burnt sienna coloured sandy material distributed on the terraces and hills in this district, is bare in fossils. According to recent studies of H. KUNO,1) the Kwantô loam in this region is composed of volcanic ashes mainly derived from Mt. Hakone and Mt. Huzi (Fuji).

The Simosueyosi series consist of the Hodogaya gravel bed and Simosueyosi sand and silt beds, which are rest on the Naganuma series and Kosiba series with unconformity, are unconformably overlain by the Kwantô loam. The sand and silt beds contain about 50 different fossils as listed in table II, III, IV. Fig. 7, 8, 9,10, 11 show the distribution of these marine deposits.

The Hodogaya gravel beds which are distributed in the terraces along the river Katabira from Hutamatagawa to Yokohama harbour, are about 30～25 m high at the base. The type locality of the Hodogaya gravel bed is that exposed on the terrace scarp south of Hodogaya railroad station. The gravels consist of pebbles derived from the mountainlands west of this region. On its southeast margin, this gravel bed is overlain by the Simosueyosi sand and silt bed.

The writer's Du terrace surface almost agrees with the depositional surface of this marine silt and sand deposits. Judging from their molluscan fauna, which is similar to that of formations containing early Pleistocene *Elephas*, the Simosueyosi series are believed to be Lower Pleistocene.

The Nagauuma series are the composite formations mostly distributed in the central part of this region, near Totuka-mati. It is subdivided into Odoriba sand, Kuratubo silt, Byobugaura sand and silt alternation, Taya gravel and sand, and Naganuma sand and silt (in descending order.)

The Odoriba sand bed is brown coloured, and bare of fossils.

The Kuratubo silt bed, which is a marine formation exposed 200 m west of Kuratubo, near Totuka-mati, is underlain by the Byôbugaura bed with erosional unconformity. Phot. 10 shows the exposure of this erosional unconformity. Table V column O and P show the fossil mollusca

---

[1] H. KUNO, *Jour. Geol. Soc. Japan*, **43**, (1936), *pp.* 225～229.

collected from this silt bed. The faunal character of this bed is similar to that of Sagami bay at a depth of about 20 m.

The Byôbugaura bed consists of brown sand and mud, upper part of which is sandy and the lower part muddy and silty. About fifty fossil mollusca have been collected from various localities of the muddy and silty part. The character of the molluscan fauna is decidedly estuarial, having been affected by the warm Kurosio (Japan) current. The faunules of loc. K, L, M, N in table V closely allied to those of the recent calm estuarial embayment in the Kii peninsula. *Umbonium decoratum* MAKIYAMA, *Theodoxus tokaidoensis* MAKIYAMA, *Batillaria multiformis* forma *yamadensis* OTUKA, and *Protapes irrediviva* MAKIYAMA are the characteristic fossils of this bed. The occurrence of fossil *Cervus* has also been reported from two localities of this bed. This bed which is partly underlain by the Kosiba series, is partly underlain by the Taya gravel and sand bed with conformity.

The Taya gravel bed is the cross-bedded sand and gravel bed exposed at Taya village, north of Oohuna railroad station. The bed is raw sienna in colour, and bare of fossils. It is underlain by the Naganuma bed with slight unconformity.

The Naganuma bed, which is the lowest formation in the Naganuma series, consists of marine sand and silt. It is underlain by the Kosiba and Kanazawa series with unconformity. Fossil mollusca collected from this bed are listed in Table V, column A, B, C, D, E. The faunal character, which is decidedly affected by the Kurosio current resembles that of recent Sagami bay at a depth of about 20 m. The faunules of the western localities of this bed show slightly deeper facies than those of the eastern localities. *Acila divaricata* (HINDS), some species of *Cymatium* and *Siphonalia* are common in the western localities, while in the eastern localities, *Pecten naganumanus* YOKOYAMA, *Crassatellites nanus* ADAMS et REEVE, *Tegula pfeifferi* PHILIPPI, *Bedeva birileffi* LISCHKE are common instead of the western ones. This ecologic fact supports the opinion that the Naganuma series was first deposited in the embayment that opens southwest.

The Kosiba series consists of Hama sand and silt alternation, Nakazato mud, and Kosiba tuffaceous sand beds.

The Hama sand and silt alternation, which is exposed near the Nagahama quarantine station, southwest of Yokohama, contains no fossils. This alternation, which is the upper most formation of the Kosiba series in this district, is overlain by the Naganuma series with such remarkable unconformity that we may still expect to find in other regions some formations lying above the Hama alternation.

The Nakazato mud bed is the basal formation exposed on the terrace scarps in the city of Yokohama. It is typically exposed at Nakazato, west of Sugita. Some pelagic molluscan remains have been collected from the mud bed. *Acila divaricata* (HINDS), *Yoldia naganumana* (YOKOYAMA), *Limopsis tokaiensis* YOKOYAMA, *Turritella fortilirata nipponica* YOKOYAMA, and *Chrysodomus phoeniseus* of YOKOYAMA are the common species in this bed. It is overlain conformably by the Hama bed and underlain by the Kosiba sand bed.

The Kosiba bed is a cross bedded tuffaceous and scoriaceous sand bed exposed at Siba near Kanazawabunko. It is underlain almost with conformity by the Kanazawa series.

M. YOKOYAMA[2] who reported some 100 species of fossil mollusca and molluscoidea from this sand bed, called this fossiliferous sand bed the Kosiba zone of his Lower Musashino formation. The fauna of this bed is mixed with fauna affected by the cold Oyasio current and the warm Kurosio current. Species common to the latter type of current found in this bed have been collected in recent seas of southwest Japan, at depth of more than 100 fathoms.

The Kanazawa series, which is overlain by the Kosiba series almost conformity, is subdivided according to its lithologic facies into three formations.

The uppermost formation, the Oohuna mud bed, which is exposed on the hill scarp west of

---

2) M. YOKOYAMA, *Jour. Coll. Sci. Tokyo Imp. Univ.*, **39**, 6 (1920).

Oohuna railroad station, the mud of which is homogenious, subconsolidated, and mineral grey in colour, and very closely resembling the Nakazato bed in its lithologic characters. The fossils in this bed have only very rarely collected. They are *Yoldia naganumana* (YOKOYAMA), *Limopsis tokaiensis* YOKOYAMA, *Trophonopsis nipponicus* (YOKOYAMA), *Chrysodomus phoeniseus* of YOKOYAMA. In this bed is found although rarely, pumice of two pyroxene dacite tuff scattered in form of intercalation.

The Nozima scoriaceous sand bed is the middle formation. This sand is rich in volcanic materials, and containing rarely deep sea mollusca, e. g. *Turcicula conveziuscula* (YOKOYAMA), *Turcicula crumpii* PILSBRY, *Dentalium yokoyamai* MAKIYAMA, and *Limopsis tokaiensis* YOKOYAMA. It gradually merges into the next underlying Uragô bed.

The Urago bed is the basal coarse sandy part of the Kanazawa series, which is typically exposed near the Oppama railroad station. It mainly consists of coarse brecciated sand of volcanic ejecta. Some horizons of this bed contain fossil mollusca.

The Uragô bed is underlain by the Dusi series with para-unconformity, its basal part being often disturbed by submarine gliding.

The Dusi series, which is an alternation of subconsolidated mud and scoriaceous sand, is underlain by the upper Hayama series with clino-unconformity. Pumices of hornblend bearing quartz andesite tuff are intercalated with this bed. Some fossil mollusca have been reported from this series, namely *Thyasira bisecta* CONRAD, *Miltha acutilineata* (CONRAD), *Chlamys miurensis* (YOKOYAMA), *Lima zushiensis* YOKOYAMA, *Nuculana yokoyamai* KURODA, and *Fusinus takatoriensis* OTUKA. Most of these species are found in the mud zone more than 100 fathoms deep in the seas of Central Japan.

The Hayama series is divided into two parts, the upper and the lower. The upper Hayama series consists of silicified shale, consolidated sandstone, and thin conglomerate. The lower part of this formation sometimes contains fossiliferous sandstone beds, from which *Trivia hayamensis* OTUKA, *Glycymeris* sp., *Cerithidea* sp., *Balanus cuculoides* (LINNAEUS), and *Astryclypeus integer* TOKUNAGA have been collected. The Sakuma series in the Bôsô peninsula may be almost contemporaneous with the upper Hayama series of the Miura peninsula.

The Lower Hayama series consists of hard black shale containing marly nodules, the tuffaceous sandstone being intruded by serpentine and other igneous rocks.

Chronologic considerations.

As previously noted, the Simosueyosi series may be lower Pleistocene. The age of the Naganuma series is a problem among the Japanese geologists. The writer is convinced that the age of the Naganuma series is either Plio-Pleistocene or Upper Pliocene, contemporaneous with the Soga bed in Siduoka prefecture and the Akimoto group in Bôsô peninsula, and the Ninomiya group in Kanagawa prefecture. Some of these groups just mentioned contain archaetypal *Elephas* and mollusca. From evolutional view point the archaetypal *Elephas* (=*Elephas matsumotoi* SAHEKI *Stegodon orientalis* OWENS) are believed to be Upper Pliocene in age. At any rate, these formations are decidedly older than the Simosueyosi series and other formations in which *Elephas namadicus naumanni* MAKIYAMA is found. *Cymatium subpyrum* (YOKOYAMA), *Umbonium naganumanum* OTUKA, *Clavatula dainichiensis muraokensis* OTUKA are the characteristic common fossil mollusca of these formations.

The Kosiba and the Kanazawa series may be Pliocene. No characteristic fossils were found in this bed. Its lithologic characters quite agree with those of the Takagohata or the Seki group in Bôsô peninsula.

The Dusi series may be Middle Neogene, and the Upper Hayama Miocene. Pumice of hornblend bearing quartz andesite tuff are usually found with the Amatu series in Bôsô peninsula and the Dusi series in the Miura peninsula.

The age of the lower part of the Hayama series may be pre-Miocene, seeing that the upper part of the Hayama series, from its foraminiferal fauna, is believed to be Miocene.

Tectonics.

Epeirogenetic movements in this district are schematically shown in Fig. 2. It may be inferred from this figure that the earth's crust in this region on the whole upheaves, with some subsidences between each period of upheaval.

Folding in this districts is marked by three phases. The first is the tectogenetic movement associated with the intrusion of Miura serpentin. The lower Hayama series was severely disturbed by this movement. This crustal disturbances will be called "the Mineoka phase."

The second is Ooyasima tectogenetic movement which was first pointed by K. WATANABE[3] from the marked structural difference between the Dusi and the upper part of the Hayama series. By this movement, the Upper Hayama series was strongly compressed in a N 45°E direction and severely folded and faulted.

The third is the Miura phase, by which the Dusi, the Kanazawa, and the Kosiba series were gently deformed, and the Ôoka, Hama, and Syakadôguti synclines, and the Gokurakuzi, and the Zyômyôzi, anticlines were formed. The folding of the Miura phase is gradually accenturated as goes southward.

Faulting. Numerous fault structure are found in the Hayama series, of which those running N45°W and EW are prominent. Most of these faults were formed by the Mineoka and Ôyasima phases.

Faulting of the Miura phase is represented by the Sugita reverse fault, the Gokurakuzi fault, the Oogigayatu faults, the Nikaidô faults, the Ikego faults, and the Takeyama reverse faults.

Beside the fault structures just described, two other faults are observed in this districts.

The one is the diagonal faulting which is finely distributed in the Dusi series, but rarely in the Kanazawa series with a trend of about N30°W and N30°E.

The other is the post-Naganuma (or Post-Simosueyosi) reverse faults, which cut the Byobugaura bed and run NS and N60°E, and are exposed at Gumyôzi and Simoôoka in Yokohama city.

K. WATANABE, *Jour. Geogr. Japan*, **37** (1925), pp. 495~500.

62. Some geologic considerations of the folded Tertiary zones in Japan (advanced paper).

By Yanosuke OTUKA,

Earthquake Research Institute, Tokyo Imperial University.

(Read March 16 th 1937, recieved Sept. 20 th, 1937.)

The writer has already published figures relating to the distribution of the contraction coefficient $\left(\frac{F-L}{F}\right)$ of the Pliocene strata in Japan,[1] and recently calculated and published the coefficients of all Tertiary strata in Japan as shown in Fig. 1. He[2] divided the seven intensely folded zones as shown in Fig. 2: (1) Karahuto-Yezo zone, (2) Miduho and Fossa Magna, (3) Ooigawa, (4) Sindi, (5) Amakusa, (6) Ryûkyû, and (7) Taiwan (=Formosa).

In this paper is discussed the manner in which these folded zones were formed through geologic ages since and before the Tertiary sediments had deposited.

The thickness of the Tertiary strata in Japan was calculated from about 140 geologic maps and reports so far published. Fig. 3 shows the distribution of the thickness of these Tertiary formations, in which the black circles mark the localities of the Tertiary formations, the thicknesses of which were measured by the writer.

Comparing the distribution of the contraction coefficients (Fig. 1) with that of the thickness of the Tertiary (Fig. 3), we find that a correlation exists between these two distributions, that is, the intensely folded area almost falls within the thickly deposited area.

In the Karahuto-Yezo folded zone, the Tertiary is some kilometers thick, but east of this zone, it is less than a few hundred meters thick.

The Miduho-Fossa Magna region is another thick deposit. The Neogene Tertiary here is some kilometers thick. The thickly deposited Tertiary extends from the western part of Hokkaidô to the western part of Northeast Japan to the Fossa Magna, while the Tertiary formations exposed on the Kitakami and Abukuma old land masses west of this region have very little thickness, with small contraction coefficients.

---

[1] Y. OTUKA, *Bull. Earthq. Res. Inst.*, **11** (1933), 4, 724~731.

[2] Y. OTUKA, *Proc. Imp. Acad. Tokyo.*, **13** (1937), 3, 78~81.

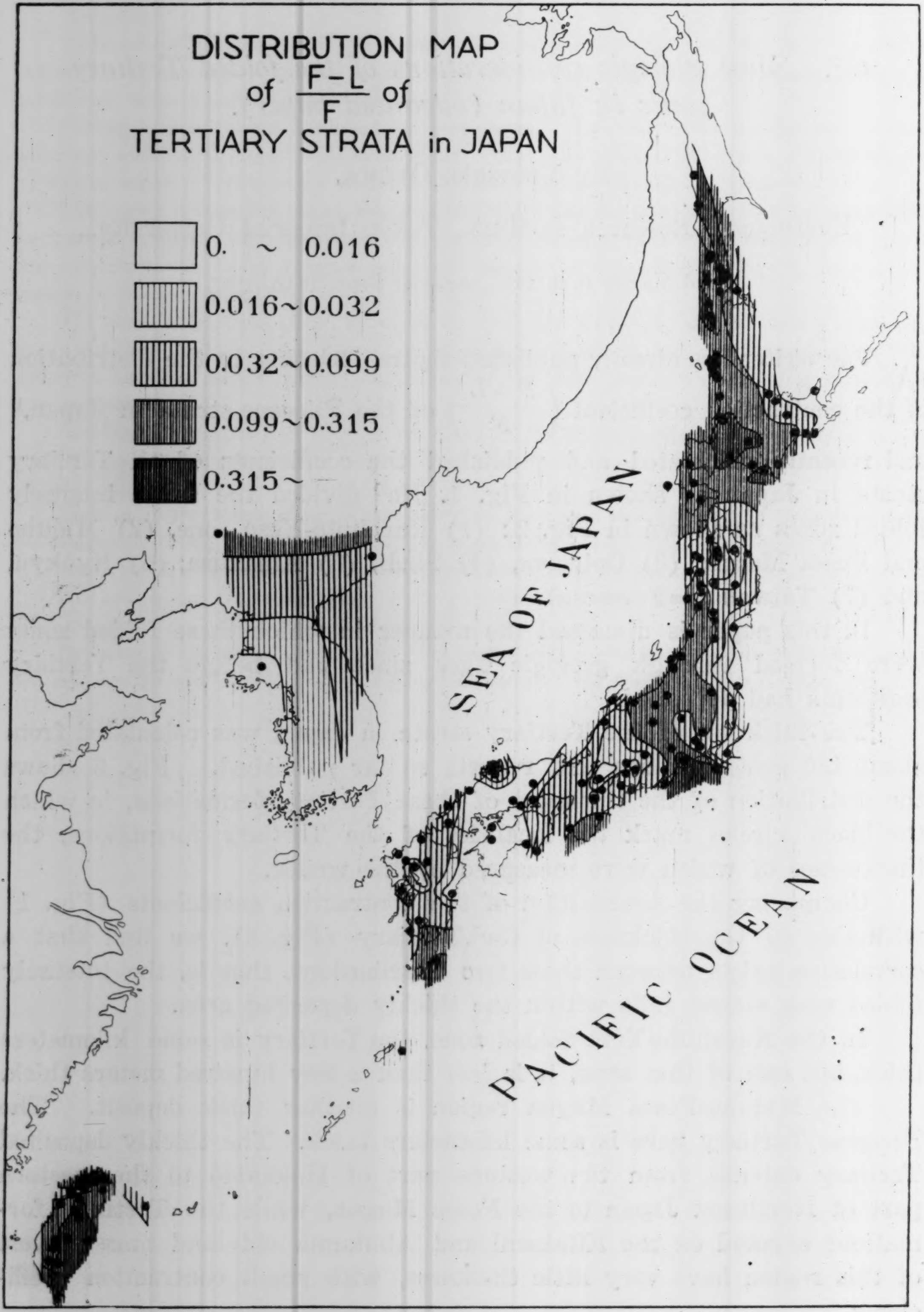
DISTRIBUTION MAP
of $\frac{F-L}{F}$ of
TERTIARY STRATA in JAPAN
0. ~ 0.016
0.016~0.032
0.032~0.099
0.099~0.315
0.315~
SEA OF JAPAN
PACIFIC OCEAN

Fig. 1. Distribution map of lines of equal $\left(\frac{F-L}{F}\right)$ of Tertiary strata in Japan. Black circles mark the localities of Tertiary measured by the writer.

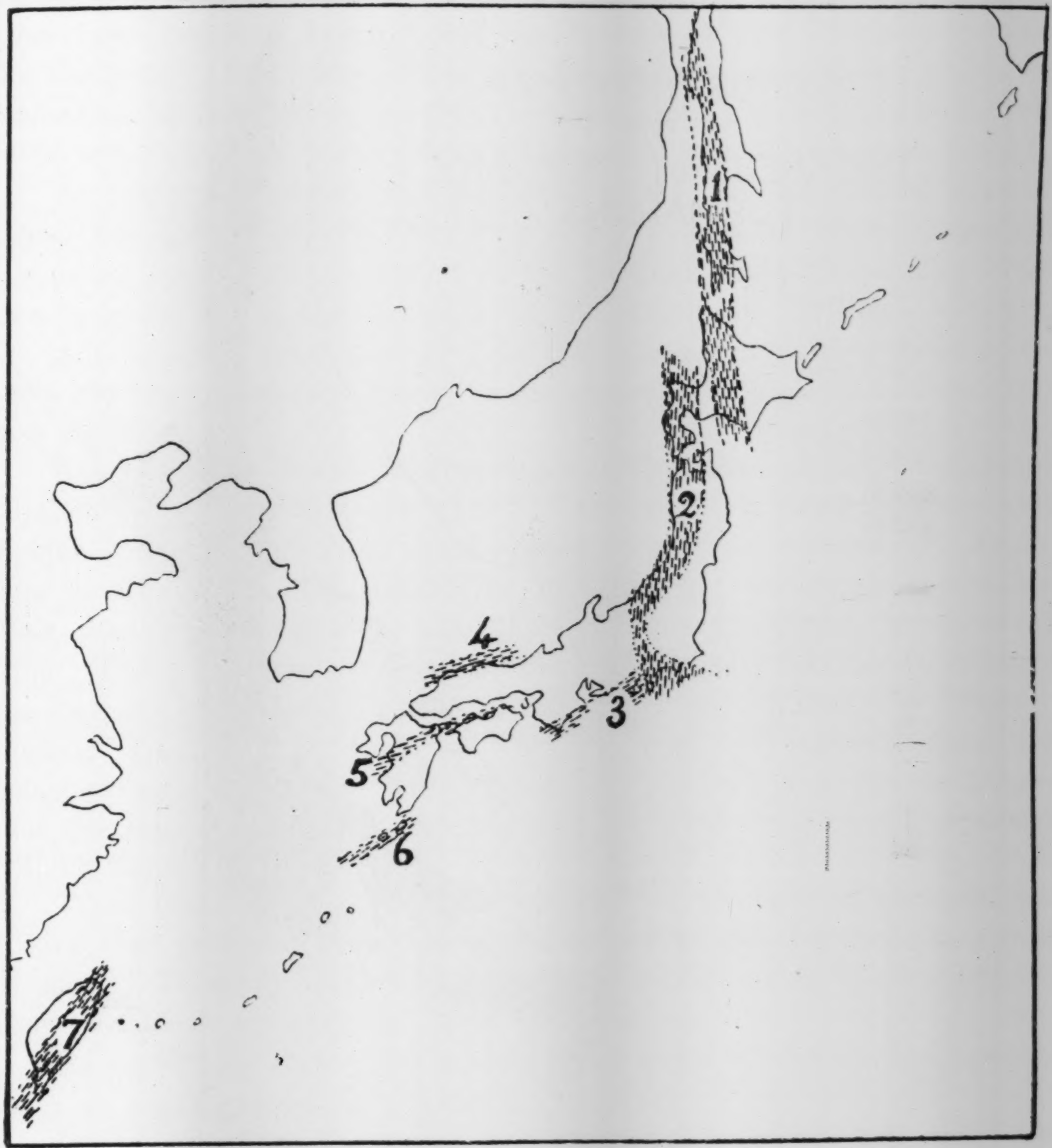

Fig 2. Distribution of folded Tertiary Zones. 1. Karahuto-Yezo zone; 2. Miduho-Fossa Magna zone; 3. Ooigawa zone; 4. Sindi zone; 5. Amakusa zone; 6. Ryûkyû zone; 7. Taiwan zone.

The writer concludes that the area on which the formation is thickly deposited deformed into a folded zone, as in the geosynclinal theory.

If this conclusion is correct, the folded region must have developed from the sedimentation area on which the formations accumulated to a great thickness.

The lithologic character of the Tertiary formation in these folded zones varies greatly. Some formations consist of cross-bedded coarse sandstone with shallow sea shells, while others consist of fine black

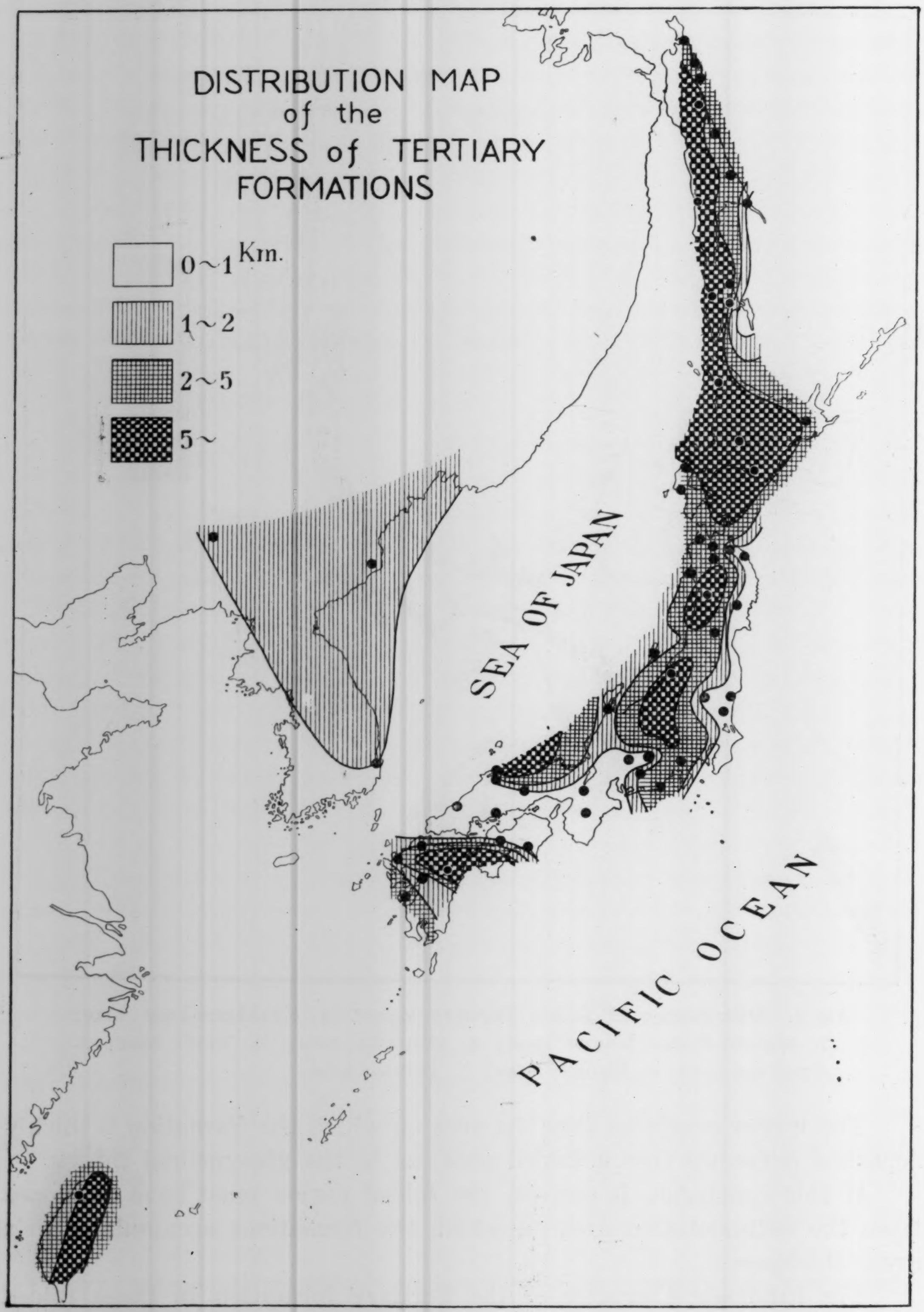
DISTRIBUTION MAP
of the
THICKNESS of TERTIARY
FORMATIONS
0~1 Km.
1~2
2~5
5~
SEA OF JAPAN
PACIFIC OCEAN

Fig. 3. Distribution of lines of equal thickness of Tertiary strata in Japan. Black circles mark the localities of the strata measured by the writer.

mud containing argillaceous foraminifera and mollusca, some of which have been reported from recent sea bottoms a few kilometers below the sea-level. Since these deep sea deposits are intercalated with the formations of these zones, the thick sedimentation area must have deepened to some thousand meters during the period of these deep sea deposits.

As previously stated, the dimension of the Tertiary folded zone in Japan was about 700~2000 km long and 100~200 km wide. Since the maximum contraction coefficient of the Tertiary formation in the folded zone is about 0·3 in the direction of the width, the original width of the sedimentation area succeeded by the folding may have been about 140~250 km as inferred from the reconstructed value of the contraction coefficient.

Recently the Naval Hydrographic Office (The Kaigun Suirobu)[3] published a new bathymetric chart of the northern Pacific. Many submarine trenches were resurveyed and their outlines corrected. According to this chart, the submarine trenches are arranged *en échelon*, their dimension being more than 2000 km long and about 150~250 km wide. These arrangements and dimensions are very similar to those of the Tertiary sedimentation area of Japan, excepting that the depth is slightly greater than that of Tertiary ones as inferred from the palaeontologic evidence. This resemblance leads the writer to believe that the recent submarine trenches may be sedimentation areas which will be succeeded by folding.

These considerations raise the question of the sort of geologic conditions that preceded these sedimentation areas later deformed to a folded zone. To study these earlier geologic conditions it is necessary to know the basal structure of these folded zones.

As previously stated, the known basal parts of the Tertiary folded zones in Japan consist of pyroclastic material.[4]

In the Karahuto-Yezo zone, T. MATSUMOTO[5] reported the occurrence of pyroclastic formation in the basal part of the Cretaceous formation in Karahuto.

In the Miduho-Fossa Magna zone, some liparitic and basaltic rocks and a thick pyroclastic formation (part of the so-called green tuff formation) extruded and deposited on the pre-Neogene and pre-Palaeogene basal rocks.

Although the folded structure of the Amakusa zone is closely related to the Median Dislocation Line and the Usuki-Yatusiro tectonic line,

---

3) *Kaigun Suirobu*, (1937).

4) Y. OTUKA, *op. cit.* (1937).

5) T. MATSUMOTO, *Jour. Geol. Soc. Japan, sp. vol.* **43** (1937).

T. MATSUMOTO[6] has reported that the Idumi sandstone in the Oonogawa basin is conformably underlain by a quartz porphyry flow which unconformably rests on the Pre-Mesozoic rocks.

In the Taiwan zone, the pre-Neogene was metamorphosed by igneous action.

As just stated, the sedimentation areas succeeded by folding are preceded by volcanic or igneous activities. The writer[7] has noted in his previous paper that volcanic activity is closely related to epeirogenetic crustal movements, and that the former was succeeded by subsidence of the earth's crust throughout the Tertiary in Japan.

From the foregoing remarks, the following scheme of the ideal tectogenesis of the Tertiary folded zones in Japan may be deduced:

1. Upheavel of land. Regression of the sea.
2. Volcanic activities; fracturing or blocking of the crust.
3. Settling of volcanically active regions.
4. Subsidence of settling areas. Transgression of the sea.
5. Formation of the sedimentation area (geosyncline or trough like depression). Accumulation of deposits.
6. Formation of the folded zone.
7. Upheaval of the folded zone.

---

62. 日本の第三紀皺曲帶の或る地質學的考察（豫報）

地震研究所 大塚彌之助

筆者は日本の第三紀皺曲帶を皺曲度によつて７つの皺曲帶に分けたが，此の論文では日本の第三系の層厚を測定して，皺曲帶の分布と層厚の大なる部分の分布とが一致することに氣付いた．之によつて地層を厚く堆積させる區域が皺曲帶になる事を知つた．今日地表に見られる海溝はその大きさ配列からみて一種の堆積區と見做せる樣である．

次にこの堆積區が如何なる地質學的經過をしたかを知るために夫々堆積層基底の性質を考究したところ基底の解つてゐる皺曲帶は何れもそれの延長方向に火成岩又は火山岩の活動の證左が見られた．斯して筆者は次の如く日本の第三紀皺曲帶成生の一般的經過を推定してゐる．

1. 地盤の隆起・海退.
2. 火山活動，地表地殼の破壞又は塊裂.
3. 火山活動の激しかつた地方の鎭靜.
4. 鎭靜區域の沈降・海進.
5. 堆積區域の形成.
6. 皺曲帶の形成.
7. 皺曲帶の隆起.

---

6) M. MATSUMOTO, *Jour. Geol. Soc. Japan.*, **43** (1937).
7) Y. OTUKA, *Disin*, **8**, 5 (1936), 221~232.

63. *Geophysical Studies of Volcano Mihara, Oosima Island; the General Aspect of Physical Conditions in the Crater.*

By Ryûtarô TAKAHASI and Takesi NAGATA,

Earthquake Research Institute.

(Read Sept. 21, 1937—Received Sept. 24, 1937)

1. The results of the topographic survey of the crater of Volcano Mihara have been reported in the previous paper.[1] According to this survey, the present pit is almost conical in shape, being about 300 m deep measured from the top of the pit wall. Although the mean diameter of the pit was only 100 m at the time of S. Nakamura's survey in 1924 and 230 m by H. Tsuya's measurement in 1933, it is about 310 m at present. These results show that the mean diameter of the crater has increased linearly with time, as shown in Fig. 1. During the period from 1924 to the present (1937), there has been no marked activity of the volcano except incessant rumblings and volcanic earthquakes. The changes in the diameter of the pit may therefore be due to collapses of the crater wall owing to these rumblings and earthquakes, while the corrosion of the rocks forming the pit wall by the effect of volcanic vapours may be indirect, but it is at the same time the most important cause of these collapses.

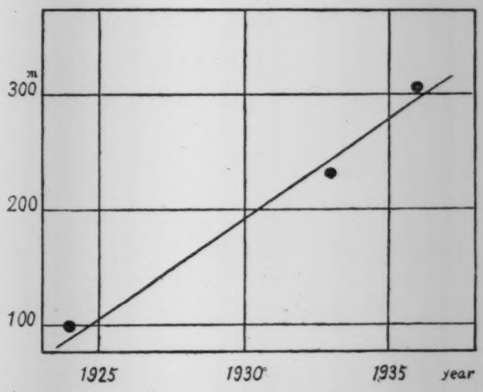

Fig. 1. Changes in the diameter of the crater of Mihara.

2. Since the changes in the topography of the interior of the pit, especially those in the depth, reflect most clearly the activity of the volcano, a re-survey of the topography of the interior of the pit was made in August, 1937. The method was exactly the same as that used in the previous case. By this re-survey it was found that the bottom of the pit has been covered with a sheet of newly formed solidified lava that flowed out probably during the minor activity of July 17, 1937.

---

[1] R. TAKAHASI and T. NAGATA, *Bull. Earthq. Res. Inst.*, **15** (1937), 441.

Except for this lava sheet, no marked change in the general topography was found to have occurred since the time of the last survey (Nov., 1936). As will be seen from Figs. 2, 3, the new lava sheet has overspread the bottom in the shape of a platter, 65 m in diameter, the molten incandescent lava being visible beneath this solidified lava sheet through its cracks. The position of the largest of these cracks was determined with the same method as mentioned in the previous paper. In Table I the results of this determination are given for comparison, together with those of Nov., 1936. These values are referred to the same coordinates as those mentioned in the previous paper. Since these values show that there has been no marked changes in the depth of the pit during the last year, we may conclude that Volcano Mihara has been quiet, and is likely to remain so for a while, seeing that a marked rise of the pit bottom must invariably precede a severe eruption

Table I.

cracks	x	y	z
	m m	m m	m m
No. 1 (Nov. 1936)	+104·6±1·7	+91·7±1·8	−267·7±3·4
No. 2 (〃)	+ 95·1±1·4	+81·3±1·3	−289·4±2·7
Aug. 1937	+114·7±1·7	+92·5±1·3	−298·7±3·6

Table II.

Reading of Current	No. of Lamp	Temperature	Condition
460 m.A.	No. 1	1020°C	Little Smoke
489	〃	1070	No Smoke
473	〃	1040	〃
498	〃	1095	〃
483	〃	1055	〃
483	〃	〃	〃
449	〃	990	Smoke
485	〃	1060	No Smoke
465	〃	1020	Little Smoke
430	No. 2	1010	〃
451	〃	1060	No Smoke
430	〃	1010	Little Smoke
439	No. 1	970	Smoke
458	〃	1010	Little smoke
465	〃	1020	〃

of this volcano,[2] just as it is the case with Asama.[3]

3. The temperature of the incandescent molten lava in the crater of a volcano is closely related to the activity of the volcano. Many reports have therefore been published on the temperature of the molten lava of such volcanoes as Vesuvius, Kilauea, Asama, Stromboli, etc. The writers measured the apparent temperature of the molten lava seen in the openings at the bottom of the pit of Mihara by means of a filament-disappearing-type pyrometer. To minimize the dispersion and absorption effects due to the emitting vapour, the measurement was made at night when there was very little or no vapour emission. These measurements are shown in Table II, in which "no smoke" means that no vadour could be seen anywhere in the whole crater, "little smoke" that the space from the bottom to the height of the shelf shown in Fig. 4 was filled with very light vapour, and "smoke" that the whole space of the pit was filled with the same very light vapour. These discontinuous changes in the conditions of the vapour are due to differences in the state of air circulation in the crater. The mean temperatures in these three states, "no smoke", "little smoke", and "smoke" were 1060°C, 1015°C, and 980°C respectively.

To reduce the dispersion effects above mentioned to the minimum, the following calculations were made.

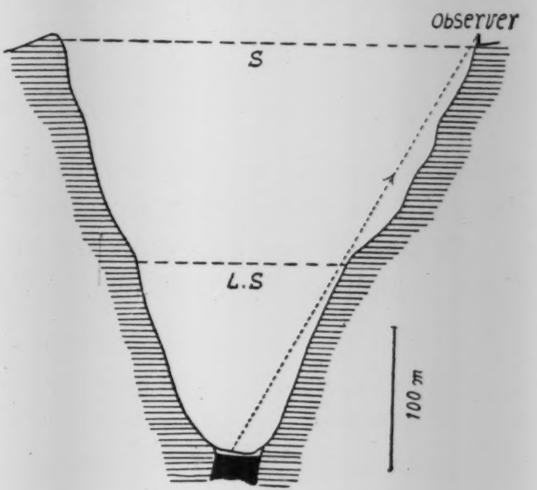

Fig. 4. Vertical section of the crater of Mihara.

Assuming that the energy change dJ of the radiation emitted from the incandescent lava is proportional to the density of the vapour in the differential interval ds of the path from the lava to the observer, we have

$$dJ = -cJ\delta ds, \qquad \cdots\cdots\cdots\cdots(1)$$

where c is a constant. Integrating (1), we get

$$J = J_0 e^{-c\int_0^s \delta ds}, \qquad \cdots\cdots\cdots\cdots(2)$$

where J is the observed energy and J_0 the true energy emitted from

---

2) F. Omori, *Rep. Earthq. Inv. Comm.*, No. 81 (1915).

3) T. Minakami, *Bull. Earth. Res. Inst.*, **15** (1937), 492.

the radiant source. As the vapour seemed to be distributed almost uniformly in the space under investigation, in both cases of "little smoke" and "smoke" we assumed that the density δ of the vapour is always constant throughout the range where the vapour is present. Of course the ranges of integration with regard to s in these two cases differ from each other. If we take

$$c\delta = k,$$
$$J = J_0 e^{-ks}, \tag{3}$$

where k is the coefficient of dispersion or absorption, and s the length of the part of the path of the radiation that is in the light vapour. As shown in Fig. 4, the lengths s are 160 m and 330 m in the cases of "little smoke" and "smoke" respectively.

Assuming further that the radiation process in our case follows Stefan-Boltzman's law, namely, $J = \sigma T^4$, we get the following relation from eqation (3):

$$4 \log T = 4 \log T_0 - ks, \tag{4}$$

where T and T_0 are the observed and true temperatures of the incandescent lava, both being expressed in the absolute temperature scale.

We shall now calculate the true temperature T_0 from our observations, which are fully shown in Table III. In determining the value of T_0, only the observed values of T that correspond to the two cases of "smoke" and "little smoke" were used. The observed temperature T in the case of "no smoke" was used only for checking the results of these determinations. The results thus calculated are

Table III.

Condition	T	S
No Smoke	1333°K (1060°C)	0 m
Little Smoke	1288 (1015 ″)	160
Smoke	1253 (980 ″)	330

$$T_0 = 1335\,^\circ K$$
$$k = 0{\cdot}00037 \text{ per meter.}$$

The magnitude of T_0 calculated above exactly agrees with the observed values in the case of "no smoke". We may therefore feel assured that this temperature of 1060°C at the surface of the incandescent lava is not very far out.

The temperature determined by us seems to be slightly higher than that found by K. Fuji[4] in 1913, just after the last severe eruption of this volcano (when $T=890°\sim1010°$C). This discrepancy may be due rather to the changes in the effect of cooling by air on the surface of the hot lava than to changes in temperature of the lava itself, for the lava in our case is in the bottom of the cone-shaped crater, 300 m deep, the greater part of which is coverd with a solidified lava shell, whereas when K. Fuji made his observation the lava had been exposed to open air at the same level as the present crater mouth.

4. During our temperature observation, we noticed that a wavy deformation had formed on the surface of the incandescent lava accompanying the intermittent vapour discharges from the lava. The deformation, which is of wave form with respect to space, makes an aperiodic motion with respect to time. The wave length λ and the amplitude of the deformation were $1{\cdot}5\sim2{\cdot}2$ m and $0{\cdot}5\sim0{\cdot}7$ m respectively. The time interval τ, in which the amplitude of the elevation becomes 1/10 of the initial value, was observed to be $1{\cdot}8\sim2{\cdot}1$ sec.

Although we have not at present any reliable knowledge of the mechanism of formation of this wavy deformation nor of its characteristics, i.e. whether it is a diverging wave or a standing wave, it is certain that this deformation is due to the disturbances caused by the intermittent gas emission, and that the surface of lava thus deformed begins to return to its stable state as soon as the gas discharges cease.

Assuming that the deformation is a standing gravity wave in a viscous fluid, we shall now estimate the magnitude of the coefficient of viscosity of the incandescent lava. For simplicity, we shall treat it as a two-dimensional problem, taking the x-axis horizontally and the y-axis upwards.

The equations of motion and the condition of continuity are

$$\frac{\partial u}{\partial t}=-\frac{1}{\rho}\frac{\partial p}{\partial x}+\nu\nabla^2 u, \qquad \frac{\partial v}{\partial t}=-\frac{1}{\rho}\frac{\partial p}{\partial y}+\nu\nabla^2 v-g, \qquad \frac{\partial u}{\partial x}+\frac{\partial v}{\partial y}=0,$$

where the notations u, v, p, ρ, t and g conform to the common usage[5] and ν donotes the kinetic coefficient of viscosity. If we take

$$u=-\frac{\partial \phi}{\partial x}-\frac{\partial \psi}{\partial y}, \qquad v=-\frac{\partial \phi}{\partial y}+\frac{\partial \psi}{\partial x},$$

---

[4] K. Fuji and T. Mizoguchi, *Proc. Tokyo. Math. Phys. Soc.*, 7 (1914), 243.

[5] See Lamb, Hydrodynamics, 4th ed. p. 591.

then
$$\left.\begin{aligned}&\Gamma^2\phi=0\,,\quad \frac{\partial^2\psi}{\partial t^2}=\nu\Gamma^2\psi\,,\\ \text{and}\quad &\frac{p}{\rho}=\frac{\partial\phi}{\partial t}-gy,\end{aligned}\right\}\tag{5}$$

where
$$\Gamma^2=\frac{\partial^2}{\partial x^2}+\frac{\partial^2}{\partial y^2}.$$

The solutions of equations (5) are

$$\phi=(Ae^{ky}+Be^{-ky})e^{ikx+\alpha t}$$
$$\psi=(Ce^{my}+De^{-my})e^{ikx+\alpha t}$$

where

$$m^2=k^2+\frac{\alpha}{\nu}.$$

In our case, $k=\dfrac{2\pi}{\lambda}$ is already given by the observation. We assume further that the depth of the fluid is infinitely large, and that the tangential and normal stresses at the free surface are zero, surface tension being neglected; whence

$$(p_{xy})_{y=0}=(p_{yy})_{y=0}=0.$$

Under these assumptions, we get the following relation after eliminating A, B, C, D;

$$(\alpha+2\nu k^2)^2+gk=4^2\nu k^3\sqrt{k^2+\alpha/\nu}\,.\tag{6}$$

Since in an extremely viscous fluid $\nu\gg 1$, we get the following approximate relation from equation (6),

$$\alpha=-\frac{g}{2\nu k}\tag{7}$$

In our case $e^{-2\cdot 0\alpha}=1/10$, and $k=2\pi/180$

that is, $\alpha=1\cdot 1$, $k=0\cdot 035$.

Putting these values in equation (7), we get

$$\nu=1\cdot 4\times 10^4\ \text{gr./cm. sec.}$$

As the mean density ρ of Mihara lava is 3·0, the cofficient of viscosity becomes $\mu=\nu\rho=5\times 10^4$ *C.G.S.*

The magnitude of the coefficient of viscosity thus obtained is near-

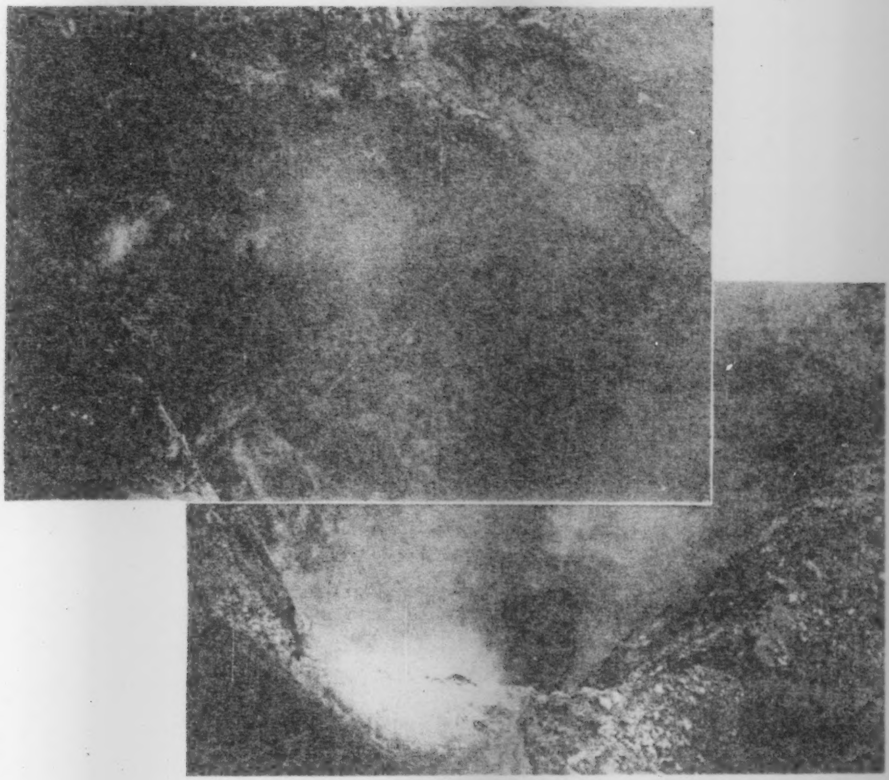

Fig. 2. The crater of Volcano Mihara.

（震研彙報 第十五號 圖版 高橋・永田）

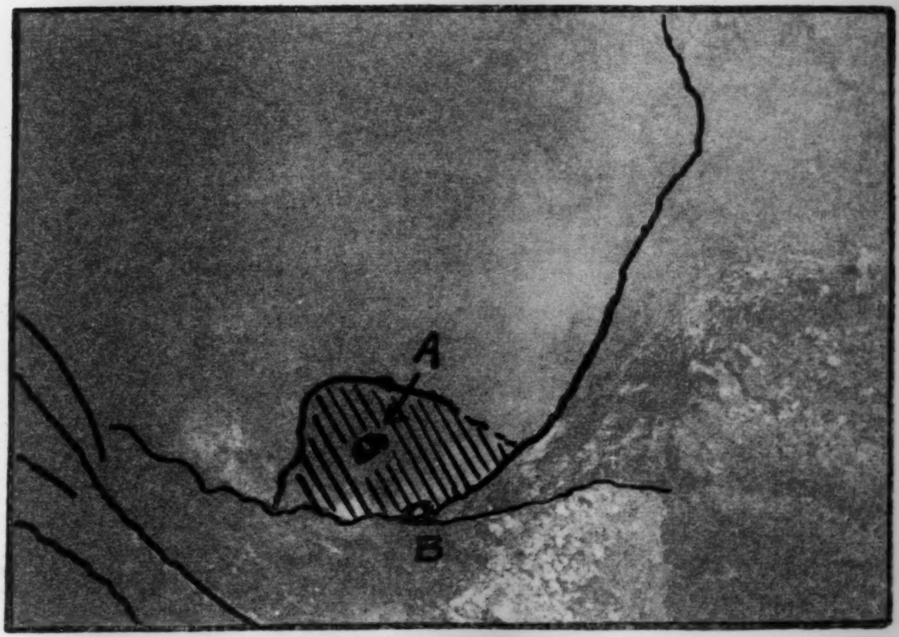

Fig. 3. The bottom of the crater of Mihara.

▨ Newly ejected and solidified lava.

A, B. Clacks, through which incandescent lava is seen.

$$\left.\begin{aligned} &\text{then} && \Gamma^2\phi=0\,, \quad \frac{\partial^2\psi}{\partial t^2}=\nu\Gamma^2\psi\,, \\ &\text{and} && \frac{p}{\rho}=\frac{\partial\phi}{\partial t}-gy, \end{aligned}\right\} \qquad (5)$$

where $$\Gamma^2=\frac{\partial^2}{\partial x^2}+\frac{\partial^2}{\partial y^2}.$$

The solutions of equations (5) are

$$\phi=(Ae^{ky}+Be^{-ky})e^{ikx+\alpha t}$$
$$\psi=(Ce^{my}+De^{-my})e^{ikx+\alpha t}$$

where

$$m^2=k^2+\frac{\alpha}{\nu}.$$

In our case, $k=\frac{2\pi}{\lambda}$ is already given by the observation. We assume further that the depth of the fluid is infinitely large, and that the tangential and normal stresses at the free surface are zero, surface tension being neglected; whence

$$(p_{xy})_{y=0}=(p_{yy})_{y=0}=0.$$

Under these assumptions, we get the following relation after eliminating A, B, C, D,

$$(\alpha+2\nu k^2)^2+gk=4^2\nu k^3\sqrt{k^2+\alpha/\nu}\,. \qquad (6)$$

Since in an extremely viscous fluid $\nu\gg1$, we get the following approximate relation from equation (6),

$$\alpha=-\frac{g}{2\nu k} \qquad (7)$$

In our case $e^{-2\alpha}=1/10$, and $k=2\pi/180$

that is $\alpha=1{\cdot}1$, $k=0{\cdot}035$.

Putting these values in equation (7), we get

$$\nu=1{\cdot}4\times10^4 \text{ g./cm. sec.}$$

As the mean density ρ of Mihara lava is 3·0, the cofficient of viscosity becomes $\mu=\nu\rho=5\times10^4$ *C.G.S.*

The magnitude of the coefficient of viscosity thus obtained is near-

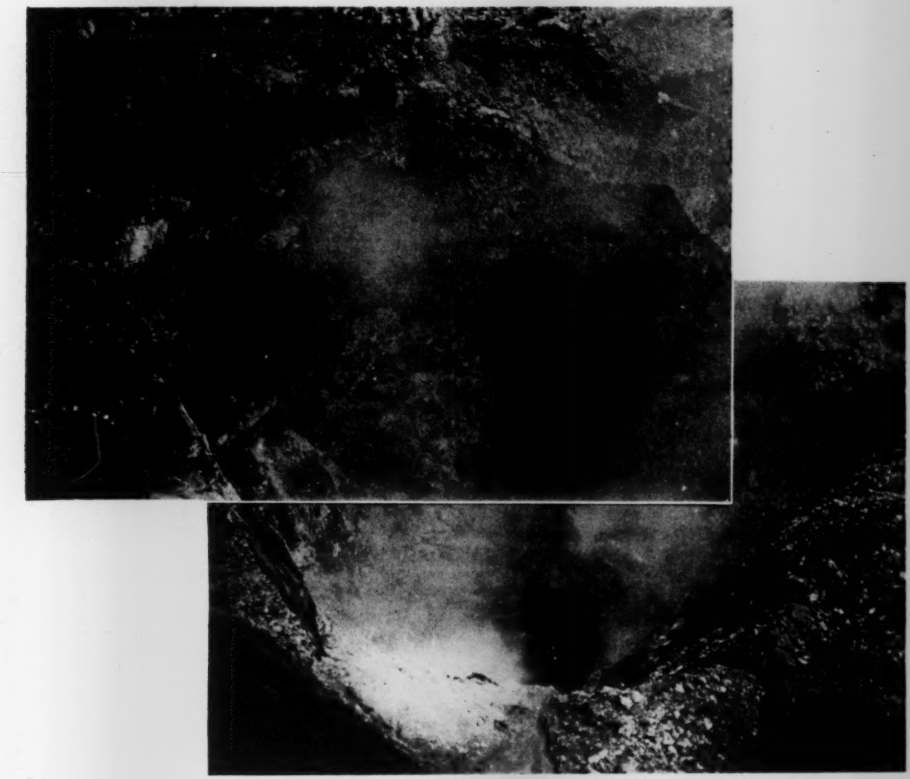

Fig. 2. The crater of Volcano Mihara.

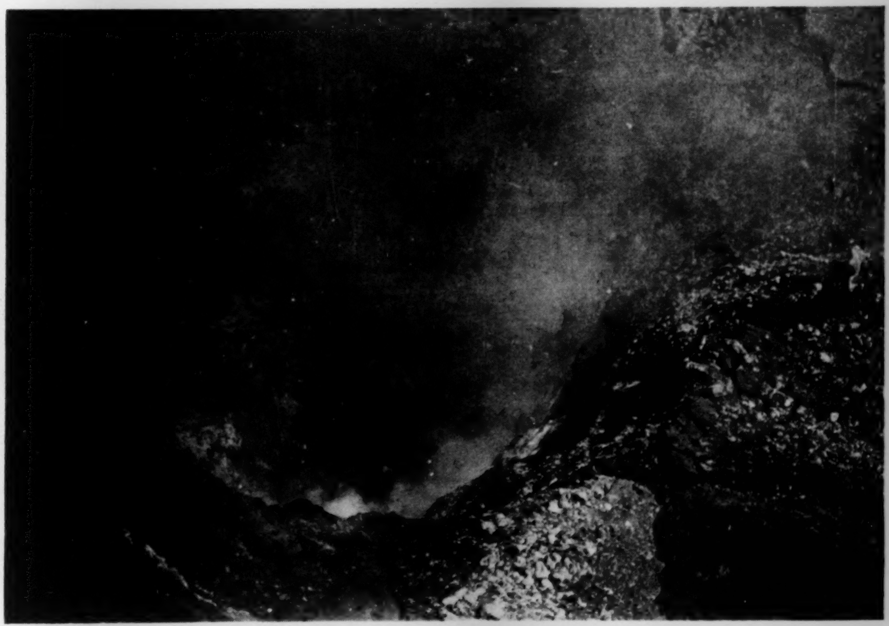

Fig. 3. The bottom of the crater of Mihara.

ly equal to that of "Miduame" at 20°C, as determined by N. Miyabe,[6] or to half of that of glycerine at 18°C.

The viscosity of the lava in the deeper part, however, will be smaller than this value obtained in the present study.

In conclusion, the writers wish to express their cordial thanks to the Hattori Hôkôkai for financial aid given, and to Prof. M. Ishimoto, the Director, for his interest in the present work.

---

63. 伊豆大島三原火山の地球物理學的研究

火口內の物理的性質の概況

地震研究所 ｛高橋龍太郎
永田武

1. 三原火山の火口內地形の再測を行つたが，1936 年 11 月の前測定から，今度の 1937 年 8 月の測定に至る間に於いては，火口底に新たな熔岩の噴出堆積があり，然も火口底は 10〜20 m 程度深くなつた他には大した變化は見られない．

2. 赤熱熔岩の表面溫度を光學高溫計で測定し，その結果に水蒸氣の吸收による影響に對する補正をして $t=1060°\mathrm{C}$ さいふ値を得た．

3. 赤熱熔岩表面の定常的波動運動から，その粘性係數を計算して，$\mu=5\times10^4$ *C.G.S.* を得た．之は 20°C に於ける水飴の粘性度に等しく Kilauea の熔岩の粘性より大いが內部に於いては更に粘性度の少い事が期待される．之等の研究は服部報公會の援助によつて行はれつゝある三原火山の地球物理學的研究の一部であつて同會に對し深謝の意を表する．

---

[6] N. Miyabe, *Bull. Earthq. Res. Inst.*, **12** (1934), 199.

——所　報——

○談話會記事

第121回談話會（昭和11年12月15日）

1. 地球内部に於けるP波の速度	本間正作
1. 北海道北見地方垂直線偏差觀測に就て	辻光之助
1. 昭和11年11月3日の地震に伴へる海水の動搖	宮部直巳 高山威雄
1. 房總半島東岸に見られる1デッケン構造	大塚彌之助 猪俣眞三
1. 根尾谷斷層に就て	津屋弘逵
1. 構造物の震動を防止する1つの方法（第1報　數理的研究）	妹澤克惟 金井清
1. 五重塔の耐震性に關する研究	妹澤克惟 金井清
1. 不連續面が彈性波の傳播に及ぼす影響（表面層の振動問題）（其の13）	西村源六郎 高山威雄
1. 振動方法による土の彈性測定　第2報　剛性率とポアソン比	石本巳四雄 飯田汲事

第122回談話會（昭和12年1月19日）

1. 伊豆伊東溫泉に就て	福富孝治 藤井次郎 鷹野政喜
1. 三原火山火口內地形の變遷	高橋龍太郎 永田武 平能金太郎
1. 北大東島試錐（第2報）	矢部長克
1. 西南日本中生代の海侵と地殼變動の概察	小林貞一
1. 球窩面に剪力が働いて起る振動とその逸散波	妹澤克惟 金井清
1. 斜めの入射波による表面層の振動とその共振れ性質	西村源六郎 高山威雄
1. 振動方法による土の彈性測定補遺	石本巳四雄 飯田汲事
1. 昭和11年12月27日の伊豆新島地震に就て	福富孝治
1. 昭和11年12月27日伊豆新島地震の餘震觀測並に踏查報告	萩原尊禮 表俊一郎
1. 淺間山に於ける12月13日の磁力變動	長岡半太郎

第123回談話會（昭和12年2月16日）

1. 本郷，丸內，三鷹村の微動の消長	石本巳四雄
1. 永久變移の在る場合の振子の振動　附 廻轉型振動臺	坪井忠二 淵田隆門

1.	日本の第三紀皺曲帶（1）	大塚彌之助
1.	新島の地質に就て	津屋弘逵
1.	新島に於ける地磁氣伏角測定結果報告	永田　武
1.	最近の淺間山の活動に現はれたる火口底の著しい昇降變化	水上　武
1.	地表層が鉛直荷重を受ける場合の彈性的變形分布は就て	妹澤克惟 金井　清
1.	斜めの入射波による表面層の振動と其の共振れ性質（補遺）	西村源六郎 高山威雄
1.	地殼內に在る空窩の破壞によつて生ずる地震波	西村源六郎
1.	淺間山活動に伴ふ急激なる磁氣變動	長岡半太郎
1.	火山熔岩の位置を如何にして測定するか	長岡半太郎

第124回談話會（昭和12年3月16日）

1.	震源距離大なる地震の東京附近卓越振動周期	石本巳四雄
1.	土の收縮に關する二三の實驗	飯田汲事
1.	伊豆地方の地殼變動に就て	山口生知
1.	昭和5年伊東地震の時間分布	岸上冬彥
1.	東京近傍水準測量	陸地測量部
1.	重力と地下構造との一關係	坪井忠二
1.	日本の第三紀皺曲帶（2）	大塚彌之助
1.	斜のディスターバンスによつて誘起する表面層の自由振動に就て 附話　先月の報告の補遺	妹澤克惟 金井　清
1.	橋梁の振動に於ける勢力の逸散性（第1報）	妹澤克惟 金井　清

第125回談話會（昭和12年4月20日）

1.	昭和5年北伊豆地震に伴ひたる蘆の湖靜振の解析	鈴木武夫
1.	蘆の湖靜振の減衰と水の粘性	鈴木武夫
1.	淺間山に於ける磁氣變動より得たる火山內熔岩の考索	長岡半太郎
1.	九州に於ける水準改測結果	宮部直巳
1.	丹後地方地殼變形の研究　補遺	宮部直巳
1.	直線源による彈性波の方位的分布に就て	井上宇胤
1.	臺灣震災地復舊測量に就て	陸地測量部
1	橋梁の振動に於ける勢力の逸散性（第2報）	妹澤克惟 金井　清
1.	琵琶湖の水位より見たる地殼變動	坪井忠二 淵田隆門
1.	重力と地下構造との關係	坪井忠二 淵田隆門
1.	玄武岩質岩漿の分別晶出作用に就て	久野　久
1.	本源岩漿の問題に就て	久野　久
1.	新島に於ける地磁氣測定結果　補遺	永田　武

第126回談話會（昭和12年5月18日）

1.	蓮臺寺の一溫泉の水位に及ぼしたる雨量氣壓並地震の影響	福富孝治

所報

1. 溫泉が湧出する場合の地表近く溫度の分布	福富孝治
1. 地震發生の一年變化	松澤武雄 仲町容 西川與志男 吉村慶丸
1. 彈性體内部に靜的歪の成立或は消失の際の過渡的現象に就て（第 1 報）	河角廣 吉山良一
1. 發震時測定精度より見たる地殼構造推定の精度に就て	河角廣
1. 發震時測定の心理的誤差に就て	河角廣 木下潤一
1. 地表層の厚さとラブ波の振幅との關係	妹澤克惟 金井清
1. 最近の淺間火山の活動と地表傾斜變化	高橋龍太郎 水上武
1. 淺間及三原火山熔岩の物理的性質（其の 1）電氣傳導度の溫度による變化	永田武
1. 清澄山地南部の地質構造	大塚彌之助
1. 名古屋城天守閣の震動	齊田時太郎

——所　報——

○談話會記事

第127回談話會（昭和12年6月15日）

1.	震源に就て	井上宇胤
2.	重力異常とゼオイドの高低	坪井忠二
3.	アイソスタシーに關するエアリー，プラットの假說に就て	坪井忠二
4.	地球の核のプラスチック性に就て	妹澤克惟
5.	構造物の震動防止法の模型實驗的確め	妹澤克惟 金井清
6.	丸ノ內に於ける表面土と基盤岩との彈性測定	飯田汲事
7.	淺間火山附近に於ける湧水及鑛泉の比重測定	柴田雄次 野口喜三雄 金子修
8.	淺間山噴火に伴ふ磁氣變動並に其機構	長岡半太郎 池邊常刀

第128回談話會（昭和12年7月6日）

1.	本鄉に於ける觀測より推定し得たる地殼表層の配列（第1報）	木下潤一
2.	百日繼續の地震計記錄裝置	石本巳四雄
3.	金時山—幕山構造線に就て	久野久
4.	橫濱—藤澤間の地質（續報）	大塚彌之助
5.	マグマ層のプラスチック性に就て	妹澤克惟
6.	振動性津浪の卓越周期に就て 附話　前回報告の補遺	妹澤克惟 金井清
7.	彈性體內に在る空窩の內面に作用する壓力變化によつて生づる彈性波	西村源六郎
8.	斜めに入射する體自由波による表面層內の彈性波振動	西村源六郎 高山威雄
9.	淺間山噴火に伴ふ磁氣變動並に其構造	長岡半太郎 池邊常刀

第129回談話會（昭和12年9月21日）

1.	本邦に於ける Composite dike 及び Composite lava flow の發見に就て	久野久
2.	本邦隆起汀線研究	尾原信彥
3.	本邦隆起汀線研究 隆起汀線の測定と夫れによつて知られた二三の事實	今村學郎
4.	本邦隆起汀線研究 樺太南部の地形隆起汀線	今村學郎
5.	伊豆式根地內島に於ける土地隆起の跡	福富孝治

6.	東京本郷に於ける短週期脈動の觀測	岸上冬彦
7.	車輛，航空機用加速度計の製作	萩原尊禮
8.	地表層の厚さと分散性レーレー波の振幅との關係	妹澤克惟 金井清
9.	(a) 極座標上から出した地球の彈性的安定の問題 (b) 前回報告の補遺	妹澤克惟 金井清
10.	短波長電波送信法を利用せる重力の比較測定	坪井忠二 淵田隆門

（昭和 12 年 9 月 22 日）

1.	餘震に就て	井上宇胤
2.	初動の振幅の方位的分布に就て（訂正）	井上宇胤
3.	建築物の強制剪斷振動による應力計算	飯田汲事
4.	弓長嶺鐵山に於ける磁力測定	高橋龍太郎
5.	三原火山及び其の活動の地球物理學的性質	高橋龍太郎 永田武 平能金太郎
6.	火口周邊に於ける地磁氣偏角の異常	永田武
7.	淺間火山の磁氣（伏角）測定	水上武
8.	草津白根火山の磁氣（伏角）測定	水上武

第15號索引

頁

淵田隆門；坪井忠二・淵田隆門　参照

藤原咲平（47）所謂椋平虹に就て（英文）……706

福富孝治（12）伊豆，熱海溫泉に就て（英文）……113

福富孝治・藤井次郎（30）伊豆伊東溫泉に就て（邦文）……506

萩原尊禮；那須信治・萩原尊禮・表俊一郎　参照

萩原尊禮・表俊一郎（33）昭和11年12月27日伊豆新嶋地震餘震觀測並に踏査報告（邦文）……559

萩原尊禮（58）車輛，航空機用加速度計の製作（邦文）……945

藤井次郎；福富孝治・藤井次郎　参照

飯田汲事；石本巳四雄・飯田汲事　参照

飯田汲事（32）土の收縮に關する二三の實驗（邦文）……544

飯田汲事（50）丸の內に於ける表面土と基盤岩との彈性係數測定（邦文）……828

井上宇胤（9）發震機構に就いて（第2報）（英文）……90

井上宇胤（14）地震回數の統計的研究（英文）……142

井上宇胤（44）發震機構に就いて（第3報）（英文）……674

井上宇胤（45）發震機構に就いて（第4報）（英文）……686

井上宇胤（59）發震機構に就いて（訂正）（英文）……956

石本巳四雄・飯田汲事（7）振動方法による土の彈性測定第2報剛性率及びポアソン比の測定（英文）……67

石本巳四雄（31）震央距離の比較的大なる地震による東京近傍卓越振動周期（邦文）……536

石本巳四雄（46）東京地方微動の觀測（佛文）……697

金井清；妹澤克惟・金井清　参照

木下潤一（5）彈性波の生成及び傳播に關する實驗（英文）……41

木下潤一（60）本鄕に於ける觀測より推定し得たる地殼表層の配列（第1報）（英文）……965

岸上冬彦（49）昭和5年伊東地震群の頻度分布（英文）……785

松澤武雄・仲町容・西川與志男・吉村慶丸（48）日本に於ける地震發生の

一年變化（獨文）………………………… 711
水上武　（6）淺間火山近傍に於ける重力偏差の觀測（共1）（英文）………………… 50
水上武　（13）淺間山麓千ヶ瀧溫泉と地下水（英文）………………… 134
水上武　（28）最近の活動に伴へる淺間火山の火口底深さの變化（英文）………… 492
水上武；高橋龍太郎・水上武　參照
宮部直巳　（10）江東地域に於ける地盤沈下の原因に就て（I）（英文）………… 102
宮部直巳　（42）丹後地方の地殼變形研究補遺（英文）………………… 654
宮部直巳　（51）昭和11年11月3日の三陸地方の地震に伴つた津浪（英文）…… 837
永田武；高橋龍太郎・永田武　參照
永田武　（17）磁氣伏角變化計（英文）………………… 185
永田武　（29）新島地震前後に於る同地方磁氣伏角測定値の比較（邦文）………… 497
永田武　（43）淺間及三原火山熔岩の物理的性質　I. 電氣傳導度及び其の溫度變化（英文）………………… 663
仲町容；松澤武雄・仲町容・西川與志男・吉村慶丸　參照
西川與志男；松澤武雄・仲町容・西川與志男・吉村慶丸　參照
那須信治・萩原尊禮・表俊一郎　（8）土壤層中に於ける人工地震波の傳播並に土壤の彈性に關する研究（共2）（邦文）………………… 87
西村源六郎・高山威雄　（25）斜めの入射波による表面層の振動とその共振れ性質（英文）………………… 394
西村源六郎　（39）彈性體內に在る球狀空窩の內面に作用する壓力變化によつて生ずる彈性波（英文）………………… 614
表俊一郎；那須信治・萩原尊禮・表俊一郎　參照
表俊一郎；萩原尊禮・表俊一郎　參照
大塚彌之助　（18）房總半島に於ける一デツケン構造（英文）………………… 193
大塚彌之助　（19）日本群島附近の古第三紀の海岸線の變化（邦文）………………… 198
大塚彌之助　（61）關東地方南部の地質構造（I）〔橫濱ー藤澤間〕（邦文）……… 974
大塚彌之助　（62）日本の第三紀褶曲帶の或る地質學的考察（豫報）（英文）……1041
妹澤克惟・金井清　（1）半無限體の振動に於ける共振現象及び逸散波（英文）…… 1
妹澤克惟・金井清　（2）球窩面の振動に於ける共振現象及び逸散波（英文）……… 13
妹澤克惟・金井清　（3）構造物の震動を防止する一つの方法（英文）………………… 21
妹澤克惟・金井清　（4）五重塔の耐震性に關する研究（英文）………………… 33
妹澤克惟・金井清　（21）地表層が鉛直荷重を受ける場合の彈性的變形分布

に就て（英文）…………………………………………………… 359
妹澤克惟・金井清 （22）震源に於ける異型の發振に伴ふその同型の定常振動（英文）…………………………………………………… 370
妹澤克惟・金井清 （23）斜のデイスターバンスによつて誘起する表面層の自由振動に就いて（英文）…………………………………… 377
妹澤克惟・金井清 （24）橋梁の振動に於ける勢力の逸散性（第1報）（英文）…… 385
妹澤克惟・金井清 （35）地表層の厚さとラブ波の振幅との關係（英文）………… 577
妹澤克惟 （36）地球の核のプラスチツク性に就て（英文）……………………… 582
妹澤克雄・金井清 （37）橋梁の振動に於ける勢力の逸散性（第2報）（英文）…… 590
妹澤克惟・金井清 （38）構造物震動の力學的制振法の模型實驗的確め（英文）… 598
妹澤克惟・金井清 （52）地表層の厚さと分散性レーレー波の振幅との關係（英文）…………………………………………………… 845
妹澤克惟・金井清 （53）極座標上から出した地球の彈性的安定の問題（英文）… 860
妹澤克惟 （54）重力を受ける地球のプラスチツク釣合（英文）…………………… 878
妹澤克惟・金井清 （55）振動性津浪の卓越周期（英文）………………………… 888
高橋龍太郎 （11）昭和11年6月19日の日食時に於ける地電流の觀測（英文）…………………………………………………… 109
高橋龍太郎・永田武 （26）伊豆大島三原火山の地球物理學的研究，火口の地形測量及大島磁氣測定（英文）………………………………… 441
高橋龍太郎・水上武 （27）最近の淺間火山の活動と地表傾斜變化（英文）……… 463
高橋龍太郎・永田武 （63）伊豆大島三原火山の地球物理學的研究，火口内の物理的性質の概況（英文）……………………………………1047
高山威雄 （16）昭和11年11月3日金華山沖地震被害調査報告（邦文）………… 179
高山威雄；西村源六郎・高山威雄 參照
坪井忠二・淵田隆門 （40）重力と地下構造との關係（英文）…………………… 636
坪井忠二 （41）鉛直線偏倚，ジオイドの凹凸と重力異常（英文）………………… 650
坪井忠二 （57）琵琶湖の水位に就いて（英文）…………………………………… 935
津屋弘逵 （20）富士火山帶の火山活動，特に伊豆及び南方諸島の地質及び岩石に就いて（英文）……………………………………………… 215
山口生知 （15）世界に於ける深層地震の分布（英文）…………………………… 170
山口生知 （56）昭和5年11月26日の北伊豆烈震に伴へる同地方の地殼變動

（英文）…………………………………………………………………… 899
吉山慶丸；松澤武雄・仲町容・西川與志男・西村慶丸　参照
（34）大分縣坂の市—鹿兒島縣伊集院村間並に宮崎縣細島町—熊本縣熊本市間の
　水準改測結果（邦文）…………………………………………………… 569

Index to Vol. XV.

Page

FUCHIDA, T., *See* TSUBOI, C. and FUCHIDA, T.

FUJIWHARA, S. (47) On the So-called Mukuhira's Arc as the Foreshadow of an Earthquake. (in English) 706

FUKUTOMI, T. (12) On the Hot Springs of Atami, Izu Peninsula. (in English) 113

FUKUTOMI, T. and HUZII, Z. (30) On the Thermal Springs of Itô, Izu Peninsula. (in Japanese) 506

HAGIWARA, T., *See* NASU, N., HAGIWARA, T. and OMOTE, S.

HAGIWARA, T. and OMOTE, S. (33) The Niizima Earthquake of December 27, 1936. (in Japanese) 559

HAGIWARA, T. (58) An Accelerograph for Measuring the Shaking of Railroad Trains, Automobiles and Airoplanes, etc. (in Japanese) 944

HUZII, Z., *See* FUKUTOMI, T. and HUZII, Z.

IIDA, K., *See* ISHIMOTO, M. and IIDA, K.

IIDA, K. (32) Some Experiments on the Shrinkage of Soil. (in Japanese) 544

IIDA, K. (50) Determination of the Elastic Constants of Superficial Soil and Base- rock at Maru-no-uti in Tôkyô. (in Japanese) 828

INOUYE, W. (9) Notes on the Origins of Earthquakes. (Second paper.) (in English) 90

INOUYE, W. (14) Statistic Investigations of Earthquake Frequencies. (in English) 142

INOUYE, W. (44) Notes on the Origin of Earthquakes. (Third paper.) (in English) 674

INOUYE, W. (45) Notes on the Origin of Earthquakes. (Fourth paper.) (in English) 686

INOUYE, W. (59) Revisions of my "Notes on the Origins of Earthquakes." (in English) 956

ISHIMOTO, M. and IIDA, K. (7) Determination of Elastic Constants of Soils by means of Vibration Methods. Part II. Modulas of Rigidity and Poisson's Ratio. (in English) 67

ISHIMOTO, M. (31) Observations des périodes prédominantes dans les secousses séismiques dont la distance épicentrale est assez grande. (en japonais) 536

ISHIMOTO, M. (46) Observations sur des secousses dûne petite amplitude. (en français) 697

KANAI, K., *See* SEZAWA, K. and KANAI, K.

KINOSITA, Z. (5) Some Experiments on the Generation and Propagation of Elastic Waves. (in English) 41

KINOSITA, Z. (60) The Arrangement of Layers in the Earth's Crust as deduced from Seismometrical Observations at Hongô, Tokyo. (first paper). (in English) 965

KISHINOUYE, F. (49) Frequency-distribution of the Itô Earthquake Swarm of 1930. (in English) 785

MATUZAWA, T., NAKAMATI, H., NISIKAWA, Y. und YOSIMURA, Y. (48) Über die Jahresschwankung der Erdbebenhäufigkeit in Japan. (in deutsch) 711

MINAKAMI, T. (6) Torsion Balance Surveys on Volcano Asama. (Part 1.) (in English) 50

MINAKAMI, T. (13) The Sengataki Thermal Spring and Underground Mineral Water at the Foot of Volcano Asama. (in English) 134

MINAKAMI, T. (28) Changes in the Depth of the Crater Floor of Volcano Asama in the Recent Activities. (in English) 492

MINAKAMI, T., *See* TAKAHASI, R. and MINAKAMI, T.

MIYABE, N. (10) The Cause of the Subsidence of the Earth's Surface in the Kôtô Region, Tokyo. I. (in English) 102

MIYABE, N. (42) Supplementary Notes to the Study of Crustal Deformation in the Tango District. (in English) 654

MIYABE, N. (51) Tunami associated with the Sanriku Earthquake that occurred on November 3, 1936. (in English) 837

NAGATA, T., *See* TAKAHASI, R. and NAGATA, T.

NAGATA, T. (17) A Dip Variometer. (in English) 185

NAGATA, T. (29) A Comparison of the Results of Magnetic Surveys before and after the Niizima Earthqurke of December, 27th, 1936. (in Japanese) 497

NAGATA, T. (43) Some Physical Properties of the Lava of Volcanoes Asama and Mihara. I. Electric Conductivity and Its Temperature-Coefficient. (in English) 663

NAKAMATI, H., *See* MATUZAWA, T., NAKAMATI, H., NISIKAWA, Y. und YOSIMURA, Y.

NISIKAWA, Y., *See* MATUZAWA, T., NISIKAWA, Y., etc.

NASU, N., HAGIWARA, T. and OMOTE, S. (8) Studies on the Propagation of the Artificial Earthquake Waves through Superficial Soil or Sand Layers and the Elasticity of Soil and Sand. (Part 2). (in Japanese) 87

NISHIMURA, G. and TAKAYAMA. T. (25) The Vibration due to Obliquely Incident Waves of a Surface Stratum Adhering Closely to the Subjacent Medium, and the Properties of its Resonance Condition. (in English) 394

NISHIMURA, G. (39) On the Elastic Waves due to Pressure Variation on the Inner Surface of a Spherical Cavity in an Elastic Solid. (in English) 614

OMOTE, S., *See* NASU, N., HAGIWARA, T. and OMOTE, S.

OMOTE, S., *See* HAGIWARA, T. and OMOTE, S.

OTUKA, Y. (18) "Decken" Structure in the Bôsô Peninsula, Japan. (in English) 193

OTUKA, Y. (19) Palaeogene Palaeogeography near Japan. (in Japanese) 198

OTUKA, Y. (61) Geologic Structure of the South Kwanto Region, Japan. (I) (Yokohama-Hudisawa districts.) (in Japanese) 974

OTUKA, Y. (62) Some geologic considerations of the folded Tertiary zones in Japan (advanced paper). (in English) 1041

SEZAWA, K. and KANAI, K. (1) Resonance Phenomena and Dissipation Waves in the Stationary Vibrations of a Semi-infinite Body. (in English) 1

SEZAWA, K. and KANAI, K. (2) Resonance Phenomena and Dissipation Waves in the Stationary Vibration of the Surface of a Spherical Cavity. (in English) 13

SEZAWA, K. and KANAI, K. (3) A Method of Minimizing the Seismic Vibrations of a Structure. (in English) 21

SEZAWA, K. and KANAI, K. (4) Further Studies on the Seismic Vibrations of a Gozyûnotô (Pagoda). (in English) 33

SEZAWA, K. and KANAI, K. (21) On the Elastic Deformation of a Stratified Body Subjected to Vertical Surface Loads. (in English) 359

SEZAWA, K. and KANAI, K. (22) The Same Stationary Vibration of an Origin Accompanying Different Types of Disturbances Therefrom. (in English) 370

SEZAWA, K. and KANAI, K. (23) On the Free Vibrations of a Surface Layer due to an Obliquely Incident Disturbance. (in English) 377

SEZAWA, K. and KANAI, K. (24) Energy Dissipation in the Vibrations of a Bridge. I. (in English) 385

SEZAWA, K. and KANAI, K. (35) Relation between the Thickness of a Surface Layer and the Amplitudes of Love-waves. (in English) 577

SEZAWA, K. (36) On the Plastic Properties of the Earth's Core. (in English) 582

SEZAWA, K. and KANAI, K. (37) Energy Dissipation in the Vibrations of a Bridge. II. (in English) 590

SEZAWA, K. and KANAI, K. (38) Model Experiment Confirmations of a Dynamic Method of Minimizing the Seismic Vibrations of a Structure. (in English) 598

SEZAWA, K. and KANAI, K. (52) Relation between the Thickness of a Surface Layer and the Amplitudes of Dispersive Rayleigh-waves. (in English) 845

SEZAWA, K. and KANAI, K. (53) The Problem of Elastic Stability of the Earth treated in Polar Coordinates. (in English)........... 860

SEZAWA, K. (54) The Plastic State of the Earth under Gravitational Forces. (in English) 878

SEZAWA, K. and KANAI, K. (55) Prevalent Periods of Oscillation in Tidal Waves. (in English) 888

TAKAHASI, R. (11) Observations on Earth Current during the Solar Eclipse of June 19, 1936. (in English) 109

TAKAHASI, R. and NAGATA, T. (26) Geophysical Studies of Volcano Mihara, Oosima Island; Topographic Survey of the Crater of Mihara and the Magnetic Survey of Oosima. (in English) 441

TAKAHASI, R. and MINAKAMI, T. (27) Tilt Observations during the Recent Activities of Volcano Asama. (in English) 463

TAKAHASI, R. and NAGATA, T. (63) Geophysical Studies of Volcano Mihara, Oosima Island; the General Aspect of Physical Conditions in the Crater. (in English) 1047

TAKAYAMA, T. (16) Report on the Field Investigation of the Earthquake of November 3, 1936. (in Japanese) 179

TAKAYAMA, T., *See* NISHIMURA, G. and TAKAYAMA, T.

TSUBOI, C. and FUCHIDA, T. (40) Relations between Gravity Values and Corresponding Subterranean Mass Distribution. (in English)... 636

TUBOI, C. (41) The Deflections of the Vertical, the Undulation of the Geoid, and Gravity Anomalies. (in English) 650

TUBOI, C. (57) The Water Surface of a Lake as an Indicator of Crustal Deformation. (in English).. 935

TSUYA, H. (20) On the Volcanism of the Huzi Volcanic Zone, with Special Reference to the Geology and Petrology of Idu and the Southern Islands. (in English) 215

YAMAGUTI, S. (15) World Distribution of "Deep" Earthquakes. (in English)... 170

YAMAGUTI, S. (56) Deformation of the Earth's Crust in Idu Peninsula in Connection with the Destructive Idu Earthquake of Nov. 26, 1930. (in English)............ 899

YOSIYAMA, Y., *See* MATUZAWA, T., NAKAMATI, H., etc.

(34) The Results of Precise Levelling along the Line between Sakanoiti and Izyuin, via Kokura, Hukuoka, and Kumamoto, and the Line between Hosozima and Kumamoto, via Nobeoka. (in Japanese) 569